

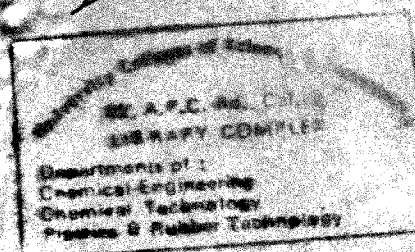
nature

Vol 299 No 5878 2-8 September 1982 £1.60 \$4.00

FLUID SECRETION IN TELEOST KIDNEYS

5883, 5885
less

14-11-83



14 NOV 1983

295

Daily Deliveries [32P]: You pick the day.

We're pleased to announce that a new and better production method enables us to make our dNTP, [α -³²P]- and ATP, [γ -³²P]- available from stock every day at catalog specifications.

Now you can order any day for shipment within 24 hours. Or order Thursday for Monday delivery. You'll get the purest and most stable ³²P nucleotides available.

Ready when you are

ATP, [γ -³²P]-

>7000Ci/mmol	Tricine
1000-3000Ci/mmol	Tricine
1000-3000Ci/mmol	Aqueous
10-50Ci/mmol	Aqueous
2-10Ci/mmol	Aqueous

dNTP, [α -³²P]-

>600Ci/mmol	Ethanol:Tricine
>600Ci/mmol	Tricine
~3000Ci/mmol	Tricine

4015

M	T	W	T	F
2	3	4	5	6
9	10	11	12	13
16	17	18	19	20
23	24	25	26	27
30	31			

HPLC makes the difference

By introducing preparative HPLC technology into our manufacturing process, we not only improved production efficiency, but purity and stability as well. In fact, extensive testing convinces us that no other manufacturer can match the reproducibility and

reliability of these nucleotides.

Send for our complete ³²P nucleotides listing.

Not for use in humans or clinical diagnosis

New England Nuclear
549 Albany Street, Boston, MA 02118
Call toll free: 800-225-1572, Telex: 94-0996
Mass. and Internat'l: 617-482-9595
Europe: NEN Chemicals GmbH, D-6072, W. Germany
Postfach 401240, Tel. (06103) 803-0, Telex 4-17993 NEN D
NEN Canada: 2453 46th Avenue, Lachine, Que H8T 3C9
Tel. 514-636-4971, Telex 05-821808 © 1982 NEN

RP425

NEN New England Nuclear®
a Du Pont company

Circle No.09 on Reader Service Card.

LEADER IN ISOTOPE
BIOTECHNOLOGY

nature

Vol. 299 No. 5877 2 September 1982

Too-easy-to-lose Wall Street blues	1
A very different game	1
Father William's jaw	2

NEWS

Pipeline embargo in new jeopardy	
EPA holds out against lead	
Affirmative action employer	
Israeli science politics	
US degrees	
Artificial intelligence	
University woos Oak Ridge laboratory	
US medical care	
Bankruptcy for interferon firm	
Spruce bark beetle	
UK medical research charities	
East German scientists	
Embarrassing admissions cause trouble	
UK academic posts	3

CORRESPONDENCE

IQ in Japan/W S Jevons returns/ Weapons treaties	8
---	---

NEWS AND VIEWS

The <i>myc</i> oncogene in man and birds (R Weiss)	
<i>Streptomyces</i> in the ascendant (K Chater)	
Stamp watching and bird collecting (R May & J May)	
Seismic triggering and earthquake prediction (W Thatcher)	
Synthetase U-turns (G Cowling)	
The first meteorite stream (D Hughes)	
Autoimmunity and the aetiology of insulin- dependent diabetes mellitus (R Kahn)	9

BOOK REVIEWS

The World Environment 1972-1982 (M W Holdgate <i>et al.</i> , eds) Timothy O'Riordan; The Molecular Biology of the Yeast <i>Saccharomyces</i> (J N Strathern <i>et al.</i> , eds) J M Mitchison and P A Fantes; The Monocotyledons: A Comparative Study (by R M T Dahlgren and H T Clifford) Peter D Moore; Crustal Evolution of Southern Africa (by A J Tankard <i>et al.</i>) H B S Cooke; Inertial Confinement Fusion (by J J Duderstadt and G A Moses) R G Evans; Clinical Aspects of Immunology, 4th Edn (P J Lachmann and D K Peters, eds) Fred S Rosen	91
---	----

MISCELLANY

Errata/Corrigenda	89
Classified advertising	xi

Cover

An isolated segment of flounder renal proximal tubule shown secreting fluid into an oil-filled lumen (see page 54)

ARTICLES

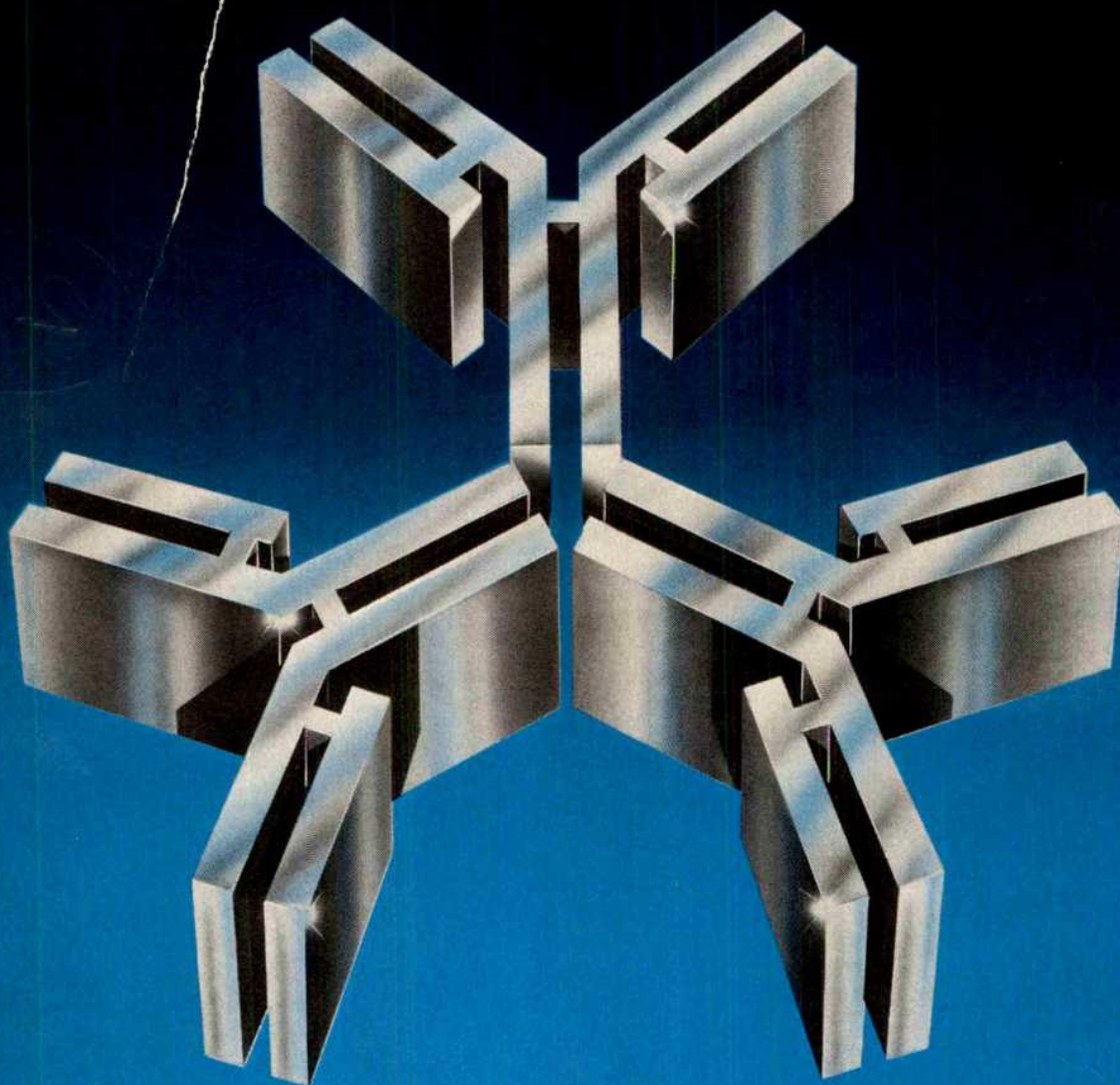
Blue sunlight extinction and scattering by dust in the 60-km altitude atmospheric region	M Ackerman, C Lippens, C Muller & P Vignault	17
Basalt genesis and mantle structure studied through Th-isotopic geochemistry	C J Allègre & M Condomines	21
A study of Si,Al ordering in thallium zeolite-A by powder neutron diffraction	A K Cheetham, M M Eddy, D A Jefferson & J M Thomas	24
Specific protein-nucleic acid recognition in ribonuclease T ₁ -2'-guanylic acid complex: an X-ray study	U Heinemann & W Saenger	27
Sequence specificity of trinucleoside diphosphate binding to polymerized tobacco mosaic virus protein	J J Steckert & T M Schuster	32

LETTERS TO NATURE

Galaxy formation by dissipationless particles heavier than neutrinos	G R Blumenthal, H Pagels & J R Primack	37
Discovery of 0.5-s oscillations in long flat top bursts from the Rapid Burster	Y Tawara, S Hayakawa, H Kunieda, F Makino & F Nagase	38
A possible resurfacing mechanism for icy satellites	J Klinger	41
Flare induced geomagnetic activity and orientation of the photospheric magnetic field	C S Wright & L F McNamara	42
Direct imaging of travelling Rayleigh waves by stroboscopic X-ray topography	R W Whatmore, P A Goddard, B K Tanner & G F Clark	44
Persistence of Subsaharan drought	P J Lamb	46
Late Palaeozoic Gondwana glaciation in Oman	J H Braakman, B K Levell, J H Martin, T L Potter & A van Vliet	48
Volatile C ₁ -C ₈ organic compounds in macroalgae	J K Whelan, M E Tarafa & J M Hunt	50
High abundance of algal 24-ethylcholesterol in Antarctic lake sediment	G Matsumoto, T Torii & T Hanya	52
Direct demonstration of fluid secretion by glomerular renal tubules in a marine teleost	K W Beyenbach	54
Absence of gonadotropin-releasing hormone receptors in human gonadal tissue	R N Clayton & I T Huhtaniemi	56
A fragment of the SV40 large T-antigen gene transforms <i>onc</i> gene amplification in promyelocytic leukaemia cell line HL-60 and primary leukaemic cells of the same patient	C E Clayton, D Murphy, M Lovett & P W J Rigby	59
	R D Favera, F Wong-Staal & R C Gallo	61

Be specific!

Choose **species-specific** labelled second antibodies from Amersham



- Reduce incidence of false positive results
- Combine high sensitivity with low backgrounds
- Choice of antibodies to: mouse, rat, rabbit, human Ig

- Choice of whole antibodies or $F(ab')_2$ fragments
- Choice of label: ^{125}I , β -galactosidase, peroxidase

Also available: Protein A labelled with ^{125}I , ^3H , β -galactosidase, peroxidase

Please call Amersham or your local representative for our booklet describing this new range of products and their applications (reference S40/82).

Amersham International plc
Amersham England HP7 9LL
telephone Little Chalfont (024 04) 4444

Amersham

Amersham Australia PTY Limited Sydney **Amersham Belgium SA/NV** Brussels **Amersham Buchler GmbH & Co. KG** Braunschweig W Germany
Amersham Corporation Arlington Heights Illinois USA **Amersham France SA** Paris **Amersham Japan** Tokyo **Amersham Nederland BV** Utrecht

Circle No.06 on Reader Service Card.



Science in France Science in West Germany

Copies of these special supplement issues are still available.

Prices (including postage): UK, £2.50 each; USA & Canada, US \$6.00 (surface), US \$9.00 (air); Rest of World, £3.00 (surface), £4.00 (air).

Orders (with payment) to:
Nature, Macmillan Journals Ltd,
Brunel Road, Basingstoke, Hants
RG21 2XS, England.

Annual Subscription including Index (51 issues)

UK & Eire		£85
USA & Canada		US\$198.50
Belgium	Airspeed only	BF7450
West Germany	Airspeed only	DM450
Netherlands	Airspeed only	G505
Switzerland	Airspeed only	SF395
Rest of Europe	Airspeed only	£100
Rest of World	Surface	£100
Rest of World*	Airmail	£150

*(not USA, Canada & Europe)

Personal subscription rates are available in some countries to subscribers paying by personal cheque or credit card.

Details can be obtained from:

UK: Nature Promotion Department,
Canada Road, Byfleet, Surrey KT14 7JL.
Telephone: Jonathan Earl: Byfleet (09323) 41459

USA: Nature, 15 East 26 Street, New York, NY 10010
Credit card orders only (in USA & Canada):
Call toll-free: (800) 824-7888 (Operator 246)

In California: (800) 852-7777 (Operator 246)

All other circulation enquiries concerning existing subscriptions please contact:

Nature Circulation Department, Macmillan
Journals Ltd., Brunel Road, Basingstoke, Hants
RG21 2XS, UK

Telephone: (0256) 29242 Telex: 858493

Back issues: (Post-paid) UK, £2.50; USA &
Canada, US\$6.00 (surface), US\$9.00 (air); Rest
of World, £3.00 (surface), £4.00 (air).

Nature Binders:

Single Binders: UK, £4.00; Rest of World, \$10.00
Set(s) of 3 Binders: UK, £10.00; Rest of World,
25.00

Nature First Issue Facsimile:

UK, 75p; Rest of World (surface), \$1.50, (air),
£2.00

Nature Annual Indexes (1971-1981):

Price (post-paid):

UK, £5.00 each; Rest of World, \$10.00

Nature Directory of Biologicals:

(Hardcover edition)
UK, £22.50; Rest of World, \$45.00

Nature Wallcharts:

How Britain Runs its Science; How the US Runs
its Science; UK, £3.50; USA, \$7.95 each

Nature in Microform:

For Information:

UK: UMI, 18 Bedford Row, London WC2R 4EJ
USA: 300 North Zeeb Road, Ann Arbor, MI
48106

Orders (with remittance) to:

Nature, Macmillan Journals Ltd.,
Brunel Road, Basingstoke, Hants RG21 2XS, UK
Tel: (0256) 29242 Telex: 858493



**Participation of myeloid leukaemic
cells injected into
embryos in haematopoietic
differentiation in adult mice**

E Gootwine, C G Webb &
L Sachs

63

**Production of a monoclonal antibody
specific for Hodgkin and Sternberg-
Reed cells of Hodgkin's disease and a
subset of normal lymphoid cells**

U Schwab, H Stein, J Gerdes,
H Lemke, H Kirchner,
M Schaadt & V Diehl

65

**HLA-restricted lymphoproliferative
responses to
MN blood group determinants**

M A Blajchman, N Heddle,
N Naipul & D P Singal

67

**Monoclonal antibody defines a
macrophage intracellular
Ca²⁺-binding protein which
is phosphorylated by phagocytosis**

D J T Vaux & S Gordon

70

**Dopaminergic supersensitivity induced
by denervation and chronic
receptor blockade is additive**

D A Staunton, P J Magistretti,
G F Koob, W J Shoemaker
& F E Bloom

72

**Enkephalin opens potassium channels
on mammalian central neurones**

J T Williams, T M Egan &
R A North

74

**Predominance of the amino-terminal
octapeptide fragment of
dynorphin in rat brain regions**

E Weber, C J Evans &
J D Barchas

77

**Dynorphin₁₋₈ and dynorphin₁₋₉
are ligands for the
 κ -subtype of opiate receptor**

A D Corbett, S J Paterson,
A T McKnight, J Magnan
& H W Kosterlitz

79

**Direct structural localization
of two toxin-recognition
sites on an ACh receptor protein**

H P Zingsheim, F J Barrantes,
J Frank, W Hämcke &
D-Ch Neugebauer

81

**The linear Onsager coefficients for
biochemical kinetic diagrams
as equilibrium one-way cycle fluxes**

T L Hill

84

**ATP-dependent unwinding of double
helix in closed circular
DNA by RecA protein of *E. coli***

T Ohtani, T Shibata,
M Iwabuchi, H Watabe,
T Iino & T Ando

86

GUIDE TO AUTHORS

Authors should be aware of the diversity of *Nature's* readership and should strive to be as widely understood as possible.

Review articles should be accessible to the whole readership. Most are commissioned, but unsolicited reviews are welcome (in which case prior consultation with the office is desirable).

Scientific articles are research reports whose conclusions are of general interest or which represent substantial advances of understanding. The text should not exceed 3,000 words and six displayed items (figures plus tables). The article should include an abstract of about 50 words.

Letters to *Nature* are ordinarily 1,000 words long with no more than four displayed items. The first paragraph (not exceeding 150 words) should say what the letter is about, why the study it reports was undertaken and what the conclusions are.

Matters arising are brief comments (up to 500 words) on articles and letters recently published in *Nature*. The originator of a Matters Arising contribution should initially send his manuscript to the author of the original paper and both parties should, wherever possible, agree on what is to be submitted.

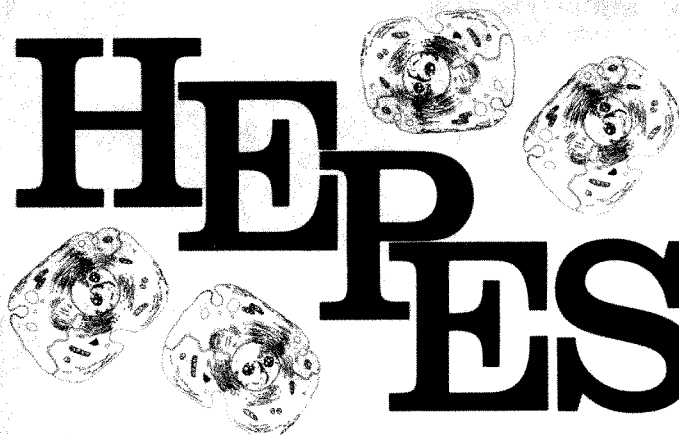
Manuscripts may be submitted either to London or Washington (decisions being made only in London). Manuscripts should be typed (double spacing) on one side of the paper only. Three copies are required, each accompanied by copies of lettered artwork. No title should exceed 80 characters in length. Reference lists, figure legends, etc. should be on separate sheets, all of which should be numbered. Abbreviations, symbols, units, etc. should be identified on one copy of the manuscript at their first appearance.

References should appear sequentially indicated by superscripts in the text and should be abbreviated according to the *World List of Scientific Periodicals*, fourth edition (Butterworth 1963-65). The first and last page numbers of each reference should be cited. References to books should clearly indicate the publisher and the date and place of publication. Unpublished articles should not be formally referred to unless accepted or submitted for publication, but may be mentioned in the text.

Each piece of artwork should be clearly marked with the author's name and the figure number. Original artwork should be unlettered. Suggestions for cover illustrations are welcome. Original artwork (and one copy of the manuscript) will be returned when manuscripts cannot be published.

Requests for permission to reproduce material from Nature should be accompanied by a self-addressed (and, in the case of the UK and USA, stamped) envelope.

HERPES



specially
tested
for
tissue culture

... and
competitively
priced!

For further details of the complete range
of very competitively priced
'Good' zwitterionic buffers
manufactured by BDH, contact Dr A T Charteris

BDH Chemicals Ltd Broom Rd Poole BH12 4NN England
Tel: 0202 745520 Ext 379 Telex: 41186 or 418123 TETRA G

Applications review now available on request



Manufacturers
of
biochemical
reagents

Circle No.03 on Reader Service Card.

Would you use the telephone without a phone directory? Neither should you do GENETICS without.

Genetic Maps

A Compilation of Linkage
and Restriction Maps of
Genetically Studied Organisms

To order:

Send prepared order (\$10.00 for individuals;
institutional and overseas rate \$15.00) or purchase
order requesting invoice to:

Stephen J. O'Brien, Editor
GENETIC MAPS
Building 560, Room 11-85
National Cancer Institute
Frederick, Maryland 21701

Edited by Stephen J. O'Brien

The second and totally revised edition of **GENETIC MAPS** is now available. **GENETIC MAPS** contains updated linkage, restriction, and mtDNA maps of over 50 organisms including λ , SV40, Φ X174, HSV1,2, E. coli, S. typhimurium, B. subtilis, N. crassa, Chlamydomonas, S. cerevisiae, C. elegans, Drosophila, mouse, cat, rabbit, 7 primates, man, corn, wheat and many more (70 maps total). Each map consists of a table of mapped loci, references for each, and an illustrated map of the 1982 status. At last, all the major gene maps are compiled in a single convenient handbook for easy reference. And, even better, **GENETIC MAPS** will be updated every two years.

The Editor:

Stephen J. O'Brien, Chief, Section of Genetics
Laboratory of Viral Carcinogenesis
National Cancer Institute, U.S.A.

The Contributors:

A distinguished list of some of the world's most eminent authorities including E.H. Coe, C.M. Rick, V.A. McKusick, P. Pearson, T. Roderick, W.W. Doane, D.L. Riddle, R.K. Mortimer, D.D. Perkins, P.C. Newell, T.M. Sonneborn, K.E. Sanderson, B.J. Bachmann, P.A. Schaffer, T.R. Broker, M. Yarmolinsky, P. Weisbeek, F.R. Blattner and many more.

nature

Vol. 299 No. 5878 9 September 1982

What kind of crisis for capitalism?	95
Paying for nuclear plants	95
Press's forgotten recipe	96

NEWS

Norway's Arctic diplomatic fix	
Two Soviets banned from Perth	
Now even MIT has troubles	
European Space technology	
Australian science politics	
More animal care	
Mexican science in money trouble	
Language a barrier	
Woods Hole laboratory	
Biotechnology index	97

CORRESPONDENCE

Japan's IQ/Disarmament/Units	102
------------------------------	-----

NEWS AND VIEWS

Kaposi's sarcoma: an oncologic looking glass (J Groopman & M Gottlieb)	
The geoid and geodynamics (B Hager)	
DNA unwinding in transcription and recombination (M Fisher)	
Murine models of multiple sclerosis (P Doherty & E Simpson)	
Haemocyanins to haemerythrins (E van Bruggen)	
Oxygen in the Earth's metallic core? (R Jeanloz)	
Poliomyelitis — epidemiology, molecular biology and immunology (P Minor, O Kew G Schild)	103

BOOK REVIEWS

East African Mammals, Vols IHC and IID (by J Kingdon) Brian Bertram; ISI Atlas of Science: Biochemistry and Molecular Biology 1978/80 A C Allison; Mitochondria (by A Tzagoloff) M J Selwyn; Ecology of Coastal Waters (by K H Mann) John H Steele; Retarded Action-at-a-Distance (by G Burniston Brown) C J S Clarke	189
---	-----

MISCELLANY

100 years ago	110
Errata	186
Books received	192
Product review	xxvii
Classified advertising	xxix

Cover

A receiver for ocean acoustic tomography being deployed on a mooring. The smaller case contains batteries and the longer case houses electronics and a magnetic tape recorder. The hydrophone is protected by a cage. (See page 121)

Molecular drive: a cohesive mode of species evolution (a review)

G Dover

111

ARTICLES

A satellite altimetric geoid in the Philippine Sea

K Horai

117

A demonstration of ocean acoustic tomography

The Ocean Tomography Group:
D Behringer, T Birdsall,
M Brown, B Cornuelle,
R Heinmiller, R Knox,
K Metzger, W Munk,
J Spiesberger, R Spindel,
D Webb, P Worcester
& C Wunsch

121

Brain spectrin, a membrane-associated protein related in structure and function to erythrocyte spectrin

V Bennett, J Davis
& W E Fowler

126

LETTERS TO NATURE

MERLIN spectral line observations of circumstellar shells around two OH/IR stars

R P Norris, P J Diamond
& R S Booth

131

Ion nucleation — a potential source for stratospheric aerosols

F Arnold

134

Ozone vertical distribution and total content using a ground-based active remote sensing technique

J Pelon & G Megie

137

Copper sulphide Cu_{1.8}S (Digenite I) precipitation in mild steel

J E Harbottle & S B Fisher

139

Pressure dependence of glass dissolution and nuclear waste disposal

R A Lewis & R L Segall

140

Origin of sulphur and geothermometry of hydrothermal sulphides from the Galapagos Rift, 86°W

R Skirrow & M L Coleman

142

Fluxes of biogenic components from sediment trap deployment in circumpolar waters of the Drake Passage

G Wefer, E Suess, W Balzer,
G Liebezeit, P J Müller,
C A Ungerer & W Zenk

145

Extreme longevity of lotus seeds from Pulantien

D A Priestley
& M A Posthumus

148

Leaf injury on wheat plants exposed in the field in winter to SO₂

C K Baker, M H Unsworth
& P Greenwood

149

Variation in genome size — an ecological interpretation

J P Grime & M A Mowforth

151

Competition of similar and non-similar genotypes

J M Pérez-Tomé & M A Toro

153

Single cortical neurones have axon collaterals to ipsilateral and contralateral cortex in fetal and adult primates

M L Schwartz
& P S Goldman-Rakic

154

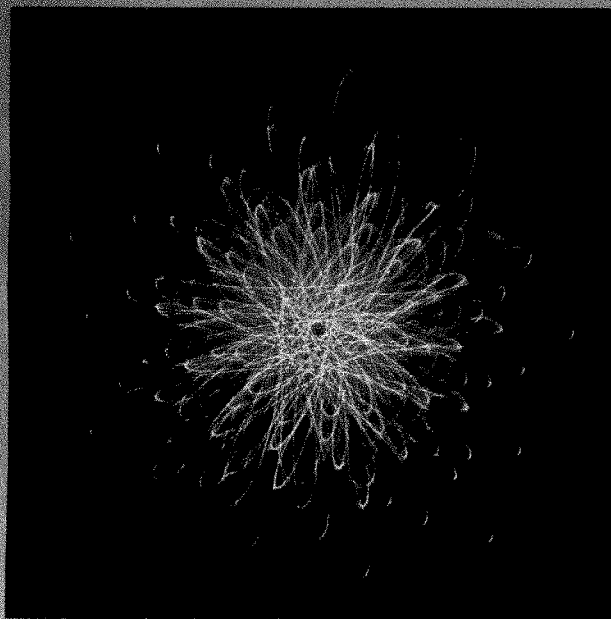
Nature® (ISSN 0028-0836) is published weekly on Thursday, except the last week in December, by Macmillan Journals Ltd and includes the Directory of Biologicals (mailed in December) and Annual Index (mailed in February). Annual subscription for USA and Canada US \$198.50 (for subscription prices elsewhere, see next page). Orders (with remittance) and change of address labels to: Macmillan Journals Ltd, Brunel Rd, Basingstoke RG21 2XS, UK. Second class postage paid at New York, NY 10010 and additional mailing offices. US Postmaster send form 3579 to: *Nature*, 15 East 26 Street, New York, NY 10010. ©1982 Macmillan Journals Ltd.



HIGH QUALITY RADIOCHEMICALS

Our **1982 catalog** lists
a wide range
of
NEW ^{14}C AND ^3H
LABELLED COMPOUNDS

For
Catalogs, Technical Information
and price quotations please
contact:



Labelled Compounds Division
CEN Saclay
91191 GIF-SUR-YVETTE CEDEX FRANCE
Tel.: (6) 908.25.56 - Telex: 690641 F
Circle No. 26 on Reader Service Card.

THE ULTIMATE IN ION-SELECTIVE MEASUREMENTS

WPI'S FD 223 DUAL/DIFFERENTIAL ELECTROMETER

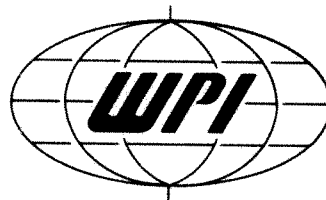


- input resistance $10^{15} \Omega$
- input capacitance 0.1 pF
- differential readings
- leakage current 10^{-14} A
- LCD readout
- independent, simultaneous readings

FD223 puts first-stage amplification close to the source with an active probe headstage minimizing noise pick up and signal loss.

FD223 DUAL/DIFFERENTIAL ELECTROMETER
... the ultimate for precision measurements from ion-selective and pH macro- and microelectrodes.

Only offered by



W-P INSTRUMENTS, INC.

60 Fitch Street • P.O. Box 3110 • New Haven, Conn.
06515 U.S.A. Tel.: (203) 389-2183 • Cables: WPINSTR •
TWX: 710-465-2638

Circle No. 16 on Reader Service Card.



Science in France Science in West Germany

Copies of these special supplement issues are still available.

Prices (including postage): UK, £2.50 each; USA & Canada, US \$6.00 (surface), US \$9.00 (air); Rest of World, £3.00 (surface), £4.00 (air).

Orders (with payment) to:
Nature, Macmillan Journals Ltd,
Brunel Road, Basingstoke, Hants
RG21 2XS, England.

Annual Subscription including Index (51 issues)

UK & Eire	£85
USA & Canada	US\$198.50
Belgium	Airspeed only BF7450
West Germany	Airspeed only DM450
Netherlands	Airspeed only G505
Switzerland	Airspeed only SF395
Rest of Europe	Airspeed only £100
Rest of World	Surface £100
Rest of World*	Airmail £150

*(not USA, Canada & Europe)

Personal subscription rates are available in some countries to subscribers paying by personal cheque or credit card.

Details can be obtained from:

UK: Nature Promotion Department,
Canada Road, Byfleet, Surrey KT14 7JL.
Telephone: Jonathan Earl: Byfleet (09323) 41459
USA: Nature, 15 East 26 Street, New York, NY 10010
Credit card orders only (in USA & Canada):
Call toll-free: (800) 824-7888 (Operator 246)
In California: (800) 852-7777 (Operator 246)

All other circulation enquiries concerning existing subscriptions please contact:

Nature Circulation Department, Macmillan
Journals Ltd., Brunel Road, Basingstoke, Hants
RG21 2XS, UK

Telephone: (0256) 29242 Telex: 858493

Back issues: (Post-paid) UK, £2.50; USA &
Canada, US\$6.00 (surface), US\$9.00 (air); Rest
of World, £3.00 (surface), £4.00 (air).

Nature Binders:

Single Binders: UK, £4.00; Rest of World, \$10.00
Set(s) of 3 Binders: UK, £10.00; Rest of World,
25.00

Nature First Issue Facsimile:

UK, 75p; Rest of World (surface), \$1.50, (air),
£2.00

Nature Annual Indexes (1971-1981):

Price (post-paid):
UK, £5.00 each; Rest of World, \$10.00

Nature Directory of Biologicals:

(Hardcover edition)
UK, £22.50; Rest of World, \$45.00

Nature Wallcharts:

How Britain Runs its Science; How the US Runs
its Science; UK, £3.50; USA, \$7.95 each

Nature in Microform:

For Information:

UK: UMI, 18 Bedford Row, London WC2R 4EJ
USA: 300 North Zeeb Road, Ann Arbor, MI
48106

Orders (with remittance) to:

Nature, Macmillan Journals Ltd.,
Brunel Road, Basingstoke, Hants RG21 2XS, UK
Tel: (0256) 29242 Telex: 858493

M MACMILLAN
JOURNALS

Similarity of unitary Ca^{2+} currents in three different species	A M Brown, H Camerer, K L Kunze & H D Lux	156
Single-channel currents in isolated patches of plasma membrane from basal surface of pancreatic acini	Y Maruyama & O H Petersen	159
Modifier role of internal H^+ in activating the $\text{Na}^+ - \text{H}^+$ exchanger in renal microvillus membrane vesicles	P S Aronson, J Nee & M A Suhm	161
Prostaglandins modulate macrophage Ia expression	D S Snyder, D I Beller & E R Unanue	163
Control of muscle and neuronal differentiation in a cultured embryonal carcinoma cell line	M W McBurney, E M V Jones-Villeneuve, M K S Edwards & P J Anderson	165
A new fucosyl antigen expressed on colon adenocarcinoma and embryonal carcinoma cells	T Miyauchi, S Yonezawa, T Takamura, T Chiba, S Tejima, M Ozawa, E Sato & T Muramatsu	168
<i>In vivo</i> surveillance of tumorigenic cells transformed <i>in vitro</i>	J L Collins, P Q Patek & M Cohn	169
A transforming gene present in human sarcoma cell lines	C J Marshall, A Hall & R A Weiss	171
The production of membrane or secretory forms of immunoglobulins is regulated by C-gene-specific signals	L Forni & A Coutinho	173
An adenovirus glycoprotein binds heavy chains of class I transplantation antigens from man and mouse	C Signäs, M G Katze, H Persson & L Philipson	175
Molecular cloning of the gene for human anti-haemophilic factor IX	K H Choo, K G Gould, D J G Rees & G G Brownlee	178
Intron-exon splice junctions map at protein surfaces	C S Craik, S Sprang, R Fletterick & W J Rutter	180
High-frequency genomic rearrangements involving archaeobacterial repeat sequence elements	C Sapienza, M R Rose & W F Doolittle	182
The helicity of DNA in complexes with RecA protein	A Stasiak & E Di Capua	185

MATTERS ARISING

Absence of thermal effects on photon mass measurements	L F Abbott & M B Gavela Reply: M A Sher & J R Primack	187
Crystal instability and melting	J L Tallon Reply: R M J Cotterill & J U Madsen	188

Nature in Poland

Readers wishing to subscribe to a weekly copy of *Nature* on behalf of a colleague in Poland (where hard currency is scarce) should send a cheque for £50 (or the equivalent in any currency), accompanied by their name and address and that of the proposed recipient, to the *Nature* office in London or New York (see addresses opposite page 95). For further details, readers are referred to *Nature* 3 June, p.354.



More Mouse/ml

MOUSE AND RAT IMMUNOCHEMISTRY REAGENTS

Let Miles be your source for mouse and rat related reagents. We offer a broad and ever-growing selection of dependable quality reagents for use in your laboratory studies of these animals, their cell lines and associated products.

Our antisera include all the major immunoglobulins, IgG subclasses and some rare ones, including anti-mouse IgD and IgE. Of course we also offer conjugates to many of these antigens. Choose from alkaline phosphatase, peroxidase, fluorescein, rhodamine and biotin labels.

Two of our newest products are immunoglobulin reference sera, for mouse and rat. These are the products you have needed to QA your quantitative procedures.

Additional mouse and rat reagents include pooled sera, albumin and gamma globulin fractions, purified immunoglobulins and quantitative RID kits.

Explore the complete listing of our vialled mouse and rat products. Call or write for our product brochure.

Research/Response/Responsibility

Research Products
Division

MILES

©1982 MILES LABORATORIES, INC.

Circle No. 13 on Reader Service Card.

HEADQUARTERS ADDRESSES:

Research Products Division
Miles Laboratories, Inc.
P.O. Box 2000
Elkhart, IN 46515
U.S.A.

Tel. Toll-free 1-800-348-7465
(in Indiana call 1-219-264-8804)

Research Products Division
Miles Laboratories, Ltd.
P.O. Box 37
Stoke Poges, Slough SL2 4LY
UNITED KINGDOM
Tel: Farnham Common 5151

RESEARCH PRODUCTS DIVISION:

Sales Offices	Telephone No.
Austria, Wien	3415160
Australia, Springvale	(03)560-5611
Belgium, Brussels	5136714
Canada,	
Rexdale, Ont.	(416)248-0771
Denmark, Birkerød	2814466
France, Paris	5385243
W. Germany,	
Frankfurt	66020
Italy, Milano	95019231
Israel, Rehovot	(054)70425
Japan, Tokyo	(03)403-9951
Netherlands, WEESP	(02940)16773
South Africa,	
Goodwood, C.P.	544531
Spain, Madrid	242-5104
United Kingdom,	Farnham
Stoke Poges	Common 5151
United States,	
Elkhart, IN	(219)264-8804

nature

Vol. 299 No. 5880 16 September 1982

Principles, policies and pipelines 193
Doing one's thing 194

US fights Canada on Videotex
Posts and statutes change at CNRS
Communication without compatibility
Canada and yellow rain
Sakharov note makes waves
European community research
Ariane in space?
UK energy consumption
Spina bifida
Helsinki agreement
Nuclear waste reprocessing
Biotechnology briefs 195

CORRESPONDENCE

Quangos/Cold war/Scrapie/etc. 200

NEWS AND VIEWS

The unacceptable face of Minoan Crete?
(K Branigan)
Of cannibals and kin (J S Jones)
Increasing atmospheric carbon dioxide
and its consequences (J G Lockwood)
A growing role for reverse transcription
(H E Varmus)
Huntington's disease: genetically
programmed cell death in the human
central nervous system (J B Martin)
Rapid environmental and climatic
changes (D Q Bowen)
A Proterozoic Pangaea? (D H Tarling)
The sunflower seed protection business
(P D Moore)
Glomar Challenger at the Cretaceous-
Tertiary boundary (A Wright, R Heath
& L Burckle) 201

BOOK REVIEWS

McGraw-Hill Encyclopedia of Science
and Technology, 5th Edn (S P Parker,
ed.) Alan Isaacs; Theory and Experiment
in Gravitational Physics (by C M Will)
Joseph H Taylor; Comparative Color
Vision (by G H Jacobs) W R A Muntz;
The Natural Coumarins (by
R D H Murray *et al.*) Leslie Crombie;
Calcium and Cellular Secretion (by
R P Rubin) O H Peterson 189

MISCELLANY

100 years ago 208
Author index, Vol. 298 xv
Books received 286
Product review: Optical physics xxviii
Classified advertising xxxi

Cover

An autoradiogram of tritium-labelled bradykinin
receptors (appearing as white dots) in the guinea pig
ileum (see page 256)

ARTICLES

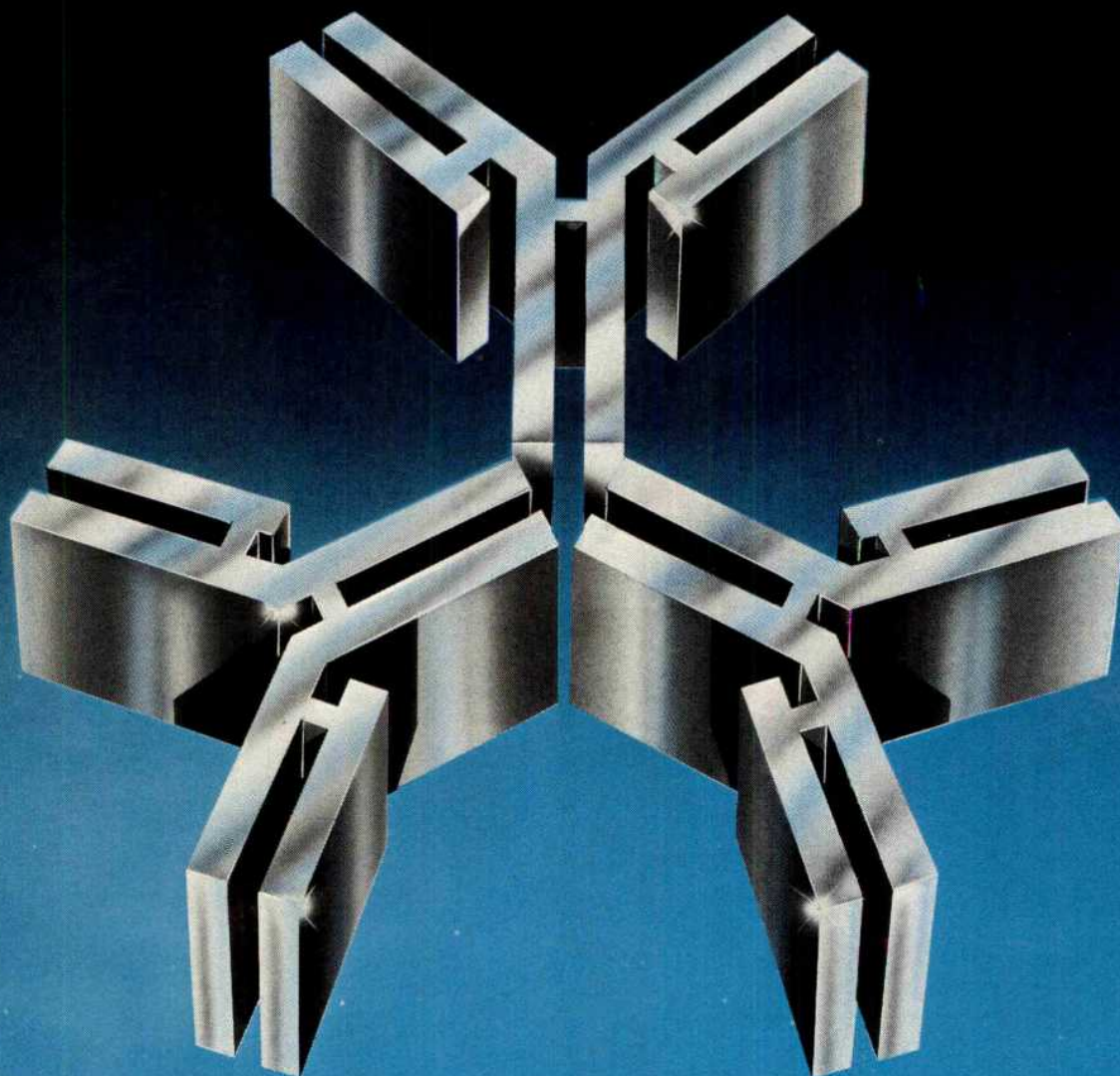
- Sharp edges of planetary rings N Borderies, P Goldreich
& S Tremaine 209
- Stratigraphical significance of the
Tulu Bor Tuff of
the Koobi Fora Formation F H Brown & T E Cerling 212
- Tuffaceous marker horizons in the
Koobi Fora region
and the Lower Omo Valley T E Cerling & F H Brown 216
- Eukaryotic ribosomes can recognize
preproinsulin initiation codons
irrespective of their
position relative to the 5' end of mRNA P T Lomedico & S J McAndrew 221
- Periodic charge distributions in the
myosin rod amino acid sequence
match cross-bridge spacings in muscle A D McLachlan & J Karn 226
- The effects of α chain mutations *cis*
and *trans* to the $\beta 6$ mutation on
the polymerization
of sickle cell haemoglobin R E Benesch, S Kwong
& R Benesch 231

LETTERS TO NATURE

- Discovery of a very red nucleus
in the radio elliptical IC5063
(PKS2048-57) D J Axon, J Bailey
& J H Hough 234
- The source of Saturn
electrostatic discharges D R Evans, J H Romig,
C W Hord, K E Simmons,
J W Warwick & A L Lane 236
- STARE observations of long
discrete echoes E Nielsen, G Sofko
& W I Axford 238
- Constancy of oceanic deposition of
 ^{10}Be as recorded in manganese crusts T L Ku, M Kusakabe,
D E Nelson, J R Southon,
R G Korteling, J Vogel
& I Nowikow 240
- <33,000-yr K-Ar dating of the
volcano-tectonic horst
of the Isle of Ischia, Gulf of Naples P-Y Gillot, S Chiesa,
G Pasquaré & L Vezzoli 242
- Unusual distribution of biological
markers in an Australian crude oil R P Philp & T D Gilbert 245
- The representation of auditory space
in the mammalian superior colliculus A R Palmer & A J King 248
- Metamorphosis of the insect nervous
system: changes in morphology
and synaptic interactions
of identified neurones R B Levine & J W Truman 250
- A transient outward current
in a mammalian central
neurone blocked by 4-aminopyridine B Gustafsson, M Galvan,
P Grafe & H Wigström 252
- Serotonergic denervation
partially protects rat
striatum from kainic acid toxicity M Berger, G Sperk
& O Hornykiewicz 254

Be specific!

Choose **species-specific** labelled second antibodies from Amersham



- Reduce incidence of false positive results
- Combine high sensitivity with low backgrounds
- Choice of antibodies to: mouse, rat, rabbit, human Ig

- Choice of whole antibodies or $F(ab')_2$ fragments
- Choice of label:
 ^{125}I , β -galactosidase, peroxidase

Also available: Protein A
labelled with ^{125}I , ^3H , β -galactosidase,
peroxidase

Please call Amersham or your local representative for our booklet describing this new range of products and their applications (reference S40/82).

Amersham International plc

Amersham England HP7 9LL
telephone Little Chalfont (024 04) 4444

Amersham

Amersham Australia PTY Limited Sydney Amersham Belgium SA/NV Brussels Amersham Buchler GmbH & Co. KG Braunschweig W Germany
Amersham Corporation Arlington Heights Illinois USA Amersham France SA Paris Amersham Japan Tokyo Amersham Nederland BV Utrecht
Circle No.36 on Reader Service Card.



Science in France Science in West Germany

Copies of these special supplement issues are still available.

Prices (including postage): UK, £2.50 each; USA & Canada, US \$6.00 (surface), US \$9.00 (air); Rest of World, £3.00 (surface), £4.00 (air).

Orders (with payment) to:
Nature, Macmillan Journals Ltd,
Brunel Road, Basingstoke, Hants
RG21 2XS, England.

Annual Subscription including Index (51 issues)

UK & Eire		£85
USA & Canada		US\$198.50
Belgium	Airspeed only	BF7450
West Germany	Airspeed only	DM450
Netherlands	Airspeed only	G505
Switzerland	Airspeed only	SF395
Rest of Europe	Airspeed only	£100
Rest of World	Surface	£100
Rest of World*	Airmail	£150

**(not USA, Canada & Europe)*

Personal subscription rates are available in some countries to subscribers paying by personal cheque or credit card.

Details can be obtained from:

UK: Nature Promotion Department,
Canada Road, Byfleet, Surrey KT14 7JL.
Telephone: Jonathan Earl: Byfleet (09323) 41459

USA: Nature, 15 East 26 Street, New York, NY 10010

Credit card orders only (in USA & Canada):

Call toll-free: (800) 824-7888 (Operator 246)

In California: (800) 852-7777 (Operator 246)

All other circulation enquiries concerning existing subscriptions please contact:

Nature Circulation Department, Macmillan
Journals Ltd., Brunel Road, Basingstoke, Hants
RG21 2XS, UK

Telephone: (0256) 29242 Telex: 858493

Back issues: (Post-paid) UK, £2.50; USA &
Canada, US\$6.00 (surface), US\$9.00 (air); Rest
of World, £3.00 (surface), £4.00 (air).

Nature Binders:

Single Binders: UK, £4.00; Rest of World, \$10.00
Set(s) of 3 Binders: UK, £10.00; Rest of World,
\$25.00

Nature First Issue Facsimile:

UK, 75p; Rest of World (surface), \$1.50, (air),
£2.00

Nature Annual Indexes (1971-1981):

Price (post-paid):

UK, £5.00 each; Rest of World, \$10.00

Nature Directory of Biologicals:

(Hardcover edition)

UK, £22.50; Rest of World, \$45.00

Nature Wallcharts:

How Britain Runs its Science; How the US Runs
its Science; UK, £3.50; USA, \$7.95 each

Nature in Microform:

For Information:

UK: UMI, 18 Bedford Row, London WC2R 4EJ
USA: 300 North Zeeb Road, Ann Arbor, MI
48106

Orders (with remittance) to:

Nature, Macmillan Journals Ltd.,
Brunel Road, Basingstoke, Hants RG21 2XS, UK
Tel: (0256) 29242 Telex: 858493



Bradykinin receptor-mediated chloride secretion in intestinal function	D C Manning, S H Snyder, J F Kachur, R J Miller & M Field	256
A new look at nonparasitized red cells of malaria-infected monkeys	C M Gupta, A Alam, PN Mathur & G P Dutta	259
Restriction of alternative complement pathway activation by sialosylglycolipids	N Okada, T Yasuda & H Okada	261
Is nasal adenocarcinoma in the Buckinghamshire furniture industry declining?	E D Acheson, P D Winter, E Hadfield & R G Macbeth	263
Loss of intervening sequences in genomic mouse α-globin DNA inserted in an infectious retrovirus vector	K Shimotohno & H M Temin	265
Ribosomal RNA genes in the replication origin region of <i>Bacillus subtilis</i> chromosome	G Henckes, F Vannier, M Seiki, N Ogasawara, H Yoshikawa & S J Seror-Laurent	268
Abnormal NAD⁺ levels in cells from patients with Fanconi's anaemia	N A Berger, S J Berger & D M Catino	271
Sulphation of tyrosine residues — a widespread modification of proteins	W B Huttner	273
Diversity of cholesterol exchange explained by dissolution into water	E Bojesen	276
Two genes for threonine accumulation in barley seeds	S W J Bright, J S H Keuh, J Franklin, S E Rognes & B J Mifflin	278

MATTERS ARISING

Zenith atmospheric attenuation measurements	H A Gebbie, D T Llewellyn-Jones & R J Knight	280
Petalona Cave dating controversy	A N Poulianos Y Liritzis M Ikeya Reply: G J Hennig, W Herr, E Weber & N I Xirotiris	280

Nature in Poland

Readers wishing to subscribe to a weekly copy of *Nature* on behalf of a colleague in Poland (where hard currency is scarce) should send a cheque for £50 (or the equivalent in any currency), accompanied by their name and address and that of the proposed recipient, to the *Nature* office in London or New York (see addresses opposite page 193). For further details, readers are referred to *Nature* 3 June, p.354.



PIERCE & WARRINER (UK) LTD
introduce

PLASMA FIBRONECTIN'S

A novel method of purification enables us to supply highly purified fibronectins at low cost.

- HUMAN
- BOVINE
- RABBIT
- RAT
- PORCINE

1 mg. £18

1 mg. £12

1 mg. £12

1 mg. £12

1 mg. £12

5 mg. £75

5 mg. £50

5 mg. £50

5 mg. £50

5 mg. £50

Packed in 10mM
caps buffer PH11

- RABBIT ANTI HUMAN PLASMA
- FIBRONECTIN ANTISERUM

1 ml. contains .01% SODIUM AZIDE £30

For cell attachment and morphology studies, serum free
tissue culture, trauma physiology, etc.

Enquiries for bulk orders welcome

PIERCE & WARRINER (UK) LTD

44 Upper Northgate Street, Chester CH1 4EF.
Telephone: Chester (0244) 382525 Telex: 617057

Circle No.26 on Reader Service Card.

Egypt

Pharmacochemical Works offer

SENDAI VIRUS CANTELL STRAIN

produced in pathogen-free-eggs purified and
concentrated haemagglutinating activity: 1×10^5
HAU/ml 5 ml recommended to use for 3×10^{10}
leucocytes in 3 1 medium

steril

Available: 5 ml vials or according to special requirement
storage: -70°C

Produced by EGYT Pharmacochemical Works
Imported by **medimpex** Hungarian Trading Company
Pharmaceutical Products
1808 Budapest, PO Box 126
Telex: 22-5477 Hungary

nature

Vol. 299 No. 5881 23 September 1982

Nothing is even more expensive	287
Health service sickness	287
Academies not international	288

NEWS

Pentagon blocks open exchange	
West German science after Schmidt	
Keyworth on fusion	
University teachers take to the streets	
Clinch River fast breeder	
SERC in South Africa	
French budget	
Council of scientific unions	
Biotechnology	
Indian space effort	
NMR tomography	289

CORRESPONDENCE

Pittdown "man"/Ball lightning/Loch Ness monster(s)/French Nobels/etc.	294
---	-----

NEWS AND VIEWS

Proton decays and high-energy speculation (L Lyons)	
Analysing the mouse <i>T/t</i> complex (P W Andrews & P N Goodfellow)	
The Hubble parameter (S van den Bergh)	
<i>In vitro</i> mutagenesis (T Harris)	
Crown gall tumours and plant growth (M Bevan)	
The American kestrel as a laboratory research animal (D M Bird)	
Multiple pathways of membrane transport (I Mellman)	295

BOOK REVIEWS

The Biology of Human Conduct: East-West Models of Temperament and Personality (by G L Mangan) C R Brand; Andesites (R S Thorpe, ed.) Richard J Arculus; Prospects for imprisoning solar energy (four recent books on solar cell science and technology) J I B Wilson; Prescott and Dunn's Industrial Microbiology, 4th Edn (G Reed, ed.) S J Pirt	377
---	-----

MISCELLANY

Books received	380
New on the market	xv
Classified advertising	xviii

Cover

Sequences and structures of viroid RNAs of the economically important cadang-cadang disease of coconuts are reported on p.316.

ARTICLES

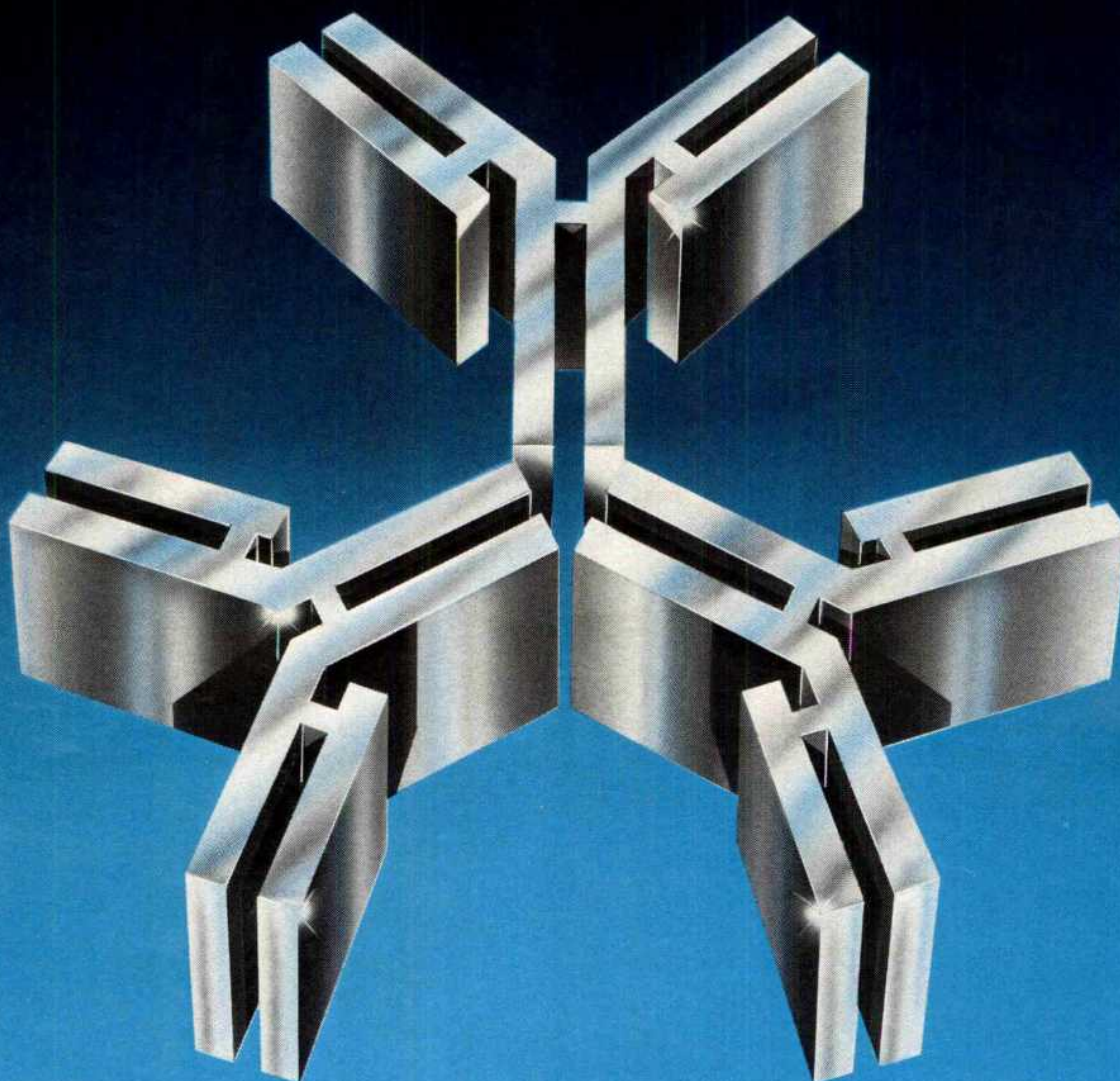
Five crucial tests of the cosmic distance scale using the Galaxy as fundamental standard	G de Vaucouleurs	303
Time-resolved X-ray diffraction studies of the structural behaviour of myosin heads in a living contracting unstriated muscle	J Lowy & F R Poulsen	308
Left-handed Z-DNA is induced by supercoiling in physiological ionic conditions	C K Singleton, J Klysik, S M Stirdivant & R D Wells	312
Viroid RNAs of cadang-cadang disease of coconuts	J Haseloff, N A Mohamed & R H Symons	316

LETTERS TO NATURE

Emission mechanism and source distances of γ -ray bursts	E P Liang	321
Neutral hydrogen associated with the planetary nebula NGC6302	L F Rodriguez & J M Moran	323
Orientation of planetary O^+ fluxes and magnetic field lines in the Venus wake	H Pérez-de-Tejada, D S Intriligator & C T Russel	325
Intergrown mica and montmorillonite in the Allende carbonaceous chondrite	K Tomeoka & P R Buseck	326
An unusual layered mineral in chondrules and aggregates of the Allende carbonaceous chondrite	K Tomeoka & P R Buseck	327
Measurement of Rayleigh-Taylor instability in a laser-accelerated target	A J Cole, J D Kilkenny, P T Rumsby, R G Evans, C J Hooker & M H Key	329
Density-driven interstitial water motion in sediments	D L Musgrave & W S Reeburgh	331
Thermal expansion effects in deep-sea sediments	T J G Francis	334
Composition of basaltic liquids generated from a partially depleted lherzolite at 9 kbar pressure	G Sen	336
Deep structure of the Scottish Caledonides revealed by the MOIST reflection profile	D K Smythe, A Dobinson, R McQuillin, J A Brewer, D H Matthews, D J Blundell & B Kelk	338
Oceanic plateaus as meteorite impact signatures	G C Rogers	341
Volcanic ash deposits of early Eocene age from the Rockall Trough	E J W Jones & A T S Ramsay	342
Evidence for earlier date of 'Ubeidiya, Israel, Hominid site	C A Repenning & O Fejfar	344
A protective function of the coacervates against UV light on the primitive Earth	H Okihana & C Ponnampereuma	347

Be specific!

Choose **species-specific** labelled second antibodies from Amersham



- Reduce incidence of false positive results
 - Combine high sensitivity with low backgrounds
 - Choice of antibodies to: mouse, rat, rabbit, human Ig
 - Choice of whole antibodies or $F(ab')_2$ fragments
 - Choice of label: ^{125}I , β -galactosidase, peroxidase
- Also available: Protein A labelled with ^{125}I , 3H , β -galactosidase, peroxidase

Please call Amersham or your local representative for our booklet describing this new range of products and their applications (reference S40/82).

Amersham International plc
Amersham England HP7 9LL
telephone Little Chalfont (024 04) 4444

Amersham

Amersham Australia PTY Limited Sydney **Amersham Belgium SA/NV** Brussels **Amersham Buchler GmbH & Co. KG** Braunschweig W Germany
Amersham Corporation Arlington Heights Illinois USA **Amersham France SA** Paris **Amersham Japan** Tokyo **Amersham Nederland BV** Utrecht

Circle No.36 on Reader Service Card.



Science in France Science in West Germany

Copies of these special supplement issues are still available.

Prices (including postage): UK, £2.50 each; USA & Canada, US \$6.00 (surface), US \$9.00 (air); Rest of World, £3.00 (surface), £4.00 (air).

Orders (with payment) to:
Nature, Macmillan Journals Ltd,
Brunel Road, Basingstoke, Hants
RG21 2XS, England.

Annual Subscription including Index (51 issues)

UK & Eire	£85
USA & Canada	US\$198.50
Belgium	Airspeed only BF7450
West Germany	Airspeed only DM450
Netherlands	Airspeed only G505
Switzerland	Airspeed only SF395
Rest of Europe	Airspeed only £100
Rest of World	Surface £100
Rest of World*	Airmail £150

*(not USA, Canada & Europe)

Personal subscription rates are available in some countries to subscribers paying by personal cheque or credit card.

Details can be obtained from:

UK: Nature Promotion Department,
Canada Road, Byfleet, Surrey KT14 7JL.
Telephone: Jonathan Earl: Byfleet (09323) 41459
USA: Nature, 15 East 26 Street, New York, NY 10010
Credit card orders only (in USA & Canada):
Call toll-free: (800) 824-7888 (Operator 246)
In California: (800) 852-7777 (Operator 246)

All other circulation enquiries concerning existing subscriptions please contact:

Nature Circulation Department, Macmillan
Journals Ltd., Brunel Road, Basingstoke, Hants
RG21 2XS, UK

Telephone: (0256) 29242 Telex: 858493

Back issues: (Post-paid) UK, £2.50; USA & Canada, US\$6.00 (surface), US\$9.00 (air); Rest of World, £3.00 (surface), £4.00 (air).

Nature Binders:

Single Binders: UK, £4.00; Rest of World, \$10.00
Set(s) of 3 Binders: UK, £10.00; Rest of World, \$25.00

Nature First Issue Facsimile:

UK, 75p; Rest of World (surface), \$1.50, (air), £2.00

Nature Annual Indexes (1971-1981):

Price (post-paid):

UK, £5.00 each; Rest of World, \$10.00

Nature Directory of Biologicals:

(Hardcover edition)

UK, £22.50; Rest of World, \$45.00

Nature Wallcharts:

How Britain Runs its Science; How the US Runs its Science; UK, £3.50; USA, \$7.95 each

Nature in Microform:

For information:

UK: UMI, 18 Bedford Row, London WC2R 4EJ
USA: 300 North Zeeb Road, Ann Arbor, MI 48106

Orders (with remittance) to:

Nature, Macmillan Journals Ltd.,
Brunel Road, Basingstoke, Hants RG21 2XS, UK
Tel: (0256) 29242 Telex: 858493



Phenotypic evolution in a poorly dispersing snail after arrival of predator	G J Vermeij	349
A molecular explanation of frequency-dependent selection in <i>Drosophila</i>	Y Haj-Ahmad & D A Hickey	350
Analysis of discrimination mechanisms in the mammalian olfactory system using a model nose	K Persaud & G Dodd	352
Corticotropin releasing activity of the new CRF is potentiated several times by vasopressin	G E Gillies, E A Linton & P J Lowry	355
Oligodendrocyte abnormalities in shiverer mouse mutant are determined in primary chimaeras	K Mikoshiba, M Yokoyama, Y Inoue, K Takamatsu, Y Tsukada & T Nomura	357
A Cl ⁻ conductance activated by hyperpolarization in <i>Aplysia</i> neurones	D Chenoy-Marchais	359
Transplacental transfer of rodent microfilariae induces antigen-specific tolerances in rats	A Haque & A Capron	361
Lithium chloride induces partial responsiveness to LPS in nonresponder B cells	S Ishizaka & G Möller	363
Random components in mutagenesis	P L Foster, E Eisenstadt & J Cairns	365
Unique cell lines harbouring both Epstein-Barr virus and adult T-cell leukaemia virus, established from leukaemia patients	N Yamamoto, T Matsumoto, Y Koyanagi, Y Tanaka & Y Hinuma	367
T4 late transcripts are initiated near a conserved DNA sequence	A C Christensen & E T Young	369
The helical hydrophobic moment: a measure of the amphiphilicity of a helix	D Eisenberg, R M Weiss & T C Terwilliger	371

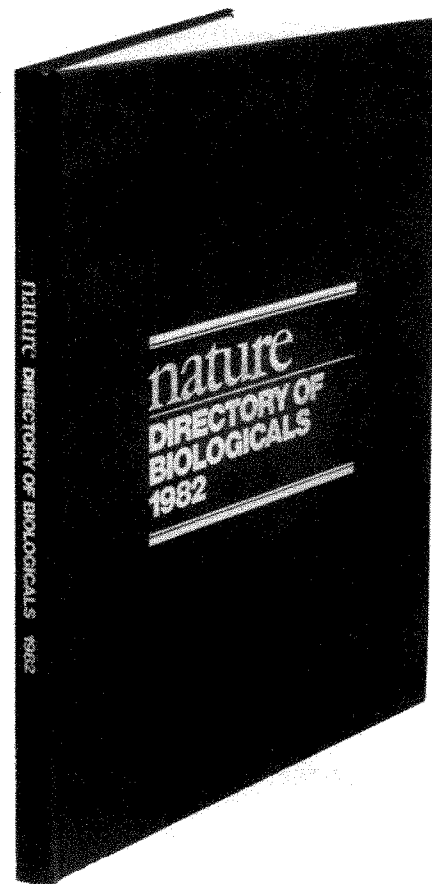
MATTERS ARISING

BVP models of nerve membrane	C J A Game Reply: J L Hindmarsh & R M Rose	375
Trophic structure of a grassland insect community	K H Lakhani	375
Thermoluminescence dating of sand dunes	K Pye Reply: A K Singhvi	376

Nature in Poland

Readers wishing to subscribe to a weekly copy of *Nature* on behalf of a colleague in Poland (where hard currency is scarce) should send a cheque for £50 (or the equivalent in any currency), accompanied by their name and address and that of the proposed recipient, to the *Nature* office in London or New York (see addresses opposite page 287). For further details, readers are referred to *Nature* 3 June, p.354.

"A unique guide to biological laboratory products."



The Directory of Biologicals offers life scientists a comprehensive listing of what is on the market and where researchers can order these materials for their work. Designed to meet the day-to-day needs of active biologists searching for the right product to use in the laboratory, its simple alphabetical listings cover all of modern life science research. Clear and easy to use, it lists more than 2,000 products commercially available, with the names and addresses of companies throughout the world that offer them for sale. Telex and telephone numbers give users direct access to sales offices in your area. Company entries also briefly describe each supplier's specialization. A separate section lists products by trade name or registered trademark, keyed to the companies in the guide.

Helpful essays on how to use the directory, safety procedures, how to purchase biological materials, and the future of modern biology, make this the most useful directory ever published for biological research workers.

All subscribers to *Nature** automatically receive a handsome paperbound version of the directory. **But if you think you need a copy to stand up against constant use in your laboratory or your library, or if you are not a subscriber, you can purchase the deluxe hardcover edition.** (No paperback editions will be available after subscribers receive their free copy.) To order a hardcover edition, all you need do is fill out the form and mail it today.

297x210mm
232 pages
ISBN: 0 333 33233 4

U.S. and Canada: *Nature*, 15 East 26th Street, New York, NY 10010

U.K. and Rest of World: *Nature*, Canada Road, Byfleet, Surrey KT14 7JL, England.

☐ **Send me _____ copies of the deluxe, hardcover edition of the Directory of Biologicals @ \$45/£22.50 each. (P&P free).** (Tax: N.Y. State Residents, please add sales tax.) (I understand that as a subscriber to *Nature* I will receive a free copy of the paperbound edition as part of my subscription.★)

Name _____

Address _____

City _____ State _____ Zip _____

Country _____

☐ I enclose \$_____/£_____
☐ I prefer to use my credit card account

Account No. _____ Expiry Date _____

☐ Visa ☐ Access/Mastercard

☐ American Express Signature _____

In the U.S. you may make your order by telephone, using our toll-free number. Our operators are on duty 7 days a week, 24 hours a day.

Call toll-free now: (800) 824-7888. Ask for operator 130 (Dept. TNA)

In California: (800) 852-7777. Ask for operator 130 (Dept. TNA)

Please allow 6 weeks for delivery.

*If your subscription was in effect on November 30, 1981, you automatically receive a paperbound copy of the 1982 Directory of Biologicals. Those who entered subscriptions after that date will receive the 1983 Directory of Biologicals next spring.

nature

Vol. 299 No. 5882 30 September 1982

The defence of Western Europe 381
La Ronde, 1982 style 382

New UK row on embryo research
Reagan no science censor
Soviet ecology
West German energy
CERN
UK nuclear power
Electronics giant
Internees in Poland
Cryo-transmission microscopy
Genetic manipulation
Greens gain in Hesse
US international cooperation
Planetary science
Video education
China's intellectuals back in fashion 383

CORRESPONDENCE

Tanks/Biotechnology/etc. 390

NEWS AND VIEWS

Twelve wise men at the Vatican
(J M Lowenstein)
Beneficial immunity (C Janeway)
Zero-momentum atoms in superfluid
helium-4 (P V E McClintock)
Changes at the crust-mantle boundary
(J Oliver)
Transgenic organisms and development
(W Petri)
Solar-terrestrial influences on weather
and climate (J Gregory)
A new type of pulsating star
(J P Cox) 395

THE AUTOMATED LABORATORY

403

BOOK REVIEWS

Night Thoughts of a Classical Physicist
(by Russell McCormmach) John
Maddox; A New View of Current Acid-
Base Theories (by H L Finston and
A C Rychtmann) John Gibson; Polymers
and their Properties, Vol. 1 (by
J W S Hearle) Paul Calvert; Idiotypes
and Lymphocytes (by C A Bona)
C A Janeway Jr; Cell Behaviour: A
Tribute to Michael Abercrombie
(R Bellairs *et al.*, eds) David I Gottlieb;
Nuclear Magnetism (by A Abragam and
M Goldman) Nicolaas Bloembergen 471

Cover

Functional subdivisions of the primate visual system
can be detected by pseudocholinesterase
histochemistry. The cover shows the reduced
contralateral-layer staining pattern in a macaque
monkey lateral geniculate body denervated for 15
days (see p. 439). The Automated Laboratory: see
pages 403-408 and Product Review, p. xxvix

COMMENTARY

Computer chess and the
humanization of technology D Michie 391

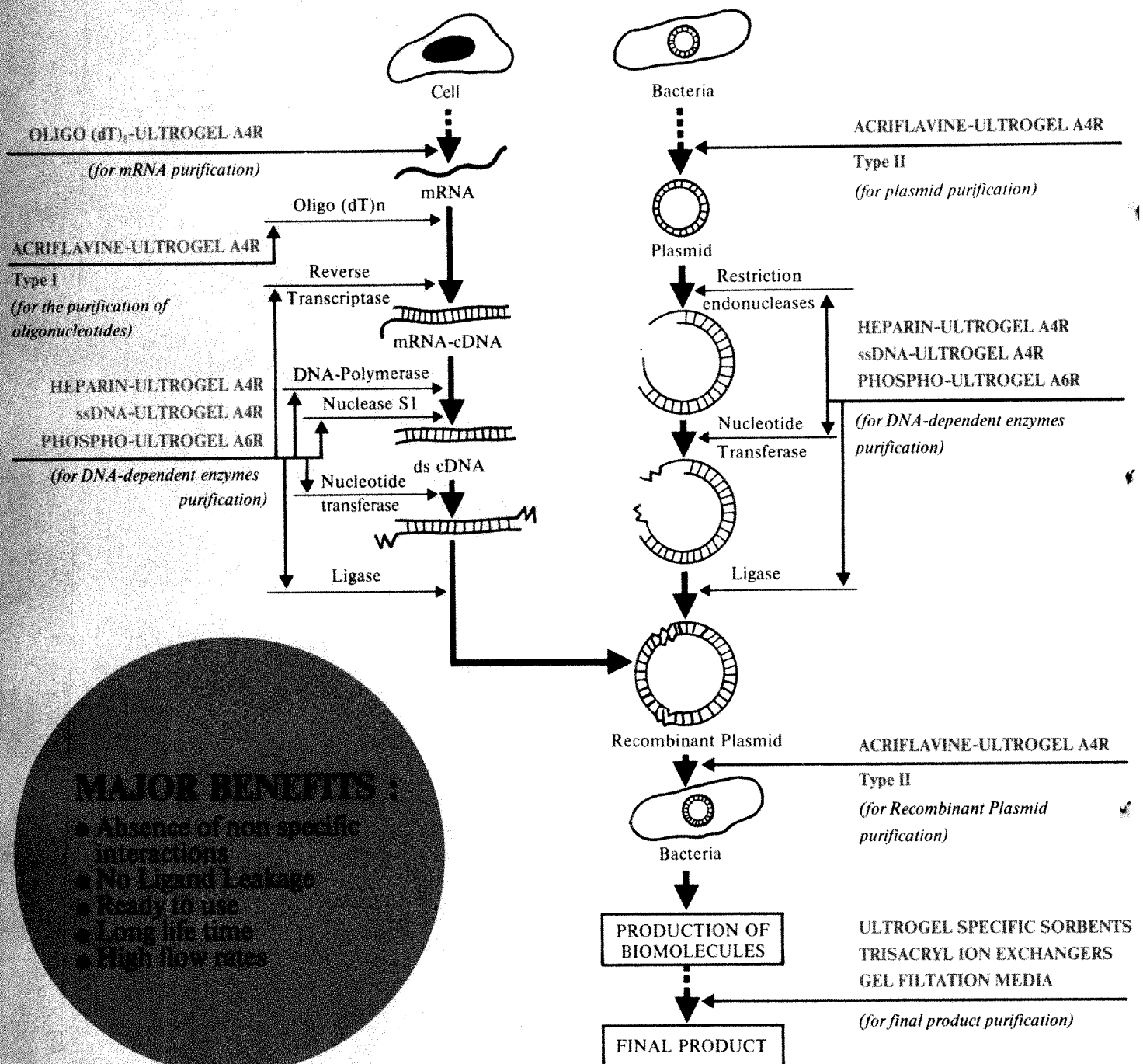
ARTICLES

Proterozoic age and cumulate origin
for granulite xenoliths, Lesotho N W Rogers
& C J Hawkesworth 409
Serotonin and cyclic AMP close single
K⁺ channels in *Aplysia* sensory neurones S A Siegelbaum, J S Camardo
& E R Kandel 413
Genomic environment of *T. brucei* VSG
genes: presence of a minichromosome R O Williams, J R Young
& P A O Majiwa 417
Stereochemistry of cooperative effects
in fish and amphibian haemoglobins M F Perutz & M Brunori 421

LETTERS TO NATURE

Neutron oscillation as a source
of excess sub-GeV
antiprotons in galactic cosmic rays C Sivaram & V Krishan 427
Intense Ly α emission from Uranus S T Durrance & H W Moos 428
Precambrian endoliths discovered S E Campbell 429
Temporal variations in dissolved
selenium in a coastal ecosystem J J Wrench & C I Measures 431
Microbial activity and bioturbation-
induced oscillations in
pore water chemistry
of estuarine sediments in spring M E Hines, W H Orem,
W B Lyons & G E Jones 433
Reappraisal of sea-ice distribution in
Atlantic and Pacific sectors
of the Southern Ocean at 18,000 yr BP L H Burckle, D Robinson
& D Cooke 435
De-A-steroid ketones and de-A-
aromatic steroid hydrocarbons in
shale indicate a novel diagenetic pathway G van Graas, F de Lange,
J W de Leeuw & P A Schenck 437
Pseudocholinesterase staining
in the primary
visual pathway of the macaque monkey A M Graybiel
& C W Ragsdale Jr 439
Functional reconnections without new
axonal growth in a partially
denervated visual relay nucleus U Th Eysel 442
Localization of β -adrenoreceptors
in mammalian lung by
light microscopic autoradiography P J Barnes, C B Basbaum,
J A Nadel & J M Roberts 444
Structural and biological properties
of a monoclonal
auto-anti-(anti-idiotypic) antibody B A Pollok, A S Bhowan
& J F Kearney 447
Chromatin changes accompany
immunoglobulin κ gene
activation: a potential
control region within the gene T G Parslow & D K Granner 449

IBF affinity chromatography for molecular genetics



MAJOR BENEFITS :

- Absence of non specific interactions
- No Ligand Leakage
- Ready to use
- Long life time
- High flow rates

— « An IBF support for every chromatographic step in Molecular Genetic » —

Réactifs
IBF

For France : **Pointet Girard** Département Réactifs IBF, 35, avenue Jean-Jaurès - 92390 Villeneuve-la-Garenne.

For other countries : please contact your local **LKB** representative.

Circle No.06 on Reader Service Card.



Science in France Science in West Germany

Copies of these special supplement issues are still available.

Prices (including postage): UK, £2.50 each; USA & Canada, US \$6.00 (surface), US \$9.00 (air); Rest of World, £3.00 (surface), £4.00 (air).

Orders (with payment) to:
Nature, Macmillan Journals Ltd,
Brunel Road, Basingstoke, Hants
RG21 2XS, England.

Annual Subscription including Index (51 issues)

UK & Eire	£85
USA & Canada	US\$198.50
Belgium	Airspeed only BF7450
West Germany	Airspeed only DM450
Netherlands	Airspeed only G505
Switzerland	Airspeed only SF395
Rest of Europe	Airspeed only £100
Rest of World	Surface £100
Rest of World*	Airmail £150

*(not USA, Canada & Europe)

Personal subscription rates are available in some countries to subscribers paying by personal cheque or credit card.

Details can be obtained from:

UK: Nature Promotion Department,
Canada Road, Byfleet, Surrey KT14 7JL.
Telephone: Jonathan Earl: Byfleet (09323) 41459
USA: Nature, 15 East 26 Street, New York, NY 10010
Credit card orders only (in USA & Canada):
Call toll-free: (800) 824-7888 (Operator 246)
In California: (800) 852-7777 (Operator 246)

All other circulation enquiries concerning existing subscriptions please contact:

Nature Circulation Department, Macmillan
Journals Ltd., Brunel Road, Basingstoke, Hants
RG21 2XS, UK

Telephone: (0256) 29242 Telex: 858493

Back issues: (Post-paid) UK, £2.50; USA &
Canada, US\$6.00 (surface), US\$9.00 (air); Rest
of World, £3.00 (surface), £4.00 (air).

Nature Binders:

Single Binders: UK, £4.00; Rest of World, \$10.00
Set(s) of 3 Binders: UK, £10.00; Rest of World,
25.00

Nature First Issue Facsimile:

UK, 75p; Rest of World (surface), \$1.50, (air),
£2.00

Nature Annual Indexes (1971-1981):

Price (post-paid):
UK, £5.00 each; Rest of World, \$10.00

Nature Directory of Biologicals:

(Hardcover edition)
UK, £22.50; Rest of World, \$45.00

Nature Wallcharts:

How Britain Runs its Science; How the US Runs
its Science; UK, £3.50; USA, \$7.95 each

Nature in Microform:

For Information:

UK: UMI, 18 Bedford Row, London WC2R 4EJ
USA: 300 North Zeeb Road, Ann Arbor, MI
48106

Orders (with remittance) to:

Nature, Macmillan Journals Ltd.,
Brunel Road, Basingstoke, Hants RG21 2XS, UK
Tel: (0256) 29242 Telex: 858493



**Genomic environment of the
expression-linked extra
copies of genes for surface
antigens of *Trypanosoma brucei*
resembles the end of a chromosome**

T De Lange & P Borst

451

**A specific replication origin in
the chromosomal
rDNA of *Lytechinus variegatus***

P M Botchan & A I Dayton

453

**Suppression of an amber mutation
by microinjection
of suppressor tRNA in *C.elegans***

J Kimble, J Hodgkin,
T Smith & J Smith

456

**When do carcinogen-treated 10T1/2
cells acquire the
commitment to form transformed foci?**

J M Backer, M Boerzig
& I B Weinstein

458

**Cytoplasmic control of preimplantation
development *in vitro* in the mouse**

A Muggleton-Harris,
D G Whittingham & L Wilson

460

**Rearrangement of mammalian
chromatin structure
following excision repair**

M E Zolan, C A Smith,
N M Calvin & P C Hanawalt

462

**Selective reinnervation of adult
mammalian muscle by axons
from different segmental levels**

D J Wigston & J R Sanes

464

**Structural evidence that myosin heads
may interact with two sites on F-actin**

L A Amos, H E Huxley,
K C Holmes, R S Goody
& K A Taylor

467

**Structure of a Zn²⁺-containing
D-alanyl-D-alanine-cleaving
carboxypeptidase at 2.5 Å resolution**

O Dideberg, P Charlier, G Dive,
B Joris, J M Frère
& J M Ghuysen

469

GUIDE TO AUTHORS

Authors should be aware of the diversity of *Nature's* readership and should strive to be as widely understood as possible.

Review articles should be accessible to the whole readership. Most are commissioned, but unsolicited reviews are welcome (in which case prior consultation with the office is desirable).

Scientific articles are research reports whose conclusions are of general interest or which represent substantial advances of understanding. The text should not exceed 3,000 words and six displayed items (figures plus tables). The article should include an abstract of about 50 words.

Letters to *Nature* are ordinarily 1,000 words long with no more than four displayed items. The first paragraph (not exceeding 150 words) should say what the letter is about, why the study it reports was undertaken and what the conclusions are.

Matters arising are brief comments (up to 500 words) on articles and letters recently published in *Nature*. The originator of a Matters Arising contribution should initially send his manuscript to the author of the original paper and both parties should, wherever possible, agree on what is to be submitted.

Manuscripts may be submitted either to London or Washington (decisions being made only in London). Manuscripts should be typed (double spacing) on one side of the paper only. Three copies are required, each accompanied by copies of lettered artwork. No title should exceed 80 characters in length. Reference lists, figure legends, etc. should be on separate sheets, all of which should be numbered. Abbreviations, symbols, units, etc. should be identified on one copy of the manuscript at their first appearance.

References should appear sequentially indicated by superscripts in the text and should be abbreviated according to the *World List of Scientific Periodicals*, fourth edition (Butterworth 1963-65). The first and last page numbers of each reference should be cited. References to books should clearly indicate the publisher and the date and place of publication. Unpublished articles should not be formally referred to unless accepted or submitted for publication, but may be mentioned in the text.

Each piece of artwork should be clearly marked with the author's name and the figure number. Original artwork should be unlettered. Suggestions for cover illustrations are welcome. Original artwork (and one copy of the manuscript) will be returned when manuscripts cannot be published.

Requests for permission to reproduce material from Nature should be accompanied by a self-addressed (and, in the case of the UK and USA, stamped) envelope.

"Our Vega synthesizer has become an extra pair of hands.

After set up, the syntheses of our oligonucleotides are done reliably 24 hours a day."

Steve Pulford,
Research
Associate,
Genex
Corporation

Genex is just one of over 60 organizations using Vega automated synthesizer equipment to increase productivity and reduce expenses. If you're doing nucleic acid research, or peptide research, or both, Vega has a synthesizer that will meet your scale and budget requirements.

The Coder™

Vega's polynucleotide synthesizer offers the ultimate in flexibility. You can use our synthetic program supplied on floppy disc, or you can program whatever additional custom methodologies you need. Proven coupling efficiency, low operating costs and variable volume capacity are among the reasons genetic researchers are using The Coder™ Model 280.

The Coupler™

Vega's peptide synthesizers are the most economical, totally automated instruments available in the

field. Sized to meet research or production requirements, The Coupler™ Model 250C or The Coupler™ Model 296 will accommodate one gram to 500 grams of resin. Through microprocessor control, the equipment automatically performs all of the washing, deblocking, neutralization and coupling steps required for addition of each amino acid to the peptide chain.

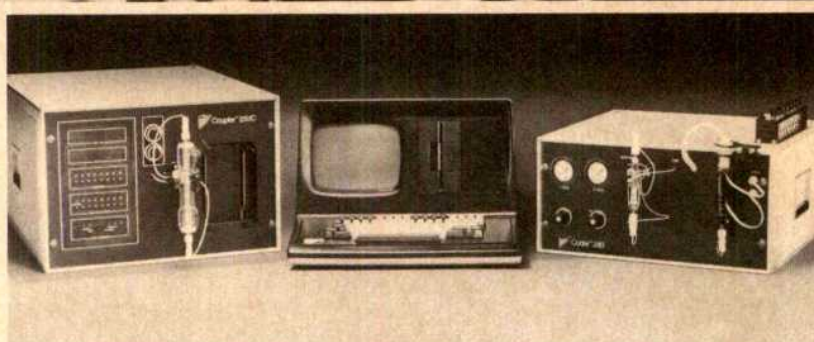
The Coder™ and The Coupler™ Combined

With the new Motorola microprocessor, you can synthesize polynucleotides and peptides simultaneously.

For maximum production capability and cost efficiency, you can operate up to four chemistry modules with one microprocessor. These modules may be all Coders™, all Couplers™, or any combination of models.

Compare The Coder™ and The Coupler™ to other synthesizers available, and you'll see why Genex and more than 60 others have selected Vega equipment. Tomorrow's generation of synthesizers is here today at Vega Biochemicals.

Call 1-800-528-4882 toll free for more information.



Vega Biochemicals

Division of Vega Biotechnologies, Inc.

P.O. Box 11648 / Tucson, Arizona 85734 / Telephone: (602) 746-1401 / Telex: 165572 (VEGA BIO TUC)



nature

Vol. 299 No. 5884 14 October 1982

What policy for West Germany?	567
London's agony (contd.)	568
Soviet science not quoted	568

NEWS

Threat to French research directors	
Few changes for West Germany	
Why the lag?	
Polish universities	
Canada's research plans	
Bilingual planners disagree	
US medical profession	
Commonwealth agriculture	
Nobel prizes 1982	
Biotechnology index	569

CORRESPONDENCE

Poland/South Africa's observatory/Japanese not so intelligent?	574
--	-----

NEWS AND VIEWS

Limitations of Maxwell's distribution	
An immunoregulatory molecular complex with five active sites (N A Mitchison)	
Mapping the Local supercluster (J Silk)	
Yet another opioid peptide? (L L Iversen)	
Plasma astrophysics at Santa Barbara (R Rosner, E Zweibel & V Trimble)	
Key structures in transposition (N Symonds)	
Survival mechanisms in wetland plants (P D Moore)	575

BOOK REVIEWS

Acceptable Risk (by B Fischhoff <i>et al.</i>) and Risk/Benefit Analysis (by R Wilson and E Crouch) Stephen Cotgrove; Tree-Ring Dating and Archaeology (by M G L Baillie) John Fletcher; Tropical Cyclones (by R A Anthes) T N Krishnamurti; Antarctic Geoscience (C Craddock, <i>ed.</i>) J F Lovering; Physics of Semiconductor Devices, 2nd Edn (by S M Sze) Andrew Holmes-Siedle; Insect Clocks, 2nd Edn (by D S Saunders) John Brady	659
---	-----

MISCELLANY

Miscellany	
100 years ago	582
New ways with magnets	663
Product Review	xxv
Classified advertising	xxix

Cover

Isomaltulose crystals under polarized light. Immobilized *Erwinia rhapsodici* cells can be used in a continuous process for converting sucrose solutions into isomaltulose (see page 628)

Postnatal developmental of the visual cortex and the influence of environment (Nobel Lecture)	T N Wiesel	583
---	------------	-----

Tapping the immunological repertoire to produce antibodies of predetermined specificity (a review)	R A Lerner	592
--	------------	-----

ARTICLES

High dynamic range mapping of strong radio sources, with application to 3C84	J E Noordam & A G de Bruyn	597
--	----------------------------	-----

Molecular structure of r(GCG)d(TATACGC): a DNA-RNA hybrid helix joined to double helical DNA	A H-J Wang, S Fujii, J H van Boom, G A van der Marel, S A A van Boeckel & A Rich	601
--	--	-----

LETTERS TO NATURE

Optical polarization position angle versus radio source axis in radio galaxies	R R J Antonucci	605
--	-----------------	-----

Distance to Crab-like supernova remnant 3C58	D A Green & S F Gull	606
--	----------------------	-----

Resolution of controversy concerning the morphology of polyacetylene	J C W Chien, Y Yamashita, J A Hirsch, J L Fan, M A Shen & F E Karasz	608
--	--	-----

Iron in north-east Pacific waters	R M Gordon, J H Martin & G A Knauer	611
-----------------------------------	-------------------------------------	-----

Radiocaesium and plutonium in intertidal sediments from southern Scotland	A B MacKenzie & R D Scott	613
---	---------------------------	-----

Detection of imogolite in soils using solid state ²⁹ Si NMR	P F Barron, M A Wilson, A S Campbell & R L Frost	616
--	--	-----

Reduction of molybdate by soil organic matter: EPR evidence for formation of both Mo(V) and Mo(III)	B A Goodman & M V Cheshire	618
---	----------------------------	-----

Isotopic variations within a single oceanic island: the Terceira case	B Dupré, B Lambret & C J Allègre	620
---	----------------------------------	-----

Source of the detrital components of uraniferous conglomerates, Quirke ore zone, Elliot Lake, Ontario, Canada	A Robinson & E T C Spooner	622
---	----------------------------	-----

Discordant layering relations in the Fongen-Hyllingen basic intrusion	J R Wilson & S B Larsen	625
---	-------------------------	-----

Arsenic in Napoleon's wallpaper	D E H Jones & K W D Ledingham	626
---------------------------------	-------------------------------	-----

Napoleon Bonaparte — no evidence of chronic arsenic poisoning	P K Lewin, R G V Hancock & P Voynovich	627
---	--	-----

The formation of isomaltulose by immobilized <i>Erwinia rhapsodici</i>	P S J Cheetham, C E Imber & J Isherwood	628
--	---	-----

Changes in muscle stiffness during contraction recorded using ultrasonic waves	Y Tamura, I Hatta, T Matsuda, H Sugi & T Tsuchiya	631
--	---	-----

[illegible]

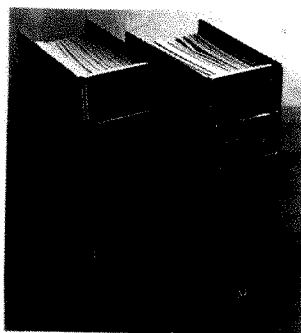
- now available to complement our wide range of radiolabelled products

Please call Amersham or your local representative for a booklet describing these products and their applications

Amersham

Circle No.29 on Reader Service Card.

Keep your copies of *Nature* protected in these tough black PVC binders



- Each binder is supplied with a set of wires for the easiest possible loading
- *Nature* logo blocked in gold on spine
- Transparent plastic pocket provided for your own reference
- Each binder takes two volumes of *Nature*; three binders will serve for a year
- Prices and address for orders are set out below

Annual Subscription including Index (51 issues)

UK & Eire		£98
USA & Canada		US\$220
Australia & NZ	Airspeed only	£137.50
Belgium	Airspeed only	BF9350
West Germany	Airspeed only	DM490
Netherlands	Airspeed only	G540
Switzerland	Airspeed only	SF420
Rest of Europe	Airspeed only	£114
Rest of World*	Surface	£115
Rest of World*	Airmail	£173

*(not USA, Canada, Europe & Japan)

Japan: For subscription details contact Nichibo, PO Box 5030 Tokyo International, 2-1 Sarugakuchō 1-chome, Chiyoda-ku, Tokyo

Personal subscription rates are available in some countries to subscribers paying by personal cheque or credit card.

Details can be obtained from:

UK: *Nature* Promotion Department, Canada Road, Byfleet, Surrey KT14 7JL. Telephone: Jonathan Earl: Byfleet (09323) 41459
 USA: *Nature*, 15 East 26 Street, New York, NY 10010
 Credit card orders only (in USA & Canada):
 Call toll-free: (800) 824-7888 (Operator 246)
 In California: (800) 852-7777 (Operator 246)

All other circulation enquiries concerning existing subscriptions please contact:

Nature Circulation Department, Macmillan Journals Ltd., Brunel Road, Basingstoke, Hants RG21 2XS, UK

Telephone: (0256) 29242 Telex: 858493

Back issues: (Post-paid) UK, £2.50; USA & Canada, US\$6.00 (surface), US\$9.00 (air); Rest of World, £3.00 (surface), £4.00 (air).

Nature Binders:

Single Binders: UK, £4.50; Rest of World, \$10.00
 Set(s) of 3 Binders: UK, £12.00; Rest of World, \$25.00

Nature Annual Indexes (1971-1981):

Price (post-paid):
 UK, £5.00 each; Rest of World, \$10.00

Nature Directory of Biologicals:

(Hardcover edition)
 UK, £22.50; Rest of World, \$45.00

Nature Wallcharts:

How Britain Runs its Science; How the US Runs its Science; UK, £3.50; USA, \$7.95 each

Nature in Microform:

For Information:

University Microfilms International, 300 North Zeeb Road, Ann Arbor, MI 48106, USA

Orders (with remittance) to:

Nature, Macmillan Journals Ltd., Brunel Road, Basingstoke, Hants RG21 2XS, UK
 Tel: (0256) 29242 Telex: 858493

M MACMILLAN JOURNALS

Induction of immortality is an early event in malignant transformation of mammalian cells by carcinogens	R F Newbold, R W Overell & J R Connell	633
Noradrenaline blocks accommodation of pyramidal cell discharge in the hippocampus	D V Madison & R A Nicoll	636
Retroviruses induce granulocyte-macrophage colony stimulating activity in fibroblasts	M J Koury & I B Pragnell	638
Differential expression of cellular oncogenes during pre- and postnatal development of the mouse	R Müller, D J Slamon, J M Tremblay, M J Cline & I M Verma	640
Ia invariant chain detected on lymphocyte surface by monoclonal antibody	N Koch, S Koch & G J Hämmerling	644
<i>uvr</i> Genes function differently in repair of acetylaminofluorene and aminofluorene DNA adducts	Moon-shong Tang, M W Lieberman & C M King	646
A protein immunologically related to erythrocyte band 4.1 is found on stress fibres of non-erythroid cells	C M Cohen, S F Foley & C Korsgren	648
Post-transcriptional control of tubulin biosynthesis during leishmanial differentiation	M Wallach, D Fong & Kwang-Poo Chang	650
Developmental inactivity of 5S RNA genes persists when chromosomes are cut between genes	J B Gurdon, C Dingwall, R A Laskey & L J Korn	652
Identification of a potential control region in bacteriophage T7 late promoters	L K Jolliffe, A D Carter & W T McAllister	653

MATTERS ARISING

Significance of ankle structures in archosaur phylogeny	R A Thulborn Reply: S Chatterjee	657
Reduction in plasma calcium during exercise in man	V A Convertino, E R Morey & J E Greenleaf Reply: J A Ruben & A F Bennett	658

GUIDE TO AUTHORS

Authors should be aware of the diversity of *Nature's* readership and should strive to be as widely understood as possible.

Review articles should be accessible to the whole readership. Most are commissioned, but unsolicited reviews are welcome (in which case prior consultation with the office is desirable).

Scientific articles are research reports whose conclusions are of general interest or which represent substantial advances of understanding. The text should not exceed 3,000 words and six displayed items (figures plus tables). The article should include an abstract of about 50 words.

Letters to *Nature* are ordinarily 1,000 words long with no more than four displayed items. The first paragraph (not exceeding 150 words) should say what the letter is about, why the study it reports was undertaken and what the conclusions are.

Matters arising are brief comments (up to 500 words) on articles and letters recently published in *Nature*. The originator of a Matters Arising contribution should initially send his manuscript to the author of the original paper and both parties should, wherever possible, agree on what is to be submitted.

Manuscripts may be submitted either to London or Washington (decisions being made only in London). Manuscripts should be typed (double spacing) on one side of the paper only. Three copies are required, each accompanied by copies of lettered artwork. No title should exceed 80 characters in length. Reference lists, figure legends, etc. should be on separate sheets, all of which should be numbered. Abbreviations, symbols, units, etc. should be identified on one copy of the manuscript at their first appearance.

References should appear sequentially indicated by superscripts in the text and should be abbreviated according to the *World List of Scientific Periodicals*, fourth edition (Butterworth 1963-65). The first and last page numbers of each reference should be cited. References to books should clearly indicate the publisher and the date and place of publication. Unpublished articles should not be formally referred to unless accepted or submitted for publication, but may be mentioned in the text.

Each piece of artwork should be clearly marked with the author's name and the figure number. Original artwork should be unlettered. Suggestions for cover illustrations are welcome. Original artwork (and one copy of the manuscript) will be returned when manuscripts cannot be published.

New

Nunc-TSP

Screening System

- Time saving
- Early screening
- No effect on cells
- Easy to handle
- Tests can be repeated under identical conditions
- No sizeable investments



The Nunc-TSP is a plate with 96 pins that have been specially produced in order to ensure high and uniform binding of polar and charged molecules (e.g. proteins).

The Nunc-TSP is based on the EIA principle, but unlike previous systems it functions »in situ«, i. e. medium is not removed from the cultured hybridoma cells. This means that the testing procedure will have no influence on the cell growth and that it can be repeated under identical conditions without changing the composition of the medium.

The Nunc-TSP provides easy handling with no or few pipetting operations, and at the same time it ensures simultaneous starting and stopping of the reactions in all 96 wells of the microtest plate.

The Nunc-TSP is used together with Nunc microtest plates. A semi-automatic or fully automatic washer are available. If only small numbers of Nunc-TSP are used, the washing can be done in the carrier-plate.



A/S NUNC
KAMSTRUP
DK-4000 ROSKILDE
DENMARK

Circle No. 17 on Reader Service Card.

References:

U. Løvborg: Monoclonal Antibodies.
Production and Maintenance. (Heinemann)

L. Olsson: Human-human Hybridomas. (In press)

Nunc – Your Partner for Progress in Immunology

nature

Vol. 299 No. 5886 28 October 1982

Cable in haste, repent at leisure	765
No future for the Greens	766
Graduate student choice	766

Belgian universities hit trouble	
Polish Academy of Sciences	
UK universities	
Cancer research	
Nuclear war games	
Asbestos hazard	
NRDC and NEB	
Celltech eyes Japanese market	
Astrophysics Laboratory	
Social sciences in France	
Spending low on France's books	
Education in Afghanistan	
FDA on overseas data	
Halley upstaged	
Nuclear fuel supply	
French nuclear power	
India embroiled in nuclear politics	767

CORRESPONDENCE

Ball lightning — a picture/ICSU	774
---------------------------------	-----

NEWS AND VIEWS

Calculating the strength of wood (John Maddox); The acetylcholine receptor cloned east and west (Charles F Stevens); A future for immobilized cell technology (John F Kennedy); Immunoregulation by gamma-interferon? (Teresa Basham & Thomas Merigan); Recent advances in optical bistability (Y R Shen); Snail shells suggest past changes in British chalk vegetation (Peter D. Moore); Chromosome rearrangements in gonococcal pathogenicity (J R Saunders); Bacterial toxins and cyclic AMP (Simon van Heyningen)	775
--	-----

BOOK REVIEWS

The Primates of Madagascar (by I Tattersall) R D Martin; Environmental History of East Africa (by A C Hamilton) A T Grove; Interplanetary Dust (by P W Hodge) David W Hughes; Hormones in Development and Aging (A Vernadakis and P S Timiras, eds) J G Phillips; Energy, Force, and Matter: The Conceptual Development of Nineteenth-Century Physics (by P M Harman) Stephen G Brush; Dynamics of Large Mammal Populations (C W Fowler and T D Smith, eds) Hans Kruuk; High Resolution Spectroscopy (by J M Hollas) Norman Sheppard	843
--	-----

Cover

Fitting a false tail to the long-tailed widowbird provides the first direct evidence for Darwin's theory that ornamental plumage of birds evolved through female preference. Males with extra long false tails attracted more females than normal males (see p.818)

Hot galactic gas and narrow line quasar absorption systems (a review)

T W Hartquist & M A J Snijders 783

ARTICLES

MERLIN observations of superluminal radio sources

I W A Browne, R R Clark, P K Moore, T W B Muxlow, P N Wilkinson, M H Cohen & R W Porcas 788

Primary structure of α -subunit precursor of *Torpedo californica* acetylcholine receptor deduced from cDNA sequence

M Noda, H Takahashi, T Tanabe, M Toyosato, Y Furutani, T Hirose, M Asai, S Inayama, T Miyata & S Numa 793

Human metallothionein genes — primary structure of the metallothionein-II gene and a related processed gene

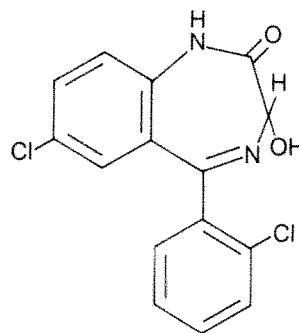
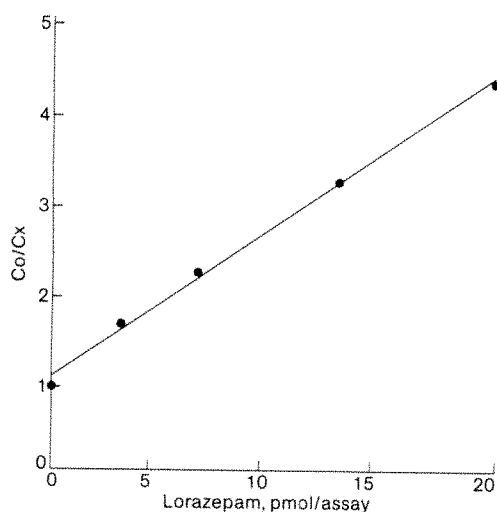
M Karin & R I Richards 797

LETTERS TO NATURE

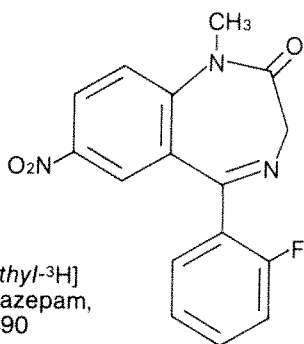
A single quantum cannot be cloned	W K Wootters & W H Zurek	802
The Crab Nebula's progenitor	K Nomoto, W M Sparks, R A Fesen, T R Gull, S Miyaji & D Sugimoto	803
Siderophiles in the Brachina meteorite: impact melting?	G Ryder	805
Terrestrial-type xenon in meteoritic troilite	G Hwaung & O K Manuel	807
Phase transition in KOH-doped hexagonal ice	Y Tajima, T Matsuo & H Suga	810
Influence of cross-diffusion on 'finger' double-diffusive convection	T J McDougall & J S Turner	812
Cyanophyte calcification and changes in ocean chemistry	R Riding	814
Evidence for a central Eurasian source area of Arctic haze in Alaska	G E Shaw	815
Female choice selects for extreme tail length in a widowbird	M Andersson	818
Self-pituitary grafts are not rejected by frogs deprived of their pituitary anlagen as embryos	L A Rollins-Smith & N Cohen	820
Clonal interaction in tumours	M F A Woodruff, J D Ansell, G M Forbes, J C Gordon, D I Burton & H S Micklem	822
Dihydroouabain is an antagonist of ouabain inotropic action	T Godfraind, J Ghysel-Burton & A De Pover	824
Hydrogen ion currents and intracellular pH in depolarized voltage-clamped snail neurones	R C Thomas & R W Meech	826
Intracellular Cl ⁻ accumulation reduces Cl ⁻ conductance in inhibitory synaptic channels	M R Gold & A R Martin	828

Benzodiazepine receptor preparation

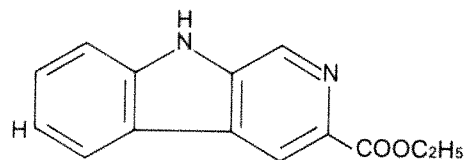
Amersham's benzodiazepine receptor preparation,* N.230, provides a specific, sensitive and rapid means for the determination of benzodiazepines and their active metabolites in biological fluids.



Lorazepam, N.232



[N-methyl-³H]
Flunitrazepam,
TRK. 590



B-[6-³H] Carboline-3-carboxylic
acid, ethyl ester, TRK.664
(non-radioactive compound, N.231)

- The receptor assay protocol is based on the competition between [N-methyl-³H] flunitrazepam and biologically active benzodiazepines.
- The sensitivity of the assay is demonstrated by the standard curve shown above constructed using lorazepam, N.232.
- The specificity of the receptor preparation is similar to that of fresh membrane-bound rat brain benzodiazepine receptors.

Please contact Amersham or your local distributor for further details.

*Manufactured for Amersham International by A/S Ferrosan, Denmark.

Circle No.11 on Reader Service Card.

Amersham International plc

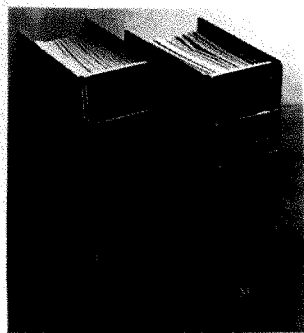
Amersham England HP7 9LL

telephone Little Chalfont (024 04) 4444

Amersham

Amersham Australia PTY Limited Sydney Amersham Belgium SA/NV Brussels Amersham Buchler GmbH & Co. KG Braunschweig W Germany
Amersham Corporation Arlington Heights Illinois USA Amersham France SA Paris Amersham Japan Tokyo Amersham Nederland BV Utrecht

Keep your copies of *Nature* protected in these tough black PVC binders



- Each binder is supplied with a set of wires for the easiest possible loading
- *Nature* logo blocked in gold on spine
- Transparent plastic pocket provided for your own reference
- Each binder takes two volumes of *Nature*; three binders will serve for a year
- Prices and address for orders are set out below

Annual Subscription including Index (51 issues)

UK & Eire	Airspeed only	£98
USA & Canada		US\$220
Australia & NZ	Airspeed only	£137.50
Belgium	Airspeed only	BF9350
West Germany	Airspeed only	DM490
Netherlands	Airspeed only	G540
Switzerland	Airspeed only	SF420
Rest of Europe	Airspeed only	£114
Rest of World*	Surface	£115
Rest of World*	Airmail	£173

* (not USA, Canada, Europe & Japan)

Japan: For subscription details contact Nichibo, PO Box 5030 Tokyo International, 2-1 Sarugakucho 1-chome, Chiyoda-ku, Tokyo

Personal subscription rates are available in some countries to subscribers paying by personal cheque or credit card.

Details can be obtained from:

UK: *Nature* Promotion Department, Canada Road, Byfleet, Surrey KT14 7JL.
Telephone: Jonathan Earl: Byfleet (09323) 41459
USA: *Nature*, 15 East 26 Street, New York, NY 10010
Credit card orders only (in USA & Canada):
Call toll-free: (800) 824-7888 (Operator 246)
In California: (800) 852-7777 (Operator 246)

All other circulation enquiries concerning existing subscriptions please contact:

Nature Circulation Department, Macmillan Journals Ltd., Brunel Road, Basingstoke, Hants RG21 2XS, UK

Telephone: (0256) 29242 Telex: 858493

Back issues: (Post-paid) UK, £2.50; USA & Canada, US\$6.00 (surface), US\$9.00 (air); Rest of World, £3.00 (surface), £4.00 (air).

Nature Binders:

Single Binders: UK, £4.50; Rest of World, \$10.00
Set(s) of 3 Binders: UK, £12.00; Rest of World, \$25.00

Nature Annual Indexes (1971-1981):

Price (post-paid):
UK, £5.00 each; Rest of World, \$10.00

Nature Directory of Biologicals:

(Hardcover edition)
UK, £22.50; Rest of World, \$45.00

Nature Wallcharts:

How Britain Runs Its Science; How the US Runs its Science; UK, £3.50; USA, \$7.95 each

Nature in Microform:

For Information:

University Microfilms International, 300 North Zeeb Road, Ann Arbor, MI 48106, USA

Orders (with remittance) to:

Nature, Macmillan Journals Ltd., Brunel Road, Basingstoke, Hants RG21 2XS, UK
Tel: (0256) 29242 Telex: 858493



Denervation of newborn rat muscles does not block the appearance of adult fast myosin heavy chain

G S Butler-Browne, L B Bugaisky, S Cuénoud, K Schwartz & R G Whalen **830**

Preferential effect of γ interferon on the synthesis of HLA antigens and their mRNAs in human cells

D Wallach, M Fellous & M Revel **833**

Direct evidence of homology between human DC-1 antigen and murine I-A molecules

M R Bono & J L Strominger **836**

Differential expression of steroid sulphatase locus on active and inactive human X chromosome

B R Migeon, L J Shapiro, R A Norum, T Mohandas, J Axelman & R L Dabora **838**

Structure of the S-Layer of *Sulfolobus acidocaldarius*

K A Taylor, J F Deatherage & L A Amos **840**

MISCELLANY

100 years ago

778

Product Review: Neurosciences

xiii

Classified advertising

xxvii

GUIDE TO AUTHORS

Authors should be aware of the diversity of *Nature*'s readership and should strive to be as widely understood as possible.

Review articles should be accessible to the whole readership. Most are commissioned, but unsolicited reviews are welcome (in which case prior consultation with the office is desirable).

Scientific articles are research reports whose conclusions are of general interest or which represent substantial advances of understanding. The text should not exceed 3,000 words and six displayed items (figures plus tables). The article should include an abstract of about 50 words.

Letters to *Nature* are ordinarily 1,000 words long with no more than four displayed items. The first paragraph (not exceeding 150 words) should say what the letter is about, why the study it reports was undertaken and what the conclusions are.

Matters arising are brief comments (up to 500 words) on articles and letters recently published in *Nature*. The originator of a Matters Arising contribution should initially send his manuscript to the author of the original paper and both parties should, wherever possible, agree on what is to be submitted.

Manuscripts may be submitted either to London or Washington (decisions being made only in London). Manuscripts should be typed (double spacing) on one side of the paper only. Three copies are required, each accompanied by copies of lettered artwork. No title should exceed 80 characters in length. Reference lists, figure legends, etc. should be on separate sheets, all of which should be numbered. Abbreviations, symbols, units, etc. should be identified on one copy of the manuscript at their first appearance.

References should appear sequentially indicated by superscripts in the text and should be abbreviated according to the *World List of Scientific Periodicals*, fourth edition (Butterworth 1963-65). The first and last page numbers of each reference should be cited. References to books should clearly indicate the publisher and the date and place of publication. Unpublished articles should not be formally referred to unless accepted or submitted for publication, but may be mentioned in the text.

Each piece of artwork should be clearly marked with the author's name and the figure number. Original artwork should be unlettered. Suggestions for cover illustrations are welcome. Original artwork (and one copy of the manuscript) will be returned when manuscripts cannot be published.

Requests for permission to reproduce material from Nature should be accompanied by a self-addressed (and, in the case of the UK and USA, stamped) envelope.

Nature in Poland

Readers wishing to subscribe to a weekly copy of *Nature* on behalf of a colleague in Poland (where hard currency is scarce) should send a cheque for £50 (or the equivalent in any currency), accompanied by their name and address and that of the proposed recipient, to the *Nature* office in London or New York (see addresses opposite page 765). For further details, readers are referred to *Nature* 3 June, p.354.

latest
addition
to our new
synthetic
peptides:

hp **GRF**

(Human Growth Hormone Releasing Factor)

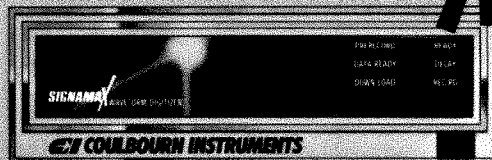
Circle No.39 on Reader Service Card.



Peninsula Laboratories, Inc.

611 Taylor Way, Belmont, California 94022
Telephone: (415) 583-5342 TELEX No. 172511

SIGNAMAX



Waveform Digitizer

Intelligent terminal for mini and microcomputers

Features:

- 100 KHz, 12 bit ADC
- Dual Channel
- 48K Byte Record
- Pre and Post Trigger Records
- Multiple Record Repeat Sweeps
- RS232-C, IEEE488 Formats

Applications:

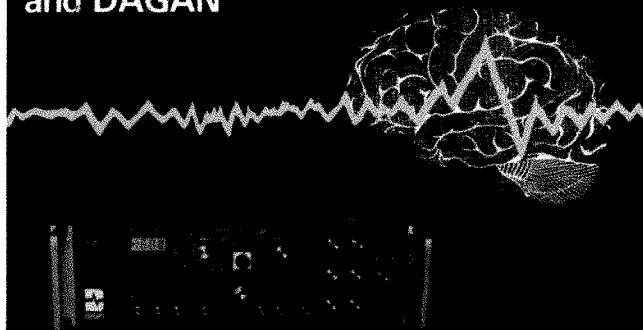
- Physical and Life Sciences
- Research and Testing
- High Speed, High Resolution Long Duration Records
- Digital Oscilloscope
- Signal Averaging

EI COULBOURN INSTRUMENTS

P.O. Box 2551 Lehigh Valley, PA 18001 (215) 395-3771

Circle No.40 on Reader Service Card.

ELECTROPHYSIOLOGY and DAGAN



PATCH CLAMP

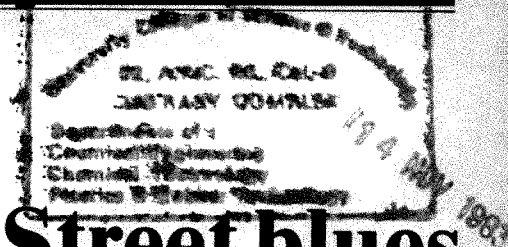
The new Dagan Model 8900 PATCH CLAMP-WHOLE CELL CLAMP provides you with the performance and operating features needed to obtain maximum results from the new giga-seal micropipette technology. The instrument has three different probes available which enables the researcher to both Voltage Clamp and observe the cellular currents of a wide range of cells. Also, cells which were too small for conventional intracellular microelectrode techniques can have their total currents recorded using the WHOLE CELL probe. For further information, contact us at our address below or circle our reader service number.

DAGAN CORPORATION
2855 PARK AVENUE
MINNEAPOLIS, MN 55407 PHONE (612) 827-5959



Circle No.28 on Reader Service Card.

2 September 1982



Too-easy-to-lose Wall Street blues

Stocks have been rallying and rates of both interest and inflation falling. Is the beginning of the end of the recession therefore in sight or is there more misery to come?

Does the recent excitement on Wall Street and the rallies that have followed on other stock exchanges, mean that the long recession is coming to an end? It is natural that people should now be asking this hopeful question just as it is natural that a man lost in a desert should mistake refraction of light in the hot air near the ground for a pool of water. For if the people who make their livings by buying and selling stocks in commercial corporations now think it worthwhile to pay more for the commodities in which they trade, does that not imply that the outlook for US industry has improved? And does it not follow that industrial economies elsewhere will soon be on the mend? Unfortunately these conclusions, welcome though they would be, are unwarrantable. This is why.

Last week's rally on the stock exchanges followed from two significant developments in the United States — a modest but steady decline in the prevailing high interest rates and the government's success in persuading Congress, on the eve of its summer holidays, to enact a package of tax increases that will bring in an extra \$98,300 million over the next three years. If the financial community had waited a few days, it would no doubt have been further cheered to know that the annual rate of inflation in the United States has now fallen to 6.7 per cent. While each of these developments is a sign of progress in the right direction, neither of them implies that the end of the recession is at hand.

The decline of interest rates to below 14 per cent (when banks lend to each other or when people lend to the government) may save many industrial corporations from bankruptcy, but there is as yet no sign that corporations will seize this opportunity to invest in new plants and equipment. Why should they when they have to pay more than 17 per cent for the funds they borrow from the money market and the bank? A decline of interest rates is rather a sign that industry has virtually dropped out of the competition for people's savings, leaving the government as the only borrower of significance. This development is therefore more a sign that the recession has begun to bite than the promise that it is coming to an end.

On present form this will remain the case for some time to come. The package of tax increases half-heartedly proposed by the government and reluctantly swallowed by Congress will not do much to help. The government's deficit for the present financial year (which ends on 30 September) will be untouched at \$110,000 million or more. The tax increases now enacted will be effective only after 1 October, and are smaller than last year's tax reductions, also then coming into effect, and will not in themselves prevent the government's deficit actually increasing in future years. The hopeful sign and the only reason why Wall Street is excited is merely that the Reagan Administration appears at last to have recognized that it cannot run deficits on this scale without also running the economy into the ground. That a Republican administration should so lightly have thrown to the wind the traditional (and old-fashioned) Republican preoccupation with balanced budgets, remains a puzzle, while Mr Reagan's support for the proposed constitutional amendment that would compel future governments to balance their books is about as easily understood as a burglar's espousal of the calls of law and order.

The chances now are high that when the November elections are safely past, the President will make another attempt to behave as he says he should and will ask Congress to agree to a more substantial reduction of the social expenditure to which it has committed him. That will be a more bloody battle than that now won. The outcome cannot be foretold, but success will mean further misery for the growing army of the unemployed, now 9.7 per cent of the working population.

Meanwhile, there is precious little evidence that the transformation of the US industry has gone far enough to provide a foundation for future prosperity. As in most of Western Europe the privations of the recession have not yet made conventional manufacturing industry competitive with similar industries elsewhere, principally in Japan. Indeed, in the manufacture of steel and motor cars for example, the chief preoccupation is still to keep some semblance of these industries alive when there is no reason to suppose that they have an important place in the world. The time to celebrate the impending end of the recession will be when tangible signs of new industries emerging and of improved productivity in conventional industries are plain for all to see.

A very different game

Can French success in boosting nuclear and space technology be repeated in electronics?

A few weeks ago, the French government announced that it was to invest FF140,000 million (£12,000 million) in the French electronics industry over the next three to five years — an apparently vast sum by all measures (see *Nature* 5 August, p.504). But now the dust is beginning to settle, it seems the amount of new government cash may not be so great. Some FF 90,000 million of the total was already due to be invested by the industry itself; and of the remaining FF50,000 million promised by the government (none of which has yet materialized) most can be accounted for by money already budgeted by the industry to be raised from the banks and other sources now nationalized.

So what is the great French electronics plan really all about? Central planning, it seems, despite President Mitterrand's insistence that the leadership of the nationalized industries would be free to manage their industries as they wished. What the President failed to emphasize was that the leadership would be chosen by the government.

So, for example, when the president of the newly-nationalized giant chemicals corporation, Rhône-Poulenc, felt obliged to resign recently (in protest against the "inconsistency" of government policy for his industry), the matter was dismissed by research and industry minister Jean-Pierre Chevènement in revealing terms. The state was in need of "good servants", he said. Jean Gandois, the resigning president, replied that he had found himself to be a "hostage" of the government.

With the leadership of much of industry in its pocket, therefore, the government must now manage industry — something that the present British government would consider to be a logical impossibility. In France, the division between government and industry is not so sharp; the leaders of both

sectors tend to come through the same somewhat military system of education — the *grandes écoles* — and interchange and interaction between civil service and industry is traditionally much stronger in France than in Britain.

Thus the change under Mitterrand is not so much a change of principle as of degree. There is, however, in this socialist government, an increased tendency to make appointments on political and ideological grounds, and voices in the electronics industry in particular are beginning to question the experience and suitability of some of their new leaders.

Moreover, the government has selected electronics to be the centrepiece of its five-year plan for the regeneration of French industry, putting the field on a par with nuclear power and space technology — the other areas very successfully championed by past French governments. But electronics is a very different game. In nuclear power, and in space, there is essentially one customer — the government — at least in the first decade or so while the business is being established. Here, a simple military regimentation of the industry towards well-defined goals will work, as all levers are in the government's hands. But in consumer electronics, for example, there are millions of customers, and there must be flexibility in response to changes in demand and competition. Even the products may change radically. It is doubtful if even the French government machine will be supple enough to deal with this by central planning, however complex the plan.

It may be, therefore, that the great government effort on electronics will work only in those areas where electronics is most like nuclear power and space, in having small, well-defined markets with few customers. This would mean that France should be watched now not for its calculators or video recorders, nor for its consumer products, but for what is called "professional electronics" — defence equipment, where there is a large French and foreign market, electronics for broadcasting and so on.

However, there is one clear thing that a great centralized plan for electronics could do. The importance of components (chips) and of software is increasing in all parts of the industry as one influential (and sceptical) director in the French electronics industry, M. Pierre Aigrain, points out. If the government can put these crucial parts of the French electronics house in order, and bring them to bear on the rest of the industry, whatever can be done by central control will have been done. Other, that is, than providing some real (rather than promised) investment.

Father William's jaw

The cost of caring for old people in the United States will grow dramatically if nothing is done.

Last week's \$98,300 million tax bill, passed by the US Congress with such fanfare, held portents of future problems for old people in the United States, for it showed the tremendous pressures that have mounted on the cost of caring for them. And while scientists like to think that the orderly world of their laboratories is far removed from political fights over Medicare and Medicaid, the research priorities of biomedical scientists in the next few years could have an impact on future costs of caring for the elderly, not to mention an impact on their well-being. US biomedical research and social policy, then, are linked.

The new law, for example, will reduce the chief health programme for the elderly, Medicare, which now costs \$53,000 million, by \$13,300 million over the next three years and increase the costs paid directly by old people by, for example, making elderly hospital patients bear some of the costs of radiology and pathology.

The move to reduce costs collides head-on with the increasing number of old people in the US population, whose government-supported health care will have to be paid from the taxes of a relatively smaller group of younger, working people (*Nature* 26 August, p.779). The resulting battle will make this year's skirmishes between the "gray lobby" seeking to retain federal

benefits, and Reagan-inspired budget cutters, look almost trivial.

Matters are not helped by the fact that the present system of Medicare and Medicaid encourages doctors to treat hospitalized patients with acute problems while most custodial care, long term care and outpatient care, is not covered.

The system reinforces what Robert N. Butler, the outgoing director of the National Institute on Aging, calls "Peter Pan Medicine": a young or middle-aged person with an acute problem but good chances of recovery is a subject of interest and is given the maximum care at no extra cost, while an older person, whose health problems are limited to outpatient visits, is not allowed to charge to the government the cost of medication and, if in hospital, is considered a less interesting case and so gets relatively little attention.

Even worse off are those in nursing homes, for long the step-children of the health care system. Federal insurance does not extend to the costs of nursing homes and Medicare pays only for those who have entered a home after an acute illness in hospital, and then only for 100 days. Meanwhile there is no evidence that nursing homes are any good, having been divorced from the mainstream of research, teaching hospitals and medical practice for so long. There are no teaching nursing homes, although the National Institute on Aging plans to try some, and there is currently only one registered nurse for every 68 residents in the country's 60,000 nursing homes. Many do not even have a regular doctor available.

Demographics will only make this worse. There were 1.3 million people in nursing homes in 1978; there will be 2.1 million in the year 2003. In the present political climate it is impossible to believe that federal benefits will be extended to include long-term care. But could not the need for long-term care be reduced by a better understanding of its medical causes? Why are people in nursing homes to begin with? Could science enable nursing homes to go the way of the TB sanatorium?

Most people enter long term care because they are senile, many of them suffering from Alzheimer's disease. Here, at least, recent progress in understanding the disease at the cellular level and its possible association with slow viruses holds out some hope. Another major reason people are sent to nursing homes is urinary incontinence, about which little is known. Next come infectious diseases, notably pneumonia and influenza, but also herpes zoster (shingles), tetanus and even tuberculosis and chickenpox, causing one in four deaths of elderly people. Here, a better understanding of the effects of ageing on the immune system could help.

Finally, there are bone fractures, encouraged by osteoporosis which could perhaps be minimized by better care in middle age and early old age, perhaps through fluoride and calcium supplements, treatments with oestrogen, progesterone, and vitamin D, and even exercise. Butler goes farther to say that biomarkers, "clocks" to detect how far organ and bodily functions have aged, may make it possible to run short clinical trials, obviating the need to wait many years for a result. This could make possible more direct study of the ageing process, and whether factors such as early diet are linked to old-age symptoms.

These are long-term goals but not far fetched ones considering the high potential social payoff. The "gray lobby", caught in yearly battles, seems unlikely to make a high priority of broad-based biomedical research, with its ifs and buts and necessarily long-term payoffs. It is the research community who hold the keys to the elderly's best hopes 20 years hence and who should take the initiative.

Only the scientists can perhaps ensure that we approach the ideal of a healthy older person, who is not senile, whose bones are not too frail, who is not humiliated by incontinence and who does not die of diseases a child would shake off.

The elderly might even come to resemble Lewis Carroll's Old Father William whose muscular jaws and hearty eating were attributed to the arguing he did as a youngster. Old Father William could stand on his head, somersault backwards, eat a goose, bones and beak, and kick his son downstairs. One thinks of him as a shrewd old fellow, who surely did not cost the state any money.

Pipeline embargo in new jeopardy

Soviet Union's technology could adapt

President Reagan's ploy to stop or delay the supply of Siberian natural gas to Western Europe may all be in vain — because of two simple technical options open to the Soviets.

Reagan's tactics have been to urge European steel manufacturers — particularly West Germany — to stop supplies of the large-diameter (1.42m) steel pipe needed for the line; and to forbid General Electric and other American suppliers from shipping key parts (for example turbine blades) to Western manufacturers making the gas turbines and compressors needed to pump the gas.

But the Soviet Union is experimenting with increasing the pressure of gas in the line from its nominal 75 atmospheres to 100 or even 120 atmospheres. At 100 atmospheres, the pipeline could be built with only two parallel pipes (the current design has three) and yet carry the same net flow of gas (40,000 million standard m³ a year). At 120 atmospheres, only one pipe would be needed, according to official reports in the newspaper *Pravda*. This would reduce the steel requirements for the line to within the capacity of Soviet industry (although the higher pressure pipes would have to be reinforced), and it would also drastically reduce the cost.

Another neglected fact is that the design capacity of the line is in excess of the contracts for gas so far signed in Europe. Since the power required to pump gas down a pipeline rises more than linearly with the rate of gas pumped, it would be possible for the Soviets to pump the contracted gas with many fewer than the 125 gas turbines of 25 MW currently on order in Europe. The 125 turbines are only necessary to pump the full design flow rate.

Exactly how many turbines the Soviet Union would need to be in place by 1984 — when the line is supposed to come on stream — depends on the detailed characteristics of the line. However, the plan is to supply just 15,000 million m³ at that date — under 40 per cent of capacity. It was never envisaged that the line would be pumping its full capacity before 1987.

In fact, according to British pipeline engineers, it would be presumptuous to assume that the Soviets would need as much as 15/40 of design pumping power by 1984, that is 47 or so 25-MW turbine and compressor sets.

It happens that there are parts available in Europe to supply 23 such sets to the Soviet Union, six at John Brown in

Scotland and the rest in France and Italy. That would leave the Soviet Union with at most 24 sets to supply from its own industry in Leningrad, as opposed to the 102 apparent from the design. According to British turbine manufacturers, the General Electric turbines are not particularly sophisticated technology — they are based on 1950s steam turbine design. The obstacle to their manufacture in the Soviet Union is primarily a matter of industrial capacity.

At present, the Soviet Union has no such capacity for 25-MW sets, but West European engineers are convinced that a working prototype is now under test in Leningrad. According to Soviet sources this prototype is "even more efficient" than the General Electric sets it is designed to replace. Whether the Leningrad works could supply 24 of these sets in working order by 1984 is open to question, but the target is a good deal more realistic than the 102 that the Reagan embargo apparently implied.

Another option open to the Soviet Union is to divert 10-MW set production, for which it has capacity, from the six national pipelines under construction. And

in Europe, the French company Alsthom-Atlantique has the capacity to build complete turbines (albeit under licence from General Electric, and so in defiance of the Reagan embargo and so in risk of penalties in America).

Thus it seems entirely conceivable that one way or another the Soviet Union will meet its 1984 deadline — and that it could develop the capacity to bring the line up to full flow by 1987, as Soviet sources continually affirm.

The pipeline design requires three 4,500 km strings to bring the gas from Siberia to the Western border of the Soviet Union. So far, 2,700 km of pipe have been delivered to the pipeline builders, according to the Soviet news agency Tass. Some 500 km of pipe have been welded into a single line, says Tass, and by mid-August 250 km had been laid in place.

Pipe laying equipment which was to have been supplied by the American Caterpillar company is also embargoed, but a new Soviet-designed pipe-layer is now under test, says Tass. The Japanese company Komatsu is also substituting for Caterpillar equipment, according to the news agency.

Robert Walgate and Vera Rich

EPA holds out against lead

Washington

The US Environmental Protection Agency (EPA) stuck to its guns last week and issued a regulation tightening limits on lead in gasoline, despite pressure from the Office of Management and Budget (OMB) to back off.

The new rule, to take effect on 1 November, limits the lead content of leaded gasoline to 1.1 grammes per gallon. EPA estimates that after eight years, airborne lead concentrations will be 31 per cent lower than they would be without the new rule.

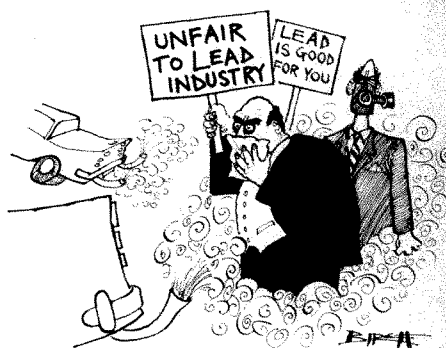
Under current regulations, refiners are allowed to average the lead content of all their gasoline, both leaded and unleaded; that pool average must not exceed 0.5 grammes per gallon. But as a result, refiners have been increasing the lead content of leaded fuel (which cannot be used in new cars with catalytic converters) as demand for it drops off. Adding lead is the cheapest way of increasing octane ratings, and EPA has found refiners using as much as 2 grammes of lead per gallon.

Earlier this year, EPA had proposed relaxing the lead regulations. This was done at the bidding of Vice President George Bush's task force on regulation. But in the face of a storm of protest — and convincing evidence that reductions to date in airborne lead have brought about real reductions in blood-levels — EPA went back to the drawing board.

By the beginning of August, EPA had

completed its about face, and in an apparent attempt to out-flank OMB, leaked its new, tougher proposal to the *New York Times*. OMB nonetheless responded by requesting EPA to reconsider the proposed 1.1 gramme limit but EPA has held its ground.

OMB did get its way, however, over the issue of the so-called small refiners.



Current regulations grant an exemption for refiners who produce less than 50,000 barrels per day; they are allowed to add from 0.8 to 2.65 grammes of lead per gallon, according to their scale of production. The new rules will narrow the exemption, reserving the "small refiner" designation for producers of less than 10,000 barrels a day who were in business before October 1976. According to EPA, this will leave only 74 companies in this category, about half the current number. They will be allowed to add up to 2.5

grammes per gallon. The losers will be the "blenders", companies that jumped into the business in the past few years to take advantage of the small-refiner loophole. They buy cheap gasoline, add lead to boost the octane, then resell it. That practice should be largely halted by the new rules.

Environmental groups are generally pleased with the new rules. The lead industry, predictably, is not. In a letter to the *New York Times* last week, Dr Jerome Cole, vice-president of the International Lead Zinc Research Organization argued that the new regulations will cost the public "millions of barrels of crude oil that lead in gasoline saves while adding billions of dollars to the US balance of payments deficit."

Stephen Budiansky

Affirmative action employer

The launch of the Soyuz-T, with a three person crew including female cosmonaut Svetlana Savitskaya, coincided neatly with the closing of Unispace-82 in Vienna and upstaged the US contribution to equal opportunities in space, the visit to the conference of Dr Anna Fisher, astronaut in training. Miss Savitskaya's visit to Salyut-7, however, should not be viewed simply as a publicity gimmick, nor an attempt to scoop the launch of Dr Sally Ride aboard the Shuttle next spring. The fact that there were female candidates training at the Gagarin space centre was announced some weeks ago. It would seem that, as far as the space planners were concerned, the launching of a woman was the next routine step.

Soviet space policy is strongly committed to the construction of large space stations,



Savitskaya and crew-mates

aboard which women would serve as scientists. ("And, of course, stewardesses", Andrian Nikolaev, the husband of the first Soviet woman cosmonaut Valentina Tereshkova, once added.) Studies of the effect of spaceflight on the female organism are an obvious prerequisite of such a programme. Yet, since Tereshkova's solo flight in 1963, no woman has been placed in orbit. The reason appears to be partly one of what a Soviet space official delicately called "the amenities". Moreover, the 1961 Soyuz-11 disaster, in which three cosmonauts died due to loss of cabin pressure during re-entry, led to a change in procedure; cosmonauts were to wear spacesuits during the re-entry, which meant that crew size had to be reduced from three to two. It was the introduction of the roomier Soyuz-T transport craft and Salyut-7, that made it possible for the multi-crew spacecraft to have a female visitor.

Israeli science politics

Physicist made Science Minister

Rehovot

Professor Yuval Ne'eman, a well known theoretical physicist and former president of Tel Aviv University has become Israel's first Minister of Science, just five years after turning down the post because he preferred to stay out of politics. Since then, though, Ne'eman has become a fully-fledged politician and now represents the nationalist Tehiya Party in the Knesset. When Tehiya joined the Begin-led coalition government, Ne'eman accepted the position of Minister of Science and Development.

Not all of Ne'eman's academic colleagues are enthusiastic about the notion of a ministry with overall responsibility for science. For one thing, they fear that it might mean an undesirable degree of government control. Ne'eman discounts such fears and claims that there are overwhelming benefits in having science represented at cabinet level. Other ministries already have their own chief scientists and research budgets and Ne'eman sees one of his chief tasks as introducing strong central coordination over these separate activities.

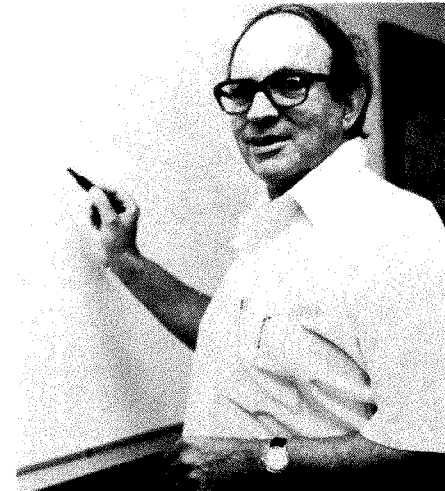
Professor Ne'eman is pleased with what has been achieved by Israeli scientists and technologists, but looks forward to a "quantum leap" in these achievements, in particular supporting the idea of creating "science cities". And he has set a target of \$5,000 million dollars a year for the annual income from exports based on local research — the current level being only \$1,000 million.

Although Ne'eman is clearly putting the emphasis on applied research, he says he will also be fighting to see that pure research gets the funds it deserves. He is particularly interested in creating more national experimental facilities like the Weizmann Institute's nuclear accelerator and the 40-inch telescope at Tel Aviv University. He also hopes to explore the possibility of Israel's becoming involved in further multi-national research bodies. Already Israel is a member of the European Molecular Biology Organization, and other candidates are the European Southern Observatory and the European Space Agency.

Only in the past 15 years, says Ne'eman, has advanced science and technology begun to have a serious impact on Israeli industry. Ne'eman himself can claim much of the credit — during the sixties he was amongst those who persuaded the government to back skill-intensive science-based industry at the expense of the labour-intensive textile industry and in the mid-seventies, as Chief Scientist in the Ministry of Defence, he had a significant impact on the country's military science.

Some Israeli scientists are sceptical about one of Ne'eman's pet projects, how-

ever. He is committed to the plan to build a canal from the Mediterranean to the Dead Sea, which among other things will provide hydroelectric power by utilizing water from the hills around the Dead Sea. Some question the value of spending an estimated \$1,000 million on a project that would only provide a few per cent of Israel's energy requirements. Ne'eman, for long a moving spirit behind the plan, maintains that the energy would be available at crucial times and that the canal



Ne'eman takes science to the cabinet

would provide much-needed cooling water for additional thermal power stations along the route.

Looking forward to his new task, the new minister says he will do his best "not to disconnect" from "real science". "I was serving as a military attaché with the Israeli Embassy in London," he recalls, "when I worked with Murray Gell-Mann on 'The Eightfold Way', the theory that led to the prediction of quarks. And if I was able to combine the purchasing of submarines with the charting of elementary particles then, I don't see why I can't maintain the same duality now."

Nechemia Meyers

US degrees

Doctoral decline

Washington

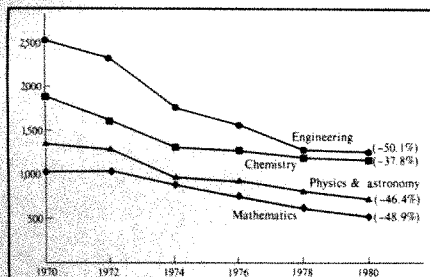
The number of US citizens who received doctorates in the "hard" science fields in the United States declined steadily during the 1970s (see chart). Some see in this trend a dangerous drift away from basic research as a career priority for young US scientists. David A. Shirley, director of the Lawrence Berkeley Laboratory, considers the figures "poignant" evidence of that US society is steering its young people away from basic science.

Another explanation is the changing environment in US university science departments, and the steady upward trend in salaries offered by industry to graduates who have made the initial four-year invest-

ment in a bachelor's degree in the hard sciences or engineering.

When US university science departments were expanding and funding was ample, a career in science was seen as the direct pursuit of a PhD and a research career on a university faculty. Young people were encouraged to consider this the most promising route — it being also the one their faculty advisers had usually followed.

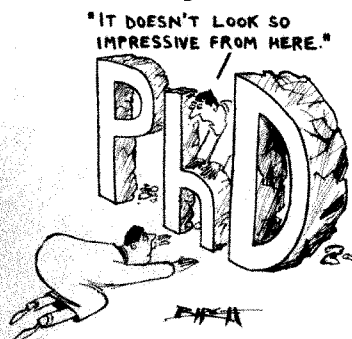
But now there are few positions available to a young PhD in university departments



The number of doctorates in science and engineering awarded to US citizens by US universities. Figures in parentheses give % decline from 1970 to 1980.

and laboratories, and still fewer with prospects of a permanent university job with tenure. Furthermore, industry pay is better. One recent survey found that industry offers geologists with a master's degree much the same salary (up to \$24,000) as they would command with a PhD as an assistant professor. So increasingly, young US researchers may not see academia as a promising or even stable place to be.

So, should they bother to get a PhD before entering industry? In June 1982, new PhDs in mathematics were offered an average of \$30,000 a year by industry, whereas new bachelors' degree holders in the field were offered, on average, \$9,000 less. Chemical engineers with a PhD were offered on average \$36,000 and again those with bachelors' degrees were offered



\$9,000 less. Since a doctorate takes seven years to earn, and the candidate earns little or no money during that time and must pay for tuition, the \$1,300 reward per year of study for the degree might seem insufficient.

So economics may be reshaping student attitudes away from the traditional career of a PhD and a university post. Of the situation, they may even be thinking, as one manpower specialist said, "why can't I do good work in industry, too?"

Deborah Shapley

Artificial intelligence

Industry beckons students

Pittsburgh

When 1,500 of the hard core among computer adepts converged upon the University of Pittsburgh campus for the National Conference on Artificial Intelligence (AI) recently, the usual talk of knowledge representation, the meaning of contradiction and many dozen other steps on the long road to a computer with human-like reasoning and perception, was supplemented by talk of entrepreneurship and commercialization. This is something new for the infant field of AI, and it has the field's old guard worried.

The change was apparent in both the exhibitors at the meeting and the audience; Dr Roger Schank of Yale University, who is also the founder of Cognitive Systems Inc, a prototype of small entrepreneurial ventures in AI, noted that ten years ago not a single venture capitalist was to be seen at AI meetings. This year, Cognitive Systems was one of several firms showing off specialized information systems for applications such as petroleum exploration, molecular genetics research and financial analysis.

Leading the charge against the new commercialism was Professor Marvin Minsky of the Massachusetts Institute of Technology, the "dean" of AI. "What I don't like about the problems most people work on is that there's too much 'do-goodism' in them," he said. Applications, such as information systems to aid in medical diagnosis or petroleum exploration draw talented people away from work that will do greater good in the long run. Minsky warned that most of the basic research in AI is done by doctoral students who then

go to work for a company, applying the AI expertise of several years ago on some very specific problem, such as signal processing (or, as Schank put it, "expert systems on paint thinners"). In so doing, Minsky said, "they rob the world of their intelligence".

The lure of industry is also attracting established university researchers in AI, just as it has in other engineering fields. A substantial number of people moving into industry are at the middle level, according to Professor Allen Newell of Carnegie-Mellon University. Newell said these are the researchers who would otherwise just be taking over their own research programmes at universities, and "we're really going to feel that loss".

According to Newell, universities should be made more competitive, both in salaries and research facilities. The average university researcher, he said, receives only one-half to two-thirds of the research support that an industry researcher receives.

To be sure, what is now happening to AI is no different from what has happened for years to computer science and engineering in general. AI, however, may be much more vulnerable. It is still a very young and speculative field, and thus pressures from industry for quick pay-backs are at once stronger and more acutely felt. The result, said Minsky, is that in the entire field there are less than 100 people who have a "license to kill" in having the freedom to spend five or ten years on a single project.

And Minsky offered a history lesson to those who expect quicker results. "It was 300 years from Galileo to Einstein," he said. "What could those fellows have been doing?"

Stephen Budiansky

University woos Oak Ridge laboratory

Last May, when the Union Carbide Corporation announced it would not renew the contract it has long held with the government to manage the Oak Ridge National Laboratory (ORNL) and three related atomic facilities, most observers expected some other corporation to take over (*Nature* 27 May, p.255).

The bidding has barely begun; indeed the US Department of Energy is only just asking all who are interested to make themselves known. Surprisingly, the local University of Tennessee at Knoxville, looks the most serious contender.

L. Evans Roth, the university's Vice Chancellor for Graduate Education, argues that the ORNL and the university are already intertwined, with ORNL scientists teaching at the university and the university programmes under way at the lab. "We already have a marriage without the contract", Roth says.

There is little doubt that acquiring the highly prestigious multi-disciplinary lab-

oratory would be a feather in the university's cap, and to that end it has a task force studying the shape of a management contract, with separate committees on administration, scientific-technical matters, and faculty liaison. Roth and other officials have toured the other national laboratories to look at other university/laboratory relationships, and Glenn Seaborg, the Nobel Prize winner and former atomic energy chief, has visited Knoxville to proffer advice.

Oak Ridge, on the other hand, may have mixed feelings about a union with the University of Tennessee — a state institution with 45,000 students and little experience in managing a giant research enterprise. Now under fire from many in Washington who are questioning the value of places like ORNL, the laboratory might be better served by a more experienced partner. The final decision may depend on what other suitors emerge in the months ahead.

Deborah Shapley

US medical care

Hospices gain

Washington

What could be a major shift in the pattern of US health care lies nearly hidden in the big tax bill Congress passed on 19 August. This is a feature allowing the federal government to pay for hospice care, that is, care of terminally ill people who have chosen not to have extreme life-prolonging measures and want to "die with dignity". Some 95 per cent of US hospice patients have cancer, and an estimated half of them are over 65.

The advent of what amounts to complete federal insurance for hospice care is sure to swell the ranks of those who chose it. Indeed, because this is a budget cutting, cost-saving year for US domestic programmes, the congressmen voted for it because of claims that it would encourage more people to use hospices, relieving pressure on acute care hospitals.

Until now, the estimated 36,000 people receiving hospice care in the United States have had to pay for many of the costs themselves, or have their families pay. Of the estimated 360,000 deaths from cancer per year in the United States, only 10 per cent are now in hospice programmes. So the potential growth of hospice usage is enormous.

According to figures provided by the Congressional Budget Office that Congress relied on heavily in its decision, this extension of Medicare benefits would cost the programme an additional \$1 million per year in the first two years. Afterwards, however, the numbers of people choosing hospices over hospitals would save \$16 million in fiscal 1985 and \$40 million in fiscal 1986. The National Hospice Organization says the cost of home hospice care is up to \$100 a day, compared with \$600 for full hospital care.

The measure's successful passage, despite opposition from the Administration, the American Medical Association, the American Hospital Association, and the Blue Cross Association, has been eclipsed by the larger fight over the tax bill.

The bill has been a focal point for national discussion of how to narrow the federal deficit and give the business community confidence in a US economic recovery. One House staffer deeply involved in the legislation noted that in normal times, something like the hospice measure would have made a big splash at the time it passed. Instead it has barely been reported, having arrived in the final bill by a strange parliamentary route.

In the house the most active proponent was Leon Panetta (Democrat, California), while Senator John Heinz (Republican, Pennsylvania) is responsible for having the Senate version included in the midst of that body's marathon debate on the overall tax bill.

Deborah Shapely

Bankruptcy for interferon firm

Washington

While Southern Biotech Inc., a Tampa, Florida, biotechnology firm that was forced to file for bankruptcy on 28 May, continues to negotiate with its creditors a plan to become solvent again, the US Food and Drug Administration has approved the company's first interferon product for clinical trials.

Approval came on 16 August for US trials of an interferon preparation of possible benefit to lymphoma patients. Although founded and promoted on the basis of its possible interferon sales, the company had not previously been able to market any in the United States, and a 50,000-million unit inventory of alpha-interferon remains unsold.

To facilitate its product reaching doctors in the Florida area, says Daphne B. Floyd, the company's vice-president for marketing, she has helped start a new organization, the Interferon Foundation of Florida, to help tell cancer patients and doctors about interferon. Southern Biotech has donated enough of the newly approved product to the foundation to treat 20 patients.

The company was formed in 1979 by former physician, John Kilgore, who sought to graft an interferon products business using genetic engineering onto a successful blood plasma business. But various deals, including one with Key Energy Enterprises of Tampa, apparently drained the company of cash. Hopes of an innovative research programme under William E. Stewart II, formerly of Memorial Sloan-Kettering Cancer Center, were dashed when Stewart, who was listed

as director of research at the time of the 18 August 1981 stock offering, was fired in September. The prospectus envisaged 17 doctoral-level scientists and a support staff of 34. At present, the scientific staff numbers 3, says Floyd.

However, the company continues to sell its blood plasmas in the United States, while a subsidiary, Southern Biotech Caribbean, located in Kingston, Jamaica, sells its interferon products locally and in West Germany.

Southern Biotech currently has applications for two other interferon products, one for treating breast carcinomas and the other for herpes, filed with FDA, says Floyd.

Deborah Shapely

Spruce bark beetle

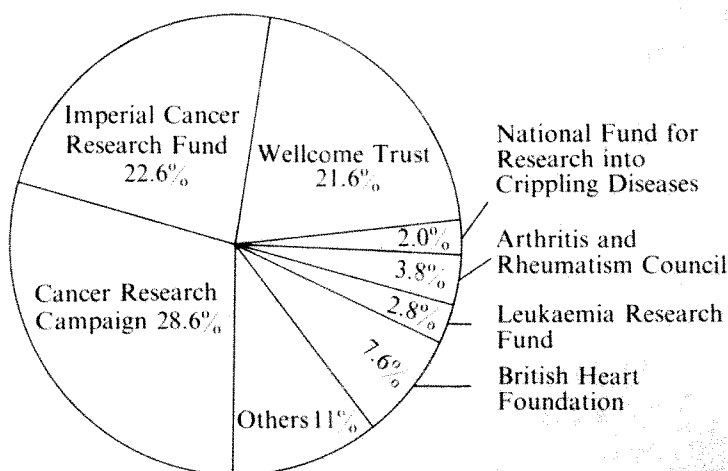
Peril imported

Despite stringent import controls which demand the stripping and spraying of imported conifers, the great spruce bark beetle (*Dendroctonus micans*) has found its way into British woodland.

Forestry Commission entomologists have identified the beetle on a private estate near Ludlow in Shropshire and the commission has implemented a monitoring programme using helicopters and foot patrols to survey the area within a 50 mile radius of Ludlow. Other counties affected are Gloucestershire, Hereford, Powys and Glamorgan. The Forestry Commission is optimistic that the pest will remain confined to this area assuming it has not already spread further afield.

Dendroctonus micans attacks and kills

Per cent distribution of UK charities' £64 million expenditure on medical research



The total annual income of the 35 principal UK medical research charities passed £100 million for the first time last year according to figures collated and just released by the Association of Medical Research Charities. Total expenditure was only £3 million less than the £103 million income but only 64 per cent of the expenditure was on "research" (the Spastics Society spent virtually all of its £18 million on such things as housing and care). The diagram shows the major contributors to research spending; none of the "others" spent more than £1 million. For comparison, the Medical Research Council was granted £102 million by Parliament for 1981-82. And in 1981 the National Society for the Prevention of Cruelty to Children collected £6.7 million and the Royal Society for the Prevention of Cruelty to Animals, £7.8 million.

conifer trees, in particular Sitka and Norway spruce, which account for a large part of British woodlands. It is endemic in Northern Europe where forestry management techniques have already been adapted to its presence. The last serious outbreak was in Holland in 1955 but after a four-year programme the beetle was eradicated.

The female great spruce bark beetle attacks spruce 20–25 years old when the bark is thick enough for her to eat out a small protective chamber where she can lay her eggs. Trees which are suffering stress are particularly vulnerable. The 100–300 eggs, laid in two broods, hatch out and the larvae feed on the edge of the chamber before emerging as adults. In serious cases grubs eat out grooves, causing ring bark.

To contain the attacks, affected trees have to be felled and stripped of their bark which is burned on site or sprayed with insecticide. The Forestry Commission has the power to ensure that owners of woodland, both private and public, take action and destroy infested trees.

It is likely that the beetle arrived in Britain in imported timber that was not properly stripped but, because the life cycle of the beetle varies from one to four years, it is impossible to know how long it has been in Britain. What seems certain is that now *Dendroctonus micans* has crossed the Channel it looks like being a pest we will have to learn to live with.

Jane Wynn

East German scientists

Too many now

Science planners in the German Democratic Republic (GDR) have failed to come up with a coherent policy for the division of labour in science, according to leading East German sociologist, Professor Manfred Loetsch. Speaking on Berlin radio, Professor Loetsch claimed that this bad planning was a major cause of the disparity between spending on science and technology and the rise in productivity in the GDR.

Part of the problem, Professor Loetsch suggested, lies in the pay structure of East German science. In general the GDR has a pay policy based on payment by results. But this principle does not apply in science, where there is a fixed pay scale according to the grade of post.

Incentives, however, are not the only requirement for increased scientific productivity. Science in the GDR, said Professor Loetsch, is greatly hampered by the lack of "intermediate personnel". Higher education was greatly expanded during the last decade, but this expansion has not been matched by a parallel growth in the training of technicians. Indeed, the science planners seem to have neglected the need for such auxiliaries, so that whereas the international average for technical research gives six auxiliaries to one scientist, in the GDR the ratio is 0.8 to one. Frequently, Professor Loetsch complained,

Embarrassing admissions cause trouble

Mathematicians and human-rights activists in the West are preparing a petition to appeal for the release of a Soviet colleague, Valerii Senderov, formerly a teacher in one of the Soviet Union's schools for mathematically gifted children. Senderov was arrested in June and is now in pre-trial detention. He will probably be charged under article 70 (anti-Soviet agitation) or article 190/1 (slandering the state).

From the official Soviet point of view, Senderov is a double offender. In 1978 he was a founder member of SMOT, the unauthorized "Inter-professional Free Trade Union" group that has recently faced increasing official hostility (founder member, Albina Vakoreva arrived in Vienna last week, after being forced to emigrate). In addition, Senderov, together with fellow mathematician Boris Kanevskii, has for the past four years been monitoring admissions to Moscow University's faculty of mechanics and mathematics.

Senderov's group claims to have established discrimination against Jews.

In 1979, the team found that of 48 applicants with no Jewish parents or grandparents, who had between them won 26 prizes in the Moscow and All-Union "Olympiads", 38 were admitted to university on the result of their entrance examinations and a further two on appeal. From a group of 40 having at least one Jewish grandparent, who between them gained 48 prizes in the Olympiads, only four were initially admitted and a further two on appeal. The group's most recent report, signed also by mathematicians Naum Meinan and Grigorii Freiman, shows the same pattern for 1980, 41 non-Jewish candidates admitted out of 49, and two "Jewish" candidates out of fifteen.

The arrest of Senderov on 17 June and of Boris Kanevskii only four days later makes a report on this year's entrance examinations, held in July, very unlikely.

Vera Rich

the lack of auxiliaries is justified on ideological grounds, so that, for example, a scientist who complains that shifting stores to the laboratory is not his job will be castigated as an "elitist". Rather than expand unduly the number of graduates, he said, existing graduates should be better deployed. At present a significant proportion of graduates (estimates range from 12 to 20 per cent) are employed in posts for which a university education is not necessary.

Vera Rich

UK academic posts

Muddy waters

Both the British Home Office and the Committee of Vice-Chancellors of British universities have made moves to try and clear up, once and for all, the confusion that persists over the appointment of overseas candidates to UK academic posts. In a recent letter to the vice-chancellors' committee, the Home Office outlined its interpretation of the immigration laws as applied to university staff. And to help universities abide by that interpretation, the vice-chancellors' committee has appointed a special officer to act as an intermediary in disputed cases.

The confusion seems to have arisen because neither universities nor immigration officials have known how to apply British immigration law to overseas students at British universities who later apply for academic posts. British immigration law is against visitors using their foothold in the country to gain permanent residence. But the Home Office also acknowledges the case for employing foreign academics who could make an outstanding contribution.

Hence, determining who should be allowed to stay has often been a lengthy procedure. Universities have taken exception to officials questioning their judgement on who is suitable for a particular job and candidates have been subjected to undue delay before hearing if their applications have been accepted. In some cases, candidates have even been told to go home to their native countries before applying for a work permit.

The Home Office letter signals no change in the law but tries to set out the criteria to be used in deciding whether someone is to get a work permit. There should be evidence, it says, that the person's employment will benefit Britain, either economically or technically, or appreciably enhance Britain's international standing in a particular field of study. The onus is on universities to convince officials that those criteria are met and that no suitable British or EEC national is available for the job.

The vice-chancellors' committee believes that the Home Office letter will help universities by providing guidelines that can be presented before immigration officials.

One further problem for universities, however, could be the Home Office's stipulation that a post must be "justifiable in its own right and not simply in terms of the candidate's abilities". In their current financial straits, not many universities are likely to be creating posts for outstanding individuals. But any that have sufficient cash should be able to hook good overseas academics simply by careful argument with the Home Office, according to David Anderson-Evans, senior administration officer at the vice-chancellors' committee.

Judy Redfearn

CORRESPONDENCE

IQ jump or trend?

SIR — Lynn¹ reported evidence of significantly higher IQ in Japan than in the United States. However, his assertion that Japanese IQ shows a "rising trend" which has resulted in a "growing disparity" is not entirely supported by his data. Statistically, a better fit is obtained by assuming that a discrete jump in IQ has occurred among Japanese born after 1945.

In his analysis, Lynn used the product-moment correlation coefficient to test for trend. This implicitly supposes a linear trend. The least-squares estimate of the trend line is shown in Fig. 1 (dashed line). In fact, Lynn was prepared to discount the 1910 data point as showing the greatest discrepancy and being possibly subject to error. The trend line without the 1910 result is shown as a dotted line. Neither of these lines seems very satisfactory. In the first place, the fitted IQ for 1910 is unreasonably low, being either 98.6 or 94.7 depending upon which line is used. Second, the deviations of the data points around the lines do not show the random pattern which a genuine trend should imply. In

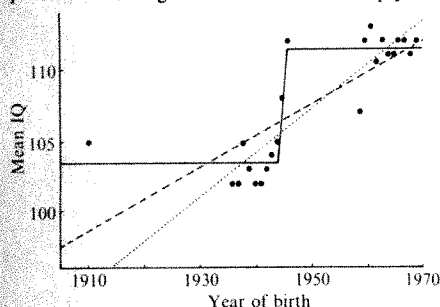


Fig. 1 Mean IQ and year of birth for 23 Japanese cohorts (data from ref. 1). The dashed line is the least-squares regression line fitted to all data points; the dotted line is the least-squares regression line fitted excluding the point for 1910. The unbroken line represents a "jump" model in which IQ is constant prior to and following 1945, but increases by a discrete step during 1945.

particular, for the 1959–69 data (mainly from a single study; see ref. 1), even though the 1959 point is low, there is little sign of a trend. If the trend was as steep as the lines suggest, it should be apparent even over a ten-year time span.

One alternative is that, instead of rising steadily, IQ has risen in a discrete jump around 1945, a time of considerable change in Japan. When the data from all cohorts are considered, the jump model (see Fig. 1) explains 89 per cent of the total variance in IQ while the linear trend accounts only for 61 per cent. If the exclusion of one outlier is permitted (jump model: 1959; trend model: 1910) these figures rise to 95 and 78 per cent, respectively. Thus, the data are much better described by a jump than by a linear trend.

Factors capable of producing a jump in the IQ results may be quite different from those which might cause a trend. In seeking reasons for the apparent rise in Japanese IQ, it may therefore be a mistake to direct too much attention to the latter.

T.B.L. KIRKWOOD

National Institute for Medical Research,
Mill Hill, London, UK

1. Lynn, R. *Nature* 297, 222–223 (1982).

... as I was saying

SIR — On 6 July 1882, I sent you a letter about "The solar commercial cycle" and I promised further elucidation about the "difficulties and objections" to my theory¹. My hope was to answer my detractors who made my theory "the subject of inconsiderate ridicule"². I was prevented from doing so by the events of 13 August 1882. On that day, intending to join my family bathing at Galley Hill beach in Sussex, I chose to descend the right side of the cliff instead of the customary left side. In the cold water I suffered a stroke and my family being on the other side of the cliff were unable to come to my aid; thus I drowned.

One hundred years have passed and all attempts to prove my correlations wrong have failed. The last three to attempt it were obliged to acknowledge that my theory should be considered as a serious hypothesis^{3–5}. After more decades of silence, a few months ago two econometricians tried their new tools and also failed. They reported whimsically: "We conclude that economic activity has an important influence on the Sun. Thus Jevons ... was right but for the wrong reason"⁶.

As the acknowledged father of econometrics⁷, let me clarify the result of their test. The seemingly absurd conclusion is due to the autoregressive mechanism of the econometric model. The sunspot influence enters through the disturbance function. The model acts as a spectral filter on the now strong frequency existing in the disturbance (the sunspot cycle). But, as it is an asymmetric filter, it produces a shift in the phase of the predominant frequency, so that the output phase reading shows up ahead of the input reading.

I also heard lately that the American SMM (Solar Maximum Mission) satellite, kept aloft for the whole year 1980, has proved through accurate instruments that the solar "constant" varies⁸. This is very exciting to me since it confirms the hunch I had in 1878 when I suggested, in your journal, that "solar observatories should be established" high in the mountains to ask the Sun himself "whether he varies or not"⁹.

For one hundred years orthodox science has been insisting that the radiation of the Sun was a "constant". Now all must agree with my 1878 hunch: it is a variable and there are significant changes from day to day, week to week, month to month ... A spectral analysis made of the SMM satellite data suggests periodicities¹⁰, and after a few more years of data, it should be possible to unravel them for forecasting purposes.

The opposition to the factual basis of my theory will crumble some day. Stubborn anomalies cannot be kept in the scientific closet forever, for sooner or later they will out.

Concerning the linking mechanism of my theory, I have very little to add. Linking solar radiation to crop yields was the obvious first choice, but I was never satisfied with it because it did not fit the data well. I have explained how, out of sheer desperation, I thought of the psychological link: "I went so far as to form the rather fanciful hypothesis that the commercial world might be a body so mentally constituted, as Mr John Mills must hold, as to be capable of vibrating in a period

of ten years. ..."¹¹.

I mentioned this idea in all my articles in the form of an inverted rhetorical question. After so much ridicule I had to be careful. My fellow scientists had barely accepted the Darwinian theory that they had vestigial parts of lower animals in their anatomy, but my fellow economists would never accept the idea that "*Homo oeconomicus*" might not have a perfectly rational psychology and is therefore somehow at the mercy of cosmic waves.

At the end of one of my articles in your esteemed journal, I forecast that the solar constant measurement was so crucial to business that, in the future, it would be "the most important news" in the daily paper¹². Living in the Victorian era, I could only insinuate my real thoughts. It is obvious that I was not referring to the effect of these daily fluctuations on crop yields but in a direct action on the solar waves on the psychological "constant" of the population. But now, after the exciting discoveries of the SMM satellite, anybody, by reading my work carefully, can get the full extent of my intuition.

A time will come when the economists will achieve the forecasting ability of the meteorologists and the vulgar will refer to us respectfully as the practitioners of the "dismal" science, the science of calculating "*dies mali*" to advise the politician and businessman properly, not so much what to do but when to do it.

WILLIAM STANLEY JEVONS

(as communicated to CARLOS GARCIA-MATA)
New Canaan, Connecticut, USA

1. Jevons, W.S. *Nature* 26, 228 (1882).
2. Jevons, W.S. *Nature* 19, 588 (1879).
3. Davis, H.T. *The Analysis of Economic Time Series*, 561–571 (Principia, Chicago, 1941).
4. King, W.I. *The Causes of Economic Fluctuations* 143–152 (Ronald, 1941).
5. Garcia-Mata, C. & Shaffner, F.I. *Q J Econ.* Nov. 1–51 (1934).
6. Sheehan, R.C. & Grieves, R. *Southern econ. J.* Jan., 775 (1982).
7. Frisch, R. *Econometrica* July, 300 (1956).
8. Willson, R.C. *et al. Science* 211, 700 (1981).
9. Jevons, W.S. *Nature* 19, 33 (1878).
10. Willson, R.C. *J. geophys. Res.* (in the press).
11. Jevons, W.S. in *Investigations in Currency and Finance* (ed. Foxwell) 226 (Macmillan, London, 1884).
12. Jevons, W.S. in *Investigations in Currency and Finance* (ed. Foxwell) 235 (Macmillan, London, 1884).

Weapons treaties

SIR — Alastair Hay (*Nature* 8 July, p.205) confuses the international treaties on chemical and biological weapons.

The 1925 Geneva Protocol outlaws the use of both chemical and biological weapons (in practice, first use, because the major parties reserved the right to use them if attacked by them).

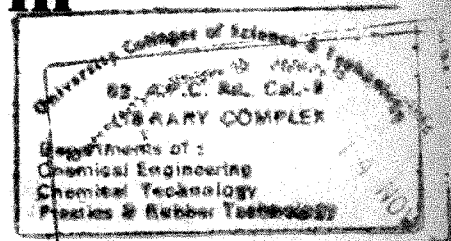
The 1972 Biological Weapons Convention — result of a British initiative taken in 1968 — bans the development, production and stockpiling of bacteriological and toxin weapons. The Committee on Disarmament is now discussing the elements of a similar convention banning chemical weapons, in which the UK delegation has made a major contribution with a draft treaty and a working paper on verification.

C.R. DEAN
Foreign and Commonwealth Office,
Arms Control and Disarmament Research
Unit, London SW1, UK

NEWS AND VIEWS

The *myc* oncogene in man and birds

from Robin Weiss



THE HL-60 cell line derived from a patient with acute promyelocytic leukaemia¹ has proved of great importance for studies of cell differentiation and transformation. The cells in culture resemble promyelocytes but can be induced to differentiate into mature granulocytes² by treatment with dimethyl sulphoxide or retinoids. The phorbol ester tumour promoter, 12-O-tetradecanoyl-phorbol-13-acetate (TPA), on the other hand, causes the cells to differentiate into macrophages³. Given this capacity to differentiate along alternative pathways, HL-60 cells are also valuable for investigating natural factors operating in myeloid cell differentiation⁴ and for delineating cell surface phenotypes during maturation.

As a leukaemic cell line, HL-60 has been examined for the expression of genes which may contribute to its neoplastic phenotype. Weinberg's laboratory⁵ showed that HL-60 DNA sequences transfected into NIH/3T3 cells caused transformation. The transfecting gene remains to be characterized. In the meantime the organization and expression of the *c-myc* gene in HL-60 cells has become a focus of interest.

The *myc* gene was first defined as the unique transforming sequence of MC29 virus and related retroviruses which cause myeloid neoplasms and other types of tumour in chickens⁶. Like other transforming genes ('oncogenes') of retroviruses, DNA sequences homologous to *myc* are found in normal chicken DNA⁶. The viral oncogene, *v-myc*, thus represents a transduced cellular gene, *c-myc*. As *c-myc* sequences have been highly conserved in evolution⁷, a cDNA probe prepared from the avian viral oncogene can be used to detect and clone the homologous gene in human DNA and to study its expression. The *c-myc* gene is expressed in a variety of neoplastic and proliferating normal human cells⁸, but mRNA levels appear to be unusually high in HL-60 cells⁹.

Two laboratories have now shown that *c-myc* DNA sequences are amplified in HL-60 cells. Collins and Groudine¹⁰, using an avian *c-myc* probe, reported in *Nature* a few weeks ago that HL-60 cells have about

16 *c-myc* copies. In this issue of *Nature* (p.61) Dalla Favera *et al.*¹¹, using cloned human *c-myc* probes, confirm this finding and show, moreover, that the leukaemic cells of the patient from whom HL-60 cells are derived were similarly amplified for *c-myc* before the cell line was established in culture. Unfortunately, normal tissue from the patient (long since dead) is no longer available so that it cannot be established whether the *c-myc* gene amplification was constitutional or was the result of somatic mutation in the leukaemia cell clone. Dalla Favera *et al.*¹¹ report that closely related pseudogenes are not amplified, suggesting that amplification might result from selection of *c-myc* function in the leukaemia cells. However, the few other patients with acute myeloid leukaemia that have been studied do not have amplified *c-myc* sequences.

Amplification of other oncogenes has been observed, but in species rather than tumours. Two related cellular genes homologous to sarcoma virus oncogenes, *Ha-ras* and *Ki-ras*, are found in markedly different copy numbers in closely related species¹². For instance, *Mus pahari* contains at least 10 copies of *c-Ha-ras*, whereas other species of mice carry only 1 or 2 copies. The transfecting gene of the human bladder carcinoma line, EJ, is now known to be the *c-Ha-ras* gene¹³, but it is not amplified in the tumour cells. It has not yet been shown whether the transfectable gene in HL-60 cells⁵ is *c-myc*; it may well be a different gene. In chicken bursal lymphomas, although *c-myc* expression is specifically elevated by adjacent provirus integration¹⁴⁻¹⁶, the gene identified by DNA transfection is quite distinct¹⁵. Similarly, the SMS-SB human pre-B leukaemia line expresses high levels of *c-abl*¹⁷, but a different transforming gene has been detected by transfection¹⁸.

The *myc* gene of MC29 is expressed in infected cells as a *gag-myc* 'fusion' protein, p110, translated from a transcript of part of the viral *gag* gene running into

myc. This was first recognized when *gag* antisera precipitated p110 from extracts of transformed cells¹⁹. Following this discovery, several other *v-onc* genes of replication-defective, transforming viruses were also found to be expressed as *gag-onc* fusion proteins. Avian retroviruses of the MC29 group, which carry *v-myc* genes, cause a bewildering variety of neoplasms — myelocytomas, endotheliomas, mesotheliomas, renal and hepatic carcinomas and sarcomas. In some elegant experiments, Graf *et al.*²⁰ showed that MC29 virus transforms both fibroblasts and macrophages in culture, but not erythroblasts, even though p110 is synthesized in infected erythroblasts. Thus, despite the variety of tumours associated with MC29 virus, there is clearly some specificity of target cells for neoplasia following infection. Furthermore, the disease spectrum can be restricted by selective passage *in vivo* of virus extracted from one type of tumour, for example, bone marrow or liver²¹, or by the isolation of *v-myc* deletion mutants *in vitro* that maintain their capacity to transform fibroblasts but are unable to transform macrophages²².

Lymphoid neoplasms are not usually caused by MC29 virus, yet the activation of *c-myc* by provirus integration in the vicinity of the cellular gene is evident in the majority of bursal lymphomas induced by avian leukosis viruses¹⁴⁻¹⁶ and also by the unrelated helper virus of reticuloendotheliosis virus²³. It is puzzling that the elevation of *c-myc* expression by the insertion of viral regulatory sequences appears to be specific to B-cell neoplasms, whereas *v-myc* inserted as part and parcel of the viral genome primarily induces other types of cancer. Hayman *et al.*²⁴, however, have now found that a transforming revertant of one of their *v-myc* deletion mutants causes a high incidence of lymphoid neoplasms with short latency. Tryptic peptide analysis of the *gag-myc* protein of this revertant indicates that the original deletion mutant may have recombined with *c-myc*. The data on deletion mutants and revertants^{22,24}, together with the evidence of selection of disease-specific strains of MC29²¹, suggest that mutations

Robin Weiss is in the Chester Beatty Laboratories, Institute of Cancer Research, Fulham Road, London SW3 6JB.

in the *myc* gene affect its target cell specificity for neoplastic transformation.

What, then, is the function of the p110 protein encoded by the *gag-myc* gene? Unlike several *v-onc* products, p110 has not been shown to have tyrosine phosphokinase activity. Recently, Moelling's²⁵ and Eisenman's²⁶ laboratories have shown both by subcellular fractionation and by immunofluorescence with *gag* antisera that the *gag-myc* protein p110 is located in the nucleus of transformed, non-virus-producing quail cells. Furthermore, purified p110 behaves as a DNA-binding protein²⁵. Since other *gag*-related polypeptides do not migrate to the nucleus or bind to DNA, it is thought that these properties relate to the transforming, *myc*-specific domain of the protein. It will be interesting, therefore, to ascertain whether the *gag-myc* proteins of the MC29 mutants²² bind to chromatin in both fibroblasts (which they transform) and macrophages (which they cannot transform), and the location and function of *c-myc* products, especially of the amplified genes in the HL-60 human leukaemia cells, also merits investigation.

The MC29 *gag-myc* protein is not the only transforming protein to have a nuclear location and DNA-binding properties. Cells transformed by Epstein-Barr virus, adenovirus and papovaviruses all express virus-coded nuclear antigens. As reviewed recently in these columns²⁷, two different viral proteins, SV40 T-antigen and a 58,000 molecular weight protein of adenovirus, both have a high affinity for p53, a host nuclear protein which may play a role in cell proliferation. Could the *myc* product be a transforming protein analogous to T-antigen or p53? □

Streptomyces in the ascendant

from K.F. Chater

DESPITE their manifest importance in antibiotic production, differentiation and soil ecology, mycelial Gram-positive bacteria of the genus *Streptomyces* have been little studied by geneticists and molecular biologists. That this situation is about to change was perhaps the major message conveyed in a recent symposium* in Kyoto on the genetics of these and many other industrial microorganisms. Various novel genetic phenomena in *Streptomyces* were documented, and the availability and use of sophisticated *in vivo* and *in vitro* *Streptomyces* recombination systems, and first steps in understanding both homologous and heterologous expression of *Streptomyces* genes were described.

A + T-rich repeated sequences (up to 12 per cent of the total DNA) are widespread in streptomycetes (R. Kirby *et al.*, University of Capetown). These sequences may have roles both in certain cases of chromosomal and plasmid structural instability, which sometimes involve the complete loss of particular DNA segments such as the tyrosinase gene of *S. reticuli* (H. Schrempf, University of Wurzburg), and in the sporadic extreme tandem amplification of functionally uncharacterized DNA sequences (H. Ono *et al.*, Institute of Microbiology, Zürich; H. Schrempf and see ref. 1). Equally unusual is the discovery of linear *Streptomyces* plasmids which have identical 611 base pair sequences at both ends of the 17 kilobase kb DNA molecules and proteins covalently bound to the 5' termini (H. Hirochika *et al.* Mitsubishi-Kasei Institute of Life Sciences, Tokyo).

Whether it will be possible to exploit these phenomena in the laboratory remains to be seen. Even without them, the *Streptomyces* geneticist has a formidable range of tools, now that endogenous *Streptomyces* DNA cloning is becoming routine. One of the most sophisticated vectors, pIJ61, which is based on the low-copy number plasmid SLP1.2, contains a selectable thiostrepton-resistance marker and a very efficiently expressed neomycin phosphotransferase gene with sites for insertional inactivation (C. Thompson *et al.*, John Innes Institute). pIJ61 was used in what is probably the first cloning of a gene involved in antibiotic production: a *para*-aminobenzoic acid synthetase gene (*pab*) involved in candidicin biosynthesis in *S. griseus* (J. Gil and D. Hopwood, John Innes Institute). Although expressed in several streptomycetes, the cloned *pab* gene was not expressed in *E. coli* unless placed under the control of an *E. coli* promoter by a deletion (it could then 'complement' mutations in both of the

unlinked *pabA* and *pabB* genes of *E. coli*). Several other *Streptomyces* genes failed to be expressed from their own promoters in *E. coli*, including genes for neomycin and viomycin phosphotransferases (D. Hopwood).

Homologous and heterologous gene expression involving *Streptomyces* DNA has been more specifically analysed with a promoter-probe vector also based on SLP1.2 (M. Bibb and S. Cohen, Stanford University). Promoters from *E. coli* (*lacUV5* and *recA*), *Serratia marcescens* (*trp*) and *Bacillus* (*penP*) all allowed the expression in *Streptomyces* of a promoterless chloramphenicol acetyltransferase gene from *E. coli*, as did a number of *Streptomyces* small DNA fragments. On the other hand, the latter fragments did not promote transcription in *E. coli*, their DNA sequences being quite unlike consensus *E. coli* promoters: their only consistent feature was a relative A + T richness (about 60 per cent G + C) in the sixty or so bases upstream of the translated regions, compared with the average G + C content of 70–73 per cent for *Streptomyces* DNA. From these results and other descriptions of the expression of R-primes among various Gram-negative bacteria (B. Holloway, Monash University, Australia) one gains the impression that promoters from low G + C DNA express in organisms with higher G + C DNA more effectively than the reverse. Together with other evidence from Bibb and Cohen that there may be less specificity for ribosomal binding to mRNA in *Streptomyces* than in *Bacillus*, streptomycetes may be uniquely suitable for studies involving heterogenic prokaryotic gene expression. No normal vegetative *Streptomyces* promoters have yet been analysed, though examples of these should soon be available for study, since highly regulated *Streptomyces* β -galactosidase and glycerol degradation genes have now been cloned (T. Eckhardt and L. Fare, Smith, Kline & French Laboratories, Philadelphia; E. Seno *et al.* John Innes Institute). As a result, antibiotic (methylenomycin A) production genes have been cloned in an attachment site deleted ϕ C31 vector carrying a viomycin resistance gene. The cloned genes were recognised because they allowed the vector to integrate into, and disrupt, the homologous genes present in a recipient, giving viomycin resistant, methylenomycin non-producing colonies (K. Chater *et al.*, John Innes Institute).

Among several λ -like *Streptomyces* phage vector systems, the most advanced is based on phage ϕ C31. An early difficulty of rather low transfection frequencies has

1. Collins, S.J., Gallo, R.C. & Gallagher, R.E. *Nature* **270**, 347 (1977).
2. Collins, S.J., Ruscetti, F.W., Gallagher, R.E. & Gallo, R.C. *Proc. natn. Acad. Sci. U.S.A.* **75**, 2458 (1978).
3. Rovera, G., Santoli, D. & Samsky, C. *Proc. natn. Acad. Sci. U.S.A.* **76**, 2779 (1979).
4. Sachs, L. *Cancer Surv.* **1**, 323 (1982).
5. Murray, M.J. *et al.* *Cell* **25**, 355 (1981).
6. Roussel, M. *et al.* *Nature* **281**, 452 (1979).
7. Sheiness, D. & Bishop, J.M. *J. Virol.* **31**, 514 (1979).
8. Eva, A. *et al.* *Nature* **295**, 116 (1982).
9. Westin, E.H. *et al.* *Proc. natn. Acad. Sci. U.S.A.* **79**, 2490 (1982).
10. Collins, S.J. & Groudine, M. *Nature* **298**, 679 (1982).
11. Dalla Favera, R., Wong-Staal, F. & Gallo, R.C. *Nature* **298**, 61 (1982).
12. Chattopadhyay, S.K. *et al.* *Nature* **296**, 361 (1982).
13. Parada, L.F., Tabin, C.J., Shih, C. & Weinberg, R.A. *Nature* **297**, 474 (1982).
14. Hayward, W.S., Neel, B.G. & Astrin, S.M. *Nature* **290**, 475 (1981).
15. Cooper, G.M. & Neiman, P.E. *Nature* **292**, 857 (1981).
16. Payne, G.S., Bishop, J.M. & Varmus, H.E. *Nature* **295**, 209 (1982).
17. Dale, B. *et al.* *Cetus-UCLA Symposium on Tumor Viruses and Differentiation* (Liss, New York, in the press).
18. Ozanne, B. *et al.* *Nature* (in the press).
19. Bister, K., Hayman, M.J. & Vogt, P.K. *Virology* **82**, 448 (1977).
20. Graf, T. *et al.* *Proc. natn. Acad. Sci. U.S.A.* **77**, 389 (1980).
21. Nagy, K. *et al.* *Archs Virol.* **68**, 81 (1981).
22. Ramsay, G., Graf, T. & Hayman, M.J. *Nature* **288**, 170 (1980).
23. Noori-Daloui, M.R. *et al.* *Nature* **294**, 574 (1981).
24. Hayman, M.J. *et al.* *Cetus-UCLA Symposium on Tumor Viruses and Differentiation* (Liss, New York, in the press).
25. Donner, P., Greiser-Wilke, I. & Moelling, K. *Nature* **296**, 262 (1982).
26. Abrams, H.D., Rohrschneider, L.R. & Eisenman, R.N. *Cell* **29**, 427 (1982).
27. Lane, D. & Harlow, E. *Nature* **298**, 517 (1982).

K.F. Chater is in the John Innes Institute, Colney Lane, Norwich NR4 7UH.

*The Fourth International Symposium on Genetics of Industrial Microorganisms, Kyoto, June 6–11 1982, was the sequel to earlier meetings in Prague (1970), Sheffield (1974) and Madison (1980).

Stamp watching and bird collecting

from Robert M. May and Judith May

AESTHETICALLY and philatelically the recent issue of US bird-and-flower stamps is remarkable; each sheet has 50 different 20 cent stamps, depicting the 'state bird' and 'state flower' of each of the 50 states. Scientists may find them additionally interesting for the way they exemplify the peculiarity of our engagement with the order Aves.

Knowing nothing about how the state birds were originally chosen, and given that there are 700 or so species to choose from, one can generate all manner of hypotheses about the diversity of bird species to be found on this set of stamps. The 'null hypothesis' would be that the states chose their birds independently and randomly, in which case we would expect only one or two pairs of states to have chosen the same bird species, and the remaining 48 or 46 states each to have made a unique choice. Of course, this null hypothesis is obviously too simple, as it overlooks biological complications in the relative abundance and geographical distribution of birds, historical and cultural factors in the founding of states, and the particular aesthetic attractions of the favoured species. The stamps in fact show the state birds to be a much less diverse assembly than would be expected on any biological grounds: 7 cardinals (for states from the east coast to Kentucky and Indiana); 6 western meadowlarks (mainly in the north-west); 6 mockingbirds (from southern states); 3 robins; 2 mountain bluebirds; 2 eastern bluebirds; 2 American goldfinches; 2 chickadees; and only 21 singletons.

Over the years, scientists too have shown that they are not immune to avian charms (though the sheer conspicuousness of birds, in comparison with most other vertebrates, undoubtedly accounts for some of this popularity). From Gilbert White's time onwards, a grossly disproportionate number of evolutionary and

ecological studies focus on birds. Many, if not most, of the subject's leading theoreticians in this century — Mayr, Lack, MacArthur and others — have been 'bird people'.

A more general reflection of this fascination is to be found in the hobby/sport/obsession of bird watching, and especially in its strange outgrowth of bird listing. We suppose some people keep life lists of the species of mammals or flowers, though surely not of insects, they have seen (after all, there do exist train listers and plane listers), but we have not met any. Bird listers, however, abound.

From their point of view, North America is a richer place than Britain; around 660 species of birds breed in North America (excluding Greenland, Bermuda and Baja California) and around 710 species are regularly seen, whereas only around 190 species of birds breed in Britain and only around 240 species are regularly seen. This difference in the number of breeding bird species is almost exactly what would be expected from the MacArthur–Wilson species–area relation, $S \sim A^z$, with $z \sim 1/4$; the ratio of the area of North America to that of Britain is roughly 80, whence we would expect roughly a ratio of 3 in the number of species. The agreement is surprising, and must surely be largely coincidental, because the underlying premises from which the species area relation is deduced pertain more to archipelagoes of islands than to large continental masses.

The list of species ever seen in North America totals around 820. In Britain the list numbers around 470, many of which are rare sightings of birds that are lost and do not want to be there. From these numbers it can incidentally be seen that membership in the '600 club' (a life list of 600 North American birds) is a substantial but not unreasonable goal. More arcane are competitions centering on the greatest number of bird species sighted in North America in one year, or simply the greatest number of species seen in any one

day, or even by turning through 360° on one spot. The record for North American bird species seen in one calendar year was until recently held by Scott Robinson, now a Princeton University graduate student, at 657. In 1979, a businessman named Vardaman spent a small fortune in pursuit of the ambition of sighting 700 species in one year. Travelling extensively and advertising widely for people to lead him to rare birds, Vardaman pushed the total number of species he had seen above 690 in the last weeks of December. The magic 700 was to elude him, however. At the year's end Vardaman's record stood at 699. God too is clearly an amateur bird lister.

Robert M. May is Class of 1877 Professor of Zoology at Princeton University, New Jersey 08544, and Judith May is an Editor at Princeton University Press.



been overcome by the surprising (and perhaps more widely applicable) finding that small positively charged, DNA-free liposomes greatly stimulate polyethylene glycol-assisted transfection of protoplasts (J. Makins, *et al.*, John Innes Institute).

Cloning systems are especially useful when allied with *in vivo* genetics. This has been made easier in *Streptomyces* by several recent developments. For example, the multicopy 8.9 kb plasmid pIJ101 is a very efficient sex factor which can be transferred into nearly all streptomycetes (D. Hopwood). Other generalized tech-

niques for achieving efficient chromosomal recombination in *Streptomyces* include protoplast fusion² and liposome-mediated transformation³. Perhaps less widely applicable is a system for Ca^{2+} -promoted transformation of competent *S. griseus* cultures by plasmid DNA (Z. Zhuang *et al.*, Institute of Microbiology, Beijing) and the discovery of a (probably narrow host range) temperate phage of *S. fradiae* which exists as a plasmid prophage and is capable of generalized transduction (S. T. Chung, The Upjohn Company, Kalamazoo).

Evidently the immediate future will see the detailed analysis of primary and secondary metabolism and differentiation in *Streptomyces*, together with a widening of our vision of prokaryotic genome structure. Some of the new techniques are sure to influence industrial programmes and may lead to the use of streptomycetes as hosts for foreign DNA expression. □

1. Robinson, M., Lewis, E. & Napier, E. *Molec. gen. Genet.* **182**, 336 (1982).
2. Hopwood, D., Wright, H., Bibb, M. & Cohen, S. *Nature* **268**, 171 (1977).
3. Makins, J. & Holt, G. *Nature* **293**, 671 (1981).

Seismic triggering and earthquake prediction

from W. Thatcher

WHILE identification of seismic gaps and the determination of earthquake recurrence intervals each provide viable means of assessing long-term earthquake potential¹, at present no comparably reliable methods exist to evaluate intermediate or short-term earthquake risk. Recent work, however, suggests that estimation of short-term risk might be improved by taking into account the potential of aseismic deformation episodes for triggering large earthquakes and incorporating this into a probabilistic assessment of earthquake risk.

The notion that aseismic movements could trigger damaging earthquakes is by no means new. Ever since Richter² pointed out the rather regular east-to-west migration of large shocks on the North Anatolian fault in Turkey, seismologists have been proposing a variety of aseismic processes that might explain this pattern and features similar to it³. What is new, however, is the accumulating evidence that transient and episodic aseismic movements are relatively common rather than extremely rare, and in several well-documented instances it appears that such movements have indeed triggered large earthquakes. The purpose of this article then is two-fold: first, to briefly review the new evidence, and second, to point out how it suggests a more integrated approach to earthquake prediction, one that draws on the evidence of studies of artificially-induced seismicity and that incorporates recently-proposed methods for the probabilistic assessment of earthquake risk⁴.

Although it has been commonly assumed that stress in seismically active regions builds up at uniform rates, geodetic survey measurements provide the evidence that this is not the case. Transient post-seismic movements of considerable size may occur over large areas for several decades after great plate boundary shocks^{5,6}, and episodic strain or elevation changes have been detected in closely monitored seismic gaps in southern California and Japan⁷⁻⁹. Uniform and non-uniform models of stress buildup are contrasted in Figure 1 and it can be seen that episodic movements could trigger a large earthquake to occur sooner than it otherwise might. Figure 2 suggests how episodic deformation could lead to the occurrence of a discernible increase in pre-earthquake minor seismicity.

Both observations and simple triggering models agree that large earthquakes can actually occur as a result of the episodic aseismic stress changes seen in geodetic

survey observations. The best evidence comes from regions where volcanic activity occurs in association with large tectonic earthquakes and triggering is the result of stress changes due to subsurface movements of liquid rock (magma) and associated gases^{10,11}. The relation between volcanism and crustal deformation on the one hand and seismicity and large earthquakes on the other is particularly well seen in Japan's Izu Peninsula¹¹.

There, two episodes of domal uplift have taken place this century (1930-33 and 1975-82), each was centred in a region of

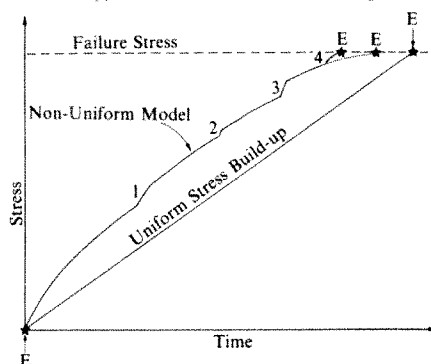


Fig. 1 Idealized modes of stress (or strain) accumulation between consecutive large earthquakes (E). Nonuniform model includes effects of both a steady postseismic decline in rate and the random occurrence of short periods of greater-than-average rates of stress increase (1-4), the last of which triggers seismic failure sooner than would otherwise have been the case (dotted curve). For simplicity the figure assumes that stress levels at any instant are everywhere the same on the eventual rupture surface. Alternatively, it can be considered that the figure shows only the stresses at the eventual earthquake hypocentre, the initiation point of failure.

Quaternary volcanism, involved uplifts of 0.2 m or more, and covered an area about 30 km in diameter. A simple magma-chamber-inflation model explains the uplift quite well¹². Near the periphery of the uplifted regions, three strike-slip earthquakes of about magnitude 7 have occurred (1930, 1978, 1980) and been preceded by one to three years of domal uplift in an adjacent region. In addition, earthquake-swarm activity was particularly marked during 1930-34 and 1975-81 and conspicuously absent during the intervening 40 years.

An inflation model shows¹¹ that shear stress increments of about a bar (0.1 MPa) were generated across the fault planes of each of these three earthquakes, in all cases acting in the correct sense to trigger seismic slippage. Of course, this increase is no more than a few per cent of the stress increment required to cause failure, the majority being supplied by regional tectonic stresses resulting from the collision of the Philippine Sea and Eurasian plates¹³.

However, because the recurrence interval for earthquakes of magnitude 7 on each of these faults is approximately 1,000 years or more¹⁴, these inflation-induced stress changes represent the equivalent of several decades of secular average stress buildup.

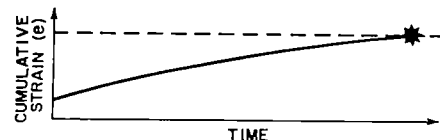
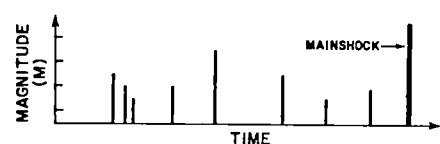
Several studies suggest that postseismic transient stress changes trigger notable earthquake activity. Utsu and Shimazaki¹⁵ have shown that in Japan, large intraplate earthquakes occur more frequently during the 10 years after a great underthrust event at the adjacent plate boundary than at other times. Studies of postseismic level changes that followed the great 1946 Nankaido earthquake demonstrate that, in contrast to interseismic secular movements, transient deformation in the several decades since 1946 extended more than 350 km inland from the plate boundary⁶. In addition, Lehner *et al.*¹⁶, following a suggestion by Anderson¹⁷, have shown that observed migrations of great earthquakes along major plate boundaries can reasonably be attributed to gradual lateral diffusion of postseismic stress away from the rupture zones of individual shocks.

Earthquakes induced by reservoir loading provide a further example of seismic triggering consistent with the mechanism sketched in Figure 1. As the graph suggests, episodic stress changes, of which the filling of a reservoir is one example, need not trigger damaging earthquakes, or indeed any earthquakes at all. Should they do so, the triggering stresses need only be a small fraction of the ambient tectonic level. Simpson¹⁸ has shown that discernible increases in post-impoundment seismicity have occurred in only a small proportion of the world's large reservoirs but further suggests that in many instances only very small stress or pore pressure changes were required to induce tectonic earthquakes of magnitude 5 or greater. Earthquakes associated with fluid injection were probably triggered by considerably larger pore pressure changes¹⁹. Swarm activity appears to precede all the well-documented large artificially-induced shocks¹⁸, and the mechanism sketched in Figure 2 may be an appropriate explanation of this activity.

While not being definite indicators of impending earthquakes, the occurrence of episodic deformation can nonetheless be taken as one indication of increased seismic risk, and several studies have suggested how they might be used to assess earthquake hazard. With respect to the strain changes observed in southern California during 1979, Raleigh *et al.*²⁰ draw attention to the non-linear character of the buildup occurring there and suggest that risk be assessed by determining whether the strain increments bring the faults of the San Andreas system closer to failure or tend to

W. Thatcher is with the US Geological Survey, Menlo Park, California 94025. A.G. Lindh, T.C. Hanks and D.J. Andrews are thanked for their helpful discussion of the paper.

① UNIFORM STRAIN BUILDUP



② EPISODIC DEFORMATION

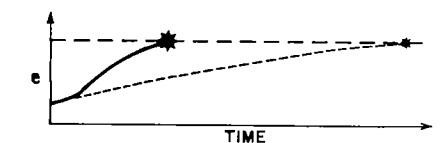
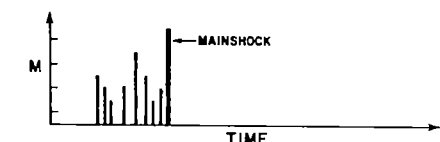


Fig 2 Possible forms of pre-earthquake seismicity

lock them, impeding slippage. They further emphasize the importance of concurrent monitoring of seismicity levels on these faults. In evaluating an earlier episode of straining that may have been related to the southern California uplift⁹, I suggested²¹ that the pattern of movements indicated relative locking of the San Andreas fault but increasing shear stresses on the bounding thrust faults of the Transverse Ranges.

Evaluation of these and other factors, as well as more concentrated monitoring, should provide rational criteria for deciding whether the probability of an earthquake has increased or decreased. Once a deformation episode has been identified, a discernible increase in micro-seismicity would provide one indicator of increased risk. The magnitude and sense of stress or strain change across candidate faults would provide another basis for deciding whether risk level should be raised or lowered. Provided areal and temporal coverage were adequate, such changes could be determined directly from geodetic data, alternatively, as was the case for the Izu Peninsula earthquakes¹¹, model calculations or indirect inferences might suffice. Earthquake focal mechanisms provide a third evaluation criterion: if micro-fault movements are in the sense expected from observed or inferred stress increments, then the probability of a damaging shock should be correspondingly increased. Even at this point, however, a large earthquake remains by no means inevitable and, in this view, no amount of positive evidence will suffice to make it so.

Nonetheless, this monitoring strategy has several advantages. It is straightforward, relies on simple physical concepts, and emphasizes well-proven methods of geodetic surveying and seismic

network operation. An emphasis on identifying episodic crustal movements and their consequences provides a rationale and focus that may be absent in a strictly empirical search for earthquake precursors. Once anomalous movements are detected, follow-up studies can begin immediately and provide risk assessments that can be continuously updated.

The ultimate importance of triggering mechanisms for earthquake prediction depends, of course, on how commonly large earthquakes are caused by detectable episodic or transient stress increases. Although this is not known, in general the probability of triggering would be expected to increase as the frequency and amplitude of episodic strain changes increase. Clearly, as Figure 1 indicates, the fault zone must already be rather close to failure.

Obvious candidates for close attention are identified seismic gaps and faults for which the time since the last large earthquake is comparable to the recurrence interval for such events. Matsuda¹⁴ has identified four such intraplate faults in Japan and refers to them as 'precaution faults'. McCann *et al.*¹ defined category 1 seismic gaps as those likely to rupture in a great earthquake 'within the next decade or few decades', and showed that seven gaps identified by this criterion since the late 1960's have subsequently been filled. From this perspective, the potential importance of triggering can perhaps best be appreciated by noting that, for many such seismic gaps, already documented episodic movements would be the equivalent of a decade or more of secular strain accumulation. □

- 1 McCann, W R, Nishenko, S P, Sykes, L R & Krause, J *Pure appl Geophys* 117, 1082 (1979); Sieh, K in *Earthquake Prediction, An International Review* (eds Simpson, D W & Richards, P G) (American Geophysical Union, 1981).
- 2 Richter, C H *Elementary Seismology* (Freeman, San Francisco, 1958).
- 3 Savage, J C *J geophys Res* 76, 1954 (1971); Scholz, C H *Nature* 267, 121 (1977); Kasahara, K *Tectonophysics* 52, 239 (1977).
- 4 Utsu, T *Rep Coord Comm Earthq Pred* 21, 164 (1979); Aki, K in *Earthquake Prediction, An International Review* (eds Simpson, D W & Richards, P G) 566 (American Geophysical Union, 1981); Lindh, A G *EOS* 61, 292 (1980).
- 5 Thatcher, W *Science* 184, 1283 (1974); Kasahara, K *Pure appl Geophys* 113, 127 (1975).
- 6 Thatcher, W & Rundle, J B *EOS* 62, 1031 (1981).
- 7 Savage, J C, Prescott, W H, Lisowski, M & King, N E *J geophys Res* 86, 6991 (1981).
- 8 Geographical Survey Institute *Rep Coord Comm Earthq Pred* 24, 152 (1980); see also Thatcher, W, Matsuda, T *J geophys Res* 86, 9237, Fig 8 (1981).
- 9 Castle, R O, Church, J P & Elliott, M R, *Science* 192, 251 (1976).
- 10 Savage, J C & Clark, M M *Science* (in the press).
- 11 Thatcher, W & Savage, J C *Geology* (in the press).
- 12 Hagiwara, in *Earthquake Precursors* (eds Kisslinger, C & Suzuki, Z) 137 (Japan Scientific Societies, 1978).
- 13 Somerville, P *Bull Earthq Res Inst Tokyo Univ* 53, 629 (1978).
- 14 Matsuda, T in *Earthquake Precursors* (eds Kisslinger, C & Suzuki, Z) 251 (Japan Scientific Societies, 1978).
- 15 Utsu, T *Rep Coord Comm Earthq Pred* 12, 120 (1974); Shimazaki, K *Bull seism Soc Am* 68, 181 (1978).
- 16 Lehner, F K, Li, V C & Rice, J R *J geophys Res* 86, 6155 (1981).
- 17 Anderson, D L *Science* 187, 1077 (1975).
- 18 Simpson, D W *Engng Geol* 10, 123 (1976).
- 19 Healy, J H, Rubey, W W, Griggs, D T & Raleigh, C B *Science* 151, 1301 (1968); Raleigh, C B, Healey, J H & Bredehoeft, J D *Science* 191, 1230 (1976).
- 20 Raleigh, C B, Anderson, D L, Sieh, K & Sykes, L R (in preparation).
- 21 Thatcher, W *Science* 194, 691 (1976).

Synthetase U-turns

from Graham Cowling

Now that the problems of gene sequence and structure are essentially solved, molecular biologists are beginning to tackle the next obstacle to a complete understanding of the translation, transcription and replication processes — the interactions between proteins and nucleic acids. The task is clearly a Herculean one and it is thus encouraging to find that advances have already been made in one area, the mechanism of aminoacyl-tRNA synthetase action.

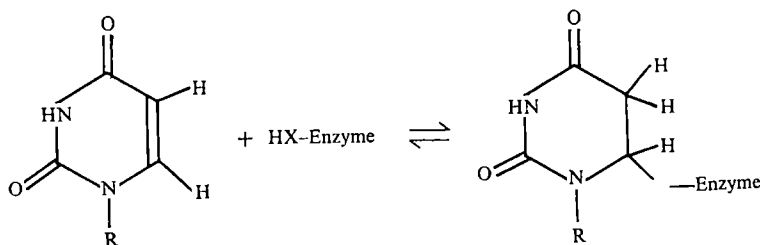
The aminoacyl-tRNA synthetases are an abundant class of cellular enzymes that assign amino acids to trinucleotide sequences (anticodons) of tRNA. They aminoacylate tRNA in a two-step reaction, first an amino acid is condensed with ATP to form an enzyme-bound aminoacyl adenylate complex and then the complex reacts with tRNA to give aminoacyl-tRNA. It is thought that there

are at least as many individual synthetases as types of amino acid and each enzyme recognizes several isoaccepting tRNAs. While each synthetase catalyses the same general type of reaction, they vary in size and quaternary structure.

The catalytic mechanism of aminoacyl-tRNA synthetase requires at least four steps, aminoacyl adenylate formation, recognition of cognate forms of tRNA, binding of tRNA to the enzyme and transfer of amino acid to tRNA. Recent work from Schimmel's group¹ has shown that at least two of these steps are related by demonstrating that a covalent bond between uridine 8 of *Escherichia coli* tRNA^{Ala} and its respective synthetase appears to be linked with enzyme activity. They further suggest that this covalent bond may be essential for active enzyme conformation.

While tRNAs vary considerably in length and nucleotide sequence, all cytoplasmic tRNAs have uridine (or 4-thiouridine) at position 8 of the nucleotide chain. This residue lies on the

Graham Cowling is at Searle Research and Development, P O Box 53, Lane End Road, High Wycombe, Bucks



Michael addition between a synthetase nucleophile and the uracil ring

inside of the vertex made by the tertiary L-shaped structure of tRNA and is well positioned to interact with synthetase. Previous observations suggest that synthetase binds tRNA by a transient, covalent bond between a uridine residue and a nucleophilic site on the protein. Synthetases seem able to catalyse the exchange of hydrogen atoms at C-5 of uridine 8 in cognate tRNAs, a reaction which involves nucleophilic attack by the enzyme on C-6 of the uracil ring to form a Michael addition product. Reversal of the reaction results in the observed H-5 exchange (see the figure). Similar mechanisms involving the formation of 5, 6-dihydropyrimidine intermediates are common with enzymes that modify pyrimidine nucleotides. Examples include thymidylate and pseudouridylate synthetases, dUMP and dCMP hydroxymethylases and DNA methylases.

Understanding of the action of thymidylate synthetase has been much helped by the use of uridine substrates with electron withdrawing groups at C-5. The substitution increases the susceptibility of C-6 to nucleophilic attack and thus allows the isolation of stable nucleoside-enzyme intermediates. This strategy has, however, failed in the case of aminoacyl-tRNA synthetase because the enzyme catalyses the breakdown of 5-bromouridine to give pyrimidine base, ribose and free enzyme. Schimmel *et al* solved this problem by finding conditions that increase both the formation and stability of 5-bromouridine-synthetase complexes. Experimentally, this involved using a greater excess of uridine derivative and omitting sulphhydryl reducing agents in the reaction. As a result a stable 'dead-end' complex between 5-bromouridine and synthetase accumulated. Each subunit of the tetrameric enzyme was found to bind one molecule of 5-bromouridine. If the site on synthetase which interacts with either 5-bromouridine or uridine 8 in tRNA is required for activity, binding the uridine derivative should block the binding of tRNA and destroy the aminoacylation activity. This seems to be the case and suggests a single uridine binding site on the enzyme.

E. coli Ala-tRNA synthetase is composed of four identical subunits each of 875 amino acids. It had already been shown that the N-terminal half of each chain (440 amino acids) is responsible for aminoacyl adenylate synthesis but cannot catalyse the

aminoacylation of tRNA². Schimmel and co-workers further demonstrate that the uridine binding site is at the C-terminal end of synthetase and 5-bromouridine does not interfere with aminoacyl adenylate formation. Data from segment directed mutagenesis experiments (unpublished) indicate that only a relatively short stretch of 30-60 residues in the C-terminal end of synthetase is required for effective tRNA binding.

Other recent studies point to a conformational change being part of the synthetase mechanism. Ebel and co-workers³ found that yeast Phe-tRNA synthetase was able to aminoacylate adenosine mononucleotide if the enzyme was conformationally triggered by binding defective yeast tRNA^{Phe} which has been stripped of its 3'-terminal adenosine (the normal site of aminoacylation). Baltzinger and Holler⁴ also concluded after kinetic studies of the catalytic mechanism of *E. coli* Phe-tRNA synthetase that a conformational change of

the nascent enzyme-tRNA complex is the rate limiting step. Whether the covalent bond between the synthetase and uridine 8 of tRNA plays a role in catalysis is less clear.

Schimmel *et al*⁵ speculate that the formation of such a bond may allow the domain responsible for adenylate formation to interact with the bound 3'-end of the tRNA. If this mechanism is correct, it will be interesting to discover how synthetases recognize the differences between cognate and non-cognate tRNAs. Although non-cognate tRNAs have been shown to bind to synthetase, this does not result in aminoacylation. Non-cognate tRNA mixtures also fail to undergo synthetase-mediated H-5 exchange. Assuming uridine binding does not occur with non-cognate tRNA, the synthetase must use other sequence or spatial criteria as part of its tRNA recognition step. These questions, as yet, remain unanswered. The abundance and heterogeneity in size and structure of synthetases suggest that the discovery of further diverse cellular functions will ensue. Already *E. coli* Ala-tRNA synthetase has been shown to bind to *alaS* promoter sequences, acting as a gene repressor of alanine biosynthesis⁶. □

- 1 Schimmel *et al* *Nature* 298, 136 (1982)
- 2 Putney *et al* *J. Biol. Chem.* 256, 198 (1981)
- 3 Ebel *et al* *Proc. Natn. Acad. Sci. U.S.A.* 78, 1606 (1981)
- 4 Baltzinger & Holler *Biochemistry* 21, 2460 (1982)
- 5 Schimmel *et al* *Trends in Biochem. Sci.* 7, 209 (1982)
- 6 Yanofsky *Nature* 289, 751 (1981)

The first meteorite stream

from David W. Hughes

METEOROID streams are common enough. Comets decay and their dust slowly spreads around the orbit forming a stream of particles in space that can be detected if the Earth intersects the stream. The August Perseids, December Geminids and January Quadrantids are examples of the displays of shooting stars produced by these intersections. The dust particles responsible usually have masses below a few grammes.

In contrast, meteorites, the rock and iron bodies that fall to the earth's surface, are much more massive and have been thought to reach the earth not in streams, but at random. Now scientists are having doubts. Seismometers left on the lunar surface by the Apollo 12, 14, 15 and 16 missions can detect meteorite impacts and as many as 150 have been recorded in a single year. Far from being random it seems that the impact rate varies throughout the year and increases between April and July.

Charles A. Wood of the Johnson Space Centre, Houston, is convinced that meteorite streams can be detected on Earth

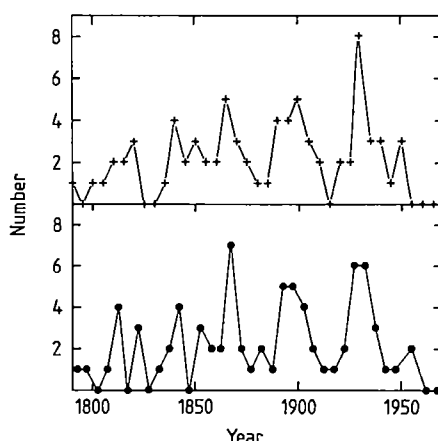


Figure 1. The number of H chondrites with cosmic ray exposure ages between 2 million and 8 million years that have been seen to fall to the Earth in a five year interval. The top data set has typical intervals 1825.5 to 1827.5, the lower data set has typical intervals 1820.0 to 1825.0. A frequency periodicity of 31.2 years can be seen with maxima in 1813, 1838, 1867, 1899 and 1929.

David W. Hughes is a Lecturer in Physics and Astronomy at The University of Sheffield, Sheffield S3 7RH.

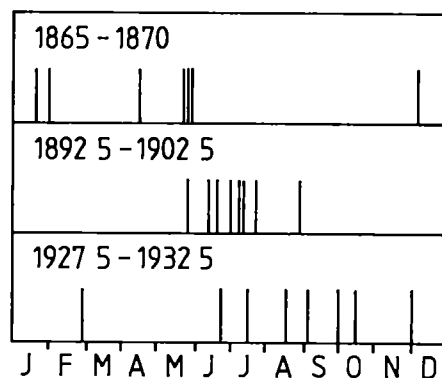
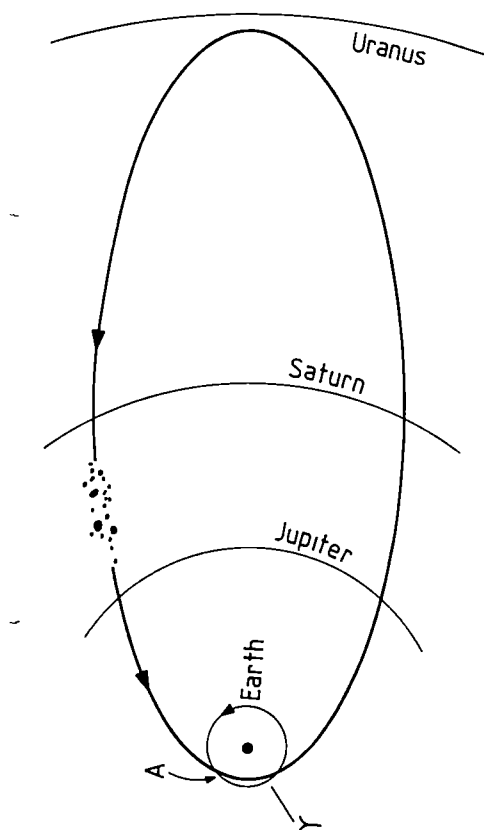


Fig 2 The meteorite stream is shown to the left. Meteorites hit the Earth at A, during June and July at a relative velocity of about 17 km s^{-1} . Impacts occur about every 31 yrs. γ represents the first point of Aries.

In the chart above the bars represent the time of fall of the meteorites that impact at the peaks of the flux curves given in Figure 1. There is a hint that the maximum flux occurs around June and July.

rate maxima are shown in the chart in figure 2. Obviously stream and sporadic meteorites are included here but still there is a hint that the maximum flux occurs around June and July, which happily agrees with the lunar seismic data. Meteorites in the orbit shown in figure 2 hit the Earth with a geocentric velocity of about 17 km s^{-1} so a reasonable amount of the meteorite survives the retardation in the atmosphere and falls to the surface.

Two major problems still await a solution. The first is the definition of the expected 1960 peak. Only 8 out of the 26 H chondrites falling between 1955 and 1970 have had their exposure ages determined.

The second problem concerns the orbit shown in figure 2. Conventional wisdom has meteorites originating from main belt asteroids. The solar gas content of

meteorites seems to require a long residence time in the inner solar system. A parent body in the asteroid belt, where about 10 per cent of the mass can be converted into regolith in $4.5 \times 10^9 \text{ yr}$, is ideal (see Anders, E., *Icarus* 24, 363, 1975). Short period comets absorb too little of the solar gases and can thus be ruled out as parent bodies, at least for all stony meteorite classes that have gas-rich members. Unfortunately, there are dynamic problems in getting meteorites from the main asteroid belt. Also, infrared observation of asteroids reveal an embarrassing lack of unambiguous parent bodies for the ordinary chondrites. Around 80 per cent of terrestrial meteorites are in this class. The orbit shown in Figure 2 however, is most unasteroid like and is typical of short period comets. It also has an aphelion distance similar to Chronos, the anomalous object orbiting between Saturn and Uranus.

Charles A. Wood and W. W. Mendell (*The Proceedings of the XIII Lunar and Planetary Science Conference* 877, 1982) conclude that the young H chondrite orbit is unstable and is representative of an orbital stage in the evolution of a small body which is moving inwards in the solar system. They propose that the H chondrite parent body was formed in the inner solar system, was ejected by Jupiter during the accretion epoch and has recently been pulled out of the Oort cloud to be reperturbed into a 'comet like' orbit that also intersects the Earth's orbit. The collision suffered by the parent body 4.45 million years ago gave the fragments very low velocities with respect to the centre of mass. This has resulted in the small spread of meteorites around the orbit and the clear indication of a 31 year period in the influx rate. The degree of spreading is shown by the narrowness of the peaks in Figure 1. □

and has published his findings in *The Proceedings of the XIII Lunar and Planetary Science Conference* 873, 1982. Wood has selected from a specific class of meteorites, ordinary chondrites with a high iron content (H chondrites), those with exposure ages between 2 and 8 million years. Cosmic rays bombarding the meteorites in space leave tracks of radiation damaged material analogous to the tracks produced by fission. Analysis of these tracks leads to an exposure age that for H chondrites peak around 4.45 ± 0.86 million years. It is generally assumed that H chondrites were part of a larger body which fragmented at the time. The falls of H chondrite in this group (figure 1) are clearly clumped in time. Neither's test for cyclical trends and the Kolmogorov-Smirnov test both confirm that the distribution is highly non-random. Power spectrum analysis gives a frequency period of 31.2 years. Maxima occur in 1813, 1838, 1867, 1899 and 1929.

The 31 year periodicity immediately indicates that the meteorites are clumped in space, in the early stages of forming a meteorite stream. An analogy is the Leonid meteoroid stream which has a period of 33 years, the small dust particles still being close to the parent comet. A period of 31 years corresponds (due to Kepler's Law) to a semi-major axis of 9.9 AU and, as the meteorites hit the Earth, it can be assumed that the perihelion distance is about 0.9 AU. The resulting orbit is shown in Figure 2. Meteorites on this orbit will hit the Earth at a specific time each year. The time of year of the fall of the meteorites from the three

Autoimmunity and the aetiology of insulin-dependent diabetes mellitus

from C. Ronald Kahn

ALTHOUGH their cause remains unknown, evidence has accumulated over the past decade that the two common types of diabetes, insulin-dependent diabetes mellitus (IDDM, also known as type I or juvenile-onset diabetes) and non-insulin-dependent diabetes mellitus (NIDDM, also known as type II or maturity-onset diabetes) may be aetiologically distinct. The damage found in IDDM appears to result from an autoimmune process which is directed at the insulin-producing β cells of the pancreas and ultimately leads to their destruction and the development of the

syndrome. The autoimmune process is probably triggered by some environmental factors in a genetically susceptible individual — exactly what these factors are is unknown but animal studies suggest viruses or toxins are likely candidates.

The first clues that an immune mechanism was involved in diabetes came from the association between IDDM and other endocrine deficiencies that had an autoimmune basis, such as those of the adrenal or thyroid glands¹. Patients with IDDM were also seen to have a remarkable increase in the prevalence of other organ-specific autoantibodies in their sera.

Direct evidence for cell-mediated autoimmunity directed against the endocrine

C. Ronald Kahn is at the Joslin Diabetes Center, Inc., Boston, Massachusetts 02215.

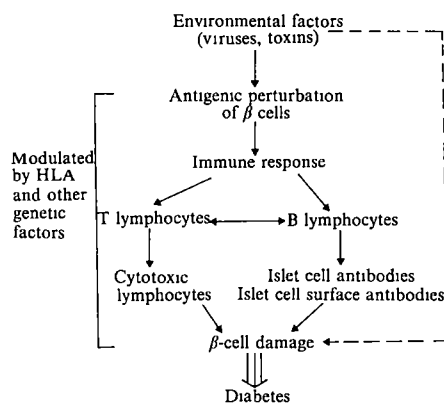
pancreas was provided in 1971 when it was found that the migration of leukocytes from patients with IDDM was inhibited by exposure to antigens prepared from endocrine pancreas². Diabetic lymphocytes also have increased adherence and cytotoxicity against cultured insulinoma cells (tumour cells of the insulin-producing β cells in the islets of Langerhans — usually benign)³. The changes in function are accompanied by alterations in the circulating lymphocyte populations in acute IDDM in both man and the BB rat, which develops an IDDM-like syndrome⁴. The passive transfer of diabetes from man to mouse and mouse to mouse using affected lymphocytes has also been reported⁵, but has been challenged as a number of groups have not been able to confirm the finding.

Despite the strong suspicion that autoantibodies might be important in IDDM, it was not until 1974 that autoantibodies against some component in the islet cell cytoplasm were detected in patients with diabetes mellitus and other autoimmune endocrinopathies⁶. Similar autoantibodies were soon confirmed in other patients and have now been found in over 2,000 diabetic patients who do not have polyendocrine failure (see review in ref 7).

As with other autoimmune features of IDDM, the exact prevalence of these autoantibodies depends on the duration of disease. Within the first one to two weeks of onset, they will be detectable in up to 85 per cent of diabetic children. This percentage rapidly declines, reaching 25 per cent by two to five years after diagnosis. The autoantibodies are present in 1–2 per cent of normal controls but their prevalence is increased in first-degree relatives of patients with IDDM and in patients with NIDDM. They are invariably of the IgG class, and, in most cases, react with the cytoplasm of all four major types of islet cells — the insulin-secreting β cells, glucagon-secreting α cells, somatostatin-secreting δ cells and pancreatic polypeptide-secreting PP cells. These autoantibodies may not be pathogenic in IDDM as only β cells are destroyed.

More recently, a complement-fixing immunofluorescence assay for detection of anti-islet cell cytoplasm autoantibodies has been used⁸. These complement-fixing antibodies seem to correlate more closely with disease. In addition, in a study currently underway, these antibodies appear to be a predictive marker of impending development of IDDM in the non-diabetic siblings of affected children.

In 1976, using a culture of insulinoma, a new class of islet cell antibodies that reacted with the surface membranes of islet cells was found⁹ and later those observations were extended using dispersed rat



Possible pathogenesis of insulin-dependent diabetes mellitus

islet cells¹⁰. Like the islet cell cytoplasm autoantibodies, the membrane autoantibodies are most prevalent in the early-onset diabetic. In the presence of complement, cell surface autoantibodies, but not cell cytoplasm autoantibodies, stimulate chromium release from radiolabelled islets and inhibit insulin release, suggesting direct cytotoxicity to islet cells¹¹. Cell surface autoantibodies, however, are also found in the sera of non-diabetic first-degree relatives of patients with IDDM.

The antigens at which the autoantibodies are directed remain to be identified. An immunoprecipitation technique¹² shows that most of the sera which contain them react with a protein of molecular weight 64,000 in ³⁵S-methionine-labelled human islet cell lysates. Hopefully, the determination of the nature of the antigen will provide a clue as to the earliest lesion in IDDM.

Circulating immune complexes have also been identified in patients with IDDM¹³. They are present not only in those patients with recent onset of disease, but also in the late phase, and in patients with NIDDM. Some of these may be immune complexes involving anti-insulin antibodies, but the widespread nature of their occurrence suggests that other antigens must be involved also.

Several animal studies suggest that virus or toxin may be the triggering factor in a genetically susceptible individual. Diabetes-like syndromes can be produced in mice by infection with encephalomyocarditis virus or reovirus^{14,15}. Reovirus also triggers production of autoantibodies that react with antigens on the surface of islet and pituitary cells, as well as antibodies that react with the hormones secreted by these cells. Likewise, insulinitis and diabetes-like syndromes can be produced by injection of low doses of β -cell toxins, such as streptozotocin¹⁴. In a series of elegant studies, Notkins and co-workers have shown that the effect of these environmental factors may be additive, and clearly varies with the genetic background of the animal¹⁵.

In humans, the precise nature of the genetic influence in the pathogenesis of

diabetes mellitus remains unclear as IDDM occurs concordantly in only about 50 per cent of identical twin pairs¹⁶. Alleles of the major histocompatibility system (the HLA system) are clearly associated with the occurrence of IDDM. Both HLA DR3 and DR4 are associated with a three- to fivefold increase in risk for IDDM¹⁷. Although there is no difference in risk between heterozygotes and homozygotes, the risk of disease to the double heterozygote — the individual with DR3/DR4 — increases almost 10-fold, suggesting that the effect of these antigens is dominant but involves independent mechanisms. HLA antigens in linkage disequilibrium with DR3 and DR4, such as B8 and B15, show similar associations. HLA B8/DR3 are associated with a persistence of islet cell surface autoantibodies in patients with IDDM^{7,8} and also appear associated with antibodies to a specific 38,000 molecular weight antigen¹². By contrast, NIDDM is not associated with any specific HLA alloantigens, but is clearly genetically influenced since it occurs in identical twins with almost total concordance¹⁶.

The recognition of the possible important role for autoimmunity in IDDM has led to attempts to suppress immune response. In mouse and rat models of IDDM, immune suppression by irradiation, neonatal thymectomy, anti-lymphocyte serum or bone marrow transplant decreases the incidence of clinical disease¹⁸. At present it is too soon to know whether these techniques will alter the course of the human disease, but they certainly present hope for the first new approach to the therapy of IDDM since the introduction of insulin over 60 years ago. □

- 1 Maccuishi, A C & Irvine, W J *Clin Endocr Metab* 4, 435 (1975)
- 2 Nerup, J., Anderson, O O., Bendixen, G., Egeberg, J. & Poulsen, J E *Diabetes* 20, 424 (1971)
- 3 Huang, S W & MacLaren, N I *Science* 192, 64 (1976)
- 4 Jackson, R., Rassi, N., Crump, T., Haynes, B. & Eisenbarth, G S *Diabetes* 30, 887 (1981); Jackson, R., Morris, M A., Haynes, B. & Eisenbarth, G S *Clin Res* 30, 395A (1982); Poussier, P., Nakhoda, A F, Jalk, J A., Lee, C. & Marliss, E B *Endocrinology* 1825 (1982)
- 5 Buschard, K., Madsbad, S. & Rygaard, J *Lancet* i, 908 (1978)
- 6 Bottazzo, G F., Florin Christensen, A. & Doniach, D *Lancet* ii, 1279 (1974)
- 7 Kahn, C R. & Flier, J S in *Clinical Immunology* Vol 2 (ed Parker, C W) 815 (1980); Irvine, W J (ed) *Immunology of Diabetes* (Teviot Scientific Publications, 1980)
- 8 Bottazzo, G F., Dean, B M., Gorsuch, A N., Cudworth, A G & Doniach, D *Lancet* i, 668 (1980)
- 9 MacLaren, N K, Huang, S W. & Fogh, J *Lancet* i, 997–1000 (1975)
- 10 Lernmark, A *et al* *New Engl J Med* 229, 375 (1978)
- 11 Dobersen, M J., Scharff, J E, Ginsberg-Fellner, F. & Notkins, A L *New Engl J Med* 303, 1493 (1980)
- 12 Baekkeskov, S *et al* *Nature*, 298, 167 (1982)
- 13 DiMario, U., Iavicoli, M. & Andreani, D *Diabetologia* 19, (1980)
- 14 Mordes, J P. & Rossini, A A *Am J Med* 70, 353 (1981)
- 15 Tomiolo, A., Onodera, T., Yoon, J W. & Notkins, A L *Nature* 288, 383 (1980); Tonodera, T *et al* *Nature* 297 (1982); Craighead, J E *Prog med Virol* 19, 161 (1975)
- 16 Barnett, A H., Eff, C., Leshe, R D G. & Pyke, D A *Diabetologia* 20, 87 (1981)
- 17 Cudworth, A G. & Woodrow, J C *Br med J* 3, 133 (1975); Rubenstein, P., Suciu-Foca, N. & Nicholson, J R *New Engl J Med* 297, 1036 (1977); Deschamps *et al* *Diabetologia* 19, 189 (1980)
- 18 Like, A A., Rossini, A A., Guberski, D L., Appel, M C. & Williams, R M *Science* 206, 1421 (1979); Like, A A. *et al* *Diabetes* 31, (Suppl 1), (1982)

ERRATUM

In *The NK cell: a phagocyte in lymphocyte's clothing?* (298, 511) an error in our labelling of a graph led to the statement that O_2^- production by NK cells exceeds that of neutrophils by two orders of magnitude: the actual production rate is about one-tenth that of neutrophils.

ARTICLES

Blue sunlight extinction and scattering by dust in the 60-km altitude atmospheric region

M. Ackerman, C. Lippens & C. Muller

Belgium Institute for Space Aeronomy, Circular Avenue 3, B-1180 Brussels, Belgium

P. Vignault

Centre d'Essais des Landes, F-40520 Biscarosse, France

Twilight data obtained photographically from a stratospheric balloon platform in the autumns of 1980 and 1981 and in the spring of 1982 are presented for blue and red light. They indicate the presence of a light absorbing layer and of a scattering layer in the mesosphere at altitudes near 60 ± 10 km with a low scattering albedo (0.1) at $0.44 \mu\text{m}$ if it is accepted that both the extinction and scattering originate from dust. The optical efficiency of the layer increases more than 10 times when the wavelength of the interacting light changes from 0.65 to $0.44 \mu\text{m}$. At the zenith and near sunset, the natural $0.44\text{-}\mu\text{m}$ extinction optical thickness and the cm^2 column scattering rate due to this layer are found to be 6.6×10^{-2} and $0.18 \text{ MR } \text{\AA}^{-1}$ respectively on 3 May 1982 above the south-west of France.

AEROSOLS have already been optically observed in the upper atmosphere from spacecrafts^{1,2} and rockets³⁻⁵. Twilight observations^{6,7} are also consistent with an upper-atmospheric particulate scattering. Other relevant experimental and theoretical work about upper atmospheric aerosols has been reviewed recently⁸ in a study of their possible continuous and sporadic extraterrestrial sources and fate. On the other hand, it has been known for more than 40 years⁹ that the atmosphere contains a source of optical extinction other than air and ozone in a supposedly transparent spectral region around $0.44 \mu\text{m}$. This extinction has been observed day and night using stars and the Sun as light sources and has caused some concern to those¹⁰⁻¹² interested in the accurate determination of the extraterrestrial solar flux who have attributed the extraextinction to aerosols. It has more recently been attributed^{13,14} entirely to NO_2 but the amount of this atmospheric constituent so deduced disagrees with observations based on the NO_2 extinction of IR radiation¹⁵⁻¹⁷ and based on the differential extinction measurement of blue light¹⁸⁻²³. Both the latter methods yield a smaller nitrogen dioxide abundance, 10–100 times less. Several authors^{20,21,23} have indicated the presence of an unattributed absorption at $0.44 \mu\text{m}$ in the upper stratosphere.

Observation method

The observation method used here has been described previously²⁴ and leads to the determination for various scattering angles, θ , of the radiance of the sunlit atmosphere in units of solar radiance as given by

$$R_\theta/R_0 = 6.79 \times 10^{-5} [Q_s n \sigma \phi_\theta / 4\pi + n_M \sigma_\theta] \quad (1)$$

where Q_s , σ , ϕ_θ and n are the aerosol scattering efficiency, the geometrical cross-section, the phase function and the number of particles on the line of sight and where n_M and σ_θ are the number of air molecules on the line of sight and the differential air scattering cross-section²⁵.

Two improvements were implemented in the gondola. A neutral density filter identical to the one used to photograph the Sun at elevation angles larger than 5° was remotely moved in front of the cameras to photograph the solar image at zenith angles from 76° to 95° allowing to perform atmospheric absorption measurements. When the Sun was at elevation angles larger than 5° , the lower neutral density screens being removed from the cameras field of view, the gondola was rotated about its

vertical axis by steps of 36° to obtain overlapping pictures of the Earth limb. The spectral bandwidths were $0.06 \mu\text{m}$ and $0.10 \mu\text{m}$ centred at $0.44 \mu\text{m}$ and $0.65 \mu\text{m}$ respectively.

The solar irradiance, I_0 , is attenuated by the atmosphere leading to the measured irradiance

$$I = I_0 e^{-\tau} \quad (2)$$

where the optical thickness

$$\tau = \sum (\sigma_g n_g) + [(Q_s + Q_a) n \sigma] \quad (3)$$

where, σ_g and n_g are the extinction cross-sections of atmospheric gases and their numbers of molecules on the optical path whereas Q_a is the absorption efficiency of the aerosol. Q_s , n and σ have been defined in equation (1). The scattering albedo of the aerosol is

$$\omega = \frac{Q_s}{Q_s + Q_a} \quad (4)$$

and the extinction efficiency of the aerosol is

$$Q_e = Q_s + Q_a \quad (5)$$

Observations

The 1981 balloon flight took place from Aire sur l'Adour in the afternoon of 19 October. During the ascent in the stratosphere and at ceiling altitude, the winds carried the balloon mainly southwards in such a way that observations took place near 43°N and $0^\circ30'\text{W}$ from 1530 to 1730 h GMT. Radar tracking was performed by the Centre d'Essais des Landes using a transponder carried with the gondola. Temperature and wind and ozone soundings were made, respectively starting at 1059 and 1336 h GMT from $44^\circ21'\text{N}$ and $1^\circ14'\text{W}$. From the beginning of the scattering measurements to the end of the absorption measurements the balloon altitude decreased from 34.3 to 33.2 km.

The observed solar irradiances, I , at $0.44 \mu\text{m}$ are plotted against solar zenith angles, χ° , in Fig. 1a as well as their theoretically evaluated evolutions from $\chi = 91^\circ$ towards smaller and larger values of χ . Rayleigh extinction by air has only been taken into account and represents fairly well the change of I from $\chi = 91^\circ$ to 94.3° . A small maximum of excess extinction is observed centred at $\chi = 92.5^\circ$. It corresponds to an optical thickness $\tau \approx 0.06$ which, if attributed to NO_2 , leads to an integrated amount on the optical path of 10^{17} molecules cm^{-2} .

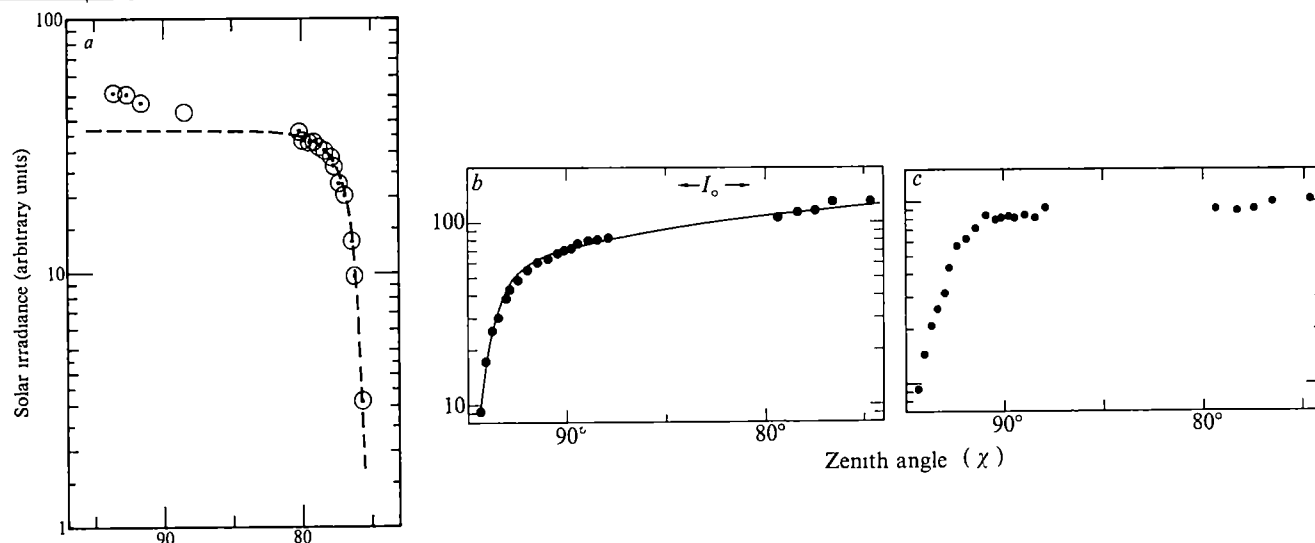


Fig. 1 *a*, Solar irradiances versus solar zenith angles observed on 19 October 1981. The circles represent the measurements while the dashed curve represents the expected variation from Rayleigh extinction, the main expected component at $0.44 \mu\text{m}$. The observed solar irradiance at $\chi = 91^\circ$ has been taken as a baseline for the computation. *b*, Solar irradiance observed on 3 May 1982 from a flight level of 6.1 mbar at $0.44 \mu\text{m}$ versus solar zenith angles χ . The values represented by the solid curve have been computed taking the extinction optical thicknesses shown in Fig. 2 and the extraterrestrial solar irradiance indicated by the arrows (I_0). *c*, As *a* but for $0.65 \mu\text{m}$. The only absorber which can be considered in this case at $\chi = 90^\circ$ is O_3 leading to a radiance reduction of 12%. No excess extinction can be detected with certainty.

at 28 km grazing altitude, a small value, if compared with previous determinations.

We wish to point out the difference between the theoretically expected and the observed evolution of I in the range $90^\circ > \chi > 76^\circ$. An excess of extinction decreasing slowly with increasing solar elevation is observed. This excess has been reported previously as shown in Table 1. Its slow evolution with zenith angle indicates that its cause lies well above flight altitude. No presently known gaseous absorber can explain the observed extinction. At $0.65 \mu\text{m}$, an optical thickness change of 0.1 can be detected in the measurements from $\chi = 76^\circ$ to 90° corresponding within experimental uncertainties to the expected variation of the ozone extinction. This leads to the first conclusion that a spectrally selective extinction takes place in the upper atmosphere at $0.44 \mu\text{m}$, of which the origin is up to now unknown. Assuming that the Chapman function is valid for $\chi < 75^\circ$, the total optical thickness at $0.44 \mu\text{m}$ on 19 October 1981 at $\chi = 90^\circ$ and at 34 km altitude may approach unity.

On 3 May 1982, another evening flight took place from Aire sur l'Adour. The gondola reached a ceiling pressure level equal to 6.1 mbar with a maximum radar measured altitude of 36.6 km. The solar extinction data are shown in Fig. 1*b*. Here again an excess extinction appears at $0.44 \mu\text{m}$ for solar zenith angles $< 90^\circ$. Figure 1*c* shows the solar extinction curve at $0.65 \mu\text{m}$. Taking into account an optical thickness of 0.1 in red light due to ozone at a zenith angle of 90° , no additional or excess absorption can be measured reliably.

The solid curve fitting the data on Fig. 1*b* is the result of a computation taking into account the optical thicknesses vari-

ation versus zenith angle shown in Fig. 2 for air (Rayleigh scattering), NO_2 and X, the unknown absorber.

To evaluate the effective altitude of X, the fraction of its maximum optical thickness τ , reached at $\chi = 90^\circ$, has been computed for various values of χ . The result is shown in Fig. 3*a*. The relative value of the extraterrestrial solar radiance indicated in Fig. 1*b* has been chosen to provide the best fit to a theoretical dependence of τ versus χ leading to an effective altitude of $60 \pm 10 \text{ km}$.

The NO_2 optical thickness shown in Fig. 2 associated with a molecular extinction cross-section of $6 \times 10^{-19} \text{ cm}^2$ leads to a total stratospheric vertical content of NO_2 of $10^{16} \text{ molecules cm}^{-2}$.

The Earth limb radiances observed in the range of zenith angles, χ° , from 86° to 93° are shown in Fig. 4 for two flights: 15 October 1981 at 37 km altitude (only mainly forward scattering is shown at $0.44 \mu\text{m}$ and at $0.65 \mu\text{m}$) and 19 October 1981 at 34 km altitude (scattering angles from 14.5° to 166° at $0.44 \mu\text{m}$ and from 10.5° to 51° at $0.65 \mu\text{m}$). The accuracy of the absolute values of R_θ/R_0 are considered to be $\pm 50\%$ from one camera to the next, mostly due to the uncertainty in the evaluation of the high extinction of the neutral density screens. The accuracy of the relative values on a single camera is $\pm 5\%$. The radiance variation observed compared with χ° on 15 October 1980 and shown here for $\theta = 13^\circ$ is the best illustration.

Table 1 List of extinctions in excess of Rayleigh scattering extinction observed at or near $0.44 \mu\text{m}$ and at solar zenith angles $\chi \approx 90^\circ$ by means of instruments flown on various dates at various altitudes in the stratosphere.

Date	Flight altitude (km)	Range of χ°	Wave-length (nm)	$\Delta\tau$	Ref
9 February 1977	40	75–80*	445	0.18	20
15 October 1980	38	81–84	440	0.28	This work ²⁴
19 October 1981	34.1	76–82	440	0.19	This work
19 October 1981	34.1	82–90	440	0.22	This work
June–July 1973	16.0	$90^\circ \rightarrow$	430	0.57	13

The changes of optical thickness, $\Delta\tau$, are indicated for various ranges of zenith angles. The observations made from Concorde in June–July 1973 lead to an absolute value of τ deduced from absolute solar irradiance data measured at 16 km altitude and at $\chi = 90^\circ$ compared with extraterrestrial solar flux values.

* τ has deduced from a least square fit to the data available in this range of χ° .

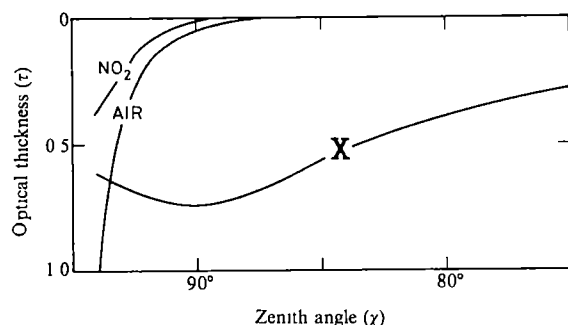


Fig. 2 Optical extinction thicknesses due to air, NO_2 and to the excess absorber, X, necessary to interpret the extinction observations of Fig. 1*b*.

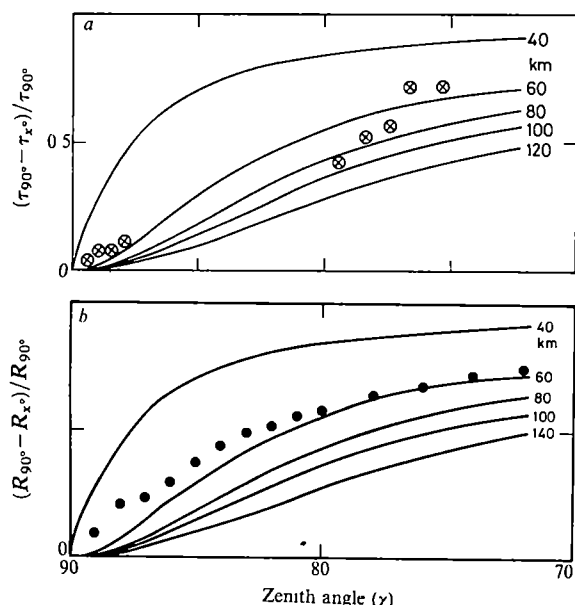


Fig. 3 *a*, Fraction of the excess extinction at $\chi = 90^\circ$ plotted against zenith angles, χ . The computed variation of this quantity versus χ for various effective altitudes (40, 60, 80, 100 and 140 km) of the X absorber. *b*, As *a*, the fraction of the excess radiance observed at $\chi = 90^\circ$ is plotted against χ . The expected variation of this quantity is also shown for various effective altitudes. It indicates an effective altitude of the excess radiance of nearly 60 km.

of the phenomenon that we wish to emphasize. Because at $0.44 \mu\text{m}$, the Rayleigh scattering should dominate the scattering, a theoretical variation of the total number of air molecules on the line of sight versus χ is fitted to the observed radiance curve at $\chi = 90^\circ$. At χ larger and smaller than 90° the observed radiance variation with χ is smaller than the theoretical one represented by the dotted curve. The cause of this difference is considered to be an excess of radiance originating from altitudes larger than the flight altitude. The dotted theoretical curve is shifted downwards to fit the observations at $\chi \approx 92.5^\circ$ where the excess of radiance becomes small compared with the air Rayleigh radiance, because lower and lower altitudes are tangentially observed at progressively larger zenith angles.

where the increasing air density must eventually dominate the scattering dependence of zenith distance. It is also observed that the excess radiance decreases slowly above the horizontal line of sight when χ° becomes $< 90^\circ$. The same phenomenon is observed on 19 October 1981 at $0.44 \mu\text{m}$ and at all scattering angles. In this case, however, the excess appears relatively smaller since the flight altitude was lower leading to a larger Rayleigh scattering due to air. A decrease of the blue and red colour ratio occurring near 1° solar depression angle, δ° , has been observed in twilight studies⁶ as well as an excess of blue light at $\delta = 0^\circ$ which was attributed to multiple scattering. In the case of our observations, however, the air observed at $\chi \leq 90^\circ$ is theoretically optically thin and multiple scattering does not explain the radiance excess, relative to pure air, linked with the anomalous radiance variation with zenith angle.

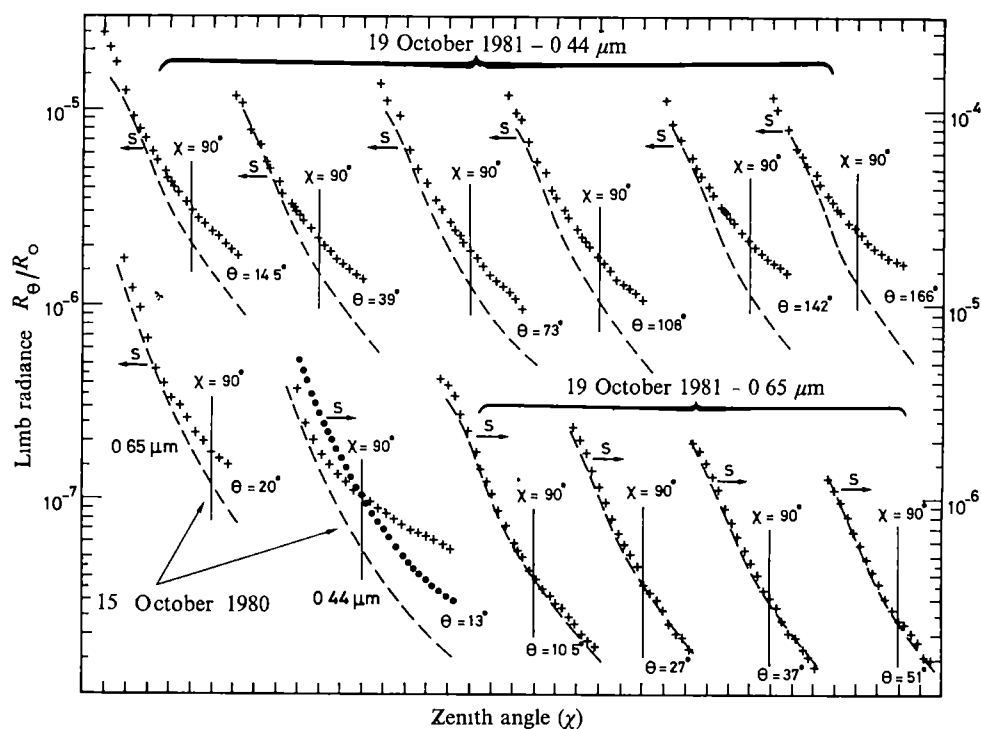
At $0.65 \mu\text{m}$, a small excess of radiance is observed at $\theta = 20^\circ$ on 15 October 1980. It is barely detectable at $\theta = 10.5^\circ$ on 19 October 1981 and it cannot be detected at larger scattering angles, being probably too small relative to Rayleigh scattering at this low flight level.

For the 3 May, 1982 flight, one of the cameras was fitted with a blue filter-equipped wide angle lens ($f = 50 \text{ mm}$) instead of the lens normally used ($f = 80 \text{ mm}$). No neutral density screen was placed in front of this camera so that the sky could be viewed over a wider range of zenith angles. The calibration of this camera was performed by comparing film optical densities of identical features simultaneously photographed by means of another blue filter, neutral density screen equipped, camera.

The limb radiances observed at two flight levels, one during the balloon ascent and the other one at ceiling altitude, are plotted in Fig. 5 against zenith angles. The variations of the number of air molecules viewed on the optical path versus zenith angles are also represented and fitted to the observations at large zenith angles ($> 90^\circ$) where pure air Rayleigh scattering must dominate.

As for the extinction in Fig. 3a, the fraction of the total excess radiance at $\chi = 90^\circ$ has been plotted against zenith angles in Fig. 3b. Here again the measurements show an effective altitude for the excess radiance near 60 km. The radiance was also observed at $0.65 \mu\text{m}$ for two flight levels as it was done in Fig. 5 for $0.44 \mu\text{m}$. The excess radiance determined in red light is 11 times smaller than in blue light. By spinning the gondola about its vertical axis by steps of 36° , the data necessary for

Fig. 4 Earth limb radiance R_θ/R_0 in units of solar radiance observed on 15 October 1980, at 37 km altitude and on 19 October 1981 at 34 km altitude versus zenith angles χ° . The observations are represented by crosses. The dashed and dotted (see text) curves represent total numbers of air molecules in arbitrary units which can be seen on the line of sight versus zenith angles χ° . The arrows marked 's' indicate the ordinate scale relevant for each graph. The scattering angles θ° , the wavelengths, $0.65 \mu\text{m}$ or $0.44 \mu\text{m}$ and the dates are also indicated. Average solar zenith angles were 78° on 19 October 1981 and 80° on 15 October 1980. For each case a vertical line indicates the $\chi = 90^\circ$ position on the abscissa where an angular difference of 1° separates two ticks, zenith angles increase towards the left-hand side of the figure.



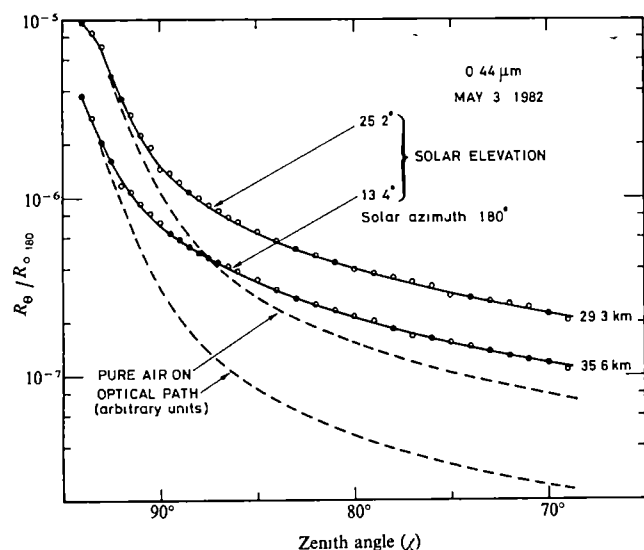


Fig. 5 Atmospheric radiance plotted against zenith angle at $0.44 \mu\text{m}$ from two flight levels on 3 May 1982. The pure air expected radiance is represented by the dashed curves.

the determination of the phase function of the excess radiance have been obtained.

The phase functions are shown in Fig. 6 for three zenith angles in the case of the excess radiance. The values for air are those measured at $\chi = 90^\circ$. However, in the latter case the angular variation reflects the phase function at zenith angles close to 93.5° , corresponding to grazing altitudes nearing 20 km. At these low altitudes the low stratospheric aerosols and perhaps the Earth sphericity induce illumination asymmetries when the solar azimuth changes from 36° to 180° . This most probably explains the deformation of the measured air phase function shown in Fig. 6 for air. At smaller zenith angles the air Rayleigh scattering becomes quickly very small compared with the excess radiance for which it becomes only a correction factor. The phase function observed at $\chi = 80^\circ$ is for this reason used to deduce its characteristics.

The value of $Q_s n \sigma$ has been evaluated from these experimental data by means of the relationship

$$Q_s n \sigma = 1.85 \times 10^5 \sum_{0^\circ}^{180^\circ} (R_\theta / R_0) (\sin \theta \sin \Delta \theta / 2) \quad (6)$$

by zonal summation every 10° between 0° and 180° . The extinction due to scattering is found to be 2.6×10^{-2} which, according to Fig. 3b, leads, at $\chi = 90^\circ$, to $Q_s n \sigma = 6.1 \times 10^{-2}$. On the other hand, the asymmetry parameter, $\langle \cos \alpha \rangle$, is found to be 0.06.

Discussion

The extinction and the excess of radiance have been shown to originate from an altitude near 60 km, in the mesosphere. They both also exhibit a large enhancement when the wavelength changes from 0.65 to $0.44 \mu\text{m}$.

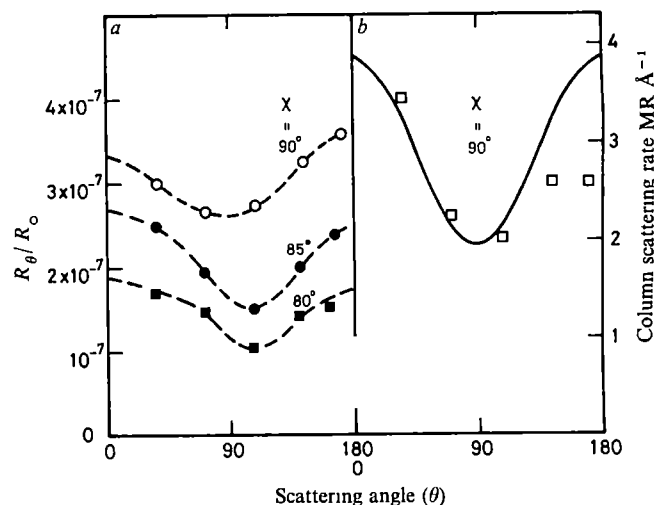


Fig. 6 Atmospheric excess radiance (a) observed at various zenith angles plotted against scattering angles θ . b, The pure air radiance phase function computed for the flight level (at 6.1 mbar) from the air differential cross-section²⁵. Solar elevation is taken as $9^\circ \pm 1.5$.

For an effective height of 60 km and an observation altitude of 35 km the optical depth factor increases 11.4 times from $\chi = 0^\circ$ to 90° . The excess extinction observed leads, according to Fig. 3, to a zenithal optical depth of 6.6×10^{-2} of which 5.4×10^{-3} is due to scattering by the dust layer. If it is accepted that the dust is responsible for both extinction and scattering in the 60-km layer, the dust scattering albedo is 0.08. This low value is compatible with very small particles exhibiting an almost symmetrical scattering phase function. One way to explain the large scattering efficiency increase when the wavelength changes from 0.65 to $0.44 \mu\text{m}$ is to consider a colour-dependent complex index of refraction in this range with a non-negligible imaginary part of the index²⁶. The dust would thus be made out of brownish matter. The complexity of the upper atmospheric dust probably having an extraterrestrial origin has already been pointed out²⁷.

Conclusion

The demonstration that a dust layer is present in the Earth's atmosphere at 60 km altitude would have a purely academic interest if it were not for its association with a non-negligible sunlight extinction and absorption *in situ* which makes it important for the Earth radiation balance, for the stratospheric and mesospheric photochemistry and energy budget and for the measurements of stratospheric trace species in blue light. These aspects justify the continued optical investigation of the layer from balloon gondola and from other platforms, and the use of other methods of investigation.

We thank the French Centre National d'Etudes Spatiales for the balloon operations and the Etablissement d'Etudes et de Recherches Météorologiques for atmospheric soundings.

Received 5 April, accepted 18 June 1982

- Giovane, F., Schuerman, D. W. & Greenberg, J. M. *J. geophys. Res.* **81**, 5388 (1976).
- Kondratyev, K. Ja., Buznikov, A. A. & Pokrovsky, O. M. *Dokl. Akad. Nauk SSSR* **235**, 53–56 (1977).
- Gray, C. R., Malchow, H. L., Merritt, D. C. & Var, R. E. *Spacecraft Rockets* **10**, No. 1 (1973).
- Cunnold, D. M., Gray, C. R. & Merritt, D. C. *J. geophys. Res.* **78**, 920–931 (1973).
- Rossler, F. *The Aerosol-Layer in the Stratosphere* (Deutsch-Französisches, St. Louis, France, 1967).
- Volz, F. & Goody, R. M. *J. atmos. Sci.* **19**, 385–406 (1962).
- Meinel, M. P. & Meinel, A. B. *Science* **142**, 582–583 (1963).
- Hunten, D. M., Turco, R. P. & Toon, O. B. *J. atmos. Sci.* **37**, 1342–1357 (1980).
- Vassy, A. & E. *J. Phys.* **10**, 403–412 (1939).
- Dunkelman, L. & Scolnik, R. *J. Opt. Soc. Am.* **49**, 356–367 (1959).
- Labs, D. & Neckel, H. *Z. Astrophys.* **69**, 1–73 (1968).
- Deluisi, J. J. *J. geophys. Res.* **80**, 345–354 (1975).
- Blamont, J., Pommereau, J. P. & Souchon, G. *C. r. hebdomadaire Séances Acad. Sci., Paris* **281**, 247–252 (1975).
- Leroy, B., Hicks, E. & Vassy, A. *Ann. Geophys.* **36**, 205–208 (1980).
- Ackerman, M. & Müller, C. *Nature* **240**, 300 (1972).
- Ackerman, M. *et al. planet. Space Sci.* **23**, 651–660 (1975).
- Cooley, M. T., Mankin, W. G. & Goldman, A. *J. geophys. Res.* **86**, 7331–7341 (1981).
- Noxon, J. F. *Science* **189**, 547–549 (1975).
- Kerr, J. B. & McElroy, C. T. *Atmosphere* **14**, 166–171 (1976).
- Goldman, A., Fernald, F. G., Williams, W. J. & Murcray, D. G. *Geophys. Res. Lett.* **5**, 257–260 (1978).
- Rigaud, P., Naudet, J. P. & Huguénin, D. *C. r. hebdomadaire Séances Acad. Sci., Paris* **284**, 331–334 (1977).
- Naudet, J. P., Rigaud, P. & Huguénin, D. *Geophys. Res. Lett.* **7**, 701–703 (1980).
- Pommereau, J. P. thesis, Univ. Paris VI (1981).
- Ackerman, M., Lippens, C. & Müller, C. *Nature* **292**, 587–591 (1981).
- Penndorf, R. *J. opt. Soc. Am.* **47**, 176–183 (1957).
- Kerker, M. *The Scattering of Light and Other Electromagnetic Radiation* (Academic, New York, 1969).
- Bigg, E. K., Kviz, Z. & Thompson, W. J. *Tellus* **23**, 247–259 (1971).

Basalt genesis and mantle structure studied through Th-isotopic geochemistry

Claude J. Allègre & Michel Condomines

Laboratoire de Géochimie et Cosmochimie, Institut de Physique du Globe et Département des Sciences de la Terre, Universités de Paris 6 et 7, 4 Place Jussieu, 75230 Paris Cedex 05, France

The relative importance of the degree of partial melting and of the composition of the source, is investigated for basalts of various origins on the basis of observed Th isotopic variations. If the oceanic island basalts (OIB) and the mid-oceanic ridge basalts (MORB) are not mutually contaminated, the Th isotopic tracers show that the difference between MORB and OIB is due to a difference in the composition of their sources rather than in the degree of partial melting. The characteristics of the island arc volcanics are completely different from those for the oceanic basalts, thereby implying a difference in both their origin and their geochemical process of petrogenesis.

THE determination of the sources and the magmatic processes for basalt genesis is a key problem in petrology^{1,2}. The relative importance of these two factors in determining the different types of volcanism is also crucial. The current (popular or accepted) ideas for the three major types of volcanism can be summarized as follows. The mid-oceanic ridge basalts (MORB) would result from a large degree of partial melting whereas oceanic island basalts (OIB) mainly alkalic or of alkalic affinity correspond to a small degree of partial melting. The difference in composition of the initial material, proposed on a geochemical basis, especially from isotope studies, seems to be secondary relative to effect of the degree of partial melting, at least for the major elements. For trace elements, especially the incompatible elements, the effect of a different source or of a different degree of partial melting would be about the same.

However, the difference between MORB and island arc basalts (or andesites) would mainly result from a major difference in the composition of the sources, the MORB originating from a depleted mantle, mainly peridotitic, whereas the island arc basalts originating either by the melting of a basic downgoing slab (in the eclogite or amphibole facies) with possible mixing with sediments of continental crust, or from the melting of an hydrated peridotitic wedge.

We attempt to show here how the use of the (²³⁰Th/²³²Th) isotopic ratios measured in volcanic rocks can help in clarifying such problems and in deciphering whether the nature of the source or the processes of formation are at the origin of the differences observed among basalts. (In what follows the ratios in parentheses are activity ratios and those between square brackets are atomic ratios.)

(²³⁰Th/²³²Th)–⁸⁷Sr/⁸⁶Sr correlation in recent volcanic rocks

The measurement of (²³⁰Th/²³²Th) ratios for recent lavas from several oceanic areas has shown the existence of an anticorrelation relative to their [⁸⁷Sr/⁸⁶Sr] ratios (Fig. 1)³. The most likely interpretation for this anticorrelation is that the source regions for the basalt volcanism of these various zones are in radioactive equilibrium, and that the (²³⁰Th/²³²Th) ratios of the lavas are representative of the (²³⁸U/²³²Th)_s ratios of the mantle source, which implies a negligible time of stay at depth and of transfer of these magmas to the surface (a few thousand years at the most) relative to the ²³⁰Th half life (75,200 yr). The (²³⁰Th/²³²Th)–[⁸⁷Sr/⁸⁶Sr] anticorrelation is then indicative of a correlation between [Th/U] and [Rb/Sr] ratios of the source regions, hence of a consistency of the Th–U, Rb–Sr and Nd–Sm chemical fractionations. A low [⁸⁷Sr/⁸⁶Sr] ratio corresponds to a mantle source with time-integrated low [Rb/Sr] and [Th/U] ratios, and thus high (²³⁰Th/²³²Th) ratio. The 'bulk Earth' value of [Th/U] ratio (~3.7) can be derived from Pb isotopic studies⁴.

This value corresponds on the correlation diagram to a [⁸⁷Sr/⁸⁶Sr] value of ~0.7048, which is precisely the 'bulk Earth' Sr isotopic ratio obtained through the Sm–Nd correlation. The consistency between these different isotopic tracers is thus confirmed. We must then admit that, in the mantle, there are depleted zones for which the [Th/U] ratio is low (high (²³⁰Th/²³²Th)) and low [⁸⁷Sr/⁸⁶Sr] ratios) they are the source regions of most of the oceanic volcanism, with a minimum [Th/U] value of around 2.3. The complement of these depleted sources is probably the continental crust which should have a [Th/U] ratio higher than 3.7.

A correlation between isotopic ratios and trace elements ratios had already been suggested previously for the MORB^{5,6}. This correlation was nonlinear. When using the Th isotopes, we do not observe any curvature in the correlation which suggests that this curvature results from a chemical fractionation in the trace element ratios created by partial melting (see Fig. 1, inset).

The comparison of the actual (²³⁸U/²³²Th) ratios of the lavas and of their (²³⁰Th/²³²Th) ratios as representative of the (²³⁸U/²³²Th) ratios of the source regions, yields a simple and unique way of determining the U–Th fractionations due to the whole magmatic processes. Because the differentiation phenomena through fractional crystallization have little effect on the [Th/U] ratio, at least for oceanic volcanism, most of the Th–U fractionation can be ascribed to partial melting³. Figure 2 illustrates this process in a (²³⁰Th/²³²Th)–(²³⁸U/²³²Th) isochron diagram⁷. The point S represents the mantle source in radioactive equilibrium. Through partial melting a magma M is produced with an identical (²³⁰Th/²³²Th) ratio but a different (²³⁸U/²³²Th). The fractionation produced may be represented by a factor

$$k = (^{238}\text{U}/^{232}\text{Th})_{\text{M}} / (^{238}\text{U}/^{232}\text{Th})_{\text{S}}$$

where M and S stand for the magma and the mantle source respectively. Since

$$(^{238}\text{U}/^{232}\text{Th})_{\text{S}} = (^{230}\text{Th}/^{232}\text{Th})_{\text{S}} = (^{230}\text{Th}/^{232}\text{Th})_{\text{M}} \\ k = (^{238}\text{U}/^{230}\text{Th})_{\text{M}}$$

Obviously, if the time of stay at depth and of transfer of the magma to the surface is significant relative to the ²³⁰Th half life then the point representative of the magma shifts along a vertical line, downwards if this point is to the left of the equiline ((²³⁰Th/²³⁸U) > 1) or upwards if the point is to its right ((²³⁰Th/²³⁸U) < 1) (Fig. 2), considering that the differentiation has no effect on the (²³⁸U/²³²Th) ratio of the magma. In this case, to determine the fractionation due to partial melting we must consider the (²³⁰Th/²³²Th)₀ initial ratio of the magma at the time of its formation. If the time of stay at depth of the

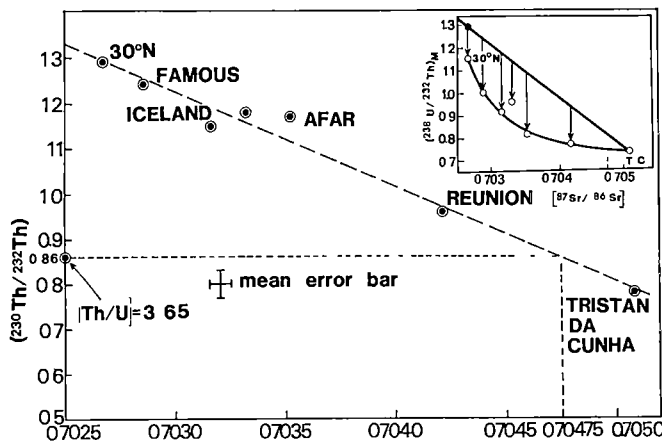


Fig. 1 Correlation diagram between $(^{230}\text{Th}/^{232}\text{Th})$ and $^{87}\text{Sr}/^{86}\text{Sr}$ ratios (from ref. 3). Inset, correlation diagram between $(^{238}\text{U}/^{232}\text{Th})_M$ ratios of the magmas and $^{87}\text{Sr}/^{86}\text{Sr}$ isotopic ratios (note the curvature of this correlation).

magma is important, its representative point on the diagram is shifted away from the $(^{230}\text{Th}/^{232}\text{Th})$ – $^{87}\text{Sr}/^{86}\text{Sr}$ correlation line because of the change in the $(^{230}\text{Th}/^{232}\text{Th})$ ratio due to radioactive decay. In this hypothesis, which may be verified through the study of the $(^{230}\text{Th}/^{232}\text{Th})_0$ initial ratios evolution of the lavas throughout the history of the volcanic region, the measurement of the $^{87}\text{Sr}/^{86}\text{Sr}$ ratio yields the $(^{230}\text{Th}/^{232}\text{Th})_0$ ratio of the initial magma through the Th–Sr isotopic correlation, hence, the fractionation parameter k for partial melting.

Characteristics of partial melting

Figure 3, in which data for recent lavas from various regions that have already been studied in detail^{3,8–12} are plotted, clearly shows that most of the regions studied plot to the left of the $(^{230}\text{Th}/^{232}\text{Th})$ – $(^{238}\text{U}/^{232}\text{Th})$ diagram. This is the case for oceanic lavas such as those from the *FAMOUS* and 30°N zones on the mid-Atlantic ridge, for lavas from Afar, from oceanic islands such as Iceland, Hawaii, Faial (Azores) and La Reunion, from Etna and Stromboli¹³ and those from the continental alkali volcanism of the Chaîne des Puys (Massif Central, France).

However, some lavas plot to the right of the equiline. These all come from subduction zone volcanism such as Costa Rica⁸ and Japan (unpublished data). This type of volcanism, thus, seems quite distinct from the general case for which $(^{230}\text{Th}/^{238}\text{U})$ is >1 .

We will now consider the case of the volcanism in oceanic regions and that in subduction zones.

Oceanic basalts

The fact that all recent oceanic lavas plot to the left of the equiline has a fundamental implication about the partial melting. The latter fractionates the $[\text{Th}/\text{U}]$ ratio (whereas crystal fractionation does not) and would produce a magma with a $[\text{Th}/\text{U}]$ ratio larger than that for the mantle source. In other words, the melt is preferentially enriched in Th relative to U ($D_{\text{Th}} < D_{\text{U}}$). Indeed, these studies demonstrate that most of the oceanic lavas originate from a mantle source with $[\text{Th}/\text{U}]$ ratios lower than the primitive value of 3.7 (ref. 3), thus, from a source which has already been depleted through previous partial melting events. This is in full agreement with the conclusions from Pb isotopic studies⁴. Thus, the oceanic tholeiites with the most depleted character in Pb isotopes (as in Sr or Nd) have the highest $(^{230}\text{Th}/^{232}\text{Th})$ ratio values hence the lowest $[\text{Th}/\text{U}]$ ratios for their source regions (Fig. 3).

Such a result shows that despite their highly magmaphile character, $[\text{Th}/\text{U}]$ ratios do fractionate during partial melting and therefore, using the $[\text{Th}/\text{U}]$ ratio measured in lavas to infer $[\text{Th}/\text{U}]$ mantle geochemistry and heterogeneities, is a risky exercise. This applies to Th and U, which are among the most magmaphile elements, but also to other elements such as rare

earth elements, Ta, Hf and, of course, to Tb, Sr, Sm, Nd (see refs 14, 15). A most important factor is the degree of partial melting which can be estimated through the parameter (k) previously defined as the Th–U fractionation factor between the mantle source and the magma. The larger this fractionation, the lower the degree of partial melting considering that the partition coefficients D_{U} and D_{Th} remain almost constant. The determination of the latter would allow a calculation of the degree of partial melting. This assumption that the partition coefficients D_{U} and D_{Th} remain constant might be an oversimplification. Indeed, we do not know which minerals are involved in Th–U fractionation during partial melting. Tatsumoto⁴ assumed that, among the main minerals of peridotite, clinopyroxene is the major phase involved in this fractionation. But, he emphasized that the experimentally determined clinopyroxene–melt partition coefficients indicate a Th–U fractionation in contradiction with the Pb isotopic data (that is a melt with a Th/U ratio lower than that of the mantle). He concluded that either the experimental clinopyroxene–melt partition coefficients were not applicable to natural conditions during partial melting, or that other minerals such as phlogopite, amphibole, (apatite) were involved in the partitioning between U and Th.

Nevertheless, it is quite obvious that the percentage of melt is rather variable for tholeiites from oceanic ridges or rift zones (for example ~ 0.9 at 30°N of the mid-Atlantic ridge, $k \sim 0.8$ for the *FAMOUS* zone and Iceland at 37°N of the mid-Atlantic ridge and $k \sim 0.7$ for a lava from Afar). In an environment of spreading centre there seems to be a relationship between the degree of alkalinity and the degree of partial melting as determined through the parameter k . Indeed, the basalts from Afar are more alkaline than those from the *FAMOUS* zone, the latter being themselves more alkaline than those from 30°N.

This relationship between the degree of alkalinity and the degree of partial melting determined through the parameter k , seems still to be valid (Fig. 3) for oceanic islands and even continental volcanism (Chaîne des Puys). For example, $k \approx 0.9$ for the tholeiites from Kilauea (Hawaii), $k \approx 0.8$ for the transitional tholeiites from La Réunion, $k \approx 0.7$ for the alkali basalts from the Grande Comore island (Indian Ocean) as well as for those from the Chaîne des Puys (Massif Central, France). Note that the k coefficients (0.9–0.7) appear to be similar to those determined for the MORB, whereas the $(^{230}\text{Th}/^{232}\text{Th})$ ratios are clearly lower and more variable, indicating different, less depleted mantle sources. The difference in the degree of melting does not seem to be the primary cause of the chemical difference between MORB and OIB. The difference between the source regions and their more or less depleted character thus appear more important than the actual percentage of partial melting.

If the OIB were actually derived from a lower degree of partial melting of mantle material than MORB, then the partition coefficients D_{U} and D_{Th} must be different in these two cases and would probably be related to two mantle sources of different chemical and mineralogical composition. As a corollary to what we know about Sr and Pb isotopic ratios, the two

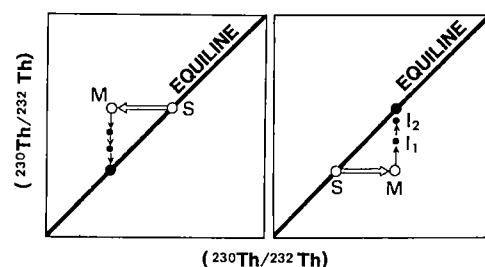


Fig. 2 Isochron diagram showing the geochemical behaviour of the ^{230}Th – ^{238}U system during partial melting and fractional crystallization (see refs 3, 11 for general explanation). S, magma source, M, primary magma, I_1 , I_2 , different lavas erupted at different times. White arrows represent partial melting, black arrows represent radioactive decay.

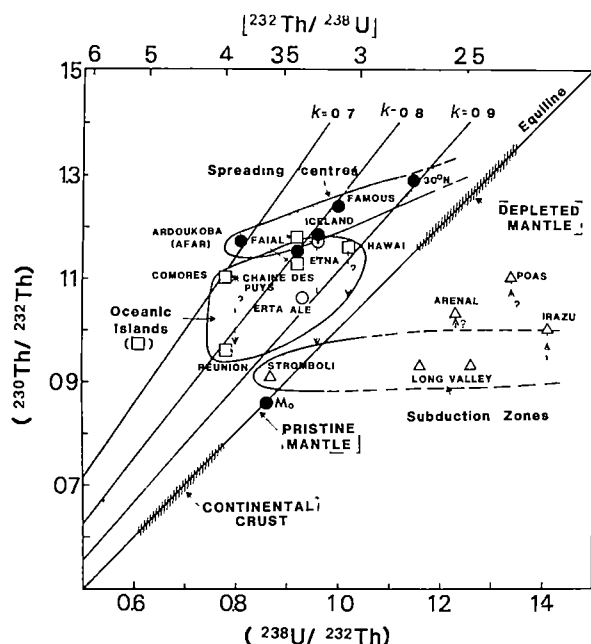


Fig. 3 Isochron diagram showing the different magmas of various sources. Data are from refs 3, 9–13, 16 and Condomines *et al* unpublished results. The lines corresponding to different fractionation coefficients k are indicated (see text). The upper horizontal axis is calibrated in $[^{232}\text{Th}/^{238}\text{U}]$ atomic ratios. The dashed arrows denote long transfer times of the magmas and the supposed positions of the primary magmas are then indicated (Etna, Chaîne des Puys, Hawaii).

domains representative of the MORB and OIB are not completely disconnected and a gradual transition does exist. Is the latter either a superficial translation of a real chemical zoning in the mantle or, conversely, an indication of mixing and contamination phenomena during the genesis and the transfer of magmas?

In the latter hypothesis, the position of the magma in the isochron diagram is no longer related to the degree of partial melting. Let us consider, for example, the following simple model⁵ an homogeneous lower mantle with a 'primitive' $[\text{Th}/\text{U}]$ ratio of 3.7 and a depleted upper mantle with a $[\text{Th}/\text{U}]$ ratio of ~ 2.3 (this is the minimum value obtained by extrapolating the oceanic trend to the equiline). The partial melting of 'blobs' from the lower mantle would yield the OIB, the partial melting in the upper mantle producing the 'normal' MORB. The mixing of these two magma types during the ascent of 'blobs' could explain the continuity of the two domains. There would be MORB more or less contaminated by the OIB magma and the reverse for OIB. In that case, the extreme values of $(^{230}\text{Th}/^{232}\text{Th})$ ratios (and Pb, Sr, Nd isotopic ratios) would be closest to the real values of these two sources. To explain the scatter of the points in the isochron diagram, each of these two mantle sources must undergo different degrees of melting (Fig. 4). It may be that the truth is in between these two extreme models (the latter simple mixing model and the model with different mantle sources for each volcanic region). The mixing model has been discussed already in the case of Iceland⁹.

It is not possible to make a definitive choice between these two models, but the ^{230}Th - ^{238}U disequilibrium data emphasize source differences among oceanic basalts. These differences might be related to chemical and mineralogical differences in the mantle composition, which would play an important part as well as the actual degree of melting, in determining the composition of the primary magmas.

Subduction zones

So far, there are only a few data available for the volcanism at subduction zones. However, a previous study of Costa Rica⁸ showed the presence of both ancient (Izaru) and recent lavas (Poas, Arenal) for which the representative points plot to the

right of the equiline in the isochron diagram (Fig. 3). This unusual behaviour is also observed for two rhyolites from the Long Valley (Sierra Nevada)¹⁶ and for lavas from the Marianas¹⁷. There are also some lavas which plot to the left of the equiline⁸ or very close to the latter (Stromboli), but it seems significant that all the lavas with $(^{230}\text{Th}/^{238}\text{U}) < 1$ come from volcanoes in subduction zone. If we admit that the partial melting fractionates the $[\text{Th}/\text{U}]$ ratio in the same manner as in oceanic basalts, then we have to find a secondary phenomenon to explain the particular position of subduction zone magmas. The arc volcanism is most probably at the origin of continental crust extraction responsible for the progressive depletion of the residual upper mantle, thus, the partial melting probably affects the $[\text{Th}/\text{U}]$ ratio in the usual way.

Another important point brought up by the magmatic evolution study of the Izaru volcano, is the variability of the $[\text{Th}/\text{U}]$ ratios of the lavas throughout the history of the volcano⁸. This is an important difference compared with the other volcanic regions studied (FAMOUS zone, Iceland, Hawaii, Etna) for which the $[\text{Th}/\text{U}]$ ratios do not vary very much. This $[\text{Th}/\text{U}]$ ratio variation for lavas from Izaru has been ascribed to a dragging of U through gas transfer during the ascent of the magma from its reservoir to the surface whereas the magma in the reservoir keeps evolving with a constant $[\text{Th}/\text{U}]$ ratio, thereby yielding an almost linear variation of the $(^{230}\text{Th}/^{232}\text{Th})_0$ initial ratios of the lavas relative to $e^{\lambda t}$ (ref. 8). If this hypothesis were correct it would demonstrate the important role of fluids in this type of volcanism and that U is far more affected than Th by the gas transfers. Would not this role of fluids, evident during the magmatic evolution, also be crucial for explaining the particular position of the magmas from subduction zones to the right of the equiline? The disequilibrium illustrated by the position of a magma to the right of the equiline may either be acquired at the time of its formation through partial melting or be the result of a source already in radioactive disequilibrium and having a similar position in the diagram.

Among the models proposed for the genesis of magmas from subduction zones, one does not seem to be compatible with the disequilibrium data: that of simple melting of the subduction oceanic crust. Indeed, oceanic crust has a quite low $[\text{Th}/\text{U}]$ ratio and hence high $(^{230}\text{Th}/^{232}\text{Th}) \geq 1.10$, after the resetting of radioactive equilibrium, inasmuch as an oceanic crust enriched in U by seawater should present even higher $(^{230}\text{Th}/^{232}\text{Th})$ ratios. Yet, most of the magmas from the subduction zones studied systematically have lower $(^{230}\text{Th}/^{232}\text{Th})$ ratios than those for oceanic tholeiites. If the oceanic crust is involved in the partial melting process there must be a mixing of the latter with another component. This other component may either be sediments dragged during the subduction, or the continental crust. Some detritic sediments (for example, clays) may have high $[\text{Th}/\text{U}]$ ratios, hence rather low $(^{230}\text{Th}/^{232}\text{Th})$ ratios when they reach radioactive equilibrium. Therefore, mixing with the oceanic crust at the time of partial melting may decrease the $(^{230}\text{Th}/^{232}\text{Th})$ ratios of the latter. Besides, the melt

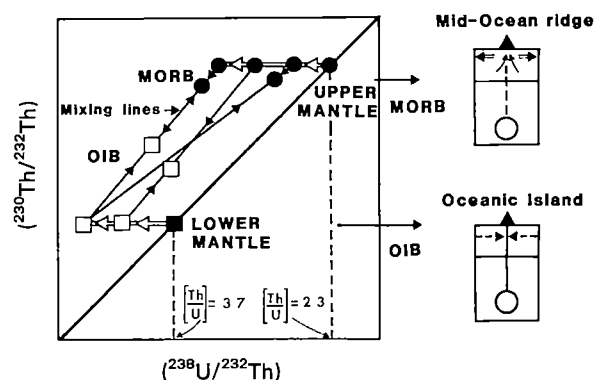


Fig. 4 Isochron diagram showing the possible genesis of MORB and OIB by cross-contamination.

must be preferentially enriched in U relative to Th. The uranium from the sediments could have been brought into the magma by the fluids during partial melting. The contamination by the continental crust (higher [Th/U] ratios) of a magma originating through the melting of the oceanic crust and the participation of fluids from the continental crust is yet another hypothesis which is compatible with the disequilibrium data for explaining the enrichment of the magma in uranium.

We may propose a simple model to account for these remarks (1) A first melting stage at ridges with creation of MORB, after the spreading, the radioactive decay occurs and the oceanic crust 'falls down' onto the equiline but in a position corresponding to a much less depleted source. (2) A second stage of mixing with sediments and a partial melting in a wet medium which yield the expected result, or interaction of the magma with continental crust and selective contamination in U by continental fluids.

Another model for the genesis of the magmas in subduction zones considers a melting of the mantle 'wedge' right above the subducting plate. This part of the mantle would have been previously enriched in some elements through dehydration of the subducting oceanic crust and through transfer by fluids of the most soluble elements such as Rb or U (mantle metasomatism). This phenomenon could provide an explanation for the

presence of sources in disequilibrium to the right of the equiline. Note that if this model of metasomatism is correct, this phenomenon must have occurred a short time before or during partial melting (the metasomatic fluid could be the cause of partial melting), before the source returned to a state of radioactive equilibrium, which could be indicated by high ($^{230}\text{Th}/^{232}\text{Th}$) ratios that most of the available data do not show.

Considering the limited available ($^{230}\text{Th}/^{232}\text{Th}$) disequilibrium data for the volcanism in subduction zones a definite choice among the above models would be premature. However, fluids would really have an important role either during the partial melting process or after (uranium enrichment of the magma) or even before the melting (uranium enrichment of the source).

A more extensive study of volcanoes from subduction zones (especially from intra-oceanic arcs) would allow confirmation of the disequilibrium position of their magmas to the right of the equiline in the isochrone diagram. In such an instance, it would set an important characteristic for this type of volcanism and yield a method to study its origin.

We thank B. Dupré for an important comment, also R. K. O'Nions and A. Zindler for helpful comments. The manuscript has been prepared by Claude Mercier-Ronnat. This is IGP contribution NS/599.

Received 30 March, accepted 14 July 1982

- 1 Yoder, H. S. Jr & Tilley, C. E. *J. Petrol.* **3**, 342–352 (1962)
- 2 Yoder, H. S. Jr *Generation of Basaltic Magma* (National Academy of Sciences, Washington DC, 1976)
- 3 Condomines, M., Morand, P. & Allegre, C. J. *Earth planet Sci. Lett.* **55**, 247–256 (1981)
- 4 Tatsumoto, M. *Earth planet Sci. Lett.* **38**, 63–87 (1978)
- 5 Allegre, C. J., Brevart, O., Dupré, B. & Minister, J. F. *Phil. Trans. R. Soc. A* **297**, 447–477 (1980)
- 6 Dupré, B. & Allegre, C. J. *Nature* **286**, 17–22 (1980)
- 7 Allegre, C. J. *Earth planet Sci. Lett.* **5**, 209–210 (1968)
- 8 Allegre, C. J. & Condomines, M. *Earth planet Sci. Lett.* **28**, 395–406 (1976)
- 9 Condomines, M., Morand, P., Allegre, C. J. & Sigvaldsson, G. *Earth planet Sci. Lett.* **55**, 393–406 (1981)
- 10 Condomines, M., Bernat, M. & Allegre, C. J. *Earth planet Sci. Lett.* **33**, 122–125 (1976)
- 11 Condomines, M., Tanguy, J. C., Kieffer, G. & Allegre, C. J. *Geochim. cosmochim. Acta* (in the press)
- 12 Morand, P., Condomines, M. & Allegre, C. J. *C. r. Acad. hebdomadaire Séances Sci. Paris* **286D**, 1845 (1978)
- 13 Capaldi, G. *et al. Bull. volcan.* **41**, 259–285 (1978)
- 14 Schilling, J. G. *Nature* **246**, 141–143 (1973)
- 15 Tarney, J., Wood, D. A., Saunders, A. D., Cann, J. R. & Varet, J. *Phil. Trans. R. Soc.* **179**–202 (1980)
- 16 Baranowski, J. & Harmon, R. S. *4th Int. Conf. Geochronol. Isotope Geol. Snow Mass, U.S.G. Open file* 22–24 (1978)
- 17 Newman, S., Finkel, R. C. & MacDougall, J. D. *EOS* **62**, 45, 1076 (1981)

A study of Si,Al ordering in thallium zeolite-A by powder neutron diffraction

A. K. Cheetham & M. M. Eddy

Chemical Crystallography Laboratory, University of Oxford, 9 Parks Road, Oxford OX1 3PD, UK

D. A. Jefferson & J. M. Thomas

Department of Physical Chemistry, University of Cambridge, Lensfield Road, Cambridge CB2 1EP, UK

The cubic structure of thallium zeolite-A has been studied by high resolution powder neutron diffraction. Refinements in which Si and Al are strictly alternating within the aluminosilicate framework (space group Fm3c) are better than those in which each Si is linked, by oxygen bridges, to three Al and one Si (space group Pn3n). This result is in accord with recent ^{29}Si (magic-angle spinning) NMR measurements on zeolite ZK-4 but at variance with previous interpretations of NMR measurements on the sodium form of zeolite-A. Our conclusions reaffirm earlier X-ray results.

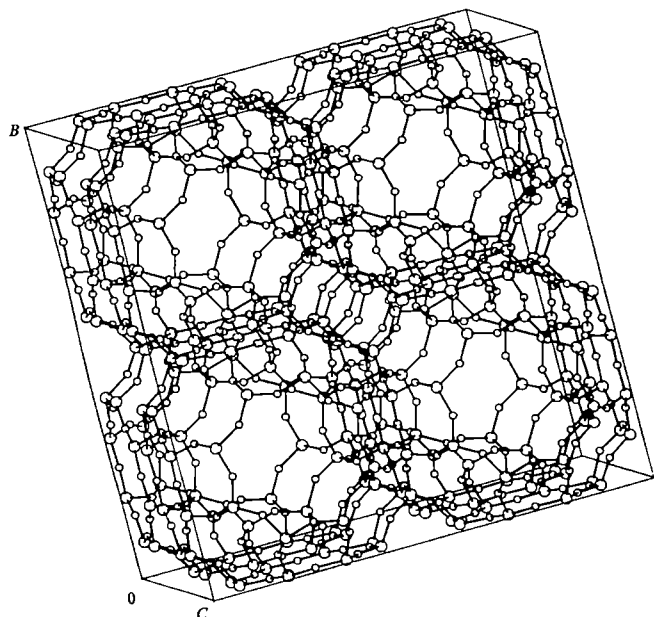
THE growing importance of zeolite materials in catalytic reactions has led to a revival of interest in their microstructure and in particular the details of their Si,Al distributions. Until recently, zeolite-A was regarded as the most definitively characterized member of the zeolite family, with the very simplicity of its structure adding to the assurance that the description was correct. The basic framework consists of silicon and aluminium atoms tetrahedrally coordinated by oxygen (Fig. 1), but the exact ordering of Si and Al has remained the subject of debate. According to Loewenstein's rules¹, a tetrahedrally coordinated aluminium atom should not be linked through oxygen to another aluminium with the same coordination geometry. Although there are exceptions to the rules^{2,3}, they nevertheless provide a good basis for describing aluminosilicate frameworks.

Strict alternation of the Si and Al, in obedience of Loewenstein's rules, leads to a cubic cell, $a \sim 24.6 \text{ \AA}$, and the space group Fm3c (refs 4, 5). In detailed single crystal X-ray studies on sodium zeolite-A⁶ and three samples of dehydrated, potassium zeolite-A⁷, Pluth and Smith obtained excellent refinements in Fm3c, although a few weak reflections violating the c -glide were observed in each case, this was also noted by Thoeni in work on hydrated samples of thallium, calcium and silver zeolite-A⁸.

The apparent violations of the c -glide condition in some of the zeolite-A data suggest the possibility that the space group Fm3c may be incorrect, and recent observations using electron diffraction, neutron diffraction, and high resolution, magic-angle spinning ^{29}Si NMR give cause for further scepticism^{9–14}.

Table 1 Final atomic coordinates for Tl zeolite-A in space group Fm3c

Atom	Position	x	y	z	Occupancy	B(Å ²)
Si	96(i)	0 0	0 0906(5)	0 1826(5)	1 0	0 11(11)
Al	96(i)	0 0	0 1852(5)	0 0884(6)	1 0	0 11(11)
O(1)	96(i)	0 0	0 1069(2)	0 2468(4)	1 0	0 68(7)
O(2)	96(i)	0 0	0 1486(3)	0 1503(3)	1 0	0 68(7)
O(3)	192(j)	0 0532(2)	0 0589(2)	0 1676(1)	2 0	0 68(7)
Tl(1)	64(g)	0 1301(3)	0 1301(3)	0 1301(3)	0 330(10)	3 10(45)
Tl(2)	96(i)	0 0	0 2272(3)	0 2273(3)	0 222(5)	3 10(45)
Tl(3)	64(g)	0 0485(9)	0 0485(9)	0 0485(9)	0 053(4)	3 10(45)
Na(1)	64(g)	0 1025(9)	0 1025(9)	0 1025(9)	0 307(26)	5 33(153)

**Fig 1** The cubic ($a \sim 12.3$ Å) sub-cell of zeolite-A, Si(Al) and oxygen atoms are shown as large and small spheres, respectively

The electron diffraction patterns of sodium zeolite-A contradict the space group Fm3c owing to the appearance of hhl reflections with $h + l = 2n$ (ref. 15), and neutron diffraction measurements on dehydrated samples of the same material show a pronounced rhombohedral distortion. The NMR studies reveal a single peak with a chemical shift (89.7 ± 0.5 ppm) in the range expected for Si surrounded by three aluminium atoms and one silicon^{12,13}. This 3:1 ordering scheme requires similar ordering for Al, in contradiction of Loewenstein's rule. A rhombohedral structural model that incorporates the 3:1 Si,Al ordering scheme has been advanced by Bursill *et al.*⁹

In an attempt to resolve the controversy surrounding the Si, Al ordering in zeolite-A, we have carried out a powder neutron diffraction study on one of the rhombohedrally distorted zeolite-A samples, having exchanged sodium for thallium. The greater neutron scattering length of Tl, compared with Na, affords the advantage of locating the exchangeable cations with greater precision.

Table 2 Bond lengths for Tl zeolite-A (Å)

Si-O(1)	1 608(14)	Al-O(1)	1 702(14)
Si-O(2)	1 628(14)	Al-O(2)	1 755(14)
2 × Si-O(3)	1 560(13)	2 × Al-O(3)	1 726(13)
Average Si-O	1 599	Average Al-O	1 728

Experimental work

The sample used in this work was prepared from the Na zeolite-A sample, Si/Al = 1:10, studied in ref. 11. Thallium was incorporated by ion-exchange at 85 °C using a saturated thallium(I) nitrate solution. The solution was changed after 24 h and the procedure repeated. Examination of the product in a Jeol 100CX TEMSCAN analytical electron microscope showed that the sodium had not been fully exchanged.

Neutron diffraction data were collected on the high resolution, powder diffractometer, D1A, at the high flux beam reactor in Grenoble, as described in ref. 14. The data were measured at room temperature in the 2θ range from 6° to 140°, with a mean neutron wavelength of 2.98 Å, and were collated using the program of Hewat¹⁵. Further data reduction and profile analysis were performed using the POWDER system¹⁶ on the Science Research Council's Interactive Computing Facility. The neutron scattering lengths used in the refinements were $b(\text{Al}) = 0.35$, $b(\text{Si}) = 0.42$, $b(\text{O}) = 0.58$, and $b(\text{Tl}) = 0.89$ (all $\times 10^{-14}$ m)¹⁷.

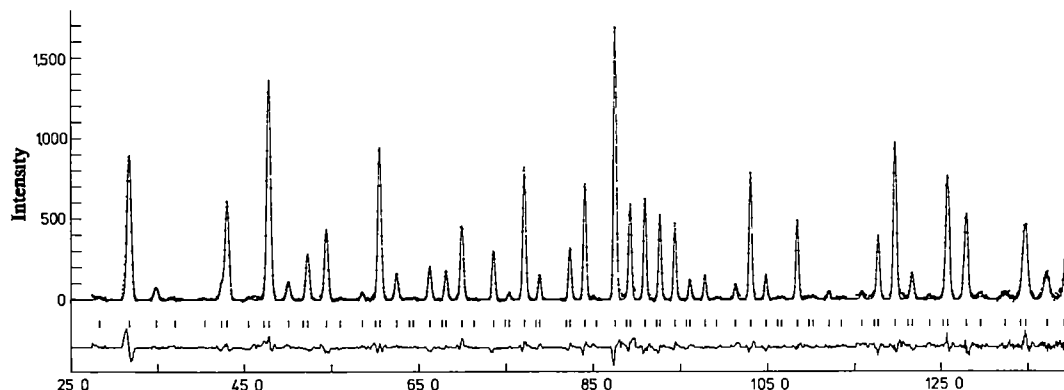
Results and discussion

The most striking aspect of the neutron powder pattern is the absence of any visual evidence for the rhombohedral distortion that was present in the anhydrous Na zeolite-A sample from which the Tl derivative was prepared. The conclusion that the sample is cubic was confirmed by the subsequent refinement that was carried out in space group Fm3c.

The Tl zeolite-A data were refined to a final R_{pr} of 11.33,

$$R_{\text{pr}} = \frac{\sum |y_i(\text{obs}) - \frac{1}{c} y_i(\text{calc})|}{\sum y_i(\text{obs})}$$

where $y_i(\text{obs})$ and $y_i(\text{calc})$ are the observed and calculated intensities, respectively, at the i th point on the profile, and c

Fig. 2 The observed (dots), calculated (solid curve) and difference profiles for Tl zeolite-A in Fm3c, reflection positions are also indicated

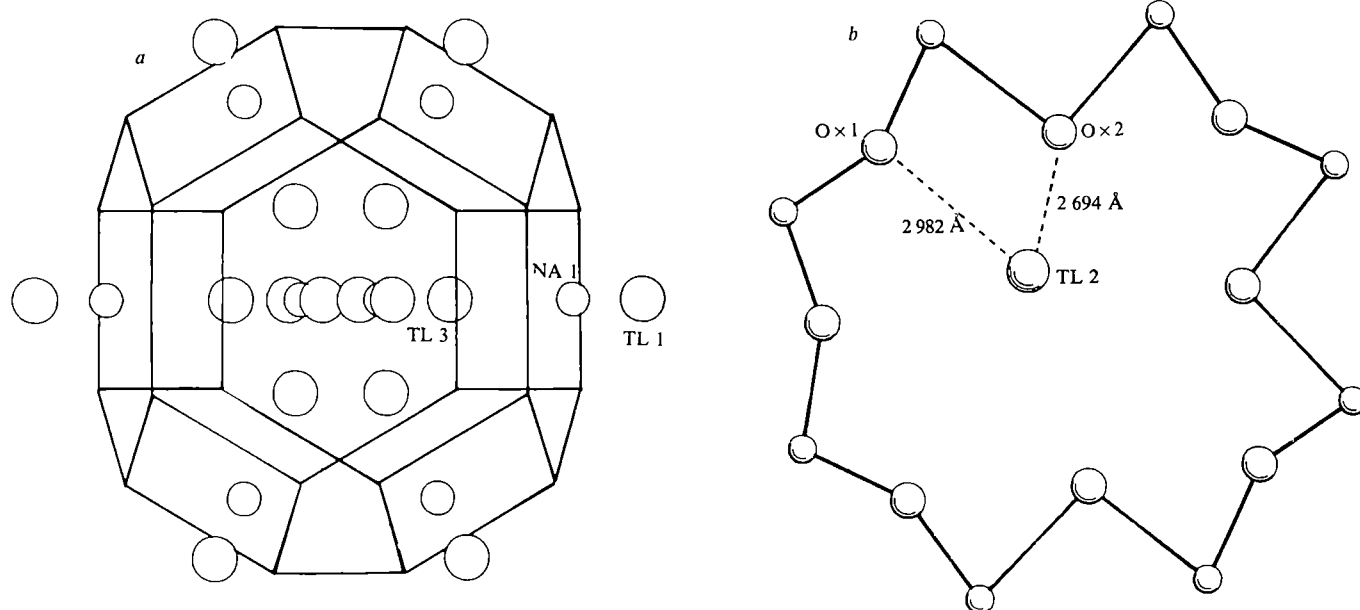


Fig. 3 a, The location of Ti(1), Ti(3) and Na(1) sites close to the 6-rings b, The location of Ti(2) in the 8-ring

is the scale factor. The final atomic coordinates and occupancy factors are given in Table 1, and the observed and calculated profiles are shown in Fig. 2. The lattice parameter obtained was 24.373 Å. The bond lengths given in Table 2 show that the Si–O and Al–O distances are unambiguously bimodal.

The ^{29}Si NMR spectrum of the Ti zeolite-A sample was essentially unchanged from that of the parent Na sample, confirming that the Si,Al distribution has been unaffected by the ion exchange reaction. The NMR result would seem to confirm the 3:1 ordering scheme for the aluminosilicate framework, and if this is indeed the case, then the neutron data should refine well in the cubic Pn3n model advanced by Bursill *et al.*, because this appears to be the only cubic model that is consistent with 3:1 ordering. The data were refined in this model to a final R_{pr} value of 13.99%. The R_{pr} value is thus >2% larger than the value obtained in Fm3c, even though four times as many atomic coordinates were refined in the Pn3n model.

The present neutron results point strongly towards the correctness of a 4:0 Si,Al ordering scheme. The bimodal Si–O and Al–O bond lengths are hard to rationalize with any other framework distribution, and the relatively poor refinement obtained in Pn3n would appear to be conclusive. If the Fm3c model is indeed correct for the Ti zeolite-A, then the position of the ^{29}Si NMR resonance at the chemical shift expected for 3:1 Si,Al ordering must be an anomaly that arises in zeolite-A because of the location of the Si in the double 4-rings. This conclusion has recently been corroborated by ^{29}Si NMR measurements on the zeolite ZK-4, which has the same aluminosilicate framework as zeolite-A^{18,19}. A further important feature of the present results is that the rhombohedral distortion is clearly dependent on the identity of the exchange-

able cations. If the 4:0 ordering scheme is correct, then the rhombohedral Na zeolite-A data should be refined in the appropriate space group for such ordering, $R\bar{3}c$. The factors influencing the rhombohedral distortion in zeolite-A, and the origin of the violations of the c -glide condition in the cubic form, remain to be elucidated.

The Ti zeolite-A structure contains two cations, Ti(1) and Ti(3), on the 3-fold axis above and below the centre of the 6-ring (Fig. 3a). These cations are trigonally coordinated by oxygens in the 6-ring at 2.715 Å and 2.923 Å, respectively, the sum of the ionic radii for Ti^{4+} and O^{2-} is ~ 2.85 Å (ref. 20). Ti(2) is coordinated by two oxygens in the 8-ring, O(1) and O(2), at 2.982 Å and 2.694 Å, respectively (Fig. 3b). Cation (4) is found surprisingly close to the centre of the 6-ring at a distance of 2.256 Å from O(3). It essentially lies between Ti(1) and Ti(3) (Fig. 3a), at the position corresponding to the cation site with the highest occupancy in sodium zeolite-A. This evidence, together with the short cation(4)–oxygen distances, the small value of the lattice parameter, and the electron microscopy results, clearly confirms that cation(4) is in fact sodium arising from incomplete cation exchange. When the scattering length of sodium is substituted for that of Ti at this site, the total cation occupancy for the compound increases from 0.72(3) to 0.91(3), the theoretical value is 0.95(2). In earlier studies²¹ of ion-exchange at 25 °C, 64% conversion from the sodium to the thallium form was obtained, our results correspond to 66% conversion. The zero-coordinated Ti atom reported by Firor and Seff²² is not found in the present work.

We thank the SERC for neutron facilities at ILL and a studentship for MME, Mr S. Heathman for experimental assistance, and the Exxon Research and Engineering Co. for a grant.

Received 28 May; accepted 8 July 1982

- Loewenstein, W. *Am. Miner.* **39**, 92–96 (1954).
- Smith, J. V. *Am. chem. Soc. Monogr.* No. 171 (1976).
- Ponomarev, V. I., Kheiker, D. M. & Belov, N. V. *Soviet Phys.-Crystallogr.* **15**, 799–801 (1971).
- Barrer, R. M. & Meier, W. M. *Trans. Faraday Soc.* **54**, 1074–1085 (1958).
- Gramlich, V. & Meier, W. M. *Z. Kristallogr.* **133**, 134–149 (1971).
- Pluth, J. J. & Smith, J. V. *J. Am. chem. Soc.* **102**, 4704–4708 (1980).
- Pluth, J. J. & Smith, J. V. *J. phys. Chem.* **83**, 741–749 (1979).
- Thoen, W. *Z. Kristallogr.* **142**, 142–160 (1975).
- Bursill, L. A., Lodge, E. A., Thomas, J. M. & Cheetham, A. K. *J. phys. Chem.* **85**, 2409–2421 (1981).
- Lodge, E. A., Bursill, L. A. & Thomas, J. M. *JCS chem. Commun.* 875–876 (1980).
- Thomas, J. M., Bursill, L. A., Lodge, E. A., Cheetham, A. K. & Fyfe, C. A. *JCS chem. Commun.*, 276–277 (1981).

- Klinowski, J., Thomas, J. M., Fyfe, C. A. & Hartman, J. S. *J. phys. Chem.* **85**, 2590–2594 (1981).
- Engelhardt, G., Zeigen, D., Lippmaa, E. & Magi, M. *Z. Anorg. Allg. Chem.* **468**, 35–38 (1980).
- Hewat, A. W. & Bailey, I. *Nucl. Instrum. Meth.* **137**, 462–471 (1976).
- Hewat, A. W. *Powder Rietveld and Refinement System* (I.L.L. Grenoble Rep., 1978).
- Rae-Smith, A. R., Cheetham, A. K. & Skarnulis, A. J. *J. appl. Crystallogr.* **12**, 485–486 (1979).
- Bacon, G. E. *Neutron Diffraction* 3rd edn (Oxford University Press, 1975).
- Thomas, J. M., Fyfe, C. A., Ramdas, S., Klinowski, J. & Gobbi, G. C. *J. phys. Chem.* (submitted).
- Melchior, M. T., Vaughan, D. E. W., Jarman, R. H. & Jacobson, A. J. *Nature* (submitted).
- Shannon, R. D. & Prewitt, C. T. *Acta crystallogr.* **B25**, 925–946 (1969).
- Sherry, H. S. & Walton, H. F. *J. phys. Chem.* **71**, 1457–1465 (1967).
- Firor, R. L. & Seff, K. *J. Am. chem. Soc.* **99**, 1112–1117 (1977).

Specific protein–nucleic acid recognition in ribonuclease T₁–2'-guanylic acid complex: an X-ray study

Udo Heinemann

Abteilung Chemie, Max-Planck-Institut für Experimentelle Medizin, Hermann-Rein-Strasse 3, D-3400 Gottingen, FRG

Wolfram Saenger

Institut für Kristallographie, Freie Universität Berlin, Takustrasse 6, D-1000 Berlin 33, FRG

RNase T₁ is folded into an α -helix of 4.5 turns, covered by a four-strand antiparallel β -sheet. Specific recognition of 2'-guanylic acid arises from hydrogen bonding between main chain peptide groups and the O-6 and N-1-H of guanine, as well as from stacking of Tyr 45 on guanine. At the active site, Glu 58, His 92 and Arg 77 are involved in phosphodiester hydrolysis.

SPECIFIC recognition of certain nucleotides or nucleotide sequences in both RNA and DNA by proteins is of central importance in various processes in molecular biology. Understanding of the mechanism by which proteins express base specificity requires structural studies of model systems like nucleases and their complexes with nucleic acid fragments. So far, crystal structures of such systems have been published for bovine pancreatic ribonuclease A^{1–3} and ribonuclease S⁴ and for the nuclease from *Staphylococcus aureus*⁵. While the staphylococcal enzyme hydrolyses both DNA and RNA, RNase S acts only on phosphodiester bonds at the 3'-terminal side of pyrimidine nucleotides in single-stranded RNA.

An even more selective enzyme, ribonuclease T₁ (RNase T₁, EC 3.1.27.3) from the fungus *Aspergillus oryzae*, degrades single-stranded RNA to yield exclusively oligonucleotides with terminal guanosine-3'-phosphate. As with RNase A, RNase T₁-catalysed cleavage involves formation of an intermediate, 2',3'-cyclic phosphate, followed by hydrolysis. Its marked specificity towards guanosine has not only made RNase T₁ an important tool in nucleic acid chemistry but it is also used extensively as a model compound to study the recognition of nucleic acids by proteins⁶.

Chemical modifications of RNase T₁, a small acidic protein, have demonstrated the importance of an active glutamic acid residue⁷ and of two histidines^{8,9} for its enzymatic activity. Participation of histidine residues in substrate binding and their interaction with carboxylate groups of the protein were also demonstrated by NMR spectroscopy^{10,11} and kinetic studies¹². However, the exact role of these residues (Glu 58, His 40 and His 92) in catalysis and/or base recognition is unknown. There is also some evidence for the side chain of the single arginine (Arg 77) being located near the active centre¹³ (see Fig. 1). The positions N-1, N-7 and the 6-oxo group of the guanine base appear to be recognized by RNase T₁.

The crystallographic investigation of the RNase T₁–2'-guanylic acid complex described here was undertaken to provide a structural basis for understanding the enzyme's remarkable base specificity, and the molecular mechanism of RNase T₁-catalysed RNA cleavage.

Structure determination

As described previously¹⁴, RNase T₁ co-crystallized with 0.25% 2'-guanylic acid from sodium acetate buffer adjusted to pH 4.0–4.4 when dialysed against 53% 2-methyl-2,4-pentanediol. Crystals used in X-ray diffraction work were orthorhombic, P2₁2₁2₁, with cell parameters $a = 46.8$ Å, $b = 50.2$ Å and $c = 40.4$ Å. Heavy atom derivatives were prepared by soaking

protein crystals in 1–5 mM solutions of the respective reagent in the mother liquor.

Diffraction data were collected by a diffractometer in the ω -scan mode with stationary background counts on both sides of each reflection. Five individual data sets of native RNase T₁ and two sets of both Pb(II) acetate and Pt(NH₃)₄Cl₂ derivatives including Friedel pairs, were measured using one single crystal for each set. Reflection standard deviations were computed from counting statistics¹⁵ and the data sets were placed on a common scale after semi-empirical absorption correction¹⁶. Corresponding structure factor amplitudes were then averaged, weighted by the inverse square of their standard deviations.

Estimates of the heavy atom structure factor amplitudes¹⁷ were used to locate the heavy atom sites by Patterson syntheses and direct methods¹⁸. Heavy atom parameters were subjected to full matrix least-squares refinement and finally the enantiomorph was selected by calculating difference Fourier maps based on protein phases derived from either hand of the sites.

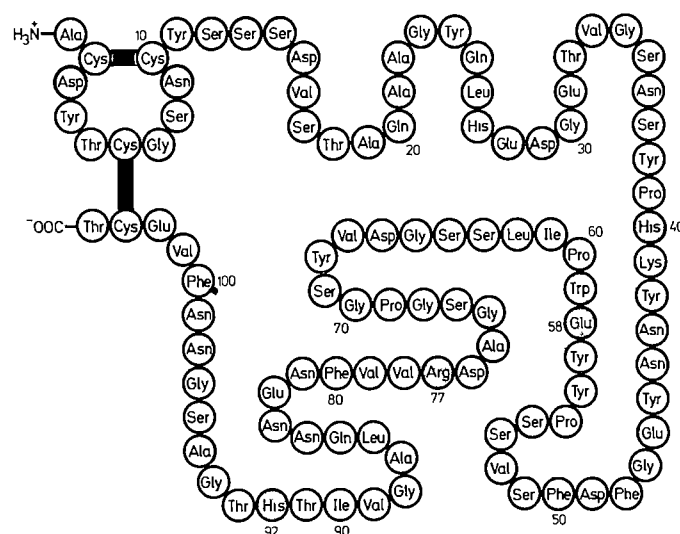


Fig. 1 Covalent structure of RNase T₁ (ref. 21). Residues shown shaded are critical for enzymatic activity. The protein used in this investigation was an isoenzyme of the sequenced species, having one additional lysine residue and lacking one glutamine or glutamate⁴⁸. Preliminary results of the amino acid analysis of iso-RNase T₁ (H. Kratzin, personal communication) suggest that Gln 25 is exchanged with Lys. The present X-ray study showed Gln 25 or Gln 85 as possible exchange positions. Enzymatic activity of the iso-RNase T₁ is the same as that of the mother protein.

Table 1 Data collection and processing statistics

Derivative	Minimum resolution (Å)	Reflections measured*	Unique reflections*	R_M	R_I	R_A	Heavy atom sites	R_{FHLE}	Phasing power
Native RNase T ₁	2.5	14,318	3,550	0.098	—	—	—	—	—
Pb(II) acetate	2.5	5,793	3,547	0.066	0.272	0.109	6	0.394	2.327
Pt(NH ₃) ₄ Cl ₂	2.5	4,897	3,139	0.051	0.159	0.125	2	0.372	2.056
Pb/Pt	3.0	1,970	1,970	—	0.149	0.108	3	0.377	2.259

Preparation of heavy atom derivatives Pb(II) acetate, crystals were soaked for 1 day in a 1 mM solution, Pt(NH₃)₄Cl₂, 2 days in a 5 mM solution, double derivative (Pb/Pt), first 1 day in 1 mM Pb(II) acetate, then 2 days in 5 mM Pt(NH₃)₄Cl₂. Individual R values are defined as

$$R_M = \frac{\sum_i |F_i - F_i^+|}{\sum_i F_i}, \quad R_I = \frac{\sum_i |F_i - F_{PH}|}{\sum_i F_i}, \quad F_A = \frac{\sum_i |F^+ - F^-|}{1/2 \sum_i (F^+ + F^-)}, \quad R_{FHLE} = \frac{\sum_i |F_{HLE} - F_{H(calc)}|}{\sum_i F_{HLE}}$$

Summations are over all reflections. F_P is the protein structure factor amplitude, F_{PH} the derivative structure factor amplitude, F^+ and F^- the positive and negative equivalents for Friedel pairs. F_{HLE} and $F_{H(calc)}$ are the estimated¹⁷ and calculated heavy atom structure factor amplitudes, respectively. The phasing power is defined as $\sum F_{H(calc)} / \sum E_{best}$, where E_{best} is the lack of closure error at the centroid protein phase.

* For derivatives, Friedel pairs were counted as one reflection.

of the platinum derivative. Conventional Blow and Crick phase determination¹⁹ yielded a mean figure of merit $\langle m \rangle = 0.75$ for all 3,547 reflections to 2.5 Å. Data processing and heavy atom refinement statistics are given in Table 1.

Map interpretation

An electron density map was calculated for protein phases obtained as described above and sampled at grid spacings of 0.9 Å. Positive density was contoured at a scale of 1 Å = 2 cm on transparent plastic sheets, which were placed in an optical comparator²⁰ for the construction of a Kendrew wire model of the RNase T₁-2'-guanylic acid complex.

From a first inspection of the map, the molecular boundaries of the ribonuclease molecule and the bound nucleotide were immediately apparent. The base, ribose and phosphate portions of 2'-GMP were well resolved. Once the chain termini were identified, tracing of the protein polypeptide chain was straightforward. In general, carbonyl 'bumps' were visible and in the pleated sheet structures, some hydrogen bonds were indicated by weak electron densities. Most amino acid side chains are clearly defined and in agreement with the published sequence²¹. The side chain of Lys 41 which points towards the solvent, however, has no density beyond its C β atom, probably a consequence of disorder. Coordinates of the 801 atoms of the complex were directly determined from the model and will be deposited with the Brookhaven Protein Data Bank.

RNase T₁ is a compact molecule

As illustrated in the schematic drawing in Fig. 2, the RNase T₁ molecule is a compact, globular protein whose shape may be defined as a slightly distorted tetrahedron with corner positions

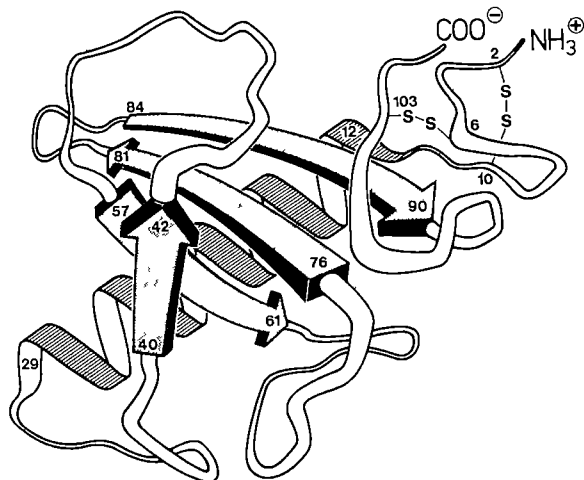


Fig. 2 Schematic drawing of the RNase T₁ polypeptide folding. Taking into account residues which occur in reverse β -turns, half the molecule consists of well-defined secondary structure. Numbers refer to amino acids in the primary sequence (see Fig. 1).

occupied by the side chains of residues Ala 1, Glu 31, Asn 83 and Ser 96. Molecular dimensions are 32 × 33 × 30 Å measured along the unit cell axes. Individual RNase T₁ molecules in the crystal lattice are largely separated by solvent regions, with only three obvious intermolecular contacts involving one hydrogen bond between the side chains of Glu 46 and Ser 35.

The polypeptide chain connecting amino acid residues adjacent to the amino-terminus almost forms a closed loop, which is held together by the disulphide bridge between residues 2 and 10. The chain then enters a regular α -helix of ~4.5 turns, followed by two wide loops separated by a stretch of extended structure to which the inhibitor is bound. Three strands of antiparallel pleated β -sheet follow, with another loop inserted after the first strand. The structure is completed by a wide turn, bringing the carboxy-terminus into the vicinity of the amino end and closing the disulphide bridge 6-103.

While the α -helix is entirely regular, the pleated β -sheet structure is severely bowed and twisted in a left-handed sense. The hydrogen-bonding pattern between backbone segments Asp 76 to Asn 81 and Asn 84 to Ile 90 is disturbed by insertion of residues in the latter strand, residue Val 79 forming a classical ' β -bulge'²² with the dipeptide Ala 87-Gly 88. Another peculiarity of RNase T₁ concerns proline residues 39 and 55 which fit the electron density best when in *cis* form.

The globular structure of the RNase T₁ molecule hides a hydrophobic core located mainly in the interface region between the long α -helix and the pleated sheet. Therefore, all hydrophobic side chains of RNase T₁ are at least partially protected against solvent contact.

Unlike bovine pancreatic ribonuclease, RNase T₁ does not provide a distinct cleft for substrate binding. In view of the outstanding specificity of RNase T₁, it is surprising that the inhibitor base is bound merely on the enzyme surface, while the 2'-GMP phosphate portion lies in a shallow concave depression. A characteristic assembly of aromatic side chains around the active site region might be involved in sub-site interactions with adjacent nucleotides along the polynucleotide chain, this would be in agreement with kinetic studies^{23,24} which have revealed differences in the hydrolysis of GpN substrates.

Positive charges cluster in a narrow zone

It is an apparent paradox that RNase T₁ is an acidic protein exhibiting an isoelectric point of 3.8 (ref. 25), while its function is to bind to and degrade negatively charged nucleic acids. It shares this property with ribonuclease U₂ (from *Usulago sphaerogena*⁶) and ribonuclease St from *Streptomyces erythreus*²⁶, but not with the ribonucleases from *Bacillus amyloquelaceus* and *Bacillus intermedius*, which belong to the same sequence-related family of enzymes²⁷. On complex formation, some of the counter-cations of the RNA must be replaced by the ribonuclease to allow close intermolecular contacts, followed by cleavage of the phosphodiester bond. Therefore it is of interest to examine the distribution of charges on the molecular surface of RNase T₁.



Fig. 3 Stereo drawings of the RNase T₁ molecule *a*, The whole RNase T₁-2'-GMP complex with the protein backbone and the nucleotide indicated by heavier lines *b*, C^α-backbone and acidic residues *c*, C^α-backbone and basic residues The side chain of Lys 41 is not visible in the electron density map and is indicated by its C^β-atom only *d*, C^α-backbone with 2'-guanylic acid shown by heavier lines

At pH values of ~ 5 , where RNase T₁ has maximum affinity for small substrate analogues²⁸, most carboxylate groups are deprotonated, while the basic residues including the histidines bear a positive charge. The resulting charge distribution of the RNase T₁ molecule is shown in Fig 3*b,c*. Except for the side chain of Glu 58, all charged residues are located on the molecular periphery, the acidic groups being equally distributed over the whole surface. The side chains of the basic residues His 40, Arg 77 and His 92, however, are arranged in a narrow zone around the active site (see below) and form the environment for the binding of the inhibitor phosphate group. On this

basis, it is tempting to deduce a function for the charged residues of RNase T₁ in promoting the attachment of its shallow active site groove to the negatively charged nucleic acid via electrostatic interactions.

Protein-nucleic acid recognition is specific

In the complex formed between RNase T₁ and 2'-GMP, the ribose moiety of the nucleotide adopts a C-3'-*endo* type puckering, the orientation about the C-4'-C-5' bond is +*gauche* and the torsion angle defined by the glycosyl link is in the *syn* range.

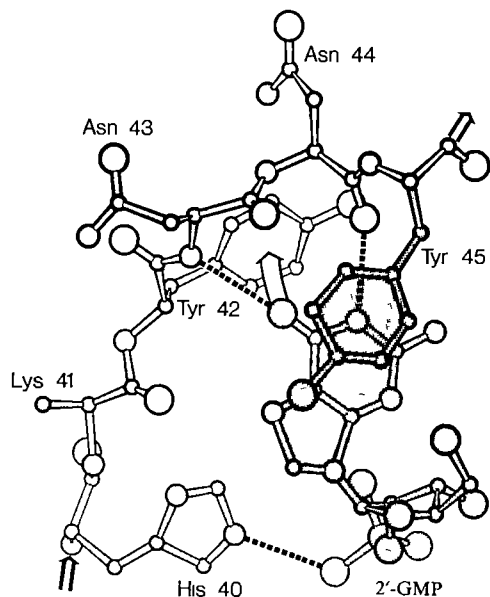


Fig. 4 Base recognition by RNase T₁. 2'-GMP is shown together with the portion of the RNase T₁ polypeptide chain from His 40 to Tyr 45. Note the hydrogen bonds (broken lines) between base positions N-1 and O-6 and the protein backbone and between the His 40 imidazole and the inhibitor phosphate moiety. The wide curved arrow indicates interactions between the O-6 of guanine and the side chain of Tyr 42. The phenyl ring of Tyr 45 stacks parallel to the guanine plane, 3.5 Å distant. The electron density map shows some evidence of an alternative, non-stacking position of the side chain of Tyr 45 which would require rotation around the C^α-C^β and C^β-C^γ bonds.

The latter conformation is unusual but not unexpected. Thus, it has been proposed earlier on the basis of circular dichroism spectra²⁹ that guanosine nucleotides bind to RNase T₁ in this particular form and there is evidence for easy conversion from *anti* to *syn* conformation of guanosine, the latter even being preferred in acidic medium.^{30,31}

The guanine base of the inhibitor is bound to the polypeptide backbone of RNase T₁ by hydrogen bonds between the N-1—H of guanine and the main-chain carbonyl of Asn 44 and between O-6 of guanine and the main-chain —NH of Asn 43 as shown in Fig. 4. This result is consistent with the requirement of the guanine N-1 and O-6 positions for base recognition by RNase T₁ (ref. 6). The geometry of the guanine-RNase T₁ interactions also suggests that substitution of the guanine base at N-7 would interfere sterically with the backbone carbonyl group of Lys 41, and that protonation of N-7 by the enzyme, as suggested on the basis of proton NMR studies¹¹, is unlikely. This is because, first, we should observe strong hydrogen bonding between guanine N-7 and RNase T₁ (this is not found) and second, the *pK_a* of guanine N-7, 2.8, is too low to induce protonation in crystallization conditions at pH 4.0–4.4. A NMR investigation of the binding of ¹⁵N-enriched 3'-GMP to RNase T₁ (ref. 32) also did not support the proposed N-7 protonation; this experiment has been interpreted in terms of a strong interaction of the amino group at guanine C-2 with RNase T₁. In the X-ray structure, however, no close contact with the guanine amino group is observed, therefore it is not essential for RNase T₁-guanine recognition. This finding is in agreement with chemical studies demonstrating that substrates in which inosine is substituted for guanosine are converted at almost the same rate.⁶

In addition to these hydrogen-bonding contacts, our model indicates interactions between guanine O-6 and the phenyl moiety of Tyr 42 and, more importantly, stacking between the guanine base and the phenyl residue of Tyr 45. The latter lies 3.5 Å 'above' the base at the very periphery of the complex. As the map shows a neighbouring portion of weak electron

density probably representing an alternative location of the Tyr 45 side chain, a conformational change of RNase T₁ on substrate binding is probable, swinging Tyr 45 over and into a stacking position with the guanine base. This movement locks in guanine after it has entered the active site following recognition, by hydrogen bonding to the main-chain atoms of Asn 43 and Asn 44. In agreement with these observations, earlier studies showed that the fluorescence of one or two tyrosines is affected when RNase T₁ is complexed with substrate analogues³³, and the above-mentioned NMR results should be reinterpreted in this light.

There is no apparent interaction between RNase T₁ and the ribose of 2'-GMP but the phosphate is involved in hydrogen bonding to the imidazole of His 40. As the phosphate group is near the side chains of His 40, Glu 58, Arg 77 and His 92 which line the active site of RNase T₁ (see below), it is possible that the more natural analogue 3'-GMP would involve other interactions of its ribose and phosphate portions. Thus, slight rotation about the glycosyl link would bring the ribose O-5' hydroxyl in hydrogen-bonding contact with Asn 98, and the 3'-phosphate would be in a position to hydrogen bond with His 92 and also with Arg 77 if this side chain were rotated into another position.

In this regard, it is of interest that the *anti*-fixed nucleotide derivative 5'-deoxy-8,5'-cyclo-guanosine-2',3'-cyclophosphate is bound to RNase T₁ and is converted to the corresponding 3'-phosphate³². As the rate of hydrolysis is rather slow compared with guanosine-2',3'-cyclophosphate, we assume that the base binds nonspecifically to the enzyme (probably promoted by stacking with Tyr 45) whereas the sugar-phosphate moiety protrudes into the active site and is cleaved. This interpretation also explains why dinucleoside phosphates with other than guanosine in the 5'-position are hydrolysed by the enzyme, although at dramatically reduced rates (a factor of $\leq 10^{-6}$) (ref. 6).

Why is the protein main chain involved in specific recognition?

When considering the specific protein-nucleic acid recognition, the often discussed side chain-base interactions spring to mind.^{34,35} In the case of guanine, these could involve Asp or Glu carboxylate accepting hydrogen bonds from guanine N-1—H and N-2—H, Arg guanidinium donating hydrogen bonds to N-7 and O-6, or Gln, Asn amide groups donating and accepting hydrogen bonds to O-6 and from N-1—H, respectively. It is surprising to find that in the RNase T₁-2'-GMP

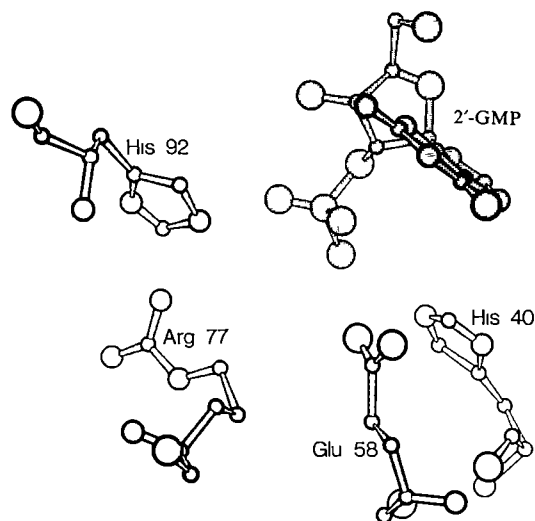


Fig. 5 Catalytic centre of RNase T₁. The plane of the guanine base is almost perpendicular to the plot.

complex none of these interactions is observed and that the nonspecific main chain peptide groups have been selected for specific recognition

Why is this so? One reason could be that amino acid side chains are floppy because of rotations about C—C single bonds, and therefore do not provide for a well-determined matrix necessary for fast, highly specific mutual recognition of the two partners. Alternatively, the main chain can be adjusted and maintained in any conceivable configuration, with peptide groups in fixed positions and ideally suited as hydrogen bonding donors and acceptors. This allows for much better fine-tuning of these interactions than utilization of amino acid side chains. Furthermore the folding of the chain can be designed to be stiff or flexible, depending on the respective needs to be served.

Catalytic site geometry suggests mechanism of RNA hydrolysis

The catalytic centre of RNase T₁ is shown in Fig 5. His 40, in the immediate neighbourhood of the side chain of Glu 58, forms a hydrogen bond or salt bridge with the 2'-GMP phosphate group. The His 92 imidazole ring points towards the phosphate portion of the inhibitor, but is too far away to interact directly with it, whereas the adjacent guanidinium group of Arg 77 is turned away from the active site. The side chain of Asn 98 is close to the 3'-hydroxyl group of the nucleotide.

Proton NMR spectroscopy has revealed unusually high *pK_a* values (7.2–7.9) for two or three histidines of RNase T₁ (refs 36–38). The interpretation that these residues interact with acidic side chains of the protein is supported by the crystal structure, which shows His 27 located close to both Glu 28 and Glu 82 and His 40 near the Glu 58 carboxyl group. Interaction of His 92 with an acidic group¹², however, would require an almost complete re-folding of the protein. The interaction of His 40 with Glu 58, as observed in the electron density map, has also been deduced from NMR studies²⁸. As the side chain of Glu 58 is close to the inhibitor phosphate moiety it is presumably protonated. This is consistent with the result of potentiometric titrations of RNase T₁, which demonstrated that the *pK* of one carboxylate group is shifted from 4.9 to 7.8 on binding of 2'-guanylic acid³⁹.

Assuming a similar binding of true substrates to RNase T₁, we propose a catalytic mechanism for the enzyme where, in the transphosphorylation step, the carboxylate group of Glu 58 acts as a base in abstracting the proton from the ribose O-2' and the imidazole of His 92 protonates the leaving O-5'. The function of His 40 is merely to activate the Glu 58 carboxylate group. Obviously, this histidine is not conserved in all members of the RNase T₁ family²⁷, because it is not essential for catalysis. This mechanism for the transphosphorylation step is consistent

with an in-line mechanism⁴⁰ for RNase T₁ action as proposed by Eckstein *et al.*⁴¹ on the basis of the methanolysis of cyclic phosphorothioates.

The situation outlined above resembles that found in bovine pancreatic RNase A, where histidine residues 12 and 119 serve as general acid and base catalysts⁴². The function of the Arg 77 of RNase T₁ could be similar to that of Lys 41 of RNase S—that is, to stabilize the pentacoordinate intermediate of transphosphorylation through electrostatic interactions⁴³.

Relationship of RNase T₁ to other nucleases

The folding of RNase T₁ bears no similarity to that of *Staphylococcus* nuclease or of RNase A from bovine pancreas. In the complex between the nonspecific staphylococcal nuclease and thymidine 3',5'-bisphosphate⁴⁴, no specific interaction between the protein and the base is observed. On the other hand, X-ray diffraction studies of several inhibitors bound to RNase S^{42, 43} have revealed that the pyrimidine base forms hydrogen bonds between its N-3 atom and O¹ of a threonine residue and between its O-2 and the backbone nitrogen of the same residue. The latter bond does not occur in all inhibitor complexes investigated⁴³. The threonine hydroxyl group serves as a hydrogen bond acceptor with uracil, where N-3 is protonated, and as a donor in the case of cytosine, thus accommodating both pyrimidine nucleotides. If mechanisms of hydrolysis of the three enzymes are compared, we find that those of RNase A and of RNase T₁ are similar to one another but different from that of staphylococcal nuclease.

Recently, the chain foldings of the ribonucleases from *S. erythraeus*²⁶ and *B. amyloliquefaciens*⁴⁵ have been elucidated by X-ray crystallography. They largely resemble that found for RNase T₁, with a long helix covered by a four-strand antiparallel pleated β -sheet. These enzymes also display sequence homologies with RNase T₁, especially around the active site residues Glu 58, Arg 77 and His 92 (ref 27) of RNase T₁, which are found in a comparable arrangement in all three proteins. The importance of the active glutamic acid for the action of the *Streptomyces* enzyme has been demonstrated⁴⁶. We conclude, therefore, that the above enzymes share a common mechanism of nucleic acid hydrolysis.

To obtain a more precise description of the processes involved in RNase T₁ action, we have commenced refinement of the present model and data collection for higher resolution. The structures of the free enzyme and of complexes with guanosine 3',5'-bisphosphate and 2'-deoxy-2'-fluoroguanlyl-(3'-5')-uridine⁴⁷ will be investigated in parallel.

All computations were carried out on the UNIVAC 1100/82 of the Gesellschaft für Wissenschaftliche Datenverarbeitung, Göttingen. We thank Professor Ruterjans and co-workers for supplying purified RNase T₁.

Received 25 May; accepted 2 July 1982

- 1 Kartha, G. *et al.* *Nature* **213**, 862–865 (1967).
- 2 Carlisle, C. H. *et al.* *J. molec. biol.* **85**, 1–18 (1974).
- 3 Wlodawer, A. *et al.* *J. biol. Chem.* **257**, 1325–1332 (1982).
- 4 Wyckoff, H. W. *et al.* *J. biol. Chem.* **245**, 305–328 (1970).
- 5 Arnone, A. *et al.* *J. biol. Chem.* **246**, 2302–2316 (1971).
- 6 Egami, F. *et al.* *Molec. Biol. Biochem. Biophys.* **32**, 250–277 (1980).
- 7 Takahashi, K. *et al.* *J. biol. Chem.* **242**, 4682–4690 (1967).
- 8 Takahashi, K. *J. Biochem., Tokyo* **67**, 833–839 (1970).
- 9 Takahashi, K. *J. Biochem., Tokyo* **80**, 1267–1275 (1976).
- 10 Fulling, R. & Ruterjans, H. *FEBS Lett.* **88**, 279–282 (1978).
- 11 Arata, Y. *et al.* *Biochemistry* **18**, 18–24 (1979).
- 12 Osterman, H. L. & Walz, F. G. *Jr Biochemistry* **18**, 1984–1988 (1979).
- 13 Takahashi, K. *J. Biochem., Tokyo* **68**, 659–664 (1970).
- 14 Heinemann, U. *et al.* *Eur. J. Biochem.* **109**, 109–114 (1980).
- 15 Stout, G. H. & Jensen, L. H. *X-Ray Structure Determination* (Collier-Macmillan, London, 1968).
- 16 North, A. C. T. *et al.* *Acta crystallogr.* **A24**, 351–359 (1968).
- 17 Matthews, B. W. *Acta crystallogr.* **20**, 230–239 (1966).
- 18 Main, P. *et al.* *MULTAN: A System of Computer Programs for the Automatic Solution of Crystal Structures from X-ray Diffraction Data* (University of York, UK and University of Louvain, Belgium, 1977).
- 19 Blow, D. M. & Crick, F. H. C. *Acta crystallogr.* **12**, 794–802 (1959).
- 20 Richards, F. M. *J. molec. Biol.* **37**, 225–230 (1968).
- 21 Takahashi, K. *J. Biochem., Tokyo* **70**, 945–960 (1971).
- 22 Richardson, J. S. *et al.* *Proc. natn. Acad. Sci. U.S.A.* **75**, 2574–2578 (1978).

- 23 Irie, M. *J. Biochem., Tokyo* **63**, 649–653 (1968).
- 24 Osterman, H. L. & Walz, F. G. *Jr Biochemistry* **17**, 4124–4130 (1978).
- 25 Kanaya, S. & Uchida, T. *J. Biochem., Tokyo* **89**, 591–597 (1981).
- 26 Yamamoto, Y. *et al.* *Nucleic Acids Res. Symp. Ser.* **10**, 227–231 (1981).
- 27 Hartley, R. W. *J. molec. Evol.* **15**, 355–358 (1980).
- 28 Takahashi, K. *J. Biochem., Tokyo* **72**, 1469–1482 (1972).
- 29 Oshima, T. & Imahori, K. *J. Biochem., Tokyo* **70**, 197–199 (1971).
- 30 Guschlbauer, W. & Courtot, Y. *FEBS Lett.* **1**, 183–186 (1968).
- 31 Son, T.-D. *et al.* *J. Am. chem. Soc.* **94**, 7903–7911 (1972).
- 32 Kyogoku, Y. *et al.* *J. Biochem., Tokyo* **91**, 675–679 (1982).
- 33 Pongs, O. *Biochemistry* **9**, 2316–2321 (1970).
- 34 Seeman, N. C. *et al.* *Proc. natn. Acad. Sci. U.S.A.* **73**, 804–808 (1976).
- 35 Helene, C. & Lancelot, G. *Prog. Biophys. molec. Biol.* **39**, 1–68 (1982).
- 36 Ruterjans, A. & Pongs, O. *Eur. J. Biochem.* **18**, 313–318 (1971).
- 37 Inagaki, F. *et al.* *J. Biochem., Tokyo* **89**, 1185–1195 (1981).
- 38 Kimura, S. *et al.* *J. Biochem., Tokyo* **85**, 301–310 (1979).
- 39 Iida, S. & Ooi, T. *Biochemistry* **8**, 3897–3901 (1969).
- 40 Usher, D. A. *Proc. natn. Acad. Sci. U.S.A.* **62**, 661–667 (1969).
- 41 Eckstein, F. *et al.* *Biochemistry* **11**, 3507–3512 (1972).
- 42 Richards, F. M. & Wyckoff, H. W. *The Enzymes* Vol. 4 (ed. Boyer, P. D.) 647–806 (Academic, New York, 1971).
- 43 Wodak, S. Y. *et al.* *J. molec. Biol.* **116**, 855–875 (1977).
- 44 Cotton, F. A. *et al.* *Proc. natn. Acad. Sci. U.S.A.* **76**, 2551–2555 (1979).
- 45 Mauguen, Y. *et al.* *Nature* **297**, 162–164 (1982).
- 46 Ohgi, K. *et al.* *J. Biochem., Tokyo* **90**, 113–123 (1981).
- 47 Ikehara, M. & Imura, J. *Chem. pharm. Bull.* **29**, 2408–2412 (1981).
- 48 Fulling, R. thesis, Univ. Munster (1980).

Sequence specificity of trinucleoside diphosphate binding to polymerized tobacco mosaic virus protein

John J. Steckert & Todd M. Schuster

Biochemistry and Biophysics Section, Biological Sciences Group, University of Connecticut, Storrs, Connecticut 06268, USA

The binding of trinucleoside diphosphates to long helical rods of tobacco mosaic virus (TMV) protein is shown to depend on base sequence, 5' AAG 3' binding being the strongest of the 25 trinucleoside diphosphate sequences measured. As TMV has a stoichiometry of three nucleotides per protein subunit, the sequence of TMV RNA suggested to be the nucleation site for self-assembly of the virus has three possible binding frames. From our binding constant data the most likely frame is predicted and shown to have two contiguous AAG sequences in a hairpin loop region.

THE mechanism of spontaneous self-assembly of tobacco mosaic virus (TMV) from its component RNA and single coat protein (TMVP) has been the subject of increasingly detailed studies. New information about the role of various TMVP aggregation states in determining the dynamics of the self-assembly process and about the molecular structure of TMVP, the whole virus and the RNA have made it possible to enquire into the chemical and structural basis for the initial recognition events between the protein and RNA.

It has been shown that TMV self-assembly proceeds by three overall processes. There is a nucleation process which involves initial binding of the protein on the RNA at a site that is $\sim 1,000$ nucleotides from the 3' end¹. Subsequent growth of the nucleoprotein complex is bidirectional and occurs by an elongation reaction involving the addition of protein to the RNA as the helical rod grows in the 5' direction, and a second elongation reaction resulting from protein addition in the 3' direction^{2,3}.

Reconstitution experiments using intact RNA and limiting amounts of TMVP, predominantly in the form of 20S two-turn (disk \rightleftharpoons helix) protein, have demonstrated the formation of short, partially assembled rods containing RNA that is nuclease-resistant and derived from the internal assembly nucleation site⁴. The nucleotide sequence of the protected portion of the RNA has been determined⁵ and overlaps much of the sequence determined in an independent effort which used a different protection strategy, that is, binding of aggregates of TMVP to

fragments of TMV RNA generated by limited ribonuclease digestion⁶. These two studies have led to two different proposals of a stable hairpin-loop secondary structure for the RNA at the nucleation site. The hairpin-loop structure is proposed to be important for the nucleation of TMV assembly because it could allow the RNA to bind from within the hole of the initiating two-turn (disk \rightleftharpoons helix) protein structure⁷. In addition, studies of the nucleotide sequences, under the constraint that the stoichiometry of the TMV particle (three nucleotides of the RNA molecule per 17,530-molecular weight (MW) protein subunit) be preserved, have led to the proposal that trinucleotide sequences at the assembly nucleation site form a reading frame for the initial binding of the 20S aggregate of TMVP^{5,6}.

We report here the results of equilibrium dialysis binding experiments utilizing various ³H-labelled trinucleoside diphosphates (trimers) and helical rods of TMVP formed in weak acid conditions. These experiments were undertaken to determine whether there are trinucleotide sequences that interact preferentially with TMV protein, and, if so, to quantitate the free energy contribution of trimer binding to helical rods of TMV protein to the total free energy of nucleation of TMV self-assembly. The binding measurements reveal a strong sequence specificity with respect to the strength of trimer binding, with AAG being the strongest ($12 \times 10^3 \text{ M}^{-1}$). These results suggest that the initial protein-nucleic acid recognition probably occurs in a hairpin-loop region of the RNA and has the binding frame —CAG/AAG/AAG—. This frame of the sequence can provide ~ 16 kcal of binding energy per mole of sites for the nucleation reaction in TMV self-assembly.

Dependence of binding on trimer sequence

Our initial attempts to measure trinucleotide binding to TMV protein, carried out in collaboration with Professor O. C. Uhlenbeck (University of Illinois), were performed at pH 7.0. At this pH the protein exists at 0 °C as a 4S species (approximately a trimer of the 17,530-MW protein subunit) or at 20 °C as an equilibrium mixture of 4S and 20S sedimenting boundaries. The latter boundary represents a mixture consisting of two-turn disks of 34 monomers⁸ and short helices, probably about two turns long⁹. In these conditions no trimer binding was detected at the lower temperature. At 20–25 °C, however, very weak binding was detected by Professor Uhlenbeck for AAG, CAG and UAG (all nucleotide sequences given here are written 5' \rightarrow 3'). Subsequent initial binding experiments at pH 6.5, 20 °C, in which the protein existed as short helical rods¹⁰, revealed that the trinucleoside diphosphates AAG, CAG, UAG and GAA bind weakly with apparent binding constants in the range $200\text{--}300 \text{ M}^{-1}$ (J. J. S. and T. M. S., unpublished results).

The pH dependence of the binding between pH 6.0 and 7.0 may result from protonation of the carboxyl groups shown in

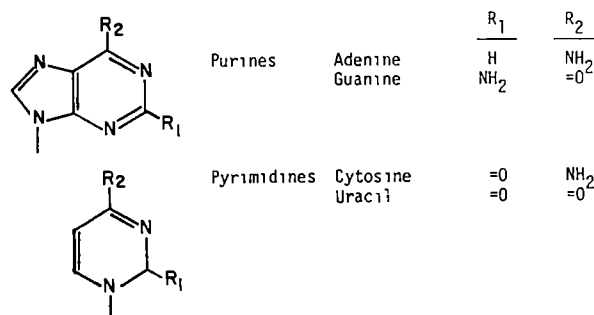


Fig. 1 Influence of single base substitutions in the trimer XAG on the apparent free energy of binding, ΔG^*

	$\Delta(\Delta G^*)$ (kcal mol ⁻¹)
GAG-UAG	-0.46 \pm 0.1
AAG-CAG	-0.42 \pm 0.1
AAG-GAG	-0.64 \pm 0.1
CAG-UAG	-0.68 \pm 0.1

For the base in the 5' position the binding energy is more sensitive to the NH₂ and the =O ring substitutions than it is to the size of the heterocyclic ring.

Table 1 Apparent binding constants, $10^{-3} \times K(M^{-1})$, of various trinucleoside diphosphates to helical rods of polymerized TMVP

Trimer (5' → 3')	Method of dialysis	
	I	II
AAA	0	0
AAG	11.7 (0.2)	12.0 (0.2)
GAA	4.4 (0.4) (pH 5.48)	4.7 (0.1)
AGA	1.0 (0.1)	1.0 (0.2)
GAG	—	4.0 (0.3)
UAG	1.7 (0.1)	1.9 (0.1)
UGA	0.8 (0.2) (pH 5–5.5)	—
GAU	0	—
AGU	0	—
AUG	—	4.1 (0.3)
CAG	5.9 (0.2)	5.8 (0.2)
CGA	0.75 (0.05) (pH 5.27)	—
GAC	0 (pH 5.31)	—
ACG	0.45 (0.05) (pH 5.46)	—
AAU	0	—
UAA	0 (pH 5.31)	—
UUU	0	—
CCU	0 (pH 5.33)	—
UUG	1.2 (0.1)	—
GUU	0 (pH 5.62)	0 (pH 5.56)
AUU	0	0
ACU	0	0
CCA	0	—
CUA	0	—
CGU	0 (pH 5.10)	—

Temperature, $20 \pm 0.1^\circ\text{C}$. Binding site concentration = $5.6 \pm 0.3 \times 10^{-4}\text{ M}$ (the error denotes the range of concentrations over which different experiments were performed and not the error in any single measurement of the protein concentration). pH values are 5.40 ± 0.05 except where indicated. In most cases the binding constants are the average of those determined in one experiment from two or more samples taken at dialysis equilibrium. The errors reported (in parentheses) represent the range of binding constants determined in this way. The K values for AGA and GAG represent averages of several equilibrium measurements in two completely separate experiments, the errors indicate the range of values over the two experiments. Equilibrium dialysis experiments were performed in two ways, binding of trimers to TMV protein rods formed during (method I) or before (method II) dialysis. Method I: a solution of TMV protein as 4S protein in a buffer of KH_2PO_4 (0.033 M), K_2HPO_4 (0.017 M), and KCl (0.12 M), pH 6.47 (24°C), was slowly warmed from 0°C to 20°C resulting in the formation of short helical rods as described by Shire *et al.*³¹ When examined in the analytical ultracentrifuge at 22°C , three boundaries were observed with sedimentation coefficients, $s_{20,w}$, and weight fractions, respectively, of 33–35S, 0.17–0.20, 23–24S, 0.72–0.74, and A-protein 4S, 0.06–0.09. A 50- μl sample of the protein was equilibrated with ~ 0.3 – $0.5\ \mu\text{Ci}$ of trimer (final total concentration at dialysis equilibrium between 0.1 and $1\ \mu\text{M}$) for 12–18 h at room temperature (23° – 25°C), then loaded into a dialysis chamber. In the opposite chamber was placed 50 μl of a pH 4.97 (23°C) buffer consisting of acetic acid (0.029 M), sodium acetate (0.071 M), KH_2PO_4 (0.050 M) and KCl (0.16 M). Method II: preformed TMV protein rods were formed as in method I but the trimer was not included with the protein. After 24 h of dialysis at 20°C , the dialysates were withdrawn from the buffer chambers and added individually to lyophilized trimers. The trimer-dialysate solutions were then loaded back individually into the empty dialysis chambers to allow the trimers to dialyse into the chambers containing the preformed protein rods. In most cases the first samples were withdrawn 4–5 days after the start of the experiment. In both methods I and II, pH values of solutions removed from the chambers at the end of an experiment were determined with a pH microelectrode. Details of the dialysis chambers used here and the method of equilibrium microdialysis are described elsewhere.³² The total molar site concentration of TMV protein was taken to be the same as the total subunit concentration at the start of dialysis. It was determined spectrophotometrically using an extinction coefficient of $1.30\ (\text{mg ml}^{-1})^{-1}\ \text{cm}^{-1}$ (ref. 33) and a molecular weight of 17,530 per subunit.³⁴ ^3H -labelled trimers of specific activity between 6 and 16 Ci mmol⁻¹ were synthesized according to the method of Thach and Doty.³⁵ Precautions were taken to prevent ribonuclease degradation of the trimers³⁶ and all samples were checked for purity by paper chromatography³⁵ after synthesis, and for degradation after equilibrium dialysis. TMV protein prepared as described by Shire *et al.*³⁷ was found by Professor Uhlenbeck to be ribonuclease-free. Because the ratio of molar concentration of sites to the molar concentration of bound plus unbound trimer at dialysis equilibrium was ≥ 500 , the binding constants were calculated from the relation, $K = (R-1)/C_0$, which assumes binding to one class of independent sites. C_0 , total molar site concentration, R , ratio of c.p.m. in 3 μl withdrawn from the chamber containing the protein to c.p.m. in 3 μl withdrawn from the opposite (dialysate) chamber. Binding constants <200 – $300\ \text{M}^{-1}$ are not measurable within experimental error by this method.

the X-ray diffraction structure of TMV to be near the nucleotide binding sites.¹¹ To enhance trinucleoside diphosphate binding we used a lower pH (5–6) to reduce the net negative charge on the protein through binding of the polymerization-linked protons.¹² The titration curve of TMV protein near 20°C shows

that one proton is bound when the pH is reduced from 8.0 to 6.5 and another on reduction of the pH from 6.5 to 5.5 (refs 13–17). As trinucleoside diphosphates are negatively charged in this pH range, a significant pH-dependence of binding was expected for weak binding.

In addition to reducing the net negative charge on the protein, the binding of the two polymerization-linked protons switches the subunit conformation in the 20S disk aggregate¹⁸ to one that is very similar to that in the helical subunit array found in the whole virus.^{19,20} On binding these polymerization-linked protons, TMVP subunits polymerize to form virus-like long helical rods.^{21,22} The greater affinity of the trimers for polymerized TMV protein at pH < 6 relative to the weak binding of some of them to the protein aggregates at pH 6.5 and 7.0 (see Table 1) is considered to result from the presence of an ordered structure that exists at pH < 6 in the polypeptide chain at low radius between the centre of the rod and the region where the RNA binds to each subunit. This ordered structure has also been found by X-ray diffraction to exist in TMV¹¹ and in helical rods of polymerized TMVP formed at pH 5.5 (refs 19,20). However, the crystal structure of the 20S disk aggregate¹⁸ reveals disorder of the polypeptide chain at low disk radius.

As TMV protein subunits polymerize extensively into helical rods at 20°C and pH < 6 (the conditions in which the present systematic binding measurements were made), we used intact virus to test for nonspecific binding. Neither of two trimers that bind to the protein, AAG or CAG, show binding to intact TMV in the same conditions. Binding of the trimers to the natural nucleotide sites on the native virus is precluded by the presence of the RNA, therefore the lack of binding of AAG and CAG to TMV means that there are no trivial trinucleotide binding sites on the coat protein of the virus. The similarity of the protein subunit packing in the virus and the helical protein rods^{19,20,23} leads us to assume that RNA-free TMV protein rods also do not have trivial trinucleotide binding sites.

Table 1 gives the apparent association equilibrium constants (K) for the binding of 25 trimers to TMV protein rods. In all cases the binding (or lack of it) was the same to preformed protein rods (method II) as to rods formed in the presence of trimers (method I), thus we can conclude that no nonspecific entrapment of trimers occurs during protein polymerization in method I. In general, the binding constants were found to be independent of the way in which the experiment was performed, indicating that the binding sites are structurally alike in both types of TMV protein rod preparation. At the concentrations of trimers used, less than 0.2% of the total trinucleotide sites on the protein rods were occupied and no site interactions were detectable.

The shape of the titration curve of TMV protein at 20°C suggests that the net charge per subunit between pH 5 and 6 depends strongly on the pH (refs 13–17). As the trinucleoside diphosphates are negatively charged in this pH range we would expect, and indeed we have observed, that the measured binding constants increase with decreasing pH. The binding constant for AGA at pH 5.25 is $1.6 \times 10^3\ \text{M}^{-1}$ (by method I, not shown), which is stronger binding than that observed at pH 5.4 ($1 \times 10^3\ \text{M}^{-1}$, see Table 1).

The results in Table 1 reveal three ranges of binding constants for the trimers studied, 0.5 – 2×10^3 , 4 – 6×10^3 and one sequence, AAG, which gives a value of $12 \times 10^3\ \text{M}^{-1}$.

Although not all possible trimer sequences have been studied, the results in Table 1 provide insights into the sequence specificity of TMV protein-RNA interactions. Various comparisons are drawn in Table 2, based on the assumption that the binding constants reported are obtained at binding equilibrium, for which there is evidence (see Table 1 legend). A further assumption underlying these comparisons is that all the trimers bind in the same frame on the protein. Although the present experiments yield thermodynamic and not structural information, the reasoning presented below argues against single base recognition as a major determinant of trimer binding, therefore at least compositional isomers such as

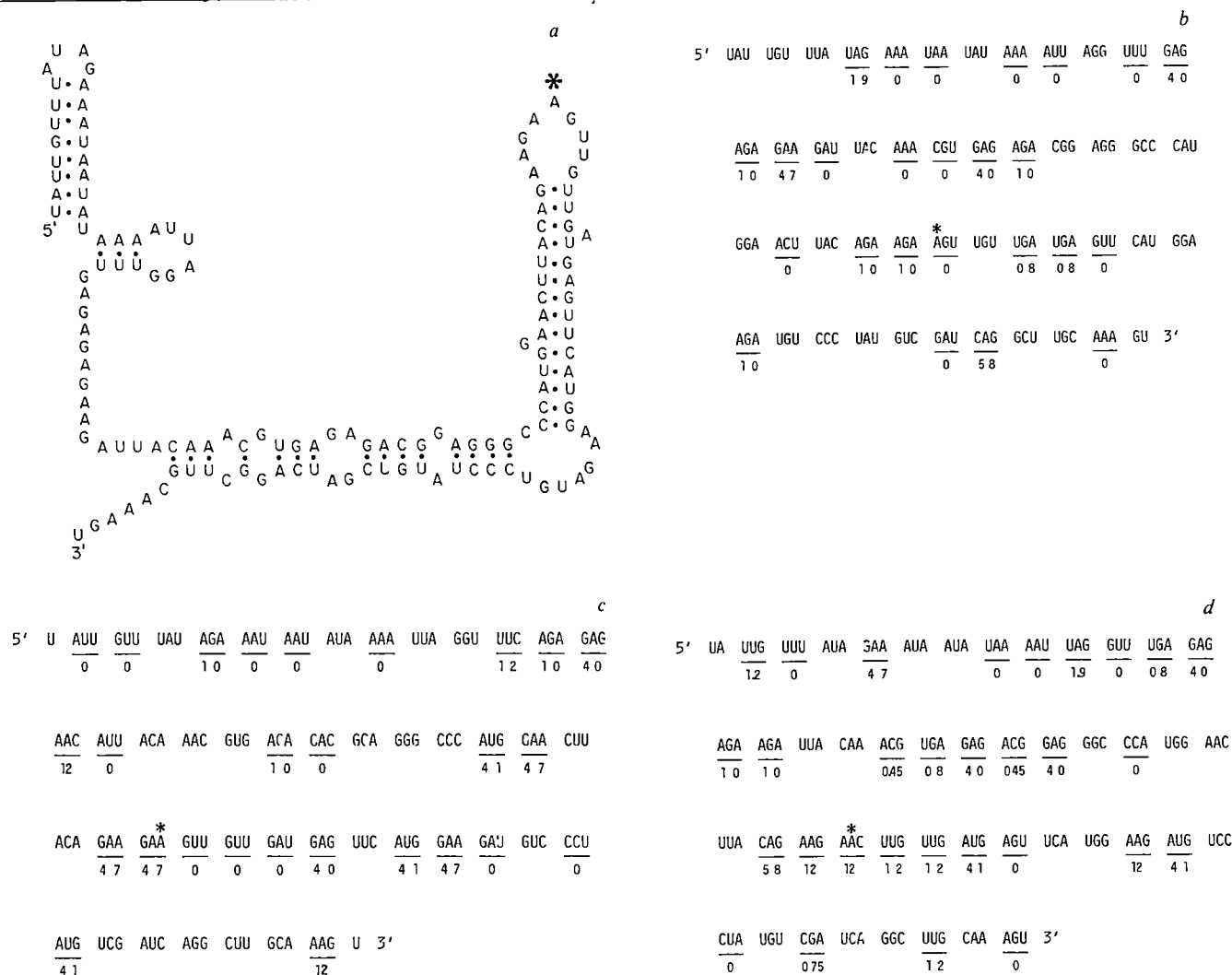


Fig. 2 *a*, Sequence of TMV RNA around the assembly nucleation region, as determined by Zimmern⁵. Secondary structure is that proposed by Zimmern. *b*, Alignment of the sequence of trinucleotides at the assembly nucleation site of TMV RNA into a binding frame for TMV protein recognition, as suggested by Zimmern⁵. Binding constants ($10^{-3} \times K (M^{-1})$) beneath the underlined trimers are for the corresponding trimers from Table 1. *c*, Trinucleotide binding frame resulting from shifting the frame in *b* one position in the 3' direction. *d*, Trinucleotide binding frame resulting from shifting the frame in *b* one position in the 5' direction.

XXY and YXX would not be expected to bind in different frames

The comparisons in Table 2 suggest the following general rules for binding. Trimer binding is highly sequence-dependent, in support of Caspar's prediction¹². Guanosine is present in every trimer that binds and appears to lead to the strongest binding when it is in the 3' position. However, an internal pyrimidine inhibits the 3' guanosine contribution to binding, with C having a stronger destabilizing effect than U. The low percentage of C at the assembly nucleation site, relative to its percentage in the whole TMV RNA molecule, has previously been interpreted to mean that C in a trinucleotide sequence exerts a destabilizing effect on binding to TMV protein^{6,24}. The pattern of binding constants in Table 1 does not reveal a simple additive contribution of single bases to the overall free energy of trimer binding, suggesting a cooperative binding mechanism. This can be seen by considering the following comparison in which the alignment of three trimers assumes that single base contributions dominate trimer binding

Protein site			Binding constant		
1	2	3	1	2	3
A	A	G			
	A	G	A		
		G	A	A	

($10^{-3} \times K (M^{-1})$)

12 0

1 0

4 7

It can be seen that each of the protein sites can be occupied identically (neglecting end effects) in the case of the three trimers examined. If single base recognition and binding determine the strength of trimer binding largely in a simple additive manner, the observed binding constants should be almost identical, clearly, this is not the case. Similar comparisons using other examples from the data in Table 1 support the conclusion that single base recognition alone does not account for the trimer binding results. This conclusion is strengthened further if the result that the trimer AAA shows no detectable binding is included in the above comparison.

The correlations described above can be summarized in the following set of rules which accurately describe the binding or non-binding of the 25 trimers tested, and predict the behaviour of the remaining 39.

Three classes of binding trimers (5' → 3') have been found: X-Y-guanosine, X-guanosine-purine, and guanosine-X-purine. Thus, the presence of a guanosine in a trimer is necessary but not sufficient for binding as trimers containing a pyrimidine in the 3' position do not bind even if there is a guanosine in either the 5' or internal position.

A comparison of the free energies of binding for the four XAG trimers, on the assumption that they bind to the protein in the same frame, leads us to conclude that for the base in the 5' position the trimer binding energy may be more sensitive to

Table 2 Dependence of apparent binding constants on trimer composition and sequence

<i>a</i>		<i>b</i>		<i>c</i>	
AUG(4 1)		AAG(12 0)		AAG(12 0)	
UAG(1 9)		GAA (4 7)		CAG (5 8)	
UGA(0 8)		AGA (1 0)		GAG (4 0)	
AGU (0)		AAA (0)		UAG (1 9)	
GAU (0)					
<i>d</i>		<i>e</i>		<i>f</i>	
AGA(1 0)		AAG(12 0)		AAG(12 0)	
UGA(0 8)		AUG (4 1)		CAG (5 8)	
CGA(0 75)		ACG (0 45)		AUG (4 1)	
				GAG (4 0)	
				UAG (1 9)	
				UUG (1 2)	
				ACG (0 45)	
					AGA(1 0)
					UGA(0 8)
					CGA(0 75)
<i>g</i>		<i>h</i>			
AAG(12 0) > AAU(0) ≡ AAA (0)		AAG(12 0) > UAG(1 9)			
AUG (4 1) > AUU(0) —		GAA (4 7) > UAA (0)			
GAG (4 0) > GAU(0) —	< GAA(4 7)	GAG (4 0) > UAG(1 9)			
UUG (1 2) > UUU(0) —		AGA (1 0) ≡ UGA(0 8)			
— AGU(0) < AGA(1 0)		AAG(12 0) > CAG(5 8)			
— GUU(0) —		AGA (1 0) ≡ CGA(0 75)			
ACG (0 45) > ACU(0) —					
— CCU(0) ≡ CCA(0)		Note however			
— CGU(0) < CGA(0 75)		GAG (4 0) < CAG(5 8)			
GAG (4 0) > GAC(0) < GAA(4 7)					

The data from Table 1 are grouped to test for the dependence of the apparent binding constants ($10^{-3} \times K(M^{-1})$) on trimer composition and sequence. The following conclusions can be drawn from these comparisons: *a*, The binding constant of a trimer depends not on nucleoside composition but on sequence (see first three entries in *b*). *b*, The presence of only purines in a trimer does not necessarily result in binding, which is seen to be strongly sequence-dependent even in a tri-purine trimer. *c*, For the trimer XAG the 5' base influences binding in the order A > C > G > U. *d*, In contrast to XAG, the binding of the trimer XGA is much less sensitive to the base in the 5' position. *e*, For the trimer AXG the internal base influences binding in the order A > U > C. *f*, All seven trimers studied which have a G in the 3' position bind. However, a G in the 5' position results in binding only if a purine is in the 3' position. All the 11 trimers which bind have a purine in the 3' position. *g*, None of the 10 trimers studied which have a pyrimidine in the 3' position bind. Ten of the possible corresponding 18 independent 3' purine-substituted trimers were measured and of these, eight exhibited binding, in contrast to the absence of binding in the parent 3' pyrimidine trimers. *h*, In most cases, a 5' purine is necessary for strong binding and substitution for a 5' pyrimidine reduces strong but not weak binding.

the NH₂ and the =O ring substituents than it is to the size of the heterocyclic ring (see Fig. 1).

As the difference in binding energies for 5' pyrimidines, $\Delta(\Delta G^*)_{py} = \Delta G^*(CAG) - \Delta G^*(UAG)$ (where R₁ is =O, see Fig. 1), is about the same as that for 5' purines, $\Delta(\Delta G^*)_{pu} = \Delta G^*(AAG) - \Delta G^*(GAG)$ (where R₁ is NH₂ or H), we assume that these substituents in the R₁ position do not influence binding and the $\Delta(\Delta G^*)$ value of $\sim 0.65 \text{ kcal mol}^{-1}$ in both reflects the NH₂ to =O substitution. Continuing on the assumption that binding is insensitive to the R₁ substituent allows a comparison of $\Delta G^*(AAG) - \Delta G^*(CAG)$ and of $\Delta G^*(GAG) - \Delta G^*(UAG)$ where the R₂ positions are the same (NH₂ and =O, respectively). This comparison yields the same value of $\Delta(\Delta G^*)$, that is, $\sim -0.45 \text{ kcal mol}^{-1}$, in both cases and suggests that this difference results from the difference in heterocyclic ring size.

These binding properties at the site for the 5' nucleoside contrast strongly with those at the 3' site. From the results for the trimer GAX (see Table 2*f, g*) it can be seen that the 3' site is more sensitive to heterocyclic ring size than is the 5' site. A detailed stereochemical interpretation of these conclusions must await elucidation by X-ray diffraction of high resolution structures of the oligonucleotide-TMV protein complex²⁵⁻²⁷ and of TMV^{11,28}.

Probable binding frame for nucleation of TMV self-assembly

Figure 2*a* shows the RNA fragment, sequenced by Zimmern⁵, which is proposed to contain the region for nucleation of *in vitro* virus assembly. The hairpin secondary structure is that proposed by Zimmern based on maximum base pairing. The non-bonded loop of the hairpin structure on the right-hand side (marked *) has been proposed to be the first part of the RNA molecule that binds to the inside of the nucleating disk^{5,7}. The three possible linear binding frames for the interaction of three nucleotides with each of the identical coat protein subunits in either the disk or helix conformation are shown in Fig. 2*b-d*.

Shown beneath each binding frame are the available binding constants for the corresponding trimers from Table 1. The frame suggested by Zimmern⁵ is shown in Fig. 2*b*. Figure 2*c* gives the trimer binding frame shifted one position in the 3' direction from Fig. 2*b*. The 5'-shifted reading frame is shown in Fig. 2*d*. A comparison of the available trimer binding constants in Table 1 with the three binding frames reveals that the trimer alignment centred around AAG (Fig. 2*d*) results in the greatest number of tight sites for protein binding.

Binding frame *d* contains the greatest number of strong binding sites and the largest total number of binding sites. Comparison of the number of trimer binding sites in the three binding frames shows that frames *b, c* and *d* have, respectively, 4, 11 and 10 binding sites with trimer affinity constants equal to or greater than $4 \times 10^3 \text{ M}^{-1}$. A more significant comparison which distinguishes between binding frames *c* and *d* is the presence of three $12 \times 10^3 \text{ M}^{-1}$ trimers in the latter and two in the former. In binding frame *d* two of the highest affinity trimers, AAG, are contiguous whereas in *c* the two AAG sequences are widely separated. To a first approximation it would be expected that trimers in such pairs contribute to binding as the product of the individual trimer binding constants. This would mean that only binding frame *d* contains a region having an affinity $\geq 10^8 \text{ M}^{-1}$. The sequence forming this region, —AAG—AAG—, is in the large loop region (marked * in Fig. 2*a*) thought to be involved in the initial binding by the disk protein aggregate^{5,7}. This loop is flanked by other trimer sequences, CAG and UUG, which bind and would thus further enhance the stability of the initial complex by $\sim 5 \text{ kcal}$ beyond the $\sim 11 \text{ kcal}$ provided by the —AAG—AAG— sequence. In general, summation of trimer binding free energies, in order to estimate free energies for larger oligonucleotides, implicitly assumes that the trimers all bind to the helical protein rods in the same binding frame. However, such an assumption is obviously not required for deriving the $\sim 11 \text{ kcal}$ provided by the hexamer —AAG—AAG— but is necessary when adding the binding energies of the adjacent trimer sequences, CAG and UUG, in the RNA loop region marked (*) in

Fig 2a Binding energies of at least ~15 kcal are probably necessary for highly specific protein-nucleic acid interactions. Co-operative binding effects between adjacent trimer sites would contribute further to the binding energy for nucleation. To estimate the minimum energy of the RNA-protein interactions, we assumed that the helical rods of TMV protein at $pH < 6$ are, to a first approximation, good representatives of TMV without the RNA^{15,19,20}. There are, however, differences in protein structure between the helical protein rods and TMV^{19,20}. Studies of the energetics of changing the protein structure in the RNA-free helical rods to that occurring in TMV in conditions of *in vitro* TMV assembly are required to define fully the energy of interaction between a trinucleotide and the RNA binding site in the final virus structure. However, the energy of this conformational change is expected to be small because the titration curves of the whole virus and the RNA-free helical protein rods are almost identical, differing by at most 0.5 kcal per mole of subunits¹⁵. Evaluation of the total free energy of assembly nucleation at $pH 7.0$ will require knowledge of the energetics of the switching of the protein conformation (disk \rightleftharpoons helix). Although there are no accurate values for the free energy of the reaction (disk \rightleftharpoons helix), one can estimate a value between 2 and 4 kcal per mole of subunits from an analysis of titration¹²⁻¹⁷ and sedimentation data⁹. The upper range of this estimate is consistent with the observed very weak binding of the AAG trimer to 20S protein which is thought to be mainly the disk aggregate at $pH 7$.

The alternative hairpin-loop structure of the nucleation region of TMV RNA proposed by Jonard *et al.*⁶ is not expected to alter the conclusion regarding the RNA binding frame for protein binding. An inspection of their structure shows that the -AAG-AAG- hexanucleotide is located at the top of the loop, and therefore is in a position on the RNA to interact with the initiating 20S protein aggregate in much the same way as is the same hexanucleotide of Fig 2d.

Discussion

These binding experiments were done in conditions that ensured a very low fractional site occupancy to avoid the complication of trimer binding to possible overlapping sites in the helical protein rods. We assume that the trimers bind to the tightest sites available to them and that they bind in an orientation similar to that of the natural RNA in the virus. There is no way of knowing from these studies alone whether the trimers were bound directly to the trinucleotide binding site of the individual protein subunits or in a site formed by two laterally adjacent subunits in the helical rods. However, based on a recent refinement of the 4 Å fibre diffraction pattern of TMV and the suggested structure of the RNA in the virus²⁸, we consider that inter-subunit trinucleotide binding would not be favoured in the conditions of our experiments. The sequence dependence of the binding affinity of trinucleoside diphosphates to TMV protein suggests that the RNA binding frame of

Fig 2d is probably the one that promotes binding to the initiating TMV protein aggregate.

The results of the binding studies described here may provide only part of the explanation for nucleation of TMV self-assembly occurring at the region of the TMV RNA molecule shown in Fig 2d, as previous studies have shown that small fragments of TMV RNA derived from parts of the molecule other than the assembly nucleation region bind to disk-like aggregates of TMV protein^{24,29}. These results have been interpreted to mean that the specificity of nucleation is defined by an RNA sequence that, once bound, promotes the quaternary conformational change of the initiating two-turn cylindrical disk to a two-turn helix⁷. However, the results reported here are consistent with the trimers binding selectively to subunits in a helical array in the (disk \rightleftharpoons helix) equilibrium.

Binding of fragments of TMV RNA can be termed non-specific if there is no concomitant switching of the protein conformation. It remains to be demonstrated whether the binding of the RNA fragments derived from the coat protein cistron of TMV RNA²⁴ (the cistron starts ~150 nucleotides from the 3' end of the assembly nucleation region³⁰) to aggregates of TMV protein results in the formation of nucleoprotein complexes having a helical structure⁶. In the three binding frames of the largest RNA fragment, T1, there are no regions of sequential binding trimers, based on the information in Table 1, that contain contiguous high-affinity AAG trimers. Tyulkina *et al.*²⁹ have shown that some of the 30S complexes formed by combining 3S fragments of TMV RNA with a preparation of TMVP containing 20S aggregates have a helical structure similar to that of TMV. Their results²⁹ and the demonstration that the T1 and P1 RNA fragments (the P1 fragment contains the assembly nucleation site sequence⁶) bind with comparable rates to the disk aggregate⁶ suggest that the secondary and tertiary structures in the TMV RNA molecule might contribute to the efficiency of the sequence specificity reported here. Certainly, the existence of higher orders of RNA structure does not sufficiently explain the sequence specificity of trinucleoside diphosphate binding to TMV protein. However, RNA folding may control the accessibility of different regions of the RNA molecule to the 20S and 4S aggregates of TMV protein. For example, it is important to know whether nonspecific binding of TMV protein to the RNA molecule is minimized by placing favourably recognized oligonucleotide sequences in the hydrogen-bonded stem regions of hairpin structures rather than in their single-stranded loops. We are confident that the sequence specificity seen for trimer binding to TMV protein is related to the specificity of nucleation as a sufficiently high concentration of AAG causes crystals of the cylindrical disk protein aggregate to dissolve²⁵. This finding suggests that the AAG trimer binds like natural TMV RNA and promotes the disk-to-helix quaternary conformational change²⁶.

We thank Dr David A. Yphantis for suggestions and discussions. This work was supported by NIH grant AI 11573.

Received 27 January, accepted 24 June 1982

- Zimmermann, D. & Wilson, T. M. A. *FEBS Lett* **71**, 294-298 (1976)
- Lebeurier, G., Nicolaieff, A. & Richards, K. E. *Proc natn Acad Sci U S A* **74**, 149-153 (1977)
- Otsuki, Y., Takebe, I., Ohno, T., Fukuda, M. & Okada, Y. *Proc natn Acad Sci U S A* **74**, 1913-1917 (1977)
- Zimmermann, D. & Butler, P. J. G. *Cell* **11**, 455-462 (1977)
- Zimmermann, D. *Cell* **11**, 463-482 (1977)
- Jonard, G., Richards, K. E., Guillely, H. & Hirth, I. *Cell* **11**, 483-493 (1977)
- Butler, P. J. G. *et al.* in *Structure-Function Relationships of Proteins* (eds Markham, R. & Horne, R. W.) 101-110 (North-Holland, Amsterdam 1976)
- Durham, A. C. H., Finch, J. T. & Klug, A. *Nature new Biol* **229**, 37-42 (1971)
- Schuster, T. M. *et al.* *Biophys J* **32**, 313-329 (1980)
- Schuster, T. M., Scheele, R. B. & Khairallah, L. H. *J molec Biol* **127**, 461-485 (1979)
- Stubbs, G., Warren, S. & Holmes, K. *Nature* **267**, 216-221 (1977)
- Caspar, D. L. D. *Adv Protein Chem* **18**, 37-121 (1963)
- Scheele, R. B. & Lauffer, M. A. *Biochemistry* **6**, 3076-3081 (1967)
- Butler, P. J. G., Durham, A. C. H. & Klug, A. *J molec Biol* **72**, 1-18 (1972)
- Scheele, R. B. & Schuster, T. M. *J molec Biol* **94**, 519-525 (1975)
- Durham, A. C. H., Vogel, D. & DeMarcillac, G. D. *Eur J Biochem* **79**, 151-159 (1977)
- Shalaby, R. A. F. & Lauffer, M. A. *J molec Biol* **116**, 709-725 (1977)
- Bloomer, A. C., Champness, J. N., Bricogne, G., Staden, R. & Klug, A. *Nature* **276**, 362-368 (1978)

- Stubbs, G., Warriner, S. & Mandelkow, E. *J supramolec Struct* **12**, 177-183 (1979)
- Mandelkow, E., Stubbs, G. & Warren, S. *J molec Biol* **152**, 375-386 (1981)
- Schramm, G. Z. *Naturf* **2b**, 112-121, 249-257 (1947)
- Durham, A. C. H. & Klug, A. *Nature new Biol* **225**, 42-46 (1971)
- Franklin, R. E. *Biochim biophys Acta* **18**, 313-314 (1955)
- Guillely, H., Jonard, G., Richards, K. E. & Hirth, I. *Phil Trans R Soc B276*, 181-188 (1976)
- Graham, J. & Butler, P. J. G. *Eur J Biochem* **93**, 333-337 (1979)
- Butler, P. J. G. & Lomonosoff, G. P. *Biophys J* **32**, 295-312 (1980)
- Bloomer, A. C., Graham, J., Hovvoller, S., Butler, P. J. G. & Klug, A. in *Structural Aspects of Recognition and Assembly in Biological Macromolecules* (eds Balaban, M., Sussman, J. L., Traub, W. & Yonath, A.) 851-864 (Balaban ISS, Rehovot, 1981)
- Stubbs, G. & Stauffer, C. J. *J molec Biol* **152**, 387-396 (1981)
- Tyulkina, L. G. *et al.* *Virology* **63**, 15-29 (1975)
- Guillely, H., Jonard, G., Kukla, B. & Richards, K. E. *Nucleic Acids Res* **6**, 1287-1308 (1979)
- Shire, S. J., Steckert, J. J. & Schuster, T. M. *J molec Biol* **127**, 487-506 (1979)
- Uhlenbeck, O. C. *J molec Biol* **65**, 25-41 (1972)
- Fraenkel-Conrat, H. & Williams, R. C. *Proc natn Acad Sci U S A* **41**, 690-698 (1955)
- Tsugita, A. *et al.* *Proc natn Acad Sci U S A* **46**, 1463-1469 (1960)
- Thach, R. E. & Doty, P. *Science* **148**, 632-634 (1965)
- Boedtker, H. *Methods Enzym* **12B**, 429-458 (1968)
- Shire, S. J., Steckert, J. J., Adams, M. L. & Schuster, T. M. *Proc natn Acad Sci U S A* **76**, 2745-2749 (1979)

LETTERS TO NATURE

Galaxy formation by dissipationless particles heavier than neutrinos

George R. Blumenthal*, Heinz Pagels†
& Joel R. Primack‡

* Lick Observatory, Board of Studies in Astronomy and Astrophysics, ‡ Board of Studies in Physics, University of California, Santa Cruz, California 95064, USA

† The Rockefeller University, New York, New York 10021, USA

In a baryon dominated universe, there is no scale length corresponding to the masses of galaxies. If neutrinos with mass < 50 eV dominate the present mass density of the universe, then their Jeans mass $M_{J\nu} \sim 10^{16} M_\odot$, which resembles super-cluster rather than galactic masses. Neutral particles that interact much more weakly than neutrinos would decouple much earlier, have a smaller number density today, and consequently could have a mass > 50 eV without exceeding the observational mass density limit. A candidate particle is the gravitino, the spin 3/2 supersymmetric partner of the graviton, which has been shown¹ to have a mass ≤ 1 keV if stable². The Jeans mass for a 1-keV noninteracting particle is $\sim 10^{12} M_\odot$, about the mass of a typical spiral galaxy including the nonluminous halo. We suggest here that the gravitino dominated universe can produce galaxies by gravitational instability while avoiding several observational difficulties associated with the neutrino dominated universe.

There is evidence that a considerable fraction of the mass in the Universe is nonbaryonic. Light element synthesis in the big bang requires that the density parameter³ $\Omega_b = \rho_b / \rho_{\text{crit}} < 0.014 H^{-2}$, where ρ_b is the present baryonic density, $\rho_{\text{crit}} = 11 \text{ keV cm}^{-3} H^{-2}$ is the closure density of the universe, and H is the Hubble parameter in units of $100 \text{ km s}^{-1} \text{ Mpc}^{-1}$ (observationally, $0.4 < H < 1$).

On the other hand, observations give a lower bound⁴⁻⁶ on the total density parameter $\Omega > 0.1$. On a galactic scale, there is also strong evidence that the mass in stars is considerably less than the mass of the nonluminous halo.

The present neutrino number density is $109 \text{ cm}^{-3} (T/2)^3$ per species. Because observationally the density parameter Ω cannot significantly exceed unity, the sum of the masses of all stable neutrino species is < 100 eV. Experimentally, the electron neutrino mass is < 50 eV, with one experiment indicating a non-zero mass⁷. Particles such as gravitinos which interact much more weakly than neutrinos decouple at a temperature T_d much higher than the neutrino decoupling temperature and long before many species have annihilated and heated (thereby increasing the number density of) the remaining interacting particles (including neutrinos). For $\Omega H^2 < 1$, the resulting upper limit on the mass of such particles (assuming two interacting helicity states) is $1.9 g(T_d) \text{ eV}$, where $g(T)$ is the effective number of interacting species including neutrinos. The standard particle physics model (QCD plus Weinberg-Salam with three quark and lepton generations) gives $g \approx 50$ above the quark deconfinement temperature of a few hundred MeV, growing slowly to $g \approx 100$ at $T \sim 100 \text{ GeV}$, with perhaps another factor of two growth due to supersymmetry. Therefore any such particle must be less massive than $\sim 1 \text{ keV}$. Here we consider the possibility that such particles dominate the Universe and, for definiteness, assume them to be gravitinos of mass $\sim 1 \text{ keV}$.

The scenarios for galaxy formation strongly depend on whether baryonic matter, neutrinos or gravitinos dominate the present Universe (see Fig. 1). Baryon condensations of galactic size are strongly damped during the radiation era by Compton drag (Silk damping)^{8,9}. For non-interacting particles of mass m ,

the maximum Jeans mass is given by^{10,11} $M_J \sim (M_{\text{Planck}})^3 / m^2$, which, for Friedmann cosmologies, is the mass within the horizon when the particles become nonrelativistic. The free streaming of dissipationless particles such as neutrinos or gravitinos destroys density perturbations on all scales smaller than the horizon until the particles become nonrelativistic. In particular, the proper free streaming distance travelled by a noninteracting particle with present momentum p_0 between time t and the present time t_0 is¹²

$$D(p_0, t) = R_0 \int_t^{t_0} dt v(t) / R(t)$$

where $R(t)$ is the scale factor of the universe and $v(t)$ is the instantaneous velocity of the particle with respect to a co-moving frame. We take the Jeans mass at time t to be the present mass of particles within a sphere of radius $D(p_0, t)$, with p_0 the characteristic momentum at the present time (ref 12, appendix).

The most important aspect of Fig. 1 is that for gravitinos the maximum Jeans mass $M_{Jg} \sim 10^{12} M_\odot$ while for neutrinos $M_{J\nu} \sim 10^{16} M_\odot$. Therefore gravitinos provide a natural scale size for galaxies, while the neutrino-dominated universe can form galaxies only by fragmentation of much larger gravitational condensations^{13,14}.

The linear growth of neutrino and gravitino perturbations, of masses $10^{16} M_\odot$ and $10^{12} M_\odot$ respectively, is illustrated in Fig. 2. The density contrast $\delta = \delta n / n$ is a gauge dependent quantity, and here we follow the standard treatment^{15,16} in time-orthogonal coordinates. Adiabatic perturbations larger than the horizon grow as $\delta \propto R^2$ in a radiation-dominated universe, while $\delta \propto R$ for nonrelativistic particles in a matter-dominated universe. Before matter (gravitino) domination, nonrelativistic gravitino perturbations with $M > M_{Jg}$ but smaller than the horizon can grow by at most a factor 2.5 (refs 17, 18), since once inside the horizon radiation oscillates and relativistic neutrinos free stream away. Thus limited growth in δ occurs for $M_{Jg} < M < M_{\text{eq}} = \text{horizon mass when matter domination first occurs} \approx 10^{16} (\Omega H^2)^{-2} M_\odot$.

If the initial perturbation spectrum is $\delta(M) \propto M^{-(3+n)/6}$, then in the matter dominated era $\delta(M)$ falls off steeply for $M < M_{Jg}$ due to free streaming of the relativistic gravitinos, is flattened with $n_{\text{eff}} \approx n - 4$ because of the effect just discussed for $M_{Jg} < M < M_{\text{eq}}$, and reflects the initial spectrum for $M > M_{\text{eq}}$. (This has been calculated in detail using the Boltzmann equation by

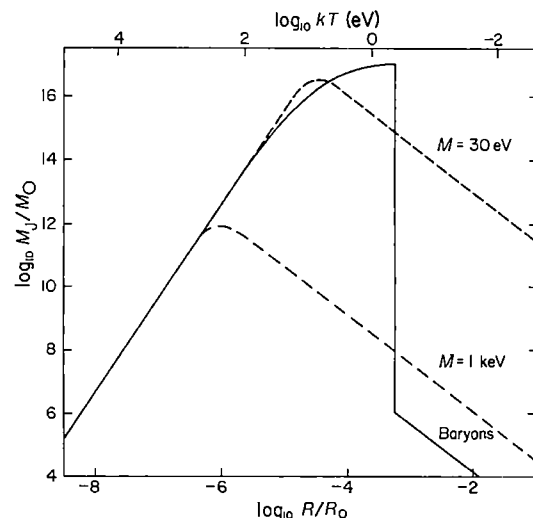


Fig. 1 The Jeans mass versus scale factor for a baryon, gravitino ($m = 1 \text{ keV}$), and neutrino ($m = 30 \text{ eV}$) dominated universe with $\Omega H^2 = 1$. Neutrino and gravitino perturbations with $M < M_J$ at any time are dissipated by free streaming.

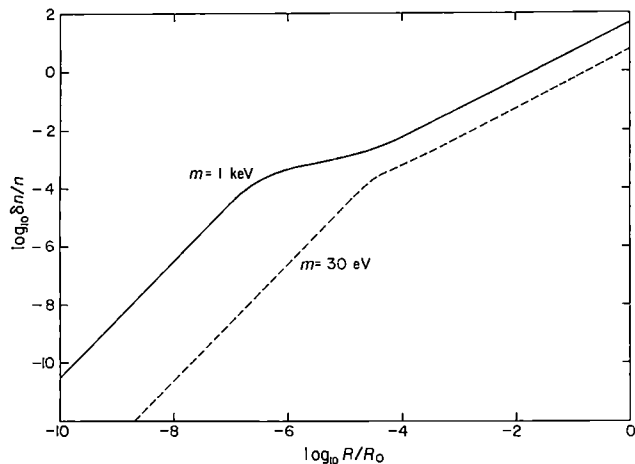


Fig. 2 The growth of linear perturbations on mass scales $> M_J$ versus the scale factor of the universe ($\Omega H^2 = 1$) for noninteracting particles of mass 1 keV and 30 eV. The overall normalizations of these curves are arbitrary.

Bond *et al.*¹⁹) Finally, after hydrogen recombination, baryon fluctuations rapidly grow towards those of the gravitinos²⁰. Consequently, in the gravitino case, an initial adiabatic perturbation spectrum with $n \approx 1$ leads to the formation of galaxies of total mass $\sim 10^{12} M_\odot$, followed by baryon dissipation on galactic scales only²¹ (consistent with cooling constraints²²), with hierarchical clustering on scales between $\sim 10^{12}$ and $\sim 10^{16} M_\odot$. Observationally²²⁻²⁴, there is little variation in matter density from small clusters to superclusters, which in the absence of dissipation implies that clusters of all sizes collapsed roughly simultaneously—that δ is nearly constant between 10^{12} and $10^{16} M_\odot$. Such a spectrum ($n_{\text{eff}} \approx -2$) follows in the gravitino scenario from the plausible initial spectrum $n \approx 1-2$. Also, in contrast to the neutrino scenario where the formation of superclusters through dissipational pancake collapse^{13,14} precedes the formation of galaxies and must therefore have occurred at $z > 3$, in the gravitino scenario supercluster collapse follows galaxy formation and is dissipationless. This is consistent²⁵ with the observed²⁶ absence of clustering of Ly α absorption lines in quasar spectra and with the lack of extreme flattening in superclusters²⁷.

The nonluminous haloes of galaxies may also distinguish between the neutrino and gravitino hypotheses. If large spiral galaxies such as our own have haloes with radius ~ 100 kpc and $M/L \approx 50$, then there is not more than about a factor of two growth in the total/baryonic mass ratio from galactic to rich cluster scales. This is expected in the gravitino picture but not in the neutrino picture, where only $\sim 10\%$ of neutrinos are cooled enough to be captured by galaxies (A. Melott, and J. R. Bond, personal communications). It has indeed been suggested recently that the data are consistent with an approximately constant ratio of 7% baryonic to total mass on all scales larger than ~ 100 kpc (refs 22, 28). Finally, the phase space constraint^{29,30} on the mass of a fermionic halo particle is strongest for dwarf galaxies, for which preliminary analysis (S. Faber and D. Lin, in preparation) suggests this mass is at least several hundred eV.

We thank J. R. Bond, M. Davis, R. Giles, W. Mathews, A. Szalay, and especially S. Faber and D. Lin for helpful discussions, and the NSF and DOE for partial support. This is Lick Observatory Bulletin no. 931.

Received 5 January, accepted 15 July 1982

- 1 Pagels, H. & Primack, J. R. *Phys. Rev. Lett.* **48**, 223 (1982).
- 2 Weinberg, S. *Phys. Rev. Lett.* **48**, 1303 (1982).
- 3 Schramm, D. N. & Steigman, G. *Astrophys. J.* **243**, 1 (1981).
- 4 Davis, M., Geller, M. J. & Huchra, J. *Astrophys. J.* **221**, 1 (1978).
- 5 Peebles, P. J. E. *Astr. J.* **84**, 730 (1979).
- 6 Davis, M., Tonry, J., Huchra, J. & Latham, D. W. *Astrophys. J. Lett.* **238**, L113 (1980).
- 7 Lubimov, V. A., Novikov, E. G., Nozik, V. Z., Tretyakov, E. F. & Kosik, V. S. *Phys. Lett.* **B94**, 266 (1980).
- 8 Silk, J. & Wilson, M. *Phys. Scr.* **21**, 708 (1980).

- 9 Rees, M. J. in *Observational Cosmology* (ed. Gunn, J. E.) 259 (Geneva Observatory, Sauverny, 1978).
- 10 Bisnovaty-Kogan, G. S. & Novikov, I. D. *Soviet Astr.* **24**, 516 (1980).
- 11 Bond, J. R., Efstathiou, G. & Silk, J. *Phys. Rev. Lett.* **45**, 1980 (1980).
- 12 Davis, M., Lecar, M., Pryor, C. & Witten, E. *Astrophys. J.* **250**, 423 (1981).
- 13 Doroshkevich, A. G., Khlopov, M. Yu., Sunyaev, R. A., Szalay, A. S. & Zeldovich, Ya. B. *Ann. N.Y. Acad. Sci.* **375**, 32 (1981).
- 14 Bond, J. R. & Szalay, A. S. *Proc. Neutrino, Maui* (1981).
- 15 Weinberg, S. *Gravitation and Cosmology* (Wiley, New York, 1972).
- 16 Peebles, P. J. E. *The Large Scale Structure of the Universe*, 304 (Princeton University Press, 1980).
- 17 Guyot, M. & Zeldovich, Ya. B. *Astr. Astrophys.* **9**, 227 (1970).
- 18 Meszaros, P. *Astr. Astrophys.* **37**, 225 (1974).
- 19 Bond, J. R., Szalay, A. S. & Turner, M. *Phys. Rev. Lett.* (in the press).
- 20 Doroshkevich, A. G., Zeldovich, Ya. B., Sunyaev, R. A. & Khlopov, M. Yu. *Soviet Astr. Lett.* **6**, 252 (1980).
- 21 White, S. M. & Rees, M. J. *Mon. Not. R. Astr. Soc.* **183**, 341 (1978).
- 22 Faber, S. M. in *Proc. Vatican Conf. on Cosmology and Fundamental Physics* (in the press).
- 23 Bhavsar, S. P., Gott, J. R. & Aarseth, S. J. *Astrophys. J.* **246**, 656 (1981).
- 24 Kirschner, R. P., Oemler, A. Jr., Schechter, P. L. & Shechtman, S. A. *Astrophys. J. Lett.* **248**, L57 (1981).
- 25 Dekel, A. *Astrophys. J. Lett.* (in the press).
- 26 Sargent, W. L. W., Young, P. J., Boksenberg, A. & Tytler, D. *Astrophys. J. Suppl.* **42**, 41 (1980).
- 27 Dekel, A. *Astrophys. J.* (submitted).
- 28 Gunn, J. in *Proc. Vatican Conf. on Cosmology and Fundamental Physics* (in the press).
- 29 Tremaine, S. & Gunn, J. *Phys. Rev. Lett.* **42**, 407 (1979).
- 30 Sato, H. & Takahara, F. *Prog. theor. Phys.* **64**, 2021 (1980).

Discovery of 0.5-s oscillations in long flat top bursts from the Rapid Burster

Y. Tawara, S. Hayakawa, H. Kunieda, F. Makino & F. Nagase

Department of Astrophysics, Faculty of Science, Nagoya University, Chikusa-ku, Nagoya, Japan

We report here a search for periodic emission of X rays from MXB1730-335 (the Rapid Burster, which is the most unusual X-ray burst source¹ out of about 30 other bursters) during the long flat top bursts². Two events from the 63 bursts showed clear peaks in the frequency power spectra at ~ 0.5 s in period. However, this is unlikely to be a pulsar period, because the periods of these two bursts are different.

The burst activity of the Rapid Burster was observed between 8 and 22 August 1979 with the X-ray astronomy satellite Hakucho. From 8 29 to 15 97 August (UT), bursts were exclusively long flat top ones. Owing to their high intensities and long durations, we were able to search for the periodicity of the X-ray intensity during these events.

We analysed 63 long flat top bursts of durations in the range 40-600 s. The power spectrum analysis was performed for the bin width of 93.75 ms, the shortest time bin available, over the frequency range 0.1-5.3 Hz. All but two bursts show no periodicity higher than statistical fluctuations. The upper limits of pulsed fractions thus obtained are 10% of the intensity during the flat tops of the bursts.

For the two long flat top bursts which occurred at A 19 h 04 min on 9 August and B 01 h 45 min on 11 August (UT), oscillations were discovered with the mean periods of 0.508 ± 0.001 s for burst A and 0.503 ± 0.001 s for burst B. Periods were determined both by the power spectrum analysis and by the folding analysis. Figure 1 shows the time profiles and the power spectra of these two events. The power spectra show clear peaks with the maximum power density of 23-24 times the average power density level of white noise, corresponding to a pulsed fraction of 30%. Statistical errors of these periods were estimated by the folding analysis. If we calculate the χ^2 defined as

$$\chi^2 = \sum_{k=1}^n (f_k(P) - \bar{f})^2 / s_k^2$$

where $f_k(p)$ is k th bin of the pulse profile folded with a trial period p , \bar{f} is the average of $f_k(p)$ over n total bins and s_k^2 is a variance of each bin, then a real period P_0 corresponds to the maximum χ^2 , $\chi^2(P_0) = \chi^2_{\text{max}}$. A statistical error of period

Table 1 Characteristics of two long flat top bursts showing 0.5-s oscillations

	A 9 August 19 h 04 min	B 11 August 1 h 45 min	C* 8-22 August
Burst			
Duration (s)	123	150	5-600
Peak luminosity† (erg s ⁻¹)	$(3.27 \pm 0.09) \times 10^{38}$	$(3.72 \pm 0.08) \times 10^{38}$	$(0.7-4.0) \times 10^{38}$
Total energy† (erg)	$(4.20 \pm 0.10) \times 10^{40}$	$(5.55 \pm 0.12) \times 10^{40}$	$(0.1-8.0) \times 10^{40}$
Black-body temperature (keV)	1.97 ± 0.06	2.00 ± 0.03	1.5-2.0
Oscillations			
Mean period (s)	$0.508 \pm 0.001 \ddagger$	$0.503 \pm 0.001 \ddagger$	
Range of period (s)§	0.50-0.52	0.50-0.52	
Mean pulsed fraction	0.28 ± 0.05	0.30 ± 0.05	
Maximum pulsed fraction in 24 s	0.52 ± 0.10	0.40 ± 0.10	

* The ranges of burst parameters for the total data

† Assuming the spherical emission at a distance of 10 kpc

‡ Statistical errors estimated by the folding analysis, see text

§ Obtained from dynamical power spectra for 24 s

ΔP is estimated as follows

$$\chi^2(P_0 \pm \Delta P) = \chi^2_{\max} - 1$$

The possibilities that these oscillations are of instrumental or geophysical origin can be excluded by the following tests (1) The period does not correspond to instrumental time constants and their harmonics that would cause the observed power spectrum peak (2) Oscillations with a period near 0.5 s are not found in the background data of 1.8 h obtained during this period of active bursts (3) The occurrence of the present oscillations have no correlation with geographical position and local time of the satellite. We therefore conclude that the observed oscillations are in the X-ray flux.

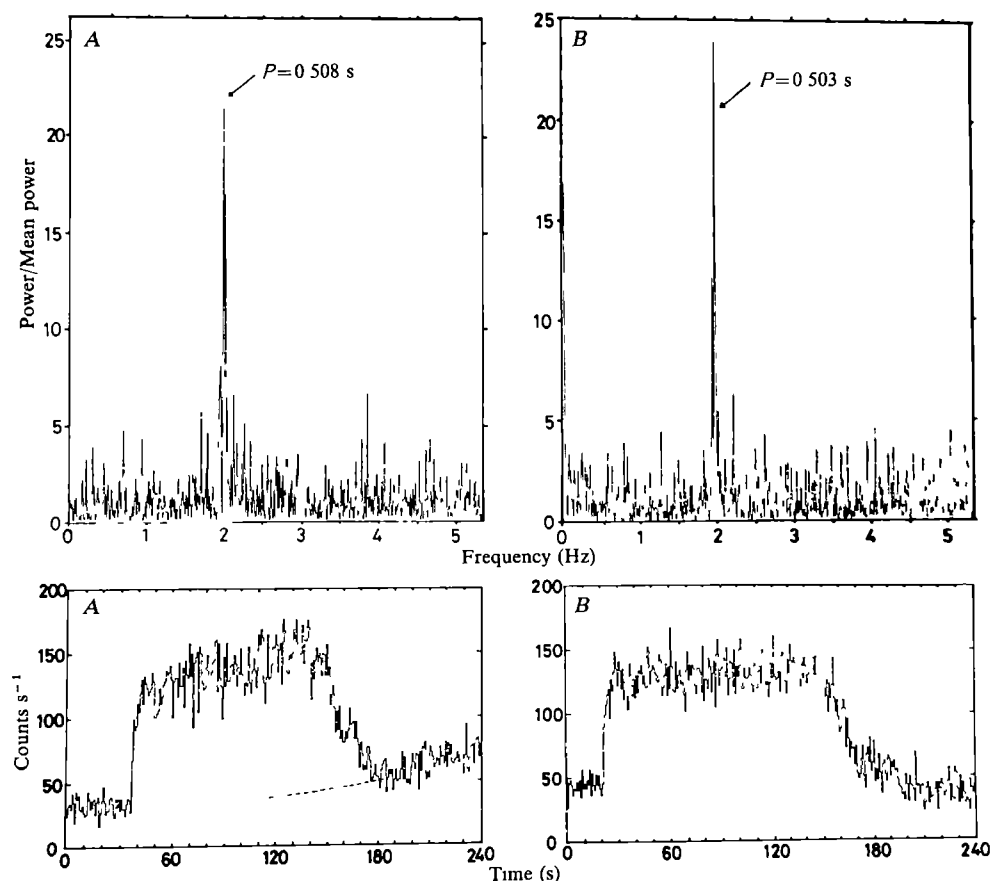
Characteristic properties of these two bursts and of the oscillations are summarized in Table 1. These two bursts occurred during the highest burst activity, the bursts during this period were of largest size, highest peak luminosity and had the hardest spectra¹. There are many bursts similar to the

oscillating events in size, luminosity and duration, but they show no oscillations. None of the 15 bursts observed between the two oscillating events A and B shows periodicity.

Several interesting properties can be noted for the observed oscillations. Figure 2 shows the power spectra of these two bursts every 24 s, where the statistical uncertainties of periods ΔP are 2 ms. Both a drift of the frequency and a variation of the pulsed fraction are clearly seen. For event A, the period of the maximum power density appears to have moved from 0.50 s to 0.52 s, the pulsed fraction increasing up to $40 \pm 10\%$, and the oscillation disappearing at ~ 20 s before the start of decay of the burst. Similar characteristics are observed for the other burst B as shown in Fig. 2.

Figure 3 shows the pulse profiles for energy band $L(1-9$ keV) and $H(9-22$ keV) respectively, obtained by folding the data of Fig. 2 Ab and Bc with periods of 0.511 s and 0.500 s for events A and B, respectively. The hardness ratios of the burst at the peak and the bottom of the folded profile are 0.296 ± 0.032 , 0.278 ± 0.046 respectively, thus they are the same within the

Fig. 1 The time profiles and the power spectra of the two long flat top bursts of 0.5 s oscillations. The time profiles start at A, 19 h 03 min 30 s on 9 August and B, 1 h 45 min 00 s on 11 August (UT) in 1979. The dashed line in the time profile of event A shows an increasing background level.



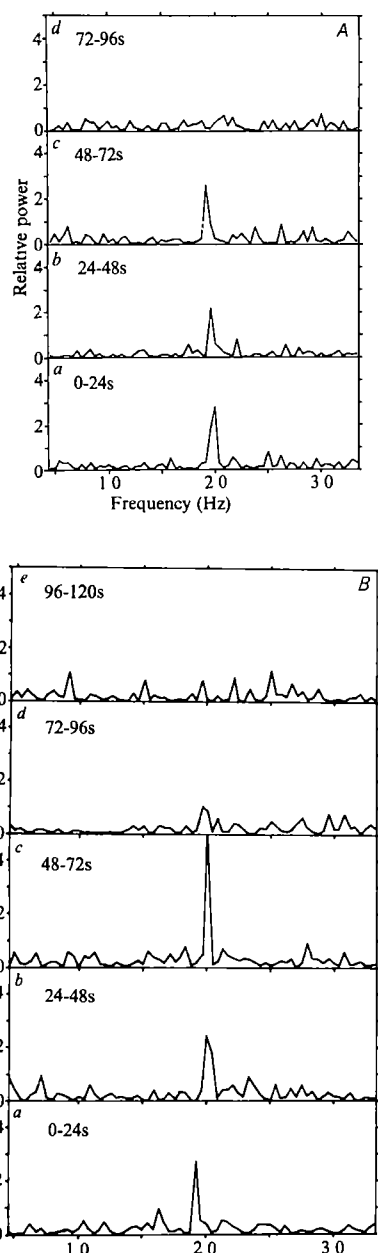


Fig. 2 The power spectra of events A and B for every 24 s, showing a drift of the period and/or phase of oscillations. Times indicated in each power spectrum in seconds are from 19 h 04 min 10 s on 9 August and 1 h 45 min 38 s on 11 August (UT), respectively

error limits. A nearly sinusoidal pulse profile is expected from the fact that the first higher harmonics is not significant in the power spectra shown in Fig. 1

As the 'rapid' bursts have been considered to be indicative of gravitational energy release by the accreting matter onto a neutron star³, the following two time scales of periodicity, within which the X-ray emission may be modulated, are conceivable (1) a stellar rotational period, (2) a keplerian period of matter orbiting around the neutron star. A 0.5-s period is an acceptable value in a pulsar period. However, a 1% change of the mean period for the two bursts separated by ~ 31 h, is too large to be accounted for by the rotating neutron star. The rotator model is also excluded by the facts that only two bursts show pulsations, that the oscillations disappear towards the end of the bursts, and that the period drifts during the burst.

The second possibility is related to a model proposed for the periodic oscillations observed in optical and X rays during outbursts from several dwarf novae such as SS Cyg (refs 4, 5)

The oscillations which are considered to take place in viscous accretion disks⁶ may also occur in an accreting neutron star with a period equal to the keplerian period at the magnetopause and then modulate the rate of accretion from the accretion disk to the neutron star. The radius of keplerian orbit with the period of 0.5 s is $\sim 10^8$ cm for a neutron star with the mass of $\sim 1 M_{\odot}$ and corresponds to the radius of the magnetopause for a magnetized neutron star with a magnetic field of $\sim 10^{12}$ G.

It is therefore conceivable that the modulation with a 0.5 s period in the matter supply from the region near the mag-

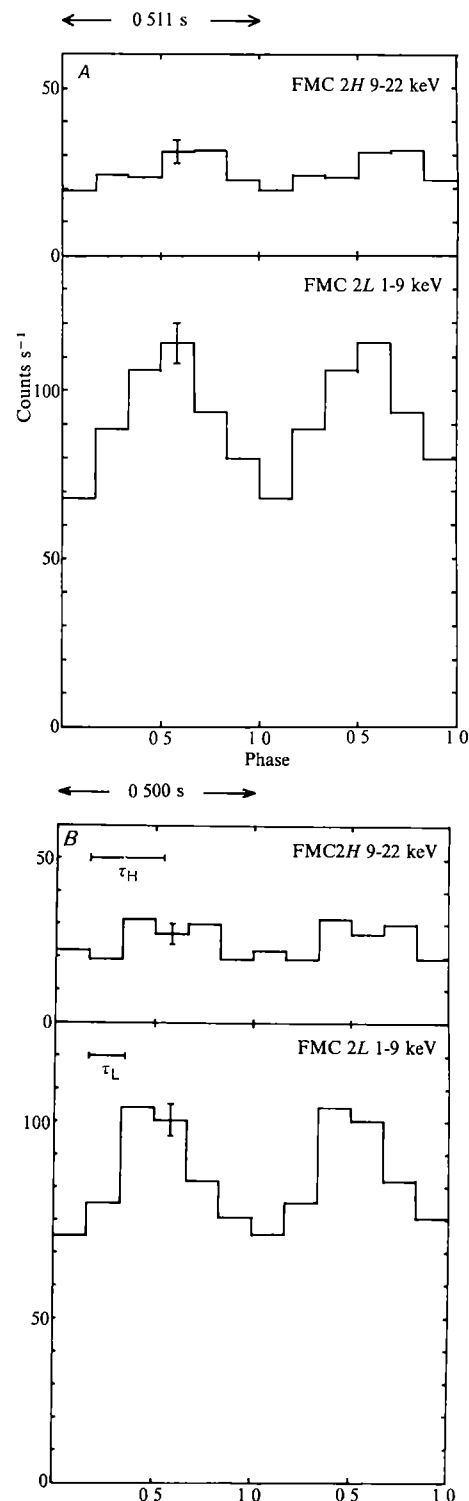


Fig. 3 The time profiles, folding the data shown in Fig. 2 A, b and B, c with periods of 0.511 s and 0.500 s, separately for L(1-9 keV) and H(9-22 keV) bands. The time, τ_L and τ_H , shown represents the data sampling time for the L and H bands, respectively

netopause to the surface of the neutron star results in the observed oscillations of the rapid burster. The fact that the hardness ratios of the bursts at the maximum and the minimum of the pulse are the same supports this possibility.

We thank the crew of the Hakucho satellite for providing observational data and to Professors Y. Tanaka and M. Matsuoka for their valuable comments.

Received 18 February, accepted 23 June 1982

- 1 Kumeda, H. *et al.* *Publ. astr. Soc. Japan* (in the press)
- 2 Inoue, H. *et al.* *Nature* **283**, 358 (1980)
- 3 Lewin, W. H. G. *et al.* *Astrophys. J. Lett.* **207**, L95 (1976)
- 4 Cordova, F. A., Chester, T. J., Tuohy, I. R. & Garmire, G. P. *Astrophys. J.* **235**, 163 (1980)
- 5 Patterson, J. *Astrophys. J. Suppl.* **45**, 517 (1981)
- 6 Van Horn, H. M., Wesemael, F. & Winget, D. E. *Astrophys. J. Lett.* **235**, L143 (1980)

A possible resurfacing mechanism for icy satellites

J. Klinger

Laboratoire de Glaciologie et Géophysique de l'Environnement,
38031 Grenoble Cedex, France

Photographs from Voyager Missions reveal a great variety of surface features for the icy satellites of Saturn¹. Mimas is covered with many old craters. Enceladus has a rather smooth surface with few and rather young craters. Some parts of Dione's surface have an important crater density, whereas other parts are relatively smooth. Thus some of Saturn's icy satellites seem to have undergone important surface modifications during their history while others did not. I suggest here that the irreversible phase transition between amorphous and cubic ice and similar phase transitions may provide a low energy resurfacing mechanism for these icy satellites.

To explain the resurfacing of Enceladus it has been suggested² that its interior may contain liquid water covered only by a thin crust of ice. For a given thickness of the crust, it is possible to estimate what the subsurface heat flux must be. For a surface temperature of 100 K, a liquid core temperature of 273 K and a heat conduction coefficient like that of normal hexagonal ice³ we obtain a heat flux in the order of magnitude of 0.1 W m^{-2} . This is comparable to the mean terrestrial heat flux ($\sim 0.063 \text{ W m}^{-2}$). If this heat flux has to be maintained permanently by tidal heating, the tidal dissipation must be at least $7 \times 10^{10} \text{ W}$ in the whole satellite. Peale *et al.*⁴ calculated the average volumetric tidal dissipation in Saturn's satellites. They found for Enceladus $2.2 \times 10^{-10} \text{ W m}^{-3}$. That corresponds to a total dissipation of $1.4 \times 10^7 \text{ W}$. So it seems difficult to maintain a liquid core by tidal heating and even more difficult to heat up a low temperature core and to melt it.

I now propose an alternative resurfacing mechanism that needs much less initial energy input. It has been shown^{5,6} that the irreversible phase transition of water ice that occurs between amorphous and cubic ice at $\sim 153 \text{ K}$ may influence the heat balance of comet nuclei. The same phase transition may in some cases be responsible for resurfacing of icy satellites. Suppose that the satellite has been condensed at temperatures sufficiently low so that the ice is in the amorphous state. As amorphous ice is a very poor heat conductor, we can assume that a large part of the heat dissipated in the interior of the icy body is used to heat it up. When in one part of the satellite the transition temperature is reached, the phase transition will start. The heat release during crystallization is about 100 J g^{-1} (ref. 7). This energy can be used to heat the neighbourhood. On the other hand the heat conduction coefficient of crystalline ice at the transition temperature seems to be about 10 times higher than that of amorphous ice³ and a growing part of the internally dissipated heat will be lost to the surface. These two mechanisms

are in competition. But as the crystallization of the amorphous ice will start in the interior the heat loss will be unimportant until the surface layers undergo the phase transition.

In the case of Enceladus the tidal dissipation calculated by Peale *et al.*⁴ is able to heat this body from 100 to 153 K in 7,000 Myr. This is evidently not realistic. But Ghormley⁷ found that amorphous ice condensed at 20 K and released 33 W g^{-1} during heating from 20 to 77 K and 92 W g^{-1} between 77 and 153 K. The heat release is smaller for ice condensed at higher temperatures. This heat will considerably speed up the process and only slight heating by tidal dissipation is necessary to initiate the temperature rise.

On the other hand, Yoder⁸ proposed that the eccentricity of Enceladus has been pumped to a higher value than the present one. This may produce some excess heating and allow a still more rapid heating from the orbital equilibrium temperature to the phase transition temperature. Evidently the mechanism described here may be combined with resurfacing mechanisms of very different nature.

Amorphous ice has a density between 1.1 and 0.94 g cm^{-3} depending on the condensation temperature⁵. During the phase transition nearly all water molecules are reoriented and the density decreases. This decrease in density may produce surface cracks and contribute to the smoothing of existing surface features.

If the heat transport to the surface due to conduction is not able to evacuate all the heat dissipated in the icy body, the internal temperature will continue to rise and might reach the transition temperature between cubic and hexagonal ice where a second resurfacing process may take place. A third resurfacing may take place when the melting temperature of hexagonal ice can be reached. When the heat loss to the surface becomes more important than the internal dissipation the satellite will cool down to the equilibrium temperature, in the case of Saturn's satellites to a temperature near 100 K. This cooling can take place after a partial or a complete resurfacing or after one or more resurfacing periods.

It is evident that similar mechanisms may apply when other materials undergo similar phase transitions. We know, for example, that the heat conduction coefficient of at least one clathrate hydrate is of the same order of magnitude and has a similar temperature dependence as amorphous substances⁹. We therefore suppose that such kind of effects will appear when clathrate hydrates reach their limits of stability.

According to Gaffney and Matson¹⁰, high pressure forms of ice may locally be produced during crater formation. Those forms are metastable at low pressures for temperatures that can be found on Jupiter's and Saturn's satellites. The lifetime of those polymorphs is evidently temperature dependent. Destruction of those ices may also contribute to a resurfacing. Gaffney and Matson suggest that icy satellites should be investigated by means of IR reflection spectroscopy. In fact, morphological studies of impact crater and other surface features combined with IR scanning reflection spectroscopy during future space missions could yield information about the chemical nature and the physical state of surface materials, on the chronology of surface smoothing, and the mechanisms involved. Those kinds of mechanism may occur on many satellites of the outer planets.

More quantitative work on the problem of the geological activity of icy satellites is planned in our laboratory. This work has been sponsored by INAG-ATP Planetologie grant 37-86.

Received 5 April, accepted 23 June 1982

- 1 Smith, B. A. *et al.* *Science* **212**, 163-190 (1981)
- 2 Mitchell Waldrop, M. *Science* **213**, 1236-1240 (1981)
- 3 Klinger, J. *Science* **209**, 271-272 (1980)
- 4 Peale, S. J., Cassen, P. & Reynolds, R. T. *Icarus* **43**, 65-72 (1980)
- 5 Smoluchowski, R. *Astrophys. J. Lett.* **244**, L31-L34 (1981)
- 6 Klinger, J. *Icarus* **47**, 320-324 (1981)
- 7 Ghormley, J. A. *J. chem. Phys.* **48**, 503-508 (1968)
- 8 Yoder, C. F. *Nature* **279**, 767-770 (1979)
- 9 Ross, R. G., Anderson, P. & Backstrom, N. *Nature* **290**, 322-323 (1981)
- 10 Gaffney, E. S. & Matson, D. L. *Icarus* **44**, 511-519 (1980)

Flare induced geomagnetic activity and orientation of the photospheric magnetic field

C. S. Wright & L. F. McNamara

Ionospheric Prediction Service, Australian Department of Science and Technology, Darlinghurst, New South Wales 2010, Australia

Attempts to determine which solar flares produce geomagnetic storms have focused attention on the importance of the direction of the magnetic field at the flare sites. Pudovkin *et al.*¹⁻³ have claimed that solar flares that occur above regions in which the photospheric magnetic fields have southward components produce geomagnetic storms whilst flares associated with northward magnetic fields do not. However, other studies have shown that geomagnetic storms are also highly correlated with energetic flares⁴, especially those accompanied by radio spectral type IV bursts⁵⁻⁸. McNamara⁸ suggested that these two sets of results were not reconcilable because they implied that nearly all type IV bursts were associated with flares with southward fields. Although this implication seemed unreasonable, recent evidence^{9,10} lends it some support. We have investigated the relationships between geomagnetic disturbances, flare energies and flare-site magnetic field directions for all large flares that occurred between 1968 and 1979. Contrary to the results of Dodson *et al.*¹⁰ we find no significant differences between the average energies of flares with northward, southward or east-west magnetic fields. Furthermore, although the inferred direction of the field at the site of a flare appears to control the geoefficiency of the flare to some extent, we find, contrary to Pudovkin *et al.*¹, that the relationship between geoefficiency and field direction is unclear.

Our study included 342 flares (with longitudes $\leq 70^\circ$) of importance 2 or greater that occurred between 1968 and 1979¹¹. Using the Mt Wilson and Kitt Peak magnetograms¹², we attempted to determine the photospheric magnetic field direction underlying the centroid of each flare under the assumption that the field was directed at right angles to the contours of magnetic intensity. Our procedure for inferring the field direction underlying the flare follows that of Pudovkin *et al.*¹. However, we make no assumptions concerning the relation between this direction and the true direction of the magnetic field within the flare site which lies above the photosphere in the chromosphere and base of the corona¹³ (Hereafter, unless otherwise stated, it is the inferred direction of the photospheric field that is implied in all discussion of the magnetic field direction at the flare site). In many cases the flare centroid was located above strongly curved contours and it was not possible to ascribe an accurate field direction. For this reason we categorized the directions into eight broad ranges (45° wide) centred on the eight cardinal directions N, NE, E, SE, S, SW, W and NW. Thus our field directions were defined with respect to the heliographic meridian of longitude at the flare site whereas Pudovkin *et al.*¹ defined their directions with respect to the projected orientation of the Earth's axis. We have compared our field directions with those determined by Pudovkin *et al.*¹ for all flares that were common to both studies and we found good agreement. In particular, nearly all flares that had northward and southward field components with respect to the Earth also had northward and southward components (respectively)

Table 1 Distribution of flares by field direction

N	NE	E	SE	S	SW	W	NW
22	33	34	35	27	17	34	35

Field direction uncertain, 72 No magnetic data, 33 Total, 342

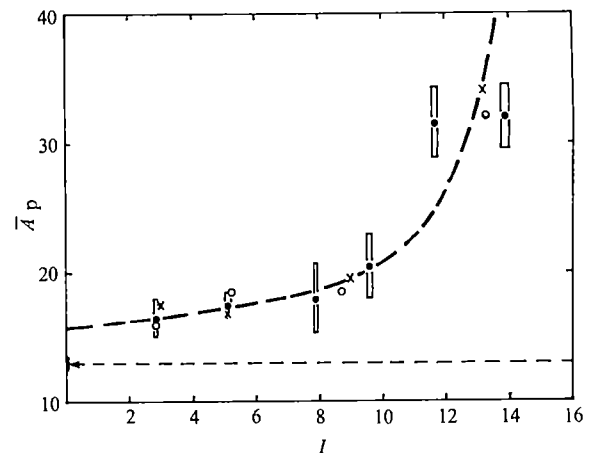


Fig. 1 The dependence of geomagnetic activity on the flare energy index. Each flare in our sample was grouped according to the magnitude of its energy index, I . The average value (\bar{A}_p) of the geomagnetic index, A_p , on the second and third days after the flares in each group was calculated. \bar{A}_p was then plotted against the average value of I for each group. The results for our entire sample of flares (●) are shown for which the magnitudes of the standard errors of the means are indicated by boxes. Also shown are the results (without error boxes) for flares in the periods 1969-76 (○) and 1977-79 (×). The mean background level of A_p is indicated by the horizontal broken line.

with respect to the Sun. Table 1 shows the distribution of the flares amongst the eight cardinal directions.

To estimate the relative energies of the flares in our sample we conceived a flare energy index, I , which is similar to the 'comprehensive flare index' (CFI) proposed by Dodson-Prince *et al.*⁴. We have introduced our own index because it is directly calculable from data to which we have ready access whereas the CFI is not. Our index takes into account flare characteristics that indicate high energy release^{13,14}, particularly those found by McNamara⁸ to be important in the flare-storm relationship. These were H α importance and intensity, X-ray class and radio spectral class. To each characteristic we attached a numerical weight in the manner shown in Table 2 and the value of the index for a given flare was then determined by summing the individual weights. Hence the least important flare in our sample, a 2F event with no radio or X-ray bursts, corresponds to a flare index of $I = 2$. The most important flare in our sample, a 3B event with X-class X-ray-ray burst, type II and strong type IV bursts, corresponds to an index $I = 15$. No X-ray data was available for 1968 so that I could not be computed for flares in that year. Also, there were a few flares in subsequent years for which I could not be computed due to incomplete data.

The level of geomagnetic activity following the flares in our sample was assessed by means of the method of superposed epochs which we applied to the daily geomagnetic index A_p . In agreement with Dodson-Prince *et al.*⁴ we found that A_p usually peaked 2-3 days after large flares. Hence to assess the geomagnetic importance of flares within any particular class we used the average value of A_p (\bar{A}_p) on the second and third days after the flares. The dependence of \bar{A}_p on the energy index, I , is shown in Fig. 1. The average level of geomagnetic activity increases slowly with I for flares with energy indices in the range $0 < I \leq 10$. However, when $I > 10$ the average level of geomagnetic activity increases rapidly with I . This is consistent with studies^{4,8} that show that very large flares nearly always produce geomagnetic storms. Figure 1 also shows that I preserves its identity over a long period of time since data for 1969-76 and 1977-79, when considered separately, define the same relationship between I and A_p . Therefore, we consider I to be a useful index with which to describe, semiquantitatively, the relative energy release of large solar flares.

Using the calculated values of I for all the flares in our sample, we were able to investigate the relative contributions

of flare energy release and magnetic field direction in the flare-storm relationship

First, we considered whether a relationship existed between energy release and flare-site field direction. For this purpose we calculated the average values of I for flares with northward, southward and east-west magnetic fields. The results are shown in Table 3. In addition to the flares in our sample we have considered the flares listed by Pudovkin *et al.*¹ Several cases are distinguished. Case 1 includes all flares described by Pudovkin *et al.*¹ for which I could be determined. All but three of these flares occurred between 1969 and 1970. In this case the subdivision of flares amongst field directions was made using the directions measured by Pudovkin *et al.*¹ Case 2 includes all flares in our sample that occurred during the same period (1969-70) and, in this case, the subdivision was made using our field directions. Case 3 includes all flares that occurred after this period, that is 1971-79, and case 4 includes our entire sample. The number of flares within each subdivision is indicated. The errors that appear against the average values of I are the standard errors of the means.

In case 1 the average value of I is significantly greater for flares with southward fields than for flares with northward fields (A similar result is obtained using the CFI of Dodson-Prince *et al.*⁴). This difference in average energies certainly would have given the flares with southward fields greater apparent geoefficiency and may partly explain the results of Pudovkin *et al.*

Table 2 Construction of flare energy index

Flare characteristic		Numerical weight
$H\alpha$ Importance,	2	2
	3	3
$H\alpha$ Intensity,	Faint	0
	Normal	1
	Bright	2
X-ray class,	No event	0
	C	1
	M	2
Radio type II,	X	4
	No event	0
	Event	2
Radio type IV,	No event	0
	$P < 100^*$	2
	$P \geq 100^*$	4

* P is the product of the intensity (1, 2 or 3) and the duration (in minutes) of the Type IV burst as listed in the radio spectral reports

*al.*¹ This also has been suggested by Dodson *et al.*¹⁰ who went further to argue, on the basis of the sample of flares used by Pudovkin *et al.*¹, that large solar flares are significantly more likely to occur over southward field regions. We suggest that this apparent bias may be due to selection effects as this sample did not include all flares of importance 2 or greater during 1967-70. Our results show no significant bias of this kind within the complete sample of flares (from the group reports¹¹) which occurred during the partially overlapping period 1969-70 (case 2). The same conclusion can be drawn from cases 3 and 4 which show that the number and the average energy of flares with southward fields do not differ significantly from the number and the average energy of flares with northward fields. These results hold even for the very largest flares. Of the flares in our sample for which $I \geq 12$, 15 had southward fields and 11 had northward fields. Of the flares for which $I \geq 8$, 34 had southward fields and 32 had northward fields. Thus our results do not support those of Dodson *et al.*¹⁰ Furthermore, even if flares with southward fields were more energetic than flares with northward fields during the period 1967-70 it is doubtful whether the magnitude of the bias (case 1) is sufficient to explain the results of Pudovkin *et al.*¹ This is clear from Fig. 1 which shows only a small difference in \bar{A}_p for flares with average indices of 5.1 and 9.3.

Next, we considered the geoefficiencies of flares of similar energies but with different field directions. Figure 2 shows the

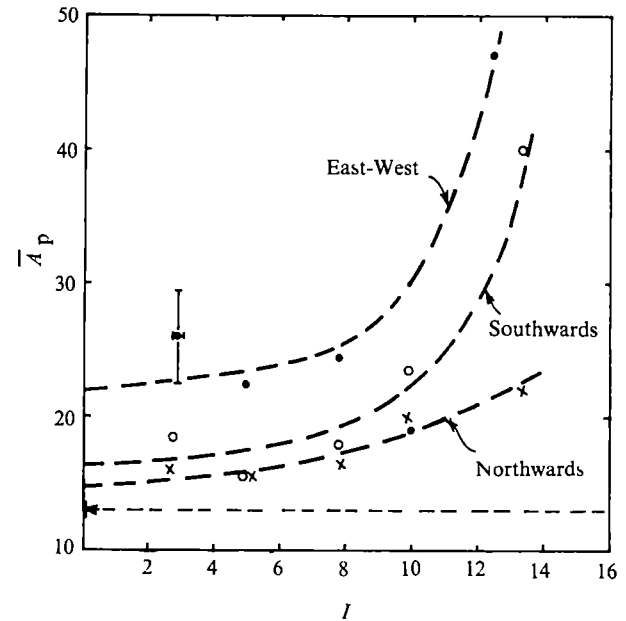


Fig. 2 Same as Fig. 1 except the data (from our entire sample) have been subdivided according to the inferred magnetic field directions at the sites of the flares. Results for flares with northward (\times), southward (\circ) and east-west (\bullet) fields are shown. The magnitude of typical r.m.s. errors of the means is indicated.

dependence of \bar{A}_p on I when the inferred magnetic field direction at the flare site is taken into account. Three curves are presented, showing \bar{A}_p plotted against I for flares with northward (N, NE, NW), southward (S, SE, SW) and east-west (E, W) magnetic fields. The scatter in the data points is larger than in Fig. 1 due to the smaller sample sizes involved. We have attempted to fit curves of the form shown in Fig. 1 to the data for each field direction. For flares with northward and southward fields, curves of this form fit the data points quite well. For flares with east-west fields, a curve of this form does not fit well but is reasonably compatible with the data points shown (note the data points at $I \approx 3$ and $I \approx 10$).

Several features of Fig. 2 are worth noting.

- (1) When $I \leq 10$, the magnitude of \bar{A}_p for flares with southward fields only slightly exceeds the magnitude of \bar{A}_p produced by flares, of similar energy, with northward fields.
- (2) When $I \geq 10$, the magnitude of \bar{A}_p is significantly greater for flares with southward fields than for flares, of similar energy, with northward fields.
- (3) Flares with eastward or westward fields tend to produce higher values of \bar{A}_p than flares, of similar energy, with either northward or southward fields.

Hence, the geoefficiency of solar flares appears to depend on the direction of the magnetic fields at the sites of those flares. However, in contrast to the results of Pudovkin *et al.*¹, flares for which the inferred field direction is southward do not

Table 3 Dependence of average flare energy on field direction

Case	Field direction					
	Southward (S, SE, SW)		East-west		Northward (N, NE, NW)	
	No	Average I	No	Average I	No	Average I
1 Pudovkin <i>et al.</i> 1969-70	12	9.3 \pm 1.4	12	6.2 \pm 1.0	21	5.1 \pm 0.5
2 This study, 1969-70	18	6.7 \pm 0.9	19	6.2 \pm 0.7	36	5.5 \pm 0.5
3 This study, 1971-79	50	8.0 \pm 0.5	31	6.5 \pm 0.5	45	1.6 \pm 0.5
4 This study, 1969-79	68	7.7 \pm 0.5	50	6.4 \pm 0.4	81	6.7 \pm 0.4

have the highest geoefficiency. Clearly the relationship between field direction and geoefficiency needs reconsideration.

Pudovkin *et al.*¹⁻³ interpreted their results in terms of the well known association¹⁵⁻¹⁷ between geomagnetic disturbances and southward field in the solar wind. They argued that the orientation of the field within the flare site was preserved in the flare stream, thus accounting for the greater geoefficiency of flares for which the inferred field was southwards. However, the flare site is not confined to a narrow height range near the photosphere but extends upwards through the chromosphere, transition region and base of the corona.¹³ The field direction may vary substantially with height within the flare. In the case of strongly sheared fields, the difference between the true magnetic field direction in the chromosphere, for instance, and the inferred direction in the underlying photosphere may be as great as $\pm 90^\circ$ (ref. 13). Thus even if the field direction within the flare is preserved in the flare stream it may not resemble

the direction inferred from the photospheric intensity contours. However, a systematic relationship may exist between the direction of the field within the flare and the orientation of the underlying photospheric field. If so it may help to explain the results of Fig. 2.

We have found no evidence to support the suggestion¹⁰ that major flares are significantly more likely to occur over regions of southward magnetic field. Therefore, we feel that it is not possible to interpret the results of Pudovkin *et al.*¹ in this way. Our results (Fig. 2) indicate that the inferred direction of the magnetic field beneath the flare controls, to some extent, the geomagnetic effects of solar flares, particularly outstanding flares. However, the relationship between the inferred field direction and the geoefficiency is not as distinct as stated by Pudovkin *et al.*¹ and needs further investigation. We suggest that the true magnetic field direction within the flare site may be more relevant to the task of predicting geomagnetic effects of solar flares.

Received 31 December 1981, accepted 2 July 1982

- 1 Pudovkin, M. I. & Chertkov, A. D. *Solar Phys.* **50**, 213-229 (1976)
- 2 Pudovkin, M. I., Zaitseva, S. A., Oleferenko, I. P. & Chertkov, A. D. *Solar Phys.* **54**, 155-164 (1977)
- 3 Pudovkin, M. I., Zaitseva, S. A. & Benevolenska, E. E. *J. geophys. Res.* **84**, 6649-6652 (1979)
- 4 Dodson-Prince, H. W., Hedeman, E. R. & Mohler, O. C. *Scient. Rep. No. 3*, (McMath-Hulbert Observatory, Pontiac, 1978)
- 5 McLean, D. J. *Aust. J. Phys.* **12**, 404-417, (1959)
- 6 de Feiter, L. D., Fokker, A. D., Van Lohuizen, H. P. Th. & Roosen, J. *Planet. Space Sci.* **2**, 223-227 (1960)
- 7 Bell, B. *Smithson. Contr. Astrophys.* **5**, 239-257, (1963)

- 8 McNamara, L. F. *Australian Ionospheric Prediction Service Rep. Ser. R*, IPS-R37 (1980)
- 9 Lundstedt, H., Wilcox, J. M. & Scherrer, P. H. *Science* **212**, 1501-1502 (1981)
- 10 Dodson, H. W., Hedeman, E. R. & Roelof, E. C. *Geophys. Res. Lett.* **9**, 199-202 (1982)
- 11 *Solar Geophysical Data, Comprehensive Reports* (US Department of Commerce, Boulder, 1968-79)
- 12 *Solar Geophysical Data, Prompt Reports* (US Department of Commerce, Boulder, 1968-79)
- 13 Svestka, Z. *Solar Flares* (Reidel, Dordrecht, 1976)
- 14 McLean, D. J. & Dulk, G. A. *Proc. Astr. Soc. Aust.* **3**, 251-252 (1978)
- 15 Fairfield, D. H. & Cahill, L. J. *J. geophys. Res.* **71**, 155-169 (1966)
- 16 Hirschberg, J. & Colburn, D. S. *Planet. Space Sci.* **17**, 1183-1206 (1969)
- 17 Svalgaard, L. in *Coronal Holes and High Speed Wind Streams* (ed. Zirker, J.) 371-441 (Colorado Associated University Press, 1977)

Direct imaging of travelling Rayleigh waves by stroboscopic X-ray topography

R. W. Whatmore

Plessey Research Ltd, Caswell, Towcester NN12 8EQ, UK

P. A. Goddard, B. K. Tanner & G. F. Clark

Department of Physics, Durham University, South Road, Durham DH1 3LE, UK

We report here the first successful experiments which exploit the time structure and single bunch mode of operation of the Daresbury Synchrotron Radiation Source (SRS). Rayleigh waves travelling on the surface of a piezoelectric crystal have been imaged by stroboscopic X-ray topography, in which the generation of the waves is synchronized with X rays emitted by the orbiting electrons in the storage ring. Interactions between the Rayleigh waves and microscopic crystalline defects have been observed and provide new insights into the factors affecting surface acoustic wave (SAW) device operation. It has been demonstrated that this novel technique has considerable potential for the study of periodic phenomena in crystals.

Piezoelectric SAW devices¹ are of great technological importance for high-frequency signal processing and filtering applications. Although the presence of crystallographic defects can have deleterious effects on the characteristics of these devices, there has been almost no study of the interactions between the Rayleigh waves and the defects concerned. Techniques such as electrostatic² and optical probes³ can be used to observe the waves, but these give no information concerning lattice strains or bulk crystal defects. Stroboscopic scanning electron microscopy has been applied to the study of piezoelectric Rayleigh waves⁴ but only surface defects and charges are imaged. X-ray topography⁵, a diffraction technique by which a two-dimensional map of the lattice strains in a crystal can be obtained, has been applied⁶ to reveal the average strain associated with a travelling Rayleigh wave but standard X-ray illumina-

tion gives no information about the periodic strains in the wave. Such strains can be revealed by generating standing waves although this gives information of limited relevance as most delay lines and filters operate by propagating travelling waves.

The unique time structure of X rays emitted from a storage ring can be exploited for stroboscopic X-ray topography in which the generation of the waves is synchronized with the illuminating pulses of radiation. Recent, independent experiments⁷ at Hamburg have demonstrated the feasibility of such a technique from studies of standing bulk waves in quartz.

Our experiments were performed with the Daresbury SRS running in the single bunch mode at 2 GeV, 1.8 mA with a lifetime in excess of 30 h, 97% of the synchrotron radiation was concentrated in a single pulse of width ~ 200 ps. A stroboscopic timing pulse was obtained from the SRS ring monitors. This 3.122 MHz square wave was frequency quadrupled, filtered and amplified to provide a 37.46 MHz, 15 V p/p sine wave to drive a 38 MHz LiNbO₃ television IF filter. White radiation X-ray topographs of the Y cut Z propagating LiNbO₃ crystal were taken using the multipurpose diffractometer at the

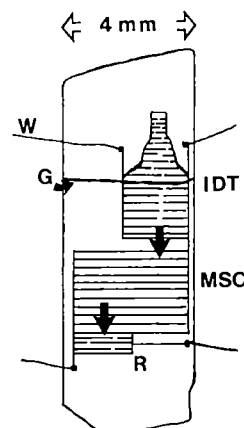


Fig. 1 Electrode configuration on the surface of the SAW device. The wave is generated in the interdigital transducer IDT and is transferred across the multistrip coupler MSC. It is detected at the receiving transducer R. W are the bonding wires, G marks the grain boundary visible in Figs 2 and 3.

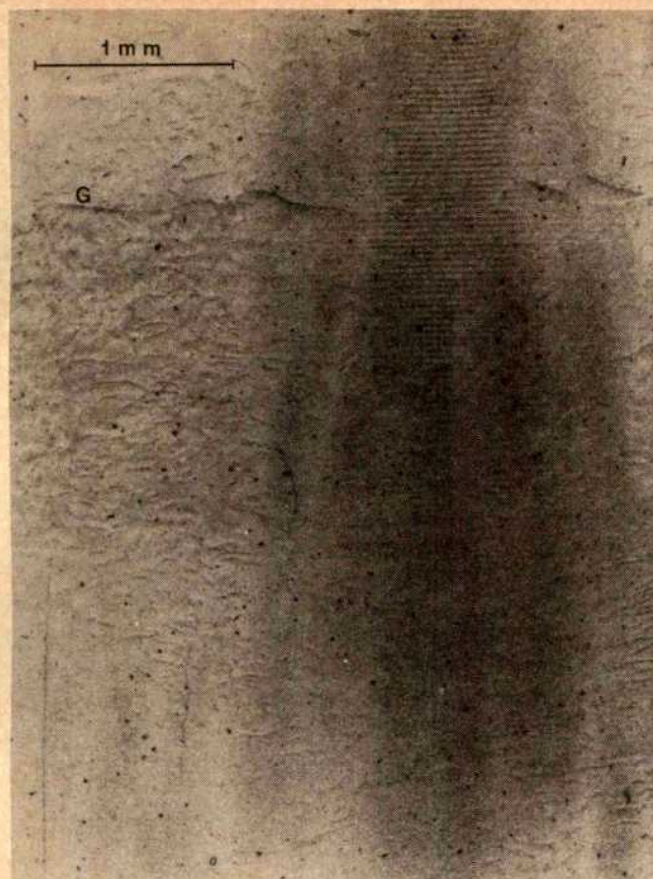


Fig. 2 X-ray topograph taken of the Rayleigh waves without synchronization to the synchrotron radiation emission. The diffuse streaks correspond to the SAW strains, the fine curved lines to dislocations. The black line G is the sub-grain boundary indicated in Fig. 1. (The measured spacing of the standing waves ($33\ \mu\text{m}$) is reduced from the half wavelength value of $46.5\ \mu\text{m}$ by a factor of $\cos 45^\circ$ due to geometrical image distortion.) 0330 reflection, 45° Bragg angle. Specimen to plate distance, 35 mm.

SRS Topography Station⁸. LiNbO_3 has a space group $R3c$ and lattice parameters $a = 5.147\ \text{\AA}$ and $c = 13.856\ \text{\AA}$. In the hexagonal indices Y corresponds to $[01\bar{1}0]$ and Z to $[0001]$. For these experiments the $[01\bar{1}0]$ direction (normal to the crystal surface) was set at 45° to the incident X-ray beam. All topographs presented were taken in the Bragg geometry on Ilford L4 Nuclear Emulsion with exposure time of $\sim 1\ \text{h}$. The many topographs simultaneously recorded correspond to a large spot size, high spatial resolution back reflection Laue pattern. A Rayleigh wave was excited by an untuned interdigital transducer visible in the upper region of Fig. 1. The electric fields associated with it are transmitted laterally along a multi-strip coupler deposited on the surface. Thus a new acoustic wave is generated which propagates, parallel to the original wave, to the receiving transducer.

Figure 2 shows an X-ray topograph taken with the Rayleigh wave propagating but without the oscillator synchronized with the electron orbit frequency. Standing waves excited within the transducer are visible in the upper region and an increase in intensity due to the mean strain associated with the travelling wave emanating from it can be observed. Figure 3a shows part of a similar topograph taken with the driving signal phase locked to the synchrotron radiation emission as described above. A periodic array of dark and light bands is visible, an image of the strains in the crystal due to the travelling Rayleigh wave at an instant in the cycle. At $37.46\ \text{MHz}$, the wavelength of the acoustic waves is $93\ \mu\text{m}$ in LiNbO_3 and it is seen that, when the appropriate geometrical correction has been made for image distortion, the contrast pattern on the topographs corresponds to a period of a half wavelength. This occurs because strains

of either sense give rise to an increase in scattered intensity in white radiation topographs taken in the present conditions. Light areas, of intensity equal to the background, correspond to regions under very small strain at that instant of the propagating cycle. Detailed study of the visibility of the SAW in the many reflections recorded simultaneously on the photographic plate will enable the strain components to be determined.

Insertion of a time delay into the driving signal line enables the strains associated with different instants in the cycle to be examined. The result of inserting a 6 ns delay is shown in Fig. 3b. Light and dark areas have now interchanged, as is expected by moving back approximately a quarter of a cycle. Comparison of Fig. 3a with 3b reveals that the wavefronts are not always continuous throughout the cycle. At points X and Y, two 'dislocations' in the wavefronts are visible in Fig. 3a which are not present a quarter of a cycle later. Clearly some form of interaction is occurring periodically, a feature which cannot be detected other than by stroboscopic methods. Careful examination of the topographs reveals a phase shift of $\pi/2$ in the

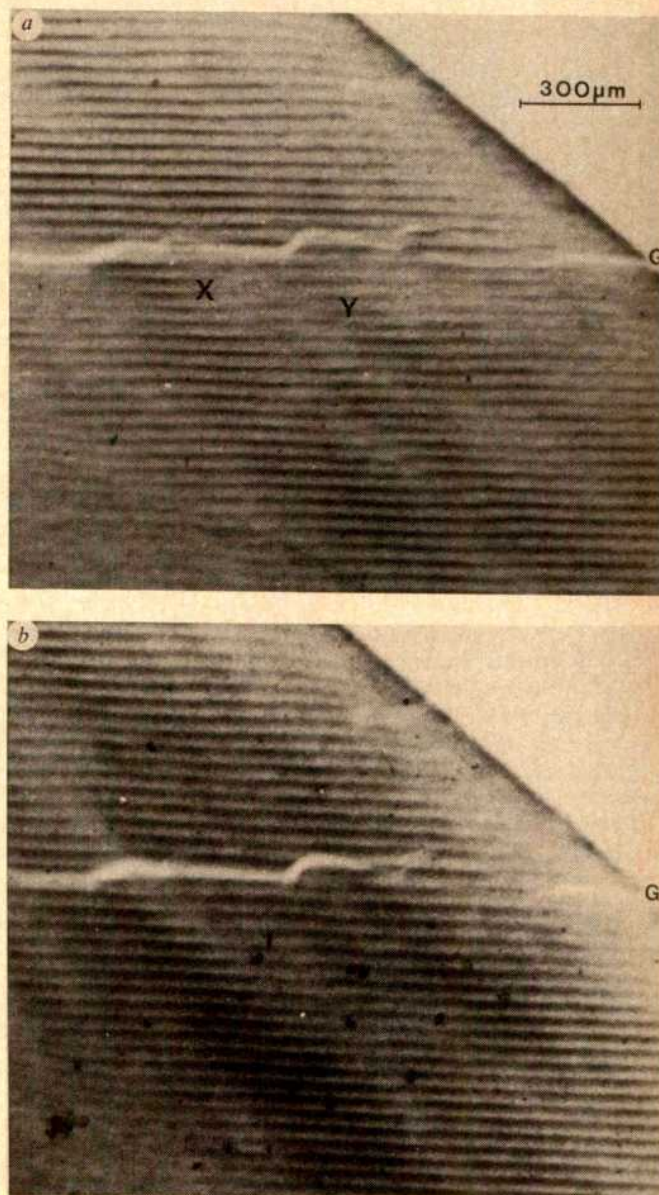


Fig. 3 Stroboscopic X-ray topographs of travelling Rayleigh waves taken with the driving signal phase locked to the synchrotron radiation emission: a, no time delay; b, additional 6 ns time delay. The broad white line G corresponds again to the sub-grain boundary marked in Figs 1 and 2. $1\bar{3}21$ reflection predominant, 33° Bragg angle. Specimen to plate distance 20 mm. Projection of the diffraction vector is parallel to the crystal edge.

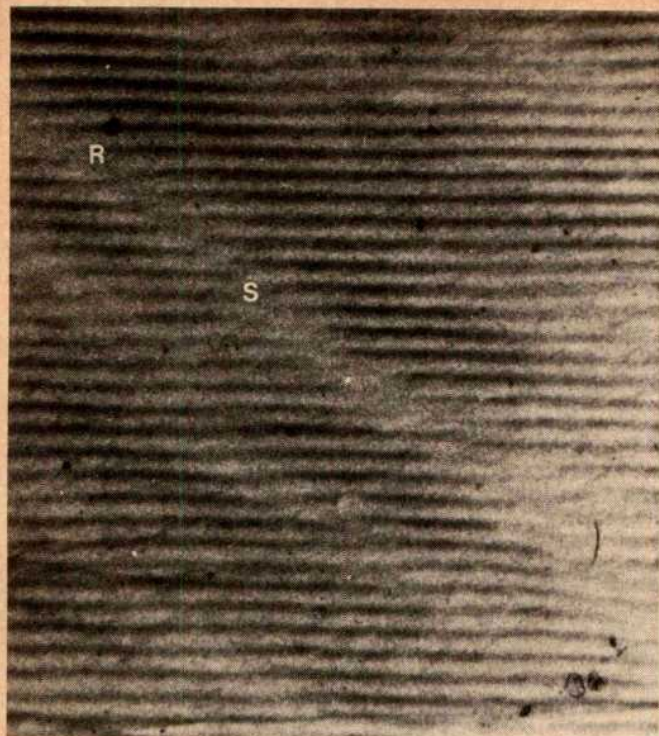


Fig. 4 Interaction of Rayleigh waves with lineal defects in the lower region of the multistrip coupler MSC. Note a phase shift of almost $\pi/2$ across the line RS. Same diffraction conditions as in Fig. 3. In both Figs 3 and 4, the wave propagates down the page.

acoustic wave along the multistrip coupler as predicted by Maerfeld⁹. In Fig. 4 we see a very strong interaction, present throughout the cycle, between a linear defect in the lower region of the multistrip coupler and the Rayleigh waves. The waves are phase shifted by about $\pi/2$ on crossing this defect, introducing another 'dislocation' into the images of the wavefronts. At present the nature of the defect has not been established.

Our experiments have established a totally new diagnostic tool for SAW device technology. Future studies will concentrate on Rayleigh wave propagation from transducers of varying configuration, the analysis of unwanted bulk modes excited by such transducers, the interactions with crystal lattice defects, the relation between diffracted intensity and wave strains, and the changes in SAW propagation as the frequency is increased. We have demonstrated that high-frequency stroboscopic X-ray scattering experiments are remarkably easy to implement with standard film recording techniques. In addition to X-ray topography, several diffraction experiments can now be envisaged to study rapid periodic phenomena in such diverse materials as thin films, ceramics, powders, fibres, polymers or even biological materials. The unique, extremely stable, time structure of the SRS running in single bunch mode has thus far not been the focus of other proposals for X-ray scattering experiments. Our present success and the availability to users of single bunch operation will hopefully stimulate many new experiments using these 200 ps width light pulses.

Financial support from SERC is acknowledged. We thank Dr P. J. Duke and Mr D. Warne for assistance in setting up these experiments.

Received 17 June; accepted 21 July 1982.

1. Matthews, H. (ed.) *Surface Wave Filters, Design, Construction and Use* (Wiley, New York, 1977).
2. Richardson, B. A. & Kino, G. F. *Appl. Phys. Lett.* **16**, 82 (1970).
3. Nakagawa, Y., Yamamuchi, K. & Shibiyama, K. *J. appl. Phys.* **45**, 2817 (1974).
4. Veith, R., Eberharter, G., Feuerbaum, H. P. & Knauer, U. *Proc. IEEE, Ultrasonics Symp.*, 348 (1980).
5. Tanner, B. K. *X-Ray Diffraction Topography* (Pergamon, Oxford, 1976).
6. Berolo, O. & Butler, D. *Proc. IEEE Ultrasonics Symp.*, 98 (1977).
7. Gluer, C.-C., Graeff, W. & Moller, H. *DESY Preprint SR-82-01* (1982).
8. Bowen, D. K. *et al. Nucl. Instrum. Meth.* **195**, 277 (1982).
9. Maerfeld, C. *Wave Electronics* **2**, 82 (1976).

Persistence of Sub-Saharan drought

Peter J. Lamb

Climatology Section, Illinois State Water Survey, Champaign, Illinois 61820, USA

The Sub-Saharan drought of the early 1970s attracted widespread attention. Particularly prominent was the suggestion that it was not likely to disappear in the near future, and could even persist into the next century¹⁻³. (The basis of this standpoint is reviewed in ref. 4.) In contrast, the post-1974 discussion of the Sub-Saharan climate has tended to the opinion that the drought ended by 1974 or 1975⁴⁻¹¹. That this may not be the case has been neglected. It was not investigated during several detailed studies of West African rainfall published since 1975¹²⁻¹⁶, because the data sets used terminated in 1974 or 1975, and is only weakly suggested by the World Meteorological Organization's annual summaries of significant meteorological events¹⁷. Strong claims that the drought continued beyond 1974 have been few, very brief, regionally focused, and qualitative¹⁸⁻²⁰. I therefore now provide a 1975-81 update of a Sub-Saharan rainfall index previously published for 1941-74²¹. This confirms the drought's persistence.

The Sub-Saharan rainfall index presented (Fig. 1) is the 1941-81 time series of the yearly average of the normalized April-October departures for 14-20 West African stations between 11 and 18°N west of 9°E. Its value for the year j is given by

$$\chi_j = \frac{1}{N_j} \sum_{i=1}^{N_j} \frac{r_{ij} - \bar{r}_i}{\sigma_i}$$

where r_{ij} is that year's April-October rainfall total at station i , \bar{r}_i and σ_i are respectively the mean and standard deviation of station i 's April-October rainfall for 1941-74, and N_j is the number of stations with complete records in year j . This index has never been evaluated before 1941 (ref. 21, Fig. 1; present Fig. 1) because only 6 of the 20 possible stations were operative then, one of which commenced in 1940. The remaining stations were established in 1941 (8), 1947 (1), 1950 (4) and 1951 (1). All 20 are located in Fig. 2 of ref. 21, which shows their adequate spatial distribution. These stations, which possess the most reliable and readily accessible records for the region, are those that appear in standard data publications²²⁻²⁶. Individual monthly station rainfall totals were obtained from these sources and various national and regional meteorological services. The April-October interval used includes both the July-September rainy season characteristic of the entire region, which on the average provides 80% of the annual rainfall²⁷, and the adjacent months that collectively contribute a further 17% (ref. 27). The continued adoption in this 1975-81 index update of the 1941-74 base period for \bar{r}_i and σ_i utilized in the original publication of the index for that period²¹, maintained the continuity of the time series in Fig. 1. For the proper use of a regional index of the present type, the rainfall departures must be statistically coherent throughout the region concerned. This has recently been strongly confirmed for Sub-Saharan West Africa^{13,15,16,18}. The statistical advantages of the particular index used here have been summarized by Kraus¹³.

The depiction of the index in Fig. 1 is complemented by the documentation in Table 1 of the consistency of the individual station departures for the years since the start of the aforementioned drought (1968), and also the dry years of the 1940s. These displays clearly suggest that the drought has not ended, despite the pronouncements to the contrary mentioned above⁴⁻¹¹. Although rainfall increased progressively from the especially severe 1972 drought year until 1975, this recovery did not reach even the 1941-74 mean value. Furthermore, it was immediately followed by a counterbalancing decrease in 1976-77. As a result, the 1977 rainfall was as deficient as that of 1972, and much more so that the other well-publicized severe drought years of the late 1960s and early 1970s (that is, 1968,

1970, 1971, 1973). While Subsaharan rainfall was clearly much greater in 1978 than a year earlier, this recovery also failed to reach the average value for 1941–74. Moreover the three most recent years have been characterized by a further progressive rainfall decline. This was sufficient to render 1979 and 1980 as dry as 1968 and 1970 and almost as rainfall deficient as 1971 and 1973, and to leave 1981 drier than all post-1967 years except for the very severe drought years of 1972 and 1977. The occurrence of the 1981 drought received little mention in the *Climatic Impact Assessment, Foreign Countries, 1981 Annual Summary* published by the United States' Center for Environmental Assessment Services (CEAS)²⁸; this organization now routinely monitors the globe's 'major anomalous meteorological events' and their 'adverse impacts'²⁸. Two of the seven 1975–81 years (1977 and 1981) also appear to have received substantially less rain than the better known drought years of the 1940s (Fig. 1). In addition, 1979 and 1980 were probably at least as dry as any year in the 1940s. Finally, it is thus clear that rainfall above the 1941–74 average has not returned to Subsaharan West Africa as a whole in the years since drought and famine made this region such a focus of attention in the early 1970s. This has extended the period since the last era of abundant rainfall (1950–58) to almost 25 yr.

The foregoing results have interesting implications. First, the suggestion that the Subsaharan drought was not likely to disappear in the near future^{1–3} has so far not been disproved. This fact, of course, does not constitute an endorsement of the basis of that prediction. Second, there is as yet no support for Faure and Gac's¹⁹ recent extrapolation-based projection of a gradual recovery from the present drought to more average rainfall during 1975–85. Third, the fact that the present drought has extended from 1968 to at least 1981 (14 yr), which is markedly longer than the three other distinct climatic epochs evident in Fig. 1 (1941–49, 1950–58, 1959–67; all of 9 yr duration), supports Kraus's¹³ findings that the Subsaharan rainfall record contains "unexpectedly long runs of wet or dry years" and that its droughts "tend to be rather persistent". This is notwithstanding Katz's²⁹ claim that the anomaly values possess "only a small degree of year-to-year persistence". Next, it should be emphasized that the occurrence of severe drought in 1977 and 1981 makes these years ideal candidates for case study investigations of the coincident (and presumably causal) tropical circulation anomalies in the manner already performed for 1972 (see ref. 10) and 1968 (see ref. 30). Finally, Glantz's³¹ 1977 belief that "with a return to above-mean rainfall levels, interest in dealing with (the) chronic (Sahelian) problems (of inadequate management practices and institutional arrangements revealed by the drought) will dissipate" now takes on added significance. The lack of publicity given to the continuation of the drought between 1975 and 1981 could well mean that such interest has

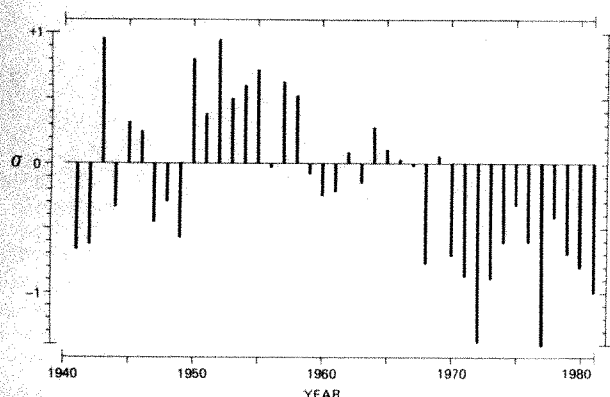


Fig. 1 1941–81 time series of the yearly average of the normalized rainfall departures (σ) for 14–20 Subsaharan stations west of 9°E. Kraus¹³, and Faure and Gac¹⁹ suggest that the largely dry epoch at the start of the time series (1941–49) commenced no more than a year or two earlier. The 1969 value of +0.06 is a correction of the +0.11 value published earlier²¹.

Table 1 April–October rainfall departure statistics for Subsaharan West Africa for 1968–81 and the drought years of 1941–49

Year	Fraction of stations with rainfall departure $\geq -1.0\sigma$ from 1941–74 mean	Fraction of stations with rainfall departure $\geq -0.6\sigma$ from 1941–74 mean	Average of all stations departures (σ)
1968	7/20	14/20	-0.78
1969	2/20	4/20	+0.06
1970	8/20	13/20	-0.72
1971	9/20	15/20	-0.88
1972	17/20	19/20	-1.39
1973	13/18	16/18	-0.91
1974	7/16	10/16	-0.60
1975	3/20	8/20	-0.27
1976	7/20	10/20	-0.62
1977	13/18	15/18	-1.42
1978	5/20	10/20	-0.42
1979	8/20	14/20	-0.70
1980	9/20	13/20	-0.80
1981	9/20	15/20	-1.00
1941	4/14	7/14	-0.67
1942	7/14	8/14	-0.63
1947	3/15	7/15	-0.46
1949	5/14	7/14	-0.58

evaporated even without a rainfall recovery. This may have been facilitated by the region's drought-induced population (human and animal) decline of the early 1970s reducing the socio-economic impact of the more recent deficient rainy seasons. The other alternatives—that the local infrastructure has dramatically improved and/or western aid has been suddenly beneficial—are more unlikely.^{9,31,32}

In view of the foregoing results and their implications, it is planned to update the present Subsaharan rainfall index towards the end of every calendar year.

Some of this material was first presented at the August 1981 Oxford Symposium on Variations in the Global Water Budget, with the aid of an award from the Legacies Fund of the Royal Meteorological Society and the encouragement of Stanley A. Changnon Jr. Grateful acknowledgment is also made of the data provided by West African regional and national meteorological services, and the assistance of P. Stone, W. Wendland, K. Hendrie and E. Kraus.

Received 30 April; accepted 29 June 1982.

- Winstanley, D. *Nature* **245**, 190–194 (1973).
- Lamb, H. H. *Drought in Africa* (eds Dalby, D. & Harrison-Church, R. J.) 28–29 (School of Oriental and African Studies, London, 1973).
- Bryson, R. A. *Ecologist* **3**, 366–371 (1973).
- Lamb, P. J. *Prog. phys. Geogr.* **3**, 215–235 (1979).
- Tanaka, M., Weare, B. C., Navato, A. R. & Newell, R. E. *Nature* **255**, 201–203 (1975).
- Hare, F. K. *Geogr. Mag.* **49**, 705–708 (1977).
- United Nations Desertification Conference Secretariat *Desertification: Its Causes and Consequences*, 4, 6 (Pergamon, Oxford, 1977).
- Grove, A. T. *Prog. phys. Geogr.* **1**, 296–310 (1977).
- Grove, A. T. *Geogr. J.* **144**, 407–415 (1978).
- Kanamitsu, M. & Krishnamurti, T. N. *Mon. Weath. Rev.* **106**, 331–347 (1978).
- Hare, F. K. *Proc. 51–87* (World Meteorological Organization Publication 537, Geneva, 1979).
- Bunting, A. H., Dennett, M. D., Elston, J. & Milford, J. R. *Q. J. R. met. Soc.* **102**, 59–64 (1976).
- Kraus, E. B. *Mon. Weath. Rev.* **105**, 1009–1018 (1977).
- Kidson, J. W. *Q. J. R. met. Soc.* **103**, 441–456 (1977).
- Motha, R. P., LeDuc, S. K., Steyaert, L. T., Sakamoto, C. M. & Stommen, N. D. *Mon. Weath. Rev.* **108**, 1567–1578 (1980).
- Stoeckenius, T. *Mon. Weath. Rev.* **109**, 1233–1247 (1981).
- Wld met. Org. Bull.* **25**, 86–93 (1976); **26**, 170–179 (1977); **27**, 242–250 (1978); **28**, 192–201 (1979); **29**, 161–170 (1980); **30**, 163–169 (1981).
- Lough, J. M. *Climate Monitor* **9**, 150–157 (1980).
- Faure, H. & Gac, J.-Y. *Nature* **291**, 475–478 (1981).
- Vermeer, D. E. *Geogr. Rev.* **71**, 281–298 (1981).
- Lamb, P. J. *Tellus* **30**, 240–251 (1978).
- Monthly Climatic Data for the World, 1957–65* (U.S. Weather Bureau, Asheville, 1957–65).
- World Weather Records, 1941–50* (U.S. Weather Bureau, Washington DC, 1959).
- Monthly Climatic Data for the World, 1966–70* (ESSA, Asheville, 1966–70).
- World Weather Records, 1951–60*, Vol. 5 (ESSA, Washington DC, 1967).
- Monthly Climatic Data for the World, 1971–81* (NOAA, Asheville, 1971–81).
- Lamb, P. J. *N.Z. J. Geogr.* **68**, 12–16 (1980).
- CEAS *Climatic Impact Assessment, Foreign Countries, 1981 Annual Summary* (Environmental Data and Information Service, NOAA, Washington DC, 1982).

29. Katz, R. W. *Mon. Weath. Rev.* **106**, 1017–1021 (1978).
 30. Lamb, P. J. *Mon. Weath. Rev.* **106**, 482–491 (1978).
 31. Glantz, M. *Bull. Am. met. Soc.* **58**, 150–158 (1977).
 32. Wade, N. *Science* **185**, 234–237 (1974).

Late Palaeozoic Gondwana glaciation in Oman

J. H. Braakman*, B. K. Levell†, J. H. Martin†,
 T. L. Potter* & A. van Vliet*

*Petroleum Development Oman LLC, PO.Box 81, Muscat,
 Sultanate of Oman

†Koninklijke/Shell Exploratie en Produktie Laboratorium, Rijswijk,
 The Netherlands

Late Carboniferous–early Permian sediments belonging to the Haushi Group in Oman have been considered to be partly of glacial origin^{1–3}. However, conclusive evidence of a continental glaciation has been lacking, and the extension of the late Palaeozoic Gondwana glaciation into the Arabian Peninsula has not been generally accepted⁴. During recent visits to outcrops of the Haushi Group in the Al Khilata area of the Huqf Massif (Fig. 1), we have found good exposures of striated pavements of Precambrian dolomite, which are directly overlain by diamictites of the Haushi Group (Fig. 2). This occurrence forms the strongest evidence so far for the presence of a continental glaciation in Oman during the late Palaeozoic.

Previous references to the occurrence of late Palaeozoic glacial sediments on the Arabian Peninsula have been summarized elsewhere^{5,6}. Roland⁵ describes the occurrence of striated and faceted pebbles and boulders of granites, gneisses and amphibolites in the Akbra shales of North Yemen and interprets them as dropstones from icebergs in a glaciomarine environment. Although no dating is mentioned, he considers the Akbra shales to be of late Palaeozoic age. McClure⁶ presents new evidence for a Stephanian to Sakmarian (late Carboniferous–early Permian) age of boulder beds in the Wajid Sandstone Formation at Khashm Khatmah and Jabal Umm Ghiran in Saudi Arabia (Fig. 1). He suggests that these boulder beds represent fluviially-reworked glacial deposits, but states, referring to the Arabian Peninsula as a whole: "Unfortunately, definitive indication of glaciation such as striated pavement and tillite is lacking".

In the context of a broader investigation into the sedimentology of the Haushi Group, exposures were studied in the outcrop area bordering the Huqf Massif (Fig. 1). Here the Haushi Group rests with an erosional unconformity on Precam-



Fig. 1 Location map: 1, Jabal Umm Ghiran; 2, Khashm Khatmah; 3, Al Khilata; 4, Haushi. (The Huqf Massif is shaded.)

brian formations of the Huqf Group. In the Al Khilata area this unconformity is well exposed in three different locations, forming a triangle of some 2 km². On the resistant surface of stromatolitic dolomites of the Huqf Group, parallel sets of striations and grooves (up to 35 cm wide and 10 cm deep) can be traced across the exposures, which are up to 30 m wide. Individual striae are up to 15 m long (Fig. 2). At this locality, 18 striae were measured (vector mean $45^\circ \pm 3^\circ$, vector magnitude 99.8%). In the other two localities, striae again have consistent mean azimuths of 45° although in one exposure a second set with an azimuth of 30° was observed. Direction of glacier movement could not be established from the striated pavements, but the consistent northeasterly foreset directions in fluviatile sandstones and conglomerates which erosively overlie the diamictite, suggest, in a simple palaeogeographical view, ice movement towards the north-east. The glacial sedimentary sequence appears to be onlapping onto the Huqf Massif, sediment transport being towards or along its margins. In two of the exposures a diamictite unit, with an average thickness of 4 m, rests directly on the striated dolomite (Fig. 2) and is therefore interpreted as a basal till. This diamictite is well exposed and correlatable over a distance of at least 1.4 km. Within a grey, fine-grained matrix it contains both igneous and sedimentary clasts. The sedimentary material consists of angular, centimetre-sized pieces of argillite and black chert (which may have been derived from the Precambrian Shuram Formation, outcropping 10 km south of Al Khilata) and fragments of dolomite probably derived from the local bedrock. The better-rounded pebbles and boulders of granite and other igneous rocks have not been related to any *in situ* occurrence in Oman. According to our present knowledge, no granites are present in surface or subsurface within a radius of 250 km of Al Khilata and hence the granite clasts are indicative of long-distance transport.

Further evidence for glacial deposition is found in several good exposures in the same area: sequences of rhythmically bedded or laminated fine sandstones and mudstones contain occasional outsize clasts (up to 240 cm), interpreted as dropstones from melting ice, floating on a body of standing water (Fig. 3a).

Table 1 Criteria for the identification of glacial deposits and their applicability in Oman

	Al Khilata	Subsurface
Abraded, striated bedrock surfaces	A	—
Stone-rich beds (diamictites)	A	A
Depositional fossil land forms	—	—
Dropstones	OP	A
Finely-graded stratification ('varves')	PP	A
Great thickness and extent of diamictites	—	PP
Association tillites/resedimented deposits	PP	OP
Variable clast lithology	A	A
Stones with wide range of shapes	A	A
Striated and faceted stones	OP	—
Clay-sized particles ('rock flour')	A	A
Fragile stones	OP	PP
Typical quartz grain textures	?	PP

A, abundant or well-defined; OP, occasionally present; PP, probably present; ? doubtful; —, not observed. Criteria after ref. 11.

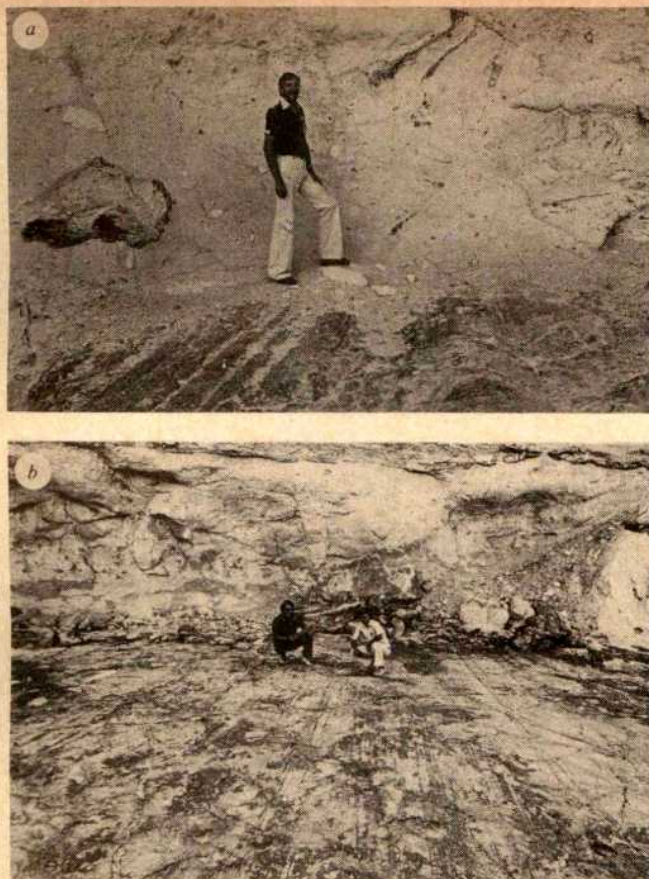


Fig. 2 a, Parallel grooves on pavement of Precambrian dolomite, overlain by a 4 m-thick diamictite (Al Khlat area). Photograph taken towards NE. b, Striated pavement in same exposure. Photograph taken towards SW.

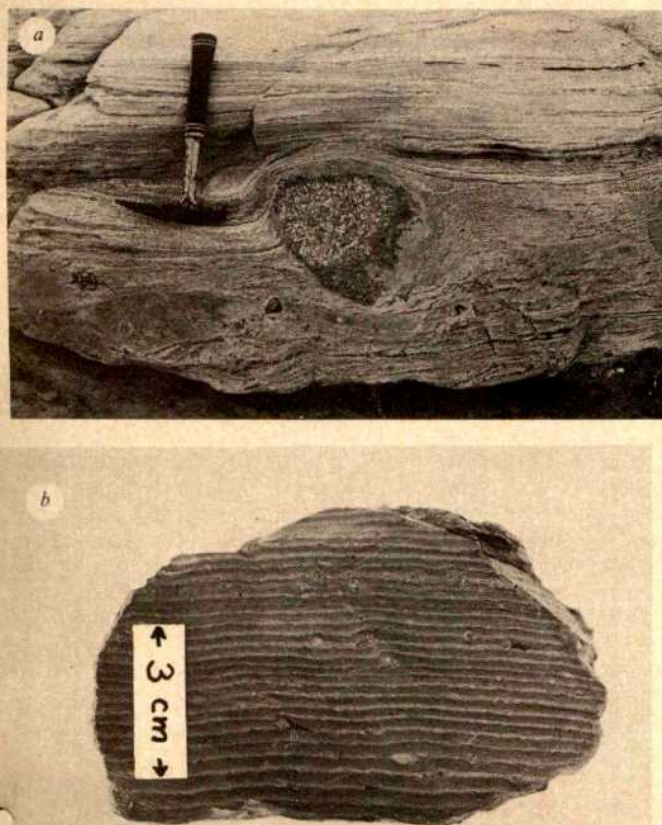


Fig. 3 a, Granite pebble and other dropstones in rhythmically bedded siltstones (Al Khlat area). b, Varved shale with dropstones from a cored well (South Oman).

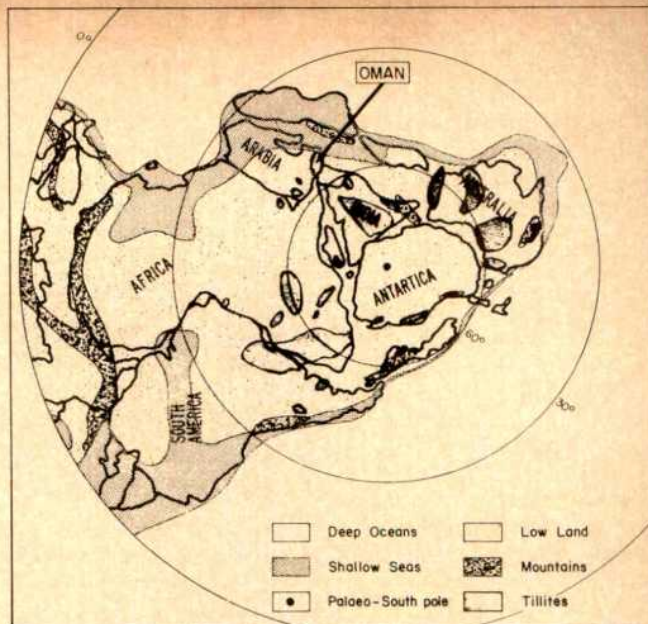


Fig. 4 Palaeogeography of the Southern Hemisphere during the late Carboniferous (after ref. 13).

Interbedded with the dropstone-laminites, discontinuous bodies of diamictite and poorly-sorted sandy conglomerates occur, some of which contain striated dolomite boulders. These units are interpreted as sub-aqueous mud flows and debris flows. Although the general appearance of these diamictites is similar to that of the basal diamictite, stratigraphical relationships favour an interpretation as subaqueously redeposited glacial debris.

Without the presence of the sedimentary units described above, which show strong evidence of a glacial environment, it would be difficult to place the bulk of the Haushi Group sequences as exposed in the Al Khlat area in a glacial setting, as it consists mainly of cross-bedded sandstones and conglomerates of fluvial or fluvio-deltaic origin.

The age of the Haushi Group in the outcrop area has been well established by palynology. The diamictites and associated claystones from the Al Khlat exposures have yielded well-preserved palynomorph assemblages. The microflora consists largely of *Cristatisporites* sp., *Parasaccites* sp., *Potoniesporites* sp., *Punctatisporites* sp., *Vallatisporites* sp. and *Verrucosporites* sp. Less common constituents include bisaccate non-striate and bisaccate striate pollen and a distinctive species, *Ahrensia* sp. The assemblages resemble those illustrated by Kemp⁷ from the Permo-Carboniferous glacial sequences of Pakistan and Brazil, and display the general characteristics of those which are assigned a latest Carboniferous age by Balme⁸. A considerable amount of reworking of palynoflora might be expected in a glacial environment; however, the presence of multistriate pollen precludes a dating older than latest Carboniferous. A bioclastic limestone interval conformably overlying the sequence containing the boulder beds in the Haushi area (Fig. 1) has been assigned an age no younger than earliest Artinskian, probably Sakmarian (early Permian)⁹, thus confirming the late Carboniferous to early Permian age of the diamictite sequence in Al Khlat.

The new evidence presented here supports the concept of a glacial to periglacial origin for the lower part of the Haushi Group in Oman as accepted and used¹⁰ by Shell and PD Oman geologists since 1976, when the occurrence of varved shales with dropstones was reported in cored wells (Fig. 3b).

Table 1 summarizes the features which are generally considered to be indicative of a glaciation, showing which of these are found in the Haushi Group of Oman. The presence of the striated bedrock and the occurrence of dropstones are considered the most diagnostic characteristics of glacial activity¹¹.

The significance of this discovery in relation to the reconstruction of Gondwanaland during the late Palaeozoic still has to be assessed. Interpretations of the palaeolatitudes of Oman during this period vary considerably. Some reconstructions¹² show a low latitude (<40°) for Oman during this period, but a 1979 reconstruction by Scotese *et al.*¹³ shows Oman at about 50° during the late Carboniferous, which is a similar palaeolatitude to that assumed for the well-documented glacial deposits in South America, South Africa and Australia (Fig. 4). Therefore, the Permo-Carboniferous glaciation in Oman could serve as support for this reconstruction of Gondwana.

Finally, we have recently learned from Thiele (personal communication) that further evidence for a late Palaeozoic glaciation has been found in North Yemen in the form of striated bedrock (granite and gabbro), overlain by tillite belonging to the Akbra Formation¹⁴. Preliminary dating of this formation by palynology suggests an age younger than Namurian and probably Permian.

Internal company reports, using data of the more than 300 subsurface well penetrations of the Haushi Group have greatly contributed to our knowledge of these glacial deposits and stimulated further studies leading to this article. Special acknowledgement is made to the work of F. J. Winkler of Shell Expro, London. We thank Shell Research B. V., The Hague, and Petroleum Development Oman LLC for their permission to publish this paper, which appears with the approval of H.E. The Minister of Petroleum and Minerals of the Sultanate of Oman.

Received 29 March; accepted 29 June 1982.

1. Hudson, R. G. S. *Q. J. geol. Soc. Lond.* **114**, 70–71 (1958).
2. Morton, D. M. *Proc. 5th World Petrol. Congr.* **1**, 277–294 (1959).
3. Tschopp, R. H. *Proc. 7th World Petrol. Congr.* **2**, 231–241 (1967).
4. Frakes, L. A. *Climates throughout Geologic Time* (Elsevier, Amsterdam, 1979).
5. Roland, N. W. *Eiszeitalter Gegenw.* **28**, 133–138 (1978).
6. McClure, H. A. *Bull. geol. Soc. Am.* **91**, 707–712 (1980).
7. Kemp, E. M. in *Gondwana Geology* (ed. Campbell, K. S. W.) 397–413 (Australian National University Press, Canberra, 1975).
8. Balme, B. E. *Palynology* **4**, 43–55 (1980).
9. Hudson, R. G. S. & Sudbury, M. *Notes et Memoires sur le Moyen Orient* Vol. 7, 19–55 (Musée Nationale d'Histoire Naturelle, Paris, 1959).
10. Murris, R. J. *Geologie Mijnh.* **60**, 467–486 (1981).
11. Hambrey, M. J. & Harland, W. B. *Earth's Pre-Pleistocene Glacial Record* (Cambridge University Press, 1981).
12. Smith, A. G., Hurley, A. M. & Briden, J. C. *Phanerozoic Paleogeographic World Maps* (Cambridge University Press, 1981).
13. Scotese, C. R., Bambach, R. K., Barton, C., Van der Voo, R. & Ziegler, A. M. *J. Geol.* **87**, 217–277 (1979).
14. Kruck, W. & Thiele, J. *Geol. Jber* (in the press).

Volatile C₁–C₈ organic compounds in macroalgae

Jean K. Whelan, Martha E. Tarafa & John M. Hunt

Woods Hole Oceanographic Institution, Woods Hole, Massachusetts 02543, USA

Small amounts of C₁–C₈ volatile organic compounds were found in macroalgae in concentrations high enough (generally in the range of 1–400 times those in sediments) to suggest that the seaweeds are a source for some of the volatile organic compounds identified in recent marine sediments. The types of compounds identified^{1–4} include alkanes, alkenes, aldehydes, ketones, furans, and sulphides. Both the light hydrocarbons and the volatile functionalized organic compounds are believed to originate from living organisms and from both biological and chemical low-temperature reactions in the sediments. Understanding their mechanism of formation may help in deciphering the thermal and biological history of the sediments. Traces of some of these compounds can be produced from bacterial degradation of naturally occurring terpenoids⁵. We consider here their occurrence in algae.

Four species of seaweeds, *Ulva lactuca*, *Ascophyllum nodosum*, *Gracilaria tikvahiae* and *Hypnea musciformis* were

grown in 1,700-l aerated tanks using circulating seawater. The macroalgae (grown and maintained by J. Ryther of Woods Hole Oceanographic Institute) were selected because of their high productivity and ease of culturing. All the species studied were shallow water species often found in tidal zones. *U. lactuca* is found from the tropics to Newfoundland, *A. nodosum* from New Jersey northward, *G. tikvahiae* is from the tropics and *H. musciformis* grows from the tropics to the south coast of Massachusetts.

Algae samples were analysed by a modified head space technique which has been used to investigate volatile organic compounds in sediments³. The plants were disaggregated in a stainless steel blending assembly equipped with Teflon gaskets and a screw cover with a sampling septum. Each sample (20–40 g wet weight) of algae was placed in the blender with distilled degassed water leaving a 118 ml gas headspace. The blender was then placed inside a glove bag which was aspirated to exclude air and filled with helium. The vessel was sealed while inside the bag, its contents were blended at high speed for ~10 min, and then heated in a 90 °C water bath for 30 min. Samples were removed through the gas chromatography (GC) septum using a syringe and analysed by GC and GC-MS⁶. Degassed distilled water and the tank water in which the algae were grown were analysed as blanks. None of the compounds reported was detected in the blanks. Compound identification was based on a comparison of GC and GC-MS data with those of commercially available standards.

Amounts of compounds present in various species of algae are shown in Table 1. Except for the sulphides, none of these compounds have previously been reported in algae. Most of the compounds found in macroalgae also occur in surface marine sediments, but usually at lower levels (~0.1–100 ng per g)^{2,3,6}. The alkenes are found most frequently in marine sediments with an oxic sediment–water interface^{2,6}. They generally decrease to trace levels (<0.1 ng per g) in the top metre of sediment.

All species of algae in Table 1 contained *n*-pentane in concentrations >10 ng per g. No other pentane isomers were detected. The discovery that recent marine sediments generally have a low isopentane to *n*-pentane ratio could be partly explained by algal contributions of *n*-pentane⁷.

The aldehydes, ketones, furans, and sulphides of Table 1 are frequently found in marine sediments—for example, on the Walvis Bay Shelf, the Peru Shelf, and the Gulf of Maine^{2,3,6}. Their levels are in the range 0.1–100 ng per g in reducing sediments. However, they also occur sporadically in smaller amounts (0.01–10 ng per g) in sediments with oxic sediment–water interface, such as the Gulf of Maine and parts of the Peru Shelf. Some of these compounds have also been detected in more deeply buried (>100 m subbottom) sediments where the geothermal gradient is low enough that the compounds have not been exposed to temperatures >20 °C, such as DSDP sites 438 and 436 in the Japan Trench⁴.

It was previously proposed that some of the volatile organic compounds in sediments may be derived from terpene precursors which occur in marine organisms³. This work supports this concept. Algae provide a rich and diverse range of these terpenes^{8,9}. Large areas of these plants can be seen in surface ocean waters in many parts of the world. Even though the occurrence of various species of macroalgae in oceanic and coastal waters is patchy, the sinking of these large plants and their fragments would provide a way of rapidly delivering small, volatile molecules to the sediments with minimal water column biodegradation. Little is known about the contribution of macroalgae to organic matter on the deep sea floor¹⁰. It has been estimated that even in deep water, large particle sinking occurs in a matter of days¹¹. The macroalgae plant structure would prevent loss of these very volatile compounds and protect the more labile functional groups, such as the aldehydes, from biodegradation at the sediment–water interface where intense microbiological activity occurs¹². Because biological activity in sediments decreases rapidly with depth¹² burial of plant

fragments to depths of even a few centimetres could provide some protection of these molecules from biodegradation.

Although much recent work has concentrated on identifying larger molecules in macroalgae¹³, the smaller, more volatile components shown in Table 1 have been largely ignored. Certain compounds seem to be restricted to particular species: methyl-1, 3-cyclopentadiene in *H. musciformis* and three compounds in *G. tikvahiae* tentatively identified as 2-ethyl-cyclobutanol, cycloheptene, and 3-cycloheptene-1-one, based on a search of the NIH 30,000 mass spectral library¹⁴. An unusual feature of the latter two compounds is their mass spectral base peak at $m/z = 54$. The 3-cycloheptene-1-one occurs in very large amounts in *G. tikvahiae*. It is either very volatile or labile as the amount measured in material which had been frozen for several months had decreased from 1 mg per g to 3,100 ng per g. In frozen samples a similar decrease in concentration over time did not occur for other compounds shown in Table 1. The literature on natural products from red algae, of which *G. tikvahiae* is a member, does not report any structures comparable to the cycloheptene, 3-cycloheptene-1-one, or the ethyl cyclobutanol, although cycloheptadiene derivatives have been reported in brown algae¹⁵. These volatile compounds would be lost in normal isolation procedures which generally involve extraction with organic solvents.

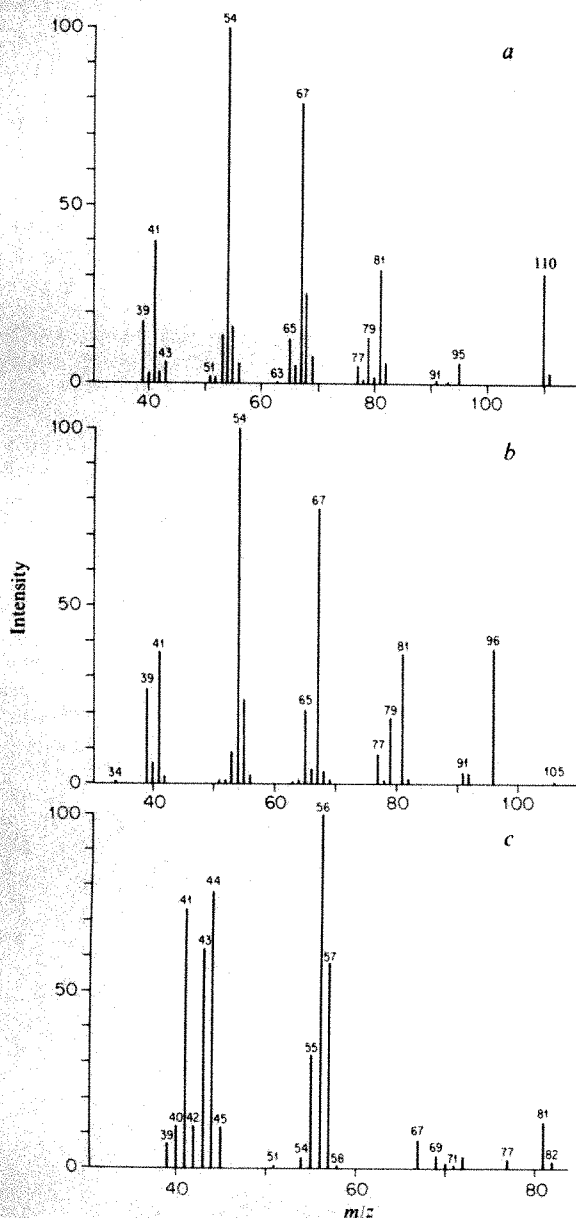


Fig. 1 Mass spectra of compounds from *Gracilaria tikvahiae*. Tentative compound identification: a, 3-cycloheptene-1-one; b, cycloheptene; and c, ethylcyclobutanol.

Table 1 Amounts of volatile organic compounds found in various species of macroalgae (units ng of compound per g dry weight of algae)

Compound	<i>Ulva lactuca</i>	<i>Hypnea musciformis</i>	<i>G. tikvahiae</i> (nutrient enriched)	<i>G. tikvahiae</i> (nutrient deprived)	<i>Asco-phylum nodosum</i>
1-Butene	0	>50	0	0	0
n-Butane	6	0	55	ND	0
1-Pentene	0	0	0	0	11
n-Pentane	10	16	171	Present	110
3-Methylpentane	0	22	0	0	0
1-Methyl-1, 3-cyclopentadiene	0	114	0	0	0
Benzene	20	20	0	0	0
Dimethylsulphide	>2,700†	>79,000	>2,000,000	0	>19,000‡
Dimethyldisulphide	0	>4	0	0	0
Propanal	0	480	0	0	0
2-Methylpropanal	190	310	0	0	0
Butanal	0	630	1,900	750	0
3-Methylbutanal	0	120	800	260	0
Pentanal	0	2,500	310	1,900	1,200
Hexanal	0	0	0	7,000	0
Acetone	0	0	0	0	>19,000‡
2-Butanone	1,200	1,800	270	2,600	0
2, 3-Butandione	0	160	0	230	0
4-Methyl-2-pentanone	0	0	0	0	2
4-Pentene-2-one	0	0	0	0	70
Furan	0	3,900	1,500	16,000	120
Dihydrofuran	0	0	900	1,600	0
2-Methylfuran	5,500	670	1,200	6,100	0
3-Methylfuran	370	270	0	1,400	0
Ethylfuran	8,300	2	70	0	0
2, 5-Dimethylfuran	0	0	0	940	0
Ethylcyclobutanol*	0	0	>240,000	14,000	0
Cycloheptene*	0	0	>40,000	0	0
3-Cycloheptene-1-one*	0	0	>1 × 10 ⁶	>100,000	0
Ethenylcyclohexane	0	0	0	200,000	0

ND, not determined.

* Preliminary identification.

† Compounds unstable in the analysis or without appropriate standards are shown as >.

‡ Total includes both dimethylsulphide and acetone.

Levels of alkanes, butanal, ethylcyclobutanol and dimethylsulphide in *G. tikvahiae* decreased in going from nutrient-enriched to nutrient-deprived cultures. However, concentrations of furans, ketones and the remaining aldehydes all increased. These differences seem to reflect a change in metabolism in the two cultures. It is known that lipid levels in organisms change in response to nutrient availability¹⁶, however, such changes have been observed only with lipids containing more than 15 carbon atoms. Our results show that changes also occur in the low molecular weight ranges.

Several species of phytoplankton (microalgae), *Thalassiosira* sp., *Gymnodinium* sp., *Emiliania huxleyi* and *Skellotenema costatum*, were analysed by the same methods as the macroalgae. Only one very volatile compound was detected which appeared to be a C₅ diene. This means that these phytoplankton cannot be directly contributing the compounds in Table 1 to sediments.

A variety of low molecular weight volatile alkanes, alkenes, ketones, aldehydes, furans, and sulphides have been found in macroalgae and the following conclusions may be made from their distribution: (1) Macroalgae are the probable source of some of these same compounds found in recent marine sediments. The low isopentane/*n*-pentane ratio of marine sediments could be partly caused by macroalgae. (2) Nutrient deprived macroalgae, such as *G. tikvahiae*, show a distinctly different volatile compound distribution from nutrient enriched algae. (3) Specific volatile compounds such as the cycloheptene and 3-cycloheptene-1-one in *G. tikvahiae* may be useful fingerprints in identification of algae. (4) Phytoplankton do not appear to be the source of volatile organic compounds in recent sediments.

This work was supported by the Oceanography Section of NSF (grant OCE 80-19508). This is Woods Hole contribution no. 5099.

Received 20 April; accepted 29 June 1982.

- Hunt, J. M. *Nature* **254**, 411–413 (1975).
- Hunt, J. M. & Whelan, J. K. *Org. Geochem.* **1**, 219–224 (1979).
- Whelan, J. K., Hunt, J. M. & Berman, J. *Geochim. cosmochim. Acta* **44**, 1767–1785 (1980).
- Whelan, J. K. & Hunt, J. M. *Init. Rep. DSDP Leg 56-57*, 1349–1365 (1980).
- Hunt, J. M., Miller, R. J. & J. K. Whelan, *Nature* **288**, 577–578 (1980).
- Whelan, J. K. *Gas Chromatography/Mass Spectrometry Applications in Microbiology* (eds Odham, G., Larsson, L. & Mardh, P. A.) (Plenum, New York, in the press).
- Hunt, J. M., Whelan, J. K. & Huc, A. Y. *Science* **209**, 403–404 (1980).
- Faulkner, D. J. & Fenical, W. H. *Marine Natural Products Chemistry* (Plenum, New York, 1977).
- Scheuer, P. J. *Marine Natural Products* (Academic, New York, 1978).
- Schoener, A. & Rowe, G. T. *Deep Sea Res.* **17**, 923–925 (1970).
- Honjo, S. J. *Mar. Res.* **38**, 53–97 (1980).
- Sorokin, Y. I. *The Changing Chemistry of the Oceans* (eds Dryssen, D. & Jangner, D.) 189–204 (Wiley, New York, 1972).
- Baker, J. T. & Murphy, V. *Handbook of Marine Science Vol. II* (CRC Boca Raton, 1981).
- Heller, S. R. & Milne, G. W. A. *EPA/NIH Mass Spectral Data Base*, Vol. 1 (U.S. Government Printing Office, 1978).
- Moore, R. E. & Yost, G. *Chem. Commun.* 937 (1973).
- Hunt, J. M. *Petroleum Geochemistry and Geology*, 91 (Freeman, San Francisco, 1979).

High abundance of algal 24-ethylcholesterol in Antarctic lake sediment

Genki Matsumoto*, Tetsuya Torii† & Takahisa Hanya*

*Department of Chemistry, Faculty of Science, Tokyo Metropolitan University, Fukazawa 2-1-1, Setagaya-ku, Tokyo 158, Japan

†Chiba Institute of Technology, Tsudanuma 2-17-1, Narashino, Chiba Prefecture 275, Japan

Sterols are one of the most widely distributed group of organic compounds in the environment, ranging in geological age from Recent to Cretaceous, and are commonly found in soils and contemporary lake and marine sediments^{1–11}. The major sterols found in lake sediments are stenols, cholest-5-en-3 β -ol (C₂₇), 24-methylcholesta-5,22-dien-3 β -ol (C₂₈), 24-methylcholest-5-en-3 β -ol (C₂₈), 24-ethylcholesta-5,22-dien-3 β -ol (C₂₉) and 24-ethylcholest-5-en-3 β -ol (24-ethylcholesterol, C₂₉) and stanols, 5 α -cholestan-3 β -ol (C₂₇), 24-methyl-5 α -cholestan-3 β -ol (C₂₈) and 24-ethyl-5 α -cholestan-3 β -ol (C₂₉) (refs. 5–8, 10, 11). C₂₉ sterols are abundant in vascular plants, whereas C₂₇ sterols are often dominant in plankton. Thus C₂₉/C₂₇ sterol ratios are believed to be indicators both of allochthonous and autochthonous contributions of organic matter for lakes and of terrigenous sources of organic matter in marine environments^{5,7,8,10,11}. In the Antarctic, vascular plants are only found in the Antarctic Peninsula¹². Thus the sterol composition of Antarctic lake sediments is expected to be considerably different from those in the temperate and tropical zones. Here we report the first analyses of sterols in Antarctic lake sediments, which are found to contain high abundances of 24-ethylcholesterol. Such sterols must arise from blue-green and green algae in lakes and surrounding soils.

During 1976–77 and 1980–81 austral summers, sediments, epibenthic algae and moss were collected from the dry valleys of Victoria Land in the Antarctic (Fig. 1, Table 1). Characteristics of the dry valley lakes are described elsewhere^{13–17}. The lakes and ponds studied are all saline. The primary productivity measurements in Lakes Vanda and Bonney yielded low values of 29 and 31 mg C m⁻² day⁻¹, respectively¹³. Lake and pond bottom sediment samples were taken with stainless steel scoop, with polyvinyl chloride pipe (length, 340 mm; i.d., 89 mm) by a diver, or using a Kitahara-type water sampler. The algae were collected from the lakeshore, which is usually covered with epibenthic algae. These samples were transferred to a glass bottle or wrapped in a Teflon sheet and stored at temperatures below 0°C until analysis. Wet samples (10–300 g) were first homogenized with an Ace Homogenizer (10⁴ r.p.m., Nihon Seiki Co. Ltd), saponified with 0.5 M potassium hydroxide in methanol solution (80°C, 2 h) and centrifuged (1,800 g). Supernatants and residues were separately acidified, extracted with

ethyl acetate after the addition of distilled water, and then concentrated under reduced pressure at temperatures below 30°C.

Part (1–1/10) of the ethyl acetate extracts was evaporated to dryness, dissolved in 50- μ l benzene: ethyl acetate (1:1) and chromatographed on a silica gel column (180 \times 4 mm i.d., 100 mesh, 5% water). After elution of 2 column volumes of hexane, 3 column volumes of benzene: ethyl acetate (95:5) fractions were evaporated to dryness, dissolved in 100 μ l benzene and rechromatographed through a silica gel column impregnated with 3% potassium hydroxide (180 \times 4 mm i.d., 100 mesh). Fractions eluted with 3 column volumes of benzene: ethyl ether (1:1) were concentrated and trimethylsilylated (TMS) with 25% N,O-bis(trimethylsilyl)acetamide in acetonitrile solution (1 h, room temperature). The TMS ethers of sterols were determined using a combined Shimadzu LKB 9000 gas chromatograph-mass spectrometer (GC-MS). The GC-MS conditions are given on Table 1 legend.

The individual sterols were identified by comparison of their retention times and mass spectra with those of authentic compounds. Stenols and stanols were quantified by measuring peak height on the mass fragmentogram carried at *m/z* 129 and 215 which are characteristic to the TMS ethers of Δ^5 -stenols and 5 α -stanols, respectively^{3,5,6,18}. The detection limits of the sterols by mass fragmentography were \sim 0.1 ng. A blank run showed the presence of possible contaminants, but only minor amounts that would not affect the analytical results. To determine the analytical reliability, four replicate experiments using authentic compounds and a lake sediment were carried out and gave recoveries of cholest-5-en-3 β -ol, 24-methylcholest-5-en-3 β -ol and 24-ethylcholesterol of 83 (standard deviation, s.d., 11), 96 (s.d., 4.0) and 99% (s.d. 4.9%), respectively.

The contents of the six stenols and three stanols identified in the sediment samples range from 0.11 to 19 and 0.0 to 7.2 μ g per g dry sediment, respectively (Table 1). The amounts of sterols in the sediment from Don Juan Pond are extremely low, while those of Lakes Fryxell and Joyce are considerably higher. However, the amounts of stanols in the sediments from Lakes Vanda, Bonney and Joyce were extremely low. The ratios of sterol carbon to the total organic carbon contents differ considerably, ranging from 0.26 to 3.9×10^{-3} , comparable with those of contemporary lake sediments from the temperate zone (0.27 – 5.2×10^{-3})^{7,8,11}.

The sources of stanols in contemporary lake sediments in the temperate zone have been widely discussed elsewhere^{4,6–8}. Our stanol composition should therefore be attributed to the hydrogenation of stenols, algal materials as shown in Table 1 and/or subsequent preferential degradation of stenols relative to stanols, as in the case of the sediments in the temperate zone.

Surprisingly 24-ethylcholesterol is the dominant sterol in all these sediment samples. It is also the most prominent sterol in some soils and water samples from the dry valley areas (G.M.,

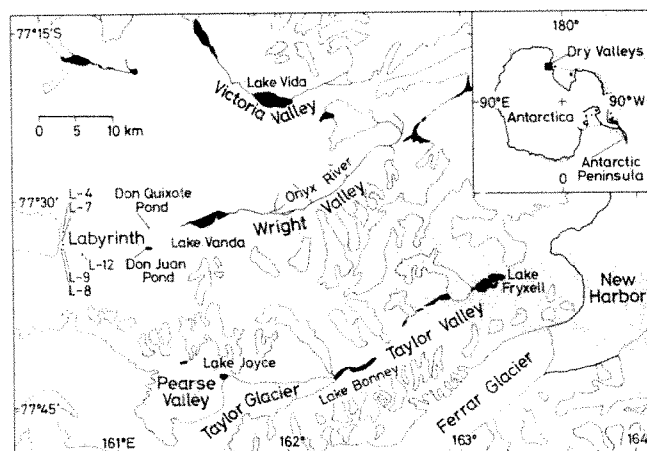


Fig. 1 Sampling locations in the dry valleys of Victoria Land in the Antarctic. L-4, L-7–L-9 and L-12 are unnamed ponds.

Table 1 Sterols found in sediments, epibenthic algae and moss from the dry valleys of Victoria Land in the Antarctic

Nature of sample†	Sediment							Epibenthic algae				Moss
	Lake Vanda G, sd	Don Juan Pond DYB, sd	L-4 pond DYO, sd	L-8 pond RB, sd	Lake Fryxell B, fsd	Lake Bonney GO, st	Lake Joyce OG, sd	L-8 pond* O	L-12 pond† O	Lake Fryxell‡ OG	Lake Bonney§ OG	Fryxell Hut Br & SG
Stenols												
Concentration (µg per g) #	4 1	0 11	1 7	1 5	19	8 2	16	6 8	14	0 56	5 8	5 1
Composition (%)												
A	2 1	2 6	0 0	1 6	2 2	7 1	1 4	3 1	0 8	3 4	2 7	0 0
B	14 6	27 6	26 0	22 1	4 1	8 8	16 9	39 0	14 4	46 7	22 3	2 7
C	2 7	9 0	0 0	2 4	24 3	30 2	19 8	5 3	3 1	8 3	9 9	3 1
D	4 9	10 4	6 0	5 4	11 1	8 8	19 4	6 0	5 8	12 4	19 2	54 7
E	10 0	6 4	3 5	7 5	8 0	8 0	0 0	6 6	13 2	6 7	4 8	3 1
F	65 7	44 0	64 5	61 0	50 3	37 1	42 5	40 0	62 7	22 5	41 1	36 4
Stanols												
Concentration (µg per g) #	0 0	0 016	0 47	0 42	7 0	0 075	0 73	ND	0 68	0 0	0 20	0 079
Composition (%)												
G	—	44	90 0	84 4	11 0	51	42 3	—	13	—	30 8	56
H	—	44	2 1	6 0	45 9	49	5 9	—	10	—	26 4	0
I	—	12	7 9	9 6	43 1	0	51 8	—	77	—	42 8	44
Sterols-C**/TOC†† (×10 ³)	1 8	0 26	1 9	0 95	1 3	3 9	3 6	0 12	0 44	0 029	0 89	0 040
C ₂₉ /C ₂₇ ‡‡	4 5	1 4	1 4	1 5	7 2	2 7	2 2	1 1	5 1	0 60	1 8	11
Stanols/Stenols	0 0	0 24	0 28	0 28	0 37	0 091	0 043	—	0 049	0 0	0 034	0 015

GC-MS conditions silanized glass column (200 cm × 3 mm i d) packed with 1% silicone OV-1 on 80-100 mesh Chromosorb W AW DMCS, temperature, injector 300 °C, column programmed from 230 to 290 °C at 5 °C min⁻¹, molecular separator 310 °C, ion source 330 °C, carrier gas, helium at 30 ml min⁻¹, accelerating voltage, 3 5 kV, multiplier gain, 3

* Blue-green algae, *Synechococcus* spp, *Phormidium* spp and *Oscillatoria* spp being the main species † Mainly *Phormidium* spp ‡ Mainly *Oscillatoria* spp § Mainly *Phormidium* spp and diatom, *Hantzschia amphioxys* || *Sarconeureum glaciale* ¶ G, grey, sd, coarse and fine sands, DYB, dull yellowish brown, DYO, dull yellow orange, RB, reddish brown, B, black, fsd, fine sand, GO, greyish olive, st, silt, OG, olive grey, O, orange, Br & SG, brown and silver green # Dry base ND, not determined ** Sterols as carbon †† Total organic carbon, which was determined by dry combustion using a CHN analyser (Yanako MT2 CHN Coder) after treatment with 6 M hydrochloric acid to remove inorganic carbon A Cholest-5,22-dien-3β-ol B Cholest-5-en-3β-ol C 24-Methylcholest-5,22-dien-3β-ol D 24-Methyl-cholest-5-en-3β-ol E 24-Ethylcholest-5,22-dien-3β-ol F 24-Ethylcholest-5-en-3β-ol G 5α-Cholestan-3β-ol H 24-Methyl-5α-cholestan-3β-ol I 24-Ethyl-5α-cholestan-3β-ol ‡‡ E + F + I/A + B + G

unpublished results) Thus the C₂₉/C₂₇ sterol ratios are high (1 4-7 2), and comparable with those of lake sediments from the temperate zone (0 48-8 5)^{6-8 10 11}, attributed to sterol inputs from vascular plants However, no vascular plants are present in the dry valley areas It is probable that there is preferential degradation in the sediments of C₂₇ relative to C₂₉ sterols, because the C₂₉/C₂₇ sterol ratios increase with increasing sediment depth in certain temperate lacustrine sediments^{6 8} However, a core sediment taken from Lake Fryxell (20 cm long) showed that the vertical changes in the C₂₉/C₂₇ ratios are small (G M, unpublished results) In addition the C₂₉/C₂₇ values of water samples through the depths from 5 4 to 65 9 m in Lake Vanda are very high (1 1-5 3, G M *et al*, unpublished results) Furthermore incubation experiments both in water and sediment have not revealed the marked changes in C₂₉/C₂₇ ratios (ref 8 and G M, unpublished results) Thus the effect of preferential degradation of C₂₇ sterols relative to C₂₉ sterols in cold dry valley lakes is small Therefore there seem to be at least three possible sources for these unusual distribution of sterols

(1) An input of aeolian dust, because small amounts of pollen have been found in the sediment cores taken by Dry Valley Drilling Project from the dry valley areas¹⁹ In addition Aeolian dusts are believed to be the principal sources of biological lipids of terrigenous materials in open ocean environments^{20 21} Normal alkanes are expected to be much more resistant to transformation than sterols in atmospheric transportation, because they are commonly found as the major constituents in atmospheric samples However, the sterol/*n*-alkane ratios calculated for aerosols from the tropical North Pacific (<0 063-<0 50)²¹ and atmospheric fallouts from the Tokyo area (0 034 and 0 13)^{22 23} are significantly lower than those of the sediment samples (0 55-750) of the dry valley areas (ref 24 and G M, unpublished results) In addition cholest-5-en-3β-ol is the most dominant sterol in these aerosols and atmospheric fallouts

These results showed that aeolian dust is not an important source for our sterols

(2) Glacial erosion of sedimentary rocks, because much of the sedimentary organic carbon in the Ross Sea is derived from the rocks being eroded by glaciers on the Antarctic continent²⁵ Very long-chain *n*-alkanoic acids found in soils from the dry valley areas are apparently originated from sedimentary rocks of Precambrian to Cretaceous ages²⁶ Stanol/stenol ratios of sedimentary rocks can be expected to be much higher than the living organisms, but these ratios of our sediment samples are rather lower than the contemporary lake sediments from common temperate lakes^{4 6-8} Further it was found that *n*-alkanes with the marked dominance of odd-carbon numbers and *n*-alkanoic acids with the great abundance of even-carbon numbers were not of ancient origin (ref 24, G M unpublished results) Thus sedimentary rocks are also unlikely sources of our sterols

(3) Biological sources, because many kinds of organisms, such as bacteria, fungi, blue-green and green algae, and mosses are found in the dry valley areas^{13 14 16 27} Certain bacteria contain sterols, but none with 24-ethylcholesterol as the most abundant sterol^{28 29} The principal sterol of fungi is ergosterol³⁰ Both organisms are therefore unlikely sources of our sterols Moss contains 24-methylcholest-5-en-3β-ol and 24-ethylcholesterol as their dominant sterols (Table 1), but the distribution of mosses in the areas studied is restricted, they only occur around Lake Fryxell in Taylor Valley Thus, mosses are also unlikely sources of the sterols in the sediments 24-Ethylcholesterol as the major sterol has been found in some Chlorophyceae³¹⁻³³, Xanthophyceae³¹ and Rhodophyceae³¹ *Synura petersenii*³⁴ and *Phormidium luridum*³⁵ also contain 24-ethylcholesterol as the most dominant sterol Our analytical results showed that 24-ethylcholesterol is the major sterols in epibenthic algae, mostly blue-green algae, which are widely distributed, collected from L-4 and L-12 ponds and Lake

Bonney Therefore algae, including green and blue-green algae, especially *Phormidium* spp are important sources of 24-ethylcholesterol in Antarctic dry valley lake sediments. In addition soil algae may contribute to the high abundances of C_{29} sterols in lake sediments²⁷

We thank the Japan Polar Research Association, Antarctic Division, DSIR, New Zealand, US NSF and US Navy for logistic support, Drs S Nakaya, T Cho, E Wada and G M Simons Jr and his research group for assistance in collecting samples, Professor H Fukushima for the identification of algae and Dr H Kanda for the identification of moss, and Drs K Ogura and T Itoh for useful suggestions

Received 25 February, accepted 8 July 1982

- 1 Comet, P A *et al* *Int Rep DSDP Leg 62*, 923-937 (1981)
- 2 Mattern, G, Albrecht, P & Ourisson, G *Chem Commun* 1570-1571 (1970)
- 3 Henderson, W, Reed, W E & Steel, G in *Advances in Organic Geochemistry 1971* (eds Gaertner, H R v & Wehner, H) 335-352 (Pergamon, Oxford, 1972)
- 4 Ogura, K & Hanya, T *Proc Japan Acad* 49, 201-204 (1973)
- 5 Huang, W-Y & Meinschein, W G *Geochim cosmochim. Acta* 40, 323-330 (1976)
- 6 Gaskell, S J & Eglinton, G *Geochim cosmochim. Acta* 40, 1221-1228 (1976)
- 7 Nishimura, M *Nature* 270, 711-712 (1977)
- 8 Nishimura, M *Geochim cosmochim. Acta* 42, 349-357 (1978)
- 9 Lee, C, Farrington, J W & Gagosian, R B *Geochim cosmochim. Acta* 43, 35-46 (1979)
- 10 Huang, W-Y & Meinschein, W G *Geochim cosmochim. Acta* 43, 739-745 (1979)
- 11 Ishiwatari, R, Ogura, K & Horne, S *Chem Geol* 29, 261-280 (1980)
- 12 Greene, S W *et al* in *Terrestrial Life of Antarctica, Antarctic Map Folio Series 5* (ed Bushnell, V C) 1-24 (American Geographic Society, New York, 1967)
- 13 Goldman, C R, Mason, D T & Hobbie, J E *Limnol Oceanogr* 12, 295-310 (1967)
- 14 Koob, D D & Leister, G L in *Antarctic Terrestrial Biology* (ed Llano, G A) 51-58 (American Geographic Union, Washington, 1972)
- 15 Torii, T *et al* *Mem natn Inst Polar Res, Spec Iss* 4, 5-29 (1975)
- 16 Siegel, B Z, McMurty, G, Siegel, S M, Chen, J & LaRock, P *Nature* 280, 828-829 (1979)
- 17 Matsumoto, G, Tanaka, Y & Torii, T *Antarct Rec* 74, 109-118 (1982)
- 18 Brooks, C J W, Horning, E C & Young, J S *Lipids* 3, 391-402 (1968)
- 19 Wrenn, J H & Webb, P N *Dry Valley Drill Proj Bull* 7, 108-109 (1976)
- 20 Simoneit, B R T, Chester, R & Eglinton, G *Nature* 267, 682-685 (1977)
- 21 Gagosian, R B, Peltzer, E T & Zafirou, O C *Nature* 291, 312-314 (1981)
- 22 Matsumoto, G & Hanya, T *Atmos Envir* 14, 1409-1419
- 23 Matsumoto, G *Atmos Envir* (in the press)
- 24 Matsumoto, G, Torii, T & Hanya, T *Mem natn Inst Polar Res, Spec Iss* 13, 103-120 (1979)
- 25 Sackett, W M, Poag, C W & Eadie, B J *Science* 185, 1045-1047 (1974)
- 26 Matsumoto, G, Torii, T & Hanya, T *Nature* 290, 688-690 (1981)
- 27 Cameron, R E, King, J & David, C N in *Antarctic Ecology Vol 2* (ed Holdgate, M W) 702-716 (Academic, London, 1970)
- 28 Schubert, K, Rose, G, Wachtel, H, Holhold, C & Ikekawa, N *Eur J Biochem* 5, 246-251 (1968)
- 29 Bird, C W *et al* *Nature* 230, 473-475 (1971)
- 30 Weete, J D in *Chemistry and Biochemistry of Natural Waxes* (ed Kolattukudy, P E) 349-418 (Elsevier, Amsterdam, 1976)
- 31 Heilbron, I M *J chem Soc* 79-89 (1942)
- 32 Dickson, L G, Patterson, G W & Knights, B A *Proc int Seaweed Symp* 1977, 9, 413-420 (1979)
- 33 Mahendran, M *et al* *J natn Sci Counc Sri Lanka* 8, 69-74 (1980)
- 34 Collins, R P & Kalnins, K *Comp Biochem Physiol* 30, 779-782 (1969)
- 35 de Souza, N J & Nes, W R *Science* 162, 363 (1968)

Direct demonstration of fluid secretion by glomerular renal tubules in a marine teleost

K. W. Beyenbach

Section of Physiology, Cornell University, Ithaca, New York 14853, USA and the Mt Desert Island Biological Laboratory, Salsbury Cove, Maine 04672, USA

The evidence for fluid secretion by the kidneys of teleosts is indirect¹⁻⁴. By using *in vitro* micropertusion of renal tubules⁵, we have observed fluid secretion in the proximal tubule of the winter flounder *Pseudopleuronectes americanus*. Unlike the isosmotic fluid transfer across most vertebrate proximal tubules, the secreted fluid in this teleost could be hyperosmotic to the bathing medium. More importantly, fluid secretion was not dependent on the transport of Mg, S or organic ions^{4,6}, but appeared to be driven by NaCl, the major solute in the secreted fluid. This mechanism of NaCl-dependent fluid secretion has been previously undetected because renal clearances showed the overall net reabsorption of NaCl and water^{4,7}.

P. americanus has a glomerular kidney containing 10,400 glomeruli on average and no aglomerular renal tubules have

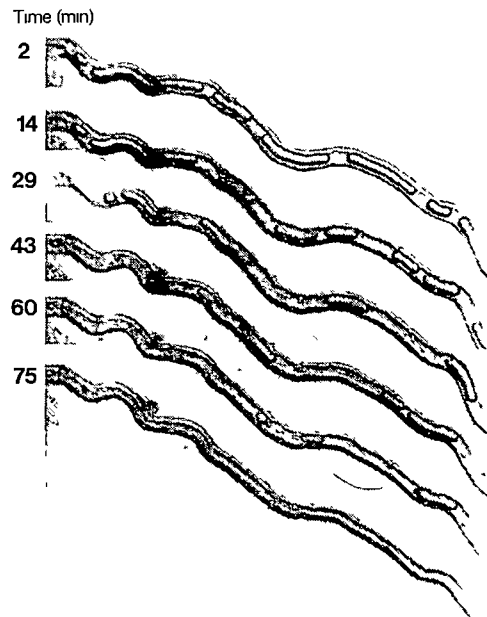


Fig 1 Fluid secretion by proximal tubule. A 1.5-mm segment of a flounder proximal tubule (outer diameter 53 μ m, inner diameter 25 μ m) is shown in serial photographs. The tubule was held by two pipettes in aerated flounder Ringer's solution ($14 \pm 1^\circ\text{C}$) containing (mmol l⁻¹) NaCl 145, NaHCO₃ 20, KCl 5, Na₂HPO₄ 1.65, NaH₂PO₄ 0.3, MgSO₄ 1, CaCl₂ 1, and glucose 10, pH 7.4. The left end of the tubule was cannulated with a perfusion pipette containing light paraffin oil, the right end of the tubule opened into a holding pipette as shown in Fig 2. Perfusion filled the lumen with oil. When perfusion was stopped, epithelial fluid secretion fractionated the column of oil in the lumen and drove the flow of oil and secreted fluid towards the open end on the right $\times 65$.

been observed⁸. Renal clearance studies do not reveal net secretion of fluid^{4,7}. However, isolated proximal tubules suspended in Ringer's solution between two glass pipettes and filled with oil can be observed to secrete fluid as in Fig 1 where fluid secretion from bath to lumen displaced the oil from the lumen.

In subsequent studies of the characteristics of fluid secretion, the lumen was not filled with oil. Instead, one end of the tubule was closed by pulling it into a narrow glass pipette and the other end (open) was drawn into a collection pipette and sealed from the bath with uncured Sylgard, a viscous silicone resin (Fig 2). In these experimental conditions secreted fluid flowed from the open end of the isolated proximal segments at rates averaging 27.1 ± 3.2 pl per min per mm tubule length ($\bar{x} \pm s$, 19 collections, 12 tubules, 12 fish). Fluid secretion ranged from 9.8 to 56.6 pl min⁻¹ mm⁻¹ with no obvious correlation of secretion rate with the tubule's appearance. A conservative estimate for flounder proximal tubule length is 3 mm (ref. 8) which gives rates of *in vitro* fluid secretion (81 pl min⁻¹) and single nephron glomerular filtration (350-650 pl min⁻¹) within the same order of magnitude. For low filtration rates, proximal fluid secretion probably exceeds glomerular filtration as was observed in another glomerular flounder, *Paralichthys lethostigma*, in which urine flow rates were substantial (0.5 ml per kg per h) in the virtual absence of glomerular filtration (0.006 ml per kg per h)⁹.

The osmolalities of secreted fluid and the peritubular Ringer's were measured by freezing point depression (Clifton nanolitre osmometer) in nine experiments. In four experiments, secreted fluid was consistently isosmotic [292.1 ± 0.9 mOsm per kg H₂O ($\bar{x} \pm s$), $n = 8$ collections] to the bathing medium (290.5 ± 3.4 mOsm kg H₂O, $n = 13$). In the other five proximal segments, secreted fluid was hyperosmotic (318.4 ± 4.6 mOsm per kg H₂O, $n = 10$) to the bathing medium ($P < 0.001$). The highest osmolality in secreted fluid was 346.8 mOsm per kg H₂O. These data are consistent with the existence of two functionally distinct segments in flounder proximal tubules, as are thought to occur in the kidneys of marine fish¹⁰. Bulger and Trump have identified a proximal tubule I and a proximal tubule II in fixed

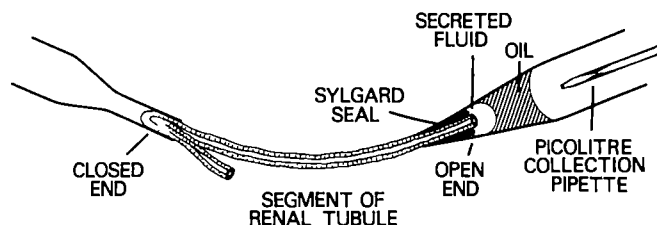


Fig 2 Collection of secreted fluid. Uncured Sylgard 124 (Dow Chemical) was used as a seal between the secreted fluid and the bath. Secreted fluid flowing from the tubule accumulated under oil and was collected every 30–40 min for analysis. Isolated segments of proximal tubules were usually between 1.2 and 2.0 mm long. Fluid secretion in any one tubule was rather constant for the duration of the experiment, in one case for as long as 18 h.

renal slices of another flounder, the English sole¹¹. In fixed renal slices of the winter flounder we have also observed two histologically distinct segments of the proximal tubule (unpublished observations). However, in the present study it was not possible to distinguish proximal tubules I and II during dissection and all data were pooled to describe the *in vitro* function of the flounder proximal tubule in general (Fig 3).

In 13 additional proximal tubule segments, the concentrations of Na, Cl, Mg and S (electron probe analysis measures the concentration of the element and not the ionic species) were measured in secreted fluid (SF), again in parallel with their corresponding concentrations in the peritubular bathing Ringer's (R)¹². Analysis of 22 SF/R sample pairs revealed that the Na concentration in SF was not significantly different from that in the bathing Ringer's, the 95% confidence interval of the Na SF/R ratio included unity (Fig 3). In contrast, the concentrations of Cl, Mg and S (SO_4^{2-} is probably secreted) in secreted fluid were significantly greater than in the bathing Ringer's. The 95% confidence intervals of these SF/R ratios did not include unity, but they were large, consistent with varying capacities for concentration in different segments of the proximal tubule. The ability of flounder renal tubules to generate and maintain transepithelial gradients for water and ions is consistent with previous measurements of their transepithelial electrical resistance¹³ which is higher ($22.3\text{--}53.0\ \Omega\text{cm}^2$) than that usually found in mammalian renal proximal tubules ($4.9\text{--}5.7\ \Omega\text{cm}^2$)¹⁴.

Previously, when evidence for fluid secretion was obtained in mammalian renal tubules⁶ and teleostean kidneys^{2,4,15}, it was thought that the secretion of organic acids⁶ or divalent ions created an osmotic driving force^{2,4,15}. However, in the isolated renal tubules described here, the presence of organic acids or divalent ions in the bathing medium was not necessary to support fluid secretion. Organic acids were not present in the flounder Ringer's solution used, and in four additional experiments in which MgSO_4 was deleted from the bathing medium fluid, secretion continued at rates ($18.2 \pm 3.1\ \text{pl min}^{-1}\text{mm}^{-1}$) that were indistinguishable from control (*t*-test, sample means).

The replacement of bath Na^+ with choline, a large cation, immediately and completely inhibited fluid secretion ($n=3$). Replacing choline-Ringer's with the original bathing medium (Na^+ -Ringer's) fully restored fluid secretion with the time course of the bath exchange ($<0.5\ \text{min}$). In contrast, when Na^+ in the bath was replaced with Li^+ , a small cation, fluid secretion continued in all tubules studied ($n=3$), but at progressively lower rates which paralleled the morphological deterioration of the tubule which occurred in Li^+ -Ringer's. Similarly, when Cl^- was replaced by a large anion (gluconate), fluid secretion immediately stopped ($n=4$). Fluid secretion returned to control rates on providing the original conditions in the bath. However, when bath Cl^- was replaced with a small substitute (Br^-), fluid secretion continued at rates indistinguishable from the control ($n=4$).

During this study some tubules were observed to constrict radially. The constrictions started as sharp invaginations of the basement membrane and extended radially towards the tubule

lumen. They occurred at single or multiple sites along the tubule. Some constrictions were sustained, others were periodic at about 3 cycles per minute. Peristalsis was not observed. Motion of axial cilia in the centre of the lumen was also occasionally seen. Solutions which stopped fluid secretion (Na^+ -free choline-Ringer's or Cl^- -free gluconate-Ringer's) also inhibited radial constrictions and ciliary motion. Solutions that restored fluid secretion (control bath) also restored tubule constrictions and ciliary motion. In tubules where radial constrictions and ciliary motion were not observed, the force of epithelial fluid secretion appeared to provide the hydrostatic pressure for axial flow. At present it is not clear whether myoepithelial cells or muscular layers^{10,16,17} are responsible for tubule constrictions. However, the constrictions were strong enough to move luminal fluid towards the open end of the tubule. Aiding axial flow in this manner might be a specialization of renal tubules that secrete fluid in glomerular kidneys having low filtration rates. In aglomerular kidneys radial constrictions might play an even greater part in the axial flow of luminal fluid.

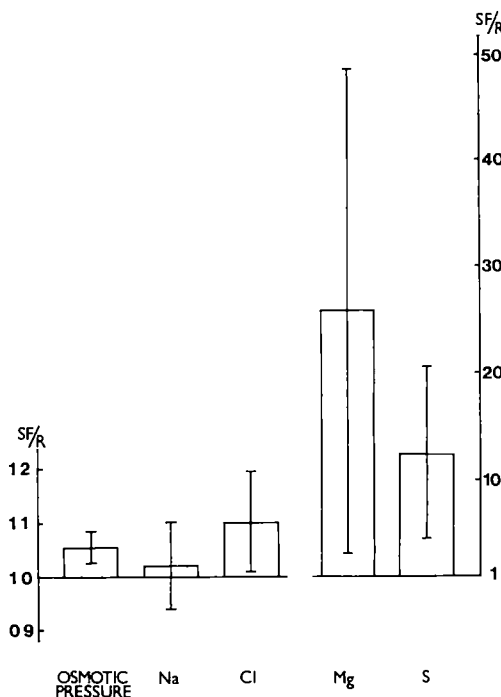


Fig 3 Osmotic pressures and the concentrations in secreted fluid (SF) and peritubular Ringer's (R) expressed as the ratio SF/R. Mean values and their 95% confidence intervals are shown for two series of experiments. In the first, the osmotic pressure was measured by freezing point depression (Clifton Nanolitre Osmometer) in 18 SF and R sample pairs collected in experiments with nine proximal tubule segments. In the second, the concentrations of Na, Cl, Mg and S were measured in 22 SF/R sample pairs obtained in the study of 13 proximal tubule segments. Concentrations were measured in $100\text{--}200 \times 10^{-12}\ \text{l}$ liquid droplets against appropriate standards (STD) of the same volume by electron probe analysis (X-ray wavelength dispersive spectroscopy, JEOL 733 Superprobe). Correlation coefficients of STD curves (chemical concentration versus X-ray counts) were high for Na, 0.97 ± 0.02 , $n=9$ STD curves, for Cl, 0.96 ± 0.02 , $n=10$, for Mg, 0.994 ± 0.005 , $n=11$, and for S, 0.998 ± 0.001 , $n=11$. Deviations of STD curves from the origin ($\pm 3\ \text{mM}$) gave rise to experimental error only in the measurement of concentrations close to zero, such as the known $1\ \text{mM}$ Mg and S concentrations in the Ringer's. Some X-ray measurements gave values less than $0.3\ \text{mM}$ for the known $1\ \text{mM}$ MgSO_4 in the Ringer's. To prevent these measurements from increasing SF/R ratios, they were rounded up to $1\ \text{mM}$, but values greater than $1\ \text{mM}$ were not rounded down, hence SF/R ratios for Mg and S are underestimates of the true ratios. All samples, SF, R and STD, were stored in Ringer's-equilibrated (alternatively in light paraffin oil equilibrated with Ringer's) light paraffin oil until they were crystallized for electron probe analysis according to the method of Bonventre *et al*.¹² Evaporation into oil occurred at rates ranging from 0.4 to $0.9\ \text{pl min}^{-1}$ for the $1\text{--}3\ \text{nl}$ volumes handled in this study and introduced experimental error ($<12\%$). However, errors due to evaporation and sample dehydration were adjusted for by taking identical volumes of SF, R and STD of each tubule experiment together through all storage and dehydration steps. The use of more than one SF/R sample pair per tubule did not affect the statistical significance of the results.

The present study has provided the first collection and analysis of fluid secreted by a proximal tubule. Although vertebrate proximal tubules usually do not generate measurable transepithelial osmotic pressure differences¹⁸⁻²⁰ these results show that some proximal segments secrete hyperosmotic fluid, which may have a bearing on the previous *in vivo* observations of hyperosmotic urine in other marine teleosts^{21,22}. While the data confirm tubular secretion of Mg and S in marine fish, they do not support the hypothesis that fluid secretion is driven by Mg and S secretion alone⁴. A NaCl-dependent mechanism of fluid secretion is also present. This mechanism was unexpected because proximal fluid secretion in conjunction with glomerular filtration does not fit the present concept of hypo-osmotic regulation through the renal conservation of water.

This work was supported in part by NIH grant AM 26633 to K W B. and NSF grant DEB 7826821 and NIH grant S07-RR-05764 to the Mt Desert Island Biological Laboratory. I thank Dr B. Schmidt-Nielsen at MDIBL for the use of the Clifton nanolitre osmometer and Mrs Linda Phelps for secretarial assistance.

Received 12 January, accepted 21 June 1982

- 1 Forster, R. P. *J. cell comp. Physiol.* **42**, 487-510 (1953)
- 2 Hickman, C. *Can. J. Zool.* **46**, 439-455 (1968)
- 3 Schmidt-Nielsen, B. & Renfro, J. L. *Am. J. Physiol.* **228**, 420-431 (1975)
- 4 Renfro, J. L. *Am. J. Physiol.* **238**, F92-F98 (1980)
- 5 Burg, M., Grantham, J., Abramow, M. & Orloff, J. *Am. J. Physiol.* **210**, 1293-1298 (1966)
- 6 Grantham, J. *J. Physiol. Rev.* **56**, 248-258 (1976)
- 7 Petzel, D. H. & DeVries, A. L. *Bull. Mt Desert Isl. Biol. Lab.* **20**, 17-18 (1980)
- 8 Nash, J. *Am. J. Anat.* **47**, 425-445 (1931)
- 9 Hickman, C. P. Jr. *Can. J. Zool.* **46**, 427-437 (1968)
- 10 Hickman, C. P. Jr. & Trump, B. F. in *Fish Physiology* Vol. 1 (eds Hoar, W. S. & Randall, D. J.) 91-239 (Academic, New York, 1969)
- 11 Bulger, R. E. & Trump, B. F. *Am. J. Anat.* **123**, 195-225 (1968)
- 12 Bonventre, J. V., Blouch, K. & Lechene, C. in *X-Ray Microscopy in Biology* (ed Mazat, M. A.) 307-366 (University Park Press, Baltimore, 1981)
- 13 Beyenbach, K. W., Booz, G. & Kleinzeller, A. *Bull. Mt Desert Isl. Biol. Lab.* **20**, 78-82 (1980)
- 14 Hegel, U., Fromter, E. & Wick, T. *Pflügers Arch. ges. Physiol.* **294**, 274-290 (1967)
- 15 Berglund, F. & Forster, R. P. *J. gen. Physiol.* **41**, 429-440 (1958)
- 16 Kinter, W. B. *Am. J. Physiol.* **211**, 1152-1164 (1966)
- 17 Townsley, P. M. & Scott, M. A. *J. Fish Res. Bd Can.* **20**, 243 (1963)
- 18 Giebisch, G. in *Physiology of Membrane Disorders* (eds Andreoli, T. E., Hoffman, J. F. & Fanestil, D. D.) 629-660 (Plenum, New York, 1978)
- 19 Morel, F. *J. Physiol., Paris* **72**, 515-530 (1976)
- 20 Schafer, J. A. *Fedn Proc.* **40**, 2450-2459 (1981)
- 21 Stanley, J. G. & Fleming, W. R. *Science* **144**, 63-64 (1964)
- 22 Vogel, V., Fischbach, H., Heinzel, W. & Bohle, A. *Pflügers Arch. ges. Physiol.* **312**, 91-98 (1969)

Absence of gonadotropin-releasing hormone receptors in human gonadal tissue

Richard N. Clayton

Department of Medicine, University of Birmingham, Edgbaston, Birmingham B15 2TH, UK

Ilopo T. Huhtaniemi

Department of Clinical Chemistry, University of Helsinki, SF-00290 Helsinki 29, Finland

The antifertility nature of the hypothalamic peptide gonadotropin releasing hormone (GnRH) and its synthetic agonist analogue (GnRH-A) has been repeatedly demonstrated in rodents, monkeys and humans (see ref. 1 for review). In all species studied, this action of GnRH was initially attributed to 'desensitization' of gonadal steroidogenesis due to loss of gonadotropin receptors in the testis and ovary, induced by high circulating levels of endogenous gonadotropins achieved following repeated administration of GnRH or GnRH-A²⁻⁵. Recently, an additional, direct inhibitory action of these peptides on ovarian granulosa^{6,7} and luteal⁸⁻¹⁰ and testicular Leydig¹¹⁻¹³ cells has been defined. This direct inhibition of gonadal steroidogenesis is mediated through specific high-affinity GnRH receptors in the respective target tissues^{8,9,12,14}. These receptors exhibit identical characteristics to GnRH receptors (GnRH-R)

in rodent anterior pituitary tissue^{9,12,14,15}. In the search for a naturally occurring ligand for gonadal GnRH-R, a biologically active 'GnRH-like' peptide has been isolated from rat ovary¹⁶ and testis^{17,18}, and from monkey testis interstitial fluid¹⁸. These findings suggest the production in rodent gonads of a GnRH-like peptide which, following interaction with gonadal GnRH-R, serves as a local modulator of steroidogenesis, and hence of reproductive capacity. If a similar situation exists in humans, GnRH-R should be detectable also in the human testis and ovary. We report here that we have been unable to detect any binding of radiolabelled GnRH-A to human corpus luteum or testis, or to the monkey testis. In contrast, GnRH-R were detected in adult and fetal human anterior pituitary tissue. Thus, we suggest that a direct inhibitory action of GnRH on primate reproductive function is unlikely. Furthermore, this important species difference highlights the need for a re-evaluation of certain rodent models designed to investigate primate, and especially human, reproductive physiology.

An area of considerable interest in reproductive biology concerns the apparently paradoxical antifertility nature of the natural hypothalamic-hypophysiotrophic hormone GnRH, responsible for the neural coordination of fertility. When administered to either laboratory animals or humans, either continuously or intermittently in high dosage, GnRH or its longer-acting agonist analogue (GnRH-A) interrupt normal cyclical ovarian activity, terminate established pregnancy, and inhibit testicular testosterone production and spermatogenesis (for review see ref. 1). In rodents, this inhibitory activity of GnRH is partly due to a direct action on ovarian and testicular steroidogenic cells. Recently, we and others (see ref. 14 for review) have reported that this extrapituitary action of GnRH and GnRH-A is mediated through specific receptor sites for the hormone either in the respective target cells, or in their cell membrane preparations.

To determine the presence of GnRH-R in primate gonadal tissue, we have used identical methods to those applied to measure rodent gonadal GnRH receptors. We used as the radioligand the iodinated GnRH agonist ¹²⁵I-GnRH-A¹⁴ which binds exclusively to high-affinity GnRH receptors in rat pituitary and gonads. Using this radioreceptor assay we have detected specific binding of the GnRH analogue to anterior pituitary membrane preparations from cadaver human glands (Table 1), despite the fact that these were removed 24-36 h postmortem at routine autopsy, and then stored at -70 °C before the assay. As considerable loss of GnRH receptors may have occurred during the time from death to freezing of the tissue, the antemortem content of pituitary GnRH receptors was probably considerably greater. We have been unable to obtain any fresh normal human pituitary tissue, although two samples of freshly obtained human pituitary adenomatous tissue were examined, neither of which contained GnRH-R (Table 1). One of these was a mixed acidophil chromophobe adenoma from a patient with acromegaly (growth hormone-secreting tumour), while the other specimen was a chromophobe adenoma secreting large quantities of prolactin. GnRH receptors were also detectable in homogenates from single human fetal pituitary glands obtained either from prostaglandin-induced abortions or at hysterotomy (Table 1). In the case of the former specimens, intra-uterine fetal death occurred 12-20 h before sample collection. However, when rat pituitaries were either collected and snap-frozen immediately after decapitation, or analysed without previous freezing and thawing, the binding of the ¹²⁵I-GnRH-A was much greater (Table 1). As this radioreceptor assay allowed detection of GnRH-R in human pituitary tissue obtained many hours after death, we used it as a method for measuring GnRH-R in fresh human gonadal tissue obtained at operation and frozen immediately. Before the radioreceptor assay, all gonadal tissues were treated in an identical manner to the human pituitaries.

There was no specific uptake of ¹²⁵I-GnRH-A by membranes prepared from corpora lutea obtained at various stages from the mid- to late-luteal phase of the menstrual cycle from six

Table 1 ^{125}I -GnRH-A binding to human and rat anterior pituitary tissue

Tissue source	mg Protein per tube	c p m Bound			Total c p m added (T)	SB/T ×100
		Bo	NSB	Specific (Bo-NSB)		
Cadaver pit (♀, 61 yrs)	1.2	1,191 ± 21(3)	788 ± 69(3)	403	16,412	2.46
Cadaver pit (♀, 30 yrs)	1.4	5,030 ± 143(2)	4,173 ± 13(2)	856	47,809	1.79
Cadaver pit (♂, 73 yrs)	1.1	4,867 ± 6(2)	4,098 ± 88(2)	769	47,809	1.61
Cadaver pit (♀, 72 yrs)	1.2	1,027 ± 12(5)	829 ± 10(5)	198	7,955	2.49
Cadaver pit (♀, 53 yrs)	0.76	797 ± 10(5)	667 ± 16(5)	129	7,955	1.62
Cadaver pit (♂, 40 yrs)	1.1	1,001 ± 14(5)	752 ± 25(3)	249	9,118	2.73
Pituitary adenoma (acidophil) (♂, 42 yrs)	0.55	2,581 ± 113(2)	2,780 ± 269(2)	ND	47,809	—
Pituitary adenoma (prolactinoma) (♀, 56 yrs)	0.69	410 ± 11(3)	395 ± 31(2)	ND	7,955	—
Fetal pit (♂, 18 weeks)*	0.19	1,045 ± 82(3)	833 ± 37(2)	217	16,412	1.32
Fetal pit (♀, 17 weeks)*	0.154	1,355 ± 130(2)	740 ± 38(2)	615	16,412	3.75
Fetal pit (♀, 18 weeks)*	0.135	909 ± 87(3)	528 ± 12(2)	381	15,525	2.45
Fetal pit (♂, 14 weeks)*	0.29	726 ± 6(2)	422(1)	303	7,955	3.8
Fetal pit (♀, 16 weeks)†	0.29	394 ± 6(2)	319 ± 11(2)	75	7,955	0.94
Rat pit ‡	0.092	7,925 ± 179(2)	1,655 ± 339(2)	6,270	47,809	13.11
Rat pit §	0.21	4,724 ± 107(3)	856 ± 73(2)	3,868	16,412	23.6
Rat pit §	0.165	4,511 ± 181(3)	1,113 ± 17(2)	3,398	15,525	21.9
Rat pit ‡	0.57	2,614 ± 48(2)	566 ± 26(2)	2,048	7,955	25.7
Rat pit ‡	0.59	1,777 ± 40(2)	515 ± 36(2)	1,261	7,955	15.86

Cadaver human pituitary (cadaver pit) tissue was obtained, from routine autopsy for non-pituitary-related disease, between 24 and 36 h post mortem, and snap-frozen following separation of the neurohypophysis. Human pituitary adenoma tissue was obtained at hypophysectomy and immediately snap-frozen in liquid nitrogen (the predominant histological staining pattern is indicated). Human fetal pituitaries were obtained after prostaglandin-induced abortion (*), or hysterotomy (†) and snap-frozen as soon as they were removed from the abortuses. Their sex and approximate gestational age are indicated in parentheses. Male rat pituitaries (Sprague-Dawley rats) were obtained immediately after decapitation and analysed without previous freezing (§), or were snap-frozen then thawed immediately before assay (‡). After snap-freezing all tissue was stored at -70°C for 1–4 weeks before assay, this does not result in any loss of rat pituitary GnRH-R¹⁴. Membrane preparations from the adult human pituitaries were prepared by homogenization (in an Ultra-Turax homogenizer) of the minced tissue in 10 mM Tris-HCl pH 7.5 containing 1 mM dithiothreitol (DTT). After initial centrifugation at 1,000g for 10 min (in a Sorval RC5B centrifuge), the membranes were precipitated from the supernatant by centrifugation at 25,000g for 30 min. The membrane pellet was re-homogenized in a small volume (1–2 ml) of 10 mM Tris-HCl and filtered through nylon gauze before use in the radioreceptor assay. All preparative procedures were performed at 4°C . Individual human fetal and rat pituitaries were homogenized, on ice, in 0.5 ml of 10 mM Tris-HCl and an aliquot of the unfractionated homogenate used for GnRH-R analysis. 100 μl of membrane or homogenate preparation were incubated with 100 μl of ^{125}I -GnRH-A ($1\text{--}3 \times 10^{-11}\text{ M}$) with (NSB, nonspecific binding) or without (total binding, Bo) a 1,000-fold excess of unlabelled GnRH-A in a total volume of 300 μl of assay buffer (10 mM Tris-HCl, 1 mM DTT, 0.1% bovine serum albumin, BSA) at 4°C for 90 min. The reaction was stopped by dilution (15-fold) with phosphate-buffered saline (PBS, pH 7.5) and the membrane fragments were separated (under vacuum) by filtration, through Whatman GF/C glass fibre filters, pre-soaked in 1% BSA to reduce nonspecific binding. After washing with 20 ml PBS, the filters were dried and counted in a γ -spectrometer with a counting efficiency of 60%. Specific binding (SB) = Bo - NSB and is expressed as a percentage (SB/T × 100) of total bindable counts added (maximum possible binding of ^{125}I GnRH-A = 50% of added c p m). Samples having the same total c p m were analysed in the same radioreceptor assay, a positive rat pituitary control was used in each assay. Values shown are the mean ± s.e., the number of replicates is shown in parentheses. Differences between Bo and NSB counts for each sample were analysed by unpaired Student's *t*-test and were considered significant if $P < 0.05$. ND, $P > 0.05$. On this basis, all human cadaver pituitary samples exhibited specific ^{125}I -GnRH-A binding. The average minimum significant difference between Bo and NSB counts (defined as 2 s.d. below the mean of Bo replicates) was $\sim 175\text{ c p m}$.

Table 2 ^{125}I -GnRH-A binding to human and rat ovarian tissue

Tissue source	mg Protein per tube	c p m Bound			Total c p m added (T)	SB/T ×100
		Bo	NSB	Specific (Bo-NSB)		
a						
Human corpus luteum 1	3.38	458 ± 11(3)	447 ± 15(4)	ND	9,625	—
Human corpus luteum 2	2.5	631 ± 27(3)	519 ± 23(4)	ND	9,625	—
Human corpus luteum 3	2.4	830 ± 74(3)	774 ± 50(4)	ND	16,194	—
Human corpus luteum 4	2.6	890 ± 28(4)	842 ± 9(5)	ND	8,491	—
Human corpus luteum 5	1.62	783 ± 68(5)	822 ± 62(5)	ND	8,491	—
Human corpus luteum 6	1.55	568 ± 26(5)	558 ± 15(5)	ND	8,491	—
b						
Human corpus luteum 7	0.43	2,830 ± 242(5)	2,748 ± 185(5)	ND	15,271	—
Human corpus luteum 8	0.77	3,999 ± 248(6)	4,057 ± 168(6)	ND	33,185	—
Human corpus luteum 9	1.07	1,794 ± 62(6)	1,919 ± 48(6)	ND	17,501	—
Human corpus luteum 10	0.13	1,541 ± 25(3)	1,548 ± 134(3)	ND	20,214	—
c						
Rat ovaries 1 (random cycle)	2.57	1,444 ± 39(4)	577 ± 17(5)	867	9,118	9.50
Rat ovaries 2 (random cycle)	2.62	2,000 ± 55(5)	841 ± 18(5)	1,159	8,491	13.65
Rat ovaries 1 (luteinized)	2.98	1,304 ± 65(3)	528 ± 33(4)	776	9,625	8.06
Rat ovaries 2 (luteinized)	2.53	1,436 ± 56(3)	528 ± 33(4)	909	9,625	9.44
Rat ovaries 3 (luteinized)	1.3	1,721 ± 76(3)	647 ± 36(3)	1,073	16,194	6.6

a, Human corpora lutea were individually excised as discrete tissue, without surrounding ovarian stroma, during laparotomy for either tubal reconstructive surgery, hysterectomy for uterine myoma, or endometriosis. Corpora lutea were obtained from the mid-late luteal phase of the menstrual cycle, the patients had not received any hormonal treatment in the 6 months before surgery. Corpus luteum tissue was immediately rinsed in ice-cold PBS, pH 7.4 to remove any adherent blood clot, snap-frozen in liquid nitrogen without further processing, then stored at -70°C for 1–4 weeks before assay. When required for assay, ovarian membranes were prepared from the frozen tissue as described in Table 1 legend **b**. As in **a** except that membranes were prepared from freshly obtained corpora lutea within 40 min of their removal from patients, without freezing or storage of the tissue, and assayed immediately. **c**, Rat ovaries were obtained from adult female animals at random stages of their oestrous cycles (random cycles) and from 25-day-old immature females treated with 50 IU of PMSG (pregnant mare serum gonadotropin, Organon) followed 5 days later by 25 IU of HCG and were killed 3 days later. These ovaries consist predominantly of luteinized follicles (luteinized ovaries). Rat ovarian tissue was frozen and thawed in the same way as for human tissue. Membrane preparations were prepared, incubated with ^{125}I -GnRH-A and the results expressed as described for Table 1. The common total c p m indicates that all tissues were analysed in the same assay, each of which incorporated positive rat ovarian membrane and pituitary homogenate controls. The average minimum significant difference between Bo and NSB counts was $\sim 170\text{ c p m}$.

Table 3 ^{125}I -GnRH-A binding to human, monkey and rat testicular tissue

Tissue source	mg Protein per tube	c p m Bound			Total c p m added (T)	SB/T $\times 100$
		Bo	NSB	Specific (Bo-NSB)		
Human testis 1	2.18	1,185 \pm 21(5)	1,141 \pm 10(5)	ND	9,439	—
Human testis 2	3.46	929 \pm 44(3)	987 \pm 25(3)	ND	9,740	—
Human testis 3	3.55	951 \pm 1(2)	974 \pm 14(2)	ND	9,740	—
Human testis 4	5.87	922 \pm 100(3)	838 \pm 25(4)	ND	14,564	—
	2.96	943 \pm 7(3)	961 \pm 54(4)	ND	14,564	—
Human testis 5	4.4	873 \pm 48(3)	838 \pm 25(4)	ND	14,564	—
	2.31	854 \pm 43(3)	960 \pm 54(4)	ND	14,564	—
Monkey testis 1	2.0	348 \pm 10(5)	334 \pm 6(5)	ND	9,439	—
Monkey testis 2	1.63	538 \pm 12(5)	573 \pm 15(5)	ND	9,439	—
Monkey testis 3	4.40	313 \pm 13(5)	283 \pm 4(5)	ND	9,439	—
Rat testis 1	4.6	767 \pm 12(5)	561 \pm 16(5)	207	9,439	2.19
Rat testis 2	5.53	888 \pm 62(3)	587 \pm 13(3)	301	14,564	2.07
Rat testis 3	4.84	751 \pm 39(3)	562 \pm 9(3)	189	14,564	1.3
Rat testis 4	5.44	742 \pm 55(6)	515 \pm 28(3)	226	9,740	2.32

Human testes were obtained from 60–80-yr-old patients at orchidectomy representing primary treatment for prostatic carcinoma. None had received previous hormone therapy with oestrogen. Monkey (*Macaca fascicularis*) testes were obtained from healthy adult animals during orchidectomy for experimental purposes. The testes were immediately snap-frozen in liquid nitrogen, without processing, and stored at -70°C for 1–4 weeks before membrane preparation and analysis. Testes from adult rats were frozen and stored in the same way as the primate specimens. Membrane preparations were prepared and incubated with ^{125}I -GnRH-A as described for Table 1. The average minimum detectable difference between Bo and NSB counts was ~ 130 c p m (2 s.d. less than the mean Bo).

individuals (Table 2), despite the presence of more membrane protein than for human cadaver anterior pituitary tissue. Fresh, unfrozen human corpora lutea analysed immediately after removal from the patients, were also devoid of GnRH receptors (Table 2). Thus, it is unlikely that the procedure of freezing and storage destroyed GnRH-R. Additionally, membrane preparations from whole, pre-menopausal human ovaries were devoid of GnRH receptors (data not shown), while identical membrane preparations from either fully luteinized rat ovaries or ovaries obtained from rats at random stages of their oestrous cycles contained many GnRH receptors. In each assay containing human ovarian tissue, at least one rat ovarian preparation and one rat pituitary homogenate preparation were included as positive controls. That the human corpus luteum membranes contained steroidogenic tissue was indicated by the presence of luteinizing hormone (LH) receptors, identified by binding of ^{125}I -HCG (human chorionic gonadotropin), in an aliquot of the preparation (data not shown).

Human and monkey testis membrane preparations also did not appear to interact with the labelled GnRH analogue (Table 3). Five different testicular preparations, obtained at orchidectomy performed as primary treatment for prostatic carcinoma, were all negative (Table 3). None of these patients had received previous hormonal (oestrogen) therapy. Similarly, no ^{125}I -GnRH-A binding was demonstrable in testis membrane preparations from three adult monkeys, obtained at orchidectomy (Table 3). Because the primate tissue had been rapidly frozen on removal, no attempt was made to separate the seminiferous tubules, which have no GnRH receptors, from the interstitial tissue, which in the rat is the only compartment exhibiting GnRH-R¹⁹. However, in one experiment in which fresh human testis was enzymatically dispersed to yield predominantly Leydig cells, there was no detectable GnRH binding, while an identical interstitial cell preparation from fresh rat testes was positive. In addition, the four rat testis membrane preparations, which were positive for GnRH-R (Table 3) comprised both tubular and interstitial cell elements as they had been stored and were prepared in an identical manner to the human samples. As with the human corpora lutea, human and monkey membrane preparations contained Leydig cell elements as evidenced by the presence of ^{125}I -HCG binding.

Thus, we have been unable to demonstrate the presence of any GnRH receptors in human corpora lutea using the most sensitive method available for detection of GnRH-R in pituitary and gonadal tissues. It is possible that the concentration of GnRH-R in human gonads is so low as to be unmeasurable by these techniques, but this seems unlikely. Indeed, using very similar methodology, Asch *et al.*²⁰ were unable to detect any GnRH analogue binding in monkey corpora lutea. Further-

more, they failed to show any effect of a GnRH agonist on progesterone production by acutely dispersed monkey luteal cells *in vitro*²¹. Similarly, human granulosa cell steroidogenesis *in vitro* was unaffected by either GnRH or an agonist analogue²². Although there has been one report²³ of direct inhibition of progesterone production for human granulosa cultured in the presence of a GnRH agonist analogue, this did not occur until after 96 h in culture. Further, the granulosa cells were exposed to concentrations of exogenous gonadotropin higher than that to which they would be exposed *in vivo* and this might alter their steroidogenic response pattern. In contrast, the inhibitory effects of GnRH peptides on steroidogenesis are observed immediately when rat luteal cells^{8,10}, rat granulosa cells^{6,7}, and porcine granulosa cells²⁴ are similarly incubated with GnRH or GnRH-A *in vitro*. Therefore, in the human and non-human primate it seems unlikely that the antifertility effect of this group of peptides involves a direct gonadal site of action. A similar conclusion might also apply to the mouse, as in this species no GnRH effect on Leydig cell function can be demonstrated *in vitro* and receptors for this peptide are also absent²⁵. It is possible that the laboratory rat is not representative of other species in respect of the direct gonadal effect of GnRH. Hence data from such studies in rats may not be applicable to primates. Specifically, we infer, from the data reported here, that human gonadal tissue may not produce any 'GnRH-like' material acting as an intragonadal modulator of reproductive function.

We thank the gynaecologists in Birmingham, Oulu and Helsinki for providing us with human ovarian tissue, and the various surgeons for providing the human testis specimens. This work was supported by grants from the MRC (to R.N.C.), the Finnish Academy (to I.T.H.) and the British Council Academic Links and Interchange Scheme (R.N.C. and I.T.H.).

Received 2 March, accepted 7 July 1982

- 1 Hsueh, A. J. W. & Jones, P. B. C. *Endocr Rev* 2, 437–461 (1981)
- 2 Hsueh, A. J. W., Dufau, M. L. & Catt, K. J. *Proc natn Acad Sci USA* 74, 592–595 (1977)
- 3 Sharpe, R. M. *Nature* 264, 644–646 (1976)
- 4 Conti, M., Harwood, J. P., Hsueh, A. J. W., Dufau, M. L. & Catt, K. J. *J biol Chem* 251, 7729–7731 (1976)
- 5 Rao, M. C., Richards, J. S., Midgley, A. R. & Reichert, L. E. *Endocrinology* 101, 512–523 (1977)
- 6 Hsueh, A. J. W. & Erickson, G. F. *Science* 204, 854–855 (1979)
- 7 Hsueh, A. J. W., Wang, C. & Erickson, G. F. *Endocrinology* 106, 1697–1705 (1980)
- 8 Clayton, R. N., Harwood, J. P. & Catt, K. J. *Nature* 282, 90–93 (1979)
- 9 Harwood, J. P., Clayton, R. N. & Catt, K. J. *Endocrinology* 107, 407–413 (1980)
- 10 Behrman, H. R., Preston, S. L. & Hall, A. K. *Endocrinology* 107, 656–664 (1980)
- 11 Hsueh, A. J. W. & Erickson, G. F. *Nature*, 281, 66–67 (1979)
- 12 Clayton, R. N., Katikineni, M., Chan, V., Dufau, M. L. & Catt, K. J. *Proc natn Acad Sci USA* 77, 4459–4463 (1980)
- 13 Hsueh, A. J. W., Schreiber, J. R. & Erickson, G. F. *Molec cell Endocr* 21, 43–49 (1981)
- 14 Clayton, R. N. & Catt, K. J. *Endocr Rev* 2, 186–209 (1981)
- 15 Reeves, J. J., Sequin, C., Lefebvre, F.-A., Kelly, P. A. & Labrie, F. *Proc natn Acad Sci USA* 77, 5567–5571 (1980)

16. Ying, S. Y., Ling, N., Böhlen, P. & Gueillemin, R. *Endocrinology* **108**, 1206, 1215 (1981).
17. Sharpe, R. M. & Fraser, H. M. *Nature* **287**, 642-643 (1980).
18. Sharpe, R. M., Fraser, H. M., Cooper, I. & Rommerts, F. F. G. *Nature* **290**, 785-787 (1981).
19. Bourne, G. A., Regiani, S., Payne, A. H. & Marshall, J. C. *J. clin. Endocr. Metab.* **40**, 407-409 (1980).
20. Asch, R. H. *et al.* *J. clin. Endocr. Metab.* **53**, 215-217 (1981).
21. Asch, R. H., Smith, C. G., Almirex, R. G. & Schally, A. V. 27th a. Meet. for Gynaecological Investigation, Denver, Abstr. 891 (1980).
22. Casper, R. F., Erickson, G. F., Rebar, R. W. & Yen, S. S. C. *Fert. Steril.* **37**, 406-409 (1982).
23. Tureck, R. W., Mastroianni, L., Blasco, L. & Strauss, J. F. *J. clin. Endocr. Metab.* **55**, 1078-1080 (1982).
24. Massicotte, J., Veilleux, R., Lavoie, M. & Labrie, F. *Biochem. biophys. Res. Commun.* **94**, 1362-1366 (1980).
25. Hunter, M. G., Sullivan, M. H. F., Dix, C. J., Aldred, L. F. & Cooke, B. A. *Molec. cell. Endocr.* **27**, 31-44 (1982).

A fragment of the SV40 large T-antigen gene transforms

Christine E. Clayton*, David Murphy, Michael Lovett† & Peter W. J. Rigby

Cancer Research Campaign, Eukaryotic Molecular Genetics Research Group, Department of Biochemistry, Imperial College of Science and Technology, London SW7 2AZ, UK

SV40-transformed cells retain and express all the sequences encoding large T antigen¹; this protein, in its entirety, appears to be essential for transformation^{1,2}. We have isolated³ a segment of integrated viral DNA (SV3T3-20-G) which encodes only the N-terminal half of T antigen but is capable of transforming rat fibroblasts. SV3T3-20-G-transformed cells synthesize a truncated T antigen of apparent molecular weight (MW) 48,000. The sequence of the virus-host junction shows that this protein is partially encoded by the flanking mouse DNA and suggests that the SV40 DNA has integrated next to a mouse gene. The mouse DNA segment of SV3T3-20-G is not required for transformation although transcription of these flanking sequences may be activated by the insertion of viral DNA.

The SV40 early transcription unit is transcribed in productively infected permissive cells into two mRNAs with identical 5' and 3' termini but different splices² (Fig. 1). The larger, 2.6 kilobase (kb) mRNA encodes small t antigen, a protein of apparent MW 17,000 which is not essential for transformation⁴⁻⁶ but which may, in some circumstances, have an enhancing role^{1,7,8}. The smaller, 2.3 kb mRNA encodes large T antigen, a protein of apparent MW 94,000 which is found predominantly in the nuclei of transformed cells and is essential for transformation^{1,2}. This protein has many functions⁹⁻²¹ but it is not clear which of its functions is directly involved in the transformation of non-permissive cells.

SV3T3-20-G is a segment of integrated viral DNA cloned from the genome of the SV3T3 C120 line of SV40-transformed BALB/c 3T3 cells³. This 8.5 kb *EcoRI* fragment (Fig. 1) contains 3.3 kb of viral DNA and 5.2 kb of mouse DNA, which includes a sequence element present many times in the mouse genome (P. Brickell, D. S. Latchman and P. W. J. R., unpublished data). The viral DNA segment extends from the *EcoRI* site (nucleotide 1,782; according to the system of ref. 2) through the 5' half of the late transcription unit and the origin of DNA replication and into the 5' half of the early transcription unit. The viral DNA is interrupted by a junction with cellular DNA located at the beginning of the region in which the *tsA* mutations map²². It thus lacks many of the viral sequences thought to be essential for transformation^{1,2}. We were therefore surprised to find that when pSV3T3-20-G (the SV3T3-20-G *EcoRI* fragment cloned into the *EcoRI* site of pAT153) was introduced into rat-1 cells by calcium phosphate-mediated DNA transfection^{23,24}, foci of morphologically transformed cells arose (Fig. 2) at a frequency of 5 per μg DNA per 10^6 cells, a frequency $\sim 1\%$ of that obtained with intact SV40 DNA²³.

* Present addresses: Department of Biochemistry, Stanford University Medical Center, Stanford, California 94305, USA; † Department of Pediatrics, University of California Medical School, San Francisco, California 94143, USA.

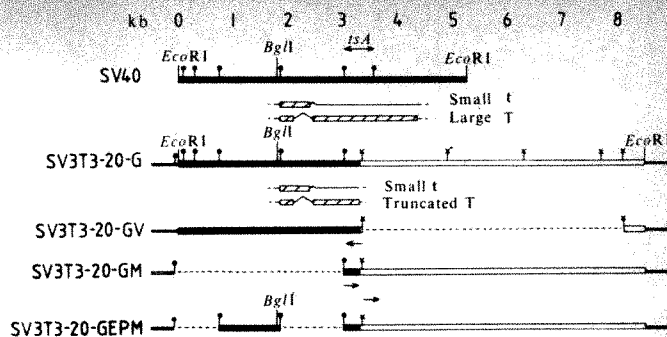


Fig. 1 Structures of pSV3T3-20-G and recombinants derived from it. At the top is shown the restriction map of SV40 DNA², linearized at the single *EcoRI* site. *HindIII* sites are marked †; the double-headed arrow indicates the *HindIII* fragment in which most *tsA* mutations map²². Also shown are the structures of the two early mRNAs found in productively infected permissive cells². \square , Translated sequences; \square , untranslated sequences; \sim , splices. The map of SV3T3-20-G is adapted from ref. 3; *XbaI* sites are marked \times . \blacksquare , SV40 DNA; \square , mouse DNA; --- , vector (pAT153) DNA. The two RNAs shown below are transcribed from the SV40 early promoter of this template (ref. 27 and M.L. and P.W.J.R., unpublished data). pSV3T3-20-GV and pSV3T3-20-GM were constructed by digesting pSV3T3-20-G to completion with *XbaI* and *HindIII* respectively, religating the digested DNA and transforming³ it into *Escherichia coli* HB101. pSV3T3-20-GEPM was constructed by inserting the *HindIII*-C fragment of SV40 DNA into the unique *HindIII* site of pSV3T3-20-GM. The DNA sequence of the virus-host junction was determined^{27,40} by sequencing from the *HindIII* and *XbaI* sites as indicated by the arrows.

Foci induced by pSV3T3-20-G appear about 10 days after those induced by the complete SV40 early region and are morphologically quite distinct, being flatter and less clearly delineated. Cells cloned from such foci are able to overgrow a monolayer of normal cells, have a more rounded morphology than the parental fibroblasts and multiply rapidly in medium containing 2% (v/v) fetal calf serum. This type of transformation has no precedent and we therefore examined the SV3T3-20-G DNA for unusual properties, first by determining the DNA sequence across the virus-host junction.

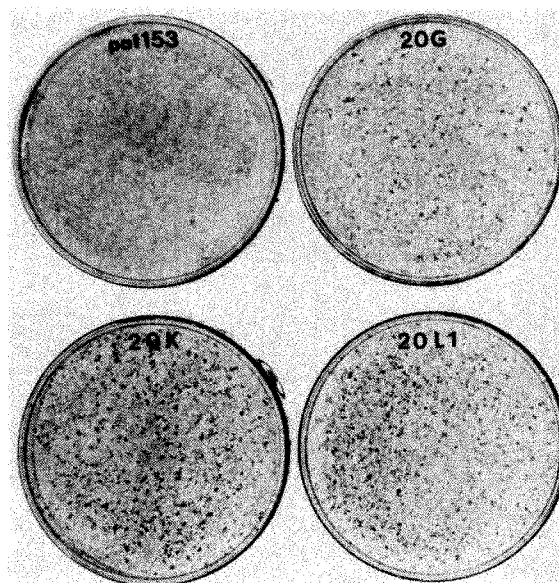


Fig. 2 Transformation by pSV3T3-20-G. Plasmid DNA (40 μg) was transfected into confluent monolayers of rat-1 cells grown on 50-mm dishes using a slight modification²³ of the calcium phosphate co-precipitation technique²⁴. Cells were maintained as monolayers in Dulbecco modified Eagle's medium supplemented with 5% (v/v) fetal calf serum and antibiotics. The dishes were fixed and stained²³ 30 days after transfection. Cells were transfected with vector (pAT153) DNA, pSV3T3-20-G and two other recombinant plasmids (pSV3T3-20-K and pSV3T3-20-L1) which contain tandem duplications in the viral early transcription unit and which transform as well as, if not better than, wild-type SV40 DNA²³.

We constructed subclones containing the virus-host junction, together with either the entire viral (pSV3T3-20-GV) or mouse chromosomal (pSV3T3-20-GM) segments, and determined the junction sequence as indicated in Fig. 1. The sequence obtained shows several interesting features (Fig. 3). An mRNA transcribed from the SV40 early promoter of SV3T3-20-G and containing the large T-antigen splice could be translated in the large T reading frame for 23 nucleotides beyond the virus-host junction, which occurs at SV40 nucleotide 3,713. Such a transcript would encode a truncated T antigen of calculated MW 45,000, the seven C-terminal amino acids of which are encoded by the flanking mouse DNA. Ten nucleotides beyond the translational stop codon is the sequence TATAAA which is one base removed from the canonical polyadenylation signal AATAAA^{25,26}. Transcripts of the size predicted if polyadenylation occurs at this site are found in SV3T3 C120 (ref. 27 and M.L. and P.W.J.R., unpublished data) and in cells transformed by pSV3T3-20-G (data not shown). In addition, cells transformed by pSV3T3-20-G contain the predicted truncated T antigen, which has an apparent MW of 48,000 (Fig. 4) and is also found in SV3T3 C120 (ref. 27). This protein may therefore be capable of inducing transformation.

An alternative explanation for our data was that the integration of the SV40 DNA had activated the adjacent DNA which contains a cellular transforming gene, a possibility strengthened by the sequence of the flanking mouse DNA (Fig. 3). Close to the virus-host junction there is a perfect consensus 'TATA' box, a feature of the 5' ends of eukaryotic RNA polymerase II transcription units²⁸. A sequence closely related to the consensus mRNA cap site²⁸ is located 34 nucleotides downstream of the first T of the 'TATA' box and this is followed, 42 nucleotides from what would be the initiating nucleotide, by an ATG triplet which marks the beginning of an open reading frame. It thus appears possible that the SV40 DNA has integrated next to a cellular gene. Neither we (D.M. and P.W.J.R., unpublished data) nor others^{29,30} have observed anything similar in other SV40-host DNA junctions.

We therefore attempted to transform cells with the viral and cellular segments in isolation. We also constructed an additional plasmid, pSV3T3-20-GEPM (Fig. 1), in which the segment of

T	Arg	Phe	Asn	Asp	Leu	Tyr	Pro	Gln	Ser	Thr
5'	AGA	TTT	AAT	GAT	CTT	TAT	CCC	GAA	AGC	ACC
3'	TCT	AAA	TTA	CTA	GAA	ATA	GGG	CTT	TCG	TGG
	3728					3713				
Poly(A) signal?										
'TATA' box										
Val	Leu	Stop								
GAG	CTT	TGA	CCA	GCT	GGC	TAT	AAA	ATG	GAG	
CTC	GAA	ACT	GGT	CGA	CCG	ATA	TTT	TAC	CTC	
Cap site??										
GCT	TCC	CCC	ATC	TCT	CTC	TGG	TCC	GCA	AAT	
CGA	AGG	GGG	TAG	AGA	GAG	ACC	AGG	CGT	TTA	
XbaI										
ACT	CTA	GAC	CGC	GCT	CGC	TCA	TCT	CTC	AGC	
TGA	GAT	CTG	GCG	CGA	GCG	AGT	AGA	GAG	TCG	

transfected DNA lacked both the termination codon for large T antigen and the polyadenylation site, so expression of a large T antigen-related protein could only occur if the integration event served to restore these control signals, a process which is certain to be extremely inefficient. In SV3T3-20-G the virus-host fusion required has already occurred.

When stained³⁷ for SV40 T antigen using the monoclonal antibody PAb419, which recognizes a determinant common to small and large T antigens³⁸, cells transformed by pSV3T3-20-G stain weakly in both nucleus and cytoplasm. The lack of nuclear retention suggests that the truncated T antigen may have a reduced ability to bind to DNA. It clearly does not bind to the cell-coded p53 protein (Fig. 4).

Colby and Shenk have recently shown³⁹ that SV40 genomes containing deletions which remove sequences coding for the C-terminal half of large T antigen, including the termination codon but not the polyadenylation signal, can immortalize rat embryo cells. Some of the cell lines thus generated have a fully transformed phenotype. The portion of the T antigen gene contained in their constructs is almost identical to that in SV3T3-20-G. However, their cell lines contain unstable T antigens whereas that encoded by SV3T3-20-G seems to be stable, a difference which may be due to the absence of the termination codon in their mutants. More surprising is the observation that their cell lines contain high levels of p53 whereas cells transformed by pSV3T3-20-G do not. These two sets of data clearly establish that the N-terminal half of large T antigen can mediate both immortalization and transformation. Our assay system is different from that used by Colby and Shenk and further studies are therefore required to explain the differences between the two sets of results.

The protein encoded by SV3T3-20-GV may transform through a hitherto unsuspected and novel property of large T antigen, perhaps by a mechanism quite distinct from that used by the intact protein. This idea is consistent with the fact that foci induced by pSV3T3-20-G are clearly distinguishable from those induced by intact SV40 DNA. The structure of SV3T3-20-G and our preliminary transcription data also raise the possibility that the integration of SV40 DNA may lead to the activation of adjacent cellular sequences.

We thank Wendy Colby and Tom Shenk for communicating unpublished data. D. M. holds a MRC research studentship and P. W. J. R. a Career Development Award from the CRC which also paid for this work.

Received 9 March; accepted 24 June 1982.

- Martin, R. G. *Adv. Cancer Res.* **34**, 1-68 (1981).
- Toozee, J. *Molecular Biology of Tumor Viruses*. Pt. 2. DNA Tumor Viruses 2nd edn (Cold Spring Harbor Laboratory, New York, 1981).
- Clayton, C. E. & Rigby, P. W. J. *Cell* **25**, 547-559 (1981).
- Lewis, A. M. Jr & Martin, R. G. *Proc. natn. Acad. Sci. U.S.A.* **76**, 4299-4302 (1979).
- Martin, R. G., Setlow, V. P., Edwards, C. A. F. & Vembu, D. *Cell* **17**, 635-643 (1979).
- Topp, W. C., Rifkin, D. B. & Sleight, M. J. *Virology* **111**, 341-350 (1981).
- Graessmann, A., Graessmann, M., Tjian, R. & Topp, W. C. *J. Virol.* **33**, 1182-1191 (1980).
- Topp, W. C. & Rifkin, D. B. *Virology* **106**, 282-291 (1980).
- Shortle, D. R., Margolske, R. F. & Nathans, D. *Proc. natn. Acad. Sci. U.S.A.* **76**, 6128-6131 (1979).
- Myers, R. M. & Tjian, R. *Proc. natn. Acad. Sci. U.S.A.* **77**, 6491-6495 (1980).
- McKay, R. & Di Maio, D. *Nature* **289**, 810-813 (1981).
- Oren, M., Winocour, E. & Prives, C. *Proc. natn. Acad. Sci. U.S.A.* **77**, 220-224 (1980).
- Tjian, R., Fey, G. & Graessmann, A. *Proc. natn. Acad. Sci. U.S.A.* **75**, 1279-1283 (1978).
- Rio, D., Robbins, A., Myers, R. & Tjian, R. *Proc. natn. Acad. Sci. U.S.A.* **77**, 5706-5710 (1980).
- Myers, R. M., Rio, D. C., Robbins, A. K. & Tjian, R. *Cell* **25**, 373-384 (1981).
- Soprano, K. J., Dev, V. G., Croce, C. M. & Baserga, R. *Proc. natn. Acad. Sci. U.S.A.* **76**, 3885-3889 (1979).
- Soprano, K. J., Rossini, M., Croce, C. & Baserga, R. *Virology* **102**, 317-326 (1980).
- Giachero, D. & Hager, L. P. *J. biol. Chem.* **254**, 8113-8116 (1979).
- Clark, R., Lane, D. P. & Tjian, R. *J. biol. Chem.* **256**, 11854-11858 (1981).
- Lane, D. P. & Crawford, L. V. *Nature* **278**, 261-263 (1979).
- Linzer, D. I. H. & Levine, A. J. *Cell* **17**, 43-52 (1979).
- Lai, C.-J. & Nathans, D. *Virology* **66**, 70-81 (1975).
- Clayton, C. E., Lovett, M. & Rigby, P. W. J. *J. Virol.* (in the press).
- Wigler, M. *et al. Proc. natn. Acad. Sci. U.S.A.* **76**, 1373-1376 (1979).
- Proudfoot, N. J. & Brownlee, G. *Nature* **263**, 211-214 (1976).
- Fitzgerald, M. & Shenk, T. *Cell* **24**, 251-260 (1981).
- Lovett, M. *et al. J. Virol.* (in the press).
- Corden, J. *et al. Science* **209**, 1406-1414 (1980).
- Botchan, M., Stringer, J., Mitchison, T. & Sambrook, J. *Cell* **20**, 143-152 (1980).
- Stringer, J. R. *J. Virol.* **38**, 671-679 (1981).
- Benoist, C. & Chambon, P. *Nature* **290**, 304-310 (1981).
- Mathis, D. J. & Chambon, P. *Nature* **290**, 310-315 (1981).
- Banerji, J., Rusconi, S. & Schaffner, W. *Cell* **27**, 299-308 (1981).

- Abrahams, P. J. & Van der Eb, A. J. *J. Virol.* **16**, 206-209 (1975).
- Abrahams, P. J., Mulder, C., Van de Voorde, A., Warnaar, S. O. & Van der Eb, A. J. *J. Virol.* **16**, 818-823 (1975).
- Mueller, C., Graessmann, A. & Graessmann, M. *Cell* **15**, 579-585 (1978).
- Lane, D. P. & Lane, E. B. *J. immun. Meth.* **47**, 303-307 (1981).
- Harlow, E., Crawford, L. V., Pim, D. C. & Williamson, N. M. *J. Virol.* **39**, 861-869 (1981).
- Colby, W. W. & Shenk, T. *Proc. natn. Acad. Sci. U.S.A.* **79**, (in the press).
- Maxam, A. & Gilbert, W. *Meth. Enzym.* **65**, 499-560 (1980).

onc gene amplification in promyelocytic leukaemia cell line HL-60 and primary leukaemic cells of the same patient

Riccardo Dalla Favera, Flossie Wong-Staal & Robert C. Gallo

Laboratory of Tumor Cell Biology, National Cancer Institute, National Institutes of Health, Bethesda, Maryland 20205, USA

Cellular *onc* genes are a group of evolutionarily conserved sequences which are homologous to the transforming genes (*v-onc*) of oncogenic retroviruses¹. Their function in normal cells is not yet known, but the sequence homology between viral and cellular *onc* genes is consistent with the idea that neoplastic transformation may, in some cases, be due to increased levels of cellular *onc* gene expression. The cellular homologue, *c-myc*, of the transforming gene of avian myelocytomatosis virus (MC29)^{1,2} is involved in the pathogenesis of chicken B-cell lymphomas induced by the non-acute leukemia virus (RAV-2)³⁻⁶, and in these tumours, *c-myc* expression is enhanced by the nearby integration of the RAV-2 terminal repeat region³⁻⁶. Transcripts from the *c-myc* gene are detectable in a variety of human cells^{7,8}, and increased levels of *myc* mRNA have been occasionally detected in some neoplastic tissues^{7,8}. The highest levels have been detected in the cell line HL-60 (ref. 8) derived from neoplastic cells from a patient with acute promyelocytic leukaemia (APL)⁹. We have now investigated whether any structural alteration at the genomic level could account for the increased expression of *c-myc* in HL-60 and report here that the *c-myc* gene is stably amplified in HL-60 DNA. Amplification was also detected in primary uncultured leukaemic cells from the same individual, suggesting that the *c-myc* amplification may have been involved in the leukaemic transformation in this case.

The genomic organization of human *c-myc* sequences has recently been studied in our laboratory¹⁰. Isolation and characterization of several recombinant phages from a human DNA library suggested the existence of at least one complete gene and several partially related sequences which may represent pseudogenes¹⁰. The complete *c-myc* gene spans ~4.5 kilobases (kb) of the human genome where two *v-myc* homologous exons are interrupted by one intron¹⁰. Three putative pseudogenes, each of which contains ~0.3 kb of *c-myc*-related sequences and lacks 3' and 5' regions of the gene, have been characterized¹⁰. Northern blotting hybridization experiments using a *v-myc* probe revealed a 2.7 kb mRNA transcript in a wide variety of human haematopoietic and nonhaematopoietic cells, including normal fibroblast and normal peripheral blood lymphocytes^{7,8}. In most of the cells, *myc* mRNA was present in 1-10 copies per cell⁸. However, at least a 10-fold increase in mRNA was observed in a few cases, including one sarcoma, two carcinomas and two haematopoietic cell lines⁸. The highest levels of *myc* RNA were present in the human promyelocytic leukaemia cell line HL-60 (ref. 8). This cell line has the capability to differentiate into mature nonproliferating granulocytes on induction with several chemical agents, including dimethyl sulfoxide (DMSO)¹¹ and retinoic acid¹². *myc* transcripts were virtually undetectable in terminally differentiated HL-60 (ref. 8). To investigate whether any structural alteration of the *c-myc* gene or adjacent regulatory regions could account for the increased *c-myc* expression in HL-60, we have now analysed the structure of *c-myc* sequences in these cells by Southern blot hybridization¹³. Our study included DNA from the HL-60 cell line,

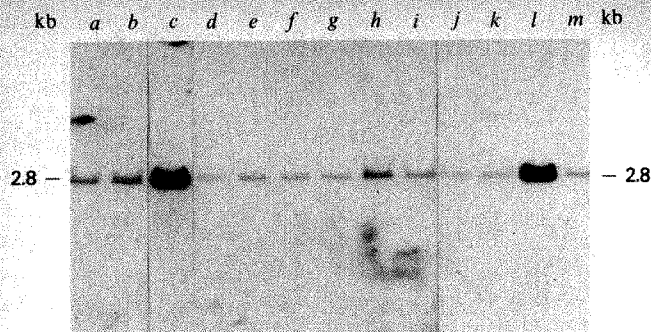


Fig. 1 Amplification of *c-myc* sequences in HL-60 DNA. DNA was extracted as previously described²⁴ from: a, peripheral blood ALL cells; b, peripheral blood CLL cells; c, HL-60 passage 70; d, peripheral blood APL cells; e, normal human spleen; f, Molt 4 cell line; g, human breast carcinoma cell line; h, peripheral blood APL cells; i, peripheral blood AMML cells; j, peripheral blood APL cells; k, peripheral blood CML cells, partial digestion; l, uncultured HL-60 cells; m, normal human peripheral blood lymphocytes; and 20 μ g were digested with *SsrI* restriction endonuclease in standard conditions recommended by the supplier. Fragments were separated by electrophoresis on a 0.8% agarose gel. DNA was denatured, transferred to nitrocellulose as described by Southern¹³ and hybridization was performed using dextran sulphate²⁵. The probe was 2×10^6 c.p.m. of nick-translated pMC41-3RC DNA. pMC41-3RC is a recombinant pBR322 plasmid derived from λ LMC41, the recombinant Charon 4A phage containing the human *c-myc* gene¹⁰. For subcloning into the plasmid, a 1.4 kb *ClqI*-*EcoRI* fragment containing the *c-myc* 3' exon¹⁰ was isolated on preparative agarose gel and ligated into *ClqI*-*EcoRI*-cleaved pBR322 (ref. 26).

from primary leukaemic cells of the same individual, from normal human tissues (peripheral blood lymphocytes and spleen) and different neoplastic cells. The latter were obtained from peripheral blood of patients with acute myelogenous leukaemia (AML; 3 cases), chronic myelogenous leukaemia (CML; two cases), APL (three cases), acute lymphocytic leukaemia (ALL; one case), chronic myelogenous leukaemia (CML; one case), acute myelomonoblastic leukaemia (AMML; one case) and from cell lines representing myeloid (KG-1 and K562: refs 14, 15 respectively) and lymphoid (Molt 4)¹⁶ leukaemia (AML; three cases), chronic myelogenous leukaemia endonuclease and hybridized to a probe (pMC41-3RC) derived from the 3' exon of the human *c-myc* gene (see Fig. 1 legend for details). This probe hybridizes to a single 2.8 kb *SsrI* fragment in human DNA and does not hybridize to any of the putative pseudogenes because they are homologous only to the 5' exon of the *c-myc* gene¹⁰.

Representative results shown in Fig. 1 indicate the intensity of the 2.8 kb band was approximately identical in DNA from all samples except the HL-60 cell line and the patient's original uncultured cells, in which cases the intensity was markedly increased. Similar results were obtained with DNAs from different passages of the HL-60 cell line and in differentiated cells after induction with DMSO (data not shown). These data suggest that the *c-myc* gene copy number is increased in HL-60 cells. To investigate the extent of amplification of *c-myc* sequences in the HL-60 genome we hybridized *EcoRI* digests of DNA from primary and cultured HL-60 cells to a probe (pMCO) containing the entire *v-myc* gene¹⁰. This probe detects all *c-myc* related sequences in the human genome, including the putative pseudogenes¹⁰. Figure 2 shows that the intensity of a 12.8 kb band, which corresponds to the entire functional gene, is markedly increased in the two HL-60 samples, confirming the results shown in Fig. 1. In contrast, the intensity of the 5.8 kb band, which corresponds to one of the *c-myc* putative pseudogenes, is uniform in all the samples, suggesting that the functional gene, but not the other related sequences, is amplified. Moreover, this band serves as an internal control, proving that the difference in intensity of the 12.8 kb band is not due to experimental artefacts such as irregular DNA transfer or non-uniform hybridization across the nitrocellulose filter. In addition, a 4.6 kb fragment appears in the two HL-60 DNA samples but not in the other samples. The origin of this fragment is unknown. We suggest that it could represent either an

unidentified pseudogene which would be part of the amplification unit or a new fragment generated during the *c-myc* amplification event in HL-60 cells. Finally, experiments were performed to quantify the amplification of *c-myc* in HL-60. Thirty μ g of *SsrI*-digested HL-60 DNA were sequentially diluted (see Fig. 3) and the intensity of the hybridization band was compared with that obtained with 30 μ g of normal human lymphocyte DNA. Hybridization to a probe derived from another human *onc* gene, *c-sis*, which is a single copy gene¹⁷, was used as a control in the same experiment. Whereas the intensity of the *c-sis* band is comparable in normal spleen and undiluted HL-60 DNA, a 16- to 32-fold dilution is necessary to bring the *c-myc* band to the same levels as the control DNA. These data indicate that the *c-myc* gene is amplified 16- to 32-fold in HL-60. Similar estimates were obtained by direct densitometric screening of X-ray films from experiments shown in Fig. 1.

Our data thus indicate that the *c-myc* *onc* gene is amplified in the genome of HL-60 cell line, as well as in the original uncultured leukaemic leukocytes which were obtained from the peripheral blood of the patient before any chemotherapeutic treatment¹⁸. The levels of *c-myc* amplification do not seem to vary during prolonged cell culture or after induction to differentiation. This result cannot be simply explained by amplification of specific chromosome(s) in these cells because they are hypodiploid and no hyperdiploidy of individual chromosomes was observed¹⁸. However, different amplified genes have been reported to be located in double minutes or homogeneous staining regions of chromosomes (for review, see ref. 19). Since double minutes have been described in the HL-60 cell line¹⁸, we are currently investigating whether these structures could contain amplified *c-myc* sequences. The *c-myc*-containing amplification unit must be larger than the 12.8 kb *EcoRI* fragment which is conserved in HL-60 DNA. The amplified fragment could be considerably larger, however, as amplified units ranging from 500 to 1,350 kb have been reported¹⁹. The amplified fragment does not contain any of the putative pseudogenes, indirectly suggesting that these are not in the immediate proximity of the *c-myc* gene in the human genome.

Although *c-myc* amplification is confirmed in HL-60 cells, we do not yet know whether *c-myc* is amplified in the other non-leukaemic cells of the same individual because tissues other than the leukaemic cells are not available from the patient. In the absence of these critical data, at least three different hypotheses can be formulated.

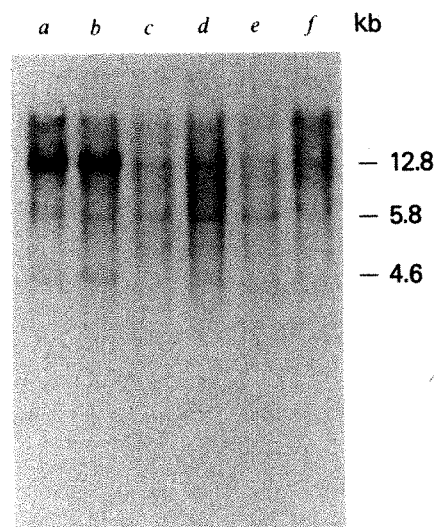


Fig. 2 Hybridization of HL-60 and other human DNAs to *v-myc* probe (pMCO). Thirty μ g of DNA from: a, HL-60 passage 70; b, uncultured leukaemic HL-60 cells; c, normal human spleen; d, peripheral blood AML cells; e, Molt 4 cell line; f, peripheral blood normal human lymphocytes; were digested with *EcoRI* and hybridized to a *v-myc* probe (pMCO)¹⁰ as described in Fig. 1 legend.

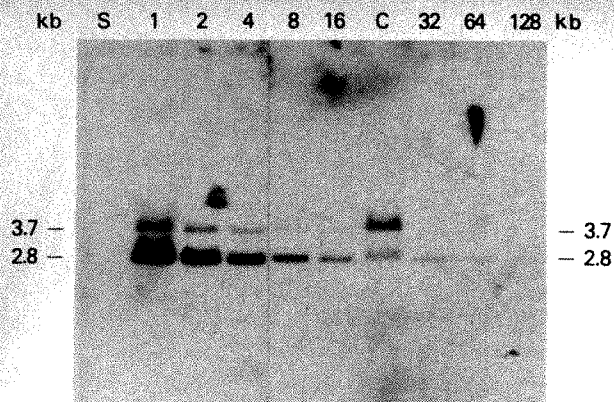


Fig. 3 Estimate of *c-myc* copy number in HL-60 DNA. For this Southern blot dilution experiment, all the DNAs listed below were digested with *Sst*I and simultaneously hybridized to pMC41-3RC and to a human *c-sis* probe (pL335)^{17,27}. *c-myc* and *c-sis* hybridization bands in 30 µg of DNA from normal human lymphocytes (lane C) were used as standards and their intensity compared with that obtained with the same amount of DNA from uncultured HL-60 cells (lane 1) and serial dilutions of the latter with equal amounts of *Sst*I-digested salmon sperm DNA. The reciprocal of the dilution factor is shown above the lanes. Salmon sperm DNA was chosen as diluting DNA as *c-myc*- or *c-sis*-related sequences are not detectable in these conditions of hybridization, as shown in lane S (30 µg). The 2.8 kb *c-myc* band in lane C is intermediate in intensity between the bands in lanes 16 and 32. The 3.7 kb band closely matches the one in undiluted NL-60 DNA. Therefore, the *c-myc* copy number is between 16- and 32-fold higher in HL-60 compared with the normal standard. In contrast, the unamplified *c-sis* gene is present as a single copy in both genomes. The slight difference in migration of diluted samples is due to decreased salt concentration after the dilution procedure.

(1) *c-myc* amplification has occurred in the germ line. As individuals of the same species usually have the same number of copies per cell of a given gene, germ-line amplification in a single individual would be novel and of, as yet, unknown significance. Another example of germ-line amplification also involves a cellular *onc* gene, *c-ras*, which is amplified in different but closely related murine species²⁰. Although this case differs from *c-myc* amplification in HL-60 as it affects an entire species²⁰, taken together, these preliminary observations could point to a relatively high genetic mobility of cellular *onc* genes.

(2) *c-myc* amplification may be present in other non-malignant myeloid cells, perhaps representing a normal event during myeloid differentiation analogous to the developmental amplifications of chorion genes during oogenesis in *Drosophila*²¹ or actin genes during myogenesis in chickens²². In this case, the 'freezing' of HL-60 cells by the transformation event in a stage when *c-myc* is amplified and thus expressed at high levels could correlate with the unique ability of HL-60 to propagate as a cell line in the absence of growth-stimulating factor(s)¹¹.

(3) *c-myc* amplification only in the leukaemic clone may have important implications for the pathogenesis of leukaemia in this patient. It has been proposed that increased expression of cellular *onc* genes may cause neoplastic transformation. Thus, the finding of *onc* gene amplification correlating with increased levels of expression in HL-60 cells suggests an alternative mechanism to the 'downstream' promotion of *onc* genes by viral promoters^{3-6,28}. The *onc* gene amplification model cannot be generally applied, at least in the case of *c-myc* and haematopoietic neoplasias, because this gene is neither amplified nor expressed⁸ above basal levels in a small group of fresh leukaemic cells or cell lines tested in this study. In particular, it is not amplified in three cases of APL tested, although no data are available on its expression in these cells. Alternatively, HL-60 cells may belong to a separate subgroup of APLs as they do not display the karyotypic abnormality involving a reciprocal translocation between chromosomes 15 and 17 (ref. 18) commonly found in this type of leukaemia²³. These observations suggest that if *c-myc* amplification is involved in leukaemic transformation in HL-60, different mechanisms, including activation of different cellular *onc* genes, may lead to transforma-

tion even in similar neoplastic diseases. The validity of the *onc* gene amplification model can be tested in several different tumours expressing high levels of any of the known cellular *onc* genes.

We thank T. S. Papas for a gift of the MC29 clone from which the pMCO probe was derived, E. P. Gelmann for preparing the pMCO recombinant plasmid, J. D. Rowley for providing leukaemic cells from some of the APL cases and Anna Mazzuca for secretarial assistance. R.D.F. is a Special Fellow of the Leukemia Society of America.

Note added in proof: Using a chicken *c-myc* probe Collins and Groudine have independently achieved similar results on *c-myc* amplification in cultured HL-60 cells (S. Collins, personal communication).

Received 28 May; accepted 17 June 1982.

1. Duesberg, P. H. *Cold Spring Harb. Symp. quant. Biol.* **44**, 13-30 (1980).
2. Lautenberger, S. A., Schulz, R. A., Garow, C. F., Tschilio, P. N. & Papas, T. S. *Proc. natn. Acad. Sci. U.S.A.* **78**, 1518-1522 (1981).
3. Hayward, W. S., Neel, B. G. & Astrin, S. M. *Nature* **290**, 475-480 (1981).
4. Neel, B. G., Hayward, W. S., Robinson, H. L., Fang, S. & Astrin, S. M. *Cell* **23**, 324-334 (1981).
5. Payne, G. S. *et al. Cell* **23**, 311-322 (1981).
6. Payne, G. S., Bishop, M. J. & Varmus, M. E. *Nature* **295**, 209-215 (1982).
7. Eva, A. *et al. Nature* **295**, 116-119 (1982).
8. Westin, E. *et al. Proc. natn. Acad. Sci. U.S.A.* **79**, 2490-2494 (1982).
9. Collins, S. J., Gallo, R. C. & Gallagher, R. E. *Nature* **270**, 347-349 (1977).
10. Dalla Favera, R. *et al. Proc. natn. Acad. Sci. U.S.A.* (in the press).
11. Collins, S. J., Ruscetti, F. W., Gallagher, R. E. & Gallo, R. C. *Proc. natn. Acad. Sci. U.S.A.* **75**, 2458-2462 (1978).
12. Breitman, T. R., Seimonick, S. E. & Collins, S. J. *Proc. natn. Acad. Sci. U.S.A.* **77**, 2936-2940 (1980).
13. Southern, E. M. *J. molec. Biol.* **98**, 503-517 (1975).
14. Koefler, H. P. & Golde, D. W. *Science* **200**, 1153-1154 (1978).
15. Lozzio, C. B. & Lozzio, B. B. *Blood* **45**, 321-334 (1975).
16. Minowada, J., Oshimura, T. & Moore, G. E. *J. natn. Cancer Inst.* **49**, 891-895 (1978).
17. Dalla Favera, R., Gelmann, E. P., Gallo, R. C. & Wong-Staal, F. *Nature* **292**, 31-35 (1981).
18. Gallagher, R. E. *et al. Blood* **54**, 713-733 (1979).
19. Schimke, R. T. (ed.) in *Gene amplification*, 317-331 (Cold Spring Harbor Laboratories, New York, 1982).
20. Chattopadhyay, S. K. *et al. Nature* **296**, 361-363 (1982).
21. Spradling, A. L. & Mahowald, A. F. *Proc. natn. Acad. Sci. U.S.A.* **77**, 1096-1100 (1980).
22. Zimmer, W. E. & Schwartz, R. S. in *Gene Amplification* (ed. Schimke, R. T.) 137-138 (Cold Spring Harbor Laboratories, New York, 1982).
23. Rowley, J. D. *Semin. Hematol.* **15**, 301-319 (1978).
24. Wong-Staal, F., Reitz, M. S. & Gallo, R. C. *Proc. natn. Acad. Sci. U.S.A.* **76**, 2032-2036 (1979).
25. Wahl, G. M., Stern, M. & Stark, G. R. *Proc. natn. Acad. Sci. U.S.A.* **76**, 3683-3687 (1979).
26. Bolivar, F. *et al. Gene* **2**, 93-113 (1977).
27. Wong-Staal, F. *et al. Nature* **294**, 273-275 (1981).
28. Noori-Daloui, M. R., Swift, R. A., Crittenden, L. B. & Witter, R. L. *Nature* **294**, 574-576 (1981).

Participation of myeloid leukaemic cells injected into embryos in haematopoietic differentiation in adult mice

Elisha Gootwine*, Cynthia G. Webb* & Leo Sachs†

Departments of *Hormone Research and †Genetics, Weizmann Institute of Science, Rehovot 76100, Israel

It is of interest to determine to what extent malignant cells are still subject to control mechanisms that govern the growth and differentiation of their normal counterparts¹⁻⁴. One approach has been the introduction of malignant cells into a normal embryo. Such studies have shown that mouse teratocarcinoma cells injected into blastocysts can participate in normal development to produce adult chimaeric animals with markers derived from teratocarcinoma cells^{1-3,5-7}. Other types of malignant cells may also be able to participate in normal morphogenesis, provided that they have the ability to differentiate and are introduced into the embryo at an appropriate stage of development. Here we have examined myeloid leukaemic cells and our results indicate that injection of these cells into embryos *in utero* at 10 days of gestation can produce apparently healthy adult mice whose granulocytes contain a marker derived from the leukaemic cells.

Table 1 Microinjection of myeloid leukaemic cells into the fetal placenta *in utero*

Survival of injected animals	Control	Experimental injected on:	
		Day 10	Day 11
Number of females operated on	13	26	58
Females dead post-operation	3	5	9
Females aborting	6	11	28
Females pregnant at term	4	10	21
Number of fetuses injected	141	268	469
Fetuses in females pregnant at term	33	94	156
Viable progeny	16	39	90
Animals dead after birth	2	7	35
Animals surviving	14	32	55

Fetuses were microinjected through the uterine wall into the fetal placenta¹². Each injection contained $\sim 5 \times 10^4$ cells and the cells were injected in the culture medium used for growing the leukaemic cells¹¹ without serum. Of 129 animals born, 70 were injected with leukaemic clone 7-M18 and 59 with leukaemic clone 1. Of 87 surviving animals, 45 were injected *in utero* with clone 7-M18 and 42 with clone 1. There was no statistically significant difference between groups receiving either of these clones and these data have therefore been pooled. Controls were injected with culture medium alone. Of the 84 females injected with leukaemic cells in these experiments, 75 were C3HeB and 9 were C57BL/6. The two apparently healthy adult mice with donor type enzyme (Table 2) were both obtained after injection of leukaemic cells into the fetal placenta of C3HeB mice.

We have used in these studies two clones of mouse myeloid leukaemic cells that grow in culture as myeloblasts to promyelocytes and which differ in their capacity to be induced to differentiate to mature macrophages and granulocytes by the normal macrophage and granulocyte differentiation-inducing protein MGI-2^{4,8-11}. One clone (7-M18) could be induced by MGI-2 to differentiate in culture to mature macrophages or granulocytes (mainly macrophages), whereas the other clone (1) could not be induced by MGI-2 to differentiate in culture to mature cells^{10,11}. To test for the incorporation of a marker from the leukaemic cells into the haematopoietic cell system, fetal mice were injected *in utero* with the myeloid leukaemic cells at 10 or 11 days of gestation. The leukaemic cells were from the strain SJL and the host animals injected were strains C3HeB or C57BL/6. Both clones of leukaemic cells contain the slow migrating glucose phosphate isomerase (GPI) isozyme GPI-1^a, whereas cells from C3H and C57BL/6 mice are homozygous for the fast migrating isozyme GPI-1^b. Leukaemic cells were microinjected into the placenta of each fetus according to the procedure described for injection of normal haematopoietic cells¹² and the numbers of viable progeny obtained are shown in Table 1.

In the first series of experiments, leukaemic cells were injected on day 10 of gestation (the day of plug was designated day 0) and 39 animals were born. One litter of four animals was cannibalized by the mother shortly after birth and another

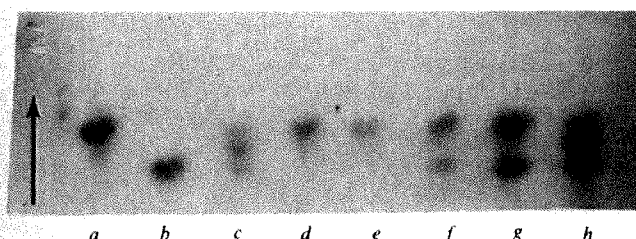


Fig. 1 Glucose phosphate isomerase isozyme analysis by starch gel electrophoresis of extracts from peritoneal exudate cells. Granulocytes or macrophages were collected from the peritoneal cavity after injection of sodium caseinate. No leukaemic cells were observed. *a*, C3H control granulocytes; *b*, SJL control granulocytes; *c*, F1 (C3H×SJL) heterozygous control macrophages; *d*, mouse 30A, granulocytes at 4 weeks after birth (no donor-type enzyme); *e*, mouse 32A, granulocytes at 4 weeks after birth (no donor-type enzyme); *f*, mouse 14A, granulocytes at 3 months after birth (host and donor-type enzymes present); *g*, mouse 24A, granulocytes at 4 weeks after birth (host and donor-type enzymes present); *h*, F1 (C3H×SJL) heterozygous control granulocytes.

three animals died, were partially eaten and could not be examined. A total of 32 animals survived after weaning at 21–28 days (18 males and 14 females); these were screened for donor type enzyme beginning at or shortly after weaning, and then at about bimonthly intervals. Granulocytes were the first cell population examined. These cells were flushed from the peritoneal cavity after injection of sodium caseinate and analysed for GPI isozyme pattern by electrophoresis¹³.

Of the 32 adult animals injected with leukaemic cells *in vivo* at 10 days of gestation, two were found to have donor type enzyme in their granulocytes. Animal 14A was a female injected with cells of clone 7-M18 and animal 24A a male injected with cells of clone 1. In both these animals there was a major contribution of donor type (GPI-1^a) enzyme in the granulocyte samples collected at the age of 1 month (Fig. 1). Densitometric analysis of the electrophoretic pattern indicated that in these samples the donor type enzyme contributed at least 25% of the GPI activity. In both animals this contribution gradually decreased with age. We found 15–20% donor-derived GPI activity in the granulocytes at 3 months of age, 10% at 5 months, and only 5% at 7 months. This isozyme was no longer detected at 8.5 months in animal 14A and 10 months in animal 24A. A minor contribution of donor type isozyme was also detected in the leukocytes isolated from the peripheral blood up to 3 months of age in the case of animal 14A and 5 months in the case of animal 24A and this could be accounted for by the granulocytes in the peripheral blood. However, this isozyme was not detected in the peritoneal macrophages in these mice (Table 2). The leukaemic cells injected into the fetuses could be readily distinguished from normal peritoneal granulocytes (Fig. 2). At least 1,000 cells per sample were examined microscopically, and no leukaemic cells were seen in the peritoneal exudate or peripheral blood cells in these or any of the other adult mice. At autopsy, when the granulocytes no longer showed donor type isozyme, there was also no detectable amount of this enzyme in the spleen, thymus, bone marrow, kidney, liver or brain.

In a second series of experiments, leukaemic cells were injected at day 11 instead of at day 10 of gestation. In this series of injections 90 viable progeny were obtained, of which only 55 survived beyond weaning. None of these 55 mice showed detectable donor type GPI in their peritoneal granulocytes or macrophages. In these experiments 39% of the injected animals died before weaning. In some cases the carcasses had been partially eaten or post mortem changes were too marked to

Table 2 Donor type GPI isozyme in adult animals microinjected *in utero* with myeloid leukaemia

Animal no.	Clone injected	Age tested (months)	% Donor-type isozyme in:			
			Peritoneal cells		Peripheral blood	
			Granulocytes	Macrophages	Leukocytes	Erythrocytes
14A	Clone 7-M18	1	25	0	3	0
		3	20	0	3	0
		5	10	ND	0	0
		7	5	ND	0	0
		8.5	0	0	0	0
24A	Clone 1	1	25	0	3	0
		3	15	0	3	0
		5	10	ND	3	0
		7	5	ND	0	0
		10	0	0	0	0

Peritoneal granulocytes and macrophages were collected at 16 and 72 h, respectively, after intraperitoneal injection of 10% sodium caseinate solution. The peritoneal cell populations contained on average ~90% granulocytes and 80% macrophages. The other cells in the peritoneal samples used were lymphocytes and no leukaemic cells were observed. Peripheral blood samples were collected from the retro-orbital sinus and the erythrocytes and leukocytes separated. Leukaemic cells were also not observed in these samples. Cell pellets were suspended in water, lysed by three cycles of freezing and thawing, and the supernatants, obtained after centrifugation for 30 min at 28,000g, were electrophoresed on starch gels and stained as described elsewhere¹³. Per cent donor-type enzyme values represent estimates based on densitometric analyses of the electrophoretic pattern of GPI. ND, not determined.

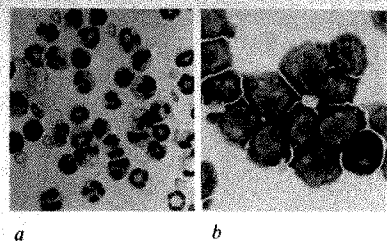


Fig. 2 *a*, Peritoneal granulocyte population collected from healthy adult mice; *b*, myeloid leukaemic cells (clone 7-M18). Cells stained with May-Grunwald-Giemsa. $\times 630$.

allow enzymatic examination. Of the remaining 18 mice that died before weaning, 9 had tumours derived from the injected leukaemic cells, as determined by GPI analysis; the rest appeared to predominantly have severe bacterial pneumonia. The animals died with tumours by 15 ± 1 days after birth, that is, 3.5 weeks after injection of the leukaemic cells. The mean survival time of the tumour-bearing animals injected *in utero* was similar to that of neonatal syngeneic mice injected within 12 h of birth with an equivalent number (5×10^4) of leukaemic cells.

The present experiments indicate that malignant cells other than teratocarcinoma cells injected into embryos may participate in normal development. In two animals injected *in utero* with myeloid leukaemic cells on day 10 of gestation, at least 25% of the glucose phosphate isomerase in the peritoneal granulocytes was donor specific at 1 month after birth. Leukaemic cells were not seen in the cell populations analysed and these adult mice seemed healthy. These results indicate that the myeloid leukaemic cells participated in haematopoietic differentiation in apparently normal adult mice. The donor type enzyme decreased gradually over a period of 7 months and was no longer detectable at the age of 8–10 months. The selection of one cell type over another has also been reported in haematopoietic chimaeric animals obtained after injection of normal haematopoietic cells¹², and in allophenic mice produced from aggregated blastomeres^{14,15}. Cells with a donor-derived marker may have a selective disadvantage compared with the host cells, resulting in a gradual decrease in their contribution to the total cell population, perhaps due to the presence of a limited number of precursors.

Injection of leukaemic cells into 10-day-old fetuses resulted in two adult mice having cells with donor type isozyme whereas injection into 11-day-old fetuses did not and gave some animals with tumours. Further experiments with larger number of animals are required to determine the importance of a specific stage of embryonic development for obtaining adult animals with a donor type marker. We injected the embryos at the stage when there appears to be considerable migration of the normal progenitors of granulocytes and macrophages¹⁶. Other tumour cells may need to be injected into blastocysts¹⁷. This has given chimaeras with teratocarcinoma^{1-3,5-7} but not with melanoma cells¹⁸. Others may need to be injected at different stages of development into the placenta¹², or directly into the fetus¹⁹. When leukaemic cells are induced to differentiate *in vitro* by the normal differentiation-inducing protein MGI-2, it is the leukaemic cells and not segregants that differentiate to mature cells^{4,9}. It has also been shown that leukaemic cells may differentiate better *in vivo* than *in vitro*²⁰. The finding of a donor cell marker in animals injected as embryos with malignant cells suggests that the malignant cells may respond to the controls that regulate normal growth and differentiation in the embryo, or the cells with a donor cell marker may be segregants with a non-malignant phenotype derived from the malignant cells, as can occur with sarcomas⁸. The use of additional donor-specific markers including chromosome markers should make it possible to distinguish between these possibilities.

We thank Professor H. B. Stein for his assistance in histopathological examination and Professor H. R. Lindner for his

helpful comments. This work was supported in part by a grant to H. R. Lindner from the Ford Foundation and the Rockefeller Foundation, New York, and to C.G.W. from the Binational Science Foundation. C.G.W. is the incumbent of the Pauline Recanati Career Development Chair in Immunology.

Received 8 March; accepted 25 June 1982.

1. Brinster, R. L. *J. exp. Med.* **140**, 1049–1056 (1974).
2. Papaioannou, V. E., McBurney, M. W. & Gardner, R. L. *Nature* **258**, 70–73 (1975).
3. Mintz, B. & Illmensee, K. *Proc. natn. Acad. Sci. U.S.A.* **72**, 3585–3589 (1975).
4. Sachs, L. *Proc. natn. Acad. Sci. U.S.A.* **77**, 6152–6156 (1980).
5. Illmensee, K. & Mintz, B. *Proc. natn. Acad. Sci. U.S.A.* **73**, 549–553 (1976).
6. Papaioannou, V. E., Gardner, R. L., McBurney, M. W., Babinet, C. & Evans, M. J. *J. Embryol. exp. Morph.* **44**, 93–104 (1978).
7. Stewart, T. A. & Mintz, B. *Proc. natn. Acad. Sci. U.S.A.* **78**, 6314–6318 (1981).
8. Sachs, L. *Harvey Lect.* **68**, 1–35 (1974).
9. Sachs, L. *Nature* **274**, 535–539 (1978).
10. Lotem, J. & Sachs, L. *Proc. natn. Acad. Sci. U.S.A.* **71**, 3507–3511 (1974).
11. Lotem, J. & Sachs, L. *Proc. natn. Acad. Sci. U.S.A.* **74**, 5554–5558 (1977).
12. Fleischman, R. A. & Mintz, B. *Proc. natn. Acad. Sci. U.S.A.* **76**, 5736–5740 (1979).
13. Pedersen, A. L., Frair, P. M. & Gordon, G. W. *Genetics* **16**, 681–690 (1978).
14. Mintz, B. & Palm, J. *J. exp. Med.* **129**, 1013–1027 (1968).
15. West, J. D. *Exp. Hemat.* **5**, 1–7 (1977).
16. Cline, M. J. & Moore, M. A. S. *Blood* **39**, 842–849 (1972).
17. Gardner, R. L. in *Methods in Mammalian Reproduction* (ed. Daniel, J. C. Jr) 137–165 (Academic, New York, 1978).
18. Pierce, G. B., Lewis, S. H., Miller, G. J., Moritz, E. & Miller, P. *Proc. natn. Acad. Sci. U.S.A.* **76**, 6649–6651 (1979).
19. Weissman, I. L., Baird, S., Gardner, R. L., Papaioannou, V. E. & Raschke, W. *Cold Spring Harb. Symp. quant. Biol.* **41**, 9–21 (1976).
20. Lotem, J. & Sachs, L. *Proc. natn. Acad. Sci. U.S.A.* **75**, 3781–3785 (1978).

Production of a monoclonal antibody specific for Hodgkin and Sternberg-Reed cells of Hodgkin's disease and a subset of normal lymphoid cells

Ulrich Schwab*, Harald Stein*, Johannes Gerdes*, Hilmar Lemke*, Hartmut Kirchner†, Michael Schaad† & Volker Diehl†

* Institute of Biochemistry and Institute of Pathology, Christian Albrecht University, D-2300 Kiel, FRG

† Department of Haematology and Oncology, Medical School of Hannover, D-3000 Hannover 61, FRG

The origins of the neoplastic cells in Hodgkin's lymphoma¹, the Hodgkin (H) and Sternberg-Reed (SR) cells, are still obscure, and these cells appear to carry no markers found on any population of normal cells^{2,3}. However the recent establishment of permanent Hodgkin cell lines^{3,4} has led to the search for tumour-specific antigens and/or for membrane markers on H and SR cells which may indicate the normal equivalent cells. Here, we describe the production of mouse monoclonal antibodies against the Hodgkin cell line L428. One hybridoma antibody, Ki-1, was found to be specific for H and SR cells of all Hodgkin's lymphomas tested and a minute, but distinct new cell population in normal tonsils and lymph nodes.

The existence of H and SR cell specific antigens was suggested by a conventional rabbit antiserum raised against the L428 cell line. After absorption with various normal human cells, the anti-L428 antiserum proved to be selectively reactive with L428 cells and H and SR cells⁵. To further investigate these apparent Hodgkin-specific tumour antigens we have started to produce hybridoma antibodies directed against H and SR cell antigens⁶.

BALB/c mice were immunized with L428 cells according to the schedule described by Stähli *et al.*⁷. Spleen cells were fused with the non-secreting myeloma line X63-Ag8.653 (ref. 8). In one fusion experiment we selected 57 pre-cloned 'resp.' highly enriched hybridomas that showed strong reactivity with L428 cells and no reactivity with a 10 times higher number of pooled normal tonsil cells. The resulting 57 monoclonal antibodies were tested by using the immunoperoxidase staining technique on frozen sections of biopsy tissue infiltrated with Hodgkin's

disease^{9,10}. One of the hybridoma antibodies reacted with H and SR cells, but not with other cells in the biopsy tissue. This clone was designated Ki-1. The constant expression of the Ki-1 antigen on H and SR cells was confirmed by immunostaining tissue from 14 cases of Hodgkin's disease of the four main histological types (Table 1). The H and SR cells of all cases stained distinctly (Fig. 1), but the intensity of the staining varied. There was no correlation between intensity of staining and histological type.

The specificity of the Ki-1 antibody for H and SR cells was further demonstrated, as the antibody did not stain cells of more than 50 cases of non-Hodgkin's lymphomas of various types, one case of osteomyelosclerosis, two cases of malignant histiocytosis and two cases of histiocytosis X. The Ki-1 antibody also did not react with cells of normal peripheral blood, skin, liver, kidney, lung or brain, or with macrophages of different types or stages of differentiation (Table 2).

Stainings with a highly sensitive three-layer immunoperoxidase labelling technique of a large series of normal or hyperplastic tonsils and lymph nodes, however, yielded unexpected results. A small population of cells located around and between cortical follicles and, to a lesser extent, at the inner rim of follicular mantles showed weak, but distinct staining for Ki-1 (Fig. 2). These cells were smaller than typical H and SR cells and had one nucleus; the nucleolus was prominent, like that of H and SR cells. Such cells could not be demonstrated with the conventional rabbit antiserum raised against L428 cells that reacted specifically with H and SR cells. There are two possible explanations for this phenomenon: (1) the conventional rabbit anti-L428 serum recognizes an antigen different from

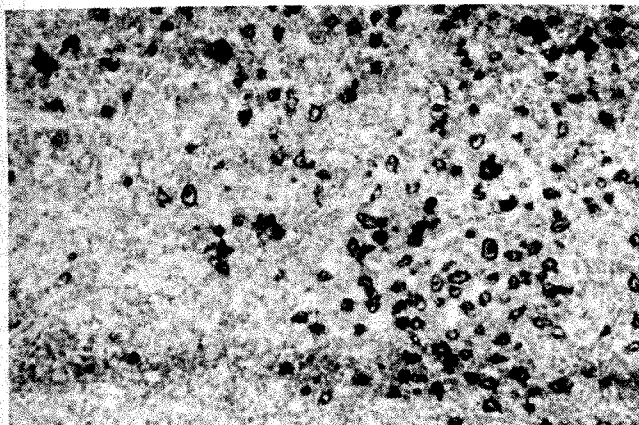


Fig. 1 Hodgkin and Sternberg-Reed cells in tissue infiltrated by Hodgkin's disease reacting selectively with the monoclonal antibody Ki-1. Lyophilized 8 μ m sections of frozen tissue biopsies were fixed in acetone for 10 min and subsequently in chloroform for 10 min, both at room temperature. The fixed sections were then incubated with undiluted hybridoma supernatants or hybridoma ascitic fluids (dilutions ranged between 1:1,000 and 1:50,000) for 30 min. After a short wash in phosphate-buffered saline (PBS) the sections were treated with peroxidase-conjugated anti-mouse Ig (Dako) for 30 min, followed by a short wash. This reagent was reabsorbed with insolubilized human serum and diluted 1:10 in PBS to which normal human serum (final dilution of 1:5) was added to block cross-reactivity against human immunoglobulin. To increase sensitivity, stainings were performed at 37 °C or the sections were incubated with a third antibody layer composed of peroxidase-conjugated goat anti-rabbit IgG antibody (Medac) diluted 1:10 in PBS to which normal human serum (final dilution of 1:10) was added. After a brief wash, peroxidase was made visible by incubating the sections with diaminobenzidine (0.6 mg per ml) and hydrogen peroxide (0.01%) for 10 min at room temperature. The sections were then washed in PBS, counterstained with haemalum and mounted for microscopic examination. Negative controls were performed with the non-reactive monoclonal antibody W6/32HK²⁵ and positive controls with a set of monoclonal antibodies reactive with IgM, IgD (Bethesda), T-cells (OKT3, Ortho) HLA-DR (Becton Dickinson) and other cells or antigens.

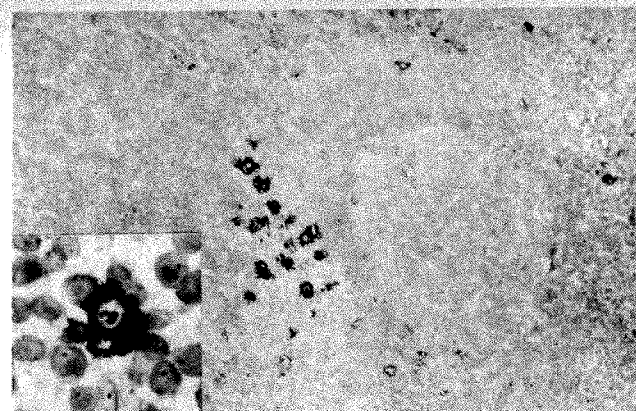


Fig. 2 A cluster of Ki-1-positive cells in a hyperplastic (non-malignant) human tonsil. They are chiefly located between, around and sometimes within the B-cell follicles. In other areas of the tonsil, there are fewer Ki-1 positive cells. Inset: Ki-1-positive cell at high power view. Note the sharply defined prominent nucleolus within the pale nucleus and the labelled abundant cytoplasm.

that detected by monoclonal antibody Ki-1, or (2) both reagents detect the same antigen, which is strongly expressed on H and SR cells but only weakly on the normal Ki-1-positive cells. The second possibility is conceivable, because the multiple-step absorbed rabbit anti-L428 serum had to be used at rather high concentrations even for the detection of H and SR cells. Thus, the titre might have been too low to produce sufficient staining of normal cells expressing only low amounts of the antigen.

We also investigated normal human bone marrow as a possible source of various precursor cells of the peripheral lymphoid tissues and blood. Stainings with a three-layer immunoalkaline phosphatase technique revealed only very few scattered Ki-1-positive cells among the haematopoietic cells. From the non-reactivity of Ki-1 antibody in a case of osteomyelosclerosis (Table 2), which is a neoplastic proliferation of cells of the granulopoiesis, erythropoiesis and thrombopoiesis, we conclude that Ki-1-positive cells in the normal bone marrow do not belong to one of those three major myeloid cell lineages.

The detection of Ki-1 antigen on a small number of normal cells in tonsils, lymph nodes and bone marrow suggests that it may be a differentiation antigen and not a virus-induced or tumour-specific antigen. The diagnostic value of the Ki-1 monoclonal antibody is not reduced by the occurrence of Ki-1 antigen on normal cells, because these cells are easily distinguishable from H and SR cells by morphological criteria. The expression of Ki-1 antigen on H and SR cells of all cases of Hodgkin's disease studied and the absence of Ki-1 antigen in non-Hodgkin's lymphomas demonstrates that this antigen may be used as a reliable marker for Hodgkin's disease. The constant expression of Ki-1 antigen on H and SR cells in all histological types of Hodgkin's disease also supports the view that H and SR cells of all variants of Hodgkin's disease are homogeneous in origin and nature and not heterogeneous as assumed by some investigators¹¹⁻¹⁴.

Table 1 Reactivity of cells of Hodgkin's disease with the antibody Ki-1

Histological type	No. of cases	No. of cases showing H and SR cells reactive with:		
		SK203 (directed at HLA-DR)	W6/32HK (inactive control)	Ki-1
Lymphocyte predominance	2	1	0	2
Nodular sclerosis	5	3	0	5
Mixed cellularity	5	4	0	5
Lymphocyte depletion	2	1	0	2
Total	14	9	0	14

Table 2 Reactivity of normal and malignant cells of various tissues with the antibody Ki-1

	No. of samples	SK203 (directed at HLA-DR)	Cells reactive with:	
			W6/32HK (inactive control)	Ki-1
Lymph nodes and tonsils	10	B-cells, macrophages, interdigitating cells	None	Usually only few, but sometimes clusters of cells showing weak reaction around, between and at inner rim of follicular mantles
Blood	5	Monocytes, B-cells	None	None
Bone marrow	2	Various cells	None	Very few, scattered cells
Thymus	1	Most of the non-lymphoid framework cells	None	Very few cells in the medulla
Lung	2	Macrophages	None	None
Kidney	3	Endothelial cells, intertubular fibrocytes, proximal tubules (weak reaction)	None	None
Liver	2	Kupffer's cells	None	None
Brain	1	Not done	None	None
Skin	2	Langerhans' cells	None	None
Piringer's lymphadenitis	1	B-cells, macrophages, interdigitating cells	None	Interfollicular areas with relatively many labelled cells
B-type chronic lymphocytic leukaemia	10	Tumour cells of all cases	None	None
Follicular lymphoma	15	Tumour cells of all cases	None	None
Lymphoblastic lymphoma of Burkitt type	5	Tumour cells of all cases	None	None
B-type large-cell lymphoma	10	Tumour cells of 4 of 5 cases	None	None
T-type chronic lymphocytic leukaemia	1	None	None	None
Lymphoblastic lymphoma of thymocytic type	3	None	None	None
Various lymphomas of peripheral T-cell type	8	None	None	None
Osteomyeloid sclerosis (containing nearly all maturation forms of the granulocyte- and thrombopoiesis)	1	Not done	None	None

So far, the cells from which H and SR cells are derived have not been identified. The small subset of cells detected by the Ki-1 antibody in normal lymphoid tissue may possibly give rise to H and SR cells in appropriate conditions. This may be the case as Hodgkin's disease usually starts to develop in those areas in which most of the small Ki-1-reactive normal cells are found, namely, the parafollicular area¹⁵. The Ki-1-positive normal cells were investigated using double immunofluorescent labelling and three-layer immunoperoxidase labelling of serial sections of tonsils and a case of Piringer's lymphadenitis, containing clusters of Ki-1-positive cells. Only the latter method was sensitive enough to obtain clear-cut results. The comparison of the single stained serial sections showed that the normal cell population expressing Ki-1 antigen does not react with antibodies directed at B cells (anti-IgM, anti-IgD), T cells (OKT11, ref. 16), macrophages (OKM1, ref. 17, monocyte.1, ref. 18 and monocyte 2, G. Nunez, *et al.*, in preparation and lysozyme), dendritic reticulum cells (R4/23, ref. 19), interdigitating reticulum cells (T-ALL 2, ref. 20), or cells of the granulopoiesis (Tü5, Tü6, Tü9, ref. 21, 3C4, ref. 22), erythropoiesis (anti-glycophorin A, ref. 23) or thrombopoiesis (J-15, AN-51, ref. 24). Thus, these data indicate that the Ki-1-positive normal cells lack markers specific to, or characteristic of all known cell types of the haemato-lymphoid system. It may be that the Ki-1 antibody detects a new, so far unidentified cell population in normal lymphoid tissue.

We thank Dr A. McMichael for the monoclonal antibodies J-15 and AN-51, Dr P. A. W. Edwards for monoclonal antibody against glycophorin A, and Dr A. Ziegler for monoclonal antibody W6/32HK. The technical assistance of Heinke Asbahr, Ilse Horn, Angela Gelhaus and Kirsten Tiemann is acknowledged. This work was supported by Deutsche Krebshilfe e.V., Schleswig-Holsteinische Krebsgesellschaft e.V. and Deutsche Forschungsgemeinschaft SFB 111, projects D7 and D8.

Received 29 March, accepted 24 June 1982.

1. Symmers, W. StC. in *Systemic Pathology* Vol. 2 (ed. Symmers, W. StC.) 767-891 (Churchill Livingstone, Edinburgh, 1978).
2. Stein, H. *et al.*, *J. Cancer Res. clin. Oncol.* **101**, 125-134 (1981).
3. Schaadt, M., Diehl, V., Stein, H., Fonatsch, C. & Kirchner, H. *Int. J. Cancer* **26**, 723-731 (1980).
4. Diehl, V. *et al.*, *J. Cancer Res. clin. Oncol.* **101**, 111-124 (1981).
5. Stein, H., Gerdes, J., Kirchner, H., Schaadt, M. & Diehl, V. *Int. J. Cancer* **28**, 425-429 (1981).
6. Köhler, G. & Milstein, C. *Nature* **256**, 495-497 (1975).
7. Stähli, C., Stachelin, T., Miggiano, V., Schmidt, J. & Häring, P. *J. immun. Meth.* **32**, 297-304 (1980).

8. Kearney, J. F., Radbruch, A., Liesegang, B. & Rajewski, K. *J. Immun.* **123**, 1548-1550 (1979).
9. Stein, *et al.*, *J. Histochem. Cytochem.* **28**, 746-760 (1980).
10. Stein, H. in *Leukaemia Markers* (ed. Knapp, W.) 99-108 (Academic, London, 1981).
11. Poppema, S. *J. Histochem. Cytochem.* **28**, 788-791 (1980).
12. Poppema, S., Kaiserling, E. & Lennert, K. *Histopathology* **3**, 295-308 (1979).
13. Poppema, S., Kaiserling, E. & Lennert, K. *Virchows Arch. B Cell Path.* **31**, 211-225 (1979).
14. Hansmann, M. L. & Kaiserling, E. *J. Cancer Res. clin. Oncol.* **101**, 135-148 (1981).
15. Lukes, R. J. *Cancer Res.* **31**, 1755-1767 (1971).
16. Verbi, W. *et al.*, *Eur. J. Immun.* **12**, 81-86 (1982).
17. Breard, J. M., Reinherz, E. L., Kung, P., Goldstein, G. & Schlossmann, S. F. *J. Immun.* **124**, 1943 (1980).
18. Ugolini, V., Nunez, G., Smith, G. R., Stastny, P. & Capra, J. D. *Proc. natl. Acad. Sci. U.S.A.* **77**, 6764-6768 (1980).
19. Naïem, M., Gerdes, J., Abdulaziz, Z., Stein, H. & Mason, D. Y. *J. clin. Path.* (submitted).
20. Stein, H., Gerdes, J., Schwab, U., Lemke, H., Mason, D. Y., Ziegler, A., Schienle, W. & Diehl, V. *Int. J. Cancer* (in the press).
21. Stein, H., Uchanska-Ziegler, B., Gerdes, J., Ziegler, A. & Wernet, P. *Int. J. Cancer* **29**, 283-290 (1982).
22. Schienle, W., Stein, H. & Müller-Ruchholtz, W. *J. clin. Path.* (in the press).
23. Edwards, P. A. W. *Biochem. Soc. Trans.* **8**, 334-335 (1980).
24. Vainchenker, W. *et al.*, *Blood* **59**, 514-521 (1982).
25. Ziegler, A. & Milstein, C. *Nature* **279**, 243-244 (1979).

HLA-restricted lymphoproliferative responses to MN blood group determinants

M. A. Blajchman*, N. Heddle†, N. Naipul† & D. P. Singal†

* The Canadian Red Cross Blood Transfusion Service and Departments of Pathology and Medicine, McMaster University, Hamilton, Ontario, Canada L8N 3Z5

† Department of Pathology, McMaster University, Hamilton, Ontario, Canada L8N 3Z5

It is well established that strong proliferative responses in mixed lymphocyte culture (MLC)¹ are controlled by gene products of the *HLA-D* locus, but stimulation between *HLA-D* identical individuals does occur and may partly be due to differences at the *HLA-A*, or *HLA-B* loci. However, many unrelated individuals who type identically for *HLA-A*, *-B*, *-C*, and *-D/DR* determinants have also been shown to be mutually stimulatory. The development of the primed lymphocyte test (PLT) provided a powerful tool in the identification of these non-*HLA* loci²⁻⁹. Using this test, we show here that significant *HLA*-restricted proliferative responses occurred in association with M or N blood group antigens.

Lymphocytes, separated from freshly drawn blood, were primed to stimulating cells from allogeneic donors in long-term MLC as described previously⁹. Lymphocytes were typed for HLA-A, -B, and -C antigens by the microdroplet lymphocytotoxicity test with a battery of highly selected typing antisera¹⁰. HLA-DR typing was performed on a B-cell enriched lymphocyte population¹⁰. HLA specificities were defined on the basis of reactivity with sera from the VIIth and VIIIth International Histocompatibility Workshops.

To investigate the role of the M and N determinants in PLT, lymphocytes from M-negative or N-negative donors were primed in long-term cultures against cells from donors mismatched for the corresponding M or N antigen. These responder-stimulator combinations were also mismatched for one or two HLA-DR antigens. Primed lymphocytes were then tested for proliferative responses against stimulating cells from third-party allogeneic donors. Data from one experiment demonstrating the role of the M determinant in PLT are given in Table 1. Lymphocytes from donor A (HLA-A2, A26; Bw16, Bw44; DRw8; Nss) were primed against cells from donor B (HLA-A1, Aw24; B8, Bw58; Cw6; DR1; MNs) in long-term MLC. Primed lymphocytes were tested for proliferative responses against stimulating cells from 10 allogeneic donors. Primed lymphocytes responded to three donors (C, D, E) who are positive for the sensitizing DR1 specificity. Primed lymphocytes also responded to three M-positive, HLA-A2-positive, HLA-DR1-negative donors (F, G, H). On the other hand, primed lymphocytes did not respond to two M-positive A2-negative, DR1-negative donors (I, J) and to two M-negative, DR1-negative donors (K, L). Similar data were observed in two other PLT experiments; (1) HLA-A3, A29; B8, Bw45; Cw6; Ns anti-A2, A28; Bw39, Bw50; DR2, DRw6; MS, and (2) HLA-A1, B7, B8; DR3, DR5; Ns anti-A2, A28; Bw39, Bw50; DR2; MS. The data from these three experiments are summarized in Fig. 1a. Primed cells responded to cells from donors who are positive for the sensitizing DR specificity. These primed lymphocytes also responded to lymphocytes from M-positive, sensitizing DR-negative individuals who shared HLA-A antigen(s) with the responder cells. However, primed lymphocytes did not respond to lymphocytes from M-positive, specific-DR-negative donors who did not share HLA-A determinant(s) with the responder cells. Primed lymphocytes did not respond to stimulating cells from M-negative, specific-DR-negative donors (data not shown).

Data from an experiment demonstrating the role of the N determinant in PLT are given in Table 2. Lymphocytes from a donor A (HLA-A2, A28; Bw39, Bw50, DR2, DRw6; MS) were primed against cells from donor B (HLA-A1, B7, B8; DR3; DR5; Ns). Primed lymphocytes were tested for proliferative responses against stimulating cells from 12 allogeneic donors. Primed lymphocytes responded to four donors (C, D, E, F) who are positive for the sensitizing DR3 or DR5

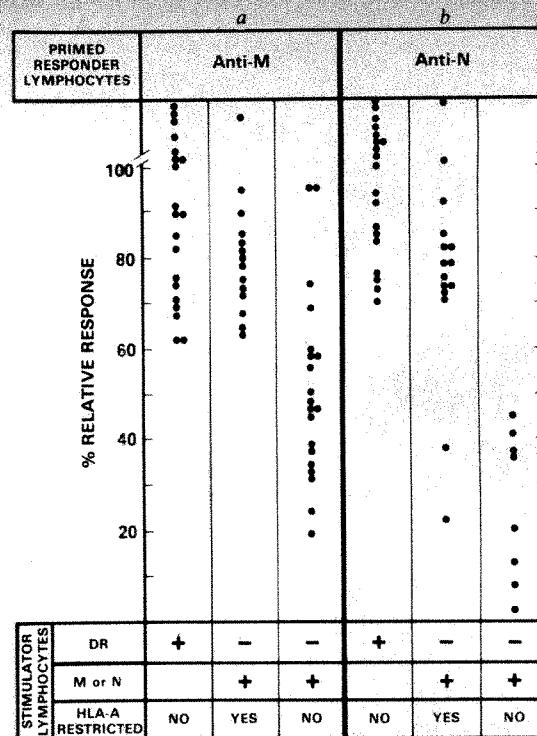


Fig. 1 Responses of primed lymphocytes to allogeneic lymphocytes in the primed lymphocyte test. *a* Shows the responses of primed lymphocytes to the sensitizing HLA-DR and M determinants (data pooled from three separate experiments); *b* shows the responses of primed lymphocytes to the sensitizing HLA-DR and N determinants (data pooled from three separate experiments). A PLT response to allogeneic donor cells was considered positive when the per cent relative response (% RR) was more than the lower limit of the mean ± 2 s.d. (95% confidence limits) of the PLT responses to the DR-specific allogeneic donors. Cut-off point for the anti-M PLT response is 61%; for anti-N 67%.

specificity. Primed lymphocytes also responded to three N-positive, HLA-A2-positive, HLA-DR3, 5-negative donors (G, H, I), but did not respond to three N-positive, A2-negative, DR3, 5-negative donors (J, K, L) or to two N-negative, DR3, 5-negative donors (M, N). No response to the s determinant was observed in this experiment. Similar data were observed in two other PLT experiments; (1) HLA-A2, A28; Bw39, Bw50; DR2, DRw6; MS anti-A3, A29; B8, Bw45; Cw6; DR3; Ns, and (2) HLA-A1, A3; Bw35, Bw52; Cw4; DR1; Ms anti-A2, A28; B14, Bw60; CW3; DR7; MNs (Fig. 1b).

Highly significant associations were found between PLT and

Table 1 Responses of primed lymphocytes to M determinant in PLT

Stimulating cell	HLA type -A, -B, -C	-DR	MNSs	% Relative response	PLT determinant
B	A1, Aw24; B8, Bw58; Cw6	1	MNs	100	+
C	Aw24, Aw33; B14, Bw63	1	MSs	145	+
D	A11, Aw33; B14, Bw44; Cw1	1	MNs	176	+
E	A1, Aw23; Bw44, Bw57; Cw6	1	MNSs	103	+
F	A1, A2; B8, Bw62; Cw3	3	MNSs	100	+
G	A1, A2; Bw39, Bw58; Cw6	7, w8	MSs	102	+
H	A2, Aw24; B7, Bw62; Cw3	4, w8	MSs	99	+
I	A1, Aw24; B8, Bw51	3, w6	MSs	58	-
J	A11; Bw62; Cw1, Cw3	3	MNs	34	-
K	A1; B7, B8	3, 5	Ns	16	-
L	A2, A3; B7, B8; Cw1	2	Ns	58	-

Lymphocytes from donor A (HLA-A2, A26; Bw16, Bw44; DRw8; Nss) were primed against cells from donor B in MLC. Primed lymphocytes were used at a concentration of 25×10^3 cells per well.

Table 2 Responses of primed lymphocytes to N determinant in PLT

Stimulating cell	HLA type -A, -B, -C	-DR	MNSs	% Relative response	PLT determinant
B	A1; B7, B8	3,5	Ns	100	+
C	A1, A2; B8, Bw62; Cw3	3	MNSs	109	+
D	A3, A29; B8, Bw45; Cw6	3	Ns	94	+
E	A11, Aw30; B13, B18; Cw6	5,7	MNS	86	+
F	A2, A29; B7, Bw60	4,5	MSs	73	+
G	A2, A3; B7, B27; Cw1	2	Ns	92	+
H	A2, A26; Bw16; Bw44	w8	NSs	73	+
I	A2, A28; B14, Bw60; Cw3	7	MNS	82	+
J	A11, Aw33; B14, Bw44; Cw1	1	MNS	45	-
K	A1, A11; Bw35, Bw37; Cw4	1	MNSs	37	-
L	A1, Aw23; Bw44, Bw57; Cw6	1	MNSs	36	-
M	Aw24, Aw33; B14, Bw63	1	MSs	22	-
N	A1, A3, Bw35, Bw52; Cw4	2	Ms	50	-

Lymphocytes from donor A (HLA-A2, A28; Bw39, Bw50; DR2, DRw6; MS) were primed against cells from donor B in MLC. Primed lymphocytes were used at a concentration of 25×10^3 cells per well.

HLA-DR determinants, and between PLT and HLA-restricted M or N determinants (Table 3). No differences were observed in the responses of responder lymphocytes to stimulator cells from homozygous or heterozygous M or N individuals. In our panel of normal healthy subjects, we have only one HLA-D/DR-identical, M- or N-mismatched pair. Primed lymphocytes (HLA-A1; B7, B8; DR3, DR5, Ns anti-A1, A3; B8, Bw35; DR3, DR5; MNS) responded to four M-positive donors who shared an HLA-A antigen with the responder lymphocytes. Primed lymphocytes did not respond to M-positive stimulators who did not share an HLA-A antigen.

To investigate the role of the S and s genes in PLT, lymphocytes were primed in responder-stimulator combinations mismatched for the S (or s) and for one or two HLA-DR antigens. Primed lymphocytes were tested for proliferative responses against stimulating cells from third-party allogeneic donors. Lymphocytes from third-party donors, who are positive for the sensitizing DR antigen, elicited strong proliferative response in PLT. However, primed lymphocytes did not respond to stimulating cells from donors who are positive for the specific S or s determinant but negative for the sensitizing DR specificity. These third-party donors included individuals who shared HLA-A determinant(s) with the responder PLT

cells. This was observed in six experiments using different responder-stimulator combinations. Thus, no effects of S or s incompatibility were observed in PLT.

The above findings demonstrate that lymphocytes from individuals mismatched for M and N determinants can cause significant HLA-restricted proliferative responses in PLT. It appears that lymphoproliferative responses in the PLT to stimulating lymphocytes from M and N mismatched individuals require the simultaneous expression of the same HLA-A antigen(s) on both stimulator and the primed responder lymphocytes. On the other hand, no effects of S and s incompatibilities were observed in the PLT.

MNSs determinants appear to be associated with two human erythrocyte membrane sialoglycoproteins¹¹⁻¹³. The M and N determinants are associated with glycophorin A, while the S and s determinants are associated with glycophorin B¹⁴. Similar sialoglycoproteins have been demonstrated in the membranes of other cells such as platelets, granulocytes and lymphocytes^{14,15}. Whether these glycoproteins are associated with the M and N antigens in these cells is unclear.

Blood group incompatibility has been shown to play a part in organ transplantation in man. Graft versus host disease in patients receiving bone marrow transplants from HLA-identical siblings has recently been correlated with MNSs incompatibility¹⁶. The present data suggest that MN determinants, or closely related genes, are expressed on lymphocytes and can cause HLA-restricted proliferative responses in PLT which may be an important consideration in organ transplantation.

This work was supported by the MRC of Canada. We thank Dr W. Rawls of McMaster University and Dr M. Schanfield of the American Red Cross for helpful suggestions during the preparation of this manuscript.

Table 3 Association between HLA-A-restricted M or N determinants and HLA-DR in PLT

	Association*				χ^2	r	P
	+/+	+/-	-/+	-/-			
PLT/M(HLA-A restricted)	14	8	0	23	18.38	0.69	$<10^{-4}$
PLT/HLA-DR	20	22	0	23	13.66	0.49	$<10^{-3}$
PLT/N(HLA-A restricted)	13	7	2	19	11.30	0.58	$<10^{-3}$
PLT/HLA-DR	19	20	0	21	12.81	0.50	$<10^{-3}$

A PLT response was considered positive or negative using the criteria given in Fig. 1. The data were analysed using 2×2 comparisons of the determinants recognized by PLT and HLA-DR. For PLT/M or N(HLA-A restricted) comparisons, allogeneic donors positive for the sensitizing HLA-DR antigens were excluded from the analysis.

* Association terminology (for example, for PLT/M(HLA-A-restricted): +/+ indicates a positive PLT test associated with the presence of the M antigen and HLA-A restriction; +/- indicates a positive PLT test associated with the absence of the M antigen and HLA-A restriction; -/+ indicates a negative PLT test associated with the presence of the M antigen and HLA-A restriction; -/- indicates a negative PLT test associated with the absence of the M antigen and HLA-A restriction.

Received 6 January; accepted 15 June 1982.

- Dupont, B., Hansen, J. & Yunis, E. *Adv. Immun.* **23**, 107-202 (1976).
- Sheehy, M. J., Sondel, P. M., Bach, M. L., Wank, R. & Bach, F. H. *Science* **188**, 1308-1310 (1975).
- Fraderlizi, D. & Dausset, J. *Eur. J. Immun.* **5**, 295-301 (1975).
- Singal, D. P. *Transplant Proc.* **10**, 771-774 (1978).
- Singal, D. P. *Transplant Proc.* **11**, 1813-1815 (1979).
- Sasportes, M., Nunez-Roldan, A. & Fraderlizi, D. *Immunogenetics* **6**, 55-68 (1979).
- Wank, R., Schendel, D. J., Hansen, J. A. & Dupont, B. *Immunogenetics* **6**, 107-115 (1979).
- Singal, D. P., Blajchman, M. A., Naipaul, N. & Josephs, S. *Hum. Immun.* **2**, 201-211 (1981).
- Singal, D. P. & Naipaul, N. *Transplant Proc.* **9**, 1755-1757 (1977).
- Terasaki, P. I., Bernoco, D., Park, M. S., Ozturk, G. & Iwaki, Y. *Am. J. clin. Path.* **69**, 103-120 (1978).
- Segrest, J. P., Kahane, I., Jackson, R. L. & Marchesi, V. T. *Archs Biochem. Biophys.* **155**, 167-183 (1973).
- Tomita, M. & Marchesi, V. T. *Proc. natn. Acad. Sci. U.S.A.* **72**, 2964-2968 (1975).
- Dahr, W., Unlenbruck, G., Janssen, E. & Schmalisch, R. *Hum. Genet.* **35**, 335-343 (1977).
- Anstee, D. J. *Semin. Hemat.* **18**, 13-31 (1981).
- Race, R. R. & Sanger, R. *Blood Groups in Man*, 92-138 (Blackwell, Oxford, 1975).
- Sparkes, R. S. *et al. Tissue Antigens* **15**, 212-215 (1980).

Monoclonal antibody defines a macrophage intracellular Ca^{2+} -binding protein which is phosphorylated by phagocytosis

David J. T. Vaux & Siamon Gordon

Sir William Dunn School of Pathology, University of Oxford, South Parks Road, Oxford OX1 3RE, UK

The macrophage is a highly phagocytic cell which has been widely used in attempts to dissect the mechanisms of endocytosis¹. In immune phagocytosis specific interactions occur between ligands on the presenting particle and Fc or C3b specific receptors expressed on the plasma membrane^{2,3}, but macrophages also avidly ingest particles such as polystyrene latex by an immunologically nonspecific mechanism. This process is guided by sequential ligand-receptor interactions^{4,5}. Biochemical studies indicate that actin, myosin and several regulatory components distinct from the troponin system of skeletal muscle, take part in phagocytosis by macrophages and polymorphonuclear leukocytes (PMN)⁶ and indirect immunofluorescence confirms the presence of these components at sites of phagocytic activity⁷. However, comparatively little is known about coupling between receptor binding and assembly of the contractile system, although electrical changes⁸ and the flux of divalent cations⁹ have been implicated. Here we report a monoclonal antibody that detects an intracellular protein from macrophages which binds Ca^{2+} in non-phagocytosing cells, and becomes phosphorylated as a result of phagocytosis. It might therefore take part in signal transduction during this process.

In an attempt to study antigenic components of the cytoplasmic face of the mouse macrophage phagolysosome membrane, rats were hyperimmunized with latex-containing phagolysosomes (LP) prepared by flotation in a discontinuous sucrose gradient¹⁰. Antibodies against LP were detected by trace indirect radioimmunoassay (RIA) and rats with high serum titres, $>1/1000$, used as spleen donors in myeloma fusions¹¹. Hybridoma supernatants containing antibodies for antigens on the cytoplasmic face of the phagolysosome membrane were screened on LP or on cells permeabilized by methanol fixation and positive cultures were cloned twice in soft agar. The present report studies PL4, one monoclonal antibody produced in this way.

The binding properties of PL4 were examined on intact or methanol-fixed thioglycollate-elicited mouse peritoneal macrophages (TPM), on LP isolated from such macrophages, and on mouse L-cell fibroblasts, which lack specific phagocytic pathways, but are able to ingest latex. The antigen it bound could be detected by RIA on LP (Fig. 1a), and in methanol-fixed, but not live TPM, even in the absence of a phagocytic stimulus (not shown). It was also detectable by RIA (Fig. 1b) and by FACS analysis (Fig. 1c) of permeabilized, but not intact (Fig. 1d) fibroblasts. Another monoclonal antibody, F4/80, which detects an external plasma membrane component of the macrophage¹², did not bind to isolated LP. Indirect immunofluorescence with fixed cells showed a granular cytoplasmic distribution, not confined to phagocytosing cells or the vicinity of phagolysosomes and the antibody recognizes a similar antigen in human and monkey, but not rat cells. We concluded that the antigen detected by PL4 is restricted to the inside of the cell and is present in macrophages as well as other cells, including cells which have not received a phagocytic stimulus.

If the inorganic phosphate pool within mouse macrophages is equilibrated with ^{32}P -labelled P_i, then a number of proteins associated with isolated LP become phosphorylated. PL4 specifically precipitates a labelled protein from lysates prepared from TPM after phagocytosis of latex microspheres (Fig. 2a,

arrow). This protein has a molecular weight of $\sim 19,000$ as estimated by SDS-polyacrylamide gel electrophoresis and was not detected as a phosphorylated molecule in control preparations without specific antibody or in the absence of a phagocytic stimulus (Fig. 2b-d).

If protein blotting techniques are used to produce nitrocellulose replicas of SDS-polyacrylamide gels then it is possible

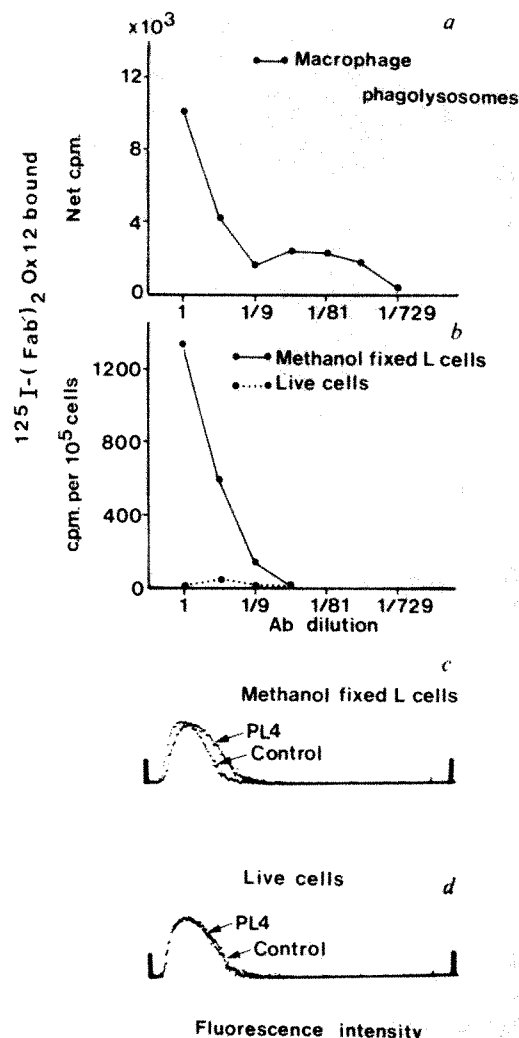


Fig. 1 PL4 detects an intracellular antigen in macrophages and fibroblasts. PL4 cells were grown in Iscove's modified minimal essential medium (MEM) supplemented with 5% fetal bovine serum (FBS), heat inactivated for 30 min at 56 °C, and antibiotics (I+5). The antibody, a rat IgG2a, was precipitated with $(\text{NH}_4)_2\text{SO}_4$, washed, dissolved in phosphate-buffered saline, pH 7.4 (PBS) and dialysed against PBS + 10 mM NaN_3 . a, LP were prepared from homogenates of TPM fed 1.1- μm latex microspheres (LB11, Sigma) 15 h previously. RIA was performed²⁰ by incubating LP with serial dilutions of PL4 in PBS + 0.1% (w/v) BSA + 10 mM NaN_3 (PBA) for 1 h at 4 °C. PL were washed twice in PBA, pelleted for 3 min and incubated for 1 h at 4 °C with 3×10^5 c.p.m., ^{125}I -F(ab')₂ fragments of MRC OX12, a monoclonal mouse antibody against the rat heavy chain b allotype¹¹ donated by Dr S. Hunt. Samples were washed three times in PBA and LP counted in clean tubes in a Packard γ -counter. Results are given as mean counts bound ($n=2$, range $<10\%$ of mean). b, Mouse L929 cells²¹ were fixed in methanol at -20 °C for 6 min or used unfixed after a wash in PBA. Binding of PL4 was done as in a. Samples were resuspended in Isoton and the number determined in a Coulter counter. Results show mean counts bound per 10^5 cells ($n=2$, range $<10\%$ of mean). c, d, Live and methanol-fixed L929 cells were incubated with PL4 and then with tetramethylrhodamine conjugated OX12, 25 μg per ml. After washing, cells were examined using a fluorescence activated cell sorter (Becton Dickinson). The profiles display relative number against rhodamine fluorescence. Cell fragments and large aggregates were excluded electronically.

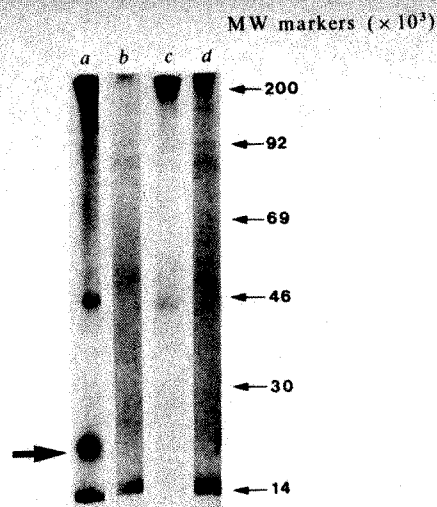


Fig. 2 PL4 precipitates a phosphorylated protein after phagocytosis. TPM were incubated for 1 day at 5×10^6 cells per 100-mm tissue culture dish (Corning 25020) in 5 ml of I+5 (see Fig. 1 legend). Adherent cells were washed twice in saline and 3 ml of MEM with 5% heat-inactivated FBS which was phosphate free, and 1 mCi per dish of $^{32}\text{P}_i$ (Amersham International). Dishes were incubated for 5 h to ensure equilibration of the phosphate pool (trichloroacetic acid-precipitable counts plateau by 90 min), the $^{32}\text{P}_i$ -containing medium was then aspirated and cells were washed with saline. Dishes were treated with 5 ml prewarmed I+5 with or without 1% latex and incubated at 37°C for 15 min. Cells were washed three times with ice-cold PBS with 10 mM NaN_3 and collected with a rubber policeman in 5 ml of ice cold collection buffer (PBS with 1% (v/v) aprotinin, 1 mM phenylmethylsulphonyl fluoride (PMSF), 2 mM EDTA and 10 mM NaN_3). Cells were centrifuged at 1,000 r.p.m. for 5 min and the pellet dissolved in 1 ml lysis buffer (PBS with 0.5% (v/v) NP40, 0.1% (w/v) SDS, 1% (v/v) aprotinin, 1 mM PMSF and 10 mM NaN_3) on ice, for 15 min. The lysate was clarified by centrifugation for 15 min and distributed to microfuge tubes for immunoprecipitation. 400 μl of lysate was incubated at 4°C for 1 h with 50 μl PL4 and then 25 μl of hyperimmune rabbit anti-rat IgG serum, heat inactivated at 56°C for 30 min and clarified by ultracentrifugation before use. The precipitate was collected by centrifuging for 10 min, washed three times in lysis buffer, and resuspended by sonication in 25 μl of 8 M urea, 5% (w/v) SDS in 25 mM Tris-HCl, pH 7.0. SDS-containing sample buffer (25 μl) was added, and the samples were boiled and analysed on 10% acrylamide SDS-polyacrylamide gels²². Gels were processed for fluorography²³, dried by vacuum and autoradiographed with Kodak X-Omat paper at -70°C for 18 days. Immunoprecipitates: a, PL4, after phagocytosis. b, PBA, after phagocytosis. c, PL4, no phagocytosis. d, PBA, no phagocytosis. ^{14}C -methylated protein markers (Radiochemical International) were run at the same time.

to detect proteins which bind $^{45}\text{Ca}^{2+}$. Figure 3 shows the major Ca^{2+} -binding species in a lysate prepared from TPM which have not received a phagocytic stimulus. When PL4 is used to immunoprecipitate unlabelled macrophage lysates insufficient protein is recovered to stain with Coomassie blue. However, after blotting and incubation with $^{45}\text{Ca}^{2+}$ it is clear that the antigen recognized by PL4 is a Ca^{2+} -binding protein (Fig. 3d) as well as a target for phosphorylation (Fig. 2a). Similar preparations of other monoclonal antibodies or heterogeneous antisera against LP do not precipitate this molecule. This novel method for detecting Ca^{2+} -binding proteins will reveal only those proteins with an affinity for Ca^{2+} below that of EDTA (otherwise EDTA will not release the unlabelled Ca^{2+} before replacement with $^{45}\text{Ca}^{2+}$) and has the disadvantage common to all nitrocellulose blotting techniques of reduced transfer efficiency with increasing molecular weight. However, the method can detect Ca^{2+} -binding proteins with molecular weight (MW) $>100,000$ (Fig. 3a).

Calcium-binding proteins of similar size have been isolated from various sources including calmodulin¹³, which is not phosphorylated, and myosin light chain¹⁴ which can be phosphorylated in certain conditions. We have found with the aid of sensitive radioimmunoassays that PL4 does not bind to highly purified vertebrate calmodulin¹⁵ or myosin light chains from bovine thymus or chicken gizzard¹⁶. As this antigen is neither species nor tissue specific we suspect that it is a different protein,

but further studies with affinity-purified material are needed to establish its identity.

The continuation of phagocytosis in the absence of extracellular calcium¹⁷ and the lack of muscle-like regulatory components of actomyosin have been used to argue against a role for Ca^{2+} in coupling ligand-receptor binding with actomyosin contraction in the macrophage. However, more recently it has

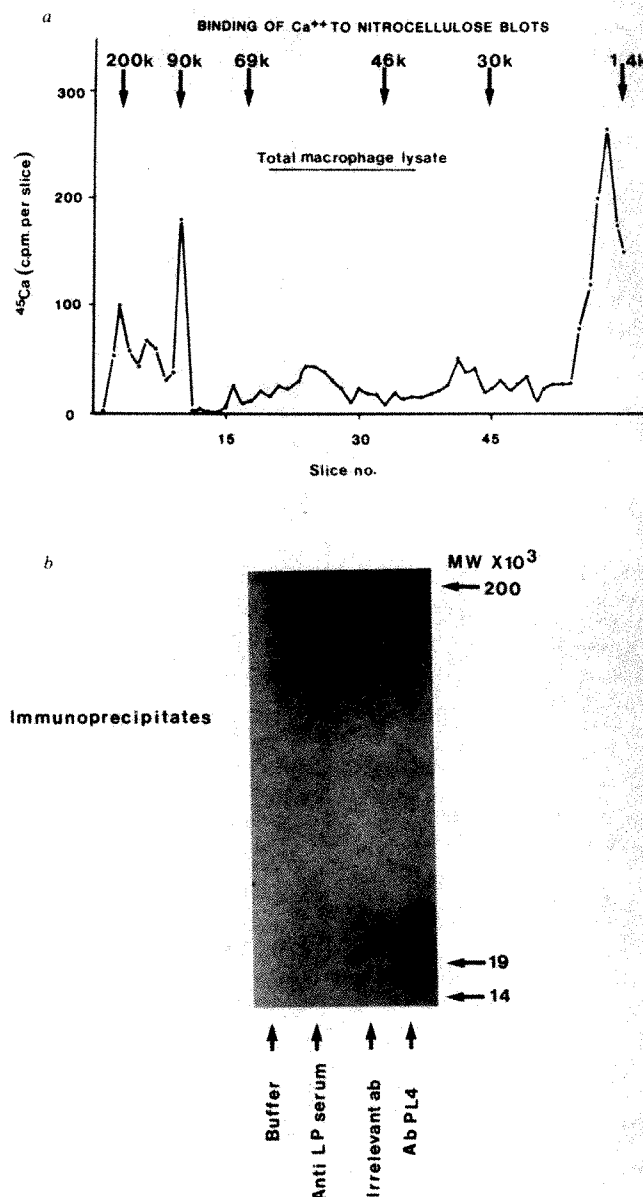


Fig. 3 The protein immunoprecipitated by PL4 binds Ca^{2+} . Unlabelled TPM were prepared without a phagocytic stimulus, as in Fig. 2. Total lysates and PL4 immunoprecipitates were processed and electrophoresed and the gel blotted on nitrocellulose filters by diffusion in transfer buffer (50 mM NaCl, 2 mM NaEDTA, 0.1 mM dithiothreitol in 10 mM Tris-HCl, pH 7.0) for 48 h²⁴. The filters were washed overnight at room temperature in PBS containing 10 mM NaEDTA, made in deionized water, and in three changes of deionized water (1 h each). Filters were incubated with $1 \mu\text{Ci cm}^{-2}$ $^{45}\text{CaCl}_2$ (Amersham International) in deionized water for 3 h at room temperature. Excess $^{45}\text{Ca}^{2+}$ was removed by washing in PBS. The filters were air dried and either autoradiographed with an intensifier screen (Fuji) using Kodak NST-1 film at 4°C for 15 days, or cut into 1-mm strips and counted in a Packard scintillation spectrometer. a, $^{45}\text{Ca}^{2+}$ -binding proteins of the macrophage lysate. Although it is possible to blot ^{14}C -methylated molecular weight markers, in this experiment the nitrocellulose blot was calibrated from markers run on an adjacent unblotted section of the parent gel. b, $^{45}\text{Ca}^{2+}$ -binding proteins after immunoprecipitation with PL4 or controls.

become clear that the macrophage does possess a molecule (gelsolin, MW ~93,000) which confers Ca^{2+} dependence on the contractile system⁶, and that this component is present at the site of phagocytosis (H. L. Yin, personal communication). It is therefore possible that the macrophage contractile machinery is ultimately under Ca^{2+} control, as in skeletal muscle¹⁸. If this is the case, then the lack of requirement for extracellular Ca^{2+} suggests that the local increased Ca^{2+} is due to some event other than an inward Ca^{2+} flux across the plasma membrane. The Ca^{2+} may be released into the cytosol from some intracellular site of sequestration, triggered by ligand-receptor binding at the cell surface. The component of the macrophage described here is a good candidate to mediate such a calcium signal and experiments are now under way to examine the kinetics of

phosphorylation and its effect on the Ca^{2+} -binding affinity of the molecule.

The antigen detected by PL4 is present in cells before phagocytosis and binds Ca^{2+} in this form, although incorporation of ^{32}P occurs only after a phagocytic stimulus. Nonphysiological stimuli which perturb the membrane such as phorbol myristate acetate¹⁹ also have this effect on the antigen. Further studies are needed to define the association between this antigen and the phagolysosomal membrane and its relation to phosphorylation by phagocytosis.

We thank Ms Maxine Bampton for technical help and Drs D. M. Watterson and J. Kendrick-Jones for purified calmodulin and myosin light chains. This work was supported by a research studentship and a grant from the MRC.

Received 24 December 1981; accepted 8 July 1982.

1. Silverstein, S. C., Steinman, R. M. & Cohn Z. A. *A. Rev. Biochem.* **46**, 669–722 (1977).
2. Unkeless, J. C. *J. exp. Med.* **145**, 931–947 (1977).
3. Bianco, C., Griffin, F. M. & Silverstein, S. C. *J. exp. Med.* **141**, 1278–1290 (1975).
4. Griffin, F. M. & Silverstein, S. C. *J. exp. Med.* **139**, 323–336 (1974).
5. Griffin, F. M., Griffin, J. A. & Silverstein, S. C. *J. exp. Med.* **144**, 788–809 (1976).
6. Stossel, T. P., Hartwig, J. H., Yin, H. L. & Stendahl, O. *Biochem. Soc. Symp.* **45**, 51–63 (1981).
7. Stendahl, O., Hartwig, J. H., Brotschi, E. A. & Stossel, T. P. *J. Cell Biol.* **84**, 215–224 (1980).
8. Kouri, J., Noa, M., Diaz, B. & Nimbo, E. *Nature* **283**, 868–869 (1980).
9. Hoffstein, S. T. *J. Immun.* **123**, 1395–1402 (1979).
10. Wetzel, M. G. & Korn, E. D. *J. Cell Biol.* **43**, 90–104 (1969).

11. Galfre, G., Milstein, C. & Wright, B. *Nature* **277**, 131 (1979).
12. Austyn, J. M. & Gordon, S. *Eur. J. Immun.* **11** (1981).
13. Klee, C. B., Crouch, T. H. & Richman, R. G. *A. Rev. Biochem.* **49**, 489–515 (1980).
14. Kendrick-Jones, J. & Scholey, J. M. *J. Muscle Res. Cell Motility* **2**, 347–372 (1981).
15. Watterson, D. M., Iverson, D. B. & van Eldik, L. H. *Biochemistry* **19**, 5762–5768 (1980).
16. Scholey, J. M., Taylor, K. A. & Kendrick-Jones, J. *Nature* **287**, 233–235 (1980).
17. Stossel, T. P. *J. Cell Biol.* **58**, 346–356 (1973).
18. Endo, M. *Physiol. Rev.* **57**, 71–108 (1977).
19. Schneider, C., Zanetti, M. & Romeo, D. *FEBS Lett.* **127**, 4–8 (1981).
20. Morris, R. J. & Williams, A. F. *Eur. J. Immun.* **5**, 274 (1975).
21. Hunt, S. V. & Fowler, M. H. *Cell Tissue Kinetics* **14**, 445–464 (1981).
22. Laemmli, U. K. *Nature* **227**, 680 (1970).
23. Bonner, W. M. & Laskey, R. A. *Eur. J. Biochem.* **46**, 83 (1974).
24. Bowen, B., Steinberg, J., Laemmli, U. K. & Weintraub, H. *Nucleic Acids Res.* **8**, 1–20 (1980).

Dopaminergic supersensitivity induced by denervation and chronic receptor blockade is additive

D. A. Staunton, P. J. Magistretti, G. F. Koob, W. J. Shoemaker & F. E. Bloom

Arthur V. Davis Center for Behavioral Neurobiology, The Salk Institute, PO Box 85800, San Diego, California 92138, USA

A persistent, severe reduction of synaptic transmission has been shown to enhance the responsiveness of postsynaptic tissue to the deficient neurotransmitter—a phenomenon called postjunctional supersensitivity^{1–4}. Regardless of whether supersensitivity is induced by removal of presynaptic nerve terminals (denervation) or by chronic postsynaptic receptor blockade, qualitatively similar adaptations in peripheral autonomic targets are usually produced, suggesting that the two types of manipulation are interchangeable and that the postsynaptic molecular alterations they produce are identical². Following bilateral destruction of dopamine-containing afferents to the nucleus accumbens in the rat, there is a pronounced behavioural hyperresponsiveness to direct dopamine agonists^{5–7}. A remarkably similar situation develops after chronic administration of antipsychotic drugs^{8–10}, such as haloperidol, which are known to be potent antagonists at putative dopamine receptors^{11–13}. We report here that a combination of these two procedures unexpectedly leads to far greater dopaminergic supersensitivity than is observed with either treatment alone. In subjects with the combined treatments, the dopamine agonist apomorphine was more effective in tests of locomotor activation, and additive elevation of the B_{max} for ^3H -spiperone binding in the nucleus accumbens was observed. These results suggest that denervation and chronic exposure to receptor antagonists can lead to independent processes of postjunctional supersensitivity.

Male Sprague-Dawley rats (Charles River Laboratories; mean weight 305 g) were used. To study denervation supersensitivity, 8 μg of 6-hydroxydopamine were injected into the nucleus accumbens on each side as previously described¹⁴. Sham-treated control subjects were prepared with bilateral

injections of the ascorbate/Ringer's 6-hydroxydopamine vehicle. On the third post-surgical day, the animals were screened for dopaminergic behavioural responsiveness to apomorphine (0.1 mg per kg = 329 nmol free base per kg; method as in Fig. 1 legend). The cumulative counts were used to rank 6-hydroxydopamine- and sham-injected subjects into two equally responsive groups of the same size.

On the day following this screening, chronic drug treatment was initiated. Haloperidol (McNeil Injectable), 2.2 μmol per kg per day, was administered subcutaneously (s.c.) to one-half of the 6-hydroxydopamine-treated and one-half of the sham-treated animals for 14 (expt 2) or 15 (expt 1) days. The control animals were injected with haloperidol vehicle¹⁵ (see Fig. 1 legend for details). None of the treatments resulted in any overt toxicity.

Seventeen days after the lesions, the rats were tested for locomotor activation by various doses of apomorphine-HCl (32.9–329 nmol per kg, s.c.). On the day following the final behavioural assessment, the animals were decapitated and catecholamine levels in the nucleus accumbens were determined (see Fig. 2 legend).

A second series of animals (expt 2) were treated for analysis of nucleus accumbens neuroleptic-binding sites. The animals were evaluated for apomorphine-induced locomotor activity (0.1 mg per kg, s.c.) as detailed above on the second day of withdrawal from chronic drug administration. On the following day, the subjects were decapitated and ^3H -spiperone-binding sites in the nucleus accumbens were measured¹⁶.

Figure 1 shows the results of behavioural testing with apomorphine-HCl at one dose (165 nmol per kg). In both sham-lesioned animals chronically treated with haloperidol and animals receiving 6-hydroxydopamine injections and vehicle, apomorphine potentiated locomotor activity ($P < 0.01$ and $P < 0.001$ respectively). When treatment with 6-hydroxydopamine and chronic haloperidol injections were combined, the response to apomorphine was considerably greater than with either treatment alone. Spontaneous locomotor activity before apomorphine injection was not significantly different between groups. The same pattern of response was observed at all doses of apomorphine (Fig. 2). There were no significant effects of the saline/ascorbate vehicle.

Additional information was obtained by determining the ED_{50} values, defined as the dose of apomorphine which led to

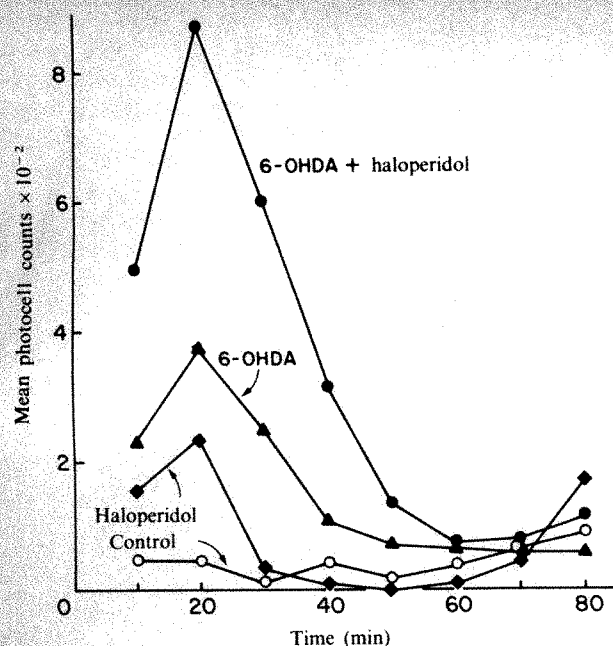


Fig. 1 Locomotor activity following interscapular subcutaneous injection (at $t=0$ min) of 165 nmol per kg apomorphine-HCl. Before injection, the animals were allowed a 70–80 min habituation period in the testing cages, during which time no effects of the various chronic pretreatments were observed. Activity was evaluated in cages containing twin photocell beams as previously described¹⁵. The values are the mean photocell counts recorded during each preceding 10 min interval for the groups represented as follows: \circ , bilateral sham nucleus accumbens injections +15 days of haloperidol vehicle ($n=7$); \bullet , sham nucleus accumbens lesion +15 days of 1 mg per kg haloperidol s.c. ($n=8$); \blacktriangle , bilateral 6-hydroxydopamine (6-OHDA; 8 μ g each side) nucleus accumbens injections +15 days of haloperidol vehicle ($n=6$); \bullet , 6-hydroxydopamine nucleus accumbens lesions +15 days of haloperidol ($n=8$). Statistical analysis was accomplished with two-factor analysis of variance, which allowed the testing for main effects of chronic haloperidol and 6-hydroxydopamine treatment as well as for their interaction, with significance assumed in each case when $P < 0.05$.

a doubling of the cumulative activity scores in one-half of the subjects in each group compared with the control group. In animals receiving prolonged haloperidol treatment alone, ED_{50} was achieved in the range 82–165 nmol apomorphine per kg, while that for subjects receiving only 6-hydroxydopamine was 33–82 nmol per kg of apomorphine. In the case of the combined treatment, the apparent ED_{50} was observed with 33 nmol apomorphine per kg. The rats receiving the combined treatment were approximately twofold more sensitive to the locomotor activating effect of apomorphine than those with the lesion alone and approximately fivefold more sensitive than those receiving chronic haloperidol alone. Moreover, our data (Fig. 2) clearly demonstrate that the magnitude of locomotor activation induced by 165 and 329 nmol per kg of apomorphine in subjects with the combined treatment is greater than the sum of the apomorphine-induced activation seen with either treatment alone. Thus, the potency and efficacy of apomorphine were both enhanced in animals with the combined treatment compared with those with either treatment alone.

Figure 3 shows a part of a Scatchard¹⁶ analysis of 3H -spiperone binding to membranes prepared from the nucleus accumbens of the similarly pretreated groups of expt 2. Statistical analysis revealed two significant effects—an elevation of B_{max} values produced by treatment with the neurotoxin ($P < 0.001$) and a separate elevation produced by chronic administration of haloperidol ($P < 0.001$). There was no significant interaction of 6-hydroxydopamine and the chronic neuroleptic. In contrast, we could not detect any effect of the pretreatments on the K_d values ($P > 0.05$). In animals with

bilateral injections of 6-hydroxydopamine into the nucleus accumbens and chronic haloperidol administration, there was a greater increase in the density of 3H -spiperone-binding sites than there was with either treatment alone, and, again, the affinity constant was not altered. The quantitatively similar effects of 6-hydroxydopamine and chronic haloperidol treatments on the B_{max} (both producing $\sim 15\%$ increase) suggested that, together, the two treatments can produce an additive increase in the receptor density.

Our findings confirm previous reports that enhanced apomorphine-induced locomotor activity follows bilateral 6-hydroxydopamine injection into the nucleus accumbens region, a phenomenon which is thought to signify post-junctional dopaminergic supersensitivity in mesolimbic targets^{6,7,17}. However, until the present study, there has been no corresponding report of an increased density of 3H -spiperone-binding sites.

Our most intriguing result is the enhancement, which is at least additive, of apomorphine-induced locomotor activity when near-total elimination of dopamine from the nucleus accumbens is coupled with prolonged exposure to haloperidol. This finding is not predicted on the basis of classical investigations of supersensitivity², because both denervation and chronic receptor blockade are thought to evoke post-junctional supersensitivity by the same route—by persistently preventing neurotransmitter action at the postsynaptic membrane. Indeed, one interpretation of our results is that chronic exposure of postsynaptic elements in the nucleus accumbens to the antagonist in the absence of any appreciable neurotransmitter could, in its own right, trigger some of the adaptations comprising supersensitivity. This is supported by the independent elevations of nucleus accumbens dopaminergic (D-2)¹⁸ receptor densities secondary to denervation and long-term receptor

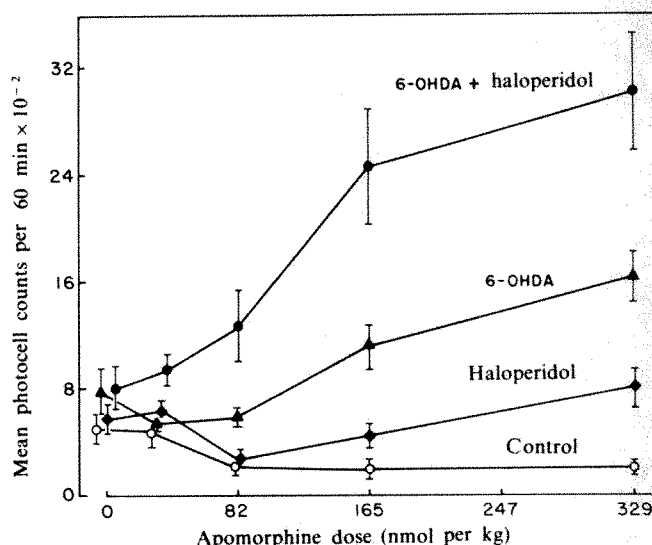


Fig. 2 Effect of various doses of apomorphine-HCl on locomotor activity. Note that the dose 329 nmol per kg corresponds to 0.1 mg per kg apomorphine-HCl. Values are the cumulative number of photocell beam interruptions (mean \pm s.e.m.) for the 60 min following apomorphine administration. Symbols and number of subjects in each group as in Fig. 1 legend. Subjects were allowed to habituate to the testing apparatus for 60–90 min before apomorphine injection. One day after the behavioural tests were completed, all subjects were decapitated for analysis of dopamine and metabolite levels in nucleus accumbens. The nucleus accumbens were dissected from a coronal slice over ice as described previously²² (wet wt ~ 8 mg) and immediately homogenized in 0.5 ml (~ 60 vols) of 0.1 M $HClO_4$ (containing 1 M $NaHSO_3$). After sonication, aliquots of each sample were centrifuged and purified by elution from alumina columns. Analysis was completed using HPLC (for details, see ref. 23). Dopamine levels (ng per mg protein) were as follows: control, 62.4 ± 5.6 ; haloperidol, 63.7 ± 3.9 ; 6-hydroxydopamine, 1.33 ± 0.21 (98% loss compared with control); 6-hydroxydopamine + haloperidol, 1.85 ± 0.52 (97% loss compared with haloperidol).

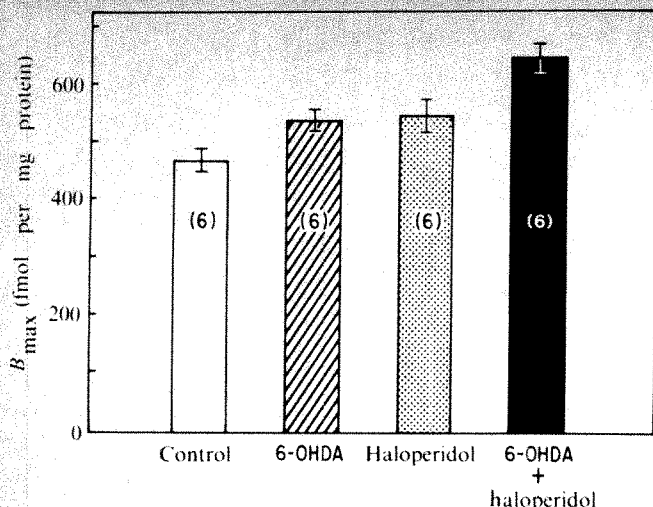


Fig. 3 Density of nucleus accumbens ^3H -spiroperone-binding sites as a function of treatment history. The nucleus accumbens were isolated (Fig. 2 legend) separately for each animal, homogenized in 1.5 ml of 10 mM Tris-maleate (with 0.9% NaCl, pH 7.5) and spun for 10 min at 20,000g at 4°C. Pellets were resuspended in 12 ml (mean final protein concentration, 60.0 μg per 900 μl) of 20 mM Tris buffer (with 0.9% NaCl, pH 7.5) using a Polytron (setting 5). An aliquot of the suspended membranes (900 μl) was combined with 100 μl of a solution containing ^3H -spiroperone (final concentrations 0.08–1.5 nM; six points in singlet for each subject) or the radioligand plus (+)butaclamol (final concentration 2 μM) to define the nonspecific binding. Further details of the binding procedure are described elsewhere²⁴. Average specific c.p.m. bound in control group binding curves were 167 and 669 for 0.08 and 1.5 nM ^3H -spiroperone respectively. B_{max} (corrected for protein²⁵) and K_d values were determined for each animal using Scatchard analysis¹⁶ and linear regression (correlation coefficients were 0.86–0.99). Control K_d values were 254 ± 24.1 pM. A recent investigation²⁶, including pharmacological characterization of ^3H -spiroperone-binding sites in the nucleus accumbens-olfactory tubercle and regional study of chronic neuroleptic-induced increases in the density of those sites strongly suggest that nucleus accumbens membrane sites labelled by this radioligand are of the dopaminergic D-2 class¹⁸ that has been characterized in the neostriatum. Thus, the nucleus accumbens sites are chiefly non-serotonergic^{27,28}. Pretreatments are as described in Fig. 1 legend, except that haloperidol was administered for 14 days. Values are the mean \pm s.e.m., n in parentheses.

blockade (see Fig. 3 legend for comments on ^3H -spiroperone binding in nucleus accumbens). It is interesting to note that acute haloperidol administration was found to decrease acetylcholine content in the corpus striatum after the elimination of the dopaminergic input¹⁹.

Because haloperidol is known to increase dopamine release which could, in part, compensate for postsynaptic receptor blockade, it could be argued that chronic haloperidol by itself does not lead to maximal supersensitivity and that dopaminergic denervation merely gives rise to the full expression of haloperidol-induced supersensitivity. However, this explanation is extremely unlikely. Because dopamine and haloperidol compete for postsynaptic receptor sites, a greater daily dose of haloperidol might be expected to produce greater postsynaptic receptor blockade and, thus, greater supersensitivity, if other factors were equal. However, it was demonstrated²⁰ that a substantially higher dose of haloperidol than we used did not produce a greater elevation of dopamine receptors, and, furthermore, haloperidol-induced dopamine utilization in rat nucleus accumbens has been shown to be reduced as the magnitude of the repeated doses is raised over a 10-fold range (0.5–5 mg per kg)²¹. Thus the idea that haloperidol-lesion-induced postsynaptic blockade is sub-maximal due to the ability of the antagonist to elevate dopamine release is unsupportable.

The marked enhancement of behavioural supersensitivity following combined denervation and chronic receptor blockade in our studies is therefore probably the result of potentiated

postjunctional supersensitivity phenomena in the nucleus accumbens. Furthermore, the increase in receptor density induced by haloperidol in 6-hydroxydopamine-treated rats cannot be located on presynaptic dopamine terminals, demonstrating that the supersensitive response to both treatments must be located on postsynaptic elements. It will be interesting to investigate the generality of these phenomena by analogous testing in other neurotransmitter systems.

We thank N. Callahan for preparation of the manuscript, Drs A. Ettenberg and S. Young for helpful discussion of data analysis, and H. Pettit and L. Randolph for technical assistance. D.A.S. was supported by grant MH 08080, P.J.M. by Swiss NSF fellowship 83.832.0.80 and W.J.S. and F.E.B. by NIMH grant 29466.

Received 24 February; accepted 1 July 1982.

1. Trendelenburg, U. *Pharmac. Rev.* **18**, 629–640 (1966).
2. Emmelin, N. *Pharmac. Rev.* **13**, 17–37 (1961).
3. Schwartz, J. C., Costentin, J., Martres, M. P., Protas, P. & Baudry, M. *Neuropharmacology* **17**, 665–685 (1978).
4. Fleming, W. W. *Trends pharmac. Sci.* **2**, 152–154 (1981).
5. Costall, B., Hui, S.-C. G. & Naylor, R. J. *Neuropharmacology* **19**, 1039–1048 (1980).
6. Kelly, P. H., Seviour, P. W. & Iversen, S. R. *Brain Res.* **94**, 507–522 (1975).
7. Kelly, P. H. & Iversen, S. D. *Eur. J. Pharmac.* **40**, 45–56 (1976).
8. Jackson, D. M., Anden, N.-E., Engel, J. & Liljequist, S. *Psychopharmacology* **45**, 151–155 (1975).
9. Gianutsos, G., Hynes, M. D., Drawbaugh, R. & Lal, H. *Prog. Neuro-Psychopharmac.* **2**, 161–167 (1978).
10. Davis, K. L., Hollister, L. E. & Fritz, W. C. *Life Sci.* **23**, 1543–1548 (1978).
11. Clement-Cormier, Y. C., Keabian, J. W., Petzold, G. L. & Greengard, P. *Proc. natn. Acad. Sci. U.S.A.* **71**, 1113–1117 (1974).
12. Miller, R. J., Horn, A. S. & Iversen, L. L. *Molec. Pharmac.* **10**, 759–766 (1974).
13. Bockaert, J., Tassin, J. P., Thierry, A. M., Glowinski, J. & Premont, J. *Brain Res.* **122**, 71–86 (1977).
14. Joyce, E. M. & Koob, G. F. *Psychopharmacology* **73**, 311–313 (1981).
15. Staunton, D. A., Magistretti, P. J., Schoemaker, W. J. & Bloom, F. E. *Brain Res.* **232**, 391–400 (1982).
16. Scatchard, G. *Ann. N.Y. Acad. Sci.* **51**, 660–672 (1949).
17. Rosenfeld, M. R., Seeger, T. F., Sharpless, N. S., Gardner, E. L. & Makman, M. H. *Brain Res.* **173**, 572–576 (1979).
18. Creese, I., Hamblin, M. W., Leff, S. E. & Sibley, D. R. *Handb. Psychopharmac.* **16** (in the press).
19. Guyenet, P. G. *et al. Brain Res.* **84**, 227–244 (1975).
20. Burt, D. R., Creese, I. & Snyder, S. H. *Science* **196**, 326–328 (1977).
21. Scatton, B. *Eur. J. Pharmac.* **46**, 363–369 (1977).
22. Koob, G. F., Stinus, L. & LeMoal, M. *Behav. Brain Res.* **3**, 341–359 (1981).
23. Staunton, D. A., Magistretti, P. J., Schoemaker, W. J., Deyo, S. N. & Bloom, F. E. *Brain Res.* **232**, 401–412 (1982).
24. Staunton, D. A., Wolfe, B. B., Groves, P. M. & Molinoff, P. B. *Brain Res.* **211**, 315–327 (1981).
25. Lowry, O. H., Rosebrough, N. J., Farr, A. L. & Randall, R. J. *J. biol. Chem.* **193**, 265–275 (1951).
26. Bacopoulos, N. G. *J. Pharmac. exp. Ther.* **219**, 708–714 (1981).
27. Enna, S., Bennett, J., Burt, D., Creese, I. & Snyder, S. H. *Nature* **263**, 338–341 (1976).
28. Marchais, D., Tassin, J. P. & Bockaert, J. *Brain Res.* **183**, 235–240 (1980).

Enkephalin opens potassium channels on mammalian central neurones

John T. Williams, Terrance M. Egan & R. Alan North

Neuropharmacology Laboratory, Department of Nutrition and Food Science, Massachusetts Institute of Technology, Cambridge, Massachusetts 02139, USA

Enkephalin and opiate analgesic drugs exert their effects on the brain by interacting with receptors located on neuronal membranes. An almost immediate consequence of this interaction is an inhibition of action potential discharge of individual nerve cells¹. This could result from a direct hyperpolarization of the neurone which bears the opiate receptors, thereby shifting its membrane away from the threshold for action potential generation. On the other hand, it is well known that opiates and enkephalin depress the release of neurotransmitters^{2,3}, and this could indirectly result in an inhibition of cell firing. Here we describe experiments which indicate that Met⁵-enkephalin and a stable analogue, D-Ala²-D-Leu⁵-enkephalin (DADLE), as well as narcotic analgesics, increase the potassium conductance of neurones in the rat locus coeruleus and thereby inhibit their spontaneous firing. This effect of the opioids results from an interaction with a receptor having a high affinity for naloxone.

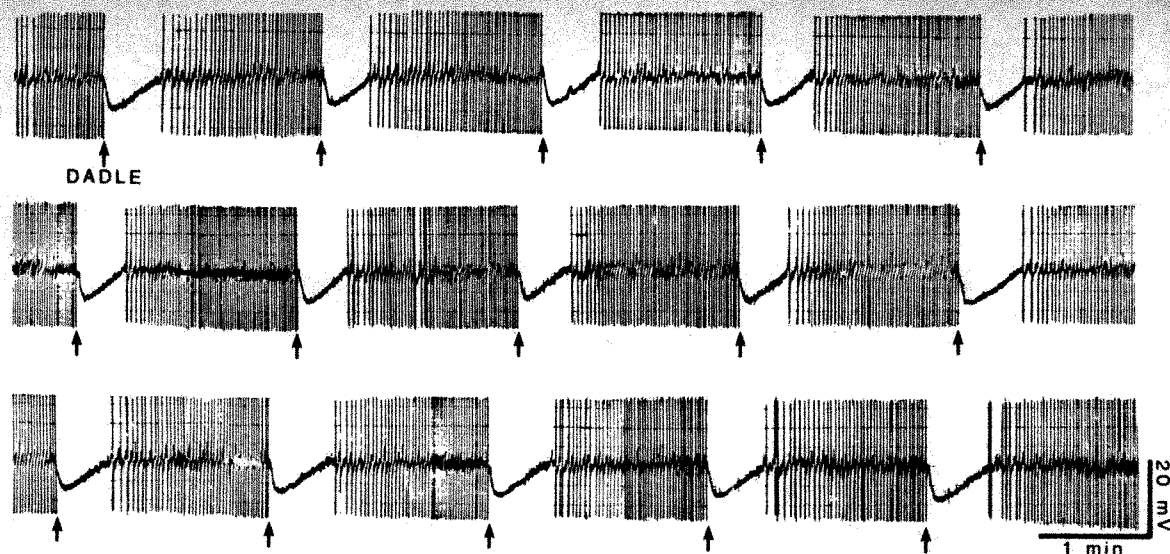


Fig. 1 Enkephalin inhibits cell firing. The figure shows an intracellular recording from a spontaneously firing locus coeruleus neurone. DADLE was applied by a brief (50 ms) pulse of pressure (70 kN m^{-2} , 10 p.s.i.) to a pipette positioned just above the brain slice at the times indicated by the arrows. The cell hyperpolarized and the action potential discharge was inhibited. The pen recorder did not reproduce the full action potential amplitude, which was 70–100 mV among different neurones. These recordings were made from a completely submerged slice of pons (thickness $\sim 300 \mu\text{m}$) continuously superfused with a solution of the following composition (nM): NaCl 126, KCl 2.5, CaCl_2 2.4, NaH_2PO_4 1.2, MgCl_2 1.3, NaHCO_3 25, glucose 11, which was equilibrated at 37°C with 95% O_2 , 5% CO_2 .

We studied the effects of opiates and enkephalin on neurones in the nucleus locus coeruleus. This is a compact group of noradrenaline-containing cell bodies which lies close to the floor of the fourth ventricle of the mammalian brain. Its widespread projections allow it to influence many brain regions, several of which have been implicated in the acute responses to opiates. Moreover, the locus coeruleus of the rat has a high density of opiate-binding sites, and enkephalin-like material has been localized in nerve terminals making synaptic contacts with locus coeruleus neurones⁴. It is known that opiates and enkephalin inhibit the firing of these neurones^{5–7}, and a previous study in the guinea pig indicated that this is due to a membrane hyperpolarization⁸. Intracellular recordings were made from locus coeruleus neurones in $300 \mu\text{m}$ -thick slices of brain tissue cut from the rat pons (see refs 8, 9). Drugs were added to the artificial cerebrospinal fluid solution which continuously superfused the brain slice (see Fig. 1 legend). In addition, normorphine, Met⁵-enkephalin and DADLE were administered by brief application of pressure to a micropipette containing the compound positioned just above the surface of the brain slice.

Most locus coeruleus neurones fired action potentials spontaneously at frequencies of 1–4 Hz, which is similar to their behaviour *in vivo*^{5,6}. Enkephalin and morphine each caused a concentration-dependent inhibition of this firing and a membrane hyperpolarization when added to the solution which superfused the slice (Fig. 1). The minimum concentration which inhibited firing was 10 nM, and the hyperpolarizations (mV, mean \pm s.e.m.) from the resting potential were: for normorphine ($1 \mu\text{M}$), 10.2 ± 1.2 ($n = 12$); normorphine ($10 \mu\text{M}$), 18.3 ± 4.4 ($n = 3$); DADLE (300 nM), 7.8 ± 1.8 ($n = 6$); and DADLE ($1 \mu\text{M}$), 15.6 ± 3.9 ($n = 7$). When the perfusion with morphine was continued for over 1 h the membrane remained hyperpolarized throughout, and rapidly recovered its original resting level when the drug was washed out. Application of Met⁵-enkephalin, DADLE or normorphine by the pressure technique gave hyperpolarizations of a more rapid time course which were dose-dependent, and which could be evoked reproducibly over periods of several hours (Fig. 1).

Several findings indicate that this inhibition of firing and hyperpolarization results from an increase in the K^+ ion conductance. (1) The conductance of the cell measured by passing small current pulses was increased during the opioid hyperpolarization (Fig. 2). This increase in conductance occurred

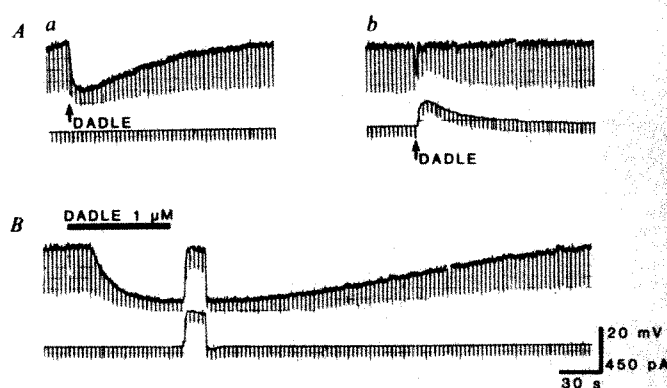


Fig. 2 Enkephalin increases membrane conductance. The upper trace is the membrane potential (resting potential -67 mV); lower trace is the transmembrane current passed by means of a bridge circuit. **A**, DADLE was applied at the arrow by pressure [two 50-ms pulses, 35 kN m^{-2} (5 p.s.i.)]. In **a**, DADLE hyperpolarized the membrane and reduced membrane resistance. In **b** the DADLE hyperpolarization was annulled by passing inward current. **B**, a similar experiment with superfusion of DADLE ($1 \mu\text{M}$) during the period indicated. The apparent delay in onset of the hyperpolarization is due to passage through the perfusion system. Restoration of the membrane potential to its control level allowed separation of the DADLE-induced resistance change and membrane rectification. In experiments of this type the amplitude of the enkephalin (or normorphine)-induced resistance changes was correlated with the potential change (ΔV) and used to estimate the response reversal potential $E_{\text{rev},R}$ from $\Delta V = (1 - R'/R)(E_{\text{rev},R} - E_m)$ where E_m is the membrane potential before application of enkephalin, R is the control input resistance, and R' is the input resistance at peak enkephalin effect, measured after restoring the potential E_m (as in **b**). $E_{\text{rev},R}$ was -135.5 ± 7.5 (mean \pm s.e.m., $n = 11$) for pressure application, and -124.0 ± 8.1 ($n = 10$) for perfusion. These values were always more negative than those estimated by changing E_m (see Fig. 3). E_{rev} was also estimated from $\Delta V = (1 - \tau'/\tau)(E_{\text{rev},\tau} - E_m)$ where τ' and τ are time constants of small hyperpolarizing current pulses. $E_{\text{rev},\tau}$ was $-103 \pm 5.9 \text{ mV}$ ($n = 10$) with application of opioids by perfusion. $E_{\text{rev},\tau}$ is relatively insensitive to the location of the conductance increase¹⁵, whereas $E_{\text{rev},R}$ will be an overestimate of E_{rev} if the conductance change significantly affects electronically distant membrane. This indicates that enkephalin increases the conductance of both the soma and the dendrites.

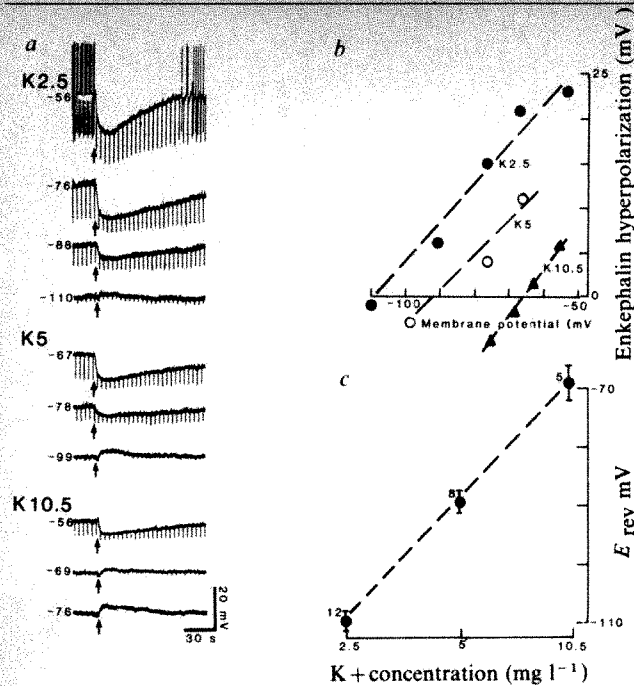


Fig. 3 Enkephalin opens potassium channels. *a* DADLE was applied by pressure [arrow, 50-ms pulse 70 kN m⁻² (10 p.s.i.)] at various membrane potentials. The potassium concentration was as indicated (K, mM). At elevated K⁺ concentrations, the enkephalin response reversed polarity with membrane hyperpolarization. Note the marked rectification occurring with hyperpolarization and with elevated K⁺ concentration. *b* Relationship between hyperpolarization amplitude and membrane potential. *c*, Enkephalin reversal potential (E_{rev}) calculated from many experiments such as those in *a* and *b*. The broken line is $E_{rev} = RT/F \ln([K]_o/[K]_i)$, where $[K]_i$, the intracellular K⁺ concentration, was taken as 145 mM. (In normal potassium solutions (2.5 mM), it was usually not possible to reverse the enkephalin hyperpolarization, therefore extrapolated values were used.) The good agreement between the observed values of E_{rev} and those predicted from the Nernst equation suggests a predominantly somatic site of action; the large steady-state conductance increase which accompanied membrane hyperpolarization would effectively remove the dendritic contribution (see Fig. 2 legend).

both on the neurone soma and dendrites (see Fig. 2 legend). (2) The enkephalin hyperpolarization became smaller when it was evoked at hyperpolarized resting membrane potentials, and the response reversed polarity at ~ -105 mV (Fig. 3). Complete reversal of the hyperpolarization was often not possible, presumably because of the dendritic site of action combined with strong rectifying properties of the membrane (Fig. 3). The extrapolated reversal potentials followed the K⁺ equilibrium potential (E_K) when the extracellular K⁺ concentration was altered (Fig. 3). (3) Intracellular injection of Cs⁺ or extracellular application of Ba²⁺ both rapidly abolished the opioid hyperpolarizations. (4) The opioids prolonged the after-hyperpolarizations which followed a burst of action potentials; this after-hyperpolarization is due to an increase in K⁺ conductance triggered by Ca²⁺ entry during the action potentials (J.T.W. and R.A.N., unpublished observations). (5) Finally, Cl⁻ movement probably does not contribute to the response because opioid hyperpolarizations were observed equally well with intracellular electrodes containing chloride, methylsulphate or citrate anions, and because chloride-dependent hyperpolarizations induced by γ -aminobutyric acid reversed to depolarizations after a period of recording with chloride-filled electrodes, whereas opiate hyperpolarizations did not change.

The opiate-induced K⁺ activation was apparently voltage-dependent: at potentials less negative than the resting potential (which was -55 to -60 mV), the amplitude of the enkephalin hyperpolarization declined sharply. This decrease in effect was not related to the fact that the cells were firing rapidly at such depolarized potentials—similar effects were observed when spontaneous firing was abolished in solutions containing tetrodotoxin and cobalt. This voltage-dependence is similar to that of the K⁺ activation by acetylcholine on autonomic ganglion cells¹⁰ and of the K⁺ activation by intracellular Ca²⁺ in myenteric neurones¹¹. It allows maximum effect of opiates at membrane potentials close to threshold.

The hyperpolarization induced by opiates was essentially unchanged in calcium-free solutions, as was previously observed^{8,12}. Thus their action is not due to release of other transmitters which then increase the K⁺ conductance of the impaled neurone.

The opiate antagonist naloxone reversibly inhibited the action of opiates. Because of the high reproducibility of the

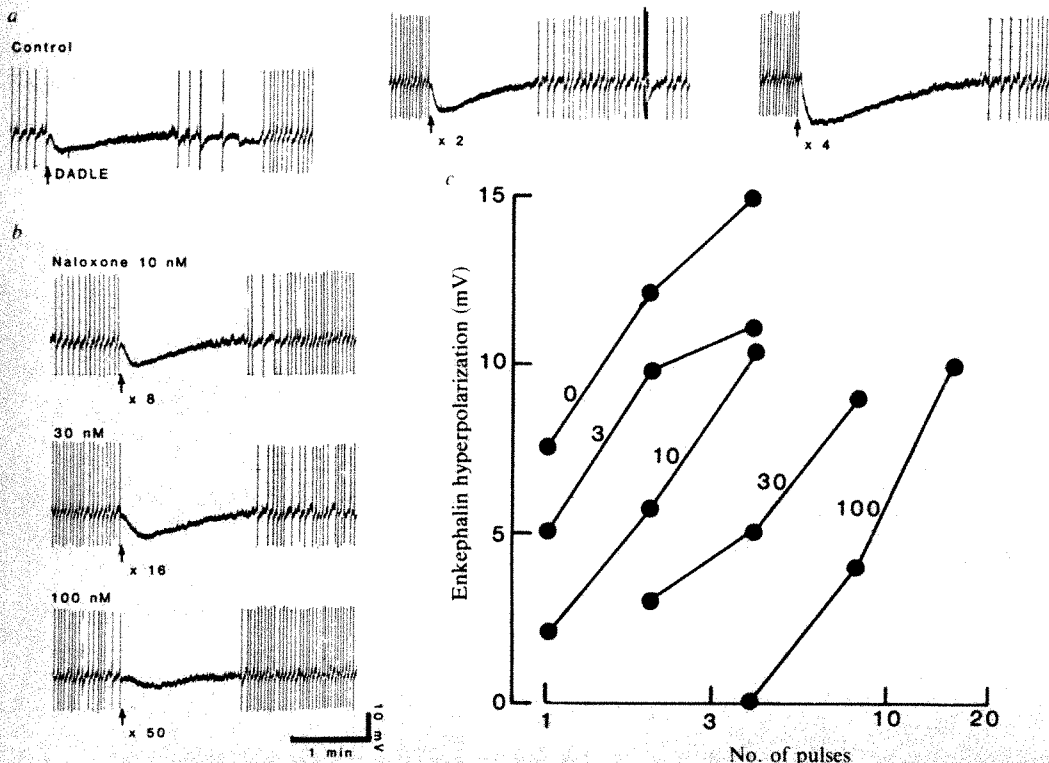


Fig. 4 Enkephalin interacts with naloxone-sensitive receptor. *a*, Control dose-response curve to DADLE applied by pressure (arrow, 24 ms, 55 kN m⁻² (8 p.s.i.), number of pulses indicated). *b*, Selected records from similar dose-response curves in the presence of various concentrations of naloxone. *c*, Dose-response curves to DADLE at the concentrations of naloxone indicated (nM). A response level was chosen so as to minimize interpolative errors and a Schild¹⁶ plot was used to calculate the dissociation equilibrium constant.

hyperpolarization induced by pressure application, we were able to demonstrate that this action of naloxone was competitive for dose ratios up to at least 64 (Fig. 4). The dissociation equilibrium constant for naloxone determined from such studies was 1.5 nM (95% confidence limits 2.1–1.1 nM, $n=4$) which is close to that found in radioactive ligand-binding studies with brain membranes prepared by homogenization. This implies that the affinity of the opiate-binding sites for naloxone determined in such biochemical experiments may be close to that found on functioning neurones.

The opening of K^+ channels by opiates may underlie not only the inhibition of cell firing but could contribute to the reduced transmitter release observed in several preparations^{2,3,13}. Transmitter release might be inhibited if the K^+ activation reduced spike duration and resulted in less Ca^{2+} entry, or if the increase in K^+ conductance caused block of impulse propagation at varicosities¹⁴. Which of these two actions predominates may depend largely on the part of the nerve cell involved, the region of the nervous system examined and on the experimental or physiological conditions, but both would contribute to the depression of the nervous system which is the hallmark of opiate action.

This work was supported by US ADAMHA grants DA 03161 (formerly 02241) and DA 03160 (formerly 01730).

Received 21 May, accepted 1 July 1982

- 1 North, R. A. *Life Sci* **15**, 1527–1546 (1979)
- 2 Yaksh, T. L., Jessell, T. M., Gamse, R., Mudge, A. W. & Leeman, S. E. *Nature* **286**, 155–157 (1980)
- 3 Kosterlitz, H. W. & Waterfield, A. A. *Rev Pharmac* **15**, 29–47 (1975)
- 4 Pickel, V. M., Joh, T. H., Reis, D. J., Leeman, S. E. & Miller, R. J. *Brain Res* **160**, 387–400 (1979)
- 5 Korf, J., Bunney, B. S. & Aghajanian, G. K. *Eur J Pharmac* **25**, 165–169 (1974)
- 6 Scott-Young, W. S., Bird, S. J. & Kuhar, M. J. *Brain Res* **129**, 366–370 (1977)
- 7 Aghajanian, G. K. *Nature* **276**, 186–188 (1978)
- 8 Pepper, C. M. & Henderson, G. *Science* **209**, 394–396 (1980)
- 9 Henderson, G., Pepper, C. M. & Shefner, S. A. *Expl Brain Res* **45**, 29–37 (1982)
- 10 Hartzell, H. C., Kuffler, S. W., Stuckgold, R. & Yoshikami, F. *J Physiol, Lond* **271**, 817–846 (1977)
- 11 Morita, K., North, R. A. & Tokimasa, T. *J Physiol, Lond* (in the press)
- 12 North, R. A., Katayama, Y. & Williams, J. T. *Brain Res* **165**, 67–77 (1979)
- 13 Mudge, A. W., Leeman, S. E. & Fischbach, G. D. *Proc natn Acad Sci USA* **76**, 526–530 (1979)
- 14 Morita, K. & North, R. A. *Neuroscience* **6**, 1943–1951 (1981)
- 15 Carlen, O. J. & Durand, D. *Neuroscience* **6**, 839–846 (1981)
- 16 Arunlakshana, O. & Schild, H. O. *Br J Pharmac Chemother* **14**, 48–58 (1959)

Predominance of the amino-terminal octapeptide fragment of dynorphin in rat brain regions

Eckard Weber, Christopher J. Evans & Jack D. Barchas

Nancy Pritzker Laboratory of Behavioral Neurochemistry, Department of Psychiatry and Behavioral Sciences, Stanford University School of Medicine, Stanford, California 94305, USA

Dynorphin is a 17 amino acid opioid peptide which was originally isolated and characterized from pig neurohypophysis and gut extracts^{1–3}. It contains a leucine-enkephalin (Leu-enkephalin) sequence at the amino terminus and has an unusually potent *in vitro* opiate activity in the guinea pig ileum longitudinal muscle/myenteric plexus preparation^{1,4}. Immunohistochemical studies have shown that perikarya, nerve fibres and terminals widely distributed throughout the central nervous system^{5,6} are immunoreactive for both dynorphin_{1–17} and α -neo-endorphin^{6,7}, another Leu-enkephalin-containing opioid peptide which is structurally related to dynorphin (Fig. 1) and was isolated from hypothalamus⁸. But although the regional distributions of α -neo-endorphin and dynorphin_{1–17} in rat brain, as measured by radioimmunoassay (RIA), are similar, the molar ratio of the two peptides seems to vary greatly from region to

region, with α -neo-endorphin being present in much higher concentrations than dynorphin_{1–17}^{9–11}. We now report that dynorphin_{1–8}, an amino-terminal fragment (Fig. 1), which has only ~3% of the opioid potency of dynorphin_{1–17}, (ref. 4), is present in up to 10-fold higher concentrations in brain than dynorphin_{1–17} immunoreactivity. We further show that dynorphin_{1–8}, but not dynorphin_{1–17}, occurs in approximately equimolar concentrations with α -neo-endorphin in all brain regions examined, suggesting a close biosynthetic relationship between α -neo-endorphin and dynorphin_{1–8}.

The various peptides were detected in acid acetone extracts of rat brain regions with three different highly specific RIAs using antibodies raised against synthetic dynorphin_{1–17}, dynorphin_{1–8} and α -neo-endorphin. All the RIAs were highly specific for their respective antigen. There was no significant cross-reactivity with related peptides or with the peptides recognized by the other RIAs (Table 1).

When extracts from rat brain regions were analysed using the α -neo-endorphin and dynorphin_{1–17} RIAs, the immunoreactivities for the two peptides were found to have a similar distribution, however, α -neo-endorphin immunoreactivity was present in much higher concentrations than dynorphin_{1–17} immunoreactivity and, more important, the molar ratio of α -neo-endorphin to dynorphin_{1–17} was extremely variable among brain regions (Table 2). This finding seemed to be inconsistent with the close biosynthetic relationship between the two peptides suggested by our initial immunohistochemical observations of the two substances in the same neurones^{6,7}.

Table 1 Specificity of RIAs used to detect dynorphin_{1–17}, dynorphin_{1–8} and α -neo-endorphin in extracts of rat brain regions

Synthetic peptide	% Cross-reactivity in RIA for		
	Dynorphin _{1–17}	Dynorphin _{1–8}	α -Neo-endorphin
Dynorphin _{1–17}	100	<0.001	0
Dynorphin _{1–8}	0	100	0
α -Neo-endorphin	0	0	100
Leu-enkephalin	0	0	0
Dynorphin _{1–6}	0	0	0
Dynorphin _{1–7}	0	0.001	0
Dynorphin _{1–9}	<0.001	0.01	0
Dynorphin _{1–13}	50	0.001	0
Dynorphin _{6–17}	0	0	0
β -Neo-endorphin	0	0	<0.01
α -Neo-endorphin _{1–8}	0	0	0

RIAs were carried out as described in Table 2 legend. The cross-reactivity was calculated based on the amounts of unlabelled peptide needed to obtain a 50% displacement of ¹²⁵I-labelled peptide from the antisera. The highest concentration of unlabelled peptide tested was 1 μ M. When the displacement was <50% at 1 μ M concentration, the cross-reactivity calculations were based on the amount of displacement obtained at this concentration. (Synthetic peptides were solid phase synthesized and purified by Dr J.-K. Chang, Peninsula Laboratories.)

Earlier studies, however, had identified an amino-terminal octapeptide fragment of dynorphin, dynorphin_{1–8}, in hypothalamus and posterior pituitary^{12,13}. We reasoned that if dynorphin_{1–8} were a major product in a biosynthetic pathway involving dynorphin_{1–17} as a precursor or intermediate, then by using antibodies to dynorphin_{1–17} we would greatly underestimate the actual amounts of dynorphin-like molecules present because the antibodies would not detect dynorphin_{1–8} (Table 1). When we measured dynorphin_{1–8} immunoreactivity in brain region extracts, it was indeed found that most of the dynorphin-like peptides corresponded to dynorphin_{1–8}-immunoreactive material with up to 10-fold more dynorphin_{1–8} than dynorphin_{1–17} immunoreactivity (Table 2). By comparing the amounts

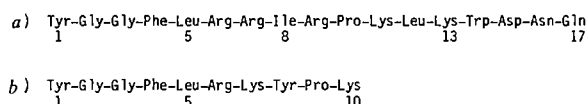


Fig 1 Amino acid sequences of the structurally related opioid peptides dynorphin_{1–17} (a) and α -neo-endorphin (b) (refs 2, 8)

of dynorphin₁₋₈ and α -neo-endorphin immunoreactivity we concluded that an approximately 1:1 molar ratio of dynorphin₁₋₈ and α -neo-endorphin immunoreactivity exists in all brain regions examined (Table 2).

We estimated the molecular size of the immunoreactive peptides by chromatographing extracts from all brain regions indicated in Table 2 on a Sephadex G-50 column in 50% acetic acid^{14,15}. In addition, immunoreactive peaks from the Sephadex G-50 profile from three regions (posterior pituitary, striatum and midbrain) were rechromatographed by reverse-phase HPLC. Figure 2a-f shows the gel-filtration profiles of hypothalamus (a-c) and striatal (d-f) extracts. In the former

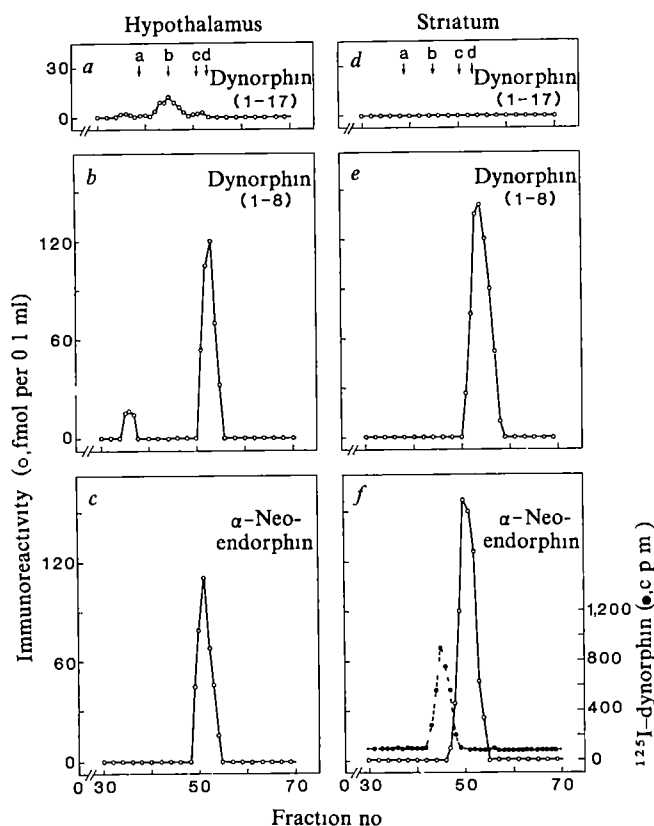


Fig 2 Gel-filtration chromatography profiles of immunoreactive dynorphin₁₋₁₇, dynorphin₁₋₈ and α -neo-endorphin in rat brain region extracts. Chromatography profiles were obtained from extracts of all brain regions indicated in Table 2. The profiles from hypothalamus (a-c) and striatal (d-f) extracts are shown. The brain regions from 10 animals were extracted with acid acetone as described in Table 2 legend. The supernatants of the acid acetone extracts were subjected to lipid extraction with 10 vol of heptane. In pilot experiments, it was found that ¹²⁵I-labelled dynorphin₁₋₁₇, dynorphin₁₋₈ and α -neo-endorphin did not enter the heptane phase but remained completely in the acid acetone phase. The heptane phases were discarded and the acid-acetone phases evaporated to dryness under a stream of air. The residues were taken up in 1 ml of 50% acetic acid and insoluble material was removed by centrifugation. The supernatants were subjected to gel-filtration chromatography at room temperature on a 120 cm × 0.9 cm column packed with Sephadex G-50 fine resin swollen and equilibrated in 50% acetic acid. Elution of Sephadex G-50 in 50% acetic acid, a strongly dissociating agent, eliminates nonspecific interactions of the peptides with the gel matrix and the elution volume on these columns is a strictly linear function of the logarithm of the molecular weight in the range 500–10,000 (refs 14, 15). Fractions (1.8 ml) were collected and 100- μ l aliquots were evaporated under reduced pressure and assayed in the three RIAs. The columns were calibrated with ¹²⁵I- α -N-acetyl β -endorphin (a), ¹²⁵I-dynorphin₁₋₁₇ (b), ¹²⁵I- α -neo-endorphin (c) and ¹²⁵I-dynorphin₁₋₈ (d). A trace amount of either ¹²⁵I-dynorphin₁₋₁₇ or ¹²⁵I- α -neo-endorphin was included in each run of tissue extract to control the reproducibility of the chromatography. The recovery of immunoreactivity from the columns was 88–92%. To determine whether dynorphin₁₋₈ can be formed from dynorphin₁₋₁₇ as an artefact during extraction, a trace amount of ¹²⁵I-labelled dynorphin₁₋₁₇ was added to the extractant immediately before homogenization of striatum, one of the regions with the largest excess of dynorphin₁₋₈ over dynorphin₁₋₁₇ (Table 2). Figure 1f shows that all the radioactivity from this experiment eluted at the position of ¹²⁵I-dynorphin₁₋₁₇. No radioactivity above background eluted at the position of ¹²⁵I-dynorphin₁₋₈.

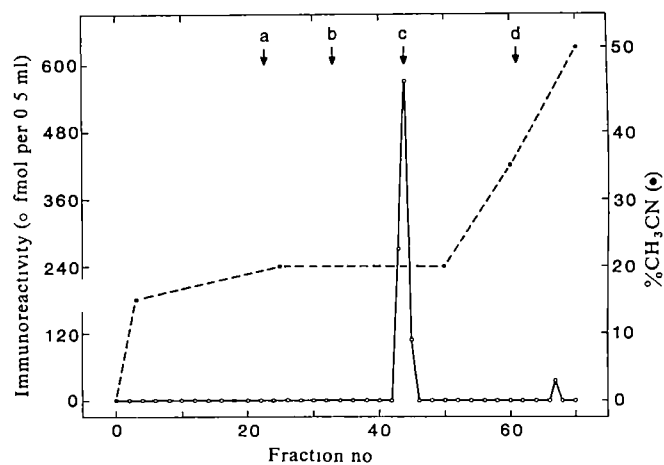


Fig 3 Reverse-phase HPLC of immunoreactive dynorphin₁₋₈ from rat midbrain extracts. Extracts were prepared and separated on a Sephadex G-50 column in 50% acetic acid as described in Fig 2 legend. A 500- μ l aliquot from the dynorphin₁₋₈ immunoreactive peak fraction was evaporated under a stream of nitrogen, taken up in HPLC buffer (see below) and chromatographed on an Altex Ultrasphere ODS column (250 mm × 4.6 mm, particle size 5 μ m). Two Altex HPLC pumps and a Beckman gradient mixing computer were used to generate a four-step acetonitrile gradient as shown in the graph. The HPLC buffer consisted of 50 mM monosodium phosphate, 1 mg ml⁻¹ phosphoric acid and 5% methanol, pH 2.7. The flow rate was 1.5 ml min⁻¹ and 1-min fractions were collected. Aliquots (500 μ l) of the fractions were evaporated first under a stream of air to remove the acetonitrile and then under reduced pressure. The residues were assayed in the dynorphin₁₋₈ RIA. Most (>95%) of the immunoreactivity eluted at exactly the same position as synthetic dynorphin₁₋₈, whereas a minor immunoreactive peak of unknown nature eluted at a higher acetonitrile concentration. The co-migration of the immunoreactivity with the synthetic standard was assessed in two ways: (1) the elution of the immunoreactive peak was compared with the elution of the synthetic peptide in a separate run as detected by optical density measurements at 210 nm, and (2) an aliquot from the immunoreactive peak fraction was 'spiked' with an equimolar amount of the synthetic peptide and rechromatographed. In the spiking experiment, the total immunoreactivity eluted as one single peak. When α -neo-endorphin immunoreactive material from the Sephadex G-50 columns was rechromatographed by reverse-phase HPLC we found, as have two other groups^{10,11}, that this material eluted at exactly the same position as synthetic α -neo-endorphin (not shown). An isocratic step was included in the elution profile between fractions 25 and 50 to improve the separation of dynorphin₁₋₈ from β -neo-endorphin. Markers: a, α -neo-endorphin; b, β -neo-endorphin; c, dynorphin₁₋₈; d, dynorphin₁₋₁₇.

extract (a-c), the material detected by the dynorphin₁₋₁₇ RIA constituted only a fraction of the material detected by the dynorphin₁₋₈ or α -neo-endorphin RIA. In the fractionated striatal extracts, dynorphin₁₋₁₇ immunoreactivity was below the detection limits of the various RIAs whereas dynorphin₁₋₈ and α -neo-endorphin immunoreactivities were readily detectable (Fig 2d-f). For all brain regions, the major immunoreactive peaks for α -neo-endorphin and dynorphin₁₋₈ eluted at exactly the same position as the respective ¹²⁵I-labelled synthetic marker peptides (Fig 2a-f). Rechromatography by reverse-phase HPLC of the major α -neo-endorphin and dynorphin₁₋₈ immunoreactive peaks from three brain regions (posterior pituitary, striatum, midbrain) showed that the immunoreactivity detected by the α -neo-endorphin and dynorphin₁₋₈ RIAs co-migrated exactly with their respective synthetic marker peptide (Fig 3).

We conclude that dynorphin₁₋₈ is neither an extraction artefact nor a product of extraneuronal metabolism of dynorphin₁₋₁₇ as (1) when ¹²⁵I-labelled dynorphin₁₋₁₇ was added to the tissue at the time of extraction, no conversion of this radioactive marker to dynorphin₁₋₈ was observed (Fig 2f), (2) the amounts of dynorphin₁₋₁₇ which we measured are similar to those reported by other groups^{9,11}, and (3) synthetic dynorphin₁₋₁₃ added to washed brain membranes or injected *in vivo* into the brain ventricles is degraded primarily at the amino terminus by aminopeptidases^{16,17}.

The results presented here suggest a precursor-product relationship between dynorphin₁₋₁₇ and dynorphin₁₋₈. It is possible that dynorphin₁₋₈ is derived from a different precursor

Table 2 Concentration and molar ratios of dynorphin₁₋₁₇, dynorphin₁₋₈ and α -neo-endorphin immunoreactivities in rat brain regions

	Immunoreactivity (pmol per g tissue)			Molar ratios		
	Dynorphin ₁₋₁₇	Dynorphin ₁₋₈	α -Neo-endorphin	D ₁₋₈ /D ₁₋₁₇	α -Neo/D ₁₋₁₇	α -Neo/D ₁₋₈
Medulla/pons	3.9 ± 0.4	22.5 ± 0.6	26.3 ± 1.1	5.7	6.6	1.2
Midbrain	6.2 ± 1.0	59.6 ± 3.7	59.7 ± 2.0	9.6	9.6	1.0
Cerebellum	<0.2	<1.2	<1.7			
Spinal cord	12.1 ± 2.3	22.7 ± 1.6	26.5 ± 2.0	1.9	2.2	1.2
Cortex	2.6 ± 0.6	21.0 ± 1.9	19.4 ± 0.9	8.2	7.6	0.9
Striatum	7.3 ± 0.7	64.1 ± 4.1	70.1 ± 4.5	8.8	9.6	1.1
Hippocampus	3.4 ± 0.7	26.5 ± 2.2	25.6 ± 1.4	7.9	7.6	1.0
Hypothalamus	10.3 ± 1.1	65.5 ± 1.8	76.7 ± 5.7	6.4	7.5	1.2
Posterior pituitary	503.6 ± 32.9	1384.0 ± 84.4	1598 ± 117.9	2.8	3.2	1.1

Brain regions were dissected from 10 male Sprague-Dawley rats (160–180 g) as described in ref. 20. The tissue was frozen immediately on dry ice. After weighing in the frozen state, each tissue sample was individually extracted by sonication in 1 ml of acid acetone (acetone/water 12 M HCl, 40:6:1). The homogenates were centrifuged at 12,000g for 10 min and supernatants were evaporated to dryness under a stream of air in silanized glass tubes. The residue was taken up in 1 ml of RIA buffer and after further centrifugation aliquots of the supernatants were appropriately diluted and assayed in the three RIAs. The RIA procedure was that described in ref. 14, with modifications: the use of a buffer pH of 7.4 rather than 6.0, and application of a double antibody separation procedure rather than a dextran-coated charcoal separation. Antiserum dilutions were 1:130,000, 1:120,000 and 1:30,000 for the dynorphin₁₋₁₇, dynorphin₁₋₈ and α -neo-endorphin RIAs respectively. Values are expressed as corrected means \pm s.e.m. from determinations of the brain regions from 10 individual animals. The measured values were corrected for recovery. The recovery for each peptide from each brain region was determined in separate experiments by adding a trace amount of ¹²⁵I-labelled synthetic peptide to the extractant immediately before homogenization of the sample. After all steps of repeated centrifugation, evaporation and rehydration, the amount of recovered radioactivity was 59 \pm 2.3%, 70 \pm 4.1% and 73 \pm 3.3% for dynorphin₁₋₁₇, dynorphin₁₋₈ and α -neo-endorphin respectively. Measurements of the three peptides were repeated twice on two groups of brains from 13 and 6 animals. Brain regions from the 13 animal group were also extracted into acid acetone while the samples from the 6 animal group were extracted into 1 ml each of 0.1 M HCl at 95 °C. The supernatant of the 0.1 M HCl extract was neutralized with an equal volume of 0.1 M NaOH and appropriate dilutions were assayed directly in the RIAs. The results from these two experiments were essentially identical to those shown in the table.

However, previous work showing that α -neo-endorphin and dynorphin₁₋₁₇ immunoreactivities occur within the same neurones^{6,7} and the finding that α -neo-endorphin and dynorphin₁₋₈, but not dynorphin₁₋₁₇, occur in equimolar concentrations throughout the brain suggest that dynorphin₁₋₁₇ is a precursor or intermediate in the formation of dynorphin₁₋₈. A precursor role of dynorphin₁₋₁₇ would explain the rather low concentrations of this peptide in brain. Furthermore, the equimolar distribution of dynorphin₁₋₈ and α -neo-endorphin in all brain regions examined raises the possibility that the two peptides are major products in the processing of a larger common precursor. However, only isolation of such a prohormone or its mRNA can assign a common biosynthetic origin of the two peptides.

The function of dynorphin₁₋₁₇ in brain as an opiate peptide must be re-evaluated in view of the present findings. Dynorphin₁₋₈, the predominant dynorphin-like peptide in brain is far less potent than its putative precursor dynorphin₁₋₁₇ (ref. 4). Given these significant differences in opiate potency of the two peptides, the finding that the ratio of dynorphin₁₋₈ to dynorphin₁₋₁₇ immunoreactivity varies greatly among brain regions, ranging from 2:1 in the spinal cord to 10:1 in the midbrain and striatum (Table 2), may reflect region-specific physiological differences in processing. Certain neuronal populations may leave relatively more dynorphin₁₋₁₇ intact in some regions, thus increasing dramatically the available pool of opiate potency and specificity towards certain receptor types^{18,19}, whereas other neuronal populations may inactivate much of this opiate activity simply by converting dynorphin₁₋₁₇ more completely into dynorphin₁₋₈. Future studies will determine whether external stimuli can significantly alter this processing pattern.

This work was supported by NIDA grant DA 01207 and a Selected Research Opportunity from the ONR (SRO 001 N00014-C-0796). We thank Pamela Angwin and Irene Inman for help with the RIAs and S. Poage for preparing the manuscript.

Received 1 March, accepted 11 May 1982

- Goldstein, A., Tachibana, S., Lowney, L. I., Hunkapillar, M. & Hood, L. *Proc. natn. Acad. Sci. U.S.A.* **76**, 6666–6670 (1979).
- Goldstein, A., Fischli, W., Lowney, L., Hunkapillar, M. & Hood, L. *Proc. natn. Acad. Sci. U.S.A.* **78**, 7219–7223 (1981).
- Tachibana, S., Araki, K., Ohya, S. & Yoshida, S. *Nature* **295**, 339–340 (1982).
- Chavkin, C. & Goldstein, A. *Proc. natn. Acad. Sci. U.S.A.* **78**, 6543–6547 (1981).
- Watson, S. J., Akil, H., Ghazarsian, V. E. & Goldstein, A. *Proc. natn. Acad. Sci. U.S.A.* **78**, 1260–1263 (1981).
- Weber, E., Roth, K. A. & Barchas, J. D. *Proc. natn. Acad. Sci. U.S.A.* **79**, 3062–3066 (1982).
- Weber, E., Roth, K. A. & Barchas, J. D. *Biochem. biophys. Res. Commun.* **103**, 951–958 (1981).
- Kangawa, K., Minamino, H., Chino, N., Sakakibara, S. & Matsuo, H. *Biochem. biophys. Res. Commun.* **99**, 871–877 (1981).

- Goldstein, A. & Ghazarsian, V. *Proc. natn. Acad. Sci. U.S.A.* **77**, 6207–6210 (1980).
- Minamino, N., Kitamura, K., Hayashi, Y., Kangawa, K. & Matsuo, H. *Biochem. biophys. Res. Commun.* **102**, 226–234 (1981).
- Maysinger, D. *et al. Neuropeptides* (in the press).
- Minamino, N., Kangawa, K., Fukuda, A. & Matsuo, H. *Biochem. biophys. Res. Commun.* **95**, 1475–1481 (1980).
- Seizinger, B., Hollt, V. & Herz, A. *Biochem. biophys. Res. Commun.* **102**, 197–205 (1981).
- Weber, E., Evans, C. J., Chang, J.-K. & Barchas, J. D. *J. Neurochem.* **38**, 436–447 (1982).
- Zakarian, S. & Smyth, D. G. *Proc. natn. Acad. Sci. U.S.A.* **76**, 5972–5976 (1979).
- Herman, B. H., Leslie, F. & Goldstein, A. *Life Sci.* **27**, 883–892 (1980).
- Leslie, F. M. & Goldstein, A. *Neuropeptides* (in the press).
- Chavkin, C., James, I. F. & Goldstein, A. *Science* **215**, 413–415 (1982).
- Hewlett, W. A., Akil, H. & Barchas, J. D. *Abstr. Proc. int. Narcotics Res. Conf. Kyoto, Japan*, 9 (Kodansha, Tokyo, 1981).
- Glowinsky, J. & Iversen, L. *J. Neurochem.* **13**, 655–669 (1966).

Dynorphin₁₋₈ and dynorphin₁₋₉ are ligands for the κ -subtype of opiate receptor

Alistair D. Corbett, Stewart J. Paterson,
Alexander T. McKnight, Jacques Magnan
& Hans W. Kosterlitz

Unit for Research on Addictive Drugs, University of Aberdeen,
Marischal College, Aberdeen AB9 1AS, UK

It is generally accepted that there are three subtypes of opiate receptor: μ , δ and κ . The main endogenous ligands for the μ - and δ -sites are Met⁵-enkephalin, Leu⁵-enkephalin and β -endorphin, whereas the putative endogenous ligands for the κ -binding site were unknown until recent observations suggested that dynorphin₁₋₁₃ might be a candidate. The most convincing evidence for this view has been presented by Goldstein and his colleagues who showed that dynorphin₁₋₁₃ is a specific endogenous ligand for the κ -receptor and has a high potency and long duration of action¹⁻³. We show here that the sequences Leu⁵-enkephalyl-Arg-Arg-Ile (dynorphin₁₋₈) and, particularly, Leu⁵-enkephalyl-Arg-Arg-Ile-Arg (dynorphin₁₋₉) are selective ligands for the κ -binding site. Whereas dynorphin₁₋₁₃ and dynorphin₁₋₁₇ are relatively resistant to the action of peptidase and have a long duration of action *in vitro* after wash-out, dynorphin₁₋₈ and dynorphin₁₋₉ are readily degraded by peptidases and their duration of action is much shorter. For this and other reasons, the possibility will have to be considered that dynorphin₁₋₈ or dynorphin₁₋₉ may be transmitters or modulators at the κ -binding site while dynorphin₁₋₁₃ and dynorphin₁₋₁₇ may act hormonally, that is, at a distance from the site of release.

Table 1 Inhibitory effects of C-terminally extended Leu⁵-enkephalins on the electrically induced contractions of the guinea pig myenteric plexus-longitudinal muscle and the vasa deferentia of the mouse, rat and rabbit

C-terminal extensions of Leu ⁵ -enkephalin	IC ₅₀ (nM)			
	Guinea pig myenteric plexus	Mouse vas deferens	Rat vas deferens	Rabbit vas deferens
—	28.6 ± 5.4	1.7 ± 0.3	550 ± 62	>10,000
Lys ⁶	107 ± 29.1	25.6 ± 4.9	720 ± 45	>10,000
Arg ⁶	102 ± 17.2	10.9 ± 1.1	790 ± 46	3,000 ± 930
Arg ⁶ -Arg ⁷	17.3 ± 2.52	25.5 ± 4.2	7,500 ± 2,000	43.0 ± 11.5
Arg ⁶ -Arg ⁷ -Ile ⁸	4.92 ± 0.53	9.2 ± 1.30	>10,000	11.7 ± 1.27
Arg ⁶ -Arg ⁷ -Ile ⁸ -Arg ⁹	2.36 ± 0.67	6.5 ± 0.34	>10,000	6.1 ± 0.45
Dynorphin ₁₋₁₃	0.31 ± 0.16	0.33 ± 0.08	>10,000	2.43 ± 0.49
Dynorphin ₁₋₁₇	0.29 ± 0.09	0.91 ± 0.13	>10,000	3.01 ± 1.6
α-Neo-endorphin	2.98 ± 0.44	7.7 ± 0.98	>10,000	21.4 ± 4.5

The values shown are the mean ± s.e.m. of three to four observations. The activity of peptidases has been inhibited by bestatin (10 μM, or 30 μM in the rat and rabbit), L-leucyl-L-leucine (2 mM), thiorphan (0.3 μM) and captopril (10 μM), in the rabbit vas deferens, this treatment increased the potency of the enzyme-sensitive peptides, but not of dynorphin₁₋₁₃ or dynorphin₁₋₁₇, 60–270-fold. The sequence of dynorphin is Tyr-Gly-Gly-Phe-Leu-Arg-Arg-Ile-Arg-Pro-Lys-Leu-Lys-Trp-Asp-Asn-Gln and of α-neo-endorphin is Tyr-Gly-Gly-Phe-Leu-Arg-Lys-Tyr-Pro-Lys. The peptides were obtained from Peninsula, Bachem and Cambridge Research Biochemicals or were gifts from Drs A. Goldstein, J. Morley and S. Udenfriend.

Our results were obtained from four *in vitro* pharmacological assays in which the preparations were made to contract by electrical stimulation. The preparations respond differently to activation of the μ-, δ- and κ-receptors. The inhibitory potencies of the peptides are given as their 50% inhibitory concentration (IC₅₀, nM) values. In the myenteric plexus-longitudinal muscle of the guinea pig ileum, an inhibitory effect is readily observed with ligands that activate μ- and κ-receptors, whereas the mouse vas deferens responds preferentially to ligands acting on δ-receptors⁴, the vas deferens of the rat has a low sensitivity to κ-ligands⁵ in contrast to the vas deferens of the rabbit in which κ-ligands, but not μ- or δ-ligands, are inhibitory^{6,7}. In these assays, the activity of peptidases was inhibited by a mixture of bestatin, L-leucyl-L-leucine, thiorphan and captopril (Table 1 and A.T.McK., A.D.C. and H.W.K., unpublished observations). The peptides used in this investigation had agonist, but no antagonist, action.

The binding of the peptides was measured by determining the inhibition constants (*K*_i, nM) in three assays on homogenates of guinea pig brain. For this purpose, ³H-labelled D-Ala², MePhe⁴, Gly-ol⁵-enkephalin was used as a highly selective μ-ligand and ³H-D-Ala², D-Leu⁵-enkephalin as a δ-ligand which, although selective, has a cross-reactivity of ~10% at the μ-binding site⁸. The most suitable ligand for the assay of the κ-binding site was found to be ³H-(−)bremazocine⁹ after suppression of the binding at the μ- and δ-sites by addition of unlabelled μ- and δ-ligands at a concentration of 100 nM each.

To reduce degradation by peptidases, the binding assays were carried out at 0 °C for 150 min (Table 2).

Two groups of C-terminal extensions of Leu⁵-enkephalin have been shown to occur in the central nervous system (CNS). They are dynorphin₁₋₈ (Leu⁵-enkephalyl-Arg-Arg-Ile, refs 10, 11) and dynorphin₁₋₁₇ (refs 12, 13), which have two arginine residues in positions 6 and 7, and α- and β-neoendorphin^{14,15}, which are nona- and decapeptides respectively, with arginine and lysine residues in positions 6 and 7.

In the pharmacological assays (Table 1), the introduction of Arg⁶ or Lys⁶ at the C-terminal end of Leu⁵-enkephalin reduced its potency without altering the relative activity pattern. However, lengthening the chain from residue 7 onwards increased the ratio of IC₅₀ for the mouse vas deferens to IC₅₀ for the myenteric plexus. The most important effects of the extensions by Arg⁶-Arg⁷ or Arg⁶-Lys⁷ and beyond are the complete loss of potency in the rat vas deferens, which probably has no κ-binding sites⁵, and the progressively increasing activity in the rabbit vas deferens which responds to ketazocine- or κ-like compounds but not to μ- or δ-like ligands^{6,7}. The most potent C-extended forms of Leu⁵-enkephalin are dynorphin₁₋₁₃, dynorphin₁₋₁₇ and dynorphin₁₋₉, Leu⁵-enkephalyl-Arg-Arg-Ile-Arg (Table 1).

These findings are confirmed by the determination of the *K*_i values at the μ-, δ- and κ-binding sites (Table 2). All C-terminal extensions have lower ratios of *K*_i at the δ-binding site to *K*_i at the μ-binding site than the ratio found for the parent Leu⁵-

Table 2 The inhibitory effects of C-terminally extended Leu⁵-enkephalins on the binding in homogenates of guinea pig brain of ³H-D-Ala², MePhe⁴, Gly-ol⁵-enkephalin (1.0 nM), ³H-D-Ala², D-Leu⁵-enkephalin (1.0 nM) and ³H-bremazocine (0.30 nM)

C-terminal extensions of Leu ⁵ -enkephalin	<i>K</i> _i (nM)		
	³ H-D-Ala ² , MePhe ⁴ , Gly-ol ⁵ -enkephalin (μ-site)	³ H-D-Ala ² , D-Leu ⁵ -enkephalin (δ-site)	³ H-(−)bremazocine after suppression of μ- and δ-binding (κ-site)
—	18.8 ± 1.77	1.18 ± 0.20	8,210 ± 1,090
Lys ⁶	12.3 ± 1.91	20.4 ± 2.42	830 ± 118
Arg ⁶	17.4 ± 1.78	10.3 ± 1.11	226 ± 14
Arg ⁶ -Arg ⁷	3.45 ± 0.11	4.45 ± 0.45	9.4 ± 1.01
Arg ⁶ -Arg ⁷ -Ile ⁸	3.83 ± 0.36	4.99 ± 0.86	1.34 ± 0.23
Arg ⁶ -Arg ⁷ -Ile ⁸ -Arg ⁹	3.64 ± 0.64	3.24 ± 0.69	0.209 ± 0.035
Dynorphin ₁₋₁₃	0.222 ± 0.035	0.485 ± 0.076	0.045 ± 0.010
Dynorphin ₁₋₁₇	0.73 ± 0.09	2.38 ± 0.61	0.115 ± 0.018
α-Neo-endorphin	1.24 ± 0.20	0.57 ± 0.086	0.196 ± 0.044

The values shown are the mean ± s.e.m. of three to four observations. The method used for the binding assays has been described previously⁹, incubation was for 150 min at 0 °C. ³H-(−)bremazocine (Dr Romer, Sandoz) was used instead of ³H-(±)ethylketazocine and the binding at the μ- and δ-sites was suppressed with 100 nM each of D-Ala², MePhe⁴, Gly-ol⁵-enkephalin (Dr Romer, Sandoz) and D-Ala², D-Leu⁵-enkephalin (Dr Wilkinson, Wellcome). ³H-D-Ala², MePhe⁴, Gly-ol⁵-enkephalin and ³H-D-Ala², D-Leu⁵-enkephalin were obtained from Amersham.

enkephalin. The most interesting observation, however, is the progressive increase in the affinity at the κ -binding site as Leu⁵-enkephalyl-Arg⁶-Arg⁷ (dynorphin₁₋₇) is extended by Ile⁸ (dynorphin₁₋₈) and by Ile⁸-Arg⁹ (dynorphin₁₋₉). Dynorphin₁₋₁₃ has the highest relative affinities at all three binding sites, the values being of an order similar to those described recently for the inhibition of the binding of ³H-dihydromorphine, ³H-D-Ala², D-Leu⁵-enkephalin and ³H-ethylketazocine by dynorphin₁₋₁₃ amide in guinea-pig brain³ or inhibition of the binding of ³H-ethylketazocine or ³H-diprenorphine by dynorphin₁₋₁₃ or dynorphin₁₋₁₇ in human brain¹⁶.

The findings with dynorphin₁₋₇, dynorphin₁₋₈ and particularly dynorphin₁₋₉ indicate that these fragments are potent and increasingly selective κ -ligands and therefore merit further analysis, particularly as dynorphin₁₋₈ has been identified in porcine hypothalamus¹⁰ and in the neurointermediate pituitary of the rat¹¹, and dynorphin₁₋₁₇ in rat pituitary¹² and in porcine duodenum¹³. The 'small' dynorphins are readily degraded by peptidases, an action which can be prevented by the mixture of peptidase inhibitors. In the myenteric plexus, the IC₅₀ values of dynorphin₁₋₇, dynorphin₁₋₈ and dynorphin₁₋₉ were, respectively, 367, 30.8 and 21.5 nM before treatment with the peptidase inhibitors and 17.3, 4.9 and 2.4 nM after treatment, an average potentiation of about 12, while there was no potentiation of either dynorphin₁₋₁₃ or dynorphin₁₋₁₇. Furthermore, in four experiments in the presence of the peptidase inhibitors, the recovery of the effect of dynorphin₁₋₉ on the contraction of the myenteric plexus-longitudinal muscle was rapid ($t_{1/2}$ = 48 ± 6 s) and the recovery after dynorphin₁₋₁₇ was slow ($t_{1/2}$ = 178 ± 8 s). Finally, in the rabbit vas deferens pretreated with peptidase inhibitors, the IC₅₀ value of dynorphin₁₋₈ is ~11.7 nM and that of dynorphin₁₋₁₃ 2.43 nM, while the corresponding K_1 values at the κ -binding site are 1.34 and 0.045, respectively. Thus, the 'small' dynorphins are liable to be degraded by peptidases, are easily washed out and have moderate potency at the κ -site while the 'large' dynorphins are peptidase resistant, do not wash out readily and are "extraordinarily potent"¹⁷. The small dynorphins seem to have the qualities of a neurotransmitter or neuromodulator of short and rapid action, whereas the large dynorphins have the characteristics of a highly potent hormonal action of long duration. Moreover, it is of interest that the small dynorphin found in neuronal tissue is dynorphin₁₋₈, which is a less selective κ -ligand than dynorphin₁₋₉. Note that the κ -binding site is very demanding in its choice of ligands as Met⁵-enkephalin, Leu⁵-enkephalin and β -endorphin have only low affinities¹⁸; thus, dynorphin₁₋₈, which has affinities to the μ - and δ -binding sites, is sufficiently selective as far as the κ -binding site is concerned.

An urgent requirement is confirmation or otherwise that dynorphin₁₋₈ and possibly dynorphin₁₋₉ are strong candidates for the role of an endogenous ligand at the κ -binding site mediating neurotransmission or neuromodulation. Lastly, it will be important to correlate the putative κ -like actions of the small dynorphins with the pharmacological effects of the ketazocine-like compounds or κ -agonists^{19,20} which are antinociceptive agents and yet do not substitute for morphine in the morphine-dependent rhesus monkey²¹⁻²³. It may now become possible to exploit the therapeutic potentials of this group of compounds⁸.

This work was supported by grants from the MRC and the US National Institute on Drug Abuse (DA 00662).

Received 17 May; accepted 14 July 1982.

1. Chavkin, C. & Goldstein, A. *Nature* **291**, 591-593 (1981).
2. Chavkin, C. & Goldstein, A. *Proc. natn. Acad. Sci. U.S.A.* **78**, 6543-6547 (1981).
3. Chavkin, C., James, I. F. & Goldstein, A. *Science* **215**, 413-415 (1982).
4. Lord, J. A. H., Waterfield, A. A., Hughes, J. & Kosterlitz, H. W. *Nature* **267**, 495-499 (1977).
5. Gillan, M. G. C., Kosterlitz, H. W. & Magnan, J. *Br. J. Pharmac.* **72**, 13-15 (1981).
6. Oka, T. et al. *Eur. J. Pharmac.* **73**, 235-236 (1980).
7. Oka, T. et al. *Eur. J. Pharmac.* **77**, 137-141 (1982).
8. Magnan, J., Paterson, S. J., Tavani, A. & Kosterlitz, H. W. *Naunyn-Schmiedeberg's Archs Pharmac.* **319**, 197-205 (1982).
9. Römer, D. et al. *Life Sci.* **27**, 971-978 (1980).
10. Minamino, N., Kangawa, K., Fukuda, A. & Matsuo, H. *Biochem. biophys. Res. Commun.* **95**, 1475-1481 (1980).

11. Seizinger, B. R., Höllt, V. & Herz, A. *Biochem. biophys. Res. Commun.* **102**, 197-205 (1981).
12. Goldstein, A., Fischli, W., Lowney, L. I., Hunkapiller, M. & Hood, L. *Proc. natn. Acad. Sci. U.S.A.* **78**, 7219-7223 (1981).
13. Tachibana, S., Araki, K., Ohya, S. & Yoshida, S. *Nature* **295**, 339-340 (1982).
14. Minamino, N., Kangawa, K., Chino, N., Sakakibara, S. & Matsuo, H. *Biochem. biophys. Res. Commun.* **99**, 864-870 (1981).
15. Kangawa, K., Minamino, N., Chino, N., Sakakibara, S. & Matsuo, H. *Biochem. biophys. Res. Commun.* **99**, 871-878 (1981).
16. Pfeiffer, A., Pasi, A., Mehraein, P. & Herz, A. *Neuropeptides* **2**, 89-97 (1981).
17. Goldstein, A., Tachibana, S., Lowney, L. I., Hunkapiller, M. & Hood, L. *Proc. natn. Acad. Sci. U.S.A.* **76**, 6666-6670 (1979).
18. Kosterlitz, H. W., Paterson, S. J. & Robson, L. E. *Br. J. Pharmac.* **73**, 939-949 (1981).
19. Martin, W. R., Eades, C. G., Thompson, J. A., Huppler, R. E. & Gilbert, P. E. *J. Pharmac. exp. Ther.* **197**, 517-532 (1976).
20. Gilbert, P. E. & Martin, W. R. *J. Pharmac. exp. Ther.* **198**, 66-82 (1976).
21. Villarreal, J. E. & Seevers, M. H. *Bull. Probl. Drug Dependence* **34**, Addendum 7, 1040-1053 (1972).
22. Swain, H. H. & Seevers, M. H. *Bull. Probl. Drug Dependence* **36**, Addendum 1168-1195 (1974).
23. Swain, H. H. & Seevers, M. H. *Bull. Probl. Drug Dependence* **38**, Addendum 2, 768-787 (1976).

Direct structural localization of two toxin-recognition sites on an ACh receptor protein

H. P. Zingsheim†, F. J. Barrantes, J. Frank*, W. Hänicke & D.-Ch. Neugebauer‡

Max-Planck-Institut für Biophysikalische Chemie (Karl-Friedrich-Bonhoeffer-Institut), D3400 Göttingen, FRG

* Center for Laboratories and Research, New York State Department of Health, Albany, New York 12201, USA

One of the most actively studied chemoreceptors is the acetylcholine receptor (AChR) in the postsynaptic membranes of neuromuscular junctions and electrocytes. The AChR from *Torpedo* is a membrane protein, each molecule comprising five polypeptide chains^{1,2}: two α -chains of molecular weight (M_r) 40,000, and three homologous chains of M_r 50,000 (β), 60,000 (γ) and 65,000 (δ). Only the α -subunits seem to carry the specific recognition sites for agonists and antagonists². As snake α -neurotoxins seem to bind highly specifically and quasi-irreversibly to these sites we performed a structural analysis to localize the α -subunits, using as marker native α -bungarotoxin (α -BTX, M_r 8,000; ref. 3). We report here the results obtained at 20 Å resolution by electron microscopy and single-particle image averaging⁴, which reveal two well-defined regions within the AChR structure^{5,6} where the mass increases significantly on binding of α -BTX. One of these (α_1) is adjacent to the region where the δ -subunit has been located⁶; the second region (α_2) is diametrically across the molecule, ~50 Å away from the δ -subunit and also from (α_1). The topography revealed by direct structural analysis can explain the results of previous nearest-neighbour cross-linking studies^{2,7}.

AChR-rich membrane fragments isolated from *Torpedo marmorata* electric organ had a specific activity of 1.9 nmol ³H-labelled α -BTX per mg protein. Aliquots (5 μ l; 7 mg protein per ml) were incubated for 60 min with 45 μ l of H₂O which had been adjusted to pH 11 by NaOH, then 120 μ l of H₂O were added and the aliquots were centrifuged in a Beckman Airfuge at 20 p.s.i. for 2 min. The pellets were resuspended and incubated for 90 min in 30 μ l of buffer (100 mM NaCl, 10 mM Na-phosphate pH 7.4, 1 mM EDTA) with α -BTX [30 μ g ml⁻¹; (+)] or without (-). Buffer was then added to 175 μ l and the samples were centrifuged as before. The final pellets were each resuspended in 20 μ l of H₂O. For the (+) sample (pre-incubated with α -BTX) no binding of ³H-labelled α -BTX was detected, indicating saturation of the available binding sites, whereas the value for the (-) sample was 1.4 nmol

† To whom correspondence should be addressed at Department of Physiology, University of Otago Medical School, Dunedin, New Zealand.

‡ Present address: Zoologisches Institut der Universität Münster, Hüfferstrasse 1, D4400 Münster, FRG.

per mg protein. Negatively-stained electron microscope specimens were prepared in parallel, with the same batch of carbon film as reported elsewhere^{5,8}.

Figure 1a,b shows average images of membrane-bound AChR. They were obtained after alignment of individual images of negatively-stained specimens of AChR-rich membrane fragments (microsacs), from which non-receptor peptides had been removed by alkaline washing⁹. These microsacs had been incubated either with [Fig. 1a, (+)] or without [Fig. 1b, (-)] α -BTX. Figure 1a,b represents average axial projections (perpendicular to the membrane plane) of the stain-excluding mass in mem-

brane bound AChR. Their difference map [$\Delta = (+) - (-)$; Fig. 1c] shows two statistically significant peaks within the stain-excluding region of the particle. Given that only about half of the mass of each AChR molecule contributes to the stain exclusion⁶, we may roughly estimate from the size of the difference peaks that the mass added to either of the two regions on binding of α -BTX amounts to less than about one-quarter of the mass of an α -subunit (M_r 40,000).

Extensive tests were done to assess the reliability of the results. As the optical density \bar{d}_{ik} in any image element (ik ; $i, k = 1, \dots, m$; $m = 32$) of an average image is the mean

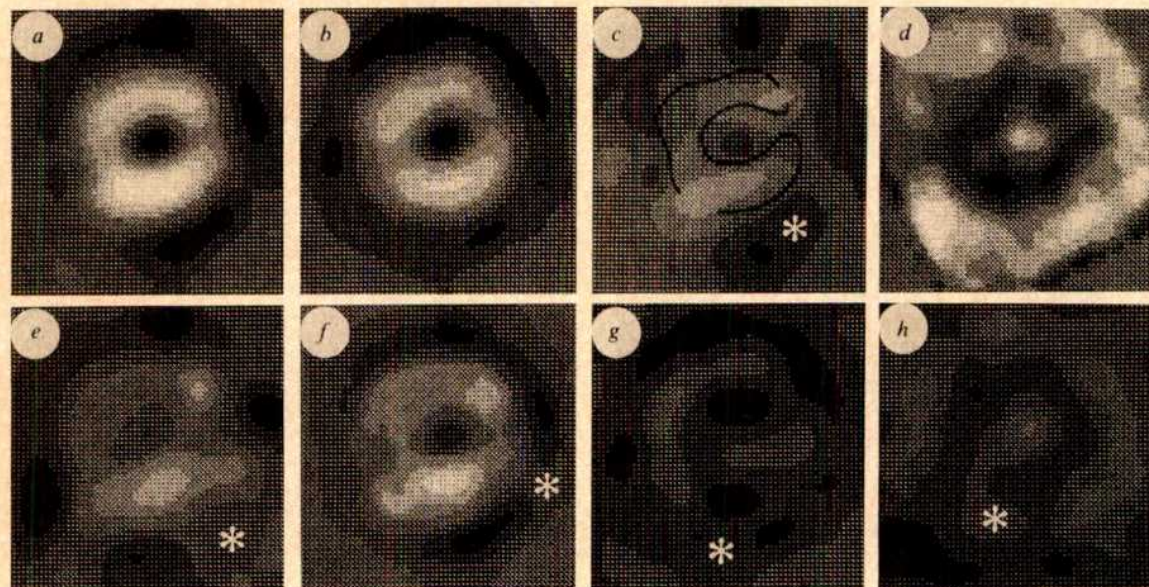


Fig. 1 Average images from negatively stained, membrane-bound AChR particles: *a*, obtained after incubation with α -BTX (+). *b*, Control [without α -BTX, (-)]. *c*, Difference [$\Delta = (+) - (-)$]. Optical density (OD) is low in bright and high in dark regions: thus, the stain-excluding mass appears bright. The density maximum of both *a* and *b* (in OD units) is 1.36. The grey levels in *a*, *b* and *c* are spaced at intervals of 0.029 OD units. Width of each map; 128 Å. *a*, *b* and *c* were low-pass-filtered to a resolution of 18 Å. For technical reasons related to image rotations and translations during alignment, only the central regions (~100 Å in diameter), but not the corners of the maps should be interpreted. The averages show the typical horseshoe-shape of the axial projections of negatively stained membrane-bound AChR particles^{5,6,21-23}. There are two regions where the stain-excluding mass increases on binding of α -BTX (*a*). This is clearly revealed by the difference map (*c*) which possesses two distinct negative peaks (-0.08 OD units) within the particle outline. The grey level closest to zero is marked by an asterisk. *d*, An unfiltered map of the standard error of the difference (s_{ik}^2 , see text) using eight grey levels spaced at intervals of one-tenth of those in *a-c*. (Low values dark, high values bright, minimum 0.017, maximum 0.031.) The lowest errors occur within the region of the stain-excluding mass of the AChR particle. Computer processing (using the SPIDER software system²⁴) of digitized micrographs taken with a scanning transmission electron microscope (STEM) was as follows^{5,6}: a large field of view was segmented into small areas, each containing a single AChR particle. A circular mask (64 Å diameter) was used to screen off the surroundings of the particles^{5,6}. The rotation angles and translation vectors relative to a reference particle were determined by correlation functions, and the individual particles aligned and averaged. Each data set [(+) and (-)] comprised 40 particles. A particle chosen at random from the (+) set was used as a common reference for both data sets. In a second cycle (refinement) each set was aligned again, its previously obtained average now acting as the reference. The masked-off regions were aligned passively and included in the final average. For imaging in the STEM the elastically scattered electrons were used ('incoherent darkfield imaging'). With this type of instrument the image recording conditions (magnification, focus, minimized electron irradiation, optical density) are the same for each set of micrographs. Moreover, images were recorded within a few hours on the same strip of film, making scaling to compensate for instrumental variations unnecessary; that is, (for symbols see text) if the scaling procedure is described by $\bar{d}_{ik}^* = a\bar{d}_{ik} + b$, then $a = 1.0$, $b = 0$. This was confirmed by measurements of the optical density on unstained parts of the carbon films. There remained the possibility that either the two preparations were not equally embedded in negative stain or the stain was not equally dense. The respective optical density characteristics (maximum, minimum, mean, s.d.), as averaged over each of the two sets of micrographs, differed by ~20%. Assuming that this did not indicate structural differences, but unequal staining, the characteristics could be closely matched by setting $a = 1.2$. Thus, it became necessary to establish the effect that scaling might have had on the difference maps. (No scaling was applied to the data shown here.) If the mean density $\bar{\Delta}$ of the difference map is given by

$$\bar{\Delta} = (1/m^2) \sum_{i,k} \Delta_{ik}^- \quad (\text{see text also})$$

and the image variance s_{Δ}^2 of the difference image by

$$s_{\Delta}^2 = \frac{\sum_{i,k} (\bar{\Delta} - \Delta_{ik}^-)^2}{m^2(m^2 - 1)}$$

we may take s_{Δ}^2 as a measure of the total amount of contrast variation (power) in the difference image. The effect of scaling on s_{Δ}^2 was investigated by varying a ($0.5 \leq a \leq 2.0$) in increments of 0.1. This indicated that the overall difference between the (+) and (-) averages within the stain-excluding region (surroundings screened off) can be minimized by setting $a = 1.3$. Nevertheless, for $0.8 \leq a \leq 1.5$, the height of the difference peaks (*c*) exceeded three times the standard error, s_{ik}^2 , of the difference ($3s_{ik}$ -criterion; see *d* and text). On increasing a from 1.0 to 1.5 the difference peak at the lower left (designated α_1 in Fig. 3) moved radially by 10 Å from its position within the main stain-excluding region to a more peripheral position. The position of the other peak (α_2 in Fig. 3) was insensitive to scaling. No additional peaks emerged. These tests show that by applying physically reasonable scaling factors, the difference peaks cannot be made to disappear below the noise level and that the difference indeed indicates a net total increase in stain-excluding matter in the (+)-image relative to the (-)-image. The effect of optical density scaling was also investigated using the phase residual (see Fig. 2) as a criterion. The results were in full agreement with those discussed above. The difference maps *e-h* were obtained in the same manner (including the investigation of scaling effects) as described for *c* and are presented using the same density increment (0.029 OD units). Again, the asterisks mark the levels closest to zero; *e* and *f* are formed between the (+)-average and averages from untreated (O) or disulphide-reduced (R; using 10 mM dithiothreitol¹⁶) membrane fragments, respectively. Thus, *e* corresponds to (+)-(O) and *f* to (+)-(R). The density minima of *e* and *f* within the stain-excluding region are -0.085 and -0.11 OD units, respectively. The reproducibility of the averages may be assessed from the difference maps *g* and *h* which correspond to (-)-(-) and (-)-(R), respectively. Within the stain-excluding regions *g* and *h* show variations of $< \pm 0.03$ OD units, which are not significant according to the $3s_{ik}$ -criterion applied throughout this work. In all difference maps, the peaks occurring in the stain regions would have to exceed ~0.1 OD units to be considered statistically significant. Note that the projection maps of the receptor particles differ from those presented earlier⁵. This is due not only to the application of a refinement cycle, but also to the inclusion of all particles in the course of the so-called '180°-decision'⁵. This applies to all data used here and is an improvement on our previous procedure, done in response to criticism raised by A. Brisson²¹, who independently confirmed the structure of the stain-excluding region by a different single-particle alignment method.

of N realizations d_{ik}^n ($n = 1, \dots, N; N = 40$)

$$\bar{d}_{ik} = (1/N) \sum_{n=1}^N d_{ik}^n$$

the standard error of the mean

$$s_{ik} = \sqrt{\frac{\sum_n (d_{ik}^n - \bar{d}_{ik})^2}{N(N-1)}}$$

was used as a criterion for assessing the significance of the difference $\Delta_{ik}^+ = \bar{d}_{ik}^+ - \bar{d}_{ik}^-$ (Fig. 1a,b) between corresponding image elements in the averages of the two sets. This difference was considered significant if it exceeded three times the standard errors (s_{ik}^+, s_{ik}^-) of the (+)– and (–)–averages. A map of the standard error of the difference

$$s_{ik}^{\Delta} = \sqrt{(s_{ik}^+)^2 + (s_{ik}^-)^2}$$

is shown in Fig. 1d. To apply this criterion we must assume that the values of d_{ik}^n have a gaussian distribution, and that the images are aligned correctly (see Fig. 1 legend). The hypothesis that the d_{ik}^n are normally distributed could not be rejected (Kolmogorov–Smirnov test¹⁰). The reliability of the alignment procedure can be deduced from a comparison of independent averages, using the phase residual as a measure of the reproducible resolution¹¹ (Fig. 2). Additionally, a non-crystallographic test¹² was developed on the basis of non-parametric statistical methods¹³ and applied to aligned and non-aligned image sets. This test requires neither gaussian distributions nor statistical independence of the data; for any image element of an average image and at any significance level it specifies a threshold to be exceeded by the contrast of nearby elements. This method established that after alignment, the density of the stain-excluding regions varied significantly (at the 95% confidence level) over distances of ~ 20 Å. When the images had been aligned merely by translation, omitting rotational alignment (so

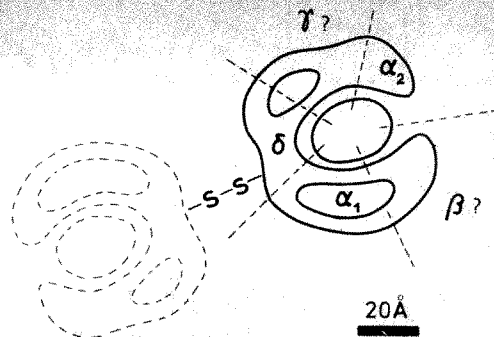


Fig. 3 Schematic representation of the subunit topography of the membrane-bound AChR protein viewed in axial projection perpendicular to the membrane plane. The approximate positions of the α_1 -, α_2 - and δ -chains have been determined directly.

that only their stain-filled centres were in register), significant density variations were lacking in the diffuse annulus representing the average stain-excluding mass.

In the preparation of the specimens, we applied an alkaline washing step⁹ to improve the image contrast of the AChR particles⁸. It extracts non-receptor peptides without either affecting the function (α -BTX binding, ion fluxes) of the AChR^{8,14} or altering the lipid composition of the microsacs¹⁵. Extraction of non-receptor peptides does not affect the internal structure of the stain-excluding mass of membrane-bound AChR¹⁶. Changes occur only near the periphery of the particles (unpublished results); they differ from the effect of disulphide reduction which abolishes a pairwise association of nearest-neighbour particles⁶. Thus, difference maps may also be formed between the average shown in Fig. 1a and averages from untreated microsacs (O) or from microsacs after disulphide reduction (R). These maps ((+)–(O); Fig. 1e, and (+)–(R); Fig. 1f) show essentially the same features as (+)–(–) (Fig. 1c); phase residuals between these maps were consistently smaller than 45° for spatial frequencies $< 1/18$ Å^{–1}. Accordingly, difference maps between the averages without α -BTX in various combinations, for example, between (–) and a corresponding average (–') from an independent data set [(–)–(–')] (Fig. 1g; see also Fig. 2) or (–)–(R) (Fig. 1h)] lacked significant peaks within the stain-excluding region.

We therefore believe that the two difference peaks in Fig. 1c are not only statistically significant, but indeed are due to bound α -BTX marking the α -subunits (α_1, α_2 ; Fig. 3). A substantial exclusion of stain by the toxin might be expected because the 'long toxins' are known to have a rather compact structure stabilized by five disulphide bridges^{3,17}. Furthermore, a compact AChR–toxin complex is suggested by the extensive surface contacts between toxin and AChR (~ 200 van der Waals contacts have been estimated¹⁸). Nevertheless, the unequal sharpness of the two difference peaks indicates that the precision of the localization is not the same for α_1 and α_2 .

Although this study provides no clues as to the location of the putative ACh-activated ion channel, it excludes the possibility that α -BTX acts by physically blocking the entrance to the central cavity of the hydrated mass in the membrane-bound AChR. From the available three-dimensional data^{6,16}, we estimate that this cavity—visualized by the densely stained pit—could accommodate a protein mass of $M_r \sim 10,000$. α -BTX (M_r 8,000) bound to this region would have been clearly revealed.

In Fig. 3 we have also indicated the previously obtained position of the δ -subunit as defined by the contact region between adjacent AChR monomers that are disulphide-linked between their respective δ -subunits⁶. As the δ – δ bond is well documented², the δ -subunit is a convenient reference point for establishing the relative topography of other subunits. The positions of $\beta?$ and $\gamma?$ in Fig. 3 are based merely on the following circumstantial evidence. Extraction of non-receptor peptides (mainly of the M_r 43,000 component (ν)⁹ by alkaline

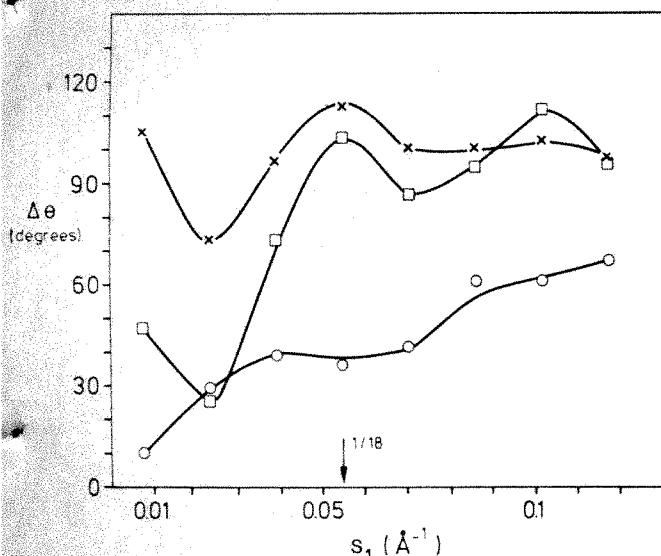


Fig. 2 Differential plots of the phase residual¹¹

$$\Delta\theta = \sqrt{\frac{(|F_1| + |F_2|)\Delta\delta^2}{(|F_1| + |F_2|)}}$$

where F_1 and F_2 denote corresponding complex Fourier coefficients of two (independent) average images and $\Delta\delta$ is their phase difference. The summations extend over a ring zone $S_1 \pm \Delta S$ of the reciprocal space. This analysis shows that $\Delta\theta$ is less than 45° when independent averages (○) taken over >20 aligned images are compared, and that presentation at 18 Å resolution is justified. The plots also illustrate the improvement achieved on alignment by comparing two arbitrarily chosen single particles before (×) and after (□) alignment. In this analysis, which was aimed at demonstrating the reproducible resolution in the stain-excluding mass of the AChR particles, a circular mask (64 Å diameter) was used to screen off the particle surroundings.

washing uncovers antigenic determinants on α , γ and δ (ref. 14). Depletion of skin-excluding mass on alkaline washing was observed (unpublished results) in the neighbourhood of the AChR, near α_2 and δ . This led to the tentative assignment of γ ? to the area between α_2 and δ (Fig. 3).

Thus, we conclude that one of the two α -chains (α_1) is situated in the immediate vicinity of a δ -chain, and that α_2 is ~ 50 Å away. Biochemical labelling and cross-linking studies (reviewed by Karlin² and Hucho⁷) have shown that all chains of the AChR are in close proximity. Despite considerable difficulties in their interpretation, such experiments provide evidence that α and δ are the species most readily cross-linked to one another, whereas cross-links between the two α -chains have not been found. Our result, while in broad agreement with these conclusions, helps to resolve the fundamental difficulty that cross-

linking experiments give equivocal results if they cannot distinguish between the two copies of the α -chain. In membrane-bound AChR the two recognition sites, one on each α -chain, are indistinguishable in their ability to bind snake α -toxins, and in the kinetics of this binding¹⁹. On the other hand, differences seem to exist with respect to affinity labelling^{2,20}. A further difference is directly manifested in the environment of each α -chain (Fig. 3): each toxin-binding region exhibits contacts with a different set of neighbouring subunits, reinforcing the evidence for the asymmetric quaternary structure of the AChR-protein.

We thank Jan de Maeyer and Angelo di Nicola for support related to computing. This work was funded by Deutsche Forschungsgemeinschaft grants DFG Zi 224/1 and DFG Zi 224/2-1. Reprint requests should be addressed to F.J.B.

Received 31 December 1981; accepted 5 July 1982.

1. Raftery, M. A., Hunkapiller, M. W., Strader, C. D. & Hood, L. E. *Science* **208**, 1454-1457 (1980).
2. Karlin, A. in *The Cell Surface and Neuronal Function* (eds Cotman, C. W., Poste, G. & Nicolson, G.) 191-260 (Elsevier, New York, 1980).
3. Karlsson, E. *Handbk exp. Pharmac.* **52**, 159-212 (1979).
4. Frank, J., Goldfarb, W., Eisenberg, D. & Baker, T. S. *Ultramicroscopy* **3**, 283-290 (1978).
5. Zingsheim, H. P., Neugebauer, D.-Ch., Barrantes, F. J. & Frank, J. *Proc. natn. Acad. Sci. U.S.A.* **77**, 952-956 (1980).
6. Zingsheim, H. P., Neugebauer, D.-Ch., Frank, J., Hänicke, W. & Barrantes, F. J. *EMBO J.* **1**, 541-547 (1982).
7. Hucho, F. *Trends biochem. Sci.* **6**, 242-245 (1981).
8. Barrantes, F. J., Neugebauer, D.-Ch. & Zingsheim, H. P. *FEBS Lett.* **112**, 73-78 (1980).
9. Neubig, R. R., Krodell, E. K., Boyd, N. D. & Cohen, J. B. *Proc. natn. Acad. Sci. U.S.A.* **76**, 690-694 (1979).
10. Massey, F. J. Jr, *J. Am. statist. Ass.* **46**, 68-78 (1951).
11. Frank, J., Verschoor, A. & Boublik, M. *Science* **214**, 1353-1355 (1981).
12. Hänicke, W. thesis, Univ. Göttingen (1981).
13. Hänicke, W., Frank, J. & Zingsheim, H. P. *Acta crystallogr.* (submitted).
14. Froehner, S. C. *Biochemistry* **20**, 4905-4915 (1981).
15. Neugebauer, D.-Ch. & Zingsheim, H. P. *Biochim. biophys. Acta* **684**, 272-276 (1982).
16. Zingsheim, H. P., Barrantes, F. J., Hänicke, W., Neugebauer, D.-Ch. & Frank, J. in *Electron Microscopy 1980 Vol. 2* (eds Brederoo, P. & de Priester, W.) 592-593 (Leiden, 1980).
17. Low, B. W. *Handbk exp. Pharmac.* **52**, 213-257 (1979).
18. Chicheportiche, R., Vicent, J. P., Kopeyan, C., Schweitz, H. & Ladzunski, *Biochemistry* **14**, 2081-2091 (1975).
19. Blanchard, S. G. *et al. Biochemistry* **18**, 1875-1883 (1979).
20. Delegeane, A. M. & McNamee, M. G. *Biochemistry* **19**, 890-895 (1980).
21. Brisson, A. thesis Univ. Grenoble (1980).
22. Wade, R. H., Brisson, A. & Tranqui, L. *J. Microsc. Spectrosc. Electron.* **5**, 699-715 (1980).
23. Kistler, J. & Stroud, R. M. *Proc. natn. Acad. Sci. U.S.A.* **78**, 3678-3682 (1981).
24. Frank, J., Shimkin, B. & Dowse, H. *Ultramicroscopy* **6**, 343-358 (1981).

The linear Onsager coefficients for biochemical kinetic diagrams as equilibrium one-way cycle fluxes

Terrell L. Hill

Laboratory of Molecular Biology, National Institute of Arthritis, Diabetes, and Digestive and Kidney Diseases, National Institutes of Health, Bethesda, Maryland 20205, USA

In a biochemical kinetic diagram¹, the various discrete states of an enzyme or enzyme complex are represented by points, and interstate transitions are represented by lines. Figure 1 is an example. I show here that, for steady states near equilibrium, the phenomenological Onsager coefficients in the linear flux-force equations that are a consequence of any such diagram have a transparent physical interpretation: these coefficients are simple combinations of one-way cycle fluxes¹ at equilibrium. The existence of this kind of relationship was pointed out recently in an appendix of a paper² on another subject. I present here the explicit connection between the phenomenological coefficients and the one-way cycle fluxes of the diagram. These coefficients are considered by many scientists to be strictly empirical and incomprehensible. My report provides a simple interpretation of them, at the molecular level, for any biochemical kinetic diagram. This is analogous to the molecular interpretation of phenomenological equilibrium thermodynamics that is provided by statistical mechanics.

Instead of treating a completely arbitrary diagram with generalized notation, the general rule can easily be deduced from a special case that has sufficient complexity. For this purpose we use the hypothetical model of the (Na⁺ + K⁺)ATPase complex shown in Fig. 1. First, cycles and one-way cycle fluxes are introduced for this model, and then their relationship to the Onsager linear coefficients is pointed out.

The hypothetical diagram (or reaction mechanism) in Fig. 1a has eight enzyme states and six cycles. The latter are shown in Fig. 1b. The anticlockwise direction is chosen as positive. The

dominant cycle is 'g'. The enzyme complex is in a membrane separating 'in' and 'out'. For each completed g cycle, in the + direction, two K⁺ ions are transported out \rightarrow in, three Na⁺ ions are transported in \rightarrow out and one ATP molecule is hydrolysed. The transitions 2 \rightleftharpoons 7 and 3 \rightleftharpoons 6 introduce some slippage and also introduce the other five cycles included in Fig. 1b: cycle a (+ direction) transports two K⁺ out \rightarrow in, cycle d (+ direction) transports two K⁺ out \rightarrow in and three Na⁺ in \rightarrow out, and so on.

The observable steady-state fluxes, per complex, are denoted J_K , J_N and J_T , for K⁺, Na⁺ and ATP, respectively. These are all chosen as positive in the normal operating directions specified above. The corresponding thermodynamic forces, per ion or molecule, are then $X_K(\text{out} \rightarrow \text{in})$, $X_N(\text{in} \rightarrow \text{out})$ and X_T , where X_K and X_N are negative, and X_T is positive. In normal operation, K⁺ and Na⁺ are driven across the membrane against their thermodynamic forces by the dominant force X_T .

There are 10 lines in the diagram and hence 20 first-order (or pseudo-first-order) rate constants (units, say, s⁻¹). If these rate constants are all specified, the three observable steady-state fluxes can be written as sums of separate cycle contributions¹:

$$\begin{aligned} J_K &= 2(J_a + J_d + J_g) \\ J_N &= 3(J_b + J_d + J_f + J_g) \\ J_T &= J_c + J_f + J_g \end{aligned} \quad (1)$$

All these fluxes are in units of s⁻¹ per complex. J_a is the net mean rate of cycle a completions in the + direction, and so on. Cycles a, d and g appear in the J_K equation because (see Fig. 1) these and only these three cycles are involved in K⁺ transport (two K⁺ per cycle). Each cycle flux J_κ ($\kappa = a, \dots, g$) above can be expressed in terms of the first-order rate constants of the diagram in the form¹

$$J_\kappa = (\Pi_\kappa^+ - \Pi_\kappa^-)F_\kappa \quad (2)$$

where Π_κ^+ is the product of rate constants around cycle κ in the positive direction, Π_κ^- is the same for the negative direction and F_κ is a positive algebraic combination of all 20 rate constants of the diagram (the details¹ of which are not needed here).

Actually, κ cycles can be completed in either direction, and J_κ can be decomposed as follows¹:

$$J_\kappa = J_{\kappa^+} - J_{\kappa^-}, \quad J_{\kappa^+} = \Pi_{\kappa^+} F_{\kappa^+}, \quad J_{\kappa^-} = \Pi_{\kappa^-} F_{\kappa^-}, \quad (3)$$

where J_{κ^+} is the mean rate (s^{-1}) at which κ cycles are completed in the + direction at steady state, and similarly for J_{κ^-} . The fluxes J_{κ^+} and J_{κ^-} are the one-way cycle fluxes for cycle κ . Both J_{κ^+} and J_{κ^-} are positive but J_κ might be negative. Separate cycle fluxes or separate one-way cycle fluxes are generally not directly observable. If a tracer were used in our example, one could observe, say, the sum

$$J_{\kappa^+} = 2(J_{a^+} + J_{d^+} + J_{g^+}) \quad (4)$$

but not J_{a^+} , J_{d^+} and J_{g^+} separately. However, as will be seen below, it is possible in some cases to determine, experimentally, equilibrium values of one-way cycle fluxes. Returning to equation (3), we note that

$$J_{\kappa^+}/J_{\kappa^-} = \Pi_{\kappa^+}/\Pi_{\kappa^-} \quad (5)$$

in which F_{κ} does not appear.

The thermodynamic force X_κ , operating in cycle κ , is determined by the processes included in cycle κ :

$$X_a = 2X_K, \quad X_b = 3X_N, \quad X_c = X_T, \quad X_d = 2X_K + 3X_N \quad (6)$$

$$X_f = 3X_N + X_T, \quad X_g = 2X_K + 3X_N + X_T$$

Each cycle force X_κ is simply related¹ to Π_{κ^+} and Π_{κ^-} for the cycle:

$$\Pi_{\kappa^+}/\Pi_{\kappa^-} = e^{X_\kappa/kT} = J_{\kappa^+}/J_{\kappa^-} \quad (7)$$

where the last relation makes use of equation (5).

The above discussion applies to an arbitrary steady state. Here, steady states near equilibrium are considered. For this we require

$$|X_K|/kT, \quad |X_N|/kT, \quad |X_T|/kT \ll 1 \quad (8)$$

However, if only cycle g is important, the near-equilibrium condition is much less stringent:

$$|X_g|/kT = |2X_K + 3X_N + X_T|/kT \ll 1 \quad (9)$$

Only the sum need be small, not the separate forces. This important special case will be referred to again below.

Returning to the general case, equation (8), remember that the model in Fig. 1 is being used here simply as a sufficiently complicated example from which to see general results. The conditions in equation (8), especially $|X_T|/kT \ll 1$, are certainly not important for the real $(Na^+ + K^+)$ ATPase (see below in this connection). Near equilibrium, the phenomenological flux-force relations are, as is well known,

$$J_K = L_{KK}X_K + L_{KN}X_N + L_{KT}X_T$$

$$J_N = L_{NK}X_K + L_{NN}X_N + L_{NT}X_T \quad (10)$$

$$J_T = L_{TK}X_K + L_{TN}X_N + L_{TT}X_T$$

where, as Onsager showed for a wide class of systems, the matrix L_{ij} is symmetric (that is, $L_{ij} = L_{ji}$). Our object is to relate the L_{ij} for a biochemical kinetic diagram to the one-way cycle fluxes. In doing this, the symmetry of the matrix will appear automatically.

At an arbitrary steady state, the rate of free energy dissipation is

$$TdS/dt = J_KX_K + J_NX_N + J_TX_T \geq 0 \quad (11)$$

Here X_K and X_N are negative and the other four factors are positive. Near equilibrium, using equations (10) and $L_{ij} = L_{ji}$,

$$TdS/dt = L_{KK}X_K^2 + L_{NN}X_N^2 + L_{TT}X_T^2 + 2L_{KN}X_KX_N$$

$$+ 2L_{KT}X_KX_T + 2L_{NT}X_NX_T \geq 0 \quad (12)$$

This is a non-diagonal quadratic form in which the last two terms are usually negative.

We turn now to a consideration of cycles. In view of equations (6) and (8), all of the $|X_\kappa|/kT \ll 1$. From equations (3) and (7),

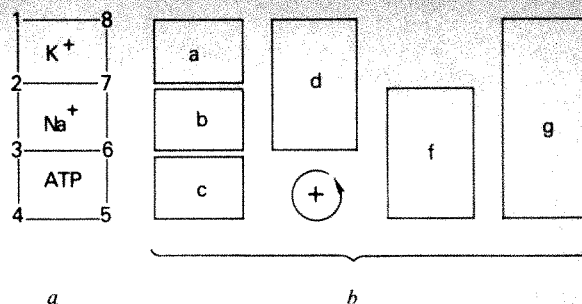


Fig. 1 Hypothetical model of $(Na^+ + K^+)$ ATPase in a membrane, in the form of a biochemical kinetic diagram (a). The enzyme complex has eight significant states, which need not be specified explicitly. The diagram has six cycles (b). All fluxes are chosen as positive in the anticlockwise direction.

we have then

$$J_\kappa = J_{\kappa^+} - J_{\kappa^-} = J_{\kappa^+}[(J_{\kappa^+}/J_{\kappa^-}) - 1]$$

$$= J_{\kappa^+}(e^{X_\kappa/kT} - 1) = J_{\kappa^+}(X_\kappa/kT) + \dots \quad (13)$$

The last form is the near-equilibrium special case. At equilibrium, the two one-way cycle fluxes for cycle κ are equal to each other, because $J_\kappa = 0$. That is, $J_{\kappa^+} = J_{\kappa^-}$. We denote either of these by $J_{\kappa^+}^e$ [as in equation (13)]. $J_{\kappa^+}^e$ is a positive quantity; it is the one-way cycle flux, at equilibrium. $J_{\kappa^+}^e$ can be expressed¹ in terms of the rate constant set of the diagram at equilibrium, using equation (3), but the physical interpretation of $J_{\kappa^+}^e$, just mentioned, is the main point of interest here.

If we now substitute the last form of equation (13), for cycles a, d and g, into the J_K equation in equations (1), and then use equations (6) to eliminate X_a , X_d and X_g , we obtain

$$J_K = 2 \left[J_{a^+}^e \left(\frac{2X_K}{kT} \right) + J_{d^+}^e \left(\frac{2X_K}{kT} + \frac{3X_N}{kT} \right) \right.$$

$$\left. + J_{g^+}^e \left(\frac{2X_K}{kT} + \frac{3X_N}{kT} + \frac{X_T}{kT} \right) \right]$$

$$= 4(J_{a^+}^e + J_{d^+}^e + J_{g^+}^e)(X_K/kT)$$

$$+ 6(J_{d^+}^e + J_{g^+}^e)(X_N/kT) + 2J_{g^+}^e(X_T/kT) \quad (14)$$

If we follow the same procedure for J_N and J_T , and then compare with equations (10), we find for the L_{ij} :

$$L_{KK} = 4(J_{a^+}^e + J_{d^+}^e + J_{g^+}^e)/kT$$

$$L_{NN} = 9(J_{b^+}^e + J_{d^+}^e + J_{f^+}^e + J_{g^+}^e)/kT$$

$$L_{TT} = 1(J_{c^+}^e + J_{f^+}^e + J_{g^+}^e)/kT \quad (15)$$

$$L_{KN} = L_{NK} = 6(J_{d^+}^e + J_{g^+}^e)/kT$$

$$L_{KT} = L_{TK} = 2J_{g^+}^e/kT$$

$$L_{NT} = L_{TN} = 3(J_{f^+}^e + J_{g^+}^e)/kT$$

The symmetry of the matrix appears at this point. The rules for the construction of equations (15), merely by inspection of the diagram and cycles, are obvious from the first form of equation (14): (1) those cycles that include process i contribute to L_{ii} ; (2) those cycles that include both process i and process j contribute to L_{ij} (hence the matrix is symmetrical); (3) the integral numerical coefficients in the L_{ij} are determined by a matrix of stoichiometric products. In the present example, the product matrix is (order K, N, T).

$$\begin{pmatrix} 2.2 & 2.3 & 2.1 \\ 3.2 & 3.3 & 3.1 \\ 1.2 & 1.3 & 1.1 \end{pmatrix} \quad (16)$$

From the simple construction of the first form of equation (14), it is clear that the above rules apply to any diagram. Thus there is a simple physical interpretation of the L_{ij} matrix for any diagram in terms of the equilibrium one-way cycle fluxes of the cycles of the diagram.

The signs of the L_{ij} ($i \neq j$) need not always be positive, as in this example. Thus, suppose we reverse the signs of J_K and X_K in equations (1) and (6) (this is a matter of convention), then we find that a minus sign appears in the expressions for $L_{KN} = L_{NK}$ and for $L_{KT} = L_{TK}$ in equations (15). This was, in fact, the choice made in ref. 1, equation (3.66). However, negative signs can be avoided by choosing all fluxes (operational and cycle) as positive in the same direction.

In principle, the L_{ij} can all be measured by observing the operational steady-state fluxes and forces in equations (10), near equilibrium. With these available, all of the J_K^* can be deduced from equations (15), in the order, for example, g, d, f, a, c, b. Thus, the equilibrium one-way cycle fluxes can be obtained from conventional flux-force measurements. This will be possible, in principle, whenever the number of cycles (with non-zero force and flux¹) in the diagram does not exceed $n(n+1)/2$ (the number of independent L_{ij}), where n is the number of operational fluxes (or forces) in the system.

If only cycle g contributes to the fluxes, we have, near equilibrium

$$J_K = 2J_g^* (X_g/kT), \quad J_N = 3J_g^* (X_g/kT), \quad J_T = J_g^* (X_g/kT) \quad (17)$$

where X_g is given in equation (6). Each linear coefficient is determined by the equilibrium one-way cycle flux of the only operative cycle and by the stoichiometry of that cycle. Here we have integral 2:3:1 stoichiometry between the observable fluxes. If other cycles participate, this exact stoichiometry will be lost.

If we substitute equations (1) into equation (11), and then use equations (6), the rate of free energy dissipation at an arbitrary steady state can be expressed in terms of cycle contributions rather than of observable process contributions:

$$Td_iS/dt = J_a X_a + J_b X_b + J_c X_c + J_d X_d + J_f X_f + J_g X_g \geq 0 \quad (18)$$

Whereas $J_K X_K$ and $J_N X_N$ in equation (11) are negative, no term in equation (18) can be negative. This follows from equations (2) and (7): J_K and X_K have the same sign. Near equilibrium, we put the last form of equation (13) into equation (18), in place of each J_K , and obtain

$$(1/k)d_iS/dt = J_a^* (X_a/kT)^2 + \dots + J_g^* (X_g/kT)^2 \geq 0 \quad (19)$$

Unlike equation (12), this is a diagonalized quadratic form, with every term positive.

Equations (18) and (19), for cycles, have the same mathematical properties as when the individual molecular transitions of a diagram are used (see, for example, equation (4.28) of ref. 1). That is, if we advance, conceptually, from the molecular level to the cycle level these properties are still retained, though they are lost if we go still further to the observable process level, as mentioned following equations (11) and (12). Thus, although cycles are composites of many molecular transitions, in some thermokinetic respects they still resemble individual transitions (for further discussion, see ref. 1).

Although the analogy to the present cycles is not close, it is interesting that Haase³ has shown that the L_{ij} for an arbitrary set of coupled homogeneous chemical reactions can be expressed in terms of one-way reaction fluxes at equilibrium.

We are here primarily concerned with the general question of the relationship between the L_{ij} and cycles for an arbitrary diagram, near equilibrium. Essentially as an addendum we note that, as is well known, many free energy transducing systems in membranes seem to be dominated by a single cycle (for example, cycle g in Fig. 1b) that operates rather near to equilibrium; other slippage cycles are probably used to a limited extent but the forces in these cycles are very far from equilibrium. Thus, if more than one (the main) cycle is used, the above uniformly-near-equilibrium treatment does not apply.

The model in Fig. 1 for $(Na^+ + K^+)ATPase$ can be used as an illustration. In normal operation, X_K and X_N are large and negative, X_T is large and positive, but $X_g = 2X_K + 3X_N + X_T$ is small and positive (cycle g is near equilibrium). Consequently,

from equations (6),

$$X_a, J_a; X_b, J_b; X_d, J_d \text{ are negative} \\ X_c, J_c; X_f, J_f \text{ are positive} \quad (20)$$

The forces in expression (20) are all large in magnitude but the fluxes are relatively small because the slippage rate constants ($2 \rightleftharpoons 7$, $3 \rightleftharpoons 6$) are relatively small. Furthermore, these cycle fluxes will be essentially one-way cycle fluxes, because of the large cycle forces [equation (7)]. Because X_g is positive, J_g is positive. Equations (1), in this case, become

$$J_K = 2[-J_a - J_d + J_g^* (X_g/kT)] \\ J_N = 3[-J_b - J_d + J_f + J_g^* (X_g/kT)] \\ J_T = J_c + J_f + J_g^* (X_g/kT) \quad (21)$$

The one-way cycle fluxes J_a^*, \dots, J_f^* that appear here are not equilibrium fluxes. The corresponding cycle forces do not enter these equations because, for these cycles, the activity is almost one-way (irreversible). The cycle g terms usually dominate; the other terms are slippage corrections which, incidentally, would spoil the exact 2:3:1 stoichiometry of cycle g. All the terms in equations (21) can be expressed¹ as functions of the rate constants of the diagram at this steady state.

I thank Dr S. R. Caplan for significant suggestions and corrections.

Received 9 March; accepted 15 June 1982.

- Hill, T. L. *Free Energy Transduction in Biology* (Academic, New York, 1977).
- Hill, T. L. *J. chem. Phys.* **76**, 1122 (1982).
- Haase, R. *Thermodynamics of Irreversible Processes*, 121–133 (Addison-Wesley, Reading, Massachusetts, 1969).

ATP-dependent unwinding of double helix in closed circular DNA by RecA protein of *E. coli*

Takuzo Ohtani*, Takehiko Shibata†, Masa-aki Iwabuchi, Hiro-omi Watabe, Tohru Iino & Tadahiko Ando

Department of Microbiology, Riken Institute (Institute of Physical and Chemical Research), Wako-shi, Saitama, 351, Japan

RecA protein is an essential component directly involved in general genetic recombination in *Escherichia coli*^{1,2}. In the presence of ATP, RecA protein promotes *in vitro* pairing of homologous DNA molecules^{3–9}, unidirectional elongation of heteroduplex joints^{7,10–12} and concerted reciprocal strand exchange^{13,14}. These activities of the protein can explain some important steps in genetic recombination (see ref. 15 for review). When negative-superhelical closed-circular double-stranded DNA (form I DNA) is a substrate, RecA protein catalyses a cycle of sequential reactions: formation and dissociation of D-loops, and inactivation and reactivation of the duplex as a substrate for D-loop formation^{16,55}. We now present evidence that, in the presence of ATP, RecA protein unwinds the double helix of form I DNA to produce positive-superhelical turns which can be relaxed by eukaryotic topoisomerase I and that, by this process, closed-circular double-stranded DNA with an extraordinarily large number of negative-superhelical turns can be formed in physiological conditions. This ATP-dependent unwinding of the double-helix might promote dissociation of D-loops in form I DNA, followed by inactivation of the form I DNA and the elongation of heteroduplex joints, as suggested by our previous studies^{16,17,55}.

* Present address: Hamari Chemicals Ltd., Higashi-Yodogawa-ku, Osaka-shi, 553, Japan.
† To whom correspondence should be addressed.

The superhelicity of DNA is thought to play a part in genetic recombination^{15,18-22}. When form I DNA was incubated with homologous single-stranded fragments, excess ATP and excess RecA protein at 37°C, D-loops were formed in the early stage of the incubation and then completely dissociated^{16,17,55} (Fig. 2a). When D-loops are completely dissociated, all form I DNA becomes an inactive substrate for D-loop formation¹⁶. These latter two processes can be explained by a model in which free RecA protein (RecA protein that does not bind to single-stranded DNA) binds to double-stranded DNA cooperatively from the site of the D-loop and unwinds the double helix unidirectionally. Unidirectional unwinding of the double helix in form I DNA in the absence of any topoisomerase activity^{23,24} results in relaxation of negative supercoiling and then the accumulation of positive supercoiling, followed by rewinding of the double helix at the trailing end of the unwound region to relax the positive supercoiling (illustrated in Fig. 1, steps from (i) to (iii) via (ii)).^{16,17,55}

To obtain direct evidence for unwinding of the double-helix in form I DNA in an inactivated state, we performed the following experiments. After the formation and subsequent complete dissociation of the D-loops by incubation of form I ³H-labelled DNA with homologous single-stranded fragments, ATP and RecA protein for 50 min (the first incubation), we treated the form I DNA for 5 min at 37°C with an eukaryotic topoisomerase I prepared from *Saccharomyces cerevisiae* (the second incubation). Eukaryotic topoisomerase I, including that from *S. cerevisiae*, is able to relax both positive and negative supercoiling (see refs 25, 26 for review, also H.W. and T.I., unpublished observation). When both the first incubation and RecA protein in the second incubation were omitted, the duplex DNA was completely converted to relaxed form (form IV) by the second incubation and exhibited a set of closely spaced bands near a band produced by nicked-circular DNA (form II

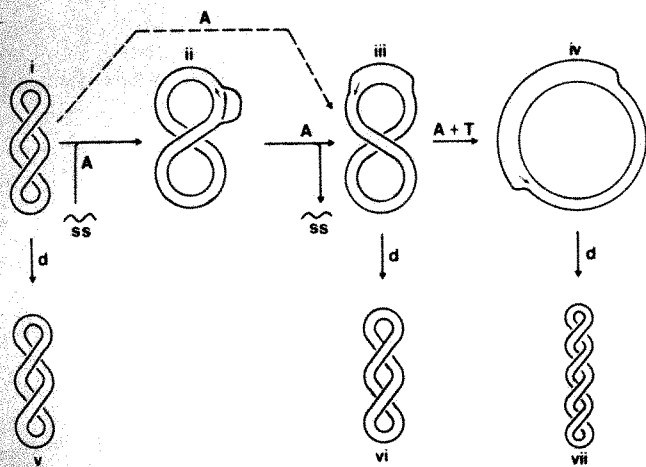


Fig. 1 Schematic diagram of the experiments to demonstrate unwinding of the double helix by RecA protein. Basically, when we compare the average linking numbers between a closed-circular DNA relaxed by topoisomerase in the presence of double helix unwinding reagents (iv) or (vii), and that relaxed in their absence, the difference directly indicates the angle of unwinding by the reagents⁴⁹⁻⁵¹. The double helix is unidirectionally unwound by RecA protein (indicated by small arrows) in (ii), (iii) and (iv). Unidirectional unwinding by RecA protein is initiated very efficiently at the site of a D-loop (small arrow in (ii)). In the case of negative-superhelical DNA (form I DNA), the initiation occurs at a very low rate even in the absence of any single-stranded DNA (indicated by broken line from (i) to (iii)), probably at transient denatured sites. Because, in the absence of topoisomerase activity, the unidirectional unwinding of the double-helix in closed-circular DNA results in the loss of negative supercoiling of form I DNA, dissociation of D-loops (steps from (ii) to (iii)) and then positive supercoiling of the form I DNA (iii). The product is then treated with eukaryotic topoisomerase I in the presence of active RecA protein (indicated by A + T). The positive supercoiling of the form I DNA (iii) is relaxed and the unwound region extended (iv). After proteins are removed (step indicated by d), product (iv) becomes a form (vii) with a larger number of negative-superhelical turns than natural form I DNA (v). When the double helix is not unwound, negative supercoiling of form I DNA is relaxed with topoisomerase I. A, T and ss denote RecA protein, topoisomerase I and homologous single-stranded fragments, respectively.

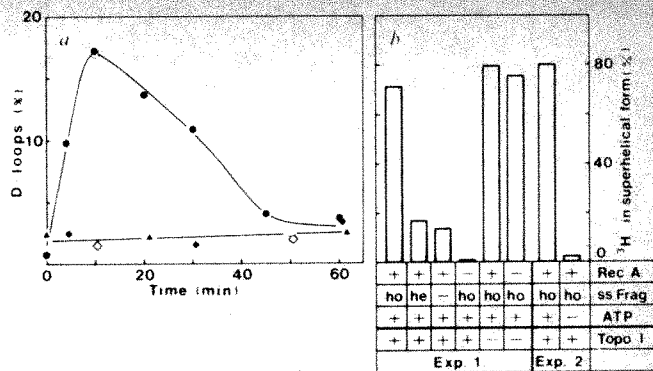


Fig. 2 Formation and dissociation of D-loops, and formation of form X. fd form I ³H DNA preparation (4 μ M, containing 75% form I DNA) and 0.05 μ M homologous single-stranded fragments were incubated with 1 μ M (in a, open symbols, and in b) or 0.5 μ M (in a, closed symbols) RecA protein (molecular weight 40,000) and 1.3 mM ATP in a reaction mixture (20.5 μ l) containing 31 mM Tris-HCl (pH 7.5), 13 mM MgCl₂, 1.8 mM dithiothreitol and 88 μ g of bovine serum albumin per ml at 37°C (the first incubation). RecA protein is a DEAE-cellulose fraction (fraction V) prepared as described previously²⁴. Preparation of DNA is described elsewhere²⁴. Amounts of DNA are expressed in moles of nucleotide residues. a, Samples were withdrawn at the indicated times and D-loops were assayed by the nitrocellulose-filter method^{16,33}. \circ , \bullet , Complete reaction mixture; \diamond , \blacklozenge , with heterologous (Φ X174) fragments; \triangle , \blacktriangle , without RecA protein. b, After treatment of fd form I DNA by the first incubation of 50 min, topoisomerase I from *S. cerevisiae*⁵² (30 μ g ml⁻¹) was added to the reaction mixture, followed by incubation for 5 min at 37°C. Reactions were terminated by chilling in an ice-water bath and by denaturing proteins with 0.5% Sarkosyl NL97 (Ciba-Geigy) and 4 μ l of phenol saturated with the buffer. Samples were then electrophoresed through 1% agarose gel in E-buffer⁵³ in the absence of dye at 20 V for 15 h at room temperature. After electrophoresis, the agarose gel (shown in Fig. 3) containing each lane was cut into several pieces, dissolved by boiling for 2-4 min with 0.1 M HCl, applied to a glass filter (Whatman GFC) and dried. Radioactivity on the filter was assayed in a Beckman LS8100 scintillation counter by using toluene scintillator. Percentage of radioactivity in bands formed by form I DNA and form X DNA to total recovered radioactivity is plotted. Topoisomerase I, with a molecular weight of 70,000 as estimated by gel filtration was purified ~8,000-fold by a series of chromatographies on an Ultrogel AcA 34 column, a double-stranded DNA-cellulose column and a hydroxylapatite column from the phosphocellulose fraction of *S. cerevisiae* IAM4274 prepared as described previously⁵⁴. This preparation of the topoisomerase is free of detectable endo- or exo-DNase, ATPase or DNA ligase activities and relaxes both positive and negative supercoiling by changing linking number in steps of one (H. W. and T.I., unpublished observation). 'ho' and 'he' indicate homologous single-stranded fragments and heterologous ones, respectively. RecA, ss frag and topo I indicate RecA protein, single-stranded fragments and the second incubation with topoisomerase I, respectively.

DNA) in the gel electrophoregram (Fig. 3, lane 9); about 99% of the recovered radioactivity of the input duplex DNA was in the bands of form IV and form II DNA. However, a large part of the duplex DNA from the complete reaction system formed a band which migrated significantly faster than the untreated form I DNA (Fig. 3, lane 14 compared with lanes 1 and 17). Here we tentatively call the form of DNA migrating faster than natural form I DNA form X, for simplicity.

We concluded from the following observations that form X is a closed-circular double-stranded DNA with an extraordinarily large number of negative-superhelical turns or much smaller linking number than natural form I DNA. Ethidium bromide is an intercalating dye which unwinds the double helix²⁷⁻²⁹. As shown in Fig. 4b, in the presence of 0.15 μ M ethidium bromide, untreated form I DNA behaved as the relaxed form in gel electrophoresis (lane 4), and form IV DNA as the positive-superhelical form (lanes 1-3). In this condition, form X DNA still behaved as a superhelical form (Fig. 4b, lanes 5-7). Form X DNA formed by the second incubation for 20 s could be relaxed by 0.7 μ M ethidium bromide in the gel (Fig. 4c, lane 5). In the presence of this concentration of the dye, both form I and form IV DNA behaved as the positive-superhelical form (Fig. 4c, lanes 1-4). The form X DNA formed by the second incubation for 5 min and that formed by the second incubation for 15 min were not relaxed by this concentration

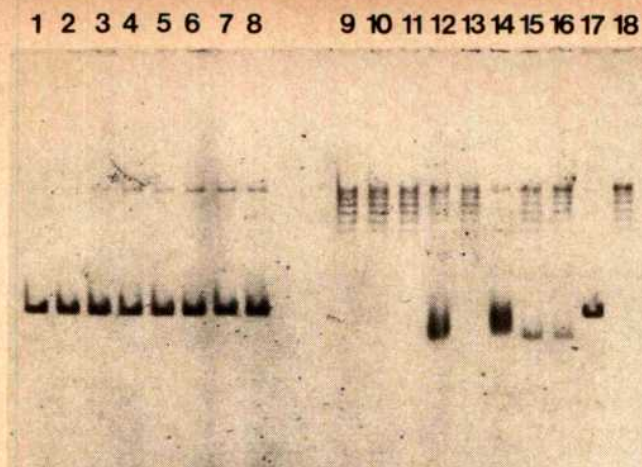


Fig. 3 Gel electrophoresis of the product formed by RecA protein and topoisomerase I. Conditions for the reaction are given in Fig. 2 legend. As the length of single-stranded fragments used in this study was about 200 nucleotides, the fd form I DNA bearing a D-loop which was formed with these fragments was not relaxed (lane 4). The band produced by the single-stranded fragments was not significant in the conditions used here, because the single-stranded fragments migrated in a broad band and their concentration was only 1/70th of the duplex DNA. For lanes 1–8, the second incubation was omitted. The period of the first incubation was as indicated. For lanes 9–16, reaction mixtures were incubated with topoisomerase I for 5 min at 37°C after the indicated period of the first incubation. Lanes 1 and 9, without RecA protein for 0 min; lanes 2 and 10, complete reaction mixture for 0 min; lanes 3 and 11, with heterologous single-stranded fragments for 0 min; lanes 4 and 12, complete reaction mixture for 10 min; lanes 5 and 13, with heterologous single-stranded fragments for 10 min; lanes 6 and 14, complete reaction mixture for 50 min; lanes 7 and 15, with heterologous single-stranded fragments for 50 min; lanes 8 and 16, without single-stranded fragments for 50 min; lane 17, untreated form I DNA; lane 18, after 50 min of the first incubation of complete reaction mixture, 3 mM ADP was added to the reaction mixture and incubated for 30 min at 37°C. Then topoisomerase I was added and incubated for 5 min at 37°C. After electrophoresis, we photographed the gel as described previously²⁴.

of ethidium bromide (Fig. 4c, lanes 6, 7); the former was relaxed by the dye at 1–3 μ M and the latter by the dye at >5 μ M. These experiments also indicate that the extent of unwinding of the double helix in the closed-circular DNA gradually increases during the second incubation. A preliminary quantitative measurement of superhelicity using the ethidium bromide-buoyant density technique³⁰ showed that the form X formed

by the second incubation for 20 s has about twofold more superhelical turns than natural form I DNA (T.O. and T.S., unpublished result). This amount of supercoiling corresponds to the unwinding of about 800 base pairs (see ref. 24). As the velocity of unwinding of the double helix in form I DNA by RecA protein was calculated to be about one base pair per second¹⁶, the above experiments suggest that during the first incubation for 50 min, positive-superhelical turns seem to be accumulated in the duplex DNA (Fig. 1, product (iii)).

The amount of topoisomerase I added in these experiments completely relaxed form I DNA in the absence of RecA protein within 20 s (Fig. 4a, lane 1). After the first incubation for 50 min, 20 s of the second incubation was enough to convert almost all of the closed-circular DNA to form X (Fig. 4a, lane 5); 74% of the recovered radioactivity of the input duplex DNA which contained 77% form I DNA was in the band of form X in the gel electrophoregram in the absence of ethidium bromide (Fig. 4a, lane 5), and 92 and 8% of the radioactivity were in the bands of relaxed form and in the band of unreacted form I DNA, respectively, in the presence of 0.7 μ M ethidium bromide (Fig. 4c, lane 5).

The yield of form X DNA was the function of the period of the first incubation. When the first incubation was omitted, no form X was formed during the second incubation (Fig. 3, lane 10), and when the first incubation was not long enough to complete the dissociation of D-loops, a smaller portion of form I DNA was converted to form X (Fig. 3, compare lanes 12 and 14; see Fig. 2a). Therefore, the double helix of all form I DNA in an inactive state is extensively unwound and this unwinding correlates with the inactivation process, as suggested by the model described above.

The formation of form X required ATP (Fig. 2b), like the formation and dissociation of D-loops^{3,8,55}. Moreover, when ADP was added to the reaction system after the complete dissociation of D-loops and incubated, the duplex DNA was completely relaxed and no form X DNA was formed during the second incubation (Fig. 3, lane 18). This correlates with our previous observation that after the inactivation of form I DNA by formation and dissociation of D-loops, addition of ADP results in the full reactivation of the duplex⁵⁵.

On the other hand, formation of form X was greatly reduced when homologous single-stranded fragments were omitted or replaced by heterologous ones (Fig. 2b). Moreover, when we compared the initial velocity, the difference between the formation of form X in the presence of homologous single-stranded

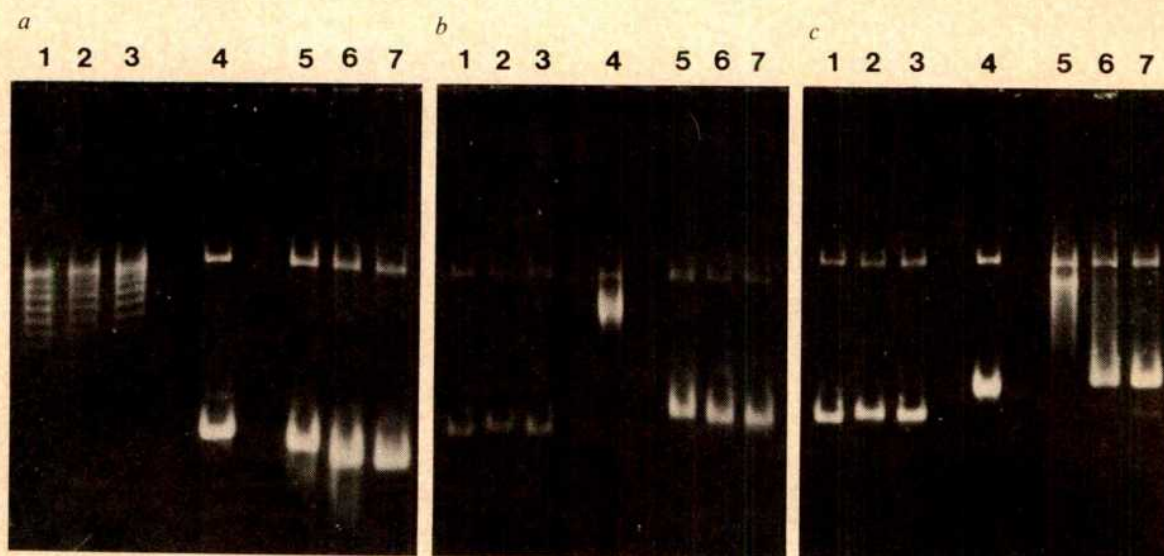


Fig. 4 Effect of ethidium bromide on the migration of the products in gel electrophoresis. Conditions for the reaction and electrophoresis are given in Figs 2 and 3 legends. Samples were electrophoresed in the absence of ethidium bromide (a), in the presence of 0.15 μ M ethidium bromide (b) or in the presence of 0.7 μ M ethidium bromide (c). For lanes 1–3, both RecA protein and the first incubation were omitted; for lanes 5–7, the first incubation in complete reaction mixture was carried out for 50 min at 37°C. The period of the second incubation with topoisomerase was 20 s (lanes 1 and 5), 5 min (lanes 2 and 6) or 15 min (lanes 3 and 7). Lane 4, untreated form I DNA.

fragments and its formation in the absence of homologous fragments was even greater, the former being 30-fold larger (M.I. and T.S., unpublished observation). However, the formation of form X DNA does occur at a very low rate in the absence of single-stranded DNA and is slightly stimulated by the addition of heterologous single-stranded fragments, but only if double-stranded DNA substrate is form I DNA (Fig. 2b and Fig. 3, lanes 15, 16). When double-stranded DNA substrate is relaxed DNA (form IV DNA), the formation of form X DNA seems to require homologous single-stranded fragments (T.S. M.I. and T.O., unpublished observation, and A. M. Wu, and C. M. Radding, personal communication). These results suggest that the unwinding of the double helix by RecA protein might be initiated at all D-loop sites and also initiated at a very low rate at the transient denatured sites in superhelical DNA³¹⁻³³. The initiation at the latter sites is stimulated by any single-stranded DNA (data not shown) as the unwinding in the presence of ATP γ S (ref. 23).

The enzymes which catalyse unwinding of the double helix in the presence of a high-energy cofactor such as ATP are called DNA helicases, and include DNA helicase I, II (refs 34-36) and III (refs 37, 38) from *E. coli*, *E. coli* Rep protein³⁹⁻⁴² and ATP-dependent DNases from *E. coli*⁴³⁻⁴⁵ and *Haemophilus influenzae*⁴⁶. As a DNA helicase, RecA protein is unique; it unwinds closed-circular DNA without strand termini, whereas all other DNA helicases require a single-stranded tail, gap or free end in the DNA to initiate the unwinding of the double helix. Moreover, RecA protein has not been found to initiate unwinding from a single-stranded tail or gap (ref. 47 and R. P. Cunningham, unpublished observation). DNA helicase activity of RecA protein seems to have a role in the elongation of heteroduplex joints by RecA protein *in vitro*¹⁰⁻¹² and in branch migration during recombination *in vivo*¹⁵.

The present study also indicates that closed-circular double-stranded DNA with an extraordinarily large number of negative-superhelical turns can be formed in physiological conditions by the two proteins, RecA protein and topoisomerase I. In eukaryotes in which gyrase activity has not been found, RecA-like protein⁴⁸ and topoisomerase I might promote a high degree of supercoiling.

We thank Dr Jean M. Michalec for reading the manuscript, Drs C. M. Radding and W. K. Holloman for communicating their results before publication and Dr C. M. Radding for stimulating discussions. This study was supported in part by a grant from the Science and Technology Agency, Japan, and by a grant from the Ministry of Education, Science and Culture, Japan.

Received 6 April; accepted 1 July 1982.

- Clark, A. J. & Margulies, A. D. *Proc. natn. Acad. Sci. U.S.A.* **53**, 451-459 (1965).
- Kobayashi, I. & Ikeda, H. *Molec. gen. Genet.* **166**, 25-29 (1978).
- Shibata, T., DasGupta, C., Cunningham, R. P. & Radding, C. M. *Proc. natn. Acad. Sci. U.S.A.* **76**, 1638-1642 (1979).
- McEntee, K., Weinstock, G. M. & Lehman, I. R. *Proc. natn. Acad. Sci. U.S.A.* **76**, 2615-2619 (1979).
- Cunningham, R. P., DasGupta, C., Shibata, T. & Radding, C. M. *Cell* **20**, 223-235 (1980).
- Cassuto, E., West, S. C., Mursallim, J., Conlon, S. & Howard-Flanders, P. *Proc. natn. Acad. Sci. U.S.A.* **77**, 3962-3966 (1980).
- DasGupta, C., Shibata, T., Cunningham, R. P. & Radding, C. M. *Cell* **22**, 437-446 (1980).
- Shibata, T. *et al. J. biol. Chem.* **256**, 7565-7572 (1981).
- Cunningham, R. P., Wu, A. M., Shibata, T., DasGupta, C. & Radding, C. M. *Cell* **24**, 213-223 (1981).
- Kahn, R., Cunningham, R. P., DasGupta, C. & Radding, C. M. *Proc. natn. Acad. Sci. U.S.A.* **78**, 4786-4790 (1981).
- Cox, M. M. & Lehman, I. R. *Proc. natn. Acad. Sci. U.S.A.* **78**, 3433-3437 (1981).
- DasGupta, C. & Radding, C. M. *Proc. natn. Acad. Sci. U.S.A.* **79**, 762-766 (1982).
- DasGupta, C., Wu, A. M., Kahn, R., Cunningham, R. P. & Radding, C. M. *Cell* **25**, 507-516 (1981).
- West, S. C., Cassuto, E. & Howard-Flanders, P. *Proc. natn. Acad. Sci. U.S.A.* **78**, 2100-2104.
- Radding, C. M. *et al. Rev. Biochem.* **47**, 847-880 (1978).
- Shibata, T., Ohtani, T., Chang, P. K. & Ando, T. *J. biol. Chem.* **257**, 370-376 (1982).
- Ohtani, T., Shibata, T., Iwabuchi, M., Nakagawa, K. & Ando, T. *J. Biochem. Tokyo* **91**, 1767-1775 (1982).
- Holloman, W. K. & Radding, C. M. *Proc. natn. Acad. Sci. U.S.A.* **73**, 3910-3914 (1976).
- Gellert, M., Mizuuchi, K., O'Dea, M. H. & Nash, H. A. *Proc. natn. Acad. Sci. U.S.A.* **73**, 3872-3876 (1976).
- Hays, J. B. & Boehmer, S. *Proc. natn. Acad. Sci. U.S.A.* **75**, 4125-4129 (1978).
- Kikuchi, Y. & Nash, H. *Cold Spring Harb. Symp. quant. Biol.* **43**, 1099-1109 (1979).

- Raina, J. L. & Ravin, A. W. *Molec. gen. Genet.* **176**, 171-181 (1979).
- Cunningham, R. P., Shibata, T., DasGupta, C. & Radding, C. M. *Nature* **281**, 191-195 (1979); **282**, 426 (1979).
- Shibata, T., Cunningham, R. P. & Radding, C. M. *J. biol. Chem.* **256**, 7557-7564 (1981).
- Champoux, J. J. *et al. Rev. Biochem.* **47**, 449-479 (1978).
- Gellert, M. *et al. Rev. Biochem.* **50**, 879-910 (1981).
- Fuller, W. & Waring, M. J. *Ber. Bunsenges. Phys. Chem.* **68**, 805-808 (1964).
- Wang, J. C. *J. molec. Biol.* **89**, 783-801 (1974).
- Pulleyblank, D. E. & Morgan, A. R. *J. molec. Biol.* **91**, 1-13 (1975).
- Bauer, W. R. *et al. Rev. Biophys. Bioneng* **7**, 287-313 (1978).
- Wiegand, R. C., Godson, G. N. & Radding, C. M. *J. biol. Chem.* **250**, 8848-8855 (1975).
- Shishido, K. & Ando, T. *Agric. biol. Chem.* **39**, 673-681 (1975).
- Beattie, K. L., Wiegand, R. C. & Radding, C. M. *J. molec. Biol.* **116**, 783-803 (1977).
- Abdel-Monem, M. & Hoffmann-Berling, H. *Eur. J. Biochem.* **65**, 431-440 (1976).
- Abdel-Monem, M., Dürwald, H. & Hoffmann-Berling, H. *Eur. J. Biochem.* **65**, 441-449 (1976).
- Kuhn, B., Abdel-Monem, M., Krell, H. & Hoffmann-Berling, H. *J. biol. Chem.* **254**, 11343-11350 (1979).
- Yarranton, G. T., Das, R. H. & Gefter, M. L. *J. biol. Chem.* **254**, 11997-12001 (1979).
- Yarranton, G. T., Das, R. H. & Gefter, M. K. *J. biol. Chem.* **254**, 12002-12006 (1979).
- Scott, J. F., Eisenberg, S., Bertsch, L. L. & Kornberg, A. *Proc. natn. Acad. Sci. U.S.A.* **74**, 193-197 (1977).
- Abdel-Monem, M., Chanal, M.-C. & Hoffmann-Berling, H. *Eur. J. Biochem.* **79**, 33-38 (1977).
- Abdel-Monem, M., Dürwald, H. & Hoffmann-Berling, H. *Eur. J. Biochem.* **79**, 39-45 (1977).
- Yarranton, G. T. & Gefter, M. L. *Proc. natn. Acad. Sci. U.S.A.* **76**, 1658-1662 (1979).
- Eichler, D. C. & Lehman, I. R. *J. biol. Chem.* **252**, 499-503 (1977).
- MacKay, V. & Linn, S. *J. biol. Chem.* **251**, 3716-3719 (1976).
- Taylor, A. & Smith, G. R. *Cell* **22**, 447-457 (1980).
- Wilcox, K. W. & Smith, H. O. *J. biol. Chem.* **251**, 6127-6134 (1976).
- West, S. C., Cassuto, E. & Howard-Flanders, P. *Nature* **290**, 29-33 (1981).
- Kmieciak, E. & Holloman, W. K. *Cell* (in the press).
- Wang, J. C. *J. molec. Biol.* **43**, 25-39 (1969).
- Germond, J. E., Hirt, B., Oudet, P., Gross-Bellard, M. & Chambon, P. *Proc. natn. Acad. Sci. U.S.A.* **72**, 1843-1847 (1975).
- Wang, J. C., Jacobsen, J. H. & Saucier, J.-M. *Nucleic Acids Res.* **4**, 1225-1241 (1977).
- Durnford, J. M. & Champoux, J. J. *J. biol. Chem.* **253**, 1086-1089 (1978).
- Sharp, P. A., Sugden, B. & Sambrook, J. *Biochemistry* **12**, 3055-3063 (1973).
- Watabe, H., Shibata, T. & Ando, T. *J. Biochem., Tokyo* **90**, 1623-1632 (1981).
- Shibata, T., Ohtani, T., Iwabuchi, M. & Ando, T. *J. biol. Chem.* (in the press).

Errata

In the letter 'Curare can open and block ionic channels associated with cholinergic receptors' by A. Trautmann *Nature* **298**, 272-275 (1982), the symbols in Table 1 representing the different types of transitions observed should be rotated through 180°.

In the letter 'Electrical stimulation of hindlimb increases neuronal cell death in chick embryo' by R. W. Oppenheim & R. Nunez *Nature* **295**, 57-59 (1982), in Fig. 2 the bars representing pooled data should be labelled CE & SE (left-hand bar) and CU & SU (right).

Corrigenda

In the letter 'Differences in the kinetics of rod and cone synaptic transmission' by J. L. Schnapf & D. R. Copenhagen, *Nature* **296**, 862-864 (1982), the plots of the equation shown in Fig. 1 legend (that is, in Figs 1c, 2c and 3) do not have large enough undershoots. This in turn leads to an overestimate of the decay time of the impulse response. The impulse response actually falls to 1/e its peak value in 80 ms for the rod synapse and 10 ms for the cone synapse (not 131 ms and 16 ms as stated in the second-to-last paragraph). The major conclusions of the paper remain unchanged: the synapses display high and low pass filter characteristics and the rod synapse is approximately 10 times slower than the cone synapse.

In the letter 'Directed effector cells selectively lyse human tumour cells' by C. B. Simone, *Nature* **297**, 234-236 (1982), line 16 on page 236 states that "direct effector cells... cause no adverse reactions *in vivo* (mice and one human)." Instead of "no adverse reactions", the author should have stated that the patient did have two fevers during the five day treatment which responded to acetoaminophen. However, no other toxicities were noted. Obviously, a full trial needs to be done to explore the efficacy of directed effector cell treatment.

BOOKS RECEIVED

Biological Sciences

- ADAMS, D.O., EDELSON, P.J. and KOREN, H.S. (eds). *Methods for Studying Mononuclear Phagocytes*. Pp.1023. ISBN 0-12-044220-5. (Academic: 1981.) \$59.50.
- AGRANOFF, B.W. and APRISON, M.H. (eds). *Advances in Neurochemistry*, Vol. 4. Pp.231. ISBN 0-306-40678-0. (Plenum: 1982.) \$32.50.
- ANDREANI, D., DE PIRO, R. *et al.* (eds). *Current Views on Insulin Receptors*. Proceedings of the Sero Symposium, Vol. 41. Pp.626. ISBN 0-12-058620-7. (Academic: 1982.) £34.80, \$71.50.
- ASSCHER, A.W., MOFFAT, D.B. and SANDERS, E. *Nephrology Illustrated: An Integrated Text and Colour Atlas*. ISBN 0-906923-01-8/0-08-028851-0. (Gower/Pergamon: 1982.) Np.
- BAKER, J.J.W. and ALLEN, G.E. *The Study of Biology*, 4th Edn. Pp.972 + appendix. ISBN 0-201-10180-7. (Addison-Wesley: 1982.) Np.
- BAREFOOT, A.C. and HANKINS, F.W. *Identification of Modern and Tertiary Woods*. Pp.189. ISBN 0-19-854378-6. (Oxford University Press: 1982.) Np.
- BLANCHARD, J.R. and FARRELL, L. (eds). *Guide to Sources for Agricultural and Biological Research*. Pp.735. ISBN 0-520-03226-8. (University of California Press: 1981.) £33.25.
- BLAXTER, J.H.S. *et al.* (eds). *Advances in Marine Biology*, Vol. 19. Pp.382. ISBN 0-12-026119-7. (Academic: 1982.) £30, \$61.50.
- HUMBER, D.P. (ed.). *Immunological Aspects of Leprosy, Tuberculosis and Leishmaniasis*. Proceedings of a Meeting held in Addis Ababa, Ethiopia, October 1980. Pp.312. ISBN 90-219-0522-1. (Excerpta Medica, The Netherlands: 1981.) \$65, Dfl.140.
- HUXTABLE, R.J. and PASANTES-MORALES, H. (eds). *Taurine in Nutrition and Neurology*. *Advances in Experimental Medicine and Biology*, Vol.139. Proceedings of a Symposium held November 1980 at the Universidad Nacional Autónoma de México, Mexico City, Mexico. Pp.551. ISBN 0-306-40839-2. (Plenum: 1982.) \$59.50.
- MCNEIL ALEXANDER, R. *Locomotion of Animals*. Pp.163. UK Hbk ISBN 0-216-91159-1; pbk ISBN 0-216-91158-3, US Hbk ISBN 0-412-00001-6; pbk ISBN 0-412-00011-3. (Blackie/Chapman & Hall: 1982.) UK Hbk £15.95; pbk £7.95. US np.
- MORRIS, C. J. and CLARK, A. (eds). *Effects of Low Temperatures on Biological Membranes*. Pp. 432. ISBN 0-12-507650-9. (Academic: 1981.) £22, \$45.50.
- MOYLE, P. B. and CECH, J. J. *Fishes: An Introduction to Ichthyology*. Pp.593. ISBN 0-13-319723-9. (Prentice-Hall: 1982.) £22.45.
- NAGASAWA, H. and ABE, K. (eds). *Hormone Related Tumors*. Pp.320. ISBN 3-540-10925-0/0-387-10925-0. (Springer-Verlag: 1981.) DM118, \$55.
- NAYAK, D.P. (ed.). *Genetic Variation among Influenza Viruses*. ICN-UCLA Symposia on Molecular and Cellular Biology, Vol. 21, 1981. Pp.672. ISBN 0-12-515080-6. (Academic: 1981.) \$56.
- NEDWELL, D.B. and BROWN, C.M. (eds). *Sediment Microbiology*. Pp.280. ISBN 0-12-515380-5. (Academic: 1982.) £14.20, \$29.50.
- NICHOLSON, B. *Plants of the British Isles*. Pp.76. ISBN 0-00-410416-1. (Collins: 1982.) £7.95.
- NOVY, M.J. and RESKO, J.A. (eds). *Fetal Endocrinology*. Pp.423. ISBN 0-12-522601-2. (Academic: 1981.) \$36.
- NUHN, P. *Chemie der Naturstoffe: Bioorganische Chemie*. Pp.660. No ISBN. (Akademie-Verlag: 1981.) Np.
- OSBOURNE, N.N. (ed.). *Biology of Serotonergic Transmission*. Pp.522. ISBN 0-471-10032-3. (Wiley: 1982.) £30, \$69.
- PEDGLEY, D. (ed.). *Desert Locust Forecasting Manual*, Vol. 1 & Vol. 2. Pp.268. ISBN 0-85135-121-2. (Centre for Overseas Pest Research, London: 1981.) Np.
- PEREZ-BERCOFF, R. (ed.). *Protein Biosynthesis in Eukaryotes*, Vol. 41. Pp.502. ISBN 0-306-40893-7. (Plenum: 1982.) Np.
- RAY, D. S. (ed.). *The Initiation of DNA Replication*. ICN-UCLA Symposia on Molecular and Cellular Biology, Vol.22, 1981. Proc. of the 1981 Symposia, Salt Lake City, Utah, March 1981. Pp.628. ISBN 0-12-583580-9. (Academic: 1981.) \$53.
- THE MACDONALD ENCYCLOPEDIA OF SHELLS. Pp.512. Pbk ISBN 0-356-08575-9. (Macdonald, London: 1982.) Pbk £4.95.
- VINCENT, T.L. and SKOWRONSKI, J.M. *Renewable Resource Management*. *Lecture Notes in Biomathematics*, Vol. 40. Proceedings of a Workshop on Control Theory, Christchurch, New Zealand, January 1980. Pp.236. Flexi ISBN 3-540-10566-2. (Springer: 1981.) Flexi DM 28.50, \$13.60.
- WALLACH, D.F.H. (ed.). *The Function of Red Blood Cells: Erythrocyte Pathobiology*. Progress in Clinical and Biological Research, Vol. 51. Proceedings of an International Symposium, Tufts University School of Medicine, Boston, Massachusetts, April 1980. Pp.404. ISBN 0-8451-0051-3. (Alan R. Liss, New York: 1981.) £25.90, DM 114.
- WEINSTEIN, B. (ed.). *Chemistry and Biochemistry of Amino Acids, Peptides, and Proteins*, Vol. 6. Pp.344. ISBN 0-8247-1363-X. (Marcel Dekker: 1982.) SwFr.148.
- WEST, D.C., SHUGART, H.H. and BOTKIN, D.B. (eds). *Forest Succession. Concepts and Application*. Pp.517. ISBN 0-387-90597-9/3-540-90597-9. (Springer-Verlag: 1981.) DM 87, \$40.50.
- WHEATER, P. R. and BURKITT, H. G. *Self-Assessment in Histology*. Pp.198. ISBN 0-443-02109-0. (Churchill Livingstone: 1982.) £3.95.
- WOOD, R. K. S. (ed.). *Active Defense Mechanisms in Plants*, Vol. 37. Pp.381. ISBN 0-306-40814-7. (Plenum: 1982.) Np.
- WOOLSEY, C. N. (ed.). *Cortical Sensory Organization*, Vol. 2. Multiple Visual Areas. Pp.237. ISBN 0-89603-031-8. (Humana Press: 1981.) \$34.50; \$44.50 (elsewhere).

- YOSHIDA, H., HAGIHARA, Y. and EBASHI, S. (eds). *CNR Pharmacology Neuropeptides*, Vol. 1. Pp.286. ISBN 0-08-028021-8. (Pergamon: 1982.) Np.
- YOSHIDA, H., HAGIHARA, Y. and EBASHI, S. (eds). *Neurotransmitter Receptors*, Vol. 2. Pp.322. ISBN 0-08-028022-6. (Pergamon: 1982.) Np.
- YOSHIDA, S. *Fundamentals of Rice Crop Science*. Pp.269. (no ISBN) (The International Rice Research Institute, Philippines: 1981.) Pbk np.
- ZABORSKY, L. *Afferent Connections of the Medial Basal Hypothalamus*. *Advances in Anatomy, Embryology and Cell Biology*, Vol. 69. Pp.107. ISBN 3-540-11067-3/0-387-11067-3. (Springer-Verlag: 1982.) DM 52, \$24.20.
- ZEITOUN, P. (ed.). *Progrès en Cancérologie*, 1. Novembre 1981. *Les Cancres de l'Appareil Digestif*. Pp.210. Pbk ISBN 2-7040-0400-5. (Doin Editeurs, Paris: 1981.) Pbk np.
- ZOPPI, G. (ed.). *Metabolic-Endocrine Responses to Food Intake in Infancy*. Workshop held September 24, 1981, Bern. *Monographs in Paediatrics*, Vol. 16. Pp.116. ISBN 3-8055-3477-9. (Karger, Basel: 1982.) SwFr.65, DM78, \$39.

Applied Biological Sciences

- ANDERSON, R. R. (ed.). *Relaxin*. *Advances in Experimental Medicine and Biology*, Vol. 143. Pp.359. ISBN 0-306-40901-1. (Plenum: 1982.) Np.
- ARNOTT, M.S., VANEYS, J. and WANG, Y-M. (eds). *Molecular Interrelations of Nutrition and Cancer*. University of Texas M.D. Anderson Hospital and Tumor Institute 34th Annual Symposium on Fundamental Cancer Research. Pp.490. ISBN 0-89004-701-4. (Raven: 1982.) \$78.88.
- BRIDGES, B. A. and HARNDEN, D. G. (eds). *Ataxia-Telangiectasia. A Cellular and Molecular Link Between Cancer, Neuropathology and Immune Deficiency*. Pp.402. ISBN 0-471-10052-2. (Wiley: 1982.) £19.75.
- BUNDGAARD, H., BAGGER HANSON, A. and KOFOD, H. (eds). *Optimization of Drug Delivery*. Proceedings of the Alfred Benzon Symposium 17, held May 31-June 4, 1981, Copenhagen. Pp.435. ISBN 87-16-08979-0. (Munksgaard, Copenhagen: 1982.) Dkr.275.
- BUSCH, H. and YEOMAN, L. C. (eds). *Methods in Cancer Research*, Vol. 19. Pp.420. ISBN 0-12-147679-0. (Academic: 1982.) \$56.
- DELANGE, F., ITEKE, F. B. and ERMANS, A. M. (eds). *Nutritional Factors Involved in the Goitrogenic Action of Cassava*. Pp.100. ISBN 0-88936-315-3. (International Development Research Centre: 1982.) \$6.
- DE SERRES, F. J. and SHELBY, M. D. (eds). *Comparative Chemical Mutagenesis*. Pp.1117. ISBN 0-306-40930-5. (Plenum: 1981.) Np.
- DIFFEY, B. L. *Ultraviolet Radiation in Medicine*. *Medical Physics Handbooks*, 11. Pp.163. Hbk ISBN 0-85274-535-4. (Adam Hilger, London: 1982.) Hbk £13.95.
- DODDS, J. H. and ROBERTS, L. W. *Experiments in Plant Tissue Culture*. Pp.178. Hbk ISBN 0-521-23477-8; pbk ISBN 0-521-29965-9. (Cambridge University Press: 1982.) Hbk £15; pbk £5.95.
- DRAPER, H. H. (ed.). *Advances in Nutritional Research*, Vol. 4. Pp.337. ISBN 0-306-40786-8. (Plenum: 1982.) \$39.50.
- EGAN, H. *et al.* (eds). *Environmental Carcinogens Selected Methods of Analysis*. Vol.4. *Some Aromatic Amines and Azo Dyes in the General and Industrial Environment*. IARC 40. Pp.347. ISBN 92-8-321140-5. (International Agency for Research on Cancer: 1981.) SwFr.60, \$30.
- FREI, R. W. and BRINKMAN, U. A. Th. (eds). *Mutagenicity Testing and Related Analytical Techniques*, Vol. 3. Pp.320. ISBN 0-677-16300-2. (Gordon & Breach: 1981.) \$46.50.
- GARLICK, D. (ed.). *Progress in Microcirculation Research*. Proceedings of the First Australasian Symposium, February 29-March 1, 1980, University of New South Wales. Pp.677. Pbk ISBN 0-85823-200-6. (The Committee in Postgraduate Medical Education: 1981.) Hbk A\$59.95, \$69.95; pbk A\$39.95, \$47.95.
- GILDENBERG, Ph. L. *et al.* (eds). *Stereotactic and Functional Neurosurgery*. Proceedings of the 8th Meeting of the World Society and 5th Meeting of the European Society, July 9-11 1981, Zurich. Pp.554. ISBN 3-8055-3501-5. (Karger: 1982.) SwFr.155, DM186, \$93.
- GLASER, R. and GOTTBIEB-STEMATSKY, T. (eds). *Human Herpesvirus Infections. Clinical Aspects*. *Infectious Diseases and Antimicrobial Agents*, Vol. 2. Pp.272. ISBN 0-8247-1536-5. (Marcel Dekker: 1982.) SwFr.105.
- GRIFFITHS, J.B., HENNESSEN, W., HORODNICEANU, F. and SPIER, R.E. (eds). *The Use of Heteroploid and other Cell Substrates for the Production of Biologicals*. Proceedings of the Joint ESACT-IABS meeting May 18-22 1981, Heidelberg. Pp.402. ISBN 3-8055-3472-8. (Karger: 1982.) SwFr.85, DM102, \$51.
- HARRIS, K. F. and MARAMOROSCH, K. (eds). *Pathogens, Vectors, and Plant Diseases: Approaches to Control*. Pp.310. ISBN 0-12-326440-5. (Academic: 1981.) \$48.
- HERMAN, A. G. *et al.* (eds). *Cardiovascular Pharmacology of the Prostaglandins*. Pp.472. ISBN 0-89004-629-8. (Raven: 1982.) \$74.80.
- KEVERLING BUISMAN, J. A. (ed.). *Strategy in Drug Research*, Vol. 4. Proceedings of the Second IUPAC-IUPHAR Symposium held August 25-28 1981, The Netherlands. Pp.420. ISBN 0-444-42053-3. (Elsevier: 1982.) Dfl.165, \$76.75.
- KLEE, M.R., LUX, H.D. and SPECKMANN, E-J. (eds). *Physiology and Pharmacology of Epileptogenic Phenomena*. Pp.432. ISBN 0-89004-599-2. (Raven: 1982.) \$67.32.
- LEE, H. J. and FITZGERALD, T. J. (eds). *Progress in Research and Clinical Applications of Corticosteroids*. Proceedings of the 6th Annual Clinical Symposium February 20-22 1981, Florida. Pp.302. ISBN 0-85501-722-8. (Heyden: 1982.) £22.
- LEWIS, G. P. and GINSBURG, M. (eds). *Mechanisms of Steroid Action*. Pp.179. ISBN 0-333-32455-2. (Macmillan Press: 1981.) £35.
- MAHESH, V. B. *et al.* (eds). *Functional Correlates of Hormone Receptors in Reproduction*. *Developments in Endocrinology*, Vol.12. Proceedings of a Conference held October 13-15 1980, Georgia. Pp.594. ISBN 0-444-00604-4. (Elsevier: 1981.) \$90, Dfl.221.

BOOK REVIEWS

World on a ledger

Timothy O'Riordan

It is worth casting one's mind back ten years. Oil prices were about \$2 a barrel; OPEC was in existence but seemingly compliant to Western interests. There had been a number of years of unprecedented economic prosperity in most Western and some Third World countries, though the Soviet bloc was experiencing its perennial economic tribulations. Prospects of widespread affluence and material comfort appeared almost a reality.

The only flies in the ointment, it seemed, were that environmental quality (however defined) was palpably worsening and fears of resource scarcity were rife: yet economists continued to tell their political masters that there need be no resource-scarcity limits to growth. This left the "environmental problem" and that was to be tackled at the United Nations Conference on the Human Environment held in Stockholm in June 1972. This conference was full of fanfare and noble rhetoric. If it did nothing else it showed that environmental protection was as much a political issue as a scientific one, and that poverty and environmental destruction were as much interlinked as affluence and environmental mismanagement.

The Stockholm Conference spawned the UN Environment Programme, a rather sickly fledgling which had to find a niche in "far off" Kenya, and a purpose. Over the past ten years UNEP has suffered setbacks as well as experienced some achievements, but in general its main problem is to convert an unwieldy bureaucracy into really meaningful action. Where it has proved its worth, however, is in the monitoring of global environmental problems and processes (notably with respect to chemical cycles and chemical transfers within these cycles) and in its encouragement of international scientific collaboration over matters of global and regional environmental concern.

This book is a fine testament to those important achievements. Its aim is to produce a scientific audit of how the global environment has altered over the ten years since the Stockholm Conference. To this end UNEP devoted considerable effort to commission reports from a large number of scientists, official and non-governmental bodies, established a Senior Scientific Advisory Board to manage the operation and asked three distinguished scholars to edit this awesome mountain of material into a comprehensive and comprehensible synthesis. A particular feature of this book

The World Environment 1972-1982: A Report by The United Nations Environment Programme. Edited by Martin W. Holdgate, Mohammed Kassas and Gilbert F. White. Pp.637. Hbk ISBN 0-907567-13-4; pbk ISBN 0-907567-14-2. (Tycooly International, Dublin: 1982.) Hbk £50, pbk £25.

lies in its almost encyclopaedic factual approach: graphs, tables and statistics abound. It also concentrates on a backward look. This is not one of the ever more prevalent "think tank scenario productions" with myriads of graphs looking like the coloured tails of an aerobatic team. Insofar as it is possible to maintain scientific objectivity, the editors have been successful, and they frequently point out when data are unavailable, difficult to interpret or based on poor experimental evidence.

The book itself is in three parts: the first is concerned with sectors of the physical environment — the atmosphere, marine water, inland water, the lithosphere and its mineral resources, the biosphere and its resources of food, fibre, timber and fuel. Trends in pollution, productivity, human use and other major features are noted, the capacity of the various environmental systems to cope with present demands upon them are also analysed, and both national and international efforts to safeguard these environmental systems are described in some detail. The second part concentrates on human use patterns — on population distribution and growth, on changing patterns of health and disease, and on the conditions of major settlements. The third section covers major human activities affecting environmental systems — industrial developments, the generation and transmission of energy, transportation and tourism.

Collectively the authors are convinced that lack of understanding rather than lack of skills is the one main reason why environmentally sustainable development cannot proceed, and devote an important chapter to recent efforts to upgrade environmental education. They are equally convinced that global survival cannot be guaranteed so long as the present diversion of resources towards military training and increasingly destructive armaments (both conventional and nuclear — though the distinction is now more blurred) continues. So they include a chapter on the ecological and economic consequences of wars

through the 1970s and to the environmental implication of both nuclear and chemical/biological warfare. The authors are not optimistic about the much-longed-for reduction in the arms race with its liberating release of resources and cash for desperately needed environmental improvements. In this chapter, as in the rest, they display an impressive grasp of the key issues and a precise analytical clarity which deserves much praise.

The editors' conclusions are both sobering and hesitant. They confess that, though much has been done over the past ten and more years to improve understanding of the main environmental systems, there are still serious gaps in both scientific understanding and the data base. They note especially the shortage of reliable quantitative information about environmental changes in the developing world. In other respects what data are available can only be described as preliminary (e.g. tropical forest loss and especially the ecological implications of this loss). Similarly detailed estimates of the increase of the desert margins are not yet available, nor are there reliable statistics on the incidence and spread of major diseases. They observe (p.623) that

even an imperfect series of environmental statistics, drawing together what we have (and, through its manifest inadequacies, providing a stimulus to better observation) would be an improvement on the present situation.

A second important conclusion from this study is the essential physical unity of the global ecosystem in terms of biochemical cycles. Each of these interact and hence each is affected by human use and misuse in a most complex manner. But how these interactions work and what will be the consequence if current alterations to these cycles continue simply are not known.

The editors' conclusions are also sobering, because enough is known to cause us all to take the matter very seriously yet the global community of nation states does not appear to want to respond. Ten years after Stockholm the world is in a very different state. Economic recession is almost universal, unemployment is growing almost everywhere and prospects for the citizens of tomorrow, in terms of jobs, wealth and leisure as conventionally defined, look dim indeed. Economic recession has also led to attempts to cut public expenditure. In such an atmosphere international organizations operating

seemingly at the periphery of global economic interests are most vulnerable. Thus UNEP itself is threatened (see *Nature* 3 June pp.348–350). Its budget is declining in real terms and it has failed to co-ordinate the efforts of the various UN agencies, jealous to protect their own sand boxes.

Sadly, this extremely valuable book is symbolic of the failure of UNEP. It is detailed and scientific, steering clear of tackling head on the political necessities for action: it looks backward most of the time but when it peers into the future it only sees uncertainty and ambiguity — two qualities that are readily exploited by politicians living for short term expediency. Finally, the book is an expensive encyclopaedia and as such inaccessible to those lay people who would most want to read it. Those wanting a more accessible document covering much the same material, though in a more political context, should read Erik Eckholm's *Down to Earth* (Pluto Books, 1982). □

Timothy O'Riordan is Professor of Environmental Sciences at the University of East Anglia, and a member of the Commission on Environmental Planning of the International Union for the Conservation of Nature and Natural Resources.

Yeast biography

J.M. Mitchison & P.A. Fantes

The Molecular Biology of the Yeast Saccharomyces: Life Cycle and Inheritance. Edited by Jeffrey N. Strathern *et al.* Pp. 751. ISBN 0-87969-139-5. (Cold Spring Harbor Laboratory: 1982.) \$75 (US), \$90 (elsewhere).

FOR at least a century, yeast has been as interesting to the biologist as it has been important to the brewer, the wine maker and the baker. This interest has increased markedly in recent years as it has become clear that yeast can provide a good model for events taking place in other and higher eukaryotic cells. In particular, genetic manipulation has become relatively easy because of the "good" genetics of yeast, the development of hybrid plasmids which will grow both in yeast and *E.coli*, and efficient methods for transformation.

This excellent book is a sign of the times — perhaps only half a sign, since the second, companion volume on metabolism and gene expression is not due until the autumn. The two books will not provide a comprehensive survey of the biology of yeast since they omit a number of topics, including the applied aspects; but they do cover many of the exciting areas of modern yeast research and there is no question of the value of this first volume. The articles are written by experts and will remain definitive statements for at least

several years, even in fast moving fields. They are a good deal more than references hung on a thin thread of text, and many of them include "overviews" which will be especially valuable to the non-specialist.

The longest article is a comprehensive account by Dujon of the dense and complex field of mitochondrial genetics. The shortest is by Roman who gives a succinct historical review of yeast genetics pointing out that it precedes the genetics of *E. coli* by more than ten years. Mortimer and Schild describe the methods of genetic mapping and provide a valuable and up-to-date map of 312 genes on the 17 chromosomes (and fragments) of *S. cerevisiae*. Fogel, Mortimer and Lusnak review the problem of meiotic gene conversion with the delightful sub-title of "Wanderings on a Foreign Stand". Their contribution is for the experts but includes a nice section on the possibility of using chromosomes modified by recombinant DNA techniques to ask direct questions about polarity and conversion. Herskowitz and Oshima give a clear and concise account of the mating type system; this is an outstanding review of the genetics and molecular biology of a fascinating aspect of yeast biology. Esposito and Klapholz deal with meiosis and ascospore development in a good article which includes a number of peripheral topics. Haynes and Kunz review the question of DNA repair and mutagenesis — a complex area which will become increasingly important in the future.

At the slightly higher level of cell physiology and cytology, Byers gives an authoritative account of the ultrastructure of the yeast life cycle where there is a real mystery in the existence of a mitotic spindle without condensed chromosomes. Perhaps this is because of the absence of H1 histone, as Fangman and Zakian suggest in their interesting review of genome structure and replication. Thorner describes the intriguing pheromones of budding yeast; these regulatory proteins "phase" cells of the opposite mating type. There is an article of high quality on the cell cycle by Pringle and Hartwell, who analyse the results from *cdc* mutants and come to a conclusion about cell cycle controls which is more complex than earlier ones. The "circuitry" of the cell cycle has proliferated into a series of parallel pathways and some of the elegant simplicity of the earlier models has been lost — but this is a criticism of life rather than of the authors.

Although the title firmly restricts the book to *Saccharomyces*, it is a little sad that there are not more comparisons both with other yeasts and with other eukaryotic cells. This, however, is a minor point. The major one is that this important book should be available to all who work with yeast and related cells. □

J.M. Mitchison is Professor and P.A. Fantes a Lecturer in the Department of Zoology, University of Edinburgh.

Monocot characters

Peter D. Moore

The Monocotyledons: A Comparative Study. By Rolf M.T. Dahlgren and H. Trevor Clifford. Pp.378. ISBN 0-12-200680-1. (Academic: 1982.) £48, \$98.50.

A COMPREHENSIVE survey of the taxonomic and phylogenetic classification of the Monocotyledones has long been needed. Perhaps it is the sheer size of the task which has deterred prospective authors, together with the wide range of techniques and evidence which is now available to those who wish to investigate evolutionary relationships.

Happily, this task has now been undertaken and it has been tackled in an ambitious and refreshingly novel manner. The bulk of this well-illustrated book is taken up with a "survey of the distribution of selected characters and their states" within the monocotyledons. Here the authors begin with vegetative morphological characters (such as bulbs, petioles, leaf-venation), progress through reproductive features (floral structures, pollen morphology, fruit types) and then consider biogeographical and physiological characteristics (salt tolerance, cyanogenesis, secondary compounds and so on). Within each of these sections the occurrence and variation of that feature within the monocots is considered and often its distribution in the group is illustrated using ordination-type diagrams of floral orders.

Finally, the classification of the monocots is considered in the light of these character analyses. The proposal of the authors is that 26 orders should be recognized, of which 11 contain just one family and a further 7 two or three families only. This may be regarded as the outcome of undue splitting, but three alternative systems are presented which permit higher levels of fusions, at the extreme recognizing only 16 orders. Also, relationships with allied dicot groups are kept firmly in mind.

This is a novel work which has broken with traditional taxonomic treatments by approaching the study of the monocots via characters rather than by dealing with proposed orders in a systematic fashion. This will prove particularly valuable to those who may have interests in specific morphological or physiological traits, from ovule types to saponins, or even in such topics as fungal or insect host-specificity. Not only does this arrangement make it possible to extract information simply and rapidly, but it also provides a rational and objective approach to the final synthesis, giving equal weight, as it does, to all of the varied lines of evidence which are now available to assist in the classification of the monocotyledons. □

Peter D. Moore is Senior Lecturer in the Department of Plant Sciences, King's College, University of London.

Interpreting the rocks of deepest Africa

H.B.S. Cooke

Crustal Evolution of Southern Africa: 3.8 Billion Years of Earth History. By A.J. Tankard *et al.* Pp.524. ISBN 0-387-90608-8/3-540-90608-8. (Springer-Verlag: 1982.) DM118, \$55.

THE systematic geological study of South Africa began before the middle of the nineteenth century and the first map of the Cape Colony by Andrew Geddes Bain appeared in 1852, by which time he had already worked out the essential Phanerozoic stratigraphy. Mineral exploitation subsequently showed the importance of the Precambrian and much attention has been devoted to unravelling the tangled skein of "basement" geology. It is only in the past decade or so that emphasis has shifted from a largely descriptive and stratigraphic attack to more detailed studies concerned with provenance and environmental interpretation. Tankard and his collaborators have produced a volume in keeping with this modern view, one that is radically different from the traditional text on regional geology; their approach is highly interpretative, strongly process-orientated and stresses the dynamic evolution of the crust. The work is dedicated to the great South African geologist and pioneer protagonist of continental drift, Alex L. du Toit, and he would certainly have enjoyed it.

The area covered is essentially the tip of the African continent south of about 16°S, embracing the Republic of South Africa and the adjoining territories of Namibia, Botswana, Lesotho, Swaziland and Zimbabwe. The introductory chapter outlines the basic tectonic framework and delimits the boundaries of major structural "provinces" that underlie the relatively undeformed cover sequences, some of the latter being as old as Late Archean. Each province is a geographical region that shares a number of geological parameters — notably the predominant radiometric age and metamorphic style — the sum of which differentiate the region from the adjoining ones. Thus the provinces are not "cratons" separated by "mobile belts", for the mobile belts of one age commonly become the cratons of a later stage. The Sand River Gneisses in the Limpopo Province south-east of Messina have been dated at 3.8 Ga and are some of the oldest rocks known on Earth; hence the subtitle of the volume. Thus the chronology of the region is a particularly long one.

For the subdivision of the Precambrian, the authors have chosen to use the standard international divisions, Archean and Proterozoic (with Early, Middle and Late subdivisions) rather than employ the regional units adopted by the South African Committee for Stratigraphy (SACS — see Handbook 8 of the Geological Survey of South Africa, 1980).

Although this may be palatable to the international readership, it is a little unfortunate as the SACS units were selected because they are "natural" local divisions and, in point of fact, correspond well with the stages into which the authors divide the evolutionary history of the South African crust. Thus their Stage 1, "Archean Crustal Evolution", does not cover the Late Archean but does correspond to the Swazian, while Stage 2 is labelled "Early Proterozoic Crustal Development" but includes the Late Archean; it corresponds to Randian plus Vaalian. In some other respects, however, the authors use of supergroup where the SACS scheme employs "sequence" (e.g. for the Karoo) is decidedly an improvement.

The text is divided into sections, each of which is devoted to one of the five major stages. Within each section the treatment is generally similar with chapters that deal primarily with a characteristic terrain and a particular province. For example, Chapter 2 is entitled "Granite-Greenstone Terrane: Kaapvaal Province" and incorporates discussion of the now classic Swaziland supergroup, although it does also include some consideration of the Zimbabwe province.

Throughout the volume there is a tendency to provide more petrologic and geochemical data for igneous and metamorphic suites than there is descriptive material for sedimentary sequences, for which only a minimum of stratigraphic or lithostratigraphic data are provided and emphasis is strongly on depositional environments and basinal analysis. The text is thus unusual in its stress on processes and causes, employing the interrelationships between observed structures to unravel the succession of events responsible for the state of the rocks that we now see. On the whole a good balance has been maintained, although the Phanerozoic may be under-played, in marked contrast to the more conventional over-emphasis on this span of geological time.

The illustrations are clear and helpful, although the quality of photographic reproduction leaves something to be desired. Literature coverage is extensive and the authors are to be congratulated on the high quality and up-to-date nature of the synthesis. Not everyone will agree with all of the conclusions and alternative interpretations are not always considered, but this is inevitable with a work of this scope and one must admire the coherence of the whole presentation. It is not easy reading and it is inevitable that many stratigraphic units are mentioned without an accompanying description, so a companion stratigraphic text (such as the recent SACS volume) would be useful for reference.

The book was written, as the preface states, "for advanced undergraduates, graduate students, and professional geologists worldwide". For all of them it should provide a new perspective and an essential tool. □

H.B.S. Cooke was until recently Carnegie Professor of Geology at Dalhousie University, and is now a geological consultant in British Columbia. He was for many years on the staff of the University of Witwatersrand, Johannesburg.

The little bang

R.G. Evans

Inertial Confinement Fusion. By James J. Duderstadt and Gregory A. Moses. Pp.347. ISBN 0-471-09050-6. (Wiley: 1982.) £36, \$64.50.

ALTHOUGH the intensive research effort now being devoted to controlled thermonuclear fusion may appear to be a consequence of the current emphasis on energy projects, the basic ideas date back to the early 1950s. The main approach to the problem of heating and confining a plasma at a temperature of one hundred million degrees has been to use a large and suitably shaped magnetic field. These magnetic confinement machines, for example the JET machine now being built at Culham, are relatively close to the conditions needed for net energy production. But there are still problems with the toroidal geometry for a reactor system, particularly regarding maintenance, and the breeding of tritium to replace that used up in the thermonuclear reactions.

An alternative approach to fusion is not to confine the plasma at all but to utilize the reactions that occur before the plasma pressure overcomes its inertia and it blows apart, hence the slight misnomer of inertial confinement fusion (ICF). At one extreme this technique has been proven with devastating efficiency in the thermonuclear or hydrogen bomb. To reduce the explosive yield of a hydrogen bomb to manageable proportions requires the rapid compression of a small pellet of deuterium/tritium fuel to densities of a few hundred grams per cubic centimetre. The technical means to do this were not available until the advent of high-power lasers in the late 1960s and the major declassification of inertial confinement fusion occurred in 1972. There was early optimism for "break even" experiments with fairly modest lasers and this spurred on laser development programmes in the United States, the Soviet Union and to a lesser extent Japan and Europe. The promise of the early theoretical predictions has been somewhat tempered in the light of experimental testing, however; the current

laser fusion projects are as expensive as the large magnetic machines.

Despite much activity in this field, it has taken ten years for the first book to appear dealing with the whole range of physics involved. *Inertial Confinement Fusion* gives a commendably comprehensive coverage of the subject dealing for instance with the thermonuclear reactions themselves, plasma physics, hydrodynamics, lasers, particle beams and reactor problems. The book is very thorough on the different driver systems and describes high power lasers, relativistic electron beams, and both light and heavy ion drivers. In dealing with such diverse topics the book will inevitably leave many readers dissatisfied with particular details. For instance the section on laser plasma interaction fails to deal adequately with the important areas of stimulated Raman and Brillouin scattering, and the problem of symmetry of compression is barely touched upon. It would also have been invaluable to have examined the reasons for the failure of laser fusion to fulfil its early promise.

Several factual errors have crept in through an apparent zeal for making the information as up to date as possible; some ICF facilities are declared to be in existence when they have yet to obtain full financial approval. The book is generally very readable, however, and has its lighter moments — for instance the definition of “anomalous” as meaning inadequately understood, and the reference to “the thrilling days of yesteryear” in relation to heavy ion fusion where the high cost of experimental hardware has so far shielded the theory and computational predictions from the rigours of reality.

Aside from these criticisms the book fills a large gap in providing graduate research workers with an up-to-date description of a wide ranging field. There is a large number of references, although these are mostly to work in laboratories in the United States, and perhaps too large a fraction are to internal laboratory reports which might not be widely available.

“The power of the stars” may not yet be with us, but at least Duderstadt and Moses have confronted us with most (though not all) of the problems of the inertial confinement approach to fusion. □

R.G. Evans is at the SERC Central Laser Facility, Rutherford Appleton Laboratory, Chilton, Oxfordshire.

Archaeoastronomy

Papers presented at the archaeoastronomy symposium held in September last year at Queen's College, Oxford (reported by Aubrey Burl in *Nature* 293, 335; 1981) have been published in book form by Cambridge University Press. The proceedings have been divided between two companion volumes, *Archaeoastronomy in the New World* (edited by A.F. Aveni) and *Archaeoastronomy in the Old World* (edited by D.C. Heggie). Prices are £16, \$29.95 and £20, \$37.50 respectively.

Gell and Coombs for the nineteen eighties

Fred S. Rosen

Clinical Aspects of Immunology, 4th Edn. Two volumes, pp.1,751. Edited by P.J. Lachmann and D.K. Peters. ISBN 0-632-00702-8. (Blackwell Scientific: 1982.) £90, \$195.

IMMUNOLOGY started as a clinical science two centuries ago in rural Gloucestershire. A hundred years later Pasteur gave the subject renewed impetus by his studies in chickens. In recent decades the greatest progress in illuminating the arcana of the immune response has come from the study of inbred strains of mice, and the clinical aspect of immunology has almost become a quiet backwater of the subject. So this revised and expanded edition of “Gell and Coombs” classic work is welcome addition to the slim space on library shelves devoted to the clinical aspects of immunology.

The first volume consists of 744 pages of basic immunology and the second of 1,006 pages of the clinically relevant applications of immunology to disease entities. Because of the nature of the subject matter the first volume is the more cohesive and satisfying of the two. It starts with six succinct chapters on the relevant globulins and cells of the immune response. The illustrations and diagrams are copious and germane to the text and each chapter ends with a useful list of references, features which remain consistently good throughout the work.

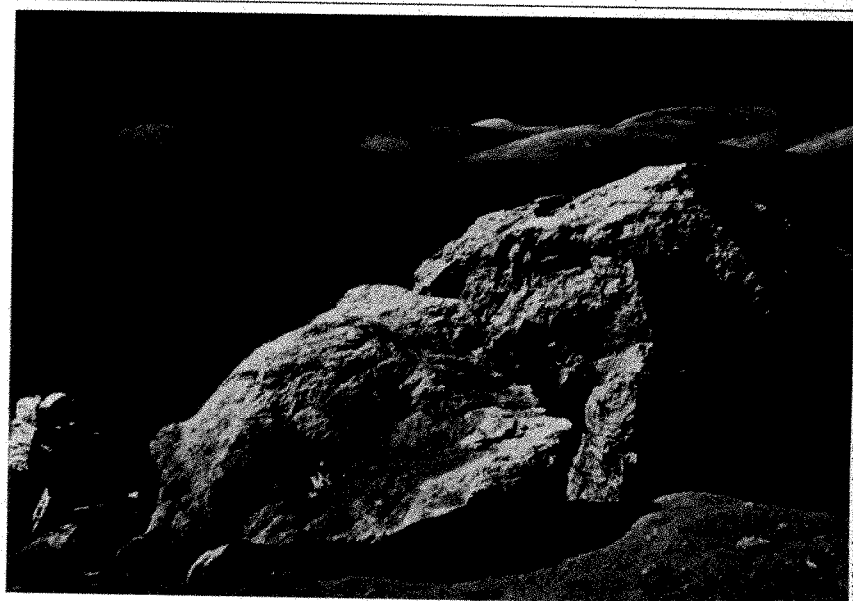
The second section in Vol. 1 is devoted to a discussion of cellular interactions and contains a unique contribution from J. H. Humphrey on the fate of antigens. Two further sections are concerned with technology that is clinically relevant, such as radioimmunoassays, rosette-forming

reactions, detection of immune complexes, tissue typing and monoclonal antibodies, and with the limited approaches to suppressing or stimulating the immune response. The final section of the first volume ends with a presentation of the pathophysiology of allergy and immune injury. Special praise is due T.A.E. Platt-Mills for his comprehensive, if not exhaustive, presentation of immediate hypersensitivity. This contribution is a mini-textbook on its own and the best current presentation of the subject matter that I know of.

The first volume is a hard act to follow, but although Vol. 2 is more uneven it in the main sustains the high quality of its companion. It deals with organ-specific immunologically-mediated disease, rheumatology, transplantation and infection. Although the text is purported to be written in English, jargon such as “... patients with NPC have high titres of anti-D, and certain patients with BL have high levels of anti-R” leave the reader groping to decipher the meaning.

This text, like all scientific and medical works these days, is expensive but it is well worth the cost to all those who practise clinical immunology. It is more current and broader in its coverage than the two other multi-volume competitors in the field. In an arena of rapidly expanding information, Lachmann and Peters have done a superb job of comprehensively assembling the diverse subject matter that constitutes the clinical aspects of immunology. □

Fred S. Rosen is the James L. Gamble Professor of Pediatrics at Harvard Medical School.



Harrison Schmitt in the valley of Taurus-Littrow during the Apollo 17 mission to the Moon. During their 22 hours of exploration Schmitt and Eugene A. Cernan investigated the major geological formations in the valley and collected 110 kg of rock and soil samples, including a 3m core — material which among other things provided new data on the early crustal history of the Moon. The picture is taken from *The Solar System and Its Strange Objects*, edited by Brian J. Skinner, a new addition to the series *Earth and Its Inhabitants: Readings from American Scientist*. The book is published by William Kaufmann, price £8.40, \$11.95 in paperback.

9 September 1982

Department of
Commercial Engineering
School of Technology
Reading, RG2 2AT, UK

What kind of crisis for capitalism?

This week's meeting of the International Monetary Fund at Toronto will avoid an immediate crisis. But more international credit will not allow rich and poor to behave as if they live on different planets.

A few weeks ago, the International Monetary Fund put out a document that argued persuasively that inflation is an evil that the international community must somehow conspire to destroy. This week, in Toronto, the members of the fund will have arranged to do the opposite. Whether they agree that the amount of credit available internationally through the fund should be doubled (as the developing countries would prefer), increased by only a fifth (as the United States has been insisting) or will compromise somewhere in between is in a sense immaterial. What matters is that any increase in the money available to the fund will be potentially inflationary. Indeed, in present circumstances, any increase of the fund's ability to lend money will probably encourage inflation. So why have the members of the fund so quickly rejected the advice their organization was putting out in August? Because they have no choice.

The International Monetary Fund, one of the last creations of John Maynard Keynes, is not a bank in the strict sense but only a kind of bank. Its objectives were originally to deal with the problems that must arise from time to time in a world in which trade is free and when governments find themselves in financial difficulties. As with any other bank, the fund will then step in with a helpful loan, usually with strings attached (devaluation, fiscal probity and so on). The fund is not however a bank in the strict sense, because people (or governments) are not forever asking it to look after their money. Instead there is an arrangement under which the fund can call on its members to stump up a contribution if it thinks the time has come to lend. For the past quarter of a century, the system has worked well, justifying Keynes's advocacy of its necessity.

This week's decision in Toronto will break new ground in the history of the fund, and may even spell its end. A little recent history is relevant. When the price of oil was first drastically increased in the second half of 1973, the world's financial community seized on two immediate problems — the huge size of the financial surpluses that would accrue to the oil exporters and the plight of those developing countries that had neither oil nor the export capacity with which to buy it. In the event, the problems cancelled each other out: the oil-exporting countries lent their surplus funds to the commercial banks in the industrialized countries which then proceeded to lend on those funds to the countries that could not afford to buy oil, or the products that oil would make. Until a few months ago, this *ad hoc* system appeared to be working well. What has gone wrong is the discovery that many Western commercial banks have lent so much money to so many shaky creditors that some of them are in danger of going bust. The reasons why the members of the International Monetary Fund will have agreed this week on some increase of its lending capacity are simply that they cannot let their own commercial banks collapse under the weight of unpaid foreign debts. The snag, of course, is that neither the fund nor its member governments will be better able to control what happens now than the commercial banks have been.

The explanation is that the debtor countries have not been living as if to qualify for a loan from the International Monetary Fund. Rather, they have been borrowing from those commercial banks gullible enough to lend to them in the hope that they might avoid trouble for another few years — latterly, months or weeks. Yet every commercial branch manager knows that it is imprudent

to lend money to help a customer pay the rent, but that helping the customer, by capital investment, so as to be better able to do so is expedient and also socially beneficial. The International Monetary Fund is no longer in a position to require such a discipline from its creditors. First, its leverage as a quasi-bank has shrunk — in twenty years, its capacity to lend has shrunk by more than a third in relation to the monetary reserves of member states. Second, habituated as they are to living beyond their means the clients of the fund are neither willing nor able to cut back.

That is why this week's decision in Toronto cannot but be inflationary. Some clients of the fund will borrow money within the next eighteen months, will use it conveniently to repay their debts to the international commercial banks, but will not be able to promise that they will also promptly put their affairs in order. Who would reasonably ask of Mexico (see page 99) that it should deal quickly with these issues when its newly elected government cannot constitutionally take office until 1 December? And what is to happen to Argentina, unable to make a deal of any kind because the British Government has not been given proof that the Falkland Islands war is over? And then, worse still, what is to happen to those countries that have been buying oil for the past decade, but which have been unable to persuade banks of any kind of their credit-worthiness? Self-deprivation has allowed them to survive so far, but only passably. How far can self-deprivation be expected to go?

The Toronto meeting of the International Monetary Fund has frequently been described as a crisis of capitalism. It is nothing of the kind. Rather, it is the opposite — the occasion of the rediscovery of what nineteenth-century economists had to say about people's (or countries') interdependence. Chase Manhattan, or some other commercial bank, might be able to make Mexico (or some other country) bankrupt, but would then have to go to the wall itself. Middling governments such as those of Britain and West Germany may embark on policies intended to cure inflation domestically but then find themselves having to fuel it because they cannot stomach the consequences. Mitterrand's France may even have to acknowledge that its alliance of socialism and the printing-press cannot endure. And Reagan's United States may have to acknowledge that a \$100,000 million deficit is a recipe for beggaring its neighbours. So what the world needs is not a substitute for capitalism but some way of melding fiscal probity with an acknowledgement that neither the poor nor the rich can these days go it alone. Keynes, where are you now?

Paying for nuclear plants

Should US utility customers pay now or later for new nuclear plants? The utilities wrongly say now.

The substantial crop of nuclear power plants due to come into service in the United States in the next few years will have an unprecedented effect on the price paid by customers for electricity. Many customers are facing rate increases of 30 per cent, customers of one utility, Kansas Gas & Electric, will be charged 60 per cent more when the Wolfe Creek reactor comes into service in 1984. The utilities are seizing on these proposed rises as an opportunity to seek a major change in the way plant construction is financed. But the change they propose — charging

consumers for construction costs as they accrue, before the plant is in operation — is short-sighted and will benefit nobody

Commercial utilities in the United States are subject to strict state regulation, in most states the time-honoured principle of charging customers only for plant equipment that is "used and useful" is the rule. The utilities argue that the rule is outmoded. When nuclear plants used to cost a few hundred dollars per kilowatt and when interest rates were a few per cent a year, the addition of a new plant barely caused a ripple. Indeed, the savings in fuel costs would often outweigh the capital costs of a new nuclear plant, resulting in a decline in the price to customers. But costs have now reached staggering heights. A new nuclear plant, with a typical capacity of 1,000 megawatts, costs more than \$2,000 million, ten times as much as in the 1960s. High interest rates and construction delays add to the cost eventually charged to the consumer — whence the 30 per cent increases. The utilities want the right to charge consumers as they go. This "Construction Work in Progress" charge (CWIP) would be used to pay the dividends due to bond and stockholders during the period of construction. It would also result in a gradual phase-in of the price increase. Without CWIP, the utilities say, they have to borrow money to pay the bonds that become due during construction, and the extra cost of borrowing is ultimately passed on to the consumer once operation begins.

The utilities seem to have overlooked the principle on which the regulation of their charges is based — that present consumers should pay only for the services available to them now and not for services that will be available only to future cohorts of consumers. That principle, which underlies the regulation of all rates charged by public services in the United States, could not be overturned just like that to suit the present convenience of the electricity utilities. Moreover, to change the rules arbitrarily would be inequitable in quite tangible ways. For while it is true that by "paying now", a consumer would avoid having to pay for the interest charges accumulating during a construction project, he would then be denied the opportunity of investing the extra payments on his own account. "Pay now" costs at least as much as "pay later".

Although "pay now" seems to solve the utilities' immediate problems (not the least of which is the public relations problem of asking for 60 per cent increases), it glosses over a more fundamental difficulty. According to Professor Michael J. Driscoll of Massachusetts Institute of Technology, "the real solution is not to play around with CWIP, it's to get back to a reasonable construction schedule". Building nuclear plants used to take six years from start to finish, in France, they still do. But in the United States they now take 10 to 12 years. And the utilities' scapegoat — government delays in issuing licences — is only partly to blame. Driscoll points to inefficient management and the practice of custom-building each new reactor. France has seen the wisdom of that American innovation, mass production. But every delay increases the interest costs accumulated during construction, and the utilities would gain more by solving this underlying problem than by covering it up with CWIP charges.

Bluntly the burden of paying a 30 per cent or 60 per cent increase in prices is less for society as a whole than paying ahead of time for a nuclear plant that is not needed. The present system has the virtue of forcing the utilities to persuade bankers and investors that future demands will justify the next 1,000 megawatt power plant. The "pay now" policy, on the other hand, allows the utility to pass off some of the risk of its venture onto its consumers. And the track record of the industry in predicting future demand suggests that the consumers would be forced to make some bad investments. The industry has been notoriously optimistic — in 1974, the Edison Electric Institute (the commercial utilities' trade group) predicted a total US energy demand of 160 quads by the year 2000. By 1976, it was 140. In 1980, Exxon Corporation was saying 105. With the demand for electricity at a near standstill (rising only 0.3 per cent in 1981, in contrast with 7 per cent per year throughout the 1960s and early 1970s), the need for cautious planning is obvious. The marketplace should be allowed to continue to exercise a check on new power plant construction.

Press's forgotten recipe

Does the US scientific community consider Dr Frank Press's cure unpalatable?

Strange as it may seem, people have been ignoring Dr Frank Press, president of the US National Academy of Sciences. Press has had the temerity in the past six months to propose a long-term cure for the ills of US science. He has been observing that in these unprecedented times, federal funding on science has become part of the vulnerable discretionary federal budget and thus vicariously liable to cuts. What has happened this year, with the executive branch and Congress still haggling over money for the year that begins on 1 October, may be symptomatic of what is to come. So, Press says, the science community should negotiate a pact with government and industry to insulate science, to stabilize funding and to ensure that talented young scientists have opportunities.

In Press's five-point plan, government would agree to assured increases each year in the budget for basic research at a rate that would cover inflation and allow an extra 2 per cent of real growth. This "base programme" would be government policy. It would not rule out larger increases, but would ensure that overall funds did not fall below this level. Government should commit a further 1 per cent each year to "targets of opportunity", for research related to national needs or for new facilities. At the same time, industry would agree to double its present total contribution of \$50 million and would also start, with the government, a new fellowship programme. A central agency, perhaps the National Academy of Sciences, might serve as a collection and distribution agent, although the funds would be spent in fields where shortages are likely and selection could rest with individual agencies. A comparatively small amount of money, say \$10 million, would buy a thousand fellowships.

The nub is in the last of Press's five points. Scientists themselves, he says, should be able to find another 2 per cent by setting priorities within their own fields and by cutting out unproductive work. Then, the argument goes, universities could persuade government to ease regulations, such as the notorious Office of Management and Budget regulation on accountability, and let them keep the savings. Based on the estimated \$7,000 million the government spends on basic science and engineering, Press's potential cure could provide an extra \$694 million, an increase of almost 10 per cent, plus the use of up to \$114 million in funds that have been reprogrammed. But where should the extra money come from? Press suggests that the government should raid the development budget where, he believes, there is a lot of waste. (The Clinch River breeder reactor programme consumes about \$600 million each year, development of the B-1 bomber about \$700 million a year.)

The weakness of the plan is Press's assumption that scientists will centralize their lobbying efforts in Washington upon the single cause of a guaranteed overall increase. (Another is that Congress is all too familiar with special groups seeking to convert appropriations into entitlements.) Success for the plan would, however, bring predictability to the support of basic research and put scientists to work setting their own priorities, not leaving that to officials in Washington. And, of course, nothing in what Press has been saying suggests that the government has at this stage agreed that the scientific community could keep whatever savings would accrue from a more rational pattern of expenditure.

So why has the scientific community neglected the challenge? In the peer-ridden US system, changing tack in any direction is difficult. Arrogant specialization does not help. But Press's message is that if the research community cannot decide priorities for itself, the accountants and the lawyers will. Press seems to be echoing what Dr George Keyworth has been saying from the Old Executive Office Building next to the White House, but he has stronger credentials for being taken seriously. Indeed, with his experience of an earlier White House, Press is uniquely well placed to make what he has been saying tell. Why does nobody respond or even listen?

Norway's Arctic diplomatic fix

Poles' defection in Spitsbergen casts shadow

The two Polish scientists who defected last month from the Polish geophysical station at Hornsund (Spitsbergen) have created a delicate diplomatic problem for their Norwegian hosts and something of a crisis for Norwegian Arctic research.

Although sovereignty over Svalbard (the island group of which Spitsbergen forms part) was granted to Norway by international treaty in 1920, by the same treaty Norway undertook that the nationals of the signatory countries (of whom, with later accessions, there are now 41) should be treated on an equal footing with regard to economic activities.

The Soviet Union thus has two coal-mining bases, one near Barentsburg and another at Pyramiden. Similarly, under a memorandum from the Norwegian government to the other signatory states, foreign expeditions have free access to carry out scientific research in Svalbard as well as free access to the information on the islands held by the Norwegian Polar Research Institute.

The Polish research base at Hornsund is staffed by a team of 10 scientists from the Institute of Geophysics of the Polish Academy of Sciences. The research programme includes geological, geophysical, glaciological and meteorological work. A relief expedition, consisting of the 1982-83 scientific team plus a group of technicians to carry out routine maintenance work at the station sailed from Gdynia in July.

On 10 August, two of the scientists (it is not clear whether from the incoming or outgoing teams) decided to ask for political asylum, and radioed the Norwegian *Sysselman* (governor), announcing their intention to report in person to file their applications at the administrative base at Longyearbyen.

This transmission was, however, picked up by the Soviet Union's mining post at Barentsburg, which sent a helicopter to intercept the two Poles who were repeatedly "buzzed". One was driven back to base while the other fled into the hills and returned to Hornsund next day.

When the *Sysselman* heard what had happened, he sent out in his own helicopter to pick up the two would-be refugees, the Soviets, however, realized what was happening and sent their own helicopter to try and reach them first. In the words of one Norwegian official, *Sysselman* won the race, confirmed that the two men still wanted political asylum and took them back with him for questioning to Long-

yearbyen, whence they were dispatched to Oslo for "safe keeping". Their requests for asylum are now being processed, their identities are for the moment being kept confidential.

A number of diplomatic questions remain to be clarified. Military activity on the islands is strictly forbidden under the Svalbard Treaty of 1920, and it could be argued that the Soviet use of their helicopter in what can only be called a third-party police action could be construed as a breach of this agreement.

Furthermore, the Soviet helicopters are supposed to ply only between Barentsburg, Pyramiden and Longyearbyen, while some 44 per cent of Svalbard (including South Spitsbergen, where Hornsund is situated) comes under nature protection orders, where any technological encroachments, including motorized vehicles, are forbidden. Noise harassment of geese and other aquatic birds during the moulting season is particularly hazardous since it can scatter flocks and separate the young prematurely from their parents.

So far, the Norwegian Foreign Office seems concerned to keep the whole incident low-key. For their part, the Soviets can have little wish to fall foul of the Norwegian environmentalists. The Soviet Union extracts some 400,000 tonnes of coal



from Svalbard each year.

At Barentsburg, however, the reserves covered by the Soviet claims patent are almost exhausted, and output is now maintained only on the basis of a leasing agreement with the Norwegian mining company which owns the adjacent areas. A Norwegian Royal Decree of 1971 stipulates that no new mining, oil drilling or other industrial operations can be initiated without a thorough preliminary study of possible environmental consequences.

Vera Rich

Two Soviets banned from Perth

Canberra

The Australian government refused two Soviet scientists visas to attend the 12th International Congress of Biochemistry in Perth on 15-21 August, organized by the Australian Academy of Science under the aegis of the International Union of Biochemistry (IUB). The scientists are Professor Y. A. Ovchinnikov, vice-president of the Soviet Academy of Sciences who was to deliver a plenary lecture, and Professor S. S. Debov, also a member of the academy. Taking umbrage, the other 25 Soviet registrants boycotted the congress. It now appears that the International Council of Scientific Unions (ICSU) may ban Australia as a venue for international conferences at its meeting on 12 September.

The Soviets singled out for exclusion were regarded by the Australian embassy in Moscow as government men rather than scientists. Consequently the banning is consistent with government policy of not allowing high-ranking Soviets into the country. Following the Soviet invasion of Afghanistan in 1979, the government announced a package of sanctions against the Soviet Union, after a cabinet decision in January 1980. These moves included the suspension of a bilateral scientific and technological agreement signed in 1975, and the banning of mutual visits by

ministers and senior officials. A cooperative expedition on a Soviet research ship was called off, Soviet scientists in Mount Stromlo Observatory were sent packing, student scholarships to the Soviet Union were cancelled and visas refused to Soviet agricultural officials. In addition universities were advised to suspend academic exchanges but not multilateral conferences.

After these events, the Australian Academy of Science found itself in the invidious position of having to provide IUB with an assurance that no scientists would be barred. It sought from the government a "form of words" considered to be acceptable to IUB — "bona fide scientists from all countries will be admitted to Australia to attend the conference subject to the normal rules and requirements for visitor entry to Australia in operation at that time." But the then minister for immigration, Mr Ian MacPhee, wrote to the then foreign secretary of the academy, Professor Gordon Ada, in June 1980 — "I should stress that if this form of words is used, it must be understood by the academy that the normal rules in operation at the time of any conference might well exclude a particular scientist, a group of scientists or scientists of a particular nationality. I could not forecast what would be normal in say 12 months or 3 years time."

These reservations were not passed on to IUB. Unfortunately the possibility of Soviet scientists being banned as officials was not considered by the organizers at any time during the interim period. A spokesman from foreign affairs believes the problem could have been overcome by consultations beforehand.

The stage was thus set for the imbroglio at the conference, the first IUB congress in Australia. The Soviet participants waited until the last minute to apply for visas, and just a few days before the conference the ban was announced. Appeals from the president of the Australian academy (Professor Arthur Birch), the premier of Western Australia (Mr O'Connor) and the Swedish Academy were all to no avail. It was too late for the government to back off gracefully.

Reactions at the congress were mixed. Professor Frank Gibson of the Department of Biochemistry, John Curtin School of Medical Research, Australian National University, says "disappointment at not hearing Professor Ovchinnikov's lecture was the main reaction". Lack of travel funds, and the relatively high cost of internal air fares and accommodation limited the number of overseas registrants, particularly from the United States.

The academy now faces the unenviable task of persuading the government to change its policy in the week before the ICSU meeting. Failing this, it will try to delay any precipitate action at the meeting. Nevertheless international censure may be just the prod the government needs to review its policy on sanctions. Significantly, the International Union of Pure and Applied Chemistry succeeded in securing the admission of Israeli scientists into India for a conference on the applications of the Mössbauer effect held in Jaipur last December. **Vimala Sarma**

European space technology

Ariane set to go

The delay to the fifth launch of Ariane, rescheduled from last April to tomorrow, has had its effects on the vehicle's future launch programme. But careful reorganization of the launch schedule up until the end of 1984 seems to have ensured minimal damage to the launcher's commercial prospects.

The five month delay has been caused by problems with Marecs B, one of two satellites that the fifth Ariane will put into geostationary orbit. Marecs B had to be modified after problems with electrostatic charging on Marecs A, the sister satellite launched by the fourth Ariane late last year. The first effect of the delay has been to reduce the number of Ariane launchers this year from four to two. The next launch now scheduled for November will put Exosat, the X-ray observatory built by the European Space Agency, into polar elliptic orbit, more or less on its target date. But the launch of ECS 1, a communications satellite, is being delayed to early next year and Intelsat, the international telecommunications satellite organization, which was to have launched the sixth Intelsat V satellite aboard Ariane in October or December this year, has taken that part of its custom elsewhere.

Intelsat, however, has not reduced its overall commitment to Ariane. The launcher will now put Intelsat V numbers 7, 8 and 9 into orbit next year instead of numbers 6, 7 and 8. Next year's launch programme has been rescheduled to include six launches, the maximum possible with the present launch pad, instead of five originally planned.

Ariane is now fully booked with firm orders until the end of 1984 according to

Arianespace, the company that will take over commercial operation of the launcher some time next year. Just two places remain to be firmly negotiated for 1985 and a number of reservations, for which customers must pay \$100,000, are apparently in hand for future years. But Ariane has now lost some early reservations from customers who have eventually plumped for US facilities and Arianespace acknowledges that the fifth launch of the shuttle in November, which will put a satellite into geostationary transfer orbit, could take the edge off Ariane's seeming attractiveness.

The next few Ariane flights will still be formally in the hands of the European Space Agency. Arianespace will take over operations and start earning revenue from launches from the middle of next year, probably after the tenth flight. The company hopes that by 1985 the capacity of the launch facilities at Kourou in French Guiana will increase from 6 to 12 when the second launch pad, now under construction, comes into operation. Arianespace expects to start showing a modest but respectable profit in 1985. But future prospects will also depend on the success of the space shuttle. The latest estimate is that customers will have little to choose between the two on price. Reliability, service and convenience could be most significant. **Judy Redfearn**

Australian science politics

Labor's policy

Canberra

The Australian Labor Party, more hopeful than ever that it will form the next federal government but less certain now than a few weeks ago that the general election will come soon, formally adopted a new policy on science and technology at its biennial conference here in July. Although the policy is vague enough not to be a constraint on Labor members of parliament, the convention that conference decisions are binding on elected representatives may yet cause trouble.

The new science policy was adopted on the nod on the last day of the conference, when most delegates were packing up to go home. On the face of things, science and technology have only low priority, at least compared with the uranium issue. The conference heard a sustained and embittered debate on the question of whether Australia under Labor would honour existing uranium contracts. That issue remains unresolved, although the conference confirmed the principle that Labor will supply uranium abroad only on tough conditions.

The cornerstone of the Labor Party's policy on science and technology is economic — government spending will bring prosperity and economic growth. Mr William Hayden, the leader of the party, and his colleague with responsibility for

Now even MIT has troubles

Washington

Even well-off US universities are not immune from the financial squeeze affecting US higher education. The Massachusetts Institute of Technology (MIT), which has an operating budget of \$500 million, reports that it had a deficit of \$2 million for the year just ended. Next year's deficit could be \$4 million. Consequently, it has now announced plans to cut costs and, among other things, to lay off 400 employees.

Unlike both the California Institute of Technology and Stanford University, with which MIT is often compared, MIT has a relatively small endowment and thus a harder cushion for hard times. The current deficit is not MIT's first, it had a deficit in the early 1970s, when it lost the extra income and overhead funds that went with the Charles Stark Draper Laboratory, from which it severed its

connections at that time.

According to provost Francis E. Low, approximately two-thirds of MIT's operating budget is composed of funds that come in each year to operate facilities such as the Lincoln Laboratory, with little control or financial benefit to the rest of the institute. To control rising costs, then, the institute must look to the \$120 or \$130 million in general funds that pay for education and its administration. To prevent rising deficits, these activities will have to be reduced. There will be some faculty reduction through normal attrition, causing a loss of approximately 30 positions. Also, 200 other people will be allowed to leave through attrition in the next few years, he says, while an additional 200 will be laid off. Low thinks the institute can afford some belt-tightening. "It [MIT] functions in some respects in a luxurious way." **Deborah Shapley**

science and technology, Mr Barry Jones, have repeatedly said as much.

Perhaps significantly, the present Liberal-Country Party coalition government has responded by increasing support for the Industrial Research and Development Incentives scheme from A\$14 million to A\$50 million. More broadly, the government has taken to justifying a more interventionist approach to Australian industry by references to "market imperfections".

More animal care

Washington

Public pressure for a change in rules governing the care of laboratory animals has prompted the National Institutes of Health (NIH) to tighten up their requirements, whether or not Congress acts on the matter this year.

NIH will require that at least one non-scientist be appointed to each research institution's animal care committee — the groups charged with overseeing the treatment of experimental animals. This echoes one of the requirements in the bill now before Congress. (The bill, renumbered HR 6928, has cleared the House Science and Technology Committee and is now before the health and environment subcommittee of the Energy and Commerce Committee.)

NIH is also planning to mount a series of site visits to check on the extent to which researchers are complying with NIH guidelines. Under current rules, recipients of NIH grants must agree to adhere to the practices outlined in NIH's *Guide for the Care and Use of Laboratory Animals*. Failure to do so can result in loss of NIH funding. A major criticism of the system, however, is that too much reliance is placed on the good-faith assurances of the researchers and too little on inspection.

But NIH is not yet ready to order on its own another change in the proposed legislation: the mandatory accreditation of all research institutions by an independent group such as the American Association for Accreditation of Laboratory Animals Care (AAALAC), which sets standards and conducts routine inspections every three years. According to Dr William Raub, NIH's associate director for extramural research, "We think the concept of accreditation makes a lot of sense. But we're not yet, at least, willing to mandate it until we know more about the costs". Universities have claimed that bringing all NIH-supported institutions up to the AAALAC standards would cost \$500 million. The legislation before Congress would eventually require all institutions to meet the AAALAC standards, but would soften the blow by allowing ten years in which to meet this goal.

Stephen Budiansky

Labor is less inhibited about intervention. The July conference undertook that research and development expenditure should increase from the present 0.9 per cent of gross national product to a level "equivalent to that in other technologically advanced countries". Prudently, Labor did not specify a target figure.

What Labor offers is more pragmatic — a promise of a new division in the Department of Science and Technology to be concerned with industrial research, development and innovation. A Labor government would be a dutiful customer for new Australian products, and would back technical innovations with hard cash. It would also provide venture capital for new kinds of industrial developments, in biotechnology for example.

On issues such as these, the parties differ only moderately. Neither will increase

spending on basic research. The best hope is that Labor would not let research funds be eroded by inflation.

Long-standing disagreements persist, however, about the role of foreign corporations in high-technology industries. Labor would require foreign corporations to carry out some research and development in Australia, but Mr Barrie Jones seems well aware that he must find a form of words not so restrictive that foreign corporations will be driven away.

The new Labor policy also promises innovations to give high relief to Australian science. The conference approved a plan for an "Australia Prize" of A\$100,000 for humanitarian scientific achievement, to be administered by the Australian Academy of Science, and an international conference on Antarctic research to reinforce Australia's claim to the largest slice of the Antarctic.

Vimala Sarma

Mexican science in money trouble

Mexico City

In the face of Mexico's present economic crisis, the country's expensive and ambitious programme for science and technology now faces shocking sudden austerity. "A crisis can be good," says Pablo Rudomín, the distinguished neurophysiologist who is president of the Mexican Academy of Sciences. "It leads you to deep thoughts about where you're going. I think it [the crisis] will give us a sense of community. We'll have to work on priorities, and quality and on preserving what we have."

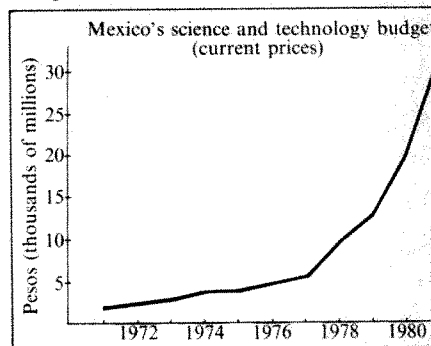
What has happened is that after a decade when the economy was flooded not just with domestic oil revenues but with loans from foreign banks (chiefly in the United States), Mexico has found that it cannot pay the instalments due on its debts, estimated at \$80,000 million. The payments were rescheduled in August, since when the Mexican banks have been nationalized. All sectors of the economy will have to be cut back, but just how will not be known until the new government of President Miguel de la Madrid Hurtado takes office on 1 December.

"Things will change, but probably for the good," echoes economist Manuel Gollás, who holds a key political post as head of the advisers to the director general of the Consejo Nacional de Ciencia y Tecnología (CONACYT), the Mexican science agency. One irony of the boom, he reflects, is that sometimes "we had more money than we did worthwhile projects".

Supported with government oil revenues and announced with a great fanfare at the beginning of President José López Portillo's 6-year term, Mexico's science and technology programme was designed to strengthen the infrastructure of science and to encourage Mexican self-sufficiency in technical matters. The programme was nothing if not ambitious. Basic research did well, but there were also

special priority programmes in fields such as agriculture and nutrition. The energy programme included work on nuclear and solar energy production. There were schemes for supporting industrial research, and the government had emphasized the importance of training graduate students.

Interviewed in their respective offices in Mexico City, both Rudomín and Gollás acknowledged that the programme had been criticized as being only a shopping list of unrelated projects, reflecting the interests of individuals and government agencies. Indeed, its execution reflected this pattern. CONACYT, which designed



the original programme and serves as the president's science adviser, actually controlled only 11–12 per cent of the total science and technology budget. The government gave the rest directly to universities (the major one being the Universidad Nacional Autónoma de México, whose main campus is in Mexico City). Money for the Instituto Politécnico Nacional, for example, comes from the Ministry of Education. Private industry and foundations play almost no part in sponsoring Mexican science.

More than half of CONACYT's budget for 1981, estimated at 3,899 million pesos, went for scholarships, another 20–30 per cent for administration, public relations, and publications. Grants for basic science directly to investigators in fact accounted

for only 5 per cent of the budget, Rudomín estimates, or 109 million pesos. With other funds, basic research claimed about 20 per cent of the total CONACYT budget.

The science programme built on a major educational effort launched by the government of President Luis Echeverría in 1970 to stress education, including science and mathematics in the Mexican schools (*Nature* 280, p.101; 1979). According to Mexican officials, in 1968–69 Mexico had around 600 PhDs. By 1982, after more than 26,000 scholarships had been awarded, it claims 15,000 technically trained graduates, of which an estimated 6,000 hold a PhD.

Language a barrier

Mexico's ambition of achieving excellence in basic science is complicated by a double-edged language barrier: few scientists in the English-speaking world read Spanish scientific journals, while not many Mexican scientists know English well enough to publish in English-language journals. Even among Latin American countries, Mexico ranks low in the prorated number of its scientific publications in English-language journals, according to one recent survey. Many Mexicans feel it is "traitorous", as one of them put it, to publish in English. The Mexican science agency was sharply criticized when it decided that its fourth publication should be in English. (This is *RD Mexico*, a colour magazine that is suspending publication because of the current crisis.)

Science Citation Index reports that of the 3,068 journals in the index, only 13 are published in Latin America. Of these, 12 are published in Spanish and one is trilingual. Three of the 13 are published in Mexico. Latin America as a whole, therefore, contributes less to the index than does East Germany, which has 40 journals, or Austria, which has 24.

Mexican scientists complain that they are damned either way. If they publish in an English-language journal, their colleagues cannot read it and if they publish in a Spanish journal, their peers abroad will not. Yet English-language journals solve this dilemma for them, they allege, by discriminating against Latin American submissions. One scientist said that he has had an easier time getting his papers accepted by English-language journals when his co-authors have had Anglo-sounding names.

In any event, Mexico has a particular disadvantage on the language question because it did not experience the waves of immigration from European countries (except from Spain) that have admixed the populations of Brazil, Argentina and Chile. Deborah Shapley

One result is that most Mexican scientists are younger than Rudomín, who is in his mid-forties, and his predecessor as president of the Academy, engineer Daniel Reséndiz, who is 42. "Mexican science is not more than 40 years old," says Rudomín. "The first thing we have accomplished is to have trust in ourselves." Rudomín himself returned to work in Mexico after a stint at the Rockefeller University in New York. He has striven, he says, to make other Mexican scientists abroad come home to do good science.

However, the science programme did not succeed in achieving its goal that 1 per cent of the Mexican gross national product (GNP) should be devoted to science and technology. Science and technology have been between 0.38 and 0.47 per cent of the Mexican GNP for the past decade, whereas in developed countries the proportion is more than 2 per cent.

On the other hand, Mexico's GNP has grown so fast that the monetary gains for science and technology have been huge. The annual increases in government spending on science and technology averaged 34 per cent in the decade 1971–81.

The present crisis has changed all this. Sitting in his modest cinderblock office, Rudomín says wistfully of the CONACYT

basic science budget, "This year it was going to be 400 million pesos. Unfortunately, we are going to have a change in the slope. Our concern now is to keep what we have achieved."

Whether that will be possible is an open question. The ambitious science programme — and the financial policies that have got Mexico into trouble were the work of the Portillo government. By custom, the new government of president-elect Hurtado will be able to reshape science policy entirely: political appointees such as Gollás are getting ready to leave their jobs. "Our programme in science and technology was oriented as far as possible to the goals of the national development programmes, the whole national economy and society. That connection should be maintained, Gollás says.

Rudomín met Hurtado in August and is on a committee of scientists appointed to advise the new president before he takes office on 1 December. "When there's an economic crisis, they will try to solve the immediate problems," Rudomín says. "I think it depends a lot on us, whether we will be able to convince them that it is important to have this [science]. I think that it's going to be a difficult task."

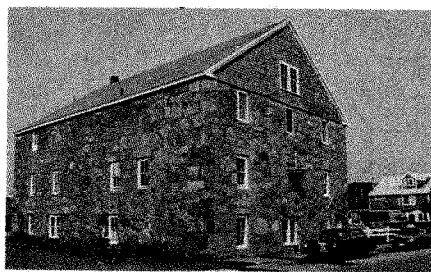
Tabitha Powledge

Woods Hole laboratory

Summer camp seeks more funds

Woods Hole, Massachusetts

The passage of Labor Day last Monday will allow the biologists' favourite summer camp, the Marine Biological Laboratory, to settle down to its year-round pre-occupation: fund-raising. By the centenary of the laboratory in 1988, the plan is to have raised \$27 million, much of which will be spent on the rehabilitation of laboratories. There are also fond hopes of augmenting the endowment fund, now more or less a pittance at just over \$3 million.



From candle-making to administration

According to Dr Paul R. Gross, director of the laboratory since 1978, money began to dry up in the early 1970s. One of the painful discoveries since then is that the laboratory has no funds with which to cover the cost of maintaining buildings, but there are also ambitions to get rid of wet laboratories immediately above parts of the library (which needs also to be extended by 10,000 square feet) and to rehabilitate the housing in which the

summer campers camp.

These anxieties seem not to have depressed this summer's visitors, more than 1,000 altogether. Clam chowder has been bounteously consumed. People have acquired a tan that should last until Thanksgiving, and the beaches have been as full as ever in the afternoons, at least until the weather turned cold towards the end of August.

The popularity of Woods Hole may be, in the long run, its most enduring asset. Gross says that the competition for places on the seven summer student courses has been as brisk this year as in the past. Three-quarters of the successful applicants turn out to be graduate students; the remainder are an interesting mixture of advanced undergraduates and postdoctoral people.

The competition from more senior people to spend the summer at the bottom right-hand corner of Cape Cod is probably, however, more influential. Some senior people turn up to help teach courses; others move their research projects lock-stock-and-barrel, bringing their assistants with them. Prudent applications to grant-making agencies specify the importance of access to fresh squid or some such animal, for the laboratory will charge bench-fees, while the cost of accommodation will be extra.

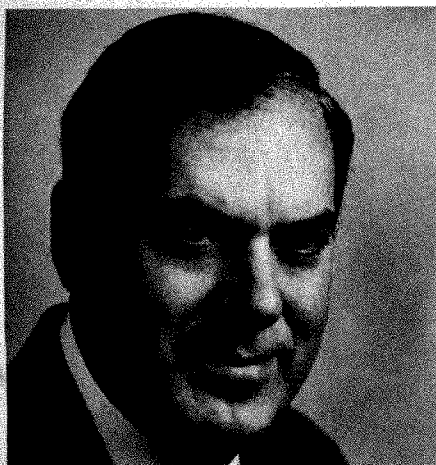
Woods Hole, a frankly elitist establishment, is thus a continuation of academic life by other means — means by which a person's knowledge of how to organize a

clam-bake or to sail a boat may partly offset his ignorance of, say, the mechanisms by which nuclear RNA is processed. Some regular summer visitors have opted out, saying that they prefer their vacations straight. The regulars remark on the importance of each evening's social encounters.

Financially, the seasonality of Woods Hole must be a serious handicap, which is why some importance is attached to two recent innovations — student courses in January (this year there were four) and the continuing research programme (which at present keeps 95 professionals active all year round). Even so, the laboratory (whose operating budget is just over \$6 million, excluding the cost of peripatetic research projects) reckons that it recovers only 42 per cent of the cost of its facilities from those who use them, and that it is at present running on a deficit of about \$750,000 a year.

Part of the problem is constitutional. Since it was established in 1888 to help young women from Boston learn some science, the laboratory has been managed by its members, of whom there are more than 650, who in turn elect the 36-member board of trustees which for practical purposes determines policy.

The climate of opinion seems slow to change (and remains unwilling to commit too much of the site to year-round activities). Indeed, Paul Gross calls himself a "one-man glue-pot" whose job is to hold the place together. Two tangible proofs of



Paul R. Gross — one-man gluepot

his success are apparent — reluctant agreement that there should be a fund-raising effort of any kind and the conversion of the candle-house left over from the New England whaling industry into a handsome administration building.

The plight of the laboratory is thus desperate but not serious. (People tend quickly to say that the Oceanographic Institute, split off from the laboratory in 1930, has greater difficulties.) Visitors nevertheless cannot help but wonder whether the first word in the laboratory's title is still apt, given that "marine" featured in the title of only one of this summer's seven courses.

Biotechnology index

Biotechnology beats bull market

Reflecting the US stock market's sudden surge in August, *Nature's* monthly index of biotechnology company stocks jumped 18.1 per cent from the base of 100 at which it began last June (*Nature* 12 August, p.599).

The *Nature* Biotechnology Index at the close of August (see box) shows that biotechnology companies outperformed two leading indicators of overall US industrial performance during the same period. The 18 per cent rise between 25 June and 27 August was greater than either the rise in the Dow Jones Industrial Average, which rose 10 per cent, or the rise in the Standard & Poor 400 Index which rose 7 per cent, as the table shows.

Biotechnology and other US stocks

Date	<i>Nature</i> Biotechnology Index	Dow Jones Industrial Average	Standard & Poor's 400 Index
25 June	100.0	803.8	122.09
30 July	102.7	808.6	119.95
27 August	118.1	883.47	130.75

Both of these general industrial indicators declined in July, whereas the Biotechnology Index rose to 102.7 in July.

The biotechnology companies as a group also did better than Standard & Poor's index of 12 leading US drug companies, which rose by only 3 per cent during the same two-month period. However, the drug index rose 11 per cent between the end of July and the end of August.

The *Nature* Biotechnology Index is weighted according to the total market value of each company's outstanding shares. It includes 15 representative biotechnology companies publicly traded in the United States. Three of the companies

are based outside the United States.

Wall Street analysts who follow the emerging biotechnology industry were not surprised that the companies as a group performed well during the sudden rally at the end of August that saw trading at record volumes. "People had been looking for refuges in this market" said one analyst at Oppenheimer and Company. "They were looking for safe stocks, buying defensively, selecting only stocks that looked like they would have high growth". More traditional US companies, in the steel, automobile and chemical industries, are unlikely to be favoured until traders think that the decline in interest rates will enable those ailing industries to recover, she said.

Among the biotechnology stocks listed in the *Nature* index, the best performance was by well-established firms, such as A/B Fortia of Sweden, Novo Industri of Denmark, and Genentech of south San Francisco, California. But the stocks of many of the smaller companies did not move at all and some declined. Analysts explained this by saying that active traders tend to avoid very small companies because a purchase can control the overall price. The fortunes of the smaller companies are affected by internal changes.

For example, Bio Logicals, of Ottawa, Canada, saw the value of its 5.9 million shares of outstanding stock decline from \$3 to \$2 per share between July and August, partly perhaps because it has been without a chief executive officer since Robert Bender left in May. Such changes make a big difference to a small company's owners, but little to the market as a whole. "It's a volatile market", as one Wall Street analyst said.

Deborah Shapley

Nature index of biotechnology stocks

1982 high	1982 low	Company (Headquarters)	Close previous month	Close 27 Aug	Change
32 3/4	16 1/8	A.B. Fortia (Sweden)	25 3/4	32 3/4	+ 7
8	2	Bio Logicals (Canada)	3	2	- 1
7	3 5/8	Bio-Response (US)	4 7/8	4	- 7/8
14 1/8	8	Cetus (US)	9	8 7/8	- 1/8
11	6 1/8	Collaborative Research (US)	8 3/8	8 3/8	0
21 7/8	14 3/4	Collagen (US)	17 3/4	17 5/8	- 1/8
8 7/8	5 3/4	Damon (US)	6 1/4	7 7/8	+ 1 5/8
17 1/4	11 1/4	Enzo-Biochem (US)	11 1/4	12	+ 3/4
28	6 5/8	Flow General (US)	7 7/8	10 5/8	+ 3
37 3/4	26	Genentech (US)	30 3/4	33 3/4	+ 3
3 3/8	2 1/4	Genetic Systems (US)	2 3/4	3 1/8	+ 3/8
17 7/8	9 7/8	Hybritech (US)	13 3/4	14 3/8	+ 5/8
10 3/4	6 1/4	Molecular Genetics (US)	6 3/8	10 3/4 *	+ 4 3/8
46 3/4	34 7/8	Novo Industri A/S (Den.)	39 7/8	46 3/4 *	+ 6 7/8
12 3/8	8	Monoclonal Antibodies (US)	9 1/4	9 3/4	+ 1/2

The *Nature* Biotechnology Index for August 1982 stands at 118.1. Base of 100 as of 25 June 1982. See *Nature*, 12 August, p.599. Close of month prices at the close of business on the last Friday of the month. Where stocks are traded over the counter, the price quoted is the bid price. For stocks traded on the American and the New York Stock Exchanges, the price quoted is the transaction price. Data courtesy of E.F. Hutton, Inc.

*High or low for this calendar year.

CORRESPONDENCE

On dotty letters

SIR — It gives your readers, I suppose, some light relief when you publish dotty letters on improbable ways of achieving peace in our time. Grey Dimond's letter (*Nature* 15 July, p.220) on the merits of an exchange of marriageable young men and women in attractive uniforms between the Soviet Union and the West has, however, a sound basis despite the more fantastic embellishments.

In the past three years or so, roughly the period since the Soviet invasion of Afghanistan and the intensification of the cold war, the numbers of people visiting the Soviet Union from the United Kingdom have increased. So too have the numbers of Soviet citizens visiting Britain — largely in parties of 500 to 700 on cruise ships and staying for only three or four days. Though the British government signs every two years an agreement with the Soviet Union which includes a commitment to facilitate cultural, scientific and educational exchange, it sometimes obstructs exchange, and paradoxically this has been happening just when it is most needed. In addition to the severe restrictions on Soviet citizens wishing to travel abroad, those who manage to obtain external passports often have much difficulty in getting UK entry visas. Travel in either direction may also have been restricted by cutting to about half by a British government body early last year of the number of flights permitted each week between the United Kingdom and the Soviet Union — primarily for commercial reasons.

Exchanges are vital precisely because of our differences with the Soviet Union. Whether the aim of a visit be business, scientific exchange, tourism, diplomacy or nuclear disarmament, there is bound to be an educational aspect, an adjustment on either side, however slight, of perceptions and understanding of the cold war enemy, and this can only be for the good.

STEWART BRITTEN

London N6, UK

Japanese IQ

SIR — Regarding possible causes of Japanese children showing a significantly higher IQ than their US and European counterparts, Magyar (*Nature* 17 June, p.532) suggested that exposure to written Japanese might play a role. I should like to point out, however, that the spoken rather than the written form of Japanese language has been found to be responsible for a characteristic, epigenetic lateralization of auditory processing in the two cerebral hemispheres of native Japanese-speakers regardless of the ethnic identity^{1,2} (but do not be misled by ref.3 based on a complete misunderstanding of the subject). In this respect, both Koreans and Chinese exhibit the same type of lateralization as do Europeans whereas the Japanese and Polynesians belong to a minor group with a different type of lateralization. A hypothesis attempting to relate IQ differences to the first language spoken during childhood could be tested with populations in Taiwan and South Korea — both of which have recently experienced remarkable leaps in economic growth.

Bhargava (*Nature* 1 July, p.8), on the other hand, suspects that a quick democratization of

education accompanying economic improvement may have been responsible for the very high IQ of Japanese children. However, literacy among the Japanese had perhaps attained a level of 45 per cent for the male and 15 per cent for the female population by the mid-nineteenth century, and at the beginning of the twentieth century practically all children in Japan were attending primary school⁴. This would indicate that the Japanese were not very much behind the Europeans in terms of literacy, and that democratization of education in Japan was neither rapid nor very recent, as suspected by Bhargava. After the war, however, competition among the young Japanese for opportunities of higher education was very much intensified. Competition now starts very early — even at the entrance examination for "elite" kindergartens which will facilitate later competition for higher education in "good" universities promising a good income and a career of life-long commitment. It is therefore conceivable that fierce competition rather than democratization in education is a more likely cause of the higher IQ among Japanese children. The IQ of Japanese children who have attended, for a number of years, Japanese schools overseas (as in London or Sydney) — and in an atmosphere much less competitive than that in Japan — could well be used to test the point.

A. SIBATANI

CSIRO Molecular and Cellular Biology Unit,
Sydney, NSW, Australia

1. Tsunoda, T. *Nipponjin no Nō* (The Japanese Brain) (Taishūkan, 1978).
2. Sibatani, A. *J. Social Biol. Struct.* 3, 255 (1980).
3. Miller, R.A. *Japan's Modern Myth* (Weatherhill, New York, 1982).
4. Reischauer, E.O. *The Japanese* (Harvard University Press, 1977).

Disarmament ideas

SIR — Among the many documents presented to the UN General Assembly at its Second Special Session on Disarmament (7 June–10 July) was one from the Medical Association for Prevention of War (MAWP) containing a completely new proposal. This calls for "a comprehensive ban on all methods and means of warfare specifically designed to kill or injure by inducing human disease, as distinct from causing mechanical and/or thermal effects". The starting point for the proposal is not the usual one of weapon-types, but the type of effect of weapons on people. The distinction between disease-inducing and mechanical or thermal effects has to be defined for the disarmament diplomats. This can be done in terms of pathology and, in lay terms, by the contrast of disease-inducing for living things only with the similarities of mechanical and thermal effects on animate and inanimate.

The MAPW proposal builds on existing agreements and negotiations on chemical, biological and toxin, and "radiological" weapons; and on agreed prohibitions on the release of "dangerous forces" from nuclear electrical generating stations, the use of environmental modification techniques for hostile purposes, and the use of conventional weapons that leave fragments in the body which are undetectable by X rays (so hindering their surgical removal and hence enhancing the risk of infection). The proposed comprehensive ban would close loopholes in

the existing agreements and extend the range of prohibitions — notably by including "neutron" weapons.

Moreover, the proposal opens up a new approach to the question of a comprehensive disarmament programme. The established approach is across-the-board disarmament of all varieties of military power. Modern versions (the United States' and the Soviet draft programmes of 1962 and the draft programme considered by the Special Session) envisage across-the-board comprehensive disarmament in three stages. This is like eating a cake in layers, and it is a proven failure.

The MAPW approach is like eating a mango. The whole of the skin ("disease-making") is peeled off first. Successive bites or cuts into the fruit can be flexible in position, size and depth. A comprehensive ban on thermal attacks on people might follow naturally from the ban on "disease-making". (If it is impermissible to inflict disease on one's enemies, one also ought not to burn them.) Reduction in the global total of the nuclear arsenals to below the theoretical level that poses a threat of species' genocide might be the next step. A prohibition on the development of any new weapons of mass destruction should be achieved without difficulty, as discussions on this subject are already in progress. Complete nuclear disarmament might have to await the introduction of objective principles for fixing ceilings on military manpower and expenditure. Current implications are that these should be proportional respectively to population size and gross national product (GNP). MAPW has found that this would have little overall effect on the present global maldistributions, which could be considerably improved, however, if the maximum permitted levels of military manpower and expenditure were made proportional to the *square roots* of populations and GNPs respectively.

The MAPW approach to comprehensive disarmament does not aspire to the ultimate UN objective of "general and complete disarmament". It leaves behind a hard core of national conventional military power. The hope must be that, having eaten the fruit, the world would decide that the only thing to do with the stone is to throw it away.

JEFFREY SEGALL

Medical Association for Prevention of War,
London NW2, UK

Units rule OK?

SIR — We view the recent letter by H.H. Rossi (*Nature* 22 July, p.320) with some disquiet. Are we witnessing the beginning of a trend towards the more widespread adoption of that Worrying Hardy Annual, The Nameless Or Unqualified Number In Today's Science (WHAT NO UNITS)?

While recognizing the practical value of bare figures for purely personal or even small group use, we believe that in all published work Units Nevertheless Incorporate Total Simplicity Regarding Unequivocal Literate Expressions Of Knowledge (UNITS RULE OK).

V.R. O'SULLIVAN
W.A. CURTIN
G.F. KAAR

Department of Anatomy,
University College,
Cork, Ireland

NEWS AND VIEWS

Kaposi's sarcoma: an oncologic looking glass

from Jerome E. Groopman and Michael S. Gottlieb

To paraphrase Lewis Carroll in *Alice in Wonderland*, Kaposi's sarcoma has become "curiouser and curiouser". It is unlikely that over a century ago when Dr Morris Kaposi¹ described patients with "multiple idiopathic pigmented sarcoma of skin" he would envision the disorder becoming an intriguing clinical puzzle that spans oncology, virology, epidemiology, public health, immunology and sexual behaviour. Indeed, the current epidemic of Kaposi's sarcoma and acquired immunodeficiency syndrome may provide important insights into the pathogenesis, prophylaxis and rational therapy of neoplasia.

In the spring of 1981 the Center for Disease Control (CDC) in Atlanta received the first of a number of reports of *Pneumocystis carinii* pneumonia occurring in young, previously healthy, homosexually-active men². Shortly thereafter, an unusual dermal malignancy, Kaposi's sarcoma (KS), was observed in similar hosts³. KS is a well recognized, rare endothelial neoplasm which generally occurs among elderly men of Mediterranean and Jewish ancestry. KS also occurs in an endemic form in certain areas of equatorial Africa. The common epidemiological link between Kaposi's sarcoma, opportunistic infection and the initial American cases was that of male homosexuality. The patients manifested a profound deficiency in cellular immunity, with anergy to recall antigens on skin testing, lymphopenia and a reversal of the normal ratio of helper to suppressor/cytotoxic T-lymphocytes^{4,5}. This ratio, although not specific for this disorder, has become a marker for the acquired immunodeficiency syndrome (AIDS). As of August 1982, there are over 500 documented cases of acquired immunodeficiency syndrome and/or Kaposi's sarcoma. There have been over 175 deaths due to this syndrome since its recognition, and the epidemic appears to be spreading⁶. In January 1982 about one case per day was reported to the CDC, since January 1982, two to three cases per day are being reported. It is estimated that KS and AIDS will account for 2-3 per cent of all deaths among men 25-40 years old in New York City, Los Angeles and San Francisco. There are now well documented cases occurring in 27 states in the United States as

well as 8 foreign countries. Ninety-five per cent of the affected persons are men, 85 per cent are either homosexual or bisexual although recently there has been an increased incidence among heterosexuals. The groups at risk for the development of Kaposi's sarcoma and AIDS now include homosexually-active men, intravenous drug users, female prostitutes, Haitian immigrants to the United States, and most recently, adult male haemophiliacs. There have been several intriguing epidemiological studies conducted by the CDC. In Los Angeles, 9 of 13 cases studied over the past year had had contact with another person who either had or later developed AIDS. It is of note that no lesbians have developed the syndrome to date. Fifty per cent of the cases come from the New York metropolitan area, about 25 per cent from California and about 7 per cent from Miami. The increasing incidence of the epidemic and its apparent transmission by sexual contact, drug apparatus and blood products strongly suggest a viral agent. Although use of various 'recreational drugs', particularly amyl and butyl nitrate, was initially believed to be important in immunodeficiency, this is now unlikely as many individuals with AIDS/KS have never used such drugs. There may be a genetic predisposition to the syndrome, as about 50 per cent of homosexually-active men in the New York area who developed Kaposi's sarcoma were positive for HLA-DR 5, nonetheless, the syndrome has clearly occurred among genetically, ethnically and socially diverse groups. Of greatest concern is the significant morbidity and mortality of the disease. Approximately 40 per cent of patients die per year with AIDS/KS, nearly 70 per cent of the patients who developed the syndrome in 1980 have died.

In the light of the occurrence of AIDS among adult male haemophiliacs, the United States government is now studying the donation and processing of blood products including hepatitis B immunoglobulin, factor VIII concentrates, cytomegalovirus (CMV) immunoglobulin,

and the new hepatitis B vaccine, all of which are frequently obtained from homosexually-active men. Recommendations from the Federal Drug Administration and the Bureau of Biologics are expected shortly.

The dimensions of this epidemic and the number of individuals at risk are unknown. Homosexually-active men who are asymptomatic have been studied and found to have a helper to suppressor-T cell ratio intermediate between that of homosexual controls and homosexually-active men with AIDS. How many of these asymptomatic men will go on to develop AIDS and/or Kaposi's sarcoma is not known. Nor is it known how the epidemic can be contained, aside from avoiding intravenous drugs and perhaps promiscuous sex. Recommendations to homosexually-active men concerning their sexual practices are difficult for the practising physician and involve complex ethical and civil rights issues.

Clinically, the opportunistic infections seen in men with AIDS are quite varied. Certain protozoa, such as *Cryptosporidium* and *Isospora*, have caused severe diarrhoeal syndromes, these are generally pathogens in livestock. In addition, certain atypical mycobacteria have caused not only severe, fatal pneumonias but a miliary pattern. Fatal fungal infections, particularly *Candida* and *Cryptococcus*, disseminated viral infections with herpes simplex, varicella zoster and adenovirus, as well as infection with toxoplasmosis, *Pneumocystis carinii* and *Legionella* have all been seen in AIDS. Therapy for many of these viral, protozoal and atypical mycobacterial infections is poor and most hosts quickly succumb.

Previous studies of endemic Kaposi's sarcoma in equatorial Africa have associated development of the neoplasm with cytomegalovirus infection⁷. A number of hypotheses have been advanced correlating the development of Kaposi's sarcoma with acquired immune deficiency syndrome. Repeated cytomegalovirus infection among homosexually-active men may 'wear down' the immune system and lead to cellular immunodeficiency. Yet why did this become apparent only during the past 2-3 years? Is there a new strain of cytomegalovirus? Although this is

Jerome E. Groopman is in the Division of Hematology-Oncology and Michael S. Gottlieb is in the Division of Clinical Immunology - Allergy, UCLA School of Medicine, Center for the Health Sciences, Los Angeles, Ca 90024

possible, preliminary studies on CMV isolates from affected hosts have not been particularly revealing. Is there a new virus? The CDC is in the process of processing sera and tissue from affected hosts and introducing filtrates into animals. Short of this, it would be difficult to identify a new virus. Because of the outbreak of AIDS among Haitian immigrants, attention has recently been turned to the Caribbean. There is preliminary information that AIDS and KS may be occurring in an epidemic fashion in Haiti. Because the

human T-cell leukaemia virus has a tropism for helper inducer T-lymphocytes and because this retrovirus is endemic in the Caribbean, AIDS patients are being studied for HTLV by Robert Gallo of the NCI.

Additionally, Burkitt's lymphoma, cloacogenic carcinoma of the rectum and immunoblastic sarcoma appear to be occurring among American homosexual men at an increased frequency. Each of these cancers has been associated with DNA viruses of the herpes family. The epidemic of AIDS and KS affords a unique opportunity to study the relationship between immune status and the pathogenesis of certain forms of neoplasia. Considering the striking mortality, clues to aetiology that lead to rational therapy are needed. □

- 1 Kaposi, M. *Archs Derm Syphilis* 4, 265 (1972)
- 2 Gottlieb, M. S. *et al* in *Morbid Mortal Weekly Rep* 30, 250 (1981)
- 3 Hymes, K. B. *et al* *Lancet* ii, 598-600 (1981)
- 4 Gottlieb, M. S. *et al* *New Engl J Med* 305, 1425-1431 (1981)
- 5 Siegal, F. P. *et al* *New Engl J Med* 305, 1439-1443 (1981)
- 6 DeWys, W. D. *et al* *Cancer Treat Rep* 66, 1387 (1982)
- 7 Boldogh, I. *et al* *Int J Cancer* 28, 469 (1981)

The geoid and geodynamics

from Bradford H. Hager

THE direct radar measurements of sea surface height from satellite GEOS 3 reported in this issue of *Nature* (p 117) by Ki-Iti Horai show that it is now possible to measure small changes in the shape of the geoid — the equipotential surface corresponding to mean sea level — with an accuracy of ± 50 cm. Detailed maps of geoid elevation with contours spaced as close as 1 m can thus be produced (see Fig 1a, p 118) and clearly show the effect of tectonic features such as deep sea trenches, outer arc rises, and oceanic ridges and troughs on the height of the geoid.

Variations in the height of the geoid are caused by horizontal variations in the density structure of the Earth. Early interpreters, assuming a rigid Earth, used the observed fluctuations of the geoid to bound the size and depth of the density contrasts that brought them about. Constraints were thus placed on the (supposed finite) strength of the Earth¹. Now, observations of the postglacial rebound and plate motions make it clear that the Earth interior behaves as a fluid, not a rigid material, over geological time, requiring interpretation of geoid anomalies in a dynamic system²⁻⁴. As is well seen in Horai's paper, the study and interpretation of the figure of the Earth is now moving from the static domain of physical geodesy to the domain of geodynamics.

Analysis of geoid anomalies in terms of density contrasts has always been hindered by the lack of a unique interpretation — an infinite family of distributions of density contrasts within a given body can satisfy

any observed gravitational potentials outside that body. Adding the extra constraint that the equations of motion in the fluid interior of the Earth must be satisfied has only recently been exploited in interpretation of the Earth's gravity field, but imposes a limit on the class of acceptable solutions.

The basic physics of the problem are relatively simple, but contain some subtleties. Consider a density contrast of spherical harmonic degree l placed at a radius r in a fluid mantle. The gravitational potential at the surface ($r = r_c$) is reduced by a factor $(r/r_c)^{l+2}$. The density contrast causes flow which leads to a downward deflection of the surface of the Earth above high density regions and upward deflection above low density regions. Trenches and oceanic ridges are the directly observable result of this type of deflection. Similar deflections occur at the core-mantle boundary and at any other internal layer boundaries which might exist. (Settling the controversial question of the existence of these boundaries⁵⁻⁷ may soon be possible using the techniques outlined here.) Solving the equations of motion within a fluid mantle⁸ shows that the deflection of the surface of the Earth is also approximately given as $(r/r_c)^{l+2}$. The gravitational effects of the surface deformation and the driving density contrast are of comparable magnitude and opposite sign and nearly cancel.

The gravitational field of the Earth thus provides the most sensitive of all experiments, the null experiment, where the net result is a small number determined by the difference of two large effects. The sign of the result depends on which of the effects is dominant.

As an example, consider the geoidal

signal resulting from the subduction of a cold, dense slab of lithosphere. If most of the stress from the sinking slab were directly transmitted to the outer surface of the Earth, the gravitational effect of surface deformation would be of greater magnitude than that from the slab itself, resulting in a net negative geoid anomaly. If the stress were transmitted more efficiently to a discontinuity deeper in the mantle, the dense slab, being closer to the surface, would dominate the gravity field, leading to a positive geoid anomaly.

Horai's geoid map shows that except for the localized area comprising the trench, the gravitational attraction of the slab is larger than that of the deformed upper surface. This shows that the weight of the slab is carried mostly by support from below such as would be provided by an increase of viscosity with depth or by the presence of a chemically induced density contrast between the upper and lower mantle. Fault plane solutions showing in general down dip compression in deep slabs are consistent with either of these interpretations⁹. An increase in effective viscosity with depth might be the result of stress-dependent rheology, as Horai suggests, or of the competing effects of increased pressure and temperature on rheology.

Many of the features of the global geoid are associated with subduction zones¹⁰, but there are many features such as the geoid lows over Siberia, Hudson Bay, and the Ross Sea, and the high over Africa, not associated with subduction. In these areas, we have no *a priori* knowledge of the sign of the causative density contrasts. They may well be the result of density contrasts not associated with present plate motions¹¹. In particular, Anderson¹² has recently suggested that the geoid highs correspond to anomalously hot mantle, with geoid lows corresponding to colder mantle. This scenario is plausible if in these regions the gravitational effects of surface deformation are large, consistent with efficient coupling of stresses to the upper surface.

How can such a hypothesis be tested? It is not possible to measure directly density contrasts in the interior of the Earth, but it is possible to measure deformation of the outer surface. The ratio of geoid height to

- 1 Jeffreys, H. *The Earth* (Cambridge University Press, 1976)
- 2 Morgan, W. J. *J Geophys Res* 70, 6175 (1965a), 70, 6189 (1965b)
- 3 McKenzie, D. P., Roberts, J. M. & Weiss, N. O. *J Fluid Mech* 62, 465 (1974), *Geophys J astr Soc* 48, 211 (1977)
- 4 Parsons, B. & Daly, S. *EOS* 60, 391 (1979)
- 5 Davies, G. F. *Geophys J astr Soc* 49, 459 (1977)
- 6 O'Connell, R. J. *Tectonophysics* 38, 119 (1977)
- 7 Richter, F. M. & McKenzie, D. J. *Geophys* 44, 441 (1978)
- 8 Richards, M. A. & Hager, B. H. *EOS* 62, 1077 (1981)
- 9 Richter, F. M. *J geophys Res* 84, 6783 (1979)
- 10 Kaula, W. M. in *The Nature of the Solid Earth* (ed Robertson, E. C.) 385 (McGraw-Hill, New York, 1977)
- 11 Chase, C. G. *Nature* 282, 464 (1979)
- 12 Anderson, D. L. *Nature* 297, 391 (1982)
- 13 McKenzie, D. P., Watts, A., Parsons, B. & Rousfosse, M. *Nature* 288, 442 (1980)
- 14 Birch, F. *Geophys J R astr Soc* 4, 295 (1961)
- 15 Nakanishi, I. & Anderson, D. L. *Bull seismol Soc Am* (in the press)

Bradford H. Hager is Assistant Professor of Geophysics in the California Institute of Technology, Pasadena, Ca 91125

surface deformation is observable and very sensitive to the distribution of viscosity^{3,8} as well as to the depth of the convecting layer. The fact that Africa (geoid high) is on average 500 m higher than Siberia or the area around Hudson Bay (geoid lows) supports the hypothesis that the geoid in these regions results from less dense and more dense mantle respectively, with stresses transmitted efficiently to the surface of the Earth. This would be consistent with the absence of a low viscosity asthenosphere in these regions. This absence would not be surprising as these areas are ancient cratons.

McKenzie and others¹³ have looked at correlations between bathymetry, interpreted as surface deformation, and geoid anomalies on a smaller scale, these anomalies are consistent with those obtained for calculations of convection in a uniform viscosity fluid. Given the sensitivity of geoid anomalies to viscosity structure, it would be of great interest to extend the calculations to include the low viscosity asthenosphere generally supposed

to exist beneath oceanic plates to see if the geoid observations are in accord with this type of rheology.

Seismology provides additional constraints. Density and seismic velocity are, in general, positively correlated¹⁴. At present, seismologists are making rapid progress in deciphering the three-dimensional distribution of lateral heterogeneities in seismic velocity in the Earth's interior¹⁵.

We are at the beginning of an exciting era in geodynamics. High quality geoid observations, combined with high quality determinations of surface deformation and new high resolution seismic data will provide powerful constraints which must be satisfied by the next generation of geodynamic models. Combining all three data sets will decrease the non-uniqueness inherent in each. The physics of the gravity field, which makes it effectively a null measurement, should make it possible in the near future to constrain variations in mantle rheology and the depth and scale of mantle convection. □

template. The sigma subunit is lost and the resulting ternary or elongation complex moves along the DNA simultaneously synthesizing the RNA transcript, which is continuously displaced from the coding DNA strand.

DNA unwinding by RNA polymerase was first unequivocally demonstrated for open promoter complexes by Wang and co-workers^{3,4}. These studies pioneered the approach of measuring DNA unwinding from the difference in linking number between DNA samples obtained by sealing a nicked circular duplex DNA with DNA ligase, in the presence and absence of the DNA binding protein⁴. Gamper and Hearst have now measured and compared DNA unwinding induced by RNA polymerase in binary, initiation and elongation complexes formed at a single prokaryotic promoter sequence in simian virus 40 DNA¹. They used gel electrophoresis to measure the change in the linking number of closed circular SV40 DNA in transcriptional complexes in which the DNA had been relaxed using a DNA nicking-closing extract. This procedure removes the overwound DNA turns arising from protein binding, thereby fixing the topological change.

The degree of DNA unwinding was found to be the same for all three transcriptional complexes and, for the elongation complex, was independent of its sequence location on DNA. The extent of DNA untwisting was deduced to be 17 ± 1 base pairs ($580^\circ \pm 30^\circ$) per polymerase molecule. The result can be compared with a value of approximately seven base pairs previously reported by Wang for open promoter complexes⁴. Although these unwinding estimates are somewhat different, the important result established by the new study is that the extent of DNA unwinding is constant throughout transcription.

Invariance of the DNA unwinding angle as the ternary complex progresses along the DNA helix suggests that the size of the unwound DNA region is tightly controlled by polymerase and is independent of the DNA sequence in the complex. A topological model that accommodates this result has been proposed to describe elongation by polymerase (Figure 1). It is suggested that RNA polymerase has two windase activities that rigidly determine the limits of the DNA unwound region and which facilitate its movement along the DNA helix. The leading unwindase opens the DNA helix which is then subsequently reformed by the lagging rewindase. These activities are coupled and result in translocation of the enzyme relative to the substrate DNA and the RNA transcript. Given the size of polymerase and that of the transcript, it seems unlikely that the ternary complex itself rotates on DNA. A more plausible and topologically feasible solution is that the DNA on either side of the unwound region rotates about the helix axis (Figure 1). Because the helix axis

DNA unwinding in transcription and recombination

from L. Mark Fisher

LOCAL unwinding of the DNA helix plays an important role in many biological processes. In transcription, opening of the DNA helix by RNA polymerase allows access to the coding DNA strand and copying of the DNA message into an RNA transcript. The formation of heteroduplex DNA structures by recombination between homologous DNA molecules, catalysed by RecA (and other) proteins, must also involve unwinding of duplex DNA. Two recent papers reveal some intriguing features of DNA unwinding by *Escherichia coli* RNA polymerase¹ and RecA protein² (see this issue of *Nature*, p 185).

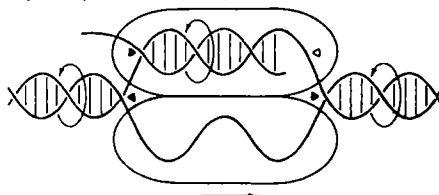
DNA helix unwinding may most conveniently be investigated by taking advantage of the topological properties of circular DNA. A closed circular duplex DNA is characterized by a topological parameter termed the 'linking number', which specifies the number of times the two complementary DNA strands are intertwined in the DNA circle. The linking number is an invariant and can be changed only by breaking and resealing the DNA. Therefore, if protein binding induces unwinding in one part of the helix in a closed duplex DNA circle, this must necessarily be accompanied by overwinding of the DNA elsewhere in the DNA molecule. The recent studies on unwinding by RecA protein and

by RNA polymerase have in different ways both exploited this phenomenon.

Unwinding by polymerase

RNA polymerase from *E. coli* is a pentameric complex of subunit structure $\alpha_2\beta\beta'\sigma$ and molecular weight 465,000. RNA synthesis by the enzyme proceeds via the sequential formation of four different enzyme-DNA complexes. The holoenzyme first binds at the promoter site forming the closed promoter complex, in which the enzyme is associated with DNA sequences in their helical conformation. This complex isomerizes, unwinding and separating the DNA strands to form the open promoter (binary) complex. Exposure of the coding DNA strand allows initiation of RNA synthesis to take place. The short RNA oligomer made in the initiation complex forms an RNA-DNA hybrid with the coding strand of the DNA

Fig. 1 Topological model for the RNA polymerase elongating complex (taken from ref 1). Filled triangles denote swivelase centres, the open triangle denotes the catalytic site for RNA synthesis. The unwound strands of the DNA are bound to polymerase, possibly to the β and β' subunits [Figure © M I T Press]



L. Mark Fisher is in the Department of Biophysics, King's College, University of London.

remains fixed, the proposed mechanism would not result in spatial revolution of the entire DNA molecule about polymerase during transcription of a circular DNA. Continuous displacement of the transcript from the DNA template is assumed to involve the rotation of the RNA-DNA hybrid. Further experimental work will be necessary to validate the details of the model and to examine its role in pausing and termination of RNA synthesis by polymerase.

Unwinding by RecA protein

The RecA protein is involved in DNA recombination and repair in *E. coli*. This 38,000 molecular weight protein has an ATP-dependent DNA strand transfer activity that promotes the formation of joint molecules between duplex DNA and either single DNA strands or double-stranded DNA with single-stranded gaps⁵. Whatever the precise mechanism of DNA strand transfer, the RecA protein must somehow unwind duplex DNA so as to catalyse the formation of heteroduplex DNA structures.

Several groups have shown that RecA protein binds cooperatively both to single-stranded and to duplex DNA⁶⁻¹¹. Complexes with duplex DNA are stabilized by the inclusion of ATPγS, a non-hydrolysable ATP analogue. These nucleoprotein complexes appear in the electron microscope as right-handed helical filaments in which the duplex DNA is elongated by about 50 per cent. This lengthening of the DNA is consistent with unwinding of the DNA helix on interaction with RecA protein¹². Stasiak and Di Capua (see p 185) have now focused on the ATPγS-stabilized cooperative binding of RecA protein to closed circular duplex DNA². Local unwinding of this DNA by RecA protein induces a compensating overwinding (positive supercoiling) of the DNA segment not complexed with protein. The countervailing positive supercoiling of the DNA constrains the extent of protein-DNA complex formation.

The amount of RecA protein that binds to DNA depends on the negative superhelical density of the starting circular DNA. Clearly, the higher the initial negative supercoiling (underwinding) of the DNA, the more protein can bind before the binding constraint is reached. Stasiak and Di Capua used electron microscopy to

measure the fraction of the DNA circle covered by protein when negatively supercoiled DNA samples with different mean linking numbers were incubated with excess RecA protein. By extrapolation, they were able to estimate the linking number of the DNA in a closed duplex circle completely covered with RecA protein. The linking number they obtained had essentially the same value as the number of visible helical turns counted for the nicked DNA molecule fully covered with the RecA protein. These elegant studies show that the DNA helix in the complex follows the protein helix seen in the electron microscope and that RecA protein unwinds the DNA helix from the usual value of about 10.5 base pairs per turn to 18.6 base pairs per turn. Studies by Shibata's group, described in *Nature* last week (299, 86), have shown that relaxation of RecA protein — closed

circular DNA complexes by a nicking-closing extract generates highly negatively supercoiled molecules consistent with RecA mediated unwinding of the DNA.

Intercalation of protein (or conceivably ATPγS) into the DNA helix could account for DNA unwinding in DNA-RecA protein filaments. Alternatively, the helix may be melted with complementary DNA strands separated and not base paired. Interestingly, RecA protein can itself form filamentous helical aggregates similar to those observed with DNA⁸. It seems possible, therefore, that the RecA protein filament provides a rigid framework to which the DNA is constrained to bind in an unwound conformation. The precise nature of RecA protein-DNA interactions in the filaments and the relevance of these structures in recombination await biochemical analysis. □

Murine models of multiple sclerosis

from Peter Doherty and Elizabeth Simpson

MULTIPLE SCLEROSIS is a chronic progressive debilitating disease which remains an intractable human problem. Despite many years of research there is no very clear indication as to aetiology, although a number of candidate viruses have been proposed. There is a tendency for people who develop multiple sclerosis (MS) early to have had several infections in childhood. There are also marked geographical variations, with the disease increasing in incidence with distance from the equator. Another clue is provided from HLA-typing studies which show a preponderance of HLA, A2, B7, DRW2 in MS patients from North America and northern Europe, but superimposed on this there is a Gm allotype linkage, an interesting finding in view of recent reports of Gm allotype- and HLA-linked control in autoimmune disease (Whittingham *et al Clin exp Immun* 43, 80, 1981, Uno *et al Nature* 292, 768, 1981).

Experimental analysis has been hampered by the lack of a generally acceptable animal model. Over the past twenty years much work has been done with the acute form of experimental allergic encephalomyelitis (EAE) although the recurrent progressive pattern of MS is not reproduced. A genetic component of EAE in rats and guinea pigs is indicated, however, since the induction of disease is dramatically strain dependent. It has also been established that EAE in these species can be induced by different fragments of myelin basic protein (MBP), and that the induction of both effector and suppressor T-cell subsets can

be separated by manipulation of the immunization schedule. A further substantial advance has been the development of experimentally induced relapsing EAE, first in rats and guinea pigs, and more recently in mice, which allows more detailed genetic and immunological analysis.

Over the same period that studies on relapsing EAE have developed, other research groups have been working on virus-induced primary demyelinating processes in mice. A recent meeting* provided a timely opportunity to bring together those studying autoimmunity and virus-induced demyelination with people concerned with analysis of basic immune mechanisms and T-cell circuits in mice.

It is apparent that the relapsing EAE model in the mouse and the chronic disease process caused by some viruses such as Theiler's virus (a picornavirus) have many features which mimic the pathology of human MS. However, there are also a number of differences. The progress of relapsing EAE is not inexorable, and substantial recovery with re-myelination commonly occurs whilst it is scarcely ever seen in humans. In progressive virus models, small amounts of virus antigen persist (H. Lipton, Northwestern University Medical School, Chicago) whereas attempts to recover viruses or detect virus coding sequences that are present in MS but absent in normal human brain have never been consistently successful. Even so, the similarities are sufficient to warrant thorough analysis of cellular

Peter Doherty is in the Wistar Institute, Philadelphia, Pennsylvania 19104 and Elizabeth Simpson in the Clinical Research Centre, Watford Road, Harrow, Middlesex HA1 3UJ.

1. Gamper, H. B. & Hearst, J. E. *Cell* 29, 81 (1982).
2. Stasiak, A. & Di Capua, E. *Nature* 299, 185 (1982).
3. Saucier, J.-M. & Wang, J. C. *Nature new Biol* 239, 167 (1972).
4. Wang, J. C., Jacobsen, J. H. & Saucier, J.-M. *Nucleic Acids Res* 4, 1225 (1977).
5. Radding, C. M. *Cell* 25, 3 (1981).
6. West, S. C., Cassuto, E., Muraslim, J. & Howard-Flanders, P. *Proc natl Acad Sci USA* 77, 2569 (1980).
7. Stasiak, A., Di Capua, E. & Koller, Th. *J molec Biol* 151, 557 (1981).
8. McEntee, K., Weinstock, G. M. & Lehman, I. R. *J biol Chem* 256, 8835 (1981).
9. Di Capua, E., Engel, A., Stasiak, A. & Koller, Th. *J molec Biol* 157, 87 (1982).
10. Flory, J. & Radding, C. M. *Cell* 28, 747 (1982).
11. Dunn, K., Chrysogelos, S. & Griffith, J. *Cell* 28, 757 (1982).
12. Cunningham, R. P., Shibata, T., DasGupta, C. & Radding, C. M. *Nature* 281, 191 (1979).

*The meeting was held at the Kroc Foundation, 22-26 June 1982, sponsored by the American Sclerosis Society and the Kroc Foundation and organized by Bryan Wakeman and Dale McFarlin.

immune regulation and effector function in affected animals. In fact, the main virtue of the meeting may have been in indicating that common pathways exist in the development of these apparently aetiologically unrelated models.

The influence of genetic factors is seen very clearly in both virally induced demyelinating disease and EAE mice. The SJL mouse, known to have both lymphoproliferative and autoimmune tendencies, is extremely sensitive to induction of demyelinating disease. However, a propensity to autoimmunity, itself multigenic, (A. Steinberg, NIH, A. Theofilopoulos, Scripps Foundation) is not responsible *per se*, since NZB and other autoimmune strains are not highly susceptible to EAE. The induction and expression of acute EAE in mouse is under the control of both H-2 and non-H-2 genes. Involvement of H-2 Ir genes is indicated by the effects of treating developing EAE with anti-Ia antisera (L. Steinman, Stanford University School of Medicine). Analysis of a set of recombinant inbred strains shows that one of the non-H-2 genes may be controlling a histamine receptor sensitivity to histamine release and thus susceptibility to rapid extravasation of fluid and cells in the central nervous system (CNS) of mice sensitized to MBP (D. Linthicum, USC Medical School, Los Angeles). Detailed studies of the susceptibility of relapsing EAE to a variety of mouse strains reveals that the disease may be induced in many strains other than STL but that the MBP fragment responsible varies from strain to strain (R. Fritz, Emory University). The absolute requirement for T cells is shown by the inability to induce the disease in SJL/hr⁻ mice, which lack a thymus.

The meeting also raised intriguing points about the nature of the pathological process of CNS damage itself. It is clear that the acute autoimmune disease at least is T cell mediated and seems to be caused principally by the Ly 1⁺ class of effector cells. This is not established for the virus models, but there is obviously an immune component. However, both sorts of experimental systems show instances in which the oligodendrocytes that synthesize the myelin remain intact and there is little evidence of neuronal death or axonal degeneration. Conventional immunological wisdom would have us believe that Ly 1⁺, Ia-restricted T cells are the instigators of demyelinating damage, but there is no evidence that Ia antigens are present on myelin, and previous claims that such determinants are present on the surface of oligodendrocytes do not seem to be generally accepted. Also, morphological evidence would suggest that cellular damage to the myelin sheath is a function of monocytes/macrophages rather than T cells. How then do T cells induce demyelination? Does this mean that the T-cell effect must be operating through a short-range product such as a lymphokine, lympho-

toxin or prostaglandin? As Cantor pointed out, Ly 1⁺ T cells can kill by activating macrophages to produce peroxidase, which then kills both macrophage and the Ly 1⁺ inducer T cell.

We may thus be looking at a final common pathway where persistent antigen in brain, whether virus, MBP or some other CNS component, is recognized on the surface of Ia-positive antigen-presenting cells (derived from invading monocytes) and where the demyelinating process itself is a bystander effect reflecting secreted products from the macrophage-lymphocyte interaction causing a physiological defect in oligodendrocyte function, or direct damage to the myelin sheath. If this analysis is correct, then MS could be a disease of multiple aetiology, with a common pathological process. One point that might make us doubt this possibility is that there are apparent Ir gene effects which may indicate the involvement of a single pathogen. However, this could equally reflect a common neurological sensitizing component regardless of the triggering.

What of the future? It seems that we now have reasonable murine models for investigating chronic demyelinating disease in the context of contemporary immunological and molecular biological concepts and

techniques. A clear understanding of suppressor and effector circuits in both the virus and EAE models can readily be developed. The possibility that non-MHC-restricted suppressor molecules from antigen-specific clones may be targeted onto relevant cell sets, as suggested by Cantor, can be analysed. A search can be made to see whether infection with various viruses causes development of brain-specific T and/or B cell populations using cloning and hybridoma techniques. This approach has been effective in the murine reovirus diabetes model (M. Haspel, NIH).

Do viruses trigger MS? Certainly the mild pleocytosis that is a common feature of many childhood infections should allow exposure of CNS components to immunologically competent cells which are non-specifically drawn into the CNS during mild inflammatory processes. We should, over the next 10 years, get the answer for one candidate virus, measles, since 90 per cent of children in the United States are given live vaccine at an early age and measles has virtually disappeared. In contrast, in the United Kingdom only about 15 per cent of children are vaccinated against measles. However, in the absence of any correlation between measles and MS there is ample scope for experimental analysis which has some hope of relevance.

Haemocyanins to haemerythrins

from E F J van Bruggen

THE invertebrate respiratory proteins include the blue, copper-containing haemocyanins of molluscs and arthropods, the haemoglobins (or erythrocruorins) from a variety of invertebrates, and the burgundy-coloured, non-haem iron haemerythrins of certain sipunculid worms. Although all have a common function — oxygen transport in the blood — they are typically giant molecules which show a beautiful but bewildering range of architectures. Because the molecules are so large many important findings come from electron microscopy. Unfortunately, extensive subunit heterogeneity has hitherto prevented detailed X-ray crystallography and sequencing. These problems are gradually being overcome, and a workshop was held in Leeds University* at which recent findings were discussed.

Arthropod haemocyanins have polypeptide subunits of molecular weight 70,000 which aggregate to form multimers containing up to 48 subunits. Three groups of workers reported extensive amino acid sequences of subunits of Cheliceratan

haemocyanin, those from horseshoe crab, *Tachyplesus* (T. Nemoto and T. Takagi, Tohoku University), *Limulus* (A. Riggs *et al.*, University of Texas), and scorpion, *Eurpelma* (B. Linzen *et al.*, University of Munich). All show extensive homologies, and are of particular interest in that all contain an unusual peptide, -His-His-Trp-His-Trp-His-, as part of their sequence, about 170 residues from the N-terminus. It seems probable that this forms a major part of the copper-containing active site. Nemoto's group reported 359 residues of the N-terminal sequence and about 100 residues of the C-terminal sequence, leaving about 100 residues to be sequenced.

It will be of great interest to correlate these data with the X-ray studies that are now coming to fruition. Thus, the X-ray structure of spiny lobster (*Panulirus interruptus*) haemocyanin at 4 Å resolution not only showed the tertiary structure of the binuclear copper centre, but also enabled a very precise model to be made for the quaternary structure of this hexameric molecule (W. Gaykema *et al.*, Rijksuniversiteit, Groningen). The model should

*The workshop was held in the Biochemistry Department, University of Leeds 19-22 July 1982 and sponsored by the European Molecular Biology Organization.

E F J van Bruggen is in the Biochemistry Laboratory of the Rijksuniversiteit Groningen, Nijenborgh 16 9747 AG, Groningen.

help interpret the different view of multi-hexameric molecules obtained by aperiodic averaging of electron microscopic images in combination with correspondence analysis (M van Heel, Rijksuniversiteit, Groningen and J Frank, New York State Department of Health, Albany) Together with information from immunoelectron microscopy using polypeptide chain-specific Fab fragments, we now have a considerably improved model for the quaternary structure of the Cheliceratan haemocyanins and their dissociation products (J Lamy *et al*, University of Tours, B Linzen *et al*, University of Munich; E van Bruggen *et al*, Rijksuniversiteit, Groningen)

A great deal of chemical spectroscopy now confirms previous ideas that the coppers in the active site of haemocyanin are held by imidazole nitrogens (E Solomon, Stanford University) Interestingly, there are a number of similarities with another copper protein, *Neurospora* tyrosinase, and the enzymatic activities, known for many years to be exhibited by haemocyanins, were discussed following their re-investigation by several groups (A Nakahara, Osaka University)

Some progress has been made with the structures of the mollusc haemocyanins and the annelid haemoglobins For the

former, elegant work using proteases has confirmed the structure of the polypeptide in gastropod haemocyanins as containing eight linked oxygen-binding units in a polypeptide of molecular weight $> 400,000$ Cephalopod haemocyanins seem to be essentially the same (C Gielen and R Lontie, Katholieke Universiteit, Leuven) One of the functional units of *Helix pomatia* haemocyanin has now been crystallized Several models for annelid haemoglobins (molecular weight up to 4×10^6) were discussed Electron microscopy shows the molecule to be a stack of two hexagonal plates 26 nm across, but many problems remain to be resolved regarding the number of subunits, their haem content, and their arrangement in the molecule

A study of the various developmental stages of the crustacean (N Terwilliger, University of Oregon) gave the first indication that there may be a 'fetal haemocyanin' This is particularly interesting as there is evidence that the variety of polypeptides which form arthropod haemocyanin (for example 12–15 in *Limulus polyphemus*) are coded by a family of mRNA molecules The polypeptides produced appear to undergo few if any post-translational modifications (E Wood and K Siggins, University of Leeds) □

doubt that compounds within the iron-oxygen system can exhibit marked changes in chemical properties at the pressures and temperatures of the Earth's deep interior To what extent these changes could decrease the miscibility gap between Fe and FeO liquids is unknown

Ringwood's model for the core has been simultaneously provocative and vexing He invokes a metallization of FeO at high pressures, such that significant amounts of the oxide can dissolve into the iron-rich core However, the electronic-bonding properties of FeO are complex and not well understood⁵ it appears that theory (for example, quantum-mechanical band calculations) cannot help us here On the other hand, wüstite exhibits a rich defect chemistry, with the result that stoichiometric FeO has virtually never been synthesized Rather, the experimentalist must work with Fe_{1-x}O ($0 < x \leq 0.15$), and it is difficult to be sure that identical wüstite compositions are reproduced from one laboratory to another Hence, not even the zero-pressure, room-temperature properties of wüstite are well documented

The only data on Fe_{1-x}O at the conditions of the core result from shock-wave experiments⁶ Indeed, the equation-of-state measurements demonstrate that wüstite transforms from its initial state (ionically bonded, NaCl-like structure) at shock-pressures above 70 GPa According to these data, up to 45 mol per cent FeO (~ 10 wt % O) dissolved in Fe satisfies the observed density of the core However, neither the crystal structure nor the bonding character is determined in the shock experiments, and numerous interpretations of the transition in FeO are possible Various authors have favoured either crystal-structured or electronic (including magnetic) changes, or both⁶⁻⁹ A definitive answer could be provided by measurement of the electrical resistivity of wüstite at high pressures and temperatures One group¹⁰ has found no resistivity anomalies to over 100 GPa (estimated) at

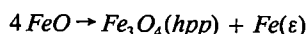
Oxygen in the Earth's metallic core?

from Raymond Jeanloz

THE outer core of the Earth has the properties of a molten iron alloy Its density, however, is nearly ten per cent less than that of iron, and considerable effort has gone into determining the 'lighter component' that is alloyed with the iron The composition of the core is of particular geochemical interest, as it provides a constraint on models of the early history of the Earth But a major question has been to what extent can (or must) one invoke unusual chemical properties for material existing at the 130–330 GPa (1.3–3.3 Mbar) and $\sim 4,000$ – $6,000$ K pressures and temperatures of the core? Several investigators have recently emphasized the degree to which chemical behaviour may change at such extreme conditions, as compared with our experience with the same materials at low pressures and temperatures

At a time when sulphur was considered by many to be the most plausible candidate, Ringwood¹, reviving earlier speculations, argued forcefully that oxygen must be the light component within

the core This might appear strange at first After all, wüstite (ideally, $\text{Fe}^{2+}\text{O}^{2-}$) is an ionic solid, with the result that most compositions in the system Fe–FeO melt (at zero pressure) to an immiscible mixture of metallic (Fe-rich) and nonmetallic (FeO-rich) liquids Therefore, one would hardly expect significant amounts of FeO to dissolve preferentially out of the Earth's oxide mantle and into the metallic core In fact, experiments had already indicated that metallic iron separates out of an oxide phase at high pressures and temperatures²



where hpp indicates a high-pressure phase (structure uncertain) and ϵ is the hexagonal-close-packed phase of iron

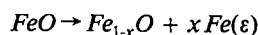
We must note, however, that FeO becomes a semiconductor in the liquid state, and Ringwood's conclusion that iron and iron-oxide liquids become miscible at high temperatures ($\geq 4,000$ K) is consistent with the available data^{1,3} That Fe in an oxide undergoes an electronic transition at high pressures has recently been verified⁴ a high-spin \rightarrow low-spin transition occurs (with no change of crystal structure) at 55 GPa in Fe_2O_3 There is no longer much

- 1 Ringwood, A E *Geochim J* **11**, 111 (1977)
- 2 Ringwood, A E *Origin of the Earth and Moon* (Springer, New York, 1979)
- 3 Mao, H K *Carnegie Inst Washington Yb* **73**, 510 (1974), Mao, H K & Bell, P M in *Energetics of Geological Processes* (eds Saxena, S K & Bhattacharji, S) **236** (Springer, New York, 1977)
- 4 Shimoji, M *Liquid Metals* (Academic, New York, 1977)
- 5 Yagi, T & Akimoto, S in *High-Pressure in Geophysics* (eds Akimoto, S & Manghnani, M H) **81** (Center for Academic Publications, Tokyo, 1982)
- 6 Fialkov, I M & Koiller, B *J Solid State Chem* **12**, 349 (1975)
- 7 Jeanloz, R & Ahrens, T J *Geophys J R astr Soc* **62**, 505 (1980)
- 8 Zou, G T, Mao, H K, Bell, P M & Virgo, D *Carnegie Inst Washington Yb* **79**, 374 (1980)
- 9 Jackson, I & Ringwood, A E *Geophys J R astr Soc* **64**, 767 (1981)
- 10 Navrotsky, A & Davies, P K *J Geophys Res* **86**, 3689 (1981)
- 11 Endo, S & Ito, K in *High-Pressure Research in Geophysics* (eds Akimoto, S & Manghnani, M H) **3** (Center for Academic Publications, Tokyo, 1982)
- 12 Liu, L, Shen, P & Bassett, W A *Geophys J R astr Soc* **70**, 57 (1982)
- 13 Shen, P, Liu, L & Bassett, W A in *High-Pressure Research in Geophysics* (eds Akimoto, S & Manghnani, M H) **421** (Center for Academic Publications, Tokyo, 1982)

Raymond Jeanloz is in the Department of Geology and Geophysics, University of California, Berkeley, Ca 94720

room temperature. This result does not support Ringwood's metallization hypothesis, but the effects of high temperature and of melting on the bonding character of FeO remain unknown at the pressures of the core¹¹.

Another dimension to the behaviour of iron oxides at extreme conditions has recently been emphasized by Liu and co-workers, who propose that the effects of nonstoichiometry have been underestimated^{12,13}. Extrapolating from earlier results, these workers suggest that wüstite becomes less stoichiometric with increasing pressure



with x increasing to a value of 0.25 with pressure. Ironically, this brings us back to Mao's conclusion³ that equation (1) proceeds to the right (it is worth noting that the nonstoichiometry of wüstite is associated with microdomains of magnetite — Fe_3O_4 , or $\text{Fe}_{0.75}\text{O}$, containing both Fe^{2+} and Fe^{3+} — within the FeO structure). At face value, it would seem that this proposal works against Ringwood's hypothesis,

with Fe separating out of the oxide phase. Nevertheless, the concept that the defect density (that is, the nonstoichiometry) could increase with pressure invites further work (the existing data in support of this are not definitive).

The significance of defects lies in the control of the nonstoichiometry by oxidation-reduction conditions (that is, Fe^{2+} – Fe^{3+} equilibria). However, the oxygen fugacity can only be poorly determined in ultrahigh pressure-temperature experiments, at present, although every expectation is that this is an important variable^{2,12}. In fact, one of the major reasons for geochemical interest in the light component of the core is to better constrain the redox state of the Earth's mantle, especially during the early history of the planet. To date, much of the research in experimental geophysics has concentrated on the effects of high pressures upon mineral properties and equilibria. We are now seeing a trend emphasizing the additional influences of high temperatures and oxidation state on the chemistry of deep planetary interiors. □

of the processing enzymes

Detailed knowledge of poliovirus genome sequences may also contribute to the development of improved live virus vaccines, with genetic determinants optimized for antigenicity and stabilized for attenuation. An important step in this direction is the recent determination of the total genome sequence of the Sabin type 1 attenuated vaccine strain⁶. When compared with that of the parental Mahoney strain, the genome of the attenuated derivative contained 57 base substitutions (total genome = 7,441 nucleotides), 21 resulting in amino acid changes. Twelve of the missense mutations occurred in the capsid proteins and were largely clustered in VP1, raising the possibility that attenuation in part involved modification of the virion surface. Gene sequencing is underway for other poliovirus strains, and some preliminary sequence data for Sabin type 3 were presented.

Poliovaccine development may be aided by progress in developing synthetic vaccines for another picornavirus, foot-and-mouth disease virus (FMDV). Synthetic vaccines offer the advantages of stability, increased economy of production and minimal containment hazards. Two approaches, based on the findings that the purified FMDV VP1 induces protective antibodies⁷, are being explored. The first involves expression in bacteria of a cloned VP1 gene⁸. Initial results were encouraging but the first generation of products had a much lower level of immunogenicity than conventional FMDV vaccines. The second approach involves the chemical synthesis of peptides⁹ representing sequences from VP1. Such products, when linked to a protein carrier, were more immunogenic than an equivalent mass of VP1 and stimulated neutralizing antibody and protection against virus challenge in experimental animals¹⁰.

The limited evidence available also suggests a role for VP1 in poliovirus antigenicity, although the antigenic structure of polioviruses appears to be quite complex. Data were presented indicating that isolated poliovirus polypeptides (VP1, VP2 and VP3) were each able to induce low levels of neutralizing antibody in animals and to prime a recipient for the production of neutralizing antibody on subsequent immunization with small amounts of intact poliovirus (A. L. Van Wezel and P. Van der Marel, personal communication).

Among the biochemical methods of poliovirus strain identification, ribonuclease T₁-oligonucleotide mapping of viral RNAs^{11–13} is the current technique of choice. Vaccine-related isolates can generally be readily distinguished from wild strains. Oligonucleotide maps are highly reproducible, such that good agreement exists in results and interpretations when different laboratories examine the same isolates. The technique is

Poliomyelitis — epidemiology, molecular biology and immunology

from P. D. Minor, O. Kew and G. C. Schild

At a recent World Health Organization meeting the current status of poliomyelitis in the world was discussed together with recent progress in molecular biological and immunological approaches to the study of polioviruses. Precise methods for strain characterization of polioviruses were seen as essential for epidemiological purposes and studies of vaccine safety and efficacy.

Participants from several countries (China, Japan, UK, US, The Netherlands, Sweden, Switzerland and USSR) reviewed their epidemiological experiences of poliomyelitis during the past triennium. These presentations and a general international review from data reported to WHO showed that poliomyelitis, although well controlled by the use of vaccines in developed countries, remains a major problem in the developing world^{1,2}. Epidemics of poliomyelitis in unvaccinated populations are chiefly caused by type 1 poliovirus, but in countries with well established vaccination programmes where paralytic cases have been reduced to a very small number, some of the few cases reported are associated with the use of live attenuated virus vaccines, particularly in cases involving poliovirus types 2 and 3.

Current research on the characterization of polioviruses emphasizes the biochemical analysis of poliovirus genomes, and the comparison of the antigenic characters of different strains using monoclonal antibodies.

A major advance has been provided by the determination of the complete nucleotide and deduced polypeptide sequence of a type 1 poliovirus (P1/Mahoney/USA/41)^{3,4}. The virus genome encodes a single large polypeptide which is specifically cleaved to produce the viral capsid proteins (VP1, VP2, VP3, VP4) and several non-capsid proteins, including an RNA polymerase, a viral protease⁵ and other proteins of yet unknown function. Complete processing of the polypeptide seems to occur by the combined action of cellular and virus-encoded proteases. Three distinct dipeptide sites are cleaved during processing⁵. Gln-Gly pairs are cleaved by the virus-encoded protease, Tyr-Gly pairs are probably cleaved by a cellular protease, and an Asn-Ser pair in VP0 is cleaved to produce VP2 and VP4 by an unidentified protease during the final stages of virion morphogenesis. Knowledge of the activities and specificities of the virus-encoded protease may open the way for development of a rational chemotherapy for poliovirus (and other picornavirus) infections by the use of specific inhibitors.

P. D. Minor and G. C. Schild are in the Division of Virology, National Institute for Biological Standards, Holly Hill, Hampstead, London NW3, and O. Kew is in the Center for Disease Control, Atlanta, Georgia.

extremely sensitive in detecting minor genome variations between strains¹⁴. The tendency of polioviruses to undergo genome variation during natural infections (an excellent example of this was presented for a type 2 vaccine strain which underwent long-term replication in an immunodeficient child)¹⁵ limits the utility of this technique in detecting distant genetic relationships between strains. This same process imposes an extreme limitation on the value for strain identification of SDS-polyacrylamide gel electrophoresis of viral polypeptides. An alternative method was suggested involving restriction mapping of cDNA transcripts of viral RNA¹⁶. This approach is expected to be less sensitive than oligonucleotide mapping and consequently may reveal more distant relationships between strains which are not apparent from T₁ maps.

Several workers continue to use strain-specific absorbed sera¹⁷ for the identification of poliovirus isolates as vaccine-derived or 'wild' and this technique was considered practicable and reliable. In general, designation of isolates as vaccine-derived by this method agree well with the results of oligonucleotide mapping.

Methods of identifying strains using monoclonal antibodies were reported^{15, 18-23}. International collaborative studies, organized through WHO, to examine the value of strain-specific monoclonal antibodies in strain identification and to compare the results obtained with those obtained by oligonucleotide mapping were proposed and this project is in progress. Preliminary observations from the US, UK, Netherlands and Japan suggested that the results obtained by serological and biochemical methods show excellent agreement.

Biochemical and immunological differences between types of polioviruses appear to be greatest in the portion of the genome coding for structural proteins²⁴. However, there appears to be extensive cross-reaction between types demonstrated by both immune precipitation and immunological study of separated viral proteins (VP1, VP2 and VP3) after electrophoretic transfer to nitrocellulose sheets (western blotting)²⁵. Cross-reactivity of poliovirus proteins (VP1) with sera specific for other picornaviruses (for example, echoviruses 11 and 16) were described.

The antigenic structure of polioviruses is complex. It has been known for many years that the mature infectious virus particle expresses an antigenic determinant termed D antigen not found in empty capsids or heat-inactivated virus. Similarly, empty capsids or heat-inactivated virus express antigenic determinants (C antigen) not found on infectious virus particles.

Monoclonal antibodies can react with epitopes unique to D antigen (represented by mature infectious virus) or unique to C

antigen (represented by denatured empty capsids or heated infectious virus). Other monoclonal antibodies react with particles expressing D antigen and also with particles expressing C antigen²⁶, showing that the two antigens are indeed distinct but particles expressing them share common antigenic determinants.

Only some 50 per cent of specifically D-reactive monoclonal antibodies neutralize virus infectivity, despite binding efficiently to virus²². In contrast, monoclonal antibodies reacting with both D and C particles generally neutralize virus to high titres. C-specific monoclonals do not neutralize infectivity. Attempts were made to identify the virus structural proteins reacting with the monoclonal antibodies²⁵. It was shown that only six of twenty C-reactive monoclonal antibodies against type 3 poliovirus reacted with poliovirus proteins separated by SDS-polyacrylamide gel electrophoresis and then subjected to electrophoretic transfer. Five reacted with VP1 and one with VP3. In contrast, none of 29 antibodies of D or D + C specificity, including several which were highly active in virus neutralization, reacted in this

system. The nature of the antigenic determinants of poliovirus mediating virus neutralization and protection thus remains elusive. Recent studies²⁷ have shown that monoclonal antibodies neutralizing poliovirus type 1 react with VP1 on the native virus but not after isolation from the virus particle. Determinants seem complex, being specified by the tertiary configuration of one or more polypeptides, rather than simply by amino acid sequences. However, the findings with foot and mouth disease and with isolated polypeptides from poliovirus mentioned above suggest that under certain circumstances, relatively simple structures may stimulate neutralizing antibody.

Further progress in the international conquest of poliomyelitis may depend on the development of new approaches to vaccine design leading to more cost-effective products. While modern biotechnologies are likely to have an important role in achieving this goal, and the meeting revealed a continuing high level of scientific interest, the problems are complex and require a multidisciplinary approach. □

- 1 Paccard, M F *Wild Hlth Statistics Annual* 32, 198 (1979)
- 2 *Wkly epidem Rec* 74, 361 (1980), 23, 180 (1981), 28, 221 (1981), 42, 329 (1981), 43, 337 (1981), 48, 377 (1981), 1, 4 (1981)
- 3 Kitamura, N *et al Nature* 291, 18 (1981)
- 4 Racanelli, V & Baltimore, D *Proc natn Acad Sci U S A* 78, 4887 (1981)
- 5 Hanecak, R *et al Proc natn Acad Sci U S A* 79, 3973 (1982)
- 6 Nomoto, A *et al Proc natn Acad Sci U S A* 79 (in the press)
- 7 Laporte, J *et al C R hebd Séanc Acad Sci, Paris* 276, 3399 (1973)
- 8 Kleid, D *et al Science* 214, 1125 (1981)
- 9 Walter, G *et al Proc natn Acad Sci U S A* 77, 5197 (1980)
- 10 Bittle, J L *et al Nature* 298, 30 (1982)
- 11 Lee, Y F & Wimmer, E *Nucleic Acids Res* 3, 1647 (1976)

- 12 Minor, P D *J Virol* 34, 73 (1980)
- 13 Nottay, B *et al Virology* 108, 405 (1981)
- 14 Aaronson, R P *et al Nucleic Acids Res* 10, 237 (1982)
- 15 Arita, M *et al Intervirology* 17 (in the press), Kew, O M *et al J gen Virol* 56, 337 (1981)
- 16 Nomoto, A *et al Virology* 113, 54 (1981)
- 17 Van Wezel, A & Hazendonk, A *Intervirology* 11, 2 (1979)
- 18 Icenogle, J *et al Virology* 115, 211 (1981)
- 19 Osterhaus, A *et al Intervirology* 16, 218 (1981)
- 20 Cramic, R *et al Dev Biol Standard* 50, 229 (1982)
- 21 Humphrey, D *et al Infect Immun* 36, 841 (1982)
- 22 Ferguson, M *et al Lancet* (in the press)
- 23 Guo Ren *et al* (in the press)
- 24 Romanova, L *et al J gen Virol* 52, 279 (1981)
- 25 Thorpe, R *et al J gen Virol* (in the press)
- 26 Schild, G C *et al* (in preparation)



100 years ago

We regret to learn of the death, at Dorpat, of Dr Kreuzwald, the publisher of old Esthonian songs and poems. He was born in 1804, and studied medicine at Dorpat. When a student he began to collect songs and tales of his country-people, and in the years 1840 to 1850 he published a series of remarkable articles on Esthonian antiquities, mythology, traditions, and tales. His principal work was the publication, with annotations, of the whole of the different parts of the great Esthonian poem, "Kalewinoey," remarkable by its fine poetical feeling for nature and analysis of human feelings. It was translated into all the chief European languages. In 1877 Dr Kreuzwald was compelled to abandon his medical practice, and died in poverty at Dorpat.

THE *Official Messenger* of St Petersburg announces, on September 1, that "by order of the Emperor the admission of new pupils to the course of medical training for women, at the Nicholas Military Hospital, will be discontinued after the present term. The students will be allowed to conclude their course, after which the clinical instruction for women at the hospital will be abolished." The Medical Academy for Women, the courses of which were quite equal to those of the old Universities, had 367 students. Since 1887, when the first lady students passed the examinations, 281 ladies have completed the whole course of studies.

THE English Government having sent to Egypt three of the Woolwich balloons, we may remind our readers that balloons were taken out by the French army in 1794. But it was impossible for Buonaparte to use them, the furnace for the preparation of pure hydrogen having been lost when the French fleet was annihilated by Nelson in Aboukir Bay. Conte, the engineer of the aéronauts, was created the head of Cairo arsenal, and Coutelle, their captain, was sent on a scientific mission to Upper Egypt.

from *Nature* 26, 470, September 7, 1882

REVIEW ARTICLE

Molecular drive: a cohesive mode of species evolution

Gabriel Dover

University of Cambridge, Department of Genetics, Downing Street, Cambridge CB2 3EH, UK

It is generally accepted that mutations may become fixed in a population by natural selection and genetic drift. In the case of many families of genes and noncoding sequences, however, fixation of mutations within a population may proceed as a consequence of molecular mechanisms of turnover within the genome. These mechanisms can be both random and directional in activity. There are circumstances in which the unusual concerted pattern of fixation permits the establishment of biological novelty and species discontinuities in a manner not predicted by the classical genetics of natural selection and genetic drift.

"THE species problem is the oldest problem in biology"¹, and it is still unresolved. Despite the impressive sophistication of the mathematics of natural selection and genetic drift, there are relatively few experimental proofs of the genetic mechanisms by which species discontinuities in ontogeny and reproductive biology have arisen. There is, however, from the activities of widespread molecular mechanisms of turnover within eukaryotic genomes, a possible genetic mechanism for the origin of evolutionary novelty that is operationally different from those of natural selection and genetic drift.

Eukaryotic (and some archaeobacterial²) genomes contain substantial numbers of multiple-copy families of genes and non-coding sequences, and it has been apparent for some years that many families exhibit unexpected sequence homogeneity within and between individuals of a species. A family that is shared between several species, on the other hand, often reveals substantial heterogeneity between the species.

Family homogeneity could be achieved by several molecular mechanisms which ensure that existing members of a family might be replaced in turn with a single new variant member. The rate of replacement seems to reflect both stochastic and directional changes operating within the genomes. The modes of operation of such mechanisms have unusual genetic consequences for the manner in which variation is distributed in nature and for the concerted evolutionary progress of a group of sexual individuals. Fixation of variants in a population as a consequence of stochastic and directional processes of family turnover is defined as molecular drive³.

The dynamics of natural selection and genetic drift are modelled on the premise that mutations are unitary and passive events that rely on the activities of selection and the vagaries of drift to increase in frequency in a population⁴⁻⁶. The two processes are considered to operate within mendelian populations and lead, by definition, to adaptive and non-adaptive modes of evolutionary change⁶, respectively. The widespread fixation of variants by molecular drive is different in that it is an outcome of a variety of sequence exchanges within and between chromosomes that give rise to persistent non-mendelian patterns of inheritance. Significantly, there are circumstances in which the activities of the genomic mechanisms, in spreading sequence information between chromosomes, would lead to the progressive increase of a variant through a family more or less simultaneously in each individual of a sexual population. This concerted pattern of fixation by molecular drive may provide an explanation for the origins of species discontinuities and biological novelty.

Genomic flux

The nuclear genomes of eukaryotes are subject to a continual turnover through unequal exchange, gene conversion and DNA

transposition. These processes operate both within and between chromosomes. Some families of sequences have been described aptly as fluid⁷ because of the continually changing nature of their composition, abundance and position. Continually changing families have been described in a wide range of plant and animal species^{3, 8-15}. Some of the families consist of sequences with unknown function (non-genic families), others are either transcribed into functional RNA (ribosomal and transfer RNAs) or translated into proteins (for example, globins, histones, immunoglobulins, MHC proteins, actins)¹⁶⁻²⁶.

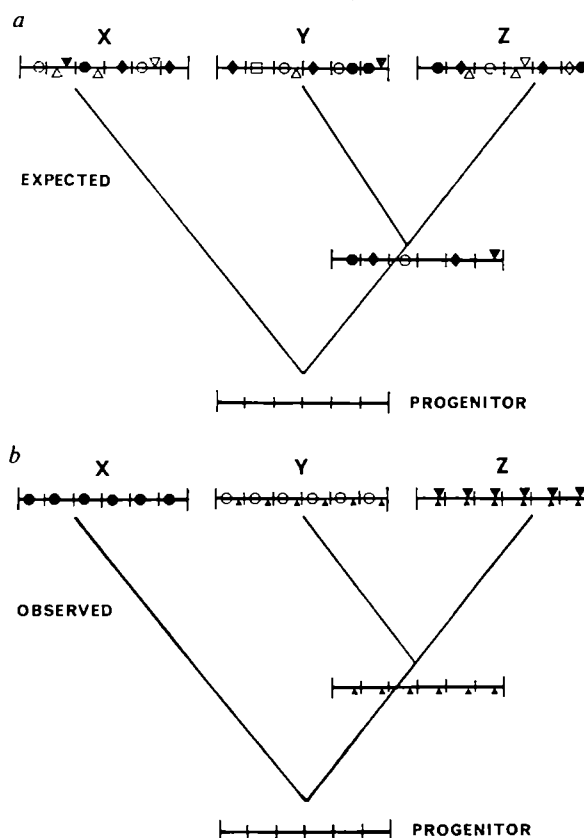


Fig 1 Schematic representation of expected (a) and observed (b) patterns of variation in a family of sequences shared by species X, Y and Z (see also refs 29, 30). If each member is free to evolve independently, then the coefficient of identity between any two randomly chosen members within a species is expected to be the same as that between two members chosen from between the species. Observed patterns reveal a high degree of within-species homogeneity. Families may be tandem (as shown) or interspersed in the genome, and may vary from two to several million members. Families may consist of copies of genes or non-coding sequences or mixtures of both.

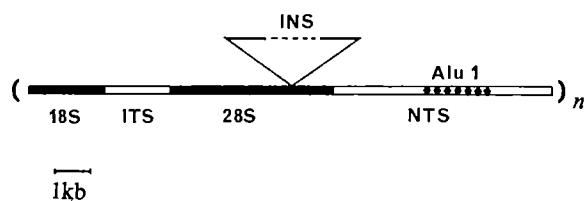


Fig 2 A repeating unit of rDNA of *D. melanogaster*.^{16 130} 18S and 28S represent regions transcribed into functional rRNAs. INS is an insert of variable length in some repeats. ITS is an internal transcribed spacer, NTS is a non-transcribed spacer within which there are *AluI* sensitive repeats with a 240-base pair periodicity. The *AluI* motif is not present in the other six sibling species, nevertheless each species contains a diagnostic sequence variant that is present throughout the X and Y chromosome rDNA arrays (Fig 3) (see text). *n* is approximately 200 in each array. There are approximately 10 *AluI* sensitive repeats in each NTS.

The molecular mechanisms of turnover help shape the patterns of variation and affect the rate of evolution of genomic families. Although there are important differences in the evolution of individual families, similarities between members of both genic and non-genic families within a species are often greater than expected if each member were evolving independently.

Figure 1 illustrates the differences between expected and observed patterns of variation in a family that is shared between three closely related species. If each member of a family is free to accumulate mutations over time then the coefficient of identity between any two members within a species would equal that of any two members chosen at random from two different species (Fig 1a). In fact, however, many families, irrespective of their copy-number, function and genomic distribution (tandem or interspersed) display a much greater within-species than between-species homogeneity (Fig 1b).

This characteristic pattern of variation was first described in the classic studies on interspecific differences in the sequence composition of tandem arrays of genes and spacers that comprise the ribosomal DNA (rDNA) in species of frog.²⁷ The spacers reveal many mutational differences between the two species and apparently are free to diverge. Nevertheless, there are no substantial differences in sequence between the several hundred copies of the spacer-gene unit within each species. Very similar features of 'concerted' evolution have been described in other genic and non-genic families (for reviews see refs 3, 16–18, 20, 28–30). A progressive homogenization of families of sequences seems to be the fate of large proportions of species' genomes.

Molecular processes of fixation

Both stochastic and directional processes of turnover occur within nuclear genomes. The stochastic component of molecular drive results from the accidental fixation of a variant in a family and in a population through random fluctuations in the frequencies of variants within the family. Three known mechanisms can produce such fluctuations: unequal chromatid (or chromosome) exchange, gene conversion and gain and loss by transposition.

Tartof³¹ and Smith³² originally proposed that the homogenization of a family that is tandemly arrayed on a single chromosome could be a consequence of unequal chromatid exchanges.

Unequal exchange is a process which creates a sequence duplication in one chromatid (or chromosome) and a corresponding deletion in the other. There is experimental verification of mitotic and meiotic unequal exchanges in the rDNA arrays of yeast^{33 34}, and it is a possible mechanism of change in the rDNA of several species.^{16 17 31 35,36} Recurrent unequal exchange within a tandem array has the effect of expanding and contracting the copy-number of the family and the process may lead to the stochastic fixation of one or another variant member throughout the array.^{30–32}

Unequal exchange is unlikely to occur often between members of a family that are interspersed with many other sequences, particularly if they are on several nonhomologous

chromosomes. Instead it has been suggested that gene conversion is a more appropriate mechanism of homogenization within such families, and possibly also within families that are tandemly arrayed.^{37–45}

Gene conversion was first inferred from deviations from the expected 2:2 ratio of alleles in the gametes of a heterozygote individual in which the four products of an individual meiotic division remain a cluster (tetrad) so that mendelian ratios can be directly observed (tetrad analysis) (for reviews see refs 38, 46–51).

Holliday⁵² proposed that deviant ratios arise by a mismatch repair within a heteroduplex DNA region, formed during recombination between two alleles *A* and *a*, and resulting in the production of either *A+A* or *a+a*. Evidence for recombinational heteroduplexes has been obtained in *Escherichia coli*.⁵³ An equal probability of conversion in each direction results in parity in the expected frequencies of *A+A* and *a+a* overall.

Gene conversion, involving up to several kilobases of DNA, has been shown by genetic and molecular analysis to occur within a chromosome,^{38 50 54} between homologous chromosomes^{45–50} and between non-homologous chromosomes.^{37 55–57} Unlike unequal exchange, gene conversion does not alter the copy-number of a family, nevertheless random fluctuations in the frequencies of the direction of conversion (*Aa* → *aa* versus *Aa* → *AA*) may lead to the accidental fixation of one variant or another throughout a family. Gene conversion has been invoked as a mechanism that achieves (1) homogeneity between pairs of relatively closely linked genes, for example pairs of mammalian globin genes^{20 41 58}, *Drosophila* heat-shock genes⁵⁹ and silk-moth chorion genes²², (2) 'switch' in the mating type genes of yeast⁵⁴, and (3) homogeneity of amplified copies of *aprt* units in mammalian cells.⁶⁰

The directional component of molecular drive is postulated to result from persistent nonrandom exchanges of sequence information both within and between chromosomes.^{3 36,61} There are two known mechanisms that may lead to a directed homogenization of a family: one is duplicative transposition and the other is biased gene conversion.

Duplicative transposition involves the duplication and movement of a sequence from one position to another. A sequence with a high propensity to duplicate with movement of one copy to another chromosome has an increased probability of spreading in a karyotype, and hence through a population.^{62–64} Eukaryote genomes contain several such families (for reviews see refs 13, 65–67).

A bias in the direction of conversion can be observed as a departure from parity in the ratios of the expected products of conversion. The frequency of *A+A* from conversions within heterozygous cells *A+a* is consistently higher than that of *a+a*, an outcome which leads to an increasingly greater proportion of *A* in succeeding generations. The extent of bias in the conversion of different mutant sites in fungi has been observed.^{39 45–47 49} In yeast, approximately half the observed mutants depart from parity, and in some cases the departure can give rise to a 2:1 ratio in favour of the conversion of one allele by another. In other species, the deviations from parity may reveal a hundred-fold preference for the conversion of one allele by another. It has been known for several years that the conversion behaviour of a mutant is dependent on its molecular nature. Whitehouse and his colleagues^{51 68}, following from the studies of Leblond⁶⁹, have observed a predominant bias in the direction of conversion in favour of frameshift mutants containing additions of sequences, whereas single base substitutions convert with about equal frequency in each direction. Additionally, there is suggestive evidence that the 'invading' strand during heteroduplex formation is preferentially favoured during mismatch repair.⁷⁰ A mutation resulting from a frameshift addition and with a high propensity to break and invade the opposing duplex might be the basis of a high conversional bias. However, the precise molecular process creating conversion disparity during recombinational mismatch repair is unknown.

Theoretical dynamics of molecular drive

Theoretical models of fixation need to consider the process of homogenizing a family of n^* copies distributed on $2n$ (diploid) number of chromosomes in a population of N_e individuals. Although the three levels of fixation are occurring simultaneously (see later), it is convenient to consider first how a variant may become fixed within an array on a single chromosome and second the fixation of the homogenized chromosomal array in the population. A thorough treatment of the dual process of fixation using the statistical dynamics of random fluctuations in unequal exchange (or gene conversion) and genetic drift has been made by Kimura and Ohta^{64,71}, and the parameters of the process have been reviewed³⁰.

It is assumed that in a randomly mating population with an effective size N_e a multiple-copy family is evolving by means of mutation, intrachromosomal unequal exchange (or unbiased gene conversion), interchromosomal recombination and genetic drift. The simplest quantity that has been studied is the 'identity coefficient' which is defined as "the probability of two randomly chosen genes belonging to the family being identical by descent"³⁰. Consideration has also been given to the expected time required to fix a variant by molecular and genetic drift (ref 72 and T. Ohta, personal communication). The identity coefficients and fixation times can be described in terms of n^* , N_e , the rate of unequal exchange (or unbiased gene conversion), and the rate of regular recombination, together with several additional parameters concerning the mean displacement of unequal exchange and the effect of selection in stabilizing family size^{30,73} (see later).

The directional component of molecular drive, arising out of nonrandom fluctuations in the direction of conversion and duplicative transposition, has the potential to accelerate the rate of fixation^{3,36,39,49,61}. Using data on conversion frequencies and disparities between alleles of single-copy genes in fungi, Lamb and Helmi⁴⁹ have shown that, for alleles that are selectively neutral, or nearly so, fixation is largely determined by the frequency and disparity in the direction of conversion.

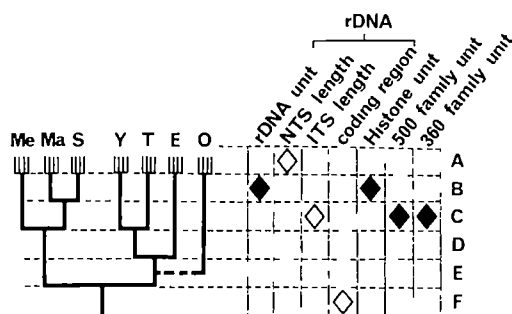


Fig 3 Phylogeny of seven sibling species of the *melanogaster* species subgroup of *Drosophila*, based on the tempo of evolution in four repetitive families, the rDNA, the histone gene family and two non-coding families, the '500' and '360'. For details of rDNA see Fig 2. The histone unit consists of five genes (H1, H3, H4, H2A and H2B) and four spacers (see ref 18 for details), of which there are approximately 100 copies per haploid genome of *D. melanogaster*. The '360' and '500' families are complex in organization, large in copy-number (up to 10,000) and can be distributed over several chromosomes^{12,61}. Some regions of a family unit (or complete family unit) are placed in the phylogeny at a level (A-F) determined by the extent to which the region (or complete unit) varies between taxa. For example, the rDNA coding region is the same in all species (level F), the NTS length (see Fig 2) of the rDNA shows intraspecific variation (level A), sequences within spacer regions of the NTS and the histone unit differ between all species but are homogeneous within each species (concerted evolution) (level B), the ITS length and various features of the '500' and '360' units vary between all species except between *D. simulans* and *D. mauritiana* (level C). \diamond Represents the rate of change in sequence or length, \blacklozenge represents the rate of fixation. For example, level B represents the minimal rate of fixation of the rDNA unit between the seven species due to the high rate of unequal exchange indicated by the high level of NTS length variation (level A). Although the rate of fixation of the complete rDNA unit is at level B, the rate of change in the coding regions within the unit is at F, probably as a result of selection limiting the number of mutational changes (see text and refs 3, 36, 61 for details). Me = *melanogaster*, Ma = *mauritiana*, S = *simulans*, Y = *yakuba*, T = *teissieri*, E = *erecta*, O = *orena*.

Conversion could be an important long-term factor even if the frequencies and disparities are smaller in organisms other than fungi. Unlike selection, fixation by biased gene conversion can take place without reduction in the number of offspring and, unlike genetic drift, it proceeds as easily in large as in small populations.

Nagylaki and Petes³⁹ have assessed recently the effect of biases in conversion on the sequence identity between members of a family within a single chromosome. The probability and mean time to fixation can be simulated for different values of n^* and different degrees of bias, on the assumption of one conversion event per generation between any two randomly chosen members of an array. A small conversional bias can have a dramatic effect on the probability and time for fixation. For example, the mean fixation time of a variant in an array of $n^* = 10,000$ decreases 100-fold with a conversion ratio (r) of 1/2 in favour of the variant (with parity $r = 1$, see ref 39 for definition of r). Small biases in the direction of interchromosomal conversion are expected, similarly, to accelerate the rate for achieving homogeneity within families of large copy-number interspersed with other sequences over many chromosomes^{3,36,61}.

Many factors influence the frequency and disparity of conversion, including the nature of the interacting sequences, the genomic location and the genetic and environmental background^{45,46,49,54}. A sequence fixed as a result of a high conversional bias could not necessarily retain its favoured place indefinitely given the constantly changing spectrum of extraneous influences.

As the molecular bases of transposition, conversion and unequal exchange are not understood, it is not possible to guess what influences the DNA sequences themselves might have on their efficiency (for discussion see refs 74-76). There are hints that certain sequences (or their organization⁷⁷) might act as either hotspots or coldspots with respect to the boundaries and frequencies of conversion and unequal exchange^{22,41}. Families are expected to differ in the extent to which new variants would influence the variety of genomic mechanisms of flux at any given moment in their history. It is probable that the stochastic and directional components of molecular drive are intimately related and vary from family to family.

A comparison of expected and observed times of fixation in well-defined groups of species for families of known size and composition permits some empirical assessment of the relative contributions of the two components of molecular drive to the evolutionary process.

Assessing the tempo of fixation

To assess empirically the rates of fixation, my colleagues Enrico Coen, Tom Strachan and Steve Brown have analysed variation in multigene and non-genic families within and between species of the *melanogaster* species subgroup of *Drosophila*^{35,36,61} and in interspersed and tandem families within closely related species of rodents^{43,78,79}. Interpretations of the data viewed *in toto*³ lead to the proposition that some supplementary mechanisms are probably acting to accelerate the fixation process. Additionally, the patterns of homogeneity within families that are distributed on two or more chromosomes reveal that there is a significant exchange of sequence information between chromosomes. The existence of interchromosomal exchanges influences the extent to which individuals of a population are evolving in unison.

Coen and Strachan have examined the extent of homogeneity within and between seven sibling species of the *D. melanogaster* sub-group, for families of rDNA, histone genes and non-genic families^{35,36,61}. The data are summarized in a phylogenetic scheme (Fig 3) based on the extent to which different regions of the families have become fixed for variants that can discriminate between the species (see ref 3) (Details of the families are given in the legends to Figs 2 and 3).

The families are homogeneous in each species in that they contain the same restriction enzyme sites in all members.

Different regions of the families evolve at different rates. For example, the gene regions of the rDNA (Fig 2) are invariant (level F, Fig 3). At the other extreme the non-transcribed spacer (NTS) of the rDNA and some coding and spacer regions of the histone repeating unit are sufficiently variant as to be different in all seven species (level B). Nevertheless, within each species the families are homogeneous for species-diagnostic sequence variants. For example, the *AluI* site present in each of the smaller repeating units within the NTS of *D. melanogaster* (Fig 2) is present throughout all the smaller repeats within the NTSs of both the X and Y chromosomes and in many populations of this species distributed worldwide. It is not present, however, in the NTSs of the other species. The rate of fixation in the rDNA and histone families is placed accordingly at level B (see refs 3, 36 for further explanation).

High variability in the lengths of NTSs and in the copy-number of each length within individual rDNA arrays³⁵ (level A) indicates that frequent unequal exchanges probably play a significant role in the fixation of variant NTSs.

Using the statistical dynamics of family and population size fluctuations, Ohta (ref 72 and personal communication) and my colleagues and I³⁶ have evaluated the number of generations required to fix a variant in the rDNA family where $n^* \approx 200$ per chromosome, $N_e = 10^5$, there is an upper limit in the rate of unequal exchange of 10^{-3} – 10^{-4} per generation³⁵ and an unequal displacement of 20%⁷² and 10%³⁶ of the array length. Both estimates arrive at a mean time for fixation of the order of 10^7 generations. The fixation time is close to estimates of a time of separation of 10^6 – 10^7 generations between *D. simulans* and *D. melanogaster*^{59, 80} which are based on genetic distances (Nei's measure, D , ref 81). The correlation between D and real time is extrapolated from the observed relationship between genetic distances of Hawaiian species of *Drosophila* and the age of the volcanic islands⁸². The fixation time estimates are probably an underestimation in that the rDNA is distributed on the X and Y chromosomes, both of which need to be maintained in equal frequencies during genetic drift. Additional retardation in the rate of fixation would result if the mean unequal displacement is similar to the 5% displacement observed in the rDNA of yeast³³. Although assessments of fixation times are accompanied by large variances, it is possible that both directional and stochastic processes have been involved in the fixation of rDNA variants in the relatively shorter time separating the appearance of *D. simulans* and *D. mauritiana*³ (see Fig 3). This possibility is open to experimental investigation.

Some directional process may also be required to fix variants in the '360' and '500' families having up to 10,000 members which can be distributed over several chromosomes⁶¹. These families have been fixed for diagnostic variants in all species except *D. simulans* and *D. mauritiana* (level C). If such non-genic families can tolerate large fluctuations in copy-number by unequal exchange then the time taken for fixation by stochastic processes is correspondingly reduced^{30, 73}. Wide polymorphic fluctuations in copy-number in these families (compare level A) are as yet unknown, but this possibility can be tested experimentally. The distributions of families to many chromosomes might pose additional problems with the effect of slowing down the rates of homogenization by drift^{3, 61}.

A family of $n^* = 20,000$ members that is interspersed with other sequences on up to 40 chromosomes and does not substantially alter in copy-number (the MIF-1 family)^{43, 83, 84} has revealed also the fixation of diagnostic variants between species of *Mus*⁴³. Palaeontological⁸⁵ and genetic distance⁸⁶ estimates put the time since separation of some of the species at 1 – 2×10^6 yr. Simulated estimates are available of the number of conversion generations within a single chromosome lineage that are needed to homogenize a family of $n^* = 20,000$ through stochastic fluctuations in unbiased intrachromosomal conversions, assuming one conversion per generation³⁹. For example, the mean time to fixation when $n^* = 20,000$ is approximately 4.00×10^8 conversion generations, or 10^8 yr, assuming four

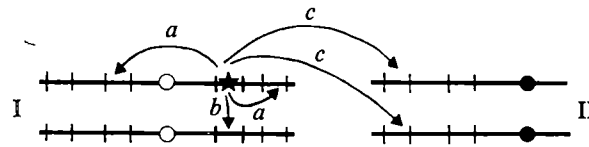


Fig. 4 Schematic representation of pathways of transfer of sequence information of a variant member *a*, Intrachromosomal homogenization either by unequal exchange or biased/unbiased gene conversion *b*, *c*, Pathways of homogenization between homologous (I) or nonhomologous (II) chromosomes. Non-reciprocal sequence transfer between chromosomes could result from either duplicative transposition or biased/unbiased gene conversion. The relative rates of transfer between *a* and *b* + *c* and the rate of chromosome turnover (generation time) determine the extent to which a simultaneous change in the ratio of new to old variants occurs in each individual of a population (see text).

generations per year in the rodent species. The model is based on an individual chromosome lineage and does not consider the requirement to fix a variant on 40 chromosomes in a population of N_e individuals³⁹. Such considerations would increase the number of conversion generations required for fixation. However, given this minimum calculation, to fix a variant in a family by stochastic processes within 10^6 yr, 100 conversions per individual per generation would be required. A small and persistent conversional advantage of a variant, for example a conversional ratio (r) of 1.2 (see ref 39 for definition), would reduce the number of required conversions per individual to one per generation, in order to fix within 10^6 yr. Such estimates clearly are open to empirical investigation.

It is reasonable to postulate, for the tandem and dispersed genic and non-genic families being considered in *Drosophila* and *Mus*, that known mechanisms of directional change may have made some contribution to the distinctive patterns of species homogeneity and may have accelerated, somewhat, the process of fixation along the lines modelled by Lamb⁴⁹ and Petes³⁹ and their colleagues. Biased conversions could be taking place within tandem arrays as well as between dispersed members. Both stochastic and directional processes could be responsible for the fixation of variants in such families in these groups of species. The relative contribution of either process has yet to be assessed. It is possible that the unexpected high levels of homogeneity of many genic and non-genic families in other species is also an outcome of a combination of stochastic and directional mechanisms of turnover within nuclear genomes.

The limited independence of chromosome evolution

The analysis of sequence identity between members of families that are distributed over several chromosomes reveals that there are considerable levels of exchange of sequence information between chromosomes in many species. For example, the occurrence of the *AluI* sensitive repeats throughout the rDNA units (Fig 2) on both the X and Y chromosomes of *D. melanogaster* must be due to exchanges between these two sex chromosomes^{35, 36}. There is molecular and cytological evidence of exchanges between the chromosomes (E. Coen and G. Dover, in preparation). Because of such exchanges the evolution of the individual arrays of rDNA are not evolving entirely independently^{3, 36}.

Restrictions on the independence of chromosome evolution are also revealed by the presence of smaller subfamilies of members within large families, identified by restriction sites not present in the rest of the family^{14, 78, 79, 87–90}. Subfamilies are generally non-overlapping and are indicative of a phenomenon in which different segments of a large family are being homogenized for different variants. Surprisingly, individual subfamilies in both an abundant tandemly-arrayed family and the interspersed MIF-1 family in rodents have been found not to be localized to a single chromosome. Most subfamilies of the two families seem to be present on several chromosomes in the same proportion (refs 43, 78, and S. Brown, unpublished results). Similarly, recent studies on the chromosomal distribution of variant subfamilies in the rDNA family of humans reveal

the presence of each subfamily on all five of the chromosomes containing rDNA⁹¹

Although there are clear examples and valid arguments for the independent evolution of either subfamilies or individual members of families that have become separated on either the same or nonhomologous chromosomes^{23,92} (for example, with respect to the organizational and functionally distinct arrays of insect chorion genes^{22,93}, sea-urchin histone genes^{18,19,94}, and *Xenopus* 5S rRNA genes^{17,95,96}), there are nevertheless many karyotypically dispersed genic and nongenic families in which interchromosomal exchanges of sequences must be taking place

Sequence homogeneity between chromosomes effected by stochastic and directional processes of unequal exchange, gene conversion and duplicative transposition, has specific and unusual genetic consequences

Unusual genetic consequences of molecular drive

To understand the unusual genetic consequences of homogenizing family members between homologous and nonhomologous chromosomes, it is necessary to appreciate changes in the frequencies of a mutation in three hierarchical sets of populations

At the lowest level is the population of sequences, often dispersed on two or more chromosomes

The second level is represented by the population of chromosomes shared between a group of sexually reproducing individuals, that is, $2n \times Ne$. In a sexual population, with a haploid/diploid alternation of generations, the chromosomes can be considered as belonging to one pool, or population, of chromosomes as a consequence of random chromosome assortment during meiosis and random fusion of gametes. How far the turnover of chromosomes generates a random population of chromosomes (that is, the frequency at which a chromosome may become associated with any other in the same individual), depends on the reproductive biology and generation time of the species

The third level is the traditionally understood population of the individual diploid organisms

Molecular drive involves changes in frequency of a variant member of a family at all three population levels. It is a process which could lead to a simultaneous increase of a variant in all individuals as a consequence of the large disparity between the rates of turnover of sequences and chromosomes

The differences in rates between intrachromosome (a) and interchromosome ($b+c$) homogenization and the generation time affect the overall rate and pattern of fixation of a variant in a population of individuals (Fig 4). It is unlikely, given the experimental assessments of the intra- and interchromosomal rates of unequal exchange and gene conversion^{33,35,36,38,49,50,57,61}, that a family would become fixed for a variant within the lifetime of an individual. The coefficient of identity between any two chromosomes taken at random from within a population, with respect to the numbers of variant repeats they have acquired, would depend on the rates of intra- and interchromosomal homogenization in relation to the rates at which chromosomes within the population are being effectively randomized at each generation. The slow rate of homogenization between chromosomes relative to the fast rate of chromosomes turnover within a population (generation time) could ensure that, at any given time, there is in each individual the same average ratio of new to old variants for a particular family^{13,97}. Hence during the period of transition the differences between individuals would be kept to a minimum with respect to the changing sequence composition of their chromosomes

Accordingly, processes of sequence homogenization between chromosomes would increase the population mean of the ratio of new to old variants (and possibly the phenotype, see below), but not the variance. Different families would experience different transition times depending on the factors affecting the rates of intra- and interchromosomal mechanisms of

homogenization and the generation times of the organisms. The dynamics of change at the three interrelated levels of population (sequences, chromosomes and individuals) are complex and a mathematical description is in preparation⁹⁸

Embodied in the concept of molecular drive is the idea of "selfishness" as previously defined^{62,63} and subsequently refined^{74,75}. Molecular drive is a more inclusive notion in that it is seen as an outcome of stochastic and directional mechanisms of turnover in the genome that aid in the fixation of all manner of sequences irrespective of their copy-number, dispersion patterns or function. The mechanism suggested as the basis for the accumulation of selfish DNA is that of duplicative transposition^{62,63}, which was originally postulated to account for the increase in copy-number of transposed (mobile) elements. Studies of mobile elements in *Drosophila* and yeast show that the copy-number of mobile families are relatively small and do not fluctuate widely^{7,13}. They are small enough to be potentially eliminated by stochastic processes^{92,100}

Biological consequences of molecular drive

Several important considerations arise from genomic mechanisms of interchromosomal sequence exchange having the potential to impart genetic cohesiveness to a large panmictic population, both during and after a period of change^{3,97}

Let us consider a family of genes or non-genic sequences affecting ontogenetic growth patterns of an organism. If the rate of intrachromosomal homogenization is high then the ensuing heterozygosity between the new and old chromosomal arrays might reduce the fitness of an individual organism, leading to the loss of the array. In this circumstance the evolutionary progress of the array, as a single unit, can be monitored by classical mendelian genetics and darwinian selection. If, however, interchromosomal family homogenization is taking place, but at a rate much slower than the rate at which the chromosomes effectively constitute a random population (short generation time), then there would be a concerted change in the ontogenetic growth patterns of a group of individuals. For example, the individuals might be turning into monsters, yet there would be no significant increase in variance in the population in the degree of monstrosity. The fixation of variant sequences on different chromosomes by stochastic and directional mechanisms would induce a concerted phenotypic change in a group of individuals without the concomitant effect of disturbing relative differences in individual fitness. This is based on the assumption that small differences between individuals in the ratio of new to old variants of a multigene family during fixation have small effects on relative fitnesses. If a progressive concerted change in phenotype were ultimately to affect the viability of the organisms, then all the individuals would be affected as a group. It is possible that some aspects of the phenotypic cohesiveness of present-day species have developed along such lines (for example, see ref 101, A. Garcia-Bellido, personal communication)

The biological consequences of molecular drive may take effect, however, at a higher level. Molecular drive may contribute to a mode of accidental speciation^{3,97,102} for maximizing the genomic and phenotypic cohesiveness within a population maximizes biological discontinuities between populations. Whether a genomic dissimilarity between any two individuals from two such populations becomes a major problem of reproductive or developmental incompatibility (speciation), depends on the nature of the sequences undergoing concerted homogenization in each population. Clearly, the widespread fixation of some variants in multigene families such as histones, rDNA, globins, immunoglobins and so on, would affect the phenotype. If, in addition, future studies confirm that many non-genic families affect DNA transcription and transcript processing^{8,103,104}, or chromatin structure and chromosome behaviour^{9,12,15,97,105-112}, then the dual process of generating intrapopulation cohesion and interpopulation discontinuities would be of considerable evolutionary significance. Hitherto, all theoretical exegeses on the genetics of species discontinuities

have considered the effects of natural selection and genetic drift operating within mendelian populations^{4-6,113-122}. A progressive concerted change in phenotype of a group of individuals effected by internal processes of genomic turnover between chromosomes could not have been foreseen in the light of classical considerations of the dynamics of population change based on individual variation and "passive" allelic mutations.

The phenomenon of "hybrid dysgenesis" between populations of *D. melanogaster* in which differential accumulation of some mobile elements has occurred^{13,100,123-125} is an example of the fixation of sequences by drive (in this case by duplicative transposition between chromosomes) leading to genomic dissimilarities and subsequent incompatibilities. Additionally, it has been known for some time that hybrids between *D. simulans* and *D. melanogaster* exhibit sterility and phenotypic disharmonies as a result of numerous small genetic differences between the chromosomes of their respective karyotypes^{126,127}. "Hybrid sterility is but one expression of this cryptic divergence, which need not in itself have had a selective value"¹²⁶.

It could be that the common ontogeny of individuals of a species is due to the unfolding effects of accidentally acquired sets of variant families and is of limited adaptive significance. The clustering of species to a remarkably few of all possible modes of development (a point expressed succinctly by Lewontin¹²⁸) might reflect in part the slow rates of production and fixation of family variants having significant ontogenetic effects. A cohesive change in species phenotype by molecular drive might be rare relative to the constancy of phenotype: an interesting parallel with 'punctuated equilibria'¹²⁹. Family turnover

is continuous and is analogous to the turnover of new for old banknotes: the introduction of a new design is, however, a rare event.

Testing the theory of the origins of evolutionary novelty and species formation by means of molecular drive requires an intense study of the modes and rates of operation of the candidate genomic mechanisms. The important differential in the rates of intra- and interchromosomal sequence homogenization relative to the rate of chromosome turnover and the relative contributions of stochastic and directional components of molecular drive needs to be analysed in depth. The numbers of affected families (genic and non-genic), their chromosomal distribution and their phenotypic effects need to be assessed in genetically well-defined groups of species and populations.

Molecular drive is not an alternative to the evolutionary processes of natural selection and genetic drift in the fixation of mutational variants of single-copy genes (although single genes are not excluded from the activities of directed conversion and may also be driven⁴⁹), it constitutes a third mode of evolution that would of necessity be subject to natural selection and genetic drift in an interesting variety of real biological situations. There is no simple solution to the species problem.

I thank Richard B. Flavell, George Miklos, John Thoday, Leslie Orgel, Richard Lewontin, Francis Crick, Michael J. D. White, Claudio Schazzocchio, Alex Jeffreys, Motoo Kimura, Tomoko Ohta, Walter Bodmer and Steve Gould for stimulating conversations, and most importantly my colleagues Enrico Coen, Steve Brown and Tom Strachan for discussing their data and their ideas on genomic turnover.

- 1 Dobzhansky, T. in *Molecular Evolution* (ed Ayala, F. J.) 95-105 (Sinauer, Boston, 1976)
- 2 Sapienza, C. & Doolittle, W. F. *Nature* **295**, 384-389 (1982)
- 3 Dover, G. A. et al. in *Genome Evolution* (eds Dover, G. A. & Flavell, R. B.) 343-374 (Academic, London, 1982)
- 4 Fisher, R. A. *The Genetical Theory of Natural Selection* (Dover, New York, 1930)
- 5 Wright, S. *Proc 6th Int Congr Genet* **1**, 356-366 (1932)
- 6 Kimura, M. *Scient Am* **251**(5), 94-104 (1979)
- 7 Young, M. W. *Proc natn Acad Sci U S A* **76**, 6274-6278 (1979)
- 8 Davidson, E. H. & Britten, R. J. *Science* **204**, 1052-1059 (1979)
- 9 Flavell, R. B. *A Rev Pl Physiol* **31**, 569-596 (1980)
- 10 Flavell, R. B. in *Genome Evolution* (eds Dover, G. A. & Flavell, R. B.) 301-324 (Academic, London, 1982)
- 11 Singer, M. F. *Int Rev Cytol* (in the press)
- 12 Brutlag, D. L. *A Rev Genet* **14**, 121-144 (1981)
- 13 Spradling, A. C. & Rubin, G. M. *A Rev Genet* **15**, 219-264 (1981)
- 14 Dover, G. A., Strachan, T. & Brown, S. D. M. in *Evolution Today* (eds Scudder, G. G. E. & Reveal, J. L.) 337-349 (Hunt Institute, Pittsburgh, 1981)
- 15 Miklos, G. L. G. in *Genome Evolution* (eds Dover, G. A. & Flavell, R. B.) 41-68 (Academic, London, 1982)
- 16 Long, E. H. & Dawid, I. B. *A Rev Biochem* **49**, 727-764 (1980)
- 17 Fedoroff, N. *Cell* **16**, 697-710 (1979)
- 18 Kedes, L. H. A. *A Rev Biochem* **48**, 837-870 (1980)
- 19 Hentschel, C. C. & Birnstiel, M. L. *Cell* **25**, 301-313 (1981)
- 20 Jeffreys, A. J. in *Genome Evolution* (eds Dover, G. A. & Flavell, R. B.) 157-176 (Academic, London, 1982)
- 21 Davidson, E. H., Thomas, T. L., Scheller, R. H. & Britten, R. J. in *Genome Evolution* (eds Dover, G. A. & Flavell, R. B.) 177-192 (Academic, London, 1982)
- 22 Jones, W. C. & Kafatos, F. C. *Cell* **22**, 855-867 (1980)
- 23 Bodmer, W. F. *Am J Hum Genet* **33**, 664-682 (1982)
- 24 Mamatis, T., Fritsch, E., Lauer, J. & Lawn, R. M. *A Rev Genet* **14**, 145-178 (1980)
- 25 Rabbitts, T. H., Bentley, D. L., Forster, A., Milstein, C. P. & Matthysens, G. in *Genome Evolution* (eds Dover, G. A. & Flavell, R. B.) 205-218 (Academic, London, 1982)
- 26 Zachau, H. G., Hochtl, J., Neumaier, P. S., Pech, M. & Schnell, H. in *Genome Evolution* (eds Dover, G. A. & Flavell, R. B.) 193-204 (Academic, London, 1982)
- 27 Brown, D. D., Wensink, P. C. & Jordan, E. J. *molec Biol* **63**, 57-73 (1972)
- 28 Dover, G. A. & Coen, E. S. *Nature* **290**, 731-732 (1981)
- 29 Hood, L., Campbell, J. H. & Elgin, S. C. R. *A Rev Genet* **9**, 305-353 (1975)
- 30 Ohta, T. *Evolution and Variation in Multigene Families* (Springer, Berlin, 1981)
- 31 Tartof, K. *Cold Spring Harb Symp quant Biol* **38**, 491-500 (1974)
- 32 Smith, G. P. *Cold Spring Harb Symp quant Biol* **38**, 507-513 (1974)
- 33 Szostak, J. W. & Wu, R. *Nature* **284**, 426-430 (1980)
- 34 Petes, T. D. *Cell* **19**, 765-774 (1980)
- 35 Coen, E. S., Thoday, J. M. & Dover, G. A. *Nature* **295**, 564-568 (1982)
- 36 Coen, E. S., Strachan, T. & Dover, G. A. *J molec Biol* **158**, 17-35 (1982)
- 37 Scherer, S. & Davis, R. W. *Science* **209**, 1380-1384 (1980)
- 38 Jackson, J. A. & Fink, G. *Nature* **292**, 306-307 (1981)
- 39 Nagyaki, T. & Petes, T. D. *Genetics* **100**, 315-337 (1982)
- 40 Baltimore, D. *Cell* **24**, 592-594 (1981)
- 41 Shen, S. H., Slightom, J. L. & Smithies, O. *Cell* **26**, 191-203 (1981)
- 42 Birky, C. J. & Skavari, R. V. *Genet Res* **27**, 249-265 (1976)
- 43 Brown, S. D. M. & Dover, G. A. *J molec Biol* **150**, 441-446 (1981)
- 44 Ohta, T. *Genet Res* **30**, 89-91 (1977)
- 45 Edelman, G. M. & Gally, J. A. in *Neurosciences Second Study Program* (ed Schmitt, F. O.) 962-972 (Rockefeller University Press, New York, 1970)
- 46 Fincham, J. R. S., Day, P. R. & Radford, A. *Fungal Genetics* 4th edn (Blackwell, Oxford, 1979)
- 47 Fogel, S. R., Mortimer, K., Lusnak, K. & Tavares, F. *Cold Spring Harb Symp quant Biol* **43**, 1325-1341 (1978)
- 48 Finnerty, V. in *The Genetics and Biology of Drosophila* (eds Ashburner, M. & Novitski, E.) Vol 1a, 331-347 (Academic, London, 1976)
- 49 Lamb, B. C. & Helms, S. *Genet Res* **39**, 199-217 (1982)
- 50 Klein, H. L. & Petes, T. *Nature* **289**, 144-148 (1981)
- 51 Whitehouse, H. L. K. *Genetic Recombination—Understanding the Mechanisms* (Wiley, New York, in the press)
- 52 Holliday, R. *Genet Res* **5**, 282-304 (1964)
- 53 Dasgupta, C., Wu, A. M., Kahn, R., Cunningham, R. P. & Radding, C. M. *Cell* **25**, 507-516 (1981)
- 54 Klar, A. J. S., Strater, J. N. & Hicks, J. B. *Cell* **25**, 517-524 (1981)
- 55 Ernst, J. F., Stewart, J. W. & Sherman, F. *Proc natn Acad Sci U S A* **78**, 6334-6338 (1981)
- 56 Munz, P. & Leopold, U. in *Molecular Genetics of Yeast* (eds Von Wettstein, D. et al.) 264-275 (Munksgaard, Copenhagen, 1981)
- 57 Mikus, M. D. & Petes, T. D. *Genetics* (in the press)
- 58 Leibhaber, S. A., Goossens, M. & Kan, Y. W. *Nature* **290**, 26-29 (1981)
- 59 Brown, A. J. L. & Ish-Horowitz, D. *Nature* **290**, 677-682 (1981)
- 60 Roberts, J. M. & Axel, R. *Cell* **29**, 109-119 (1982)
- 61 Strachan, T., Coen, E. S., Webb, D. A. & Dover, G. A. *J molec Biol* **158**, 37-54 (1982)
- 62 Orgel, L. E. & Crick, F. H. C. *Nature* **284**, 604-607 (1980)
- 63 Doolittle, W. F. & Sapienza, C. *Nature* **284**, 601-603 (1980)
- 64 Kimura, M. & Ohta, T. *Proc natn Acad Sci U S A* **76**, 4001-4005 (1979)
- 65 Moveable Genetic Elements *Cold Spring Harb Symp quant Biol* **45** (1981)
- 66 Finnegan, D. J., Will, B. M., Bayev, A. A., Bowcock, A. M. & Brown, L. in *Genome Evolution* (eds Dover, G. A. & Flavell, R. B.) 29-40 (Academic, London, 1982)
- 67 Young, M. W. & Schwartz, H. E. *Cold Spring Harb Symp quant Biol* **45**, 629-640 (1981)
- 68 Yu-Sun, C., Wickramaratne, M. R. T. & Whitehouse, H. L. K. *Genet Res* **29**, 65-81 (1977)
- 69 Leblon, G. *Molec gen Genet* **115**, 36-48 (1972)
- 70 Markham, P. & Whitehouse, H. L. K. *Nature* **295**, 421-423 (1982)
- 71 Ohta, T. *Genet Res* **31**, 13-28 (1978)
- 72 Ohta, T. *Genet Res* (submitted)
- 73 Ohta, T. *Genetics* **99**, 555-571 (1982)
- 74 Orgel, L. E., Crick, F. H. C. & Sapienza, C. *Nature* **288**, 645-646 (1980)
- 75 Dover, G. A. & Doolittle, W. F. *Nature* **288**, 646-647 (1980)
- 76 Dover, G. A. *Nature* **285**, 618-620 (1980)
- 77 Hentschel, C. C. *Nature* **295**, 714-716 (1982)
- 78 Brown, S. D. M. & Dover, G. A. *Nucleic Acids Res* **8**, 781-792 (1980)
- 79 Brown, S. D. M. & Dover, G. A. *Nature* **285**, 47-49 (1980)
- 80 Eisses, K. T., Van Dijk, H. & Van Delden, W. *Evolution* **33**, 1063-1068 (1979)
- 81 Nei, M. *Molecular Population Genetics and Evolution* (North-Holland, Amsterdam, 1975)
- 82 Carson, H. L. *Nature* **259**, 395-396 (1976)
- 83 Maniatis, T. *Nucleic Acids Res* **8**, 3247-3259 (1980)
- 84 Heller, R. & Arnheim, N. *Nucleic Acids Res* **8**, 5031-5042 (1980)
- 85 Brothwell, D. in *Biology of the House Mouse* (ed Berry, R. J.) 1-11 (Academic, London, 1981)
- 86 Thaler, L., Bonhomme, F. & Britton-Davidian, J. in *Biology of the House Mouse* (ed Berry, R. J.) 27-39 (Academic, London, 1981)
- 87 Scheller, R. H. et al. *J molec Biol* **149**, 15-39 (1981)
- 88 Horz, W. & Zachau, G. G. *Eur J Biochem* **45**, 501-510 (1977)
- 89 Dennis, E. S., Dunsmuir, R. & Peacock, W. J. *Chromosoma* **79**, 179-198 (1980)
- 90 Southern, E. M. *J molec Biol* **94**, 51-69 (1975)
- 91 Krystal, M., D'Eustachio, P., Ruddle, F. H. & Arnheim, N. *Proc natn Acad Sci U S A* **78**, 5744-5748 (1981)
- 92 Selker, E. U. et al. *Cell* **24**, 819-828 (1981)
- 93 Jones, W. C. & Kafatos, F. C. *J molec Biol* (in the press)
- 94 Simpson, R. T. *Proc natn Acad Sci U S A* **78**, 6803-6807 (1981)
- 95 Ford, P. J. & Brown, R. D. *Cell* **48**, 485-493 (1976)
- 96 Ford, P. J. & Southern, E. M. *Nature new Biol* **241**, 7-12 (1973)
- 97 Dover, G. A. in *Mechanisms of Speciation* (eds Barigozzi, C., Montalenti, G. & White, M. J. D.) (Liss, New York, in the press)
- 98 O'Donald, P., Friday, A. & Dover, G. A. (in preparation)
- 99 Fink, G., Farabaugh, P., Roeder, G. & Chaleff, D. *Cold Spring Harb Symp quant Biol* **45**, 575-580 (1981)

100. Engels, W. R. *Cold Spring Harb. Symp. quant. Biol.* **45**, 561-565 (1981).
101. Garcia-Bellido, A. *Symp. Soc. dev. Biol.* (in the press).
102. Dover, G. A. *Nature* **272**, 123-124 (1978).
103. Jelinek, W. R. *et al. Proc. natn. Acad. Sci. U.S.A.* **77**, 1398-1402 (1980).
104. Davidson, E. H. & Posakony, J. W. *Nature* **297**, 633-635 (1982).
105. Bennett, M. D. in *Genome Evolution* (eds Dover, G. A. & Flavell, R. B.) 239-262 (Academic, London, 1982).
106. Macgregor, H. C. in *Genome Evolution* (eds Dover, G. A. & Flavell, R. B.) 325-342 (Academic, London, 1982).
107. Hotta, Y. & Stern, H. *Cell* **27**, 309-320 (1981).
108. Manuelidis, L. in *Genome Evolution* (eds Dover, G. A. & Flavell, R. B.) 263-286 (Academic, London, 1982).
109. Smith, G. R. *Cell* **24**, 599-600 (1981).
110. Wittig, S. & Wittig, B. *Nature* **297**, 31-38 (1982).
111. Weisbrod, S. *Nature* **297**, 289-295 (1982).
112. Darnell, J. E. *Nature* **297**, 365-371 (1982).
113. White, M. J. D. *Modes of Speciation* (Freeman, San Francisco, 1978).
114. Dobzhansky, T. *Genetics of the Evolutionary Process* (Columbia University Press, New York, 1970).
115. Lande, R. *Am. Nat.* **116**, 463-479 (1980).
116. Templeton, A. R. *A. Rev. ecol. Syst.* **12**, 23-48 (1981).
117. Thoday, J. M. *Proc. R. Soc. B* **182**, 109-143 (1972).
118. Maynard-Smith, J. *Am. Nat.* **100**, 637-650 (1966).
119. Clarke, B. *Am. Nat.* **100**, 389-402 (1966).
120. Stebbins, G. L. & Ayala, F. J. *Science* **213**, 967-971 (1981).
121. Lewontin, R. C. *The Genetic Basis of Evolutionary Change* (Columbia University Press, New York, 1974).
122. Mayr, E. *Animal Species and Evolution* (Harvard University Press, Cambridge, Massachusetts, 1963).
123. Bregliano, J. C. & Kidwell, M. C. in *Mobile Genetic Elements* (ed. Shapiro, J. A.) (Academic, New York, in the press).
124. Rubin, G. M., Kidwell, M. G. & Bingham, P. M. *Cell* **29**, 987-994 (1982).
125. Bingham, P. M., Kidwell, M. C. & Rubin, G. M. *Cell* **29**, 995-1004 (1982).
126. Muller, H. J. & Pontecorvo, G. *Genetics* **27**, 157 (1941).
127. Muller, H. J. & Pontecorvo, G. *Nature* **146**, 199-200 (1940).
128. Lewontin, R. C. *Am. Nat.* (in the press).
129. Gould, S. J. & Eldridge, N. *Palaeobiology* **3**, 23-40 (1977).
130. Glover, D. M. *Cell* **26**, 297-298 (1981).

ARTICLES

A satellite altimetric geoid in the Philippine Sea

Ki-iti Horai

Lamont-Doherty Geological Observatory of Columbia University, Palisades, New York 10964, USA

A detailed geoidal map of the Philippine Sea, constructed from GEOS 3 altimeter data, revealed that the average geoidal height in the basins of the Philippine Sea decreases as the age of the basins increases. The geoidal height-age relationship is comparable with that of mid-oceanic ridges, suggesting that the cooling of the marginal sea basin's lithosphere after its formation is similar to that of the oceanic lithosphere created at the mid-oceanic ridges. The data appear to be consistent with the back-arc opening model. However, the corner flow model is also compatible with the smoothly varying geoid over the entire Philippine Sea.

THE advent of satellite altimetry has allowed a detailed delineation of sea-surface height in oceanic areas. In sea areas where oceanographic disturbances do not predominate, the height of the sea surface measured from the Earth's standard ellipsoid provides an excellent approximation of a marine geoid. As a first step in studying the mechanical and thermal characteristics of the marginal basins of the West Pacific, a geoid map of the Philippine Sea was constructed using GEOS 3 altimeter data. The Philippine Sea was chosen because it developed behind the Mariana Island Arc that is, "in many respects, the simplest and easiest of all island arc systems to study"¹.

Data adjustment

The altimeter data consist of a set of sea-surface height values measured along the satellite's track. At cross-overs between northbound (ascending) and southbound (descending) tracks, sea-surface height values are expected to coincide. In reality, however, they disagree owing to the satellite's orbit tracking error, the altimeter's instrumental bias and the noise due to variable sea-surface condition. A consistent field of sea-surface

height is obtained by making corrections for the track data's erroneous bias and tilt, so that the r.m.s. residual from all intersections in the area becomes minimal². In the area of study covering the Philippine Sea, there are 1,575 intersections among 48 ascending and 58 descending tracks. The r.m.s. cross-over residual was more than 15 m for the original uncorrected data. That was decreased to 1.5 m by removing the data's erroneous bias by a method of iterative correction³. Further tilt correction brought the r.m.s. residual to 46 cm. A geoidal map with a contour interval of 1 m was prepared based on this final corrected data (Fig. 1a).

Figure 1b is a map of the 'residual'⁴ geoid that was derived from the total geoid, as shown in Fig. 1a, by removing the spherical harmonic component of GEM-10 geoid⁵ expanded to the order of $n = 12$ and degree $m = 12$. The lower spherical harmonics of the standard geopotential model such as GEM-10 are considered to have originated from sources deeper than the Earth's asthenosphere⁶. Therefore, the residual geoid map is appropriate for the discussion of structural anomalies in the lithosphere and asthenosphere. Note that the shortest

Table 1 Average residual geoid in the marginal sea basins of the Philippine Sea

Basin	Water depth (m)	Grid for average computation		Residual* geoid		
		Grid size (deg)	No. of grids	Average and s.d. for the basin $\Delta h \pm \sigma(\Delta h)$ (m)	Reference values from undisturbed Western Pacific Δh_0 (m)	Reduced residual geoid $(\Delta h - \Delta h_0) \pm \sigma(\Delta h)$ (m)
Bonin Trough	>3,000	0.5	13	4.1 ± 1.5	0.6	3.5 ± 1.5
Shikoku Basin	>4,000	1.0	33	1.8 ± 2.1		1.2 ± 2.1
Mariana Trough	>3,000	1.0	16	7.0 ± 2.4		5.7 ± 2.4
Parece Vela Basin	>4,000	1.0	85	1.1 ± 2.7	1.3	-0.2 ± 2.7
Northern West Philippine Basin	>5,000	1.0	77	-3.5 ± 1.4		-4.8 ± 1.4
Okinawa Trough	>1,000	0.5	33	1.5 ± 0.8	-3.5	5.0 ± 0.8

* Lower harmonics of GEM-10 geoid, expanded up to order $n = 12$ and degree $m = 12$, removed from the total geoid.

wavelength contained in the removed component is 30° , about the same as the width of the Philippine Sea. Physiographic provinces necessary for the following discussion are summarized in Fig. 1c.

Geoidal distribution

As expected, the geoid distribution has many features in common with the gravity field which primarily reflects the bottom topography. In particular, the similarity between the distributions of the residual geoid and the free-air gravity anomaly⁷ is

remarkable. Conspicuous geoidal depressions exist on the Bonin, Mariana, Yap, Palau, Philippine and Ryukyu trenches. Geoidal bulges, corresponding to outer highs of topography and gravity seaward of the trenches⁸ are well developed along the Bonin, Mariana and Philippine trenches. All major topographic features in the Philippine Sea have geoidal signatures. The Nankai Trough is associated with a notable geoidal low. The north-south trending South Honshu (West Mariana and Iwo-jima) and Kyushu-Palau ridges are seen as disturbances to the generally smoothly varying geoid of the Philippine Sea;

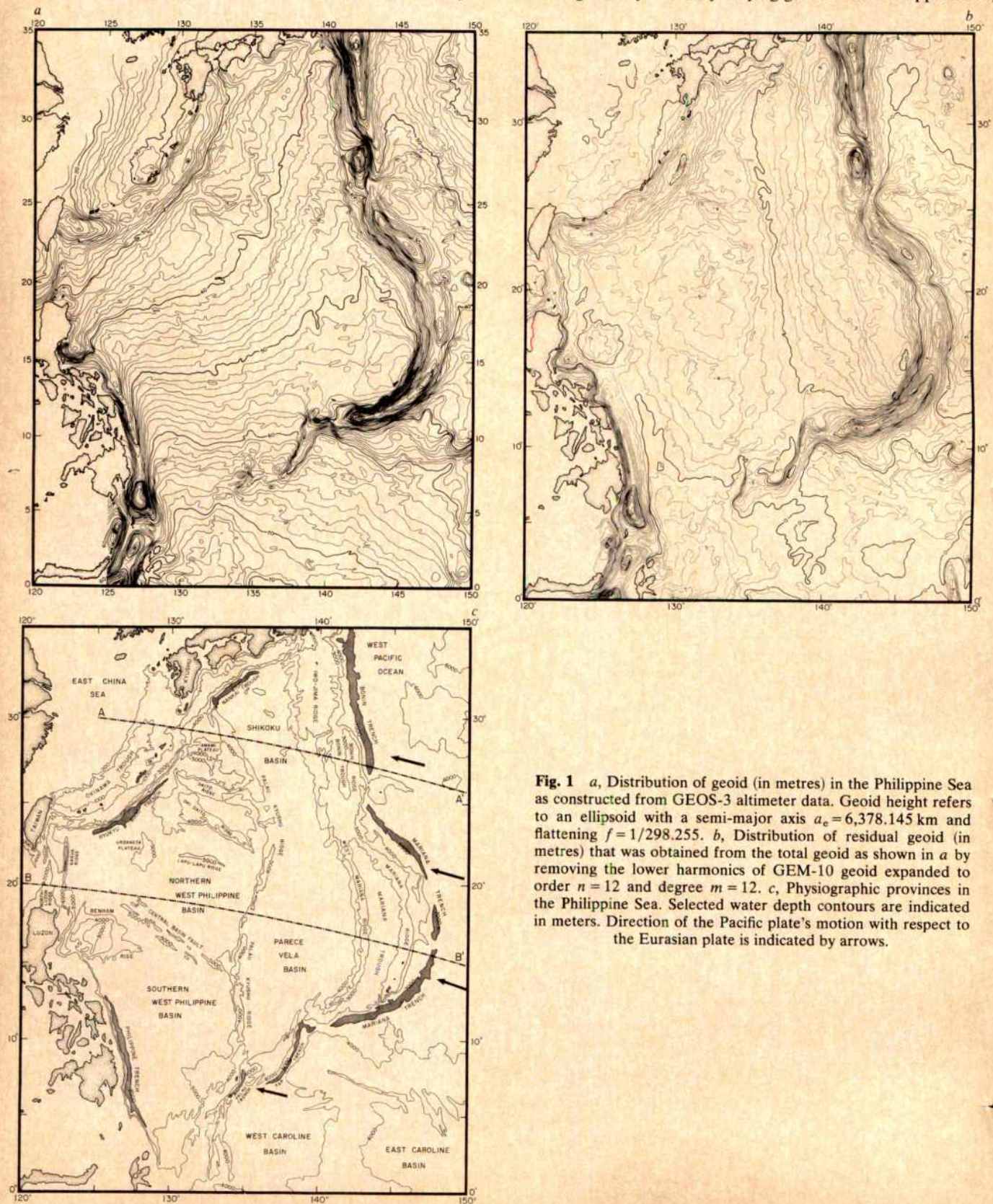


Fig. 1 *a*, Distribution of geoid (in metres) in the Philippine Sea as constructed from GEOS-3 altimeter data. Geoid height refers to an ellipsoid with a semi-major axis $a_e = 6,378.145$ km and flattening $f = 1/298.255$. *b*, Distribution of residual geoid (in metres) that was obtained from the total geoid as shown in *a* by removing the lower harmonics of GEM-10 geoid expanded to order $n = 12$ and degree $m = 12$. *c*, Physiographic provinces in the Philippine Sea. Selected water depth contours are indicated in meters. Direction of the Pacific plate's motion with respect to the Eurasian plate is indicated by arrows.

so are the Daito, Oki-Daito, Lapu-Lapu, Gagua and the Central Basin ridges that are oblique (except Gagua that is parallel) to the trend of the South-Honshu and Kyushu-Palau ridges. Over the Benham Rise and the Urdaneta Plateau, the geoidal anomalies reflect their topography, which is generally smooth, flat and shallower than the surrounding oceanic floors⁹. Quasi-circular negative geoidal anomalies are observed off Taiwan and Luzon where the Ryukyu and the Philippine trenches abutt, respectively, against the Gagua Ridge and its extension.

Geoidal height-age relationship

The distribution of the residual geoid in the Philippine Sea (Fig 1b) shows that the Philippine Sea basin's geoidal height decreases as the basin's age increases. Over the active Mariana Trough (Quaternary), the residual geoid is the highest in spite of its local topographic depression. The geoid is lower in the inactive Shikoku (early Miocene-middle Miocene) and Parece Vela (early Oligocene-middle Miocene) basins. A further decrease of the geoid from the Parece Vela Basin to the Northern West Philippine Basin (Palaeocene-Eocene) seems to reflect the difference in age as well as the mean water depth, which increases substantially from east to west across the Palau-Kyushu Ridge. It can readily be inferred that the source of the residual geoid anomaly, localized in the lithosphere and asthenosphere, is closely related to the mechanism of basin formation.

To substantiate the argument, the Philippine Sea basins' average residual geoid heights were calculated (Table 1). The basins were defined by water depth, and were divided into a set of grids of equal area. Then, at each grid point, an expected geoidal height value was computed by the weighted average method³. A GEOS 3 autocovariance was used as a weight and the range of data collection was set to 1.5 arc deg. This implies that all adjusted GEOS 3 sea-surface height values, within 167 km of a grid point, were used to estimate the expected residual geoid height at that point. The basin's average is simply an arithmetic mean of these expected values.

The average residual geoid heights of the Philippine Sea basins were then normalized against that of the Pacific Ocean floor off the Bonin and Mariana trenches. Formation of marginal sea basin is causatively closely related to the oceanic lithosphere's subduction under the arc-trench system. It is postulated that the marginal sea basin's residual geoid anomaly is meaningful only when compared with the residual geoid over the normal oceanic floor where it is free from the effect of bending due to subduction. Average residual geoid height of the Western Pacific margin was calculated with the aid of $1^\circ \times 1^\circ$ grids "in the region 400 to 500 km seaward of the trench beyond the outer rises in topography where the ocean floor is regionally undisturbed and of normal depth for its age"¹⁰. The results obtained from the latitude range from 20°N to 35°N and from 10°N to 25°N were subtracted, respectively, from the Bonin Trough-Shikoku Basin data and the Mariana Trough-Parece Vela Basin-Northern West Philippine Basin data as shown in Table 1. For the data in the Okinawa Trough, that of the Northern West Philippine Basin was used as a reference.

Figure 2 illustrates the reduced residual geoid heights of the Philippine Sea basins plotted against their ages determined from dating of the oldest sediments from DSDP Legs 6 (ref 11), 31 (ref 12), 58 (ref 13), 59 (ref 14) and 60 (ref 15) drillings and the ages estimated from the basin's magnetic lineations^{9,16,17}. The data indicate a linear relationship with a slope of 0.26 m Myr^{-1} . This is a somewhat higher slope than observed on the mid-oceanic ridges, which ranges from 0.11 to 0.19 m Myr^{-1} (W. Haxby, personal communication, see also ref 18). As McAdoo pointed out¹⁹, the geoidal anomaly over the marginal sea basins includes the effect of a dense subducting lithosphere. In the Bonin and Mariana island arc systems, the dip of Benioff-Wadati zone is among the steepest (70° – 90° in thrust angle) and its downthrust the deepest (500–700 km)²⁰ of the world's subduction systems²¹. The result is a broad and smoothly varying geoidal anomaly with its maximum located

immediately landward of the fore-arc axis. Therefore, it can be assumed that a substantial part of the anomaly due to the subducting lithosphere has already been removed as lower harmonics of GEM-10 geopotential. The anomaly's remaining component, if any, being subtracted from the observation, the slope of the geoid height-age relationship may become indistinguishable from the values exhibited by the mid-oceanic ridges.

Back-arc opening model

The Philippine Sea basin's geoid height-age relationship as summarized in Fig 2 seems to imply that the marginal sea basin's mode of cooling after its formation is similar to what the oceanic lithosphere experiences in the vicinity of the mid-oceanic ridge. The steeper slope of the linear relationship for the marginal sea basin indicates that the cooling is faster for the lithosphere of marginal sea. This is conceivable because, compared with the oceanic lithosphere created at the mid-oceanic ridge, marginal sea basin's lithosphere has a much smaller extent and in contact with adjacent lithospheres that are generally older, and hence colder, than the newly created lithosphere of the marginal basin.

The data seem to be consistent with the theory of back-arc opening^{22,23}. According to Karig²³, the basins of the Philippine Sea were created by crustal extension. After the formation of the West Philippine Basin, the Shikoku and Parece Vela basins opened and these were, in turn, followed by the opening of the Mariana Trough. An opening occurs by separating a remnant arc, formerly an active arc-trench system, from a continuously active arc-trench system that migrates seaward as spreading of the marginal sea proceeds. The opening is not a continuous

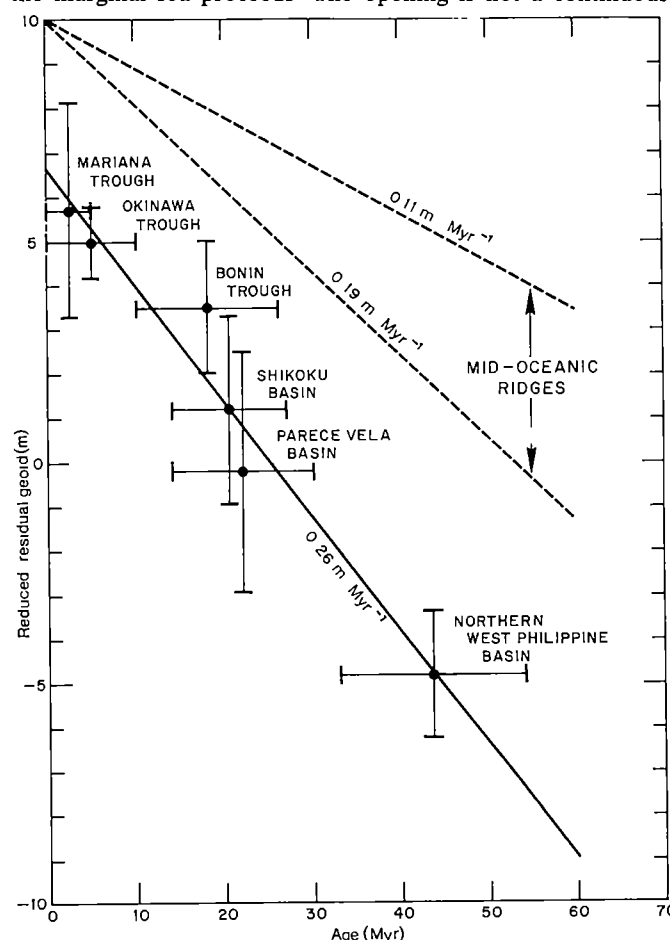


Fig 2 Average reduced residual geoid height-age relationship in marginal sea basins of the Philippine Sea. Ranges of uncertainties (error bars) of each datum point are for geoid height, standard deviation as shown in Table 1, for age, ranges of values as indicated by either direct measurement on DSDP samples or inference from magnetic lineations. Ages of the Bonin and the Okinawa troughs are uncertain. Based on the arguments of structural geology of these areas^{27,31}, the ages of Miocene (10–26 Myr) and Pliocene (0–10 Myr) were assigned, respectively, to the openings of the Bonin and the Okinawa troughs.

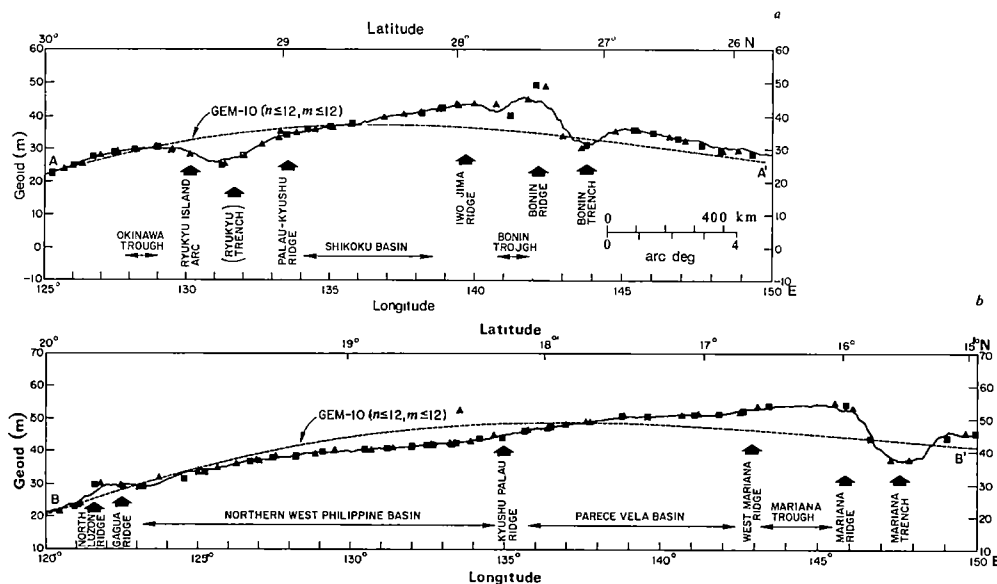


Fig. 3 Profiles of geoid along traverses across the Philippine Sea, *a*, a Bonin Trough-Shikoku Basin-Okinawa Trough traverse, *b*, a Mariana Trough-Parece Vela Basin-Northern West Philippine Basin traverse. Solid line, a profile of expected values calculated as a weighted average of data distributed within 167 km of the traverse. Dashed line, lower harmonics of GEM-10 geoid expanded to order $n=12$ and degree $m=12$. Adjusted GEOS-3 track data \blacksquare , ascending, \blacktriangle , descending at intersection with the traverse

process, but two successive openings are separated by a period of quiescence spanning 10–15 Myr. Thus, the Palau-Kyushu Ridge is a remnant arc associated with the openings of the Shikoku and Parece Vela basins and the West Mariana Ridge with that of the Mariana Trough.

Karig²³ modelled the crustal extension of marginal sea as caused by a thermal diapir, supposedly generated at the frictional upper surface of the subducting lithosphere. That the sinking slab's upper surface is the locus of thermal diapir generation has since been questioned²⁴. An equally important problem is whether the crustal extension due to intrusion of thermal diapir is a cause or an effect of the marginal sea's opening. In mid-oceanic ridge areas, the regional tectonic stress field is known to be tensional and the crustal accretion is believed to be due to passive upwelling of basaltic magma that is undoubtedly generated in the upper mantle. In marginal sea areas that are the zones of plate convergence, the tectonic stress is generally compressional. Recent studies tend to indicate, however, that a change of regional tectonic stress pattern from compressional to tensional²¹, or at least a release of compressional stress²⁵, is necessary for a marginal sea to open. It could be safely assumed that the mode of ascent of the thermal diapir in the marginal sea basin is similar to the passive upwelling of magma in the mid-oceanic ridges. In fact, an active spreading centre, comparable with that in the mid-oceanic ridges, has been identified and located in active marginal sea basins such as the Mariana Trough²⁶.

Among the basins of the Philippine Sea that were formed by back-arc opening, the Bonin Trough is anomalous in its mode of formation²⁷. The Bonin Trough is situated seaward of the Iwo-jima Ridge (active fore-arc) that is a complex of *en-echelon* ridge and trough systems with signs indicating nascent rifting. The Bonin Trough's frontal arc is the Bonin Ridge, an uplifted trench slope break. The Bonin Trough itself has no evidence of recent activity, but there is no doubt about its crustal extensional origin. Thus, the Bonin Trough cannot be classified as a back-arc basin, but is better termed a fore-arc basin. In spite of this fact, the Bonin Trough's geoid height-age datum appears to be consistent with the data of back-arc basins (Fig. 2). We conclude that the linear relationship between the reduced residual geoid and the age holds for the marginal sea basin of extensional origin, irrespective of whether the basin is situated fore-arc or back-arc.

Geoidal slope over marginal sea basins

Another remarkable feature of the Philippine Sea's geoidal distribution (Fig. 1*a, b*) is a uniform horizontal space gradient of the geoid over the marginal sea basins. This is best illustrated by the profiles of geoid along the traverses across the sea (Fig. 3*a, b*). Recognizing the causative relationship between the

marginal basin formation and the subduction of oceanic lithosphere, the traverses were chosen in the direction parallel to that of the Pacific plate's convergence to the Philippine Sea²⁸. The profiles show that both the total and the residual geoids' horizontal space gradients are uniform and tilt eastward on the Shikoku and Parece Vela basins. Part of the eastward tilt of the geoid is undoubtedly due to the water depth, which increases to the west in both the Shikoku and Parece Vela basins. The eastward tilt of the geoid could be explained most easily if the openings of the Shikoku and Parece Vela basins were unilateral, with their spreading centres migrated eastward with the advancing fore-arc. Then, it becomes likely that the westward decreasing geoid height is due to the age of the basin floor which increases progressively from east to west.

There is evidence, however, that both basins were formed by bilateral spreading. Based on magnetic lineation and bottom topography, Watts and Weissel¹⁶ traced a N-S trending remnant spreading centre in the middle of the Shikoku Basin. The data are highly disturbed in the eastern half of the basin, and the authors retained a possibility that the basin's mode of opening could be unilateral. A later study¹² confirmed a bilateral spreading as a more likely cause of the Shikoku Basin's opening. In the Parece Vela Basin, Mrozowski and Hayes¹⁷ located the N-S trending Parece Vela Rift and identified it as the approximate location of a remnant two-limbed spreading centre, indicating a similarity of structure and history with the Shikoku Basin.

Although a bilateral spreading in the Shikoku and Parece Vela basins is thus undeniable, the geoidal distribution of these basins shows no sign of geoidal height-age relationship within the basins. The geoid's slope is constant despite the age difference of 8–13 Myr between the centre and the margins of these basins. Analogy with the mid-oceanic spreading centre predicts a decrease of geoid of 1–2 m from the basin's centre to the margins. This is a detectable amount in the light of the nominal precision of 50 cm for the GEOS 3 altimeter measurement. There are some structural anomalies peculiar to these basins. The remnant spreading centre of the Shikoku Basin is not as morphologically prominent as the active spreading centre of the mid-oceanic ridge. In the Parece Vela Basin, the remnant spreading centre is identified as a rift rather than a ridge. In both basins, the sediment thickness increases substantially from the basin's centre towards the margins. A combined effect of these may be large enough to offset the effect of the ageing lithosphere.

In the West Philippine Basin, the NW-SE trending Central Basin Fault was believed to be a remnant two-limbed spreading centre. A recent study⁹ showed that its exact position does not precisely coincide with the Central Basin Fault. Nevertheless, the generally NNE-SSW trending spreading direction was

inferred from magnetic lineation. Figure 1b shows a symmetric distribution of residual geoid with respect to the West Philippine Basin's remnant ridge crest. In its vicinity, a decrease of the geoid for the age increment of 10 Myr is 2 and 1 m, respectively, to the NNE and SSW directions. The slope is steeper for the former, but the data for both limbs agree with that exhibited by the active mid-oceanic ridges.

Corner flow model

The eastward tilt of the total geoid over the entire Philippine Sea and that of the residual geoid over the basins east of the Palau-Kyushu Ridge (Fig 3a, b) seem to lack a correlation with the basin's lithospheric structure. They must have originated from some causes in the asthenosphere underneath or deeper. As one such cause, a corner flow looks most pertinent. Corner flow is a flow of visco-elastic material in the asthenosphere induced by the subducting oceanic lithosphere. Of the two flow systems induced along the sinking slab's upper and lower sides, that on the upper side (landward) is the more important in the present discussion. McKenzie²⁹ showed that the maximum stress heating of the viscous flow is localized in the vicinity of the island arc, directly beneath the marginal sea's lithosphere. This suggests that the thermal diapir, as a cause of marginal sea opening, is generated in the asthenosphere where the corner flow's viscous stress heating is a maximum. Thus, the corner flow model, an apparent alternative to the thermal diapir model, can actually be compatible with, as well as complementary to, it. Rheology of mantle material is, however, generally not well known. In McKenzie's calculation, the asthenosphere's viscous flow was assumed to be newtonian. It was recently shown³⁰ that the regional geoid depends strongly on the power of non-newtonian constitutive equation ($\epsilon = \eta \sigma^n$, $\eta = \text{constant}$) which gives the strain rate (ϵ) as a function of

stress (σ). McAdoo's model calculation with a sinking slab's dip of 60° showed that the exponent (n) of the constituent equation must be >3 for the slope of geoid over the marginal sea basin to tilt towards the fore-arc. Apparently, simulations for a sinking slab with much steeper thrust angles are needed to compare the numerical result with the data obtained from the Philippine Sea. The slope of the total geoid ranging from 0.8 to 1.6 m per 100 km over the Philippine Sea basin should impose an effective constraint on the rheological property of the model. It is not clear whether the corner flow is restricted within the mobile asthenosphere or, as the depth of deep-focused earthquakes indicates, penetrating into the Earth's deep interior. If the corner flow's convective cell is shallow, the slope of the residual geoid will be more appropriate for the theory.

Conclusion

In addition to the bottom topography, marine geology, magnetic anomaly and heat flow, the geoid derived from satellite altimeter data has proved useful in studying the marginal sea's history. The idea of comparing the geoid of marginal sea basins with that of the oceanic floor, where the lithosphere is in a pre-subduction state and is undisturbed from the bending effect, is probably the most important. Data of bottom topography and heat flow processed in a similar fashion will serve to develop a systematic theory of marginal sea formation. This study will be extended to other marginal seas in the Western Pacific Ocean.

The original draft of this article has been revised substantially by constructive criticisms given by Dr D. E. Karig of Cornell University. This work was supported by the Office of Naval Research under contract N00014-80-C0098-B. Lamont-Doherty Geological Observatory Contribution No. 3666.

Received 13 January, accepted 16 June 1982

- 1 Karig, D. E. *Bull. geol. Soc. Am.* **82**, 323-344 (1971)
- 2 Rapp, R. H. *J. geophys. Res.* **84**, 3784-3792 (1979)
- 3 Horai, K. *J. geophys. Res.* (in the press)
- 4 Watts, A. B. & Daly, S. F. *A. Rev. Earth planet. Sci.* **9**, 415-448 (1981)
- 5 Lerch, F. J., Klosko, S. M., Laubscher, R. E. & Wagner, C. A. *J. geophys. Res.* **84**, 3897-3916 (1979)
- 6 Kahn, M. S. *Geophys. J. R. astr. Soc.* **48**, 197-209 (1977)
- 7 Watts, A. B., Bodine, J. H. & Bowin, C. O. *A Geophysical Atlas of the East and Southeast Asian Seas: Free Air Gravity Field* (Geological Society of America, MC-25, Boulder, 1978)
- 8 Watts, A. B. & Talwani, M. *Geophys. J. R. astr. Soc.* **36**, 57-90 (1974)
- 9 Mrozowski, C. L., Lewis, S. D. & Hayes, D. E. *Tectonophysics* **82**, 1-24 (1982)
- 10 Watts, A. B., Talwani, M. & Cochran, J. R. *Geophys. Monogr.* **19**, 17-34 (1976)
- 11 Fisher, G. A. *et al. Init. Rep. DSDP Leg 6*, 293-387 (1971)
- 12 Karig, D. E. *et al. Init. Rep. DSDP Leg 31*, 25-350 (1975)
- 13 Klein, G. de V. *et al. Init. Rep. DSDP Leg 58*, 21-545 (1980)
- 14 Kroenke, L. *et al. Init. Rep. DSDP Leg 59*, 21-483 (1981)
- 15 Hussong, D. M. *et al. Init. Rep. DSDP Leg 60*, 101-249 (1982)

- 16 Watts, A. B. & Weisell, J. K. *Earth planet. Sci. Lett.* **25**, 239-250 (1975)
- 17 Mrozowski, C. L. & Hayes, D. E. *Earth planet. Sci. Lett.* **46**, 49-67 (1979)
- 18 Haxby, W. F. & Turcotte, D. L. *J. geophys. Res.* **83**, 5473-5478 (1978)
- 19 McAdoo, D. C. *J. geophys. Res.* **86**, 6073-6090 (1981)
- 20 Katsumata, M. & Sykes, L. R. *J. geophys. Res.* **74**, 5923-5984 (1969)
- 21 Uyeda, A. & Kanamori, H. *J. geophys. Res.* **84**, 1049-1061 (1979)
- 22 Packham, G. H. & Falvey, D. A. *Tectonophysics* **11**, 79-109 (1971)
- 23 Karig, D. E. *J. geophys. Res.* **76**, 2542-2561 (1971)
- 24 Sleep, N. & Toksoz, M. N. *Nature* **233**, 548-550 (1971)
- 25 Scholz, C. H., Barazangi, M. & Sbar, M. L. *Bull. geol. Soc. Am.* **82**, 2979-2990 (1971)
- 26 Karig, D. E., Anderson, R. N. & Bibee, L. D. *J. geophys. Res.* **83**, 1213-1226 (1978)
- 27 Karig, D. E. & Moore, G. F. *Tectonophysics* **27**, 97-118 (1975)
- 28 Minster, J. B., Jordan, T. H., Molnar, P. & Heines, E. *Geophys. J. R. astr. Soc.* **36**, 541-576 (1974)
- 29 McKenzie, D. P. *Geophys. J. R. astr. Soc.* **18**, 1-32 (1969)
- 30 McAdoo, D. C. *On the Compensation of Geoid Anomalies due to Subducting Slabs* (Technical memorandum TM82157, Goddard Space Flight Center, Greenbelt, 1981)
- 31 Herman, B. M., Anderson, R. N. & Truchan, M. in *Am. Ass. petrol. Geol. Mem.* **29**, 199-208 (1979)

A demonstration of ocean acoustic tomography

The Ocean Tomography Group: D. Behringer*, T. Birdsall†, M. Brown‡, B. Cornuelle§, R. Heinmiller§, R. Knox‡, K. Metzger†, W. Munk‡, J. Spiesberger‡, R. Spindel||, D. Webb||, P. Worcester‡ & C. Wunsch§

* Atlantic Oceanic and Meteorological Laboratory of NOAA, Miami, Florida 33149, USA

† Cooley Electronics Laboratory, University of Michigan, Ann Arbor, Michigan 48109, USA

‡ Scripps Institution of Oceanography, IGPP, La Jolla, California 92093, USA

§ Department of Earth and Planetary Sciences, Massachusetts Institute of Technology, Cambridge, Massachusetts 02139, USA

|| Woods Hole Oceanographic Institution, Woods Hole, Massachusetts 02543, USA

Over the past decade oceanographers have become increasingly aware of an intense and compact ocean 'mesoscale' eddy structure (the ocean weather) that is superimposed on a generally sluggish large-scale circulation (the ocean climate).

Traditional ship-based observing systems are not adequate for monitoring the ocean at mesoscale resolution. A 1981 experiment mapped the waters within a 300×300 km square south-west of Bermuda, using a peripheral array of moored midwater acoustic sources and receivers. The variable acoustic travel times between all source-receiver pairs were used to construct the three-dimensional (time-variable) eddy fields, using inverse theory. Preliminary results from inversions are consistent with the shipborne and airborne surveys.

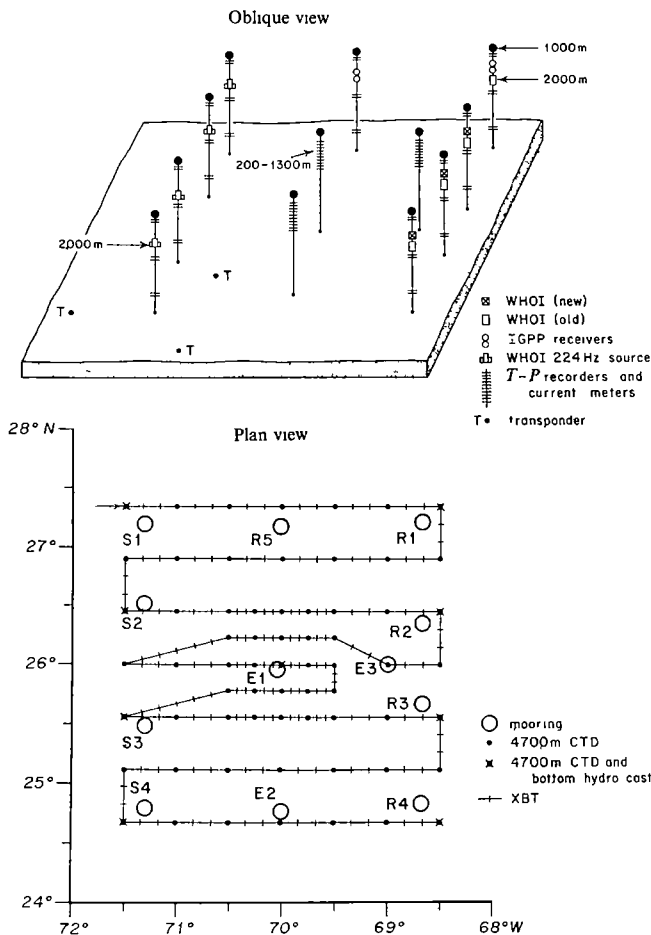


Fig 1 Geometry of the 1981 Ocean Tomography Experiment S1 to S4 designate the acoustic source moorings, R1 to R5 the acoustic receiver moorings, and E1 and E2 the environmental moorings with current meters and temperature-pressure (T-P) recorders E3 is a current meter mooring set by F Schott Acoustic moorings also carried T-P recorders The receivers R1 and R5 consisted of short vertical arrays Floats at 1,000 m depth with 1,000 lb buoyancy provided taut moorings, thus eliminating wave forces and reducing horizontal excursions The position of each acoustic source and receiver was monitored by a 10-kHz source (placed just beneath the low-frequency tomographic sources and receivers) which interrogated three bottom transponders T dropped a few kilometres from the mooring (shown for S4) The plan view shows the grid for CTD/XBT surveys in March, May and July In addition, AXBT drops at the CTD positions were carried out in April and June The experimental area is over the Hatteras abyssal plain with depths varying between 5,300 and 5,600 m

THE chief obstacle to understanding the ocean circulation is the overwhelming difficulty in observing it The ocean is an enormous turbulent fluid fluctuating on all space and time scales Largely as a result of the MODE expedition¹ in 1973, it has become clear that a 'mesoscale' variability, closely analogous to weather systems in the atmosphere, is superimposed on the large-scale ('climatic') flow field But the mesoscales are disparate a few months and several hundred kilometres in the oceans as compared with a few days and several thousand kilometres in the atmosphere

There has been no perceived national or international requirement to lead towards a large-scale ocean observation network The cost in ship time is prohibitive (10 full-time vessels for 1 Mm² (1,000 × 1,000 km, about one-third the Mediterranean) Interior *in situ* sensors cannot transmit data by conventional means because the ocean is opaque to electromagnetic radiation For the same reason remote sensors in space cannot penetrate the ocean interior

But the ocean is transparent to sound Acoustic tracking of submarines goes back to World War I and tracking of neutrally buoyant floats from ships or shore stations is now a widely used oceanographic tool However, there has been no previous

attempt to exploit the properties of the sound field itself as a way of attacking the fundamental observation problem

The present experiment derives from a proposed scheme² for measuring the field of sound-speed fluctuations within a volume by acoustic transmission through the volume along many diverse paths It was called 'ocean acoustic tomography', in analogy with the medical X-ray procedure CAT (for computer-assisted tomography) The procedure is best illustrated by reference to the 1981 experiment (Fig 1) We chose a 300-km square in the same general area occupied by the MODE experiment¹ with a known mesoscale variability (MODE involved six ships and 25 conventional moorings) The 300-km dimension permitted adequate mapping from a ship in three weeks' time for comparison with the acoustic method, and the use of existing acoustic hardware Sound pulses emitted at each of the four sources S were recorded at each of the five receivers R Sound-speed in the ocean is predominantly a function of temperature, a cold eddy within the observation square will delay the arrival of any transmission through the eddy

There is a minimum in sound-speed (Fig 2) around 1 km depth forming a 'sound channel' which traps some of the acoustic energy This waveguide, which is the dominant feature of mid-latitude acoustic propagation, is useful here in two ways (1) acoustic rays that are refracted back towards the axis before intersecting the surface and bottom lose little energy through the boundaries and thus can be detected over several thousand kilometres (megametres), and (2) steep rays which sample the entire water column and generally arrive early can be distinguished from flat late rays which remain nearer the axis, and in this way something can be learned about the depth dependence of the ocean disturbances A very shallow disturbance affects only the very steep rays with shallow upper turning points, a deep disturbance alters the travel times of both steep and shallow rays

For each of the 20 source-receiver pairs (Fig 2 represents one of these) we record roughly 10 multipaths, giving a total of about 200 travel times for each transmission The number of data points grows geometrically with the product $R \times S$, as compared with the sum $R + S$ for conventional spot measurements and the path integration reduces the noise from local finestructure

One needs a procedure for converting this information into maps or spectra (or other interesting representations) of the ocean temperature field Generally the system is underdetermined, and there is an infinity of solutions 'Inverse theory' can be used to constrain the solution by solving for the smoothest field, or finding the unique solution consistent with *a priori* knowledge of the field covariance (The procedures of medical tomography are a specialized subset of the available mathematical tools)

The procedure depends critically on the resolution, identification and stability of multipaths over large ranges The scheme² proposed in 1979 depended on theoretical estimates, but there was no direct experimental evidence that any one of the three requirements could be met Positive results, rather

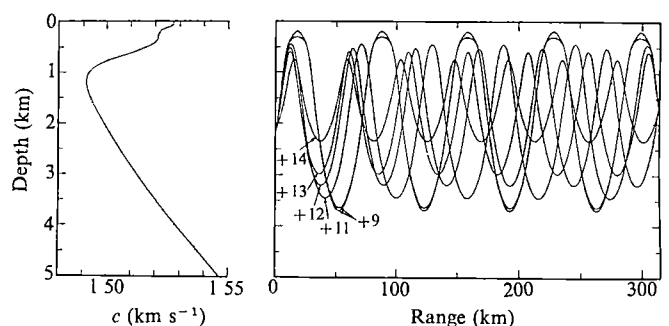


Fig 2 Ray (multipath) diagram from source S1 to receiver R3 for upward (+) launch angles only The identifier gives total (upper plus lower) number of ray turning points The associated measured and predicted arrival structures are plotted in Fig 3 The range-averaged sound-speed profile from S1 to R3 is shown to the left

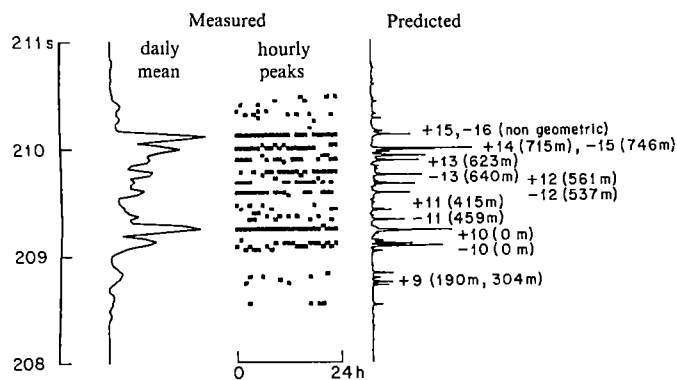


Fig 3 Comparison of measured arrival pattern with the WKBJ predicted impulse response on year day 64 for S1 to R3 transmissions. The daily mean pattern is formed from 24 hourly transmissions. Travel times for the peak arrivals are shown for each hour. Only peaks with signal-to-noise ratios exceeding 15 dB are plotted. Selected arrivals are identified, for example, +14 (715 m) refers to an upward launch angle with 14 ray turning points, the upper turning point being at 715 m depth. Some of the associated rays are identified in Fig 2. The non-geometric arrival refers to a ray with a turning point just above the receiver. Surface reflected a non-geometric arrivals are not included in Fig 2.

better than expected, were subsequently obtained during 48 days of transmissions at 10-min intervals over a 900 km path eastwards from a source moored near Bermuda³. A northward 300-km transmission that was intersected by a southern meander of the Gulf Stream gave similar results⁴. These experiments also provided experience for solving two crucial engineering problems: mooring position keeping and time keeping.

Measurements

The acoustic sources are patterned after the neutrally buoyant SOFAR floats that have been used extensively to track subsurface circulation in the Atlantic^{5,6}. Each source consists of four parallel 1-ft diameter aluminium tubes that are tuned for resonance at 224 Hz and have a bandwidth of 20 Hz. They are driven at the closed end by a flat circular plate of piezoelectric material. A microprocessor controls all source timing (on-off scheduling), including the phase modulation of its 224-Hz carrier. Briefly, the modulation is a 127-digit maximal length shift register sequence⁷. The autocorrelation function of the sequence is sharply peaked and has no sidelobes. Each digit comprises 14 cycles of the carrier and therefore has a duration of 62.5 ms. This is the width of the correlation peak and establishes the multipath resolution of the system. A sequence of 127 digits lasts nearly 8 s, which more than covers the time spread between the first and last arrivals (Fig 3). A transmission consisting of 24 consecutive sequences lasts nearly 192 s, which is roughly the decorrelation time of the ocean due to internal waves for this experiment. Coherent averaging of the 24-sequence receptions affords signal-to-noise gain. One can think of each transmission as being equivalent to the transmission of 62.5 ms pulses at 8 s intervals repeated 24 times. Coherent summation produces a single intense pulse^{8,9}. The transmitted power level is quite low, about 14 W ($186 \text{ dB } \mu\text{Pa}^{-1}$ at 1 m), for a total of 2,700 J per transmission (about the same energy as in the prolonged grunt of a blue whale heard off the coast of Chile¹⁰) but when this energy is 'compressed' into 62.5 ms pulses it can be recorded at typically 25 dB signal-to-noise ratios, leading to a theoretical travel time precision of 2 ms for a resolved arrival.

The acoustic receivers are microprocessor controlled devices. The arrival time structure of the multipath field between source and receiver is obtained by cross-correlating the coherently averaged incoming signal with a stored replica of the transmitted signal. Some receivers performed the cross-correlation *in situ* and stored only the time of arrival of multipath peaks, while others simply stored signal samples for later on-shore processing. Reception times were synchronized to source transmission times. Transmissions were at hourly intervals (for tidal correc-

tion and to suppress internal wave noise) on every third day only (to conserve batteries).

To provide a time base accurate to better than 10 ms, each source and receiver was equipped with a rubidium atomic frequency standard to make daily measurements of the frequency offset of a considerably less stable (but of lower power) continuously running quartz crystal clock. The frequency offsets are integrated to yield time corrections. It is necessary also to correct the travel times for mooring excursions. These were measured with bottom transponders to a precision of $\sim 1.5 \text{ m}$ (1 ms for a line-of-sight displacement).

Travel times

The procedure depends critically on the resolution, identification and stability of multipaths over large ranges³. The predicted arrival pattern (Fig 3) is derived from a generalization to ray theory¹¹, and it matches the measured pattern rather well. This identification, based on travel time, was checked for ray inclination at receivers R1 and R5 which were equipped with vertical arrays¹², and in no instance did the difference between measured and predicted inclination exceed the experimental error.

Figure 4 shows this arrival pattern on a reduced scale over a 100-day period. Multipath peaks are plotted as single points, and only those paths whose signal-to-noise ratio exceeded 15 dB are shown. The relative pattern is stable, some weak late arrivals are surface and bottom reflected and have not been used in the analysis. The 2 s drift of the raw pattern towards

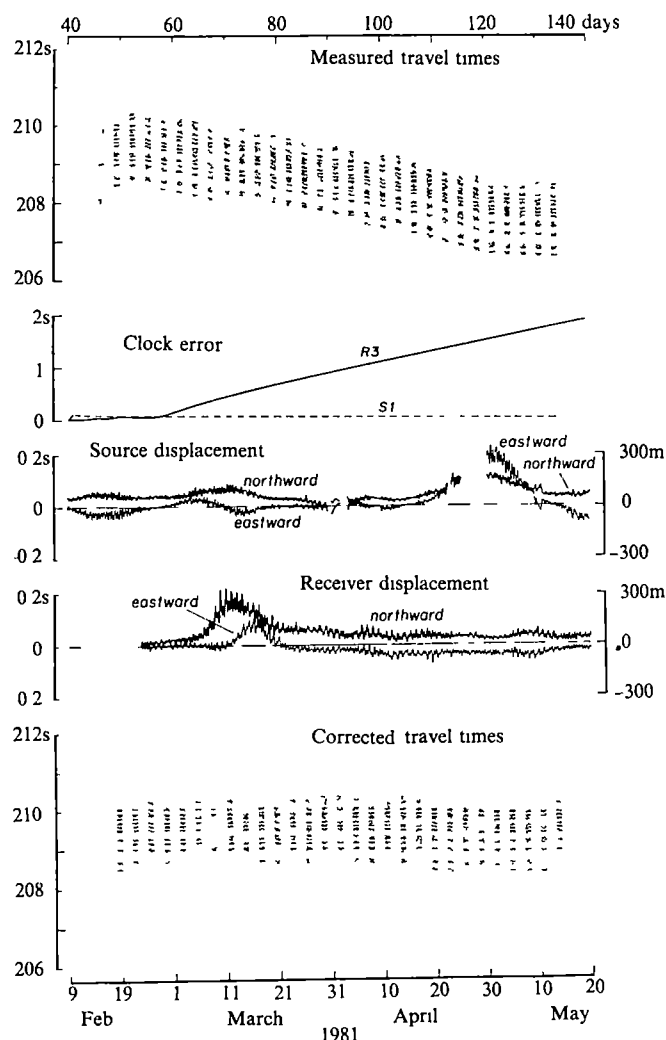


Fig 4 Multipath arrival structure S1 to R3, before and after corrections for clock drifts and mooring displacements. Transmissions were over 24 h on each third day, starting 18 February (year day 49). The unstructured patterns on days 43 and 46 (before transmission) show processed noise. Gaps in the source displacement are due to missing data.

earlier arrival is almost entirely associated with the gain of the receiver clock (as measured by the rubidium standard). Horizontal excursions of the moorings provide a lesser correction. The high frequency excursions can be related to tidal motion. The arrival pattern corrected for clock drift and mooring motion provides the database for the tomographic inversion.

Comparison of tomographic with traditional measurements

There is a basic problem of comparing two fields that are not the same. The CTD (conductivity/temperature/depth) surveys took almost three weeks (during which time the fields changed), the acoustic surveys provided almost synchronous snapshots (one can think of them as surveys conducted at 3,000 knots).

Panels *b*, *e*, *f*, *i* of Fig 5 show the sound-speed maps from the first two CTD/XBT cruises¹³. Nominal station spacing was 50 km but near the centre the spacing was halved (Fig 1). During the second cruise 10 additional 1,500-m CTD casts extended the grid 100 km westward. Panel *a* was inferred (using representative *T-S* relations) from AXBT drops on 13–14 April at positions of the CTD stations. (The AXBT's were from P-3 aircraft supported by NAVOCEANO Standard AN/SSQ36 probes (to 300 m depth) were used, with temperature calibrations (to $\pm 0.15^\circ\text{C}$) as described in ref 14.) Sound-speed was computed¹⁵ and then contoured using an objective interpolation scheme like that used in MODE¹⁶. The necessary weights were computed using a gaussian correlation function of 100-km scale.

The March map (days 66–85) shows a cold eddy nearly in the centre, evidently embedded in a background gradient with warmer water to the north. The May map (days 120–139) shows the same cold eddy displaced about 200 km to the west, weakened, and perhaps split in two. A new cold eddy, smaller than the original, has appeared in the south-eastern corner.

The four central charts are from the tomographic inversion. The sound-speed field is modelled by specifying a covariance function for the perturbations around a basic state. The horizontal covariance function is homogeneous, isotropic and gaussian with a decay scale of 100 km. The vertical structure is made up of empirical orthogonal functions calculated from the MODE dataset¹.

The tomographic maps show a slow westward movement and slight weakening of the central cold eddy, and the appearance of a new cold centre in the south-east corner, consistent with the CTD surveys. A premature failure of receiver R4, followed by R2 and R3, has so far prevented the plotting of the tomographic chart for the time of CTD II, as had been intended. (The failures were the result of a faulty battery batch, the remaining receivers and all sources functioned normally and will eventually permit limited inversions through the full experimental period.) The chart sequence as shown implies a remarkably stable pattern for the first 40 days, followed by rapid changes in the subsequent 20 days. This interpretation of a 'jumpy' eddy movement is consistent with the observed stability in travel time to R1 until day 110, with rapid changes thereafter in the sense indicated by the charts in Fig 5. Similarly, 'stick charts' of the measured currents at the environmental moorings E1 and E2 are uneventful until day 110 and then change rapidly¹³. The indicated sequence is as follows¹³.

- Days 62–91 A large cold eddy remains nearly stationary at a position north-east of E1 where it was observed during CTD I. Under its influence the E1 currents flow generally to the south-east and the E2 currents flow to the east.
- Days 91–110 The cold eddy moves slowly WSW to a position west of E1, near where it was seen during the AXBT flight on day 103. (This corresponds to the times of the tomographic inversions.) As a result the flow of the shallow E1 current meter (137 m) turns counterclockwise to the north, and the

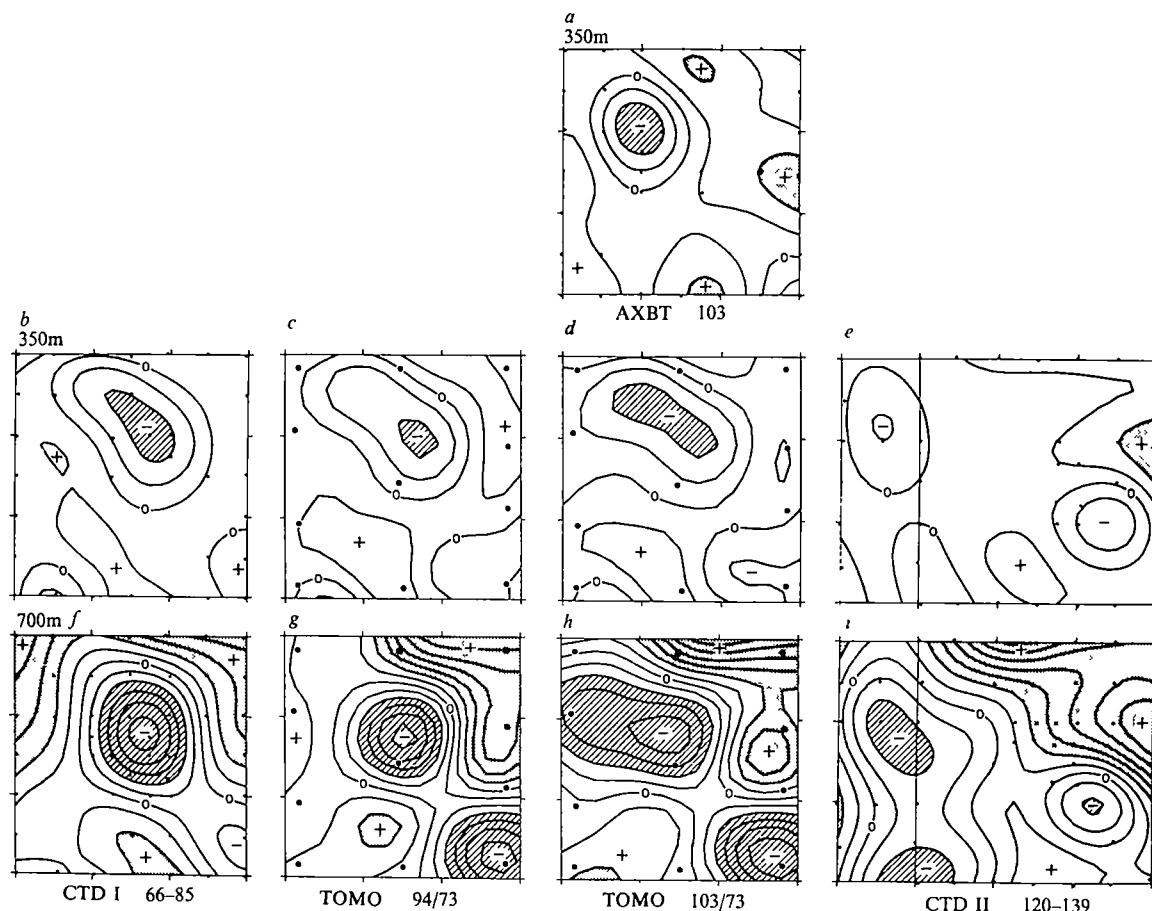


Fig 5 Mosaic of sound-speed anomaly charts in the 300×300 km square (centred at 26°N , 70°W). *b*, *f* are from the first CTD survey (CTD II includes an additional 100 km strip to the west), *a* is from the AXBT survey. The four central charts are from the tomographic inversions, assuming travel time error bars of 10 ms. Year days 1981 are indicated below, the tomographic inversions are referenced to the travel time on day 73. *f*–*i* at 700 m depth gives sound-speed departures δC relative to $1,505.9 \text{ m s}^{-1}$, *a*–*e* at 350 m depth relative to $1,521.7 \text{ m s}^{-1}$, with contour interval 1 m s^{-1} , departures above $+2 \text{ m s}^{-1}$ and below -2 m s^{-1} are shaded. Points give positions of CTD and AXBT casts, and of acoustic and environmental moorings (see Fig 1 for mooring identification).

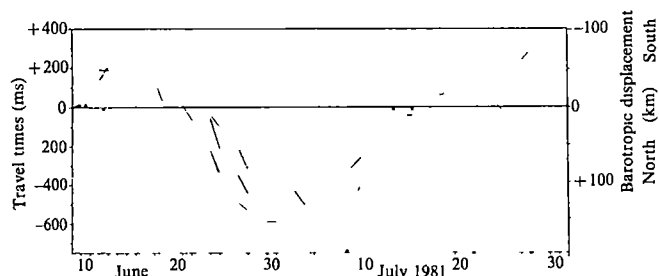


Fig. 6 Relative travel times at hourly intervals for every third day (transmission day) from two sources to north station are portrayed by the sloping line segments, short or missing lines are the result of low signal-to-noise levels. The right-hand scale shows the corresponding barotropic displacement of the Gulf Stream. *, Positions of the North wall of the Gulf Stream inferred from sea-surface temperature measured by NOAA-6 satellite.

flow of the deep (835 m) current meter turns completely around to the west (The different degrees of turning of the shallow and deep current meters are caused by the north-east tilt of the eddy axis). The flow of E2 turns slightly clockwise to the ESE.

- Days 110–130 The first cold eddy rapidly moves west to the edge of the experimental box and a second cold eddy appears in the south-east quadrant, where they are seen during CTD II. The flow is generally to the north-west at E1 and south-west at E2.

The above interpretation is supported by the good agreement between the measured currents and those from the dynamic height maps during CTD I and CTD II. We conclude that the tomographic inversions are consistent with the CTD and current meter observations.

The tomographic charts in Fig. 5 are the result of preliminary inversion for a few transmission days, using only a few paths per source–receiver pair. Work is in progress to optimize the procedure and to attempt inversions subsequent to day 103 with the degraded array (unfortunately the number of data points not only grows but also declines geometrically with the number of moorings).

There are two basic problems with the inversion process: initialization and linearization. Work on these problems has started. In this preliminary report we follow the simplest initialization procedure: for each source–receiver pair we use only the difference in travel time reckoned from the (known) ocean state on day 73 to compute perturbation fields relative to day 73, and map the combined (initial plus perturbation) fields. For very long time series one would refer the perturbation maps to a climatological mean state which (probably) suffices for ray identification purposes (Doubtful cases could be tied down with AXBT flights). Any errors in the assumed mean state will, of course, be retained in the combined maps.

An equivalent (and better) procedure is to use absolute travel time for the known initial (or mean) ocean state to correct the array configuration for a navigational error of ± 0.5 km, and to use absolute travel times in the subsequent inversions. (This involves only 15 independent constants, for example, the x , y positions of eight moorings relative to some arbitrary reference mooring, plus an arbitrary coordinate rotation. The present procedure involves 20 independent constants, for example, the absolute travel times on day 73 for each source–receiver pair.)

Formally, the tomographic procedure is independent of CTD surveys, these are used only to remove navigational errors. It

is expected that the GPS satellite system and sea floor localization procedures¹⁷ will determine the configuration of future arrays to within ± 1 m. At this point a knowledge of the climatological state is required only for ray identification, and the perturbation maps are free from initialization error.

In our linearized inversion procedure we ascribe perturbations in travel time to perturbations in sound-speed along the unperturbed ray paths. But rays emerging from mesoscale eddies have turning depths that may differ sufficiently from the unperturbed turning depths so that a significant part of the travel time perturbation is accumulated outside the eddy¹⁸. Generally the errors are too large to be neglected, yet sufficiently small to suggest an iteration procedure¹⁹. This has not yet been attempted.

Remote stations

The sources were monitored at remote facilities to assure their proper functioning, and to gain experience with long-range transmissions. In this connection we observed a systematic fluctuation in travel time over a northward 2,000-km path across the Gulf Stream (Fig. 6). (On calendar days 52, 55, 58 the receptions from source S2 were poor, on day 61 this source was recovered, found faulty, and another source deployed. No other source anomalies were seen during the remaining six months.) At the midpoint of the 50 days record, the travel time was shortened by 0.8 s. This is the result of a 200-km northward displacement of the Gulf Stream, with the associated decrease in the amount of cold slope water over the path²⁰. (Satellite sea surface temperatures support this interpretation.)

Discussion

The preliminary report of the 1981 experiment indicates that ocean mapping with mesoscale resolution can be performed tomographically over substantial areas. There is, of course, a shortcoming in measuring only the sound-speed field. But in regions of tight T - S relations, or where the disturbances are associated mostly with vertical displacements of the isopycnals, the sound-speed perturbation can be mapped into density perturbations with accuracies adequate for computing geostrophic currents²¹.

Two developments are planned for the future. In the autumn of 1982 we plan to make reciprocal transmissions²² at 300 km ranges and use the difference in the oppositely directed travel times to infer the water velocity along the ray paths (velocity tomography). Subsequently we plan to establish an array of megametre dimensions to measure the variability of an ocean gyre²³. Here the tomographic principle would be used to obtain vertical resolution, in the horizontal directions advantage is taken of the integrating properties of long range sound transmissions, opening the way to true ocean-basin scale measurement programmes.

We thank C. Spofford for discussion and advice. J. Dahlen furnished the T - P recorders. Many people have helped, but we are particularly indebted to Paul Boutin, S. Liberatore, F. Schuler, A. Bradley, J. Kemp and M. Jones of Woods Hole, to F. Dormer, K. Hardy, B. Ma, D. Peckham and R. Truesdale at Scripps, and to B. Grant and S. Johnson at MIT. The work has been supported by the Office of Naval Research and by the NSF. The Atlantic Oceanographic and Meteorological Laboratory of NOAA provided support for three CTD/XBT cruises of the ship *Researcher* and for J. S. The US Navy Oceanographic Office supported the two AXBT flights.

Received 21 June, accepted 7 July 1982

- 1 The MODE Group *Deep-Sea Res.* **25**, 859 (1978)
- 2 Munk, W. & Wunsch, C. *Deep-Sea Res.* **26A**, 123 (1979)
- 3 Spiesberger, J. L., Spindel, R. C. & Metzger, K. *J. acoust. Soc. Am.* **67**, 2011 (1980)
- 4 Spindel, R. C. & Spiesberger, J. L. *J. acoust. Soc. Am.* **69**, 982 (1981)
- 5 Webb, D. C. *Proc. Oceans '77 Conf. Rec. MTS-IEEE* **2**, 44B (1977)
- 6 Spindel, R. C., Porter, R. P. & Webb, D. C. *IEEE J. Oceanic Engng* **OE-2**, 331 (1977)
- 7 Golomb, S. W. *Shift Register Sequences* (Holden-Day, San Francisco, 1967)
- 8 Spindel, R. C. *Proc. IEEE Electron. Aerospace Convnt.* **80 CH**, 1587-4AES, 165 (1980)
- 9 Spindel, R. C. *IEEE Trans. Acoustics, Speech Signal Processing* **ASSP-27**, 723 (1979)
- 10 Cummings, W. C. & Thompson, P. O. *J. acoust. Soc. Am.* **50**, 1198 (1971)
- 11 Brown, M. G. *J. acoust. Soc. Am.* (in the press)
- 12 Worcester, P. F. *J. acoust. Soc. Am.* **70**, 1743 (1981)

- 13 Behringer, D. W., Heinmiller, R., Knox, R. & Thomas, G. *NOAA Technical Rep.* (1982)
- 14 Sessions, M. H. & Barnett, T. P. in *Near Surface Ocean Experimental Technology Workshop* (Proc. NORDA, 125 (1980))
- 15 Chen, C. T. & Millero, F. J. *J. acoust. Soc. Am.* **62**, 1129 (1977)
- 16 Bretherton, F. P., Davis, R. E. & Fandry, C. B. *Deep-Sea Res.* **23**, 559 (1976)
- 17 Spiess, N. F. (Chairman), *Panel on Ocean Bottom Positioning of the Committee of Geodesy* (National Academy of Sciences, Washington, DC, 1982)
- 18 Mercer, J. A. & Booker, J. R. *J. geophys. Res.* (submitted)
- 19 Spiesberger, J. L. & Worcester, P. F. *J. acoust. Soc. Am.* (submitted)
- 20 Spiesberger, J. L. *et al. J. phys. Oceanogr.* (submitted)
- 21 Worcester, P. F. & Cornuelle, B. *Proc. 2nd Working Conf. on Current Measurements* (in the press)
- 22 Worcester, P. F. *J. acoust. Soc. Am.* **62**, 895 (1977)
- 23 Munk, W. & Wunsch, C. *Phil. Trans. R. Soc.* (in the press)

Brain spectrin, a membrane-associated protein related in structure and function to erythrocyte spectrin

Vann Bennett, Jonathan Davis & Walter E. Fowler

Department of Cell Biology and Anatomy, The Johns Hopkins University School of Medicine, 725 North Wolfe Street, Baltimore, Maryland 21205, USA

An immunoreactive analogue of erythrocyte spectrin has been purified from brain membranes. This protein co-sediments with and cross-links actin filaments, associates with spectrin-binding sites on erythrocyte membranes, and has been visualized by rotary shadowing as an extended, flexible rod. The brain spectrin comprises 3% of the total membrane protein, and may have a major role in mediating linkage of actin to membranes.

MEMBRANE-associated forms of actin have been observed in many types of cells and are thought to participate in cell motility, adherence of cells to surfaces, determination of cell shape and in the organization of cell-surface integral proteins (for review see ref 1). A direct linkage has been demonstrated between actin and integral membrane proteins in lymphocytes^{2,3}, but the polypeptides required for these associations are unknown. Actin is a component of erythrocyte membranes^{4,5} and its mechanism of association with this simple membrane has been established in detail (reviewed in refs 6, 7). Erythrocyte actin is bound to spectrin in a complex perhaps involving band 4.1 (refs 8–10). Spectrin is an extended rod-like molecule present as a tetramer formed by head-to-head association of dimers¹¹, spectrin dimers consist of two different subunits, arranged as parallel chains. The β -subunit of spectrin is bound to ankyrin^{12–16}, which in turn is associated directly with the cytoplasmic domain of band 3, the major membrane-spanning protein in erythrocytes^{17–19}.

It has been assumed that the association of actin with erythrocyte membranes is not relevant to the arrangement of actin in other cell types, where spectrin could not be detected by radioimmunoassay²⁰. However, polypeptides immunologically related to erythrocyte spectrin^{21,22} and ankyrin^{23,24} have been detected in brain and other tissues. These cross-reacting proteins include soluble and membrane-associated forms. A class of soluble analogues of ankyrin and spectrin have been identified as high-molecular weight microtubule-associated proteins (MAPs)^{22,24}. MAP1, a group of polypeptides of molecular weight (M_r) ~370,000 (370K), contains a component which is related to ankyrin, while MAP2, a polypeptide of M_r 300,000, shares antigenic sites with the α -subunit of spectrin. MAP2 shares with spectrin the ability to bind to actin²⁵ and the shape of an extended rod²⁶, but lacks membrane-binding activity. Here we describe another immunoreactive analogue of spectrin from brain which binds to actin, associates with spectrin-binding sites in erythrocyte membranes, and is an extended rod-like molecule. This spectrin analogue comprises 3% of the total membrane protein, and is a suitable candidate for having a major role in mediating linkage of actin to membranes.

Purification of spectrin analogue from brain membranes

Brain membranes contain a prominent pair of polypeptides of M_r ~260K and 265K which cross-react with affinity-purified antibody against erythrocyte spectrin (Fig 1). Membrane fractions from kidney, liver and testes also contain polypeptides of similar molecular weight which cross-react with anti-spectrin antibody, but brain membranes were the richest source of these polypeptides (not shown). In liver, cross-reacting polypeptides of M_r 260K and 265K were localized exclusively in the plasma

membrane fraction (Fig 2). The mitochondria, nuclei and soluble fractions all contain polypeptides unique for each fraction which cross-react with anti-spectrin antibody, but none are of molecular weight 260K or 265K. The significance of multiple cross-reacting polypeptides is unknown, and further studies with each polypeptide are required. The reactions are specific in that there was no cross-reaction of these polypeptides with non-immune antibody (Figs 1, 2) or with antibody against ankyrin or band 3 (not shown). A possible explanation is that functional domains of spectrin are conserved as discrete amino acid sequences in other polypeptides and have been combined with other activities to form proteins distinct from spectrin. Here we present a detailed study of the 260K and 265K cross-reacting polypeptides.

Fractionation of brain membranes by differential centrifugation or sedimentation on gradients of sucrose or sucrose-Ficoll did not yield membranes significantly enriched in these polypeptides, and only myelin lacked the polypeptides (not shown). Therefore, total membranes depleted of myelin were used as starting material for purification procedures. These membranes contained ~75% of the 260K/265K polypeptide present in total brain homogenates. The 260K/265K polypeptides can be solubilized from brain membranes by extraction with 1 M KCl or at low ionic strength with 0.2 mM Na-EGTA (not shown). Extraction with low salt was more selective, and was therefore used to solubilize the protein for purification. The immunoreactive 260K/265K polypeptides were purified to homogeneity by precipitation with ammonium sulphate, gel filtration and finally rate zonal sedimentation on sucrose gradients (Fig 1).

To examine the cross-reaction between spectrin and the brain protein, ¹²⁵I-labelled brain protein was immunoprecipitated by antibody against spectrin, and this binding was displaced completely by unlabelled spectrin (Fig 1B). The brain protein displaced binding of ¹²⁵I-labelled spectrin to antibody by a maximum of 20% (Fig 1C). The limited displacement achieved by the brain protein occurred in the same range of concentration as displacement by erythrocyte spectrin. Thus, only 20% of the antigenic sites recognized by our antibody in erythrocyte spectrin are shared by the brain protein, but those sites which are common between these proteins are well conserved. The fact that the brain and erythrocyte proteins are only partially cross-reactive could explain previous negative results of radioimmunoassay for spectrin²⁰.

The possibility that our antibody was reacting with a minor contaminant which co-migrated with the brain polypeptides was excluded by comparing peptide maps of each brain polypeptide with maps of polypeptides immunoprecipitated by the antibody (Fig 3). The total brain polypeptides and the fraction immunoprecipitated with anti-spectrin antibody produced almost identical peptide maps. Thus, the antibody recognizes a major constituent of each polypeptide.

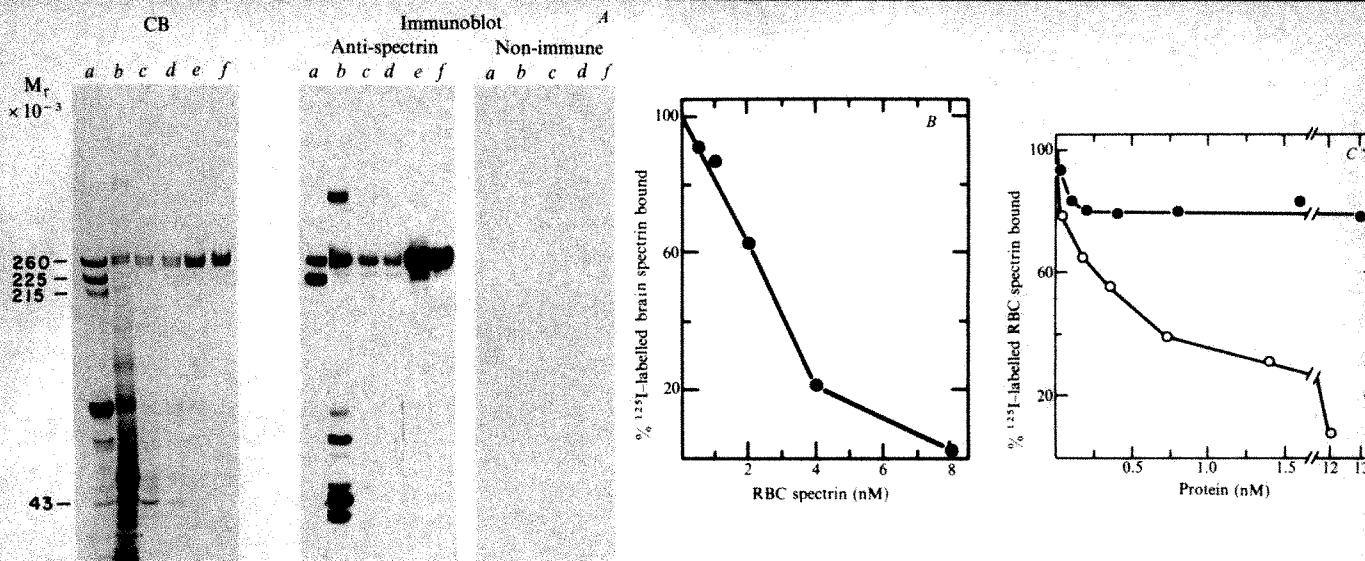


Fig. 1 Purification from brain membranes of a protein which shares antigenic determinants with erythrocyte spectrin. Fractions at various stages of purification were analysed by SDS-polyacrylamide gel electrophoresis on 3.5–17% exponential gradient gels^{22,24} (A). Polypeptides were visualized by staining with Coomassie blue (CB); those cross-reacting with erythrocyte spectrin were identified by electrophoretic transfer from polyacrylamide gels to nitrocellulose paper, followed by overlay of the nitrocellulose with $1 \mu\text{g ml}^{-1}$ affinity-purified rabbit antibody against human erythrocyte spectrin or with non-immune antibody followed by ^{125}I -labelled Protein A^{22,24}. Immunoreactive bands were then detected by autoradiography. Samples are: a, pig erythrocyte ghosts; b, pig brain membranes; c, low ionic strength extract of brain membranes; d, soluble protein recovered from ammonium sulphate precipitation of sample c; e, pooled fractions from gel filtration; f, pure protein from sucrose gradients. Immunoprecipitation of ^{125}I -labelled pure protein (lane f) and ^{125}I -labelled pig erythrocyte spectrin by anti-spectrin antibody were measured as described elsewhere^{22,23}. Binding of ^{125}I -labelled brain protein by anti-spectrin antibody (100 nM IgG) was displaced by unlabelled erythrocyte spectrin (B). C, binding of ^{125}I -labelled erythrocyte spectrin by anti-spectrin antibody (7 nM IgG) was displaced by unlabelled erythrocyte spectrin (○) and partially displaced by unlabelled pure brain protein (●). Frozen grey matter from pig brain (125 g) was homogenized in 800 ml of 0.32 M sucrose, 2 mM Na-EGTA, 200 $\mu\text{g ml}^{-1}$ phenylmethylsulphonyl fluoride (PMSF) (v/v) diisopropylfluorophosphate, 3 $\mu\text{g ml}^{-1}$ pepstatin A, pH 7.0. The 900g supernatant of this suspension was pelleted at 30,000g for 25 min to collect the crude membrane fraction. This fraction was depleted of myelin by centrifugation for 40 min at 30,000g through 0.8 M sucrose. The myelin-depleted membranes were washed successively by centrifugation for 25 min at 30,000g with homogenization buffer, followed by 10 mM sodium phosphate, 2 mM Na-EGTA, 50 $\mu\text{g ml}^{-1}$ PMSF pH 7, and finally 2 mM Na-EGTA, 50 $\mu\text{g ml}^{-1}$ PMSF pH 7. The washed membranes (1.6 g protein) were extracted at 37°C for 60 min in 800 ml of 0.2 M Na-EGTA, 0.5 mM dithiothreitol (DTT), 50 $\mu\text{g ml}^{-1}$ PMSF pH 7. The suspension was pelleted at 200,000g for 30 min and the supernatant (120 mg extracted protein) was adjusted to 45% saturation with solid ammonium sulphate. The precipitated proteins were dialysed overnight against 1 M urea, 20 mM glycine, 2 mM Na-EGTA, 1 mM NaN_3 , 0.2 mM DTT, and centrifuged at 200,000g for 3 h. The supernatant was applied to a Sephacryl S400 gel filtration column (2.6 × 90 cm) equilibrated with urea buffer. Fractions containing the 260K polypeptides eluted near the void volume. The protein was precipitated with ammonium sulphate, dialysed extensively against 0.2 M Na-EGTA, 0.5 mM NaN_3 , 0.2 mM DTT pH 7, then centrifuged at 200,000g for 90 min. The supernatant was fractionated on 10–30% linear sucrose gradients in dialysis buffer using a Beckman V Ti 50 rotor (14 h at 36,000 r.p.m.). The gradient fractions with the purest protein (at about a sedimentation rate of 11S) contained 1.2 mg of protein. An additional 2 mg of less pure protein was recovered from adjacent fractions.

A feature which distinguishes spectrin from other high-molecular weight actin-binding proteins, such as filamin and MAP2, is the presence of two distinct polypeptide chains. In this respect, the brain protein resembles spectrin as the 265K and 260K polypeptides are clearly different by peptide mapping (Fig. 3). The two chains co-purify in a 1:1 molar ratio, and both polypeptides co-sediment with actin (see below). The brain protein has a molecular weight of 1,090,000, calculated from preliminary hydrodynamic values ($R_s = 240 \text{ \AA}$, $s_{20,w} = 10.8$, \bar{v} assumed to be 0.73). This protein is therefore a tetramer with two copies of each subunit.

The peptide maps of α - and β -chains of erythrocyte spectrin are dissimilar from either chain of the brain protein (Fig. 3). It is of interest that peptide maps of human and pig erythrocyte spectrin differ by at least 60% and that antibody against human spectrin binds with a lower affinity to pig erythrocyte spectrin (not shown). Erythrocyte spectrin evidently does not have a highly conserved amino acid sequence. The fact that the peptide fingerprints of the brain protein differ from those of erythrocyte spectrin does not rule out functional homology between these proteins or a possible common evolutionary origin. The difference in peptide maps between the immunoprecipitated brain polypeptides and spectrin does, however, exclude the possibility of contamination by erythrocyte spectrin in the brain protein.

Spectrin analogue has similar morphology to erythrocyte spectrin

Erythrocyte spectrin is distinctive in that the tetramer appears in rotary-shadowed preparations as a highly extended rod almost 200 nm long¹¹. In similar preparations, the brain protein also appears as an extended rod with average length 195 nm and width 4–6 nm (estimated without compensating for the

additional mass of platinum) (Fig. 4). Occasionally, the rods open in the middle to reveal two parallel chains. The chains are most often closely apposed or helically entwined along the length of the molecule. Pig erythrocyte spectrin tetramers are slightly shorter with an average length of 175 nm, but otherwise are quite similar to the brain protein (Fig. 4). One significant difference between the two proteins is that, on average, the brain protein is straighter and there are fewer cases of separation of individual chains than observed for erythrocyte spectrin (Fig. 4A; compare with ref. 11). A more rigid conformation for the brain protein tetramer is indicated also by its lower sedimentation coefficient (10.8S) compared with that of the spectrin tetramer (12.5S). The brain protein tetramer was not converted to dimer by warming at 37°C (not shown) and thus is more stable than tetramers of erythrocyte spectrin. However, a limited conversion of tetramer to dimer was achieved by prolonged exposure to 1 M NaBr (Fig. 4). The dimers produced by this treatment exhibit a R_s of $\sim 110 \text{ \AA}$ and are comparable in length to erythrocyte spectrin dimers.

An important similarity between brain and erythrocyte proteins is that at concentrations less than 2 mg ml^{-1} , oligomers larger than tetramers were observed only rarely. Thus, it is likely that dimers of the brain protein have a polarity and are associated head-to-head, as has been suggested for erythrocyte spectrin^{11,27,28}. Otherwise, with a non-polar or a head-to-tail association, polymerization could occur to form extended filaments.

The spectrin analogue binds to erythrocyte membranes and to F-actin

Important criteria for a spectrin-like protein, in addition to structural similarities, are functions of binding to membranes and association with actin filaments. The brain protein remains

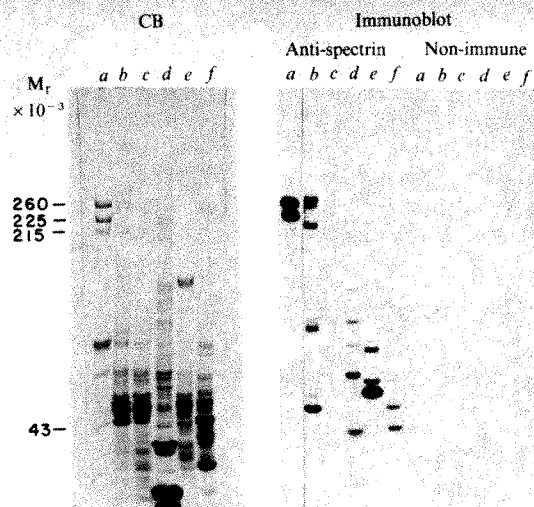


Fig. 2 Polypeptides (265K and 260K) cross-reacting with anti-spectrin antibody are localized in plasma membranes of liver. Plasma membrane sheets from blancher livers were isolated by two steps of upward flotation through 1.42 M sucrose essentially as described elsewhere⁴⁰ except that the buffers contained 7.5 mM sodium phosphate, 1 mM $MgCl_2$ pH 7.5, and protease inhibitors (200 $\mu g\ ml^{-1}$ PMSF and 0.01% (v/v) diisopropylfluorophosphate). Mitochondria were isolated as described elsewhere⁴¹ with the same buffer and protease inhibitors as above. The total microsomal and soluble fractions were isolated by pelleting (200,000g, 45 min) the 25,000g supernatant from liver homogenized in 0.25 M sucrose, 7.5 mM sodium phosphate, 1 mM $MgCl_2$ pH 7.5 and protease inhibitors. The microsomal pellet was washed once in 7.5 mM sodium phosphate, 1 mM Na-EGTA pH 7.5. Nuclear membranes were prepared essentially by the procedure of Dwyer and Blobel⁴² except that 0.5 mM Na-EGTA and protease inhibitors were included in the buffers, and the nuclei were digested with RNase and DNase. The samples were analysed on SDS-polyacrylamide gels; polypeptides were visualized by staining with Coomassie blue (CB; left) and immunoreactive polypeptides (right) identified as described in Fig. 1 legend. a, Erythrocyte ghosts; b, plasma membranes; c, microsomal membranes; d, nuclear envelopes; e, mitochondria; f, soluble proteins.

associated with membranes during repeated washes, and presumably is involved in a stable linkage with some membrane component(s). The brain protein also contains a binding site for erythrocyte ankyrin, as it displaces binding of ^{125}I -labelled erythrocyte spectrin to inside-out spectrin-depleted vesicles from erythrocyte membranes (Fig. 5). This assay measures association of spectrin with ankyrin, as spectrin binding to the membrane is displaced entirely by a spectrin-binding proteolytic fragment of ankyrin²⁹ and by antibody against this fragment of ankyrin¹². The brain protein is less active than erythrocyte spectrin, with 50% displacement at 60 nM compared with 30 nM for erythrocyte spectrin dimer. ^{125}I -labelled brain protein associates with erythrocyte membrane vesicles (not shown); this binding is blocked by unlabelled erythrocyte spectrin with 50% displacement at 10–15 nM (Fig. 5). The brain protein and erythrocyte spectrin thus bind to the same membrane site but erythrocyte spectrin binds with approximately twofold higher affinity. The lower affinity of the brain protein may be explained by a difference in its ankyrin-binding site, and/or may be a consequence of steric restrictions resulting from its more rigid conformation.

The brain protein associates with actin filaments, as demonstrated by co-sedimentation with actin through sucrose barrier gradients (Fig. 6). Over 60% of the brain protein was pelleted in the presence of actin, compared with <7% in the absence of actin, in conditions of 60 nM brain protein and 5 μM actin monomer. The brain protein greatly increased the low-shear apparent viscosity of F-actin, with an apparent gel point in the range of 60 nM (Fig. 6). Pig erythrocyte spectrin (tetramer/dimer ratio of ~3) exhibited a comparable activity (Fig. 6). The gel point for the brain protein varied with the actin preparation used and was as low as 20 nM when tested with actin purified further by gel filtration (V. Fowler, unpublished data).

Previous studies of cross-linking of actin filaments by human erythrocyte spectrin have noted the requirement for band 4.1 (refs 9, 10). We have also observed that human spectrin alone is not active in cross-linking actin, but that pig erythrocyte spectrin purified in the same way and compared in the same assay is not dependent on band 4.1 (V. Fowler and V.B., unpublished data). The results with pig spectrin agree with those of Brenner and Korn⁸ who observed that pure sheep erythrocyte spectrin was also capable of cross-linking actin

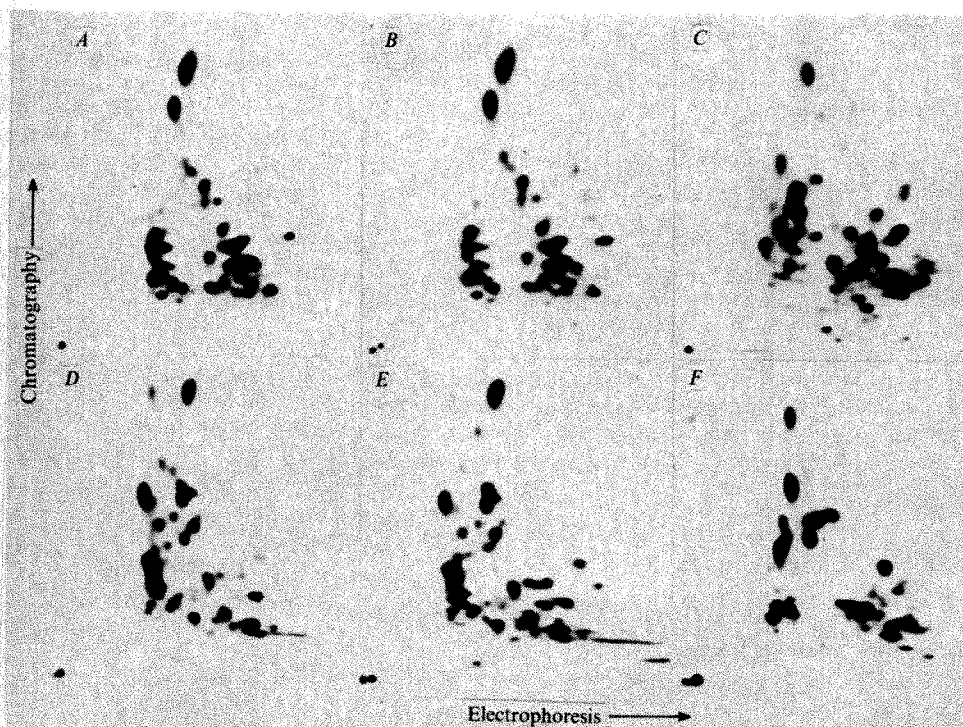
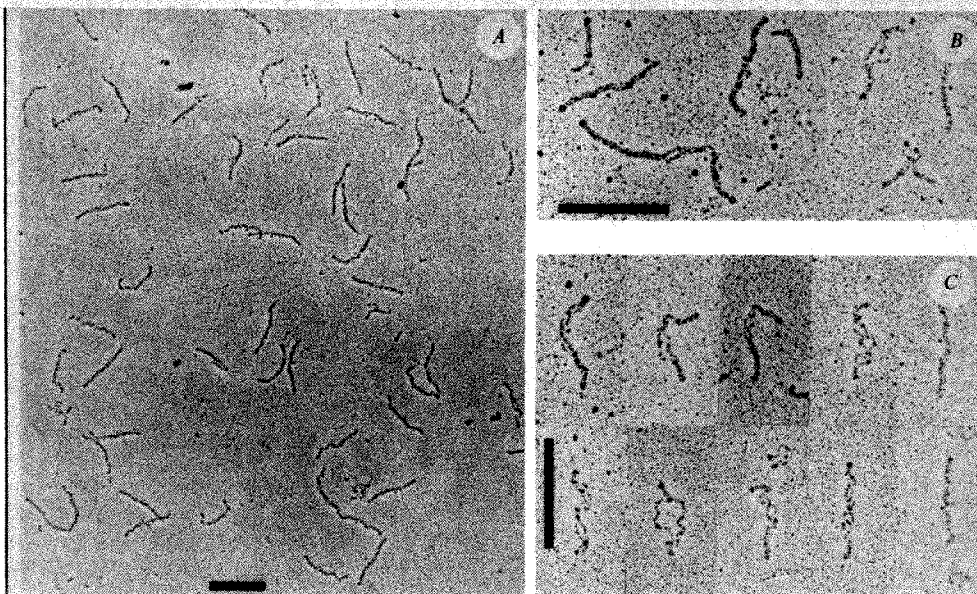


Fig. 3 Two-dimensional maps of ^{125}I -labelled α -chymotryptic peptides from α - (A–C) and β - (D–F) subunits of brain spectrin (A, D), brain spectrin immunoprecipitated by anti-erythrocyte spectrin antibody (B, E) and pig erythrocyte spectrin (C, F). ^{125}I -labelled brain spectrin (Fig. 1; 4×10^7 c.p.m.), ^{125}I -labelled brain spectrin immunoprecipitated by antibody against erythrocyte spectrin (Fig. 1; 2×10^6 c.p.m.) and pig erythrocyte spectrin (3×10^7 c.p.m.) were mixed with 2 μg unlabelled brain spectrin or erythrocyte spectrin and then electrophoresed on a SDS-polyacrylamide gel (see Fig. 1 legend). The gel was stained lightly with Coomassie blue, and equilibrated with 50 mM ammonium acetate, 1 mM sodium azide, pH 7. The protein bands were excised, suspended in 0.5 ml ammonium acetate buffer and incubated at 37 °C for 20 h with two additions of 25 μg α -chymotrypsin. The digests were lyophilized, and analysed by electrophoresis and chromatography as described elsewhere^{22,43}.

Fig. 4 Electron micrographs of rotary-shadowed brain spectrin (A, B and top row of C) and pig erythrocyte spectrin (bottom row of C). A, representative field of purified brain spectrin molecules which were diluted to $10 \mu\text{g ml}^{-1}$ in 100 mM ammonium formate (pH 7), mixed with 1/3 vol of glycerol, sprayed on to mica, dried under vacuum at room temperature and rotary-shadowed with platinum at an angle of 1 in 10 (refs 11, 44). Scale bar, 200 nm. B, brain spectrin molecules from a different less pure preparation, which was treated with 1 M NaBr for several days before dialysis against 100 mM ammonium formate and rotary shadowing as described for A; the field on the left includes an 'octamer' and two 'dimers', as well as two 'tetramers'. The two-stranded character of the molecules is seen more clearly in the field on the right and in C. Scale bar, 200 nm. C, selected brain spectrin molecules are shown in the top row and pig erythrocyte spectrin tetramers in the bottom row. These molecules were selected to demonstrate structural similarities between the two spectrin species, such as their two-stranded, double-helical nature. Scale bar, 200 nm.



filaments. Overloaded gels of brain spectrin exhibited contaminating polypeptides, but each polypeptide contributed no more than 1–2% of the total protein. Furthermore, the contaminating polypeptides were not specifically adsorbed by F-actin (Fig. 5). It is therefore unlikely that additional proteins are required in a 1:1 ratio with spectrin for association of brain spectrin with actin. The possibility that a protein may act in sub-stoichiometric ratios cannot be excluded.

Discussion

Here we have described the purification from brain membranes of an immunoreactive analogue of erythrocyte spectrin which closely resembles spectrin in structure and shares functions of binding to erythrocyte membranes and to actin filaments. The brain analogue of spectrin comprises 3% of the total membrane protein, and it would be surprising if this protein had not been noticed previously. An actin-binding protein containing two polypeptides of molecular weight ~240K and 235K has been purified partially from brain and has been termed brain actin-binding protein³⁰. An axonally transported protein with two polypeptide chains of molecular weight ~250K and 240K has been isolated from the particulate fraction of brain, and demonstrated to bind to actin³¹. This protein was named fodrin and was localized by immunofluorescence in the cortical cytoplasm of cultured fibroblasts, neurones and intestinal epithelial cells. It was concluded that fodrin was not related to spectrin as antibody against fodrin did not form a precipitin reaction with erythrocyte spectrin. However, this result does not exclude cross-reactivity that is partial or of reduced affinity.

It is possible that several groups have discovered the same protein and named it differently. We suggest that, in view of the similarity to erythrocyte spectrin, this protein be referred to as brain spectrin. Polypeptides of similar molecular weight to brain spectrin which cross-react with spectrin antibody are present in liver plasma membranes (Fig. 2) and membranes from other tissues (not shown). These proteins are probably also spectrin analogues and can be named according to the cell or tissue of origin.

The extent of structural homology between erythrocyte spectrin and the brain analogue is of the order of 20% as determined by immunoreactivity (Fig. 1). This is much less than the homology observed in other families of proteins such as actins, calmodulins and intermediate filament polypeptides. It should be kept in mind that spectrin polypeptides are unusually large and a homologous region could have a molecular weight of as

much as 60,000. Furthermore, the extended rod-like conformation of spectrin may be compatible with more variation in amino acid sequence than the folding of a globular protein. It is pertinent in this regard that peptide maps of erythrocyte spectrin from different species are substantially different (see above), even though the proteins are almost identical in morphology. In view of these considerations and the demonstration of functional homology, we suggest that the spectrins are a multigene family of proteins with a common evolutionary origin. Erythrocyte spectrin is probably the most deviant member of

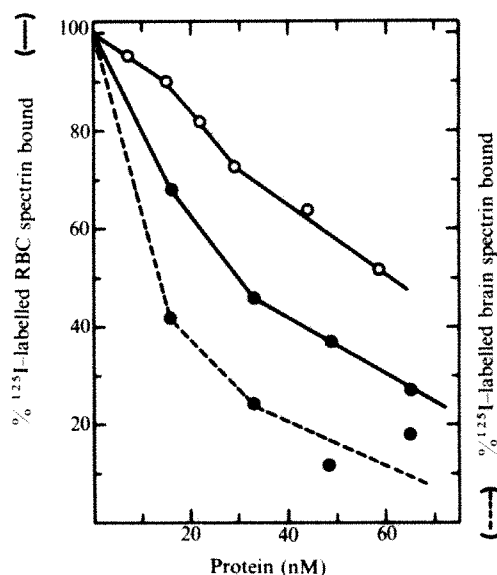


Fig. 5 Displacement of binding of ^{125}I -labelled erythrocyte (—) and brain (---) spectrin to spectrin-depleted erythrocyte membranes by unlabelled erythrocyte (●) and brain (○) spectrin. Binding of ^{125}I -labelled erythrocyte spectrin dimer (1 nM , $2 \times 10^6 \text{ c.p.m. pmol}^{-1}$) and ^{125}I -labelled brain spectrin (1 nM , $8 \times 10^5 \text{ c.p.m. pmol}^{-1}$) to spectrin-depleted inside-out vesicles from human erythrocytes ($20 \mu\text{g}$ membrane protein per assay) was measured as described elsewhere⁴⁵, in the presence of increasing concentrations of unlabelled brain spectrin (○) and pig erythrocyte spectrin dimer (●). The data are expressed as per cent binding in the absence of added proteins, and are corrected for nonspecific binding at each concentration of unlabelled proteins by subtracting values for ^{125}I -labelled proteins that were heat-denatured (10 min at 70°C).

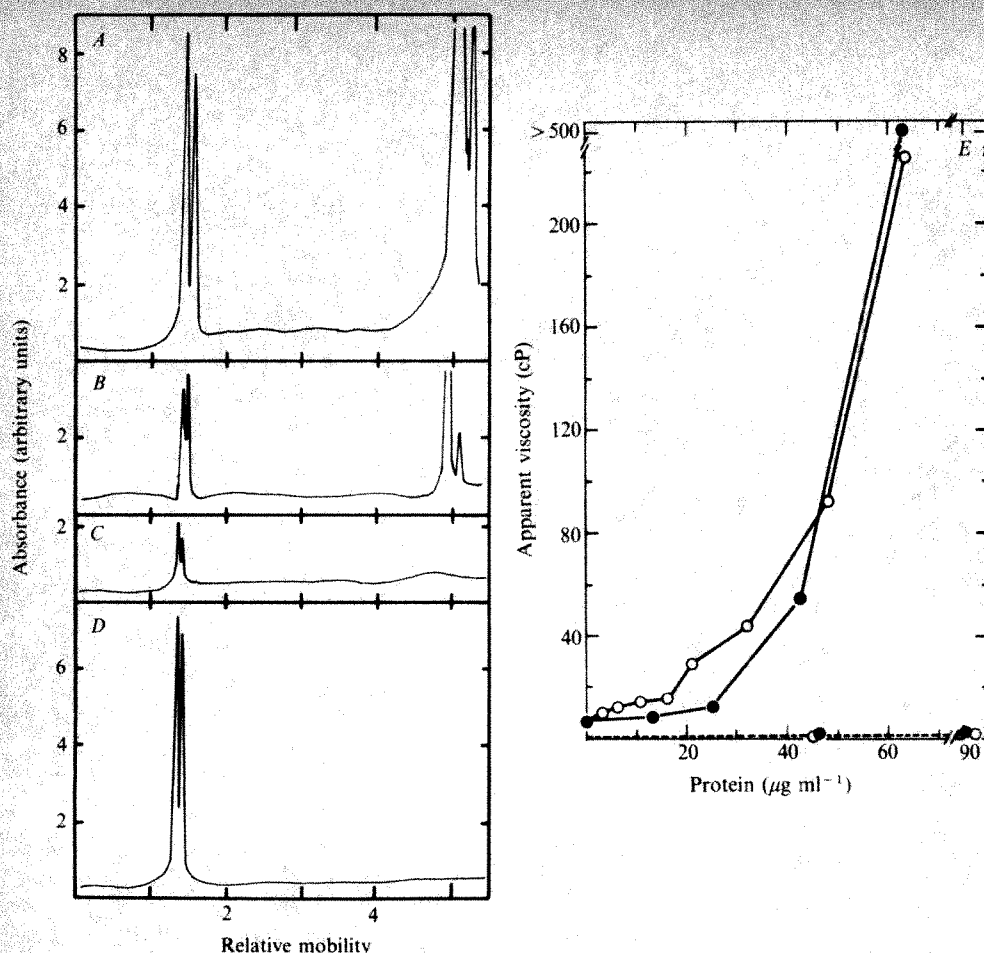


Fig. 6 Brain spectrin co-sediments with F-actin and increases the low-shear viscosity of F-actin. Brain spectrin ($60 \mu\text{g ml}^{-1}$) was incubated (60 min at 30°C) in the presence or absence of rabbit muscle actin⁴⁶ ($200 \mu\text{g ml}^{-1}$) in buffer containing 40 mM PIPES pH 6.8, 20 mM KCl, 1 mM MgCl_2 , 5 mM Na-EGTA. The proteins were layered over 10% (w/v) sucrose in the same buffer and centrifuged at $200,000g$ for 60 min. The pellets were resuspended in the original volume, and equal aliquots of pellets and supernatants analysed by SDS-polyacrylamide gel electrophoresis (see Fig. 1). The polypeptides were visualized with Coomassie blue, and the gels were scanned in a densitometer (left): A, pellet, brain spectrin and actin; B, supernatant, brain spectrin and actin; C, pellet, brain spectrin alone; D, supernatant, brain spectrin alone. E, effect of increasing concentrations of brain spectrin (\circ) on the low-shear viscosity of actin (0.8 mg ml^{-1}) was determined in the same buffer with a falling ball viscometer^{10,47}. For comparison, pig erythrocyte spectrin (tetramer/dimer ratio = 3) was tested in the same assay (\bullet). In the absence of actin the proteins had very low viscosity (---).

this family, as the functional constraints in these specialized cells are quite different from those in more complex cell types.

The widespread distribution of spectrins implies that functional analogues of ankyrin and band 3 should also be present in other cell types. A polypeptide of $M_r \sim 200,000$ that cross-reacts with antibody against ankyrin is associated with membranes of brain and the plasma membrane fraction of liver (not shown; ref. 32). Immunoreactive forms of band 3, detected with antibody against the cytoplasmic domain of band 3, are also present in the same membrane fractions as ankyrin and spectrin (not shown). It will be essential to purify and characterize these cross-reacting polypeptides to verify possible functions.

Spectrin in association with actin and band 4.1 forms a supportive lattice on the inner surface of the plasma membrane in erythrocytes, and spectrin may also participate in a similar structure in plasma membranes of other cells. Actin is associated with a detergent-insoluble matrix underlying the plasma membrane^{33,34}, and has been identified in association with the inner surface of the plasma membrane in several cases¹. Cells in tissues also have specialized regions of cell-cell contact such as zonula adherens and postsynaptic densities where actin filaments are attached to the membrane. Spectrin may function in these areas to couple actin to the membrane and to form a two-dimensional meshwork adjacent to the membrane analogous to the matrix in erythrocytes.

The spectrins are large enough to be visualized by high resolution electron microscopy of cells and tissues, and would appear as flexible filaments 2–4 nm wide. Filaments having these dimensions and lengths up to 300 nm have been observed in whole mounts of cells by high voltage electron microscopy

and seem to link actin to other cell structures³⁵. Filaments 4 nm wide have also been reported in postsynaptic densities—these were visualized by rapid freezing and rotary shadowing³⁶, and appear to interact with actin filaments as well as intramembrane particles. The narrow filaments do not correspond to previously studied structural proteins and may, at least in part, be composed of spectrin.

The widespread distribution of proteins closely related to erythrocyte spectrin and possibly other erythrocyte proteins suggests it will soon be possible to define in detail at least one generally occurring type of linkage of actin filaments to membranes. This information may explain how integral membrane proteins are organized and directed in their motions and will also be important in understanding how membranes are integrated with the cytoplasm.

Following submission of this article, a protein of similar structural features to brain spectrin has been purified from brain and intestine³⁷. Immunoreactive forms of spectrin and their distribution have also been observed in several tissues³⁸. A brain protein having similar properties to brain spectrin has been isolated³⁹.

This research was supported by grants to V.B. from the NIH (1 RO1 AM29808-1 and a Research Career Development Award) and the Muscular Dystrophy Association. W.E.F. was supported by a postdoctoral fellowship from the Muscular Dystrophy Association. Facilities for electron microscopy were funded in part by grants to Dr Ueli Aepli from the Muscular Dystrophy Association and the NIH (GM2-7765). We thank Drs Ann Hubbard and Larry Gerace for advice on the preparation of plasma membranes and nuclear envelopes from liver. Dr V. Fowler provided muscle actin and advice on measurement of low-shear viscosity.

Received 14 April; accepted 11 June 1982.

1. Weihing, R. B. *Meth. Achiev. exp. Path.* **8**, 42–109 (1979).
2. Koch, G. & Smith, M. *Nature* **273**, 274–278 (1978).
3. Flanagan, J. & Koch, G. *Nature* **273**, 278–281 (1978).
4. Ohnishi, T. *J. Biochem.* **52**, 307–308 (1963).

5. Tilney, L. G. & Detmers, P. J. *Cell Biol.* **66**, 508–520 (1975).
6. Branton, D., Cohen, C. M. & Tyler, J. *Cell* **24**, 24–32 (1981).
7. Bennett, V. *J. cell. Biochem.* **18**, 49–66 (1982).
8. Brenner, S. L. & Korn, E. D. *J. biol. Chem.* **254**, 8620–8627 (1979).
9. Ungewickell, E., Bennett, P. M., Calvert, R., Ohanian, V. & Gratzner, W. *Nature* **280**, 811–816 (1979).

10. Fowler, V. & Taylor, D. L. *J. Cell Biol.* **85**, 361–376 (1980).
11. Shotton, D. M., Burke, B. E. & Branton, D. *J. molec. Biol.* **131**, 303–329 (1979).
12. Bennett, V. & Stenbuck, P. *J. biol. Chem.* **254**, 2533–2541 (1979).
13. Luna, E., Kidd, G. & Branton, D. *J. biol. Chem.* **254**, 2526–2532 (1979).
14. Yu, J. & Goodman, S. *Proc. natn. Acad. Sci. U.S.A.* **76**, 2340–2344 (1979).
15. Calvert, R., Bennett, P. & Gratzner, W. *Eur. J. Biochem.* **107**, 355–361 (1980).
16. Litman, D., Hsu, C. J. & Marchesi, V. T. *J. Cell Sci.* **42**, 1–22 (1980).
17. Bennett, V. & Stenbuck, P. *J. biol. Chem.* **255**, 2540–2548 (1980).
18. Hargreaves, W. R., Giedd, K. M., Verkleij, A. & Branton, D. *J. biol. Chem.* **255**, 11965–11972 (1980).
20. Hiller, G. & Weber, K. *Nature* **266**, 181–183 (1977).
21. Goodman, S., Zagon, I. S. & Kulikowski, R. *Proc. natn. Acad. Sci. U.S.A.* **78**, 7570–7574 (1981).
22. Davis, J. & Bennett, V. *J. biol. Chem.* **257**, 5816–5820 (1982).
23. Bennett, V. *Nature* **281**, 597–599 (1979).
24. Bennett, V. & Davis, J. *Proc. natn. Acad. Sci. U.S.A.* **78**, 7550–7554 (1981).
25. Sattilaro, R. F., Dentler, W. L. & LeCluyse, L. *J. Cell Biol.* **90**, 467–473 (1981).
26. Votr, W. A. & Erickson, H. P. *J. Cell Biol.* **91**, 331a (1981).
27. Tyler, J. M., Reinhardt, B. & Branton, D. *J. biol. Chem.* **255**, 7034 (1980).
28. Morrow, J., Speicher, D., Knowles, W., Hsu, C. & Marchesi, V. T. *Proc. natn. Acad. Sci. U.S.A.* **77**, 6592–6597 (1981).

29. Bennett, V. *J. biol. Chem.* **253**, 2292–2299 (1978).
30. Shimo-Oka, T. & Watanabe, Y. *J. Biochem.* **90**, 1297–1307 (1981).
31. Levine, J. & Willard, M. *J. Cell Biol.* **90**, 631–643 (1981).
32. Bennett, V., Davis, J. & Fowler, W. E. *Phil. Trans. R. Soc. B* (in the press).
33. Luna, E., Fowler, V., Swanson, J., Branton, D. & Taylor, D. L. *J. Cell Biol.* **88**, 396–409 (1981).
34. Mescher, M., Jose, M. & Balk, S. *Nature* **289**, 139–144 (1981).
35. Schliwa, M. & van Blerkom, J. *J. Cell Biol.* **90**, 222–235 (1981).
36. Gulley, R. L. & Reese, T. S. *J. Cell Biol.* **91**, 298–302 (1981).
37. Glenney, J., Glenney, P. & Weber, K. *Cell* **28**, 843–854 (1982).
38. Repasky, E., Granger, B. & Lazarides, E. *Cell* **29**, 821–833 (1982).
39. Burridge, K., Kelly, T. & Connel, L. *Phil. Trans. R. Soc. B* (in the press).
40. Toda, G., Oka, H., Oda, T. & Ikeda, Y. *Biochim. biophys. Acta* **413**, 52–64 (1975).
41. Fleischer, S. & Kervina, M. *Meth. Enzym.* **31A**, 15 (1974).
42. Dwyer, N. & Blobel, G. *J. Cell Biol.* **70**, 581–591 (1976).
43. Elder, J. H., Pickett, R. A., Hampton, J. & Lerner, R. A. *J. biol. Chem.* **252**, 6510–6516 (1980).
44. Fowler, W. E. & Erickson, H. P. *J. molec. Biol.* **134**, 241–249 (1979).
45. Bennett, V. & Branton, D. *J. biol. Chem.* **252**, 2753–2763 (1977).
46. Spudich, J. A. & Watt, S. J. *J. biol. Chem.* **246**, 4866–4871 (1971).
47. MacLean-Fletcher, S. & Pollard, T. D. *Biochem. biophys. Res. Commun.* **96**, 18–27 (1980).

LETTERS TO NATURE

MERLIN spectral line observations of circumstellar shells around two OH/IR stars

R. P. Norris, P. J. Diamond & R. S. Booth

University of Manchester, Nuffield Radio Astronomy Laboratories, Jodrell Bank, Macclesfield, Cheshire SK11 9DL, UK

The OH maser emission from OH/IR stars shows structure on an arc second scale, and is therefore ideally suited to observation by the new Jodrell Bank Multi Element Radio Linked Interferometer Network (MERLIN)¹ operating in the spectral line mode². Here we present MERLIN observations of two OH/IR stars: OH127.8–0.0 and OH104.9+2.4. The spatial structure of OH127.8–0.0 revealed by Booth *et al.*³ using three single base line interferometers was consistent with a simple expanding shell model. Our maps of OH127.8–0.0 confirm this interpretation, whereas the circumstellar shell that we find around OH104.9+2.4 exhibits a more complex motion, which we interpret in terms of rotation.

The sources OH127.8–0.0 and OH104.9+2.4, hereafter called OH127.8 and OH104.9 respectively, were observed at 1612.231 MHz with four telescopes of MERLIN in March 1981. The measured cross-correlation functions on the six baselines were recorded every 30 s and then Fourier transformed off-line to yield a spectrum of 80 frequency channels on each baseline. The unresolved source BL Lac was also observed to calibrate and correct the data for both amplitude and phase variations across the bandpass. During the observations on each source, additional phase variations occur which are common to all channels. These are corrected as follows.

The emission in one channel, the reference channel, containing strong emission which need not be spatially simple or unresolved was mapped using the closure phase technique⁴. The resulting spatial distribution was then Fourier transformed to obtain ϕ_{ss} , the phase due to the source structure. The phases ϕ in the other frequency channels were then corrected using the relation

$$\phi' = \phi - \phi_{ref} + \phi_s - \phi_{BP}$$

where ϕ_{ref} is the observed phase of the reference channel and ϕ_{BP} is a small correction term describing the phase response of the instrument. The corrected phases ϕ' and the observed amplitudes were processed using the CLEAN algorithm⁵ to produce maps of the brightness distribution integrated over suitable velocity intervals.

The OH maser emission from OH/IR stars is characterized by a double-peaked spectrum, demonstrated by Fig. 1a, which

shows the autocorrelation spectrum of OH127.8. Neither OH127.8 nor OH104.9 have been detected optically, but they have been identified with the IR sources CRL230 and CRL2885 respectively. The stellar velocity is assumed to lie roughly at the midpoint of the velocities of the OH maser peaks, and the double-peaked spectrum may then be produced by expansion, contraction or rotation of circumstellar material containing the OH.

By analogy with OH/IR stars which do have optical identifications, the central star is probably an *M* giant star, but its mass may lie anywhere in the range from $\sim 1 M_{\odot}$, corresponding to a Mira variable, to $\sim 30 M_{\odot}$, corresponding to an *M* supergiant.

Figure 1a demonstrates that the flux density has decreased by approximately a factor of 3 compared with that measured in 1980³. Such variations in intensity are well known in OH/IR

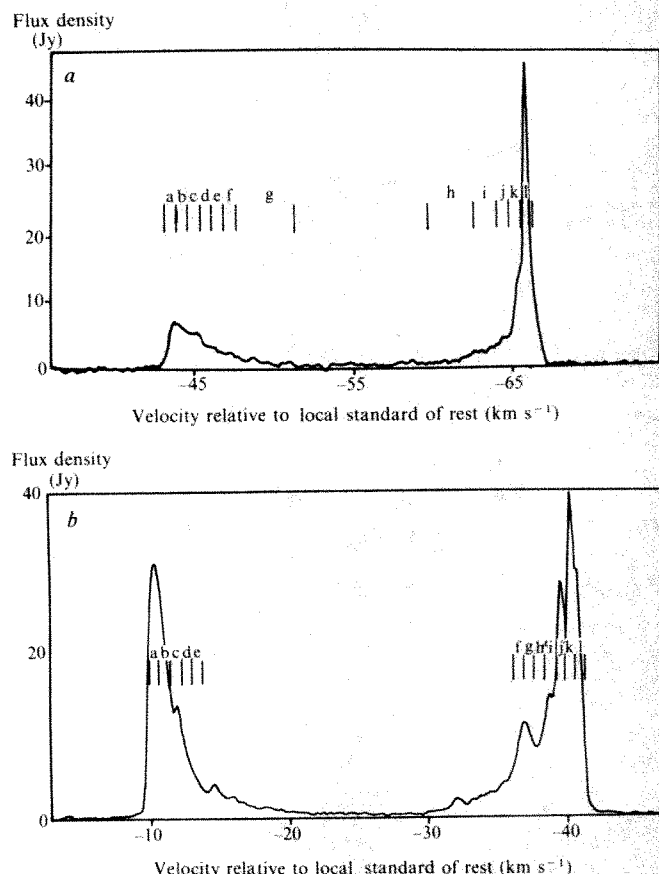
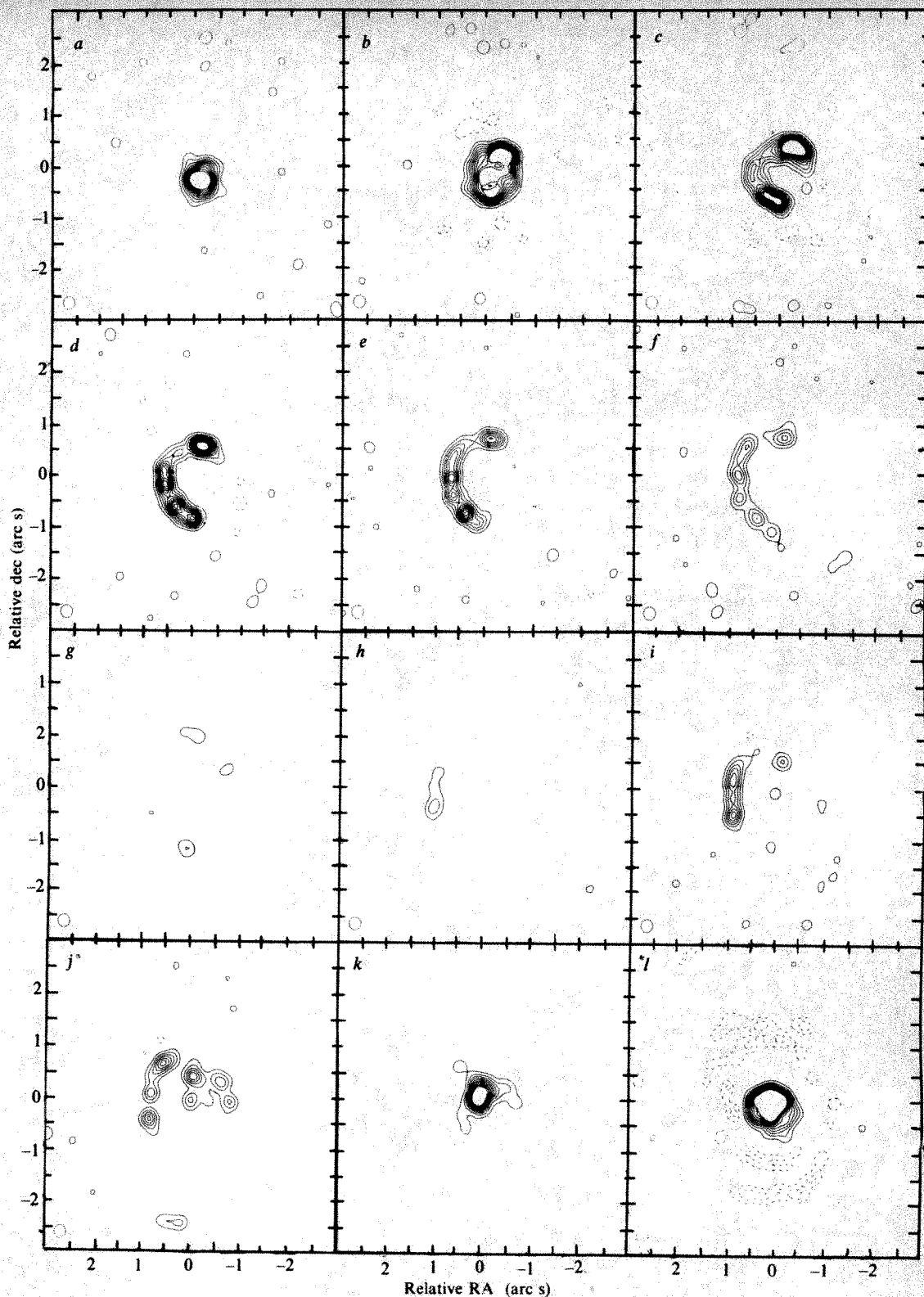


Fig. 1 Autocorrelation spectrum of: a, OH127.8; b, OH104.9 measured in July 1981.

Fig. 2 Maps of the emission in each of the 12 frequency channels shown in Fig. 1a. The lowest contour level and the contour spacing are 0.1 Jy per beam area, except for maps *k* and *l* in which the lowest contour level is 0.3 Jy. Map *l* is the reference feature mapped using the closure phase technique. Only the lowest 10 contours are shown in each case.



stars^{6,7}. Unfortunately, this reduction in brightness precludes our detecting the weaker emission detected by Booth *et al.*, preventing a detailed correspondence between the two sets of maps.

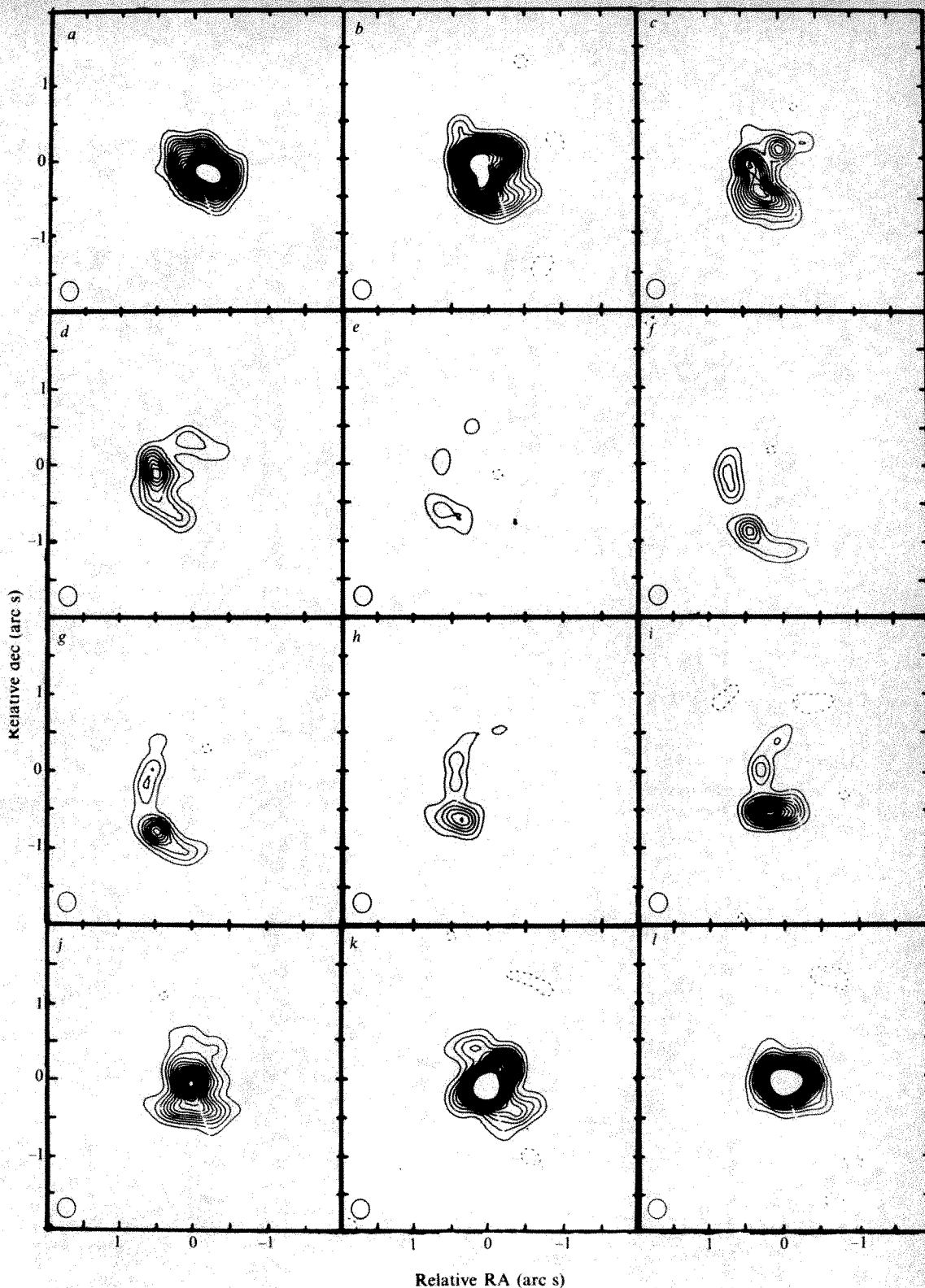
Also shown in Fig. 1a are 13 velocity ranges. Each of the maps in Fig. 2 represents the spatial distribution of the masing gas within the corresponding velocity interval in Fig. 1a. These maps have greater frequency resolution than those published by Booth *et al.*³ and confirm their earlier interpretation. The similarity of these maps to those of Booth *et al.*, despite the variation in intensity, confirms that the variations are a result of changes in the brightness of the star's IR radiation which

pumps the OH masers, rather than changes within the masing gas.

The maps show that the emission at each of the two ends of the spectrum emanates from two spatially coincident compact regions at the centre of the source, whilst the weaker emission towards the centre of the spectrum shows a roughly annular distribution. The radii of the annuli increase with decreasing velocity separation from the centre of the spectrum, in the way expected for a uniformly expanding shell of OH. The knots and gaps in the annuli indicate some turbulence or inhomogeneities in the expanding shell.

The spectrum of OH104.9, shown in Fig. 1b has a similar

Fig. 3 Maps of the emission in each of the 12 frequency channels shown in Fig. 1b. The lowest contour level and the contour spacing are 0.5 Jy per beam area. Contours above a flux density of 10 Jy have been suppressed.



overall form to that of OH127.8 but is not as smooth and indicates a more complex motion. This is reflected in the maps shown in Fig. 3 in which no complete annuli are observed. However, the strong emission at each end of the spectrum again emanates from a region close to the centre of the source.

Note that there is no detectable emission in a region to the west of the source. However, because the maser requires a uniform line of sight velocity along its length, the maser process is extremely sensitive to inhomogeneities and anisotropies in the gas dynamics. Therefore the absence of emission may be explained as a random perturbation or non-uniformity in the gas dynamics. Such irregularities have already been seen in OH26.5 (ref. 9).

Relative RA (arc s)

A detailed study of the components in the maps shows a further systematic departure from a simple expanding shell model. For example, in the regions to the north and south of the centre, components in the front and back of the shell which appear spatially coincident have a mean velocity of -25.8 km s^{-1} , whereas similarly coincident components to the east have a mean velocity of -25.3 km s^{-1} .

For a uniformly expanding shell, the radius $a(v)$ at which the line of sight component of the expansion velocity is v is given by

$$a(v) = R[1 - (v/v_e)^2]^{1/2}$$

where v_e is the expansion velocity and R is the shell radius.

Table 1 Parameters of the model for OH127.8 and OH104.9

	OH127.8	OH104.9
RA of centre relative to coordinate centre (arc s)	-0.11 ± 0.01	-0.12 ± 0.01
Dec. of centre relative to coordinate centre (arc s)	-0.15 ± 0.01	-0.21 ± 0.01
Position angle of rotation axis (deg)	10 ± 5	0 ± 5
Stellar velocity relative to the local standard of rest (km s^{-1})	-55.4 ± 0.2	-25.8 ± 0.2
Expansion velocity (km s^{-1})	10.9 ± 0.2	14.3 ± 0.2
Rotation velocity (km s^{-1})	0.2 ± 0.1	-0.9 ± 0.1
Shell radius (arc s)	1.53 ± 0.02	1.44 ± 0.02

These values assume that the rotation axis is perpendicular to the line of sight, because the fit is insensitive to this parameter. The quoted errors are estimated 1σ uncertainties.

For material in a uniform expanding shell, therefore, a plot of $\log a$ against $\log[1 - (v/v_e)^2]$ should yield a straight line with a gradient of 0.5. A plot of these quantities for some of the components of OH104.9 is shown in Fig. 4. The components to the north and south of the centre follow the uniform expanding shell model, but the components to the east, which are shown in Fig. 4, do not. Departure from a gradient of 0.5 may be caused either by an error in the assumed position of the expansion centre or by an incorrect value of v_e . Similarly, separation on the plot of high and low velocity components which are spatially coincident may be caused by an incorrect value of the central (stellar) velocity. However, even if all these parameters are allowed to vary, there is still no solution for a uniformly expanding, non-rotating shell which fits all the observed data.

We conclude that the kinematics of the components depart from a simple expanding shell model not only because of small-scale turbulence as mentioned above, but also because of a large scale non-radial motion. The simplest explanation of the non-radial motion is that the shell is rotating about the star as well as expanding from it. The kinematics of a rotating, expanding, thin shell are easily modelled and we have used a computer least squares program to fit such a model to the data on OH127.8 and OH104.9, resulting in the parameters given in Table 1. In each case, there is excellent agreement between the model and the data, and the r.m.s. error in velocity is $\sim 0.3 \text{ km s}^{-1}$, which is less than half our velocity resolution of 0.8 km s^{-1} . The model for OH127.8 shows no significant rotation, but the shell around OH104.9 is rotating with an equatorial speed of 0.9 km s^{-1} .

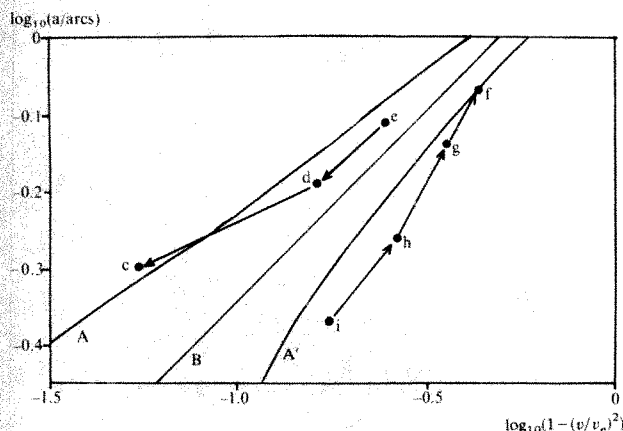


Fig. 4 A plot of $\log_{10} a$ against $\log_{10}(1 - (v/v_e)^2)$ for components at position angle 90° (see text). Line B is the curve expected from a simple expanding shell model. Lines A and A' are the curves expected from a rotating expanding shell. ●, The observed data, and the arrows connecting them are in the direction of increasing velocity. Despite the large scatter in the data points, they show clearly the bifurcation expected from a rotating expanding shell. Small letters against data points correspond to the maps in Fig. 3.

The angular momentum of the shell may be derived either from rotation of the star or from the orbital angular momentum of a binary companion. The former explanation implies a high rate of angular momentum loss from the star, leading us to favour the second explanation. A plausible model would separate the binary companion from its primary by $\sim 10^{15} \text{ cm}$, implying an orbital period of the order of hundreds of years. The current position of the companion, which may destroy the conditions for maser emission, may lie to the west of the source, where there is no detectable OH maser emission. These models are developed and discussed in more detail in ref. 10.

The evaluation of the mass loss rate from long period variable stars is of great importance in understanding stellar evolution. By assuming³ a molecular hydrogen number density of $2 \times 10^4 \text{ cm}^{-3}$, we derive a mass loss rate of $8 \times 10^{-5} M_\odot \text{ yr}^{-1}$ for OH127.8 and $5 \times 10^{-5} M_\odot \text{ yr}^{-1}$ for OH104.9. Such high mass loss rates agree well with the IR properties of OH/IR stars¹¹, although they imply a short lifetime for a star in this state.

We have produced further evidence for the evidence of a simple expanding shell around OH127.8, and have shown that OH104.9 possesses a shell which is rotating as well as expanding, and may be a member of a binary system. It is clearly necessary to extend these results to other sources, and such work is in progress.

Received 13 May; accepted 2 July 1982.

1. Davies, J. G., Anderson, B. & Morison, I. *Nature* **280**, 64–66 (1980).
2. Norris, R. P., Booth, R. S. & Diamond, P. J. *Mon. Not. R. astr. Soc.* (in the press).
3. Booth, R. S., Kus, A. J., Norris, R. P. & Porter, N. D. *Nature* **290**, 382–384 (1981).
4. Cornwell, T. J. & Wilkinson, P. N. *Mon. Not. R. astr. Soc.* **196**, 1067–1086 (1981).
5. Hogbom, J. A. *Astr. Astrophys. Suppl.* **15**, 417–426 (1974).
6. Jewell, P. R., Webber, J. C. & Snyder, L. E. *Astrophys. J. Lett.* **242**, L29–L31 (1980).
7. Herman, J. & Habing, H. in *Proc. Workshop on Physical Processes in Red Giants*, Erice (1980).
8. Norris, R. P. & Booth, R. S. *Mon. Not. R. astr. Soc.* **195**, 213–226 (1981).
9. Baud, B. *Astrophys. J. Lett.* **250**, L79–L83 (1981).
10. Diamond, P. J., Norris, R. P., Booth, R. S., Withington, S. W. & Rowland, P. R. 1982 (in preparation).
11. Werner, M. W. *et al. Astrophys. J.* **239**, 540–548 (1980).

Ion nucleation—a potential source for stratospheric aerosols

F. Arnold

Max-Planck-Institut für Kernphysik, Postfach 103 980, 6900 Heidelberg, FRG

The stratospheric aerosol layer is of considerable interest for its potential influence, at least temporarily, on the Earth's radiation budget and climate¹. While the nature of the aerosol is now reasonably well established the mechanisms leading to the formation of new particles are poorly understood^{2–4}. It is thought that the aerosols are formed by heterogeneous heteromolecular condensation involving sulphuric acid and water vapour and pre-existing condensation nuclei (CN) of tropospheric or meteoric origin. The resulting supercooled solution droplets which are composed of $\sim 75\%$ (by mass) H_2SO_4 and 25% H_2O undergo condensational and coagulational growth and are ultimately removed from the stratosphere by gravitational sedimentation. CN-formation in the stratosphere by homogeneous or ion nucleation (IN) has largely been found to be inefficient^{2–6}. I have now investigated the role of recent progress in both the areas of stratospheric ion composition⁷ and sulphuric acid vapour^{8–10} measurements. In contrast to previous conclusions ion nucleation is found to be a potential source for stratospheric aerosols.

Ion nucleation involves growth of ions by association of gas molecules to a critical size at which the resulting molecular cluster is stable against evaporational destruction after neutralization of its net charge by ion-ion recombination. In

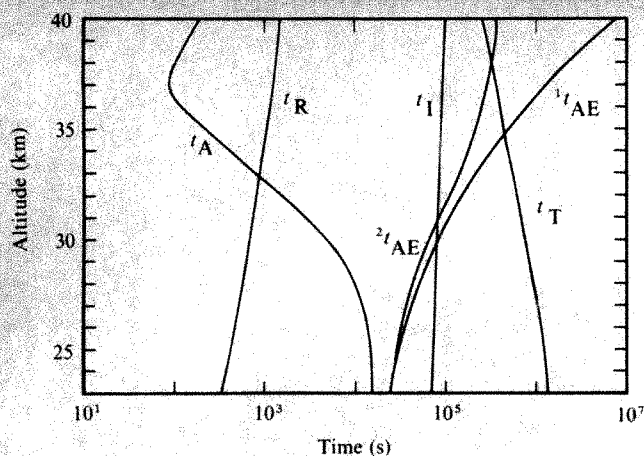


Fig. 1 Typical time scales for ion growth (t_A), ion-ion recombination (t_R), H_2SO_4 attachment to ions (t_I) and aerosols (t_{AE}) and vertical turbulent transport (t_T). For t_A two cases, H_2SO_4 - H_2O aerosols ($^1t_{AE}$) and, in addition to these, meteoric smoke particles ($^2t_{AE}$) (7% recondensation of meteor vapour) are given¹⁷. For details see text. For t_R evaluation measured α and n_{\pm} values were taken.

stratospheric conditions only molecular clusters containing H_2SO_4 and H_2O molecules can form CN. Consequently only ions containing H_2SO_4 and H_2O molecules can be involved in IN. It has been found recently⁷ from balloon-borne composition measurements of stratospheric negative ions that the most abundant ion species above 27 km are H_2SO_4 (H_2SO_4) $_n$ (H_2O) $_m$ and that these already develop properties similar to H_2SO_4 - H_2O solution droplets for $n \geq 3$. The time scale for addition of an H_2SO_4 molecule to an ion is $t_A = (k[H_2SO_4])^{-1}$ where k is a phenomenological binary rate coefficient for H_2SO_4 association being typically of the order of $10^{-9} \text{ cm}^3 \text{ s}^{-1}$ in the conditions considered^{11,12} and $[H_2SO_4]$ is the concentration of H_2SO_4 -vapour molecules.

The ion lifetime compared with ion-ion recombination is $t_R = (\alpha n_{\pm})^{-1}$ where α is the effective ion-ion recombination coefficient and n_{\pm} is the total charged particle concentration.

The abundance ratio $R_{n+1,n}$ for ions containing $n+1$ and n H_2SO_4 molecules is obtained from a simple steady state treatment

$$R_{n+1,n} = (1 + t_A/t_R)^{-1} \quad (1)$$

accordingly one obtains the approximation

$$R_{n_c,0} = (1 + t_A/t_R)^{-n_c} \quad (2)$$

where n_c is the number of H_2SO_4 molecules contained in an ion cluster which also remain stable against evaporational destruction after neutralization.

Thus the ion nucleation rate is

$$J = Q(1 + t_A/t_R)^{-n_c} \quad (3)$$

where Q is the galactic cosmic ray ionization rate, being of the order of $10 \text{ cm}^{-3} \text{ s}^{-1}$ in the middle stratosphere¹³.

The critical quantity n_c may be set equal to the number of H_2SO_4 molecules contained in an electrically neutral drop which is just stable and whose size may be obtained from the Kelvin expression¹⁴. The latter relates the droplet radius r_c to the supersaturation ratio $S = p/p_0$ where p and p_0 are the partial and equilibrium saturation pressures for sulphuric acid vapour. For $S \leq 6$, n_c becomes larger than ~ 10 and increases steeply as S increases. This is consistent with laboratory studies¹⁵ of IN suggesting that IN becomes efficient for $S \geq 4-6$. However, usually in these studies $t_A \ll t_R$, in contrast to the stratospheric situation.

Typical t_A and t_R values are shown in Fig. 1. Measured α and n_{\pm} were taken (ref. 16, and D. Smith, personal communication) and k was set equal to $10^{-9} \text{ cm}^3 \text{ s}^{-1}$. Values for $[H_2SO_4]$ were taken from recent measurements⁸⁻¹⁰ (Fig. 2) where it was

found that $[H_2SO_4]$ below ~ 27 km is similar to the lower limit curve predicted by the theoretical model case of Turco *et al.*¹⁷ which neglects H_2SO_4 re-evaporation from the aerosol. Above ~ 35 km, $[H_2SO_4]$ is similar to the upper limit curve CHA 75) predicted by a purely photochemical diffusive model¹⁸ which neglects H_2SO_4 condensation. In the intermediate altitude range (27-35 km) $[H_2SO_4]$ is similar to $[H_2SO_4]_e$, the expected equilibrium saturation pressure for H_2SO_4 over the aerosol^{9,10}.

Thus it appears that $S < 1$ above ~ 35 km, $S = 1$ between ~ 27 and 35 km and $S > 1$ below ~ 27 km. That implies that aerosols are unstable above ~ 35 km and that IN can occur only at heights below ~ 27 km. Since $[H_2SO_4]_e$ increases strongly as temperature increases, the $[H_2SO_4]_e$ curves are different for winter and summer due to seasonal temperature changes. Corresponding $[H_2SO_4]_e$ curves for winter (45 W) and summer (45 S) and 45° latitude are also shown in Fig. 2.

Ion nucleation rates J calculated from equation (3) for average winter and summer temperatures at 45° latitude are shown in Fig. 3. Here the curve T80 (Fig. 2) was taken as a lower limit to $[H_2SO_4]$.

Generally the calculated J values increase as height increases and decrease abruptly above a certain height where S becomes smaller than ~ 10 and where consequently n_c becomes large. This is due to the large t_A/t_R ratios in this height region. Maximum J values of about $3 \times 10^{-3} \text{ cm}^{-3} \text{ s}^{-1}$ (winter) and $5 \times 10^{-4} \text{ cm}^{-3} \text{ s}^{-1}$ (summer) are reached around 29 km and 24 km respectively. Corresponding column IN rates J_c are $\sim 9.3 \times 10^2 \text{ cm}^{-2} \text{ s}^{-1}$ (winter) and $1.6 \times 10^2 \text{ cm}^{-2} \text{ s}^{-1}$ (summer). By comparison, the globally averaged J_c required to maintain the stratospheric aerosol layer is only of the order of $0.01 \text{ cm}^{-2} \text{ s}^{-1}$.

Thus IN apparently has the potential to form more CN than required to seed the stratospheric aerosol layer.

However, a large fraction of the newly formed CN may become removed before they can grow a new aerosol solution droplet. Loss processes may involve mostly CN attachment to aerosols. The lifetime of a gas molecule (molecular weight 29) against collision with aerosols t_{AE} is given in Fig. 1. Below 30 km it is of the order of only 10^4 - 10^5 s. In comparison, the time scale for adding an H_2SO_4 -gas molecule to a CN having a radius of 10^{-7} cm is of the order of 10^4 s. Thus a newly formed CN can pick up a few more H_2SO_4 -vapour molecules before it collides with an aerosol solution droplet. This is particularly true as the CN lifetime against collision with aerosols should be much larger than t_{AE} due to the large CN mass.

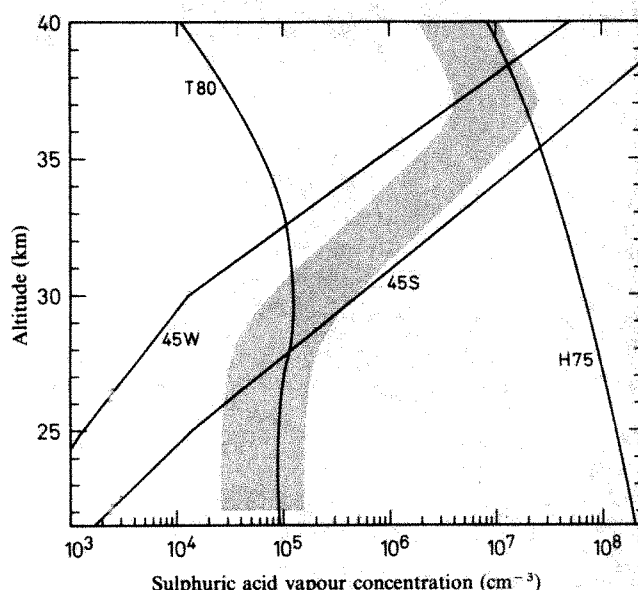


Fig. 2 Sulphuric acid vapour concentrations. Measured values⁸⁻¹⁰ are indicated by the shaded area. Extreme cases as obtained from theoretical model calculations are indicated by H75 (all sulphuric acid in the gas phase¹⁷) and T80 (no re-evaporation of sulphuric acid vapour¹⁶) for average winter and summer temperatures at 45° latitude are also shown.

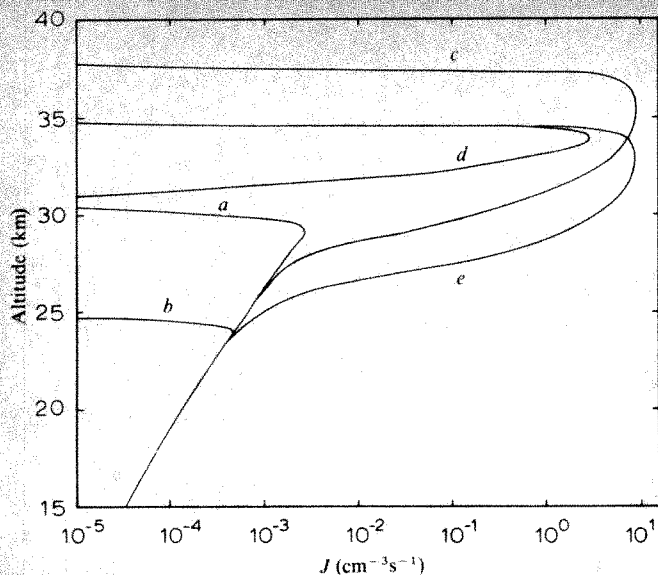


Fig. 3 Calculated ion nucleation rates J : a , average winter temperatures (T_w); b , average summer temperatures (T_s); c , cooling from T_s to T_w ; d , cooling from $T_s + 5$ to T_s ; e , cooling from $T_s + 10$ to T_s .

Assuming a CN lifetime against attachment to aerosols of 10^5 s and a yearly averaged J of the order of 10^{-3} $\text{cm}^{-3} \text{s}^{-1}$ around 25–30 km one obtains an average CN concentration $[\text{CN}]$ of the order of 100 cm^{-3} for the 25–30-km region and 10 cm^{-3} for 20 km.

Measured¹⁹ $[\text{CN}]$ are about $1\text{--}100 \text{ cm}^{-3}$ (25–30 km) and $1\text{--}10 \text{ cm}^{-3}$ (20 km) and compare reasonably well with the above model predictions for altitudes below about 25–30 km.

However, no CN formation occurs above 25–30 km in the conditions considered and therefore CN must be transported, mostly by turbulent diffusion, to this height range. The time scale for vertical turbulent diffusion t_T (per kilometre) is given in Fig. 1, being $\sim 10^5\text{--}10^6$ s (1–10 days). Thus it is much larger than the CN lifetime against collision with aerosols, which implies that little vertical CN transport should occur below ~ 35 km. Consequently, CN observed above 25–30 km can hardly be explained by the above IN model.

In the stratosphere, however, dramatic departures from a condensation–evaporation equilibrium for sulphuric acid can occur. These should be induced by short-term temperature changes which are quite common, particularly at latitudes $>45^\circ$ during local winter²⁰. An example of temperature changes at 35 km in Fig. 4 shows measured temperatures along with average summer (S), spring–autumn (SA) and winter (W) values. Typical amplitudes and time scales are about $5\text{--}10^\circ$ and one to a few days respectively in winter; occasionally, dramatic temperature enhancements, ‘sudden stratospheric warmings’, occur²⁰ during which temperatures may even exceed summer values. These events are thought² to arise mostly from large amplitude planetary waves pumping heat energy from the tropical troposphere and stratosphere to the polar regions. Thus, the radiative imbalance in the atmosphere arising from the smaller amount of solar radiation absorbed at high latitudes is compensated through adiabatic processes.

As the temperature increases, $[\text{H}_2\text{SO}_4]$ increases (by about a factor of 10 per 10° (refs 22, 23). Eventually the entire $\text{H}_2\text{SO}_4\text{--H}_2\text{O}$ aerosol may evaporate, depending on the maximum temperature reached, in which case $[\text{H}_2\text{SO}_4]$ would be equal to curve H75 (Fig. 2). As the temperature falls again, sulphuric acid vapour may become highly supersaturated with respect to the condensed $\text{H}_2\text{SO}_4\text{--H}_2\text{O}$ phase.

The time scale for H_2SO_4 -vapour recondensation on aerosols is larger than t_{AE} (Fig. 1), being ~ 1 day around 30 km. This implies that high supersaturations may persist for at least 1 day.

A typical case for a major winter warming would be a temperature rise to average summer values and a subsequent cool-

ing to average winter values which implies a maximum S of ~ 3 (Fig. 2). Corresponding J values are shown in Fig. 3 (curve c). Around 35 km they become comparable to Q ($10 \text{ cm}^{-3} \text{s}^{-1}$) and fall off steeply above and less steeply below this height. The thickness of the IN layer is ~ 5 km. The fall-off towards larger heights is mostly due to a decrease of S causing a steep increase of n_c . The fall-off towards smaller heights is mostly due to the decrease of $[\text{H}_2\text{SO}_4]$ causing an increase of t_A/t_R .

Summer IN events for temperature increases of 5° and 10° and subsequent coolings to average summer values are also shown in Fig. 3 (curves d and e). These IN layers peak around 34 and 33 km respectively and are ~ 1.5 and 5 km thick respectively.

For curves c , d and e maximum J values are sufficiently large to allow for a rapid build-up of a limiting $[\text{CN}]$, being of the order of 10^5 cm^{-3} within <1 day. For $[\text{CN}] \geq 10^5 \text{ cm}^{-3}$ the lifetime of a CN against mutual CN coagulation becomes ≤ 1 day. For $[\text{CN}] = 10^5 \text{ cm}^{-3}$ the lifetime of an H_2SO_4 -vapour molecule against attachment to a CN is of the order of $10^4\text{--}10^5$ s. Consequently the supersaturated H_2SO_4 vapour should become consumed by condensation onto the newly formed CN within a day or less, leading to an average aerosol corresponding to only $10^3\text{--}10^4$ H_2SO_4 molecules or $\sim 4\text{--}8 \times 10^{-7}$ cm in radius.

In the days after their formation the CN undergo further mutual CN coagulation until $[\text{CN}]$ has fallen to a level of $\sim 10^3\text{--}10^4 \text{ cm}^{-3}$, at which the time scale for coagulation becomes weeks to months. At these time scales vertical turbulent diffusion becomes efficient, having a time scale t_T of the order of a few days per kilometre. Vertical turbulent diffusion leads to a broadening of the CN layer and a further decrease of the peak $[\text{CN}]$ value.

Upward diffusion carried the CN into a region where $S < 1$ leading to CN evaporation. Downward diffusion carries CN into a region of large S where they are safe from evaporational destruction by subsequent warming events.

It appears then that IN due to warming–cooling events is an efficient CN source at heights around 27–37 km. It may give rise to average $[\text{CN}]$ values of the order of $10^3\text{--}10^4 \text{ cm}^{-3}$, corresponding to average CN sizes of 1.6×10^{-6} cm and 8×10^{-7} cm respectively.

The column IN rates J_c corresponding to curves c , d and e (Fig. 3) are $\sim 4 \times 10^7 \text{ cm}^{-2} \text{s}^{-1}$, $1 \times 10^7 \text{ cm}^{-2} \text{s}^{-1}$ and $4 \times 10^7 \text{ cm}^{-2} \text{s}^{-1}$.

The column IN production for long-lived CN only (lifetime >1 day) are $\sim 6 \times 10^{10} \text{ cm}^{-2}$, $1 \times 10^{10} \text{ cm}^{-2}$ and $6 \times 10^{10} \text{ cm}^{-2}$. In comparison, the persistent IN source existing below

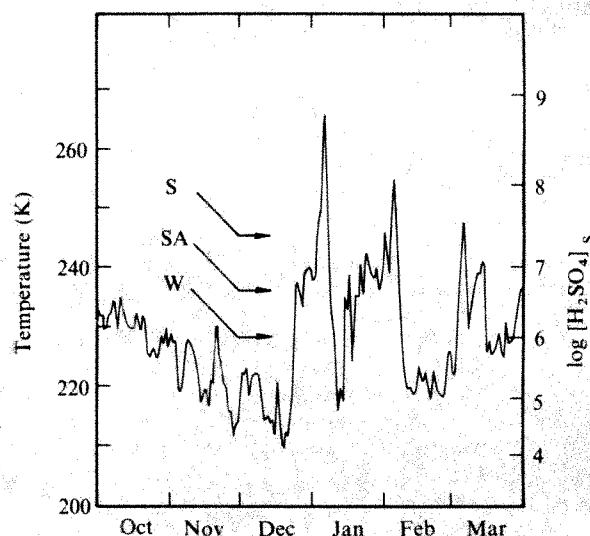


Fig. 4 Stratospheric temperatures (E. Pantzke, personal communication) as measured at 35 km altitude over Berlin (52°N , 14°E) during the winter 1975–76. Corresponding saturation concentrations for sulphuric acid vapour and average winter-, spring–autumn- and summer temperatures²⁴ are also given.

25–30 km leads to a column production of $\sim 2 \times 10^{10} \text{ cm}^{-2}$ for an entire year.

Thus the warming-cooling events contribute substantially to, or even dominate, the overall CN production. Regionally and during certain periods of time they give rise to large CN concentrations in the 27–37 km range.

Note that there is a possible influence of solar activity on the CN production by IN. Galactic cosmic radiation, the only important source of ionization in the undisturbed stratosphere, is partly shielded by the interplanetary magnetic field which gives rise to an anticorrelation of Q and solar activity. Typically Q values by about a factor of 4 over a solar sunspot cycle at middle latitudes. Since $n_{\pm} = (Q/\alpha)^{1/2}$, t_R varies by a factor of about 2. The t_R curve shown in Fig. 1 and used for the above calculations corresponds to solar sunspot maximum conditions (large t_R).

For solar sunspot minimum, t_R is smaller by a factor of 2, leading to smaller IN rates, particularly in conditions where $t_A/t_R \gg 1$. For example, the maximum value of curve a (Fig. 3) would be smaller for solar sunspot minimum conditions by about a factor of 10.

Thus the global CN production by IN may be substantially smaller during conditions of low solar activity. As a consequence the aerosol size distribution may shift towards larger sizes as fewer CN compete for the available sulphuric acid. As a change of the aerosol size distribution may affect the radiation properties of the stratospheric aerosol layer, solar activity changes may modulate the possible influence of the stratospheric aerosol layer on the Earth's radiation budget and climate.

Finally possibilities for observational tests of the ion nucleation hypothesis will be discussed. Observable quantities are [CN], [H₂SO₄] and the ion composition. Concerning [CN] the IN model seems to be in harmony with measurements. In particular the CN layer recently detected by Hofmann and Rosen¹⁹ around 30–35 km is readily explained and its major features are reasonably well reproduced by the IN model.

It seems, however, that predicted [CN] values are larger than observed ones. As far as [H₂SO₄] and ion composition measurements are concerned only few data exist. It would be desirable to carry out coordinated measurements of [CN], [H₂SO₄] and ion composition during a major winter warming-cooling event. During the early phase of the cooling large S values and very complex ion clusters should occur while large [CN] values should persist for days after the onset of the cooling.

Note that the above model calculations of IN are only rough approximations and that extensive model calculations of stratospheric IN should be carried out.

I thank D. J. Hofmann, P. Hamill, K. Labitzke and B. Naujokat for helpful discussions, and E. Pantzke for providing stratospheric temperature data.

Received 3 March; accepted 8 June 1982.

- Pollack, J. B. *et al.* *J. geophys. Res.* **81**, 1971 (1976).
- Cadle, R. D. & Grams, G. W. *Rev. Geophys. Space Phys.* **13**, 475 (1975).
- Toon, O. B. & Farlow, N. H. *A. Rev. Earth planet. Sci.* **9**, 19 (1981).
- Castleman, A. W. Jr *A. Rev. Earth planet. Sci.* **9**, 227 (1981).
- Hamill, P., Turco, R. P., Toon, O. B., Kiang, C. S. & Whitten, R. C. *J. Aerosol Sci.* (submitted).
- Mohnen, V. A. *Proc. 4th Conf. on CIAP* (US Department of Transportation, 1975).
- Arnold, F., Viggiano, A. & Schlager, H. *Nature* **297**, 371–376 (1982).
- Arnold, F. & Fabian, R. *Nature* **283**, 55 (1980).
- Arnold, F., Fabian, R. & Joos, W. *Geophys. Res. Lett.* **8**, 293 (1981).
- Arnold, F., Fabian, R., Ferguson, E. E. & Joos, W. *Planet. Space Sci.* **29**, 195 (1981).
- Viggiano, A. A., Perry, R. A., Albritton, D. L., Ferguson, E. E. & Fehsenfeld, F. C. *J. geophys. Res.* **85**, 4551 (1980).
- Webber, W. J. *Geophys. Res.* **67**, 5091 (1962).
- Thomfor, G. & Volmer, M. *Ann. Phys.* **5**, 109 (1939).
- Castleman, A. W. Jr *Adv. Colloid Interface Sci.* **10**, 73 (1979).
- Gringel, W., Hofmann, D. J. & Rosen, J. M. *Rep. No AP-47* (University of Wyoming, Laramie, 1978).
- Turco, R. P., Toon, O. B., Hamill, P. & Whitten, R. C. *J. geophys. Res.* **86**, 113 (1981).
- Harker, A. B. *J. geophys. Res.* **80**, 3399 (1975).
- Hofmann, D. M. & Rosen, J. M. *Nature* **297**, 120 (1982).
- Labitzke, K. *J. geophys. Res.* **86**, 9665 (1981).
- Schoeberl, M. R. *Rev. Geophys. Space Phys.* **16**, 521 (1978).
- Ayers, G. F., Gillett, R. W. & Gras, J. L. *Geophys. Res. Lett.* **7**, 433 (1980).
- Rödel, W. *J. Aerosol Sci.* **10**, 375 (1979).
- U.S. Standard Atmosphere Supplements* (US Government Printing Office, Washington DC 1966).

Ozone vertical distribution and total content using a ground-based active remote sensing technique

J. Pelon & G. Megie

Service d'Aéronomie du CNRS, BP 3, 91370-Verrieres-Le-Buisson, France

The evaluation of possible perturbations of anthropogenic origin on the Earth environment has become increasingly important with the development of industrial and agricultural activities. Among these the depletion of the ozone layer under the influence of chemically active minor constituents produced by anthropogenic sources is still under question, thus emphasizing the importance of ozone monitoring in the atmosphere. Beside classical systems, such as the Dobson spectrometer and Brewer or ECC sondes, new techniques of ozone monitoring are being developed which include passive IR and microwave spectrometry and active IR and UV laser soundings¹. They should soon allow complementary routine measurements. We have previously described² the UV lidar system set up at the Observatoire de Haute Provence (44° N, 6° E) in the south of France and the methodology of the differential absorption laser technique (DIAL) which provide routine measurements of the ozone vertical distribution from the ground up to 25 km. We report here the first active ground-based measurements of the ozone distribution at higher altitudes up to 40 km and of the total ozone content using the same system.

Attempts to measure ozone number density above its maximum using a ground-based UV system are complicated because the extinction of the laser emitted light is high due to the absorption in the lower altitude layers. Furthermore the rapid decrease in ozone number density above 28 km requires very rapidly increasing acquisition times for the measurement². To overcome these major problems, a different wavelengths pair B (305.8–310.8 nm) was chosen to probe the upper levels (13–38 km) as compared with the one A (288.8–294.5 nm) previously adopted for the lower altitude range. These wavelengths choices minimize the interferences by other absorbing gases (SO₂–NO₂) and by aerosol particles and optimize the signal-to-noise ratio². Whereas ozone distribution measurements in the boundary layer can be performed using the DIAL method³, we have restricted our measurements to the altitude range above 3 km to avoid any problem related to geometrical effects and to the large dynamic of the backscattered signals in the first few kilometres. Compared with the previously reported measurements², a factor of 5 reduction in the acquisition time has been obtained by increasing the receiving telescope diameter from 36 to 80 cm. The parameters of the lidar system are listed in Table 1. Adopted values for the ozone absorption cross-sections are those of Inn and Tanaka⁴ corrected for temperature dependence as given by Vigroux⁵.

Figure 1 represents two lidar measured ozone profiles as obtained on 1 and 2 December 1981 at 00 h UT. The acquisition time for each profile is 90 min. The vertical resolution varies between 360 m in the troposphere, 1.2 km at 25 km and 3.6 km

Table 1 Parameters of the lidar system

Emitted wavelengths		
A pair	$\lambda_1 = 288.80 \text{ nm}$	$\lambda_2 = 294.50 \text{ nm}$
B pair	$\lambda_1 = 305.80 \text{ nm}$	$\lambda_2 = 310.80 \text{ nm}$
Spectral width $\Delta\lambda < 5 \text{ pm}$		
Emitted energy $E = 40 \text{ mJ-10 Hz}$		
Divergence $< 0.5 \text{ mrad}$		
Telescope $\phi 80 \text{ cm}$		
Field of view 0.7 mrad		

at 35 km and above. A moving parabolic least-square regression is used to fit the experimental data². The 1σ -standard deviation is better than 5% up to 25 km and decreases down to 20% at the uppermost level. To avoid systematic errors due to the aerosol particles extinction, the aerosol layers were detected by simultaneously recording the lidar backscattered signals at 532 nm. No enhanced aerosol layer was detected during these measurements and no further correction was performed on the 0.3- μ m lidar signals². As a comparison, the ozone distribution measured using a classical Brewer-Mast sonde launched by the Météorologie Nationale at Biscarrosse (44° N, 0.5° W) on 30 November at 13 h 30 UT is also shown in Fig. 1. The agreement between the various profiles can be considered as satisfactory above 20 km, only a systematic bias <1.5% between the Brewer and lidar measurements was detected. At lower altitudes the variations observed in the ozone number density can be attributed to horizontal inhomogeneities due to dynamical motions as they are frequently observed in this altitude range: a north-south circulation was established at the 100-mbar level over western Europe in early December⁶ which could explain the variations observed. In any case, previous comparisons of lidar and ECC measured ozone profiles below 25 km have shown the reliability of the DIAL remote sensing technique⁷.

Both wavelengths pairs A and B were used to measure the ozone number density between 13 and 15 km: considering several profiles obtained during successive nights a systematic bias was detected showing ozone values 2% higher when measured using the A pair. This discrepancy can be related (1) to uncertainties in the absolute values of the cross-sections and (2) to the very high spectral resolution of the laser measurements as compared with the spectrometric ones^{4,5}. Due to experimental uncertainties, the detected bias between the A, B pairs and Brewer measurements could only be considered as estimations in this first approach; as the overall bias was not larger than 2% no final adjustment was performed.

The total ozone content can be derived from the measured vertical distribution. Various sources of uncertainty then have to be considered²:

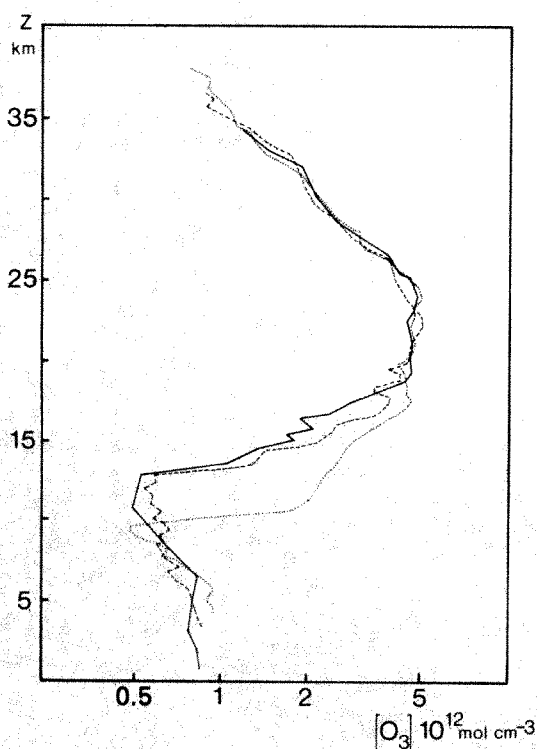


Fig. 1 Ozone concentration profiles measured by lidar at the OHP on 1 December 1981 (dashed line) and 2 (dotted line) at 0 h UT compared with the profile obtained by a Brewer sonde launched at Biscarrosse on 30 November 1981 at 13 h 30 UT (solid line).

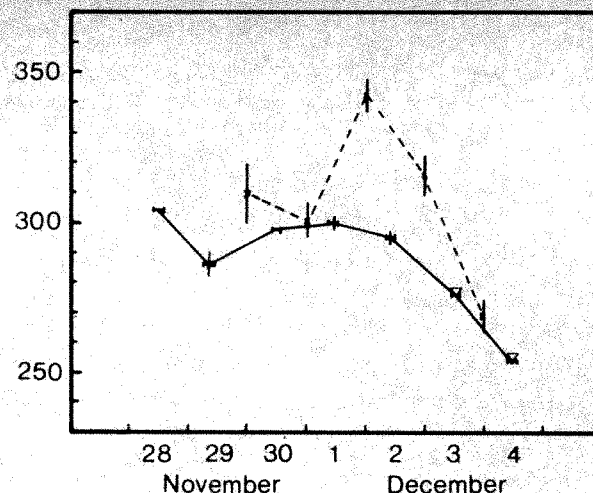


Fig. 2 Total ozone measured by lidar at the OHP (dashed line) and Dobson spectrometers at Biscarrosse (solid line) and Arosa (∇).

- (1) The statistical fluctuations of the detected signals which constitutes the major error source estimated to be <10 Dobson units in a 95% confidence interval. This error can be further reduced by increasing the acquisition time.
- (2) The Rayleigh extinction by the atmospheric gas molecules: this uncertainty is reduced below 0.1 Dobson unit by correcting the lidar data using the pressure, temperature and humidity distribution as measured by radiosonde at the nearby meteorological station of Nîmes (44° N, 5° E).
- (3) The Mie differential extinction by aerosol particles: this uncertainty which can be large at lower altitudes² is reduced when using the A wavelength pair to measure the total content up to 15 km which leads to high ozone optical thickness as compared with the aerosol contribution. It can be estimated to be <1 Dobson unit whereas the use of the B pair in the same altitude range will have resulted in a one order of magnitude higher uncertainty.
- (4) A systematic bias due to the discrepancies already pointed out between the two wavelength pairs and the absolute cross-sections determinations.
- (5) A constant value of 10.4 Dobson units which corresponds to the average ozone content above 40 km (ref. 8): the 2σ -standard deviation results in a 3.2 Dobson units uncertainty similar to that introduced at the lower boundary by the extrapolation of the ozone distribution down to the ground level.

The lidar derived values of the ozone total content have been plotted on Fig. 2 together with the values obtained from the Dobson spectrometer measurements performed at Arosa (46° N, 10° E) and Biscarrosse. The values obtained on 29 and 30 November and 3 December are in a good agreement with a maximum difference of 3%. On 1 December a difference of 47 Dobson units is observed which decreases down to 25 Dobson units on 2 December. It corresponds to the variations measured between 10 and 18 km when considering the vertical distributions (Fig. 1) and can thus be related as already pointed out, to the horizontal transport. Further validation of the lidar system's ability to measure the total ozone content will imply correlative measurements with a Dobson spectrometer set up at the same location which is within the scope of future developments of the geophysical station at the Observatoire de Haute Provence.

The main advantage of the remote sensing technique described above is the direct determination of the ozone number density with an independent instrument which does not require any internal or inter-calibration. This advantage can then be extended to the measurement of the total ozone content. The preliminary measurements presented here will be improved: the development of new laser sources such as excimer lasers

providing higher output energy in the same wavelength range could thus be a further determining step.

This work was supported under contract 79-71020 from the Délégation Générale de la Recherche Scientifique et Technique. The development of the O.H.P. lidar facility is supported by CNRS and INAG. We thank Professor C. Fehrenbach, Director of the Observatoire de Haute Provence for hospitality, also Dr H. Dütsch and A. Lovisa for providing the results of the Dobson spectrometers and Brewer sonde measurements.

Received 20 May; accepted 7 July 1982.

1. Global Ozone Research and Monitoring Project, Rep. 9 (WMO, Boulder, 1980).
2. Pelon, J. & Mégie, G. *J. geophys. Res.* **87**, 4947-4956 (1982).
3. Browell, E. V., Carter, A. F. & Shipley, S. T. *Proc. Quadrennial int. Ozone Symp.*, Boulder, 99-107 (1981).
4. Inn, E. C. Y. & Tanaka, Y. *J. opt. Soc. Am.* **43**, 870 (1953).
5. Vigroux, E. *Ann. Phys.* **8**, 709 (1953).
6. *European Meteorological Bulletin*, Frankfurt (1981).
7. *Upper Atmospheric Programs Bulletin*, D.E.E. (AEE 300) 81-2, 5 (Washington DC, 1981).
8. Krueger, A. J. & Minzer, R. A. *J. geophys. Res.* **81**, 4477-4481 (1976).

Copper sulphide $\text{Cu}_{1.8}\text{S}$ (Digenite I) precipitation in mild steel

J. E. Harbottle & S. B. Fisher

Central Electricity Generating Board, Berkeley Nuclear Laboratories, Berkeley, Gloucestershire GL13 9PB, UK

The microstructure of mild steel pressure vessel plate and weldments has recently been examined by transmission electron microscopy (TEM) to characterize certain numerous small ($<1,000 \text{ \AA}$) matrix precipitates and relate them to the bulk mechanical properties of the steel. The TEM examination was undertaken using in-line energy dispersive (EDAX) spectrometry. In view of the strong influence of Cu on radiation hardening and embrittlement in steels¹ particular emphasis was placed on the identification of any copper-bearing precipitates within the grains. We report here the first observation of discrete particles of copper sulphide, positively identified as $\text{Cu}_{1.8}\text{S}$ (Digenite I), and found only in the matrix of the mild steel weld specimens. In spite of having a similar copper content to the plate, the precipitation of copper sulphide uniquely in the welds is thought to arise from the high temperature oxidizing environment experienced during welding. This favours the formation of $\text{Cu}_{1.8}\text{S}$ in the presence of soluble copper from the less stable FeS commonly found in sulphur-bearing steels. The importance of this observation in relation to the mechanical properties of the steel is briefly discussed.

Examination of the microstructure of mild steel plate and weld materials, similar to those used for reactor pressure vessels, is aimed at identifying and measuring the matrix precipitate populations and relating their presence to the bulk mechanical properties. As the most numerous precipitates, and therefore those having the greatest hardening effect, are also the smallest ($<100\text{--}1,000 \text{ \AA}$) they require for identification micro-probe TEM with in-line EDAX and EELS spectrometers. These instruments permit concurrent convergent beam electron diffraction together with energy dispersive and energy-loss analyses. Electron microscope specimens in the form of extraction replicas of the steels were specially prepared and mounted to reveal precipitates having a wide compositional range. The composition typical of all the steels is: C 0.1, Mn 1.0-1.8, Si 0.1-0.4, Cr 0.05, Cu 0.05-0.2, S 0.01-0.03 wt %.

In view of the marked effect of small amounts of copper on certain post-irradiation mechanical properties^{2,3}, such as increases in yield stress and the ductile-brittle transition temperature, particular emphasis was placed on the detection and identification of copper-bearing precipitates in the grains. Special precautions were taken to eliminate stray copper signals from within the microscope. Before this study observations

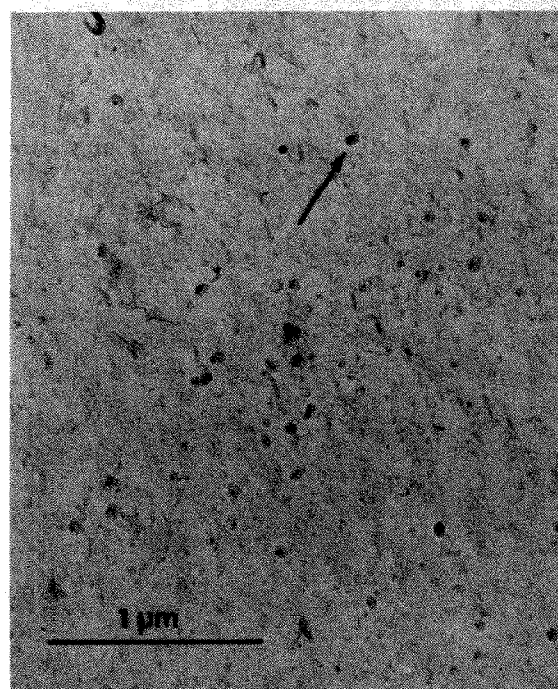


Fig. 1 Bright-field micrograph of copper sulphide $\text{Cu}_{1.8}\text{S}$ precipitation in a mild steel weld grain.

have been reported on the presence⁴, but not the crystallographic identity, of small copper-bearing precipitates in the matrix of mild steels. Small unidentified precipitates have been seen on dislocations and in the grains following ageing^{5,6} and irradiation⁷ of Fe-Cu alloys. These were assumed to be either copper precipitates or copper-vacancy complexes.

In the present study, irregularly shaped precipitates having sizes in the range $100\text{--}360 \text{ \AA}$ and a density of $\sim 10^{11} \text{ mm}^{-3}$ were observed throughout the grains of the as-welded specimens. A typical bright-field micrograph is shown in Fig. 1. These precipitates were not present in the plate material. Energy dispersive analysis indicated the presence of only copper and sulphur (Fig. 2) and the associated electron diffraction patterns (Fig. 3) consistently fitted data from the f.c.c. copper sulphide phase $\text{Cu}_{1.8}\text{S}$ (Digenite I). Copper sulphide precipitation was also found after a typical stress-relieving anneal at 600°C for 6 h, demonstrating its stability at this temperature and indicating that it was formed at high temperature during the welding process. This result is the first experimental proof of the existence of copper sulphide in steels, the crystallographic structure having been originally determined from a sample of the naturally occurring digenite mineral⁸.

The possibility that copper sulphide may form in mild steels was first suggested by Melford⁹ in a study of surface hot shortness. A feature of this effect is the localized enrichment of certain residual elements (Cu, Ni, S, Sn) that occurs below the surface scale during heating in an oxidizing environment to temperatures in excess of $\sim 1,200^\circ\text{C}$. Similar conditions will prevail during welding. A microprobe analysis of a section through the scale showed⁹ that the copper peak often coincided with an enrichment of sulphur, suggesting the presence of copper sulphide. The close association of these two elements for an individual particle near the scale was verified by mapping, although no electron diffraction pattern was obtained to provide positive identification of the particular compound.

Due to its relative insolubility ($<0.03 \text{ wt \%}$ at $1,200^\circ\text{C}$) any sulphur present in iron during steel manufacture combines to form either MnS or FeS depending on the Mn:S ratio¹⁰. Copper on the other hand is soluble up to 9 wt % in γ -iron¹¹, varying little in the temperature range $1,050\text{--}1,250^\circ\text{C}$, and therefore remains free to combine with other elements during welding, for example. Free energy calculations⁹ show that, in the

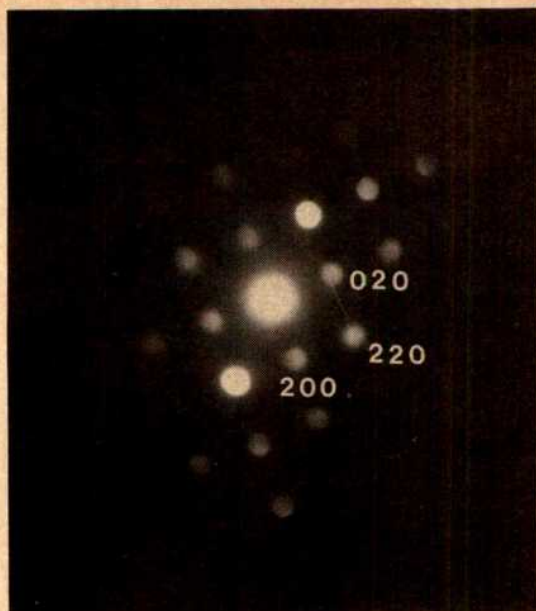
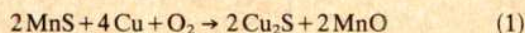
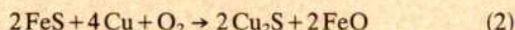


Fig. 2 Electron diffraction pattern from the arrowed particle in Fig. 1. The zone axis is [001] and the camera constant = 23.61 mm Å.

presence of oxygen and at temperatures approaching melting, copper sulphide should form from either FeS or MnS, following the reactions



and



Although we have found MnS in the large weld product inclusions but not in the weld matrix, the presence of MnO is never detected. However, FeO is commonly found throughout the matrix. This suggests that reaction (2) is the most likely to account for the observed $\text{Cu}_{1.8}\text{S}$ and FeO in the weld metal, where the high temperature, oxidizing environment would favour the transformation of FeS and the formation of copper sulphide. These conditions are not met in general in the plate material and explains the absence of both copper sulphide and wüstite in these specimens.

This result contributes principally to the understanding of copper's role in changing the yield stress of irradiated or aged ferritic steels. Previously it has been assumed that the increased hardening (or DBTT) is due to all the copper, initially in solid solution, being free to form either copper-vacancy complexes during irradiation or precipitates during thermal ageing. This

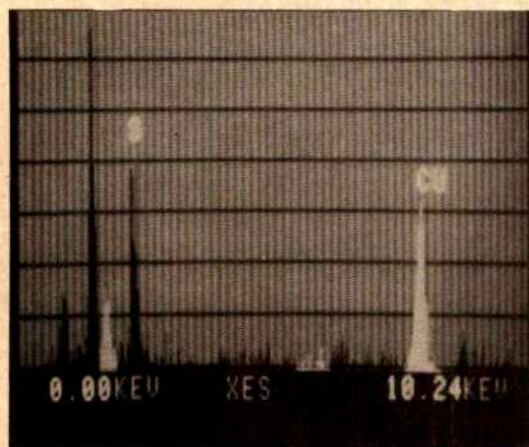


Fig. 3 EDAX spectrum from $\text{Cu}_{1.8}\text{S}$ particle. The highest peak arises from the aluminium grid holding the replica.

result shows that a proportion (up to 100% in some welds) of the total copper is precipitated as $\text{Cu}_{1.8}\text{S}$ and is therefore no longer available as free copper atoms. This can significantly reduce its influence in causing subsequent increases in yield stress. Hawthorne's¹² recent measurements support these results by showing that the addition of sulphur always reduces the detrimental effect of copper on radiation sensitivity in steels. The net change in yield stress depends on the relative quantities of free and precipitated copper. By taking the latter into account a good correlation may be obtained between the yield stress increase of various irradiated steels and (soluble copper content)^{1/2} based on a barrier hardening model.

This letter is published by permission of the Central Electricity Generating Board.

Received 9 June; accepted 13 July 1982.

1. Potapovs, U. & Hawthorne, J. R. *Nucl. Apps.* **6**, 27-46 (1969).
2. Wullaert, R. A., Sheckherd, J. W. & Smith, R. W. *Am. Soc. Testing Mater. Spec. Tech. Publ.* **611**, 400 (1976).
3. Biemiller, E. C. & Byrne, S. T. *Am. Soc. Testing Mater. Spec. Tech. Publ.* **611**, 418-433 (1976).
4. Lott, R. G., Brenner, S. S., Miller, M. K. & Wolfenden, A. *Trans. Am. nucl. Soc.* **38**, 303-304 (1981).
5. Hornbogen, E. & Jung, H.-P. *Acta Metall.* **10**, 525-533 (1962).
6. Fujii, A., Nemoto, M., Suto, H. & Monma, K. *Trans. J. Inst. Metals* **9**, 374-380 (1968).
7. Takaku, H. & Tokiwai, M. *J. Nucl. Mats.* **80**, 57-68 (1979).
8. Morimoto, N. & Kullerud, G. *Am. Miner.* **48**, 110-123 (1963).
9. Melford, D. A. *J. Iron Steel Inst.* **200**, 290-299 (1962).
10. Mann, G. S. & Van Vlack, L. H. *Metall. Trans.* **B7**, 469-475 (1976).
11. Melford, D. A. *Phil. Trans. R. Soc. A295*, 89-103 (1980).
12. Hawthorne, J. R. *Trans. Am. nucl. Soc.* **38**, 304-305 (1981).

Pressure dependence of glass dissolution and nuclear waste disposal

R. A. Lewis & R. L. Segall

School of Science, Griffith University, Nathan 4111, Australia

Schemes to dispose of high-level radioactive waste by vitrification and subsequent burial call for an appraisal of the consequences of groundwater encountering the waste glass¹. Glass dissolution rates are influenced not only by properties of the glass and solvent themselves but also by properties of the combination such as the glass surface area to solvent volume ratio². Although pressure may affect glass dissolution rates, it has not received unambiguous explicit experimental investigation. A simple experiment has been designed to determine dissolution rates at room temperature of glass samples subject to very high pressure in a centrifuge. The results reported here show that the dissolution rates for Na and Si increase slightly with pressure, but that at a pressure of 160 MPa (>1,500 atm) these dissolution rates are still of the same order as those at atmospheric pressure.

Thermodynamic principles have been used to explain dissolution and redeposition under pressure in solutions at equilibrium³ but are not pertinent to dissolution kinetics which are dealt with here. Pressure effects on the solvent are not likely to be important in the dissolution double layer where large electric fields dominate⁴. Likewise, throughout this experiment, dissolution is not rapid enough for the diffusion of ions away from the surface to be a rate limiting factor. On the other hand, mass transport by diffusion in the glass might well be restricted by compression. Modification of the electronic surface states of the glass by pressure will alter their position relative to states in the solvent⁵. The application of pressure to elucidate electronic properties of semiconductors is well-known. Pressure may introduce a new, less stable phase in the glass or, in the extreme, devitrification. Hence, the study of the overall effect of pressure is germane to the development of a comprehensive theory of glass dissolution as well as having considerable practical relevance to high-level radioactive waste disposal.

Table 1 Glass composition (wt %)

SiO ₂	55.53
B ₂ O ₃	29.26
Li ₂ O	4.94
Na ₂ O	10.27
	100.00

The glass utilized was the precursor of a radioactive waste storage glass (designated 189 or M5) fabricated at AERE Harwell; its composition is given in Table 1. The stability of this simple glass in water is relatively poor. The complete high-level waste glass, which contains metallic oxides such as MgO and Al₂O₃ from Magnox waste, is considerably more durable. Beads of 2.5 mm diameter formed under surface tension by heating cubes of glass on graphite were used. The annealing sequence consisted of heating from 20 to 727 °C at 320 °C min⁻¹, holding at 727 °C for 2 min, cooling to 427 °C at 5 °C min⁻¹ and then to 20 °C at 80 °C min⁻¹. The surface is therefore well-annealed and, essentially, flame-polished. A bead was placed with 12.5 ml of deionized distilled water in each of three cellulose nitrate centrifuge tubes. The base of each tube was 152 mm from the centrifuge axis and the depth of water in each tube was 86 mm. These tubes, together with three tubes containing water alone, were spun at 20 °C in an ultracentrifuge for 45 h. The experiment was performed at centrifugation speeds 28, 35 and 40 × 10³ r.p.m. which correspond to pressures of 80, 120 and 160 MPa respectively. A control experiment consisting of six tubes was also left for 45 h without spinning. The liquid in each of the tubes was analysed for Na and Si in solution by flame atomic absorption spectrophotometry. The behaviour of the other glass constituents namely Li, an alkali and B, a glass former, would be expected to follow that of Na and Si respectively. The mean and the best estimate of the standard deviation, $\sigma(n/(n-1))^{1/2}$, for each set of data were calculated. The results for Na are presented in Fig. 1.

A small increase in the Na loss with pressure, is evident in Fig. 1. Using the Student's *t* statistic, the hypothesis that the amounts of Na measured in solution after attack at 0.1 and 160 MPa are the same is first rejected at a level of significance of 0.04. At the same level of significance the hypothesis can be rejected that the amount of Na in solution for the 160 MPa experiment compared with the one at 0.1 MPa is greater by a factor of two. It is plausible, therefore, to argue that Na leaching is slightly enhanced at the higher pressure. The analysis for Si in solution by flame atomic absorption is less accurate than that for Na, but Si exhibits a similar small increase in loss with pressure. Clearly no marked effect occurs.

Scanning electron micrographs of the glass beads before aqueous attack are basically featureless. After attack at both ambient and elevated pressures scanning electron micrographs show typical features of glass surfaces following aqueous treat-

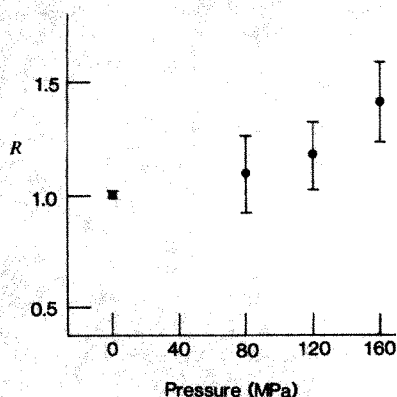


Fig. 1 The effect of pressure on glass dissolution rates, measured by the ratio, *R*, of Na loss at pressure to ambient loss.

ment—fissuring and erosion. However, there is no systematic alteration in the surface features with increasing pressure.

A general theory of the progress of glass dissolution has yet to be developed, but three stages of aqueous attack may be distinguished. For short times, the loss of material from the glass is largely the product of alkali leaching and varies as $t^{1/2}$. This regime is conveniently described by diffusion theory⁵. During intermediate times, the amount of material in solution varies as t^1 , being the result of the constant break down of the glass network. Chemical kinetics are often used to explicate the pertinent mechanisms⁶. Over long times, when the glass is either completely dissolved or the saturation of the liquid ensures redeposition at the same rate as dissolution, the amount of material in solution is constant. This state is dealt with by thermodynamics⁷.

In the present case, considering the 0.1 MPa results, the extent of Na loss is $1.42 \pm 0.03\%$ and for Si the loss is $0.7 \pm 0.3\%$. Evidently the loss of Na by exchange with H⁺ has at least occurred, and may still be occurring, when the experiment was terminated. The comparable loss of Si indicates that network break down has also been taking place. The concentrations of these ions in solution—Na, $0.59 \pm 0.01 \mu\text{g ml}^{-1}$; Si, $0.9 \pm 0.4 \mu\text{g ml}^{-1}$ —is well below saturation. In relation to the three stages of attack outlined above, in the conditions of this experiment the glass has been subject to the first and the second, but not the third stage. This may appear surprising for aqueous attack at such a low temperature (20 °C) and for such a short duration (45 h). This glass, however, is known to be very easily corroded. Other experiments in our laboratory have shown that a 10 mm × 2 mm disk of the glass dissolves entirely in <48 h at 170 °C in 15 ml of water. A variety of nuclear waste glasses show only 0.5–2% dissolution when subject to these conditions.

A difficulty in interpreting glass dissolution measurements is the large number of variables which influence the glass-solvent interaction. These include properties of the glass, such as its composition, homogeneity, melt history, environmental history, surface preparation and physical form; properties of the solvent such as its pH and species in solution; and properties of the glass-solvent system, such as the duration of contact, nature of solvent flow and temperature⁸. While it cannot be asserted that the effect of pressure will be negligible in conditions different from those of the present experiment, a knowledge of the mechanisms of the attack contributes to confidence that this is so. No conspicuous difference in the amount of Na present as a result of ambient and high pressure attack is apparent. A difference would be expected if pressure grossly affected the mechanisms occurring at the $t^{1/2}$, or diffusion stage. Likewise, the lack of marked change in the Si concentrations indicates no large effect of pressure on the mechanisms operating at the t^1 , or network break down stage.

The maximum pressure considered in this experiment is more than seven times the pressure of water at the critical point (374 °C, 22 MPa) and well above that expected in underground high-level waste repositories⁹. This experiment provides no evidence that pressure effects will be of importance in the disposal of high-level waste in glass. Absence of a pronounced pressure effect on dissolution kinetics makes a useful simplification to the complex set of variables in the glass-solvent interaction.

We thank S. Myhra, R. St. C. Smart and P. S. Turner for helpful comments. This research was supported by the Australian Institute for Nuclear Science and Engineering.

Received 17 March; accepted 6 July 1982.

- McCarthy, G. J. *et al.* *Nature* **273**, 216–217 (1978).
- Clark, D. E. & Yen-Bower, E. Lue. *Surface Sci.* **100**, 53–70 (1980).
- Durney, D. W. *Nature* **235**, 315–317 (1972).
- Morrison, S. R. in *The Chemical Physics of Surfaces*, 263–277 (Plenum, New York, 1977).
- Doremus, R. H. *J. Non-Crystalline Solids* **19**, 137–144 (1975).
- Budd, S. M. *Phys. Chem. Glasses* **2**, 111–114 (1961).
- Paul, A. *J. Mater. Sci.* **12**, 2246–2268 (1977).
- Cousens, D. R. *et al.* *Radioactive Waste Management* **2**, 143–168 (1981).
- Donath, F. A. *Nucl. Chem. Waste Management* **1**, 103–110 (1980).

Origin of sulphur and geothermometry of hydrothermal sulphides from the Galapagos Rift, 86° W

Russell Skirrow

Applied Geochemistry Research Group,
Department of Geology, Royal School of Mines, Imperial College,
London SW7 2BP, UK

Max L. Coleman

Isotope Geology Unit, Institute of Geological Sciences,
64 Gray's Inn Road, London WC1X 8NG, UK

Polymetallic hydrothermal massive sulphides from a mid-ocean ridge were first recovered in 1978^{1,2}, from the East Pacific Rise (EPR) at 21° N, and later 'black smokers' were found³ debouching fluids at 380° ± 30 °C. The Galapagos Rift and Fracture Zone Intersection (GRAFZI) Project of 1980 discovered sulphides in inactive mounds with up to 27% Cu and 31% Fe at 86° W on the Galapagos Rift⁴, that are chemically very different from the EPR 21° N sulphides (up to 50% Zn). Stable isotope studies were initiated in an attempt to find the origin of the sulphide sulphur, to determine the temperature of formation of an equilibrium assemblage of chalcopyrite (CuFeS₂) and pyrite (FeS₂), and to understand the operative seawater/rock ratio, and therefore the controls on permeability of the oceanic crust responsible for producing hydrothermal sulphides. There has been relatively little similar work on samples from 21° N (refs 5–7). We report here results which indicate sulphide formation at 390° ± 20 °C that is almost identical to that of the 21° N black smokers which were measured directly by temperature probe. The seawater sulphate contribution to the sulphur of the sulphides was much more dominant than at 21° N (ref. 7), and suggests a more fractured crust and/or more rapid hydrothermal solution flow rates, induced from higher seawater/rock ratios.

Reflected light microscopy was used to select samples in which the finely intergrown pyrite and chalcopyrite appeared to have precipitated in isotopic equilibrium. The samples were subjected to quantitative X-ray diffraction⁸ to check their purity and the relative proportions of the two minerals of interest were determined to an accuracy of ±10%. Isotopic analyses of eight samples of sulphide and two of amorphous hydrated silica were carried out in late 1981.

The two samples of amorphous silica were subjected to a citrate/dithionite-buffered leach⁹ to remove contaminant iron oxides, and then heavy mineral separation to remove intermixed sulphides, before oxygen isotope analysis. After standard preparation of sulphur dioxide¹⁰ and oxygen (by fluorination¹¹), $\delta^{34}\text{S}$ and $\delta^{18}\text{O}$ results were produced using two separate VG Micromass mass spectrometers, a 602-C double collector and a 903 triple collector, respectively. Raw data were corrected for change-over valve leakage and for isobaric interference¹² and expressed relative to the Canon Diablo Meteorite, troilite phase (CDT) for sulphur, and standard mean ocean water (SMOW) for oxygen.

The inactive hydrothermal massive sulphides were recovered from the southern margin of the northern rift valley of the double-rifted system at 86° W, and were associated with a faulted perched block⁴ (Fig. 1). The hydrothermal vent system was located at a water depth of 2,850 m and extended for at least 1 km along the base of the fault scarp. The morphological and tectonic setting of this massive Fe–Cu sulphide bears many

similarities to the ophiolite sulphide deposits of the Troodos Complex^{4,13}. Chalcopyrite-rich samples were taken from a hydrothermal veinlet at the top of the inactive sulphide mound (Fig. 2). The samples rich in pyrite were taken from the mound middle, as were the amorphous silica samples. Paragenetic relations between chalcopyrite and pyrite indicate that they precipitated in equilibrium as was suggested by Styrer *et al.*⁷ for EPR 21° N sulphides.

Mineralogy exerts a control on $\delta^{34}\text{S}$ values and there is a linear relationship for samples 4, 6, 7 and 8 of high pyrite or chalcopyrite purity (Fig. 3). The isotopic data plotted against the chalcopyrite/pyrite composition (Fig. 3) show a spread of the eight data points with values for $\delta^{34}\text{S}$ between +5.42‰ and +6.34‰. The highest isotopic values came from pyrite-rich samples from the mound middle, while the lowest values were produced by mound-top chalcopyrite-rich samples. On extrapolation to pure end-member pyrite, (100% FeS₂) a value of +6.42‰ is obtained while 100% CuFeS₂ yields +5.38‰. The isotopic fractionation factor (α) of one sulphide species with respect to the other varies as a function of temperature. The calibration of Kajiura and Krouse¹⁴,

$$1,000 \ln \alpha_{\text{pyr}}^{\text{pyr}} = 4.5 (10^5 T^{-2})$$

yields a temperature of formation of 388° ± 20 °C for the GRAFZI pyrite/chalcopyrite mineral assemblage. The analytical precision averages 0.04‰, but values for individual samples have been indicated by error bars in Fig. 3.

The great spread of results, with four samples deviating from linearity (Fig. 3), may be explained in terms of the mechanism of transport of subsurface hydrothermally convected seawater. In a dynamic system of convectively circulated seawater, continuously interacting with igneous rocks at different temperatures at various seawater/rock ratios, in which H₂S and SO₄²⁻ are lost from solution by precipitation of sulphide and sulphate minerals, the budget of sulphur in the hydrothermal solutions must be changing constantly. Consequently, there are two possible explanations for the isotopic composition of the samples rich in pyrite (samples 1, 2 and 5 in Fig. 3) which fall below the best-fit straight line, and are therefore depleted of ³⁴S. Biological and diagenetic activity could reset and reduce the $\delta^{34}\text{S}$. The presence of organic debris was common in both GRAFZI sulphides (data not shown) and at the EPR 21° N (ref. 2). The second mechanism would involve augmenting the hydrothermal fluids with an increased amount of basaltic sulphur ($\delta^{34}\text{S} = +0.5$ to +1.0‰)¹⁵ as the fluids became progressively depleted in their seawater sulphate content ($\delta^{34}\text{S} = +20\%$)¹⁵, due to precipitation of sulphide and sulphate minerals within the upper crust.

The one isotopically heavy $\delta^{34}\text{S}$ value (sample 3) is problematical. This sample may have formed as a hydrothermal solution became isotopically heavier with time, possibly due to addition of more seawater sulphate from entrained seawater or due to operation of a simple closed reservoir where residual hydrothermal solutions became enriched in ³⁴S, as the ³²S isotope preferentially left solution on sulphide precipitation. The possibility of apparent ³⁴S-enrichment in GRAFZI samples due to the presence of micro-inclusions of isotopically heavy anhydrite can be ruled out as this mineral was not found, although Arnold and Sheppard⁵ noted anhydrite in EPR sulphides.

The two samples rich in amorphous silica gave the following $\delta^{18}\text{O}$ results: sample 9, +25.2 ± 0.8‰; sample 10, +17.0 ± 0.4‰. The large errors presumably are due to the presence of water in hydrated silica which may be retained to varying extents during analysis. These results imply formation at different temperatures or mixing of a high and low temperature amorphous silica product. It is interesting to calculate the range of temperatures from these values either in equilibrium with pure seawater (SMOW) or a heavier seawater representing exchange with hot basaltic material as at 21° N for example, +1.64‰ (ref. 16). The variability in published calibrations of this equilibrium fractionation^{17,18} produce further uncertainties in the temperature calculation. If all these variations are included,

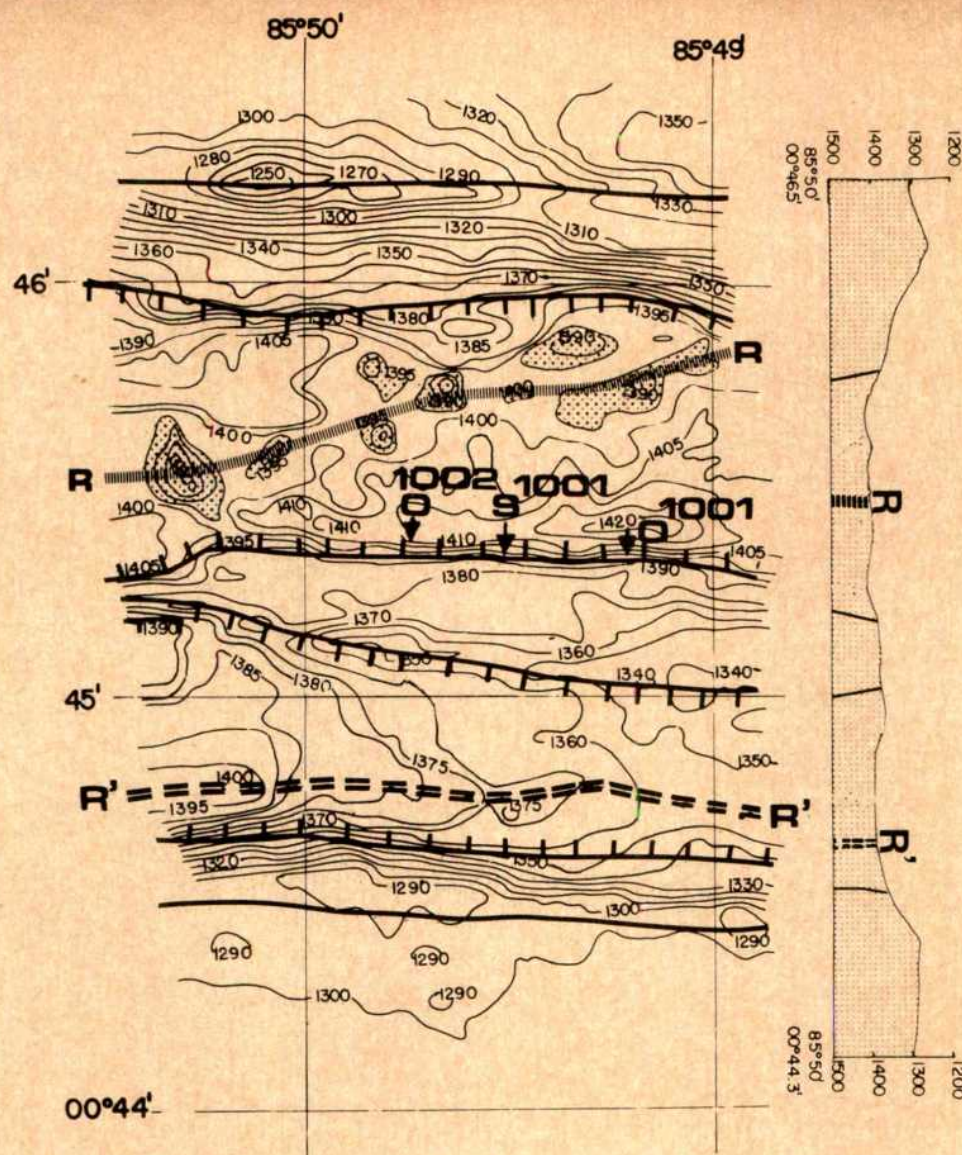


Fig. 1 High-resolution bathymetric map of the Galapagos Double Rift Area. R, principal rift axis; R', 'jumped' rift axis. The solid line delineates high crest on the tilted block and dotted areas indicate axial volcanic piles. Hashures indicate down-thrown side of normal faults; O, location of hydrothermal iron oxides; S, location of hydrothermal sulphide deposit mapped on dive 1001. (Depths in uncorrected fathoms.) After Malahoff *et al.*

the range of temperature for the two samples is from 60° to 172 °C. This suggests the possibility of considerable low temperature diagenetic additions of SiO₂ augmenting much lower temperature emissions than produced the sulphides, as has been noted for EPR 'white smokers'⁵. Amorphous silica probably formed at the periphery of the venting plume of hydrothermal water where mixing with ambient seawater occurred.

A comparison of $\delta^{34}\text{S}$ values between Recent and ancient submarine hydrothermal sulphides formed from modified seawater solutions¹⁹⁻²² reveals a similarity of composition (Fig. 4), although Kuroko deposits are associated with calc-alkaline volcanism rather than with deep-ocean tholeiitic basalts.

To compare Recent deposits in more detail, the hottest hydrothermal vents on the EPR at 21° N, at 380° ± 30 °C are actively debouching fluids which are precipitating mainly chalcopyrite, and these are very similar in temperature to GRAFZI inactive Cu-Fe sulphides which formed at 390° ± 20 °C. The overall chemistry of the two sulphide deposits is distinctively different, with the 21° N sulphides dominated by Zn, while GRAFZI deposits are richest in Cu and Fe. It is interesting to speculate whether the hottest 21° N hydrothermal vents,



Fig. 2 Hydrothermal veinlet from the mound-top rich in 'brecciated' chalcopyrite grains (up to 3 mm). The chilled margin of the veinlet with the rapid decrease in grain size and the gossan surface are particularly noteworthy features. Scale of veinlet, 18 mm long × 12 mm wide.

previously depositing Zn sulphide, but now Cu sulphide, are sealing themselves up, as GRAFZI sulphides once did.

$\delta^{34}\text{S}$ values for 21°N sulphides range from +1.3 to +4.1‰ and the sulphides received a 10% seawater sulphate sulphur contribution with 90% from basaltic leaching^{5,7}. Both experimental evidence²³ and now GRAFZI sulphide evidence have shown that the total hydrothermal $\delta^{34}\text{S}$ in a modern submarine deposit can exceed +5‰, and here ranges from +5.4 to +6.3‰. Styrer *et al.*⁷ observed that H_2S entirely of seawater origin may have $\delta^{34}\text{S}$ values as low as +5‰. If this is true, the entire sulphur of the GRAFZI sulphides may have a seawater sulphate origin. These sulphides are considerably enriched in ^{34}S compared with 21°N sulphides, suggesting a more dominant seawater source of sulphur at 86°W. This observation has profound implications, in that higher seawater/rock ratios than have been realised previously, can be responsible for the production of seabed hydrothermal sulphides. In terms of subsurface crustal structure, this would be manifested by a permeable, well-fractured oceanic crust and/or rapid flow rates for the hydrothermal solutions, which would allow great fluxes of seawater into the upper oceanic crust for convection and possible sea floor sulphide precipitation, on mixing with ambient bottom waters.

The analogy between GRAFZI and Cyprus-type sulphide ores can be carried further when considering stockwork hydrothermal fluid temperatures. These were found to range between 250°C and 350°C (ref. 24), and 300°C (ref. 25) by different workers on Cyprus-type sulphides of the Troodos ophiolite complex. Heaton and Sheppard²⁵ postulated a seawater/rock ratio of between 1 and 5 responsible for producing disseminated stockwork cupriferous pyrites with $\delta^{34}\text{S}$, +5.1‰ (Fig. 4), while massive pyrite gave $\delta^{34}\text{S}$, +4.3‰. These values are similar to GRAFZI pyrites (up to +6.3‰) but are generally slightly lower. Spooner²⁴ suggested a major component of sulphur for the sulphides from reduced seawater sulphate at Troodos, that is,

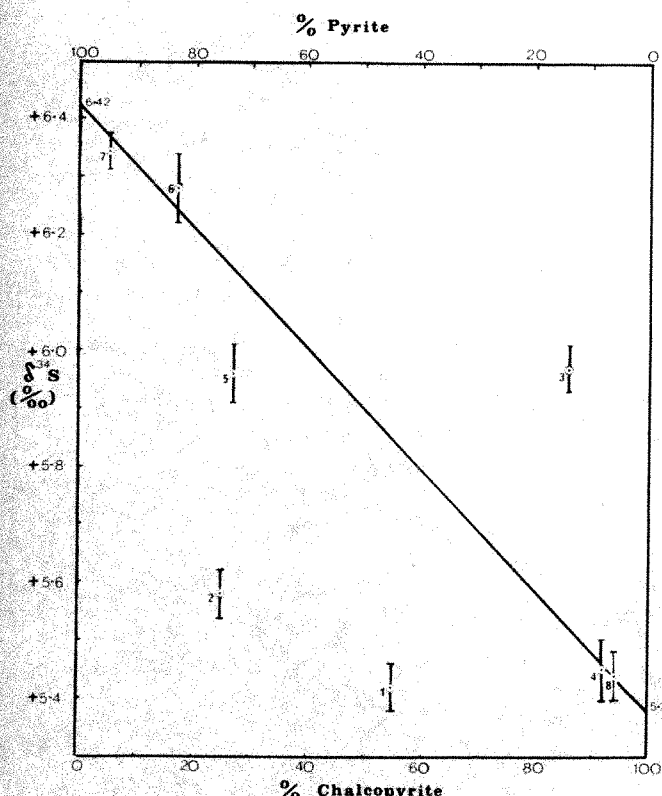


Fig. 3 $\delta^{34}\text{S}$ plotted against % chalcopyrite/pyrite mineralogy. Samples 1, 3, 4 and 8 from chalcopyrite-rich mound top. Samples 2, 5, 6 and 7 from pyrite-rich mound middle. The line is the best-fit straight line.

$$\Delta^{34}\text{S}_{\text{Pyr-Cpyr}} = \delta^{34}\text{S}_{\text{Pyr}} - \delta^{34}\text{S}_{\text{Cpyr}} = 6.42 - 5.38\text{‰} = 1.04\text{‰}$$

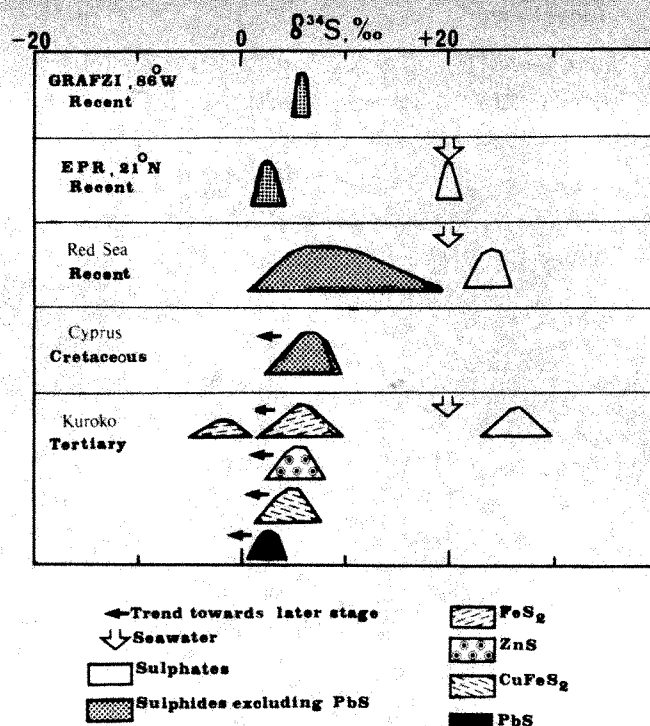


Fig. 4 Comparative sulphur isotopic data of some stratiform massive sulphide deposits associated with submarine volcanism, adapted from Ohmoto and Rye¹⁹. The sources of data on Cyprus and Kuroko are summarized in Rye and Ohmoto²⁰. The data on the Red Sea are from Kaplan *et al.*²¹, and Shanks and Bischoff²². EPR, 21°N, data are from Arnold *et al.*⁵ and Styrer *et al.*⁷.

10% and possibly up to 100%. Therefore, this seems to confirm our hypothesis of a major source of sulphur derived from seawater rather than basalt at 86°W, on the Galapagos Rift.

We thank NERC for provision of research funds and a research studentship to R.S.; Dr A. Malahoff of the National Ocean Survey; NOAA for donation of samples; Dr D. S. Cronan for invaluable discussions; Mrs M. A. Cox for analytical assistance; and Miss P. Raymond for preparation of the typescript.

Received 7 May; accepted 20 July 1982.

- Francheteau, J. *et al.* *Nature* **277**, 523–528 (1979).
- Hekinian, R., Fevrier, M., Bischoff, J. L., Picot, P. & Shanks, W. C. *Science* **207**, 1433–1444 (1980).
- Spies, F. N. *et al.* *Science* **207**, 1421–1433 (1980).
- Malahoff, A., Cronan, D. S., Skirrow, R. & Embley, R. W. *Mar. Mining* (in the press).
- Arnold, M. & Sheppard, S. M. F. *Earth planet. Sci. Lett.* **56**, 148–156 (1981).
- Haymon, R. M. & Kastner, M. *Earth planet. Sci. Lett.* **53**, 363–381 (1981).
- Styrer, M. M. *et al.* *Earth planet. Sci. Lett.* **53**, 382–390 (1981).
- Tatlock, D. B. *U.S. geol. Surv. Bull.*, 1209 (1966).
- Jackson, M. L. *Soil Chemical Analysis* (Constable, London, 1958).
- Robinson, B. W. & Kusakabe, M. *Analyst. Chem.* **47**, 1179–1181 (1975).
- Clayton, R. N. & Mayeda, T. K. *Geochim. cosmochim. Acta* **27**, 43–52 (1963).
- Coleman, M. L. *IGS Stable Isotope Rep. No. 45* (1980).
- Adamides, N. G. *Proc. Int. Ophiolite Symp., Geol. Surv., Cyprus*, 117–127 (1979).
- Kajiwar, Y. & Krouse, H. R. *Can. J. Earth. Sci.* **8**, 1397–1408 (1971).
- Sakai, H., Veda, A., & Field, G. W. *U.S. Geol. Surv. Open-File Rep.* 78–101 (1978).
- Craig, H. *et al.* *EOS* **61**, 392 (1980).
- Bottinga, J. & Javoy, M. *Earth planet. Sci. Lett.* **20**, 250–265 (1973).
- Matsuhisa, Y., Goldsmith, J. R., & Clayton, R. N. *Geochim. cosmochim. Acta* **43**, 1131–1140 (1979).
- Ohmoto, H. & Rye, R. O. in *Geochemistry of Hydrothermal Ore Deposits*, 2nd edn (ed. Barnes, H. L.) 509–567 (Wiley, New York, 1979).
- Rye, R. O. & Ohmoto, H. *Econ. Geol.* **69**, 826–842 (1974).
- Kaplan, I. R., Sweeney, R. E. & Nissenbaum, A. in *Hot Brines and Recent Heavy Metal Deposits in the Red Sea* (eds Degens, T. & Ross, D. A.) 474–498 (Springer, New York, 1969).
- Shanks, W. C. & Bischoff, J. L. *Geol. Soc. Am. Ann. Mig. Abstr.* 1266 (1975).
- Ohmoto, H., Cole, D. R. & Mott, M. J. *EOS* **57**, 342 (1976).
- Spooner, E. T. C. in *Volcanic Processes in Ore Genesis* 58–71 (Institute of Mining and Metallurgy, London, 1976).
- Heaton, T. H. E. & Sheppard, S. M. F. in *Volcanic Processes in Ore Genesis*, 58–71 (Institute of Mining and Metallurgy, London, 1976).

Fluxes of biogenic components from sediment trap deployment in circumpolar waters of the Drake Passage

Gerold Wefer*, Erwin Suess†, Wolfgang Balzer‡, Gerd Liebezeit‡, Peter J. Müller*, C. André Ungerer† & Walter Zenk‡

* Geologisches Institut, Olshausenstrasse 40–60, 2300 Kiel, FRG

† School of Oceanography, Oregon State University, Corvallis, Oregon 97331, USA

‡ Institut für Meereskunde, Düsternbrooker Weg 20, 2300 Kiel, FRG

Circumpolar surface waters dominate the circulation of the Southern Ocean and sustain one of the ocean's largest standing stocks of biomass thereby producing a significant output of biogenic components, mainly diatoms, to the bottom sediments. Generally transit of biogenic matter from the sea surface to the sea floor affects nutrient regeneration fuels benthic life and transfers signals to the sediment record^{1–5}. Reliable quantification of the relationship between biological production, fractionation of skeletal and tissue components and bottom sediment accumulation depends on direct vertical flux measurements from sediment trap deployments^{6–9}, which have proved to be most scientifically productive^{10–13}. We now present data on vertical mass fluxes from the Southern Ocean and evidence for strong biogeochemical fractionation between organic carbon-, nitrogen- and phosphorus-containing compounds, siliceous and calcareous skeletal remains, and refractory aluminosilicates.

Results are from the first deployment of sediment traps in Antarctic waters. Our traps, with a collection area of 314 cm² (ref. 14), were attached to a moored array located at 60°54.6' S and 57°06.0' W in 3,625 m of water depth for 52 days from 2 December 1980 to 25 January 1981. During that time the integrated mean primary production in the study area was 0.1 g C m⁻² day⁻¹ (ref. 15). Current and temperature observations at 400 m, 1,500 m and 3,590 m of water depth revealed some unexpected results. The upper two current meters showed a general tendency of eastward water movement, although the short time series yielded no reasonable mean current vectors. The mean temperatures recorded were 1.76 °C and 1.20 °C at 400 m and 1,500 m, respectively. In both cases the standard deviation was 0.09 °C from 5,165 individual values.

In contrast to these mid-water current observations, which characterize the southern extension of the Antarctic Circumpolar Current in the Drake Passage, an unexpectedly persistent undercurrent was measured at abyssal depth. This movement feeds near-bottom water from the Scotia Sea continuously into the deep South Pacific Ocean, has a mean vector of 20.9 ± 5.3 cm s⁻¹ towards 222° relative to true north and maximum velocities of 32 cm s⁻¹ with an average temperature of -0.02 ± 0.06 °C. The countercurrent was also noted north of Livingston Island during the Dynamic Response and Kinematic Experiment (DRAKE) in 1979¹⁶.

Material in the sediment traps was recovered from water depths at 965 m and 2,540 m; the samples are designated M 269–965 and M 269–2540, respectively. Chloroform for preservation was released into the collecting vessel during trap deployment from an imploding glass vial. Surface particulate matter was also collected at the mooring site on 25 January 1981 for 8 h. About 3 m³ of sea-surface waters from the RV *Meteor*'s contamination-free pumping system were continuously filtered through a 75-µm mesh sieve to concentrate enough material for individual component analyses; this sample is designated M 8101–38.

On recovery the sediment trap material and the surface particulate matter were split into 10 aliquots by pipetting from a suspension in filtered seawater which was kept homogenous

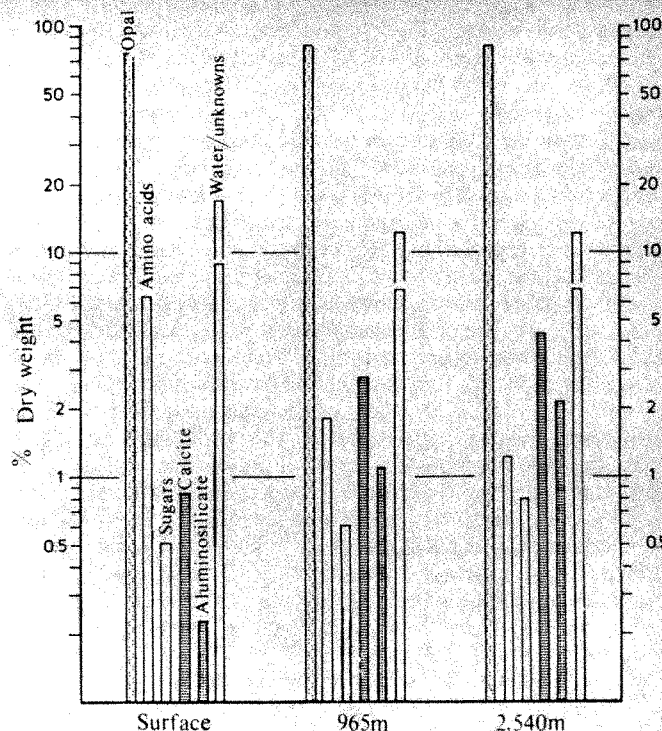


Fig. 1 Relative changes in major phase composition of particulate matter with water depth in the Drake Passage.

by continuous agitation. To minimize bacterial degradation, splits were immediately poisoned with 100 p.p.m. HgCl₂ and frozen. Just before analysis, the samples were thawed and de-salted by repeated washings in distilled water, then they were freeze-dried. The wash water was retained for labile phosphorous determinations. The yields of 8 out of 10 splits gave total dry weights, estimated to be accurate to within 5 mg. These estimates were then used to calculate the total mass fluxes of 143 ± 1 g m⁻² yr⁻¹ at 2,540 m, 163 ± 2 g m⁻² yr⁻¹ at 965 m and 471 ± 6 g m⁻² yr⁻¹ at the surface. The measure for the mass flux at the surface is the product of the mean organic carbon fixation rate¹⁵ multiplied by the bulk mass of the surface particulate matter divided by the concentration of organic carbon, and is considered a first approximation of the net bulk production. All individual component fluxes will be calculated from these bulk flux estimates.

Individual splits were analysed for elemental and phase composition, amino acid, amino sugar and carbohydrate contents and foraminiferal counts, using methods described elsewhere¹⁷. In addition, hand-picked foraminifera were analysed for their stable isotope composition as described elsewhere¹⁸. Results of the major element and stable isotope compositions are listed in Table 1.

Most of the material collected in the traps, and virtually all of the surface particulate matter, was biogenic with a very minor portion of aluminosilicates. Figure 1 illustrates the relative changes in the major particulate phases with water depth. Whole individuals of diatoms, fragments and molds of crustaceans and tests of foraminifera were most abundant. The tests were almost exclusively of the left-coiling variety of the species *Globoquadrina pachyderma*. Faecal pellets were also common.

Quantitatively, diatomaceous debris is the dominant constituent as seen in the high SiO₂-content (Table 1, Fig. 1). Hereby the percentages listed refer to anhydrous SiO₂ only, thus the H₂O of diatomaceous opal, estimated to be between 6 and 9 wt%, may largely account for the unknown portion of the total biogenic matter.

The next most important phase is organic matter which shows a change from the surface particulates to the deep trap material in decreasing protein and labile phosphorus and increasing carbohydrate contents. Calcium carbonate and the aluminosilicate fractions increase in relative importance with water depth, obviously due to the more rapid disappearance of opal and

Table 1 Major element and stable isotope composition of sediment trap material and surface plankton

	(wt%) de-salted and freeze-dried material									$\delta^{18}\text{O}$	$\delta^{13}\text{C}$
	C-total C-carb C-org	N-total	P-sum P-leach P-HCl P-total	Ash SiO ₂	Ca-sol Ca-res	Mg-sol Mg-res	Al-sol Al-res	Ba-sol Ba-res		(‰ PDB) >300* ~200 ~125	
M 8101-38, sea surface											
Split (1)	8.00 ND ND	1.35 1.39	0.655 0.578 0.015 0.077	78.0 74.9	0.194 0.014	0.155 0.024	0.010 0.023	0.002 0.007	ND	ND	ND
Split (8)	7.78 0.14 7.12†	1.34 1.32	0.589 0.513 0.014 0.076	78.5 75.5	0.197 0.016	0.140 0.022	0.005 0.021	0.002 0.003	ND	ND	ND
M 269-965, 965 m depth											
Split (1)	3.36 ND ND	0.48 ND	0.064 0.024 0.005 0.041	86.4 81.5	0.832 0.095	0.067 0.098	0.005 0.106	0.023 0.094	3.26 3.08 3.39	0.74 0.83 0.80	
Split (8)	3.85 0.33 2.85†	0.51 ND	0.066 0.026 0.007 0.041	86.2 80.0	0.737 0.058	0.072 0.060	0.021 0.122	0.021 0.124	ND	ND	ND
M 269-2540, 2540 m depth											
Split (1)	4.19 ND ND	0.48 ND	0.090 0.046 0.008 0.044	85.8 79.7	1.18 0.152	0.088 0.110	0.041 0.198	0.033 0.045	3.28 3.44 3.04	1.06 0.67 0.76	
Split (8)	3.49 0.55 2.76†	0.42 ND	0.102 0.064 0.010 0.038	86.7 78.4	1.38 0.167	0.096 0.122	0.048 0.223	0.034 0.076	ND	ND	ND

In each column the sequence of numbers for one sample split refers to the sequence of components as listed in the column heading: N-total, duplicate Kjeldahl determinations; C-total, CO₂ liberated by heat combustion; C-carb, CO₂ liberated by phosphoric acid; C-org, CO₂ liberated by dichromate/sulphuric acid digestion; P-HCl, hydrochloric acid-soluble; P-leach, water soluble; P-total, after water leach by nitric/fluoric acid digestion; P-sum, water soluble plus total phosphorus (calculated); ash, after ignition at 400 °C for 2 h; sol, hydrochloric acid soluble; res, residual (not hydrochloric acid soluble); for analytical scheme see ref. 17. ND, not determined.

* Splits (3)(6); shell size in μm .

† C-org contents used in carbon budget of Table 2.

organic matter. This is evident when comparing the respective changes in component flux rates with water depth.

The total calcium carbonate flux (determined from Ca and CO₂ analyses) into the traps was 4.5 and 6.6 g m⁻² yr⁻¹, respectively; whereas the *G. pachyderma* test flux (determined from test counts) was $\sim 10 \times 10^5$ individuals for each trap. For the test sizes 125, 200 and 300 μm , individual weights ranged from 1.1 to 8.9 μg with a mean test weight of 5.2 μg , thus when comparing both fluxes, it appears that *G. pachyderma* may account for the entire calcium carbonate flux.

The stable isotope values of *G. pachyderma* for three size fractions are also listed in Table 1. The tests in both traps showed mean $\delta^{18}\text{O}$ values of 3.25‰ PDB and appear unchanged during growth. This is in contrast to results from other neritic environments where, in general, for the same species the larger (older) shells are enriched in ^{18}O (ref. 19). The constant $\delta^{18}\text{O}$ values may be due to the rather small temperature variation within the euphotic zone of the study area. Depth migration during growth, if it occurs in the life cycle of *G. pachyderma*, does not lead the organism to encounter large temperature changes in circumpolar waters. The mean $\delta^{18}\text{O}$ value of 3.25‰ PDB indicates an equilibrium precipitation temperature of +1.8 °C based on the 'calcite' palaeotemperature equation of Epstein²⁰ and assuming -0.65‰ for the circumpolar surface water²¹. The calculated temperature is in good agreement with measured ones which we have recorded; that is +3.0 °C at the sea surface, -0.26 °C at 100 m, +1.44 °C at 203 m and +2.01 °C at 446 m of water depth (R. Wittstock, personal communication). The salinity varies over this same depth range between

Table 2 Organic carbon, nitrogen and phosphorus budgets of surface plankton and sediment trap material

	Sea surface M 8101-38	965 m depth M 269-965	2,540 m depth M 269-2540
	(μmol g ⁻¹ dry wt)		
Organic carbon	5,930	2,380	2,300
Amino acid carbon	2,895	713	531
Amino sugar carbon	46	42	40
Carbohydrate carbon	170	207	256
Carbon accounted for	52%	40%	36%
Organic nitrogen	964	357	321
Amino acid nitrogen	748	193	145
Amino sugar nitrogen	7.7	7.1	6.6
Ammonia nitrogen	83	33	25
Nitrogen accounted for	87%	65%	55%
Total phosphorus*	201	21	31
Water-soluble	176	8	18
HCl-soluble*	5	2	3
Insoluble	20	11	10
Phosphorus accounted for	100%	100%	100%

Amino acid carbon and nitrogen, sum of 22 individual amino acids; amino sugars, sum of galactosamine and glucosamine; carbohydrate carbon, sum of 11 hexoses; results of individual amino acid and sugar spectra will be published elsewhere (P.J.M. and G.L. in preparation).

* Organic + apatitic phosphorus, whereby HCl-soluble fraction may be considered apatitic²⁴.

Table 3 Mean annual production and flux rate estimates of individual biogenic components and aluminosilicates at the sea surface, at 965 m and 2,540 m of water depth at station M 269

Particulates	Sea surface M 8101-38	965 m depth M 269-965	2,540 m depth M 269-2540
		(g m ⁻² yr ⁻¹)	
Total mass flux	471	163	143
Organic carbon	36.5	5.41	4.78
Amino acid carbon	16.4	1.39	0.91
Carbohydrate carbon	0.96	0.40	0.44
Amino sugar carbon	0.26	0.08	0.07
Organic nitrogen	6.36	0.81	0.64
Amino acid nitrogen	4.93	0.44	0.29
Ammonia nitrogen	0.55	0.075	0.050
Amino sugar nitrogen	0.05	0.016	0.013
Organic phosphorus			
Water soluble	2.57	0.041	0.079
Insoluble	0.29	0.057	0.046
Silica, anhydrous	354	132	113
Calcium carbonate	5.5	4.5	6.6
Barite	0.06	0.36	0.23
Aluminosilicates	1.08	1.79	3.00
Al ₂ O ₃	0.20	0.35	0.57
MgO	0.18	0.21	0.27
CaO	0.10	0.17	0.32

Organic phosphorus (insoluble), P-total minus P-hydrochloric acid soluble; calcium carbonate, mixed Ca-Mg-carbonate probably also containing SrCO₃; barite, soluble plus residual barium plus stoichiometric SO₄; aluminosilicates, sum of residual oxides plus 3 × (Al₂O₃) as aluminosilicate SiO₂; flux rates do not include quartz-SiO₂; the individual component fluxes are calculated by averaging the compositions.

33.7 and 33.5‰ S, therefore our data indicate that *G. pachyderma* precipitates its tests close to isotopic equilibrium. The carbon isotope values also do not vary with shell size and thus do not show the 'normal' trend of ¹³C enrichment with increasing age¹⁹, again the rather homogeneous water column properties seem responsible for this low variability in the stable carbon isotope signature of *G. pachyderma*.

Dramatic qualitative and quantitative changes with water depth were observed for the organic matter fraction (Table 2). Whereas in surface plankton 52% of the total organic carbon may be accounted for as being tied up in polypeptides, proteins and polysaccharides, these portions decrease with depth to 40% and 36%, respectively. The non-characterized fraction probably contains hydrocarbons, wax esters and other lipid material as well as 'humic matter'; its proportion increases with depth from ~50 to ~65% of the total organic carbon pool.

Because only < 1 μmol g⁻¹ of ammonia-N could be contained in the aluminosilicate fraction as fixed NH₃ (ref. 22), we assume that all nitrogen is organically bound. The free ammonia-N listed in Table 2 is also organically bound but is liberated from the protein fraction during hydrolysis.

The decrease in amino yield and the increase in carbohydrate contents with water depth reflect the preferential degradation of proteinaceous material²³. This is supported by a decrease in both amino acid-C and amino acid-N, whereas the relative increase in the non-characterized organic nitrogen fraction might reflect a pronounced abundance of nucleic acid bases and/or 'humic material'. Amino sugars on the other hand, comprise a relatively stable fraction of both organic-C and organic-N at all depths, indicating that they may be derived from poorly degradable chitinous matter.

For phosphorus we attempted partitioning by a methodology based on fractional solubilization. This approach explains why we account for the entire phosphorus budget. Hereby the water-soluble portion probably represents very labile organic phosphorus compounds such as ATP and related energy storage compounds and nucleic acids, released from living cells. We then defined a small fraction of phosphorus, soluble in hydro-

chloric acid, which could come from apatitic biogenous skeletons²⁴. Consequently, the calculated difference between P-sum minus P-HCl and P-leach represents an insoluble organic phosphorus fraction such as phospholipids from cell walls or similar tissue structures. The relative increase of this fraction from 10% at the sea surface to ~40% at depth also indicates it to be of a more refractory nature.

We may now compare flux rate changes of organic phases with mineral phases during transit through the water column (Table 3), because ultimately, fractionation resulting from such differential flux rates transforms surface particulate matter into bottom sediments. From Table 3, four types of biogeochemical regeneration can be differentiated. (1) Labile organic phosphorus is the most rapidly recycled; only < 5% of that fraction escapes recycling within near-surface waters and reaches depths of ~1,000 m, below which its flux remains essentially constant. (2) Polypeptides, presumably proteinaceous material of surface plankton are at first rapidly recycled between the surface and ~1,000 m of depth and thereafter at a slower rate. This exponential degradation is seen in changes of amino acid-C, amino acid-N and ammonia-N fluxes; it essentially affects the entire particulate nitrogen pool. (3) Fluxes of skeletal silica, polysaccharides, amino sugars and insoluble organic phosphorus show a slight tendency of refractory chemical behaviour which is marked by imperceptibly small flux rate changes in deep water. This is not surprising, as all are 'residual' components of biogenic matter: opal of diatom tests, carbohydrates and insoluble phosphorus of cell walls and amino sugars of chitinous skeletons. (4) Finally, the behaviour of calcium carbonate, barite and aluminosilicates cannot be adequately assessed from our flux data, because their sources are not restricted to surface waters of the same region as indicated by the deep countercurrent. Therefore, the bulk production rate assumed for the surface is a poor estimate. All three components of this group may have sources farther to the east of the sampling site and thus are not included in our production rate estimate from surface particulate matter. Similarly, aluminosilicates are advected horizontally and vertically throughout the water column, and the deeper the traps are deployed, the larger the aluminosilicate fluxes will be. But at least our flux data indicate that calcium carbonate, barite and aluminosilicates are very refractory and will undergo little, if any, recycling in the water column below ~1,000 m due to rapid transit.

This work was supported by the Deutsche Forschungsgemeinschaft and the US Office of Naval Research through grant N00014-79-C-0004, Project NR083-1026 to Oregon State University. We thank especially B. von Bodungen and R. Wittstock for help in deployment and recovery of the mooring in the Drake Passage. This is contribution no. 394 from the Sonderforschungsbereich 95, University of Kiel.

Received 5 April; accepted 7 June 1982.

- Schrader, H.-J. *Science* **174**, 55-57 (1971).
- Hinga, K. R., Sieburth, J. & Heath, G. R. *J. mar. Res.* **37**, 557-579 (1979).
- Cobler, R. & Dymond, J. *Science* **209**, 801-802 (1980).
- Suess, E. *Nature* **288**, 260-263 (1980).
- Thunell, R. & Honjo, S. *Mar. Geol.* **40**, 237-253 (1981).
- Honjo, S., Manganini, S. J. & Cole, J. J. *Deep-Sea Res.* **29**, 609-625 (1982).
- Deuser, W. G., Ross, E. H. & Anderson, R. F. *Deep-Sea Res.* **28**, 495-505 (1981).
- Knauer, G. A., Martin, J. H. & Bruland, K. W. *Deep-Sea Res.* **26**, 97-108 (1979).
- Starecnic, N. *J. mar. Res.* (in the press).
- Wakeham, S. G. *et al. Nature* **286**, 798-800 (1980).
- Deuser, W. G. & Ross, E. H. *Nature* **283**, 364-365 (1980).
- Knauer, G. A. & Martin, J. H. *Limnol. Oceanogr.* **26**, 181-186 (1981).
- Urrere, M. A. & Knauer, G. A. *J. Plankton Res.* **3**, 3-19 (1981).
- Zeitzschel, B., Uhlmann, L. & Diekmann, P. *Mar. Biol.* **45**, 285-288 (1978).
- Tilzer, M. & von Bodungen, B. *Berichte aus dem Institut für Meereskunde* No. 80 (1981).
- Whitworth, T., Nowlin, W. D. Jr & Worley, S. J. *J. Phys. Oceanogr.* (in the press).
- Suess, E. & Ungerer, C. A. *Oceanol. Acta* **4**, 151-160 (1980).
- Berger, W. H. & Killingley, J. S. *Science* **197**, 563-566 (1977).
- Berger, W. H., Killingley, J. S. & Vincent, E. *Oceanol. Acta* **1**, 203-216 (1978).
- Epstein, S., Buchsbaum, H. A., Lowenstamm, H. A. & Urey, H. C. *Bull. geol. Soc. Am.* **64**, 1315-1325 (1953).
- Craig, H. & Gordon, L. I. *Stable Isotopes in Oceanographic Studies* (ed. Tongiorgi, E.) 9-130 (Consiglio Nazionale delle Ricerche, Rome, 1965).
- Müller, P. J. *Geochim. cosmochim. Acta* **41**, 765-776 (1977).
- Handa, N. & Yanagi, K. *Mar. Biol.* **4**, 197-207 (1969).
- Black, C. A. *Methods of Soil Analysis* Pt II, 1038-1040 (American Society of Agronomy, Madison, 1965).

Extreme longevity of lotus seeds from Pulantien

David A. Priestley*† & Maarten A. Posthumus‡

* Department of Plant Physiology, Agricultural University, Arboretumlaan 4, 6703 BD Wageningen, The Netherlands

† Boyce Thompson Institute, Tower Road, Cornell University, Ithaca, New York 14853, USA

‡ Laboratory of Organic Chemistry, Agricultural University, De Dreijen 5, 6703 BC Wageningen, The Netherlands

In 1923 Ohga¹ first brought to general scientific attention the existence of a cache of viable seeds of East Indian lotus (*Nelumbo nucifera* Gaertn.), contained within an ancient lakebed deposit at Pulantien in southern Manchuria. From the geological and historical evidence available, Ohga suggested a possible age in excess of 400 years^{1,2}. Libby³ radiocarbon dated some of Ohga's material at 1040 ± 210 years BP. This evidence of great antiquity for viable seeds has been controversial⁴⁻⁶. The main hindrance to the resolution of the problem has been the paucity of available Pulantien seeds following the dissipation of Ohga's original collection⁷. Recently we have received four Pulantien seeds, three of which were viable, albeit lacking in vigour. The lipids of the unimbibed seeds were examined and found to be still highly polyunsaturated, suggesting that they had undergone little atmospheric autoxidation. Radiocarbon dating of one of the viable seeds suggested a probable age of about 466 years at the time of germination. This is the oldest viable seed for which an age has been directly determined.

The four seeds supplied to us (designated P1 to P4) were collected in 1952 at Pulantien (Hsinchin, Liaoning Province, People's Republic of China)⁸. Following collection they were stored under herbarium conditions. For comparative purposes, we have also analysed freshly grown lotus seeds (designated W1 to W3) obtained from a colony in Washington D.C. that had been derived from two Pulantien lotus seeds germinated in 1951⁵. Each of the Pulantien seeds had the morphological peculiarities described by Ohga⁹ as distinguishing them from recently grown lotus seeds—a waxless, dark-brown pericarp, slightly pitted and lacking a styler protuberance at the apical end. It should be noted that lotus 'seeds' are technically dry fruits, since the seeds in the strict sense are surrounded by an extremely hard pericarp. This massively thickened structure is highly impervious to water and gases unless it is radically scarified^{1,10}. In our investigations, the extreme basal tip of the pericarp was sawn off to expose a small cavity where the cotyledons had shrunk away from the inner pericarp wall. Approximately 10 mg of dry cotyledonous material was excised for lipid analysis and the remainder of the seed was subjected to a germination test. In all the seeds examined the cotyledons were white, except P3 which had dull yellow cotyledons. Germination was initiated by imbibing in tap water at 20 °C for 15 min. The seeds were then placed semi-submerged on cotton wool and left in darkened conditions at approximately 25 °C. All the seeds (except P3) showed some signs of germination within 72–96 hours. After 96 hours the 'fresh' Washington material had plumules extending 39–44 mm beyond the tip of the seed. The corresponding extensions for the Pulantien seeds were less than 20 mm for P1 and less than 10 mm for P2 and P4. During the same period P3 took up water, though the cotyledons did not maintain turgidity and its plumule showed no evidence of growth. After 96 hours, seeds P3 and P4 were heated in an oven at 110 °C for 2 days to kill and dry the material for radiocarbon dating. The seeds were dated at 340 ± 80 BP (GrN-11012) and 430 ± 100 BP (GrN-11013) respectively, which correspond historically (after calibration against dendrochronologically dated tree-rings¹¹) to AD 1440–1640 and AD 1410–1620. Seeds P1 and P2 were allowed to continue germinating and, after transplanting, they developed into

apparently normal plantlets possessing three or four leaves, at which stage observations were terminated.

One common hypothesis of seed ageing identifies the oxidation of polyunsaturated fatty acid as a possible primary lesion during dry long-term storage¹². Lipids from the lotus seeds were analysed, therefore, as important indicators of the extent of autoxidation in the tissue. The Washington seeds (W1, W2 and W3 of Table 1), which had all presumably matured under rather similar conditions, had very similar fatty acid contents. The degree of polyunsaturation was high, dienoic (C18:2) and trienoic (C18:3) fatty acids accounting for almost half of the total. The total lipid content of the seed was approximately 1% of dry weight. The Pulantien seeds had a more variable fatty acid content than their Washington counterparts, although their similarity to the latter is obvious (Table 1). The much lower linoleic acid (C18:2) content of P3 and P4 compared to P1 and P2 is unlikely to be due to oxidation during isolation. Linolenic acid (C18:3), which is much more sensitive to oxidative degradation, was still quite evident. Most likely, P3 and P4 matured in warm summers, whereas P1 and P2 developed under colder conditions favouring a higher degree of polyunsaturation. Such effects are known to occur in other species^{13,14}.

The oldest documented age for seed viability is for a lotus seed collected in China in 1705 which germinated in 1942, a lifespan of 237 years^{6,15}. Our own data for the Pulantien material suggests that an even greater longevity for this species is possible and that lotus seeds can maintain their high degree of polyunsaturation despite very long periods of quiescence. The situation in lotus is in contrast to that in maize (*Zea mays* L.), for example, which loses the bulk of its polyunsaturated fatty acid within about 100 years¹⁶. The two factors most in favour of prolonged longevity in the Pulantien seeds are probably the extremely thick pericarp and the generally reducing environment present in the peat within which they were deposited. It should be noted that enzymatic repair mechanisms are unlikely to operate in such seeds, which have a moisture content of approximately 11%¹. The lack of extensive lipid autoxidation in the Pulantien material probably accounts for the relatively well-preserved membrane profiles seen in ultrastructural studies^{17,18}. On the basis of such limited data it is difficult to speculate on the causes of viability loss in seed P3. Some lipid autoxidation may have occurred, but not enough to eliminate linolenic acid (C18:3) or to reduce the total level of polyunsaturation below that of the (viable) seed P4. The yellowing of the cotyledons of P3 is probably significant. In a previous study we noted similarly enhanced yellowing in corn seed that had lost viability during thirty to forty years of long-term storage, although this could not always be convincingly linked to fatty acid autoxidation¹⁹.

As noted by Godwin²⁰ complete credibility for claims of

Table 1 Fatty acid contents of Pulantien and Washington lotus seeds

	% Of total fatty acid						
	16:0	18:0	18:1	18:2	18:3	20:0	22:0
P1	25.0	1.3	11.7	49.2	4.5	2.5	5.7
P2	23.7	1.4	12.9	48.0	4.2	3.4	6.4
P3	34.7	2.4	11.8	39.5	2.6	2.5	6.5
P4	31.5	2.8	17.3	36.3	2.6	2.7	6.7
W1	21.6	2.1	19.6	42.4	5.1	3.5	5.6
W2	21.0	1.4	20.5	41.7	4.7	4.0	6.7
W3	22.7	1.3	20.4	43.0	4.6	3.5	4.4

Lipids were extracted from approximately 10 mg of cotyledonary material using 10 ml of chloroform:methanol (2:1, v/v). The solvent extract was filtered and washed once against 2 ml of 0.9% (w/v) NaCl. Fatty acid methyl esters were prepared according to ref. 24. Analyses were made using a Pye Series 204 gas chromatograph coupled to a VG Micromass 70–70 mass spectrometer system. The separations were on a 1.5 m × 2 mm column packed with 3% Silar 10-C on Chromosorb W-HP (100/120 mesh) using a temperature programme of 140–220 °C at 4 °C min⁻¹ or 120–220 °C at 6 °C min⁻¹. (16:0, palmitic; 18:0, stearic; 18:1, oleic; 18:2, linoleic; 18:3, linolenic; 20:0, arachidic; 22:0, behenic). Seeds P1–P4, Pulantien; W1–W3, Washington.

† Address for correspondence.

extreme seed longevity can come only from dating of the seed itself, preferably of a completely inert part such as the coat⁵. The mere dating of an object or structure associated with the seed is insufficient. With the possible exception of a reputedly 620-year-old *Canna compacta*²¹ seed, all other circumstantial claims for long lifespan are seriously suspect⁶. It is worth noting that not only are the lotus seeds among the oldest viable seeds recorded, but also their tissues must contain some of the longest-lived post-mitotic plant cells known. Although some trees such as *Sequoia sempervirens* and *Pinus longaeva* may attain ages of several millennia, the living cells in such structures are unlikely to exceed in lifespan a few decades at most^{22,23}. The cryptobiotic nature of well-protected dehydrated seeds such as the lotus assures their constituent tissues of a potentially much greater longevity.

We thank Dr Pei-sung Tang (Institute of Botany of the Chinese Academy of Sciences) and Dr Liu Shen-cheng (Beijing Botanical Garden) for providing seeds and Dr Horace V. Wester (National Parks Service, Washington DC) for donating freshly grown lotus seeds. Radiocarbon dating was carried out by Dr W. G. Mook (Laboratory of General Physics, State University of Groningen). We thank Professors Johan Bruinsma and Carl Leopold for encouragement. D.A.P. acknowledges the provision of a fellowship by the Netherlands Organization for the Advancement of Pure Research.

Received 25 March; accepted 15 June 1982.

- Ohga, I. *Bot. Mag., Tokyo* **37**, 87-95 (1923).
- Ohga, I. *Bot. Mag., Tokyo* **41**, 1-6 (1927).
- Libby, W. F. *Science* **114**, 291-296 (1951).
- Godwin, H. & Willis, E. H. *New Phytol.* **63**, 410-412 (1964).
- Wester, H. V. *Hortscience* **8**, 371-377 (1973).
- Justice, O. L. & Bass, L. N. *Principles and Practices of Seed Storage* (USDA Agriculture Handbook No. 506, Washington, D.C., 1978).
- Chaney, R. W. *Gdn. J. N.Y. bot. Gdn* **1**, 137-139 (1951).
- Krishtofovich, A. N. *Priroda, Mosk.* Part 1, 76-78 (1953).
- Ohga, I. *Jap. J. Bot.* **3**, 1-20 (1926).
- Ohga, I. *Am. J. Bot.* **13**, 754-759 (1926).
- Stuiver, M. *Radiocarbon* **24**, 1-26 (1982).
- Villiers, T. A. in *Seed Ecology* (ed. Heydecker, W.) 265-288 (Pennsylvania State University, University Park, 1973).
- Howell, R. W. & Collins, F. I. *Agron. J.* **49**, 593-597 (1957).
- Harris, H. C., McWilliam, J. R. & Mason, W. K. *Aust. J. agric. Res.* **29**, 1202-1212 (1978).
- Anonymous *Nature* **149**, 658 (1942).
- Priestley, D. A., Galinat, W. C. & Leopold, A. C. *Nature* **292**, 146-148 (1981).
- Hallam, N. D. & Osborne, D. J. in *Eighth International Congress on Electron Microscopy, Canberra, 1974*, Vol. 2 (eds Sanders, J. V. & Goodchild, D. J.) 598-599 (Australian Academy of Science, Canberra, 1974).
- Zhukova, G. Ya. & Yakovlev, M. S. *Bot. Zhur.* **61**, 869-872 (1976).
- Priestley, D. A., McBride, M. B., Galinat, W. C. & Leopold, A. C. *Pl. Physiol. (Suppl.)* **67**, 115 (1981).
- Godwin, H. *Nature* **220**, 708-709 (1968).
- Lerman, J. C. & Cigliano, E. M. *Nature* **232**, 568-570 (1971).
- MacDougal, D. T. & Smith, G. M. *Science* **66**, 456-457 (1927).
- Fritts, H. C. *Tree Rings and Climate* (Academic, London, 1976).
- Douce, R. & Lance, C. *Physiol. Vég.* **10**, 181-198 (1972).

Leaf injury on wheat plants exposed in the field in winter to SO₂

C. K. Baker, M. H. Unsworth* & P. Greenwood

Department of Physiology and Environmental Science,
University of Nottingham School of Agriculture, Sutton Bonington,
Loughborough LE12 5RD, UK

The combined stresses of air pollution and low temperatures have been suspected as a cause of difficulty in establishing grasses¹ and trees² in upland areas of northern England. Davison and Bailey³ recently showed in controlled environment studies that exposure to SO₂ predisposed grasses to frost injury, and Keller⁴ has established that exposure to SO₂ of young spruce trees kept in cabinets outdoors over winter enhanced their sensitivity to frost injury the following spring. We report here the first observations of injury of winter wheat exposed in the field to controlled concentrations of SO₂ during the severe winter weather of December 1981 to January 1982. We conclude that the injury was probably caused by cold-stress after SO₂ exposure had rendered the plants cold-sensitive.

* Present address: Department of Botany, North Carolina State University, Raleigh, North Carolina 27650, USA.

A microcomputer-controlled system has been designed to release SO₂ from the upwind edge(s) of a square of pipes so that an area 20 m × 20 m in a normally-managed field of winter wheat can be exposed continuously to elevated concentrations of SO₂ from crop emergence in the autumn to harvest in the summer of the following year. The system, described fully elsewhere⁵, has been operated so that, independent of wind speed and direction, the SO₂ concentration at the centre of the square is maintained at a mean value of 100 p.p.b. (267 µg m⁻³ at 20 °C) above ambient, which is typically 10-20 p.p.b. at this site. Plants closer to the upwind edge are exposed to higher concentrations, typically 400 p.p.b. at 2 m from the gas release lines, whereas plants near the downwind edge experience lower concentrations, typically 20 p.p.b.⁵. Thus exposure in the treated area, other than close to the centre, depends on wind direction. By regarding the exposed area as a grid of 25 squares of 4 × 4 m and by combining measured SO₂ concentrations with a numerical diffusion model, the accumulated pollution dose in each grid square (concentration × time) is calculated by the computer.

The field was sown with winter wheat (*Triticum aestivum* L. cv. Bounty) on 23 September 1981. After emergence, the field exposure system was installed and release of SO₂ began on 27 November when the plants were ~4-5 cm high and had four leaves on the main stem. Exposure to SO₂ was continuous apart from breaks for system development and maintenance. Up to 11 December there were no significant differences between exposed plants and controls which were taken from an area ~60 m distant in which SO₂ concentrations did not differ from background values and where soil properties and microclimate were similar to those in the exposed area. On 11 and 14 December ~20 cm of snow fell, covering the plants completely. Gas release continued during the period of snow cover. On 23 December samples of snow (top few mm) were collected at the exposure and control sites for chemical analysis. The snow thawed on 31 December. During the period 12-30 December the mean daily maximum and minimum air temperatures at a Meteorological Office site ~400 m from the wheat field were 1.2 and -6.4 °C, respectively. After a brief mild period, very cold weather returned on 6 January and ~20 cm of snow fell on 8-9 January 1982, remaining until 16 January. Snow samples were collected on 12 January. In the period 6-15 January, mean daily maximum and minimum air temperatures were -1.7 and -9.2 °C, respectively.

A few days after the rapid thaw on 16 January it was clear that leaves of plants within the exposed zone had substantially more injured area than plants in the rest of the field. These injuries, which did not differ significantly throughout the 20 × 20 m zone, consisted of senescing tissue at the leaf tips; injured leaves appeared waterlogged and translucent. An independent assessment revealed no signs of disease. Table 1 shows the percentage of senescing tissue (lamina length) on leaves 4, 5 and 6 of exposed and control samples harvested on three different dates after the thaw. Data for leaf 3 are omitted because these leaves were senescing rapidly throughout the field at this period. Leaves 4 and 5 were injured significantly more in the exposed area; it seems that the injury on leaf 4 developed after the thaw, but injury on leaf 5 did not increase significantly after it was first recorded. A small amount of injury was observed on leaf 6 which emerged mainly after the thaw. Leaves emerging subsequently showed no injury.

We have examined three hypotheses to account for the injury observed:

(1) Leaves were injured due to 'acid' snow resulting from absorption of SO₂ at the snow surface. Injury would have been most likely when the snow thawed and plants were bathed in an acid solution.

(2) The injury was a response to SO₂ uptake by leaves after the plants had been made susceptible to SO₂ injury by low temperatures.

(3) Plants were injured by low temperatures after exposure to SO₂ had reduced their cold-hardiness.

The 'acid snow' hypothesis is not supported by our observations. Analyses of the two sets of snow samples showed insignificant differences between chemical composition of samples from the SO₂-exposed site and the control site. On 12 January the pH of the top few mm of snow ranged from 5.7 to 7.2 in the exposed area and from 6.4 to 7.6 in the control. Sulphate concentration in the snow was 9.5–14.4 µg ml⁻¹ and 9.3–10.8 µg ml⁻¹ at the exposed and control sites, respectively. Analyses of samples collected on 23 December also showed little difference between pH and sulphate concentration at the two sites. The lack of accumulation of sulphate in the snow at the exposed site is consistent with the low deposition velocity reported for SO₂ to snow⁶.

To investigate whether injury could have been caused to roots by a 'pulse' of acid or concentrated sulphate solution leached by melting snow from previously deposited sulphur on plants or soil, we analysed samples of soil solution collected by suction sampling from porous cups at 15 cm depth on 21 January. There were no significant differences in sulphate concentration in the soil solution between exposed and control areas.

It is more difficult to test retrospectively hypotheses (2) and (3). In support of the hypothesis that SO₂ uptake caused the injury is the observation that leaves harvested from near the centre of the exposed area on 21 January contained substantially more total sulphur than controls (8.4 ± 0.2 mg per g dry wt as opposed to 5.1 ± 0.1 mg per g). Dissolved SO₂ dissociates to phytotoxic sulphite and bisulphite forms⁷ and injury is more likely in cold conditions when oxidation to sulphate and other detoxification mechanisms are slow⁸. However, it is necessary to account for the uniformity of injury over the treated area where the dose experienced was very variable. Table 2 shows the computed SO₂ dose for each grid square during daylight hours in the period from 27 November until the injury was observed, excluding periods of snow cover. This dose, which varies by a factor of four across the exposed area would be expected to correlate well with absorbed SO₂ (ref. 9). Thus, unless there was a threshold sulphur content above which injury occurred independent of further sulphur uptake, or unless only leaf tips were susceptible to injury, it is impossible to explain the uniformity of injury. In addition, the symptoms of injury did not resemble the typical well-defined bleached areas attributed to SO₂ injury¹⁰.

The hypothesis that plants were injured by low temperatures after exposure to SO₂ had reduced their cold-hardiness, seems the most probable explanation for the injury, because at least two known mechanisms of SO₂ action on plants are likely to influence cold-hardiness in ways which could account for the uniformity of injury. Black and Black¹¹ observed that brief exposure of bean leaves to SO₂ concentrations similar to those in our experiment decreased the survival of cells on epidermal strips; survival rates did not depend strongly on concentration above ~80 p.p.b. If SO₂ exposure weakened membranes on wheat leaves, it seems likely that resistance to cold stress would be reduced. Alternatively, it is known that in plants where

Table 1 Injury on wheat plants harvested on three dates at a site exposed to SO₂ and a control site

Date	Site	Leaf no.		
		4	5	6
21/1	Control	12 ± 4	6 ± 3	0
	Exposed	16 ± 4	36 ± 5	0
3/2	Control	8 ± 2	10 ± 5	0
	Exposed	40 ± 5	44 ± 4	2 ± 1
12/2	Control	8 ± 2	6 ± 1	0
	Exposed	40 ± 2	40 ± 2	3 ± 1

Values shown are the mean percentage (±s.d.) leaf length injured for plants harvested on the dates shown from a site exposed to SO₂ and a control site. The first two harvests consisted of 6 plants from a larger sample of 0.25 m of two adjacent rows. The third harvest was 60 plants from each site.

Table 2 Cumulative SO₂ dose (p.p.m. h⁻¹) calculated for each 4 × 4 m grid square in the experimental area for the daylight hours of 27 November 1981 to 16 January 1982

51.3	28.5	25.8	26.9	40.4
49.0	20.0	16.0	17.2	31.2
49.5	20.1	16.0	16.9	30.3
51.0	24.1	21.3	21.0	31.7
68.7	54.1	51.1	49.7	52.2

Periods when plants were covered with snow are not included.

photosynthetic rates have been reduced or respiration increased, cold-hardiness may be reduced¹². Black and Unsworth¹³ demonstrated that SO₂ concentration > 50 p.p.b. reduced net photosynthesis in beans, and the reduction was independent of SO₂ concentration at low irradiance. Dark respiration was increased, also independent of SO₂ concentration.

We observed no injury after the first cold period even though the lowest night-time air temperature (–15.3 °C) was comparable with the lowest in the second period (–15.8 °C). Temperatures at the surface would have been even colder than these values. It may be that the intervening warm weather with maximum temperatures of 10–12 °C reduced cold-hardiness. On the other hand, day-time temperatures in January were much lower than in December, therefore a threshold for injury may have been exceeded, perhaps because repair mechanisms or replenishment of assimilates could not proceed at the lower temperature.

As with all post mortems, it is difficult to be conclusive about causes of injury. In particular the lack of replication of our treatment and control sites makes definitive interpretation of the causes of injury difficult. It seems essential, therefore, to test our hypotheses of the mechanisms of plant response by experiments in more controlled environments.

Whereas cereals are likely to recover from injury during winter, the delay in establishing leaf area could reduce yield if growth was limited later in the season, for example, by nutrition, drought or high temperatures. Frost injury enhanced by SO₂ exposure could not only reduce quality of horticultural crops but also, by delaying harvest, could cause large financial losses.

This work was supported by the Department of the Environment. We thank Sue Gregson and Geoff Dollard for chemical analyses and Colin and Valerie Black for helpful discussions.

Received 6 May; accepted 24 June 1982.

1. Bell, J. N. B. & Mudd, C. H. in *Effects of Air Pollutants on Plants* (ed. Mansfield, T. A.) 87–103 (Cambridge University Press, 1976).
2. Lines, R. in *Rep. Forest Research 1977*, 18–19 (HMSO, London, 1977).
3. Davison, A. W. & Bailey, I. F. *Nature* **297**, 400–402 (1982).
4. Keller, T. *Gartenbauwissenschaft* **46**, 170–178 (1981).
5. Greenwood, P. et al. *Atmos. Envir.* (in the press).
6. Barrie, L. A. & Walmsley, J. L. *Atmos. Envir.* **12**, 2321–2332 (1978).
7. Puckett, K. J. et al. *New Phytol.* **72**, 141–154 (1973).
8. Schiff, J. A. & Hodson, R. C. A. *Rev. Pl. Physiol.* **24**, 381–414 (1973).

9. Fowler, D. & Cape, J. N. in *Effects of Gaseous Air Pollution in Agriculture and Horticulture* (eds Unsworth, M. H. & Ormrod, D. P.) 3–26 (Butterworths, London, 1982).
10. *Diagnosing Vegetation Injury Caused by Air Pollution* (Air Pollution Training Institute, Research Triangle Park, North Carolina, 1976).
11. Black, C. R. & Black, V. J. *J. exp. Bot.* **30**, 291–298 (1979); *Pl. Cell Envir.* **2**, 329–333 (1979).
12. Alden, J. & Hermann, R. K. *Bot. Rev.* **37**, 37–142 (1971).
13. Black, V. J. & Unsworth, M. H. *J. exp. Bot.* **30**, 473–483 (1979).

Variation in genome size—an ecological interpretation

J. P. Grime & M. A. Mowforth

Unit of Comparative Plant Ecology (NERC), Department of Botany, The University, Sheffield S10 2TN, UK

Previous attempts to explore the significance of variation in genome size have involved comparisons with respect to life history^{1–4}, taxonomic and evolutionary affiliations^{5–9} and geographical distribution^{10,11}. Here we examine variation in the British flora. Large genomes are particularly associated with Mediterranean geophytes and grasses in which growth is confined to the cool conditions of winter and early spring. We suggest that large genomes have evolved under circumstances in which growth is limited by the effect of low temperature on rates of cell division and are part of a mechanism whereby growth at low temperature is achieved by rapid inflation of large cells formed during a preceding warm dry season. Where moisture supply allows growth to occur in the summer, temporal separation of mitosis and cell expansion confers no advantage and the longer mitotic cycle of large cells is likely to restrict rates of development; here the effect of natural selection has been to reduce cell and genome size.

Figure 1 describes the distribution with respect to genome size of various classes of flowering plants represented by 162 native or naturalized species of the British flora. Contrary to earlier observations^{1,11}, no consistent difference is apparent

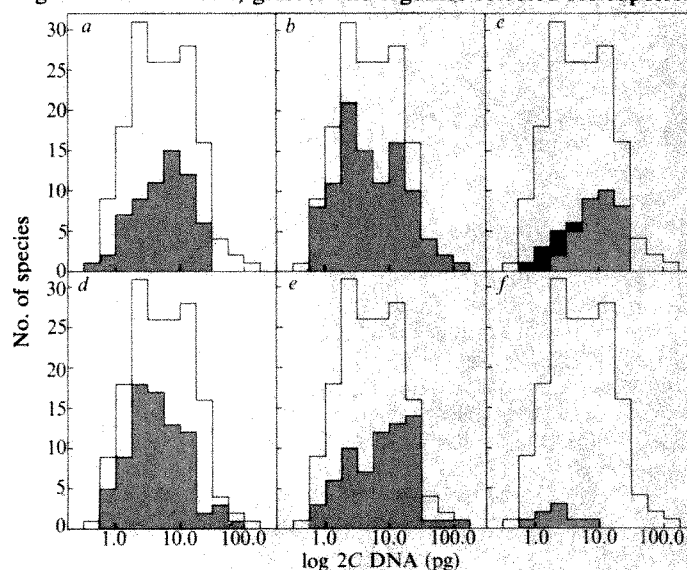
between annuals and perennials. This is due to inclusion in the analysis of common perennial herbs, trees and shrubs, many of which (for example, *Epilobium hirsutum*, *Chamaenerion angustifolium*, *Salix caprea*, *Eriophorum vaginatum*) have comparatively small genomes. Grasses include many species with large (2C DNA >10 pg) genomes whereas low values are more typical of woody plants. Monocotyledons (mean 2C DNA = 17.28 pg) have significantly larger genomes ($P < 0.001$) than dicotyledons (mean 2C DNA = 6.86 pg). If comparison is restricted to herbaceous plants (Table 1) the difference in mean genome size between monocotyledons and dicotyledons is still observed but no consistent differences are associated with life history. When maps¹² are used to classify the species it is evident that plants found in southern Britain have markedly larger genomes. The mean genome size for the 69 southern species (mean 2C DNA = 13.31 pg) is significantly greater ($P < 0.05$) than that for the 80 species of widespread distribution (mean 2C DNA = 7.96 pg). Although data are available for only eight species, it is interesting that the mean value for plants of northern distribution is low (mean 2C DNA = 2.55 pg).

The species combining southern distribution and large genome size in Fig. 1 include a high proportion of geophytes and grasses with geographical ranges centred on the Mediterranean region. In most of these species, growth occurs during cool winter conditions and survival during the dry summer involves dormancy of both seeds and established plants. Similar phenologies are also common among the species of large genome size and widespread distribution in the British Isles. Here, however, the early development of species such as *Endymion non-scriptus*, *Ranunculus ficaria* and *Caltha palustris* occurs in relatively moist habitats and appears to provide a mechanism of evading competition from productive summer-green trees and herbs¹³.

The correlation between large genome size and the capacity for growth at low temperature is consistent with the enlarged genomes of cereals, grasses and legumes selected for superior

Fig. 1 Genome size in 162 flowering plants occurring in the British Isles.

a, Annuals; b, perennials (including biennials); c, grasses (stippled) and trees and shrubs (shaded); d, widespread distribution; e, southern distribution; f, northern distribution. The distribution for all 162 species is also reproduced in each subsection. In the following key to species and 2C DNA values (pg), original data (obtained by Feulgen microdensitometry on 10 nuclei from each of three seedlings) are distinguished by* from that collated by Bennett and Smith². *Achillea millefolium** (14.4), *Agrostis tenuis** (6.6), *Alliaria petiolata* (3.9), *Allium ursinum** (63.0), *Anthoxanthum odoratum** (11.8), *Anthyllus vulneraria** (1.0), *Aphanes arvensis* (1.1), *Arabidopsis thaliana* (0.5), *Arrhenatherum elatius** (16.0), *Artemisia absinthium* (7.3), *Arum maculatum* (21.8), *Avena fatua* (28.3), *Avena ludoviciana* (27.5), *Beta maritima* (2.6), *Betula pubescens** (1.4), *Brachypodium pinnatum** (2.3), *Brassica napus* (3.2), *Brassica nigra* (1.6), *Brassica oleracea* (1.8), *Briza media* (16.9), *Bromus commutatus* (21.7), *Bromus erectus** (22.6), *Bromus interruptus* (16.8), *Bromus lepidus* (15.7), *Bromus madritensis* (9.7), *Bromus pseudohominii* (19.7), *Bromus racemosus* (27.0), *Bromus rigidus* (17.2), *Bromus sterilis* (6.7), *Bryonia dioica* (3.3), *Caltha palustris* (33.0), *Campanula rotundifolia* (4.9), *Capsella bursa-pastoris* (1.4), *Cardamine flexuosa** (1.6), *Carex caryophyllaea** (1.5), *Chamaenerion angustifolium** (0.7), *Convallaria majalis* (49.3), *Crepis biennis* (16.9), *Crepis capillaris* (4.7), *Dactylis pilosa* (0.6), *Daucus carota* (2.5), *Digitalis purpurea** (2.3), *Drosera intermedia* (2.0), *Drosera rotundifolia* (1.8), *Endymion non-scriptus* (42.4), *Epilobium hirsutum** (0.6), *Eranthis hyemalis* (18.6), *Eriophorum angustifolium** (1.2), *E. vaginatum** (1.0), *Festuca ovina** (9.5), *Fritillaria meleagris* (141.4), *Fumaria muralis* (1.1), *Helianthemum chamaecistus** (4.5), *Helleborus niger* (22.8), *Holcus lanatus** (3.4), *Hordeum jubatum* (21.7), *Hordeum marinum* (11.0), *Hordeum murinum* (11.1), *Hordeum secalinum* (22.4), *Ilex aquifolium** (2.2), *Impatiens glandulifera** (2.2), *Lactuca serriola* (3.7), *Lamium album* (2.2), *Lamium purpureum* (2.2), *Lathyrus aphaca* (13.8), *Lathyrus maritimus* (15.6), *Lathyrus montanus* (16.5), *Lathyrus nissolia* (13.0), *Lathyrus sylvestris* (23.0), *Lathyrus tuberosus* (18.6), *Leontodon autumnalis* (2.7), *Leontodon hispidus** (5.2), *Lilium pyrenaicum* (65.5), *Lolium italicum* (9.8), *Lolium perenne* (9.9), *Lolium temulentum* (13.6), *Lotus corniculatus** (2.2), *Lotus tenuis* (1.0), *Lotus uliginosus** (1.1), *Lupinus arboreus* (1.6), *Luzula multiflora* (1.9), *Luzula sylvatica* (1.6), *Luzula sylvatica* (1.6), *Matricaria matricarioides* (4.6), *Matricaria recutita* (7.8), *Medicago lupulina** (1.6), *Melilotus alutissima** (2.5), *Mercurialis perennis* (4.7), *Mibora minima* (5.5), *Molinia caerulea** (4.6), *Montia perfoliata* (4.4), *Myosurus minimus* (2.2), *Origanum vulgare** (1.3), *Ornithogalum longibracteatum* (15.2), *Oxalis acetosella* (6.4), *Papaver dubium* (9.0), *Papaver rhoeas* (5.2), *Papaver somniferum* (7.6), *Petasites hybridus** (1.8), *Phalaris arundinacea* (11.4), *Phalaris canariensis* (7.7), *Pheum bertolonii* (3.4), *Picris echioides* (2.4), *Picris hieracioides* (3.1), *Pimpinella saxifraga** (9.5), *Plantago lanceolata** (2.3), *Poa annua** (3.8), *Poa infirma* (2.4), *Poa trivialis* (5.6), *Ranunculus acris* (10.7), *Ranunculus arvensis* (12.2), *Ranunculus auricomus* (18.0), *Ranunculus baud* (8.4), *Ranunculus bulbosus* (11.2), *Ranunculus ficaria* (18.6), *Ranunculus flammula* (12.7), *Ranunculus hederaceus* (4.2), *Ranunculus lingua* (50.2), *Ranunculus ophioGLOSSIFOLIUS* (11.3), *Ranunculus paludosus* (16.5), *Ranunculus parviflorus* (12.5), *Ranunculus repens* (22.4), *Ranunculus sardous* (6.4), *Ranunculus scleratus* (8.0), *Ranunculus trichophyllus* (9.7), *Ranunculus tripartitus* (9.0), *Rhinanthus minor* (7.9), *Rumex acetosa** (3.1), *Rumex obtusifolius** (2.7), *Salix caprea** (0.8), *Sambucus nigra** (2.9), *Sarothamnus scoparius** (1.7), *Senecio aquaticus* (3.6), *Senecio squalidus* (1.8), *Senecio vulgaris* (3.0), *Scirpus sylvaticus** (1.3), *Sieglingia decumbens** (5.9), *Silene dioica** (5.0), *Sonchus asper* (3.7), *Stellaria media* (2.1), *Taraxacum officinale* (2.6), *Thymus drucei** (2.6), *Trifolium arvense** (1.4), *Trifolium campestre** (0.9), *Trifolium medium** (6.7), *Trifolium pratense** (1.3), *Trifolium repens** (3.0), *Tripleurospermum maritimum* (5.3), *Tussilago farfara** (4.6), *Urtica dioica** (2.9), *Urtica urens* (0.6), *Veronica persica* (1.5), *Vicia bithynica* (9.1), *Vicia cracca** (11.4), *Vicia hirsuta** (7.2), *Vicia lathyroides* (5.2), *Vicia lutea* (14.8), *Vicia orobus* (10.7), *Vicia sativa* ssp. *angustifolia** (4.0), *Vicia sepium* (9.4), *Vicia sylvatica* (17.2), *Vicia tetrasperma* (7.4).



yield at high latitudes or elevations¹⁰ and with the low values reported for cacti² and tropical plants^{2,9,11}. It is at first surprising that the genomes measured in native plants of northern distribution in Britain (for example, *Eriophorum* spp., *Drosera rotundifolia*) are small. However, at high latitudes winter and spring are severe and unpredictable and the vegetation tends to be dominated by species in which both shoot growth and germination are delayed until the onset of warmer summer conditions^{14,15}.

The massive genomes reported for *Fritillaria* spp. ($2C$ DNA = 96.5–254.8 pg) and *Tulipa* spp. ($2C$ DNA = 39.9–90.6 pg)² are associated with the capacity for early and rapid expansion of relatively short-lived shoots and it is noticeable that their development precedes that of the spring grasses of more moderate genome size with which they are often associated in meadows and gardens respectively. Figure 2 provides a more objective test of the relationship between genome size and phenology. Measurements of the seasonal change in the shoot biomass of species established in natural herbaceous vegetation of the Sheffield region^{13,16,17} have been used to relate the timing of shoot growth in the spring to the genome sizes of individual species. Figure 2 includes all species for which quantitative measurements of both shoot phenology and genome size are available. The results indicate that from early spring to mid-summer changes in the identity of the most actively growing species are associated with a progressive reduction in genome size.

We suggest that the selective force determining this relationship between genome size and season of growth arises from a

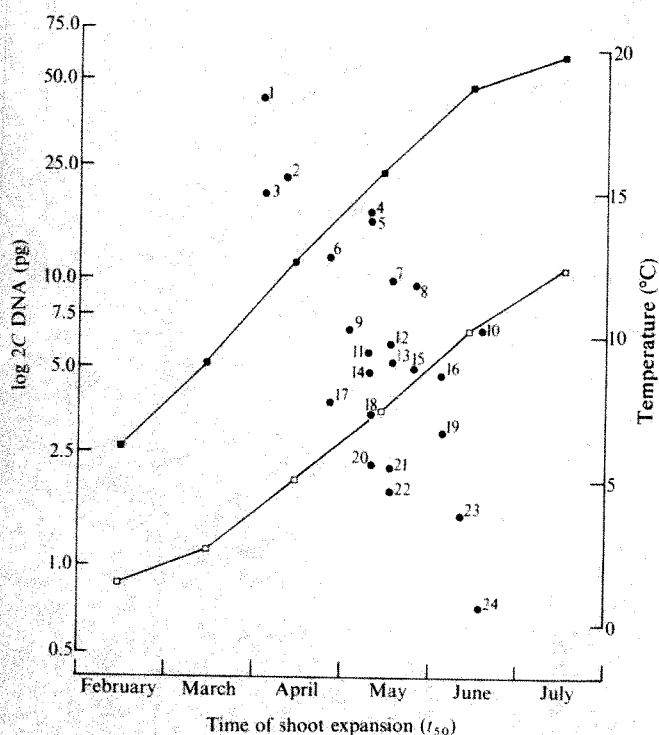


Fig. 2 Relationship between genome size and time of shoot expansion in plant species commonly found in the Sheffield region (correlation coefficient significant at <0.001). The time of shoot expansion is calculated as the date to the nearest quarter-month at which 50% of the maximum shoot biomass was attained^{13,16,17}. Temperature in Sheffield is expressed as the long-term averages for each month of daily minima (□) and maxima (■) in air temperature 1.5 m above the ground surface. 1, *E. non-scriptus*; 2, *R. repens*; 3, *R. ficaria*; 4, *B. media*; 5, *A. elatius*; 6, *A. odoratum*; 7, *L. perenne*; 8, *F. ovina*; 9, *T. medium*; 10, *A. tenuis*; 11, *S. decumbens*; 12, *P. trivialis*; 13, *L. hispidus*; 14, *C. rotundifolia*; 15, *M. perennis*; 16, *M. caerulea*; 17, *P. annua*; 18, *H. lanatus*; 19, *U. dioica*; 20, *B. pinnatum*; 21, *L. corniculatus*; 22, *P. hybridus*; 23, *C. caryophylla*; 24, *C. angustifolium*.

Table 1 Comparison of mean genome size (pg) in various classes of herbaceous plant of the British flora

	Annual	NS	Perennial	Total
Monocotyledons	14.07 ***		18.10 **	17.29 ***
Dicotyledons	5.76	NS	8.17	7.17

Probability of significant difference *** <0.001 , ** <0.01 . NS, not significant.

differential effect of low temperature on cell division and cell expansion. As temperature rises during the spring the advantage of growth dominated by cell enlargement is likely to give way to that of growth involving high rates of cell division. Evidence supporting this hypothesis is available from studies¹⁸ in which mitosis has been shown to be inhibited at temperatures which permit high rates of cell expansion. Variation in genome size is implicated in this proposed mechanism by both our own unpublished observations which confirm that species which habitually grow by cell enlargement at low temperatures have relatively large cells and measurements^{19–23} establishing that potentially large cells have large nuclear volumes and high DNA contents. The mechanism dictating the strong correlation between cell size and nuclear volume remains obscure, although it has been suggested^{3,4} that large cells require an enlarged nuclear envelope to maintain adequate rates of nucleocytoplasmic transport of RNA. It is also possible that cells growing and functioning at low temperatures require more enzymes to sustain adequate metabolic rates. This may necessitate cell enlargement to accommodate extra protein, and higher DNA content could arise from 'dosage repetition'²⁴ of genes coding for proteins and ribosomes²⁵.

As the minimum duration of the mitotic and meiotic cycles is inescapably long in large cells^{19–23} the advantage of growth by cell enlargement would not be expected to pertain at warm temperatures. Thus, small genomes are observed^{2,26} not only in species of continuously warm tropical or arid environments but also in plants in which growth is restricted to the summer period in temperate, continental or arctic zones.

In the geophytes of very large genome size (such as *Fritillaria*, *Tulipa*, *Endymion*), growth occurs mainly by expansion of cells formed during warm relatively dry conditions of the preceding year²⁷. A similar, if less extreme, temporal separation of cell division and expansion may occur in grasses such as *Briza media* and *Anthoxanthum odoratum*, which in Fig. 2 follow the geophytes in the phenological sequence. Here spring growth involves the expansion of relatively large cells but it is less determinate and includes some cell division. In these species, we suggest that spring development may be sustained by the capacity for growth by cell expansion during intermittent cold periods and in the cooler parts of the daily temperature cycle. We suspect also that an integral part of this mechanism may be the accumulation of unexpanded cells during periods in which cell expansion but not cell division is restricted by moisture stress.

Patterns of variation in genome size may be useful in predicting plant response to climate, in crop breeding and in the analysis of niche-differentiation in plant communities. The data compiled by Britten and Davison²⁸ suggest that temperature may have played a major part in the determination of genome size in animals also. As might be expected, small genomes are characteristic of warm-blooded animals and it is particularly interesting that reptiles which flourish in dry hot conditions have uniformly small genomes whereas amphibians include species with exceptionally large genomes and cells. The respiratory system of amphibians depends on the maintenance of a moist permeable skin, so the ecology and behaviour of most species involve avoidance of insulation and maintenance of low body temperature. We suspect that particularly in amphibians exploiting temporary water bodies in a Mediterranean climate, there may be some temporal separation of cell division and expansion; in these conditions natural selection acting on rates of develop-

ment may have followed a course similar to that proposed for vernal plants.

We thank Drs M. D. Bennett, D. Goldstein, T. T. Elkington,

Received 13 April; accepted 2 July 1982.

- Bennett, M. D. *Proc. R. Soc. B* **181**, 109–135 (1972).
- Bennett, M. D. & Smith, J. P. *Phil. Trans. R. Soc. B* **274**, 227–274 (1976).
- Cavalier-Smith, T. *J. Cell Sci.* **34**, 247–278 (1978).
- Cavalier-Smith, T. *Bio Systems* **12**, 43–59 (1980).
- Rothfels, K., Sexsmith, E., Heimburger, M. & Krause, M. O. *Chromosoma* **20**, 54–74 (1966).
- Chooi, W. Y. *Genetics* **68**, 195–211 (1971).
- Smith, J. P. & Bennett, M. D. *Heredity* **35**, 231–239 (1975).
- Price, H. J. *Bot. Rev.* **42**, 27–52 (1976).
- Jones, R. N. & Brown, L. M. *Heredity* **36**, 91–104 (1976).
- Bennett, M. D. *Envir. exp. Bot.* **16**, 93–108 (1976).
- Levin, D. A. & Funderburg, S. W. *Am. Nat.* **114**, 784–795 (1979).
- Perring, R. H. & Walters, S. M. *Atlas of the British Flora* (Nelson, Edinburgh, 1962).
- Al-Mufti, M. M., Sydes, C. L., Furness, S. B., Grime, J. P. & Band, S. B. *J. Ecol.* **65**, 759–791 (1977).

B. C. Jarvis, D. L. Lewis, R. Law and D. Watts, and Messrs J. P. Smith, S. Band and C. Mathieson for advice and encouragement. This research was supported by the NERC.

- Billings, W. D. & Mooney, H. A. *Biol. Rev.* **43**, 481–529 (1968).
- Wein, R. W. & Maclean, D. A. *Can. J. Bot.* **51**, 2509–2513 (1973).
- Al-Mashhadani, Y. D. thesis, Univ. Sheffield (1979).
- Furness, S. B. thesis, Univ. Sheffield (1980).
- Haber, A. H. & Luippold, H. J. *Pl. Physiol.* **35**, 168–173 (1960).
- Bradley, M. V. *Am. J. Bot.* **41**, 398–402 (1954).
- Van't Hof, J. & Sparrow, A. *Proc. natn. Acad. Sci. U.S.A.* **49**, 897–902 (1963).
- Commoner, B. *Nature* **202**, 960–968 (1964).
- Darlington, C. D. *Cytology* (Churchill, London, 1965).
- Bennett, M. D. *Proc. R. Soc. B* **178**, 277–299 (1971).
- Finnegan, D. J., Rubin, G. M., Young, M. W. & Hogness, D. S. *Cold Spring Harb. Symp. quant. Biol.* **42**, 1053–1063 (1977).
- Long, E. O. & Dawid, I. B. *Rev. Biochem.* **49**, 727–764 (1980).
- Avdulov, J. P. *Trudy prikl. Bot. Genet. Selek.* **44**, Suppl. 4, 1–428 (1931).
- Hartsema, A. M. *Handb. PflPhysiol.* **16**, 123–167 (1961).
- Britten, R. J. & Davidson, E. H. *Q. Rev. Biol.* **46**, 111–133 (1971).

Competition of similar and non-similar genotypes

J. M. Pérez-Tomé

Colegio Universitario Arcos de Jalón, Arcos de Jalón s/n, Madrid-32, Spain

M. A. Toro

Departamento de Genética Cuantitativa, Instituto Nacional de Investigaciones Agrarias, Carretera de la Coruña km 7, Madrid-35, Spain

It has been well established that the fitness of a genotype is often a function of the presence and relative frequencies of other genotypes coexisting with it^{1–3}. Facilitation or interference between individuals of like genotypes is suggested by some experiments^{4–9}, and it is commonly accepted that competition is an important element in agricultural practice^{10,11}. However, most such studies, at least those that use *Drosophila* as the experimental organism, involve strains which carry different mutations or chromosomal rearrangements. Here we demonstrate that competition of similar as opposed to non-similar genotypes can be detected in a random mating population not subject to genetic manipulation.

In the experiments reported here we used a population of *Drosophila melanogaster* founded from a cross of 70 isofemale lines derived from flies collected by E. Torroja in Carbonera (Almería) in September 1981. Since then the population has been maintained on Lewis food medium. The flies were kept in an incubator room at $25 \pm 1.5^\circ\text{C}$ under continuous illumination. All handling was at room temperature using ether anaesthesia.

Virgin males and females were collected within 6 h of emergence and placed in plastic or glass vials containing *Drosophila* medium, in groups of 20–30 of the same sex. The matings were set up when the flies were 3 days old by placing each one of 80 males with 10 females in a vial for 96 h, after which the male was removed. Two series of vials were then established. In the first, called the homogeneous series, the 10 females that had mated with the same male were placed in a 9×3 cm vial with 2 ml of medium. In the second, called the heterogeneous series, 10 females chosen randomly, but excluding any females

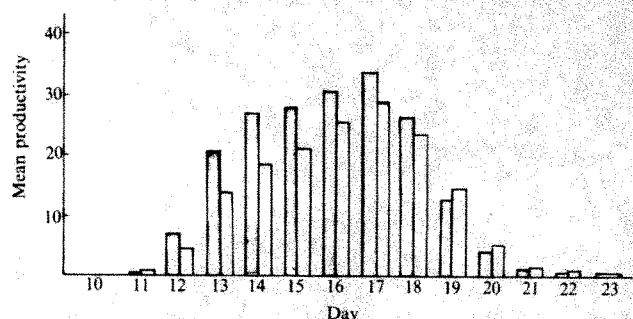


Fig. 1 Mean number of flies emerging daily for the homogeneous (□) and heterogeneous (▨) series.

mated with the same male, were placed in the same vial. All the females were transferred to fresh vials every 24 h for a total of four egg-laying periods. The progeny emerging in each vial were removed and counted daily until the cultures were exhausted.

The only difference between the homogeneous and the heterogeneous series is that in the first the full-sib families that compete are related as half-sibs whereas in the second these full-sib families are randomly assorted. However, the genotypes sampled in the two series are the same, thus explanations such as heterozygote advantage can be disregarded when interpreting the experiment.

Table 1 shows the mean productivity (number of flies emerging per vial) for the different egg-laying periods and the series. Figure 1 shows the daily mean productivity for the two series. This productivity is clearly greater in the heterogeneous than in the homogeneous series; and the difference between the total productivity of the flies in the two series is highly significant ($P < 0.005$).

The results presented here demonstrate clearly that in highly competitive conditions larval viabilities of *D. melanogaster* depend on the similarity of the genotypes coexisting. The productivity can be decreased by 17% merely by modifying the way in which the full-sib families compete.

There are two basically different mechanisms by which some larvae may affect the survival of others: (1) by diffusible metabolic products that affect the survival of other larvae; and (2) by differential utilization of niches by the different genotypes.

Table 1 Mean number of *Drosophila* emerging per vial for the different egg-laying periods and experimental series

Series	Period				Total
	1	2	3	4	
Heterogeneous	58.46 ± 3.16	53.62 ± 2.41	42.62 ± 1.93	37.49 ± 2.04	192.20 ± 5.3
Homogeneous	51.88 ± 3.41	39.88 ± 3.33	38.51 ± 3.00	32.86 ± 2.35	159.69 ± 9.90
t	1.43	3.38	1.16	1.49	2.94
P	<0.20	<0.001	<0.30	<0.20	<0.005

Approximately 35 vials were examined per period for each series; 10 flies per vial. Values shown are mean ± s.d.

It is not clear whether interference or facilitation is involved in these mechanisms.

These results have a bearing on the importance of frequency-dependent selection as an explanation for the maintenance of polymorphism, and are also relevant to the competition between genotypes important in agricultural practice. If this phenomenon is a general one it would also provide a mechanism for the maintenance of recombination through sib-competition¹². The simplicity of the experimental design presented here should allow us to explore more easily the nature of competition between genotypes.

We thank B. Charlesworth, John Maynard Smith, C. Lopez-Fanjul, L. Silveira, J. Malpica and E. Torroja for helpful advice and criticism.

Received 7 June; accepted 5 July 1982.

1. Ayala, F. J. & Campbell, C. A. *A. Rev. Ecol. Syst.* **5**, 115-138 (1974).
2. Lewontin, R. *The Genetic Basis of Evolutionary Change* (Columbia University Press, 1974).
3. Clark, B. *Proc. R. Soc. B* **205**, 453-474 (1979).
4. Dobzhansky, T. & Spassky, B. *Genetics* **29**, 270-290 (1944).
5. Lewontin, R. *Evolution* **9**, 27-41 (1952).
6. Mather, K. & Cooke, P. *Heredity* **17**, 381-407 (1962).
7. Lewontin, R. & Matsu, Y. *Proc. natn. Acad. Sci. U.S.A.* **49**, 270-278 (1963).
8. Seaton, A. P. C. & Antonovics, J. *Heredity* **22**, 19-33 (1967).
9. Caligari, P. D. S. *Heredity* **45**, 219-231 (1980).
10. Donald, C. M. *Adv. Agron.* **15**, 1-118 (1963).
11. Allard, R. W. & Adams, J. *Am. Nat.* **103**, 621-645 (1969).
12. Maynard Smith, J. *The Evolution of Sex* (Cambridge University Press, 1978).

Single cortical neurones have axon collaterals to ipsilateral and contralateral cortex in fetal and adult primates

Michael L. Schwartz & Patricia S. Goldman-Rakic

Section of Neuroanatomy, Yale University School of Medicine, New Haven, Connecticut 06510, USA

In the adult brain, cortical neurones that project to other cortical areas have traditionally been classified as either 'associational' (having connections within the ipsilateral hemisphere) or 'callosal' (projecting to areas in the contralateral hemisphere). Using double-labelling with fluorescent dyes^{1,2}, we have now identified a novel category of mature cortical neurone that has both an 'associational' and a 'callosal' axon. Such neurones can direct their callosal axons either to a cytoarchitectonic area homotopic to the one in which their cell bodies reside or to an entirely different heterotopic region in the contralateral hemisphere. These cortical neurones with divergent axon collaterals in the adult neocortex differ from recently described neurones that have two axons only transiently during development³⁻⁵.

Our evidence is based on data from two fetal (embryonic ages E132 and E137 respectively), two infant (4 and 12 days old respectively) and two adult rhesus monkeys. Each monkey received injections of one dye [Fast blue (FB), Nuclear yellow (NY) or propidium iodide (PI)] in the dorsal bank of the principal sulcus in the left hemisphere and injections of a second dye in the posterior bank of the intraparietal sulcus of the right hemisphere. In addition, one of the monkeys was injected with a third dye in the posterior cingulate cortex of the right hemisphere. Twenty to 72 h after the last injection, the animals were killed and their brains were immediately sectioned and prepared for microscopic examination. The distribution and morphology of labelled callosal neurones were determined in the principal sulcus, the intraparietal sulcus and the cingulate cortex (see outlined areas, Fig. 1). All three regions of association cortex receive projections from each other⁶⁻¹¹ as well as from the corresponding homotopic area in the opposite hemisphere^{6,7,12}.

Over 95% of fluorescent neurones in the areas examined were single-labelled with FB, NY or PI in all animals (Fig. 2a, b, e). Many of these were callosal neurones, retrogradely filled by dye injections in the corresponding cortical region of the opposite hemisphere. In agreement with previous studies^{10,13-15}, callosal neurones were concentrated in layer III, although some were also found in layers V and VI. All other single-labelled cells, also concentrated in layer III, were association neurones. For example, neurones in the principal sulcus were retrogradely filled by dye injections into the intraparietal cortex in the same hemisphere. Association and callosal neurones were generally intermixed rather than segregated into distinct laminar or radial groupings.

The remaining fluorescent neurones ($\leq 5\%$) were double-labelled and their percentage was no greater in fetuses or infants than in adults. This small population could be divided into two classes: (1) homotopic callosal neurones, which project one axon across the callosum to the same cytoarchitectonic cortex in the contralateral hemisphere (for example, left principal sulcus to the right principal sulcus) and a second axon to a distant cortical target in the same hemisphere (such as left principal sulcus to left intraparietal sulcus) (Fig. 2c, d); and (2) heterotopic callosal neurones which, like their homotopic counterparts, also have axon collaterals in both hemispheres. However, in this case, the target in the contralateral hemisphere is an area different from the homotopic site of origin. For example, double-labelled neurones were found in both anterior and posterior cingulate cortex in each hemisphere, indicating that a cingulate neurone can project simultaneously to the frontal cortex of one hemisphere and the parietal cortex of the other. In one animal injected with PI in the posterior cingulate cortex, several retrogradely labelled PI cells were found in the ipsilateral anterior cingulate cortex; some of them also contained FB which had been injected in the prefrontal cortex of the opposite hemisphere (Fig. 2e, f). Thus, these anterior cingulate neurones projected to both the posterior cingulate cortex of one hemisphere and the prefrontal cortex of the other.

Recent studies of cortical sensory areas in kittens³ and neonatal rats^{4,5} have suggested that, at early stages of postnatal

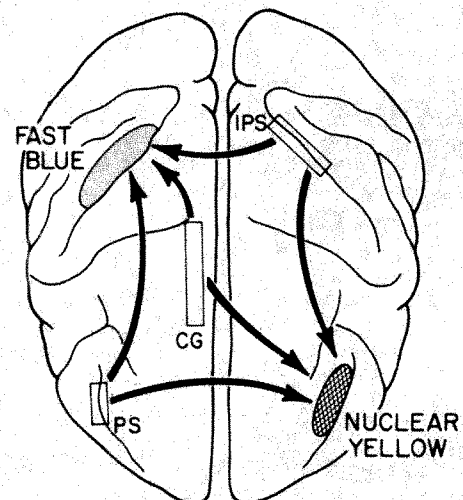
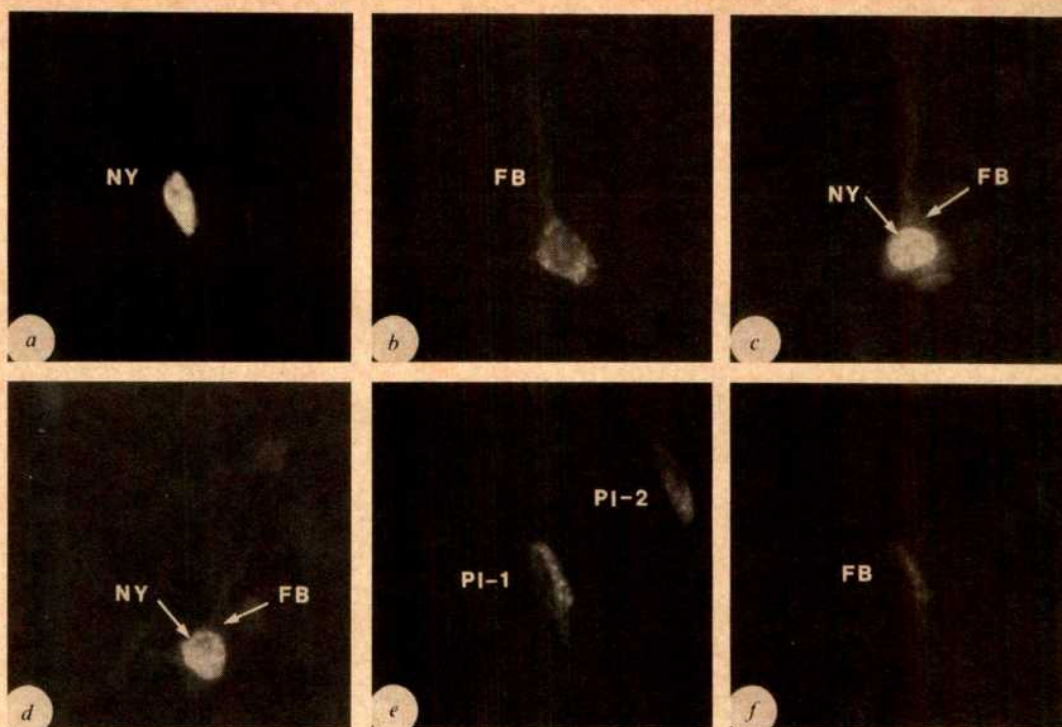


Fig. 1 The basic experimental procedure. Three monkeys received multiple 0.5- μ l injections of 5% FB in the posterior bank of the intraparietal sulcus (IPS) of the right hemisphere and multiple 0.5- μ l injections of 1% NY in the dorsal bank of the principal sulcus (PS) in the left hemisphere. One animal was injected with the same dyes but in reversed locations. The remaining two animals received injections of 3% PI and 5% FB, respectively, in the principal sulcus of the left hemisphere and 1% NY and 3% PI in the intraparietal sulcus, respectively, of the right hemisphere. Shaded areas represent injection sites; areas outlined by open rectangles indicate principle regions examined for cell labelling. Arrows indicate direction of projection of labelled neurones.

Fig. 2 Single- and double-labelled neurones photographed on a Leitz Orthoplan fluorescent microscope equipped with filter cubes D and M. With filter cube D both NY and FB can be simultaneously visualized in the nucleus and cytoplasm, respectively, of retrogradely labelled neurones¹. Filter cube M allows the visualization of PI in the cytoplasm of labelled cells². *a*, Layer III cell in the dorsal bank of the principal sulcus single-labelled with NY injected in contralateral principal sulcus (excitation wavelength 390 nm). Note that only the nucleus is labelled with this dye. *b*, Neurone single-labelled with FB following injection of FB in ipsilateral intraparietal sulcus. With this dye only the cytoplasm is labelled. *c*, *d*,



Double-labelled neurones in layer III from principal sulcus, where the nucleus shows intense yellow labelling with NY while the cytoplasm is labelled blue by FB. These neurones have both a callosal (contralateral) axon collateral to the homotopic principal sulcus and a divergent associational (ipsilateral) axon collateral to the intraparietal sulcus. Note that no significant NY labelling of glia was observed in the areas examined, indicating that, at the survival times used, the NY dye did not leech from labelled cells for re-uptake by nearby neurones and glial cells. *e*, Neurones situated in the anterior cingulate cortex labelled with PI following an injection in the posterior cingulate cortex of the same hemisphere (excitation wavelength 550 nm). *f*, The same field as in *e*, photographed at a different excitation wavelength (390 nm), showing that the neurone labelled PI-1 in *e* is labelled with both PI and FB. Thus, this double-labelled neurone projects to the contralateral principal sulcus and the ipsilateral posterior cingulate cortex.

development, a cortical neurone with intrahemispheric connections issues a callosal collateral which is later lost by selective elimination. In the present study, the density and distribution of double-labelled cortical neurones was the same in fetal, newborn and adult monkeys. It should be emphasized that our injections in monkey fetuses were made 1 month before birth at about the time that cortical axons penetrate the cortical plate in this species¹⁶. Thus, the difference between our findings and those previously reported in other animals cannot be easily attributed to differences in the stages of development examined. A more plausible explanation for the discrepancy between the present results and those of others³⁻⁵ is that there may be a genuine difference in the development of cortical connectivity in acallosal cortical areas such as primary visual cortex, on the one hand, and richly callosal regions of association and limbic cortex, on the other. In either case, our findings clearly demonstrate that for some cortical neurones, collateralization is not a transient developmental state but rather a permanent feature of their adult morphology.

The functional significance of the mature collateralized cortical neurones is not known. Obviously, the simultaneous influence of a single neurone on cytoarchitecturally distinct areas in the two hemispheres is an efficient means for coordinating the activity and transfer of information between widely divergent territories in the two halves of the brain. Such neurones could play a part in interhemispheric transfer by which information is made available to both hemispheres at once^{17,18}. In the present study less than 5% of all neurones were double-labelled, but the territories injected are only a fraction of the total callosal and intrahemispheric targets of the examined areas. Furthermore, although we did not find any triple-labelled neurones in the monkey with injections of three dyes, it is possible that some neurones have more than the two branches identified here. Indeed, future studies may reveal that the two classes of double-labelled neurones described here are actually

members of a single class of callosal neurone with multiple projections to both homotopic and heterotopic callosal targets plus one or more associational targets. Thus, the number of cortical neurones and the number of axon collaterals connecting regions within the same and opposite hemispheres may be considerably larger than indicated by the present results. Accordingly, these results provide new information for interpreting the functions, development and plasticity of the cerebral cortex and alter traditional views of cortical circuitry based on the existence of separate populations of associational and callosal neurones.

This work was supported by USPHS grants NS16666 and MH00298 and fellowship award MH08308. We thank Professor H. G. J. M. Kuypers and Dr Heinz Loewe for providing NY and FB.

Received 10 May; accepted 6 July 1982.

1. Kuypers, H. G. J. M., Bentivoglio, M., Catsman-Berrevoets, C. E. & Bharos, A. T. *Expl Brain Res.* **40**, 383-392 (1980).
2. Kuypers, H. G. J. M., Bentivoglio, M., Van Der Kooy, D. & Catsman-Berrevoets, C. E. *Neurosci. Lett.* **12**, 1-7 (1979).
3. Innocenti, G. M. *Science* **212**, 824-827 (1981).
4. Killackey, H. P. & Ivy, G. O. *Neurosci. Abstr.* **7**, 178 (1981).
5. O'Leary, D. D. M., Stanfield, B. B. & Cowan, W. M. *Dev Brain Res.* **1**, 607-617 (1981).
6. Goldman, P. S. & Nauta, W. J. H. *Brain Res.* **122**, 393-413 (1977).
7. Goldman-Rakic, P. S. & Schwartz, M. L. *Science* **216**, 755-757 (1982).
8. Chavis, D. A. & Pandya, D. N. *Brain Res.* **117**, 369-386 (1976).
9. Jacobson, S. & Trojanowski, J. Q. *Brain Res.* **132**, 209-233 (1977).
10. Hedreen, J. C. & Yin, T. C. T. *J. comp. Neurol.* **197**, 605-621 (1981).
11. Baleyrier, C. & Mauguier, F. *Brain* **103**, 525-554 (1980).
12. Jacobson, S. & Trojanowski, J. Q. *Brain Res.* **132**, 235-246 (1977).
13. Jones, E. G. & Wise, S. P. *J. comp. Neurol.* **175**, 391-438 (1977).
14. Mesulam, M. M., Van Hoesen, G. W., Pandya, D. N. & Geschwind, N. *Brain Res.* **136**, 393-414 (1977).
15. Tigges, J. et al. *J. comp. Neurol.* **202**, 539-560 (1981).
16. Goldman-Rakic, P. S. *The Organization of Cerebral Cortex* (eds Schmitt, F. O., Worden, F. G., Dennis, S. G. & Adelman, G.) 69-97 (MIT Press, Cambridge, 1981).
17. Sperry, R. W. *Science* **133**, 1749-1759 (1961).
18. Gazzaniga, M. S. *Scient. Am.* **217**, 24-29 (1967).

Similarity of unitary Ca^{2+} currents in three different species

A. M. Brown*, H. Camerer, D. L. Kunze* & H. D. Lux

Max-Planck-Institut für Psychiatrie, Kraepelinstrasse 2, D-8000 München 40, FRG

* University of Texas Medical Branch, Galveston, Texas 77550, USA

Membrane Ca^{2+} currents are the triggers for numerous cellular activities such as secretion, contraction, and oscillations in neural discharge. Different Ca^{2+} channels are assumed to subserve the various functions¹; this does not apply to Na^+ currents for which there is thought to be only one type of channel. We have examined single Ca^{2+} channels in cells from three very different species (bird, snail and rat) using the patch-clamp method², and report here that unitary events consisted of small, brief current pulses that often occurred in bursts and were similar for all three species. Thus, reported differences among various Ca^{2+} currents¹ must have other origins.

In our experiments, invertebrate neurones were represented by identified pacemaker cells³ of *Helix pomatia*, vertebrate neurones by cultured dorsal root ganglion (DRG) cells from chick (*Gallus gallus*)⁴, and vertebrate secretory cells by the PC12 line of cultured rat (*Rattus rattus*) adrenal medullary tumour cells^{5,6}. The cultured neurones have macroscopic Ca^{2+} currents that are similar to those of snail neurones^{3,4,7}. Snail neurones were isolated as described elsewhere³ and DRG cells

were prepared using a method that results in glia-free preparations⁸. At least 24 h elapsed before these cells were studied. PC12 cells grown according to Lucas *et al.*⁹ were studied 4–8 h after sub-culture. During experiments, cultured cells were viewed with phase-contrast optics through an inverted microscope. All experiments were done at 20–22 °C. Patch-clamp recordings were made using cell-attached patches and isolated patches in the inside-out configuration². The snail neurones were simultaneously voltage-clamped using a two-microelectrode method^{3,10}. Whole-cell clamping with the patch pipette was done in some DRG and PC12 cells.

Single channel Ca^{2+} currents were separated using solutions which suppressed Na^+ and K^+ currents. Osmotic strengths were 250 and 320 mosM for snail and vertebrate cells, respectively. In bath and patch pipettes, Na^+ and K^+ ions were replaced with (mM): Tris 60–100 or Cs 60–100, and tetraethylammonium (TEA) 10–60. The anions were Cl^- and/or gluconate. Tetrodotoxin (TTX), 2–5 μM and 4-aminopyridine (4-AP), 5 mM were added in most experiments. Ca^{2+} was present in concentrations of 20 or 40 mM in the patch pipette, except in some experiments where 20 mM BaCl_2 replaced CaCl_2 ; pH was buffered to 7.4 by Tris or HEPES (Serva). For inside-out patches the bath solutions contained (mM): Cs gluconate (60–80 for snail; 130 for vertebrate cells), hemi-Mg gluconate 20–40, EGTA (Titrplex VI; Merck) 1.0, and TEA-Cl 10–20; pH was buffered to 7.2 using Tris. Similar 'intracellular' solutions were used in the patch pipettes when whole-cell recordings from vertebrate cells were made. In the case of snail neurones, TEA was electrophoresed³ to produce estimated intracellular concentrations of 20–50 mM.

Voltage and current data were recorded on analog tape. Currents were low pass-filtered at 1 or 2.5 kHz by a 4-pole active filter and were digitized at 0.15–0.25 ms per point using a PDP 11/34 minicomputer. Control and test records were

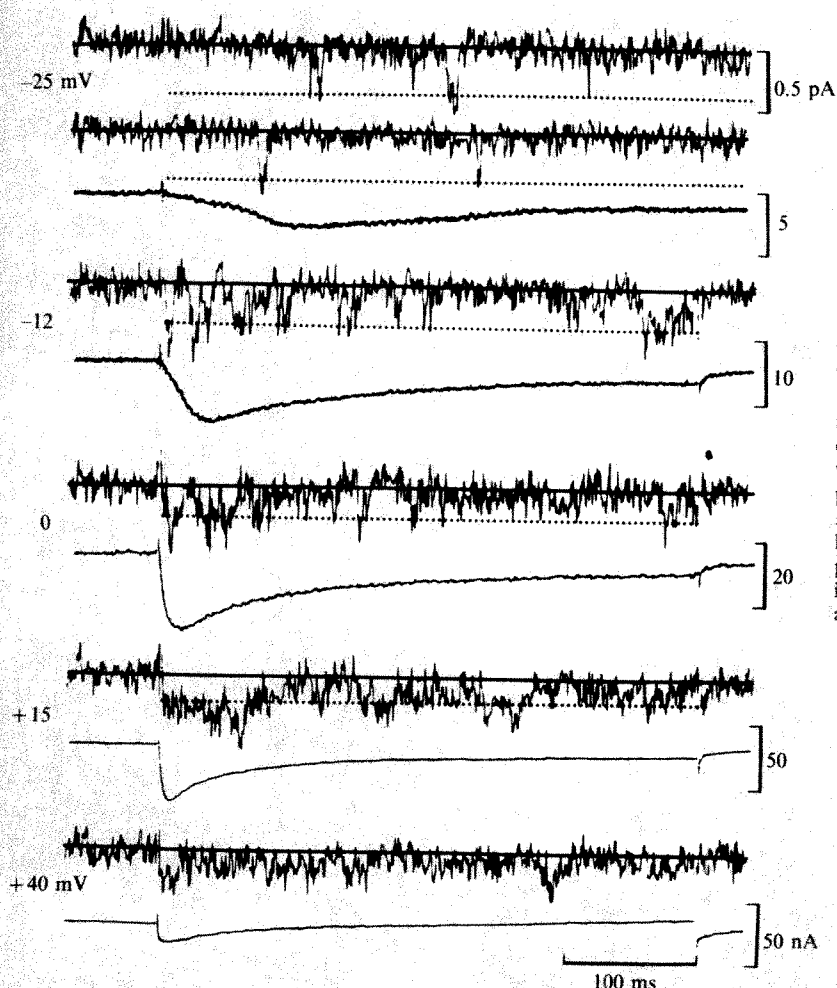
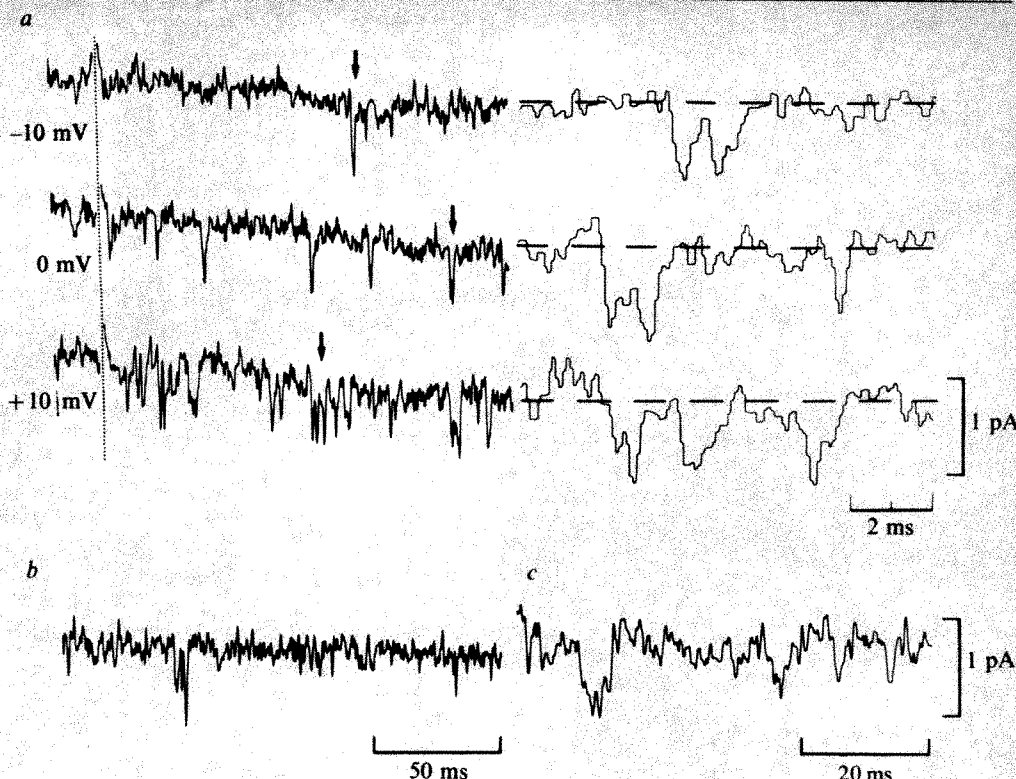


Fig. 1 Unitary membrane Ca^{2+} currents from a snail neurone. The entire neurone was voltage-clamped. Top traces show the patch Ca^{2+} currents and bottom traces the whole-cell membrane Ca^{2+} current during steps to indicated membrane potentials from a holding potential of -50 mV. Linear components of leakage and capacitance have been subtracted. Ca^{2+} concentrations in the patch pipette and bath solution were identical (40 mM). Average unit current amplitude is indicated by dotted lines, and baseline values by the solid lines. As the potential was increased, the frequency of channel openings increased, simultaneous openings from 2 units appeared and unit amplitudes decreased. The data were filtered at 1 kHz.

Fig. 2 *a*, Unitary Ba^{2+} currents from a DRG cell-attached patch at different potentials. The dotted line indicates the time of the voltage step. Components of leakage and capacitance have been subtracted. A resting membrane potential of -50 mV was assumed. The threshold for activation of unitary Ba^{2+} currents was -20 mV. With increasing potential, the frequency of channel openings increased. Openings that occur in a burst were observed. Sections of the current records marked with an arrow in the left-hand panel are shown on an expanded time scale and bandwidth in the right-hand panel; the data were filtered at 1 kHz and 2.5 kHz, respectively. *b*, Unitary Ba^{2+} currents from a PC12 inside-out patch at $+30$ mV. Note a burst of openings with a superimposed single opening. Holding potential, -50 mV. *c*, Unitary Ca^{2+} currents from a DRG inside-out patch at $+20$ mV. Holding potential, -50 mV. Data were filtered at 1 kHz (*b*, *c*). 20 mM Ba^{2+} (*a*, *b*) or Ca^{2+} (*c*) was present in the patch pipette.



0.3–1.0 s long, and sets of at least 12 records were used for unit analysis.

Background noise was 0.1–0.2 pA r.m.s. at d.c. to 1.0 kHz bandwidth. As the signal-to-noise ratio was low, we used two different methods of measuring amplitudes and open and closed times. With the first method an interactive program was used to excise unitary currents that occurred singly or in bursts. Mean values for the background current were computed and used as reference levels. This method required subjective estimates of the unitary currents. A more objective method was to apply threshold levels at $\sim 2/3$ and $1/3$ of the expected current amplitude to mark the beginning and end of a channel current. When necessary, time-varying mean currents were removed before computing the histograms. The different methods were applied to two sets of identical data and were found to give similar results.

In snail neurones, the membrane potential was recorded directly together with macroscopic currents. Unitary patch currents which appeared similar were recorded repeatedly from different parts of the same neurone) this apparently caused no

damage to the cell, although an inward current often appeared transiently on removal of the patch electrode. Membrane potential was not recorded in DRG and PC12 cells. However, the resting potentials^{6,11} were probably similar to the holding potential of -50 mV used for snail neurones.

Unitary currents were observed following $G\Omega$ seals in 13 patches from DRG cells, 16 patches from PC12 cells, and > 200 patches from snail neurones. In all cases, these currents were characterized by the appearance of brief current pulses of small amplitude (0.5 ± 0.1 pA) at potentials that were depolarized by 20–30 mV from the resting potential. The openings occurred throughout steps of 1.0 s duration, but appeared to be less frequent at longer times. The openings occurred singly or in bursts (see Figs 1, 2). Long openings without evidence of any closure were also observed. Occasionally, amplitudes of about twice the unit height (Figs 1, 2b) were observed; these were interpreted as simultaneous openings of two channels. Openings became more frequent with increased depolarization (Figs 1, 2a), and the unitary current amplitudes decreased. In snail neurones the slope conductance was calculated to be 6–7 pS.

Table 1 Ca^{2+} channel characteristics

	Snail neurone	Rat PC12 cell	Chick DRG neurone
Current amplitude \pm s.d. (pA)	-0.47 ± 0.11 (120)	-0.53 ± 0.12 (1115)	-0.53 ± 0.10 (790)
Closed time (ms)			
within bursts	1.3 (15)	0.9 (543)	0.7 (274)
between bursts	46.2 (94)	21.9 (550)	20.7 (484)
Open time (ms)	2.8 (120)	2.7 (1115)	0.5 (790)
Duration of bursts (ms)	3.4 (106)	6.8 (577)	1.5 (516)
No. of openings per burst	1.2 (106)	1.9 (577)	1.5 (516)
k_2 (ms^{-1})	0.64	0.58	0.95
k_3 (ms^{-1})	0.13	0.53	0.48
k_4 (ms^{-1})	0.36	0.37	2.00

Mean values of Ca^{2+} channel characteristics from cell-attached patches of snail neurone (-20 mV), rat PC12 cell (-10 mV) and chick DRG neurone (10 mV). For analysis, we selected recordings which showed a discrete amplitude level on opening, presumably from one channel, and came from 1, 3 and 2 cell-attached patches for snail, rat and chick cells, respectively. The resting potential of DRG and PC12 cells was assumed to be -50 mV; that of snail neurone was -50 mV. Patch pipettes contained 40 mM Ca^{2+} for snail neurone and 20 mM Ba^{2+} for PC12 and DRG cells. The standard deviation of current amplitudes was due almost completely to the background noise current. In the calculation of the duration of bursts and number of openings per burst, single openings have been included. k_2 , k_3 and k_4 are the rate constants estimated according to the three-state model¹⁸. Numbers in parentheses represent the numbers of measurements from which the values shown were calculated. In the case of the closed times, the numbers were estimated from the integrals of the fast and slow components. The amplitude and open time values for the snail neurone patch are similar to values from larger samples, recorded previously¹⁰.

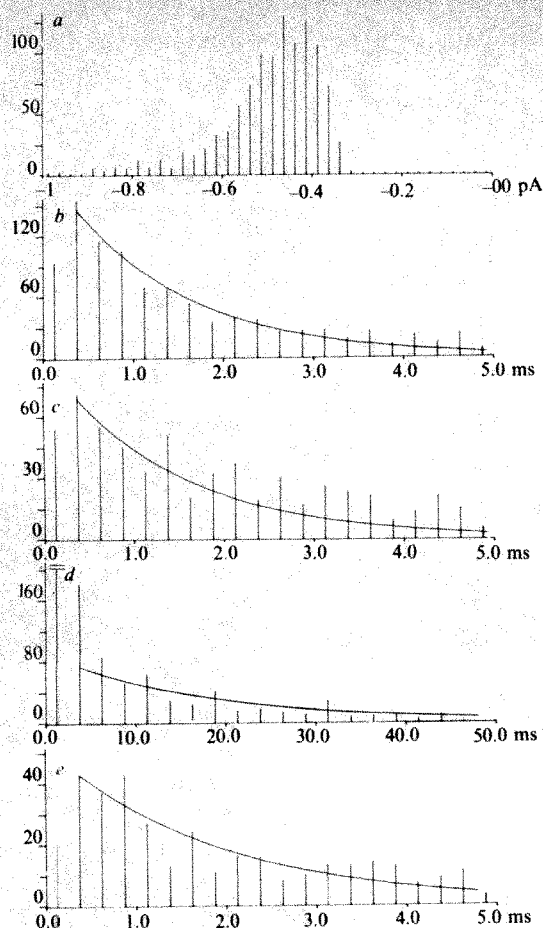


Fig. 3 Histograms of amplitude (a), open time (b), closed time (c, d) and burst duration (e) distributions for unitary Ba^{2+} currents from a PC12 cell-attached patch. Ba^{2+} concentration was 20 mM. The closed time distribution is shown on two different time scales to allow the two exponential components to be distinguished easily. Holding potential was assumed to be -50 mV and the patch potential was stepped to -10 mV. The histograms were computed from 21 records, each of 500 ms duration. Data were filtered at 1 kHz and sampled at 4 kHz. Values were obtained by the threshold method described in the text. The exponential curves in the histograms have time constants of b, 1.3; c, 1.8; d, 17.0; and e, 1.9 ms.

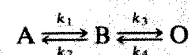
The inward currents became slightly larger when Ba^{2+} replaced Ca^{2+} (Fig. 2a, b). For inside-out patches the pipette interior was made positive by 50–70 mV. In the case of cell-attached patches, channels were activated with depolarizing steps ranging from 30 to 100 mV, and openings became more frequent at larger depolarizations. The currents remained almost unchanged for 10–15 min, which was the usual survival time of the inside-out patches in our solutions.

Table 1 gives the similarities in average amplitudes of the unitary currents for the different cells from the three species examined. Open times for snail neurones and PC12 cells showed similar distributions; the values for DRG cells were shorter, possibly because of differences in resting and activating potentials. The properties of the bursts were similar (see Fig. 3). The open times were described by a single exponential function. The closed times were similar among the different cell groups and could be separated into two exponential functions having short and long time constants. The short time constants are due to the intervals associated with bursts of activity, which were more prominent for Ba^{2+} currents. The longer time constants are due to the intervals between bursts.

The unitary activity could not have been produced by the flow of Ba^{2+} or Ca^{2+} through Na^+ or K^+ channels as the former

were blocked by TTX and the latter by TEA, 4-AP and Cs substitution. TTX-resistant Na^+ channels can be excluded as they do not conduct Ca^{2+} ions¹². The present inward currents were never observed when 10 mM Mg^{2+} or Co^{2+} replaced Ba^{2+} or Ca^{2+} , consistent with observations on macroscopic Ca^{2+} currents. The unitary Ba^{2+} currents were rather larger, a result also predicted from the macroscopic currents⁷. The unitary current amplitudes agree with those reported previously¹⁰ but are larger than values estimated from noise measurements^{13,14}. The present data are insufficient to allow any significant conclusion to be made regarding differences between divalent cations or the effects of changes in divalent concentration.

Our data do, however, indicate that open Ca^{2+} channels have only one conduction level. The bursting activity points to the fact that activation is more complicated than a simple first-order process; see also ref. 10. Further evidence for this is the delayed turn-on of Ca^{2+} currents which can be fitted by an m^2 model¹⁵ and the bi-exponential nature of Ca^{2+} tail currents^{16,17}. The simplest kinetic scheme consistent with our data is



where A and B are closed states and O is open. The rate constants k_2 , k_3 and k_4 can be estimated from the histograms¹⁸ and are given in Table 1. This model was also used by Fenwick *et al.*¹⁷.

The units of Ca^{2+} conduction were similar in the three different species studied here. The unitary currents produced in isotonic Ba^{2+} solutions in bovine chromaffin cells¹⁷ and in neonatal rat heart cells¹⁹ also resemble the units described here. It is possible that, as the cells from two of the species were cultured, the units might not be representative of the original cells. This possibility cannot be excluded, but the fact that the Ca^{2+} currents and action potentials recorded from these cultured cells^{4,11} are very similar to those recorded from a wide range of species and tissues renders such a suggestion unlikely. Hence, we conclude that Ca^{2+} channels everywhere are basically the same. The reported differences among macroscopic Ca^{2+} currents may be due to, among other factors, the variety of receptors associated with Ca^{2+} channels^{4,20} and the second-messenger actions of Ca^{2+} ions²¹.

We thank Drs C. Lucas, Y. Barde and R. Deisz, Ms G. Schuster and Ms S. Messerschmidt, and Mr R. Childers. We especially thank Mr H. Zucker for help with the computer programs and Drs E. M. Fenwick, A. Marty and E. Neher for providing us with a preprint of their paper. A.M.B. was supported by a Josiah Macy Fellowship and NIH grant NS 11453. H.C. was supported by DFG grant HE 1120/2-2.

Received 14 April; accepted 29 June 1982.

- Hagiwara, S. & Byerly, L. A. *Rev. Neurosci.* **4**, 69–125 (1981).
- Hamill, O. P., Marty, A., Neher, E., Sakmann, B. & Sigworth, F. J. *Pflügers Arch. ges. Physiol.* **391**, 85–100 (1981).
- Hofmeister, G. & Lux, H. D. *Pflügers Arch. ges. Physiol.* **391**, 242–251 (1981).
- Dunlap, K. & Fischbach, G. D. *J. Physiol., Lond.* **317**, 519–535 (1981).
- Greene, L. A. & Tischler, A. S. *Proc. natn. Acad. Sci. U.S.A.* **73**, 2424–2428 (1976).
- O'Leary, P. H. & Huttner, S. L. *Proc. natn. Acad. Sci. U.S.A.* **77**, 1701–1705 (1980).
- Brown, A. M., Morimoto, K., Tsuda, Y. & Wilson, D. L. *J. Physiol., Lond.* **320**, 193–218 (1981).
- Barde, Y. A., Edgar, D. & Thoenen, H. *Proc. natn. Acad. Sci. U.S.A.* **77**, 1199–1203 (1980).
- Lucas, C. A., Edgar, D. & Thoenen, H. *Expl. Cell Res.* **121**, 79–86 (1979).
- Lux, H. D. & Nagy, K. *Pflügers Arch. ges. Physiol.* **391**, 252–254 (1981).
- Spector, I. in *Excitable Cells in Tissue Culture* (eds Nelson, P. G. & Lieberman, M.) 247–274 (Plenum, New York, 1981).
- Kostyuk, P. C., Veselovsky, N. S. & Tsyndrenko, A. Y. *Neuroscience* **6**, 2423–2430 (1981).
- Akaike, N., Fishman, H. M., Lee, K. S., Moore, L. C. & Brown, A. M. *Nature* **274**, 379–382 (1978).
- Krishtal, O. A., Pidoplichko, V. I. & Shakhvalov, Yu. A. *J. Physiol., Lond.* **310**, 423–434 (1981).
- Kostyuk, P. G., Krishtal, O. A. & Shakhvalov, Yu. A. *J. Physiol., Lond.* **270**, 545–568 (1977).
- Tsuda, Y., Wilson, D. L. & Brown, A. M. *Biophys. J.* **37**, 181a (1982).
- Fenwick, E. M., Marty, A. & Neher, E. *J. Physiol., Lond.* (in the press).
- Colquhoun, D. & Hawkes, A. G. *Proc. R. Soc. B211*, 205–235 (1981).
- Reuter, H., Stevens, C. F., Tsien, R. & Yellen, G. *Nature* **297**, 501–503 (1982).
- Yatani, A., Tsuda, Y., Akaike, N. & Brown, A. M. *Nature* **296**, 169–171 (1982).
- Rasmussen, H. & Goodman, D. B. P. *Physiol. Rev.* **57**, 421–509 (1977).

Single-channel currents in isolated patches of plasma membrane from basal surface of pancreatic acini

Y. Maruyama & O. H. Petersen*

The Physiological Laboratory, University of Liverpool, PO Box 147, Brownlow Hill, Liverpool L69 3BX, UK

Precise localization and characterization of conductance pathways in glandular epithelia have so far proved difficult¹. The patch-clamp technique for high resolution current recording²⁻⁴, which has already been applied successfully to a number of electrically excitable cells^{3,4}, can in principle overcome these difficulties. We now report measurements of single-channel currents from isolated patches of plasma membrane (inside-out) from the baso-lateral surface of collagenase-isolated rat and mouse pancreatic acini. We have identified a cation channel having a conductance of ~ 30 pS and a mean open time in the range 0.3–1 s which is dependent on internal calcium. The single-channel current–voltage relationship is linear and the mean open time independent of the membrane potential. These channels may, at least in part, account for the Ca^{2+} -mediated neural and hormonal control of pancreatic acinar membrane conductance, which is probably responsible for the Ca^{2+} -dependent acinar fluid secretion⁵⁻⁷.

We used collagenase-isolated rat or mouse pancreatic acini prepared as described previously⁸⁻¹⁰. With this procedure, clusters of acinar cells (5–20) retaining intact tight junctions and the normal morphological polarity are obtained⁸⁻¹⁰. Fabrication of patch recording pipettes, isolation of inside-out membrane patches and high-resolution current recording were carried out as described in detail by Neher and collaborators^{3,4,11}. The total Ca^{2+} concentration in the bath and pipette solutions used was measured by atomic absorption spectroscopy.

Figure 1a shows current recordings from a single patch of plasma membrane with Na-sulphate solution on both sides of the membrane. We observed unitary events of constant amplitude at the same numerical membrane potential (–20 and +20 mV), but with a larger amplitude at a higher membrane potential (–40 mV). In the absence of a membrane potential, no unitary steps were detected. Unit current steps of this type were observed in 47 patches from 28 batches of isolated rat pancreatic acini. Similar experiments performed on pancreatic acini from mice revealed the same type of unit current steps (8 membrane patches from 4 batches of acini).

There was a linear relationship between the amplitude of the unitary current steps and the membrane potential, with reversal of current polarity at 0 mV. At zero membrane potential we observed no channel opening or closure using the same NaCl or Na_2SO_4 solutions on both sides. The existence of a Ca^{2+} gradient, typically 1.28 mM in the pipette and 40 μM in the bath, did not change the reversal potential. Figure 1b shows plots of single-channel current–voltage relationships from one series of experiments in which NaCl or Na_2SO_4 solutions (same concentration on both sides of the membrane) were used. As the single-channel conductance was independent of the presence of Cl^- , these channels seem to be cation-selective. Figure 1b also includes data from experiments in which $\sim 50\%$ of the Na_2SO_4 was replaced by K_2SO_4 , this did not change the conductance. It seems reasonable therefore to assume that the channels do not discriminate very well between Na^+ and K^+ . The mean value of the single-channel conductance in the three experiments carried out in NaCl solutions was 27 pS, whereas in one series with Na_2SO_4 solutions a mean of 33 pS (10 patches) was obtained.

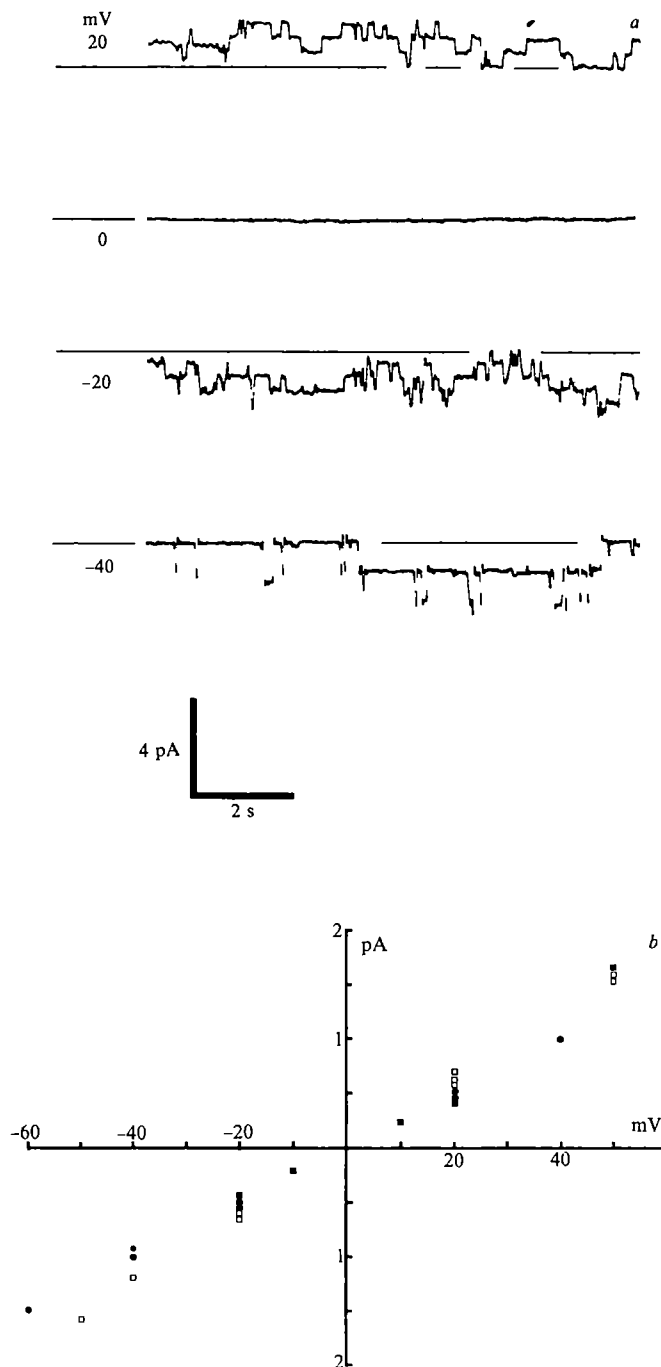


Fig 1 Single-channel current–voltage relationship. *a*, Recordings of single ion channel currents from isolated membrane patch taken from the baso-lateral surface of collagenase-isolated rat pancreatic acinus. Short segments of the recordings from the same patch at four different membrane potentials are shown. The isolated membrane patch was 'inside-out', that is, the physiological inside of the membrane faced the bath, whereas the outer surface of the membrane faced the interior of the pipette. Outward currents (current from the intracellular to the extracellular side of the membrane) are represented by upward deflections. The membrane potentials indicated are conventional in that, for example, a potential of –40 mV denotes that the physiological inside of the membrane is 40 mV negative with respect to the outside. The patch resistance was 5 G Ω . In this experiment the same solution was present on both sides of the membrane and had the following composition (mM): Na_2SO_4 , 80, KCl, 4.7, CaCl_2 , 1.28, MgCl_2 , 1.15, glucose, 10, HEPES, 10. The pH of the solution (titrated by NaOH) was 7.3 and the temperature 22 °C. 20 Hz filtering (low pass) was applied. *b*, Relationship between the single-channel current and membrane potential. Values shown are from experiments in which (●) a solution with 110 mM NaCl, 10 mM HEPES, 10 mM glucose, 1.15 mM MgCl_2 and 4.7 mM KCl was present on both sides of the membrane; (□) a Na_2SO_4 solution (NaCl replaced isosmotically by Na_2SO_4) was present on both sides; and (■), a solution with 40 mM Na_2SO_4 and 45 mM K_2SO_4 was used on both sides. In these three series of experiments the external total Ca^{2+} concentration (pipette fluid) was in the range 1.28–2.56 mM, while the internal total Ca^{2+} concentration (bath fluid) ranged from 40 μM to 1.28 mM.

* To whom correspondence should be addressed

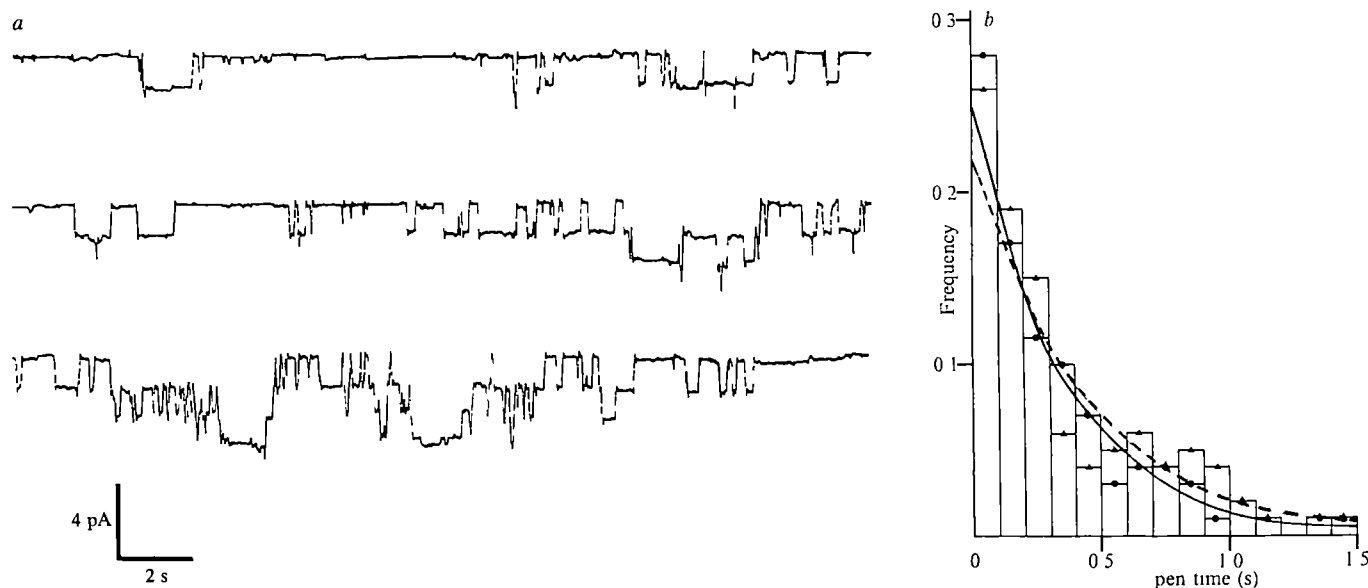


Fig. 2 Temporal characteristics of channel opening and closure *a*, Continuous trace of single-channel current recording from an inside-out patch exposed to Na-sulphate solution on both sides with 2.56 mM Ca^{2+} in the pipette fluid and 40 μM Ca^{2+} in the bath fluid. The Mg concentration on both sides was 1.15 mM, membrane potential, -50 mV, patch resistance, 15 G Ω . The frequency distributions of both the open and closed times for all the events in the entire recording ($n = 94$ and 77, respectively) were similar to exponential distributions with a single-channel mean open time of 0.93 s and a mean closed time of 0.83 s, if we assume that there are three mutually independent channels and that opening and closure of each of these is a Poisson-type phenomenon. Clamping the membrane potential at 0 mV abolished unitary current steps in this and all other experiments. *b*, Histograms obtained from one membrane patch at membrane potentials of -40 mV (\bullet , $n = 108$) and +40 mV (\blacktriangle , $n = 110$), showing the relative (normalized) frequency distribution of the open times. The curves (\bullet — \bullet) (-40 mV) and (\blacktriangle — \blacktriangle) (+40 mV) represent the theoretical exponential distributions for mean open times of 0.36 s and 0.43 s, respectively. In this case the patch apparently only contained one channel.

In one patch for which a relatively long continuous recording was obtained (Fig. 2*a*), the mean single-channel open time was calculated to be 0.93 s whereas the closed time was 0.83 s. We also investigated the effect on the mean open time of changing the membrane potential. In one patch the relative frequency density distribution was compared for membrane potentials of -40 and +40 mV. Figure 2*b* shows the two histograms superimposed on each other. For comparison, the theoretical exponential (Poisson) curves are shown. The two distributions are clearly very similar.

In one series of experiments we investigated the internal calcium dependence of the single-channel currents. Varying the total Ca^{2+} concentration in the bath fluid between 10 μM and 1.25 mM did not markedly affect the current recordings. However, complete removal of bath fluid Ca^{2+} (no Ca^{2+} added, 1 mM EGTA) stopped unitary current activity (Fig. 3). The effect of Ca^{2+} removal was reversible in that the unitary current steps reappeared after Ca^{2+} addition, however, the open time was much shorter and the frequency of opening reduced compared with the first control period. In all five experiments (on five different patches) in which Ca^{2+} was removed from the bath fluid during continued recording, the unitary current steps disappeared.

The channels we have found in the acinar membrane patches seem in many respects similar to the Ca^{2+} -dependent inward current channels recently described in cultured cardiac cells¹² and neuroblastoma cells¹³. This type of channel, so far found in muscle, nerve and gland cells, may be an important feature of many different cells, having a number of roles in various tissues.

The existence of Ca^{2+} -dependent cation permeation pathways in the baso-lateral surface membrane of pancreatic acinar cells was postulated previously on the basis of indirect evidence^{5,14,15}. It is probable that this channel, which has now been directly demonstrated, is important in the stimulus-secretion coupling sequence of acinar cells. Internal Ca^{2+} by simultaneously activating exocytosis and Na^+ entry through

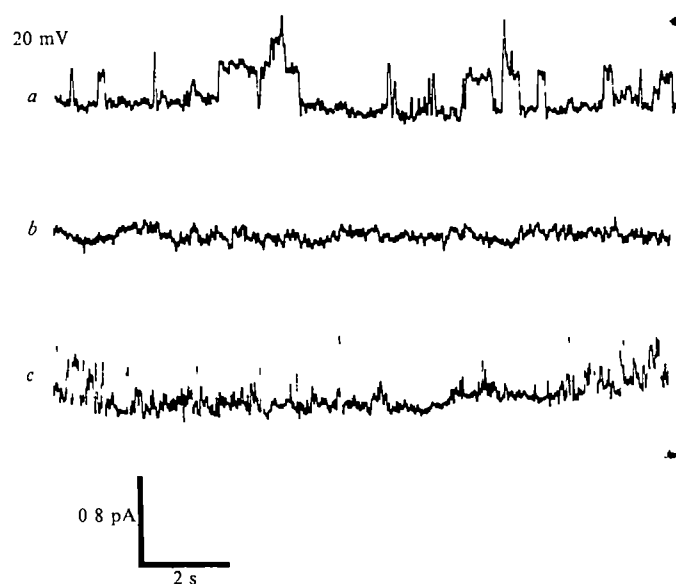


Fig. 3 Ca^{2+} dependency of single-channel currents *a-c*, Consecutive traces from a continuous recording from the same inside-out membrane patch. In this experiment (patch resistance, 3 G Ω) a Na_2SO_4 solution with 1.15 mM MgCl_2 , 4.7 mM KCl, 10 mM glucose and 10 mM HEPES (pH 7.3) was used on both sides. The external (pipette) solution contained 1.28 mM Ca^{2+} . The bathing fluid total Ca^{2+} concentration was 1.28 mM in *a*, while trace *b* was obtained 2 min after changing the bath solution to one without Ca^{2+} but with added EGTA (1 mM). Trace *c* was obtained ~5 min after return of the control solution (1.28 mM Ca^{2+}). The unitary outward current steps seen in *a* disappeared after removal of internal Ca^{2+} , but returned again in *c* after restoration of Ca^{2+} , however, in this period open times were severely shortened. In other experiments recordings were made of inward current steps at membrane potentials of -20 or -40 mV. Removal of Ca^{2+} from the bath fluid always abolished the unitary current steps.

these Ca^{2+} -dependent channels, will couple the two physiologically important processes in the acinar cells, fluid and enzyme secretion, to hormone-receptor interaction. Several other important elements in the stimulus-secretion coupling sequence still remain to be positively identified, that is, the link between hormone-receptor interaction and activation of the Ca^{2+} -effector^{6,14} and the Cl^- (anion) permeation mechanism and its activation¹⁶. Further work with the patch-clamp technique should help in the characterization of the transepithelial transport mechanism and its control.

We thank Dr E. Neher for practical advice and demonstration of the techniques for high-resolution current recording, and Dr I. Schulz for help in the preparation of isolated pancreatic acini. This work was supported by a project grant from the MRC.

Received 20 May, accepted 11 June 1982

- Petersen, O. H. *The Electrophysiology of Gland Cells* (Academic, London, 1980).
- Neher, E. & Sakmann, B. *Nature* **260**, 799–802 (1976).
- Neher, E. in *Techniques in Cellular Physiology* (ed. Baker, P. F.) 121, 1–16 (Elsevier, Amsterdam, 1982).
- Hamill, O. P., Marty, A., Neher, E., Sakmann, B. & Sigworth, F. J. *Pflügers Arch. ges. Physiol.* **391**, 85–100 (1981).
- Iwatsuki, N. & Petersen, O. H. *Nature* **268**, 147–149 (1977).
- Petersen, O. H., Nishiyama, A., Laugier, R. & Philpott, H. G. in *Drug Receptors and Their Effectors* (ed. Birdsall, N. J. M.) 63–73 (Macmillan, London, 1981).
- Petersen, O. H. *et al.* *Phil. Trans. R. Soc. B296*, 151–166 (1981).
- Williams, J. A., Korce, M. & Dormer, R. L. *Am. J. Physiol.* **235**, E517–E524 (1978).
- Peikin, S., Rottman, A. J., Batzri, S. & Gardner, J. D. *Am. J. Physiol.* **235**, E743–E749 (1978).
- Wakasugi, H. *et al.* *J. Membrane Biol.* **65**, 205–220 (1982).
- Neher, E., Sakmann, B. & Steinbach, J. H. *Pflügers Arch. ges. Physiol.* **375**, 219–228 (1978).
- Colquhoun, D., Neher, E., Reuter, H. & Stevens, C. F. *Nature* **294**, 752–754 (1981).
- Yellen, G. *Nature* **296**, 357–359 (1982).
- Petersen, O. H. & Iwatsuki, N. *Ann. N.Y. Acad. Sci.* **307**, 599–617 (1978).
- Schulz, I. & Heil, K. *J. Membrane Biol.* **46**, 41–70 (1979).
- Petersen, O. H. & Philpott, H. G. *J. Physiol., Lond.* **306**, 481–492 (1980).

Modifier role of internal H^+ in activating the Na^+-H^+ exchanger in renal microvillus membrane vesicles

Peter S. Aronson, Jeannette Nee & Marjorie A. Suhm

Departments of Medicine and Physiology, Yale University School of Medicine, New Haven, Connecticut 06510, USA

The intracellular pH in animal cells is generally maintained at a higher level than would be expected if H^+ were passively distributed across the plasma membrane¹. In a wide variety of cells including sea urchin eggs², skeletal muscle³, renal and intestinal epithelial cells^{4,6}, and neuroblastoma cells⁷, plasma membrane Na^+-H^+ exchangers mediate the uphill extrusion of H^+ coupled to, and thus energized by, the downhill entry of Na^+ . Plasma membrane vesicles isolated from the luminal (microvillus, brush border) surface of renal proximal tubular cells possess a Na^+-H^+ exchanger^{4,5} that seems to be representative of the Na^+-H^+ exchangers found in other tissues. For example, the renal microvillus membrane Na^+-H^+ exchanger, like other Na^+-H^+ exchangers, mediates electroneutral cation exchange^{4,5}, is sensitive to inhibition by the diuretic drug amiloride^{5,8}, and has affinity for Li^+ in addition to Na^+ and H^+ (refs 5, 9). Here we have examined the effect of internal H^+ on the activity of the Na^+-H^+ exchanger in renal microvillus membrane vesicles. Our results suggest that internal H^+ , independent of its role as a substrate for exchange with external Na^+ , has an important modifier role as an allosteric activator of the Na^+-H^+ exchanger. Allosteric behaviour with respect to internal H^+ is a property that would enhance the ability of plasma membrane Na^+-H^+ exchangers to extrude intracellular acid loads and thereby contribute to the regulation of intracellular pH.

Microvillus membrane vesicles were isolated from rabbit renal cortex by a modification¹⁰ of the Mg-aggregation method of Booth and Kenny¹¹. For membranes prepared in this manner, the enrichment in specific activity (final pellet/homogenate) of

luminal membrane markers, such as γ -glutamyl transpeptidase, is >10-fold, whereas those of markers for basolateral membranes and mitochondria, such as $(\text{Na}^++\text{K}^+)\text{ATPase}$ and succinic dehydrogenase, respectively, are <1.0 (refs 10, 11). Electron microscopy reveals that this membrane preparation consists predominantly of right-side-out microvilli with intact core structures¹². Studies using freeze-fracture techniques and immunological methods have also demonstrated that >85% of renal microvillus membrane vesicles are oriented right-side-out¹³.

The effect of internal pH on the Na^+ uptake rate is illustrated in Fig. 1. In this experiment, the vesicles were pre-equilibrated (120 min at 20°C) in media of pH 7.47–6.16 and then the 5-s uptake of 1 mM Na^+ was assayed at external pH 7.26. We have previously shown that equilibration of imposed pH gradients occurs within 120 min in these membrane vesicles⁵. The rate of Na^+ uptake was progressively stimulated as internal pH was lowered. This stimulation of Na^+ uptake by internal H^+ was almost completely abolished by 1 mM amiloride, as earlier observed⁸. Amiloride is a specific, competitive inhibitor for the Na^+-H^+ exchanger in these membrane vesicles⁸. However, the K_i of 3×10^{-5} M for amiloride inhibition of the renal microvillus membrane Na^+-H^+ exchanger is considerably higher than the apparent K_i (10^{-8} – 10^{-7} M) for inhibition of Na^+ channels in tight epithelia¹⁴. Consequently, drug concentrations of 10^{-3} M must be used to abolish Na^+-H^+ exchange in these membrane vesicles⁸. The finding that amiloride-sensitive Na^+ uptake was stimulated by internal H^+ certainly represented the behaviour expected for a Na^+-H^+ exchange process. If the stoichiometry

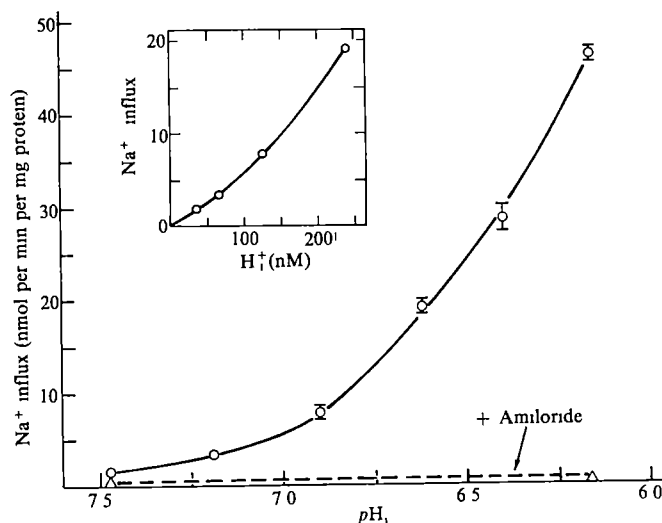


Fig. 1 Effect of internal pH on Na^+ influx rate. Membrane vesicles were isolated and initially suspended in 200 mM mannitol, 41 mM K^+ , 80 mM HEPES pH 7.47, and then pre-equilibrated for 120 min at 20°C in 157 mM mannitol, 74 mM K^+ , 52 mM Cl^- , 42 mM HEPES pH 7.47 or with isosmotic replacement of mannitol by 9, 17, 26, 35 or 52 mM 2-(*N*-morpholino)ethane sulphonate (MES) at pH 7.19, 6.90, 6.62, 6.40 or 6.16, respectively. The membrane vesicles were then incubated for 5 s at 20°C with 1.0 mM ^{22}Na , 45 mM K^+ , 11 mM Cl^- , 178 mM mannitol, 67 mM HEPES, 10 mM MES pH 7.26 in the absence (○) or presence (Δ) of 1.0 mM amiloride. These incubations were performed in a volume of 50 μl, containing 0.1 μCi ^{22}Na (NEN) and 100–200 μg membrane protein. The incubations were terminated by rapid addition of 3.5 ml of an iced (0–4°C) 'stop' solution consisting of 160 mM KCl, 2.5 mM Tris, 4 mM HEPES pH 7.5. The mixture was immediately poured on a 0.65 μm Millipore filter (DAWP) and washed with an additional 10.5 ml of 'stop' solution. Filters were placed in vials containing 3.0 ml Ready Solv HP (Beckman) and counted by scintillation spectroscopy. Values for the nonspecific retention of radioactivity by the filters were subtracted from the values for the incubated samples. Each datum represents the mean ± s.e. for three determinations. The inset shows a plot of Na^+ influx versus internal H^+ concentration for the pH range 7.47–6.62.

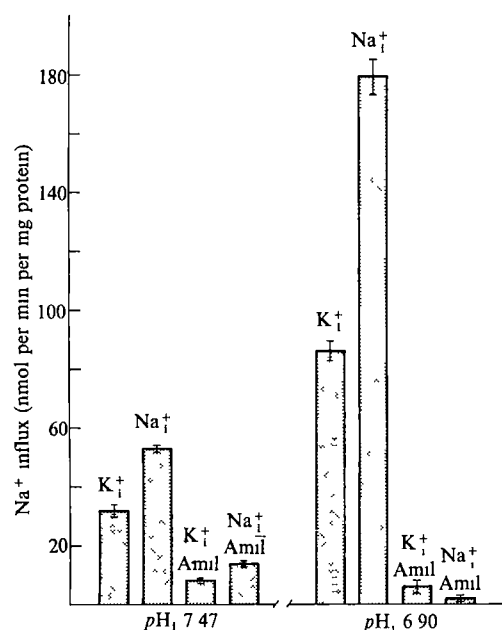


Fig. 2 Effect of internal pH on Na⁺ influx via Na⁺-Na⁺ exchange. Membrane vesicles were pre-equilibrated for 120 min at 20 °C either in 157 mM mannitol, 22 mM K⁺, 42 mM HEPES and 52 mM KCl ('K⁺') or 52 mM NaCl ('Na⁺') at pH 7.47, or in 140 mM mannitol, 22 mM K⁺, 42 mM HEPES, 17 mM MES and 52 mM KCl ('K⁺') or 52 mM NaCl ('Na⁺') at pH 6.90. Using the same filtration method as for Fig. 1, the 5-s uptake of ²²Na was then assayed in the presence of 10 mM ²²Na, 43 mM K⁺, 21 mM Cl⁻, 175 mM mannitol, 63 mM HEPES, 3.5 mM MES pH 7.39 with ('Amil') or without 2.0 mM amiloride. Each datum represents the mean \pm s.e. for three determinations.

of exchange were 1 H⁺ : 1 Na⁺, one would expect the Na⁺ uptake rate to increase linearly with increasing internal H⁺ (first order kinetics) and then to plateau (zero order kinetics) as the internal H⁺ transport site became saturated with H⁺. As indicated in the inset to Fig. 1, however, in the pH range 7.47–6.62 the Na⁺ uptake rate has a greater than first order dependence on the internal H⁺ concentration. This finding raised two possibilities. First, the Na⁺-H⁺ exchanger might possess more than one transport site for internal H⁺. Given that Na⁺-H⁺ exchange in these vesicles seems to be electroneutral^{4,5} with a H⁺ : Na⁺ coupling ratio¹⁵ of 1.0, this would imply that the stoichiometry of Na⁺-H⁺ exchange, rather than 1 : 1, is 2 : 2, 3 : 3, etc. However, arguing against this possibility, the dependence of the Na⁺ uptake rate on the external Na⁺ concentration conforms to simple Michaelis-Menten kinetics^{8,9}. Second, the Na⁺-H⁺ exchanger might possess only a single transport site for internal H⁺ but, in addition, possess one or more modifier sites at which internal H⁺ could bind and thereby activate the exchanger without being transported. Therefore, additional experiments were performed to attempt to demonstrate that internal H⁺, independent of its role as a transportable substrate for exchange, could actually activate the Na⁺-H⁺ exchanger.

Previous studies have suggested that the renal microvillus membrane Na⁺-H⁺ exchanger can mediate Na⁺-Na⁺ exchange⁹. In the experiment shown in Fig. 2, we examined the effect of internal pH on the rate of ²²Na uptake occurring via exchange for internal Na⁺. Membrane vesicles were pre-equilibrated with 52 mM KCl or 52 mM NaCl at pH 7.47 or 6.90, and then the 5-s uptake of 10 mM ²²Na was assayed at external pH 7.39. Because the renal microvillus membrane Na⁺-H⁺ exchanger has no detectable affinity for K⁺ (refs 5, 9), ²²Na uptake into vesicles containing K⁺ should occur only by Na⁺-H⁺ exchange, whereas ²²Na uptake into vesicles preloaded with unlabelled Na⁺ could occur by both Na⁺-H⁺ exchange and Na⁺-Na⁺ exchange. Thus, at any given internal pH, the difference between the ²²Na influx rates of vesicles preloaded with Na⁺ and those preloaded with K⁺ should represent the

component of ²²Na uptake occurring via Na⁺-Na⁺ exchange. As indicated in Fig. 2, the difference between the ²²Na influx rates of Na⁺-preloaded and K⁺-preloaded vesicles was much greater at internal pH 6.90 than at 7.47. That is, internal H⁺ stimulated the component of ²²Na uptake occurring via Na⁺-Na⁺ exchange. This internal H⁺-stimulated Na⁺-Na⁺ exchange was amiloride sensitive, consistent with the concept that it represented a mode of operation of the Na⁺-H⁺ exchanger. Accordingly, this experiment strongly suggested that internal H⁺, independent of its transport role, could indeed activate the Na⁺-H⁺ exchanger. Figure 2 appears to indicate that the amiloride-insensitive Na⁺ influx was not the same in all conditions. However, the actual values for Na⁺ uptake in the presence of amiloride were less than twice the nonspecific retention of ²²Na by the Millipore filters, probably accounting for the observed variability. No consistent relationship between amiloride-insensitive Na⁺ uptake and either internal H⁺ or internal Na⁺ was clearly evident on replications of this experiment.

The renal microvillus membrane Na⁺-H⁺ exchanger can mediate net Na⁺ transport in either direction^{8,15}. When $[Na^+]_o/[Na^+]_i$ exceeds $[H^+]_o/[H^+]_i$, there is net influx of Na⁺ in exchange for internal H⁺, when $[Na^+]_i/[Na^+]_o$ exceeds $[H^+]_i/[H^+]_o$, there is net efflux of Na⁺ in exchange for external H⁺ (ref. 15). In the experiment illustrated in Fig. 3, we tested the effect of internal pH on the rate of net Na⁺ efflux occurring via exchange for external H⁺. Membrane vesicles were pre-equilibrated with 52 mM Na⁺ at pH 7.47 or 6.90, diluted 1 : 100 into a Na⁺-free medium at pH 7.47, and the net efflux of Na⁺ was assayed over the subsequent 30-s period. As indicated in Fig. 3, the net efflux of Na⁺ from vesicles with internal pH 7.47. This internal H⁺-stimulated Na⁺ efflux was amiloride sensitive, consistent with the fact that it represented transport via the Na⁺-H⁺ exchanger. Clearly, the thermodynamic driving force for net Na⁺ efflux via Na⁺-H⁺ exchange ($\Delta\mu_{Na^+} - \Delta\mu_{H^+}$)¹⁶ was less favourable at internal pH 6.90 than at 7.47. Accordingly, the findings in Fig. 3 indicated that internal H⁺ had activated the Na⁺-H⁺ exchanger sufficiently to more than compensate for the inhibitory effect of a diminished driving force for net Na⁺ efflux. This experiment thus provided further support for the concept that internal H⁺ was a potent activator of the renal microvillus membrane Na⁺-H⁺ exchanger.

Because our studies were performed using isolated plasma membrane vesicles rather than intact cells, we can conclude

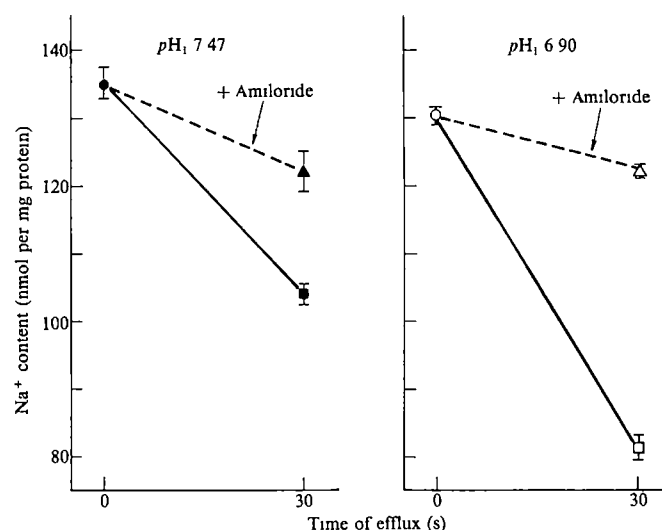


Fig. 3 Effect of internal pH on Na⁺ efflux. Membrane vesicles were pre-equilibrated for 120 min at 20 °C in 52 mM ²²NaCl, 22 mM K⁺, 42 mM HEPES and either 157 mM mannitol at pH 7.47 (●, ▲, ■) or 140 mM mannitol and 17 mM MES at pH 6.90 (○, △, □). Intravesicular ²²Na content was then assayed before (●, ○) and after 1 : 100 dilution and reincubation of the vesicles for 30 s at 20 °C in 200 mM mannitol, 41 mM K⁺, 80 mM HEPES pH 7.39 with (▲, △) or without (■, □) 1.0 mM amiloride. Each datum represents the mean \pm s.e. for three determinations.

that the observed activation of the Na^+-H^+ exchanger by internal H^+ must have arisen from an interaction at the level of the microvillus membrane. The simplest molecular model to explain our findings is that the Na^+-H^+ exchanger is a transmembrane protein with one or more inwardly facing titratable groups to which internal H^+ can bind and thereby cause a conformational change resulting in an increased transport activity. In experiments not illustrated, we found that the initial rate of Na^+ -dependent glucose uptake in renal microvillus membrane vesicles was not affected by a change in intravesicular pH from 7.47 to 6.90. Thus, whatever the precise molecular mechanism by which internal H^+ activates the Na^+-H^+ exchanger, this activation must not represent a general, nonspecific alteration of microvillus membrane transport function.

In almost all animal cells, a steep inwardly directed Na^+ gradient is maintained across the plasma membrane due to the active extrusion of Na^+ via the $(\text{Na}^++\text{K}^+)\text{ATPase}$. Because $[\text{Na}^+]_0/[\text{Na}^+]_i$ exceeds $[\text{H}^+]_0/[\text{H}^+]_i$ in most conditions, the net driving force acting on plasma membrane Na^+-H^+ exchangers generally favours the net exchange of external Na^+ for internal H^+ . Thus, allosteric activation by internal H^+ would enhance

the ability of plasma membrane Na^+-H^+ exchangers to protect intracellular pH against intracellular acid loads. Recent studies suggest that activation of plasma membrane Na^+-H^+ exchangers may also have a role in such other physiological processes as the regulation of cell volume and the control of cell proliferation^{17,18}. It has been proposed that elevations in intracellular Ca^{2+} may induce this activation¹⁸. We have found that preloading renal microvillus membrane vesicles with 10^{-7} – 10^{-3} M Ca^{2+} has no significant effect on Na^+-H^+ exchange activity (Barrett and P. S. A., unpublished observations). Because of mitochondrial $\text{Ca}^{2+}-\text{H}^+$ exchange, perturbations that induce a rise in intracellular Ca^{2+} can cause a fall in intracellular pH¹. Our studies raise the possibility that the apparent activation of plasma membrane Na^+-H^+ exchangers by intracellular Ca^{2+} could actually represent allosteric activation by intracellular H^+ .

We thank Ginger James for secretarial assistance. This work was supported by USPHS Research grant AM-17433 and an Established Investigatorship from the American Heart Association (P. S. A.).

Received 2 April, accepted 7 July 1982

- 1 Roos, A. & Boron, W. F. *Physiol Rev* **61**, 296–434 (1981)
- 2 Johnson, J. D., Epel, D. & Paul, M. *Nature* **262**, 661–664 (1976)
- 3 Aicken, C. C. & Thomas, R. C. *J Physiol, Lond* **273**, 295–316 (1977)
- 4 Murer, H., Hopfer, U. & Kinne, R. *Biochem J* **154**, 597–604 (1976)
- 5 Kinsella, J. L. & Aronson, P. S. *Am J Physiol* **238**, F461–F469 (1980)
- 6 Rindler, M. J. & Sauer, M. H. Jr *J Biol Chem* **256**, 10820–10825 (1981)
- 7 Moolenaar, W. H., Boonstra, J., van der Saag, P. T. & de Laat, S. W. *J Biol Chem* **256**, 12883–12887 (1981)
- 8 Kinsella, J. L. & Aronson, P. S. *Am J Physiol* **241**, F374–F379 (1981)
- 9 Kinsella, J. L. & Aronson, P. S. *Am J Physiol* **241**, C220–C226 (1981)
- 10 Aronson, P. S. *J Membrane Biol* **42**, 81–98 (1978)
- 11 Booth, A. G. & Kenny, A. J. *Biochem J* **142**, 575–581 (1974)
- 12 Aronson, P. S. & Kinsella, J. L. *Fedn Proc* **40**, 2213–2217 (1981)
- 13 Haase, W., Schafer, A., Murer, H. & Kinne, R. *Biochem J* **172**, 57–82 (1978)
- 14 Cuthbert, A. W. & Shum, W. K. *Proc R Soc B189*, 543–575 (1975)
- 15 Kinsella, J. L. & Aronson, P. S. *Biochim biophys Acta* **689**, 161–164 (1982)
- 16 Aronson, P. S. *Am J Physiol* **240**, F1–F11 (1981)
- 17 Kregonow, F. M. A. *Rev Physiol* **43**, 493–505 (1981)
- 18 Benos, D. J. *Am J Physiol* **242**, C131–C145 (1982)

Prostaglandins modulate macrophage Ia expression

David S. Snyder, David I. Beller & Emil R. Unanue

Department of Pathology, Harvard Medical School, Boston, Massachusetts 02115, USA

Prostaglandins are important modulators of inflammation and of humoral and cellular immune responses^{1–8}. In order to evaluate a possible mechanism for the regulation of immune responses we have studied the effects of prostaglandins on the expression of I-region-associated (Ia) antigens by macrophages. The expression of these glycoproteins is essential for macrophages to function as antigen-presenting cells during the induction of immune responses⁹. The synthesis and membrane expression of Ia, however, is not a constitutive property of the phagocyte¹⁰ but is under regulation and a positive regulation of this process is exhibited by activated T cells¹¹. In contrast, a negative regulation is conspicuously found in the neonate where a product from a young replicating macrophage inhibits the expression of Ia by the mature macrophages¹². We show here that prostaglandins of the E series (PGE) are potent inhibitors of the expression of Ia-antigens on macrophages and that thromboxane B₂ (TXB₂) antagonizes the effect of PGE.

The effects of PGE₁ and PGE₂ on the surface Ia expression of cultured macrophages were tested initially. Macrophages were obtained from normal mice or from mice previously injected with proteose-peptone or infected with *Listeria monocytogenes*. Resident macrophages from normal mice contained 5 to 10% Ia-positive cells, those from peptone-induced exudates had 5 to 15% positive, while those from *Listeria*-infected mice had 40 to 80% positive at the start of the culture. We had previously shown that these macrophages rapidly lost the capacity to synthesize Ia, and became Ia-negative after 24 to 48 hours of culture¹⁰. The addition of a lymphokine-containing conditioned medium from immune T cells at the start of the culture resulted in the progressive expression of Ia

so that most of the macrophages were positive after 4 to 7 days regardless of the initial level of Ia-positive cells¹³. This expression of Ia was markedly inhibited by PGE₁ and PGE₂ in a dose-dependent manner with 50% inhibition (I₅₀) at 1.5×10^{-10} M and 8.6×10^{-10} M, respectively (Fig. 1). The dose of PGE required to inhibit Ia was dependent on the amount of T cell-conditioned medium. A fivefold increase in the amount (v/v) of conditioned medium relative to that used in the experiment reported in Fig. 1 did not change the per cent of macrophages that became Ia-positive but resulted in a 10-fold increase in the I₅₀ dose of PGE₁ or E₂. PGE at concentrations of 10^{-7} M or less had no effect on macrophage viability, morphology, adherence properties, or on the per cent expressing IgG Fc receptors, or H-2K glycoproteins (Table 1). Identical results were found testing resident macrophages or those from exudates induced with peptone or following *Listeria* infection. It appears that PGE inhibition is associated with suppression of Ia biosynthesis (unpublished observation). The time of addi-

Table 1 Effects of PGE₂ on expression of macrophage surface proteins

Treatment		% Of cells positive for		
Lymphokine	PGE ₂	Ia	H-2K	Fc receptors
–	–	1	78	>98
+	–	37	83	>98
+	10^{-9} M	18	82	>98
+	10^{-7} M	5	82	>98
+	10^{-6} M	2	77	>98

Macrophages were prepared and cultured exactly as described in Fig. 1. Macrophages were cultured for 6 days with 2% conditioned media (lymphokine). Prostaglandins were added during the last 2 days of culture. Ia expression was assessed by immunofluorescence as in Fig. 1. H-2K expression was similarly determined using a monoclonal anti-H-2K^b antibody (clone line 11–4.1, from Dr L. Herzenberg), followed by fluorescein-labelled F(ab')₂ rabbit anti-mouse immunoglobulin. The cells were fixed after staining for H-2K. Fc receptors were detected by standard techniques of erythrocyte rosetting, using sheep red blood cells coated with rabbit IgG antibody.

tion of PGE to the cultured macrophages was important. Addition for only the first 2 days retarded the appearance of Ia-positive cells by 1 to 2 days but did not affect the ultimate level of Ia expression, addition at the time when most macrophages were Ia-positive resulted in loss of expression within 48 h.

As PGE is known to increase intracellular cyclic AMP levels in macrophages¹⁴, we tested the effects of cyclic AMP analogues

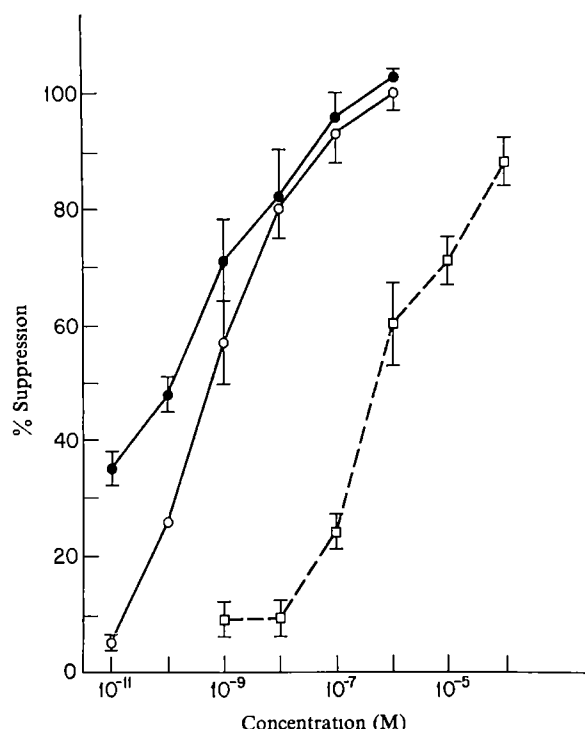


Fig. 1 Suppression of macrophage Ia expression by PGE₁ (●), PGE₂ (○), and dibutyryl cyclic AMP (□) in culture. Macrophages were obtained from the peptone-elicited peritoneal exudates (1 ml 10% proteose-peptone, 3 days before cells were collected) of adult A/St mice previously infected with 2×10^4 live *Listeria monocytogenes* organisms intraperitoneally²². The exudates were collected 3 to 4 days later by lavaging with 5 ml of Hank's balanced salt solution containing 0.6% g bovine serum albumin, 10 mM HEPES, and 10 units per ml heparin. Peritoneal exudate cells (2×10^5) were plated on glass coverslips placed in flat-bottom, Costar wells, in 1 ml of RPMI 1640 containing 5% fetal calf serum for 2.5 h at 37°C, 5% CO₂, then non-adherent cells were washed off. The medium was replaced with RPMI 1640 containing 10% fetal calf serum, plus or minus 2% conditioned media from a *Listeria*-immune T-cell line¹³. This medium was washed off on day 3 or 4 and replaced with fresh RPMI with or without the drugs. Prostaglandins were the gift of Dr John Pike (Upjohn). They were stored as stock solution at 10 mg per ml of absolute ethanol at 4°C, then diluted before each experiment with a 0.2 M phosphate buffer. On day 4 or 5, the macrophages were given a 24-h pulse of 5×10^6 heat-killed *Listeria* organisms and were then fixed in 1% paraformaldehyde and stained for surface Ia on day 5 or 6²². Cells on glass coverslips were exposed to a monoclonal anti-I-A^k antibody (clone 10-2-16) (5 µg per ml) mixed with a 1:5 dilution of decomplexed normal rabbit serum, at 4°C for 15 min. Fluorescent labelling was carried out as described in ref. 22. The % of Ia-positive macrophages was determined by counting 200 cells with a fluorescent microscope. Macrophages cultured in RPMI alone were 0 to 5% Ia-positive, those cultured in T-cell lymphokine were 40 to 80% positive. Per cent suppression was calculated as

$$\frac{\% \text{ Ia-positive control} - \% \text{ Ia-positive experimental}}{\% \text{ Ia-positive control} - \% \text{ Ia-positive background}} \times 100$$

Data represent the mean \pm s.e.m. These results are similar to those from radiolabelled antibody binding.

or agonists. Figure 1 shows that dibutyryl cyclic AMP inhibited Ia expression with an I_{50} of 9×10^{-7} M. (In other experiments, isoprenaline inhibited in the dose range of 10^{-5} M to 10^{-6} M and theophylline in the range 10^{-3} to 10^{-4} M.)

The concentrations of PGE inhibiting Ia are well within the physiological range found in tissues, which varies from about 10^{-11} M in basal states¹⁵ to as high as 10^{-7} M in inflammatory sites¹⁶. The inhibitory effects of PGE on macrophage Ia could be shown *in vivo* under two circumstances (Table 2). First, intraperitoneal injection of PGE₁ inhibited the lymphokine-induced development of peritoneal exudates rich in Ia-positive macrophages¹¹. Second, injection of indomethacin not only augmented the response to lymphokines but increased the basal number of Ia-positive macrophages as well. Further indication of the role of PG *in vivo* comes from an earlier study in which we showed that repeated injection of resident peritoneal macrophages—the phagocyte population producing the highest basal level of PGE¹⁷—interfered with the lymphokine-induced development of Ia-positive macrophages¹². Additionally, there are reports that indomethacin stimulates monocytopoiesis resulting in increased numbers of peripheral blood monocytes and tissue macrophages¹⁸ and that PGE inhibits monocytopoiesis¹⁹. Taken together, these examples suggest that PGE-mediated inhibition of Ia expression may be one of several regulatory effects exerted by arachidonic acid metabolites on the macrophage lineage.

Another important aspect of PGE regulation of Ia expression is the possibility that other arachidonic acid metabolites can antagonize the effects of PGE. We, therefore, looked at the effect of TXB₂, a stable metabolite of thromboxane A₂. Thromboxane A₂, which is produced by activated macrophages²⁰, has been shown to lower intracellular cyclic AMP levels²¹. Although TXB₂ is known to be less active than thromboxane A₂ it exerted an effect in our system. Figure 2 indicates that TXB₂ was a surprisingly potent antagonist to the effects of PGE₂ but had a small and inconsistent effect on Ia expression in the absence of T-cell stimulation. PGE₁ had no effect, either *in vitro* or *in vivo*. We are now investigating products of the lipoxygenase pathway. In preliminary studies, we have tested three monohydroxyicosatetraenoic acids (5-HETE, 11-HETE, and 15-HETE provided by Dr E. Goetzl). In the presence of lymphokines, these lipoxygenase metabolites increased the number of Ia-positive macrophages by 13 to 60%.

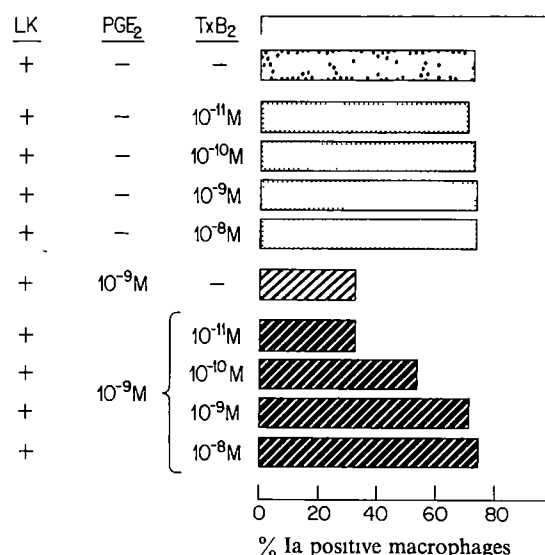


Fig. 2 TXB₂ and PGE₂ are antagonists. Macrophages were prepared and cultured as described in Fig. 1. On day 3, RPMI plus or minus 2% T-cell lymphokine (LK) was replaced with fresh RPMI containing PGE₂, TXB₂, or both. Cells were pulsed with heat-killed *Listeria* organisms on day 4, then fixed and stained for Ia on day 5.

Table 2 Effects of indomethacin and PGE₁ on peritoneal exudate macrophages

Experiment no.	Injected material	Macrophages per mouse ($\times 10^{-5}$)	Ia-positive (%)	Ia-positive macrophages per mouse ($\times 10^{-5}$)
1	Indomethacin, 50 μ g in 5% ethanol 5% Ethanol	10.0	5	0.5
		24.3	28	7.0
		19.3	8	1.5
2	Indomethacin, 50 μ g in 5% ethanol Lymphokine, 1:20 Indomethacin, 50 μ g, plus lymphokine, 1:20	5.5	9	0.5
		26.0	23	6.0
		11.6	38	4.4
		26.2	50	13.1
3	Lymphokine, 1:2 Lymphokine, 1:2, plus 15-methyl PGE ₁ , 1 μ g	8.6	4	0.3
		30.2	35	10.6
		26.0	15	3.9
4	15-Methyl PGE ₁ , 1 μ g PGE ₁ , 50 μ g Lymphokine, 1:2 Lymphokine, 1:2, plus 15-methyl PGE ₁ , 1 μ g Lymphokine, 1:2, plus PGE ₁ , 50 μ g	8.8	4	0.35
		24.8	9	2.2
		15.4	7	1.1
		35.0	45	15.8
		57.8	8	4.6
		47.5	5	2.4

A/St or B10.A adult mice were injected intraperitoneally with 0.5 ml of the materials every 12 h, six times, as previously reported¹¹. Peritoneal exudate cells were collected 12 h after the last injection, then plated on coverslips in RPMI for 2.5 h as described in Fig. 1. Non-adherent cells were washed off and counted, and the per cent adherent cells was calculated. Adherent cells were fixed and stained for Ia as described in Fig. 1.

Overall, our results suggest that prostaglandins can regulate the expression of Ia antigens on macrophages induced by lymphokines (Fig. 1, Table 1) as well as the T-cell-independent development of the basal levels of Ia-positive macrophages in tissues. Our results also suggest that the relative concentration of different arachidonic acid metabolites influences the level of Ia expression (Fig. 2). The finding that indomethacin increased Ia expression *in vivo* in the absence of exogenous lymphokine suggests either that PGE interferes with the spontaneous expression of Ia by some macrophages or that it influences the response to environmental stimuli. The basal level of Ia-positive macrophages, however, was not inhibited by injection of PGE (Table 1), implying that there may be some heterogeneity among macrophages with respect to PGE sensitivity. Finally, we suggest that the regulation of Ia expression by prostaglandins could be an important control mechanism in the inductive phase of immune responses. We have recently found that the loss of Ia by macrophages after exposure to PGE is associated with reduced antigen presentation to immune T cells (unpublished observations).

This work was supported by grants from the US NIH and the Council for Tobacco Research Inc.

Control of muscle and neuronal differentiation in a cultured embryonal carcinoma cell line

M. W. McBurney, E. M. V. Jones-Villeneuve,
M. K. S. Edwards & P. J. Anderson

Departments of Medicine, Biology and Biochemistry,
University of Ottawa, Ottawa, Canada K1H 8M5

Pluripotent murine embryonal carcinoma cells can differentiate in culture into many tissue types similar to those normally found in early embryos¹ and may be useful in investigating some developmental events^{1,2}. Central to our understanding of embryonic development are explanations of cellular determination, that is, the commitment of early embryonic cells to form divergent cell types. Of relevance is recent work with the F9 line of embryonal carcinoma cells which suggests that certain extra-embryonic cell types are specifically formed following treatment of undifferentiated cells with drugs^{3,4} and the manipulation of culture conditions⁵. We report here that the P19 line of embryonal carcinoma cells⁶ may provide an analogous system in which drugs can be used to manipulate the formation of tissues which normally comprise the fetus. In the presence of dimethyl sulphoxide (DMSO) aggregates of P19 cells differentiate rapidly to form large amounts of cardiac and skeletal muscle but no neurones or glia. We have previously shown that in the presence of high concentrations of retinoic acid ($>5 \times 10^{-7}$ M), aggregates of these same cells develop into neuronal and glial tissues but not muscle⁷. Thus, drugs can be used to generate two quite different spectra of embryonic tissue types from the same population of embryonal carcinoma cells.

P19 is a euploid (40:XY) embryonal carcinoma cell line derived from a teratocarcinoma induced in C3H/He strain mice⁶. For the experiments described below, we used P19S1801A1, a ouabain-resistant and 6-thioguanine-resistant subclone of P19 isolated without mutagenesis. Suspensions of dispersed cells were plated onto bacterial-grade plastic surfaces to which cells do not adhere⁸. Cells adhere to each other to form small aggregates. These aggregates were cultured in suspension for 4–5 days in the presence or absence of DMSO.

Received 5 April; accepted 28 June 1982.

- Kueh, F. A. Jr & Egan, R. W. *Science* **210**, 978–984 (1980).
- Goldyne, M. E. & Stobo, J. D. *CRC Crit. Rev. Immun.* **2**, 189–223 (1981).
- Stenson, W. F. & Parker, C. W. *J. Immun.* **125**, 1–5 (1980).
- Scott, W. A., Zrike, J. M., Hamill, A. L., Kempe, J. & Cohn, Z. A. *J. exp. Med.* **152**, 324–335 (1980).
- Rouzer, C. A., Scott, W. A., Kempe, J. & Cohn, Z. A. *Proc. natn. Acad. Sci. U.S.A.* **77**, 4279–4282 (1980).
- Kurland, J. I. & Bockman, R. J. *exp. Med.* **147**, 952–957 (1978).
- Leung, K. H. & Mihich, E. *Nature* **280**, 597–600 (1980).
- Webb, D. R. & Nowowiejski, I. *Cell. Immun.* **33**, 1–10 (1977).
- Unanue, E. R. *Adv. Immun.* **31**, 1–136 (1981).
- Beller, D. I. & Unanue, E. R. *J. Immun.* **126**, 263–269 (1981).
- Scher, M. G., Beller, D. I. & Unanue, E. R. *J. exp. Med.* **152**, 1684–1698 (1980).
- Snyder, D. S., Lu, C. Y. & Unanue, E. R. *J. Immun.* **128**, 1458–1465 (1982).
- Beller, D. I. & Ho, K. *J. Immun.* **129** (in the press).
- Bonta, I. L., Adolfo, M. J. P. & Parnham, M. J. *Prostaglandins* **22**, 95–103 (1981).
- Samuelsson, B. in *Advances in the Biosciences* (ed. Bergstrom, S.) 7–23 (Pergamon, Oxford, 1973).
- Higgs, G. A. & Salmon, J. A. *Prostaglandins* **17**, 737–746 (1979).
- Humes, J. L. *et al. J. Immun.* **124**, 2110–2116 (1980).
- Razin, E., Hayari, Y. & Globerson, A. *Prostaglandins Med.* **6**, 613–620 (1981).
- Pelus, L. M., Broxmeyer, H. E., Kurland, J. I. & Moore, M. A. S. *J. exp. Med.* **150**, 277–292 (1979).
- Brune, K., Glatt, M., Kalin, H. & Peskor, B. A. *Nature* **274**, 261–263 (1978).
- Moncada, S. & Vane, J. R. *New Engl. J. Med.* **300**, 1142–1147 (1979).
- Beller, D. I., Kiely, J.-M. & Unanue, E. R. *J. Immun.* **124**, 1426–1432 (1980).

They were then plated into tissue culture-grade plastic dishes.

In the absence of drug, the plated aggregates contained undifferentiated embryonal carcinoma cells along with small numbers of extra-embryonic endodermal cells⁷ (Fig. 1a). The presence of DMSO in the culture medium produced effects which became clear 1–2 days after plating, that is, 6–7 days after initiation of the experiment. In cultures exposed to 0.25% (v/v) DMSO, most plated aggregates contained embryonal carcinoma cells, rhythmically contracting muscle and fibroblast-like cells. At concentrations of 0.5, 0.75 and 1.0% DMSO, none of the plated aggregates contained embryonal carcinoma cells (identified by morphology), virtually all contained areas of rhythmically contracting muscle, and all contained cells with fibroblast-like morphology (Fig. 1c). By 10–12 days the amount of contracting muscle had increased (Fig. 1d, e). Also at this time many of the DMSO-treated aggregates developed areas of bipolar myoblasts which fused into myotubes (Fig. 1f). These myotubes were usually non-contractile but often developed spontaneous twitching activity by 14 days.

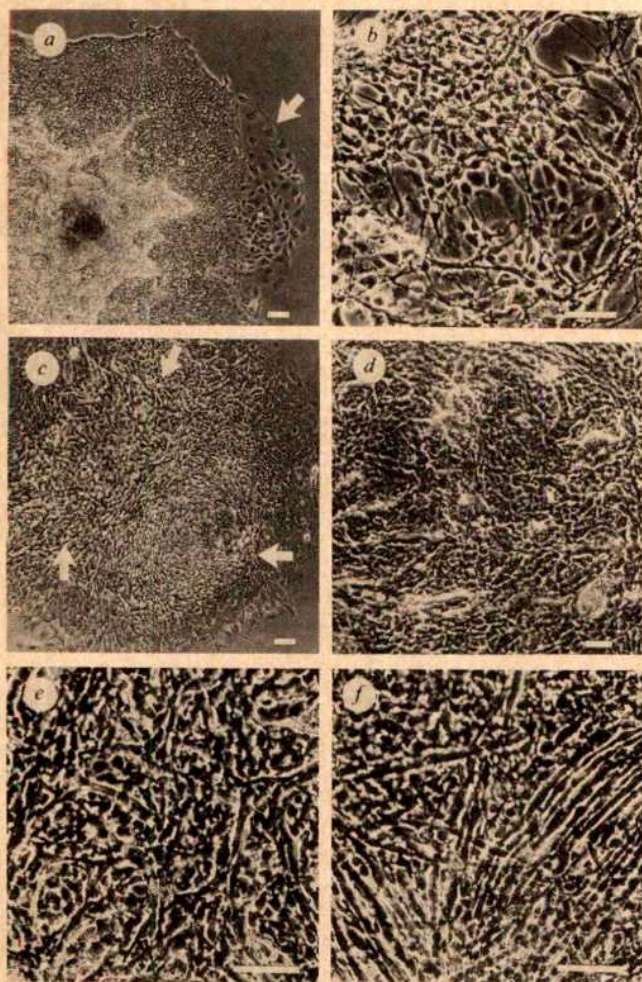


Fig. 1 Phase contrast photomicrographs of live teratocarcinoma cells. The conditions for cell culture^{7,12} and aggregation⁸ have been described previously. Cell aggregates were formed from a stock culture of P19S1801A1 cells and parallel cultures were carried in: *a*, normal medium (α -medium plus 10% fetal bovine serum¹²); *b*, in medium containing 5×10^{-7} M retinoic acid; and *c–f*, in medium containing 0.5% (v/v) DMSO. Aggregates were cultured in suspension in bacterial-grade Petri dishes for 5 days before being plated on to tissue culture-grade plastic surfaces. Photographs were taken 2 days (*a–c*) or 9 days (*d–f*) later. *a*, Untreated aggregates contain embryonal carcinoma and a few extra-embryonic endoderm cells (arrow). *b*, Aggregates of cells which had been cultured in the presence of 5×10^{-7} M retinoic acid contain neurones and astrocyte glial cells⁷. *c–f*, Aggregates cultured continuously in the presence of 0.5% DMSO contain small areas of rhythmically contracting cardiac muscle (arrows in *c*) which become more extensive with time (*d*). At higher magnification are: *e*, areas of rhythmically contracting mononucleate cardiac muscle and, *f*, multinucleate skeletal muscle. Scale bars, 200 μ m.

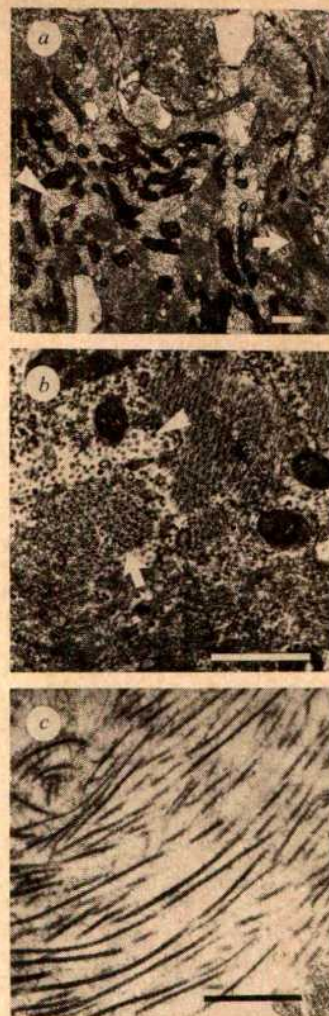


Fig. 2 Electron micrographs of some of the tissues formed in DMSO-treated cultures. *a*, A section through cardiac muscle shows bundles of thick and thin filaments in longitudinal section (arrows), glycogen granules (arrowhead) and numerous mitochondria. *b*, A section through a multinucleate myotube shows the thick and thin filaments in cross section (arrow) and glycogen (arrowhead). Many of the non-muscle cells in these cultures secreted collagen (*c*) which was often seen forming part of an intercellular matrix. Scale bars, 0.5 μ m.

Electron microscopy of the cells in DMSO-treated cultures indicated that the rhythmically contracting cardiac muscle cells contained glycogen granules, large numbers of mitochondria, and numerous areas of thick and thin filaments which were not organized into mature myofibrils (Fig. 2a). The multinucleate skeletal muscle cells were similar in appearance (Fig. 2b). Thus both muscle types seemed to be immature. Many of the non-muscle cells had abundant rough endoplasmic reticulum and some were surrounded by extracellular matrix which included collagen fibres (Fig. 2c).

The DMSO-treated aggregates of P10S1801A1 cells developed muscle but neither neurones nor glia. Treatment of the same cells with retinoic acid resulted in the development of neurones (Fig. 1b), glial cells, fibroblast-like cells, but no muscle. Cultures exposed to both retinoic acid (5×10^{-7} M) and DMSO (0.5 or 1.0%) developed as if exposed only to retinoic acid, that is, neurones and glia but no muscle were formed.

Differentiated cultures contained more actin than did untreated cultures (Table 1). Much of the actin in DMSO-treated cultures was α -actin, the type present only in skeletal and cardiac muscle cells⁹. Muscle-specific myosin was also detected in both cardiac and skeletal muscle by immunofluorescence using monoclonal antibodies directed against muscle myosin. About 15% of all cells were muscle myosin positive in these cultures by 8 days but none were detected in untreated or in retinoic acid-treated cultures.

When 10 μ M adrenaline was added to DMSO-treated cultures, the cardiac muscle responded by a 2–2.5-fold increase in contraction frequency and some previously quiescent areas of the culture were stimulated into rhythmic activity. Therefore β -adrenergic receptors were present. Such receptors are apparently acquired by cardiac muscle after the acquisition of spontaneous contractility¹⁰.

DMSO was not demonstrably cytotoxic to the P19S1801A1 cells at concentrations effective in differentiation experiments. Figure 3 shows that the efficiency of colony formation was unaffected by DMSO at concentrations up to 1.0%. Virtually all colonies formed in DMSO contained only embryonal carcinoma cells. In other experiments, monolayers of cells were cultured for 20 days in 1% DMSO without change in growth rate or morphology. At the end of this 20-day period, the DMSO-treated cells were aggregated in the presence or absence of DMSO (0.5%). Those aggregates formed in the absence of DMSO did not differentiate while those cultured in the drug formed muscle and fibroblasts in the usual way. Thus, it seems that the DMSO had no effect on the P19S1801A1 cells cultured as monolayers and that both the drug and cell aggregation are necessary for muscle differentiation. DMSO could be removed after 2–3 days but cardiac muscle still developed at 6–7 days as in the continuous presence of the drug.

The effects of DMSO described above were observed not only on P19S1801A1 cells, but also on the parental P19 cells and on all of the subclones from this line which were tested. However, DMSO had no effect on the differentiation of the embryonal carcinoma cell lines F9¹¹, OC15S1¹² and C86S1¹² whereas some clones of P10 cells¹³ appear to form an excess of neurones in the presence of DMSO (G. D. Paterno and M.W.M., unpublished). Variation has also been observed in the response of different embryonal carcinoma lines to retinoic acid^{3,7} and to aggregation in the absence of drugs^{1,2}.

DMSO is an inducer of Friend cell differentiation¹⁴ as are 6-thioguanine¹⁵, butyrate¹⁶ and ouabain¹⁷. The effects reported above for DMSO have also been observed with non-toxic concentrations of 6-thioguanine and butyrate but not with ouabain. Another Friend cell inducer, hexamethylene bisacetamide (HMBA), has previously been shown to influence the differentiation of some other embryonal carcinoma cell lines^{18,19} but we have not tested this compound with P19 cells.

Many papers have reported the formation of a limited range of cell types following spontaneous or induced differentiation of lines of teratocarcinomas and of embryonal carcinoma cells^{20–23}, but it is not clear whether this is the result of differential selection or of the occurrence of a limited number of determinative events. We think it is unlikely that differential selection can account for our observations because: (1) the cells

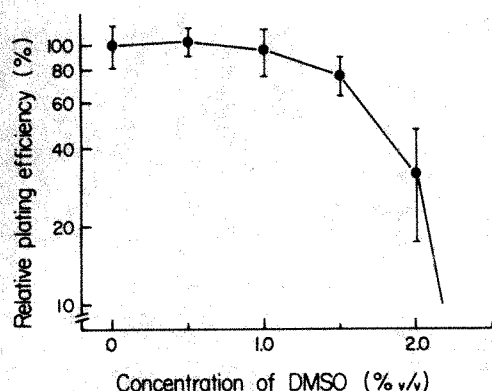


Fig. 3 The efficiency of colony formation of P19S1801A1 embryonal carcinoma cells in the presence of DMSO indicates the absence of toxicity at concentrations of less than 1% (v/v). About 200 cells were introduced into replicate 60-mm diameter dishes containing various concentrations of DMSO dissolved in α -medium supplemented with 10% fetal bovine serum and 10^{-6} M β -mercaptoethanol. Incubation was for 8 days at 37°C. All colonies consisted of cells with embryonal carcinoma morphology. Those colonies formed in 1.5% DMSO were smaller than control colonies, indicating that at these concentrations, the rate of cell proliferation was decreased.

Table 1 Presence of α -actin in DMSO-treated cultures

Treatment	Total actin*	α -actin*	% Muscle actin
Untreated, day 7	1.91 \pm 0.07	0.16 \pm 0.02	8.4
Retinoic acid, day 7	2.31 \pm 0.03	0.30 \pm 0.02	13.0
DMSO, day 7	2.62 \pm 0.15	0.52 \pm 0.01	19.8
DMSO, day 11	3.05 \pm 0.14	0.68 \pm 0.02	22.3

Aggregated cultures were prepared as described in Fig. 1 legend. Two days after plating (day 7) or 6 days after plating (day 11) the cultures were collected for analysis. The DMSO-treated day 7 culture contained rhythmically contracting but not multinucleate muscle. By day 11 both muscle types were present. Protein and peptide isolation was carried out as previously described²⁴ except for the use of trypsin instead of chymotrypsin for peptide generation. The actin contents were calculated by measuring the amounts of material which co-purified during electrophoresis at pH 6.5, 2.1 and 3.5 with tryptic peptides generated from muscle actin. Total actin values were calculated from the amounts of radioactive material co-migrating with the two chemically modified peptides CmCys-Asp-Ile-Asp-Ile-Arg and CmCys-Phe. All known actins contain peptides which should co-purify with these two. α -Actin values were calculated from the amount of material co-purifying with an 18-residue CmCys-containing peptide generated from the N-terminal region of α -actin. Actins from other tissues differ from α -actin in this region⁹ so should not co-purify with this peptide. Total actin is higher in differentiated than in undifferentiated cultures and there is more muscle-specific α -actin in DMSO-treated cultures. The 8–13% of muscle actin present in untreated and in retinoic acid-treated cultures may represent a background of radioactive label derived from non- α -actin peptides which co-purify with the legitimate peptide.

* mg actin per 100 mg total protein.

did not differentiate into embryonic cell types in the absence of drugs, (2) the cell types formed in DMSO-treated cultures were substantially different from those formed by the same cells in parallel cultures exposed to retinoic acid, (3) neither drug appeared to be toxic, (4) all subclones responded to both drugs, (5) the drugs were effective even when cultures were exposed to them for 48 h at the beginning of an experiment, and (6) DMSO did not inhibit the formation of neurones in cultures exposed to both retinoic acid and DMSO. The simplest interpretation of these data seems to be that each drug acts by 'inducing' uncommitted embryonal carcinoma cells to differentiate along a limited number of developmental avenues. If the drugs act by bringing about intracellular changes which mimic the results of certain embryonic decisions, it may be possible to use the drugs to identify parts of the cellular decision-making apparatus.

This work was supported by grants from the NCI of Canada and the MRC of Canada. We thank Irwin Schweitzer and Kem Rogers for their help. Antibody to glial fibrillar protein was the gift of Dr V. Kalnins and antibody to muscle-specific myosin was provided by Drs D. Morgenstern, D. A. Fischman and P. Merrifield.

Received 10 January; accepted 15 June 1982.

- Graham, C. F. in *Concepts in Mammalian Embryogenesis* (ed. Sherman, M. I.) 313–394 (MIT Press, Cambridge, 1977).
- Martin, G. R. *Science* **209**, 768–775 (1980).
- Strickland, S. & Mahdavi, V. *Cell* **15**, 393–403 (1978).
- Strickland, S., Smith, K. K. & Marotti, K. R. *Cell* **12**, 347–355 (1980).
- Hogan, B. L. M., Taylor, A. & Adamson, E. *Nature* **291**, 235–237 (1981).
- McBurney, M. W. & Rogers, B. J. *Dev Biol.* **89**, 503–508 (1982).
- Jones-Villeneuve, E. M. V., McBurney, M. W., Rogers, K. A. & Kalnins, V. I. *J. Cell Biol.* (in the press).
- Martin, G. R. & Evans, M. J. *Proc. natn. Acad. Sci. U.S.A.* **72**, 1441–1445 (1975).
- Vandekerckhove, J. & Weber, K. *Eur. J. Biochem.* **113**, 595–603 (1981).
- Lipshultz, S., Shanfeld, J. & Chacko, S. *Proc. natn. Acad. Sci. U.S.A.* **78**, 288–292 (1981).
- Bernstine, E. G., Hooper, M. L., Grandchamp, S. & Ephrussi, B. *Proc. natn. Acad. Sci. U.S.A.* **70**, 3899–3903 (1973).
- McBurney, M. W. *J. cell. Physiol.* **89**, 441–456 (1976).
- McBurney, M. W. & Strutt, B. J. *Cell* **21**, 357–364 (1980).
- Friend, C., Scher, W., Holland, J. G. & Sato, T. *Proc. natn. Acad. Sci. U.S.A.* **68**, 378–383 (1971).
- Gusella, J. F. & Housman, D. *Cell* **8**, 263–269 (1976).
- Leder, A. & Leder, P. *Cell* **5**, 319–322 (1975).
- Bernstein, A., Hunt, D. M., Crichtley, V. & Mak, T. W. *Cell* **9**, 375–381 (1976).
- Jakob, H., Dubois, P., Eisen, H. & Jacob, F. *C. r. hebdom. Séanc. Acad. Sci., Paris* **286D**, 109–111 (1978).
- Speers, W. C., Birdwell, C. R. & Dixon, F. J. *Am. J. Path.* **97**, 563–584 (1979).
- Gearhart, J. G. & Mintz, B. *Cell* **6**, 61–66 (1975).
- Vandenberg, S. R., Herman, M. M., Ludwin, S. K. & Bignami, A. *Am. J. Path.* **79**, 147–168 (1975).
- Pfeiffer et al. *J. Cell Biol.* **88**, 57–66 (1981).
- Darmon, M., Bottenstein, J. & Sato, G. *Dev Biol.* **85**, 463–473 (1981).
- Anderson, P. J. *Biochem. J.* **179**, 425–430 (1979).

A new fucosyl antigen expressed on colon adenocarcinoma and embryonal carcinoma cells

Teruo Miyauchi*, Suguru Yonezawa†, Tsukasa Takamura‡, Taku Chiba‡, Setsuzo Tejima‡, Masayuki Ozawa*, Eiichi Sato† & Takashi Muramatsu*

Departments of *Biochemistry and †Pathology, Kagoshima University School of Medicine, 1208-1 Usukicho, Kagoshima 890, Japan

‡Department of Hygienic Chemistry, Faculty of Pharmaceutical Sciences, Nagoya City University, 3-1 Tanabedori, Mizuhoku, Nagoya 467, Japan

Carbohydrate antigens on the surface of mammalian cells have recently gained renewed interest because some are specifically expressed at certain stages of cellular differentiation¹⁻⁴. Most of the useful antibodies detecting such carbohydrate antigens have been monoclonal antibodies produced by the hybridoma technique using whole cells as the immunogen¹⁻³ or the antibodies in the sera of some of human patients⁴. Here we report that an antiserum raised against an unusual carbohydrate linkage prepared by organic synthesis can preferentially react with certain tumour cells. Thus, an antiserum against the Fucal→3Gal linkage reacted with human colon adenocarcinoma cells and murine teratocarcinoma cells but reacted only with severely restricted regions in normal tissues.

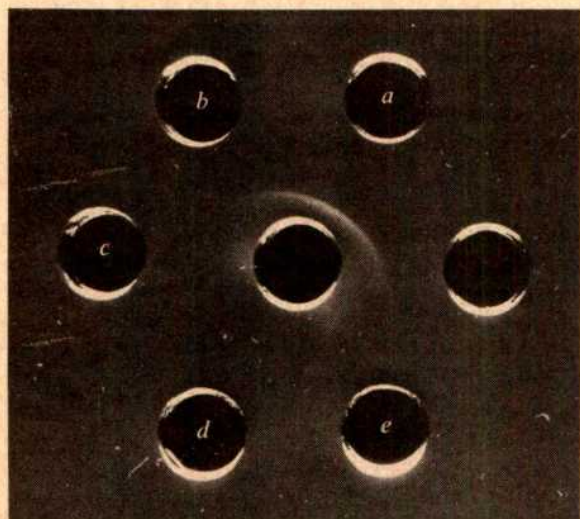


Fig. 1 Ouchterlony double-diffusion analysis on the specificity of the rabbit antiserum against 3'-fucosyllactose-PIP-BSA. The antigen (0.4 mg) was mixed with Freund's complete adjuvant and injected into the footpads of a rabbit. After 3 and 5 weeks, the rabbit received two booster injections using half the amount of antigen. The rabbit was bled 10 days after the last immunization. The double-diffusion analysis was performed in 1% agar gel containing 2% Triton X-100, 0.15 M NaCl, 50 µg ml⁻¹ of phenylmethanesulphonyl fluoride and 0.05% sodium azide in 0.01 M Tris-HCl buffer, pH 7.6, on a slide glass. The central well contained the antiserum and the peripheral wells contained 20 µg each of the following materials: a, 3'-fucosyllactose-PIP-BSA, b, 4'-fucosyllactose-PIP-BSA, c, 6'-fucosyllactose-PIP-BSA, d, lactose-PIP-BSA, e, BSA. Preparation of 4'-fucosyllactose and 6'-fucosyllactose has been described elsewhere¹². Carbohydrate contents of the PIP-BSA derivatives were determined by the phenol-H₂SO₄ reaction¹³, and were found to be 20 mols per mol of BSA in 3'-fucosyllactose-PIP-BSA, 25 mols per mol of BSA in the 4'-fucosyl compound and 23 mols per mol of BSA in the 6'-fucosyl compound.

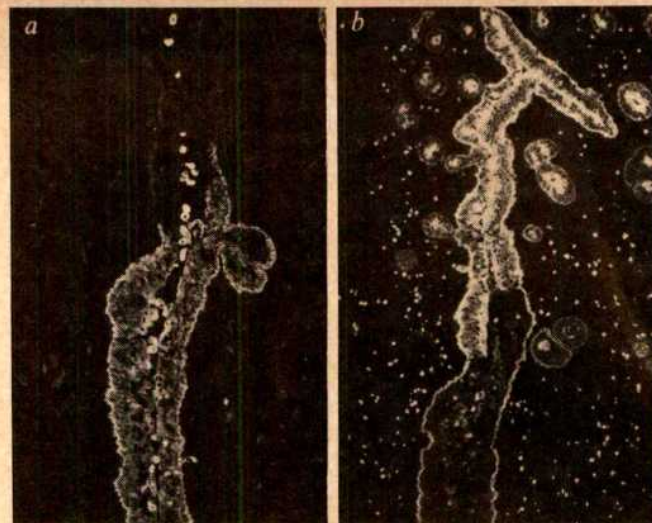


Fig. 2 Reaction of the serial tissue sections from a mouse uterus with the anti-Fucal→3Gal serum or with UEA-1. The organs were taken from a 3-month-old female 129/SV mouse, quick frozen and sectioned in a cryostat. The section was fixed for 1 min with acetone. a, Immunofluorescence staining with the antiserum showing the presence of the antigen in the squamous epithelium of the uterine cervix. The section was incubated with the antiserum diluted 20-fold with phosphate-buffered saline and then with FITC-conjugated F(ab')₂ fragment of goat anti-rabbit IgG (Cappel), and was observed by a fluorescence microscope using epillumination (Olympus, Model BH-RFL-LB). ×80. Very similar results were also obtained using BALB/c, ICR and ddY mice. No staining was observed in control experiments where rabbit non-immune serum, rabbit anti-BSA or rabbit anti-lactose-PIP-BSA was used instead of the specific antiserum. b, Staining with FITC-UEA-1. The tissue sections were incubated with 25 µl of FITC-UEA-1 at 1 mg ml⁻¹. ×80.

3'-Fucosyllactose (Fucal→3Galβ1→4Glc) was synthesized as described previously⁵, converted to the *p*-isothiocyanate-phenethylamine (PIP) derivative and coupled with bovine serum albumin (BSA) according to Smith *et al.*⁶. The product (3'-fucosyllactose-PIP-BSA), which contained 20 mols of 3'-fucosyllactose per mol of BSA, was injected into a rabbit. The resulting antiserum formed a sharp precipitation line with the antigen, but not with BSA, lactose-PIP-BSA, 4'-fucosyllactose-PIP-BSA nor with 6'-fucosyllactose-PIP-BSA (Fig. 1). Furthermore, these BSA derivatives without the Fucal→3Gal linkage were unreactive to the antiserum even in a binding assay, in which Sepharose coupled with the derivatives were stained with the antiserum by indirect immunofluorescence technique used in Fig. 2.

The reactivity of the antiserum to normal cells was also studied. Frozen sections of organs of adult mice were incubated with the diluted antiserum, and then fluorescein isothiocyanate (FITC)-labelled F(ab')₂ fragment of goat anti-rabbit IgG. We found that the antiserum stained squamous epithelium of the uterine cervix (Fig. 2a), ciliated border of the oviduct, epithelium of the bronchus, ependyma lining the ventricles of the brain and spermatocytes of the testis. The following organs were negative for the antigen: small intestine, proximal and distal colons, liver, spleen, kidney, epididymis, ovary and endometrium. The extremely restricted distribution of the antigen in the mouse suggests that the antiserum does not cross-react with H antigen whose determinant is Fucal→2Gal linkage⁷ or with SSEA-1 whose determinant involves Fucal→3GlcNAc linkage^{2,3}. SSEA-1 is known to be present in the epididymis and in the endometrium but not in squamous epithelium of the uterine cervix. It is also present in a portion of epithelial cells of the oviduct but not in ciliated border of the oviduct⁸. H antigen detected by staining with FITC-conjugated *Ulex europaeus* agglutinin 1 (UEA-1) was expressed in a variety of the adult tissues including endometrium of the uterus (Fig.

2b), small intestine, proximal and distal colons. Furthermore, the present antiserum did not stain erythrocytes of a number of human subjects whose blood types included H and Le^a. The failure to react with Le^a erythrocytes excluded the possibility that the antiserum cross-reacts with Fuc α 1 \rightarrow 4GlcNAc linkage⁷. From all these results, we propose that the antiserum specifically recognized Fuc α 1 \rightarrow 3Gal linkage. The antigen recognized by the antiserum was termed as FG3 antigen.

The antigen was detected in human colonic adenocarcinoma (Fig. 3a). The staining reaction was inhibited by 0.2 M 3'-fucosyllactose, but not by 0.2 M lactose, 0.2 M fucose, nor by 10 mg ml⁻¹ BSA. So far frozen sections of 17 human colonic adenocarcinoma have been examined. Of these, seven cases expressed the antigen in intracytoplasmic granules (Fig. 3a) and five cases expressed it along the cell apex. As the antigen was present not only on the luminal surface of the carcinoma but also in the invasive nests of the carcinoma in deep layers of intestinal wall (Fig. 3a), we considered that the antigen was produced by the carcinomas themselves. Only tumour cells

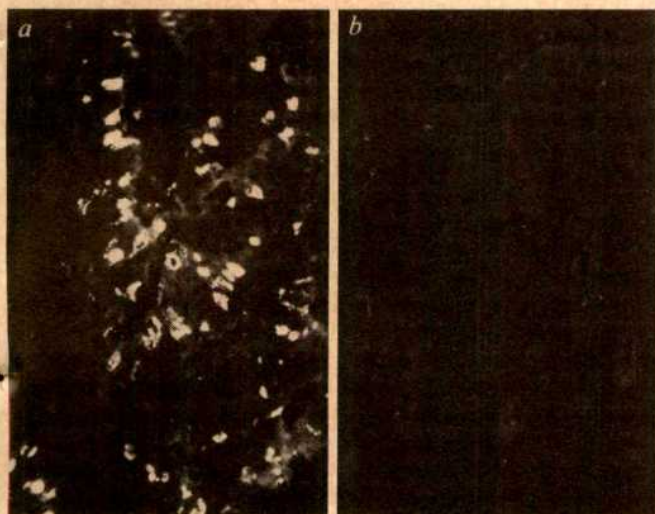


Fig. 3 Immunofluorescent staining of a human colonic adenocarcinoma using the anti-Fuc α 1 \rightarrow 3Gal serum. The tissue section was prepared from surgically removed specimen of a human colon adenocarcinoma of 44-year-old female Japanese patient (Blood group B type). Staining was performed as described in the legend of Fig. 2. *a*, Cancerous lesion. $\times 160$. *b*, Non-neoplastic mucosa of this patient. $\times 80$.

within the colonic tissue section were positive for the antigen (Fig. 3b). Antiserum against lactose-PIP-BSA did not react with the tumour region. FG3 antigen was undetectable in tissue sections of normal human duodenum, liver, gallbladder, pancreas, lung, thyroid, thymus, lymph node, muscle, connective tissue and blood vessels. Although further studies are needed to examine the distribution of the antigen in other normal tissues and also in other neoplastic conditions, the tumour-specific expression of the antigen in human colon is of significant interest.

As stem cells of teratocarcinoma are known to express unusual fucosyl glycopeptides^{9,10}, we examined the expression of FG3 antigen in a stem cell line, F9 and found it (Fig. 4). The antigen was also detected on stem cells of teratocarcinoma OTT6050 and on another stem cell line, STT-M. Therefore, some embryonic antigens expressed on teratocarcinoma stem cells may contain this unusual fucosyl linkage.

However, the Fuc α 1 \rightarrow 3Gal linkage is not found in glycoproteins and glycolipids isolated from diverse sources, but its presence has been reported in mixtures of higher homologues of human milk oligosaccharides¹¹. The present results suggest

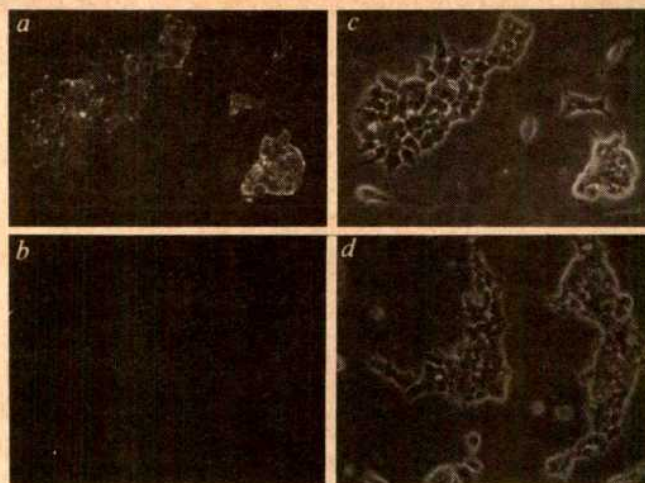


Fig. 4 Immunofluorescent staining of F9 embryonal carcinoma cells using the anti-Fuc α 1 \rightarrow 3Gal serum. F9 cells were cultured on a glass coverslip in Dulbecco's modified minimum essential medium containing 15% fetal calf serum. Cells on the coverslip were stained as described in the Fig. 2 legend, except that acetone treatment was omitted. *a*, Specific staining. $\times 120$. *b*, Control staining using non-immune serum. $\times 120$. *c*, Phase contrast microscopic observation of the cells shown in *a*. $\times 120$. *d*, Phase contrast microscopic observation of the cells shown in *b*. $\times 120$.

that the unusual fucosyl linkage is expressed in certain cancerous and embryonic tissues. It is possible that such carbohydrate linkages are involved in intercellular communication during early embryonic life but are expressed aberrantly in certain cancerous cells.

We thank Miss Kumiko Sato for secretarial assistance.

Received 8 March; accepted 14 June 1982.

1. Stern, P. L. *et al. Cell* **14**, 775-783 (1978).
2. Solter, D. & Knowles, B. B. *Proc. natn. Acad. Sci. U.S.A.* **75**, 5565-5569 (1978).
3. Gooi, H. C. *et al. Nature* **292**, 156-158 (1981).
4. Kapadia, A., Feizi, T. & Evans, M. J. *Expl Cell Res.* **131**, 185-195 (1980).
5. Takamura, T., Chiba, T. & Tejima, S. *Chem. Pharm. Bull.* **29**, 1076-1082 (1981).
6. Smith, D. F., Zopf, D. A. & Ginsburg, V. *Meth. Enzym.* **50**, 169-177 (1978).
7. Watkins, W. M. *Science* **152**, 172-181 (1966).
8. Fox, N., Danjanov, I., Martinez-Hernandez, A., Knowles, B. B. & Solter, D. *Dev. Biol.* **83**, 391-398 (1981).
9. Muramatsu, T. *et al. Proc. natn. Acad. Sci. U.S.A.* **75**, 2315-2319 (1978).
10. Muramatsu, T., Gachelin, G., Dammonville, M., Delarbre, C. & Jacob, F. *Cell* **18**, 183-191 (1978).
11. Yamashita, K., Tachibana, Y. & Kobata, A. *Archs Biochem. Biophys.* **174**, 582-591 (1976).
12. Chiba, T., Nishio, M., Takamura, T., Matsuda, H. & Tejima, S. *Proc. 3rd Symp. Carbohydrate Chemistry, Japan*, 90-91 (Japan Society Carbohydrate Chemists, 1980).
13. Dubois, M., Gilles, K. A., Hamilton, J. K., Rebers, P. A. & Smith, F. *Analyt. Chem.* **28**, 350-356 (1956).

In vivo* surveillance of tumorigenic cells transformed *in vitro

John Leslie Collins, Paul Q. Patek & Melvin Cohn

Salk Institute, PO Box 85800, San Diego, California 92138, USA

Any theory of surveillance against cancer requires that cells susceptible to host protective mechanisms exist as intermediates on the pathway from normal to cancer¹. The failure to demonstrate a significant frequency of such intermediates as a result of chemical carcinogenesis has cast serious doubt on the validity of the surveillance hypothesis². Here we report the conditions in which such intermediates can be identified as the major class of transformed cells resulting from *in vitro* chemical carcinogenesis of a cloned fibroblastic cell line.

We have previously reported the isolation and identification of cells that are intermediates between normal and cancerous cells³. We treated cloned cell lines (N-type) *in vitro* with

Table 1 Classification of cells by their tumorigenic potential

Type	Growth as a tumor in:	
	ATxFL mice	normal mice
N	-	-
I	+	-
C	+	+

chemical carcinogens and selected transformants by their anchorage-independent growth in agarose (Table 1). These transformants were then tested for their ability to grow as tumours in normal and surveillance-deficient mice; thymectomized, irradiated, and fetal liver restored (ATxFL). We found: (1) a correlation of 0.9 between the ability of these cells to grow in agarose and as tumours in ATxFL mice; (2) two classes of transformants, those which were tumorigenic in ATxFL mice but not in normal mice (I-type) and those which were tumorigenic in both (C-type); and (3) 20% of the chemically transformed cells were of the I-type and 80% of the C-type. The existence of I-type cells shows that a surveillance mechanism operates in normal mice to prevent the growth of some transformed cells and this surveillance mechanism is deficient in ATxFL mice.

The principle of the experiment described here is to treat N-cells *in vitro* with a chemical carcinogen and select transformants, not by their ability to grow in agarose, but by their ability to grow as tumours in ATxFL and normal mice. By testing the tumorigenic potential of carcinogen-treated N-cells in ATxFL and normal mice we were able to estimate the frequency with which transformation results in the I or C phenotype. Further, we demonstrated that transformants of N-cells selected for their tumorigenicity were anchorage-

Table 2 The tumorigenic potential of N-cells treated *in vitro* with BPE

Treatment	No. of dishes containing cells which were:		Tumorigenic only in ATxFL mice (I-type)	Tumorigenic in ATxFL and normal mice (C-type)
	Non-tumorigenic	Tumorigenic in ATxFL		
Expt 1				
THF control	6	1		
BPE	1	23		
Expt 2				
THF control	2	0		0
BPE	1	7		1
Expt 3				
THF control	10	1		0
BPE	9	8		7

The N-cell line, B/C-N 7.1, was grown in Dulbecco's modified Eagle's minimum essential medium (DMEM) plus 10% fetal calf serum (FCS). Cells (10^6 per 60 mm dish) in DMEM were treated with benzo(a)pyrene-*trans*-7,8-dihydrodiol-9,10-epoxide (BPE; supplied by NCI) dissolved in THF. The final concentration of BPE was 20 ng ml^{-1} in 1% THF. The control dishes were treated with DMEM containing 1% THF. One week later the cells were removed from the dishes with trypsin, washed, and injected into two normal mice and two mice which had been thymectomized as adults, lethally irradiated (750 rad) and restored with 10^7 syngeneic liver cells from 14-15-day-old-fetuses (ATxFL). Animals were examined weekly for tumours, which appeared between 45 and 120 days after injection. Tumours were excised when they reached approximate volumes of $1-2 \text{ cm}^3$, mechanically dissociated, and re-established in *in vitro* culture. In all experiments tumours were derived from the injected parental N-cell populations and not from *in situ* transformation of host cells as shown by the fact that all the excised tumours were hypoxanthine-guanine phosphoribosyltransferase-negative, a marker introduced into the parental N-cells.

independent, the converse of our previous experiment³ where cells selected for anchorage independence were tumorigenic. Thus, starting with this cloned non-tumorigenic, anchorage-dependent cell line, not only does selection for anchorage independence result in tumorigenicity but selection for tumorigenicity results in anchorage independence.

Benzo(a)pyrene epoxide (BPE) dissolved in tetrahydrofuran (THF) was added to culture dishes containing 10^6 cloned N-cells in media without serum. The final concentration of BPE was 20 ng ml^{-1} , the medium contained 1% THF. Serum was added after 1 h of exposure to BPE; after 1 week the cells were collected, counted, and 10^6 cells injected into ATxFL mice (experiment 1, Table 2) or ATxFL and normal mice (experiments 2 and 3, Table 2). As a control, an equal number of N-cells treated only with medium containing 1% THF were injected into mice.

Two points emerge from the results shown in Table 2. First, BPE dissolved in THF is much more effective than THF alone in transforming N-cells to grow as tumours; 46/57 dishes treated with BPE plus THF resulted in tumours compared with only 2/20 in the THF-treated dishes. Assuming that the number of transformants per dish follows a Poisson distribution, then the frequency of transformation by BPE plus THF is 40 times that of THF alone. Second, N-cells transformed by BPE can be divided into two classes based on their tumorigenicity, I-type growing as tumours in ATxFL but not normal mice and C-type growing as tumours in both ATxFL and normal mice. In the two experiments where the I or C phenotype of the transformants in 23 dishes was determined, 15 were I-type and 8 C-type. From the distribution of these data, I-type transformants appear at least three times more frequently than C-type.

The excised tumour cells were re-established in culture and then analysed for their ability to grow anchorage-independently. All of them expressed anchorage-independent growth (colony forming efficiencies³ between 1 and 30%) relative to the parental anchorage-dependent N-line (colony forming efficiency $<0.01\%$) from which they were derived. The plating efficiency in agarose was independent of whether the tumour cells were derived from ATxFL or normal mice or whether tumours resulted from the injection of BPE-treated N-cells or from the few tumours formed by injecting control THF-treated N-cells. There is no correlation between the colony-forming efficiency of a transformant and its I or C phenotype.

The fact that all tumours, when re-established in culture, are anchorage-independent is complementary to our previous observation that anchorage-independent fibroblasts are tumorigenic³. Thus, for fibroblastic cell lines, tumorigenicity and anchorage independence are coordinately expressed whether the selection pressure used to isolate them is anchorage independence or tumorigenicity.

The major difference between the transformants selected by their ability to grow as tumours and those selected by their ability to grow in agarose is the frequency with which the transformations result in the I or C phenotype. By using transformants selected for their expression of anchorage independence, we previously estimated the frequency of transformation resulting in a cell of the I-type to be $\sim 20\%$ (ref. 3). In the experiments reported here the frequency of I-type transformants is much greater than 50%.

There are two possible explanations for the differences in the proportion of I- and C-type transformants in these two experiments. First, the *in vitro* selection for anchorage independence selects against anchorage-dependent transformants which grow as I-lines in mice. This means that there are both anchorage-independent and dependent transformants which grow as I-type cells in mice. When the transformants are tested directly in mice, both anchorage-independent and dependent transformants are revealed as I-type. When transformants are first selected for anchorage independence, then analysed in mice, only those which express anchorage independence are revealed. This reduces the total number of cells which express the I phenotype. It follows that if, in addition, there were

anchorage-dependent and independent transformants which were capable of growing as C-lines *in vivo*, the proportion of the I-type relative to the C-type would be the same in these two experiments. As the proportion of I-type varies, it seems that most transformants which express the C phenotype *in vivo* are anchorage-independent and most anchorage-dependent transformants are of the I phenotype.

Because no tumours were anchorage-dependent, any anchorage-dependent transformants must be at a stage on the pathway to cancer that allows the *in vivo* selection of anchorage-independent variants at a high frequency.

Second, the proportion of I- and C-type cells depends on the chemical carcinogen used to transform the N-line. When transformants were selected for anchorage independence before testing in mice, they were induced with various chemical carcinogens. All of the transformants tested directly in mice were induced with BPE. If BPE influences the tumorigenic phenotype of the transformants, then it must induce more I-type transformants than several other carcinogens that were analysed collectively.

The existence of the I phenotype shows that at least some transforming events result in cells which are sensitive to a tumour surveillance mechanism operating in normal but not ATxFL mice. ATxFL mice are severely depressed with respect to both immunological (cell-mediated and humoral immunity) and non-immunological (natural killer (NK) and natural cytotoxic (NC) cells) host protective mechanisms. Although it is possible that one (or both) of these host protective mechanisms is responsible for the destruction of I-lines by normal mice, we cannot ascribe the surveillance measured here to either mechanism. Regardless of the mechanisms of surveillance, the frequency with which transformation by a chemical carcinogen results in the I phenotype is at least three times that of the C phenotype. This is important because the efficacy of any surveillance mechanism is a function of the proportion of newly transformed cells which are susceptible to surveillance.

We acknowledge the contribution of the Armand Hammer Cancer Workshops and the technical assistance of Ms Scotti Brauer. This work was supported by NCI grant CA 19754-07.

Received 26 April; accepted 15 July 1982.

1. Burnet, M. *Immunological Surveillance* (Pergamon, London, 1970).
2. Prehn, R. T. *Am. J. Path.* **77**, 119-122 (1974).
3. Patek, P. Q., Collins, J. L. & Cohn, M. *Nature* **276**, 510-511 (1978).

A transforming gene present in human sarcoma cell lines

C. J. Marshall, A. Hall & R. A. Weiss

Chester Beatty Laboratories, Institute of Cancer Research, Fulham Road, London SW3 6JB, UK

Morphological transformation of NIH/3T3 cells by transfection with DNA has been used to identify transforming sequences in human tumours^{1,2}. Transforming activity has been reported for DNAs isolated from bladder, mammary, colon and lung carcinomas, neuroblastoma, lymphoid and myeloid tumours¹⁻⁶. Each of these tissues seems to contain different transforming sequences except for the colon and lung tumours where the same sequence seems to be involved⁵. We now report that in two different human sarcoma cell lines, a fibrosarcoma and an embryonal rhabdomyosarcoma, the DNAs have transforming activity. The transforming gene is the same in both sarcomas but differs from the activated sequences detected in other tumours. We have also found that the transforming gene has no detectable homology to eight retrovirus oncogenes tested.

High molecular weight DNA was prepared from three different types of human sarcoma cell lines and assayed for transforming activity on NIH/3T3 cells using the calcium phosphate co-precipitation technique⁷. Table 1 shows that DNA

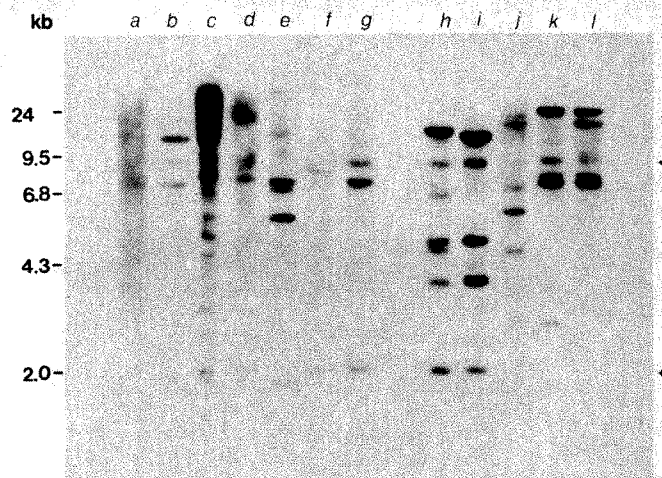


Fig. 1 Presence of human repetitive sequences in secondary transformants derived from RD and HT1080. DNAs (20 µg) were digested with *EcoRI*, phenol-extracted and loaded on a 1-cm thick, 0.8% agarose gel. After electrophoresis the DNA was transferred to nitrocellulose and the blot was hybridized essentially as described by Wahl *et al.*²⁰ except that the formamide concentration was 30%, the hybridization temperature 60 °C and mouse DNA was used as carrier. The probe used was fetal liver DNA (previously sonicated to an average length of 4 kb) nick-translated to a specific activity of 2×10^8 c.p.m. per µg. The filter was washed in $0.4 \times \text{SSC}/0.1\%$ SDS for 30 min at 60 °C, and subjected to autoradiography with an intensifying screen at -70 °C for 5 days. Lanes a, NIH/3T3; b, c, secondaries derived from HT1080 primary 125; d, e, secondaries derived from HT1080 primary 144; f, g, secondaries derived from HT1080 primary 120; h, i, secondaries derived from RD primary 145; j, secondary from RD primary 149; k, l, secondaries derived from RD primary 148. Arrows show the position of the 8.8 kb band conserved in all transfectants and the 1.8 kb band present in some transfectants. (In lane e of the blot shown the 8.8 kb band is poorly visible, however in other blots of this DNA the band is present though faint.)

from embryonal rhabdomyosarcoma cell line RD (ref. 8) and from one of two fibrosarcomas, HT1080 (ref. 9), was able to transform NIH/3T3 cells. DNA extracted from a second fibrosarcoma cell line, HS10CL7, and from an osteogenic sarcoma, MG63 (ref. 10), as well as normal human DNA did not cause morphological transformation. The transforming efficiencies of RD and HT1080 DNAs were similar, though lower than that of the T24 bladder carcinoma cell line. Individual cells in sarcoma DNA-induced foci were morphologically similar to those produced by the bladder line, but the foci themselves were smaller. This suggests that the transfectants produced using sarcoma DNA grow more slowly than those derived using T24 DNA. The morphologically altered cells were found to initiate rapidly growing tumours with short latent periods (10 days) when injected into nude mice whereas the clone of untransformed 3T3 cells did not produce tumours over a 2-month observation period (Table 1). The transfectants differed from the NIH/3T3 cell line in being able to grow in low-serum and in anchorage-independent conditions. Furthermore, DNA isolated from primary transfectants was able to transform NIH/3T3 cells, demonstrating that the transforming activity could be passaged serially (Table 1).

To determine whether the transforming activity of the human sarcoma cell lines was related to sequences previously identified in other tumour types or to known viral oncogenes the following experiments were performed.

First, DNAs from the sarcoma cell lines, or from primary transfectants, were digested with various restriction endonucleases before transfection of NIH/3T3 cells. Enzymes having sites in the transforming sequence should destroy the transforming activity of the DNA. Digestion of DNA from primary transfectants with six enzymes that cut DNA on average every 3-7 kilobases (kb) completely destroyed the transforming

Table 1 Transfection of NIH/3T3 cells with DNAs from human sarcoma cell lines

Donor DNA	Efficiency of transfection* (no. foci per μg DNA)	Tumorigenicity of transfectants†	Efficiency of secondary transfection*‡ (no. foci per μg DNA)
RD (rhabdomyosarcoma)	0.07 (16/12)	2/2, 2/2 (10 days)	0.14 (11/4), 0.16 (13/4), 0.13 (10/4)
HT1080 (fibrosarcoma)	0.16 (58/18)	3/3, 3/3 (10 days)	0.13 (10/4), 0.28 (22/4), 0.73 (44/3)
HS10C17 (fibrosarcoma)	0 (0/10)	—	—
MG63 (osteogenic sarcoma)	0 (0/12)	—	—
T24 (bladder carcinoma)	1.45 (348/12)	3/3, 3/3 (10–12 days)	6
Normal human DNA from fetal liver	0 (0/12)	—	—
NIH/3T3 cells	0 (0/30)	0/8 (8 weeks)	—

RD, HT1080 and MG63 (refs 8–10 respectively) cells were obtained from the American Type Culture Collection via Flow Laboratories. HS10C17 cells were a gift of Dr G. A. Currie.

* DNA (20 μg) co-precipitated with calcium phosphate was applied to a 60-mm culture dish seeded 24 h previously with 3×10^5 NIH/3T3 clone D4 cells. The medium was changed after 4 h and then every other day and foci were scored after 16–17 days. Values are the mean of several experiments. The number of foci scored/number of plates examined is given in parentheses.

† 10^6 cells from two independent transfectants were suspended in 0.2 ml of medium and injected subcutaneously into two or three 8–12 week old CBA *nu/nu* mice. The mean time for cells to produce 0.5 cm diameter tumours was also recorded. Each value represents the takes from a different independent primary transfectant.

‡ Each set of values represents the transfection efficiencies for a different primary transfectant.

activity (Table 2). Digestion of DNA from a primary transfectant induced by the bladder carcinoma line T24 showed a different sensitivity to digestion, so the sarcoma transforming sequence is not identical to that of the bladder carcinoma¹¹. Similarly, comparison with published data shows that the transforming sequence of the sarcoma DNAs is not the same as that present in mammary³ or lymphocyte⁶ neoplasms. In addition, none of four enzymes (*XhoI*, *Clal*, *SalI* and *SmaI*) having restriction sites that contain the rare dinucleotide CpG and which therefore cut human DNA relatively occasionally inactivated the sarcoma transforming activity. The restriction enzyme sensitivity profiles of RD and HT1080 DNAs are identical for 10 enzymes, suggesting that the transforming activity is associated with the same sequence in both tumours (Table 2).

To characterize the transforming sequence further, we analysed the DNA of secondary transfectants for the presence of human repetitive sequences. After two consecutive rounds of transfection only a small amount of human DNA remains in the transformed cells; any repetitive DNA sequences that are conserved in all secondary transfectants would therefore be expected to be closely linked to or contained in the transforming

Table 2 Effect of restriction endonuclease digestion on the transforming activity of sarcoma DNAs

Enzyme	No. of foci per μg DNA		
	HT1080-f125	RD-f145	T24-f106
No enzyme	0.2	0.28	1.0
<i>EcoRI</i>	0	0	1.0
<i>BamHI</i>	0	0	ND
<i>HindIII</i>	0	0	0.51
<i>BglII</i>	0	0	0.4
<i>PvuII</i>	0	0	0
<i>PstI</i>	0	0	0
<i>XhoI</i>	0.1	0.2	ND
<i>SalI</i>	0.22	0.18	ND
<i>ClaI</i>	0.32	0.18	ND
<i>SmaI</i>	0.13	0.07	ND

DNA (100–200 $\mu\text{g ml}^{-1}$) was digested according to the manufacturers' instructions but using a 10-fold excess of enzyme. After addition of enzyme an aliquot containing 1 μg of DNA was removed and added to 1 μg of λ DNA. Complete digestion of λ DNA was taken to correspond to complete digestion of cellular DNA. 60 μg of digested DNA were added to 120 μg of high molecular weight mouse DNA and calcium phosphate co-precipitates were divided between six plates of NIH/3T3 cells. For all cell lines, DNAs of primary transfectants were used for restriction digests because their transforming activity was higher than that of the original cell lines. In confirmatory experiments, digests of DNA from the original human cell lines gave similar results.

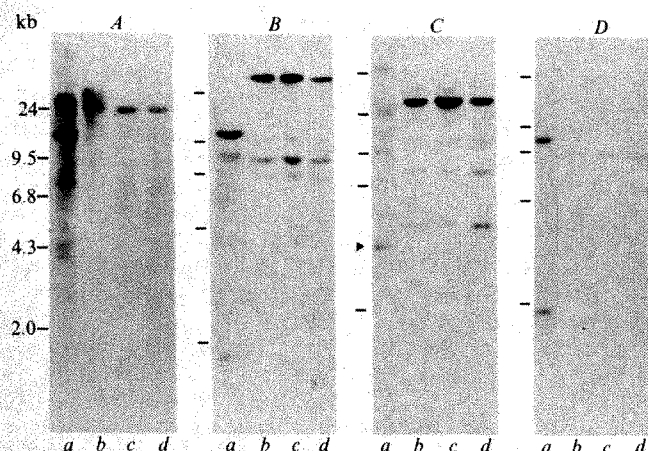


Fig. 2 Southern blots of *EcoRI* (A–C) or *BamHI* (D) digestions of the following DNAs: a, human fetal liver; b, NIH/3T3; c, a primary HT1080 transfectant; and d, a primary RD transfectant. The blots were hybridized with the following ^{32}P -labelled viral oncogene probes: A, a 1.5 kb *PstI* fragment containing *v-myc*; B, a 2.5 kb *PvuII* fragment containing *v-erb-A* and *v-erb-B*; C, a 1.8 kb *PvuII* fragment containing *v-Ki-ras* and flanking sequences (the arrow indicates the position of the human 3 kb *EcoRI* fragment homologous to the viral oncogene and identified in NIH/3T3 cells transfected with human lung carcinoma DNA¹⁶); D, a 0.9 kb *PstI/XbaI* fragment containing *v-sis*. All four blots were hybridized in 50% formamide, $5 \times \text{SSC}$ at 42°C except D which was at 50°C . The filters were washed as follows: A, $0.3 \times \text{SSC}$, 65°C ; B, $0.1 \times \text{SSC}$, 45°C ; C, $0.3 \times \text{SSC}$, 60°C ; and D, $0.6 \times \text{SSC}$, 50°C .

sequence^{4,5}. A Southern blot¹² profile of such conserved repetitive sequences can be used to distinguish different transforming sequences^{4,5}. Accordingly, DNAs were isolated from secondary transfectants derived from RD and HT1080 DNAs, digested with *EcoRI* and probed on Southern blots with nick-translated total human DNA¹³. In the conditions of hybridization used, only human repetitive sequences can be detected. Although several fragments are present in each transfectant, only a single 8.8 kilobase pair (kbp) *EcoRI* fragment is conserved in all secondary transfectants (Fig. 1). Identical Southern blots probed with the plasmid BLUR-8 (ref. 14), which contains a cloned repetitive sequence from the human *Alu* family, show a similar pattern of hybridization (data not shown). However, the band corresponding to the 8.8 kbp *EcoRI* fragment is less intense than the other bands. We assume that the repetitive sequence present in this fragment is only distantly related to the *Alu* repetitive element contained in BLUR-8. Many of the secondary transfectants also contain a second fragment of 1.8 kbp (Fig. 1). However, as this fragment is not conserved in all secondary transfectants, it is probably not contained in the transforming sequence but may be linked to it. The observation that an 8.8 kbp *EcoRI* fragment is conserved in all secondary transfectants derived from both RD and HT1080 DNAs again strongly suggests that the transforming sequence in the two

DNAs is the same. Furthermore, the size of the *EcoRI* fragment is different from the fragments found by other investigators in secondary transfectants from DNAs of colon, lung, neuroblastoma and promyelocytic leukaemia^{4,5}.

Recently it has been shown that the transforming sequence activated in bladder carcinoma cell lines is a human cellular homologue of *v-Ha-ras*, the oncogene of Harvey sarcoma virus¹⁵. The transforming sequence of a lung carcinoma cell line is homologous to *v-Ki-ras*, the oncogene of Kirsten sarcoma virus¹⁶. Furthermore, Eva *et al.*¹⁷ have reported that human sarcoma cells contain high levels of RNA transcribed from the cellular homologue of *v-sis*, the oncogene of simian sarcoma virus. It was therefore important to determine whether the sarcoma transforming sequence is related to these or other retrovirus oncogenes. We have probed Southern blots of transfectants to see whether they contain human sequences homologous to *v-erb-A*, *v-erb-B*, *v-Ki-ras*, *v-myc*, *v-sis* (Fig. 2) and to *v-abl*, *v-Ha-ras* and *v-src* (data not shown). None of these probes detected any human sequences in the transfectants although the conditions used detected the mouse homologues

in the transfectants and the human homologues in human DNA.

We conclude from these experiments that the same transforming sequence is present in cell lines derived from the two different types of sarcoma, a rhabdomyosarcoma and a fibrosarcoma. (Recently other workers¹⁸ noted that HT1080 DNA has transforming activity.) We have shown that this sarcoma sequence is different from transforming sequences identified in other human tumour lines and in eight RNA tumour viruses. These data therefore support the idea that different transforming sequences are activated in different tumour types and that these sequences may have a role in both the normal physiology and the neoplastic transformation of those tissues^{3-6,19}. Further characterization of the transforming sequence and the elucidation of its mode of action will depend on the isolation of molecular clones of the transforming gene and its normal allele.

We thank James Christie and Micaela Fairman for technical assistance, R. Avery, J. M. Bishop, R. C. Gallo, J. Neil and B. Ozanne for cloned retrovirus oncogenes and C. Schmid for the BLUR-8 clone. Financial support was generously provided by the Cancer Research Campaign and MRC.

Received 21 June; accepted 26 July 1982.

1. Shih, C., Padhy, L. C., Murray, M. & Weinberg, R. A. *Nature* **290**, 261-264 (1981).
2. Krontiris, T. G. & Cooper, G. M. *Proc. natn. Acad. Sci. U.S.A.* **78**, 1181-1184 (1981).
3. Lane, M.-A., Saiten, A. & Cooper, G. M. *Proc. natn. Acad. Sci. U.S.A.* **78**, 5185-5189 (1981).
4. Murray, M. J. *et al. Cell* **25**, 355-361 (1981).
5. Perucho, M. *et al. Cell* **27**, 467-476 (1981).
6. Lane, M.-A., Saiten, A. & Cooper, G. M. *Cell* **28**, 873-880 (1982).
7. Graham, F. L. & Van der Eb, A. J. *Virology* **52**, 456-467 (1973).
8. McAllister, R. M., Melnyk, J., Finklestein, J. Z., Adams, E. C. & Gardner, M. B. *Cancer* **24**, 520-526 (1969).
9. Rasheed, S., Nelson-Rees, W. A., Toth, E. M., Arnstein, P. & Gardner, M. B. *Cancer* **33**, 1027-1033 (1974).

10. Billiau, A. *et al. Antimicrob. Ag. Chemother.* **12**, 11-15 (1977).
11. Goldfarb, M., Shimizu, K., Perucho, M. & Wigler, M. *Nature* **296**, 404-409 (1982).
12. Southern, E. M. *J. molec. Biol.* **98**, 503-517 (1975).
13. Gusella, J. F. *et al. Proc. natn. Acad. Sci. U.S.A.* **77**, 2829-2833 (1980).
14. Rubin, C. M., Houck, C. M., Deininger, P. L. & Schmid, C. W. *Nature* **284**, 372-374 (1980).
15. Parada, L. F., Tabin, C. J., Shih, C. & Weinberg, R. A. *Nature* **297**, 474-478 (1982).
16. Der, C. J., Krontiris, T. G. & Cooper, G. M. *Proc. natn. Acad. Sci. U.S.A.* **79**, 3637-3640 (1982).
17. Eva, A. *et al. Nature* **295**, 116-119 (1982).
18. Pulciani, S. *et al. Proc. natn. Acad. Sci. U.S.A.* **79**, 2845-2849 (1982).
19. Weiss, R. A., Teich, N., Varmus, H. E. & Coffin, J. *RNA Tumor Viruses* (Cold Spring Harbor Laboratory, New York, 1982).
20. Wahl, G. M., Stern, M. & Stark, G. R. *Proc. natn. Acad. Sci. U.S.A.* **76**, 3683-3687 (1979).

The production of membrane or secretory forms of immunoglobulins is regulated by C-gene-specific signals

Luciana Forni & Antonio Coutinho*

Basel Institute for Immunology, 487 Grenzacherstrasse, Postfach, 4005 Basel, Switzerland

* Department of Immunology, Umeå University, 90185 Umeå, Sweden

Selective patterns of antibody isotypes are produced in response to thymus-dependent and thymus-independent antigens and mitogens¹⁻⁵. Together with information on the organization of immunoglobulin C_H genes in myelomas^{6,7}, various models on the control of C-gene expression and switch in normal B cells have been proposed but only secreted products or secretory cells have been considered. We report here a dissociation between expression of membrane-bound immunoglobulins and secretion of the same isotype, and in this case describe C-gene specific signals which regulate the production of membrane versus secretory forms of immunoglobulin. These results indicate that regulation of isotypic patterns operate at levels other than immunoglobulin gene structure, and suggest that the secretory phenotype alone is inadequate as the measure of C-gene expression.

Spleen cells were exposed to either the T-independent mitogen lipopolysaccharide (LPS)⁸ or helper T cells which specifically activate a large set of B cells⁹. Activation of B cells under these two conditions results in two distinct patterns of γ -isotype secretion although activation of μ secretion is comparable in both cases. T-independent induction results in pre-dominant secretion of $\gamma 2b$ and $\gamma 3$, while helper cells induce primarily $\gamma 1$ and $\gamma 2a$, but here we have also studied the expression of membrane-bound immunoglobulins. As shown in Table 1, following T-independent induction, $\gamma 1$ is the pre-dominant membrane isotype, indicating a clear discrepancy between the expression and the secretion of this particular

isotype. The dissociation between expression of membrane and secretory form of $\gamma 1$ cannot be explained by different kinetics, as high frequencies of $\gamma 1$ -bearing blasts are observed from days 3 to 7 of culture. Passive adsorption of $\gamma 1$ on LPS blasts is unlikely because the concentration of this isotype in culture supernatants remains low (A.C. and L.F., in preparation), and therefore would require the presence of Fc receptors with exquisite specificity and high affinity for $\gamma 1$, which is not the case for B lymphocytes¹⁰. In contrast, no dissociation of membrane and secretory isotypes was observed after exposure to T helper cells.

We addressed the question of the fate of such LPS-induced, $\gamma 1$ -bearing cells, and of the mechanisms responsible for the dissociation between expression and secretion observed in LPS cultures. We attempted to correct the secretory defect of LPS-activated populations by exposure to specific T-cell help. LPS-activated blasts re-exposed to either LPS or to helper cells produce 3 days later quite distinct isotypes (Table 2). The T-dependent re-stimulation resulted in: the appearance of a high number of $\gamma 1$ secretors which are missing in LPS culture (the number of these is very close to the one of $\gamma 1$ -bearing cells in the starting population); decrease of $\gamma 3$ and $\gamma 2b$ secretors (although at values still higher than in helper cultures) and a significant increase of α plaque-forming cells (PFC). Note that in both cases a comparably high fraction (40%) of all recovered cells are high rate secretors and, of these, a similar proportion (57% and 56%) secrete γ ; both stimuli seem therefore to be equally competent in inducing switch and terminal maturation. The differences are isotype specific and relate to the quality of the stimulus controlling terminal maturation in the same population of activated cells.

To define further the specificity of the maturation signals, we analysed similar cultures both for cells expressing membrane-bound immunoglobulins and PFC. Table 3a shows that LPS is fully competent to induce $\gamma 3$ secretion, and ineffective with regards to $\gamma 1$ secretion. On the other hand, helper activity does induce $\gamma 1$ secretion. As, however, it also doubles the number of $\gamma 1$ -bearing blasts, LPS-activated, $\gamma 1$ -bearing blasts may remain nonsecretory in the presence of helper cells, which

Table 1 Isotype distribution of secreted and membrane-bound immunoglobulin molecules

C _H isotype	Isotype distribution (%) [*]			
	Cultures stimulated with LPS		Cultures stimulated with specific helper T cells	
	Secreted [†]	Membrane bound [‡]	Secreted [†]	Membrane bound [‡]
γ3	35.9	21.3	2.6	0.4
γ1	3.3	35.4	66.0	67.2
γ2b	51.1	27.0	4.6	9.1
γ2a	8.1	14.7	19.0	16.2
α	1.3	1.7	7.4	7.1

Normal spleen cells from C3H/Tif mice were cultured in RPMI medium supplemented with 5×10^{-5} M 2-mercaptoethanol, 10 mM glutamine, 10 mM HEPES, antibiotics and 20% fetal calf serum (Gibco) (5×10^5 ml⁻¹, 2 ml⁻¹ per culture). The cultures were stimulated with either $50 \mu\text{g ml}^{-1}$ lipopolysaccharide from *Salmonella abortus equi* (Difco) or 2×10^5 helper cells from C3H/HeJ anti-C3H/Tif cell lines that were established and maintained in continuous growth *in vitro* over the last 16 months by weekly stimulation with irradiated C3H/Tif spleen cells, according to methods previously described in detail¹⁹. The helper cells used in these experiments were from clones isolated by limiting dilution in suspension cultures which activate C3H/Tif spleen cells as described, but are MHC-restricted (unpublished), in contrast to uncloned lines reported before in this strain combination^{19,20}. The 'effector helper to target spleen cell' ratios used here (1:5) had previously been found optimal in these conditions.

^{*} The values are expressed as percentages of the total numbers of cells expressing the isotypes listed in the table. These are mean values of two independent experiments.

[†] Assays for secreting cells were performed after 6–7 days of culture when non-IgM PFC accounted for 50–60% of all PFC, representing 20–25% of all viable cells. Plaque-forming cells (PFC) were detected in a Protein A plaque assay using isotype-specific rabbit antisera^{21,22} raised by injection of purified myeloma proteins of the different isotypes.

[‡] Assays for membrane-bound isotypes were performed at days 3–4 of culture. Cells bearing membrane isotypes other than μ accounted for 25–30% of all cells. When tested in double staining with anti- μ , most cells were found also to bear IgM in conjunction with another C_H isotype. Rabbit antisera raised against purified myeloma proteins were made specific by adsorption of Sepharose-coupled myeloma proteins of different isotypes, as well as F(ab')₂ fragment prepared by pepsin digestion of total IgG from pooled mouse sera. The specificity of the antisera was assayed in solid-phase enzyme immunoassay²³. Conjugation with fluorochromes as well as staining for membrane-bound immunoglobulins was performed as described²⁴.

independently induce γ3-bearing cells to switch to γ1 expression and secretion, thus accounting for the disappearance of γ3 producers on the whole. To distinguish between the two possibilities we examined single cells for the presence of membrane-bound and intracytoplasmic immunoglobulins by double immunofluorescence. This was done soon after restimulation because with the half lives of message and proteins, it should be possible to determine the isotype persisting on the membrane of cells that were newly activated to secretion. Table 3b shows that about half of the γ1-bearing blasts, which in this short period had not greatly increased in number, had been activated to produce intracytoplasmic γ1 by helper cells. This resulted in a proportion of secretors, out of the total γ1 population, which is one order of magnitude higher than in parallel LPS

cultures. The switch from γ3 to γ1, measured as cells with intracytoplasmic γ1 and membrane γ3, was proportionally more frequent in LPS than in helper cell-stimulated cultures. On the other hand, the decay of γ3 cells, both membrane-positive and secretors, was observed after 20 h of restimulation. As the proportion of secretors out of the total γ3 population remains unaffected, the decay of γ3-producing cells can only be explained by inability of helper cell signals, in contrast to LPS, to maintain proliferation and/or viability of γ3-bearing cells and to activate them to secretion. Preliminary experiments indicate that comparable results can be obtained with supernatants of the T-cell clones used in these experiments, which suggests that neither of the T-cell effects, induction of γ1 secretion and inability to support γ3 production, requires cell-to-cell contact.

To confirm that γ1 secretors in helper cell-restimulated cultures derive from γ1-bearing blasts present in LPS cultures, positive selection in a fluorescence-activated cell sorter (FACS II) was carried out. As shown in Table 4, a large number of γ1 high-rate secretors were induced within 15 h by T helper cells in the γ1-enriched but not in the γ1-depleted population, indicating that few, if any γ1 PFC are newly derived from either μ or γ3 to γ1 switches. As the majority of the γ1-bearing blasts in LPS cultures switched from μ (and δ) production after mitogen stimulation (only 2% or less of spleen cells are γ1 positive) we conclude that thymus-independent B-cell activation can induce switches to γ1 expression but is very inefficient in activating γ1 secretion. This operates in a strict C-gene specific manner, because the mitogen is fully competent to induce secretion not only of γ3, but also of γ2b and γ2a, which are coded by genes located distally from γ1. Table 4 also shows that helper cells are much less efficient than LPS in inducing γ3 secretion in the γ1-depleted population and this, in view of the short subculture period, is unlikely to be the result of preferential survival or expansion of γ3 cells in LPS cultures.

The present observations show that measurements of antibodies and secreting cells is insufficient when considering C-gene expression. They also point out that isotype commitment in antibody responses^{1–3} is regulated at levels other than DNA rearrangements and gene structure. In the example described here, the regulation of membrane-versus-secretory forms of immunoglobulins is intimately connected to the control of terminal maturation to high-rate secretion and dependent on the quality of the activating signal. It has been known for some time that the carboxy terminus of membrane μ is encoded in a separate exon, distinct from the C μ 4 domain¹¹, and it is now established that all other C_H genes exhibit the same type of structure^{12–14}. Models based on differential nuclear RNA splicing and/or selective termination of transcription, as well as post-translational controls, have been proposed to explain the production of membrane-bound or secretory heavy chains. The physiological mechanisms regulating these processes are unknown, but the present experiments prove the existence of

Table 2 Differential effects of LPS and helper T cells on secretion of γ isotypes

	PFC per 10 ⁵ B cells [*]						Total PFC	Total non-IgM PFC
	μ	γ3	γ1	γ2b	γ2a	α		
Input cells	12,214	292	62	699	211	84	13,462	1,348
(day 3 LPS blasts)	(ND)	(5,900) [†]	(10,400)	(5,800)	(3,200)	(ND)		
Subculture with LPS	15,927	5,236	211	11,345	4,282	44	37,045	21,118
Subculture with TH	18,391	1,242	10,881	7,645	3,434	479	42,072	23,681
Isotype distribution (%)								
Input cells	90	2	0.5	5	2	0.5		
Subculture with LPS	43	14	0.5	31	12	0.1		
Subculture with TH	44	3	26	18	8	1		

C3H/Tif spleen cell cultures were stimulated with LPS and assayed after 3 days of culture for the presence of membrane-bound immunoglobulins by immunofluorescence and of plaque-forming cells of different C_H isotypes (see Table 1 legend). Such 3-day LPS blasts were then subcultured in Microtitre II plates (Falcon) at 2×10^4 cells in 0.2-ml cultures in the same medium with either LPS ($50 \mu\text{g ml}^{-1}$) or with C3H/HeJ anti-C3H/Tif helper cells (4×10^3 per culture) and isotype-specific PFC were determined after an additional 3 days of culture.

^{*} The values are expressed per 10⁵ initial cells, and per 10⁵ recovered cells, to facilitate the comparison between the results obtained with the different assays. The total number of B cells recovered per culture was very similar after exposure to LPS or to T helper cells (1.8 ± 0.2 and $1.65 \pm 0.18 \times 10^5$ respectively).

[†] Figures in parentheses represent the number of cells in the starting population positive on the membrane by immunofluorescence. ND, not determined.

Table 3 Effect of LPS and T helpers on expression and secretion of $\gamma 3$ and $\gamma 1$

a	LPS day 3	% Blasts in culture		3 days LPS +3 days TH
		3 days LPS	3 days LPS	
$\gamma 3$ membrane	5.8	3.1	0.35	
$\gamma 3$ PFC	0.5	5.3	0.45	
$\gamma 1$ membrane	10.4	9.1	20.4	
$\gamma 1$ PFC	0.4	0.35	8.9	

b	LPS		% Blasts in culture		TH	
	day 3	day 4	3 days LPS +1 day LPS	3 days LPS +1 day TH	day 3	day 4
$\gamma 3$ membrane	2.5	6.6	7.0	2.0	0.1	0.1
$\gamma 3$ membrane	ND	3.4	3.6	1.5	ND	0.05
$\gamma 3$ cytoplasm	ND	0.85	0.9	0.95	ND	0.05
$\gamma 1$ membrane	5.7	8.6	7.1	8.1	12.5	15.6
$\gamma 1$ membrane	ND	0.3	0.3	4.3	ND	11.4
$\gamma 1$ cytoplasm	ND	0.3	0.3	4.3	ND	11.4

Proportion of secretors out of the total membrane-positive population						
$\gamma 3$	—	0.51	0.51	0.75	—	—
$\gamma 1$	—	0.035	0.042	0.53	—	0.73

Day 3 LPS blasts subcultured with either LPS or T helper cells (TH) and assayed in the conditions described in the legends to Tables 1 and 2. *a*, 3 days subculture. Separate samples of the same cultures were stained by immunofluorescence for membrane-bound immunoglobulins, or assayed for $\gamma 3$ and $\gamma 1$ PFC. *b*, 20 h subculture. The same cell samples were stained by double immunofluorescence for membrane-bound and intracytoplasmic $\gamma 3$ and $\gamma 1$ (ref. 24). ND, not determined.

Table 4 Early effects (15 h subculture) of LPS and T helper cells on secretion of $\gamma 3$ and $\gamma 1$ by selected membrane $\gamma 1^+$ and $\gamma 1^-$ LPS blasts

Cell population	Isotype of PFC	PFC per 10^5 recovered cells Mitogen in subculture		
		None	LPS	T helper cells
Membrane $\gamma 1^+$	$\gamma 1$	915	900	6,450
LPS blasts	$\gamma 3$	375	550	300
Membrane $\gamma 1^-$	$\gamma 1$	<15	<15	300
LPS blasts	$\gamma 3$	650	9,150	2,750

Day 3 LPS-activated blasts were stained with fluorescein-labelled anti- $\gamma 1$ and separated in the fluorescence-activated cell sorter (Becton and Dickinson FACS II). The $\gamma 1^+$ and $\gamma 1^-$ populations represent the 10% brightest and 10% dimmest cells, respectively. Conditions of primary and secondary cultures and assays were as described in the legends to Tables 1 and 2.

such controls and demonstrate that they are C-gene specific.

Our results stress that such C-gene specificity concerns terminal maturation (high rate production of secretory form), and not switch, as implied before¹⁻⁵ and might operate independently of whether the cell has undergone¹⁵⁻¹⁷ a switch recombination or not¹⁸. Whatever the precise mechanism involved here, it is clear and quite astonishing that the ability to produce the secretory form of immunoglobulins is related to the quality of the activating signal in a C-gene specific manner. As we have studied polyclonal B-cell responses that proceed independently of immunoglobulin (V-region) specificity, it is likely that such C-gene specific regulation is mediated by cellular structures other than immunoglobulin receptors.

The Basel Institute for Immunology was founded and is supported by Hoffmann-La Roche, Basel. This work was partly supported by the Swedish MRC. We thank Ms M. Tuneskog for technical help, Ms W. Breisinger and Ms M. Bühler for typing the manuscript, all participants in the Second Umeå Seminar on Immunobiology for discussion, and Chris Paige for critical reading of the manuscript.

Received 29 March; accepted 22 July 1982.

- Pearlmuter, R. M. *et al.* *J. exp. Med.* **149**, 993-998 (1979).
- Slack, J., Der-Balian, G. P., Nahm, M. & Davie, J. M. *J. exp. Med.* **151**, 853-862 (1980).
- Mongini, P. K. A., Stein, K. E. & Paul, W. E. *J. exp. Med.* **153**, 1-12 (1981).
- Martinez-A. C., Coutinho, A. & Augustin, A. A. *Eur. J. Immun.* **10**, 698-702 (1980).
- Martinez-A. C. & Coutinho, A. *Eur. J. Immun.* (in the press).
- Kataoka, T., Kawahara, T., Takahashi, N. & Honjo, T. *Proc. natn. Acad. Sci. U.S.A.* **77**, 919-923 (1980).
- Roeder, W., Maki, R., Traunecker, A. & Tonegawa, S. *Proc. natn. Acad. Sci. U.S.A.* **78**, 474-478 (1981).
- Andersson, J., Sjöberg, O. & Möller, G. *Transplant. Rev.* **11**, 131-177 (1972).
- Augustin, A. A. & Coutinho, A. *J. exp. Med.* **151**, 587-598 (1980).
- Dickler, H. P. *Adv. Immun.* **24**, 167-214 (1976).
- Early, P. *et al.* *Cell* **20**, 313-319 (1980).
- Tyler, B. M., Cowmann, A. F., Adams, J. M. & Harris, A. W. *Nature* **293**, 406-408 (1981).
- Maki, R. *et al.* *Cell* **24**, 353-365 (1981).
- Tucker, P. W., Liu, C., Mushinski, J. F. & Blattner, F. R. *Science* **206**, 1353-1360 (1980).
- Sakano, H., Maki, R., Kurosawa, Y., Roeder, W. & Tonegawa, S. *Nature* **286**, 676-683 (1980).
- Takahashi, N., Kataoka, T. & Honjo, T. *Gene* **11**, 117-217 (1980).
- Liu, C.-P., Tucker, P. W., Mushinski, G. F. & Blattner, F. R. *Science* **209**, 1348-1353 (1980).
- Alt, F. W., Rosenberg, N., Casanova, R. J., Thomas, E. & Baltimore, D. *Nature* **296**, 325-331 (1982).
- Coutinho, A. & Augustin, A. A. *Eur. J. Immun.* **10**, 535-541 (1980).
- Coutinho, A., Augustin, A. A., Forni, L. & Fischer Lindahl, K. *J. Immun.* **127**, 21-25 (1981).
- Gronowicz, E., Coutinho, A. & Melchers, F. *Eur. J. Immun.* **6**, 588-590 (1976).
- Bernabé, R. R. *et al.* *Immun. Meth.* **2**, 187-197 (1981).
- Engvall, E. & Perlmann, P. *Immunochimistry* **8**, 871-874 (1971).
- Forni, L. *Immun. Meth.* **1**, 151-167 (1979).

An adenovirus glycoprotein binds heavy chains of class I transplantation antigens from man and mouse

Christer Signäs, Michael G. Katze*, Håkan Persson* & Lennart Philipson*

Department of Microbiology, University of Uppsala, The Biomedical Center, Box 581, S-751 23 Uppsala, Sweden

The successful killing of virus-infected cells by cytotoxic T lymphocytes (CTL) is dependent on the recognition of both a viral product and class I antigens of the major histocompatibility complex (MHC) on the infected cell surface¹⁻⁹. Whether these two entities are found independently on the cell surface and therefore recognized by two different CTL receptors, or whether they are associated together and can therefore be recognized by a single receptor is not known¹⁰. The association between an adenovirus-encoded glycoprotein expressed on the cell surface early after infection and class I antigens has been investigated and it has been found that antisera against class I antigens can co-precipitate the antigen and the viral glycoprotein from an adenovirus-transformed cell line from the Hooded-Lister rat strain^{11,12}. We show here by *in vitro* affinity chromatography and *in vivo* immunoprecipitation that the viral glycoprotein specifically binds to the heavy chain of class I antigens in both man and mouse.

An adenovirus glycoprotein E3/19K (ref. 13), encoded in region 3 of the adenovirus genome, is found soon after infection. When the glycoprotein fraction from cytoplasmic extracts of infected HeLa cells or a human adenovirus-transformed epithelial cell line (293)¹⁴ superinfected with adenovirus type 2 (Ad2) was immunoprecipitated with anti-HLA antisera both the E3/19K and the heavy chain of the HLA were immunoprecipitated in infected but not in uninfected cells (Fig. 1). From counting the radioactivity in the bands it appears that the two moieties are present in almost equimolar amounts and that most of the HLA chains are bound to E3/19K (not shown). However, in productive infection with Ad2 the E3/19K is overproduced and only around 5-10% of the viral glycoprotein

*Present addresses: Molecular Biology and Genetics, Unit of the Graduate School, Memorial Sloan-Kettering Cancer Center, New York, New York 10021, USA (M.G.K.); Laboratory of Molecular Genetics, National Institute of Child Health, and Human Development, Bethesda, Maryland 20205, USA (H.P.); European Molecular Biology Laboratory, Postfach 10-2209, D-6900 Heidelberg, FRG (L.P.).

is associated with the class I antigens but in transformed rat cells more than 80% of the viral E3/19K is associated with the class I antigen¹¹. Control experiments showed that artificial mixtures of purified E3/19K and cells did not result in co-precipitation of the complex. The E3/19K protein can thus bind strongly to human transplantation antigen *in vivo* as previously demonstrated for the class I antigen of rats^{11,12}. Given these results we analysed whether this complex could also be formed *in vitro*. Purified E3/19K (Fig. 2h) was coupled to CNBr Sepharose 4B. The glycoprotein fraction from ³⁵S-methionine-labelled cytoplasmic extracts from two human established lymphoid cell lines (Ingemar B7 and IM-199), which express mainly the class I antigens B7 and A2, were passed over the column. A column prepared with coupled bovine serum albumin (BSA) was the control. Figure 2 shows that a polypeptide of the same molecular weight as the heavy chain of the HLA-B7 allotype specifically bound to the E3/19K column but not to the BSA column. This polypeptide represents the heavy chain of the HLA as revealed by immunoprecipitation (Fig. 2e). It can also be seen that the amount of this polypeptide

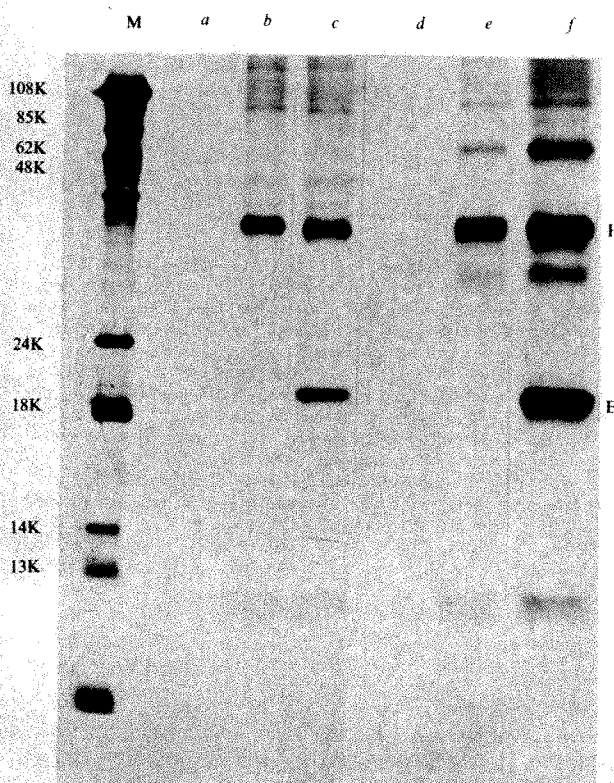


Fig. 1 Immunoprecipitation from uninfected and adenovirus-infected HeLa and 293 cells with anti-HLA serum. Suspension cultures of HeLa cells were labelled overnight with ³⁵S-methionine (10 μ Ci ml⁻¹) to enhance labelling of the class I MHC antigens, in methionine-free spinner medium (M) supplemented with 2.5% normal medium and 7% calf serum. Monolayers of 293 cells were labelled similarly using Eagle's medium and 10% fetal calf serum. The cells were washed twice and infected with adenovirus type 2 (ref. 18). Cycloheximide (25 μ g ml⁻¹) was added 2 h post-infection and removed 3 h later in order to enhance early viral mRNA accumulation¹⁹. The cells were then labelled for an additional 3 h with ³⁵S-methionine (10 μ Ci ml⁻¹) in the presence of cytosine arabinoside (25 μ g ml⁻¹). The cells were washed in phosphate-buffered saline (PBS) and lysed in 0.5% NP40, 150 mM KCl, 1.5 mM MgCl₂, 10 mM Tris-HCl pH 8.0. The cytoplasmic extracts (2 ml from 2×10^8 cells) were passed over a lentil lectin Sepharose column (4 ml) (Pharmacia) equilibrated with PBS, 0.1% Triton X-100, 1 mM phenylmethylsulfonyl fluoride (PMSF) (buffer A). Elution was performed with buffer A containing 0.1 M α -methylmannoside. The glycoprotein eluate was immunoprecipitated after preprecipitation with an unrelated immune complex and analysed on 13% SDS-polyacrylamide gels²⁰. The anti-HLA serum used was a mixture of a monoclonal antiserum that recognizes HLA-A, -B or -C antigens²¹ and a rabbit antiserum made against papain-solubilized HLA. Lanes a, d, immunoprecipitation with normal rabbit serum; b, c, e and f, immunoprecipitation with anti-HLA serum. a, c, infected HeLa cells; b, uninfected HeLa cells. d, f, infected 293 cells; e, uninfected 293-cells. In this and subsequent figures ³⁵S-labelled adenovirus proteins were used as size markers M.

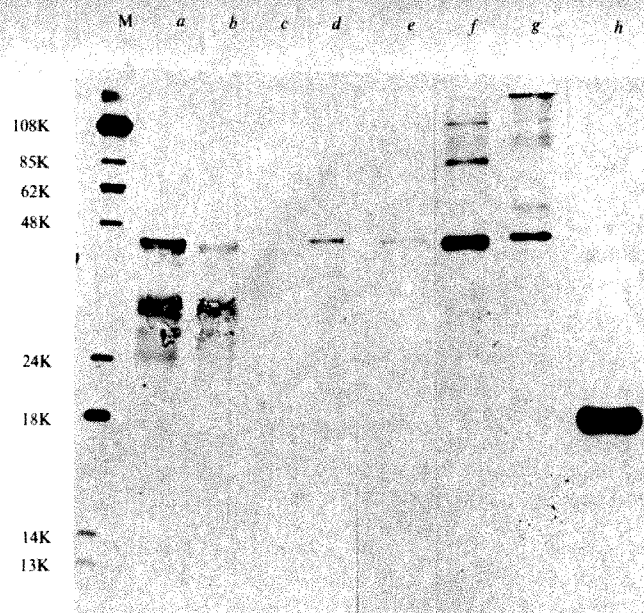


Fig. 2 Affinity chromatography of human class I antigens on the adenovirus glycoprotein. The adenovirus E3/19K protein (100 μ g) or bovine serum albumin (100 μ g) was coupled to 1 ml cyanogen bromide-activated Sepharose 4B (Pharmacia). Two different lymphoid cell lines, HLA-A2 and HLA-B7, were labelled overnight with ³⁵S-methionine (10 μ Ci ml⁻¹), cytoplasmic extracts were prepared, and the glycoproteins isolated by lentil lectin chromatography as described in Fig. 1 legend except that 2 mM dithiothreitol (DTT) was included in the buffers. The lentil lectin eluate was dialysed against buffer A (see Fig. 1), divided in two aliquots and passed over the BSA and the E3/19K columns respectively at 4 °C. The columns were washed thoroughly and eluted with buffer A containing 2 M NaCl and 2 mM DTT. Each fraction was analysed by SDS-polyacrylamide gel electrophoresis and immunoprecipitated as described in Fig. 1 legend. a, Percolate of HLA-B7 from the BSA column; b, percolate of HLA-B7 from the E3/19K column; c, eluate BSA column; d, eluate E3/19K column; e, eluate from E3/19K column immunoprecipitated with anti-HLA serum. No precipitate was observed with normal serum. f, g Show the percolate and eluate fractions of HLA-A2 glycoproteins; h, purified E3/19K. The size marker M is described in Fig. 1 legend.

is decreased in the eluate of the E3/19K column compared with the BSA column. The same results were obtained with the HLA-A2 cells (Fig. 2f, g). These results suggest that the E3/19K can specifically bind to different allotypes of the class I transplantation antigens of man.

We also examined *in vitro* binding of mouse class I antigens using the cell line YAC1 (H-2^a derived from a H-2^k/H-2^d hybrid). Figure 3 shows that a polypeptide of a similar size to that from humans specifically bound to the E3/19K column. Immunoprecipitation with anti-H-2-serum established that this polypeptide corresponded to the heavy chain of the H-2 antigen (not shown). It appears therefore, that the binding of E3/19K to the heavy chain class I transplantation antigens does not show species specificity.

To localize the site of interaction between the two molecules we attempted to perform enzymatic digestions of plasma membranes in order to release the complex. The heavy chain of the class I antigens can be released from membranes with papain, creating the 32,000 (32K) and 34,000 (34K) molecular weight (M_r) subspecies¹⁵. However, papain treatment of infected HeLa cells could not release a complex containing both moieties when analysed by immunoprecipitation with anti-HLA serum. Instead the viral glycoprotein remains in the plasma membrane pellet together with uncleaved or partially cleaved antigen (Fig. 4). The use of an affinity chromatography column with papain released fragments of the human HLA-B7 antigen confirmed this. Figure 4b demonstrates that very few papain fragments are bound to the E3/19K column even though the columns were loaded with material carrying eight times more radioactivity than in the previous experiments. These results suggest that the major interaction occurs either close to the cell membrane or on the cytoplasmic side of the membrane but a

configurational change in the papain fragments cannot be excluded. It is also possible that nonspecific hydrophobic interactions occur between the proteins where they penetrate the membrane, but we consider this unlikely as Triton X-100 was used in all the buffers and a nonspecific interaction may not give the selectivity observed.

If a cytoplasmic interaction guides the complex formation, considerable variation in this region of the transplantation antigens could account for the diversity in CTL recognition. Recent analyses of the genomic structure of the HLA and H-2 genes indeed suggest that the cytoplasmic portions of the class I transplantation antigens are complex and contain at least three exons with varying splice patterns for the H-2 genes^{16,17}.

The strong complex formation between adenovirus glycoprotein and the transplantation antigens appears to be unique among the viral systems investigated so far. The influenza virus haemagglutinin⁹, the vesicular stomatitis virus glycoprotein⁵ and several other identified virus determinants for the T-cell mediated cytotoxicity⁵⁻⁹ do not appear to be co-precipitated with the heavy chain of the class I antigens. The adenovirus system, including the mouse adenovirus, where an S-antigen is firmly complexed to the class I transplantation antigens of the mouse⁸, may therefore be a model for the altered self hypothesis of virus-induced T-cell cytotoxicity. We have previously demonstrated that this complex in rat cells is recognized by syngeneic rat cytotoxic T cells and that this reaction can be inhibited by syngeneic antibodies to the cells and allogeneic

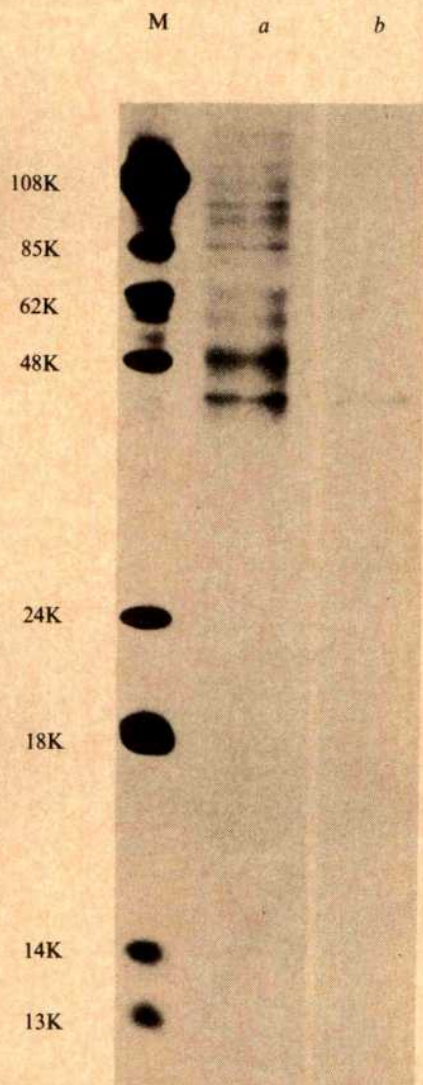


Fig. 3 Affinity chromatography of mouse class I antigens on the adenovirus glycoprotein. A labelled cytoplasmic extract from the YAC (H-2^{kd}) cells was treated exactly as in Fig. 2. *a*, Percolate from the E3/19K column; *b*, eluate. The size marker M is described in Fig. 1 legend.

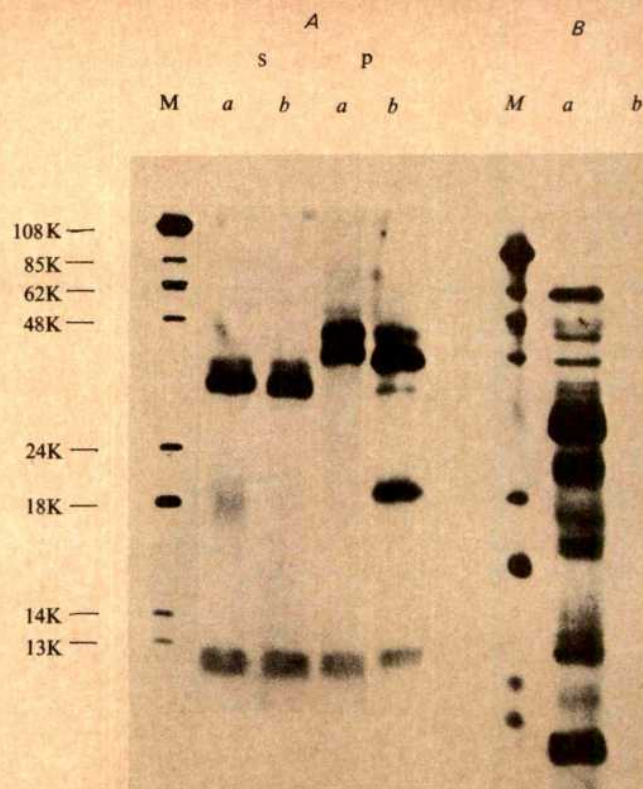


Fig. 4 Immunoprecipitation of papain-treated membranes from infected and mock-infected HeLa cells (*a*) and affinity chromatography of papain-released HLA-B7 on the E3/19K column (*b*). HeLa cells were labelled and infected as described in Fig. 1 legend. The cells were collected by centrifugation and membrane preparation and papain treatment was performed as previously described²². The supernatant after papain digestion was dialysed against PBS, 1% Triton X-100, 1 mM PMSF and immunoprecipitated. The pellet was dissolved in PBS, 1% Triton X-100, 1 mM PMSF by stirring overnight at 4 °C. The dissolved pellet was also immunoprecipitated and the samples were analysed by SDS-gel electrophoresis. HLA-B7 cells were labelled as described in Fig. 1 legend. Membrane preparation and papain treatment was performed as described above. The supernatant after papain treatment was dialysed against PBS, 0.1% Triton X-100, 1 mM PMSF and added to the E3/19K column was described in Fig. 2 legend. *A*, Immunoprecipitation with anti-HLA serum from the supernatant (*s*) and pellet (*p*) after papain digestion of HeLa cells; *a*, uninfected; *b*, infected cells. *B*, Affinity chromatography on E3/19K protein column. Lane *a*, percolate, and lane *b*, high salt eluted fraction. The size marker M is described in Fig. 1 legend.

antibodies to the class I transplantation antigen¹². By using the complexes, which are retained on the affinity columns, as immunogen for the production *in vivo* of both specific antibodies and cytotoxic T cells, we hope to be able to define the T-cell receptor and the role of the CTL in virus infection.

We thank B. M. Johansson for technical assistance and Marianne Gustafson for secretarial help. The HLA and H-2 antisera were provided by Drs W. Bodmer and P. Peterson. We also thank Dr J. Andersson, for the YAC-1 cell line and critical comments. M.G.K. was supported by a postdoctoral fellowship from the EMBO. This work was supported by grants from the Swedish MRC and the Swedish Society against Cancer.

Received 5 April; accepted 5 July 1982.

1. Paul, W. E. & Benacerraf, B. *Science* **195**, 1293-1300 (1977).
2. Zinkernagel, R. M. & Doherty, P. C. *Adv. Immun.* **27**, 51-177 (1979).
3. Doherty, P. C., Blanden, R. V. & Zinkernagel, R. M. *Transplant. Rev.* **29**, 89-123 (1976).
4. Langman, R. E. *Rev. Physiol. Biochem. Pharmac.* **81**, 1-37 (1978).
5. Hale, A. H., Witte, O. N., Baltimore, D. & Eisen, H. N. *Proc. natn. Acad. Sci. U.S.A.* **75**, 970-974 (1978).
6. Lawman, M. J. P. *et al. Infect. Immunity* **30**, 451-461 (1980).
7. Finberg, R., Weiner, H. L., Burakoff, S. J. & Fields, B. N. *Infect. Immunity* **31**, 646-649 (1981).
8. Inada, T. & Uetake, H. *Microbiol. Immun.* **24**, 525-535 (1980).
9. Effros, R. B., Doherty, P. C., Gerhard, W. & Bennink, J. J. *exp. Med.* **145**, 557-568 (1977).
10. Zinkernagel, R. M. & Doherty, P. C. *Cold Spring Harb. Symp. quant. Biol.* **41**, 505-510 (1977).
11. Persson, H., Kvist, S., Östberg, L., Peterson, P. A. & Philipson, L. *Cold Spring Harb. Symp. quant. Biol.* **44**, 509-517 (1980).

12. Kvist, S., Östberg, L., Persson, H., Philipson, L. & Peterson, P. A. *Proc. natn. Acad. Sci. U.S.A.* **75**, 5674–5678 (1978).
13. Persson, H., Jansson, M. & Philipson, L. *J. molec. Biol.* **136**, 375–394 (1980).
14. Graham, F. L., Smiley, J., Russell, W. C. & Nairn, R. J. *gen. Virol.* **36**, 59–72 (1977).
15. Krangel, M. S., Orr, H. T. & Strominger, J. L. *Scand. J. Immun.* **11**, 561–571 (1980).
16. Malissen, M., Malissen, B. & Jordan, B. R. *Proc. natn. Acad. Sci., U.S.A.* **79**, 893–897 (1982).
17. Steinmetz, M. *et al. Cell* **25**, 683–692 (1981).
18. Persson, H., Öberg, B. & Philipson, L. *J. Virol.* **28**, 119–139 (1978).
19. Craig, E. A. & Raskas, H. J. *J. Virol.* **14**, 26–32 (1974).
20. Hérisse, J., Courtois, G. & Galibert, F. *Nucleic Acids Res.* **8**, 2173–2192 (1980).
21. Barnstable, C. J. *et al. Cell* **14**, 9–20 (1978).
22. Turner, M. J. *et al. J. biol. Chem.* **250**, 4512–4519 (1975).

Molecular cloning of the gene for human anti-haemophilic factor IX

K. H. Choo, K. G. Gould, D. J. G. Rees & G. G. Brownlee

Sir William Dunn School of Pathology, University of Oxford, South Parks Road, Oxford OX1 3RE, UK

A functional deficiency of factor IX, one of the coagulation factors involved in blood clotting¹, leads to the bleeding disorder known as Christmas disease², or haemophilia B. Both this disease and haemophilia A (factor VIII (C) deficiency) are X chromosome-linked and together occur at a frequency of ~1 in 10,000 males. The molecular basis for the functional alteration of factor IX in Christmas disease is not clearly understood. As a first step towards the elucidation of the molecular events involved, we have attempted molecular cloning of the factor IX gene. We used a bovine factor IX cDNA clone, isolated using synthetic oligonucleotides as probes, to screen a cloned human gene library. Here we report the isolation and partial characterization of a λ recombinant phage containing the human factor IX gene.

As a first step in the isolation of a cDNA clone for bovine factor IX, bovine liver was used to prepare total mRNA by the guanidine hydrochloride method³. A preparation enriched in factor IX-specific mRNA was obtained by oligo (dT)-cellulose chromatography, followed by two successive separations by sucrose gradient centrifugation. The enrichment was monitored by a specific immunological assay based on cell-free translation using rabbit reticulocyte lysates (Fig. 1). A sucrose gradient fraction sedimenting at 20–22S was found to be enriched (about 10-fold) for the bovine factor IX mRNA, and was therefore used in the following cloning experiments.

Synthetic oligonucleotides were used⁴ to produce a cloned cDNA library. From the available amino acid sequence data for bovine factor IX⁵, two different sets of oligonucleotides were synthesized. The first set [designated oligo (N-1)] was deduced from the amino acid sequence residues 348–352 (His-Met-Phe-Cys-Ala) and was synthesized, using the solid phase phosphotriester method⁶, as a mixture of eight different sequences (5'-GC₆CA₆AACAT₆TC-3'). The second set of oligonucleotides [oligo (N-2)] was deduced from amino acids 70–75 (Glu-Cys-Trp-Cys-Gln-Ala); this was synthesized as two mixtures of eight different sequences each (5'-GCTTG₆CACCA₆CA₆TC-3' and 5'-GCCTG₆CACCA₆CA₆TC-3').

From a knowledge of the concentration of factor IX in blood plasma (~2–4 $\mu\text{g ml}^{-1}$) and of the amount of ³⁵S-cysteine counts precipitable by anti-factor IX antibodies, the abundance of factor IX mRNA was estimated to be as low as 0.01%. Therefore, to achieve further enrichment for factor IX mRNA, oligo (N-1) was used as a primer to synthesize cDNA from the sucrose gradient-enriched poly(A)-mRNA preparation. A library of 7,000 colonies was prepared and screened using ³²P-labelled oligo (N-2) (see Fig. 2 legend). One colony (designated BIX-1) gave a positive hybridization signal above background. Characterization of this colony by restriction endonuclease cleavage

(data not shown) indicated that it contained a DNA insert of ~430 base pairs (bp). Figure 2 shows part of the nucleotide sequence, that is, 304 residues of the BIX-1 insert, and confirms that it is a bovine factor IX sequence. It is interesting that only part of the insert sequence (amino acid residues 52–139) corresponds directly to the nucleotide sequence predicted from the known bovine amino acid sequence data⁵. Over this region, there are no discrepancies between BIX-1 and the published data for factor IX, except at nucleotides 38–40 which code for Asp instead of Thr. This amino acid change was also observed in a second, independent cDNA clone. (This latter clone, which

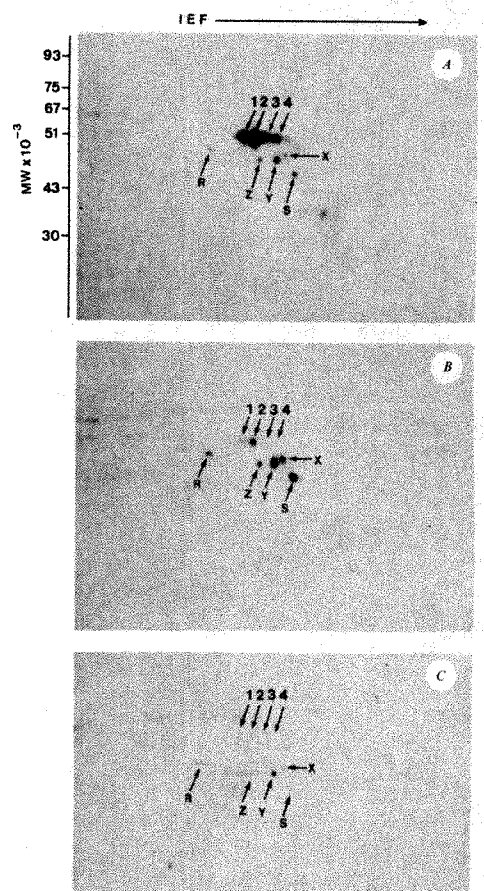


Fig. 1 Two-dimensional polyacrylamide gel electrophoretic analysis of immunoprecipitated cell-free translation products of bovine liver mRNA. mRNA purified through an oligo (dT)-cellulose column¹¹ was translated in a rabbit reticulocyte cell free system¹² in the presence of ³⁵S-cysteine. After incubation at 29°C for 90 min, samples were treated for immunoprecipitation as described previously¹³. Crude antiserum against pure bovine factor IX was raised in rabbit. Specific anti-factor IX immunoglobulins used for immunoprecipitation were purified as described previously¹⁴ by passage of the crude antiserum through a Sepharose 4B column to which pure bovine factor IX had been coupled. After incubation, the antibody-antigen complex was precipitated by the addition of protein A-Sepharose CL-4B resin (Pharmacia), washed and resolved on a two-dimensional polyacrylamide gel¹⁵. A, immunoprecipitation was performed in the presence of purified antibodies; B, same as for A, except that immunoprecipitation was performed in the presence of both antibodies and a competing amount of unlabelled pure bovine factor IX; C, same as for A, except that immunoprecipitation was performed in the presence of a control antiserum from a rabbit which had not been immunized with factor IX. 1–4, Factor IX polypeptide spots; evidence for this comes from the fact that (1) these are the predominant spots immunoprecipitated by the specific antibody; (2) their molecular weight (~50,000, a single polypeptide chain plus a possible pre-peptide signal sequence) is compatible with published data⁵; (3) the spots are specifically competed for by pure factor IX; and (4) they are absent from the gel when control serum is used. (Partial chymotryptic digestion of polypeptide spots 1 and 2 (data not shown) suggests that they are related and may have arisen as a result of post-translational modification; the amount of material recovered from spots 3 and 4 was insufficient for these to be compared.) R, S, X, Y, and Z designate nonspecific background polypeptide spots which form useful reference points on the two-dimensional gel. The molecular weights (MWs) of the polypeptide markers on the second dimension gel are shown on the left. IEF designates isoelectric focusing in the first dimension¹³, SDS, polyacrylamide gel electrophoresis in the second dimension¹³.

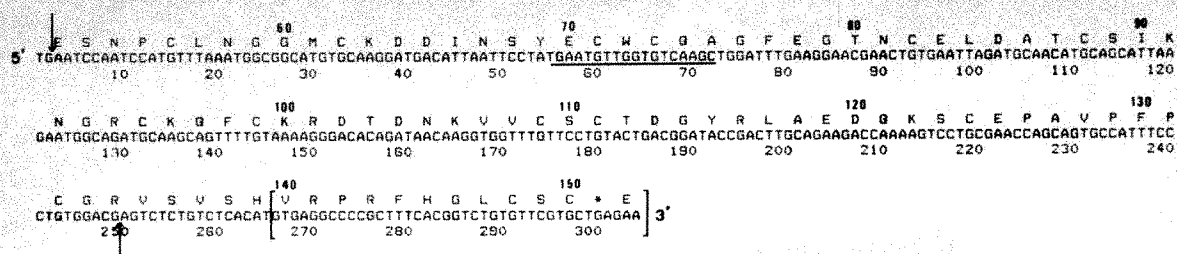


Fig. 2 Isolation and characterization of bovine BIX-1 clone. A library of clones containing bovine cDNA inserts was prepared as follows. First, cDNA strands were synthesized as described elsewhere¹⁵ except that 2 μ g of oligo (N-1), 20–30 μ g of sucrose gradient-enriched poly (A)⁺ mRNA, 10 μ Ci [α -³²P]dATP (3,000 Ci mmol⁻¹; Amersham) and 50 U of reverse transcriptase were used in a 50 μ l reaction mixture. The cDNA was phenol-extracted, desalted on a Sephadex-G100 column, then treated with alkali (0.1M NaOH, 1mM EDTA) at 60 °C for 30 min to remove the mRNA strand. Second strand DNA was synthesized as described elsewhere¹⁵. The double-stranded DNA was then cleaved with the restriction enzyme *Mbo*I and ligated to pBR322 which had been cut with *Bam*HI and treated with calf intestinal alkaline phosphatase to minimize vector self-religation. The ligated DNA was used to transform *Escherichia coli* strain MC1061 (ref. 16). A library of 7,000 ampicillin-resistant colonies was obtained. Of these, ~85% were tetracycline-sensitive. The library of colonies were transferred in an unordered fashion to 13 Whatman 541 filter papers, amplified with chloramphenicol, and prepared for hybridization as described by Gergen *et al.*¹⁷. The filters were prehybridized at 65 °C for 4 h in 6 \times NET, 5 \times Denhardt's, 0.5% NP-40 and 1 μ g ml⁻¹ yeast RNA described by Wallace *et al.*⁴. Hybridization was at 47 °C for 20 h in the same solution, containing 3 \times 10⁵ c.p.m. (0.7 ng) ml⁻¹ of labelled oligo (N-2) probe. Labelling was achieved by phosphorylating the oligonucleotides at the 5' hydroxyl end using [γ -³²P]ATP and T₄ phosphokinase (Boehringer)¹⁸. At the end of the hybridization, filters were washed successively at 0–4 °C (2 h), 25 °C (10 min), 37 °C (10 min) and 47 °C (10 min). On fluorography of the filters from this screening, one colony showed a positive signal above background; this clone was designated BIX-1 and part of the DNA insert was characterized by sequencing performed according to Maxam and Gilbert⁸. Only the coding strand is shown and this is numbered in the opposite orientation to the tetracycline resistance gene of the plasmid. The deduced amino acid sequence (top row) has been numbered according to Katayama *et al.*⁵. The 5' *Sau*3AI cloning site in the BIX-1 clone is eight nucleotides to the left of the start of the above sequence. The arrows indicate two *Hinf*II sites which give rise to a 247-nucleotide fragment (see text). Brackets indicate the start of a sequence which does not correspond to published amino acid data* (see text). The region corresponding to the oligo (N-2) probe is underlined. * Designates a nonsense codon. IXNET is 0.15 M NaCl, 1 mM EDTA, 15 mM Tris-chloride, pH 7.5.

has a DNA insert spanning nucleotides 7–108 as shown in Fig. 2, was isolated using the procedure described for the BIX-1 clone, except that oligo (dT)_{12–18} was used to initiate cDNA synthesis, and the cloned cDNA library was prepared following the homopolymer tailing method of Roychoudhury and Wu⁷. The origin of the adjacent sequence starting at residue 140 (see Fig. 2) which codes for an amino acid sequence unrelated to factor IX is not clear.

A DNA fragment (see Fig. 3 legend) was isolated from the bovine BIX-1 clone and used as a hybridization probe to screen a cloned human gene library; a positive clone, λ HIX1b, was isolated and characterized by restriction endonuclease cleavage and Southern blotting (see Fig. 3). From these results, a partial restriction map for λ HIX1b was constructed (Fig. 4A). A segment of the DNA insert containing the region that hybridizes to the bovine cDNA probe, was identified and isolated for

direct sequencing⁸. The results (Fig. 4B) reveal that, for the 96 nucleotides determined, there is 85% nucleotide sequence homology between λ HIX1b and bovine factor IX. Comparison of the amino acid sequences deduced from the nucleotide sequences shows 78% homology between the two species; note that three of the nucleotide changes are not accompanied by an amino acid change and are therefore silent changes. The degree of homology is compatible with the cross-hybridization observed between the bovine factor IX cDNA probe and the λ HIX1b clone in the rather stringent conditions used, and provides direct evidence that the latter carries an authentic DNA sequence coding for the human factor IX gene.

The present data are equivocal as to whether the λ HIX1b clone carries a complete factor IX gene. The restriction map (Fig. 4A) shows however, that the cloned segment includes more than six kilobases (kb) of DNA on one side and >10 kb

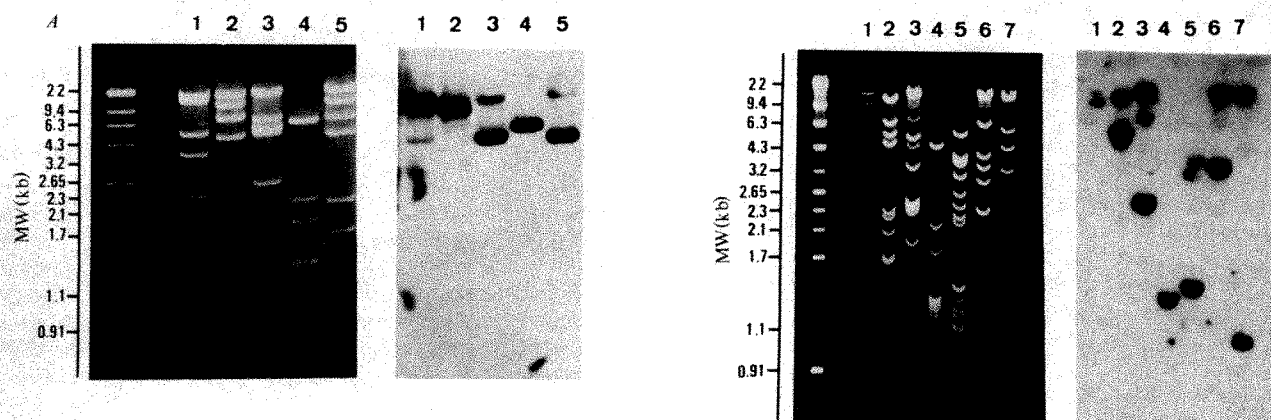


Fig. 3 Isolation and characterization of the human λ HIX1b clone. The cloned human DNA library used was a *Hae*III/*Alu*I λ Charon 4a library prepared by Lawn *et al.*¹⁸. Phage recombinants (10⁶) from this library were screened using the *in situ* plaque hybridization procedure described previously¹⁸. Prehybridization and hybridization were carried out at 42 °C in 50% formamide. After hybridization, filters were washed at room temperature with 2 \times SSC, 0.1% SDS, then at 65 °C with 1 \times SSC, 0.1% SDS. A 325-nucleotide fragment from the bovine BIX-1 cDNA clone was initially used as a probe in the hybridization. This fragment corresponds to nucleotides –8 to 317 as shown in Fig. 2, and was isolated by *Sau*3AI digestion of BIX-1 plasmid DNA. The isolated DNA was labelled to high specific activity by incorporation of [α -³²P]ATP using Amersham's nick-translation kit; 10 clones were isolated. These were plaque-purified and re-screened with a 247-nucleotide fragment from BIX-1 clone. This fragment, derived from nucleotides 3–249 (see Fig. 2), contains only sequences corresponding to the published bovine factor IX amino acid sequence⁵, and was isolated by *Hinf*II digestion of BIX-1 plasmid DNA. Only a single clone gave a positive hybridization signal with this probe. This clone was further plaque-purified and the resulting clone (designated λ HIX1b) characterized by digestion with various restriction endonucleases. Ethidium bromide-stained gels are shown on the left and their corresponding fluorograms after Southern transfer¹⁹ and hybridization with factor IX-specific 247-nucleotide probe are shown on the right. A, 1–5, cleavage pattern with *Bam*HI, *Bgl*II, *Hind*III, *Hpa*II and *Eco*RI, respectively. The sizes of the fragments showing predominant hybridization signals for these endonucleases are ~16, 11, 5.5, 6.5 and 5.5 kb respectively. B, 1, cleavage with *Bgl*II alone; 2–7, cleavage with *Bgl*II in combination with *Bam*HI, *Hind*III, *Hpa*II, *Pvu*II, *Sst*I and *Eco*RI, respectively. The sizes of the fragments showing predominant hybridization signals for these endonucleases (1–7) are ~11, 5.5, 2.5, 1.4, 1.5, 3.4 and 1.0 kb, respectively. The MW markers (kb) shown on the left are fragments from pBR322 plasmid DNA cleaved with *Alu*I, *Bam*HI + *Pvu*II and *Bam*HI + *Pst*I, plus λ DNA cleaved with *Hind*III.

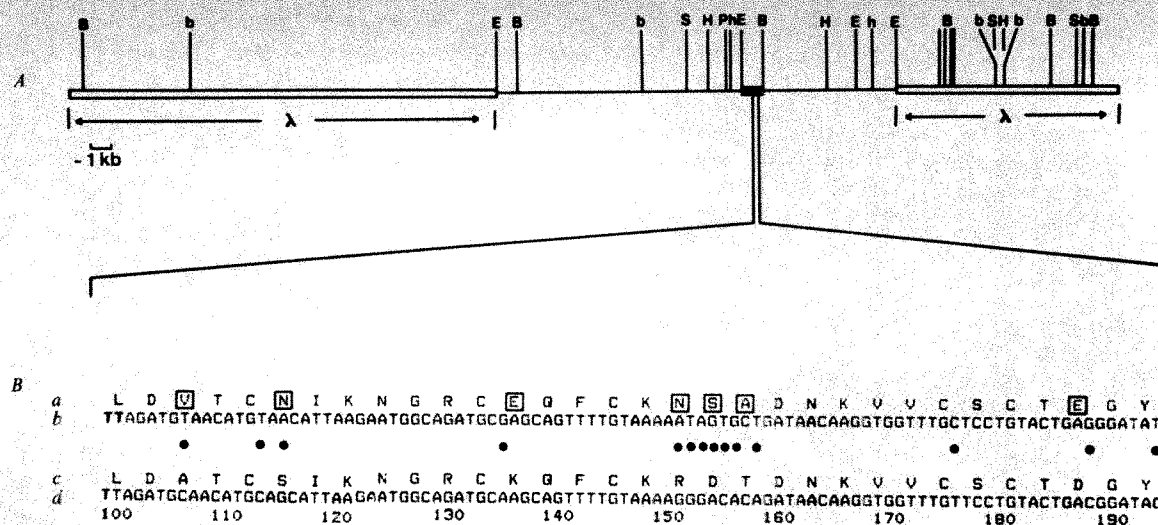


Fig. 4 A, partial restriction map of λHIX1b phage DNA. B = BglII; b, BamHI; E, EcoRI; S, SstI; H, HindIII; h, HpaII; P, PvuII. The Charon 4A λ vector long arm is on the left and the short arm is on the right. Restriction sites for BglII, BamHI, EcoRI, SstI and HindIII on the vector arms are shown. The smallest fragment (~1 kb) within the human DNA insert which hybridizes to the bovine cDNA probe (Fig. 3) is a BglII-EcoRI fragment (indicated by a solid box). The construction of this map was based on the data shown in Fig. 3 and that derived from restriction analysis of a pBR322 subclone of the 10–12-kb BglII fragment containing the 1-kb BglII-EcoRI probe region. This map shows the approximate positions of the nearest restriction sites to the left and right of the probe region (with the exception of SstI and PvuII where their sites to the right have not been determined). B, Sequence of 96 nucleotides located within a region of the human DNA insert which hybridizes to the bovine cDNA probe. a, Amino acid sequence deduced from the nucleotide sequence b, for λHIX1b. These two sequences are compared with the amino acid c and nucleotide d sequence of bovine factor IX. The bovine nucleotide sequence has been numbered similarly to that shown in Fig. 2. • Indicates a nucleotide difference between the human and bovine sequences. □ Indicates a difference in amino acid between the two species. Note that the orientation of this sequence within the genomic clone is 5' to 3' from right to left.

on the other side of the sequenced region (or the 'connecting peptide region')⁵, and suggests that this segment potentially contains a complete human factor IX gene. Further sequencing should clarify this and also elucidate the structure of this gene.

Recent reports^{9,10} have described the use of specific gene probes for prenatal and antenatal diagnosis of genetic disorders. These methods are based on the observation of the existence of polymorphisms for restriction endonuclease sites which are closely linked to a particular gene locus. It is hoped that the genomic clone reported here will be similarly useful for the diagnosis and understanding of the mutations in patients with haemophilia B, as well as of heterozygote mothers who are carriers of the factor IX mutation.

We thank Dr M. P. Esnouf for gifts of the crude anti-bovine factor IX antiserum and pure bovine factor IX; Drs F. E. Baralle, N. J. Proudfoot and F. Giannelli for their help and useful discussion; and Dr M. C. Carroll for providing the BamHI-cut and phosphatase-treated pBR322 vector. This work was supported in part by MRC project grant G8103835 to G.G.B. K.H.C. is a recipient of Uncle Bobs Travelling Scholarship and a C. J. Martin Research Fellowship from the National Health and MRC of Australia.

Note added in proof: Further sequence of clone λHIX1b suggests that there is a splice point after residue 101 of the sequence (Fig. 4B, line d). The TTAG (nucleotides 98–101) may therefore derive from an intron and may not code for the amino acids L and D.

The origin of the sequence unrelated to factor IX mRNA shown within square brackets in Fig. 2 could reflect either a cloning artefact or may derive from an intron region assuming we have cloned a region of a pre-mRNA molecule. Further sequencing of the genuine clone should resolve this.

Received 12 May; accepted 23 June 1982.

- Jackson, C. M. & Nemerson, Y. A. *Rev. Biochem.* **49**, 765–811 (1980).
- Ratnoff, O. D. in *The Metabolic Basis of Inherited Disease* (eds Stanbury, J. B., Wyngaarden, J. B. & Frederickson, D. S.) 1755–1791 (McGraw-Hill, New York, 1978).
- Chirgwin, J. M., Przybyla, A. E., MacDonald, R. J. & Rutter, W. J. *Biochem.* **18**, 5294–5299 (1979).
- Wallace, R. B. *et al. Nucleic Acids Res.* **9**, 879–894 (1981).
- Katayama, K. *et al. Proc. natn. Acad. Sci. U.S.A.* **76**, 4990–4994 (1979).
- Duckworth, M. L. *et al. Nucleic Acids Res.* **9**, 1691–1706 (1981).
- Roychoudhury, R. & Wu, R. *Meth. Enzym.* **65**, 43–62 (1980).
- Maxam, A. & Gilbert, W. *Proc. natn. Acad. Sci. U.S.A.* **74**, 560–564 (1980).
- Kan, Y. W., Lee, K. Y., Furbetta, M., Angius, A. & Cas, A. *New Engl. J. Med.* **302**, 185–188 (1980).
- Little, P. F. R. *et al. Nature* **285**, 144–147 (1980).

- Caton, A. J. & Robertson, J. S. *Nucleic Acids Res.* **7**, 1445–1456 (1979).
- Pelham, H. R. B. & Jackson, R. J. *Eur. J. Biochem.* **67**, 247–256 (1976).
- Choo, K. H., Cotton, R. G. H., Danks, D. M. & Jennings, I. G. *Biochem. J.* **181**, 285–294 (1979).
- Choo, K. H., Jennings, I. G. & Cotton, R. G. H. *Biochem. J.* **199**, 527–535 (1981).
- Huddleston, J. A. & Brownlee, G. G. *Nucleic Acids Res.* **10**, 1029–1038 (1981).
- Casadaban, M. J. & Cohen, S. N. *J. molec. Biol.* **138**, 179–207 (1980).
- Gergen, J. P., Stern, R. H. & Wensink, P. C. *Nucleic Acids Res.* **7**, 2115–2136 (1979).
- Lawn, R. M., Fritsch, E. F., Parker, R. C., Blake, G. & Maniatis, T. *Cell* **15**, 1157–1174 (1978).
- Southern, E. M. *J. molec. Biol.* **98**, 503–517 (1975).

Intron-exon splice junctions map at protein surfaces

Charles S. Craik, Stephen Sprang, Robert Fletterick & William J. Rutter

Department of Biochemistry and Biophysics, University of California, San Francisco, California 94142, USA

There have been several suggested explanations for the presence of noncoding intervening sequences in many eukaryotic structural genes. They may be examples of 'selfish DNA'^{1,2}, conferring little phenotypic advantage, or they may have some importance in gene expression and/or evolution. It has been suggested that each exon (coding sequence) may represent a structural or functional unit of the encoded protein^{3,4}, for which there is good evidence in the case of immunoglobulin⁷ and haemoglobin^{8,9} genes. Exon modification, duplication and recombination may thus be general mechanisms for the rapid evolution of eukaryotic structural genes. In many cases, however, it is not apparent that an exon corresponds to some specific feature of the encoded protein^{10,11}. We describe here evidence that intron-exon junctions usually map to amino acid residues located at the protein surface, suggesting a restriction on the permitted positions of introns within a gene.

For several proteins, proteolysis cleavage points are observed at the region of the splice junctions. This implies that the junctions correspond to a location at the protein surface. For example, clostripain specifically cleaves the three arginines which exist at the splice junctions, whereas another arginine, presumably buried, is less labile⁸. Similarly, the amino acids that are cleaved in the maturation of chymotrypsin correspond

to one of the splice sites (see Table 1). In addition, in immunoglobulins and proinsulin, proteases recognize surface amino acids mapping at or near splice junctions. We therefore have examined those proteins for which both genomic sequence and protein tertiary structure are known. Unfortunately the number of examples for which these data are available is limited. We have listed in Table 1 all those proteins that we know of for which both the gene structure and tertiary structure have been determined. This data set contains 31 splice junctions for 10 protein chains containing 1,928 amino acids. For all the splice junctions in Table 1, except one (the exon A boundary of lysozyme), the splice junctions map at the surface of the protein structure (for stereo views of dihydrofolate reductase and chymotrypsinogen, see Fig. 1).

We have quantified this observation by comparing the solvent-accessible surface area of amino acids encoded at intron-exon boundaries with those located elsewhere in the protein, a residue with $\leq 20 \text{ \AA}^2$ accessible surface being defined as interior¹². Note that this calculation does not always distinguish residues at the protein surface from those within its interior. For example, in a β -sheet core or inward facing surface of a helix, the immediate environment of a residue could be exposed to a solvent channel, or a surface amino acid can be buried by the side chains of neighbouring peptides. The calculation¹³ of the solvent-accessible surface for the amino acids that map at the splice junction shows that in every case except for lysozyme, at least one and usually both amino acids that map at the splice junctions are solvent-accessible.

A statistical analysis of these data can be made by assuming we have a random sample of events for which there are two possible states; that is, the splice junction maps either at the surface or at the interior of the protein molecule. Furthermore, the junction may fall either within (class I) or between (class II) codons. In the first case, accounting for 9 of the 31 samples, the intron-exon boundary maps to a single amino acid. The solvent-accessible surface calculation was used to find the fraction of buried amino acids (Table 1, column 6). Of the 1,928

amino acids represented, 745 are not accessible to the solvent. Thus for this sample, on average 0.389 of the amino acids are buried. Class II (the remaining 22) splice junctions map between two residues, thus the accessibility of both must be considered. Here position is determined to be interior only if both residues are inaccessible. Of the 1,918 adjacent pairs in the data set, 381 or 0.199, are buried by this criterion. However, none of the pairs at intron-exon boundaries are buried. Assuming that a binomial distribution describes the probability of a splice junction mapping to the protein interior, we can calculate the expected probability for the event that up to 1 out of 9 class I, and 0 out of 22 class II junctions, are buried by chance using the formula:

$$P = \sum_{y=0}^1 \binom{9}{y} p_1^y q_1^{9-y} \binom{22}{0} p_{11}^0 q_{11}^{22}$$

where $p_1 = 0.389$, $p_{11} = 0.199$ and q_i , the probability of the junction being on the surface, is $1 - p_i$. This calculation shows that the probability P of observing only one (or zero) buried splice site for these samples is 6×10^{-4} . This calculation strongly suggests that the observed surface location of splice junctions is not coincidental.

The above observations might be explained by the restricted nucleotide composition observed around the splice junction¹⁴. This could result in a skewed amino acid composition that, in turn, might influence the location of this site within the tertiary structure of the protein. Thus, if charged amino acids were favoured there would be a 90% probability that they appear on the protein surface¹⁵. Similarly, as two-thirds of the amino acids in the hydrophobic core of proteins are Phe, Cys, Val, Ile, Leu or Met a choice from this set would tend to yield an interior splice junction. RNA sequence analysis¹² has shown that the sequence GT is nearly always found at the 5' junction, and AG at the 3' junction. We have translated in all reading frames the nucleotide sequence at the 5' and 3' side of all known splice junctions (refs 16, 17, Table 1 and unpublished data). The results show no particular constraints on the amino acid

Table 1 Solvent-accessible surface areas for intron-exon junctions in coding regions

Protein*	Intron	Intron-exon* splice position	Amino acid position	Amino acid solvent-accessibility (\AA^2)	Fraction of residues buried	Fraction of residue pairs buried
Cytochrome c ¹⁸		Gly	56	66	0.330	0.127
Immunoglobulin ¹⁹	A	Arg	103	150		
Fab λ light						
Immunoglobulin ¹⁹	A	Ser Gly	384 385†	90 46	0.356	0.183
Fab γ heavy	B	Glu Pro	423 424†	96 44		
Haemoglobin α ²⁰	A	Glu Arg	30 31	43 81	0.326	0.121
	B	Lys Leu	99 100	142 17		
Haemoglobin β ²⁰	A	Arg Leu	30 31	83 11	0.294	0.110
	B	Arg Leu	104 105	135 23		
Lysozyme ²¹	A	Trp	28	18	0.370	0.188
	B	Ser Ala	81 82†	74 33		
	C	Trp Val	108 109†	11 86		
Trypsinogen ²²	B	Ser	59	85	0.470	0.237
	C	Thr	144	91		
	D	Gln Gly	189 190	137 13		
Chymotrypsinogen	B	Gln Asp	34 35	25 38	0.443	0.278
B ²³	C	Thr	61	62		
	D	Lys Val	87 88	110 25		
	E	Ala Asn	146 147	126 48		
	F	Met Gly	192 193	105 24		
Dihydrofolate reductase ²⁴	A	Arg	28	159	0.338	0.151
	B	Gly	45	51		
	C	Lys	80	171		
	D	Lys Ala	122 123	114 54		
	E	Glu Tyr	161 162	105 32		
Carboxypeptidase	C	Asp Glu	16 17	87 59	0.464	0.278
A ²⁵ §	D	Asn Arg	58 59†	68 38		
	E	Lys Lys	84 85†	15 36		
	F	Trp Arg	126 127†	36 43		
	G	Ala Ser	156 157†	23 30		
	H	Lys Thr	216 217†	86 108		
	I	Asn Gln	260 261	62 54		

* The amino acid residues represented are those of the protein crystal structure.

† Where the intron-exon boundary splits a codon a single residue is shown; otherwise residues on both sides of the junction are listed (see below).

‡ The precise position of the splice is sometimes equivocal due to the ambiguities of the DNA sequence around the intron-exon boundary so two amino acids are shown.

§ Five of the seven splice junctions were determined by detailed restriction and heteroduplex mapping (ref. 11 and C.S.C., unpublished).

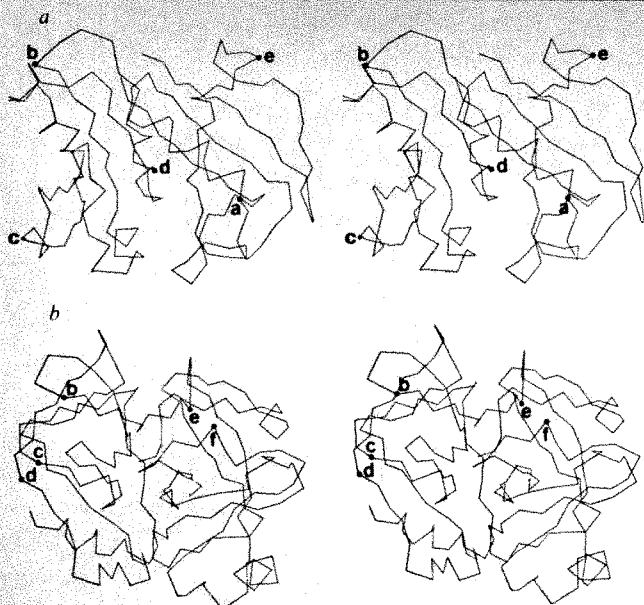


Fig. 1 Stereo views of the α -carbon chain tracing of dihydrofolate reductase (a) and chymotrypsinogen (b) showing the location of the splice junctions mapped on the protein sequence.

composition at that 3' side of the AG at the splice site. However, at the 5' side of the GT at the splice junctions, the extremely hydrophobic, and usually buried, amino acids (Phe, Cys, Val, Ile, Leu and Met) are underrepresented by a factor of 2.1 (expected from a natural abundance of 27%, that observed here being 13%) and the extreme hydrophilic and usually surface amino acids (Lys, Arg, Glu, Gln and Asp) are overrepresented by a factor of 1.6 (expected 28%, observed 44%). We have also tabulated the codons actually used at the junction sites. Again there was no strong bias in the amino acids present at the 3' side of the splice junction, but at the 5' side, the extremely hydrophobic amino acids are underrepresented by a factor of 4.1 (expected 27%, observed 6.6%) and the extremely hydrophilic amino acids are overrepresented by a factor of 2.3 (expected 28%, observed 64%). These data indicate that a hydrophilic amino acid is indeed more common near the intron-exon splice junction and provides a bias for the location of intron junctions at protein surfaces.

It is possible that the relationship between the location of the splice junction in the gene at the surface of the protein confers a biological advantage and hence is a result of natural selection. Introns and their associated splicing systems could be exploited in many ways during the evolution of a protein. We now realize that introns do not always mark large domains of protein structure, but often mark subdomains or segments of protein structure with some function. A further generalization can be made about the location of introns from the data reported here—usually the intron positions map outside the hydrophobic core and near the surface of the proteins. The cytoplasmic proteins used here are presumably exposed to a hydrophilic environment, thus the amino acids in the region of surface splice junctions are largely hydrophilic. If the rule is general, then proteins exposed to a hydrophobic environment should have hydrophobic amino acids near the surface splice junctions. That the 'seam' of a protein should appear on its surface is not surprising from an engineering viewpoint; if we consider the consequences of joining protein segments by cavalier recombination of exons, any novel amino acid sequences that might result from the new splicing would be isolated on the surface of the protein. This provides a means for change without forfeiting the pre-existing three-dimensional structure. It might therefore be expected that protein sequences contain additions or deletions in the region encompassing the splice junction. We have shown elsewhere that the region of major variation in the serine protease family occurs at or near splice junctions¹⁷.

Our findings are in accord with previous speculations on function or nonfunction and placement of introns, but set a requirement for their location with respect to protein structure. If the surface rule for intron-exon junctions is general, then the location of splice points in genomic DNA sequences also provides useful tertiary structural information about the gene product, as certain regions of the primary sequence can be reliably predicted to reside at the surface. Thus these data might be used in part to predict aspects of tertiary structure as well as provide a strategem for the design of new proteins.

We thank David Standing and Pat O'Farrell for discussions; Graeme Bell, Carmen Quinto, Qui Lim Choo and Robert T. Schimke for communicating their sequencing data on chymotrypsin, trypsin and dihydrofolate reductase before publication; Raymond MacDonald for providing the trypsin cDNA; and Leslie Spector for preparation of the manuscript. This research was supported by NSF grant PCM 8001950 (to R.J.F.) and NIH grant AM 21344 (to W.J.R.). C.S.C. is a recipient of an American Cancer Society postdoctoral fellowship.

Received 21 January; accepted 13 July 1982

1. Doolittle, W. F. & Sapienza, C. *Nature* **284**, 601–603 (1980).
2. Orgel, L. S. & Crick, F. H. C. *Nature* **284**, 604–607 (1980).
3. Gilbert, W. *Nature* **271**, 501 (1978).
4. Blake, C. C. F. *Nature*, **273**, 267 (1978); **277**, 598 (1979).
5. Tonegawa, S., Maxam, A., Tizard, R., Bernard, O. & Gilbert, W. *Proc. natn. Acad. Sci. U.S.A.* **75**, 1485–1489 (1978).
6. Sakano, H. *et al.* *Nature* **277**, 627–633 (1979).
7. Bernard, O., Hozumi, N. & Tonegawa, S. *Cell* **15**, 1133–1144 (1978).
8. Craik, C. S., Buchman, S. R. & Beychok, S. *Proc. natn. Acad. Sci. U.S.A.* **77**, 1384–1388 (1980).
9. Craik, C. S., Buchman, S. R. & Beychok, S. *Nature* **291**, 87–90 (1981).
10. Stein, I. P., Catterall, J. F., Kristo, P., Means, A. R. & O'Malley, B. W. *Cell* **21**, 681–687 (1980).
11. Quinto, C. *et al.* *Proc. natn. Acad. Sci. U.S.A.* **79**, 31–35 (1982).
12. Janin, J. *Nature* **277**, 491–492 (1979).
13. Lee, B. & Richards, F. M. *J. molec. Biol.* **55**, 379–400 (1981).
14. Breathnach, R., Benoist, C., O'Hara, K., Gannon, F. & Chambon, P. *Proc. natn. Acad. Sci. U.S.A.* **75**, 4853–4857 (1978).
15. Sprang, S., Yang, D. & Fletterick, R. J. *Nature* **280**, 333–335 (1979).
16. Breathnach, R. & Chambon, P. *A. Rev. Biochem.* **50**, 349–383 (1981).
17. Craik, C. S. *et al.* in *Gene Regulation* (O'Malley, B. & Fox, C. F. (1982); *UCLA Symp. molec. cell. Biol.* **26**, (in the press).
18. Swanson, R. *et al.* *J. biol. Chem.* **252**, 759–776 (1977).
19. Amzel, L. M. & Poljak, R. J. *A. Rev. Biochem.* **48**, 961–997 (1979).
20. Ten Eyck, L. F. & Arnone, A. *J. molec. Biol.* **100**, 3–29 (1976).
21. Blake, C. C. F. *et al.*, *Nature* **206**, 757–763 (1965).
22. Chambers, J. L. & Stroud, R. M. *Cryst.* **B35**, 1861–1874 (1979).
23. Matthews, B. W., Sigler, P. B., Henderson, R. & Blow, D. M. *Nature* **214**, 652–660 (1967).
24. Volz, K. *et al.* *J. biol. Chem.* (in the press).
25. Lipscomb, W. N. *Acc. chem. Res.* **3**, 81–89 (1970).

High-frequency genomic rearrangements involving archaeobacterial repeat sequence elements

Carmen Sapienza*, Michael R. Rose† & W. Ford Doolittle*

Departments of *Biochemistry and †Biology, Dalhousie University, Halifax, Nova Scotia, Canada B3H 4H7

Halobacterium halobium is an obligately halophilic archaeobacterium¹ of interest to molecular biologists for many reasons^{2–5}, one of which is the unexplained high frequency (10^{-4} – 10^{-2} mutants per cell plated) at which it yields readily identifiable and unstable mutants⁴. We showed previously⁵ that the genome of *H. halobium* contains many (>50) families of repeated sequences whose members are dispersed on both chromosome and plasmid. Here we report that most if not all of the members of most of these repeat sequence families effect or are affected by spontaneous genomic rearrangements. Quantitative analyses show that such repeat sequence-associated rearrangements (which may be of several kinds) occur at high frequencies (> 4×10^{-3} events per family per cell generation), while unique-sequence DNAs are physically stable. The presence of so many families of elements of such great instability in the halobacterial genome gives it an unusual degree of structural and perhaps functional plasticity.

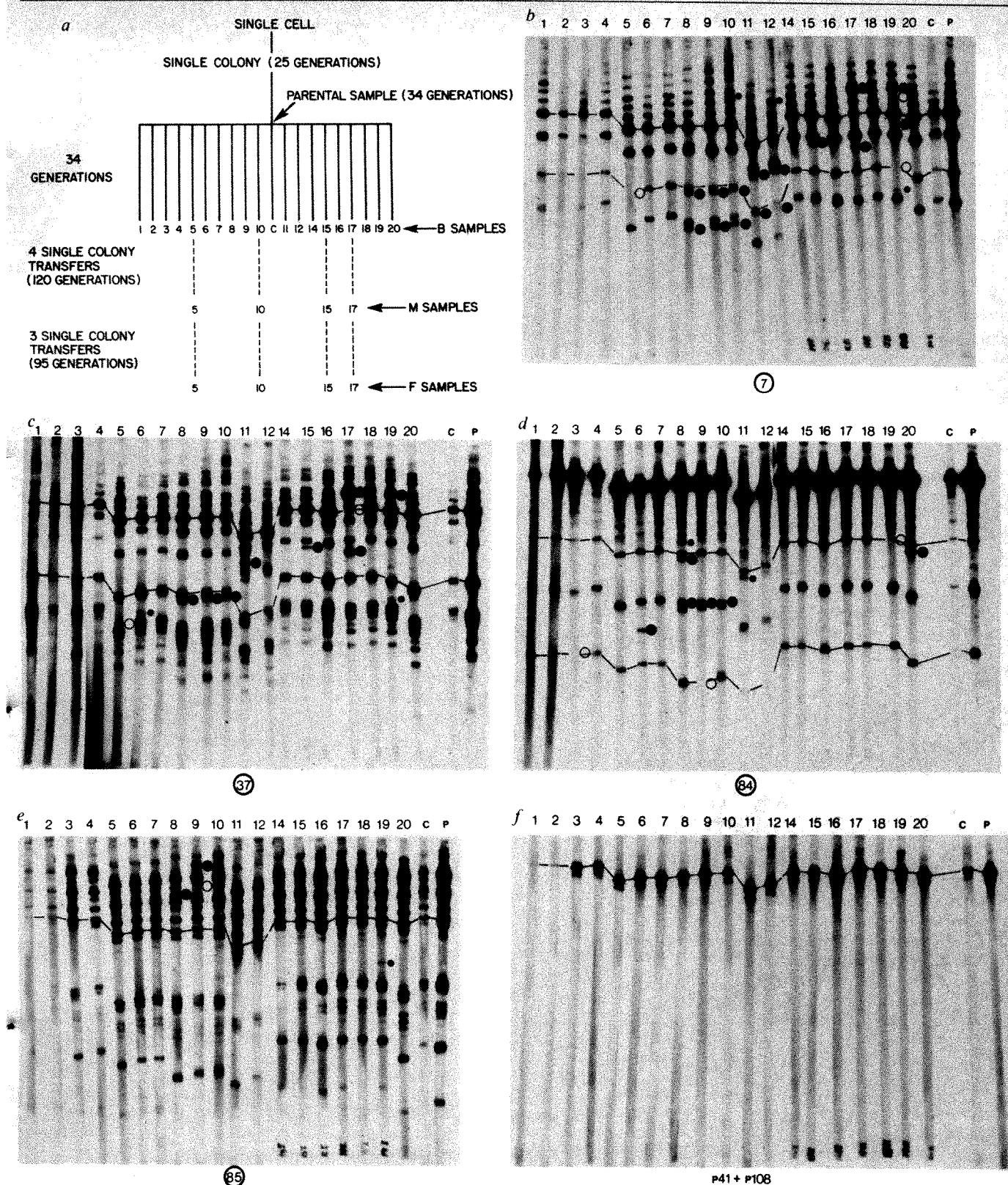


Fig. 1 *a*, Experimental protocol. A single cell of *H. halobium* wild-type strain NRC-1 was plated to give a single colony (25 generations), and cultured in liquid for a further nine generations. Most of this culture was used to prepare DNA taken to be representative of the first 'parental' cell (tracks labelled P in *b-f*). (A portion of the culture was diluted and grown in liquid for a further 34 generations, without re-plating. DNA prepared from this subculture appears in tracks labelled C of *b-f*). The rest of the culture was plated out to give single colonies; 19 of these which showed no visible phenotypic alteration were picked into liquid and grown for DNA preparation (tracks 1-19 in *b-f*). Again, 34 generations elapsed between initial plating and collection. Then four isolates (5, 10, 15 and 17) were re-plated and carried through seven additional platings and single-colony isolations. DNA was prepared from samples after four platings (120 generations, tracks labelled M in Fig. 2) and again after seven platings (215 generations, tracks labelled F in Fig. 2). The methods used for culture and DNA isolation are described in ref. 5. *b*, Results of probing *Eco*RI digestion products of the DNAs described above with cloned *H. halobium* repeat sequence element 7. ●, Hybridizing fragments present in the DNA of one of the 19 isolates which were absent from the DNA of the initial cell from which they derive (represented by tracks labelled P). ○, Hybridizing fragments absent from the DNA of one of the 19 isolates but present in the DNA of the initial cell. Hybridizations were performed as described previously⁵. *c-e*, Results for cloned repeat sequences 37, 84 and 85, respectively. *f*, Results for two cloned *Pst*I fragments of *H. halobium* DNA bearing only unique sequences.

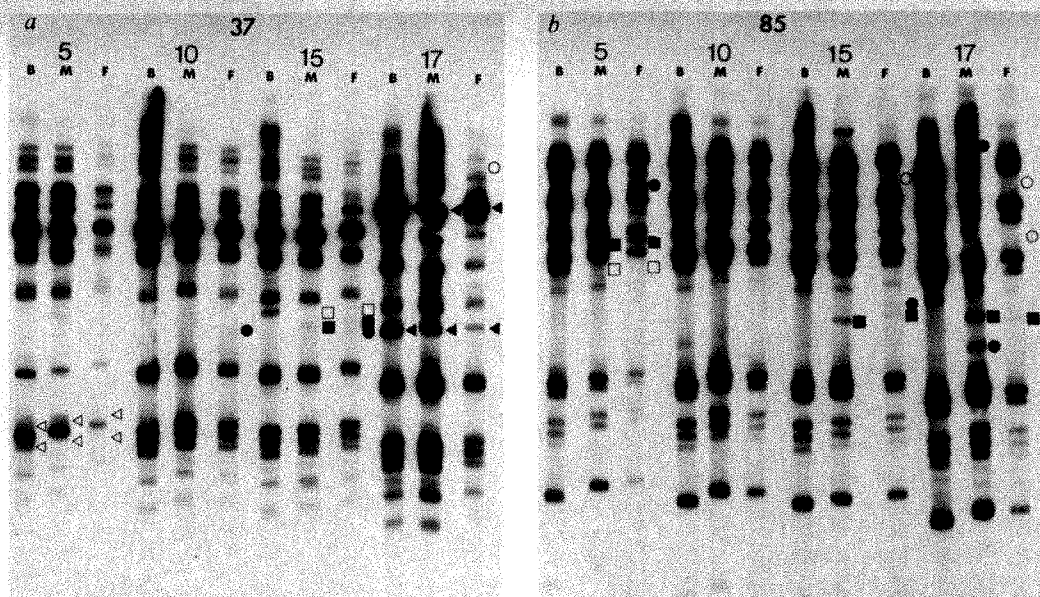


Fig. 2 *Eco*RI-cleaved DNAs from isolates 5, 10, 15 and 17 probed with 32 P-labelled cloned repeat sequence DNAs from strain NRC-1. ◀ Indicates the position of a fragment absent from the parental DNA sample (lane P in Fig. 1b-f) but present in B, M and F DNA samples. ◁ Indicates the absence of fragments from the B, M and F DNA samples that were present in the parental DNA sample. ■, Hybridizing fragments in the M and F DNA samples not present in B DNA samples; □, fragments hybridized in B DNA samples but absent from M or F DNA samples. ●, Fragments hybridized in only M or F DNA samples; ○, fragments absent from F but present in B and M DNA samples. a and b are results of probing with repeat sequence clones 37 and 85, respectively.

We described previously⁵ the molecular cloning and characterization of small (~3 kilobase pair, kbp) *Eco*RI fragments of *H. halobium* DNA bearing members of one or more repeat sequence families of small family size (2 or 3 to perhaps 20 members). Preliminary experiments with two of these fragments suggested that such repeated elements could be affected by spontaneous genomic rearrangements. These experiments provided no information, however, on the frequency or nature of those rearrangements, nor did they elucidate whether such instability is associated only with repeated elements and, if so, whether all families, or all members of any family, exhibit instability.

The experiments shown schematically in Fig. 1a measured rates of spontaneous rearrangement in 19 cell lines separated from a common ancestor by only that minimum number of generations (in practice, 34) required for the preparation of sufficient DNA for Southern blot analyses^{5,6}. *Eco*RI-digested total DNAs from each of these 19 isolates were resolved on agarose gels, transferred to nitrocellulose filters and probed with 32 P-labelled, *Eco*RI-cloned *H. halobium* fragments bearing members of seven distinct repeat sequence families⁵. Results obtained with four of these probes are shown in Fig. 1b-e. Many changes in both number and position of hybridizing fragments are apparent. If each independent appearance or disappearance of a hybridizing fragment is defined as an event, there were 56 different events among the 19 isolates which were uniquely detected by one or another of the seven repeat sequence probes. All such probes detected events in at least one of the isolates and we believe that all repeat sequences are associated with genomic rearrangements occurring at high and roughly comparable frequencies. On the other hand, two unique-sequence DNA probes detected few if any changes in any of the isolates (Fig. 1f).

If genomic rearrangements involving repeat sequences occur independently, then the observed frequency of events (roughly 10^{-2} per repeat sequence family per cell generation) could be taken as the probability of such rearrangements occurring in any cell line (isolate). However, events were not randomly distributed among isolates. Four isolates together accounted for about half the events and one showed alterations with five of the seven repeat sequence probes, while seven isolates showed no changes with any probe. If we assume that one event is usually coupled with others, then the probability of that first

event (assumed to be the same for all repeat sequence families) provides the most conservative estimate of rearrangement frequency. This can be calculated from the observed frequency of isolates exhibiting no changes using the zero-term of the binomial distribution. That is, the probability of change, P , can be calculated from the observed frequency ($7/19 = 0.368$) of isolates showing no alterations in 34 generations, using the equation $0.368 = [(1 - P)^{34}]^7$. This use of the binomial distribution assumes that rearrangements depend on independent Bernoulli trials over seven families. If rearrangements can arise at any time, however, a similar calculation using the zero-term of the Poisson formula is more realistic⁷. Both calculations give values for P of 4×10^{-3} events per repeat sequence family per cell generation (or from 4×10^{-4} to 1×10^{-3} per repeat sequence element). This is not remarkably lower than 10^{-2} , our observed frequency irrespective of order, because events are only partially coupled. From these values, we predict that about one-tenth of all isolates will experience rearrangements affecting at least one of the seven repeat sequence families during the first three or four divisions after their establishment from single cells. Such rearrangements will give rise to restriction site polymorphisms detectable as weakly hybridizing fragments in the DNA prepared after 34 generations. Weak bands were indeed detected for several isolates and with several probes and were, as far as possible, excluded from our calculations.

Of the nine *Eco*RI fragments probed strongly by the repeat sequence family member carried on clone 7, five have been deleted in one or another of the isolates characterized here (Fig. 1a) or previously⁵. This suggests that all members of at least this repeat sequence family are equally liable to exhibit genomic rearrangement. To determine whether the 'new' hybridization patterns produced by rearrangement are as stable as 'old' ones, 4 of the 19 isolates (Fig. 1a) were carried through seven further single-colony isolations, with DNA prepared as above after the fourth (120 generations) and seventh (215 generations) platings. These DNAs were probed with five cloned *H. halobium* repeat sequence DNAs and two cloned repeat sequence DNAs from *Halobacterium volcanii* previously shown to be homologous with two different *H. halobium* repeats⁵ (Fig. 2 and data not shown). In none of the three cases in which one of these four isolates had lost a hybridizing fragment during the first 34 generations was that fragment regained during 215 subsequent generations; vacated sites

appear not to be selectively reoccupied. In only one of the four cases in which one of these four isolates had gained a new hybridizing fragment during the first 34 generations was that fragment lost during the subsequent 215; newly-occupied sites do not appear to be uniquely unstable. Other changes observed during the propagation of these four isolates occurred with a frequency ($\sim 2 \times 10^{-3}$) in reasonable agreement with that obtained from the more extensive survey reported above.

The events observed result in either: (1) the appearance of a new hybridizing fragment without the loss of pre-existing fragments; (2) the loss of a pre-existing fragment without the appearance of a new one; or (3) the appearance of a new fragment and the loss of a pre-existing fragment, at about the frequency expected for independent occurrences of events of the first two types in the same cell line.

There is substantial indirect qualitative evidence^{4,8} for the transfer of discrete DNA sequences between plasmid, phage and chromosomal DNAs and we believe that many of the events whose frequency we have measured here are probably at least formally analogous to transpositions, although we cannot exclude alternative interpretations invoking deletions and duplication via unequal cross-over events between repeats of the same family. Whatever the nature of these events, the high frequency with which they occur in all repeat sequence families tested, and the large number of such families, must give the halobacterial genome an unusual degree of structural plasticity. It is easy to calculate that two daughter cells produced by a single division have only an 80% chance of bearing identical genomes, and that of the 10^{11} progeny in a 1-l culture established from a single cell, only 3×10^7 will bear genomes identical to that of the first cell, if all rearrangements are selectively neutral. They are not likely to be, and questions about the functional significance of this genomic plasticity and its relationship to the observed high frequency of spontaneous mutation are of considerable interest.

We thank the MRC of Canada for support, A. Cohen for technical assistance and N. Kleckner for critical advice.

Received 17 May; accepted 8 July 1982.

1. Woese, C. R. *Scient. Am.* **244**(6), 94-106 (1981).
2. Bayley, S. T. & Morton, R. A. *CRC crit. Rev. Microbiol.* **6**, 151-205 (1978).
3. Weidinger, G., Klotz, G. & Goebel, W. *Plasmid* **2**, 377-386 (1979).
4. Pfeifer, F., Weidinger, G. & Goebel, W. *J. Bact.* **145**, 375-381 (1981).
5. Sapienza, C. & Doolittle, W. F. *Nature* **295**, 384-389 (1982).
6. Southern, E. M. *J. molec. Biol.* **98**, 503-517 (1975).
7. Feller, W. *An Introduction to Probability Theory and its Applications* 3rd edn (Wiley, New York, 1968).
8. Schnabel, H. *et al. EMBO J.* (in the press).

The helicity of DNA in complexes with RecA protein

Andrzej Stasiak & Elisabeth Di Capua

Institute for Cell Biology, Swiss Federal Institute of Technology, Hoenggerberg, CH-8093 Zürich, Switzerland

The RecA protein of *Escherichia coli* is involved in recombination (for review see ref. 1). The protein binds transiently to double-stranded DNA in the presence of ATP. In the presence of ATP γ S, a non-hydrolysable analogue of ATP, recA-DNA complexes are stable^{2,3}. Duplex DNA in these complexes is stretched by a factor 1.5 (ref. 4), and the complexes appear in the electron microscope as helical filaments with a pitch of ~ 100 Å and 6.2 recA units per turn covering 18.6 base pairs (bp)⁵. RecA crystals have a space group of similar helical parameters⁶. In order to understand the function of recA, it is necessary to describe the conformation of the DNA in the recA complex. Using a topological method, the present work determines the helicity of DNA in the complex. We find that the DNA helix follows the protein helix visible in the electron microscope and has 18.6 bp per turn, which corresponds to an unwinding of the DNA double helix by 15° per bp.

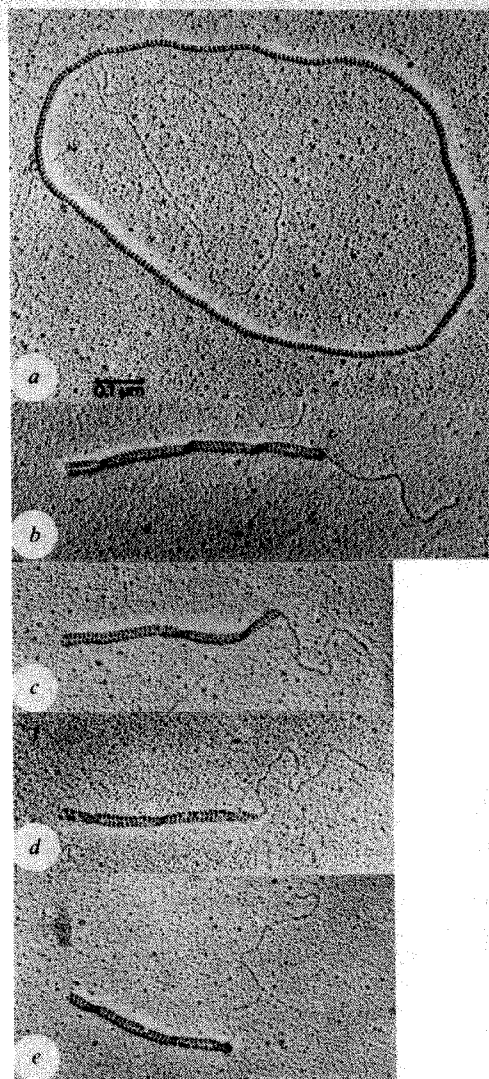


Fig. 1 Nicked circular DNA fully covered with RecA protein (a) and topoisomers of different linking numbers α reacted with RecA protein, $\alpha = 432$ (b), 445 (c), 459 (d), 472 (e). Note that in b to e the rod-like striated structures arise from side-by-side aggregation of neighbouring segments of the same circular RecA-DNA complex, while the thin filaments represent the highly positively supercoiled segments not covered by RecA. The cross-striations visible are due to the helical structure of the RecA-DNA complexes described in more detail in ref. 5. This helical structure is identical by our criteria whether the complexes are made with relaxed or cccDNA. The plasmid used is a pBR322 derivative of 4,961 bp. The topoisomers were produced by reacting plasmid DNA (100 μ M bp) with nicking-closing extract from rat liver nuclei¹³ in the presence of 0 μ M (b), 6 μ M (c), 12 μ M (d), 18 μ M (e) ethidium bromide. The recA-DNA complexes were obtained by incubating 50 ng DNA with 2.5 μ g RecA protein and 2 mM ATP at room temperature in 20 μ l 25 mM triethanolamine chloride (pH 7.6) and 5 mM magnesium acetate, conditions which seem to permit initiation of binding of RecA to cccDNA. After 20 min, ATP γ S to 0.5 mM was added to stabilize the complexes and the reaction was continued for 1 or 24 h at room temperature. The extent of reaction was the same after both times of reaction, thus implying that the reaction was complete after 1 h. Control experiments with different RecA-DNA ratios gave the same extent of DNA covering by RecA for a given DNA sample. Thus, in our experimental conditions, the extent of reaction is not a function of RecA:DNA ratio (see also ref. 4).

Double-stranded DNA has been shown⁷ to be unwound to some extent by RecA. We have now found conditions that allow the formation of complexes with covalently closed circular (ccc) DNA, and this enables us to determine the extent of this unwinding by a topological approach. A cccDNA molecule is characterized by its linking number which is fixed⁸; thus, reac-

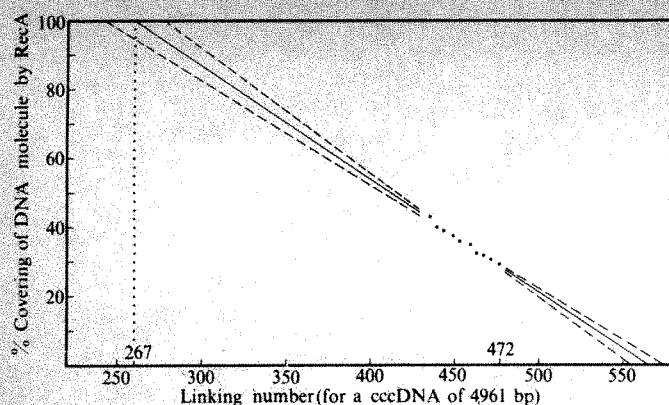


Fig. 2 Determination of the linking number of a cccDNA fully covered with RecA. The linking numbers were calculated by assuming 10.5 bp per turn of B-DNA in solution^{10,11}, which results in 472 turns for 4,961 bp, and subtracting from this value the number of superturns determined from the maximum of the distribution on band-counting gels⁹. For each topoisomer family the extent of covering with RecA was determined from 15–25 molecules. The standard deviation for each point was 2–3%, which is compatible with the presence of 7–8 topoisomers in each sample as seen on the band-counting gels. Extrapolation to 100% covering with RecA leads to a value of 267 ± 19.2 for the linking number of a totally covered molecule. The confidence interval was drawn assuming 95% confidence.

tion with an unwinding agent will lead to a topological constraint in the molecule, and it is to be expected that the binding of the unwinding agent will stop when this constraint reaches a limit. The linking number will then be the sum of the underwound and overwound turns. In the case of RecA protein, which covers the DNA cooperatively⁴, we found (Fig. 1) that the underwound and the overwound regions are distinct and easily recognizable as striated complexes and highly supercoiled tails, respectively. Thus, the fraction of the molecule that is allowed to undergo complex formation can be measured. The linking number α is related to this complexed fraction by

$$\alpha = \frac{f_c n + f_t (N - n)}{360}$$

where n is the number of base pairs complexed with RecA, f_c the topological winding angle of the DNA complexed with RecA, N the total number of base pairs of the molecule and f_t the topological winding angle of the DNA not covered with RecA (recognized as a tail in Fig. 1).

If we now determine the extent of covering by RecA on cccDNA molecules of different α , the values of f_c and f_t can be determined by extrapolating the relationship to $n = N$ (completely reacted), and $n = 0$, respectively (Fig. 2). The angles f_c and f_t are assumed to be independent of α , that is, the constraint in the tail will be constant per unit length. We assume that this tail takes up a limit value of positive supercoils. Note that the values of f_c and f_t are the result of two orders of helicity, the primary helix of the DNA (in the covered part and in the naked tail respectively), and a secondary helix. In the case of f_t (uncovered tail) the second order helix is the positive supercoiling caused by torsional stress. In the case of f_c (complex) the second order helix is inherent in the structure of RecA-DNA complexes associated side by side (visible as turning-over points⁵) and is not caused by torsional stress; since this second-order helicity in the complexed part contributes only 2.6% to the linking number we do not take it into account here, and consider simply the overall unwinding.

cccDNA molecules of various linking numbers were obtained by reacting plasmid DNA with nicking-closing enzyme in the presence of various amounts of ethidium bromide. After purification of the products, the amount of unwinding was determined by estimating the supercoiling on band-counting gels⁹. Unfortunately, using the band-counting technique it is

difficult to determine precisely the linking number of highly supercoiled molecules above a superhelical density of 0.1. This limited the range in which the linking number and the extent of RecA covering could be related precisely. A series of cccDNA molecules of various linking numbers complexed with RecA protein is shown in Fig. 1; a relaxed complex formed with nicked DNA (thus allowing 100% complex formation) is shown for comparison. It is seen that the lower the linking number, the more RecA is bound. In Fig. 2, the extent of covering with RecA is plotted against the linking number. Least-squares analysis fits the data to a straight line with a correlation factor of 0.99. Extrapolation shows that 100% covering of DNA by RecA would require a linking number of 267 ± 19.2 (confidence 0.95). From our previous work, we know that a relaxed circular molecule of 4,961 bp will form a complex with 267 or 268 visible helix turns (ref. 5, and Fig. 1a). The linking number calculated above from Fig. 2 is very close to this number. We thus conclude that the RecA-helix seen in the electron microscope reflects the helix of the DNA molecule within the complex.

It is interesting to point out that the RecA self-complexes (that is, filaments formed in the absence of any DNA) form a similar helix as far as we can judge from our electron micrographs (see also ref. 2). By interaction with RecA protein, double-stranded DNA is unwound from about 10.5 bp per turn^{10,11} to 18.6 bp per turn. This corresponds to an unwinding of 15° per bp, a value similar to the unwinding by ethidium bromide (26° per 2 bp¹²) and is thus compatible with the intercalation type of interaction we suggested to explain the stretching of DNA in the complex⁴. We cannot exclude, however, the possibility that the DNA in the complex is melted and the single strands are wound around each other without forming a base-stacked helix.

We thank Professor Theo Koller for his help and support, Philipp Bucher for help with the calculations and Dr Martin Gellert for stimulating comments. This work was supported by Schweizerischer Nationalfonds zur Förderung der wissenschaftlichen Forschung (grant to Th. Koller).

Received 10 May; accepted 15 July 1982.

1. Radding, C. M. *Cell* **25**, 3–4 (1981).
2. McEntee, K., Weinstock, G. M. & Lehman, I. R. *J. biol. Chem.* **256**, 8835–8841 (1981).
3. West, S. C., Cassuto, E., Mursallim, J. & Howard-Flanders, P. *Proc. natn. Acad. Sci. U.S.A.* **77**, 2569–2573 (1980).
4. Stasiak, A., Di Capua, E. & Koller, Th. *J. molec. Biol.* **151**, 557–564 (1981).
5. Di Capua, E., Engel, A., Stasiak, A. & Koller Th. *J. molec. Biol.* **157**, 87–103 (1982).
6. McKay, D. B., Steitz, T. A., Weber, L. T., West, S. C. & Howard-Flanders, P. *J. biol. Chem.* **255**, 6662 (1980).
7. Cunningham, R. P., Shibata, T., Das Gupta, C. & Radding, C. M. *Nature* **281**, 191–195 (1979).
8. Crick, F. H. C. *Proc. natn. Acad. Sci. U.S.A.* **73**, 2639–2643 (1976).
9. Keller, W. *Proc. natn. Acad. Sci. U.S.A.* **72**, 4876–4880 (1975).
10. Wang, J. C. *Proc. natn. Acad. Sci. U.S.A.* **76**, 200–203 (1979).
11. Rhodes, D. & Klug, A. *Nature* **286**, 573–578 (1980).
12. Baase, W. A. & Johnson, W. C. *Jr Nucleic Acids Res.* **6**, 797–814 (1979).
13. Champoux, J. J. & McConaughy, B. L. *Biochemistry* **15**, 4638–4632 (1976).

Errata

The cover photograph on the issue of 22 July, relating to the letter 'Monoclonal antibodies against human T lymphocytes label Purkinje cells of many species' by J. A. Garson *et al.* *Nature* **298**, 375–377 (1982), was reproduced in only two colours so that orange and green staining was not sufficiently differentiated. The photomicrograph shows neonatal mouse cerebellar cortex stained with two monoclonal antibodies simultaneously. The Purkinje cells are stained orange by Leu-4/biotin/avidin/rhodamine, while basket fibres and other axons are stained green (fluorescein conjugate) with the antineurofilament monoclonal RT97 (donated by B. Anderton).

In the article 'Dynamic observation of defect annealing in CdTe at lattice resolution' by R. Sinclair *et al.* *Nature* **298**, 127–131 (1982), parts *c* and *e* of Fig. 3 have been transposed thus interrupting the movement of the arrowed dislocation across the frame. The figure is correct on reprints.

MATTERS ARISING

Absence of thermal effects on photon mass measurements

THE mass of the photon^{1,2} is known to be less than 10^{-16} eV. However, in a letter to *Nature*, Primack and Sher³ have questioned the validity of this result. They suggest that electrodynamics may undergo a phase transition at low temperature, and point out that all of the photon mass experiments took place at temperatures above a few degrees Kelvin. Thus, they claim that the above mass limit may only apply to a high-temperature phase ($T > T_c$ where T_c could be as large as a couple of degrees Kelvin), and that when measured at lower temperatures the photon mass could be as large as about 10^{-4} eV. Apparently, low-temperature photon mass experiments are presently being considered⁴. We explain here why we believe that the scenario proposed by Primack and Sher³ is, in fact, impossible. We find that the limit of 10^{-16} eV on the mass of the photon is unaffected by the fact that the relevant experiments were performed at finite temperature. It is therefore completely valid and applies to experiments regardless of whether they are carried out at room temperature or at absolute zero.

To analyse thermal effects on measurements of the photon mass we must define what is meant by a phase transition in finite temperature field theory⁵⁻⁷. At zero temperature, the vacuum and the various particle states are described by definite state vectors. We can study vacuum expectation values of different field operators and we can measure the photon mass by examining how a photon propagates through the vacuum. At non-zero temperature, the system is described by a density matrix. We can no longer consider vacuum expectation values, but instead we deal with thermal expectation values. At finite temperature space is filled with thermal radiation and to measure the photon mass we must determine how a photon propagates through this thermal radiation. It is important to note that the vacuum does not change with temperature. However, quantities like field expectation values or particle masses can change because at non-zero temperatures they are measured not in the vacuum but in a thermal ensemble.

Therefore, we must ask what is the nature of the thermal fluctuations which occur at or below room temperature, and how can these affect the measured value of the photon mass? In particular, are the interactions of the photon with the thermal fluctuations at these temperatures strong enough to make a massive photon appear massless? The mass of a field sets a lower limit on the energy of its small fluctuations so a field of mass m will only experience significant fluctuations at tem-

peratures $kT \geq m$. At room temperature or below the only relevant thermal radiation consists of blackbody photons. Note that if there existed a fundamental or composite scalar field with a small vacuum expectation value which gave the photon a mass, then this field would only experience significant thermal fluctuations at normal temperatures if it produced a charged scalar particle with a mass of a fraction of an eV. If the associated charge scalar were heavier than this then thermal fluctuations of this scalar field would be exponentially suppressed. Since no such light charged particle exists we conclude that there is no way for thermal fluctuations to change the expectation value of such a field and thereby change the photon mass from some non-zero low-temperature value to zero at room temperature. However, we must still consider the effect of thermal photons on the photon mass at finite temperature.

The real-time thermal propagator for a particle of mass μ is

$$\frac{i}{k^2 - \mu^2} + \frac{2\pi}{e^{E/kT} - 1} \delta(k^2 - \mu^2) \quad (1)$$

The temperature-dependent term in this propagator is multiplied by $\delta(k^2 - \mu^2)$ so thermal effects are completely absent, to lowest order in α , for off-shell, virtual photons. The best limits on the photon mass come from measurements of the static magnetic field produced by Jupiter and these involve virtual photons. The second term in equation (1) is only relevant for real, on-shell photons of energies $E \leq kT$. For these photons this term represents the stimulated emission effect which the presence of thermal photons produces. Equation (1) is of course modified by order α corrections due to the interactions between thermal photons and a propagating virtual photon. However, such interactions occur only through loops of charged particles and are suppressed by a factor $e^{-m/kT}$ where m is the mass of the charged particle. The lightest charged particle is the electron and it produces polarization factors,

$$\Pi_{\mu\nu} \propto e^2 m_e^2 \left(\frac{m_e}{kT} \right) e^{-m_e/kT} \quad (2)$$

At temperatures of order room temperature or below, the factor $e^{-m_e/kT}$ is a gigantic suppression factor so these thermal effects are completely negligible. Thus, a virtual photon propagating through thermal radiation at normal experimental temperatures is completely unaffected by the presence of that radiation simply because no mechanism exists for it to interact in any appreciable way with the thermal photons. It follows that experiments which determine how a virtual photon propagates, like the photon mass experiments, will be unaffected as well. The photon mass limit of 10^{-16} eV is therefore valid at low temperature.

We wish to thank Alvaro DeRujula for

helpful discussions. This work was supported in part by the US Department of Energy under contract DE-AC02-76ER03230-A005.

L. F. ABBOTT

M. B. GAVELA*

*The Martin Fisher School of Physics,
Brandeis University,
Waltham,
Massachusetts 02254, USA*

* Permanent address: Laboratoire de Physique Theorique et Hautes Energies, University Paris-Sud, 91405 Orsay, France.

1. Goldhaber, A. S. & Nieto, M. N. *Rev. mod. Phys.* **43**, 277-296 (1971).
2. Davis, L., Goldhaber, A. S. & Nieto, M. N. *Phys. Rev. Lett.* **35**, 1402-1405 (1975).
3. Primack, J. R. & Sher, M. A. *Nature* **268**, 680-681 (1980).
4. Dombey, N. *Nature* **288**, 643-644 (1980).
5. Dolan, L. & Jackiw, R. *Phys. Rev. D* **9**, 3320-3341 (1974).
6. Weinberg, S. *Phys. Rev. D* **9**, 3357-3378 (1974).
7. Linde, A. D. *Prog. theor. Phys.* **42**, 389-435 (1979).

SHER AND PRIMACK REPLY—In our paper, we explained that neither spontaneous nor dynamical symmetry breaking could lead a mass for the photon at low temperature; but we speculated that some other physical mechanism could conceivably do it, and we pointed out that the question could be decided experimentally. Abbott and Gavela argue again that spontaneous symmetry breaking (the 'Higgs mechanism') will not work. The essential physical point they make is that "... a field of mass m will only experience significant fluctuations at temperatures $kT \geq m$." We agree. The question is whether the absence of charged particles (either bosons, mentioned by Abbott and Gavela, or fermions) lighter than the electron excludes an electromagnetic phase transition at $kT < m_e$, even one arising from a hitherto unknown mechanism. We are persuaded that their argument indeed excludes this possibility.

It should be noted that this argument could affect other, more realistic calculations. There have been many calculations of supercooling in both SU_5 and the Weinberg-Salam model. In some of these, the mass (at $T=0$) of the scalar before the transition vanishes (Coleman-Weinberg); the field can then experience significant fluctuations. In some, however, the scalar does have a small but non-zero mass m (see ref. 1). The argument of Abbott and Gavela appears to rule out a transition at $T \ll m$; completing a transition at such a temperature may not be possible (if only the Higgs potential is considered; massless fermions could condense and drive the transition if the coupling constant is large enough).

MARC A. SHER

JOEL R. PRIMACK

*Physics Department,
University of California,
Santa Cruz,
California 95064, USA*

1. Cook, G. P. & Mahanthappa, K. T. *Phys. Rev. D* **23**, 1321-1336 (1981).

Crystal instability and melting

COTTERILL AND MADSEN¹ argue against an essential connection between thermodynamic melting and crystal instability. Their molecular dynamics simulation of a 336-particle Lennard-Jones (LJ) assembly revealed the existence of a dislocation-mediated mechanical instability in the superheated crystalline phase at a density ($\rho_{\text{inst}} = 1.22$) lying just outside the melting interval ($\rho_{\text{cryst}} = 1.38$, $\rho_{\text{liq}} = 1.24$) determined by Hansen and Verlet² for the same isotherm. Moreover, with increasing temperature, the instability was progressively further removed from the melting interval. We suggest, however, that contrary to their hypothesis, these results add further to an already substantial weight of evidence for the essential connection between crystal instability and melting^{3,4}.

Born⁵ was among the first to propose that melting occurs as a mechanical instability when one of the crystal shear moduli falls to zero. Of course, experiment demonstrated that the shear moduli remained finite up to the melting point, but we have shown^{6,7} that extrapolation of one of the shear moduli as a function of density beyond the melting point, reveals that it would fall to zero at the freezing density for a wide range of ionic, metallic and molecular crystals. We interpreted this as implying the universal existence of an instability concealed between the melting and freezing lines but lying close to the latter. This is confirmed by theoretical calculations for alkali halides⁸ and, indeed, is what one would expect from a proper interpretation of Born's melting criterion. If the crystal were superheated to the critical density, ρ_c , of vanishing static shear modulus, the resultant localization of shear modes would contribute an additional amount, $R \ln 2$, to the entropy⁸, so that the system would be able thermodynamically to make an isothermal jump from a lower density, ρ_{cryst} , to the density, ρ_c . Thus the instability, in normal circumstances, would be concealed by the first-order transition, and to a first approximation ρ_c ($= \rho_{\text{inst}}$) may be equated to ρ_{liq} .

The molecular dynamics result of Cotterill and Madsen seems to confirm our original interpretation of Born's melting criterion, since the freezing density and instability density are almost coincident. Both the suppression of long-wavelength phonons in their finite (336-particle) system and critical slowing would serve to delay the instability and thus it lies a little beyond the melting interval, and is displaced further away with increasing temperature.

Note also that the single-cell occupancy system simulated by Hansen and Verlet to obtain a reversible path between liquid and solid, probably has a first-order transition (L. V. Woodcock, personal communication) rather than the second-

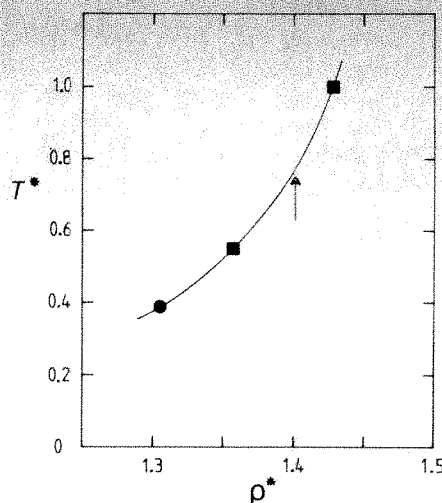


Fig. 1 LJ glass transition temperature (T^*) as a function of density (ρ). The expected transition temperature on Cotterill and Madsen's isotherm is indicated by the arrow.

order transition assumed by Hansen and Verlet. Their phase boundaries may not therefore be altogether reliable. We note that the actual freezing line for argon is displaced progressively away from the Hansen and Verlet line in the same manner as the instability line.

Finally, Cotterill and Madsen's location of the glass transition between the melting and freezing lines at $\rho_g = 1.29$ seems incorrect. Their procedure of finding the intersection of extrapolated linear fits of the extremes of their isothermal pressure-density data ignores the fact that the isotherms are naturally curved in any one phase. Figure 1 shows LJ glass transition temperatures as a function of density reported by Abraham⁹ (squares) and Damgaard-Kristensen¹⁰ (circle) and this predicts a glass transition on Cotterill and Madsen's 0.77 isotherm at $\rho_g = 1.401$; that is, well above their value $\rho_g = 1.29$, and outside the melting interval. That their glassy pair and bond angle distribution functions (pdf and adf, respectively) are actually evaluated for supercooled liquid is evidenced by the lack of a fully developed split-second peak in the pdf. Presumably the incipient splitting in their adf at 110° and 120° would be fully developed in a true glass.

J. L. TALLON

Physics and Engineering Laboratory,
DSIR, Private Bag, Lower Hutt,
New Zealand

1. Cotterill, R. M. J. & Madsen, J. U. *Nature* **288**, 467 (1980).
2. Hansen, J.-P. & Verlet, L. *Phys. Rev.* **184**, 151 (1969).
3. Jelinek, G. E. *Phys. Rev.* **B3**, 2724 (1971).
4. Boyer, L. L. *Phys. Rev. Lett.* **45**, 1858 (1980).
5. Born, M. *J. chem. Phys.* **7**, 591 (1939).
6. Tallon, J. L., Robinson, W. H. & Smedley, S. I. *Nature* **266**, 337 (1977).
7. Tallon, J. L. *Phil. Mag.* **39A**, 151 (1979).
8. Tallon, J. L. *Physics and Engineering Laboratory Rep. No.* 705 (1981); *Phys. Lett.* **87A**, 361 (1982).
9. Abraham, F. F. *J. chem. Phys.* **72**, 359 (1980).
10. Damgaard-Kristensen, W. *J. Non-Cryst. Solids* **21**, 303 (1976).

COTTERILL AND MADSEN REPLY—Tallon considers our instability density for $T = 0.75$ to be indistinguishable from the freezing density, within computational error, and dismisses the disparate temperature dependencies with a reference to real argon, despite its differences from the pseudoinfinite Lennard-Jones matter studied by Hansen and Verlet¹ and ourselves². Moreover, the discrepancy between the two materials is opposite to Tallon's claim. We cannot see why model-dependent stabilization, beyond the instability point, should be more effective at higher temperature. Melting is a reversible first-order transition, the location of which depends on the properties of both liquid and crystal. Instability theories attempt comprehensive treatment of the transition, including projections of liquid properties, using exclusively crystalline characteristics. Such unilateral approaches are inferior to those incorporating more realistic concepts of liquid structure.

Because the properties of all three condensed states are nevertheless determined by the same interatomic interactions, empirical correlations between properties are inevitable; the proximity of the instability and freezing densities²⁻⁴ is thus hardly surprising. But vacancy⁵ and dislocation⁶ parameters both also correlate with the melting temperature, even though melting theories based on these two defects are mutually exclusive⁷. We show elsewhere⁸ that the excess entropy of liquids over crystals is associated with fluidity, not disorder, and stems from conversion of transverse phonons to diffusive modes⁹. Tallon's rather nebulous analysis¹⁰ fails through, amongst other things, neglecting the entropy associated with perfect crystal oscillatory modes. The location of the glass transition density is subject to a choice of convention, but a density of 1.4 for $T = 0.77$ is irreconcilable with our findings; the pressure varies linearly with density in the range 1.35–1.45. Applying Abraham's convention¹¹ to our data, or vice versa, produces no contradiction.

R. M. J. COTTERILL
J. U. MADSEN

Department of Structural
Properties of Materials,
The Technical University of Denmark,
DK-2800 Lyngby, Denmark

1. Hansen, J. P. & Verlet, L. *Phys. Rev.* **184**, 151 (1969).
2. Cotterill, R. M. J. & Madsen, J. U. *Nature* **288**, 467 (1980).
3. Ross, M. & Alder, B. J. *Phys. Rev. Lett.* **16**, 1077 (1966).
4. Hoover, W. G. & Ree, F. H. *J. chem. Phys.* **49**, 3609 (1968).
5. Gorecki, T. Z. *Metallkunde* **65**, 426 (1974).
6. Cotterill, R. M. J., Jensen, E. J., Damgaard-Kristensen, W., Paetsch, R. & Esbjörn, P. O. *J. Phys.* **36**, 35 (1975).
7. Cahn, R. W. *Nature* **273**, 491 (1978).
8. Madsen, J. U. & Cotterill, R. M. J. *Phys. Lett.* **83A**, 219 (1981).
9. Madsen, J. U. & Cotterill, R. M. J. *Physica Scripta* **24**, 959 (1981).
10. Tallon, J. L. *Phys. Lett.* **87A**, 361 (1982).
11. Abraham, F. F. *J. chem. Phys.* **72**, 359 (1980).

BOOK REVIEWS

A disappearing breed

Brian Bertram

WITH the publication of Vols IIIC and IIID of *East African Mammals*, Jonathan Kingdon has completed his *tour de force*. These final volumes deal with most of the artiodactyls — the bovines and antelopes whose numbers and diversity contribute so much to the array of East Africa's mammals.

The format is the same as in the earlier volumes. For each tribe the author presents an introductory profile covering topics such as structure, coat colouring, the form of the horns, body size, evolutionary history, signalling and ecological niches. For each species he then describes its past and present distribution, its distinguishing features, its feeding and predators, its behaviour and breeding. Again, the author's superb illustrations abound, and contribute greatly to the information presented; Kingdon can convey so much more with a few pencil lines than anyone could say in many pages of text. There are always beautiful and meticulously accurate drawings of the whole animal, and there are often equally accurate drawings of the skinned animal, revealing the underlying musculature, and of the skeleton. In addition, there are countless thumbnail sketches which capture the essence of an animal's appearance or behaviour.

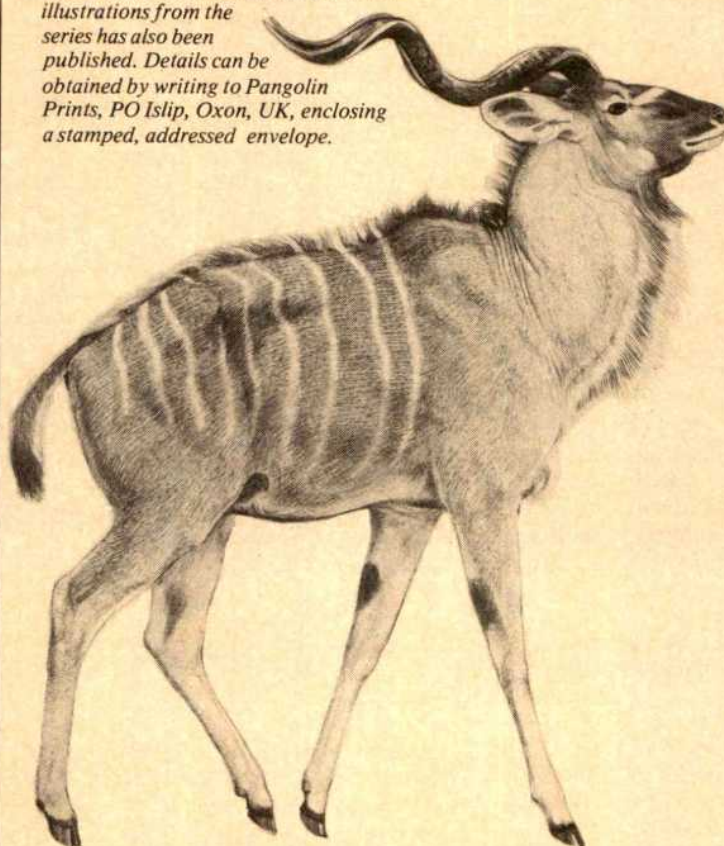
Unlike earlier volumes in the series, neither of these final volumes can stand on its own. Volume IIIC includes the bovines and the smaller antelopes, while Vol. IIID has the larger antelopes, four appendices, the bibliography and indexes for these last two volumes, and a species checklist for all seven volumes. The first appendix outlines the fundamental problems of conservation, and the ethic, the threats, and the meagreness of the response. The second, by David M. Jones, summarizes current knowledge of the feeding and handling of mammals in captivity. Appendix III lists the various parasites and diseases known to infect

East African Mammals: An Atlas of Evolution in Africa, Vols IIIC and IIID. By Jonathan Kingdon. Vol. IIIC, pp.393, ISBN 0-12-408344-7; Vol. IIID, pp.353, ISBN 0-12-408345-5. (Academic: 1982.) Each volume £49.95, \$99.50.

East African mammals, and Appendix IV considers briefly the potential for commercial exploitation of wildlife.

We can now look back on the whole series, and we must do so with considerable awe. The 2,900 pages contain a vast wealth of information and discussion. They also contain hundreds of fascinating and often most beautiful illustrations. Particularly in the earlier volumes, more guidance could have been given to help the reader to make use of the illustrations, noting important features or explaining what an animal was doing. But it remains indisputable that these seven books constitute a remarkable work.

The art of Jonathan Kingdon — a Greater Kudu from Vol. IIIC of East African Mammals. A limited edition of full-size illustrations from the series has also been published. Details can be obtained by writing to Pangolin Prints, PO Islip, Oxon, UK, enclosing a stamped, addressed envelope.

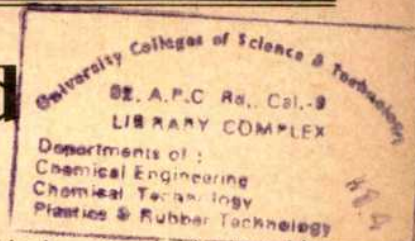


The series has expanded in the writing. "This is the first of a three volume work" announced the flysheet to Vol. I, in 1971. By geometrical progression, this was followed by IIA and IIB, and by IIIA, IIIB, IIIC and IIID. It has been a somewhat unplanned growth, resulting in some awkward anomalies of arrangement: thus the page numbers in Vols IIB and IIID, but only these, continue from where the previous volumes' numbers left off; the bibliographies are sometimes split up according to subject and sometimes not; and what is essentially the same gazetteer appears in Vols I, IIB, IIIA and IIID.

Expansion plus inflation have had an alarming effect. On publication eleven years ago, the 446 pages of Vol. I cost £12 (about £38 at today's prices), and a reprint can still be bought for £34.40. The 353 pages of Vol. IIID will cost you £49.95, and the whole series £255 (\$534.50), which means that what started as a set of three, which keen private naturalists could just hope to afford, has ended as a series mainly for libraries. It is well worth making sure you have access to it somehow, because it contains so much of value as well as of beauty.

Valuable beautiful things are rare, and so may well prove to be good investments. On their current form these books will be. But I fear that the series, like its author and like several of the species it describes, is a disappearing breed. The very high standard of production, the generous use of space, the large typeface and the ample illustrations all allow what have become increasingly reference works for the specialist and the professional to retain the attractiveness of coffee table books. What a pity it is that other continents and other faunas have yet to be so well served by anyone as East Africa has by Jonathan Kingdon and Academic Press. □

Brian Bertram is Curator of Mammals at the Zoological Society of London.



And citation begat co-citation . . .

A.C. Allison

ISI Atlas of Science: Biochemistry and Molecular Biology 1978/80. Pp.540. ISBN 0-941708-00-4. (Institute for Scientific Information, Philadelphia: 1982.) \$45 (individual), \$90 (institution).

THE information explosion is daunting to most people but challenging to others, including Eugene Garfield and his colleagues of the Institute for Scientific Information (ISI) in Philadelphia, who have devoted themselves to the systematic collection and organization of information. First came *Current Contents*, the usefulness of which is universally acknowledged. The commercial success of *Current Contents* allowed the production of the *Science Citation Index*, which is widely but less generally used. More recently the Institute has published *Research Fronts in ISI/Biomed* and now the *ISI Atlas of Science*, a reference work to 102 Research Fronts or "Specialties" within the fields of biochemistry and molecular biology.

The Research Fronts included in the *Atlas* were identified by frequent citations in the *Science Citation Index*. The central process of selection of papers was the process termed "co-citation clustering". This is when an author, in citing the works of two other authors, establishes an intellectual link between them. The papers quoted in the *Atlas* were both highly cited and frequently co-cited. This computer analysis is supposed to reveal sets of papers that are important, because of the attention they have received from colleagues of the authors, and highly related because of the co-citation linkage. For each specialty, maps are constructed in which the documents are arranged graphically according to a mathematical treatment of co-citation patterns. The same treatment is also used to construct a Global Map, which shows the relationships among the various specialties in biochemistry and molecular biology.

For each specialty there is a section entitled "Citation Core Documents" which comprises the main citations and co-citations constituting the cluster. This is intended to provide objective assessment of clustering and case documentation, instead of the usual subjective assessment by individual scientists. There is a short, one-page mini-review of each specialty.

The unique feature of the *Atlas* is the Specialty Maps and the Global Map, but it can be questioned whether this is the most useful way to employ computers. The value of computers for information retrieval, especially for recovering associated information (e.g. on prostaglandins in a particular cell type) is well established and has lightened this burden for most scientists. Listing the Citation Core Documents for each specialty is helpful,

although similar information can be obtained through the *Index Medicus* and other compilations. A brief perusal of these documents will often establish their relatedness more surely than the maps, which are for the most part statements of the obvious and are at times misleading.

It can also be questioned whether, for persons intending to go into a field seriously, reviews of specialties by various experts, such as are found in the *Annual Review of Biochemistry*, do not provide

equally accessible and more authoritative and up-to-date sources of information than the data in the *Atlas* (most of the analyses in the *Atlas* were completed before 1980, but supplements refer to major citations in 1980).

The general conclusion is that the thirst for information is not easily satisfied, and that the *Atlas* does provide a ready source of information on a range of subjects. Certainly, it is likely to be widely sold and used. □

Anthony Allison is Director of the Institute of Biological Sciences, Syntex Research, Palo Alto, California.

Mitochondria: the cell's paying guests?

M. J. Selwyn

Mitochondria. By Alexander Tzagoloff. Pp.342. Hbk ISBN 0-306-40799-X; pbk ISBN 0-306-40778-7. (Plenum: 1982.) Hbk \$42.50, £26.78; pbk \$19.95, £12.57.

MITOCHONDRIA have provided interesting and challenging subjects for study by biochemists and cell physiologists ever since it became possible, in the early 1950s, to isolate them in quantity and quality. The reason for this interest is that the organelles have an integrated set of functions which, although complex, is more simple than that of a whole cell; for instance it was soon recognized that they contained complete sets of enzymes for the citric acid cycle and fatty acid oxidation. In his new book, Alexander Tzagoloff appropriately describes these metabolic pathways in brief, in only one of the eleven chapters; most readers can be expected to be well acquainted with them.

The central chapters of *Mitochondria* deal with the properties and functions of the membrane-bound enzymes and carrier systems, including the vital function of regenerating ATP by oxidative phosphorylation. The story of the investigation of these systems should be a fascinating and salutary tale. The classical techniques and concepts of aqueous phase biochemistry failed to resolve the mechanisms, and new methods and ideas for membrane biochemistry had to be developed. Sad to say I found this, the longest and a very important section, somewhat disappointing. The author appears to give unenthusiastic acceptance to the chemiosmotic coupling theory and these chapters are not as up-to-date as they should be, few papers after 1978 being cited. The treatment is patchy and sometimes falls far short of what is needed. For example, descriptions of ions simply as "permeant" can be misleading, as is describing uncouplers as "blocking" reactions; and are we really not sure that

valinomycin is a mobile carrier and gramicidin a pore-former? The failure to describe the proton-conducting function of the membrane-embedded component detracts seriously from the treatment of the ATPase complex.

The last two chapters, on mitochondrial biogenesis and genetics, make more exciting reading. Over the past 20 years mitochondria have been found to contain not only their own DNA but a complete apparatus for synthesizing a few polypeptides. And whilst a decade ago the mitochondrial protein synthesizing system appeared to be very similar to that of prokaryotes, major differences are now being discovered — not only between the mitochondrial and prokaryotic systems but also between mitochondrial systems from different organisms. The idea that mitochondria are the descendants of symbiotic prokaryotes which paid for their keep in the ancestral eukaryote cell by regenerating ATP is now no more plausible than the alternative that mitochondria arose by segregation of certain functions and some DNA within the eukaryote. Whichever is the case, it is clear that mitochondria are now set to be a testing ground for fundamental investigations in molecular genetics and into the evolution of eukaryotic cells.

Tzagoloff helps to fill the gap left by the failure to revise Lehninger's *The Mitochondrion* since it first appeared in 1964. He provides much of the basic material which a research student working with mitochondria will need to know. Teachers of advanced undergraduate courses will also want a copy, and one or two in the library, but they will have to supplement and comment on the bioenergetics chapters. □

M. J. Selwyn is Dean and Senior Lecturer in Biochemistry in the School of Biological Sciences, University of East Anglia.

On the edges of the sea

John H. Steele

Ecology of Coastal Waters A Systems Approach By K H Mann Pp 322 Hbk ISBN 0-632-00669-2, pbk ISBN 0-632-00953-5 (Blackwell Scientific/University of California Press 1982) Hbk £25, \$36, pbk £10 80, \$18

COASTAL ecosystems are very diverse, reflecting the many different ways in which the land interacts with the sea. This coastal zone has always fascinated biologists and, more recently, has become subject to increasing pressure for recreational and commercial uses. Thus, for both scientific and practical reasons, we need to generalize about these environments. Dr Mann's book approaches the problem in two ways — by description of the principal types of coastal ecosystem and by considering the application to these systems of various modelling techniques.

Coastal waters are often considered as the most accessible parts of the pelagic ocean. Here only one chapter is given to phytoplankton-based systems, while most of the text is devoted to excellent analyses of major features such as marshes, mangroves and coral reefs. There is also an emphasis on the sediment communities and their microflora which play a critical role in exchange of materials across the sediment-water interface and from land to sea.

In particular, Mann focuses on general patterns of energy flow and on average conditions within each system. Although a chapter on water movements is included, there is little on the consequences for these coastal areas of the highly episodic nature of physical changes. Instead, the homeostatic properties of coastal ecosystems are a central feature of the approach used in this book. As Mann acknowledges, further work will be needed to assess these properties in the context of extremes of variability to which they are exposed.

The final chapter, "Models and Management", brings together methods of synthesizing and using ecosystem studies in the coastal zone. The author discusses several computer simulations which attempt to reconstruct the system numerically from its physical, chemical and biological components. The general conclusion is that these exercises give valuable insights, but are far from being a predictive tool for environmental managers. Mann points out that the managerially useful models, such as those for biological oxygen demand in estuaries, would be considered by many researchers as unrealistic simplifications. The broad question he raises is whether simpler holistic models without explicit formulation of organism behaviour are not merely of empirical value, but a recognition of a general feature of the hierarchies within and between

ecosystems. This question is not new, nor confined to the coastal area, but it is central to both the future research and management philosophy for this part of our environment.

Ecology of Coastal Waters combines sound descriptive chapters with proper speculative flavouring. It is aimed at advanced students and professionals, and will be useful and interesting to all concerned with the edges of the sea. □

John H Steele is Director of the Woods Hole Oceanographic Institution, Massachusetts

Galileo rules, OK?

C. J. S. Clarke

Retarded Action-at-a-Distance The Change of Force with Motion By G Burniston Brown Pp 145 ISBN 0-904378-14-4 (Cortney Publications, 95-115 Windmill Road, Luton, UK 1982) £9 95

It is in the nature of science to question, to refuse to treat anything as unalterable dogma, and so there is nothing improper in questioning the correctness of Maxwellian electrodynamics, special relativity and general relativity, as does the author of this book. In their place he proposes Euclidean space and time, with Galilean relativity, combined with retarded inter-particle action at a distance using unconventional force-laws. It is a polemical book, and so one looks for a clear critique of the central philosophical and experimental points where he differs from conventional wisdom. But one looks in vain: the experimental evidence is ignored, the philosophical arguments evaded.

For example, in his theory electromagnetic interactions are linear and linked to the Euclidean geometrical relations between the particles involved, thus it is crucial that a null result be obtained for the "gravitational bending of light" experiment. And so it is astonishing that his only reference on this subject is to a 1930 article criticizing the "early claims that the effect of gravitation on light at eclipses had been proved", as if the author were unaware of the work of Counselman, Fomalont and Sramek that improved on the early eclipse observations by an order of magnitude in accuracy.

Gaia anew

J E Lovelock's *Gaia A New Look at Life on Earth* (reviewed in *Nature* 282, 154, 1979) has now appeared in a paperback edition. The book is published by Oxford University Press, price £2 95.

The crucial difficulty with any direct action theory is the explanation of radiation-reaction, as manifested in the behaviour of charged particles in accelerators. It was this difficulty that led Wheeler and Feynman to propose their time-symmetric direct action theory, explicitly rejected by the author. Yet he concerns himself almost exclusively with phenomena such as current electricity, where it is possible to avoid the problem, and nowhere gives a clear account of radiation-reaction on individual particles.

The treatment of philosophical issues is no more satisfactory. The author is proposing a Galilean structure for space-time, but without any serious philosophical justification whatever. One supposes that he holds to the Kantian view that the Euclidean nature of space is part of its *a priori* status, but Kant was writing before Poincaré, Reichenbach and Gruenbaum, and before the Eötvös-type experiments of Dicke and Braginsky on which the relativistic concept of space is nowadays based. Dr Burniston Brown is writing after these writers and experimentalists have shown that it is far from obvious that the "space" used by astronomers is necessarily Euclidean. In 1880 this book might have been a useful contribution. In 1982 it is conspicuous only by its omissions. □

C J S Clarke is a Lecturer in Mathematics at the University of York

"THE MOST COMPLETE HISTORY OF THE ATOM TO BE PUBLISHED" *Energy Daily*

The Atomic Complex

by Bertrand Goldschmidt is an accurate, complete and fascinating worldwide political history and personal memoir of nuclear energy — from the development of the bomb in World War II to today's nuclear energy complex and proliferation problems.

Goldschmidt, a leading French scientist turned international statesman, reviews half a century of political moves, counter-moves, international intrigue and manipulation. *The Atomic Complex* is a pragmatic look at the nuclear world today, carefully examining the terror nuclear weapons represent, but at the same time stressing the benefits of nuclear energy.

Order this 500 page best seller today "superbly done and reads easily"

**\$31 Hardbound
\$24 Softbound**

American Nuclear Society
555 North Kensington Avenue
La Grange Park, IL 60525 USA

Circle No 12 on Reader Service Card

BOOKS RECEIVED

Applied Biological Sciences

- MITCHELL, M S and OETTGEN, H F (eds) *Hybridomas in Cancer Diagnosis and Treatment Progress in Cancer Research and Therapy*, Vol 21 Pp 282 ISBN 0-89004-768-5 (Raven 1982) \$40 80
- NAJJAR, V A (ed) *Immunologically Active Peptides Developments in Molecular and Cellular Biochemistry*, Vol 2 Pp 135 ISBN 90-6193-842-2 (Junk, The Netherlands 1981) \$55, Dfl 125
- PALTI, J *Cultural Practices and Infectious Crop Diseases Advanced Series in Agricultural Sciences*, Vol 9 Pp 243 ISBN 3-540-11047-X/0-387-11047-X (Springer-Verlag 1981) \$39 80
- PONTIFEX, G (ed) *Lung Cancer Proc of the 1st European Symposium held September 7-13, 1980, Chalkidiki* Pp 381 ISBN 90-219 0499-3/0-444-90224-4 (Excerpta Medica/Elsevier 1981) \$90 75, Dfl 195
- ROBINSON, R *Genetics for Dog Breeders* Pp 264 ISBN 0-08-025917-0 (Pergamon 1982) £9 95, \$19 95
- RYMAN, N (ed) *Fish Gene Pools Preservation of Genetic Resources in Relation to Wild Fish Stocks Proc of an International Symposium held January 23-25, 1980, Stockholm Ecological Bulletins*, 34 Pp 111 ISBN 91-546-0299-8 (Swedish Council for Planning and Coordination of Research 1981) Np
- SALEM, M R (ed) *Pediatric Anesthesia Current Practice*, Vol 1 Pp 158 ISBN 0-12-615201-2 (Academic 1981) \$27 50
- SCHULTZ, V and WARD WHICKER, F *Radioecological Techniques* Pp 298 ISBN 0-306-40797-3 (Plenum 1982) Np
- A SCIENTIFIC AMERICAN BOOK *Industrial Microbiology and the Advent of Genetic Engineering* Pp 108 Hbk ISBN 0-7167-1385-3, pbk 0-7167-1386-1 (Freeman 1981) Np
- SORENSEN, J R, SWAZEY, J P and SCOTCH, N A *Reproductive Pasts Reproductive Futures Genetic Counseling and Its Effectiveness Birth Defects Original Article Series*, Vol XVII, 4 Pp 214 ISBN 0-8451-1044-6 (Alan R Liss 1981) £21, DM 96
- SUTHERLAND, R L and JORDAN, V C (eds) *Non-steroidal Antioestrogens Molecular Pharmacology and Antitumour Activity* Pp 496 ISBN 0-12-677880-9 (Academic 1982)
- SZARA, S I and LUDFORD, J P (eds) *Benzodiazepines A Review of Research Results, 1980 NIDA Research Monograph*, 33 Pp 101 ISBN 017-024-01108-8 (DHHS, Rockville 1981) \$4 75
- THOMPSON, T and JOHANSON, C E (eds) *Behavioral Pharmacology of Human Drug Dependence NIDA Research Monograph*, 37 Pp 294 ISBN 017-024-01109-6 (DHHS, Rockville 1981) \$6 50
- VAN DEN BOSCH, R, MESSENGER, P S and GUTIERREZ, A P *An Introduction to Biological Control* Pp 247 ISBN 0-306-40706-X (Plenum 1982) Np
- WEISSMANN, G (ed) *Advances in Inflammation Research*, Vol 4 Pp 208 ISBN 0-89004-669-7 (Raven 1982) \$28 56
- YOSHIDA, H, HAGIHARA, Y and EBASHI, S (eds) *Biochemical Immunological Pharmacology*, Vol 4 Pp 280 ISBN 0 08-028024-2 (Pergamon 1982) Np
- YOSHIDA, H, HAGIHARA, Y and EBASHI, S (eds) *Cardio-renal and Cell Pharmacology*, Vol 3 Pp 340 ISBN 0-08-028023-4 (Pergamon 1982) Np
- YOSHIDA, H, HAGIHARA, Y and EBASHI, S (eds) *Clinical Pharmacology Teaching in Pharmacology*, Vol 6 Pp 315 ISBN 0-08-028026-9 (Pergamon 1982) Np
- YOSHIDA, H, HAGIHARA, Y and EBASHI, S (eds) *Toxicology and Experimental Models*, Vol 5 Pp 355 ISBN 0-08-028025-0 (Pergamon 1982) Np

Psychology

- COLES, E M *Clinical Psychopathology An Introduction* Pp 502 Hbk ISBN 0-7100-0864-3, pbk ISBN 0-7100-0867-8 (Routledge & Kegan Paul 1982) Hbk £15, pbk £8 95
- OLSEN, P (ed) *Comprehensive Psychotherapy*, Vol 3 Pp 156 ISBN 0-677-16369-A (Gordon & Breach 1981) \$45
- SOLOMON, J (ed) *Alcoholism and Clinical Psychiatry* Pp 238 ISBN 0-306-40794-9 (Plenum 1982) Np
- USDIN, E (ed) *Clinical Pharmacology in Psychiatry* Pp 352 ISBN 0-444-00556-0 (Elsevier 1981) \$59, Dfl 135
- WOLBERG, L R *The Practice of Psychotherapy 506 Questions and Answers* Pp 416 ISBN 0-87630-290-8 (Brunner/Mazel, New York 1982) \$30

Sociology

- AULIN, A *The Cybernetic Laws of Social Progress Towards a Critical Social Philosophy and a Criticism of Marxism* Pp 218 ISBN 0-08-025782-8 (Pergamon 1981) £22 50, \$45
- BLALOCK, A B and BLALOCK, H M Jr *Introduction Social Research*, 2nd Edn Pp 153 Hbk ISBN 0-13-496810-7, pbk ISBN 0-13-496802-6 (Prentice Hall 1982) Hbk £8 95, pbk £5 95
- EVANS, B and WAITES, B *IQ and Mental Testing An Unnatural Science and its Social History* Pp 228 Hbk ISBN 0-333-25648-4, pbk ISBN 0-333-25649-2 (Macmillan Press, London & New York 1981) Hbk np, pbk £4 95
- KONEČNI, V J and EBBESEN, E B (eds) *The Criminal Justice System A Social-Psychological Analysis* Pp 418 Hbk ISBN 0-7167-1312-8, pbk ISBN 0-7167-1313-6 (Freeman 1982) Hbk np, pbk np
- REYNOLDS, P D *Ethics and Social Science Research* Pp 191 ISBN 0-13-290965-0 (Prentice Hall 1982) £7 45

Anthropology

- STEIN, P L and ROWE, B M *Physical Anthropology*, 3rd Edn Pp 482 ISBN 0-07-061151-3 (McGraw-Hill 1982) \$18 95
- WOOLFSON, C *The Labour Theory of Culture A Re-examination of Engels' Theory of Human Origins* Pp 124 ISBN 0-7100-0997-6 (Routledge & Kegan Paul 1982) £4 95

General

- CHARALAMBOUS, G and INGLET, G (eds) *The Quality of Foods and Beverages Chemistry and Technology*, Vol 2 *Proceedings of a Symposium of the 2nd International Flavor Conference, July 1981, Athens, Greece* Pp 383 ISBN 0-12-169102-0 (Academic 1981) \$26 50
- CHIGIER, N A (ed) *Progress in Energy and Combustion Science*, Vol 6 Pp 395 ISBN 0-08-027153-7 (Pergamon 1981) £51, \$118
- COOPER, W E and SORENSEN, J M *Fundamental Frequency in Sentence Production* Pp 213 ISBN 3-540-90510-3 (Springer-Verlag 1981) DM 48, \$22 90
- McMAHAN, J *British Nuclear Weapons For and Against* Pp 165 Hbk ISBN 0-86245-047-0, pbk ISBN 0-86245-049-7 (Junction Books, London 1981) Hbk £9 95, pbk £3 95
- MEEKS, L B and HEIT, P *Human Sexuality Making Responsible Decisions* Pp 503 ISBN 0-03-058366-7 (Saunders 1982) Np
- ORTNER, S B and WHITEHEAD, H (eds) *Sexual Meanings The Cultural Construction of Gender and Sexuality* Pp 435 Hbk ISBN 0-521-23965-6, pbk ISBN 0-521-28375-2 (Cambridge University Press 1982) Hbk £25, pbk £7 95
- POLMAR, N and ALLEN, T B *Rickover Controversy and Genius A Biography* Pp 744 ISBN 0-671-24615-1 (Simon & Schuster, New York 1982) \$20 75
- RAYNOR, J O and ENTIN, E E *Motivation, Career Striving, and Aging* Pp 406 ISBN 0-89116-189-9 (Hemisphere Publishing 1982) \$24 95
- RICHMOND, C R, WALSH, P J and COPENHAVER, E D (eds) *Health Risk Analysis Proceedings of the 3rd Life Sciences Symposium, Gatlinburg, Tennessee, October 1980* Pp 483 ISBN 0-89168-042-X (Franklin Institute Press, Pennsylvania 1981) \$40
- RIEPE, D (ed) *Asian Philosophy Today* Pp 291 ISBN 0 677-15490-9 (Gordon & Breach 1981) \$24
- ROBERTS, M J and BLUHM, J S *The Choices of Power Utilities Face the Environmental Challenge* Pp 458 ISBN 0-674-12780-3 (Harvard University Press 1981) £17 50
- ROSS, S D *Learning and Discovery* Pp 134 ISBN 0-677-05110-7 (Gordon & Breach 1981) \$29 50
- SALOMON, J-J *Prométhée Empêtré La Resistance au Changement Technique* Pp 174 Pbk ISBN 0-08-027064 6 (Pergamon 1981) Pbk np
- SAXENA, J and FISHER, F (eds) *Hazard Assessment of Chemicals Current Developments*, Vol 1 Pp 461 ISBN 0-12-312401-8 (Academic 1981) \$49 50
- SAYERS, J *Biological Politics Feminist and Anti-Feminist Perspectives* Pp 235 Hbk ISBN 0-422-77870-2, pbk ISBN 0-422-77880-X (Tavistock, London 1982) Hbk £10 95, pbk £4 95
- SHAFFER, M *Life after Stress* Pp 273 ISBN 0-306-40869-4 (Plenum 1982) \$15 95
- SHARPE, R S (ed) *Research Techniques in Nondestructive Testing*, Vol 5 Pp 332 ISBN 0-12-639055-X (Academic 1982) £28 40, \$58 50
- SIGMON, B A and CYBULSKI, J S (eds) *Homo erectus Papers in Honor of Davidson Black Based on the Proceedings of an International Symposium, Cedar Glen, Ontario, October 1976* Pp 271 ISBN 0-8020-5511-7 (University of Toronto Press 1982) £21, \$37 50
- SOFER, S S and ZABORSKY, O R (eds) *Biomass Conversion Processes for Energy and Fuels* Pp 420 ISBN 0-306-40663-2 (Plenum 1981) \$49 50
- STEPHENSON, R M *Living with Tomorrow A Factual Look at America's Resources* Pp 280 ISBN 0-471-09457-9 (Wiley 1981) £16 75, \$29 95
- SWERN, D (ed) *Bailey's Industrial Oil and Fat Products*, Vol 2 4th Edn Pp 603 ISBN 0-471-83958-2 (Wiley 1982) £44, \$80
- UN ECONOMIC COMMISSION FOR EUROPE *Protein and Energy Supply for High Production of Milk and Meat A Symposium of the UN Economic Commission for Europe and the Food and Agriculture Organization* Pp 191 ISBN 0 08-028909-6 (Pergamon 1982) £15, \$30
- WATERS, M D *et al* (eds) *Short-Term Bioassays in the Analysis of Complex Environmental Mixtures II Environmental Science Research*, Vol 22 *Proceedings of the 2nd Symposium held in Williamsburg, Virginia, March 1980* Pp 524 ISBN 0-306-40890-2 (Plenum 1981) \$59 50
- WATLING, R *Three Bolbitaceae Agrocye, Bolbitus & Conocycbe* Pp 139 ISBN 0-11-491750-7 (HMSO 1982) £8
- WEATHERS, W *The Broken Word The Communication Pathos in Modern Literature Communication and the Human Condition*, Vol 1 Pp 226 ISBN 0-677-04990-0 (Gordon & Breach 1981) \$62 50
- WEBBER, B L and NILSSON, N J (eds) *Readings in Artificial Intelligence* Pp 557 ISBN 0-935382-03-8 (W H Freeman 1982) £17 50
- WEISSMAN, R F E *Ritual Brotherhood in Renaissance Florence Population and Social Structure* Pp 254 ISBN 0-12-744480-7 (Academic 1982) Np
- WILFORD, J N *The Mapmakers* Pp 414 ISBN 0-86245-041-1 (Junction Books, London 1981) £9 95
- WINITZ, H (ed) *Native Language and Foreign Language Acquisition*, Vol 379 Pp 378 Hbk ISBN 0-89766-147-8, pbk ISBN 0-89766-148-6 (New York Academy of Science 1981) Hbk \$75, pbk np

nature

16 September 1982

Department of
 Communications
 Cambridge University
 Cambridge CB2 3RQ
 Planned to receive Technology

8 NOV 1983

Principles, policies and pipelines

The great Siberian pipeline row has caught out most Western governments (and the Reagan Administration in particular). The need is for a compromise. But intellectual work is also necessary.

The quarrel between the United States and Western Europe about the Siberian pipeline is another vivid illustration that nothing so confounds international relations as incomprehension, a failure to appreciate that other parties to a dispute may also have a case. But even when the origins of such disputes are insubstantial, the consequences may be as damaging as when the conflict is about some tangible issue, say a disputed piece of territory. Already, four European companies (three French, one British) have been put on an unprecedented blacklist to which United States corporations will be forbidden to supply goods. More European companies will no doubt soon join them, for there has so far been no break in the seeming determination of Western European governments that their domestic manufacturers should honour contracts for supplying equipment for the pipeline project. But in the long run, the financial damage to the companies concerned will be negligible compared with the damage done to relations between Europe and the United States. Paradoxically, even those in the Soviet Union who may at present be delighted at the apparent discomfiture of the Atlantic alliance may in the end themselves be discomfited (Soviet readers, as important a part of any international journal's readership as any other, please note).

Responsibility

President Ronald Reagan and his advisers must shoulder the prime responsibility for incomprehension. That Mr Reagan should have turned out to be a more zealous advocate than his predecessor of the use of economic sanctions to bring political pressure on the Soviet Union is not of course surprising, for it was well advertised in advance, but even Mr Jimmy Carter followed a similar course after the appearance of Soviet forces in Afghanistan at the beginning of 1980. The US government's present calculation is that economic sanctions against the Soviet Union, and in particular the denial of specialized supplies for the Siberian pipeline, will indirectly bring about a relaxation of the martial law regulations imposed in Poland last December. The questions whether the calculation is correct, whether the United States has reason to expect Western European governments to share its conclusions and objectives — and why President Reagan appears to have passed up the opportunity to find out at the June summit meeting at Versailles — are important but do not touch the central principle. It is the same with the questions that have been raised about the wisdom of the Western European governments agreeing to buy natural gas from the Soviet Union — strategic dependence in energy supply and the provision of a steady flow of hard currency over the decades ahead (see *Nature* 22 July, p 313). What matters, and what the United States appears to be incapable of understanding, is that these arrangements were concluded during Mr Carter's presidency, were then widely regarded in a very different light and could not now be abrogated retrospectively without causing serious legal difficulties for Western European corporations and even for their governments.

Mr Reagan's government is now busily making matters worse by insisting that one of the objectives of its present policy is to demonstrate to all concerned, Europeans as well as the Soviet Union, that the United States has reassumed the leadership of the Atlantic alliance. While, after several years of US indecision, that

message would ordinarily be welcome in Western Europe, its timing and its manner are inappropriate, not to say inept. For the governments in Western Europe that Mr Reagan now wishes to have follow the United States in being tough with the Soviet Union are, like his own, governments by the grace of their electors. And it has not been forgotten in Western Europe that the long and painful decline of Chancellor Helmut Schmidt's coalition government in West Germany dates from the time when he put his political future on the line in favour of President Carter's proposal to base neutron bombs in Europe — and then found that Mr Carter had climbed down without telling him in advance. Mr Reagan's present position on the pipeline, whether justifiable or not, is bound to seem to many as a reversal of previous policies without consultation, let alone agreement, and will thus strengthen the Gallic line towards the Atlantic alliance that has been rife in Europe for decades — the view that, over the long run, the interests of the United States are unlikely always to coincide with those of Western Europe, for which reason Western Europe had better plan for self-sufficiency.

European governments, whatever their political colour, will not be able to overlook the growth of this opinion, even if it should be misconstrued, to fail to do so might be to risk electoral defeat, even replacement by gallically-inclined successors. But even governments not now at risk, or which (like the British government, with the Falklands war behind it) keenly appreciate the importance of assistance from the United States, may find it impolitic to stomach the style of leadership now on offer. Unless the quarrel about the pipeline is quickly patched up, it is not entirely far-fetched that it could mark the beginning of the end of transatlantic arrangements for the defence of Western Europe. Strange though it may seem, that would not be the unmixed benefit for the Soviet Union that it would seem at first sight to be, for there is every chance that Western Europe living more by its own devices than at present would be a more awkward, if less predictable, customer than it is now.

Retreat

Retreating from the present position will demand more diplomatic skill than either the United States or Western Europe has shown in the past few months. Although the pipeline issue has been rumbling on since the beginning of the year, neither of the parties seems to have done what prudence would have required at the Versailles meeting — insisting that it should know for sure what was in the other's mind. Instead, the official communique includes a vague reference to the need for caution in dealing with the Soviet Union, given the troubling events in Poland in previous months. President Reagan seems diffidently not to have asked for a commitment to boycott the Siberian pipeline, and the governments of Western Europe to have been content to let sleeping dogs lie. Since then, embarrassment, indolence and more recently bad temper have been substituted for rational discussion. Until the imposition in mid-August of sanctions by the United States on French pipeline suppliers, it would have sufficed that the United States should have demanded of Western Europe an account of what it planned to do to implement the loose wording of the Versailles communique. Now, with opinions on both sides hardened, the only hope for a resolution of the quarrel is that there should be a serious attempt to hammer out a policy on

economic relations with the Soviet Union on which the governments concerned can agree, or agree to disagree. The more public that process, the more easily the United States could abandon as it must its sanctions against companies in Western Europe without losing face.

Agreement is too much to ask for, but a basis for civilized disagreement should be attainable. The underlying issue is what kind of relationship should obtain between the industrialized West and the industrialized East, partners in a more vexing dispute than over a mere pipeline. A few things are agreed, at least formally: there should be negotiations on strategic arms control, and neither side will sell defence equipment to the other. Two other issues are more fuzzy: the extent to which personal freedom is subordinate to or the basis for the integrity of the state, and the part that should be played in such a tense relationship by what would otherwise be considered normal commercial and cultural relationships. Broadly speaking, the governments of West and East differ radically on the first question (which is why they are at loggerheads), but the West is divided among itself on the second. It is possible to argue that the restraint of commerce will force illiberal regimes to become more liberal, but also that the opposite is the truth. The perplexity of British governments about the encouragement of sport in the Republic of South Africa is a proof that historical precedent is not a sure guide.

In such circumstances, the only acceptable basis for an understanding between the disputants of the West is that they should all know clearly where they stand on the restraint of commerce and of cultural relations and (knowing the hazards of ballot-box democracy) should be able to lay odds about where they may stand in future. On the face of things, there is much to be said for Andrei Sakharov's position (see page 199) that the questions of strategic arms control and of human rights (the nature of democracy) should be uncoupled and that the principle should also be extended to uncouple commercial relations on non-military commodities (such as natural gas) from the issue of personal liberty. For once restraint has gone so far that the provision of pipeline equipment is not allowed, the time would soon arrive when even the sale of ostentatiously unstrategic commodities (cereals, say) to the Soviet Union would be disallowed. Paper clips could just as easily be embargoed.

Ostensibly, none of this has much to do with the scientific community, but the contrary is the truth. The tale of how Sir Humphry Davy went on a scientific jaunt (with his new bride) through mainland Europe at the height of the Napoleonic Wars is almost too well known, while the fact that Pugwash could safely meet in Warsaw this August can easily be discounted on the grounds that it is no longer in a position to risk giving offence. Protests among Australian biochemists and other professional people that the federal government should not have put last month's meeting of biochemists at Perth in hazard by denying visas to two Soviet officials travelling as scientists are more to the point, if only because they illustrate how intimately government officials rather than professionals are now involved in the judgement of what should be done. (To its credit, the Australian National Academy of Sciences has done everything that might have been expected of it to protest.)

But such issues are too important to be left to government officials. Professional people in the strict sense should have more say. Natural scientists could (and therefore should) argue that their lives would be more interesting and therefore more productive if there were less, not more restraint. Economists (regarded as scientists proper in many places) have much to say about the fructifying all-round benefits of more trade, whatever its nature or with whom. Historians (also still considered to be professional scientists in most of mainland Europe) have important information to contribute about the unfolding of enduring events. If professional people are serious in their protestations that the present world is dangerous, they would be well-advised to turn their energies from saying that nuclear war would be cataclysmic to showing how to solve the more subtle but more urgent problem of East-West relations which has so perplexed the most powerful governments in the past few months.

Doing one's thing

What do the British Association, ICSU and the Falkland Islands have in common? Distraction.

Crisis is not everybody's agenda, and the British Association for the Advancement of Science duly met last week at the University of Liverpool for its annual jamboree. To nobody's surprise after 150 similar occasions, there were few surprises. Thus Dr Beverly Halstead rehearsed his previously advertised objections to cladistics, Dr W. Eldridge (Gould's collaborator on punctuated equilibrium, and now curator of fossils at the New York Museum of Natural History) replied and the London *Times* earned a familiar rebuke from Sir Andrew Huxley for having reported the affair as if it had sprung up anew. Most of those listening to the debate, like those attending the meeting as a whole, will have found the experience rewarding (for otherwise they would not have chosen to go). The British Association itself is in a more serious dilemma: it purports to carry the message from research laboratories to the world at large (and many daily newspapers still behave as if that were the case). For next year's meeting, the association is promising that it will have forged stronger relationships with learned societies in the United Kingdom, in the hope that its message will be more pointed. (There will still, of course, be anxieties about money.) Why does not this venerable institution stick to what it does well and have the courage to let others judge whether there are wider benefits and what they are?

The meeting of the International Council of Scientific Unions (ICSU) at Cambridge (England) this week will have seemed to its participants to be in quite a different case. Should mainland China be admitted in preference to Taiwan (yes) and if so how (no terms specified in advance)? What should be done about the prospect that thoroughly international conferences will henceforth be impossible because of the assumption by governments that they should be consulted in advance? (The government of Australia last week gave the Australian delegation to the ICSU meeting terms of reference wide enough to be a basis for almost any negotiation at Cambridge, but added the proviso that in future it should have a hand in planning conferences of this kind.) And Sir John Kendrew (once secretary-general of the union) was duly appointed president for the next three years. The international union is also short of money, partly at least because it is trying to accomplish goals for which it was not created.

The Falkland Islands are in much the same case. Earlier this week in London, Lord Shackleton (truly a relative of the polar explorer) produced for the British government (and the public gaze) his latest report on the economic prospects for these recently disputed islands. (The British government seems to have gone to war earlier in the year without having read the earlier version of the report, published in 1976.) Some of the recommendations are predictable — the only usable runway on the islands, for example, should be extended to 8,500 feet, thus allowing high-performance military aircraft as well as heavy civil transports to land safely. The proposed deep-water jetty is more of a surprise, as is the proposal that the ownership of land should be transferred, as is only just, to those who work it. In present circumstance, Lord Shackleton's proposal that there should indefinitely be a military garrison on the Falklands and that there should be a development agency modestly to encourage low-technology industries (fishing, knitting and the like) will similarly not cause consternation.

Predictably what remains unsaid is that the Falkland Islands, like the British Association for the Advancement of Science and the International Council of Scientific Unions, cannot be allowed to find their own level in the scheme of things (serving the membership or making arrangements that enable science to function internationally) because of external circumstances, the recent conflict, the shortage of money and the ubiquity of political considerations respectively. Is it not high time that such institutions (even islands) were allowed to get on with what they can do, and were not expected to do what is beyond them?

US fights Canada on Videotex

Moynihan plans retaliation for Ottawa law

Washington

An international war of nerves between the Canadian government and Senator Daniel Patrick Moynihan (Democrat, New York) may break into the open in September, affecting the fates of the Canadian, British and French videotext and teletext systems now competing for a prime position in the huge US market.

When the Senate's Finance Committee meets in late September, to take up a rather parochial bill dealing with US-Canadian broadcasting relations, it could well adopt a policy that would cripple Canada's videotext system, Telidon, as a contender in the US market — thus improving the chances of Britain's Prestel and France's Antiope, which until now had seemed dim.

The *agent provocateur* is Moynihan, who announced in June that he would try to introduce a clause into the bill (S.2051) that would prevent the treatment of any monies spent by US businesses to adopt Canada's Telidon system as a business expense. Many major US news organizations, such as Time-Life Inc., are well along the road towards adopting Telidon. Moynihan's clause has been denounced by an association of 100 US companies and individuals, the Videotext-Industry Association, as "an unprecedented and unreasonable kind of trade warfare".

Moynihan's clause is intended as a stick to beat the Canadian government and make it bend on a completely different issue. Moynihan's home state of New York includes several US broadcasting stations near the Canadian boarder that derive large audiences and considerable advertising revenue from Canada. The stations have been up in arms ever since 1976, when the Canadian parliament adopted a law, known as C58, that attempted to gain "cultural sovereignty" over what is broadcast in Canada. As Canada could not legally prevent incoming broadcasts (which are picked up by cable networks), it used the only legal means at its disposal and deprived Canadian companies of the right to treat as a business expense the cost of advertising on these US stations. The stations promptly called on Washington to do something. They estimate they have lost \$20 million annually in advertising.

Thus began what is now called the "border broadcaster's war". Both President Jimmy Carter and the office of the US Special Trade Representative have criticized the Canadian action. Congressmen from states along the border

have introduced legislation depriving US companies that advertise on Canadian broadcasting stations of the right to deduct their advertising revenues. But the Senate's bill (S.2051) is an insufficient weapon: the Canadian stations stand to lose only about \$3 million in advertising revenues, compared to the \$20 million lost to US stations under the Canadian law.

Thus Moynihan has hit on Telidon as an additional means of bringing Canada to the negotiating table. Canadian engineers worked closely with AT&T, NBC Inc, RCA Corporation and others to develop the "North American Standard" as a common standard to which all videotext and teletext systems should adhere. A key element in the system is the concept for

drawing graphics that is at the heart of Telidon. AT&T's own videotext system, which is not as fully developed as Telidon, would be compatible with this standard as would the French Antiope. These and other companies have jointly protested to Moynihan, citing the "severe negative consequences on the development of electronic publishing in the United States".

So far, the Canadian government had refused to be drawn on Moynihan's proposed action against Telidon but Canada will probably protest to the State Department if and when the clause seems likely to become US law.

The gigantic Times-Mirror newspaper empire, Time-Life Inc. has also protested strongly against the Moynihan proposal

Posts and statutes change at CNRS

A close henchman of Jean-Pierre Chevènement, the highly political French minister for research and industry, is to take up the top job in the management of basic science in France — the director-generalship of the Centre National de la Recherche Scientifique (CNRS). CNRS has a budget of FF6,000 million (£500 million) and a staff of 20,000, and most French scientists aspire to be supported by it. The appointment and major reforms in the statute of CNRS were announced last week in moves described by the minister as marking a "great change" in French science.

Some people, however, fear an increase in the political control of French science, something the CNRS directorate has long resisted on the principle that scientists are the best managers of science.

Certainly, there are some grounds for concern. Last year, the then president and director-general of CNRS resigned over the issue — when the minister tried to appoint his own nominee as director of social sciences. That post remains unfilled, as Chevènement appeared (remarkably) to have misconstrued the CNRS constitution.

But the constitution is now changed, so that CNRS scientific directors appointed only on the advice of the director general, rather than on his instruction and their powers will be increased in a general devolution of power in the CNRS management.

The new appointee to the CNRS director-generalship, 43-year-old physicist Professor Pierre Papon, denies, however, that the powers of his new post will be reduced. The increase in ministerial power "is only formal" he said on Monday. In practice, there will be constant discussion between CNRS and the ministry "as always". As for the great changes, CNRS will protect basic science, said Papon, but will now take more account of national cultural, economic and social needs.

Further, the powers of the director-

general will be increased in relation to the CNRS council, which will no longer make appointments and is renamed the council of administration. Claude Fresjacques remains president of CNRS and of this reduced council. One important power remains with the council, however: deciding the budget.

It is stressed at CNRS that there was no disagreement between Chevènement and the man Papon will succeed, Professor Jean-Jacques Payan. Although only ten months in his post, Payan has been enticed to a key job at the ministry of national education — where he will be responsible



Payan — universities. Papon — science.

for universities and research. Payan's move, in fact, may help to strengthen Chevènement's hold on university research (which, except through the research councils such as CNRS, is strictly outside his control) insofar as Payan himself is a one-time Chevènement nominee (for the CNRS director-generalship).

Other reforms in CNRS announced include the establishment of new, partially elected committees to advise the scientific directors and the creation of two new scientific directorates, one for the application of CNRS results, and one for publications and popularization. The constitution is also changed to allow profitable liaisons to be made between laboratories and industry. The changes are closely in line with the "law for research" voted by the National Assembly earlier this year (*Nature* 8 July, p.110).

Robert Walgate

fearing that the clause may be more destructive of US than of Canadian economic interests.

Moynihan's staff counters that the market for videotext and teletext is still so fluid in the United States that the big customers, who plan to use these systems to bring newspapers and news services into homes within a decade, can still choose the French or British system, that under development by AT&T or some other.

The US Federal Communications Commission (FCC), which has the legal power to affect the outcome by developing standards for this new industry or by endorsing some industry-proposed standard, is standing aside. In October 1981, FCC announced that the market should decide which systems were the best. The announcement, not yet a formal notice, heartened British Videotex and Teletex of New York, the company responsible for marketing Prestel in the United States. So long as FCC does not endorse a North American standard, Prestel still has a fighting chance. Senator Moynihan's clause would give it even a better one.

Deborah Shapley

Canada and yellow rain

UN expert group asked to act

Washington

This autumn will see a test of the United Nations' ability impartially to examine allegations of Soviet-inspired use of toxin weapons in South-East Asia. The Canadian government has submitted a report to the United Nations that gives credence to the charges and explains how they could be resolved. It will be up to the Group of Experts convened by the General Assembly to recommend to the Assembly whether or not to take up the report's suggestions. So far the Group of Experts has failed to reach any conclusion. The Soviet Union has denied that there is any toxin warfare in South-East Asia.

Canada has strongly supported the extension of the Group of Experts' mandate last year when its first investigation did not decide the matter. Refugees from Laos and Kampuchea say that helicopters and fixed-wing aircraft have been spraying poisonous gas that causes death to humans, animals and plants. If this is true, the Vietnamese, who

are presumably flying the planes and helicopters, would be in violation of the 1925 Geneva Protocol prohibiting the use of poisons in warfare. If, as is suspected, the Soviet Union is the source of the toxin weapons, it is in violation of the 1972 Convention on Biological and Toxin Weapons.

Independently of its active role on the issue in the United Nations, the Canadian government commissioned its own study of the matter. In February it asked Dr H. Bruno Schiefer, chief of the toxicology group in the Western College of Veterinary Medicine at the University of Saskatchewan, to try and resolve the veracity of the charges. Dr Schiefer made a two-week visit to Thailand — neither he nor the Group of Experts were allowed into Laos or Kampuchea to check reports first-hand or take samples. Like the Group of Experts, Schiefer interviewed refugees through an interpreter and took samples from border areas near the sites of the alleged attacks.

Schiefer concluded that the events reported to have taken place at the time of the alleged attacks "cannot be explained on the basis of naturally occurring phenomena". He corroborates an assessment made by the US Department of State earlier this year that toxin warfare was indeed being conducted there (*see Nature* 25 March, p291).

Schiefer first sought to resolve an apparent inconsistency. The poisons found in border areas, the particular tricothecene mycotoxins involved, act slowly and would have to occur in massive quantities to cause human death. Yet refugees seemed to say that clouds of "yellow gas" sprayed from the air caused death immediately. After close questioning of refugees, Schiefer concluded that the human deaths were not occurring immediately but that humans, animals and plants in the vicinity were dying 10 to 14 days afterwards. This would be consistent with the level of poison reaching the ground in sprays.

Another problem has been that the tricothecene mycotoxins involved could not alone penetrate the human skin in such a fashion as to cause death. Schiefer began searching for possible agents that might be combined with the tricothecene to facilitate entry through the human skin. Because some of the refugees reported a garlic-like smell after the attacks, Schiefer suspects that dimethyl sulphoxide (DMSO) could be such an agent. The report suggests future field searches for DMSO and other possible agents.

The report also urges that a search should be made for the only known mycotoxin that could kill through ingestion, macrocyclic tricothecene, which thus would not need any additional agent to penetrate the skin.

Communication without compatibility

None of the six main videotex standards is fully compatible with any other. Each offers a different solution to the central problem of balancing quality of display against the cost of the terminal.

At the cheap end of the scale are the systems with "alpha-mosaic" graphics, producing pictures on the screen with a crude building-block appearance. The memory of alpha-mosaic terminals stores a limited repertoire of basic mosaic shapes, from which an incoming byte of data can extract a particular shape and place it in a particular slot on the screen. The result, although inelegant, is economic in the use of memory and transmission bandwidth. But the description of information in the database is terminal-dependent.

"Alpha-geometric" systems specify pictures in terms of basic geometric figures and coordinates of a point on the screen. Almost any shape can be created and placed anywhere on the screen, while picture descriptions are not generally terminal-dependent. But greater memory and processor requirements raise the cost of such terminals.

The leading videotex systems have the following characteristics:

● **Prestel:** An alpha-mosaic standard established in 1974 by the British Post Office (now British Telecom) in cooperation with the broadcasting authorities BBC and IBA. Internationally, there are more Prestel-type terminals than others. Extended graphics capability is being developed.

● **Antiope:** The alpha-mosaic standard developed by the French tele-

communications and broadcast authorities (DGT and TDF).

● **Telidon:** The first alpha-geometric standard (produced by the Canadian Department of Communications) has attracted much attention for its superior display capability.

● **32×16 US alpha-mosaic:** The central characteristic of this system — 16 lines of 32 characters — is based on the low-cost Motorola VDG microchip. It has been adopted by US cable television and microprocessor manufacturers.

● **CEPT:** An attempt by the Association of European Telecommunications Administrations to establish a unified European alpha-mosaic standard. The standard can interpret data according to either the Prestel or the Antiope schemes, depending on the terminal.

● **PLP:** AT&T's Presentation Level Protocol is not a standard in itself but is a vast package of options, from which AT&T will select a subset to be included in a terminal for mass production. The range of capability offered is so great that a comprehensive terminal would be of prohibitive cost. The importance of PLP is its flexibility and AT&T's formidable powers for production and marketing. Other suppliers are willing to modify their standards to be compatible with PLP. The CEPT standard is compatible with the PLP alpha-mosaic subset, but is restrained from change because of the many videotex and teletex sets already in use in Europe. Discussions with AT&T to modify its alpha-mosaic subset may prevent a permanent split between US and European standards. **Bronwen Maddox**

Schiefer also found that tricothecene mycotoxins do not occur naturally in the environment in the region — as they do in other places (such as Saskatchewan). Nor did he find evidence of the human illnesses that are associated with naturally-occurring tricothecene mycotoxins. His report recommends more systematic questioning of refugees so that a proper epidemiological survey can be made.

The mycotoxins in question are toxin weapons, whose production, development, stockpiling and transfer is forbidden by the 1972 Convention. Use of the weapons in warfare is prohibited by the 1925 Geneva Protocol. There has been some confusion about whether to count the

mycotoxins as chemical or biological weapons because although chemicals they are the products of living fungi.

Schiefer's report suggests that the agent involved may be not only the pure chemical but the chemical and fungus mashed together. It recommends that future field work should look for evidence of the fungi that produce the poisons.

The Canadian government has not formally endorsed Schiefer's report but has forwarded it to the Group of Experts. Its own study of the matter will continue, it says. The Group of Experts is due to report to the next General Assembly, which opens in mid-October and will stay in session about six weeks.

Deborah Shapley

Sakharov note makes waves

Pugwash survives Warsaw

Last month's Pugwash Conference in Warsaw — the thirty-second in the twenty-five year history of the Pugwash movement — stressed, once again, the special responsibility of scientists to help "devise means to limit and eventually reverse" the arms race, and their "major responsibility" for disseminating knowledge about the meaning and implication of their work. As is customary, the conference concentrated on major issues of arms proliferation and control, destabilizing factors such as the possible use of food and energy strategies for political means and current or recent world conflicts — Namibia, the Falklands, Iraq-Iran, Afghanistan and Lebanon. But what the council's concluding statement called "the deteriorating international climate" was reflected in two topics which did not appear on the official agenda — a letter to the Pugwash movement from Academician Andrei Sakharov and the meeting of council members with General Jaruzelski.

The Sakharov letter was not originally intended for the Warsaw meeting but for the Pugwash Silver Jubilee Conference in Canada earlier this year. It seems to have been delayed in transmission, however, and shortly before the Warsaw meeting came into the hands of one of the intending participants, Dr Joel Primack from the University of California.

Under Pugwash procedure, because Sakharov had not himself been invited to the conference, the letter could only be circulated as a background document. Not surprisingly, there was considerable Soviet opposition — one Russian proclaiming that since twenty million Soviet citizens had died during the Second World War, it was inappropriate for "anti-Soviet propaganda" to be distributed at a Pugwash meeting. Finally, however, normal procedure prevailed.

The Sakharov letter in fact contained little new. It censured the negative stance taken by Soviet delegations at international meetings where "in all discussions of critical problems, they always behave as

well-disciplined functionaries of one gigantic bureaucratic machine".

As in several previous statements, Sakharov gave "absolute priority" to the achievement of international security and disarmament. In spite of his known opinion that there should be no absolute linkage between disarmament and human rights, he also appealed to the participants to speak out in defence of prisoners of conscience in the Soviet Union.

While generally sympathetic, the conference could not agree with Sakharov's view that "the West would be unable to withstand the forces of the USSR and its camp if nuclear and thermonuclear weapons were excluded from the balance". Rather, the conference concluded, the concept that the Warsaw Pact conventional forces are significantly more powerful than those of NATO needs "searching reexamination".

The problem of linkage seems to have underlain many of the doubts expressed by participants about the meeting of the Pugwash Council with General Jaruzelski but meetings with the head of state or government of the host country are a Pugwash tradition.

Pugwash participants say they put a number of searching questions to the general on the implications of martial law, the future of Solidarity and the fate of internees, and that he predictably replied that the present "state of war" was necessary to defend the state and economy from anarchy, but that "a number of democratically orientated social, political and economic mechanisms" had nevertheless arisen.

Even so, some participants felt that the very fact of the meeting might in some sense be interpreted as conferring a kind of approval on the current military regime. Jaruzelski, himself, however, carefully avoided any such claim, saying only that the choice of Warsaw for the Pugwash meeting was an expression of respect for the Polish nation, and of trust in its wisdom.

Vera Rich

European community research

Spending money

Brussels

The brief Belgian summer has not distracted officials at the European Commission from putting together plans for the new European science strategy agreed at the ministerial meeting on 30 June. Three papers have been presented to the Council of Ministers, EEC's decision-making body, covering the reform of the research and development programme of the joint research centres, the preliminary phase of the Esprit programme on information technologies and the first phase, for 1983, of the long-term plan to stimulate the scientific and technical potential of the European Community.

The last of these projects, however tentative, is the most interesting. The Commission is proposing that the Community should spend \$5 million to stimulate research in seven selected fields, thus paving the way for spending on a larger scale in the period 1984-87. For next year, the plan is that funds should be spent on a handful of fashionable fields of enquiry — new applications of cell and molecular biology, composite materials, mathematical analysis applied to optical problems, the behaviour of materials in the presence of combustion, non-destructive testing, interface phenomena and transitory effects in climatology. Information technology is already catered for by the Esprit programme.

If the Commission's proposals are accepted by the Council of Ministers, the research ministers at their meeting arranged for 30 November will invite applications for research funds in respect of both the pilot programme for research and development and for Esprit.

One of the attractive features of the pilot programme is that funds will be available for multi-national projects, including seminars and workshops, as well as for the travel and research expenses of scientists working at foreign laboratories.

The research ministers are unlikely to be as pleased with the Commission's paper on the joint research centres, the latest revision of the rolling three-year programme. The rising cost of the Super-Sara project on reactor safety is the perennial stumbling-block, especially for those governments that were dubious about the project at the beginning. The Commission now argues that work on this project should be pushed ahead so that the past investment in it will at least yield some information in time for it to be used in the design of light-water reactors, but it is not yet clear whether these arguments will prevail. For the rest, however, the Commission has proposed that the work of the four joint centres should be brought more into line with the new framework proposed for the general support of research and development.

Jasper Becker

Ariane in space

What next?

Last week's failure of the fifth Ariane flight is bound to have repercussions on the launcher's commercial prospects. But officials at the European Space Agency (ESA) are still hopeful that the fault that caused the failure in the rocket's third stage will prove to be no more than a manufacturing error, thus reassuring customers of Ariane's basic soundness. Three previous successful flights are taken as testimony that the fault probably does not lie with the design.

ESA is keen to point out that the rocket's first and second stages worked perfectly. But the third stage, which was carrying two satellites into geostationary transfer orbit, suddenly lost power after about 4 seconds and brought the satellites back down to Earth. A preliminary analysis of telemetry data recorded at a station in north-east Brazil has revealed a sudden failure in a gear controlling the flow of cryogenic propellant from the liquid oxygen and liquid hydrogen pumps. Nobody yet knows, however, precisely what went wrong with the gear.

Whether the failure was due to a simple error or to a more ominous design fault, sorting it out is bound to delay the future Ariane launch programme. A lengthy delay could postpone the launch of Exosat, ESA's X-ray astronomy observatory, from its scheduled date of next November to June or July next year. Exosat can only be launched during specific launch windows around December and midsummer.

Although a delay to Exosat could upset Europe's hard-done-by X-ray astronomers, ESA is bound to be more worried about the effects of delay and uncertainty over Ariane's reliability on the launcher's potential commercial customers. Intelsat, the international owner of the Intelsat series of telecommunications satellites, for

example, is due to launch three of the Intelsat 5 series on Ariane next year. Although the organization has made little response yet to last week's failure it will be watching the next Ariane launch keenly before making any firm commitments.

Meanwhile, ESA is having to decide how to make amends for Marecs B and Sirio 2, the two satellites lost last week. Sirio 2, a telecommunications satellite of primarily Italian design was uninsured, but the insurance money from Marecs B could be used to assemble quickly Marecs C, possibly for launch at the end of 1983 or the beginning of 1984. Inmarsat, the International Maritime Satellite Organization which had planned to lease channels on Marecs B for maritime communications in the Pacific, says that it can continue its present service in the area with the US Marisat satellite. But it is likely to take up ESA's offer to assemble and launch as quickly as possible the Marecs C replacement.

Amendments to the launch programme could delay the transition of the Ariane programme from ESA's control to that of Arianespace arranged before last week for July or August next year. Arianespace seems likely to take longer than expected before earning money. The company's prospects also seem to depend more than it must have hoped on the success or otherwise of the space shuttle, due to make its fifth (and first operational) flight in November.

Judy Redfearn

Spina bifida

Trials ahead

The Medical Research Council (MRC) is soon to start trials to investigate the role of folic acid and other multivitamin supplements in the prevention of neural tube defects (NTD). The programme is controversial because of its ethical implications. Women invited to participate will already have conceived one spina bifida baby and are therefore at risk of conceiving another. In order to understand the effects of dietary supplements, women in the control group will not be given multivitamin and folate supplements.

The government is to give £300,000 for the first three years of the trials. Although many scientists and doctors believe that multivitamin supplementation is important in the reduction of NTD, MRC says that new trials are necessary because previous experiments have not provided strong enough evidence for such a link. Experiments on folate and multivitamin supplementation at the Universities of Cardiff and Leeds are considered not to have been properly randomized. The women who participated were mainly from the middle classes and therefore at lower risk anyway.

The MRC programme will involve 3,000 women at 20 centres. There will also be centres in Israel and Australia. The women

will be offered full antenatal screening facilities and the centres will have to be approved by local ethical councils. The volunteers, who are planning a pregnancy (pills are taken before and after conception), will be randomized and divided into four groups. The first will receive pills containing minerals plus multivitamins, the second minerals, multivitamins and folate, the third minerals and folate and the control group minerals only. This design will permit a comparison between the multivitamin effect and the folic acid effect.

The National Childbirth Trust has written to the Minister of Health, Mr Kenneth Clarke, expressing its worries about the trials. It says that there is already sufficient evidence to link folic acid deficiency with spina bifida and point out that the women participants will have a one in four chance of being in the control group and therefore at risk. In Britain one in 20 women who have already conceived an NTD baby conceive another.

Ethical worries about the trial's implications hang on how well the women will be briefed. The Association of Spina Bifida and Hydrocephalus (ASBAH) agrees that there is a need for more scientific evidence and that this cannot be done without further trials. Its support is qualified, however, by the proviso that the participants must be adequately briefed. At present MRC decides what information is given to women volunteers.

Dr Nicholas Wald of the Radcliffe Infirmary in Oxford, who is to coordinate the trials, stresses that the women will be invited to participate. But he points out that even if they were not fully briefed the trials would not necessarily be unethical. He argues that the trial is ethical primarily because there is a broad balance between the likely good of the treatment and the possible harm.

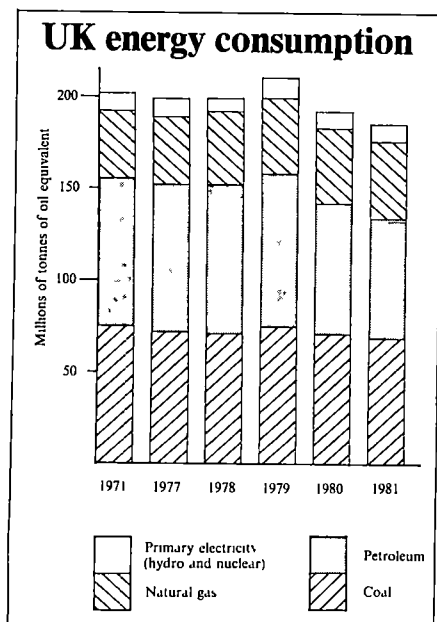
No one is willing to be explicit about what volunteers will be told. While women in the control group will not receive multivitamin or folate supplements, it should however be pointed out that such supplements would not necessarily be recommended by a general practitioner or by ASBAH in any case. ASBAH hopes that the MRC trials will establish what dietary advice should be given to women at risk who plan to become pregnant again.

Jane Wynn

Helsinki agreement

Monitoring stops

The formal disbanding, last week, of the Moscow "Helsinki Monitoring Group" is little more than an acknowledgement of a *fait accompli*. Since its foundation, six years ago, to monitor Soviet observance of the Helsinki Accords, the group has been subject to ever-increasing official pressure. In 1978, its founder and original chairman, Dr Yuri Orlov the physicist, was sentenced



to seven years in a labour camp, plus five years Siberian exile, for his part in the group's activities. Since Dr Orlov's conviction the active membership of the group has been whittled down by successive arrests to, effectively, two persons, Elena Bonner, the wife of Academician Andrei Sakharov, and Sofia Kallistratova, an elderly lawyer. It was apparently an official warning to Mrs Kallistratova last week that she might soon be arrested and charged with anti-Soviet activities that led to the disbanding.

The Moscow Helsinki group has not been the only victim of repression. Other Helsinki groups throughout the Soviet Union, and in particular the Ukrainian group founded by Mykola Rudenko the science fiction writer, have been similarly obliterated by the imprisonment of their members. So has the Moscow "Working Group for the Investigation of the Misuse of Psychiatry for Political Purposes". The founder members of SMOT, the "Inter-professional Free Trade Union", have all been either taken into custody or expelled from the Soviet Union. Since the arrest of Dr Viktor Brailovskii on the opening day of the Madrid "Helsinki Review" conference in November 1980, the Moscow Sunday Seminar for refusenik scientists has been able to meet only on very rare occasions, and regular participants have been subjected to harassment. Brailovskii himself is now eligible for early release from his exile in Beineu (Kazakhstan), but has so far been unable to obtain the necessary character reference from the local authorities, which, it is understood, want specific authorization from Moscow.

Some forms of grass-roots dissent do seem to have survived, however. Mrs Albina Yakoreva, a computer specialist and founder member of SMOT, who was put on a plane to Vienna last month, reported that the free trade union movement has decentralized, but that at least twenty-one grass-roots branches are active, their main object now being the building up of a climate of opinion that will accept such fundamental democratic concepts as worker self-management. In Byelorussia, which was relatively passive during the upsurge of dissent of the early 1970s, underground initiatives protesting against the russification of Byelorussian culture have been reported. The three Baltic republics, Lithuania, Latvia and Estonia, which have developed their own traditions of dissent (the *Chronicle of the Lithuanian Catholic Church* has long been one of the most prestigious underground Soviet journals, while Estonia has staged protest marches and token strikes) have, in the past year, begun to coordinate their efforts on fundamental issues. Their most significant effort so far is a letter to the governments of the Nordic and Baltic countries expressing their support for the proposed Nordic nuclear-free zone, but urging that the ban be extended to the relevant areas of the Soviet Union.

Vera Rich

Nuclear waste reprocessing

Germans divide

Heidelberg

The reprocessing of nuclear waste has predictably become an issue in the Hesse and Bavaria elections, now in full swing. The Social Democrats, the major partners in the Bonn coalition with the Free Democrats but fighting separately in the elections for the *Länder* governments, shoulder the chief responsibility for having declared that each *Land* includes a candidate site. The Free Democrats, party to these decisions but united electorally with the more powerful Christian Democrats, are more or less immune from the attacks with which the "Greens" (the environmentalist party) threaten to enliven the elections.

The 14 nuclear power plants in West Germany now produce some 350 tonnes of spent fuel-rods a year. By 1990, 25 power plants will be producing 750 tonnes a year. Under contracts with the French state-controlled Cogema, the rods will be reprocessed at the Cap de la Hague plant in Normandy until 1985, after which the outlook is unclear. Pending the completion of a second 800 tonne per year unit at Cap de la Hague, West Germany will in any case have to take back the highly reactive waste

and put it somewhere.

At present, Cap de la Hague and Sellafield (as Windscale is now called) are the only two commercial reprocessing plants functioning, but there is a chance that the smaller plant at Mol in Belgium may reopen soon (see *Nature* 26 August, p 783). Worldwide, however, there is a desperate shortage of reprocessing facilities, with 200 nuclear power reactors operating and 150 under construction. Only the US interdiction of the reprocessing of spent fuel bridges the gap.

In West Germany, after the abandonment last year of the plan for a 1,400-tonne reprocessing plant at Gorleben in Lower Saxony for political reasons and after massive environmentalist protest, the industry-run organization responsible for reprocessing is considering three 350-tonne per year sites at Frankenberg (Hesse), Schwandorf (Bavaria) and Kaisersesch (Rheinland-Pfalz).

The final storage of wastes, however, remains the responsibility of the federal government. Geologists estimate that salt deposits underlie about a quarter of Northern Europe and in spite of protests and a recent controversial study which revealed unexpected depths of erosion of the salt dome during the last ice age, investigations continue.

Sarah Toozee

Biotechnology briefs

The Cetus Corporation announced last week the first lay-offs in its history and a substantial refocusing of its research and development on projects that would be likely to pay off in the short term. Forty employees have been laid off, and projects dealing with the production of high-purity fructose and energy and chemical processing have been stopped. Cetus raised a record \$107 million with its public offering of shares in March 1981, but Standard Oil of California, a major shareholder, has declined to continue supporting fructose work at the company.

Another biotechnology company with ambitions in the artificial sweetener field is about to make a public stock offering. The Genex Corporation of Rockville, Maryland, is expected to offer 2.5 million shares in late September or early October, which could raise as much as \$33 million according to documents that Genex has filed with the US Securities and Exchange Commission (SEC). Genex already has a production plant for L-aspartic acid, which is used in the production of aspartame, a sweetener marketed by the Searle Corporation that was recently approved by the US Food and Drug Administration. Genex is also interested in genetically-engineered production of calf rennin, bovine, porcine and ovine animal growth hormones and various industrial chemicals. The company is 45 per cent owned by the Kopper Co. Inc. of

Pittsburgh, a major chemical concern. The company, which is one of the largest genetic engineering companies in the United States, has grown steadily through contract research, the income from which rose from zero in 1977 to \$3.9 million in 1981.

Eli Lilly and Co. of Indianapolis is expected to announce later in the month the availability of the first genetically-engineered product for human use, human insulin. The work has been carried out by Genentech Corporation of South San Francisco.

Meanwhile, Amos Corporation, also of South San Francisco, a company founded in June 1980 by Brian T. Sheehan, formerly of Genentech, has filed for bankruptcy in the San Francisco courts. Sheehan says that this will enable the company to reorganize and that several investors are interested in its potential.

Another Canadian entry into the biotechnology field is Allelix of Mississauga, Ontario, whose scientific director, Derek C. Burke, is leaving the University of Warwick in the United Kingdom to work full-time for the company. Allelix is a joint venture between the Canada Development Corporation, John Labatt Limited and the province of Ontario. Burke says that the assurance of Can\$100 million over the next ten years will prevent the company from having to "panic" in the quest for short-term genetically-engineered products.

Deborah Shapley

CORRESPONDENCE

No to quangos

SIR — Your leading article in *Nature* of 5 August ("James Watt and biotechnology", p 501) asks some important questions, which you imply that only the government can answer. The difference between James Watt's doings and ours is that he was free from committees and we are not. I agree that to go back to James Watt would do no harm, provided that in going back we dismantle the bureaucratic structure that strangles our communications. Mr G H Fairtlough may understand the links between the Medical Research Council and the British Technology Group (and the National Enterprise Board and National Research and Development Corporation) and Celltech, but few others do. Things would work so much better without these complicated bureaucracies and we and Mr Fairtlough would be free to compete or collaborate with each other, and free to collaborate with the research scientists.

You ask how the government can give British industry a sporting chance of survival. The answer (towards which the present government is working) is to leave it alone. Take the committees and the quangos (and the formal channel of communication between the Department of Industry and the University Grants Committee) off our backs.

S J STARKIE
(Managing Director)

Xoma (UK) Ltd,
London SW17, UK

Cold war

SIR — I am afraid that E G Dimond's suggestion to exchange ¼ million young people between the United States and the Soviet Union as an alternative to arms race (*Nature* 15 July, p 220) would be more unacceptable to the Soviet Union than a tenfold increase in arms buildup by the United States. Why? It would be labelled as a "philistine ploy (1) for mass infiltration of the Soviet Union by CIA agents and (2) for infecting Soviet youth with decadent bourgeois ideology to use them later as a Trojan horse to disrupt the fabric of the socialist society". This is the essence of the tragedy why every effort to reduce tensions, promote detente and so on must inevitably end in deadlock.

VIT KLEMES

National Hydrology Research Institute,
Ottawa,
Ontario, Canada

China syndrome

SIR — In *Nature* of 19 August (p 746) you published a paper entitled "Age of the Lufeng, China, hominoid locality". One of the authors, Qi Guo-qin, appears on the contents page as Q Guo-qin, which wrongly assumes Guo-qin to be the surname, and is a common mistake among Westerners.

The convention in Chinese names places the surname first, followed by the given names, which are usually hyphenated. The author is therefore Mr Qi not Mr Guo-qin. The Chinese tend to use their names in full, and the shortened form is made by dropping the given names for well known people, as in "Chairman Mao".

There is, however, a tendency among Chinese exposed to the West to adopt our convention and place the initials of their given names before their family name. Perhaps they have become fed up with our getting their names mixed!

As scientists, the Chinese name convention should not strike us as odd — it is, after all, the same as the Linnean nomenclature!

J A IRVING

Dulwich, London, UK

Scrapie a "gene"?

SIR — In *News and Views*¹ R H Kimberlin commented on the recent suggestion by Stanley B Prusiner of the University of California, San Francisco, that the scrapie agent is a novel proteinaceous infectious particle².

The search for the scrapie virus proposed by Cuille and Chelle in 1938³, has been continuous. An early trickle of papers became a torrent when Chandler transmitted the disease to mice in 1961⁴. There have been so many variations on a virus theme that the virus hypothesis now lacks absolutely nothing, except a virus. One response to this impasse has been to call the virus "unconventional"⁵, an ingenious solution, for is not a square an unconventional circle?

In pursuing our suggestion in 1967 that the scrapie agent might be a small protein⁶, my colleagues and I applied fractionation procedures to scrapie tissues. Every experiment included control inocula of normal tissue treated precisely as the scrapie tissue, and diagnosis of scrapie was rigidly based on the presence of characteristic histological lesions in the brain⁷. These technical points are emphasized for two reasons. First, because few other investigators of the disease have used normal tissue controls in more than the occasional experiment, and very few have examined histologically the brain of every animal in every experiment, whether or not it showed clinical evidence of scrapie, this latter procedure is important in detecting scrapie agent in high dilution, or in unexpected circumstances. Second, because use of this experimental routine may explain why we apparently detected scrapie agent in tissues of some non-scrapie animals.

Our findings were published in *Nature* in 1968⁸. In brief, in over 150 experiments scrapie did not occur in any of 2,640 mice injected with unfractionated tissue from normal sheep, goats or mice (an observation matching that of many other investigators). By contrast, scrapie occurred occasionally, and unpredictably, in mice injected with fractionated tissue from non-scrapie animals. The possibility existed, therefore, that fractionation had released a scrapie-producing factor from non-scrapie tissue.

The obvious interpretation of our findings was that normal tissue had been contaminated with scrapie. To examine this criticism, we carried out further experiments in which attempts were made purposely to contaminate normal tissue inocula. By using unwashed glassware etc. we certainly produced some contamination, but the distribution of scrapie was different from that observed after injection of fractionated normal tissue⁹.

If, for a moment, it be accepted that we did

indeed detect scrapie agent in normal tissue, an explanation can be offered for the apparent enigma of replication without nucleic acid that faced us initially, and now faces Prusiner. The agent may not, in fact, replicate as the disease progresses, instead — as we suggested in 1968 — replication may be simulated by an unmasking process of a particle already present. Again, if scrapie agent were a component of normal tissue, there would be a simple explanation for the widely observed but obscure phenomenon that the scrapie agent does not apparently stimulate antibody. If the agent were "self" no antibody would be expected.

In recent years, research on scrapie in sheep has largely been bypassed in favour of the experimentally-produced disease in laboratory animals, for the obvious reason that few laboratories are equipped to handle large numbers of sheep. In consequence, it is not widely recollected that many outbreaks of naturally-occurring scrapie in sheep have been associated with close mating to improve agriculturally desirable breed characteristics¹⁰. In 1974 I reported the apparently spontaneous occurrence of scrapie in sheep selectively bred, for high susceptibility to experimental scrapie¹¹. The significance of genetic make-up in susceptibility to scrapie in sheep is beyond dispute (for example ref. 12).

It may not be far-fetched, therefore, to suggest that the scrapie agent is an inhibited particle in normal tissue, released genetically in the naturally-occurring disease in sheep.

I H PATTISON

Newbury, Berks, UK

- 1 Kimberlin, R H. *Nature* 297, 107–108 (1982).
- 2 Prusiner, S B. *Science* 216, 136 (1982).
- 3 Cuille, J & Chelle, P L. *C r hebdomadaire Seances Acad Sci, Paris* 206, 1687 (1938).
- 4 Chandler, R L. *Lancet* i, 1378 (1961).
- 5 Gajdusek, D C. *Science* 197, 943 (1977).
- 6 Pattison, I H & Jones, K M. *Vet Rec* 80, 2 (1967).
- 7 Pattison, I H & Smith, K. *Res vet Sci* 4, 269 (1963).
- 8 Pattison, I H & Jones, K M. *Nature* 218, 102 (1968).
- 9 Pattison, I H, Jones, K M & Jebbett, J N. *Res vet Sci* 12, 30 (1971).
- 10 M'Gowan, J P. *Investigation into the Disease of Sheep Called Scrapie* (Blackwood, Edinburgh, 1914).
- 11 Pattison, I H. *Nature* 248, 594 (1974).
- 12 Nussbaum, R E, Henderson, W M, Pattison, I H, Elock, N V & Davies, D C. *Res vet Sci* 18, 49 (1975).

To the point

SIR — Having read Cedric A B Smith's letter proposing a new system for representing numbers (*Nature* 12 August, p 600), I am afraid that it cannot go unchallenged. He not only suggests a totally confusing system of numbers and letters, but goes on to contradict himself.

He states "0 700 means exactly the same as 7", but is wrong since 7 is correct to one decimal place and 0 700 is correct to three places. And surely "7" can be easily confused with "7" — referring back to an earlier paragraph in his letter "what makes it worse is that especially in handwriting (and sometimes also in print) not only may dots and commas be difficult to distinguish reliably but also they may be so faint as to escape notice altogether".

MOHAMED S. NANJİ

Department of Biochemistry,
National Heart Hospital,
London W1, UK

NEWS AND VIEWS

The unacceptable face of Minoan Crete?

from Keith Branigan

THE Minoans were a civilized people, by soon after 2000 BC they were living in spacious houses with bathrooms, toilets and drains, and they decorated their living rooms with colourful frescoes depicting the birds, animals and fish which inhabited their beautiful island and the seas around it. Only the legend of the Minotaur, half man, half bull, which annually devoured twelve Athenian youths sent as tribute to King Minos, has cast a shadow on this idyllic scene — until the summer of 1979 when two dramatic discoveries were made in excavations only a few miles apart in central Crete.

At Knossos, the home of the Minotaur, the butchered remains of two young lads were found in a basement room of a Minoan house. Careful study of the bones suggested that cannibalism provided the only satisfactory explanation of all the evidence. Meanwhile, at Arkhanes, less than 10 km to the south, below the fallen walls of a Minoan temple destroyed by earthquake at about 1700 BC, the skeleton of a boy aged about 18 years was found sprawled across an altar, a bronze knife lying on the body. Again, a careful examination of all the evidence led the excavators to the inescapable conclusion that here was a Minoan human sacrifice. These two remarkable discoveries have naturally attracted a great deal of attention and comment, and alternative explanations to cannibalism and sacrifice have been offered, but do the alternatives fit the observed facts?

Details of the Arkhanes temple were published by S. Elliott in 1980 (*The Athenian*, 22 March 1980), with extensive quotes from an interview with the excavators, I. and E. Sakellarakis. Altogether four skeletons were found in the temple: one, a man, in the antechamber, and three (including the sacrificial victim) in the western of the three cult chambers. The other two skeletons in this room were those of a woman, lying face down and legs splayed, and of a man, fallen on his back and with his arms raised to his chest. These three skeletons are thought to be the remains of people (priests?) struck down in the temple at the time of its destruction by a major earthquake, which is well evidenced elsewhere in central Crete around 1700 BC. The fourth victim is thought to have died in

a different manner for four reasons.

First, unlike the others, he lay not on the floor but on a stone platform or altar. Second, he was not spreadeagled like the others but lay on his side with his legs tucked tightly up against the body — an unusual position suggestive perhaps of his being trussed up, but certainly not the position of someone caught by falling masonry or timber while trying to escape the building. Third, the ceremonial bronze dagger lying across his body is suggestive of sacrificial activity. Finally, the bones on the lower side of the body were stained a much darker colour than those on the upper side, and it has been suggested that this preserved traces of the manner in which the man died — from a severed artery on his left side, through which the blood drained, first from his upper right side, and eventually from his left side.

The collective evidence is impressive but not incontrovertible. In particular, pathologists in this country are unconvinced by the differential discoloration of the bones, which cannot be ascribed to the position of any supposed wound. The sacrificial weapon, too, presents some difficulties because it is not a dagger but a spearhead, and although it could be used to kill someone, it would be a cumbersome implement to use for sacrifice, particularly in the manner suggested — piercing the carotid artery of a person lying on their side on a raised altar. It might also be argued that the body fell, rather than lay, on the altar or platform where it was found. Only the position of the body is difficult to reconcile with this person being a fourth victim of the earthquake rather than of a priest's sacrificial knife, and until we have definitive reports with photographs of that position, we cannot be certain how critical to the interpretation the position of the skeleton really is. At present, the case for human sacrifice at Arkhanes has to remain 'unproven'.

The evidence from Knossos is well documented in articles and photographs published by the excavator, Peter Warren [in *Sanctuaries and Cults in the Aegean Bronze Age* (eds Hagg, R. & Marinatos,

N) 155, 1981, *Archaeological Reports for 1980–81*, 73, 1981]. A small basement room contained a deposit dating from about 1500–1450 BC, amongst which were 300 fragments of human bone. On analysis, these proved to be the remains of two boys, aged 8 and about 11 years respectively. Although examination of the skulls and bones suggested both children were in good health at the time of death, it also revealed 27 bones on which there were clear knife marks, several of them well away from the ends of bones. The bones were subjected to microscopic examination and it was concluded that the marks had been made by repeated cutting or sawing (possibly with a sharp obsidian blade rather than a bronze knife) and there was no evidence for either chopping the bones or for scraping the bones longitudinally.

The discovery of these gruesome remains in the basement of a house raises three obvious possibilities. The first is that the bodies result from an undiscovered crime. This proposition can be repudiated by observing the nature and position of the cut marks. None results from chopping or slashing, none results from blows struck with a heavy implement. Apart from marks on the torso, there are also cut marks on the legs and arms, which are difficult to explain in terms of murder wounds. Most significant, however, are the multiple cut marks at a single point — one clavicle, for example, has five marks criss-crossing each other at one point, and another three 1 cm away, these must represent repeated and careful cutting or sawing rather than eight very precisely aimed blows on the single collar bone. A second explanation is that we have in this basement the remains of two secondary burials — that is, the bones removed from an initial burial place for burial elsewhere or perhaps for use in ritual. Secondary burial was certainly practised in Crete, but there are no other examples of children being subject to this treatment, and such evidence as we have for the practice is found, not surprisingly, in Minoan cemeteries, not in town houses. In any case, how does secondary burial explain the cut marks?

Warren plumps, somewhat unwillingly, for the third possibility — that we have the first evidence of Minoan cannibalism. He argues persuasively that the only explanation consistent with the nature and

Keith Branigan is in the Department of Prehistory and Archaeology, University of Sheffield, Sheffield S10 2TN

position of the cut marks is that flesh was being cut from the bodies, and although in this case it cannot be demonstrated, the likelihood is that the flesh would be eaten. There are some further clues which support the proposal. For example, among the childrens' bones there were also some sheep bones, including a third cervical vertebra bearing cut marks consistent with the sheep having had its throat cut. In a room across the corridor from the childrens' bones, a storage jar was found containing burnt earth, snails and more childrens' bones, including one with cut marks. Are these too food remains? The ritual nature of the deposit in this second room is undoubted, with a remarkable collection of miniature vases of various shapes, each with a small hole perforating their base — typical libation vessels. Certainly, if we have evidence for cannibalism, we should look for a ritual setting (see, for example, Harris, M. *Cannibals and Kings*, 1978), whatever the real reason for the eating of human flesh may have been.

There are, however, some unusual features of the discovery which ritual cannibalism cannot explain. The first is the incompleteness of the skeletons, neither skeleton was anywhere near entire and, in particular, in neither case was there evidence for the lower legs. If the bodies had flesh removed for eating, obviously the bodies must have been newly dead, the absence of substantial parts of the skeletons cannot be explained by advanced decomposition and disarticulation. The bodies must have been slaughtered and butchered elsewhere, with only parts of the bodies being brought here, or, the butchering was done here and the missing parts removed to other places. Such events are possible, but they raise many new questions if we accept them. Second, some of the bones bearing cut marks come from parts of the body unlikely to have been eaten. Thus, all three shoulder blades, one of the two collar bones and two of the jaw bones show cut marks. If we recall that the evidence of the marks clearly points to cutting or sawing rather than chopping, and that we are therefore thinking not of butchery but of removing meat from the bone, then it is difficult to believe that in these instances we are looking at evidence for cannibalism, this is particularly true of the jaw bones.

The most economical explanation of all the observed facts that can at present be offered is that we have here evidence for post-funerary ritual involving human bones, that is, that the bones had been removed from a primary burial area and were being used in, or prepared for use in, a further ritual. The removal of bones from funerary contexts for further ritual use is attested elsewhere in prehistory (Piggott, S. *The West Kennet Long Barrow*) and there are hints of this activity in Crete by the third millennium BC (Blackman *Kretika Chronika*, 199, 1973). In particular,

Blackman refers to bones found at the Aya Kyriaki tholos tomb (*Annual of the British School at Athens*, 77, in the press) which were clearly and cleanly cut through at both ends. The cutting or sawing marks on the bones from Knossos could be traces of similar activity, although none of the bones

found in the basement has been completely cut through.

On the evidence from Knossos, we cannot assert that the Minoans did not practise human sacrifice or cannibalism, but the onus of proof must still be with those who believe that they did. □

Of cannibals and kin

from J S Jones

THERE has grown up in biology the comforting supposition that nature is not really red in tooth and claw, that animals behave, in general, in an altruistic or at least a polite fashion to other members of their own species, and that animals belonging to the same species rarely do serious damage to each other. Just how far this is from the truth is revealed in a recent account of cannibalism in natural populations¹.

Cannibalism has been recorded in more than 1,300 species, and is often the primary cause of mortality. Ninety per cent of fish fry may be eaten by conspecifics, three-quarters of crow eggs and nestlings cannibalized by adults, and a quarter of all lion cubs killed and eaten by older animals. In viviparous salamanders, a few young develop teeth which they use, while still unborn, to devour their less well-endowed sibs, and adult hyaenas often eat the corpses of others which they have killed in territorial battles. The female of most species is more cannibalistic than the male. The flesh of one's own species may be a major source of food, even in man — where anthropophagy has been recorded in some sixty cultures — human flesh was sometimes the second most important item of dietary protein. Some animals are particularly enthusiastic cannibals. Walleye fish, *Stizostedion*, eat each other 'tail first', and chains of up to four fish engaged in simultaneous cannibalism have been seen².

How can this apparently unadaptive behaviour evolve? The answer is no doubt complex and involves a variety of selective forces which differ from case to case. The individual benefits are obvious enough, for a cannibal not only obtains food but also reduces the competition. In ground squirrels, *Spermophilus beldingi*, for example, infanticide by unmated females leads to previously occupied nest burrows becoming available³. There may also be population benefits as cannibalism enables populations of desert scorpions and other animals to persist when food is short in a fluctuating environment⁴. However, the most interesting aspect of cannibalism is the insight it may give into evolution by kin selection.

It is often claimed that the behaviour of

J S Jones is in the Department of Genetics and Biometry, University College London.

animals towards other members of their own species is influenced by their degree of genetic relatedness. Altruistic behaviour, in which one individual decreases his own fitness in order to increase that of others, is believed to be particularly likely to occur when donor and recipient have a high proportion of their genes in common. Unfortunately, it is usually difficult to identify a particular behaviour as altruistic, and impossible to assess the costs and benefits to the individuals involved in the interaction. Cannibalism epitomizes selfishness. It is hence the converse of altruism, and many prove a better test of the theory of kin selection, as it is easier to identify cannibalism and to measure the nutritional or other benefit gained by the attacker.

In some circumstances, patterns of genetic relatedness do seem to influence the evolution of cannibalism. Adult eggs of the flour beetle, *Tribolium confusum*, are often eaten by larvae and pupae by adults. Crosses between populations with different cannibalistic tendencies show that the behaviour has a genetic basis⁵. Experimental populations founded by members of the same large and variable base population attain very different population size under identical conditions — largely because of differences in the rate of pupal cannibalism⁶. In high-productivity populations, 85 per cent of pupae survive to become adults, while in populations with low productivity and equilibrium size the survival rate is only 5 per cent.

Wade⁷ has recently made use of this genetic variation in behaviour to show that the evolution of cannibalism is affected by degree of relatedness as predicted by kinship theory. Laboratory populations of *T. confusum* larvae were offered eggs from full sibs, from half sibs or from unrelated individuals. Larval females which ate eggs laid on the average one egg more per day on reaching adulthood than did non-cannibals. After eight generations, the egg cannibalism rate was lowest in the full-sib group, intermediate in the half-sib and highest in the populations in which the larvae had been offered eggs from unrelated beetles.

Kin selection may also be involved in controlling cannibalism in vertebrates. In

the lemming *Dicrostonyx groenlandicus*, males kill the offspring of unrelated males, but do not attack their own young⁸. Young males of the gerbil *Meriones unguiculatus* will normally kill and eat any pups. However, experimental exposure to a pregnant female inhibits this behaviour⁹. As gerbils are monogamous and territorial, any pups which a male meets after an encounter with a pregnant female in nature are likely to be his own and hence to share a high proportion of his genes. In mice, however, in which males will mate with any available female, destruction of young by adult males continues throughout life. Pregnant female mice exposed to a novel male reabsorb the fetuses which have resulted from a previous mating, this 'prenatal cannibalism' may have evolved in response to the high probability of the young being eaten at birth by the unrelated male¹⁰. Such kinship effects may influence the demography of vertebrate populations. In pike, attacks on unrelated individuals mean that fewer young are produced in ponds founded by mixing two full-sib families than when members of only one family are used¹¹.

Kin selection is particularly likely to reduce cannibalism in organisms whose local populations are relatively inbred, so that their members have a rather high proportion of genes in common. Wade's experiments on *Tribolium* show this clearly, as an avoidance of sibling cannibalism evolved only in inbred populations. In experiments in which there was random mating among the evolving stocks, no differences appeared among populations offered related or unrelated eggs. Computer simulations show that even a small amount of inbreeding greatly hastens the evolution of altruistic behaviour¹². It is often assumed that the social groups found in large mammals represent locally inbred populations and that their close kinship leads to the evolution of altruism and the avoidance of cannibalism among their members. However, detailed observation of individual mating patterns or the analysis of relatedness using genetic markers in lions and primates show that the members of a social group are not always particularly closely related to each other^{13,14} so that their behaviour cannot be explained simply by assuming that kin selection is operating.

A less ambiguous method of testing the importance of kinship effects has recently

become available with the realization that many hermaphrodite animals reproduce by self-fertilization¹⁵. This represents very close inbreeding. It might therefore provide an unusually direct way of examining the role of kinship in aggression and cannibalism, as in those species in which both selfing and outcrossing forms occur in the same population, outbreeders should be more likely to attack their relatively distant relations than are selfers

to destroy their close kin.

It is already clear that to cannibalize unrelated animals may increase the probability of survival of an aggressor's own genes. This may be an important factor in the evolution of behaviour, however much it conflicts with the widespread view that the struggle for existence is usually tempered by avoiding fatal interactions between members of the same species. □

Increasing atmospheric carbon dioxide and its consequences

from John G. Lockwood

NUMEROUS forecasts of the increase in atmospheric CO₂ that will result from the burning of fossil fuels have been made. The IIASA Energy Systems Programme¹ predicts an atmospheric CO₂ concentration of 430 to 500 p.p.m.v. in 2030 while The World Climate Programme² suggests values of 410 to 490 p.p.m.v. in 2025. Concentrations as low as 200 p.p.m.v. have been estimated for the end of the last glacialiation^{3,4}, even though levels may have been considerably higher in the more remote geological past. Recent observations show that the global mean CO₂ concentration in the atmosphere has increased from about 315 p.p.m.v. in 1958 to about 335 p.p.m.v. in 1979, a considerable increase over nineteenth century pre-industrial levels estimated at about 290 p.p.m.v.

Armed with forecasts of future fossil fuel needs and CO₂ production, how do we estimate the effect that these increasing concentrations will have? At a recent gathering in Norwich*, Gates (Oregon State University) argued that the problem is best approached using general circulation models (GCMs), which have the ability to portray many of the nonlinear feedback processes which serve to regulate atmospheric (and hence climatic) changes. The first application of a GCM to the CO₂ climate problem⁵ used an idealized geography with a swamp-like ocean and annually averaged insolation, and predicted that a doubling of atmospheric CO₂ would result in a 2–3K increase of globally averaged surface air temperature. This first attempt also showed the warming to be several times larger in high latitudes than at the Equator, and the globally averaged precipitation to be increased by a few per cent.

In subsequent simulations with GCMs

including more realistic geography and seasonal variations, generally similar results (global temperature increases of about 2K for a doubling of CO₂) have been found, such GCMs indicate that the largest warming will occur in the winter in high latitudes, with the summer precipitation shifted slightly polewards along with increased surface dryness in mid-latitudes. Flohn (University of Bonn) noted that high-latitude warming could lead to the disappearance of the perennial Arctic sea-ice and changes in the mass balance of the Antarctic ice sheet. In contrast, the zero-order, purely optical effect of doubling atmospheric CO₂, according to Kandel (CNRS), would be an increase of about 0.2K in surface temperature, but depending on what is assumed about various feedback mechanisms, such as atmospheric temperature, humidity, lapse rate, evaporation and clouds, this zero-order sensitivity may be multiplied by a factor ranging from 0.1 to 50.

Detection studies are now being directed by Wigley and Kelly (University of East Anglia) towards isolating those parts of observed climate fluctuations that are attributable to increasing atmospheric CO₂. This involves detecting what is at present a relatively weak signal in the presence of considerable noise. Climatic changes during the past century can partly be explained by increasing atmospheric CO₂ with contributions from volcanic activity. However, on the basis of the results so far it seems unlikely that a CO₂ signal will be detected with high confidence before 1990. Nevertheless, it looks as though CO₂-induced warming could become a major climatic factor by the middle of the next century. □

1. Polis, G. A. *Rev. Ecol. Syst.* **12**, 225 (1981).
2. Cuff, W. R. *Can. J. Zool.* **58**, 1504 (1980).
3. Sherman, P. in *Natural Selections and Social Behaviour* (eds Alexander, R. D. & Tinkle, D.) (Chiron, New York, 1980).
4. Polis, G. A. *Behav. Ecol. Sociobiol.* **7**, 25 (1980).
5. Wade, M. J. & McCauley, D. E. *Evolution* **34**, 799 (1980).
6. McCauley, D. E. & Wade, M. J. *Evolution* **34**, 813 (1980).
7. Wade, M. J. *Evolution* **34**, 844 (1980).
8. Mallory, F. F. & Brooks, R. J. *Nature* **273**, 144 (1978).
9. Elwood, R. W. *Anim. Behav.* **28**, 1188 (1980).
10. Hardy, S. B. *Ethol. Sociobiol.* **1**, 13 (1979).
11. Bry, C. & Gillet, C. *Reprod. Nutr. Dev.* **20**, 173 (1980).
12. Wade, M. J. & Breden, F. *Evolution* **35**, 844 (1981).
13. Packer, C. & Pusey, A. E. *Nature* **296**, 740 (1982).
14. Melnick, D. J. *Genetics* **100**, s46 (1982).
15. Foltz, D. W. *et al. Biol. J. Linn. Soc.* **17**, 225 (1982).

John G. Lockwood is in the School of Geography, University of Leeds, Leeds LS2 9JT.

1. IIASA Energy Systems Program *Energy in a Finite World* (Ballinger, 1981).
2. World Climate Program *On the Assessment of the Role of CO₂ on Climate Variations and their Impact* (WMO, Geneva, 1981).
3. Oeschger, H. *et al. in Interactions of Energy and Climate* (eds Bach, W., Pankrath, J. & Williams, J.) 107 (Rendel, 1980).
4. Delmas, R. *et al. Nature* **284**, 155 (1980).
5. Manabe, S. & Wetherald, R. T. *J. Atmos. Sci.* **32**, 3 (1975).

A growing role for reverse transcription

from Harold E Varmus

THE viruses resembling human hepatitis B virus that were recently discovered in other animals — woodchucks¹, ground squirrels² and domestic ducks³ — have begun to yield their anticipated harvest. In the June issue of *Cell*, J Summers and W Mason (Institute for Cancer Research, Philadelphia) make a strong case, based upon work with the duck virus, for the novel idea that RNA-directed DNA synthesis ('reverse transcription') is central to the life cycle of hepatitis B viruses⁴. The claim that RNA tumour viruses (retroviruses) are not the only animal viruses to use a reverse transcriptase may have implications that reach well beyond virology, since a growing constellation of eukaryotic genetic elements — various pseudogenes^{5,6} and repetitive sequences⁷ — appear to depend upon reverse transcriptases of unknown provenance for their existence or amplification. It is not necessary, however, to venture beyond the human hepatitis B virus itself to appreciate the significance of the new findings: this virus is currently replicating in about 200,000,000 people⁸ and infection is strongly associated with the most common

reactions *in vitro*. In infected duck livers, on the other hand, Mason, Summers and their colleagues recently observed that single-stranded putative intermediates in DNA synthesis were composed exclusively of 'minus' strands¹³. The asymmetrical properties of the two strands of hepatitis B viruses appear inconsistent with semi-conservative patterns of DNA replication, instead, the picture more closely mimics retroviral DNA synthesis, in which a virion-associated enzyme synthesizes a 'minus' DNA strand from an RNA template and a 'plus' strand from the 'minus' strand¹⁴.

Past efforts to understand the life cycle of hepatitis B viruses and make sense of such asymmetries have been frustrated in part by the failure of any member of this virus class to grow in cultured cells. Summers and Mason⁴ have circumvented this problem using materials from ducks naturally infected with the duck hepatitis B virus (DHBV). Their experiments required two crucial reagents isolated from cytoplasmic extracts of infected livers: viral cores that exhibit 'endogenous' DNA polymerizing activities, and deproteinized viral nucleic acids that work as templates in reactions 'reconstructed' with a retroviral reverse transcriptase. Synthesis of DHBV 'minus' strand DNA, in either the 'endogenous' or the 'reconstructed' reaction is resistant to the DNA intercalating agent, actinomycin D, whereas synthesis of the 'plus' strands in either reaction is sensitive to the drug. Furthermore, the growing 'minus' strands are partially associated with RNA and largely sensitive to a single-strand-specific nuclease, whereas the 'plus' strands are present entirely in DNA-DNA duplexes. These findings have been interpreted to mean that 'minus' strands are synthesized from templates of DHBV RNA and that 'plus' strands are synthesized from templates of 'minus' strand DNA.

The general picture that emerges from this work reveals the life cycles of hepatitis B and retroviruses to be temporally permuted versions of each other. Infectious particles of retroviruses contain viral RNA, viral DNA is synthesized in the cytoplasm early after infection and used in turn as a template for repeated synthesis of genomic RNA later in the infection. Infectious hepatitis B virus particles, in contrast, contain incompletely double-stranded DNA, the product of reverse transcription, viral RNA must be made during an early step in the life cycle and used as template for reverse transcription within cytoplasmic cores in the late phase.

The gross similarities in replication strategy, however, should not obscure a host of intriguing questions that address contrasting aspects of DNA synthesis, viral persistence and oncogenesis by these two

classes of viruses. Unlike retroviral reverse transcriptases, the hepatitis B DNA polymerases have not yet been solubilized to allow the enzymological study they deserve, so these proteins and their activities remain basically unknown. (The enzymes, incidentally, are probably virus-coded, since both the human¹⁵ and woodchuck¹⁶ hepatitis B genomes maintain a large unassigned open reading frame adequate for a protein of molecular weight about 90,000.) One clue to the enzymatic differences may reside in the mechanism of priming. Retroviruses use host tRNA to prime synthesis of the first strand of DNA, hepatitis B viruses, on the other hand, have an unidentified protein linked to the 5' end of 'minus' strand DNA¹⁷. Is it possible that the primer is a protein, as in the synthesis of adenovirus DNA^{18,7}?

Both retroviruses and hepatitis B viruses establish persistent infections, but again important differences are evident. Retroviruses perpetuate their genomes in infected cells by efficient and precise integration of DNA that resembles a transposable element and forms a suitable template for long-term synthesis of viral

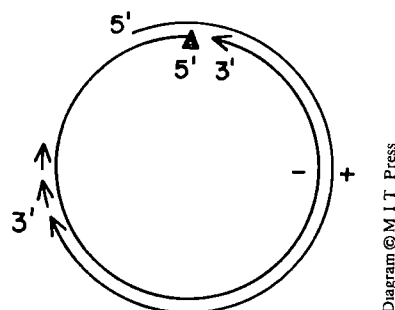


Fig. 1 Genome structure of hepatitis B-like viruses. Δ , covalently bound protein

fatal cancer of man, primary hepatic carcinoma⁹.

Among the clues that led Summers and Mason to consider a replicative mechanism involving reverse transcription were the asymmetrical features of hepatitis B virus DNA, identified in both virus particles and infected cells. The viral DNA genome, as found in particles isolated from sera, is composed of one 3.2 kilobase strand of fixed chemical polarity (the 'minus' strand) base-paired with a shorter 'plus' strand of variable length¹⁰. (Because the 5' ends of these two strands invariably overlap by about 300 bases¹¹, the genome is in a circular configuration, although neither strand is itself a closed circle, see Fig. 1.) A DNA polymerizing activity in virus particles, first discovered in the human virus several years ago by Kaplan *et al.*¹², extends only the 'plus' strand during

Harold E Varmus is a Professor in the Department of Microbiology and Immunology, School of Medicine, University of California, San Francisco, California 94143

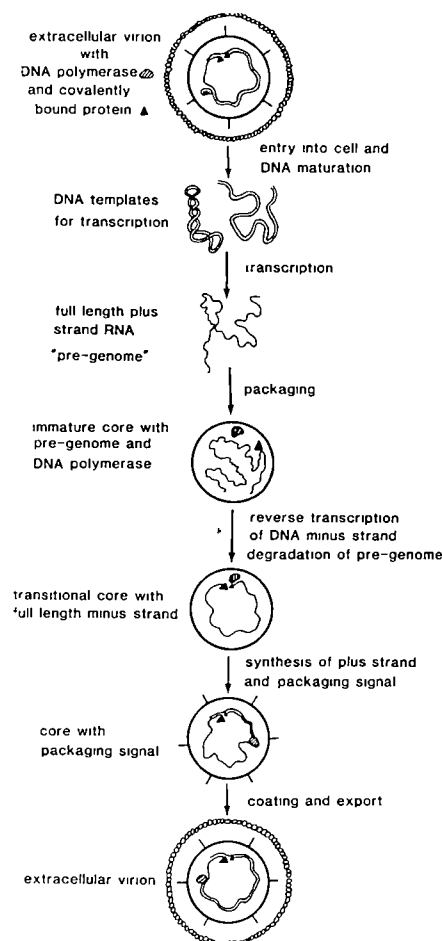


Fig. 2 The pathway for replication of the genome of hepatitis B-like viruses proposed by Summers and Mason⁴

RNA¹⁴ Little is known about the integration of hepatitis B DNA during productive infection of the liver, but the first detailed account of integrated viral DNA in woodchuck liver tumours, again by Summers and his colleagues¹⁹ in the same issue of *Cell*, reveals complex rearrangements within multimeric viral inserts. Similar rearrangements have been found in integrated DNA from a human hepatoma cell line (W. Rutter, personal communication). This picture is not conducive to a belief that integrated DNA

has a role in the life cycle. But if ordered integration does not occur, how is the genome maintained during persistent infection? In particular, what is the template for synthesis of valid copies of viral RNA?

A final comparison of retroviruses and their new cousins is at once the most obvious and the most mysterious: are the hepatitis B viruses truly oncogenic agents and do they use mechanisms recently discovered to influence the development of tumours by retroviruses? □

serotonin, noradrenaline, thyrotropin-releasing hormone and somatostatin — are preserved, indicating that death of nerve cells, rather than a change in afferent inputs, initiates the disease.

Attempts to produce animal models to mimic the pathology, the movement disorder, or the neurochemistry of the disease have received wide attention in recent years. Despite the large number of neurologic mutations that have been described in rodents, particularly mice, none has been identified which shows the key pattern of normal development, followed by cell death in a selected region of the central nervous system. Such mutants, if discovered, might provide a useful clue to the factors that lead to maintenance of cell integrity and an opportunity to study local trophic influences or lack thereof.

The local injection of neurotoxins, the most important of which is kainic acid^{2,3}, has provided a way of mimicking some of the effects of Huntington's disease. There is evidence that the principal neurotransmitter in the corticostriatal pathway, which forms a major input to the striatum, is glutamate, an excitatory neurotransmitter. Kainic acid, a rigid, cyclic analogue of glutamate, has potent excitatory effects, and when injected locally into brain tissues that contain glutamate receptors, causes neuronal death. Cells die, but incoming terminals survive, and many of the biochemical changes of Huntington's disease are seen. Because the effects of kainate require an intact corticostriatal system (the drug is less effective in animals that have previously had surgical corticectomy), it has been proposed that an endogenous kainate-like substance may overstimulate the corticostriatal system with cell death arising from an excitotoxic effect. Kainic acid receptors have been described in the brain and Coyle and his associates³ are currently searching for an endogenous substance with kainate receptor binding capacity. Additional evidence for the importance of afferent inputs to the striatum in determining the neurotoxic effects of kainic acid is provided in the paper by Berger *et al* in this issue of *Nature* (p 254). Depletion of serotonin by injection of 5,7-dihydroxytryptamine, a serotonergic neurotoxin, into the brain stem is shown to make striatal cells more resistant to kainic acid. The kainic acid model, although unlikely to provide a clue to the basic genetic defect in Huntington's disease, does hold some promise for assessing the effects of striatal lesions and perhaps for testing the effectiveness of various therapies.

An alternative approach has been to search for evidence of a generalized defect in cellular functions in Huntington's disease by investigation of peripheral non-neuronal cells more accessible to study. Initial indications of *in vitro* abnormalities in fibroblast growth rates and sus-

- 1 Summers, J., Smolec, J. M. & Snyder, R. *Proc natn Acad Sci U S A* 75, 4533 (1978)
- 2 Marion, P. L. *et al* *Proc natn Acad Sci U S A* 77, 2941 (1980)
- 3 Mason, W. S., Seal, G. & Summers, J. *J Virol* 36, 829 (1980)
- 4 Summers, J. & Mason, W. S. *Cell* 29, (1982)
- 5 Marx, J. *Science* 216, 969 (1982)
- 6 Denison, R. A. & Weiner, A. M. *Molec cell Biol* 2, 815 (1982)
- 7 Jagadeeswaran, P., Forget, B. G. & Weissman, S. M. *Cell* 26, 141 (1981)
- 8 Zuckerman, A. J. *Nature* 287, 483 (1980)
- 9 Beasley, R. P., Lin, C. C., Hwang, L.-Y. & Chien, C.-S. *Lancet* ii, 1129 (1981)
- 10 Summers, J., O'Connell, A. & Millman, I. *Proc natn Acad Sci U S A* 72, 4597 (1975)
- 11 Sattler, F. & Robinson, W. S. *J Virol* 32, 226 (1979)
- 12 Kaplan, P. M., Greenman, R. L., Gerin, J. L., Purcell,

- R. H. & Robinson, W. S. *J Virol* 12, 995 (1973)
- 13 Mason, W. S., Aldrich, C., Summers, J. & Taylor, J. M. *Proc natn Acad Sci U S A* 79, 3997 (1982)
- 14 Varmus, H. E. *Science* 216, 812 (1982)
- 15 Galibert, F., Mandart, E., Fitoussi, F., Tiollais, P. & Charnay, P. *Nature* 281, 646 (1979), Pasck, M. *et al* *Nature* 282, 575 (1979), Valenzuela, P., Quiroga, M., Zaldivar, J., Gray, P. & Rutter, W. J. in *Animal Virus Genetics* (eds Fields, B., Jaenisch, R. & Fox, C. F.) 57 (Academic, 1980)
- 16 Galibert, F., Chen, T. N. & Mandart, E. *J Virol* 41, 51 (1982)
- 17 Gerlich, W. H. & Robinson, W. S. *Cell* 21, 801 (1980), Ganem, D., Greenbaum, L. & Varmus, H. E. *J Virol* (in the press)
- 18 Chalberg, M. D., Desiderio, S. V. & Kelly, T. J. Jr *Proc natn Acad Sci U S A* 77, 5105 (1980)
- 19 Ogston, C. W., Jonak, G. J., Rogler, C. E., Astrin, S. M. & Summers, J. *Cell* 29, 385 (1982)

Huntington's disease: genetically programmed cell death in the human central nervous system

from Joseph B. Martin

HUNTINGTON'S DISEASE, characterized by involuntary movements and progressive dementia, is transmitted as an autosomal, dominant trait whose effect is not seen until the third or fourth decade of life. The tragedy of the disorder lies not only in the effects of the disease itself, but in the absence of any genetic marker to diagnose those at risk, hence transmission of the disease to offspring commonly occurs before symptoms develop. Any inquiry into the cause of the disease must tackle this central issue of how a gene mutation can permit normal development, integration and function of neuronal systems for some thirty to forty years and yet then bring about the relentless, regionally selective, premature death of neurones.

The caudate nucleus and putamen (striatum) are the most severely affected, but other regions of the basal ganglia, hypothalamus and brain stem are also involved. The loss of neurones in the striatum has not been seen to be accompanied by any cytopathology or tissue reaction and cells appear to die without inducing a local

response. Other cells and systems of the body appear unaffected. Dementia becomes severe, but its characteristics are strikingly different from those of the more common Alzheimer's disease, and at autopsy, although the cerebral cortex is diminished in overall size, no certain decrease in total numbers of cells has been unequivocally demonstrated.

How can one account for such a course of events and how can research strategies approach a solution to the problem? The discovery that the symptoms of Parkinson's disease are due to a dopaminergic deficiency secondary to degeneration of the pigmented nigrostriatal system provided strong grounds for investigating biochemical changes in Huntington's disease. Within the striatum and often in the neural projections from it, there is a decrease in the concentrations of the neurotransmitters, acetylcholine and GABA, and of the neuropeptides, substance P, enkephalin and cholecystokinin¹. These decreases in transmitter concentrations appear to be associated with the cell death since their concentrations remain normal in other regions of the brain. Tissue concentrations of other transmitters in the afferent pathways to the striatum — including dopamine,

Joseph B. Martin is Bullard Professor of Neurology in the Massachusetts General Hospital, Harvard Medical School, Boston 02114

ceptibility to irradiation have not been adequately confirmed⁵ Studies of differences in red cell membranes by electron spin resonance and of abnormalities in $(Na^+ + K^+)ATPase$ have not been replicated^{6,7} To date one cannot point to any described abnormality of other cells which provides an indication or marker of the genetic defects

Perhaps the answer will ultimately come from the new techniques of molecular genetics The Huntington's disease gene is considered to have a penetrance of 100 per cent and the mutation rate is exceedingly low, indeed, no proven cases of sporadic mutation have ever been described which satisfy the criteria of proven parentage, with parents surviving to an old age without symptoms, pathologically proven Huntington's disease in the new case, and subsequent transmission to a child The low mutation rate makes it possible and practicable to search for a DNA polymorphism which might be useful as a genetic linkage marker⁸ So far the

chromosomal localization of the defect is unknown but restriction endonuclease digests of DNA collected from the peripheral white blood cells of patients with the disease, combined with somatic cell hybridization, are being used to localize the polymorphisms to a specific chromosome In the long term, it should be possible to survey each chromosome in the human genome sequentially, first for a polymorphism to provide a genetic linkage and ultimately to localize the gene itself There will then be a real possibility of identifying the metabolic defect □

- 1 Bird, E D A *Rev Pharmacol Tox* 20, 511 (1980)
- 2 Coyle, J T & Schwarcz, R *Nature* 263, 244 (1976)
- 3 Ferkany, J W, Zaczek, R & Coyle J T *Nature* 298, 757 (1982)
- 4 Berger, M, Sperk, G & Hornykiewicz, O *Nature* 299, 254 (1982)
- 5 Goetz, J E, Roberts, E & Warren, J *Am J Hum Genet* 33, 187 (1981)
- 6 Fung L W M & Ostrowski, M S *Am J Hum Genet* 34, 469 (1982)
- 7 Comings, D E, Pekkala, A, Schuh, J R, Kuo, P C & Chan, S I *Am J Hum Genet* 33, 166 (1981)
- 8 Houseman, D E & Gusella, J F *Molecular Genetic Neuroscience* (eds Schmitt, F O, Bird, S J & Bloom, F E) 415-424 (Raven, New York, 1982)

Rapid environmental and climatic changes

from D Q Bowen

THE successful characterization and evaluation of past rapid changes in the environment and climate depend largely on the integrity and sensitivity of dating methods All too often imprecision in the climatic record stems from dating uncertainties, with bioturbation and a variety of lag effects providing additional problems Given these constraints, it is little wonder that much of a recent meeting* on the character and timing of rapid environmental and climatic changes was devoted to the comparatively well-dated Holocene record and, to a lesser extent, to that of the later part of the last glaciation Small-scale systems of generally short duration, but for which detailed data were available, received far more attention than the larger systems with somewhat coarser data available over longer time scales

At the larger end of the scale it is difficult to identify specific climatic causes for changes in climate (R V Barry, University of Colorado, Boulder) Among the many uncertainties are whether fluctuations on the 100-1,000 year scale are due to longitudinal and/or latitudinal changes in circulation, whether particular regimes persist for long periods and what the circulation

variability of different regimes is It is not even possible to ascribe the quasi-persistent types of circulation regime to external or internal forcings, to atmospheric auto-variation or to internal feedback mechanisms between land, ocean and atmosphere Barry stressed, however, that the intensity and timing of climatic change will show considerable geographical variation step-like in some areas but more gradual in others

R Bryson (University of Wisconsin, Madison) further stressed that in regarding climatic change as essentially nonlinear, a major break with tradition had now occurred, while J Mitchell (Environmental Data Service, Silver Spring, Maryland) emphasized the role of the oceans as a global climatic fly-wheel which limits change more strictly over shorter than over longer periods Deep water formation in the North Atlantic may also play an important part in speeding glacial events, sea-level changes can lead to perturbations in oceanic thermocline circulation processes which may enhance oceanic heat transportation to higher latitudes during periods of glacial growth (C Rooth, University of Miami)

Global data show considerable glacial fluctuations during the last glaciation, mostly reflecting local or anomalous conditions (S Porter, University of Washington, Seattle) and the glacier response to rapid climatic change is best assessed from Holocene examples where

lead and lag effects can be partially quantified Sea-level data for the past 140 kyr (T Cronin, US Geological Survey, Reston) demonstrate the many pressing problems still extant, where was the last glacial maximum sea level? Where was sea level during the mid-Wisconsin? How rapid were sea-level changes? The possibility of a high sea-level event between 130 and 140 kyr received much attention but was strongly questioned by W Ruddiman (National Science Foundation) on the basis of the oxygen-18 record

The most sensitive indications of climatic change are provided by the oxygen-18 record in ice sheets followed by sea-surface temperatures (H Wright, University of Minnesota, Minneapolis) Most pollen records are beset by persistent difficulties in interpretation due to their proximity to ice sheets Sensitivity and response times might thus be better detected at very low latitudes or in the Southern Hemisphere, free from such influences Furthermore the climatic signal from pollen data fails to provide a clear record of climatic change of short duration even when its amplitude is large (M Davis, University of Minnesota) for example, the 'Little Ice Age' is only recorded clearly by pollen at a few sites, despite the considerable impact on human culture Except in a few cases it is difficult to infer from pollen data whether climatic change is step-wise or gradual and unidirectional (W Watts, Trinity College Dublin) Relationships between climatic change and the pollen record are only indirect because plant populations generally become established long after causal climatic events There is thus an urgent need to identify sensitive ecotonal areas at the margins of plant ranges where pollen data and climate can be linked directly Most rapid of all may be the response of lake sediments to climatic change (R Anderson, University of New Mexico, Albuquerque) Seasonal control is dominant and gives a clear signature, while cumulative changes in seasonal components demonstrate rapid climatic change It should be possible to design transfer functions expressing linkages between climate and sedimentation, with eventual application to non-varied sediments

In summing up the proceedings, J Mitchell predicted that climate will change over a transitional period of the next 200 years because of an increased carbon dioxide content in the atmosphere, then settle into a 1,000 year equilibrium state The rapidity of this transition could be comparable to that at the Younger Dryas to Holocene change some 10,000 years ago. □

Erratum

In K F Chater's article 'Streptomyces in the ascendant' (*News and Views* 299, 10, 2 September 1982), the last eleven lines of paragraph four (beginning 'As a result,') should have appeared at the end of paragraph five

*The 7th Biennial Conference of the American Quaternary Association on 'Character and Timing of Rapid Environmental and Climatic Changes' was held at the University of Washington, Seattle, 28-30 June 1982

D Q Bowen is in the Department of Geography, The University College of Wales, Aberystwyth SY23 3DB

A Proterozoic Pangaea?

from D.H. Tarling

IN a recent review of palaeomagnetic data (*Earth planet. Sci. Lett.* **59**, 61; 1982), Piper concludes that a single huge continent, Pangaea, existed throughout the Proterozoic period of the Earth's history (2,600–570 Myr ago). Such a conclusion is consistent with many geological features that indicate extensive continental stability during this period, yet Piper's analyses also require that this Pangaeian supercontinent was in motion relative to the Earth's axis of rotation. Such motion must, presumably, be associated with the same mantle convective motion that currently results in continental splitting and ocean-floor spreading. Piper's conclusions are thus of fundamental importance in testing some of the basic assumptions in both palaeomagnetism and plate tectonics.

Palaeomagnetic studies allow the determination of the palaeolatitude and orientation (relative to the palaeomagnetic pole) of the sampled area. Where sufficient data are available, they can be used to construct a palaeomagnetic polar wandering curve, indicating the changing position of the pole relative to the stable tectonic block from which the samples were obtained. Such curves do not, in fact, mean that the pole is moving, as this is fixed relative to the ecliptic, but results from a movement of the sampled region relative to the pole. The fact that polar wandering curves exist for the Proterozoic is thus of the utmost importance as it clearly indicates that the continent, or continents, were in motion and were presumably driven by mantle convection.

If polar wandering paths for the same period of time can be matched between different tectonic units, then the relative positions of these tectonic units can be precisely defined. Thus the palaeomagnetic data from the different cratonic blocks of the world can be used to determine the existence, or not, of one or more continental units during the Proterozoic. Piper finds that he can define Pangaea throughout the Proterozoic as a cigar-shaped continent comprising Australia, China, India and Antarctica backing onto western South America–Africa, with Kazakhstan–Siberia against North Africa and bordering onto western Laurentia (North America, Greenland and Europe). Piper finds that such a continent is not only required by the palaeomagnetic data but is also consistent with the available geological evidence.

It is only too easy to be sceptical about the data base on which any such model is

erected. Even with a single craton, the radiometric dating of any intrusive event is uncertain within 100–200 Myr, even ignoring problems of open chemical systems, during which time major continental motions could have occurred. It is also worrying that much Precambrian data are based on alternating magnetic field demagnetizations — a technique that is 'noisier' than thermal demagnetization — yet thermal demagnetization is often apparently ineffective in determining discrete components of remanence. Even when such components can be isolated, there is doubt about their age. There is a tendency to assume that the component with the highest stability is, in fact, the oldest — yet this may simply reflect the presence of haematite that may have formed very much later than the rock itself. Even when such components have been isolated and dated, it is rare for there to be adequate tectonic control of subsequent movements, although the Proterozoic crust appears to have been little deformed as the overlying sediments tend to have only shallow dips. The uncertainties involved are thus immense and require subjective evaluation. Unfortunately, this

can lead to the syndrome in which scattered data are examined and the odd points that are near to previous observations are accepted for publication and the remainder appear, if at all, in the inaccessible appendix of a thesis. Despite Piper's attempts to be objective, therefore, the data may well already have been subjectively selected to conform to previous data or models. However, the only way in which such problems can be resolved is by the erection of specific models which can then be tested by a variety of methods and by new data.

This is not Piper's first model and it seems unlikely to be his last. However, the fact that he can make a very plausible case for support of his model is, in itself, of great importance. It demonstrates, for example, that continental motions occurred, thus indicating the action of mantle convection currents. This is no great surprise in view of the much higher radiogenic heat production in the past, but raises the problem of why such motions did not cause continental splitting, as they do now and also did in pre-Proterozoic times. The implication is that the continental lithosphere, in Proterozoic times, was too strong or too thick to be split by such motions. But how did such a thickness develop suddenly at the end of Archaean times and what caused the change to present-day continental splitting? □

The sunflower seed protection business

from Peter D. Moore

The consumption of the seeds of plants by invertebrate and vertebrate predators is a serious problem for the agronomist, and much effort has been devoted to finding ways of limiting the predators' numbers. There is, however, a quite different way of tackling the problem. In a recent paper¹, field trials are reported of attempts to protect economically important seeds by buying off the predators with an abundant supply of another seed.

In many North American forests, small mammals have often been found responsible for seed predation and depression of woodland regeneration, in particular the douglas fir (*Pseudotsuga menziesii*) has been much studied. That seed predators may limit the regeneration of plant species has been known for some time. As long ago as 1919 Watt's² records of the fate of acorns in oakwoods showed that high mortality of acorns in oakwoods could be largely put down to predation by birds and mammals. He also found that in the case of beech², invertebrates were involved and concluded that the low level of regeneration found in British woodland was a consequence of

seed predation. The high population density of mice and voles, regarded by him as major culprits, could in turn be related to rearing of game birds and consequent destruction of predators, a view supported and popularized by Tansley³.

The possibility that the problem might be overcome through providing an alternative food source was first approached experimentally by Sullivan⁴ who supplied deer mice (*Peromyscus maniculatus*, a major seed predator of douglas fir) with sunflower seed in order to distract it from the conifer seed. He found that very large quantities of sunflower seed had to be provided (seven sunflower seeds for every douglas fir seed) in order to reduce predation significantly.

Sullivan and Sullivan⁵ have now repeated these experiments with lodgepole pine (*Pine contorta*) in an area of British Columbia from which the pine had been

D.H. Tarling is Reader in Palaeomagnetism in the Department of Geophysics, The University, Newcastle upon Tyne NE1 7RU.

Peter D. Moore is Senior Lecturer in the Department of Plant Sciences at King's College, University of London.

felled in 1978. Lodgepole pine was seeded at a density of 45,000 ha⁻¹ and, in some experimental plots, sunflower seed was added at twice this density (90,000 ha⁻¹). Damage by mice was very high in plots without the sunflower additive (often less than 5 per cent survival after 5 months), but where sunflower seed was also sown, pine seed survival was around 25 per cent after 5 months. This fivefold increase in the rate of survival is obviously of great interest to the forester.

There are two complications, however, which lead to a certain degree of apprehension. The first, which has received emphasis from Harper⁶, is that compensating factors may be operating so that when one cause of mortality is reduced another assumes prominence. The second is the fear that a rich new resource of sunflower seeds may cause an increase in mouse population density, which will subsequently lead to greater predation upon the pine seeds. Sullivan and Sullivan claim that such increases in mouse density were observed in the sunflower plots only where initial densities were below 5 mice ha⁻¹, so other population limits are evidently in operation. It also appears from their data that no other cause of pine seed mortality has replaced that due to predation, so the technique seems to warrant more extensive trials.

Ecological, or perhaps ethical, attitudes have evidently changed since the days of Watt and Tansley. Instead of shooting the predators we now feed the mice. □

1. Watt, A.S. *J. Ecol.* 7, 172 (1919).
2. Watt, A.S. *J. Ecol.* 1 (1923).
3. Tansley, A.G. *The British Islands and their Vegetation* (Cambridge University Press, Cambridge, 1939).
4. Sullivan, T.P. *J. appl. Ecol.* 16, 475 (1979).
5. Sullivan, T.P. and Sullivan, D.S. *J. Appl. Ecol.* 19, 95 (1982).
6. Harper, J.L. *Population Biology of Plants* (Academic, London, 1977).

Glomar Challenger at the Cretaceous-Tertiary boundary

from Audrey Wright, Ross Heath and Lloyd Burckle

THE drilling vessel *Glomar Challenger* reached Yokohama on 20 June 1982, after sampling six sites in the western North Pacific. Major objectives of this leg were to determine the chronology and extent of late Neogene through Pleistocene migrations of the subarctic front; to acquire a Cenozoic record of aeolian and authigenic sedimentation in the North Pacific; and to collect an undisturbed sample of the Cretaceous-Tertiary boundary on Shatsky Rise.

Hydraulic piston cores taken at four sites located along a north-south transect from 34° to 44°N latitude and centred at about 155°E longitude recovered a suite of siliceous sediments for in-depth palaeoceanographic and palaeoclimatic reconstructions for the past five million years. Sediments from two 'red clay' sites, located east and west of Shatsky Rise, provide an excellent basis for resolving Cenozoic North Pacific authigenic sedimentation as well as for detailing the depositional history of wind-blown sediment from Asia.

At Site 577 on the Shatsky Rise, a complete and expanded sequence containing the Cretaceous-Tertiary (K-T) boundary was collected. Triplicate hydraulic piston cores were successfully taken through this critical interval, guaranteeing complete coverage and sufficient material for detailed study of floral and faunal changes as well as palaeomagnetic and geochemical properties across the K-T boundary. Studies of the foraminifers, nannofossils, palaeomagnetic signature and aeolian debris from this section, begun at sea, will be continued

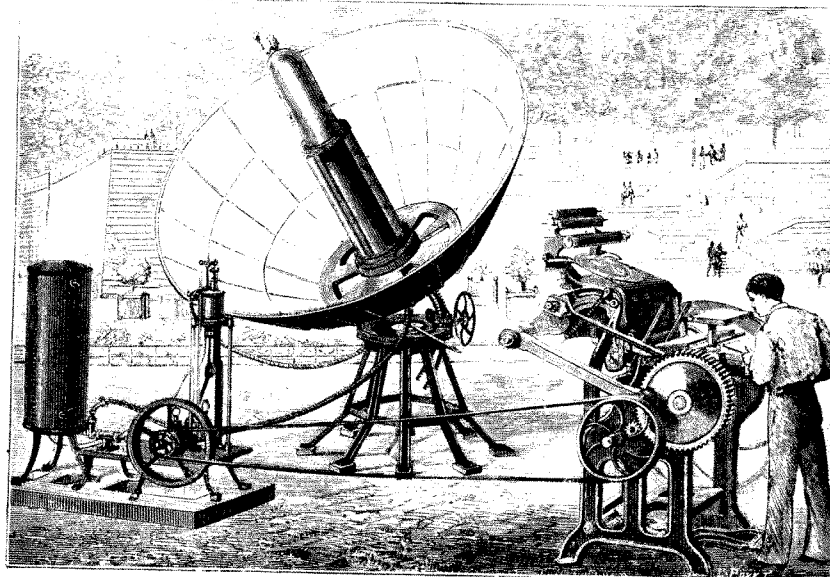
on-shore in the laboratories of cruise participants.

Initial examinations of the calcareous nannofossils and planktonic foraminifers suggest that the K-T boundary, located at a sub-bottom depth of 109.7 m, is continuous and complete. The abundance of the late Maestrichtian *Micula mura* nannofossil assemblage decreases abruptly at the boundary. Above it, Cretaceous species are replaced by a less diverse, less abundant and moderately preserved assemblage characterized by the genera *Thoracosphaera* and *Cyclagelosphaera*, as well as *Markalius astroporus* and the very small *Cruciplacolithus primus*. Few reworked Cretaceous forms were found 20 cm above the boundary.

Preservation of foraminifers is moderate to good throughout the boundary interval. The K-T boundary is marked by the extinction of all Cretaceous planktonic forms and the first appearance of the early Palaeocene foraminifer *Chiloguembelina taurica*. Rare reworked Cretaceous foraminifers are found at least 20 cm above the boundary. The first appearance of the primitive globigerinid foraminifer, *Globigerina eugubina*, occurs 40 cm below the boundary. At this point the specimens are few in number and very tiny. They become abundant and of a consistently larger size at the boundary. These preliminary findings are in contrast with the section at Gubbio, Italy, in which the first appearance of *G. eugubina* marks the K-T boundary. □

Audrey Wright, Ross Heath and Lloyd Burckle are members of the DSDP 86 scientific staff.

100 years ago



A SOLAR PRINTING PRESS

It was mentioned in a recent number of this journal that a printing press worked by solar heat had been exhibited in the Tuileries Garden in Paris on the occasion of a *fête*. The solar generator was devised by M. Abel Pifre. The insolator, shown in the middle of the picture, measured 3'50 m. diameter at the aperture of the parabolic mirror. It was set up in the garden, near the large basin, at the foot of the flight of steps of the Jeu de Paume. The steam from the boiler placed in its focus was utilised by means of a small vertical motor (shown on the left), having a power of 30 kilogrammetres, which actuated a Marinoni press (on the right). Though the sun was not very ardent, and the radiation was hindered by frequent clouds, the press was worked with regularity from 1 p.m. till 5.30 p.m., printing on an average 500 copies an hour, of a journal specially composed for the occasion, viz., the *Soleil Journal*. This result, though not indicating a revolution in the art of printing, may enable one to judge of the services these *insolators* may render in climates with a radiation more powerful and constant. From *Nature* 26, 503; September 21, 1882.

ARTICLES

Sharp edges of planetary rings

Nicole Borderies & Peter Goldreich

Division of Geological and Planetary Sciences, California Institute of Technology, Pasadena, California 91125, USA

Scott Tremaine

Department of Physics, Center for Space Research and Center for Theoretical Physics, Massachusetts Institute of Technology, Cambridge, Massachusetts 02139, USA

The ring systems of Saturn and Uranus exhibit several sharp edges across which the optical depth drops from order unity to essentially zero. At least two and perhaps all of these features are associated with the location of orbital resonances between a satellite and the ring particles. It is remarkable that the optical depth varies on a distance scale which is much finer than that over which angular momentum can be transferred between a satellite and the ring material. The important features of this phenomenon are (1) A perturbed band of width $\Delta a/a \approx (M_s/M_p)^{1/2}$ adjacent to the edge within which the angular momentum transfer occurs (2) Streamlines perturbed such that the angular momentum luminosity decreases smoothly across the band to zero at the edge even though the optical depth remains constant (3) Dynamical equilibrium requires a relation between the random velocity, the rate of deformation and the optical depth

SHARP edges are common features of planetary rings¹. Stellar occultation observations of the rings of Uranus revealed edges which are sharp at a resolution of a few kilometres². Stellar and radio occultations carried out by the Voyager spacecraft revealed several sharply defined gaps and ringlets in the saturnian ring system (refs 3, 4 and L. Tyler, personal communication). Of these, perhaps the most interesting are the outer boundaries of the classical A and B rings which are sharp on a scale of hundreds of metres. Voyager discovered that the outer boundary of the A ring is virtually coincident with the 7:6 resonance of the larger co-orbital satellite⁴ and confirmed the prediction that the outer boundary of the B ring is located at the 2:1 resonance with Mimas^{5,6}. On the basis of these two examples, we adopt the hypothesis that a satellite resonance is associated with every sharp edge across which the optical depth falls to zero.

Here we consider the dynamics in several stages. First, we review some relevant material about periodic orbits and particle disks, and then we prove that the ring particle velocity dispersion is greatly enhanced near a sharp edge. Next, we show how the angular momentum luminosity gradually decays to zero even though the surface density and velocity dispersion do not vary appreciably. Finally, we indicate why the surface density remains high until it drops abruptly to zero over a distance from the edge comparable to the vertical thickness of the ring.

The semi-quantitative arguments presented here are, in part, based on numerical calculations of ring equilibria near an edge, the results of which we shall publish elsewhere. For ease of notation, and because the outer A and B ring boundaries are among the best studied examples of sharp edges, we have concerned ourselves only with outer edges; the discussion can be translated easily to render it applicable to inner edges.

Periodic orbits

The perturbation potential near an isolated resonance is characterized by an azimuthal wavenumber m and a pattern speed Ω_p . In a reference frame which rotates with the pattern speed, the potential varies as $\cos m\varphi$ with longitude φ .

There is a set of test particle orbits, referred to as periodic orbits, which are closed in the rotating frame. In the inertial frame the periodic orbits are precessing ellipses. For small

eccentricity, the shapes of the orbits in the rotating frame satisfy

$$r = a \left[1 + \Gamma \frac{M_s a}{M_p (a - a_r)} \cos m\varphi \right] \quad (1)$$

where r is the radial distance from the centre of the planet, a is the semi-major axis, M_s and M_p are the masses of the satellite and planet, respectively, and Γ is of order unity. The eccentricity increases with decreasing distance from the resonance which is at semi-major axes a_r . In a region of width

$$\Delta a \approx a_r (M_s/M_p)^{1/2} \quad (2)$$

around a_r , the periodic orbits intersect

Streamlines

The ring particle streamlines are described by

$$r = a \{ 1 - e(a) \cos m[\varphi + \Delta(a)] \} \quad (3)$$

in the rotating frame. Here a and e are the semi-major axis and eccentricity of the ring particle orbits and Δ is a phase lag. The determination of e and Δ from the viscous stress and gravitational perturbations due to the satellite and the ring material is described later. The outer edge a_0 is near a_r , and for $(a_0 - a)/\Delta a \gg 1$, the streamlines are well approximated by periodic orbits. Closer to a_0 , the self-gravity of the ring material and the interparticle stress modify the streamlines so that they do not cross.

For later use, we define

$$J(a, \varphi) = \frac{\partial r}{\partial a} \bigg|_{\varphi} = 1 - q \cos [m(\varphi + \Delta) + \gamma] \quad (4)$$

where

$$q^2 = \left(\frac{a de}{da} \right)^2 + \left(\frac{mae d\Delta}{da} \right)^2, \quad \text{sgn } q = \text{sgn} \left(\frac{de}{da} \right) \quad (5)$$

and

$$\tan \gamma = \frac{me d\Delta/da}{de/da}, \quad -\frac{\pi}{2} \leq \gamma \leq \frac{\pi}{2} \quad (6)$$

Viscosity

A rigorous treatment of the viscous stress in a particle disk of modest optical depth requires the derivation of the full stress tensor from kinetic theory. The Boltzmann equation with col-

isions has been solved for perturbed particle disks⁷ We rely on this calculation for guidance but for simplicity we use the hydrodynamical approximation and relate the viscous stress to the deformation rate tensor by a single parameter, the kinematic viscosity, ν

For an unperturbed keplerian disk it is a good approximation to take

$$\nu \approx 0.5 \frac{v^2 \tau}{\Omega(1+\tau^2)} \quad (7)$$

where v is the one-dimensional r.m.s. random velocity⁸ For simplicity, we ignore the real complications introduced by anisotropic random velocities and the distribution of particle sizes It is qualitatively acceptable but quantitatively inaccurate to extend the use of equation (7) to regions perturbed by resonances

The rate of dissipation of mechanical energy per unit mass is expressed macroscopically by

$$\frac{dE_v}{dt} \approx 2\nu |S|^2 \quad (8)$$

and microscopically by

$$\frac{dE_v}{dt} \approx (1-\varepsilon^2) \nu^2 \Omega \tau \quad (9)$$

Here S is the rate of deformation tensor and ε is the coefficient of restitution for particle collisions Equating the two expressions for viscous dissipation and using equation (7) for ν , we obtain

$$\varepsilon^2 \approx 1 - \frac{G(q^2)}{1+\tau^2} \quad (10)$$

where

$$G(q^2) \approx |S/\Omega|^2 \quad (11)$$

If $\varepsilon(\nu)$ were known, equation (10) would determine ν as a function of q^2 and τ Unfortunately, we can be confident only that $d\varepsilon/d\nu < 0$, $dG/d|q| > 0$ and $G \rightarrow \infty$ as $|q| \rightarrow 1$ However, we can draw one important conclusion from equation (10) that is, in steady state the magnitude of the rate of deformation is bounded such that

$$|S| \lesssim \Omega(1+\tau^2)^{1/2} \quad (12)$$

An external stress might temporarily drive $|S|$ above the upper limit However, the random velocity would then grow exponentially, with rate constant $\Omega\tau$, until the viscous stress was large enough to reduce $|S|$ to an acceptable steady-state level

Angular momentum and energy fluxes

The angular momentum and energy fluxes, $F_H(a, \varphi)$ and $F_E(a, \varphi)$, are the rates at which these quantities cross a unit length of the streamline with semi-major axis a and longitude φ The luminosities $L_H(a)$ and $L_E(a)$ are the integrals of the fluxes around the streamline

The ring divides naturally into two regions, an inner unperturbed portion with $a < a_1$ and an outer perturbed part with $a_1 \leq a \leq a_0$ The location of a_1 need not be specified beyond the requirement that $\Delta a \ll a_0 - a_1 \ll a$

Unperturbed inner region. In the inner, or keplerian, region the streamlines are circles, $\Omega^2 a^3 = GM_p$, and

$$L_H(a) = 2\pi a F_H(a) = 3\pi \Sigma \nu \Omega a^2 \quad (13)$$

$$L_E(a) = \Omega L_H(a) \quad (14)$$

with Σ the surface density⁹ The radial drift velocity of a ringlet is

$$\frac{da}{dt} = -\frac{1}{\pi a^2 \Omega \Sigma} \frac{dL_H}{da} \quad (15)$$

and vanishes if L_H is conserved The viscous dissipation of energy per unit mass is

$$\frac{dE_v}{dt} = -\frac{1}{2\pi a \Sigma} \left[\frac{dL_E}{da} - \frac{\Omega dL_H}{da} \right] = \frac{3\Omega L_H}{4\pi a^2 \Sigma} = \frac{9\nu \Omega^2}{4} \quad (16)$$

Note that L_E decreases outwards even where L_H is conserved **Perturbed outer region.** Here the streamlines are not circular and the fluxes are functions of φ as well as of a The hydrodynamical approximation yields

$$F_H(a, \varphi) = 2\nu(a) \Sigma(a) \Omega a (1-q^2)^{1/2} \left[\frac{1}{J} - \frac{1}{4J^2} \right] \quad (17)$$

where $\Sigma(a)$ is the mean surface density averaged over φ and $\Omega(a)$ is the mean orbital angular velocity As $e(a) \ll 1$, $F_E = \Omega F_H$ If ν is assumed to be a function of a but not of φ , then

$$L_H(a) = 4\pi \nu \Sigma \Omega a^2 K(q^2) \quad (18)$$

where

$$K(q^2) = \frac{3-4q^2}{4(1-q^2)} \quad (19)$$

Of course, $L_E = \Omega L_H$

Two values of $|q|$ are of particular significance For $|q| = q_1 = 3/4$, $F_H = 0$ where $\cos[m(\varphi + \Delta) + \gamma] = \text{sgn } q$ For $|q| < q_1$, $F_H > 0$ for all φ and for $|q| > q_1$, there is an interval of φ in which $F_H < 0$ The inward flux of angular momentum arises because the angular velocity increases outwards in this longitude range For $|q| = q_2 = \sqrt{3}/2$, $L_H = 0$ For $|q| < q_2$, $L_H > 0$ and for $|q| > q_2$, $L_H < 0$

The existence of two transitional values of $|q|$ is established by our solution of the Boltzmann equation⁷ The particular numerical values, $q_1 = 3/4$ and $q_2 = \sqrt{3}/2$, are special consequences of the hydrodynamical approximation The more appropriate kinetic theory yields values which are functions of optical depth

Conditions near edges

Enhanced velocity dispersion. An outer edge may remain fixed at a resonance if the angular momentum which flows out from the unperturbed inner region, $L_H(a_1)$, is completely absorbed by the satellite Then, it follows from the Jacobi relation that energy is transferred to the satellite at a rate $\Omega_p L_H(a_1)$ The rate of energy dissipation in the perturbed region must be $L_E(a_1) - \Omega_p L_H(a_1) = (\Omega - \Omega_p) L_H(a_1)$ Most of this dissipation takes place in the narrow outer band of width Δa in which the streamlines are severely distorted The average dissipation rate per unit mass in this band is

$$\frac{dE_v}{dt} = \frac{(\Omega - \Omega_p)}{2\pi a \Delta a \Sigma} L_H(a_1) \quad (20)$$

Comparison of equations (16) and (20) shows that dE_v/dt is enhanced in the outer band by a factor $2a(\Omega - \Omega_p)/(3\Omega \Delta a)$ relative to its unperturbed value Use of the resonance condition $m(\Omega - \Omega_p) = \Omega$ and $\Delta a/a \approx (M_s/M_p)^{1/2}$ allows us to simplify the enhancement factor to $m^{-1}(M_p/M_s)^{1/2}$

It is apparent from equation (8) that either or both ν and $|S|$ must increase in the outer band However, the upper limit on $|S|$ given by equation (12) proves that for $\tau = 0(1)$, most of the enhanced dissipation is due to an increased ν Since ν is proportional to v^2 , it follows that ν is enhanced by a factor

$$F \approx \left[\frac{1}{m^2} \frac{M_p}{M_s} \right]^{1/4} \quad (21)$$

Decay of L_H . It might seem peculiar that L_H would decay in the outer band where Σ is constant and ν is enhanced above its unperturbed value However, there is no paradox here

$L_H = 0$ for any values of Σ and ν if $|q| = q_2$. Thus $q_2 - |q| \ll 1$ in the outer band and $|q| = q_2$ at the edge

Sharp edges. We have seen how L_H can decay to zero in the outer band at constant Σ . However, one question remains why does Σ maintain a constant value right up to the edge?

To answer this, we refer to equation (10) which relates ε , τ and $|q|$. Since ε is a function (admittedly unknown) of ν , and τ is directly proportional to Σ , equation (10) may be viewed as connecting ν , Σ and $|q|$. But in the outer band, $|q| \approx q_2$ and ν is enhanced by a factor F above its unperturbed value. Thus, in principle, equation (10) determines Σ in the outer band as a function of the resonance parameter $m^{-1}(M_p/M_s)^{1/2}$ and the unperturbed ν .

The precise distance over which Σ drops to zero is probably of the order ν/Ω which is the vertical thickness of the ring and, for $\tau = 0(1)$, is also the mean free path for particle collisions. Our use of the hydrodynamical model is not valid closer than ν/Ω to the ring edge.

Numerical results

The dynamical state of the ring may be modelled by dividing it into narrow ringlets whose shapes are determined by the three variables a , e and Δ . The perturbation accelerations are due to the satellite gravity, the self-gravity of the ring and the viscous stress. We have derived the differential equations which govern the variations of a , e and Δ for each ringlet. The evolution equations are supplemented by equations (7) and (10) and one of several plausible relations for $\nu(\varepsilon)$.

Equilibrium solutions have been obtained with up to 20 ringlets. They exhibit the features discussed above. In particular, there is an outer band of width approximately Δa in which ν is greatly enhanced, $|q| = q_2$, Σ is fairly constant and L_H decays to zero. With some forms of $\varepsilon(\nu)$ we were unable to obtain equilibrium solutions for which Σ varies smoothly with a in the outer band. Presumably, the smooth equilibria suffer from a secular instability of the kind proposed to explain the multiple ringlet structure of Saturn's rings¹⁰⁻¹².

Single ringlet model for the outer band. Several characteristics of the numerical solutions may be illustrated by a crude model in which the entire outer band is represented by a single ringlet.

We balance the satellite torque on the ringlet

$$T_s = -(ma\Omega)^2 e \frac{M_s}{M_p} \Sigma a \Delta a |\sin m\Delta| \quad (22)$$

against the angular momentum luminosity which enters it, $L_H(a_1)$, to obtain

$$|\sin m\Delta| = \frac{\nu}{\Omega(ma)^2} \left(\frac{M_p}{M_s} \right)^2 \quad (23)$$

where ν is the unperturbed viscosity. In deriving equation (23) we have set $e = \Delta a/a \approx (M_s/M_p)^{1/2}$. The condition that the satellite is capable of opening a gap at the resonance is equivalent to $|\sin m\Delta| \leq 1$ (ref. 13).

The values a_0 and e_0 for the outer edge depend on the parameters m , M_s/M_p and $\Sigma a^2/M_p$. At a strong resonance,

$|\sin m\Delta| \ll 1$ so that $q \approx a \, de/da$. Now $q \approx |q_2|$ in the outer band and, for our hydrodynamical mode, $q_2 = \sqrt{3}/2$. The expression

$$e \approx \left(\frac{M_s}{M_p} \right)^{1/2} \left[1 + \frac{\sqrt{3}}{2} \right] + \frac{\sqrt{3}}{2} \left[\frac{a - a_r}{a_r} \right] \quad (24)$$

takes into account the fact that the streamlines are well approximated by periodic orbits for $a < a_r - \Delta a$ and that $a \, de/da \approx \sqrt{3}/2$ for $a \geq a_r - \Delta a$. The condition that the outer edge streamline does not precess in the rotating frame is

$$\frac{\Sigma a^2}{M_p e_0} - \frac{m M_s}{e_0 M_p} \approx \frac{3(m-1)}{2} \left[\frac{a_0 - a_r}{a_r} \right] \quad (25)$$

The first and second terms on the left-hand side are due to the gravitational perturbations from the ring and the satellite, which force the apsidal line to advance and regress, respectively. For $p \equiv \Sigma a^2/(m M_s) \geq 0(1)$, equations (24) and (25) may be solved for $(a_0 - a_r)/a$ and e_0 . Both e_0 and $(a_0 - a_r)/a$ are proportional to $(p M_s/M_p)^{1/2}$ for $p \gg 1$.

Discussion

The Voyager 2 images show that the outer boundary of the B ring is an ellipse centred on Saturn whose short axis points approximately towards Mimas⁵. A calculation of the periodic orbits near the 2:1 resonance with Mimas indicates that the first orbits which cross have $ae = 30$ km. The observations yield $ae \geq 70$ km for the B-ring outer edge. This information may allow a local determination of Σ from more precise versions of equations (24) and (25).

The velocity dispersion and the vertical thickness should be enhanced by between one and two orders of magnitude in the outer band of the B ring relative to their unperturbed values. It is reasonable to assume that the enhanced collision velocities associated with resonance features such as sharp edges and density wavetrains would result in the copious production of small particles. These particles might account for the peaks in optical depth found near resonances in the UV spectrometry occultation data⁴. These peaks should then be absent from the radio occultation data.

The arguments presented in this article are based on the implicit assumption that outside a sharp edge $L_H = 0$, or at least is reduced far below its value in the unperturbed part of the ring. The possibility remains that although τ drops by one or even two orders of magnitude, ν might rise by a similar factor, thus maintaining L_H at its unperturbed value in a region which is apparently empty. The juxtaposition of high and low optical depth regions separated by a sharp boundary would then be an extreme limit of the secular instability proposed to account for the fine structure in Saturn's rings¹⁰⁻¹².

We thank E. Danielson, A. Lane, J. Lissauer, R. Terrile and L. Tyler for helpful discussions. During this research N.B. held a NSF US-France exchange postdoctoral fellowship and a grant from ATP Planétologie 1981. P.G. acknowledges support from NSF grant AST 80-20005 and NASA grant NGL-05-002-003. S.T. acknowledges support from NASA grants NSG-7643 and NGL-22-009-638. This work is contribution 3797 from the Division of Geological and Planetary Sciences, California Institute of Technology.

Received 23 June, accepted 29 July 1982

- 1 Smith, B. A. *et al Science* **212**, 163 (1981)
- 2 Elliot, J. L., Dunham, E., Wasserman, L. H., Millis, R. L. & Churms, J. *Astr. J.* **83**, 980 (1978)
- 3 Lane, A. L. *et al Science* **215**, 537 (1982)
- 4 Holberg, J. B., Forrester, W. T. & Lissauer, J. J. *Nature* **297**, 115-120 (1982)
- 5 Smith, B. A. *et al Science* **215**, 504 (1982)

- 6 Goldreich, P. & Tremaine, S. *Icarus* **34**, 240 (1978)
- 7 Borderes, N., Goldreich, P. & Tremaine, S. (in preparation)
- 8 Goldreich, P. & Tremaine, S. *Icarus* **34**, 227 (1978)
- 9 Lynden-Bell, D. & Pringle, J. E. *Mon. Not. R. Astr. Soc.* **168**, 603 (1974)
- 10 Lin, D. N. C. & Bodenheimer, P. *Astrophys. J. Lett.* **248**, L83 (1981)
- 11 Luukkari, J. *Nature* **292**, 433-435 (1981)
- 12 Ward, W. R. *Geophys. Res. Lett.* **8**, 641 (1981)
- 13 Goldreich, P. & Tremaine, S. *Astrophys. J.* **241**, 425 (1980)

Stratigraphical significance of the Tulu Bor Tuff of the Koobi Fora Formation

F. H. Brown & T. E. Cerling

Department of Geology, University of Utah, Salt Lake City, Utah 84112, USA

The Tulu Bor Tuff, a major marker horizon in the Koobi Fora Formation, has been misidentified in previous studies. Identification of this tuff in sediments previously mapped as the Kubi Algi Formation requires re-evaluation of the existing stratigraphical framework of the Koobi Fora region

DURING the past 2 yr we have investigated the chemistry of tuffs from Plio-Pleistocene deposits east of Lake Turkana in northern Kenya. The stratigraphy at Koobi Fora is based on marker beds and their supposed correlatives¹. We state specific locations where particular stratigraphical marker beds may be observed. This is necessary because miscorrelations have been made in erecting the type sections of formally defined formations, and because several stratigraphical terms now in use are defined only vaguely. In addition, we find that considerable stratigraphical revision is needed at Koobi Fora.

Stratigraphical problems at Koobi Fora have been evident for some time. By 1977 it had been shown² that chemical differences between the Tulu Bor Tuff in area 129 and what had been called the Tulu Bor Tuff in areas 15, 102 and 116 were significant. Identification of two distinct tuffs which had been previously mapped as the KBS Tuff also indicated that some miscorrelations had been made^{2,3}. Also in 1977 White and Harris⁴ stated that "suids from the lower Member of the Koobi Fora Formation (below the Tulu Bor Tuff) equate well with those from Member B. The Koobi Fora Formation lacks fossiliferous horizons equivalent in age to Shungura Members C through F, although there are indications that the Kubi Algi fauna may, in part, fill this hiatus", implying the Kubi Algi Formation must be partly equivalent to the Koobi Fora Formation^{5,6}. In 1981 Williamson⁷ defined 10 molluscan range zones in the type sections of the Kubi Algi, Koobi Fora and Guomde Formation must be partly equivalent to the Koobi Fora Formation^{5,6}. In 1981 Williamson⁷ defined 10 molluscan range zones horizons had been called the Tulu Bor Tuff and advocated substantial stratigraphical revision of the Kubi Algi and Koobi Fora Formations. Despite these disturbing observations, the same stratigraphical sections were published⁸ in 1981 as were published in 1973, with no comments about possible problems.

Stratigraphy and stratigraphical nomenclature

The stratigraphy of the Koobi Fora region has been widely discussed^{1,2,4,7-18}. In a reconnaissance study from 1970 to 1973 Bowen^{1,12} recognized three Plio-Pleistocene lithological units, the Kubi Algi Formation, the Koobi Fora Formation and the Guomde Formation. Only the Koobi Fora Formation was studied in detail, and was divided into the Upper, Lower and Ileret Members. Three stratigraphical levels were mapped during this study: the Suregei Tuff, the transition between the laminated siltstone facies and the facies above it (near the level of the KBS Tuff), and the Chari Tuff where it is overlain by the Guomde Formation¹²⁻¹⁴. Detailed mapping of the region followed (1972-80), and many additional marker horizons were recognized by Findlater¹⁵⁻¹⁸ and mapped throughout the region. In many cases the horizons mapped by Bowen were mapped differently by Findlater, but no reasons were stated for the changes.

In 1977 White and Harris⁴ published a tuff indexing system, and recorded the type areas of the named marker beds. Vondra and Bowen¹⁴ eliminated the Ileret Member in 1978, and redefined the lower boundary of the Upper Member of the

Koobi Fora Formation as the first channel conglomerate above the KBS Tuff.

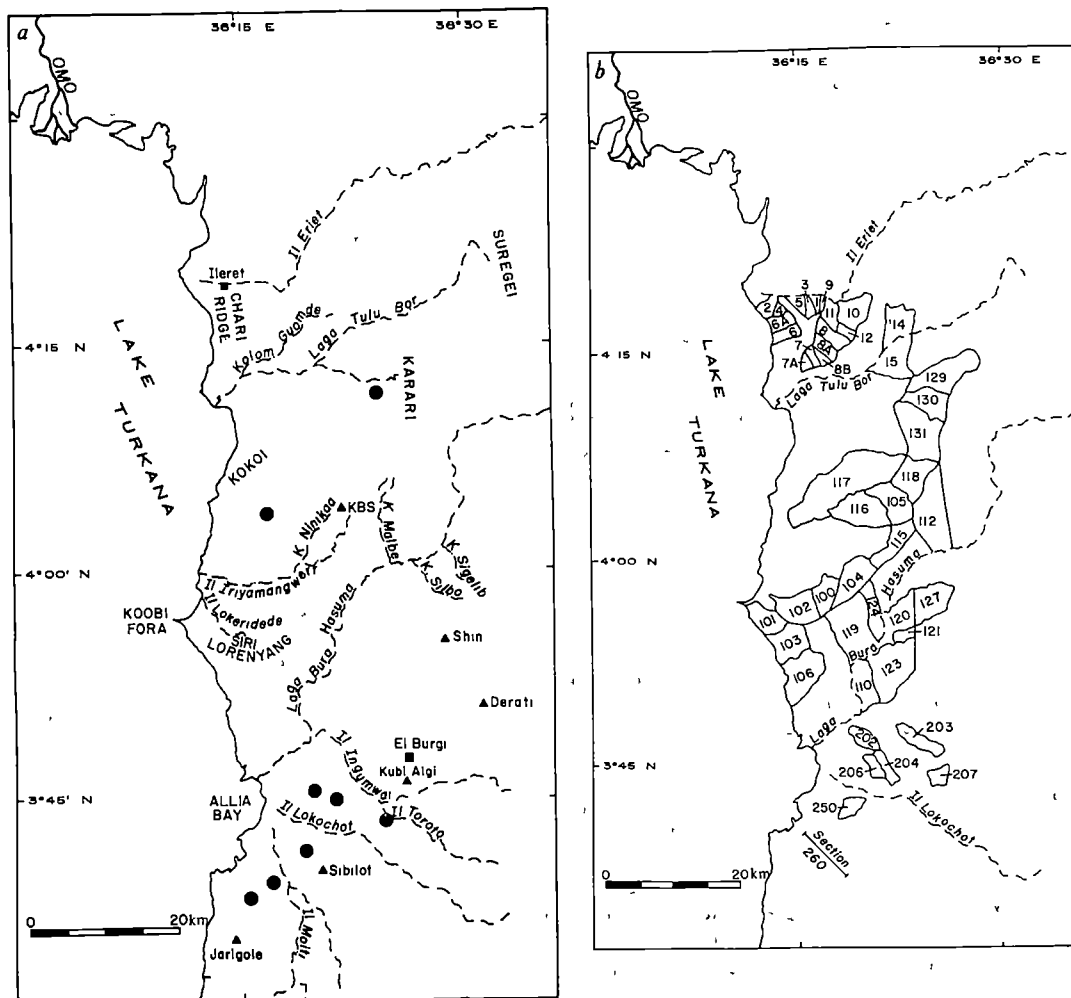
The three Plio-Pleistocene formations were defined using the Suregei, Tulu Bor, KBS and Chari Tuffs either as defining horizons or as horizons useful for correlation from one part of the basin to another. The Kubi Algi Formation (the oldest) was defined as "those strata that lie below the basal contact of the Suregei Tuff Complex"¹. The Koobi Fora Formation was defined as "those sedimentary strata which lie between the basal contact of the Suregei Tuff Complex and the upper contact of the prominent tuff exposed along the Ileret ridge, here named the Chari Tuff, or the basal contact of the Holocene gray tuffaceous predominantly lacustrine siltstones which represent a late stage rise in the level of Lake Rudolf"¹. The Guomde Formation was defined as "those strata which lie between the top of the Chari Tuff on the Ileret ridge and the overlying gray tuffaceous siltstones which represent a late stage rise in the lake level"¹. To understand clearly what is meant by the stratigraphy, we must determine what was meant by each of the marker beds when the formations were defined.

Suregei Tuff Complex: What was originally referred to as the Suregei Tuff Complex has recently been called the Suregei Diatomite Complex⁸ following demonstration that the Suregei Tuff Complex is not tuffaceous². Most of the diatoms in this unit are recrystallized, however, and therefore we refer to this unit as the Suregei Complex. Bowen and Vondra¹ state that

Table 1 Analyses of the Tulu Bor Tuff, and of tuffs thought to be the Tulu Bor Tuff

Area	Sample no	Fe ₂ O ₃	CaO	Ba	Mn	Nb	Ti	Y	Zn	Zr
117	80-183	1.51	0.65	491	330	70	1,533	49	58	380
129	77-26	1.54	0.66	480	336	68	1,513	50	70	388
129	77-27	1.46	0.61	452	326	70	1,452	50	55	388
129	80-212	1.37	0.58	448	287	68	1,378	50	75	388
129	77-24	1.25	0.61	427	240	72	1,437	52	53	280
s 260	80-288	1.31	0.58	419	274	77	1,482	54	57	298
s 260	80-289	1.29	0.50	419	265	74	1,319	55	55	276
s 260	80-290	1.25	0.47	407	250	77	1,250	54	62	280
204	81-635	1.26	0.48	407	250	77	1,185	53	56	272
204	81-636	1.29	0.49	406	275	76	1,202	55	59	290
117	75-117C	1.55	0.40	152	364	82	940	61	74	349
207	81-460	1.45	0.33	143	372	81	925	61	87	351
117	80-182	1.52	0.33	140	372	84	975	62	73	373
117	80-179	1.56	0.32	135	387	83	930	63	79	366
117	80-181	1.55	0.31	135	381	81	925	63	88	360
117	80-177	1.56	0.31	134	392	85	962	63	73	386
117	80-778	1.52	0.32	130	362	84	1,045	62	79	389
204	81-437	1.46	0.30	122	351	85	877	62	68	357
102	72-38	2.36	0.16	9	1,408	154	1,012	84	149	809
102	80-104	2.20	0.15	5	1,448	156	900	84	153	823
102	80-123	2.07	0.15	5	1,408	154	898	85	150	807
110	77-32	3.16	0.20	26	881	201	1,197	130	243	1,284
116	75-116LT	4.05	0.39	285	1,889	129	3,725	72	173	784
116	75-116DK	4.27	0.19	448	1,757	109	4,477	57	153	626
15	72-188	3.23	0.41	182	1,169	132	2,444	79	140	982
15	80-136	2.53	1.13	464	1,075	119	3,119	77	111	825

Fig. 1 *a*, Map of the Koobi Fora Formation region showing names of principal geographical features ●, Points at which the Tula Bor Tuff has been positively identified *b*, Map of the Koobi Fora Formation region showing palaeontological collection areas



this complex "extends from immediately east of the Ileret area to about 15 km to the south along the Suregei". Thus the type area lies within areas 14 and 15 (Fig 1*b*), and the complex takes its name from the Suregei highlands. In this area the Suregei Complex consists of pale tan to pale grey siltstones and claystones with prominent white bands which contain cristobalite. This unit lies about 80 m below the Tulu Bor Tuff near the boundary between area 15 and area 129 (ref 12).

Tulu Bor Tuff: The type area of the Tulu Bor Tuff lies in what is now area 129. Vondra and Bowen¹⁴ state that the Tulu Bor Tuff "outcrops extensively between the Laga Tulu Bor and the southern margin of the Kokoi". This tuff is light grey, and most of the shards are flat bubble-wall fragments. It contains a variety of sedimentary structures including parallel lamination and cross-bedding. Occasionally it contains lenses of small pumice pebbles. In the southern part of the Koobi Fora region it is generally ~10 m thick, whereas in the north it is only ~3 m thick.

KBS Tuff: The type locality of the KBS Tuff is unequivocal. It is a tuff exposed at the KBS archaeological site, a location clearly marked on Fig 1 of ref 11 in what is now area 105. This tuff is light grey, and consists of medium to fine glass shards ~10–30% of which are usually brown, often giving the tuff a salt-and-pepper appearance, although sometimes the basal portion has only clear shards. In many localities the tuff contains pumice clasts up to 30 cm in diameter. The thickness of this bed is variable but generally approximates 1 m, in many areas it is absent.

Chari Tuff: Bowen and Vondra¹ define this tuff as a prominent tuff exposed along the Ileret Ridge, however, there is more than one prominent tuff along the Ileret Ridge. We propose that the prominent tuff exposed in area 5 be regarded as the

type locality of the Chari Tuff. It is light grey, and consists of fine to medium glass shards, with elongate tubules. The Chari Tuff is 1–2 m thick, often has a tuffaceous clay layer at the base, and is thinly bedded at the base and top. In most exposures it contains pumice clasts which may be up to 50 cm in diameter.

In addition to these marker beds, it will be necessary to use names of two other beds in the Koobi Fora region, the Allia Tuff (or 4/5 tuff) and the Hasuma Tuff (or 3/9 tuff), both of which were defined by Findlater¹⁷. It will also be convenient to refer to the Lokochot Tuff and Ingumwai Tuff, which are defined in ref 19.

Correlation methods and analytical procedures

Bowen and Vondra¹ correlated three marker beds from the northern part of the region to other parts of the basin on the basis of internal stratigraphical consistency. From lowest to highest these levels were (1) the Suregei Tuff, recognized by its white colour and fine grained nature, and by the fact that the enclosing sediments were silty claystones, (2) the Tulu Bor Tuff, recognized by its distance 80 m above the Suregei Tuff and by its 3 m thickness, and (3) the KBS Tuff, recognized by its 30 m distance above the Tulu Bor Tuff, its fluvial nature, its position several metres above the highest beds of laminated siltstone facies, and its 'salt-and-pepper' appearance. These horizons were originally recognized in the northern part of the Koobi Fora region, later three similar horizons in area 102 were correlated with them. Additional support for the correlation of the Tulu Bor Tuff from area 129 to area 102 was provided by oxygen isotope analyses²⁰, although other proposed correlations were negated by the same data.

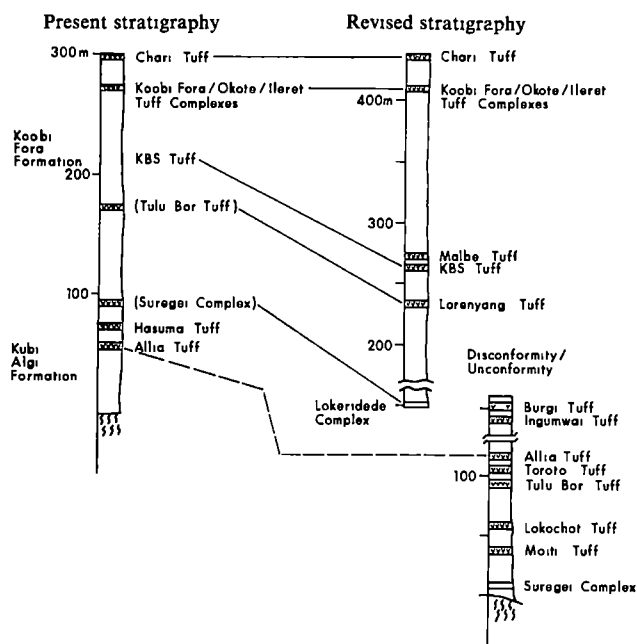


Fig. 2 Comparison of existing and revised stratigraphical nomenclature of Plio-Pleistocene sediments of the Koobi Fora region. See ref. 19 for additional discussion.

Our approach to stratigraphical correlation in the Koobi Fora region is based on chemical characterization of the tuffs, a method used successfully in many other studies²¹⁻²³. In many cases tuffs of the Koobi Fora region are very impure, sometimes consisting of only 10–20% glass shards. Bulk analyses yield meaningless results for purposes of correlation, and early attempts at using this method were discouraging²⁴. For this reason, we produced glass separates from the tuffs using heavy liquids and magnetic separation, calcite was removed with 10% HNO₃, clay films and limonitic staining were removed with 5% HF in conjunction with ultrasonic vibration. Each sample was checked optically to ensure that the separates consisted of >99% glass before analysis. In general the only remaining impurities in the glass were minute feldspar microlites in the shards.

The samples were analysed by X-ray fluorescence techniques on pressed pellets of the glass mixed with cellulose in a 4:1 ratio. Because these tuffs are alkaline or possibly peralkaline²⁵, they are rather different in trace element chemistry from most standard rocks. Two samples were analysed by the standard addition method, and were then used as standards for determination of Nb, Zr, Y, Sr, Rb and Zn on all other samples. Absorption corrections for these elements were made using the reciprocal of background. Analyses for Ti and Ba were made using United States Geological Survey standard G-2, correction for absorption was made using a regression based on potassium content. Iron and manganese were determined colorimetrically on a series of samples spanning the total range of concentration observed; other samples were analysed by X-ray fluorescence for these elements using the colorimetrically analysed samples as standards. Absorption corrections for iron and manganese were estimated by determination of absorption of CrK β . Precision and accuracy for all elements except barium are estimated to be ~2% and 5%, respectively, barium values are within 10% except those below 100 p.p.m., when the values are ± 25 p.p.m.

Our method of correlation depends primarily on the ability to recognize tuffs which are chemically distinct, rather than on the character of the sediments which enclose the tuffs. We have described problems which might be encountered in this method of correlation in a separate paper²⁶. Here only analyses of the Tulu Bor Tuff and tuffs formerly correlated with the Tulu Bor Tuff are presented (Table 1). However, analyses of more than

200 samples of some 30 distinct tuffs from the region are consistent with the correlations proposed below, and none of our correlations are inconsistent with correlations which might be made from stratigraphical considerations, although they differ from those proposed by earlier workers.

Identification of the Tulu Bor Tuff does not rest on analyses of that unit alone. In both the northern and southern part of the region the Lokochot Tuff¹⁹ underlies the Tulu Bor Tuff. The Tulu Bor Tuff and the Lokochot Tuff are correlative with Tuffs B and A of the Shungura Formation, respectively¹⁹.

Distribution of the Tulu Bor Tuff

We have analysed the Tulu Bor Tuff in area 129, its type locality, in area 117, and in areas 204, 207 and section 260 where it had not been previously recognized. We have also analysed samples of what was said to be the Tulu Bor Tuff in areas 15, 102, 110 and 116. The tuffs in areas 15, 102, 110 and 116 which were thought to be the Tulu Bor are not.

The tuff described as the Tulu Bor Tuff in area 102 is here named the Lorenyang Tuff after the local name for part of the Koobi Fora Ridge (Siri Lorenyang). The type locality of this tuff is in area 102, where it is best exposed in the centre of an anticline located in the north central part of the area. Here it is 3 m thick, is grey, fine grained, contains disrupted small scale cross-beds and has a sharp basal contact with a gradational upper one. The shards are frothy and quite distinct from the flat shards of the Tulu Bor Tuff. It also occurs in area 104, where it had been mapped¹⁸ as the KBS Tuff.

The tuff previously mapped as the Tulu Bor Tuff in area 110 is the KBS Tuff. This is sensible as the section above it is very similar to the section above the KBS Tuff in area 102.

The tuff in area 116 is the source of material dated at 3.18 Myr (ref. 27), a number generally associated with the Tulu Bor Tuff. This tuff is the uppermost of three tuffs in a continuous section ~10 m thick, and is here designated the Nimikaa Tuff. It consists of medium to fine cross-bedded grey ash and contains pumice clasts up to 20 cm in diameter. About 30% of the shards are brown, and shard shapes include bubble junction, stretched and frothy types. It appears to be confined to a channel.

The stratigraphical position of the Nimikaa Tuff has not been satisfactorily determined, however, it is very similar in composition to one sample of a tuff mapped as the Hasuma Tuff¹⁵. At least two different tuffs have been mapped as the Hasuma Tuff, and stratigraphical relations between these have not been determined. The particular sample similar to the Nimikaa Tuff lies ~25 m above the Tulu Bor Tuff in area 204.

Significance of the distribution of the Tulu Bor Tuff

Bowen¹² places the Suregei Complex about 80 m below the Tulu Bor Tuff in his section 130-1 along the western margin of the Suregei Cuesta. Findlater¹⁵ places the Allia Tuff 74 m below what Bowen and Vondra¹ identified as the Suregei Complex in areas 202 and 204. Acuff²⁸ finds a different thickness, but agrees on the stratigraphical order. We were therefore surprised to find that the Tulu Bor Tuff lies stratigraphically below the Allia Tuff in areas 204 and 207, and therefore must also underlie the so-called Suregei Complex of area 202. As the Suregei Complex lies below the Tulu Bor Tuff in the type area of both units, it is evident that the unit mapped as the Suregei Complex in area 202 must be a different stratigraphical horizon from that in area 15. Thus two different stratigraphical horizons have been correlated and mapped as the Suregei Complex. One of these lies near the base of the Plio-Pleistocene sequence in the Koobi Fora region, the other is much younger and lies nearer the middle of the sequence.

In order that these two units no longer be confused, we designate the white siltstones in area 102 as the Lokeridede

Complex, after the name of a small stream nearby. This unit lies below a major topographical break in slope and thus lies below the well exposed section in area 102. The nature of the contact is obscure, but the trend of the Lokeridede Complex differs from that of the overlying sediments, suggesting that it may lie below a slight angular unconformity. We accept the correlation of Williamson⁷ of this unit with the unit designated 'Suregei Tuff Complex' in area 202 because it seems to be situated in roughly the same position with respect to the KBS Tuff in area 110, and is lithologically similar. This complex is at about the level of the Burgi Tuff which is defined in the accompanying article. This unit is a very light grey montmorillonitic claystone containing cristobalite with parallel bedding. It is saline, with gypsum at the surface, and contains abundant recrystallized diatoms.

The base of the Suregei Complex is defined as the base of the Koobi Fora Formation. What has been erroneously identified as the Suregei Complex in area 202, however, overlies the Tulu Bor Tuff, furthermore, the Tulu Bor Tuff is widely exposed in what has been mapped as the Kubi Algi Formation, but in its type area belongs to the Koobi Fora Formation. Here a choice must be made, either the Koobi Fora Formation and the Kubi Algi Formation must be redefined, or the Kubi Algi Formation must be regarded as a very small part of the sedimentary sequence in the Koobi Fora region. At present we leave the definitions of the formations as they are, and apply those definitions throughout the Koobi Fora region—strata everywhere in the region which lie between the Suregei Complex and the Chari Tuff must be assigned to the Koobi Fora Formation.

Although we have not redefined the Koobi Fora Formation, certain strata formerly placed in the Kubi Algi Formation are now assigned to the Koobi Fora Formation. Figure 2 shows a composite section of the Koobi Fora Formation in which the old stratigraphical nomenclature is compared with the revised nomenclature. Stratigraphical terms in parentheses are formerly named units which were miscorrelated from their type localities. Stratigraphical thicknesses shown on the revised diagram are only our best estimates at present.

Discussion and conclusions

The most important implication of this work is that the type section of the Koobi Fora Formation includes neither of the marker horizons which were used to define the formation. The present type section begins at the Lokeridede Complex, not the Suregei Complex, and extends upward to levels above the Koobi Fora Tuff Complex, but not to the Chari Tuff. The

existing type section near the Koobi Fora spit requires correction, because the interval between the KBS Tuff and the Koobi Fora Tuff Complex (shown as ~80 m)¹⁴ is far too thin, and must be increased by nearly a factor of two^{2,29}. New sections which extend the present type section of the Koobi Fora Formation must be established which include the defining marker beds. It may be desirable to redefine the Koobi Fora Formation when such sections are established so that it includes the small sections below the Suregei Complex and above the Chari Tuff. As defined at present, the Kubi Algi Formation is only ~5 m thick, and is not lithologically distinct from the strata immediately above the Suregei Complex, thus there is no good reason for retaining that formation as a stratigraphical unit. Similarly, most of those strata presently assigned to the Guomde Formation should be included as part of the Koobi Fora Formation, because the two formations are not lithologically distinct². Strata belonging to the Guomde Formation as presently defined¹ have been mapped as part of the Upper Member of the Koobi Fora Formation in one area, and as part of the lower member of the Koobi Fora Formation in others^{12,15}.

The stratigraphical revisions proposed above are based solely on tuff correlation, but many of the same revisions, or variations on them, were proposed independently on the basis of palaeontological considerations^{4,6,7}. With the proposed revisions, most faunal correlation problems disappear without having to call on ecological differences to explain them. Fossil mammal assemblages in the Turkana basin appear, indeed, primarily to reflect age, as noted earlier³⁰, ecological effects seem subordinate.

Mapping, palaeomagnetic interpretations, definition of isotopic trends of carbonates and volcanic glass in time, and palaeogeographical reconstructions^{8,14,31} are all dependent on the lithostratigraphy, and earlier studies in these areas will have to be reconsidered (or amended). Although the revisions proposed above are important to the geological history of the area, the geographical positions of invertebrate and mammalian (and hominid) fossil specimens are not affected, and since they are recorded on aerial photographs³², their stratigraphical attributions can be checked. The Koobi Fora region is well known for its fossil hominids, but as most of these come from levels near or above the KBS Tuff, the present revisions will affect few of them.

We thank R. E. Leakey, M. G. Leakey and G. L. Isaac for support, J. M. Harris and P. Williamson for critically reading the manuscript, B. E. Bowen for copies of his field notes, B. W. Cerling, D. Norman and T. Haig for sample preparation, and P. Onstott for drafting the figures. Principal financial support of this work was provided by the NSF, grant BNS-8007354. We also acknowledge support from grant BNS-80-14139, and the National Museums of Kenya.

Received 12 February, accepted 7 June 1982

- Bowen, B. E. & Vondra, C. F. *Nature* **242**, 391–393 (1973).
- Cerling, T. E. thesis, Univ. California, Berkeley (1977).
- Cerling, T. E., Brown, F. H., Cerling, B. W., Curtis, G. H. & Drake, R. E. *Nature* **279**, 118–121 (1979).
- White, T. D. & Harris, J. M. *Science* **198**, 13–21 (1977).
- Boaz, N. T., Brown, F. H., de Heinzelin, J. & Howell, F. C. *Science* **202**, 1309 (1978).
- White, T. D. & Harris, J. M. *Science* **202**, 1309 (1978).
- Williamson, P. G. *Nature* **295**, 140–142 (1982).
- White, H. J., Burggraf, D. R., Bainbridge, R. B. & Vondra, C. F. in *Hominid Sites: Their Geological Settings* (eds Rapp, G. & Vondra, C. F.) (Westview Press, Boulder, 1981).
- Leakey, R. E. F. in *Koobi Fora Research Project Vol. 1* (eds Leakey, M. G. & Leakey, R. E. F.) 1–13 (Clarendon, Oxford, 1978).
- Behrensmeyer, A. K. *Nature* **226**, 225–226 (1978).
- Vondra, C. F., Johnson, G. D., Bowen, B. E. & Behrensmeyer, A. K. *Nature* **231**, 245–248 (1971).
- Bowen, B. E. thesis, Iowa State Univ. (1974).
- Vondra, C. F. & Bowen, B. E. in *Earliest Man and Environments in the Lake Rudolf Basin* (eds Coppens, Y., Howell, F. C., Isaac, G. L. & Leakey, R. E. F.) 24–49 (University of Chicago Press, 1976).
- Vondra, C. F. & Bowen, B. E. in *Geological Background to Fossil Man* (ed. Bishop, W. W.) 395–414 (Scottish Academic, Edinburgh, 1978).
- Findlater, I. C. thesis, Univ. London (1976).
- Findlater, I. C. in *Earliest Man and Environments in the Lake Rudolf Basin* (eds Coppens, Y., Howell, F. C., Isaac, G. L. & Leakey, R. E. F.) 94–104 (University of Chicago Press, 1976).
- Findlater, I. C. in *Geological Background to Fossil Man* (ed. Bishop, W. W.) 415–420 (Scottish Academic, Edinburgh, 1978).
- Findlater, I. C. in *Koobi Fora Research Project Vol. 1* (eds Leakey, M. G. & Leakey, R. E. F.) 14–31 (Clarendon, Oxford, 1978).
- Cerling, T. E. & Brown, F. H. *Nature* **299**, 216–221 (1982).
- Cerling, T. E. in *Earliest Man and Environments in the Lake Rudolf Basin* (eds Coppens, Y., Howell, F. C., Isaac, G. L. & Leakey, R. E. F.) 105–114 (University of Chicago Press, 1976).
- Sarna-Wojcicki, A. M. *US geol. Surv. Prof. Pap.* **972** (1976).
- Smith, D. G. W. & Westgate, J. A. *Earth planet. Sci. Lett.* **5**, 313–319 (1969).
- Izett, G. A., Wilcox, R. E. & Borchardt, G. A. *Quat. Res.* **2**, 554–578 (1972).
- Luedtke, N. A. M.S. thesis, Univ. of Rhode Island, Kingston (1975).
- Martz, A. M. & Brown, F. H. *Quat. Res.* **16**, 240–257 (1981).
- Cerling, T. E., Cerling, B. W. & Brown, F. H. *Quat. Res.* (in the press).
- Fitch, F. J. & Miller, J. A. in *Earliest Man and Environments in the Lake Rudolf Basin* (eds Coppens, Y., Howell, F. C., Isaac, G. L. & Leakey, R. E. F.) 123–147 (University of Chicago Press, 1976).
- Acuff, H. thesis, Iowa State Univ. (1976).
- Johnson, G. D. & Reynolds, R. in *Earliest Man and Environments in the Lake Rudolf Basin* (eds Coppens, Y., Howell, F. C., Isaac, G. L. & Leakey, R. E. F.) 115–122 (University of Chicago Press, 1976).
- Shuey, R. T., Brown, F. H., Howell, F. C. & Eck, G. G. in *Geological Background to Fossil Man* (ed. Bishop, W. W.) 103–124 (Scottish Academic, Edinburgh, 1978).
- Burggraf, D. R., White, H. J., Frank, H. J. & Vondra, C. F. in *Hominid Sites: Their Geological Settings* (eds Rapp, G. & Vondra, C. F.) (Westview, Boulder, 1981).
- Leakey, R. E. F., Leakey, M. G. & Behrensmeyer, A. K. in *Koobi Fora Research Project Vol. 1* (eds Leakey, M. G. & Leakey, R. E. F.) 86–182 (Clarendon, Oxford, 1978).

Tuffaceous marker horizons in the Koobi Fora region and the Lower Omo Valley

T. E. Cerling & F. H. Brown

Department of Geology and Geophysics, University of Utah, Salt Lake City, Utah 84112, USA

Eight tuffs can now be correlated between the Shungura Formation in the Lower Omo Valley, Ethiopia, and the sediments in the Koobi Fora region, Kenya. Re-evaluation of the stratigraphy shows that at least 475 m of sediment was deposited in the Koobi Fora region

BOTH the Lower Omo Valley, Ethiopia, and the Koobi Fora region, Kenya, have been extensively studied geologically, and for their mammalian remains¹⁻³, we now consider the correlation of tuffs in Plio-Pleistocene strata. The Shungura Formation in the Lower Omo Valley is a sequence of fluvial and lacustrine sediments deposited by the proto-Omo River which drained the Ethiopian highlands. Its good exposure and relatively simple stratigraphy have resulted in a well-calibrated Plio-Pleistocene section. This 760-m thick section ranges in age from ~3.5 to ~0.8 Myr in age⁴. Twelve members have been recognized and are defined on the basis of widespread tuffs, labelled A to L from the lowest to the highest member. In addition to the tuffs used to define members, >100 other tuffs have been recognized in the section.

Plio-Pleistocene strata in the Koobi Fora region are only slightly tilted, and have fewer long stratigraphical sequences

exposed than does the Lower Omo Valley. Large areas of late Quaternary alluvium separate exposures of the Plio-Pleistocene strata. These strata appear to have had a more complicated erosional history that has resulted in discontinuities in the section. However, the Plio-Pleistocene strata in the Koobi Fora region span approximately the same time interval as those in the Lower Omo Valley. The Plio-Pleistocene strata of the Koobi Fora region have been divided into the Kubi Algi, Koobi Fora and Guomde Formations in stratigraphical order from oldest to youngest^{5,6}. Of these formations, only the Koobi Fora Formation has been studied in detail⁵⁻¹⁴.

Procedure

Samples from the Shungura Formation were collected in 1972-74, most samples from the Koobi Fora region were collected from 1977 to 1981, although a few were collected earlier.

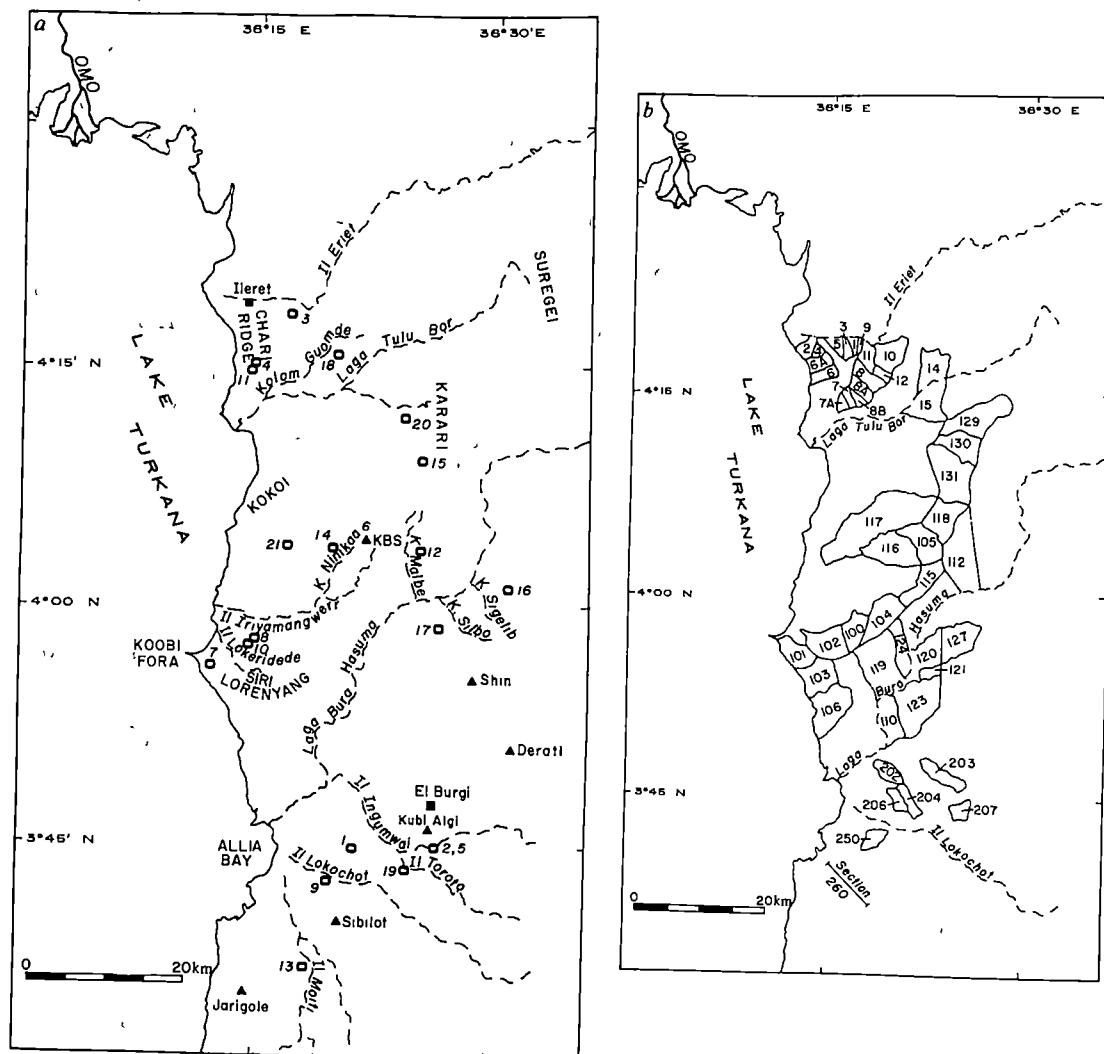


Fig. 1 a, Geographical localities in Koobi Fora region. Numbers refer to type localities of marker horizons (Table 3). b, Fossil collection areas.

Table 1 Trace and minor element compositions of some tuffs in the Koobi Fora region and in the Shungura Formation

Area	Tuff	Sample	Fe ₂ O ₃	CaO	Ba	Mn	Nb	Ti	Y	Zn	Zr
Omo	Tuff A	F-133	3 70	0 21	109	824	153	1,285	140	253	1,419
117	Lokochot	75-117B	3 77	0 19	115	863	160	1,269	145	252	1,470
250	Lokochot	K80-295	3 58	0 19	123	837	152	1,263	141	239	1,403
251	Lokochot	77-30	3 62	0 18	114	809	152	1,201	135	250	1,407
260	Lokochot	K80-291	3 51	0 18	121	809	146	1,233	135	233	1,360
Omo	Tuff B- α	F-134	1 30	0 48	412	267	74	1,165	53	48	274
Omo	Tuff B- α	F-135	1 41	0 55	416	283	75	1,364	55	55	288
117	α -Tulu Bor	K80-183	1 51	0 65	491	350	70	1,533	49	58	380
129	α -Tulu Bor	77-24	1 25	0 61	427	240	72	1,437	52	53	280
129	α -Tulu Bor	77-27	1 46	0 61	452	326	70	1,452	50	55	353
204	α -Tulu Bor	K81-635*	1 26	0 48	407	250	77	1,185	53	56	272
260	α -Tulu Bor	K80-288	1 31	0 58	419	274	77	1,482	54	57	298
Omo	Tuff B- β	F-136	1 64	0 43	219	393	85	1,128	64	83	449
117	β -Tulu Bor	75-117c	1 55	0 40	152	364	82	940	61	74	349
117	β -Tulu Bor	K80-179	1 52	0 31	130	387	84	1,045	62	79	379
207	β -Tulu Bor	K81-460	1 45	0 33	143	372	81	925	61	87	351
204	Toroto	K80-307	4 65	0 15	286	932	78	1,626	98	209	905
207	Toroto	K80-279	4 68	0 21	296	1,017	86	1,705	104	211	947
204	Allia	77-31†	0 84	0 25	163	196	50	782	39	34	151
207	Allia	K81-694	0 84	0 38	168	188	52	775	39	37	156
Omo	C4	F-140	2 62	0 31	17	744	94	1,063	82	151	803
207	Ingumwai	K80-273	2 66	0 25	1	836	100	1,008	80	142	871
Omo	H2	F-101	3 22	0 22	27	832	201	1,467	131	236	1,306
Omo	H2	76-H2B‡	3 00	0 17	89	825	191	1,205	131	230	1,319
12	KBS	K80-134	3 12	0 18	7	887	204	1,215	137	253	1,276
15	KBS	K80-141	3 15	0 21	17	881	200	1,190	131	253	1,276
102	KBS	72-44§	3 07	0 19		850		1,080			
105	KBS	77-17	3 09	0 23	30	843	194	1,292	129	252	1,239
106S	KBS	K80-238	3 10	0 18	14	874	200	1,217	131	241	1,276
110	KBS	77-32¶	3 16	0 20	26	881	201	1,197	130	243	1,284
129	KBS	K80-222P#	3 25	0 38	30	891	196	1,564	127	228	1,314
130	KBS	K80-285	3 00	0 17	10	862	198	1,215	133	241	1,265
131	KBS	77-10	3 08	0 18	21	859	199	1,174	130	257	1,240
Omo	H4	F-105	4 78	0 38	70	1,907	143	3,578	83	204	1,007
112	Malbe	77-18**	4 81	0 43	120	1,921	139	3,360	84	196	990
112	Malbe	K80-225**	4 70	0 38	60	1,897	139	3,353	82	194	996
Omo	J7	228-11	2 46	1 12	740	989	80	2,731	60	95	661
119		K80-195	2 50	1 01	785	978	83	2,715	61	99	679
Omo	L	L‡	2 76	0 18	257	603	99	1,124	100	192	1,053
Omo	L	76-L‡	2 70	0 20	225	518	102	1,056	101	183	1,106
1	Chari	77-23	2 81	0 18	223	564	103	1,093	102	190	1,085
6A	Chari	K80-127	2 83	0 19	216	574	107	1,182	103	196	1,107
108	Chari	108-1‡	2 66	0 19	291	482	97	1,019	98	182	1,028
131	Chari	77-19	2 90	0 23	306	643	100	1,219	100	192	1,059
7	Silbo	7-106††	3 57	0 16	1	1,238	138	1,139	105	208	1,169
Kokoi	Silbo	K80-151	3 53	0 14	1	1,236	126	1,194	98	203	1,084
Shun	Silbo	K80-248**	3 52	0 20	18	1,219	131	1,264	99	200	1,101
Shun	Silbo	K80-251‡‡	3 66	0 17	5	1,231	134	1,281	99	203	1,109

* 15 m below Allia Tuff (77-31)

† Allia Tuff of Findlater^{7,9}

‡ Pumice

§ Analysis by electron microscope

|| Previously mapped as Surgaei Tuff^{7,9}¶ Previously mapped as Tulu Bor Tuff^{7,9}

Composite pumice sample. Previously unmapped as any tuff

** Previously mapped as KBS Tuff^{7,9}†† Previously mapped as Chari Tuff^{7,9}‡‡ Previously mapped as Okote Tuff^{7,9}

Samples were prepared and analysed as described in ref 15. New standards more similar in composition to our samples than the USGS rock standards have resulted in analytical results that are more accurate and more precise than those reported earlier¹⁶. Where statements are made concerning individual shards, the analyses were done by electron microprobe.

Results

Eight pairs of horizons in the two regions can be correlated on the basis of chemical compositions (Table 1). Tuffs A, B- α , B- β , C4, H2, H4, J7 and L from the Lower Omo Valley correspond to the Lokochot Tuff, the α -Tulu Bor Tuff, the β -Tulu Bor Tuff, the Ingumwai Tuff, the KBS Tuff, the Malbe Tuff, an unnamed tuff near the level of the Koobi Fora Tuff, and the Chari Tuff in the Koobi Fora region, respectively. These correlations together with definitions of new tuff names and complications are discussed below.

Tuff A-Lokochot Tuff: Tuff A is the lowest major tuff in the Shungura Formation, situated ~30 m above the lowest exposed sediments of the Shungura Formation. The Lokochot Tuff, in the Koobi Fora region, is named for a major ephemeral

stream channel, Il Lokochot, in the area east of Allia Bay, this tuff crops out extensively in this region and is also exposed in area 117, south of the Kokoi (see Fig 1 for area designations and geographical names). The type exposure is located 200 m west of the point where the road crosses Il Lokochot. Here, the Lokochot Tuff is a 2.0-m thick bed of poorly stratified, grey, coarse to medium ash, with calcified rootcasts in its lower part. The glass shards are very light grey and clear or slightly frosted, they are stretched, bubblewall and platey shards. This tuff rests on a bed of greyish brown silty claystone with polyhedral fracture, irregular subvertical carbonate fillings occur in the upper part of the silty claystone. It is overlain by sandy siltstones and clayey siltstones. The strata in which it is located were formerly assigned to the Kubi Algi Formation⁵⁻¹⁴, although we believe that these beds should be assigned to the Koobi Fora Formation¹⁵. Analysis of glass separates (Table 1) from Tuff A and from the Lokochot Tuff are indistinguishable. This tuff is of interest because analyses of individual shards by electron microprobe fall into two distinct compositional groups (Fig 2), both of which differ from the bulk composition of the glass separates. Tuff A also has this characteristic. It is possible

Table 2 Representative chemical analyses of some trace and minor elements from pure glass separates from marker tuffs at their type localities (see Table 3) in the Koobi Fora region

Tuff	Area	Sample	Fe ₂ O ₃	CaO	Ba	Mn	Nb	Rb	Ti	Y	Zn	Zr
Allia	204	77-31	0.84	0.37	163	196	50	129	782	39	34	151
Burgi	207	K80-274	3.56	0.22	28	1,357	211	157	1,548	104	192	1,254
Chari	1	77-23	2.81	0.18	223	564	103	102	1,093	102	190	1,085
Ileret Complex	6A	K80-144	4.91	0.23	5	1,732	239	162	1,993	131	318	1,653
	6	72-8	4.74	0.19	53	1,651	152	127	2,074	96	217	1,066
Ingumwai	207	K80-273	2.66	0.25	1	836	100	145	1,008	80	142	871
KBS	105	77-17	3.09	0.23	30	843	194	165	1,297	129	253	1,239
Koobi Fora Complex	101	K80-108	4.70	0.46	8	1,610	214	118	2,494	114	241	1,396
	101	K80-115	5.39	0.19	1	1,899	256	127	1,969	131	282	1,656
Lokochot	250	K80-295	3.58	0.19	123	837	152	132	1,263	141	239	1,403
Lorenyang	102	K80-104	2.20	0.15	1	1,448	56	152	900	84	153	823
Lower Ileret	6A	77-20	5.78	0.15	1	2,023	357	182	1,492	192	403	2,542
Malbe	112	K80-225	4.70	0.38	61	1,897	139	103	3,353	82	194	996
Moti	260	K81-602	2.70	0.18	401	618	122	97	1,063	114	235	1,099
Nimikaa	116	75-116it	4.05	0.39	285	1,889	129	85	3,725	72	173	784
	116	75-116dk	4.27	0.19	448	1,757	109	87	4,477	57	153	626
Okote Complex	131	77-9	4.76	0.20	34	1,595	215	149	1,847	124	256	1,493
	131	77-106B	3.81	0.72	1,048	1,183	137	79	1,470	102	184	1,179
Sigilib	—	K80-244	6.69	0.47	507	2,208	154	100	2,699	106	284	1,228
Silbo	—	K80-251	3.66	0.17	5	1,231	134	105	1,281	99	203	1,109
Toroto	207	K80-279	4.68	0.21	296	1,017	86	84	1,705	104	211	947
α -Tulu Bor	129	77-27	1.46	0.61	452	326	70	112	1,452	50	55	353
β -Tulu Bor	117	K80-179	1.56	0.32	135	387	83	112	930	63	79	366

Only one analysis is given for each tuff unless additional analyses of pure glass separates from the tuff showed compositional variability. Concentration is given in parts per million, except calcium and iron which are reported as the oxide in per cent. Total iron as Fe₂O₃.

that two tuffs erupted at different times may have very similar compositions, but the unique combination of finding two tuffs with identical bulk analyses and having two shard compositions mixed in the same ratio is very unlikely to have happened twice. Consequently, we regard the correlation of Tuff A and the Lokochot Tuff as one of the strongest ties between the Shungura Formation and the Plio-Pleistocene strata at Koobi Fora.

Tuff B-Tulu Bor Tuff: Tuff B of the Shungura Formation was divided into several units when it became clear that it represented several depositional events. We have analysed glass separates from tuffs from only the lowest two units, Tuff B- α and Tuff B- β . Although they differ slightly in composition they are chemically related (Table 1).

Several different stratigraphical horizons have been called the Tulu Bor Tuff⁵. Here, we use this name only for the tuff in area 129 (where it was originally named), and for those tuffs that have similar or indistinguishable compositions. The Tulu Bor Tuff in the Koobi Fora region has at least two variants, two of these correspond to Tuff B- α and Tuff B- β of the Shungura Formation (Table 1), and we refer to these as the α -Tulu Bor Tuff and β -Tulu Bor Tuff, respectively. Where a distinction is not necessary the term Tulu Bor Tuff is used. The type Tulu Bor Tuff in area 129 corresponds to Tuff B- α of the Shungura Formation (Table 1), this tuff is also found in areas 117, 204, 207 and 260. The tuff mapped as the Tulu Bor Tuff in area 117 (refs 8, 10) is in most places equivalent to Tuff B- β of the Shungura Formation (Table 1). However, in area 117 ~10% of the shards are compositionally similar to those of

the α -Tulu Bor Tuff, indicating that it has some older shards reworked into it.

In addition to the compositional similarity there are several other favourable points of comparison between Tulu Bor Tuff and Tuff B. Both are of normal polarity^{4,16}, and composed dominantly of flat bubble wall shards. The Tulu Bor Tuff lies ~35 m above the Lokochot Tuff, a distance comparable with the 40 m that separates Tuff B from Tuff A in the Shungura Formation. The intervening section of fluvial sediments is also similar.

Tuff C4-Ingumwai Tuff: Tuff C4 in the Shungura Formation lying ~110 m above Tuff B has normal polarity. Table 1 shows that sample K80-273 is chemically similar to Tuff C4. This is a sample of the lowest of four tuffs exposed in a cliff along Il Ingumwai (Fig. 1a). At this locality it lies ~50 m above the Tulu Bor Tuff. This tuff is here defined as the Ingumwai Tuff. It has a maximum thickness of ~0.5 m in this exposure, and is lenticular, pinching out to the west. It is pinkish grey to very pale yellowish grey, and consists of silt to medium sand sized glass shards. Most shards are light grey to greyish white, a few are very light brown. They are generally frosted. Most are stretched or frothy.

Tuff H2-KBS Tuff: Tuff H2 of the Shungura Formation has previously¹⁷ been correlated with the KBS Tuff in the Koobi Fora region on the basis of trace and minor element contents of glass separates from pumice, compositions of phenocrysts in pumice, and on the major and minor element content of glass shards analysed by the electron microprobe. We have since analysed glass separates from tuffs by X-ray fluorescence, and can now positively identify the KBS tuff in areas 10, 15, 130, 131, 105, 110 and south of area 106 (Table 1). Glass shards from the KBS Tuff are fairly distinctive. In general, the shards are clear 60–90% are very light grey or colourless. The remainder grade from light grey to dark brown. This gives the tuff a 'salt-and-pepper' appearance in many localities. Occasionally the basal portion does not have the dark shards, Tuff H2 also lacks dark shards. The shards are a subequal mixture of bubble-wall stretched, platy and frothy types. Occasionally this tuff has <30% glass and should properly be called a tuffaceous sandstone (for example, area 102). Chemical analysis by electron microprobe indicates its presence in area 102 (ref. 17). The samples from area 110 and south of area 106 are from tuffs which had previously been mapped as the Tulu Bor Tuff and the Suregei Tuff, respectively^{7,9}, other tuffs mapped as the KBS Tuff can be shown to be different on the basis of their chemistries (see discussion below). Both Tuff H2 and the KBS Tuff lie in sections of normal polarity^{4,17}, the KBS Tuff has

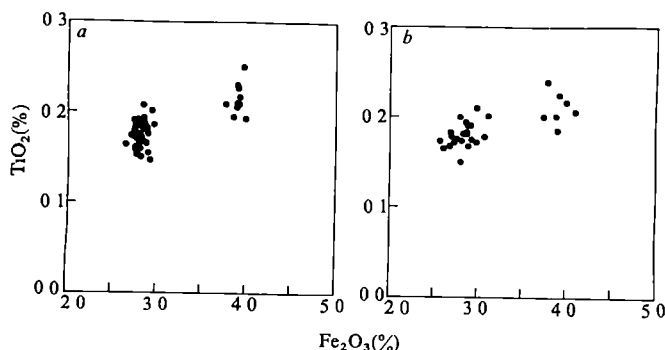


Fig. 2 Iron and titanium contents of individual glass shards from *a*, the Lokochot Tuff (59 shards) and *b*, from Tuff A (30 shards). Each point represents the average composition of an individual shard.

been dated at 1.89 ± 0.02 Myr (samples from areas 105 and 131 in ref 19), a date comparable with that of Tuff H2 (1.88 Myr).

Tuff H4-Malbe Tuff: Tuff H4 occurs 15 m above Tuff H2 in the Shungura Formation. Tuff H4 has previously¹⁷ been correlated with a tuff in the Koobi Fora region, which we now designate as the Malbe Tuff, named for Kolom Malbe, along which this tuff is well exposed. This tuff occurs ~15 m above the KBS Tuff in the eastern portion of area 105. Analyses of glass separates from this tuff are given in Table 1. This tuff has pumice clasts of variable composition, which are not included in Table 1, but which are discussed elsewhere^{17,18}. Glass separates from these pumices fall on a single compositional trend, and may represent eruptive products of different portions of a compositionally variable magma chamber¹⁸. Electron microprobe studies of individual shards show that the entire range of glass compositions spanned by the pumice glasses is present in the tuff¹⁸. Although McDougall *et al.*¹⁹ do not distinguish this tuff from the KBS Tuff, samples of this tuff give a K/Ar age of 1.88 ± 0.02 Myr (samples from area 112 of ref 19).

In its type area the Malbe Tuff is confined to a channel, and reaches a maximum thickness of ~2 m. It can be distinguished from the KBS Tuff in the field wherever it contains pumice, because the pumice clasts of the Malbe tuff are an assemblage of very dark brown (nearly black), medium grey and white types, whereas those of the KBS Tuff are dominantly grey or white, with very rare (<1%) dark pumice.

Tuff J7-Koobi Fora Tuff (*sensu lato*): Tuff J7 of the Shungura Formation occurs in sediments of reversed polarity. An unnamed tuff in area 119 (K80-195) has essentially the same composition as Tuff J7 (Table 1). This tuff is at about the same level as the Koobi Fora Tuff, which also has reversed polarity¹⁶. This sample is ~5 m below a tuff which is compositionally the same as a sample from the Koobi Fora Tuff in area 101.

The Ileret Tuff Complex, the Okote Tuff Complex and the Koobi Fora Complex, or variations on these names, are found near Ileret, along the Karari Ridge and near Koobi Fora spit, respectively. These tuffs have been correlated^{9,10} because they are tuffaceous intervals above the KBS Tuff. We have analysed over 30 glass separates from pumice and tuffs from these localities and have found only one compositionally distinct set of samples. They are found at the base of the Ileret Tuff

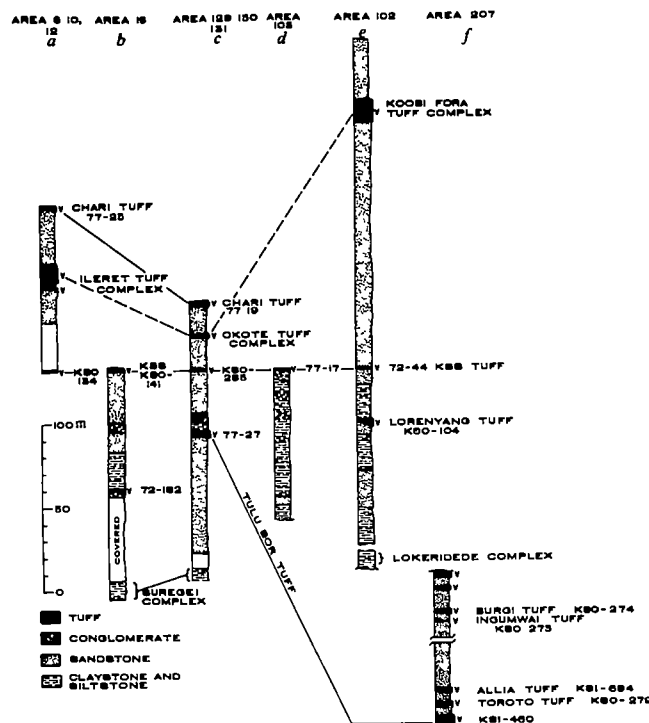


Fig. 3 Stratigraphical sections of Plio-Pleistocene sediments in the Koobi Fora region. Section a by Bowen⁵ and T E C, section b by Bowen⁵, section c by Bowen⁵ and T E C, section d by T E C, section e by T E C, section f by F H B and T E C.

Complex. Thus, we designate this tuff as a separate unit, the Lower Ileret Tuff. This tuff is medium to dark grey, has fine to medium shards, and is ~1 m thick. The shards are dark grey and are dominantly frothy. It has an abrupt basal contact and overlies a brown mudstone with prismatic structure. It is overlain by 3–4 m of interbedded sandstones and siltstones, which give way to the tuffaceous sand and silts of the Ileret Tuff Complex.

The Ileret, Koobi Fora and Okote Tuff Complexes have variable chemistries as shown by major, minor and trace element analyses of glass separates from pumice and from tuff

Table 3 Type localities of marker horizons in the Koobi Fora region

Marker horizon	Type area	Sample	Locality*	Photo	X	Y	Bowen and Vondra ⁶	White and Harris ²⁵ Harris ²⁶	Findlater ⁸	Findlater ¹⁰	Findlater ⁹
1 Allia Tuff	204	77-31	1,574	167-056	—	—	—	Allia	45	Allia	Allia
2 Burgi Tuff	207	K80-274	1,729	083-093	—	—	—	—	—	—	—
3 Chari Tuff	1	77-23	1,467	077-122	—	—	Chari	Chari	Chari†	Chari	Karari
4 Ileret Tuff Complex	6A	K80-144	1,398	135-145	—	—	—	Lower/Middle	Middle	Okote	Okote
5 Ingumwai Tuff	207	K80-273	1,729	083-093	—	—	—	—	—	—	—
6 KBS Tuff	105	77-17	1,591	142-109	—	—	KBS	KBS	KBS	KBS	KBS
7 Koobi Fora Tuff	101	K80-108	1,343	103-174	—	—	—	Koobi Fora	BBS	Okote	Okote
8 Lokeride Complex†	102	K80-126	1,414	120-168	—	—	Suregei	102/T II	Surgaei	Suregei	Surgaei
9 Lokochot Tuff	250	K80-295	1,550	042-138	—	—	—	250/T I	—	—	—
10 Lorenyang Tuff	102	K80-104	1,413	150-022	—	—	Tulu Bor	102/T IV	Tulu Bor	Tulu Bor	Tulu Bor
11 Lower Ileret Tuff	6A	77-20	1,397	127-043	—	—	—	Lower/Middle	Lower†	Okote	Okote
12 Malbe Tuff	112	K80-225	1,656	040-102	—	—	—	—	—	—	KBS
13 Motti Tuff	260	K81-602	1,435	143-096	—	—	—	—	—	—	—
14 Ninikaa Tuff	116	75-1,161	1,589	057-115	—	—	—	116/T II	Tulu Bor	Tulu Bor	Tulu Bor
15 Okote Tuff Complex	131	77-9	1,750	049-124	—	—	—	Okote	BBS	Okote	Okote
16 Sigelb Tuff	—	K80-244	1,815	035-152	—	—	—	—	—	—	KBS
17 Silbo Tuff	—	K80-251	1,741	155-072	—	—	—	—	—	—	Okote
18 Suregei Complex†	15	K80-138	1,600	074-033	—	—	Suregei	Suregei	Surgaei	Suregei	Surgaei
19 Toroto Tuff	207	K80-279	1,729	035-160	—	—	—	—	—	—	—
20 α-Tulu Bor Tuff	129	77-27	1,648	055-114	—	—	Tulu Bor	Tulu Bor	Tulu Bor	Tulu Bor	Tulu Bor
21 β-Tulu Bor Tuff	117	K80-179	1,456	086-152	—	—	—	117/T III	Tulu Bor	Tulu Bor	Tulu Bor

Representative compositions of tuffs from the type locality are given in Table 2. Other names that have been used for these horizons in their type localities are also included. The type localities are shown in Fig. 1.

* Localities are given by coordinates of type locality on 9×9-inch photographic prints of area taken in December 1970 by Hunting Surveys, London. X and Y coordinates are in millimetres from the left edge and from the top edge of print, respectively.

† Contains diatoms. Probably recrystallized diatomite.

‡ Captions for Figs 3 and 5 in ref. 8 are transposed.

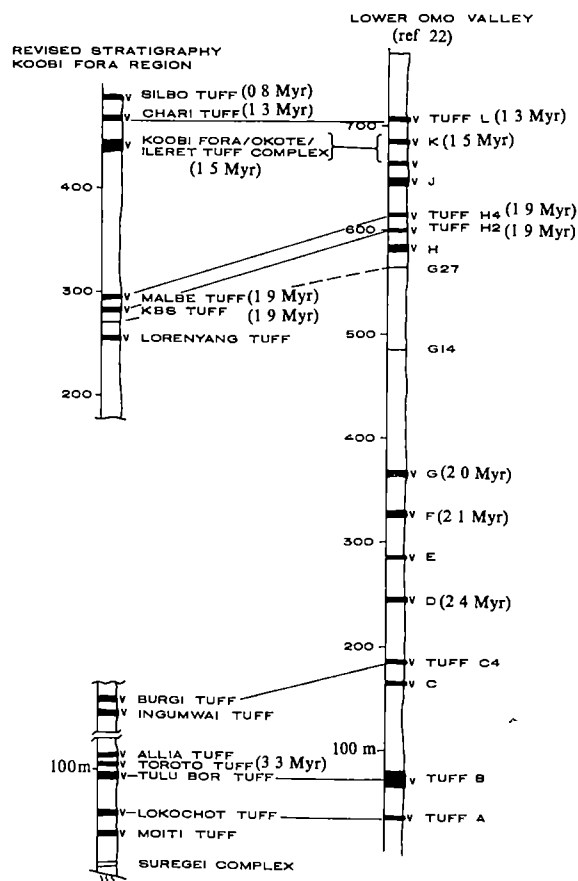


Fig. 4 Correlations of marker horizons in the Koobi Fora region with those in the Shungura Formation. Revised total thickness based on section *a*, *e* and *f* of Fig. 3. Sediment thickness above the Chari Tuff and stratigraphical positions of the Lokochot and Moiti Tuff are based on unpublished field notes. The Ninikaa Tuff occurs about 25 m above the Tulu Bor Tuff, the Lokeridede Complex lies at about the level of the Burgi Tuff, the position of the Sigelb Tuff is not yet known.

Electron microprobe studies of individual shards from each of these tuff complexes show that each tuff is heterogeneous. The X-ray fluorescence and electron microprobe studies both suggest that all samples are genetically related in that the variations fall on well defined compositional trends. Thus, we feel that although these tuffs complexes are of about the same age, they should be considered as three separate units. In no case can one show that any individual subunits from two different complexes are correlative. These complexes are equivalent in age to upper Member J and Member K of the Shungura Formation. The distinction between correlation of these as general units versus as individual beds is important. If the time-mesh required for a particular study is on the order of 10,000–100,000 Myr, they can be considered as correlative. However, if a study requires a more narrow time-mesh (for example, a palaeoecological studies), then they cannot be considered to be time-stratigraphical units. We hope that we will soon be able to define more finely the relationship between the Ileret, Okote and Koobi Fora Tuff Complexes. Until then, they should retain their distinctive names.

Tuff L–Chari Tuff: Tuff L of the Shungura Formation has previously¹⁷ been correlated with the Chari Tuff of the Koobi Fora Formation, and the Chari Tuff was thought to be the same as the Karari Tuff of Findlater^{7,9} (see Table 1). Since the name Chari Tuff has precedence over the name Karari Tuff, only the former name should be retained.

Other tuffs

In addition to these tuffs, there are other tuffs which are fairly widespread, or of importance because they have been dated. Some of these were previously thought to be the Tulu Bor Tuff,

but in an accompanying article, we show that previous correlations of the Tulu Bor Tuff to areas 15, 102, 110 and 116 are in error¹⁵. One of these is the KBS Tuff (area 110). The Tuff in area 15 remains unnamed, the tuff in area 102 has been named the Lorenyang Tuff¹⁵. The tuff in area 116 is of importance because it has been dated by K/Ar at ~3.1 Myr (ref. 20 and G. H. Curtis, unpublished data) and has been named the Ninikaa Tuff¹⁵.

In the southern part of area 204, where the Allia Tuff was mapped^{7,9}, there are three tuffs in ~15 m of section. The uppermost tuff is the most prominent, and its outcrop pattern corresponds most closely to the Allia Tuff on these maps^{7,9}, therefore we have assigned it the name Allia Tuff. The lowest tuff in this sequence is the Tulu Bor Tuff (Table 1), the intermediate tuff in this sequence is here named the Toroto Tuff. These three tuffs are quite distinctive and descriptions of the Toroto and Allia Tuffs are given below, the Tulu Bor Tuff is described in the accompanying article¹⁵.

The Toroto Tuff takes its name from Il Toroto, a tributary stream to Il Ingumwai. It is dark grey tuff ~2.3 m thick with conspicuous pumice clasts in its upper part. The lower part (0.8 m) is an impure tuff with many flat glass shards of fine to coarse sand size.

The Allia Tuff is a massive 2-m thick tuff in area 204, the uppermost of three tuffs in a 15-m stratigraphical interval. It is white, the glass shards are coarse to medium in grain size and are predominantly stretched in shape. They are similar to the stretched variety of shards observed in the Koobi Fora Tuff, but the walls of the tubules are more massive in the Allia Tuff.

The Moiti Tuff outcrops extensively in the southern part of the sedimentary sequence in the Koobi Fora region. It is the lowest of five widespread tuffs in the Allia Bay region, which are the Allia, Toroto, Tulu Bor, Lokochot and Moiti Tuffs, in descending order. It is ~20 m below the Lokochot Tuff. The tuff is medium grained, has bubble-junction shards and sometimes contains pumice up to 20 cm in diameter. Locally it is extremely pure. The pure basal portion is from 0 to 50 cm in thickness and is overlain by up to 5 m of impure tuff.

The Burgi Tuff occurs ~5 m above the Ingumwai Tuff along Il Ingumwai near Kubi Algi. It takes its name from a waterhole, El Burgi, ~3 km north of Kubi Algi. It is the lower of two tuffs of similar composition, these two tuffs are found in several localities south and east of Laga Bura Hasuma. The Burgi Tuff is ~1 m thick in its type locality, the shards are light grey and are predominantly stretched, although a few frothy shards are also present. In area 202 it occurs just below the level of a Zone 3 molluscan fauna of Williamson²¹, in area 102 the Lokeridede Complex occurs above a Zone 3 molluscan fauna²¹. Thus the Burgi Tuff lies near the level of the Lokeridede Complex.

The Silbo Tuff refers to a tuff whose type area is near Shin, just south of Kolom Silbo for which it is named. It is also exposed in area 7, and along the western margin of the Kokoi (Table 1). It has been variously mapped as the Chari, Okote, and KBS Tuffs^{7,9}, and lies within the Guomde Formation⁵. The Silbo Tuff is massive, up to 2 m thick, greyish white, and composed dominantly of stretched and bubble-wall shards. It often contains isolated pumice clasts up to 50 cm in diameter, in its type locality it has a pumice channel that has pumice clasts up to 100 cm in diameter.

The Sigelb Tuff is a massive, 6-m thick tuff that is exposed on the basin margin and was previously mapped as the KBS Tuff^{7,9}. It is dark grey, has medium to fine grained shards which are predominantly bubble-wall fragments or stretched varieties. Its age and stratigraphical position have not been established.

Discussion

We have analysed over 200 glass separates from tuffs in the Koobi Fora region. We have found more than 40 chemically distinct tuffs. We have also observed additional tuffs whose weathered aspect does not allow them to be purified. Thus, there are more than 40 tuffs in the Koobi Fora region. We have

also analysed numerous tuffs in the Shungura Formation, although we have done less than one-third of the total. There are now eight positive ties between the Koobi Fora region and the Lower Omo valley and more correlations are expected with analysis of additional samples from the Shungura Formation. Thus, many tuffs occur in both sequences, and approximately the same number of tuffs occur in any given interval in both sequences, contrary to earlier belief²².

If stratigraphical sections from different localities in the Koobi Fora region are examined in detail, several significant features are noted (Fig 3). In area 129, some 30 m of section separates the KBS Tuff (1.89 Myr in age¹⁹) and the Tulu Bor Tuff (> 3 Myr age⁴). In area 102, there is > 100 m of lacustrine section below the KBS Tuff; the Tulu Bor Tuff is not found in area 102. This lacustrine sequence (the laminated siltstone facies of Bowen^{5,11}) is about the same age and thickness as the lacustrine interval from G14 to G28 of the Shungura Formation, and so should be considered as broadly correlative, as suggested by Brown *et al.*²³ However, in area 207, south of Kubi Algi, ~70 m of section occurs above the Tulu Bor Tuff; these sediments are not similar to the laminated siltstones in area 102, but rather represent fining-upward fluvial cycles, and are in fact equivalent to members B and C of the Shungura Formation which is also characterized by fining-upward cycles. This suggests that a considerable thickness of sediment was deposited in the Koobi Fora region between Tulu Bor and KBS times.

However, in some areas (such as area 129) almost the entire thickness was removed before deposition of the KBS Tuff. In area 129, we believe that erosion exposed the Tulu Bor Tuff and that the present dip slope of the Tulu Bor Tuff may represent an exhumed land surface. In area 15, erosion probably removed the Tulu Bor tuff entirely. Based on correlation with the Shungura Formation, this erosion must have taken place between the time represented by member D and that represented lower part of member G, or between ~2.4 and ~2 Myr ago.

We can now account for much of the sediment thought to be missing in the Koobi Fora region²³. Stratigraphical thicknesses between marker beds in the Shungura Formation and the Koobi Fora Formation are often quite similar (Fig 4). This, combined with the presence of tuffs in both the Koobi Fora region and the Lower Omo Valley, implies that the two sequences were probably part of the same depositional system. Differences in thicknesses can sometimes be attributed to erosion, as well as to primary differences in thicknesses.

We thank B. W. Cerling and D. Norman for laboratory assistance, R. E. Leakey, M. G. Leakey and G. L. Isaac for support and encouragement, P. G. Williamson and J. M. Harris for critical comments on the manuscript, and B. E. Bowen for copies of his field notes. This work was supported by NSF grant no. BNS-8007354, the foundation for Research into the Origin of Man, and the National Museums of Kenya.

Received 12 February, accepted 7 June 1982

- 1 Bishop, W. W. (ed.) *Geological Background to Fossil Man* (Scottish Academic, Edinburgh, 1978).
- 2 Coppens, Y., Howell, F. C., Isaac, G. L. & Leakey, R. E. (eds) *Earliest Man and Environments in the Lake Rudolf Basin* (University of Chicago Press, 1976).
- 3 Leakey, M. G. & Leakey, R. E. *Koobi Fora Research Project Vol 1* (Clarendon, Oxford, 1978).
- 4 Brown, F. H., Shuey, R. T. & Croes, M. K. *Geophys. J. R. astr. Soc.* **54**, 519–539 (1978).
- 5 Bowen, B. E. thesis, Iowa State Univ. (1974).
- 6 Bowen, B. E. & Vondra, C. F. *Nature* **242**, 391–393 (1973).
- 7 Findlater, I. C. thesis, Univ. London (1976).
- 8 Findlater, I. C. in *Earliest Man and Environments in the Lake Rudolf Basin* (eds Coppens, Y., Howell, F. C., Isaac, G. L. & Leakey, R. E. F.) 94–104 (University of Chicago Press, 1976).
- 9 Findlater, I. C. in *Geological Background to Fossil Man* (ed. Bishop, W. W.) 415–420 (Scottish Academic, Edinburgh, 1978).
- 10 Findlater, I. C. in *Koobi Fora Research Project Vol 1* (eds Leakey, M. G. & Leakey, R. E.) 14–31 (Clarendon, Oxford, 1978).
- 11 Vondra, C. F. & Bowen, B. E. in *Earliest Man and Environments in the Lake Rudolf Basin* (eds Coppens, Y., Howell, F. C., Isaac, G. L. & Leakey, R. E.) 79–93 (University of Chicago Press, 1976).
- 12 Vondra, C. F. & Bowen, B. E. in *Geological Background to Fossil Man* (ed. Bishop, W. W.) 395–414 (Scottish Academic, Edinburgh, 1978).
- 13 Vondra, C. F. & Burggraf, D. R. in *Fluvial Sedimentology* (ed. Miall, A. D.) 511–529 (Canadian Society of Petroleum Geologists, Mem. 5, 1978).
- 14 Vondra, C. F., Johnson, G. D., Behrensmeier, A. K. & Bowen, B. E. *Nature* **231**, 245–248 (1971).
- 15 Brown, F. H. & Cerling, T. E. *Nature* **299**, 212–215 (1982).
- 16 Hillhouse, J. W., Ndombi, J. W. M., Cox, A. & Brock, A. *Nature* **265**, 411–415 (1977).
- 17 Cerling, T. E., Brown, F. H., Cerling, B. W., Curtis, G. H. & Drake, R. E. *Nature* **279**, 118–121 (1979).
- 18 Cerling, T. E., Cerling, B. W. & Brown, F. H. *Quat. res.* (submitted).
- 19 McDougall, I., Maier, R., Sutherland-Hawkes, P. & Gleadow, A. J. W. *Nature* **284**, 230–234 (1980).
- 20 Fitch, F. J. & Miller, J. A. in *Earliest Man and Environments in the Lake Rudolf Basin* (eds Coppens, Y., Howell, F. C., Isaac, G. L. & Leakey, R. E.) 123–147 (University of Chicago Press, 1976).
- 21 Williamson, P. G. *Nature* **295**, 140–142 (1982).
- 22 Bishop, W. W. in *Earliest Man and Environments in the Lake Rudolf Basin* (eds Coppens, Y., Howells, F. C., Isaac, G. L. & Leakey, R. E.) 585–589 (University of Chicago Press, 1976).
- 23 Brown, F. H., Howell, F. C. & Eck, G. G. in *Geological Background to Fossil Man* (ed. Bishop, W. W.) 473–498 (Scottish Academic, Edinburgh, 1978).
- 24 Cerling, T. E. thesis, Univ. California, Berkeley (1977).
- 25 Fitch, F. J., Findlater, I. C., Watkins, R. T. & Miller, J. A. *Nature* **251**, 213–215 (1974).
- 26 White, T. D. & Harris, J. M. *Science* **198**, 13–21 (1977).
- 27 Harris, J. M. in *Koobi Fora Research Project Vol 1* (eds Leakey, M. G. & Leakey, R. E.) 32–63 (Clarendon, Oxford, 1978).

Eukaryotic ribosomes can recognize preproinsulin initiation codons irrespective of their position relative to the 5' end of mRNA

Peter T. Lomedico & Stephen J. McAndrew

Department of Molecular Genetics, Hoffmann-La Roche Inc., Nutley, New Jersey 07110, USA

The functional assay of a eukaryotic mRNA, into which additional AUG codons have been introduced by in vitro mutagenesis, shows that a translational initiation site need not necessarily be the nearest AUG codon to the 5' end of a mRNA. Hence, the sequence surrounding the AUG, and not simply its position relative to the 5' end of mRNA, appears to be important in determining initiation efficiency.

How does a ribosome decide where to begin translation on a eukaryotic messenger RNA? In prokaryotic mRNAs, initiation codons are preceded by a conserved, purine-rich sequence which plays some part in directing the ribosome to the correct AUG codon. In contrast, comparison of 5'-noncoding regions

of eukaryotic mRNAs fails to reveal any sequence homology or conservation, casting doubts on the existence of a sequence functionally analogous to the bacterial ribosome binding site¹. One simple hypothesis to explain initiation codon selection by the eukaryotic ribosome is that translation begins at the first

a

Coding Region Start
▽

3' End of Mature mRNA
▽

119 bp Intron in 5' Noncoding Region
▽

499 bp Intron in Coding Region
▽

(Hpa II)
Eco RI

Hind III

Bgl I

Late mRNA

Early mRNA

Bam HI

Probe 1

Hha I

Eco RI

Probe 2

Bam HI

Dde I

Probe 3

b

H

253

255

268

250

410

418

248

218

41

48

T T T T G C A A A A A G C T T G G T A A G T G A C C A C T A C A T C G G A A A C C A T C A G C A A G C A G G T A T G

A C T C T C C A A G G T G G C C T T G G C T T C C C C A G T C A A G A C T C C A A A T T T G A G G A C G C T G T

G G C T C T T C T C T T A C A T G T A C C T T T T G C T A G C T C A A C C C T G A C T A T C T T C C A G G T C A T T

G T T C C A A C A T G G C C C T G

c

H

A T G

A T G

A T G

A T G

T T T T G C A A A A A G C T T G C C A T G C T G T C C A G G C A G G T A G A T G A C G A C C A T C A G G G A C A G C T T

C A A G G A T C G C T C G C G G C T C T T A C C A G C C T A A C T T C G A T C A T T G G A C C G C T G A T C G T C A C G

G C G A T T T A T G C C G C C T C G G C G A G C A C A T G G A A C G G G T T G G C A T G B A T T G T A G G C G C C G C C

C T A T A C C T T G T C T G C C T C C C C G C G T T G C G T C G C G G T G C A T G G A G C C G G G C A A G C T T G G C T

A C A G T C G G A A A C C A T C A G C A A G C A G G T C A T T G T T C C A A C A T G G C C C T G

S

d

H

A T G

A T G

A T G

A T G

T T T T G C A A A A A G C T T G C C C G G C T C C A T G C A C C G C G A C G C A A C G C G G G A G G C A G A C A A G G

A T A G G G C G G C G C C T A C A A T C C A T G C C A A C C C G T T C C A T G T G C T C G C C G A G G C G G C A T A A

T C G C C G T G A C G A T C A C G G T C C A A T G A T C G A A G T T A G G C T G G T A A G A G C C G C G A G C G A T

C T T G A A G C T G T C C C T G A T G T C G T C A T C T A C C T G C C T G G A C A G C A T G G C A A G C T T G G C T

C A G T C G G A A A C C A T C A G C A A G C A G G T C A T T G T T C C A A C A T G G C C C T G

S

H

A T G

A T G

A T G

A T G

T T T T G C A A A A A G C T T G C T G T C C C T G A T G T C G T C A T C T A C C T G C C T G G A C A G C A T G G C C

C A A C G C G G G C A T C C C G A T G C C G C C G G A A G C G A G A A G A A T C A T A T G G G G A A G G C C A T C

G C C T C G C G T C G C G A A C G C C A G C A A G A C G T A G C C C A G C G C G T C G G C C G C C A T G C C G G C A

A T G G C C T G C T T C T C G C C G A A A C G T T T G G T G G C G G G A C C A G T G A C G A A G G C T T G A G C G A

G G C G T G C A A G A T T C G A A T A C C G C A A G C G A C A G G C C G A T C A T C G T C G C G C T C C A G C G A A

G C G G T C C T C G C C G A A A A T G A C C C A G A G C G C T G C C G G C A C C T G T C C T A C G A G T T G C A T G A

A A G A A G A C A G T C A T A A G T G C G G C G A C G A T A G T C A T G C C C C G C G C C C A C C G G A A G G A G C

G C T T G G C T A C A G T C G G A A A C C A T C A G C A A G C A G G T C A T T G T T C C A A C A T G G C C C T G

S

quences. The cloned deletion mutants were characterized by sequence analysis. The end point of each deletion is ample, the sequence across the *Hind*III site of mutant $\Delta 255$ and *Alu*I (403 bp) is TGCAAAAAGCTTGGCTACA, ion mutants were created by attaching *Hind*III linkers to *Hae*III (213 bp) fragments of pBR322, and inserting these. Individual clones were characterized by restriction analysis and the inserts were completely sequenced. The *Hae*III orientations in Apr12/SVO 255J2 (c) and Apr12/SVO 255J5 (d) and the *Alu*I fragment in one orientation, Apr12/SVO nows both *Hind*III sites (H), the preproinsulin initiation codon (boxed ATG), and the ATG triplets in the insert ity, the 5'-noncoding region intron is deleted (s denotes where this intron resides in the plasmid DNA), hence, e predicted sequence of the spliced mature mRNA. For convenience, these plasmids will be abbreviated as $\Delta 255J2$,

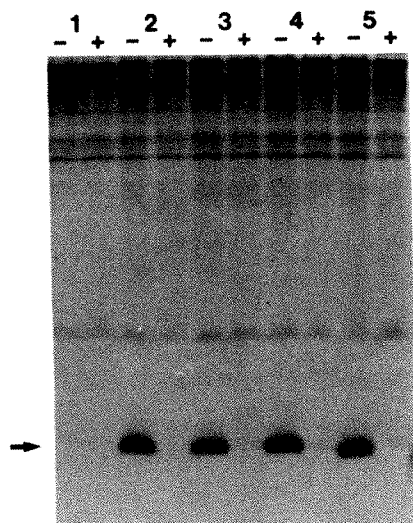


Fig. 2 Calcium phosphate DNA precipitate suspensions were formed²¹ using plasmid DNA at $20 \mu\text{g ml}^{-1}$ and presented to COS cells as described by Chu and Sharp²². One-fifth of the cells were plated in a 6-cm dish and the remainder in a 15-cm dish. Following a 5-h incubation at 37°C in 5% CO_2 , the DNA supernatant was removed and the cells were shocked with 25% glycerol in media for 1 min²², rinsed and returned to the incubator with fresh media. After 3 days, RNA was isolated from the 15-cm dish, and the cells in the 6-cm dish were labelled with ^{35}S -cysteine²³ for 4 h and solubilized with detergents²⁴. Equal amounts of solubilized proteins were reacted with antiserum to bovine insulin (Miles) in the presence (+) and absence (-) of an excess of bovine insulin (Sigma; $10 \mu\text{g}$) as competitor²⁵. The antigen-antibody complexes were recovered²⁶ using *Staphylococcus aureus* bacteria (Pansorbin; Calbiochem), extracted with 8 M urea/1% SDS/0.1 M dithiothreitol at 100°C and electrophoresed on 15% acrylamide/SDS gels²⁷. The acrylamide gel was impregnated with fluor (Enhance, NEN), dried down and exposed to X-ray film at -80°C . 1, pSV0; 2, prI2/SV40-46; 3, $\Delta 250$; 4, $\Delta 255$; 5, $\Delta 268$. Plasmid pSV0 is a pBR322 derivative which contains only the 416-bp SV40 origin of replication. Insulin antigen released into the culture media from transfected cells was measured by radioimmunoassay (Amersham; this assay uses human insulin as a standard and expresses concentrations in $\mu\text{U ml}^{-1}$ where pure insulin is ~ 25 units per mg); 23, 270, 206, 214 and $144 \mu\text{U ml}^{-1}$ were found in cultures 1-5, respectively.

AUG codon at the 5' end of the mRNA. As embodied in the scanning ribosome model², this hypothesis explains many characteristics of initiation by eukaryotic ribosomes (for example, the absence of polycistronic eukaryotic mRNAs). The 'first AUG' hypothesis predicts that there is no eukaryotic equivalent of a bacterial ribosome binding site, and that the 5'-proximal AUG triplet alone, with no influence from surrounding sequences, signals where polypeptide chain synthesis will initiate. We have directly tested this hypothesis by analysing mutations introduced in the 5'-noncoding region of the rat insulin II gene.

Experimental strategy

For a particular eukaryotic mRNA, if an AUG triplet is introduced into the 5'-noncoding region (upstream of the normally used initiation codon), the simple interpretation of the 'first AUG' hypothesis predicts: (1) if this new AUG codon is in the normal reading frame with no intervening termination codons, then translation will result in the expected polypeptide with an N-terminal extension; or (2) if this new AUG codon is out of the normal reading frame, then translation will not generate the expected protein. To test these predictions, we have used a rapid expression assay to evaluate rat (pre)proinsulin synthesis programmed by mutants of plasmid prI2/SV40-46³. This recombinant plasmid (see Fig. 1a) was constructed by connecting the 5'-noncoding region of the SV40 large T/small T antigen gene to the 5'-noncoding region of the rat insulin II gene. We

have previously shown that when introduced into COS cells (simian cells transformed by origin-defective SV40 mutants)⁴, the SV40 early region promoter in this construct functions to drive transcription yielding a correctly spliced hybrid SV40-insulin mRNA in which the 5'-proximal AUG triplet is the normally used rat preproinsulin initiation codon. This mRNA is translated to generate preproinsulin, which is rapidly processed to proinsulin. This system permits the rapid analysis of cloned, *in vitro* engineered mutations necessary to test the 'first AUG' hypothesis.

Construction of deletion mutants

Plasmid prI2/SV40-46 carries a unique *Hind*III site, which facilitates the engineering of AUG codons into the 5'-noncoding region of the hybrid SV40-insulin mRNA. Unfortunately, downstream from this *Hind*III site is a termination codon that is in the preproinsulin reading frame. To correct this, deletion mutants were generated using exonuclease *Bal*31 (Fig. 1b). Mutants $\Delta 255$, $\Delta 268$ and $\Delta 250$ all carry small deletions (11, 17 and 30 base pairs (bp), respectively) in the insulin 5'-noncoding region, which remove this in-frame termination codon. In COS cells, these mutants, and the parental plasmid, all programme (pre)proinsulin synthesis to similar levels (Fig. 2), demonstrating that the deleted nucleotides have no obligatory role in initiation codon selection.

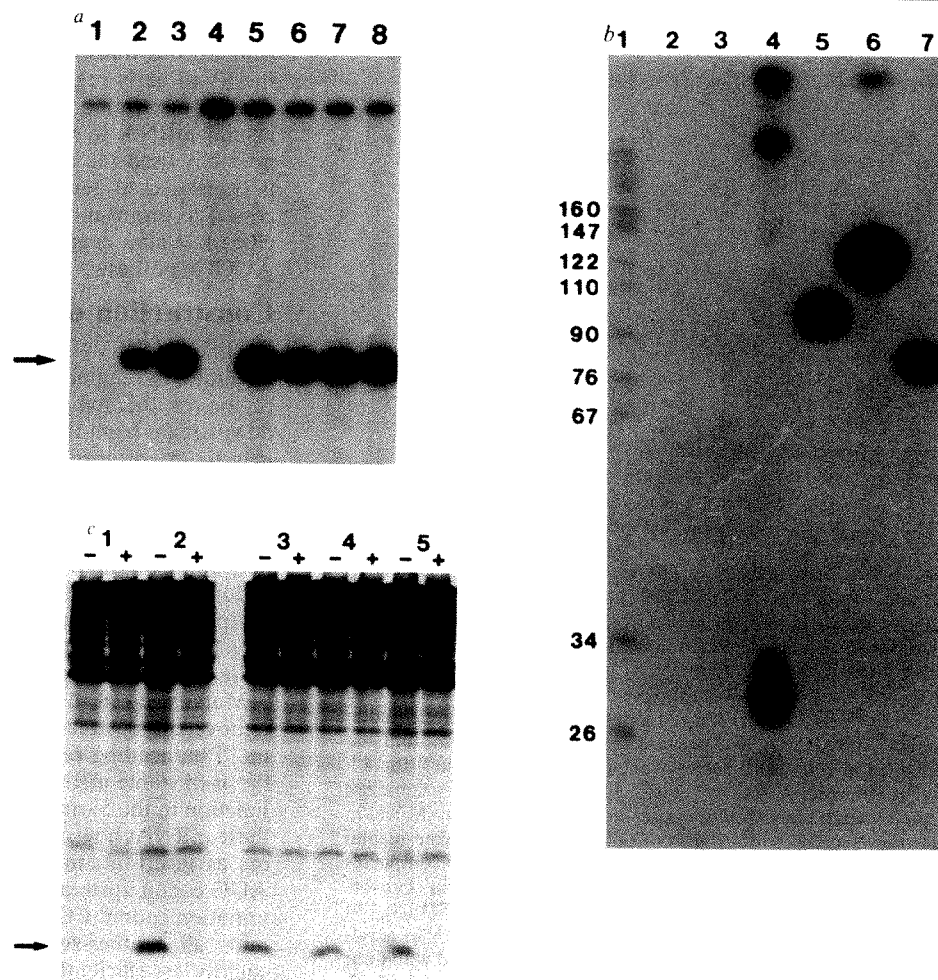
Mutants $\Delta 418$, $\Delta 41$ and $\Delta 419$ carry larger deletions, which remove the upstream splice junction from the intron lying in the 5'-noncoding region. These mutants programme the synthesis of stable mRNA (Fig. 3a), in which the remaining splice junction in the 5'-noncoding region is not used (Fig. 3b). Thus, these mRNAs now carry the previously excised intronic sequences as insertions in the 5'-noncoding region, creating a new AUG codon upstream, but out of frame with the normally used initiation codon. COS cells transfected with these mutant plasmids all synthesize and secrete proinsulin (Fig. 3c), albeit slightly less efficiently than the parental plasmid. Hence, in spite of the upstream AUG, ribosomes still recognize the normally used initiation codon, clearly violating a prediction of the 'first AUG' hypothesis.

Construction of insertion mutants

To create mutants with upstream, in-frame AUG codons, fragments of pBR322 were cloned into the *Hind*III site of $\Delta 255$. Mutants $\Delta 255\text{J5}$ and $\Delta 255\text{J2}$ contain a 213-bp *Hae*III fragment, carrying six AUG codons, cloned in both orientations (Fig. 1c and 1d). Mutant $\Delta 255\text{L3}$ contains a 403-bp *Alu* fragment, carrying nine AUG codons, inserted in one orientation (Fig. 1e). The mRNAs produced by $\Delta 255\text{J5}$ and $\Delta 255\text{L3}$ will have the 5'-proximal AUG in the insulin reading frame with no intervening termination codons; all other AUG triplets are out of frame. For the mRNA produced by $\Delta 255\text{J2}$, only the sixth AUG triplet from the 5' end will be in the insulin reading frame. These mutants programme the synthesis of stable, correctly spliced mRNA (Fig. 4a) which contain the inserted pBR322 sequences intact (Fig. 4b). COS cells transfected with these mutant plasmids all synthesize proinsulin, but much less efficiently than the parental plasmid (Fig. 4c). A large insulin-immunoreactive protein (molecular weight (M_r) $\sim 21,000$) is seen in $\Delta 255\text{J5}$ transfected cells (Fig. 4c). Pulse-chase experiments (Fig. 4d) indicate that this larger protein is somewhat unstable (because of incorrect processing?) and does not chase into proinsulin.

These experiments indicate that ribosomes can recognize the normally used insulin initiation codon, in spite of it being the 7th (in $\Delta 255\text{J2}$ and $\Delta 255\text{J5}$) or 10th (in $\Delta 255\text{L3}$) AUG from the 5' end. This conclusion is supported by the ability to generate preproinsulin in a cell-free translation using mRNA from all three transfected cells (data not shown). Apparently, the first AUG is also being used on the $\Delta 255\text{J5}$ mRNA, leading to the synthesis of an $\sim 21,000$ - M_r which probably consists of preproinsulin (110 amino acids) with an N-terminal extension (87 amino acids). Thus, there are two functional initiation codons

Fig. 3 COS cells were transfected with different plasmids as described in Fig. 2. RNA was prepared³ from the 15-cm dish and examined by S_1 mapping²⁸ using end-labelled probes²⁹. *a*, Probe 1 (see Fig. 1*a*) is a 750-bp fragment uniquely 3'-end-labelled at a *Bam* site in the coding region, extending to a *Hha* site on the other side of the 499-bp intron in the coding region. If a correctly spliced mRNA anneals to the labelled anti-sense DNA strand, nuclease S_1 will digest the unhybridized intronic sequences, leaving protected a 170-nucleotide labelled fragment (designated by the arrow on the photograph of the X-ray film). 1, No RNA; 2, 10 ng of rat insulinoma poly(A⁺)RNA³; 3, 50 ng of rat insulinoma poly(A⁺)RNA; 4–8, equal amounts of RNA (1/10th of the sample) from cells transfected with pSVO, prI2/SV40-46, Δ 41, Δ 418, and Δ 419, respectively. There are $\sim 5 \times 10^7$ molecules of preproinsulin II mRNA in 10 ng of rat insulinoma poly(A⁺)RNA³. *b*, Probe 2 (see Fig. 1*a*) is a 600-bp fragment from prI2/SV40-46 uniquely 5'-end-labelled at a *Bam* site in the coding region, extending upstream to the SV40 *Eco*RI site. If a correctly spliced mRNA anneals to the labelled anti-sense DNA strand, nuclease S_1 will digest the unhybridized intronic sequences, leaving protected a 29-nucleotide labelled fragment. In the deletion mutants, if the intronic sequences are not spliced out, then S_1 will digest at the deletion end point. 1, 32 P-pBR322/*Hpa*II molecular weight numbers (chain length in nucleotides shown alongside); 2, no RNA; 3–7, equal amounts of RNA (1/10th of the sample) from cells transfected with pSVO, prI2/SV40-46, Δ 41, Δ 418 and Δ 419, respectively. *c*, Transfected cells (6 cm dish) were labelled with 35 S-cysteine and the solubilized proteins processed as described in Fig. 2. 1–5, pSVO, prI2/SV40-46, Δ 41, Δ 418 and Δ 419, respectively. Radioimmunoassay revealed 27, 288, 95, 83 and 124 μ U ml⁻¹ of insulin antigen in the spent media from cultures 1–5, respectively.



on the Δ 255J5 mRNA; the initiation codon closer to the 5'-terminus appears to be used more frequently (Fig. 4*d*) even though it probably does not function in *E. coli*⁵. No larger proteins are detected in Δ 255J2 and Δ 255L3 transfected cells, implying that these upstream in-frame AUG triplets are not used as initiation codons. It is possible that these undetected proteins might be rapidly degraded, incapable of reacting with insulin antibodies, or rapidly processed to proinsulin, but we consider this unlikely based on the properties of the 21,000-*M_r* protein programmed by Δ 255J5, the immunological characteristics of preproinsulin⁶, and the cell-free translation results which confirm the *in vivo* findings.

Implications for initiation codon selection

These data demonstrate that eukaryotic ribosomes are capable of initiating polypeptide chain synthesis at internal AUG codons, that multiple initiation sites can be used on the same mRNA, that some AUG triplets never function as initiation codons and that proximity to the 5' end modulates the efficiency of initiation codon utilization. The mere presence of an AUG triplet at the beginning of a mRNA, as predicted by the 'first AUG' hypothesis, is simply not enough information to signal translation initiation. It is likely that the structure surrounding an AUG triplet, as well as its location, are important for efficient initiation. Possibly the system described here could be used to study systematically the sequence requirements involved in initiation codon selection. Also, more experiments are necessary to see if inefficient initiation at internal AUG codons

is the result of the presence of multiple upstream AUG triplets, the increased distance between the internal initiation codon and the 5' end of the mRNA, or an altered structure around the AUG codon.

Other work lends support to the notion that the 'first AUG' hypothesis is not tenable, and that initiation codon proximity to the 5'-terminus has some role in translational efficiency. There are several eukaryotic mRNAs in which translation appears to initiate at an internal AUG triplet^{7–10} or which appear to possess two functional initiation codons^{11,12}. Mulligan and Berg¹³ have shown using a SV40 vector system that an internal AUG codon is used in bacterial xanthine-guanine phosphoribosyl transferase synthesis in mammalian cells; deletion of the upstream AUG triplets results in more efficient translation. Rosenberg and Paterson have demonstrated that the 5'-proximal coding sequence in a polycistronic prokaryotic mRNA can be translated in a eukaryotic cell-free system if this RNA carries a 5'-terminal cap structure^{14,15}; genes encoded by internal cistrons can be expressed if they are moved closer to the 5'-terminus^{15,16}. Finally, Young *et al.*¹⁷ have suggested that the different lengths of the 5'-noncoding region of mouse α -amylase mRNA may be responsible for differential amylase expression in liver and salivary gland.

If ribosomes can initiate at internal AUG codons, why are there no polycistronic mRNAs and why is the first AUG triplet used as an initiation codon on the vast majority of mRNAs? Kozak, in a modified scanning model^{7,8}, suggests that a 40S ribosomal subunit moves along the mRNA, starting from the

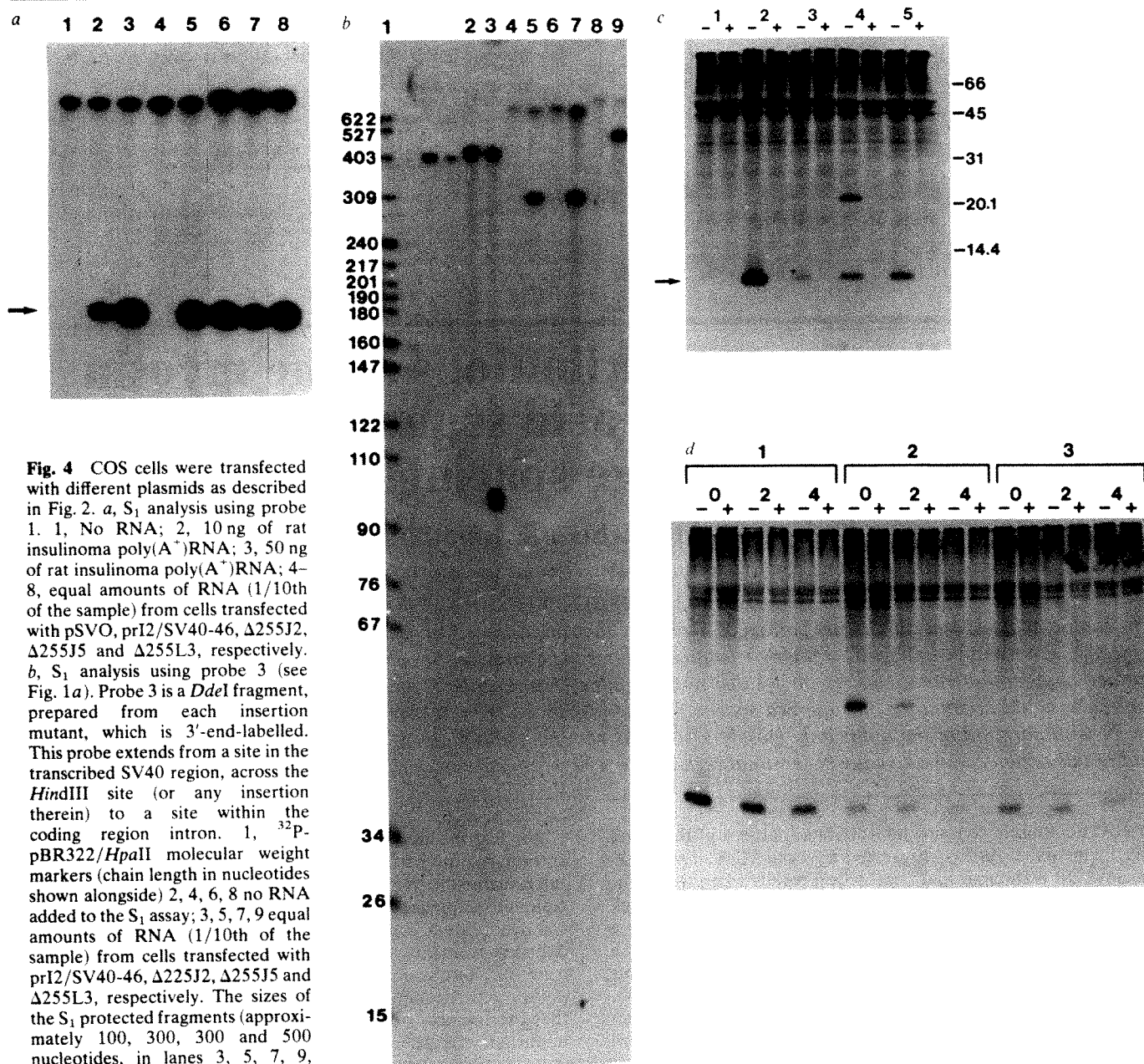


Fig. 4 COS cells were transfected with different plasmids as described in Fig. 2. *a*, S₁ analysis using probe 1. 1, No RNA; 2, 10 ng of rat insulinoma poly(A⁺)RNA; 3, 50 ng of rat insulinoma poly(A⁺)RNA; 4-8, equal amounts of RNA (1/10th of the sample) from cells transfected with pSVO, prI2/SV40-46, Δ255J2, Δ255J5 and Δ255L3, respectively. *b*, S₁ analysis using probe 3 (see Fig. 1*a*). Probe 3 is a *Dde*I fragment, prepared from each insertion mutant, which is 3'-end-labelled. This probe extends from a site in the transcribed SV40 region, across the *Hind*III site (or any insertion therein) to a site within the coding region intron. 1, ³²P-pBR322/*Hpa*II molecular weight markers (chain length in nucleotides shown alongside) 2, 4, 6, 8 no RNA added to the S₁ assay; 3, 5, 7, 9 equal amounts of RNA (1/10th of the sample) from cells transfected with prI2/SV40-46, Δ225J2, Δ255J5 and Δ255L3, respectively. The sizes of the S₁ protected fragments (approximately 100, 300, 300 and 500 nucleotides, in lanes 3, 5, 7, 9, respectively) indicate that S₁ is

attacking at the 5'-noncoding region upstream splice junction, and that the inserted sequences are preserved intact within these mRNA. Analysis using probe 2 confirms that the 5'-noncoding region intron is spliced normally in all these mRNAs. *c*, Transfected cells (6 cm dish) were labelled with ³⁵S-cysteine and the solubilized proteins processed as described in Fig. 2. 1-5, pSVO, prI2/SV40-46, Δ255J2, Δ255J5 and Δ255L3, respectively. Molecular weight markers (weight in daltons × 10⁻³) were run in a parallel lane and visualized by Coomassie blue staining. Radioimmunoassay revealed 22, 117, 29, 89 and 42 μU ml⁻¹ of insulin antigen in the spent media from cultures 1-5, respectively. *d*, Transfected cells were labelled with ³⁵S-cysteine for 15 min and collected immediately (0 h), or subjected to a 2 or 4 h chase (the radioactive media were removed and the monolayer was rinsed several times with complete media). The solubilized proteins were processed as described in Fig. 2. 1, prI2/SV40-46; 2, Δ255J5; 3, Δ255L3.

5' end, searching for AUG codons. The model predicts that flanking sequences modulate the recognition of functional AUG initiation codons by the migrating ribosomal subunit; if synthesis is not initiated at a particular AUG triplet, the scanning process continues until a functional initiation site is encountered. Functional initiation codons are found most frequently in the sequence $\hat{C}XXAUGG$. Kozak proposes that this process works most efficiently when the first AUG triplet is the functional initiation codon, thus there is a strong selective pressure against mutations that create new AUG triplets in the 5'-noncoding region. Furthermore, nature may use this process as a translational control mechanism: by placing a particular polypeptide's synthesis under the control of an internal AUG initiation codon, this polypeptide will not be produced as abundantly (the bacterial XGPRT experience¹³ fits this hypothesis). With respect to the data presented here (for example, with

Δ255J5), it seems that initiation at a particular AUG codon does not preclude initiation at a downstream AUG codon. Hence, if ribosomes do scan, initiation is curiously leaky. This problem is most notable in the Δ255L3 mRNA which possesses many potential initiation sites, as defined by the modified scanning model, upstream of the functional insulin initiation codon. In support of the modified scanning model, we find that some AUG triplets never function as initiation codons and that initiation at an AUG codon appears more efficient when this is the first AUG at the 5' end. We favour a model where eukaryotic ribosomes directly recognize certain AUG triplets which have favourable structures at the 5' end of a mRNA; proximity to the 5'-cap structure may modulate this recognition affecting the rate of polypeptide chain initiation.

We thank A. Shatkin and M. Kozak for comments on the manuscript and D. Andriola for typing.

Received 21 May; accepted 2 July 1982.

1. Baralle, F. E. & Brownlee, G. G. *Nature* **274**, 84–87 (1978).
2. Kozak, M. *Cell* **15**, 1109–1123 (1978).
3. Lomedico, P. T. *Proc. natn. Acad. Sci. U.S.A.* (in the press).
4. Gluzman, Y. *Cell* **23**, 175–182 (1981).
5. Sutcliffe, J. G. *Cold Spring Harb. Symp. quant. Biol.* **43**, 77–90 (1979).
6. Lomedico, P. T., Chan, S. J., Steiner, D. F. & Saunders, G. F. *J. biol. Chem.* **252**, 7971–7978 (1977).
7. Kozak, M. *Nucleic Acids Res.* **9**, 5233–5252 (1981).
8. Kozak, M. *Biochem. Soc. Symp.* **47** (in the press).
9. Dhruva, B. R., Shenk, T. & Subramanian, K. N. *Proc. natn. Acad. Sci. U.S.A.* **77**, 4514–4518 (1980).
10. Hendy, G. N., Kronenberg, H. M., Potts, J. T. Jr & Rich, A. *Proc. natn. Acad. Sci. U.S.A.* **78**, 7365–7369 (1981).
11. Jay, G., Nomura, S., Anderson, C. W. & Khoury, G. *Nature* **291**, 346–349 (1981).
12. Bos, J. L. *et al. Cell* **27**, 121–131 (1981).
13. Mulligan, R. C. & Berg, P. *Molec. cell. Biol.* **1**, 449–459 (1981).
14. Paterson, B. M. & Rosenberg, M. *Nature* **279**, 692–696 (1979).
15. Rosenberg, M. & Paterson, B. M. *Nature* **279**, 696–701 (1979).
16. Schumperli, D., Howard, B. H. & Rosenberg, M. *Proc. natn. Acad. Sci. U.S.A.* **79**, 257–261 (1982).
17. Young, R. A., Hagenbuchle, O. & Schibler, U. *Cell* **23**, 451–458 (1981).
18. Lomedico, P. *et al. Cell* **18**, 545–558 (1979).
19. Roberts, T. M., Bikel, I., Yocum, R. R., Livingston, D. M. & Ptashne, M. *Proc. natn. Acad. Sci. U.S.A.* **76**, 5596–5600 (1979).
20. Legerski, R. J., Hodnett, J. L. & Gray, H. B. *Nucleic Acids Res.* **5**, 1445–1464 (1978).
21. Graham, F. L. & van der Eb, A. J. *Virology* **52**, 456–467 (1973).
22. Chu, G. & Sharp, P. A. *Gene* **13**, 197–202 (1981).
23. Gruss, P. & Khoury, G. *Proc. natn. Acad. Sci. U.S.A.* **78**, 133–137 (1981).
24. Mulligan, R. C., Howard, B. H. & Berg, P. *Nature* **277**, 108–114 (1979).
25. Lomedico, P. T. & Saunders, G. F. *Nucleic Acids Res.* **3**, 381–391 (1976).
26. Kessler, S. W. *J. Immun.* **115**, 1617–1624 (1975).
27. Laemmli, U. K. *Nature* **227**, 680–685 (1970).
28. Berk, A. J. & Sharp, P. A. *Proc. natn. Acad. Sci. U.S.A.* **75**, 1274–1278 (1978).
29. Weaver, R. F. & Weissmann, C. *Nucleic Acids Res.* **7**, 1175–1193 (1979).

Periodic charge distributions in the myosin rod amino acid sequence match cross-bridge spacings in muscle

Andrew D. McLachlan & Jonathan Karn

Laboratory of Molecular Biology, University Postgraduate Medical School, Hills Road, Cambridge CB2 2QH, UK

The amino acid sequence of the rod portion of nematode myosin, deduced from the sequence of the unc-54 heavy chain gene of Caenorhabditis elegans, is highly repetitive and has the characteristics of an α -helical coiled coil. The molecular surface contains alternate clusters of positive and negative charge. Interactions between charge clusters on adjacent molecules could account for the observed spacings of the myosin cross-bridges in muscle. Calculations also suggest that the N-terminal third of the rod is only loosely associated with the thick filament backbone. Bending of the rod near the end of this region could allow the N-terminal section to act as a hinged arm during muscle contraction.

STRIATED muscle contains interdigitated lattices of thick and thin filaments^{1,2}. As first suggested by both H. E. and A. F. Huxley^{3,4}, it is thought that contraction results when the actin-containing thin filaments slide past the myosin-containing thick filaments. The myosin molecule is adapted to perform both a structural task, in the assembly of the thick filament, and enzyme reactions, which generate tension. The native molecule contains two heavy chains^{5,6} each of molecular weight (MW) ~200,000. Long regions of these chains nearest the carboxyl end form an α -helical coiled coil, known as the rod, and these rods form the backbones of the thick filaments. The myosin molecule also has two globular heads^{6,7} composed of the amino ends of each heavy chain combined with the four light chains⁵. The heads act as movable cross-bridges^{1,2} between the thick and thin filaments.

Interactions between the rod segments of the myosin molecules are necessary for the assembly of thick filaments. Although the structural details vary considerably in different organisms, the general features are conserved and these are outlined in Fig. 1a. The thick filament is bipolar and contains myosin molecules assembled in an antiparallel arrangement in the central 'bare zone', which is about 1,600 Å wide^{8,9}. Throughout the rest of the filament the rods form two parallel arrays in which the heads project away from the surface, with an axial stagger of ~143 Å between heads^{10–13} and a helix repeat in vertebrates of 429 Å. These spacings give rise to the familiar X-ray diffraction pattern of muscle^{10–12}. Proteolysis of thick filaments^{5,14} and isolated myosin suggests that the backbone of the thick filament is largely formed by interactions between the C-terminal two-thirds of the myosin rod (light meromyosin or LMM), while the N-terminal third of the sequence, or subfragment-2 (S-2) region, is only loosely attached. Bending of the myosin rod in the region of the S-2–LMM junction has been postulated^{11,15} as a critical feature for the movement of the myosin cross-bridge during contraction.

We describe here how features of myosin rod sequences may account for the patterns of assembly of myosin molecules into thick filaments. We have based our analysis primarily on the complete sequence of the rod of a myosin heavy chain¹⁶ of the soil nematode, *Caenorhabditis elegans*, which we have recently deduced from DNA sequence studies of the cloned *unc-54* gene^{17–19}, but comparison of the nematode sequences with myosin rod sequences from mammals and *Drosophila* suggests that the features of the rod which we take to be structurally important are indeed maintained in all striated muscle types.

Myosin rod sequences are conserved

The complete 1,117-residue amino acid sequence of the nematode myosin rod is shown in Fig. 2. The proteolytic cleavage site at the N-terminus of the rod (the S-1–S-2 junction) is well defined and lies close to the proline residue which seems to mark the N-terminal boundary of the regular helical rod sequence (see below). Aligned with the nematode sequence are partial amino acid sequences for rabbit S-2 and LMM determined by Elzinga and his colleagues^{20,21} using protein chemistry, as well as LMM sequences of rat and *Drosophila* deduced from cDNA sequence analysis of clones by Mahdavi *et al.*²² and S. Bernstein *et al.* (personal communication). The rod sequences are homologous along their entire lengths and show high levels of matching amino acids. For example, there are 42.5% matching amino acids between the nematode and rabbit sequences from the beginning of the rod to residue 463, and 48.1% matching amino acids between nematode and rat from residues 673 to the end of the rod sequence at residue 1,100. The two mammalian sequences are even more highly conserved and show 75.9% amino acid homology from residues 787 to 1,098. Most of the sequence alterations are conservative, particularly at positions in the molecule where charged or hydrophobic residues are preferred, so that the chemical characteristics of the sequences are preserved.

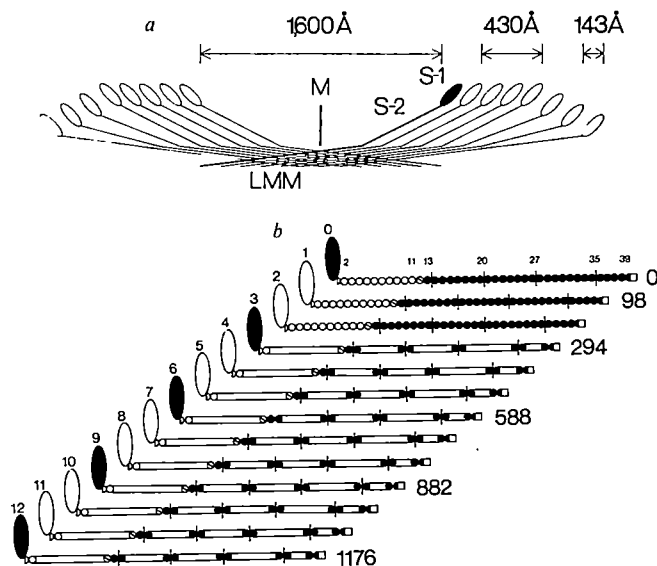


Fig. 1 *a*, Schematic drawing of the bipolar arrangement of myosin molecules in the thick filament. The filaments extend in both directions from the mid-line (M) and the globular heads form a regular array of cross-bridges with an axial separation of ~ 143 Å in vertebrate striated muscle and a helix repeat of 430 Å. The central bare zone, free of cross-bridges, is $\sim 1,600$ Å wide. Each molecule contains two chains (one only shown here) composed of the head, S-1, a helical rod-like arm, S-2, and a rod-like core segment, LMM. The width is not to scale. A typical complete vertebrate thick filament is $\sim 15,700$ Å long, with 49 levels of cross-bridges on each end and three cross-bridges emerging at each level^{2,8}. *b*, Parallel array of staggered myosin rods, drawn to show the relationship between the 143 Å (or 98-residue) and 430 Å (294 or 295 residues) displacements and the 28-residue zones in the amino acid sequence, as shown in Fig. 2. In rods numbered 0-2, open circles represent the zones in short S-2, ending within zone 12, and closed circles are zones in long S-2 or LMM. Vertical bars mark skip residues and the open square beyond zone 40 is the non-helical tailpiece. Rods 3-12 emphasize the half-staggered arrangement of skip residues. The diagram is a two-dimensional view of the stagger and should not be taken literally. The numbers at the right of the ends of the rods show the staggers in amino acid residues 0, 98, 294... A cross section through one such staggered array contains approximately 12 rods if S-2 is bound to the backbone or 8 rods when S-2 is bent away in zone 12. Vertebrate striated muscle probably has the equivalent of three such arrays in each cross-section.

28-Residue repeat units and helical structure of the myosin rod

The myosin rod sequence is highly repetitive and shows features typical of an α -helical coiled-coil protein. Between residues 2 and 1,088 the predicted α -helix probability profile²³ is high almost everywhere, with levels of 70-90% except for 15 local weak spots with a level below 50%. This whole region contains no proline. Beyond residue 1,088 the helix seems to end, leading into a tailpiece, Pro 1,095-Phe 1,117, with an apparently irregular secondary structure.

Many α -helical coiled-coil proteins²⁴⁻²⁶, especially tropomyosin^{27,28}, fibrinogen^{29,30} and α -keratin³¹, have a characteristic regular 7-residue pattern *a, b, c, d, e, f, g*, in which hydrophobic residues are concentrated at alternate intervals of three and four residues along the lengths of the chain at positions *a* and *d* (refs 24, 32). The residues at positions *a* and *d* form a closely packed hydrophobic interface or 'core' of knobs and holes between the two strands of the coiled coil³³. Fragments of the rabbit skeletal myosin rod sequence have already been found^{21,34} which show a marked 7-residue hydrophobic repeat, though less regular than that in tropomyosin²⁸. The histograms in Fig. 3 show how the complete nematode rod sequence has hydrophobic residues strongly concentrated in the core positions *a* and *d*. The helix surface is highly charged, with acidic and basic residues clustered mainly in the outer positions *b, c* and *f*.

Several fibrous proteins^{35,36} have longer repeated structural units which are important in the assembly and function of these molecules. The myosin rod shows strong evidence for a 28-

residue unit with a repetitive sequence as suggested originally by Parry³⁷ in his analyses of the rabbit myosin sequence determined by Elzinga *et al.*^{20,21,34}. Comparison of the sequence with itself shows that the entire helical sequence of the coil can be mapped out as a cyclical pattern of 28 amino acids. The statistical analysis of the pattern and its significance will be given elsewhere. We stress here two features which appear relevant to the rod structure. First, the repeat pattern is interrupted at four positions by the insertion of one extra residue which we call a 'skip residue'. As will be discussed below, these residues probably modulate the pitch of the coiled coil, a possibility previously proposed by Elzinga and Trus³⁸. Second, the distribution of the charges on the helix surface suggests that the rods are held in the thick filament structure by electrostatic forces between rods which lie side by side.

The positions of the skip residues are narrowly defined to within one or two turns of α -helix, and we have assigned them to residues 351, 548, 745 and 970, which are separated by regular intervening regions with lengths which are exact multiples of 28—196, 196 and 224, respectively. When aligned in this way, the coil region divides into 41 zones, 38 of which show a complete 28-residue cycle composed of four 7-residue sections with the characteristic coiled-coil pattern, beginning at position *d*. The 28 positions in a zone can thus be labelled 1*d*, 1*e*, ... 1*c*, 2*d*, 2*e*, ... 4*b*, 4*c*. With this convention the skip residues all occur at the end of a zone after position *c*, and the next zone begins at position *d*. The arrangement of repeat units and skip residues suggests that the whole sequence has evolved from a primitive 28-residue segment by a series of gene multiplication steps, perhaps involving a longer 197-residue structural unit in the later stages.

Each zone has a characteristic pattern of hydrophobic residues and a remarkable distribution of charges. The histograms in Fig. 3 show these patterns, which are drawn more realistically on a helical net diagram in Fig. 4. A typical 28-residue zone divides into six alternating bands of positive and negative charge which are spaced so that the strongest peak of positive charge (position 1*b*) is exactly 14 residues (or one half-zone) away from the strongest peak of negative charge (position 3*b*). A Fourier analysis of the charge distribution shows very intense peaks at periods of 28 and 28/3 residues in both the acidic and basic amino acids. Parry detected some of these peaks in earlier sequence fragments³⁷.

The hydrophobic residues are not uniformly distributed throughout the 28-residue zones and some positions such as 1*a* and 4*d* are particularly weak, because of the displacement of hydrophobic residues by charged amino acids. Lysine and arginine often appear in the *a* core positions (31 examples). The negatively charged side chains of aspartic and glutamic acid are, however, totally excluded from position *a* and are rare in position *d* (15 examples) except near the maxima of the negative charge pattern.

Although individual zones differ, the character of a typical 28-amino acid zone may be summed up in a 'consensus' sequence derived by taking the most common residue at each position:

<i>d</i>	<i>e</i>	<i>f</i>	<i>g</i>	<i>a</i>	<i>b</i>	<i>c</i>	<i>d</i>	<i>e</i>	<i>f</i>	<i>g</i>	<i>a</i>	<i>b</i>	<i>c</i>
L-E-K-Q-K-K-K-L-E-Q-E-L-E-E	(1-14)												
L-Q-E-Q-L-D-E-E-E-R-A-L-A-K	(15-28)												

Skip residues and the coiled-coil pitch

The skip residues appear at homologous positions in each of the species studied so far, and break the 7-residue pattern of the coiled-coil sequence. We built space-filling models of the skip regions and several comparable 56-residue lengths of the regular coil to test whether the extra residue produced a complete break in the coiled coil or merely a minor deformation. Reasonable limits for the pitch of the regular supercoil range

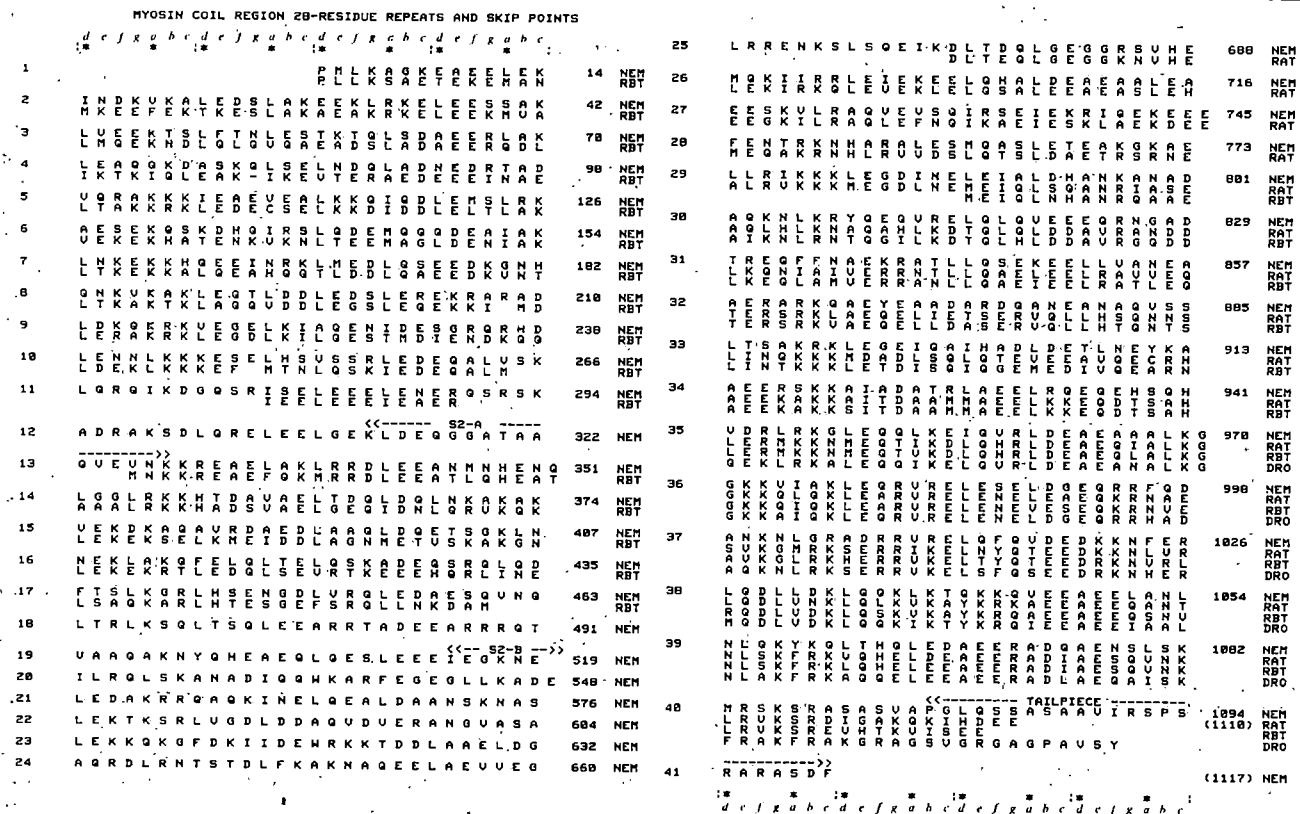


Fig. 2 28-Residue repeats and skip points in the coil region sequence. Complete sequence from nematode (NEM), with aligned fragments from rabbit (RBT), rat and *Drosophila* (DRO) myosins. The sequence divides into 41 zones. The first zone is short, with only 14 residues, and the helical region ends near residue 1,094 in zone 40. Above the 28 columns letters *d*, *e*, *f*, *g*, *a*, *b*, *c* indicate positions in the 7-residue coiled-coil repeat; Asterisks mark positions *a*, *d* on the inner face of the coil which often contain hydrophobic amino acids. Skip residues are shown on the right-hand margin at positions 351, 548, 745 and 970. Special features are: S2-A, junction of short S-2 with long LMM; S2-B, junction of long S-2 with short LMM; the non-helical tailpiece, residues 1,095-1,117.

from 92 amino acids (137 Å) in tropomyosin^{28,39} through 90–120 in paramyosin^{40,41} up to 126 for an ideal α -helix with 3.6 residues per turn. In our models we assumed a twist of $\sim 90^\circ$ over each regular 28-residue zone, corresponding to a pitch of 112 residues.

All the models of regular regions confirm that the hydrophobic core of the supercoil is well packed together when the chains are in register. In each skip region the models suggest that the supercoil can accommodate the extra residues by yielding to local distortions without any severe alteration of the structure. The seam of hydrophobic residues shifts across the helix surface over a stretch of 14–21 residues and resumes its regular zig-zag pattern at the far side of the region. Figure 4 shows an example of this near residue 351 (the models will be described in more detail elsewhere). The main overall effect is to flatten out the twist of the supercoil and make the helices run parallel to one another for a few turns. The local pitch distortions produced by the skip residues could have important effects on the way myosin molecules pack in the cross-sections of the thick filaments.

Electrostatic interactions between the rods

The regular bands of charge on the rod suggest that strong attractions and repulsions will arise when two molecules are placed side by side. We have analysed these interactions for parallel chains using a linear model⁴², as if the charge distributions were averaged round the circumference of the helix surface. A more realistic analysis based on a three-dimensional model would certainly be preferable, but at present this is not possible, as the pitch of the coiled coil is unknown. The zone structure of the myosin rod sequence suggests³⁷ that there should be strong repulsions when the stagger is zero or a multiple of 28 residues, and strong attractions when it is an odd multiple of 14 residues. Our calculations confirm this and show that particularly strong attractions are expected for staggers of 98 or 294 residues.

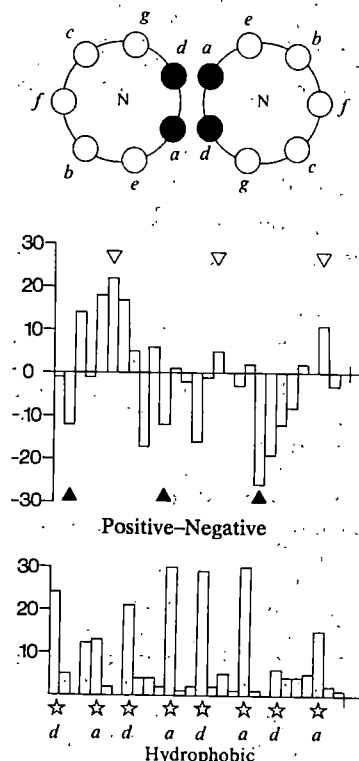


Fig. 3 Histograms of amino acid distributions in the 28-residue zones. The data are for the 38 complete zones in the nematode only. The 28 bars correspond to the 28 columns in Fig. 2, with the skip residues omitted. The heights of the bars were obtained by counting the amino acids in the columns. The upper histogram shows the net charge (positive minus negative). Triangles show the positions of the six main bands of charge in the average zone. Asterisks mark the core positions in the hydrophobic residue pattern. The cross-section of the coiled coil (above) shows how the positions *a-g* appear when viewed from the amino end of the parallel helices:

Figure 5 shows how the net electrostatic interaction between two parallel rod sequences depends on the axial stagger. A pair of molecules was treated as two linear arrays of charged and uncharged amino acids shifted successively by 0, 1, 2, ... n residues. Two charges were considered to interact if they lay nearly opposite one another, within a range of 0, ± 1 , ± 2 residues. In these calculations only the acidic and basic amino acids were considered and the coil was taken to have a length of 1,094 residues, ignoring the non-helical tailpiece, at residues 1,095–1,117. The energy oscillates strongly with stagger, showing a 28-residue period, and has peaks close to the odd multiples of 14. The amplitude decreases as the molecular overlap is reduced, but not uniformly, and several peaks stand out. The most prominent are at odd multiples of staggers of 98—for example, 98, 294 (98×3) and 490 (98×5). A stagger of 98 residues or $3\frac{1}{2}$ complete zones would correspond to a distance of 145.5 Å, assuming a helical rise of 1.485 Å per residue⁴³ in the α -helical coiled coil. This distance is close to the cross-bridge translation of 143–146 Å observed in muscle. A small correction is required for an average of one skip residue every 196 residues, so that the theoretical step length would be 98.5 residues or 146.3 Å. A further unknown correction is needed if the rods bend, or if they run at a small angle to the thick filament axis. The interactions seen at staggers that are odd multiples of 98 allow for several kinds of nearest neighbour in the close-packing of myosin rods in three dimensions. Thus, the stagger of 294 residues accounts for the interactions between ideal straight molecules translated by 436.5 Å or between real molecules at the axial helical repeat distance of 430 Å seen in muscle. Similarly, the interactions at a 490-residue stagger reflect potential interactions between molecules further apart in the helix.

This overlap calculation does not show which portions of the rod interact most strongly, nor whether attractions and repulsions are equally important. A more detailed picture was built up by calculating local interactions between shorter segments of staggered rods with a certain span length. Trials showed that the clearest results were obtained when attractions and repulsions had equal weights and when interactions were averaged over long spans of 99–589 residues.

Significant interactions appear at most staggers which are half-integer multiples of 28, especially in the first half of the molecule, but the strongest and most persistent interaction is at a stagger of 98. In Fig. 6 the interaction density summed over a span of 99 residues is plotted along the length of the rod for staggers of 294, 100, 98 and 96 residues. The favourable interactions for a stagger of 98 stand out clearly. The strong peak centred on residue 320 corresponds to the attraction between residues 271–369 of one rod and 173–271 of its neighbour, displaced 98 residues towards the carboxyl end. The pairing persists strongly down to the shoulder near residue 880. The interactions at a stagger of 294 residues are generally weaker and they appear mainly in the second half of the molecule. The high plateau from residues 740–1,008 in Fig. 6 corresponds to a strong averaged interaction in the LMM fragment between residues 691–1,057 and 593–959, with a stagger of 294 residues which corresponds to the helix repeat distance in vertebrate muscle.

Search for a hinge between S-2 and LMM

It has been suggested that myosin contains flexible sections or hinges. A hinge in the rod between S-2 and LMM could allow the cross-bridge to move in or out from the thick filament backbone^{10,15}. Electron microscope observations of sharp bends in isolated myosin rods^{7,44} support this notion. Also, proteolysis of myosins from a wide variety of species^{5,6,14} shows that the rod tends to cleave at narrowly localized points, which may reflect the presence of hinges. In rabbit skeletal muscle either a 37,000-MW fragment (short S-2) or a 59,000-MW one (long S-2) can be cleaved from the amino end of the rod. Analysis of the rabbit fragments^{21,38,45,46} suggests that the C-terminus of short S-2 is homologous to a region in the nematode between

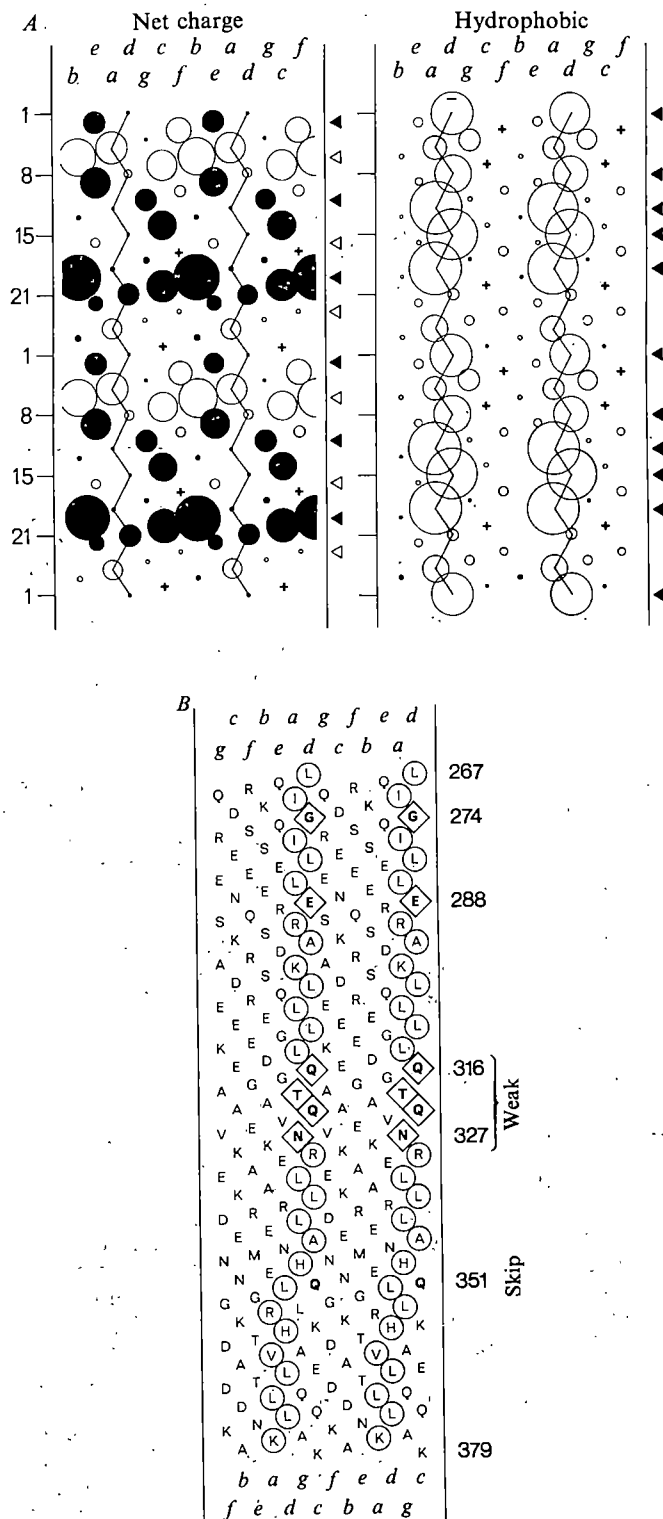


Fig. 4 A, charge distribution and hydrophobic residues for the averaged 28-residue zone plotted on the supercoil surface of two paired α -helices. A section of coil 56 residues long has been projected onto a cylinder and unrolled so that each section of sequence appears twice side-by-side, first on one helix and then on the other. The sequence reads across from right to left with a slight downward slant and is drawn with a pitch of $3\frac{1}{2}$ residues per turn. Inner positions a, d are connected by a zig-zag line. Circles have radii proportional to the numbers in Fig. 3, with white and black to represent positive and negative charges. A (+) sign marks points of zero net charge. Triangles at the side mark six bands of charge in the typical zone. Hydrophobic residues are plotted in a similar way with triangles to mark the major sites and (+) signs to mark forbidden positions. B, helical net of part of the coiled-coil sequence to illustrate the interrupted pattern of hydrophobic residues in the core. Hydrophobic or basic amino acid side chains are ringed, while diamonds enclose acidic, polar or glycine side chains, which are likely to weaken the core. At skip residue Gln 351 the pattern shifts across the helix surface. Residues 316–327 may form an unusually weak part of the coil and they lie near the short S-2–LMM junction.

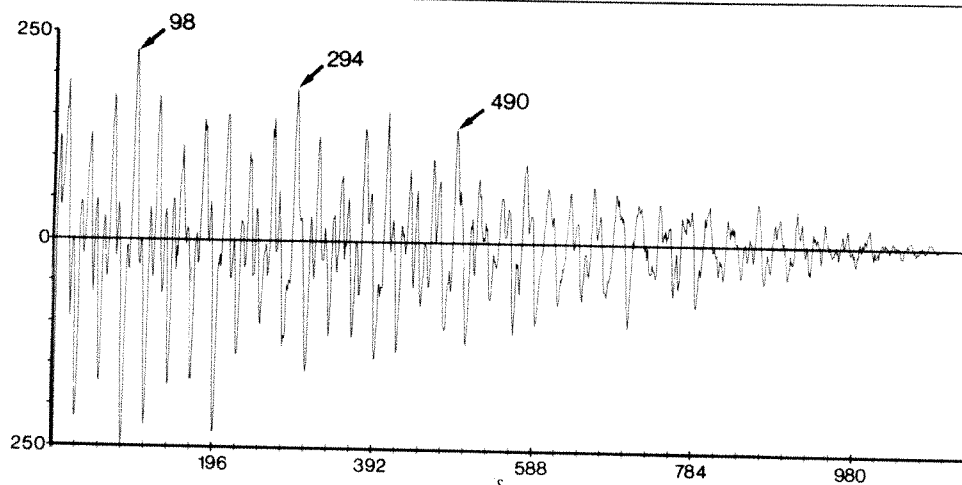


Fig. 5 Charge interactions between parallel rods 1,094 residues long. The stagger, s , is plotted horizontally and the net number of interactions (attractions minus repulsions) vertically. Amino acids are counted within an axial range of ± 2 residues, taking each rod as a single chain, because only one side at a time can interact with its neighbour. Note the peaks at staggers which are odd multiples of 98.

lysines 312 and 328, which would give a molecular weight of between 36,173 and 37,783. The remainder of the rod, possibly the longest LMM fragment, would then have a MW of 91,386 or 89,776. Lu and Wong⁴⁵ have also demonstrated that fragments of rabbit myosin homologous to residues 326–386 are present in long but not short S-2. The long S-2–LMM junction⁴⁶ is near Lys 517. Cleavage at this point would lead to a 59,313-MW fragment and a corresponding form of LMM with MW 68,246.

There is no part of the nematode rod or the vertebrate sequence fragments which seems at all likely to form a specific non-helical molecular hinge distinct from the coiled coil. The short S-2 region and LMM are predicted to be α -helical to the same extent and the 28-residue repeat pattern is strong in both regions. The total net charge differs little. The skip regions do not seem to correspond to the hinges defined by proteolysis. The first skip residue, at position 351, and the second at 548 lie well to the C-terminal sides of the likely cleavage sites for short and long S-2. There is no evidence for specific cleavages near the third and fourth skip residues.

We searched the nematode sequence for potential weak spots where several consecutive missing hydrophobic residues in the core might disturb the coiled-coil structure. The sequences in Fig. 2 and the histograms in Fig. 3 suggest that Ala can substitute satisfactorily for Leu, Val or Ile in the core positions a and d , while the hydrophobic basic groups Arg and Lys are tolerated more readily than Asp and Glu. Therefore, we looked for regions with polar, negatively charged, or glycine residues in positions a and d . With this rule the weakest sections of the coil seem to be positions 316–327, with four consecutive defects, and 176–183 and 823–830 with three each. The section 316–327, which is one of the most pronounced of these potential weak points, lies close to the point of division between the short and long S-2 fragments in rabbit^{45,46}. We have also obtained (J. K. and L. Barnett, unpublished) the sequences of two other nematode heavy chains in the region 316–327. In one gene the sequence is identical to *unc-54*, but the second shows an apparently stronger structure in which Leu replaces Thr 320 and strengthens the core.

The freedom of movement of the S-2 region must also depend on its interactions with the rest of the filament. Our analysis of the electrostatic interactions between parallel rods (Fig. 6) suggests that the N-terminal part of the short S-2 region has a weakened attraction, or even repulsion, for other molecules aligned with staggers close to 98 residues, whereas the middle section, residues 173–271, has a strong attraction for residues 271–369 of an adjoining molecule. At certain staggers the tip of S-2 can be attracted to other sections of the myosin rod. A particularly strong interaction appears when the stagger is 95 or 96.

Our analysis suggests that the S-2 region is held against the rest of the thick filament by a comparatively weak 'electrostatic spring' which allows the tip of the rod to bend outwards under stress. Residues 316–327 may be a 'soft spot' in the coiled coil

where the α -helix can bend or even unravel and extend locally⁴⁷ to accommodate the movement.

Structure of thick filaments

The high density of charged groups on the outer surface of the myosin rod and the lack of hydrophobic groups on the surface suggest that ionic interactions are by far the most important forces involved in the assembly of thick filaments. We have seen that the rod sequence is made up of structurally similar repeat units which are 28 residues (or 41.6 Å) long, which have a characteristic charge distribution and attract one another strongly when they are half-staggered by half-integer multiples of their length. Our one-dimensional model calculations suggest that direct interactions between complementary charges on parallel rods staggered by 98 or 294 residues may account for the 143 and 430 Å axial spacings found in muscle. Our result

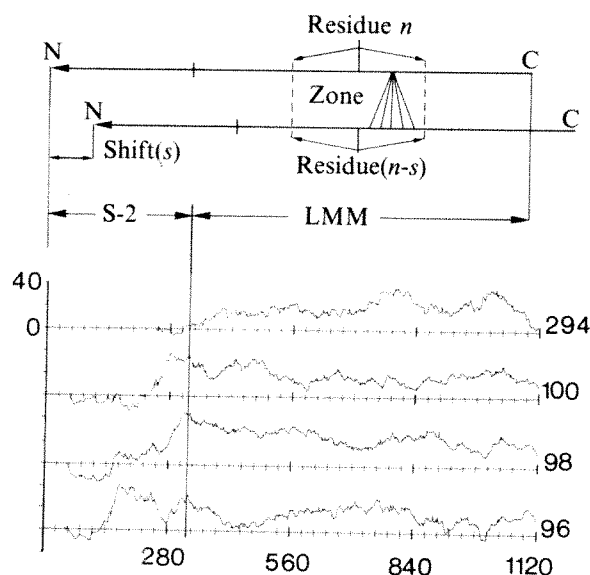


Fig. 6 The distribution of charge interactions along the length of a pair of parallel rods. The upper rod is fixed and the lower rod has been shifted s residues to the right. The curves are drawn for shifts of 96, 98, 100 and 294 residues and the positions of the rods shown here correspond to the 98-residue shift. The height of the graph under residue n of the upper rod is equal to the sum (attractions–repulsions) of a 99-residue section centred on residue n and the adjacent 99-residue section of the lower rod centred on residue $(n-s)$. When residue n nears the end of the sequence the 99-residue active zone becomes shortened and the interactions gradually decrease at each end. Thus, the top curve for a shift of 294 residues reaches its peaks between residues 343 and 1,045. The interactions are scored in the same way as in Fig. 5. Inside each 99-residue section the charge pairs are counted within an axial range of ± 2 residues. The relationship between the zone and the scoring is shown schematically in the upper diagram (not to scale). The S2–LMM junction has been placed at residue 322 and refers to the upper rod.

that the 294-residue stagger leads to strong attractions in the LMM segment agrees with some observations on LMM paracrystals^{48,49}. The 430 Å stagger often coexists in a phase equilibrium with the 143 Å stagger. The 143 and 430 Å spacings associated with the myosin molecule are both close to half-integral multiples of 286 Å and suggest³⁷ that the long spacings in muscle are produced by electrostatic interactions between larger-scale structural units ~196 or 197 residues long, which form a variety of half-staggered fibrous arrays. The two 197-residue sections of myosin rod, 351–547 and 548–744, bounded by the first three skip residues, may therefore be discrete structural units in the assembly of the thick filament. If this type of structural scheme is correct, it would suggest that paramyosin⁵⁰, which assembles with a long spacing of 725 Å ($2\frac{1}{2}$ times 290 Å), also contains 28-residue zones and skip residues, and that the shorter 290 Å network spacing in paramyosin results from a combination of opposed half-integer spacings of 725 and 435 Å.

We have not yet extended our calculations to analyse the three-dimensional packing of myosin rods in the thick filaments. All such models² depend crucially on the pitch of the supercoil, and in myosin the presence of skip residues which probably modulate the pitch is an added complication. Two funda-

mentally different types of attraction are possible; direct salt bridges⁵¹ or indirect ion-bridged couplings between clusters of like charges⁵². Packing schemes which only allow direct salt bridges are quite restricted. A cross-section through the filament at each level must contain a lattice of alternating positive and negative charges with nearest neighbours formed into even-membered sub-assemblies of 2, 4, 6, ... two-stranded myosin rods. The simplest regular assemblies of this type have square or hexagonal cross-section lattices. The presence of 28-residue zones throughout the sequence suggests that the packing may originally have evolved from a regular crystalline lattice in which amino acids separated by 28 residues occupied equivalent sites.

Finally, we note that numerous mutants of the *unc-54* gene have been isolated which show defects in the thick filament assembly. Analysis of the sequence alterations in these strains should provide an experimental framework for testing the ideas presented here.

We thank M. Elzinga, S. Tong, R. C. Lu, V. Moldavi, B. Nadal-Ginard and S. Bernstein for allowing us to use their unpublished sequence data; M. Stewart, R. W. Craig, A. G. Weeds, H. E. Huxley, P. Goelet and L. Barnett for helpful discussions; and S. Brenner for his enthusiastic support.

Received 14 May; accepted 13 July 1982.

- Huxley, H. E. in *Fibrous Proteins: Scientific Industrial and Medical Aspects* Vol. 1 (eds Parry, D. A. D. & Cremer, L. K.) 71–95 (Academic, New York, 1979).
- Squire, J. M. *The Structural Basis of Muscular Contraction* (Plenum, New York, 1981).
- Huxley, H. E. & Hanson, J. *Nature* **173**, 973–976 (1954).
- Huxley, A. F. & Niedergerke, R. *Nature* **173**, 971–972 (1954).
- Lowe, S., Slayter, H. S., Weeds, A. & Baker, H. *J. molec. Biol.* **42**, 1–29 (1969).
- Lowe, S. in *Fibrous Proteins: Scientific Industrial and Medical Aspects* (eds Parry, D. A. D. & Cremer, L. K.) 1–26 (Academic, New York, 1979).
- Elliott, A. & Offer, G. *J. molec. Biol.* **123**, 505–519 (1978).
- Craig, R. W. *J. molec. Biol.* **109**, 69–81 (1977).
- Sjostrom, M. & Squire, J. M. *J. molec. Biol.* **109**, 49–68 (1977).
- Huxley, H. E. & Brown, W. *J. molec. Biol.* **30**, 383–434 (1967).
- Miller, A. & Tregear, R. T. *J. molec. Biol.* **70**, 85–104 (1972).
- Wray, J. S. *Nature* **277**, 37–40 (1979).
- Offer, G. & Elliott, A. *Nature* **271**, 325–329 (1978).
- Weeds, A. & Pope, B. *J. molec. Biol.* **111**, 129–157 (1977).
- Pepe, F. A. *J. molec. Biol.* **27**, 227–236 (1967).
- MacLeod, A. R., Waterston, R. H., Fishpool, R. M. & Brenner, S. *J. molec. Biol.* **114**, 133–140 (1977).
- Karn, J., Brenner, S., Barnett, L. & Cesareni, G. *Proc. natn. Acad. Sci. U.S.A.* **77**, 5172–5176 (1980).
- MacLeod, A. R., Karn, J. & Brenner, S. *Nature* **291**, 386–390 (1981).
- Karn, J., McLachlan, A. D. & Barnett, L. in *Molecular and Cellular Control of Muscle Development* (eds Epstein, H. F., Garrels, J. I., Kaufman, S. J. & Pearson, M. L.) (Cold Spring Harbor Laboratory, New York, in the press).
- Elzinga, M. & Collins, J. H. *Proc. natn. Acad. Sci. U.S.A.* **74**, 4281–4284 (1977).
- Trus, B. L. & Elzinga, M. in *Structural Aspects of Recognition & Assembly in Biological Macromolecules* Vol. 1 (eds Balaban, M., Sussman, J. L., Traub, W. & Yonath, A.) 361 (International Science Services, Tel-Aviv, 1981).
- Mahdavi, U., Periasamy, M. & Nadal-Ginard, B. *Nature* **297**, 659–664 (1982).
- McLachlan, A. D. *Int. J. quant. Chem.* **12**, Suppl. 1, 371–385 (1977).
- Crick, F. H. C. *Acta crystallogr.* **6**, 689–697 (1953).
- Wilson, I. A., Skehel, J. J. & Wiley, D. C. *Nature* **289**, 366–373 (1981).
- Geisler, N. & Weber, C. *Proc. natn. Acad. Sci. U.S.A.* **78**, 4120–4123 (1981).
- Stone, D., Sodek, J., Johnson, P. & Smillie, L. B. *Proc. 9th FEBS Meet. Budapest* **31**, 125–136 (1975).
- McLachlan, A. D. & Stewart, M. *J. molec. Biol.* **103**, 271–298 (1976).
- Parry, D. A. D. *J. molec. Biol.* **120**, 545–551 (1978).
- Doolittle, R. F., Goldbaum, D. M. & Doolittle, L. R. *J. molec. Biol.* **120**, 311–326 (1978).
- Parry, D. A. D., Crewther, W. G., Fraser, R. D. B. & MacRae, T. P. *J. molec. Biol.* **113**, 449–454 (1977).
- McLachlan, A. D. & Stewart, M. *J. molec. Biol.* **98**, 293–304 (1975).
- Parry, D. A. D. in *Fibrous Proteins: Scientific Industrial and Medical Aspects* Vol. 1 (eds Parry, D. A. D. & Cremer, L. K.) 393–427 (Academic, New York, 1979).
- Capony, J. P. & Elzinga, M. *Biophys. J.* **33**, 148a (1981).
- Hoffmann, H., Fietzek, P. P. & Kuhn, H. *J. molec. Biol.* **141**, 293–314 (1980).
- McLachlan, A. D., Stewart, M. & Smillie, L. B. *J. molec. Biol.* **98**, 281–291 (1975).
- Parry, D. A. D. *J. molec. Biol.* **153**, 459–464 (1981).
- Elzinga, M. & Trus, B. L. in *Methods in Peptide and Protein Sequence Analysis* (ed. Birr, Chr.) 213–224 (Elsevier, Amsterdam, 1980).
- Phillips, G. N., Fillers, J. P. & Cohen, C. *Biophys. J.* **32**, 485–502 (1980).
- Elliott, A. & Lowe, J. *J. molec. Biol.* **53**, 181–203 (1970).
- Cohen, C. & Holmes, K. C. *J. molec. Biol.* **6**, 423–432 (1963).
- Hulmes, D. J. S., Miller, A., Parry, D. A. D., Piez, K. A. & Woodhead-Galloway, J. *J. molec. Biol.* **79**, 137–148 (1973).
- Fraser, R. D. B. & MacRae, T. P. *Conformation in Fibrous Proteins* (Academic, New York, 1973).
- Takahashi, K. *J. Biochem. Japan* **83**, 905–908 (1978).
- Lu, R. C. & Wong, A. *Biophys. J.* **37**, 52a (1982).
- Lu, R. C. *Proc. natn. Acad. Sci. U.S.A.* **77**, 2010–2013 (1980).
- Ueno, H. & Harrington, W. F. *Proc. natn. Acad. Sci. U.S.A.* **78**, 6101–6105 (1981).
- Bennett, P. M. *J. molec. Biol.* **146**, 201–221 (1981).
- Katsura, I. & Noda, H. *J. Biochem. Japan* **73**, 257–268 (1973).
- Cohen, C., Szent-Györgyi, A. G. & Kendrick-Jones, J. *J. molec. Biol.* **56**, 223–237 (1971).
- Bloemer, A. C., Champness, J. N., Bricogne, G., Staden, R. & Klug, A. *Nature* **276**, 362–368 (1978).
- Stewart, M. & McLachlan, A. D. *J. molec. Biol.* **103**, 251–269 (1976).

The effects of α chain mutations *cis* and *trans* to the $\beta 6$ mutation on the polymerization of sickle cell haemoglobin

Ruth E. Benesch, Suzanna Kwong & Reinhold Benesch

Department of Biochemistry, Columbia University, College of Physicians and Surgeons, New York, New York 10032, USA

*The solubility of polymers formed by haemoglobins with one β^S chain and one mutant α chain, either *cis* or *trans* to each other, has revealed three distinct regions on the surface of the tetramer which participate in intermolecular bonding within the haemoglobin S fibre.*

It has become increasingly clear that the polymer formed from concentrated solutions of deoxygenated sickle cell haemoglobin (HbS) is a multi-stranded helix, the basic unit of which is the double-stranded structure described for HbS crystals by Wishner *et al.*¹. This is supported by the spontaneous transfor-

mation of fibres into crystals that show the same diffraction pattern as those studied by Wishner *et al.*, which has been demonstrated for fibres stored for very long periods of time², and also for fibres stirred to accelerate their transformation to crystals^{3–5}—in which case a considerable polymorphism of the

intermediate structures formed during crystallization can be observed.

The link between the HbS fibre structure and that of the Wishner double strand is also supported by the demonstration that many of the mutations that interfere with HbS gelation are located at residues that form contacts between the haemoglobin molecules in the Wishner crystal⁶⁻⁹. The significance of the double strands as the basic unit from which the fibres are constructed is also illustrated by the observation that specific pairs of strands are missing from the fibre structure in certain conditions. This was found in minor forms of HbS fibres¹⁰ as well as in the principal form of the fibres of the double mutant haemoglobin $\alpha_2^{\text{Sealy}} \beta_2^{\text{S}}$ (ref. 11).

In HbS crystals the molecules are arranged in paired strands with tetramers in adjacent strands staggered by half a molecular diameter¹. The lateral contact between members of a pair involves the HbS mutation in only one of the β chains of a tetramer—a hydrophobic bond between valine 6 of the β_2 chain of a tetramer in one strand with residues on the haem pocket of the β_1 chain of a molecule in the adjacent strand. It follows that in the crystal (and therefore also in the fibre) the two β chains, and hence also the two α chains, are not equivalent and that residues on the surface of the α_1 and the α_2 chain will be involved in different groups of intermolecular contacts. The different role of the two β chains in the polymerization was first demonstrated in solution by the effect of HbA on the polymerization of HbC-Harlem¹², and later by the finding that tetramers containing only one β^{S} chain can form gels^{13,14}.

As the structure of the fibres of deoxy HbS has not been solved unequivocally, several models have been proposed for

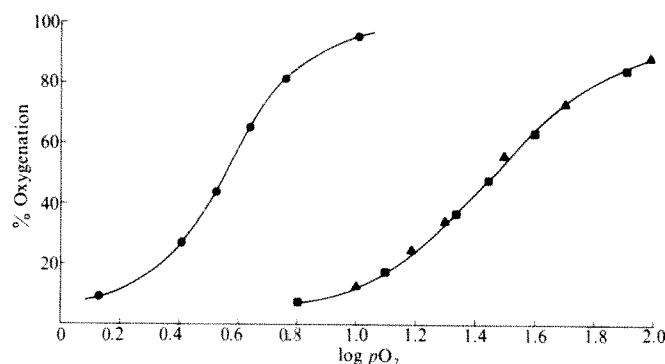


Fig. 1 The effect of the cross-link on oxygenation curves. These were determined spectrophotometrically as described elsewhere^{29,30}. ●, HbS; ▲, cross-linked HbS; ■, cross-linked HbAS. 0.05 M bis Tris buffer, pH 7.3, 0.1 M chloride, 20 °C.

fibres composed of four¹⁵, seven^{10,16,17} or eight¹⁸ 'Wishner double strands'. Of these, the eight-stranded one is the most unlikely, having been proposed before the non-hollow structure of the fibres was recognized. The 16-stranded model was proposed on the basis of the fibre to crystal transformation^{3,18}, but only the 14-stranded structure results from direct image reconstruction of the fibre itself^{10,16,17}.

In such a multi-stranded helix at least three classes of intermolecular contacts can be distinguished: (1) The axial contact between molecules within a single strand. These contacts will be similar in all strands throughout the fibre. (2) The lateral contact between members of a double strand, described above. Again, this contact will exist throughout the structure, and β_1 6 valines do not participate. (3) A much more diverse group of contacts are those that hold the double strands together to form the multi-stranded helix. They are not only much less well characterized, but are necessarily of several different kinds, particularly in the case of the 14-stranded structure. These contacts must be different from the inter-pair ones in the crystal, and they are, of course, especially relevant for the stability of the fibre structure.

Double mutants, containing the β^{S} mutation and an additional one on the α chains, have previously been used to define regions on the α chain that participate in the intermolecular contacts⁶⁻⁸. As pointed out by Nagel *et al.*⁹, the conclusions that can be reached by this approach are limited from a stereochemical point of view, as both α chains and both β chains are substituted in these tetramers.

As only one of the β 6 valines participates in the bonding between the two partners of a double strand, the effect of an α chain mutation will depend on its position relative to the contact-forming β^{S} chain (β_2). With this in mind we have prepared tetramers containing only one β^{S} chain (the other one being β^{A}) so that an α chain mutation could be placed either on the same dimer as the β^{S} mutation (*cis*) or on the opposite one (*trans*). Because such haemoglobin tetramers, consisting of two different $\alpha\beta$ dimers, disproportionate to homogeneous ones during aerobic chromatography, they were isolated by using a specific covalent cross-link between the β chains^{19,20}.

The results presented here show that these molecules could be used to test some of the predictions which emerge from the proposed models of the sickle fibre.

Preparation of mixed tetramers

The general approach was to mix equal amounts of the two haemoglobins in aerobic conditions to allow for $\alpha\beta$ dimer exchange which results in a mixture containing 50% of the hybrid and 25% of each of the parent haemoglobins. The mixture was deoxygenated to freeze the equilibrium, and an intra-dimeric cross-link was introduced by reaction with 1.4 mols of 2-nor-2 formylpyridoxal 5' phosphate per mol of haemoglobin, followed by reduction with NaBH_4 as described previously^{19,20}.

Table 1 Effect of α 16 and α 47 mutations on gel solubility

Expt	c_{sat} (g per 100 ml)	γ	a_{sat} (g per 100 ml)	$\frac{(a_{\text{sat}})\alpha\text{mutant}}{(a_{\text{sat}})\alpha\text{A}}$
a				
$\beta^{\text{S}}\alpha^{\text{A}}$	14.5 ± 1.3 (22)	3	44	—
$\beta^{\text{S}}\alpha^{\text{A}}$	26.5 ± 1.2 (10)	15	405	9.2
$\beta^{\text{S}}\alpha^{\text{Sealy}}$	20.2 ± 1.3 (10)	6.5	135	3.1
b				
$\beta^{\text{S}}\alpha^{\text{A}}$	12.3 ± 0.5 (6)	2.5	33	—
$\beta^{\text{S}}\alpha^{\text{A}}$	22.8 ± 0.1 (2)	8.5	194	5.9
$\beta^{\text{S}}\alpha^{\text{Sealy}}$	14.9 (1)	3.1	46	1.4
c				
$\beta^{\text{S}}\alpha^{\text{A}}$	20.0 ± 1.8 (11)	5.5	110	—
$\beta^{\text{S}}\alpha^{\text{A}}$	31.1 ± 0.7 (2)	29.5	917	8.3
$\beta^{\text{S}}\alpha^{\text{Sealy}}$	21.0 ± 0.3 (3)	6.6	139	1.3

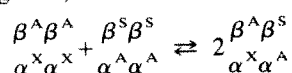
HbA was obtained from normal human blood as described previously²³. HbS ($\alpha_2\beta_2^{\text{S}}$), Hb^{Sealy} ($\alpha_2^{\text{Sealy}}\beta_2^{\text{S}}$) and Hb¹ ($\alpha_2^{\text{16Lys}}\beta_2^{\text{S}}$) were isolated from the blood of heterozygous donors using the chromatographic system of Abraham *et al.*²⁴ on a preparative scale²⁵. Polymerization was induced by reduction with two equivalents of deoxygenated dithionite per haem, the gels were centrifuged and the haemoglobin concentration was determined in the supernatant as described elsewhere²⁶. For many of the experiments the volume of haemoglobin solution necessary was decreased to 80–100 μ l by using centrifuge tubes 45 mm in length made from Pyrex capillary tubing (i.d. 2 mm, o.d. 5 mm). The supernatant concentration (c_{sat}) is independent of the initial concentration²⁵. Because these concentrated solutions are highly non-ideal, c_{sat} must be multiplied by the activity coefficient (γ)²⁷ to obtain a thermodynamic measure of the polymerizing tendency (a_{sat}).

Table 2 Gel solubility of tetramers with *cis* and *trans* $\alpha 16$ mutations

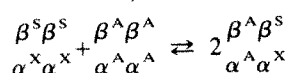
	c_{sat} (g per 100 ml)	γ	a_{sat} (g per 100 ml)	$(a_{\text{sat}})_{\alpha \text{ mutant}} / (a_{\text{sat}})_{\alpha \text{ A}}$
$\left[\begin{smallmatrix} \beta^S \alpha^A \\ \beta^A \alpha^A \end{smallmatrix} \right]$	20.0 ± 1.8 (11)	5.5	110	—
$\left[\begin{smallmatrix} \beta^S \alpha^I \\ \beta^A \alpha^I \end{smallmatrix} \right]$	31.1 ± 0.7 (2)	29.5	917	8.3
<i>cis</i> $\left[\begin{smallmatrix} \beta^S \alpha^I \\ \beta^A \alpha^A \end{smallmatrix} \right]$	31.3 ± 0.1 (3)	31	973	8.8
<i>trans</i> $\left[\begin{smallmatrix} \beta^S \alpha^A \\ \beta^A \alpha^I \end{smallmatrix} \right]$	19.7 ± 0.2 (3)	5.5	108	1.0

Following the NaBH_4 reduction, all haemoglobins were converted to the metcyanide form by oxidation at pH 7.0 and room temperature with 1.2 equivalents of $\text{K}_3\text{Fe}(\text{CN})_6$ per haem in the presence of 2.0 equivalents of KCN. Ferri cyanide and ferrocyanide were removed by passage through Sephadex G-25 in 0.1 M phosphate buffer pH 7.3 containing 10^{-2} M KCN. The three cross-linked species (the hybrid and the two parent haemoglobins) were then separated from uncross-linked haemoglobins by passage of the mixture through a 4×52 cm Sephadex G-100 column in 1 M MgCl_2 , 0.1% Tris pH 7.0, 10^{-2} M KCN at 18 ml h^{-1} (ref. 28). The isolation of the desired cross-linked haemoglobins was again accomplished by the Abraham method²⁴ using sectional columns²⁵. This method resulted in excellent separations of all the components of the mixtures except in the case of the *trans* isomer of the Hb^{Sealy} :HbS hybrid. Since HbS, Hb^{Sealy} and the hybrid all have the same charge in neutral solution, a lower pH to protonate the $\alpha 47$ histidine of Hb^{Sealy} was used to resolve this mixture. This was done by chromatography on CM-Sephadex in 0.05 M phosphate buffer pH 6.0 with a gradient of NaCl from 0 to 0.1 M. After elution all haemoglobin solutions were dialyzed to equilibrium against 0.1 M phosphate buffer pH 7.3 containing 0.01 M KCN. They were then concentrated as described previously²⁵.

(1) *Trans* tetramers, with the α and β chain mutations on different $\alpha\beta$ dimers. These are made by mixing HbS and the α mutant haemoglobin, thus:



(2) *Cis* tetramers, with the α and β chain mutations on the same $\alpha\beta$ dimer. The starting material for this kind of tetramer was the double mutant, $\alpha^X \beta^S$, prepared by previously described methods⁶⁻⁸. The *cis* tetramer is formed by subunit exchange of this double mutant with HbA, thus:



The structure of these mixed tetramers is unequivocally determined by their method of preparation, as the dissociation of haemoglobin in neutral solution does not proceed beyond the $\alpha\beta$ dimer stage.

The pyridoxal phosphate dialdehyde used throughout this investigation for stabilizing the mixed tetramers provides a single covalent bridge between the N-terminal amino group of one β chain and lysine 82 of the other β chain, across the polyphosphate binding site²¹. This cross-link greatly lowers the

O_2 affinity (Fig. 1) to values similar to those found in the presence of excess inositol hexaphosphate. Furthermore, the cross-link does not appear to alter the structure of the fibres, as cross-linked HbS fibres are typical of those of normal HbS in the presence of organophosphates (Fig. 2).

Polymerization studies

The effect of the two mutations in the α chain ($\alpha 16$ and $\alpha 47$) on the gel solubility of tetramers that also carry the β^S mutation is compared in Table 1. Three types of tetramers were initially studied: (1) Uncross-linked tetramers in which both α chains and both β chains are substituted. (2) The same tetramers cross-linked between the β chains. (3) Cross-linked tetramers in which both α chains are mutant ones, but only one β chain is β^S .

It is clear that in all cases the solubilizing effect of the $\alpha 16$ substitution far exceeds that at $\alpha 47$. Both these mutations were previously reported to increase the solubility in concentrated phosphate, but with their relative effectiveness reversed. This was probably due to the influence of the high ionic strength used in this assay on the electrostatic interactions responsible for these contacts⁶. A comparison of the results for (2) and (3) shows that the tetramers containing only one β^S chain behave similarly to the ones with two β^S chains except for a higher solubility. The somewhat lowered gel solubility of cross-linked compared with uncross-linked HbS (Table 1) also shows that this modification does not interfere with polymerization but actually favours it, probably because it fits so well into the deoxyconformation of the central cavity²¹.

The results in Table 2 show the dramatic difference in the effect of the $\alpha 16$ mutation in the *cis* compared with the *trans* configuration. The tetramer in which both mutations are present on the same $\alpha\beta$ dimer (*cis*) is almost 10 times as soluble as the *trans* tetramer, which has the same solubility as the one in which both α chains are normal (Table 2). As substitution of glutamate for lysine at position 16 in the *trans* α chain has no effect on polymerization, the mutation in the *cis* position must be responsible for the whole solubilizing effect observed when both α chains are mutant ones.

The corresponding data for the $\alpha 47$ mutation are shown in Table 3. In this case substitution of mutant for normal α chains in both positions affects polymerization, but in opposite directions. While the mutation in the *cis* α chain causes an increase in solubility, the same substitution in the *trans* α chain actually decreases it (Table 3). The extent to which these two opposing effects neutralize each other evidently depends on the kind of tetramer into which the two α chain mutations are introduced. In uncross-linked HbS the solubilizing effect prevails (Table 1a) whereas in the cross-linked ones the two effects largely cancel each other (Table 1b, c).

Discussion

The striking difference in the solubility of the *cis* and *trans* isomers of both mutations testifies to the different role that each of the α chains has in the formation of the HbS fibre.

In the case of the $\alpha 16$ mutation, substitution of the normal

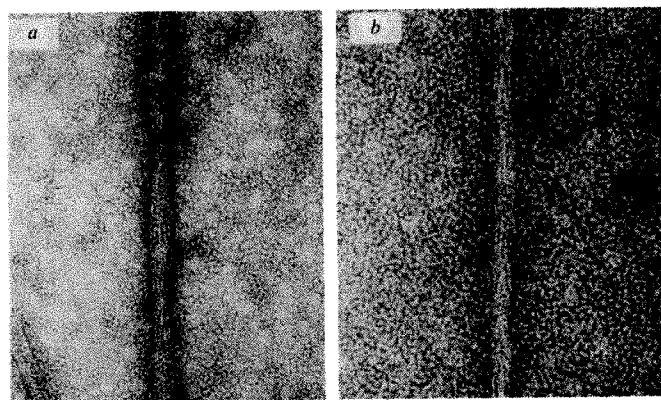


Fig. 2 Electron micrographs of HbS and cross-linked HbS fibres. a, HbS; b, cross-linked HbS. 2% Phosphotungstic acid. $\times 280,000$.

Table 3 Gel solubility of tetramers with *cis* and *trans* $\alpha 47$ mutations

	c_{sat} (g per 100 ml)	γ	a_{sat} (g per 100 ml)	$(a_{\text{sat}})_{\alpha \text{ mutant}} / (a_{\text{sat}})_{\alpha \text{ A}}$
$\left[\begin{smallmatrix} \beta^S \alpha^A \\ \beta^A \alpha^A \end{smallmatrix} \right]$	20.0 ± 1.8 (11)	5.5	110	—
$\left[\begin{smallmatrix} \beta^S \alpha^{\text{Sealy}} \\ \beta^A \alpha^{\text{Sealy}} \end{smallmatrix} \right]$	21.0 ± 0.8 (3)	6.6	139	1.3
<i>cis</i> $\left[\begin{smallmatrix} \beta^S \alpha^{\text{Sealy}} \\ \beta^A \alpha^A \end{smallmatrix} \right]$	23.8 ± 0.5 (2)	9.8	233	2.1
<i>trans</i> $\left[\begin{smallmatrix} \beta^S \alpha^A \\ \beta^A \alpha^{\text{Sealy}} \end{smallmatrix} \right]$	12.7 ± 0.8 (5)	2.7	34	0.3

Experimental details were as for Table 2.

lysine by a glutamate in the α_2 chain causes a very large increase in gel solubility, whereas the same substitution in the α_1 chain has no effect at all. According to Wishner *et al.*¹ lysine α_2 16 is situated in the axial contact between the molecules along a single strand, and the normal attraction between this lysine and glutamate β 22 in the next molecule would then be replaced by a repulsion in the mutant. Lysine α_1 16, on the other hand, is not involved in any of the contacts of the Wishner-Love structure. Our results with the α 16 mutation therefore strongly support the Wishner-Love double strand as a basic unit of the HbS fibre.

The significance of the α 16 locus for the polymerization of HbS raises the possibility of using it as a receptor site for antisickling modifications. In this connection it is of interest that Acharya and Manning found that lysine α 16 was the most reactive residue in the α chain towards glyceraldehyde²².

The situation is quite different for the α 47 mutation. Neither α_1 47 nor α_2 47 is involved in intra double strand contacts¹, but in both cases substitution of the normal aspartate by a histidine

changes the stability of the fibre (Table 3). The observed effects must therefore be due to contacts between the double strands. Since these results thus identify two separate regions on the tetramer, (α_1 47 and α_2 47) as being involved in inter double-strand contacts, they provide much needed constraints for the orientation of the double strands within the HbS fibre. It was shown earlier that the presence of this mutation in both α chains of a HbS tetramer leads to fibres with a loss of two specific pairs of strands, 'capped' by a ring of 16 new strands¹¹. Hopefully electron microscopy of the *cis* and *trans* isomers will resolve the question of the relative roles of the mutation in the two different α chains in causing these structural alterations.

We thank Drs Richard Crepeau and Stuart Edelstein for providing us with the micrographs of native and cross-linked HbS, Drs Stuart Edelstein and Jonathan Greer for helpful suggestions and comments, and especially Dr J. S. Wilkenfeld for gifts of blood containing haemoglobin Sealy. This work was supported by NIH grant HL-17552 and NSF grant PCM-7911610.

Received 7 April; accepted 2 July 1982.

1. Wishner, B. C., Ward, K. B., Lattman, E. E. & Love, W. E. *J. molec. Biol.* **98**, 179-194 (1975).
2. Magdoff-Fairchild, B. & Chiu, C. C. *Proc. natn. Acad. Sci. U.S.A.* **76**, 223-226 (1979).
3. Welles, T. E., Vasser, R. J. & Josephs, R. *J. molec. Biol.* **153**, 1011-1026 (1981).
4. Pumphrey, J. G. & Steinhardt, J. *Biochem. biophys. Res. Commun.* **69**, 929-931 (1976).
5. Pumphrey, J. G. & Steinhardt, J. *J. molec. Biol.* **112**, 359-375 (1977).
6. Benesch, R. E., Yung, S., Benesch, R., Mack, J. & Schneider, R. G. *Nature* **260**, 219-221 (1976).
7. Benesch, R. E., Kwong, S., Benesch, R. & Edalji, R. *Nature* **269**, 772-775 (1977).
8. Benesch, R., Kwong, S., Benesch, R. E. & Edalji, R. *INSERM Symp. on Molecular Interactions of Hemoglobin* **70**, 221-230 (1977).
9. Nagel, R. L. *et al. Nature* **283**, 832-834 (1980).
10. Dykes, G. E., Crepeau, R. H. & Edelstein, S. J. *J. molec. Biol.* **130**, 451-472 (1979).
11. Crepeau, R. H. *et al. Proc. natn. Acad. Sci. U.S.A.* **78**, 1406-1410 (1981).
12. Bookchin, R. M. & Nagel, R. L. *J. molec. Biol.* **60**, 263-270 (1971).
13. Bookchin, R. M., Balazs, T., Nagel, R. L. & Tellez, I. *Nature* **269**, 526-527 (1977).
14. Benesch, R. E., Benesch, R., Edalji, R. & Kwong, S. *Biochem. biophys. Res. Commun.* **81**, 1307-1312 (1978).

15. Josephs, R., Jarosch, H. S. & Edelstein, S. J. *J. molec. Biol.* **102**, 409-426 (1976).
16. Edelstein, S. J. *J. molec. Biol.* **150**, 557-575 (1981).
17. Edelstein, S. J. *Texas Rep. Biol. Med.* **40**, 221-232 (1981).
18. Welles, T. E. & Josephs, R. *J. molec. Biol.* **137**, 443-450 (1980).
19. Benesch, R., Benesch, R. E., Yung, S. & Edalji, R. *Biochem. biophys. Res. Commun.* **63**, 1123-1129 (1975).
20. Benesch, R. E. & Benesch, R. *Meth. Enzym.* **76**, 147-159 (1981).
21. Arnone, A., Benesch, R. E. & Benesch, R. *J. molec. Biol.* **115**, 627-642 (1977).
22. Acharya, A. S. & Manning, J. M. *J. biol. Chem.* **225**, 1406-1412 (1980).
23. Benesch, R. E., Benesch, R., Renthal, R. D. & Maeda, N. *Biochemistry* **11**, 3576-3582 (1972).
24. Abraham, E. C., Reese, A., Stallings, M. & Huisman, T. H. *Haemoglobin* **1**, 27-44 (1976).
25. Benesch, R. E., Kwong, S., Edalji, R. & Benesch, R. *J. biol. Chem.* **254**, 8169-8172 (1979).
26. Benesch, R. E., Edalji, R., Benesch, R. & Kwong, S. *Proc. natn. Acad. Sci. U.S.A.* **77**, 5130-5134 (1980).
27. Ross, P. D., Briehl, R. W. & Minton, A. P. *Biopolymers* **17**, 2285-2288 (1978).
28. Macleod, R. M. & Hill, R. J. *J. biol. Chem.* **248**, 100-103 (1973).
29. Benesch, R., Macduff, G., & Benesch, R. E. *Anal. Biochem.* **11**, 81-87 (1965).
30. Benesch, R. E., Benesch, R. & Yung, S. *Analyt. Biochem.* **55**, 245-248 (1973).

LETTERS TO NATURE

Discovery of a very red nucleus in the radio elliptical IC5063 (PKS2048-57)

D. J. Axon*, Jeremy Bailey† & J. H. Hough‡

* Department of Physics and Astronomy, University College London, Gower Street, London WC1E 6BT, UK

† Anglo-Australian Observatory, PO Box 296, Epping, New South Wales, Australia

‡ School of Natural Sciences, Hatfield Polytechnic, Hatfield, Hertfordshire AL10 9AB, UK

We report here the discovery of an extremely red IR source in the nucleus of the elliptical galaxy IC5063 (PKS2048-57). The observed (2.2-3.8) μ m colour index within a 5 arc s aperture is 2.1 mag while the colours at shorter wavelengths and in the 5-10 arc s annulus around the nucleus are close to those of normal elliptical galaxies. The IR excess could arise from a BL LAC type nucleus with a steep non-thermal spectrum ($\alpha \sim -4.5$ defined by $F \propto \nu^\alpha$), similar to the recently identified 'red QSOs' typified by 1413+135 (refs 1, 2).

Low luminosity BL Lac objects are predominantly associated with the nuclei of elliptical galaxies which possess flat radio spectra for example, Mkn 421 (refs 3, 4). Many of the nearby E/S0 galaxies have similar radio properties, suggesting that they may also contain nuclei of this type^{5,6}. There are, however, good observational reasons for suspecting that most of this population would not have been recognized as BL Lac objects. The presence of a nuclear source embedded in a bright elliptical galaxy could be almost completely hidden in the visible and near IR by the stellar component. This would arise either

because it was of low luminosity like Mkn 421 or if it had a steep non-thermal spectrum similar to 1413+135, even if the spectrum only steepened at much shorter wavelengths. As most interest has centred on the stellar populations of elliptical galaxies there has been little attention directed at wavelengths longer than 2.2 μ m where radiation from the nuclei is expected to dominate.

NGC1052 is probably the best known example of a radio elliptical which could fit into this category with its large 10- μ m excess⁷ and its recently observed near IR polarization⁸. Other galaxies whose excess 10- μ m fluxes⁹ may qualify them as objects of this type are M87, NGC3894 and NGC4552.

The existence of 'BL Lac' nuclei in the class of active gas-rich ellipticals would be particularly important. These ellipticals are characterized at one extreme by the galaxies NGC1052 and PKS0349-27, which show shock excited line spectra^{10,11} and IC5063, PKS2158-380 at the other, whose optical spectrum is more likely to be due to photoionization by a non-thermal nuclear source^{12,13}. A detailed knowledge of the shape of the non-thermal spectrum of the nuclei of these galaxies would be a vital step in understanding both the physical processes at work in them, and their relationship to the origin of radio galaxies.

Observations of IC5063 and the three other active ellipticals mentioned above (NGC1052, PKS2158-380 and PKS0349-27) were obtained on 16 December 1981 using the IR photometer on the 3.9-m Anglo-Australian telescope. Photometry at J (1.20 μ m), H (1.64 μ m), K (2.2 μ m) and L (3.8 μ m) was obtained through 5 and 10 arc s circular apertures. In all cases the galaxies were centred in the beam by maximizing the 1.2 μ m signal. A chopper throw of 12 arc s in a north-south direction was used.

The results of the photometry are given in Table 1, together

Table 1 Observed K magnitudes and IR colours of the four active ellipticals

IC5063	K	$J-H$	$H-K$	$K-L'$
5 arcs	11.32 ± 0.03	0.92 ± 0.04	0.48 ± 0.04	2.15 ± 0.05
10	10.58 ± 0.03	0.85 ± 0.04	0.40 ± 0.04	1.66 ± 0.08
5-10	11.34 ± 0.04	0.80 ± 0.06	0.31 ± 0.06	0.72 ± 0.09
NGC1052				
5 arcs	10.12 ± 0.03	0.77 ± 0.04	0.35 ± 0.04	0.70 ± 0.04
10	9.30 ± 0.03	0.78 ± 0.04	0.32 ± 0.04	0.57 ± 0.08
5-10	9.98 ± 0.04	0.79 ± 0.06	0.29 ± 0.06	0.23 ± 0.09
PKS2158-380				
5 arcs	12.33 ± 0.03	0.76 ± 0.04	0.39 ± 0.04	$\leq 0.8 (2\sigma)$
10	11.71 ± 0.03	0.73 ± 0.04	0.36 ± 0.04	$\leq 0.7 (2\sigma)$
5-10	12.61 ± 0.04	0.70 ± 0.06	0.32 ± 0.06	
PKS0349-27				
5 arcs	14.14 ± 0.03	0.76 ± 0.07	0.46 ± 0.04	
10	13.30 ± 0.03	0.73 ± 0.04	0.52 ± 0.04	
5-10	13.97 ± 0.04	0.71 ± 0.08	0.49 ± 0.06	
Normal elliptical		0.75	0.22	~ 0.3

with the calculated magnitudes and colours within the 5-10 arc s annulus surrounding the nucleus. The colours (on the AAO-Johnson system¹⁴) of normal elliptical galaxies¹⁵ are given for comparison.

Clearly the colours of PKS2158-380 and PKS0349-27 are very similar to those of normal elliptical galaxies, whereas the results on NGC1052 show the excess IR radiation in the nucleus which has been reported previously⁷.

However, IC5063 shows a very much larger ($K-L'$) colour of 2.1 mag within the 5 arc s aperture, while its ($J-H$) and ($H-K$) colours are close to those of normal ellipticals. This indicates the presence of a very red source which begins to dominate the light of the galaxy only at wavelengths longer than $3 \mu\text{m}$. Furthermore, the colours measured for the 5-10 arc s annulus do not show the large excess, implying that it predominantly originates within the 5 arc s aperture. The ($K-L'$) colour of the annulus is slightly larger than those of normal ellipticals, but a combination of aperture misplacement and seeing could cause a slight spillage of light from the nucleus outside our 5 arc s aperture, so we regard these data as being consistent with a compact source for the IR excess.

We have used two methods to attempt to separate the colours of the IR source from the stellar component of IC5063. First, because the IR colour gradients in normal elliptical galaxies are small¹⁵, we can assume that the ratio of the flux from the stellar component in the 5 arc s aperture and the 5-10 arc s annulus is the same at all colours. Assuming the contribution of the nucleus is negligible at J , we can then estimate the stellar contribution within the 5 arc s aperture for each colour (see Table 2).

The second method is shown in Fig. 1, which is a plot of the observed colours in the form of a flux ratio diagram^{4,16}. On this diagram the observed colours must lie on a straight line joining the colours of the component sources. The colour of the nucleus must therefore be on the line through the 5 and 10 arc s points. A further assumption about the nature of the sources spectrum is needed to define its colours uniquely. The two natural choices for the nuclear spectrum are, non-thermal radiation represented by a power law $F_\nu \propto \nu^\alpha$, and re-radiation by hot dust in the form of a black-body spectrum; although a range of dust temperatures can mimic a power law. For a true power law spectrum the intersection of the line with the locus of possible power law spectral indices, α , indicates a value for α of ~ -4.5 , whereas in the case of a black body, by a similar procedure we find that its colour temperature is $\sim 650 \text{ K}$. If the IR excess is non-thermal in origin this analysis shows that the nuclear source has an extremely steep spectrum, similar to those observed in NGC1052 and the red QSOs. The spectrum of NGC1052 is much shallower, $\alpha = 1.7$ longward of $3 \mu\text{m}$, but must steepen to at least $\alpha = -2.7$ below $2.2 \mu\text{m}$ to account for its weakness in the optical⁸. The spectra of the red QSOs also start shallower

than observed in IC5063 but again steepen rapidly to $\alpha \sim -3$ below $5 \mu\text{m}$ (ref. 17). Observation of these objects^{1,2,18} and brighter flat spectrum sources¹⁹ have shown that they possess many of the characteristics of BL Lac objects. The detection of appreciable linear polarization in 1413+135 (ref. 1) strongly supports their identification as steep spectrum BL Lac objects and the rapid steepening of their spectra has been convincingly explained as a sudden high energy cutoff in the distribution of synchrotron emitting electrons^{1,2}. If the luminosity range of the red QSOs approaches that of normal BL Lac objects then we might expect to find low luminosity counterparts to Mkn 421 in nearby elliptical galaxies. The nuclear IR source in IC5063 may well be just such an object.

The alternative possibility of emission from hot dust arises because the Wein tail of a black body curve can readily mimic a steep spectral index source. This explanation has proved very attractive for the IR continua of Seyfert galaxies as it avoids the physical problems associated with producing the observed spectral changes with non-thermal spectra^{20,21}. Inspection of the SRC Southern Sky Survey shows there is dust in IC5063 which could be heated by the intense UV source invoked as the origin of the photoionization of the gas. However, the high excitation of the gas at large distances from the nucleus argues that the UV source cannot be obscured as heavily as a typical Seyfert nucleus. With the limited range of our data we cannot rule out either option directly although we find the need for an alternative mechanism is capable of producing steep spectrum sources far less compelling since the discovery of the red QSOs. Observations of variations in the near IR with time scales of the order of a day would indicate the presence of a non-thermal source. Another test to distinguish between the

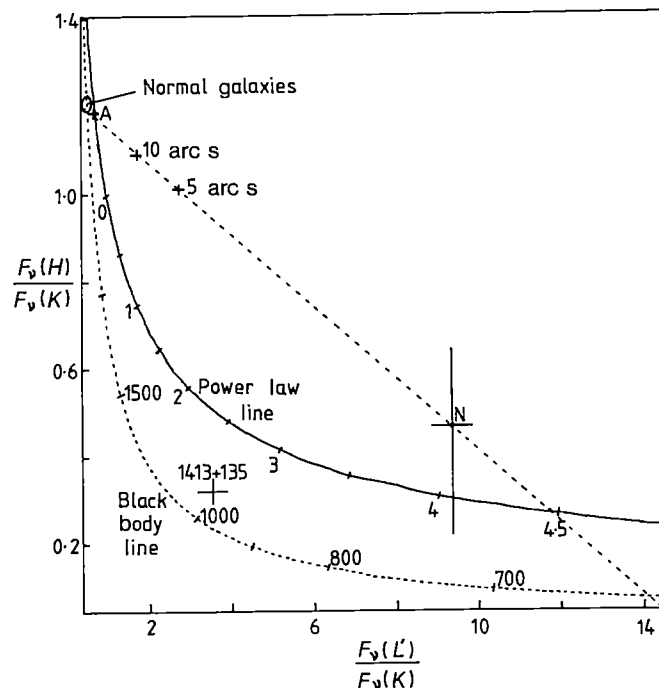


Fig. 1 Flux ratio diagram plotting the ratio of flux at H ($1.64 \mu\text{m}$) to K ($2.19 \mu\text{m}$) against ratio of fluxes at L' ($3.8 \mu\text{m}$) to K ($2.19 \mu\text{m}$). On this diagram, the point representing a composite object must lie on the straight line joining the colours of the two component sources. We have plotted the observed points for IC5063 in 5 and 10 arc s apertures and in the 5-10 arc s annulus (marked A). These points represent varying contributions from the elliptical galaxy and the central IR source. The line through these points passes through the region of the normal elliptical galaxies when extrapolated to the left. The colours of the nucleus must lie on the same line extrapolated to the right. Thus if the source is a power law it must have $\alpha \sim -4.5$. If it is a black body it must have $T \sim 650 \text{ K}$. The colours deduced for the nucleus given in Table 2 are also marked (N). The approximate position of the very red QSO 1413+135 is marked. This source lies below the power law line as its spectrum is becoming less steep by $3.5 \mu\text{m}$.

Table 2 IR colours of the stellar and nuclear components of IC5063

	5–10 arcs annulus	5 arcs aperture	Mag. of galaxy inside 5 arcs (assumed)	Mag of central IR source
<i>J</i>	12.45	12.72	12.72	—
<i>H</i>	11.65	11.80	11.92	14.3
<i>K</i>	11.34	11.32	11.61	12.89
<i>L'</i>	10.62	9.17	10.89	9.41

two alternatives in IC5063 would be IR polarimetry. The presence of significant linear polarization in the IR would firmly establish the non-thermal origin of the continuum. It is also important to determine the shape of the spectrum at longer wavelengths to search for either evidence of re-radiation by warm dust or the flattening which characterizes the continuum of BL Lac objects. If the IR source is non-thermal in origin then its spectrum must flatten dramatically towards the UV if it is to be responsible for photoionizing the gas. We should also stress that our observations do not preclude the existence of bright non-thermal nuclei in PKS2158–380 and PKS0349–27 provided their spectra steepen at longer wavelengths than in IC5063.

Similar observations for a complete sample of radio ellipticals would establish the frequency of this type of nucleus.

We thank Bob Fosbury and Bill Sparks for stimulating our interest in this class of galaxy, and David Aitken for valuable discussions about the IR spectra of active galaxies, also the technical staff of the Anglo-Australian observatory for support and SERC for funding these observations. J.B. is the recipient of an SERC fellowship.

Received 5 May; accepted 14 July 1982.

1. Bregman, J. N. *et al.* *Nature* **293**, 714–717 (1981).
2. Beichman, C. A. *et al.* *Nature* **293**, 711–713 (1981).
3. Ulrich, M. H. *et al.* *Astrophys. J.* **198**, 261–266 (1975).
4. Bailey, J. *et al.* *Mon. Not. R. astr. Soc.* **197**, 627–632 (1981).
5. Disney, M. J. & Wall, J. V. *Mon. Not. R. astr. Soc.* **179**, 235–254 (1977).
6. Condon, J. J. & Dressel, L. L. *Astrophys. J.* **221**, 456–469 (1978).
7. Rieke, G. H. & Low, F. J. *Astrophys. J. Lett.* **176**, L95–100 (1972).
8. Rieke, G. H. *et al.* *Astrophys. J. Lett.* **252**, L53–L56 (1982).
9. Puschell, J. J. *Astrophys. J.* **247**, 48–51 (1981).
10. Fosbury, R. A. E. *et al.* *Mon. Not. R. astr. Soc.* **183**, 549–568 (1978).
11. Fosbury, R. A. E. *ESO Messenger* **21**, 11–13 (1980).
12. Danziger, I. J. *et al.* *Mon. Not. R. astr. Soc.* **196**, 845–856 (1981).
13. Caldwell, N. & Phillips, M. M. *Astrophys. J.* **244**, 447–457 (1981).
14. Jones, T. J. & Hyland, A. R. *Mon. Not. R. astr. Soc.* **192**, 359–364 (1980).
15. Frogel, J. A. *et al.* *Astrophys. J.* **220**, 75–97 (1978).
16. Wade, R. A. thesis, California Institute of Technology (1980).
17. Reike, G. H. *et al.* *Astrophys. J. Lett.* **232**, L157–L154 (1979).
18. Beichman, C. A. *et al.* *Astrophys. J.* **247**, 780–786 (1981).
19. Impey, C. D. & Brand, P. W. J. L. *Nature* **292**, 814–816 (1981).
20. Reike, G. H. & Lebofsky, M. J. *Nature* **284**, 410–412 (1980).
21. Cutri, R. M. *et al.* *Astrophys. J.* **245**, 818–828 (1981).

The source of Saturn electrostatic discharges

D. R. Evans*, J. H. Romig*, C. W. Hord†, K. E. Simmons†, J. W. Warwick* & A. L. Lane‡

* Radiophysics Inc., 5475 Western Avenue, Boulder, Colorado 80301, USA

† Laboratory for Atmospheric and Space Physics, University of Colorado, Boulder, Colorado 80309, USA

‡ Jet Propulsion Laboratory, California Institute of Technology, Pasadena, California 91109, USA

During both Voyager encounters with the saturnian system, the Planetary Radio Astronomy (PRA) experiment detected strong discrete episodic bursts of radio emission, termed Saturn electrostatic discharges (SED)^{1–3}. An examination of Voyager 2 photopolarimeter (PPS) data now reveals a narrow feature (possibly a gap) in Saturn's B ring. A single, unique object appears to be responsible for both the SED and this feature.

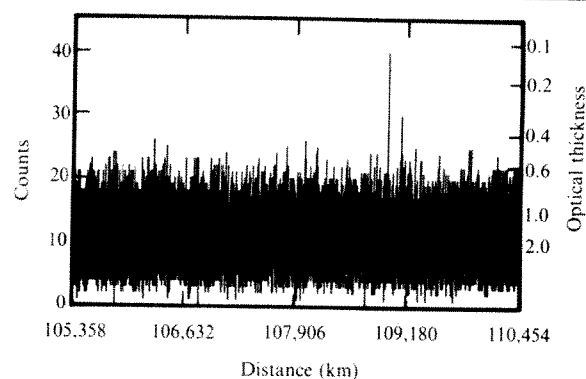


Fig. 1 Optical thickness of 5,000 km of the outer B ring at 2,650 Å (300 Å bandwidth), as determined by the Voyager 2 photopolarimeter during the Delta Scorpii occultation. The optical thickness is calculated from the number of counts received at the instrument in a given 10-ms sample time.

The episodic nature of SED was well defined at both Voyager 1 and Voyager 2 encounters, the mean period being 10 h 10 ± 5 min and 10 h 11 ± 5 min, respectively, after spacecraft motion was taken into account. The simplest, but by no means only, explanation of this episodic behaviour is that the SED source is an object in a circular, equatorial orbit 107,990–109,200 km from the centre of Saturn. For this hypothetical object to be the source of SED, it must be distinct from its environment by virtue of physical, chemical and/or electrical properties. Such an object should have an effect on surrounding ring material. Indeed, both the Voyager 2 high-resolution (100 m) photopolarimeter and the lower-resolution (~5 km) imaging aboard both spacecraft show remarkable features in this region of the rings.

The PPS occultation data, which are taken at a wavelength of 2,650 Å, show a relatively opaque region from 105,000 to 110,000 km within the B ring (Fig. 1). This region has a mean optical depth in excess of 1.8; however, embedded within this part of the B ring there is a single feature ~150 m wide in which the apparent optical thickness is much less than this value (Fig. 2). This feature is located at $108,942 \pm 6$ km [based on a best fit to experimental values of the Saturn pole position by J. Holberg (personal communication)]. The apparent optical depth in the middle of the feature is 0.15. Like all experimental measurements, this number has an associated error; we calculate that the true optical depth at this point is less than 0.50, with 99.5% certainty. In fact, due to the finite instrument response time and thickness of the ring at this point, these numbers are very much upper limits; the data are certainly not inconsistent with a narrow region of much lower optical depth. To ascertain the reality of this feature, as opposed to the possibility of a statistical fluctuation occurring in the PPS instrument, we have plotted the frequency distribution of the PPS counting rate for 48,000 points in the vicinity of the feature (Fig. 3). The number of counts recorded by the PPS instrument in a given 10-ms sample is proportional to the number of photons received at the instrument in that time. The recorded number of counts is thus related to optical thickness in a logarithmic manner.

The frequency distribution displayed in Fig. 3 has a mean of 11.745 counts and a standard deviation of 3.2935 counts. For comparison, Fig. 3 also shows a gaussian curve with these parameters. Generally, the two curves agree closely, except in the wings. Using this gaussian as a model, we can at least estimate the probability that the feature is produced by statistical fluctuation, within an order of magnitude or so. The feature comprises two adjacent points, with readings of 40 and 25 counts. The combined probability of obtaining two such adjacent points is of the order of 10^{-22} . We have nearly 48,000 possible adjacent pairs, so the probability of obtaining the

observed result by chance somewhere in the data is about 10^{-17} ; even allowing for the lack of accuracy in the model gaussian, this result clearly shows that the feature is almost certainly not statistical in origin. In addition, we have examined over 100,000 independent data points taken by the PPS instrument in its occultation mode at other times, and we find no trace of a similar event anywhere in this enormous data set.

A second peak, of 30 counts, is also visible in Fig. 1. Applying similar statistics, we obtain a probability of 5×10^{-4} of chance occurrence. However, in this instance, only a single data point is significantly different from background values, and, as we have already noted, the gaussian model does not fit the data exactly in the wings, so we feel that this second feature may well be statistical in origin.

The PPS occultation data therefore indicate that at a radial distance of $\sim 108,942$ km there is a region of lowered optical thickness some 150 m wide. As our best estimate of the optical thickness in the middle of the feature is 0.15, we believe that it is reasonable to describe the feature by the term 'gap'.

The radial distance of $108,942 \pm 6$ km corresponds to an orbital period of $10 \text{ h } 9 \text{ min } 4 \text{ s} \pm 3 \text{ s}$ (J. Anderson, personal communication), after planetary oblateness is taken into account. This level of accuracy of period determination permits us to combine unambiguously the Voyager 1 and Voyager 2 SED databases, thus providing an effective baseline of some 290 days from which to estimate the period of the SED source. The PRA data alone provide us with a 'comb' of possible periods with 'tooth' separation of ~ 54 s. If we assume that the SED source may be uniquely identified with the PPS gap, the PPS data should permit us to identify a particular tooth which is consistent with both experimental results. We have indeed found that the data identify a tooth with a period of $10 \text{ h } 9 \text{ min } 12 \text{ s} \pm 6 \text{ s}$, which is consistent with the orbital period above. It is reassuring that the two different sets of data are consistent with a single period, although this fact cannot be described as statistically significant, as the chance probability of this being possible is quite high— $12/54$, or $\sim 22\%$. Bearing in mind our previous argument concerning the uniqueness of the SED source, we believe that it is highly likely that there is a single cause of both SED and the PPS occultation gap observation.

In addition to the PPS data, Voyager images of this region show two intense azimuthal bands which appear bright in forward scattered light, indicating that they comprise a local enhancement of the micrometre-sized dust population, which is ubiquitous throughout the outer two-thirds of the B ring. These bands are each roughly 300 km wide and are $\sim 2,000$ km apart. Although it is true that unusual features are to be seen on Voyager images throughout this region, these two bands are

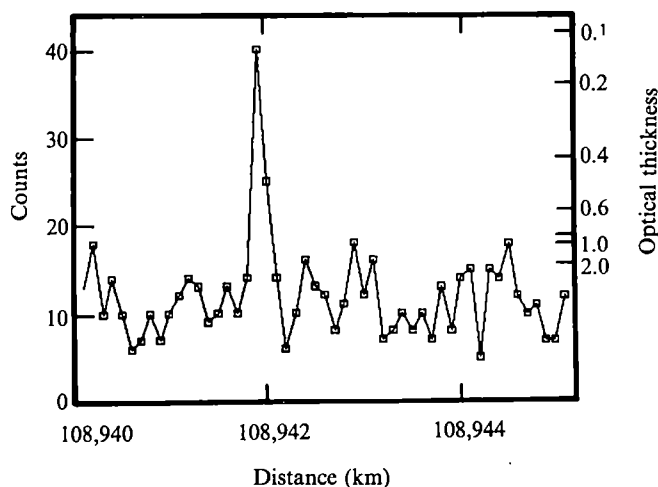


Fig. 2 Detailed structure of the B ring near the large spike in Fig. 1; this structure indicates a narrow (~ 150 m) gap of low optical thickness.

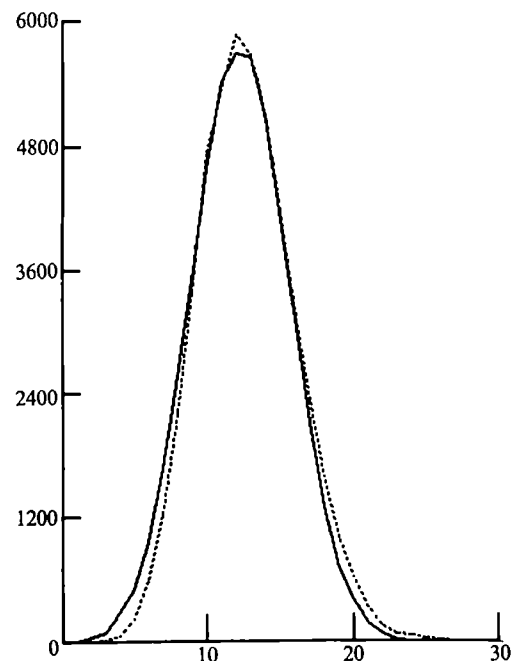


Fig. 3 Occurrence frequency versus counts for 48,000 data points obtained in the region shown in Fig. 1. Experimental data are shown dotted. The solid line is a gaussian with mean 11.745, s.d. 3.2935.

the most prominent features in wide-angle images of this part of the ring system. Furthermore, enhanced colour images of the ring system indicate a change in particle population characteristics at or near the region in question. This change, and indeed the very existence of micrometre-sized dust in the outer B ring, may be a direct result of the presence of the object and/or the associated SED.

Voyager 2 also carried a UV spectrometer which was boresighted with the PPS instrument and simultaneously observed Delta Scorpii in the range $900\text{--}1,700$ Å. This spectrometer failed to detect any reduction in optical depth at the PPS gap location (with 99.9% confidence) (J. Holberg, personal communication). It is possible that the 'gap' is in fact populated with small Rayleigh scatterers (of the order of ≤ 100 Å in diameter; several theories indicate that there may be substantial numbers of such scatterers in the rings—see, for example, ref. 4). Whether or not this is the true reason for the UV spectrometer null result, the observation that the optically dense outer B ring seems capable of sustaining a very narrow gap (at least to $2,650$ Å radiation) is important in developing a theoretical understanding of the ring.

Thus, Voyager PRA and PPS data indicate the presence of a single, unique object in the B ring at a distance of $\sim 108,942$ km from the centre of Saturn. This object exerts an influence on material adjacent to its orbit, resulting in the formation of a 150-m gap along that orbit. In addition, Voyager imaging data suggest that the object may influence micrometre-sized dust hundreds of kilometres away. The interaction between this object and its environment seems to be the source of SED.

Received 19 April; accepted 19 July 1982.

1. Warwick, J. W. *et al.* *Science* **212**, 239–243 (1981).
2. Evans, D. R., Warwick, J. W., Pearce, J. B., Carr, T. D. & Schauble, J. J. *Nature* **292**, 716–718 (1981).
3. Warwick, J. W. *et al.* *NASA tech. Mem.* 83856 (1981).
4. Northrop, T. G. & Hill, J. R. *J. geophys. Res.* (submitted).

STARE observations of long discrete echoes

E. Nielsen*, G. Sofko† & W. I. Axford*

*Max-Planck-Institut für Aeronomie, D-3411 Katlenburg-Lindau 3, FRG

†University of Saskatchewan, Saskatoon, Saskatchewan, Canada S7N 0W0

Early studies of auroral radar echoes by Unwin^{1,2} showed the existence of a particular class of 'long discrete' echoes, distinguished as being weak and relatively long-lasting (1–60 min). The backscatter usually consists of several narrow (~20 km) bands which drift slowly in latitude, and the height of the backscattering region appears not to exceed 100 km. Here, we report on observations of this type of radar aurora made during the past few years with the Scandinavian Twin Auroral Radar Experiment (STARE). Whereas Unwin's observations covered the range of geomagnetic latitudes corresponding to I -values ~3–5, the present study is concerned with higher latitudes, corresponding to the range $I \sim 5.7$ –8.

The STARE system³ provides measurements of the backscatter intensity and irregularity drift velocity over a large area (~200,000 km²) with good spatial resolution (20 × 20 km²) and a temporal resolution of ~20 s. The twin radar system permits Doppler velocities of E-region ionospheric irregularities to be measured stereoscopically. Aliasing around the time base is avoided by the use of a low pulse repetition frequency (0.05 Hz). Measurements from a given volume of space are combined to yield the irregularity drift velocity vector, assuming that the Doppler velocity measured in a given direction equals the component of the irregularity velocity in that direction. The operating frequencies of the two radars are ~140 MHz, so that they are sensitive to irregularities with wavelengths of the order of 1 m. The system has an automatic gain control which is adjusted to the strongest backscatter detected; thus regions of relatively weak scatter cannot be detected in the presence elsewhere of regions of strong signal-to-noise ratio, which, of course, can effect the apparent probability of occurrence of the former.

The characteristics of the long discrete auroral radar echoes, as observed by STARE, are as follows: (1) On a range-time-intensity plot (Fig. 1a) the echoes appear as a series of striations

which may persist for an hour or more (time interval II in Fig. 1a). (2) The striations are rather straight and are narrow in range (~20–100 km) in contrast with the spread, diffuse appearance of the more intense backscatter associated with strong auroral activity (time interval I in Fig. 1a). (3) The backscatter intensities are weak, with a typical signal-to-noise ratio of only a few decibels. (4) The speed of the irregularities as obtained from Doppler measurements (0–400 m s⁻¹) and the speeds of the apparent motions in range of the backscattering regions (100–300 m s⁻¹) are much smaller than the speeds usually associated with radar aurora (~300–3,000 m s⁻¹). (5) The echoes commonly occur following periods of intense radar auroral activity associated with magnetic disturbances, as indicated in the Fig. 1. (6) The echoes appear to be most prevalent in the early morning and late afternoon hours and in winter rather than summer.

The clear distinction between the properties of intense radar aurora occurring during disturbed periods and the long discrete echoes is evident in Fig. 1b, c where the distributions of the signal-to-noise ratio (SNR) and Doppler-determined velocity (speed and direction) are shown for the intervals I and II. It is evident from Fig. 1b that the backscatter intensity of discrete echoes (average SNR ~5 dB) is in general much less than that from ordinary radar aurora (average SNR ~18 dB). As emphasized above, discrete echoes might also be present in interval I but they would be masked in the presence of the more intense and diffuse radar aurora associated with very active periods and as a result of the automatic gain control of the STARE receivers.

There is a very clear difference in the speed distributions between intervals I and II, shown in Fig. 1c. During the strongly disturbed period, which includes interval I, the observed speed distribution shows an almost complete cut-off at speeds below 300 m s⁻¹, whereas in the period dominated by discrete echoes the average speed is only 150 m s⁻¹ and hardly ever exceeds 300 m s⁻¹. It is interesting that during interval II in Fig. 1 the speed of the polewards motions of the backscatter striations is comparable with but not exactly the same as those obtained from the simultaneous Doppler measurements. The angular distribution of the Doppler velocities measured during the two intervals is shown in Fig. 1c; in interval I the directions lie in the sector 0–90° east of north with a maximum at ~75°; in contrast, the angular distribution during interval II is much broader, being predominantly northwards but with deviations of 70° and more, both east and west of north.

The diurnal and seasonal distributions of the occurrence of discrete echoes observed during 5 yr between 1977 and 1981 are shown in Fig. 2. It is clearly evident that this type of radar

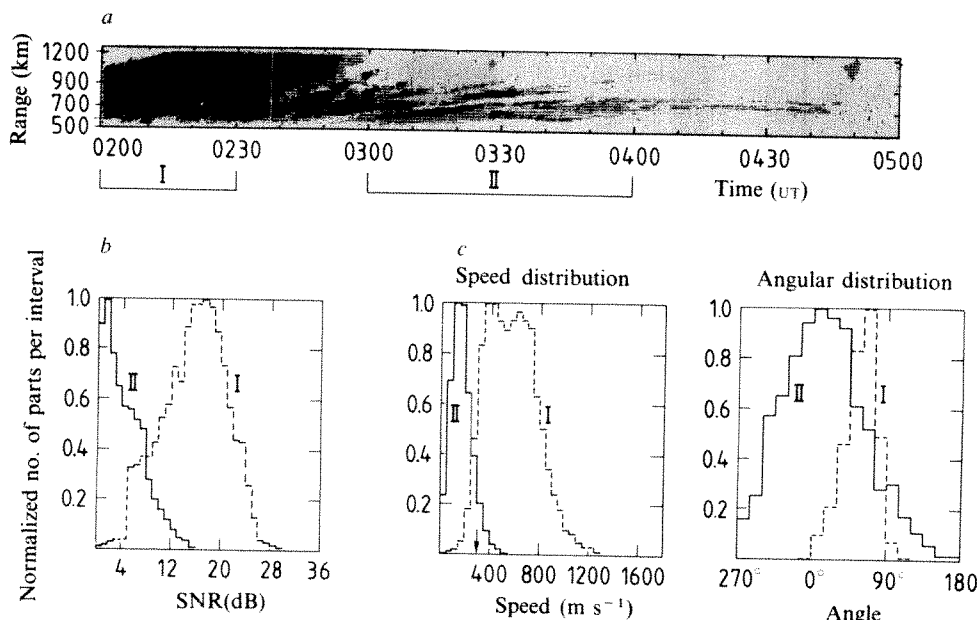


Fig. 1 a, A range-time-intensity plot showing ordinary radar aurora and long discrete echoes detected by a single narrow antenna beam pointing 24.5° E of geographic north (beam B). The signal in time interval I is representative of the radar aurora associated with auroral electrojet activity. The striated appearance of the record in interval II indicates the presence of long discrete echoes. b, Statistical distributions of the signal-to-noise ratios measured during intervals I and II. The long discrete echoes are significantly weaker than the ordinary radar aurora. c, Distributions of the irregularity drift speeds and directions in intervals I and II. The long discrete echoes have drift speeds which are less than the threshold of the two-stream instability (arrow).

aurora is almost entirely confined to periods of EUV 'darkness' at E-region altitudes and is predominantly an early morning phenomenon. Note, however, that the presence of intense backscatter would tend to mask the presence of any discrete echoes during the period 2000–0200 h and hence there is a possible bias in the diurnal distribution.

The most remarkable feature of the discrete echoes is the speed distribution. It is usually assumed, on the basis of linear instability theories of plasma processes occurring in the auroral ionosphere, that the Doppler velocities determined by STARE measurements are essentially the same as the electron drift velocities and hence provide a measurement of the E-region electric field^{4–6}. The two-stream instability⁷ is the most likely candidate for producing the density irregularities observed to occur in regions of strong auroral zone electric currents such as observed during interval I, for example. However, this instability has a threshold such that the electron drift speed relative to the ions must exceed the ion sound speed, which is typically 300 m s^{-1} (equivalent to $\sim 15 \text{ mV m}^{-1}$). The speed distribution observed during the period of occurrence of discrete echoes shown in Fig. 1c, is clear evidence that the electron density irregularities cannot be due to the two-stream instability. Because we do not know the nature of the electron density irregularities we cannot assert that the measured apparent speeds represent electron drift speeds and hence they may not necessarily constitute a measurement of the ionospheric electric field strength.

It is possible that the electron density irregularities associated with striated radar aurora are due to an instability other than the two-stream instability, for example the gradient-drift instability⁸. However, to produce this instability with an eastwards directed electric field a strong eastwards directed electron density gradient is required. This is difficult to accept in view of the fact that the striations are evidently narrow in north-south extent and persist for upwards of an hour. The length scales involved ($\sim 20 \text{ km}$) do not in any case suggest that the electron density gradient is large.

It is difficult to argue that the electron density irregularities which produce the discrete echoes observed by STARE are associated with magnetospheric effects. A mapping to ionospheric levels of small-scale magnetospheric motions (or, equivalently, electric fields) must be ruled out as a possible cause of the irregularities because for such small-scale lengths perpendicular to the magnetic field, as required in this case, the mapping is quite ineffective⁹. It is also unlikely that the source of the ionization produces electron density irregularities of the required scale directly, as the gyroradii of electrons with energies of the order of 10 keV (necessary to penetrate to altitudes of $\sim 100 \text{ km}$) are $\sim 10 \text{ m}$, which is much larger than the irregularity scale size required. It is also conceivable, however, that a combination of a strongly inhomogeneous source distribution and the gradient drift instability, together with some cascading in irregularity scale could be effective¹⁰.

If the discrete echoes are associated with enhanced electron precipitation it is conceivable that the irregularities are due to unstable electron velocity distributions resulting from a relatively high density of secondaries. If the secondary electron distribution function is indeed unstable, such irregularities should be present in all regions of intense electron precipitation, especially around arcs; in general an anticorrelation of backscattering and precipitation regions is observed (G. Keys and M. Scourfield, personal communication), although this could be affected by the automatic gain control in the STARE system. Such an explanation would be consistent with the slow, polewards drift observed in the early morning post-substorm aurora¹¹; however it is not obvious that field-aligned irregularities can be produced at relatively low altitudes by this means.

In view of the fact that both the magnetospheric and ionospheric explanations for the origin of the irregularities producing the discrete echoes are not completely satisfactory, it is interesting to consider whether or not an atmospheric origin is a

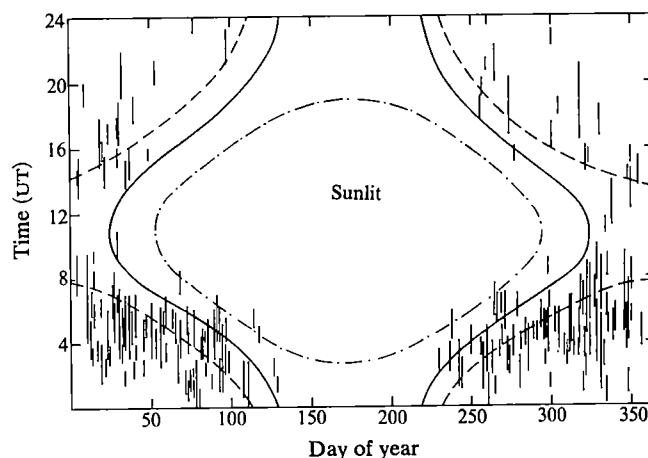


Fig. 2 The diurnal and seasonal occurrence of long discrete echoes. Contours of constant solar elevation ($0^\circ \pm 10^\circ$) in the middle of the STARE field of view are shown and indicate that the discrete echoes are not present, within the limits of the system sensitivity, for solar elevation angles $\geq 10^\circ$. ---, -10° ; —, 0° ; ····, 10° .

possibility. In this case, the echoes would be similar to those observed by mesosphere-stratosphere-troposphere radars such as the SOUSY system¹². The electron density irregularities are then most likely to be the result of an interaction between turbulent motions of the neutral gas and steep electron density gradients, although other processes such as density fluctuations associated with the turbulence itself, which produce corresponding fluctuations in the electron density (by entrainment or as a result of the ionizing processes), are also possibilities^{13–15}. In this case however, the backscatter must occur at much lower altitudes than usually assumed to be the case for radar aurora, as the STARE scattering scale length of $\sim 1 \text{ m}$ is equal to the mean free path in the neutral atmosphere at an altitude of $\sim 112 \text{ km}$. To produce a reasonable level of fluctuations in the neutral density the mean free path should be $\ll 1 \text{ m}$, which suggests that the scatter should originate at altitudes $\leq 100 \text{ km}$, and even then the length scale would lie in the viscous subrange of the atmospheric turbulence. This explanation has certain attractive features, notably that it does not require a velocity threshold and, indeed, the observed speeds are comparable with the speeds of atmospheric motions. To test this hypothesis it will be necessary to determine more accurately the height of the region from which the echoes come, which, according to Unwin^{1,2}, is "100 km or less".

The disappearance of E-region irregularities after sunrise could be explained as a consequence of an enhanced recombination rate. It can be shown that the decay time of an irregularity is $1/2\alpha\bar{n}$, where α is the (dissociative) recombination coefficient and \bar{n} the mean electron density. As \bar{n} may increase by a factor of 10 or more after sunrise, it is clear that the effects of any source of electron density fluctuations must be strongly suppressed in such circumstances. However, if the irregularities occur at much lower (D-region) altitudes, this argument is not necessarily correct, because photodissociation of negative ions may have an important role during sunrise. In this case the disappearance of the echoes would be more easily accounted for on the basis of a complete change in the electron density profile as well as a possibly enhanced loss rate.

To make further progress in understanding the phenomenon of discrete radar echoes in the auroral zone, further observations are required. For example, it will be necessary to determine whether or not striations as shown in Fig. 1 correspond to regions of enhanced optical emission and enhanced ionospheric plasma density. The latter can be determined using the EISCAT system, now being brought into operation, and this will also allow us to determine whether or not the Doppler velocities measured by STARE are related to electric field drifts. More extensive latitude coverage will also be required,

for example, to determine the relationship of the discrete echoes to phenomena occurring near the auroral electrojet. This is now possible using STARE together with the new SABRE system, which is similar to STARE but operates in a lower latitude range ($4.2 \leq l \leq 5.6$).

Finally, direct measurements of the altitude of the echo-producing irregularities should be possible by using the partial reflection system existing at the EISCAT site and other backscatter radars which are available, including the EISCAT VHF system.

Received 10 May; accepted 5 July 1982.

1. Unwin, R. S. *Ann. Geophys.* **15**, 377–394 (1959).
2. Unwin, R. S. *J. atmos. terr. Phys.* **28**, 1183–1194 (1966).
3. Greenwald, R. A., Weiss, W., Nielsen, E. & Thomson, N. R. *Radio Sci.* **13**, 1021–1039 (1978).
4. Baumjohann, W., Untiedt, J. & Greenwald, R. A. *J. geophys. Res.* **85**, 1963–1977 (1980).
5. Cahill, Jr., L. J., Greenwald, R. A. & Nielsen, E. *Geophys. Res. Lett.* **5**, 687–690 (1978).
6. Nielsen, E. & Whitehead, J. D. *Proc. COSPAR Meet.*, Ottawa, (in press).
7. Sudan, R. N., Akinrimisi, J. & Farley, D. T. *J. geophys. Res.* **78**, 240–248 (1973).
8. Rogister, A. & D'Angelo, N. *J. geophys. Res.* **76**, 7754–7760 (1971).
9. Farley, D. T. *J. geophys. Res.* **65**, 869–877 (1960).
10. Sofko, G. J., Greenwald, R. A., Nielsen, E. & André, D. *EOS* **60**, 357 (1979).
11. Meng, C. I. *J. geophys. Res.* **86**, 2149–2174 (1981).
12. Rettger, J., Klostermeyer, J., Czechowsky, P., Ruster, R. & Schmidt, G. *Naturwissenschaften* **65**, 285–296 (1978).
13. Booker, H. S. *J. atmos. terr. Phys.* **8**, 204–211 (1956).
14. Booker, H. S. *J. geophys. Res.* **61**, 673–705 (1956).
15. Dungey, J. W. *Cosmic Electrodynamics*, 167 (Cambridge University Press, 1958).

Constancy of oceanic deposition of ^{10}Be as recorded in manganese crusts

T. L. Ku & M. Kusakabe

Department of Geological Sciences, University of Southern California, Los Angeles, California 90089-0741, USA

D. E. Nelson, J. R. Southon, R. G. Korteling, J. Vogel & I. Nowikow

Archaeology and Chemistry Departments, Simon Fraser University, Burnaby, British Columbia, Canada V5A 1S6

Recent developments in the use of nuclear accelerators as high-energy mass spectrometers^{1,2} has renewed interest in the study of cosmogenic ^{10}Be (half life 1.5 Myr) as a geophysical time tracer. The accelerator techniques enable us to measure ^{10}Be with a sensitivity of 10^7 atoms or less. The potential age dating span with ^{10}Be is extended back to at least 15 Myr BP, providing that the ^{10}Be production and deposition rates remain constant or nearly constant over that time period. A knowledge of the long-term constancy in the ^{10}Be deposition rate is thus very important. We report here the first detailed measurements of ^{10}Be and ^9Be in two ferromanganese oxide crusts from the sea floor of the equatorial Atlantic (sample no. K-9-21) and the North Pacific (SCHW-1D), each representing >10 Myr of accumulation history. We have found in these crusts that the deposition of ^{10}Be and $^{10}\text{Be}/^9\text{Be}$ during the past 7–9 Myr has been constant. Averaged over time intervals of ~1 Myr, the variation is within $\pm 6\%$. Before that time, both crusts show similar significant deviations. The 7–9 Myr demarcation may be related to the reported late Miocene global abyssal circulation change in the ocean³.

The extent of variation in the oceanic deposition rate of ^{10}Be during the past 2.5 Myr has been assessed based on the ^{10}Be distribution in sediment cores^{4,5}. An upper limit of $\pm 10\%$ has been placed on the variation when the deposition is integrated over time periods of $2\text{--}7 \times 10^5$ yr. For shorter periods of 1×10^5 yr (roughly corresponding to climatic cycles), the limit is placed⁵ at $\pm 30\%$. The record can be extended by examining ^{10}Be distribution in deep-sea ferromanganese deposits as these materials, in addition to being relatively free of terrestrial detrital input, contain very long depositional records due to their slow accretion rates⁶. Manganese crust K-9-21 was

dredged from a fracture zone scarp on the Sierra Leone Rise. It rested on an altered foraminifera ooze. The substrate of SCHW-1D was a large basaltic rock. These crusts were chosen over the more commonly occurring manganese nodules for the study because the crusts were: (1) relatively flat, so that sampling of contiguous layers perpendicular to the growth axis could be accurately done; (2) fixed in their growth position with respect to top and bottom orientations relative to the sea floor.

Thin layers parallel to the growth surface were carefully taken throughout the whole thickness of the crusts for analyses of ^{10}Be , ^9Be , Mn, and Fe. The thickness of each layer was estimated using caliper and/or from the area, weight and density of material scraped off⁷. In the accelerator analyses of ^{10}Be , milligramme-to-gramme-sized samples were leached with hot 8 M HCl, and then to the leachate was added a $^9\text{BeSO}_4$ carrier (equivalent to 1–10 mg BeO). A simplified version of the procedures of Ku *et al.*⁸ involving only the ion exchange steps was used in the separation of Be from the leachate, as strict chemical purity is not required by the accelerator technique. Measurements of $^{10}\text{Be}/^9\text{Be}$ were carried out using the McMaster University tandem Van de Graaff accelerator modified for this purpose⁹. The sensitivity achieved was $\sim 5 \times 10^{-13}$, and background intensities from reagent blank runs were <10% of the weakest sample signals measured. Mn, Fe and total Be were measured by atomic absorption spectrophotometry; to measure Be, flameless atomization with a deuterium background corrector was used.

The analytical results are presented in Table 1, with errors shown as $\pm 1\sigma$. For Mn and Fe, the measurement precisions are about $\pm 1\%$. The concentration values are listed on a residue-free basis, as the Mn, Fe, and Be will be mainly associated with the HCl-leachable oxide phase of the crusts²⁴.

The temporal variation of ^{10}Be deposition can be assessed by examining the depth distribution of ^{10}Be and the other chemical constituents. As the major constituents in ferromanganese deposits, Mn and Fe are often anti-correlated, and their ratios can be used as a measure of chemical and growth rate variability^{10,11}. In this regard, the two samples studied both show narrow limits of variability. As seen in Table 1, concentrations of Mn and Fe in the two specimens are comparable and show variations of about $\pm 10\%$, with Mn/Fe ratios ranging only from 0.7 to 1.0. Except for the low values in surface layers of SCHW-1D, ^9Be also shows minor temporal fluctuations of about $\pm 10\%$. These narrow limits of variation suggest overall uniformity in the deposition of the two crusts. The log-linear distribution of ^{10}Be shown in Fig. 1 supports this uniformity: the straight lines are weighted least-squares fits to an exponential function, as obtained through iterations¹². The effective measurement depth for each sample is calculated iteratively to account for the radioactive decay taking place during the deposition period represented by each sample interval. The fittings are made over the 'linear' segments of the plots (see legend to Fig. 1), covering major portions of both samples. The slopes of the straight-line fits, which yield accretion rates for the crusts, have standard errors of $\pm (4\text{--}7)\%$ (averaging $\pm 5.5\%$). These errors denote the scatter of data about an exponential curve, and therefore limits the constancy of the ^{10}Be flux and of the flux ratio ^{10}Be to ^9Be into the deposits.

Both the growth rate (~ 1.5 mm Myr) and the Mn/Fe ratio (< 1) are near the lower end of their reported ranges of values for Mn nodules^{6,11}, suggesting minimum influence of diagenesis as a source for Mn. The crusts have received $\sim 2 \times 10^4$ atoms $\text{cm}^{-2} \text{yr}^{-1}$ of ^{10}Be , which is $\sim 4\%$ of the global average ^{10}Be production rate^{13,14}. A similar situation applies to the Mn inventory: $\sim 0.05 \text{ mg cm}^{-2} \text{Kyr}^{-1}$ in the crusts compared with $1.3 \text{ mg cm}^{-2} \text{Kyr}^{-1}$ as the average Mn flux into 38 deep-sea cores¹⁵. Thus most of the ^{10}Be and Mn must have deposited in the adjacent sediment, or the accretion process is not continuous; that is on average, the crusts were actually growing for $\sim 4\%$ of their lifetime^{8,16}.

A decrease of ^{10}Be concentration toward the surface from a near-surface maximum occurs in SCHW-1D (Fig. 1). The

Table 1 Analytical data on Mn crusts

Depth in crust (mm)	HCl insoluble residue (%)	Mn (%)	Fe (%)	⁹ Be (p.p.m.)	¹⁰ Be ($\times 10^8$ atoms g ⁻¹)	¹⁰ Be/ ⁹ Be atom ratio (= 10^{-9})
K-9-21 (7°58'N, 21°02'W; 1,800 m)						
0-1.5	2.1	16.8	22.3	9.89 ± 0.22	488 ± 49	74.0 ± 7.6
1.5-3	2.8	17.8	25.4	10.4 ± 0.7	387 ± 28	55.6 ± 5.5
5-7	7.4	19.2	26.8	13.2 ± 0.5*	107 ± 11	12.2 ± 1.3
10-13	4.9	19.6	24.9	12.3 ± 0.8	15.7 ± 1.6	1.85 ± 0.23
13-17	2.7	17.3	18.3	9.23 ± 0.92	10.3 ± 0.6	1.66 ± 0.19
17-23	4.0	17.6	21.5	9.88 ± 0.99	2.95 ± 0.58	0.45 ± 0.10
Weighted average	4.0	18.0	22.3	10.6	—	—
SCHW-1D (30°N, 140°W; 3,840 m)						
0.00-0.09	29.5	20.1	23.7	3.86 ± 0.35	479 ± 23	186 ± 19
0.09-0.16	25.2	16.7	22.7	2.91 ± 0.21	276 ± 27	142 ± 17
0.16-0.29	24.1	16.7	24.0	5.05 ± 0.21	372 ± 21	110 ± 8
0.29-0.48	18.0	16.7	22.6	4.82 ± 0.26	384 ± 17	119 ± 8
0.48-0.85	9.6	17.7	22.2	6.00 ± 0.60	377 ± 32	94.0 ± 12.3
0.85-1.66	5.2	17.0	20.1	5.87 ± 0.45	361 ± 17	91.9 ± 8.3
1.66-3.16	10.7	18.1	20.7	6.43 ± 0.50	269 ± 13	62.4 ± 5.7
3.16-4.66	15.4	20.3	24.8	8.23 ± 0.04	151 ± 5	27.5 ± 0.9
4.66-6.16	16.7	21.0	24.1	7.70 ± 0.50	116 ± 7	22.6 ± 1.4
6.16-7.66	20.2	21.8	22.3	7.69 ± 0.50	69.4 ± 2.3	13.5 ± 1.0
7.66-9.16	27.4	21.8	23.1	8.11 ± 0.24	50.1 ± 2.5	9.24 ± 0.55
9.16-10.7	22.4	21.6	21.9	7.99 ± 0.28	35.8 ± 1.6	6.70 ± 0.38
10.7-12.2	24.6	22.9	23.2	9.81 ± 0.60	31.0 ± 1.6	4.73 ± 0.38
12.2-14.7	24.2	20.7	22.2	9.10 ± 0.70	26.4 ± 1.7	4.33 ± 0.43
14.7-17.2	31.7	18.6	23.7	9.55 ± 0.45	20.4 ± 1.2	3.19 ± 0.24
Weighted average	21.2	20.2	22.7	8.1	—	—

Concentrations are reported on a residue-free basis.

* Dr C. Measures (MIT) obtained a value of 12.8 ± 0.5 p.p.m. using a gas chromatographic technique.

sampling resolution is not sufficient to detect such a feature in K-9-21. But we have found this feature to be rather ubiquitous among the other deep-sea ferromanganese deposits we have studied. This ¹⁰Be 'inversion' occurs at a depth corresponding to ~0.5 Myr in age. Whether it reflects a change in the ¹⁰Be input or a diagenetic phenomenon remains to be resolved. Noting a surface depletion of ⁹Be as well as ¹⁰Be (Table 1), two of us (M.K. and T.L.K. in preparation) have proposed a post-depositional Be fixation process whereby both Be isotopes are released from a labile phase (or phase with exchangeable Be) at the seawater-solid interface and transferred to the oxide phase through diffusion and adsorption reaction in pure fluid.

As pelagic sediment and shale contain only 2-3 p.p.m. of Be (ref. 17), most of the Be in the samples, like many other elements in ferromanganese deposits, must be authigenically precipitated rather than of detrital origin. Recent studies have described the particulate cycling of ¹⁰Be and ⁹Be in the sea¹⁸⁻²⁰. Information on the extent to which the oceanic reservoirs of these two isotopes are equilibrated in time and space is germane to the ¹⁰Be geochronology. If isotope equilibrium is achieved, the use of the ¹⁰Be/⁹Be ratio in lieu of ¹⁰Be concentration would circumvent the latter quantity's being affected by factors other than radioactive decay, such as changes in sedimentary composition and deposition rate. The present data suggest that for periods of the order of 1 Myr the oceanic ¹⁰Be/⁹Be reservoir as well as ¹⁰Be deposition has remained constant to within ±6% for approximately the past 8 Myr (represented by the first 10-13 mm of the crusts; Fig. 1).

It should also be of interest to determine the spatial constancy of the ¹⁰Be and ⁹Be reservoirs. This information would be best obtained from simultaneous measurements of ¹⁰Be and ⁹Be in water columns from various parts of the ocean. But these have yet to be done. A less rigorous alternative would be to compare reported values for the isotope ratio ¹⁰Be/⁹Be (extrapolated to zero age) in manganese nodules and crusts from different areas²¹. These values range over one order of magnitude²². To eliminate any interlaboratory discrepancies, we list in Table 2 the extrapolated ratios in six ferromanganese samples based

on measurements made only at our own laboratories, including the two crusts reported here. The data scatter is outside the experimental uncertainties of about ±15%, suggesting variability of ¹⁰Be/⁹Be with location and water mass. This is plausible, in view of the fact that the residence time of Be in the sea has been estimated¹⁸⁻²³ as being comparable with or shorter than the oceanic overturn time of ~10³ yr. If so, the temporal constancy in ¹⁰Be/⁹Be for the past 7-9 Myr deduced in this study would imply considerable stability (on a Myr time scale) in oceanic circulations during the period. However, conditions before 7-9 Myr BP could be significantly different, as shown by the deviations from the log-linear fits deeper in both crusts (Fig. 1). According to Ciesielski *et al.*³, the abyssal circulation then was very different due to the absence of a true Antarctic Bottom Water similar to that produced today in the Weddell Sea.

The Fig. 1 deviations are such that they can be explained by an approximately twofold increase in the accretion rate of the crust. Although possible, such a large increase seems unlikely considering the following. A near-synchronous accretion rate change occurring in two different major ocean basins would call for events affecting the global supply of Mn and/or Fe, such as changes in submarine hydrothermal activity and sea floor redox condition. And one would expect the samples to show a major change in their Mn/Fe ratio and perhaps ⁹Be

Table 2 Extrapolated (to zero age) atom ratio ¹⁰Be/⁹Be in six ferromanganese deposits

Sample no.	Lat., long.	¹⁰ Be/ ⁹ Be ($\times 10^{-7}$)
K-9-21	7°58'N, 21°02'W	0.96
K79-05-47BC	11°01'N, 140°03'W	3.0
Mn 139	20°01'N, 136°36'W	2.3
Aries-13D	20°45'N, 173°40'E	1.2
SCHW-1D	30°N, 140°W	1.2
Rama 1-24GC	30°N, 158°W	1.3

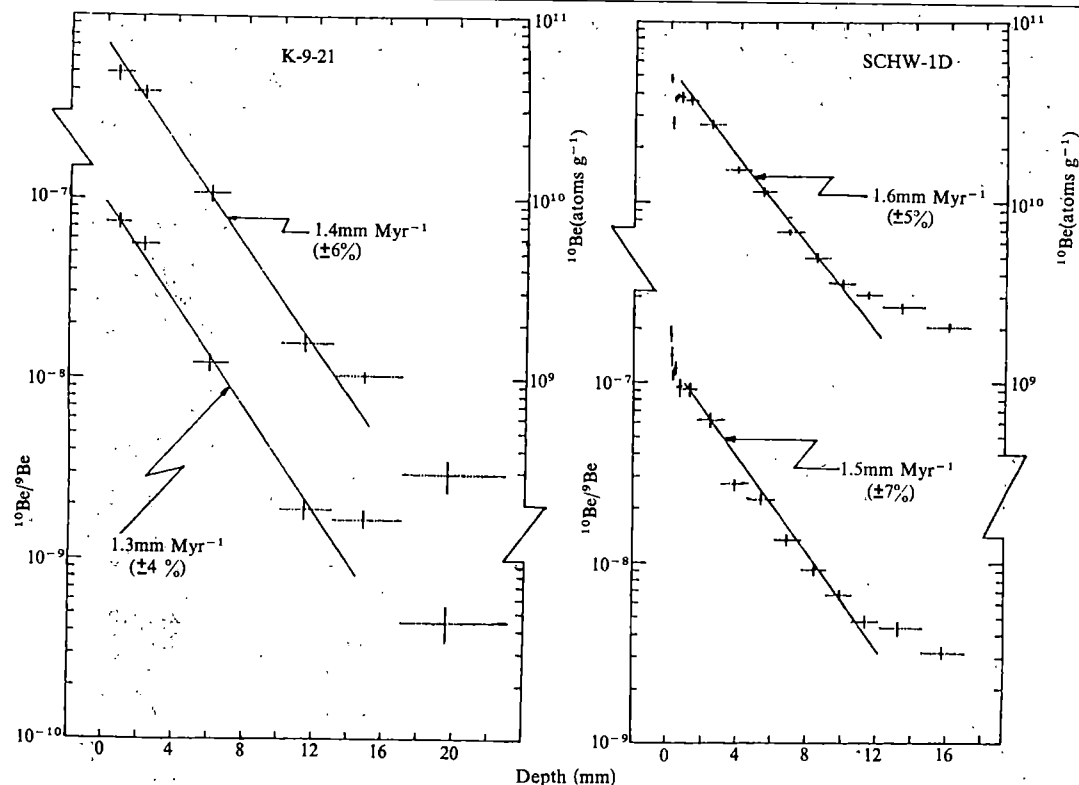


Fig. 1 Depth plots of ^{10}Be concentration (on a residue-free basis) and $^{10}\text{Be}/^9\text{Be}$ in two Mn crusts. Least squares fits for the 'linear' segments of the plots give estimates for the accretion rates (and their standard errors) of the crusts. The linear segment for sample K-9-21 includes the top four data points; for SCHW-1D, data points 6–12 from the crust surface. The horizontal dotted lines denote the depth intervals analysed, and the positions of the vertical lines (error bars) are placed at the effective measurement depths.

and residue concentrations across the 7–9 Myr boundary. We do not discern such a change. We thus favour the possibility that those deviations were caused by a shift in the initial $^{10}\text{Be}/^9\text{Be}$ ratio resulting mainly from a shift in the ^{10}Be input. While the primary atmospheric supply of ^{10}Be might have varied, we consider it more likely that the ^{10}Be input change is related to the modification of oceanic mixing patterns 7–9 Myr ago³, as mentioned above. During that time, the major production of the Antarctic Bottom Water began. This event marks the initiation of the modern global circulation, and has led to shifts in such oceanic properties as carbonate compensation level and carbon isotopic composition³. It could also have influenced the Be records observed here, by exposing the crusts to bottom waters bearing different ^{10}Be contents and $^{10}\text{Be}/^9\text{Be}$ ratios before and after the 7–9 Myr event. Studies of sedimentary deposits (such as Deep-Sea Drilling Project sediments) as well as other Mn crusts would be required to test this possibility further.

We thank J. Kuehner and his staff at the McMaster accelerator for assistance, W. S. Moore and T. Walsh for supplying the samples which were the collections of Lamont-Doherty Geological Observatory (K-9-21) and Scripps Institution of Oceanography (SCHW-1D), C. Measures for checking our ^9Be analyses, and K. Johnson for making available the atomic absorption facilities at the University of California, Santa Barbara. J. Sheppard and N. Bohna assisted in the ^9Be and data analyses. This research was supported by the NSF Manganese Nodule Program (MANOP), by the NSERC of Canada, and by Simon Fraser University.

Received 9 June; accepted 14 July 1982.

1. Muller, R. A. *Science* **196**, 489–494 (1977).
2. *Proc. Symp. on Accelerator Mass Spectrometry* (Argonne National Laboratory, 1981).
3. Ciesielski, P. F., Ledbetter, M. T. & Ellwood, B. B. *Mar. Geol.* **46**, 1–51 (1982).
4. Inoue, T. & Tanaka, S. *Nature* **277**, 209–210 (1979).
5. Tanaka, S. & Inoue, T. *Earth planet. Sci. Lett.* **45**, 181–187 (1980).
6. Ku, T. L. in *Marine Manganese Deposits* (ed. Glasby G.) 249–267 (Elsevier, Amsterdam, 1977).
7. Bender, M. L., Ku, T. L. & Broecker, W. S. *Science* **141**, 325–328 (1966).
8. Ku, T. L., Omura, A. & Chen, P. S. in *Marine Geology and Oceanography of the Pacific Manganese Nodule Province* (eds Bischoff, J. L. & Piper, D. Z.) 791–814 (Plenum, New York, 1979).
9. Southon, J. R. et al. *Nucl. Instrum. Meth.* (in the press).
10. Margolis, S. V. & Burns, R. G. A. *Rev. Earth planet. Sci.* **4**, 229–263 (1976).
11. Lyle, M. *Geol. Soc. Am. Mem.* **154**, 269–293 (1981).
12. Wolberg, J. R. *Prediction Analysis* (Van Nostrand, Princeton, 1967).

13. Somayajulu, B. L. K. *Geochim. cosmochim. Acta* **41**, 909–913 (1977).
14. Reyss, J. L., Yokoyama, Y. & Guichard, F. *Earth planet. Sci. Lett.* **53**, 203–210 (1981).
15. Bender, M. L., Ku, T. L. & Broecker, W. S. *Earth planet. Sci. Lett.* **8**, 143–148 (1970).
16. Bhat, S. G., Krishnaswami, S., Lal, D., Rama & Somayajulu, B. L. K. *Proc. Symp. Hydrogeochem. Biogeochem.* **1**, 443–462 (Clarke, Washington DC, 1973).
17. Krishnaswami, S. & Lal, D. *Nobel Symp. No. 20* (eds Dyrssen, D. & Jagner, D.) 307–320 (Wiley, New York, 1972).
18. Raisbeck, G. M. et al. *Earth planet. Sci. Lett.* **51**, 275–278 (1980).
19. Measures, C. I. & Edmond, J. M. *Nature* **297**, 51–53 (1982).
20. Kusakabe, M. et al. *Nature* (submitted).
21. Yokoyama, Y., Guichard, F., Reyss, J. L. & Nguyen, H. V. *Science* **201**, 1016–1017 (1978).
22. Krishnaswami, S. et al. *Earth planet. Sci. Lett.* **59**, 217–234 (1982).
23. Merrill, J. R., Lyden, E. F. X., Honda, M. & Arnold, J. R. *Geochim. cosmochim. Acta* **18**, 108–129 (1960).
24. Guichard, F. thesis, Univ. Paris VII (1982).

<33,000-yr K–Ar dating of the volcano–tectonic horst of the Isle of Ischia, Gulf of Naples

P.-Y. Gillot

Centre des Faibles Radioactivités, Laboratoire mixte CNRS-CEA, 91190 Gif-sur-Yvette, France

S. Chiesa, G. Pasquare & L. Vezzoli

Istituto di Geologia, Università di Milano, sezione di Bergamo, 23100 Bergamo, Italy

The Gulf of Naples corresponds to a tectonic sink connected with recent volcanic activity in the South-Campanian area (Phlegrean Fields, Ischia and Vesuvius). At its extreme north-west, the Isle of Ischia was early recognized as a volcano-tectonic horst by Rittmann¹. Previous data² concluded that its uplift ended around 300,000 yr, and that the Green Tuff formation, of which it is predominantly composed, had an age of some 700,000 yr. But tectonic and morphological studies, together with original tephrostratigraphical observations on the slope of the horst, led us to do some new K–Ar datings. These revealed that the 780 m uplift of the horst from the sea level is younger than 33,000 yr; the Green Tuff, which was considered to be the oldest volcanic unit in the island is now dated at 56,000 yr, its eruption following the dismantlement of a first volcanic complex now dated as not older than 130,000 yr.

Rittmann¹ recognized that the principal structure of the Isle of Ischia is a volcano-tectonic horst (Monte Epomeo, 787 m) and not a central volcano as had previously been believed^{3,4}.

The horst of Monte Epomeo is part of a system of faults running north to south and from east to west, describing a quadrilateral between the villages of Lacco Ameno, Casamicciola, Barano and Panza (Fig. 1); it is formed of a trachytic ignimbrite: Green Tuff. Although of subaerial origin, this unit was totally covered by the sea before the uplift of the horst, as attested by the overlay of marine deposits and the existence of diffuse 'glauconite' giving it its green colour. Rittmann considers Green Tuff as the oldest formation found outcropping on the island, on which all the products of subsequent volcanic activity occurring along the horst faults were deposited. K-Ar chronometric studies of volcanic units from the Isle of Ischia have dated Green Tuff at 6.0 ± 0.14 Myr (biotite)⁵ later corrected to 0.7 ± 0.1 Myr (sanidine and biotite)². According to these data, the most important phase in the activity of the island goes back to ~ 0.3 Myr and it would be around that period when the uplift of the horst ended. However, Evernden and Curtis⁶ have obtained a K-Ar dating of 83,000 yr on sanidine from a sample of Green Tuff, and an attempt at U-Th dating the Tuff of Citara^{7,8}, which is the product of an important explosive event of Ischia, gave a probable age of $41,500 \pm 3,000$ yr.

New tephrostratigraphical⁹, tectonic and morphological studies have been undertaken on the Isle of Ischia, as part of the research into the evaluation of volcanic risk in active volcanic regions. They revealed that lava units associated with breccia can be individually identified under the Green Tuff at the foot of the Western slope of Monte Epomeo (Rione Bocca), bearing witness to the existence of a phase of activity before the formation of the Green Tuff. However, they also reveal that the formation of the horst of Ischia is very recent, without doubt still active and directly correlatable with the historical volcanic activity attested by archaeological observations¹⁰ of which the latest manifestation is the Arso lava flow (December 1301–January 1302). The disparity of ages and the new data available prompted us to renew the chronometric study of the main eruptive phases on the island. The techniques used have been described elsewhere^{11,12}. Argon was analysed using a 180° , 6-cm radius, 500 V accelerating potential mass spectrometer operated in the static mode. The sensitivity of the machine was 4×10^9 atoms mV⁻¹ using a $10^{11} \Omega$ resistor in the vibrating reed electrometer. For the ^{36}Ar peak, the output was typically 30–100 mV and the noise level was around 0.03 mV. The accurate correction for contamination necessary when dating such young rocks was obtained by avoiding any discrimination effect in the mass spectrometric measurements, that is, unspiking, and consequent successive measuring of 36 and 40 ion beam intensities for sample argon, atmospheric argon and the standard argon amount in the same working conditions in the mass spectrometer (with $<0.3\%$ fluctuation of any of the parameters—accelerating potential, arc voltage, electron beam current, background of the mass spectrometer with masses other than argon and the amount of argon present in the mass spectrometer when doing the comparison of sample argon with atmospheric argon)¹². In these conditions it is possible to date to within 10,000 yr (refs 12–14) lavas containing 1% of potassium. Therefore Ischia's rocks can be dated to within a few thousand years, being classified between latites and alkali-trachytes with a potassium content of at least 4%. This accuracy corresponds typically to a limit of detectability of 0.2% on the level of radiogenic ^{40}Ar . It makes possible a 10% accurate dating at a contamination level of 98%. Confirmation that such precision of measurement can be attained was provided by analyses of air argon samples measured at the same working point of the mass spectrometer; the uncertainty in $^{40}\text{Ar}/^{36}\text{Ar}$ ratio was $0.12\%/(2\sigma)$ for a single analysis calculated from about 12 runs). Data on 11 samples from historic or radiocarbon dated volcanic units presented in Table 1 reveal a fairly good agreement and confirm the reliability of K-Ar data down to 0.2% of radiogenic argon. Among the analysed samples is one from the Arso flow from Ischia which erupted in AD 1302. Note that the dispersion observed for replicate measurements on the same sample was always within the range of the predicted error.

Sixteen samples of volcanic units of the Isle of Ischia were then dated. They were selected as a function of their stratigraphical position and corresponded to the different activities developed in the island: before the horst uplift, old volcanic remains outcropping on its periphery and volcanic units affected by the faults of the horst; recent volcanic activities developed along the faults of the horst, contemporaneously to the uplift. Ages obtained are reported in Table 2. All these results are in agreement with the available stratigraphical control: the trachyte of the Costa Sparaina (sample 2) flowed over the lava of the Selva del Napolitano (sample 3) both lying on Green Tuff (samples 8, 9) on the eastern flank of the horst; a trachytic block (sample 10) included in the Green Tuff and the lava flow at Rione Bocca (sample 11), overlain by Green Tuff, gave ages slightly older and coherent with other ages obtained for the oldest volcanic units outcropping on the Isle between 130,000 and 75,000 yr; also, samples 4, 5 and 6 corresponding to the products of the Campotese volcano and the Citara pumice level are directly superimposed. Moreover ages obtained on separated mineral phases (sanidine and groundmass) of the same unit, with various potassium contents and various levels of contaminant argon, gave the same ages within the limit of the predicted accuracy. Under the pumice deposit associated with the trachytic lava of Fondo d'Oglio crater (sample 1), which erupted during the historic period according to our K-Ar results ($<2,000$ yr), we have sampled shells in a palaeo-beach level to crosscheck our result with radiocarbon dating. We also found a piece of ceramic indicating that the pumice flowed over historical deposits, in good agreement with our result: this pottery could be attributed to the third century AD (G. Marinelli, personal communication).

Our K-Ar measurements confirm that Green Tuff, $56,000 \pm 4,000$ yr, is not the oldest volcanic formation outcropping on the Isle of Ischia. The dating of volcanic units between 130,000 yr (Castello d'Ischia lava, sample 16, $132,000 \pm 2,600$ yr; Monte di Vezzi lava flow, sample 15, $128,000 \pm 5,000$ yr) and $75,000 \pm 2,000$ yr (dome of Monte Vico, sample 12) shows that volcanic centres were active before the Green Tuff's eruption. These centres correspond to volcanic units which are at present partly dismantled and visible at the

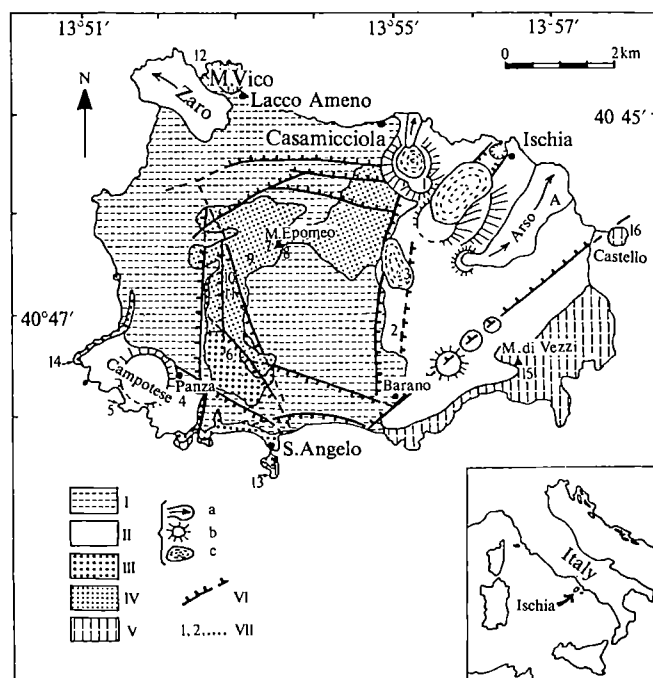


Fig. 1 Geological sketch map of the Isle of Ischia. I, scree and mud flows; II, volcanic units younger than 30,000 yr, a, lava flow; b, crater; c, dome; III, Citara Tuff; IV, Green Tuff of Monte Epomeo; V, formations of the first volcanic complex, dismantled; VI, faults; VII, samples location (same numbers as in Table 2 and the text).

periphery of the Epomeo's horst; this is also the case at Castello d'Ischia in the east, Monte Vico in the north, the peninsula of S. Angelo (sample 13, $97,000 \pm 5,000$ yr) in the south and Monte di Vezzi in the south-east. The first complex probably extended beyond the boundaries of the present island and dating indicates that it was built up over at least 60,000 yr. The major part of the old volcano has indeed been eroded and disappeared following former collapses and the Green Tuff's eruption. In the south-west part of Ischia, near Panza, the recent products of the complex volcanic centre of the Campotese are

superimposed on the remnants of old structures almost completely submerged and outcropping along the coast at Punta Imperatore (sample 14, $118,000 \pm 3,000$ yr), Capo Negro and S. Angelo. A level of pumice (the Citara Tuff) divides the old flows from the recent products of the Campotese⁹. Citara Tuff also overlaps the Green Tuff on the south-west slope of Monte Epomeo, where it is affected by the faults of the horst, and passes laterally into a facies of fine cinerites, which are intercalated with marine deposits. Hence, this pumice level (sample 6, $33,000 \pm 2,000$ yr), younger than the Green Tuff and the

Table 1 Analytical K-Ar data on volcanic rocks of known ages

	Material (K%)	$^{40}\text{Ar}^*$ (%) (± 0.2)	$^{40}\text{Ar}^*$ (10^{10} atoms g^{-1})	K-Ar age (kyr)	Known age (yr)
A	Groundmass (6.00)	0.04	<3.2	<5.1	AD 1302
		0.00	<2.5	<4.0	
	Sanidine (9.00)	0.18	1.1	1.2 ± 1.3	
		0.00	<1.3	<1.5	
B	Sanidine (10.55)	0.90	3.6	3.3 ± 0.8	$3,700 \pm 200$ ^{14}C (ref. 15)
		1.18	4.7	4.2 ± 0.8	
C	Sanidine (10.54)	10.43	17.0	15.4 ± 0.7	Between 11,000 and 12,000 yr ^{14}C (ref. 15)
		8.80	15.5	14.1 ± 0.7	
		3.55	16.7	15.1 ± 0.9	
D	Sanidine (11.19)	8.90	40.7	34.8 ± 0.9	Between 28,000 and 35,000 yr ^{14}C (ref. 16)
		9.70	39.8	34.0 ± 0.9	
E	Groundmass (5.00) Leucite (15.00)	0.05	<2.1	<4.0	AD 1944
		0.00	<7.9	<5.0	
F	Glass (5.00)	0.00	<1.1	<2.0	Late Roman decade, about 1,400 yr BP (ref. 17)
		0.08	<1.6	<3.0	
G	Groundmass (5.00) Sanidine (10.00)	0.25	0.8	1.5 ± 1.2	Flank of modern Vulcano
		0.29	0.9	1.7 ± 1.2	
		0.00	<1.6	<1.5	
H	Groundmass (4.03)	0.20	2.1	5.0 ± 5.0	Base of modern Stromboli
		0.25	2.7	6.5 ± 5.0	
I	Groundmass (1.50)	0.00	<1.1	<7.0	AD 1971
Mean value of 5 measurements ranging between -0.04 and 0.07% radiogenic level					
J	Groundmass (1.50)	0.00	<0.8	<5.0	Sixteenth century AD
		Mean value of 5 measurements ranging between -0.05 and 0.09% radiogenic level			
K	Groundmass (1.35)	0.60	1.9	13.0 ± 4.3	$7,800 \pm 300$ ^{14}C (ref. 18)
		0.35	1.3	9.5 ± 5.4	

A, Arso flow of Ischia (sample 36 I), drilled in the core of the flow at the international camping of Ischia Porto; B, trachytic dome of Caprara (sample CF 27), connected with Astroni crater, Phlegrean Fields, Campania, Italy; C, Pumice level (sample 36 O), connected with Neapolitan Yellow Tuff, Phlegrean Fields, Italy; D, Campanian Ignimbrite (sample 35 P) sampled at S. Agata dei Goti, Campania, Italy; E, AD 1944 Vesuvius tephritic flow (sample 35 H); F, Obsidian flow of Rocche Rosse (sample 28 X), Lipari Island, Italy; G, Grotta dei Palizzi trachytic flow (sample 38 T) southern flank of modern Vulcano, Aeolian Islands, Italy; H, Punta Frontone shoshonitic flow (sample 37 P) base of modern Stromboli (Filo dell'Arpa), Aeolian Islands, Italy; I, Mount Etna AD 1971 flow (sample 29 C) fine grained light grey facies of the core of the flow; J, Mount Etna (Sicily) sixteenth century AD flow (sample FLG 3) sampled in the quarry of Nicolosia; K, basaltic flow of Puy de la Vache (sample 30A, sampled at St Saturnin, Chafne des Puys, Massif Central, France. The errors are calculated according to:

$$\frac{\sigma^2 \text{Age}}{\text{Age}^2} = \left(\frac{1-T}{T} \right)^2 \frac{\sigma^2 \text{Ar}}{\text{Ar}^2} + \frac{\sigma^2 \text{Cal}}{\text{Cal}^2} + \frac{\sigma^2 \text{K}}{\text{K}^2}$$

where T is the radiogenic argon proportion in total argon;

$$(\% \text{ error in radiogenic Ar})^2 + (\% \text{ error in calibration})^2 + (\% \text{ error in K})^2$$

Its value tends to $\pm 2\%$ when the radiogenic argon level becomes $>10\%$, taking into account a 0.5% (2σ) error on the calibration for a definite value of standards¹⁹ and an error of 1.5% on K content dosed by atomic absorption spectrophotometry. The error in the radiogenic argon was determined using the expression:

$$\left(\frac{1-T}{T} \right)^2 \left(\frac{\sigma^2 r}{r^2} + \frac{\sigma^2 r'}{r'^2} \right)$$

where r and r' are the $^{40}\text{Ar}/^{36}\text{Ar}$ ratios in sample argon and atmospheric argon. This expression is comparable with the formulation in refs 20-22. Because of the steadiness of the different argon signals measured in our machine and because of the simultaneous collection of ^{36}Ar and ^{40}Ar signals, the error in radiogenic ^{40}Ar corresponds to the errors in the measurements of isotopic ratios, and, essentially, to the error on ^{36}Ar measurements. In our case of very low radiogenic level, $r \sim r'$; the error on radiogenic argon can be written:

$$\left[2 \left(\frac{100 - ^{40}\text{Ar}^* \%}{^{40}\text{Ar}^* \%} \times \% \text{ error in } ^{40}\text{Ar}/^{36}\text{Ar} \right)^2 \right]^{1/2}$$

This is the major uncertainty in the calculated age because of the error magnification associated with the small proportion of radiogenic argon found in the analyses ($0-10\%$).

Sample weight: $5-10$ g per argon analysis; $^{40}\text{Ar}^*$ = radiogenic ^{40}Ar ; the following decay constants were used in the ages calculation²³: $\lambda_B = 4.962 \times 10^{-10} \text{ yr}^{-1}$, $\lambda_e = 0.581 \times 10^{-10} \text{ yr}^{-1}$, $^{40}\text{K}/\text{K} = 1.167 \times 10^{-4}$.

Table 2 Analytical K-Ar data on Ischia's lavas

Material (K%)	$^{40}\text{Ar}^*(\%)$	$^{40}\text{Ar}^*$ (10^{10} atom g^{-1})	Apparent age (kyr)
1 Groundmass (5.53)	0.20	0.5	1.0 ± 1.0
	0.27	0.8	1.6 ± 1.1
Feldspar (6.95)	0.15	0.8	1.0 ± 1.3
	0.29	1.5	2.0 ± 1.4
2 Groundmass (5.90)	0.39	2.3	3.7 ± 1.9
	0.65	2.9	4.5 ± 1.5
	0.31	1.9	3.0 ± 2.0
Feldspar (6.51)	0.42	2.9	4.1 ± 2.0
	0.47	3.9	5.6 ± 2.5
3 Groundmass (5.20)	1.28	5.7	10.2 ± 1.6
	1.17	4.9	9.0 ± 1.5
	1.26	4.1	7.6 ± 1.2
Feldspar (7.94)	1.42	8.6	10.3 ± 1.5
	1.45	8.7	10.4 ± 1.5
4 Sanidine (8.80)	2.86	21.7	23.7 ± 1.7
	2.82	21.5	23.5 ± 1.7
5 Sanidine (8.83)	1.66	25.9	28.1 ± 3.3
	1.80	27.3	29.6 ± 3.2
	1.95	27.0	29.3 ± 3.0
6 Sanidine (7.54)	3.55	25.6	32.5 ± 1.8
	3.86	26.4	33.5 ± 1.7
7 Sanidine (9.70)	3.28	57.4	56.7 ± 3.5
	3.51	55.0	54.2 ± 3.0
	1.79	58.8	58.0 ± 6.5
8 Sanidine (9.51)	2.69	56.5	56.8 ± 4.0
9 Sanidine (10.40)	2.59	55.7	51.5 ± 4.0
	3.03	61.6	56.7 ± 4.0
10 Groundmass (6.03)	0.60	71.1	113.0 ± 37.0
	0.54	62.3	97.0 ± 36.0
11 Groundmass (6.08)	3.34	85.7	135 ± 8.0
	3.42	82.4	130 ± 8.0
Feldspar (6.18)	8.19	78.7	122.0 ± 3.0
12 Groundmass (5.19)	16.39	41.4	76.0 ± 1.9
Feldspar (5.70)	15.55	43.5	73.0 ± 1.8
	16.51	45.2	76.0 ± 1.9
13 Groundmass (5.85)	2.09	60.6	99.0 ± 9.0
	2.20	61.3	100.0 ± 9.0
Feldspar (6.04)	6.17	59.1	95.0 ± 3.0
14 Groundmass (5.93)	7.95	72.7	117.0 ± 3.3
	13.92	73.1	118.0 ± 3.0
Feldspar (6.35)	18.41	77.0	116.0 ± 2.9
	21.52	81.2	123.0 ± 3.1
15 Whole rock (5.37)	4.96	71.6	128.0 ± 5.0
16 Groundmass (5.85)	23.02	80.9	132.0 ± 3.3

1, Fondo d'Oglio trachytic flow (sample 35 V); 2, Costa Sparaina trachytic flow (sample 35 Y); 3, trachytic lava at Selva del Napolitano (sample 35 W); 4, trachytic lava flow near Panza (sample 35 M); 5, trachytic lava, base of the cliff of Grotta del Mavone (sample 35 N); 6, Citara trachytic Tuff sampled at Ciglio (sample ISH 85); 7, Green Tuff at S. Nicola (sample 38 Eb), near the top of Monte Epomeo; 8, Green Tuff, real top of Monte Epomeo (sample 38 Ea); 9, Green Tuff at Pietra dell'Acqua (sample ISH 114 B); 10, trachytic block included in the Green Tuff, Rione Bocca (sample 36 D); 11, Rione Bocca trachytic flow (sample ISH 84), under the Green Tuff; 12, Monte Vico latitic dome (sample 35 J) at Baia S. Montano; 13, S. Angelo latitic dome (sample ISH 103), at the base of the mount; 14, trachytic lava, at the base of the cliff at Punta Imperatore (sample ISH 118); 15, Monte di Vezzi trachytic flow (sample 36 H); 16, Castello d'Ischia latitic lava (sample ISH 113). Same analytical conditions as presented in Table 1.

ancient lavas of the south and south-west part of the island, was deposited close to sea level before the formation of the horst of Monte Epomeo; consequently the amplitude of this uplift of at least 800 m can be dated back to <33,000 yr. The formation of the horst was accompanied by volcanic activity which developed at its periphery during the past 30,000 yr. In

particular, the north-east sector of Ischia, described by the eastern marginal fault of the horst of Epomeo and by the fault running south-west north-east Barano-Castello, appears to consist of pyroclastics and lavas, recently emitted by domes, explosion craters and spatter cones (for example, Selva del Napolitano lava, sample 3, $9,000 \pm 1,500$ yr; Costa Sparaina trachytic flow, sample 2, $4,000 \pm 1,800$ yr; Fondo d'Oglio trachytic flow, sample 1, $1,500 \pm 1,000$ yr). In this sector, it was possible, by dating, to link an important phase of activity to the prehistoric and historic period. Besides the formation of the flows and the trachytic domes, the pumice layers which extend over the whole eastern sector of the island also originated during this phase. The data from our study indicate that the volcanic and tectonic history of the Isle of Ischia is perceptibly different from that which was previously accepted and reveal the important seismic and volcanic risks in this zone. The age of the volcanic activity of Ischia is much younger than was thought. From ~130,000 yr ago, a first complex was built which was partly eroded and dismantled by a tectonic phase which finished by a collapse, following the eruption of the Green Tuff, dated at $55,000 \pm 3,500$ yr. The uplift of the volcano-tectonic horst of Monte Epomeo is <33,000 yr old, as given by the age of the Citara Tuff. It occurred at the same time that the modern volcanic activity developed.

The study was supported by CNR (Progetto Geodinamica—Rischio Vulcanico) and the Programme Interdisciplinaire de Recherche pour la Prevision et la Surveillance des Eruptions Volcaniques, CNRS. We thank J. Labeyrie and J. C. Duplessy for useful criticism, and Dominick Christie for translating the manuscript.

Received 11 March; accepted 6 July 1982.

- Rittmann, A. Z. *Vulk. Ergbn.* 6 (1930); *Bull. Suisse Miner. Petrogr.* 28, 643–698 (1948).
- Capaldi, G., Civetta, L. & Gasparini, P. *Bull. Volcan.* 40, 1–12 (1976).
- Fonseca, F. *Annali Accad. Asp. Natural. Napoli* 1, 163–200 (1847).
- Fuchs, C. W. C. *Mem. pr Servire alla Descrizione della Carta Geologica d'Italia* vol. 2, 1–59 (1873).
- Gasparini, P. & Adams, J. A. S. *Earth planet Sci. Lett.* 6, 225–230 (1969).
- Evernden, J. F. & Curtis, G. H. *Curr. Anthropol.* 6, 343–385 (1965).
- Federici, C. & Taddeucci, A. *Soc. ital. Miner. petrogr.* 30, 695–704 (1974).
- Delitala, M. C., Federici, C. & Taddeucci, A. *Bull. Volcan.* 38, 1015–1022 (1974).
- Forcella, F., Gnaccolini, M. & Vezzoli, L. *Riv. Ital. Paleont.* 87, 329–366 (1981).
- Buchner, P. *Nature* 34, 39–62 (1943).
- Cassignol, C., Cornette, Y., David, B. & Gillot, P.-Y. *Rapport CEA-R-4908 CEN Saclay* (1978).
- Cassignol, C. & Gillot, P.-Y. in *Numerical dating in stratigraphy* (ed. G. S. Odin) 160–179 (Wiley, New York, 1982).
- Gillot, P.-Y. *et al. Earth planet Sci. Lett.* 42, 444–450 (1979).
- Gillot, P.-Y. & Nativel, P. J. *Volcan. Geotherm. Res.* 13, 131–146 (1982).
- Alessio, M. *et al. R. Soc. ital. Miner. Petrogr.* 27–II, 305–308 (1971).
- Di Girolamo, P. & Keller, J. *Ber. naturf. Ges. Freiburg* 61/62, 85–92 (1972).
- Pichler, H. R. *Soc. ital. Miner. Petrogr.* 36, 415–440 (1980).
- Pelletier, H., Delibrias, G., Labeyrie, J., Perquis, M. T. & Rudel, A. C. R. *Acad. heb. Séanc. Sci., Paris* 214, 2221 (1959).
- Cassignol, C., David, B. & Gillot, P.-Y. *Geostandard Newslett.* 1, 105–106 (1977).
- Cox, A. & Dalrymple, G. B. J. *geophys. Res.* 72, 2603–2614 (1967).
- McDougall, I., Pollach, H. A. & Stüpp, J. J. *Geochim. cosmochim. Acta* 33, 1485–1520 (1969).
- Baksi, A. K. *Chem. Geol.* 35, 167–172 (1982).
- Steiger, R. H. & Jäger, E. *Earth planet. Sci. Lett.* 36, 359–362 (1977).

Unusual distribution of biological markers in an Australian crude oil

R. P. Philp & T. D. Gilbert

CSIRO Division of Fossil Fuels, PO Box 136, North Ryde, New South Wales, 2113, Australia

The stereochemical configuration of hopane-type triterpanes in source rock extracts or crude oils is normally determined by the maturity of the sample¹. Naturally occurring precursors of the hopane hydrocarbons are dominated by the $17\beta\text{H}$, $21\beta\text{H}$ stereochemistry with only one diastereomer at the C22 position in the C₃₁ and higher homologues². Note that the $17\beta\text{H}$, $21\beta\text{H}$ -C₂₈ homologue has never been reported in any sample. Mature crude oils in general contain hopane hydrocarbons dominated by the thermally more stable configuration of $17\alpha\text{H}$, $21\beta\text{H}$ stereochemistry and a mixture of the two diastereomers at the

C22 position for C₃₁ and higher homologues in the ratio of ~3/2. We present here evidence for the presence of an unusual distribution of hopanes in an Australian crude oil. A study by computerized gas chromatography-mass spectrometry (C-GC-MS) designed to determine whether different oils from the same basin have similar sources has revealed the presence of the thermally unstable 17 β H, 21 β H isomers of hopane-type triterpanes in conjunction with C22 diastereoisomers in the unusual ratio of 1:9. We propose that there are two possible explanations for this unusual distribution of the triterpanes. (1) The oil is immature or (2) these compounds have accumulated in the oil as it migrated through coals in the region of the reservoir which are also known to contain the unusual hopane distribution.

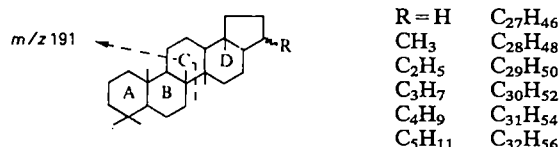


Figure 1a, which is a portion of the *m/z* 191 chromatogram obtained from the GC-MS analysis of an Australian crude oil, illustrates the use of the technique of single-ion monitoring (SIM) to determine the distribution of the triterpanes³. This ion corresponds to the A/B ring fragment of the hopane structure shown above. Examination of complete spectra showed that the predominant hopane components in this sample (1, 2, 5-10) all have the 17 α H, 21 β stereochemistry as has been previously reported for crude oils¹. The ratio of the C₃₁ 22S and R isomers is ~60/40, previously reported by Seifert *et al.*⁴ to be the equilibrium ratio for these isomers in crude oils. The second eluting isomer possesses the naturally occurring stereochemistry (22R). It was previously thought that crude oils with a 22R/22S ratio of >1 have never been observed since such a distribution would indicate lack of sufficient maturity for petroleum generation⁴.

We now report the first observation for Australian crude oils of a higher proportion of the C₃₁-22R diastereomer than the C₃₁-22S diastereomer. This unusual distribution has been observed in at least two oils from the Gippsland Basin, one from the Surat Basin and one from the Carnarvon Basin but is most pronounced in the Turrum 2 oil discussed in detail here. Thus from a total of ~40 oils examined, 10% had a higher concentration of C₃₁-22R epimer than the C₃₁-22S epimer and several others had a 1:1 ratio of the 22R and S isomers. Shi Ji-Yang *et al.*⁵ have recently reported a similar occurrence in one oil from China and Seifert *et al.*⁴ reported oils from one basin where the 17 α (H), 21 β H 22R:22S ratio was greater than the proposed equilibrium ratios and where ratios as low as 1.2 were observed in the least mature oils. However, the present study suggests that such a distribution is not uncommon in crudes from several Australian basins.

The most striking example of this unusual ratio was observed in an oil from the Turrum well in the Gippsland Basin for which the *m/z* 191 chromatogram is shown in Fig. 1b. In this example the ratio for 22S and R is 10/90 compared with the 60/40 predicted by Seifert *et al.*⁴ for mature oils, where the 22S and R isomers are supposedly in thermodynamic equilibrium. Furthermore, the ratio for the C₃₂-22S and R diastereomers is analogous to the C₃₁ ratio in that the 22R diastereomer is present in higher concentrations than the 22S diastereomer. Examination of complete spectra taken over the peak from the second eluting isomer showed no evidence for the presence of gammacerane which has been reported to co-elute with the C₃₁-22R-homohopane on non-polar columns⁵. Comparison of this oil with that taken from a reservoir 2,000 ft deeper in the same well illustrates a significant difference in distribution of the hopanes (Fig. 1c). The deeper oil has a more characteristic hopane distribution pattern dominated by the 17 α H, 21 β H-C₂₉ component and with the C₃₁-22S and R isomers present in a

53/47 ratio. It is generally thought, though not unequivocally proven, that the oils from this part of the basin have the same or very similar sources⁶. If this is the case for these two oils, what explanations are available for the unusual ratio of C₃₁-22S and R diastereomers in the shallower oil plus several other differences in individual hopane distributions?

The location of the Gippsland Basin and the onshore Victorian brown coal deposits prompted a re-examination of the triterpanes present in Yallourn lignite. The sample of Yallourn lignite used in this study was taken from the onshore area of the Gippsland Basin. Most of the offshore areas of the basins contain relatively high proportions of dispersed coaly material

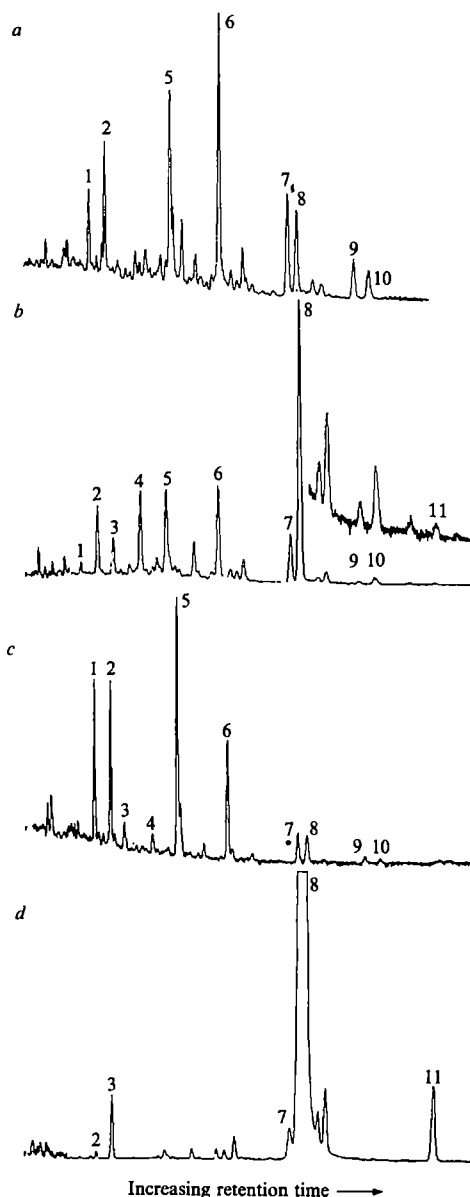


Fig. 1 Partial single-ion chromatograms of *m/z* 191 for Kingfish (a) and Turrum (b, 5,177 ft; c, 7,624 ft) oils from the Gippsland Basin and an extract from Yallourn lignite (d). Samples were analysed on a Finnigan 4023 GC-MS system. GC conditions were: 40 m fused silica WCOT column programmed from 10 to 200 °C at 20 °C min⁻¹ and then 4 °C min⁻¹ to 280 °C. The mass spectrometer was operated in multiple-ion detection mode at an electron energy of 70 eV and ion current of 250 μ A. Peak identification: 1, 18 α (H)-22,29,30-trisnorhopane; 2, 17 α (H)-22,29,30-trisnorhopane; 3, 17 β (H)-22,29,30-trisnorhopane; 4, 17 α (H),21 β (H)-28,30-bisnorhopane; 5, 17 α (H),21 β (H)-30-norhopane; 6, 17 α (H),21 β (H)-hopane; 7 and 8, 22S and R 17 α (H),21 β (H)-30-homohopane; 9 and 10, 22S and R 17 α (H),21 β (H)-30,31 bishomohopane; 11, 17 β (H),21 β (H)-30-homohopane. Inset in b is $\times 10$ magnification.

that is very similar to the onshore lignite and brown coal deposits although of a slightly higher maturity. Figure 2a shows a cross-section through this part of the Gippsland Basin and illustrates the presence of non-marine sands, shales and coals in the reservoir areas of the Turrum well. Figure 2b shows the stratigraphical sequence through the Turrum 2 well, again indicating the presence of interspersed coals in the reservoir zones. In this study the Yallourn lignite is used as a concentrated example of the type of material that is typically dispersed throughout the basin.

Van Dorsselaer *et al.*⁷ found that the major triterpane component in Yallourn lignite is the $17\alpha(\text{H})$, $21\beta(\text{H})$ - $22\text{R}-\text{C}_{31}\text{H}_{54}$ homohopane diastereomer. The m/z 191 chromatogram (Fig. 1d) for the hydrocarbon fraction from a sample of Yallourn lignite demonstrates that in addition to the $17\alpha(\text{H})$, $21\beta(\text{H})$ - $22\text{R}-\text{C}_{31}$ -homohopane, $17\beta(\text{H})$ - C_{27} -trisorhopane and $17\beta(\text{H})$, $21\beta(\text{H})$ - C_{31} -homohopane were also present as very minor components. Note that this sample of lignite is only being used to demonstrate the unusual hopane distribution; it is unlikely that it is specifically responsible for the unusual hopane distributions in the shallow Turrum oil because it does not contain the C_{32} -homohopanes. Detailed analysis of the Turrum 2 oil showed that the two $17\beta(\text{H})$ -hopanes mentioned above were also present in the oil. The presence of $17\beta(\text{H})$ -hopanes in crude oils is in itself a very unusual observation. It is generally considered that at the maturity levels required for the formation of petroleum, the $17\beta(\text{H})$ isomers will be converted into their $17\alpha(\text{H})$ analogues, although trace amounts of the $17\beta\text{H}$ C_{27} -hopane are present in genuine source rocks and petroleum⁸. If this is the case, the only explanation for the presence of the two $17\beta(\text{H})$ hopanes plus the predominance of the $22\text{R}-\text{C}_{31}$ -homohopane seems to be that they are derived directly from an immature brown coal source, similar to the Yallourn lignite, which has been in contact with the oil.

There are alternative explanations for this unusual distribution of triterpanes. MacKenzie *et al.*^{9,10} have proposed that an oil can appear immature on the basis of one type of biological marker parameter but be apparently mature, or 'normal', in terms of another type of measurement. In other words, a measurement of the extent to which one reaction type has occurred will correspond to different values of a measurement based on a different reaction type. Determination of the % $20\text{S}/20\text{R} + 20\text{S}-24\text{-ethyl}-5\alpha(\text{H}), 14\alpha(\text{H})17\alpha(\text{H})$ -cholestane for the two Turrum oils from the m/z 217 chromatogram gives values of 23% and 43% for the shallow and deep oils, respectively. The value for the shallow oil is similar to that observed by Shi Ji-Yang *et al.*⁵ for samples of immature Chinese oils.

The immaturity of the Turrum 2 oil based on the % $20\text{S}-\text{C}_{29}$ -sterane combined with the hypothesis of Mackenzie *et al.*^{9,10} would suggest that the Turrum 2 oil is an immature oil similar to those first observed by them in samples from China. Whilst agreeing in general with their hypothesis, we feel that the Turrum 2 oil, and possibly other Australian oils are exceptions to this hypothesis. We propose that the unusual distribution of the 22R and $\text{S}-\text{C}_{31}$ -homohopanes in the Turrum 2 oil arises as a result of oil coming into contact with relatively immature brown coal zones in the reservoir areas. Many of the reservoirs in the Gippsland Basin contain significant quantities of dispersed coaly material (Fig. 2a, b) and hence the oil would be in contact with this material for a relatively long period of time. The strongest pieces of supportive evidence for this theory are the presence of the $17\beta(\text{H}), 21\alpha(\text{H})-\text{C}_{27}$ and C_{31} -hopanes in both the oil and a sample of onshore Yallourn lignite and the predominance of the $22\text{R}-\text{C}_{31}$ -homohopane in both the oil and the extract of the Yallourn lignite. The results of this study suggest that, in certain cases, the biological markers in crude oils may not always be derived directly from major source rocks but may be acquired during migration or after accumulation in the reservoir. Such an observation may be unique for Australian basins where the content of coal is generally much higher than for other oil-bearing basins around the world.

We thank Esso Australia Ltd for samples of the Gippsland

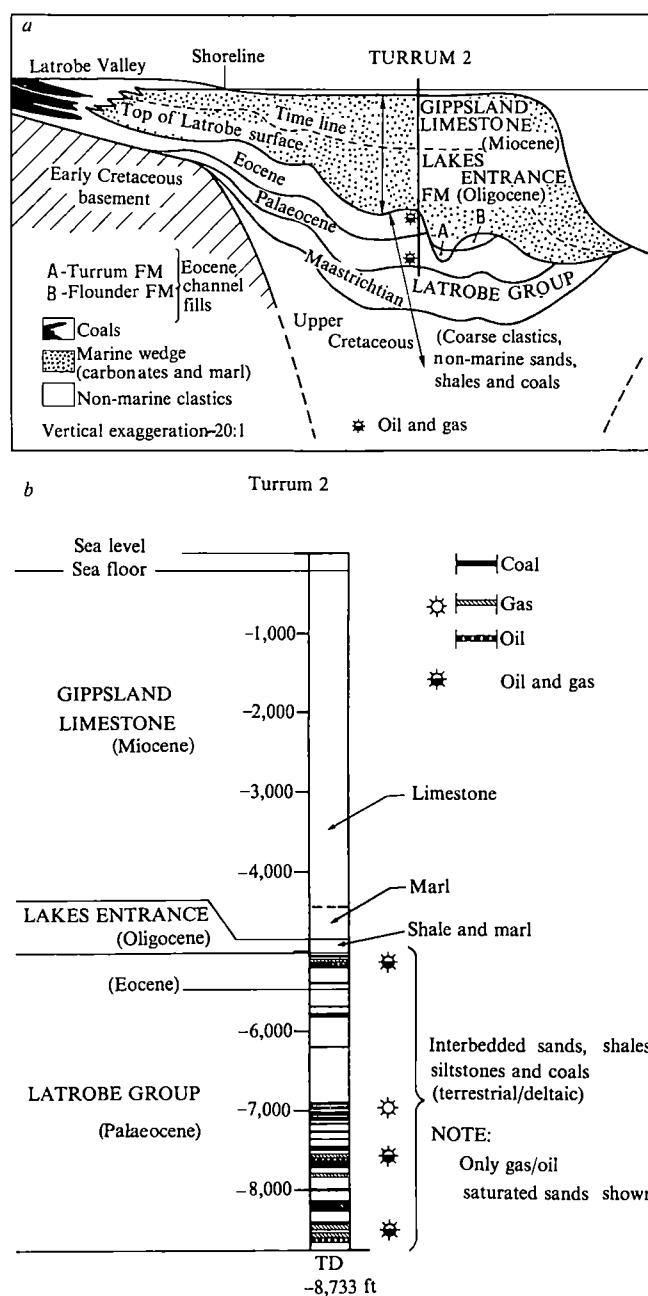


Fig. 2 a, Cross-section through part of the Gippsland Basin in the vicinity of the Turrum 2 well. b, Stratigraphical sequence through the Turrum 2 well.

oils and Dr J. R. Maxwell for his constructive criticisms and for providing preprints, also Esso Australia Ltd and Hematite Petroleum Pty Ltd for permission to reproduce the diagrams shown in Fig. 2. Fig. 2a was originally drawn by A. D. Partridge of Esso Australia Ltd.

Received 19 February; accepted 29 June 1982.

- Seifert, W. K. & Moldowan, J. M. *Geochim. cosmochim. Acta* **45**, 783-794 (1981).
- Ensminger, A., Van Dorsselaer, A., Spyckerelle, Ch., Albrecht, P. & Ourisson, G. *Advances in Organic Geochemistry 1973* (eds Tissot, B. & Biennier, F.) 245-260 (Editions Technip, Paris, 1974).
- Philp, R. P. & Gilbert, T. D. *Australian Petrol. Explor. Ass. J.* **20**, 221-228 (1980).
- Seifert, W. K., Moldowan, J. M. & Jones, R. W. *Proc. 10th World Petroleum Congr., Bucharest; Paper SP8*, 425-440 (Heyden, New York, 1980).
- Shi Ji-Yang *et al. Chem. Geol.* **35**, 1-31 (1982).
- Threlfall, W. F., Brown, B. R., & Griffith, B. R. *Economic Geology of Australia and Papua New Guinea Vol. 3* (eds Leslie, R. B., Evans, H. J. & Knight, C. L.) 41-67 (Australasian Institute of Mining and Metallurgy, Melbourne, 1976).
- Van Dorsselaer, A., Albrecht, P. & Connan, J. *Advances in Organic Geochemistry 1975* (eds Campos, R. & Goni, J.) 53-59 (Enadimsa, Madrid, 1977).
- Seifert, W. K., & Moldowan, J. M. *Advances in Organic Geochemistry 1979* (eds Douglas, A. G. & Maxwell, J. R.) 229-237 (Pergamon, Oxford, 1980).
- Seifert, W. K., Lamb, N. A. & Maxwell, J. R. *Nature* **295**, 223-226 (1982).
- Mackenzie, A. S., Lewis, C. A. & Maxwell, J. R. *Geochim. cosmochim. Acta*, **45**, 2369-2376 (1981).

The representation of auditory space in the mammalian superior colliculus

A. R. Palmer & A. J. King

National Institute for Medical Research, The Ridgeway, Mill Hill, London NW7 1AA, UK

The superior colliculus (SC) is involved in orienting responses to sensory stimuli¹ and contains detailed sensory and motor maps¹⁻³. The visual and somatosensory maps have been well documented⁴⁻¹⁵ and are topographic representations of the primary receptor surfaces. However, the formation of an ordered map of auditory space is rather more problematic as it requires either reorganization of monaural information or combination of information from both ears^{16,17}. Nevertheless, such an ordered map has been demonstrated in the midbrain of the barn owl¹⁸ and there have been indications that a similar map occurs in mammals^{7-9,12,13,19-21}, although a recent study suggests that this is not the case in the cat²². Here we report briefly the results of our study, showing that auditory space is precisely represented in the deep layers of the guinea pig SC. This map of auditory space resembles the visual map in that cells responding to sounds in the anterior contralateral field are located rostrally, while those responding to sounds in the posterior contralateral field are located in caudal SC.

We have recorded auditory evoked responses of 155 cells throughout the deep layers of the guinea pig SC. After anaesthetizing the animals²³, the tracheae were cannulated and rectal temperature was maintained at 37 °C. A craniotomy was performed above the cortex overlying the SC and recordings were made with cortex intact using glass-coated tungsten microelectrodes. The animals were held from behind in a normal position with a minimal head-holder screwed to the skull. The pinnae, which were reflected by the initial incision, were carefully repositioned by sutures. The animal was placed at the centre of an anechoic chamber on a small table around which, level with the interaural plane at a radius of 1.1 m, was an array of loudspeakers at 22.5° intervals. A small flashing light was used to locate the centre of the visual receptive fields (RFs) of cells in the superficial layers. Electrodes were positioned to traverse the representation of the horizontal visual meridian so that auditory fields, if in register, would occur within the arc of speakers. A 100-ms burst of noise with a bandwidth of 100–20,000 Hz was presented repeatedly once every 1–2 s, while

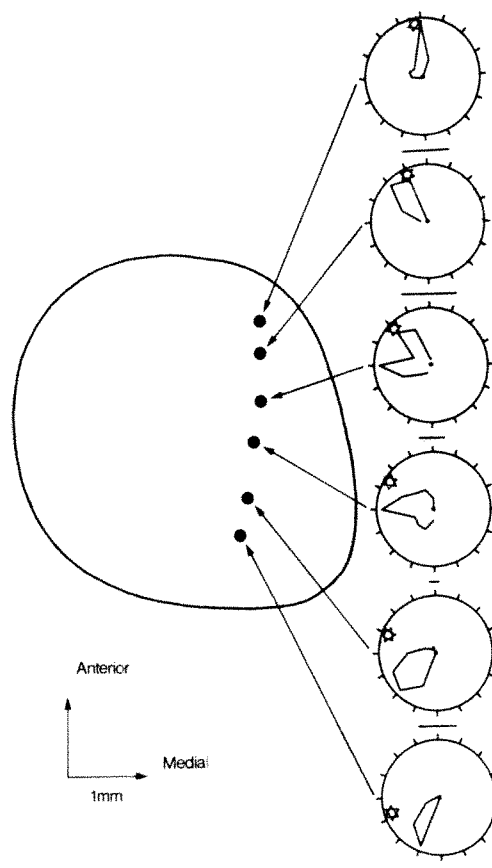


Fig. 2 Surface view of the guinea pig SC showing the location of six electrode penetrations at successive positions along the rostro-caudal axis. Polar diagrams are shown for six SC cells recorded in the electrode penetrations indicated. Each graph shows only responses at one sound level, at which the field was well defined, near threshold for each cell. Bars indicate 0.5 spikes per stimulus. Stars indicate the position of the RF of superficial layer visual cells. The cell showing two lobes could not be allocated a single preferred sound location and does not appear on the subsequent figure.

the recording electrode was being advanced through the deep layers of the colliculus. Once a single cell was isolated, its average discharge was measured in response to sound from the 11 speakers. Electrolytic lesions were placed in each electrode track to enable accurate identification of the recording site from histological reconstructions.

Of the cells we have studied, 75% showed a preference for sound originating from a particular direction. The effect of stimulus intensity on this directional preference was examined

Fig. 1 Number of spikes evoked from a SC cell per presentation of a 100-ms wideband noise stimulus, as a function of the horizontal location of the sound source and its level. Each value plotted on the radial axis of the polar graph is the mean response to 32 presentations. The repetition rate of the stimulus was decreased until an optimal response was obtained which usually occurred at one presentation every 1–2 s. In *a* the repetition rate was one every 1,800 ms and in *b* one every 1,600 ms. Only spikes occurring during a time window 10–70 ms after the stimulus onset were counted to minimize the contribution of spontaneous discharges. The bar represents a radial extent equal to 0.5 counts per presentation. It is clear that the discharge rates measured are extremely low. Although habituation in the SC deep layers has been well documented, increase in the inter-stimulus interval beyond those used did not increase the discharge probability. Such poor responsiveness has been attributed by several authors to the use of inappropriate stimuli. For example, cells in deep SC are known to be more responsive to moving stimuli which were not possible with the present apparatus. The angle of the polar plot represents the angular horizontal position of the loudspeaker. The star symbol indicates the position of the centre of the visual RF of cells in the superficial layers encountered in the same electrode penetration. Note that the highest sound level did not evoke the biggest response. Such non-monotonic responses were frequently encountered.

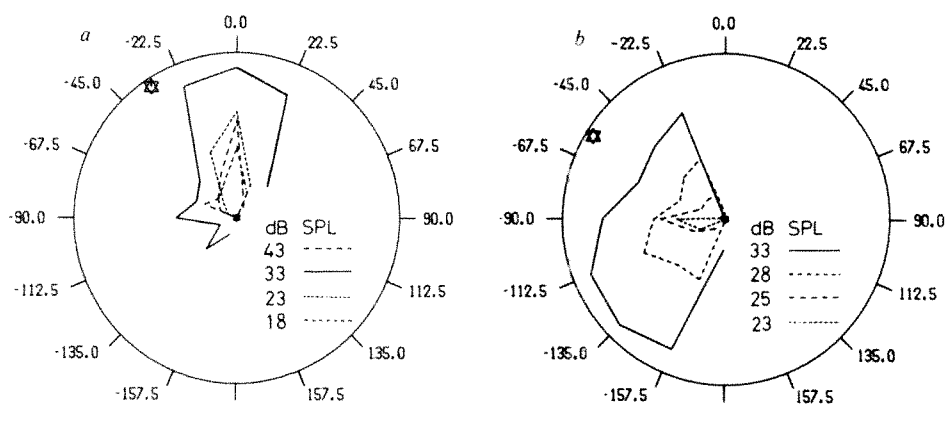
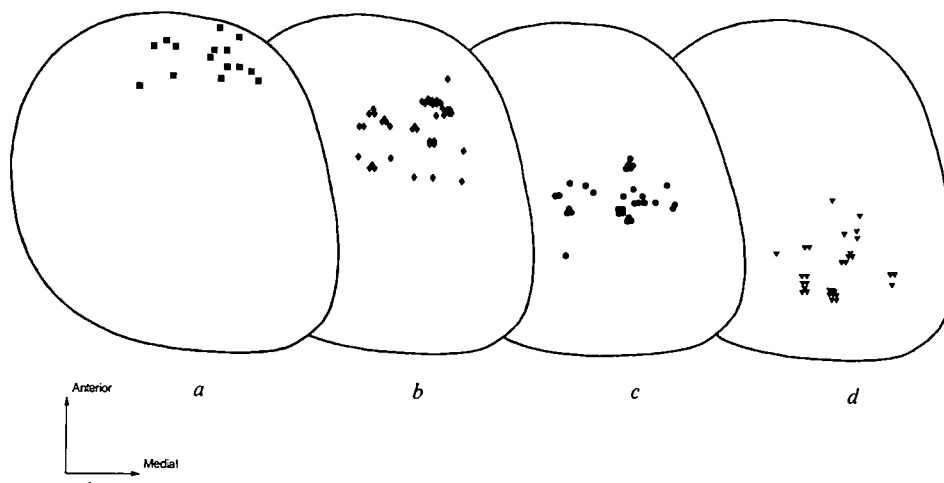


Fig. 3 Four identical surface views of the guinea pig SC. *a* Shows the position of electrode penetrations in which visual responses in the superficial layers were observed, but no auditory responses could be detected in the deeper layers. *b-d* Show respectively the position of cells which showed a preference for sounds located at 0–45°, 67.5–90° and 112.5–157.5°.



in 92 cells. Of these, 39% were narrowly tuned to a particular direction regardless of the sound level used, whereas the directional tuning of the remaining 61% broadened markedly with increasing stimulus intensity. Two examples of cells showing these characteristics are illustrated in Fig. 1. The cell shown in Fig. 1*a* responded to sound emanating from a limited spatial angle in front of the animal, even when noise levels were more than 25 dB above its minimum threshold. Figure 1*b* shows the response of a cell which preferentially responded to sounds from a particular direction only for noise levels near threshold. For levels even a few dB above this, however, the range of effective sound locations expanded, particularly in the caudal direction, in some cases occupying the whole contralateral field. The only cells which were driven by sounds in the ipsilateral auditory field were those with preferred sound locations at or near 0° (see Fig. 1*a*). Of 54 penetrations in which auditory responses were observed, more than one cell was found in 40. Tuned cells in a single penetration responded optimally to sounds from the same direction.

As the site of the recording electrode was moved from the anterior to the posterior part of the superior colliculus, the location of sounds to which the cells responded most vigorously shifted from the anterior to the posterior auditory field of the animal. This spatial representation of auditory space is analogous to the visual map over the collicular surface. Figure 2 shows data from a single animal in which responses from six electrode positions were analysed. The cells at each electrode site attended to a narrow region of space and formed an ordered array including the entire hemifield. Whether the vertical axis is also represented in the medio-lateral axis of the colliculus remains to be investigated.

That cells in a particular region of the superior colliculus are tuned to a specific location can also be illustrated using pooled data from different animals. Figure 3 illustrates the collicular position of 117 cells which showed a preference for sound location, grouped according to spatial location of their auditory receptive fields. These data indicate a reasonably strict topographical mapping of the auditory projection onto the deep layers of the SC over most of its rostro-caudal dimension (pooling of data and other unavoidable inaccuracies obscures the monotonic progression shown in Fig. 2). We did not find any cells responsive to auditory stimulation in 15 penetrations through the rostral pole of the SC (as indicated in Fig. 3*a*) even though these tracks certainly traversed both deep and superficial layers (in which visual responses were recorded).

Having demonstrated a well organized auditory map in the SC an obvious question is whether this map is in register with those of other modalities. Certainly, the visual maps found in other rodents^{4,8–10,12–14} resemble the topographic arrangement shown in Fig. 3. More direct evidence is, however, provided by our own visual RF data. In each penetration we routinely determined the centre of the RFs of cells in the superficial layers. The positions of these were in register with the auditory

fields ($\pm 11^\circ$) in 43% of cases, but often severe discrepancies of up to 60° occurred, particularly for auditory fields in front or behind the animal. Three main factors contributed to this discrepancy: (1) the abnormal position of the eye due to anaesthesia (on average the eye was 10.5° forward and 22° downward of the central orbit position). (2) The rostral and caudal curvature of the SC caused sampling from different topographical regions in the superficial and deeper layers. (3) The absence of auditory responses in the rostral SC. Allowing for these it appears that when the eye is in a normal position the maps of visual and auditory space are in register. Registration has also been indicated by previous authors^{7–9,12,13,19–21}, but final resolution of this question awaits detailed simultaneous mapping of the different modalities.

It is generally accepted that the auditory system localizes sound by comparing time and intensity differences between the two ears, although significant monaural localization has been demonstrated¹⁷. As we have shown here, cells within the SC are sensitive to the cues associated with a specific spatial location and are arranged to produce an internal representation of these locations. We do not yet know either the cues used by the guinea pig in localizing sound or the developmental strategies used in ordering the neural connections. For these reasons directional hearing is and has been a particularly challenging research problem, the ultimate solution of which will depend on understanding the nature of the excitatory and inhibitory interactions between the two ears and the detailed circuitry of the auditory projections.

We thank S.-H. Chung, M. J. Keating and S. Grant for discussion and G. E. Goldsmith and particularly S. J. Caidan for technical assistance. A.J.K. is a MRC scholar.

Received 25 May; accepted 30 July 1982.

- Wurtz, R. H. & Albano, J. E. *A. Rev. Neurosci.* **3**, 189–226 (1980).
- Sprague, J. M., Berlucchi, G. & Rizzolatti, G. in *Handbook of Sensory Physiology* Vol. VII/B (ed. Jung, R.) 27–101 (Springer, Berlin, 1972).
- Gordon, B. in *Physiology* Ser. 1, 3 (ed. Hunt, C. C.) 185–231 (Butterworth, London, 1975).
- Siminoff, R., Schwassmann, H. O. & Kruger, L. *J. comp. Neurol.* **127**, 435–444 (1966).
- Feldon, S., Feldon, P. & Kruger, L. *Vision Res.* **10**, 135–143 (1970).
- Cynader, M. & Berman, N. *J. Neurophysiol.* **35**, 187–201 (1972).
- Gordon, B. *J. Neurophysiol.* **36**, 157–178 (1973).
- Dräger, U. C. & Hubel, D. H. *Nature* **253**, 203–204 (1975).
- Dräger, U. C. & Hubel, D. H. *J. Neurophysiol.* **38**, 690–713 (1975).
- Dräger, U. C. & Hubel, D. H. *J. Neurophysiol.* **39**, 91–101 (1976).
- Stein, B. E., Magalhães-Castro, B. & Kruger, L. *J. Neurophysiol.* **39**, 401–419 (1976).
- Tiao, Y. C. & Blakemore, C. *J. comp. Neurol.* **168**, 483–504 (1976).
- Chalupa, L. M. & Rhoades, R. W. *J. Physiol., Lond.* **270**, 595–626 (1977).
- Finlay, B. L., Schneps, S. E., Wilson, K. G. & Schneider, G. E. *Brain Res.* **142**, 223–235 (1978).
- Stein, B. E. & Dixon, J. P. *J. comp. Neurol.* **183**, 269–284 (1979).
- Erulkar, S. D. *Physiol. Rev.* **52**, 237–360 (1972).
- Durlach, N. I. & Colburn, H. S. in *Handbook of Perception* Vol. 4 (eds Carterette, E. C. & Friedman, M. P.) 365–456 (Academic, New York, 1978).
- Knudsen, E. I. & Konishi, M. *Science* **200**, 795–797 (1978).
- Wickelgren, B. G. *Science* **173**, 69–72 (1971).
- Updyke, B. V. *J. Neurophysiol.* **37**, 896–909 (1974).
- Harris, L. R., Blakemore, C. & Dohaghy, M. *Nature* **288**, 56–59 (1980).
- Wise, L. Z., Irvine, D. R. F., Pettigrew, J. D. & Calford, M. B. *Neurosci. Lett. Suppl.* **8**, S88 (1982).
- Evans, E. F. *Archs Otol.* **105**, 185–186 (1979).

Metamorphosis of the insect nervous system: changes in morphology and synaptic interactions of identified neurones

Richard B. Levine* & James W. Truman

Department of Zoology, University of Washington, Seattle, Washington 98195, USA

The nervous system of holometabolous insects directs the behaviour of three radically different stages, the larva, pupa and adult. In some cases, larval neurones degenerate during metamorphosis and are replaced in the adult by neurones derived from retained embryonic neuroblasts^{1,2}, but many larval neurones are retained and undergo a morphological and synaptic reorganization which allows them to perform new functions in the adult^{3,4}. This cellular rearrangement, however, creates a problem in that the developing adults continue to display pupal-like behaviour even after the neurones attain their adult form. We show here that in the tobacco hornworm, *Manduca sexta*, the adult function of a neurone is prevented from being expressed precociously by the persistence of inhibitory influences that are removed abruptly at adult emergence.

We have investigated the changes that occur during metamorphosis in the relatively simple abdominal portion of *M. sexta*. During adult development several external muscle groups differentiate and are innervated by motoneurones whose larval targets have degenerated shortly after the larval-to-pupal molt⁴. The motoneurone MN-1 controls dorsal external oblique muscle DEO 2 in the larva, but loses this target in the pupal stage, innervating a new dorsal external muscle (DE 4) in the adult (Fig. 1). During this transition the cell undergoes considerable anatomical reorganization⁵. Figure 1 shows that the growth of new processes was most vigorous between days 4 and 12 of development and the adult morphology was essentially established by day 14.

The structural reorganization of MN-1 is correlated with changes in the pattern of synaptic inputs to the neurone. We chose to study a stretch receptor, specifically SR-3, which is located bilaterally in each abdominal segment and is present throughout the life of the insect⁵ (Fig. 1). Each sensory cell sends an axon into the central nervous system (CNS) and responds to stretch of its segment with a burst of action potentials⁶. Its central processes, which are similar at all stages, branch in the dorsal region of the neuropil and are confined totally to the hemiganglion in which they enter (Fig. 1).

During the larval stage we observed that MN-1 received excitatory input from the SR-3 ipsilateral to its axon and target muscle (Fig. 2). A single electrical stimulus to the stretch receptor resulted in a constant-latency excitatory postsynaptic potential (e.p.s.p.) in the motoneurone. After subtracting the portion of this latency due to conduction of the SR-3 spike into the CNS (obtained by recording from SR-3 in the periphery and within the CNS), the remaining latency was less than 1 ms, a delay consistent with the pathway being monosynaptic. The processes of both neurones extended through similar regions of the dorsal neuropil and simultaneous cobalt backfills revealed areas of potential contact. This pathway remained unchanged throughout metamorphosis.

The larval MN-1 was inhibited by the SR-3 contralateral to its target. Stretch of this SR-3 or trains of electrical stimuli to its axon caused inhibition of tonic MN-1 activity, which was associated with a hyperpolarization and a conductance increase in the motoneurone (Figs 2, 3). The inhibitory postsynaptic

potential (i.p.s.p.) evoked by a single spike in the contralateral SR-3 had a long, variable latency and decreased rapidly in an all-or-none fashion during repeated stimulation. The terminal branches of the contralateral SR-3 were anatomically separated from the main dendritic arborization of MN-1. The only point of possible contact between the two neurones—the neurite leading from the soma of MN-1—passed ventral to the processes of SR-3. These data suggest that the inhibitory influence of the contralateral SR-3 is mediated by a polysynaptic pathway.

In the early pupal stage (days 1 and 2 after pupal ecdysis), the contralateral SR-3 continued to inhibit MN-1, but the relationship changed dramatically during metamorphosis. In the adult moth (1–2 days post-emergence), trains of stimuli to the contralateral SR-3 evoked a large depolarization and firing of the motoneurone (Fig. 3). Single stimuli resulted in an e.p.s.p. with a short, constant latency (Fig. 2). The i.p.s.p. which resulted from stimulation of the same SR-3 in earlier stages was not revealed by hyperpolarization or depolarization of the adult MN-1. On reexamination of the pathway in the larva, it was found that hyperpolarization of MN-1 caused reversal of the i.p.s.p. in a single step, and failed to reveal a hidden, short latency excitatory component in the interaction (Fig. 2). This change in the functional relationship of SR-3 with MN-1 coincides with the morphological changes shown by the motoneurone. The proximity of the new adult-specific dendrites to the terminal branches of the contralateral SR-3, together with the short, constant latency of the new e.p.s.p., suggests that the SR-3 makes direct contacts with these new dendrites.

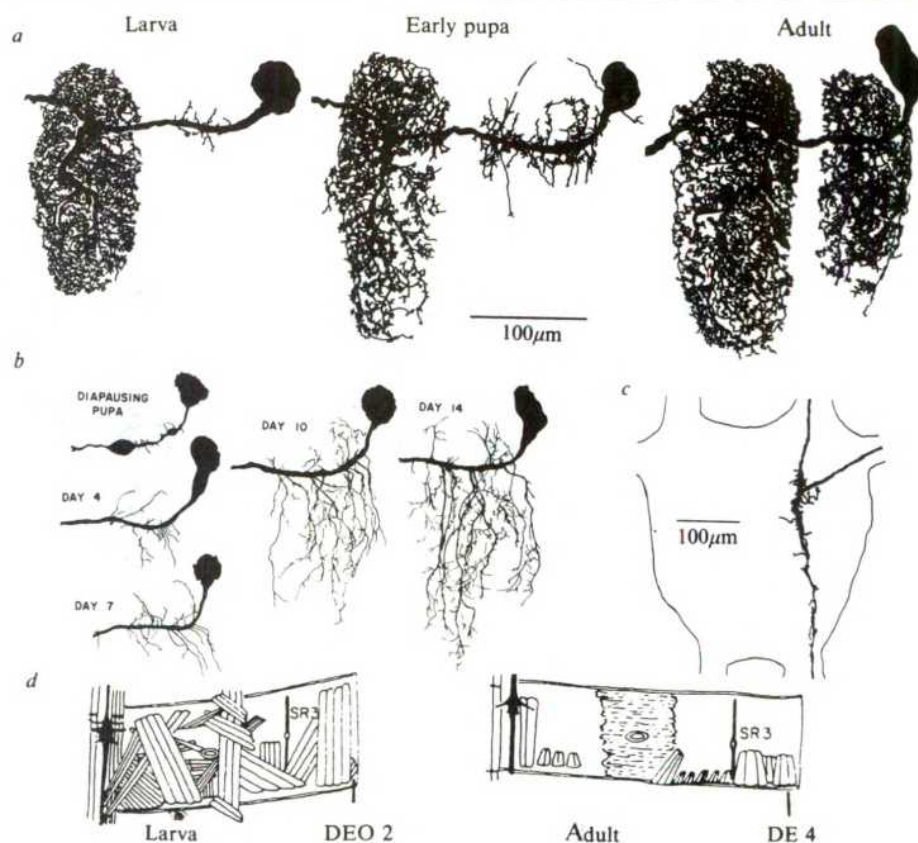
MN-1 attains its adult morphology and has full control of its new target 3–4 days before adult emergence. Despite these changes, however, the behaviour of the animal (which is covered by a pupal cuticle), is pupal in character until the time of adult emergence, when its behaviour abruptly switches to that of the adult⁷. Certain behaviours such as the defensive gin-trap reflex are unique to the pupal stage⁸, and new neuronal pathways must develop without disrupting them. On the last day of adult development, individual SR-3 impulses evoked a biphasic response in the contralateral MN-1, a short latency e.p.s.p. followed by an i.p.s.p. (Fig. 2). Occasionally the e.p.s.p. was sufficient to evoke an action potential in MN-1, but trains of stimuli or stretch of the receptor resulted in inhibition of the motoneurone (Fig. 3). The inhibitory component disappeared abruptly following adult emergence. Within 30 min of emergence, bursts of stimuli to the contralateral SR-3 evoked a pure excitatory response in MN-1 and single stimuli produced a short latency e.p.s.p., without an i.p.s.p. (Fig. 2). Furthermore, depolarization of the motoneurone revealed no i.p.s.p., and spontaneous activity was not inhibited during the period formerly associated with the i.p.s.p.

The functional and anatomical reorganization of MN-1 is reasonable in terms of its behavioural roles in the three stages of insect life. Both the larval and adult targets of MN-1 are near the dorsal midline of the abdominal segment. In the larva and pupa many behaviours depend on the ability of the abdomen to flex laterally. The right and left targets of MN-1 would be antagonists in this situation. Within a day after adult emergence, however, the abdomen of the moth becomes relatively rigid, and flexion is confined to the dorso-ventral plane. This lack of lateral movements makes asymmetric SR-3 inputs relatively pointless, as the only movements that are possible are ones for which the two DE 4 muscles must contract or relax together. Indeed, in the adult the right and left MN-1s often fire together in synchronous bursts. This synchrony is not due to direct coupling between the cells, which suggests that they share numerous common inputs.

A simple model for the change in the relationship of MN-1 to the contralateral SR-3 is shown in Fig. 3. In the larva, the contralateral SR-3 inhibits MN-1 through an unidentified interneurone. During adult development MN-1 grows new dendritic branches and accepts excitatory synapses from the contralateral SR-3. Before adult emergence, however, this excitatory connection is not behaviourally effective because the persisting parallel

*Present address: Department of Biology, Rice University, Houston, Texas 77001, USA.

Fig. 1 Structural reorganization of MN-1. *a*, Camera lucida drawings of MN-1 in the larval, early pupal and adult stages. Neurones were stained by passing positive current through an intracellular micropipette filled with 10% cobalt nitrate, and the stain enhanced in whole mount with a modification of the Timm's silver intensification procedure¹¹. In the larval and adult stages, MN-1 was identified by correlating activity recorded intracellularly from the motoneurone with that recorded extracellularly or intracellularly from the target muscle. In addition, action potentials in the MN-1 axon may be identified unambiguously in extracellular records from the third branch of the 'dorsal' segmental nerve, which allows MN-1 identification in the pupal stage. Note that during adult development MN-1 acquires a new dendritic field ipsilateral to its soma. *b*, Growth of the dendritic field ipsilateral to the MN-1 cell body. Neurones were stained at various times during adult development by back-diffusion of cobalt through the cut axon, followed by silver intensification of sectioned material. Although the period of adult development is 18 days, dendritic growth is essentially complete by day 14. *c*, Morphology of the stretch receptor (SR-3) sensory cell within the abdominal ganglion of an adult. The cell's morphology is similar throughout the animal's life. Note that its processes do not cross the midline of the ganglion. Although not shown, the processes of the sensory cell extend into the adjacent abdominal ganglia. *d*, Abdominal musculature in the larva and adult. In each case half of one abdominal segment is shown as though the animal had been cut along the dorsal midline and pinned open. The ventral nerve cord is on the left. The intersegmental muscles have been dissected away to reveal the external muscles, all of which die at the end of the larval stage and are replaced by newly generated muscles in the adult. The motoneurone MN-1 innervates a dorsal external oblique muscle (DEO 2) in the larva, and a dorsal external muscle (DE 4) in the adult. The right-hand stretch receptor (SR-3) is shown at each stage.

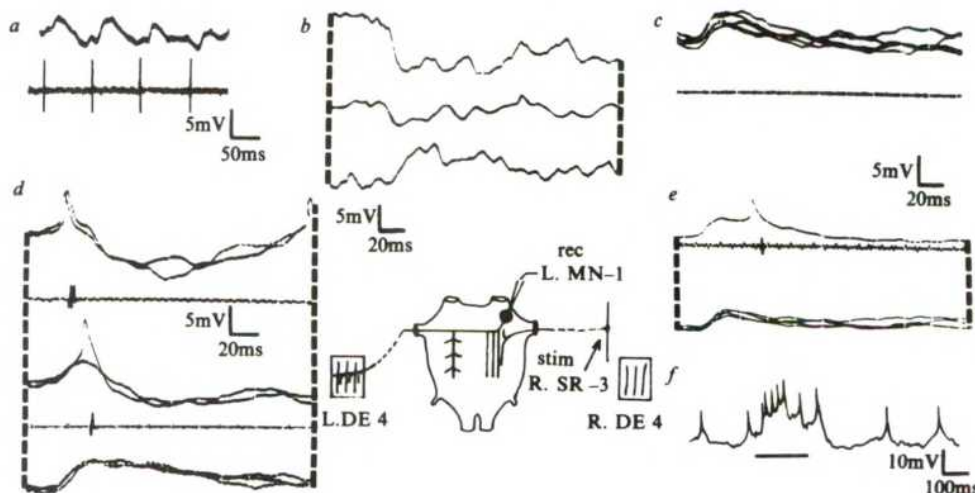


inhibitory pathway is always co-activated. An alternative interpretation is that the inhibitory synapse of the larval stage becomes excitatory and passes through a bifunctional stage⁹. Our data suggest, however, that the larval pathway is polysynaptic, while the adult pathway is direct.

The inactivation of the inhibitory pathway may be triggered

by eclosion hormone, which is released at the end of adult development and acts on the nervous system to release the emergence behaviours¹⁰. A second possible signal is the steroid 20-hydroxyecdysone, the reduction of which late in adult development triggers the death of many motoneurons and interneurons (J.W.T. and L. M. Schwartz, in preparation).

Fig. 2 Influence of SR-3 on MN-1 at different stages in the life cycle. *a*, The larval MN-1 is excited by the SR-3 ipsilateral to its target muscle. Each action potential in the SR-3 sensory cell (bottom, recorded near the sensory organ) causes an e.p.s.p. in the ipsilateral MN-1 (top). *b*, Inhibition of the larval MN-1 by the contralateral SR-3. A single electrical stimulus to the contralateral SR-3 (at the start of each trace) caused an i.p.s.p. in MN-1. The i.p.s.p. was enhanced by depolarization of MN-1 (top), and reversed by hyperpolarization (bottom). Note that a short-latency e.p.s.p. is not present (compare with *c-e*). *c*, Influence of the contralateral SR-3 on MN-1 in an adult 30 h after emergence. Intracellular (top), and extracellular (bottom) records from MN-1. Single stimuli to the SR-3 (at the start of the trace) evoked a constant-latency e.p.s.p. in the contralateral MN-1 (multiple trials, compare with *b*). *d*, Traces same as in *c*. About 5 h before adult emergence, single stimuli to SR-3 evoked a biphasic response in the contralateral MN-1. The later, inhibitory component was enhanced by depolarization of the motoneurone (top), and reversed by hyperpolarization (bottom). The early component may lead to an action potential (also visible in the extracellular records). *e*, Single stimuli to SR-3 30 min after emergence evoked only the short-latency depolarizing response in the contralateral MN-1 (bottom). Depolarization of the motoneurone revealed no inhibitory component (top). Note that action potentials were not blocked during the period formerly associated with the i.p.s.p. *f*, Bursts of stimuli to the contralateral SR-3 (bar) 30 min after emergence excited the MN-1. The insert shows the experimental set-up for *b-e*. The adult morphology of MN-1 is drawn schematically. rec, Recording electrode; stim, stimulating electrode.



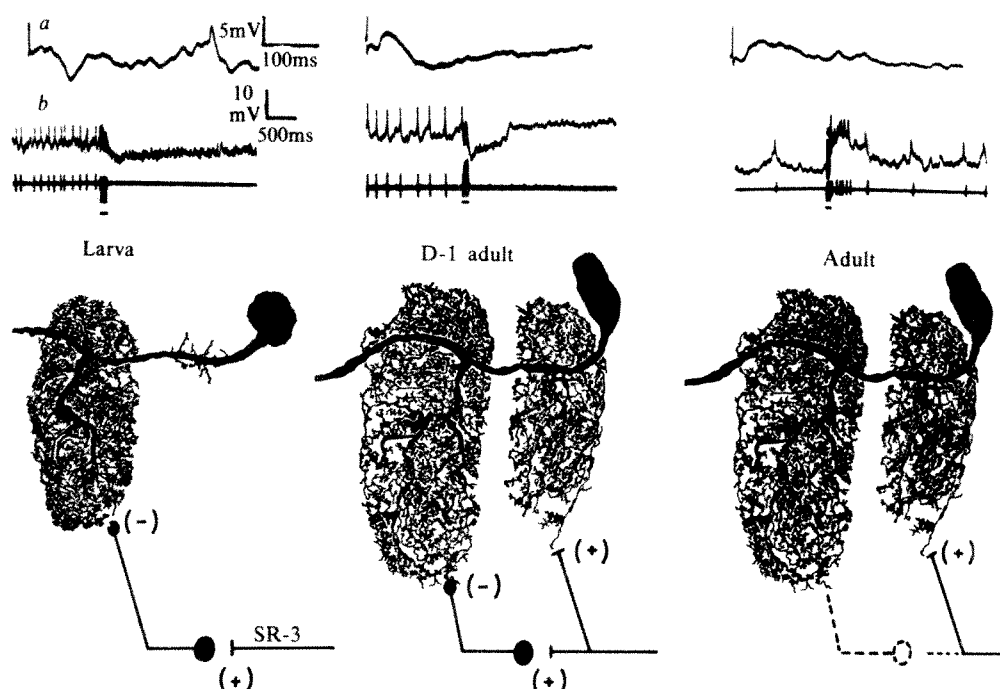


Fig. 3 Model for the changes observed in the interaction between MN-1 and SR-3. *a*, Response of MN-1 to single stimuli delivered to the contralateral SR-3. *b*, Response of MN-1 to a burst of stimuli (100 Hz) to the contralateral SR-3, which mimics the response of the receptor to natural stretch. Intracellular (top) and extracellular (bottom) records from MN-1. In the larva MN-1 is inhibited by the contralateral SR-3 through a polysynaptic pathway. The processes of SR-3 do not cross the midline of the ganglion, and lie in a different region of neuropil from the main neurite of MN-1. Single stimuli evoked long-latency i.p.s.p.s. On the day before adult emergence (D-1 adult) SR-3 evoked a biphasic response in the contralateral MN-1; the original inhibitory path was co-activated with a new direct excitatory path. Bursts of receptor spikes, however, still inhibited MN-1. The new dendritic processes of MN-1 overlapped with those of SR-3. After adult emergence, the inhibitory component was lost, and the SR-3 evoked a pure depolarizing response in the contralateral MN-1.

The inhibitory interaction between SR-3 and MN-1 is permanently inactivated after adult emergence. However, a reversible inactivation of parallel inhibition might be applicable to other situations in which hormones or other factors alter markedly the function of a particular neural pathway.

Received 6 April; accepted 7 July 1982.

1. Nordlander, R. H. & Edwards, J. S. *Wilhelm Roux's Arch. dev. Biol.* **164**, 247–260 (1970).
2. Matsumoto, S. G. & Hildebrand, J. G. *Proc. R. Soc. B* **213**, 249–277 (1981).
3. Truman, J. W. & Reiss, S. E. *Science* **192**, 477–479 (1976).
4. Truman, J. W. & Levine, R. B. in *Current Methods in Cellular Neurobiology* (eds Barker, J. & McKelvey, J.) (Wiley, New York, in the press).

This work was supported by grants from the NIH (R01-NS13079), NSF (PCM-8029975) and the McKnight Foundation. R.B.L. was supported by a NIH postdoctoral fellowship. Figure 1d was modified from unpublished drawings of S. E. Reiss, who also provided valuable assistance with the histology.

5. Libby, J. L. *Ann. ent. Soc. Am.* **54**, 887–896 (1961).
6. Weevers, R. de G. *J. exp. Biol.* **44**, 177–194 (1966).
7. Truman, J. W. *J. comp. Physiol.* **107**, 39–48 (1976).
8. Bate, C. M. *J. exp. Biol.* **59**, 95–107 (1973).
9. Watclet, H. & Kandel, E. R. *Science* **158**, 1206–1208 (1967).
10. Truman, J. W. in *Insect Biology in the Future* (eds Locke, M. & Smith, D. S.) 385–401 (Academic, New York, 1980).
11. Bacon, J. P. & Altman, J. S. *Brain Res.* **138**, 359–363 (1977).

A transient outward current in a mammalian central neurone blocked by 4-aminopyridine

B. Gustafsson*, M. Galvan†, P. Grafe† & H. Wigström*

* Department of Physiology, University of Göteborg, PO Box 33031, S-400 33 Göteborg, Sweden

† Department of Physiology, University of Munich, Pettenkoferstrasse 12, 8000 Munich 2, FRG

It is becoming increasingly clear that nerve cells in the mammalian central nervous system (CNS) have a very complex electroresponsiveness. They exhibit not only time- and voltage-dependent Na^+ and K^+ conductances, analogous to those in the squid giant axon¹, but also a variety of other conductances that have a significant role in the control of cell excitability. Of the outward currents, there are, in addition to the delayed rectifier, the Ca^{2+} -activated K^+ current^{2,3} which underlies the long-lasting spike afterhyperpolarization, and the M current⁴, a non-inactivating K^+ current evoked by membrane depolarization and blocked by muscarinic, cholinergic agonists. We demonstrate here the existence in a mammalian central neurone (hippocampal CA3 pyramidal cells) of yet another outward current, which is transient and may be carried by K^+ ions. Further, the experiments show that this current is substantially reduced by the convulsant 4-aminopyridine (4-AP)⁵, resulting in a marked increase in cell excitability.

The experiments were performed on transverse slices (400–600 μm thick) of guinea pig hippocampus. The slices were kept either half or totally immersed (see below) in an experimental chamber perfused with a solution containing (in mM): NaCl, 123; KCl, 3.0; CaCl_2 , 2.0; MgSO_4 , 2.0; NaHCO_3 , 26; glucose, 10. The temperature was kept constant at either 33 °C or 26 °C. Neurones in the CA3 region were impaled with 3 M KCl-filled microelectrodes and voltage-clamped using a single electrode switched clamp circuit (a DAGAN 8100 or a custom-built amplifier of similar design⁶); the switching frequency was 3 kHz and the duty cycle was 10–25%. Possible artefacts involved in the use of these instruments have been discussed elsewhere⁷. Drugs were applied in fixed concentrations to the bathing solution and the data collected were either computer-averaged or photographed from the oscilloscope screen using Polaroid film.

Figure 1a illustrates that in control solution, constant-current pulses applied to CA3 neurones at a resting potential of -70 mV evoked electrotonic potentials (ETPs) which were smaller in the depolarizing than in the hyperpolarizing direction. Closer examination of these depolarizing ETPs shows that they increased rapidly, then suddenly levelled off in a manner which suggests that an opposing outward current had been activated. This behaviour was more clearly seen when Na^+ and Ca^{2+} action potentials were blocked by addition of tetrodotoxin (TTX) and Mn^{2+} ions (Fig. 1b). A similar outward-going rectification (albeit at more depolarized membrane potentials) has been observed in sympathetic and hippocampal CA1 neurones and attributed to depolarization-activation of M channels^{4,8,9}. However, addition of muscarine in sufficient concentrations to block M channels, did not noticeably affect the observed outward rectification (Fig. 1c). Thus it seems that, in these

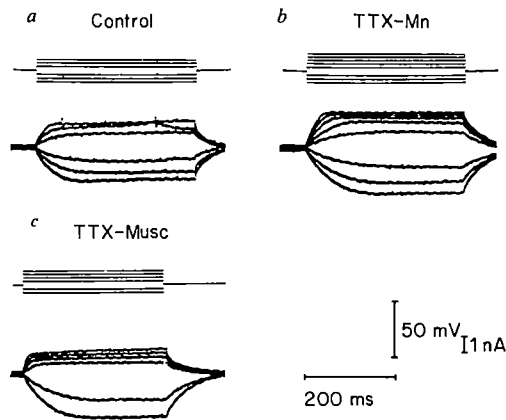


Fig. 1 Recordings of electrotonic potentials (ETPs) in CA3 neurones at 26°C. *a*, Control solution; *b*, in solution containing 3 μ M TTX and 4 mM $MnCl_2$; *c*, in solution containing 1 μ M TTX and 25 μ M muscarine chloride. (Slices were kept totally immersed in the solutions.) The membrane potential was set at -70 mV by passing steady d.c. current through the recording microelectrode, and the amplifier was set in the switched (sample-and-hold) current clamp mode. The top traces show rectangular constant current pulses and the lower traces the resulting membrane potential deflections. *a* and *b* were recorded from the same cell and illustrate the marked attenuation of the amplitude of depolarizing ETPs. Note the slow depolarizing 'creep' of the second largest depolarizing ETP leading to an action potential towards the end of the pulse. This creep was also often observed in the presence of inward current blockers. As judged from the amplitude of the smallest depolarizing and hyperpolarizing pulses, membrane resistance increased in the TTX-Mn solution, possibly due to blockade of tonic synaptic activity. *c* was recorded from another neurone and illustrates that the outward rectification was still present after blockade of possible M-currents by muscarine (Musc).

neurones, there is an outward rectifying current operating in the threshold range, that is distinct from M-channel activation.

Figure 2 shows voltage-clamp recordings from a CA3 neurone in a solution containing TTX. From a holding potential of -70 mV (Fig. 2*a*), hyperpolarizing voltages elicited small inward currents, which were relatively linear and time independent. When the cell was depolarized to potentials greater than -60 mV, a rapidly activating outward current was observed, which decayed over the next several hundred milliseconds. The peak amplitude of this transient outward current was increased as the cell was stepped to more positive potentials. This current-

voltage relationship is plotted in Fig. 2*c* (closed circles); it is nonlinear, indicative of voltage-dependent activation. It was also observed that the current amplitude varied with the holding potential, increasing with membrane hyperpolarization (-70 to -100 mV) and decreasing to zero at holding potentials more positive than -55 mV. Thus, when the same cell was held at -40 mV and subjected to step hyperpolarizations, only steps to potentials more negative than -55 mV were followed, on return to the holding potential, by a transient outward current (Fig. 2*b*). The relationship between the hyperpolarizing step and the resulting outward current is shown in Fig. 2*c* (open circles) and is an approximate measure of the inactivation characteristic of this current.

The transient outward current was observed in all CA3 neurones examined ($n = 35$), and had an amplitude of 4.2 ± 1.5 (\pm s.d.) nA ($n = 9$) as measured 30 ms following a 50–55 mV, 1–1.5 s hyperpolarizing voltage step from -30 mV, and back again. The activation kinetics were too rapid to be resolved using the single electrode clamp technique; our data show only that the current appears to have peaked within 10–15 ms. The inactivation consisted of an initial rapid phase followed by a very slow second phase, which lasted for up to several seconds (Fig. 2*b*); this form of decay could not be described by first-order kinetics.

A transient current having these characteristics has been described in invertebrate^{10,11} and vertebrate¹² neurones and has been shown to be mainly carried by K^+ ions. In the present experiments, an increase in the external K^+ ion concentration (40–60 mM with totally immersed slices) always decreased or abolished the transient outward current. A clear reversal was not obtained but this may simply reflect poor diffusion of K^+ ions into the slice, resulting in only a small positive shift of the K^+ reversal potential. Outward rectification, probably caused by activation of the transient outward current, persisted in solutions containing Ca^{2+} -channel blockers (Mn^{2+} ions) (Fig. 1*b*). Under voltage-clamp, it was also observed that the current was not blocked by Mn^{2+} , although the activation-voltage curve seemed to be shifted ~ 10 mV in the positive direction. This is, to a lesser extent, evident also from Fig. 1*b*. Thus, the results demonstrate the presence of a transient outward current in CA3 neurones, which induces a marked rectification in the current-voltage relation at membrane potentials close to threshold. This current is probably a K^+ -current that is not dependent on Ca^{2+} ion movements.

It has been shown previously that the convulsant agent 4-AP can (at mM concentrations) selectively reduce the amplitude of transient outward currents in invertebrate neurones¹³ as well

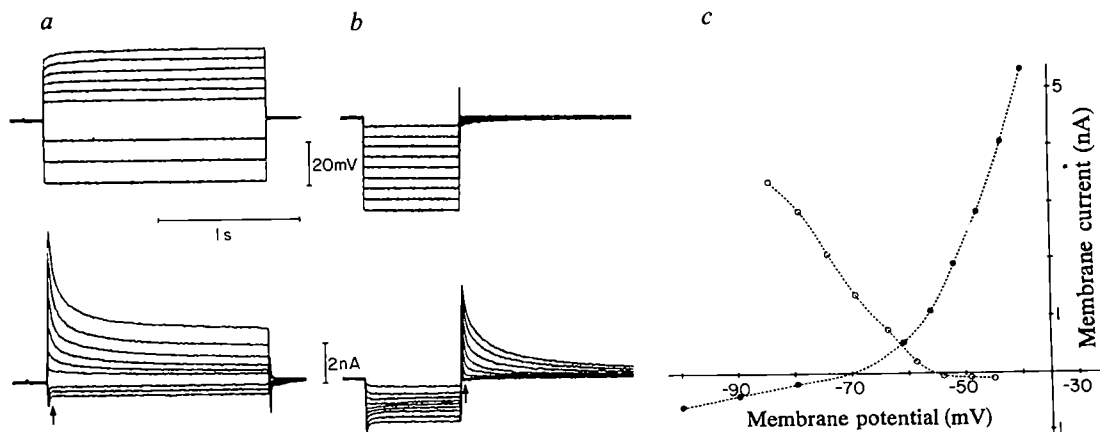
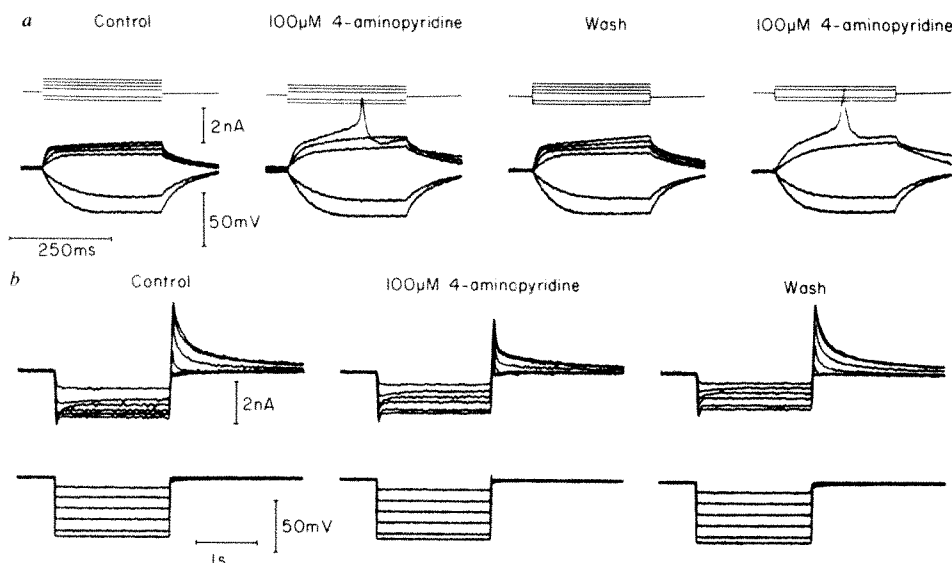


Fig. 2 Computer-averaged recordings of membrane voltage (upper traces) and current (lower traces) from a single CA3 neurone held at -70 mV (*a*) and -40 mV (*b*). Temperature, 33°C. Slices were kept half-immersed in the solutions. Transient outward currents were elicited by step depolarizations from -70 mV or following hyperpolarizations from -40 mV. Note that for large pulses, the membrane voltage attained initially deviated from the command level. This results from inadequate feedback gain—a consequence of single electrode clamping with relatively high resistance microelectrodes. In *b*, small inward current relaxations can be observed during small hyperpolarizing commands, suggesting the presence of M-current. Measurements of membrane voltage and current, made at the times indicated by the arrows in *a* and *b*, respectively, are plotted in *c*. ●, The current-voltage curve from -70 mV; ○, the relationship between hyperpolarizing command potential and the resulting post-pulse current.

Fig. 3 Effect of 4-AP on electrotonic potentials (*a*) and transient outward currents (*b*) measured in two separate CA3 neurones. The experiment illustrated in *a* (26 °C) was performed in the presence of 1 μ M TTX and 25 μ M muscarine chloride; *b* (33 °C) was performed in 0.5 μ M TTX. The slices in *a* were kept totally immersed, while those in *b* were kept half-immersed. In *a* the membrane potential was manually set at -70 mV; in *b* the holding potential was -30 mV. The current clamp records in *a* show electrotonic potentials before, at the end of and 60 min after bath application (8 min) of 100 μ M 4-AP. After a substantial recovery had been obtained, 4-AP was applied again for a longer period (20 min). Note that a maximum effect was not achieved during the first application, as evidenced by the much larger change from outward rectification resulting from the second, longer application. The amplitude of hyperpolarizing ETPs was almost unaltered by 4-AP as was the current necessary to hold the membrane at -70 mV. In *b*, the voltage clamp records illustrate that a brief (5 min) application of 100 μ M 4-AP substantially and reversibly reduced transient outward currents.



as in mammalian cardiac muscle fibres¹⁴. Figure 3*a* demonstrates that in CA3 pyramidal cells, 100 μ M 4-AP can reversibly reduce the outward rectification, resulting in a considerable increase in cell excitability; evidence for this comes from the appearance of a Ca^{2+} action potential. Furthermore, Fig. 3*b* shows that in voltage-clamp, the transient outward current was substantially blocked by 4-AP. These effects were evident after only a few minutes of 4-AP application at times when it was unlikely that the 4-AP concentration equalled that in the bathing solution. The classical K^+ -channel blocker tetraethylammonium chloride (TEA), which blocks delayed rectifier channels¹⁵ and Ca^{2+} -activated K^+ channels in vertebrate neurones¹⁶, did not (at 3 mM) have any significant effect on this current. Note, however, that even in the presence of high concentrations (500 μ M) of 4-AP (in which no transient outward currents were observed), some outward rectification from -70 mV remained. This may be related to the presence of M currents, which were also observed in these cells.

Thus, hippocampal CA3 pyramidal cells exhibit a transient outward current distinct from the delayed rectifier K^+ current, the Ca^{2+} -activated K^+ current and the M current. The activation-inactivation characteristics as well as the pharmacology are similar, in principle, to those of the so-called A current in invertebrate neurones and it seems reasonable to extend this terminology to mammalian central neurones. We cannot, however, be certain that the current described here is similar in all respects to that of invertebrates. Connor and Stevens¹⁷ proposed that the A current controls repetitive firing in gastropod neurones. Its long duration and large amplitude in CA3 neurones also suggest that A currents in these cells, together with the Ca^{2+} -activated K^+ conductance, could serve such a role. More importantly, our data show that A currents are capable of controlling the approach of membrane potential to spike threshold and thus contribute to the control of cell excitability. The activation kinetics suggest that A currents may even affect the action potential (see ref. 18) and excitatory postsynaptic potential trajectories. The postsynaptic excitatory effect of 4-AP can probably be explained by blockade of A currents, although other contributory mechanisms cannot yet be excluded¹⁹. The presence of such currents also in vertebrate nerve terminals might explain the facilitatory actions of aminopyridines on neurotransmitter release¹⁹. Nevertheless, it certainly seems that the postsynaptic effects of 4-AP may contribute to its convulsant action.

This work was supported by grants from the Swedish MRC (projects 05180 and 05954), the Deutsche Forschungsgemein-

schaft (Ga 277/2-4) and the European Science Foundation (European Training Programme in Brain and Behaviour Research).

Received 19 April; accepted 5 June 1982.

- Hodgkin, A. L. & Huxley, A. F. *J. Physiol., Lond.* **117**, 500-544 (1952).
- Hotson, J. R. & Prince, D. A. *J. Neurophysiol.* **43**, 409-419 (1980).
- Krnjevic, K., Puil, E. & Werman, R. *J. Physiol., Lond.* **275**, 199-223 (1978).
- Adams, P. R., Brown, D. A. & Halliwell, J. F. *J. Physiol., Lond.* **317**, 29P (1981).
- Galvan, M., Grafe, P. & Bruggencate, G. *ten. Brain Res.* **241**, 75-86 (1982).
- Djorup, A., Jahnson, H. & Laursen, M. *Brain Res.* **219**, 196-201 (1981).
- Galvan, M. & Adams, R. *Brain Res.* (in the press).
- Brown, D. A. & Adams, P. R. *Nature* **283**, 673 (1980).
- Constanti, A. & Brown, D. A. *Neurosci. Lett.* **24**, 289-295 (1981).
- Adams, D. J., Smith, D. J. & Thompson, S. H. *A. Rev. Neurosci.* **3**, 141-167 (1980).
- Connor, J. A. & Stevens, C. F. *J. Physiol., Lond.* **213**, 21-30 (1971).
- Adams, P. R., Brown, D. A. & Constanti, A. in *Physiology and Pharmacology of Epileptogenic Phenomena* (eds Klee, M. R., Lux, H. D. & Speckmann, E.-J.) 175-187 (Raven, New York, 1982).
- Thompson, S. H. *J. Physiol., Lond.* **265**, 465-488 (1977).
- Kenyon, J. L. & Gibbons, W. R. *J. gen. Physiol.* **73**, 139-157 (1979).
- Hille, B. *J. gen. Physiol.* **50**, 1287-1302 (1967).
- Constanti, A., Adams, P. R. & Brown, D. A. *Soc. Neurosci. Abstr.* **7**, 14 (1981).
- Connor, J. A. & Stevens, C. F. *J. Physiol., Lond.* **213**, 31-53 (1971).
- Shimohara, T. *Neurosci. Lett.* **24**, 139-142 (1981).
- Thesleff, S. *Neuroscience* **5**, 1413-1419 (1980).

Serotonergic denervation partially protects rat striatum from kainic acid toxicity

Michael Berger, Günther Sperk & Oleh Hornykiewicz

Institute of Biochemical Pharmacology, University of Vienna, Borschkegasse 8a, A-1090 Vienna, Austria

We report here observations indicating that the rat striatum can be partially protected from the neurotoxic action of locally applied kainic acid (KA, a rigid structural analogue of glutamic acid¹) by procedures resulting in reduced serotonergic brain activity. This observation may be important because the striatal damage produced by KA shows morphological and neurochemical similarities to the changes seen in the striata of patients dying of Huntington's chorea^{2,3}, an hereditary brain disorder, and because functional and morphological brain changes induced by KA have been proposed as a close model for human epilepsy⁴. Our observations thus suggest that serotonergic brain mechanisms influence the development of neuropathological changes accompanying certain neurological disorders.

Half-maximal lesion of the striatum (with respect to marker enzymes for acetylcholine and γ -aminobutyric acid neurones, see Fig. 1*b*; for enzyme assays, see Fig. 1 legend) was reproducibly obtained by applying stereotactically (David Kopf apparatus) 2 nmol of KA dissolved in 1 μ l 0.9% buffered saline into the rostral part of the striatum (coordinates A: 7.9, L: 2.5, D: 0.9, according to the rat brain atlas of König and Klippel¹⁵) at a rate of 0.33 μ l min⁻¹. For all experiments male albino rats (Sprague-Dawley; Versuchstierzuchtanstalt Himberg, Austria) weighing 250–350 g were used. For stereotaxic operations the animals were anaesthetized with 50 mg per kg intraperitoneal (i.p.) pentobarbital; intracisternal (i.c.) injections were performed under ether anaesthesia.

The experimental results are expressed as percentage of enzyme activity related to the contralateral striatum (into which no KA was injected). This strategy seemed justified as the various drug pretreatments, which always affected both striata, had no statistically significant effect on the absolute enzyme activities, and the striatal KA-induced lesion did not influence the enzyme levels in the contralateral striatum. The use of each animal as its own control permitted the detection of even small drug effects on the KA-induced changes. In this respect, direct comparison between the means of absolute enzyme activities of the different groups yielded identical results; however, due to inter-individual variation, the degree of statistical significance between the groups was, as expected, correspondingly smaller.

As shown in Fig. 1*a*, administration of 200 μ g 5,7-dihydroxytryptamine (5,7-DHT) into the cisterna magna (i.c.)⁶ 10 days before intrastriatal microinjection of 2 nmol KA, reduced the effect of KA on the activity of the striatal marker enzymes glutamic acid decarboxylase (GAD) and choline acetyltransferase (CAT). The difference between the group of animals receiving KA alone and that pretreated with 5,7-DHT was statistically significant at the 0.1 per cent level (Student's *t*-test). The striatal serotonin level in the 5,7-DHT-injected animals was reduced to 40% of control value.

The same degree of protection of the striatum from KA toxicity as that attained by 5,7-DHT, could be achieved

Table 1 Effect of manipulations influencing brain serotonin on striatum lesioned with 2 mol kainic acid (injected intrastrially)

	% CAT \pm s.e.m.	(n)	% GAD \pm s.e.m.	(n)
5, 7-DHT i.c. + KA	68.9 \pm 2.4	(14)*	79.3 \pm 3.7	(14)*
KA	54.7 \pm 1.7	(15)	59.0 \pm 2.0	(15)
<i>p</i> -Cl-Phe i.p. + KA	74.0 \pm 6.4	(4)†	79.9 \pm 5.1	(4)†
KA	57.0 \pm 4.0	(6)	59.8 \pm 4.4	(6)
Metergoline i.p.				
+ KA	70.4 \pm 1.9	(6)†	70.6 \pm 2.6	(6)†
Solvent + KA	59.1 \pm 3.6	(7)	58.7 \pm 4.4	(7)
5,7-DHT i.str.				
+ KA	71.4 \pm 3.2	(8)†	73.9 \pm 4.0	(7)†
Saline + KA	62.0 \pm 2.6	(7)	59.0 \pm 4.5	(7)
Pargyline + 5-OH-Trp i.p. + KA	62.3 \pm 3.9	(15)	65.0 \pm 2.9	(15)
KA	57.3 \pm 2.7	(12)	58.2 \pm 3.0	(12)
5-MDMT + KA	58.2 \pm 5.9	(7)	65.3 \pm 5.0	(7)
KA	61.1 \pm 3.4	(8)	62.8 \pm 3.4	(8)

5,7-Dihydroxytryptamine (5,7-DHT) was administered intracisternally (i.c.) or intrastrially (i.str.) in N₂-bubbled 0.9% NaCl containing 0.05% ascorbic acid, 10 days before kainic acid (KA); the rats were pretreated with desipramine (25 mg per kg, i.p.), controls to i.str. 5,7-DHT injections received i.str. saline. *p*-Chlorophenylalanine (*p*-Cl-Phe; 300 mg per kg, in saline) was injected i.p. 6 days before KA. Metergoline (12 mg per kg) was dissolved in 5% polysorbate 80 and injected i.p. 1 h before KA; controls received 5% polysorbate 80 i.p. Pargyline (25 mg per kg, in saline) and L-5-hydroxytryptophan (5-OH-Trp; 5 mg per kg, in saline neutralized with acetic acid) were injected i.p. 30 and 15 min, respectively, before KA, and 5-methoxy-*N,N*-dimethyltryptamine (5-MDMT; 3 mg per kg, in saline) 15 min before KA. Only animals showing typical 'serotonin related symptoms'¹⁸ (especially 'wet dog shakes') were used for KA injection. Values are means \pm s.e.m., expressed as percentage of enzyme activity related to the contralateral non-injected striatum. Ranges of enzyme activities in the contralateral striata were for CAT, 24–38 nmol ¹⁴C-acetylcholine and for GAD, 11–16 nmol ¹⁴CO₂ formed per and mg wet tissue weight. Significance of the difference between corresponding groups was calculated using Student's *t*-test. Number of animals is given in parentheses.

* *P* < 0.001; † *P* < 0.05 compared with controls.

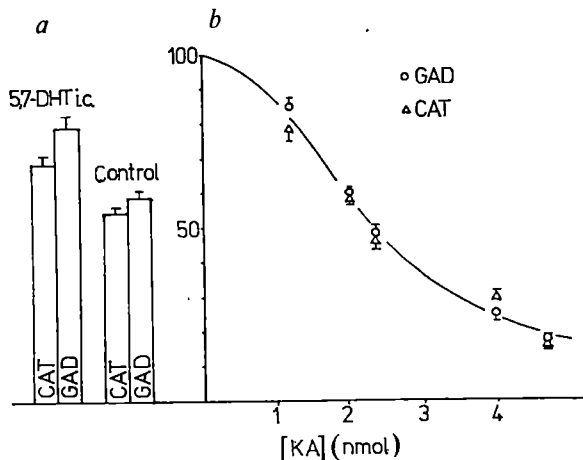


Fig. 1 Protective effect of i.c. injections of 5,7-dihydroxytryptamine (5,7-DHT) against the striatal toxicity of 2 nmol kainic acid (KA) (*a*), compared with the dose dependency of striatal KA-induced lesions (*b*). Activities of the striatal marker enzymes, measured 7 days after KA injection, are indicated on the ordinate as percentage of the contralateral non-injected striatum (means \pm s.e.m.). Glutamic acid decarboxylase (GAD) was assayed by trapping ¹⁴CO₂ formed from radiolabelled glutamic acid following the procedure of Miller *et al.*¹⁹. L-[1-¹⁴C]glutamic acid (4 nM), 0.5 mM pyridoxal phosphate and 1 h incubation at 37 °C were used. Choline acetyltransferase (CAT) was assayed by the Fonnum method²⁰ using [1-¹⁴C]acetyl-CoA (0.2 mM), 8 mM choline chloride, 0.1 mM physostigmine and 30 min incubation at 37 °C. ¹⁴C-acetylcholine was extracted with heptanone (3) containing 1% Na-tetraphenylborate. In the 5,7-DHT-treated rats striatal levels of serotonin were reduced by 60%, whereas dopamine levels remained unchanged, as determined by HPLC with electrochemical detection^{15,21}.

by i.p. pretreatment with *p*-chlorophenylalanine (*p*-Cl-Phe, 300 mg per kg), a serotonin-depleting agent⁷, or metergoline (12 mg per kg), a serotonin receptor blocker⁸ (Table 1). Although the protective effect of these drugs was of the same magnitude as that of 5,7-DHT, the statistical significance of the achieved differences was lower (0.02 < *P* < 0.05). However, taken together, these results strengthen the conclusion that the protective effect of i.c. 5,7-DHT against the striatal toxicity of KA was based on a reduction of serotonin levels in the brain.

Because 5,7-DHT given i.c. reduced not only the striatal serotonin but also the serotonin in the thalamus (–75%) and frontal cortex (–90%) (both brain regions are major sources of striatal input neurones), we tested the striatal specificity of the protective effect of 5,7-DHT. Thus, in a separate experiment, injection of 5 μ g 5,7-DHT (dissolved in 1 μ l 0.9% saline) bilaterally into the medial part of the striatum (coordinates⁵ A: 6.8, L: 3.6, V: 0.2) reduced the striatal serotonin levels by 65% whereas those in the frontal cortex were reduced by only 35%, with the thalamic serotonin remaining unchanged. Dopamine levels in the striatum were moderately reduced (–35%). The intrastriatal 5,7-DHT pretreatment, similar to the i.c. application, again afforded the same degree of protection against striatal KA toxicity, as judged by striatal GAD and CAT activities (Table 1). This indicates that the serotonergic system of the striatum itself was involved in the observed 5,7-DHT effect.

On the other hand, we have been unable to render intrastriatal KA more neurotoxic by i.p. pretreatment of the rat with pargyline plus 5-hydroxytryptophan (5-OH-Trp) or 5-methoxy-*N,N*-dimethyltryptamine (5-MDMT, Table 1), although both procedures can be expected to increase brain serotonin activity. This suggests that serotonin may influence

KA toxicity indirectly, especially as the correlation between kainate-induced neuronal degeneration and 5,7-DHT-induced striatal serotonin depletion was only moderately significant ($r = 0.50$ with 20 degrees of freedom, $0.02 < P < 0.05$).

In search of an explanation for our results, it is interesting that iontophoretically applied serotonin is generally assumed to exert an inhibitory influence on striatal neurone activity⁹⁻¹¹. Cortical ablation, which interrupts the excitatory glutamatergic input to the striatum, results in a dramatic reduction of striatal KA toxicity¹², so that we cannot exclude the possibility that deafferentation of the striatum as such may exert some protective effect, regardless of whether the transmitter involved is excitatory (as the cortico-striatal glutamatergic input is supposed to be) or not. However, in contrast to iontophoretically applied serotonin, the synaptically released amine may indeed have a net excitatory effect on striatal neurones. This is indicated by observations showing that lesion of the raphe-striatal serotonin pathway results in a substantial reduction of acetylcholine turnover in the striatum¹³. In fact, our present results, seen in conjunction with the effect of interruption of the glutamatergic cortical input to the striatum, may be taken

as indirect support for an excitatory role of striatal serotonin. Regardless of the nature of the neurophysiological effect of striatal serotonin, our results strengthen the notion that KA, in addition to its direct excitotoxic activity, triggers circuits of neuronal hyperactivity including the area injected and some particular afferents as essential components¹⁴. The dramatic rise in striatal serotonin (and dopamine) turnover observed after local injection of KA^{15,16} could reflect the involvement of these afferents in KA-elicited hyperactivity circuits. In this respect, it may be noteworthy that in Huntington's disease the severe loss of the intrinsic and output neurones population of the affected striatum results in a relative predominance of striatal input systems including those containing serotonin and dopamine¹⁷. It would be interesting to know if this relative and progressive predominance of striatal serotonin and dopamine exerts any detrimental influence on the time course of the morphological and functional deterioration of the Huntington striatum.

We thank Waltraud Krivanek for technical help and for typing the manuscript. This work was supported by the Austrian Science Research Fund, project S-25/02.

Received 19 January; accepted 1 July 1982.

1. Olney, J. W., Rhee, V. & Ho, O. L. *Brain Res.* **77**, 507-512 (1974).
2. Coyle, J. T. & Schwarcz, R. *Nature* **263**, 244-246 (1976).
3. McGeer, E. G. & McGeer, P. L. *Nature* **263**, 517-519 (1976).
4. Ben-Ari, Y., Tremblay, E. & Ottersen, O. P. *Neuroscience* **5**, 515-528 (1980).
5. König, J. F. R. & Klippel, R. A. *The Rat Brain: A Stereotaxic Atlas of the Forebrain and Lower Parts of the Brainstem* (Krieger, Huntington, New York, 1970).
6. Stewart, R. M., Gerson, S. C., Sperk, G., Campbell, A. & Baldessarini, R. J. *Ann. N.Y. Acad. Sci.* **305**, 198-207 (1978).
7. Koe, B. K. & Weissman, A. J. *Pharmac. exp. Ther.* **154**, 499-516 (1966).
8. Hamon, M. *et al.* *J. Neurochem.* **36**, 613-626 (1981).
9. Miller, J. J., Richardson, T. L., Fibiger, H. C. & McLennan, H. *Brain Res.* **97**, 133-138 (1975).
10. Olpe, H.-R. & Koella, W. P. *Brain Res.* **112**, 357-360 (1977).
11. Davies, J. & Tongroch, P. *Eur. J. Pharmac.* **51**, 91-100 (1978).
12. McGeer, E. G., McGeer, P. L. & Singh, K. *Brain Res.* **139**, 381-383 (1978).
13. Butcher, S. G., Butcher, L. L. & Cho, A. K. *Life Sci.* **18**, 733-744 (1976).
14. Nadler, J. V. & Cuthbertson, G. J. *Brain Res.* **195**, 47-56 (1980).
15. Sperk, G., Berger, M., Hörtnagl, H. & Hornykiewicz, O. *Eur. J. Pharmac.* **74**, 279-286 (1981).
16. Anderson, K., Schwarcz, R. & Fuxe, K. *Nature* **283**, 94-96 (1980).
17. Hornykiewicz, O. *Adv. Neurol.* **23**, 679 (1979).
18. Gersen, S. C. & Baldessarini, R. J. *Life Sci.* **27**, 1435-1451 (1980).
19. Miller, L. P., Martin, D. L., Mazumder, A., Walters, J. R. J. *J. Neurochem.* **30**, 361-368 (1978).
20. Fonnum, F. J. *Neurochem.* **24**, 407-409 (1975).
21. Sperk, G. J. *Neurochem.* **38**, 840-843 (1982).

Bradykinin receptor-mediated chloride secretion in intestinal function

Donald C. Manning & Solomon H. Snyder*

Departments of Neuroscience, Pharmacology and Experimental Therapeutics, Psychiatry and Behavioral Sciences, Johns Hopkins University School of Medicine, 725 North Wolfe Street, Baltimore, Maryland 21205, USA

James F. Kachur, Richard J. Miller & Michael Field

Departments of Pharmacological and Physiological Sciences and Medicine, University of Chicago, Chicago, Illinois 60637, USA

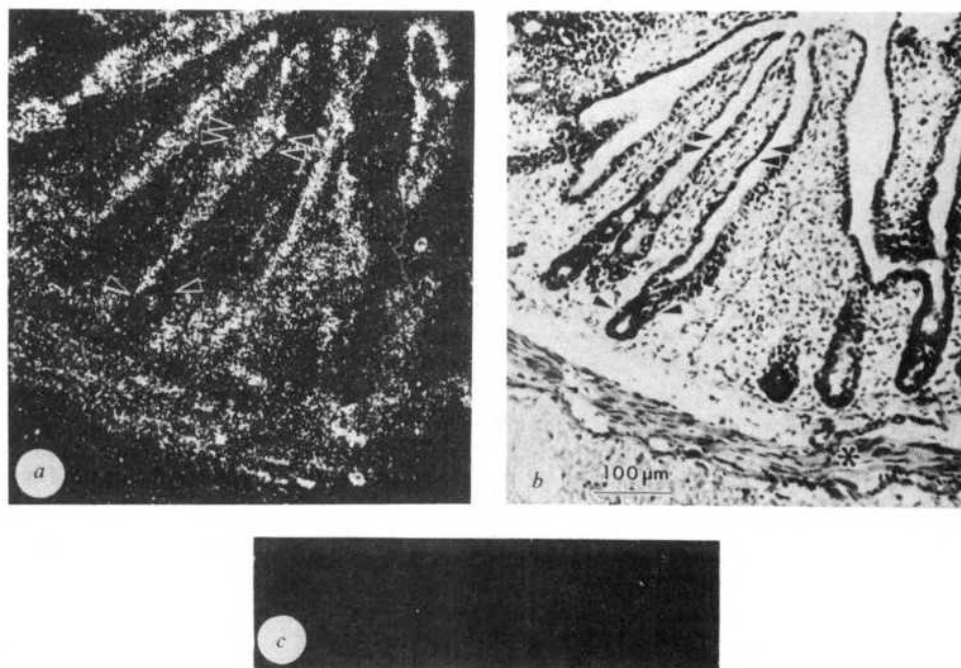
The nonapeptide bradykinin (Arg-Pro-Gly-Phe-Ser-Pro-Phe-Arg) and the decapeptide kallidin (Lys-bradykinin) are released during tissue damage and cause vasodilation, increased vascular permeability, altered gut motility and pain¹⁻⁴. Accordingly, they have been implicated in several pathological processes, including carcinoid tumours and postgastrectomy dumping syndrome. Symptoms of these two syndromes include flushing, light-headedness, headaches and diarrhoea⁵⁻⁹. Increased blood levels of bradykinin^{5,7-9} and kallikrein⁹, the bradykinin-releasing enzyme, have been noted in such patients and may explain these symptoms. However, while kinin-forming and -destroying activity has been noted in the gut¹⁰⁻¹⁴, bradykinin itself has not been directly demonstrated. Moreover, while bradykinin influences gut motility and electrical activity^{15,25,26}, most clinical diarrhoea is due to ion and fluid secretion into the gut lumen rather than altered motility¹⁶. We describe here specific bradykinin receptors in intestinal mucosa and muscle. We also report that bradykinin and several peptide analogues potently stimulate chloride secretion in the gut with a peptide specificity indicative of specific receptor interactions. These findings suggest a physiological and a pathological role for kinins in intestinal function. Throughout this report the term kinin will indicate both bradykinin and kallidin activities since in several cases the true active form is unknown.

Previously, we demonstrated specific ³H-bradykinin receptor-binding sites in guinea pig ileum¹⁷. The potencies of peptides at these binding sites correlated with their potencies in contracting smooth muscle, suggesting that the binding sites might be localized to muscle. The results shown in Table 1 demonstrate that specific bradykinin receptor-binding sites occur in the mucosa as well as in the muscle area. The relative potencies of bradykinin and six analogues listed in Table 1 are quite similar in both mucosa and muscle and correspond well with those observed previously in the total ileal tissue¹⁷. The 25-fold-enhanced potencies of the peptides observed in this study, compared to our earlier work, are due to enhanced specific activity and diminished degradation of the ³H-bradykinin. The relative potencies of bradykinin and its analogues at the ³H-bradykinin receptor-binding site closely parallels their potency in stimulating active chloride secretion. Removal of the arginine in the 9 position, forming Des-Arg⁹-bradykinin, destroys receptor-binding affinity and eliminates biological activity. Replacement of proline in position 3 with α -aminoisobutyric acid (AIB), forming AIB³-bradykinin reduces receptor-binding potency markedly in parallel with a decrease in biological activity. In contrast to internal changes in the bradykinin structure, addition of lysine to the amino-terminal only reduces the receptor-binding and secretory activity slightly. While Met-Lys-bradykinin is 30-50% as potent as bradykinin in affecting short-circuit current, it is only 10% as potent at ³H-bradykinin receptor-binding sites. It is possible that in the short-circuit current assay, Met-Lys-bradykinin is metabolized to the more potent Lys-bradykinin while conditions of the binding assay retard such metabolism (see Table 1 legend).

The localization of bradykinin receptors to both the mucosa and muscle layers of the ileum was confirmed by light microscopic autoradiographic studies (Fig. 1). Autoradiographic grains were apparent in highest density over the lamina propria surrounding both villus and crypt epithelial cells. Grains were also concentrated over the circular and longitudinal muscle layers. By contrast, grain density was sparse or absent over lymphatic tissue, as well as the myenteric ganglia. Inclusion of 1 μ M unlabelled bradykinin in incubations greatly reduced

* To whom correspondence should be addressed.

Fig. 1 Autoradiographic localization of ^3H -bradykinin (BK) receptor binding in guinea pig ileum. The dark-field photomicrograph (a) shows the autoradiographic grain distribution over the same tissue as the bright-field photomicrograph (b). Note that grains are concentrated over muscle layers (*) and also over the villi (between double arrows). Grains are almost entirely localized over the centre or lamina propria of the villi and are sparse or absent over the luminal surface of the epithelium. Grains are also absent inside the crypts of Lieberkuhn (single arrows) but are concentrated over the serosal side of the crypt epithelial cells. The dark-field photomicrograph (c) shows the absence of specific receptor binding in an adjacent 10- μM section when 1 μM unlabelled BK was included in the incubation buffer. The coverslip method of Young and Kuhar³³ was used. Guinea pigs were perfused through the heart with 500 ml of 0.1% formaldehyde in a mixture of equal parts of phosphate-buffered saline and 20% sucrose, pH 7.4. The ilea were then removed, embedded in homogenized calf cerebral cortex and flash-frozen in liquid nitrogen. Sections (10 μm thick) were cut in a cryostat at -12°C , thaw-mounted onto chrome alum gelatin subbed microscope slides and stored frozen at -20°C . Slides were warmed to room temperature, then incubated for 120 min at 4°C in medium containing 25 mM trimethylaminoethanesulphonic acid (TES) pH 6.8, 1 μM 1,10-phenanthroline, 0.2% bovine serum albumin (BSA) (protease-free), 1 mM dithiothreitol, 0.1 mM bacitracin, 1 μM captopril (SQ 14,225), 300 mM sucrose, and 0.2 nM ^3H -BK (52 Ci mmol⁻¹). Blanks were incubated in the same medium with the addition of 1 μM unlabelled BK. After incubation tissue sections were washed in 25 mM TES pH 6.8, and 1 mM 1,10-phenanthroline for 60 min (2×30 min) at 4°C . Sections were then dried rapidly in cold, dry air, NTB-2 emulsion-coated coverslips were apposed and the sections were exposed to the emulsion for 1 month.



grain density with the remaining grains being distributed diffusely. The pharmacological specificity was also indicated by biochemical experiments using the six bradykinin analogues listed in Table 1 and slide-mounted tissue sections. After incubation and washing, the tissue section was wiped off the slide with a circle of filter paper and the bound radioactivity assessed

by scintillation counting. In these experiments the affinity of bradykinin receptors was the same as in homogenate estimations. Also, ^3H -bradykinin binding is displaced by peptides with the same potencies as in homogenate experiments.

Bradykinin receptors in the muscle layers presumably mediate the contractile effects of bradykinin. To investigate the

Table 1 Relative potencies of bradykinin (BK) and several related peptides in receptor binding and short-circuit current assays

Kinin	Structure	Stimulation of short-circuit current EC ₅₀ (nM)	Inhibition of ^3H -BK binding	
			Mucosa IC ₅₀ (nM)	Muscle layer IC ₅₀ (nM)
	1 2 3 4 5 6 7 8 9			
Bradykinin (BK)	H-Arg-Pro-Gly-Phe-Ser-Pro-Phe-Arg-OH	1.0 ± 0.2	0.2	0.2
Kallidin (Lys-BK)	Lys-Arg-Pro-Gly-Phe-Ser-Pro-Phe-Arg-OH	2.8 ± 0.5	0.4	0.2
Met-Lys-GK	Met-Lys-Arg-Pro-Gly-Phe-Ser-Pro-Phe-Arg-OH	2.6 ± 0.8	1.8	2.2
AIB ³ -BK		183.0 ± 44	5.0	5.0
Hydroxyproline ³ -BK		3.1 ± 0.3	0.4	0.6
β-(2-Thienyl)-Ala ^{5,8} -BK		5.8 ± 1.4	0.5	0.4
Des-Arg ⁹ -BK		No response	>10 ⁻⁶	>10 ⁻⁶

^3H -BK was prepared (by NEN) by reduction of 2,3-dehydroproline-BK with tritium gas, resulting in a specific activity of either 27 or 52 Ci mmol⁻¹. The radiochemical purity of the ligand was determined by HPLC both before and after binding assay. The HPLC system used separates all partial sequence fragments of BK including BK₂₋₉, BK₁₋₈ and BK₁₋₇. A μ Bondapak C₁₈ (Waters Ass.) column (4 mm i.d. \times 30 cm) was used with a linear gradient solvent system (a, H₂O + 0.2% H₃PO₄, pH 2.4; b, CH₃CN + 0.2% H₃PO₄; 12% B \rightarrow 24% B) over 20 min with a flow rate of 2.0 ml min⁻¹. Fractions (30-s) were collected and the radioactivity measured by liquid scintillation counting. Using this HPLC system we were able to monitor the metabolism of the ^3H -ligand after the binding assay and thus develop a mixture of peptidase inhibitors effective in stabilizing BK. This increase in BK stability and use of a ligand of 2-4 times higher specific activity accounts for the almost 10-fold greater detected affinity of BK for its receptor than published previously¹⁷. In all assays mucosa was separated from the muscle layers by scraping gently with a glass slide. Crude membranes were prepared by homogenizing tissues in 20 vol 25 mM TES, pH 6.8 + 1 mM 1,10-phenanthroline with a Brinkmann Polytron PT10 (setting 6 for 30 s). The homogenates were centrifuged twice at 50,000g for 10 min with an intermediate rehomogenization in buffer. For routine studies the final pellets were resuspended in 300 vol of incubation buffer (25 mM TES pH 6.8, 1 mM 1,10 phenanthroline, 0.2% BSA (Sigma; crystallized, lyophilized), 0.1 mM bacitracin, 1 mM dithiothreitol, 1 μM captopril). To triplicate polypropylene incubation tubes were added (in a total volume of 4 ml); 850 μl of freshly resuspended tissue, 25,000 d.p.m. of ^3H -BK (final concentration 0.05 nM) and competing agents. After incubation for 90 min at 4°C the samples were rapidly filtered over GF/B filters previously coated with 0.1% aqueous polyethyleneimine solution, then the filters were washed three times with 3 ml ice-cold buffer. Filter-bound radioactivity was determined by liquid scintillation counting at 40% efficiency in 10 ml Formula 947 (NEN). Typical c.p.m. were 1,000 total and 35 blank with a tissue concentration of 1 ml tissue wet weight per ml. For metabolism studies, samples were centrifuged after incubation and the supernatant analysed by HPLC. E_{max} ; maximal effect; EC₅₀, concentration to elicit 50% maximal effect relative to bradykinin E_{max} in stimulating I_{sc} in guinea pig ileum; IC₅₀, concentration of nonradioactive BK or BK analogue required to displace 50% of specifically bound ^3H -BK from its receptor EC₅₀ values represent mean \pm s.e.m.

Table 2 Effect of bradykinin on chloride fluxes

	m→s	Cl ⁻ flux s→m	Net
Control	8.2±0.8	8.7±0.8	-0.5±1.6
Bradykinin (10 ⁻⁵ M)	8.3±0.4	12.1±1.1*	-3.8±1.3*

Values are the μ equiv. $\text{cm}^{-2} \text{h}^{-1} \pm \text{s.e.m.}$ for six paired experiments. Two 10-min samples were taken starting 15–20 min after the addition of $^{36}\text{Cl}^-$ and 5 min after adding bradykinin. * $P < 0.025$. Fluxes were measured with tissues short-circuited as described previously¹⁸. Flux is from mucosa to serosa (m→s) or serosa to mucosa (s→m).

possible function of the mucosal receptors, we evaluated the influence of bradykinin on the transepithelial potential difference (p.d.) and short-circuit current (I_{sc}) of the mucosal layer of the guinea pig ileum using techniques previously described¹⁸ (Fig. 2, Table 1). Tissue conductance showed no appreciable change and therefore the change in I_{sc} was proportional to the change in p.d. There was no effect on p.d. or I_{sc} when bradykinin in concentrations up to 10 μM was added to the mucosal bathing solution. In striking contrast, addition of nanomolar concentrations of bradykinin to the serosal surface rapidly increased p.d. and I_{sc} , with maximal effects within 2 min (Fig. 2). The finding that bradykinin acts only when added to the serosal surface agrees with the localization of bradykinin receptors to the serosal surface of villus and crypt epithelium. These effects resemble those produced in this tissue by other peptides such as vasoactive intestinal peptide¹⁹, substance P²⁰, neurotensin²⁰ and bombesin²¹.

After quickly becoming maximal, the I_{sc} diminished with a rather slower time course similar to that observed for the 'fading' of the smooth muscle-contacting effects of bradykinin⁴. Whether it is related to tachyphylaxis or peptide metabolism is unclear. In the absence and presence of the kininase II inhibitor, captopril, 50% of the maximal response occurs at 10 and 1.0 nM bradykinin, respectively. With this 10-fold enhancement of potency, bradykinin has a similar potency in altering I_{sc} and binding to receptors (Table 1).

Several experimental results suggest that the bradykinin-induced increase in I_{sc} is due to stimulation of anion secretion. Thus, the effects of bradykinin on p.d. and I_{sc} are reduced by 86% when Cl^- and HCO_3^- are replaced by sulphate (data not shown). Other evidence derives from direct measurement of unidirectional Cl^- fluxes across the short-circuited ileal mucosa in the presence and absence of bradykinin (Table 2). In control tissues there is a mean net Cl^- secretion of 0.5 $\mu\text{equiv. cm}^{-2} \text{h}^{-1}$. In the presence of bradykinin, net Cl^- secretion increases to +3.8 $\mu\text{equiv. cm}^{-2} \text{h}^{-1}$. These experiments used high concentrations of bradykinin to obtain maximal and prolonged effects.

The effects of bradykinin do not seem to be mediated by influences on neuronal conduction, as they are not affected by tetrodotoxin (Table 3); calcium movements may be involved, as verapamil, a Ca^{2+} channel blocker, markedly inhibits the influences of bradykinin on I_{sc} (Table 3). Bradykinin stimulation of I_{sc} is also completely blocked following the addition of the Ca^{2+} channel blocker CoCl_2 (1 mM). A possible role of Ca^{2+} agrees with data that Ca^{2+} regulates intestinal secretion²² and bradykinin receptor binding¹⁷.

It also seems that the effects of bradykinin on Cl^- secretion may be mediated by arachidonic acid and its metabolites. We have found that the action of bradykinin can be inhibited by a variety of agents that act as inhibitors of cyclooxygenase (for example, indomethacin) and phospholipase A_2 (for example, mepacrine). Moreover, exogenously added arachidonic acid or prostaglandin E_2 (PGE_2) are both powerful secretory stimuli and bradykinin can stimulate the *in vitro* release of PGE_2 (ref. 23). Interestingly, phospholipase A_2 , the enzyme that releases arachidonic acid from membrane phospholipids, is dependent on calcium. Conceivably, bradykinin alters the availability of

calcium to phospholipase A_2 by opening calcium channels as indicated by the inhibitory effects of Ca^{2+} channel blockers.

The present results suggest that bradykinin may have both a physiological and pathological role in the intestine. Our *in vitro* findings are consistent with the observations of Hardcastle *et al.*¹⁵ that bradykinin causes a transient increase in transcolonic and transjejunal p.d. in the rat. Independently Cuthbert and Margolius^{24,25} have also found potent enhancement of gut chloride secretion by kallidin and have also suggested a role for prostaglandins. The bradykinin receptors in the crypts might regulate this anion secretion. Bradykinin may enhance intestinal absorption of amino acids and glucose^{25,26}, effects that could involve bradykinin receptors in the tips of the intestinal villi where such absorption takes place.

Autoradiography at the light microscopic level does not allow the precise determination of the cellular location of receptors. Bradykinin receptors in the lamina propria are probably located on the basolateral membranes of the epithelial cells, however, receptors may also occur on smooth muscle cells, blood vessels and/or sensory nerve fibres in the villi.

Excessive kinin activity might account for some pathological conditions. In carcinoid syndrome, serotonin may be responsible for some of the symptoms⁵⁻⁷. However, although serotonin does elicit diarrhoea²⁸, it causes vasoconstriction⁷ rather than the vasodilatation and the associated flushing, light-headedness and headache that typically occurs in carcinoid patients. Moreover, while some increase of blood level of serotonin occurs in certain patients with carcinoid syndrome, there is no correlation with the onset of their symptoms⁷. By contrast, increase blood levels of kinins have been detected in carcinoid patients in the course of their symptoms⁵⁻⁷.

Kinins could also play a part in inflammatory bowel disease. In these conditions the plasma levels of kinins correlate very closely with the onset of vasomotor and gastrointestinal symptoms⁶⁻⁹. As inflammation is associated with the formation of kinins²⁹, one would expect kinins to be released into the local or systemic circulation. Indeed, inflamed intestinal tissue

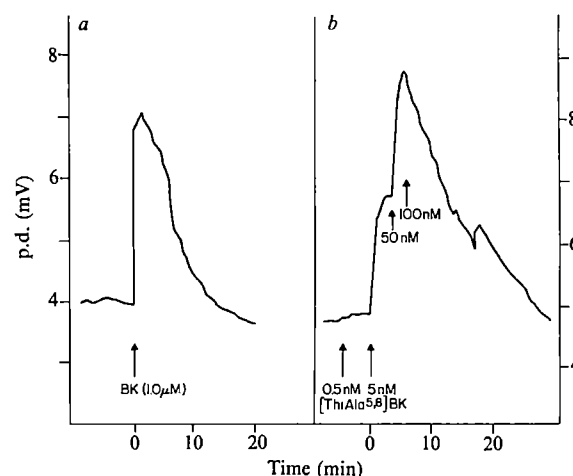


Fig. 2 Effect of BK on intestinal potential difference (p.d.). Ileal mucosa was obtained from female Hartley guinea pigs weighing 400–600 g. Segments of distal ileum, ~10–15 cm long, were excised 5 cm above the ileo-caecal junction. The segments were cut along their mesenteric border and placed in oxygenated ice-cold Ringer's. After stripping off the serosa and underlying longitudinal muscle layer, each tissue was mounted between two Leucite half chambers, the exposed areas being 0.64 cm^2 . The apparatus for measuring p.d. and I_{sc} was as described previously¹⁸. *a*, Effect of single dose of BK on transepithelial p.d. across guinea pig ileal mucosa. *b*, Effect of increasing concentrations of BK analogue (ThiAla^{5,8}) on p.d. Peptides were added at \uparrow . Tracings are from single experiments, but are characteristic of tracings from at least 10 other experiments.

Table 3 Effect of verapamil and tetrodotoxin on peak increments in I_{sc} elicited by bradykinin

	n	Response to 1.0 μ M bradykinin Change in I_{sc} on drug addition (μ A cm ⁻²)	(% of control response)
Tetrodotoxin	4	-44.4 \pm 4.8	119.4 \pm 17.1
Verapamil	4	-24.6 \pm 5.2	29.9 \pm 10.3*

Values are mean \pm s.e.m.; n, number of paired experiments. Negative values reflect decreases in I_{sc} . * $P < 0.01$ compared with control.

from patients with ulcerative colitis contains abnormally high levels of active kallikrein, the kinin-releasing enzyme¹⁴. Plasma and tissue levels of peptidyl dipeptidase which degrades kinins, are depressed in patients with regional enteritis; this would elevate kinin levels^{30,31}. Also, in regional enteritis plasma levels of α_2 -macroglobulin are reduced³². α_2 -Macroglobulin inhibits the bradykinin releasing enzyme kallikrein, thus reduced levels of the inhibitor should facilitate kinin synthesis. If indeed kinins are associated with symptoms of carcinoid syndrome or inflammatory bowel disease, then administration of the peptidyl dipeptidase inhibitor captopril to such patients may be contraindicated.

We thank Lynda Hester for technical assistance and Dr John Stewart, University of Colorado, for the gift of the bradykinin analogues. This work was supported by USPHS grants DA 02121, AM 21345, DA 00266 and NS 16374, and grants from the National Foundation of Ileitis and Colitis, the McKnight Foundation and RSA award DA 00074 to S.H.S.

Received 9 February; accepted 13 July 1982.

1. Rocha Y, Silva, M. & Rosenthal, S. R. *J. Pharmac. exp. Ther.* **132**, 110-116 (1961).
2. Juan, H. & Lembeck, F. *Naunyn-Schmiedeberg's Archs Pharmac.* **283**, 151-164 (1974).
3. Copley, A. L. & Tsulcuva, V. *Biochem. Pharmac.* **10**, 67-85 (1962).
4. Regoli, D. & Barabe, J. *Pharmac. Rev.* **32**, 1-45 (1980).
5. Oates, J. A., Pettinger, W. A. & Doctor, R. B. *J. clin. Invest.* **45**, 173-178 (1966).
6. Oates, J. A., Melmon, K., Sjoerdsma, A., Gillespie, L. & Mason, D. T. *Lancet* **i**, 514-517 (1964).
7. Zeitlin, I. J. & Smith, A. N. *Lancet* **ii**, 986-991 (1966).
8. Cuschieri, A. & Onabanjo, D. A. *Br. med. J.* **3**, 565-566 (1971).
9. Wong, P. Y., Talamo, R. C., Babior, B. M., Raymond, G. G. & Colman, R. W. *Anns int. Med.* **80**, 577-581 (1974).
10. Amundsen, E. & Nustad, K. *J. Physiol., Lond.* **179**, 479-488 (1965).
11. Fasth, S., Hulten, L., Johnson, B. J., Nordgren, S. & Zeitlin, I. J. *J. Physiol., Lond.* **285**, 471-478 (1978).
12. Zeitlin, I. J. in *Bradykinin and Related Kinins: Cardiovascular, Biochemical and Neural Actions* (eds Scutieri, F., Rocha Y Silva, M. & Bock, N.) 329-339 (Plenum, New York, 1970).
13. Zeitlin, I. J. *Br. J. Pharmac.* **42**, 648-649 (1972).
14. Zeitlin, I. J. & Smith, N. *Gut* **14**, 133-138 (1973).
15. Hardcastle, J., Hardcastle, P. T., Flower, R. J. & Sanford, P. A. *Experientia* **34**, 617-618 (1978).
16. Sodeman, N. A. & Watson, D. W. in *Pathologic Physiology: Mechanisms of Disease* (eds Sodeman, W. A. & Sodeman, W. A.) 767-789 (W. B. Saunders, Philadelphia, 1974).
17. Innis, R. B., Manning, D. C., Stewart, J. M. & Snyder, S. H. *Proc. natn. Acad. Sci. U.S.A.* **78**, 2630-2634 (1981).
18. Field, M., Fromm, D. & McColl, I. *Am. J. Physiol.* **220**, 1388-1396 (1971).
19. Schwartz, C. J., Kimberg, D. V., Sheerin, H. E., Field, M. & Said, S. I. *J. clin. Invest.* **54**, 536-544 (1974).
20. Kachur, J. F., Miller, R. J., Field, M. & Rivier, J. *J. Pharmac. exp. Ther.* **220**, 456-463 (1982).
21. Kachur, J. F., Miller, R. J., Field, M. & Rivier, J. *J. Pharmac. exp. Ther.* **220**, 449-455 (1982).
22. Bolton, J. & Field, M. *J. Membrane Biol.* **35**, 159-174 (1977).
23. Musch, M., Kachur, J., Miller, R., Stoff, J. & Field, M. *Gastroenterology* **82**, 1257 (1982).
24. Cuthbert, A. W. & Margolius, H. S. *J. Physiol., Lond.* **319**, 45 (1981).
25. Cuthbert, A. W. & Margolius, H. S. *Br. J. Pharmac.* **75**, 587-598 (1982).
26. Moriaki, C., Fujimori, H., Moriaki, H. & Kizuki, K. *Chem. Pharmac. Bull.* **25**, 1174-1178 (1977).
27. Moriaki, C. & Fujimori, H. *Chem. Pharmac. Bull.* **29**, 804-809 (1981).
28. Donowitz, M., Charney, A. N. & Tai, Y. H. in *Mechanisms of Intestinal Secretion* (ed. Binder, H.) 217-230 (Liss, New York, 1979).
29. Lewis, G. P. in *Bradykinin, Kallidin and Kallikrein* (ed. Erdos, E. G.) 516-530 (Springer, New York, 1970).
30. Silverstein, E., Fierst, S. M., Simon, M. R., Weinstock, J. V. & Friedland, J. *Am. J. clin. Path.* **75**, 175-178 (1981).
31. Weaver, L. J., Simonowitz, D., Driscoll, R. & Solliday, N. *J. surg. Res.* **29**, 475-478 (1980).
32. Brown, D. J. C., Khan, J. A., Copeland, G. & Jewell, D. P. *J. clin. Lab. Immun.* **4**, 53-57 (1980).
33. Young, W. S. & Kuhar, M. J. *Brain Res.* **179**, 255-270 (1979).

A new look at nonparasitized red cells of malaria-infected monkeys

C. M. Gupta, A. Alam, P. N. Mathur & G. P. Dutta

Divisions of Biophysics & Microbiology,
Central Drug Research Institute, Lucknow-226001, India

Many reports have shown that malarial parasites can produce distinct morphological and molecular alterations in the membranes of the parasitized erythrocytes¹⁻⁸, but few studies have been carried out on nonparasitized erythrocytes of infected animals⁹⁻¹¹. We report here that the outer leaflet of the membrane bilayer of nonparasitized erythrocytes contains significantly larger amounts of aminophospholipids (phosphatidylethanolamine (PE) and phosphatidylserine (PS)), than the normal red cell membrane. This alteration in nonparasitized red cells is probably caused by Ca²⁺-induced cross-linking of spectrin, and gradually disappears after chloroquine treatment. The external localization of PS in these cells together with defective structure of their cytoskeletal network provide a strong basis for the complications associated with malaria infection like thrombosis, infarction and severe anaemia.

The transbilayer distributions of the diacylglycerophospholipids, phosphatidylcholine (PC), PE and PS, in the membranes of normal erythrocytes of uninfected monkeys as well as nonparasitized red cells of *Plasmodium knowlesi*-infected monkeys were investigated using phospholipase A₂ and 2,4,6-trinitrobenzenesulphonic acid (TNBS) as external membrane probes^{12,13}. The results shown in Table 1 reveal marked differences between the two types of cells after treatments with phospholipase A₂. Unlike the normal intact cells, PE (~31%) and PS (~15%) in nonparasitized erythrocytes from infected monkeys were readily accessible to the enzyme. Almost complete (92-100%) hydrolysis of all the glycerophospholipids occurred when unsealed ghosts of the normal and nonparasitized cells were separately treated, in identical conditions, with phospholipase A₂.

Treatments of both types of cells with TNBS also reflected notable differences (Table 2). In the nonparasitized cells, TNBS

Table 1 Erythrocyte phospholipid degradation by phospholipase A₂

Sample	n*	PC (%)	PE (%)	PS (%)
Normal red cells	15	57.35 \pm 4.11	0	0
Nonparasitized red cells	12	48.31 \pm 4.23	31.31 \pm 2.40	15.19 \pm 2.32

Synchronous infections of *Plasmodium knowlesi* (WI strain) were maintained in healthy rhesus monkeys as described earlier⁸. The monkeys were bled when parasites were at the schizont stage. Blood was drawn into heparinized glass tubes and washed three times with phosphate-buffered saline (pH 7.2). Leukocytes and platelets from normal blood and leukocytes, platelets and schizonts from infected blood were removed by means of a Ficoll-Hypaque gradient²⁶. The nonparasitized red cells thus obtained were invariably contaminated with <1% erythrocytes that were infected with early ring stage of *P. knowlesi*, as determined by Giemsa staining. Erythrocytes were treated with phospholipase A₂ (purified from *Naja naja* snake venom, Haefkin Institute, Bombay) essentially in the conditions described earlier⁸. After inhibiting the enzyme activity by addition of o-phenanthroline and EDTA²⁷, lipids were extracted from cells. The lipid mixture was chromatographed on silica gel G-60 TLC plates as described previously⁸ and the total phosphorus content in each spot was determined²⁸. The percentage of the total phospholipid hydrolysed after treatment of red cells with the enzyme was determined by measuring the ratio of remaining diacylglycerophospholipids to the corresponding lyso derivative. Values are expressed as mean \pm s.d. <5% cells were lysed under the experimental conditions. Unsealed ghosts, prepared²⁹ from both the normal and nonparasitized cells, were also treated with the enzyme in identical conditions. Almost complete (92-98%) hydrolysis of all the diacylglycerophospholipids was observed in both the cases. n, Number of determinations.

* Three determinations on each blood sample of five uninfected monkeys and four infected monkeys (parasitaemia 10-20%).

Table 2 Labelling of erythrocyte aminophospholipids with TNBS

Sample	n*	PE (%)	PS (%)
Normal red cells	12	18.55 ± 2.87	0
Nonparasitized red cells	9	34.89 ± 2.81	16.10 ± 2.43

Labelling of erythrocytes with TNBS was carried out according to the reported procedure³⁰. The incubations were done at 20° ± 2 °C for 4, 6 and 10 h. No differences in the percentage of labelling in these experiments were observed. No detectable cell lysis occurred in all these experiments. The percentage of TNBS labelling was determined by the total phosphorus determinations and also by measuring absorbance of yellow colour at 340 nm. Values shown are mean ± s.d.. All the aminophospholipids were completely labelled when unsealed membrane ghosts from both the normal and nonparasitized cells were treated with TNBS under identical conditions. n, Number of determinations.

* Three determinations on each blood sample of four uninfected monkeys and three infected monkeys (parasitaemia 10–20%).

modified both PE (~35%) and PS (~16%) whereas in the normal cells, only PE (~19%) was labelled by the reagent. The increased amounts of PE in the outer surface of the nonparasitized cells, as compared with the normal cells, did not arise from the transmembrane movement¹⁴ of this lipid from the inner to the outer surface of the cell membrane because almost equal amounts of PE were labelled when the cells were treated with TNBS for 4, 6 and 10 h. Also, the observed differences in the amounts of labelled aminophospholipids were not due to a partial reaction with reagents, as PE and PS were completely labelled when unsealed ghosts of the two types of cells were reacted with TNBS in identical conditions. Attempts were also made to use these methods to study the nonparasitized cells obtained from blood of monkeys which developed >30% parasitaemia. Invariably, extensive haemolysis of cells occurred on

exposing them to similar concentrations of phospholipase A₂ for relatively short periods of time and also during their treatment with TNBS for >4 h. However, the amounts of PS labelled by TNBS in 4 h in such cells were significantly larger (~40%) than those observed in the nonparasitized cells of monkeys with parasitaemia (10–20%).

Accessibility of different phospholipids to phospholipases and TNBS in intact red cells has been correlated with their localization in the external leaflet of the membrane bilayer^{11,12}. From this study, it appears that parasitization of erythrocytes by the malarial parasite not only alters the phospholipid asymmetry in the parasitized cell membrane⁸, but also leads to an enormous change in the transbilayer distributions of various phospholipids in nonparasitized erythrocyte membrane. As shown in Table 1, the amounts of PC in the outer surface of the nonparasitized cells seem to be less than in normal cells. This redistribution of PC may have occurred to compensate for the increased amounts of PE and PS in the outer surface.

The above studies were carried out on a group of four infected monkeys. The same monkeys were treated with chloroquine (20 mg per kg for 3 days). This treatment completely removed circulating parasites. Similar doses of chloroquine were also given to a group of three uninfected monkeys. Determinations of transbilayer phospholipid distributions in the erythrocyte membrane on day 30 after treatment of the infected monkeys with the drug, revealed that appreciable amounts of PS (5–8%) were still present in the outer surface whereas amounts of the external PE (18–22%) in these cells were similar to those of the normal erythrocytes. Unlike the normal erythrocytes, phospholipase A₂ could still degrade PE (9–14%) in these cells.

Table 3 Concentrations of GSH in erythrocytes

Sample	n	GSH (μmol per ml packed cells)
Normal red cells	10	2.2 ± 0.7
Nonparasitized red cells*	6	1.9 ± 0.3

Concentrations of GSH in red cells were determined by the procedure of Beutler *et al.*³¹. Values are expressed as mean ± s.d.; n, number of animals.

* Parasitaemia 10–20%.

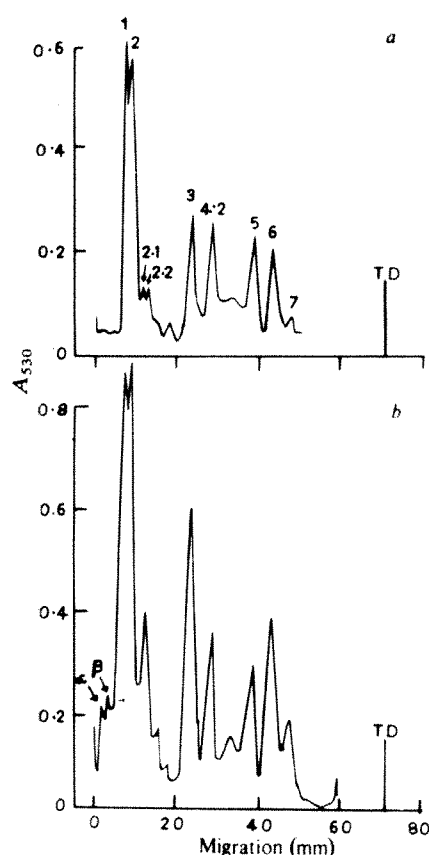


Fig. 1 Densitometer scans of gels stained for proteins with Coomassie blue after electrophoresis of red cell ghosts on polyacrylamide gels in the presence of SDS (ref. 22). *a*, Normal monkey erythrocyte ghosts; *b*, ghosts of nonparasitized erythrocytes of *P. knowlesi*-infected monkey (parasitaemia ~12%). The protein bands of the normal monkey erythrocyte are numbered according to the nomenclature of Fairbanks *et al.*²². TD, tracking dye.

However, by day 60, the amounts of PE (16–20%) and PS (none) in the external surface were normal. Chloroquine treatments of uninfected monkeys had no effect on red cell membrane phospholipid asymmetry.

Recent studies have shown that strong interactions between aminophospholipids and cytoskeletal proteins (specifically spectrin) probably determine phospholipid asymmetry in the erythrocyte membrane^{15–17}. This asymmetry in red cells is lost if the spectrin component of the cytoskeletal network becomes defective^{14,15}. Defects in the structure of spectrin may originate from decreased concentrations of glutathione (GSH) or from elevated levels of Ca²⁺ in cells^{18–21}. To look at this, membrane proteins of nonparasitized red cells were analysed by SDS-polyacrylamide gel electrophoresis²². Similar studies were also carried out on normal red cells of a group of six uninfected monkeys. The gel profiles of membrane proteins of nonparasitized erythrocytes from five different monkeys (parasitaemia 10–20%) invariably showed two additional high molecular weight protein bands (α and β , Fig. 1*b*) of variable intensity, which were absent in the gel profiles of the normal cell ghosts (Fig. 1*a*). No correlation was found between the intensity of the two bands and the extent of parasitaemia in monkeys. From a comparison between the relative intensities of protein bands present in the gel profiles of normal and nonparasitized erythrocyte ghosts, it appears that the two protein bands arise from cross-linking of spectrin. To examine whether these bands originate from oxidation of sulphhydryl groups of the protein¹⁵, the nonparasitized cell ghosts were incubated with dithiothreitol at 37 °C for 60 min before their extraction. This treatment had no effect on these bands, implying that the two high molecular weight proteins did not arise from oxidation of sulphhydryl

Table 4 Ca^{2+} contents of normal red cells of uninfected monkeys and non-parasitized erythrocytes of *P. knowlesi*-infected monkeys

Sample	n	Ca^{2+} (μg per ml packed cells)
Normal red cells	5	0.61 ± 0.39
Nonparasitized red cells*	6	2.36 ± 1.67

Ca^{2+} content in red cells was determined by atomic absorption spectrophotometry as described by Harrison and Long²².

* Parasitaemia 10–20%.

groups of spectrin. This is further supported by our finding that almost equal concentrations of GSH were present in normal as well as nonparasitized cells (Table 3). Nevertheless, the Ca^{2+} levels in the two types of cells were significantly different (Table 4). The elevated levels of Ca^{2+} present in the nonparasitized cells are compatible with earlier findings that malaria infection in animals results in diminished levels of ATPase activity in parasitized as well as nonparasitized red cells¹⁰. A partial (or complete) deactivation of ATPase in these cells would result in the elevated levels of Ca^{2+} and consequently activation of transglutaminase which may induce cross-linking of spectrin in the nonparasitized cells^{18–20}.

Normal structure of spectrin seems essential for the invasion of red cells by the malarial parasite²³. This means that if the structure of this protein becomes defective in the total population of nonparasitized erythrocytes in a malaria-infected animal then further invasion would not proceed. That parasitaemia does regularly increase in the infected monkeys suggests that only a fraction of the total population of the nonparasitized cells becomes abnormal. This conclusion is supported by the observation that unlike the nonparasitized cells, erythrocytes containing malarial parasite at the early ring stage have PS located exclusively in the inner leaflet of the membrane bilayer⁸.

Previous findings^{9,10} indicate that the serum of malaria-infected animals contains some unknown factors which induce changes in the nonparasitized cells. We, therefore, incubated normal erythrocytes with serum of heavily infected monkeys at 37 °C for 2–3 h. Treatments of such cells with TNBS and phospholipase have so far not revealed any effect of the serum but further studies are in progress.

These observed abnormalities suggest that externalization of PS in these cells could enhance blood coagulation^{24,25} and, therefore, may cause thrombosis. Also these cells, because of their defective cytoskeletal network, would be rapidly cleared from the circulation by the spleen¹⁸, making the animals more anaemic.

We thank Dr Nitya Nand for his help and the Council of Scientific and Industrial Research, New Delhi, for award of a fellowship to A.A. The *Plasmodium knowlesi* strain was a gift from Professor P. Garnham. This report is communication No. 3139 from CDRI, Lucknow.

Received 7 June; accepted 22 July 1982.

- McLaren, D. J., Bannister, L. H., Trigg, P. I. & Butcher, G. A. *Parasitology* **79**, 125–139 (1979).
- Aikawa, M., Miller, L. H., Rabbege, J. R. & Epstein, N. *Cell Biol.* **91**, 55–62 (1981).
- Schmidt-Ullrich, R. & Wallach, D. F. H. *Proc. natn. Acad. Sci. U.S.A.* **75**, 4949–4953 (1978).
- Howard, R. J. & Sawyer, W. H. *Parasitology* **80**, 331–342 (1980).
- Vincent, H. M. & Wilson, R. J. M. *Trans. R. Soc. trop. Med. Hyg.* **74**, 449–451 (1980).
- Hommel, M. & David, P. H. *Infect. Immunity* **33**, 275–284 (1981).
- Kilejian, A. *Proc. natn. Acad. Sci. U.S.A.* **77**, 3695–3699 (1980).
- Gupta, C. M. & Mishra, G. C. *Science* **212**, 1047–1049 (1981).
- Zuckerman, A. *Expl. Parasit.* **15**, 138–183 (1964).
- Seed, T. M. & Kreier, J. P. *Proc. helminth. Soc. Wash.* **39**, 387–411 (1972).
- Howard, R. J. & Day, K. P. *Expl. Parasit.* **51**, 95–103 (1981).
- Etemadi, A.-H. *Biochim. biophys. Acta* **604**, 423–475 (1980).
- van Deenen, L. L. M. *FEBS Lett.* **123**, 3–15 (1981).
- Lubin, B., Chiu, D., Bastacky, J., Roelofsens, B. & van Deenen, L. L. M. *J. clin. Invest.* **67**, 1643–1649 (1981).
- Haest, C. W. M., Plasa, G., Kamp, D. & Deuticke, B. *Biochim. biophys. Acta* **509**, 21–32 (1978).
- Mombers, C., Verkleij, A. J., deGier, J. & van Deenen, L. L. M. *Biochim. biophys. Acta* **551**, 271–281 (1979).
- Mombers, C., deGier, J., Demel, R. A. & van Deenen, L. L. M. *Biochim. biophys. Acta* **603**, 52–62 (1980).
- Marchesi, V. T. J. *Membrane Biol.* **51**, 101–131 (1979).
- Branton, D., Cohen, C. M. & Tyler, J. *Cell* **24**, 24–32 (1981).
- Gratzer, W. B. *Biochem. J.* **198**, 1–8 (1981).

- Thompson, S. & Maddy, A. H. *Biochim. biophys. Acta* **649**, 38–44 (1981).
- Fairbanks, G., Steck, T. L. & Wallach, D. F. H. *Biochemistry* **10**, 2606–2617 (1971).
- Wilson, R. J. *Nature* **295**, 368–369 (1982).
- Zwaal, R. F. A., Comfurius, P. & van Deenen, L. L. M. *Nature* **268**, 358–360 (1977).
- Chiu, D. *et al. Blood* **58**, 398–402 (1981).
- Wallach, D. F. H. & Conley, M. J. *molec. Med.* **2**, 119–136 (1977).
- Verkleij, A. J. *et al. Biochim. biophys. Acta* **323**, 178–193 (1973).
- Ames, B. N. & Dubin, D. T. *J. biol. Chem.* **235**, 769–775 (1960).
- Bjerrum, P. J. J. *Membrane Biol.* **48**, 43–67 (1979).
- Gordesky, S. E., Marenetti, G. V. & Love, R. J. *Membrane Biol.* **20**, 111–132 (1975).
- Beutler, E., Duron, O. & Kelly, B. M. *J. lab. clin. Med.* **61**, 882–888 (1963).
- Harrison, D. G. & Long, C. J. *Physiol., Lond.* **199**, 367–381 (1968).

Restriction of alternative complement pathway activation by sialosylglycolipids

Noriko Okada*, Tatsuji Yasuda† & Hidechika Okada‡

* Department of Bacteriology, The Kitasato Institute, Shirokane, Tokyo 108, Japan

† Department of Cell Chemistry, Institute of Medical Science, University of Tokyo, Shirokanedai, Tokyo 108, Japan

‡ Virology Division, National Cancer Center Research Institute, Tsukiji, Tokyo 104, Japan

Although sheep erythrocytes do not activate the alternative complement pathway (ACP) of human serum, the erythrocytes gain a capacity to activate human ACP following removal of membrane sialic acid by neuraminidase treatment^{1–3}. Therefore, asialoglycoconjugates generated from sialosylglycoconjugates by neuraminidase treatment might be responsible for this type of ACP activation on cell membrane⁴. Alternatively certain sialosylglycoconjugates on the cell membrane might restrict the activation of ACP and removal of the terminal sialic acid from the glycoconjugates would abolish this restricting capacity and result in activation of the ACP on the cell membrane⁵. To determine which of the above two possible mechanisms is the case, we used a liposome model membrane in which glycolipids could be artificially inserted, and our results suggest that the latter of the two possible mechanisms is the case.

A standard liposome preparation was prepared with cholesterol and dimyristoylphosphatidylcholine (DMPC) at an equimolar ratio. To prepare liposomes with test glycolipids inserted, cholesterol, DMPC and the test glycolipid were mixed in chloroform/methanol (2:1) at a molar ratio of 1.0:1.0:0.1 and the solvent evaporated, leaving a lipid film in a rotatory evaporation flask. On the dried film of lipid, 0.2 M carboxyfluorescein (CF) was added and the lipid dispersed at 60 °C by vigorous shaking. Thus prepared liposomes were washed with gelatin veronal-buffered saline (GVB, pH 7.4) by centrifugation at 15,000 r.p.m. for 20 min. The liposomes with inserted

Table 1 Chemical structures of glycolipids used

Glycolipid	Chemical structure
GM3	NA-Gal-Glc-ceramide
GM1	Gal-GalNac-Gal-Glc-ceramide
	NA
SPG	NA-Gal-GlcNac-Gal-Glc-ceramide
CMH	Gal-ceramide
CDH	Gal-Glc-ceramide
CTH	Gal-Gal-Glc-ceramide
GA2	GalNac-Gal-Glc-ceramide
GA1	Gal-GalNac-Gal-Glc-ceramide
Globoside	GalNac-Gal-Gal-Glc-ceramide
PG	Gal-GlcNac-Gal-Glc-ceramide

SPG, sialosylparagloboside; CMH, galactocerebroside; CDH, lactosylceramide; CTH, ceramidetrihexoside; GA2, asialo-GM2; GA1, asialo-GM1; PG, paragloboside; NA, neuraminic acid; Gal, galactose; Glc, glucose; GalNac, N-acetylgalactosamine; GlcNac, N-acetylglucosamine.

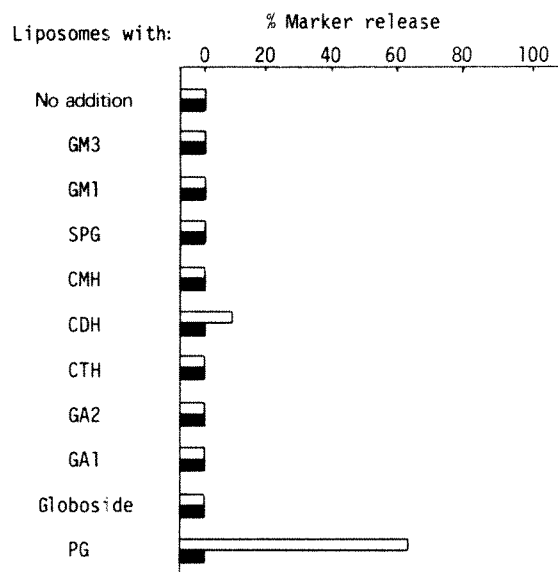


Fig. 1 Lysis of liposomes incorporated with glycolipids induced by 1:4 dilution of C4D-GPS (open bars) or human serum (solid bars) in Mg^{2+} -EGTA-GVB. To 50 μ l of a 1:4 dilution of C4D-GPS or human serum in Mg^{2+} -EGTA-GVB, 5 μ l of liposome solution (the concentration of liposome was adjusted to correspond to 0.05 mM phosphorus) in GVB were added and the mixture incubated at 25 °C for 60 min. After incubation, 2.0 ml of EDTA-VBS were added to each reaction mixture and the fluorescent intensity of CF release determined by excitation at 490 nm and emission at 520 nm. The 100% marker release was achieved by lysing liposomes with Triton X-100 as described previously⁷. Human serum did not lyse liposomes incorporated with any of the glycolipids. Although C4D-GPS lysed liposomes with paragloboside (PG), antibody against PG was detected. After heat inactivation at 56 °C, the C4D-GPS was diluted in GVB²⁺ (GVB containing 0.15 mM $CaCl_2$ and 0.5 mM $MgCl_2$) and incubated with PG-inserted liposomes in the presence of fresh human serum to detect antibody activity to PG by classical complement pathway-mediated liposome lysis. Antibody against PG was detected up to a 1:263 dilution of the heated C4D-GPS. Therefore, no glycolipids were found which induce ACP-mediated liposome lysis by C4D-GPS or human serum in the absence of antibody reaction.

glycolipids were then incubated at 25 °C for 60 min with C4-deficient guinea pig serum (C4D-GPS) or human serum diluted 1:4 in Mg^{2+} -EGTA-GVB (GVB containing 2 mM $MgCl_2$ and 10 mM ethyleneglycol-bis(β -aminoethyl ether) N,N' -tetraacetate, pH 7.4). Mg^{2+} -EGTA-GVB was used to inhibit complement activation via the classical pathway which requires Ca^{2+} at the reaction of the first component of complement, C1. After incubation, the amount of CF marker released from the liposomes was determined by excitation at 490 nm and emission at 520 nm following dilution with EDTA-VBS (veronal-buffered saline containing 10 mM EDTA pH 7.4) as described elsewhere^{6,7}. However, no glycolipid including the asialo-type glycolipids such as CDH, GA1 and GA2 (see Table 1 for their structure) made liposomes reactive with guinea pig or human complement via the alternative pathway except where the serum used for the complement source contained natural antibody against the glycolipid inserted (Fig. 1). These results indicated that glycolipids including asialo-type glycolipids have no capacity to activate ACP in the absence of specific antibody.

Recently we found that liposomes inserted with trinitrophenylaminocaproyldipalmitoylphosphatidylethanolamine (TNP-Cap-DPPE) can be lysed by guinea pig complement via ACP activation⁷. Therefore, glycolipids were inserted onto the membrane of liposomes with TNP-Cap-DPPE (TNP-Cap-liposomes) to examine the effect of the glycolipids on the ACP-activating capacity of TNP-Cap-liposomes. TNP-Cap-liposomes with inserted test glycolipids were composed of cholesterol, DMPC, TNP-Cap-DPPE and the test glycolipids at a molar ratio of 1.0:1.0:0.05:0.1, respectively. The reactivity

of the liposomes with guinea pig ACP was examined by the release of CF marker from liposomes as described previously⁷. Sialosylglycolipids [GM3, GM1 and sialosylparagloboside (SPG)] inserted onto the liposome membrane of TNP-Cap-liposomes markedly inhibited the lysis of the liposomes by C4D-GPS in Mg^{2+} -EGTA-GVB (Fig. 2). It was possible that sialosylglycolipids such as GM3 made the liposomes resistant to complement attack and that the TNP-Cap-liposomes with the said glycolipids were not lysed by complement although they activated guinea pig ACP. However, this was not the case as the insertion of GM3 to TNP-Cap-liposomes also suppressed the capacity of the liposomes to consume guinea pig complement. Briefly, C4D-GPS diluted 1:2 in Mg^{2+} -EGTA-GVB was mixed with an equal volume of TNP-Cap-liposomes, TNP-Cap-liposomes with GM3, TNP-Cap-liposomes with CDH, and liposomes composed of only DMPC and cholesterol. Those liposomes were not carrying the CF marker and had been suspended at 5 mM phosphorus of DMPC. After incubation at 25 °C for 60 min, the reaction mixtures were centrifuged at 15,000 r.p.m. for 20 min. The supernatants were diluted in Mg^{2+} -EGTA-GVB and incubated with TNP-Cap-liposomes to determine the residual lytic activity on the liposomes via ACP activation. Preincubation of C4D-GPS with TNP-Cap-liposomes and TNP-Cap-liposomes containing CDH consumed over 90% of the complement activity while pretreatment with

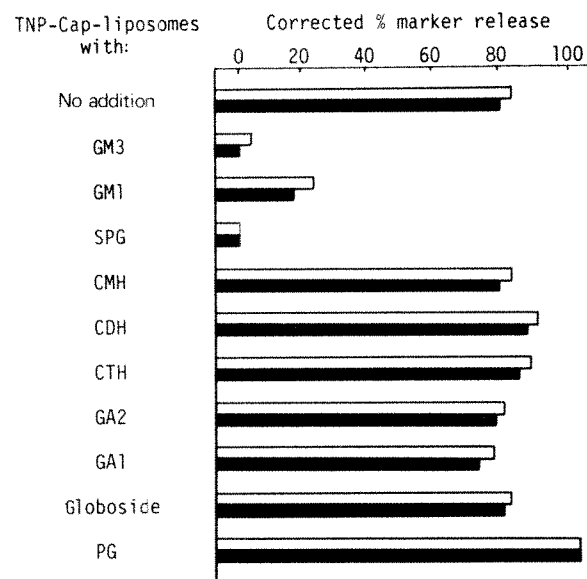


Fig. 2 Lysis of TNP-Cap-liposomes with inserted glycolipids by 1:4 (open bars) or 1:8 (solid bars) dilutions of C4D-GPS in Mg^{2+} -EGTA-GVB. Liposomes were incubated at 25 °C for 60 min with C4D-GPS and CF marker release was determined as described in Fig. 1 legend. The extent of liposome lysis was expressed as the corrected per cent marker release which was calculated as a percentage of the maximum release of CF by complement-mediated liposome lysis. The maximum release was determined by lysing liposomes with a 1:10 dilution of Hartley guinea pig serum in the presence of heat-inactivated rabbit anti-serum to TNP in GVB²⁺. The maximum release was approximately 70% of the total releasable CF in the liposomes by Triton X-100. We used the corrected per cent marker release, as the extent of possible release by complement attack varied to some degree among liposome preparations. Sialosylglycolipids (GM3, GM1 and SPG) exhibited remarkable inhibition of lysis in Mg^{2+} -EGTA-GVB by C4D-GPS in liposomes to which sialosylglycolipids were inserted. Enhanced lysis of TNP-Cap-liposomes with PG was due to the presence of antibody to PG in the C4D-GPS. TNP-Cap-liposomes also activate the classical complement pathway (CCP) of guinea pig⁷ as well as ACP. Therefore, TNP-Cap-liposomes with glycolipids were also incubated with Hartley guinea pig serum in GVB²⁺ to determine the effect of glycolipids on CCP-mediated liposome lysis. However, no inhibition of the CCP-mediated liposome lysis was noted upon insertion of the sialosylglycolipids, indicating that they inhibit complement activation via the ACP but not by the CCP.

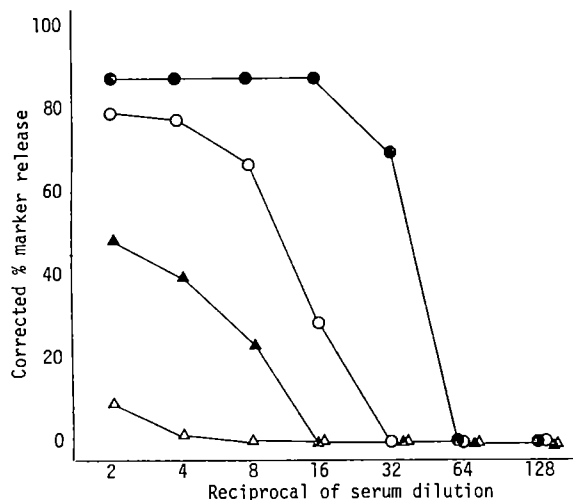


Fig. 3 Lysis by C4D-GPS of TNP-Cap-liposomes having incorporated varying amounts of GM3 onto the membrane. The membrane compositions of the liposomes were cholesterol/DMPC/TNP-Cap-DPPE/GM3 = 1.0:1.0:0.05:0.1 (Δ), 1.0:1.0:0.05:0.03 (▲), 1.0:1.0:0.05:0.01 (○), or 1.0:1.0:0.05:0 (●). Liposomes were incubated with C4D-GPS serially diluted in Mg^{2+} -EGTA-GVB and lysis was determined by CF marker release. GM3 incorporated liposome lysis was inhibited in a dose-dependent manner.

TNP-Cap-liposomes containing GM3 consumed only 40% of the complement activity. This result indicated that incorporation of GM3 onto TNP-Cap-liposomes inhibited the ACP activation on the liposomes.

On the other hand, CDH and GA1 which were asialo-type glycolipids of GM3 and GM1 respectively, did not affect the ACP-activating capacity of TNP-Cap-liposomes to which they were inserted. This suggests that sialosylglycolipids on cell membranes restrict the activation of ACP, and that removal of sialic acid from the glycolipid abolishes the restricting capacity which allows the activation of ACP on cell membrane.

To examine the amount of GM3 required for the restriction of ACP activation on TNP-Cap-liposomes, varying quantities of GM3 were inserted onto the liposomes. GM3 incorporated onto TNP-Cap-liposomes at a molar ratio to DMPC of as low as 0.01 can still inhibit ACP activation by TNP-Cap-liposomes (Fig. 3).

As sialosylglycolipids create a negative potential on the liposome surface, it was considered that the negative potential might play some part in the restriction of ACP activation on TNP-Cap-liposomes. However, positively charged amphiphiles such as stearylamine, and negatively charged ones such as dicetylphosphate and dipalmitoylphosphatidic acid, had no effect on ACP activation by the TNP-Cap-liposomes to which they were inserted⁷. Therefore, the restricted ACP activation on TNP-Cap-liposomes with sialosylglycolipids was not merely due to the negative potential on the membrane caused by the glycolipids. Sialosylglycolipids might interact with C3b molecules generated by the initial C3 convertase, C3(H₂O)Bb, which is made in serum in physiological conditions by the reaction of spontaneously hydrolysed C3 (at thiolester bond in α -chain) with factor B (ref. 8), and the C3b molecules interacted with sialosylglycolipids might be promptly inactivated by regulatory proteins in serum, factors H and I, resulting in the inhibition of the amplification reaction of C3b molecules which would otherwise form new C3 convertases with factor B, causing a positive feedback circuit in ACP activation^{9,10}.

As demonstrated above, sialosylglycolipids, and possibly sialosylglycoproteins, are thought to have a role in restricting undesirable amplification of ACP reaction, especially on self cell membranes. However, in addition to the glycolipid-mediated restriction of ACP activation on the cell membrane, some other mechanisms in the regulation of ACP activation on cell membranes such as C3b receptor-mediated restriction¹¹⁻¹³ remains

to be studied, as neuraminidase-treated cells do not activate homologous ACP^{11,14} although they activate heterologous ACP¹⁻³. This may lead to the clarification of the mechanism(s) by which complement recognition of the normal self cell membrane is achieved and how restriction of the complement reaction is maintained.

We thank Professors T. Tsumita and A. Gohda for encouragement, and Miss Y. Koga for editorial assistance. This work was supported by Grants-in-Aid from the Japanese Ministry of Education, Science and Culture, and the Adult Disease Clinic Memorial Foundation.

Received 15 April; accepted 30 July 1982.

1. Lauf, P. K. *J. exp. Med.* **142**, 974-988 (1975).
2. Fearon, D. T. *Proc. natn. Acad. Sci. U.S.A.* **75**, 1971-1975 (1978).
3. Pangburn, M. K. & Müller-Eberhard, H. J. *Proc. natn. Acad. Sci. U.S.A.* **75**, 2416-2420 (1978).
4. Pangburn, M. K., Morrison, D. C., Schreiber, R. D. & Müller-Eberhard, H. J. *J. Immun.* **124**, 977-982 (1980).
5. Kazatchkine, M. D., Fearon, D. T. & Austen, K. F. *J. Immun.* **122**, 75-81 (1979).
6. Yasuda, T., Naito, Y., Tsumita, T. & Tadokuma, T. *J. immun. Meth.* **44**, 153-158 (1981).
7. Okada, N., Yasuda, T., Tsumita, T. & Okada, H. *Immunology* **45**, 115-124 (1982).
8. Pangburn, M. K., Schreiber, R. D. & Müller-Eberhard, H. J. *J. exp. Med.* **154**, 856-867 (1981).
9. Nicol, P. A. E. & Lachmann, P. J. *Immunology* **24**, 259-275 (1973).
10. Whaley, K. & Ruddy, S. J. *exp. Med.* **144**, 1147-1163 (1976).
11. Fearon, D. T. *Proc. natn. Acad. Sci. U.S.A.* **76**, 5867-5871 (1979).
12. Fearon, D. T. *J. exp. Med.* **152**, 20-30 (1980).
13. Iida, K. & Nussenzweig, V. *J. exp. Med.* **153**, 1138-1150 (1981).
14. Okada, H., Tanaka, H. & Okada, N. *Immunology* (submitted).

Is nasal adenocarcinoma in the Buckinghamshire furniture industry declining?

E. D. Acheson, P. D. Winter, E. Hadfield & R. G. Macbeth

MRC Environmental Epidemiology Unit, University of Southampton, Southampton General Hospital, Southampton SO9 4XY, UK and the Department of Ear, Nose and Throat Surgery, High Wycombe General Hospital, Buckinghamshire HP11 2TT, UK

Since adenocarcinoma of the epithelium of the nasal cavity and accessory sinuses was recognized to occur more commonly in woodworkers in the British furniture industry than in other men^{1,2} and was prescribed as an industrial disease³, it has been found to occur in the furniture industry in many other countries. Here we review the incidence of the disease in Buckinghamshire up to the end of 1981 and report that skilled furniture makers such as wood machinists and cabinet and chair makers have experienced a cumulative lifetime risk of having nasal adenocarcinoma of at least 1 in 120 during the period studied. An analysis according to birth cohorts suggests that the disease may have reached its peak in men who entered the industry in the years 1915-24 but the apparent decline in incidence in men entering thereafter is not statistically significant. We argue that the carcinogen is almost certainly present in wood dust and point to the absence of recent quantitative data about dust levels in British furniture factories.

We studied the cases of nasal adenocarcinoma registered with the Oxford Regional Cancer Register between 1945 and the end of 1981. The Register includes data from the county of Buckinghamshire and the town of High Wycombe, one of the centres of the British furniture industry. Our estimates of the working population at risk have been derived from a register of 5,371 past and present workers in the Buckinghamshire furniture industry⁴ assembled (with the cooperation of the High Wycombe Furniture Manufacturers Association) by means of a letter sent to all member firms. Nine firms kept records containing sufficient identifying data to allow a follow-up. The

Table 1 SCIR for nasal adenocarcinoma in four birth cohorts of Buckinghamshire furniture workers

Birth cohort	Median year of entry to industry	Observed cases	Expected cases	SCIR (95% confidence intervals)
1890-99	1910	5	9.26	54 (18-126)
1900-09	1920	23	17.33	133 (84-199)
1910-19	1930	16	15.03	106 (61-173)
1920-29	1940	4	6.38	63 (17-161)
Total		48	48.00	100

register consists of men whose details had been recorded and retained by at least one of the nine firms and who had worked in one or more of these firms before the end of 1968. Men born after the beginning of 1940 were excluded. The nine firms comprise only 40% of the workforce in the Buckinghamshire furniture industry but are assumed to be representative of age, occupation and duration of service.

Man-years at risk were calculated for the periods 1945-68 and 1969-81, in 10-yr age groups. As the men on the register have so far only been followed up in respect of death from all causes to the end of 1968, the man-years at risk for 1969-81 were adjusted by the Buckinghamshire age-specific death rates taken from the 1969-73 Area Mortality Tables. The man-years at risk in the Buckinghamshire furniture industry for the period 1945-81 were then obtained by multiplying adjusted data from the register by the factor 2.5.

Standardized cohort incidence ratios (SCIR) were computed after Beral *et al.*⁵. Overall age-specific incidence rates were applied to the man-years at risk for individual cohorts to obtain expected numbers of cases, and confidence intervals were computed by assuming the observed number of cases to be a Poisson variable with expectation equal to the expected number of cases.

A total of 53 men who had worked at some time in the Buckinghamshire furniture industry are known to have developed nasal adenocarcinoma between the end of the Second World War and the end of 1981. Three of these (two cabinet makers and a machinist) had left Buckinghamshire before developing the tumour and were considered further only in computing the cumulative life risk of nasal adenocarcinoma in skilled furniture workers. Of the 50 men remaining, 16 were cabinet or chair makers, 22 were wood machinists including 2 turners, 5 were veneers, 3 were sanders or benchmen and 2 were French polishers. Two were unskilled: a labourer in the sawmill of a furniture factory and a man who maintained woodworking machinery.

Although there were more cases of nasal cancer in 1960-69 (20 cases) and 1970-79 (17 cases) than in 1950-59 (8 cases), the age at which the tumours were diagnosed increased over the period. The proportions of patients over 55 yr old for the periods 1945-64 and 1965-81 were significantly different ($\chi^2 = 11.4$, 1 d.f.; $P < 0.01$).

In Table 1 the 48 skilled men have been allocated to birth cohorts. The results show that the incidence ratio for nasal adenocarcinoma increased to a maximum for the men born

during 1900-09 (whose median year of entry to the industry was ~1920) and has declined thereafter. However, the decline is not statistically significant ($\chi^2 = 2.14$, 1 d.f.; $P > 0.1$)⁶. Neither computing the expected numbers on the basis of 5-yr as opposed to 10-yr age groups, nor excluding the 1890-99 cohort from the analysis alters the conclusion that there was a decline in the incidence experienced in the last three cohorts, but that it is not statistically significant.

The incidence of nasal adenocarcinoma among skilled woodworkers in the furniture industry—SCIR 147 (95% confidence interval = 108-194)—was more than 12 times that among the other employees in the industry (SCIR 12; 95% confidence interval = 0-32). No significant difference was found between the incidence in the two principal groups of skilled woodworkers, cabinet makers and wood machinists. Those affected were all men who had worked in close proximity to cutting or sanding, which creates large quantities of wood dust. The risk of a skilled woodworker in the Buckinghamshire furniture industry suffering from a nasal adenocarcinoma in his lifetime during the period of study has thus been about 1 in 120. This value is probably an underestimate as it is unlikely to include all the men who developed the tumour after leaving the area. During 1945-81 no case of adenocarcinoma is known to have occurred in a carpenter or joiner or in a wood machinist working outside the furniture industry in Buckinghamshire, although there are at least as many such woodworkers as in the furniture industry. Only five cases of adenocarcinoma occurred in Buckinghamshire men in other occupations during the same period.

For 40 of the 48 skilled woodworkers who developed nasal adenocarcinoma, we were able to obtain information about the period of time spent in the furniture industry. Two men had worked less than 5 yr, three between 5 and 20 yr, and 35 had worked more than 20 yr in the industry (Table 2). A comparison of those who had spent less than 20 yr in the industry with those who had worked 20 yr or more, revealed SCIR of 31 (95% confidence interval = 10-72) and 147 (confidence interval = 102-204), respectively. The risk of nasal cancer is thus significantly greater in men who have served longer in the industry.

None of the cases reported in Buckinghamshire presented less than 25 yr after first exposure. In the 42 patients for whom there was sufficient information, the average period from first exposure to diagnosis was 43.9 yr. Our best estimate of the temporal pattern of nasal adenocarcinoma occurrence in the Buckinghamshire furniture industry (Table 1) suggests that the epidemic reached its peak in skilled men born during the years 1900-09 (who entered apprenticeship between 1915-25) and has begun to decline in those entering in 1924-35 and 1935-44. This pattern will have been distorted if the ascertained proportion of the total number of cases occurring altered during the period. As the Oxford Cancer Register was not fully effective until 1956, it is possible that our estimate of the incidence in the 1890-99 cohort is low. However, a search of the High Wycombe death registers suggests that the disease was extremely rare before the Second World War². In any event, exclusion of the 1890-99 cohort from the analysis does not alter the apparent decline in the incidence of nasal cancer in those entering the industry since 1925.

It is possible also that the proportion of cases brought to our attention has increased recently; such a distortion would reduce the impact of a real decline in the disease. One of us (R.G.M.) has offered a screening service to furniture workers in the High Wycombe area since 1969; as a result of this, 4 of 19 patients with nasal adenocarcinoma in furniture workers resident in Buckinghamshire have been diagnosed since 1970. It seems likely that these tumours would otherwise have been diagnosed later in the illness. The fact that, recently, nasal cancer has occurred in older men is in part explained by the aging of the workforce. Another possible source of bias is our assumption that the age distribution of the men who worked for the nine firms is representative of Buckinghamshire furniture workers as a whole.

Table 2 Cases of nasal adenocarcinoma observed and expected and SCIR in Buckinghamshire furniture workers by duration of work in the industry

Years of work in industry	Observed cases 1945-79	Expected cases	SCIR (95% confidence intervals)
Under 5	2	5.56	36 (4-130)
5-9	1	3.47	29 (1-161)
10-19	2	7.14	28 (3-101)
20+	35	23.84	147 (102-204)
Total	40	40.00	100

See text for method of computation of man-years at risk.

The fact that the furniture workers with nasal cancer whose cases are reported here had first entered the furniture industry before the Second World War does not necessarily mean that the carcinogen is no longer present in the working environment. Three cases of nasal adenocarcinoma in men who entered the furniture industry in other areas of England shortly after the Second World War have been reported to us and cases in men who entered the industry during the war have been reported in France and Italy^{7,8}.

Nasal adenocarcinoma is now known to have been a special risk to furniture makers elsewhere for several decades and in Britain since 1920 and possibly earlier. This widespread occurrence, together with the fact that woodworking machinists (who saw the timber) and the cabinet and chair makers (who shape, finish, sand and assemble the furniture) experience similar risks make it unlikely that the tumours are due to a chemical agent applied to the wood at a particular stage of the process but more probably to a substance in wood dust itself. Occupational histories show that men exposed exclusively to beech and oak have developed tumours, but a wider range of hardwoods is probably implicated. It is unknown whether the absence of an excess risk of tumours in carpenters and joiners is due to the exposure of these men to low concentrations of dust particles of the appropriate size or because the carcinogen is absent from soft woods.

Prolonged inhalation of dust by furniture workers has been shown to impair mucociliary clearance and to lead to squamous metaplasia. Deposits of dust have been observed in the noses of furniture workers, on the mucosa close to the ethmoid bulla where the tumours are believed to originate⁹. The nature of the substances in wood dust which bring about these changes and which initiate carcinogenesis is unknown. Far from being an inert material as was believed previously, wood contains a wide range of biologically active substances including flavonols, other phenolic compounds and many terpenoids, some of which probably exert a protective function in timber as natural insecticides and fungicides. It is possible that one or more of these may be carcinogenic. Another possibility is that carcinogens may be formed by pyrolysis during machining. As nasal cancer in boot and shoe operatives is limited to men and women exposed to dust associated with preparing and finishing leather for heels and soles—which is usually tanned with vegetable extracts including extracts of wood—it is possible that these cancers also may be caused by a carcinogen derived from wood¹⁰. Systematic studies of the carcinogenicity of wood and leather dust are needed.

Although nasal cancer in furniture makers was prescribed as an industrial disease in 1969, there are no data indicating whether dust levels in British furniture factories have subsequently declined. A study of Buckinghamshire furniture factories published in 1974 showed that the average dust concentration was $\geq 5 \text{ mg ml}^{-1}$ (ref. 11). In 1976 a regulation was introduced in the United Kingdom requiring 'efficient exhaust ventilation' in furniture factories¹² but it is unknown whether this regulation has brought an improvement in dust levels.

We thank Miss Corinne Hunt and the staff of the Oxford Regional Cancer Register and the High Wycombe Furniture Makers Association for their help with this study.

Received 10 March 1981; accepted 28 July 1982.

1. Macbeth, R. G. *J. Lar. Otol.* **79**, 592–612 (1965).
2. Acheson, E. D., Cowdell, R. H., Hadfield, E. & Macbeth, R. G. *Br. med. J.* **2**, 587–596 (1969).
3. Statutory Instrument No. 619 (1969).
4. Rang, E. H. & Acheson, E. D. *Int. J. Epidemiol.* **10**, 253–261 (1981).
5. Beral, V., Fraser, P. & Chilvers, C. *Lancet* **i**, 1083–1086 (1978).
6. Berry, G. *The Analysis of Mortality by the Subject-years Method* (paper read to the Biometric Society, 1980).
7. Desnos, J. & Martin, A. *Cahiers d'O.R.L.* **8**(4), 367–374 (1973).
8. Fombeur, J. P. *Archs. Mal. prof. Méd. trav.* **33**, 454–5 (1972).
9. Hadfield, E. *Ann. R. Coll. Surg.* **46**, 301–319 (1970).
10. Acheson, E. D., Cowdell, R. H. & Jolles, B. *Br. med. J.* **1**, 385–393 (1970).
11. Hounam, R. F. & Williams, J. *Br. J. ind. Med.* **31**, 1–9 (1974).
12. *Woodworking Machines Regulations, 1974* Statutory Instrument No. 903, Pt 8 (1974).

Loss of intervening sequences in genomic mouse α -globin DNA inserted in an infectious retrovirus vector

Kunitada Shimotohno* & Howard M. Temin

McArdle Laboratory, University of Wisconsin, Madison, Wisconsin 53706, USA

Genes lacking the intervening sequences that are present in otherwise apparently homologous genes have been found in some highly oncogenic retroviruses (some viral oncogenes) and in the normal cell genome (cDNA genes, pseudogenes or processed genes)^{1–10}. Such cDNA genes might have arisen by reverse transcription of the spliced (intervening sequences removed) RNA transcript of the homologous genes. Another possible way for genes with intervening sequences to lose such sequences would be during replication in a retrovirus vector. To test this hypothesis we inserted genomic mouse α -globin DNA containing two intervening sequences¹¹ into the DNA of an infectious retrovirus vector¹² and report here that the intervening sequences were removed from DNA of progeny virus during virus replication.

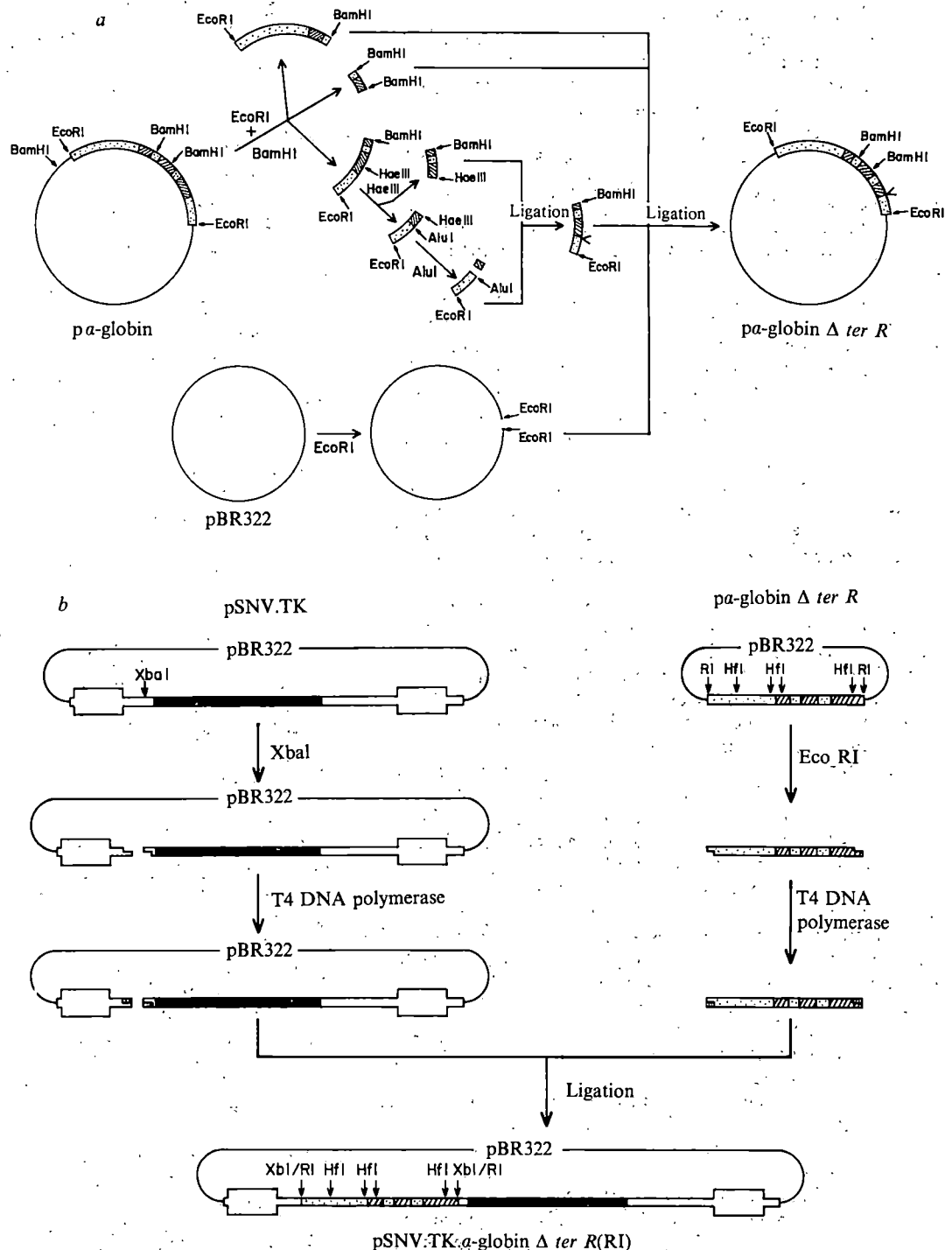
We previously found that removal of the 3' terminus of a thymidine kinase (TK) gene before its insertion in our infectious spleen necrosis virus (SNV) vector increased the recovery of infectious virus¹². Therefore, we prepared DNA of mouse α -globin without 3'-terminal sequences including the site of poly(A) addition (α -globin Δ terR gene) by removing 130 base pairs (bp) from the gene. The sequences removed were from 25 bp after the end of the coding sequences for protein (*Hae*III cleavage site) to 65 bp after the end of the sequences for mRNA (*Alu*I cleavage site) (Fig. 1a, also see map in Fig. 3).

The *Eco*RI- or *Hin*FI-digested α -globin Δ terR was then inserted into the *Xba*I cleavage site 40 bp (13 amino acids) inside the *gag* gene¹³ of a herpes simplex virus thymidine kinase Δ terR gene-containing retrovirus vector in which retrovirus sequences from approximately 1 to 7 kbp had been deleted¹⁴. (This vector is produced in mixed infection at approximately the same rate as a non-defective helper retrovirus¹⁴.) The strategy used for this insertion maintained both the *Xba*I and the *Eco*RI cleavage sites, pSNV-TK- α -globin Δ terR (RI), or *Hin*FI cleavage sites, pSNV-TK- α -globin Δ terR (*Hin*FI), at the ends of the vector and the α -globin Δ terR DNA (map in Fig. 1b).

To recover infectious virus carrying the α -globin DNA, pSNV-TK- α -globin Δ terR (RI) DNA was co-transfected into chicken cells with one tenth as much DNA of a provirus clone of a non-defective helper virus, reticuloendotheliosis virus strain A (REV-A). The virus produced was first assayed by its thymidine kinase transforming activity in buffalo rat liver (BRL) TK⁻ or chicken TK⁻ cells¹². SNV-TK- α -globin Δ terR (RI) was recovered at ~10% the yield of the parental SNV-TK; and SNV-TK α -globin Δ terR (*Hin*FI) was produced at about 30% of the yield of SNV-TK (data not shown). Therefore, sufficient recombinant thymidine kinase-containing virus was produced for a direct examination of its structure. Virus recovered 5 days after transfection with pSNV-TK- α -globin Δ terR (RI) $\sim 10^4$ – 10^5 TK-forming units per ml) was used to infect fresh chicken embryo fibroblasts. Three days later unintegrated linear viral DNA was prepared, digested with *Hin*FI, *Xba*I or *Eco*RI, and analysed (Fig. 2). Two bands, of 1.9 and 1.7 kbp, that hybridized to α -globin DNA were found after digestion with *Xba*I or *Eco*RI. The upper band is the same size as the parental α -globin Δ terR; the lower band about 250 bp smaller (see maps in Fig. 3). This difference in size is consistent with the absence of both intervening sequences from the DNA in the lower band (IVS-1 is 122 bp and IVS-2 is 134 bp¹¹). Digestion with *Hin*FI also resulted in two bands, of 810 and 560 bp, that hybridized

* Present address: National Institute of Genetics, Mishima, 411 Japan.

Fig. 1 Construction of recombinant DNAs. **a**, Construction of α -globin: $\Delta terR$: α -globin (200 μ g) was digested with *Eco*RI (New England Biolabs) at 37 °C for 10 h. The digest was analysed by electrophoresis into a 1% agarose gel at 30 V for 12 h. A fragment of 2 kbp (α -globin) was isolated from the gel²¹, digested with *Bam*HI (New England Biolabs), and the digest analysed by electrophoresis into a 1% agarose gel. DNA fragments of 1.2 (*Eco*RI/*Bam*HI), 0.3 (*Bam*HI/*Bam*HI), and 0.6 (*Bam*HI/*Eco*RI) kbp were isolated from the gel. The 0.6-kbp (*Bam*HI/*Eco*RI) fragment was digested then with *Hae*III (New England Biolabs), which digests between the C-terminal end of the protein and AATAAA in the untranslated region of the sequence (see map in Fig. 3), and the digest was analysed by electrophoresis into a 6% acrylamide gel. DNA fragments of 0.3 (*Bam*HI/*Hae*III) and 0.32 (*Hae*III/*Eco*RI) kbp were isolated from the gel. The fragment of 0.32 kbp (*Hae*III/*Eco*RI) was digested with *Alu*I (New England Biolabs), which digests after the site of poly(A) addition (ref. 11, also see map in Fig. 3), and the digested DNA was analysed by electrophoresis into a 6% acrylamide gel. A DNA fragment of 0.2 kbp (*Alu*I/*Eco*RI) was isolated from the gel. Equimolar amounts of the *Bam*HI-*Hae*III fragment of 0.3 kbp and the *Alu*I-*Eco*RI fragment of 0.2 kbp were ligated with T4 DNA ligase (NEN) at 24 °C for 17 h to allow ligation between the *Alu*I and *Hae*III sites. The ligated DNA (concatamers) was digested with *Bam*HI and *Eco*RI to produce a 0.5-kbp fragment having *Bam*HI and *Eco*RI sites at its ends. Equimolar amounts of a 4.3-kbp *Eco*RI-digested pBR322, which had been treated with alkaline phosphatase (BRL), the 1.2-kbp *Eco*RI-*Bam*HI fragment, the 0.3-kbp *Bam*HI-*Bam*HI fragment and the 0.5-kbp *Bam*HI-*Eco*RI fragment were ligated together. The ligated DNA was introduced into *Escherichia coli* HB101 cells and transformants carrying plasmids were grown in the presence of 25 μ g ml⁻¹ of ampicillin. Colonies which hybridized to mouse α -globin DNA were isolated and grown in L-broth to prepare plasmid DNA. The DNAs were characterized by mapping with restriction endonucleases *Pst*I, *Bam*HI and *Eco*RI (data not shown). Symbols: line, pBR 322; cross-hatched bar, α -globin mRNA coding sequences; stippled bar, noncoding sequences; V indicates deletion of 128 bp from the 3' terminus of the mouse α -globin DNA. **b**, Construction of pSNV-TK- α -globin $\Delta terR$ (RI): α -globin $\Delta terR$ DNA (100 μ g) was digested with *Eco*RI. A 2-kbp (*Eco*RI/*Eco*RI) α -globin-containing fragment from the digest was isolated after electrophoresis in a 1% agarose gel. pSNV-TK DNA (20 μ g) was digested with *Xba*I (New England Biolabs). The ends of these DNAs were filled in with T4 DNA polymerase (Bethesda Research Laboratories). The reaction mixture consisted of 330 μ M of dATP, dCTP, dGTP and dTTP, 167 μ g ml⁻¹ of bovine serum albumin, 16.6 mM of ammonium sulphate, 1 mM dithiothreitol, 6 mM MgCl₂, 50 mM Tris-HCl (pH 8.5), 5 μ g DNA fragment and 2 U of T4 DNA polymerase in 40 μ l. The reaction was carried out for 1 h at 37 °C. The reaction mixture was passed through a Sephadex G-50 column (0.7 \times 12 cm) to separate unreacted materials from DNA and the DNA was then precipitated with ethanol. Equimolar amounts of these DNA fragments were ligated together. The ligated DNA was introduced into *E. coli* HB101 cells and the transformants were grown in L-broth in the presence of 50 μ g ml⁻¹ ampicillin. Plasmids carrying α -globin $\Delta terR$ DNA were isolated from the transformants and the structures of the plasmid DNAs were characterized by mapping with restriction endonucleases (data not shown). Clones prepared in this manner with T4 DNA polymerase retain the cleavage sites of both *Xba*I and *Eco*RI. Construction of pSNV-TK- α -globin $\Delta terR$ (HinfI): α -globin $\Delta terR$ DNA was digested with *Hinf*I (New England Biolabs), which cuts 20 bp 3' to the sequences for the 5' end of globin mRNA, 118 bp 3' to the sequences for the carboxy-end of α -globin, and at two other sites in the 5'-noncoding region (see map in Fig. 3)¹¹. A DNA fragment of ~800 bp (*Hinf*I/*Hinf*I) containing α -globin sequences was isolated after electrophoresis in a 1% agarose gel. The ends of the *Hinf*I fragment were filled in by T4 DNA polymerase as described above. The filled-in DNA fragment and pSNV-TK that was digested with *Xba*I and had its ends filled in with T4 DNA polymerase were ligated together with T4 DNA ligase. Transformed *E. coli* HB101 cells carrying the plasmid were isolated and the plasmid DNA was mapped by restriction endonuclease digestion (data not shown). Cleavage sites of both *Xba*I and *Hinf*I were retained by this method of construction. Symbols: open bar, SNV; filled bar, herpes simplex thymidine kinase gene; other symbols as in Fig. 1a. (The sequences 3' of exon 3 are now shown cross-hatched to indicate the removal of the sequences for the 3' end of globin mRNA. The pBR322 sequences are not drawn to scale.)



to α -globin DNA (other hybridizing bands ran off the gel). The upper band contains the parental α -globin $\Delta terR$ coding sequences (A); the lower band contains 5' non-translated DNA sequences (B) and the progeny (smaller) α -globin $\Delta terR$ sequences (C). The increase in relative amount of the lower band locates the decreased size of the α -globin $\Delta terR$ DNA to the coding sequences.

Similar results were found after co-transfection with pSNV-TK- α -globin $\Delta terR$ (HinfI) and REV-A DNAs (data not shown).

To confirm the loss of intervening sequences in the progeny virus, molecular clones were made of the insert recovered from progeny virus. Closed circular viral DNA was prepared 3 days after infection of chicken cells with virus that was recovered 5 days after transfection with pSNV-TK- α -globin $\Delta terR$ (RI). This closed circular DNA was digested with *Xba*I and the α -globin $\Delta terR$ insert was cloned in the modified λ vector Charon 4A as described in Fig. 3 legend. Globin DNA-containing phage were then isolated and the inserts characterized by digestion with *Hinf*I and *Bam*HI. The results of restriction enzyme mapping are consistent with loss of the two intervening sequences in the α -globin DNA (Fig. 3). DNA sequencing then directly demonstrated that the two intervening sequences were precisely removed (data not shown).

To determine the rate of loss of intervening sequences in progeny virus, virus was collected 4–9 days after transfection and used to infect fresh chicken cells. Unintegrated linear viral DNA was then prepared 3 days after infection (7–12 days after transfection). Multiple cycles of infection had occurred in this time.

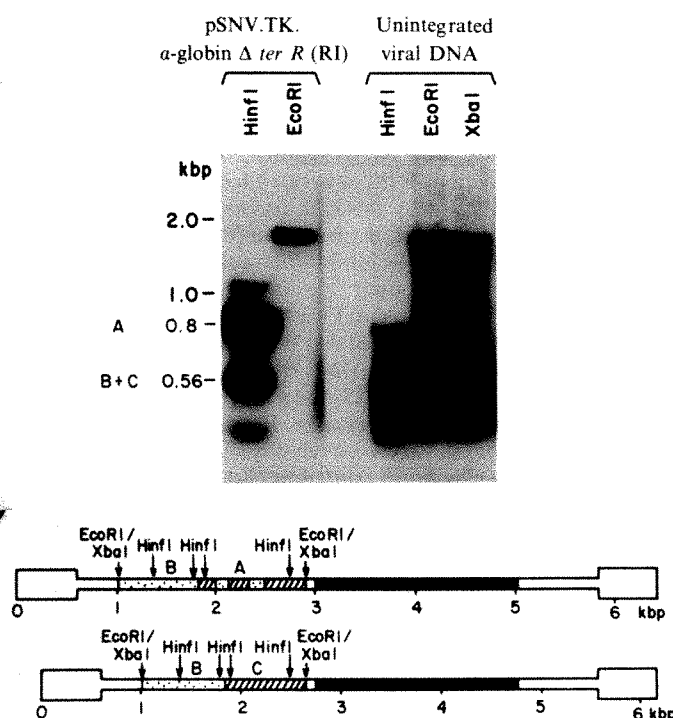


Fig. 2 Recovery of unintegrated viral DNA from chicken cells infected with recombinant virus. pSNV-TK- α -globin $\Delta terR$ (RI) DNA (10 μ g) and REV-A DNA (1 μ g) as helper were introduced into chicken fibroblastic cells in 100-mm Petri dishes in the presence of calcium phosphate. After 5 days, virus was collected from the medium and fresh chicken cells (30–100-mm Petri dishes) were infected with undiluted virus. Three days after infection, the cells were collected and unintegrated viral DNA was isolated by the Hirt procedure^{22,23}. The unintegrated viral DNA was digested with *Hinf*I, *Xba*I or *Eco*RI and analysed by electrophoresis in a 1.3% agarose gel. Each lane contained DNA from four Petri dishes. The gel was blotted onto nitrocellulose filter paper and the filter was hybridized with nick-translated ³²P-labelled globin-containing *Eco*RI fragment from α -globin $\Delta terR$ (RI). pSNV-TK- α -globin $\Delta terR$ (RI) DNA was used as a control (left two lanes). The maps of unintegrated viral DNA at the bottom represent the parental virus and progeny virus without globin intervening sequences. The smearing seen in the unintegrated viral DNA lanes is probably a result of degradation in cells killed by the virus infection²⁴. A distinct 0.56-kbp band is visible in the *Hinf*I lane of the original.

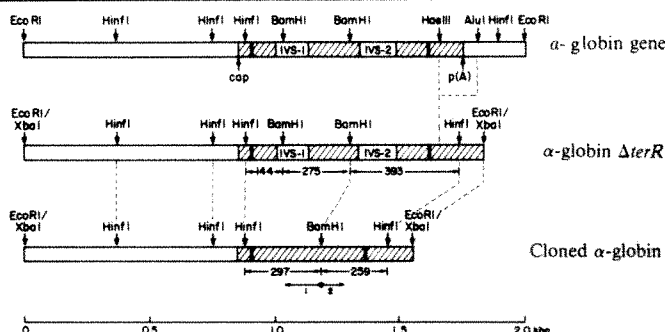


Fig. 3 Cloning and characterization of an α -globin DNA fragment from SNV-TK- α -globin $\Delta terR$ (RI). Isolation of circular unintegrated viral DNA from chicken cells infected with virus produced by chicken cells transfected with SNV-TK- α -globin $\Delta terR$ (RI) and REV-A DNAs: Virus-infected chicken cells (60–100-mm Petri dishes) were lysed with SDS 3 days after infection. Unintegrated viral DNA was isolated by the Hirt procedure. The Hirt supernatant fraction was treated with proteinase K (20 μ g ml⁻¹; Beckman) for 2 h at 37 °C and then with phenol and chloroform. One gramme of CsCl was added per ml of the preparation, and ethidium bromide was added to a final concentration of 0.1 mg ml⁻¹. The solution was centrifuged for 48 h in the Beckman 50 Ti rotor at 35,000 r.p.m. and 40 fractions were collected from the bottom of the centrifuge tube. 5 μ l of each fraction were spotted on to nitrocellulose filter paper, the DNA was denatured with 0.1 M NaOH and the filter was neutralized, heated at 80 °C for 2 h, and hybridized with ³²P- α -globin DNA. Fractions containing circular unintegrated viral DNA were collected and ethidium bromide and CsCl were removed by extraction with isopropanol and dialysis, respectively. The viral DNA was then digested with *Xba*I. Charon 4A DNA²⁵ was digested first with *Xba*I and then with alkaline phosphatase to remove terminal phosphate residues. Four molar equivalents of the insert DNA were added and the DNAs were ligated together. The ligated DNA was packaged, and the phage were used to infect *E. coli* DP50supF on NZYDT agar plates²⁵. The efficiency of isolation of positive plaques was about 10⁻³. The α -globin-containing phage were purified by serial dilution of the plaques containing the phage. DNA was extracted from purified phage, digested with *Xba*I and electrophoresed into a 1% agarose gel. The cleavage map of one of the clones is shown compared with the α -globin $\Delta terR$ DNA and the original α -globin gene¹¹. The thick vertical lines in exons 1 and 3 represent the ends of protein coding sequences. The numbers beneath the maps represent the sizes of the fragments found. Strategy used for sequencing the *Xba*I-digested globin DNA clone: the *Xba*I-digested DNA clone was digested with *Bam*HI followed by digestion with alkaline phosphatase. The DNA was labelled at its 5' ends with ³²P by T4 polynucleotide kinase (P-L Biochemicals) and then digested with *Hinf*I. DNA fragments of 300 and 260 bp were isolated and sequenced by the method of Maxam and Gilbert²⁶. The regions sequenced are indicated by arrows under the map of the cloned α -globin DNA and agree with the published sequence¹¹. IVS-1 is intervening sequence 1; IVS-2 is intervening sequence 2; 1 and 2 are the sequences of the regions corresponding to IVS-1 and IVS-2 after recovery from virus; cap is the 5' end of mouse α -globin mRNA; p(A) is the poly(A) addition site for mouse α -globin mRNA.

Figure 4 shows that virus with inserts containing intervening sequences was still present 7 days after transfection. Thus, the probability of losing the intervening sequences per replication cycle is less than 100%. However, by 9 days after transfection essentially all the viral DNA lacked the globin intervening sequences.

In a parallel experiment, virus was collected 4 days after transfection and passaged at 3-day intervals in fresh chicken cells. Before each passage, the unintegrated viral DNA was analysed as in the experiments described in Figs 2 and 4. Virus containing unspliced inserts was still detected after the first passage (7 days after the initial transfection) (data not shown). By the second passage all virus recovered contained only spliced globin DNA.

We believe that the loss of intervening sequences from these retroviral vectors occurred from genomic RNA for the following reason. In one of our constructions, pSNV-TK- α -globin $\Delta terR$ (HinfI), the *Hinf*I cleavage is ~20 bp 3' to the 5' end of sequences for globin mRNA¹¹ and so removes any promoter for globin mRNA synthesis. Progeny virus containing α -globin DNA without intervening sequences was recovered after transfection with pSNV-TK- α -globin $\Delta terR$ (HinfI) DNA (data not shown). Since no subgenomic RNA could be made, this finding indicates that splicing took place in genomic RNA rather than in globin mRNA followed by recombination with genomic RNA.

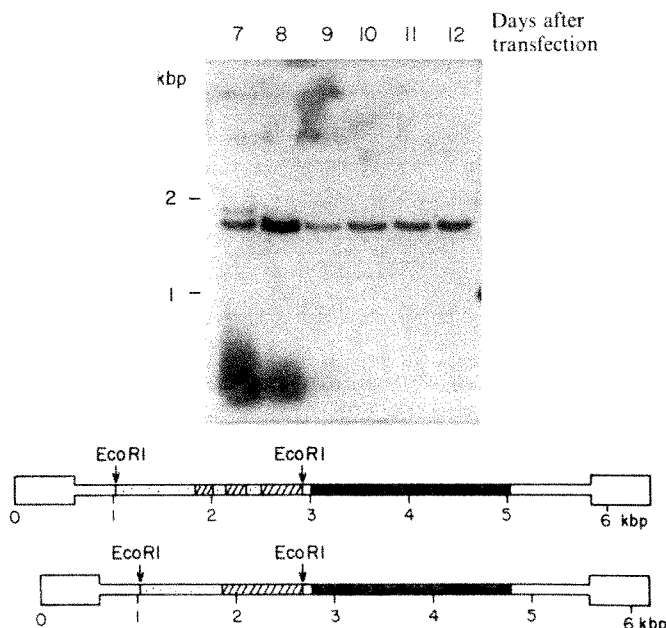


Fig. 4 Kinetics of loss of intervening sequences in recombinant virus. Virus produced by chicken cells transfected with pSNV-TK- α -globin Δ terR(R1) and REV-A DNAs was collected 4, 5, 6, 7, 8 and 9 days after transfection. Fresh chicken cells were infected with these viruses. Three days after infection (days 7–12 after transfection), unintegrated viral DNA was extracted by the procedure of Hirt^{22,23}. The DNAs were digested with *Eco*RI and analysed by electrophoresis in a 1.3% agarose gel. The gel was blotted onto a nitrocellulose filter and the filter was hybridized with nick-translated ³²P- α -globin DNA. Parallel preparations of DNA from uninfected chicken cells did not hybridize to mouse α -globin DNA (data not shown).

The difference between the normal 100% splicing of globin gene transcripts¹⁵ and the less efficient (~10%) splicing of the same sequences seen here may reflect the requirements of the retrovirus life cycle. Retroviruses normally synthesize some subgenomic mRNAs¹⁶. If all viral RNA were spliced, only subgenomic RNA and no progeny genomic RNA would be made. The retrovirus may therefore control the rate of splicing, perhaps through their 5' sequences which also control numerous other processes including encapsidation^{14,17,18}. Alternatively, the difference in cells or secondary structure of the RNA could be responsible for the difference in efficiency of splicing.

No virus containing DNA with one intervening sequence spliced out and the other remaining was found. Because the rate of loss of intervening sequences is less than 100%, this result indicates that loss of the two intervening sequences is not independent. Normal splicing of mouse β -globin mRNA precursor involves a partially spliced intermediate¹⁹.

The results reported here clearly demonstrate information transfer from DNA through spliced RNAs to DNA. They thus support the hypothesis that cDNA genes arose by reverse transcription of spliced RNA^{6–10,20}. However, it would not be correct to conclude that the results reported here indicate that retrovirus transfer is necessary for the formation of cDNA genes although it may well account for the origin of some viral oncogenes. In any case, our data illustrate how retroviruses can be used to delete intervening sequences from genomic DNAs, a process that would allow the expression of eukaryotic genes in prokaryotes.

We thank D. Hamer, NIH, for the α -globin plasmid, T. Schedl for help with cloning, I. Chen for advice, S. Watanabe for the DNA sequencing and our colleagues for helpful comments on the manuscript. This work was supported by NCI grants CA-07175 and CA122443. H.M.T. is an American Cancer Society Research Professor.

Received 28 May; accepted 14 July 1982.

1. Parker, R. C., Varmus, H. E. & Bishop, J. M. *Proc. natn. Acad. Sci. U.S.A.* **78**, 5842–5846 (1981).
2. Goff, S. P., Gilboa, E., Witte, O. N. & Baltimore, D. *Cell* **22**, 777–785 (1980).
3. Favera, R. D., Gelmann, E. P., Gallo, R. C. & Wong-Staal, F. *Nature* **292**, 31–35 (1981).
4. Vennström, B. & Bishop, J. M. *Cell* **28**, 135–143 (1982).

5. Chen, I. S. Y., Wilhelmsen, K. & Temin, H. M. *J. Virol.* (in the press).
6. Vanin, E. F., Goldberg, G. I., Tucker, P. W. & Smithies, O. *Nature* **286**, 222–226 (1980).
7. Nishioka, Y. & Leder, A. *Proc. natn. Acad. Sci. U.S.A.* **77**, 2806–2809 (1980).
8. Hollis, G. F., Hieter, P. A., McBride, D. W., Swan, D. & Leder, P. *Nature* **296**, 321–325 (1982).
9. Sharp, P. A. *35th Ann. Symp. Fundamental Cancer Research* (Raven, New York, in the press).
10. Wilde, C. D., Crowther, C. E., Cripe, T. P., Lee, M. G. S. & Cowan, N. J. *Nature* **297**, 83–84 (1982).
11. Nishioka, Y. & Leder, P. *Cell* **18**, 875–882 (1979).
12. Shimotohno, K. & Temin, H. M. *Cell* **26**, 67–77 (1981).
13. O'Rear, J. J. & Temin, H. M. *Proc. natn. Acad. Sci. U.S.A.* **79**, 1230–1234 (1982).
14. Watanabe, S. & Temin, H. M. *Proc. natn. Acad. Sci. U.S.A.* (in the press).
15. Ross, J. *J. molec. Biol.* **106**, 403–420 (1976).
16. Varmus, H. & Swanstrom, R. in *RNA Tumor Viruses, Molecular Biology of Tumor Viruses* Pt 3 (eds Weiss, R. A. et al.) 369–512 (Cold Spring Harbor Laboratory, New York, 1982).
17. Temin, H. M. *Cell* **27**, 1–3 (1981).
18. Temin, H. M. *Cell* **28**, 3–5 (1982).
19. Kinniburgh, A. J. & Ross, J. *Cell* **17**, 915–921 (1979).
20. Temin, H. M. *J. cell. Biochem.* (in the press).
21. Tabak, H. F. & Flavell, R. A. *Nucleic Acids Res.* **5**, 2321–2332 (1978).
22. Hirt, B. *J. molec. Biol.* **26**, 365–369 (1967).
23. Chen, I. S. Y. & Temin, H. M. *J. Virol.* **41**, 183–191 (1982).
24. Weller, S. K. & Temin, H. M. *J. Virol.* **39**, 713–721 (1981).
25. Williams, B. G. & Blattner, F. R. *J. Virol.* **29**, 555–575 (1979).
26. Maxam, A. M. & Gilbert, W. *Meth. Enzym.* **65**, 499–560 (1980).

Ribosomal RNA genes in the replication origin region of *Bacillus subtilis* chromosome

G. Henckes*, F. Vannier*, M. Seiki†, N. Ogasawara‡, H. Yoshikawa‡ & S. J. Seror-Laurent*§

* Institut de Microbiologie, Bâtiment 409, Université Paris XI-91405, Orsay Cedex 05, France

† Department of Viral Oncology, Cancer Institute, Toshimaku, Tokyo, Japan

‡ Cancer Research Institute, Kanazawa University, Kanazawa, Japan

In *Bacillus subtilis*, DNA replication proceeds bidirectionally, commencing in the *Bam*HI fragment, B7 (see Fig. 4). The middle *Eco*RI fragment E19, generated from B7, is the first to be replicated, followed by the E22 fragment in one direction and by the E6' fragment in the other direction^{1,2}. The B7 fragment was also shown to inhibit the replication of a plasmid which carried this fragment^{3,4} and the minimal essential sequence for the inhibition (*sar*) was located to a 200-base pair (bp) region of E19, which contains two promoters, as deduced by the sequence analysis⁵. Previous studies showed that the E6' fragment was unique while E19 and E22 fragments hybridized to multiple sites on the chromosome. In addition, in the course of the analysis of an RNA covalently linked to DNA and synthesized at specific times related to chromosome initiation⁶, we found that this RNA was complementary both to the E19 and E22 fragments and to ribosomal RNA genes⁷. We show here that a ribosomal RNA gene set (*rrnO*) overlaps the first replicating fragments in one direction. The promoters for these genes are in fact the promoters of the *sar* sequence.

B. subtilis chromosomal DNA was digested to completion by *Bam*HI and *Sma*I restriction endonucleases, separated electrophoretically, and the resulting fragments were assayed by hybridization with ³²P-labelled E19 and E22. The patterns presented in Fig. 1 show that the E19 and E22 fragments hybridized with at least 7 different fragments on the chromosome, in agreement with earlier results⁴. A similar hybridization experiment was performed with the total chromosomal DNA using 16S and 23S RNA probes. The results presented in Fig. 2 showed that the E19 and E22 fragments hybridized with restriction fragments which are specific for the 16S RNA or for both 16S and 23S RNA. The bands corresponding to 14, 11 and 3.5 kbp *Bam*HI fragments, and to 7.2 and 5.4 kbp *Sma*I fragments, which are specific for the 23S RNA⁸, were absent in both E19 and E22 hybridization patterns.

To determine the precise homology between the E19 and E22 fragments and the ribosomal RNA genes, we took advan-

§ To whom correspondence should be addressed.

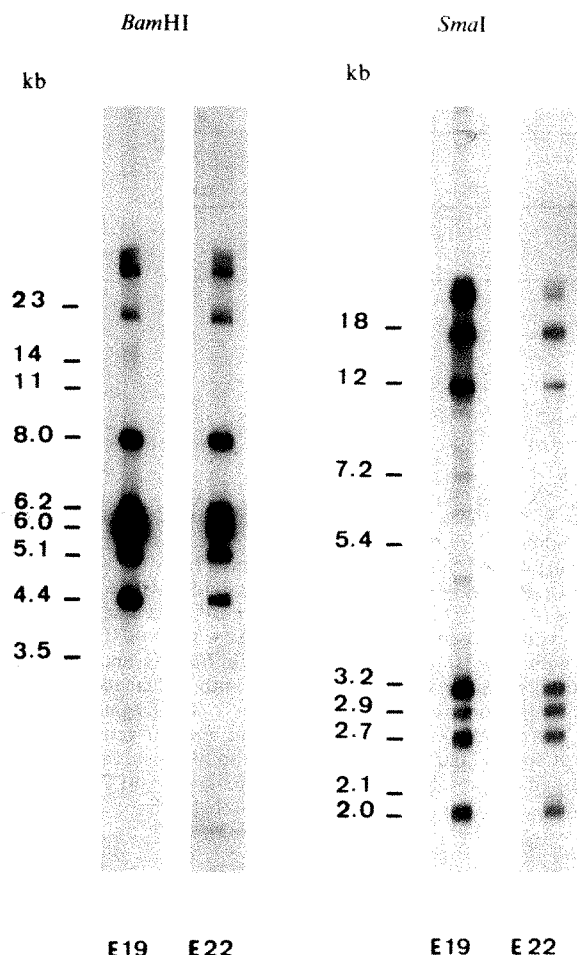


Fig. 1 Southern hybridization of E19 and E22 fragments with the *Bam*HI and *Sma*I *B. subtilis* DNA digests. Chromosomal DNA from *B. subtilis* 168 (*thy*, *trp*) was digested to completion either with *Bam*HI or with *Sma*I (New England Biolabs), electrophoresed in 0.7% agarose, transferred and fixed on nitrocellulose sheets (Millipore) according to the method of Southern¹⁹. DNA from plasmid pKY2700 containing E19 or E22 fragments⁴ was purified by caesium chloride-ethidium bromide equilibrium centrifugation followed by sedimentation on sucrose gradients and finally digested with *Eco*RI and electrophoresed in 1% agarose. After extraction from the gel, the E19 and E22 fragments were nick translated with [α -³²P]dCTP (400 Ci mmol⁻¹, Amersham France). Before mixing with ³²P-DNA the Southern transfers were incubated for 1 h at 65 °C in 0.02% Ficoll, 0.02% polyvinyl pyrrolidone, 0.02% bovine serum albumin, 100 μ g ml⁻¹ yeast tRNA 4 \times SSC. Then the ³²P-labelled E19 or E22 DNA was added and, after 18 h at 65 °C, the sheets were washed in 2 \times SSC, 0.5% SDS for 2 h at 65 °C, then for 1 h at 25 °C and finally in 2 \times SSC for 1 h at 25 °C. After washing the sheets were exposed to X-ray film.

tage of the restriction map of a ribosomal RNA gene set recently obtained by Bott *et al.*⁹. DNA from plasmid p14B1 containing the DNA sequence coding for one of the ribosomal RNA gene clusters, was completely digested as detailed in Fig. 3. The resulting fragments were separated electrophoretically and assayed by hybridization with ³²P-labelled E19 and E22 fragments. The E19 fragment showed homology with the fragment limited by the *Hind*III and *Eco*RI sites and containing the coding sequence for the 5'-terminus of 16S RNA (Fig. 3). The E22 fragment showed homology with the fragment limited by *Eco*RI sites and containing the coding sequence for the 3'-terminus of 16S RNA.

The restriction maps independently constructed by Bott *et al.*⁹ and Seiki *et al.*¹, for one of the ribosomal RNA gene clusters and the replication origin region respectively are remarkably similar, as shown in Fig. 4. Most of the differences could be explained by a small displacement of several of the sites. In fact, some heterogeneity has been observed in the organization of the different ribosomal RNA genes (ref. 10 and G. C. Stewart,

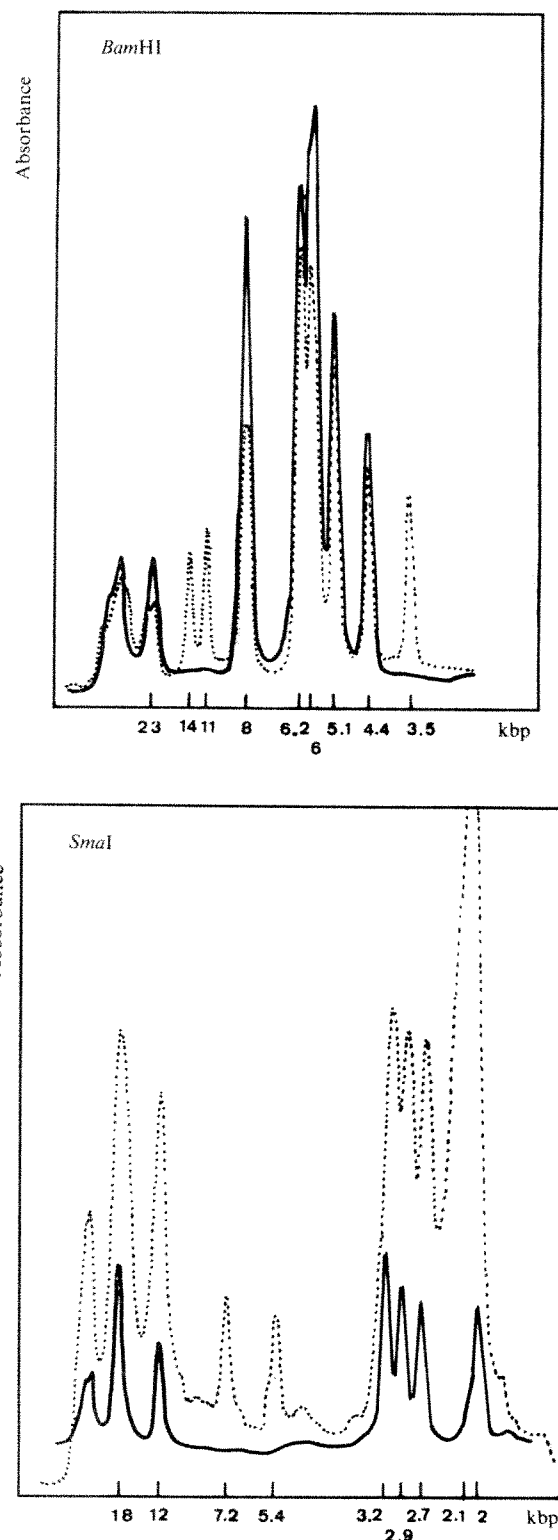


Fig. 2 Comparison of hybridization patterns obtained with ³²P-E19 and E22 fragments and ³²P-ribosomal RNA (16S+23S). E19 and E22 fragments were labelled with ³²P and hybridized with the *Bam*HI and *Sma*I *B. subtilis* DNA digests as described in Fig. 1 legend. The 16S and 23S ribosomal RNAs were purified from a nucleic acid extract by sedimentation through 15–30% sucrose gradients and labelled at their 5' termini with [α -³²P]ATP (3,000 Ci mmol⁻¹, Amersham France) and T4 polynucleotide kinase. The ³²P-labelled 16S and 23S were incubated with the Southern transfers for 18 h at 68 °C in 3 \times SSC and 0.1% SDS. After hybridization the sheets were washed in 3 \times SSC for 1 h at 37 °C, then in 3 \times SSC for 4 h at 48 °C. The sheets were exposed to X-ray film and the absorbance of the film image was measured using a densitometer (Kipp et Zonen). ³²P-E19 or ³²P-E22 fragments (—); ³²P-ribosomal RNA (16S+23S) (....).

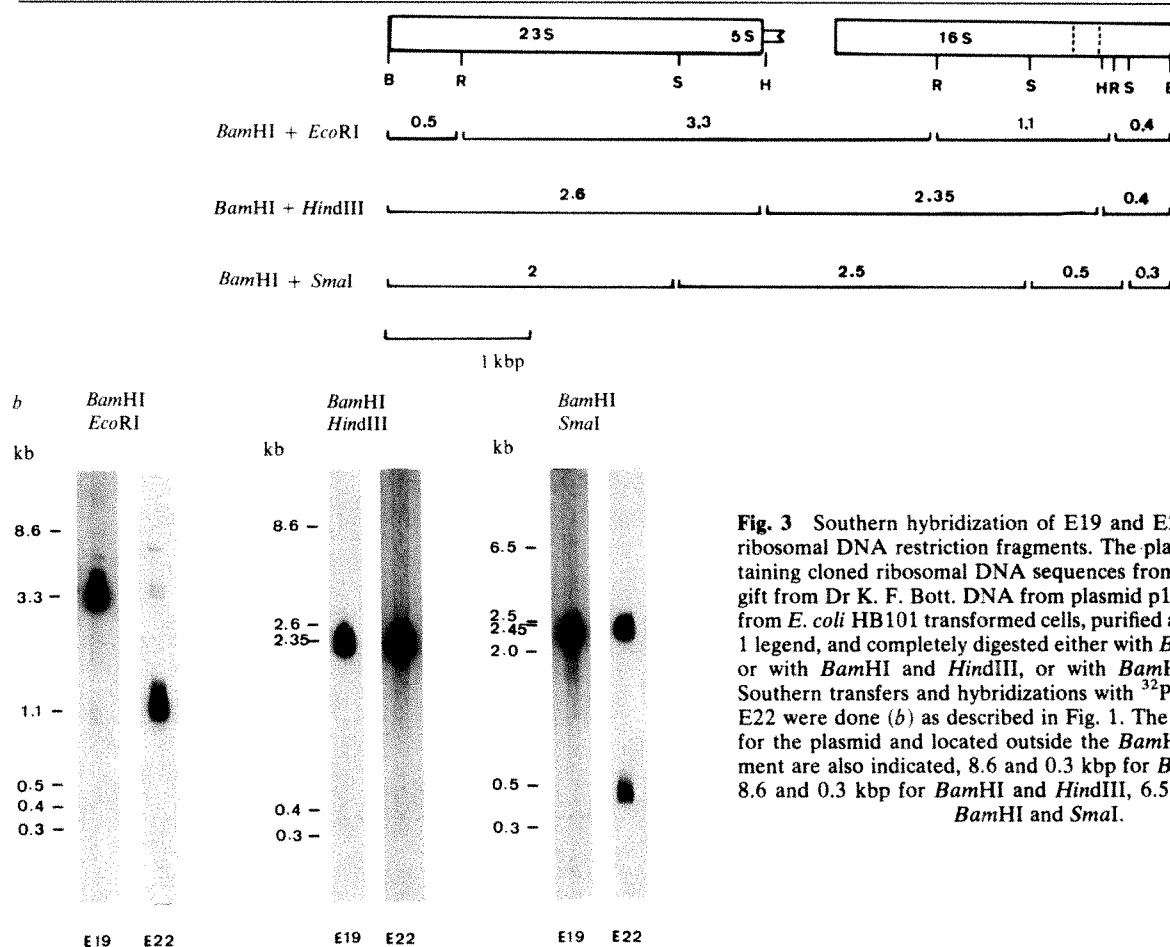


Fig. 3 Southern hybridization of E19 and E22 fragments with ribosomal DNA restriction fragments. The plasmid p14B1, containing cloned ribosomal DNA sequences from *B. subtilis*, was a gift from Dr K. F. Bott. DNA from plasmid p14B1 was prepared from *E. coli* HB101 transformed cells, purified as described in Fig. 1 legend, and completely digested either with *Bam*HI and *Eco*RI, or with *Bam*HI and *Hind*III, or with *Bam*HI and *Sma*I (a). Southern transfers and hybridizations with 32 P-labelled E19 and E22 were done (b) as described in Fig. 1. The fragments specific for the plasmid and located outside the *Bam*HI-generated fragment are also indicated, 8.6 and 0.3 kbp for *Bam*HI and *Eco*RI, 8.6 and 0.3 kbp for *Bam*HI and *Hind*III, 6.5 and 2.45 kbp for *Bam*HI and *Sma*I.

personal communication). Moreover, the similarity observed concerns not only the region covering the E19 and E22 fragments but also the region beyond the E22 fragment, suggesting the presence of a complete ribosomal RNA gene set in the region of the chromosome origin.

From the data obtained in this study, it seems likely that a 500-bp region, which has been shown to be responsible for the inhibitory effect on plasmid replication⁴, could include the ribosomal RNA promoters and a sequence of nucleotides which is normally removed from the precursor 16S RNA to form the mature molecule¹¹. Recently, the nucleotide sequence of this region has been determined and has revealed the presence of two tandem promoters located 98 bp apart⁵. The sequence of the analogous region of the ribosomal RNA genes cloned in p14B1 has been determined by K. F. Bott (personal communication). Comparison of the two regions shows two identical sequences of about 80 nucleotides located downstream from the second promoter, the second one coding for the 5' end of the mature 16S ribosomal RNA. These data strongly support

the homology reported here. Interestingly, there are some differences in the region of the second promoter and the sequence containing the first promoter is absent in the ribosomal RNA genes set cloned in p14B1.

Within the 500-bp region, the *sar* sequence (suppressor for autonomous replication) has been found to be essential for the *cis*-inhibition of plasmid replication⁵. This sequence contains the two promoters described above. The elimination of the second promoter dramatically affected both the inhibitory effect and *in vitro* transcription, suggesting that the transcriptional activity of the second promoter is involved in the *cis*-inhibition of DNA replication⁵. The location of the *sar* sequence very close to or overlapping the replication origin could explain the failure to isolate an autonomous replicative sequence from the *B. subtilis* chromosome. The *sar* sequence has been assumed to control negatively the initiation of the chromosome and this effect should be removed during initiation. It is of particular interest to note the isolation of an RNA covalently linked to DNA and synthesized at specific times related to

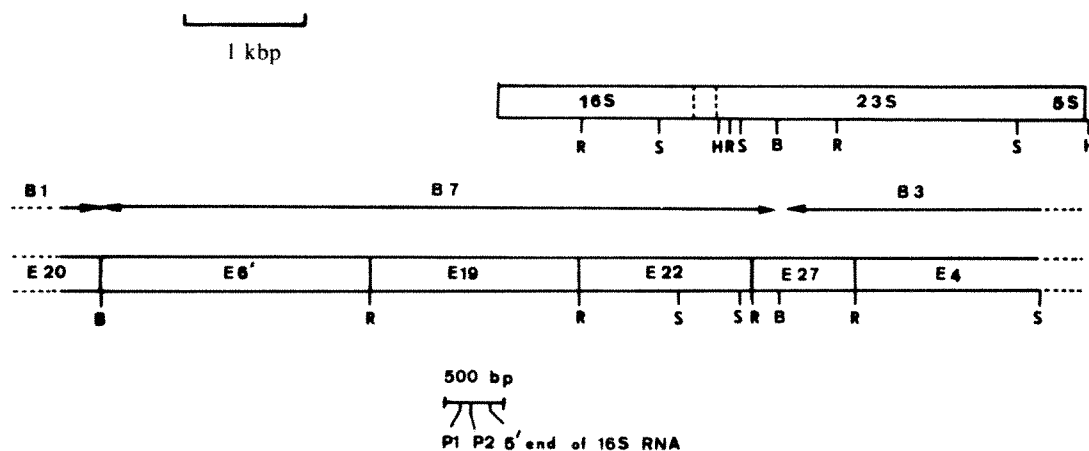


Fig. 4 Comparison of the restriction maps of the ribosomal RNA operon and the region of the replication origin. This figure also shows the location of the 500 bp sequenced segment of E19. P1 and P2 are the two promoters identified in the *sar* sequence. Data from Bott *et al.*⁹ and from Seiki *et al.*¹.

chromosome initiation⁹. Recently this RNA has been found to be homologous to the first replicating fragments E19 and E22 and thus appears as a possible candidate for the primer role at the replication origin (data not shown).

The chromosome replication origin has been located on the genetic map near *purA*, probably between *rec F15* and *ts8132* loci¹². A DNA-protein complex which is known to be related to the cells' ability to initiate chromosome replication has been located near the origin, on the B1 fragment contiguous to the B7 fragment^{13,14}. In addition, the *gua* gene has been found by transformation to be present in the B3 fragment, which is adjacent to B7 (data not shown). The identification of a ribosomal RNA sequence on the first replicating fragment E19 provides more precise information on the organization of the replication origin region. From the results presented here, it can be concluded that the region covered by the two promoters and the 16S RNA sequences must contain the origin or be located within a few hundred nucleotides of the origin.

The ribosomal RNA genes are probably present in 10 copies in *B. subtilis*^{8,10,15} and some of these genes have been mapped^{16,17}. This study reports the location of a new ribosomal

RNA gene set, which we call *rrnO*, close to the replication origin. The promoters and the leading sequence of the *rrnO* gene set may be unique and responsible for the specific properties associated with the replication origin of the chromosome. This is the first indication in prokaryotes that ribosomal RNA cistrons may be located at the replication origin. However, studies on eukaryotic chromosomes indicate that replication origins occur in each repeating unit of the ribosomal RNA clusters¹⁸.

A major question in understanding the regulation of DNA replication is how the number of chromosomes is maintained in the cell at a certain value, through successive generations and through changes in the environment that alter growth rate. The finding in *B. subtilis*, of a ribosomal gene set in the region of the replication origin may throw light on this question.

We thank Dr Kenneth F. Bott for his gift of plasmid p14B1, for communicating the sequence of the coding region for the 16S RNA and for helpful discussion. We also thank Dr I. Barry Holland for a critical reading of the manuscript. This work was supported by grants from the CNRS (L.A. 136) and from ATP Microbiologie.

Received 20 April; accepted 30 July 1982.

- Seiki, M., Ogasawara, N. & Yoshikawa, H. *Nature* **281**, 699–701 (1979).
- Ogasawara, N., Seiki, M. & Yoshikawa, H. *Nature* **281**, 702–704 (1979).
- Seiki, M., Ogasawara, N. & Yoshikawa, H. *Molec. gen. Genet.* **183**, 220–226 (1981).
- Seiki, M., Ogasawara, N. & Yoshikawa, H. *Molec. gen. Genet.* **183**, 227–233 (1981).
- Seiki, M., Ogasawara, N. & Yoshikawa, H. *Proc. natn. Acad. Sci. U.S.A.* (in the press).
- Henckes, G., Vannier, F., Buu, A. & Seror-Laurent, S. *J. Bact.* **149**, 79–91 (1982).
- Seror-Laurent, S. *et al.* (in preparation).
- Moran, C. P. & Bott, K. J. *J. Bact.* **140**, 99–105 (1979).
- Bott, K. F., Wilson, F. E. & Stewart, G. C. in *Sporulation and Germination* (eds Levinson, H. C., Soneishein & Tipper, D. J.) 119–122 (American Society for Microbiology, Washington DC, 1981).

- Loughney, K., Lund, E. & Dahlberg, J. E. *Nucleic Acids Res.* **10**, 1607–1624 (1982).
- Hecht, N. B. & Woese, C. R. *J. Bact.* **95**, 986–990 (1968).
- Harford, N., Lepesant-Kejzarova, J., Lepesant, J., Hamers, R. & Dedonder, R. *Microbiology* 1976, 28–34 (American Society for Microbiology, Washington DC, 1976).
- Yoshikawa, H., Yamaguchi, K., Seiki, M., Ogasawara, N. & Toyoda, H. *Cold Spring Harb. Symp. quant. Biol.* **43**, 569–576 (1978).
- Yoshikawa, H., Ogasawara, N. & Seiki, M. *Molec. gen. Genet.* **179**, 265–272 (1980).
- Smith, I., Dubnau, D., Morell, P. & Marmur, J. *J. molec. Biol.* **33**, 123–140 (1968).
- Chow, L. T. & Davidson, N. *J. molec. Biol.* **75**, 265–279 (1973).
- Wilson, F. E., Hoch, J. A. & Bott, K. J. *Bact.* **146**, 624–628 (1981).
- Bozzoni, I., Baldari, C. T., Amaldi, F. & Buongiorno-Nardelli, M. *Eur. J. Biochem.* **118**, 585–590 (1981).
- Southern, E. M. *J. molec. Biol.* **98**, 503–517 (1979).

Abnormal NAD⁺ levels in cells from patients with Fanconi's anaemia

Nathan A. Berger, Sosamma J. Berger & Donna M. Catino

Hematology/Oncology Division, Departments of Medicine and Pharmacology, The Jewish Hospital of St Louis, and Washington University School of Medicine, St Louis, Missouri 63110, USA

Poly(ADP-ribose) is synthesized from NAD⁺ in the nuclei of eukaryotic cells and the activity of the chromatin-bound enzyme, poly(ADP-ribose) polymerase, is markedly stimulated by DNA strand breaks^{1–7}. Recent studies suggest that poly(ADP-ribose) is associated with the repair of DNA damage^{8–10} and the process of cellular differentiation^{11,12}. Hence, abnormalities in the metabolism of poly(ADP-ribose) could be aetiologically related to some of the human genetic disorders of DNA repair, especially those that are characterized by congenital and developmental anomalies. Defects in poly(ADP-ribose) metabolism could arise from abnormalities in the enzyme poly(ADP-ribose) polymerase, abnormalities in levels of its substrate NAD⁺, the proteins that act as acceptors for poly(ADP-ribose) or polymer stability. We have examined cells from patients with genetic disorders of DNA repair to determine whether they contain the enzyme poly(ADP-ribose) polymerase, whether the enzyme increases its activity in response to DNA damage and whether the cells maintain normal levels of NAD⁺. We demonstrate here that cells from patients having Fanconi's anaemia have lower NAD⁺ levels than cells from normal donors. This abnormality may contribute to the disorders of DNA repair and congenital anomalies that characterize this disease^{13,14}.

Table 1 shows the NAD⁺ levels found in a series of normal and repair-deficient human skin fibroblasts. The normal cells maintained a mean NAD⁺ level of 1,140 ± 304 pmol per 10⁶ cells with a range from 870 to 1,570 pmol per 10⁶ cells. Cells from patients in two of the subgroups of xeroderma pigmen-

tosum maintained NAD⁺ levels that were slightly higher than normal. Cell lines from two patients with Cockayne's syndrome were examined; one had low and the other high NAD⁺ levels.

Cell lines derived from seven patients with Fanconi's anaemia (2061, 646, c111, 1196, c114, 368 and 1746) had low NAD⁺ levels compared with normal cells, while Fanconi's anaemia cell lines 2361, 369 and 449 maintained NAD⁺ levels that were in the low-normal range. The mean level of NAD⁺ in the Fanconi's fibroblasts was approximately half that of normal cells.

We then compared NAD⁺ levels in freshly prepared human lymphocytes derived from normal donors and from patients with Fanconi's anaemia. Normal human lymphocytes are resting intermitotic cells with low levels of pyridine nucleotides^{15,16}; when stimulated by phytohaemagglutinin (PHA), they undergo a marked expansion of their pyridine nucleotide pools, reaching peak levels on the third or fourth day of culture¹⁶. In the present study, NAD⁺ levels were measured in lymphocytes within 2–3 h of their preparation from fresh human blood and again after 3 days of PHA stimulation. Table 2 shows that the mean NAD⁺ level in resting lymphocytes from 35 normal donors was 80 ± 28 pmol per 10⁶ cells. Cells stimulated with PHA always showed marked increases in NAD⁺ levels, ranging from 3 to 16 times the NAD⁺ in resting cells.

Lymphocytes were prepared from five patients with Fanconi's anaemia and NAD⁺ levels were determined before and 3 days after PHA stimulation. Microscopic examination showed that the lymphocytes obtained from such patients underwent a normal agglutination reaction after PHA treatment. These cells also showed a normal increase in DNA synthesis as measured by ³H-thymidine (³H-TdR) incorporation on the third day after PHA stimulation. Initial NAD⁺ levels in freshly isolated lymphocytes from patients with Fanconi's anaemia were usually within the normal range. On PHA stimulation, the NAD⁺ levels increased; however, in the first four patients with Fanconi's anaemia, they were still below normal. Patient 4, whose PHA-stimulated lymphocytes exhibited an NAD⁺ level, at the lower limit of normal, was a 16-yr-old boy whose pancytopenia had partially responded to androgen therapy. Patient 5, who showed

Table 1 NAD⁺ levels (pmol per 10⁶ cells) in human fibroblasts

Normal cells		Xeroderma pigmentosum		Fanconi's anaemia	
Cell line	NAD ⁺	Cell line	NAD ⁺	Cell line	NAD ⁺
CRL1119	870 ± 247	CRL1223 (XPA)	2,210 ± 981	GM2061	245 ± 122
325	914 ± 281	CRL1160 (XPD)	1,470 ± 741	GM0646	286 ± 196
CRL1141	983 ± 217	Mean	= 1,840 ± 522	c111	398 ± 179
CRL1220	1,010 ± 361	Cockayne's syndrome		CRL1196	453 ± 107
CRL1121	1,480 ± 691	Cell line	NAD ⁺	c114	512 ± 533
AG1518	1,570 ± 458			GM0368	699 ± 440
Mean	= 1,140 ± 304			GM1746	789 ± 325
				GM2361	892 ± 540
		GM0739	684 ± 363	GM0369	907 ± 214
		GM1856	2,290 ± 4	GM0449	973 ± 454
		Mean	= 1,490 ± 1,140	Mean	= 614 ± 239

The sources of the human skin fibroblasts were as follows: AG1518, GM0739, GM1856, GM2061, GM0646, GM0368, GM1746, GM2361, GM0369 and GM0449 were all from the Human Genetic Mutant Cell Repository, Camden, New Jersey. CRL1119, CRL1141, CRL1220, CRL1121, CRL1223, CRL1160 and CRL1196 were from the American Type Culture Collection, Rockville, Maryland. Cell lines c111 and c114 were from Dr M. Swift, University of North Carolina. Cell line 325, from a patient with β -glucuronidase deficiency, was obtained from Dr W. Sly, Washington University Medical School. As these cells have no known disorder of DNA repair they are included in this series with the normal cell lines. All lines were maintained in alpha modified Eagle's medium supplemented with 20% heat-inactivated fetal calf serum (FCS) 100 U ml⁻¹ penicillin, 100 μ g ml⁻¹ streptomycin and 25 mM HEPES, pH 7.2 at 37 °C. All studies were performed with three batches of FCS, both normal and abnormal cells were processed with each batch of serum and results were independent of the batch used. Most of the cell lines were examined for mycoplasma by independent assays at Flow Laboratories and all those examined were found to be free of contamination. For NAD⁺ determinations, confluent cultures in T75 flasks were split 1:3 into 100-mm Petri dishes with 15 ml medium and incubated at 37 °C. NAD⁺ assays were performed on the second day after plating. Cells were quickly scraped from plates, suspended in their growth medium by vortexing and the cell samples were processed for NAD determination by extraction and enzymatic cycling techniques as described previously^{16,24}. Additional samples of cell suspension were diluted into 5% Cetrimide and cell numbers counted electronically on a Coulter counter model F. All assays were performed in duplicate on duplicate samples taken at each time point. All assays were therefore performed in quadruplicate with less than 10% variation between separate assays. Results for each cell line are presented as the mean \pm s.d. for assays performed at multiple passages between 7 and 20 except for cell lines CRL1220 and CRL1121 which were studied between passages 19 and 24. Differences between NAD⁺ values in normal and Fanconi's anaemia cells are significant at $P < 0.01$.

a completely normal increase in NAD⁺ in response to PHA, was a 20-yr-old woman whose pancytopenia was in a spontaneous partial remission. The mean NAD⁺ level in PHA-stimulated lymphocytes from all patients with Fanconi's anaemia was approximately half that detected in normal cells.

Table 2 NAD⁺ levels (pmol per 10⁶ cells) in human lymphocytes

Normal donors	Control	PHA
FA patients	80 ± 28	470 ± 180
1	59	176
2	27	66
	71	191
3	59	99
	74	244
4	39	252
5	98	693
Mean	61 ± 23	245 ± 208

Peripheral blood lymphocytes were prepared on Ficoll-Hypaque gradients as described previously^{16,17} from fasting normal donors and patients with Fanconi's anaemia. None of these donors were the same as those used in Table 1. The cells were diluted into alpha modified Eagle's medium supplemented with 2 mM glutamine, 100 U ml⁻¹ penicillin, 100 μ g ml⁻¹ streptomycin, 10% heat-inactivated FCS and 25 mM HEPES, pH 7.2. For PHA studies, cells were incubated at 3×10^5 cells ml⁻¹ in a 20 ml T flask at 37 °C with 2 μ g ml⁻¹ sterile L-phytohaemagglutinin (Sigma). Control values were determined within 2–3 h of the time that cells were isolated from peripheral blood; PHA-stimulated values were determined after 3 days' incubation at 37 °C. At each time point cells were collected for NAD extraction and determination by enzymatic cycling assays as previously described^{16,24}. Additional samples were diluted into 5% Cetrimide for cell counting. All assays were performed in duplicate on duplicate samples taken at each time point; values shown are the means of assays performed in quadruplicate, with less than 10% variation between replicate assays. The five patients were all diagnosed as having Fanconi's anaemia (FA) based on pancytopenia, chromosomal abnormalities, typical skin changes, retarded growth and congenital anomalies of kidneys and bones. Their ages and sexes are as follows: 1, 10 yr (F); 2, 9 yr (F); 3, 11 yr (F); 4, 16 yr (M); 5, 20 yr (F). Patients 2 and 3 are sisters; cells from each of these two patients were examined on two separate occasions. Patient 4 was taking 2.5 mg oxymethalone every other day. The other patients were not receiving any drugs. Cells from 35 normal donors were used to establish the NAD⁺ level in control lymphocytes and cells from 25 of these donors were stimulated with PHA to determine the NAD⁺ levels in PHA-stimulated cells. There was no significant difference in NAD⁺ levels in resting lymphocytes between normal donors and patients with Fanconi's anaemia. The difference in NAD⁺ levels in PHA-stimulated cells between normal and Fanconi's anaemia patients was significant at $P < 0.01$.

As the highest NAD⁺ levels in the mitogen-stimulated lymphocytes from Fanconi's anaemia patients occurred in those two whose diseases were in partial remission, it is possible that their defect in maintaining NAD⁺ levels was improved. Alternatively, it is possible that the ability to achieve normal NAD⁺ levels contributes to the attainment of remission.

Additional studies were performed in which lymphocytes from normal donors were mixed with cells from patients with Fanconi's anaemia before extraction and measurement of NAD⁺ levels. The cells from patients with Fanconi's anaemia contained no substances that interfered with either the extraction or the measurement of NAD⁺. Furthermore, when lymphocytes from normal donors were co-cultivated with lymphocytes from Fanconi's anaemia patients, the final NAD⁺ values were those expected from the sum of the cells grown independently. Thus, Fanconi's anaemia cells contain no factors capable of reducing NAD⁺ levels in normal cells in the same culture system. Furthermore, the presence of normal cells does not correct the decreased NAD⁺ levels in the Fanconi's anaemia cells.

Freshly prepared human lymphocytes were also used to assay for the presence of poly(ADP-ribose) polymerase in Fanconi's anaemia and to determine whether its activity increased in a normal manner in response to DNA damage¹⁷. These studies were performed in lymphocytes that were untreated (control cells), or treated either with UV irradiation (50 J m⁻²) or with *N*-methyl-*N'*-nitro-*N*-nitrosoguanidine (MNNG; 20 μ g ml⁻¹), incubated for 3 h at 37 °C, then permeabilized and supplied with ³H-NAD to measure the activity of poly(ADP-ribose) polymerase¹⁷. Table 3 shows that the enzyme was present and its activity increased in normal cells in response to treatment with UV irradiation or MNNG. Similarly, it was present in cells from patients with Fanconi's anaemia and its activity increased in response to UV irradiation and treatment with MNNG. While the latter cells showed less enzyme activity than the normal cells, they nevertheless did respond to DNA damage as did normal cells with an increase in activity of poly(ADP-ribose) polymerase.

As a result of the increase in poly(ADP-ribose) polymerase activity that occurs in response to DNA damage, cellular pools

Table 3 Poly(ADP-ribose) synthesis (pmol per 10^6 cells per 30 min) in DNA-damaged lymphocytes

	Normal donors	Donors with Fanconi's anaemia
Control	36 ± 18 (n = 15)	17 ± 4 (n = 2)
UV-irradiated (50 J m ⁻²)	179 ± 70 (n = 12)	90 ± 0 (n = 2)
MNNG (20 µg ml ⁻¹)	511 ± 235 (n = 5)	260 ± 171 (n = 2)

Immediately after preparation of peripheral blood lymphocytes from normal donors or patients with Fanconi's anaemia, the cells were suspended at 3×10^5 ml⁻¹ in the same medium as described in Table 2. Control cells received no further treatment. UV-irradiated cells received 50 J m⁻² as previously described¹⁷ and MNNG-treated cells were adjusted to contain final concentrations of 20 µg ml⁻¹ MNNG and 0.2% dimethyl sulphoxide (DMSO). Previous studies have shown that mock-irradiation or DMSO treatment has no effect on poly(ADP-ribose) synthesis²⁰. Cells were incubated in tissue culture medium at 37 °C for 3 h, then permeabilized; 10^6 cells were then incubated with ³H-NAD (NEN) for 30 min and treated with 20% cold trichloroacetic acid to measure incorporation into poly(ADP-ribose) as described previously¹⁷. The result for each donor is the mean of assays performed in triplicate which agreed within 10%. The results for normal cells are expressed as the mean ± s.d. of assays performed on cells from the number of donors is indicated in parentheses. The values for the patients with Fanconi's anaemia were obtained for lymphocytes from two donors, patients 1 and 5 in Table 2.

of NAD⁺ can be rapidly consumed¹⁸⁻²¹. Table 4 shows that NAD⁺ levels decreased in normal and Fanconi's anaemia cells after UV irradiation and treatment with MNNG. This fall in NAD⁺ levels serves as an independent demonstration that DNA damage activates poly(ADP-ribose) polymerase in Fanconi's anaemia cells as it does in normal cells^{20,21}. Although these determinations were only performed on cells from two donors, it is interesting that the residual NAD⁺ levels in Fanconi's anaemia cells were lower than in normal cells. These exceptionally low NAD⁺ levels may severely impair the ability of Fanconi's anaemia cells to maintain their energy metabolism during the period required for the normal DNA repair processes. For example, when the NAD⁺ levels of L1210 and 3T3 cells are depleted by growth in nicotinamide-deficient medium, they lose their ability to perform unscheduled DNA synthesis and to reseat DNA strand breaks^{8,9}. Thus, the low NAD⁺ levels in cells from some patients with Fanconi's anaemia may contribute to their decreased ability to recover from DNA damage.

Many studies have identified NAD⁺ levels and poly(ADP-ribose) synthesis as important factors in the normal process of differentiation. Nicotinamide analogues that interfere with NAD⁺ synthesis prevent normal differentiation and result in congenital anomalies in developing embryos²². Incubation of chick mesenchymal cells in high levels of nicotinamide induce high intracellular NAD⁺ levels and cause cells to differentiate into myoblasts, whereas incubation in medium with low nicotinamide result in NAD⁺-depleted cells and cause differentiation into cartilage cells¹¹. Poly(ADP-ribose) polymerase activity increases when myoblasts differentiate into myotubes and when Friend erythroleukaemic cells are induced to synthesize haemoglobin^{12,23}. Thus, the pleiotropic abnormalities that occur in patients with Fanconi's anaemia may be explained by abnormalities in the sizes of their NAD⁺ pools.

More studies are clearly required to determine whether decreased NAD⁺ pools in patients with Fanconi's anaemia are due to underproduction or over-utilization. In addition, it will

Table 4 NAD⁺ levels (pmol per 10^6 cells) in DNA-damaged lymphocytes

	Normal donors	Donors with Fanconi's anaemia
Control	79 ± 20 (n = 19)	80 ± 28 (n = 2)
UV-irradiated (50 J m ⁻²)	11 ± 7 (n = 15)	0.7 ± 0.1 (n = 2)
MNNG (20 µg ml ⁻¹)	6 ± 7 (n = 6)	0.4 ± 0.5 (n = 2)

Control and DNA-damaged cells were treated as described in Table 3 then incubated in tissue culture medium at 37 °C for 3 h. Cells were collected for NAD assays and cell counts as described in Table 2. The values represent the mean ± s.d. of assays performed on cells from the number of donors given in parentheses. The assays using cells from patients with Fanconi's anaemia were performed on lymphocytes from two donors, patients 1 and 5 in Table 2.

be necessary to determine whether the low NAD⁺ levels are the cause or consequence of the DNA repair defect. Finally, longitudinal studies will be required to investigate the relationship of NAD⁺ levels to the severity of the disease and the possibility that some of the abnormalities may be ameliorated by correcting NAD⁺ levels.

This work was supported by NIH grant GM26463 and American Cancer Society grants CH134 and BC4W. Some of the cell culture media used in these experiments were prepared in a Cancer Center Facility funded by the NCI. N.A.B. is a Leukemia Society of America Scholar. We thank Drs W. Sly and M. Swift for cell cultures, and Drs G. Broun, V. Land and H. Zarkowsky for allowing us to study their patients.

Received 23 March; accepted 30 June 1982.

1. Hayaishi, O. & Ueda, K. A. *Rev. Biochem.* **46**, 95-116 (1977).
2. Hiltz, H. & Stone, P. *Rev. Physiol. Biochem. Pharmac.* **76**, 1-57 (1976).
3. Purnell, M. R., Stone, P. R. & Whish, W. J. D. *Biochem. Soc. Trans.* **8**, 215-227 (1980).
4. Mullins, D. W., Giri, C. P. & Smulson, M. *Biochemistry* **16**, 506-513 (1977).
5. Miller, E. G. *Biochim. biophys. Acta* **395**, 191-200 (1975).
6. Benjamin, R. C. & Gill, D. M. *J. biol. Chem.* **255**, 10493-10501 (1980).
7. Cohen, J. J. & Berger, N. A. *Biochem. biophys. Res. Commun.* **98**, 268-274 (1981).
8. Durkacz, B. W., Omidiji, O., Gray, D. A. & Shall, S. *Nature* **283**, 593-596 (1980).
9. Jacobson, E. L., Juarez, D. & Sims, J. L. *Fedn Proc.* **39**, 1739 (1980).
10. Berger, N. A. & Sikorski, G. W. *Biochemistry* **20**, 3610-3614 (1981).
11. Caplan, A. I. & Ordahl, C. P. *Science* **201**, 120-130 (1978).
12. Farzaneh, F., Shall, S. & Zalin, R. in *ADP-Ribosylations of Regulatory Enzymes and Proteins* (eds Smulson, M. E. & Sugimura, T.) 217-224 (Elsevier, Amsterdam, 1980).
13. German, J. *Med. Genet.* **8**, 61-101 (1972).
14. Poon, P. K., O'Brien, R. L. & Parker, J. W. *Nature* **250**, 223-225 (1974).
15. Blomquist, C. H., Larson, K. E. & Taddei, L. *Expl Cell Res.* **100**, 447-450 (1976).
16. Berger, N. A., Berger, S. J., Sikorski, G. W. & Catino, D. M. *Expl Cell Res.* **137**, 79-88 (1982).
17. Berger, N. A., Sikorski, G. W., Petzold, S. J. & Kurohara, K. K. *J. clin. Invest.* **63**, 1164-1171 (1979).
18. Skidmore, C. J. *et al. Eur. J. Biochem.* **101**, 135-142 (1979).
19. Juarez-Salinas, H., Sims, J. L. & Jacobson, M. K. *Nature* **282**, 740-741 (1979).
20. Sims, J. L., Berger, S. J. & Berger, N. A. *J. supramolec. Struct.* **16**, 281-288 (1981).
21. Sims, J. L., Sikorski, G. W., Catino, D. M., Berger, S. J. & Berger, N. A. *Biochemistry* **21**, 813-821 (1982).
22. Caplan, A. I. *Dev Biol.* **28**, 71-83 (1972).
23. Rastl, E. & Swetly, P. *J. biol. Chem.* **253**, 4333-4340 (1978).
24. Kato, T., Berger, S. J., Carter, J. A. & Lowry, O. H. *Analyt. Biochem.* **53**, 86-97 (1973).

Sulphation of tyrosine residues—a widespread modification of proteins

Wieland B. Huttner

Department of Neurochemistry, Max-Planck-Institute for Psychiatry, D-8033 Martinsried/Munich, FRG

Of the many known covalent modifications of proteins¹, few have been recognized as widespread. Among these modifications, protein phosphorylation has been extensively studied²⁻⁴. Recently, phosphorylation of tyrosine residues has been implicated in regulatory events such as cell transformation and hormone-induced cell growth⁵⁻⁷. The present study explores the possibility that another modification of tyrosine residues in proteins, tyrosine sulphation, may be widespread. This modification is particularly interesting because of the molecular resemblance of tyrosine-O-sulphate and tyrosine-O-phosphate. Protein sulphation on tyrosine residues was found to occur in all cell types in culture and all tissues *in situ* so far examined. Moreover, for each cell type and tissue, proteins containing tyrosine-O-sulphate were found in distinct electrophoretic patterns throughout the molecular weight range studied. Thus, protein sulphation on tyrosine residues appears to be a widespread covalent modification, and may have an important role in cell function.

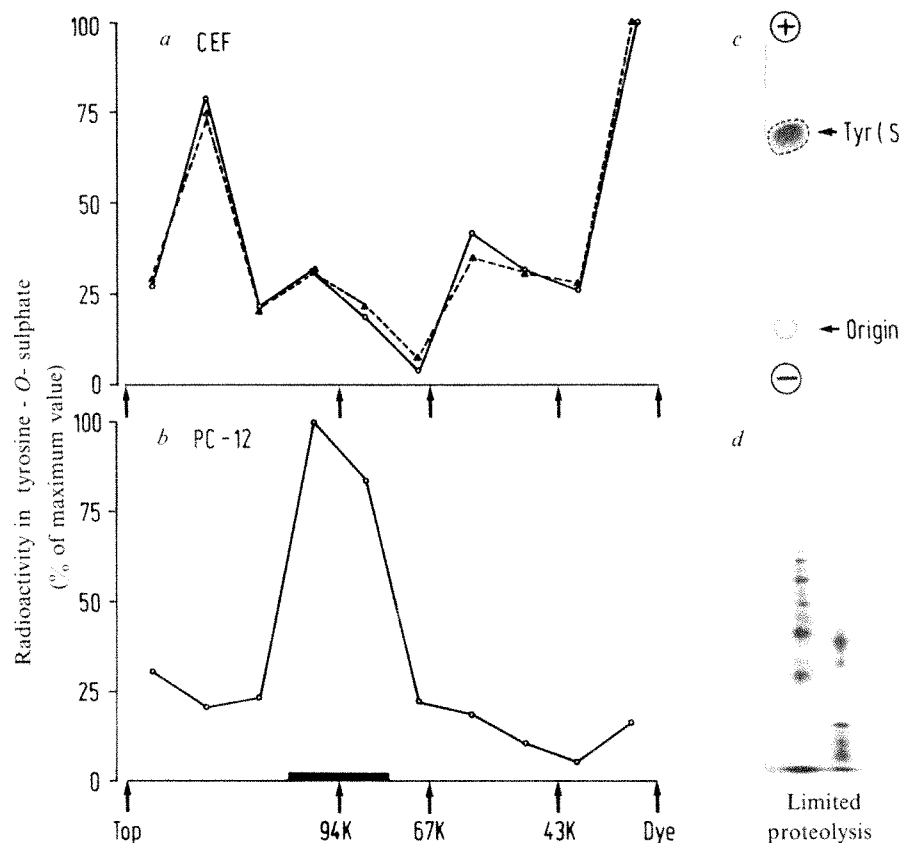
Protein sulphation on tyrosine residues was studied in the following cells in culture: bovine adrenal cells, chicken embryo fibroblasts, chicken embryo muscle cells, chicken embryo retina cells, rat brain cells and rat pheochromocytoma cells. Cell cultures were incubated with either ³⁵S-sulphate or ³⁵S-sulphate plus ³H-tyrosine (see Fig. 1 legend for experimental details).

Cellular proteins were then separated by SDS-polyacrylamide gel electrophoresis. The gels were divided from the top to the dye front into 10 equal portions containing the cellular proteins of high molecular weight to low molecular weight, respectively. Proteins from the individual gel pieces were hydrolysed, and the hydrolysates were analysed for radioactive tyrosine-*O*-sulphate by thin-layer electrophoresis at pH 3.5 followed by autoradiography. A typical autoradiogram of ^{35}S -labelled material obtained from one of the gel pieces is shown in Fig. 1c. The following lines of evidence, taken together, indicate that the radioactive substance migrating towards the anode on electrophoresis at pH 3.5 was indeed tyrosine-*O*-sulphate. (1) The radioactive substance migrated exactly as authentic tyrosine-*O*-sulphate⁸ in this one-dimensional separation (Fig. 1c) and on two-dimensional electrophoresis at pH 1.9 and pH 3.5. The migration of the radioactive substance was clearly different from that of methionine and cysteine (neither of which migrated towards the anode at pH 3.5) and from that of cystic acid (which migrated ~1.5 times faster towards the anode than tyrosine-*O*-sulphate). (2) The radioactive substance appeared to be an amino acid since it could also be generated by extensive pronase digestion alone. (3) The radioactive substance appeared to have the same pH-stability⁹ as authentic tyrosine-*O*-sulphate since the sulphate group was not removed by alkali treatment but was removed by treatment with 1 M HCl for 5 min at 100 °C. (4) The radioactive substance, when obtained from double-labelled cells, contained both ^{35}S -sulphate and ^3H -tyrosine (Fig. 1a).

The radioactivity in the tyrosine-*O*-sulphate spot obtained after thin-layer electrophoresis of the protein hydrolysates was quantitated for all 10 gel pieces of each cell type studied in culture. The electrophoretic patterns of protein-incorporated radioactive tyrosine-*O*-sulphate thus obtained are illustrated in Fig. 1 for chicken embryo fibroblasts (CEF, panel a) and rat pheochromocytoma cells (PC-12, panel b). For both CEF and PC-12 cells, proteins that had incorporated ^{35}S -sulphate on tyrosine residues were found in all gel pieces, that is throughout the molecular weight range studied. However, the electrophoretic pattern of protein-incorporated ^{35}S -tyrosine-*O*-sulphate observed for CEF (Fig. 1a, solid line) was clearly different from that observed for PC-12 cells (Fig. 1b, solid line). Since the CEF proteins had been double-labelled with both ^{35}S -sulphate and ^3H -tyrosine, it was also possible to analyse the sulphation of tyrosine residues by counting the tyrosine-*O*-sulphate spot for ^3H -label present on the benzene ring of tyrosine. The electrophoretic pattern of protein-incorporated ^3H -tyrosine-labelled tyrosine-*O*-sulphate (Fig. 1a, dashed line) was found to be almost identical to that of ^{35}S -sulphate-labelled tyrosine-*O*-sulphate (Fig. 1a, solid line). Using the experimental approach illustrated in Fig. 1, the other cell types studied in culture (adrenal, brain, muscle and retina cells) also gave distinct electrophoretic patterns of cellular proteins containing tyrosine-*O*-sulphate throughout the molecular weight range studied.

In the analysis of PC-12 cells (Fig. 1b), the 120K-80K molecular weight region of the gel (indicated in Fig. 1b by the

Fig. 1 Protein sulphation on tyrosine residues in chicken embryo fibroblasts (CEF) and rat pheochromocytoma cells (PC-12) in culture. Cells were incubated for 18 h in sulphate-free Dulbecco's modified Eagle's medium (DMEM) containing 0.3 mCi ml^{-1} of ^{35}S -sulphate and, in the case of CEF, $25 \mu\text{Ci ml}^{-1}$ of L-[3, 5- ^3H]tyrosine. (The concentration of 'cold' sulphate in normal DMEM was sufficient to reduce radioactive sulphate incorporation markedly.) The medium was then removed, the cells were solubilized in Laemmli sample buffer¹⁶, and cellular proteins separated on a 7.5% SDS-polyacrylamide gel. The gel was fixed in 50% methanol/10% acetic acid, stained with Coomassie blue, and dried. Each lane of the dried gel, containing either CEF or PC-12 cell proteins, was then cut from the top to the dye front into 10 equal portions representing different molecular weight regions. The individual gel pieces were reswollen in 50 mM ammonium bicarbonate containing $100 \mu\text{g ml}^{-1}$ of pronase and incubated for 24 h at 37 °C. The eluates were lyophilized, dissolved in 0.2 M barium hydroxide, evacuated, incubated for 24 h at 110 °C, neutralized with sulphuric acid, and centrifuged. The supernatants were lyophilized, dissolved in a solution containing $5 \mu\text{g}$ of tyrosine-*O*-sulphate standard⁸, spotted on TLC-cellulose sheets, and subjected to electrophoresis in 5% acetic acid/0.5% pyridine, pH 3.5. Panel c shows a typical autoradiogram after thin-layer electrophoresis of ^{35}S -labelled material obtained from one of the gel pieces. The dashed line indicates the position of the tyrosine-*O*-sulphate standard, detected by ninhydrin staining. For each of the 10 gel pieces of CEF (panel a) and PC-12 cells (panel b), the radioactivity in the tyrosine-*O*-sulphate spot was determined by liquid scintillation counting and is expressed as per cent of that obtained from the gel piece giving the maximum value (100%): ^{35}S (solid lines) CEF 3,925 c.p.m., PC-12 cells 2,405 c.p.m.; ^3H (dashed line) CEF 294 c.p.m. Values are from left to right for gel pieces containing high molecular weight proteins to gel pieces containing low molecular weight proteins. Arrows indicate the positions of molecular weight marker proteins. The solid bar on the abscissa of panel b indicates the region of the gel that was subjected to peptide mapping after limited proteolysis¹⁰ ($1.5 \mu\text{g}$ of *Staphylococcus aureus* V8 protease) with the modifications described elsewhere¹⁶. Panel d shows an autoradiogram of the proteolysis gel.



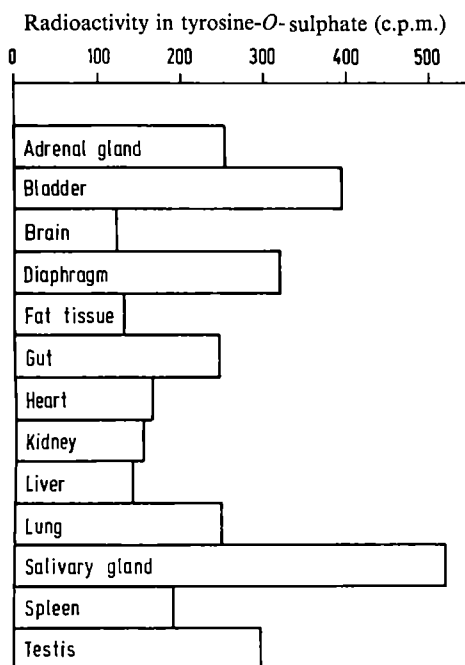


Fig. 2 Protein sulphation on tyrosine residues in various rat tissues *in situ*. At 18 h after an intraperitoneal injection of 20 mCi of ^{35}S -sulphate, rat tissues were freed of blood by perfusion with saline and were then rapidly homogenized in 3% SDS. Aliquots of each tissue containing equal amounts of protein (300 μg) were subjected to SDS-polyacrylamide gel electrophoresis and analysed for protein-incorporated ^{35}S -tyrosine-*O*-sulphate as described in Fig. 1 legend. The radioactivity in tyrosine-*O*-sulphate is given for tissue proteins from a whole lane of the gel.

solid bar) contained the highest amounts of protein-incorporated ^{35}S -tyrosine-*O*-sulphate. The same region of a duplicate gel was subjected to limited proteolysis¹⁰ during a second SDS-polyacrylamide gel electrophoresis step. Subsequent autoradiography of the proteolysis gel showed that the proteins from the 120K–80K region yielded two distinct patterns of ^{35}S -labelled fragments (Fig. 1*d*). Extensive pronase treatment of individual gel pieces containing these fragments yielded ^{35}S -tyrosine-*O*-sulphate in each case.

Since sulphation of proteins on tyrosine residues occurred in a variety of cell types in culture, it was of interest to determine whether this modification could also be observed after *in vivo*-labelling of tissues *in situ*. For this analysis (see Figs 2 and 3 legends for experimental details), 20 tissues were dissected from a rat 18 h after the animal had been injected intraperitoneally with inorganic ^{35}S -sulphate. With a single injection of 20 mCi of inorganic ^{35}S -sulphate into a 150 g rat, one would expect a marked dilution of the radioactive label and a great reduction in its specific activity because of the presence of endogenous inorganic sulphate in the body fluids. Nevertheless, radioactive sulphate incorporation into proteins on tyrosine residues could be detected in all 20 rat tissues examined. The results for 13 tissues are given in Fig. 2.

In addition, the electrophoretic pattern of proteins containing ^{35}S -tyrosine-*O*-sulphate was also determined for each tissue, using the experimental approach described above for cultured cells. These results are illustrated in Fig. 3 for three of the tissues examined, adrenal gland, gut and lung. These three tissues contained similar amounts of the total protein-incorporated ^{35}S -tyrosine-*O*-sulphate. However, the electrophoretic patterns of tissue proteins containing ^{35}S -tyrosine-*O*-sulphate were distinct for the three tissues. In fact, all the other tissues examined also gave distinct electrophoretic patterns of proteins containing ^{35}S -tyrosine-*O*-sulphate throughout the molecular weight range studied.

Only one protein, fibrinogen⁹, and a few biological peptides^{11–15} have so far been demonstrated to contain tyrosine-*O*-sulphate. The results of this study provide evidence that in all

cell types in culture and all tissues *in situ* so far examined, many proteins are sulphated on tyrosine residues. Two observations could help to explain why this widespread occurrence of protein sulphation on tyrosine residues has not been reported so far. First, the ester bond of tyrosine-*O*-sulphate is remarkably acid-labile⁹. The sulphate group is therefore likely to be hydrolysed in some of the common protein-chemical procedures. Second, ^{35}S -sulphation of proteins and other macromolecules on carbohydrate moieties tends to obscure the presence of proteins containing ^{35}S -tyrosine-*O*-sulphate, for example on autoradiography of SDS-polyacrylamide gels.

The widespread occurrence of protein sulphation on tyrosine residues suggests that this modification may have an important role in cell function. The distinct electrophoretic patterns of proteins containing tyrosine-*O*-sulphate that were observed in many different cell types raise the possibility that protein sulphation on tyrosine residues may be involved in a variety of cellular processes.

If protein sulphation on tyrosine is found to occur in the same subcellular compartment as phosphorylation on tyrosine, then the possibility should be considered that tyrosine residues which are physiologically *O*-sulphated may be subject to 'false' modification by becoming *O*-phosphorylated (and vice versa). Such false modification may have significant biological consequences. The false modification of tyrosine residues may not be fully recognized as such by the cell, since there is a molecular resemblance of tyrosine-*O*-sulphate and tyrosine-*O*-phosphate. The false modification of tyrosine residues may, however, be dissimilar enough from the physiological modification to perturb the balance of cellular regulation.

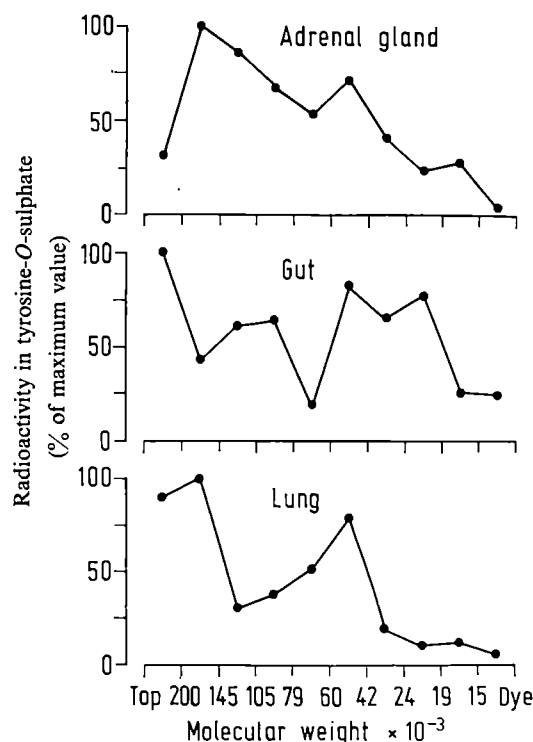


Fig. 3 Electrophoretic patterns of proteins containing tyrosine-*O*-sulphate in rat adrenal gland, gut and lung. The tissues were labelled *in situ* with ^{35}S -sulphate and tissue proteins were subsequently solubilized as described in the legend to Fig. 2. Aliquots containing equal amounts of proteins (3 mg) were subjected in duplicate to SDS-polyacrylamide gel electrophoresis on either 7.5% or 15% gels. Each of the gels was cut into five portions, representing different molecular weight ranges as indicated on the abscissa. Gel pieces containing molecular weight ranges above 60,000 were obtained from the 7.5% gels, the other gel pieces were obtained from the 15% gels. Analysis of individual gel pieces for protein-incorporated ^{35}S -tyrosine-*O*-sulphate was performed as described in the legend to Fig. 1. Maximum values (100%) were: adrenal gland 583 c.p.m., gut 477 c.p.m., lung 616 c.p.m.

I thank Professor H. Thoenen for his continuous support and advice, Dr K. von der Helm for donating CEF cells, H. Thorun for PC-12 cells, C. Suchanek for technical assistance, and Dr L. DeGennaro, Professor G. Gerisch, Professor D. Oesterhelt and my colleagues Dr R. Lee and Dr S. Por for their helpful comments on the manuscript.

Received 30 March; accepted 26 July 1982.

1. Wold, F. A. *Rev. Biochem.* **50**, 783-814 (1981).
2. Greengard, P. *Science* **199**, 146-152 (1978).
3. Krebs, E. G. & Beavo, J. A. *A. Rev. Biochem.* **48**, 923-959 (1979).
4. Cohen, P. in *Molecular Aspects of Cellular Regulation* Vol. 1 (ed. Cohen, P.) 255-268 (North-Holland, Amsterdam, 1980).
5. Hunter, T. *Cell* **22**, 647-648 (1980).
6. Erikson, R. L., Purchio, A. F., Erikson, E., Collett, M. S. & Brugge, J. S. *J. Cell Biol.* **87**, 319-325 (1980).
7. Ushiro, H. & Cohen, S. *J. biol. Chem.* **255**, 8363-8365 (1980).
8. Reitz, H. C., Ferrel, R. E., Fraenkel-Conrat, H. & Olcott, H. S. *J. Am. chem. Soc.* **68**, 1024-1031 (1946).
9. Bettelheim, F. R. *J. Am. chem. Soc.* **76**, 2838-2839 (1954).
10. Cleveland, D. W., Fischer, S. G., Kirschner, M. W. & Laemmli, U. K. *J. biol. Chem.* **252**, 1102-1106 (1977).
11. Gregory, H., Hardy, P. M., Jones, D. S., Kenner, G. W. & Sheppard, R. C. *Nature* **204**, 931-933 (1964).
12. Anastasi, A., Bertaccini, G. & Erspamer, V. *Br. J. Pharmac. Chemother.* **27**, 479-485 (1966).
13. Anastasi, A., Erspamer, V. & Endean, R. *Experientia* **23**, 699-700 (1967).
14. Mutt, V. & Jorpes, J. E. *Eur. J. Biochem.* **6**, 156-162 (1968).
15. Unsworth, C. D., Hughes, J. & Morley, J. S. *Nature* **295**, 519-522 (1982).
16. Laemmli, U. K. *Nature* **227**, 680-685 (1970).
17. Huttner, W. B. & Greengard, P. *Proc. natn. Acad. Sci. U.S.A.* **76**, 5402-5406 (1979).

Diversity of cholesterol exchange explained by dissolution into water

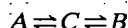
Eigil Bojesen

Institute of Experimental Hormone Research, University of Copenhagen, 71 Nørre Alle, DK-2100 Copenhagen, Denmark

It is usually considered that the stability of lipid bilayers results from the elastic resistance of water to the dissolution of hydrophobic compounds^{1,2}. However, attempts to describe this unique property of water in more detail^{2,3} have been difficult and some authors⁴⁻⁷ believe that the dispersion attraction of apolar molecules (London-van der Waals forces) is the most important factor. Details of the transfer kinetics into water of apolar compounds may elucidate this. Here I describe an analysis of the kinetics of cholesterol exchange between erythrocytes and lipoproteins that makes it possible to calculate precisely the widely differing specific rate constants of cholesterol dissolution from both kinds of structures. The analysis also accounts qualitatively for the different exchange kinetics reported for homologous and heterologous dispersed systems in water.

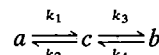
The fairly rapid exchange of cholesterol between erythrocytes and lipoproteins⁸ was originally assumed to reflect the dissolution of cholesterol from both dispersed phases. However, this has been questioned as the rate of exchange in this and other heterologous binary systems depends on the concentrations of the lipid particles⁹⁻¹², suggesting a collision frequency limitation, and transfer during collision. However the surfaces of lipoproteins and erythrocytes in rats are, on average, more than 100 Å apart¹³, closer contact being prevented by the cell glycocalyx. Furthermore, the kinetics of cholesterol exchange in pure homologous binary systems of artificial lipid vesicles is incompatible with a collision limitation¹⁴⁻¹⁶. The problem remains of why the kinetics are so different in heterologous and homologous systems.

Consider a closed system containing the amounts *A* and *B* of cholesterol in two dispersed lipid phases in equilibrium. If the exchange of cholesterol between the two phases is mediated solely by the amount, *C*, of cholesterol in water the scheme of equilibrium becomes:



In a homologous system *A* and *B* could be present in two separable types of liposomes and in a heterologous system, such as erythrocytes in serum, they represent the cholesterol of the cell membranes and in the lipoproteins, respectively.

In the tracer experiments in which *A* or *B* is labelled initially, the most simple corresponding scheme for the time-dependent amounts of *a*, *b* and *c* of tracer is



In this scheme it is assumed that only one pair of rate constants describes the transfer of the tracer in and out of each of the dispersed phases. As *c* is very small compared with *a* and *b* the scheme describes an experiment with monophasic exchange kinetics eventually leading to isotopic equilibrium. As such it does not differ from a simple two pool model, but whereas the two pool model is only a mathematical concept, the above scheme includes rate constants of real physical significance. As the processes are slow compared with diffusion equilibria within distances of ~100 Å, the tracer is evenly distributed in the aqueous phase with the concentration *c_w*. If *α* and *β* represent the reactive surface areas of the two kinds of dispersed phases the system approaches tracer equilibrium according to the two rate equations

$$-da/dt = k_1a - k_2c_w\alpha \quad (1)$$

$$-db/dt = k_3b - k_4c_w\beta \quad (2)$$

Thus *k₁* and *k₃* are first order whereas *k₂* and *k₄* are second order rate constants.

By eliminating *c_w* and using the substitution

$$Q = \frac{k_2\alpha}{k_4\beta}$$

we get

$$da/dt + k_1a = Q(db/dt + k_3b) \quad (3)$$

At equilibrium, when *t* → ∞, the ratio *a_∞/b_∞* is determined by

$$\frac{a_\infty}{b_\infty} = Q \frac{k_3}{k_1} = f_\infty \quad (4)$$

The low water solubility of cholesterol¹⁷ means that the total amount of tracer, *R*, in the system is equal to (*a* + *b*) and that *da/dt* = -*db/dt*.

Thus one of the two variables in (3) can be eliminated. Written in terms of *a* we get

$$da/dt + k_1a = -Qda/dt + k_3QR - k_3Qa \quad (5)$$

As *Q* and *R* are time-independent this equation can be solved by separation of the variables; followed by integration between the limits of *t* from 0 to *t* and of *a* from *a₀* to *a_t*. Using the identities (*R* - *a₀*) = *b₀*, (*R* - *a_t*) = *b_t*, and *Q* = *f_∞*(*k₁/k₃*), we get

$$\ln \left[\frac{a_t - f_\infty b_t}{a_0 - f_\infty b_0} \right] = -t \left[\frac{k_1(1 + f_\infty)}{1 + (k_1/k_3)f_\infty} \right] \quad (6)$$

This equation defines a rate constant *ε*

$$\epsilon = \frac{k_1(1 + f_\infty)}{1 + (k_1/k_3)f_\infty} \quad (7)$$

Table 1 The specific rate constants of cholesterol dissolution from red cells and lipoproteins

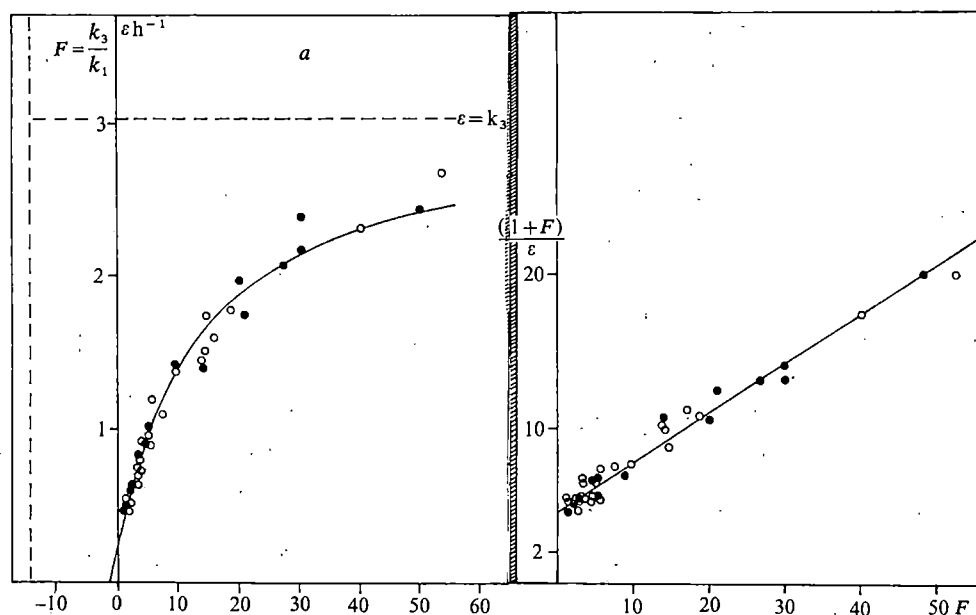
Type of experiment	No. of experiments	Correlation coefficient	<i>k₃</i> (h ⁻¹) (mean ± s.e.m.)	<i>k₁</i> (h ⁻¹) (mean ± s.e.m.)
Cell → Serum	18	0.988	3.10 ± 0.12	0.224 ± 0.012
Serum → Cell	24	0.985	3.30 ± 0.12	0.203 ± 0.007
Both types, all <i>F</i>	42	0.986	3.21 ± 0.087	0.211 ± 0.006
Both types (1.15 < <i>F</i> < 5.8)	25	0.70	2.82 ± 0.61	0.225 ± 0.014

k₁ and *k₃* are the rate constants for dissolution of cholesterol from red cells and from lipoprotein, respectively, calculated on the basis of the linear regression (1 + *F*)/*ε* = *F*/*k₃* + 1/*k₁*.

Fig. 1 a, The time constant (h^{-1}) of the exchange of cholesterol at 37°C between rat erythrocytes and serum lipoproteins as a function of the cell: cholesterol pool ratio F . ●, Results of cells \rightarrow serum assays; ○, results of serum \rightarrow cells assays. F values < 9 were obtained by variation of the haematocrit whereas higher values required dilution of serum. A special washing procedure¹³ was applied in order to preserve the disk shape of cells isolated from EDTA blood of fasted rats. The final medium was an oxygenated 1:1 mixture of isotonic sucrose and a slightly hypotonic 2 mM phosphate buffer with 5 mM glucose and 1 mM CaCl_2 , pH 7.4. Serum from the same rat was heated at 50°C for 45 min to block ester formation and then labelled with $\sim 0.5 \mu\text{Ci}$ purified ^3H cholesterol (specific activity 50 Ci mmol^{-1} ; Amersham) deposited on small glass beads²⁵. 4 ml of serum were labelled and used directly in the serum \rightarrow cells assays. 1 ml of labelled serum diluted twofold with the sucrose buffer medium was incubated for 2 h with 2.5 ml of packed cells for cells \rightarrow serum assays. The labelled cells were stored at 5°C overnight in the sucrose buffer medium after numerous washings. The assay was made with a vigorously shaken 2 ml cell suspension in serum or diluted serum with a 5% CO_2 atmosphere. The time intervals between collections of 6 or 7 aliquots (200 μl) were increased progressively to approach a linear change in fractional equilibria from < 0.1 to > 0.9 . After quantitative separation of cells from the serum by centrifugation and washing, the lipids were extracted after haemolysis and dilution of the two fractions. The extracts were used either for tracer measurements, liquid scintillation counting, or for chemical analyses of cholesterol, separated quantitatively from cholesteryl esters by column chromatography²⁵. Two additional aliquots per assay were used for this purpose. The time constant and tracer equilibrium for the assays were computed as described in the text. The curve shows the hyperbolic relationship between ϵ and F according to

$$\epsilon = \frac{k_1(1+F)}{1+(k_1/k_3)F}$$

with k_1 and k_3 of Table 1 computed on the basis of all the 42 assays. Also, the two asymptotes are drawn: $\epsilon = k_3$ and $F = -k_3/k_1$. **b** Shows the same data plotted according to the linear regression $1 + F/\epsilon = F(1/k_3) + 1/k_1$. The drawn regression line is $y = x(0.312 \pm 0.0084) + (4.74 \pm 0.143)$.



In a homologous system ϵ is independent of f_∞ , as $k_1 = k_3$; however ϵ is a function of f_∞ in heterologous systems, for which $k_1 \neq k_3$. Equation (7) describes an equilateral hyperbola, with $\epsilon = k_3$ and $f_\infty = -(k_3/k_1)$ as the asymptotes. The equation can be transformed into

$$\frac{1+f_\infty}{\epsilon} = f_\infty/k_3 + 1/k_1 \quad (8)$$

and k_1 and k_3 can therefore be obtained by a linear regression analysis of (ϵ, f_∞) data, using a suitable wide range of f_∞ values.

For the system of erythrocytes in serum we assign A and a to the cells, and B and b to the lipoproteins. With the cells initially labelled (cells \rightarrow serum assays) we have $a_0 = R = (a_i + b_i)$, and $b_0 = 0$. The specific rate constants of tracer dissolution, k_1 and k_3 are then assigned to the cells and the lipoproteins, respectively. In such assays, performed as described in Fig. 1 legend, the two parameters ϵ and f_∞ were computed from the b_i or $f_i = a_i/b_i$ values of a time series of aliquots. Two transforms of the left-hand side of (6) were used: $\ln(1 - b_i/b_\infty)$ or $\ln[(f_i - f_\infty)/(1 + f_i)]$. From computed values of b_∞ one immediately gets f_∞ , as $f_\infty = (R/b_\infty - 1)$. The optimal values of f_∞ (or b_∞) were obtained as the values which in the regression analysis resulted in a minimum of standard error of the time constant. The left-hand side of (6) was weighted according to the computed variances¹⁸, assuming that the coefficient of variation in the determination of f_i or b_i is equal to that of the total counts of the aliquots (3%).

This analysis has demonstrated the validity of the basic assumptions expressed in equations (1) and (2). The exchange kinetics were monophasic, within the analytical error as the data always defined the rate constant ϵ with a coefficient of variation smaller than 4% and a numerical value of the intercept of the regression line smaller than ± 0.04 . Furthermore, the regression line describes the approach to complete tracer equilibrium. The mass ratio of cholesterol, $F = A/B$, obtained by chemical analysis of cholesterol^{13,19}, and the computed f_∞ were identical, within analytical errors ($f_\infty/F = 1.001 \pm 0.045$ ($n = 14$)). Therefore F can replace f_∞ in equations (7) and (8).

In the reverse experiments (serum \rightarrow cell assays) only the

tracer uptake was used in the computation of ϵ . The procedure for labelling the lipoproteins resulted directly in the formation of a small amount of unexchangeable tracer ($< 10\%$) and therefore in erroneous f_∞ values. Thus only the chemically determined F is available for this type of assay.

The results obtained at 37°C for both types of assays are presented in Fig. 1a; the same data, plotted according to equation (8) are shown in Fig. 1b. This linear regression was used to calculate the specific rate constants k_1 and k_3 as the scatter of the 42 points of $(F, (1-F)/\epsilon)$ does not vary with F . The coefficients of variation of the reciprocal values of the two constants were obtained directly and used to calculate the s.e.m. in the estimation of rate constants. Table 1 shows the results of this analysis for all the 42 data points covering the whole range of F values and for the 18 cells \rightarrow serum as well as the 24 serum \rightarrow cells experiments separately. Clearly it makes no difference whether the initially labelled partner is serum or cells. Table 1 also shows that assays with F confined to the lower range give a well defined value for k_1 but a crude value for k_3 which is not significantly different from that calculated on the basis of all the data. The result that k_3 was much larger than k_1 was expected. According to some authors^{20,21} the hydroxyl group of cholesterol is hydrogen-bonded to the carbonyl group of lecithin, and others^{22,23} have observed that the mobility of cholesterol is less restricted in the lipoproteins. The observation that k_3 has a well defined value is perhaps surprising, considering the chemical diversities of lipoproteins. The observed monophasic exchange kinetics and the identity of the calculated f_∞ with F over the whole range of F values demonstrate; however, that the variation in k_3 within lipoproteins must be relatively small. However, the sensitivity of this criterion should not be overrated²⁴ and assays with separated lipoproteins are needed.

Equation (7) predicts that the time constant of exchange is only independent of F if $k_1 = k_3$. This is in accordance with the difference in the kinetics of homologous and heterologous systems as referred to above. If k_1 is much smaller than k_3 in heterologous systems the term $(k_1 F)/k_3$ vanishes provided the two dispersed phases contain about equal amounts of

cholesterol. The time constant of exchange then varies in proportion to $(1 + F)$, and approaches the limiting value of k_1 as F approaches zero. This prediction is again, at least qualitatively, in agreement with reported observations^{9,10,12}.

Thus the phase partition theory⁸ accounts for the exchange kinetics of homologous artificial systems as well as for the natural heterologous system in blood. The idea of transfer by collision is therefore redundant. Since the specific rate constants

k_1 and k_3 can be estimated quite accurately (Table 1) the effect of temperature will provide information on the energy by which cholesterol and probably other apolar compounds are bound in different dispersed phases.

Inge Norby Bojesen, Institute of Experimental Hormone Research and Erik Sjøntoft, Institute of Experimental Surgery, have contributed significantly to the applied mathematics and statistics. I thank Dr G. Bojesen for revising the manuscript.

Received 9 February; accepted 2 July 1982.

1. Tanford, C. *Science* **200**, 1012–1018 (1978).
2. Pratt, L. R. & Chandler, D. J. *chem. Phys.* **67**, 3683–3704 (1977).
3. Chan, D. Y. C., Mitchell, J., Ninham, B. W. & Pailthorpe, B. A. *J. chem. Soc. Farad. Trans. 74*, 2050–2062 (1978).
4. Hildebrand, J. H. *Proc. natn. Acad. Sci. U.S.A.* **76**, 194 (1979).
5. Cramer, R. D. J. *Am. chem. Soc.* **99**, 5408–5412 (1977).
6. Amidon, G. L., Pearlmann, R. S. & Anik, S. T. *J. theor. Biol.* **77**, 161–170 (1979).
7. Salem, L. *Can. J. biochem. Physiol.* **40**, 1287–1298 (1962).
8. Hagerman, J. S. & Gould, G. *Proc. Soc. exp. Biol. Med.* **78**, 329–332 (1951).
9. Quarfordt, S. H. & Hilderman, H. L. *J. Lipid Res.* **11**, 528–535 (1970).
10. Gottlieb, M. H. *Biochim. biophys. Acta* **600**, 530–541 (1980).
11. Jonas, A. & Maine, G. T. *Biochemistry* **18**, 1722–1728 (1979).
12. Giraud, F. & Claret, M. *FEBS Lett.* **103**, 186–191 (1979).
13. Bojesen, E. & Bojesen, I. N. *Acta physiol. scand.* **114**, 513–523 (1982).
14. Nakagawa, Y., Inoue, K. & Nojima, S. *Biochim. biophys. Acta* **553**, 307–319 (1979).
15. Backer, J. M. & Dawidowicz, E. A. *Biochemistry* **20**, 3805–3810 (1981).
16. McLean, L. R. & Phillips, M. C. *Biochemistry* **20**, 2893–2900 (1981).
17. Gilbert, D. B., Tanford, C. & Reynolds, J. A. *Biochemistry* **14**, 444–448 (1975).
18. Armitage, P. *Statistical Methods in Medical Research*, 319–320 (Blackwell, Oxford and Edinburgh, 1971).
19. Zlatkis, A., Zak, B. & Boyle, A. J. *J. Lab. clin. Med.* **41**, 486–492 (1953).
20. Huang, C. *Nature* **259**, 242–243 (1976).
21. Bicknell-Brown, E. & Brown, K. G. *Biochem. biophys. Res. Commun.* **94**, 638–645 (1980).
22. Lund-Katz, S. & Phillips, M. C. *Biochem. biophys. Res. Commun.* **100**, 1735–1743 (1981).
23. Hamilton, J. A. & Cordes, E. H. *J. biol. Chem.* **253**, 5193–5198 (1978).
24. Zuppiroli, L. *Le Traitement Statistique des Données Experimentales*, Rapport CEA-R-4802 (Service de Documentation, CEN, Saclay, France, 1976).
25. Bojesen, E. *Scand. J. clin. Lab. Invest.* **38**, Suppl. 150, 26–31 (1978).

Two genes for threonine accumulation in barley seeds

Simon W. J. Bright, Joseph S. H. Kueh,
Julian Franklin, Sven Erik Rognes*
& Benjamin J. Mifflin

Biochemistry Department, Rothamsted Experimental Station,
Harpenden AL5 2JQ, UK

* Botanical Institute, University of Oslo, Blindern, Oslo 3, Norway

Cereal seed protein is the major direct source of dietary protein for man and also serves as an indirect source through the feeding of livestock. For non-ruminant animals, such as man, swine and poultry, most cereal seed proteins are deficient in lysine and threonine and much effort has been devoted to their improvement¹. Supplementation of barley diets for pigs with lysine and threonine is sufficient to produce a feed with protein of high biological value². Mutant lines that accumulate these amino acids in the seed could therefore be of agricultural value. The synthesis of lysine, threonine and methionine, which are all derived from aspartic acid, is regulated in plants by a series of feedback loops^{3,4}. This regulation is such that when barley embryos are germinated on a medium containing lysine plus threonine (LT medium) the plants are starved of methionine and fail to grow⁵. Plants which do grow in these conditions may contain enzymes that are no longer feedback-regulated and that may allow enhanced amounts of end-product amino acids to accumulate. We report here the identification of two genes in barley, mutations in which lead to decreased feedback sensitivity of the enzyme aspartate kinase, resistance to lysine plus threonine and, in some cases, to accumulation of soluble threonine in the seed.

From an M_2 population of 10^4 mature embryos (M_1 treated with sodium azide) three mutants resistant to lysine plus threonine (2–3 mM) were selected for further study. These were R(Rothamsted) 2501 (ref. 6), R3004 and R3202 which produced sensitive and resistant progeny in the M_3 generation. Pure-breeding resistant lines were obtained from R3004 and R3202 and, with difficulty, from R2501. The designation R3004 or R3202 refers henceforth to the M_3 and subsequent generations of such lines.

Both R3202 and R3004 plants grew better than controls in a range of concentrations of lysine and threonine (Fig. 1). R3202 plants were generally larger and had better root growth than R3004. Both mutant lines had lost the synergistic inhibition of growth by lysine plus threonine (Fig. 2) but were still slightly inhibited by lysine alone. This was reduced by addition of arginine. Neither R3202 nor R3004 were resistant to the lysine analogue S-(2-aminoethyl)cysteine.

To characterize the genetic basis of resistance, mutant plants were crossed among themselves and with normal barley cv. Golden Promise. Crosses with Golden Promise (Table 1) showed a segregation of three resistant to one sensitive in the F_2 generation, consistent with resistance in each case being due to the action of a single dominant nuclear gene. When R3202 and R3004 were reciprocally crossed, in the F_2 generation a ratio of 15 resistant plants to 1 sensitive plant was observed (Table 1), suggesting that the two genes *Lt1b* and *Lt2* are unlinked. Progeny of single F_1 plants of reciprocal crosses of heterozygous R2501-derived plants (*Lt1a/+*) with R3202 (*Lt1b/Lt1b*) were scored in the same way for resistance (Table 1). Three plants (C, D and E) gave no sensitive progeny in the F_2 generation, suggesting that they had received a resistance gene from each parent and that these two genes are allelic or closely linked. However, two plants (A and B) produced sensitive progeny, suggesting that they had received the wild-type sensitive gene from R2501; this hypothesis is supported for A by the segregation ratio of 33:8 (not significantly different from 3:1) and for B by the finding that, when 13 of the 15 resistant F_2 plants were self-pollinated and their F_3 progeny tested, 9 of them gave rise to some sensitive plants (pooled data 108:44 not significantly different from 3:1). No segregation data are available for the cross R2501 × R3004.

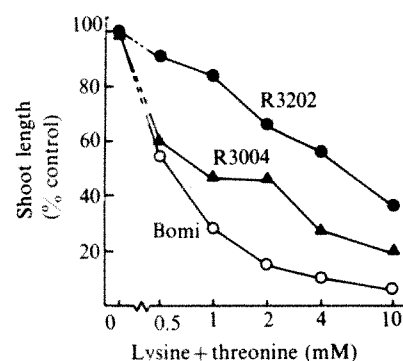


Fig. 1 Growth of two mutants R3004 (▲) and R3202 (●) and their parent cultivar Bomi (○) in a range of equimolar concentrations of lysine and threonine. Mature embryos were hand dissected and grown on a basal medium containing agar, salts, sucrose and vitamins in Petri dishes under lights at 25 °C as in ref. 5. Amino acids were filter sterilized before addition to autoclaved medium. After 7 days, 7–16 plants were removed and the length of the shoot from the tip of the first leaf to the base was measured. Results are expressed as percentages of the mean value of each genotype in the absence of lysine and threonine. 100% values ranged from 46 to 61 mm with standard error values less than 5 mm.

Table 1 Genetics of resistance to lysine plus threonine in three mutants crossed amongst themselves and with cv. Golden Promise

F ₁ parents female × male	F ₁ genotype at two loci		No. of F ₂ plants	
	<i>lt1</i>	<i>lt2</i>	resistant	sensitive
R2501 × Golden Promise	<i>Lt1a/+</i>	<i>+/+</i>	92	28
Golden Promise × R2501	<i>+/Lt1a</i>	<i>+/+</i>	50	18
R3004 × Golden Promise	<i>+/+</i>	<i>Lt2/+</i>	131	44
Golden Promise × R3004	<i>+/+</i>	<i>+/Lt2</i>	113	36
R3202 × Golden Promise	<i>Lt1b/+</i>	<i>+/+</i>	37	15
Golden Promise × R3202	<i>+/Lt1b</i>	<i>+/+</i>	74	27
R3004 × R3202	<i>+/Lt1b</i>	<i>Lt2/+</i>	183	13
R3202 × R3004	<i>Lt1b/+</i>	<i>+/Lt2</i>	151	10
R2501 × R3202	A	<i>+/Lt1b</i>	33	8
	B	<i>+/Lt1b</i>	15	1
	C	<i>Lt1a/Lt1b</i>	110	0
	D	<i>Lt1a/Lt1b</i>	61	0
R3202 × R2501	E	<i>Lt1b/Lt1a</i>	58	0

Mature embryos were germinated for 1 or 2 days on basal medium before transfer to LT medium. Resistance was scored after 7 days' total growth. Resistant plants, when grown in the presence of lysine plus threonine, had long green shoots and pale scutella, whereas sensitive plants, derived either from the original selections or from control plants of several cultivars, had short yellow shoots and dark pigmentation on the scutellum and at the base of the leaf. The absence of darkening of the scutellum was used as an absolute indicator of resistance. Ratios were analysed by χ^2 test. In crosses with cv. Golden Promise the R2501-derived plant used was homozygous (*Lt1a/Lt1a*), in crosses with other mutants the R2501-derived plants were heterozygous (*Lt1a/+*). R3202 (*Lt1b/Lt1b*) and R3004 (*Lt2/Lt2*) plants were homozygous for resistance at the *Lt1* and *Lt2* loci, respectively. Crosses were performed with glasshouse grown plants. Flowers on plants of the female parents were emasculated and enclosed in cellophane bags for 2–4 days before pollination with anthers from selected male parents. Bags were kept over the ears until collected.

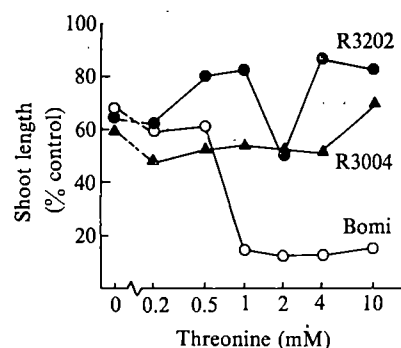
Aspartate kinase (AK) in barley can be separated into the three isoenzymatic forms AKI, AKII and AKIII (ref. 6); the latter two are sensitive to feedback inhibition by lysine. Analysis of the properties of these isoenzymes⁷ has shown that R2501 and R3202 both have an AKII with greatly decreased sensitivity to inhibition by lysine and a normal AKIII, whilst R3004 has an unchanged AKII but an AKIII that is relatively unaffected by lysine. These results, taken with the genetic data, suggest that resistance to lysine plus threonine in R2501 and R3202 is due to mutations in a gene *lt1* causing altered feedback sensitivity of AKII and in R3004 is due to a mutation in a gene *lt2* which decreases lysine inhibition of AKIII. The genes *lt1* and *lt2* are, therefore, likely to be structural loci for the two aspartate kinase isoenzymes. The absence of tight regulatory control of aspartate kinase would allow sufficient flux down the pathway to satisfy the methionine requirement in LT medium.

It has been suggested that mutants having such altered regulatory feedback properties might produce cereal plants with grains

Table 2 Soluble amino acids in grains of normal barley and three mutants

Amino acid	Soluble content (nmol per mg-nitrogen)				
	Pooled controls		R3004	R3202	R2501
	I	II			
Thr	9 ± 3	12 ± 5	116 ± 36	16 ± 5	147 ± 21
Lys	12 ± 5	12 ± 5	15 ± 3	18 ± 5	19 ± 8
Ala	49 ± 13	47 ± 10	41 ± 6	68 ± 14	29 ± 5
Val	18 ± 10	28 ± 12	17 ± 5	38 ± 10	19 ± 4
Glx	143 ± 25	140 ± 36	122 ± 20	199 ± 39	112 ± 22
Asx	167 ± 27	181 ± 28	122 ± 18	237 ± 45	131 ± 24
Total (17/20)	580	740	745	905	743
Seed nitrogen (mg N per g dry wt)	14–18	22–27	22–27	16–19	24–29

Milled grain samples were extracted with 5% cold trichloroacetic acid plus 10 mM 2-mercaptoethanol as in ref. 6 and analysed on a Technicon TSM autoanalyser. Values are expressed as mean ± s.d. for at least eight analyser runs and four grain samples. Tryptophan and cysteine were not determined; methionine peaks were always too small to quantify as they were overlapping with a small unidentified peak. Glutamine and asparagine were hydrolysed to the free acid before analysis. Data for R2501 are taken from ref. 6 for comparison and are for pooled seeds from heterozygous *Lt1a/+* individuals. Nitrogen was determined by Kjeldahl analysis. The two control groups were: I, Bomi and sensitive lines segregating from the original R3202 selected plant; II, sensitive lines segregating from the original R2501 selected plant.

**Fig. 2** Growth of two mutants R3004 (▲) and R3202 (●) and Bomi (○) in a range of threonine concentrations with lysine held constant at 3 mM. Mature embryos were grown and 12–19 plants measured as in Fig. 1. 100% values ranged from 49 to 67 mm with standard error values less than 5 mm.

of improved nutritional quality^{8,9}. Analyses of the soluble amino acids of seeds (Table 2) showed that the mutation in R3004 caused a greater than 12-fold increase in threonine. Similar increases have been previously observed in R2501 (ref. 6). The absence of such accumulation in R3202 may be because there was less of the mutant enzyme form⁷. An increase in threonine of 100 μ mol per g nitrogen would be sufficient to increase the total threonine content of the seed (~1,400 μ mol per g nitrogen) by about 7%. Increases of this order have been measured. This would decrease the amount of extra threonine required for optimum nutrition of monogastric animals fed on barley meal plus vitamins¹⁰. Seed of R3004 has been multiplied and will be used to test this in rat feeding trials. The agronomic performance of the R3004 line, even in the absence of outcrossing and reselection, is not markedly affected when compared with the parent Bomi.

None of the mutants has enhanced levels of soluble lysine. This is consistent with the lack of resistance to the lysine analogue aminoethylcysteine and is probably because the activity of the first enzyme unique to lysine biosynthesis—dihydrodipicolinic acid synthase—is also tightly regulated by lysine¹¹.

Variant plant cells accumulating tryptophan¹² and threonine¹³ as a consequence of altered enzymatic regulation have been selected. However, it is only possible to examine the effects of such changes on seed composition by using fertile plants. Our results confirm the view that it is possible to select mutants with relaxed feedback control which can accumulate nutritionally essential amino acids in the seed. A maize mutant which accumulates threonine in the seed¹⁴ has also been identified. We view these mutants as a significant step towards the development of a barley grain of balanced amino acid content.

Parts of this work were supported by EEC contract 473 to B.J.M. and NATO grant RG255.80 to S.W.J.B. and S.E.R. M₂ seed was donated by V. Haahr, Risø, Denmark.

Received 5 April; accepted 13 July 1982.

- Seed Protein Improvement in Cereals and Grain Legumes Vol. 1 (STI/PUB/496, IAEA, Vienna, 1979).
- Fuller, M. F., Livingstone, R. M., Baird, B. A. & Atkinson, T. *Br. J. Nutr.* **41**, 321–331 (1979).
- Bryan, J. K. in *The Biochemistry of Plants: a Comprehensive Treatise* Vol. 5 (ed. Mifflin, B. J.) 403–452 (Academic, New York, 1980).
- Rognes, S. E., Lea, P. J. & Mifflin, B. J. *Nature* **287**, 357–359 (1980).
- Bright, S. W. J., Wood, E. A. & Mifflin, B. J. *Planta* **139**, 113–117 (1978).
- Bright, S. W. J., Mifflin, B. J. & Rognes, S. E. *Biochem. Genet.* **20**, 229–243 (1982).
- Rognes, S. E., Bright, S. W. J. & Mifflin, B. J. *Planta* (submitted).
- Mifflin, B. J. in *Genetic Improvement of Seed Proteins*, 135–158 (National Academy of Science, Washington, DC, 1976).
- Green, C. E. & Phillips, R. L. *Crop Sci.* **14**, 827–830 (1974).
- Fuller, M. F., Mennie, I. & Crofts, R. M. J. *Br. J. Nutr.* **41**, 333–340 (1979).
- Wallsgrove, R. M. & Mazelis, M. M. *Phytochemistry* **20**, 2651–2655 (1981).
- Widholm, J. M. *Biochim. Biophys. Acta* **279**, 48–57 (1972).
- Hibberd, K. A., Walter, T., Green, C. E. & Gengenbach, B. G. *Planta* **148**, 183–187 (1980).
- Hibberd, K. A. & Green, C. E. *Proc. natn. Acad. Sci. U.S.A.* **79**, 559–563 (1982).

MATTERS ARISING

Zenith atmospheric attenuation measurements

ZAMMIT and Ade¹ have made a valuable contribution to observations of millimetre wave attenuation and rightly argue its importance in locating telescopes. In finding a linear relationship between attenuation and measured total water, they question the results of Llewellyn-Jones *et al.*² who reported from laboratory measurements a quadratic dependence of absorption on the amount of water. We believe that the two results may not be in conflict when the difference in degree of saturation of the vapour in the two experiments is recognized. In the laboratory the vapour sample was homogeneous in temperature and was measured over a wide range of relative humidity including values close to saturation. In the zenith sky experiment, the measurements represented integrated absorption from layers at different temperatures and of unknown relative humidity, the only other quantity known being the total amount of water. It was therefore possible for all layers to be sufficiently far from saturation so that the millimetre wave absorption was in the range of linear dependence on water amount. That this is realistic has been verified by modelling millimetre wave absorption for various atmospheric columns specified by radiosonde data taken as a function of height. These show that integrated absorption in real atmospheric columns can be an insensitive measurement from which to deduce molecular behaviour. We believe, therefore, that a monomeric water model is not proven to be adequate for the prediction of millimetre wave attenuation.

Zammit and Ade find that their measured absorption values exceed the

predictions of accepted standard models and while the validity of these must always be questioned, the procedure of simply reassigning parameters to fit a given set of experiments may obscure new effects. Any observed absorption in excess of a physically acceptable molecular model may mean that some additional mechanism has been overlooked. From the aspect of choosing telescope sites it then becomes important to see if meteorological conditions can be found when the additional mechanism is inoperative and the excess becomes zero.

Specifically, from what is known about excess absorption, there is a strong case for investigating continental sites surrounded by deserts such as Kitt Peak, Arizona or Sacramento Peak, New Mexico for comparison with maritime sites like Izana, Tenerife and Mauna Kea, Hawaii. It is possible that in dry regions the relative humidity values at all levels of the atmosphere would be lower and that telescope sites located in them would be free from the effects of local high humidity sources which were found at Mauna Kea³. Such a benefit would not be revealed by simply measuring the total amount of water above the site.

H. A. GEBBIE

Department of Electrical Engineering
Imperial College of Science
and Technology,
London SW7 2BT, UK

D. T. LLEWELLYN-JONES
R. J. KNIGHT

Rutherford-Appleton Laboratory,
Chilton, Didcot,
Oxon OX11 0QX, UK

1. Zammit, C. C. & Ade, P. A. R. *Nature* **293**, 550-552 (1981).
2. Llewellyn-Jones, D. T., Knight, R. J. & Gebbie, H. A. *Nature* **274**, 876-878 (1978).
3. Moffat, P. H., Bohlander, R. A., Macrae, W. R. & Gebbie, H. A. *Nature* **269**, 676-677 (1977).

Petralona Cave dating controversy

IN their investigation of the fossil hominid cranium from Petralona Cave, Greece, Henning *et al.*¹ have neglected some of the relevant literature data. They state that the skull was lying on the cave floor. However, I² and all six men who found the skull³ report that the skull "was adhering to a rock"⁴ through a stalagmitic column, while the skeleton of the same individual was buried under a stalagmitic cover ~5 cm thick. The skeleton had apparently been separated from the skull during a dry period; the soil, having shrunk, moved the skeleton, while the skull remained attached by stalagmites about 20-24 cm above the skeleton. The skull belonged to a human who died there

before the formation of the travertine layer. Samples from the stalagmitic cover of the rock to which the skull adhered and from the travertine layer covering the skeleton, have been ESR-dated by Ikeya⁵ who obtained an age of 670 kyr BP (where the archaeological dose was 0.1 rad yr⁻¹) and 340 kyr BP (where the dose was 0.2 rad yr⁻¹). The same stalagmite tested by U/Th (sample 75 GR4-2) by Schwarcz *et al.*⁶ "actually yields a finite age of 440 kyr".

Henning *et al.* state that the skull was covered only with a brown calcite layer. However, I maintain that the skull was covered with pale whitish stalagmite, similar to that which is still found on the rock of the 'Mausoleum' and which was adhering to the skull. The brown calcite was overlying the whitish encrustation of the skull⁷, which protruded by 7-10 cm.

The stratigraphy of the cave indicates an age for the skull and the skeleton of the Petralonian man older than 700 kyr. This is supported also by faunal evidence, macro and micro, preserved in the cave⁸⁻¹⁰ and by the lithic technique^{11,12} proving that man did live in the cave as early as the Lower Pleistocene.

ARIS N. POULIANOS

*Anthropologike Hetaireia Hellados,
Daphnomele 5
Athens 706, Greece*

1. Hennig, G. J., Herr, W., Weber, E. & Xirotiris, H. L. *Nature* **292**, 533-536 (1981).
2. Poulanos, A. *Anthropos* **4**, 37-46 (1977).
3. Malkotsis, Y. *et al. Makedonia* 19 Sept., p. 1 (1960).
4. Malkotsis, Y. *et al. Cur. Anthropol.* **22**, 287 (1981).
5. Ikeya, M. *Anthropos* **7**, 144 (1980).
6. Schwarcz, H. P., Liritzis, Y. & Dixon, A. *Anthropos* **7**, 152-173 (1980).
7. Malkotsis, Y. *Anthropos* **7** (front cover January, 1980).
8. Kurtén, B. & Poulanos, A. N. *Anthropos* **4**, 47-130 (1977).
9. Kretzoi, M. *Anthropos* **4**, 131-142 (1977).
10. Fortelius, M. & Poulanos, N. *Anthropos* **6**, 15-43 (1979).
11. Poulanos, A. *Anthropos* **5**, 74-80 (1978).
12. Poulanos, A. & Ganapayya, B. P. *Anthropos* **7**, 260-273 (1980).

IN their recent investigation of the age of the Petralona skull using electron spin resonance (ESR), Hennig *et al.*¹ compared the results of ²³⁴U/²³⁰Th dating², of the top travertine floor in the area where the skull rested. It is hoped that the contribution of the ²³⁴U/²³⁰Th dates (corrected for its detrital residues) to ESR results will clarify matters and be a step forward in resolving this controversy.

Their statement that practically all previous age determinations were done on samples from deeper strata, but not from the thin brown top layers of the travertine floor, was inaccurate. I have studied the top, brownish layer of the Mausoleum by the ²³⁴U/²³⁰Th dating method. Three samples in this investigation contribute to the ESR dates^{2,3}: P-12, P-13 and P-6 (Table 1).

P-12 had an obvious multi-layered appearance (consisting of an upper series of lime-reddish grey layers), ~0.6 cm thick which presumably implies different times of deposition. (A similar description applies to a further five samples throughout the cave.)

The age of P-12 drops from 250 kyr to 154⁺¹⁹ kyr using a mode of correction which calculates the different U and Th leachable radioisotopes, by analysing the detritus insoluble residues after total carbonic dissolution^{2,4}. This corrected age, due to the interstratified nature of the sample, indicating as it does a very slow deposition of calcite, (thin section analysis has confirmed this), represents the average of the intermittent stages of this 0.6 cm layer. That is, the upper surface layer could be as young as 80 kyr and the deeper part as old as 259 kyr, which would

Table 1 Radiometric data of uncorrected and corrected $^{230}\text{Th}/^{234}\text{U}$ ages of Petralona Cave travertines

Sample no.	Description	$^{230}\text{Th}/^{234}\text{U}$	$^{234}\text{U}/^{238}\text{U}$	$^{230}\text{Th}/^{232}\text{Th}$	U (p.p.m.)	Th (p.p.m.)	Age (kyr)*
P-12	Travertine (smooth and pale reddish brown), from upper part of Mausoleum calcitic floor	0.953 ± 0.045	1.272 ± 0.049	3	0.75	0.91	250^{+49}_{-34}
(U, Th) corr*		0.780 ± 0.042	1.171 ± 0.053	∞	0.59		$154.4^{+19.1}_{-16.4}$
P-13	Thick (1-cm) monocrystalline travertine from the upper part of Mausoleum calcitic floor	0.980 ± 0.046	1.315 ± 0.031	15	2.7	0.73	269^{+58}_{-39}
(U, Th) corr		0.781 ± 0.037	1.297 ± 0.032	∞	2.51		$150.2^{+15.2}_{-13.5}$
P-6		0.540	1.005	8	8.12†	1.70	84^{+46}_{-32} (130 kyr, +1 σ)

* (U, Th) corr, mode of correction and corrected ages.

† Severe bone contamination as determined by X-ray diffraction renders an age of at least 150 kyr + 1 σ the most probable. Small clay residue plus contaminant bone prevented (U, Th) corrections.

suggest an average growth rate of $\sim 0.003 \text{ cm kyr}^{-1}$.

The 4-cm travertine beneath (thick, un laminated sheet of prismatic calcite), ranged in age from at least 750 kyr to 280 kyr (ref. 5).

P-13 gave an uncorrected age of 269^{+38}_{-39} kyr, which, when corrected for its detrital residue isotope ratios, became $\sim 150 \pm 40$ kyr.

Another indicative sample (P-6) presumably from the burial site of the skull, gave an age of 130 kyr (including 1 σ ; bone contamination noted). The appearance of this sample has many features in common with the material which encrusted the skull. The above age sequence was found to be typical for certain other parts of the cave.

However, any material, for example of prismatic calcite (colourless to pale brownish-grey), still remaining on the skull beneath the red-brown ESR-dated layer, would imply further that the skull is even older than 250 kyr.

From the above, we can see an obvious correlation, within the errors, between the U/Th series dates for the top travertine layer and the ESR dates for the stalagmitic encrustation on the Petralona cranium.

Y. LIRITZIS

Physics Laboratory II,
Patras University,
Patras, Greece

1. Hennig, G. J., Herr, W., Weber, E. & Xirontiris, H. L. *Nature* **292**, 633–636 (1981).
2. Liritzis, Y. thesis, Edinburgh Univ. (1979).
3. Liritzis, Y. *Anthropos* **7**, 215–249 (1980).
4. Liritzis, Y. & Galloway, R. B. (in preparation).
5. Schwarcz, H., Liritzis, Y. & Dixon, A. *Anthropos* **7**, 152–173 (1980).

THE determination of the age of the hominid cranium from Petralona by Hennig *et al.*¹ is remarkable because it is the first to date the carbonate encrust and cranium itself by the ESR method². However, there are uncertainties in their age derivation.

They assumed that the brown calcite encrusted the cranium soon after the death of the hominid. If this carbonate had been growing linearly up to recent time, the age of the cranium must be doubled to 400 kyr using their ESR age

for the carbonate. It must be stressed that the carbonate encrust age is just a minimum age of the cranium.

The high external dose rate of $190 \pm 20 \text{ mrad yr}^{-1}$ on the cave travertine floor is too high and is very close to that in the soil at Petralona. The dose rate in a limestone cave is generally highly affected by the flow-in soils nearby³. The high dose rate would be due to the soil mixed up by excavations in 1960–62 or recently.

The response of CaSO_4 to low energy γ rays is also high, leading to an apparently high dose rate. Furthermore, the carbonate encrust was presumably about a few centimetres above the cave floor and shielded by the cranium against the floor. Thus, it would not be appropriate to use the dose rate of 190 mrad yr^{-1} . If the external dose rate of 87 mrad yr^{-1} with thermoluminescent dosing of $\text{CaSO}_4(\text{Tm})$ or the $50\text{--}80 \text{ mrad yr}^{-1}$ of Liritzis *et al.*⁴ with $\text{NaI}(\text{Tl})$ at Petralona cave were used as the external dose rate, the total dose rate would be $\sim 100 \text{ mrad yr}^{-1}$. The average age of the carbonate encrust could then be 420–600 kyr which is close to those obtained for some carbonates and bones at Petralona with ESR⁵. Careful assessment of the radiation environment must be made using ESR dating before a large scale excavation proceeds.

We have used ESR to study Choukoutien bones. The total dose of natural radiation (TD) of Choukoutien bones estimated with ESR ranged from 20 to 40 krad. The TDs for Petralona bones range from ~ 10 krad for bones embedded in pure calcite to 80 krad in the soil sediment. The latter age would be ~ 400 kyr considering the high dose rate of 200 mrad yr^{-1} . The TDs of the cranium of 27 krad yr^{-1} obtained by Hennig is very close to that of bones of layer 17 at Petralona (21 krad) where Petralona man was originally located, according to Poulianos. There are some problems of apatite recrystallization in ESR dating of bones⁶. We might obtain a younger age than the real age for bones with ESR. However, these results may have some bearing on the stratigraphy. The bones at Arago, Tautavel fall in nearly the same

range of TDs.

Note added in proof: ESR dating of fossil bones are being determined taking ^{238}U -series disequilibrium and a model of constant uranium accumulation rate into account. Tentative ages neglecting the loss of gaseous radon are 810 kyr and 550 kyr (Kabuh and Pucangan Layer, Jawa), 335–480 kyr (Mauer, Heidelberg), 330–440 kyr (Petralona) and 240–200 kyr (Steinheim). Actual ages are older when a 30–50% loss of gaseous radon is taken into account.

MOTOJI IKEYA

Technical College,
Yamaguchi University,
Ube 755, Japan

1. Hennig, G. J., Herr, W., Weber, E. & Xirontiris, H. L. *Nature* **292**, 533–536 (1981).
2. Ikeya, M. *Nature* **255**, 48–51 (1975).
3. Ikeya, M. *Anthropos* **5**, 54–59 (1978); *Hlth Phys.* **31**, 76–77 (1976).
4. Liritzis, Y. & Poulianos, A. N. *Anthropos* **7**, 252–259 (1980).
5. Ikeya, M. *Archaeometry* **20**, 147–153 (1978); *Anthropos* **7**, 143–151 (1980).
6. Ikeya, M. & Miki, T. *Science* **207**, 977–979 (1980).

HENNIG *ET AL.* REPLY—With regard to the above comments we will keep our replies to each author distinct.

The statement by Poulianos in his own publications in *Anthropos* and *Current Anthropology* that there exists a skeleton which belongs to the same individual as the hominid cranium, that is said to have been “buried under a stalagmitic cover $\sim 5 \text{ cm}$ thick”, clearly contradicts what he has published elsewhere²; “Unfortunately, the skeleton was not preserved and lost forever for science. Only the skull was preserved due to the fact that it was covered with stalactitic material”.

As far as we know, there is no indication that any bone fragments under the 5-cm thick stalagmitic floor are related to hominids, and even less to the hominid skull. Until now no proof for the existence of a hominid skeleton has been presented.

Poulianos furthermore quotes age data of 340 kyr and 670 yr derived by Ikeya (optionally for dose rates of 0.2 rad yr^{-1} and 0.1 rad yr^{-1} respectively³). Curiously, there is no detailed description of the colour, texture, thickness and exact sampling location of these samples in Ikeya's paper. Thus, it is almost impossible to

reconstruct a reliable stratigraphical relationship of these samples to the hominid skull. It is important to know that the skull was removed from Petralona Cave many years before Poulianos became involved.

With respect to the age cited by Poulianos of 440 kyr, which had been derived by Schwarcz *et al.*⁴, everybody can verify that this sample originates from a depth of >1.5 cm below the surface of the travertine floor at the discovery site of the cranium. Altogether four different samples of this clear, massive base layer have been dated by Schwarcz *et al.* (ref. 4, Table 1, samples 75 GR-4) and yielded the U-series ages 272.9^{+122}_{-68} , 451^{+90}_{-150} , 283^{+84}_{-57} and >450 kyr.

Based on these data, Schwarcz *et al.* have derived a growth interval for this clear base layer "from at least 450 to 260 kyr BP" (ref. 4, p. 161). Consequently, the overlaying (1.5-cm thick) calcite should be younger than 260 kyr, which is particularly true for the thin brown surface layer covering the hominid skull also. It must be stressed that Schwarcz *et al.* have only dated samples from the clear prismatic layer, but none from above this massive stratum (ref. 4, p. 155). Therefore, the age data of Schwarcz *et al.* cited above can only set upper limits for the age of the hominid cranium and its thin brown encrustation. (This is also true for the quoted ages derived by Ikeya³, provided he used the same stalagmite sample, as Poulianos maintains.) In this context, the lower ages of 273 and 283 kyr, respectively, and 260 kyr deduced by Schwarcz *et al.*⁴ are in agreement with our ESR age of $\approx 200 \pm 40$ kyr for the hominid skull and its covering brown calcite¹.

Regarding Poulianos' next point, one of us (N.I.X.) was involved in the preparation of the skull and removed the calcite encrustation that was adhering to the bone surface. Fortunately, on a few of these brown calcite pieces tiny bone fragments were attached, which we separated and used for an ESR-age determination¹. Poulianos obviously does not know that a part of the cranium base was intentionally left unprepared and is still today encrusted with the thin brown calcite layer. Here one can clearly see that this brown encrustation is directly in contact with the lamina externa of the skull bone.

As to his final point, we do not think that a stratigraphy alone can indicate any absolute ages, particularly as the hominid cranium is a surface finding. Any interrelation of the hominid cranium and the cave fauna is, therefore, very questionable. Moreover, the fauna at Petralona cave has also been described as Riss/Würm⁵.

Dealing with the comment by Liritzis, we are pleased to know that he also has studied the thin brown top layer at the site of the discovery of the hominid skull. He has recently given, for the first time,

details of three samples, P-12, P-13 and P-6, which were formerly only associated with the word 'Mausoleum' in his quoted publication⁶, in which, however, any further sample description is missing. Consequently, it was impossible to interrelate these three speleothem samples and thus they were not mentioned in our paper¹. We are, however, now pleased to recognize that samples of the thin brown top layer of the travertine floor were independently dated by the uranium series method. Certainly it is most remarkable that all three samples dated by Liritzis yield $^{230}\text{Th}/^{234}\text{U}$ ages in best agreement with our ESR ages of the hominid skull and its encrustation, even within the limits of error.

With respect to Ikeya, he doubts the temporal relation between the brown calcite encrustation and the skull itself and he further suggests we should double our age of 200 kyr by assuming linear growth until today. Surely it should be noted that here he does not rely on his own experimental data.

There are at least four arguments which point to a relatively rapid conservation of the skull by the brown calcite encrustation:

- (1) The excellent conservation of the osteological material of the cranium was recently confirmed by histological studies⁷ demonstrating that the skull was covered a relatively short time after the death of the hominid.
- (2) The ESR-dating of the skull bone material itself has yielded about the same age as its covering calcite layer¹.
- (3) A stratigraphically older calcite (sample(d)) which does not appear on the skull was taken 3–4 mm below the thin brown surface layer. Being older than the skull itself, it allows us to set an upper limit of 198 ± 50 kyr for the age of the hominid¹.
- (4) Ikeya's suggestion of a linear growth for the 1–2 mm-thick encrustation from 400 kyr until the present would imply a highly unrealistic growth rate of 1–2 mm per 400 kyr ($\approx 2.5\text{--}5 \times 10^{-3} \mu\text{m yr}^{-1}$) which is about three orders of magnitude lower than typical experimentally determined growth rates of 1–10 $\mu\text{m yr}^{-1}$ (ref. 8). Here, it may also be of interest that Ikeya published vertical growth rates of 0.3–0.6 $\mu\text{m yr}^{-1}$ and 0.45–0.9 $\mu\text{m yr}^{-1}$ for two different floor travertines of Petralona Cave³. In addition, the lack of lamination in the brown calcite encrustation indicates a relatively rapid and uninterrupted depositional event.

Another point is Ikeya's opinion that "the high external dose rate of 190 ± 20 mrad yr^{-1} on the cave travertine floor is too high". This contradicts his previous assertion⁹. "We are using the tentative annual dose of natural radiation of ~ 0.2 rad yr^{-1} for the Petralona stalagmite from U/Th measurements using low background Ge(Li)-detector"³.

With respect to our measured radiation

dose of 190 ± 20 mrad yr^{-1} , Ikeya recommends an external dose rate of 87 mrad yr^{-1} and a total dose rate of 100 mrad yr^{-1} . On the basis of this dose rate one would obtain ages between 270 and 420 kyr from our EDs of 27–42 krad (ref. 1) and not—as he claims—ages of 420–600 kyr. Obviously, there is an error in his simple estimation.

Furthermore, Ikeya does not say that he has measured his recommended dose rate of 87 mrad yr^{-1} —as far as we know—at some location in another branch of the cave, but not in the place where the hominid skull was found. Our dose rate of 190 ± 20 mrad yr^{-1} was established directly on the surface of the travertine floor at the site of the discovery.

In fact, relatively high dose rates on the surface of some cave floors are not unusual and similar values have been observed at other sites. For example, Ikeya reports a much higher archaeological dose for the surface layer of a Petralona cave floor as compared with deeper strata. His comment on this effect is simply: "Too much exposure at the surface?"³.

This effect of a comparably higher dose rate on cave floors was explained mainly by airborne radionuclides (for example radon and daughter products¹). Accumulation of atmospheric radon in calcite caves has been reported, and radon activities up to 13.2 mCi m^{-3} were for example, measured at Akiyoshi cave, Japan¹⁰. Such high radon concentrations will enhance the external α -, β - and γ -dose rates of surface layers in caves.

Furthermore, Ikeya reports a total dose (TD) that is an archaeological dose of 21 krad for "bones at the layer 17 at Petralona (21 krad) where Petralona man originally was according to Poulianos".

It is not surprising that using this measured TD value of 21 krad (determined by Ikeya) in connection with his suggested dose of 0.1 rad yr^{-1} yields an ESR-age for the Petralona hominid of 210 kyr.

On closer inspection, Liritzis' and Ikeya's data turn out to be consistent with our ESR-age determination of $\sim 200 \pm 40$ kyr for the Petralona skull.

G. J. HENNIG
W. HERR
E. WEBER
N. I. XIROTIRIS

*Institut für Kernchemie
der Universität Köln,
Zùlpicher Strasse 47, 5000 Köln-1, FRG*

1. Hennig, G. J., Herr, W., Weber, E. & Xirotiris, N. I. *Nature* **292**, 533–536 (1981).
2. Poulianos, A. N. *Archaeology* **24**, 11 (1971).
3. Ikeya, M. *Anthropos* **7**, 144 (1980).
4. Schwarcz, H. P., Liritzis, Y. & Dixon, A. *Anthropos* **7**, 152–173 (1980).
5. Sickenberg, O. *Geol. Geophys. Res. Inst. Athens* **9**, 1–16 (1964).
6. Liritzis, Y. *Anthropos* **7**, 221 (1980).
7. Schultz, M. & Xirotiris, N. I. *J. Med. Anthropol. Archaeol.* **1**, 308–331 (1982).
8. Harmon, R. S., Thompson, P., Schwarcz, H. P. & Ford, D. *Nat. speleol. Soc. Bull.* **27**, 21–33 (1975).
9. Ikeya, M. *Anthropos* **7**, 145 (1980).
10. Miki, T. & Ikeya, M. *Phil. Phys.* **39**, 351–354 (1980).

BOOK REVIEWS

Science and technology, A to Z

Alan Isaacs

UNLIKE their editors, the reviewers of large reference books are not expected to read every word of the works they are asked to discuss. In the case of the new (fifth) edition of the *McGraw-Hill Encyclopedia of Science and Technology* one would have a full-time job for 2.4 years reading its 8.9 million words (assuming a 35-hour week and a reading rate of 2,000 words per hour). These figures highlight the enormous task of the editors, who have had to commission, edit, illustrate and index its 7,700 articles, which occupy some 12,700 A-4 pages arranged in 15 volumes. There were, so the blurb tells us, 3,500 contributors, 18 of whom were Nobel-prize winners. The result of this massive endeavour could have been a fiasco. In fact it is a *tour de force* of which its publishers have every right to be proud. It is extremely well illustrated and has been typeset and printed to a very high standard indeed.

Accepting the professionalism and authority of the work the first question that springs to mind — a £500 question — is “Who is it for?”. McGraw-Hill’s publicity suggests that libraries, teachers, students and general readers, not to mention scientists, engineers, technical writers, and industrial and business managers, will find it indispensable. This is a fairly high proportion of the population. But, as everyone knows, advertising copy cannot be taken seriously. Who *really* will find it useful?

Before attempting to answer this question one has to ask two others. At what level is it written and what does it contain? The editor, Sybil P. Parker, goes some way to answering the first of these questions in her preface:

The level of writing is, of course, consistent with the degree of complexity inherent in each subject, but is geared to nonspecialists.

The whole question of the level and style of writing is of the greatest importance in assembling works such as this. In this century the explosive growth of science in general, and the technology of communication in particular, has been accompanied by a blunting of the primary tool of communication — language. Technical language requires a technical vocabulary; scientists use a large number of words and expressions that are not found in the general language. Non-scientists find this puzzling and unacceptable. All too often they expect an intelligible explanation of,

The McGraw-Hill Encyclopedia of Science and Technology, 5th Edn. Edited by Sybil P. Parker. 15 volumes, pp.12,700. ISBN 0-07-079280-1. (McGraw-Hill: 1982.) £495, \$850.

say, quantum theory, in the vocabulary of the general language.

Another aspect of the same problem is syntactical. A writer needs a grasp of syntax that will enable his readers to understand his sentences after reading them only once. A scientist who does not have an inherent ability to say precisely what he means often loses confidence in himself and plunges into an ugly jargon, which he makes uglier still with impenetrable syntax.

Ms Parker and her team have managed to cope with both problems more than adequately. I am quite certain that not all the contributors presented typescripts containing the impeccable prose that has reached print. This is not to say that the layman will find many of the entries useful, or even intelligible. Ms Parker’s warning that the level is “consistent with the degree of complexity inherent in each subject” is appropriate and honest. No attempt has been made to simplify to an extent that involves either distortion or trivialization. For example, the section on special relativity uses such expressions as galilean transformation, inertial frame, ether drift, Lorentz-Fitzgerald contraction and Michelson-Morley experiment with either no explanation at all or a brief gloss. The article therefore does not pretend to inform the layman. Rather it is a summary that could be very useful to a physical scientist whose main field of study does not include relativistic mechanics. I am not sure what engineers would make of it; probably not much. This does not mean that the set is not a good investment for engineers. The civil engineer, for example, will find plenty of information in, say, mechanical, electrical and chemical engineering that he will undoubtedly find valuable. In general, then, the articles are designed for scientists and engineers trained in one discipline who are seeking information in another.

“Scientists”, in this context, should be taken to mean “hard” scientists, for the “soft” sciences do not find much place here. The publishers say that the work encompasses “all the physical, life, and earth sciences, as well as engineering. . .”. It is, therefore, something of a surprise to find

that one of the 75 headings in the useful subject index is *physiological and experimental psychology*. However, the remaining 74 sections together provide a detailed coverage of all of the hard sciences and of technology. The entries themselves are arranged in one alphabetical sequence opening with the inevitable and omnipresent *aardvark* at the beginning of Vol. 1 and closing with the obscure group of fungi *Zythiaceae* at the end of Vol. 14. Between these alphabetical extremes the reader can learn about such a diversity of subjects as antisubmarine warfare, emotion, laser welding, open-pit mining, quantum chemistry, petrochemicals and the Wentzel-Kramers-Brillouin method (which may sound like an invention of Saki but is, in fact, a technique for solving the Schrödinger equation). Volume 15 contains a list of contributors, the topical index and the analytical index.

So, who should be spending £500 on the set. Clearly, at this price one is talking to librarians rather than individuals. One can say at once that for all libraries of science, technology and engineering it is an obvious must. But what about general libraries? How much of interest to the general reader does it contain that is not available in the latest edition of, say, *Encyclopaedia Britannica*? This is a critical question for individual librarians, and one to which there is no definitive answer. While *Encyclopaedia Britannica* is strong and authoritative in the sciences, the *McGraw-Hill Encyclopedia* is much more detailed and almost a decade more up-to-date. One can only generalize: any library that has a serious intention of catering for scientists, technologists and engineers needs a copy of this edition of the McGraw-Hill opus.

Finally, a few words of criticism, in the hope that they may be helpful in preparing future editions. I was surprised to find no mention of the now widely current expressions *electric constant* and *magnetic constant*; the articles under permittivity and permeability are adequate except for the omission of these modern terms. In the article on the plant kingdom the proof-reading has not been as good as it should have been, and the somewhat controversial classification provided is, I am told, not acceptable to all plant scientists, but the article does not say so.

The alphabetical index can sometimes be very helpful and sometimes not. For

example, in view of the current controversy I tried to find what the *Encyclopedia* had to say about Darwinism. I was surprised to find that it was an entry neither in the main text nor in the index. There are, it is true, 11 references in the index under *Darwin, Charles*. None of these proved helpful, however, and the reference to the *Origin of Species* turned out to be no more than a brief mention in an article on plant taxonomy. After an inordinate amount of time I found what I was looking for in the article on speciation. But, incidentally, the set is silent on cladistics — at least I think it is, because it does not appear in the index. □

Alan Isaacs is editor of the Macmillan Encyclopedia, the Penguin Dictionary of Science, Longman's New Dictionary of Physics, and science editor of Collins English Dictionary. He has contributed to many other dictionaries and encyclopaedias.

Tests of gravity

Joseph H. Taylor

Theory and Experiment in Gravitational Physics. By Clifford M. Will. ISBN 0-521-23237-6. (Cambridge University Press: 1982.) £37.50, \$75.

GRAVITATION, the only one of nature's basic forces that we ordinarily feel, has been the centre of renewed research effort in the past quarter of a century — largely because improved experimental techniques have made possible ever more precise tests of theory. In a concise and meaty book, Clifford Will has summarized the recent developments in the field, and has brought together a store of information not otherwise available in one place. It is a truism that the fate of a physical theory lies in its successful prediction of the results of experiments. With this fact clearly in mind, Professor Will presents his material by concentrating on the methods and results of both laboratory and astronomical tests of the subtleties of gravity, and on the theoretical tools used for interpreting the experiments.

The first quarter of the book presents the theoretical foundations of the subject, from the Einstein Equivalence Principle (in a sufficiently small, freely falling enclosure, it is impossible to tell whether gravitational forces are present) to the detailed mathematical framework of gravitation as geometry. We then encounter the Parametrized post-Newtonian (PPN) formalism, a theory of gravitational theories developed by Kenneth Nordvedt towards the end of the 1960s and later extended in collaboration with Professor Will. The PPN framework is well suited to the analysis of the slow-motion, weak-field experiments that can be performed in the

laboratory or with Solar System astronomical objects; in such a post-Newtonian limit, any metric theory of gravity can be characterized by the values of a set of ten parameters, the so-called PPN parameters. For general relativity, two of the parameters have value unity and the rest are zero; in the post-Newtonian limits of other theories, the parameters have other values. The book presents detailed recipes and examples of how the parameters can be calculated within a given theory.

The middle section of the book develops the equation of motion for bodies moving under post-Newtonian conditions, and then uses this formalism to analyse the "classical" tests of general relativity: the deflection of starlight near the limb of the Sun, the time-delay of radar signals in the vicinity of the Sun and the perihelion shift of the orbit of Mercury. Together with the results of some less famous experiments involving lunar laser ranging, geophysical effects, the orbits of planets and the constancy of the Newtonian G , these tests establish a set of experimental constraints on the PPN parameters. We learn that "viable theory space" is squeezed to the extent that in the post-Newtonian limit, any gravitation theory must agree with general relativity to within fractional margins of error ranging from 1 to 10^{-7} per cent.

Unfortunately, perhaps, there are a number of distinct theories of gravity which can, by suitable adjustments of arbitrary parameters, accommodate all of the Solar System experiments. Consequently, the last quarter of the book deals with tests which probe beyond the weak-field, post-Newtonian limits. These tests involve gravitational radiation, the structure and motion of neutron stars and other inherently relativistic compact objects, timing measurements of the orbiting pulsar discovered in 1974 and, finally, observations of cosmological significance. Only the binary pulsar experiment has yet produced results of quantitative significance; again, the results are consistent with general relativity, while constraining other theories rather severely.

Why so much ado about "other" possibly viable theories of gravity, when relativity remains uncontradicted by experiment and stands alone in its freedom from arbitrarily adjustable constants? True, the failure of all attempts to quantize relativity still segregates it from the rest of modern physics, but then the other theories being discussed are not quantum theories either. So the motivation for undertaking the hard labours involved in developing or mastering the PPN machinery seems obscure. Nevertheless, I find Professor Will's book a valuable addition to my library, and a most useful reference work. Other researchers and serious students of gravitation should be pleased with it, too.

J.H. Taylor is Eugene Higgins Professor of Physics at Princeton University.

Seen in colour

W. R. A. Muntz

Comparative Color Vision. By Gerald H. Jacobs. Pp.209. ISBN 0-12-378520-0. (Academic: 1982.) £16, \$24.

THE opening words of the preface to *Comparative Color Vision* describe how the author received a telephone call some years ago asking how to go about studying colour vision in the American elk. Anyone who has worked on comparative colour vision will have received similar requests, and will have shared Dr Jacobs's frustration that no convenient and up-to-date source of information is available on the methods and results of work in this area.

The present book is Dr Jacobs's response to this situation, and about half of it does indeed give the required information both clearly and concisely. Thus an initial chapter sets out the necessary techniques, dealing particularly with the bugbear problem of brightness, and should help anyone designing experiments to avoid the major pitfalls. Two further chapters late in the book present a comparative survey of colour vision in vertebrates (invertebrates are specifically excluded). These chapters are especially comprehensive in their coverage of the mammals, particularly the primates: 36 of the 58 pages of the survey deal with the mammals, and of these 20 are devoted to the primates. This emphasis is not a defect, for it is only reasonable for a book to reflect the author's interests, but it inevitably results in the "lower" vertebrates being more sketchily covered. With this minor proviso, these chapters provide a valuable introduction to the field.

The rest of the book is mostly devoted to background information on vision in general, with accounts of the structure of the eye, photopigments, basic electrophysiology, the psychophysics of human colour vision and so on. I feel these sections are less useful, since many other publications exist which deal with these subjects well. It is also impossible, in a book of this length, to cover such a range of topics in any depth, and it seems to me that in this part of the book the author has fallen between two stools: the information is so condensed that it would be difficult for anyone who is not already familiar with the field to understand it, and yet for those who are experienced it will add little to their knowledge or understanding.

In spite of these reservations the book serves a useful purpose. Anyone working within the general area it covers will find both interest and a number of new facts, and it should in particular provide a very useful introduction for someone who knows the basic data of vision, and now wishes to pursue the subject in colour. □

W.R.A. Muntz is Professor of Biology at the University of Stirling.

Everything you wanted to know about . . .

Leslie Crombie

The Natural Coumarins: Occurrence, Chemistry and Biochemistry. By Robert D.H. Murray, Jesus Mendez and Stewart A. Brown. Pp.702. ISBN 0-471-28057-7. (Wiley: 1982.) £70, \$160.

MORE than 800 natural coumarins are known today, many from higher plants, but a number are important compounds from microbial sources and include antibiotics as well as the more notorious group of aflatoxins. With the appearance of this large and well-printed volume there can be few groups of natural products which have so modern and extensive a documentation; indeed if there were more volumes of this type natural products study would become much more accessible, and some order brought to a massive and rather sprawling area of science.

The volume should attract more than one type of reader and in some ways it is two books in one. Chapters 1-8 will be of special interest to natural products organic chemists interested in the themes of structure, synthesis and biosynthesis. These chapters are particularly impressive for their depth of coverage, bringing together much scattered information. The style of writing is pleasant, and older information is integrated with newer material in a way which gives the reader confidence in the judgement and scholarship of the authors. There is much here in the chemistry, synthesis and use of spectroscopic and other techniques to attract the non-coumarin specialist.

Chapters 9-13, the second part of the text, have biochemically orientated themes which tend to concentrate on certain biologically active structures such as the aflatoxins, dicoumarol, novobiocin and the furanocoumarins. All these compounds have interesting biochemical interactions which lend themselves well to an essay-type of treatment. Some are of more recent discovery, but knowledge of the effects of the furanocoumarins (e.g. from rue) goes way back in time, and photosensitization reactions in skin by their linear members are now well studied. An indication of what our ancestors thought about the biological activity of certain plant furanocoumarins is given in the concise lines,

Rue maketh chast and eke preserveth sight,
Unfuseth wit, and Fleas doth put to flight.

These claims, however, are perhaps somewhat excessive.

Despite a careful exposition of the different numbering systems for coumarins given early in the book, it is unsettling that two systems are employed in different parts of the text for furanocoumarins, one intended for chemists, one for biochemists and biologists. There are instances of interesting but unreferenced items, such as chlorflavonin (p.101), but few errors jar

the reader's pathway. Nonetheless the strong recommendation, in heavy black type, of a total ban on benzene for extraction and chromatography on the grounds of toxicity hazards, does seem a little excessive. If professional chemists cannot handle toxic materials by safe working, who then will?

Impressive features of this book are the indexes and tables which must have involved a remarkable amount of work. These cover 379 pages of the 702-page book. Natural coumarins are tabulated according to chemical type along with trivial name, empirical formula, melting point, rotation and references. There are then separate indexes of melting point, molecular weight, trivial names, botanical occurrence, and families and genera, together with a general index and 3,383 references — we shall henceforth have little excuse for not being able to find specific pieces of information on natural coumarins. This is a massive work, with strong elements of original treatment, which will become a valued and well-known book among scientists in the natural product area. □

Leslie Crombie is Sir Jesse Boot Professor of Organic Chemistry at the University of Nottingham.

Reprise of calcium and secretion

O. H. Petersen

Calcium and Cellular Secretion. By Ronald P. Rubin. Pp.276. ISBN 0-306-40978-X. (Plenum: 1982.) \$35, £22.05.

THE importance of calcium in the control of secretion has not been in dispute for many years. However, the realization of the key role played by calmodulin, the demonstrations of the internal calcium control of membrane conductance, the characterization of calcium channels and the availability of much improved methods for measuring the internal free calcium concentration, together with many other important findings made in the past ten years, is certainly justification for a new book on the subject. This monograph is a much improved version of *Calcium and the Secretory Process* by the same author, which appeared in 1974 (for review see *Nature* 255, 265; 1975).

The present book is only slightly longer than its predecessor, but contains much new material reflecting the rapid growth of

this research field. There are four main chapters. The first deals with a mixture of general problems such as analytical techniques, subcellular calcium distribution and its redistribution during stimulation. There is a wealth of useful information including a critical assessment of calcium antagonists. Unfortunately the sections on calcium channels and the effects of internal calcium on other ion channels are already out of date, since there is no mention of single-channel current recordings with the Neher/Sakmann patch clamp technique. Dr Rubin can hardly be blamed for this, since the results of the application of this powerful technique to secretory cells have only recently been appearing in print. More worrying is the author's tendency to quote reviews rather than original papers. This can have unfortunate consequences as seen in the discussion of the calcium-evoked potassium release, where no reference to Gardos is found although this phenomenon is generally associated with his name.

The second chapter is a survey of calcium actions covering all the main secretory cell types. The historical development of the stimulus-secretion coupling concept is traced by considering first the cholinergic nerves and then the adrenal medulla and the neurohypophysis, but perhaps because these three systems are discussed mainly in a historical context one looks in vain for even a brief description of the Baker-Knight experiments with permeabilized adrenal medulla cells (*Nature* 276, 620-622; 1978). It is sad that an otherwise fine chapter, which is on the whole up to date, should be marred by the failure to discuss one of the most direct approaches to the question of intracellular control of secretion.

Chapter 3 is a brief consideration of possible mechanisms by which calcium acts to control secretion. There is rightly emphasis on calcium-binding proteins and in particular calmodulin, but it is clear that many important pieces of the puzzle are still missing. Finally, the author deals with the interactions of calcium with other putative intracellular mediators, in particular cyclic AMP and cyclic GMP. The picture is far from clear, but this again is not Dr Rubin's fault. These are muddy waters and much remains for research workers to discover and probably also "undiscover".

Dr Rubin's compact monograph will be useful to the many students of this exciting research field. It is not yet the ideal book on the topic, but considering the difficulties in compressing the vast amount of available material into what has become a very readable book, we must be grateful for this effort. □

O. H. Petersen is George Holt Professor of Physiology at the University of Liverpool, and author of *The Electrophysiology of Gland Cells* (Academic, 1980).

BOOKS RECEIVED

Physics

BONIFACIO, R. (ed.). Dissipative Systems in Quantum Optics: Resonance Fluorescence, Optical Bistability, Superfluorescence. Topics in Current Physics, Vol.27. Pp.151. ISBN 3-540-11062-3/0-387-11062-3. (Springer-Verlag: 1982.) DM 48, \$22.40.

BRUESCH, P. Phonons: Theory and Experiments I. Lattice Dynamics and Models of Interatomic Forces. Series in Solid-State Sciences, Vol.34. Pp.261. ISBN 3-540-11306-1/0-387-11306-1. (Springer-Verlag: 1982.) DM 63.50, \$28.20.

BUECHE, F. Principles of Physics, 4th Edn. Pp.837. ISBN 0-07-008867-5. (McGraw-Hill: 1982.) £19.50.

JAROS, M. Deep Levels in Semiconductors. Pp.302. Hbk ISBN 0-85274-516-8. (Adam Hilger: 1982.) Hbk £24.

SVELTO, O. and HANNA, D.C. Principles of Lasers, 2nd Edn. Pp.375. ISBN 0-306-40862-7. (Plenum: 1982.) Np.

VONSOVSKY, S.V., IZYUMOV, Yu. A. and KURMAEV, E.Z. Superconductivity of Transition Metals: Their Alloys and Compounds. Pp.512. ISBN 3-540-11382-7/0-387-11382-7. (Springer-Verlag: 1982.) DM 95, \$42.20.

WHITTEN, R.C. (ed.). The Stratospheric Aerosol Layer. Topics in Current Physics, Vol.28. Pp.152. ISBN 3-540-11229-4/0-387-11229-4. (Springer-Verlag: 1982.) DM 54, \$25.20.

WILKINSON, D. (ed.). Progress in Particle and Nuclear Physics, Vol.8. Quarks and the Nucleus. Proceedings of the International School of Nuclear Physics held April 1981. Pp.446. ISBN 0-08-029103-1. (Pergamon: 1982.) £36.50, \$84.

Chemistry

ATKINS, P.W. and CLUGSTON, M.J. Principles of Physical Chemistry. Pp.246. ISBN 0-273-01774-8. (Pitman: 1982.) Np.

BAIULESCH, G.E., PATROESCU, C. and CHALMERS, R.A. Education and Teaching in Analytical Chemistry. Pp.190. ISBN 0-85312-384-5/0-470-27283-X. (Ellis Horwood/Halsted: 1982.) £15, \$32.85.

BOSCHKE, F.L. New Trends in Chemistry. Topics in Current Chemistry, Vol.100. Pp.213. ISBN 3-540-11287-1/0-387-11287-1. (Springer-Verlag: 1982.) DM 98, \$45.70.

CHANEY, J.F., RAMDAS, V. *et al.* (eds). Thermophysical Properties Research Literature Retrieval Guide 1900-1980, Vol.3. Organic Compounds and Polymeric Materials. ISBN 0-306-67223-5. (Plenum: 1982.) Np.

CHANEY, J.F., RAMDAS, V. *et al.* (eds). Thermophysical Properties Research Literature Retrieval Guide 1900-1980, Vol.4. Alloys, Intermetallic Compounds, and Ceramics. ISBN 0-306-67224-3. (Plenum: 1982.) Np.

FINSTON, H.L. and RYCHTMAN, A.C. A New View of Current Acid-Base Theories. Pp.216. ISBN 0-471-08472-7. (Wiley: 1982.) Np.

LATNER, A.L. and SCHWARTZ, M.K. (eds). Advances in Clinical Chemistry, Vol.22. Pp.306. ISBN 0-12-010322-2. (Academic: 1981.) \$38.

LEJA, J. Surface Chemistry of Froth Flotation. Pp.758. ISBN 0-306-40588-1. (Plenum: 1982.) \$69.50.

SENNING, A. (ed.). Sulfur in Organic and Inorganic Chemistry, Vol.4. Pp.456. ISBN 0-8247-1350-8. (Marcel Dekker: 1982.) SwFr. 214.

Technology

NEMETH, K. (ed.). Application of Electro-Ultrafiltration (EUF) in Agricultural Production. Proceedings of 1st International Symposium held May 1980, Budapest. Pp.128. ISBN 90-247-2641-7. (Martinus Nijhoff, The Netherlands: 1982.) Dfl.50, \$22.

TRAPPL, R., DE P. HANIKA, F. and TOMLINSON, R. (eds). Progress in Cybernetics and Systems Research, Vol.10. Pp.562. ISBN 0-89116-239-9. (Hemisphere: 1982.) \$88.

TRAPPL, R., FINDLER, N.V. and HORN, W. (eds). Progress in Cybernetics and Systems Research, Vol.11. Pp.601. ISBN 0-89116-240-2. (Hemisphere: 1982.) \$88.

TRAPPL, R., KLIR, G.J. and PICHLER, F.R. (eds). Progress in Cybernetics and Systems Research, Vol.8. Pp.529. ISBN 0-89116-237-2. (Hemisphere: 1982.) \$88.

TRAPPL, R., RICCIARDI, L. and PASK, G. (eds). Progress in Cybernetics and Systems Research, Vol.9. Pp.532. ISBN 0-89116-238-0. (Hemisphere: 1982.) \$88.

Earth Sciences

DREVER, J.I. The Geochemistry of Natural Waters. Pp.388. ISBN 0-13-351403-X. (Prentice-Hall: 1982.) £23.95.

GILLEN, C. Metamorphic Geology: An Introduction to Tectonic and Metamorphic Processes. Pp.144. Hbk ISBN 0-04-551057-1; pbk ISBN 0-04-551058-X. (George Allen & Unwin: 1982.) Hbk \$9.95, £4.95; pbk np.

HUGHES, C.J. Igneous Petrology, Vol.7. Pp.552. ISBN 0-444-42011-8. (Elsevier/North Holland: 1982.) \$28.00, Dfl.70.

McCONNELL, A. No Sea too Deep: The History of Oceanographic Instruments. Pp.162. ISBN 0-85274-416-1. (Adam Hilger, Bristol: 1982.) £19.50.

Biological Sciences

BOCK, P. The Paranganglia. Pp.315. ISBN 3-540-10978-1/0-387-10978-1. (Springer-Verlag: 1982.) DM 268, \$124.80.

BONNER, J.T. (ed.). Evolution and Development. Report of the Dahlem Workshop held May 10-15, 1982, Berlin. Life Sciences Research Report, Vol.22. Pp.357. ISBN 3-540-11331-2/0-387-11331-2. (Springer-Verlag: 1982.) DM 46, \$21.50.

CRAIL, T. Apetalk and Whalespeak: The Quest for Interspecies Communication. Pp.298. ISBN 0-87477480-3. (Tarcher, Los Angeles: 1981.) \$14.95.

DEWBURY, D.A. (ed.). Mammalian Sexual Behavior: Foundations for Contemporary Research. Benchmark Papers in Behavior, Vol.15. ISBN 0-87933-396-0. (Hutchison Ross: 1981.) \$48.

EHRlich, P. and EHRlich, A. Extinction: The Causes and Consequences of the Disappearance of Species. Pp.305. ISBN 0-575-03114-X. (Gollancz, London: 1982.) £9.95.

FARNER, D.S. and LEDERIS, K. (eds). Neurosecretion. Molecules, Cells, Systems. Pp.531. ISBN 0-306-40760-4. (Plenum: 1981.) Np.

FLETCHER, W.W. and KIRKWOOD, R.C. Herbicides and Plant Growth Regulators. Pp.400. ISBN 0-246-11266-2. (Granada, London: 1982.) £25.

FRAENKEL-CONRAT, H. and KIMBALL, P.C. Virology. Pp.406. ISBN 0-13-942144-0. (Prentice-Hall: 1982.) £24.70.

GANTEN, D., PRINTZ, M. *et al.* (eds). The Renin Angiotensin System in the Brain: A Model for the Synthesis of Peptides in the Brain. Experimental Brain Research Supplement 4. Pp.385. ISBN 3-540-1344-4/0-387-1344-4. (Springer-Verlag: 1982.) DM78.40, \$36.50.

GRIFFIN, D.R. (ed.). Animal Mind-Human Mind. Report of the Dahlem Workshop held March 22-27, 1981, Berlin. Life Sciences Research Report, Vol. 21. Pp.427. ISBN 3-540-11330-4/0-387-11330-4. (Springer-Verlag: 1982.) DM54, \$25.20.

GUDE, W.D., COSGROVE, G.E. and HIRSCH, G.P. Histological Atlas of the Laboratory Mouse. Pp.151. ISBN 0-306-40686-1. (Plenum: 1982.) Np.

LAJTHA, A. (ed.). Handbook of Neurochemistry, 2nd Edn. Vol. 1, Chemical and Cellular Architecture. Pp.496. ISBN 0-306-40861-9. (Plenum: 1982.) Np.

MARKHAM, K.R. Techniques of Flavonoid Identification. Pp.114. ISBN 0-12-472680-1. (Academic: 1982.) £9.40, \$19.50.

MAYER, A.M. and POLJAKOFF-MAYER, A. The Germination of Seeds, 3rd Edn. Pp.211. Hbk ISBN 0-08-028854-5; pbk ISBN 0-08-028853-7. (Pergamon: 1982.) Hbk np; pbk £9.50, \$19.

MÜLLER, E.E. and MACLEOD, R.M. (eds). Neuroendocrine Perspectives, Vol. 1. Pp.405. ISBN 0-444-80365-3. (Elsevier/North Holland: 1982.) \$99.50, Dfl.214.

NEWMAN, E.I. (ed.). The Plant Community as a Working Mechanism: Special Publication Number 1 of the British Ecological Society produced as a Tribute to A.S. Watt. Pp.128. ISBN 0-632-00839-3. (Blackwell Scientific: 1982.) £4.50.

O'RIORDAN, J.L.H., MALAN, P.G. and GOULD, R.P. (eds). Essentials of Endocrinology. Pp.230. ISBN 0-632-00643-9. (Blackwell Scientific: 1982.) £7.50.

ROBERTS, M.B.V. Biology: A Functional Approach, 3rd Edn. Pp.655. ISBN 0-17-448015-6. (Nelson: 1982.) £9.50.

RUSE, M. Darwinism Defended. A Guide to the Evolution Controversies. Pp.356. ISBN 0-201-06273-9. (Addison-Wesley: 1982.) £6.95.

RUSSELL, R.S., IGUE, K. and MEHTA, Y.R. (eds). The Soil/Root System in Relation to Brazilian Agriculture. Pp.372. No ISBN. (Fundação Instituto Agronômico do Paraná, Brazil: 1981.) Np.

SAFE DRINKING WATER COMMITTEE. Drinking Water and Health, Vol. 4. Pp.299. ISBN 0-309-03198-2. (National Academy Press: 1982.) \$15.95.

SAMUELSSON, B. and PAOLETTI, R. (eds). Leukotrienes and Other Lipooxygenase Products: Advances in Prostaglandin, Thromboxane, and Leukotriene Research Series, Vol. 9. Pp.384. ISBN 0-89004-741-3. (Raven: 1982.) \$59.84.

SAUNDERS, D.S. Insect Clocks, 2nd Edn. Pp.409. Hbk ISBN 0-08-028848-0; pbk ISBN 0-08-028847-2. (Pergamon: 1982.) Hbk £45, \$90; pbk £24, \$48.

SEARS, T.A. (ed.). Neuronal-Glial Cell Interrelationships. Report of the Dahlem Workshop held November 30-December 5, 1980, Berlin. Life Sciences Research Report, Vol. 20. Pp.375. ISBN 3-540-11329-0/0-387-11329-0. (Springer-Verlag: 1982.) DM48, \$22.40.

SEEBERG, E. and KLEPPE, K. (eds). Chromosome Damage and Repair. Pp.623. ISBN 0-306-40886-4. (Plenum: 1981.) Np.

TANZER, J.M. Animal Models in Cariology. (A Special Supplement to Microbiology Abstracts-Bacteriology). Proceedings of a Symposium and Workshop, Sturbridge, Massachusetts, April 1980. Pp.458. Pbk ISBN 0-917000-09-9. (Information Retrieval, Oxford: 1981.) Pbk \$25, £10.

TAVOLGA, W.N., POPPER, A.N. and FAY, R.R. (eds). Hearing and Sound Communication in Fishes. Proceedings in Life Sciences. Pp.608. ISBN 3-540-90590-1. (Springer-Verlag: 1981.) DM 118, \$55.

TER MEULEN, V., SIDDELL, S. and WEGE, H. (eds). Biochemistry and Biology of Coronaviruses. Advances in Experimental Medicine and Biology, Vol.142. Proceedings of an International Symposium held in October 1980 at the University of Würzburg, FRG. Pp.438. ISBN 0-306-40806-6. (Plenum: 1981.) \$52.50.

TURNER, P.D. Oil Palm Diseases and Disorders. Pp.280. ISBN 0-19-580468-6. (Oxford University Press: 1981.) £27.50.

VINNIKOV, Y.A. Evolution of Receptor Cells. Molecular Biology Biochemistry and Biophysics, Vol.34. Pp.142. ISBN 3-540-11083-6. (Springer-Verlag: 1982.) DM 88, \$41.

WHITTEN, T. The Gibbons of Siberut. Pp.207. ISBN 0-460-04476-1. (Dent, London: 1982.) £9.50.

YEOMAN, M.M. and TRUMAN, D.E.S. (eds). Differentiation *In Vitro*. The 4th Symposium of the British Society for Cell Biology. Pp.286. ISBN 0-521-23926-5. (Cambridge University Press: 1982.) £30.

23 September 1982

LIBRARY COMPLEX

 Departments of:
 Chemical Engineering
 Chemical Technology
 Physics & Rubber Technology

Nothing is even more expensive

The international Atomic Energy Agency (celebrating its 25th anniversary) has a tenable niche on nuclear power but it is not the only custodian of peace.

The outlook for the international nuclear power business seems to have improved a little at last week's meeting of the board of governors of the International Atomic Energy Agency (IAEA) at Vienna. That, at least, is what the public noises mean. For one thing, the authority has been able to spell out in its annual budget a prospectus for a much more meticulous procedure for accounting for fissile material ostensibly under international safeguards that might be used for making bombs. For another, in spite of the deteriorating economics of nuclear power enterprises in countries such as the United States, the economic outlook in countries such as West Germany is not nearly as parlous even with a change of government in the offing. And then the authority had the wit to put up Dr Sigvard Eklund, its director-general until last year, to make the keynote speech at its annual public meeting this week on experience with nuclear power and to echo the late Homi Bhabha in saying "No energy is more expensive than no energy". That message will be remembered.

At the same time, the recognition that countries differ enormously among themselves in their assessment of the importance of nuclear power will begin to sink in. With hindsight, it is entirely credible that, in the United States, the nuclear power industry should have been made uneconomic by the public protests (on the grounds of amenity and safety) of people who are broadly speaking assured of electricity supplies at reasonable cost from conventional fuel sources. In fuel-importing countries such as left-wing France, it is understandable that the balance should lie the other way — and that it should be exaggerated by M. Chevènement's enthusiasm for the future. It is more of a surprise that Mr Helmut Schmidt's chancellorship should have been brought to an end partly on the issue of nuclear power, when West Germany is more dependent on imported fuel than most other European countries except Denmark and Sweden.

The truth, of course, is that the nuclear issue in West Germany springs not from the federal republic's need of energy of some kind (on the grounds that no energy would cost more) but from Mr Schmidt's advocacy of President Carter's fleeting belief that there should be neutron bombs in West Germany. Paradoxically, Mr Schmidt's opponents on the nuclear issue, the wayward "Greens", may be more willing to toe the line when the Christian Democrats are in office. The conventional but cynical wisdom that it takes a left-wing government to accomplish right-wing goals (and the other way round) is undermined by the way in which the expectations of those who oppose the policies of their own governments diminish when their governments are replaced. In the end, what will matter is that the countries most in need of nuclear power (and able to afford it) will build nuclear power stations (and, given their need, will be able to do so cheaply); the others will wait.

The problem for the International Atomic Energy Agency that should occupy its new director, Mr Hans Blix, is therefore what has occupied him in his short tenure of his post — how to arrange that countries buying fissile material from others do not use it for making nuclear weapons or, by threatening to do so, disturb the peace. Outwardly, he must be seen to worry. But the nations most often canvassed as the leading members of the next nuclear generation, Israel for example, live so dangerously already that they are more likely to be constrained by conventional diplomacy than by anything a United Nations agency could accomplish

(witness this week's withdrawal from West Beirut). The trick, for the next year or so, must be to repeat the demonstration in the past year that international safeguards function effectively while showing that they are consistent with, for example, the reprocessing of spent fuel. Mr Blix appears to have the spirit even for that enterprise.

Health service sickness

The British government is heading for a row on nationalized medicine; it should reorganize.

The British National Health Service, variously regarded as a triumph of social engineering and as an embodiment of "socialized medicine", is in trouble. The underlying problems are financial. Since the creation of the health service in 1948, the assumption that the cost of medical care should be a charge on public funds has increasingly been challenged by the disappointing growth of the British economy and by the rapid increase (in real terms) of the cost of medical care, itself a measure of the advance of medical technology. The cost of the National Health Service, £14,500 million in 1982–83, is roughly six per cent of the Gross Domestic Product and has increased by some 5 per cent (in real terms) since 1979–80. While the total cost is less than the proportion of national income spent on health care in, for example, West Germany and the United States, successive British governments of all colours have been increasingly perplexed to know how to pay the bills wished on them three decades ago. Although they have differed in their generosity towards the National Health Service, they seem all to have agreed that the salaries paid to those working in it should be kept as low as possible. The consequences have now caught up with Mrs Thatcher's government.

After decades of parsimony, many health service workers are now paid much less than they would be paid in comparable jobs elsewhere. That trainee nurses earn less than they would be paid if they were unemployed is a relic of the days when nursing was considered a kind of extension of voluntary social work, but the nurses are no longer the genteel profession they once were, and have formally rejected, as would have a trades union, this year's offer of a 7.5 per cent salary increase. Those nurses belonging to the Royal College of Nurses (perhaps 60 per cent of all student and qualified nurses) were prevented by their charter from joining this week's one-day strike by other health service workers. The possibility that the self-denying ordinance may be removed from their charter is, however, a sign that gentility has gone for good. (The decision of the Trades Union Congress to urge that other trades unionists should strike in sympathy for at least an hour is, by contrast, more probably a sign of its eagerness to test the effectiveness of the legislation that makes secondary strikes illegal, and those engaging in them susceptible to civil actions by their employers.) So British governments must steel themselves for annual confrontations over health service pay, for there is no prospect of paying proper salaries to those most deprived while keeping the total cost of the National Health Service commensurate with the likely growth of the British economy. But such a state of affairs could not continue for long without damaging the capacity of the health services to care for the sick;

for those who work for the National Health Service for too little pay, but whose services are essential, will in due course choose to work elsewhere.

The dilemma is familiar, not only in the United Kingdom. Whether medical services are provided free by the state or by some combination of free market and medical insurance, the experience of the past several decades shows that total costs increase more quickly than most other economic indicators. This is only to be expected. The ageing populations of most countries inevitably make greater demands on medical services — but the ageing has itself been made possible by the diligent application of novel medical technology. The old dream of Mr Aneurin Bevan, the architect of the National Health Service, that a comprehensive (and free) health service would reduce the real cost of health care is plainly an illusion. Most probably, the real resources spent by prosperous societies will continue to grow in comparison with other kinds of expenditure (as on food, for example). It is not surprising that the present British government should already be casting round for other ways of financing health services than from direct taxation — and, politics being what they are, that this should have provoked fierce protests from its political opponents. How then should the government proceed?

The time has long since gone when the principle of the National Health Service — free medical care for all — was an ideological issue in the United Kingdom. The past three decades have shown that the mere existence of the National Health Service has been a civilizing and enlightening social influence in Britain. That indigent people and the chronically sick have been cared for well and sympathetically has had a powerfully beneficent influence on the temper of society. The British government, which has been flirting with the notion that medical costs should be to some extent met from insurance schemes, cannot now abandon the principle that medical treatment should be provided for children, the indigent, the chronically sick and the elderly and that, at least for the first three groups, that it should be free, with no questions asked. Once this is accepted, the choice between methods of financing — say from general revenue or health insurance — is logically unimportant. Thus if, as in West Germany, health insurance were compulsory, people with jobs would be unaffected — their insurance premiums would presumably be met out of the income tax they would save. The reality, of course, would be more complicated. Changing the system by which British health services are financed would replace one set of inequities by another, perhaps more burdensome. But changing the system would not of itself improve the quality of medical care.

The now bitter argument about nurses' pay is powerful evidence of that. The immediate complaint is that 7.5 per cent extra is all too modest. Many would agree that qualified nurses should be paid twice as much. The trouble is that such largesse is ruled out not merely by the straitened state of the public finances but also because the nurses' pay is linked with that of the substantial army of ancillary health service workers whose jobs might often just as well be done by private contractors or even by computers. The strongest argument for changing the financial basis of the service as a whole is that there would then be a natural opportunity for looking again at the necessity for this huge workforce — and probably for dispensing with a large part of it.

But why should not the managers of the National Health Service undertake that task off their own bat, without waiting for the financial basis of their operations to be changed? Because there are no managers. Most British nationalized industries are run by public corporations whose members can (in theory) be fired for incompetence. The National Health Service, by contrast, is technically the ultimate responsibility of the Secretary of State for Health and Social Security, who no doubt delegates day to day responsibility to his civil servants. The result is that even administrative issues are, by definition, political questions. If physicians seek a pay increase, or wish to change their terms of service, they must negotiate with identifiable parts of the Whitehall machine, staffed by different officials every few years. Titularly, the hospital service is the responsibility of regional health authorities, large committees consisting of representatives

of the great and the good (retired vice-chancellors are conspicuous) and of regional political interests with chairmen chosen for their neutrality rather than for their managerial skills. The consequence is that radical questions (such as whether the health services would be more efficient if hospitals were financially autonomous, with incomes somehow linked with the numbers of patients treated) can never be considered. In such circumstances, the wonder is not that the British health services are so inefficient (and so badly paid) but that they have survived at all. The present government is right to look for different ways of paying for the same job, but it must also find better ways of arranging that the whole system is properly administered — and not by itself.

Academies not international

How can the International Council of Scientific Unions make best use of the opportunities ahead?

The International Council of Scientific Unions is one of those organizations that would have to be invented if it did not exist but which, once invented, is almost incapable of doing the job its inventors planned. The logic goes like this. National scientific academies are in a particular sense representative of what is best in national scientific communities; they are not elected in a democratic sense, but they perpetuate themselves by electing their own members (who are usually their successors). When, and, if so, because the criteria for election involve intellectual attainment, the resulting national academies can be unexpectedly influential. Over the years, such undemocratic academies have demonstrated that their influence can extend beyond the interests of those who happen to be their members to the interests of the national scientific community at large. So is it not reasonable to expect that a consortium of such academies might exert its collective influence in the interests of the international scientific community, however defined? That is the argument from which ICSU springs.

The calculation is, of course, deficient. And the products of ICSU's work fall far short of what they would be if the calculation were correct, as last week's general assembly at Cambridge showed. That there should have been an argument of any kind about the terms on which the People's Republic of China should belong, and whether Taiwan should have to withdraw if membership were granted on politically unpalatable terms, is absurdly inconsistent with ICSU's ultimate objectives. Why not both? That (see page 292) is how it was decided. The vague form of words on which the compromise is based will not, however, serve as a model for deciding what to do when similar issues arise in more politically contentious international settings. (Chinese membership of most United Nations organizations now habitually takes precedence over that of Taiwan, but the question whether Israel should belong to the European or Middle Eastern section of the World Health Organization was a running sore even before the events of the past few weeks.) International organizations with more clout will debate these forms of words even more exhaustively than at Cambridge last week. ICSU's success on the Chinese question is a measure of its impotence.

ICSU should be worrying more than it does about that state of affairs. Uncontentious good sense (such as the proposal that short-lived radioactive isotopes should be free from import duty) will sweep all before them in due course, but governments (to judge only by the innocent Australian government's performance) are still some way from recognizing that ICSU should have a right to say who from overseas should attend the conferences its member unions sponsor. But is there a chance that ICSU might have more clout if it set about transforming its way of working so as to replicate the ways in which national academies function? For the past several decades, such questions have been overlain by ICSU's liking for paperwork (no doubt acquired by infection from UNESCO, its UN sponsor) and by its lack of funds. Has the time come to break that mould? And does the new leadership have the courage or even the inclination?

Pentagon blocks open exchange

Weinberger in optics meeting censorship

Washington

In the latest crackdown by the Reagan Administration on what it says is a dangerous flow of US scientific information to the Soviet Union, Secretary of Defense Caspar Weinberger last month authorized an eleventh-hour move that prevented approximately 100 scientific papers from being given at a San Diego meeting and caused confusion and even "panic", according to one account, when the meeting was held.

The 26th annual international technical symposium of the Society of Photo-Optical Instrumentation Engineers (SPIE) opened on 18 August on schedule, in spite of the fact that immediately before that, military officials had warned many participants that their papers were too sensitive to be given. The Pentagon had expected 28 Soviet scientists to attend, and it concluded, after checking with the armed services and on the basis of a memorandum to Mr Weinberger, that they represented "a major security problem or disaster". The authors were warned that many papers might not have had proper clearance from the Department of Defense, and about one-sixth of those who had planned to give papers voluntarily withdrew them.

The resulting confusion about clearance procedures led to worried engineers at the meeting badgering military officials to find out whether they would be in trouble if they delivered their papers. Most participants who had carried out their work on defence grants, contracts or subcontracts had cleared their papers through local contracting offices or military bases, in accordance with past procedure. They were apparently unaware of a new rule promulgated in April requiring papers that contain "technical data" of a sensitive nature to be cleared by the Pentagon.

The Pentagon learned of the contents of the meeting only by chance, when an official read a copy of the programme and showed it to Dr Stephen D. Bryen, Deputy Assistant Secretary of Defense for international economics, trade and security policy. "Even if you were a zoologist you would have found that program disturbing", says one military official. "They were going to describe the reconnaissance capabilities of the F-18 fighter and how to see a US guy through the army's obscurants." (Obscurants are smoke or gases used to hide troop movements.) "We didn't withdraw any papers", the official said. "We just warned people they might be in violation of the April rules."

According to the Department of Defense, the authority for the withholding of technical information — regardless of whether or not it should be classified — is the 1954 Arms Export Control Act, as a result of which the State Department issued the International Traffic in Arms Regulations (ITAR) which prohibit the export of certain kinds of equipment or of "technical data" about its use. In addition, the 1979 Export Administration Act calls for development of a list of strategically important technologies and goods that should not go to the Soviet Union.

SPIE is the principal professional group in a field with many military applications. SPIE officials were upset by what

happened at its meeting and by the resignation over the incident of some of its members. Richard Wollensack, a vice-president of the Itek Corporation and president of SPIE, spent three hours talking to defence officials last week. The society stressed its interest in avoiding future problems with the Department of Defense as well as in the continued freedom of its members to present papers at meetings. Military officials stressed that no blame attached to the society.

But the cure for the problem may be more drastic than the disease. The Department of Defense may form a committee of Pentagon officials to monitor more systematically material to be presented at

West German science after Schmidt

Heidelberg

What are the prospects for science and technology in West Germany if a Christian Democratic administration emerges in Bonn? As described in the party's document on research, *Technologische-politisches Konzept*, the strategy will be to restore the prestige and credibility of research and development in science and technology as keys to future prosperity.

Christian Lenzer, spokesman for the Christian Democratic Union/Christian Social Union (CDU/CSU) on research and technology, emphasizes the need for more basic research, but sponsorship and direction would continue within the existing self-administering framework of the Deutsches Forschungsgemeinschaft, the Max Planck Society, the foundations and large institutions.

In the areas of applied research and development, however, CDU/CSU would change the emphasis from direct to indirect support, thus returning to the pattern of the 1960s for which employers' organizations have been asking.

Industrial research would be primarily self-financed and government support would take the form of indirect financial incentives such as tax concessions (to be assessed by the tax authorities), quicker depreciation of research and development investments, provision of risk capital and tax allowances for patenting and licensing. CDU stresses the importance of free market forces, decentralization and reduction in state control in creating the right climate to encourage performance, risk-taking and entrepreneurial innovation. In particular, small and middle-sized businesses would receive preferential support.

Applied research in public institutions would focus on complex long-term research in transport, communications, aerospace and defence. A better balance would have to be found between the need to protect these areas from short-term political and economic influences and the con-

sequent dangers of bureaucracy and institutionalized decreases in effectiveness and creativity. In general, however, support would be for institutions rather than for projects, partly to reduce the administrative costs involved in assessment. Lenzer points out that the Ministry of Research and Technology employs more than 1,200 advisers at a cost of more than DM600 million. Many members of assessing committees come from large industries and have tended to channel funds away from smaller businesses.

With an eye to French competition, Heinz Riesenhuber, CDU/CSU spokesman on energy, stresses the role of nuclear power in the West German energy programme. CDU/CSU would be more aggressive in the application of proven techniques and development of reprocessing facilities. Highly critical of the ambivalence and delays of the Social Democratic Party (SPD), CDU/CSU would increase state participation in innovative developments such as the prototype reactors, in spite of soaring costs (see *Nature* 26 August, p.783).

In microelectronics, besides software and systems technologies, emphasis would be on widening the technological basis and development and production techniques for highly integrated elements and instruments in communications. CDU/CSU recognize the potential of biotechnology and promise increased state support for work in the field.

On environmental problems, stress is laid on the necessity for providing early anticipatory legal frameworks and also on the possibility of reconciling protection of the environment and economic growth by, for example, investment in energy saving technologies.

A deteriorating economic situation has resulted in no growth in gross national product in the first half of 1982, an increase in unemployment of 49 per cent over 1981 and hard times in the universities and elsewhere.

Sarah Tooze

scientific and technical meetings. The committee would not include outside academics. "We want to be sure that the US taxpayer benefits from this research and that the Soviet Union doesn't", says one official.

The academic community has been predictably alarmed by the incident. Officials of the Association of American Universities, the National Association of State Universities and Land Grant Colleges and the American Council on Education raised the matter at a meeting on 1 September

with Under-Secretary of State Richard D. De Lauer, the Pentagon's chief scientist. The Defense Science Board, which advises De Lauer, has made a series of studies on which scientific information should be withheld and has helped to compile the militarily critical technologies list, which is considered so sensitive that even the list of headings remains classified. Thus, so far, scientists and engineers have no idea what subjects the Department of Defense considers too sensitive for presentation in public.

Deborah Shapley

Keyworth on fusion

US seeks more foreign links

Washington

The Reagan Administration's alarm about the outflow of scientific information from the United States seems not to have interfered with its little-noticed plan to promote international cooperation in fusion. The architect of the policy is George A. Keyworth III, the presidential science adviser, who says that the next generation of fusion devices should be jointly agreed by the United States, the European Community and Japan, perhaps even jointly funded and operated by them.

Fusion advocates in Congress think the strategy too risky, citing the strains that might arise if construction of the \$1,000 million-dollar devices become subject to other strains among the allies. Another problem is whether the Administration would agree to the participation of the Soviet Union. The Soviet Union has an advanced fusion programme and a long history of cooperation with US fusion scientists. But President Reagan has been allowing bilateral science agreements with the Soviet Union to expire, and the agreement which covers fusion cooperation is due to end next March.

The White House's logic was explained recently by John Marcum, assistant director of Keyworth's office for energy and natural resources. "We are spending nearly half a billion dollars a year on fusion, which is the most challenging project man has ever undertaken including the Moon landing and the Manhattan project", says Marcum. "Yet we don't expect fusion to generate significant quantities of commercial electricity until the middle of the next century. Devices will cost in the billion dollar range and several different prototypes will have to be built before we find the one that is most practical.

"Let's face it, the United States, Japan and Europe can't afford independently to build their own tokamaks, stellarators and tandem mirror devices."

The JT-60 tokamak being built in Japan is now the most expensive fusion device under construction; it will cost an estimated \$1,000 million. The Joint European Torus (JET) that the European Community is building at Culham in the

United Kingdom will cost approximately \$500 million. The largest US device under construction is the TFTR at Princeton University, which will cost approximately \$300 million. Another device, the long-pulse length Torsupra being built by France, will also be expensive. Keyworth and others in the fusion community argue that by the time the next generation comes to be designed the costs will be too great for any single country to bear.

Keyworth has reportedly visited the most advanced example of US cooperation in fusion research, the US-Japanese Doublet III, built by the General Atomic Company in San Diego, California, and funded and operated on a 50:50 basis. The United States also participated with the EEC, Japan and the Soviet Union in an International Atomic Energy Agency design workshop known as INTOR (for International Tokamak Reactor).

As a result of the Versailles summit meeting in June, Keyworth has a chance to make his influence felt. He is the President's representative to the summit working group on cooperation in science and technology, and fusion is one area the group is studying.

The Department of Energy (DoE), which runs the US fusion programme, is following the Keyworth policy. Last week,

fusion programme officials met representatives of three foreign programmes in Washington: Donato Palumbo, the director of the EEC's fusion programme; S. Mori, a director of the Japanese Atomic Energy Research Institute; and R.S. Pease, programme director of the UK Atomic Energy Authority fusion programme. The purpose was to "look for areas of mutual technical interest" according to Mike Roberts of DoE. The foreign fusion officials also met officials of the White House, since they were in Battimore attending a world fusion conference.

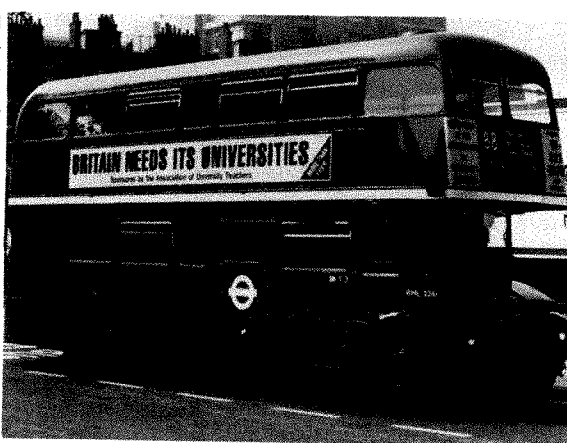
But Congresswoman Marilyn Lloyd Bouquard (Democrat, Tennessee), who hosted a workshop last week where international fusion scientists met congressmen and their staffs, is sceptical of Keyworth's enthusiasm for international cooperation on future devices. One of her staff pointed out that it took two years of negotiations to get US-Japanese agreement on the Rotating Target Neutron Source machine at Lawrence Livermore Laboratory. "If you don't want to spend money, it's nice to throw this idea out", he went on. "On the other hand, there's more to international cooperation than good intentions. When we have some friction with our allies over steel or the pipeline, its going to be tough to go on building billion dollar machines."

It is not yet clear whether the Soviet Union would be deliberately excluded from future planning to decide which country builds a stellarator, or a mirror, or a tokamak. Keyworth's office makes it clear that it wants to enhance cooperation in EEC and Japanese projects, rather than in the International Atomic Energy Agency's joint project which includes the Soviet Union. Although Keyworth has not said publicly that he would exclude the Soviet Union, the Administration's overall denial of advanced technology to that country would make such a policy likely. It remains to be seen what Keyworth's would-be partners in fusion cooperation think on the question of Soviet participation.

Deborah Shapley

University teachers take to the streets

Politicians in Britain are well aware that further cuts in spending on the universities will be met with indifference or approval from the majority of their constituents. That, at least, is the thinking behind a new advertising campaign launched by the Association of University Teachers (AUT) last week. To give added weight to the AUT's political lobbying the association is buying advertising space on buses on London's 88 route, which passes the AUT's headquarters and, as it happens, goes down Whitehall. AUT sees this as a beginning to the process of making the general public more aware of the value of the universities. Further exploits being considered include advertising on London's underground trains and spreading the bus campaign to provincial cities.



Clinch River fast breeder

Now the crunch

Washington

Opponents of the Clinch River Breeder Reactor project in the US Congress seem well placed this year to bring the project to an end. Ever since the Clinch River project began a decade ago, scarcely a year has passed without an attempt to kill it. President Carter tried, congressional committees have repeatedly tried and last year the House fell just 20 votes short — and the Senate just two votes short — of withdrawing funds.

This year congressional opponents are trying again and have put together an unusual alliance of liberals and conservatives that seems likely to prevail. The rallying point for this alliance is economics, an issue that the breeder's opponents believe has been strengthened by several developments:

- The breeder's competitiveness. A study by Los Alamos National Laboratory concluded last year that uranium would have to rise from its present price of about \$25 per pound to \$165 per pound before the breeder would break even. According to the Department of Energy (DoE), the price will have reached only half that break-even point by the year 2020.

- Cost overruns. Clinch River was initially supposed to cost \$400 million but the official projection now is \$3,570 million. In addition, all of the costs overruns are to be borne by the government, while industry's contribution is fixed at a maximum of \$257 million. Thus the project, which was supposed to be an industry-government partnership, is now government-supported to the tune of more than 90 per cent.

- Cheaper alternatives. The efficiency of conventional light-water reactors can be increased by 20 to 25 per cent through modifications to allow so-called "extended burn-up" of fuel. Breeder opponents say this is a far more cost-effective way to stretch existing supplies of uranium. Both Westinghouse and General Electric are already collaborating with Japanese firms on the design of these advanced reactors.

- Budget cuts and tax increases. Many members of Congress — including Republicans — are finding it difficult to justify expenditures on the breeder in the face of massive budget cuts in social programmes and the recent tax increase.

Among the most visible opponents this year are such staunchly conservative groups as the Heritage Foundation, which find the Reagan Administration's support for Clinch River inconsistent with its often-stated free-market policy. Even strongly pro-nuclear legislators are coming out against it; Senator Gordon Humphrey (Republican, New Hampshire) recently called it "nothing but a plutonium pork-barrel", a reference to the growing conviction that the Administration's support for

the project is a political favour to Senator Howard Baker, the Republican majority leader from Tennessee, in whose state the Clinch River site lies.

The showdown will come in Congress before 30 September, the end of the fiscal year. Any appropriations bills that are not passed by that date will be incorporated into what is known as a "continuing resolution", a stop-gap measure that continues spending at current levels. So far, not a single appropriating bill has been acted on; and it is thus very likely that the Clinch River appropriations will end up in such a continuing resolution.

That is exactly what Clinch River's supporters want. Continuing resolutions are usually not subject to amendment, but are presented to the Congress as a take-it-or-leave-it package. By incorporating appropriations for Clinch River into a bill that includes many vital appropriations, it is much more likely to go through.

Opponents, led by Representative Claudine Schneider (Republican, Rhode Island), have already anticipated that and are seeking a special rule that would allow a separate vote on the House floor on the \$252 million request for Clinch River. (The remaining \$500 million or so budgeted for the breeder programme is not at issue. Those funds are for research and for the Fast Flux Test Facility, a small experimental breeder at the Hanford Reservation in Washington state.)

Meanwhile, supporters of Clinch River suffered another blow recently when a federal district judge in Atlanta issued an injunction preventing initial site preparation for the project. The order had been sought by the Natural Resources Defense Council, an environmental group, which charged that the Environmental Protection Agency broke the law by allowing construction to begin without an environmental impact statement and a water permit. The DoE, which is managing the project, had been eager to start on the actual construction before Congress took up the matter.

Still, supporters maintain that it makes no sense to turn back now. According to the American Nuclear Energy Council (ANEC), an industry lobbying group, research and development on Clinch River is 96 per cent complete while 60 per cent of the plant's major components are either completed or on order. Industry is also threatening to demand a refund on the \$122 million it has already contributed should the project be terminated.

The supporters have also sought to make Clinch River a symbol of nuclear power and American technical superiority in general. Yet even nuclear "hawks" are far from enthusiastic about Clinch River. And the "keeping up with the Joneses" (in this case France) argument is piling beside the economics. France's Super Phénix breeder, says one Clinch River opponent, has become the "nuclear Concorde".

Stephen Budiansky

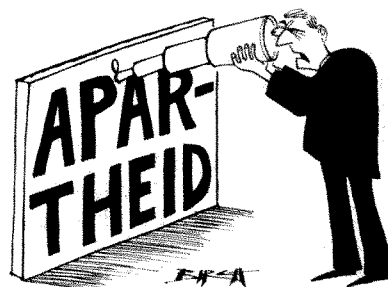
SERC in South Africa

British astronomers seeking to sever links with the South African Observatory near Sutherland, Cape Province, seized another opportunity to put their case at a symposium arranged by the Science and Engineering Research Council (SERC) two weeks ago. But the balance of opinion still seems to rest with those who claim that the link with South Africa is scientifically invaluable.

At the symposium, held at the University of Sussex and arranged to assess future commitments to the Anglo-Australian Telescope (AAT) and the South African Observatory (SAO), Dr Michael Rowan-Robinson of Queen Mary College, London, argued that if British astronomers did not face up to the moral and political problems occasioned by continued collaboration with SAO, they might find the decision taken out of their hands.

At present SERC is a major user of the observatory, buying 35 per cent of the total viewing time at an annual cost of about £240,000. SAO is a valuable

"I STILL CAN'T MAKE IT OUT..."



facility for British astronomers because of its geographical and climatic position; most of the work done there could not be reallocated to AAT.

The only feasible alternative facility for the optical and infrared photometry work largely done at SAO would be the European Southern Observatory in Chile. But, as Professor Michael Disney, one of the members of the SERC working party which has been examining the case of renewing the contract with the SAO, points out, this alternative may well prove more politically unsavoury to astronomers, as well as more expensive.

When the SERC working party questioned the groups likely to want to use SAO, however, it received only four objections on political grounds to its continued use, whereas 43 other groups wanted to carry on working there. So, in spite of the protests of Dr Rowan-Robinson and others who argued at the symposium in favour of abandoning SAO, it seems likely that the Astronomy, Space and Radio Board, when it meets in December, will make its decision primarily on the scientific merits of SAO.

David Millar

French budget

Science pluses

Paris

The French science budget really is on the up and up: FF32,500 million (£2,650 million) in 1983, 28 per cent more in 1982, according to figures released last week by the ministry of research and industry.

This figure, which includes all government civil research and development, must be corrected for inflation (now 12 per cent and optimistically projected to be 8 per cent next year). But even so the increase is impressive and seems even more remarkable when set against the present parlous state of the French economy, propped up last week by a \$4,000 million international loan, and against the average government budget increase for next year — a meagre 5 per cent in real terms.

How does Jean-Pierre Chevènement, the minister for research and industry, do it? From the left of the socialist party now in power, he appears to have formed a remarkable liaison with a man from the right, Jacques Delors, the finance minister, who is constantly urging budgetary restraint and the control of inflation. Both, it seems, are seized with a kind of constructive realism: they agree that France must renew and rebuild its wealth-generating industry, to which end science and technology are essential.

This is an economic objective, however, not a "scientific" one, and its implications run right through the 1983 budget. Moreover, Chevènement has stealthily adopted, without ever quite announcing it, a means of science funding akin to the British "Rothschild principle": the customer pays, and the contractor does what the customer wants, to the best of his ability. In France this is now called budget management "*par programme*".

The ministry identified seven major strategic areas, and four key technologies (called "*programmes mobilisateurs*" and "*programmes de développement technologique*", see below). The only difference from Rothschild's historic adjustment to the accounting of British research council cash in 1972 is that, in France, no precise figure has been set aside for the research councils to manage by themselves.

The seven *programme mobilisateurs* are:

- Rational use of energy and diversification of sources
- Biotechnology
- Development of the electronics industry
- Science and technology for the Third World
- Research on employment and work conditions.
- Promotion of French as a scientific language, and the spread of scientific culture
- The penetration of technology into industry

The four *programmes de développement technologique* are: Nuclear power; Space; Civil aeronautics; Oceans.

The whole sum, effectively, is in the hands of the customer — the ministry.

This shows up particularly clearly if the FF32,500 million civil research budget is divided into two parts: money directly controlled by the ministries or sent to industry, and money "processed" through the *grands organismes* (on which French university and *grands organismes* researchers can exert the greatest pressure). The first category is more applied, and more easily controlled politically; the second more basic, and less easily controlled.

The easily controlled category includes: FF1,500 million directly available to Chevènement for his own research priorities (up 29 per cent on this year); FF1,800 million for industrial research support (up 78 per cent); and FF7,200 million spent on research and development by other ministries under Chevènement's guidance (up to 65 per cent). Altogether, this category totals FF10,500 million in the 1983 budget, compared with only FF6,500 million in 1982: a rise of 62 per cent. The remainder of the budget, sullied — from the political point of view — by the inertia of the *grands organismes*, amounts to FF22,000 million, a rise of only 17 per cent on this year.

These global figures, however, conceal important differences in treatment among the different *grands organismes*. Here it is also important to distinguish between money credited — actually to be spent next year — and authorized, which equals the credits plus sums, usually for capital equipment, which can be committed but not spent. A third accounting category is "ordinary spending", essentially salaries. All the figures so far given apply to the authorized sums plus ordinary spending, as this is the best long-term indicator.

In the 1983 budget, the most dramatic differences are in the credits, which for the *grands organismes* rise 26 per cent over the last year to FF8,900 million. (The fact that authorizations rise only 16 per cent indicates perhaps that the ministry is taking care not to over-commit itself to basic research for 1984, should the French budget collapse entirely.)

Within these credits to the *grands organismes*, the Centre National de la Recherche Scientifique (CNRS), which does most basic research and has the greatest prestige, will see a 28 per cent rise in 1983 and — almost uniquely, a larger rise in authorizations: 36 per cent. CNRS will do well. INSERM, which supports medical research, gets a rise of 37 per cent in credits, but only 21 per cent in authorizations.

This year, Chevènement has been able to amass enough cash essentially to insulate basic scientists from the impact of technological priorities, which are appearing as additions to budgets rather than alterations. But whether this will be so next year (that is, in 1984) may depend on the performance of the French economy in the interim.

Robert Walgate

Council of scientific unions

Enter China

The admission of the People's Republic of China to the International Council of Scientific Unions (ICSU) was the highlight of this year's general conference, held last week in Cambridge, England. China will be represented by the China Association for Science and Technology (CAST).

During the past few years, science — a major casualty of the cultural revolution — has been considerably rehabilitated in China. The prestigious journal *Scientia Sinica* has resumed publication and the admission of China to ICSU was so little in doubt that a seven-person delegate from Beijing was already in Cambridge, waiting for two days while a suitable formula was worked out. The main problem was to ensure the admission of CAST without excluding the academy in Taipei (Taiwan), whose contribution to science has of recent year been considerably larger than the modest size of the population would suggest.

Apart from excitement over the Chinese issue, which some delegates felt had become too political, this ICSU conference, like its predecessors, consisted largely of reports on continuing activities rather than startling innovations. There were no real controversies, even on such sensitive subjects as the storage of high-level radioactive wastes on or near the Earth's surface; the main controversy was whether they should be so stored for 50 or 100 years. There was, however, general agreement that an ICSU-sponsored survey of nuclear war scenarios would be useful.

In the Committee on the Safeguarding of the Pursuit of Science, there were some sharp remarks on recent cases of Soviet Jews deprived of their academic degrees for political reasons. On the other hand, the case reported to the Committee for the Free Circulation of Scientists of the two Soviet scientists refused visas for an international conference in Australia in August was finally resolved, after an exchange of telexes, by a pledge from the Australians that no such difficulties would arise in the future for Soviet scientists wishing to attend multi-national conferences in Australia.

A number of routine matters were brought to a satisfactory conclusion. The Committee on Science and Technology in Developing Countries (COSTED) was reorganized to give it a wider orientation (recently it has concentrated almost entirely on India). A long-term plan by the Committee on Publications and Communications (COPAC) for the establishment of an ICSU press was accepted, and COPAC was authorized to proceed to the projected first phase of that plan — the discussion of ways and means with the presses of member national academies and the like, as well as with commercial presses where academies do not have their own press.

Vera Rich

Biotechnology

Insulin on tap

Insulin has become the first product of genetically manipulated bacteria to be marketed for human use. Now that Eli Lilly has official approval for sale in the United Kingdom of bacterially-produced human insulin, it will try to wrest from Novo Industry some of the £20 million annual market for insulin in the United Kingdom.

Approval has come one month after publication in *The Lancet* of a double-blind clinical trial involving five UK hospitals and 94 insulin-dependent diabetics. The trial demonstrated only slight differences between Lilly's new insulin, which has the exact structure of the human hormone, and conventional preparations purified from pig or cow pancreas. Probably because it is absorbed slightly more rapidly from the site of injection, rather more of the new insulin was needed to produce the same reduction of blood sugar. That slight disadvantage, however, is offset by corresponding advantages, according to Professor Harry Keen of Guy's Hospital Medical College in London.

The possible advantages are two-fold. First, the few diabetics who develop an allergy to animal insulins may not do so to human insulin. And second, the new insulin is slightly better than the old at hastening the removal of ketones from the bloodstream.

Availability and cost, therefore, will determine the choice of insulin in the market. On the basis of a 1978 report of the US National Diabetes Advisory Board, Eli Lilly believes that the demand for insulin will outstrip conventional supplies before the end of the century, mainly because of the likely increase in insulin-dependent diabetes.

As regards cost, Eli Lilly claims to be undercutting by about 10 per cent the cost of Novo Industry's "humanized" insulin. Novo, which dominates the European insulin market, recently perfected the trick of chemically converting purified pig insulin into human insulin. Its "humanized" insulin beat Lilly's human insulin to the marketplace when it received UK approval last June.

In an attempt to beat off the opposition from Lilly, Novo had contemplated withdrawing all its conventional animal insulins, thereby forcing a switch to its human version. If that had happened, one reason for not switching to the Lilly insulin — that it was human in structure — would have been removed before it arose. However, Novo's mooted switch would have meant an increase in price, and for that reason at least the idea was dropped.

Eli Lilly will now try to muscle in on the UK insulin market with its new product, having spent a great deal of money on softening up the medical consumers by

ostentatious image advertising in medical journals before approval was granted. It is less clear what will happen in the United States where Lilly has about 85 per cent of the market already. A spokesman for Lilly said he could not comment on the question of whether approval for its new insulin has yet been sought in the United States.

It has taken just four years for Lilly to scale up the process developed by Genentech for the production of human insulin from two bacterially-produced fragments. The bacteria are supplied with synthetic genes for either the A or the B fragment of insulin. After the two fragments are produced by the bacteria at Lilly's Indianapolis site they are chemically combined either there or at the site in Speke, near Liverpool. Final purification is carried out at Speke. **Peter Newmark**

Indian space effort

Falling flat

New Delhi

from a correspondent

India's grandiose scheme for satellite-based domestic communications and direct television broadcasts has received a jolt following the sudden demise of the INSAT-1A satellite. The \$60 million multi-purpose satellite, which had a design life of seven years, was abandoned on 5 September after only four months in space. The Indian Space Research Organization (ISRO), which was responsible for its operation, said the satellite had become useless because it had no more fuel left for on-orbit control.

Ever since its launch from Cape Canaveral on 10 April, INSAT-1A had been plagued by a series of problems. For several days, the INSAT control team at Hassan near Bangalore struggled with the jammed C-band antenna and a stuck solar sail. The antenna was deployed after much expenditure of fuel but the team had no luck with the solar sail, an umbrella-shaped device meant to offset the imbalance caused by INSAT-1A's asymmetrical solar panels. In the absence of the solar sail, on-board thrusters were fired more frequently to keep the satellite balanced, so depleting the fuel. ISRO estimated in mid-June that the fuel would last until the middle of 1984, but this calculation was upset by yet another problem detected early in September. The isolation valve in the fuel manifold got stuck and the fuel simply vented into space, leaving ISRO with no alternative but to abandon the satellite.

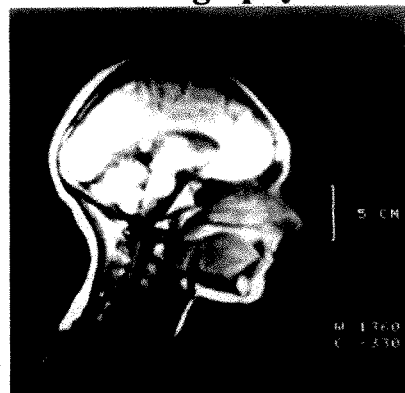
The satellite had been partly operational since 15 June from its geostationary parking slot at 74°E, although its capacity was largely under-utilized because of problems on board the spacecraft and non-readiness of the ground segment. INSAT-1A was used to provide 200 long-distance telephone circuits (against its capacity of 4,000) and television relaying was restricted to four hours a day because of overheating

of the television transponder on board.

The loss of INSAT-1A has placed the Indian government in a difficult position. Apart from the monetary loss (part of which is covered by insurance) the country faces the prospect of keeping idle the 31 Earth stations set up at a cost of more than \$60 million. The enormous preparations for live television broadcasts of the Asian Games scheduled for November have also been jeopardized by the failure of INSAT-1A. While the radio and television networking should await the launching of INSAT-1B, the impact on the Indian Meteorological Department is minimal as it continues to get cloud pictures and cyclone warnings from the United States weather satellites.

To restore a semblance of domestic communications and to lessen the impact of INSAT-1A's failure on the Asian Games coverage, India is planning to lease two transponders of Intelsat's Indian Ocean satellite at a cost of about \$16 million a year.

NMR tomography



One of the latest images produced by the rapidly developing technique of nuclear magnetic resonance (NMR) tomography. This image was obtained in the Erlangen Laboratories of the German company Siemens AG, which hopes to market a machine for hospital use early next year, some months after the first machines are expected to be sold by Picker International. The images reflect the precessing movement and dipole characteristics of protons subjected to a high frequency magnetic field. The relaxation time of protons so affected depends upon their environment. Different environments are imaged as different shades of grey. Because it detects protons, NMR tomography provides a different picture from that of the X-ray tomography used in current brain and body scanners. Furthermore, there are no known hazards of magnetic fields to rival those of X-rays. On the other hand, the resolution of NMR tomography is inherently less good than that of the X-ray scanners (and it will wipe out credit cards — including those of potential customers with about £0.5 million to spare).

CORRESPONDENCE

Piltdown jaw confirmed as orang

SIR — When the specimens from Piltdown were "discovered" in 1912, the combination of the human skull with an ape-like jaw caused immediate controversy^{1,2}. Smith Woodward, G.E. Smith, A. Keith and others accepted the association, but G. Miller (1915) thought that the jaw represented a new species of chimpanzee, *Pan vetus*³. Hooton accepted the association but described the jaw as "almost indistinguishable from that of a young

the canine tooth into the gravel pit must have known that the jaw was also that of an orangutan.

The positive identification of the Piltdown jaw and tooth as orangutan, after 70 years of often acrimonious debate, is of more than academic interest. Although the Piltdown "fossil" was a forgery, many primate fossils have been broken and largely destroyed by natural causes. The relations of human beings

this phenomenon before, even when the house was struck, as it was on several occasions. We therefore continued with our practice of leaving all the windows open. But during the same rainy season the same thing happened again with the same startling effect. After that we always kept the windows on one side of the room closed and we never experienced the phenomenon again.

J.D. GILLET

London School of Hygiene and Tropical Medicine, London WC1, UK

Collagen reactions: Piltdown jaw and canine

	Human	C. chimp	P. chimp	Orang	Rhesus	Elephant	Bovine
Jaw	0.61	0.56	0.76	1	0.35	0.01	0.04
Canine	0.66	0.62	0.42	1	0.34	0.02	0.04

The numbers represent relative binding of antisera to various collagen species by extracts of Piltdown jaw and canine. Maximum binding is taken to be 1. Antiserum to orang collagen is more strongly bound by the Piltdown extracts than antisera to any of the other collagens. The pattern of cross-reactions is also characteristic for orangutan collagen.

chimpanzee". There were doubters, however, and Weidenreich (1946) believed that the jaw did not belong with the skull and that it was the jaw of a fossil orangutan⁴. Weidenreich spoke of *Eoanthropus* as the result of reconstruction by "English authors". Clearly, distinguished scholars could make the facts fit any of the suggested theories. In retrospect, it is surprising that the fragmentary mandible could be diagnosed at all.

Overconfidence in comparative anatomy led prominent scientists astray. Weiner (1955) describes the story of the discovery of the forgery¹. It was chemistry, not anatomy, which led to the proof that the jaw and skull did not belong together⁵. Weiner¹ makes a strong case that the jaw and canine tooth are those of an orangutan, but he must resort to comparisons of the same kind that led Keith, Hooton and many others to conclude that they were like those of a chimpanzee. We report here the results of a collagen radioimmunoassay which proves that both the Piltdown jaw and the canine tooth are those of an orangutan.

Collagen radioimmunoassay¹ permits identification of species-specific proteins in very small samples of tissue. The method has been used to investigate the relations of fossil to living species^{6,7}. Collagen identification was performed using 50 mg of bone from the Piltdown jaw and 0.9 mg from the canine tooth. Antisera to orangutan collagen were bound by extracts from the jaw and tooth more strongly than antisera to the collagens of man (*Homo sapiens*), common chimpanzee (*Pan troglodytes*), pygmy chimpanzee (*Pan paniscus*), rhesus monkey (*Macaca mulatta*), Indian elephant (*Elephas maximus*) or cow (*Bos taurus*), as shown in the table.

These results confirm that the jaw is that of an orangutan and that it did not belong with the human skull. The canine tooth was found a year after the jaw, and it has been suggested that it was introduced into the gravel by a second forger. But at the time of the "discoveries", everyone was stressing the chimpanzee-like characteristics of the jaw. It was more than 15 years before the similarities with the orangutan were noticed. Unless one assumes, as Matthews⁸ does, coincidental use of orangutan material by two different forgers, it would seem likely that whoever put

to other primates are still debated, and neither anatomy nor currently available fossils are likely to settle the problem of "man's place in Nature". Whenever possible, such problems should be settled, or at least bounded, by the findings of molecular biology.

JEROLD M. LOWENSTEIN

Department of Medicine,
University of California,
San Francisco, California, USA

THEYA MOLLESON

British Museum (Natural History),
London SW7, UK

SHERWOOD L. WASHBURN

Department of Anthropology,
University of California,
Berkeley, California, USA

1. Weiner, J.S. *The Piltdown Forgery* (Oxford University Press, 1955).
2. Reader, J. *Missing Links* (Little Brown, Boston, 1981).
3. Miller, G.S. *Smithsonian misc. Collns* **65**, 1-31 (1915).
4. Weidenreich, F. *Apes, Giants and Man* (University of Chicago Press, 1946).
5. Weiner, J.S., Oakley, K.P. & Le Gros Clark, W.E. *Bull. Br. Mus. nat. Hist.* **A2**, 141-146 (1953).
6. Lowenstein, J.M. *Phil. Trans. R. Soc.* **B292**, 143-149 (1981).
7. Lowenstein, J.M., Sarich, V.M. & Richardson B.J. *Nature* **291**, 409-411 (1981).
8. Matthews, L.H. *New Scientist*, **90-91** (series of 10 articles on Piltdown; 30 April-2 July 1981).

Ball of fire

SIR — I was interested to read Professor Pippard's letter on his experience with lightning (*Nature* 19 August, p.702). Thunderstorms are frequent in the Entebbe Peninsula, Lake Victoria (Uganda). During one of these storms, which usually come at night time, there was a simultaneous flash of lightning and its associated clattering crash of thunder. A second or less later, several balls of brilliant blue light, about 4-6 cm diameter, entered the room through a window on the south side and "floated" across the room to leave by a window on the east side. My wife and I were already awake (it would have been difficult not to be) and independently exclaimed aloud on what we had just seen.

The incident occurred during the pre-independence period of Uganda and so there was no air conditioning. We therefore left all the windows open at night, protected only by the anti-mosquito metal screening. During many hundreds of storms we had never seen

Monstrous outrage

SIR — Since it appears to be the season for arguing about names, permit us to point out that Jeremy Greenwood¹ does not really appear to have a valid case for complaint under the International Rules for Zoological Nomenclature when a contributor to *Science*² uses the name *Prion*, otherwise applied to a group of birds, to Proteinaceous Infective Particles, since these can clearly only be classified as animals when they appear in them as inclusions. *Nature* itself has in fact committed a much more serious nomenclatorial offence in the past by publishing a new name *Nessiteras rhombopterix* for the Loch Ness monster⁴, when *Nessum monstrosum* had at least 40 years' priority⁴, unless, as Gregory's pictures suggest⁴, there is more than one type of monster in the loch. In the present case would it not be simpler just to call the particles "pips", or would this lead to further complaints from botanists?

W. R. BOURNE

Department of Zoology,
University of Aberdeen

S. HOWE

BP Petroleum Development Ltd,
Aberdeen, UK

1. Greenwood, J.J.D. *Nature* **298**, 510 (1982).
2. Prusiner, S.B. *Science* **216**, 136 (1982).
3. Scott, P. & Rines, R. *Nature* **258**, 466-468 (1975).
4. Gregory, W.K. *Nat. Hist.* **89**, 130-131 (1980, reprinted from 1934).

Which war?

SIR — There is a minor error in your editorial "Rules for limited war" (*Nature* 27 May, p.253). Surely you mean that it was the 1967 "six day war" and not the 1973 "Yom Kippur war" in which the Israelis took the Sinai Desert. The Yom Kippur war was the one in which the Israelis, already in possession of the Sinai, were the victims of a surprise attack that resulted in no real net gain of territory for anyone. Nonetheless, thank you for a timely and interesting editorial.

BERT ATSMIA

Montclair, New Jersey, USA

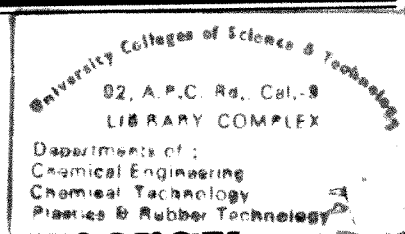
French Nobels

SIR — In the article "Language of love" (more like *The Sun* than *Nature*, but let it pass) in *Nature* of 26 August (p.780) you describe Alfred Kastler as "France's sole Nobel physicist". May I remind you that Louis de Broglie, the discoverer of wave mechanics and 1929 Nobel Laureate is still with us and that Louis Néel got the Nobel in 1970 for his discovery of antiferromagnetism.

ANATOLE ABRAGAM

Collège de France, Gif-sur-Yvette, France

NEWS AND VIEWS



Proton decays and high-energy speculation

from Louis Lyons

A HIGHLIGHT of the recent International Conference on High Energy Physics* was the suggestion that catalysed decay of protons might occur. It has long been realized that protons must be extremely stable. As Maurice Goldhaber has said: "You can feel it in your bones that protons do not decay"; for, if their lifetime was shorter than 10^{17} years, the damage to bones would be serious. Recent grand unified theories (which unite the weak force responsible for β decay with the strong one which confines quarks within protons) suggest, however, that protons could decay with a lifetime of around 10^{31} years. Such a value would give a reasonable chance of the decay of just one proton in a human being in a lifetime. Experiments looking for proton decays, necessarily involving hundreds of tons of material situated deep underground, are currently being run.

The new suggestion, originally put forward by V. Rubakov (Institute for Nuclear Research, Moscow) and independently developed by C. Callan (Princeton University) is that, if magnetic monopoles exist, they could, in their passage through matter, fairly readily stimulate proton decays. Grand unified theories do suggest that magnetic monopoles exist, although the number near the Earth and at this stage of the Universe's development is unknown.

In passing through a large detector, a monopole could produce a string of proton decays, separated from each other by perhaps tens of centimetres. Such a sequence of events correlated in time to within a few microseconds would be a very characteristic experimental signature, and has provided an extra motivation for the proton decay experiments. It has also led to the somewhat tongue-in-cheek suggestion that if only such monopoles could be collected, the ensuing catalysed proton decays may provide a source of energy.

Such exciting chains of decays have not yet been observed. Present experiments

merely set limits on the product of the flux of monopoles times the probability of their catalysing proton decay. The observation of decays would be a major development, shedding light both on the existence of monopoles and on the instability of the proton.

Meanwhile, experiments are accumulating events which could contain examples of the ordinary decay of the proton. The main difficulty is that the expected decay rate is so low that all sorts of background effects can be confused with genuine decays. An experiment at the Kolar Goldfield in India has three candidates, while another inside Mont Blanc has one. More data and further studies of backgrounds are now required. If the results are confirmed, it would open a whole new field for experimental study, and would be a major success for the grand unified theories which predicted the decays.

Four groups working at the new $\bar{p}p$ collider reported their results at the conference. The supersynchrotron (SPS) at CERN in Geneva is used to accelerate simultaneously protons and antiprotons circulating in opposite directions around the machine. When both particles reach 270 GeV, they are brought into head-on collision, resulting in interactions at the highest artificially produced energies. Because of relativistic effects, head-on collisions are very much more effective than those of a single beam with a stationary target. With the extra energy available, hitherto unobserved phenomena could take place. Until now, however, the low intensity of the beams has resulted in only a few thousand interactions being observed, so that only the gross features of the reactions have been studied. Thus, although the heavy W and Z bosons responsible for transmitting the weak interactions (in much the same way as the photon transmits electromagnetic phenomena) can be produced in $\bar{p}p$ reactions, they have yet to be observed.

Although free quarks have not been produced in experiments at accelerators (and perhaps have not been seen elsewhere — see L. Lyons *Nature* 291, 534; 1982), the

existence of quarks has a readily apparent effect on many types of high-energy reactions. Thus, in electron-positron annihilations, the various types of quarks contribute once the beam energies are high enough. Data presented at the conference provided new information concerning the properties of the bottom quark (*b*), especially concerning its decays to lighter quarks. Searches for evidence of the expected top quark (*t*) have still been unfruitful.

High-mass particles usually decay faster than light ones, so techniques for detecting tracks corresponding to such particles and for measuring their lifetimes need continual improvement. Whereas the weakly decaying strange particles have lifetimes down to 10^{-10} seconds, the heavier charmed particles live for less than 10^{-12} seconds. This corresponds to a distance of 2 mm for a charmed particle travelling at 99 per cent of the speed of light. The lifetime of the τ particle, the heavier version of the electron and the muon, is also in the latter range. The conference saw a series of measurements of these lifetimes, which now begin to look reliable, with the systematic effects better controlled. An interesting question for the future is whether the lifetimes of particles incorporating the *b* quark will be similarly amenable to direct measurement, after further improvements in the techniques.

Another impressive result came from the measurements of the forward-backward asymmetries in the reactions $e^+e^- \rightarrow e^+e^-$, $\mu^+\mu^-$ and $\tau^+\tau^-$ at high energies. The main contribution to these processes comes from a virtual-photon intermediate state, which on its own would result in a symmetric angular distribution. However, its interference with virtual weak boson Z^0 results in an expected asymmetry, whose magnitude is consistent with observations. This, together with the observation of parity violation in an atomic physics experiment, provides further confirmation

*The XII International Conference on High Energy Physics was held in Paris, in July 1982. Some 1,200 theorists and experimenters from 45 countries gathered to hear over 100 talks.

Louis Lyons is in the Nuclear Physics Laboratory, University of Oxford, Keble Road, Oxford OX1 3RM.

of Weinberg and Salam's model of electromagnetic and weak interactions.

As usual, theoretical speculation abounded. One relatively new approach is the idea of supersymmetry, relating $\frac{1}{2}$ -integer spin fermions and integer spin bosons. Experiments are already setting limits on the possible existence of the new objects which are expected in such models, although in most cases these are, as yet, not particularly stringent. Another series of models deals with the possible non-elementary nature of quarks and leptons (see L. Lyons *Nature* 298, 601; 1982).

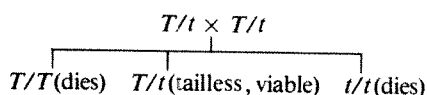
By and large the rest of the conference was devoted to clarification of experimental issues. Each on its own may seem, at the time, not particularly significant, but the increase in our appreciation (if not understanding) of elementary particle phenomena from one conference to the next is impressive. Certainly the prospects of new results to come from the proton decay experiments and from the $\bar{p}p$ collider make it look as if the next couple of years could bring excitement and surprises in an already fast-moving field. □

Analysing the mouse *T/t* complex

from P.W. Andrews and P.N. Goodfellow

RECENT experiments, reported by Artzt and colleagues in *Cell*^{1,2}, show that progress is being made in the detailed genetic analysis of the organization of the mouse *T/t* gene complex. Ever since the dominant mutation *Brachyury*, or *T*, was first described³ in 1927, the *T/t* complex has been a puzzle for geneticists and developmental biologists. The *T* mutation, located on chromosome 17, about 15 cM from the *H-2* region, is of itself unremarkable: it behaves as a single mutation that obeys the laws of Mendel, producing a shortened tail in heterozygotes and causing death of homozygotes after about 10 days of embryonic development. It is when *T* mutants are outcrossed to laboratory and wild mice that the strange properties of the mutation become apparent.

With a surprising frequency many such crosses yield offspring that completely lack a tail, and when intercrossed breed true, producing only tailless offspring⁴. The tailless condition is caused by interaction of *T* with a *t* haplotype; each *t* haplotype consists of a series of chromosome 17-linked genetic alterations which are responsible for a bizarre range of phenotypes. The *t* haplotypes isolated from wild mice carry recessive lethal mutations which complement the lethal effect of *T* so that intercrossing *T/t* (tailless) heterozygotes constitutes a balanced lethal system⁵:



Many such *t* haplotypes have been isolated and their lethal factors have been found to fall into several different complementation groups, each of which causes death at a particular stage of embryonic development^{6,7}. A number of other peculiar genetic traits are often exhibited by the *t* haplotypes, including segregation distortion in males but not females (*t/+* heterozygous males often transmit the *t* and '+' chromosomes in non-mendelian proportions), sterility in males but not

females doubly heterozygous for two complementing *t* haplotypes, and suppression of crossing-over in the interval between the centromere and *H-2* on chromosome 17 (see refs 8–10 for general reviews of the *T/t* complex). This suppression of recombination is of particular practical significance for it has made the genetic dissection of the *T/t* gene complex extremely difficult.

Over the years, various proposals have been made to explain the properties of the *T* locus. Gluecksohn-Waelsch and Erickson^{8,11} suggested, by analogy with *H-2*, that genes of the *T/t* complex control the expression of cell-surface molecules that are important in mediating cellular interaction, in embryonic development and perhaps also during spermiogenesis and fertilization. Bennett and her colleagues have presented data indicating that the *T/t* complex does control the expression of cell-surface molecules on sperm and early embryos^{12–14}, possibly through the activity of glycosyl transferases¹⁵. However, others have failed to detect such specific antigens on sperm¹⁶ and data indicating that at least some of the *T/t* gene complex effects are associated with metabolic disturbances have been reported^{17,18}. An alternative view of the *T/t* complex is that it consists of a random selection of lethal mutations maintained in the population because of their association with a gene causing segregation distortion.

Despite suppression of crossing-over by *t* haplotypes, the occasional recombinant does occur in the *T* region when a *t* haplotype is present (about 0.2 per cent compared with about 7 per cent recombination between *T* and the coat morphology marker *tf* in the absence of a *t*-haplotype). Lyon and her colleagues used this phenomenon to study the genetic organization of

the *t*-haplotype *t*⁶ (refs 19–23). They isolated reciprocal recombinants and showed that the factor which interacts with *T* to produce the tailless condition (*t*⁶) is separable from the factor(s) which causes embryonic death (*L*) and male sterility (*S*). The factors causing segregation distortion were more difficult to analyse but seemed to result from the interaction of several different factors mapping to the regions carrying *t*⁶, *L* and *S*. Another factor, segregation distorter *A*, mapping separately from these was also detected.

A similar conclusion was reached by Styrna and Klein²⁴ who also noted a striking parallel with the genetics of transmission distortion and male sterility seen in the segregation distorter (*SD*) system of *Drosophila melanogaster*²⁵. In *Drosophila*, segregation distortion results from the interaction of two closely linked loci, *Rsp* and *Sd*, with effects on segregation and male fertility²⁶, that are very similar to those of the *t*-haplotype *A* and *S* factors. Many other parallels between the *T/t* complex and *SD* have been noted²⁷ and it is perhaps not a very big leap of imagination, given that the spermiogenesis must have originated early in phylogeny, to suppose that fundamental aspects of this process may be highly conserved and subject to similar genetic aberrations in such widely different species as *Drosophila* and mice.

A notable new advance in the analysis of the *T/t* complex was made a year ago with the report by Silver and Artzt that much higher levels of recombination occur between two complementary *t*-haplotypes than between a *t*-chromosome and a normal chromosome²⁸. This supports the idea, originally suggested by Lyon²⁹, that recombination suppression results from mismatching of *t*-haplotype and normal chromatin. Since all *t*-haplotypes are thought to have evolved from a common ancestor, the cause of such mismatching would be common to all *t*-haplotypes. Matching and recombination can occur between two *t*-chromosomes but not between a *t*-chromosome and a normal chromosome. This report opened the way for much more detailed genetic analyses of the *T/t* complex than had previously been possible.

Artzt and her colleagues have now studied recombination between four *t*-haplotypes, *t*^{w12}, *t*^{w32}, *t*^{w5} and *t*^{w18}. In the first of two articles¹, they provide evidence that the lethal factors of these *t*-haplotypes map to quite different positions and hence are not allelic. They also found in one case, *t*^{w32}, that embryonic lethality may be due not to one but to two interacting mutations at two different but closely linked loci.

One unexpected observation was the higher than normal recombination seen between *T* and *tf*. For example, between a *T tf t*^{w12} chromosome and *t*^{w5} or *t*^{w32} chromosome, 15 per cent recombination in the *T-tf* interval was recorded, compared with 10 per cent in the normal case (only

P.W. Andrews is in the Wistar Institute, Philadelphia, Pennsylvania 19104 and P.N. Goodfellow in the Imperial Cancer Research Fund Laboratories, Lincoln's Inn Fields, London WC2A 3PX.

females studied). In combination with t^{w18} , less recombination was measured (8.1 per cent) but this was interpreted in terms of a shorter region of t -chromatin in this t -haplotype — as suggested by the fact that recombination between tf and the t^{w18} lethal factor is not normally suppressed when t^{w18} is in *trans* to a normal chromosome 17. These abnormal recombination frequencies need to be viewed in the light of evidence for abnormal location of genetic loci in the t -haplotypes. The authors recall the suggestion that the locus, *Tcp1*, coding for the p63 protein, which is defined by two-dimensional gel electrophoresis, is differently located in t -haplotypes and the normal chromosome 17 (ref. 30). Furthermore, in their second article², they report evidence that the H -2 region in t -haplotypes is located between T and tf (about 6 centiMorgans proximal to tf) compared with its usual location about 10–15cM distal to tf . The simplest explanation for this finding would be a chromosomal inversion in the t -haplotypes. In the *SD* system of *Drosophila*, suppression of recombination is known to be associated with inversions. However, as yet, no karyologically detectable inversions associated with t -bearing chromosomes have been found. Thus the authors suggest a chromosomal transposition; unfortunately the haplotypes so far studied are deficient in polymorphic variants of other loci, the study of which could help to clarify this problem.

Despite the early progress made by Lyon and her colleagues the suppression of recombination associated with the t -haplotypes bedevilled attempts to make a detailed dissection of the pleiotropic effects of these mutant chromosomes into their component parts. The new finding that high-frequency recombination may be obtained between different t -haplotypes should now permit the isolation, in congenic stocks, of the various mutant loci of the t -haplotypes. These will become important tools in analysing how the different effects of the T/t complex on segregation, infertility and embryonic death

come about, and whether any of these have common genetic causes. For example, coupled with the development of monoclonal antibodies they should allow a clear analysis of whether any of the effects are mediated by specific cell-surface molecules.

The results also suggest new ways for investigating the genetic organization of the t -haplotypes. For example, the finding that the H -2 locus lies close to the lethal factors for t^{w5} , t^{w18} and t^{w32} means that cloning of these genes using cosmids and 'walking' from the H -2 region is a feasible proposition. □

In search of the Hubble parameter

from Sidney van den Bergh

New techniques of determining the distances of galaxies, and recent results using some of the more traditional methods of distance determination have, as de Vaucouleurs points out in this issue of *Nature* (p303), resulted in discordant estimates of the Hubble parameter. These apparent discrepancies are important because the global Hubble parameter is a measure of the scale-size and hence the age of the Universe.

Efforts to calibrate the extra-galactic distance scale have proceeded along two parallel tracks. One class of methods employs objects of known luminosity within galaxies, such as Cepheids, novae and the brightest red giants, as standard candles. A second more robust approach uses the galaxies themselves as luminosity indicators. Baum¹ first showed that the colours and luminosities of elliptical galaxies were correlated and subsequently van den Bergh^{2,3} devised a system of luminosity classification for spirals. Both methods suffer from the relatively low precision with which the luminosities of individual galaxies can be determined and further uncertainties in the extent to which environmental factors, such as membership in clusters, might affect the colours of ellipticals or the morphology of spirals. A particularly exciting new technique for the distance determination of spiral galaxies stems from the recent discovery by Tully and Fisher⁴ that the luminosity of a spiral is highly correlated

with its 21-cm line width. The correlation between velocity dispersion and luminosity of ellipticals also promises to provide distances for early-type galaxies.

The nature of the controversy that has arisen from these new measurements is perhaps best illustrated by comparing the results of three of the best-known recent determinations of the Hubble parameter.

De Vaucouleurs^{6,7} used traditional distance indicators such as Cepheids, RR Lyrae stars and novae to calibrate the 21-cm line width versus blue luminosity relation for galaxies. Aaronson, Mould and Huchra⁸⁻¹⁰ used the nearby Local Group galaxies M 31 and M 33, which have very well-determined distances, to calibrate the 21-cm line width versus infrared luminosity relation for spirals. Finally, Sandage and Tammann¹¹ used the luminosity of the brightest red supergiants (calibrated using Cepheids) to determine the maximum luminosity of type I supernovae. The apparent brightnesses of SN I then allowed them to find the distances to galaxies in and beyond the Virgo Cluster. The results obtained by these three techniques are compared in Table 1.

The distances for the relatively nearby M

Sidney van den Bergh is the Director of the Dominion Astrophysical Observatory, 5071 West Saanich Road, Victoria, BC V8X 4M6, Canada.

Table 1 Comparison of Hubble parameters and distances

Distance to:	Aaronson, Mould & Huchra ⁸⁻¹⁰	De Vaucouleurs ^{6,7}	Sandage & Tammann ¹¹
NGC2403/M81 group	3.6 ± 0.3 Mpc	3.2 Mpc	3.25 Mpc
M 101 group	6.8 ± 1.0 Mpc	5.0 Mpc	6.9 Mpc
Virgo Cluster	15.7 ± 0.6 Mpc	15.0 ± 0.6 Mpc	21.7 ± 3.1 Mpc
H_0 (local)	62 ± 4 km s ⁻¹ Mpc ⁻¹	64 km s ⁻¹ Mpc ⁻¹	45 ± 7 km s ⁻¹ Mpc ⁻¹
H_0 (global)	95 ± 4 km s ⁻¹ Mpc ⁻¹	95 km s ⁻¹ Mpc ⁻¹	50 ± 7 km s ⁻¹ Mpc ⁻¹
Infall velocity	509 ± 99 km s ⁻¹	250 km s ⁻¹	118 ± 223 km s ⁻¹

- Artzt, K., McCormick, P. & Benoit, D. *Cell* 28, 463–470 (1982).
- Artzt, K., Shin, H.-S. & Bennett, D. *Cell* 28, 471–476 (1982).
- Dobrovolskaia-Zawadskaia, N. *Cr. Séanc. Soc. Biol.* 97, 114–119 (1972).
- Dobrovolskaia-Zawadskaia, N. & Kobozieff, N. *Cr. Séanc. Soc. Biol.* 110, 728–784 (1932).
- Chesley, P. & Dunn, L.C. *Genetics* 21, 525–526 (1936).
- Bennett, D. *Science* 144, 263–267 (1964).
- Guenet, J.-L., Condamine, H., Gaillard, J. & Jacob, F. *Genet. Res.* 36, 211–217 (1980).
- Gluecksohn-Waelsch, S. & Erickson, R.P. *Curr. Topics dev. Biol.* 5, 281–316 (1970).
- Bennett, D. *Cell* 6, 441–454 (1975).
- Sherman, M.I. & Wudl, L.R. in *Concepts in Mammalian Embryogenesis* (ed. Sherman, M.I.) 136–234 (MIT Press, 1977).
- Gluecksohn-Waelsch, S. & Erickson, R.P. *Proc. Symp. Immunogenet. of the H-2 System*, Liblice-Prague, 120–122 (1970).
- Yanagisawa, K., Bennett, D., Boyce, E.A., Dunn, L.C. & Dimeo, A. *Immunogenetics* 1, 57–67 (1974).
- Artzt, K., Bennett, D. & Jacob, F. *Proc. natn. Acad. Sci. U.S.A.* 71, 811–814 (1974).
- Marticorena, P., Artzt, K. & Bennett, D. *Immunogenetics* 7, 337–347 (1978).
- Cheng, C.C. & Bennett, D. *Cell* 19, 537–543 (1980).
- Goodfellow, P.N., Levinson, J.R., Gable, R.J. & McDevitt, H.O. *J. Reprod. Immun.* 1, 11–21 (1979).
- Ginsberg, L. & Hillman, N. *J. Embryol. exp. Morph.* 33, 715–723 (1975).
- Wudl, L.R. & Sherman, M.I. *Cell* 9, 523–531 (1970).
- Lyon, M.F. & Phillips, R.J.G. *Heredity* 13, 23–32 (1959).
- Lyon, M.F. & Meredith, R. *Heredity* 19, 301–312 (1964).
- Lyon, M.F. & Meredith, R. *Heredity* 19, 313–325 (1964).
- Lyon, M.F. & Meredith, R. *Heredity* 19, 327–330 (1964).
- Lyon, M.F. & Mason, I. *Genet. Res.* 29, 255–266 (1977).
- Styrna, J. & Klein, J. *Genet. Res.* 38, 315–325 (1981).
- Sandler, L., Hiraizumi, Y. & Saudler, I. *Genetics* 44, 232–250 (1959).
- Hartl, D.L. *Genetics* 73, 613–629 (1973).
- Braden, A.W.H. et al. in *Edinb. Symp. Genetics of the Spermatozoon* (eds Beatty, R.A. & Gluecksohn-Waelsch, S.) 310–312 (1982).
- Silver, L.M. & Artzt, K. *Nature* 290, 68–70 (1981).
- Lyon, M.F., Evans, E.P., Jarvis, S.E. & Sayers, I. *Nature* 279, 38–42 (1979).
- Silver, L.M., White, M. & Artzt, K. *Proc. natn. Acad. Sci. U.S.A.* 77, 6077–6080 (1980).

81 and M 101 groups are seen to be in reasonable agreement with each other. Differences first appear at the distance to the Virgo Cluster where many kinds of distance indicators begin to fade below the plate limit. Errors quoted for each distance do not fully take into account external and systematic errors so it is probable the distances obtained for the Virgo Cluster are actually consistent with one other. Hopefully, observations of novae in Virgo ellipticals obtained with CCD cameras and of Cepheids with the space telescopes will soon reduce the remaining uncertainty in the distance to the Virgo Cluster.

From 160 radial velocities of Virgo Cluster members, Kraan-Korteweg¹² finds a mean velocity (corrected for solar motion) $V_0 = 967 \pm 53 \text{ km s}^{-1}$ from which the values of H_0 (local) given in the table may be derived. Many, but not all, available data appear consistent with H_0 (local) = $55 \pm 10 \text{ km s}^{-1} \text{ Mpc}^{-1}$.

Because clusters of galaxies contain so much 'missing mass' they exert a significant gravitational pull on galaxies in their neighbourhood. As a result, our Milky Way System appears to be falling towards the Virgo Cluster. Direct evidence for even larger-scale anisotropies in the galaxian velocity field is provided by giant holes¹³ in the distribution of galaxies. Peebles¹⁴ points out that velocity anomalies at the edges of such holes probably lie in the range 100 to 350 km s^{-1} .

To minimize the effects of such deviations from a smooth Hubble flow the global value of the Hubble parameter has to be determined from distant galaxies that are situated well beyond the Local Supercluster. In such distant galaxies, standard candles are dim and standard meter sticks have characteristic sizes close to that of stellar seeing disks. Accurate measurement of the distances to such objects is therefore one of the most difficult problems in observational astronomy. Traditionally only the most daring and optimistic observational cosmologists have ventured into this difficult area. It is then surprising that some of them are, at times, also a bit optimistic concerning the influence of various selection effects and about their own observational errors? It is this that probably explains the apparent discrepancies in published values of H_0 (global). □

In vitro mutagenesis

from Tim Harris

CLONING techniques are now allowing the isolation and direct structural analysis of a large number of prokaryotic and eukaryotic genes and their regulatory regions, without recourse to classical genetic techniques. The ability to introduce changes into these cloned DNAs at predetermined sites and to assess the effect of these changes biologically (sometimes described as 'genetics in reverse') is rapidly becoming a routine part of gene manipulation technology. This was demonstrated quite clearly at a recent Cold Spring Harbor symposium entitled '*In Vitro* Mutagenesis'.

In theory, the present techniques allow deletions, insertions or point mutations to be introduced at almost any location in a cloned DNA molecule¹. In practice, the type of mutation introduced depends largely on what is already known about the DNA and what biological questions are being asked. Several groups, for example, have analysed the promoter regions of cloned eukaryotic genes by the successive deletion of sequences upstream of the coding region, using exonuclease III and nuclease S_1 or the double strand-specific nuclease *Bal*-31. The effect of the deletion on the level of transcription of the gene can then be measured either *in vitro* or *in vivo*.

One disadvantage of exonucleases commonly used to generate deletions is that they act at both ends of a linear DNA molecule simultaneously. Unidirectionality can be achieved, however, by incorporating an α -thio deoxynucleotide at the 3' end of one strand to prevent the action of exonuclease III (ref. 2). The functional domains of the alanyl-tRNA synthetase gene are being examined in this way by deletion of 3' portions of the coding sequence without affecting the 5' end of the gene³.

In addition to deletion mutations, single base changes can also be generated at or near restriction enzyme sites. In the presence of ethidium bromide, some restriction enzymes nick DNA in one strand rather than cutting both strands. This nick can be extended to a gap by exonuclease treatment and base transitions introduced into the remaining single-stranded DNA by bisulphite treatment⁴. Bisulphite specifically deaminates cytosine to uracil in single stranded nucleic acids⁵, resulting in a transition mutation during repair. Obviously, restriction sites are not always conveniently placed for gap or deletion mutagenesis. This limitation has been overcome to some extent by utilizing the fact that in the presence of *Escherichia coli* RecA protein, small single-stranded DNAs will efficiently displace a complementary sequence in a supercoiled double-stranded DNA molecule forming a D-loop. The displaced single-stranded

loop is then available for mutagenesis using nuclease S_1 and bisulphite⁶. In this way a number of point mutations can be introduced into a target area defined by the size of the DNA used to form the D-loop. The ease of cloning DNA in single-stranded phage cloning vectors (such as M13) has extended the versatility of this approach; the formation of specific heteroduplexes allows the displacement and mutagenesis of defined regions of DNA and the efficient recovery of the mutants by transfection. Mutations have been introduced into the early promoters of both SV40⁷ and adenovirus⁸ by this technique and this kind of segment-specific mutagenesis has also been used to analyse functional sequences in the *lac* promoter⁹.

Besides introducing mutations into single-stranded DNA directly, mutations can also be introduced by misincorporation of nucleotides during repair synthesis with DNA polymerase. The simplest system is to nick (and gap) at a restriction site and 'fill in' with DNA polymerase in the absence of a nucleotide or in the presence of a nucleotide analogue¹⁰. Base exchange during repair can be prevented either by incorporation of α -thio deoxynucleotides¹¹ or by using reverse transcriptase, which lacks a proofreading activity. DNA ligase is used to freeze mutations after repair by sealing across the nick.

There is no doubt that the most powerful method for obtaining defined single base changes is the oligonucleotide-directed method championed by M. Smith and applied initially to the single-stranded phage ϕ X174¹². In this method, an oligonucleotide with a mismatch or small deletion is annealed to a single-stranded template and used to prime the synthesis of a complementary strand. Theoretically, 50 per cent of the progeny molecules arising after transfection should be mutant. The power of the method lies in the fact that there is virtually no constraint on the target, provided the nucleotide sequence of the DNA is known. Moreover, the identification of the progeny is now relatively straightforward since the primer which was used to introduce the mutation can also be used as a probe to search for mutants under stringent hybridization conditions¹³. The method is also very versatile; it can be used on plasmid DNA rendered single stranded by nicking and extensive exonuclease III digestion as well as on DNA cloned in M13 or other single-stranded vector. One possible drawback is the need for a supply of well characterized synthetic oligonucleotides. If nothing else,

Tim Harris is a group leader in Molecular Biology at Celltech Ltd, Slough, UK.

1. Baum, W. A. *Publ. astr. Soc. Pacif.* **71**, 106 (1959).
2. van den Bergh, S. *Astrophys. J.* **131**, 215 (1960a).
3. van den Bergh, S. *Astrophys. J.* **131**, 558 (1960b).
4. Tully, R. B. & Fisher, J. R. *Astr. Astrophys.* **54**, 661 (1977).
5. Faber, S. M. & Jackson, R. E. *Astrophys. J.* **204**, 668 (1976).
6. De Vaucouleurs, G. *Astrophys. J.* **224**, 710 (1978).
7. De Vaucouleurs, G. *Astrophys. J.* **253**, 520 (1982).
8. Aaronson, M., Mould, J. & Huchra, J. *Astrophys. J.* **237**, 655 (1980).
9. Mould, J., Aaronson, M. & Huchra, J. *Astrophys. J.* **238**, 458 (1980).
10. Aaronson, M. *et al.* *Astrophys. J.* **239**, 12 (1980).
11. Sandage, A. & Tammann, G. A. *Astrophys. J.* **256**, 339 (1982).
12. Kraan-Korteweg, R. C. *Astr. Astrophys.* **204**, 280 (1981).
13. Kirshner, R. P. *et al.* *Astrophys. J. Lett.* **248**, L57 (1981).
14. Peebles, P. J. E. *Astrophys. J.* **257**, 438 (1982).

this should provide an additional stimulus to the development of rapid oligonucleotide synthesis methods.

Several examples of the application of oligonucleotide site-directed mutagenesis are available. It has been used to resolve the functions of two overlapping spliced adenovirus mRNAs made early in infection — a question which could not have been answered unequivocally by random or target-directed mutagenesis¹⁴. At least two groups have used the procedure to alter the anticodon of a cloned tRNA gene (for example, tRNA^{Lys} or tRNA^{Tyr}) to that of a suppressor tRNA gene. The function of the tRNA was then tested by its ability to suppress various amber mutations (see, for example, ref.15). Finally, the method has been used to probe the function of the signal peptide present on secreted proteins. Changing the charge of the amino acids at the NH₂ terminus of the *E. coli* outer membrane protein affected the ability of the protein to be assembled in the membrane¹⁶.

Clearly, there are a wide variety of biological problems which will benefit from the application of both target- and site directed *in vitro* mutagenesis. It is now

possible to introduce specific changes into cloned DNA; when coupled with high-level gene expression vectors it should also be possible to assay the effect of these changes in several prokaryotic and eukaryotic systems. For certain proteins, for which there is detailed structural information and a cloned gene available, it is not too fanciful to consider that specific mutations could be introduced to produce molecules with altered or novel activities. □

1. Shortle, D., DiMaio, D. & Nathans, D. *A. Rev. Genet.* 15, 265-294 (1981).
2. Putney, S.D., Benkovic, S.J. & Schimmel, P.R. *Proc. natn. Acad. Sci. U.S.A.* 78, 7350-7304 (1981).
3. Jasin, M. & Schimmel, P. Abstract of the meeting.
4. Shortle, D. & Nathans, D. *Proc. natn. Acad. Sci. U.S.A.* 75, 2170-2174 (1978).
5. Hayatsu, H. *Prog Nucleic Acid Res. molec. Biol.* 16, 75-124 (1976).
6. Shortle, D. *et al. Proc. natn. Acad. Sci. U.S.A.* 77, 5375-5379 (1980).
7. Everett, R.D. & Chambon, P. *EMBO J.* 1, 433-437 (1982).
8. Hearing, P. & Schenk, T. Abstract of the meeting.
9. Weiher, H. & Schaller, H. *Proc. natn. Acad. Sci. U.S.A.* 79, 1408-1412 (1982).
10. Müller, W. *et al. J. molec. Biol.* 124, 343-358 (1978).
11. Shortle, D. *et al. Proc. natn. Acad. Sci. U.S.A.* 79, 1588-1592 (1982).
12. Smith, M. & Gillam, S. *Genet. Engng* 3, 1-32 (1981).
13. Wallace, R.B. *et al. Nucleic Acids Res.* 9, 3647-3656 (1981).
14. Montell, C. *et al. Nature* 295, 380-384 (1982).
15. Temple, G.F. *et al. Nature* 296, 537-540 (1982).
16. Inouye, S. *et al. Proc. natn. Acad. Sci. U.S.A.* 79, 34438-3441 (1982).

Crown gall tumours and plant growth regulators — any connection?

from Mike Bevan

CROWN gall tumour cells produced by infection with *Agrobacterium tumefaciens* can grow in culture in the absence of endogenous auxins such as indole acetic acid (IAA), in contrast to normal plant cells. Transformation takes place when part of the giant Ti, or tumour-inducing, plasmid is stably integrated into the nuclear DNA of the host plant. It is not clear whether the tumorous state is caused by the insertion of T-DNA into plant sequences, or if T-DNA encodes control or structural genes for plant growth regulators. Recently, Lui *et al.*¹ presented evidence for the presence of an IAA gene on the Ti plasmid. Although mutations in the IAA locus render the bacteria harbouring the plasmid avirulent, the locus itself is in a part of the plasmid that is not stably maintained in tumours.

The gene, *iaaP*, responsible for IAA synthesis was identified on the tumour-inducing plasmid by inserting the plasmid into an avirulent, plasmid-free mutant that did not synthesize IAA (*A. tumefaciens* cells themselves normally produce large amounts of IAA). The *iaaP* locus, which may encode enzyme(s) responsible for the conversion of indolepyruvate to IAA, was

mapped by transposon (Tn5) mutagenesis to a region of the Ti plasmid known to be involved in oncogenesis. These sequences, called the virulent region, have been delineated by transposon mutagenesis to a region of about 30 kilobases (in pTiB6806^{2,3}) which may mean that many traits other than IAA production are involved in virulence. It remains to be demonstrated that this Tn5 insertion does not have polar effects on adjacent virulence genes. The question now remains, how do these virulence genes, in particular the *iaaP* locus, incite tumour formation when it is only the T-DNA, some 20 kb from the virulent region, that is stably maintained in the plant tumour?

Lui *et al.* have three suggestions. First, IAA secreted by virulent bacteria may 'pre-condition' a wounded plant cell by inciting cell wall changes and DNA synthesis which would allow subsequent transformation. This is reminiscent of gall induction on olive and oleander stems by *Pseudomonas savastanoi*, which harbours a plasmid-encoded enzyme that converts indoleacetic acid to IAA. Virulence, as measured by gall formation, is directly related to IAA levels⁴, and no transfer of plasmid DNA to the host plant has been observed. Second, the authors speculate that IAA may be a 'second messenger' that activates other virulence genes when the bacterium

encounters a suitable plant cell. Finally, it is suggested that some sort of DNA arrangement may integrate the IAA gene(s) into T-DNA in an early transient stage of crown gall formation.

Recent evidence from extensive transposon mutations in T-DNA indicates that several genes in a highly conserved region of T-DNA are involved in tumour growth and morphology. Two genes, when mutated, give rise to a shooty phenotype, and one gene gives rise to a rooty phenotype when mutated⁵. These findings can be formally explained by postulating that the rooty locus regulates cytokinin levels, and the two shooty loci regulate auxin (IAA?) levels. Ooms *et al.*⁶ demonstrated that exogenous auxin reversed the shooty phenotype and exogenous cytokinin reversed the rooty phenotype in mutated octopine tumours. Interestingly, nearly all of T-DNA can be deleted without affecting the ability of remnant left and right border fragments to be transferred into plant DNA⁷. These 'transformed' cells are, of course, non-tumorous. The virulence region, which maps outside T-DNA, has been implicated in the transfer of T-DNA to plant cells.

In the light of these findings there may be no need to postulate the integration of the non-T-DNA auxin gene into plant DNA to explain oncogenesis, as Lui *et al.* suggest. Indeed, the significance of IAA production by *Agrobacterium* is unclear as in the absence of endogenous tryptophan, both virulent and avirulent mutants failed to accumulate IAA⁸. Perhaps there is adequate tryptophan present in the cell sap of the wound where gall formation is initiated to induce IAA synthesis by virulent *Agrobacterium*, but this has not been investigated.

What does seem clear is that it is profitable to consider auxin and cytokinin autotrophy, regulated by loci on conserved sequences in T-DNA, as being important, if not the basis, for the autonomous growth of crown gall tumours. Endogenous growth regulator levels in plant cells are known to vary widely, and it is reasonable to assume that both sources of growth regulators contribute to the final growth rate and morphology of tumours. The search for a definite connection between the shooty and rooty loci and growth regulator production has been confounded by the very low concentrations of mRNA and proteins encoded by this region of T-DNA. A promising approach has been to direct the expression of T-DNA-encoded genes in *Escherichia coli* minicells⁹, and identify the activity of T-DNA-encoded proteins. □

1. Lui, S.-T., Perry, K.L., Shardi, L.L. & Kado, C.I. *Proc. natn. Acad. Sci. U.S.A.* 79, 2812-2816 (1982).
2. Garfinkel, D.J. & Nester, E.W. *J. Bact.* 144, 732-743 (1980).
3. Ooms, G., Klapwijk, P.M., Poulsen, J.A. & Schilperoort, R.A. *J. Bact.* 144, 82-91 (1980).
4. Smidt, M.L. & Kosuge, T. *Physiol. Pl. Path.* 13, 203-214 (1978).
5. Garfinkel, D.J. *et al. Cell* 27, 143-153 (1981).
6. Ooms, G., Hooykaas, P.J.J., Moolenaar, G. & Schilperoort, R.A. *Gene* 14, 33-50 (1981).
7. Leemans, J. *et al. EMBO J.* 1, 147-152 (1982).

Mike Bevan is in the Plant Breeding Institute, Mavis Lane, Trumpington, Cambridge CB2 2LQ.

The American kestrel as a laboratory research animal

from David M. Bird

AMERICAN KESTRELS (*Falco sparverius*) were first bred in the laboratory unintentionally by Morris¹ in 1850 and later gained acclaim as laboratory animals when they were used to help indict DDT as a significant cause of reproductive failure in wild birds². Since then, the kestrel has been used extensively in laboratory studies, for example, toxicology³, behaviour⁴ and physiology⁵, and has also proved useful as a model species to develop management techniques for endangered species such as the peregrine falcon (*Falco peregrinus*)⁶.

Two large captive colonies have been

established in North America, one in Laurel, Maryland for toxicological research⁷, and a pedigree one of over 200 individuals at McGill University, Montreal in a diverse research programme. Here, I shall outline some of the advantages of the American kestrel as a laboratory animal.

This kestrel nests commonly in most

David M. Bird is the Director of the Macdonald Raptor Research Centre of McGill University, 21,111 Lakeshore Rd, Ste Anne de Bellevue, Quebec H9X 1C0.



100 years ago

PROFESSOR HAECKEL IN CEYLON

THE great black scorpion (nearly a foot long) is so common in Ceylon that I once collected half a dozen in the course of an hour. Snakes exist also in great numbers. Slender green tree-snakes hang from almost every bough, and at night the great rat-snake (*Coryphodon Blumenbachii*) hunts rats and mice over the roofs of the huts. Although they are harmless and their bite not poisonous, it is by no means a pleasant surprise when one of these rat-snakes, five feet long, suddenly drops through a hole in the roof into one's room, occasionally alighting on the bed.

On the whole, however, my nights in Belligam were but little disturbed by animal intruders, although I was often kept awake by the howling of jackals and the uncanny cry of the Devil-bird (a kind of owl, *Syrnium Indrani*) and other night-birds. The bell-like cry of the pretty little tree-frogs which make their dwelling in the cups of large flowers, acted rather as a slumber song. But I was far oftener kept awake by the whirl of my own thoughts, by the recollection of the many events of the past day, and the anticipation of that which was to come. A brilliant succession of lovely scenes, of interesting observations and varied experiences mingled in my brain with plans of fresh enterprise and new discoveries for the morrow.

At seven o'clock my boatmen appeared to carry down my nets and glasses for the daily canoe expedition. This lasted from two to three hours, and on my return I busied myself in disposing my captures in glasses of different sizes, and saving such as could be saved among the few survivors. The more important specimens were microscopied and drawn at once. Then I had my second bath, and at eleven o'clock appeared my so-called 'breakfast', consisting chiefly of curry and rice. The rice was simply boiled, but in the preparation of the curry my old cook, Babua, exerted all the ingenuity with which nature had endowed his diminutive brain to present me with a fresh

combination every day. Sometimes the curry was 'sweet', sometimes 'hot'; sometimes it appeared as an undefinable *mixtum compositum* of vegetables, sometimes as a preparation of the flesh of various animals. Babua seemed to divine that as a zoologist I was interested in every class of animal life, and that he could not do better than turn my curry into a sort of daily zoological problem. . . . He was apparently a staunch upholder of the theory of the near relationship of birds and reptiles, and held it to be immaterial what particular species of *Saurian* were prepared for the table.

It is estimated by Prof. Dufour (*Arch. des Sciences*) that in a disastrous hailstorm on August 21 last year, about 100,000 cubic metres of ice fell in the district of Morges alone in a few minutes, and probably more than 1,000,000 cubic metres in the whole canton de Vaud that afternoon. Yet this is a small matter compared with the terrible hailstorm of July 13, 1788 (regarding which he makes some calculations). He gives some interesting facts, which seem to have been overlooked, in the history of *paragrêles*, or hail-preventers. Old men in the Canton de Vaud remember such apparatus, of lightning-rod character, being set up in several vineyards in 1825; the object being to hinder the formation of hail, by withdrawing electricity from the clouds. A hailstorm in July 1826 devastated, it is said, the best protected vineyards, and the *paragrêles* were then removed. Yet it was on receipt of encouraging and credible testimony from Italy and France (Prof. Dufour shows by extracts) that this brief experiment was made. Considering the distance of hail-forming clouds from the highest *paragrêles*, it is difficult, the author considers, to admit an influence of such apparatus; yet it must be remembered that electricity is '*un véritable fluide à surprises*'; often showing new and unexpected properties. Lately it is said to have been observed in some Swiss cantons, that showers of hail are more rare near forests than in unwooded districts. Prof. Dufour notes this as a matter calling for investigation. A forest may be regarded as a collection of *paragrêles*, and should it be proved to have the influence referred to, the theories which prevailed in 1824 and 1825 would gain new support.

From *Nature* 26, 503; 21 September 1882.

rural and urban areas. In North America, two subspecies exist: *F.s. sparverius* and *F.s. paulus*. *F. s. sparverius* weighs 85–140 g, the female being approximately one-third heavier than the male. This species can be easily sexed by plumage after 12 days of age: males have blue-grey wings and female rufous-brown. The kestrel is sexually mature in its first spring and breeds readily in captivity. Unmated captive-raised females can often be induced to lay eggs simply by providing a nestbox during the breeding season, thus facilitating studies on artificial insemination⁶. Ninety per cent of randomly selected pairs lay an egg every two to three days to produce a first clutch of five eggs. If the first clutch is removed within a week of the laying of the last egg, 95 per cent of the females recycle 11 days later to lay a second clutch⁸. Replacement clutches, though, may have one less egg, longer eggs and eggs with thicker shells than first clutches⁸. If eggs are removed as they are laid, up to 26 eggs can be produced.

The overall fertility of randomly selected pairs is about 65 per cent, but rises to 80 per cent in compatible pairs⁹. The kestrel can be easily inseminated artificially, as males massaged every two days will give, on average, 0.01 ml of semen containing about 400,000 spermatozoa⁶. The mean duration of fertility in females after one insemination averages 8 days with a maximum of 12 days¹⁰. Motile sperm can be obtained after freezing and thawing in a glycerol medium.

The breeding season usually begins in early April in temperate regions, peaks at about 13.5 h of daily light and is strongly influenced by the photoperiod. Pairs can be induced by changing the photoperiod to undergo an extra breeding season during freezing temperatures between two successful spring seasons¹¹. Hatchability with either natural or artificial incubation averages between 60 and 70 per cent, decreasing as the season progresses. The large variation in hatchability from year to year is being investigated¹². Eggs take 28–30 days to hatch. For artificial incubation, a temperature of 37.5°C, 50–60 per cent humidity and turning at least four times daily is ideal. Young hatching from artificially incubated eggs can be hand-reared or fostered to natural parents with eggs or young. Kestrels hand-reared in family groups do not exhibit abnormal reproductive behaviour when sexually mature, but hand-reared females do lay larger clutches with heavier eggs¹³. Hand-rearing, that is, feeding to satiation four times daily, should be used with caution, however, as it may result in physically smaller birds¹³. The sex ratio at hatching is 1:1. Nestlings take 25–30 days to fledge.

The McGill colony is sustained on an *ad libitum* diet of day-old cockerels, usually one per bird daily, supplemented by SA-37 (Rogar-STB Ltd, Montreal) vitamin/mineral supplements and dietary lime-

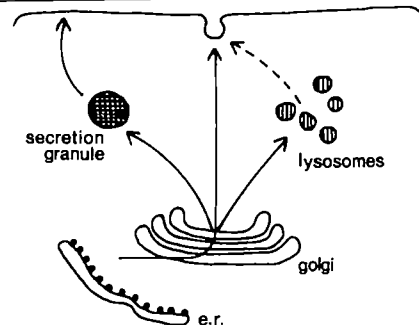
stone, and occasionally laboratory mice. Falcons do not require water for drinking, but do enjoy bathing. Pen design has varied from cages of wire mesh⁷, 15.2 × 6.1 × 1.8 m (L × W × H), to cages of polyethylene or cardboard, 1.5 × 1.2 × 1.2 m. The standard design now preferred at McGill is a plywood box, 2.4 × 1.2 × 2.4 m, with wire mesh roof and floor. Each pen is equipped with a nestbox, 25 × 25 × 46 cm, accessible by a trap-door, several sisal rope perches 1.3 cm in diameter and a wooden feeding perch 5 cm wide.

The colony is usually wintered in flocks of about 20 birds housed in unheated flight pens, 6.1 × 6.1 × 2.4 m, with rope perches. Annual mortality may be up to 10 per cent, and results mainly from intraspecific aggression and winter temperatures of -30°C. Several birds are still breeding successfully after 9 years in captivity.

Approximately 1 ml (10 per cent of total blood volume) of blood can be removed weekly from the brachial vein with no ill effects. Haematological data have been reported^{14,15} and assay techniques for determining the levels of six reproductive steroid hormones are almost complete in our laboratory. We are now investigating factors influencing mate selection in

falconiformes using mate choice tests¹⁶, as well as the influence of diet quality versus frequency of feedings during nestling growth on subsequent body size and reproductive performance. A pedigree colony enhances its value in genetic research for wild-type birds. A wild colony of at least 25 pairs of kestrels has been established using nestboxes within a 10 mile radius of our laboratory to permit comparative studies between wild and captive birds. The use of the McGill University colony is extended to other interested scientific institutions. □

1. Morris, F.O. *Zoologist*, 2648 (1850).
2. Wiemeyer, S.N. & Porter, R.D. *Nature* 227, 737 (1970).
3. Lincer, J.L. & Peakall, D.B. *Nature* 228, 783 (1970).
4. Mueller, H.C. *Nature* 233, 345 (1971).
5. Fox, R. *et al. Science* 192, 263 (1976).
6. Bird, D.M. *et al. Can. J. Zool.* 54, 1183 (1976).
7. Porter, R.D. & Wiemeyer, S.N. *J. Wildl. Mgmt* 34, 594 (1970).
8. Bird, D.M. & Laguë, P.C. *Can. J. Zool.* 60, 71 (1982).
9. Bird, D.M. & Laguë, P.C. *Can. J. Zool.* 60, 80 (1982).
10. Bird, D.M. & Buckland, R.B. *Can. J. Zool.* 54, 1595 (1976).
11. Bird, D.M. *et al. Can. J. Zool.* 58, 1022 (1980).
12. Bird, D.M. in *Recent Advances in Raptor Diseases* (Chiron, UK, 1981).
13. Bird, D.M. & Laguë, P.C. *Can. J. Zool.* 60, 89 (1982).
14. Snyder, J. *et al. in Recent Advances in Raptor Diseases* (Chiron, UK, 1981).
15. Rehder, N.B. *et al. Comp. Biochem. Physiol.* 72A, 105 (1982).
16. Bird, D.M. & Goldblatt, C. in *Recent Advances in Raptor Diseases* (Chiron, UK, 1981).



In eukaryotic cells, integral plasma membrane proteins and proteins destined for secretion share a common origin: translation on membrane-bound polysomes concomitant with vectorial insertion into (or across) the membrane of the endoplasmic reticulum (ER)^{18,21}. The first post-translational modification of these proteins, glycosylation, also occurs at this stage²². This often involves the transfer of a branched, mannose-rich oligosaccharide to an asparagine residue on the nascent peptide. Processing of the carbohydrate chain begins within minutes of its addition. First, glucose residues are removed, followed sequentially by the trimming of several mannoses and the addition of a new complement of terminal sugars (G1cNAc, fucose, galactose and sialic acid) via the activity of several different glycosyl transferases. Terminal glycosylation and at least some mannose removal occurs following the transfer of newly synthesized proteins from the ER to the Golgi². Membrane vesicles then form which transport lysosomal, secretory and plasma membrane proteins to their appropriate destinations.

Multiple pathways of membrane transport

from Ira Mellman

INSIDE the cell a complex pattern of membrane traffic is generated by the intake and secretion of proteins and the manufacture and recycling of membrane components. Recent experiments suggest that the biosynthesis and transport of membrane, lysosomal and certain secretory proteins have a great deal in common, and may share parts of the same constitutive pathway. At the same time, there is also biochemical evidence that at least those secretory proteins which are sequestered in secretion granules before exocytosis are transported along a distinct pathway once they have left the Golgi apparatus.

The Golgi apparatus plays a central part in the post-translational processing of the carbohydrate moieties of membrane and secretory glycoproteins. It is a complex structure consisting of several flattened cisternae, usually with dilated rims, and its mode of operation is the topic of considerable debate. Central to this question is an understanding of the pathway(s) of membrane transport into, through and out from the Golgi stack. Traditionally, movement through the Golgi has been thought to be in one direction, with newly synthesized proteins (both membrane and secretory) entering at the *cis* face (the side defined

morphologically as being closest to the endoplasmic reticulum (ER) and/or nucleus) and exiting as mature glycoproteins at the opposite or *trans* face¹. While the existence of such directionality is not yet proved, Rothman² has recently postulated that individual cisternae of the stack could act like units of a distillation apparatus. Proteins destined for transport to the plasma membrane would be successively processed and enriched relative to contaminants (for example, components of the ER membrane) as the former move by vesicular transport from *cis* to *trans* cisternal elements.

Recent experiments from Rothman's laboratory³ suggest the existence of at least two temporally and functionally distinct components within the Golgi which are involved in the processing of carbohydrates of membrane glycoproteins. Homogenates of CHO cells were centrifuged in sucrose density gradients and, among the fractions, the putative 'early-acting' processing enzyme α_2 -mannosidase, which trims mannose residues from the oligosaccharide, was

found to be slightly separated from the 'late-acting' enzymes involved in terminal glycosylation, galactosyl transferase and sialyl transferase (see Fig. 1 legend). Interestingly, when labelled homogenates of cells infected with vesicular stomatitis virus were centrifuged, the mature (that is, galactose-labelled) form of the viral spike glycoprotein G was found to co-sediment with galactosyl transferase, while a more immature form of G protein sedimented with mannosidase.

If, as these findings imply, early events, such as mannose-trimming, take place in one compartment while later stages, such as terminal glycosylation, take place in another, then it is appealing to speculate that the two compartments correspond to the *cis* and *trans* Golgi cisternae. Such an interpretation must, however, remain speculative given the lack of available corroborative morphological data. Although it has been demonstrated that cisternal elements are cytochemically heterogeneous, most of the activities relevant to glycosylation have yet to be localized to *cis* or *trans* Golgi elements. Indeed, evidence for heterogeneity within single cisternae has been found^{4,5}. In addition, it is also not at all certain to what extent Golgi subcompartments retain their integrity after homogenization.

Further progress requires specific markers that will permit the separation and

Ira Mellman is Assistant Professor of Cell Biology in the School of Medicine, Yale University, New Haven, Connecticut 06510.

identification of Golgi subcompartments, particularly in experiments in cell-free systems⁶⁻⁸ where the morphological features which characterize the Golgi are usually lost.

Some first steps in this direction come from recent experiments by Roth and Berger in which a terminal glycosyltransferase has been immunocytochemically localized to the *trans* aspect of the Golgi apparatus of HeLa cells⁹. An antiserum against human milk galactosyltransferase was used and the antigen visualized on fixed, embedded material by protein A-colloidal gold staining. Gold was localized to two or three cisternae, coincident with a second Golgi cytochemical marker thiamine pyrophosphatase that is usually detected in *trans* elements. However, the '*trans*-most' Golgi cisternae, marked cytochemically by acid phosphatase activity, were not labelled with gold.

A novel approach to the identification of Golgi subcompartments has recently been taken by Louvard *et al.*¹⁰. They immunized rabbits with a rat liver Golgi fraction and obtained an antiserum which exhibited significant anti-Golgi activity. Following sequential adsorptions against rat blood plasma and microsomal membranes, the serum showed highly specific Golgi reactivity as judged by immunofluorescence and by immunoperoxidase labelling in the electron microscope. The antiserum labelled many, but not all, of the stacks of the Golgi complex in rat NRK cells. Whether these were *cis* or *trans* cisternae could not be determined. Many Golgi-associated vesicles were also labelled, some of which had clathrin coats. The antigenic determinant appeared to be on the luminal surface of both cisternae and vesicles. Rather surprisingly, the antiserum recognizes only a single 135,000 molecular weight polypeptide, in both NRK cells and rat liver. While this particular protein may not prove to be useful for Golgi isolation and identification in cell fractions (for example, by immunoadsorption, as demonstrated by Ito and Palade¹¹), the value of the approach is clear. In fact, another paper¹² in the same issue of *Journal of Cell Biology* reports the isolation of a monoclonal antibody against another Golgi-associated protein. A crude (Triton-insoluble) extract of cells was used as the immunogen. However, the antibody's specificity was defined only at the level of immunofluorescence, thus the actual localization of its antigen must await further study.

The fact that both membrane and secretory proteins undergo proximal and terminal glycosylation implies that they may take the same or similar routes through the Golgi apparatus. Once proteins have left the Golgi, though, it seems membrane and secretory proteins do not always take the same pathway to the plasma membrane (Fig. 1). Two general types of secretory activity can be dis-

tinguished. The first, which presumably occurs in many cell types, mediates an apparently continuous and non-concentrative exocytosis of secretory products. In the second, newly synthesized secretory proteins are concentrated and stored in intracellular granules, as in exocrine cells. The granules can be induced to fuse with the plasma membrane by specific secretagogue stimuli. This latter pathway is unlikely to be responsible for delivering new plasma membrane components to the cell surface since the polypeptide composition of the secretion granule is considered quite 'simple' and turns over more slowly than the contents it delivers¹³.

Direct evidence consistent with the existence of at least two separate pathways has now been provided by Gumbiner and Kelly¹⁴. They have studied a pituitary tumour cell line (AtT-20) which synthesizes the polypeptide hormone ACTH and the gp70 envelope glycoprotein of an endogenous murine leukaemia virus. Both are glycosylated during synthesis. Proteolytically processed (mature) ACTH is sequestered intracellularly in secretion granules¹⁵ and is released only slowly in the absence of secretagogues ($t_{1/2}$ = 3–4 h). In contrast, gp70 appears on the cell surface and/or is released (secreted?) much more rapidly ($t_{1/2}$ < 30 min). Incompletely processed ACTH precursors (polypeptides of molecular weights 23,000 and 30,000) were also continuously released with kinetics identical to gp70. These presumably represent hormone which escaped complete proteolytic processing and condensation in granules.

The differential rates of gp70 and mature ACTH release suggest that these molecules are transported by distinct mechanisms. Supporting evidence comes from the effect of secretagogues such as cyclic AMP, which cause a rapid increase in the rate of

ACTH secretion but have relatively little effect on ACTH precursor or gp70 release. Similarly, the membrane of isolated secretion granules was found to contain only an insignificant fraction of total cellular gp70. It obviously must be shown that the same cells actually secrete both ACTH and gp70, but these observations do suggest the existence of at least two separate pathways from the Golgi to the cell surface. Mature ACTH is probably transported by a route found only in specialized secretory cells. In contrast, gp70 transport may occur via a pathway which is involved in the continuous delivery of secretory products and new (or recycling) membrane components to the cell surface.

Recent evidence has also suggested that, at least in certain conditions, newly synthesized lysosomal hydrolases take the continuous route followed by gp70 and ACTH precursors. Like membrane and secretory proteins, lysosomal hydrolases are synthesized and glycosylated on the ER and then processed during transit through the Golgi complex^{16,17}. However, as shown by Kornfeld, Von Figura and others, processing results in the attachment of terminal mannose phosphate residues^{1,18}. These are recognized by a specific membrane receptor which may be involved in the delivery of mannose phosphate-containing enzymes to lysosomes¹⁹. The delivery system seems only partially efficient since some newly synthesized hydrolases are usually secreted into the medium. Also, as Rosenfeld *et al.*¹⁷ show, virtually all the cathepsin D and β -glucuronidase synthesized by cultured rat hepatocytes are secreted when glycosylation is inhibited by tunicamycin.

Thus, lysosomal hydrolases may be transported from the Golgi via two distinct pathways, the first directed towards lysosomes, the other towards the cell surface (Fig. 1). Tunicamycin might inhibit the former route by preventing the formation of the mannose phosphate recognition marker. An alternative explanation, however, might be that most vesicles coming from Golgi which are bound for the plasma membrane first fuse with lysosomes (or another acidified vacuole) before continuing to the cell surface. Since low pH is known to dissociate mannose phosphate glycoproteins from their receptor, this pathway could still account for the delivery of newly synthesized hydrolases to lysosomes. Moreover, this interpretation is appealing since it provides an interface between the pathways of membrane transport during lysosomal biogenesis and during endocytosis, the latter being a process which generates an extensive bidirectional flow of membrane between lysosomes and the cell surface. Endocytosis is already known to transport a wide variety of plasma membrane proteins²⁰, including cell surface mannose phosphate receptors, which mediate the uptake and delivery of extracellular hydrolases to lysosomes¹⁹. □

1. Farquhar, M.G. & Palade, G.E. *J. Cell Biol.* 991, 77s (1981).
2. Rothman, J.E. *Science* 213, 1212 (1981).
3. Dunphy, W.G., Fries, E., Urbani, L.J. & Rothman, J.E. *Proc. natn. Acad. Sci. U.S.A.* 78, 7453 (1981).
4. Farquhar, M.G., Bergeron, J.J.M. & Palade, G.E. *J. Cell Biol.* 60, 8 (1974).
5. Cheng, H. & Farquhar, M.G. *J. Cell Biol.* 70, 660 (1976).
6. Quinn, P.S. & Judah, J.D. *Biochem. J.* 172, 301 (1978).
7. Bergeron, J.J.M., Rachubinski, R.A., Siktstrom, R.A., Posner, B.J. & Paielement, J. *J. Cell Biol.* 92, 139 (1982).
8. Rothman, J.E. & Fries, E. *J. Cell Biol.* 89, 162 (1981).
9. Roth, J. & Berger, E.G. *J. Cell Biol.* 93, 223 (1982).
10. Louvard, D., Reggio, H. & Warren, G. *J. Cell Biol.* 92, 92 (1982).
11. Ito, A. & Palade, G.E. *J. Cell Biol.* 79, 590 (1978).
12. Lin, J.J.-C. & Queally, S.A. *J. Cell Biol.* 92, 108 (1982).
13. Meldolesi, J., Borgese, N., DeCamilli, P. & Ceccarelli, B. in *Membrane Fusion* (eds Poste, G. & Nicolson, G.L.) 509 (Elsevier, Amsterdam, 1978).
14. Gumbiner, B. & Kelly, R.B. *Cell* 28, 51 (1982).
15. Gumbiner, B. & Kelly, R.B. *Proc. natn. Acad. Sci. U.S.A.* 78, 318 (1981).
16. Erickson, A.H. & Blobel, G. *J. biol. Chem.* 254, 11771 (1979).
17. Rosenfeld, M.G., Kreibich, G., Popov, D., Kato, K. & Sabatini, D.D. *J. Cell Biol.* 93, 135 (1982).
18. Sabatini, D.D., Kreibich, G., Morimoto, T. & Adesnik, M. *J. Cell Biol.* 92, 1 (1982).
19. Gonzalez-Noriega, J.H., Grubb, Talkad, V. & Sly, W.S. *J. Cell Biol.* 85, 839 (1980).
20. Mellman, I.S., Steinman, R.M., Unkeless, J.C. & Cohn, Z.A. *J. Cell Biol.* 87, 712 (1980).
21. Blobel, G. *Proc. natn. Acad. Sci. U.S.A.* 77, 1496 (1980).
22. Hanover, J.A. & Lennarz, W.J. *Archs Biochem. Biophys.* 211, 1 (1981).

ARTICLES

Five crucial tests of the cosmic distance scale using the Galaxy as fundamental standard

G. de Vaucouleurs

Department of Astronomy and McDonald Observatory, University of Texas, Austin, Texas 78712, USA
Mount Stromlo and Siding Spring Observatories, Australian National University, Canberra

Five crucial tests of the 'long' and 'short' extragalactic distance scales based on a new approach using our Galaxy as the fundamental calibrator are presented. All confirm the short scale within 0.1–0.2 mag and the corresponding value of the Hubble constant $H_0 = 95 \pm 10 \text{ km s}^{-1} \text{ Mpc}^{-1}$. All reject the long scale ($H'_0 = 50 \text{ km s}^{-1} \text{ Mpc}$) at very high significance levels.

THE traditional approach to the extragalactic distance scale rests on a pyramid of primary, secondary and tertiary indicators of increasing range and decreasing accuracy. This multi-step procedure, fraught with the danger of cumulative errors, has led to two main, widely diverging scales: the 'long' scale¹ implying a Hubble constant $H'_0 \approx 50 \text{ km s}^{-1} \text{ Mpc}^{-1}$, and the 'short' scale² leading to $H_0 \approx 100 \text{ km s}^{-1} \text{ Mpc}^{-1}$. Several authors have shown that the long scale rests on very precarious foundations²; counter-arguments have been offered in its defence and to criticize the short scale¹. A conclusive test was needed.

Such a test (actually five different ones) is now possible through direct quantitative comparison of our Galaxy with other galaxies: (1) by comparing the two competing scales with a third, independent scale, calibrated only by the Galaxy, or (2) by comparing with the known value of the basic scale factor of our Galaxy, the galactocentric distance of the Sun, R_0 , with those implied by the distances of the Virgo cluster in the two scales.

The direct calibration of tertiary indicators by means of the Galaxy, without recourse to the galaxies of the Local Group and nearby groups as stepping stones, bypasses most of the difficulties (particularly the propagation of errors) of the classical approach.

Various tests are possible by means of the main metric, photometric and kinematic parameters of the Galaxy (Table 1) which are known with sufficient precision (10–20%) to allow a clear cut choice between two distance scales which differ by a factor of 2.

The morphological type of our Galaxy, SAB(rs)bc, determined by a multiplicity of converging indications^{3,4}, corresponds, in the numerical scale of the *Second Reference Catalogue* (RC2)⁵, to stage $T = 4 \pm 0.5$ of the revised Hubble sequence. The galactocentric distance of the Sun, $R_0 = 8.5 \pm 0.5 \text{ kpc}$, is now established to within 10–15%; it rests on two independent primary distance indicators: the variable stars of the RR Lyr type and those of long periods (Mira-type) whose absolute magnitudes are both fixed by fundamental methods with mean errors of 0.1–0.2 mag (ref. 6). Their agreement greatly strengthens the usefulness of R_0 the basic scale length of the galactic system, as a standard yardstick of extragalactic distances.

The rotation velocity of the Galaxy at the Sun's distance, $V(R_0) = 220 \pm 15 \text{ km s}^{-1}$, is also well determined by several recent investigations⁶. So is the central velocity dispersion $\sigma_v(0) = 130 \pm 7 \text{ km s}^{-1}$ of the galactic bulge⁶. The total absolute magnitude of the Galaxy seen face-on by an external observer, $M_T^0 = -20.2 \pm 0.15$ (in blue light) if $R_0 = 8.5 \text{ kpc}$, can be surprisingly well determined by numerical integration of galactic

models based on star counts and direct photometry of the galactic bulge^{4,7}. (Note that this absolute luminosity scales as R_0^2 , hence M_T^0 varies as $-5 \log R_0/8.5$.) The metric (effective) and photometric (isophotal) diameters of the Galaxy in the standard RC2 system can also be calculated from the photometric models⁴. Finally, several indications suggest that an incomplete ring structure exists in the inner regions of our Galaxy⁴ whose radius is indicated by the '3-kpc arm' feature observed in the 21-cm line of hydrogen out to 20° from the galactic centre⁴, which would give it a diameter of 5.8 kpc.

These basic galactic parameters may be used to calibrate the various correlations between the global properties of galaxies that can serve as distance indicators.

First test: Tully–Fisher relations

The linear correlations discovered by Tully and Fisher (T–F)⁸ between absolute magnitude and maximum rotation velocity V_M (or width W of the 21-cm line) can be used to build extragalactic distance scales. [Traditionally the calibration of these scales (or in practice the zero point of the corresponding distance modulus $\mu = m - M = 5 \log \Delta + 25$, if the distance Δ is in megaparsecs) has been based on a few nearby galaxies whose distances derived from primary or secondary indicators, are presumed to be known. This calibration can be checked now by the zero point independent established by the Galaxy alone.] The most recent version of the T–F relation⁹ for total

Table 1 Fundamental constants of the Galaxy

a, Galactic constants	
Morphological type, SAB(rs)bc	$T = 4 \pm 0.5$
Galactocentric distance of Sun (kpc)	$R_0 = 8.5 \pm 0.5$
Total absolute magnitude (face-on, $i = 0^\circ$)	$M_T^0(B) = -20.2 \pm 0.15$
Total colour index ($i = 0^\circ$)	$(B - V)_T^0 = +0.53 \pm 0.04$
Absolute magnitude of spheroidal component	$M_1^0(B) = -18.2 \pm 0.3$
Colour index of spheroidal component	$(B - V)_1^0 = +0.65 \pm 0.05$
IR absolute magnitude	$M^*(H) = -22.55 \pm 0.23$
Circular rotation velocity (km s^{-1})	$V(R_0) = 220 \pm 15$
Central velocity dispersion (km s^{-1})	$\sigma_v(0) = 130 \pm 7$
Photometric diameter (at $\mu_B = 25.0$)	$D_0/2R_0 = 1.44$
Metric (effective) diameter	$D_e/2R_0 = 0.63$
Diameter of (rs) structure ('3 kpc-arm')	$D_r/2R_0 = 0.34$
b, Stellar constants	
Mean absolute magnitude of RR Lyr variables ($P > 0.42$ days)	$\langle M_v(\text{RR}) \rangle = +0.8 \pm 0.15$
Zero point of bolometric period-luminosity relation of long period variables	$\langle M_{\text{bol}}(0) \rangle = +0.76 \pm 0.1$
Mean absolute magnitude of globular clusters	$\langle M_v(\oplus) \rangle = -7.2 \pm 0.2$

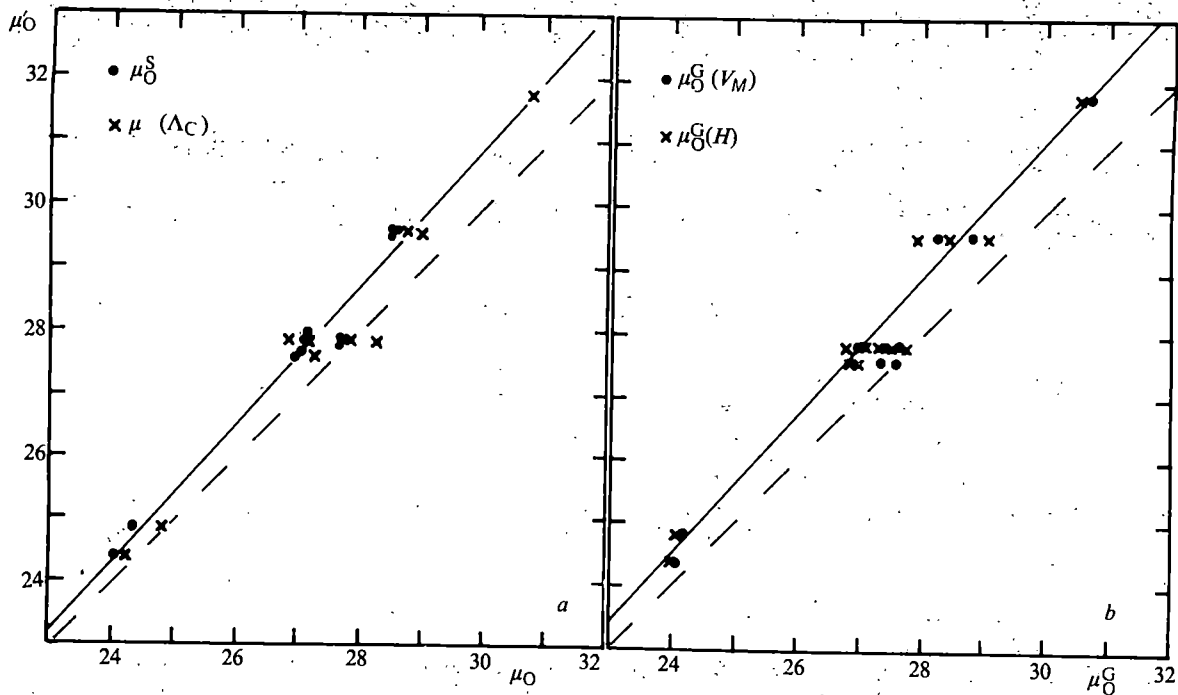


Fig. 1 Comparison of distance moduli on the long distance scale μ_0' and on several other scales: *a*, primary and secondary calibrators μ_0^T and luminosity index $\mu_0(\Lambda_c)$ on the short scale; *b*, revised *B*-band T-F relation, $\mu_0(V_M)$ and *H*-band relation, $\mu_0(H)$ with galactic zero points. Both panels show closely similar zero point and scale errors in the long scale. Solid lines, least squares solutions; dashed lines, equality of scales.

magnitudes in the B_T^0 system of RC2 is of the form

$$-M_T^0 = a(B) + 5(\log V_M - 2.2) \quad (1)$$

where V_M (km s^{-1}) is derived from the widths W of the 21-cm line (measured at the 20, 40 and 50% levels of the line profile), corrected for the effects of inclination and velocity dispersion. To calculate the corrected (geometric) distance modulus, $\mu_0 = B_T^0 - M_T^0$, one needs only to fix the zero point, $a(B)$. With the values adopted in Table 1 for the Galaxy, and assuming that $V_M \approx V(R_0)$, as the Sun is on the $V = \text{constant}$ branch of the rotation curve⁶, one finds $a^G(B) = 19.5 \pm 0.27$. This value is in excellent agreement with that (19.40 ± 0.15) derived earlier⁹ from 11 calibrating galaxies of the Local Group and nearby groups on the short distance scale. It follows that a correction of -5% only is sufficient to reduce the value of H_0 derived previously¹⁰ from $\mu_0(V_M)$ to the scale whose zero point is fixed solely by the Galaxy, that is $H_0^G = 98 \pm 13 \text{ km s}^{-1} \text{ Mpc}^{-1}$. This value is independent of the supergalactic anisotropy of the velocity field since the value of μ_0 in ref. 10 ($H_0 = 103$) resulted from simultaneous solutions for solar motion and Hubble constant based on 300 galaxies in the distance range $2 < \Delta < 29 \text{ Mpc}$ and well-distributed over both hemispheres.

A second version of the T-F relation applicable to IR magnitudes in the $H^c \equiv H_{c,0.5}^c$ system¹¹ is of the form

$$-M^c(H) = a(H) + 10(\log W - 2.5) \quad (2)$$

where $W = W_{20}^1$ is the width of the 21-cm line (at 20% level), corrected only for the effect of inclination. To calculate the distance modulus $\mu_0 = H^c - M^c$, one needs only to fix the zero point, $a(H)$. The absolute magnitude $M^c(H)$ of our Galaxy can be computed by correcting $M_T^0(B)$ for the mean value $\langle Y \rangle = 2.35 \pm 0.15$ of the differences $Y = B_T^0 - H^c$ for galaxies of its type *T* (ref. 12), whence $M^c(H) = -22.55 \pm 0.23$. Then, with

$W = 485 \text{ km s}^{-1}$, one finds $a^G(H) = 20.69 \pm 0.33$. With this zero point, application of equation (2) to 12 nearby galaxies and to the Virgo cluster (see below) defines a modulus scale (μ_0^G) in excellent agreement (± 0.1 – 0.2 mag) with both the scale based on equation (1) and with the short scale (μ_0), but in strong disagreement with the long scale (μ_0') (Fig. 1). The mean relations

$$\mu_0' - 28.18 = (1.133 \pm 0.026)(\mu_0 - 27.61) \quad (3)$$

$$\mu_0' - 28.18 = (1.120 \pm 0.025)(\mu_0^G - 27.45) \quad (4)$$

confirm the presence of a scale error in the μ_0' scale, of 12–13% per magnitude in the interval $24 < \mu_0' < 32$, which had already been suggested by analyses of the foundation and indicators of the long scale².

Application of equations (1) and (2) with their galactic zero points to a sample of 13 spirals of the Virgo cluster (or more precisely the Virgo S Cloud)¹³ leads to mean distance moduli $\langle \mu_0^G(B_T^0, V_M) \rangle = 30.70 \pm 0.12$ (dispersion 0.42 mag) and $\langle \mu_0^G(H, W) \rangle = 30.50 \pm 0.11$ (dispersion 0.40 mag) respectively. This is in good agreement with the short scale: the mean modulus of nine spirals of the Virgo cluster previously derived from their luminosity indices^{13,14} is $\langle \mu_0(\Lambda_c) \rangle = 30.77 \pm 0.16$ (dispersion 0.46 mag). The general mean of a variety of determinations by various methods (all based on the primary and secondary calibrators of the short scale) is $\langle \mu_0 \rangle = 30.71 \pm 0.2$ (refs 2, 15).

The disagreement with the long scale is conspicuous: the distance modulus of the Virgo cluster on the long scale^{1,2} is $\langle \mu_0' \rangle = 31.5 + 0.26 = 31.76$, where the correction $+0.26$ reflects the revision of the Hyades modulus². If this value were correct, it would imply for the zero point of the scale defined by equation (1), the value $a'(B) = a(B) + (31.76 - 30.70) = 19.5 + 1.06 = 20.56$. In such case equation (1) shows that if $V_0 = 220$ were correct, the absolute magnitude of the Galaxy should be -21.26 (instead of -20.2); and, since M_T^0 scales with $-5 \log R_0/8.5$, it would follow that $R_0' = 13.8 \text{ kpc}$ (instead of 8.5). Furthermore, the absolute magnitude of the RR-Lyr variables should be -0.26 (instead of $+0.8$) and that of the long period variables -0.3 (instead of $+0.76$) which is impossible. Or, if $R_0 = 8.5$

Table 2 Zero points of Faber-Jackson relations

Type	E	L	SO/a	Sa	Sab	Sb	Sbc	Sc	Scd
<i>T</i>	-5	-2	0	1	2	3	4	5	6
$\alpha(B)$	18.98	19.18	20.70	20.88	21.12	21.45	21.88	22.24	23.15
$\alpha(V)$	19.95	19.95	21.52	21.65	21.84	22.12	22.50	23.01	23.67

kpc were correct, one would have to conclude that the rotation velocity of the Galaxy at R_0 is $V'_0 = 135 \text{ km s}^{-1}$ (instead of 220), a totally inadmissible value. Or again, if one were to split the corrections between R_0 and V_0 to minimize the errors, one would have to suppose that $R'_0 = 10.85 \text{ kpc}$ and $V'_0 = 172 \text{ km s}^{-1}$. This combination, which implies errors of 4.2σ in $\log R_0$ and simultaneously of 3.7σ in V_0 , has a total probability (calculated for the normal law) $P(\mu'_0) = 1.5 \times 10^{-9}$. The same reasoning applied to equation (2) and to the modulus $\langle \mu_0^G(H) \rangle = 30.53$ leads to similar conclusions.

Second test: Faber–Jackson relations

The linear correlations discovered by Faber and Jackson (F–J)¹⁶ between the absolute magnitude M and the central velocity dispersion σ_v in elliptical galaxies or in the spheroidal components of lenticular and spiral galaxies¹⁷ can also be used to build extragalactic distance scales. It is now possible to obtain an independent determination of the zero point by means of the spheroidal component of our Galaxy.

It has been shown recently^{17,18} that the slope, but not necessarily the zero point, of the F–J relation is very nearly the same for galaxies of all three principal classes (E, L, S). The simplest relation is of the form

$$-M_T^0 = \alpha + \beta(\log \sigma_v - 2.3) \quad (5)$$

where M_T^0 is the total magnitude (E, L galaxies) and $\beta(B) = 9$ in the B band, or $\beta(V) = 8.5$ in the V band. In the case of spirals M_T^0 must be replaced by the magnitude M_i^0 of the spheroidal component only. The latter can be deduced from the total magnitude, corrected for the mean systematic difference $\Delta m_i(T) = M_i^0 - M_T^0$, which varies rapidly with morphological type T (ref. 19), and for the colour index $(B - V)_i^0$ of the spheroidal component, which varies also (but little) with T .

For the Galaxy ($T = 4 \pm 0.5$) with $M_T^0(B) = -20.2 \pm 0.15$ (Table 1) and $\Delta m_i(4) = 2.0 \pm 0.1$ (ref. 19), one finds $M_i^0(B) = -18.2 \pm 0.3$ with $(B - V)_i^0 = 0.65 \pm 0.05$. Then with $\sigma_v^G = 130 \pm 7 \text{ km s}^{-1}$ (Table 1) equation (5) gives $\alpha(4, B) = 21.88 \pm 0.40$ (B band) and $\alpha(4, V) = 22.50 \pm 0.42$ (V band). The distance modulus of a galaxy of type T , apparent total magnitude B_T^0 (or V_T^0) and velocity dispersion σ_v is given by

$$\mu_0(B_T^0, \sigma_v) = \alpha(T, B) + B_T^0 + 9(\log \sigma_v - 2.3) \quad (6a)$$

or

$$\mu_0(V_T^0, \sigma_v) = \alpha(T, V) + V_T^0 + 8.5(\log \sigma_v - 2.3) \quad (6b)$$

with the zero points of Table 2. (Note that equations (6) apply to total magnitudes, Δm_i^0 is taken into account in Table 2.)

Table 3 The Galaxy and its 'sosie'

a, Taxonomic parameters								
Parameter	T	L	Λ_c	$(B - V)_T^0$	ΔM_i	C_{31}	$m_s'(B)$	H_1
	(1)	(2)	(3)	(4)	(5)	(6)	(7)	(8)
Galaxy	4	2.5	0.65	0.53	(2.0) [†]	<3.7	13.14	(2.1) [‡]
Sosie*	4.25	2.25	0.67	0.51	2.25	3.1	13.19	2.2
b, Parameters on two distance scales								
Parameter	$M_T^0(B)$	D_0	D_e				O–C	
	(9)	(10)	(11)	(12)			(13)	
Galaxy ($R_0 = 8.5 \text{ kpc}$)	-20.2	24.4	10.8	5.8				
Sosie*, if $\langle \mu_0 \rangle = 30.21$	-20.0	22.7	10.3	5.75	+0.2		+0.1	
—, if $\langle \mu_0 \rangle = 31.73$	-21.5	46.5	21.6	11.4	-1.3		-1.4	

Columns: (1) type; (2) luminosity class; (3) luminosity index; (4) colour index; (5) relative magnitude of spheroidal component¹⁹ $\Delta M_i = M_i^0 - M_T^0$; (6) concentration index²¹; (7) mean effective surface brightness (mag arc min⁻²) (ref. 5); (8) hydrogen index^{5,19}; (9) total absolute magnitude; (10) photometric diameter (kpc) at isophotal level 25.0 mag arc s⁻²; (11) effective diameter (kpc); (12) diameter of (r_s) ring (kpc); (13) O–C in magnitudes (see text).

* Mean of NGC 1073, 4303, 5921 and 6744.

† Mean for $T = 4$.

‡ Mean for $\Lambda_c = 0.65$.

Table 4 Implications of two estimates of the distance to the Virgo E cluster

Parameters	Long scale ($H_0 = 50$)	Short scale ($H_0 = 95$)	Observed
Distance of Virgo E cluster	22.5 (E, S)	11.8 (E)	
True distance modulus μ_0	31.76 (μ'_0)	30.37 (μ_0)	
Galactic extinction A_v	0.00	0.15	
Apparent modulus μ_v	31.76	30.52	
Mean apparent magnitude of globular clusters	$\langle m_v \rangle$ m.e.		23.3 ± 0.04
Mean absolute magnitude of globular clusters	$\langle M_v(\oplus) \rangle$ m.e.	-8.46 -7.22	-7.2 ± 0.2
Mean absolute magnitude of RR Lyr variables	$\langle M_v(RR) \rangle$ m.e.	-0.46 +0.78	+0.8 ± 0.15
Distance of galactic centre	R_0 (kpc) m.e.	15.2 ± 3.1	8.4 ± 0.5
Zero point of P–L relation of Mira variables	$\langle M_{bol}(0) \rangle$ m.e.	-0.5 ± 0.4	+0.74 ± 0.1

The validity of these relations has been verified by application to four nearby spirals (M31, M81, NGC 4594 and 7793) covering a wide range of types and a large interval of σ_v . Equations (6) were then applied to a sample of 15 spirals having velocity dispersions $130 < \sigma_v < 180 \text{ km s}^{-1}$. The distance moduli so calculated were compared with those previously derived, on the short scale, from primary and secondary indicators, μ_0^s , from the luminosity index, $\mu_0(\Lambda_c)$ (ref. 14), from the T–F relations in the B -band, $\mu_0(V_M)$ (ref. 9), and from the diameter of the r , r_s inner rings, $\mu_0(r)^2$. There is excellent agreement ($\pm 0.2 \text{ mag}$) and no appreciable divergence of the scales in the interval $24 < \mu_0 < 32$ covered by the data. The mean systematic difference $\langle \mu_0^G(\sigma_v) - \mu_0 \rangle = +0.10 \pm 0.17$ is insignificant and the dispersion of the differences (0.78 mag) is consistent with the estimated errors (0.5–0.6 mag) of the various indicators.

A comparison with the moduli (μ'_0) of the same galaxies on the long scale leads to very different results. In the interval $24 < \mu'_0 < 32$, the mean ratio is $(\mu'_0 - 30.07)/(\mu_0^G(\sigma_v) - 29.22) = 1.088 \pm 0.084$ (Fig. 2b), which confirms the presence of zero point and scale errors in the μ'_0 moduli, in agreement with the conclusions drawn from equations (3) and (4).

To apply equations (6) to the galaxies of the Virgo E cluster²⁰ the differences of zero points reflecting the fundamental differences in shape and internal dynamics between elliptical galaxies and the bulges of spirals must be taken into account. At $\sigma_v = \text{constant}$, ellipticals are on average less luminous than the bulges of spirals by $\sim 0.7 \text{ mag}$ according to Whitmore *et al.*¹⁷ which corresponds to 0.9 mag in the system of Simien and de Vaucouleurs¹⁹; it follows that $\alpha = 18.98$ (B) and 19.95 (V) for $T = -5$. These constants are subject to revision because the magnitude difference at $\sigma_v = \text{constant}$ between elliptical and spiral bulges is still in doubt, mainly as a result of different methods in decomposing spirals into disk and spheroidal components. Hence the present application of the F–J relations to the Virgo E cluster carries a lower weight than the other tests. Rejecting it would make no difference to the conclusions (see Table 5). According to de Vaucouleurs and Olson¹⁸ elliptical and lenticular galaxies are equally luminous (at $\sigma_v = \text{constant}$) in the V_T^0 system of total magnitudes, but lenticulars are brighter by 0.2 mag in the B_T^0 system. This implies $\alpha = 19.18$ (B) and 19.95 (V) for $-3 \leq T \leq -1$ (Table 2).

With the zero points so fixed (indirectly) by the Galaxy equations (6) have been applied to 17 early-type galaxies ($T < 0$) of the Virgo E cluster²⁰. The mean modulus $\langle \mu_0^G(\sigma_v) \rangle = 30.32 \pm 0.10$ (internal m.e.) is in excellent agreement with the mean value $\langle \mu_0 \rangle = 30.37 \pm 0.2$, previously derived from a variety of indicators on the short scale^{2,15}.

Both values are in sharp disagreement with the modulus of the Virgo cluster, $\mu_0 = 31.76$ (with the corrected Hyades zero point)^{1,2} postulated by the long scale. The discrepancy $\langle \mu'_0 - \mu_0^G(\sigma_v) \rangle = +1.44 \text{ mag}$ is far in excess of any plausible error in the galactic calibration of the σ_v scale. A propagation of error analysis shows that if the difference were distributed among the four parameters R_0 , T , σ_v and the correction $\Delta M(E-S)$, so

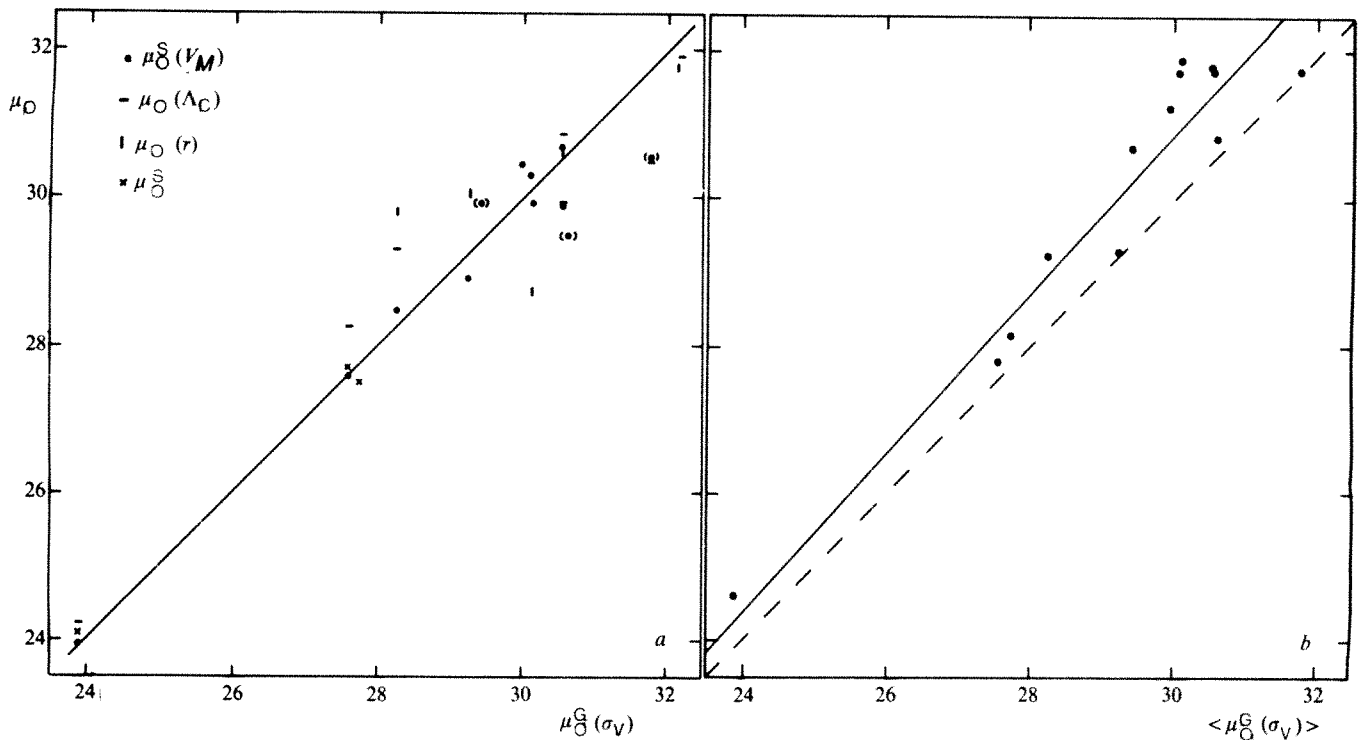


Fig. 2 Comparison of distance moduli: *a*, on the short scale (see text); *b*, on the long scale, with the mean values $\mu_0^G(\sigma_V)$ derived from the F-J relations. Note good systematic agreement in *a* and zero point and scale error in *b*.

as to minimize the errors, a reconciliation of the long scale with the galactic parameters would require changing simultaneously (and in the right direction) each of the four parameters by more than 1.4σ . This combination of errors has a total probability $P(\mu_0') < 10^{-5}$.

Third test: zero point of the luminosity index scale

The tertiary index on which the short distance scale was initially based^{2,14} is the corrected 'luminosity index', $\Lambda_c = (T + L_c)/10$, where T is the morphological type and L_c the luminosity class, corrected for inclination effects¹⁴. In the interval $|\Lambda_c - 1| < 0.65$, the correlations between Λ_c and the total absolute magnitude, M_T^0 , or the linear photometric (isophotal) diameter, D_0 , both in the RC2 system⁵, are essentially linear:

$$-M_T^0 = \gamma - 3.0(\Lambda_c - 1) \quad (7)$$

and

$$\log D_0 = \delta - 0.6(\Lambda_c - 1) \quad (8)$$

The constants γ, δ fixing the zero points of the distance scales were first determined by means of 16 'calibrating galaxies', that is, nearby galaxies whose distances had been previously derived from primary and secondary indicators^{2,15}. The slopes of the relations are well determined and the linearity of the scale of distances based on Λ_c has already been verified by comparison with a variety of independent indicators^{2,9,15}. It remained to confirm the adopted values of γ, δ by direct application of equations (7) and (8) to our Galaxy whose type, Sbc ($T = 4 \pm 0.5$), is well established. Its luminosity index is not directly observable, but can be inferred indirectly by three methods: (1) the statistical relation $\langle T \rangle = \langle L \rangle + 1$ (ref. 21) suggests $L^G \approx 3$ and $\Lambda_c^G \approx 0.7 \pm 0.1$; (2) according to all available evidence^{3,4} our Galaxy is intermediate between M31 ($T = 3, L = 2, \Lambda_c = 0.45$) and M33 ($T = 6, L = 4, \Lambda_c = 1.00$) (ref. 14), but closer to the former, whence $\Lambda_c^G \approx 0.63 \pm 0.07$; (3) the statistical relation²¹ between Λ and the maximum rotation velocity V_M , \log

$V_M = 2.15 - \frac{1}{2}(\Lambda - 1)$, implies $\Lambda_c^G \approx 0.61 \pm 0.1$, if $V_M \approx V_0 = 220 \pm 15 \text{ km s}^{-1}$. On average $\Lambda_c^G = 0.65 \pm 0.05$. Then, with the adopted values of $M_T^0 = -20.2 \pm 0.15$ and $\log D_0 = 4.39 \pm 0.03$ (D_0 in parsecs) for $R_0 = 8.5 \text{ kpc}$ (Table 1), equations (7) and (8) give $\gamma^G = 19.15 \pm 0.25$ and $\delta^G = 4.18 \pm 0.05$.

These values, which happen to coincide with those, $\gamma = 19.15 \pm 0.16$ and $\delta = 4.18 \pm 0.045$, previously derived from the 16 calibrating galaxies¹⁴, confirm precisely the linear formulae adopted to calculate the distances of 458 galaxies¹⁴ on the short scale and the value of the Hubble constant $H_0 = 96 \pm 10 \text{ km s}^{-1} \text{ Mpc}^{-1}$ derived from them²². [Actually two different forms of interpolating formulae were used in ref. 14, and the resulting weighted mean moduli $\mu_0^G(\Lambda_c)$ are -0.07 less than those calculated from equations (7) and (8) with the γ^G, δ^G zero points; hence, with the latter, distances would be 3.2% greater and H_0 3.2% smaller, that is $H_0 = 93 \pm 11 \text{ km s}^{-1} \text{ Mpc}^{-1}$. This value is independent of the supergalactic anisotropy of the velocity field because the value of μ_0 in ref. 22 ($H_0 = 96$) resulted from simultaneous solutions for solar motion and Hubble constant based on 200 galaxies in the distance range $2 < \Delta < 32 \text{ Mpc}$ and well-distributed over both hemispheres.

Clearly the probability that $H_0 = 50 \text{ km s}^{-1} \text{ Mpc}^{-1}$ is very small calculated for a one-tail normal error law in $\log H_0$ it is $P(\mu_0') < 10^{-7}$.

Table 5 Probabilities $P(\mu_0')$ that the fundamental constants of the Galaxy are consistent with the long distance scale

Tests	Parameters	$P(\mu_0')$
Tully-Fisher relation in Virgo S cluster	R_0, V_0, M_T^0 B-band	1.5×10^{-9}
	H-band	2×10^{-6}
Faber-Jackson relations in Virgo E cluster	$R_0, \sigma_v(0), M_T^0, T$	$< 10^{-5}$
Magnitude-diameter-luminosity index relations for 458 spirals	$R_0, M_T^0, D_0, \Lambda_c$	$< 10^{-7}$
Magnitude and diameters of Galaxy compared with its 'sosie'	$R_0, M_T^0, D_0, D(r)$	$< 10^{-8}$
Mean magnitudes of globular clusters in Virgo E cluster	$R_0, M_T^0, m_v(\oplus), M_v(RR)$	$< 10^{-5}$
	$M_{bol}(0)$ (Miras)	

Fourth test: Galaxy and its 'sosies'

The concept of galactic 'sosies' has recently been introduced by Paturel²³ to describe galaxies that look essentially identical with respect to all available taxonomic criteria (such as type, colours, bulge-to-disk ratio, maximum rotation velocity and hydrogen-luminosity ratio). By application of Hubble's 'principle of the uniformity of nature', it is reasonable to expect them to have also closely similar luminosities and sizes.

According to numerous indices the four galaxies NGC 1073, 4303, 5921 and 6744, appear closely to resemble our Galaxy^{4,24}. The composite galaxy defined by the average of these four galaxies is a good 'sosite' of our Galaxy (Table 3a). On this basis the plausibility of proposed distance scales can be tested by comparison of the known values of the absolute magnitude and linear diameters of our Galaxy (Table 1) with those calculated for its 'sosite' in each of the two following cases: (1) $\langle\mu_0\rangle = \langle\mu_0^*(\Lambda_0)\rangle = 30.21$ on the short scale and corresponding to $H_0 = 95 \text{ km s}^{-1} \text{ Mpc}^{-1}$ (ref. 22), and (2) $\langle\mu_0'\rangle = 31.73$ on the long scale (with corrected Hyades zero point) and assuming $H_0' = 50$ (ref. 25). Table 3b shows that on the average the 'sosite' appears only 0.2 mag fainter than our Galaxy on the short scale, but 1.3 mag brighter on the long scale. Likewise, the diameters of the 'sosite' are $\sim 4\%$ less (corresponding to 0.1 mag fainter) on the short scale, but $\sim 96\%$ larger (corresponding to ~ 1.4 mag brighter) on the long scale. It is obvious that while the short scale implies a quasi-equality between the Galaxy and its 'sosite', as suggested by the taxonomic criteria, the long scale leads to a contradiction. To reconcile the metric and photometric parameters of the Galaxy and its 'sosite' on the long scale, one would need to change R_0 from 8.5 to ~ 16 kpc which would require a 4.5σ change in M_0^2 . It would also imply that the mean absolute magnitudes of the RR Lyr and long period variables are both 1.3–1.4 mag brighter than the best current estimates (Table 1), which is out of the question.

Fifth test: distance of the Virgo cluster and its implications

A final verification of the short scale and an independent confirmation of the impossibility of the long scale rest on a comparison of the implications of the distances proposed for the Virgo cluster, particularly the Virgo E cluster, in which many globular star clusters associated with spheroidal galaxies have been observed. According to Hanes²⁶ the mean apparent magnitude of these clusters, derived from their luminosity function, on the plausible assumption that it is gaussian with dispersion $\sigma_M = 1.1 \pm 0.1$ mag (ref. 27), is $\langle m_v \rangle = 23.3 \pm 0.4$. As shown in Table 4 this implies $\langle M_v(\oplus) \rangle = -7.22$, if Virgo E is at the distance (11.8 Mpc) corresponding to the mean distance modulus $\langle \mu_0 \rangle = 30.37 \pm 0.2$ on the short scale, but $\langle M_v(\oplus) \rangle = -8.46$, if it is at the distance (22.5 Mpc) corresponding to the mean modulus $\langle \mu_0' \rangle = 31.76$ postulated by the long scale^{1,2}.

Now, the mean magnitude difference between the globular clusters and the RR Lyr variables is $\langle M_v(\text{RR}) - M_v(\oplus) \rangle = 8.0 \pm 0.1$ (ref. 15). It follows that the short scale implies $\langle M_v(\text{RR})(\mu_0) \rangle = -7.22 + 8.0 = +0.78 \pm 0.4$, in excellent agree-

ment with the average of modern determinations of this primary indicator, $\langle M_v(\text{RR}) \rangle = +0.8 \pm 0.15$ (Table 1). But the long scale implies $\langle M_v(\text{RR})(\mu_0') \rangle = -8.46 + 8.0 = -0.46 \pm 0.4$, which is $1.26 \text{ mag} \approx 3\sigma$ brighter than the adopted value.

Furthermore, because the values of R_0 derived from RR Lyr and Mira-type variables are in excellent agreement (Table 1)⁶, one would also have to conclude that the zero point of the (bolometric) period-luminosity relation of the long period variables should be changed from $+0.76$ to -0.5 ± 0.4 , which would be another 3σ correction. The combined probability of such errors, that is of the hypothesis that the long scale is correct, is $P(\mu_0') < 2 \times 10^{-6}$.

Discussion and conclusions

The results of the five tests above, summarized in Table 5, singly and collectively demonstrate that reconciling the long scale with the known values of the basic metric, photometric and kinematic parameters of the Galaxy is practically impossible.

A detailed discussion of the various *ad hoc* hypotheses that might be advanced to escape this conclusion and 'save' the long scale (a different galactic extinction model, a large cosmic scatter about the T-F and F-J relations, large errors in the adopted values of the galactic parameters, systematic differences between the globular cluster luminosity functions in the Virgo cluster and the Galaxy) shows that none is plausible nor capable of quantitatively accounting for the 1.1–1.4 mag discrepancies. The conclusion seems inescapable that first on the short scale all galactic data fit in naturally within their known errors and there is no need to invoke special circumstances, and second the long scale fails all available tests by a large margin and cannot be reconciled with the galactic data.

The essentially independent scales based on the traditional approach, that is on primary, secondary and tertiary indicators², and the new approach using the Galaxy alone as a fundamental calibrator, are in near perfect agreement and the most probable value of the Hubble constant derived from them is $H_0 = 95 \text{ km s}^{-1} \text{ Mpc}^{-1}$.

The time scale argument often invoked in support of $H_0' = 50 \text{ km s}^{-1} \text{ Mpc}^{-1}$ and as an objection to the Hubble time, $T_H = H_0^{-1} \approx 10^{10} \text{ yr}$, associated with $H_0 = 95 \text{ km s}^{-1} \text{ Mpc}^{-1}$, rests entirely on the arbitrary (often implicit) hypothesis that a Friedmann model without cosmological constant is applicable to the real Universe. It is interesting that recent studies of the space distribution of quasars²⁸ lead, independently of any assumption on H_0 , to a Lemaître model with a small positive curvature parameter ($k = K/H_0^2 = +0.22$), a reasonable density parameter ($\Omega_0 \approx 0.07$) and a well-determined positive cosmological constant ($\Lambda = \Lambda/3H_0^2 = +1.15$), which implies a satisfactory value for the age of the Universe, $T_U \approx 1.8 \times 10^{10} \text{ yr}$ if $T_H = 10^{10} \text{ yr}$.

This work was supported by a visiting fellowship of the Australian National University while G. de V. was on research leave from the University of Texas. I acknowledge the support of both institutions and the hospitality of Mount Stromlo and Siding Spring Observatories.

Received 10 May; accepted 24 June 1982.

1. Tammann, G. A., Sandage, A. & Yahil, A. in *Physical Cosmology*, Les Houches, Sess. XXXII, 53 (North Holland, Amsterdam, 1979).
2. de Vaucouleurs, G. in *10th Texas Symp. in Relativistic Astrophysics*, 90–122 (New York Academy of Sciences, 1981).
3. van den Burgh, S. *The Galaxies of the Local Group* (Preprint, David Dunlap Observatory, No. 195, 1968).
4. de Vaucouleurs, G. & Pence, W. D. *Astr. J.* **83**, 1163–1173 (1978).
5. de Vaucouleurs, G., de Vaucouleurs, A. & Corwin, H. G. *Second Reference Catalogue of Bright Galaxies* (University of Texas Press, Austin, 1976).
6. de Vaucouleurs, G. *Astrophys. J.* (submitted).
7. Bahcall, J. & Soneira, R. M. *Astrophys. J. Suppl.* **44**, 73–110 (1980).
8. Tully, R. B. & Fisher, R. *Astr. Astrophys.* **54**, 661–673 (1977).
9. Bottinelli, L., Gouguenheim, L., Paturel, G. & de Vaucouleurs, G. *Astrophys. J. Lett.* **242**, L153–L156 (1980).
10. de Vaucouleurs, G., Peters, W. L., Bottinelli, L., Gouguenheim, L. & Paturel, G. *Astrophys. J.* **248**, 408–422 (1981).
11. Aaronson, M., Mould, J. & Huchra, J. *Astrophys. J.* **229**, 1–13 (1979); **237**, 655–665 (1980).
12. Tully, R. B., Mould, J. & Aaronson, M. *Astrophys. J.* (in the press).

13. de Vaucouleurs, G. *Astrophys. J.* **253**, 520–525 (1982).

14. de Vaucouleurs, G. *Astrophys. J.* **227**, 380–390, 729–755 (1979).

15. de Vaucouleurs, G. *Observatory* (in the press).

16. Faber, S. & Jackson, R. *Astrophys. J.* **204**, 668–683 (1976).

17. Whitmore, B. C., Kirshner, R. P. & Schechter, P. L. *Astrophys. J.* **234**, 68–75 (1979); **250**, 43–54 (1981).

18. de Vaucouleurs, G. & Olson, D. W. *Astrophys. J.* **256**, 346–369 (1982).

19. Simien, F. & de Vaucouleurs, G. *IAU Symp.* No. 100 (submitted).

20. de Vaucouleurs, G. *Astrophys. J. Suppl.* **6**, 213–234 (1961).

21. de Vaucouleurs, G. *The Evolution of Galaxies and Stellar Populations*, 43–94 (Yale University Observatory, New Haven, 1977); *Astr. J.* **85**, 182 (1980).

22. de Vaucouleurs, G. & Peters, W. L. *Astrophys. J.* **248**, 395–407 (1981).

23. Paturel, G. thesis, Univ. Lyon (1981); *Astr. Astrophys.* (submitted).

24. de Vaucouleurs, G. *IAU Symp.* No. 38, 18–25 (1970).

25. Sandage, A. & Tammann, G. A. *A Revised Shapley-Ames Catalogue of Bright Galaxies* (Carnegie Institution Publ. 635, Washington, 1981).

26. Hanes, D. A. *Mon. Not. R. astr. Soc.* **180**, 309–321 (1977); **188**, 901–909 (1979).

27. de Vaucouleurs, G. *Nature* **266**, 126–129 (1977).

28. Fliche, H. H. & Souriau, J. M. *Astr. Astrophys.* **78**, 87 (1979).

Time-resolved X-ray diffraction studies of the structural behaviour of myosin heads in a living contracting unstriated muscle

J. Lowy & F. R. Poulsen

Open University, Oxford Research Unit, Foxcombe Hall, Boars Hill, Oxford OX1 5HR, UK

The intensities of three regions of the low-angle X-ray diffraction pattern from a molluscan unstriated muscle have been followed during tension generation at a time resolution of 0.5–1 s using synchrotron radiation. The observed intensity changes can be reasonably interpreted in terms of myosin cross-bridge movements during the contractile cycle. A model that accounts for the intensity changes suggests that myosin heads move out from the thick filament during activation and attach to actin sites to produce tension with a small delay. During relaxation from both phasic and tonic contractions the heads remain attached to actin sites longer than it takes for tension to decay.

THERE is now general agreement that the transformation of chemical to mechanical energy in muscle is associated with a calcium-controlled interaction between actin and myosin during which ATP is split. The globular head of the myosin molecule is believed to attach and detach from actin in a cyclical manner and this is called the 'cross-bridge cycle'^{1,2}. We have used X-ray diffraction techniques to obtain time-resolved data about the behaviour of myosin heads during the mechanical contractile cycle in an unstriated muscle, the anterior byssus retractor (ABRM) of *Mytilus edulis*. Such investigations aim to produce structural information from normally functioning living muscles which is not only interesting for its own sake but can also help in the interpretation of biochemical data and formulation of kinetic schemes. The choice of the ABRM as our experimental material was motivated by the fact that it possesses certain unique structural and mechanical properties.

We define a contractile unit in the ABRM as the thick filament with its surrounding actin filaments. The unique structural feature of this muscle is that its thick filament diameter shows a wide variation^{3,4} which means that its contractile units cannot form a well-ordered lattice. This feature is also responsible for the smooth, streak-like appearance of the central equatorial diffraction (Fig. 1a).

Previous X-ray studies of the ABRM⁵ have demonstrated that the sideways packing of actin filaments produces a strong equatorial peak (Fig. 1a) at 14 nm. Our present interpretation of changes in the intensity of the peak is based on the assumption that the actin filaments are packed into a one-dimensional lattice (rosette) which surrounds the thick filament. This is supported by evidence from electron micrographs from this laboratory and by numerical modelling of the intensity distribution of the equatorial peak.

In addition to diffraction from the thick and thin filaments, we describe here for the first time the diffuse background (disk) diffraction (Fig. 1a) and show that this is likely to be associated with disordered myosin heads.

Stimulation of the ABRM with alternating current produces a phasic contraction⁶. After stimulation stops tension decays to zero somewhat more slowly than tension rise⁶. Treatment with acetylcholine⁷ gives a tonic response known as a catch contraction. After washing out the drug, relaxation can be up to two orders of magnitude slower than in a phasic contraction. From the physiological viewpoint the muscle is unique in that in catch contractions a high level of tension is maintained in the absence of active state (that is, ability for redevelopment of tension after a release^{8,9}) and energy turnover as measured by oxygen consumption¹⁰ is so low that the amount of ATP split must be insignificant.

Another drug, serotonin, exerts its most important effect on relaxation⁷. Thus, with increasing concentration, serotonin

speeds up tension decay in both phasic and catch contractions^{7,8}, until the rate reaches a value nearly as high as tension rise⁸. With natural seawater as a bathing solution, different muscles produce contractions with different relaxation rates. To obtain standardized muscles, serotonin was applied at a concentration of $10^{-4.5}$ M, which produces a completely reproducible relaxation rate¹¹.

In a standardized ABRM the half time of tension rise is ~ 1.5 s at 10 °C, about 50 times slower than the corresponding time at the same temperature for twitches of the striated frog's sartorius used by Huxley *et al.* in similar time-resolved X-ray experiments¹². In phasic contractions we were able to obtain useful data with a time resolution of 0.5–1 s. A time resolution of 1–3 min was adequate for the relaxation phase in catch contractions.

The preparation of the ABRM has been described previously, as have optimal methods of stimulation¹¹. The muscles used were about 25 mm long and 1 mm thick. They were maintained in oxygenated natural seawater (osmolarity about 600 mosmol) in a Perspex cell with mylar windows for the passage of X rays. The cell was fitted into a copper frame through which liquid from a heating/cooling bath was circulated in order to control the temperature of the muscle's bathing solution. Muscles were mounted isometrically with one end attached to a force transducer.

The experiments were carried out at the EMBL Outstation at DESY, Hamburg, using the electron-positron storage ring DORIS as the X-ray source. Both tension and X-ray data were transmitted into a computer. Details of the Hamburg set-up are given elsewhere¹³.

All our results were obtained with a muscle-to-detector distance of 3 m. Phasic contractions were produced by applying a.c. (50 Hz) via transverse electrodes for 6 s and an interval of 3 min was allowed between contractions¹¹. Three features of the low-angle X-ray diffraction pattern were studied using two placements of a position-sensitive detector (Fig. 1a, at P and Q). The X-ray features are the equatorial streak, the 14-nm equatorial peak and the central diffuse disk (Fig. 1a). All subsequent references to streak intensity mean the intensity at the 38-nm equatorial spacing (Fig. 1a, at Q).

Results

The equatorial streak and central diffuse disk were recorded together by placing the detector in the meridional direction at an equatorial spacing of 38 nm (Fig. 1a, at Q). The resting intensity profile thus obtained is shown in Fig. 2a together with the difference profile at peak tension. The boundary between streak and disk is indicated by the double arrows. At peak tension the streak has increased and the disk decreased in

intensity. Figure 3a shows the time course of the streak intensity integrated after subtraction of the disk-background. The intensity increases with an initial rate appreciably higher than that of tension which itself follows a sigmoidal time course. This gives the streak a 1.5-s lead in reaching half-maximum. About 3 s ahead of tension it reaches a plateau 25% above its resting intensity where it stays for about 12 s before returning with a 5-s lag behind tension at half-maximum. The intensity change recorded in the central disk (Fig. 3a) shows a decrease of about 35% which follows much the same time course as tension rise; it returns to its resting value more slowly than tension.

Two other ways of presenting the disk data are useful. First, the time dimension can be eliminated by plotting disk intensity against tension. This reveals a linear relationship during the rising phase but not during relaxation (Fig. 4a). It also allows pooling of results from experiments with different time courses. Second, to determine the relative number of scattering units

(see below) the intensity data can be drawn as Guinier plots¹⁴ (Fig. 5). To record the 14-nm equatorial peak the detector was oriented in the horizontal direction and placed as shown at P in Fig. 1a. The intensity profile thus obtained at rest and peak tension is seen in Fig. 2b.

During the rising phase, the intensity of the 14-nm peak decreases by maximally 50% with much the same time course as tension; it returns to its resting value appreciably more slowly than tension (Fig. 3b). The 14-nm peak does not broaden in the equatorial direction (Fig. 2b).

Plotting intensity against tension gives a linear relation during the rising phase but not during relaxation (Fig. 4b). Except for a difference in time scale the same results were obtained in catch contractions (Fig. 4c).

Structural interpretation of intensity changes

We consider models for the contractile units like that shown in Fig. 1b and take into account the known variation in their size. We assume constancy in the axial projection of the structure of the paramyosin core and the location of the actin filaments. Hence, the change in the location of the myosin heads will account for all the intensity changes. The reason for assuming constancy in the paramyosin core structure is that we observe no changes in intensity of the 36-nm paramyosin layer line during contraction. Arguments for a constant actin filament location are given in the discussion of the 14-nm equatorial peak.

Quantitative interpretation of the equatorial intensity changes is greatly assisted by knowing the relative masses of the proteins involved. To this end we calculate the masses of the proteins in a 72-nm long section for the various sizes of the contractile units. It is assumed that the number n_P of paramyosin molecules per nm² of cross-sectional area and the number n_M of myosin molecules per nm² of surface area of the core is independent of the core diameter, and that n_P and n_M are the same in the ABRM and in the opaque adductor of the oyster which has thick filaments of a similar type¹⁵. For the opaque adductor the frequency of occurrence f_i (expressed as a fraction of the total) of core diameter D_i has been determined using electron microscopy¹⁶. We calculate n_P to be 0.184 from X-ray data on the intermolecular distance extrapolated to the dehydrated state of the muscle^{17,18} (tetragonal unit cell side taken as 1.65 nm), and from the molecular repeat length of 144 nm (ref. 19). Taking the molecular weights (M_s , in daltons) for paramyosin (220,000) and myosin (470,000), and 8 as the mass ratio paramyosin/myosin for the opaque adductor²⁰, we find that n_M comes to 0.00302. We can now calculate the paramyosin and myosin masses in a contractile unit of length 72 nm as a function of core diameter.

We also want to know the average masses per 72 nm in the ABRM. Using f_i from ref. 4, we find that these values for paramyosin and myosin are 5.670 and 1.277×10^7 daltons, respectively. Then, taking the M_r of the myosin head as 121,000 (ref. 21), the myosin head mass comes to 0.658×10^7 daltons.

Taking the M_s of actin (42,000) and tropomyosin (70,000), a 2.75-nm axial repeat between actin monomers, and 7 actin monomers per tropomyosin molecule, we calculate that the mass m_A in a 72-nm long actin filament is 1.361×10^6 daltons. The number of actin filaments N_A surrounding a given thick filament can be determined from the core diameter (see Fig. 1b) and the spacing of 14 nm between actin filaments. However, due to the sharing of actin filaments between thick filaments, only the fraction $s = N_0 / \sum f_i \cdot N_A$ of their mass belongs to the contractile unit. N_0 is the observed average number of actin filaments per thick filament. Knowing that $N_0 = 16.7$ (ref. 4), we find that $s = 0.848$. The average mass of actin filament per 72 nm length is $N_0 \times m_A = 2.274 \times 10^7$ daltons. Thus, the mass ratio myosin head/actin filament comes to 0.29.

Taking into account the variation in the size of the contractile units, our calculations show that if all heads move from r to d in Fig. 1b, the average streak intensity at 38 nm increases by 11%; if they move to f the increase is 46%. In our experiments

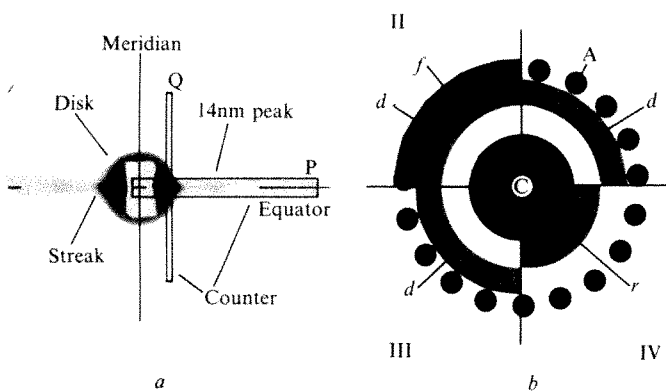


Fig. 1 a, Low-angle X-ray diffraction pattern of resting ABRM muscle in natural seawater recorded on film with an exposure time of 2.5 min and a muscle-to-film distance of 3 m. Note the equatorial streak, central diffuse disk and 14-nm equatorial peak. The two positions (P and Q) of the one-dimensional position-sensitive detector are shown in terms of the effective window used in the time-resolved experiments with contracting muscles. Detector position Q is at an equatorial spacing of 38 nm. The boundary between the streak and the 14 nm peak is at an equatorial spacing of about 20 nm. b, Model of contractile unit used for the interpretation of equatorial intensity changes. Division into four quadrants represents phases in the mechanical contractile cycle which are referred to in the text. In the ABRM a variety of thick filament diameters are present³ and the frequency of occurrence f_i has been determined⁴ ($\sum f_i = 1$). The paramyosin core C of radius r_{Ci} is surrounded by a rosette of $N_{Ai} = 2\pi r_{Ai}/14$ nm evenly spaced actin filaments A (centre-to-centre distance 14 nm) of 8 nm diameter and at a radial position $r_{Ai} = r_{Ci} + 24$ nm. The radial position r_{Si} of the centres of mass of the myosin heads can vary from $r_{Ci} + 5$ nm at r , to $r_{Ci} + 15$ nm at d , to $r_{Ci} + 24$ nm at f . The intensity of the equatorial streak is $\sum f_i \cdot I_i$, where I_i is the intensity from the i th size of unit: $I_i = (F_{Ci} + F_{Ai} + F_{Si})^2$, where $F_{Ci} = w_{Ci} \cdot 2J_1(2\pi r_{Ci}R)/(2\pi r_{Ci}R)$, $F_{Ai} = w_{Ai} \cdot J_0(2\pi r_{Ai}R)$ and $F_{Si} = w_{Si} \cdot J_0(2\pi r_{Si}R)$. These formulae are explained by Vainshtein²⁴. w_{Ci} , w_{Ai} and w_{Si} are the respective masses of paramyosin, actin plus tropomyosin, and myosin head in a 72-nm long section of a contractile unit of the i th size. The equatorial position R is $1/38$ nm. At this value of R higher order Bessel functions can be omitted in the expression for F_{Ai} as can the contribution from the shape factors for the various molecules. The calculations show that if all myosin heads move from r to d , the streak intensity at 38 nm increases by 11% and that if they move to f , the increase is 46%. The 14-nm peak comes basically from the evenly spaced actin filaments. Its intensity is reduced as myosin heads enter the spaces between actin filaments. In our model practically all actin filaments are part of the rosettes, and this, together with our two-state structural model (see text), means that the intensity of the 14-nm peak is of the following form: $I = I_0 \cdot (\mu_A - x\mu_{Si})^2$, where I_0 is the intensity with no myosin heads in the rosette spaces, μ_A and μ_{Si} are, respectively, the total masses of actin filaments and of myosin heads, and x is the fraction of the myosin heads present in the rosette spaces. As shown in the text, μ_{Si}/μ_A is 0.29. This means that the maximum possible intensity decrease is to 50%. Although the above expression for the intensity as a function of number of myosin heads in the rosette spaces is parabolic, the relation is practically linear over the range where the intensity is reduced by a factor of two. In our model the myosin heads are disordered in locations r and d . They produce the central diffuse disk which will have an intensity directly proportional to the number of disordered heads. The intensity of the disk will be independent of the radial position of the myosin heads, but as they enter the rosette spaces, they will become sufficiently ordered not to contribute to the disk.

the actual intensity increase at peak tension ranges from 25 to 50%. This indicates that during tension rise myosin heads move radially outward from the thick filament surface and at least partly into the rosette spaces.

Our finding that during contraction the intensity decrease in the 14-nm peak is not accompanied by any change in its equatorial width (Fig. 2b) means that the intensity decrease is

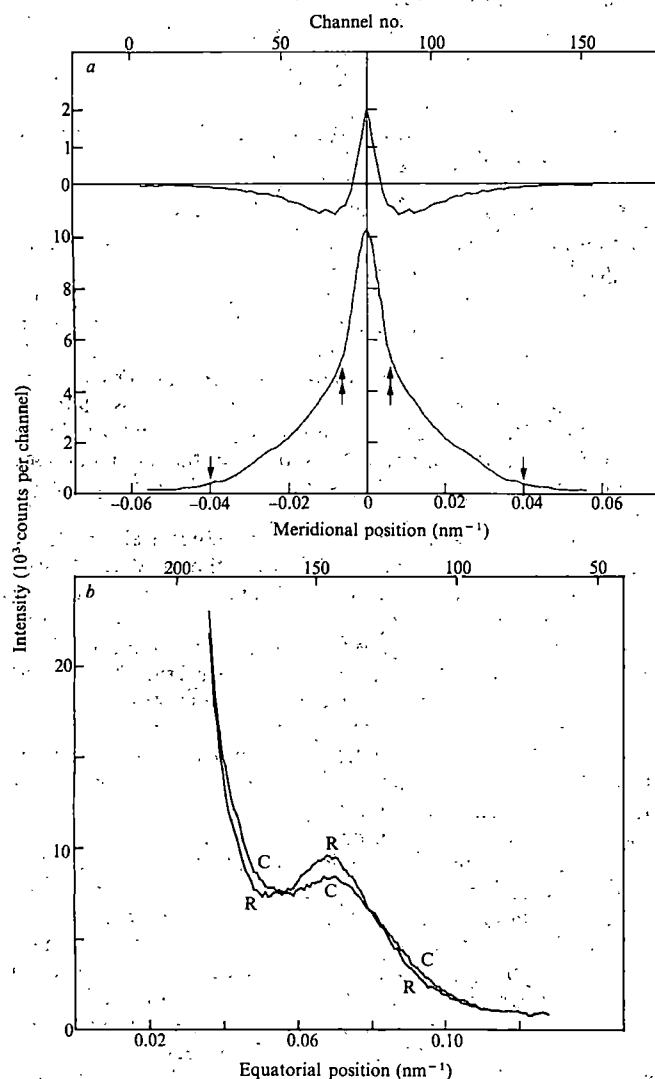


Fig. 2 *a*, Intensity profiles obtained with the detector in the meridional direction and located at an equatorial spacing of 38 nm (position Q in Fig. 1a) where the streak and disk are recorded together. Resting profile (lower curve) and change in profile (upper curve) at peak of tension in a phasic ABRM contraction at 28 °C in sea water with serotonin. Note that the disk intensity (between single and double arrows) has decreased and that the streak intensity (inside double arrows) after subtraction of the disk background has increased. The justification for dividing the data into two components is that during contraction the intensity at any point outside the double arrows follows one particular time course (equal to that shown in Fig. 3a, \diamond) and at any point inside it follows a completely different time course. (The main features of the latter are a sharp peak that occurs about 2 s after the beginning of stimulation, followed by a pronounced minimum which practically coincides with peak tension and after that there occurs a second broader peak.) After subtraction of the background formed by the disk, the time course is equal to that shown in Fig. 3a, Δ . The disk background was estimated as the intensity in 10 channels just outside the double arrows on both sides of the profile. *b*, Intensity profiles recorded with the detector along the equator (position P in Fig. 1a) and at rest (R) and at peak of tension in phasic contractions (C). These data were accumulated from experiments on four different muscles. The 14-nm peak appears on a fairly steep background, coming mainly from the streak and the disk. The time course of the integrated intensity of the peak after background subtraction during phasic contraction is shown in Fig. 4b. The background was defined as the best second-order polynomial fitted to the intensity on either side of the peak. Further analysis of the peak profile shows that as its intensity decreases, no changes in its equatorial width take place but that its spacing can decrease up to 3%. The latter indicates that the actin rosette moves closer to the thick filament surface when cross-bridges are formed during generation of tension.

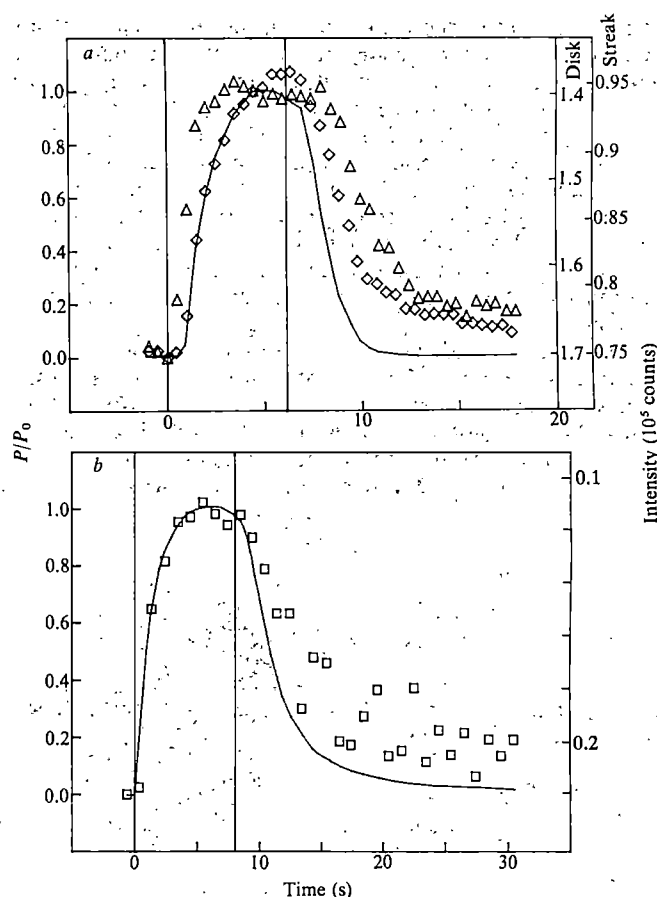


Fig. 3 *a*, Time courses of tension (—), streak intensity (Δ) and disk intensity (\diamond) recorded with the detector as shown in Fig. 1a at position Q during a phasic contraction at 28 °C in seawater containing serotonin. The period of stimulation is indicated by two vertical lines. The time resolution was 0.5 s. Streak intensity was integrated between the double arrows shown in Fig. 2a after subtraction of the background defined by the disk (outside double arrows). Disk intensity was integrated between the single and double arrows as shown in Fig. 2a. Note that the streak intensity increases much faster than tension and has reached a plateau within 2 s of the start of stimulation. Streak intensity remains at this plateau value until tension has decayed to about 20%. When tension is zero the streak intensity is only halfway back to its resting value. Disk intensity also takes longer than tension to return to its resting value but during the rising phase disk intensity decreases with a time course close to that of tension. *b*, Time course of tension (—) and integrated intensity of the 14-nm equatorial peak after background subtraction (\square) during a phasic contraction in natural seawater at 14 °C. The period of stimulation is indicated by two vertical lines. The time resolution was 1 s. Note that during the rising phase the intensity decreases with the same time course as tension increases whereas during relaxation the intensity recovers much more slowly than tension decays.

not due to a decrease in the packing order of the actin filaments. This is because analytical arguments¹⁴ show that in small one-dimensional lattices a decrease in intensity caused by disorder also leads to a widening of the peak in the equatorial direction. We have confirmed this argument by numerical modelling. Thus, it may be concluded that the observed intensity decrease is produced entirely by the extra mass added to the actin filaments as myosin heads.

The extent of the intensity decrease in the 14-nm peak depends on the peak tension. The maximal observed decrease was by 50%. To explain such a large change with the available myosin head mass relative to the actin filament mass (which as shown above is 0.29:1), the myosin heads must move to their most effective position, namely fully into the space between the actin filaments as shown in Fig. 1b at *f*. In that location we calculate that a mass ratio of 0.29 will cause a 50% decrease in the intensity of the 14-nm peak. This interpretation of the movement of myosin heads into the rosette spaces is supported by the data on the streak intensity changes.

The circular symmetry of the disk (Fig. 1a) indicates that the scatter is due to completely disordered units. The Guinier plot¹⁴

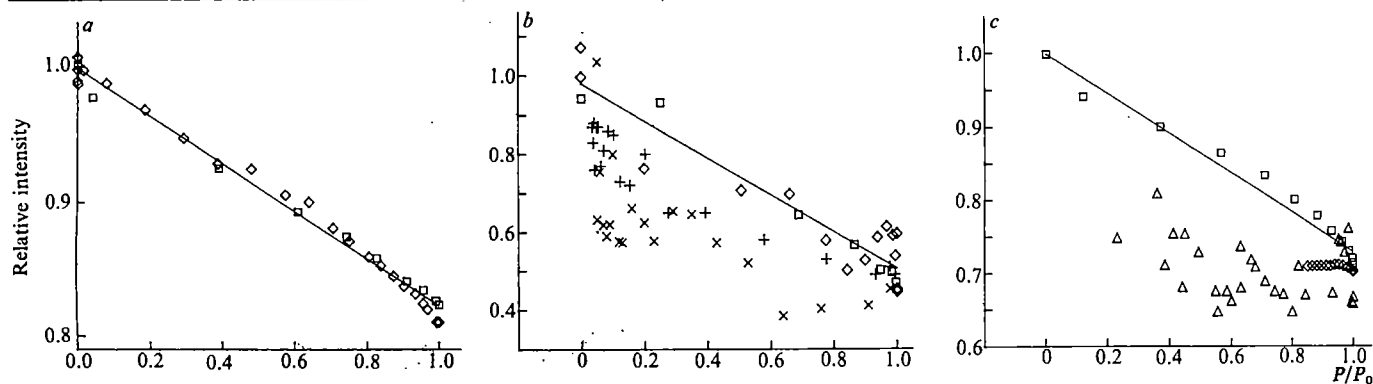


Fig. 4 *a*, Relationship between disk intensity and tension during the rising phase. Data taken from Fig. 3*a* (\square) and from an experiment carried out at 10 °C where the time course was about a factor of two slower (\diamond). Here and in *b* and *c* the regression line of intensity of tension is shown during the rising phase. *b*, Relationship between intensity of the 14-nm equatorial peak and tension during phasic contractions. Data for tension rise and relaxation phase (\square , +), respectively, were taken from Fig. 3*b* and from one other similar experiment (\diamond , \times) where the time resolution was 0.5 s and the time course of tension rise was identical to that shown in Fig. 3*b*. *c*, Relationship between intensity of the 14-nm equatorial peak and tension during tonic contraction produced by application of acetylcholine (5.5×10^{-6} M). In one experiment the time resolution was 2 s during both the rising phase (\square) and the catch phase of relaxation (\diamond) which follows washing out of acetylcholine. Further data from the relaxation phase of three other muscles are shown (\triangle) where the time resolution was 3 min. Except for the difference in time scale, the relationship between intensity and tension closely resembles that observed in phasic contractions illustrated in *b*.

gives a straight line (Fig. 5), indicating that the disk is due to one kind of scattering unit. The zero-angle intensity can be estimated by extrapolation of the line to its intercept with the intensity axis and is a measure of the number of scattering units¹⁴. In the experiment illustrated (Fig. 5), the observed change in the zero-angle intensity corresponds to a 35% decrease in that number at peak tension. The slope of the line is directly related to the radius of gyration R_g (ref. 14). As the slope does not change during contractions it follows that this also applies to the size of the scattering unit. Moreover, it means that the integrated intensity of any section of the disk gives a direct measure of the number of scattering units.

The close similarity between the time course of tension and change of intensity of the disk during the rising phase of contraction (Fig. 3*a*) suggests that the scattering units are composed of disordered myosin heads that become ordered on attachment to actin sites. The R_g values determined from the slope of the Guinier plots ranged from 8 to 16 nm. These values are similar to those obtained for heavy meromyosin from light scattering studies (14.7–18.5 nm, ref. 22) and suggest that in the ABRM the scattering unit is a dimer of myosin heads.

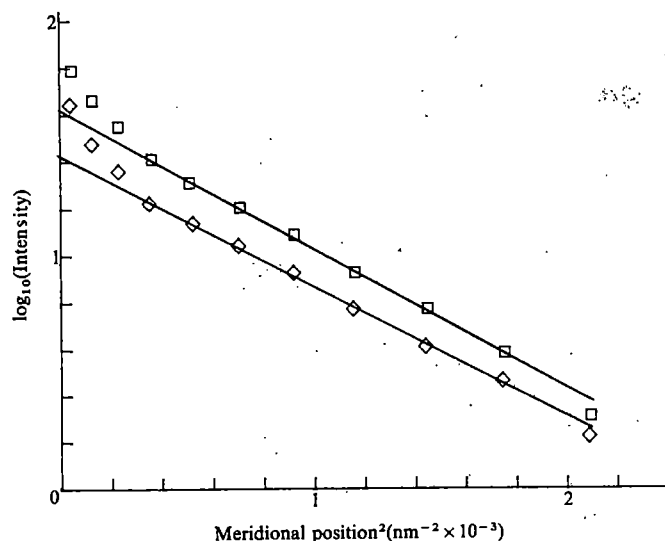


Fig. 5 Guinier plots¹⁴ of intensity profiles recorded with detector positioned as shown in Fig. 1*a* at Q; before stimulation (\square) and at peak tension (\diamond) in a phasic contraction at 14 °C in the presence of serotonin. The linear parts of the plots correspond to the diffuse disk. See text for summary of evidence on which it is suggested that the disk is due to disordered myosin heads. The deviation from the linear relation at small values of the square of the meridional position is caused by the superposition of the streak on the disk (see Fig. 2*a*). The slope of the straight line we have determined from the off-centre section through the disk is the same as that which would be derived from a section through the centre. Since the slope does not change during contraction, the intercept of the line with the intensity axis is directly proportional to the zero-angle intensity.

Discussion

Having reached *d* in Fig. 1*b*, the myosin heads could move into the rosette spaces in various different ways. Two extreme possibilities are that all heads move simultaneously towards their final position at *f* or that they move one-by-one fully into this position. Any significant contribution from the first mode of movement can be excluded because this would lead to a severe distortion of the shape of the 14-nm equatorial peak during tension rise. Our results during tension rise show no shape changes from those illustrated in Fig. 2*b*. Thus, we arrive at a structural mechanism for the movement of myosin heads in and out of the rosette spaces which can be represented by a two-state structural model where cycling myosin heads spend most of their time being either fully inside or fully outside the rosette spaces. Assuming that our identification of the disordered scattering units as myosin heads is correct, further support for the proposed model can be deduced from the finding that the number of disordered scattering units decreases during tension rise with the same time course as that of the increase in the number of myosin heads accumulating in the rosette spaces (Fig. 3*a,b*). This would indicate that during tension rise the myosin heads go directly from the disordered state into the ordered state in the rosettes.

The change in intensity of the equatorial streak has a significant lead over tension (Fig. 3*a*). In muscles like the ABRM it is known that the myosin heads are switched on by an action of Ca^{2+} on the light chains²³. We suggest that in this system, Ca^{2+} release also has a direct effect on the transfer of myosin heads from the thick filament surface to actin and that this effect is active and unidirectional. In other words, Ca^{2+} release does not bring about the transfer of myosin heads by shifting a passive equilibrium towards actin as an initial small fraction of myosin heads (already at actin) are switched on and attach. If that happened the rate of myosin head transfer would not exceed that of tension rise. It therefore appears that the time course of the streak intensity increase could give a direct measure for the spread of activation.

During the rise of tension it seems likely that the fall of intensity in both the 14-nm peak and in the disk are due to the close attachment of myosin heads to the actin filaments, and our model (Fig. 1*b*) suggests that the heads are then located between neighbouring filaments. The close similarity of time course of the tension and intensity changes implies that tension rises in direct proportion to the number of attached myosin heads.

Our results suggest an interesting structural explanation for the catch mechanism. During catch relaxation (Fig. 4*c*) the 14-nm peak intensity–tension relation is completely different from the linear one observed during tension rise. It appears that myosin heads remain in the rosette spaces for a

considerable time after they stop their chemical cycle, and this could explain how passive tension is held during catch^{8,9}. If, but for a difference in time scale, the same happens during phasic relaxation (Fig. 4b), this would also explain why here 'active state' decays faster than tension⁸. Serotonin would then act to speed up the release of passive myosin heads from the rosette spaces in both catch and phasic contractions.

On our interpretation of the disk scattering, the results presented in Figs 3a and 4a show that during tension rise the number of disordered myosin heads decreases with the same time course as the number of attached ones increases. From this it is conceivable that the disordered myosin heads could represent the detached phase of the cross-bridge cycle. If that can be confirmed, further analysis of our data will produce estimates for rate constants of attachment and detachment of myosin heads in the cross-bridge cycle.

Taking all the results and interpretations, the sequence of structural events during the mechanical contractile cycle may be summarized as follows (Fig. 1b, quadrants I–IV). On activation, disordered myosin heads move away from the paramyosin core surface towards the actin filaments (IV–I), causing an

increase in streak intensity but no change in disk intensity. As myosin heads start cycling they move into the spaces between the actin filaments (I–II), causing a decrease in intensity of both the 14-nm peak and the disk because such myosin heads are no longer disordered enough to contribute to the disk; a further increase in the streak intensity will also occur. When tension has decayed to a low level myosin heads leave the rosette spaces (II–III), causing the 14-nm peak and disk intensities to recover. Eventually, myosin heads move back to the core surface (III–IV) and streak intensity returns completely to its resting level.

We thank Drs J. Bordas and M. H. J. Koch (EMBL Outstation, Hamburg) for their most effective and enthusiastic collaboration in carrying out the experimental work and data reduction; Drs R. H. Abbott, H. E. Huxley and R. M. Simmons for many useful discussions; and Professor R. H. Stülmann (Head of Outstation, Hamburg), Dr D. A. Blackburn (Director of Oxford Research Unit), Professor G. F. Elliott (Head of Biophysics Group, Oxford Research Unit) and other members of the staff in Hamburg and Oxford for their support. This work was supported by the MRC and the Muscular Dystrophy Association of the USA.

Received 27 October 1981; accepted 1 July 1982.

1. Huxley, H. E. *Science* **164**, 1356–1366 (1969).
2. Huxley, A. F. *Prog. Biophys. biophys. Chem.* **7**, 255–318 (1957).
3. Lowy, J. & Hanson, J. *Physiol. Rev.* **42**, 34–47 (1962).
4. Sobieszek, A. J. *Ultrastructure* **43**, 313–343 (1973).
5. Lowy, J. & Vibert, P. J. *Nature* **215**, 1254–1255 (1967).
6. Fletcher, C. M. J. *Physiol., Lond.* **91**, 172–185 (1937).
7. Twarog, B. M. J. *cell. comp. Physiol.* **44**, 141–163 (1954).
8. Lowy, J. & Millman, B. M. *Phil. Trans. R. Soc. B246*, 105–148 (1963).
9. Jewell, B. J. *Physiol., Lond.* **149**, 154–177 (1959).
10. Baguet, F. & Gillis, J. M. J. *Physiol., Lond.* **198**, 127–143 (1968).
11. Cornelius, F. & Lowy, J. *Acta physiol. scand.* **102**, 167–180 (1978).
12. Huxley, H. E., Faruqi, A. R., Milch, J. R., Bordas, J. & Koch, M. H. J. *Nature* **284**, 140–143 (1980).

13. Bordas, J., Koch, M. H. J., Clout, P. N., Boulin, C. & Gabriël, A. J. *Phys. scient. Instrum.* **E13**, 938–944 (1980).
14. Guinier, A. in *X-Ray Diffraction* 326–333 (Freeman, San Francisco and London, 1963).
15. Hanson, J. & Lowy, J. *Proc. Roy. Soc. B154*, 173–196 (1961).
16. Elliott, G. F. *J. molec. Biol.* **10**, 89–104 (1964).
17. Elliott, A., Lowy, J., Parry, D. A. D., & Vibert, P. J. *Nature* **218**, 656–659 (1968).
18. Elliott, A. & Lowy, J. *J. molec. Biol.* **53**, 181–203 (1970).
19. Elliott, A. *J. molec. Biol.* **132**, 323–341 (1979).
20. Elliott, A. *Proc. R. Soc. B186*, 53–66 (1974).
21. Mendelson, R. & Kretzschmar, K. M. *Biochemistry* **19**, 4103–4108 (1980).
22. Holtzer, A., Lowey, S. & Schuster, T. in *The Molecular Basis of Neoplasia* 259–280 (University of Texas Press, Austin, 1962).
23. Kendrick-Jones, J., Lehman, W. & Szent-Györgyi, A. *J. molec. Biol.* **54**, 313–326 (1970).
24. Vainshtein, B. K. in *Diffraction of X-Rays by Chain Molecules* 125–143 (Elsevier, Amsterdam, 1966).

Left-handed Z-DNA is induced by supercoiling in physiological ionic conditions

Charles K. Singleton*, Jan Klysik*, Steven M. Stirdivant* & Robert D. Wells*

Department of Biochemistry, College of Agricultural and Life Sciences, University of Wisconsin-Madison, Madison, Wisconsin 53706, USA

In physiological ionic conditions (200 mM NaCl), the (dC–dG)₁₆ and (dC–dG)₁₃ blocks in plasmid pRW751 are in a left-handed state when the negative superhelical density of the plasmid is greater than 0.072. As the salt concentration decreases or when (d^mC–dG) sequences are present, less negative supercoiling is required to induce the right- to left-handed DNA transition. Furthermore, the single strand-specific nuclease, S₁, recognizes and cleaves aberrant structural features at the junction between neighbouring right- and left-handed DNA regions.

RECENT studies^{1–3} have demonstrated that alternating (dC–dG) sequences can adopt a left-handed helical conformation in negatively supercoiled plasmids in high salt (several molar) conditions. Furthermore, the torsional strain of superhelical DNA can enhance the salt-induced transition from a right-handed to a left-handed helical state². This is consistent with the unfavourable free energy of superhelix formation^{4,5}. Thus, processes which bring about relaxation of negative superhelical density such as a right- to left-handed helical transition have a favourable free energy input from the reduction of this torsional strain.

Alternating (dC–dG) sequences also are self-complementary (that is they have inverted repeat symmetry) and thus in principle are able to form hairpin loops or cruciforms. It has been shown recently that supercoiling can stabilize and bring about the formation of cruciforms at inverted repeats of several circular DNAs^{6–8}. Thus, it was of interest to determine if the 32-

and 26-base pair (bp) (dC–dG) stretches of pRW751 (ref. 1) would adopt a cruciform structure in low salt conditions. This was tested by using single strand-specific nucleases (S₁ and gene 3 product of phage T₇) as probes for the cruciform state^{6–8}. Surprisingly, we found that cruciforms are not formed in the two (dC–dG) blocks but instead, a right- to left-handed primary helical transition is induced solely by the torsional strain of supercoiling at millimolar salt concentrations. This transition is sensitive to the salt concentration and C5 methylation within the (dC–dG) blocks such that decreasing salt concentrations and methylation allow the transition to occur at lower negative superhelical densities. Also, we show that S₁ nuclease recognizes structural features of the junction between adjacent left-handed and right-handed helical segments.

S₁ nuclease treatment of pRW751

The plasmid pRW751 has been characterized previously^{1,9}. Briefly, this plasmid is a pBR322 derivative containing an insert of 157 base pairs into the *Bam*HI site. The insert consists of a 95-bp *Escherichia coli* *lac* operator DNA fragment flanked by

* Present addresses: University of Alabama, Birmingham, Schools of Medicine and Dentistry, Department of Biochemistry, Birmingham, Alabama 35294, USA (C.K.S., J.K., R.D.W.); The Biological Laboratories, Harvard University, Cambridge, Massachusetts 02138, USA (S.M.S.).

alternating (dC-dG) stretches of 32 and 26 bp (Fig. 2). Samples of this plasmid with various negative superhelical densities were generated and characterized as described previously¹⁰. Agarose gel electrophoresis of several of these samples is shown in Fig. 1a, and the calculated mean negative superhelical density of each is listed in Fig. 1 legend. As the negative density increases, the gel mobility increases.

Each sample was treated with *S*₁ nuclease, followed by *Ava*II restriction digestion, to determine whether supercoiling could induce any single strand structural feature(s) which *S*₁ nuclease might recognize and cleave. Figure 1b illustrates that several

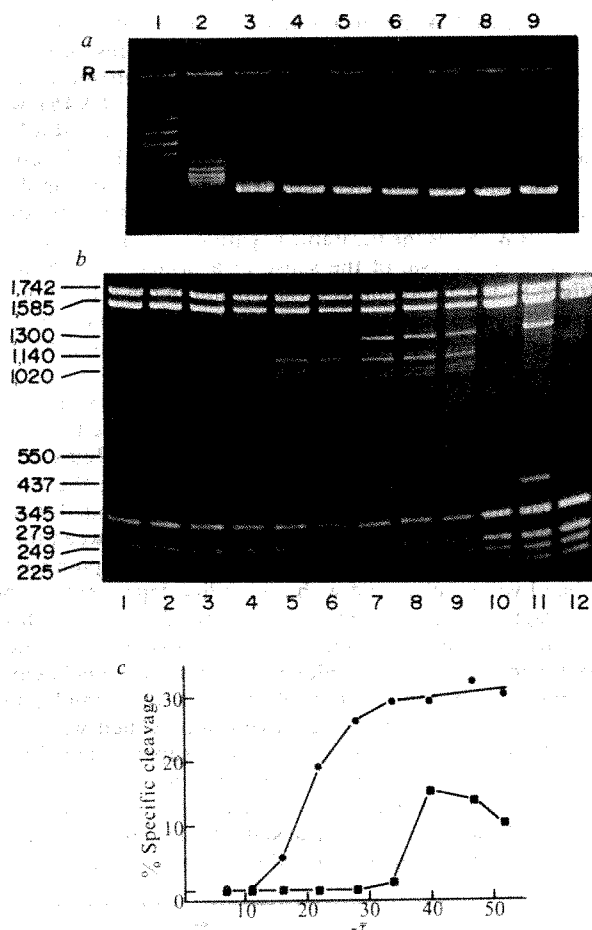


Fig. 1 Cleavage of pRW751 with *S*₁ nuclease followed by *Ava*II digestion. **a**, 1% agarose gel electrophoresis (80 mM Tris-acetate, 40 mM Na acetate, 2.5 mM EDTA pH 8.3, 85 V, 18 h) of various supercoiled samples of pRW751. The samples were generated and characterized as described elsewhere¹⁰. Plasmid DNA was isolated as described previously⁹. The mean negative titratable superhelical density in *S*₁ digestion conditions was: 1, 0.015; 2, 0.024; 3, 0.035; 4, 0.048; 5, 0.062; 6, 0.075; 7, 0.088; 8, 0.104; 9, 0.115 (calculated using 10 bp per turn and pRW751 = 4,518 bp). **R**, relaxed plasmid. **b**, Aliquots (1.5 μ g) of each sample shown in **a** were treated with 0.08 units of *S*₁ nuclease²⁸ in 50 μ l of 40 mM Na acetate, 50 mM NaCl, 1 mM ZnSO₄, pH 4.6. Reactions were carried out at 37°C for 50 min then stopped by addition of 2 μ l of 500 mM EDTA-2Na, pH 8. Following dialysis against 15 mM Tris-HCl, 6 mM NaCl, 6 mM MgCl₂, 2.5 mM dithiothreitol, pH 7.7, one unit of *Ava*II (BRL) was added and digestion was carried out at 37°C for 5 h. The DNA fragments were then separated by 2% agarose gel electrophoresis (same buffer as above, 175 V, 5 h). Lanes 1–9 correspond to the supercoiled pRW751 samples shown in **a**; lane 10 is pRW751 without *S*₁ treatment; lanes 11 and 12 are control plasmid pRW451 (ref. 1) treated with and without *S*₁, respectively. 1,140, 1,020 and 550 bp represent the approximate centre for each doublet. **c**, Specific cleavage by *S*₁ nuclease plotted against $-\sigma$ (mean number of negative superhelical turns). A photographic negative of **b** was traced using a Joyce-Loebl microdensitometer, and the area of each peak was determined in conditions of linearity. Specific cleavage near the (dC-dG) blocks was obtained from the ratio of the 1,585-bp band (containing the (dC-dG) inserts) to the 1,742-bp band relative to this ratio for the sample not treated with *S*₁ (●). Specific cleavage at the major pBR322 cruciform site^{6,7} was determined analogously after *Taq*I digestions and analysis of loss of the fragment containing this site (■).

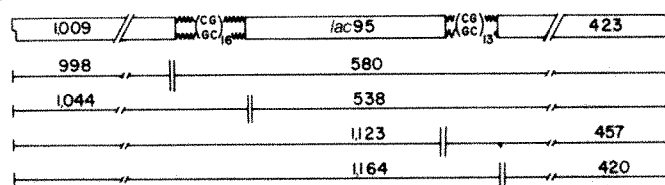


Fig. 2 Fragment sizes generated by *S*₁ nuclease-specific cleavages near the (dC-dG) blocks of pRW751. Sample 9 of Fig. 1a, b was digested first with *S*₁ nuclease and then with *Ava*II as described in Fig. 1 legend. The resulting fragments were separated by 2% agarose gel electrophoresis together with the appropriate size markers. The top line represents the (dC-dG)-containing 1,585-bp *Ava*II restriction fragment. Within this fragment, the sizes of non-(dC-dG) as well as the (dC-dG) sequences are indicated. The sizes of the *S*₁-specific bands derived from the *Ava*II 1,585-bp band were determined²⁹ and are illustrated by the bottom four lines. The larger bands are correct to within ± 10 bp, while the accuracy for the smaller bands is ± 7 bp. The known length of fragments possessing an *Ava*II terminus and ending at a non-(dC-dG)/(dC-dG) interface (junction) are (from left to right): 1,009 + 576; 1,041 + 544; 1,136 + 449; 1,162 + 423. Mapping of the bands arising from *S*₁ cleavage at the major pBR322 cruciform gave 1,300 bp (1,306 expected) and 437 bp (436 expected).

*S*₁-specific bands appear as the negative density increases. These bands were not present in the controls which were not treated with *S*₁ nuclease (Fig. 1b, lanes 10, 12).

The first bands which appeared were four sets of doublet bands centred around 1,140, 1,020, 550 and 430 base pairs. Concomitant with the appearance of these bands, the *Ava*II 1,585-bp band decreased in intensity compared with the other *Ava*II bands. The 1,585-bp band contains the (dC-dG)-flanked insert of pRW751. Also, as the doublet bands were not seen when pRW451 (ref. 1; control plasmid of about the same size as pRW751 but not containing any alternating (dC-dG) sequences) was treated with *S*₁ nuclease, these bands are specific for the (dC-dG)-containing insert. At higher negative superhelical densities, two new bands appeared; these can be assigned to *S*₁ cleavage at the major pBR322 cruciform site^{6,7} based on their mobilities and their production when the control plasmid, pRW451, was treated with *S*₁ nuclease (Fig. 1b, lane 11).

The per cent specific cleavage (relative loss of the restriction fragment containing the 157-bp insert or the pBR322 cruciform site) by *S*₁ nuclease at these sites was plotted against the number of mean negative superhelical turns for each sample (Fig. 1c). Specific cleavage within the 1,585-bp band reached a maximum at a negative superhelical density of ~ 0.07 and remained at this level as the negative density increased.

Mapping of *S*₁ nuclease-specific cleavage sites

The *S*₁ nuclease-specific fragments shown in Fig. 1b were sized by gel electrophoresis of an *S*₁ nuclease-treated, *Ava*II-digested sample, together with markers of the appropriate lengths. The results of this mapping are illustrated in Fig. 2. For the eight bands derived from the *Ava*II 1,585-bp fragment, *S*₁ nuclease cleavage occurred in the regions flanking the (dC-dG) blocks, within 2–13 bp of the first alternating (dC-dG) residues. This pattern of cleavage explains the appearance of doublet bands; the larger band of each doublet represents cleavage near the boundary of a (dC-dG) block distal to an *Ava*II site while the smaller band resulted from cleavage near the proximal boundary. The average length difference for the two bands of each doublet was 44 bp for the doublets corresponding to cleavage around the 32-bp (dC-dG) block and 39 bp for those flanking the 26-bp (dC-dG) block. Mapping of the *S*₁ nuclease cleavage sites with other restriction endonucleases (*Pst*I, *Eco*RI and *Alu*I) was in complete agreement with the *Ava*II mapping data.

Models consistent with doublet pattern

At least two models are consistent with this pattern of cleavage. The first would be cleavage by *S*₁ nuclease at the junction between the normal helix and the stem of a cruciform. This model seems unlikely, however, as *S*₁ nuclease cleavage at cruciforms has, so far, always mapped as a single band consistent

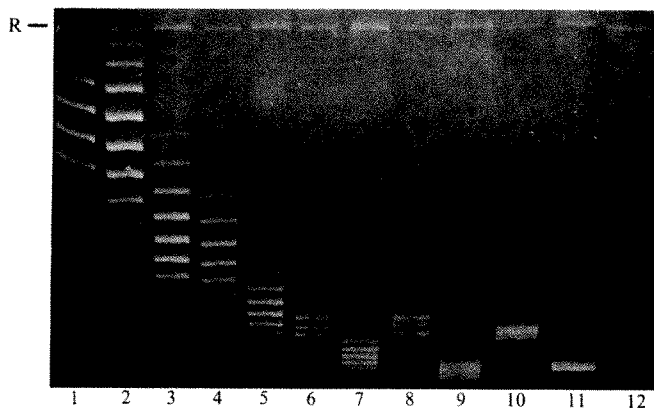


Fig. 3 Gel electrophoretic analysis of supercoiled samples of pRW751 (even-numbered lanes) and pRW451 (odd-numbered lanes). 2% Agarose gel electrophoresis was carried out using the buffer system described in Fig. 1 legend. Electrophoresis was at 140 V for 29 h. The calculated mean number of negative supercoils (and that determined by gel electrophoresis) is: lane 1, 5.3(5); 2, 5.3(5); 3, 9.1(9); 4, 10(10); 5, 13.3(13.5); 6, 14.6(14); 7, 17(18); 8, 18.1(15); 9, 22(21.5); 10, 23.9(16); 11, 26.5(-); 12, 29.4(18.5). A value for sample 11 was not obtained due to the lack of resolution of topoisomers at this high density. R, relaxed plasmid.

with cleavage within the single strand loop region (Fig. 1b)^{6,7}. Even though alternating (dC-dG) sequences are not interrupted with a region of non-inverted symmetry, steric constraints argue that a loop of at least four bases must occur^{11,12}. A cruciform within the (dC-dG)₂₆ block would thus have a loop of 4 bases and a stem of 11 bp; such a cruciform should be comparable in stability to the pBR322 major cruciform. However, the results presented in Fig. 1 show that the S₁ nuclease-specific bands corresponding to cleavage at the 26-bp (dC-dG) boundaries appear at much lower negative superhelical densities than the bands corresponding to cleavage at the pBR322 cruciform site.

A second model consistent with the cleavage pattern observed is that the torsional strain of supercoiling induced a right- to left-handed helical transition of the (dC-dG) blocks. Such a transition would partially relieve this torsional strain. As the unfavourable free energy of superhelix formation increases quadratically with increasing negative superhelical density^{4,5}, this transition would be more favourable at higher negative densities. Because only the (dC-dG) sequences in the plasmid can undergo this transition^{1,2,13}, a junction must be present between the left-handed helical (dC-dG) sequences and the right-handed helical flanking sequences¹. If this junction possesses any single-strandedness, S₁ nuclease may be recognizing and cleaving at these sites. Although little is known about the structural details of a right-handed-left-handed helical junction, model building studies have suggested that at least one base pair 'slip-out' is required within the junction due to steric constraints¹⁴. As discussed below, other data support this second model.

Gel analysis reveals relaxation of negative supercoils

pRW751 samples possessing a gaussian distribution of about eight topoisomers were used to obtain the results presented in Fig. 1. These samples were produced and characterized by a method which, in essence, determines the average amount of unwinding of the two DNA strands relative to the normal amount of winding for the relaxed plasmid¹⁰. The unwinding is brought about by intercalation of ethidium molecules into the DNA duplex in the presence of a topoisomerase. By determining the amount of bound ethidium, the level of unwinding can be calculated by assuming each ethidium unwinds the primary helix by 26° (ref. 15). This unwinding represents the mean linking difference¹⁶ for the plasmid sample and is partitioned between twist, writhe and other structural features in a

manner that minimizes the free energy of the unwound state¹⁷⁻¹⁹ once the ethidium is removed. The mean superhelical density (or number of superhelical turns) of each sample is calculated assuming that the DNA is in a normal B helix and all unwinding is partitioned into negative superhelical turns¹⁰. Thus, these values are the classical titratable superhelical densities²⁰.

When samples of pRW751 having different superhelical densities were analysed by 2% agarose gel electrophoresis (Fig. 3, even-numbered lanes), a discrepancy arose for the samples that were more highly supercoiled; gel analysis gave a lower estimate of the mean negative superhelical density than the calculated values. Such a discrepancy was not seen for the control plasmid, pRW451, for which the mobilities of the samples increased as the titratable negative density increased, in agreement with the calculated values, until resolution of individual topoisomers was lost (Fig. 3, odd-numbered lanes). The mobility pattern of supercoiled samples of pRW451 was as expected^{10,21}, whereas the mobility pattern of the pRW751 samples was atypical. This result is consistent with the relaxation of negative supercoils brought about by a partial or complete transition to a left-handed helix within the alternating (dC-dG) blocks of pRW751 as the titratable negative superhelical density increases. The reversal of the sense of a primary helical turn from right-to-left-handedness should result in the relaxation of approximately two negative supercoils. Thus, a complete transition within the two (dC-dG) blocks of pRW751 (total 58 bp) will result in the loss of 10.5 supercoils².

Stirdivant *et al.*² observed that individual topoisomers of pRW751 undergo relaxation when the right- to left-handed helical transition is induced by titration with NaCl. Relaxations of <10.5 supercoils were interpreted as reflecting the time-averaged equilibrium between the right- and left-handed states. Indeed, for a given topoisomer, if the transition between these two states is fast compared with the time of electrophoresis, a sharp band will be observed with a mobility dependent on the time-averaging of the superhelical density of the two states⁵. As the samples used here consisted of a gaussian distribution of about eight topoisomers, following the relaxation behaviour was slightly more complicated. Within a given sample, the topoisomers which are more negatively supercoiled will relax to a greater extent than those having less supercoiling. Thus, the expected pattern would be a compaction and apparent smearing of the topoisomer population as the equilibrium shifts in favour of the left-handed helical state (that is, as the negative superhelical density increases). Finally, the gaussian distribution

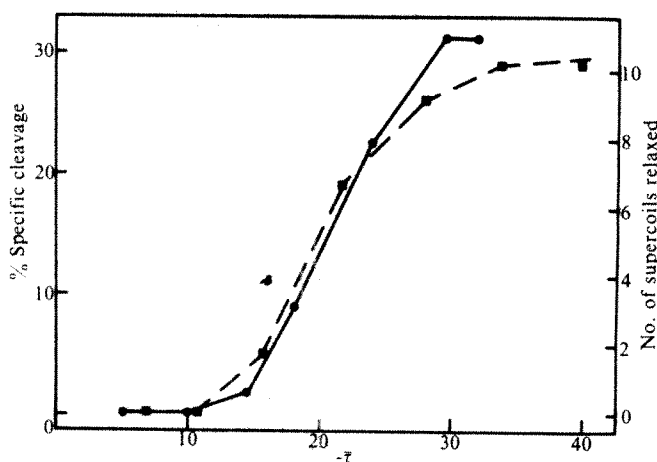


Fig. 4 Average number of negative supercoils relaxed plotted against the mean number of titratable superhelical turns, $-\tau$. The number of supercoils relaxed for pRW751 was obtained by determining the median position of the topoisomer distribution from Fig. 3, and subtracting this value from the expected median position based on the calculated titratable superhelical density (●). The transition end points are based on analysis of the behaviour of individual topoisomers within a given sample. The broken line (■) illustrates S₁ nuclease-specific cleavage versus $-\tau$ (see Fig. 1c).

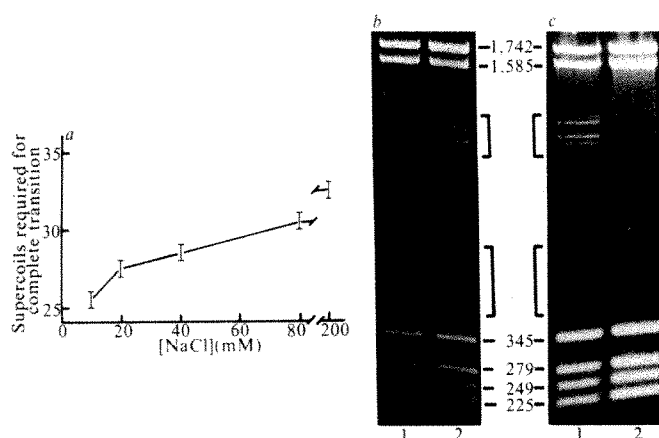


Fig. 5 Effect of Na^+ and methylation on formation of left-handed DNA in pRW751. *a*, Mean number of titratable supercoils required to give the complete right- to left-handed transition plotted against NaCl concentration of the electrophoresis buffer. The electrophoresis buffer (40 mM Tris-HCl pH 8.3, 1.25 mM EDTA, 10–200 mM NaCl) was continuously circulated. Electrophoresis of supercoiled pRW751 samples was carried out on a 2% agarose slab gel for 27–52 h. The current was regulated such that the temperature of each gel was $\sim 28^\circ\text{C}$. The transition end point was determined as described in Fig. 4 legend. *b*, *Ava*II digest of S_1 nuclease-cleaved pRW751 samples was carried out on a 2% agarose slab gel for 27–52 h. The current was regulated such that the temperature of each gel was $\sim 28^\circ\text{C}$. The transition end point was determined as described in Fig. 4 legend. *c*, *Ava*II digest of S_2 -cleaved methylated (lane 1) and unmethylated (lane 2) pRW751. Methylation was carried out essentially as described elsewhere³⁰ with *Hha*I methylase (G^mC-G-C). Methylation was monitored by observing loss of cleavage with *Hha*I restriction endonuclease (J. K., unpublished). Brackets denote S_1 nuclease-specific bands.

should reappear at a position indicative of a loss of ~ 11 negative supercoils once the mean superhelical density is sufficient to cause the complete transition.

Compaction and smearing of the topoisomer population was found for the pRW751 samples 6–10 of Fig. 3. The population of topoisomers shown in Fig. 3, lane 12 appears as a normal distribution of topoisomers; however, the average number of negative supercoils is about 11 less than the expected, calculated value. The average number of supercoils for the first two pRW751 samples shown in Fig. 3 (and all but the two highest supercoiled topoisomers of sample 3) were as expected, indicating that these topoisomers are of insufficient superhelical density to induce the right- to left-handed helical transition.

Figure 4 illustrates the supercoil-induced relaxation behaviour of pRW751. Relaxation of pRW751 plateaus after a loss of about 11 negative supercoils. This degree of relaxation correlates well with the expected value for a complete transition from a right- to a left-handed helix within the (dC-dG) blocks, but is inconsistent with cruciform formation at these sites, a process which would result in the relaxation of only about six supercoils as 58 bp would be unwound on cruciform formation.

These results demonstrate that at or above a titratable negative superhelical density of 0.064, the (dC-dG) blocks within pRW751 are completely in a left-handed helical state in the gel buffer conditions. This result is also consistent with the levelling off of S_1 nuclease-specific cleavage around a density of ~ -0.07 . Indeed, as shown in Fig. 4, specific cleavage by S_1 nuclease correlates well with relaxation as revealed by gel analysis.

When isolated from *E. coli* cells, pRW751 possesses a lower negative superhelical density than the control plasmid, pRW451, and other pBR322 derivatives as revealed by gel electrophoretic analysis². By direct comparison with the gel results presented here (Fig. 3), we have determined that part of the reduced density can be attributed to a relaxation of supercoils due to formation of left-handed DNA within the (dC-dG) blocks (data not shown). This is also consistent with

pRW751 as isolated from *E. coli* cells showing S_1 nuclease-sensitivity at the (dC-dG) blocks.

Salt effects

When the supercoiled samples of pRW751 were electrophoresed in different ionic conditions, the number of negative supercoils required to induce complete relaxation decreased as the NaCl concentration decreased (Fig. 5a). This effect is greatest at low salt concentrations and appears to level off in the 200 mM range. Figure 5b illustrates that specific cleavage by S_1 nuclease is also enhanced at a lower Na^+ concentration. The enhancement of specific cleavage on decreasing the Na^+ level was observed only for samples which had not undergone the complete transition. Thus, this effect results in a shift to the left of the curves in Fig. 4.

This salt effect was unexpected as Stirdivant *et al.*² found the opposite relationship between salt concentration and superhelical density for the formation of left-handed DNA in pRW751. However, this previous study focused on the salt-induced transition from right- to left-handed DNA and thus used much higher concentrations (several molar) of NaCl. The results presented in this paper focus on the right- to left-handed DNA transition which is driven by the relief of the torsional strain of supercoiling at relatively low levels of sodium ions. Thus, the ionic environment of the DNA in the two studies was very different, which could account for the apparent discrepancy. Furthermore, the salt effect described here levelled off at higher Na^+ concentrations, suggesting a loss in the trend observed at lower salt concentrations.

Effect of methylation

It was demonstrated recently that C5-methylation of cytidine residues in $(\text{dC-dG})_n \cdot (\text{dC-dG})_n$ greatly facilitated the formation of a left-handed structure for this polymer^{22,23}. We have found that, although not as dramatic as with the polymer, methylation of the cytidine residues of the (dC-dG) blocks of pRW751 by *Hha*I methylase facilitates formation of left-handed DNA in the plasmid. Figure 5b illustrates that S_1 nuclease-specific cleavage is enhanced when the fully methylated plasmid is used as template. Gel analysis of the methylated plasmid DNA also demonstrated that less supercoiling is required to bring about formation of left-handed DNA relative to the unmethylated plasmid (data not shown). In general, the effect of methylation on left-handed DNA formation in pRW751 is equivalent to increasing the number of negative supercoils by four to five.

Conclusions

We have demonstrated that left-handed DNA can exist in plasmids in physiological conditions of ionic strength and superhelical density. Furthermore, we have shown that S_1 nuclease can serve as a probe for the conformational junction which must exist between adjacent left-handed and right-handed helical DNA regions. Specific cleavage within the junction region suggests that some degree of single strandedness exists within this region, which is consistent with model building studies¹⁴. It is apparent, though, that S_1 nuclease binds to and cleaves within the junction region rather inefficiently. This is reflected in the fact that specific cleavage by S_1 nuclease levels off at $\sim 30\%$ even though gel analysis of the plasmid samples demonstrates that the (dC-dG) blocks are completely stabilized in a left-handed helical state. That a relatively large region of single strandedness is not present is also consistent with the fact that we have been unable to demonstrate junction recognition by another single strand-specific nuclease, the gene 3 product of phage T₇ (data not shown).

The S_1 nuclease-specific fragments which correspond to cleavage near the 32-bp (dC-dG) block appear at lower negative superhelical densities than the bands corresponding to cleavage at the 26-bp block (Fig. 1b, lanes 3, 4). This is consistent with the previous finding² that salt-induced left-handed DNA formation within the 32-bp (dC-dG) region occurs at

lower salt concentrations than left-handed DNA formation within the 26-bp region. Note also that one junction (third from the left in Fig. 2) is recognized and cleaved by S_1 nuclease more readily than the other three, as judged by the band intensities in Fig. 1b. This result suggests significant differences between various junction regions, perhaps due to sequence effects. Finally, we wish to emphasize that S_1 nuclease cleavage apparently occurs outside the (dC-dG) blocks, implying that the complete (dC-dG) sequences are in a left-handed state, in agreement with previous studies^{1,2,24}.

The S_1 nuclease and gel analyses on samples of pRW751 containing different superhelical densities demonstrate that formation of left-handed DNA within the (dC-dG) blocks of this

plasmid begins at a negative superhelical density of ~ 0.039 and is completely stabilized at a density of -0.072 (18–32/33 negative supercoils) in physiological ionic conditions (200 mM NaCl). The range of superhelicity required to stabilize left-handed DNA in these conditions is well within the range of physiological superhelical densities typically found for most plasmids²⁰. If *in vitro* supercoiling is a true reflection of that occurring *in vivo*^{25–27}, our results indicate that left-handed DNA within (dC-dG) regions exists *in vivo* under the torsional strain of supercoiling.

This work was supported by NIH grant CA 20279 and NSF grant PCM-8002622. C.K.S. was supported by a postdoctoral fellowship (PF-1904) from the American Cancer Society.

Received 23 March; accepted 7 June 1982.

1. Klysik, J., Stirdivant, S. M., Larson, J. E., Hart, P. A. & Wells, R. D. *Nature* **290**, 672–677 (1981).
2. Stirdivant, S. M., Klysik, J. & Wells, R. D. *J. biol. Chem.* (in the press).
3. Zacharias, W., Larson, J. E., Klysik, J., Stirdivant, S. M. & Wells, R. D. *J. biol. Chem.* **257**, 2775–2782 (1982).
4. Pulleyblank, D. E., Shure, M., Tang, D., Vinograd, J. & Vosberg, H.-P. *Proc. natn. Acad. Sci. U.S.A.* **72**, 4280–4284 (1975).
5. Depew, R. E. & Wang, J. C. *Proc. natn. Acad. Sci. U.S.A.* **72**, 4275–4279 (1975).
6. Panayotatos, N. & Wells, R. D. *Nature* **289**, 446–470 (1981).
7. Lilley, D. M. J. *Proc. natn. Acad. Sci. U.S.A.* **77**, 6468–6472 (1980).
8. Singleton, C. K. & Wells, R. D. *J. biol. Chem.* **257**, 6292–6295 (1982).
9. Klysik, J., Stirdivant, S. M. & Wells, R. D. *J. biol. Chem.* (in the press).
10. Singleton, C. K. & Wells, R. D. *Analyt. Biochem.* **122**, 253–257 (1982).
11. Tinoco, I., Uhlenbeck, O. C. & Levine, M. D. *Nature* **230**, 362–367 (1971).
12. Haasnoot, C. A. G., den Hartog, J. H. J., de Rooij, J. F. M., van Boom, J. H. & Altona, C. *Nucleic Acids Res.* **8**, 169–181 (1980).
13. Wells, R. D. *et al. J. biol. Chem.* (in the press).
14. Drew, H. R. & Dickerson, R. E. *J. molec. Biol.* **152**, 723–736 (1981).

15. Wang, J. C. *J. molec. Biol.* **89**, 783–801 (1974).
16. Wang, J. C. *Trends biochem. Sci.* **5**, 219–221 (1980).
17. Benham, C. J. *J. molec. Biol.* **150**, 43–68 (1981).
18. Camerini-Otero, R. D. & Felsenfeld, G. *Proc. natn. Acad. Sci. U.S.A.* **75**, 1708–1712 (1978).
19. Vologodski, A. V., Anshelevich, V. V., Lukashin, A. V. & Frank-Kamenetskii, M. D. *Nature* **280**, 294–298 (1979).
20. Bauer, W. R. A. *Rev. Biophys. Bioengng* **7**, 287–313 (1978).
21. Keller, W. *Proc. natn. Acad. Sci. U.S.A.* **72**, 4876–4880 (1975).
22. Behe, M. & Felsenfeld, G. *Proc. natn. Acad. Sci. U.S.A.* **78**, 1619–1623 (1981).
23. Behe, M., Zimmerman, S. & Felsenfeld, G. *Nature* **293**, 233–235 (1981).
24. Wartell, R. M., Klysik, J., Hillen, W. & Wells, R. D. *Proc. natn. Acad. Sci. U.S.A.* **79**, 2549–2553 (1982).
25. Gellert, M. A. *Rev. Biochem.* **50**, 879–910 (1981).
26. Pettijohn, D. E. & Pfinninger, O. *Proc. natn. Acad. Sci. U.S.A.* **77**, 1331–1335 (1980).
27. Sinden, R. R., Carlson, J. O. & Pettijohn, D. E. *Cell* **21**, 773–783 (1980).
28. Dodgson, J. B. & Wells, R. D. *Biochemistry* **16**, 2374–2379 (1977).
29. Southern, E. M. *Analyt. Biochem.* **100**, 319–323 (1979).
30. Mann, M. B. & Smith, H. O. in *Transmethylation* (eds Usdin, E., Borchardt, R. T. & Creveling, C. R.) 483–492 (Elsevier, New York, 1979).

Viroid RNAs of cadang-cadang disease of coconuts

James Haseloff, Nizar A. Mohamed*[†] & Robert H. Symons

Adelaide University Centre for Gene Technology, Department of Biochemistry, University of Adelaide, Adelaide, South Australia 5001
* FAO/UNDP Coconut Research Project, Philippine Coconut Authority, Albay Research Center, Guinobatan, Albay, Philippines 4908

Cadang-cadang is a serious lethal disease of coconut palms in the Philippines. Infectivity is associated with four viroid RNAs (ccRNAs) which are from 246 to 574 residues in size but do not vary in sequence complexity. They share sequence and structural homology with other viroids. Variant ccRNAs found in nine isolates sequenced may have arisen as by-products or intermediates of viroid replication.

CADANG-CADANG is a serious and economically important disease of coconut palms which was first reported in 1927 on San Miguel Island in the Philippines¹. By 1962, all but 100 of the 250,000 palms on this island had died from the disease². Cadang-cadang disease has spread rapidly and now, 56 years after its first known occurrence, it is widespread over the south-east part of Luzon and many neighbouring islands (Fig. 1). It is estimated that cadang-cadang is responsible for the death of 500,000 palms each year in the Philippines (B. Zelazny, personal communication). Recent work has indicated that tinangaja disease of coconuts on Guam, an island in the Pacific 1,500 miles east of the Philippines, has the same aetiology as cadang-cadang³. However, cadang-cadang disease has not been found in any other coconut growing area.

Four low-molecular weight RNA species (ccRNAs) are found associated with cadang-cadang disease⁴. Two of these RNAs, called ccRNA 1 fast and ccRNA 2 fast, of ~ 250 and 500 nucleotides⁵ respectively, are present in infected palms at early stages of the disease⁴. As infection progresses over a period of years, two additional RNAs, ccRNA 1 slow and ccRNA 2 slow (of ~ 300 and 600 nucleotides, respectively), characterized by their slower electrophoretic mobilities on polyacrylamide gels,

appear and then predominate⁵. Ribonuclease fingerprinting showed that the ccRNAs, although differing in size, contain common repeated sequences, suggesting that the ccRNA 2 fast and slow species may be dimers of the respective ccRNA 1 species⁵ and that the three larger RNAs are closely related to ccRNA 1 fast.

All four ccRNA species have been shown recently to be infectious⁶. They are single-strand covalently closed circular RNAs with high degrees of secondary structure^{7,8} and so possess properties similar to those of a small group of infectious plant pathogens, the viroids⁹. Thus, the ccRNAs can now be classed definitely as the coconut cadang-cadang viroid (CCCV) in view of the recent infectivity data. The other viroids characterized each consist of single infectious RNA species which do not seem to code for functional polypeptide products but are capable of autonomous replication^{9,10}.

We report here the primary sequences and secondary structures of the four RNAs of several CCCV isolates. The results are compared with the structures of other viroids and are discussed in terms of the possible origin of cadang-cadang disease and mechanisms for the replication of viroids.

RNA sequence and structure determination

The approaches we have used successfully for the determination of the sequences and structures of chrysanthemum stunt viroid

[†] Present address: National Health Institute, PO Box 50348, Porirua, New Zealand.

Table 1 Properties of RNAs of various ccRNA isolates

ccRNA isolate*	Relative proportions of sequence variants†		Total length of ccRNA (residues)	Length of sequence duplication (residues)
	C	CC		
ccRNA 1 fast				
Baao 54	1.0	0	246	
Tinambac	1.0	0	246	
Ligao 14B	0.8	0.2	246/247‡	
Ligao 620C	0.6	0.4	246/247	
Ligao 191D	0.4	0.6	246/247	
Ligao T1	0.2	0.8	246/247	
ccRNA 2 fast				
Baao 54	1.0	0	492	
Ligao T1	0.2	0.8	492–494§	
ccRNA 1 slow				
Baao 54	1.0	0	287	41
Ligao 14B	1.0	0	296	50
Ligao 620C	1.0	0	296	50
Ligao 191D	1.0	0	296	50
Ligao T1	1.0	0	301	55
Ligao 5	1.0	0	296	50
Guinayangan	1.0	0	296	50
San Miguel	1.0	0	296	50
San Nasciso	0	1.0	297	50
ccRNA 2 slow				
Baao 54	1.0	0	574	41

* ccRNA isolates were purified⁴ from nucleic acid extracts³³ of single, infected coconut palms.

† Relative proportions of sequence variants were determined by sequence analysis of RNase T₁-digested, 5'-³²P-radiolabelled full-length linear ccRNAs. If a ccRNA consisted of a mixture of variants, band doubling was observed on sequencing gels¹⁰ after ccRNA 1 fast residue 197. Relative proportions of the two sets of band doublets were taken as estimates of the molar proportions of the two variant ccRNA species.

‡ These ccRNA 1 fast species consisted of a mixture of two species, one of 246 and the other of 247 residues.

§ Ligao T₁ ccRNA 2 fast species contained sequence heterogeneity at the positions corresponding to ccRNA 1 fast residue 198. Due to limitations of sequencing technique, we did not determine whether dimeric ccRNA 2 fast consisted of a 492(2×246)-residue species together with a 494(2×247)-residue species or only a 493(246+247)-residue species.

(CSV)¹⁰, avocado sunblotch viroid (ASBV)¹¹, citrus exocortis viroid (CEV)¹², and the viroid-like RNAs (virusoids) of velvet tobacco mottle virus (VTMOV)¹³ and solanum nodiflorum mottle virus (SNMV)¹³ were applied to the four ccRNAs. Native circular ccRNAs were subjected to limited digestion either by ribonuclease T₁, which catalysed cleavage of ccRNA 1 species at single sites and ccRNA 2 species at either or both of two sites to produce specific full-length linear ccRNAs, or by ribonucleases A or U₂, which produced smaller overlapping RNA fragments. These linear RNA molecules were 5'- or 3'-radiolabelled and then purified by polyacrylamide gel electrophoresis^{10,14}. The sequences of these 5'- or 3'-labelled fragments were determined by partial enzymatic digestion¹⁰. The use of fragments labelled separately at both the 5'- and 3'-ends allowed the sequence determination of long RNA fragments up to 574 residues long and, with shorter fragments, resolved gel compression artefacts¹⁵ when the relevant nucleotide sequences were determined from both directions. The sequences of overlapping fragments were assembled to construct the complete primary structures of the circular RNA molecules.

Secondary structure models for the native ccRNAs were constructed using the base pairing matrix procedure of Tinoco *et al.*¹⁶, values for the thermodynamic stability of predicted RNA structures (G. Steger, H. J. Gross, J. W. Randles, H. L. Sänger and D. Riesner, personal communication), and experimental evidence for the location of ribonuclease-sensitive single-stranded regions on the native molecules. In addition, specific full-length linear ccRNAs, produced by ribonuclease T₁ cleavage, were either 5'- or 3'-labelled with ³²P and the

single-strand regions in the native structures located by the nuclease S₁ mapping procedure¹⁷. The sites of cleavage were determined by co-electrophoresis of the radiolabelled fragments of the nuclease S₁ digest with products of sequencing reactions using the partial enzymatic digestion procedure¹⁰.

ccRNAs differ in size but not sequence complexity

The sequences and predicted structures of the ccRNA 1 fast and slow forms isolated from a single infected coconut palm (isolate Baao 54) are shown in Fig. 1 together with the known structures of four viroids, potato spindle tuber viroid (PSTV)¹⁸, CSV¹⁰, CEV¹², and ASBV¹¹. The two native ccRNAs 1 possess extensive regions of intramolecular base pairing and can form rod-like native structures similar to other viroids. The ccRNA 1 fast and ccRNA 1 slow possess 246 and 287 residues, respectively, and have calculated thermodynamic stabilities of -320 and -360 kJ mol⁻¹, respectively. ccRNA 1 slow contains the entire sequence and structure of the smaller ccRNA 1 fast but differs by an additional duplicated sequence and structure of 41 residues (residues 103–143 in ccRNA 1 fast) which is added at the right-hand end of the native molecule between residues 123 and 124 of ccRNA 1 fast (Fig. 2). Thus, the rod-like, base-paired native structure is maintained in the larger molecule.

The nucleotide sequences of ccRNA 2 fast and ccRNA 2 slow, consisting of 492 and 574 residues, respectively, are perfect dimers of the respective ccRNA 1 forms. A schematic summary of the relationships between the primary structures of all four ccRNAs and their predicted secondary structures is given in Fig. 3. While each of the monomeric ccRNA 1 forms can base pair intramolecularly to form a single rod-like conformer, the ccRNA 2 forms, due to their dimeric nature, can form either of two rod-like conformers (A or B, Fig. 3) and a large number of intermediate cruciform-shaped structures, one of which is given in Fig. 3.

The ccRNA 1 fast and ccRNA 1 slow molecules each possess, in experimental conditions, a highly accessible site for cleavage by ribonuclease T₁ at the right-hand terminal hairpin loop of the predicted native structure (between residues 124 and 125 in Baao 54 ccRNA 1 fast and between residues 145 and 146 in Baao 54 ccRNA 1 slow). Limited ribonuclease T₁ digestion

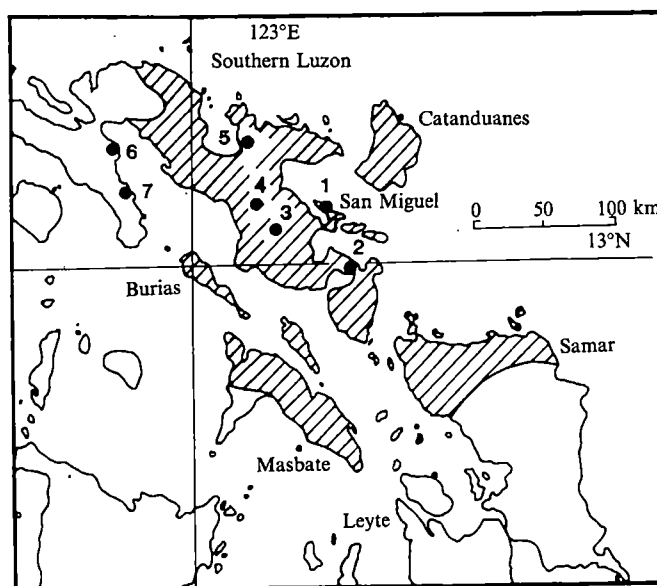


Fig. 1 Incidence of cadang-cadang disease of coconuts. Regions of the Philippine islands where the disease is widespread are shown cross-hatched, while isolated incidences of the disease occur in surrounding areas³². The different ccRNA isolates used in this work were each obtained from separate diseased coconut palms in one of the following locations: 1, San Miguel Island; 2, Sorsogon; 3, Ligao; 4, Lake Baao; 5, Tinambac; 6, Guinayangan; and 7, San Nasciso.

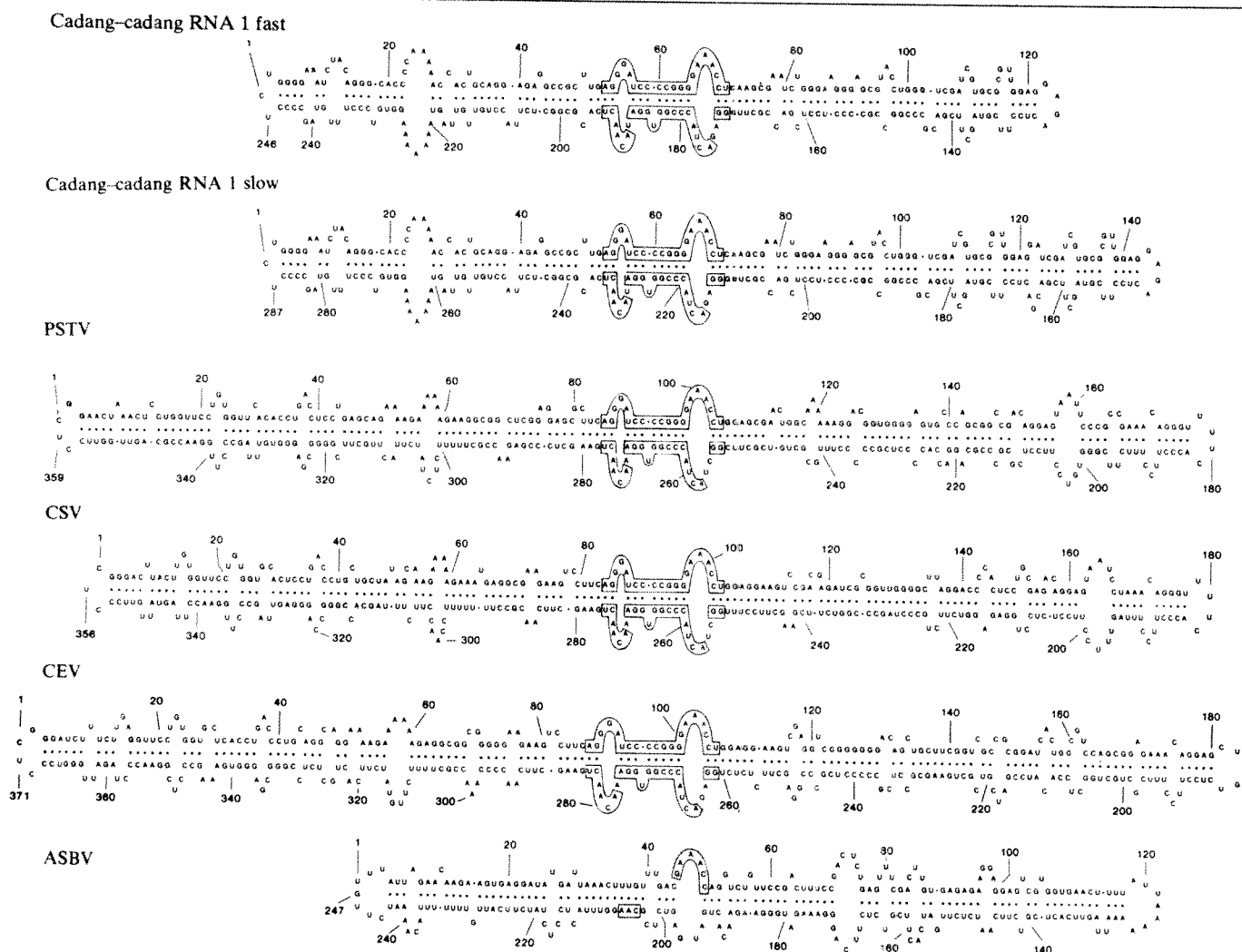


Fig. 2 Sequences and predicted secondary structures of the Baoo 54 isolate of ccRNA 1 fast and ccRNA 1 slow are shown with those of PSTV¹⁸, CSV¹⁰, CEV¹² and ASBV¹¹. The structures are aligned under the central conserved regions of these viroids (boxed). For sequence determination, nucleic acids were extracted from the fronds of a single infected coconut palm³³, and ccRNAs purified by preparative polyacrylamide gel electrophoresis⁴. Purified ccRNAs were sequenced essentially as described in ref. 10. Thus, 5 µg circular ccRNA in 20 µl 600 mM NaCl, 10 mM MgCl₂, at 0 °C was digested with RNase T₁ (Sigma) at 2,000 units ml⁻¹ to produce specific full-length linear molecules, or with 3 units ml⁻¹ RNase U₂ (Sankyo) or 5 ng ml⁻¹ RNase A (Sigma) to produce smaller linear fragments. These fragments were 5'-radiolabelled using [γ -³²P]ATP and T4 polynucleotide kinase or, after treatment with calf intestinal phosphatase³⁴, 3'-radiolabelled using [γ -³²P]dpCp and T4 RNA ligase¹⁴, and fractionated on a 80 × 20 × 0.05 cm 6% polyacrylamide gel containing 8 M urea and TBE buffer (90 mM Tris-borate pH 8.3, 2 mM EDTA). Bands located by autoradiography were excised and eluted¹⁰, and sequenced using partial enzymatic cleavage¹⁰. The sequences of numerous overlapping fragments were assembled to give the complete primary structure of each circular molecule. For S₁ nuclease mapping of the secondary structures¹⁷, 5'- or 3'-radiolabelled full-length linear fragments, obtained as described above by RNase T₁ digestion, were suspended in 20 µl 200 mM NaCl, 0.5 mM ZnSO₄, 50 mM sodium acetate pH 4.6, containing 5 µg *Escherichia coli* tRNA carrier, and incubated at 37 °C for 10 min with 0.1, 1 or 10 units of S₁ nuclease (Boehringer). The reaction mixture was extracted with phenol, the RNA precipitated with ethanol and fractionated by polyacrylamide gel electrophoresis in TBE, 8 M urea. Products of partial enzymatic sequencing reactions of the same ccRNA were run as markers, thus allowing sites of S₁ nuclease sensitivity to be located. Data so derived were used to construct the secondary structure models of ccRNA 1 fast and ccRNA 1 slow.

of each ccRNA 2 species produced specific linear RNA fragments corresponding to both the respective full-length ccRNA 2 and ccRNA 1 molecules. Sequence determination of these fragments showed that cleavage of the ccRNA 2 molecules occurred at two sites located at the same sequences as for the two ccRNA 1 molecules. This suggests that either the predicted conformer A of the two ccRNA 2 molecules or possible cruciform intermediates exist in solution whereby the terminal hairpin loops are exposed. However, the existence of type B conformers cannot be precluded.

Variation in sequence between different ccRNA isolates

Different isolates of cadang-cadang RNAs were each obtained from single infected coconut palms from different localities in the Philippines (Fig. 1). Sequence differences between the different isolates consist of two types. First, the sequences of

the ccRNA 1 slow forms can differ. While all ccRNA 1 fast forms are essentially identical (see below), ccRNA 1 slow forms can differ in the length of the repeated sequence inserted between residues 123 and 124 of ccRNA 1 fast. Three different repeated sequences found in nine sequenced isolates of ccRNA 1 slow are given in Fig. 4; these vary in length from 41 to 55 residues but they are internally base-paired to produce duplicated structures as well as sequences at the right-hand ends of the molecules. Interestingly, the right-hand ends of the native molecules of PSTV, CSV, CEV and ASBV (Fig. 2) are at a similar distance from the central conserved regions of these molecules. In contrast, the right-hand side of the ccRNA 1 fast molecule is shorter while those of the elongated ccRNA 1 slow molecules are closer in size to those of PSTV, CEV and ASBV.

Second, four of the six isolates of ccRNA 1 fast sequenced each consist of two populations of molecules, one of 246 residues and the other of 247 residues, which differ in the

presence or absence of a C at residue 198 (Fig. 5, Table 1). Similar sequence heterogeneities have also been reported for CEV¹⁹ and the viroid-like RNA of VTMOV¹³. The relative proportions of the two ccRNA 1 fast subspecies vary between different isolates as listed in Table 1. For the two ccRNA 2 fast isolates sequenced, the relative proportions of the two forms are the same as those of the corresponding ccRNA 1 fast. In contrast to the ccRNA 1 and 2 fast species, no similar sequence heterogeneity has been observed in nine isolates of ccRNA 1 slow and the one sequenced isolate of ccRNA 2 slow (Table 1). Each isolate of the ccRNA slow species thus consists entirely of either one subspecies or the other; in all except one case, the C at the position corresponding to ccRNA 1 fast residue 198 was absent. The various sequence differences between the ccRNA isolates do not seem to correlate with differences in geographical location.

Structural similarities between ccRNAs, viroids and virusoids

The ccRNAs share two regions of sequence homology, each of about 20 nucleotides, with the viroids PSTV, CSV and CEV

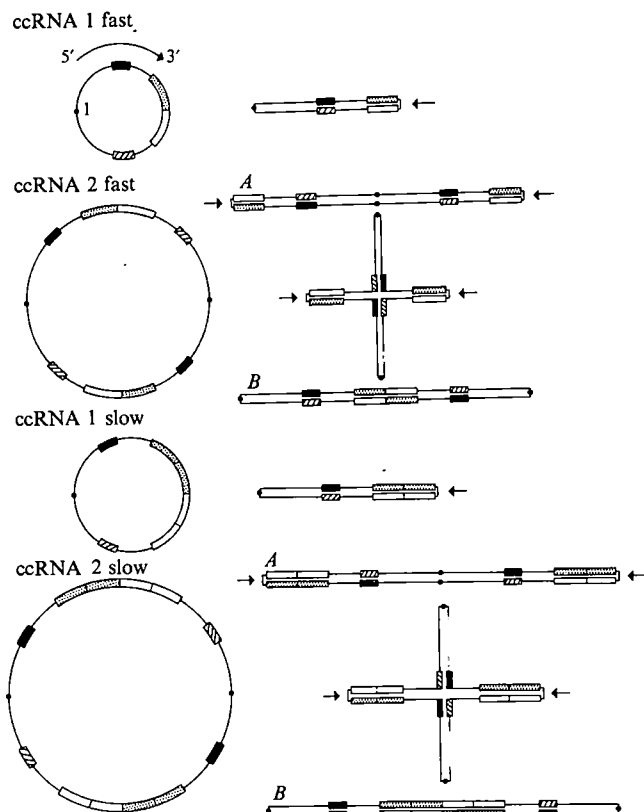


Fig. 3 Schematic representation of the sequences and predicted structure relationships between the ccRNAs. The circular sequences of the four ccRNAs are shown with black boxed and cross-hatched boxed regions representing the sequences highly conserved between the ccRNAs, PSTV, CSV and CEV (Baao 54 ccRNA 1 fast residues 52–71 and 171–194, respectively). The white boxed and stippled boxed regions represented those sequences duplicated within the ccRNA 1 slow species (Baao 54 ccRNA 1 fast residues 103–123 and 124–143, respectively). Positions corresponding to residue 1 of ccRNA 1 fast or ccRNA 1 slow are indicated by black dots. Both ccRNA 1 fast and ccRNA 2 slow molecules are dimers of their respective ccRNA 1 forms. Each ccRNA 2 can potentially form either of two rod-like conformers, A or B, as well as a large number of cruciform-shaped intermediates of which one is shown for ccRNA 2 fast and ccRNA 2 slow. Each ccRNA 1 species possesses a single, highly accessible site for RNase T₁ cleavage located on a hairpin loop (between Baao 54 ccRNA 1 fast residues 124 and 125 and between ccRNA 1 slow residues 145 and 146); these sites are indicated by arrows. Each ccRNA 2 species possesses two such accessible sites for RNase T₁ cleavage and arrows indicate where these sites also occur on hairpin loops in the different ccRNA 2 conformers.

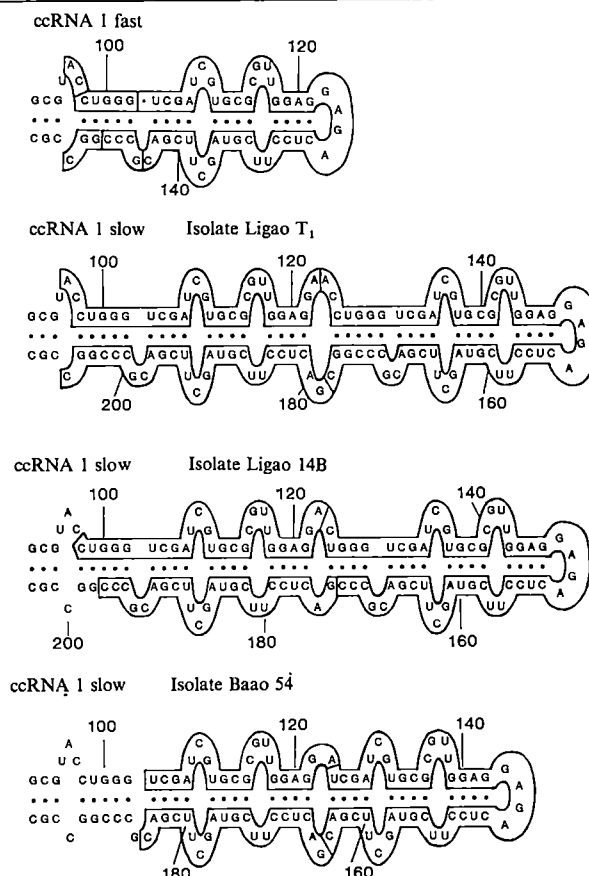


Fig. 4 Sequence variation between ccRNA 1 slow of three ccRNA isolates. The sequences and structures of various ccRNA 1 fast and ccRNA 1 slow isolates were determined as described in Fig. 2 legend. As essentially all sequence variation occurred at the right-hand end of the ccRNA 1 slow molecules, only this region is shown. Boxed regions represent those sequences which are duplicated in the ccRNA 1 slow molecules and which are 41 (isolate Baao 54), 50 (isolate Ligao 14B) or 55 residues (isolate Ligao T₁) long. All sequenced ccRNA 1 slow isolates correspond to one of these forms (Table 1).

(Fig. 2). The latter three viroids are closely related, sharing about 50% sequence homology. These two conserved regions are base-paired in the predicted structures of the native molecules to form highly conserved secondary structures.

The conserved regions shared by the ccRNAs correspond to regions of PSTV, CSV and CEV postulated to be involved in base pairing of viroid complementary RNAs with a plant small nuclear RNA (snRNA) in a manner analogous to that proposed for the interaction of mRNA intron-exon splice junctions with mammalian Ula snRNA^{19,20}, and in the formation of a stabilizing stem-loop structure in the viroid complements¹⁹. The proposed interaction between viroid complements and snRNA is postulated to reflect the origin of viroids from an intron ancestor²⁰ or as a basis for pathogenesis^{19,20} but not to be directly involved in viroid replication. However, the complementary RNA of at least one viroid, ASBV, is incapable of base pairing with a Ula-like snRNA or of formation of the conserved stem-loop structure, despite up to 18% sequence homology between ASBV and other viroids¹¹. It is possible that the central conserved regions of native viroids reflect functional similarities related to viroid replication rather than to the postulated snRNA binding.

Interestingly, the virusoids (encapsidated viroid-like RNAs) of VTMOV¹³, SNMV¹³, and subterranean clover mottle virus (J.H., C. Davies and R.H.S., unpublished data) also contain highly conserved sequences which are central to their rod-like native structures and which share only the pentanucleotide sequence, GAAAC, with all sequenced viroids, including ASBV.

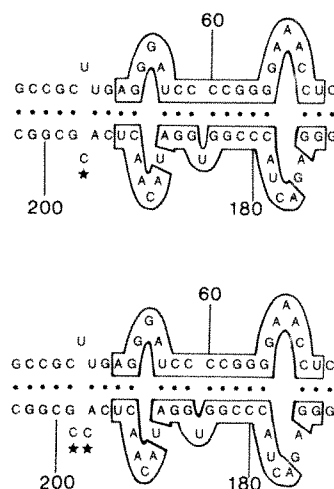


Fig. 5 Portions of the predicted native structures for the two forms of ccRNA 1 fast molecules. Purified ccRNA isolates were found to consist of either one or a mixture of two RNA species which differed in the presence or absence of an extra C residue at the position corresponding to ccRNA 1 fast residue 197 or 198. Stars indicate the sequence differences. Boxed regions indicate those sequences common to PSTV, CSV and CEV.

Replication of ccRNAs

As PSTV, CSV, CEV and the ccRNAs are capable of autonomous replication, the enzymes involved are of considerable interest. However, no viroid-encoded translation products have been found *in vitro*^{21,22} or *in vivo*²³. Although PSTV, CSV and CEV share ~50% sequence homology, none of these viroids nor their putative complementary RNAs can theoretically encode similar translation products^{10,12}, even assuming the existence of translatable linear viroid RNAs *in vivo*^{24,25}. Possible protein-coding regions similar to those of other viroids are not found in the ccRNAs or their complements nor are there any AUG initiation codons present. As a 5'-proximal AUG initiation codon seems essential for initiation of translation of eukaryotic RNA^{26,27}, it seems highly unlikely that the ccRNAs can code for any functional polypeptide product. All evidence, therefore, indicates that ccRNAs and other viroids must rely entirely on host components for their replication.

Larger than unit-length complementary (-) RNA intermediates have been detected in PSTV- and CEV-infected tissues²⁸⁻³⁰, and recently an oligomeric series of RNAs of ASBV (+) have been detected in infected avocado tissue (G. Bruening, A. R. Gould, P. J. Murphy and R.H.S., unpublished results). Rolling circle mechanisms have been postulated for the synthesis of oligomeric complementary RNAs from circular viroid templates^{28,30}, and oligomeric viroid (+) sequences could be simply generated by transcription of multimeric (-) strand templates. Unit-length linear viroid produced by either specific transcription or cleavage of oligomeric viroid RNAs must be ligated to produce the final circular product. Such a model for viroid replication, involving oligomeric RNA intermediates, could readily account for the formation of the dimeric forms of both ccRNA 1 fast and ccRNA 1 slow; that is, ccRNA 2 fast and ccRNA 2 slow, respectively. Rate-limiting steps during the transcription or the possible processing of viroid transcripts would allow the dimeric ccRNAs 2 to accumulate over the

monomeric ccRNA 1 species. The presence or absence of higher multimers of (+) ccRNAs or the complementary (-) ccRNAs in infected tissue has yet to be determined.

ccRNA slow variants and the time course of infection

In the initial stages of cadang-cadang disease, only the fast forms of ccRNA 1 and ccRNA 2 are present in infected palms and it is only after a further 24-30 months that the slow variants of ccRNA 1 and ccRNA 2 first appear and in the following years predominate⁵. These data, plus preliminary evidence that the ccRNA fast species are more infectious than the ccRNA slow species⁴, are consistent with the *de novo* generation of the ccRNA slow variants during each cadang-cadang disease infection. This proposition is supported by the following sequence data.

- (1) The ccRNA 1 slow forms differ from ccRNA 1 fast by the insertion of a single repeated sequence (Fig. 2) and could be simply generated from the ccRNA 1 fast by processing and/or transcription mechanisms.
- (2) The ccRNA 1 slow isolates can differ in the size of their inserted sequence repeats (Fig. 4, Table 1) suggesting separate origins for these ccRNA slow variants.
- (3) While most ccRNA fast isolates contain a sequence heterogeneity at residue 198, and consist of varying ratios of the 246- and 247-residue species, each of the nine sequenced ccRNA slow isolates consists of a single homogeneous population, either with or without a C residue at the position homologous to ccRNA 1 fast residue 198, and with only one size of repeated sequence (Table 1).

These data are consistent with the generation of ccRNA slow forms from ccRNA fast by single, rare sequence duplication events occurring separately in each cadang-cadang-infected palm. All ccRNA slow molecules would, therefore, originate from single parent molecules and may accumulate in preference to ccRNA fast species due to a competitive advantage in replication.

Origin of cadang-cadang disease

The ccRNAs share biological properties and sequence and structural homology with viroids so that application of the term coconut cadang-cadang viroid is fully justified. However, whereas other viroids consist of a single predominant infectious RNA species, CCCV consists of several variant RNA species. It is feasible that CCCV may have arisen from a pre-existing viroid and that mutation or infection of new hosts, such as the coconut palm and related species³¹, resulted in production of the variant ccRNAs by aberrant transcription and/or processing mechanisms which normally occur faithfully in the replication of other viroids. The outbreak and subsequent apparent rapid spread of cadang-cadang disease in the Philippines this century³² is consistent with such an origin of the ccRNAs. Future work with coconut palms inoculated with purified ccRNA species should allow a study of the generation of the ccRNA variants and may help elucidate the nature of viroid replication.

This work was supported by the Australian Research Grants Scheme and the UNDP/FAO Coconut Research Project. We thank Dr B. Zelazny for advice, Dr D. Riesner for unpublished data, Dr A. J. Gibbs for suggesting the term virusoids for encapsidated viroid-like RNAs, and Jenny Rosey, Lisa Waters and Julita Imperial for assistance.

Received 28 June; accepted 16 August 1982.

1. Ocfemia, G. P. *Philipp. Agric.* **26**, 338-340 (1937).
2. Bigornia, A. E. & Philipp, J. *Coconut Stud.* **2**, 5-33 (1977).
3. Boccardo, G., Beaver, R. G., Randles, J. W. & Imperial, J. S. *Phytopathology* **71**, 1104-1107 (1981).
4. Imperial, J. S., Rodriguez, J. B. & Randles, J. W. *J. gen. Virol.* **56**, 77-85 (1981).
5. Mohamed, N. A., Haseloff, J., Imperial, J. S. & Symons, R. H. *J. gen. Virol.* (in the press).
6. Mohamed, N. A. & Imperial, J. S. (in preparation).
7. Randles, J. W., Rillo, E. P. & Diener, T. O. *Virology* **74**, 128-139 (1976).
8. Randles, J. W. & Hatta, T. *Virology* **96**, 47-53 (1979).
9. Gross, H. J. & Riesner, D. *Angew. Chem. int. Edn.* **19**, 231-243 (1980).

10. Haseloff, J. & Symons, R. H. *Nucleic Acids Res.* **9**, 2741-2752 (1981).
11. Symons, R. H. *Nucleic Acids Res.* **9**, 6527-6537 (1981).
12. Visvader, J. E., Gould, A. R., Bruening, G. E. & Symons, R. H. *FEBS Lett.* **137**, 288-292 (1982).
13. Haseloff, J. & Symons, R. H. *Nucleic Acids Res.* **12**, 3681-3691 (1982).
14. England, T. E. & Uhlenbeck, O. C. *Nature* **275**, 560-561 (1978).
15. Kramer, F. R. & Mills, D. R. *Proc. natn. Acad. Sci. U.S.A.* **75**, 5334-5338 (1978).
16. Tinoco, I., Uhlenbeck, O. C. & Levine, M. D. *Nature* **230**, 362-367 (1971).
17. Wurst, R. M., Vournakis, J. N. & Maxam, A. M. *Biochemistry* **17**, 4493-4499 (1978).
18. Gross, H. J. *et al. Nature* **273**, 203-208 (1978).
19. Gross, H. J. *et al. Eur. J. Biochem.* **121**, 249-257 (1982).
20. Diener, T. O. *Proc. natn. Acad. Sci. U.S.A.* **78**, 5014-5015 (1981).

21. Davies, J. W., Kaesberg, P. & Diener, T. O. *Virology* **61**, 281–286 (1974).
22. Semancik, J. S., Conjero, V. & Gerhart, J. *Virology* **80**, 218–221 (1977).
23. Conjero, V. & Semancik, J. S. *Virology* **77**, 221–232 (1977).
24. Kozak, M. *Nature* **280**, 82–85 (1979).
25. Konarska, M., Filipowicz, W., Domdey, H. & Gross, H. J. *Eur. J. Biochem.* **114**, 221–227 (1981).
26. Baralle, F. E. & Brownlee, G. G. *Nature* **274**, 84–87 (1978).
27. Kozak, M. *Cell* **15**, 1109–1123 (1978).
28. Branch, A. D., Robertson, H. D. & Dickson, E. *Proc. natn. Acad. Sci. U.S.A.* **78**, 6381–6385 (1981).
29. Rohde, W. & Sanger, H. L. *Biosci. Rep.* **1**, 327–336 (1981).
30. Owens, R. A. & Diener, T. O. *Proc. natn. Acad. Sci. U.S.A.* **79**, 113–117 (1982).
31. Randles, J. W., Boccardo, G. & Imperial, J. S. *Phytopathology* **70**, 185–189 (1980).
32. Zelazny, B. *Acta phytopathol. Acad. Sci. Hung.* **14**, 115–126 (1979).
33. Randles, J. W. *Phytopathology* **65**, 163–167 (1975).
34. Efstratiadis, A. *et al. Nucleic Acids Res.* **4**, 4165–4174 (1977).

LETTERS TO NATURE

Emission mechanism and source distances of γ -ray bursts

Edison P. Liang

Lawrence Livermore National Laboratory, University of California, Livermore, California 94550, USA and *Institute for Plasma Research, Stanford University, Stanford, California 94305, USA

The reported continuum spectra (~ 20 keV–2 MeV) of most γ -ray bursts resemble a simple exponential^{1–4}. Hence, the conventional view is that they are the optically thin free-free (bremsstrahlung) emission of a hot thermal plasma ($kT \geq 100$ keV with the exception of a few soft events, notably the 5 March 1979 event). I show here that: (1) independent of the source distance, there is an inherent difficulty with the free-free interpretation if the sources are indeed neutron stars with magnetic field $B \geq 10^{12}$ G, because the synchrotron emissivity of these hot thermal electrons would greatly exceed their free-free emissivity for any reasonable electron density consistent with $\tau_{\text{es}} \ll 1$ required by observations; (2) the spectral data can be fitted equally well, if not better, by optically thin thermal synchrotron spectra of mildly relativistic ($kT \sim mc^2$) electrons; (3) the absence of observable low-energy turnover due to synchrotron self-absorption (or high energy Compton distortion) puts interesting upper limits to the source of luminosity and distance. Most sources are noncosmological (< 10 kpc–1 Mpc) but not necessarily as nearby as some authors have suggested using the free-free spectral interpretation (see, for example, ref. 2).

The essential arguments only are outlined here and illustrated with a few examples. Systematic analyses of a large collection of reported γ bursts have been performed and will be reported elsewhere⁵. Throughout this letter $T \equiv kT_e/mc^2$ (T_e = electron temperature; m = electron mass); $\nu_L \equiv eB/2\pi mc = 11.6$ keV ($B/10^{12}$ G) and $\nu_c \equiv \nu_L T^2$.

In the optically thin limit, the total free-free luminosity is given by⁶

$$L_{\text{ff}} = 1.2 \times 10^{-22} n_e^2 V Z T^{1/2} \text{ erg s}^{-1} \quad (1)$$

where n_e is electron density, Z is atomic number and V is emission volume, while the synchrotron luminosity from a thermal plasma is⁷ (compare with refs 8, 9)

$$L_{\text{syn}} \approx 2.7 \times 10^9 n_e V T^2 \mathcal{F}(T) B_{12}^2 \text{ erg s}^{-1} \quad (2)$$

where $\mathcal{F} = T^{-1}$ for $T \ll 1$; $\mathcal{F} = T^2/K_2(1/T)$ for $T \geq 1$, (K_2 = Bessel function); $B_{12} \equiv B/10^{12}$ G. Hence, $L_{\text{ff}} \approx L_{\text{syn}}$ only if

$$n_e \geq 2.3 \times 10^{31} T^{3/2} \mathcal{F}(T) B_{12}^2 Z^{-1} \text{ cm}^{-3} \quad (3)$$

independent of source distance. The absence of any Compton tail or 'Wien hump' implies that $\tau_{\text{es}} = \sigma_{\text{es}} h n_e \ll 1$ where σ_{es} is the (Klein–Nishina) Compton cross-section and h is the thickness of the emission region. Hence, equation (3) requires

$$h < 2 \times 10^{-7} T^{-3/2} \mathcal{F}^{-1} B_{12}^{-2} Z \text{ cm} \quad (4)$$

Since $T \sim 1$ for most bursts¹, h is inconceivably small even for fields much below 10^{12} G, keeping in mind that typical bursts

last longer than seconds. (The gravitational scale height is, of course, huge: $h_G \sim 3.6 \times 10^3 T$ cm, but even magnetic confinement has difficulty because equation (3) says that gas pressure often exceeds magnetic stress: $P_{\text{gas}}/P_{\text{mag}} \geq 10^3 T^{5/2} Z^{-1} \mathcal{F}$. The above difficulty is actually much more acute if we concentrate on the specific emissivities of the observed frequency range (20 keV–2 MeV) instead of the total emitted power. This is because much of the free-free emission contained in equation (1) comes out at X-ray energies, whereas the synchrotron spectrum has more power in γ -ray energies (compare with equation (5)).

There is now widespread belief that most γ -ray bursts originate from neutron stars with strong magnetic fields (see ref. 10 for review). The discovery of cyclotron absorption lines by Mazets *et al.*¹, if they can be confirmed, would also give support to the presence of strong fields in the sources. The above arguments thus force us seriously to consider thermal synchrotron as the universal emission mechanism of γ -ray bursts. (See refs 11, 12 on the 5 March event. This has also been emphasized by Lamb¹⁰ and Katz¹³.)

The specific synchrotron emissivity of mildly relativistic electrons ($T \sim 1$) assume a simple analytical form in the regime $\nu \gg \nu_L/T$ (refs 7, 8)

$$j_\nu(\theta) = \left(\frac{2\pi e^2}{3c} \right) \nu n_e \cdot K_2^{-1}(1/T) \cdot \exp(-(4.5\nu/\nu_c \sin \theta)^{1/3}) \quad (5)$$

Hence, the photon number spectrum has the form

$$n_\nu \text{ (photons cm}^{-2} \text{ s}^{-1} \text{ sr}^{-1} \text{ keV}^{-1}) \propto \exp(-(4.5\nu/\nu_c \sin \theta)^{1/3}) \quad (6)$$

where θ is the angle between the observer direction and the (average) field direction. Figure 1 shows the spectral fits with equation (6) to several representative γ -ray spectra reported by Mazets *et al.*¹ and Gilman *et al.*². It is clear that the synchrotron fits are at least as good as the free-free exponential^{1,2}. In each case the fit gives the value of $\nu_c \propto BT^2$ (assuming that the flux is dominated by emissions near $\theta = \pi/2$) but no direct information on B or T separately. For most of the spectra we have studied, ν_c lies in the range 1–20 keV, with a clustering around 5–10 keV (see Table 1, also ref. 5). Because in almost all cases the rise of the continuum continues down to the detector limit, say 20–30 keV (ref. 1), we can only suppose that the cyclotron first harmonic lies below the detector limit, so that $B \leq 2\text{--}3 \times 10^{12}$ G, and $T \geq 0.2\text{--}1$ for the hot emission region. On the other hand, if the narrow absorption dips reported by Mazets *et al.*¹ are real and due to cyclotron absorption, there must exist colder ($kT < 100$ keV) regions with stronger fields ($B \sim 4\text{--}6 \times 10^{12}$ G) located between the continuum emission region and us. The asymmetry in many of Mazets' line profiles¹ with the absorption spreading towards the red (weaker fields in the cyclotron interpretation) may indeed suggest that the field is quite inhomogeneous, with the field strength increasing from the hot emission region to the (initially) cold absorption region. One may therefore visualize the 'expulsion' of the field by the hot emitting plasma (see ref. 14 for this scenario arising in the thermonuclear model). But how such a configuration can hold up for seconds is a significant problem.

It is reasonable to assume that the electrons can maintain a thermal (maxwellian) distribution in the first place? The synchrotron cooling time is extremely short:

$$t_{\text{syn cool}} \approx 4 \times 10^{-16} B_{12}^{-2} T^{-2} \mathcal{F} \text{ s}^{-1} \quad (7)$$

* Address for correspondence.

Table 1 Parameters corresponding to the spectra of Fig. 1

Spectra	ν_c (keV)	ν_{\min} (keV)	$T(\nu_L \leq \nu_{\min})$	τ_{es}^*	$L_{syn}^{*†}/A$	Flux [†] (observed)	d_{max}^* (kpc) $A^{1/2}$
a	10.1	20	≥ 0.71	8.6×10^{-4}	1.1×10^{41}	5.6×10^{-6}	12.6
b	4.6	30	≥ 0.39	4.3×10^{-4}	4.6×10^{40}	1.5×10^{-6}	15.9
c	0.9	20	≥ 0.21	5.8×10^{-5}	2.2×10^{39}	7.4×10^{-7}	5.0
d	5.8	50	≥ 0.34	5.3×10^{-4}	1.4×10^{41}	6.4×10^{-6}	13.5

Note that the small τ_{es} is consistent with the lack of a 'Wien hump'.

* Upper limits assuming $\nu_L \cong \nu_{\min}$, A is emission area in km^2 .

† Integrated over frequencies $\geq \nu_{\min}$, L_{syn} and flux are in erg s^{-1} and $\text{erg s}^{-1} \text{cm}^{-2}$, respectively.

and energy must be continuously supplied to the electrons on this time scale. Coulomb collisions are obviously too slow to thermalize the electrons:

$$t_{coul} \sim 6 \times 10^{-12} T^{3/2} n_{24}^{-1} \text{ s} \quad n_{24} = n_e / 10^{24} \text{ cm}^{-3} \quad (8)$$

However, at least in laboratory situations it is widely believed that even collisionless plasmas can maintain near-maxwellian distributions via collective processes which operate on time scales of the order of plasma instability (for example, two-stream, beam-plasma, cyclotron resonance) growth times which are tied to the plasma or the cyclotron frequency¹⁵. Without delving into the controversy of whether such processes are indeed relevant, especially in strong fields, we only point out here that both the plasma oscillation time

$$\nu_p^{-1} \sim 10^{-16} n_{24}^{-1/2} \text{ s} \quad (9)$$

and electron gyration period

$$\nu_{cyc}^{-1} \sim 3 \times 10^{-19} B_{12}^{-1} \text{ s} \quad (10)$$

can be much shorter than $t_{syn cool}$. Thus a maxwellian electron distribution via collective processes is conceivable, at least for fields much below the quantum limit ($B_{crit} = 4.4 \times 10^{13} \text{ G}$).

The total synchrotron emissivity (ϵ) above a minimum frequency $\nu_{\min} > \nu_L/T$ can be obtained by integration of

equation (26) of ref. 7 (see also ref. 9) and is given approximately by the formula:

$$\epsilon = 2.7 \times 10^9 \text{ erg cm}^{-3} \text{ s}^{-1} n_e B_{12}^2 T^4 \cdot K_2^{-1}(1/T) e^{-x_m} (1 + x_m + \frac{x_m^2}{2!} + \frac{x_m^3}{3!} + \frac{x_m^4}{4!} + \frac{x_m^5}{5!}) \quad (11)$$

where $x_m \equiv (4.5 \nu_{\min}/\nu_c)^{1/3}$. On the other hand, the lack of synchrotron self-absorption turnover down to a frequency ν_{\min} means that (see ref. 9):

$$\frac{h j_{\nu_{\min}}}{m \nu_{\min}^2 T} \leq 1 \quad (12)$$

where we again assume $\langle \theta \rangle \cong \pi/2$ for the strongest constraint. Substituting the explicit form of j_ν (see equation (5)) we obtain

$$n_e h \leq 4.8 \times 10^{19} \nu_{\min \text{ keV}} T K_2(T^{-1}) e^{+x_m} \quad (13)$$

Since $L_{syn}(\nu \geq \nu_{\min}) = 10^{10} \cdot \epsilon h A$ where A is the emission surface area in units of km^2 , we obtain an upper bound to L_{syn} :

$$L_{syn} \leq 9.5 \times 10^{36} A T \nu_{\min \text{ keV}} \nu_c^2 \text{ keV} (1 + x_m + \frac{x_m^2}{2!} + \frac{x_m^3}{3!} + \frac{x_m^4}{4!} + \frac{x_m^5}{5!}) \text{ erg s}^{-1} \quad (14)$$

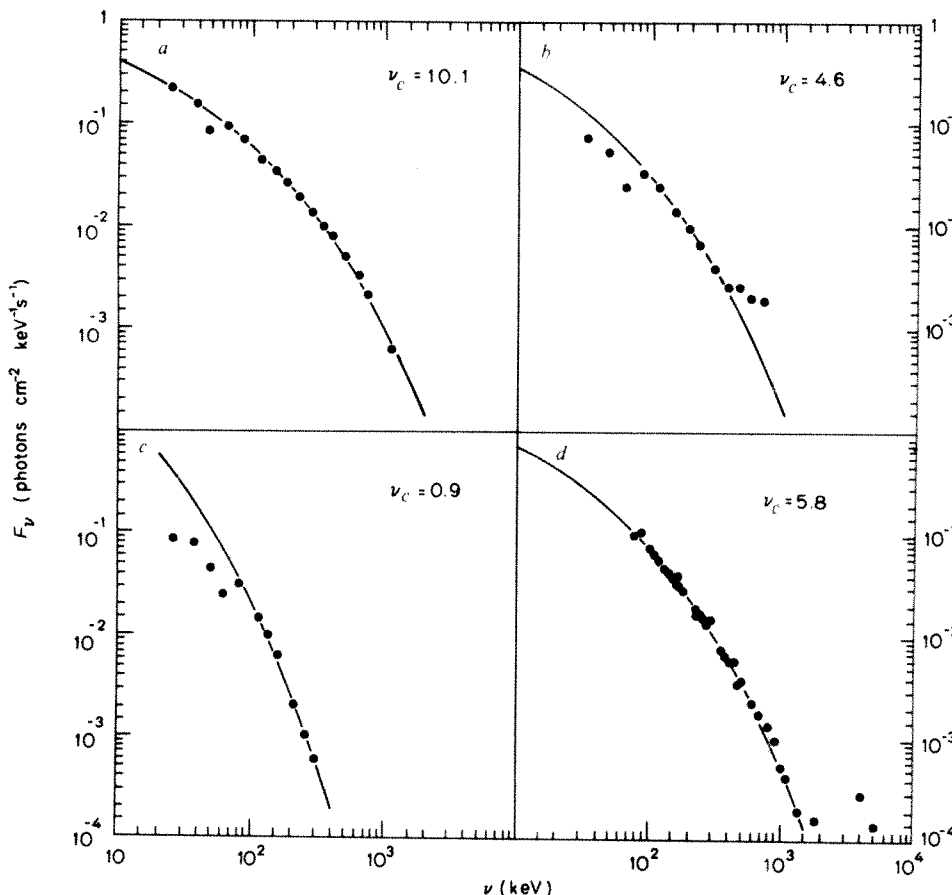


Fig. 1 Representative γ -ray burst spectra fitted with the thermal synchrotron formula (equation (6)). Spectra a, b correspond to Fig. 1a and 1b respectively of Mazets *et al.*¹. Spectrum c corresponds to Fig. 2d of Mazets *et al.*¹. Spectrum d corresponds to Fig. 3 of Gilman *et al.*². ν_c of the theoretical curves are in keV. The dips on the upper left of a, b, c were interpreted by Mazets *et al.*¹ as due to cyclotron absorption. The significance of the high energy excess is unclear because of huge error bars. For observational error bars and widths of energy bins readers should refer to the original articles^{1,2}.

For example, if we use the representative values of $\nu_{\min} = 20$ keV, $\nu_c = 10$ keV, and an observed flux of $\sim 6 \times 10^{-6}$ erg cm $^{-2}$ s $^{-1}$, then $x_m \approx 2$ and $L_{\text{syn}} \leq 1.5 \times 10^{41} T_A \text{ erg s}^{-1}$. If we further assume that $\nu_L \approx 20$ keV, then $T \approx 0.7$ and the upper bound to the intrinsic luminosity is $\sim 10^{41} A \text{ erg s}^{-1}$ and the source distance is $\leq 12 A^{1/2}$ kpc. Table 1 lists the upper bounds corresponding to the four examples of Fig. 1. Since L_{syn} decreases with ν_{\min} (see equation (14)), it is therefore important for future γ -burst observations to lower their detector energy limits to search for possible self-absorption turnover. We should also emphasize that equation (14) is almost definitely a lenient overestimate because in reality anisotropic pitch angle distributions will make the synchrotron luminosity less than that of an isotropic maxwellian plasma with the emission rate governed by pitch angle scattering rates.

We have discovered that optically thin thermal synchrotron from mildly relativistic electrons fits most observed γ burst spectra very well. The absence of self-absorption turnover down to 20–30 keV in most cases then suggests they lie within our local group of galaxies (≤ 1 Mpc). This, of course, does not contradict the suggestion from log N –log S analyses that most sources are likely galactic, since ours are upper limits which could be tightened by future observations at low energies. What is new is that these limits allow the possibility of some sources (for example, the 5 March event) being outside the galaxy. This

would not be possible using a free-free spectral interpretation (see refs 2, 16) since free-free luminosities are many orders of magnitude lower than synchrotron.

It has also been suggested recently that inverse Comptonization (of a soft photon source by hot electrons) may be the origin of the γ burst continuum¹⁷. While inverse Compton spectra may fit better than synchrotron or free-free in isolated cases, a preliminary survey of the Mazets catalogue shows that most of the spectra do not fit as well, since unsaturated inverse Compton spectra tend to have a more prominent 'knee' at $h\nu \sim 3kT_e$. More importantly, such fits would give lower electron temperatures ($T_e \leq 100$ keV) and a τ_{es} close to unity. For electrons in a 10^{12} G field, such large τ_{es} (compare with τ_{es} in Table 1) then leads to unacceptably large cyclotron luminosity. We would have to give up the strongly magnetized neutron star picture altogether.

We emphasize that no single spectral interpretation is binding in itself. But thermal synchrotron is physically more consistent with the conventional picture of strongly magnetized regions of neutron stars as the burst source. Confirmation of the synchrotron mechanism (for example, through the discovery of the first harmonics at low energies) will strongly affect future models of the bursts.

I thank Vahe Petrosian, Reuven Ramaty and George Chapline for useful discussions and Don Lamb for interesting comments.

Received 8 March; accepted 20 July 1982.

1. Mazets, E. P., Golenetskii, S. V., Aptekar', Guryan, Yu. A. & Ilinskii, V. N. *Nature* **290**, 378 (1981).
2. Gilman, D., Metzger, A. E., Parker, R. H., Evans, L. G. & Trombka, J. I. *Astrophys. J.* **236**, 951 (1980).
3. Cline, T. L. *Ann. N.Y. Acad. Sci.* **262**, 159 (1975).
4. Cline, T. L. & Desai, U. D. *Astrophys. J. Lett.* **196**, L43 (1975).
5. Liang, E. P. *Astrophys. J.* (submitted).
6. Tucker, W. *Radiation Processes in Astrophysics* (MIT Press, Cambridge, 1981).
7. Petrosian, V. *Astrophys. J.* (submitted).
8. Trubnikov, B. A. *Phys. Fluids* **4**, 195 (1961).

9. Bekefi, G. *Radiation Processes in Plasmas* (Wiley, New York, 1966).
10. Lamb, D. Q. *Proc. La Jolla Workshop on Gamma-Ray Transients and Related Astrophysical Phenomena* (ed. Lingenfelter, R. (AIP, 1981).
11. Ramaty, R., Lingenfelter, R. E. & Bussard, R. W. *Astrophys. Space Sci.* **75**, 193 (1981).
12. Liang, E. P. T. *Nature* **292**, 319 (1981).
13. Katz, J. *Astrophys. J.* (submitted).
14. Woosley, S. E. & Wallace, R. K. *Astrophys. J.* (submitted).
15. Mikhailovskii, A. B. *Theory of Plasma Instabilities* (Consultants Bureau, New York, 1974).
16. Helfand, D. J. & Long, K. S. *Nature* **282**, 589 (1979).
17. Fenimore, E. E. *et al. Nature* **297**, 665 (1982).
18. Mazets, E. P. *et al. Astrophys. Space Sci.* **80**, 119 (1981).

Neutral hydrogen associated with the planetary nebula NGC6302

Luis F. Rodríguez

Instituto de Astronomía, UNAM, Apdo. Postal 70-264, 04510 Mexico DF, Mexico

James M. Moran

Harvard-Smithsonian Astrophysical Observatory, 60 Garden Street, Cambridge, Massachusetts 02138, USA

Observations of the 21-cm line of neutral hydrogen in absorption made with the Very Large Array (VLA) towards the thermal radio source in the planetary nebula NGC6302 show two velocity components at 6 and -40 km s $^{-1}$ (radial velocity with respect to the local standard of rest). The 6 km s $^{-1}$ component is probably due to a line-of-sight cloud, while the -40 km s $^{-1}$ component is most likely associated with NGC6302. We interpret this latter absorption component as coming from the neutral, outer part of an expanding (~ 10 km s $^{-1}$) ring whose inner part is ionized and produces the absorbed thermal continuum radiation. The mass in atomic hydrogen of the outer (neutral) part of the ring is $\sim 0.06 M_{\odot}$. NGC6302 is probably in an evolutionary stage intermediate to those of protoplanetary nebulae such as GL2688 and evolved planetary nebula such as NGC7293. This is the first detection of H I associated with a planetary nebula.

Planetary nebula are believed to form from the expanding envelopes of red giants and supergiants¹. These stars have mass loss rates in the range 10^{-7} – $10^{-4} M_{\odot} \text{ yr}^{-1}$ with flow velocities of 10–20 km s $^{-1}$ (ref. 2). There is evidence that in many cases the outflow is not isotropic, but rather occurs preferentially in an equatorial plane³, presumably leading to a thick, expanding

disk around the star. It is not known how the final phases of mass loss occur. In a short time, which depends strongly on the stellar mass, the stellar radius decreases to only $\sim 0.02 R_{\odot}$ and the effective temperature of the star increases to $\sim 10^5$ K (ref. 4). The ionizing photons produced by the star will ionize the inner regions of the gaseous envelope. As the envelope expands and becomes less dense, it requires fewer UV photons to be ionized completely. Once complete ionization occurs, a classical planetary nebula, such as NGC6720 or NGC7293, formed by

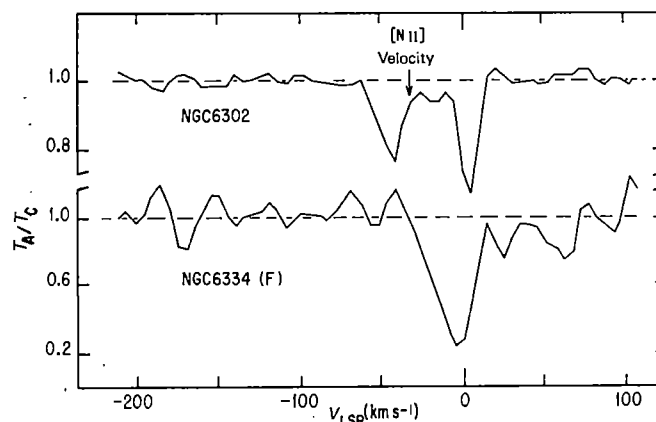


Fig. 1 H I absorption spectra towards the planetary nebula NGC6302 and the compact H II region NGC6334(F). The arrow marks the systemic velocity of NGC6302 from optical observations of [N II] (ref. 13). The absorption component at $V_{\text{LSR}} = -40$ km s $^{-1}$ is interpreted as coming from the outer region of an expanding ring around the planetary nebula. The horizontal axis is the radial velocity with respect to the local standard of rest and the vertical axis is the antenna temperature (T_A ; line plus continuum) over the continuum temperature T_C .

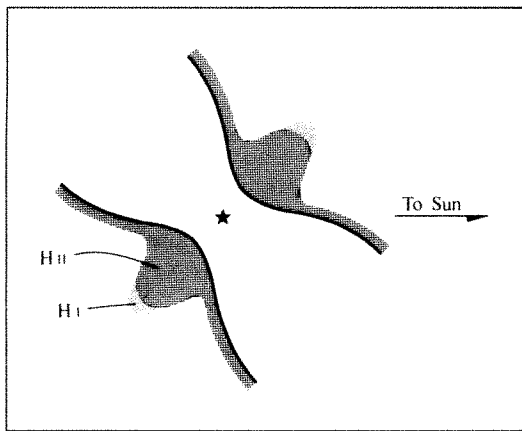


Fig. 2 A possible model for NGC6302. The central star is surrounded by an expanding ring of gas. The inner part of the ring is ionized and produces thermal continuum emission^{20,23}. The outer part of the ring is still neutral and causes the H I absorption that we observed.

an expanding ring of ionized gas, becomes visible. This last stage is the best studied and understood. Recently, considerable advances have been made in the understanding of the earlier evolutionary stages of forming planetary nebulae, mainly from radio and IR observations⁵. Particularly relevant to this understanding has been the identification of small nebulous objects as protoplanetary nebulae⁶⁻⁸, characterized by a predominance of molecular gas. When ionized gas is detected optically, it is found to originate from small regions with dimensions of $\sim 10^5$ cm or less, and consequently the radio flux is undetectable or weak^{9,10}. There should be objects between the protoplanetary nebula and the evolved planetary nebula stages which should have relatively strong thermal radio emission from the ionized gas, while retaining outer regions of neutral gas. A possible example is NGC7027, which is associated with a molecular cloud¹¹. However, the nature of this cloud is unclear as its mass exceeds $5 M_{\odot}$ (ref. 2), very large for a planetary nebula ($0.1-0.2 M_{\odot}$).

During 1982 February we made observations of the 21-cm line of H I in absorption against several compact radio sources in the molecular cloud complex NGC6334 (ref. 12) with the VLA of the National Radio Astronomy Observatory, located near Socorro, New Mexico. Details of the instrumental settings will be given elsewhere¹². We used 13 antennas of the VLA which was in the process of being moved from the C to A configuration. The angular resolution of the interferometer was ~ 10 arc s and the spectral window was ~ 330 km s⁻¹ with a resolution of 10.3 km s⁻¹. As a check source we observed NGC6302, which is only $\sim 2^{\circ}$ from NGC6334. NGC6302 has galactic coordinates of $l^{\text{II}} = 349^{\circ}$, $b^{\text{II}} = 1^{\circ}$ and we expected to detect absorption components only in the ± 10 km s⁻¹ range from local clouds. The observed spectrum is shown in Fig. 1. We detected an absorption component at $V_{\text{LSR}} = 6$ km s⁻¹, probably due to a line-of-sight cloud. A second component at -40 km s⁻¹ is also evident in the spectrum. This component is probably associated with NGC6302 for two reasons. First, the spectrum towards the nearby H II region NGC6334, also shown in Fig. 1, has no detectable absorption at -40 km s⁻¹. Absorption at such a velocity would be expected only from clouds farther than 5 kpc from the Sun. Second, the absorption feature is blueshifted by ~ 9 km s⁻¹ with respect to the radial velocity of the ionized gas in NGC6302, which is $V_{\text{LSR}} = -31 \pm 1$ km s⁻¹ (ref. 13). As the optical emission from the ionized gas originates from gas expanding symmetrically from the star, it can be considered to give a reliable estimate of the systemic velocity. Thus, the H I absorption appears to be due to gas that is expanding away from the nebula at 9 km s⁻¹. This expansion velocity is typical of planetary nebulae. In particular, the expansion velocity for NGC6302 derived from [O III] observa-

tions is 10 km s⁻¹ (ref. 14). However, the total dynamical picture is more complex. For example, higher velocity flows of ~ 100 km s⁻¹ have been seen in the ionized material¹⁵. To our knowledge this is the first detection of H I associated with a planetary nebula. Observing H I in absorption in planetary nebula is difficult as it requires the presence of a substantial amount of ionized gas to provide the background source and, at the same time, the presence of neutral gas. Probably, H I can be detected only during a transition phase, lasting $\sim 10^3$ yr, where the envelope changes from being neutral to being fully ionized. In 1970 Thompson and Colvin¹⁶ attempted to detect H I in six planetary nebulae, including NGC6302, but the sensitivity of their instrument was insufficient for this purpose. The presence of neutral gas in NGC6302 was already evident from the optical observations of Evans¹⁷, who detected strong [O I] line emission from it. Also, his short exposure photograph shows a dark lane separating the two lobes of NGC6302.

Our results can be combined with those of other authors^{15,17,18} to produce a model for NGC6302. Around the star there is a toroidal gaseous structure expanding at a velocity of ~ 10 km s⁻¹. The inner part of this toroid is ionized. Observations of the continuum of NGC6302 made with the VLA²⁰ show a ring-shaped structure with outer dimensions of $\sim 6 \times 9$ arc s. The outer part of the toroid is neutral (Evans' obscuring lane) and causes the H I absorption. The bipolar appearance of the nebula is due to the emission from ionized gas pushed out along the poles of the toroidal configuration. Figure 2 shows a schematic representation of this model, which is similar to that proposed by Canto *et al.*²¹ to explain bipolar outflows in pre-main-sequence objects.

Although the thermal source is ring-shaped with outer angular dimensions of 6×9 arc s, we will approximate it as a sphere of ~ 7 arc s diameter as this allows us to use the formulation of Milne and Aller²² to derive the distance of NGC6302. For a 6-cm flux of 2.8 Jy (refs. 20, 23), assuming the source is optically thin, a reasonable assumption based on the electron temperature, and an angular radius of ~ 3.5 arc s we obtain a distance of 2.4 kpc. Implicit in this derivation is the assumption that the mass in ionized hydrogen is $0.16 M_{\odot}$, the typical total mass of a planetary nebula. As we shall see, this assumption is reasonable since the mass in H I is smaller than the mass in H II. For an expansion velocity of 10 km s⁻¹ and a radius of $\sim 10^{17}$ cm (3.5 arc s at 2.4 kpc) we obtain a kinematic age of $\sim 4 \times 10^3$ yr for NGC6302.

Finally, we estimate the mass in H I. If we assume an excitation temperature of 100 K for the H I, then the column density is $N_{\text{H I}} \sim 8 \times 10^{20}$ cm⁻². If the H I covers the thermal continuum source, the mass of the foreground H I is $\sim 0.03 M_{\odot}$. Multiplying by 2 to account for the H I on the far side of the nebula gives $\sim 0.06 M_{\odot}$ for the total mass in H I. We ignore molecular hydrogen.

The several planetary nebulae which have characteristics similar to those of NGC6302 should be examined for H I. They probably are relatively young planetary nebulae with characteristics intermediate between those of protoplanetary nebulae and evolved planetary nebulae.

NRAO is operated by Associated Universities Inc., under contract with the NSF. We thank J. Meaburn and Y. Terzian for helpful comments.

Received 24 June; accepted 13 July 1982.

- Shklovsky, I. S. *Astr. Zh.*, **33**, 315-329 (1956).
- Knapp, G. R. *et al. Astrophys. J.* **252**, 616-634 (1982).
- Morris, M. *Astrophys. J.* **249**, 572-585 (1981).
- Paczynski, B. *IAU Symp.* **76**, 201-205 (1978).
- Zuckerman, B. A. *Rev. Astr. Astrophys.* **18**, 263-288 (1980).
- Zuckerman, B. *et al. Astrophys. J. Lett.* **205**, L15-19 (1980).
- Calvet, N. & Cohen, M. *Mon. Not. R. astr. Soc.* **182**, 687-704 (1978).
- Lo, K. Y. & Bechis, K. P. *Astrophys. J. Lett.* **205**, L21-25 (1976).
- Westbrook, W. E. *et al. Astrophys. J.* **202**, 407-414 (1975).
- Kwok, S. & Purton, C. R. *Astrophys. J.* **229**, 187-195 (1979).
- Mufson, S. L., Lyon, J. & Maronni, P. A. *Astrophys. J. Lett.* **201**, L85-89 (1975).
- Moran, J. M., Rodríguez, L. F. & Backer, D. (in preparation).
- Minkowski, R. & Johnson, H. M. *Astrophys. J.* **148**, 659-662 (1967).
- Robinson, G. J., Reay, N. K. & Atherton, P. D. *Mon. Not. R. astr. Soc.* **199**, 649-657 (1982).

15. Meaburn, J. & Walsh, J. R. *Mon. Not. R. astr. Soc.* **193**, 631-640 (1980).
16. Thompson, A. R. & Colvin, R. S. *Astrophys. J.* **160**, 363-368 (1970).
17. Evans, D. S. *Mon. Not. R. astr. Soc.* **119**, 150-156 (1959).
18. Elliot, K. H. & Meaburn, J. *Mon. Not. R. astr. Soc.* **181**, 499-507 (1977).
19. Barral, J. F., Canto, J., Meaburn, J. & Walsh, J. R. *Mon. Not. R. astr. Soc.* **199**, 817-832 (1982).
20. Rodríguez, L. F. *et al.* (in preparation).
21. Canto, J., Rodríguez, L. F., Barral, J. F. & Carral, P. *Astrophys. J.* **244**, 102-114 (1981).
22. Milne, D. K. & Aller, L. H. *Astr. Astrophys.* **38**, 183-196 (1975).
23. Terzian, Y., Balick, B. & Bignell, C. *Astrophys. J.* **188**, 257-277 (1974).

Orientation of planetary O^+ fluxes and magnetic field lines in the Venus wake

H. Pérez-de-Tejada*, D. S. Intriligator†
& C. T. Russell‡

* Instituto de Geofísica, Universidad Nacional Autónoma de México, México 20 DF, México

† Carmel Research Center, PO Box 1732, Santa Monica, California 90406, USA

‡ Institute of Geophysics and Planetary Physics, University of California, Los Angeles, California 90024, USA

The presence of 'contaminant' heavy ions of planetary origin in the solar wind has long been the subject of intense theoretical and experimental research. Studies of their abundance, acceleration, and direction of motion are important because of their implications on the composition and dynamics of planetary and cometary plasma wakes. The plasma and magnetic field observations made with the Pioneer Venus Orbiter (PVO) at Venus have provided the opportunity to examine the conditions in which planetary ions are picked up by the solar wind. We show here that in the outer regions of the venusian far wake the displacement of planetary O^+ particles, characteristic of the Venus upper ionosphere, does not occur necessarily along the magnetic field lines but approximately in the direction of the shocked solar wind.

The mass loading of the solar wind plasma with atmospheric ions in non-magnetic planets was first examined in connection with the limited capacity of the flow to accommodate added mass¹. Contaminant material is expected to arise from photo-ionization processes and charge exchange collisions of the solar wind particles with exospheric atoms². In most studies^{3,4} the motion of the planetary ions is believed to result from electric $E \times B$ drifts superimposed on the Larmor gyration around the magnetic field lines. Wave-particle interactions associated with turbulent processes in the plasma^{5,6} may modify this motion, however, and produce a viscous-like acceleration of the planetary ions⁷.

The observation of heavy ions of planetary origin in the Venus wake was first reported⁸ from the low latitude orbital passes of the Venera 9 and 10 spacecraft. These ions were identified as a cool low-energy component directed into the umbra behind the terminator. The results of the spectral analyses of other Venera plasma data⁹ were also consistent with the presence of a component of planetary ions within the umbra.

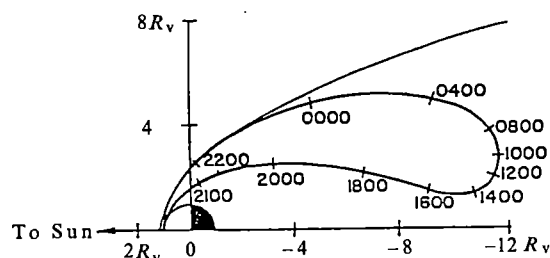


Fig. 1 Two-dimensional projection of the trajectory of the PVO in orbit 189, 11 June 1979.

The more recent measurements carried out with the PVO plasma probe^{10,11} have now revealed the detection of significant fluxes of O^+ ions of planetary origin in the Venus far wake. The energies of these ions are consistent with their having been accelerated to solar wind speeds, and their angular distributions imply that their direction of motion differs, at most, by only a few degrees ($\leq 5^\circ$) from that of the shocked solar wind. In addition, they seem to represent only a contaminant population because of the low ($\sim 1\%$) concentrations observed in the ambient shocked solar wind plasma. With such low densities their mass and momentum flux is significantly smaller than that of the shocked solar wind.

Simultaneous measurements of the magnetic field in the Venus wake carried out with the PVO magnetometer¹² have also indicated the existence of a peculiar magnetic geometry in that region. Most notable is a characteristic increase in the magnitude and fluctuation level of the magnetic field vector, which is predominately oriented along the Sun-Venus direction. Significant departures from this orientation may occur in the outer regions of the wake, however, and in particular at locations where the O^+ fluxes are detected.

From the comparison of the plasma and magnetic data in such regions, it is possible to examine the relative orientation of the magnetic field lines with respect to the direction of motion of the planetary heavy ions. Figure 1 shows the trajectory of the PVO during orbit 189 in a two-dimensional projection where the vertical coordinate is the distance perpendicular to the Sun-Venus axis. The spacecraft probed the magnetic wake between ~ 1230 and ~ 1730 UT and measured intense O^+ fluxes beginning at ~ 1210 UT. The aberrated azimuthal angle of these fluxes¹³ during the 1200-1400 UT time interval is illustrated in Fig. 2 together with the orientation of the local magnetic field (positive values result from directions with a component opposite to the orbital motion of the planet in a coordinate system where the x -axis is directed to the Sun).

The time interval shown is particularly useful because of the fairly persistent orientation of the magnetic field vector away from the solar direction between 1200 and 1300 UT. As shown in Fig. 2, this is predominately along directions which make appreciable negative angles with respect to that of the motion of the planetary ions. During this period the plasma probe measurements showed O^+ fluxes arriving from directions $\leq 5^\circ$ away from the x -axis, and thus with no apparent agreement with the orientation of the magnetic field lines. Simultaneous measurements of the direction of the shocked solar wind plasma showed that this differs at most by a few degrees from that of the O^+ fluxes (both traces would be, in fact, practically indistinguishable at the scale shown). A similar situation is observed between 1300 and 1400 UT despite the fact that during this time interval the magnetic field vector is significantly more variable. Thus, with the exception of the orientation seen near 1300 and 1350 UT, the magnetic field vector again makes large angles with respect to the direction of motion of the planetary ions. Further analysis of the data obtained later in this orbit also indicates significant differences between the direction of the plasma fluxes and the magnetic field orientation. Deeper within the wake, however, the observation of the O^+ particles is more sporadic and the magnetic field vector is seen to suffer frequent and sudden changes in magnitude and direction. In these conditions it is more difficult to establish a clear identification with respect to the direction of motion of the O^+ particles.

The overall tendency of the planetary ions to move in the direction of the shocked solar wind flow is indicative of the type of mechanism that should be responsible for their acceleration. Most notable is the fact that the direction of motion of the O^+ ions appears to be uncorrelated with changes in the direction of the magnetic field vector. Thus, the differences in the orientation of the particle and magnetic fluxes are important not only because they reveal that the displacement of the planetary particles is not necessarily along the field lines, but also because the observations show that the same drift velocity

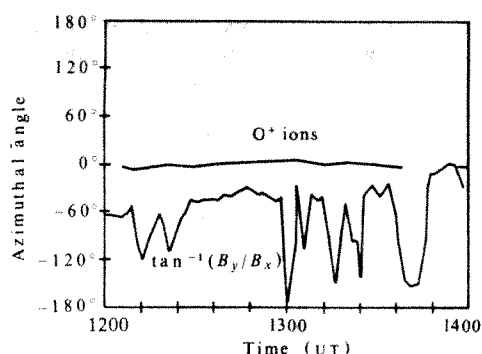


Fig. 2 Azimuthal angle of the magnetic field vector and of the direction of motion of the (peak intensity) O^+ fluxes in the Venus wake between 1200 and 1400 UT in orbit 189.

(nearly coincident with the shocked solar wind velocity) is measured consistently. This behaviour would not be expected if $E \times B$ drifts were solely responsible for the motion of the planetary O^+ ions. If this were the case, their direction of motion would reflect the changes of direction of the magnetic field encountered along the trajectory of the PVO. This circumstance seems to indicate that $E \times B$ pick up processes are not sufficient to account for the acceleration and direction of motion of the planetary ions.

As indicated above, the effects of wave-particle interactions associated with the turbulent character of the ionosheath flow, as revealed by the PVO plasma wave measurements¹⁴, should give place instead to stochastic motions, and enhance the fluid-like behaviour of the local plasma. In these conditions the acceleration process should result from collective interactions between the solar wind and the ionospheric particles, and produce an effective viscous drag between both particle populations⁷. This should set the O^+ particles into motion with speeds and directions nearly coincident with that of the streaming solar wind flow, and independent of the direction of the magnetic field. The PVO observation of heavy ion fluxes in this latter direction, and of the different orientation of the magnetic field vector, is consistent with that interpretation and indicates that wave-particle interactions should have an important role in the acceleration of the ionospheric particles.

As the interaction between the solar wind and the Venus environment is primarily with the atmosphere-ionosphere and not with a planetary magnetic field, the above results are also probably relevant to cometary plasma wakes. If this is the case, then downstream of a comet we should expect to observe accelerated cometary ions flowing in a direction similar to that of the solar wind and independent of the local orientation of the magnetic field.

Services and facilities provided by the Centro de Investigación y Educación Superior de Ensenada, Baja California, Mexico are gratefully appreciated. Partial support by NASA under research contracts: NAS2-10926 at the Carmel Research Center, NAS2-9491 at the University of California and A-80608B(DDA) for the PVO guest investigator programme is acknowledged.

Received 4 March; accepted 18 June 1982.

1. Michel, F. C. *Planet. Space Sci.* **15**, 19 (1971).
2. Wallis, M. K. & Ong, R. S. B. *Planet. Space Sci.* **23**, 713 (1975).
3. Cloutier, P. A., Daniell, R. E. Jr. & Butler, D. M. *Planet. Space Sci.* **22**, 967 (1974).
4. Cloutier, P. A. *Solar Wind Interaction with Planetary Ionospheres*, 111 (NASA SP-397, 1976).
5. Daniell, R. E. Jr. *J. geophys. Res.* **86**, 10094 (1981).
6. Curtis, S. A. *J. geophys. Res.* **86**, 4715 (1981).
7. Pérez-de-Tejada, H. *J. geophys. Res.* **85**, 7709 (1980).
8. Vaisberg, O. L. et al. *Physics of Solar Planetary Environments* vol. 2 (ed. Williams, D. J.) 904 (American Geophysical Union, Washington, DC, 1976).
9. Verigin, M. I. et al. *J. geophys. Res.* **83**, 3721 (1978).
10. Mihalov, J. D., Wolfe, J. H. & Intriligator, D. S. *J. geophys. Res.* **85**, 7613 (1980).
11. Intriligator, D. S. *Geophys. Res. Lett.* **9**, 727, 1982.
12. Russell, C. T., Luhmann, J. G., Elphic, R. C. & Scarf, F. L. *Geophys. Res. Lett.* **8**, 843 (1981).
13. Intriligator, D. S., Wolfe, J. H. & Mihalov, J. D. *IEEE Trans. Geosci. Remote Sensing* **GE-18**, 39 (1980).
14. Scarf, F. L., Taylor, W. L., Russell, C. T. & Elphic, R. C. *J. geophys. Res.* **85**, 7599 (1980).

Intergrown mica and montmorillonite in the Allende carbonaceous chondrite

Kazushige Tomeoka & Peter R. Buseck

Department of Geology and Chemistry, Arizona State University, Tempe, Arizona 85287, USA

Calcium-, aluminium-rich inclusions (CAIs) in carbonaceous chondrites such as Allende are of considerable interest because of their primitive character. There are, however, differences of opinions as to whether they formed directly by condensation from the early solar nebula¹ or by the evaporation of primitive dust². The mineralogy of the CAIs potentially bears on this question and therefore much effort has been devoted to detailed petrographic studies. We present here high-resolution transmission electron microscopy (HRTEM) observations of a complex mixture of mica and montmorillonite that occurs within a fine-grained CAI in the Allende C3(V) meteorite. In spite of previous intensive petrographic investigations of this and related meteorites, the existence of such CAIs bearing mica and montmorillonite has not been reported previously, and there have been no previous positive identifications of these minerals in carbonaceous chondrites.

We extracted part of an ordinary petrographic thin section that includes a CAI, and ion-thinned it for electron microscope observations. The inclusion, round and ~0.4 mm in largest dimension, consists of fine-grained fragments ranging in diameter from <1 to 50 μ m. Electron microprobe analyses show that the inclusion contains considerable Mg, Fe and Na in addition to major Si, Al and Ca, and that it exhibits extreme local compositional variations. The fine-grained fragments are mostly Fe-containing spinels that are characteristically enclosed by fine-grained rim material. These textural and chemical characteristics indicate that the inclusion corresponds to a fine-grained alkali-rich spinel aggregate in Wark's³ classification of CAIs and Type 3 in Kornacki's⁴ classification of fine-grained CAIs in Allende. The fine-grained CAIs are rich in alkali and volatile elements in addition to the refractory Ca-Al-rich minerals, which makes it difficult to explain their origin by simple condensation models⁵. Studies of petrographic characteristics of the fine-grained inclusions in the Allende meteorite are reported elsewhere^{3,6}.

In low magnification TEM images, we have observed phyllosilicate that shows a complex, fluffy texture. It occurs along two cavities that appear to be interstitial to spinel grains and are located close to the margin of the inclusion. Investigation by HRTEM has shown that much of the phyllosilicate has a (001) basal fringe spacing of ~10 Å (Fig. 1). This feature clearly distinguishes it from serpentine-type phyllosilicates that are now widely accepted as major constituents of the C2 matrix phases. Possible candidates for the phyllosilicates having such (001) spacings include mica, dehydrated montmorillonite-type clay minerals, and talc⁷.

The phyllosilicate grains display characteristic features in their morphologies and arrangements of lattice planes. Some crystals have a straight or sub-parallel arrangement of their lattice fringes. On the other hand, most crystals commonly show bending, terminating and overlapping fringes (Fig. 1). In some areas, fringes vary in spacing between 10 and 15 Å. These structural characteristics indicate a strong similarity to those observed in terrestrial mixed layered mica and montmorillonite⁸⁻¹⁰.

Chemical analyses were performed with an energy dispersive X-ray spectrometer (EDS) on our TEM and scanning electron microscope (SEM). EDS spectra from the phyllosilicate reveal large Si and Al peaks and less intense K, Mg, Ca and Fe peaks. Sodium was detected in significant but variable amounts, and minor Cl and Ti were also encountered. These results preclude the possibility of talc. Based on data from imaging and chemical analyses, we conclude that the phyllosilicate is a complex

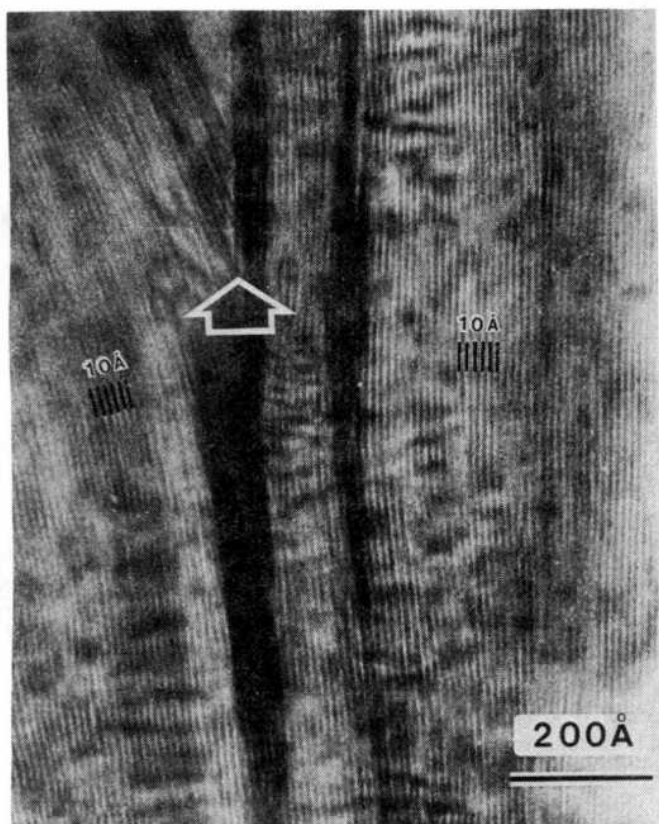


Fig. 1 An HRTEM image of an intergrown mica and montmorillonite crystal occurring along Ca-, Al-rich silicate grains within a fine-grained CAI of the Allende carbonaceous chondrite. The crystal exhibits bending, terminating and overlapping fringes (indicated by an arrow) and has a characteristic modulation in intensity along the length of the fringes.

mixture of mica and montmorillonite. Here the names are used as representing minerals having rather broad compositional ranges in these groups and not particular species.

The nature of the distribution of the Allende mica and montmorillonite along the walls of micro-cavities suggests that the phyllosilicate is genetically related to the surrounding alkali- and Ca-Al-rich silicate grains; owing to their fine-grained nature, the quality of chemical data from the surrounding crystals are not adequate to identify mineral species. They are probably feldspathic minerals, which constitute a rim material surrounding the spinel cores⁹. Recently, unusual unidentified phases have been reported to occur within rim material surrounding spinel grains in the fine-grained type of CAIs in Allende and Mokoia C3 meteorites^{11,12}; these phases have strikingly similar composition and texture to the present mica and montmorillonite assemblage. Aluminium-rich phyllosilicate was also reported from an inclusion within a C2-like clast in the Plainview (H5) meteorite¹³.

It is significant that the Allende mica and montmorillonite occur close to the boundary between the inclusion and matrix, and that the boundary is highly irregular in that region. Furthermore, a small spinel grain that is apparently related to the inclusion, occurs isolated within the matrix near the boundary. These observations suggest that reaction occurred between the inclusion and the matrix, and also that favourable conditions for producing the mica and montmorillonite existed near the boundary. McSweeney studied many C3(V) type meteorites and showed that there is apparent petrographic evidence of relatively mild metamorphism in several of those meteorites, and fine-grained olivine inclusions and CAIs in Allende may have undergone partial Fe/Mg exchange with matrix¹⁴. Our identification of mica and montmorillonite supports his view and suggests, as inferred from terrestrial analogues, that the metamorphism included aqueous alteration at a relatively low temperature.

Montmorillonite had been proposed as one of the possible phyllosilicate types that constitute a major portion of the matrix of C1 and C2 meteorites¹⁵⁻¹⁷. Recently, Barber reported fairly convincing evidence of the presence of montmorillonite in the matrix of the Nawapali C2(M) meteorite¹⁸. Bass suggested that montmorillonite replaces serpentine, providing for random mixed layering between them¹⁵. However, we did not encounter any evidence of serpentine intergrown with the mica and montmorillonite in Allende. On the contrary, the present results indicate that montmorillonite could be related to the Ca-Al-rich inclusions.

Armstrong *et al.*¹⁹ based on a detailed study of a hibonite-, calcite-bearing inclusion in the Murchison C2(M) meteorite, suggested that extensive alteration of CAIs may have occurred by aqueous alteration and thermal metamorphism before final meteorite formation. The scarcity of CAIs, especially the fine-grained type of inclusions in the C2 meteorites, could be explained by the susceptibility of CAIs to hydrothermal alteration. Oxygen isotopic data for fine-grained CAIs in the C2 meteorites would be useful for verifying whether or not such a hypothetical reaction had been widespread.

We thank John Larimer, Ian Mackinnon and David Veblen for helpful discussions and James Clark for assistance with electron microprobe analyses. The microprobe was obtained partly with funds provided by the Chemistry Instrumentation Program of the NSF. Electron microscopy was performed at the electron microscope facility in the Center for Solid State Science at Arizona State University. This work was supported by NASA grant NAGW-143.

Received 20 May; accepted 9 July 1982.

- Grossman, L. *Geochim. cosmochim. Acta* **39**, 433-454 (1975).
- Wood, J. A. *Earth planet. Sci. Lett.* **56**, 32-44 (1981).
- Wark, D. A. *Astrophys. Space Sci.* **65**, 275-295 (1979).
- Kornacki, A. S. *Lunar planet. Sci.* **XII**, 562-564 (1981).
- Grossman, L. & Ganapathy, R. *Geochim. cosmochim. Acta* **40**, 967-977 (1976).
- Kornacki, A. S. *Geochim. cosmochim. Acta* (submitted).
- Veblen, D. R. & Buseck, P. R. *Science* **206**, 1398-1400 (1979).
- McKee, T. R. & Buseck, P. R. *Electron Microscopy* **1**, 272-273 Intern. (1978).
- Page, R. & Wenk, H. R. *Geology* **7**, 393-397 (1979).
- Kobutsugaku Zasshi Spec. Issue* **14**, 205-227 (Appendix) (1979).
- Wark, D. A. & Lovering, J. F. *Proc. 8th Lunar Sci. Conf.* 95-112 (1977).
- Cohen, R. E. *Meteoritics* **16**, 304 (1981).
- Nozette, S. & Wilkening, L. L. *Geochim. cosmochim. Acta* **46**, 557-563 (1982).
- McSweeney, H. Y. Jr *Geochim. cosmochim. Acta* **41**, 1777-1790 (1977).
- Bass, M. N. *Geochim. cosmochim. Acta* **35**, 139-147 (1971).
- Caillière, S. & Rautureau, M. C. *r. Acad. hebdom. Séanc. Sci., Paris* **D279**, 539-542 (1974).
- Fanale, F. P. & Cannon, W. A. *Geochim. cosmochim. Acta* **38**, 453-470 (1974).
- Barber, D. J. *Geochim. cosmochim. Acta* **45**, 945-970 (1981).
- Armstrong, J. T., Meeker, G. P., Huneke, J. C. & Wasserburg, G. J. *Geochim. cosmochim. Acta* **46**, 575-595 (1982).

An unusual layered mineral in chondrules and aggregates of the Allende carbonaceous chondrite

Kazushige Tomeoka & Peter R. Buseck

Departments of Geology and Chemistry, Arizona State University, Tempe, Arizona 85287, USA

Olivine-rich chondrules and aggregates in the Allende C3(V) carbonaceous chondrite are characterized by abundant opaque spherules of metal, sulphide and magnetite grains. This assemblage has been explained as resulting from the crystallization of immiscible metal-sulphide-oxide liquids, suspended as droplets within the chondrules¹. Petrographic evidence indicates a significant metasomatic effect in a highly oxidizing condition in a later cooled stage^{2,3}. We have found that an unusual Fe-, Ni- and O-rich layered mineral, related to serpentine, occurs within the opaque assemblage; it is formed by alteration of olivine. The textural and compositional features are clearly distinct from terrestrial phyllosilicates. This is the first report of a serpentine-related mineral in the Allende meteorite. Our observations suggest that aqueous conditions occurred in Allende before the final stage of meteorite formation.

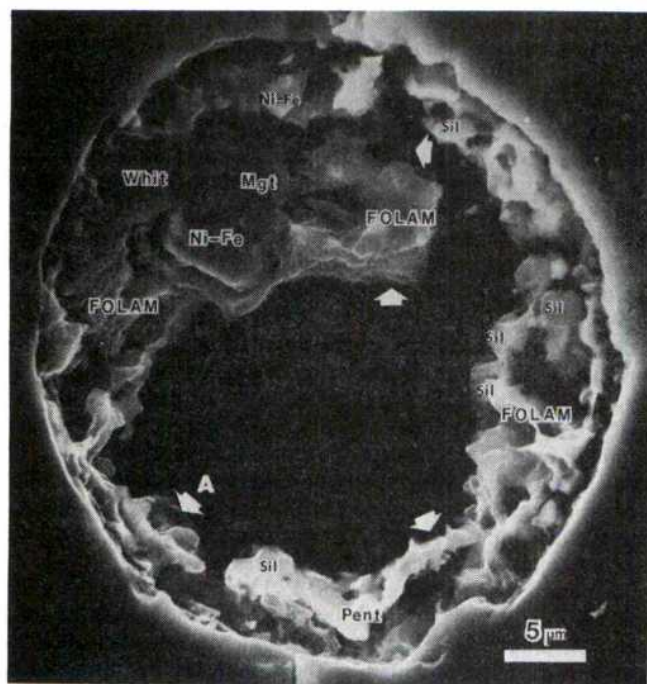


Fig. 1 SEM photograph of one of the ion-etched opaque spherules existing inside chondrules. The spherule contains Ni-Fe metal, magnetite (Mgt), pentlandite (Pent), whitlockite (Whit) and Fe-Mg silicate (Sil). The large central black region is a hole made by ion-thinning. The new phase, FOLAM, is observed at the positions indicated by white arrows. Along the right side of the spherule, fine-grained silicate grains (0.5–2 μm across) are intergrown with FOLAM.

The opaque spherules in the Allende chondrules and aggregates are commonly complex assemblages of troilite, pentlandite, magnetite and Ni-Fe metal in varying combinations and proportions¹. Silicates, chromite, heazlewoodite, and whitlockite are also finely disseminated in the opaque phases. Because of their intimately intergrown and fine-grained character, the mineralogical relationships are more complex than can be determined by conventional petrographic techniques.

The combined techniques of transmission electron microscopy (TEM) and scanning electron microscopy (SEM), with energy dispersive X-ray (EDS) and electron energy loss (EELS)

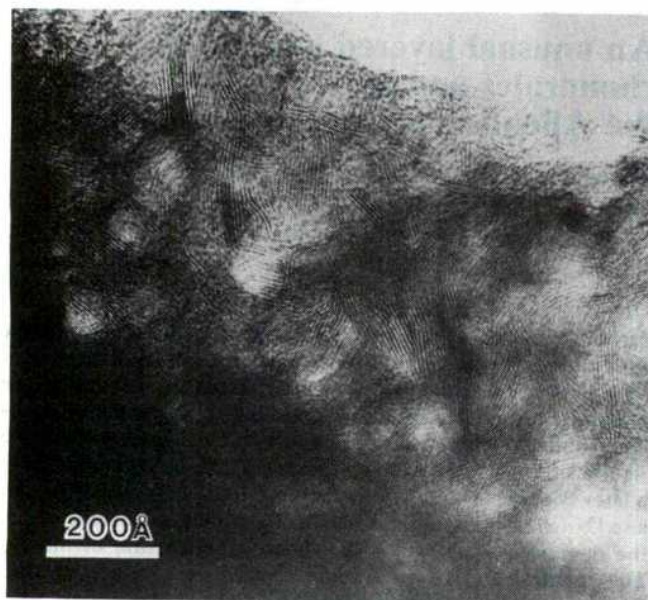


Fig. 2 A high-resolution TEM photo of FOLAM showing a complex arrangement of fringes, typical of materials having layer-structures.

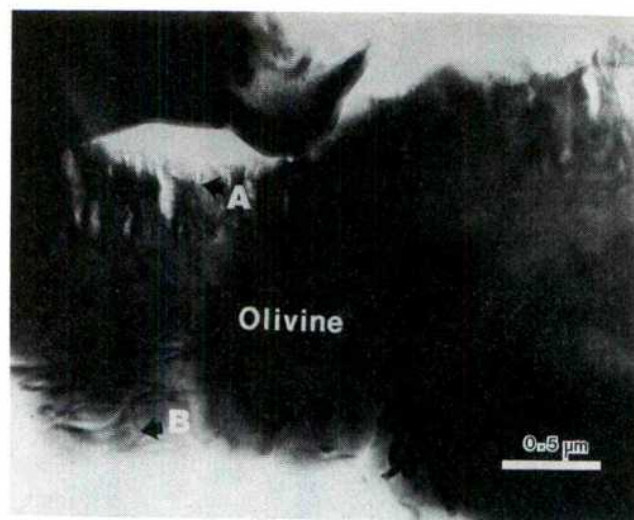


Fig. 3 A low-magnification TEM photo of an olivine grain showing the partial alteration to FOLAM at the top side of the grain. The grain occurs in an opaque spherule consisting of Ni-Fe, magnetite and pentlandite, within a barred olivine chondrule.

spectroscopy have been used to study the microstructures and phase relationships of the minerals in the opaque spherules. Chondrules and aggregates enclosing opaque spherules were extracted from a petrographic thin section and ion-thinned. The opaque minerals are softer than the surrounding silicate grains, and thus can be preferentially thinned for TEM observations.

Figure 1 shows an SEM photomicrograph of one of the ion-thinned opaque spherules. An unusual Fe-, Ni- and O-rich layered material (here called 'FOLAM' for brevity) is observed by TEM along the edges of the central hole. It commonly occurs in complex intergrowths with small silicate grains, as seen in Fig. 1. A low-magnification TEM image of FOLAM shows an extremely complicated, fluffy, 'cotton'-like texture. Each fragment appears to consist of a bundle of fine fibres entangled in complex ways. Submicrometre-sized chromite grains (<0.1 μm in diameter) commonly occur in association with FOLAM.

In most areas FOLAM is poorly crystalline and does not give clear diffraction patterns, but characteristically exhibits fairly strong powder rings at positions corresponding to spacings of 2.5, 2.0 and 1.5 \AA . Diffuse scattering characterizing spacings >2.5 \AA suggests a wide variety of spacings in that range. Rarely, however, did we observe lattice fringe images (Fig. 2). Such images also exhibit extremely complex textures. The fringe spacings vary widely, but average $\sim 6.8 \text{ \AA}$ which is close to but slightly smaller than the serpentine spacing (7.3 \AA). Most FOLAM crystallites consist of <10 layers and curve and diverge in various ways. The abundant overlapping and crossing fringes are especially prominent. The layers in these images are approximately parallel to the viewing direction; overlapping fringes therefore indicate that individual layers are not extended in the direction of the axes of each roll⁴. This unusual fringe texture can be best described as a 'ribbon'-structure resembling that in some graphitic carbons⁵. Based on the similarity of appearance in TEM images and spacings, we assume that FOLAM has a structure similar to that of serpentine.

EDS spectra from FOLAM show, without exception, large Fe and Ni and small Si, S, Cr and Mg peaks. Chlorine and Ca also occur, but in very small amounts. EELS spectra reveal a large oxygen peak in addition to the above elements. These compositional features differ from those observed in terrestrial phyllosilicates. Of special significance is the extremely small Si content, relative to the large amount of Fe, and the invariable presence of Ni, S and Cr. To explain the low Si content, we assume that FOLAM has a structure related to cronstedtite, an Fe-rich end member of the septeclorite series; cronstedtite is unique as a sheet silicate mineral, as it has Fe^{3+} substituting

for Si in tetrahedral sites⁶. It has been reported to occur in the Cochabamba C2(M) meteorite⁷.

As far as its chemical composition is concerned, FOLAM appears similar to 'PCP'⁸, a phase that is ubiquitous in C2 carbonaceous chondrites but has not yet been properly characterized. Previous petrographic studies suggest that PCP also has a layer structure and is closely related to phyllosilicates^{9,10}.

During our TEM study, we encountered evidence regarding the origin of FOLAM. Figure 3 shows an olivine grain that is partly altered to FOLAM along the top side. EDS analyses (Fig. 4) indicate that the olivine is distinctly more fayalitic than the olivines surrounding the opaque spherule. On the other hand, Si and Mg are strongly depleted while Fe and Ni are greatly enriched in the FOLAM. These observations show that FOLAM has been produced by alteration of olivines that are finely disseminated among the opaque phases.

Phyllosilicates are known to be major constituents of C1 and C2 carbonaceous chondrites, but relatively little is known about their occurrence and character in C3 carbonaceous chondrites. The matrix in Allende consists mostly of fine-grained olivines, and phyllosilicate has not been reported previously. It is significant that the FOLAM is restricted to the opaque spherules in chondrules and aggregates. Its occurrence suggests that conditions were once favourable for the formation of a serpentine-like mineral within the opaque spherules; presumably, low temperature and a somewhat hydrous condition were required. It seems improbable that the whole meteorite experienced such an environment, because otherwise fine-grained olivines, abundant in the matrix, would also have been affected and altered to sheet silicates.

Armstrong *et al.*¹¹ based on a detailed study of a hibonite-bearing inclusion in the Murchison C2(M) meteorite, showed

that aqueous alteration occurred before that inclusion was incorporated into its present location. Our observations provide an independent set of data that suggest an alteration stage may also have occurred in Allende before the final stages of meteorite formation. Either the environment required to produce FOLAM was unique to the opaque spherules, or the conditions needed to produce FOLAM occurred before the time that chondrules were trapped within the Allende matrix.

Haggerty and McMahon¹ argued that the presence of the unusually high Ni-content alloy coexisting with magnetite resulted from a highly oxidizing condition. The unusual composition of FOLAM presumably results from the oxidizing environment that the opaque spherules experienced during or after the formation of FOLAM. In these conditions, Fe would exist in the ferric state and thus be able to substitute for Si in the tetrahedral as well as octahedral sites of the cronstedtite structure. Ni²⁺ and Cr³⁺ must also enter the octahedral sites. Sulphur is conceivably incorporated into the structure as a sulphate ion. The occurrence of the large amount of Fe³⁺ could account for the smaller basal fringe spacing of FOLAM than those of the serpentine minerals. However, we are uncertain about the extent to which these ions can enter the structure without a breakdown of the lattice. In any case, the unusual characteristics of FOLAM reflect undetermined extraterrestrial conditions experienced by some chondrules and aggregates.

We thank John Larimer, Ian Mackinnon and David Veblen for helpful discussion and James Clark and Brian McIntyre for assistance with electron microprobe analyses and scanning electron microscopy. The microprobe was obtained partly with funds provided by the Chemistry Instrumentation Program of the NSF and the SEM is supported by NSF grant ATM 8022849. The electron microscopy was performed at the electron microscope facility in the Center for Solid State Science at Arizona State University. This work was supported by NASA grant NAGW-143.

Received 7 June; accepted 5 July 1982.

- McMahon, B. M. & Haggerty, S. E. *Proc. 11th Lunar planet. Sci. Conf.* 1003-1025 (1980).
- Haggerty, S. E. & McMahon, B. M. *Proc. 10th Lunar planet. Sci. Conf.* 851-870 (1979).
- McSweeney, H. Y. *Geochim. cosmochim. Acta* **41**, 1777-1790 (1977).
- Veblen, D. R. & Buseck, P. R. *Am. Miner.* **66**, 1107-1134 (1981).
- Ban, L. L., Crawford, D. & Marsh, H. J. *Appl. Crystallogr.* **8**, 415-420 (1975).
- Hendricks, S. B. *Am. Miner.* **24**, 529-539 (1939).
- Müller, W. F., Kurat, G. & Kracher, A. *Tschermaks miner. petrogr. Mitt.* **26**, 293-304 (1979).
- Fuchs, L. H., Olsen, E. & Jensen, K. J. *Smithson. Contr. Earth Sci.* **10**, 1-39 (1973).
- Ramdohr, P. *The Opaque Minerals in Stony Meteorites* (Elsevier, Amsterdam, 1973).
- Bunch, T. E. & Chang, S. *Geochim. cosmochim. Acta* **44**, 1543-1577 (1980).
- Armstrong, J. T., Meeker, G. P., Huneke, J. C. & Wasserburg, G. J. *Geochim. cosmochim. Acta* **46**, 575-595 (1982).

Measurement of Rayleigh-Taylor instability in a laser-accelerated target

A. J. Cole & J. D. Kilkenny

The Blackett Laboratory, Imperial College of Science and Technology, London SW7 2BZ, UK

P. T. Rumsby, R. G. Evans, C. J. Hooker
& M. H. Key

Rutherford Appleton Laboratory, Chilton, Didcot,
Oxfordshire OX11 0QX, UK

The classical Rayleigh-Taylor (R-T) instability of a fluid supporting a higher-density fluid^{1,2} in a gravitational field is expected to occur in laser-driven compression³. A laser produces a high-pressure plasma that accelerates a higher-density solid shell of thickness Δr at a rate a . The effective gravitational acceleration— a would cause shell perturbations of wavenumber k to grow at the R-T rate $\gamma = (ka)^{1/2}$. However, ablation effects³⁻⁵ are predicted to damp short-wavelength modes, giving rise to a maximum growth rate at $k \sim 1/\Delta r$ and implying a maximum aspect ratio $r/\Delta r$ for a stable implosion. We present here the first clear experimental evidence for the growth of the

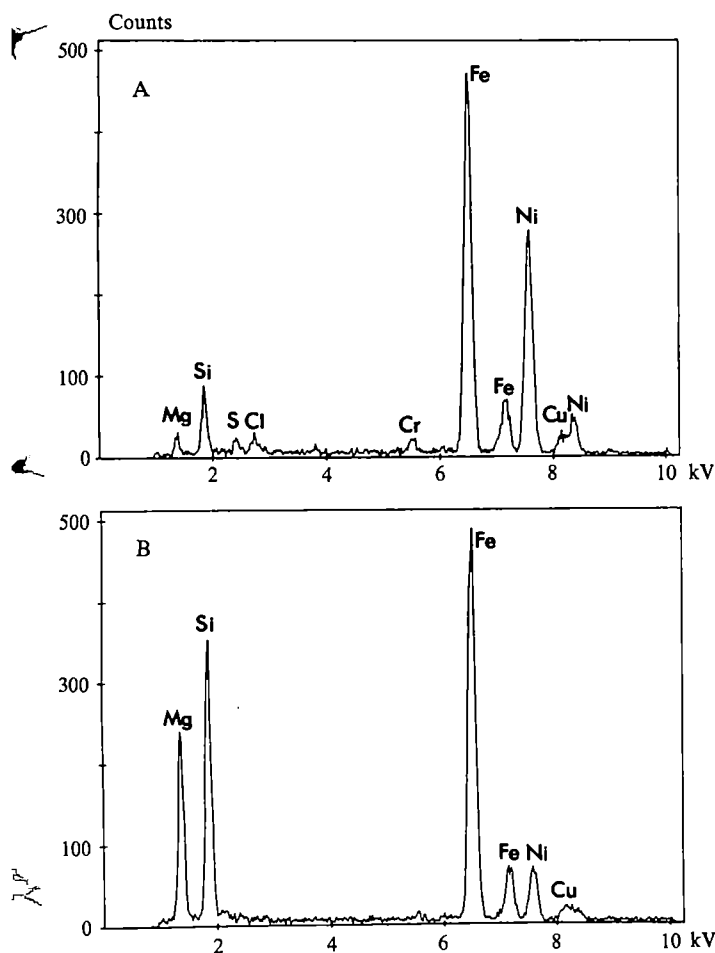


Fig. 4 EDS spectra from the areas of altered FOLAM (A) and olivine (B) in Fig. 3. The copper peaks result from the supporting grid.

R-T instability in a laser-accelerated plane target. These results were obtained by a novel technique using a target with an initial corrugation of known k . Streak X-ray radiography allows direct measurement of the growth of mass modulations in the target caused by this initial perturbation. The time-averaged growth rate of an imposed perturbation is measured as $(0.3 \pm 0.05) \times (ka)^{1/2}$, in close agreement with a numerical simulation.

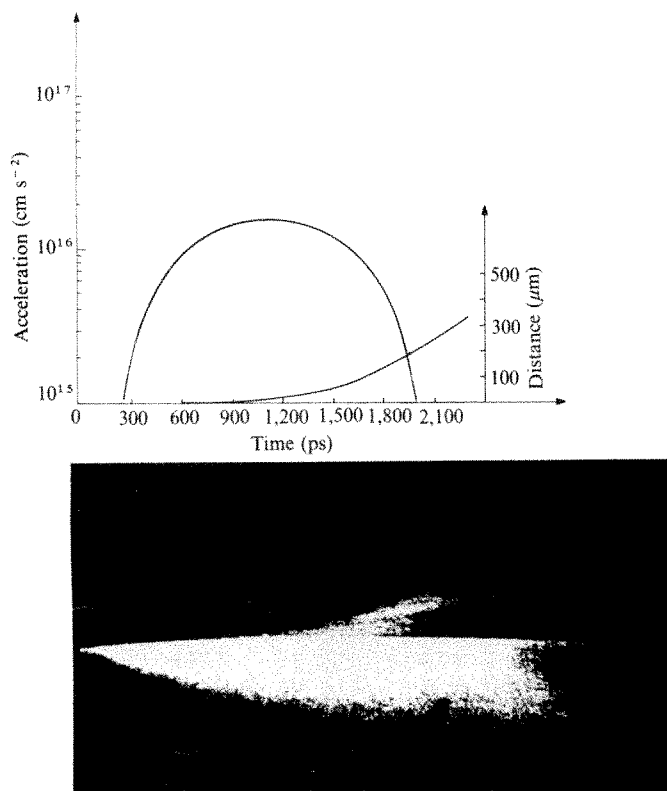


Fig. 1 X-ray streak camera photograph of a laser-accelerated microdisk target. The target is viewed edge on and is irradiated from below. The X-ray self emission of the accelerated material can be seen moving vertically away from the absorbing edge of unirradiated material. Also shown (above) is the target trajectory and the derived acceleration.

The accelerated target was a plane aluminium disk of diameter 550 μm and thickness 3 μm , symmetrically irradiated with three of the six orthogonal 0.53- μm beams of the Science and Engineering Research Council's Central Laser Facility⁶. Each of the beams was focused with an $f/1$ lens at an angle of incidence of 56°, allowing the target normal direction to be used for diagnosis by streaked X-ray radiography.

To measure their acceleration, the targets were positioned edge on and accelerated transversely across the field of view of an X-ray pinhole camera which had a 5- μm pinhole filtered with 3 μm of Al and 15 μm of Be. Images were recorded on an X-ray streak camera with 10 ps and 10 μm time and spatial resolution, respectively. The three beams with 32 J in total in 1.2 ns were focused 250 μm beyond the targets, thus only illuminating and accelerating the central 300 μm of the target. The streaked X-ray emission is shown in Fig. 1, where the accelerated central part of the target can be clearly seen moving away from the absorbing edge of the unaccelerated outer ring of the target. From knowledge of the laser irradiation-time profile and independently measured ablation pressure-irradiance scaling relationships⁷, it was possible to determine the acceleration of the target as shown in Fig. 1. This acceleration profile is compatible with the measured target trajectory also shown in Fig. 1 and could be scaled to match the irradiance of the transmission measurement described below.

To observe the R-T instability, the targets were turned so as to face away from the streak camera, and a different cluster of three beams was used to accelerate the target towards the camera. A more uniform illumination at approximately the same peak irradiance was used, by focusing 550 μm beyond the targets and increasing the laser energy to 87 J on target.

The R-T instability of the Al target was initiated by using a target with a corrugation of wavelength 20 μm and amplitude 0.5 μm . Behind the Al disk targets a separate Cu target was irradiated by a fourth synchronous backlighting laser beam. This produced a plasma 500 μm across and 100 μm high in the streak direction. In the spectral region of observation the X-ray emission from this target was several times brighter than that from the Al disk, as shown by an experiment with deliberately delayed backlighting. The Cu plasma provided a source with which to make an X-ray absorption picture of the accelerated Al disk. The spectrum of the Cu backlighting target, measured with two crystal spectrometers, showed a peak at a wavelength

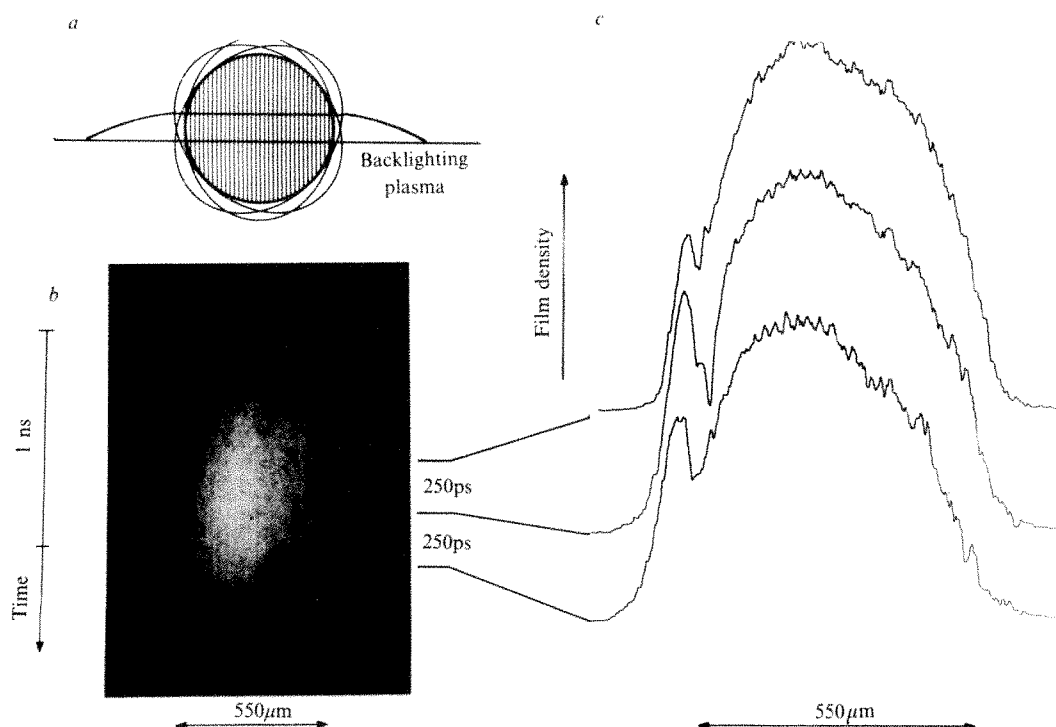


Fig. 2 *a*, Corrugated microdisk target illumination geometry showing location of backlighting plasma. *b*, X-ray streak photograph of backlighting emission through an irradiated microdisk target with 20 μm corrugation. *c*, Microdensitometer tracings of *b* at times 700, 950 and 1,200 ps, showing increasing modulation with time.

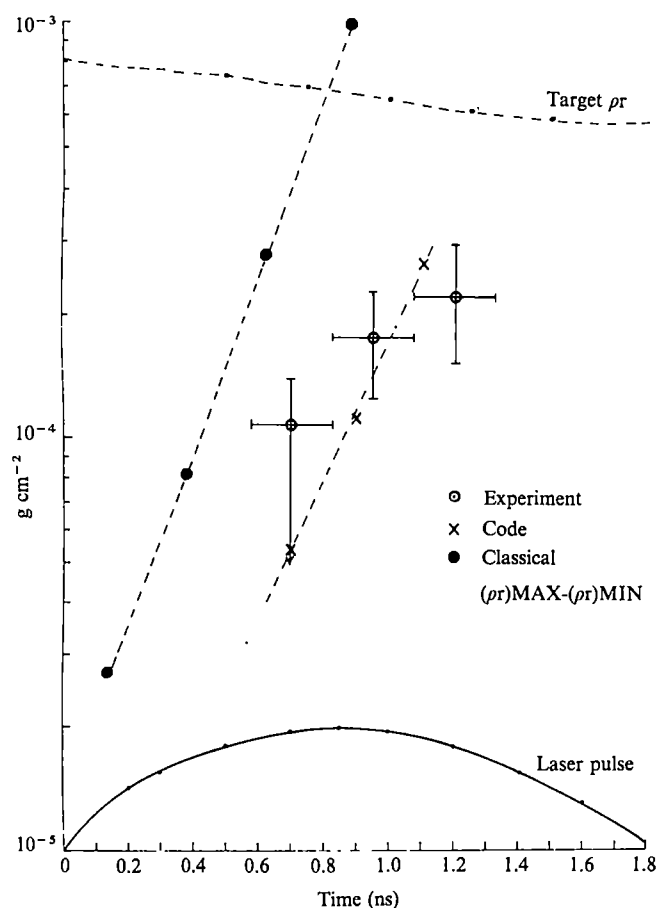


Fig. 3 Graph of modulation in target areal density from the three experimental measurements in Fig. 2c. Also shown are the results of two-dimensional fluid simulations and the modulation expected of a classically growing instability.

of 10 Å (in I_A), with a rapid fall at shorter wavelength. The variation of the X-ray intensity reaching the streak camera with Al target thickness was calculated from the spectrum and the transmission of the filters, giving agreement with the 55% transmission observed through a 3- μ m Al foil in a separate experiment.

An X-ray streak photograph of the transmission of such an accelerated target is shown in Fig. 2, with the corrugation parallel to the direction of streaking. Initially there is, as expected, no variation of transmission across the target, but as the instability grows, mass is redistributed and modulations in the transmission with a period of 20 μ m can be seen. In control experiments with no initial corrugation, no such regular modulation is observed.

The film density modulations evident in Fig. 2 were converted to mass per unit area modulation by using the calculated variation of spectrally integrated transmission with Al thickness as described above. The amplitude of the modulation is shown in Fig. 3 as a function of time, the errors representing the spread in the amplitude of the eight modulations evident at late time in Fig. 2.

The average growth rate from Fig. 3 is $1.6 \pm 0.5 \times 10^9 \text{ s}^{-1}$, with some evidence of saturation. Figure 3 also shows the classical growth, taken from $(ka)^{1/2}$ and the acceleration scaled from the measurements shown in Fig. 1. The classical growth is started, in Fig. 3, at the onset of target motion with an initial amplitude determined by projecting back the slope of the experimental observations to zero time. The initial surface perturbation is not an R-T eigenmode, as there is no initial velocity perturbation, and this can cause some delay in the growth of an R-T mode⁸. However, it can be seen that the observed growth rate is $\sim 0.3 \times (ka)^{1/2}$.

The experiment has been simulated using a two-dimensional Eulerian fluid code⁹. An absorbed irradiance of $2.0 \times$

$10^{13} \text{ W cm}^{-2}$ was used so that the distance moved by the foil in the simulation matched the observed motion. A corrugated target as used in the experiment seeded the growth of an instability at the desired wavelength. The code predictions of growth in mass-density modulations (after convolving with a pinhole response) are also shown in Fig. 3.

The experimental measurements of Fig. 3 are lower than both the classical value and the simulated value. This is not due to ablating too much material from the target: the initial areal density is 0.8 mg cm^{-2} and the decrease due to ablation⁷ is shown in Fig. 3. The analysis of the Al transmission assumes the cold X-ray mass attenuation coefficients. However, the code values for the temperature and a local thermodynamic equilibrium ionization equation shows that this produces a negligible error. However, several phenomena are omitted or modelled inaccurately in the simulation, including radiation transport, equation of state, ion viscosity and magnetic field generation.

In conclusion, observations of the growth of area density modulations at a rate of $0.3 \times (ka)^{1/2}$ have been observed. Although these results are incomplete, in that data have so far only been obtained for one k value, it is nevertheless encouraging for laser-driven compression that the growth rate is so low, significantly less than classical, as has been predicted by numerical simulation⁵.

We acknowledge helpful conversation with W. C. Mead. A.J.C. was supported by a SERC studentship.

Received 13 May; accepted 14 July 1982.

1. Lord Rayleigh, *Theory of Sound* 2nd edn, Vol. 2 (Dover, New York, 1945).
2. Taylor, G. I. *Proc. R. Soc. A* **201**, 192 (1930).
3. Nuckolls, J. H., Wood, L., Thiessen, A. & Zimmerman, G. *Nature* **239**, 139 (1972).
4. McCrory, R. L., Monteith, L., Morse, R. L. & Verdon, C. P. *Phys. Rev. Lett.* **46**, 336 (1981).
5. Emery, M. H., Gardner, J. H. & Boris, J. P. *Phys. Rev. Lett.* **48**, 677 (1982).
6. Ross, I. et al. *IEEE J. Quant. Elect.* **QE17**, 1653 (1981).
7. Goldsack, T. J. et al. *Opt. Commun.* **42**, 55 (1982).
8. Lindl, J. D. & Mead, W. C. *Phys. Rev. Lett.* **34**, 1273 (1975).
9. Pert, G. J. *comp. Phys.* **43**, 111 (1981).

Density-driven interstitial water motion in sediments

D. L. Musgrave & W. S. Reeburgh

Institute of Marine Science, University of Alaska, Fairbanks, Alaska 99701, USA

Sediment depth distributions and fluxes of dissolved chemical substances have been interpreted as being a result of reaction, diffusion, bioturbation and irrigation^{1,2}. However, several studies suggest that density-driven convection³ can alter the depth distribution and increase the fluxes of dissolved substances when density decreases below the sediment surface⁴⁻⁷. We present here temperature-time series measurements for a freshwater lake undergoing autumn cooling. These are the first *in situ* observations of heat transport due to motion of interstitial waters over periods of less than 1 hour. Density, calculated from temperature, decreases with depth at the time and place that this motion occurs.

Temperature was measured by inserting a multi-thermistor plastic probe into the sediments. The probe was made of 2.5-cm PVC pipe with glass bead thermistors mounted along its length. The thermistors were pushed through drilled 2-mm diameter holes until the sensing element protruded at least 1 mm beyond the exterior wall of the pipe. Electrical leads from each thermistor were fed through the interior of the pipe to resistance bridges at the top of the probe. The probe was filled with polyurethane foam to reduce its thermal mass. Self-heating of the thermistors was negligible. Time response of the probe to temperature changes was <30 s. The voltage output from each thermistor was recorded on magnetic tape at 5-min intervals with a 12-bit Datel DL-2 data logger. All thermistors were corrected for

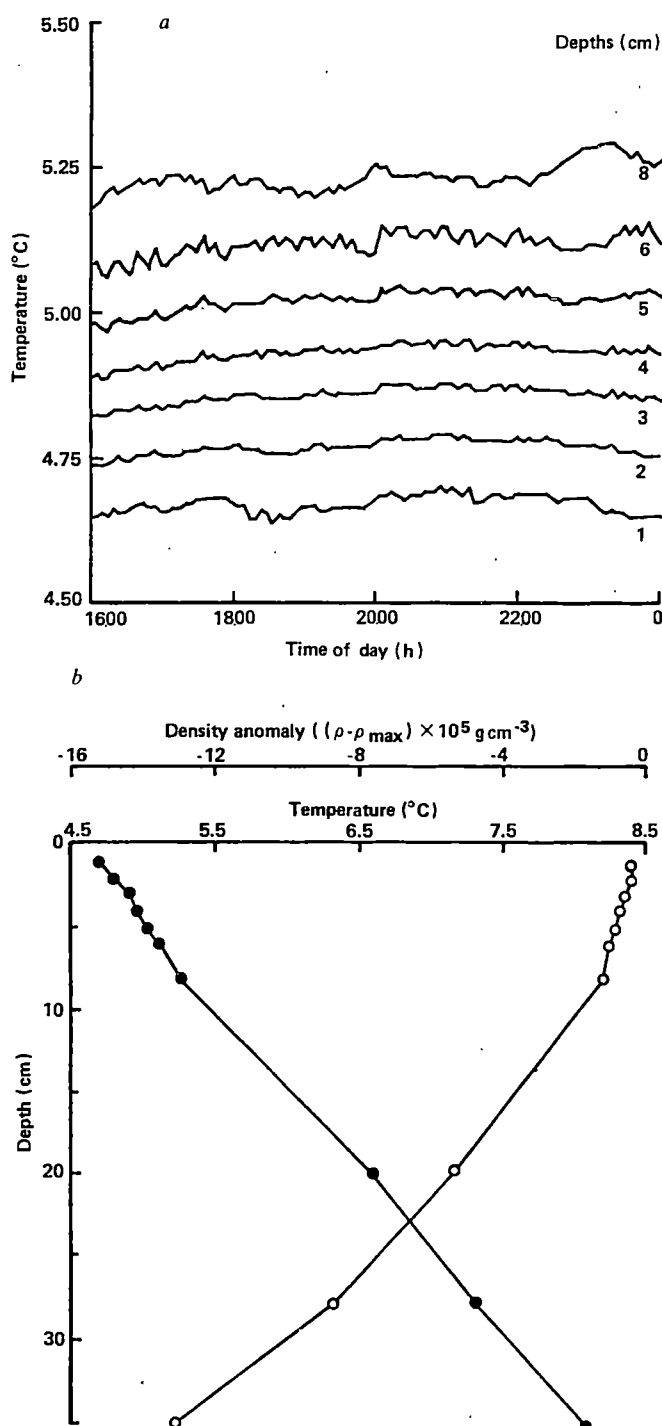


Fig. 1 *a*, Temperature records at depths below the sediment surface (27 October 1979; 0.75 m water depth). The record at 20 cm showed no temperature fluctuations. *b*, Temperature (●) and density (○) profiles in sediments (27 October 2000 CST). Density was calculated from temperature⁹.

gain and supply voltage changes by monitoring a reference voltage and the bridge supply voltage. The probes were calibrated at 2 °C intervals between 0 and 20 °C in a temperature bath controlled to 0.001 °C (Northwest Regional Calibration Centre). Although the probes were not recalibrated immediately after deployment, comparisons between calibrations indicated long-term (6-month) accuracy for each thermistor bridge of 0.01 °C. Short-term (1-day) stability is determined by the resolution of the data logger (1 bit in 12 over 27 ° = 0.007 °C), so changes in temperature can be resolved to this limit. The *in situ* temperature distributions were disturbed by the initial insertion of the probe for 4 hours. All temperatures reported here were from periods several days after the probe insertion.

We placed three probes in the sediments of Lake 227 of the Experimental Lakes Area, Ontario, Canada, at water depths of 0.75, 1.25, and 1.75 m. These sediments have high, nearly constant porosity (0.85) and organic content (48% dry weight measured by loss of weight on ignition at 900 °C)^{4,8}. The particle size data for two similar, nearby lakes at ELA show the following distribution⁸: sand (>50 μ m) 13%; silt (2–50 μ m) 75%; clay (<2 μ m) 12%. The probes were in place from mid- to late-October 1979, in anticipation of bottom-water density increases due to autumn cooling. The diurnal temperature range at the sediment surface of Lake 227 was <1 °C. The temperature increased with depth into the sediments (Fig. 1*b*). Temperatures varied smoothly at all depths until 25 October. At this time the temperatures in the upper 8 cm of the sediments at 0.75 and 1.25 m water depth developed transient perturbations that were independent of temperature variations at the sediment surface (Fig. 1*a*). The perturbations continued (with maximum amplitudes of 0.06 °C at depths of 6 and 8 cm) until the probes were retrieved.

The observed temperature fluctuations are probably caused by interstitial water motion due to buoyancy forces. However, they may be caused by other mechanisms, namely: (1) noise generated by the data acquisition system; (2) interstitial water motion caused by biological processes such as bioturbation and irrigation; and (3) interstitial water motion due to physical forces other than buoyancy.

We rely on our own calibration data and the long-term behaviour of the data acquisition system (as indicated by the temperature-time series) to address questions of noise due to instabilities of the acquisition system. Any noise-like error due to electronic instabilities of the data logger should appear in all channels because all input signals are processed in serial mode and thus employ the same circuitry. Visual inspection of the time series shows that the temperature fluctuations occur simultaneously only over a few adjacent thermistors. The relative stability of thermistors at other depths indicates that the electronics were introducing no sources of noise (and that the probe was not being physically moved in to or out of the sediment). There are two facts that indicate that the fluctuations are not caused by failure of electronics outside of the data logger: (1) before 25 October, fluctuations in the frequency range of the observed fluctuations do not occur in any channel; (2) the fluctuations in adjacent thermistors are coherent. Therefore, we are quite confident that we are observing *in situ* temperature fluctuations.

The possibility that the fluctuations are caused by bulk sediment redistribution or irrigation by infauna is not consistent with this environment. Hesslein⁴ showed that the solid phase of these sediments has not been redistributed after deposition. Infauna, if present, would disturb the sediment solid phase and therefore we take Hesslein's remarks as evidence that no infauna exist in these sediments. The absence of temperature fluctuations before 25 October corroborates this conclusion. We rule out the possibility of bubble ebullition for the same reasons.

Physical mechanisms that could cause interstitial water motion include ground water seepage, surface wave phenomena and buoyancy. Ground water flow is negligible, which is consistent with absence of the fluctuations for long intervals of time. In any case, we do not expect fluctuations of ground water flow with the regularity or high frequency of the observed fluctuations. Forced convection in the sediments due to surface waves or seiches is precluded by the lack of coherent temperature fluctuations in the upper sediments and concomitant attenuation of the surface fluctuations with depth in sediments.

The temperature gradient is destabilizing below the sediment surface due to autumn cooling of the bottom waters (Fig. 1) and may cause density-driven convection, leading to the observed temperature fluctuations. Quay¹⁰ shows that dissolved solids can significantly affect water density in Lake 227. The main effect in this context would be an offset in the density

since all solute gradients are above depths of 10 cm. The density gradients would not be affected.

The possibility of density-driven (free) convection leads us to consider the Rayleigh number³, Ra , defined by

$$Ra = \frac{\alpha \Delta T K (\rho c)_i H}{\lambda_B}$$

where K is the hydraulic conductivity, α is the thermal expansion coefficient, $(\rho c)_i$ is the heat capacity of the interstitial water, λ_B is the bulk thermal conductivity coefficient of the saturated porous medium, and H and ΔT are the scale depth and temperature difference, respectively. This dimensionless number is a measure of the ratio of the destabilizing buoyancy force to the stabilizing process of diffusion. According to theory and laboratory experiments, the thermal Rayleigh value must exceed a critical value ($Ra_c = 40$) before the motions induced by small horizontal temperature perturbations can maintain free convection. This critical value is derived assuming a saturated, homogenous, porous medium of depth H bounded above and below by impermeable, isothermal plates across which a destabilizing temperature difference, ΔT , is imposed. The equation of state relating density to temperature is linear and the system is assumed to be time independent. Nonlinear density-temperature relationships¹¹, periodic boundary conditions¹², nonhomogeneous¹³ or anisotropic porous medium¹⁴ or permeable boundaries¹⁵ can all act to reduce the critical Rayleigh number, although probably not by a factor of 10. Therefore, we take the value of 40 as an order of magnitude estimate for the critical Rayleigh number.

The Rayleigh number was estimated using the following assumptions. The high porosity permits the use of the thermal diffusivity, κ , of water ($1 \times 10^{-3} \text{ cm}^2 \text{ s}^{-1}$) for the quotient $\lambda_B/(\rho c)_i$. Our efforts at measuring *in situ* hydraulic conductivity failed in Lake 227 so we estimated it to be 10^{-1} cm , which is similar to the value for sands. This is a high value but we think it is justified by the flocculent nature of Lake 227 sediments. The amplitude of the annual temperature cycle at the 1 m water depth is 20°C which we take for ΔT and the sediment depth, H , is 10 m. Using these values the maximum value of the Rayleigh number is 200, which is realized only when the amplitude of the annual temperature cycle is realized across the whole depth of the sediments. When this happens the interstitial water is freely convecting.

However, there is a period of time after autumn cooling begins when ΔT is not realized over the whole sediment depth. In transient systems, a time-dependent Rayleigh number can be calculated based on the product $H\Delta T$ where H and ΔT are scaled according to diffusion theory and both change with time. When this time-dependent Rayleigh number first exceeds the critical value at time t_c convection ensues over the depth $H(t_c)$ (ref. 16). The convecting layer erodes the stable layer below and H increases faster than purely diffusive transport would allow until the convecting layer reaches the sediment basement and ΔT is realized across the entire sediment depth.

Since we do not have temperatures below 35 cm we estimate H and ΔT as a function of time as follows. The temperature of the bottom water in contact with the sediments at 1 to 2 m water depth was 22°C from 1 June to 1 September. For this time interval we calculate the diffusive scale length to be 200 cm, which is the depth to which summer heating occurs. We assume that on 1 September the sediments to 200 cm are at 22°C , and the sediment surface begins cooling linearly with time to the observed temperature of 4.4°C on 30 October. The temperature-depth distribution as a function of time, for a system undergoing surface cooling at a linear rate, is given by Carslaw and Jaeger¹⁷. If we define the scale depth, H , as the depth at which the temperature is 0.0567 times the temperature difference between the temperature much deeper in the sediment and the temperature at the surface, then H is given by $H = 2\sqrt{\kappa t}$ where t is the time after 1 September. The scale temperature difference, ΔT , is then given by $\Delta T = mt$ ($0.0567 - 1$), where m is the rate of cooling. The product $H\Delta T$ increases

as the $3/2$ power of time and on 28 October is estimated to be $2 \times 10^3^\circ \text{C cm}$.

The Rayleigh number on this date is 20 and certainly within the range of the critical value, considering that this estimate is valid over an order of magnitude. The appearance of the temperature fluctuations at this time indicates that the estimate is fairly good.

Although we think the temperature fluctuations are due to free convection, they are not characteristic of linear, steady-state, convection. Horne and O'Sullivan¹⁸ have shown that oscillatory convection occurs at Rayleigh numbers above 240. Our estimate of the Rayleigh number is lower by 10 times, although we think that it could be an underestimate. However, the absence of temperature fluctuations below 15 cm is not consistent with the oscillatory systems described by Horne and O'Sullivan.

The density calculated from temperature shows negligible gradients in the upper few centimetres due to the density extremum at 4°C . So at the time the fluctuations occur, the unstable convecting layer is bounded above by a stable quiescent layer. Free fluids near the density extremum at 4°C show large temperature fluctuations at the boundary between the stable and convecting layers¹⁹. These fluctuations have been interpreted as internal waves propagating along the interface²⁰. The dynamics of flow in porous media do not allow inertial effects, and phenomena such as internal waves do not exist. However, we think that the convecting layer, beneath a shallow stable layer, causes the observed fluctuations in some manner whose details have been examined theoretically.

The increase in heat transport due to convection is quantified by the Nusselt number which is the ratio of heat flux across a convecting layer to the heat flux across the same layer assuming purely diffusive transport. The Nusselt number does not strictly apply to transient convection but we can get an order of magnitude of the increased transport from theoretical and experimental studies which give the Nusselt number as a function of the Rayleigh number³. Near the critical Rayleigh number the Nusselt number is just greater than 1. In Lake 227 the Rayleigh number continues to grow with time until the convecting layer intersects the impermeable rock below the sediments at 10 m. The Rayleigh number based on this depth is 200 and the maximum Nusselt number is then 4. The increase in transport of solutes cannot be readily estimated. In systems that are undergoing circular motion, there is no net water transport across any horizontal surface and net transport of solutes occurs only if vertical gradients in concentration exist. This implies that the increase in solute transport will also depend on the strength of the solute sink (or source) in the sediments. We know of no theory to describe the increase in transport of a passive solute as a function of the Rayleigh number and sink strength. We only mention that solute diffusivities are typically 10^{-2} – 10^{-3} times the thermal diffusivity and therefore seem more susceptible than heat to increased transport by convection.

This work was supported by NSF grants OCE 78-20896, OCE 80-26046 and a Jessie Smith Noyes Foundation Fellowship to D.L.M. We thank R. H. Hesslein and D. W. Schindler for their assistance, and W. D. Harrison for helpful discussions. Contribution no. 489 from the Institute of Marine Science, University of Alaska.

Received 21 December 1981; accepted 9 July 1982.

1. Berner, R. A. *Principles of Chemical Sedimentology* (Princeton University Press, 1971).
2. Berner, R. S. *Early Diagenesis. A Theoretical Approach* (Princeton University Press, 1980).
3. Combarous, M. A. & Bories, S. A. *Adv. Hydrosci.* **10**, 232-309 (1974).
4. Hesslein, R. H. *Can. J. Fish. Aquat. Sci.* **37**, 545-551 (1980).
5. Thorstensen, D. C. & Mackenzie, F. T. *Geochim. cosmochim. Acta* **28**, 1-19 (1974).
6. Harrison, W. D. & Osterkamp, T. E. *J. geophys. Res.* **83**, 4707-4712 (1978).
7. Smetacek, V. F., von Bedungen, F., von Brockel, K. & Zeitzschel, B. *Mar. Biol.* **34**, 373-378 (1976).
8. Brunsell, G. J., Povolo, D., Graham, B. W. & Stainton, M. P. *J. Fish. Res. Bd Can.* **28**, 277-294 (1971).
9. Kell, G. S. *J. Chem. Engng Data* **12**, 66-69 (1967).
10. Quay, P. D. thesis, Columbia Univ. (1977).
11. Ray-shing Wu, Cheng, K. C. & Craggs, A. *Numerical Heat Transfer* **2**, 303-318 (1979).
12. Chhuon, B. & Caltigione, J. P. *J. Heat Transfer* **101**, 244-248 (1979).
13. Green, T. & Frechill, R. L. *J. appl. Phys.* **40**, 1759-1762 (1969).

14. Wooding, R. A. *Proc. 2nd Workshop Geotherm Reservoir Engng*, 339-345 (Stanford University Press, 1976).
15. Nield, D. A. *Wat. Resour. Res.* **4**, 553-560 (1968).
16. Elder, J. W. *J. Fluid Mech.* **32**, 69-96 (1968).
17. Carslaw, H. S. & Jaeger, J. C. *Conduction of Heat in Solids* 2nd edn (Oxford University Press, 1959).
18. Horne, R. N. & O'Sullivan, M. J. *J. Fluid Mech.* **66**, 339-352 (1974).
19. Townsend, A. A. *Q. J. R. met. Soc.* **90**, 248-259 (1964).
20. Townsend, A. A., *J. Fluid Mech.* **24**, 307-319 (1966).

Thermal expansion effects in deep-sea sediments

T. J. G. Francis

Institute of Oceanographic Sciences, Brook Road, Wormley, Godalming, Surrey GU8 5UB, UK

Understanding how *in situ* heating affects unlithified deep-sea sediments is important for both geological and practical reasons. Deep-sea drilling by *Glomar Challenger* over the past decade has revealed several places where magma has intruded sediment to form sills and the heat released by a large sheet of molten rock has been shown to produce substantial changes on the sediments in its vicinity¹. Another example is the burial of hot canisters of high-level radioactive waste within the sediments of the ocean floor, which has been proposed as a solution to the problem of disposing of this material². I consider here the physical effects which high temperatures might produce in deep-sea sediments. Substantial chemical effects are also likely, but these are not discussed. In practice, the physical and chemical effects would work together in modifying the original sediment.

The individual thermal behaviour of the components of a sediment is straightforward and well understood. The pressure-volume-temperature relations for seawater differ very little from those for pure water³. The specific volume of pure water as a function of temperature and pressure has been tabulated by Burnham *et al.*⁴ and can be corrected with the work of Saunders⁵ to give values for seawater. The resulting thermal expansion of seawater at pressures of 200 and 500 bar is shown in Fig. 1. It is clear that the volume thermal expansion coefficient, defined as $1/V(\partial V/\partial T)_P$ is not constant but increases with increasing temperature. In contrast, the thermal expansion of most rock-forming minerals can be adequately described by a constant coefficient in the temperature range 0-400 °C (ref. 6). The thermal expansion of one particular solid material, quartz, is also shown in Fig. 1 to illustrate the contrast in thermal expansivity between the solid and liquid components of the sediment. One can conclude that the thermal expansivity

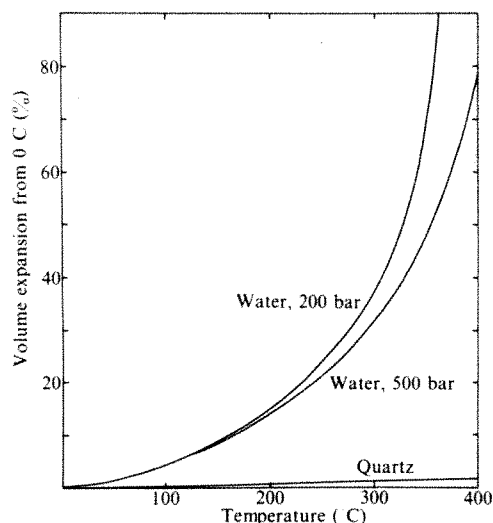


Fig. 1 The thermal expansion of water/seawater at 200 and 500 bar. The expansion of quartz, measured at atmospheric pressure, is shown for comparison. As a general rule the thermal expansivity of sedimentary pore water is two orders of magnitude greater than that of the solid component.

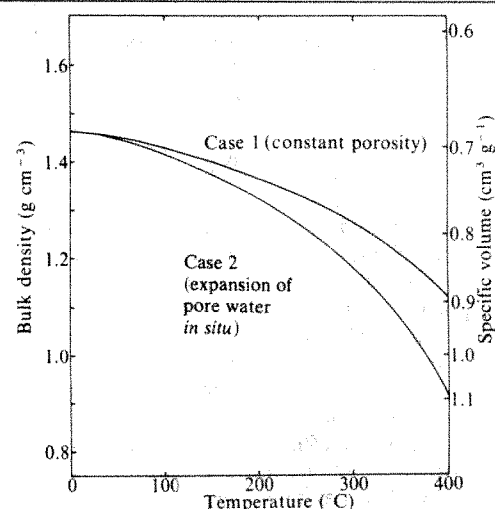


Fig. 2 The effect of thermal expansion on the density of a sediment at an ambient pressure of 500 bar. Initial porosity of sediment 0.75; grain density 2.7 g cm^{-3} .

of sedimentary pore water is some two orders of magnitude greater than that of the solid component. For the present purposes, the expansion of the solid component of the sediment is regarded as negligible.

The manner in which a sediment expands will be affected by the way in which heat is applied. The heating of sediment *in situ* is unlikely to be a uniform process. With magma intrusion and the burial of radioactive waste strong temperature gradients are likely to exist, both during the development of the temperature field and in the steady state. Two limiting cases to the way in which a sediment responds to heating can be considered. The first is the fully drained case, where the sediment matrix remains unchanged and expanding pore water is accommodated by flowing away from the source of heat. The porosity of the sediment is unchanged, but the bulk density of the heated sediment is reduced because of the reduced density of the pore water. The bulk density ρ is related to the solid particle density ρ_s and the fluid density ρ_f by $\rho = (1 - \phi)\rho_s + \phi\rho_f$ where ϕ is the fractional porosity. This expression can be used to calculate the density of the heated sediment since ρ_f is known as a function of temperature and ρ_s and ϕ are unchanged (case 1, Fig. 2). The second limiting case is where the pore water remains in place as it expands, disrupting the sedimentary matrix in the process. The bulk density of the heated sediment will be reduced both because of its increased porosity and because the density of the pore water is reduced. If a volume of sediment V weighs W and the weights of the solid and fluid components are W_s and W_f respectively, then

$$V = \frac{W_s}{\rho_s} + \frac{W_f}{\rho_f} = \frac{W}{\rho}$$

where in the undrained case W , W_s , W_f and ρ_s are constants. For a sediment of initial porosity 0.75 and grain density 2.7 g cm^{-3} , the expression becomes

$$\rho = \frac{1.4633}{0.25 + (0.7883)/(\rho_f)}$$

Values obtained from this equation corresponding to an ambient pressure of 500 bar are shown as case 2 in Fig. 2.

The behaviour of a sediment in reality will fall between these two limiting cases. One would expect a highly permeable sand to behave in a fully drained manner (case 1). A uniformly heated, impermeable clay might tend to follow case 2. As already mentioned, however, uniform heating is unlikely and strong temperature gradients are probable. In the second case, these would give rise to pore pressure gradients, pore water flow would occur to relieve the pressure and collapse of the expanded sediment matrix back towards its original porosity would result. Pore water flow will be facilitated by the increase

in permeability which accompanies an increase in porosity. Measurements of permeability as a function of porosity or void ratio have now been made on a range of deep-sea sediments (refs 7, 8, and P. J. Schultheiss, personal communication). These indicate that the increase in porosity associated with case 2 thermal expansion would be accompanied by an increase in permeability of at least an order of magnitude. Thus, although case 2 behaviour may be the instantaneous or short-term response of a sediment to heating, case 1 is more likely to reflect its longer-term behaviour. Nevertheless, case 2 is worth considering to determine the maximum reduction in density that a sediment might undergo.

Consider now the cooling of a sediment. When a highly permeable, coarse-grained sediment cools, the process of expansion is likely to be reversed. Water will flow back to fill the space created by the pore water contracting and the overall effect of the thermal cycle will be nil. But for fine-grained, impermeable sediments reversibility seems less likely. Thermal contraction of pore water will reduce pore pressure which, if not compensated by the return flow, will lead to collapse of the sedimentary matrix. Any collapse of the matrix will reduce its permeability, making return flow of pore water more difficult and further collapse of the sediment more likely. Thus the overall effect of heating and cooling sediment will be to produce a more compacted, less permeable sediment—a process which can conveniently be called 'thermal tamping'. Fine-grained sediments can be regarded as acting like a non-return valve, opening to allow increased pore water pressure to dissipate itself but closing to prevent pore water flowing towards zones of reduced pore pressure.

If thermal tamping is 100% efficient, the reduction in porosity or void ratio can be calculated as a function of temperature. If V_s is the volume of the solid component and V_v the volume occupied by the fluid component of the original sediment, then the original void ratio is defined by $e_{\text{orig}} = V_v/V_s$. If heating the sediment to $T^\circ\text{C}$ from its ambient value causes the pore water to expand by 100%, then the volume V_v occupied by fluid at $T^\circ\text{C}$ becomes $V_v/(1+m)$ on cooling back to 0°C . Thus the final void ratio on completion of the thermal cycle is given by $e_{\text{final}} = e_{\text{orig}}/(1+m)$, or in terms of porosity $\phi_{\text{final}} = \phi_{\text{orig}}/(1+m(1-\phi_{\text{orig}}))$.

Values of m taken from Fig. 1 have been used to compute the reduction in void ratio which thermal tamping would bring about to a sediment with original void ratio 3.0 (porosity 75%) at an ambient pressure of 500 bar and are shown in Fig. 3. Clearly, the higher the temperature to which the sediment is heated the greater the reduction in void ratio. Heating to 350°C reduces void ratio by ~ 1 , corresponding to a decrease in

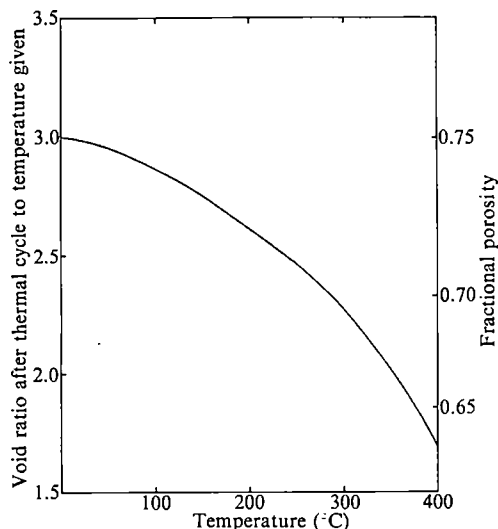


Fig. 3 Thermal tamping. The reduction in void ratio of a sediment, originally close to 0°C , when heated to a given temperature and then allowed to cool back to its original temperature. Original void ratio 3.0 (porosity 75%); ambient pressure 500 bar.

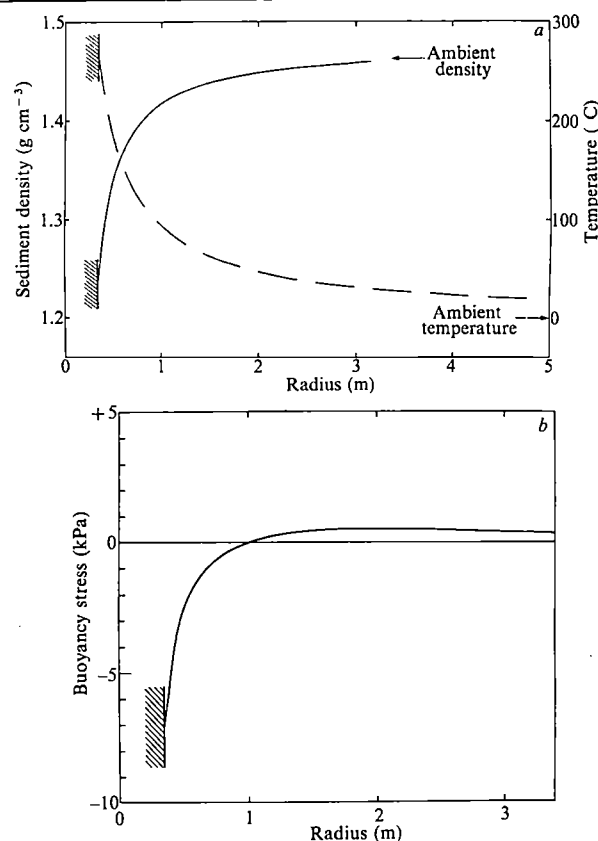


Fig. 4 *a*, The steady state temperature field around a spherical canister of radius 0.35 m, heat output $1,000\text{ W}$, embedded in sediment of thermal conductivity $0.85\text{ W m}^{-1}\text{ K}^{-1}$ (dashed line). The solid line shows the corresponding sediment density, assuming that the sediment expanded with the pore water *in situ* (case 2 in Fig. 2). *b*, The corresponding buoyancy stress of the canister and surrounding shell of sediment as a function of radius. Density of the canister, 3.0 g cm^{-3} . For comparison, the shear strength of a typical oceanic sediment at 30 m burial depth is $\sim 30\text{ kPa}$ (ref. 7).

permeability of approximately an order of magnitude.

Evidence for thermal tamping was obtained on Leg 64 of the Deep Sea Drilling Project, when *Glomar Challenger* drilled sites in the Gulf of California where basaltic sills had penetrated highly porous sediments at shallow depths⁹. The intrusion was found to reduce the porosity of the sediment in the vicinity of the sills¹. At hole 481A, for example, the original porosity of the sediment immediately above the sill is estimated at 0.7 and the final porosity is observed to be 0.3. The formula relating final to original porosity given above indicates that the pore fluid expanded by 444%. At an ambient pressure of 200 bar this requires that the temperature close to the sill reached $\sim 370^\circ\text{C}$ (ref. 1) (offscale on Fig. 1). Although the temperature of the molten rock must have been close to $1,200^\circ\text{C}$, a value in the region of 370°C is reasonable because this is about the temperature at which water boils at 200 bar. Furthermore, the relatively rapid contraction of the pore water in the region of 370°C may have aided the process of thermal tamping.

The ideas outlined above also allow us to calculate the physical properties of the sediment around a buried canister of radioactive waste. Immediately after emplacement the temperature field will develop, reaching an effectively steady-state configuration in a time of the order of a year¹⁰. Thereafter the temperature follows the decay of the radioactive waste contained in the canister. The peak temperature to which the canister wall rises must be restricted if a canister lifetime of 500–1,000 yr is to be achieved. At present, peak wall temperatures in the range $100\text{--}250^\circ\text{C}$ are thought appropriate¹¹. To understand the effect of thermally induced density changes in the sediment surrounding the canister, it is sufficient to rely on the peak temperature field developed around it. Making the following simplifying assumptions, this is easily calculated:

- (1) The canister is assumed to be a sphere of radius 0.35 m, making it comparable in volume with the more realistic cylindrical canisters proposed¹².
- (2) The heat output of the canister, Q , is taken to have a constant value of 1,000 W.
- (3) The thermal conductivity of the sediment, K , is taken as $0.85 \text{ W m}^{-1} \text{ K}^{-1}$ and assumed to be independent of the temperature. This is a good assumption up to 200°C and a reasonable one up to 400°C (ref. 12).
- (4) Hickox *et al.*¹⁰ have shown that thermally induced convection of the pore water is negligible and that conduction theory is sufficient to calculate the steady-state temperature field around the canister.
- (5) The ambient temperature of the sediment before emplacement is taken as 0°C .

With the above assumptions, the steady-state temperature of the sediment at radius r from the centre of the canister is given by

$$T = \frac{Q}{4\pi Kr}$$

For the values of Q and K given, this gives rise to the temperature distribution shown in Fig. 4a. Using the relationship of sediment density to temperature where the sediment expands with the pore water *in situ* (case 2 in Fig. 2), the corresponding density of the sediment as a function of radius has been obtained.

It has been suggested that heat from the canister would reduce the density of the sediment to such an extent that convective upwelling would occur which might carry the buried canister back to the sea bed (the 'Burp' effect). For this to be possible, the effective density of the canister and surrounding sediment must be less than the density of the unaffected sediment. The sediment density distribution shown in Fig. 4a allows this effect to be examined quantitatively.

Considering a spherical shell of heated sediment and outer radius r surrounding the canister of radius r_0 . Assuming that the canister remains fixed within the shell of heated sediment a buoyancy force, F , can be defined:

$$F = \frac{4}{3}\pi r^3 \rho_s - \frac{4}{3}\pi r_0^3 \rho_c - \int_{r_0}^r 4\pi r^2 \rho \, dr$$

where ρ_s is the density of unaffected sediment; ρ_c the mean density of canister; ρ the density of heated sediment $= \rho(r)$.

A positive buoyancy force will tend to move the canister upwards, a negative one to make it sink. To appreciate whether the buoyancy force developed is ever big enough to actually move the canister, it must be converted into a stress which can be compared with the strength of the sediment. A buoyancy stress can be obtained simply by dividing the buoyancy force by the cross-sectional area of the sphere: $S = F/\pi r^2$. S has been evaluated numerically taking values of ρ from Fig. 4a, $\rho_s = 1.463 \text{ g cm}^{-3}$ and $\rho_c = 3.0 \text{ g cm}^{-3}$ (see ref. 13) and is plotted in Fig. 4b. Beyond a radius of $\sim 1 \text{ m}$ the combined volume of canister and heated sediment is positively buoyant. The maximum buoyancy stress developed, however, is small, $\sim 0.6 \text{ kPa}$. In contrast the shear strength which the sediment can be expected to have at a burial depth of 30 m (ref. 13) is about 30 kPa (ref. 7). Because positive buoyancy is only developed beyond $\sim 1 \text{ m}$ radius and the maximum buoyancy stress at $\sim 2 \text{ m}$ radius, where the sediment is unlikely to be weakened either by temperature or by the mechanical effects of emplacement, positive buoyancy of the canister upwards seems very unlikely. This conclusion supports the results of the finite element modelling of Dawson and Chavez^{14,15}.

In conclusion, a hot body buried in deep-sea sediments will substantially modify the physical properties of the sediments adjacent to it. Cooling of the sediment is unlikely to be simply the reverse of heating, but could lead to collapse of the sediment matrix if pore water cannot flow back fast enough. This process, 'thermal tamping', would create a compacted shell of sediment around the body once it has cooled whose permeability would

be less than that of the unaffected sediment. The process could have important implications for the burial of hot canisters of radioactive waste beneath the ocean floor:

- (1) Thermal tamping would enhance the ability of the sediment to retain the radionuclides once the canister has corroded away. Since most of the thermal tamping would occur within 100 yr of burial, a canister life of $500\text{--}1,000 \text{ yr}$ may not be necessary.
- (2) The higher the peak temperature the more effective thermal tamping is likely to be. This would favour either a higher loading of radionuclides within the canister or a shorter period before disposal.
- (3) Thermal tamping would also be more effective at shallower sites, as the thermal expansivity of water decreases with pressure (Fig. 1). In this respect, therefore, a $4,000\text{-m}$ disposal site would be marginally more effective than a $6,000\text{-m}$ one.

An experimental investigation of the effects of temperature cycling on deep-sea sediments in *in situ* conditions is needed to confirm the existence and magnitude of thermal tamping.

I thank Peter Schultheiss and Hugh St John for helpful discussions. This research has been carried out under contract for the Department of the Environment, as part of its radioactive waste management research programme. The results will be used in the formulation of government policy, but at this stage they do not necessarily represent government policy.

Received 1 March; accepted 5 July 1982.

1. Einsele, G. *et al.* *Nature* **283**, 441–445 (1980).
2. Hollister, C. D. *Oceanus* **20**, 1, 18–25 (1977).
3. Bischoff, J. L. *Science* **207**, 1465–1469 (1980).
4. Burnham, C. W., Holloway, J. R. & Davis, N. F. *Geol. Soc. Am. spec. Pap.* No. 132 (1969).
5. Saunders, P. M. *J. Phys. Oceanogr.* **11**, 573–574 (1981).
6. Skinner, B. J. *Geol. Soc. Am. Mem.* **97**, 75–96 (1966).
7. Silva, A. J. *Oceanus* **20**, 1, 31–40 (1977).
8. Silva, A. J., Laine, E. F., Lipkin, J., Heath, G. R. & Akers, S. A. *Proc. Marine Technology '80*, Washington DC (1980).
9. Curran, J. R. *et al.* *Geotimes* **24**, 7, 18–20 (1979).
10. Hickox, C. E., Gartling, D. K., McVey, D. F., Russo, A. J. & Nuttall, H. E. *Proc. Marine Technology '80*, Washington DC (1980).
11. Waste Form and Canister Task Group Report *Proc. 6th Annual NEA-Seabed Working Group Meet.* SAND-81-0427 (Sandia Laboratories, 1981).
12. Hadley, G. R., McVey, D. F. & Morin, R. *Proc. Marine Technology '80*, Washington DC (1980).
13. Systems Analysis Task Group Report *Proc. 6th Annual NEA-Seabed Working Group Meet.* SAND-81-0427 (Sandia Laboratories, 1981).
14. Dawson, P. R. *Buoyant Movements of Nuclear Waste Canisters in Marine Sediments*, SAND-78-0841 (Sandia Laboratories, 1978).
15. Chavez, P. F. & Dawson, P. R. *Thermally Induced Motion of Marine Sediments Resulting from Disposal of Radioactive Wastes*, SAND-80-1476 (Sandia Laboratories, 1981).

Composition of basaltic liquids generated from a partially depleted lherzolite at 9 kbar pressure

Gautam Sen*

Department of Geosciences, University of Texas at Dallas, Richardson, Texas 75080, USA

Two contrasting views exist regarding the nature and origin of mid-ocean ridge basalts (MORB): first, that these olivine-tholeiites with $\text{Mg}/(\text{Mg} + \text{Fe}) = 0.70\text{--}0.72$ are primary and are generated by partial fusion of plagioclase + spinel lherzolite at around 30-km ($\approx 9 \text{ kbar}$ pressure) in the mantle¹. Others^{2–8} suggest that even the most primitive MORBs are not primary but are derived by fractionation of olivine ± pyroxene from picritic parental magmas that are generated at depths of 45 km or more. Duncan and Green^{2,3} argued for the existence of a second primary magma, a high-MgO quartz-normative or olivine-poor tholeiite, which is produced at depths $\leq 25 \text{ km}$ beneath the ocean ridges. This problem, concerning the composition and depth of origin of primary MORBs, has been approached here by experimentally melting a plagioclase + spinel lherzolite xenolith from Hawaii at 9 kbar pressure. The experimental melts are very similar to some mid-ocean ridge basalts, which suggests that the latter are probably primary and are generated at shallow depths in the mantle.

* Present address: Department of Earth and Space Sciences, University of California at Los Angeles, Los Angeles, California 90024, USA.

The plagioclase + spinel lherzolite 77PAII-1 was collected from the Pali no. 2 vent⁹ on Oahu. The partially depleted character of this xenolith is reflected in its lower FeO, Na₂O and higher MgO contents relative to some of the least-depleted upper mantle peridotites (Table 1). Table 1 also shows that this xenolith is chemically similar to the plagioclase lherzolites of the Troodos ophiolite and the Trinity ultramafic complex. These bodies presumably represent mid-ocean ridge-type upper mantle^{2,10-16}, and therefore the results of the present study should be applicable to the problem of generation of mid-ocean ridge basalts.

The experiments were carried out in graphite capsules sealed within Pt-foil in a piston-cylinder apparatus. A piston-out technique was used, and no friction-correction was applied to the nominal pressure. The near-solidus and higher temperature runs were held for 26 and 6 h, respectively. The run products were analysed using an automated electron microprobe: 1–2 μ m diameter electron beam, 15 kV accelerating potential, and 0.15 μ A beam current. 10,000 or more counts were obtained for most major elements. Na-loss by volatilization was checked by simultaneously analysing three different Na-bearing standards. Quench crystals of pyroxenes were present in minor amounts; their abundance in the 1,400 °C and 1,600 °C runs made it impossible to obtain representative glass compositions for these runs. Fifteen or more spot analyses were obtained on glass (without quench crystals) from different parts of the capsule in each run. Although no reversal runs were made, general absence of zoning in the mineral phases, compositional homogeneity in the glasses, and overall correspondence between the analysed olivine and calculated equilibrium olivine compositions for the runs (Table 2) suggest that equilibrium was achieved in each of the runs. Results of a few runs performed with Ni and NiO starting materials, and the absence of metallic Fe in the run products suggest that the oxygen fugacity for these runs was between Ni/NiO and Fe/FeO buffers.

77PAII-1 begins to melt at a temperature of 1,210 °C, which is almost 100 °C lower than the solidus temperature in the CaO(C)–MgO(M)–Al₂O₃(A)–SiO₂(S) system¹ (Fig. 1). With increase of temperature, and degree of partial fusion, clinopyroxene (cpx) disappears at a temperature between 1,225 and 1,250 °C (Fig. 1, Table 1). Spinel (sp) continues to remain in the residue up to a temperature of ~1,290 °C. Olivine (ol) and orthopyroxene (opx) persist in the residue, until a temperature of ~1,600 °C where the residue becomes dunite, composed entirely of olivine (Fo₉₄).

Table 2 shows a comparison of compositions of the experimental melts with those of some proposed primary/primitive/parental magmas in mid-oceanic environments. B₁ and B₂ were postulated by Bryan¹⁷ to represent magmas allegedly

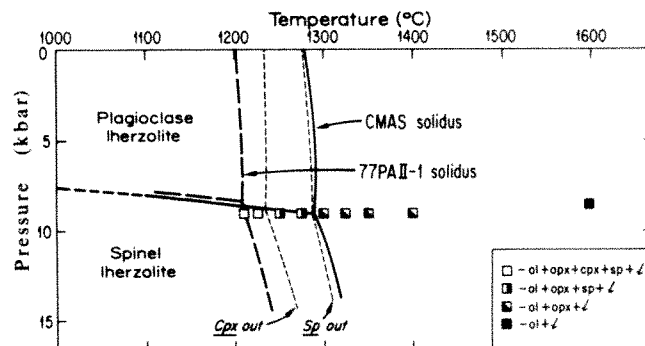


Fig. 1 Melting relations of the plagioclase + spinel lherzolite (77PAII-1) are compared with that of the CMAS system¹.

parental to the *Famous* (Mid-Atlantic ridge) basalt glasses. His "high-ol parental liquid" (B₁ in Table 2) appears to be a good candidate for a primary magma, following the definition of Presnall *et al.*¹. Note that B₁ is lower in SiO₂ and higher in Na₂O than the experimental melts, and this difference is manifested in the significantly higher content of normative olivine in B₁. Bryan's "low-ol parental liquid" (B₂ in Table 2) is much closer in composition to the melts produced at temperatures between 1,210 and 1,250 °C. B₂ is, however, higher in Na₂O than the experimental melts, which causes the former to be slightly olivine-normative. The "second-stage melts" of Duncan and Green², which were postulated to have been produced at a depth of ≤ 25 km, are also similar to B₂ and have more Na₂O than the experimental melts.

The difference in Na₂O between experimental melts of this study and the proposed primary/primitive/parental mid-ocean ridge magmas is not surprising in view of lower Na₂O content (that is, partially depleted composition) of the starting material than most relatively less-depleted peridotites (Table 1). Phase equilibria considerations of compositions and phenocryst assemblages of MORBs from different geographical localities¹⁸, major- and trace-element chemical studies, and isotopic studies^{19,20}, suggest that MORBs are likely to be derived from compositionally heterogeneous source lherzolites in the oceanic upper mantle. Noting that oceanic peridotites exhibit minor variations in FeO/MgO ratio but significant variations in Na₂O, CaO, Al₂O₃, and TiO₂, Bryan and Dick¹⁸ further argued that primary MORBs may show considerable spread in Na₂O, CaO, Al₂O₃, and TiO₂ contents but a very narrow range of FeO/MgO. Considering such major element heterogeneities in the ocean upper mantle and the Na₂O-poor composition of the starting material, the overall chemical similarity between the lower temperature experimental melts and the second-stage

Table 1 Compositions of the starting material and least depleted peridotites

	(1)	(2)	(3)	(4)	(5)	(6)	(7)	(8)	(9)	(10)
SiO ₂	43.46	45.20	44.95	43.70	42.90	45.00	45.10	42.86	42.75	43.45
TiO ₂	0.07	0.71	0.08	0.25	0.20	0.07	0.50	0.33	0.02	0.04
Al ₂ O ₃	3.66	3.54	3.22	2.75	5.80	3.01	4.10	6.99	3.63	2.03
FeO*	7.60	8.52	7.67	10.19	9.20	7.98	9.90	9.33	8.25	8.23
MgO	42.42	37.50	40.03	37.22	37.20	39.70	36.70	35.07	40.34	43.78
CaO	2.00	3.08	2.99	3.26	3.70	3.15	2.30	4.37	3.46	1.67
MnO	0.12	0.14	0.13	0.14	0.11	0.11	0.20	0.14	0.18	0.14
Na ₂ O	0.02	0.57	0.18	0.33	0.40	0.24	0.60	0.45	0.06	0.06
K ₂ O	0.00	0.13	0.02	0.14	0.00	0.04	0.02	0.00	0.01	0.00
Cr ₂ O ₃	0.30	0.43	0.45	0.28	0.20	0.41	0.30	0.18	0.65	0.52
NiO	0.27	0.20	0.26	n.d.	0.20	0.25	0.20	0.20	0.25	0.24

(1) Plagioclase-spinel lherzolite 77PAII-1 (starting material used in this study); composition obtained from X-ray fluorescence.

(2) Pyrolite model composition⁵.

(3) Tinaquillo lherzolite⁵.

(4) PHN 1611, garnet lherzolite xenolith in South African kimberlite.

(5) Model upper mantle composition estimated by Carter²¹ for Kilbourne Hole.

(6)–(8) Analyses of lherzolites given by Ernst²².

(9) Average of three plagioclase lherzolites from the Troodos ophiolite¹¹.

(10) Average of six plagioclase lherzolite from the Trinity complex (source ref. 14).

Table 2 Comparisons of basalt compositions

Temperature (°C)§	9 kbar† melts (present study)							MORB ¹⁷		Second-stage melts ²			Plagioclase-rich vein ¹⁶ 9W21
	1,210	1,225	1,250	1,275	1,300	1,325	1,350	B ₁	B ₂	(3)	(4)	(11)	
SiO ₂	50.61 (0.7)¶	51.64 (0.8)	51.44 (0.7)	51.65 (0.8)	51.18 (0.8)	51.34 (0.6)	51.12 (0.4)	48.53	51.20	54.20	52.40	53.30	49.31
TiO ₂	0.36 (0.06)	0.34 (0.08)	0.31 (0.06)	0.34 (0.08)	0.24 (0.07)	0.20 (0.07)	0.19 (0.04)	0.62	0.87	0.40	0.30	0.60	0.12
Al ₂ O ₃	17.73 (0.8)	15.53 (0.5)	15.08 (0.5)	15.06 (0.7)	13.98 (0.7)	13.50 (0.6)	11.25 (0.8)	16.65	15.03	15.40	11.70	14.40	15.59
FeO*	7.14 (0.3)	7.84 (0.5)	7.23 (0.4)	7.50 (0.5)	8.69 (0.4)	9.30 (0.6)	9.44 (0.8)	8.41	8.39	7.90	8.40	9.90	8.09
MgO	8.52 (0.5)	10.6 (0.3)	11.63 (0.7)	12.03 (0.6)	14.38 (0.4)	15.39 (0.5)	15.91 (0.4)	10.25	9.21	8.70	15.80	7.80	12.78
CaO	13.26 (0.6)	13.51 (0.4)	12.87 (0.8)	13.29 (0.4)	11.12 (0.5)	10.03 (0.5)	10.10 (0.6)	12.68	12.73	11.50	10.70	12.40	13.30
Na ₂ O	0.48 (0.09)	0.48 (0.05)	0.48 (0.04)	0.44 (0.04)	0.41 (0.05)	0.33 (0.07)	0.21 (0.03)	2.26	1.87	1.60	0.70	1.70	0.52
K ₂ O	0.10 (0.04)	0.07 (0.04)	0.09 (0.03)	0.05 (0.03)	0.05 (0.03)	0.07 (0.04)	0.07 (0.04)	0.06	0.10	0.10	0.10	0.10	0.02
Cr ₂ O ₃	0.03 (0.01)	0.03 (0.01)	0.02 (0.01)	0.29 (0.04)	0.36 (0.04)	0.47 (0.03)	0.48 (0.04)	0.03	0.07	n.d.	n.d.	n.d.	
CIPW norm													
q	4.92	3.28	3.11	2.28	0.36	0.14	0.97	—	—	5.47	—	3.59	—
or	0.60	0.41	0.54	0.29	0.29	0.41	1.42	0.25	0.57	0.59	0.59	0.59	0.12
ab	4.14	4.06	4.10	3.71	3.49	2.79	1.81	17.71	15.80	13.57	5.92	14.36	4.31
an	46.32	39.99	39.11	38.50	36.10	35.09	29.74	35.84	32.31	34.61	28.45	31.30	49.30
di	8.23	10.94	10.59	10.95	7.82	5.88	8.74	22.10	25.20	9.20	9.88	12.40	10.46
hy	26.54	29.73	29.25	32.41	43.96	49.32	49.34	—	21.65	26.61	44.65	24.31	27.66
ol	—	—	—	—	—	—	—	21.64	2.36	—	0.065	—	6.40
il	0.50	0.64	0.59	0.64	0.46	0.38	0.37	1.02	1.60	0.76	0.57	1.14	0.22
[Mg/													
(Mg+Fe)]*	0.887	0.902	0.903	0.909	0.910	0.914	0.916						
[Mg/													
(Mg+Fe)]†	0.876	0.889	0.905	0.905	0.908	0.909	0.910						

* [Mg/(Mg+Fe)] ratio in olivine analysed with the electron microprobe.

† [Mg/(Mg+Fe)] ratio in equilibrium olivine calculated on the basis of $K_D = (Fe/Mg)^{olivine} / (Fe/Mg)^{melt} = 0.3$ (ref. 23).‡ An uncertainty of ± 0.5 kbar exists.§ The nominal temperature values quoted are good within ± 10 °C.

¶ Standard deviation given in parentheses.

melts is remarkable. Such compositional resemblance possibly suggests that at least some MORBs (second-stage melts) are primary and that they may be generated at shallow depths (~30 km).

A final comparison can be made with a proposed primary magma from the Trinity mafic-ultramafic complex¹⁶. These 'melts'¹⁶ occur as plagioclase-rich veins in host plagioclase lherzolite. Using compositional, field and phase equilibria arguments, Quick suggested that these melts were generated at pressures of <10 kbar. Table 2 shows that these veins are compositionally similar, including Na₂O contents, to some of the experimental melts, which supports the conclusion of Quick. It is further suggested that the source lherzolite for such melts must have undergone previous partial fusion and depletion in elements such as Na.

Application of the results of this experimental study to the MORBs and possible primary melts of the Trinity complex therefore supports the contention that the high-MgO, high-SiO₂ basalts of the mid-ocean ridges are primary, and are generated at relatively shallow mantle depths, possibly from plagioclase + spinel lherzolite.

This research was carried out at the University of Texas at Dallas. Financial support was received from NSF grants EAR74-22571A01, EAR8018359, and EAR7822766 to D. C. Presnall, and NSF grant EAR7923615 to W. G. Ernst. Reviews by Ernst and Presnall helped in revision of the original manuscript. Discussions with Presnall, Ernst, and J. E. Quick are gratefully acknowledged. G. Stummer provided the XRF analysis. C. McCann and V. Jones helped in preparation of the manuscript. This is Department of Geosciences, University of Texas at Dallas, contribution no. 427.

Received 19 April; accepted 29 June 1982.

- Presnall, D. C., Dixon, J. R., O'Donnell, T. H. & Dixon, S. A. *J. Petrol.* **20**, 3–35 (1979).
- Duncan, R. A. & Green, D. H. *Geology* **8**, 22–28 (1980).
- Duncan, R. A. & Green, D. H. *Geology* **8**, 562–563 (1980).
- Green, D. H., Hibberson, W. O. & Jaques, A. L. in *The Earth: its Origin, Structure, and Evolution* (ed. McElhinny, W. H.) 265–299 (Academic, New York, 1979).
- Jaques, A. L. & Green, D. H. *Contr. Miner. Petrol.* **73**, 287–310 (1980).
- O'Hara, M. J. *Nature* **220**, 683–686 (1968).
- Elthon, D. *Nature* **278**, 514–518 (1979).
- Stolper, E. *Contr. Miner. Petrol.* **74**, 13–28 (1980).
- Sen, G. thesis, Univ. Texas at Dallas (1981).
- Moore, E. M. & Vine, F. J. *Phil. Trans. R. Soc.* **268**, 443–466 (1971).
- Menzies, M. & Allen, C. *Contr. Miner. Petrol.* **45**, 197–213 (1974).
- Smewing, J. D., Simonian, K. O. & Gass, I. G. *Contr. Miner. Petrol.* **51**, 49–64 (1975).
- Smewing, J. D. & Potts, P. J. *Contr. Miner. Petrol.* **57**, 245–258 (1976).
- Quick, J. E. *Contr. Miner. Petrol.* **78**, 413–422 (1981).

15. Lindsley-Griffin, N. *North American Ophiolites*, Bull. 95 (Department of Geology & Mineral Industries, Oregon 1977).16. Quick, J. E. *J. geophys. Res.* **86**, 11837–11863 (1981).17. Bryan, W. B. *J. Petrol.* **20**, 293–325 (1979).18. Bryan, W. B. & Dick, H. J. B. *Earth planet. Sci. Lett.* **58**, 15–26 (1982).19. Langmuir, C. H., & Hanson, G. *Phil. Trans. R. Soc. A297*, 383–407 (1980).20. Wilkinson, J. F. G. *Earth-Sci. Rev.* **18**, 1–57 (1982).21. Carter, J. L. *Bull. geol. Soc. Am.* **81**, 2021–2034 (1970).22. Ernst, W. G. *Petrologic Phase Equilibria* (Freeman, San Francisco, 1976).23. Roeder, P. L. & Emslie, R. F. *Contr. Miner. Petrol.* **29**, 275–289 (1970).

Deep structure of the Scottish Caledonides revealed by the MOIST reflection profile

David K. Smythe*, Alan Dobinson*, Robert McQuillin*, Jonathan A. Brewer†, Drummond H. Matthews‡, Derek J. Blundell‡ & Brian Kelk§

* Institute of Geological Sciences, Murchison House, West Mains Road, Edinburgh EH9 3LA, UK

† Department of Earth Sciences, University of Cambridge, Madingley Road, Cambridge CB3 0EZ, UK

‡ Department of Geology, Chelsea College, University of London, 552 Kings Road, London SW10 0UA, UK

§ Natural Environment Research Council, Polaris House, North Star Avenue, Swindon, Wilts SN2 1EU, UK

The Moine and Outer Isles Seismic Traverse (MOIST) is a deep crustal reflection profile shot at sea off the north coast of Scotland in 1981. Spectacular reflections are observed from the Moho and from thrust zones within the Caledonian fold belt and foreland. Deep reflection profiling of the continental crust of the United States under the direction of the COCORP group, has amply demonstrated the value of this technique when applied to suitable geological problems (see, for example, refs 1, 2). A similar group, the British Institutes Reflection Profiling Syndicate (BIRPS), has now been set up in the UK to organize such projects. Funds are provided by the Natural Environment Research Council (NERC) through the core group based at Cambridge University. However, a preliminary experiment, of which MOIST is the result, was organized through the Institute of Geological Sciences (IGS).

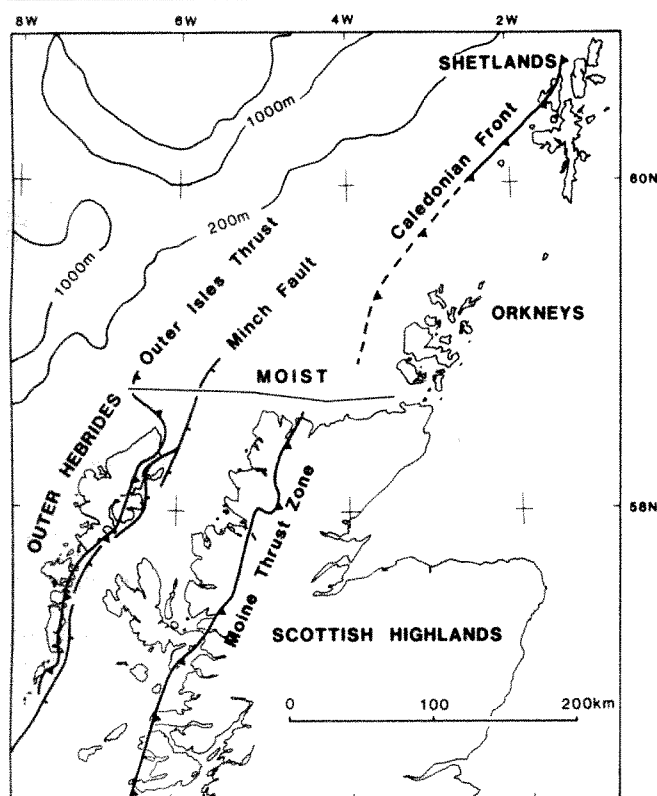


Fig. 1 Location of MOIST in relation to the Caledonian orogenic front off northern Scotland.

The strategy of recording reflection profiles offshore was adopted because a number of areas of basement outcrop around the United Kingdom are known to give rise to good upper- and mid-crustal reflections on confidential commercial reflection data³⁻⁵. Furthermore, shooting at sea is nearly an order of magnitude cheaper, mile for mile, than on land, as well as giving better quality data, although the obvious drawback is that reflections cannot be tied in directly to exposed outcrop.

One of the most important targets for reflection profiling in the UK is the Caledonian orogenic front (Fig. 1), which runs the length of north-west Scotland, trending north-east offshore from the Scottish mainland towards the Shetlands⁶. The nature of the front and the deeper crustal structure of the Moine Thrust zone and Outer Isles Thrust are the subject of several conflicting hypotheses, referred to below. There is a good coverage of industry reflection data offshore, recorded mainly to 5 s two-way time (TWT)—up to 15 km of crustal penetration—and several major crustal refraction profiles have been observed both offshore and onshore⁷⁻¹⁰. Although in many respects these long refraction profiles have proved disappointing in their lack of resolution of crustal problems, they do at least define well the Moho depth, which is about 25 km below the foreland.

MOIST crosses the offshore extrapolation of the Caledonian fold belt and runs onto the foreland to the west (Fig. 1). Its precise location was fixed with the help of the commercial data³, avoiding as far as possible the complicating effects of plutons and other intrusions. The survey comprised one line running from the Pentland Firth to 30 km NW of the Butt of Lewis, a total of 181 km (Fig. 1). The line consisted of three straight segments run close to and parallel to the coast for best possible correlation with known land geology, but sufficiently far offshore to minimize side swipe interference from charted coastal features.

The survey was conducted by Western Geophysical Company of America, using essentially the same equipment as for conventional oil industry surveys, except that the source and detector were towed at a greater depth to optimize the lower frequency signal content. The source was a 905 in³ tuned airgun array

operating at 4,500 p.s.i. pressure, towed at a depth of 12 m. The 3-km hydrophone streamer, comprising 60 × 50 m sections, was towed at a depth of 15 m. Shot interval was 50 m. Sixty channels were recorded at a 4-ms sampling rate to a record length of 15 s. Positioning was by satellite navigator integrated with bottom tracking Doppler sonar.

A conventional basic processing sequence was followed to produce final stacked sections with 30-fold subsurface coverage at a 25-m common depth point interval. In addition, array simulation techniques were used before stacking, to enhance the continuity of events deep in the section. The operator lengths were equivalent to a 200-m source array and a 100-m

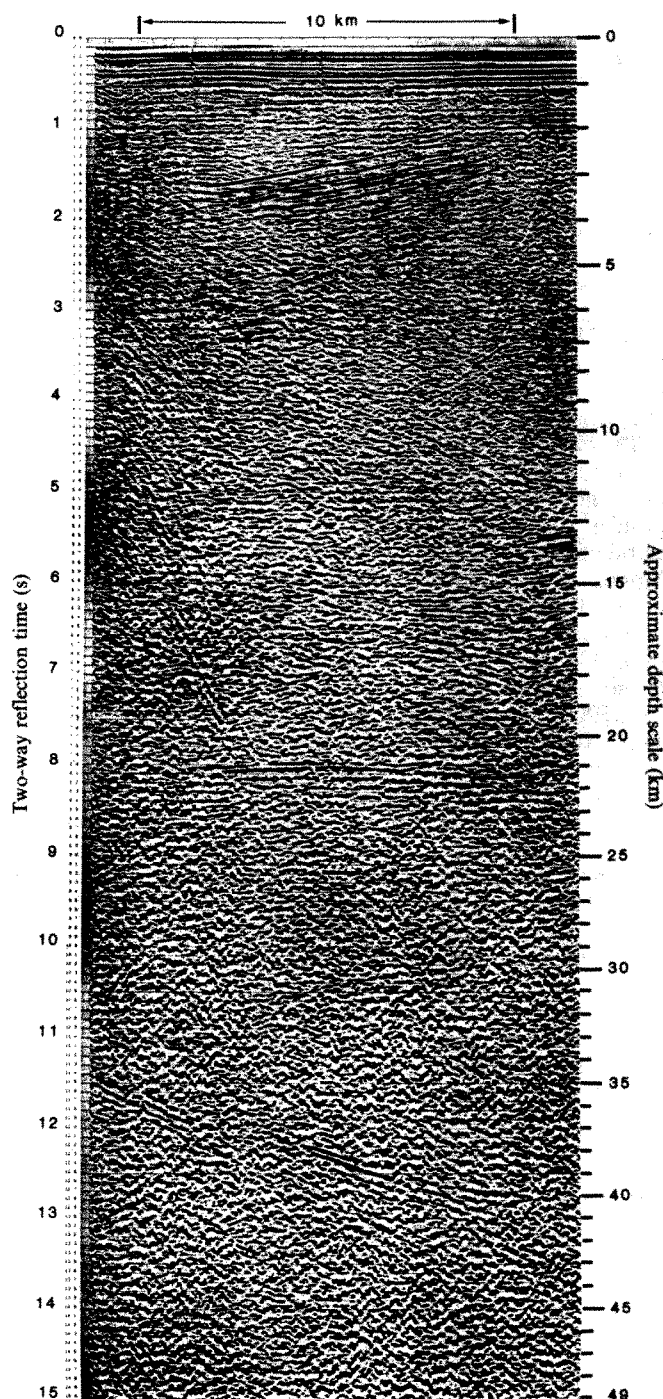


Fig. 2 Part of the final equalized stack section processed by Western Geophysical (located in Fig. 3). Strong reflectors at 1.4–1.8 s TWT are from Permo-Triassic redbeds below Jurassic shales. The Moho is at 8.0 s TWT and the 'Flannan Thrust' reflectors dip east between 12 and 13 s TWT. Depth scale on right is approximate.

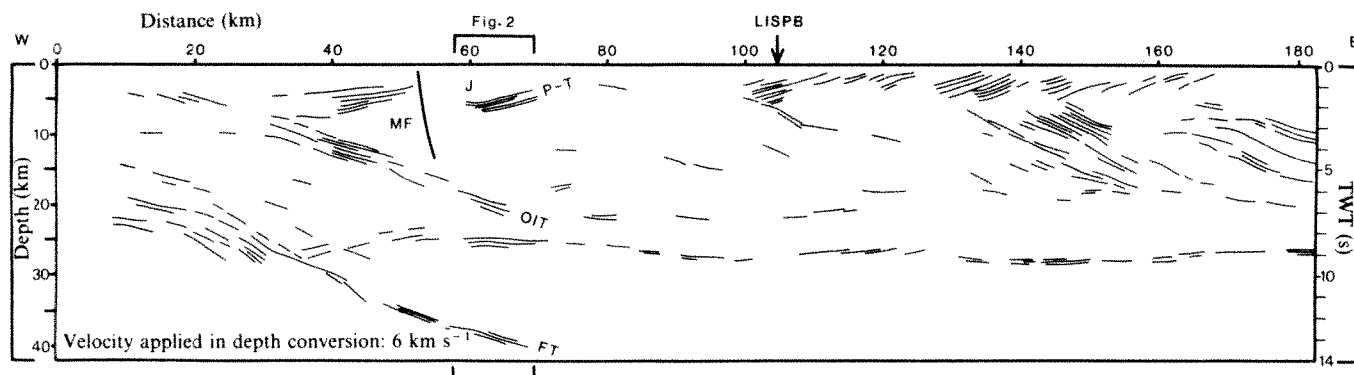


Fig. 3 Line drawing of MOIST profile, based on migrated sections but also using data from unmigrated stacks. Vertical depth scale assumes a constant velocity of 6 km s^{-1} ; no vertical exaggeration. LISP intersection near Cape Wrath is shown. MF, Minch Fault (drawn from other data); J, Jurassic; P-T, Permo-Triassic; OIT, Outer Isles Thrust; FT, Flannan Thrust.

receiver array. Velocity analyses were computed at 3-km intervals.

Figure 2 shows part of the equalized stack section resulting from the above processes, showing the excellent data quality. Figure 3 is a line drawing based on a migrated section produced for BIRPS by Shell Expro UK Ltd, but also using the information from the conventional stack (for example, Fig. 2) together with other migrations subsequently produced by one of us (J.A.B.) on the COCORP computer at Cornell University.

The base of the crust is well defined by an almost continuous Moho reflector along most of the section, 35–181 km, at a depth of around 25 km, in good agreement with the LISP and NASP profiles^{7,8}. Apparent vertical offsets in TWT, for example, astride the Minch fault, may be due to structural offsets in the Moho, although pull-up effects due to lateral variations in crustal P-wave velocity cannot be ruled out. The W-dipping reflectors in the uppermost 2–3 s TWT are from sediments in half-grabens of ages ranging from Proterozoic (?Stoer Group, 990 Myr) to Jurassic. Lewisian basement of Laxfordian (~1,700 Myr) or older age, forming the sub-sedimentary crop along the westernmost two-thirds of the profile, is the apparently autochthonous foreland. It generally lacks coherent reflectors, but in the western half of the profile is cut by two sequences of reflectors dipping east at around 20° . The upper of these corresponds to the northward offshore extension³ of the Outer Isles Thrust, a major intra-foreland thrust zone cropping out along the eastern coastline of the Outer Hebrides. The thrust appears either to flatten out at ~20 km depth or to cut and displace the Moho (Fig. 3, 70–90 km along profile). In either case, it has clearly been reactivated as a low-angle normal fault, permitting deposition of the westward dipping sediments above. Comparisons with the geologically better controlled geophysical data in the Minches and Sea of the Hebrides^{11–14} suggest that the Stoer Group (~990 Myr) and/or Torridon Group (~810 Myr) piedmont fan and fluvial deposits^{15–17} may form the base of these sedimentary prisms, in which case the Outer Isles Thrust would be of Grenville or earlier age.

The deeper sequence of eastward-dipping reflectors was totally unexpected. It appears to truncate the Moho (Fig. 3, 35 km along profile) and can be traced convincingly to 13 s TWT (Figs 2, 3)—about 40 km depth. The reflectors are primary, not multiple, events; their apparent termination of the Moho, and their parallelism with the overlying Outer Isles Thrust, suggest that the reflector group lies approximately in the plane of section, and that it is due to another thrust. We call it the Flannan Thrust, since it may crop out along the western margin of the Flannan Trough^{18–20} west of the Hebrides.

The west-dipping half-grabens seen along the eastern part of the section (Fig. 3, 100–170 km along profile) contain red beds of late Palaeozoic age. The easterly-downthrowing faults bounding the sedimentary prisms presumably flatten out into

the group of prominent east-dipping reflectors beneath, which have been interpreted³ as due to intra-orogenic belt structure. Our new interpretation of these requires a fuller discussion (J.A.B. and D.K.S., in preparation) than can be given here; however, the data suggest that thrust structures flatten out at 17–20 km depth. Thus, thin-skinned models^{21–23} of the Moine Thrust Zone and 'duplex' models of full crustal thickness²⁴ appear to be incorrect.

In conclusion, MOIST demonstrates that conventional marine seismic reflection techniques are indeed now capable of profiling the whole continental crust, contrary to pessimistic theoretical predictions²⁵, and also, that reflection profiling, even when located offshore, can be an extremely powerful tool for testing *a priori* hypotheses. We stress, however, that line drawings such as that in Fig. 3 cannot simply be 'coloured in' with a geological interpretation; new and better-constrained hypotheses can only emerge from a synthesis of all available geological and geophysical data.

We thank Western Geophysical, especially David Skidmore, for providing us with help and advice above their contractual obligations. We also thank Shell Expro UK Ltd, and particularly Gordon Robson and Rodney Calvert, for giving us both the benefit of their experience and for supplying us with a migrated version of the line.

Received 13 July; accepted 4 August 1982.

1. Cook, F. A. *et al.* *Geology* **7**, 563–567 (1979).
2. Ando, C. J., Cool, F. A., Oliver, J. E., Brown, L. D. & Kaufman, S. *Mem. geol. Soc. Am.* (in the press).
3. Smythe, D. K. *Geophys. J. R. astr. Soc.* **61**, 199 (1980).
4. Blundell, D. J. & Smythe, D. *Geophys. J. R. astr. Soc.* **61**, 216–217 (1980).
5. Blundell, D. J. in *Petroleum Geology of the Continental Shelf of North-west Europe* (eds Illing, L. V. & Hobson, G. D.) 58–64 (Heyden, London, 1981).
6. Flinn, D., Frank, P. L., Brook, M. & Pringle, I. R. in *The Caledonides of the British Isles—Reviewed* (eds Harris, A. L., Holland, C. H. & Leake, B. E.) 109–115 (Scottish Academic, Edinburgh, 1979).
7. Smith, P. J. & Bott, M. H. P. *Geophys. J. R. astr. Soc.* **40**, 187–205 (1975).
8. Bamford, D., Nunn, K., Prodehl, C. & Jacob, B. *Geophys. J. R. astr. Soc.* **54**, 43–60 (1978).
9. Hall, J. J. *geol. Soc.* **135**, 555–563 (1978).
10. Bott, M. H. P., Armour, A. R., Himsforth, E. M., Murphy, T. & Wylie, G. *Tectonophysics* **59**, 217–231 (1979).
11. Smythe, D. K., Sowerbutts, W. T. C., Bacon, M. & McQuillin, R. *Nature phys. Sci.* **236**, 87–89 (1972).
12. McQuillin, R. & Watson, J. *Nature phys. Sci.* **245**, 1–3 (1973).
13. Binns, P. E., McQuillin, R. & Kenolty, N. *Rep. Inst. Geol. Sci.* no. 73/14 (1974).
14. Smythe, D. K., Chesser, J. & Bishop, P. *Rep. Inst. Geol. Sci.* (in the press).
15. Stewart, A. D. *Mem. Am. Ass. petrol. Geol.* **12**, 595–608 (1969).
16. Williams, G. E. *Mem. Am. Ass. petrol. Geol.* **12**, 609–629 (1969).
17. Stewart, A. D. *Spec. Rep. geol. Soc. Lond.* **6**, 43–51 (1975).
18. Jones, E. J. W. *Nature* **272**, 789–792 (1978).
19. Smythe, D. K., Kenolty, N. & Russell, M. J. *Nature* **276**, 420–421 (1978).
20. Jones, E. J. W. *J. geophys. Res.* **86**, 11, 533–511, 574 (1981).
21. Elliot, D. & Johnson, M. R. W. *Trans. R. Soc. Edinb. Earth Sci.* **71**, 69–96 (1980).
22. Coward, M. P. *J. struct. Geol.* **2**, 11–17 (1980).
23. McClay, K. R. & Coward, M. P. *Geol. Soc. Lond. Spec. Publ.* No. 9, 241–260 (1981).
24. Soper, N. J. & Barber, A. J. *J. geol. Soc.* **139**, 127–138 (1982).
25. Backus, M. M., Stoffa, P. L., Tsai, C. J. & Stark, T. J. *Geophysics* **47**, 454 (1982).

Oceanic plateaus as meteorite impact signatures

Garry C. Rogers

Pacific Geoscience Centre, Earth Physics Branch, Sidney, British Columbia, Canada V8L 4B2

The oceanic plateaus are an enigmatic set of deep ocean structures¹⁻⁵. Could these be signatures of ancient meteorite impacts? While numerous confirmed and suspected impact sites, ranging in age from Precambrian to Recent, have been identified on the continents⁶, none has thus far been identified in the oceans. The ocean floor is relatively young compared with most of the continental land masses and is constantly being renewed at spreading centres and destroyed in subduction zones. Nevertheless, roughly half of the ocean basins are of Cretaceous age or older (the Pacific ocean floor is shown in Fig. 1) and they represent geologically very stable platforms. Noting, for example, the number of major continental impacts documented to be less than 100 Myr old (15 craters with diameters >10 km including two >50 km in the Soviet Union⁶), a significant number of oceanic impact structures of this age should also be present. A recurrence relation derived from impact structures on land, when correlated for the size and average age of the ocean basins, indicates that impact structures should be more numerous in the oceans (Fig. 2). The key problem is what to look for. I discuss here reasons for considering the sparsely scattered deep ocean plateaus to be likely candidates.

Deep ocean plateaus can be divided into two categories⁴: continental type and oceanic type. The former seem to be rifted segments of continents and are not of concern here. The origin of the oceanic type of plateaus is much more difficult to explain. They are few in number and most are away from plate margins in older ocean floor. They are broad, high standing, aseismic features, with little relief in the crestal zone. The largest is several hundred kilometres in dimension. Their crustal structure differs markedly from the relatively uniform three-layer model which applies to most of the oceanic crust. They seem to be equivalent to thickened sections of oceanic crust³, with a notably thick basal layer having a compressional wave velocity in the 7.1–7.6 km s⁻¹ range⁴. Most plateaus do not exhibit significant isostatic anomalies, implying almost complete compensation⁵. The larger plateaus are capped by thick calcareous sediments, some of which are now below the calcite compensation depth, suggesting significant subsidence since formation. Sampling from the Deep Sea Drilling Project (DSDP) has confirmed a shallow water origin by the presence and size of abundant vesicles in the basalts cored and the presence of shallow water fauna in the fossil record⁷⁻⁹. The magnetic signature of the plateaus is confused and different from the lineations which characterize typical oceanic crust⁵, suggesting that normal seafloor spreading was not involved or that they were formed during one polarity interval of the Earth's magnetic field. Although recent authors agree that oceanic plateaus have been caused by unusually voluminous basaltic eruptions^{2,3}, no complete explanation for their origin has yet been published²⁻⁵.

With the properties of the plateaus in mind, suppose that a large extraterrestrial body (5–10 km in diameter) collided with the Earth in an oceanic area. The energy-absorbing effect of a few kilometres of water has been estimated to be negligible in a collision with a body of this size^{10,11}. The impact would be large enough to cause a crater of the order of 100 km in diameter¹⁰⁻¹¹ and fracture completely through the oceanic lithosphere, causing an initial ballistic structural uplift that would upwarp the asthenosphere, distort the geothermal

gradient and raise the deep ocean floor to near or above sea level. (A central uplift of 1/10th the crater diameter is not uncommon for large craters on land¹³⁻¹⁵.) If the impact was large enough, the upwarping of the asthenosphere might be sufficient to cause the formation of a long-lived thermal plume in the mantle¹⁰. In any case, massive outpouring of basalt and significant melting of the upper mantle might be expected if the bolide targeted on young ocean floor^{10,11}. (The plateaus of the western Pacific all have ages within a few tens of millions of years of the surrounding sea floor^{3,7,9,16}.) The volcanism would extend much beyond the original crater because of extensive fracturing of the thin oceanic lithosphere, and the original impact structure would thus probably be obliterated. The basalts erupted in shallow water on the top of the uplifted central structure would contain many vesicles, and the time constant for viscoelastic response of the lithosphere (of the order of 10⁶ or 10⁷ yr)^{17,18} would allow a large body of calcareous sediment to build up as it sank slowly back to equilibrium position. The mixture of water with the melted and uplifted mantle would cause widespread serpentinization, resulting in a net volume increase (and a thick, high velocity basal layer in the crust^{1,4}) which would make the final structure a plateau significantly above the abyssal sea floor. Thus, the properties of the oceanic plateaus are not inconsistent with what could be expected for structures caused by the impact of a large extraterrestrial body.

Consistency, however, is not proof. The diagnostic features of astroblemes on land^{13,19}—large circular structure, meteorite

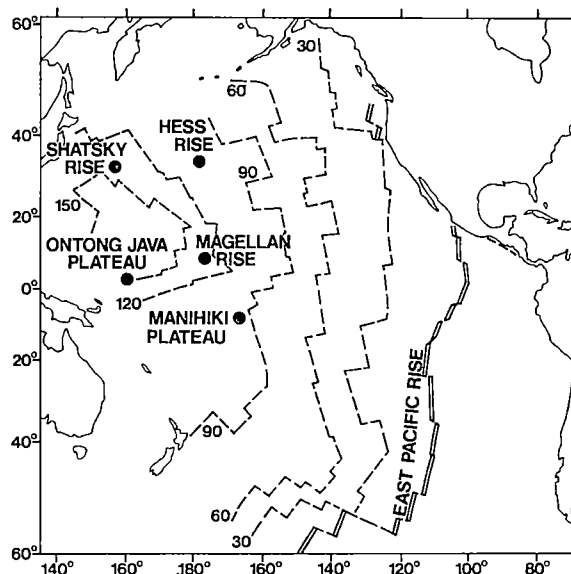


Fig. 1 Location of the larger oceanic plateaus in the Pacific with the age of the ocean floor in Myr.

fragments and evidence of shock metamorphism—are considerably more difficult to apply to the ocean bottom, particularly to a structure covered with abundant tholeiitic basalts and thick calcareous sediments. However, detailed geophysical surveys of plateaus may reveal remnants of arcuate structure and drilling in the central portion, dredging on the flanks and sampling in the surrounding sediments may reveal evidence for the petrographic effects of shock metamorphism. In addition, if large meteorite impacts prove to have widespread geochemical signatures²⁰, then the correlation of such signatures with the times of plateau formation would be very convincing evidence.

In light of the hypothesis put forward here, an obvious corollary question to ask is whether one of the large oceanic plateaus could be the topographic evidence of the Cretaceous–Tertiary boundary event. There is increasing evidence that this sudden and widespread extinction of the majority of species of flora and fauna on the Earth about 65 Myr ago was due to the

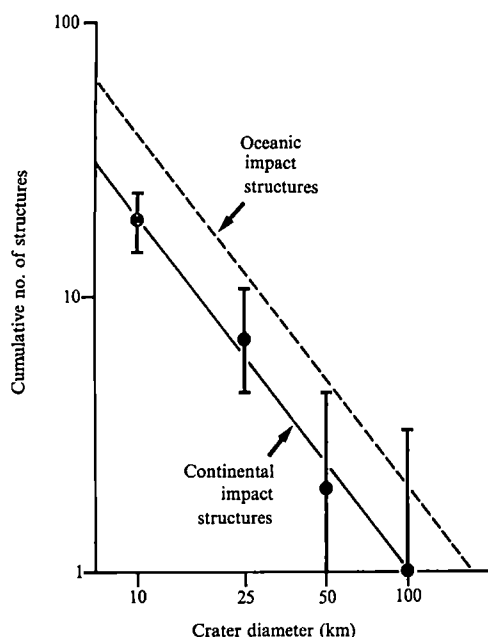


Fig. 2 The data points represent the cumulative number of probable impact structures on land greater than a given diameter for the last 150 Myr⁶. Error bars are 67% confidence limits for a poissonian distribution²⁴. The dashed line represents the number of structures expected in the ocean basins assuming the average age of the oceans is half the maximum of 150 Myr and that the area has been consistently three times that of the land mass.

impact of a giant meteorite^{11,12,20,21}. Preliminary investigation of ages in DSDP cores on the three largest oceanic plateaus, the Shatsky Rise, the Manihiki Plateau and the Ontong Java Plateau, rule them out because they are all older than 100 Myr^{3,7,9,16}. However, an oceanic impact marking this massive biological extinction could be represented by a large plateau that has now been subducted or coupled to a bordering continental margin. This plateau would have had to be much larger than the largest of the contemporary plateaus because there was not the same order of biological extinction at the time of initiation of formation of the three largest plateaus. The difficulty in subducting such a huge area of thickened crust should be a recognizable tectonic event in the ocean basins or in some of the ophiolite sequences at their margins. If the localized Cretaceous-Tertiary extinction of higher plants around the present day North Pacific²² surrounds the impact site¹¹, then the northwestern Pacific margin is a region in which to search for evidence of an anomalous tectonic event, occurring since the Cretaceous, that could represent the difficulty in subducting a massive plateau. A tectonic event of the appropriate magnitude might be the abrupt change in the motion of the Pacific plate about 45 Myr ago²³.

Received 7 June; accepted 21 July 1982.

- Den, N. et al. *J. geophys. Res.* **74**, 1421-1434 (1969).
- Winterer, E. L., Lonsdale, P. F., Mathews, J. L. & Rosendahl, B. R. *Deep Sea Res.* **21**, 793-814 (1974).
- Hussong, D. M., Wiperman, L. K. & Kroenke, L. W. *J. geophys. Res.* **84**, 6003-6010 (1979).
- Carlson, R. L., Christensen, N. I. & Moore, R. P. *Earth planet. Sci. Lett.* **51**, 171-180 (1980).
- Ben-Avraham, Z., Nur, A., Jones, D. & Cox, A. *Science* **213**, 47-54 (1981).
- Grieve, R. A. F. & Robertson, P. B. *Icarus* **38**, 212-229 (1979).
- Moberly, R. & Larsen, R. L. *Init. Rep. DSDP Leg 32*, 945-956 (1975).
- Jackson, E. D. & Schlanger, S. O. *Init. Rep. DSDP No. 33*, 915-927 (1976).
- Packham, G. H. & Andrews, J. E. *Init. Rep. DSDP No. 30*, 691-705 (1975).
- Grieve, R. A. F. *Precamb. Res.* **10**, 217-247 (1980).
- Emiliani, C., Kraus, E. B. & Shoemaker, E. M. et al. *Earth planet. Sci. Lett.* **55**, 317-334 (1981).
- Napier, W. M. & Clube, S. V. M. *Nature* **282**, 455-459 (1979).
- Dence, M. R., Grieve, R. A. F. & Robertson, P. B. in *Impact and Explosion Cratering*, 247-275 (Pergamon, New York, 1977).
- Dence, M. R. & Grieve, R. A. F. *Lunar planet. Sci.* **10**, 282-294 (1979).
- Grieve, R. A. F., Robertson, P. B. & Dence, M. R. *Proc. Lunar Planet. Sci.* **12A**, 37-57 (1981).

- Douglas, R. G. & Moullade, M. *Bull. geol. Soc. Am.* **83**, 1163-1168 (1972).
- Beaumont, C. *Geophys. J. R. astr. Soc.* **55**, 471-497 (1978).
- Lambeck, K. & Nakiboglu, S. M. *J. geophys. Res.* **86**, 6961-6984 (1981).
- Dence, M. R. 24th int. geol. Congr. Sect. 15, 77-89 (1972).
- Alvarez, L. W., Alvarez, W., Asaro, F. & Michel, H. V. *Science* **208**, 1095-1108 (1980).
- Smit, J. & Hertogen, J. *Nature* **285**, 198-200 (1980).
- Hickey, L. J. in *Catastrophes in Earth History: The New Uniformitarianism* (Princeton University Press, 1982).
- Morgan, W. J. *Mem. geol. Soc. Am.* **132**, 7-22 (1972).
- Weichert, D. H. *Bull. seism. Soc. Am.* **70**, 1335-1346 (1980).

Volcanic ash deposits of early Eocene age from the Rockall Trough

E. J. W. Jones

Department of Geology, University College London, London WC1E 6BT, UK

A. T. S. Ramsay

Department of Geology, University College of Swansea, Singleton Park, Swansea SA2 8PP, UK

The stratigraphy of the Rockall Trough (Fig. 1) has proved difficult to elucidate because a mantle of Recent sediments usually prevents piston corers and dredges from sampling older accumulations. Although a seismic stratigraphy has been erected^{1,2}, considerable uncertainty surrounds the history of sedimentation and, consequently, the petroleum potential of the region. The upper 500-1,000 m of the succession are clearly Cenozoic deposits whose distribution has been strongly influenced by movements of Norwegian Sea overflow water¹. Deeper in the section, major current-controlled accumulations are absent, a feature observed elsewhere in the Atlantic¹. In view of the paucity of samples from these older deposits³, we report here the recovery of sediments that were laid down in the northern Rockall Trough before polar waters radically changed the depositional regime. The sediments record a period of explosive volcanicity during the early Eocene in the vicinity of the Wyville-Thomson Ridge.

The rock specimens were obtained from RRS *Shackleton* in 1979 during dredging operations at three locations in a trough separating the Wyville-Thomson Ridge and Faeroe Bank from Ymir Ridge (S1-S3, Fig. 1). This narrow depression acts as an important, although probably intermittent, entry point for dense Norwegian Sea overflow water into the Rockall Trough⁴. It was anticipated that the overflow had inhibited deposition locally and even caused sufficient erosion to expose formations normally deeply buried within the sediment pile. Figure 2 shows a complex pattern of current-controlled drift deposits associated with the overflow. These accumulations are absent south-west of kilometre 16 and along dredge tracks S1 and S2 on the side of Faeroe Bank, which is underlain by strongly reflecting, layered material pre-dating the drift sediments. A refraction profile on the crest of Faeroe Bank (V28-61; Fig. 1) suggests that the highly reflective sequence has a seismic velocity exceeding 4 km s⁻¹ and is therefore probably correlative with the 3.9-4.9 km s⁻¹ shallow volcanics of the Faeroes (Fig. 2).

Over 200 rocks, weighing a total of ~100 kg, were recovered at each dredge site (Fig. 1). The principal constituent is an indurated, manganese-stained, calcareous tuff, olive-green or grey in colour, containing a high proportion of unaltered glass shards. At sites S2 and S3 the tuffaceous components make up about 65% of the specimens. The striking lithological similarity between the tuffs indicates a local derivation from outcrops on the flanks of Faeroe Bank and Ymir Ridge. With the possible exception of some basaltic blocks, the remaining rocks at S2 and S3 consist of a diverse collection of glacial erratics. The dredge haul from S1 (Figs 1, 2) is more heavily contaminated with obvious glacial material.

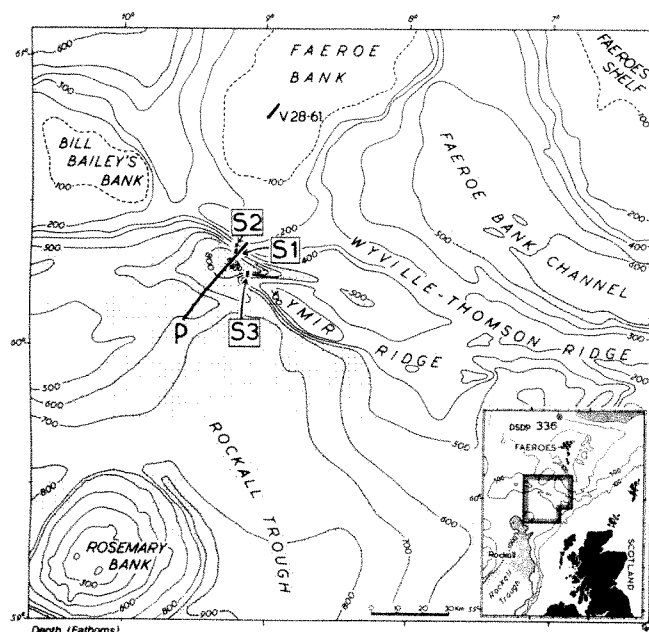


Fig. 1 The locations of Shackleton dredge sites S1–S3 at the northern end of the Rockall Trough. Bathymetric contours are based on a map of Ellett and Roberts⁴ and unpublished Shackleton soundings (100 fathoms = 183 m). The mid-points and depths of the sampling tracks are as follows: S1, 60°19.1' N, 9°13.2' W (986–1,450 m); S2, 60°20.3' N, 9°13.5' W (790–892 m); S3, 60°14.7' N, 9°08.6' W (1,223–1,602 m). An airgun reflection profile along track P is reproduced in Fig. 2. V28-61 is an unreversed seismic refraction profile shot with a sonobuoy receiver at the southern termination of the line. The refraction results are presented in Fig. 2.

The tuffaceous samples have been dated on the basis of calcareous nannofossils. All assemblages examined from the three dredge sites are Ypresian (early Eocene) in age and are assigned to the *Marthasterites tribrachiatus* zone of Brönnimann and Stradner⁵. The following species were recorded in each assemblage: *Braarudosphaera bigelowi*, *Chiasmolithus consuetus*, *Chiasmolithus grandis*, *Cyclococcolithus neogammation*, *Chiphragmalithus calathus*, *Discoaster barbadiensis*, *Discoasteroides kuepperi*, *Sphenolithus radians*, *Zygrhablithus bijugatus* and *Zygodolites dubius*. The datum indicator *M. tribrachiatus* occurs in two samples from dredge S1, one specimen from S2 and five samples from S3. *Discolithina plana* and various species assigned to the genus *Micrantholithus* are found in most specimens. The presence of *B. bigelowi* and *Micrantholithus* indicates sedimentation at relatively shallow depths. The former is most abundant in the near-shore waters of the

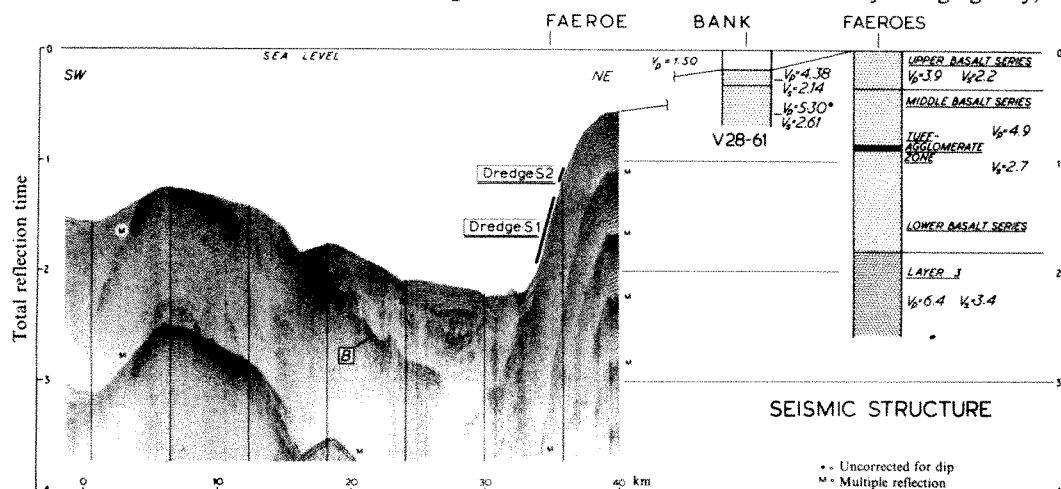
present Atlantic, while in Eocene sediments from the North Atlantic it is limited to deposits recovered from depths of less than 1,600 m (ref. 6).

The *M. tribrachiatus* zone is equivalent to NP12 of the standard calcareous nannoplankton zonation scheme proposed by Martini⁷. The numerical age of the zone is still a matter for debate. It is dated at 52–50 Myr BP by Hardenbol and Berggren⁸ (53–52 Myr adopting the 1976 ICC atomic abundance and decay constants). Odin and Curry⁹, however, argue that the zone is appreciably younger (49–47 Myr BP; ICC constants).

As the three dredges traversed a depth range of several hundred metres on both sides of the channel (Fig. 1), the restriction of the tuffaceous samples to zone NP12 suggests that a substantial thickness of Ypresian volcanogenic sediments outcrops in the area. Petrographic examinations and the major element contents of 19 specimens reveal compositions corresponding to tholeiitic basalts. The tuffs could have been derived from several volcanic regions which were active in the early Eocene. An oceanic rift to the west of the Faeroes and the Rockall Plateau is one possible area, as magnetic lineations of early Eocene age occur in the Greenland–Rockall Basin¹⁰. Rosemary Bank to the south¹¹, the Scottish Hebridean region and the Faeroese province, which we take to include the Wyville–Thomson Ridge, Faeroe Bank and Ymir Ridge, are other likely sources¹². A plot of the abundances of the elements Y, Zr and Ti, which are relatively insensitive to alteration processes¹³, shows the dredge samples clustering in the field normally occupied by within-plate basalts (Fig. 3). They are quite distinct from the basic lavas of Rosemary Bank¹¹ and from ocean-floor basalts, suggesting that Rosemary Bank and the oceanic rift to the west did not provide the volcanogenic material. The Hebridean area is an unlikely source of supply because winds with a strong easterly component probably prevailed in this region during the Lower Tertiary¹⁴. Local volcanic centres in the Faeroese province are therefore considered to be the provenance of the Ypresian tuffs reported here.

In the Faeroes a significant period of pyroclastic activity is recorded by the tuff–agglomerate zone separating the Lower from the Middle Basalt Series (Fig. 2)¹². According to Schilling and Noe-Nygaard¹⁵, the lavas below the tuff–agglomerate zone have compositions typical of plume basalts, whereas the volcanics above are of oceanic character, like the late Eocene basalts at Deep Sea Drilling Project (DSDP) Site 336 on the Faeroe–Iceland Ridge¹⁶ (Fig. 3). A palynological study by Laufeld¹⁷ suggests that the tuffs are Eocene in age, although they cannot be dated very precisely. As these are the only indications of substantial pyroclastic activity the tuff–agglomerate sequence may be coeval with the Ypresian volcanogenic sediments exposed on the flanks of Faeroe Bank and Ymir Ridge. The lower Eocene tuffs recovered by dredging may, as

Fig. 2 Shackleton dredge sites S1 and S2 shown in relation to the shallow seismic structure recorded using an airgun reflection profiler along track P in Fig. 1. Water-layer multiples are labelled M. The edge of Faeroe Bank is underlain by well stratified material which appears to outcrop on the southern slope. Between the 16 and 34 km positions on the horizontal scale, thick and irregular sedimentary drift deposits occur above the strong reflector B. The seismic structure of the upper portion of Faeroe Bank has been derived from refraction data recorded along track V28-61 in Fig. 1. The structure of the Faeroese volcanic pile is taken from the results of Pálmason²⁶. Seismic velocities are given in km s⁻¹.



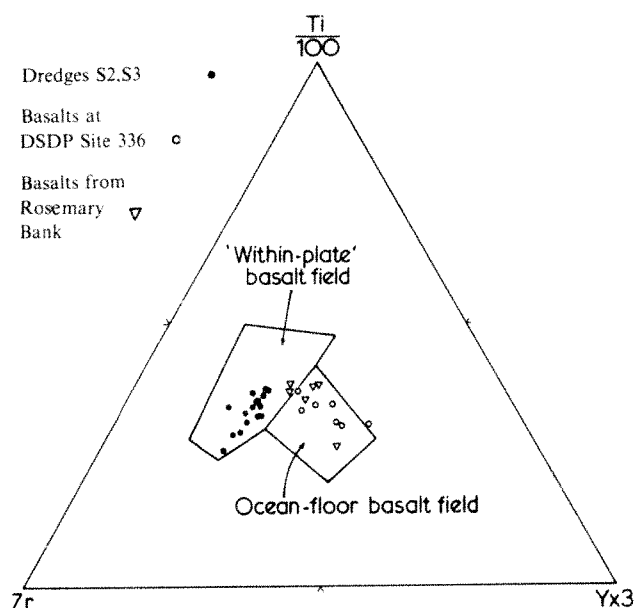


Fig. 3 Trace element variations in the Ypresian tuffs from dredge sites S2 and S3 shown on a Ti-Zr-Y discrimination diagram. Compositional fields are derived from Pearce and Cann¹³. The tuffs are quite distinct from the basaltic rocks dredged from Rosemary Bank¹¹ and from ocean-floor basalts such as the late Eocene lavas drilled at DSDP Site 336¹⁶ north of the Faeroes (Fig. 1).

in the Faeroes, be interbedded with thick basalt units, for seismic reflection profiles show layering beneath Faeroe Bank and Ymir Ridge, while high-amplitude, short-wavelength magnetic anomalies^{18,19} imply strongly magnetic, probably basaltic rocks, close to the seabed.

Correlation can be made further afield with the Rockall Plateau and the North Sea where Lower Tertiary ash falls are recorded. An early Tertiary ash sequence, much of it derived from basaltic sources, is widespread in the North Sea and forms an important seismic marker²⁰. The same tuffaceous interval also appears in wells recently drilled west of the Shetlands²¹. According to Jacqué and Thouvenin²⁰, the climax of the pyroclastic activity occurred in the late Palaeocene, at the time of deposition of the Woolwich Formation in southern England (zone NP9). The dredged tuffs are somewhat younger, but Ypresian ash layers have been encountered in wells in the northern North Sea²⁰. In East Anglia, over 40 thin ash beds of Ypresian age, considered by Jacqué and Thouvenin to be slightly younger than the main North Sea tuffs, have been discovered at the base of the London Clay^{22,23}. These are believed to be contemporaneous with ash bands in the Mo Clay Formation of Denmark²⁴. Furthermore, Harrison *et al.*²⁵ have found tuffaceous sediments in the late Palaeocene-early Eocene (NP9 to NP12) sections drilled on the western side of the Rockall Plateau, thus extending considerably the known limits of the Lower Tertiary ash falls. The volcanogenic deposits from Faeroe Bank and Ymir Ridge clearly form part of the widespread ash series which accumulated around Britain during late Palaeocene-early Eocene time. The provenance of these extensive ash accumulations is problematical. However, as Faeroe Bank and Ymir Ridge appear to be underlain by thick pyroclastic sequences of Ypresian age, the Faeroese province was probably an important source for an appreciable proportion of the lower Eocene volcanic ash in the North Sea and surrounding areas.

We thank the officers, crew and scientific party aboard RRS *Shackleton*, the staff of the NERC Research Vessel Services, Robert Houtz of the Lamont-Doherty Geological Observatory and Professor Dennis Curry for their help in this study, and Anthony Osborn for carrying out chemical analyses. Financial support was provided by the NERC.

Received 19 January; accepted 19 July 1982.

1. Jones, E. J. W., Ewing, M., Ewing, J. I. & Eittreim, S. L. *J. geophys. Res.* **75**, 1655-1680 (1970).
2. Roberts, D. G. *Phil. Trans. R. Soc. A* **278**, 447-509 (1975).
3. Jones, E. J. W., Ramsay, A. T. S., Preston, N. J. & Smith, A. C. S. *Nature* **251**, 129-131 (1974).
4. Ellett, D. J. & Roberts, D. G. *Deep-Sea Res.* **20**, 819-835 (1973).
5. Brönnimann, P. & Stradner, H. *Erdöl-Z. Bohr- u. Fördertechnik* **76**, 364-369 (1960).
6. Ramsay, A. T. S. *Nature* **236**, 67-70 (1972).
7. Martini, E. *Proc. 2nd int. Conf. Planktonic Microfossils*, Rome 739-805 (Tecnoscienza 1971).
8. Hardenbol, J. & Berggren, W. A. *Contributions to the Geologic Time Scale* (eds Cohee, G. V., Glaessner, M. F. & Hedberg, H. D.) 213-234 (American Association of Petroleum Geologists, Tulsa, 1978).
9. Odin, G. S. & Curry, D. C. *r. hebdom. Séanc. Acad. Sci., Paris* **293**, 1003-1006 (1981).
10. Vogt, P. R. & Avery, O. E. *J. geophys. Res.* **79**, 363-389 (1974).
11. Dietrich, V. J. & Jones, E. J. W. *Mar. Geol.* **35**, 287-297 (1980).
12. Rasmussen, J. & Noe-Nygaard, A. *Geology of the Faeroe Islands* (Geological Survey of Denmark I, Ser. No. 25, Copenhagen, 1970).
13. Pearce, J. A. & Cann, J. R. *Earth planet. Sci. Lett.* **19**, 290-300 (1973).
14. Donn, W. L. & Ninkovich, D. J. *J. geophys. Res.* **85**, 5455-5460 (1980).
15. Schilling, J.-G. & Noe-Nygaard, A. *Earth planet. Sci. Lett.* **24**, 1-14 (1974).
16. Talwani, M. & Shipboard Scientific Party *Init. Rep. DSDP Leg 38*, 23-116 (US Govt Printing Office, Washington DC, 1976).
17. Laufeld, S. *Geol. Föreningens Stockholm Förhand.* **87**, 231-238 (1965).
18. Bott, M. H. P. & Stacey, A. P. *Deep-Sea Res.* **14**, 7-11 (1967).
19. Avery, O. E., Burton, G. D. & Heirtzler, J. R. *J. geophys. Res.* **73**, 4583-4600 (1968).
20. Jacqué, M. & Thouvenin, J. in *Petroleum and the Continental Shelf of North-West Europe*, I (ed. Woodland, A. W.) 455-465 (Applied Science Publishers, London, 1975).
21. Ridd, M. F. in *Petroleum Geology of the Continental Shelf of North-West Europe*, (eds Illing, L. V. & Hobson, G. D.) 414-425 (Institute of Petroleum, London, 1981).
22. Elliott, G. F. *Nature phys. Sci.* **230**, 9 (1971).
23. Knox, R. W. O'B. & Harland, R. J. *geol. Soc. Lond.* **136**, 463-470 (1979).
24. Pedersen, A. K., Engell, J. & Rønsbo, J. G. *Lithos* **8**, 255-268 (1975).
25. Harrison, R. K., Knox, R. W. O'B. & Morton, A. C. *Init. Rep. DSDP Leg 48*, 771-785 (1979).
26. Palmason, G. *Tectonophysics* **2**, 475-482 (1965).

Evidence for earlier date of 'Ubeidiya, Israel, hominid site

Charles A. Repenning

United States Geological Survey, Menlo Park,
California 94025, USA

Oldrich Fejfar

Geological Survey of Czechoslovakia, Praha, Czechoslovakia

It has been suggested that the evolution of man took place in Africa. This suggestion results from the unusual abundance of fossil material in Africa that is quite ancient in comparison with what is known elsewhere. The theory of an African origin has influenced the interpretation of the age of some non-African archaeological sites. A case in point is the 'Ubeidiya locality in Israel, which is generally considered to be about 700,000 yr old because it has been assumed by a few that the associated Early Acheulian tool industry, and the persons who used it, would have taken considerable time to disperse from Olduvai Gorge to this non-African site in Israel. Here we evaluate fossil mammals from 'Ubeidiya, which are stratigraphically and directly associated with Early Acheulian artefacts, and find no substantial reason for considering the locality younger than 2 Myr, and possibly as much as 500,000 yr older than any record of Early Acheulian artefacts or *Homo erectus* in Africa.

Abundant Early Acheulian artefacts¹ with associated extinct mammals have been known from the 'Ubeidiya area, 3 km south of the Sea of Galilee on the west side of the valley of the Jordan River, since agricultural clearing exposed the site in 1959^{2,3}. A few fragmentary remains have been referred to *Homo erectus*, although Tobias⁴ felt that they were too incomplete for specific designation. Haas⁵ has described the mammalian fauna from 'Ubeidiya, which is most recently summarized by Tchernov⁶. The site is usually considered to be older than 700,000 yr but probably not much older^{7,8}.

Early Acheulian artefacts and remains of *Homo erectus* first occur in Olduvai Gorge, Tanzania, in the deposits above the

Lemuta Member in the lower part of Bed II. The Lemuta Member is dated as about 1.5 Myr in age. In Koobi Fora, Kenya, ~800 km closer to Israel, skull KNM-ER 3733 appears to predate the 1.5 Myr Okote Tuff⁹. The abrupt appearance of *Homo erectus* and Early Acheulian artefacts in Bed II of Olduvai has suggested to some the possibility of an invasion¹⁰. "Most, if not all, students consider it likely that *H. erectus* gave rise to *H. sapiens*."¹¹

Although many authors accept the African origin of man the toolmaker, others have suggested that the development of man took place in more temperate environments¹². The question of how much older than 700,000 yr the 'Ubeidiya Acheulian archaeological record thus becomes of interest: is it older than Bed II in Olduvai Gorge and, if so, is it possible that *Homo erectus* evolved elsewhere than Africa and invaded Africa more than 1.5 Myr ago¹²?

As listed by Tchernov⁶, the 'Ubeidiya fauna contains several mammals that present a 'late Villafranchian' aspect, comparable with that at Seneze, France¹³, as well as that at St Vallier, France, and Kislang, Hungary. In the micromammal bio-chronology of Europe¹⁴, it is a fauna characteristic of the Villanyian age which has been dated as being at least as old as 2.5 Myr (Roca Neyra, France) and at least as young as about 1.9 Myr (Le Coupet, France). (There is and will probably always be inconsistency in the use of the term Villafranchian age. In micromammal chronology the latest Villafranchian is separable as a distinct mammalian age, the Villanyian.) The Seneze fauna itself is from the top of a sequence of lake sediments overlying a basalt dated 2.3 Myr old and is immediately upsection from one of the Reunion polarity events¹⁵, so the fauna must be between 2.12 and 2.0 Myr old. A Villanyian age assignment corresponds approximately to some previous mammalian age assignments for the 'Ubeidiya fauna^{5,16}, but reflects subsequent refinement and temporal calibration of the biochronology (see Fig. 1). Extraordinary support for the calibration of the temporal limits of the Villanyian micromammal age (as used by Fejfar and Heinrich¹⁴) comes from the correlation of Holarctic microtine rodent dispersal events that mark the beginning and end of this age¹⁷.

The correlation of the 'Ubeidiya fauna with the Villanyian age of Europe is very good, although not perfect. On the basis of Tchernov's listing⁶, the following mammals of the 'Ubeidiya fauna are of particular significance.

The zebrine horse, *Equus stenonis*, is reported from 'Ubeidiya as the earliest record from Israel; it is first known in Europe from 'late Villafranchian' (or Villanyian) faunas and the earliest occurrence is in the Roca Neyra fauna (2.5 Myr). The earliest East African records of zebrine horses are 2.01–2.14 Myr old^{18,19}, and much older than the first record of Early Acheulian artefacts and *Homo erectus*, even though they indicate a later immigration than that of Europe. The zebras had to pass 'Ubeidiya en route to Africa and dispersed rapidly across the continent¹⁸.

The pig *Sus* sp. cf. *Sus strozzii* is a typical 'late Villafranchian' or Villanyian form and is believed to derive from *Sus minor* of the early Pliocene of Europe (earlier Villafranchian or older). *S. strozzii* was replaced by *Sus scrofa* (the modern domestic pig) in the early Biharian faunas of Europe. In Israel, *S. strozzii*, but no zebrine horses, is also present in the older Bethlehem fauna⁶ and its presence in 'Ubeidiya could have been as a relict, but *S. scrofa* also replaced *S. strozzii* in younger faunas of Israel⁶ and it dispersed westward along the southern shore of the Mediterranean where it is present in the Ternifine fauna, Algeria²⁰.

Cervid artiodactyls (deer and elk) appear in Israel for the first time in the 'Ubeidiya fauna^{5,6,21}. They are present in this fauna in a greater number of specimens than any other large mammal except *Hippopotamus*⁵ and are assigned to four forms. *Cervus* sp. cf. *Cervus ramosus* (= *Croizetoceros ramosus* or *Anoglochis ramosus*) is a species first known from the Villaroya fauna of Spain (Villanyian age) and possibly last known from the Saint Esteve-Janson fauna of France (less than 450,000 yr

old. *Euctenoceros senezensis* was described from the Seneze fauna and is also known from the Roca Neyra fauna of France (2.5 Myr old); it is possibly last known from the Cromer Forest Bed, England (600,000–730,000 yr old). *Dama* sp. is known from the Villanyian faunas of Europe into the recent fauna. The oldest (Villanyian? equivalent) *Dama* known from Africa occurs with zebrine horses near Wadi Halfa, Sudan²². *Megaloceros* sp. (giant deer) is reported on the basis of a single large deciduous last premolar⁵ of questionable value in identification. The genus is first known without question from European early Biharian faunas but is questionably present in faunas as old as Kislang.

Bison priscus (steppe wisent), to which two tooth fragments are assigned⁵, is known in Europe only from early Biharian and younger faunas but is reported from Villanyian-equivalent faunas in Siberia²³. Its distinction from the Villafranchian genus *Leptobos* on two tooth fragments is questioned.

Crocota crocuta (spotted hyaena) is first known in latest Biharian faunas of Europe. However, *Crocota* sp., often referred to as *Crocota crocuta*, is present in African deposits at least as old as Member G of the Shungura Formation²⁴, Ethiopia, and Bed I at Olduvai, Tanzania. These records are as old as those of zebrine *Equus* in Africa.

Ursus etruscus (primitive bear) is primarily, or entirely, known from Villanyian faunas including Seneze, France. It derives from an earlier Villafranchian form and is ancestral to Biharian bears of Europe and Asia, one of which, *Ursus arctos*, is known from younger faunas in Israel and westward along the northern coast of Africa to the Ternifine fauna, Algeria, and in Morocco. The specific identity of the 'Ubeidiya material is dependent on Tchernov's⁶ note that the premolars have a primitive construction.

Megantereon megantereon (sabre- or dirk-tooth tiger) is a form characteristic of the Villafranchian in Europe and the youngest records are of Villanyian age, although the lineage persisted later in Asia and survived in North America until the early Holocene. *Megantereon* is known from late Pliocene (Villanyian) faunas throughout Africa and is reported in East Africa²⁴ in members B to G of the Shungura Formation of Ethiopia.

The micromammals of the 'Ubeidiya fauna also indicate a Villanyian age; 18 (ref. 5) to 20 (ref. 6) forms have been identified in the fauna. In adjacent articles Janossy¹⁶ and Jaeger²⁵ provide interpretations of the age of the 'Ubeidiya micromammals. Jaeger indicates that the absence of the Quetta mole-vole, *Ellobius fuscicapillus*, and the grass rat, *Arvicanthis ectos* (an African immigrant), in the 'Ubeidiya fauna and their presence in the younger Oumm Quatafa fauna of Israel and in the Ternifine fauna of Algeria indicate that the 'Ubeidiya fauna is older than that from Ternifine, a suggestion noted above in connection with the presence of *S. scrofa* and *U. arctos* from Ternifine.

Janossy¹⁶ presented an outline of the micromammal bio-chronology of Europe, on the basis of microtine rodents and soricid insectivores. He pointed out that the 'Ubeidiya fauna of Israel correlated with the beginning of the Biharian micromammal age (as then used), and with the Brielle fauna, Netherlands (which correlates with the earliest Biharian as now used, as well as in 1975 usage).

Of the many micromammals in the 'Ubeidiya fauna, only *Hypolagus* sp. (primitive hare), *Jordanomys pusillus* and *Lagurodon arankae* (primitive steppe lemmings) need discussion here. Around the Holarctic world the primitive archaeolagine *Hypolagus* is replaced by advanced leporids, primarily *Lepus* (modern hare), when these appear. In North America large species of *Hypolagus* vanish, apparently instantaneously, with the introduction of advanced leporids from Asia ~2.5 Myr ago. In Europe *Hypolagus* survives at least until the early part of the Biharian micromammal age in such faunas as Kamyk, Poland, that are more or less the temporal equivalent of the Brielle fauna of the Netherlands and the Olduvai event (~1.7–1.9 Myr ago). In Africa, *Hypolagus* is not known, but

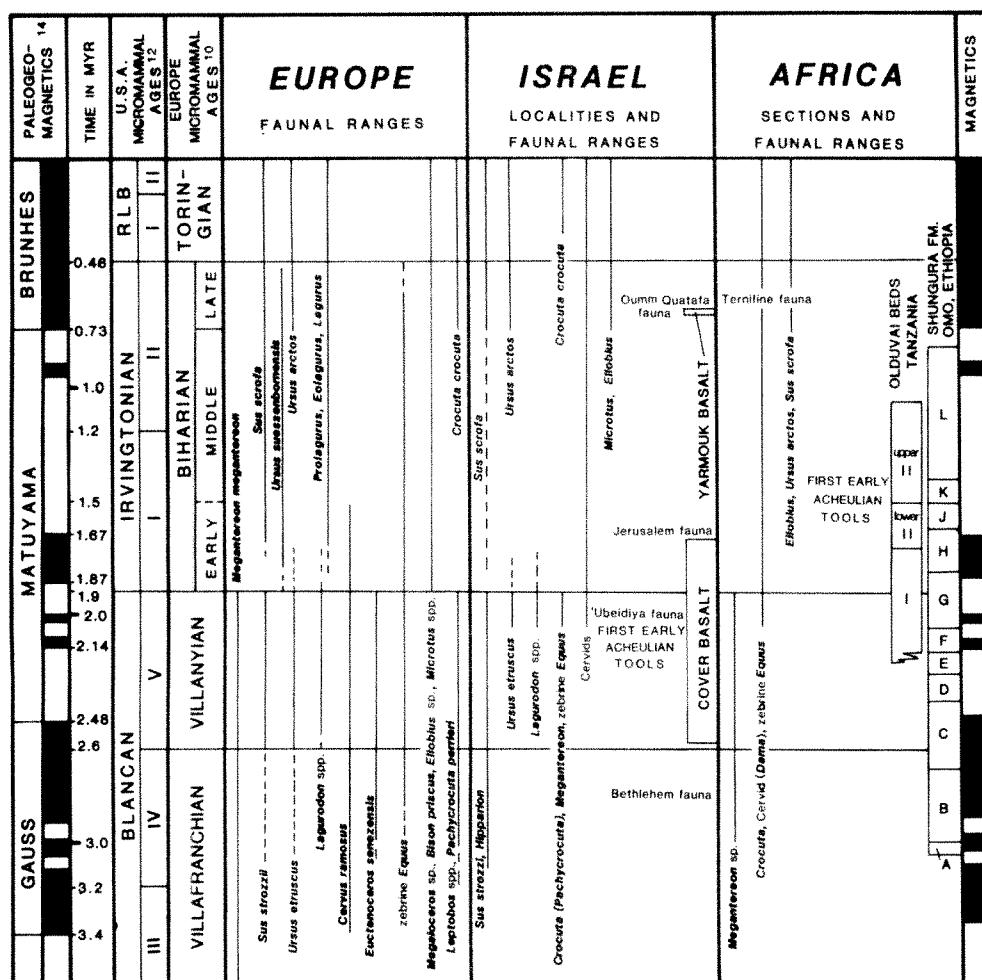


Fig. 1 Biochronology of species found in Europe, Israel and Africa.

Lepus appears in the early Pleistocene (= Biharian) of South Africa²⁶. It has to pass 'Ubeidiya to get to Africa. Although the lack of *Lepus* in the 'Ubeidiya fauna may not reflect its absence in the Levant, the presence of *Hypolagus* certainly suggests that if *Lepus* was present, it had not been there very long.

With regard to the microtine rodents, Israel is near the southern limits of their distribution today and apparently was so in the past. Beyond, only *Microtus socialis* (= *Microtus guntheri*²⁷) and *Ellobius fuscicapillus* succeeded in invading Africa but they do not appear in Israel until the Oummu Quatafa fauna, of an age appreciably younger than 'Ubeidiya. In view of the rarity of microtines in Israel, it is somewhat surprising that two genera and three species are present in the 'Ubeidiya fauna. Haas⁵ named *J. pusillus* and *Arvicola(?) jordanica* from the fauna and also recognized *L. arankae* in it. As Haas notes, *A. (?) jordanica* has too many alternating triangles on the first lower molar to be assigned to the genus *Arvicola*; at present, it is of little value in the interpretation of the age of the fauna.

J. pusillus is a lagurine microtine related to the steppe lemmings and is the junior synonym of *Lagurodon praepannonicus* named by Topachevski²⁸ one year before Haas named *J. pusillus*. *L. praepannonicus* and *L. arankae* belong to one of the better known lineages of microtine rodents and are known to occur first in the earliest Villanyian faunas of Europe. They are also present in earliest Biharian faunas of Europe (associated with *Microtus* and *Ellobius*), but by mid-Biharian time both are extinct and are replaced by more advanced steppe lemmings.

L. praepannonicus and *L. arankae* thus could be either Villanyian (2.5–1.9 Myr old) or earliest Biharian (1.9 to possibly as young as 1.7 Myr old). If earliest Biharian in age, they should be replaced shortly, in somewhat younger faunas, by more advanced genera. Tchernov²⁹ has named a second species of

Jordanomys (= *Lagurodon*), *Jordanomys haasi* from the younger-than-'Ubeidiya (but pre-*Microtus* and *Ellobius*) fauna in the karst breccia near Jerusalem. Because the 'Ubeidiya species are not replaced by a different genus in younger faunas, it would seem that they are more probably of Villanyian age.

Thus, *M. megantereon*, *E. stenonis*, *U. etruscus*, *S. strozzii*, and *E. senezensis* indicate a Villanyian or older age; if the 'Ubeidiya fauna is younger, these represent remarkable records. *L. praepannonicus* and *L. aranke* indicate a Villanyian or slightly younger age, although the presence of *Lagurodon* in the younger Jerusalem fauna favours the older part of this time range for the 'Ubeidiya fauna. *C. ramosus* and *Dama* sp. suggest a Villanyian or younger age. The presence of a large species of *Hypolagus* favours the absence of modern *Lepus*, which is known from South Africa in Biharian-equivalent faunas, thus suggesting that *Hypolagus* in the 'Ubeidiya fauna may be pre-Biharian. *C. crocuta* would suggest a much younger late Biharian age, but the specimens are few and the specific identity is questioned; *Crocuta* sp. (or *Pachycrocuta* sp.) is known from Villanyian and older deposits in both Africa and Europe. *Megaloceros* sp. and *B. priscus* suggest a younger-than-Villanyian age but *Megaloceros* sp. is known from the Villanyian Kislang fauna of Hungary³⁰ (type locality of *Lagurodon aranke*) and it is questionable whether the 'Ubeidiya tooth fragments assigned to *B. priscus* could be separated from Villafranchian *Leptobos*.

On the basis of the associated mammal fauna, the possible age range of the fauna from 'Ubeidiya, Israel, is between 2.6 and ~1.7 Myr old, but an age of less than 1.9 Myr would necessitate an age-range extension for five well-known mammalian species and make difficult the explanation of *Hypolagus* in the fauna and of *Lagurodon* in the Jerusalem fauna.

We thank Annie H. Walton for assistance in library research and for preparation of the illustration, and especially F. C.

Howell for his remarkable efforts in providing a technical review of a preliminary draft. L. L. Jacobs, K. R. Lajoie, E. S. Lowell, J. D. Lowell and H. Merrick also reviewed the manuscript and

Received 6 May; accepted 21 July 1982.

1. Bar-Yosef, O. in *After the Australopithecines* (eds Butzer, K. W. & Isaac, G. L.) 571-604 (Mouton, The Hague, 1975).
2. Stekelis, M. *Israel Acad. Sci. Humanities* (1966).
3. Stekelis, M., Bar-Yosef, O. & Schick, T. *Israel Acad. Sci. Humanities* (1969).
4. Tobias, P. V. *Nature* **211**, 130-133 (1966).
5. Haas, G. *Israel Acad. Sci. Humanities* (1966).
6. Tchernov, E. in *The Quaternary of Israel* (ed. Horowitz, H.) Sect. 7 (Academic, New York, 1979).
7. Siedner, G. & Horowitz, A. *Nature* **250**, 23-26 (1974).
8. Horowitz, H. (ed.) *The Quaternary of Israel* (Academic, New York, 1979).
9. Walker, A. & Leakey, R. E. F. *Scient. Am.* **239**(2), 54-66 (1978).
10. Leakey, M. D. *Olduvai Gorge 3. Excavations in Beds I and II, 1960-1963*, 272 (Cambridge University Press, 1971).
11. Howell, F. C. in *Evolution of African Mammals* (eds Maglio, V. J. & Cooke, H. B. S.) 154-248 (Harvard University Press, Cambridge, 1978).
12. Kretzoi, M. *Anthrop. kozl.* **20**, 3-11 (1976).
13. Schaub, S. *Ecol. geol. Helv.* **36**, 270-289 (1943).
14. Fejfar, O. & Heinrich, W.-D. *Ecol. geol. Helv.* **74**, 997-1006 (1981).
15. Prevot, M. & Dalrymple, G. B. *C. r. heb. Séanc. Acad. Sci., Paris* **271**, 2221-2224 (1970).

provided many helpful suggestions. Marion E. Anderson typed the manuscript.

16. Janossy, D. in *After the Australopithecines* (eds Butzer, K. W. & Isaac, G. L.) 375-397 (Mouton, The Hague, 1975).
17. Repenning, C. A. *Can. J. Anthropol.* **1**, 37-44 (1980); *Acta zool. fennica* (in the press).
18. Churcher, C. S. & Hooijer, D. A. *Zoöl. Meded., Leiden* **55**, 265-280 (1980).
19. Mankinen, E. A. & Dalrymple, G. B. *J. geophys. Res.* **84**, 615-626 (1979).
20. Cooke, H. B. S. & Wilkinson, A. F. in *Evolution of African Mammals* (eds Maglio, V. J. & Cooke, H. B. S.) 435-482 (Harvard University Press, Cambridge, 1978).
21. Bar-Yosef, O. & Tchernov, E. *Israel Acad. Sci. Humanities* (1972).
22. Lydekker, R. Q. *Jl. geol. Soc. Lond.* **43**, 161-164 (1887).
23. Vangengeim, E. A. *Acad. Sci. U.S.S.R. Geol. Inst.* (1977).
24. Howell, F. C. in *Early Hominids of Africa* (ed. Jolly, C. J.) 85-130 (Duckworth, London, 1978).
25. Jaeger, J.-J. in *After the Australopithecines* (eds Butzer, K. W. & Isaac, G. L.) 399-418 (Mouton, The Hague, 1975).
26. Cooke, H. B. S. in *African Ecology and Human Evolution* (eds Howell, F. C. & Bouliere, F.) 65-116 (Aldine, Chicago, 1963).
27. Corbet, G. B. *The Mammals of the Palaearctic Region* (British Museum (N.H.), London, 1978).
28. Topachevski, V. O. *Acad. Sci. Ukrain. S.S.R., Inst. Zool.*, 1-164 (1965).
29. Tchernov, E. *Verh. naturf. Ges. Basel* **79**, 161-185 (1968).
30. Kretzoi, M. *Föld. Intézet, Evi jelentesei*, 239-265 (1954).

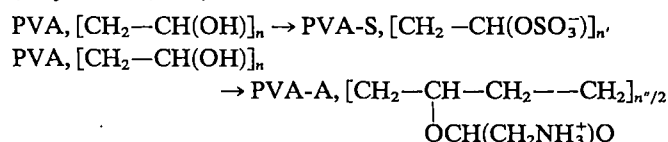
A protective function of the coacervates against UV light on the primitive Earth

Hiroyuki Okihana & Cyril Ponnampuruma*

Laboratory of Chemical Evolution, University of Maryland, College Park, Maryland 20742, USA

Results from simulation experiments in the laboratory support the Oparin-Haldane hypothesis of chemical evolution¹⁻⁴. The organic compounds produced may have accumulated in the primitive sea, constituting the so-called 'primordial soup' of organic molecules. Beyond this primordial stage, however, many developments were required before the emergence of the first cellular organism. The first cell need not necessarily have been a modern cell, complete with a membrane, a chromosome, ribosomes, enzymes, a metabolism, and the property of self-replication; the primary requirement of the protocell would have been the ability to evolve into a complete cell. There are many models of the protocell: for example coacervate droplets⁵⁻⁹, proteinoid microspheres^{10,11}, micelles (lipid vesicles)¹², and marigranules^{13,14}. Of these, the coacervate droplets are of interest as they are dynamic^{6,7} and because their mechanism of formation is perhaps better understood¹⁵⁻¹⁶. Coacervate droplets are essentially small bounded spaces in which the concentration of substances is higher than in the surrounding medium and in which the distribution of the substances differs from that in the solutions. Their essential functions in the protocell model are: (1) selection; (2) concentration; (3) production of hypohydrous effects; (4) interaction; and (5) organization⁵⁻⁹. Here we report another possible function of the coacervate. We added glycine or diglycine to the coacervate system, then irradiated the system with an argon lamp. We report that the coacervate droplets concentrated glycine or diglycine, thus protecting them from decomposition by irradiation. These results suggest a protective function of the coacervate against UV light on the primitive Earth.

Partially sulphated polyvinyl alcohol (PVA-S) and a partially amino-acetylated alcohol (PVA-A) were obtained by the esterification¹⁷ of commercially available polyvinyl alcohol (Polysciences, Inc.):



The products were dialysed against water and deionized by

passage through mixed-bed Rexyn I-300 ion-exchange resin (Fisher Science). The degree of esterification was estimated by conductimetric titration¹⁷. One of the six PVA-A and one of the five PVA-S compounds were used in this study. The molecular weights of the PVAs from which the PVA-A-6 and PVA-S-1 compounds were derived were 3,000 and 78,000, respectively. The degrees of esterification were 4.99 mol % and 34.1 mol %, respectively.

PVA-A-6 and PVA-S-1 were mixed at equal charge density ratio in sodium phosphate buffer (0.025 M, pH 7.5) at room temperature. On mixing of the two compounds, the solution became turbid and coacervate droplets were observed under the microscope. Some of them coagulated into larger ones having vacuoles and others assembled to form colonies.

Glycine or diglycine (0.2 μmol) was added to 1 ml of the system at the time of formation of the coacervate droplets (experiment 1) or after their formation (experiment 2). After incubation for 30 min, the coacervate droplets were separated from the surrounding medium (equilibrium liquid) by low-speed centrifugation (3,000 r.p.m. for 10 min). In experiment 2, the mixture of PVA-A-6 and PVA-S-1 was incubated in buffer for 10 min before the addition of glycine or diglycine. Glycine and diglycine were concentrated more in the coacervate droplets than in the surrounding equilibrium liquid; that is, about three times more for glycine and about twice for diglycine (Table 1). There were no differences between the two experiments. Equilibrium between the coacervate droplets and the equilibrium liquid was completed within the 30 min of incubation.

Concentration of substances from the surrounding medium is one of the most essential functions of the coacervate droplets. The droplets used in this study were the simplest ones, that is, having no membranes at the surface nor any enzymes within. The concentrations of glycine and diglycine achieved must, therefore, be due to their solubilities between the concentrate phase (the coacervate droplets) and the dilute phase (the equilibrium liquid), that is, the partition equilibrium, and not due to any active transport on the part of the coacervate droplets.

As an irradiation source for the photochemical decomposition experiments, a high pressure argon lamp¹⁸ (15 atm; Gianini, Photon Flux) (UV range from $\sim 5 \times 10^{16}$ to 10^{18} with visible range at $\sim 5 \times 10^{18}$ photons cm⁻² s, 50 Å) was used because of the similarity of its spectrum to that of the Sun. The coacervate droplets were separated by low-speed centrifugation, washed once with buffer without both PVA-A-6 and PVA-S-1, and were used in the following experiments. The reaction mixture consisted of 0.025 M sodium phosphate buffer pH 7.5 and 0.5 mM of glycine or diglycine, with or without the coacervate droplets. Quartz cells for UV spectroscopy (1 cm × 1 cm) were used as the irradiation cells. These were attached to an emission window of the argon lamp. The systems were closed with caps, and were gently agitated by convection during the irradiation.

*To whom correspondence should be addressed.

The effects of irradiation on glycine and diglycine are shown in Fig. 1. For the first 2 h, the reaction mixtures were held in the reaction cells without any irradiation; no decomposition occurred. Then the samples containing glycine and diglycine were irradiated for 4 h and 1 h, respectively. In the systems without the coacervate droplets, 84% of the glycine decomposed after 4 h of irradiation (Fig. 1*b*), while 97% of the diglycine decomposed in 1 h (Fig. 1*f*). In the coacervate droplets

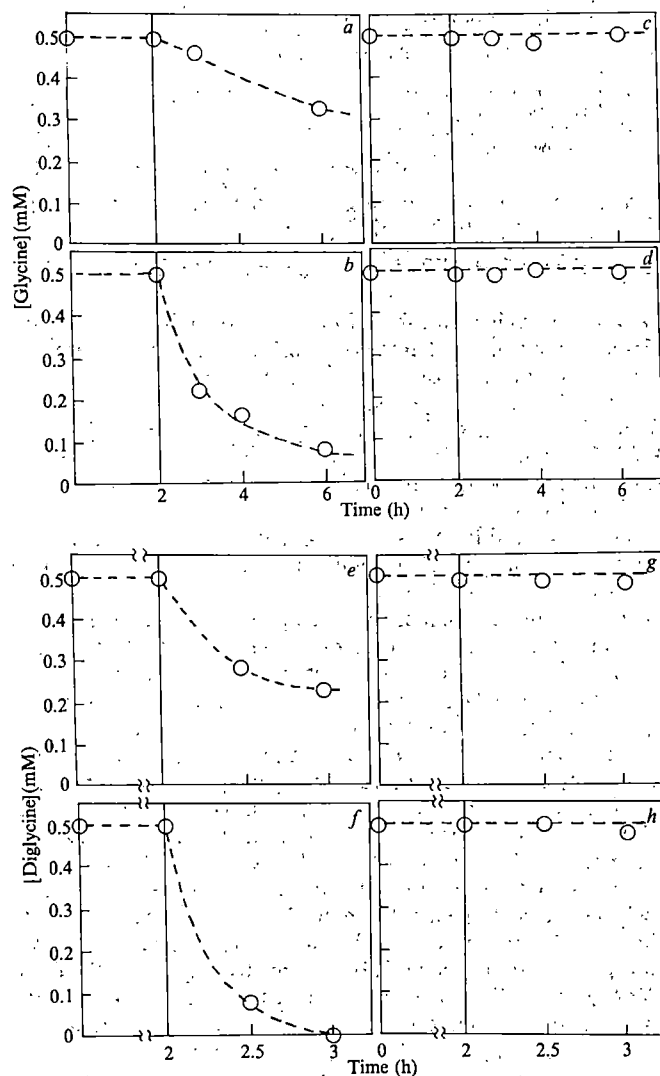


Fig. 1 *a-d*, Time course of glycine irradiation. The concentrations of glycine in the systems were plotted against time. Every sample was kept in the absence of irradiation for the first 2 h. The samples with (*a*) and without (*b*) coacervate droplets were irradiated for 4 h. The same samples with (*c*) and without (*d*) coacervate droplets were also kept in the absence of irradiation. *e-h*, Time course of irradiation of diglycine. Except for the irradiation time, conditions were the same as described for glycine.

systems, 34% of glycine (Fig. 1*a*) and 52% of diglycine (Fig. 1*e*) decomposed within the same periods of irradiation.

The decomposition processes appeared to be those of a first-order reaction (see Fig. 2). The kinetic constants were estimated from the slopes of $\ln(A_0/A_t)$ plotted against time, where A_t and A_0 represent the amounts of reactants at time t and at $t=0$, respectively. The constants for reactions without the coacervate droplets were 0.44 h^{-1} for glycine and 3.5 h^{-1} for diglycine. With the coacervate droplets both constants decreased to 0.093 h^{-1} and 1.8 h^{-1} for glycine and diglycine, respectively.

The products of the diglycine solution were analysed after 1 h of irradiation. The analyser was equipped with a normal ninhydrin detection system so that only compounds containing an NH_2 group were detected. As judged from the retention time, 0.24 mM of diglycine, 0.16 mM of methylamine, 0.071 mM of ammonia and 0.029 mM of α -aminobutyric acid were detected in the case of the coacervate droplets system, and 0.015 mM of diglycine, 0.11 mM of methylamine, 0.061 mM of ammonia and 0.026 mM of α -aminobutyric acid were detected in the absence of the coacervate droplets system. There were no peaks at the position of glycine. Some other small peaks were present which have not been identified. The photochemical products of diglycine are quite different from the thermal hydrolysed ones.

Although the detailed photochemical mechanisms are unknown, the coacervate droplets protected glycine and digly-

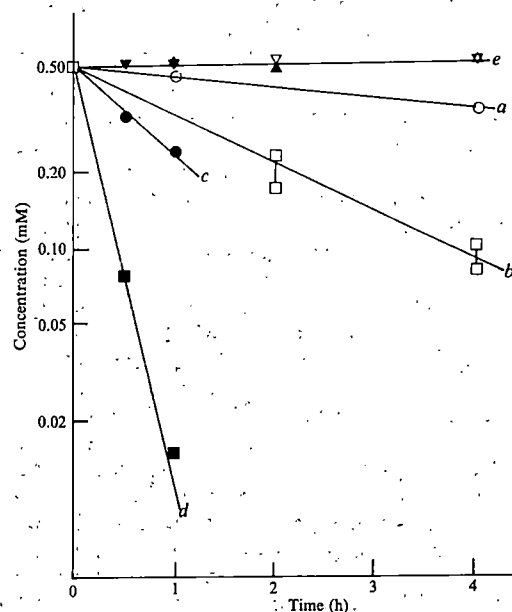


Fig. 2 Semi-log plots of the reactions. *a*, Glycine, with coacervate droplets; *b*, glycine without coacervate droplets; *c*, diglycine with coacervate droplets; and *d*, diglycine without coacervate droplets (shown in Fig. 1*a*, *b*, *e*, and *f*, respectively). Line *e* represents all the experiments without irradiation. Δ , Gly; \blacktriangle , gly with coacervate; \star , digly; \star , digly with coacervate.

Table 1 Concentrations of glycine and diglycine in the experimental systems

Equilibrium liquid					Coacervate droplets			
		Concentration (mM)	Volume (ml)	amount (μmol)	Concentration (mM)	Volume (ml)	amount (μmol)	Concentration ratio
Expt 1	Gly	0.164 ± 0.02	0.87	0.143	0.435 ± 0.01	0.13	0.057	2.7
	(Gly) ₂	0.169 ± 0.02	0.82	0.139	0.340 ± 0.1	0.18	0.061	2.0
Expt 2	Gly	0.167 ± 0.02	0.89	0.149	0.479 ± 0.06	0.11	0.053	2.9
	(Gly) ₂	0.171 ± 0.01	0.84	0.144	0.356 ± 0.01	0.16	0.057	2.1

Glycine or diglycine ($0.2 \mu\text{mol}$) were added to the systems (1) at the time of coacervate formation or (2) after their formation. Total volume of each of the systems was 1 ml. Amounts of glycine or diglycine are the product of the concentration and the volume.

cine from decomposition by irradiation. There are two possible explanations for this effect: (1) the coacervate droplets concentrated glycine or diglycine from the surrounding medium. These concentrated substances would be much less susceptible to irradiation, decomposing considerably less than those in the homogeneous solution or in the surrounding medium. (2) The coacervate droplets screened light, because transmitted light through the coacervate system was much less intensive than that through the homogeneous solution. Glycine and diglycine even in the surrounding medium were decomposed less than in the homogeneous solution. Thus, equilibrium is established between the coacervate droplets and the surrounding medium. As the decomposition of glycine or diglycine in the surrounding medium occurs, these substances are released from the coacervate droplets into the surrounding medium and vice versa.

We do not propose that the very same molecules as the

synthetic polyelectrolytes used here might have existed in the primitive sea, but they represent compounds having similar molecular weight and charge density. The molecular weights and charge densities of PVA-S-6 and PVA-S-1 are similar to those of some proteins, and of DNA or RNA. It is reasonable to assume that polyelectrolytes in the primitive sea, such as oligonucleotide-like polymers and oligopeptide-like polymers could have interacted much like the synthetic ones used in this study.

Water in the primitive sea has been said to protect the ingredients in the primordial soup from decomposition by irradiation. The coacervate droplets enhanced this effect and also selectively concentrated these ingredients. This function might have been one of the most important attributes of primitive microsystems, leading to further development and ultimately to the first living organism.

Received 20 April; accepted 16 June 1982.

1. Miller, S. L. *Science* **117**, 528–529 (1953).
2. Ponnampetuma, C. *Cosmochemistry* (ed. Milligan, W. O.) 137–197 (Robert A. Welch Foundation, Houston, 1978).
3. Miller, S. L. & Orgel, L. E. *The Origins of Life on the Earth* (Prentice-Hall, New Jersey, 1974).
4. Dillon, L. S. *The Genetic Mechanism and the Origin of Life* Ch. 1 (Plenum, New York, 1974).
5. Bungenberg de Jong, H. G. *Colloid Science* Ch. 10 (Elsevier, Amsterdam, 1949).
6. Oparin, A. I. *The Origin of Life* (Macmillan, New York, 1938).
7. Evreinova, T. N. *Coacervates* (Kyoritsu, Tokyo, 1974).
8. Mizutani, H., Okihana, H., Hasegawa, M., Yano, T. & Noda, H. *The Origin of Life and Evolutionary Biochemistry* (eds Dose, K., Fox, S. W., Deborin, G. A. & Pavlovskaya, T. E.) 339–354 (Plenum, New York, 1974).
9. Noda, H., Mizutani, H. & Okihana, H. *Origins of Life* **6**, 139–146 (1975).
10. Fox, S. W., Harada, K. & Kendrick, J. *Science* **129**, 1221–1223 (1959).
11. Fox, S. W. *The Origins of Prebiological Systems and of Their Molecular Matrices* (ed. Fox, S. W.) 361–373 (Academic, New York, 1965).
12. Goldacre, R. J. *Surface Phenomena in Chemistry and Biology* (eds Danielli, J. R., Pankhurst, K. G. A. & Riddiford, A. C.) 276–278 (Pergamon, London, 1958).
13. Yanagawa, H. & Egami, F. *Proc. Japan Acad.* **53**, 42–45 (1977).
14. Okihana, H. *Viva Origino* **8**, 19–22 (1979).
15. Okihana, H. & Noda, H. *Origin of Life* (ed. Noda, H.) 375–383 (Japan Scientific Press, Tokyo, 1978).
16. Tainaka, K. *Biopolymers* **19**, 1289–1298 (1980).
17. Okihana, H. & Nakajima, A. *Bull. Inst. chem. Res.* **54**, 63–71 (1976).
18. Rushbrook, P., Ponnampetuma, C. & Reinisch, R. F. *Abstr. Pacific Conf. Chemistry and Spectroscopy*, Am. Chem. Soc. Meet., San Francisco (1970).

Phenotypic evolution in a poorly dispersing snail after arrival of a predator

Geerat J. Vermeij

Department of Zoology, University of Maryland, College Park, Maryland 20742, USA

The phenotypic stability of many species in the face of changing conditions suggests that adaptive evolution can occur only under limited circumstances. One of the necessary conditions may be the lack of genetic mixing between dispersed populations inhabiting different environments. Intertidal molluscs on the east coast of North America between Cape Cod and Nova Scotia were exposed to an increase in the abundance of shell breaking predators when the green crab *Carcinus maenas* spread gradually northward from Cape Cod in the first half of the twentieth century¹. The periwinkle *Littorina littorea*, which produces larvae that become widely dispersed, did not show an increase in shell thickness as an adaptation to shell-breaking predation¹. However, I show here that the dog whelk *Nucella lapillus*, which is poorly dispersed in the bottom-dwelling juvenile phase, did adapt phenotypically after establishment of the green crab. This suggests that phenotypic stasis and gradual change are alternative responses depending on the degree of genetic mixing between populations.

Experiments show that *N. lapillus* co-occurring with predaceous crabs have slender, heavy, strong shells with a small aperture and a thick adult outer lip, whereas individuals from sites without crabs have thinner, weaker, stouter shells with a broader aperture and a thinner adult lip^{2–4}. Comparisons among populations further show that the degree of development of breakage-resistant traits is greatest where the abundance and strength of predators are greatest^{3,4}. Although shell shape is influenced by food availability and is size-dependent^{5–7}, it is at least in part determined genetically⁸. If *N. lapillus* was affected by the arrival of the green crab and if it responded adaptively to this change, spire height (shell height divided by aperture height) and mean adult lip thickness would be expected to increase through time.

Proof that the establishment of the green crab north of Cape Cod represented an increase in the importance of breakage as a component of selection in *N. lapillus* comes from data on the incidence of repaired shell injuries. The presence of a repaired injury provides evidence that the gastropod encountered a shell-breaking agent and that the shell was sufficient to withstand the agent's attack^{9,10}. The frequency of repaired injury (number of scars per shell) is probably an underestimate of the incidence of unsuccessful attack by shell-breaking agents in *N. lapillus*, because the thick lip of the adult may remain undamaged after an attack, so that no record of the encounter is preserved¹⁰. An increase in the frequency of repaired injury through time would mean that a greater proportion of individuals was exposed to potential selection in favour of resistance to breakage.

I examined 44 samples of *N. lapillus* (US National Museum of Natural History, Washington; Academy of Natural Sciences, Philadelphia; Museum of Comparative Zoology, Harvard University, Cambridge; and personal collections) from sites between Cape Cod and Halifax, the current northern limit of the green crab in North America¹¹. Samples were designated as pre-*Carcinus* or post-*Carcinus* depending on whether they were collected before or after the first known occurrence of the green crab at the locality in question^{12–14}. The 22 post-*Carcinus* samples were collected a minimum of 7 years after the arrival of the green crab. Scars resulting from repaired breaks of the outer lip were counted on the last whorl of each shell. The frequency of scars (Table 1) rose from 0.025 ± 0.021 in pre-*Carcinus* samples to 0.044 ± 0.028 in post-*Carcinus* samples ($P < 0.006$, one-tailed Mann-Whitney *U*-test). Scars increased in frequency at each of six sites where both pre-*Carcinus* and post-*Carcinus* samples were available.

N. lapillus evidently responded adaptively to the arrival of the green crab north of Cape Cod. Spire height increased from 1.385 ± 0.039 to 1.412 ± 0.061 ($P < 0.02$), and mean adult lip thickness increased from 1.92 ± 0.54 to 2.15 ± 0.49 ($P < 0.05$) after the appearance of the green crab (Table 1). At sites where both pre-*Carcinus* and post-*Carcinus* samples were available, spire height and lip thickness either increased (three sites) or remained about the same (three sites). These changes were not associated with a general increase in body size, and occurred despite the probable action of such other selective agents as wave surge^{2,15}, visual predators^{16–18} and parasites¹⁹.

Table 1 Differences in *N. lapillus* collected before and after the arrival of the green crab

Locality and date	n	Frequency of repaired injury	Adult shell slenderness	Adult lip thickness
Pre-Carcinus samples				
Beverly Farms, Massachusetts, 1876	60	0.017	1.365	1.86
Harborsville, Nova Scotia, 1850s	27	0.037	1.334	2.33
Isle Au Haut, Maine, 1897	143	0.014	1.347	1.20
Eastport, Maine, 1872	41	0.024	1.390	2.01
Eastport, Maine, before 1918	33	0.060	1.405	1.24
St George, Maine, 1863	51	0.020	1.385	2.56
Island near Rockland, Maine, 1912	59	0.018	1.411	2.24
Kittery, Maine, 1877	56	0.036	1.380	2.84
Castine, Maine, 1878	50	0.020	1.359	1.20
Salem, Massachusetts, 1870s	64	0	1.472	2.16
Peak's Island, Maine, 1873	160	0.044	1.416	2.30
Ten Pound Island, Massachusetts, 1878	40	0.025	1.413	2.00
Newcastle, New Hampshire, 1877	36	0.028	1.368	1.60
Beverly Bridge, Massachusetts, 1870s	36	0.056	1.454	2.28
Grand Manana, New Brunswick, 1920	95	0.032	1.370	1.04
Blue Hill Bay, Maine, 1915	167	0.036	1.403	2.24
Gloucester, Massachusetts, before 1900	17	0	1.337	1.76
Mount Desert, Maine, around 1920	374	0.017	1.309	2.26
St Andrews, New Brunswick, 1920	157	0.038	1.369	0.94
Wells, Maine, 1915	19	0.053	1.375	2.62
Islesboro, Maine, 1894	17	0	1.423	1.50
Somes Sound, Maine, around 1920	373	0.011	1.390	2.44
Post-Carcinus samples				
Kennebunkport, Maine, 1925	44	0.070	1.392	2.32
Cape Neddick, York, Maine, 1951	74	0.066	1.320	1.44
St Andrews, New Brunswick, 1963	79	0.051	1.408	1.44
Kittery, Maine, 1951	85	0.048	1.449	2.86
Biddeford, Maine, 1938	36	0.083	1.400	2.28
Squirrel Island, Maine, 1971a	13	0	1.344	1.21
Squirrel Island, Maine, 1971b	11	0.091	1.527	2.50
Harbourville, Nova Scotia, 1960	40	0.075	1.513	2.86
Lincolntonville, Maine, 1941	62	0.016	1.424	1.46
North Weymouth, Massachusetts, 1914	21	0.14	1.473	2.44
Salisbury Bay, New Brunswick, 1957	21	0.048	1.475	2.26
Gloucester, Massachusetts, 1925	107	0.036	1.324	2.54
Queensland, Nova Scotia, 1960	68	0.044	1.499	2.00
Marblehead, Massachusetts, 1927	78	0.013	1.415	2.70
Lynn, Massachusetts, 1938	15	0.067	1.456	1.56
Lawrencetown, Nova Scotia, 1960	44	0	1.312	2.36
Kelly's Cove, Nova Scotia, 1959	68	0.044	1.396	2.32
Alma, New Brunswick, 1960	31	0	1.422	2.50
Ogunquit, Maine, 1941	53	0.038	1.435	1.62
Eastport, Maine, 1981	50	0.040	1.399	1.72
Nahant, Massachusetts, 1981	65	0.091	1.431	2.90

n, Number of shells in the sample.

Insufficient material of *N. lapillus* was available to test whether shell shape and frequencies of repair remained constant over time in Canada north of the range of the green crab. For *L. littorea*, however, both shell thickness and the frequency of repair have remained the same over at least the last 100 years¹. Although the arrival of the green crab was associated with an increase in the frequency of repair in both *L. littorea* and *N. lapillus*, only the latter species showed signs of adaptive phenotypic change. These results suggest that genetic mixing was in part responsible for phenotypic stasis, and support the view²⁰ that limited dispersal permits relatively rapid evolutionary change. They also point to the importance of monitoring

the phenotypes of species as major changes in the biological environment are being brought about by man.

Received 11 May; accepted 3 August 1982.

- Vermeij, G. J. *Evolution* **36**, 561-580 (1982).
- Kitching, J. A., Muntz, L. & Ebling, F. J. *J. Anim. Ecol.* **35**, 113-126 (1966).
- Hughes, R. N. & Elner, R. W. *J. Anim. Ecol.* **48**, 65-78 (1979).
- Currey, J. D. & Hughes, R. N. *J. Anim. Ecol.* **51**, 47-56 (1982).
- Moore, H. B. *J. mar. Biol. Ass. U.K.* **21**, 61-89 (1936).
- Spight, T. M. *J. exp. mar. Biol. Ecol.* **13**, 215-228 (1973).
- Phillips, B. F., Campbell, N. A. & Wilson, B. R. *J. exp. mar. Biol. Ecol.* **11**, 27-69 (1973).
- Largen, M. D. *Proc. Malac. Soc.* **39**, 383-388 (1971).
- Vermeij, G. J. *Malacologia* **23**, 1-12 (1982).
- Vermeij, G. J., Schindel, D. E. & Zipser, E. *Science* **214**, 1024-1026 (1981).
- Bousfield, E. L. & Laubitz, D. R. *Nat. Mus. Canada Publ. Biol. Oceanogr.* **5**, 1-51 (1972).
- Dow, R. L. & Wallace, D. E. *Fish. Circ.* **8**, Bull. Dept Sea Shore Fish., Augusta, Maine, 11-15 (1952).
- Scattergood, L. W. *Fish. Circ.* **8**, Bull. Dept Sea Shore Fish., Augusta, Maine, 2-10 (1952).
- Welch, W. R. *Fish. Bull.* **67**, 337-345 (1968).
- Berry, R. & Crothers, J. H. *J. Zool.* **155**, 5-17 (1968).
- Colton, H. S. *Ecology* **3**, 146-157 (1922).
- Berry, R. J. & Crothers, J. H. *J. Zool.* **162**, 293-302 (1970).
- Berry, R. J. & Crothers, J. H. *J. Zool.* **174**, 123-148 (1974).
- Feare, C. J. *Bird Study* **18**, 121-129 (1971).
- Scheltzema, R. S. *Marine Organisms* (eds Battaglia, B. & Beardmore, J. A.) 303-322 (Plenum, New York, 1978).

A molecular explanation of frequency-dependent selection in *Drosophila*

Yousef Haj-Ahmad

Department of Biological Sciences, Brock University, St Catharines, Ontario, Canada L2S 3A1

Donal A. Hickey

Department of Biology, University of Ottawa, Ottawa, Ontario, Canada K1N 6N5

Frequency-dependent selection provides a means for maintaining genetic variability within populations, without incurring a large genetic load^{1,2}. There is a wealth of experimental evidence for the existence of frequency-dependent changes in genotypic fitness among a wide variety of organisms. Examples of traits which have been shown to be subject to frequency-dependent selection include the self-incompatibility alleles of plants³, chromosomal rearrangements in *Drosophila*⁴, visible mutations⁵, enzyme variants⁶⁻¹¹ and rare-male mating advantage in *Drosophila*¹²⁻¹⁴. These experiments have been interpreted in a number of different ways¹⁵. Principally, frequency dependence of genotype fitness may result from intergenotype facilitation due to the production of biotic residues¹⁶⁻²⁰, or from the differential use of resources by the competing genotypes²¹. However, it has proved extremely difficult to isolate and identify any biotic residue of importance or, alternatively, to understand the manner in which genotypes partition the environment. Thus, the difficulty in the interpretation of experiments which show frequency-dependent selective effects stems largely from our lack of understanding of the exact physiological mechanisms which produce these frequency-dependent effects². The principal aim of this study was to investigate the mechanisms associated with frequency-dependent selection at the amylase locus in *Drosophila melanogaster*. The excretion of catalytically active amylase enzyme and its effects on food medium composition were correlated with the outcome of intraspecific competition between amylase-deficient and amylase-producing genotypes. Amylase-producing genotypes were shown to excrete enzymatically active amylase protein into the food medium. The excreted amylase causes the external digestion of dietary starch; this accounts for the frequency-dependent increase in the viability of the amylase-deficient mutants in mixed cultures, maintained on a starch-rich diet.

The results described here involved two homozygous amylase genotypes, one which produces active amylase enzyme, *Amy*¹ (refs 22, 23); and another which has no detectable amylase activity, *Amy*^{null} (Haus and Hickey, unpublished data). Our

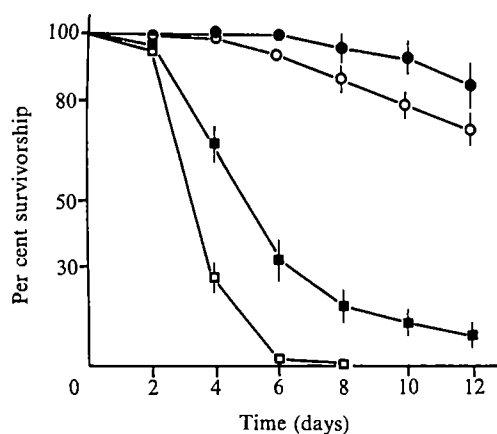


Fig. 1 Relationship between initial frequency and per cent survivorship of *Amy*^{null} flies, when grown in mixed culture with individuals of the *Amy*¹ genotype. Culture vials (8 dram shell vials) contained 15 ml of a starch-rich medium (8% soluble starch+0.5% killed brewer's yeast). In mixed cultures, genotypes were usually identified by an association with visible genetic markers (*curved* wings and *Lobe* eyes). Experiments were repeated using reversed marker associations, to eliminate the possibility of marker effects. Initially, a total of 100 one-week-old flies were added to each vial. Dead flies were removed every 24 h. Survivors were transferred to fresh vials every 48 h. Initial *Amy*^{null} frequencies were: 1.0 (□), 0.9 (■), 0.6 (○) and 0.1 (●). These data represent the means of seven replicate experiments. Bars indicate s.e.m.

prediction was that the *Amy*^{null} flies would be unable to use dietary starch as an energy source. This prediction was tested by measuring the viability of adult flies of both genotypes at 2-day intervals over a 12-day period. Three different dietary regimes were used: one food medium containing 8% starch; a second medium containing 8% glucose in place of starch; and a third medium containing no carbohydrate. Table 1 shows the per cent survivorship recorded on day 12 of the experiment. The survivorship of both genotypes on the food which contained glucose was over 95%; the survivorship of both strains in the absence of all carbohydrates was less than 1%. This indicates that the dietary sugar is essential for the survival of both genotypes. When dietary sugar was replaced by starch, the survivorship of the *Amy*¹ homozygotes remained high (over 90%) but the survivorship of the *Amy*^{null} genotype fell to zero (Table 1). Thus, as expected, the *Amy*¹ flies can use dietary starch as an energy source, but the *Amy*^{null} individuals are unable to do so.

The next set of experiments followed the same general procedure as outlined above, but the two genotypes were main-

Table 1 Per cent survivorship of two amylase genotypes on three food media

Genotype	Food type		
	Glucose (8%)	No carbohydrate	Starch (8%)
<i>Amy</i> ¹	96.0±1.1	0.2±0.1	92.1±1.9
<i>Amy</i> ^{null}	96.3±1.3	0	0

All foods contained 0.5% killed brewer's yeast and 0.8% propionic acid (as a mould inhibitor), and 1.5% agar. In these conditions of dietary deprivation (low yeast) the supplementary carbohydrates were essential for survival. In contrast, in the presence of high levels of yeast (5%), the survivorship of both strains in the absence of supplementary carbohydrates was quite high. Before the experiments were begun, all flies were aged for one week on a nutritionally rich diet (5% killed yeast, 10% sucrose). All cultures were maintained in 8 dram shell vials at 25 °C. Experiments were initiated with 100 one-week-old flies of each genotype. Dead flies were removed every 24 h and survivors were transferred to a fresh medium every 48 h. Data represent survivorship on day 12 of the experiment. Each value represents the mean of 10 replicate experiments ± s.e.m.

tained in mixed rather than pure cultures. Figure 1 shows that the survivorship of *Amy*^{null} on starch food in mixed culture was greater than in pure cultures, with survivorship increasing as the initial frequency of the *Amy*^{null} genotype decreased; that is, the fitness of the *Amy*^{null} genotype in mixed cultures shows a pattern of negative frequency dependence. However, at low frequency, the *Amy*^{null} survivorship only approaches that of *Amy*¹, but does not surpass it. The survivorship of *Amy*¹ flies in mixed culture was high, and comparable with that seen in pure cultures, regardless of the initial genotype frequencies; therefore, one would not expect that this particular example of frequency-dependent selection would result in a stable genetic polymorphism. The high survivorship of the *Amy*¹ flies in all conditions indicates that the general level of competition must be rather low.

As the survival of the *Amy*^{null} genotype depends on the availability of dietary sugar (Table 1), it seemed likely that sugar was being made available to these flies in mixed cultures fed dietary starch. This hypothesis was tested directly by assaying the free sugar concentration in a food medium containing 8% added starch, after it had been exposed to varying numbers of amylase-producing flies. Figure 2 shows that as the number of *Amy*¹ flies was increased, the sugar content of the food medium also increased. Therefore, when the frequency of the *Amy*^{null} genotype was low in mixed cultures and the frequency of the *Amy*¹ genotype was correspondingly high, the sugar content of the starch containing medium was elevated. This explains the frequency-dependent survival of the *Amy*^{null} flies in mixed cultures (Fig. 1).

Amylase-producing flies may modify their environment by either direct excretion of sugars or excretion of active amylase which, in turn, causes the external digestion of starch. Amylase activity was measured at the surface of a medium exposed to *Amy*¹ males for 48 h. A significant amount of amylase activity (about 20% of that recorded in the flies themselves) was detected. We cannot deduce the actual rate of amylase excretion, however, as we do not know the stability of the enzyme over the 48-h period. There was no detectable increase in the amylase activity of food media which were exposed to *Amy*^{null} flies.

Finally, we checked that the external amylase activity that was associated with amylase-producing genotypes was indeed *Drosophila* amylase, and not due to microbial contamination.

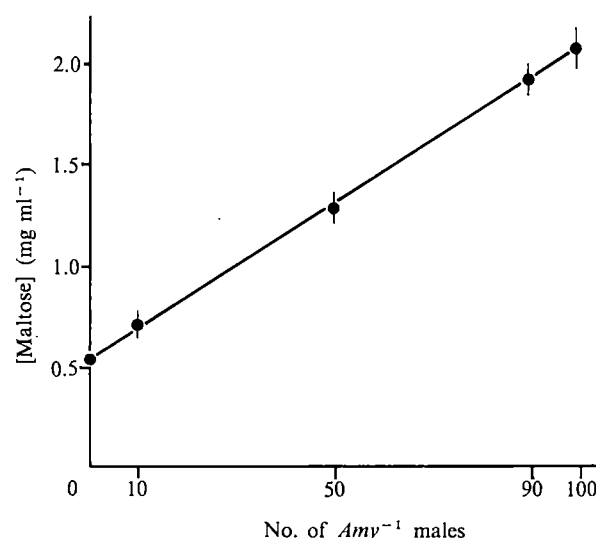


Fig. 2 Relationship between sugar concentration in the food medium and exposure to amylase producing flies (genotype *Amy*¹). The food medium contained 8% soluble starch and 0.5% killed brewer's yeast. Varying numbers of flies (males only) were maintained on the medium for 48 h. Sugar concentration is expressed in maltose equivalents, as measured by the DNSA assay²⁴. Values given are the means of 12 replicate experiments. Bars indicate s.e.m.

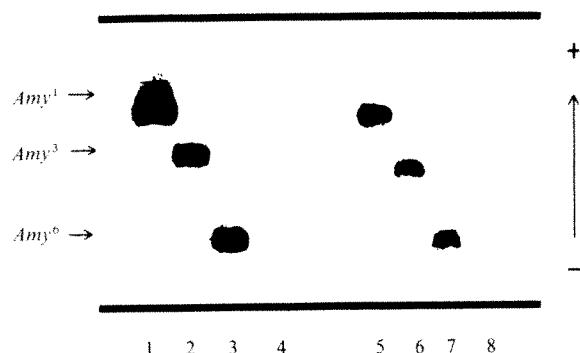


Fig. 3 Comparison of electrophoretic patterns for four amylase genotypes and the enzymes which were recovered from their respective substrates. One hundred males (one week old) were maintained in clean glass vials for 10 h. At the end of this period flies were homogenized and the excretion recovered in 0.4 ml of electrophoresis buffer. Samples of both the crude fly homogenates and their respective excretions were electrophoresed in vertical polyacrylamide gels. Gels were incubated in a starch solution and stained with iodine-potassium-iodide to visualize amylase activity²³. Electromorph designations are indicated to the right of the figure. Gel samples 1 to 4 are homogenates of *Amy*¹, *Amy*³, *Amy*⁶ and *Amy*^{null} flies, and samples 5 to 8 are their respective excretions. This is a negative print of a gel photograph.

This was done by electrophoresis of a number of electrophoretically distinct amylase variants; flies of each genotype were homogenized and electrophoresed along with a sample of the associated food medium. It can be seen that, in each case, the amylase which was recovered from the substrate was electrophoretically identical to that of the flies maintained on this substrate (Fig. 3). Therefore, it seems that the modification of the starch-containing medium by the amylase-producing flies is due to the excretion of active enzyme molecules. Thus, the enzymatic products of one genotype positively enhances the survivorship of the other genotype which lacks this enzyme.

In summary, frequency-dependent selection is a potentially powerful mechanism for the maintenance of genetic polymorphism^{1,2}. However, as pointed out by Clarke², despite the success of many researchers in detecting frequency-dependent selection and the power of that selective mode in maintaining genetic variations, the mechanisms involved are still largely unknown. The results presented here provide a unique example of a noncompetitive intergenotype interaction, one which has a frequency-dependent effect on the viability of one of the genotypes and one where we fully understand the underlying physiological mechanisms. However, the particular form of frequency-dependent selection discussed here will not necessarily maintain a polymorphism, because the fitness of the null allele is always less than, or equal to, the fitness of the wild-type amylase-producing allele.

We thank Dr Winifred Doane for providing the *Amy*¹ stock. Financial support was provided by a grant from NSERC, Canada. Y.H.-A. was the recipient of an Ontario Graduate Scholarship.

Received 5 May; accepted 13 July 1982.

- Lewontin, R. C. *The Genetic Basis of Evolutionary Change* 256-260 (Columbia University Press, New York, 1974).
- Clarke, B. C. *Proc. R. Soc. B* **205**, 453-474 (1979).
- Mather, K. *Genetical Structure of Populations* (Chapman and Hall, London, 1973).
- Levene, H., Pavlovsky, O. & Dobzhansky, T. *Evolution* **8**, 335-349 (1954).
- Clarke, B. *Heredity* **24**, 347-352 (1969).
- Kojima, K. & Huang, S. L. *Evolution* **26**, 313-321 (1972).
- Kojima, K. & Tobari, Y. N. *Genetics* **61**, 201-209 (1969).
- Nassar, R. *Genetics* **91**, 327-338 (1979).
- Snyder, M. & Ayala, F. J. *Genetics* **92**, 995-1003 (1979).
- Tosic, M. & Ayala, F. J. *Genetics* **97**, 679-701 (1981).
- Morgan, P. *Nature* **263**, 765-766 (1976).
- Petit, C. *Bull. Biol. Fr. Belg.* **92**, 248-329 (1958).
- Ehrman, L. *Am. Nat.* **101**, 415-424 (1967).
- Spies, E. B. *Am. Nat.* **102**, 363-379 (1968).
- Ayala, F. J. & Campbell, C. A. *Rev. ecol. Syst.* **5**, 115-138 (1974).

- Lewontin, R. C. *Evolution* **9**, 27-41 (1955).
- Ayala, F. J. *Science* **171**, 820-824 (1971).
- Dolan, M. & Robertson, A. *Heredity* **35**, 311-316 (1975).
- Bos, M. *Evolution* **33**, 768-771 (1979).
- Caligari, P. D. S. *Heredity* **45**, 219-231 (1980).
- Ayala, F. J. *Am. Sci.* **60**, 348-357 (1972).
- Doane, W. W. J. *exp. Zool.* **171**, 321-341 (1969).
- Hickey, D. A. *Biochem. Genet.* **19**, 783-793 (1981).
- Noelting, G. & Bernfield, P. *Helv. chim. Acta* **31**, 286-290 (1948).

Analysis of discrimination mechanisms in the mammalian olfactory system using a model nose

Krishna Persaud & George Dodd

Warwick Olfaction Research Group, Department of Chemistry and Molecular Sciences, University of Warwick, Coventry CV4 7AL, UK

Olfaction exhibits both high sensitivity for odours and high discrimination between them¹. We suggest that to make fine discriminations between complex odorant mixtures containing varying ratios of odorants without the necessity for highly specialized peripheral receptors, the olfactory systems makes use of feature detection using broadly tuned receptor cells organized in a convergent neurone pathway. As a test of this hypothesis we have constructed an electronic nose using semiconductor transducers and incorporating design features suggested by our proposal. We report here that this device can reproducibly discriminate between a wide variety of odours, and its properties show that discrimination in an olfactory system could be achieved without the use of highly specific receptors.

The morphology of the olfactory system in mammals is remarkably homogeneous² (Fig. 1). Typically, the sensing mucosa has some tens of millions of sensing cells, which act as the primary neurones and synapse with the secondary neurones in the olfactory bulb. The receptor cells in all mammals show a small range of variation, are broadly tuned and respond to a wide variety of odorant types². Cells responding to a single class of odours, for example musks, have not been found. The molecular transducers have not been identified; the sensory

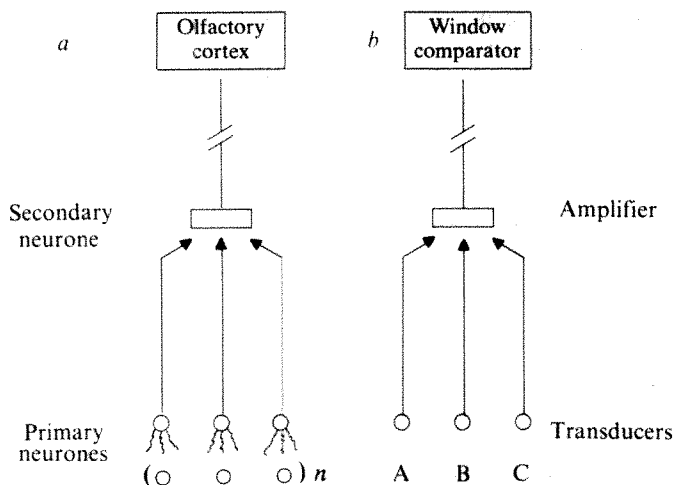


Fig. 1 Diagrammatic comparison of the mammalian olfactory system and the model nose. *a*, Olfactory system. The sensing cells are the ciliated primary neurones. The axons of these neurones pass back through the cribriform plate into the olfactory bulb where they synapse with the secondary neurones, the mitral cells. The signal from the mitral cells passes through the higher olfactory pathways into the olfactory cortex. There is a striking convergence in the peripheral pathway; the ratio of primary to secondary neurones is of the order of $2 \times 10^4:1$. *b*, Model nose. The sensing elements are semiconductor devices with overlapping odorant response distributions. The amplifier, an analogue of the secondary neurone, measures the ratio of the response of selected transducers using a defined algorithm. The signal passes to the window comparator and associated memory circuits. A particular type of odour activates a designated light-emitting diode.

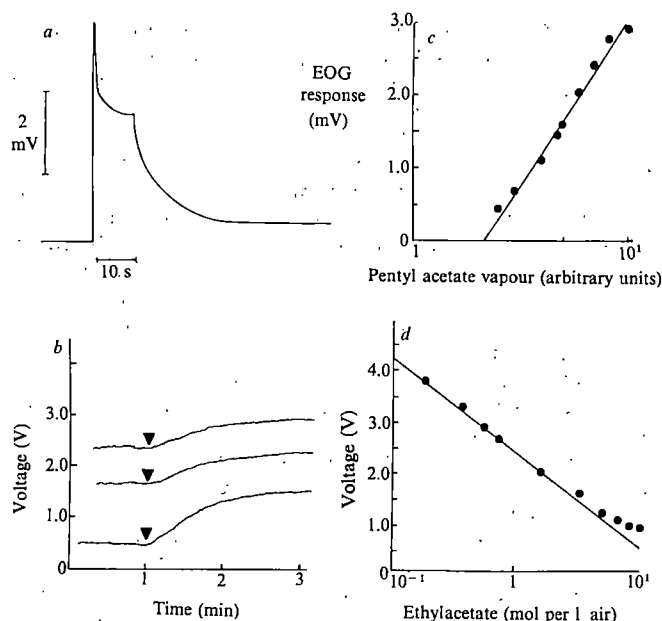


Fig. 2 Comparison of the response characteristics of the olfactory system and model nose. *a*, The summated receptor potential (electro-olfactogram) in olfactory mucosa to a square-wave pulse of pentyl acetate. The electro-olfactogram was recorded as described previously²¹. *b*, The voltage change of a Figaro 812 semiconductor gas sensor in response to the odorant ethyl trimethylacetate. The sensor was located at the top of a 5 l flask immersed in a water bath at 25 °C. The humidity in the flask was maintained at 100% and the air in the flask was mixed using a paddle stirrer. The odorant, 0.1 µl, was injected into the flask through a glc septum using a Hamilton syringe and vaporized in these conditions. Time of injection is marked ▼. *c*, The electro-olfactogram from sheep olfactory mucosa as a function of odorant concentration. The odorant was pentyl acetate. The odorant was delivered using a precision olfactometer and the odorant concentration was determined using a flame ionization detector as previously described^{21,22}. Ten-second odour pulses with a pulse interval of 2 min were used. In these conditions, there was no adaptation of the response. An ascending concentration series was used to avoid adaptation. *d*, The voltage response of the Figaro 812 sensor as a function of odorant concentration. The response was measured as described in *b*, using an ascending concentration series. Sufficient time was allowed for the response to reach the plateau region (see *b*).

membranes contain many particles which may be receptor proteins³. On average, 10–20,000 primary neurones synapse with a single secondary neurone. The secondary neurones show a fairly specific response to odour classes but the response specificities of the primary neurones connected to any particular secondary neurone are unknown. There are other neurone types in the olfactory bulb which cross-connect the secondary neurones.

It is clear that the discrimination properties of the olfactory system are a property of the system as a whole. The higher centres process the pattern of signals from lower centres and the pattern is used to encode a particular type of odour. It should be possible to stimulate this process using some of the principles of pattern classification which have come from studies on artificial intelligence^{4–6}. Extensive mathematical modelling of pattern recognition systems has been carried out^{4,5} and a specific model for the recognition of chemical stimuli has been formulated⁷.

To construct an electronic model olfactory system, we have selected two fundamental characteristics of all mammalian olfactory systems: (1) the odorant detectors, the primary neurones, respond to a wide range of chemical types; and (2) the output from the detectors is processed in a convergent feature detection system which has, at least in part, parallel feature detection. Thus, we have made the following assumptions for the design of an electronic nose which can learn to discriminate between smells: there is no requirement for odour-specific transducers; and the ratio of the signals from the transducers can be processed to identify an odour.

The electrical response of the primary neurones (R) is proportional to the logarithm of the odorant concentration, $[O]$, over a range of concentrations (Fig. 2c) and can be described by the equation

$$R = \alpha \log [O] \quad (1)$$

where α is the odorant constant and is characteristic of a particular odorant. Because the neurones are generalist detectors in a parallel detection system, the generator potential of the receptor cells must contain information about both the quality and intensity of an odour and this information must be encoded in the odour constant, α . The information on odour quality can be separated from that on odour intensity by an analysis of the ratios of the responses from the transducers. The simple method we have selected for the nose is described in Fig. 3. This shows the hypothetical frequency distribution of the responses of a sensing cell to different odours. Such a distribution has not been measured, both because of technical difficulties arising in recording from the small olfactory neurones and because of the lack of an appropriate physico-chemical parameter for the abscissa in this type of plot. The actual distributions may be non-gaussian and multi-modal. The odorants giving the maximum response for a cell may have the optimum fit to the binding sites on the sensory membranes and such odorants may be regarded as 'primary' odorants.

In the example shown (Fig. 3), the two transducers have overlapping response distributions and respond differentially to the two odorants. The ratio of the responses of each transducer (T) towards the two odorants is given by the expression

$$\frac{T_1}{T_2} = \frac{R_1/R_2}{R_4/R_3} = \frac{\alpha_1 \log [O]_A}{\alpha_2 \log [O]_B} = \beta \quad (2)$$

Table 1 Response of the artificial nose to a wide variety of odours

α , Odorant	Selectivity constants using the following pairs of transducers:		
	812/813	812/817	711/813
Isojasnone	0.12	1.58	—
Undecanaldehyde	0.13	1.85	—
Methanol	0.14	1.60	—
Clove bud oil	0.18	1.68	—
Rose oil (synthetic)	0.23	1.49	—
Phenylethanol	0.33	0.88	—
Acetophenone	0.40	1.90	—
Cineole	0.42	1.24	—
Lilac (synthetic)	0.48	—	—
Benzyl methyl ketone	0.71	—	—
Coriander oil	1.43	—	—
Amyl alcohol	1.51	2.43	—
Amyl acetate	1.73	—	1.25
Jasmin oil (synthetic)	1.80	1.95	—
Clary sage oil	1.89	—	—
Isobutyl acetate	1.95	2.33	1.81
Vetival	1.96	1.90	—
Ethanol	2.14	2.33	1.98
Diethyl ether	2.34	2.33	2.27
Pulegone	—	—	1.06
2-Acetyl-3-methylpyrazine	—	0.72	0.11

b, Relationship between sensor response and odorant concentration for different odours for a single transducer

Odorant	$-\alpha$
Butyl propionate	1.54
Ethyl acetate	1.64
Pentyl acetate	1.65
Ethyl trimethylacetate	1.92
Ethyl bromoacetate	1.94
Ethyl propionate	1.95
Cineole	2.06

The reproducibility of the measurements in *a* can be judged from the data in Fig. 4. The selectivity constant (β) is defined in equation (2). The voltage response of a Figaro 812 gas sensor was measured as a function of the odorant concentrations as described in Fig. 2 legend. A plot of the response against the log odorant concentration was linear (Fig. 2). The slope of this line gives the odour constant, α .

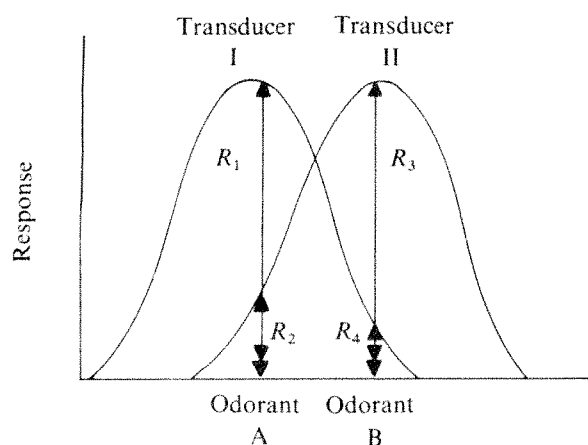


Fig. 3 The odour frequency response for a fixed concentration of odour of two hypothetical odour transducers. The odorants A and B respectively elicit responses R_1 and R_4 from the first transducer and responses R_2 and R_3 from the second transducer.

if the transducers respond to the odorants like the olfactory neurones (equation (1)). The selectivity constant, β , is independent of the odorant concentration and can be used as an index to describe an odour. This analysis is easily extended to N transducers with overlapping frequency distributions and the ratio of the responses for a particular odour computed with the appropriate algorithm will occupy a unique point in a multi-dimensional space. This extension is necessary in the case of the real nose where there are tens of millions of primary neurones and each secondary neurone, on average, is synapsed to about 2×10^4 sensing cells. The model nose can explore the discrimination by following these principles and using the minimum number of transducers (two).

Several odour-detector systems have previously been described⁸⁻¹⁴, but they have a limited application. More recently, n -type semiconductor devices have been described which show a conductance change when they adsorb combustible gases^{15,16}. An important feature of the semiconductor devices is that the response spectrum to vapours can be slightly altered by doping with suitable materials.

Odour sensors based on copper-doped tin oxide semiconductors were constructed exactly as described by Ohno¹⁵. These devices responded to a wide variety of odours. The relative responses of one particular device to ethanol, ammonia, diethyl-ether and iodomethane were respectively 1.0, 0.17, 0.07 and 0.05.

The commercially available semiconductor gas detectors are more stable than the devices we constructed and were used as the transducers for the nose. These transducers, like the sensory neurones, gave a voltage change proportional to the log of the odorant concentration (Fig. 2a), but the response time (Fig. 2a, b) was considerably slower than the response time of the olfactory system. The transducers, in contrast to the neurones, decrease their voltage in response to an odorant stimulus; this difference does not affect the pattern recognition mechanism. A single type of transducer responds differentially to different odours and this is reflected in the odour constants shown in Table 1. Over a period of 6 months the transducers gave a consistent response with most odorants tested and duplicate measurements agreed to within $\pm 5\%$. Some odorants, including 1,8-cineole, 5- α -androstan-3-one and pyridine, produced irreversible changes in the detector and were excluded from the main experiments.

Three Figaro gas sensors were used as the transducers: the 812(A), a general purpose combustible gas sensor; the 813(B), which is more sensitive for alcohols; and the 711(C), which is more sensitive for carbon monoxide. The relative sensitivities of these transducers towards ethanol are 1.0, 0.4 and 10.0 respectively. Thus, they fulfill our requirement of a differential response spectrum. The transducers were arranged in a circuit so that the ratio of their outputs could be derived (Fig. 1). The

precision of the measurements was satisfied by a simple analog circuit¹⁷ which was modelled on a published circuit¹⁸.

The device responds to a wide variety of odours, but since it has no odour memory it will not identify the odour. Thus the nose has to be calibrated by exposing it to various odours and locating the response in the memory. The human olfactory system appears to have similar properties. The selectivity constants determined for a variety of odorants cover a range of values (Table 1a) and allow the nose to discriminate between a large variety of odours. This discrimination is indicated in our system by the operation of a numbered light-emitting diode. The nose reliably discriminates between odours (Fig. 4).

Using three transducers, the system can mimic the discrimination of the mammalian olfactory system at a gross level. An electronic nose which can make fine discriminations, and which will be of interest as a quality control device in industries concerned with flavours, perfumes and smells is feasible using the principles we have used for the simple nose, together with recent developments in microelectronics¹⁹.

The implications of the model nose for olfactory receptor mechanisms are interesting. The model shows that discrimination between odours may be effected by the olfactory system amplifying the small differences in the responses from the detector cells. These small differences in the responses of the primary cells may arise from relatively nonspecific interaction of the odorants with the sensory membranes. Specific receptor proteins such as are found for many hormones and neurotransmitters and some odorants^{3,14,20} may exist only for odorants of special biological importance such as sexual pheromones.

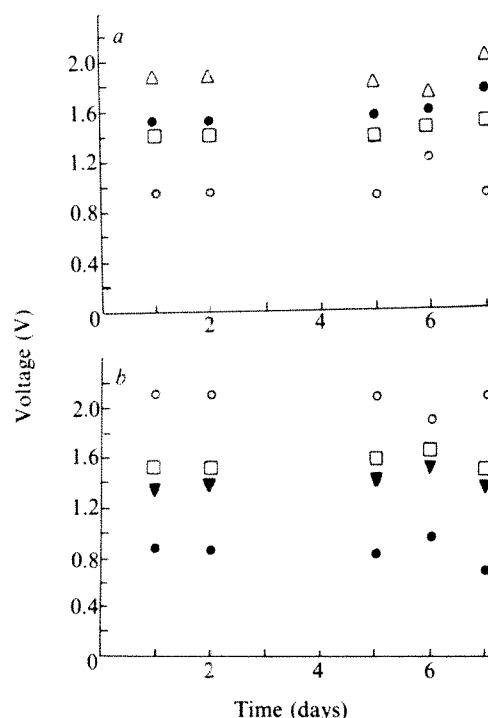


Fig. 4 Reproducibility of the response of the model nose to selected odorants. The odorants had significantly different selectivity constants (Table 1). Response bands were selected on the voltage comparator with limits of $\pm 10\%$ of the appropriate ratio (selectivity constant). a, Responses measured by taking the ratios of the outputs from sensors A (812) and B (813). Δ , Amyl acetate; \bullet , ethanol; \square , ether; \diamond , octanol. b, Responses measured by taking the ratios of the outputs from sensors A (812) and C (711). \circ , Valeric acid; \square , methylpyrazine; ∇ , lemon oil; \bullet , isojaosmone. Each transducer had its own zero circuitry which allowed us to compensate the response for changes in humidity or background odours and which converted the drop in resistance of the transducer to a positive voltage increase. The voltages were fed to individual temperature-stabilized logarithmic amplifiers. The ratio of the signals from the transducers was derived by subtracting the outputs of the logarithmic amplifiers using a differential amplifier. The ratioed signal, after passage through an anti-logarithmic amplifier, was fed into a window comparator. In the experiments reported here we measured the ratio of the signals from transducers A and B, and A and C respectively (Fig. 1).

The work of the Warwick Olfactory Research Group is supported by grants from the SERC, MRC and the Royal Society. We thank Dr H. Mykura for help with the construction of the semiconductor transducers.

Received 24 March; accepted 13 July 1982.

1. Stoddart, D. M. (ed.) *Symp. zool. Soc., Lond.* **45**, (1980).
2. Dodd, G. H. & Squirrell, D. J. *Symp. zool. Soc., Lond.* **45**, 35–56 (1980).
3. Dodd, G. H. & Persaud, K. in *Biochemistry of Taste and Olfaction* (eds Cagan, R. & Kare, M.) 333–357 (Academic, New York, 1981).
4. Holden, A. V. *Lect. Notes Biomath.* **32** (Springer, Heidelberg, 1976).
5. Sampson, J. R. *Adaptive Information Processing* (Springer, Berlin, 1976).
6. Uttal, W. R. *The Psychobiology of Sensory Coding* (Harper & Row, New York, 1973).
7. Deutsch, S. *Models of the Nervous System* (Wiley, New York, 1967).
8. Cherry, R. J., Dodd, G. H. & Chapman, D. *Biochim. biophys. Acta* **211**, 409–416 (1970).
9. Wilkens, W. F., Hartman, J. D. & Rosano, H. *Ann. N.Y. Acad. Sci.* **116**, 608–612 (1964).
10. Moncrieff, R. W. J. *appl. Physiol.* **16**, 742–749 (1961).
11. Dravnieks, A. & Trotter, P. J. *J. Scient. Instrum.* **42**, 624–627 (1965).
12. Sawateri, K. *Chem. Abstr.* **83**, P 35757 T (1975).
13. Tanyolac, N. N. & Eaton, J. R. *J. Am. pharmac. Ass.* **39**, 10–14 (1950).
14. Persaud, K., Pelosi, P. & Dodd, G. H. *Olfaction & Taste* **7**, 101 (1980).
15. Ohno, Y. *Chem. Abstr.* **85**, 28276Y (1976).
16. T.G.S. *Gas-Sensing Semi-Conductor* (Figaro Engineering Inc., Osaka, 1974).
17. Dodd, G. H. & Persaud, K. C. *Provisional UK Patent No.* 8035806 (1980).
18. *Electronics Today International* 62–65 (January 1979).
19. Roberts, G. G., Pande, K. P. & Barlow, W. A. *Electron. Lett.* **13**, 581–583 (1977).
20. Persaud, K., Wood, P., Squirrell, D. J. & Dodd, G. H. *Biochem. Soc. Trans.* **9**, 107–108 (1981).
21. Menevse, A., Dodd, G. H. & Poynder, T. M. *Biochem. J.* **176**, 845–854 (1978).
22. Squirrell, D. J. thesis, Univ. Warwick, UK (1978).

Corticotropin releasing activity of the new CRF is potentiated several times by vasopressin

G. E. Gillies, E. A. Linton & P. J. Lowry

Pituitary Hormone Laboratory, Department of Chemical Pathology, St Bartholomew's Hospital, London EC1A 7BE, UK

Initially the hypothalamic factor responsible for the release of corticotropin (CRF), was thought to be a simple peptide^{1–6}. More recent work has led to the conclusion that CRF is a multifactorial complex^{7–9}. In 1979 we proposed¹⁰ that vasopressin, much disputed as a CRF candidate, was a major constituent of the complex, interacting with and potentiating the CRF activity of the other component(s). The recent characterization of a 41 residue ovine hypothalamic peptide capable of releasing adrenocorticotrophic hormone (ACTH) in a dose-related manner¹¹ has allowed us to compare its CRF bioactivity with that of vasopressin and simple extracts of the hypothalamus, and to investigate any interaction it may have with vasopressin and other hypothalamic factors in the release of ACTH. We report here that the new CRF is more potent than vasopressin in releasing ACTH. When given simultaneously with vasopressin a fourfold potentiation of CRF activity with steep dose-response characteristics was observed. It also potentiated vasopressin-free hypothalamic extracts, suggesting that the new CRF does not account for all the non-vasopressin portion of the CRF complex.

The bioassay used in this study was that described previously¹², except that the antioxidant, ascorbic acid, was added to all physiological media (60 µg ml⁻¹) and peptide solutions under storage (1 mg ml⁻¹) for two reasons. First, we have observed synergism between chromatographically separated hypothalamic fractions only when ascorbic acid was included in the eluant¹⁰. Second, Vale *et al.*¹¹ observed that the synthetic 41 residue CRF was 10 times more potent than purified native ovine CRF. This was attributed to the presence of the methionine sulphoxide in the latter peptide and this oxidized form, which may have been spontaneously generated during purification, may not display all the biological characteristics of the native unoxidized form.

In agreement with Vale *et al.*¹¹, we observed that the new CRF was more potent than vasopressin in releasing ACTH (Fig. 1). However, the most active CRF in our system is still a rat stalk-median eminence extract (SME) which we have generally adopted as our CRF standard¹². A linear response to this extract begins around 0.01 SME ml⁻¹ (refs 12, 13) and at the

maximum concentration we have tested (0.2 SME ml⁻¹) ACTH release was at least 20-fold that of basal secretion (unpublished observations). In view of this large response, and for fear of nonspecific effects due to tissue extracts, our investigations have been routinely carried out in the linear range of responses observed for 0.01–0.1 SME ml⁻¹. We have never reached a plateau response with SME. Figure 1b illustrates that the response to CRF-41 plateaus by 60 ng ml⁻¹. The log dose-response curve to vasopressin is characteristically shallow and significantly non-parallel to that for SME with an ED₅₀ in the 5–10 ng ml⁻¹ range¹⁴. The highest dose of SME used here (0.1 SME ml⁻¹), however, contains only 1 ng of vasopressin by radioimmunoassay. Small-scale chromatography of rat SME has shown that at least three CRFs can be separated by gel filtration, one of which has the characteristics of vasopressin on chromatography, immunoassay and CRF bioassay¹⁰. The individual CRF peaks showed only a small fraction of the total CRF bioactivity, which was restored on recombination of the three partially purified CRF peaks, resulting in a log dose-response curve identical to that for crude SME. These results suggested that CRF consists of vasopressin plus at least two other factors which interact synergistically for full CRF bioactivity. We therefore tested synthetic vasopressin and CRF-41 simultaneously in our bioassay and observed a dramatic potentiation (Fig. 1b). A threefold elevation of ACTH release above background when either peptide was given alone became an 11-fold elevation at a dose of 10 ng ml⁻¹ of each peptide, and the resulting log dose-response curve was as steep as that for crude SME. Thus the combination of vasopressin and the new CRF clearly constitutes a potent stimulator of ACTH release from the anterior pituitary corticotropes in our assay system.

Next we investigated whether the CRF activity of SME was simply due to vasopressin plus the new CRF or whether other factors are involved. When the new CRF was added to rat SME a considerable potentiation of CRF bioactivity was observed with the higher doses of CRF tested (Fig. 2). This suggests that it is synergizing with vasopressin present in the extract and/or other factors. To investigate this interaction further we tested the effects of adding the new CRF to SME which has its ACTH-releasing activity quenched by vasopressin antiserum (Fig. 2). The potentiating ability of the new CRF at 10 ng ml⁻¹ was reduced by almost one-half, with the observed responses

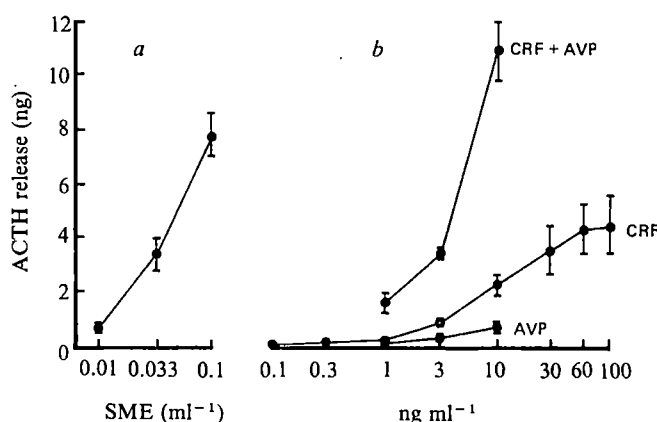


Fig. 1 Rat isolated pituitary cells, prepared by gentle mechanical agitation in Earle's balanced salt solution (EBBS; Gibco Biocult) containing trypsin (2.5 mg ml⁻¹), were mixed with swollen BioGel P2 (200–400) mesh, packed into a 2-ml plastic column and perfused (0.5 ml min⁻¹) with EBBS containing human serum albumin (0.25%), streptomycin (25 µg ml⁻¹), benzylpenicillin (15 µg ml⁻¹) Trasylol (100 kallikrein inactivator units per ml) and ascorbic acid (60 µg ml⁻¹). No significant losses of vasopressin or ACTH occur in passage of these peptides through the system. CRF bioactivity was measured by ACTH release in excess of background as monitored by immunoassay of 1-ml (2 min) fractions of cell column effluent. *a*, Rat SME (1 SME = 3–4 mg wet weight tissue¹²); *b*, synthetic vasopressin and 41 residue ovine hypothalamic CRF (Universal Biologicals Ltd, Cambridge) tested separately and simultaneously. Results are mean \pm s.e.m. of *n* = 3 experiments.

exceeding the additive responses 4-fold for untreated SME compared with 2.4-fold for vasopressin antibody-quenched SME. This suggests that a considerable part of the CRF's activity was due to its interaction with vasopressin. The residual potentiation could be due to interaction with remaining free vasopressin or with a completely different factor. In our original antibody quenching experiments¹³, we did not include ascorbic acid in the media as its importance was not then appreciated. In more recent experiments performed up to 2 yr later, with ascorbic acid in the media, dilutions of antiserum which had been capable of quenching SME CRF activity below the sensitivity of our bioassay, now produced a 60–70% reduction of activity. It is impossible to deduce whether this is due to a deterioration of the antiserum so that all the vasopressin was not fully quenched, or, as we feel more probable, the ascorbic acid stabilizes a third factor^{9,14}. This point was clarified by using SME from the Brattleboro rat which is completely deficient in vasopressin and which has reduced ACTH-releasing activity^{13,15}. A significant potentiation was observed when synthetic CRF was added to Brattleboro SME (Fig. 3) although the extent of potentiation was again considerably less than that observed with untreated normal SME. Therefore it appears that the new CRF is synergizing with other factors apart from vasopressin in the CRF complex.

We have already presented some evidence that a molecule with free thiol groups is necessary for full CRF bioactivity of SME¹⁴ and that vasopressin in some way confers stability on the CRF complex¹³. It is unlikely that vasopressin interacts with the cysteine-free 41 residue hypothalamic peptide, so we postulate that the CRF complex consists of vasopressin, the 41 residue CRF plus another factor(s).

The multi-molecular nature of CRF has been reported by ourselves¹⁰ and by other workers^{7–9}, but the identity of one of the factors as vasopressin is controversial^{9,14}. Evidence in favour of the role of vasopressin includes immunohistochemical identification of vasopressinergic neurones terminating at the portal capillary bed of the zona externa of the median eminence, which respond to manipulations of the pituitary–adrenal axis^{16–18}; high levels of vasopressin in portal blood¹⁹; observations from this laboratory using the perfused isolated rat anterior pituitary cell column bioassay coupled with chromatography^{2,9,10,12–14}; and potentiation of Brattleboro rat CRF by addition of synthetic vasopressin^{13,20}. Furthermore, CRF activity from porcine and ovine hypothalamic extracts which chromatographs as vasopressin has the amino acid com-

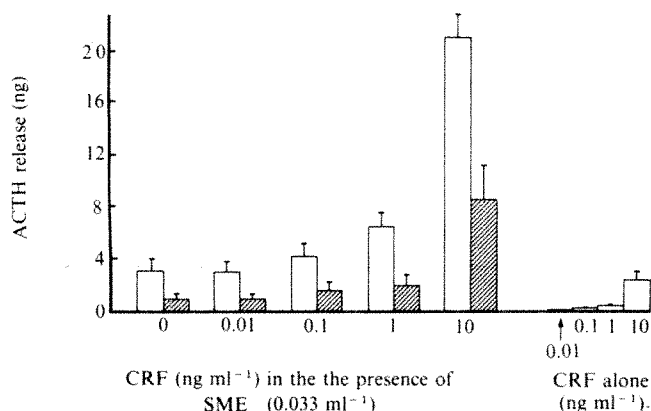


Fig. 2 CRF bioactivity of different doses of synthetic CRF combined with rat SME (0.033 SME ml⁻¹) compared with synthetic CRF alone. SME had been preincubated overnight at 4 °C in bioassay perfusion buffer in the presence (▨) and absence (□) of vasopressin antiserum² (final dilution 1:1,000). Vasopressin antiserum had no effect on synthetic CRF given alone. As controls (not illustrated), normal rabbit serum and a somatostatin antiserum (final dilution 1:1,000) were substituted for vasopressin antiserum. Responses were superimposable on those for synthetic CRF and SME preincubated in the absence of vasopressin antiserum (□) with no effect on the potentiating ability of synthetic CRF. Results are mean ± s.e.m. (*n* = 5).

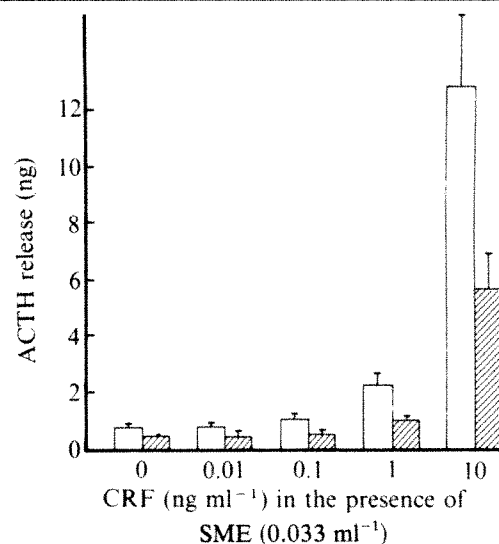


Fig. 3 CRF bioactivity of varying doses of synthetic CRF combined with normal (□) and Brattleboro (▨) rat SME (0.033 SME ml⁻¹) (*n* = 4).

position of lysine-vasopressin LVP⁹ and arginine-vasopressin¹¹ respectively. Despite some evidence to the contrary^{7,21} (see ref. 9 for review), a role for vasopressin as a physiological CRF is now being reconsidered more carefully^{15,22}.

The 41 residue peptide of ovine hypothalamic origin recently characterized by Vale *et al.*¹¹ as a potent CRF has enabled us to investigate its interaction with vasopressin. We found that although the new CRF is more potent in releasing ACTH in our bioassay than is vasopressin, it is still not as active a CRF at the rat anterior pituitary corticotrope as is rat SME. However, we have demonstrated a dramatic synergism between vasopressin and the new CRF over the linear portion of their individual log dose–response curves. Although the resultant curve is qualitatively identical to that for an extract of the rat stalk median eminence region, the amount of peptides required appear to be relatively high. In 0.1 SME, we would expect to find 1 ng immunoactive vasopressin, whereas recombination of 1 ng ml⁻¹ of both vasopressin and CRF produces a response far less than that observed for 0.1 SME ml⁻¹ (Fig. 1). Until a radioimmunoassay for the 41 residue CRF is established and the amounts of the new CRF (or related substance) in our extract can be measured, the concentration of the synthetic CRF used in our experiments remains arbitrary. On the basis of our chromatographic evidence that CRF consists of vasopressin plus at least two other synergizing factors, we previously added vasopressin to normal rat SME, but found only additive responses, suggesting that the other factors are present in limiting amounts. This was borne out to a large extent when vasopressin added to Brattleboro rat SME in amounts found in normal SME significantly potentiated CRF bioactivity¹³. Furthermore, potentiation of CRF bioactivity by addition of synthetic 41 residue CRF to normal SME supports this idea and suggests that a peptide similar to the synthetic CRF may play a significant part in controlling ACTH secretion in the rat. From the results with vasopressin antiserum-quenched SME and vasopressin-free SME from Brattleboro rats (Figs 2, 3) we deduce that at least one other substance besides vasopressin and the 41 residue CRF will be required for full CRF bioactivity in our system. We have evidence that, apart from vasopressin and a CRF which co-elutes with it on Sephadex G-50 (but not on Biogel P2), the rat and pig hypothalamic CRF complex contains a material of apparent molecular weight 5,000–8,000 which can be generated from a higher molecular weight precursor and which potentiates the CRF activity of vasopressin⁹. An antiserum to the 41 residue CRF may allow us to study its relationship to these CRFs and to the many other reported partially purified CRFs (see ref. 9 for review).

This work was supported by the MRC.

Received 11 January; accepted 28 July 1982.

1. Burgus, R. & Guillemin, R. A. *Rev. Biochem.* **39**, 499–526 (1970).
2. Gillies, G., Greidanus, T. B. V. W. & Lowry, P. J. *Endocrinology* **103**, 528–534 (1978).
3. Pearlmutter, A. F., Dokas, L., Kong, A., Miller, R. & Saffran, M. *Nature* **283**, 698 (1980).
4. Royce, P. C. & Sayers, G. *Proc. Soc. exp. Biol. Med.* **142**, 842–845 (1960).
5. Schally, A. V. & Guillemin, R. *Proc. Soc. exp. Biol. Med.* **112**, 1014 (1963).
6. Schally, A. V., Arimura, A. & Kastin, A. J. *Science* **179**, 341–350 (1973).
7. Pearlmutter, A. F., Rapino, E. & Saffran, M. *Endocrinology* **97**, 1336–1339 (1975).
8. Sayers, G., Hanzmann, E. & Bodansky, M. *FEBS Lett.* **116**, 236–238 (1980).
9. Gillies, G. & Lowry, P. J. in *Frontiers in Neuroendocrinology* Vol. 7 (eds Martini, L. & Ganong, W. F.) 45–74 (Raven, New York, 1982).
10. Gillies, G. & Lowry, P. J. *Nature* **278**, 463–464 (1979).
11. Vale, W., Spiess, J., Rivier, C. & Rivier, J. *Science* **213**, 1394–1397 (1981).
12. Gillies, G. & Lowry, P. J. *Endocrinology* **103**, 521–527 (1978).
13. Gillies, G. & Lowry, P. J. *J. Endocr.* **84**, 65–73 (1980).
14. Gillies, G. & Lowry, P. J. in *Interactions within the Brain-Pituitary-Adrenocortical System* (eds Jones, Gilham, Dallman & Chattopadhyay) 51–61 (Academic, New York, 1979).
15. Sokol, H. W., & Zimmerman, E. A. *Ann. N.Y. Acad. Sci.* (in the press).
16. Watkins, W. B., Schwabedal, P. & Bock, R. *Cell Tissue Res.* **152**, 411–421 (1974).
17. Zimmerman, E. A. in *Frontiers of Neuroendocrinology* Vol. 4 (eds Martini, L. & Ganong, W. F.) 25–62 (Raven, New York, 1976).
18. Zimmerman, E. A. *et al. Ann. N.Y. Acad. Sci.* **297**, 405–419 (1977).
19. Goldman, H. & Lindner, L. *Separatum Experientia* **18**, 279–281 (1962).
20. Buckingham, J. C. *J. Physiol., Lond.* **312**, 9–16 (1981).
21. Lutz-Butcher, B., Koch, B., Miahle, C. & Briaud, B. *Neuroendocrinology* **30**, 178–182 (1980).
22. Baertisch, A. in *Neuroendocrinology of Vasopressin, Corticotropin and Opiomelanocortin* (eds Baertisch, A. & Driefuss, J.-J.) (Academic, London, in the press).

Oligodendrocyte abnormalities in *shiverer* mouse mutant are determined in primary chimaeras

K. Mikoshiba*, M. Yokoyama†, Y. Inoue‡, K. Takamatsu*, Y. Tsukada* & T. Nomura†

* Department of Physiology, Keio University School of Medicine, 35 Shinano-machi, Shinjuku-ku, Tokyo 160 Japan

† Central Institute for Experimental Animals, 1430 Nogawa, Miyamae-ku, Kawasaki 213, Japan

‡ Department of Anatomy, Hokkaido University, School of Medicine, 15–7, Kita-ku, Sapporo, Hokkaido, Japan

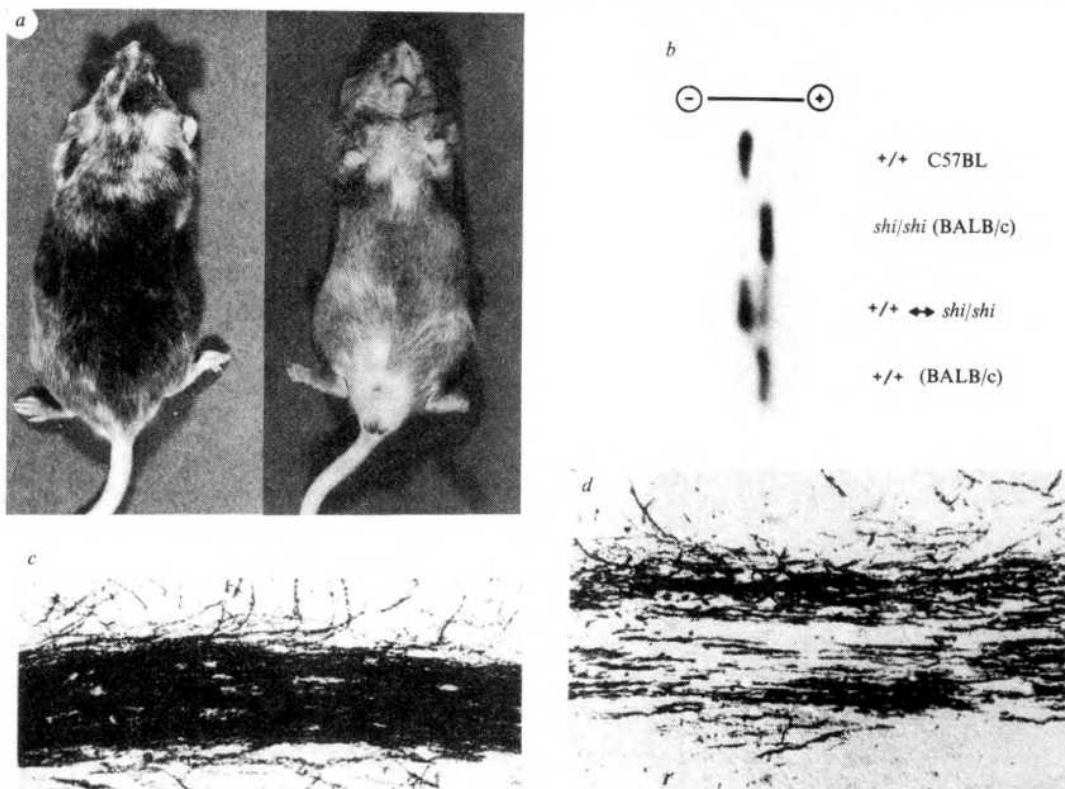
There is increasing interest in hereditary dysmyelinating mutant mice such as *jimpy*, *quaking*, *shiverer* and *twitcher*, as animal models for leukodystrophy in man^{1–3}. These mutants are characterized by severe tremor and tonic convulsions. *Shiverer* is an autosomal recessive mutant which displays abnormal and poor myelination of the central nervous system^{4–9} and is genetically different from the other dysmyelinating mutants. Despite many reports on the morphological and chemical changes which occur in *shiverer* mice, the pathogenesis of the abnormal and poor myelin formation is unknown. We have now produced chimaeras by aggregation of eight-cell-stage embryos from wild-type and *shiverer* mutants. Analysis of the white matter of the chimaera suggests that the oligodendrocyte is responsible for the abnormal and poor myelination in *shiverer*.

Chimaeras were produced by the aggregation method^{10–13}, which makes it possible to know the interactions among cells. To facilitate the judgement of mosaicism of different genotypes in the brain, C57BL/6N mouse strain (black coat colour) was used as wild-type control, as they have a different isozyme pattern of glucose phosphate isomerase (GPI) which is distinct from that of *shiverer* mutant mice on the BALB/c background (white coat colour). We have obtained six chimaeras, and selected for analysis the chimaera shown in Fig. 1a. Examination of the strain-specific GPI isozyme pattern of brain tissues in the chimaera shows chimaerism of both genotypes as well as coat colour. The gel electrophoretic pattern of GPI isozyme revealed that brain tissue in the chimaera was composed of isozymes of both BALB/c and C57BL/6N (Fig. 1b). In the several *shiverer* mice examined so far, we have observed a clear correlation between the mosaicism of coat colour and that of the GPI isozyme pattern.

A neurochemical characteristic of the *shiverer* mutation is the absence of myelin basic protein (MBP), which is a major component of the myelin sheath. The immunohistochemical reaction using antiserum against MBP also shows the absence of MBP^{4,14}. Here we have used the immunohistochemical reaction of MBP as a marker to distinguish *shiverer*-type myelin from that of the wild-type control.

If all myelin formation was abnormal in the chimaera central nervous system, we would suspect the presence of an extrinsic harmful factor derived from the *shiverer* which could not be neutralized by the normal tissue. Conversely, if myelin formation in the central nervous system of the chimaera was similar

Fig. 1 Mosaics of coat colour, brain tissue GPI isozyme pattern and brain MBP-positive and -negative fibres from the normal-*shiverer* chimaera mouse. *a*, Chimaera mouse (*shi/shi* ↔ *+/+*) produced by the aggregation technique. *b*, Cellulose acetate electrophoresis of mouse strain-specific enzyme variants of GPI from homogenates of part of the brain. The chimaera was produced from the *+/+* (C57BL) and *shi/shi* (BALB/c) mice. *c*, Immunohistochemical staining of the white matter of the control (*+/+*) cerebellum using anti-MBP serum. *d*, Immunohistochemical staining of the white matter of the chimaera by anti-MBP serum. MBP-positive fibres and MBP-negative fibres are mixed in the white matter of the chimaera, indicating the absence of humoral factors which might cause abnormal and poor myelin formation.



to that of the control, we would assume that the abnormal myelin formation of the *shiverer* had been resolved by the diffusion of some extrinsic humoral factor from the normal tissue to the *shiverer*, or by the removal by the control tissue of an extrinsic humoral factor responsible for abnormal myelin formation in *shiverer*. If the mutation were expressed intrinsic to the *shiverer* cells themselves, it seems probable that both normal and abnormal *shiverer*-type myelin would occur as a mixture or as patches.

In fact, we observed MBP-positive and -negative fibres mixed in the white matter (Fig. 1d, compare with Fig. 1c, which is a control section), thus eliminating the possibility that humoral factors caused the abnormal myelin formation of the *shiverer*. We therefore suggest that the *shiverer* mutation occurs intrinsic to the cells themselves, namely neuronal or glial cells.

Myelination is a process of interaction of neuronal and glial cells. Oligodendrocytes send out their processes to search for the axon to myelinate³. There are thus two possible causes of dysmyelination in *shiverer* mice: abnormalities in the neuronal cells which are to be myelinated or abnormalities in the glial cells responsible for the myelination. In fact, morphological abnormalities have been detected in both the neurone, using the silver impregnation technique¹⁵, and the glial cell (abnormal myelin formation in oligodendrocytes^{5,8,9,16} and a hypertrophy of astrocytes¹⁴).

If the cause of dysmyelination is primarily on the neuronal side, *shiverer*-type axon would always have *shiverer*-type myelin (Fig. 2b) and normal axon would have normal myelin (Fig. 2a). In such a case, the type of myelin observed in Fig. 2c would not be present. However, if dysmyelination in *shiverer* is due to an abnormality of the oligodendrocyte rather than the neurone, *shiverer*-type myelin would be seen adjacent to normal myelin on the same axon; this feature is often observed under the electron microscope.

We therefore suggest that the cause of abnormal myelination in *shiverer* mutant mouse is not of neurogenic origin, but rather that the oligodendrocyte itself is responsible.

Chimaeric analysis has proved successful in analysing the pathogenesis of the photoreceptor cells degeneration in the retinal dystrophy mutant¹⁷, the degeneration of Purkinje cells in the Purkinje cell degeneration mutant¹⁸, in muscular dystrophy¹⁹ and also in other neurological mutants²⁰. The

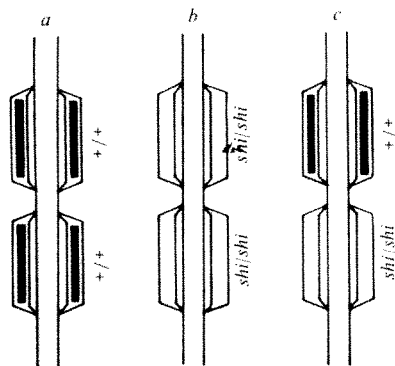


Fig. 2 Three hypothetical models of myelin formation in the central nervous system of the *shiverer*-normal chimaera. The dense bar in the myelin indicates the major dense line which is absent in the *shiverer*-type myelin. If the *shiverer* mutation acts on the axons in the chimaera, all the myelin formed on the axon originated from *shiverer* would be *shiverer*-type (b), and the myelin sheaths on the control axon would all be normal (a). If the *shiverer*-type myelin is observed adjacent to the control-type myelin (c), it is the oligodendrocyte that is affected by the *shiverer* mutation. In the *shiverer*-normal chimaera, all three types of myelin formation were observed.

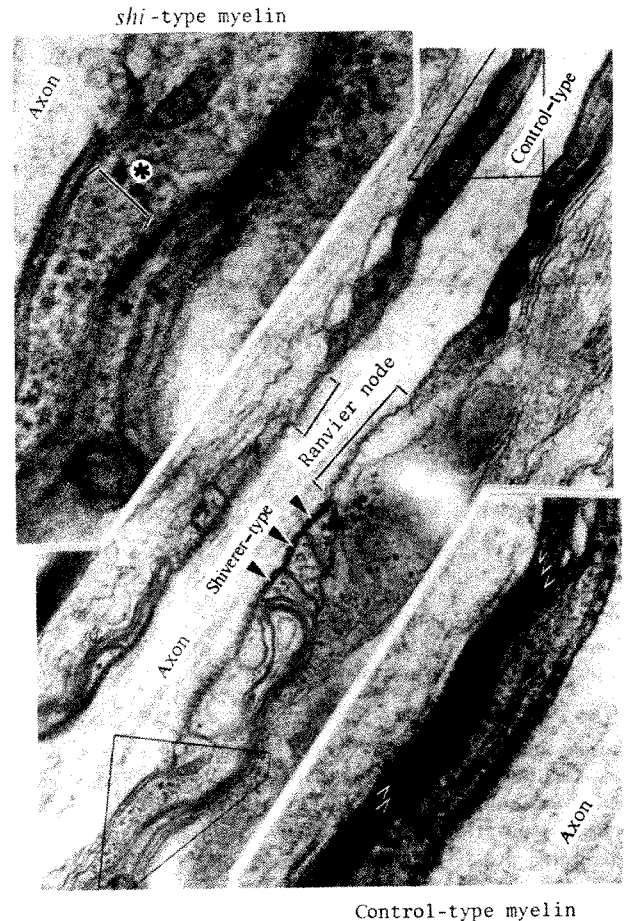


Fig. 3 An axon with control and *shiverer*-type myelin in the white matter of the chimaera mouse. Electron microscopic demonstration of the sagittal section of the myelinated axon in the corpus callosum. In the typical myelin lamella, major dense lines (indicated by small arrowheads) are clearly observed (lower inset) and paranodal cytoplasmic pockets lose their cytoplasm immediately to form the major dense line (central figure), while in the myelin of the lower left (central figure) and upper inset, which is believed to be of *shiverer* origin, the paranodal cytoplasmic pockets are enlarged and irregular in form and isolated pockets (indicated by larger arrow heads) are often observed. In the *shiverer*-type myelin, cytoplasm of the oligodendrocyte (indicated by *) is found where the major dense line would form in normal myelin.

present results demonstrate the site at which the *shiverer* mutation is acting, and future work should establish whether the inability of the oligodendrocyte to synthesize MBP is controlled by other cells (for example, astrocytes) through short-distance diffusible factors or by fibres attached to oligodendrocytes in *shiverer*. Double immunohistochemical staining using antisera against MBP and strain-specific GPI should elucidate whether or not MBP-synthesizing activity in control oligodendrocytes (the origin of which can be detected by the GPI antiserum) is converted to *shiverer*-type (which can be detected by MBP antiserum) by the adjacent *shiverer* cells.

We thank Drs F. Lachapelle and N. Baumann for their generous supply of *shiverer* mutant mice, and Dr J.-L. Guenet, Dr M. Katsuki and N. Ohsawa for valuable discussions.

Received 20 April; accepted 21 July 1982.

1. Baumann, N. *Neurological Mutations Affecting Myelination, Research Tools in Neurobiology Correlations to Human Neurological Diseases* (Elsevier, Amsterdam, 1980).
2. Sidman, R. L., Green, M. C. & Appel, S. H. *Catalog of the Neurological Mutants of the Mouse* (Harvard University Press, Cambridge, 1965).
3. Morell, P. *Myelin* (Plenum, New York, 1977).
4. Dupouey, O. et al. *Neurosci. Lett.* **12**, 113-118 (1979).
5. Privat, A., Jacque, C., Bourre, J. M., Dupouey, P. & Baumann, N. *Neurosci. Lett.* **12**, 107-112 (1979).
6. Mikoshiba, K., Nagaoka, K., Kohsaka, S., Takamatsu, K. & Tsukada, Y. *Bull. Japan. neurochem. Soc.* **18**, 200-203 (1979).

7. Mikoshiba, K., Aoki, E. & Tsukada, Y. *Brain Res.* **192**, 195–204 (1980).
8. Mikoshiba, K., Nagaike, K. & Tsukada, Y. *J. Neurochem.* **35**, 465–470 (1980).
9. Inoue, Y., Nakamura, R., Mikoshiba, K. & Tsukada, Y. *Brain Res.* **219**, 85–94 (1981).
10. Mintz, B. *Science* **138**, 594–595 (1962).
11. Mintz, B. *Am. Zool.* **2**, 432 (1962).
12. Mintz, B. in *Methods in Mammalian Embryology* (ed. Daniel, J. C. Jr.) 186–214 (Freeman, Toppan 1971).
13. Mullen, R. J. & Whitten, W. K. *J. exp. Zool.* **178**, 165–176 (1971).
14. Mikoshiba, K., Takamatsu, K., Kohsaka, S., Tsukada, Y. & Inoue, Y. in *Genetic Approaches to Developmental Neurobiology* (ed. Tsukada, Y.) 195–221 (Tokyo University Press, 1982).
15. Friedrich, V. L., Koniecki, D. L. & Massa, P. T. in *Neurological Mutations Affecting Myelination* (ed. Baumann, N.) 141–146 (Elsevier, Amsterdam, 1980).
16. Rosenbluth, J. J. *comp. Neurol.* **194**, 639–648 (1980).
17. Mullen, R. J. & LaVail, M. M. *Science* **192**, 801–799 (1976).
18. Mullen, R. J. in *Approaches to the Cell Biology of Neurons* Vol. 2. (eds Cowan, W. M. & Ferendelli, J. A.) 47–65 (Society for Neuroscience, Bethesda, Maryland, 1976).
19. Peterson, A. C. *Nature* **248**, 561–564 (1974).
20. Bray, G. M., Rasminsky, M. & Aguayo, A. J. *A. Rev. Neurosci.* **4**, 127–162 (1981); *Neurology* **31**, 118 (1981); *Soc. Neurosci. Abstr.* **7**, 545 (1981).

A Cl^- conductance activated by hyperpolarization in *Aplysia* neurones

Dominique Chenoy-Marchais

Laboratoire de Neurobiologie, École Normale Supérieure,
46 rue d'Ulm, 75005 Paris, France

Although many voltage-gated cation channels have been described and extensively studied in biological membranes, there are very few examples of voltage-gated anion channels. Chloride conductances activated by depolarization have been observed in skate electroplaque^{1,2} and in frog and chick skeletal muscle^{3–5}. A Cl^- conductance activated by hyperpolarization has been suggested both for frog muscle treated with acid (pH 5) solutions³, and for crayfish muscle^{6,7} where it could account for the fact that the pronounced inward-going rectification of the $I-V$ curve disappears if the fibres have been soaked in a Cl^- -free solution. More recently, voltage-dependent anion channels extracted from biological membranes have been incorporated^{8–10} into artificial membranes. I now report that in *Aplysia* neurones, and in particular those in which the internal Cl^- concentration has been increased, a Cl^- conductance can be observed which is slowly activated by hyperpolarization and shows a very steep voltage dependence. This time- and voltage-dependent Cl^- conductance probably exists also in many other cells. Its presence might explain why it is difficult when using KCl-filled microelectrodes to maintain prolonged hyperpolarizations¹¹. This Cl^- conductance constitutes a new type of inward-going rectification distinct both from the classical 'anomalous rectification' which involves selective K^+ channels^{12,13} and from the current termed i_t in heart muscle that is presently attributed to a cationic conductance¹⁴.

Most experiments were performed on identified *Aplysia* neurones (the A neurones of the cerebral ganglion) which were voltage-clamped using two intracellular microelectrodes filled with either K_2SO_4 (0.5 M) or KCl (1–3 M)¹⁵. These neurones respond to acetylcholine by a rapid conductance increase specific for Cl^- ions and a slower conductance increase specific for K^+ ions¹⁵: the reversal potentials of these two responses provide direct measurements of the Cl^- and K^+ equilibrium potentials (E_{Cl} and E_{K}). The neurones were held near the resting potential, at -45 or -50 mV, and were then hyperpolarized for a few seconds by a square voltage jump to -100 mV. When the intracellular electrodes were filled with K_2SO_4 , the current change during the pulse was usually square, although sometimes the inward current recorded at -100 mV showed a slight and slow increase during the pulse (Fig. 1a). On the other hand, when the recording electrode was a leaky electrode filled with KCl, or when chloride ions were injected iontophoretically through an additional intracellular KCl electrode, I observed, after the hyperpolarizing jump, in addition to the instantaneous current change, a very large inward current which increased slowly for a few seconds. A large slow tail current was observed after repolarization from -100 to -50 mV. The fact that at -100 mV all the currents crossing the ionic channels of the

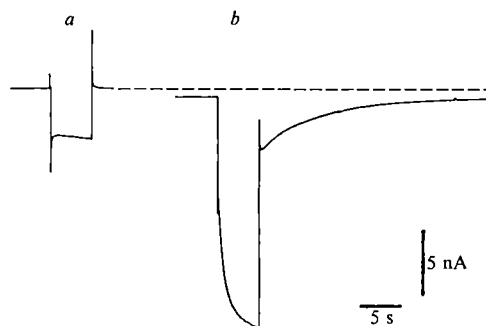


Fig. 1 Increasing the intracellular Cl^- concentration reveals a large slow hyperpolarization-induced inward current which slowly deactivates on repolarization. The cell was impaled with two microelectrodes filled with K_2SO_4 (0.5 M) plus one double-barrelled micropipette containing K_2SO_4 (0.5 M) in one barrel and KCl (1 M) in the other. The cell was maintained at -50 mV between hyperpolarizing pulses (5 s to -100 mV) which were applied every 3 min. The current recorded during such a voltage jump is shown before (a) and after (b) the internal Cl^- concentration had been raised. In a, a braking current of 10 nA was applied to the double-barrelled micropipette to avoid leakage of Cl^- into the cell; in b, Cl^- ions had been injected iontophoretically with a current of 30 nA for 15 min. The steady-state current at the holding potential was slightly altered by the chloride injection, suggesting that, after the injection, the voltage-dependent inward current in this cell was slightly activated at -50 mV.

membrane were inward currents (all the ionic equilibrium potentials were more depolarized than -100 mV), suggested that the slow inward current observed at -100 mV was due to the slow activation of an ionic conductance induced by hyperpolarization and that the tail current was due to the slow deactivation of this conductance.

The ionic specificity of these slow voltage-dependent currents was investigated. As larger currents could be obtained by loading the neurones with Cl^- , I used systematically a KCl voltage recording microelectrode and only started the analysis after E_{Cl} had reached a stable value. The currents activated by the hyperpolarizing jumps were clearly not due to the activation of a selective K^+ conductance, as in cells in which E_{K} was measured precisely (as the reversal potential of the slow cholinergic response), large slow increases in inward current were triggered by voltage jumps from -50 mV to E_{K} , and slow tail currents were observed after repolarization from -100 mV to E_{K} (E_{K} was always found very close to -80 mV). I considered the possibility that the current is similar to the i_t of heart cells (ref. 14; see also ref. 16): these currents, which resemble the current described here in that they are activated by hyperpolarization, are attributed to an increased cationic conductance to both Na^+ and K^+ and have been shown to be blocked by Cs^+ . Neither of these properties applies to the current observed in *Aplysia* neurones: (1) Complete substitution of external Na^+ by Tris, which is usually not permeant through cationic channels, did not induce any change in the current, either in amplitude or in kinetics. (2) Addition of Cs^+ ions (1–50 mM) did not modify the current (provided Co^{2+} ions (10 mM) were present both in control and Cs^+ -containing solutions to prevent Cs^+ -induced changes in synaptic activity). (3) In two experiments, slow hyperpolarization-activated inward currents very similar to those usually observed in control seawater, were recorded in an isotonic CsCl extracellular solution, after replacement (by treatment with nystatin¹⁷) of intracellular monovalent cations by Cs^+ ions. (The extracellular CsCl solution was Na^+ -free and K^+ -free (517 mM CsCl , 10 mM CaCl_2 , 50 mM MgCl_2 , 5 mM HEPES- CsOH , pH 7.6.) For treatment with nystatin, the ganglion was perfused with a Cs^+ -loading solution (300 mM CsCl , 394 mM sucrose, 100 mM MgSO_4 , 5 mM HEPES- CsOH); nystatin (20 mg l^{-1}) was applied in this solution for 30 min. The ganglion was then washed for 30 min with the nystatin-free Cs^+ -loading solution before being perfused with the isotonic CsCl solution; before recording, the cell bodies were isolated

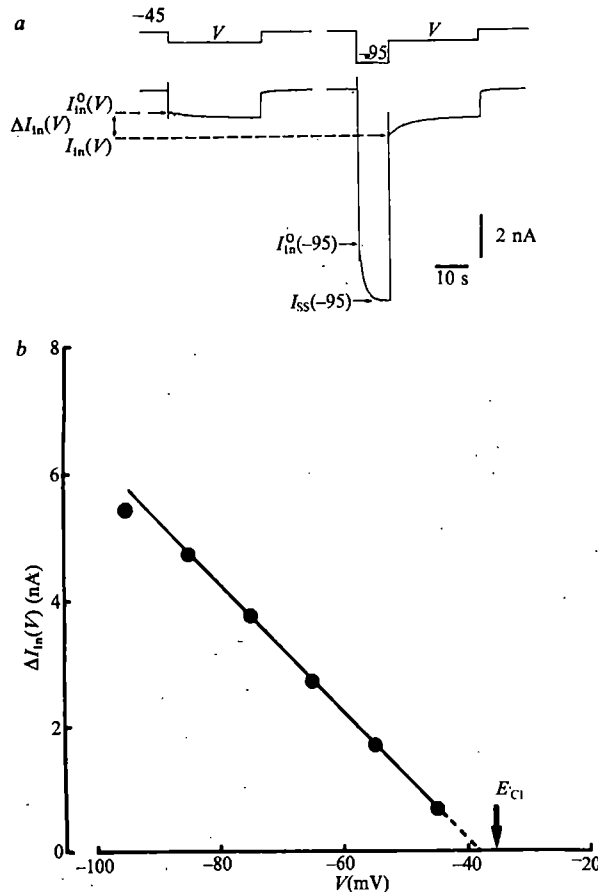


Fig. 2 Extrapolation of the instantaneous current-voltage curve to zero current gives a reversal potential close to E_{Cl} (b). In a are shown the voltage jumps which were used to establish the curve in b (the records presented come from an experiment similar to that reported for b). Arrows in a indicate the measured current values. $I_{in}^0(V)$ is the instantaneous current at V after a hyperpolarizing jump from -45 mV to V . At the holding potential (-45 mV) the current under investigation was not activated: pulses from -35 to -45 mV did not induce any slow time-dependent inward current at -45 mV. Thus, $I_{in}^0(V)$ is the 'resting' current at V . $I_{in}(V)$ is the instantaneous current at V after a depolarizing jump from a hyperpolarized level (-95 mV) at which the inward current was activated for 10 s. $I_{in}^0(V)$ and $I_{in}(V)$ were measured by extrapolation to time zero of the exponential kinetics of the currents recorded at V . $\Delta I_{in}(V)$, the difference between $I_{in}(V)$ and $I_{in}^0(V)$, is plotted in b. E_{Cl} (indicated by an arrow) was measured as the reversal potential of the Cl^- response to ionophoretically applied carbachol. It was not modified by the hyperpolarizing pulses applied in this experiment. $I_{ss}(V)$ is the steady-state value of the current at V .

by cutting the axons in order to avoid synaptically-induced changes in conductance. The intracellular microelectrodes were filled with CsCl (0.5 M) or CsSO₄ (0.5 M).

These results, together with the fact that the currents were very sensitive to the intracellular Cl^- concentration (Fig. 1) suggested that the observed currents were due to a voltage-gated Cl^- conductance. This was further demonstrated by comparing the reversal potential of the fast cholinergic response (E_{Cl}) with the reversal potential (E_r) of the tail currents observed after repolarization to various membrane potentials after a given hyperpolarizing pulse. Direct measurement of this reversal potential was difficult because in order to have large hyperpolarization-induced currents, it was necessary to load the cell with Cl^- thus bringing E_{Cl} within a range (more depolarized than -40 mV) where many currents are activated by a sudden depolarization. (The problem was further compounded by the fact that the kinetics of the tail currents becomes rapid in this range (see Fig. 3a).) The reversal potential of the

tail currents was therefore estimated by extrapolating values measured at various levels below the reversal potential (Fig. 2). The extrapolated reversal potential (E_r) was very close to E_{Cl} ($E_r - E_{Cl} = -2.3 \pm 2.0$ (7) (mean \pm s.d. (n)). Furthermore, in four experiments in which half the extracellular chloride was replaced by isethionate, both E_r and E_{Cl} shifted by similar values, that is, 10 ± 2 mV and 9.3 ± 0.9 mV, respectively. In another experiment, the intracellular Cl^- concentration was increased in two steps, by two successive iontophoretic injections of Cl^- ; E_{Cl} shifted from -30 mV to -20 mV while E_r shifted from -32 mV to -22 mV.

Thus, the hyperpolarization-induced slow inward current and the corresponding tail current appear to result from a voltage-gated Cl^- conductance slowly activated by hyperpolarization and slowly deactivated by repolarization.

To characterize the activation and deactivation of this Cl^- conductance, I analysed the kinetics and the amplitude of the ON relaxations induced by square hyperpolarizing pulses from -50 mV to various test potentials, and the kinetics of the OFF relaxations induced by repolarization to a variable test potential after a 10-s hyperpolarizing pulse from -50 to -100 mV. In some experiments, these relaxations could be described by single exponentials. (In other experiments which were disregarded, the relaxations presented an additional slower component which may have resulted from an imperfect clamp of the membrane potential). The time constants of the exponential relaxations ($\tau_{ON}(V)$ and $\tau_{OFF}(V)$) are plotted in Fig. 3a. For membrane potentials which allowed accurate measurement of both $\tau_{ON}(V)$ and $\tau_{OFF}(V)$ the values of these two time constants were found to be identical. This was confirmed in six other such experiments. Figure 3a shows that the kinetics of activation is much more rapid at -100 mV than at -70 mV, varying by a factor e per 14 mV. Figure 3b illustrates the amplitude of the conductance change during each hyperpolarizing pulse. In this cell, the voltage-gated Cl^- current did not seem to be activated at -50 mV as a pulse from -40 to -50 mV did not trigger any slow time-dependent inward current. (Preliminary experiments (not shown) indicate that the threshold for activation of this Cl^- conductance becomes lower as the intracellular Cl^- concentration is increased. This may explain why in the experiment of Fig. 1, the Cl^- conductance is already activated at -50 mV, whereas this is not so in the experiment of Fig. 3.) Figure 3b therefore gives the voltage-dependence of the steady-state Cl^- conductance. It is very steep between -50 and -70 mV (e -fold increase per 9 mV) and saturates at highly hyperpolarized membrane potentials.

Most of the results presented here were obtained on intact A cells, but similar results were obtained from cell bodies isolated by cutting off the axons. The Cl^- conductance described

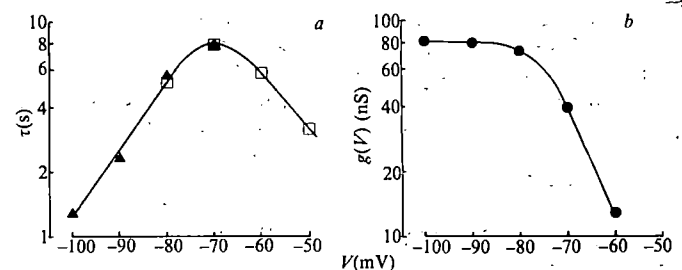


Fig. 3 Voltage-dependence of the kinetics of activation and deactivation and of the steady-state conductance. a, $\tau_{ON}(V)$ (▲) and $\tau_{OFF}(V)$ (□); b, steady-state conductance $g(V)$. $g(V)$ was calculated as follows:

$$g(V) = \frac{I_{ss}(V) - I_{in}^0(V)}{V - E_{Cl}}$$

where $I_{ss}(V)$ is the steady-state value of the current at the potential V and $I_{in}^0(V)$ is the instantaneous current at V after a jump from a potential at which the Cl^- conductance was not activated. In the experiment illustrated, the jump started from -50 mV; E_{Cl} was -35 mV.

is therefore not synaptic and is at least partially located on the soma. Preliminary results indicate that this voltage-gated Cl^- conductance described in A cells exists in many other *Aplysia* neurones.

In conclusion, I have described a neuronal non-synaptic Cl^- conductance in which both the steady-state conductance and the kinetics of activation are highly voltage-dependent (Fig. 3) while the instantaneous current-voltage curve is approximately linear (Fig. 2). These properties resemble those of some voltage-gated Cl^- conductances previously described in non-neuronal systems^{3,7,10}. It is possible that such a conductance exists in many other neurones. It may coexist with other inward rectifying conductances like the classical 'anomalous rectification' of the K^+ -conductance. Indeed, two different mechanisms have already been suggested¹⁸ to account for the anomalous rectification of molluscan neurones¹⁹. The functional role of this Cl^- conductance may be partly to stabilize membrane potential and prevent excessive hyperpolarization. It could also be a mechanism of regulating the intracellular Cl^- concentration, helping to maintain it at low levels in cells which, like *Aplysia* neurones, are normally very impermeant to Cl^- (ref. 20) but which may become loaded with Cl^- during repeated activation of Cl^- inhibitory synapses.

I thank Professor P. Ascher for his encouragement and help during this work and D. Paupardin-Tritsch for isolation of cell bodies. This work was supported by grants from the CNRS, the DGRST and the Université Pierre et Marie Curie.

Received 13 April; accepted 7 July 1982.

- Grundfest, H., Aljure, E. & Janiszewski, L. *J. gen. Physiol.* **45**, 598 A (1962).
- Hille, B., Bennett, M. V. L. & Grundfest, H. *Biol. Bull.* **129**, 407-408 (1965).
- Warner, A. E. *J. Physiol., Lond.* **227**, 291-312 (1972).
- Fukuda, J. *Science* **185**, 76-78 (1974).
- Fukuda, J. *Nature* **257**, 408-410 (1975).
- Reuben, J. P., Girardier, L. & Grundfest, H. *Biol. Bull.* **123**, 509-510 (1962).
- Ozeki, M., Freeman, A. R. & Grundfest, H. *J. gen. Physiol.* **49**, 1335-1349 (1966).
- Schein, S. J., Colombini, M. & Finkelstein, A. *J. Membrane Biol.* **30**, 99-120 (1976).
- Colombini, M. *Nature* **279**, 643-645 (1979).
- White, M. M. & Miller, C. *J. Biol. Chem.* **254**, 10161-10166 (1979).
- Coombs, J. S., Eccles, J. C. & Fatt, P. *J. Physiol., Lond.* **130**, 326-373 (1955).
- Adrian, R. H. *Prog. Biophys. molec. Biol.* **19**, 341-369 (1969).
- Ohmori, H., Yoshida, S. & Hagiwara, S. *Proc. natn. Acad. Sci. U.S.A.* **78**, 4960-4964 (1981).
- Di Francesco, D. *J. Physiol., Lond.* **314**, 377-393 (1981).
- Ascher, P. & Chesnoy-Marchais, D. *J. Physiol., Lond.* **324**, 67-92 (1982).
- Adams, P. R. & Halliwell, J. V. *J. Physiol., Lond.* **324**, 62 P (1982).
- Russell, J. M., Eaton, D. C. & Brodwick, M. S. *J. Membrane Biol.* **37**, 137-156 (1977).
- Marmor, M. F. *J. Physiol., Lond.* **218**, 573-598 (1971).
- Tauc, L. & Kandel, E. R. *Nature* **202**, 1339-1341 (1964).
- Ascher, P., Kunze, D. & Neild, T. O. *J. Physiol., Lond.* **256**, 441-464 (1976).

Transplacental transfer of rodent microfilariae induces antigen-specific tolerance in rats

Azizul Haque & André Capron

Centre d'Immunologie et de Biologie Parasitaire, Institut Pasteur, 15, rue Camille Guérin, 59019-Lille, France

Microfilariae are the smallest form in the life-cycle of filarial nematode parasites. They are released by the adult female worms and migrate through the blood and extracellular fluids where they can be transmitted by vectors. A few reports have indicated the possibility of the transmission of microfilarial infection from mother to offspring¹⁻³. We have infected rats with adult females of the rodent filaria, *Dipetalonema viteae*, and report here that the transfer of *D. viteae* microfilariae does indeed occur through the placenta. Exposure to specific antigens early in development can readily induce immune tolerance⁴⁻⁶. We observed that a state of reversible immune unresponsiveness occurred in rats as a result of pre- and post-natal exposure to microfilariae and this was associated with impairment of T-cell responses. The induction of tolerance allowed *D. viteae* infective larvae to reach maturity in the Fischer rat which is otherwise innately resistant to this parasite.

All experiments were performed in inbred Fischer/ICO rats. Infant rats were bred in our animal facility and the adults were obtained commercially (IFFA CREDO). Infective larvae of *D. viteae* cannot reach maturity in Fischer rats but surgically transplanted female adults of *D. viteae* will establish and release microfilariae which circulate in the peripheral blood for about 120 days⁷.

In the present investigation, 10 mature female worms were collected under sterile conditions from hamsters infected 90 days previously and were transferred individually with blunt forceps or a probe within a few minutes of collection, into a subcutaneous pocket in the back of the anaesthetized female animals. A microfilaraemia was first detected on day 2, reaching a peak around day 20 to 30 and then declining and remaining at a low level until about days 120-130 after implantation. Seven days after infection, pairs of non-infected males and microfilaraemic females were mated and litters were born between 21 and 35 days later. All offspring irrespective of sex showed the presence of microfilariae in their peripheral blood. The number of microfilariae remained steady in the circulation until day 100 after birth and declined thereafter, disappearing from the peripheral blood at about days 120-130 after birth. The duration of microfilaraemia was much the same in the mothers and their offspring. The microfilaraemia resulting in the mother rats and in their offspring is shown in Table 1.

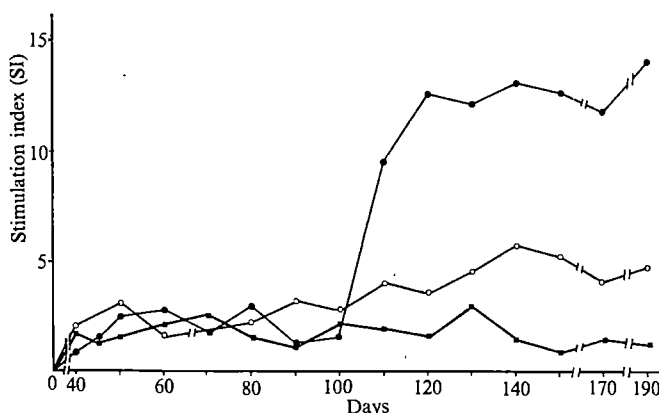


Fig. 1 *In vitro* lymphocyte proliferation in response to *D. viteae* antigens (prepared as described previously¹²) by spleen cells obtained from rats born to microfilaraemic (MR) or noninfected rats (NR). The degree of lymphocyte stimulation is expressed by the stimulation index (SI)

$$SI = \frac{\text{average c.p.m. in stimulated cultures}}{\text{average c.p.m. in unstimulated (control) cultures}}$$

The level of incorporation in unstimulated cultures was variable but within the range of $1,125 \pm 377$ to $3,322 \pm 764$ c.p.m. for normal spleen cells and within the range of $1,265 \pm 585$ to $3,698 \pm 798$ c.p.m. for spleen cells from infected animals. Each point represents the mean value and standard deviations were below 10% in all groups. Two rats were tested at each point. The optimal conditions for lymphocyte transformation towards parasite antigens, T and B cell mitogens were predetermined in both infected and noninfected Fischer rats (data not shown). Spleen cells were incubated for 96 h with parasite antigens ($250 \mu\text{g ml}^{-1}$). Proliferation response of spleen cells taken from MR either towards filarial antigens (●) or to *Ascaris lumbricoides* antigens (○). The response of spleen cells from NR toward filarial antigens (■) was measured at the same time. Glass bead fractionation was performed on each occasion. A few fibres of nylon-wool was placed into the barrel of a 5 ml glass syringe and cleaned glass beads ($150 \mu\text{m}$ size unispheres, Sigma) were added up to the 3 ml mark. It was then preincubated in RPMI plus 5% fetal calf serum (FCS) for 45 min at 37°C . Spleen cells ($0.75-1 \times 10^8$) in 2 ml of the same medium, prewarmed to 37°C , were run into the column, which was incubated for a further 30 min at 37°C . Non-adherent cells were then eluted with 25 ml of warmed medium and were washed three times with RPMI only to remove FCS and finally resuspended in RPMI supplemented with the synthetic tripeptide glycyl-histidyl-lysine (20 ng ml^{-1}), L-glutamine ($29 \text{ mg per } 100 \text{ ml}$) and antibiotics. Lymphocyte transformation studies were performed in microtitre plates (Nunc) utilizing triplicate 0.1 ml cultures containing 0.5×10^6 spleen cells per culture well. Four hours before the end of the culture period $1 \mu\text{Ci}$ of [^3H]thymidine (1 Ci mmol^{-1} , CEA) was added to each culture. Microcultures were collected on a Titertek cell collector (Skatron). Filter disks were dried and transferred to scintillation vials with 10 ml of scintillation fluid (Lipo Luma) and assayed with a Nuclear Chicago liquid scintillation counter.

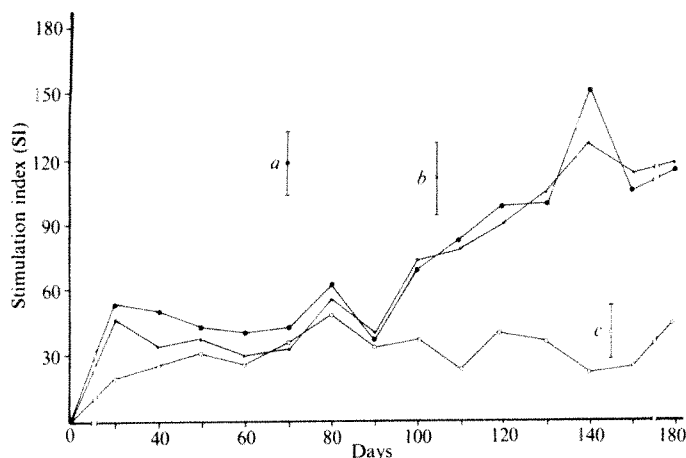


Fig. 2 The proliferative responses to PHA (*), Con A(●) and LPS(○) of spleen cells from rats born to microfilaraemic mothers, plotted as a function of time after infection. Spleen cells non-adherent to glass beads were used throughout as described in the legend to Fig. 1. SI values were calculated as described for Fig. 1. The level of incorporation in control cultures was variable but within the range of $1,052 \pm 309$ c.p.m. to $4,398 \pm 844$ c.p.m. for normal spleen cells and within the range of $1,013 \pm 586$ to $6,741 \pm 756$ for cells from infected animals. Each point represents the mean value from the rats and standard deviations were below 12% in all groups. Spleen cells (0.5×10^6) were incubated for 72 h with PHA, Con A ($100 \mu\text{g ml}^{-1}$) and for 96 h with LPS ($250 \mu\text{g ml}^{-1}$). The response of spleen cells from control rats (NR) to Con A (a), PHA (b) or LPS (c) was assayed at the same time as for rats born to microfilaraemic mothers (MR). [^3H]thymidine incorporation was measured as in Fig. 1. a, b, and c are the mean \pm one standard deviation stimulation indices for normal spleen cells in response to Con A, PHA and LPS respectively.

Further experiments were undertaken to examine whether the transfer of microfilariae from mothers to the litter occurs through the placenta during gestation or via the milk during lactation. The litters born to microfilaraemic mothers were removed immediately after birth and kept with non-infected foster mothers for suckling. They always showed the presence of microfilariae in their circulation. In contrast, microfilariae were never observed in any of the litters born to non-infected mothers and kept with microfilaraemic foster mothers for nursing. The body fluids from the fetus removed from microfilaraemic mothers by caesarian delivery always contained microfilariae. These data strongly suggest that the transfer of microfilariae occurs through the placenta and not through the milk.

The possible tolerizing effect of the transplacentally transferred microfilariae was tested by measuring the immune response of the offspring towards filarial antigen *in vitro* and *in vivo*. Antigens prepared from *D. viteae* adult worms had no effect

on spleen cells from normal Fischer rats *in vitro*. They were able to stimulate cells from rats in which transplacental transfer of microfilariae had occurred but only when the microfilariae had disappeared from the peripheral blood (Fig. 1). There was no significant response of spleen cells from normal or infected rats towards antigens of *Ascaris lumbricoides* at any time following birth. The spleen cells from normal or microfilariae infected rats immunized with ovalbumin (OA, a total of $200 \mu\text{g}$ with complete Freund's adjuvant per rat) at day 70 after birth were, however, stimulated in the presence of OA (data not shown). In the studies with bancroftian⁸ and brugian⁹ filariases or with various experimental filariases¹⁰⁻¹² in which both adult worms and microfilariae coexist, it has been shown that the infected individuals or animals with microfilaraemia respond poorly or not at all to filarial antigens. The results of the present study indicate that the causative agent for the antigen-specific cellular unresponsiveness towards *D. viteae* antigens may be due to microfilariae or their derived factors.

The response of spleen cells, obtained from rats born to microfilaraemic mothers and showing the presence of microfilariae in the circulation, to phytohaemagglutinin (PHA) and concanavalin A (Con-A) was depressed but their response to lipopolysaccharide (LPS) was unaffected (Fig. 2). This suggests that the function of the T lymphocytes that respond to PHA and Con-A was impaired. However the significance of the depressed response of spleen cells to mitogens is controversial, although it has often been observed in diseases where defects in cellular immunity (antigen specific or nonspecific) have been documented¹³.

Antibodies and soluble filarial antigens may be transferred from mother to fetus across the placenta. We were, however, unable to detect a significant level of *D. viteae* circulating antigens in the serum obtained from rats born to microfilaraemic mothers at any period after birth using anti-*D. viteae* hyperimmune rabbit serum in the radioimmunoprecipitation PEG assay (data not shown). This could have been due to the dilution of circulating antigens (present in the mothers at a relatively low level) after transfer. Alternatively, it may be that the numbers of microfilariae present in the offspring were too low to produce detectable circulating antigen or that the adult worm is the only source of such antigen. Antibodies to *D. viteae* filarial antigens or to microfilariae were not detected by haemagglutination or the immunofluorescence assay in the serum from the offspring as long as microfilariae circulated in their peripheral blood (data not shown). The results show that although the response of B lymphocytes to LPS was not affected, the production of parasite specific antibodies was impaired.

The effects of acquired tolerance on the susceptibility or resistance to *D. viteae* infection were also investigated. The

Table 1 Microfilaraemia and adult worm recovery on various days after infection or birth

Infection	Mean microfilaraemia \pm s.d. per 100 mm ³ on various days after infection										Mean no. of adults recovered from 3 rats on day	
	7	20	30	40	60	70	90	110	120	130	45	60
Female rats implanted with 10 <i>D. viteae</i> female worms	90 \pm 40	680 \pm 210	650 \pm 140	210 \pm 80	240 \pm 72	190 \pm 56	70 \pm 32	40 \pm 20	10 \pm 6	0	5 \pm 3*	ND
Rats born to microfilaraemic	20 \pm 8	24 \pm 10	18 \pm 6	16 \pm 6	18 \pm 8	16 \pm 4	16 \pm 6	10 \pm 4	4 \pm 2	0	—	—
Rats born to noninfected mothers	0	0	0	0	0	0	0	0	0	0	—	—
MR infected with <i>D. viteae</i> stage-3 larvae†	18 \pm 6	18 \pm 6	16 \pm 4	18 \pm 8	24 \pm 6	60 \pm 12	70 \pm 10	20 \pm 8	4 \pm 2	0	7 \pm 3‡	4 \pm 2‡
NR infected with <i>D. viteae</i> stage-3 larvae†	0	0	0	0	0	0	0	0	0	0	0	0

Samples of blood in duplicate (10 or 20 μl) were taken with a glass disposable microsampling pipette from the retroorbital plexus of rat, spread directly onto a slide, covered with a cover slip and immediately examined under the microscope and counted. As the number of microfilariae decreased, blood samples were treated with distilled water and microfilariae were isolated on 5 μm Millipore membranes. Microfilariae were then resuspended in Hanks Wallace solution and counted. Rats born either to microfilaraemic or non-infected mothers were infected at day 75 after birth with 100 *D. viteae* stage-3 larvae. Ticks (*Ornithodoros tartakowskyi*) infected 4 weeks previously were washed briefly in 70% alcohol, rinsed in sterile saline and then dissected with fine sharpened needles in Ringer's solution containing antibiotics. The stage-3 larvae obtained were washed free of tick tissues, counted and injected subcutaneously into rats. Five rats per group were used. ND, not determined.

* Worms were calcified.

† Infection rate with *D. viteae* was 80%. This includes 3 \pm 2 which were dead and encapsulated in a granulomatous nodule.

‡ This includes 2 \pm 1 which were dead and encapsulated in a granulomatous nodule.

male rats born to microfilaraemic mothers and harbouring microfilariae in their circulation became susceptible to *D. viteae*. A varying percentage of infective larvae of *D. viteae* became established and developed into adult worms. These worms produced microfilariae which were observed in the peripheral blood of the rats from about day 55 after infection. In contrast, no microfilariae were seen in the peripheral blood and no worms were found at post-mortem in rats, age-matched and born to non-infected mothers, following inoculation with *D. viteae* infective larvae 75 days after birth (Table 1). On the other hand, when rats born either to microfilaraemic or to non-infected mothers were exposed to *Schistosoma mansoni* cercariae there were no differences between the numbers of *S. mansoni* worms (immature) recovered at day 21 after infection from each group (data not shown). These results suggest that a state of antigen-specific immune unresponsiveness had developed in the animals as a result of prior sensitization with specific parasite antigens in the early stages of their life. In this investigation, we have shown that the suppression of the host's immune responsiveness also suppresses innate resistance and permits a filarial nematode to establish itself in an otherwise refractory host.

We thank Bernadette Bonnel, Jean-Paul Lejeune, Anita Caron and Pierre Billaut for technical assistance and maintenance of the animal colony. This work was supported by CNRS (ERA 422) and INSERM(U 167).

Received 20 April; accepted 12 July 1982.

1. Mantovani, A. *Parasitologia* 6, 1-3 (1964).
2. Bloomfield, R. D., Suarez, J. R. & Malangit, A. C. *J. natn. med. Ass.* 70, 587-598 (1978).
3. Sucharit, S. & Rongsriyam, Y. S. *E. Asian J. trop. Med. publ. Hlth* 11, 416 (1980).
4. Dresser, D. & Mitchison, N. *Adv. Immun.* 8, 129-181 (1968).
5. Etlinger, H. & Chiller, J. *J. Immun.* 122, 2558-2563 (1979).
6. Hasek, M. & Chutna, J. *Immun. Rev.* 46, 3-26 (1979).
7. Haque, A. *et al. Clin. exp. Immun.* 43, 1-9 (1981).
8. Ottesen, E. A., Weller, P. F. & Heck, L. *Immunology* 33, 413-421 (1977).
9. Piessens, W. F. *et al. J. Clin. Invest.* 65, 172-179 (1980).
10. Portaro, J. K., Britton, S. & Ash, L. R. *Expl. Parasit.* 40, 438-446 (1976).
11. Weller, P. F. *Cell Immun.* 37, 369-382 (1978).
12. Haque, A. A., Ogilvie, B. M. & Capron, A. *Expl. Parasit.* 52, 25-34 (1981).
13. Bryceon, A. in *Prog. Immun.* 2, 161-170 (1974).

Lithium chloride induces partial responsiveness to LPS in nonresponder B cells

Shigeaki Ishizaka & Göran Möller

Department of Immunobiology, Karolinska Institute, Wallenberg Laboratory, Lilla Frescati 7, S-104 05 Stockholm 50, Sweden

The lipopolysaccharide (LPS)-nonresponder mouse strains C3H/HeJ, C57BL/10ScCR and C57BL/10ScN do not respond to LPS acting as a polyclonal B-cell activator^{1,2}, a mitogen¹⁻⁵, or an adjuvant^{6,7}. The genetic basis for the defective LPS responses has been extensively studied in C3H/HeJ and C57BL/10ScCR mice, in which it was demonstrated that a single gene locus on chromosome 4 was responsible for LPS unresponsiveness^{8,9}. Lithium chloride, a potent inhibitor of adenylate cyclase, not only improved lymphocyte activity in a patient with adenosine deaminase deficiency^{10,11} but also enhanced the phytohaemagglutinin (PHA)-induced responses of normal human lymphocytes^{12,13}. Therefore, we investigated whether LiCl could restore LPS responsiveness in spleen cells of C3H/HeJ mice. We show here that LPS, in the presence of LiCl, induced polyclonal IgM and IgG antibody formation and DNA synthesis in C3H/HeJ mouse spleen cells *in vitro*. Moreover, LiCl (10 mM), which by itself is non-mitogenic, increased RNA synthesis in spleen cells from both LPS-nonresponder and high responder strains; in contrast, LPS failed to increase RNA synthesis in cells from such LPS-nonresponder strains as C3H/HeJ and B10ScCR mice.

C3H/HeJ mouse spleen cells (10^7 cells ml^{-1}) were cultured with LPS in the presence of (10 mM LiCl) to determine whether LiCl affects the B-cell nonresponsiveness to LPS in these cells.

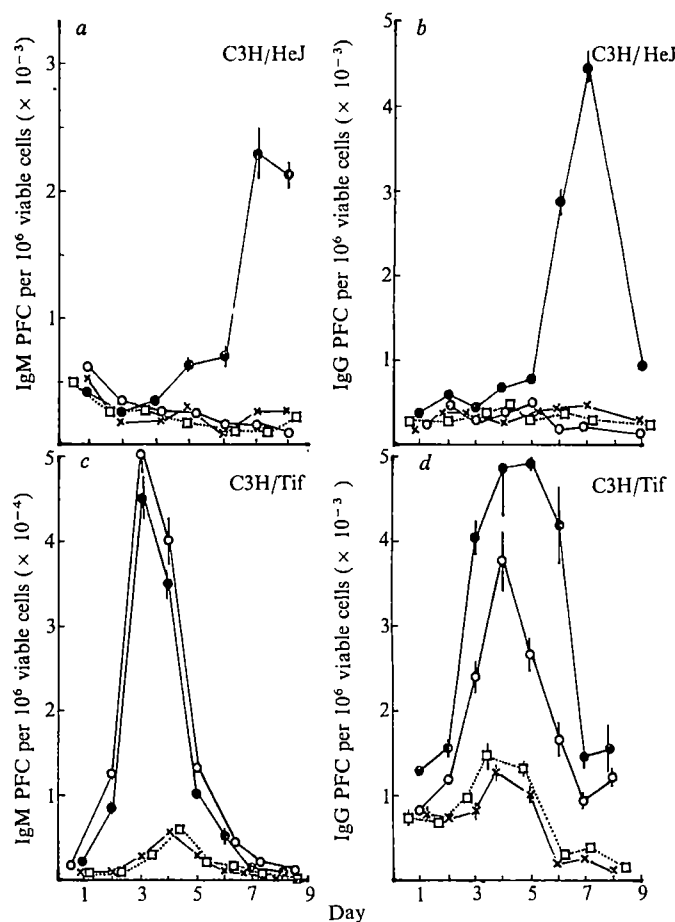


Fig. 1 Kinetics of polyclonal IgM and IgG antibody production induced by LPS in the presence of LiCl in C3H/HeJ and C3H/Tif spleen cells. Spleen cells (10^7 cells ml^{-1}) from unprimed C3H/HeJ or C3H/Tif mice were cultured for 9 days with $150 \mu\text{g ml}^{-1}$ of LPS extracted from *Escherichia coli* 055:B5 by the phenol-water method (given by T. Holme, Karolinska Institute) in the presence or absence of LiCl (10 mM) in RPMI 1640 medium (Gibco) plus 10% fetal bovine serum. IgM and IgG PFC per 10^6 viable cells were counted after the indicated days by using the protein A plaque assay²⁴. *a, b*: IgM and IgG PFC in C3H/HeJ cells induced by $150 \mu\text{g ml}^{-1}$ LPS + 10 mM LiCl (●), $150 \mu\text{g ml}^{-1}$ LPS (○), or 10 mM LiCl (□); ×, unstimulated control. *c, d*: IgM and IgG PFC in C3H/Tif cells induced by $150 \mu\text{g ml}^{-1}$ LPS + 10 mM LiCl (●), $150 \mu\text{g ml}^{-1}$ LPS (○) or 10 mM LiCl (□); ×, unstimulated control. Each point represents the mean \pm s.e. (vertical bars) of triplicate experiments.

(Preliminary tests suggested that 10 mM is the optimal concentration of LiCl.) In the presence, but not the absence, of LiCl, LPS induced polyclonal IgM and IgG antibody responses in the spleen cells that peaked after 6-7 days of culture. LiCl alone did not stimulate polyclonal IgM and IgG antibody responses (Fig. 1), and was non-toxic to cultured spleen cells, as judged by Trypan blue exclusion. On the other hand, LPS induced a polyclonal IgM response in spleen cells from high responder strain C3H/Tif that peaked on day 3. LPS plus LiCl did not affect the magnitude of the IgM response, whereas the IgG response was increased compared with that induced by LPS alone (Fig. 1*c, d*). Thus, the magnitude of the observed stimulation by LPS plus LiCl in spleen cells from C3H/HeJ mice (indices of maximal stimulation of IgM and IgG were 14.2 and 9.4 plaque-forming cells (PFC) respectively) was very similar to that induced by LPS alone in C3H/Tif spleen cells (maximal stimulation indices of IgM and IgG were 17.5 and 7.9 respectively), because the background PFC of high responder cells was higher than that of nonresponder cells (Fig. 1). LiCl plus LPS also stimulated DNA synthesis in C3H/HeJ and C3H/Tif spleen cells, although the response was smaller with C3H/HeJ cells. Neither LiCl nor LPS alone stimulated DNA synthesis in C3H/HeJ spleen cells (Table 1).

Table 1 Effect of LiCl on LPS-induced DNA synthesis in C3H/HeJ and C3H/Tif spleen cells

Strain	Addition to culture	1	2	c.p.m. on day: 3	4	5
C3H/HeJ	None	402 ± 26	281 ± 14	200 ± 87	185 ± 82	226 ± 82
	LPS	570 ± 63	242 ± 13	311 ± 34	304 ± 57	347 ± 22
	LiCl	531 ± 61	147 ± 6	146 ± 36	142 ± 12	245 ± 52
	LiCl + LPS	662 ± 62	580 ± 19	1,052 ± 175	748 ± 58	800 ± 107
C3H/Tif	None	186 ± 33	167 ± 18	307 ± 50	902 ± 115	999 ± 35
	LPS	407 ± 86	2,432 ± 248	5,338 ± 261	10,897 ± 815	5,969 ± 224
	LiCl	253 ± 55	192 ± 52	369 ± 30	1,579 ± 223	1,167 ± 258
	LiCl + LPS	366 ± 51	5,387 ± 492	11,441 ± 370	17,494 ± 745	7,606 ± 232

C3H/HeJ spleen cells (10^6 cells ml^{-1}) were cultured in RPMI 1640 medium containing 5% fetal bovine serum. LPS was added to a final concentration of $30 \mu\text{g ml}^{-1}$. LiCl was also added to a final concentration of 10 mM per well of a round-bottomed microtitre plate (Nunc). At appropriate times, the wells were then pulsed with $1 \mu\text{Ci ml}^{-1}$ of ^3H -thymidine for 6 h. The cells were collected using a multiple automated sample collector and processed for scintillation counting. Results are the mean c.p.m. \pm s.e. of triplicate experimental cultures.

Polyclonal IgM antibody responses induced by LPS in cells from high responder mice peaked at day 3 of culture in the conditions used, whereas the peak response of cells from LPS-nonresponder mice occurred at day 6 (Fig. 1). There was a kinetic difference between LPS-high responder and nonrespon-

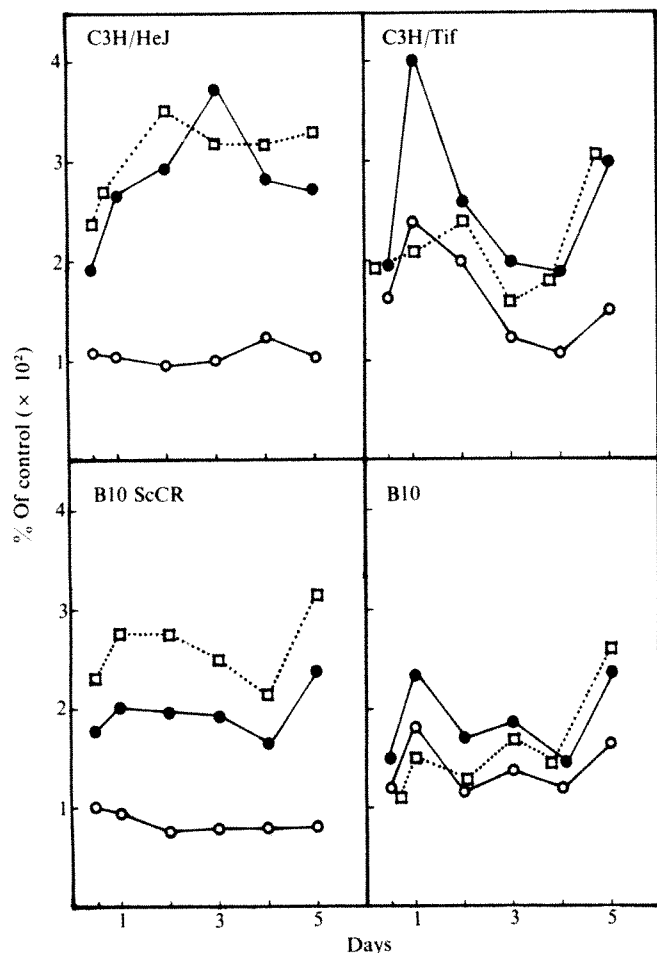


Fig. 2 Time course of RNA synthesis in spleen cells from LPS-nonresponder and high responder mice induced by LPS plus LiCl. Spleen cells (2×10^6 cells per 0.2 ml) from C3H/HeJ, B10ScCR, C3H/Tif and B10 mice were cultured for 5 days with $150 \mu\text{g ml}^{-1}$ LPS, 10 mM LiCl, or $150 \mu\text{g ml}^{-1}$ LPS plus 10 mM LiCl per well of microplates (Nunc) in RPMI 1640 medium supplemented with 5% fetal bovine serum. These cell cultures were pulsed with $0.2 \mu\text{Ci } ^3\text{H}$ -uridine (specific activity 37 Ci mmol^{-1} ; NEN) for 3 h at various times. The reactions were stopped by adding cold 5% trichloroacetic acid, and cells were collected with a multisample collector for analysis. RNA synthesis induced by LPS (○), LiCl (□), or LPS plus LiCl (●) are expressed as the mean experimental c.p.m. per control c.p.m. $\times 10^{-2}$.

der mice with respect to LPS-induced polyclonal IgM responses. It seems unlikely that the polyclonal IgM responses induced by LPS in spleen cells from C3H/HeJ mice was secondary to polyclonal T-cell activation induced by LiCl, as LiCl did not stimulate DNA or RNA synthesis in T cells and thymocytes from C3H/HeJ mice (data not shown). Furthermore, LPS non-responsiveness in B cells from C3H/HeJ mice is due to a B-cell defect rather than the activation of suppressor T cells or the dysfunction of helper T cells and macrophages^{14,15}. It is possible that LiCl induces the expression of a LPS receptor in B cells from C3H/HeJ mice, but it is unknown whether there are any differences in the binding of LPS to B cells from LPS-high responder and nonresponder mice^{16,17}. Therefore, the possibility of B-cell activation in LPS-nonresponder mice induced by this mechanism remains open.

LiCl did not induce DNA synthesis or IgM and IgG antibody synthesis in cells from C3H/HeJ mice, but increased ^3H -uridine incorporation in cells from C3H/HeJ mice; LPS did not have this effect. LPS plus LiCl increased DNA, RNA and IgM antibody synthesis in C3H/HeJ spleen cells and B cells (Table 2), suggesting that nonresponsiveness to LPS in C3H/HeJ spleen cells was partly overcome by the new RNA synthesis induced by LiCl. LiCl produced greater stimulation of RNA synthesis in cells from the LPS-nonresponder strains C3H/HeJ and B10ScCR than in cells from the LPS-high responder strains C3H/Tif and B10. Furthermore, LPS plus LiCl induced later RNA synthesis in cells from LPS-nonresponder mice than in cells from high responder mice (Fig. 2). These results show that the increase in RNA synthesis and polyclonal antibody synthesis induced by LPS plus LiCl occurs later in C3H/HeJ cells than in cells from a LPS-high responder strain.

LPS induced a relatively low rate of RNA synthesis in LPS-high responder strains compared with DNA and IgM synthesis, in contrast to results obtained with other polyclonal B-cell activators¹⁸. Furthermore, recent cell fusion studies indicate that LPS nonresponsiveness of C3H/HeJ cells is due to a dysfunction of the cytoplasm and not the nucleus¹⁹. Therefore, it seems possible that LPS stimulates translation of mRNA rather than new mRNA synthesis. Although LPS failed to induce RNA synthesis in spleen cells of LPS-nonresponder mice, the nonresponsiveness to LPS is probably alleviated by direct or indirect effects of LiCl on murine chromosomes^{20,21} leading to induction of new RNA synthesis, perhaps through the modification of cyclic AMP-dependent events in cells. In addition, there is indirect evidence that α -amanitin, an inhibitor of RNA synthesis, inhibited polyclonal antibody responses induced by κ -carrageenan²², but not LPS-induced responses at an early stage of the response. Also, actinomycin D, an inhibitor of ribosomal RNA synthesis, suppressed polyclonal antibody formation induced by both LPS and κ -carrageenan¹⁸. This suggests that LPS stimulates the translation of RNA by ribosomes in B cells of LPS-nonresponder mice and that LiCl may

Table 2 DNA, RNA and IgM synthesis in C3H/HeJ B cells induced by LPS and LiCl

Addition	C3H/HeJ spleen cells		C3H/HeJ B cells		
	DNA (c.p.m.)	RNA (c.p.m.)	DNA (c.p.m.)	RNA (c.p.m.)	IgM PFC per 10^6 viable cells
None	564 ± 109	189 ± 11	356 ± 26	473 ± 63	170 ± 15
LPS	625 ± 59 (1.1)	207 ± 8 (1.1)	485 ± 36 (1.4)	260 ± 22 (0.5)	180 ± 20 (1.1)
LiCl	571 ± 133 (1.0)	753 ± 88 (4.0)	268 ± 33 (0.8)	2,721 ± 197 (5.8)	202 ± 15 (1.2)
LPS + LiCl	2,019 ± 247 (3.6)	790 ± 207 (4.2)	805 ± 69 (2.3)	2,328 ± 204 (4.9)	513 ± 11 (3.0)
Con A	42,786 ± 1,342 (75.9)	NT	498 ± 22 (1.4)	NT	NT

C3H/HeJ B-cell suspensions were prepared by treatment of spleen cells with monoclonal anti-Thy 1.2 antibody (final concentration 10^{-3} ; NEN) and complement²³, followed by removal of adherent cells in plastic Petri dishes as described previously²². C3H/HeJ B cells (2×10^6 cells per 0.2 ml) were cultured with $150 \mu\text{g ml}^{-1}$ LPS, 10 mM LiCl, $150 \mu\text{g ml}^{-1}$ LPS plus 10 mM LiCl or concanavalin A (Con A) in RPMI 1640 medium supplemented with 5% fetal bovine serum for 3 days. Synthesis of DNA and RNA was measured by pulsing with $1 \mu\text{Ci ml}^{-1}$ ^3H -thymidine and $1 \mu\text{Ci ml}^{-1}$ ^3H -uridine for 3 h. IgM PFC were estimated by using the protein A plaque assay²⁴. The values in parentheses are stimulation indexes. NT, not tested.

induce the production of ribosomal RNA rather than mRNA and then elicit polyclonal antibody synthesis. In LPS-nonresponder mice, LPS could not efficiently stimulate translation due to insufficient polyribosome formation, without the produc-

tion of new ribosomal RNA induced by LPS, thereby resulting in nonresponsiveness to LPS. The alteration in LPS-nonresponder cells by LiCl may be important in the analysis of the biochemical events of B-cell activation by LPS.

Received 25 March; accepted 20 July 1982.

1. Watson, J. & Riblet, R. *J. exp. Med.* **140**, 1147–1161 (1974).
2. Coutinho, A., Forni, L., Melchers, F. & Watanabe, T. *Eur. J. Immun.* **7**, 325–328 (1977).
3. Sultzer, B. M. *Infect. Immunity* **5**, 107–113 (1972).
4. Vogel, S. N., Hansen, C. T. & Rosenstreich, D. L. *J. Immun.* **122**, 619–622 (1979).
5. Coutinho, A., Gronowicz, E. & Sultzer, B. M. *Scand. J. Immun.* **4**, 139–143 (1975).
6. Skidmore, B. J., Chiller, J. M., Morrison, D. S. & Weigle, W. O. *J. Immun.* **114**, 770–775 (1975).
7. Talcott, J. A., Ness, D. B. & Grumet, F. C. *Immunogenetics* **2**, 507–515 (1975).
8. Watson, J., Riblet, R. & Taylor, B. A. *J. Immun.* **118**, 2088–2093 (1977).
9. Coutinho, A. & Meo, T. *Immunogenetics* **7**, 17–24 (1978).
10. Polmar, S. H. in *Inborn Errors of Immunity and Phagocytosis* (eds Guttie, F., Seakins, J. W. T. & Harkness, R. A.) (MTP Press, Lancaster, 1979).

11. Gelfand, E. W. & Dush, H.-M. in *In Vitro Induction and Measurement of Antibody Synthesis in Man* (eds Fauci, A. S. & Ballieux, R. E.) 309 (Academic, New York, 1979).
12. Gelfand, E. W., Dush, H.-M., Hastings, D. & Shore, A. *Science* **203**, 365–367 (1979).
13. Shenkman, L., Borkowsky, W. & Shopin, B. *Med. Hypotheses* **6**, 1–6 (1980).
14. Glode, L. M., Scher, I., Osborne, B. & Kern, M. J. *Immun.* **125**, 102–107 (1980).
15. Coutinho, A. *Scand. J. Immun.* **5**, 129–140 (1976).
16. Gregory, S. H., Zimmerman, D. H. & Kern, M. J. *Immun.* **125**, 102–107 (1980).
17. Forni, L. & Coutinho, A. *Eur. J. Immun.* **8**, 56–62 (1978).
18. Ishizaka, S. & Morisawa, S. (in preparation).
19. Watanabe, T. & Ohara, J. *Nature* **290**, 58–59 (1981).
20. Szabo, K. T. *Lancet* **ii**, 849 (1969).
21. Szabo, K. T. *Nature* **225**, 73–75 (1970).
22. Ishizaka, S., Otani, S. & Morisawa, S. *J. Immun.* **118**, 1213–1218 (1977).
23. Gorczynski, R. M., Miller, R. G. & Phillips, R. A. *J. Immun.* **108**, 547–551 (1972).
24. Gronowicz, E., Coutinho, A. & Melchers, F. *Eur. J. Immun.* **6**, 588–590 (1976).

Random components in mutagenesis

P. L. Foster*, E. Eisenstadt†‡ & J. Cairns†

* Interdisciplinary Programs in Health,

† Department of Microbiology and ‡ Laboratory of Toxicology, Harvard School of Public Health, 665 Huntington Avenue, Boston, Massachusetts 02115, USA

The mutability of DNA varies enormously from one base pair to another. Part of this variation is due to the specificity of the reaction between mutagen and base, but much of the variation is due to unknown causes. A genetic system developed by Miller and colleagues¹ allows the mutation frequencies of a large number of different base pairs in the *lacI* gene of *Escherichia coli* to be compared. For example, Coulondre and Miller² found that the sites most readily mutated by UV light are almost 100 times more often mutated than the least susceptible sites. A recently completed study³ of mutagenesis with neocarzinostatin (NCS) in the *lacI* gene has prompted us to re-examine some previous studies^{2,4,5} of mutagenesis in this gene. Our analysis, reported here, suggests that the mutations induced by certain mutagens fall into two classes: mutations in one class are clearly distributed non-randomly, that is, they are very common at some sites and significantly less common at others; mutations in the second class, however, occur at low frequency and appear to be randomly distributed. Both classes of mutations seem to occur only at damaged bases.

One of the largest collections of fully characterized point mutations is a set of about 600 nonsense mutations generated in the *lacI* gene by UV light². There are 64 sites in this gene that can yield amber (TAG) or ochre (TAA) codons by single base changes. Overall, the distribution of UV-induced mutations among these sites is obviously non-random; 3 of the 64 possible nonsense codons were each represented more than 50 times, 3 did not appear in the collection at all and many occurred

only once or twice. Because UV-mutagenesis clearly involves non-random elements, it has often been assumed that the entire process is non-random and that each base pair occupies some unique position in a continuum of mutability. However, if we disregard both the base substitutions being monitored and the distribution of events over the genetic map, and instead simply look at the distribution of frequencies, it becomes apparent that the rarer mutations form a Poisson distribution (that is, their frequencies appear to be randomly distributed) with a mean of 2.7 occurrences per site (Fig. 1a). Of the 64 sites, 41 fall into this distribution. (We have included in this set the 3 codons in which no nonsense mutations were detected, because a mean occupancy of 2.7 would be expected to leave 3 out of 41 sites unoccupied.)

Solely on the basis of the frequencies of the different mutations, we therefore conclude that UV-induced mutations arise from two classes of events: apparently random, low-frequency occurrences (LFOs) that account for about one-third of the mutations, and non-random, high-frequency occurrences (HFOs) that account for the rest. This conclusion is greatly strengthened when we consider the base sequences at the 64 sites. As pointed out by Coulondre *et al.*⁵, all of the dozen or so 'hotspots' for UV-induced G·C to A·T transitions found in the *lacI* gene are at sites of adjacent pyrimidines. Based on our analysis, we find that all 23 of the sites for HFOs are base pairs at which the pyrimidine has a pyrimidine next to it; in contrast, 15 of the 41 LFO sites involve base pairs where the pyrimidine has purines on both sides of it. This difference between the sites for HFOs and LFOs is highly significant ($\chi^2 = 9.4$, $P < 0.005$). Thus, it seems likely that UV-induced HFOs require interaction between adjacent pyrimidines (for example, they may be due to pyrimidine dimers⁶ or some other lesion involving a pyrimidine pair⁷) whereas LFOs do not. As the UV-induced LFOs occur at every monitorable site in the *lacI* gene and can generate each of the five base pair changes that yield nonsense codons (G·C to A·T, T·A or C·G; A·T to T·A or C·G), it seems likely that UV light is producing, at

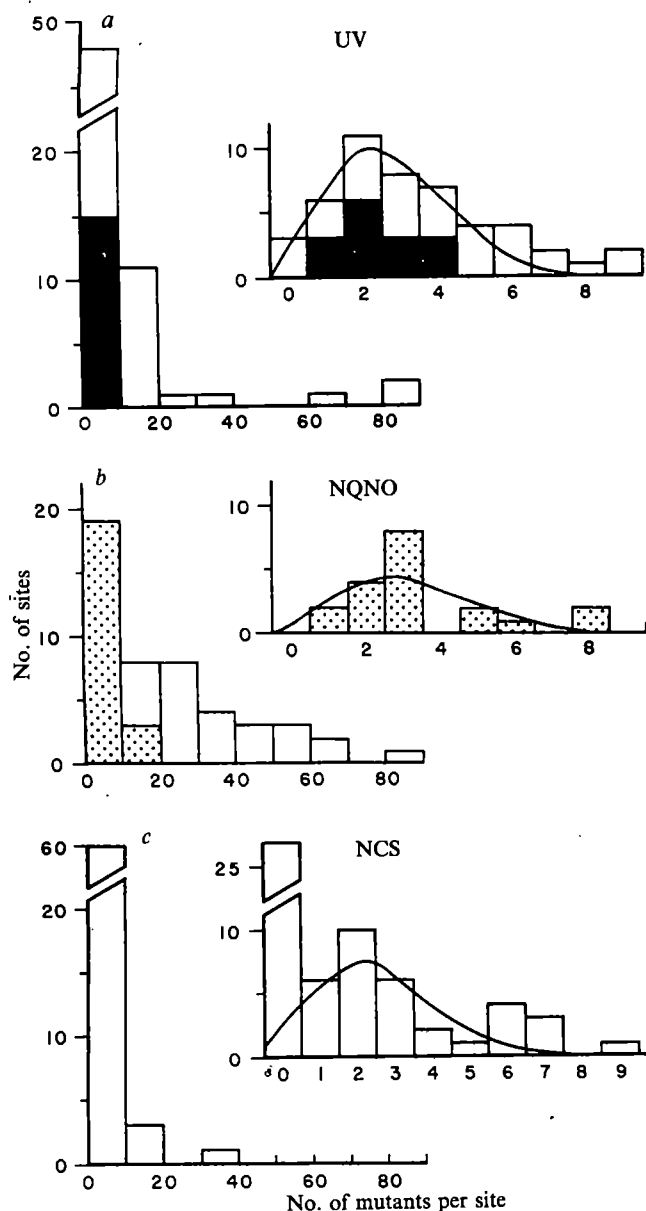


Fig. 1 The frequency distributions of approximately 600 UV-induced² (a), 1,000 NQNO-induced² (b) and 200 NCS-induced³ (c) amber and ochre mutations in the *lacI* gene of *E. coli*. The histograms show the number of sites at which k mutations were found. The inset histograms show the lower end of the distributions for individual values of k from 0 to 9. These have been matched to Poisson distributions, whose means were estimated using the relationship:

$$m = (k+1) \frac{N_{k+1}}{N_k}$$

where N_k and N_{k+1} are the number of sites at which occurred k and $k+1$ mutations, respectively. The observed values of N_k for several consecutive classes were used to calculate m . The total number of sites (N_T) expected to fall into the Poisson distribution was calculated from the observed values of N_k using the relationship:

$$N_T = \frac{\sum_{k=0}^{\infty} N_k}{e^{-m} \sum_{k=0}^{\infty} m^k / k!}$$

The total number of mutations (T) in the Poisson distribution was then calculated as:

$$T = mN_T$$

a, UV-induced mutations at all sites are shown; sites where the pyrimidine of the target base pair is not adjacent to another pyrimidine are shaded. The Poisson distribution includes 111 mutations at 41 sites ($N_k \leq 6$); $m = 2.7$ was estimated from N_0 to N_2 . b, NQNO-induced mutations at G-C sites only are shown; sites where G-C transversions occur are stippled. The Poisson distribution included 63 mutations at 18 sites ($N_k \leq 8$); $m = 3.3$ was estimated from N_1 and N_2 . c, NCS-induced mutations at all sites are shown. The Poisson distribution included 72 mutations at 29 sites ($N_k \leq 6$); $m = 2.5$ was estimated from N_1 and N_2 .

random, all possible base substitutions at every base pair.

For a base pair to be a site for UV-induced HFOs, it clearly is not enough that its pyrimidine be adjacent to another pyrimidine. Of the 49 base pairs in the *lacI* gene that involve adjacent pyrimidines and are capable of generating nonsense codons, only 23 were sites for HFOs. For example, of the 14 Py-C-A-G and Py-C-A-A sequences in the *lacI* gene where transition of the C to a T yields a nonsense codon, 10 are sites for HFOs and cover a 10-fold range of mutability; the remaining 4 are sites for LFOs only. So some factor other than neighbouring base sequence must be important in determining the frequency of mutation at these sites. As the loss of the *uvrB*-dependent excision repair pathway has no effect on the relative UV mutability of most sites⁴, accessibility to this repair pathway cannot account for most of the variation in mutation frequency. We conclude, therefore, that the mutability of different pairs of adjacent pyrimidines is probably determined by the effect that some factor, such as DNA secondary structure, has on the frequency of formation of premutational lesions.

Mutagenesis by UV light requires induction of the 'SOS response'⁸. Because LFOs seem to be random and indiscriminate, it was conceivable that they represent untargeted mutagenesis due to error-prone DNA repair or replication. We therefore extended our analysis to the published results for 4-nitroquinoline-*N*-oxide (NQNO), which is also an SOS-dependent mutagen⁹. Coulondre and Miller² have shown that NQNO is highly specific for G-C base pairs, with a strong preference for producing G-C to A-T transitions. We see here that NQNO, like UV light, produces a non-random distribution of HFOs plus an apparently random distribution of LFOs (Fig. 1b). However, in contrast to the UV results, the mutations that are produced by the NQNO-induced HFOs and LFOs are distinguishable—all the G-C transitions arise from HFOs, whereas nearly all the G-C transversions arise from LFOs (any G-C transitions produced by LFOs cannot be detected because the sites for transitions are dominated by HFOs). Since untargeted mutagenesis would be expected to include base substitutions of A-T sites, the failure of NQNO to mutate A-T base pairs implies that both HFOs and LFOs result from targeted events. We can conclude, therefore, that the low level of apparently random mutagenesis following treatment with mutagens such as NQNO or UV light cannot be accounted for by untargeted mutagenesis.

Another SOS-dependent mutagen that we have examined is NCS (Fig. 1c). Like UV light and NQNO, it produces both HFOs and LFOs; the LFOs include examples of each of the five kinds of base changes that can be detected as nonsense mutations. However, NCS mutates only 37 of the 64 sites in the *lacI* gene; the sites it fails to mutate include examples of all monitorable base changes³. As in the case of NQNO, the failure of NCS to mutate nearly half the monitorable sites in the *lacI* gene would be difficult to explain if untargeted mutagenesis were making a major contribution to SOS-dependent mutagenesis.

Although we have looked at only a few mutagens, we now realize that the available data are less informative than they seem at first sight. For example, because of the nature of the genetic code, an analysis of nonsense mutations cannot distinguish which of the four pyrimidine pairs (T-T, T-C, C-T, or C-C) is the best target for UV mutagenesis; any effect attributable to the pyrimidine pair is confounded by the constraints on both the event being monitored (which can be transitions or transversions at cytosines, but only transversions at thymines) and the reading frame (for example, substitutions for thymine cannot be monitored at the first position of a codon). To separate these factors would require an analysis of missense mutations, which are not subject to the same base sequence restrictions. But there is yet another problem. In any mutant collection, the rarer events (LFOs) will be present in rather small numbers and, because of this, their frequency distribution will be dominated by the variance of the Poisson distribution. Thus, although we have said that LFOs appear to be randomly

distributed, this suggestion needs to be confirmed by a much larger collection of LFOs.

We can, however, draw some important conclusions about LFOs. First, like HFOs, they are likely to be targeted, that is, to occur only at damaged bases. Second, they can account for a significant proportion of the mutations arising after exposure to a mutagen (for example, one-third of the UV-induced mutations). Last, they seem to be able to induce all base changes—the LFO lesion seems to be non-informational and to allow the insertion of a base at random. These conclusions suggest that, unlike HFO lesions, which are clearly specific to each mutagen, the LFO lesion may be the same for a number of mutagens; one example of such a common lesion would be an apurinic or apyrimidinic site.

P.L.F. was a fellow of the Interdisciplinary Programs in Health and was supported by grant CR807809-01-1 from the US Environmental Protection Agency. E.E. was supported in part by US NIH grant CA26135.

Received 12 April; accepted 26 July 1982.

1. Miller, J. H. in *The Operon* (eds Miller, J. H. & Reznikoff, W. S.) 31–88 (Cold Spring Harbor Laboratory, New York, 1978).
2. Coulondre, C. & Miller, J. H. *J. molec. Biol.* **117**, 557–606 (1977).
3. Foster, P. L. & Eisenstadt, E. *J. Bact.* (submitted).
4. Todd, P. A. & Glickman, B. W. *Proc. natn. Acad. Sci. U.S.A.* **79**, 4123–4127 (1982).
5. Coulondre, C., Miller, J. H., Farabaugh, P. J. & Gilbert, W. *Nature* **274**, 775–780 (1978).
6. Fisher, G. J. & Johns, H. E. in *Photochemistry and Photobiology of Nucleic Acids* Vol. 2 (ed. Wang, S.-Y.) 225–295 (Academic, New York, 1976).
7. Lippke, J. A., Gordon, L. K., Brash, D. E. & Haseltine, W. A. *Proc. natn. Acad. Sci. U.S.A.* **78**, 3388–3392 (1981).
8. Witkin, E. M. *Bact. Rev.* **40**, 869–907 (1976).
9. Kondo, S., Ichikawa, H., Iwa, K. & Kato, T. *Genetics* **66**, 187–217 (1970).

Unique cell lines harbouring both Epstein-Barr virus and adult T-cell leukaemia virus, established from leukaemia patients

Naoki Yamamoto, Tadashi Matsumoto*, Yoshio Koyanagi, Yuetsu Tanaka & Yorio Hinuma

Institute for Virus Research, Kyoto University, Sakyo-ku, Kyoto 606, Japan

* Institute of Cancer Research, Faculty of Medicine, Kagoshima University, Kagoshima 880, Japan

Members of three distinct classes of animal virus have been associated with naturally occurring neoplasias in man: Epstein-Barr virus (EBV)¹, a DNA virus belonging to herpesvirus group, papillomavirus², and a novel human RNA (retro) virus^{3–8}, human T-cell leukaemia virus or adult T-cell leukaemia (ATL) virus. We have established seven continuous cell lines from ATL patients and 0.1–7% of these cells consistently express ATL-specific antigens (ATLA)^{8,9}. EBV-associated nuclear antigen (EBNA)¹⁰ is also found in more than 90% of these cells. We have cloned cells from two of these lines and show here that both ATLA and EBNA were present in the same B-cell clone carrying surface immunoglobulin (sIg).

Patients with ATL investigated in this study were admitted from September 1980 to December 1981 to the hospitals in the Kagoshima Prefecture, where ATL is endemic¹¹. Clinical features and some of the data from laboratory investigations of the patients are shown in Table 1. Most frequently they reveal leukocytosis, with a high percentage of leukaemic cells showing indented or lobulated nuclei. Most of these cells spontaneously form rosettes with sheep erythrocytes (E). The percentage of cells with sIg is usually very low. All patients tested had antibodies against EBV and ATL.

Peripheral leukocytes separated by Ficoll-Conray gradient centrifugation were cultured in 10-cm plastic tubes (1 ml per tube) with RPMI 1640 medium supplemented with 10–20% fetal calf serum and antibiotics. The initial cell density was adjusted to 5×10^6 cells per ml. The cultures were incubated at 37 °C in a humidified 7.5% CO₂ atmosphere for 1 week without any change of medium. Thereafter, they were fed twice weekly. After 1 month of culture, they started to grow continuously and the number of cells increased rapidly. The originating cell lines were designated ATLB 1–7. They grew in suspension forming clumps of cells and have been maintained in continuous culture for 6–22 months. Morphologically, they were lymphoblastoid cell lines with a doubling time of about 24–48 h. The cells unexpectedly had sIg in 5–75% of the population (sIgG + sIgM) and were mostly negative for E-receptors as shown in Table 2. No T-cell growth factor¹² was used throughout these experiments. The establishment and more detailed characteristics of these lines will be reported elsewhere.

The acetone or methanol fixed cells were examined for EBNA and for ATLA by indirect immunofluorescence as described previously^{7–10}. For EBNA tests, standard sera obtained from healthy persons were used. For ATLA staining, human sera from ATL patients were used initially but it was impossible to detect ATLA because of the presence of cytoplasmic IgG in cells of these lines. Therefore, mouse monoclonal antibodies (GIN-14 and GIN-2) raised against one (p28) of at least six polypeptides of ATLA in MT-2 cells¹³ used in combination with fluorescein isothiocyanate (FITC)-conjugated goat anti-mouse IgG. These monoclonal antibodies reacted with ATLA-positive but not -negative cell lines. (Y.T. *et al.*, in preparation.) All seven ATL-derived cell lines gave a positive reaction in both EBNA and ATLA staining with three reference sera from anti-EBV reactive healthy persons and with two monoclonal antibodies to ATLA, respectively. They failed to react with three negative control sera or with supernatants from control cultures. From 0.1 to 7% cells were consistently ATLA positive, whereas more than 90% of cells showed EBNA staining. The sera did not react with cells of 17 ATL-unrelated lines of haematopoietic origin⁴.

These data demonstrate that all lines established from the seven patients with ATL express ATLA in a small fraction of the cells and EBNA in the majority of cells. This could indicate that ATLA was expressed in a small number of T cells, although most of the cells in these lines were negative for E rosettes, whereas EBNA was present in a much larger number of B cells. To clarify this, cells of two lines, ATLB 1 and 2, were cloned by using Seaplaque agarose (Marine Colloids) as described previously¹⁴. Three weeks after inoculation colonies of varying size were obtained in soft agarose. Cloning efficiencies ranged from 0.1% and 3.1% in ATLB 1 and 2 lines, respectively. Clones of ATLB 2 cells were isolated by Pasteur pipette and subcultured for 7 days in liquid medium. Then, they were stained for ATLA and EBNA. Table 3 clearly shows that two-thirds of the clones are positive for ATLA and they are all positive for EBNA at the same time. Most of them had sIg (IgG + IgM) ranging from 0.1 to 60% of the total cell population (data not shown). Analogous results were obtained by analysing clones of ATLB 1 cells. These data show that ATLA and EBNA are not mutually exclusive and present in the same B-cell population expressing sIg.

It is interesting to analyse the infection of B lymphoblasts with ATL and EBV. It is well established that EBV is present in B lymphocytes *in vivo* and can infect them *in vitro*¹. However infectivity of ATL seems not to be restricted to T cells in view of the following preliminary observations: (1) Not only T but also B, non-T and non-B cells either of primary or of established cell lines were infectable with ATL by cocultivation with an ATL-producer T-cell line, MT-2 (ref. 9 and N.Y. unpublished observation). (2) Proviral DNA of ATL was found after cell fractionation in B-cell-enriched fractions as well as in T-cell fractions of the blood from ATL patients (M. Yoshida, personal communication).

Table 1 Clinical and laboratory data of patients with ATL

Case no.	Specimen	Sample date	Age/sex	White blood count	% Leukaemic cells	% Cells with		Antibodies against	
						E-RFC	sIg	EBV-VCA	ATLA
1	PB	9/80	54/F	66,400	80	94.6	1.2	160	160
2	PB	1/81	39/F	148,600	83	93.1	0.7	ND	ND
3	PB	5/81	65/F	23,300	40	95.6	2.8	80	10
4	LN	2/81	63/F	6,800	1	74.9 (84.6)	2.7 (0.9)	160	160
5	PB	12/81	55/M	35,700	62	43.0	0.4	ND	NS
6	LN	12/81	66/F	121,600	87	76.0 (14.2)	6.3 (0.4)	160	80
7	PB	12/81	67/F	12,000	75	85.8	2.0	80	40

PB, peripheral blood; LN, lymph node; ND, not done; NS, nonspecific fluorescence. Number in parentheses shows a result of lymph node.

Table 2 Characteristics of ATL cell lines from ATL patients

Cell line	Months after establishment	% Cells with			% Of fluorescent cells	
		E-R	sIgG	sIgM	ATLA*	EBNA
ATLB 1	20	<1	<1	55	1~2	>90
ATLB 2	15	<1	35	5	2~4	>90
ATLB 3	10	<1	18	40	3~4	>90
ATLB 4	13	<1	<1	67	5~7	>90
ATLB 5	5	<1	<1	5	0.1~0.2	>90
ATLB 6	5	<1	ND	ND	0.1~0.2	>90
ATLB 7	5	<1	<1	75	<0.1	>90

E-R, receptor for sheep erythrocytes.

* ATLA-positive cells were determined by mouse monoclonal antibodies (GIN-14 and GIN-2) as described in the text. The use of both antibodies resulted in very similar percentage of immunofluorescence-positive cells.

Available data indicate that it is hard to obtain continuous cultures of ATL-positive T-cell lines from patients with ATL. On the other hand, it is well established that EBNA-positive B-cell lines are easily obtained from patients with African Burkitt's lymphoma and infectious mononucleosis or even from normal EBV-seropositive persons by the activation of residential EBV genomes¹. These data suggest that ATL-positive T cells do not have the growth capacity in the present conditions of *in vitro* cultivation while EBV-positive B cells grow easily in tissue culture. It is likely that proliferation of ATL-positive leukaemic T cells *in vivo* are fully sustained by factors present in the serum whereas EBNA-positive B cells are strictly suppressed in ATL patients as in normal EBV-seropositive donors.

Van der Loo *et al.*³ and later Gallo and his colleagues independently found the C-type virus from patients with T-cell malignancies, mycosis fungoides and Sézary's syndrome⁴⁻⁶. The latter group named their virus isolates human T-cell leukaemia

virus (HTLV) and characterized them extensively. Importantly, HTLV was reactive with serum from Japanese ATL patients. They also showed that Japanese ATL and Western ATL were clinically and haematologically indistinguishable, and that the retrovirus of Japanese ATL was also indistinguishable from Western isolates in serological studies¹⁵⁻¹⁷. These data indicate that HTLV is closely related, if not identical, with ATL. A worldwide survey of the distribution of the virus is required.

The monoclonal antibody (GIN-14) used in the present studies only reacted with ATLA-positive but not -negative cell lines. This mouse antibody precipitated at least the p28 polypeptide of the ATLA complex from ATL-positive cells. The p28 polypeptide was shown to be precipitated consistently from ³⁵S-methionine-labelled ATL-positive cells when anti-ATLA-positive human sera were reacted¹³. Moreover, another monoclonal antibody (GIN-2) precipitated both the p28 and p19 polypeptides at the same time. This suggests that p28 and p19 polypeptides are related antigenically. Tryptic peptide analysis of these polypeptides are in progress. Preliminary data by the use of metabolic labelling also showed that one of the ATL 2 clones synthesized p24 which is a major protein of ATL^{7,13} by the use of human anti-ATLA-positive sera.

Our data may raise the suspicion that B cells act as the ATL reservoir in infected individuals. ATL may initially infect any class of lymphocyte or stem cell of haematopoietic origin before or after the EBV infection but an interaction between type C and herpes viruses occurs as suggested by previous observations^{1,18,19}. So far ATL patients without antibodies to EBV have not been detected in our laboratory where sera from more than 100 cases have been examined. Further studies will clarify whether or not the interaction of EBV and ATL is important in the etiology of ATL.

We thank H. zur Hausen for critical review of the manuscript. This work was supported by grants-in-aid from the Ministry of Education, Science and Culture, and from the Ministry of Health and Welfare of Japan.

Table 3 Per cent of ATLA- and EBNA-positive cells in cloned ATL 2 cells

Clone no.	% Cells with		Clone no.	% Cells with	
	ATLA	EBNA		ATLA	EBNA
1	35	>90	16	<1	>90
2	<1	>90	17	35	>90
3	0	>90	18	3	>90
4	5	>90	19	0	>90
5	0	>90	20	<1	>90
6	<1	>90	21	40	>90
7	40	>90	22	<1	>90
8	<1	>90	23	40	>90
9	2	>90	24	<1	>90
10	4	>90	25	0	>90
11	0	>90	26	0	>90
12	0	>90	27	8	>90
13	8	>90	28	40	>90
14	0	>90	29	0	>90
15	<1	>90	30	13	>90

Received 25 May; accepted 4 August 1982.

- Epstein, M. A. & Achong, B. G. (eds) *The Epstein-Barr Virus* (Springer, Berlin, 1979).
- zur Hausen, H. & Gissmann, L. *Viral Oncology* (ed. Klein, G.) 433-447 (Raven, New York, 1980).
- Van der Loo, E. M. et al. *Virchows Arch. B Cell Path.* **31**, 193-203 (1979).
- Poiesz, B. J. et al. *Proc. natn. Acad. Sci. U.S.A.* **77**, 7415-7419 (1980).
- Reitz, M. S., Poiesz, B. J., Ruscetti, F. W. & Gallo, R. C. *Proc. natn. Acad. Sci. U.S.A.* **78**, 1887-1891 (1981).
- Poiesz, B. J., Ruscetti, F. W., Reitz, M. S., Kalyanaraman, V. S. & Gallo, R. C. *Nature* **294**, 268-271 (1981).
- Hinuma, Y. et al. *Proc. natn. Acad. Sci. U.S.A.* **78**, 6476-6480 (1981).
- Yoshida, M., Miyoshi, I. & Hinuma, Y. *Proc. natn. Acad. Sci. U.S.A.* **79**, 2031-2035 (1982).
- Yamamoto, N., Okada, M., Koyanagi, Y., Kannagi, M. & Hinuma, Y. *Science* **217**, 737-739 (1982).
- Reedman, B. M. & Klein, G. *Int. J. Cancer* **11**, 499-520 (1973).
- The T- and B-Cell Malignancy Study Group Japan. *J. clin. Oncol.* **11**, 11 (1981).
- Morgan, D. A., Ruscetti, F. W. & Gallo, R. C. *Science* **193**, 1007-1008 (1976).
- Yamamoto, N. & Hinuma, Y. *Int. J. Cancer* (in the press).
- Yamamoto, N. & zur Hausen, H. *Nature* **280**, 244-245 (1979).
- Catovsky, D. et al. *Lancet* **i**, 639-643 (1982).
- Robert-Guroff, M. et al. *Science* **215**, 975-978 (1982).
- Gallo, R. C. et al. *Lancet* **i**, 683 (1982).
- Kufe, D. et al. *Proc. natn. Acad. Sci. U.S.A.* **70**, 737-741 (1973).
- Markham, P. D., Ruscetti, F. W., Salahuddin, S. Z., Gallagher, R. E. & Gallo, R. C. *Int. J. Cancer* **23**, 148-156 (1979).

T4 late transcripts are initiated near a conserved DNA sequence

Alan C. Christensen & Elton T. Young

Department of Biochemistry SJ-70, University of Washington, Seattle, Washington 98195, USA

Bacteriophage T4 late transcription is unusual, among prokaryotes, in its complexity. Late transcription requires the host RNA polymerase, the products of T4 genes 33, 45 and 55, and other small polypeptides, the genes of which have not been identified¹. In addition the DNA template must be 'competent' for late transcription. First the DNA must contain the substituted base 5-hydroxymethyl cytosine in place of cytosine (this requirement is eliminated by a mutation in the T4 *alc* gene)^{1,2}. Second, the DNA must be replicating, although late transcription can be uncoupled from DNA replication by mutations in the T4 genes coding for DNA ligase (gene 30) and DNA exonuclease (gene 46)^{1,3}. We report here the location of the initiation sites of the messenger RNAs (mRNAs) synthesized *in vivo* from four late genes (genes 21, 22, 23 and 36) by S₁ nuclease mapping and we have determined the DNA sequences at these sites. We have found strong homology to the sequence TATAAATAC-TATT immediately upstream from the 5' ends of the late messages and we suggest that this sequence is specifically recognized by the complex responsible for late transcription. Also, we have examined gene 23 mRNA synthesized in the absence of DNA replication using the 30⁻ 46⁻ mutant described above and find that it is identical to the true late transcript synthesized in normal infections.

Previous work has suggested that gene 23 (which codes for the major capsid protein) is transcribed into a monocistronic message and into two or more polycistronic messages⁴. Transcription has been shown to be initiated upstream from genes 21, 22 and 23, with all these transcripts extending into gene 23 (refs 4, 5). Much of the DNA of this region has been sequenced (our unpublished data, ref. 6; M. Parker, personal communication; M. Showe, personal communication). It has also been suggested that genes 36, 37 and 38 are cotranscribed⁷ and part of this group of genes has also recently been sequenced⁸. These regions of the T4 genome are shown in Fig. 1, with locations of the genes indicated. The restriction fragments used as probes for S₁ nuclease mapping^{9,10} and DNA sequencing are indicated, and are labelled 1 to 4. These fragments were isolated, strand separated, 5' end-labelled, and subjected to the Maxam and Gilbert¹¹ sequencing reactions.

Portions of the same labelled DNA preparation were hybridized to RNA extracted 20 min after infection from T4-infected *Escherichia coli*. The DNA-RNA hybrids were then treated with S₁ nuclease to digest all of the DNA that was not in a

hybrid form with an RNA molecule. The DNAs were then resolved on a DNA sequencing gel and the gel was subjected to autoradiography (Fig. 2). Lanes G, A, T and C represent the results of Maxam and Gilbert sequencing reactions. DNA in the O lanes was incubated without S₁. In all cases there is a low level of background at every position in these lanes with the majority of the radioactivity remaining in the full length fragment. DNA in the N lanes was incubated in the absence of RNA and then digested with S₁. There was no radioactivity evident in these lanes, except for a variable amount of completely undigested probe remaining at the top of the lane due to the incomplete digestion by S₁. DNA in the R lanes was hybridized with late RNA and treated with S₁. These lanes have bands corresponding to 5' ends of RNA molecules. The bands are of an intensity that correlates with the amount of RNA added (data not shown). There is generally a cluster of bands in the R lanes which is probably due to variable cleavage at the junction between single-stranded DNA and DNA-RNA hybrid. It is, therefore, impossible to determine exactly which nucleotide corresponds to the first nucleotide of the mRNA, but it is probably within two or three nucleotides of the major band of each cluster. A correction must also be made because the sequencing reactions remove the base in question and leave a 3'-phosphate, while S₁ leaves the base intact and creates 3'-hydroxyl ends¹². The sense strand sequences surrounding the 5' ends of the late transcripts are shown in Fig. 3. The sense strand was independently sequenced in every case. The lengths of the tails of the arrows in the figure are proportional to the intensity of the corresponding band as measured by densitometry.

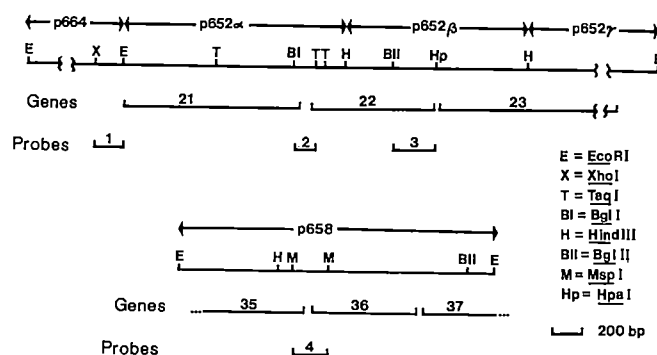
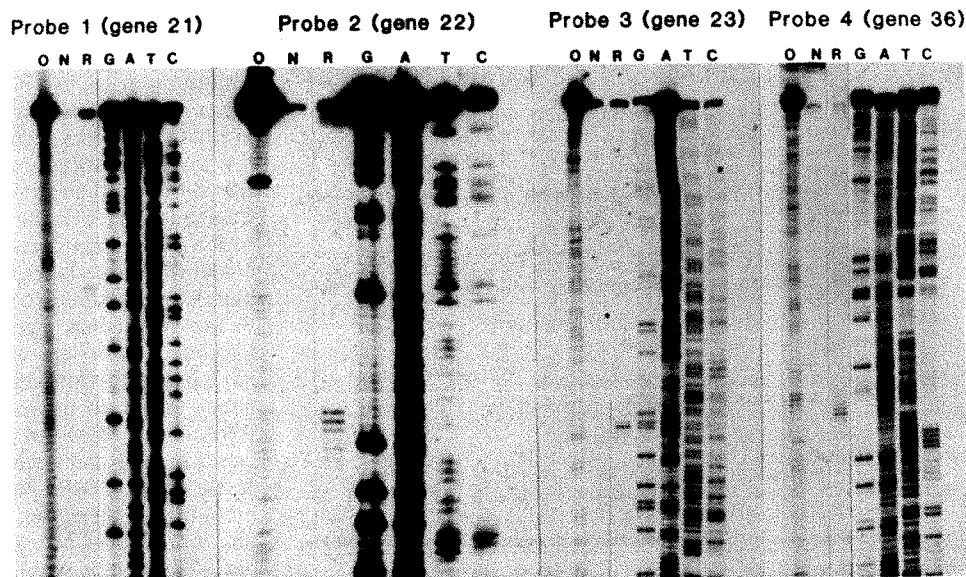


Fig. 1 Restriction maps. Clones were isolated as described in Mattson *et al.*²¹ and Young *et al.*²². The *EcoRI* fragment containing genes 18, 19, 20, PIP (ref. 23) and part of 21 is called 664. The *EcoRI* fragment containing genes 21 to 23 is 652. This fragment was subcloned with *HindIII* into pBR313, forming 652A, 652B and 652C as previously described^{4,22}. The T4 inserts of 652A, 652B and 652C were transferred into pBR322 and renamed 652α, 652β and 652γ. The *EcoRI* fragment containing genes 35 to 37 is 658. Genes 22 and 23 are placed by DNA sequence data (for gene 22, M. Parker, personal communication and our unpublished data; for gene 23, ref. 6). Genes 35, 36 and 37 are placed by comparison to published DNA sequence data⁸. The location of gene 21 is estimated from genetic data and the size of the polypeptide (M. Showe, personal communication and ref. 24). Fragments used for sequencing and S₁ mapping were isolated as described below. Enzymes were obtained from Bethesda Research Labs or New England Biolabs. Agarose was from SeaKem; acrylamide and bisacrylamide were from Bio-Rad. Probe 1: Plasmid 664 was digested with *XhoI* and *EcoRI* and the 170-base pair (bp) band purified by electrophoresis in a 5% polyacrylamide gel (20:1 acrylamide:bisacrylamide) in TBE buffer (90 mM Tris, 90 mM Boric Acid, 1 mM EDTA) followed by electroelution in 1/2×TBE buffer at 50 V overnight. The electroeluate was loaded onto a Whatman DE-52 column (1 cm diameter, bed volume 1 ml) in 50 mM Tris, 10 mM EDTA, 150 mM NaCl, pH 7.4. The DNA was eluted from the column with 50 mM Tris, 10 mM EDTA, 1M NaCl, pH 7.4, ethanol precipitated, washed with 80% ethanol, dried in vacuum and resuspended in 10 mM Tris, 1 mM EDTA, pH 8.0. Probe 2: Plasmid 652α was digested with *BglII* and *TaqI* and the 140-bp fragment was isolated from a 5 per cent polyacrylamide gel as described above. Probe 3: Plasmid 652β was digested with *HpaI* and *BglII* and the 275-bp fragment was isolated from a 5 per cent polyacrylamide gel as described above. Probe 4: Plasmid 658 was digested with *HindIII* and *BglII*. The 1,200-bp fragment was resolved on a 1% agarose gel and electroeluted as above. The purified fragment was then digested with *MspI* and the 220-bp fragment was isolated from a 5% polyacrylamide gel as described above.

Fig. 2 Maxam–Gilbert sequencing and S_1 nuclease mapping. Probes were obtained as described in Fig. 1 legend. DNA fragments were strand separated on a 5% polyacrylamide gel as described in Maxam and Gilbert¹¹. Single-stranded DNA fragments were identified by staining the gel in $0.5 \mu\text{g ml}^{-1}$ ethidium bromide, and the gel slices were cut out and electroeluted as described in Fig. 1 legend. The electroeluate was precipitated with isopropanol, washed with 80% ethanol, dried in vacuum, resuspended in 0.3 M sodium acetate and transferred to a 1.5 ml Eppendorf tube. Single-stranded DNA fragments were 5' end-labelled as follows: DNA (about 10–20 pmol of 5' ends) was ethanol precipitated and washed with 80% ethanol. $100 \mu\text{Ci}$ [γ - ^{32}P]ATP (specific activity 1,000–3,000 Ci mmol⁻¹ in aqueous solution, NEN) was added to the wet DNA pellet and the mixture was dried in vacuum. The DNA and ATP were resuspended in water and stock solutions were added to give a final volume of 50 μl and final concentrations of 50 mM Tris pH 7.6, 10 mM MgCl_2 , 100 μM EDTA, 50 mM dithiothreitol, 1 mM spermidine HCl, 300 μM ADP. Final concentrations of DNA 5' ends and [γ - ^{32}P]ATP were approximately 0.2 μM and 1 μM , respectively. Five units of polynucleotide kinase (New England Biolabs) was then added. Incubation was at 37°C for 1 h, followed by addition of 200 μl 2.5 M ammonium acetate and 750 μl ethanol. The sample was precipitated (at -70°C) twice, washed with 80% ethanol and dried. The DNA was then resuspended in 10 mM Tris, 1 mM EDTA, pH 8.0 and distributed into tubes for S_1 mapping and DNA sequencing. The G and C reaction tubes received half as much of the DNA sample as any of the other tubes. DNA sequencing reactions were done as in Maxam and Gilbert¹¹, except that the samples were transferred to fresh tubes following the 90°C incubation and four drying steps were done with the addition of 40 μl H_2O before the last three. T4 late RNA was prepared by infecting *E. coli* B^E at 4×10^8 cells ml⁻¹ with T4D at a multiplicity of infection of 10, at 30°C. RNA was extracted 20 min after infection by the method of Hagen and Young²⁵. S_1 nuclease mapping was done by the method of Nasmyth *et al.*¹⁰ using 192 U of S_1 nuclease (Bethesda Research Labs) per reaction. Samples were run on 35 cm \times 43 cm \times 0.4 mm gels (Bethesda, sequencing gel apparatus SO) consisting of 7.6 per cent acrylamide, 0.4 per cent bisacrylamide, 50 per cent urea in TBE buffer at 65 W per gel. Probes numbered as in Fig. 1 were used as indicated at the top of the figure. Lanes G, A, T and C are DNA sequencing reactions G, G+A, T+C and C, respectively. Lanes O, N and R are S_1 mapping experiments. Lane O is a no S_1 control using 30 μg of late RNA, lane N is a no RNA control and lane R was a reaction done with 30 μg of late RNA. Autoradiography was on Kodak XAR film.



The sequences are aligned to emphasize the absolutely conserved sequence TATAAATA and the highly conserved CTATT immediately following. The sequences were determined further upstream (to at least -80 with respect to the 5' end of the mRNA) and no significant homology was observed (data not shown). Nor is there any similarity at -35 , either to one another or to the -35 sequence of *E. coli* promoters. As far as we are aware, this conserved sequence is not found anywhere in the T4 DNA sequenced to date, with the following exceptions: (1) the four cases mentioned here; (2) in front of the late genes 24 (M. Parker, personal communication; T. Elliott, personal communication), and *e* (lysozyme)¹³; and (3) in front of gene 32 (ref 26).

That these 5' ends are due to transcription initiation rather than mRNA processing has been shown in two of these cases. Kassavetis and Geiduschek⁵ have shown that there are RNA molecules with 5'-diphosphate or triphosphate termini, that have most likely arisen through initiation, whose 5' ends map at essentially the same positions as the 5' ends mapped in Fig. 2, lanes 2R and 3R (upstream of genes 22 and 23, respectively).

We have examined the mRNA produced in an infection with the T4 triple mutant *tsL56* (gene 43, DNA polymerase) *amH39X* (gene 30, DNA ligase) *amN130* (gene 46, DNA exonuclease). When this mutant infects *E. coli* at 30°C, DNA replication and late transcription both occur. At the restrictive temperature of 43°C, DNA replication is blocked but late transcription occurs even in the absence of replication because of the mutations in genes 30 and 46 (ref. 3). One hypothesis to explain this uncoupling of late transcription from DNA replication is that nicks are transiently formed in the DNA during replication. The absence of ligase mimicks this aspect of DNA replication by allowing nicks which form in the DNA to remain unsealed. The mutation in DNA exonuclease merely serves to prevent degradation of the infecting DNA³. S_1 nuclease mapping using probe 3 (gene 23) and RNA extracted from T4 *tsL56 amH39X amN130*-infected cells is shown in

Fig. 4. It can be seen that there is no homologous RNA produced at early times at 30°C (lane W) or at 43°C (lane Y) and that the RNA synthesized at late times at 43°C (lane Z) appears identical to the late RNA of the wild-type infection (lane R) or the mutant infection at 30°C (lane X). This shows that 5' ends of gene 23 late transcripts in the replication uncoupled mutant *tsL56 amH39X amN130* are identical to those of normal replication-dependent transcripts. This means that random nicks in the DNA do not serve as sites for initiation of transcription. Assuming that this is the case for all late genes, two possible conclusions can be drawn: (1) there is an enzyme which nicks the DNA at specific sites. These nicks serve as initiation sites for RNA polymerase¹⁴. DNA ligase seals these nicks, thereby preventing transcription initiation and DNA replication either prevents the ligase-mediated sealing or greatly increases the occurrence of these nicks; (2) either DNA replication, or random nicking of the DNA in the absence of both replication and ligase, alters the topology of the DNA template, allowing initiation of late transcription at specific promoter sequences.

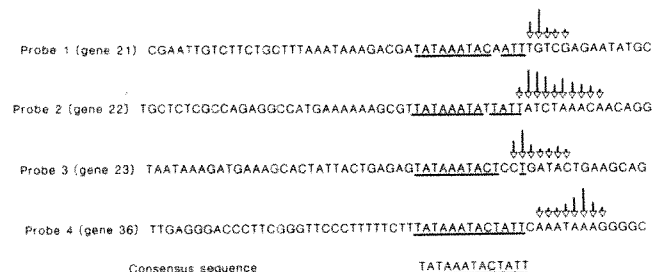


Fig. 3 DNA sequences of the mRNA identical (sense) strand near the positions of 5' ends revealed by S_1 mapping. Densitometry of the bands in lanes R of Fig. 2 was done using a Joyce-Loebl scanning densitometer with integrator. The lengths of the tails of the arrows are proportional to the measured band density. The consensus sequence is indicated at the bottom of the figure and bases identical to it are underlined in the DNA sequences.

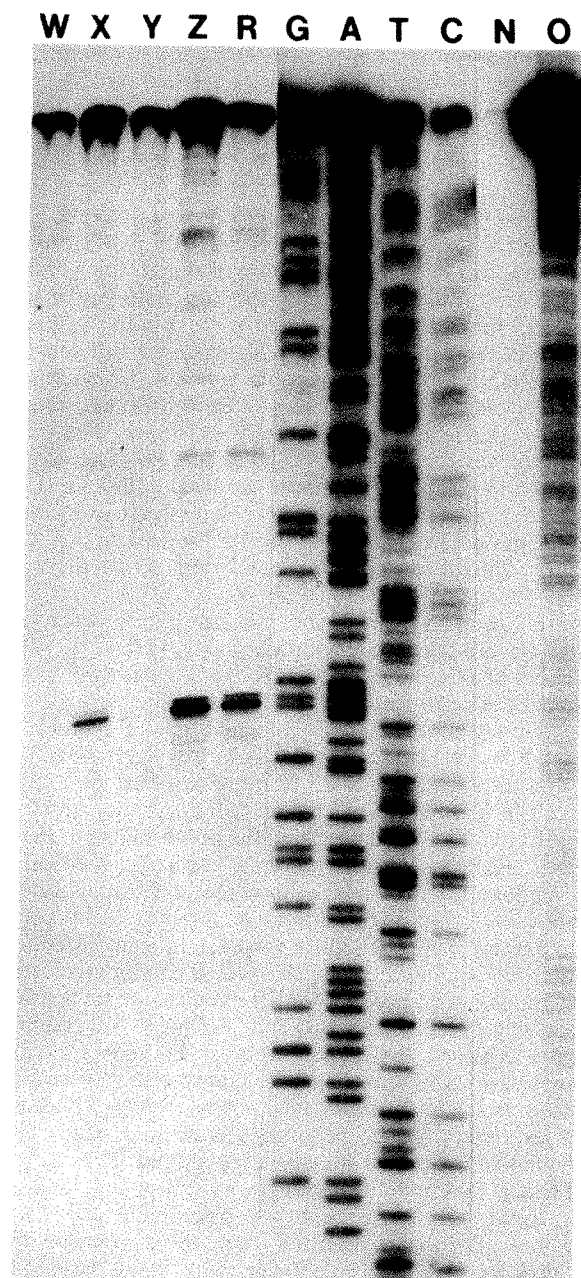


Fig. 4 Replication-uncoupled transcription. Probe 3 was used (gene 23). Lanes G, A, T, C, N, O and R are as described in Fig. 2. Lanes W, X, Y and Z are S_1 mapping experiments performed as described in Fig. 2 using RNA extracted from *E. coli* infected with the T4 mutant *tsL56 amH39X amN130*. Lanes W and X are from an infection of *E. coli* B^F at 30 °C with RNA extracted at 5 and 20 min after infection, respectively. Lanes Y and Z are from an infection of *E. coli* B^F at 43 °C with RNA extracted at 3 and 18 min after infection, respectively.

Transcriptional specificity in prokaryotes is conferred in large part by DNA sequences at -10 (Pribnow box) and -35 relative to the initiation site¹⁵⁻¹⁷. Temporal control of gene expression in the bacteriophage life cycle can be achieved by synthesis of a new RNA polymerase molecule with different specificity. For example, T7 directs the synthesis of an RNA polymerase which does not recognize the -35 and -10 regions of *E. coli* or T7 class I promoters, but instead recognizes a specific 23-base pair sequence¹⁸. Alternatively, phage-specified proteins can modify the existing RNA polymerase, altering its DNA sequence specificity. This phenomenon is well documented in *Bacillus subtilis*. For example, phage SP01 synthesizes gp 28 which displaces the σ subunit of the host RNA polymerase. This activates middle promoters which have -35 and -10 sequences different from those of *B. subtilis* promoters or SP01 early promoters¹⁹. T4 is similar to SP01 in that it modifies the host RNA polymerase rather than synthesizing a new enzyme. Like SP01

middle promoters, the DNA sequence which is well conserved among the T4 late transcripts examined here is different from the sequences recognized by the unmodified RNA polymerase. Although the first five bases of the conserved sequence are identical to the first five bases of the Pribnow box (TATAA), the sixth base of the Pribnow box is a 100 per cent conserved T (refs 15-17) while the 100 per cent conserved A found here is actually more similar to eukaryotic promoter sequences²⁰. The consensus sequence is also longer and closer to the 5' end of the mRNA than the Pribnow box recognized by the host enzyme and there is apparently no specific sequence recognized at -35. The change in transcriptional specificity that occurs at late times is thus not only a substitution of one set of specific DNA-protein interactions with another, but also a fundamental change in the geometry of the interactions.

We thank M. Parker, G. Kassavetis, T. Elliott, E. P. Geiduschek, M. Showe, G. Smith and H. Krisch for communicating results before publication, G. Stormo and L. Gold for access to T4 DNA sequences, M. Parker, A. H. Doermann and C. Furlong for help and technical advice, and the NIH for support (grant AI-09456).

Received 28 April; accepted 13 July 1982.

1. Rabussay, D. & Geiduschek, E. P. in *Comprehensive Virology* Vol. 8 (eds Fraenkel-Conrat, H. & Wagner, R. R.) 1-196 (Plenum, New York, 1977).
2. Snyder, L., Gold, L. & Kutter, E. M. *Proc. natn. Acad. Sci. USA* **69**, 603-607 (1972).
3. Wu, R., Geiduschek, E. P. & Cascino, A. J. *molec. Biol.* **96**, 539-562 (1975).
4. Young, E. T., Menard, R. C. & Harada, J. J. *Virology* **40**, 790-799 (1981).
5. Kassavetis, G. A. & Geiduschek, E. P. *EMBO J.* **1**, 107-114 (1982).
6. Parker, M., Christensen, A. C., Young, E. T. & Doermann, A. H. (in preparation).
7. King, J. & Laemmli, U. K. *J. molec. Biol.* **62**, 465-477 (1971).
8. Oliver, D. B. & Crowther, R. A. *J. molec. Biol.* **153**, 545-568 (1981).
9. Berk, A. J. & Sharp, P. A. *Cell* **12**, 721-732 (1977).
10. Nasmyth, K. A., Tatchell, K., Hall, B. D., Astell, C. & Smith, M. *Cold Spring Harb. Symp. quant. Biol.* **45**, 961-981 (1980).
11. Maxam, A. M. & Gilbert, W. *Meth. Enzym.* **65**, 499-560 (1980).
12. Sollner-Webb, B. & Reeder, R. H. *Cell* **18**, 485-499 (1979).
13. Emrich-Owen, J., Schultz, D. W., Taylor, A. & Smith, G. R. *J. molec. Biol.* (submitted).
14. Lewis, M. K. & Burgess, R. R. *J. biol. Chem.* **255**, 4928-4936 (1980).
15. Pribnow, D. in *Biological Regulation and Development* Vol. 1 (ed. Goldberger, R. F.) 219-278 (Plenum, New York, 1979).
16. Rosenberg, M. & Court, D. A. *Rev. Genet.* **13**, 319-353 (1979).
17. Siebenlist, U., Simpson, R. B. & Gilbert, W. *Cell* **20**, 269-281 (1981).
18. Rosa, M. D. *Cell* **16**, 815-825 (1979).
19. Lee, G. & Pero, J. *J. molec. Biol.* **152**, 247-265 (1981).
20. Grosfeld, G. C., deBoer, E., Shewmaker, C. K. & Flavell, R. A. *Nature* **295**, 120-126 (1982).
21. Mattson, T., Van Houwe, G., Bolle, A., Selzer, G. & Epstein, R. *Molec. gen. Genet.* **154**, 319-326 (1977).
22. Young, E. T. *et al. J. molec. Biol.* **183**, 423-445 (1980).
23. Völcker, T. A. & Showe, M. K. *Molec. gen. Genet.* **177**, 447-452 (1980).
24. Showe, M. K., Isobe, E. & Onorato, L. *J. molec. Biol.* **107**, 35-54 (1976).
25. Hagen, F. & Young, E. T. *J. Virol.* **26**, 793-804 (1978).
26. Krisch, H. *et al. Proc. natn. Acad. Sci. USA* (in the press).

The helical hydrophobic moment: a measure of the amphiphilicity of a helix

David Eisenberg, Robert M. Weiss & Thomas C. Terwilliger

Molecular Biology Institute and Department of Chemistry, University of California at Los Angeles, Los Angeles, California 90024, USA

The spatial distribution of the hydrophobic side chains in globular proteins is of considerable interest. It was recognized previously¹ that most of the α -helices of myoglobin and haemoglobin are amphiphilic; that is, one surface of each helix projects mainly hydrophilic side chains, while the opposite surface projects mainly hydrophobic side chains. To quantify the amphiphilicity of a helix, here we define the mean helical hydrophobic moment, $\langle \mu_H \rangle = |\sum_{i=1}^N \vec{H}_i|/N$, to be the mean vector sum of the hydrophobicities H_i of the side chains of a helix of N residues. The length of a vector \vec{H}_i is the signed numerical hydrophobicity associated with the type of side chain, and its direction is determined by the orientation of the side chain about the helix axis. A large value of $\langle \mu_H \rangle$ means that the

helix is amphiphilic perpendicular to its axis. We have classified α -helices by plotting their mean helical moment versus the mean hydrophobicity of their residues, and report that transmembrane helices, helices from globular proteins and helices which are believed to seek surfaces between aqueous and non-polar phases, cluster in different regions of such a plot. We suggest that this classification may be useful in identifying helical regions of proteins which bind to the surface of biological membranes. The concept of the hydrophobic moment can be generalized also to non-helical protein structures.

Schiffer and Edmundson² represented helix amphiphilicity by a two-dimensional 'helical wheel' diagram: a projection down the idealized helix axis shows side chains protruding from a circle every 100°. Non-polar residues were mainly on one side of the circle, polar and charged residues on the other. Helical wheels have since been used to represent other amphiphilic helices: for example, it has been noted that portions of apolipoprotein chains³⁻⁵ and a synthetic melittin-like peptide⁶ can be built into helices having one polar face and one non-polar face. The notion of amphiphilic helices has also been helpful in studying the folding of proteins (for example, see ref. 7).

The concept of amphiphilic helices can be quantified by combining a hydrophobicity scale with the helical wheel. Figure 1 shows portions of two helices viewed in projection down their axes. The hydrophobicity of each amino acid residue is represented by a vector directed radially from the projected helix centre to the idealized projected α -carbon position. The length of each vector is H_i , the hydrophobicity of the residue; as this is a signed quantity, hydrophobic residues on one face of the helix reinforce contributions of hydrophilic residues on the other face. For the calculations described in Figs 1 and 2, the values of H_i are those proposed by Janin⁸ on the basis of

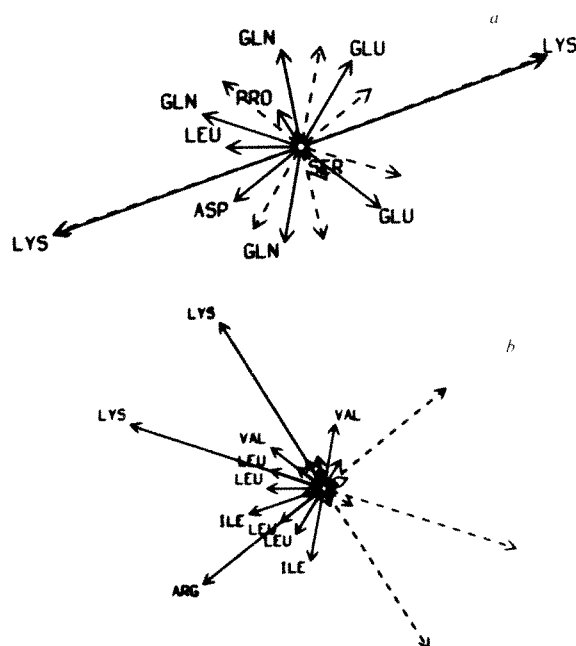


Fig. 1 Graphical representation of the contributions, by residue, to the helical hydrophobic moment, $\bar{\mu}_H$. *a*, The 11-residue stretch of a helix in lactate dehydrogenase starting at residue 308. Hydrophobic residues have positive values for the hydrophobicity, H_i , and are represented as vectors extending out from the centre of the axial projection of the α -helix. Hydrophilic residues have negative values of H_i and their positions about the helix axis are represented by dashed vectors extending from the centre. Their vector contributions are represented by solid lines 180° away. The vector sum of the \bar{H}_i is $\bar{\mu}_H$. As the distribution of solid lines is relatively symmetric, this segment has a small hydrophobic moment, $\langle\mu_H\rangle=0.10$. *b*, Residues 5–22 of melittin, the most amphiphilic 18-residue segment ($\langle\mu_H\rangle=0.40$). Residues of small contribution are represented by vectors but are not labelled. The resulting hydrophobic moment would be off the page to the upper left.

observed distributions of each amino acid between the surface and interior of proteins. We also performed calculations with other sets of hydrophobicity values, including those proposed by Wolfenden *et al.*⁹, von Heijne and Blomberg¹⁰ and Chothia¹¹, as well as with our own set. The general features of the results described below do not depend on the hydrophobicity scale used.

We define the degree of amphiphilic character of a helix perpendicular to its axis by the helical hydrophobic moment, μ_H , the magnitude of the vector sum of the \bar{H}_i for N residues of an α -helix: $|\bar{\mu}_H| = \sum_{i=1}^N \bar{H}_i$. To compare moments of helices of different lengths, it is convenient to work with the intensive form of the moment, $\langle\mu_H\rangle = |\bar{\mu}_H|/N$, which we will sometimes refer to simply as the hydrophobic moment. In much of our work, a stretch of 18 residues was chosen because an ideal α -helix of this length makes exactly five turns; thus the side chains are distributed uniformly about its circumference. However other lengths were also studied. Although the real vectors calculated from atomic coordinates (see below) can also be used, the present approach can be used when the tertiary structure is unknown, but the secondary structure can be predicted.

Figure 2 shows a hydrophobic moment plot in which $\langle\mu_H\rangle$ is plotted against the mean hydrophobicity, $\langle H \rangle = (\sum_{i=1}^N H_i)/N$, for helices of N residues, where N is always greater than 10. For helices of ≥ 19 residues, the largest value of $\langle\mu_H\rangle$ for any 18-residue segment is also plotted with a related symbol. Thus, for each helix of 11–18 residues, there is a single point on the plot, and for each helix of 19 or more residues there are two points. The abscissa value of Fig. 2 reflects the solubility of each helix in a non-polar medium, the points falling to the right representing helices which prefer a non-polar medium to a polar medium. The ordinate reflects the tendency of a helix to assume a preferred orientation at an interface between polar and non-polar media. The plot shows data from 64 helices in 26 proteins. Of these helices, 28 have 19 or more residues (up to a maximum of 53 residues for the haemagglutinin membrane glycoprotein of influenza virus) and 36 have 11–18 residues.

Figure 2 shows that different types of helices cluster in different regions of the diagram. Transmembrane sequences are found in the lower right; this is to be expected because, as noted by others¹², such sequences have high mean hydrophobicities which render them soluble in lipid. They also have small helical hydrophobic moments, indicating that all orientations about the helix axis are essentially energetically equivalent. We have assumed that these transmembrane sequences are in α -helical conformations on the basis of Henderson's argument¹³ that this conformation is strongly favoured in a membrane. The common length of 18–24 hydrophobic residues also suggests that these sequences bridge the apolar portion of the bilayer (~ 30 Å) in α -helical conformations (1.5 Å per residue along the helix axis).

In the left and lower central regions of Fig. 2 are clustered α -helical segments from globular proteins. These segments (Table 1) include every representative α -helix of known conformation having 18 or more residues, and every helix of 11–17 residues in the same proteins, after Feldman¹⁴. Of course, other regions of these polypeptide chains are generally not α -helical (and therefore are not plotted). Because these helices are from soluble proteins, it is not surprising that their mean hydrophobicities are smaller than those of membrane-penetrating sequences (that is, they are more hydrophilic). The helical hydrophobic moments for these helices vary substantially, but are often small.

In the upper right of Fig. 2 is a group of helices (represented by triangles and arrowheads) which have both high helical moments and large mean hydrophobicities. The main members of this group are 26-residue peptides known to be both lytic and surface-active. Two are melittins, the main protein components of venom from bees^{15,16}, another is a synthetic melittin-like peptide⁶ and two others are δ -haemolysins, lytic peptides secreted by *Staphylococcus aureus* which are similar to melittin

Table 1 Helices included in the hydrophobic moment plot of Fig. 2

Protein	Organism/organ	1st residue	No. of residues	Evidence for helix*	Protein type	Ref. for sequence or structure
Adenylate kinase	Pig	69(Leu)	15	X ray	Globular	14
		123(Glu)	11			
		144(Glu)	21			
		179(Val)	16			
Alcohol dehydrogenase	Horse	170(Cys)	18	X ray	Globular	14
		202(Gly)	11			
		324(Ser)	13			
		353(Glu)	13			
Carboxy-peptidase A	Cow	14(Thr)	15	X ray	Globular	14
		112(Asn)	11			
		173(Glu)	15			
		215(Asp)	17			
		285(Gln)	22			
Chymotrypsin	Cow	230(Arg)	16	X ray	Globular	14
HA2 haemagglutinin	Influenza virus	77(Glu)	53	X ray	Globular	22, 23
Lactate dehydrogenase	Dogfish	33(Val)	12	X ray	Globular	14
		55(Met)	16			
		107(Glu)	13			
		120(Phe)	11			
		165(Cys)	17			
		249(Trp)	15			
		308(Lys)	22			
Myoglobin	Sperm whale	1(Val)	19	X ray	Globular	14
		20(Asp)	16			
		58(Ser)	20			
		100(Pro)	19			
		125(Ala)	24			
Myohaemerythrin	Marine worm	18(Tyr)	21	X ray	Globular	14
		40(Ser)	23			
		69(Glu)	19			
		93(Ala)	18			
Ribonuclease S	Cow	3(Thr)	11	X ray	Globular	14
		24(Asn)	11			
Thermolysin	<i>Bacillus thermo-proteolyticus</i>	67(Asp)	21	X ray	Globular	14
		137(Ile)	14			
		160(Glu)	20			
		235(Gly)	12			
		260(Arg)	15			
		281(Phe)	16			
		301(Gln)	12			
TMV coat protein	Tobacco mosaic virus	20(Pro)	13	X ray	Globular	24, 25
		38(Gln)	11			
		74(Ala)	15			
		114(Val)	21			
Triose phosphate isomerase	Chicken	17(Lys)	15	X ray	Globular	14
		44(Pro)	12			
		105(Ser)	16			
		138(Ile)	17			
		177(Thr)	20			
		213(Thr)	11			
Glycophorin	Human erythrocyte	12(Ile)	23	Length	Membrane	26
Glycoprotein	Vesicular stomatitis virus	51(Ser)	24	Length	Membrane	27
HA2 haemagglutinin	Influenza A/Victoria or A/Aichi	185(Trp)	24	Length	Membrane	28
HA2 haemagglutinin	Influenza A/Japan	527(Val)†	24	Length	Membrane	23
IgM	B lymphocyte	569(Asn)	26	Length	Membrane	29
Isomaltase	Small intestine	10(Ile)	22	Length	Membrane	30
M13 coat	M13 virus	20(Tyr)	18	Length	Membrane	31
M13 procoat	M13 virus	-20(Ser)	21	Length	Membrane	31
δ-Haemolysin	<i>S. aureus</i>	1(Met)	26	Analogy	Surface	17
	<i>S. aureus</i> (canine strain)	1(Met)‡	26	Analogy to melittin	Surface	17
Melittin	<i>Apis mellifera</i>	1(Gly)	26	X ray	Surface	15, 19
	<i>Apis florea</i>	1(Gly)§	26	Analogy to above	Surface	16
Cytotoxic peptide with melittin-like activity	Synthetic	1(Leu)	26	CD	Surface	6
Diphtheria toxin peptide	Diphtheria toxin	7(Leu)	26	Prediction from sequence	Surface	20

* X ray means that an α -helical conformation has been established by X-ray crystallographic studies; CD, evidence for helicity comes from examination of circular dichroism; length, for a transmembrane protein, the length of the hydrophobic sequence is suitable for spanning the hydrophobic portion of a lipid bilayer as an α -helix.

† Corresponds to residue 185 in the enumeration of ref. 28.

‡ The sequence differs from that of the above strain of *S. aureus* in four residues.

§ The sequence differs from that of *A. mellifera* in five residues.

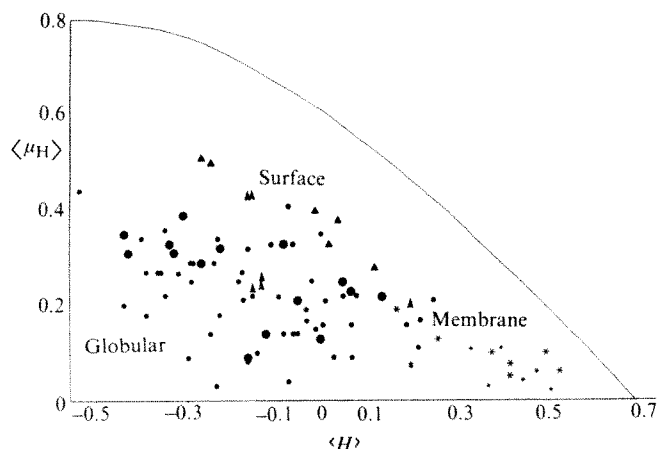


Fig. 2 A hydrophobic moment plot for 64 α -helical segments from the 26 proteins listed in Table 1. The abscissa gives the mean hydrophobicity of each segment and the ordinate gives the corresponding value of $\langle \mu_H \rangle$, as defined in the text. Helices from proteins having different functions plot in various regions of the diagram, as explained in the text. Membrane, membrane-penetrating helices: * represents the average of the entire helix (present for all helices) and * the 18-residue segment having the largest hydrophobic moment (present only for helices of ≥ 19 residues). Globular, helical segments from globular proteins: ●, average and ●, largest moment, Surface, surface-seeking helices: ▲ and ▲. The curve shows the largest possible value of $\langle \mu_H \rangle$ for each value of $\langle H \rangle$, as described in the text.

in both properties and sequence¹⁷. One of the melittins is known from X-ray diffraction studies to have an α -helical conformation^{18,19}; the synthetic melittin is α -helical as judged by circular dichroism⁶. By analogy to these two peptides, we assume here that the δ -haemolysins are also α -helical. The final member of this group is a 26-residue peptide, fragment B from diphtheria toxin. This peptide has been predicted to have an α -helical conformation and is part of a larger CNBr peptide that induces conductance changes in lipid bilayers²⁰. We include it in this group only to suggest that some peptides from larger proteins may have relatively large hydrophobic moments related to special functions.

Also shown in Fig. 2 is the maximum possible helical hydrophobic moment for each value of the hydrophobicity, represented by a curve which meets the abscissa at 0.70, the value for a hypothetical polyisoleucine α -helix. (Cysteine was excluded from the calculations of the maximum hydrophobic moment because the procedure used⁸ to determine hydrophobicities may overestimate that of cysteine.) Note that even the highly amphiphilic δ -haemolysins are far less amphiphilic than some hypothetical helices.

The amphiphilic helical portions of melittin, as well as similar helical regions in other proteins, might be termed 'surface-seeking helices' because their large hydrophobic moments tend to align them at the surface between polar and non-polar phases¹⁹. Another class of proteins believed to function as amphiphilic helices is the apolipoproteins^{3,4}; these have not been included here because even less direct information on their three-dimensional structures is available than for the melittins.

Although proteins of different functional types cluster in different regions of Fig. 2, these regions do not have absolute boundaries. This is expected as the various types of helices do not have entirely distinct functions. For example, the solubility of melittin in aqueous solution is believed¹⁸ to be achieved in part by the highly charged C-terminal segment of the helix. This segment projects polar groups uniformly to all sides¹⁹ and hence lowers the value of $\langle \mu_H \rangle$ for the entire melittin chain below that of the most amphiphilic 18-residue segment. For the two types of melittin and the synthetic melittin-like peptide, this results in arrowheads near the coordinates $\langle H \rangle = -0.15$,

$\langle \mu_H \rangle = 0.25$. Other helical segments that plot in intermediate regions include some of those from the purple membrane protein model described by Engelman *et al.*²¹; these plot between the 'membrane' and 'surface' regions because of the charged and polar residues in the sequence (they are not included in Fig. 2). Such membrane helices with large hydrophobic moments may pair in the membrane, thereby reducing the net hydrophobic moment of the pair. More generally we suspect that segments from a helix that plot in a region of Fig. 2 occupied mainly by another type of helix may have a specialized function.

A potential limitation in the calculation of the helical hydrophobic moment $\langle \mu_H \rangle$ is that amino acid side chains deviate significantly from the idealized positions we have used (spaced 100° apart perpendicular to the helix axis). To clarify this point, we have investigated the properties of the structural hydrophobic moment, $\bar{\mu}_s$; the most convenient definition for this comparison is $\bar{\mu}_{s1} = \sum_{i=1}^N H_i \bar{s}_i$, where \bar{s}_i is a unit vector pointing from the α -carbon atom of the i th residue to the centre of the residue side chain. This quantity can be calculated for any protein segment whose structure is known; when calculated for the idealized helices used in obtaining the mean hydrophobic moment, the angular deviation between the idealized \bar{s}_i and the corresponding vectors perpendicular to the helix axis for a real helix averaged 30°. The difference in magnitude between the mean and structural moments, after scaling the latter by the length of the helix, averaged 25%. When computed for a helix, the structural hydrophobic moment $\bar{\mu}_{s1}$, like $\bar{\mu}_H$, emphasizes the amphiphilicity perpendicular to the helix axis. An alternative definition is $\bar{\mu}_{s2} = \sum_{i=1}^N (H_i \bar{R}_i - \langle H \rangle \bar{R}_i)$, in which \bar{R}_i is a vector from any origin to the centre of the side chain of the i th residue. This definition of the hydrophobic moment represents amphiphilicity in directions both parallel and perpendicular to a helix axis and may have applications in energetics calculations.

We conclude that hydrophobic moment plots can reveal correlations between amino acid sequence and protein function; in particular, they can identify sequences particularly well suited for forming surface-seeking helices.

We thank L. Aha for discussions, and acknowledge support from the NSF (PCM 80-03725) and the NIH (GM 16925). T.C.T. was the recipient of a NSF graduate fellowship.

Received 25 February; accepted 24 June 1982.

- Perutz, M. F., Kendrew, J. C. & Watson, H. C. *J. molec. Biol.* **13**, 669–678 (1965).
- Schiffer, M. & Edmundson, A. B. *Biophys. J.* **7**, 121–135 (1967).
- Morrisett, J. D., Jackson, R. L. & Gotto, A. M. Jr *Biochim. biophys. Acta* **472**, 93–133 (1977).
- Segrest, J. P., Jackson, R. L., Morrisett, J. D. & Gotto, A. M. Jr *FEBS Lett.* **38**, 247–253 (1974).
- Segrest, J. P. & Feldman, R. J. *Biopolymers* **16**, 2053–2065 (1977).
- DeGrado, W. F., Kezdy, F. J. & Kaiser, E. T. *J. Am. chem. Soc.* **103**, 679–681 (1981).
- Pitts, O. B. & Rashin, A. A. *Biophys. Chem.* **3**, 1–20 (1975).
- Janin, J. *Nature* **277**, 491–492 (1979).
- Wolfenden, R., Andersson, L., Cullis, P. M. & Southgate, C. C. B. *Biochemistry* **20**, 849–855 (1981).
- von Heijne, G. & Blomberg, C. *Eur. J. Biochem.* **97**, 175–181 (1979).
- Chothia, C. *J. molec. Biol.* **105**, 1–14 (1976).
- Segrest, J. P. & Feldman, R. J. *J. molec. Biol.* **87**, 853–858 (1974).
- Henderson, R. *Soc. gen. Physiol.* **33**, 3–15 (1979).
- Feldman, R. J. *Atlas of Macromolecular Structure on Microfiche* (Tracor Jitco, Rockville, Maryland, 1976).
- Habermann, E. *Science* **177**, 314–322 (1972).
- Kriel, G. *FEBS Lett.* **33**, 241–244 (1973).
- Fitton, J. E., Dell, A. & Shaw, W. V. *FEBS Lett.* **115**, 209–212 (1980).
- Terwilliger, T. C. & Eisenberg, D. *J. biol. Chem.* **257**, 6016–6022 (1982).
- Terwilliger, T. C., Weissman, L. & Eisenberg, D. *Biophys. J.* **37**, 353–361 (1982).
- Kayser, G. *et al. Biochem. biophys. Res. Commun.* **99**, 358–363 (1981).
- Engelman, D. M., Henderson, R., McLachlan, A. D. & Wallace, B. A. *Proc. natn. Acad. Sci. U.S.A.* **77**, 2023–2027 (1980).
- Wilson, I. A., Wiley, D. C. & Skehel, J. J. *Nature* **289**, 366–373 (1981).
- Porter, A. G. *et al. Nature* **282**, 471–477 (1979).
- Bloomer, A. C., Champness, J. N., Bricogne, G., Staden, R. & Klug, A. *Nature* **276**, 362–368 (1978).
- Dayhoff, M. O. *Atlas of Protein Sequence and Structure* Vol. 5, D283 (National Biomedical Research Foundation, Washington DC, 1972).
- Furthmayr, H., Galardy, R. E., Tomita, M. & Marchesi, V. T. *Archs Biochem. Biophys.* **185**, 21–29 (1978).
- Rose, J. K., Welch, W. J., Sefton, B. M., Esch, F. S. & Ling, N. C. *Proc. natn. Acad. Sci. U.S.A.* **77**, 3884–3888 (1980).
- Verhoeyen, M. *et al. Nature* **286**, 771–776 (1980).
- Rogers, J. *et al. Cell* **20**, 303–312 (1980).
- Frank, G. *et al. FEBS Lett.* **96**, 183–188 (1978).
- Wickner, W. *Science* **210**, 861–868 (1980).

MATTERS ARISING

BVP models of nerve membrane

HINDMARSH and Rose¹ propose, for use in simulating networks containing small numbers of neurones, a phenomenological model based on their experimental data, and notable for its simple numerical integrability. Inspection of their paper shows that their experimental data do not in fact extend into the region $x < -15$ mV, yet it is just this region that contains the novel feature of their model, a positive gradient for the isocline $\dot{y} = 0$. Others (for example, see ref. 2) have collected data in this region which do not support the positive gradient used by Hindmarsh and Rose for $\dot{y} = 0$ (see Fig. 1). Thus, their slow variable y has less physical meaning than the usual BVP (Bonhoeffer-van der Pol) slow variable³. Furthermore, for constructing models of this kind, there already exists a method^{4,5} which gives explicitly solvable equations and requires no numerical integration. Over the full range of experimental data, this method gives a better fit than that of Hindmarsh and Rose. The method is as

follows: divide the voltage range into three segments; fit the data in each segment with a straight line (making $f(x)$ and $g(x)$ continuous and step-wise linear); and solve the resulting second-order linear system of ordinary differential equations.

Real nerve cell membranes, the Hodgkin-Huxley system⁶, and the usual BVP models⁴ are made relatively more excitable by an anode break shock. In contrast, its novel feature makes the Hindmarsh-Rose model relatively refractory after such a stimulus.

C. J. A. GAME

Department of Neurology,
Academic Hospital of Leiden,
2333 AA Leiden, The Netherlands

1. Hindmarsh, J. L. & Rose, R. M. *Nature* **296**, 162-164 (1982).
2. Hodgkin, A. L., Huxley, A. F. & Katz, B. *J. Physiol., Lond.* **116**, 424-448 (1952).
3. Game, C. J. A. *Biol. Cybernet.* (in the press).
4. Scott, A. C. *Rev. mod. Phys.* **47**, 487-533 (1975).
5. Perkel, D. H. *Comput. biomed. Res.* **9**, 31-43 (1976).
6. Hodgkin, A. L. & Huxley, A. F. *J. Physiol., Lond.* **117**, 500-544 (1952).

HINDMARSH AND ROSE REPLY—The novel feature we wished to draw attention to was not the positive gradient of the isocline $\dot{y} = 0$ in the region $x < 0$, but rather the close proximity of the isoclines $\dot{x} = 0$ and $\dot{y} = 0$. This proximity is determined by $z_{sp}(\infty)$, which is small according to both the Hodgkin-Huxley data for x_p between 0 and -65 mV and our data for x_p between 0 and -20 mV. On the other hand, the location of these isoclines is determined by $z_{sp}(0)$. Few points were obtained for $z_{sp}(0)$ for $x_p < 0$ because by using the single electrode voltage clamp, the initial responses were obscured by a capacitive current. We therefore followed Fitzhugh¹ in taking a cubic form for $z_{sp}(0)$. Due to this, both isoclines have a positive gradient in the region $x < 0$ which, as both Game and Fitzhugh (personal communication) have pointed out, means that our model is relatively refractory after an anode break shock. Although this positive gradient is thus a disadvantage in our model, it is consistent with the following experiment (tail current reversal) performed numerically with the Hodgkin-Huxley² equations.

If the voltage is held at +50 mV until a steady state is reached, and then stepped back to various negative potentials, it is found that when the potential is sufficiently negative, the tail current changes direction. This property is shown, at least qualitatively, by our model, as can be seen from our phase plane diagram³. Given the choice between explanations of tail current reversal or anode break, we chose the former, because we saw that this would also predict the long interspike interval. This suggests that $z_{sp}(0)$ for $x_p < 0$ should be constructed from such

tail current data rather than from negative voltage steps from zero. Such a determination seems more relevant to the time course of the membrane potential during firing.

Clearly, if $z_{sp}(0)$ is determined from voltage clamp steps from zero and the Hodgkin-Huxley data is used (Fig. 1a), then straight lines will provide a better fit than a cubic. In this case both isoclines will still have a small positive gradient in the region $x < 0$, which will mean that the phase state on the limit cycle travels far to the left before returning to the origin between the isoclines, resulting in a large undershoot of the membrane potential. In our case, replacing the cubic by three straight lines does not lead to a significant deterioration in accuracy of prediction of the time course of the membrane potential, and does, as Game points out, offer the advantage of explicit solutions.

J. L. HINDMARSH
R. M. ROSE

Department of Applied
Mathematics and Astronomy and
Department of Physiology,
University College,
Cardiff CF1 1XL, UK

1. Fitzhugh, R. *Biophys. J.* **1**, 445-466 (1961).
2. Hodgkin, A. L. & Huxley, A. F. *J. Physiol., Lond.* **117**, 500-554 (1952).
3. Hindmarsh, J. L. & Rose, R. M. *Nature* **296**, 162-164 (1982).

Trophic structure of a grassland insect community

FROM a detailed study of insect species in a grassland community, Evans and Murdoch¹ concluded that the ratio of herbivorous insects to entomophagous insects remained fairly constant throughout the growing season. They suggested that this reflected an underlying trophic pattern that persisted despite continuing turnover of species. Cole² rejected this claim by showing that an appearance of constancy can be generated by samples taken from a fixed pool of all available species.

It is true that in the absence of exact knowledge of the community structure through the season it is not possible to assert that species turnover occurs. However, it is equally impossible to assert that species turnover does not occur. Nevertheless, this is precisely the arbitrary assumption made by Cole.

He assumes that all species listed by Evans and Murdoch (131 herbivorous, 80 entomophagous) are present throughout the season, and treating the total number of species observed each fortnight as a random sample (r) from the population of 211 species, he demonstrates that the expected number of herbivores agrees

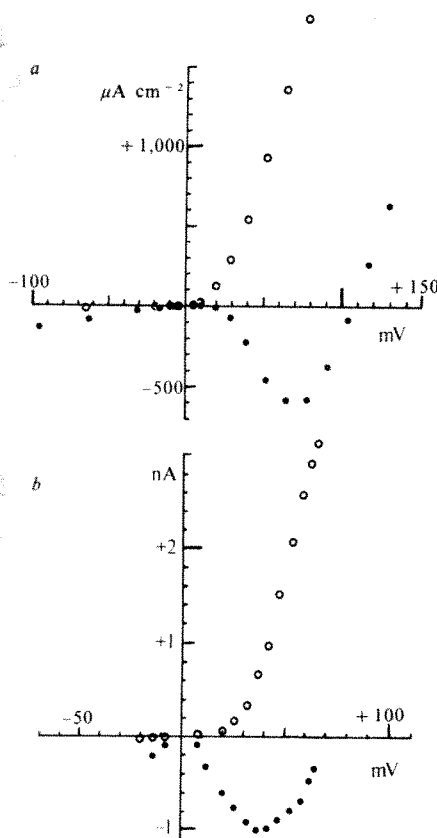


Fig. 1 Schematic summary of the data under consideration. Ordinates show the membrane current supplied by the clamping electrode; the abscissae show the membrane potential at which the clamp is set. ○, Steady-state current; ●, initial current. a, Based on the data of ref. 2 for squid giant axon; b, based on the data of ref. 1 for snail neurone soma.

Table 1 Community structure

Time period	Herbivorous species	Entomophagous species	Total no. of species
1	H ₁ , H ₂	E ₁ , E ₂ , E ₃ , E ₄	6
2	H ₃ , H ₄ , H ₅	E ₅ , E ₆ , ..., E ₁₀	9
3	H ₆ , H ₇ , H ₈ , H ₉	E ₁₁ , E ₁₂ , ..., E ₁₈	12
			27

well with the observed number for each fortnight. However, such an agreement can equally arise if the insect community did in fact possess a stable trophic structure. For example, consider the season divided into (say) three time periods and let the exact community structure be as shown in Table 1. Here, each H_i and E_j is a distinct species. There is a complete and known turnover of species, and for each time period the ratio of the number of herbivorous to entomophagous species is exactly 1/2. An assumption like Cole's, that all species are present at all times, will give $n = \text{total species} = 27$, $n_1 = \text{number of herbivores} = 9$, $r_1 = 6$, $r_2 = 9$, $r_3 = 12$; and, for each time period, the expected and observed number of herbivorous species will agree exactly.

Cole's conclusion that the ratio of herbivores to predators, in the insect community studied by Evans and Murdoch, is maintained at a constant level by no other force than a statistical one is thus possible but not proven. The value of Cole's letter is that it gives a warning that an apparent observed trophic structure may not only be due to the background fact of nature, it can also arise for other reasons.

Obviously, much detailed work on the life history of individual species is required before it is possible to assess adequately the extent of species turnover in a given community. Also, even if energy, biomass or nutrients are undeniably transferred from one trophic level to another, it is perhaps an oversimplification to search for general patterns in terms of the number of species, ignoring abundance, average size and requirements of the members of each species.

K. H. LAKHANI

*Institute of Terrestrial Ecology,
Monks Wood Experimental Station,
Abbots Ripton,
Huntingdon PE17 2LS, UK*

1. Evans, F. C. & Murdoch, W. W. *J. Anim. Ecol.* **37**, 259–273 (1968).
2. Cole, B. J. *Nature* **288**, 76–77 (1980).

Thermoluminescence dating of sand dunes

SINGHVI ET AL.¹ have recently suggested that the thermoluminescence (TL) technique can be used successfully to date aeolian sand dunes. These authors use the TL signal from the 1–8 µm fraction of dune sediments in Rajasthan to suggest dune ages of between 2,000 and 20,000 yr. This procedure implicitly

assumes that the 1–8 µm particles are entirely a primary detrital component, and that secondary additions of fines after dune stabilization are unimportant. This assumption warrants close examination, since significant secondary input could result in TL dates which are too young.

Active desert dunes usually contain <3% silt, whereas stabilized and weathered dunes may contain >30%. Goudie *et al.*² have reported 20–30% fines in stabilized dunes from Rajasthan. Post-depositional addition of fines may reflect aeolian dust input^{3–5}, introduction by surface wash from higher ground^{6,7}, surficial deposition of biogenic silica⁸ or the effects of *in situ* weathering on sand grains⁹. Dust input is probably the most significant factor in terms of errors in TL dating of desert dune deposits. The dust, deposited on a dune surface, may be rapidly eluviated by rainwater percolating through the dune sand column. Wright and Foss¹⁰ demonstrated experimentally that 8 g of fine silt placed on top of a 33-cm column of medium sand was completely leached by <1 litre of water. In sealed sand columns the eluviated fines are deposited as an illuvial sub-surface horizon which grows vertically with time.

As a result of the efficacy of this process, TL dating of 1–8 µm-sized particles may simply reflect rates of aeolian dust addition rather than the age of a dune sand body in which they occur. Where such dust eluviation and deposition occurs, a TL age gradient up the profile is to be expected. Singhvi *et al.* demonstrate such an age gradient in the dunes they studied, but suggest that it may reflect slow vertical accretion of aeolian sand over a substantial period of time. However, in the absence of independent supportive evidence it would be equally valid to suggest that the dune sand bodies were formed entirely in the late Pleistocene, and that TL dates on the upper parts of the dune profiles investigated are artificially low due to contamination. Geomorphological and palaeoenvironmental evidence also suggest that dune formation in Rajasthan has occurred as a series of discrete events in response to periodic climatic changes in the late Pleistocene and Holocene, rather than by slow vertical accretion^{2,11}.

¹⁴C and TL dates on associated archaeological artefacts are of limited value as a cross-check on the reliability of TL dates of silt particles because of the uncertainty surrounding the time relationship between the artefacts and adjacent or surrounding sediment. The best solution to the problem would be to apply the TL dating technique to the sand grains themselves. Both quartz and alkali feldspar inclusions in pottery have been dated using various grain sizes in the range 0.1–0.5 mm and the methodology could be adapted for application to sand dunes. Indeed, several TL laboratories involved in sediment dating already use grains of

≥0.1 mm (ref. 12). Singhvi *et al.* should examine the TL of sand grains at various levels in the dune profiles to establish whether or not they indicate increasing age with depth.

I thank Ann Wintle for comments and discussion.

K. PYE

*Department of Earth Sciences,
University of Cambridge,
Downing Street,
Cambridge CB2 3EQ, UK*

1. Singhvi, A. K., Sharma, Y. P. & Agrawal, D. P. *Nature* **295**, 313–315 (1982).
2. Goudie, A. S., Allchin, B. & Hegde, K. T. M. *Geogr. J.* **139**, 243–257 (1973).
3. Yaalon, D. H. *Soil Sci.* **116**, 146–155 (1973).
4. Syers, J. K., Jackson, M. L., Berkheiser, V. E., Clayton, R. N. & Wex, R. W. *Soil Sci.* **107**, 421–427 (1969).
5. Goudie, A. S. *J. Arid Envir.* **1**, 291–310 (1978).
6. Bigarella, J. J. *Bol. Para. Geosci.* **33**, 133–167 (1975).
7. Walker, T. R., Waugh, B. & Crone, A. J. *Bull. geol. Soc. Am.* **89**, 19–32 (1978).
8. Wilding, L. P. & Drees, L. R. *Clays Clay Miner.* **22**, 295–306 (1974).
9. Goudie, A. S., Cooke, R. U. Doornkamp, J. C. *J. Arid Envir.* **2**, 105–112 (1979).
10. Wright, W. R. & Foss, J. E. *Proc. Soil. Sci. Soc. Am.* **32**, 446–448 (1968).
11. Verstappen, H. T. Z. *Geomorph. Suppl.* **10**, 104–120 (1970).
12. Wintle, A. G. & Huntley, D. J. *Q. Sci. Rev.* **1**, 31–53 (1982).

SINGHVI REPLIES—I thank Dr Pye for his valued comments. In fact, some of the studies he suggested are already in progress and the results will be presented at the Third International Specialist Seminar on Thermoluminescence Dating (Denmark, July 1982) and will be published elsewhere¹. In the meantime, I hope the following information will suffice:

(1) In the field, the permeability of a stabilized dune is circumscribed by factors such as vegetation, carbonate crust and the original fine grain population of the dune sand. In such an arid environment, the experiments of Wright and Foss² (where almost 15 cm of standing water was constrained to move unidirectionally), do not have much relevance. In fact, at Amarpura the average rainfall is <300 mm yr⁻¹.

(2) The archaeological evidence of a habitation and radiocarbon/TL dates indeed validate fine-grain TL dates as being the dates of accumulation of dune sand. Certainly the archaeological material (pottery, charred bone, and so on) cannot percolate down to 1–2 m depths and therefore the overlying sediment has to be post-archaeological debris.

(3) We agree that a comparison between the coarse-sand fraction and the fine-grain TL dates is useful. The same has been attempted with encouraging results for Langhnaj samples. These analyses will be completed shortly and the results will be presented at the TL seminar in Denmark.

A. K. SINGHVI

*Physical Research Laboratory,
Ahmedabad 380 009, India*

1. Singhvi, A. K., Sharma, Y. P. & Agrawal, D. P. *PACT* **9** (in the press).
2. Wright, W. R. & Foss, J. E. *Soil. Sci. Soc. Am. Proc.* **32**, 446–448 (1968).

BOOK REVIEWS

Traits of empire

C.R. Brand

STANDING in an African flower-pot, a pop-eyed, stick-figured ET — displaying an enviable claim to masculinity — looks out from the cover of *The Biology of Human Conduct*. Browsers will presume that some kind of sociobiology or anthropology is in store, and that the Western models of the sub-title are to encounter yet another challenge from the mysterious East. The only clue that matters are otherwise is provided by the author's position in the Department of Experimental Psychology at the University of Oxford — several of whose members are to be put in, together with H. J. Eysenck, to bat for the West, while Pavlov, Teplov, Nebylitsyn and Strelau (in Warsaw) represent the trait-psychology of the East. Thus, in the hope of a crowd, are British psychometrician-psychologists and Russian psychophysiologicalists made to confront each other.

The match turns out to be something of a friendly. All the contestants certainly accept as ground-rules the importance of such questions as: "What are the major (independent) dimensions of personality?"; "What individual differences in psychophysiological mechanisms and processes underlie these behavioural dimensions?"; and "Are such differences partly genetic in origin?". Nor is there radical disagreement as to methods: indeed, some Western readers will be surprised by the prevalence of twin-studies in the countries of the Eastern bloc. As the humanistic fashion of Western psychology decrees, Mangan frequently steps aside to admit that the agreed questions are simple and that reality is complex; but, though Freud, Jung, Piaget and Wilhelm Reich are occasionally called upon to plug holes, the bulk of the book is concerned with the laboratory investigation of Extraversion (alias strength, or non-reactivity, of the nervous system), Neuroticism (alias dynamism) and similar putative dimensions of personality such as "mobility", "lability" and "irradiation of inhibition". Quotations provide the occasional diversion: "Only idealists can speak of thinking without language" (J. V. Stalin, 1951).

Regrettably, the contest staged by the author is a colossal disappointment. Not only does the reader quickly realize that the result is going to be a messy draw, but he learns that Mangan will not even allow there to be a Man of the Match. The preface itself sets the depressive tone by announcing that the book contains "the detritus" of Mangan's 20-year interest in

The Biology of Human Conduct: East-West Models of Temperament and Personality. By G.L. Mangan. Pp.571. ISBN 0-08-026781-5. (Pergamon: 1982.) £35, \$72.

personality; and Mangan soon makes it clear that his regard for the theorists whose work he considers is so beset with scholarly inhibition that he cannot allow the reader the luxury of having any of their theories set out at length. Even his own favourite theme — the importance of the "mobility" dimension — is forever the subject of allusion rather than development; so he can hardly afford to indulge Gray and Strelau. That psychological scientists will have to refer to this reference-packed work or to dismiss the East altogether is the best that can be said.

Mangan's lack of panache may be of situational rather than personological origin. Although the Russians have lately relaxed Stalin's ban on IQ-testing, Soviet typological theory of personality seems to be in a Lysenkoist mess. The fact is that the firmly materialistic and "biological" work that Mangan reports has been tolerated over the years only on the understanding

that it has nothing to do with important psychological differences between people — which differences are considered in the East to be matters of nurture rather than of nature. As Mangan politely puts it when discussing work at the Kiev Institute, "There is no suggestion, of course, of any relationship between nervous system properties and intellectual endowment ...". Thus Soviet differential psychophysiologicalists are left to play with somewhat hypothetical variants of Eysenck's E and N, since these dimensions repeatedly manifest themselves even in laboratories that draw on Soviet sophomores for their subjects. But General Intelligence (g) is denied them, and they have no certain method for discovering dimensions of personality just because, if they did have one, they might discover g for themselves. Mangan's tolerance of this state of affairs allows him to be the dispassionate, if dispiriting, reporter of years of Soviet endeavour — so perhaps the problem with this book is personological after all. □

C.R. Brand is a Lecturer in the Department of Psychology at the University of Edinburgh.

A mixed bag of andesites

Richard J. Arculus

Andesites: Orogenic Andesites and Related Rocks. Edited by R. S. Thorpe. Pp.724. ISBN 0-471-208034-8. (Wiley: 1982.) \$134, £59.50.

ANDESITIC volcanoes are forced to the attention of the general public in sometimes unpredictably violent ways involving loss of livelihood and even life. In developed nations, like Japan and the United States, advanced technology is applied to monitoring and forecasting of dangerous eruptions, but given the lengthy repose cycles typical of these volcanoes a great deal remains to be learnt of their behaviour.

In other ways, the products of andesitic volcanoes are fascinating in that their composition and isotopic characteristics provide clues to the nature of the processes that occur in the upper mantle and crust of the Earth during the collision of lithospheric plates. It is possible that the magmatic activity associated with these plate collisions has been an important

agent in the extraction on a geological timescale of continent-forming material from the mantle.

In *Andesites*, R. S. Thorpe has assembled contributions from over 50 authors reviewing many of the intriguing aspects of this type of magmatism. Subjects covered range through classification of andesitic rock types, petrology and mineralogy, chemical and isotopic features, and description of the distribution and characteristics of active andesitic volcanoes excluding only the Vanuatu, Solomon Islands, Philippine and Soviet Union segments of the Pacific rim. Eruptive styles, evolution of andesitic volcanism through time, major types of andesite-associated mineral deposits and experimentally-based studies of petrogenesis are also included.

Clear diagrams and print make the book visually pleasing, and the reader will emerge from the whole volume with an appreciation of some of the main points of current debate on the sources and

evolutionary history of andesites. Unfortunately, the multi-authored approach results in an incoherent overall presentation of the relevant data. For example, several different hypotheses are advanced by individual authors suggesting that andesites are formed from partial melts of subducted lithosphere, from primary melts of metasomatized and hydrated mantle peridotite, or from derivative melts from precursor basaltic magmas. So there is a fair cross-section of expert views, but no balanced, editorial presentation of the defects and successes of these individual hypotheses. Even the definitions of the qualifying terms applied to different types of andesite — "calcalkaline", for instance — are not consistently employed throughout the text.

Uneven coverage of the important aspects of andesitic volcanoes extends unfortunately into one of the most potentially useful parts of the book, that occupied by descriptions of individual arc segments. There is no consistent presentation of information on basement age and character, evolution of volcanism, volumetric abundance of rock types, average and representative chemical and isotopic analyses, mineralogical data and petrogenetic interpretation. Text length devoted to individual arcs is even-handed but unbalanced when the complexities in the 7,000km length of Andean volcanic and plutonic activity merits the same space as the 700km long Lesser Antilles, even if allowance is made for the stimulating variety of oddities that is compressed into the eastern Caribbean Arc.

Nevertheless, the book does contain a number of useful and provocative contributions. Ewart has produced a comprehensive summary of the regional variation of chemistry and mineralogy present in continental and island arc volcanoes, which is a much-needed comparative data base for further study. (However inclusion of the hinterland of the western United States seems unwise in this exercise.) Also instructive is the comparison between the documentation by Ewart that most Cenozoic andesites contain plagioclase phenocrysts with a median composition of 50–60 mole per cent anorthite, and the drastically more sodic plagioclase (25–35 mole per cent anorthite) reported by Condie in Archean andesites. Given other compositional differences such as elevated Ni, Co and Zr contents in Archean andesites, it would appear that direct analogies drawn between modern and ancient, magmatic and tectonic processes are suspect.

The sections describing the contrasts in chemistry of erupted rocks consequent upon changes in tectonic environment in areas of Africa–Arabia collision (Innocenti *et al.*), and collision and rifting in the Antarctic Peninsula (Tarney *et al.*), are important for our understanding of the interplay of tectonic and magmatic

processes. Further in this vein, the summaries of trace element and isotopic characteristics by Pearce and Hawkesworth provide a number of constraints on petrogenetic hypotheses attributing significant roles for the different tectonic elements involved in plate collision zones. Some of these constraints are not recognized by authors of other segments of the book.

Space devoted to the role of andesites in the evolution of continental crust and the

types of mineral deposits found in arc environments could have been expanded, but at least serves as an introduction to these subjects. Overall, then, this is not a book for the beginner, but a number of important contributions and ideas are included which make for fascinating reading. □

Richard J. Arculus is a Research Fellow in the Research School of Earth Sciences, Australian National University, Canberra.

Prospects for imprisoning solar energy

J.I.B. Wilson

Solar Cells: Operating Principles, Technology, and System Applications. By Martin A. Green. Pp.274. ISBN 0-13-822270-3. (Prentice-Hall: 1982.) £22.35, \$27.95. *Solar Cell Device Physics.* By Stephen J. Fonash. Pp.332. ISBN 0-12-261980-3. (Academic: 1982.) \$35, £23.20. *Photovoltaic and Photo-electrochemical Solar Energy Conversion.* NATO Advanced Study Institute Series, B69. Edited by F. Cardon, W.P. Gomes and W. Dekeyser. Pp.422. ISBN 0-306-40800-7. (Plenum: 1981.) \$49.50, £31.19. *Photochemical Conversion and Storage of Solar Energy.* Proceedings of the Third International Conference, Boulder, USA. Edited by John S. Connolly. Pp.444. ISBN 0-12-185880-4. (Academic: 1982.) \$34.50, £23.

THE photochemical and photovoltaic approaches to energy conversion are often linked, as a contrast to the mechanical-engineering-based photothermal converters of solar energy. Photochemical converters — including photosynthetic systems — and photovoltaic cells are similar in that both use high quantum energy from a radiant source to produce high-grade energy. Of the two technologies, however, only photovoltaic cells have reached technical maturity. The problems which still prevent the practical application of photochemistry are electrode degradation and too low a power conversion efficiency, but these drawbacks are countered by the ease with which liquid systems can be increased in area and by the possibility of combined energy storage, benefits which together offer the prospect of cheaper large-scale energy conversion than high-technology, solid-state solar cells.

An accurate impression of the state of play in both the solar chemical and electrical conversion techniques can be gained from the list of contents of these four books. Solar cells are now included in some undergraduate courses and so a number of teaching texts are appearing, of which this one by Green is the most comprehensive; the author uses few

equations and his book is one of the best introductions to solar cell technology for anyone with some knowledge of physical science. At the same time, priorities in solar cell research are changing from meeting the requirements of space technology for high-efficiency cells to an emphasis on lower costs; thus the basic physics is being examined in detail for possible alternative device structures and for additional solid-state phenomena which might add appreciably to power output. Fonash's research-level monograph considers *all* sources of photocurrent and photovoltage in a generalized model of solar cells, and it should provide the theoretical basis for any future development. The book can be recommended as a specialist theoretical text for semiconductor device engineers.

The other two books reviewed here are essentially the records of conferences and contain chapters based on lectures from experts on a range of specialized topics. This format usually appeals only to those who went to the meetings, or would have liked to attend, but both volumes do contain sections of broad appeal.

The NATO Advanced Study Institute, held in Ghent late in 1980, was restricted to energy systems which were not then commercially viable, or not even technically proven. Thus economics, the ultimate arbiter of success in this field, was not included. The Boulder conference had much more emphasis on biological aspects of photochemistry and on the attempts to produce an *in vitro* photosynthetic system, but there is some overlap with the contents of the NATO volume — even to the extent of containing an identical chapter by A.J. Nozik.

Since the first question to be asked about a new solar energy device is: "what is its efficiency?", the chapter by J.R. Bolton and colleagues in the Boulder conference proceedings should be prerequisite reading for those wanting to understand the limitations of the answers they receive. Although there is a strict thermodynamic limit to the solar energy conversion efficiency of a two-level quantum converter of about 31 per cent, various

researchers have paid particular attention to the ultimate physical limitations of selected converters, and Bolton *et al.* compare these calculations. Of especial value is the authors' comparison of similar quantities in chemistry, photovoltaics and thermodynamics. They also show that the two-photon process of photosynthesis provides a greater excess potential to overcome energy losses than the simple one-photon system. This may well be a significant indicator for attempts to build an efficient artificial system simulating natural photosynthesis.

Such attempts are described in some detail by M. Calvin in the critical review which opened the Boulder conference, and the fundamental problems are stated quite clearly: although effective optical absorption is achieved easily enough, conversion of the photon energy to a separable chemical product creates considerable difficulties. Usually two coupled systems are required for separate oxidation and reduction reactions in a closed cyclic system, and it has proved difficult to connect the two parts without excessive energy loss. This is well demonstrated by the breadth of attempts to photolyse water using sensitized absorbing aqueous liquids or photosensitive semiconductor electrodes. Also in the Boulder volume is a detailed description of *in vivo* chlorophyll research through which we may eventually assemble an artificial system; this section, however, will be difficult going for the non-specialist.

Of more general interest is the problem of physically containing chemicals and photoactive surfaces, since all photochemical systems, whether generating electricity or chemical fuel, rely on active interfaces to separate the various functions. In a green plant the sunlight-absorber, chlorophyll, is contained in a thylakoid membrane which apparently separates the initially reactive oxidation and reduction products. Some of the experiments in generating hydrogen and oxygen from water by photolysis use analogous artificial membranes to separate the two balanced reactions without impeding the transfer of electrons and protons. In the alternative "single cell systems", the redox catalysts generate hydrogen and oxygen together, but these must be separated afterwards.

This sort of research requires a blend of semiconductor physics and inorganic and organic chemistry; it relies heavily on the design of new chemical compounds with specific molecular structures. In this

context, the more successful sections in both of the symposium volumes come from the photochemical side. In contrast is the brief chapter by S. Wagner (Boulder conference) on photovoltaic cells which fails to put forward any interesting problems requiring a chemistry solution (for instance in the application of amorphous semiconductors).

Recent calculations suggest the possibility of a solar energy converter whose efficiency is limited only by that of an infinite array of separate absorbers with different bandgaps. This possible efficiency limit of 66 per cent (which also exceeds the 52 per cent efficiency of an ideal thermal converter) was only mentioned during discussions at the Boulder conference, but details have since been published by R.T. Ross and A.J. Nozik (*J. Appl. Phys.* 53, May 1982). The trick is to inject "hot" charge carriers from the semiconductor into the electrolyte before they can thermalize and come into equilibrium with the other free carriers, in a manner analogous to negative electron affinity photocathodes for vacuum photodiodes. In this way less of the excess photon energy above the semiconductor bandgap is lost as heat. In his chapters in the books under review, Nozik describes some systems which may be showing these hot-carrier injection effects, but a viable energy converting cell remains to be produced.

I have selected only a few topics for discussion here, but it should be clear that photovoltaic cells use sophisticated semiconductor technology to provide an efficient, reliable source of electrical energy: such research is now concentrated on reducing production costs without undue sacrifice of efficiency. Some of the cells which have this objective are covered in detail in the NATO book, but there is no description of conventional crystalline silicon cells and no account of amorphous silicon cells. Photochemical cells providing either chemical or electrical energy using solid-liquid interfaces are more difficult to make as well as to understand. Since they are mostly too inefficient or too short-lived because of electrode corrosion to compete with existing energy sources, their application is some years hence. In view of the overlap between the treatment of these devices in the NATO volume and in the proceedings of the Boulder conference, I prefer the latter for its wider spread of subjects, more attractive format and for its inclusion of photosynthetic processes. It is to be hoped that some of the current photochemical research which appears in this book as abstracts of contributed papers may attract sufficient further study to lead to the cheap, efficient solar energy converter which we all await. □

J.I.B. Wilson is Senior Research Fellow in the Physics Department, Heriot-Watt University, Edinburgh.

Science in ferment

S.J. Pirt

Prescott and Dunn's Industrial Microbiology, 4th Edn. Edited by Gerald Reed. ISBN 0-333-33630-5. (Macmillan, London: 1982.) £40.

FERMENTATION technologists need a source book of descriptions of the fermentation processes used in industry. For this purpose one of the first choices has for many years been Prescott and Dunn's manual, first published in 1940. Originally the book was a straightforward account of information of practical use in virtually every industrial fermentation, with emphasis on the traditional high-volume, low-cost products.

The development of our understanding of the scientific basis of fermentation has proceeded apace in the 20 years since the appearance of the third edition of Prescott and Dunn. This development probably constitutes the greater part of what is known today of the quantitative expression of fermentation processes, metabolic regulation and the application of genetic manipulation to fermentation. A further consequence of two decades of activity has been the unification of the diverse technologies depending on microbial action — brewing, dairy and other food fermentations, secondary metabolite production, vaccine production and biological purification of effluents. The provision of a common basis for all of these processes is one of the strengths of biotechnology.

All of this has meant that the updating of Prescott and Dunn presented a considerable challenge. The editor, appreciating the magnitude of this task, coupled with the increased range of fermentations, has solved the problem by restricting the scope of the fourth edition to fermentations related to the food and beverage industries. In addition, the original monograph style with two authors for the whole book has been replaced by the edited text with contributions by many authors. Essentially the only thing left of the original book is the title.

Although the aim has been to provide a descriptive account of the various fermentations, within this format there is wide coverage of the scientific basis on which the various technologies rest, and a good coupling of the science with the technology. There is a liberal sprinkling of important details which could be crucial to technologists who are concerned with the industrial operation of the processes; thus the authors seriously attempt "technology transfer". In all the tradition of Prescott and Dunn has been preserved, albeit with the inclusion of only some rather than all industrial fermentations. □

S.J. Pirt is Professor in and Head of the Department of Microbiology at Queen Elizabeth College, University of London.

The business of solar cells

Finance and Utilization of Solar Energy published by the Center for Innovation and Entrepreneurial Development at the University of California, Santa Cruz, contains the proceedings of a conference on the topic held at the Center in October of last year. The publication costs \$10 plus postage.

BOOKS RECEIVED

Chemistry

- BOCKRIS, J.O'M., CONWAY, B.E. and WHITE, R.E. (eds). *Modern Aspects of Electrochemistry*, No.14. Pp.661. ISBN 0-306-40845-7. (Plenum: 1982.) \$55.
- CHANEY, J.F., RAMDAS, V., RODRIGUEZ, C.R. and WU, M.H. (eds). *Thermophysical Properties Research Literature Retrieval Guide 1900-1980*. Vol. 2. *Inorganic Compounds*. ISBN 0-306-67222-7. (Plenum: 1982.) Np.
- COYLE, J.D., HILL, R.R. and ROBERTS, D.R. (eds). *Light, Chemical Change and Life: A Source Book in Photochemistry*. Pp.406. ISBN 0-335-16100-6. (Open University: 1982.) £6.95.
- DENNEY, R.C. *Key Definitions in Chemistry*. Pp.144. ISBN 0-584-10559-2. (Muller, London: 1982.) £3.95.
- FRANKEL, M. *Chemical Risk. A Workers' Guide to Chemical Hazards and Data Sheets*. Pp.96. ISBN 0-86104-362-6. (Pluto: 1982.) £1.95.
- FRIED, B. and SHERMA, J. *Thin-Layer Chromatography: Techniques and Applications*. *Chromatographic Science Series*, Vol. 17. Pp.320. ISBN 0-8247-1288-9. (Marcel Dekker: 1982.) SwFr.148.
- FURTER, W.F. (ed.). *A Century of Chemical Engineering*. Pp.463. ISBN 0-306-40895-3. (Plenum: 1982.) Np.
- GIANURCO, F.A. (ed.). *Atomic and Molecular Collision Theory*. Pp.505. ISBN 0-306-40807-4. (Plenum: 1982.) \$59.50.
- KORYTA, J. *Ions, Electrodes and Membranes*. Pp.197. Hbk ISBN 0-471-10007-2; pbk ISBN 0-471-10008-0. (Wiley: 1982.) Hbk £17, \$39.60; pbk £7.90, \$18.75.
- KUMAKHOV, M.A. and KOMAROV, F.F. *Energy Loss and Ion Ranges in Solids*. Pp.296. ISBN 0-677-21220-8. (Gordon & Breach: 1981.) \$93.50.
- LESKE, A.M. *Introduction to Physical Chemistry*. Pp.746. ISBN 0-13-492710-9. (Prentice-Hall: 1982.) Np.
- LÉVY, M., LE GUILLLOU, J.-C. and ZINN-JUSTIN, J. (eds). *Phase Transitions*. *Cargèse 1980*. Pp.462. ISBN 0-306-40825-2. (Plenum: 1982.) Np.
- MATJEVIC, E. (ed.). *Surface and Colloid Science*, Vol. 12. Pp.473. ISBN 0-306-40616-0. (Plenum: 1982.) \$55.
- MILLER, J.S. (ed.). *Extended Linear Chain Compounds*, Vol. 1. Pp.481. ISBN 0-306-40711-6. (Plenum: 1982.) \$52.50.
- PATAI, S. (ed.). *The Chemistry of Functional Groups Part I and Part II*. Part I ISBN 0-471-27871-8; Part II ISBN 0-471-27872-6. (Wiley: 1982.) £150, \$295 (Part I and II).
- RODRIGEZ, F. *Principles of Polymer Systems*, 2nd Edn. Pp.575. ISBN 0-07-053382. (McGraw-Hill, Berkshire: 1982.) £22.50.
- SEYMOUR, R.B. and STAHL, G.A. (eds). *Macromolecular Solutions: Solvent-Property Relationships in Polymers*. Pp.233. ISBN 0-08-026337-2. (Pergamon: 1982.) £21.25, \$42.50.
- TAYLOR, J.B. and KENNEWELL, P.D. *Introductory Medicinal Chemistry*. Pp.202. UK Hbk ISBN 0-85312-207-5; pbk ISBN 0-85312-311-X; US ISBN 0-470-27252-X. (Ellis Horwood, Chichester/Wiley/Halsted Press: 1981.) Hbk £20; pbk £7.50, \$16.45.

Technology

- ATHERTON, D.R. *Nonlinear Control Engineering*. Pp.470. ISBN 0-442-30486-2. (Van Nostrand Reinhold: 1982.) £8.95.
- MILLHON, J.P. and WILLIS, E.H. (eds). *New Energy Conservation Technologies and Their Commercialization*. In 3 Volumes. (Not available separately). *Proceedings of an International Conference held April 6-10 1981, Berlin*. Pp.3269. ISBN 3-540-11124-7/0-387-11124-7. (Springer-Verlag: 1981.) DM 320, \$149.
- MORGAN, R.P. and ICERMAN, L.J. *et al.* *Renewable Resource Utilization for Development*. Pp.394. ISBN 0-08-026338-0. (Pergamon: 1981.) £19.75, \$39.50.
- NATIONAL RESEARCH COUNCIL. *Outlook for Science and Technology: The Next Five Years*. Pp.788. Hbk ISBN 0-7167-1345-4; pbk ISBN 0-7167-1346-2. (W.H. Freeman: 1982.) Np.
- SAHA, S.K. and BARROW, C.J. (eds). *River Basin Planning: Theory and Practice*. Pp.357. ISBN 0-471-09977-5. (Wiley: 1981.) £19.
- WILLIAMS, J.C. and BELOV, A.F. (eds). *Titanium and Titanium Alloys. Scientific and Technological Aspects*, Vol. 1. Pp.798. ISBN 0-306-40191-6. (Plenum: 1982.) \$195.
- WISEMAN, A. (ed.). *Topics in Enzyme and Fermentation Biotechnology*, Vol. 6. Pp.232. UK ISBN 0-85312-372-1; US ISBN 0-470-27304-6. (Ellis Horwood, Chichester/Wiley/Halsted Press: 1982.) £21.50.

Earth Sciences

- BONNEAU, M. and SOUCHIER, B. *Constituents and Properties of Soils*. Pp.496. ISBN 0-12-114550-6. (Academic: 1982.) £36.20, \$74.50.
- CUMBERLAND GEOLOGICAL SOCIETY. *The Lake District. Rocks and Fossils No. 4*. Pp.136. ISBN 0-04-554007-1. (Unwin, London: 1982.) £3.95.
- LEEDER, M.R. *Sedimentology. Process and Product*. Pp.344. Hbk ISBN 0-04-551053-9; pbk ISBN 0-04-551054-7. (George Allen & Unwin: 1982.) Np.
- MONMONIER, M.S. *Computer-Assisted Cartography. Principles and Prospects*. Pp.214. ISBN 0-13-165308-3. (Prentice-Hall: 1982.) £15.70.
- SALTZMAN, B. (ed.). *Advances in Geophysics*, Vol. 23. Pp.391. ISBN 0-12-018823-6. (Academic: 1981.) \$48.50.
- SIMPSON, I.M. *The Peak District. Rocks and Fossils, No. 3*. Pp.120. ISBN 0-04-554006-3. (Unwin, London: 1982.) £3.95.
- STIRLING, R. *The Weather of Britain*. Pp.270. ISBN 0-571-11695-7. (Faber & Faber: 1982.) £12.50.

VON RAD, U., HINZ, K. *et al.* (eds). *Geology of the Northwest African Continental Margin*. Pp.703. ISBN 3-540-11257-X/0-387-11257-X. (Springer-Verlag: 1982.) DM 110, \$51.20.

WILSON, G. and COSGROVE, J.W. *Introduction to Small-Scale Geological Structures*. Pp.160. Hbk ISBN 0-04-551051-2; pbk ISBN 0-04-551052-0. (George Allen & Unwin: 1982.) Hbk £10; pbk £4.95.

Applied Biological Sciences

- ALTSCHUL, A.M. and WILCKE, H.L. (eds). *New Protein Foods*, Vol.4, *Animal Protein Supplies. Part B: Food Science and Technology*. Pp.378. ISBN 0-12-054804-6. (Academic: 1981.) \$49.
- ASHTON, H. and STEPNEY, R. *Smoking: Psychology and Pharmacology*. Pp.222. ISBN 0-422-77700-5. (Tavistock, London: 1982.) £9.95.
- BECKER, F.F. (ed.). *Cancer 1. A Comprehensive Treatise*. 2nd Edn. *Etiology: Chemical and Physical Carcinogenesis*. Pp.714. ISBN 0-306-40701-9. (Plenum: 1982.) \$69.50.
- BENDER, A.E. and BENDER, D.A. *Nutrition for Medical Students*. Pp.380. ISBN 0-471-28041-0. (Wiley: 1982.) £16.
- BINDRA, J.S. and LEDNICER, D. (eds). *Chronicles of Drug Discovery*, Vol.1. Pp.283. ISBN 0-471-06516-1. (Wiley: 1982.) £24, \$43.
- BRUSHKE, A.V.G., VAN HERPEN, G. and VERMEULEN, F.E.E. (eds). *Coronary Artery Disease Today: Diagnosis, Surgery and Prognosis. Proceedings of an International Symposium held in Utrecht, May 1981*. Pp.455. ISBN 90-219-0503-5. (Excerpta Medica, Amsterdam: 1982.) \$107, Dfl.230.
- COHEN, J.S. (ed.). *Noninvasive Probes of Tissue Metabolism*. Pp.270. ISBN 0-471-08893-5. (Wiley: 1982.) £36.50, \$166.
- COMISION DE ONCOLOGIA. *Protocolos Terapeuticos Del Cancer De La Clinica Universitaria De Navarra*. Pp.354. ISBN 84-313-0724-2. (Ediciones Universidad de Navarra, S.A. Pamplona: 1981.) Np.
- CONSEILLER, C. *et al.* (eds). *Postgraduate Course 12th International Meeting of Anaesthesiology and Resuscitation 1980: Anaesthesia and Postoperative Care in Uncommon Diseases*. Pp.441. ISBN 9-0219-0473-X. (Excerpta Medica, Amsterdam: 1981.) \$74.50, Dfl.160.
- CONSEILLER, C. *et al.* (eds). *Postgraduate Course 12th International Meeting of Anaesthesiology and Resuscitation 1980: Volatile Halogenated Anaesthetics*. Pp.241. ISBN 9-0219-0474-8. (Excerpta Medica, Amsterdam: 1981.) \$55.75, Dfl.120.
- COSOFRET, V.V. *Membrane Electrodes in Drug-Substances Analysis*. Pp.362. ISBN 0-08-026264-3. (Pergamon: 1981.) £29.50, \$60.
- DE DATTA, S.K. *Principles and Practices of Rice Production*. Pp.618. Pbk ISBN 0-471-09760-8. (Wiley: 1981.) Pbk np.
- DENIS, L., SMITH, P.H. and PAVONE-MACALUSO, M. (eds). *Clinical Bladder Cancer. Proc. of an International Symposium presented at the Antwerp Medical Days held September 1980 in Antwerp, Belgium*. Pp.202. ISBN 0-306-40835-X. (Plenum: 1982.) \$29.50.
- DI CHIARA, G. and GESSA, G.L. (eds). *GABA and the Basal Ganglia. Advances in Biochemical Psychopharmacology*, Vol.30. Pp.252. ISBN 0-89004-752-9. (Raven: 1981.) \$28.

Psychology

- APTER, M.J. *The Experience of Motivation: The Theory of Psychological Reversals*. Pp.420. ISBN 0-12-058920-6. (Academic: 1982.) £16.80, \$34.50.
- BRENNAN, J.F. *History and Systems of Psychology*. Pp.374. ISBN 0-13-392209-X. (Prentice-Hall: 1982.) £15.70.
- GRAY, J.A. *The Neuropsychology of Anxiety: An Enquiry into the Functions of the Septo-Hippocampal System*. Pp.548. ISBN 0-19-852109-X. (Oxford University Press: 1982.) £27.50.
- WAGNER, D.A. and STEVENSON, H.W. (eds). *Cultural Perspectives on Child Development*. Pp.315. Hbk ISBN 0-7167-1298-X; pbk ISBN 0-7167-1290-3. (Freeman: 1982.) Hbk £14.80; pbk £7.60.

Sociology

- CAFAGNA, A.C., PETERSON, R.T. *et al.* (eds). *Child Nurture: Vol. 1. Philosophy, Children, and the Family*. Pp.377. ISBN 0-306-41003-6. (Plenum: 1982.) Np.
- GAUTIER, J.-Y. *Socioecologie: L'animal Social et Son Univers*. Pp.267. ISBN 2-7089-8702. (Privat, France: 1982.) F.79.70.
- HERFURTH, M. and HOGEWEG-DE HAART, H. (eds). *Social Integration of Migrant Workers and Other Ethnic Minorities: A Documentation of Current Research*. Pp.265. ISBN 0-08-028957-6. (Pergamon: 1982.) £48, \$96.

History of Science

- ATHA, A. (ed.). *A Scottish Naturalist: The Sketches and Notes of Charles St John 1809-1856*. Pp.192. ISBN 0-233-97390-7. (André Deutsch: 1982.) £10.95.
- CANNON, J.T. and DOSTROVSKY, S. *The Evolution of Dynamics: Vibration Theory from 1687 to 1742. Studies in the History of Mathematics and Physical Sciences*, Vol. 6. Pp.184. ISBN 3-540-90626-6. (Springer-Verlag: 1981.) DM 98, \$45.70.
- CHRISTEN, Y. *Le Dossier Darwin*. Pp.252. No ISBN. (Editions Copernic, Paris: 1982.) F.75.

30 September 1982

The defence of Western Europe

High-tech warfare is all the rage, and the US Army is saying that the conventional defence of Europe may again be possible. The message (which may be wrong) should not be overlooked.

Must the defence of Western Europe rest for ever on nuclear weapons, mostly made in the United States? The usual answer (yes) is a recurrent embarrassment to many of the governments concerned. In Belgium, the Netherlands and West Germany, politicians now have ample experience of the risks of defending nuclear defence. And the assumption that nuclear weapons are a necessity for Western Europe is an impediment in arms control negotiations. So it is welcome, and may be important, that in the past year there has been a revival of interest in conventional (non-nuclear) forces as a means of defending Western Europe. The interest has come from many quarters, from German military experts, from the US Army, from among technologists who are studying how the job could be done and from those more thoughtful advocates of the nuclear freeze who recognize that the West without nuclear weapons must still defend itself. The outcome could be refreshing and important.

The belief that the defence of Western Europe must be based on nuclear weapons stems from the Lisbon conference of 1952, when the embryo NATO alliance agreed that the number of troops and armaments required to counter a possible Soviet invasion were, literally, unsupportable — 96 divisions and 9,000 aircraft. To circumvent this weakness, NATO made a Faustian pact with the nuclear genie. Soviet leaders were warned that if they ever flexed their considerable muscle in the direction of Western Europe, the United States would consider its vital interests threatened and might respond with nuclear weapons — at the outset, clumsy devices carried by long-range aircraft. Since then, the basic conundrum has remained but the weapons have changed. The US weapons laboratories developed smaller nuclear weapons that could fit into guns and short-range aircraft, making tactical engagements credible, if only just, later they invented the neutron bomb, to make nuclear weapons more acceptable both to battlefield commanders and to Europeans. The most recent development was to put small but very accurately directed nuclear warheads on longer-range weapons, such as the Pershing II missile and the ground-launched cruise missile, to persuade everyone that nuclear war in Europe could be neat and precise. The US Army even called its neutron bomb the "cookie cutter".

Weapons

But no trick of technology or public relations could change the basic problem: NATO countries had mostly to rely on nuclear weapons controlled by the United States to defend themselves, and the weapons would destroy the very territory they were meant to protect.

So far, the conventional alternative has made very little headway. West European governments have consistently resisted on the grounds of cost, while the United States has pleaded in turn its commitment in Vietnam and, more recently, cost again. Only in the late 1970s did the Carter Administration exact from West European governments a commitment to increase defence spending by 3 per cent a year — handsome by past standards but still inadequate, given the build-up in conventional weapons by the Warsaw Pact countries throughout the 1960s and 1970s. So the Lisbon strategy has remained, but weakened by the Soviet strategic nuclear build-up, it can no longer be assumed that US arms will serve as Western Europe's shield.

Developments in technology and in military thinking could

now change all this quite soon. Manfred Worner, a likely candidate for the post of defence minister in any Christian Democrat government in West Germany, said in Washington last summer that NATO's previous conventional option, to increase its present 26 divisions to 36 forward divisions with 9–12 in reserve, would entail an unacceptable doubling of the West German army, the Bundeswehr. But technology, he said, may offer an alternative. An arsenal of remotely piloted vehicles, cruise missiles and shorter-range ballistic missiles, all armed with conventional munitions and terminal homing, could do much damage to the Warsaw Pact's follow-on forces that give a potential Soviet offensive punch and staying power. Such stand-off weapons could be attached to NATO's JABO-class fighter-bomber aircraft, extending the defence for hundreds of kilometres behind the main line of advance. By counter-attacking in depth, Worner argued, NATO could perhaps hold off and even turn back an invasion.

War games

US Army war games recently played at Fort Leavenworth appear to confirm this view. Using an extended counter-attack strategy with the weapons the US Army plans to have in the field by 1986, the game showed that the defence could hold an invasion through the Fulda Gap — one of the passes near the border, without resort to nuclear weapons (or to chemical weapons either). Likewise, the US Defense Advanced Research Projects Agency (DARPA) has just finished a test called "Assault Breaker" which explored what kinds of radars, missiles, munitions and terminal homing systems are available, and which combinations could defeat putative Soviet second echelon forces 100 kilometres behind the battle front. These forces, which would be expected to roll along after the first invaders in enormous timed masses, could have as many as 600 tanks, 500 armoured vehicles, 50 artillery batteries, 200 surface-to-air missiles and 300 trucks.

With the old technology, it might have taken 5,500 air sorties and 33,000 tonnes of bombs to destroy such a force. Assault Breaker showed, however, that sufficiently accurate conventional weapons with ranges from 100 to 200 kilometres could do the job as well. Tentatively, the agency estimates that to equip Central Europe with these things — many of which are already in existence but would have to be fitted onto existing planes, guns and rocket launchers — could cost a mere \$2,300 million. The calculation is that only the US forces would have to be re-equipped, allied conventional forces would be unchanged.

Such talk about the conventional defence of Europe has not been heard since the 1930s when the Maginot Line was built. An improved conventional defence, that substitutes technology and strategy for large standing armies and nuclear bombs, is an intriguing new theme. In the United States, people are talking about using dirt and concrete to fortify the passes at Fulda, Meiningen and elsewhere, forcing an invader onto the northern or southern flanks, where he would be more vulnerable. Simple things, like the construction of more short runways near the German border so that F-5s and other short-range aircraft could be brought into battle, are similarly calculated to make a big difference. If further study shows that these conventional means of defence could be effective, the result may be to liberate Western Europe from the Lisbon understanding, now thirty years

old The consequences of that would be profound

First, it may be possible to put the nuclear genie back into its bottle, at least where Central Europe is concerned. The governments that have struggled with opposition parties over the siting of nuclear weapons on their territory, but under US control, will jump at the prospect that conventional defence might instead suffice. And since no European government can foretell the state of public opinion after 1986, the earliest that a new-style conventional defence could be in place, even those that hitherto have been most hospitable to nuclear arms are bound prudently to look again at the new conventional alternative. Everything will depend on the degree to which they are persuaded that some version of the conventional alternative will be effective — and that the present wave of enthusiasm for it in the United States is not a blind for the withdrawal of other than strategic nuclear weapons.

Second, an improved conventional defence of Western Europe would not overnight make Central Europe free from danger. If it were possible to rely on new conventional forces to repel conventional attacks, Western Europe could still be browbeaten into submission by the threat of nuclear attack. So the promise of strategic nuclear support from the United States would still be necessary for the security of Western Europe. And those states in Europe that consider independent nuclear forces essential to their security, France and the United Kingdom, would presumably continue as at present.

The most hopeful consequence of the new interest in conventional defence is, however, in arms control. Bilateral negotiations will be resumed this week in Geneva on the Soviet and US proposals that intermediate-range nuclear weapons on either side of the German frontier should be limited, but the prospect of rapid progress is slim. The Soviet side has a tactical advantage in stringing the United States along until late next year, when the Pershing II and cruise missiles are due to be installed in Western Europe, but both sides are also genuinely perplexed to know how to strike a balance between their qualitatively very different nuclear forces. If the conventional defence of Western Europe is feasible, economically as well as technically, the bargaining position of the United States in these negotiations would be strengthened, as would the prospect that Central Europe could be made substantially safer than it is at present.

La Ronde, 1982 style

The French government may have bargained for less than it will get from a job-switch.

Will all the reforms and reorganizations of French science, which appear to have been almost continuous since May 1981, when President Mitterrand came to power, amount come to much in the end? There are two clear views in France: the cynical and the refreshing. But each observer is ambivalent.

"We've had so many, we know how to resist reforms", they say, "but there has also been a *prise de conscience*". Something does seem to have happened, but it is not so much in the rules and regulations, as in attitudes. The shift, which realigns the bulk of scientists and university staff with the economy and with industry, rather than against it as a kind of intellectual resistance movement, was under way before the socialists came to power. But Jean-Pierre Chevènement, as minister of science and now of research and industry (note the change) has confirmed the move and is attempting to institutionalize it, and with some success.

Take the National Colloquium on Science and Technology last January. "What a mess it was," said a polytechnicien the other day, "but how important!" Very little of practical importance was concluded, the committee on finance, for example, did not even consider figures, and a recommendation to preserve the French *troisième cycle* form of higher degree was ignored in Chevènement's subsequent law for research (it is billed for change). But people met at the colloquium who had never met before — in particular the universities and industry — and found they had something useful to offer each other. This is the *prise de*

conscience that led earlier this year to a large majority of university lecturers saying in response to a questionnaire that they would like more involvement with industry. This is the *prise de conscience* that is leading industry actually to pay visits to university laboratories ("I've had four visits from industry this year" said one researcher recently "It just wouldn't have happened two years ago") and also encouraging French scientists to seek contracts with industry.

Moreover, the recent changes at the head of the Centre National de la Recherche Scientifique (CNRS), which funds the cream of basic science in France, and of the higher education division of the Ministry of National Education, seem likely to confirm the trend. Pierre Papon, a chemist who takes over at CNRS, is somewhat quieter than his predecessor, Jean-Jacques Payan, and he has been much closer to Chevènement as a member of the minister's policy-making cabinet. Payan, at a little leaving party at CNRS headquarters a couple of weeks ago, said that "like Nelson, I know how to disobey". Papon may not be so resistant to Chevènement's plans for, say, the social sciences, where Chevènement would like to impose essentially his own view of the subject as something more akin to a tool of policy. Papon has refrained from appointing Chevènement's *protégé*, the marxist M. Godelier, to the post of director of social sciences. But clearly Papon by conviction, by inclination and by personality is likely to allow Chevènement a somewhat greater influence over CNRS than hitherto — and that will imply an inclination towards industry.

At the Ministry of National Education, the new director of higher education is Jean-Jacques Payan, the man who could disobey Chevènement. Will he protect the old interests of the universities there? Probably not. He did, after all, encourage most of the reforms of CNRS (social sciences aside), he believes in the new government, he understands the need for improving French industry, he understands the universities (he was president of the University of Grenoble) and he understands power. He is going to use that power to reform the universities along the lines of the "*prise de conscience*". The universities are highly centralized in France, and that gives Payan weapons he is not going to relinquish easily. His power is very great: he largely controls appointments and the budgets of all the universities, effectively, he is in the position of the former Minister of the Universities (when such a ministry existed), Alice Saunier-Seïté, who so appalled the universities with her dirigism, her dismantling of many *troisième cycle* degrees and what are now seen as arbitrary acts of vindictiveness.

Payan has almost the same weapons (the control of appointments has recently been made a little more democratic) and the same reforming zeal. So where does he differ from his reviled right-wing predecessor? The difference is that he is optimistic, he says, about the future of the universities whereas Alice Saunier-Seïté was ultimately pessimistic.

So the universities should, in principle, enjoy the forthcoming Payan reforms whereas they hated Saunier-Seïté's. Payan would however like to do away with the *troisième cycle*, and the subsequent *thèse d'état* (one basically a little lower, the other a little higher, than a PhD), and substitute a PhD system, and there is going to be a lot of resistance to that, unless Payan handles the situation with enormous tact — and muscle. (Many comfortable livings in French universities depend on the existence of the *troisième cycle*, which requires fewer lectures but brings in more cash than undergraduate teaching.)

However Payan is limited by one thing — the forthcoming "law for the universities", a reform of the 1968 act which established the French university system after the student rebellion of that year. This law was almost ready when Payan moved across to the Ministry of National Education from CNRS, and he may be able to make only minor changes to the existing text. But, he says, he was "pleasantly surprised" with the present version and he may have to do little to suit his taste. As for the Mitterrand government, and its use of science and technology as an economic engine "I shall do everything in my power to make it succeed" he says.

New UK row on embryo research

Edwards in fresh ethical contretemps

Yet another public controversy has erupted in Britain about the *in vitro* fertilization of human ova and the practices associated therewith. At the weekend and in the following days, many British newspapers reported that Dr Robert Edwards, of the physiology department at the University of Cambridge, had told a weekend conference that he had been carrying out experiments on viable human embryos surplus to the requirements of *in vitro* fertilization operations.

Dr Edwards and the surgeon Mr Patrick Steptoe were the first British exponents of this technique. Most comments this week were accompanied by condemnations of what is supposed to be going on from various public figures, including Dr John Havard, secretary of the British Medical Association.

So far as can be learned, none of the popular reports so far published includes an account of what Dr Edwards actually said, first in the Galton Lecture of the Eugenics Society and then by telephone to a conference improbably held at Gatwick Airport, south of London, organized by the British Medical Journalists' Association and sponsored by the Ciba Foundation.

The occasion may nevertheless be important because of the appointment by the British government last July of a committee under Dr Mary Warnock to examine the ethical problems arising from *in vitro* fertilization. A spokesman for the Department of Health said on Monday that the newspaper reports merely confirmed that the government had foresight in setting up the committee, which is due to report two years from now. He could not immediately say whether the committee had yet met.

On the telephone earlier this week, Dr Edwards gave an account of his paper. After the Galton Lecture, the same discourse was given by telephone to the Medical Journalists' Association. He says that he explained how, in the process of *in vitro* fertilization, more than a sufficient number of fertilized ova (two or three) may be produced.

What seems not to be widely appreciated about the technique is that it is conventional to maintain these embryos in culture for between two and five days, before implanting them in the uterus of the putative mother. Dr Edwards said that he had reported to the conferences that "spare" embryos had on some occasions

been observed to provide further information on the optimum time for implantation.

Dr Edwards also reported that he told the conference that he had maintained some embryos in culture for longer than five days — nine days is the maximum so far. He said that while the primary objective of this work has been to improve the efficiency of *in vitro* fertilization, he is also interested in more distant possibilities, and told the conferences as much.

Dr Edwards said that while conventional wisdom has it that unwanted fertilized ova should be kept in a deep-freeze, but not allowed to die, until their future could be decided, there are good reasons for making use of them in studies of fertilization, differentiation and genetic abnormality.

He said, however, that there should first be "strong ethical advice" on the subject, and that those wishing to maintain human embryos for longer than a fixed period — five or nine days perhaps — should be required to have a licence to do so.

If those hurdles could be surmounted, however, Dr Edwards believes there are

substantial medical benefits ahead. While "dead against" the use of surrogate mothers to provide uterine hospitality for genetically unrelated embryos, he argues that freeze-dried congenic embryos grown at some future time to the stage at which heart or brain tissue differentiate (12-14 days) would provide adult human beings with access to compatible "spare part tissue" and thus offer an escape from immunological barriers in transplantation.

Dr Walter Hedgcock (73), a former deputy secretary of the British Medical Association, was reported by the London *Standard* on Monday as having been "horrified" by Dr Edwards's disembodied speech as received at Gatwick Airport, and to be looking for a parliamentary ban on such experiments.

Dr Edwards, not for the first time in trouble with the British popular press, considers he may have been unwise to talk to an audience without being able to look its members in the eye. The incident is nevertheless potentially important because it may prompt the British government to preempt the Warnock inquiry. ●

Reagan no science censor

Washington

President Ronald Reagan denied last Friday that his Administration sought to "close off legitimate transfer of knowledge and information" when his appointees in the Pentagon caused some hundred papers to be withdrawn in the name of national security at a symposium of the Society of Photo-Optical Instrumentation Engineers in San Diego, California, last month (see *Nature* 23 September, p 289).

At a meeting with a group of business publishers at the White House, President Reagan told me that the Soviet Union has acquired an enormous amount of US technology because of "carelessness". He defended the censorship as "just an attempt to close off those avenues where, just by reason of attendance at scientific forums and seminars, they have gone home with things that they have then turned to military advantage and the sophistication of their military build-up."

"Their technological sophistication is a threat to the whole peace-loving world so that is what is back of that — not any desire on our part to close off legitimate transfer of knowledge and information."

The President continued by saying that "if, here and there, something goes too far, we will rectify that" — an apparent acknowledgement that the Administration has sometimes gone too far in censorship.

There is, however, no evidence that the withdrawal of the papers at the San Diego meeting was done with presidential knowledge, even though Secretary of Defense Caspar Weinberger had been informed in

advance of what his staff considered an impending "disaster" at the photo-optical society meeting. In view of the attendance of Soviet scientists, Mr Weinberger then asked his staff to warn those due to read papers that they might be in violation of Pentagon review procedures if they did so.

"The situation is in total confusion", says Hakime Sakai, professor of physics at the University of Massachusetts at Amherst, who withdrew his paper in response to warnings from his sponsor, the Air Force's Geophysical Laboratory at Hanscomb Field. Sakai, like others, has now submitted his paper for Pentagon review, a requirement he was unaware of until days before the meeting.

While the president stressed the importance of stopping the "careless" transfer of information to the Soviet Union, he also indicated an equal interest in preserving "legitimate" transfer of information. But neither the President nor his science adviser, Dr George A. Keyworth (who, in a statement at the time, called the photo-optical society incident "unfortunate and ill-timed"), said how these two goals will be met.

It is not yet clear which procedures cover the presentation of unclassified scientific material at international meetings or, for that matter, publication in the open literature. The office of Stephen D. Bryen in the Pentagon, which issued the warnings, cited a "new" regulation issued in April (numbered 5230.9) which requires central Pentagon clearance (instead of clearance

by contractors and sponsors locally) for any papers containing "technical data" relating to equipment having military uses. Export of such equipment and related data is regulated by the 1954 International Traffic in Arms Regulations (ITAR). But the provision has previously been applied only to such things as directions for using a machine-tool device.

The Department of Commerce, which administers ITAR, sent a telegram to scientists before the meeting warning them of possible violations of ITAR, but Professor Sakai and others were unaware of this new Pentagon regulation, or that ITAR could apply to unclassified basic research, much of it based on work already published in the open literature. Sakai believed he was in compliance with another order of the Pentagon (numbered 12356), also issued in April, which said that unclassified basic research could not be classified unless it had a "direct" relationship to national security (Professor Sakai's paper was on infrared atmospheric emissions).

The Department of Defense now hopes to establish a steering committee to decide what to do about future scientific meetings. Professor Sakai notes that hundreds of scientific papers are presented in the United States each week that describe work funded by the Department of Defense. "It will be a monumental problem", he says, if the Reagan Administration imposes another review requirement on all those papers, as an addition to the regular peer review that the papers now receive.

Deborah Shapley

West German energy

Two reactors in need of help

Bonn puts pressure on public utilities

Heidelberg

The West German parliamentary commission of inquiry into future atomic energy policy reported last week on the comparative safety of the 300-MW prototype fast breeder reactor under construction at Kalkar (SNR 300) and a conventional 1,300-MW high-pressure light-water reactor, Biblis B, in Hesse. Nationally, opinion about the future use of nuclear energy in West Germany and in particular about the prototype reactors is deeply divided. The commission, which included seven members of parliament and was under the chairmanship of Harald Schäfer (Social Democratic Party), reflected this split by voting 11/5 that SNR 300 does not carry greater safety risks and should be put into operation. Because there is still much to be learned about the prototype, they recommend stepwise construction and careful training of personnel. The minority view was that a maximal meltdown accident with the fast breeder reactor would have far worse effects than a similar event in a conventional reactor, and the probability of its occurrence was unknown. Political, economic and security aspects should also be taken into account.

The sodium-cooled fast breeder has been 20 years in gestation. Its first project leader

was Wolf Häfele, then at the Karlsruhe Atomic Energy Research Center, now a member of the commission. The construction firm is Interatom and the scheme is financed by the federal government, various utility companies and to a lesser extent the Belgians and Dutch.

The other prototype reactor in West Germany is the thorium high-temperature reactor (THTR 300) at Schmehausen in the Ruhr, which was originally planned to produce high-grade heat for the chemical industry and for coal distillation and which is being constructed by Brown-Boveri & Co. Although the federal government is providing 75 per cent of the costs, these have risen high enough to dampen the interest of the chemical industry, especially because the reactor seems unlikely to provide the 1,000°C needed for coal distillation.

The construction of both reactors has been dogged by bureaucracy, litigation and political prevarication. Delays cost money and it is the escalating costs that are likely to decide the final fate of the reactors.

Andreas von Bulow, the Social Democrat minister of research and technology, has been asking industry to help make up the rising deficits. He emphasized that he could not allow two projects that have got out of hand to jeopardize basic research and the support of innovations which are more important for the German economy. The total ministry research and development budget for 1982 is DM6,500

Soviet ecology

Caspian water level drops

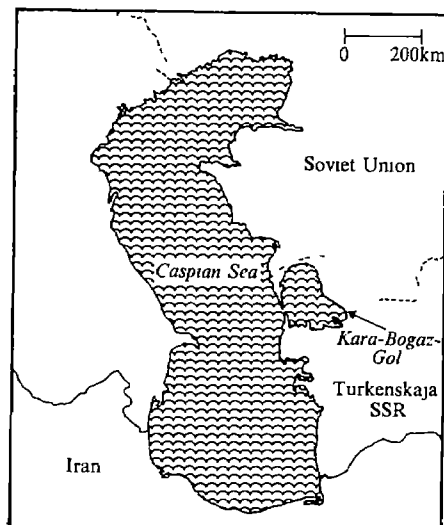
Soviet plans to exploit the mineral resources under the Kara-Bogaz-Gol gulf have run into trouble with conservationists working on the protection of the Caspian Sea. Beneath the Kara-Bogaz-Gol lies an underground brine lake rich in sodium sulphate — an estimated 16,000 million tonnes. Long-term development plans for the Turkmenian SSR see the brines as vital feedstocks for the rapidly expanding chemical industry of the republic.

Unfortunately, the prevailing arid conditions are rapidly reducing the water level in the Caspian. The sea has an annual intake of some 300 km³ from precipitation, but loses some 355 km³ from evaporation and 30 km³ to the needs of industry and desalination plants. The Caspian thus has a net loss of 15 km³ per year. During the past 50 years its level has sunk by 2.6 m and in places the shoreline has receded by several hundred metres.

Shallow areas near the shore are primarily responsible for the high level of evaporation — in particular, the Kara-Bogaz-Gol, from which some 5 km³ of water is lost annually. Accordingly, in 1979

it was suggested that a dyke should be constructed across the entrance to the gulf, which would then be allowed to dry out without depleting the Caspian of water.

In spite of Moscow's enthusiasm for the scheme, others are not so keen. The leading Ashkhabad newspaper, *Turkmenkaya*



Iskra recently carried a major attack on the dam project by G. Bagirov, laboratory chief of Karabogazsulfat, the organization that exploits the brines. The dam, he said, would do immeasurable damage to the brine resources. The balance between deep and surface brines, he claims, has already been upset, so that the concentration of harmful chlorides in the deep brines is constantly rising, while that of sulphates is dropping. Moreover, if the Kara-Bogaz-Gol were allowed to dry out completely, the salts could be picked up by strong winds and ruin fertile land and fishspawning grounds for hundreds of kilometres. Meanwhile, the Caspian would gradually become more saline, as the gulf's role as a natural desalinator would be ended.

All these problems would be overcome, Bagirov claimed, if a sluice were constructed to allow limited entry of water into the gulf from the Caspian, to maintain a water balance in the gulf with at least 1 km² of saturated natural brine. A plan for such a sluice, he claimed, has already been drawn up by the All-Union Ministry of Land Reclamation and Water Conservancy, but was shelved by the Turkmenian Ministry on the grounds that more surveys were needed.

Vera Rich

million (£1,500 million), and universities and research throughout the country are on short commons

It is relevant that in July the US General Accounting Office contested on economic grounds the priority set by the Reagan Administration on the first US fast breeder planned at Clinch River, Tennessee, at an estimated cost of \$3,500 million

Heinz Riesenhuber, Christian Democrat spokesman on energy, has emphasized the importance of both West German reactors

CERN

Electrons collide environmentally

The European Centre for Nuclear Research (CERN, near Geneva) is still battling with the politics of its next big project the large electron-positron collider, LEP. Although LEP was officially approved at the international CERN Council last December, local French opposition has again reared its head. But CERN is in such a hurry to get LEP built that it seems prepared to ignore opposition, and even, effectively, to 'gag' members of its own staff.

The problem is "environmental" approval. LEP must meet the regulations of France and Switzerland, through both of which it passes. Swiss law is already satisfied. But the French environmental hearings have only just started, and strenuous objections are already coming from the little village of Echevenex, tucked under the Jura Mountains six miles from the present CERN site.

Some 30 CERN staff live in the village, which is a well-known thorn in the CERN flesh. Last year the mayor, M Honorat, managed to halt construction of a pilot tunnel under the Jura, and was finally overruled by the highest French legal body, the Conseil d'Etat. Since then both LEP and M Honorat have changed their positions — LEP to avoid construction problems under the Jura, eliminating the need for the tunnel, and M Honorat for reasons of his own. LEP appeared to be safe.

However, the new path of LEP, although out of the Jura, comes much closer to Echevenex — and brings with it one of the four primary experimental halls, which will appear on the surface like a 400-metre-long factory, only 250 metres from the edge of the village, which looks down on the site across a valley. "It's a beautiful spot" said one resident last week. "The hall would go where the children like to play, and where we pick nuts." The site would be an eyesore in what is essentially a rural retreat, say the villagers — and it would bring noise.

The objections may be dismissed as romantic — unless one lives there — but CERN director-general Professor Herwig Schopper wrote recently that "We should aim not merely at LEP being tolerated by the local inhabitants, but at making them proud supporters of CERN as a positive

asset in their neighbourhood." Echevenex villagers see little sign of those ideals. At a meeting with CERN officials in the village on 2 July this year, the CERN reply to a question about noise was "you'll get used to it".

This apparently unhelpful attitude incensed even CERN employees in the village, and one of them, say the villagers, began to raise technical questions. For his pains, however, the employee was carpeted, and his attention drawn to a clause in the CERN employment contract which reads "Members of the personnel shall refrain from an act or activity which is incompatible with their functions or which would be materially or morally prejudicial to the organization." Clearly frightened for his future, he withdrew from the discussion. Since then, CERN has published a notice which indicates that employees are free to act in their interests, within the national law of their place of residence — but that they must also take note of their conditions of employment, thus, if they criticize CERN they are in danger.

What happens next depends on how CERN chooses to react, and on the process of French law. According to CERN foreign relations director, M Lévy-Mandl, CERN is likely to make "only small adjustments" to its plans. It would be technically possible to move buildings, he said, but this would slow the rate at which experiments could be moved in and out, compromise safety and increase costs. Representations to this effect would be made to the Commission of Inquiry, a body of six local personalities now taking local views on LEP according to French law. This commission will present its conclusions to the French government, which must then decide whether or not to give LEP the status of being "in the public interest", construction could then go ahead.

It seems inconceivable, now, that approval will not be given — so the question facing the government, with its professed concern for regionalism, is simply how far to take into account the objections of the little village of Echevenex. Will the Echevenex halls be just where CERN says they should be? Or where the villagers would like them?

Robert Walgate

UK nuclear power

Decision time

The management style of the United Kingdom Atomic Energy Authority may be subtly changed from 1 October, with the accession of Sir Peter Hirsch, the Oxford metallurgist, as the authority's part-time chairman. Since 1967, the successive chairmen of the authority (Sir John Hill and Sir Walter Marshall) have been full-timers from the nuclear industry.

Most immediately, the change will probably mean more responsibility for Mr A M Allen, deputy chairman of the authority for the past year and previously responsible for finance and administration. Mr Allen, who describes himself as a "lapsed historian", is now the authority's chief executive. Whether and to what extent Sir Peter Hirsch will think it politic to follow his predecessors in outspoken advocacy of a strong British nuclear programme remains to be seen.

In the public inquiry on the proposed pressurized water reactor for Sizewell (Suffolk), which is due to get under way early next year, the running is likely to be made by the Central Electricity Generating Board, the purchaser of the plant. The authority's chief concern is the programme of fast reactor development centred on the Prototype Fast Reactor at Dounreay, now costing close on half the authority's net budget (£201 million in the year ending last March).

The Department of Energy has made encouraging noises in the House of Commons about the continuation of this programme, which among other things is an important source of employment in the north of Scotland. The authority's annual report, published this week, says that problems with leaks in the steam evaporators (through which molten sodium from the reactor core circulates) continued during the past year, reducing the power output of the reactor and thus the amount of spent fuel available for reprocessing through the experimental plant at Dounreay.

The next milestone for the British fast reactor programme will be the government's decision on the proposal to build a commercial demonstration reactor, the capital cost of which is now estimated at 20 per cent more than the Advanced Gas Cooled Reactor being built at Heysham. The government has been brooding about this decision for at least the past two years.

The possibility of partnership with the Commissariat à l'Energie Atomique on the Superphénix programme seems to have receded as the French programme itself has faltered. Nobody seems to know how to devise a framework for Anglo-American collaboration that would survive the confusion about the Clinch River fast breeder reactor.

In the end, much will depend on how much the Central Electricity Generating

Board offers to contribute to the cost. Meanwhile, the authority plans to use the prototype reactor, commissioned in 1974, for further studies of the fast reactor fuel cycle.

Against the general trend, the authority increased its skilled work-force by a hundred to 2,925 during the past year, but expects now to be stationary. There seems to be some concern that the Harwell establishment may not be able to sustain its

present level of contract work for industry, worth more than £25 million a year.

The authority's annual accounts, traditionally among the most laconic of public corporations', are further made obscure this year by the large increase (of

£40 million) in the net cost of operations in the year ending last March, partly attributable (to the tune of £12.5 million) to the cost of writing off the capital cost of miscellaneous fissile material and equipment.

Internees in Poland

Psychiatric abuse claim

Four political internees in Poland have appealed to the World Psychiatric Association, claiming to be victims of psychiatric repression. The four had been temporarily transferred from internment camp to the municipal hospital in Lodz for treatment in the departments of surgery, internal medicine and laryngology respectively. On 18 August, however, their treatment was discontinued, and they were transferred to the psychiatric wing of a hospital at Zgierz (near Lodz) and placed in the ward for alcoholics. Their letter appeals to the World Psychiatric Association for "speedy intervention".

As the claimants themselves point out, this appears to be the first case of psychiatric reprisals against internees. One Solidarity activist, the logician Jan Waszkiewicz, who was arrested on charges of organizing a strike in the Lenin shipyard in Gdansk and of continuing union activities after the proclamation of martial law, was sent by the court to a mental hospital after the major charge of organizing the strike had been dropped. Friends of Waszkiewicz have said, however, that he seemed to be in a genuinely disturbed state, and that there was nothing sinister in his being transferred to the hospital, where he seems to be undergoing a normal rest cure. He is not receiving any medication or other treatment and is allowed to leave the hospital once a week.

The use of psychiatry as a means of political reprisal has always been abhorrent to Polish psychiatrists. In 1975 there was considerable concern that proposed new mental health legislation would make easier the incarceration of political dissidents in mental hospitals. But after a public outcry, the proposed bill was dropped and Polish psychiatrists — unlike their colleagues in the Soviet Union — avoided the possibility of having to diagnose political dissent or religious enthusiasm as a symptom of schizophrenia.

During its five years' existence (1976–1981), the Workers' Defence Committee KOR, which documented abuses of human and civil rights in Poland, recorded only one attempt at psychiatric confinement — the case of a young man petitioning for the broadcasting of Sunday Mass — and this fell through because psychiatrists were unwilling to certify him.

Under martial law, however, the security services have taken renewed interest in the possibility of psychiatric internment. After

the demonstrations over the May Day weekend, according to underground Solidarity sources, the commandant of one of the departments of the mid-town district of Warsaw, Magistrate Czepinski, applied to Dr Zielinski, director of the Nowowiejski hospital, for facilities for the hospitalization by the civil police of "mentally deviant persons who exhibit a tendency to disrupt public order when various festivities are organized".

Dr Zielinski refused to comply with this request, and reminded Czepinski that the law on psychiatric admissions permits the hospitalization of a mentally sick patient only at his own request, the request of a close relative, or, under carefully defined conditions, by a general practitioner.

The Zgierz incident, however, indicates that not all Polish doctors have the courage and quick-wittedness to follow his example.

Vera Rich

Cryo-transmission microscopy

Fading hopes

Bonn

The three German laboratories developing an electron microscope to operate at the temperature of liquid helium have jointly agreed that at least one of the supposed advantages of their machine is not nearly as great as originally thought. That conclusion, however, is based on observations with only one crystalline sample, and opinions differ as to how serious a setback it represents.

At 4 K, the cryo-transmission electron microscope (cryo-TEM) has the theoretical advantages over conventional machines that molecular movement should be damped and damage to the sample from the beam of electrons minimized. Initially, the reduction in beam damage was estimated to be only modest, so that there was considerable excitement a few years ago when Dr I. Dietrich's laboratory at Siemens AG in Munich — where the superconducting lens for the cryo-TEM was developed — claimed that beam damage at 4 K could be reduced by as much as several hundredfold.

Now the Siemens group has agreed with Dr Jacques Dubochet's group at the European Molecular Biology Laboratory (EMBL) in Heidelberg that the protection gained by working at 4 K compared with room temperature is not more than tenfold for standard samples of L-valine.

A few weeks ago, the two groups

Electronics giant

Brussels

While Mrs Margaret Thatcher was in Japan expressing the United Kingdom's concern at Japan's excessive imbalance between imports and exports and attempting to encourage cooperation between Japanese and British high technology companies, another strategy for coping with Japan's exports of electronic goods was under discussion in Brussels. Max Grundig, the founder of the German electronics group that carries his name, recently put before EEC Industry Commissioner Etienne Davignon and Karl-Heinz Narjes, the European Commissioner from West Germany responsible for innovation and the internal market his own solution for improving the competitiveness of the European electronic components industry.

Grundig proposed that the European Commission should support a European company for the development and production of electronic components, bringing together the resources of Grundig-Telefunken, Blaupunkt-Bosch and ITT-Schaub-Lorenz. Other European producers would be welcome to join in, with the exception of The Netherlands' Philips and the French group Thompson — the company might be too large and unwieldy if such industrial giants were included.

Grundig is anxious to gain EEC support for his idea in order to side-step both German and EEC anti-trust and monopoly laws. Grundig argues, however, that something must be done soon to meet the threat of Japan's rapidly growing dominance, otherwise he fears there will be grave repercussions for both the consumer electronics industry and for Europe's defence technology companies. He would like his project to be launched as soon as next spring.

The idea of an aggressive new European electronics company met with a warm reception in EEC circles, although there will have to be many further discussions before anything is decided. A meeting has, however, already been arranged of representatives of leading European manufacturers at which Davignon will take the chair.

Jasper Becker

together with that of Dr E Zeitler of the Fritz Haber Institute in Berlin (the only other recipient of a Siemens superconducting lens) agreed, within limits, on a revised estimate of L-valine beam damage at 4 K. A brief statement of their measure of agreement has been sent to the *Journal of Molecular Biology* which in 1980 published an estimate (by Dr E Knapik of Siemens and Dubochet) of a cryoprotection factor of about 70 for L-valine.

The note implies that beam damage can vary greatly with specimen preparation, and especially with the characteristics of the material that supports the sample. Dr Knapik also believes that orientation of the sample and support relative to the electron beam is important, and may account for the discrepancy between the original and revised cryoprotection factors. A more

rigorous test of cryoprotection will come, he feels, from a planned comparison of four further compounds whose orientation is known.

One of these specimens will be the "purple membrane" of a peculiar bacterium. The results will be anxiously awaited at EMBL, which has devoted much time and effort to the development of a cryo-TEM. Even if the cryoprotection factor turns out to be minimal, the decrease in molecular movement at 4 K should still improve resolution to a worthwhile degree.

But nobody now confidently predicts that the cryo-TEM will be much better than existing electron microscopes for the study of biological samples. And it is hard to know if the scanning version of the cryo-electron microscope will be any better.

Peter Newmark

Genetic manipulation

What future for regulation?

UK committee's role disputed

The future of the UK Genetic Manipulation Advisory Group (GMAG) remains uncertain, its third report, published on 24 September (Cmd 8665, HMSO, £7.75), concludes that health risks involved in recombinant DNA technology are and are likely to remain negligible. GMAG's terms of reference remain the same as when it was set up in 1976 except that it must now submit annually, and not when the fancy seems to take it. Despite a formal pat on the back in the foreword from Sir Keith Joseph, Secretary of State for Education and Science, and a note in the report that long-term monitoring is still necessary, GMAG seems on the point of working itself out of a job.

The Association of Scientific, Technical and Managerial Staffs (ASTMS), which has three members on GMAG, is clearly alarmed not only that GMAG will not survive but that its terms of reference are no longer appropriate. A delegation of six members of parliament sponsored by ASTMS and the three ASTMS representatives on GMAG — Donna Haber, Professor Derek Ellwood and Professor Bob Williamson — met Mr William Shelton, the minister responsible for GMAG, last week to put the union's case.

The delegation pointed out that GMAG had played an important role in ensuring the safe development of genetic manipulation and in reassuring public opinion. It argued that despite the successful identification of potential health and safety risks, there remained some areas where knowledge is limited and which would need to be carefully scrutinized case by case.

The delegation also pressed for an extension of GMAG's role to cover the

ethics of human genetic engineering. ASTMS says that gene replacement therapy will affect the population as a whole and should not be decided by hospital ethical committees alone. ASTMS also wants GMAG's function to include problems of environmental contamination which could result from the large-scale use of genetically manipulated organisms. The union feels that GMAG has kept up a dialogue with industry and is well placed to advise on the safety of industrial biotechnology.

The minister appears to have told the delegation that the government is fully aware of the issues in genetic engineering, especially because biotechnology would make an important impact on industry in the next five years. But he insisted that GMAG is not an appropriate body to advise on ethical issues.

The GMAG report notes that the group's advice on the large-scale use of genetically manipulated organisms would be restricted to the biological properties of the organisms in use. The Health and Safety Executive (HSE) will be concerned with the physical aspects of safety. In this spirit, GMAG seems to have delegated responsibility for site visits to laboratories in the past year entirely to HSE.

On the future of GMAG, it is planned that a full meeting of the group will discuss various options in November. GMAG members are themselves divided. Some see the group's importance as residing in its capacity as public watchdog and reassurer. Many feel that GMAG was set up to advise on the safety of certain experiments and that its remit should end there. Others point to the existence of local safety committees and their dwindling workload as evidence that the group has become redundant. The government may well share this view and reorganize GMAG into an expert committee.

Jane Wynn

Greens gain in Hesse

Heidelberg

The Hesse election on 26 September provided the latest in a string of surprising events in West German politics. Upsetting all predictions, the Christian Democrats (CDU) and Social Democrats (SPD) emerged neck and neck with 52 and 49 seats respectively in the regional parliament. The Green environmentalist party (see *Nature* 17 June, p 528) will be represented in the Hesse parliament for the first time with a crucial minority of nine seats. The Free Democrats (FDP), whose decision to withdraw from national coalition with the SPD may cause the collapse of Schmidt's government, have lost their seats. SPD, under Ministerpresident Holger Börner, continue as a minority administration, but the likelihood of Green/SPD administrative and legislative cooperation are slimmer in Hesse than in Hamburg.

The Greens' success rests mainly on local environmental issues, of which Hesse has more than its fair share. The new runway addition to what is already Europe's largest airport at Frankfurt, plans for a reprocessing plant for nuclear waste, plans for a third 1,350-MW nuclear power plant at Biblis where a 2,600-MW capacity plant already exists, US military poison gas depots, pollution of all kinds and so on.

The Hesse result has much to do with contrast between Helmut Schmidt's cool statesmanship and the less dignified politicking and fiscal sabre-rattling among FDP, CDP and CSU since the SPD/FDP coalition broke up nine days earlier, nevertheless, the Greens, now represented in six regional parliaments, are indisputably the third national party. The establishment is beginning to take them seriously — after the election result was announced, Willy Brandt talked about a left-wing alliance between the Greens, the trade unions and the SPD left. The Greens themselves, however, are unwilling to compromise on what they consider to be the key issues, such as nuclear power, armaments and industrial development, and are wary of being absorbed and corrupted by the corridors of power and by the blandishments of SPD in particular.

There are clear national implications. CDU/CSU and SPD have no electoral mandate for even a temporary administration, national elections must take place soon and there will be Green seats in the tense Deutschen Bundestag. The date for the federal election may be determined on 1 October and an outcome like that in Hesse and Hamburg is a real possibility, with the balance of power lying with the environmentalists.

Sarah Tooze

US international cooperation

Science board's other voice

Washington

The National Science Board, the governing body of the National Science Foundation (NSF), has just issued a stirring but gently worded plea for continued scientific contacts between the United States and other countries, including the communist bloc. The board also called on NSF director, Mr John B Slaughter, to "play a significant role, with the Department of State and the Executive Office of the President, in development and implementation of international science policy".

The board thus authorized Slaughter (who plans to leave his post at the end of the year) to become involved in decisions on international science that are now usually made by the State Department and the White House without consultation with NSF. Although NSF manages several major international science programmes, such as the Deep Sea Drilling Project and the US Antarctic Program, historically NSF has had little influence over diplomatic and policy decisions, such as that made by the President after the imposition of martial law in Poland last December to terminate bilateral US-Soviet scientific agreements as they came up for renewal. The decision effectively ended most US-Soviet scientific contact.

The National Science Board, which is second only to the White House Science Advisory Committee in authority and prestige, has only rarely played a role in these decisions. "The board's options are quite limited" explained one member involved in drafting the recent statement. On the one hand, he explained, it advises NSF and is part of the executive branch of government. In this capacity it recognizes that there are situations in which the government might legitimately want to classify scientific data. On the other hand, the board is made up of, and reflects the thinking of, US university scientists, who believe that science fares best when it has plenty of international freedom.

The statement reflected this difficulty, noting that "restrictions which diminish that openness are likely to have serious costs to science and, ultimately, to national security. Such costs should be carefully considered before implementing any actions that would compromise the traditionally open environment that has served us so well in the past."

The board's plea for internationalism comes just a month after the Department of Defense blocked the reading of about 100 papers at a San Diego conference (see this issue, p 383, and *Nature* 23 September, p 289) — the most recent example of the Reagan Administration's campaign against the flow of scientific information to communist countries.

● The number of US participants in international scientific congresses has been declining, even as US science has become more dependent on work done abroad, as the table and figure show. Moreover, the latest data, for 1980, shown in the table, exclude information on the growing list of international congresses at which no US scientists participated.

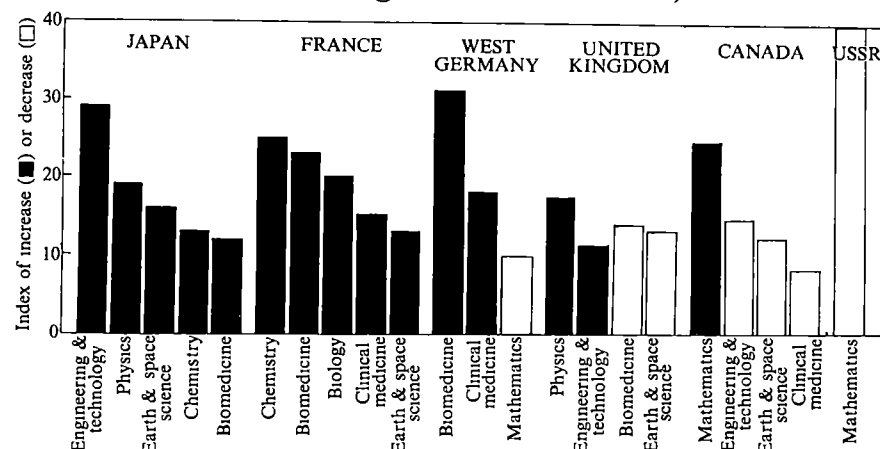
US participation in international scientific congresses			
Year	No of congresses	Total participants	No of US participants
1960-62	23	33,082	9,033 (27%)
1963-65	28	37,964	10,012 (26%)
1966-68	42	59,748	12,297 (21%)
1969-71	38	55,711	12,956 (23%)
1972-74	73	73,819	18,630 (25%)
1975-77	52	59,658	12,767 (22%)
1978-80	37	55,358	7,975 (14%)

Source: *Science Indicators-1980* and NSF unpublished data for 1980.

At the same time, US scientists are depending more and more on foreign scientific work in selected fields, as indicated by citation data shown in the figure. The board's action, therefore, comes at a time when US scientists are relying more than ever on their foreign colleagues — but are seeing less and less of them.

Deborah Shapley

Changes in US use of foreign scientific literature, 1973-79



Planetary science

Shopping list

Planetary scientists in Europe have been getting together. Under the umbrella of the space science committee of the European Science Foundation (ESF), they have recently published a report which recommends that the European Space Agency and national organizations take action to strengthen their subject.

Europe's planetologists seem somewhat surprised at their own level of expertise, given that they have had fewer opportunities than their Soviet or US colleagues to participate in deep space missions. Their report is an attempt to ensure that they at least maintain their international status. But the Executive Council of ESF, which has yet to decide how to advocate the report's recommendations to ESA and national governments, may have a tough task. Funding agencies, now everywhere short of cash, will be asking what level of priority to assign to planetary science compared with other branches of space science and astronomy.

The planetologists, however, seem aware that straightforward requests for more missions will fall on stony ground. Hence, they recommend that ESA, for example, conduct more preliminary studies of missions, thus ensuring that final decisions on which to argue are well-founded. Money might also be saved, says the report, if the spacecraft design for Giotto, the European mission to Halley's comet, is adopted wherever possible in deep space missions.

Planetary science could also be strengthened from the ground, says the report. There should be better access to optical and radio telescopes and long-baseline interferometry. New instruments should be developed through greater collaboration between research laboratories and manufacturing industry and cooperation between space scientists should be encouraged to "take full advantage of facilities such as the space telescope".

ESF itself may have the power to act on two of the report's recommendations: that studentships be set up for young planetologists in centres of excellence and that a system of travel grants be available for European planetary scientists to visit each others' laboratories.

But the most significant outcome of the European planetary scientists' recent get-together may be apparent after a meeting with their US counterparts next October. Under discussion will be joint missions probably too costly for one agency to carry out alone. Ideas, which are still very preliminary, include missions to Venus and Mars and a mission to Saturn and the outer planets. The plan is to make a choice within the next year in time for launch in 1991.

Judy Redfearn

Video education

US engineers forge ahead

Washington

The poor track record of video-based education in the United States is showing signs of improvement. Mid-career engineers employed in US companies are now benefiting from the country's first widely successful experiment in video education.

Orders have been mushrooming for engineering and related courses to be taught by video this year and compiled and catalogued by a little-known group based in Atlanta, Georgia. Although the Association for Media-Based Continuing Education (AMCEE) is only two months into its current fiscal year, it has as many orders now as it had halfway through the previous year. John T. Fitch, the group's executive director, estimates that some 30,000 to 40,000 people, most of them engineers although they include businessmen and secretaries, are taking AMCEE-offered courses.

AMCEE serves as a nonprofit-making clearinghouse for courses produced at universities around the country. Its member universities now number 22 and include many state institutions and private schools.

To qualify, a school must have a campus-based media-based continuing education programme. The programme films the professor lecturing to students — or in a campus studio — packages the cassettes and related text material, and distributes them, weekly or biweekly, to companies, usually in the immediate area. This year's AMCEE catalogue contains 448 courses in 18 disciplines given at 21 universities. Course contents range from "Grammar for Secretaries" to "Advanced Heat Flow Analysis".

The latter course, taught by Professor W. Edwards Deming of Massachusetts Institute of Technology and consisting of 14 videocassettes and a textbook, has been a best-seller. In it, Deming teaches, according to the AMCEE catalogue, why "productivity increases as quality improves" in industrial production, and explains the "14 steps that must be adapted to achieve this result". There have been at least 4,000 orders for this course.

Some of the participating schools have raised continuing education for engineers by video to an advanced art. Colorado State University, for example, offers 76 video courses, most taken by students who are employed at companies in the Denver-Boulder area. Couriers drive the taped cassettes around to the locations where the students are taking the courses — usually at their employers' offices — and pick up homework assignments, questions, and the like.

AMCEE's success — which is in marked contrast to many other attempts at systematized video learning for credit — is based, says Fitch, on a tradition in engineering that calls for working engineers to go back to school, to catch up on basic knowledge that has advanced since they graduated, or to retrain for new specialties. Traditionally, companies give their employees leave to go back to school for this retraining, but this is expensive in terms of lost pay, commuting costs, and tuition. The video system means that the engineer can take the course at his office, while remaining employed.

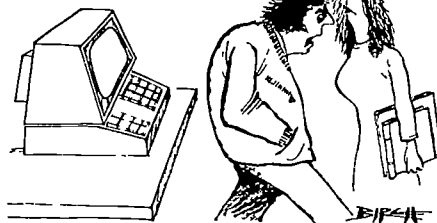
So far, AMCEE does not offer any courses for undergraduate engineers. However, it does have big plans. Under Dr. Lionel Baldwin, dean of engineering at Colorado State University, AMCEE is drawing up plans for schools to offer courses by satellite in real time, so that the engineer who has moved with his job to Massachusetts can take a course offered at Stanford and talk to his teacher by satellite. The proposed "National Technical University" could offer an accredited degree — all by video.

If the plan materializes, it will be a big step for AMCEE, which was embryonic after its founding in 1976 until grants from the National Science Foundation and the Alfred P. Sloan Foundation helped it get started gathering and vetting course materials.

Although a study by the Corporation for Public Broadcasting published last year estimated that half a million people around

the United States take some kind of course using television, specific programmes of video education have not usually fared well. At the end of this month, for example, the University of Mid-America (UMA) goes out of business, it was an

"IT'S SENT ME TO THE BACK OF THE CLASS AGAIN!"



eight-year attempt, funded by the federal government and supported by 11 state universities, to make and distribute video courses around the mid-west. At present, says Milan Wall of UMA, around 8,000 students take courses that use UMA-developed materials, which range from a history of the Great Plains to subjects in the humanities. But UMA's market — housewives seeking more learning and adults who dropped out of college but who now want to complete their degrees — has not materialized. Even direct distribution of British Open University programmes has not been extensive, Wall says, "not because they're not of high quality but because they're designed for a totally different educational system."

Deborah Shapley

China's intellectuals back in fashion

China's new policy of eliminating traces of "leftism" which led to the recent abolition of the post of Party Chairman, will mean an upgrading of both status and living standards for intellectuals. A number of party and government documents, mostly at provincial level, have recently called for educational campaigns, intended to "surmount the traditional stance of looking down on intellectuals".

Proposed measures include

- The complete rehabilitation of all intellectuals unjustly or falsely persecuted during the cultural revolution, including the restoration of or compensation for lost salaries, and the "education" of those involved in the "mishandling" of such cases.

- Opportunities for employment for intellectuals in accordance with their talents and qualifications. Intellectuals with "ability and integrity" who are in the "prime of life" should be selected for key posts, and their opinions on economic policy listened to "conscientiously". Party cadres are instructed to respect non-party intellectuals, while factories and other organizations assigned new graduates "must not haggle" about giving them

appropriate employment.

- Intellectuals should be able to spend five sixths of their working time on professional activity, facilities (including study leave) must be provided for them to keep up their knowledge.

- The system of examinations and promotions for professional and technical grades and titles should be improved. Allowances for education and research in provincial budgets should be gradually increased and the provision of equipment, instruments, books and auxiliary staff ensured. Party schools should offer scientific and technical courses. Administrators in key posts whose own academic or technical background is not up to standard should be sent on refresher courses.

Some officials, it is noted, have not recognized the importance of intellectuals in the community, considering that once the intellectuals in their particular area have been rehabilitated, all is well. Parents, however, have been quick to grasp the new trend and a recent article in the party journal *Red Flag* criticizes parents who have already started cramming their three- and four-year old children in preparation for university entrance.

Vera Rich

CORRESPONDENCE

Tanks are unsafe

SIR — The discussion about the effectiveness of “enhanced radiation weapons” (ERWs) against vehicles such as tanks brought up the question of whether advanced radiation shields in the armour of tanks could substantially improve the protection factor^{1,2} against radiation from ERWs

Tables 1–3 give the results of a series of shielding calculations. Based on the methods used in ref. 3 (for example, the use of code ANISN), we assumed an explosion height of 500 m

Three different shields have been proposed¹ incorporating a strong neutron poison into the sandwich structure of the armour of modern tanks. Each shield is based on a layer of a strong neutron absorber (B_{nat} and 6Li), and they differ only by the amount of neutron absorber present in the shield (0.1 cm B, 0.5 cm B and 1 cm 6Li_2O)

Total shielding is defined by

$$C_{tot} = \frac{(D_n + D_\gamma)_F}{(D_n + D_\gamma)_B}$$

where D_n and D_γ are the neutron and gamma radiation dose rates in rads and subscript F refers to the layer in front of the shield and B, that behind the corresponding layer. Neutron and gamma shielding are defined by

$$C_n = \frac{(D_n)_F}{(D_n)_B} \quad \text{and} \quad C_\gamma = \frac{(D_\gamma)_F}{(D_\gamma)_B}$$

The tables clearly show that the neutron

radiation determines the total radiation dose in all cases

To determine what effect various cross section libraries have on the shielding factors, three different cross section libraries were used (ENDFB IV, VITAMIN C and LASL), and the differences were insignificant (Table 1)

The total protection factors of the classical armour of tanks (about 10 cm steel wall) lay in the range 2–2.5, and the relatively complicated and heavy shields considered here exhibit a total protection factor between 6 and 7. Even for a 1-cm thick 6Li_2O layer, the shielding factor does not increase substantially. The physical reason is, of course, that the neutron spectrum is too broad to make the neutron poison an effective absorber in all energy levels

Thus still more moderator material would be necessary to guarantee a sufficiently high protection factor. The protection factor should be of the order of magnitude of 1,000 to reduce a dose of 20,000–30,000 rads to a few tens of rads. This dose could be survived without the biological and psychological effects of a radiation illness

Water is a cheap and practical shield material for protection against radiation from ERWs. Assuming an explosion height of 500–1,000 m, the half-value thickness of water is about 15 cm and a very thick water shield would be needed for the required protection factor

In conclusion, it seems impossible to design a practical shield for manoeuvrable tanks with a sufficiently high protection factor — such a

shield would be too heavy. This confirms our previous findings³ that protection against radiation from an enhanced neutron weapon is much easier (and cheaper) for the civilian population than for tank crews

W SEIFRITZ

P KÖHLER

J STEPANEK

Swiss Federal Institute
for Reactor Research,
Würenlingen, Switzerland

1 Baruch, J. E. F. *Nature* 292, 792 (1981)

2 Gsponer, A. *La Bombe à Neutrons est-elle une arme antichar vraiment efficace?* (Geneva International Peace Research Institute, GIPRI 82-05, 28 February 1982)

3 Köhler, P., Seifritz, W. & Stepanek, J. Protection against Enhanced Radiation Weapons in *Atomkernenergie* (in the press)

Falling stock

SIR *Nature* has decided to apply one of its news pages to a biotechnology stock report (*Nature* 12 August, p. 599). As a financial analyst who specializes in biotechnology, I must question the need for printing information such as this in a professional journal of science. It would be rather like a drug stock index in *The Lancet*. In addition, I find the selection of stocks arbitrary. Collagen Corporation is a superior company and a good investment, but what does conversion of two cowhides per month into pure, injectible collagen have to do with “biotechnology”? And in the chauvinism department, why exclude such Japanese Corporations as Ajinomoto, Kyowa Hakko and Green Cross? More seriously, the stock index is so heavily weighted by Novo Industri A/S and AB Fortia, two Scandinavian companies, that perhaps you could perhaps call it the “*Nature* ScandIndex”

SCOTT R. KING

Brooklyn, New York, USA

Polish defection

SIR — The article “Norway’s Arctic diplomatic fix” (*Nature* 9 September, p. 97) grossly misrepresents the development in connection with the defection of two members of the Polish geophysical station in Svalbard in August 1982

According to a report to the local newspaper in Svalbard, the “*Sysselmannen*” — governor of Svalbard — sent a helicopter to the station on 3 August to collect a station member who had asked for political asylum in Norway. On 10 August another member defected. There was no “race” between Norwegian and Soviet helicopters, and no intervention by Soviet helicopter crews or by the Soviet authorities in Barentsburg in order to prevent the defections

Since the article also refers to the duties of our institute in relation to foreign expeditions, we would like to point out that it provides information on the scientific activity in Norwegian Polar areas and also on governmental laws and regulations, but has no obligation to give free access to its scientific material. In due time, the data are published in our own scientific series, a monograph series, *Skifter*, and a bulletin, *Polar Research*, or in international periodicals

TORÉ GJELSVIK
(Director)

Norwegian Polar Research Institute,
Oslo, Norway

Table 1 Neutron-, gamma- and total shielding factors of a 0.1-cm boron-containing shield

Material sequence of shield	C_n			C_γ			C_{tot}			D_n/D_γ		
	A	B	C	A	B	C	A	B	C	A	B	C
500 m air	1	1	1	1	1	1	1	1	1	7.72	7.38	6.23
5 cm steel	1.94	1.93	1.94	1.27	1.35	1.31	1.83	1.84	1.81	6.03	5.15	4.21
10 cm water	6.05	6.16	6.17	1.87	1.96	1.99	4.82	4.91	4.78	2.38	2.35	2.00
0.1 cm boron	6.15	6.35	6.37	1.91	2.01	2.03	4.91	5.05	4.92	2.4	2.33	1.99
1 cm lead	6.53	6.75	6.75	3.83	4.11	4.01	6.04	6.27	6.17	4.52	4.5	3.7

Values assume an ERW explosion at a height of 500 m. Three different cross section libraries were used in the calculations (A, ENDFB IV, B, VITAMIN C, C, LASL). The last column gives the neutron- to gamma dose ratios at the various positions within the shield

Table 2 Neutron-, gamma- and total shielding factors of a 0.5-cm boron-containing shield

Material sequence of shield	C_n	C_γ	C_{tot}	D_n/D_γ
500 m air	1	1	1	7.39
5 cm steel	1.94	1.35	1.84	5.16
10 cm water	6.20	1.96	4.93	2.33
0.5 cm boron	6.53	2.17	5.27	2.46
1 cm lead	7.03	4.30	6.53	4.52

Values assume an ERW explosion height of 500 m. VITAMIN C nuclear cross sections were used. The last column gives the neutron- to gamma dose ratios of the various positions within the shield

Table 3 Neutron-, gamma- and total shielding factors of 6Li -containing shield

Material sequence of shield	C_n	C_γ	C_{tot}	D_n/D_γ
500 m air	1	1	1	7.39
5 cm steel	1.94	1.37	1.85	5.24
10 cm water	6.28	2.21	5.15	2.6
1 cm 6Li_2O	6.77	2.48	5.61	2.71
1 cm lead	7.29	4.47	6.78	4.54

Values assume an ERW explosion height of 500 m. VITAMIN C nuclear cross sections were used. The last column gives the neutron- to gamma dose ratios at the various positions within the shield

COMMENTARY

Computer chess and the humanization of technology

Donald Michie*

THE first serious proposal to have a machine play chess was made by Babbage¹, the British pioneer of digital computing, but was never executed. In the early years of this century the Spanish engineer Quevedo demonstrated an electro-mechanical device for mating with king and rook versus king². But it was not until the late 1940s that serious experiments with the complete game were conducted. The British logician and computation theorist Turing³, in collaboration with Champenowne and others, constructed and tested various 'paper machines' embodying mechanized strategies for chess⁴. Play was poor. In 1950 the American founder of information theory Claude Shannon⁵ published the classic paper for the theoretical ideas. During the same period de Groot's⁶ study of the thought processes of chess masters revealed that their special ability does not derive from 'computer-like' qualities of memory or of accurate, fast and sustained calculation, but from powers of conceptualization. This result has been foreshadowed by Binet's⁷ investigation in 1900 of the ability of chess masters to play many games of blindfold chess simultaneously. He concluded that in addition to *la mémoire* this accomplishment rested on *l'érudition* (the use of accumulated chess knowledge to form meaningful descriptions of positions) and *l'imagination* (ability mentally to reconstruct a position from a description). Progress has been made in mechanizing the 'computer-like' mental attributes, but little in respect of *l'érudition* and *l'imagination*.

Developments

The earliest chess programs, developed in the 1950s, have been reviewed by Samuel⁸. The modern era dates from the 1967 entry into human tournaments of the Greenblatt-Eastlake-Crocker⁹ program under the playing name MacHack. This program played at the level of a weak-to-middling club player — Category III, USCF rating 1,400–1,600 (Candidate

Master level begins at 2,000, National Master at 2,200, International Master at 2,400, Grandmaster at 2,500).

Computer chess tournaments, in which all games are program-against-program, are now organized annually in the United States by the Association for Computing Machinery (ACM). The first took place in 1970 in New York. In addition, every three years a World Computer Chess Championship sponsored by the International Federation of Information Processing Societies is held. The first¹⁰, in Stockholm in 1974, resulted in a victory for

BELLE, CHESS 4.9, NUCHESS and CRAY BLITZ, were all in the Candidate Master (2,000–2,199) range of play. The same year saw the emergence of several commercially available portable chess machines claimed by their manufacturers to rate at least 1,900 (Category I).

Computer chess has been described as the *Drosophila melanogaster* of machine intelligence. Just as Thomas Hunt Morgan and his colleagues were able to exploit the special limitations and conveniences of the *Drosophila* fruit fly to develop a methodology of genetic mapping, so the game of

Chess provides the opportunity for studying the representation of human knowledge in machines, but it took more than a century since its conception for chess playing by machines to become a reality. The World Computer Chess Championship and other computer chess tournaments where program is matched against program occur regularly. But how far can the less clever but more intelligent human master rely on the computer's brute force technology?

the program KAISSA developed in Moscow by V.L. Arlazarov, G.M. Adelson-Velskiy, A.R. Bitman and M.V. Donskoy. Chess 4.0, entered by L. Atkins and D. Slate of Northwestern University, United States, came second. Standards of play corresponded approximately to USCF 1,600–1,650. In 1975 the ACM tournament evoked play at the same general level, but produced one game, between Chess 4.4 and CHAOS, of a more distinguished standard.

In the late 1970s most progress in computer play resulted from a combination of improvements in the efficiency of deep tree-searching methods with faster speeds of available computing hardware. Chess 4.6 won the Second World Computer Chess Championship at Toronto 1977, and domination of the ACM by updated versions of CHESS continued until BELLE (Bell Labs) won in 1979. The Third World Computer Chess Championship at Linz, Austria in 1980 was also won by BELLE. The program¹¹ ran on an LSI 11/23 micro-computer linked to a hard-wired chess machine and could 'see' of the order of 100,000 board positions per second.

In 1981 the four strongest programs,

chess holds special interest for the study of the representation of human knowledge in machines. Its chief advantages are: (1) chess constitutes a fully defined and well-formalized domain; (2) the game challenges the highest levels of human intellectual capacity; (3) the challenge extends over the full range of cognitive functions such as logical calculation, rote-learning, concept-formation, analogical thinking, imagination, deductive and inductive reasoning; (4) a massive and detailed corpus of chess knowledge has accumulated over the centuries in the form of chess instructional works and commentaries; (5) a generally accepted numerical scale of performance is available in the form of the US Chess Federation and International ELO rating system.

Computational and cognitive mechanisms

The fundamental procedure, proposed independently by Turing and by Shannon, involves *lookahead* from the current position along a branching tree of possibilities. Of course, chess-masters also look ahead (concrete analysis) but on a severely restricted scale. According to de Groot, 30 positions is around the limit of

*Machine Intelligence Research Unit, University of Edinburgh, Meadow Lane, Edinburgh EH8 9NW, UK.



Would the onlooker be as interested at a computer championship?

what is normally held in lookahead memory. By contrast chess programs commonly grow lookahead trees comprising millions of nodes.

Branching of the lookahead tree ranges from around 25 branches per node (if no pruning is applied) down to less than two branches per node for Masters. The number, variety and severity of pruning rules varies from one program to another. In one or two of the stronger programs all but the alpha-beta rule are effectively absent. In such a case the program seeks to make up in brute-force calculation what it lacks in selectivity. All programs apply termination rules to halt growth of the tree beyond certain limits. The main factor in termination is the occurrence of quiescent positions (Turing's 'dead' positions) in which no capture or other violent changes are in immediate prospect. At the deeper levels of the lookahead tree quiescence is taken as a sufficient indication to discontinue forward analysis.

In the Turing-Shannon scheme on completion of the lookahead tree the program applies an *evaluation function* to the terminal positions, labelling them with computed estimates of their degree of strategic strength or weakness. The labels are then *backed up* the tree by the minimax rule: that is, a node for which it is white's turn to play is credited with the maximum-valued of the labels attached to its successors, while a black-to-play node receives its label from the minimum-valued of its successors. The wave of labelling thus spreads through the tree from the terminal nodes towards the root node (representing the current position) until all its successors are labelled. The program then selects the move leading to the highest-valued of these successors, if it is white's turn to move; otherwise the move leading to the lowest-

valued successor.

The functioning of this basic mechanism can be improved by various devices aimed at eliminating redundant calculations and redundant storage. In favourable conditions the alpha-beta rule¹² for pruning almost doubles the realized depth of lookahead without altering the final result of the computation: the spirit animating this rule is that once the search has found that a particular line falls short of being selected there is no point in exploring its further ramifications to determine by just how far it falls short. Lookahead depths attained in modern computer chess lie in the range 6-15, somewhat in excess of the typical depths to which Masters and Grandmasters look (average 6-7 as found by de Groot). In spite of this the standard of computer chess remains far below Grandmaster levels. Some of the reasons are as follows:

(1) **Horizon effect.** The computer scientist and former World Correspondence Chess Champion, Hans Berliner¹³, has pointed out that reliance on the unaided Turing-Shannon procedure renders a program oblivious to all events which may occur beyond its lookahead horizon. Even though a post-horizon loss, or a post-horizon gain, may appear inevitable and obvious to the human onlooker, the program plans from hand to mouth, foolishly sacrificing material to delay a loss which cannot indefinitely be averted; alternatively it may forfeit an eventual large expectation by grabbing at a small gain.

(2) **Lack of long-range ideas.** A Master plans at the conceptual level, linking the main milestones with detailed steps as a separate operation. Contemporary

programs have no corresponding capability. In the end-game in particular, where long-range reasoning of this kind is at a premium, programs can flounder aimlessly, promoting small disconnected goals with no unifying strategic thread.

For these reasons, computer programs make a poorer showing in the end-game than in the opening and mid-game, performing like club players rather than candidate masters. Advances in sheer computer power, even micro-millisecond processors or mega-megabyte memories, are not expected in themselves materially to improve this situation. Remedies must take their departure from an appreciation of the ability of the chess-master to utilize very large bodies of highly conceptualized and cross-referenced chess knowledge. But in programs of the Turing-Shannon type the only significant repository of chess knowledge is in the evaluation function, typically a linear combination of terms measuring such features as material advantage (conventional scores: 9 for Q, 5 for R, 3 for B, 3 for N, 1 for P), king safety, piece mobility, pawn structure, rook control of files and so on. Typically the number of features contributing terms to the evaluation function in state-of-the-art tournament programs lies in the range 30-50.

So simple a scheme is too weak to represent the fine structure of human knowledge marshalled in the standard expository works such as Reuben Fine's *Basic Chess Endings*. Contemporary research is directed towards buttressing the Turing-Shannon paradigm along a line sometimes described as the 'knowledge approach'. Essential to this approach is the extension of studies like Binet's and de Groot's to the discovery of the basic concepts (properties and relations of pieces, files, ranks and so on which the Master uses as the bricks and mortar of his mental descriptions). Chase and Simon¹⁴ found that the relations of defence of one piece by another, proximity of pieces, and being of the same denomination or colour were all used as mental building-blocks, and that a particularly important relation for binding together clusters of pieces held as a unit in memory was combination of pieces of the same colour to converge on the opponent's king position.

Tan¹⁵ formalized the process of conceptualization for the special case of pawn structures. His computer program was able to describe pawns-only positions in terms of 'islands' and 'fronts' forming pawn-relations graphs, from which 'attack-defence-diagrams' are automatically constructed. The dynamic potentialities of the position are thus summarized. More recently a computer induction algorithm¹⁶ derived from Hunt's 'Concept Learning System'¹⁷ has been used to synthesize complete machine-executable theories for the endings king and pawn versus king¹⁸ and king and pawn (on a7) versus king and rook¹⁹.

Chess is a two-person finite game with perfect information which satisfies the zero-sum condition — an outcome which is good for one player is bad in equal measure for the other. For any such game it is theoretically possible exhaustively to calculate backwards from the terminal (checkmate or drawn) positions in such a way as to determine for every position whether it is drawn, won or lost and in the latter two cases what continuations correspond to best strategy. In practice such computations, even if performed on the fastest conceivable computers, are infeasible except for end-games simple enough to contain less than a billion or so legal positions. Such computations were first done²⁰ for elementary endings such as king and rook versus king (K RK) and king and pawn versus king (K PK) which consist respectively of 50,015 and 179,656 legal positions. They have been extended to all the non-trivial four-piece endings, such as K QKR, K RKN and so on and to a subset of K PKP (M.R.B. Clarke, personal communication). The most complex enumerations to have been performed in this way are K QPKQ²¹ and K RPKR²², of which the first is notable for having been consulted with good effect by Bronstein during adjournment of a master tournament in Kiev. Significant findings have been made with the use of these end-game 'databases', including the previously unsuspected prevalence of serious error in master texts on the end-game. Thus Fig. 1 shows a derivative of the celebrated position given by al-Adli in the ninth century, re-discovered and (incorrectly) analysed in *The Chess-Players' Chronicle* in 1859, and repeatedly (and incorrectly) re-analysed since then. Among errors of Grandmaster Fine's analysis in *Basic Chess Endings* is his classification of the position in Fig. 1 as a draw. Computer analysis shows that knight-capture or mate can be forced in 12 further moves²³.

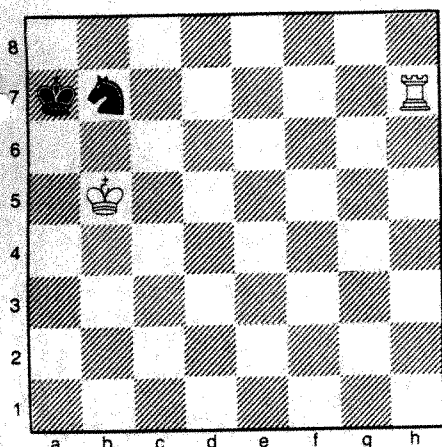


Fig. 1 One of two positions generated in Fine's analysis of the al-Adli position (see text) to which the wrong won/drawn status is assigned. Fine states that, after black's Kb8, white can only draw. Computer analysis reveals that by Kc6 white can then win in 12 moves. As shown in ref. 23, lesser errors abound.

Brute-force computing in technology

The available power of computation advances at the rate of almost tenfold every five years. For today's large machines one hundred million calculations per second is not abnormal. Measured on a comparable scale, the human brain musters perhaps five per second. The brain, being able to deploy a large associative store of pattern-based concepts, is not normally used in this restricted sequential way. Otherwise feats such as recognizing a person from a photograph, or understanding his speech, would be impossible for a device with such weak calculational powers. On the other hand computing systems still rely primarily on brute force. So long as the present rate of advance in hardware technology continues, they can afford to. But can we, their less clever but more intelligent masters, afford to let them?

Several recent incidents have involved complex computer control systems. The suggestion is that reliance on the escalating power of brute force may be heading towards danger. However effective and reliable such systems may be in normal conditions, use of brute force may not be worth the price paid during the rare episodes when a computer-controlled power station or military installation or air-traffic control system malfunctions. On these occasions a new factor becomes paramount: the human operator or supervisor needs to follow what the computing system 'thinks it is doing'.

The computer's processes are measured in millions of steps per second. The human's proceed very slowly — but in a richly furnished space of descriptive concepts. These concepts are not mirrored in any way in the machine's relatively small memory. So when operating conditions stray from the norm, useful dialogue between the two breaks down. In its report on the Three Mile Island accident the Kemeny Commission concluded that the main failures were operator failures, and that the main cause of operator failure was bewilderment by the stream of messages, warning displays and the like from the control computer²⁴.

If such unsettling phenomena deserve laboratory analysis, then we could hardly find better material than the game of chess. The current world computer chess champion examines a tree of more than ten million possibilities in lookahead analysis before selecting a move, and is able on this basis to stand up to Grandmasters in purely tactical play. The Grandmasters, by virtue of their associative stores of conceptualized chess knowledge, have the edge in strategic, or positional play. But as earlier stated a Grandmaster's mental investigation of lookahead positions averages at most 30. So the kind of mismatch that was noted by the Kemeny Commission, namely between the calculation-rich but concept-poor computer and the calculation-poor but

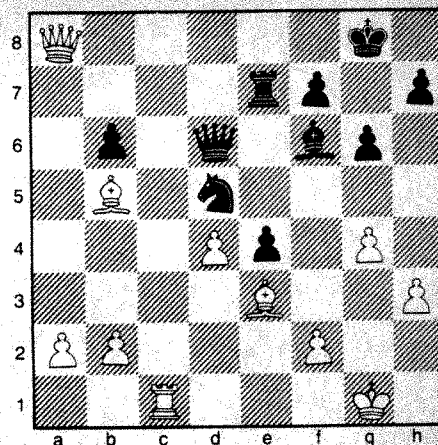


Fig. 2 Position in the Toronto game DUCHESS against KAISSA after white had played Qa8+. Black's play of the apparently meaningless rock sacrifice Re8 was seen by an audience which included several strong chess-masters as a grotesque blunder. Overnight analysis by KAISSA's programmers showed otherwise.

concept-rich human, should be reproducible in the computer chess laboratory. This is indeed the case, as has already been shown through an analysis of the mechanisms employed in state-of-the-art computer chess and its theoretical basis²⁵.

Machine penetration

Machine penetration into complex positions began to reach beyond the human horizon as early as 1977. In the Second World Computer Chess Championship held that year in Toronto, the position shown in Fig. 2 arose in a game between the then reigning champion KAISSA, a Moscow program running on an IBM 168 computer, and the North Carolina program DUCHESS. DUCHESS had just given check with the queen. To the several hundred computer scientists and chess players in the auditorium the only reasonable option was to move the king out of check. KAISSA instead interposed a rook, promptly losing to QxR check. With a whole rook advantage DUCHESS had no difficulty in crushing KAISSA in another 15 or so moves, and the Russian team handed in KAISSA's resignation in the conviction that they had been robbed by an unsuspected program error.

Next morning Arlazarov and Donskoy announced the result of a retrace operation which had occupied them half the night and had revealed no evidence of error. On the contrary, deep-going scrutiny showed KAISSA's apparent blunder to have been a brilliancy which purchased an extended lease of life for a program which had already arrived in a hopelessly lost position. The rook sacrifice had cleverly averted a mating combination which both KAISSA's and DUCHESS's lookaheads were deep enough to spot, but which eluded onlookers who included former world champion Grandmaster Mikhail Botvinnik.



Chess — the classroom for decision making

Expert versus martian systems

Now consider chess as a laboratory model of real-life decision-taking. Imagine KAISSE's brute-force computations to be those of an automated control system for a nuclear power station. Let Grandmaster Botvinnik be the engineering supervisor, highly knowledgeable about the domain, assigned to monitor the system's decisions and to intervene with manual over-ride when he judges malfunction to have occurred. The machine makes an unexpected decision. Does the supervisor intervene? Lacking the calculational power fully to probe the system's martian mentality, let us suppose that he does. Disaster follows. Yet had he been able to interrogate the system he would have realized that the seemingly aberrant action was really geared to buying vital time — time in which staff could be evacuated, population warned, ambulances and fire engines summoned and so forth. Yet he has to decide on the basis of his knowledge and best judgement. Not being a martian, he decides wrongly.

This problem cannot be brushed aside by improvements to the program's surface features, such as better trace and diagnostics and more 'user-friendly' command languages. For the particular case, chosen from 1977 vintage computer chess, this might suffice. But as the depth of calculation increases, a point is reached at which mere surface modifications will not do. Radical reconstruction of the program becomes necessary, using as building-blocks machine representations for the very same concepts as those which the knowledgeable human brings to bear on the problem.

This approach leads to a new form of computing system, known as the 'expert

system', which is deliberately built in the human rather than martian mental mould. The use of such systems to act as interpretative buffers between the two mentalities was first demonstrated at the Rand Corporation in RITA, a computer program knowledgeable both about the intricacies of the ARPA trans-continental computer network and about the limitations of non-programming personnel desirous of using the network²⁶.

Brute-force computing is pushing information technology towards regions of complexity which only machines will be able to penetrate. To make it possible for them to report back what they see, RITA-like developments in human-interface software will be required. An eight-year programme of research and development in advanced computing technology recently announced by the Japan Information Processing Development Center is based in part on this conception, namely on the design and construction of intelligent knowledge-based systems²⁷. Their role will be to mediate between the world of machines and the world of people.

Future work and prospects

Large-scale transfer of human knowledge from books (or brains) to computers has not been achieved in any human intellectual domain. Computer chess is at the leading edge of experimental attempts to achieve it. Endeavours centre round three foci:

(1) The design of data-structures in forms suitable for representing conceptualized knowledge (descriptions, patterns and theories) which are also convenient for the human user to modify and increment interactively.

(2) Improved facilities for inductive

inference, so that programs can acquire new knowledge both from illustrative examples supplied by human tutors, and also from the results of their own internal generation of examples for self administration.

(3) The engineering of conceptual interfaces between program and human expert, making it easier for the latter to 'teach' the machine.

Advances under all of the above headings are required before the goal of Grandmaster play by machine can be seriously envisaged. By the same token, few investigators doubt the ultimate attainment during the present decade of Grandmaster levels. Apart from benefits to the arts of programming, such an extension of technique also has a bearing on the study of cognition.

I thank Senior Master Danny Kopec for helpful comments.

1. Babbage, C. *Passages from the Life of a Philosopher* (Longman, Green, Longman, Roberts & Green, London 1864). Reprinted in *Babbage and his Calculating Engines* (Dover, New York, 1961).
2. Vigneron, H. *La Nature* 56-61 (1914).
3. Turing, A.M. *Faster than Thought* (ed. Bowden, B.V.) 286-310 (Pitman, London, 1953).
4. Maynard Smith, J. & Michie, D. *New Scientist* 12, 367-369 (1961).
5. Shannon, C.E. *Phil. Mag.* 41, 256-275 (1950).
6. de Groot, A. *Thought and Choice in Chess* (ed. Baylor, G.W.) (Mouton, Paris, 1965).
7. Binet, A. *Psychologie des Grands Calculateurs et Joueurs d'Echecs* (Hachette, Paris, 1894).
8. Samuel, A. *IBM J. Res. Dev.* 3, 210-229 (1959).
9. Greenblatt, R.D., Eastlake, D.E. & Crocker, S.D. *Proc. FJCC* 801-810 (1967).
10. Hayes, J.E. & Levy, D.N.L. *The World Computer Chess Championship* (Edinburgh University Press, 1976).
11. Condon, J.H. & Thompson, K. *Advances in Computer Chess* Vol. 3 (ed. Clarke, M.R.B.) 45-54 (Pergamon, Oxford, 1982).
12. Knuth, D.E. & Moore, R.W. *Artificial Intelligence* 6, 293-326 (1975).
13. Berliner, H. thesis, Carnegie-Mellon University, Pittsburgh (1974).
14. Chase, W.G. & Simon, H.A. *Cognit. Psychol.* 4, 55-81 (1973).
15. Tan, S.T. *Advances in Computer Chess* Vol. 1 (ed. Clarke, M.R.B.) 74-88 (Edinburgh University Press, 1977).
16. Quinlan, J.R. *Machine Intelligence* Vol. 10 (eds Hayes, J.E., Michie, D. & Pao, Y-H) 159-172 (Horwood, Chichester, 1982).
17. Hunt, E.B., Marin, J. & Stone, P. *Experiments in Induction* (Academic, New York, 1966).
18. Shapiro, A. & Niblett, T.B. *Advances in Computer Chess* 3 (ed. Clarke, M.R.B.) 73-92 (Pergamon, Oxford, 1982).
19. Shapiro, A. thesis, Machine Intelligence Research Unit, University of Edinburgh (in preparation).
20. Clarke, M.R.B. *Advances in Computer Chess* Vol. 1 (ed. Clarke, M.R.B.) 108-115; Appendix: King and rook against king, 116-118 (Edinburgh University Press, 1977).
21. Komissarchik, E.A. & Futer, A.L. *Problemy Kybernet* 29, 211-220 (1974).
22. Arlazarov, V.L. & Futer, A.L. *Machine Intelligence* Vol. 9 (eds Hayes, J.E., Michie, D. & Mikulich, L.L.) 361-371 (Horwood, Chichester, 1979).
23. Kopec, D. & Niblett, T. *Advances in Computer Chess* 2 (ed. Clarke, M.R.B.) 57-81 (Edinburgh University Press, 1982).
24. Kemeny, J.G. et al. *Report of the President's Commission on the Accident At Three Mile Island*, Washington D.C. (1979).
25. Michie, D. *SIGART Newsl.* No. 80, 64-70 (1982).
26. Waterman, D.A. *Pattern-Directed Inference Systems* (eds Waterman, D.A. & Hayes-Roth, F.) (Academic, New York, 1978).
27. JIPDEC Fifth Generation Computer Committee Preliminary Report on Study and Research on Fifth-Generation Computers 1979-1980 (Japan Information Processing Development Centre, Tokyo, 1981).

NEWS AND VIEWS

Twelve wise men at the Vatican

from J.M. Lowenstein

A RECENT meeting* of twelve scholars at the Pontifical Academy of Sciences in the Vatican Gardens proved historic in two respects. First, the group, which consisted of palaeontologists, geneticists and molecular biologists and which had been specifically assembled to reconcile the palaeontological evidence of primate evolution with that from molecular biology, was able to agree on a scenario for primate evolution over the past 30 million years. To many protagonists of the two disciplines this will seem something of a miracle. Second, the highest scientific body of the Catholic Church produced a strong statement supporting the evolutionary hypothesis as the explanation for the origin and diversity of living primates — just a few weeks after the hundredth anniversary of Darwin's death.

Presiding over the working group was the President of the Pontifical Academy, Carlos Chagas, a neurophysiologist from Brazil and scientific adviser to Pope John Paul II. The pope reportedly takes a keen interest in the activities of the Academy.

Palaeontologists and molecular biologists have been divided over whether the various living apes and man diverged early on (20 Myr BP) or late (5–7 Myr BP). Some fossil evidence, particularly the dating of *Ramapithecus*, considered by many palaeoanthropologists to be hominid, supports the earlier date. A mass of biochemical data showing about 99 per cent identity between the DNA and proteins of chimpanzee, gorilla and man implies, from inferred rates of DNA and protein change, that the separation occurred at the later date.

The working group was able to reconcile the fossil and biochemical evidence by taking into account evidence that *Ramapithecus* is not hominid but is more probably related (along with *Sivapithecus*) to the orang-utan lineage. Particularly important are the recent discovery of a *Sivapithecus* face which has many orang-

utan-like features (see Pilbeam *Nature* 295, 232; Andrews *News and Views* 295, 185; 1982) and the finding that limb bones attributed to *Ramapithecus* or *Sivapithecus* (but not found in association with jaws and teeth) strongly suggest an arboreal adaptation. Supporting evidence comes from a new radioimmunoassay technique. Preliminary results (Lowenstein) show the fossil proteins of *Ramapithecus/Sivapithecus* to be most like the serum proteins of orang-utan, gibbon and gorilla, less like those of man and chimpanzee and least like those of monkey and other mammals — suggesting the Miocene genera *Ramapithecus/Sivapithecus* were hominoid (ancestral to apes or to apes and humans) rather than hominid.

The first true hominids were agreed to be the australopithecines of East and South Africa, dated from about 4 Myr BP. Coppens, who with Johanson and White named the species *Australopithecus afarensis*, now considers that the observed large variation in size may not be due to sexual dimorphism as previously thought, but may indicate that more than one species was present at that early time. In the period between 4 and 14 Myr, when the common ancestor of man, chimpanzee and gorilla probably lived, there is no significant African fossil record of hominids or hominoids and no fossil record at all for chimpanzee and gorillas. Fossils from this period are badly needed to decide the path of human evolution.

The earliest record of monkey-like and ape-like primates, known from the Fayum formation of Egypt, was reviewed by Simons, who also described a new genus, *Qatrania*. *Aegyptopithecus*, earlier discovered in the Fayum by Simons, has teeth resembling those of apes but limb bones resembling those of New World howling monkeys. *Aegyptopithecus*, dated at 25–35 Myr, may be ancestral either to Old World monkeys and hominoids or to hominoids only, depending on the dating of the monkey–hominoid split. Molecular data suggest the split occurred 20–25 Myr BP which would make *Aegyptopithecus*

ancestral to both groups. Palaeoanthropologists commonly date the split much earlier, so that in their view, *Aegyptopithecus* is a hominoid ancestor only. Here, as in so much of primate evolution, accurate dating of divergences between lineages becomes critical.

One characteristic proposed as evidence of a phylogenetic relationship between *Ramapithecus* and *Australopithecus* is the presence of thickly enamelled molars. In Greenfield's opinion, this trait has very limited phylogenetic significance and does not support the inferred relationship. Rather, bipedalism and not small canines or an enlarged brain appears to be the emergent hominid trait — although what ecological conditions encouraged bipedalism is not at all clear.

Molecular biology can be expected to prove of increasing value in providing information about the relationships of extant higher primates. Doolittle pointed out that the study of pseudogenes, which change rapidly without any apparent selection pressures to restrict base pair substitutions, may provide particularly useful data.

Many other controversial areas of primate evolution were discussed. Tobias put forward the view that *Homo habilis* may have been capable of speech (albeit rudimentary) on the basis of an inferred well-developed vocal tract, endocast evidence of possible Broca's and Wernicke's areas, and a stone tool technology reflecting learned technical skills requiring speech for their transmission.

Overall, though, the working group was able to agree on its conclusion:

"We freely acknowledge that there is room for differences of opinion on such problems as species formation and the mechanisms of evolutionary change. Nonetheless, we are convinced that masses of evidence render the application of the concept of evolution to man and other primates beyond serious dispute". □

J. M. Lowenstein is Clinical Professor of Medicine at the University of California, San Francisco, California 94143.

*Participants at the conference, held 24–27 May 1982, were E. Bone (Belgium), Y. Coppens and J. Lejeune (France), R. Doolittle, L. Greenfield, J. Lowenstein, D. Pilbeam and E. Simons (USA), C. Pavan (Brazil), G. Sermoniti (Italy) and P. Tobias (S. Africa).

Beneficial autoimmunity?

from Charlie Janeway

THE immune system has a difficult part to play in the biology of vertebrate species for it must recognize and respond to a great variety of microorganisms which have a short generation time and can evolve more rapidly than the animals they invade. The immune system appears to have solved this problem by a general strategy of generating and amplifying the expression of those members of the very large set of recognition molecules or antibodies that are suitable for binding the potentially pathogenic organisms in its environment. At the same time, a complex series of regulatory mechanisms has been developed to prevent autoimmunity, the activation of such responses towards constituents of self. One type of autoimmune response, however, may have a central role in immune regulation: since each specific antibody molecule has a chemically and hence antigenically unique structure, recognition of that structure by the immune system could be used to control immune responses¹. Whether it does indeed have such a role is a matter of contention. A paper in this week's issue of *Nature* (p.447) provides an important piece of evidence supporting the existence of this form of autoimmune response and its potential regulatory function².

The general term for an antigenic determinant borne on the portion of the antibody molecule involved in specific antigen binding is an idiotype: the collection of idiotopes on a molecule make up its idiotype. Since most idiotypes are present at very low levels in normal serum, it appears that animals are not tolerant of these idiotypes, as they are of other serum protein antigens present at far higher concentrations. When an animal is immunized, the concentration of the idiotypes carried on the antibodies specific for the immunizing antigen undergoes a dramatic increase. In some cases, it has also been possible to demonstrate directly that the increase in those idiotypes is also accompanied by production of antibodies against them (anti-idiotype antibody)³. This occurs at a time at which the antibody

response is being reduced, and, since injection of anti-idiotype antibody is also suppressive of specific antibody responses⁴, the logical conclusion has been that the anti-idiotype antibody has an immunoregulatory role. Over the past few years, similar observations have been made in several experimental systems and have frequently employed monoclonal idiotypes and monoclonal anti-idiotypes as probes for regulation⁵. In addition, anti-(anti-idiotype) and anti-(anti-anti-idiotype) antibodies have been produced by artificial immunization schemes, and shown to affect the expression of idiotype in antibody responses⁶. It is thus clear that animals are able to make such responses, and that such antibodies, once produced, do affect the expression of antigenically related immunoglobulins.

What Pollok *et al.*² have shown is that, during the course of a normal immune response to a bacterial antigen, phosphorylcholine (PC), anti-(anti-idiotype)-specific B lymphocytes are activated, as demonstrated by making hybridomas that secrete monoclonal antibodies of this specificity from spleen cells of immunized mice. Furthermore, when the monoclonal antibody produced is injected into syngeneic mice before immunization with PC, it profoundly alters the expression of idiotype and of anti-PC antibody. While such an observation falls short of demonstrating an actual regulatory role for such auto-anti-(anti-idiotype) antibodies, it is certainly consistent with such a role and, since the antibodies were induced by immunization with antigen (PC) with which the anti-(anti-idiotype) antibodies do not react, it suggests that some intervening anti-idiotype response must also occur.

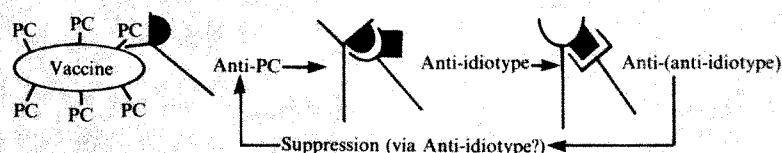
A number of questions are left unanswered by these studies. Some are technical, but important: while the anti-(anti-idiotype) antibodies do not react with PC, the immunization was actually performed with intact bacteria; do the putative anti-(anti-idiotype) antibodies react with the vaccine? If so, they would represent another example of the sharing of idiotope by two antibodies directed at distinct determinants on an antigenic particle^{7,8}. More

important, one would not, then, need to postulate anti-idiotype as the *sole* stimulus for production of the putative anti-(anti-idiotype) antibody. A second question needs further examination: is the anti-(anti-idiotype) actually secreted during this response, or has the fusion itself allowed expression of a B cell product that is normally not secreted? It is not known whether B cells giving rise to hybridomas are actually in a secretory or pre-secretory phase of activation when fusion occurs.

If one allows that the experiments of Pollok *et al.* demonstrate the presence of a *bona fide* auto-anti-(anti-idiotype) response, and that the antibody produced does play a part in normal regulation, several obvious questions need to be answered. First, how is anti-(anti-idiotype) antibody production induced by an antigen with which the anti-(anti-idiotype) does not react? Many types of anti-idiotypic elements have been described: B cells², two distinct classes of helper T cells^{9,10} and various cells in suppressive pathways¹¹⁻¹⁴. Which, if any, of these anti-idiotype cells or molecules activate production of anti-(anti-idiotype) needs to be determined; a first choice might be the anti-idiotypic helper T cell described by Cerny and Caulfield¹⁰ which appears to act directly on idiotype B cells in the absence of antigen, although activation of the B cell by anti-idiotype antibody may also be required¹⁵.

Second, and equally important, what cell is the target of the anti-(anti-idiotype) antibody in modulating expression of the original idiotype? Again, the same cell types may be involved, since anti-(anti-idiotype) antibody presumably affects anti-idiotypic cells or molecules. However, since the effect in the present case is suppression, the logical choice is either direct suppression of an anti-idiotype helper by anti-(anti-idiotype), or activation of a suppressor T cell that is anti-idiotypic, as demonstrated by Owen and Nisonoff¹¹ in the response to azophenylarsonate.

A major difficulty confronting advocates of anti-idiotypic immunoregulation is demonstrating the importance of such



Schematic representation of the experiment of Pollok *et al.* Immunization with a phosphorylcholine-bearing bacterial vaccine induces production of antibody marked by a particular idiotope. B cells from these mice, isolated as monoclonal antibody-secreting hybridomas, produce an antibody reacting with anti-idiotype, but not binding to PC. The authors propose that production of this antibody is stimulated by an anti-idiotype, here represented as anti-idiotype antibody. This anti-(anti-idiotype) can also feedback, again presumably via an anti-idiotype antibody or cell, to prevent production of anti-PC bearing the original idiotype.

Charlie Janeway is in the School of Medicine, Yale University, Connecticut 06510.

1. Jerne, N.K. *Ann. Immun. Inst. Pasteur (Paris)* **125**, 373 (1974).
2. Pollok, B.A., Bhowan, A.S. & Kearney, J.F. *Nature* **299**, 447 (1982).
3. Cosenza, H. *Eur. J. Immun.* **6**, 114 (1976).
4. Cosenza, H. & Kohler, H. *Science* **176**, 1027 (1972).
5. Kelsoe, G., Reth, M. & Rajewsky, K. *Immun. Rev.* **52**, (1981).
6. Urbain, J. *et al. Prog. Immun.* **4**, 81 (1980).
7. Oudin, J. & Cazenave, P.A. *Proc. natn. Acad. Sci. U.S.A.* **71**, 4500 (1971).
8. Metzger, D.W., Miller, A. & Sercarz, E.E. *Nature* **287**, 541 (1980).
9. Bottomly, K. in *Immunoglobulin Idiotypes* (eds Janeway, C., Sercarz, E. & Wigzell, H.) 517 (Academic, New York, 1981).
10. Cerny, J. & Caulfield, M.J. *J. Immun.* **126**, 2262 (1981).
11. Owen, F.L. & Nisonoff, A. *J. exp. Med.* **148**, 182 (1978).
12. Pierce, S.K. & Klinman, N.R. *J. exp. Med.* **146**, 509 (1977).
13. Eardley, D.D., Shen, F.W., Cantor, H. & Gershon, R.K. *J. exp. Med.* **150**, 44 (1979).
14. Germain, R.N. *et al. in Immunoglobulin Idiotypes* (eds Janeway, C., Wigzell, H. & Sercarz, E.) 709 (Academic, New York, 1981).
15. Eichmann, K., Falk, I. & Rajewsky, K. *Eur. J. Immun.* **8**, 853 (1978).

effects during immune responses *in vivo*. Previous experiments have often employed heterogeneous antisera raised by vigorous immunization regimes. The studies of Pollok *et al.* avoid this difficulty, but do not answer the quantitative question of whether the responses are crucial to the biology of the immune system, or whether they represent largely an experimental curiosity. The extraordinary capabilities of

the immune system to produce antibodies of virtually any specificity, as well as the heterogeneity of these antibodies, make this question enormously difficult to approach, let alone to answer. The finding of one element of a putative idiotypic regulatory network as a result of immunization with antigen is, however, a further incentive to pursue this line of investigation to its conclusion. □

Zero-momentum atoms in superfluid helium-4

from P.V.E. McClintock

ONE of the many oddities of liquid helium is that it often seems to behave as though it were a gas. It does not, of course, expand to occupy all the available space in its container — it could not be described as a liquid at all, if this were the case — but in terms, for example, of its very low density, its refractive index close to unity, its feeble interatomic forces, its tiny surface tension and its extremely small viscosity (less than that of air at room temperature, even for normal, non-superfluid helium-4), its properties often seem more gas-like than liquid-like.

The natural question to ask, therefore, is just how far this analogy can be taken. In particular, given that helium remains fluid down to the lowest attainable temperatures, does it fall into the sort of exotic ground state predicted for ideal gases at very low temperatures? For 'real' gases, of course, the question does not arise, because they would no longer be gaseous at the low temperatures in question; but for liquid helium . . . ? These questions, first posed more than four decades ago by F. London (*Nature* 141, 643; 1938), have remained central to any fundamental discussion of the liquid heliums ever since. It has, in fact, been known for some time that the profound differences which exist between the low-temperature properties of liquid helium-3 (the rare isotope) and those of liquid helium-4 can mostly be accounted for quite well if the two liquids are considered by analogy with gases. What has remained extremely uncertain, however, is whether or not a finite proportion of the atoms in liquid helium-4 exist in the peculiar zero-momentum state (so-called Bose-Einstein condensate) which is predicted for an ideal gas in the same conditions. It is this crucial question which seems now to have been answered as a result of work at Chalk River, Canada, by Sears, Svensson, Martel and Woods, published in a recent issue of *Physical*

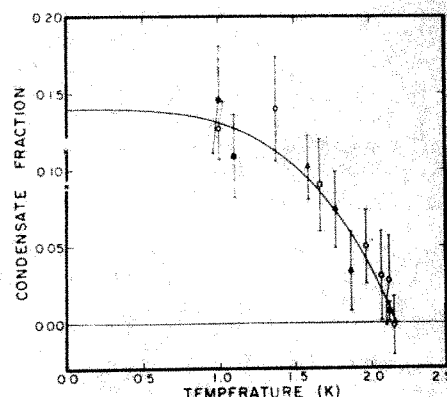
Review Letters (49, 279; 1982).

Bose-Einstein condensation represents one of the most intriguing predictions of quantum-statistical mechanics. The phenomenon is expected to occur in a gas which (1) consists of bosons (made from an even number of fundamental particles) and (2) is ideal (point particles with zero interatomic forces). Helium-4 clearly satisfies criterion (1) because the atom consists of two protons, two neutrons and two electrons; but the same cannot be said of criterion (2). There has been a continuing debate about the extent to which the existence of the interatomic forces, albeit very weak ones in the case of liquid helium, would modify the behaviour of the assembly. In an ideal gas, it is expected that there will exist a critical temperature, T_c , below which atoms will start to condense into the zero-momentum state. The de Broglie wavelength of atoms in this state is infinite (in practice, equal to the dimensions of the container) so that the more familiar concept of atoms as 'particles' becomes, to say the least, a little strained. The onset of the condensation phenomenon is predicted to occur with extreme suddenness as the temperature is lowered. It turns out that, as T falls below T_c , the requirements of quantum statistics can be satisfied only if some of the atoms are 'forced' into the zero-momentum ground state. As a result, the occupation number of this state should suddenly start to shoot up from a quite negligible value above T_c to a finite value as T falls below T_c ; and it should approach unity for $T \ll T_c$, corresponding to almost all the atoms in the assembly being in the zero-momentum state. The existence of interatomic forces is expected to modify this picture to a considerable extent, however. In particular, it can be shown that the condensate fraction at $T=0$ should be reduced to a value lower than the 100 per cent characteristic of an ideal gas.

One of the great attractions of applying these ideas to liquid helium is that the superfluid transition, observed at the so-called lambda point of $T_\lambda = 2.2\text{K}$, may then

be identified with the onset of Bose-Einstein condensation — albeit in a modified form because of the interatomic forces. This identification is supported by the facts that the superfluid transition occurs very suddenly, just as predicted for Bose-Einstein condensation; that it takes place at approximately the calculated temperature; and that many of the strange properties exhibited by liquid helium below T_λ , for example its quantized rotational modes, can readily be accounted for if it is assumed that some condensate is present. The variation of the specific heat with T near T_λ and many other properties of the liquid are, however, entirely different from those predicted for an ideal Bose-Einstein gas. Thus, although all such discrepancies may be attributed — reasonably plausibly — to the influence of the interatomic forces, there has remained a nagging doubt as to whether the liquid really does have a finite condensate fraction or not.

Attempts to test London's ideas through a direct determination of the magnitude of the condensate fraction have been based on neutron and X-ray scattering from the liquid. For technical reasons, both the experiments and their interpretation have been rather difficult. Part of the problem arises from the fact that the condensate fraction is evidently quite small, thus necessitating a measurement of relatively high precision. Some of the earlier experimental results were, in fact, quite consistent with the condensate fraction being zero, a most discouraging conclusion. There has also been some degree of controversy about the validity of one of the (apparently) most successful techniques which has been used, based on measuring the temperature dependence of the two-



The condensate fraction in liquid helium-4 plotted as a function of temperature (from V.F. Sears, E.C. Svensson, P. Martel & A.D.B. Woods *Phys. Rev. Lett.* 49, 279; 1982). The filled symbols represent new measurements based on inelastic neutron scattering. The open symbols correspond to values determined from the measured temperature dependence of the two-particle correlation function, including some earlier measurements (squares) by H. N. Robkoff, D. A. Ewan & R. B. Hallock (*Phys. Rev. Lett.* 43, 2006; 1979). X represents theoretical predictions for $T=0$.

P.V.E. McClintock is in the Department of Physics at the University of Lancaster, Lancaster LA1 4YW.

particle correlation function $g(r)$.

The new results now presented by the Chalk River group, shown by the filled symbols in the figure, are based on inelastic neutron scattering, a completely different technique the validity of which has not been impugned. The open symbols represent data derived from the temperature dependence of $g(r)$. Agreement between results obtained by these two techniques would appear to be excellent and there is really no longer any room for serious doubt as to the existence of a Bose-

Einstein condensate in liquid helium-4 below T_λ . It appears that the magnitude of the condensate fraction rises from zero at T_λ and approaches a limiting low-temperature value of about 14 per cent below 1K, a value which is in quite reasonable accord with recent theoretical predictions.

The principal conclusion, that London's imaginative suggestions of 44 years ago are indeed correct, will provide a source of considerable satisfaction for all those with an interest in liquid helium. \square

indicate a simpler boundary zone at that locality, but one with evidence for a fault that may be traced through the entire crust to the surface. Three COCORP reflection lines crossing the Quachita-Appalachian orogen in the USA suggest that modern continental Moho to the seaward ends of the lines may, in fact, be former oceanic Moho buried during major thrusting. Or perhaps Moho is the base of the former oceanic sedimentary layer now overlying oceanic crust eclogitized to display mantle properties.

Other geophysical techniques are providing different types of evidence on Moho. Studies of the earthquake-generated phases Pn and Sn reveal major lateral variations in velocity and attenuation in the uppermost mantle. In some places, such as the shallow mantle of the Atlantic and the Pacific and the down-going slab of subduction zones, this zone enigmatically forms perhaps the most efficient transmitter of high-frequency seismic waves within the Earth; in others it is a severe attenuator.

Gravity data are being used in conjunction with seismic data to explore lateral variations in the Moho⁵, and new kinds of computer handling of these data will facilitate this approach^{6,7}. Drilling seems limited to depths of 15 km or less for the near future and hence could penetrate Moho only in anomalous places or in the ocean basins.

Seismic refraction studies have long shown spatial variations in sub-Moho velocities that could be, but rarely have been, interpreted geologically. The Soviet DSS method uses refractions and wide-angle reflections in a particularly comprehensive fashion, and important new methods of analysis of refraction data, such as the τ/p method and ray tracing through arbitrary structures, are being developed to minimize bias to special geometries and to facilitate incorporation of geological information and concepts.

The Moho at sea has been best observed by seismic refraction measurements, but occasionally vertical reflections are obtained⁸ and improved techniques may produce more such information. Geochemical studies of igneous rocks indicate consistent lateral variations of the source rocks in the mantle⁹.

In the transition zone between continents and oceans, observations of Moho are characteristically difficult, and the structure of the mantle there is usually derived by inference. This situation is unfortunate because some evidence, such as the general uniformity of thickness of the continental crust, suggests substantial ductile flow near the base of the crust, whereas the inferred configuration of the transition zones is sufficiently abrupt to suggest that such flow is resisted.

Perhaps best of all, former Moho can now be seen, touched and sampled. Within the last 15 years, many pieces of former oceanic Moho have been re-

Changes at the crust-mantle boundary

from Jack Oliver

MANY recent observations indicate that the current view of the Moho, the crust-mantle boundary, needs revision. In particular, the widely held concept of the Moho as a sharp and laterally uniform boundary appears misleading in its simplicity, and may even be a major barrier to a better understanding of the nature and evolution of continents.

A brief look at the history of ideas about the Moho reveals how concepts can sometimes facilitate, and sometimes inhibit, understanding of the Earth. The Moho was discovered by the Serbian seismologist A. Mohorovičić in 1909. His evidence, seismic waves generated by nearby earthquakes and refracted to the surface, indicated a zone of rapid increase of seismic velocity at depth. Since then, innumerable seismic refraction surveys have shown that the velocity increase is nearly always found in continental areas at depths of 30 to 50 km and in ocean basins at depths of perhaps 10 to 12 km.

Until recently, the only method used for analysing seismic refraction data was, in essence, that employed by Mohorovičić. The method, based on ray theory and the time-distance plot, is biased strongly towards abrupt discontinuities and plane-bounded layers. Although the biases are well known to seismologists, results are often presented to others in a way that inadvertently overemphasizes these characteristics.

At some point, Mohorovičić's zone of rapid velocity increase became the crust-mantle boundary. The attractions of this step were many. The velocity increase could be readily observed. It implied a major density increase and hence a possible place for isostatic compensation and for the sources of certain gravity anomalies. It could conveniently be assigned to mark the boundary between acidic and basic rocks

of the crust and the ultrabasics of the mantle.

Some awkward scientific and semantic problems arose from this step, but they aroused little attention. For example, it was first thought that lateral variations were absent below the Moho. However, as mantle thickness is different under continents and oceans, the velocities and the velocity gradients cannot be identical. Later, plate tectonics called for, and observations demonstrated, a more dynamic and heterogeneous mantle.

The simple concept of the Moho has been so appealing and so emphasized that it may have become repressive. Sometimes sub-Moho rocks with velocities of 8.4 km s⁻¹ at one site have been lumped as 'mantle' with sub-Moho rocks at 7.6 km s⁻¹ from another site without attracting much attention to the lateral differences. A change of this magnitude in the vertical direction could form a spectacular 'low-velocity layer' and command astonishment and imaginative interpretation! The concept of a uniform mantle has been so ingrained that some have risked circular reasoning and interpreted all variations from the standard 8.1 km s⁻¹ as effects of anything but composition.

Now, new kinds of observations, and reconsidered old ones, are demonstrating that much more is to be learned about the Moho. In a recent paper, Hale and Thompson¹, following the lead of Fuchs² and Meissner^{3,4}, draw attention to the complexity of the boundary zone in the vertical dimension. They describe a laminated zone several kilometres thick revealed at five sites by recent seismic reflection profiling, noting only minor lateral variations at any one site and similarity among all five sites. The laminated structures are variously interpreted as cumulates, metasediments, tectonic banding, or lenses of partial melt. Other reflection studies, such as the BIRPS profile on the shelf north-east of Britain,

Jack Oliver is in the Department of Geological Sciences, Cornell University, Ithaca, NY 14853.

cognized on land as parts of ophiolite sequences that have been moved onto continents as oceans closed¹⁰. The boundary zone between the gabbros of the oceanic crust and the peridotite overlying harzburgite of the mantle is evident and informative about the generation of lithosphere at oceanic spreading centres.

Furthermore, as shown by Berkhemer¹¹, the former continental Moho and associated deep crustal rocks are exposed in the Ivrea zone of the Alps, and, in a recent paper, Fountain and Salisbury¹² list areas on four continents where former continental Moho may be at or near the surface. In general, the rocks from near the Moho have a layered structure that is much more complex than most geophysical observations suggest, and they have a special attraction for detailed study at this time of increasing emphasis on understanding the deep continental crust.

Within the last few decades, the name of the boundary under discussion has grown simpler, going from 'Mohorovičić discontinuity' to 'Moho' to, sometimes, 'M'. Our knowledge of the boundary itself is moving in the opposite direction. □

1. Hale, L.D. & Thompson, G.A., *J. geophys. Res.* **87**, 4625 (1982).
2. Fuchs, K. Z. *Geophys.* **35**, 133 (1969).
3. Meissner, R. *Geophys. Prospect* **15**, 598 (1967).
4. Meissner, R. *Geophys. Surv.* **1**, 195 (1973).
5. Cook, F.A. & Oliver, J.E. *Am. J. Sci.* **281**, 993 (1981).
6. Arvidson, R.E., Guineess, E.A., Strebeck, J.W., Davies, G.F. & Schulz, K.J., *EOS* **63**, 261 (1982).
7. Simpson, R.W. Jr, Hildenbrand, T.G., Godson, R.H. & Kane, M.F., *U.S. geol. Surv. Open-file Rep.* 82-477 (1982).
8. Stoffa, P.L., Buhl, P., Herron, T.J., Kan, T.K. & Ludwig, W.J. *Mar. Geol.* **35**, 83 (1980).
9. Allegre, C.J., *Tectonophysics* **81** 109 (1982).
10. Hopson, C.A., Coleman, R.G., Gregory, R.T., Pallister, J.S. & Bailey, E.H. *J. geophys. Res.* **86**, 2527 (1981).
11. Berkhemer, H. *Tectonophysics* **8**, 97 (1969).
12. Fountain, D.M. & Salisbury, M.H. *Earth planet. Sci. Lett.* **56**, 263 (1981).

Transgenic organisms and development

from William Petri

DEVELOPMENTAL biologists have claimed that the secret of cell differentiation in higher organisms is differential gene expression. Unfortunately, documentation of the molecular mechanisms involved has been sparse and superficial and lagged far behind that for prokaryotic systems such as *lac* and λ . However, the mood at a recent meeting on molecular aspects of development* was optimistic that real progress towards understanding the control of gene expression during development may be at hand. Much of the progress will be due to the application of the recombinant DNA technologies and the recently acquired ability to create completely¹ transgenic organisms (organisms all of whose cells contain a copy of an experimentally introduced DNA).

In a transgenic organism, a copy of an experimental gene is inserted very early in development; ideally the gene will be integrated into the germ line. If this occurs, progeny will be produced that will carry the foreign gene in every cell, and the expression of the gene can be assayed throughout development in every tissue. Comparisons among organisms containing systematically modified variants of the same gene and nucleotide sequences associated with it (for example, ref. 2) should allow identification of the genetic elements responsible for controlling tissue-specific and developmental stage-specific

gene expression. Such elements are the core of developmental regulation, and their elucidation has not been possible using the previously available test systems involving cell-free transcription, injection of amphibian oocytes and transfection of cultured cells since they are primarily limited to investigation of cellular and genetic factors necessary for gene expression *per se* or those influencing transcriptional efficiency. Hence, completely transgenic organisms should form the basis of a boom in our understanding of developmental control mechanisms. Fortunately, such organisms are now not only possible but apparently more easily obtained than expected.

B. Mintz (Institute for Cancer Research) reported two routes of entry for cloned DNAs (in particular, a plasmid containing both the human β -globin and herpes simplex virus thymidine kinase genes) into the mouse germ line: egg pronuclear injection and transfection of totipotent teratocarcinoma cells followed by blastocyst implantation. Both methods succeeded at experimentally usable frequencies (up to 20 per cent in preliminary experiments). However, expression of the HSV-TK gene was observed in only one of five parental transgenic mice³. Importantly, the introduction of exogenous DNA via a recently developed totipotent mouse euploid teratocarcinoma culture cell line will allow pre-selection and pre-characterization of genetic changes before re-introduction into the mouse.

Using microinjection into mouse eggs, R. Palmiter (University of Washington)

reported successful non-homologous integration of cloned fusion genes (5' mouse metallothionein-1 promoter and 3' HSV-TK structural gene) into the germ line⁴. In most transgenic mice capable of expressing the HSV-TK activity, the gene was inducible by heavy metals, the normal inducers of metallothionein, indicating the successful introduction of functional controlling elements into recipient mice. Fusion gene expression in induced progeny is, however, highly variable, often extinguished, and unrelated to parental levels and to gene dosage. The unpredictable expression of introduced genes seen in both groups may hinder the usefulness of transgenic mice as assay systems for developmental control elements; however, it may also provide insights into the ways gene expression can be modulated or extinguished.

Fortunately these problems may not plague all transgenic systems. G. Rubin (Carnegie Institute), in collaboration with A. Spradling, reported the successful germ-line incorporation of cloned *rosy*⁺ (xanthine dehydrogenase) into *rosy*⁻ *Drosophila* by injection into the poleplasm of fertilized eggs using the P element responsible for hybrid dysgenesis as a vehicle. A very high proportion of fertile adults resulting from injected *rosy*⁻ eggs produced *rosy*⁺ progeny (20–50 per cent), and *rosy*⁺ segregants always contain extra *rosy* material whereas *rosy*⁻ segregants do not. Hence, in contrast to the mouse results, here it seems that at least some incorporated genes are expressed in each transgenic line. Although integration of the injected *rosy*⁺ genes is non-homologous, two features of the system are intriguing. First, six of twelve *rosy*⁺ insertion sites are very close to the normal *rosy* locus and second, integration occurs with the precise exclusion of the plasmid cloning vector. Overall, transgenic *Drosophila* appear to provide a promising system for the study of developmental control elements and effects of gene location on expression.

The key difficulty of where and how important changes in gene activity occur in the long and increasingly complicated process of development received much attention (and see refs 5 & 6, for example). Selected points brought out at the meeting follow.

Contrary to previous notions, few genes seem to turn on sharply in early development. Most sequences prevalent in the pluteus of the sea urchin (E. Davidson, Caltech)⁷ or the gastrula of *Xenopus* (I. Dawid, NIH) are already present in maternal RNA. Yet these sequences do not simply represent housekeeping functions since most are not found in adults (Davidson). Generally, an important level of control in early development seems to be variable turnover rates of cytoplasmic

William Petri is Associate Professor of Biology at Boston College, Chestnut Hill, MA 02167.

* The 41st Annual Symposium of the Society for Developmental Biology entitled 'Gene Structure and Regulation in Development' was held at Harvard University on 17–19 June 1982.

The author thanks Peter Cherbas and Arlene Wyman for comments on the manuscript.

transcripts (Davidson)⁸. Curiously, a major portion of the egg cytoplasmic poly(A)-containing RNA in sea urchins and in *Xenopus* contains interspersed repeat sequences in relatively long transcripts reminiscent of nuclear RNA (Davidson, Dawid)⁹. They could result from a failure of termination, as seems to be the case in the unusually long transcription units characteristic of lampbrush chromosomes (J. Gall, Yale University)¹⁰, or perhaps from lack of intron splicing (Davidson). The role of these molecules, if any, remains speculative. It is unlikely that they are translated without further processing since many of the repeated elements contain multiple stop codons (Davidson); hence, it is possible a type of developmental control could reside in tissue- and stage-specific completion of RNA processing.

Genetic transcriptional control elements are known to exist upstream from the TATA box in cases such as dimethyl sulphoxide induction of β -globin (Maniatis, Harvard University) and heavy-metal induction of metallothionein (Palmiter) and sometimes quite far upstream^{11,12}, but their developmental role is equivocal. Other possible developmental controls include tissue-specific differential splicing of primary transcripts as may occur in the *Drosophila bithorax* system (M. Goldsmith-Clermont, Stanford University), tissue- and stage-specific differential gene amplification as evidenced in the *Drosophila* chorion system (F. Kafatos, Harvard University) and tissue-specific differences in protein kinase levels (R. Erikson, Harvard University). So far, cascades of sigma

factors seem limited to prokaryotic and viral developmental systems (J. Pero, Harvard University).

Importantly, in a number of cases control is not simply an 'on-off' affair, but rather quantitative changes may be critical. For example, P. Cherbas (Harvard University) reported the early protein level response to ecdysone in *Drosophila* K₁ cells involves an increase in the amounts of three proteins (EIP 28, EIP 29 and EIP 40) already present before induction. The main effect of Rous sarcoma virus *src* gene may be to increase the level of cellular protein kinase by 20-fold in order to cause a gross change in cellular morphology (Erikson). The pattern of gene expression can also be affected by the changing location of transposable genetic elements, as documented in maize (B. Burr, Brookhaven National Laboratory)¹³, *Drosophila* (Ruben) and yeast (I. Herskowitz, University of California, San Francisco)¹⁴. It remains to be seen what part such genomic instabilities routinely play in

developmental processes outside the vertebrate immune system.

Appropriately, Kafatos cautioned that developmental biologists should not assume that the way things are controlled in one system will be the way they are controlled in another. For example, compare two insects: the silk moth and *Drosophila*. The former constructs its eggshell using germ-line repeated gene pairs while the latter employs differential gene amplification of single-copy genes. Yet, perhaps one should not be too surprised by the difference since the lepidoptera and diptera diverged evolutionarily almost 300 million years ago, about the same time that human and reptilian lines split.

The conference ended with an appealing model from H. Weintraub (Hutchinson Cancer Research Center) concerning activation of chromatin structure¹⁵. He pointed out that concomitant with the activation of globin genes during chick erythropoiesis, DNase-hypersensitive regions appear at the 5' ends of the genes due to the formation of single-stranded stem-loop structures. Once induced these hypersensitive sites remain even after removal of the inducer and even through DNA replication. Interestingly, these sites can be induced by salt shock. Changing the salt concentration drastically alters the places where S₁ nuclease will cut. Hence, Weintraub speculates, if the early embryo contains a salt gradient perhaps this could activate different chromatin regions in cells occupying different positions within the gradient. In short, Weismann's determinants could be differential salt concentrations! □

1. Gordon, J.W. & Ruddle, F.H. *Science* **214**, 1244 (1981).
2. McKnight, S.L. & Kingsbury, R. *Science* **217**, 316 (1982).
3. Wagner, E.F., Stewart, T.A. & Mintz, B. *Proc. natn. Acad. Sci. U.S.A.* **78**, 5016 (1981).
4. Palmiter, R.D., Chen, H.Y. & Brinster, R.L. *Cell* **29**, 701 (1982).
5. Darnell, J.E. *Nature* **297**, 365 (1982).
6. Brown, D.D. *Science* **211**, 667 (1981).
7. Flytzanis, C.N., Brandhorst, B.P., Britten, R.J. & Davidson, E.H. *Devl Biol.* **91**, 27 (1982).
8. Davidson, E.H., Hough-Evans, B.R. & Britten, R.J. *Science* **217**, 17 (1982).
9. Davidson, E.H. & Posakony, J.W. *Nature* **297**, 633 (1982).
10. Diaz, M.O., Barsacchi-Pilone, G., Nahon, K.A. & Gall, J.G. *Cell* **24**, 649 (1981).
11. Shermoen, A.W. & Bechendorf, S.K. *Cell* **29**, 601 (1982).
12. Muskavitch, M.A.T. & Hogness, D.S. *Cell* **29**, 1041 (1982).
13. Burr, B. & Burr, F.A. *Cell* **29**, 977 (1982).
14. Herskowitz, I. & Oshima, Y. in *Molecular Biology of Yeast Saccharomyces: Life Cycle & Inheritance*, 181 (Cold Spring Harbor Laboratory, New York, 1981).
15. Larsen, A. & Weintraub, H. *Cell* **29**, 609 (1982).



100 years ago

ELECTRIC NAVIGATION

THE idea of propelling a boat through water by the motive power of electricity is no new one. The invention of the electromagnet showed the power of an electric current to produce a mechanical force. It was no very difficult matter, therefore, for the electricians of fifty years ago to utilise the force of the electromagnet to drive small electromagnetic engines; and from the small beginnings of Dal Negro, Henry, Ritchie, and Page, grew up a group of electric motors which only awaited a cheap production of electric currents to become valuable labour-saving appliances. Nor was it a very long stride to foresee that if a sufficiently powerful battery could be accommodated on board a boat, it might be possible to propel a vessel with electromagnetic engines drawing their supply of currents from the batteries. This suggestion — one of the earliest, indeed, of the many applications of the electromagnet — was made by Prof. Jacobi of St. Petersburg, who, in

1838, constructed an electric boat. This machine was worked at first by a Daniell's battery of 320 couples, containing plates of zinc and copper, 36 square inches each, and excited by a charge of sulphuric acid and sulphate of copper. The speed attained with this battery did not reach so much as 1 1/4 miles per hour. But in the following year, 1839, the improvement was made of substituting 64 Grove's cells, in each of which the platinum plates were 36 square inches in area. The boat, which was about 28 feet long, 7 1/2 broad, and not quite 3 feet in depth, was propelled, with a convoy of fourteen persons, along the River Neva, at a speed of 2 1/4 (English) miles per hour.

The electric launch *Electricity*, which made its trial trip on Thursday, September 28, 1882, on the waters of the Thames, is certainly a great advance upon that which had been previously attained. This boat, is of iron, and is a trifle less in length than the wooden boat which Jacobi propelled. She will carry twelve persons, though at the trial trip but four were on board. After a few minutes' run down the river and a trial of the powers of the boat, to go forward, slacken, or go astern at will, her head was turned Citywards, and she sped — I cannot say steamed — along the southern shore, running about eight knots an hour against the tide.

From *Nature* 26, 554, 5 October 1882.

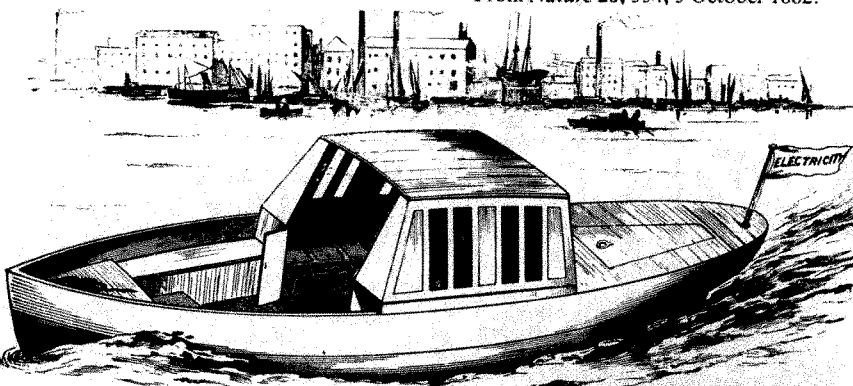


FIG. 2.—The Electric Launch.

Solar-terrestrial influences on weather and climate

from John Gregory

No longer is it appropriate to ask, as did one book reviewer, whether the subject of links between the Sun and weather and climate is a fit one for scientific study. The topic has now become respectable and, in the next quarter-century, will take its place among new and revised studies of solar-terrestrial relationships. These are the overall impressions gained at the recent Second International Symposium on Solar-Terrestrial Influences on Weather and Climate*. There are three main reasons for these developments; first, some previous evidence for solar-climate relations has withstood continued scrutiny; second, the variability of solar output is at last being measured; and third, new physical effects linking the Earth and Sun are being observed in the terrestrial system.

At the first symposium in 1979, Mitchell (NOAA), Stockton and Meko (University of Arizona) had used tree ring data to show that the incidence of droughts on the Great Plains west of the Mississippi is linked to the Hale (22 yr) solar cycle¹. The result has been generally approved^{2,3} and at the conference the original authors incorporated additional data in a new analysis and the 22 yr period was confirmed; though as earlier reported, it is not consistently present in all regions. Evidence for an 18–19 yr period was found, as noted by Currie⁴, in the interval 1850–1962. The phase linkage, which places drought maxima about 2 yr after Hale minima, was also confirmed, but at higher significance from 1700 to 1850 than at other epochs. The authors concluded that the variance of drought area indices may follow both the 18.6 yr lunar cycle and the 22 yr solar cycle, but that the latter is the predominant periodic component.

The best historical evidence for the short-term cyclic nature of climate continues to be the Precambrian distal varves (annual deposits of sediment) found in the Elatina formation of South Australia⁵. G. Williams, noting similarities between the 700 Myr rock and modern records, ventured a prediction of a ~300 yr cycle of solar activity, into the trough of which the Sun is now entering (see the table).

For more recent times, cores drilled in compacted snow at the South Pole and Vostok show evidence of 11 and 22 yr periodicity over about 1,000 yr. G. Dreschoff, E. Zeller and B. Parker (University of Kansas) examined nitrate

concentrations in the cores from the Pole, and incidentally found an unambiguous decrease coincident with the Maunder minimum.

Comparison of periods of solar activity (years)		
Elatina formation	Tree rings	Solar records
11	—	11
22	22	22
90	—	90
145	142–157	—
290	270–300	—

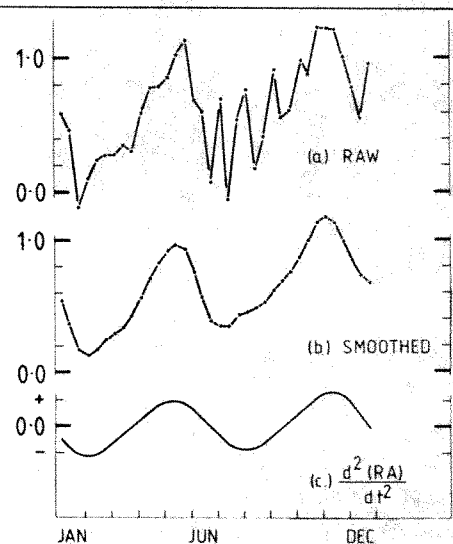
What processes might link solar activity and weather-climate? The opening speaker, J. Eddy (NCAR), asked for 'strong hints' as to mechanism and three speakers can be selected as providing answers.

D. Page (European Space Agency) analysed magnetic indices interpreted in terms of torques exerted by the interplanetary magnetic field on the magnetosphere. By subtracting magnetic indices for northern and southern hemispheres ($A_n - A_s$), and ordering them according to the polarity of the solar field, positive (away) and negative (towards), temporal variations of the quantity ($A_n - A_s$) positive – ($A_n - A_s$) negative were studied. The figure shows a basic result, which is well substantiated in subsets of data. There is an evident connection with the acceleration of the Sun in Right Ascension. To link angular accelerations back to torques, magnetospheric interaction with the interplanetary field is invoked. Temporal variations are interpreted as indicating that the torque on the magnetosphere is maximum when the north magnetic pole is closest to the Sun. Effects in the terrestrial system include characteristic differences in the recovery of magnetic storms, the phase

of the semi-diurnal atmospheric pressure tide at near-equatorial stations, which shifts about 15 minutes, and also shifts when magnetic sector boundaries are crossed, changes in average daily pressure differences between stations north and south of the equator by 1 mbar with change of polarity of the interplanetary field (the range of daily mean pressure at these locations being 2.5 and 9 mbar respectively) and the temporal occurrence of earthquakes. The build-up of torque to a maximum at about one day before a magnetic storm is also inferred from the behaviour of the D_{ST} index. A new mechanism is proposed for the origin of the semi-diurnal atmospheric tide, which would become a dynamical, not a thermal, response. No detailed mechanism which transmits torque on the magnetosphere to the neutral atmosphere and solid earth was proposed. Page points out that his interpretation requires that orbital energies be involved, and these are some 4×10^3 larger than rotational energy for a mass at the equator, in comparison with which solar radiation is much less significant. His interpretation may lead to considerable discussion as to the physics involved, but this should not be allowed to obscure the importance of the new terrestrial responses which he has established.

The second paper relates to a more familiar difficulty, the momentum balance of the stratosphere and mesosphere, which is coming closer to solution⁶. J. Gregory, A. Manson and C. Meek (University of Saskatchewan) showed, from wind measurements at 60–110 km altitude, that mean winter zonal speeds at 52°N have increased from solar minimum to maximum by a factor of at least two, the increase being largest a little above the mesopause (85 km). Little-known measurements at 95 km altitude, taken in the GDR and USSR for eighteen years⁷, support the interpretation of the Canadian data as an 11 yr cycle. In all the records, the increase in speeds is greater in winter than summer, by a factor of at least two to four in the mesosphere. To account for this,

The quantity ($A_n - A_s$) post – ($A_n - A_s$) neg plotted at 10-day intervals averaged over 1959–74. (a) gives the single 10-day values and (b) is obtained from (a) by taking 3-point moving averages. Curve (c) is the acceleration of the Sun in Right Ascension.



*The symposium, organized by B.M. McCormac and W.O. Roberts, was held at Boulder, Colorado, on 2–6 August 1982.

John Gregory is Professor of Physics at the University of Saskatchewan, Saskatoon, Canada.

Gregory proposed that increased heating, due to enhanced UV radiation around solar maximum, is most effective in the summer tropics and hemisphere. The meridional flow from summer to winter hemispheres is enhanced, and the solar modulation is thus transferred via Coriolis torque into the winter circulation, itself inherently variable. Other work^{8,9} shows that this effect is detectable in the winter stratosphere and troposphere.

The third paper involves long-wave radiation. G. Reid and K. Gage (NOAA) have extended their work¹⁰ on the annual variation of the height of the tropical tropopause to model an 11 yr variation, with change in solar 'constant' as a key factor. They showed that there is considerable sensitivity of that height to mean sea surface temperatures, via absolute humidity and deep cumulus convention. To establish agreement with observations, an increase in the solar 'constant' on the 11 yr basis is required. Reid reminded listeners that the decreases so far observed, of a few tenths of 1 per cent, are for shorter periods, and that the

change in solar irradiance over the 11 yr cycle is not yet established.

The symposium heard substantial papers on the variations of solar input to the atmosphere, induced effects in the upper atmosphere, responses of climate models to solar perturbations and also many papers on short-term effects and favoured mechanisms. These will appear in the proceedings. Special mention may be made of a survey by M. Nicolet (Pennsylvania State University) of photochemical responses affecting ozone: this comprehensive study will be a valuable reference source. □

1. Mitchell, J.M. Jr, Stockton, C.W. & Meko, D.M. in *Solar-Terrestrial Influences on Weather and Climate* (eds McCormac, B.M. & Seliga, T.A.) 125 (Reidel, Dordrecht, 1979).
2. Dickinson, R.E. *Bull. Am. met. Soc.* **61**, 611 (1980).
3. Pittock, A.B. *Rev. Geophys. Space Phys.* **16**, 400 (1978).
4. Currie, R.G. *J. geophys. Res.* **86**, 11055 (1981).
5. Williams, G.E. *Nature* **292**, 624 (1981).
6. Holton, J.R. *J. atmos. Sci.* **39**, 791 (1982).
7. Portnyagin, Yu. I., Kaydalov, O.V., Greisiger, K.M. & Sprenger, K. *Phys. Solar-Terris.* **5**, 91 (1977).
8. Nastrom, G.D. & Belmont, A.D. *Geophys. Res. Lett.* **7**, 457 (1980).
9. Nastrom, G.D. & Belmont, A.D. *J. geophys. Res.* **85**, 443 (1980).
10. Reid, G.C. & Gage, K.S. *J. atmos. Sci.* **38**, 1928 (1981).

A new type of pulsating star

from John P. Cox

A NEW type of pulsating star has been found by astronomers at the McDonald Observatory in Texas. The newly discovered variable star, known as GD358, is unique in that it is the first variable star to have been predicted as variable before its discovery^{1,2}.

The discovery, made by D.E. Winget, E.L. Robinson, R.E. Nather and G. Fontaine, was announced at the recent conference on 'Pulsations in Classical and Cataclysmic Variable Stars' held in Boulder, Colorado³. A more detailed account will be published soon in the *Astrophysical Journal*.

The new variable star is a kind of white dwarf — a DB white dwarf — whose outermost layers are composed of nearly pure helium. The surface temperature of GD358 is probably close to 30,000K. Several periods have been observed in GD358, ranging from a little more than 2 minutes up to about 16 minutes.

White dwarfs are extremely dense stars, with a mass equal to about that of the Sun and a radius comparable with the Earth's. Hence their densities are quite large — some 10⁶ times the density of water — and their surface gravities approximately 10⁵ times that of the Earth. White dwarfs are thought to represent the end stages in the evolution of at least certain kinds of stars.

Consequently, the interiors of the white dwarfs are likely to be devoid of hydrogen and, in most cases, of helium also. The hydrogen and helium often observed on the surfaces of white dwarfs is thought to be present only in thin 'films' formed when these lighter elements float to the surface under the influence of the strong gravitational field. In contrast, in most ordinary stars, the hydrogen and helium is believed to be distributed fairly uniformly throughout the interior.

The DB white dwarfs comprise only a small fraction, some 10 per cent, of all white dwarfs. Most, perhaps 80 per cent, have predominantly hydrogen in their outermost layers, and are called DA white dwarfs.

In the past decade or so, a number of variable DA white dwarfs have been found⁴. All have surface temperatures in the range 10,000–12,000K and are called 'ZZ Ceti' stars. Their periods range from about 2 to 20 minutes. The pulsations are thought to be nonradial, with different parts of the stellar surface moving out of phase with each other. The variable DA white dwarfs are thought to be ordinary DA white dwarfs which have slowly evolved into a condition where they pulsate for a time, perhaps a few million years — like temporary 'sickness' — and then become ordinary, nonvariable DA white dwarfs again.

Although less than 20 ZZ Ceti stars are known, they are probably by far the most

numerous kind of variable star in the Galaxy, in large part because white dwarfs themselves are so numerous (perhaps 10 per cent of all stars in the Galaxy). The variable DB white dwarfs may turn out to be the second most numerous kind of variable star in the Galaxy.

The new discovery is particularly significant because it confirms many of our ideas regarding stellar pulsation and its causes in general, and variable white dwarfs in particular. By applying pulsation theory to certain details of the observed period structures, it is possible to infer, for example, the rotation periods of the white dwarfs of interest, something that has been difficult to do by other methods. This has now been done for several variable white dwarfs. For the GD358 the method yields a rotation period of about 1.5 hours, which is quite representative of periods for white dwarfs whose rotations have been studied.

By applying pulsation theory to other aspects of variable white dwarfs, it is possible to study their internal structure in much the same way geophysicists use seismic waves to study the interior of the Earth. For example, that only certain periods are present in the variable white dwarfs strongly suggests that the outer regions have a layered structure — the thin hydrogen and/or helium layers can 'trap' certain pulsation modes⁵. The layered structure had previously been inferred on the basis of other elements of stellar evolution theory⁶. Since nearly all DA white dwarfs are expected to go through a variable phase sometime in their evolution, the layered structure is probably found in white dwarfs in general.

Similarly, it should be possible in the future to use the pulsations of GD358 to infer something about the interiors of the DB white dwarfs. It is interesting that the 'driving agent' for the pulsations of the DB white dwarfs is second helium ionization, as is thought to be mainly responsible for pulsations in the classical Cepheids. On the other hand, the same theory that led to the prediction that GD358 should be variable has identified the main physical cause of the pulsations of the ZZ Ceti stars as hydrogen ionization^{1-3,7,8}. This is the same physical agent that is believed to be mainly (or at least largely) responsible for the pulsations of the Mira variables⁹, among the largest stars known. □

1. Winget, D.E. thesis, Univ. Rochester (1981).
2. Winget, D.E. *et al. Astrophys. J. Lett.* **251**, L65 (1982).
3. Winget, D.E. & Fontaine, G. in *Pulsations in Classical and Cataclysmic Variable Stars* (eds Cox, J.P. & Hansen, C.J.) (Joint Institute for Laboratory Astrophysics, University of Colorado, in the press).
4. Good reviews of variable DA white dwarfs, or ZZ Ceti stars are: Robinson, E.L. *IAU Colloq.* **53**, 343 (1979); McGraw, J.T. *Space Sci. Rev.* **22**, 601 (1980).
5. Winget, D.E., Van Horn, H.M. & Hansen, C.J. *Astrophys. J. Lett.* **245**, L33 (1981).
6. *IAU Colloq.* **53** (1979).
7. Dolez, N. & Vauclair, G. *Astr. Astrophys.* **102**, 375 (1981).
8. Starrfield, S., Cox, A.N., Hodson, S. & Pesnell, W.D. in *Pulsations in Classical and Cataclysmic Variable Stars* (eds Cox, J.P. & Hansen, C.J.) (Joint Institute for Laboratory Astrophysics, University of Colorado, in the press).
9. Wood, P.R. in *Pulsations in Classical and Cataclysmic Variable Stars* (eds Cox, J.P. & Hansen, C.J.) (Joint Institute for Laboratory Astrophysics, University of Colorado, in the press).

John P. Cox is at the Joint Institute for Laboratory Astrophysics, University of Colorado, Boulder, Colorado 80309.

THE AUTOMATED LABORATORY

A load off the mind

AUTOMATION in the laboratory is like automation anywhere, but more so. Immediately after the Second World War, it seemed in all kinds of laboratories to be sensible that the repetitive measurement of the same properties of similar samples should be made by using the techniques developed by mechanical engineers for assembling bits and pieces of motor cars into standard structures — plastic bottles containing predetermined amounts of solutions doped with known radioactive isotopes would in this spirit be carried within the range of suitable detectors, scintillation counters perhaps. Other repetitive laboratory jobs — the chemical analysis for specified elements of broadly similar specimens of material, for example — were made more or less automatic once there had been developed reliable devices for measuring small amounts of chemical reagents (usually in liquid form). Economically, such devices were easily justifiable; better that routine measurements and assays should be carried out by standardized procedures undisturbed by the personal equations of the experimenters, while the cost of employing laboratory assistants to carry out tasks that could be delegated to machines was often higher than that of the interest paid on large sums of money borrowed from some bank. Production-line automation in this style remains as productive of improved efficiency as at any time in the past three decades. Automatic amino acid analysers, or machines that will assemble some predetermined nucleotide sequence from its component nucleotides, have become essential components of many laboratories' equipment.

The notes in the pages that follow show, however, that the ambitions of those who would make laboratories automatic have now transcended those fashionable in earlier decades. At the bench, or at the control panel of some large telescope, people are now rightly concerned to ask whether the arrival of microprocessors provides an opportunity for delegating to machines tasks that can in principle be carried out only by people, but which are in practice likely to be performed only hesitantly, even inefficiently. Of all automatic laboratory instruments, the machine-driven telescope (dating from the early nineteenth century) is the prototype: even clockwork machinery is usually more dependable than a human being at following the rotation of the Earth on its axis.

Traditionally, astronomers have supposed that only human beings (people like themselves) can decide for how long a telescope should be locked onto some celestial object of particular interest before the equipment they are using can be pointed at something else. (Given the logarithmic response of the photographic emulsion to integrated light intensity, mistakes have traditionally been commonplace.) Fortunately, the high cost and, more to the point, the competition for access to machines such as the Einstein X-ray observatory have reminded astronomers of the need to work out in advance of the collection of radiation from a nominated celestial object the amount of radiation (the number of quanta) that will yield a significant result. One obvious snag, of course, is that the significance of a data-set thus collected automatically may depend critically on the quality of the data, so that it will not be possible to specify in advance how many quanta should be collected but only to work out as the data accumulate when an observation should be stopped. That is a problem that those who design experiments in high-energy physics have lived with for several years. What they have found is that the automated laboratory brings severe and

unusual disciplines. The hypothesis to be tested must be clearly specified, and there must be explicit criteria for deciding what constitutes a significant test. Not unnaturally, in fields where the choice between manual and automatic experimentation is not overwhelmingly determined by the decrease of cost that automation brings, people resent the need to be this clear in advance.

These uncharted fields happen also to be those in which there is at present most interest, among manufacturers and their customers, in the automation of laboratory equipment. Two important influences have helped to bring about this state of affairs. First, the proportions of working scientists now reasonably skilled at writing computer programs has surreptitiously increased so that the notion that an experimental program might with advantage be delegated to a machine is more likely to come up than not. Second, the microprocessor has become ubiquitous and at the same time cheap. It is therefore natural enough that there should be a rash of laboratories concerned with traditional fields of research, muscle physiology or old-fashioned biochemical investigations, in which ingenious people have found it worthwhile (or at least fun) to latch together a microprocessor (perhaps in the form of a "home" computer) and an experimental rig in such a way as to avoid the need for telling when one "run" is at an end, and that it is time for another to begin. It is more of a surprise that equipment manufacturers rightly alert to the opportunities for adding to their catalogues equipment incorporating microprocessors should so often have found it necessary or at least expedient to quote substantially increased prices for automatic equipment compared with the traditional variety. Although users appreciate the need to amortize the cost of new developments, and even appreciate that their own increased efficiency is worth paying for, there is also a danger that manufacturers will rob themselves of valuable opportunities, and deprive their customers of important benefits, if they persist in seeking for themselves the whole of the value that can be added by automation.

In reality, the developments of the past few decades in the automation of experimental work are probably no more than a modest and even grudging concession to the practical importance of computing machinery. So much, it is hoped, will be apparent from Professor Donald Michie's article on computer chess (see page 391). This game is properly regarded as a kind of simulation of the problem of understanding how the natural world is put together. There is a qualitative correspondence between the search for winning strategies and that for successful hypotheses about the origins of natural phenomena. Computationally, chess is for the time being beyond the reach of even very large computers, implying that the understanding of natural phenomena is even less likely to be turned over to machines. But the past decade has seen such remarkable improvements in the capacity of machines to play the mechanical game of chess respectably, and the way ahead so clearly points to the utility of abstract definitions of useful strategies, that it is not unreasonable to hope that the practice of science may in due course be rid of the tedium by which generations of students (and even their teachers) have been oppressed. The drift towards the automation of the laboratory may be sustained by economic calculations turning on the salaries of technicians, but the long-term objective must be to free the imagination, not to cramp it.

The manufacturers' approach

THE means to automate laboratory instruments have been available for some years. Laboratories with large mainframe computers or minicomputers have been able to use them to automate certain aspects of instrument control and data processing. But developing such systems around large computers is costly. Automation has only really been feasible for many applications in the few years since the development and availability of cheap microprocessors. Manufacturers of scientific equipment nowadays are always keen to point out that their newly-developed instruments, even the cheapest, are in some way microprocessor controlled.

Researchers and technicians on the whole have welcomed automation, although some notable problems do exist (see opposite). Automated instruments are often easier and quicker to use than old methods and in many cases they make feasible experiments and measurements that would otherwise have taken too long to be seriously contemplated.

Control or data handling

Microprocessors or complete computer systems can be used in scientific instruments for two different but related functions — instrument control and data processing. The way in which the computer unit is incorporated into the instrument is crucially important for it determines the degree of control the user has over what the instrument will do. In general, microprocessor units pre-programmed in read-only memory cannot be easily re-programmed. Thus, the user has to accept the instrument functions that the manufacturer has decided he or she will want to do. Many users are only too willing for the microprocessor to take over the tedium of setting

up and continually adjusting instruments. Others find the manufacturers' programs too limited for their purposes.

Manufacturers have attempted to overcome the problem of satisfying different types of user in different ways. They are still searching for solutions. But in general, cheaper instruments include a microprocessor unit, pre-programmed in unerasable read only memory, that is responsible for both instrument control and, where applicable, data processing.

Pre- and re-programming

Moderately-priced instruments, worth up to a few tens of thousands of pounds, may include a pre-programmed microprocessor unit for instrument control and a standard interface for feeding data output from the instrument into a computer for data processing. Although the microprocessor unit may not be designed to be re-programmed, manufacturers can often program it to perform a wide range of functions including the sophisticated control of several parameters by dynamic feedback. Theoretically at least, users can connect their instrument to any computer for data analysis but in practice the choice of computer is often limited to those for which the manufacturer has written software for data analysis. Writing software from scratch for a different computer operating system is usually far too expensive — almost certainly more expensive than modifying the manufacturers' software considerably.

Manufacturers normally offer users the capability to re-program all aspects of instrument control and data processing only for costly instruments at the top end of their ranges. The reason is not too difficult to appreciate. A microprocessor unit pro-

duced as pre-programmed hardware is cheap and can be made to satisfy the bulk of users who may be technicians working in industrial or testing laboratories. Offering the researcher access to all aspects of instrument control may involve providing an interface for a separate microcomputer to over-ride programs written into the microprocessor unit. That is costly.

One example of a medium- to high-priced instrument is the X-ray spectrometer developed by the Division of Science and Industry at Philips in Eindhoven, the Netherlands. A pre-programmed microprocessor unit controls the instrument and a standard interface is provided for outputting data to a stand alone computer. The user selects the control program by answering a series of questions that the instrument displays on a screen. Safeguards are included so that user cannot enter a potentially dangerous command. Once a program has been selected it can be stored for recall later, perhaps by a completely inexperienced operator.

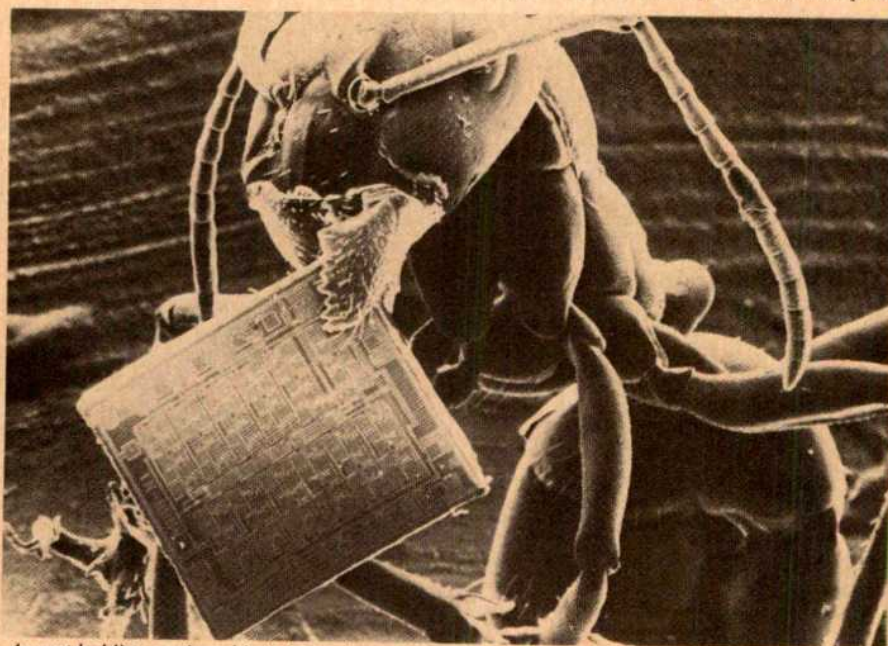
Until recently, Philips has always regarded its ultraviolet and atomic absorption spectrophotometers as falling into the cheaper category of instrument. Hence it has provided them with only a single microprocessor pre-programmed for instrument control and data analysis. Now, however, the scope of the instruments can be extended by adding a programmable calculator and automatic sample changer.

Investment in software

Before the advent of the cheap microprocessor, an instrument manufacturers' investment in developing automated systems would have been mainly on hardware. Now, it is not surprising that most effort goes into software development. The instruments that have perhaps been most successfully automated are those concerned with analytical chemistry. A large market for analytical equipment that is cheap and easy to operate exists not only in routine testing laboratories but also in research. Chromatography, mass spectrometry and liquid scintillation, for example, have many uses.

A look at the development of liquid scintillation counters by Philips illustrates how microprocessor development has influenced the way in which the company regards future instrument development. Not so many years ago, the instrument's computer control system was a series of boxes piled on top of each other, the system taking more space than the liquid scintillation counter itself. Now the microcomputer unit is housed in a small box under the instrument.

Although the basic instrument has changed little in outward appearance, the miniaturization of the control system has meant that more features can be programmed into it. Today's instrument contains a pre-programmed unit containing 16 programs corresponding to the most commonly used isotope labels in



An ant holding a microchip (photomicrograph courtesy Philips)

samples. The user can load several trays, each containing ten samples, into the instrument. Each tray carries instructions on the program by which its samples are to be analysed. The instrument can be connected to a microcomputer for data analysis if desired. Philips envisages further development in this range of instruments occurring when a new generation of microprocessor chips is available. The instrument will probably look much the same but more microprocessor power should make it faster or give it extended capabilities.

Mechanical limitations

But more advanced automation does not depend simply on the advent of the 16 bit or even 64 bit microprocessor. For some applications, advances in mechanical engineering seem to be lacking behind computer control. High performance liquid chromatography, for example, has reached the stage where further improvement will only be made if mass spectrometers can be used as detectors. And that involves using microbore columns with very slow flow rates. The development of microbore columns, which must be packed with suitable phases, now limits further improvements in the sensitivity of HPLC.

The bane of many laboratories especially those involved in routine testing, is the preparation of large numbers of samples. Unfortunately, however, few instrument manufacturers have either had the expertise or considered it economically worthwhile to develop automatic sample preparation. Hence, for example, the user of Philips liquid scintillation counter may be able to load up the machine to analyse several hundred samples in one batch but someone probably still has to put each sample into its bottle in the first place. Sample preparation could ultimately be the automation log-jam.

Judy Redfearn

When to go it alone

THE laboratory microcomputer and the automation of laboratory instruments have, in general, been welcomed by potential users — although some will always prefer to exercise their hard-won skills in setting up difficult experiments by manually adjusting knobs, carefully measuring angles and the like. The general enthusiasm for automation, however, does not always extend to the equipment on offer. The more a laboratory or organization is involved in fundamental research, the less likely it seems to be satisfied with the automated laboratory instruments that can be bought off the shelf. Such organizations are likely to devote considerable resources to custom-built instruments and computer systems.

Instrument manufacturers, not surprisingly, have developed equipment that will do the job of the majority of users as cheaply as possible. Thus, much analytical equipment is geared, for example, towards the needs of the testing laboratory in industry or medicine. Researchers may find that the commercially-available equipment of the type they are looking for does not have the flexibility of operation they desire. Only in the case of the most costly instruments may it be in the manufacturer's commercial interest to devote resources to altering the instrument to meet the customer's specific needs. In the majority of cases the task, then, is up to the research customer.

Assessing the economics of do-it-yourself automation is complex and, it seems, not often undertaken. Off-the-shelf equipment is undoubtedly much cheaper than custom-built. But to what extent should a laboratory strive to make do with off-the-shelf at the risk of compromising a

piece of research? Some university departments seem to think never — instrument development is often seen as an integral part of a piece of research and as much is said in grant applications. Industrial research laboratories, with their more mission-oriented approach to research, however, may be more willing to use what equipment is available and to try to adapt it if necessary.

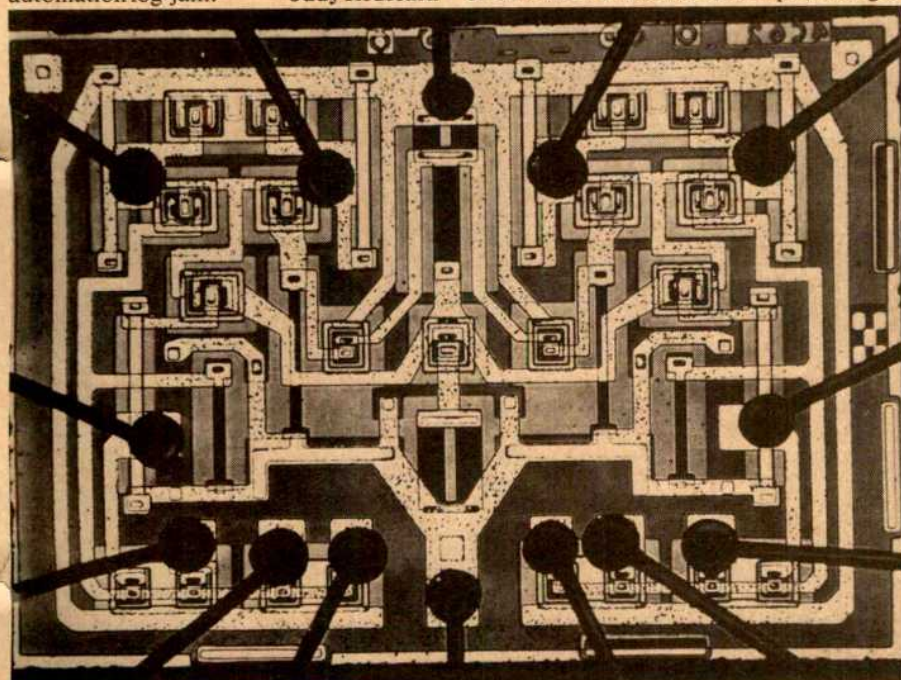
The problem is that the relatively cheap ranges of instrument, those that are most commonly used, often contain pre-programmed read only memories that cannot be re-programmed. The ideal, according to Dr Nick Goddard from the chemistry department at Imperial College in the University of London, would be for manufacturers to incorporate an interface into their instruments allowing users to feed their own programs into the built-in microprocessor. As that rarely happens with cheap instruments, users resort to building their own using standard subsystems and modules wherever possible. Occasionally, a research team may embark on designing a microprocessor system from scratch (see p.406), but generally it makes far more sense to control a custom-designed instrument using a standard microcomputer.

Custom-building

Two examples of custom-built automated instruments at the Imperial College chemistry department illustrate very different reasons for designing instruments. In one, the team is trying to devise a relatively cheap method of measuring very small concentrations of copper in solution by relying on the fact that copper will plate out on an electrode. The electroconductivity equipment used is controlled by a program written for a Research Machines microcomputer. Various programs for data analysis have also been written. The idea is to measure small concentrations of heavy metals as accurately as and more cheaply than spectroscopy.

The other development is driven by the need to measure transient effects in an electrode, which no commercially-available spectrometer can apparently do at present. The team is combining electrochemistry and spectroscopy in a technique to record a spectrum in a matter of microseconds.

An industrial research laboratory's problems with automation may be very different from those of a university, chiefly because research is mission-oriented and often on a large scale. Sample preparation and handling, for example, can be limiting. The Wellcome Research Laboratories at Beckenham in Kent, part of the Wellcome Foundation, have tackled custom-designed automation by establishing a



Photomicrograph of a double-gate silicon integrated circuit

special automation department of 50 or so people, nominally linked to the physical chemistry laboratory, but now acting as consultants to other laboratories on the Wellcome site. Eleven of the team are specialists in electronics or mechanical engineering, the rest being physical chemists.

Among the systems developed by the team and now operating is a method of controlling and measuring fluorescence polarization spectra, using an Apple microcomputer interfaced to the fluorescence instrument and a DEC PDP 11 34 minicomputer. The system basically speeds up the analysis of fluorescence polarization data. The Apple microcomputer logs data and controls the basic functions of the instrument. Data can be analysed slowly on the Apple or more rapidly on the PDP 11 34.

In another development, the team claims to have completely automated a Fourier transform nuclear magnetic resonance spectrometer made by Bruker. The mechanical engineering division devised an automatic sample changer made from non-ferromagnetic material and the electronics division wrote programs to control the sample changer and certain of the spectrometer functions with an Apple. Final data are analysed with software written for a PDP-11/15. The chief advantage of the modification is that an otherwise standard Bruker instrument now operates untended outside working hours.

Not all the Wellcome group's automation projects, however, have involved the application of computers or microprocessors in novel ways to established instruments. The skills of the mechanical engineering department have in some cases been sufficient to automate a process fully usually by automating sample handling or preparation. One notable example, still under development, is an automatic technique for preparing a sample for infrared spectroscopy. The key to the technique involves grinding the sample in a small pot with a vane that works like a reverse Archimedean screw and then automatically compressing it into a thin flat disk.

The automation group, according to Dr A. Everett, head of the department of physical chemistry, has had such success with some of its projects that instrument manufacturers, not often keen to modify instruments for one particular customer's needs, have been keen to help. The laboratories' policy is to encourage manufacturers' assistance in developing a technique rapidly — manufacturers, of course, benefit from the improvements they can subsequently make to their instrument. Dr Everett is convinced that his laboratory has developed sufficient automated techniques to set up in the instrument business on its own. But the practical difficulties involved have persuaded Wellcome to concentrate instead on forming comfortable symbiotic relationships with existing instrument makers.

Judy Redfearn

Astronomy — by proxy

ONE of the perks that makes it worthwhile being an astronomer in the United Kingdom — the chance to visit Hawaii — may be harder to come by as a result of a new 7,000-mile computer link-up. On 6 September an astronomer sitting at a computer terminal at the Royal Observatory in Edinburgh used the UK Infrared Telescope at Mauna Kea in Hawaii to take an infrared photometric measurement and a spectrophotometric scan of the star HR 8824.

As well as saving on travel costs between Britain and Hawaii (the initial 3-hour test cost only £80), the new system will make the operation of the telescope much more flexible, with night-time observations in Hawaii being carried out during normal working hours in Edinburgh.

The route between Edinburgh and

Hawaii is complex and instructions take around 6 seconds to make the trip. Messages pass from the observatory's computer console via the Edinburgh Regional Computer Centre to the Science and Engineering Research Council's Rutherford Appleton Laboratory in Oxfordshire.

British Telecom then takes the signal to the International Packet Switching Service and via transatlantic satellite link to the American packet switching network Telenet. The message emerges from the Telenet network at Honolulu in Hawaii and then goes by telephone line to the Mauna Kea laboratory's remote control room at the foot of the mountains. Only then does the message travel the final 14,000 feet to the observatory in the clear seeing conditions on the mountain peak.



Telescope installations on Mauna Kea — the 150-inch UK Infrared Telescope is on the right

Microprocessors — what are they?

THE basic elements of a microprocessor system are fourfold: the central processor unit (CPU), the program control unit (PCU), the memory and the input/output devices (or 'peripherals').

The input/output devices usually encountered with mainframe and minicomputers are visual display units, keyboard writers and printer. All of these devices can be connected to microprocessors, but the advantage and cheapness of microprocessors for the experimenter are perhaps more significant with less sophisticated peripherals. For instance, the pressure of a gas, normally relayed electrically to a chart-recorder or some other analog device, can be fed directly via an analog-digital convertor

into the input of a microprocessor. A trivial task for the microprocessor might be to adjust the frequency of measurement according to the rate of change in pressure. The output of the microprocessor might be connected to a gas heater, so that the 'boundary condition' of the experiment could be altered depending on the results obtained.

This interactive system exemplifies the flexibility and usefulness of microprocessors: only a few chips are needed to handle such a system — memory chips and processor chips.

There are two principal types of memory chip: random access memories (RAMs) and read only memories (ROMs). The former are used for storage and recall of

data during the running of a program, while the latter are pre-programmed before incorporation into the microprocessor system. The ROMs are programmable in several ways. Mask programmable ROMs are programmed during construction by the manufacturer and, being economic only in large production runs, are unlikely to be of use to the individual experimenter seeking a tailor-made system.

The field-programmable and erasable-programmable ROMs (EPROMs) can be programmed by the user although usually this involves specially designed

Abbreviations

CPU	Central processor unit
PCU	Central control unit
RAM	Random access memory
ROM	Read only memory
EPROM	Erasable-programmable ROM

programming devices. Once programmed, however, the chip remains so, whether or not it is plugged into the system, until erased by a particular type of voltage pulse, or by shining ultraviolet light through a window above the integrated circuit in the case of some EPROMs. Of course, once the system is developed and working the microprocessor program is fixed, so that such time-consuming procedures are limited only to construction and development.

Computer games

RAMs incorporate a two-dimensional matrix of semiconductor on-off switches, each of which acts as a unit (1 or 0) of digital memory and each of which is accessible by combining their 'x' and 'y' coordinates into a digital word. As miniaturization proceeds so the size of matrix that can be incorporated into a single chip increases. This is one of the important battlegrounds of today's micro-computing manufacturers. [As the size of memory increases, so does the number of 'bits' (binary digits) required to access it. For instance, a 256 bit memory requires 8 bits to access its individual locations, that is, physically speaking, 8 wires connecting it to the central control processor ($256 = 2^8$).] Currently RAMs are available with memories of 16K (16,000 bits), 32K and 64K and the 246K RAM is just around the corner. The 1M RAM is on the horizon (Nippon Electric Company recently unveiled a 1M ROM). The CPU carries out the arithmetic instructions stored in the ROM, as coordinated by the PCU. Typical operations are ADD, SUBJECT, SHIFT (left and right), logical AND, OR etc. Such operations are not only essential for calculation but can be used with ingenuity, by manipulating or monitoring individual digits within binary numbers to produce very fast and efficient programming. As with much programming, the development of such lateral thinking is great fun and becomes an enjoyable means of procrastination.

The final component of the microprocessor system is the PCU. This undergoes a cycle of process that coordinates and instructs the other components in a sequence which is maintained by an internal clock. This 'cleaning house' activity is managed via several 'registers' inside the PCU. A typical cycle might be as follows:

- (1) A program control counter, whose current value defines the memory 'address' of the next program instruction within the appropriate memory (usually a ROM), feeds its number into the memory access register of the PCU.
- (2) The instruction at this address (which will be coded as a single binary number) is transferred from the memory into the 'instruction register' of the PCU.
- (3) The instruction register is read and appropriate semiconductor switches in the central processor unit are either

opened or closed.

- (4) The program control counter is incremented by 1.

The programming 'language' used with a microprocessor system can be a standard language (for example, FORTRAN) which is translated into the unique code of the microprocessor system via a compiler. The advantage is the relative ease and familiarity with the programming but the disadvantages are the necessity of a compiler and an inefficient (in terms of memory space and speed) use of the microprocessor. By using the direct code of the microprocessor on the other hand, the system will be more efficient but will be correspondingly more difficult to develop and 'de-bug'. Whichever route one takes, and whether or not one asks a consulting agency to do the job completely, will depend on experience, time and money available, and the complexity of the required system.

Philip Campbell

Microcomputers for all

NOT so long ago, researchers had very little option other than to communicate with a mainframe computer when they wanted to analyse data from their experiments. The experiments themselves could be controlled by computer, either by a mainframe or a minicomputer available for the use of, say, one laboratory — but only if someone was available with the necessary expertise to do the hard wiring and write the software. Now, however, cheap, powerful microcomputers are altering the balance of computing power in research organizations and universities.

Microcomputers have fallen so much in price in recent years that many researchers, even apparently in Britain's financially hard-pressed universities, can afford to buy one out of their research grants or general budgets. Groups of two or three researchers with their own shared microcomputer are commonplace and even the sole researcher with his or her own personal computer is not uncommon. Microcomputers may not be able to do everything a mainframe computer can — their reduced power, for example, means that they are far slower at detailed and lengthy calculations — but they do contain substantial computing power packaged in a very useful form. Microcomputers can be used, for example, far more easily than mainframe computers, to control laboratory experiments. They can also be converted to word processors simply by buying suitable software.

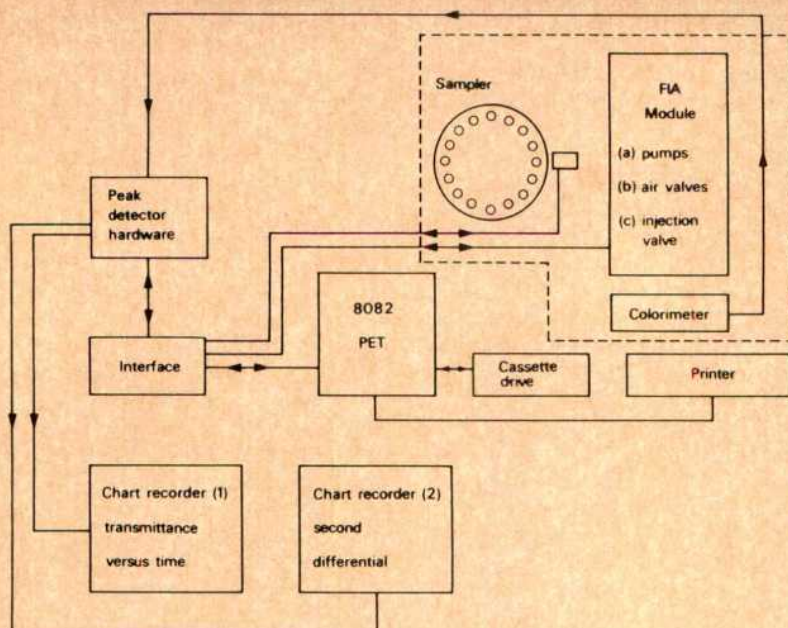
Proven software

The microcomputer's usefulness to laboratory scientists stems largely from the fact that they are proven systems for which a lot of software has been written, not only of the type needed, say, for word proces-

sing, but also for statistical analysis and even for control of experiments. Even if the specific software for a particular application is not available, writing it or adapting old software is not usually too much of a problem given that the popular ranges of microcomputer, at least, use standard and proven operating systems. Some researchers will always believe that nothing is available off the shelf that would do the job they want. They will probably design a microcomputer system from scratch, perhaps contributing to microprocessor development in the process. But for most researchers who have no special expertise in microprocessor design and whose aim is to spend as much time as possible on research in their particular discipline, adapting standard microcomputers to their singular needs is undoubtedly most cost effective.

The researcher with a microcomputer, however, may not necessarily find life plain sailing. He or she would normally rely on the services of a central computing unit to help with problems on the mainframe. Now, however, the computing power is entirely within the researcher's control and specialist computer staff may not be available to help with problems. The researcher needs to know at least the basics of computing and to understand the capabilities of his or her microcomputer.

Universities have started to run courses aimed at the researcher who would benefit from using a microcomputer but knows little about them. One such course, run by the chemistry department and computer centre at Imperial College in the University of London, has attracted support from the British Department of Industry which needed a means of training scientists in government laboratories, especially the



An example of a layout for microcomputer control of hardware

Laboratory of the Government Chemist, to make better use of microcomputers. The course, held twice a year, runs for one week and is open to anybody who can pay the £300 attendance fee. The industry department provided £60,000 to set the course up eighteen months ago under its Microcomputers Applications Programme (MAP). Most of the money was spent on setting up demonstration experiments and writing course software.

According to Edward James of Imperial College computer centre, the course has two aims: to help people who know nothing of microcomputers, even those who have difficulty understanding the manufacturer's unpacking instructions, and to make them realize the microcomputer's full capability. Another aim is to help researchers choose the right microcomputer system — the wrong system could cause chaos, says Mr James.

The course begins with an introduction to how a microcomputer stores and transfers information and how it executes programs. Participants learn how to program in BASIC. The capabilities and limitations of standard interfaces such as the IEEE-438, a favourite with manufacturers of scientific instruments, are discussed — and so too are the practicalities of converting analog signals to digital and vice versa. Participants are also introduced to programming languages other than BASIC, including machine codes.

Practical help

Nick Goddard from Imperial College's chemistry department designed a special non-standard interface for the course which allows the user to interface up to 16 of any combination of function boards into a microcomputer. He and other members of the chemistry department also devised a series of experiments showing

participants how microcomputers can be used in practice and inviting them to write their own simple programs.

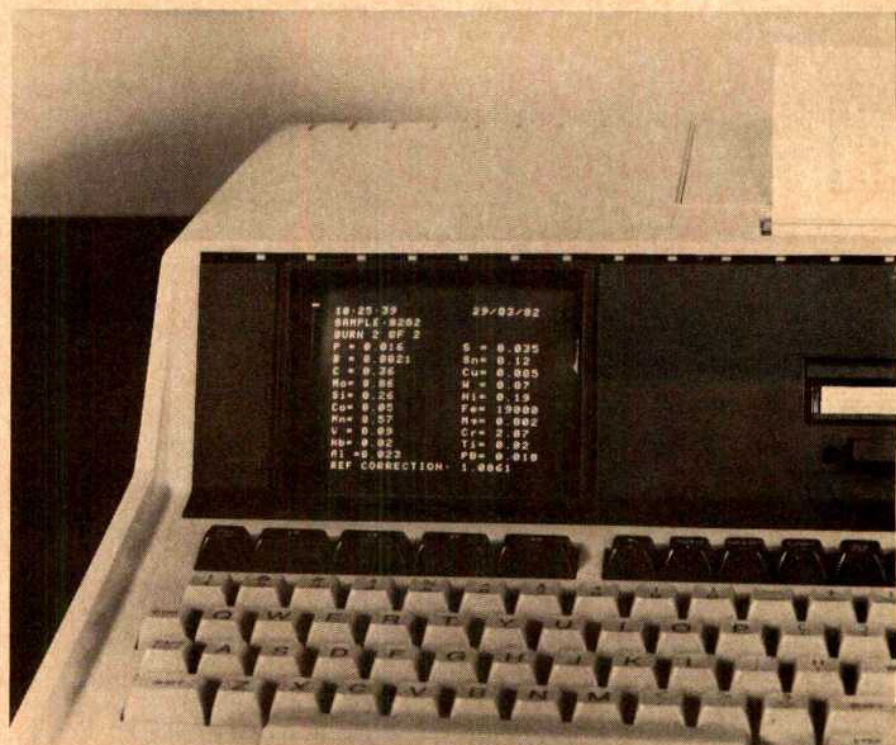
One experiment, for example, introduces course participants to computer controlled experiments by inviting them to perform acid-base titrations using standard alkali solutions delivered by a computer-controlled dispenser. Programs for calibrating the pH electrode, sampling and displaying its output at regular intervals and creating a user file containing pH results are provided. Participants are

invited to write their own programs for finding the end-points from the pH data and calculating the number of moles of acid in a sample.

The idea is that participants will return to their laboratories able to control simple experiments and analyse data with their own microcomputers. Those who do not have a "micro", but are contemplating buying one, will have a better idea of what type of system they need for their purposes and what limitations to expect. The course philosophy seems to be to recommend to those who have little computing experience systems that are well-proven with plenty of written software, even though the system capabilities may be less in theory than those of other systems. Microcomputers based on the new 16-bit processor, for example, would probably be recommended only for those who need the extra computing power and who have sufficient experience to write software from scratch. Others would be wiser to choose one of the standard 8-bit machines, for which plenty of software now exists.

One problem encountered by the Imperial College team is that of researchers who have bought instruments containing pre-programmed microprocessors only to find that the programs are not suitable for their purposes and that nothing can be done about re-programming. Another function of the course is to help researchers interface their own micros to computerized instruments where that is possible and where it is not, at least to make them aware of the pitfalls to be avoided when purchasing new equipment.

Judy Redfearn



A mission-oriented computer: A Hewlett-Packard HP-85 personal computer is incorporated in the Philips PV8020 emission spectrometer. The computer produces results in element concentrations on the built-in video screen as well as hard-copy printout.

ARTICLES

Proterozoic age and cumulate origin for granulite xenoliths, Lesotho

N. W. Rogers* & C. J. Hawkesworth

Department of Earth Sciences, Open University, Walton Hall, Milton Keynes MK7 6AA, UK

Rare earth element (REE), $^{143}\text{Nd}/^{144}\text{Nd}$ and $^{87}\text{Sr}/^{86}\text{Sr}$ analyses on a range of granulite xenoliths from kimberlite pipes in Lesotho demonstrate that useful whole rock ages can be obtained from such lower crustal material. The characteristic positive Eu-anomalies, relatively low REE abundances and large variation in Sr contents suggest that many of the xenoliths are crystal cumulates rather than residua after partial melting. They yield an Sm–Nd whole rock age of $1,400 \pm 100$ Myr and are unrelated to the younger magmatic rocks of the Karoo.

COMPARATIVELY little is known about the age and composition of the lower crust, particularly in apparently stable continental areas. The Cretaceous kimberlites of southern Africa contain a large range of crustal material included as xenoliths, and thus offer a unique opportunity to investigate the chemical and temporal variations within a relatively large segment of continental crust. Kimberlites occur both on the Archaean craton and in the surrounding Proterozoic mobile belts, but controversy exists over the nature of the belts and the position of their boundaries within the craton beneath the Karoo cover. Kröner¹ has argued that such mobile belts are formed by reworking of pre-existing crust, but Barton *et al.*² have recently demonstrated that in both Natal and East Namaqualand a considerable amount of new crustal material was generated in these late Proterozoic events (1,300–1,100 Myr). Similarly it has been postulated that diamondiferous kimberlites tend to occur above old, cold and thick lithosphere and should therefore be confined to the cratonic areas³, and that anhydrous granulites are only found around the edges of the craton⁴ (Fig. 1). Yet in Lesotho, diamonds and granulite xenoliths are typically found in the same kimberlite pipes.

We report $^{143}\text{Nd}/^{144}\text{Nd}$, $^{87}\text{Sr}/^{86}\text{Sr}$, and trace element abundances on a suite of granulite xenoliths from Lesotho in an attempt to determine (1) whether these meta-igneous rocks represent 'liquid' compositions, cumulates or residua after partial melting; (2) the age of the lower crust in this area, and (3) any relationship with the widespread magmatic rocks of the Karoo.

The Lesotho granulite xenolith suite has been extensively analysed for both whole rock major element and mineral compositions^{4–6}. The mineralogy is predominantly clinopyroxene, garnet and plagioclase, although orthopyroxene and amphibole do occur in some samples, and accessory minerals include mica, rutile, scapolite and occasional apatite. Application of standard geothermometers and geobarometers to minerals in the samples analysed here gives temperatures and pressures in the range 500–700 °C and 5–13 kbar (ref. 4); although pressures of 15–20 kbar were also inferred from similar Lesotho granulite xenoliths by Jackson and Harte⁶, who suggested that some may therefore have been derived from depths below that of the present day Moho (~37 km)⁷. Major element analyses of most xenoliths listed in Tables 1 and 2 are similar to transitional olivine basalt with minor nepheline or hypersthene in the norm: the exception is LT 2 which is a more leukocratic granulite of intermediate composition, with significant modal and normative quartz⁴. From a consideration of the densities of the xenoliths and crustal seismic velocities beneath southern Africa, Griffin *et al.*⁴ suggested that the Lesotho lower crust comprises 50–70% basic garnet granulite and 50–30% intermediate granulite.

Trace element analyses of the xenoliths were undertaken by Griffin *et al.*⁴, and the REE abundances of five samples were reported previously⁵. In both cases it was shown that the trace elements are much more variable than the major elements, and that this variation was not caused by contamination from the trace element enriched host kimberlite. Although the granulite xenoliths were interpreted as a coherent suite of meta-igneous rocks it remained unclear whether the geochemical variations were due primarily to partial melting or fractional crystallization. In addition, the more immobile trace elements offered no unambiguous indication of the petrogenetic affinities of the xenoliths; for example, on a Ti–Zr–P discriminant diagram three of the xenoliths plot as alkali basalts, 10 as tholeiites, and the remainder fall outside any defined field⁴.

Rare earth elements

The results of the REE analyses are listed in Table 1 and illustrated in Fig. 2. The basic granulites appear to fall into two groups on the basis of their total REE abundance. Those in one group have Sm contents of 25–35 × chondrite and no significant Eu anomalies, whereas the remainder have much lower REE contents (Sm = 3–11 × chondrite) and typically exhibit marked positive Eu anomalies. Both groups include LREE enriched and LREE depleted samples. Interestingly, however, three rocks in the second group combine low middle REE concentrations with a slightly curious enrichment in the

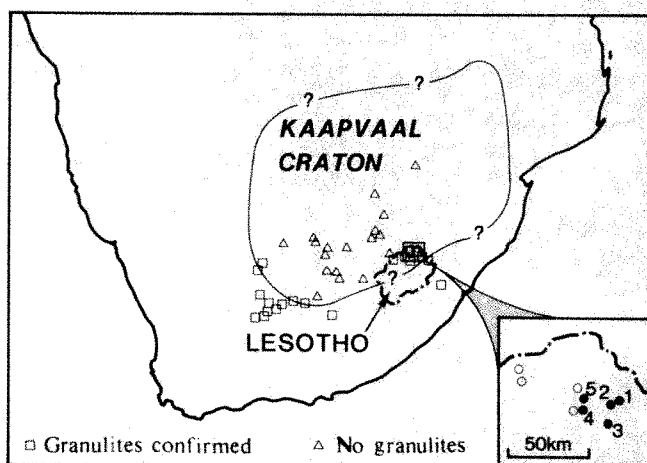


Fig. 1 Distribution of granulite xenoliths in kimberlite pipes in relation to the boundary of the Kaapvaal Craton (after ref. 4). Inset shows the xenolith localities in North Lesotho; 1, Letseng-la-Terae; 2, Mothae; 3, Matsoku; 4, Pipe 200; 5, Liqhobong.

* Present address: Goldsmith's College, Creek Road, London SE8 3BU, UK.

light rare earths (samples L 13, PHN 2533 and PHN 1670, Fig. 2) and at least two of them are believed on isotopic grounds to have been affected by interaction with the host kimberlite (see Fig. 4, and discussion). Thus the LREE enrichment in such samples may be due to contamination en route to the surface. The felsic granulite LT 2 is again different from the other samples in that it possesses a more fractionated REE pattern (higher La/Yb ratio), and a slight positive Eu anomaly similar to many felsic granulites from regional metamorphic terrains⁸.

Previous discussions have accepted that the granulites are of igneous origin^{4,5}, and while those with the higher REE contents and no Eu anomalies may represent near-liquid compositions, the others are likely to be either residua after partial melting or cumulates. The characteristic positive Eu anomalies indicate that plagioclase was an important residual mineral, and the variation in the abundance of heavy REE with relatively little change in Sm/Yb suggests that garnet was not. Moreover, analyses of separated minerals have shown that in xenoliths with the distinctive positive Eu anomalies, all the constituent minerals (garnet and clinopyroxene, as well as plagioclase) display similar anomalies⁹. This emphasizes the metamorphic nature of the present mineral assemblage, implies that the REE patterns were established before granulite-facies metamorphism, and suggests that petrogenetic models should be based on an inferred low pressure (garnet-free, plagioclase-rich) igneous mineralogy. As the low pressure mineralogy of basic rocks is often comparable with their CIPW norms, the following models use normative, and not modal, assemblages.

Various models have been proposed in which the lower crust is residual after large-scale anatexis, and the melt contributes to the more siliceous upper crust^{10,11}. In these models, the lower crust is rich in residual plagioclase and so acquires a positive europium anomaly to balance the negative anomaly characteristic of upper crustal rocks¹⁰. However, such a model does not readily explain the composition of the Lesotho basic granulites. First, they exhibit a relatively restricted range of SiO₂ (42–51%) and those with the higher values tend to have lower REE contents. This is the opposite of what might be expected during intracrustal partial melting when a reduction in SiO₂ is likely to be accompanied by lower total REE contents. Second, during partial melting plagioclase tends to melt more rapidly than any co-existing mafic minerals, and yet the low REE granulites which exhibit the distinctive positive Eu anomalies contain 40–60% normative plagioclase, together with 15–17% olivine and 9–34% clinopyroxene. This compares with <45% normative plagioclase in more REE enriched basic granulites. Finally, the relative variations in compatible and incompatible trace elements (Table 1, and refs 4, 5) appear contrary to that predicted for residua after partial melting. Frey and Prinz¹² have argued that compatible trace elements in such residua will have a limited range in concentration, whereas the abundance of incompatible elements may be highly variable. Their model was based on the extraction of basic melts from the mantle but the principles of their approach can be applied to partial melting within the crust. In this case pyroxene and plagioclase feldspar would be the major residual phases so that Sr would have been compatible and Rb and Nd incompatible. Their concentrations in the residual xenoliths vary by factors of 18, 6 and 6 respectively (Table 2). This is the opposite of that expected in residua

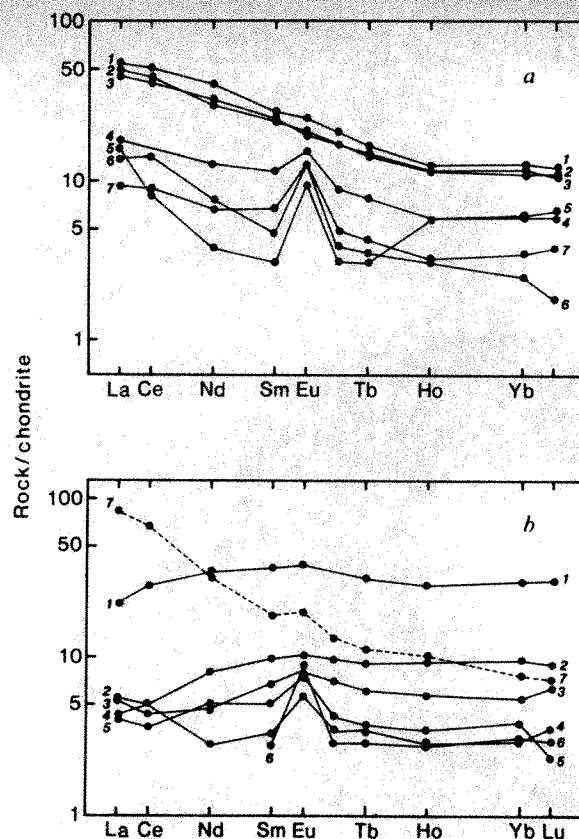


Fig. 2 Chondrite normalized REE abundances for the Lesotho granulite xenoliths. Normalizing values from ref. 24. REE determined by INAA²⁵. a: 1, MAT 12; 2, L 20; 3, PHN 1646; 4, PHN 1919; 5, PHN 2533; 6, PHN 1670; 7, PHN 2852. b: 1, LQ 4; 2, L 12b; 3, L 12a; 4, L 13; 5, OVK F 10303; 6, PHN 2855; 7, LT 2 (felsic granulite).

after partial melting, but it is consistent with a cumulate origin¹² which we shall now consider in more detail.

Trace element abundances of cumulates were calculated using the normative mineralogy of the residual basic xenoliths and assuming that the minerals had crystallized from particular magmas. It is clearly extremely difficult to obtain a realistic value for the amount of intercumulus liquid, so it was decided simply to re-calculate the norms of the xenoliths in terms of plagioclase, olivine and clinopyroxene, and recast all other normative components as trapped liquid and assign them a K_D value of 1. By treating the model in this way, the amount of intercumulus liquid is bound to be underestimated as it will contain some of the normative pyroxene and plagioclase components. Bulk distribution coefficients for these normative assemblages were calculated from published K_D values (REE^{13,14}, TiO₂ and Zr (ref. 15), Sr (ref. 14) and the trace element abundances of the hypothetical cumulates were estimated assuming that the crystals had been in equilibrium with liquids which were either LREE enriched or slightly LREE depleted (for example, L 20 and LQ 4, Fig. 3). Such calculations produce trace element patterns similar to, but slightly lower

Table 1 Rare earth element analyses of granulite xenoliths

	MAT 12	L 20	PHN 1646	PHN 1919	PHN 2533	PHN 1670	PHN 2852	LQ 4	L 12b	L 12a	L 13	F 10303	PHN 2588	LT 2
La	17.8	16.1	14.9	5.74	5.25	4.53	3.07	7.27	1.84	1.76	1.33	1.39	—	27.3
Ce	44.6	38.3	35.2	13.8	7.19	12.4	7.74	24.6	4.32	3.84	3.13	4.29	—	58.4
Nd	25.2	18.9	20.0	8.1	2.33	4.88	4.25	21.5	5.07	2.97	3.15	1.74	—	21.2
Sm	5.46	4.78	4.95	2.30	0.63	0.97	1.39	7.42	1.99	1.38	1.04	0.68	0.58	3.71
Eu	1.93	1.57	1.52	1.20	0.72	0.96	0.97	2.96	0.79	0.65	0.58	0.44	0.64	1.48
Tb	0.88	0.75	0.77	0.40	0.16	0.18	0.22	1.63	0.48	0.33	0.20	0.18	0.15	0.59
Ho	1.00	0.90	0.88	0.45	0.46	—	0.25	2.23	0.73	0.45	0.27	0.22	0.22	0.80
Yb	2.87	2.62	2.49	1.30	1.32	0.56	0.77	6.61	2.11	1.21	0.87	0.67	0.68	1.72
Lu	0.41	0.36	0.37	0.20	0.22	0.06	0.13	1.04	0.31	0.22	0.08	0.12	0.10	0.25

Table 2 Nd- and Sr-isotope results

Sample*	Pipe†	SiO ₂ ‡	Rb‡	Sr‡	⁸⁷ Sr/ ⁸⁶ Sr§	Sm	Nd	¹⁴⁷ Sm/ ¹⁴⁴ Nd	¹⁴³ Nd/ ¹⁴⁴ Nd¶
MAT 12	M	42.9	5	268	0.70408 ± 4	4.73	20.68	0.138	0.512092 ± 14
LQ 4	Li	44.0	21	283	0.70423 ± 5	8.11	27.72	0.177	0.512464 ± 16
PHN 1919	Mo	45.2	14	195	0.70483 ± 3	1.96	7.86	0.151	0.512281 ± 20
PHN 1646	M	45.6	25	1050	0.70396 ± 4	4.30	18.12	0.143	0.512101 ± 14
PHN 2495	Li	47.0	1	163	0.70590 ± 4	7.56	33.60	0.136	0.512265 ± 12
PHN 2852	M	47.1	12	860	0.70412 ± 3	1.30	5.65	0.139	0.512322 ± 16
PHN 1670	M	49.2	30	3556	0.70372 ± 3	0.97	4.94	0.118	0.512307 ± 12
F 10303	M	49.3	8	1250	0.70365 ± 4	0.59	2.23	0.160	0.512570 ± 14
L 12A	M	49.5	11	812	0.70359 ± 3	1.17	3.18	0.223	0.512951 ± 22
L 12B	M	49.7	5	698	0.70376 ± 3	1.52	4.46	0.206	0.512819 ± 10
L 13	M	49.9	10	882	0.70374 ± 4	0.88	2.72	0.196	0.512696 ± 26
M1	M	50.4	13	1081	0.70373 ± 4	1.18	5.12	0.139	0.512232 ± 14
PHN 2533	P	50.4	31	700	0.70373 ± 3	0.59	2.76	0.129	0.512472 ± 18
PHN 2588	Li	51.2	23	625	0.70507 ± 4	0.52	1.30	0.242	0.513019 ± 24
LT 2	L	59.9	3	294	0.70700 ± 4	3.42	20.50	0.101	0.511764 ± 14

* All basic granulites, except PHN 2495 (pyroxenite) and LT 2 (felsic granulite).

† Kimberlite pipes: L, Letseng; Li, Lihobong; M, Matsoku; Mo, Mothae; P, Pipe 200.

‡ Analyses from refs 4 and 5, except MAT 12 which is a new analysis.

§ NBS987 = 0.71015 ± 2. || Isotope dilution, ± 0.5%. ¶ Normalized to ¹⁴⁶Nd/¹⁴⁴Nd = 0.7219, BCR-1 = 0.51262 ± 2.

than, those observed in the low REE granulites (Fig. 3). Moreover, it is very striking that in both the analysed and calculated patterns those with lower REE abundances tend to have larger positive Eu anomalies. The relatively low concentrations in the calculated patterns are probably due to the fact that our model tends to underestimate the amount of intercumulus liquid. Because the latter is enriched in incompatible elements, any underestimate of the amount of trapped liquid will also cause the calculated incompatible element contents of the cumulates to be too low. Such models can only be expected to provide minimum values for the concentrations of incompatible elements in cumulates. Thus the similarities between the observed and calculated trace element patterns, and even the slightly low abundances of the latter, are considered to be strong evidence for a cumulate origin for the igneous protoliths of the basic garnet granulite xenoliths.

Nd and Sr isotopes

Nd and Sr were separated using standard two- and one-column ion exchange techniques, and analysed as metal species on triple and single filament assemblies in a VG 54E mass spectrometer with on-line computer control. Chemical blanks are better than 0.5 ng for Nd and 3 ng for Sr, and the means of repeated analyses of BCR-1 ¹⁴³Nd/¹⁴⁴Nd = 0.51262 ± 2, and NBS 987 = 0.71015 ± 2. The measured ⁸⁷Sr/⁸⁶Sr ratios of the basic granulites are low, 0.7036–0.7051 (Table 2), with all but two being < 0.7043. This is consistent with their low Rb/Sr ratios (9 of the 13 analysed are < 0.024) but no clear isochron relationship was observed, and two have Rb/Sr ratios which are too high to have been responsible for their low ⁸⁷Sr/⁸⁶Sr in the period of time indicated by the Sm–Nd system. The pyroxenite and felsic granulite have significantly higher ⁸⁷Sr/⁸⁶Sr ratios of 0.7059 and 0.7070, but their Rb/Sr ratios are low (0.006 and 0.01 respectively), suggesting that they too had a more complex multi-stage history.

In contrast the Sm–Nd system is much more informative. The measured ¹⁴³Nd/¹⁴⁴Nd ratios vary from 0.51176 to 0.51302, and 10 of the granulites analysed scatter about an errorchron corresponding to an age of 1,400 ± 100 Myr (MSWD = 28), with an initial Nd ratio slightly higher than that of the Earth, or CHUR (ref. 16), at that time (Fig. 4). The four remaining granulites plot above the errorchron, and because they have the lowest Nd contents of those samples whose ¹⁴³Nd/¹⁴⁴Nd ratios were less than those of typical kimberlites at the time of emplacement¹⁷, the observed scatter probably reflects contamination en route to the surface. The age of 1,400 Myr compares with the model Sr age of 1,300 Myr obtained from the average composition of the seven basic granulites with > 800 p.p.m. Sr (Table 2), and represents the

best estimate for the maximum age of the lower crust in Lesotho. Mineral results from similar material include ages of 1,500 and 1,050 Myr from U–Pb on zircons¹⁸, and 1,000 and 714 Myr K/Ar on a mica and hornblende respectively¹⁹; and they encouraged Harte *et al.*¹⁹ to reconsider the possibility that the observed mineral assemblages reflect metamorphic conditions which were present in the late Proterozoic.

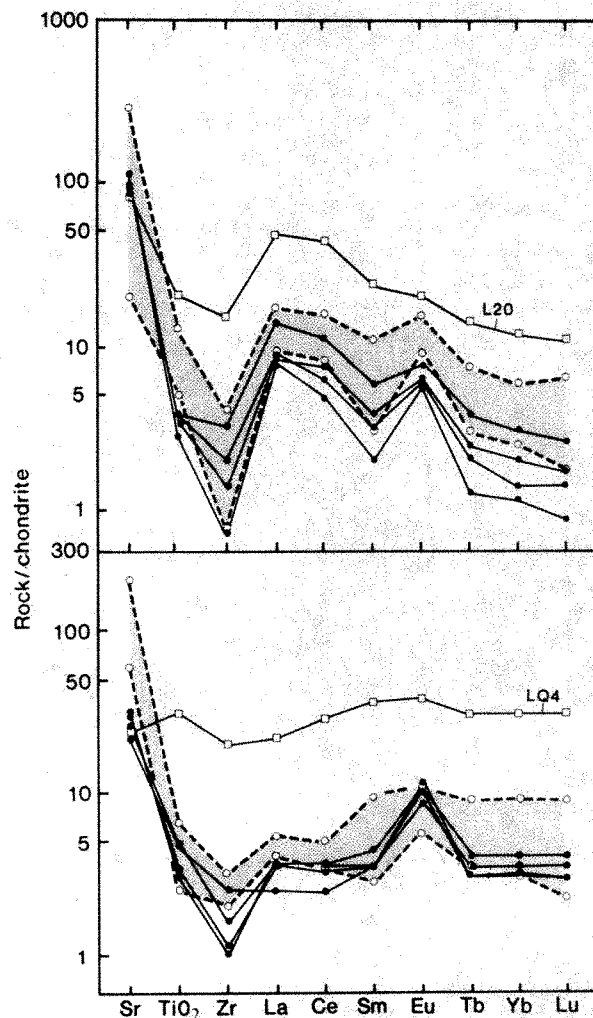


Fig. 3 Comparison of model cumulates (●), based on normative mineralogies, with the xenolith analyses (○). REE normalization values as in Fig. 2, Sr = 11.8 p.p.m., Ti = 620 p.p.m. and Zr = 6.84 p.p.m. □, Liquid compositions used in model.

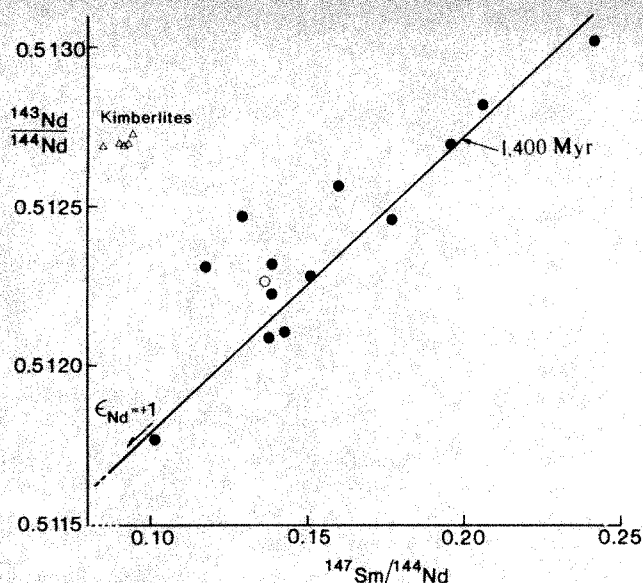


Fig. 4 Sm-Nd isochron diagram illustrating the data on Lesotho granulite xenoliths and representative kimberlites¹⁷ (Δ), \circ , Pyroxenite PHN 2495.

Discussion

The results presented here suggest that the basic lower crustal xenoliths from Lesotho represent metamorphosed basalts and cumulates which were derived from the upper mantle $\sim 1,400$ Myr ago. This Upper Proterozoic age is consistent with the suggestion that granulite xenoliths of this type are characteristic of kimberlite pipes around the edge of the Archaean craton⁴ (Fig. 1), and it would appear in conflict with the idea that diamondiferous kimberlites are unlikely to occur in the Proterozoic mobile belts. However, it has been argued that many of the upper crustal gneisses and metasediments in the Lesotho kimberlites are lithologically similar to those exposed in Archaean terrains²⁰, and it may be that Archaean upper crustal rocks overlie a Proterozoic lower crust in this area.

Cox²¹ has recently argued that most continental flood basalts are probably derived by fractional crystallization from more

picritic parental magmas, and that consequently significant volumes of cumulates may occur within the lower continental crust. One of the best examples of such a volcanic province is the Karoo of southern Africa, and as the Lesotho basic granulites are found in kimberlites which intrude but are some 100 Myr younger than the local Karoo volcanics, they were likely candidates for such cumulate material. Moreover, combined Nd- and Sr-isotope work on a variety of Karoo volcanic rocks indicates that many were derived from upper mantle source regions which had been enriched in incompatible elements for almost 1,000 Myr before their eruption at 190 Myr (ref. 22). Hence it might be argued that the granulite Sm/Nd whole rock results (Fig. 4) represent some form of erupted, or source isochron, rather than the time of their separation from the upper mantle. A test of this hypothesis is provided by a plot of ϵ_{Nd} against ϵ_{Sr} in which the initial $^{143}Nd/^{144}Nd$ and $^{87}Sr/^{86}Sr$ ratios of Karoo volcanics are compared with the Nd- and Sr-isotope ratios of the basic granulites at the time of Karoo volcanism, 190 Myr (Fig. 5).

In Fig. 5 a few Karoo volcanic rocks plot on the mantle array, but most fall in the bottom right-hand quadrant which is where rocks (or source regions) with higher Rb/Sr and lower Sm/Nd than the 'bulk Earth' evolve with time. (Note also that 25 of the analysed Karoo rocks have initial ϵ_{Sr} greater than +45 and so plot to the right of Fig. 5.) The basic granulites by contrast have a relatively restricted range in ϵ_{Sr} and a large variation of ϵ_{Nd} , and so plot in a near vertical trend down into the bottom left quadrant. None of the basic garnet granulites analysed fall with most of the Karoo volcanics in the bottom right quadrant, strongly suggesting that these two rock suites are not genetically related. The two xenoliths which do plot in the bottom right quadrant are the felsic granulite LT 2 (an improbable cumulate), and the pyroxenite PHN 2495 which, on the basis of the arguments presented here, is the one xenolith which might be a cumulate of Karoo age.

Accepting that the Sm/Nd whole rock age (Fig. 4) reflects the time of crystallization of the granulite protoliths then they presumably represent a magmatic episode early in the evolution of the Natal mobile belt. Sr-isotope studies on granites and gneisses within the belt yield ages of 1,000–1,300 Myr and low initial $^{87}Sr/^{86}Sr$ ratios suggesting that any crustal precursors were $<1,500$ Myr old². If crustal reworking took place it seems

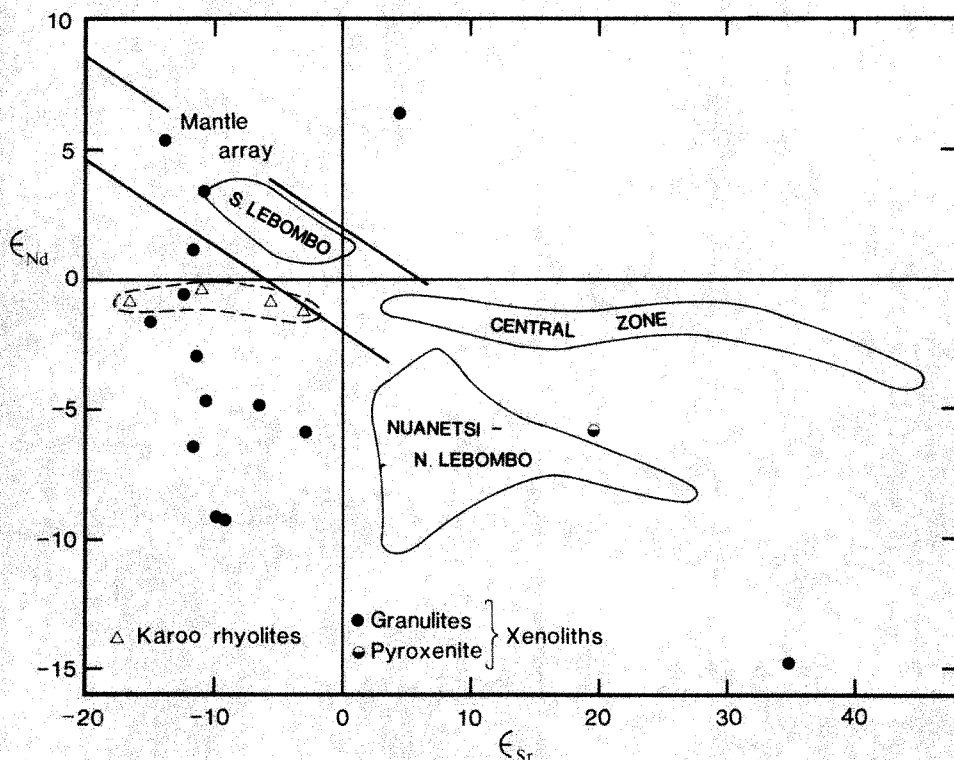


Fig. 5 $\epsilon_{Nd}/\epsilon_{Sr}$ for the Lesotho granulite xenoliths and Karoo volcanic rocks²² at 190 Myr.

only to have involved comparatively young material, there is as yet no indication from either lower crustal xenoliths or surface exposures that significant quantities of Archaean crust were remobilized in this area. However, the recognition that considerable volumes of new continental crust was generated in the period 1,400–1,000 Myr (ref. 2 and this work) raises the intriguing question of whether there is a relationship between that event and the fact that the isotopic variation observed in both Karoo lavas²² and diopsides in garnet peridotites from the Kimberley area²³ reflect chemical variations which may have persisted for ~1,000 Myr. The formation of a belt of new, and probably thicker continental crust around an old cratonic nucleus clearly increases the area of stable continental crust (Fig. 1), and that in turn should increase the volume, and perhaps even the thickness, of mantle material incorporated in

this segment of continental lithosphere. Thus it is envisaged that the formation of the Natal–Namaqua belt may have ultimately stabilized a 'late Proterozoic' lithosphere beneath this area of southern Africa, which was to be sampled some 1,000 Myr later by Karoo magmatism and the xenoliths in kimberlite pipes.

Samples were provided by P. H. Nixon, W. L. Griffin, D. A. Carswell and P. Suddaby. N. W. R. acknowledges the tenure of a NERC Research Fellowship and A. R. Gledhill and P. W. van Calsteren are thanked for their assistance in the isotope laboratories at the Open University. Drs K. G. Cox, and B. Harte critically appraised the manuscript. The REE analyses were carried out at the University of London Reactor Centre. John Taylor prepared the diagrams, and Janet Dryden typed the manuscript.

Received 29 April, accepted 2 August 1982

- 1 Kroner, A. *Tectonophysics* **40**, 101–135 (1977)
- 2 Barton, E. S., Harmer, R. E. & Burger, A. J. *Geotectonics 81 Abstr. geol. Soc. S. Afr.* 12–13 (1981)
- 3 Gurney, J. J. & Harte, B. *Phil. Trans. R. Soc. A* **297**, 273–293 (1980)
- 4 Griffin, W. L., Carswell, D. A. & Nixon, P. H. in *The Mantle Sample: Inclusions from Kimberlites and other Volcanics* (eds Boyd, F. R. & Meyer, H. O. A.) 59–86 (American Geophysical Union, Washington DC, 1979)
- 5 Rogers, N. W. *Nature* **270**, 681–684 (1977)
- 6 Jackson, P. M. & Harte, B. *2nd int. Kimberlite Conf. Extended Abstr.* (1977)
- 7 Hales, A. L. & Sacks, I. S. *Geophys. J. R. Astr. Soc.* **2**, 15–33 (1959)
- 8 Weaver, B. & Tarney, J. *Earth planet. Sci. Lett.* **55**, 171–180 (1981)
- 9 Rogers, N. W. thesis, Univ. London (1980)
- 10 Jakes, P. & Taylor, S. R. *Geochim. cosmochim. Acta* **38**, 739–745 (1974)
- 11 Fyfe, W. S. *Geol. J. Spec. Iss.* **2**, 201–216 (1970)

- 12 Frey, F. A. & Prinz, M. *Earth planet. Sci. Lett.* **38**, 129–176 (1978)
- 13 Arth, J. G. & Henson, G. N. *Geochim. cosmochim. Acta* **39**, 325–362 (1975)
- 14 Hanson, G. N. *A. Rev. Earth planet. Sci.* **8**, 371–406 (1980)
- 15 Pearce, J. A. & Norry, M. J. *Contr. Miner. Petrol.* **69**, 33–47 (1979)
- 16 DePaolo, D. J. & Wasserburg, G. J. *Geophys. Res. Lett.* **3**, 249–252 (1976)
- 17 Kramers, J. D., Smith, C. B., Lock, N. P., Harmon, R. S. & Boyd, F. R. *Nature* **291**, 53–56 (1981)
- 18 Davis, G. L. *2nd int. Kimberlite Conf. Extended Abstr.* (1977)
- 19 Harte, B., Jackson, P. M. & Macintyre, R. M. *Nature* **291**, 147–148 (1981)
- 20 Nixon, P. H. & Gray, A. *19th A. Rep. Res. Inst. Afr. Geol., Univ. Leeds* 42–44 (1975)
- 21 Cox, K. G. *J. Petrol.* **21**, 629–650 (1980)
- 22 Hawkesworth, C. J., Marsh, J. S., Norry, M. J. & Duncan, A. R. *Geotectonics, '81 Abstr. geol. Soc. S. Afr.* 105–106 (1981)
- 23 Menzies, M. & Rama Murthy, V. *Nature* **283**, 634–636 (1980)
- 24 Nakamura, N. *Geochim. cosmochim. Acta* **38**, 757–775 (1974)
- 25 Borley, G. D. & Rogers, N. W. *Geostandards Newslett.* **3**, 89–92 (1979)

Serotonin and cyclic AMP close single K⁺ channels in *Aplysia* sensory neurones

Steven A. Siegelbaum, Joseph S. Camardo & Eric R. Kandel

Center for Neurobiology and Behavior, Departments of Pharmacology and Physiology, Columbia University, College of Physicians and Surgeons, and The New York State Psychiatric Institute, New York, New York 10032, USA

We have identified a serotonin-sensitive K⁺ channel with novel properties. The channel is active at the resting potential, its gating is moderately affected by membrane potential and is not dependent on the activity of intracellular calcium ions. Application of serotonin to the cell body or intracellular injection of cyclic AMP causes prolonged and complete closure of the channel, thereby reducing the effective number of active channels in the membrane. The closure of the channel can account for the increases in the duration of the action potential, Ca²⁺ influx, and transmitter release which underlie behavioural sensitization, a simple form of learning.

SINGLE-CHANNEL current recordings¹ have been used to analyse the properties of ion channels that are directly gated by voltage^{2–5}, intracellular Ca²⁺ (refs 6–9) and chemical transmitters^{10–12}. Previous analyses of synaptic transmission, for example those of the acetylcholine-activated channels at the neuromuscular junction¹³, have focused on synaptic potentials of brief duration where the action of the transmitter leads directly to the opening of a channel coupled to a receptor. These channels are relatively independent of voltage and open only in the presence of transmitter, and so do not normally contribute to the resting or action potential.

Transmitters can also produce slow synaptic actions, often, this does not lead directly to the opening of a channel but modulates the gating of a voltage-dependent channel that contributes to the resting or action potential^{14–16}. Thus, slow synaptic actions can alter the cell's resting and active electrical properties. Alterations in the configuration of the action potential can affect Ca²⁺ influx and modify transmitter release from the neurone presynaptic terminals¹⁷. Furthermore, with some slow synaptic actions, the receptor for the transmitter is often not directly coupled to the channel but to an adenylate cyclase that

activates a series of biochemical steps leading to a cyclic AMP-dependent phosphorylation of the channel or a protein related to it¹⁸.

Serotonin elicits a long-lasting excitatory postsynaptic potential (e.p.s.p.) in certain molluscan neurones^{19–21}. In *Aplysia* sensory neurones it produces a slow e.p.s.p. and facilitates transmitter release²² through a cyclic AMP-dependent phosphorylation²³ that leads to a decrease in a specific K⁺ conductance²⁴. This action of serotonin is thought to underlie behavioural sensitization, an elementary form of short-term memory. The serotonin-sensitive K⁺ conductance differs from the four previously identified neuronal K⁺ currents^{25–27, 31}. Using single-channel recording techniques, we have now identified in *Aplysia* sensory neurones a serotonin-sensitive K⁺ channel with novel properties. The channel is active at the resting potential. Its gating is not affected by the activity of intracellular Ca²⁺ ions and is only moderately dependent on membrane potential. Application of serotonin to the cell body or intracellular injection of cyclic AMP causes prolonged and complete closure of the channel. As a result, serotonin appears to reduce the effective number of active channels in the membrane.

Serotonin closes outward current channels

The most frequently observed channel in a membrane patch from a sensory cell gives rise to an outward elementary current of ~ 3 pA at 0 mV. This channel is modulated by serotonin (Fig 1). In the absence of serotonin (Fig 1a), the net patch membrane current fluctuates among several discrete levels, reflecting the superposition of the random openings and closings of several individual ion channels that are active in the patch. The unit current steps are, in general, all of a similar amplitude, suggesting that a single type of channel predominates. The probability that a given number of channels is open at any one time follows the binomial distribution, indicating that channels open and close independently of one another. The channels display two types of closures: brief closures lasting only a few milliseconds or less (the closings appear as frequent downward spikes in Fig 1a), and much longer closures lasting for tens or hundreds of milliseconds (apparent as the step changes in current level).

Application of serotonin caused a dose-dependent increase in the cell input resistance and a reduction in channel activity. As Fig 1b shows, the addition of ~ 30 μ M serotonin to the bath reduced the number of active channels from five to two. With ~ 60 μ M serotonin in the bath, the remaining channels closed (Fig 1c) and remained largely closed for the remainder of the drug application (4 min). On superfusion of the ganglion with serotonin-free artificial seawater (ASW), the activity of the channels partially recovered within the next 5–10 min (Fig 1d).

Serotonin seems to act on individual channels in an all-or-nothing manner (Fig 1). Channels once closed by serotonin remain closed, while channels which still open in the presence of serotonin seem to open and close normally. Thus, serotonin does not promote the appearance of channels with a reduced current amplitude or channels that open for periods of time that are briefer than normal. Rather, the transmitter causes channels to close for prolonged times (≥ 1 min) and, therefore, on the time scale of normal channel gating, seems to reduce the number of channels active in the membrane patch. Four experiments using fluctuation analysis of single-channel currents²⁸ confirmed that there is no change in the gating kinetics of channels which remain active in the presence of transmitter.

Power spectra of single-channel currents (determined between 10 and 1,000 Hz) displayed two lorentzian kinetic components with average time constants of 1 ± 0.1 and 29 ± 8 ms (at 0 to +10 mV). In the presence of serotonin, there was a reduction in total outward patch current but no significant change in the time constants of the two lorentzian components.

In 10 out of 13 experiments, serotonin produced a clear reduction in channel activity. In five of these experiments, serotonin almost completely inhibited channel openings and in the other five it reduced the average activity (defined as average patch current, see Fig 3c) by 50–90%. In two of the three experiments where it did not affect channel currents, serotonin also had no effect on the cells' input resistance.

Single channel current is voltage dependent

We next examined the effects of membrane potential on current flow through the serotonin-sensitive channels (Fig 2). The channel contributes outward current and is open for a large fraction of the time, even at potentials negative to the resting level. As the membrane is depolarized, the size of the unit current step increases, although there is only a small change in channel kinetics and in the probability that the channel is in the open state (see Fig 3c).

The single-channel current-voltage (i - V) relationship displays outward rectification (Fig 3b). A linear extrapolation of the i - V curve yields an estimate for the reversal potential, E_{rev} , that is negative to -65 mV, suggesting that K^+ is the major charge carrier of this current. Moreover, the i - V curve can be fitted by the Goldman-Hodgkin-Katz²⁹ constant field current equation for a K^+ current. In two experiments the K^+ dependence of current flow through the channel was tested directly. Normal-sized single-channel currents were recorded from cell-free (inside-out)¹ membrane patches where the 'intracellular' surface of the membrane was exposed to a bath solution containing 360 mM K^+ and 10 mM Na^+ . When the solution was changed to normal Na^+ ASW (10 mM K^+), current flow through the channels was dramatically reduced.

The time-averaged current through the serotonin-sensitive channel, $\langle I \rangle$, also displays outward-going rectification (Fig 3c, open symbols). This largely reflects the voltage dependence of

Fig 1 Action of serotonin (5-HT) on single-channel current. Patch clamp current recorded from mechanoreceptor sensory neurones in the abdominal ganglion of *Aplysia californica*. Trace a, current in the absence of serotonin. Left-hand ordinate shows the number of open channels, right-hand ordinate shows current magnitude. Individual current steps are 2.6 pA. The current record was well fitted by a binomial distribution assuming that five channels are active in the patch and that each channel opens with a probability of 0.84. Trace b, current obtained 2 min after addition of 30 μ M serotonin to the bath. Trace c, 1 min after addition of a further dose of serotonin, raising the total concentration to 60 μ M. The two traces are a continuous recording. The downward current deflection at the end of the bottom trace is from an intracellular current pulse used to monitor cell resistance. Trace d, current record obtained about 5 min after superfusion with serotonin-free ASW. The small reduction in unit current was probably due to a slight hyperpolarization of the cell resting potential as the intracellular microelectrode was withdrawn from the cell before solution change. The single-channel currents were recorded in response to steady depolarizations of the patch membrane to 0 mV (defined as patch pipette potential minus cell resting potential) produced by changing the potential inside the patch pipette. The use of steady-state recording conditions minimizes interference from inactivating K^+ , Na^+ and Ca^{2+} currents²⁷. In contrast, serotonin-sensitive K^+ current is active during steady-state depolarizations^{26,33}. The bath ASW had the following composition: 470 mM Na, 10 mM K, 10 mM Ca, 55 mM Mg, 600 mM Cl, 10 mM HCO_3^- , 10 mM Tris buffer at pH 7.4. Abdominal ganglia were pretreated with 0.2% trypsin (Sigma, type 1X) in ASW for 10–20 min. Current records were filtered at 1.0 kHz. Temperature, 23 °C.

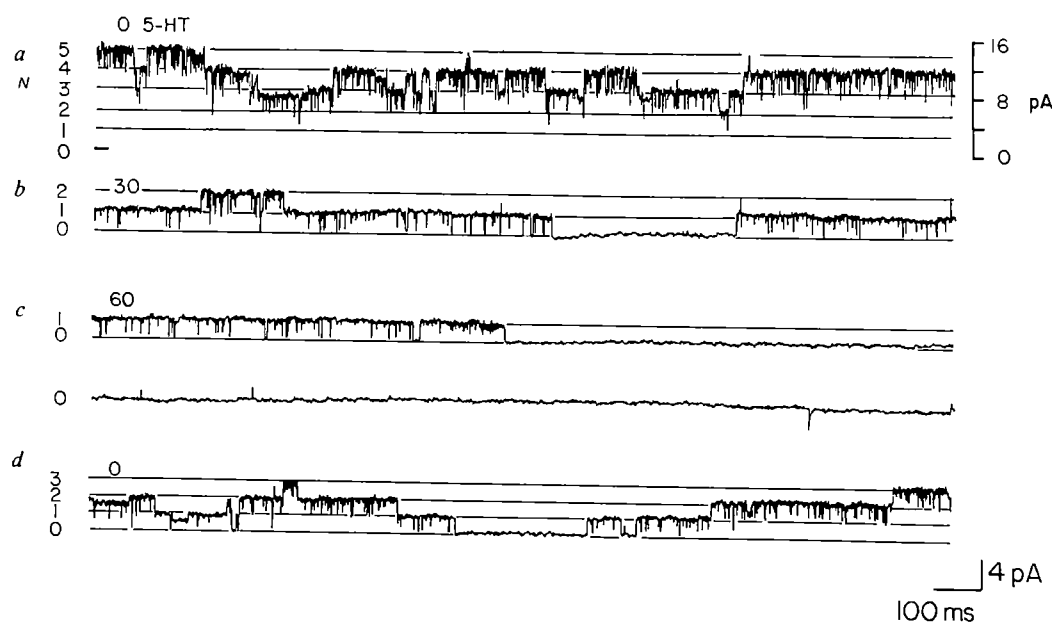
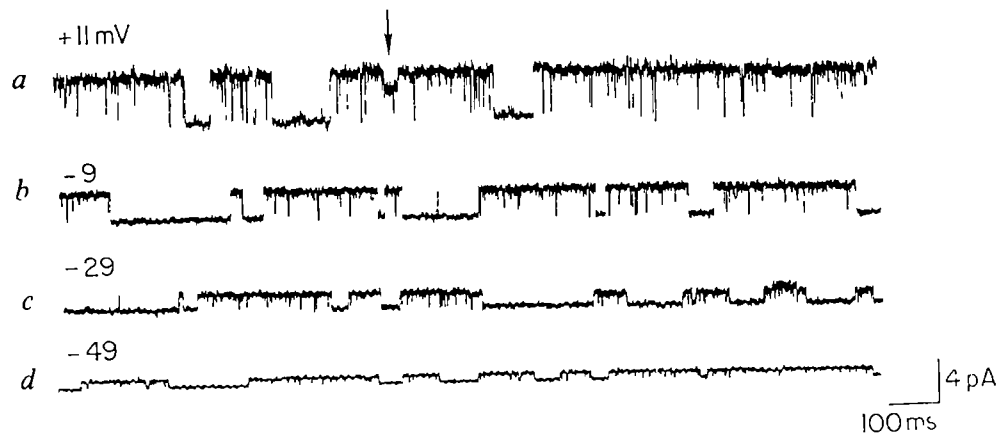


Fig. 2 Single-channel current at different membrane potentials. Current records shown are at four different patch membrane potentials (indicated at the left of each trace). Cell resting potential = -39 mV. Channel openings appear as step increases in outward current. The current fluctuates between two levels corresponding to closed and open channel. At all potential levels the channels show both brief and long closures but spend most of the time in the open state. The arrow indicates a partial closure. Addition of $10 \mu\text{M}$ serotonin to the bath caused the prolonged closure of this channel (not shown). Current records *a-c* were filtered at 16 kHz, record *d* was filtered at 10 kHz. Temperature, 23°C .



the i - V relation, as the probability, P , that the channel is open, obtained from $\langle I \rangle = P_i$, shows only a modest dependence on voltage (Fig. 3c, filled symbols). The voltage dependence of the probability of channel opening varied among different membrane patches. The maximum steepness of the relationship between P and voltage ranged over 25 – 100 mV (average 52 ± 35 mV, $N = 6$) for a two-fold change in P . Some of this variability may be related to the fact that the channels can switch between different kinetic states which may exhibit different degrees of voltage dependence (see Fig. 4). The average value for the single-channel conductance (defined as slope conductance at 0 mV) was 55 ± 6 pS ($N = 12$).

The histogram of channel current amplitudes measured at $+11$ mV from the experiment of Fig. 2 shows a single peak, with a mean channel step size of 3.9 pA, indicating that most opening and closing transitions involve current steps of a fixed amplitude (Fig. 3a). However, channels occasionally show partial closings to an intermediate current level (Figs 2a, 4a,c at arrows, see also ref. 30). The conductance of this partially open state is roughly two-thirds that of the fully conducting state. Such events do not represent the opening of a channel which carries a small inward current because the amplitude of the intermediate current step is increased on depolarization of the membrane (compare Fig. 4a and b at arrows). In addition, no inward channels (of similar amplitude and duration as the intermediate current step) were observed during periods of closure of the serotonin-sensitive outward current channel.

Non-stationary gating of channels

The kinetic behaviour of the serotonin-sensitive channels is quite complex, channels can display a low ($P < 0.1$) probability of being open or show a much higher ($P > 0.5$) opening probability. In the records of Fig. 4 (taken from the same experiment as Fig. 2), the channel was initially closed for most of the time (Fig. 4a,b). It then underwent an abrupt, apparently spontaneous, transition (Fig. 4c) to a state which displayed a much higher open probability and remained in this high open probability state for the next 5 min (during which time the records of Fig. 2 were obtained). At this time serotonin ($10 \mu\text{M}$) was added to the bath and the channel closed. The effect of serotonin does not reflect a switching of the channel back to the low open probability state, as serotonin caused channel closures (mean closed time = 64 s) lasting 300 times longer than the mean closed time observed with the channel in the low open probability state. In patches which display more than one active channel, channels can coexist in both high and low open probability states (see, for example, Figs 1b, 5a), suggesting that the different states do not reflect generalized changes in membrane properties or metabolic state of the cell. Serotonin causes closure of channels regardless of whether they are in the high or low probability state of opening.

Channel is insensitive to intracellular Ca^{2+}

The serotonin-sensitive channel seems to be insensitive to changes in intracellular calcium. In four experiments, tetanic stimulation of the cell, which is known to increase intracellular Ca^{2+} in these cells, did not noticeably alter the probability of channel opening or closing. In addition, intracellular injection of EGTA using hyperpolarizing iontophoretic current pulses (up to 33 nC of total charge into a cell of $\sim 3 \times 10^{-11}$ l volume), had no effect on channel activity. To obtain more direct evidence on the effects of intracellular Ca^{2+} on channel gating, we carried out four experiments in isolated cell-free membrane patches in which the intracellular surface of the membrane was exposed to the bath (inside-out patch). Channel opening and

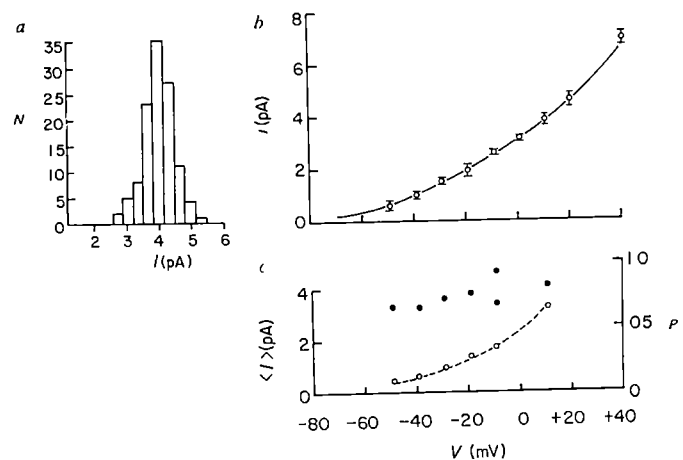
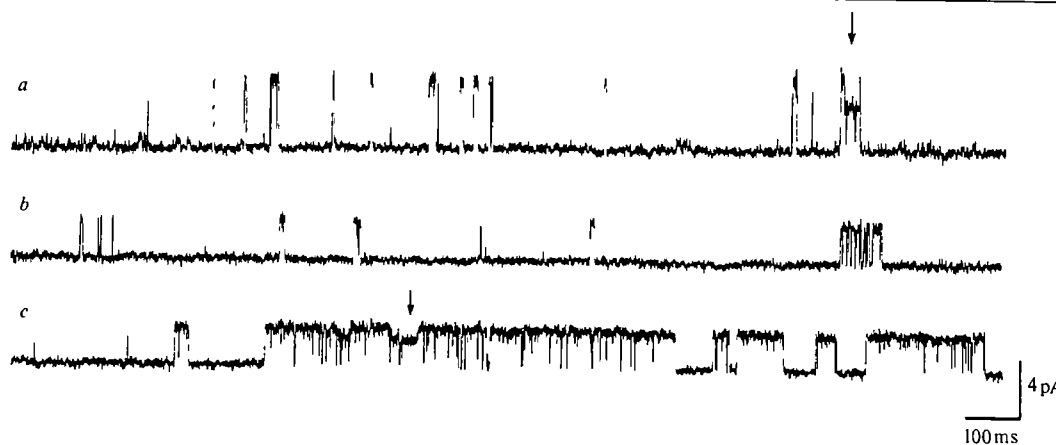


Fig. 3 Voltage dependence of current flow through serotonin-sensitive channel. The three panels are from the same experiment as in Fig. 2. *a*, Histogram of single-channel current amplitudes measured at $+11$ mV. *b*, Single-channel current-voltage relation. Single-channel current amplitudes (i) were measured over a potential range from -49 mV to $+41$ mV and are plotted as a function of membrane potential. The solid curve represents the prediction from the Goldman-Hodgkin-Katz equation for a K^+ current, fitted to the points assuming an intracellular K^+ concentration of 360 mM and a channel K^+ permeability of $8.7 \times 10^{-14} \text{ cm}^3 \text{ s}^{-1}$. *c*, Current records were digitally sampled at various potentials (at 20 kHz sampling frequency) and analysed using an LSI 11/23 computer. Average current flow ($\langle I \rangle$) through the channel was calculated by integrating current flow during channel openings and dividing the integral by the total time of the sample (generally 10 – 20 s of data at each potential). The open symbols show the dependence of $\langle I \rangle$ on membrane potential (left-hand ordinate). Average current is given by $\langle I \rangle = NP_i$, where N is the number of channels in the patch, P is the probability that a single channel is open and i is the amplitude of the single-channel current. Since $N = 1$ in this experiment, $P = \langle I \rangle / i$ (plotted as the filled symbols in *c*, right-hand ordinate).

Fig. 4 Spontaneous transition in channel kinetics. Records show patch membrane current from the same patch as Fig 2 but slightly earlier in the experiment. *a*, Channel currents at a patch membrane potential of +21 mV. Channels are closed for most of the time. Average probability of channel opening, P , is 0.05. *b*, Channel currents at a potential of -9 mV, $P = 0.025$. *c*, Current record is continuous with the end of trace *b* and shows an abrupt increase in channel open probability, after transition $P = 0.67$. Arrows indicate partial closures.



closing were unchanged when the calcium activity at the intracellular face of the membrane was varied from less than 10^{-9} M free Ca^{2+} (0 Ca, 10 mM EGTA) to ~ 10 μM free Ca^{2+} .

Cyclic AMP causes channel closure

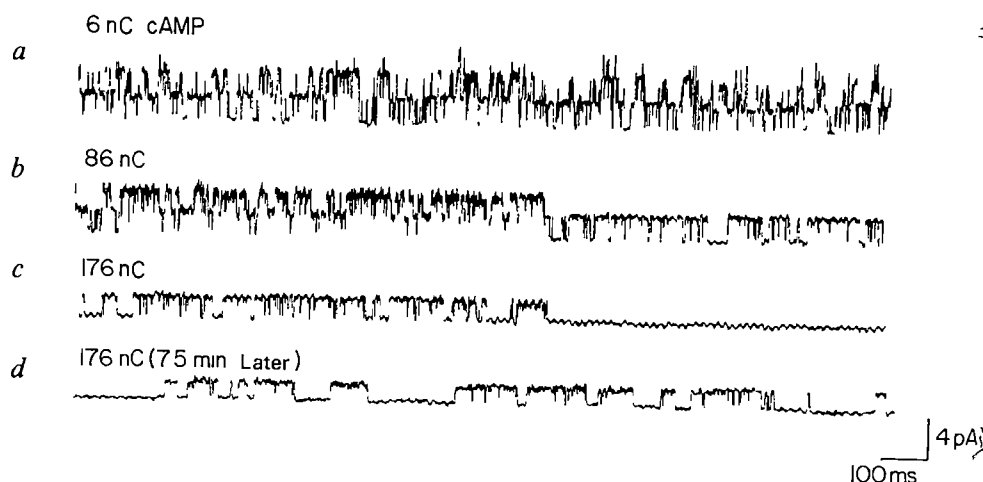
The patch pipette forms a very stable and high-resistance seal with the membrane which is thought to prevent diffusion of transmitters or other ligands from outside to inside the pipette. As a result, in the acetylcholine-activated channels of muscle, the transmitter has to be introduced in the patch pipette to affect the channels under the patch pipette¹. By contrast, serotonin consistently decreased channel opening in the patch when applied to the bathing solution outside the pipette. This finding is consistent with the notion that the modulation of the K^+ channel is mediated by means of an intracellular messenger that can act on the patch from within the cell. To test this idea directly, we injected into the cell cyclic AMP, the second messenger thought to modulate the serotonin-sensitive K^+ current (J S C and E R K, unpublished observation). Intracellular injection of cyclic AMP, by means of current pulses, causes channels to close in an all-or-none manner similar to the action of serotonin. In the experiment of Fig 5, three channels are initially active before the start of the current injection (Fig 5*a*). After the onset of the current pulses, these channels drop out one at a time (Fig 5*b,c*). Channel activity partially recovered a few minutes after the cyclic AMP electrode had been removed from the cell (Fig 5*d*). A similar reduction in channel activity on injection of cyclic AMP was observed in four out of six experiments. The effect is not due to the iontophoretic procedure, as similar injections of charge from KCl- or K^+ -EGTA-filled pipettes produced no change in channel gating.

Serotonin-sensitive channels represent a new class of channel

The frequency with which we observe the serotonin-sensitive outward channel suggests that it represents a major K^+ conductance in the cell body of the sensory neurone. The fact that the opening probability of the channels shows moderate sensitivity to membrane potential and no dependence on intracellular Ca^{2+} indicates that the serotonin-sensitive channel is distinct from previously described K^+ currents, including the early K^+ current, delayed rectification, the Ca^{2+} -activated K^+ current and the M current. These findings on the level of single channels are consistent with studies of the macroscopic properties of the serotonin-sensitive current^{24,31}. Because the channel is open at rest and throughout the whole physiological range of membrane potential, the serotonin-sensitive channel may best be described as a background K^+ channel. The inhibition of such a channel is consistent with the physiological effects of serotonin, including depolarization of the resting potential, increase in resting membrane resistance and an increase in the duration of the action potential.

Our results provide direct evidence that serotonin and cyclic AMP modulate the gating of a specific and novel K^+ channel and indicate possible mechanisms whereby this modulation is achieved. The modulatory action does not involve a change in the channel's ionic specificity or detectable changes in single channel conductance or the lifetime of the channel in the open state. Rather, serotonin and cyclic AMP, presumably acting through cyclic AMP-dependent protein phosphorylation, seem to increase the lifetime of the channel in the closed state. This

Fig. 5 Effect of intracellular injection of cyclic AMP on single-channel current. Following establishment of the seal between patch electrode and membrane, the cell was impaled with a microelectrode filled with 1 M cyclic AMP (Sigma) and cyclic AMP was injected into cells by hyperpolarizing current pulses (0.5–2.5 nA). Total charge (nanocoulombs) injected into the cell is indicated above each trace. *a*, Current obtained soon after impalement of the cell with the cyclic AMP electrode. *b*, *c*, Current records after subsequent injection periods. During the record shown in *c* the remaining active channel closed. The cyclic AMP electrode was withdrawn from the cell and no channel openings were observed for 5 min. Channel activity then partially recovered (trace *d*). Cell membrane potential hyperpolarized during the experiment. Patch membrane potential was $\sim +14$ mV in *a*, $+11$ mV in *b*, $+7$ mV in *c* and $+2$ mV in *d*. The time bar in *d* equals 125 ms. Current records were filtered at 1.0 kHz in *a–c* and 800 Hz in *d*. Temperature, 22 °C.



may simply represent the modification of the normal channel gating process whereby one of the normal rate constants of channel opening is dramatically decreased. Alternatively, serotonin may induce new closed states of the channel (perhaps corresponding to the channel in a phosphorylated form) in which the channel is not available to the normal gating process. In contrast, it has been shown recently that isoprenaline seems to act on the Ca^{2+} channel in heart muscle by increasing the probability that the channel will remain open³².

The ability to record the activity of the serotonin-modulated

channel in cell-free inside-out patches, invites the *in vitro* biochemical study of the steps involved in the cyclic AMP-mediated phosphorylation of single ionic channels. It will be interesting to determine whether the catalytic subunit of the cyclic AMP-dependent protein kinase can phosphorylate the channel in the isolated patch, and whether this phosphorylation can be reversed by a specific phosphatase. These questions are all the more interesting because they lead to a molecular understanding of transmitter modulation that underlies a simple form of learning.

Received 17 May, accepted 19 July 1982

- 1 Hamill, O., Marty, A., Neher, E., Sakmann, B. & Sigworth, F. J. *Pflügers Arch ges Physiol* **391**, 85–100 (1981)
- 2 Conti, F. & Neher, E. *Nature* **287**, 140–143 (1980)
- 3 Sigworth, F. J. & Neher, E. *Nature* **291**, 426–428 (1981)
- 4 Horn, R., Patlak, J. & Stevens, C. *Nature* **291**, 426–428 (1981)
- 5 Lux, H. D. & Nagy, K. *Pflügers Arch ges Physiol* **391**, 252–254 (1981)
- 6 Marty, A. *Nature* **291**, 497–500 (1981)
- 7 Pallotta, B. S., Magleby, K. K. & Barrett, J. J. *Nature* **293**, 471–474 (1981)
- 8 Colquhoun, C., Neher, E., Reuter, H. & Stevens, C. F. *Nature* **294**, 752–754 (1981)
- 9 Yellen, G. *Nature* **306**, 357–359 (1982)
- 10 Neher, E. & Sakmann, B. *Nature* **260**, 799–802 (1976)
- 11 Patlak, J. B., Gratton, K. A. F. & Usherwood, P. N. R. *Nature* **278**, 643–645 (1979)
- 12 Miledi, R., Parker, I. & Cull-Candy, S. *J Physiol, Lond* **321**, 195–210 (1981)
- 13 Colquhoun, C. & Sakmann, B. *Nature* **294**, 464–466 (1981)
- 14 Tsien, R. W. & Siegelbaum, S. in *Physiological Basis of Membrane Disorders* (Plenum, New York, 1978)
- 15 Kehoe J. & Marty A. *A Rev Biophys Bioengng* **9**, 437–465 (1980)

- 16 Hartzel, H. C. *Nature* **291**, 539–544 (1981)
- 17 Klein, M., Shapiro, E. & Kandel, E. R. *J exp Biol* **89**, 117–157 (1980)
- 18 Greengard, P. *Harvey Lect* **75** (1981)
- 19 Gershenfeld, H. M., Paupardin-Tritsch, D. & Deterre, P. in *Serotonin Neurotransmission and Behavior* (MIT Press, 1981)
- 20 Pellmar, T. C. & Carpenter, D. O. *Nature* **277**, 483–484 (1977)
- 21 Klein, M. & Kandel, E. R. *Proc natn Acad Sci USA* **75**, 3512–3516 (1978)
- 22 Brunelli, M., Castellucci, V. & Kandel, E. R. *Science* **194**, 1178–1181 (1976)
- 23 Castellucci, V. F. et al. *Proc natn Acad Sci USA* **77**, 7492–7496 (1980)
- 24 Klein, M. & Kandel, E. R. *Proc natn Acad Sci USA* **77**, 6912–6916 (1980)
- 25 Camardo, J., Klein, M. & Kandel, E. R. *Soc Neurosci Abstr* **7**, 836 (1981)
- 26 Adams, D. J., Smith, S. J. & Thompson, S. H. A. *Rev Neurosci* **3**, 141–163 (1980)
- 27 Brown, D. A. & Adams, R. P. *Nature* **283**, 672–676 (1980)
- 28 Anderson, C. R. & Stevens, C. F. *J Physiol, Lond* **235**, 665–692 (1973)
- 29 Hodgkin, A. L. & Katz, B. *J Physiol, Lond* **108**, 37–77 (1949)
- 30 Hamill, O. & Sakmann, B. *Nature* **294**, 462–464 (1981)
- 31 Klein, M., Camardo, J. S. & Kandel, E. R. *Proc natn Acad Sci USA* **79** (in the press)
- 32 Reuter, H., Stevens, C. F., Tsien, R. W. & Yellen, G. *Nature* **297**, 501–504 (1982)
- 33 Paupardin-Tritsch, D., Deterre, P. & Gershenfeld, H. M. *Brain Res* **217**, 201–206 (1981)

Genomic environment of *T. brucei* VSG genes: presence of a minichromosome

Richard O. Williams, John R. Young & Phelix A. O. Majiwa

International Laboratory for Research on Animal Diseases, PO Box 30709, Nairobi, Kenya

Restriction endonuclease maps of some trypanosome variant surface glycoprotein (VSG) genes have a site 3' to the gene where many enzymes appear to cut. This site is sensitive to Bal31 exonuclease, indicating a natural double-strand break in the DNA. One VSG gene exists in several cell clones as a non-integrated minichromosome.

ANTIGENIC variation in *Trypanosoma brucei* involves switching on and off the expression of members of a large family of genes coding for the variable surface glycoproteins (VSGs)¹. In some cases switching of expression of a VSG gene is closely linked to duplication and transposition of the gene^{2–4}. For other VSG genes a similar rearrangement is probably involved in the production of a copy which can be expressed (manuscript in preparation). This copy however, is stable and its expression must be controlled by a mechanism other than the duplication and transposition event itself^{5–7}. Previous work has shown length variations in restriction enzyme fragments extending into 3'-flanking sequences of VSGs genes whose expression is not linked to duplication^{6,8} but similar length variation has also been observed in independently isolated trypanosome clones expressing the same VSG gene whose expression is closely linked to duplication⁴.

We have been studying four VSG genes from the ILTaR 1 antigen repertoire. Of these, only one (ILTat 1.1)⁷ undergoes a rearrangement whose expression appears to be controlled by duplication⁹. There are four distinct copies of the ILTat 1.3 gene, and three of the ILTat 1.4 gene⁶ in each member of a closely related group of trypanosome clones but the number of copies of these genes does not vary with expression. Variation in length of restriction enzyme fragments extending into 3'-flanking regions has been observed for two copies of the ILTat 1.3 gene and one copy of the ILTat 1.4 gene. No rearrangements have been detected in the genomic environment surrounding two copies of each of these genes.

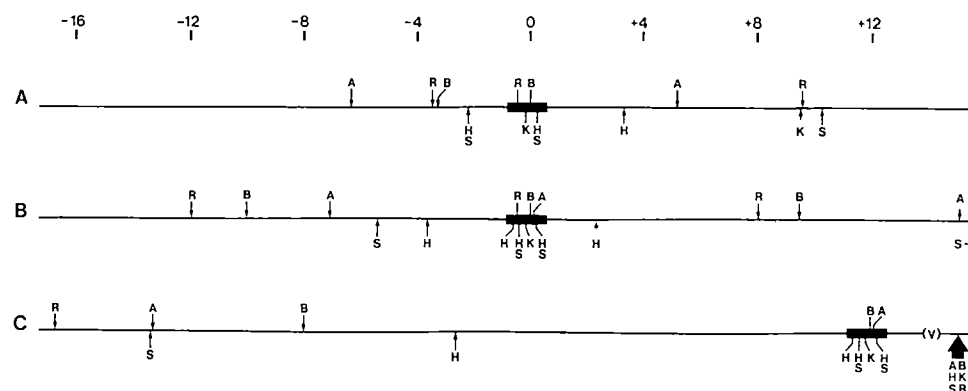
In a comparison of two expressed copies of the *T. brucei* VSG 118 gene, each resulting from different duplication events,

Michels *et al.*⁴ observed a similar variation in the length of 3'-flanking restriction enzyme fragments. However, in this case there were also changes in the length of 5'-flanking fragments. They also reported an apparent cluster of enzyme sites beyond the 3' end of the gene which, they suggested, might be at the end of a chromosome^{4,10}. We have found a similar cluster of enzyme sites beyond the 3' end of those copies of the ILTat 1.3 and 1.4 genes which undergo rearrangement. The cluster is located at the 3'-distal end of the enzyme fragments containing the 3'-flanking sequences. We present here further evidence that these clusters are probably at the ends of chromosomes, and that this location of a VSG gene is not necessarily related to its expression. We also show that one copy of the ILTat 1.3 gene is located near the end of a small linear DNA molecule in native DNA preparations.

Terminal location of VSG genes

The derivation of the ILTaR 1 trypanosome clones used here has been described previously. All clones were derived from a single parent clone (ILTat 1.1) by no more than two relapse infections⁸. Figure 1 shows restriction enzyme maps of the three genomic copies of the ILTat 1.4 gene present in all clones of the ILTaR 1 antigen repertoire so far tested. Restriction enzyme sites internal to the regions of homology with the cloned ILTat 1.4 cDNA (thick bars) were found to be different in the three copies. The sites marked in copy C were identical with those found in the cDNA¹¹. Copies A and B contain an *EcoRI* site not present in the cDNA. In copy A other sites are absent. It therefore seems probable that copy C is the template for transcription of ILTat 1.4 mRNA. The finding of further sequence

Fig 1 Map of restriction enzyme sites in the vicinity of the three copies of the ILTat 1.4 gene. The scale is in kilobases. The solid bar represents the regions occupied by sequences homologous with the ILTat 1.4 cDNA in plasmids pcBD1 and pcBD2 (J E Donelson, J R Y and R O W, manuscript in preparation). A = *Ava*I, B = *Bgl*II, H = *Hinc*II, K = *Kpn*I, R = *Eco*RI, S = *Sal*I (V) indicates a region of variable length in different trypanosome clones. The orientation of the coding sequence (5' to 3') is left to right. The large arrow represents a group of restriction enzyme sites which map to the same position within the accuracy of the measurements made (~200 bp, see Fig 2). Enzyme sites mapping at this position include *Eco*RI, *Ava*I, *Bgl*II, *Sau*3A1, *Sal*I, *Kpn*I, *Hinc*II, *Hae*III, *Msp*I and *Rsa*I. DNA from different trypanosome clones was digested completely with one or more enzymes and used in Southern transfer experiments as described elsewhere⁶, using 5' and 3' cDNA probes from either side of the central *Bgl*II site (J E Donelson, J R Y and R O W, manuscript in preparation). The results of double and triple digestion experiments allowed the allocation of particular 5' and 3' fragments to the appropriate genomic copy. Where cloned genomic DNA was available, this allocation was confirmed by analysis of these genomic clones (J E Donelson, J R Y and R O W, manuscript in preparation). Differences in restriction enzyme sites within the cDNA region were also revealed in these experiments, for example, the 5' *Hinc*II fragment of copy A also hybridized to the 3' probe, showing that the 5' two *Hinc*II sites were absent from this copy.



differences between the cDNA sequence and cloned fragments of copies A and B supports this conclusion (J E Donelson, J R Y and R O W, manuscript in preparation).

For copies A and B in Fig 1, no differences were detected in their flanking sequences in eight trypanosome clones, three expressing and five not expressing ILTat 1.4. In comparing expressing and non-expressing clones, no differences were found in enzyme sites on the 5' side of the copy C gene in a region of 25 kilobases (kb). This implies that any transposition involved in modulating the expression of this gene would have to involve a transposed section much greater than that observed for other VSG genes¹⁰.



Fig 2 Illustration of the close mapping of restriction enzyme sites distal to the 3' end of copy C of the ILTat 1.4 gene. DNA from trypanosome clone ILTat 1.2 was completely digested with restriction enzymes M = *Msp*I, K = *Kpn*I, R = *Rsa*I, B = *Bgl*II, A = *Ava*I and S = *Sal*I. Tracks MS, RS and AS are double digests with the indicated enzymes. Fragments were resolved by electrophoresis in a 0.75% agarose gel, transferred to nitrocellulose and hybridized to pcBD1 as described elsewhere⁶. Molecular weight markers (m) are various fragments of known length hybridizing to pBR322.

The large arrow in Fig 1 on the 3' side of copy C represents a cluster of enzyme sites that cannot be resolved within the accuracy of the mapping technique used. Figure 3 illustrates the proximity of these sites for six restriction enzymes, in one trypanosome clone. Each track of this gel contains a hybridizing fragment between 5.5 and 5.9 kb which is known from mapping data to come from the 3' end of copy C. There is a recognition site for each of these enzymes between 75 (*Msp*I) and 472 (*Sal*I) base pairs (bp) from the 5' end of the pcBD1 cDNA insert (J E Donelson, J R Y and R O W, manuscript in preparation). The 5.9 and 5.5 labels indicate the size of the *Msp*I and the *Sal*I fragments determined from measurements on this and other autoradiographs, using the size markers shown. The difference of 400 bp between 3' fragments with these two enzymes is exactly as expected from the position of the sites in the cDNA if the 3' distal sites are at identical positions. The fragments found with the other enzymes are of intermediate length, showing that their 3' ends also map at the same position. Double-digestion experiments like those shown on the right in Fig 2 did not reveal any site mapping even closely inside the apparent cluster. This experiment resolved differences of less than 200 bp, making this the upper limit on the length of the cluster. Significantly, we did not find a site for any enzyme mapping beyond the position of the cluster. These data suggest that the 'cluster' is in fact a natural double-strand break in the trypanosome DNA. The region of the genome between this break and the gene is unusual in that none of the enzymes we used recognized a site within this region.

We have found a similar cluster of restriction enzyme sites distal to the 3' ends of the two copies of the ILTat 1.3 gene which are subject to 3' length variation (manuscript in preparation). To rule out the possibility that the clustering of enzyme sites was coincidental, we tested the susceptibility of the flanking regions of the ILTat 1.3 gene in intact ILTat 1.3 DNA to the double-stranded exonuclease *Bal*31 (ref 12). Intact DNA was treated with *Bal*31 for varying times and then cut with *Ava*I. The nearest *Ava*I sites in the flanking regions of the ILTat 1.3 genes have been mapped and are shown in Fig 3. The 3' fragments of copies C and D (12.0 and 7.2 kb) are the fragments for which length variation is observed in different trypanosome clones, and at the end of which is the cluster of enzyme sites. The top of Fig 3 shows that pretreatment with *Bal*31 results in progressive shortening of these two fragments while the other fragments are unaffected. The 80-kb band is faint because of shearing in this DNA preparation. This band is the 5' fragment of copy D. Its intensity decreases, but with such a large fragment it is not possible to distinguish between exonucleolytic shortening and cleavage by any contaminating endonuclease. This experiment demonstrates that the ends of the 3'-flanking

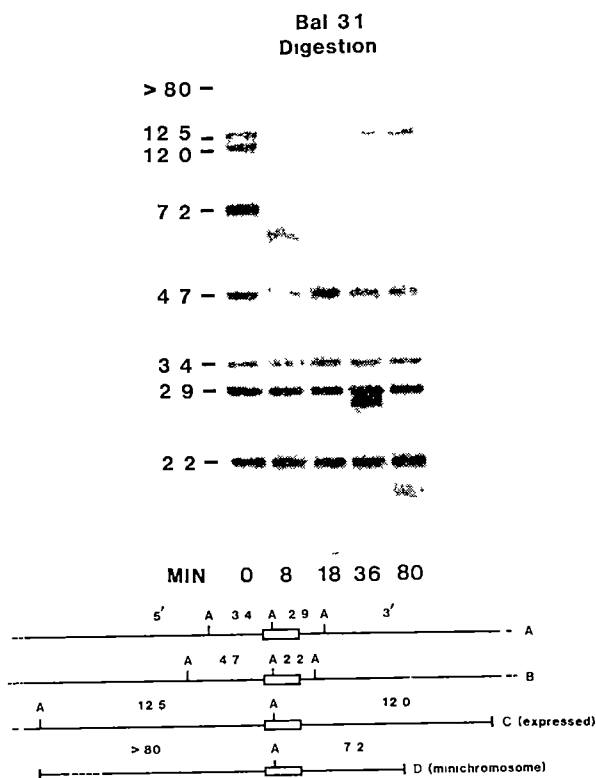


Fig. 3 *Bal31* digestion of nuclear DNA. 40 μ g of nuclear DNA was digested with 13 units of *Bal31* enzyme in 600 mM NaCl, 12 mM CaCl_2 , 12 mM MgCl_2 , 20 mM Tris-HCl pH 8 and 1 mM EDTA. The reaction was incubated at 30 °C and aliquots were taken at the times shown by pipetting into water-saturated phenol. Each DNA was precipitated with ethanol and subsequently digested with *AvaI* restriction endonuclease. The digested DNAs were electrophoresed in a 0.8% agarose gel and transferred to nitrocellulose paper as described previously⁶. Preparation of plasmid pcBC1 containing the complete coding sequence for VSG ILTat 1.3 has been described elsewhere⁶. The plasmid was nick-translated and hybridized as described elsewhere⁶. The upper portion of the figure shows the results of the blotting experiments. The lower portion shows a map of the *AvaI* sites in the vicinity of the four copies of the ILTat 1.3 genes.

sequences of copies C and D are accessible to exonuclease digestion in intact DNA. This observation cannot be explained by random breakage as this should affect all fragments equally. It could be the result of a site-specific cleavage by a trypanosome endonuclease during DNA isolation, or the result of a specific region of DNA being unusually susceptible to shearing. Site-specific cleavage of DNA has not been observed in trypanosomes. We are not aware of any DNA structures hypersensitive to shearing. Therefore we prefer the simpler explanation that the restriction enzyme site clusters observed in our work are in fact the site of natural double-strand breaks in the trypanosome genome, and are probably the ends of chromosomes. In ILTat 1.4 DNA, the same two fragments of the ILTat 1.3 gene are susceptible to *Bal31* (data not shown), so that telomeric location of this gene is not correlated with expression.

A VSG gene on a minichromosome

The observation of two copies of the ILTat 1.3 gene, each adjacent to the end of a DNA molecule, led us to investigate whether these genes might be located on unusual extrachromosomal DNA structures similar to the small non-integrated pieces of DNA which carry the ribosomal RNA genes in the macronucleus of *Tetrahymena*¹³. To test this possibility minimally sheared DNA was prepared from three trypanosome clones expressing VSGs ILTat 1.2, 1.3 and 1.4 and fractionated on sucrose density gradients. Figure 4 shows the distribution of the four copies of the ILTat 1.3 genes in these gradients. *HincII*

does not cut the gene and the single *HincII* fragment corresponding to each gene copy in these clones is known from restriction enzyme mapping data (manuscript in preparation). We reported previously that the ILTat 1.3 clone contains a minor cell population in which a copy D of the ILTat 1.3 gene is on a different-sized *HincII* fragment⁶. This is the larger fragment seen in fraction 16 of the ILTat 1.3 gradient and is smaller than the copy C *HincII* fragment seen in fractions 20 to 30. In all three clones the DNA carrying copy D was clearly separated from the bulk of the DNA which was sedimented to the bottom of the tube. Copy D is located on a DNA molecule that is not integrated into, and is smaller than, the bulk of

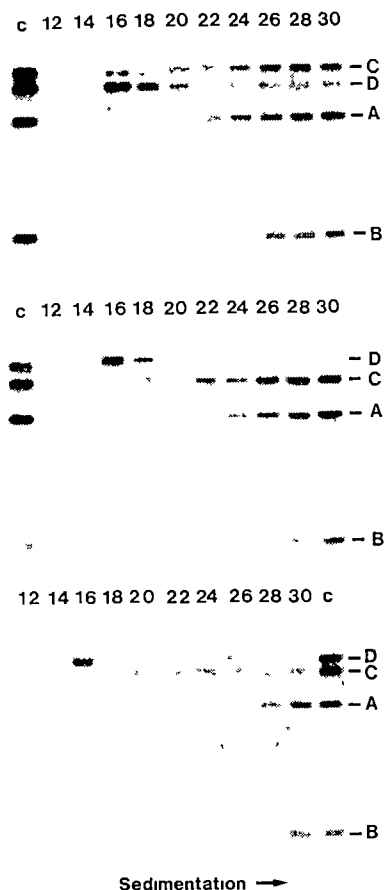


Fig. 4 Location of ILTat 1.3 genes in fractions from intact trypanosome DNA sedimented through a sucrose density gradient. Trypanosomes homogeneously expressing different VSGs were isolated by Percoll density gradient centrifugation¹⁸, and suspended at $2-4 \times 10^8$ cells per ml in 25 mM Tris-HCl, 100 mM NaCl, 5 mM EDTA, pH 8.0 (TNE) in 30-ml centrifuge tubes. Trypanosomes were lysed by addition of SDS to 0.5%. The lysate was incubated for 2 h with 100 mg ml^{-1} RNase A (previously heated to 70 °C for 60 min), then for 4 h with 1 mg ml^{-1} of Pronase (preincubated at 37 °C for 2 h), both at 37 °C. The lysate was extracted with an equal volume of phenol (redistilled, saturated with TNE) in 125-ml conical flasks in a gyratory incubator at ~ 60 r.p.m. at room temperature overnight. The aqueous phase was transferred to 30-ml centrifuge tubes and centrifuged at 5,000 r.p.m. for 10 min in a Heraeus-Christ minifuge. The extremely viscous DNA solution ($10-20 \mu\text{g ml}^{-1}$) was transferred with a wide-mouthed pipette tip into dialysis tubing and dialysed against four changes of 50 volumes of TNE. 5 ml of the dialysed DNA was layered onto a 10-40% sucrose gradient in 10 mM Tris-HCl, 5 mM EDTA, pH 8.0 and centrifuged at 24,000 r.p.m. for 10 h in a Beckman SW27 rotor at 20 °C. The gradient was fractionated with an ISCO gradient fractionator (30 \times 1.2-ml fractions). The DNA was precipitated by addition of NaCl to 0.2 M and 2.5 volumes of ethanol, recovered by centrifugation, washed in 75% ethanol and resuspended in 10 mM Tris-HCl, 0.1 mM EDTA, pH 8.0. The position of the ILTat 1.3 genes in the gradient was determined by a Southern blot analysis of DNA from alternate fractions digested with *HincII*, using pcBC1 as a probe. Direction of sedimentation was from left to right. Tracks marked C are digests of unfractionated DNA. Top, clone ILTat 1.3, middle, clone ILTat 1.4, bottom, clone ILTat 1.2. A, B, C and D mark the *HincII* fragments from the four distinct copies of the ILTat 1.3 gene (manuscript in preparation). The gradient of the ILTat 1.2 DNA contained half the amount of DNA used in the others reducing the extent of trailing due to aggregation.

16 19 23 16 18
Gradient fraction

Fig. 5 Electrophoresis of intact minichromosome DNA. DNA recovered from the gradients shown in Fig. 4 was electrophoresed in a 0.55% agarose gel at 1 V cm^{-1} for 40 h. The DNA was transferred to nitrocellulose, and hybridized with ^{32}P -labelled pcBC1 as described elsewhere⁶. The three left-hand fractions were from the gradient of ILTat 1.3 DNA. The right-hand two fractions were from the ILTat 1.4 gradient. Fraction numbers are indicated beneath the figure.

trypanosome DNA. This small DNA molecule is present whether the ILTat 1.3 gene is expressed or not. This molecule is a discrete entity in isolated DNA. Our interpretation, that it exists *in vivo* as a minichromosome, depends on the same arguments as made above for the conclusion that the gene is located next to a natural double-strand break.

In all three gradients copy D is located in fractions 16 and 17. We have calculated a sedimentation coefficient ($s_{20,w}$) of 41S for these fractions corresponding to a length of ~80 kb (ref. 14). The small amount of copy D which sedimented further is not due to size heterogeneity of the minichromosome as shown by the data in Fig. 5. A hybridizing fragment, the same size as the minichromosome, is present in all fractions in this figure. This minichromosome is clearly resolved from the bulk of the DNA. Presumably aggregation accounts for the trailing of the minichromosome peak. By comparison with partially cohered λ bacteriophage DNA we have estimated the minichromosome size to be just less than two λ DNA molecules, which agrees with the estimate made from the sedimentation coefficient (80 kb).

The same gradient fractions were analysed for the presence of three other VSG genes (ILTats 1.1, 1.2, 1.4). None of these genes was found to sediment more slowly than the bulk of trypanosome DNA (80S). All copies of these genes are on very large DNA molecules even though some are located near the ends, as is copy C of the ILTat 1.3 gene. In the gradient of the ILTat 1.2 DNA, the pcBC1 probe detected two faintly hybridizing fragments in slowly sedimenting DNA (fractions 16 and 20). These bands are barely visualized in unfractionated DNA (track C). The pcBC1 probe contains sequences which hybridize to the 3' ends of other VSG genes⁶. These bands may result from different VSG genes on other small DNA molecules. Fraction 20 corresponds to a sedimentation coefficient of 53S.

(160 kb). A proportion of molecules carrying copy C also appears to sediment more slowly than copies A and B. This may be a result of its proximity to the end of the chromosome which would lead to a smaller average size of the sheared DNA in which it appears. If this gene were also located on a minichromosome we would expect to have found a definite peak rather than the broad distribution evident in this gradient.

A number of restriction enzyme sites in and around the ILTat 1.3 gene in the minichromosome have been mapped. These are shown in Fig. 6. All 20 enzyme sites within the gene are identical with sites in the cDNA and in copy C. Five sites 5' of the gene, and the *Ava*II site 3' of the gene are also identical with sites around copy C. It appears that either copy C or D could serve as the template for the transcription of mRNA. However the preferential sensitivity of copy C to DNase I digestion (manuscript in preparation) suggests that copy C is the template in clone ILTat 1.3.

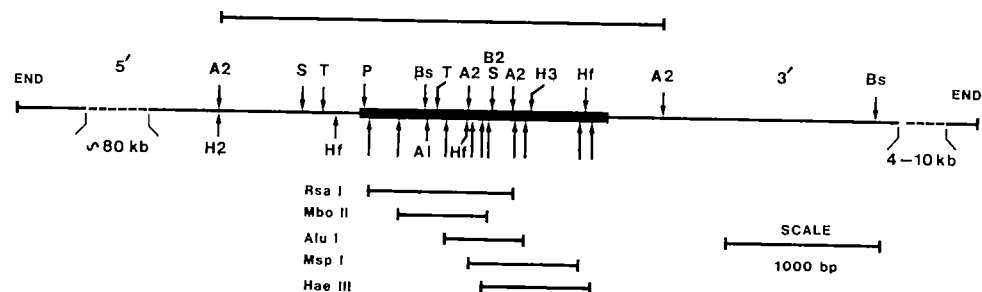
The region of length variation between the *Bst*EII enzyme site and the 3' end of the minichromosome is not cut by 14 different restriction enzymes, including 4 that have 4 base recognition sequences. This suggests that this region is composed of a repetitive sequence, similar to the region adjacent to expression-linked copies of other VSG genes¹⁰ and copy C of the ILTat 1.3 gene. This characteristic region in the 3'-flanking sequences represents another similarity between the minichromosome copy and the expressed copy C.

We have not detected sites 5' of the gene in the minichromosome for 10 different restriction enzymes. For the enzymes *Eco*RI, *Eco*RV, *Bam*HI and *Sal*I, prolonged electrophoresis was used to detect cutting of the intact minichromosome. We would have detected any reduction of more than 20 kb in the length of the minichromosome. Thus we have found no sites for these enzymes more than 20 kb from the 5' end of the minichromosome. For the other six enzymes, listed in Fig. 5 legend, the very large fragments from the 5' end of this gene copy are not detectably shorter than the intact minichromosome. However, the shorter electrophoresis used in these experiments only allows us to conclude that there are no sites less than 40 kb from the gene. Even a region of 40 kb in length uncut by any of these 10 enzymes is remarkable. It seems likely, therefore, that the central region of the minichromosome is also composed of a highly repetitive sequence.

Discussion

Borst *et al.*¹⁵ found several kinds of large DNA molecules after digestion of *T. brucei* DNA with *Hae*III enzyme. These consisted mainly of long linear DNA molecules, but also some circles and lariat-shaped molecules with duplex stems. Because the DNA was cut with *Hae*III, these molecules may have been cut from intact DNA by the enzyme, or may have been present before digestion as discrete molecules. Fractions containing

Fig. 6 Restriction enzyme map of the minichromosome copy of the ILTat 1.3 gene. The thickened bar represents the region of homology with the cDNA in pcBC1. The sites marked by letters were located by Southern hybridization experiments with whole DNA, isolated minichromosome, and cloned genomic DNA from copies A and B, using 5' and 3' probes. The bars beneath the map indicate internal fragments which are of identical size in this copy, copy C and the cDNA. Copy D *Hinc*II fragments from a clone expressing and a clone not expressing ILTat 1.3 were separated by sucrose gradient centrifugation. Southern blot experiments with the enzymes shown at the left of the bars demonstrated the presence of these fragments in both copies. The longer arrows show the position of the ends of these fragments in the cDNA sequence¹¹. The bar above the map spans a region where all enzyme sites are identical in both the minichromosome and copy C (manuscript in preparation). All labelled sites within the region of homology with the cDNA are identical to those in the cDNA. The broken line 5' of the gene represents a region of DNA (~80 kb) that is not cut by *Eco*RI, *Ava*I, *Msp*I, *Bgl*II, *Eco*RV, *Bst*EII, *Hind*III, *Hgr*AI, *Bam*HI or *Sal*I. The broken 3' of the gene is a region of variable length in different ILTat 1 trypanosome clones. This region is not cut by *Ava*I, *Bgl*II, *Sau*3AI, *Hha*I, *Hae*II, *Pst*I, *Eco*RI, *Sal*I, *Hinc*II, *Bst*NI, *Bam*HI, *Rsa*I, *Eco*RV or *Hind*III. Enzyme labels are A1 = *Ava*I, A2 = *Ava*II, B2 = *Bgl*II, Bs = *Bst*EII, H2 = *Hinc*II, H3 = *Hind*III, Hf = *Hinf*I, P = *Pst*I, S = *Sau*3AI, T = *Taq*I.



these molecules were shown to have a 180-bp *AluI* repeated sequence. The repeated sequence was also frequently cut by *HindIII* as its recognition sequence is related to *AluI*. Since the central region of the minichromosome is not cut by *HindIII*, it appears unlikely that it contains the same repetitive element. As we have demonstrated *Bal31* sensitivity at only one end of the minichromosome, we cannot rule out the possibility that it is one of the lariat molecules observed by Borst. If so this would change the estimated size of the minichromosome.

We have found a minichromosome copy of the ILTat 1.3 gene in all ILTaR 1 clones investigated. The minichromosome appears to be a more stable component of the trypanosome genome than the expression-linked copies of some VSG genes^{3,4}. The ILTat 1.3 VSG gene in the minichromosome is identical to the expressed gene, by restriction enzyme mapping, over a range of at least 2.7 kb, and is similarly situated close to the 3' end of a DNA molecule. Both of these copies (C and D) have probably arisen by mechanisms similar to the generation of expressed copies of other VSG genes (manuscript in preparation). This involves recombination within the 3' end of the coding sequence⁹. The fact that both copies appear to be recombined with the same 3' end, unlike independently duplicated expression-linked copies, suggests that they were both derived from a single recombination event. It may be that one

gene is the precursor of the other. If the minichromosome copy is the precursor of the expressed copy it suggests a role for this unusual structure. The minichromosome may be an intermediate in the production of expressed copies of VSG genes. If this is the case, then our failure to find such a minichromosome copy of other VSG genes suggests that the stability of this particular one is unusual.

There are alternative possibilities. It is interesting to note that the ILTat 1.3 VSG is expressed in metacyclic parasites from the ILTaR 1 antigen repertoire (J. D. Barry, personal communication). Metacyclic VSGs are expressed in the tsetse fly in conditions very different from the blood stream of the mammalian host. It is possible that metacyclic VSG gene expression is controlled by a different mechanism. The minichromosome could be involved in such a mechanism.

Genetic recombination in trypanosomes has been implied from the results of Tait¹⁶. The minichromosome may be a structure involved in intercellular genetic exchange. Of course, until our observations are extended to other VSG genes, it remains possible that the minichromosome is the product of an unusual process within this trypanosome stock.

The success of the trypanosome in presenting the molecular biologist with unusual and interesting phenomena¹⁷ nearly equals its success as a parasite.

Received 16 June, accepted 19 July 1982

- 1 Turner, M. J. & Cordingley, J. S. in *Molecular and Cellular Aspects of Microbial Evolutions* (eds Carlile, M., Collins, J. & Moseley, B.) 313–347 (Cambridge University Press, 1981).
- 2 Hoijmakers, J. H. J., Frasch, A. C. C., Bernards, A., Borst, P. & Cross, G. A. M. *Nature* **284**, 78–80 (1980).
- 3 Pays, E., van Meirvenne, N., Le Ray, D. & Steinert, M. *Proc. natn. Acad. Sci. USA* **78**, 2673–2677 (1981).
- 4 Michels, P. A. M., Bernards, A., Van der Ploeg, L. H. T. & Borst, P. *Nucleic Acids Res.* **10**, 2353–2366 (1982).
- 5 Williams, R. O., Young, J. R. & Majiwa, P. A. O. *Nature* **282**, 847–849 (1979).
- 6 Young, J. R., Donelson, J. E., Majiwa, P. A. O., Shapiro, S. Z. & Williams, R. O. *Nucleic Acids Res.* **10**, 803–819 (1982).
- 7 Majiwa, P. A. O., Young, J. R., Englund, P. T., Shapiro, S. Z. & Williams, R. O. *Nature* **297**, 514–516 (1982).

- 8 Williams, R. O., Young, J. R., Majiwa, P. A. O., Doyle, J. J. & Shapiro, S. Z. *Cold Spring Harb. Symp. quant. Biol.* **45**, 945–949 (1980).
- 9 Bernards, A. *et al.* *Cell* **27**, 497–505 (1981).
- 10 Van der Ploeg, L. H. T., Bernards, A., Rijsewijk, F. A. M. & Borst, P. *Nucleic Acids Res.* **10**, 593–609 (1982).
- 11 Rice-Ficht, A. C., Chen, K. K. & Donelson, J. E. *Nature* **294**, 53–57 (1981).
- 12 Legerski, R. J., Hodnett, J. L. & Gray, H. B. *Nucleic Acids Res.* **5**, 1445–1464 (1978).
- 13 Karren, K. M. & Gall, J. G. *J. molec. Biol.* **104**, 421–453 (1976).
- 14 Studier, F. W. *J. molec. Biol.* **11**, 373–390 (1965).
- 15 Borst, P., Fase-Fowler, F., Frasch, A. C. C., Hoijmakers, J. H. J. & Weijers, P. J. *Molec. Biochem. Parasit.* **1**, 221–246 (1980).
- 16 Tait, A. *Nature* **287**, 537–538 (1980).
- 17 Englund, P. T., Hajduck, S. J. & Marini, J. C. A. *Rev. Biochem.* **51** (in the press).
- 18 Grab, D. J. & Bwayo, J. J. *Acta tropica* (in the press).

Stereochemistry of cooperative effects in fish and amphibian haemoglobins

M. F. Perutz

MRC Laboratory of Molecular Biology, Hills Road, Cambridge CB2 2QH, UK

M. Brunori

Institute of Chemistry, Medicine, I University, and Department of Biochemistry, Medicine, II University, Rome, Italy

↪ The low oxygen affinity of many fish haemoglobins at low pH is suggested to be due to the replacement by serine of the reactive cysteine F9 β found in mammalian haemoglobins. Model building shows that hydrogen bonds between this serine and the C-terminal histidine stabilize the quaternary deoxy(T) structure. A stereochemical model for the binding of the allosteric effectors ATP or GTP is also advanced.

LACTIC ACID, secreted into the blood by a gland attached to the swim bladder, causes teleost fish haemoglobins to discharge oxygen into the bladder, and thus to raise the buoyancy of the fish¹. This acid-activated discharge is known as the Root effect, but in fact it represents no more than an enhanced version of the alkaline Bohr effect exhibited by mammalian haemoglobins. Both effects consist in a reciprocating action of protons and oxygen uptake of protons causes release of oxygen and vice versa. They arise because all vertebrate haemoglobins are in an equilibrium between two structures: the deoxy or tense (T) structure and the oxy or relaxed (R) structure. The former has a low affinity for oxygen and a high one for protons, chloride, organic phosphate and CO₂. In the latter these relative affinities are reversed. The factors that affect the oxygen affinity are known collectively as heterotropic ligands. Structural analysis

has shown that they stabilize the T structure by forming salt bridges within or between the subunits. These salt bridges are absent in the R structure². The transition between the two structures in the course of oxygen uptake gives rise to the cooperativity of oxygen binding. Hill's coefficient *n* provides a measure of the degree of cooperativity.

The response of fish haemoglobins to heterotropic ligands is markedly different from that of most mammalian haemoglobins³. While in human haemoglobin *n* remains at or just below 3.0 independent of pH, in fish haemoglobins it drops to unity, or even below unity, near pH 6. This disappearance of cooperativity at acid pH is due to inhibition of the allosteric transition from the T to the R structure and is now widely used as a diagnostic of the Root effect. *n* rises to a maximum of only just above 2.0 near neutral pH and in many, but not all fish,

Table 1 Important Amino-Acid Replacements Distinguishing Mammalian, Amphibian and Fish Haemoglobins

Position of amino acid residue†	Human	Rat II and III	Carp	Trout IV	Trout I	Aquatic frog <i>Xenopus</i>	Terrestrial frogs <i>R. esculanta</i> (Europe)	<i>R. catesbeiana</i> (America)	Tadpole of <i>R. catesbeiana</i>	Shark (<i>Heterodontus portusjacksoni</i>)	Lungfish (<i>Lepidosiren paradoxa</i>)
β chain											
NA2	His	His	Glu	Asp	Glu	Gly	—	—	His	His	His
EF6	Lys	Lys	Lys	Lys	Leu	Lys	Lys	Lys	Lys	Lys	Lys
F6	Glu	Glu	Val	Val	Glu	Lys	Glu	Glu	Glu	Lys	His
F9	Cys	Cys	Ser	Ser	Ala	Ser	Ser	Ser	Ala	Ala	Ser
FG1	Asp	Asp	Glu	Glu	Asn	Glu	Asn	Gly	Asn	Glu	Glu
H21	His	His	Arg	Arg	Ser	His	Lys	Lys	His	Lys	Arg
HC1	Lys	Lys	Gln	Gln	Arg	Gly	Ala	Gly	Ser	Glu	Glu
HC3	His	His	His	His	Phe	His	His	His	His	His	His
α chain											
NA1	Val	Val	Ac-Ser	Ac-Ser	Ac-Ser	Leu	Gly	?	Ac-Ser	Ac-Ser	Met-Arg
C3	Thr	Thr	Gln	Gln	Gln	Lys	?	?	Gln	Ala	Gly
Root effect	—	?	+	+	—	+	—	—	—	—	—
Allosteric effector	DPG	DPG	ATP	ATP	—	DPG	?	?	?	?	ATP
Bohr effect	Normal	Normal	Strong	Strong	Absent	Normal	Weak	Weak-Normal	Reversed	Weak	Normal
Refs	40	40–42*	43	44	45	46†	47	48, 49	50, 51	52, 53	54

* Also L. M. Garrick and M. D. Garrick, unpublished

† Also R. M. Kay, R. Harris and J. G. Williams, unpublished

‡ For meaning of the symbols see Figs 3–5

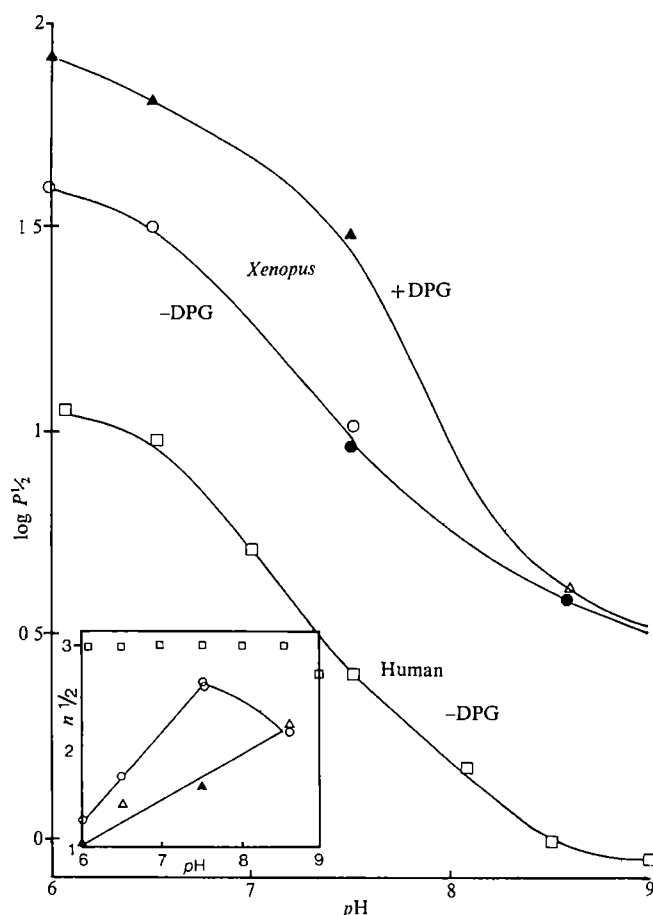


Fig. 1 Oxygen Bohr effect from two different preparations (open and closed symbols) of *Xenopus* haemoglobin at 20 °C. O, Stripped in 0.1 M bis-Tris or Tris-HCl+0.1 M NaCl; Δ , Same+5 mM DPG. Haemoglobin concentration 180–300 μ M haem. The insert shows the pH dependence of $n_{1/2}$. Blood from various animals was pooled and washed with 0.7% NaCl. The packed cells were lysed with distilled water, and stroma and nuclei were spun down. The haemoglobin was stripped as described in ref. 55 and dialysed against 0.1 M NaCl and water. The haemolysate was analysed by starch gel electrophoresis at pH 8.6 before and after incubation with 2 mM mercaptoethanol, but no evidence of polymerization was found. Oxygen dissociation curves were determined spectrophotometrically. \square , Stripped human haemoglobin in 0.05 M bis-Tris+0.1 M NaCl.

falls again at higher pH. Both the span of oxygen affinities covered by the pH range 6–9 and the magnitude of the alkaline Bohr effect ($\Delta \log p_{50}/\Delta \log pH$) are larger in fish than in mammalian haemoglobins. For instance, in carp haemoglobin k_1 , the association constant of the first oxygen molecule to be taken up, rises 100-fold between pH 6.5 and 9, compared to eight-fold in human haemoglobin. Over the same pH range k_4 , the association constant of the last oxygen, rises 10-fold in carp compared to 1.2-fold in human. On oxygenation, human haemoglobin in deionized water releases no more than one proton per tetramer, while carp releases 3.6. On the other hand, the enhancement of the alkaline Bohr effect by chloride or phosphate is smaller in carp than in human haemoglobin. Most mammalian red blood cells contain 2,3-disphosphoglycerate as an allosteric effector, while those of fish contain ATP or GTP instead.^{4–11}

What makes the allosteric properties of these fish haemoglobins so different from those of mammalian haemoglobins? Seeing that the fraction of amino acid replacements between, say, human and carp haemoglobin is of the order of 50%, this seems a forbidding problem, but experience has shown that the great majority of replacements between species is functionally neutral, while a few in key positions dominate the allosteric functions. At a meeting on allostery at Cambridge in August 1980, these thoughts led Perutz to suggest that a single replacement, namely that of cysteine F9(93) β in mammalian haemoglobins by serine in fish, may be sufficient to explain most of the Root effect. The recent discovery of serine in the same position of *Xenopus* haemoglobin then led him to predict that it should also exhibit a Root effect. The results reported below confirm this. Model building and study of amino acid sequences now lead us to propose a detailed stereochemical mechanism for the cooperative effects in fish and amphibian haemoglobins.

Ligand binding by *Xenopus* haemoglobin

Xenopus haemoglobin has a range of oxygen affinities below those of human haemoglobin, suggesting greater stability of its T structure. We have found its alkaline Bohr to be similar in magnitude to that of human haemoglobin, but its Hill's coefficient to approach unity at pH 6.0, as in fish haemoglobins that exhibit the Root effect, suggesting that acid pH inhibits the transition from T to the R structure (Fig. 1). This inference is confirmed by the kinetics of carbon monoxide recombination after flash photolysis. In mammalian haemoglobins this reaction accelerates as combination of successive CO molecules is accompanied by the T \rightarrow R transition, but in fish haemoglobins at pH 6.0 that acceleration is absent, because the T \rightarrow R transi-

tion is inhibited⁶ In *Xenopus* haemoglobin the kinetics of CO recombination were obscured at first by partial dissociation into non-cooperative, fast-reacting dimers. We therefore determined the dependence of the fraction of dimers on protein concentration, pH and organic phosphates and corrected our measurements of the time course of recombination accordingly. The corrected curves are shown in Fig 2. After complete photolysis at pH 7.2 recombination is autocatalytic, because the flash is followed by conversion from the R to the T structure within the dead time of the instrument, and recombination is accompanied by reconversion to the R structure, which accelerates the reaction. After partial photolysis initial recombination is much faster, which indicates that Hb(CO)₃ remains in the R structure (Fig 2a). In human haemoglobin the overall kinetic behaviour is similar to this at both pH 7.2 and 6.0, with and without organic phosphates.

In *Xenopus* haemoglobin at pH 6.0 with inositol hexaphosphate (IHP) full photodissociation produced a time course that no longer accelerated, indicating that the tetramers of *Xenopus* haemoglobin remained in the T structure as they took up CO. On partial photolysis the time course of CO recombination was no faster than on complete photolysis. This is the decisive result, because it suggests the absence of a significant fraction of Hb(CO)₃ tetramers in the R structure, and is characteristic of haemoglobins exhibiting the Root effect (Fig 2b).

The discovery of dissociation into dimers in the kinetic experiments raised the question of whether this could have contributed to the absence of cooperative oxygen binding in our equilibrium measurements at pH 6. However, the haemoglobin concentrations used for these were 9–15 times higher than for the kinetic measurements, and the fraction of dimers present was no more than 5%.

Stereochemical interpretation of the Root effect

In the T structure of all haemoglobins that exhibit a Bohr effect, the imidazole of the C-terminal histidine HC3 β forms a salt bridge with Asp or Glu FG1 or Glu F6. Formation of that salt bridge raises the *pK* of the histidine such that protons are bound. The C-terminal carboxyl of the same histidine forms a salt bridge with the invariant Lys C5 α in the T structure of all haemoglobins, regardless of whether they show a Bohr effect or not³. Previous electron density maps of the R structure have shown no density for His HC3 β , whence it was believed to be waving about freely, but a recent high resolution map of human oxyhaemoglobin at -2°C shows that it is in fact anchored, and that its density may previously have been smeared out by its high temperature factor (B. Shaanan, personal communication). The new map shows that its carboxyl group forms a salt bridge with Lys HC1 of the same β chain and that its imidazole is free, the distance between its N ϵ and the carboxyl of Asp FG1 has increased from 2.8 Å in the T structure to 9 Å in the R structure. Lys HC1 β , to which the terminal carboxyl binds in the R structure, is invariant in mammals, but in those fish haemoglobins that exhibit a Root effect it is replaced by glutamine, and in *Xenopus* by glycine, neither of which would bind the carboxyl (Figs 3 and 4, Table 1). Thus less energy is needed to move His HC3 β towards Asp FG1 β on going from the R to the T structure.

In mammals, position F9 β is occupied by cysteine whose sulphhydryl group takes up one of two alternative positions. In one of them it is tucked away in the pocket between helices F and H, in close contact with the side chain of Tyr HC2 with which it shares the pocket, in the other it is external. In the R structure the SH group oscillates between the two positions, and the equilibrium varies with the spin state of the haem. Low spin favours the internal, high spin the external position (Fig 3b)¹². In the T structure the sulphhydryl group is out of the tyrosine pocket, but now it is screened from access to reagents by the C-terminal histidine HC3 β , it is in contact with that oxygen of the C-terminus that is not bonded to Lys C5 α (Fig

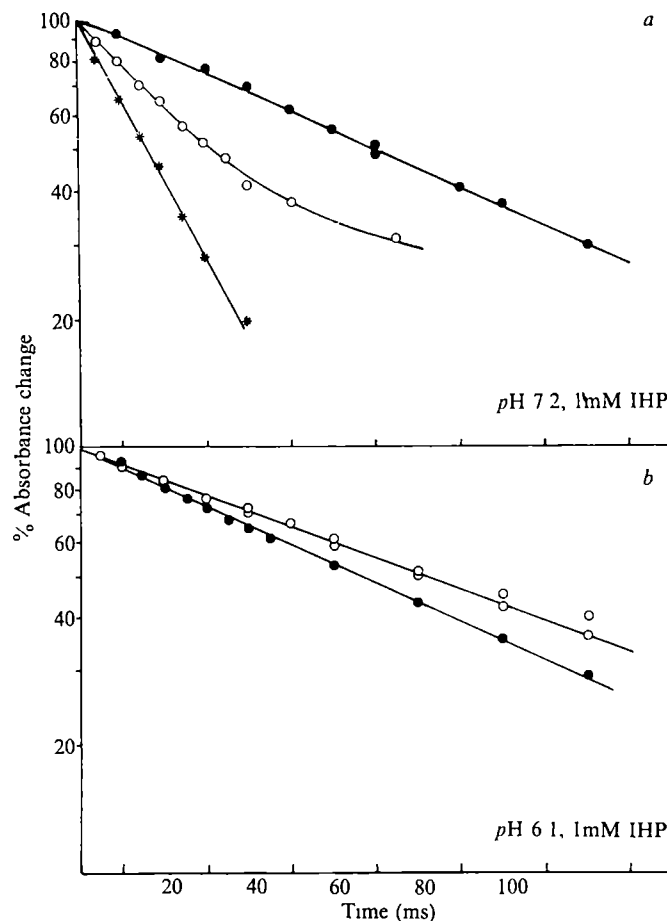


Fig. 2 Recombination of *Xenopus* haemoglobin with CO at 20°C . The time course of the reaction was followed at 436 nm, using a flash photolysis apparatus similar to that described previously^{5,6}. The intensity of the flash for the partial photolysis experiments was reduced by interposing appropriate neutral density filters. Haemoglobin (concentration = $20\ \mu\text{M}$ haem) in 0.1 M bis-Tris buffer + 0.1 M NaCl + 1 mM IHP, total CO $100\ \mu\text{M}$. *Xenopus* haemoglobin is partially dissociated into dimers in the ligated form, and the dissociation is pH dependent. At $5\ \mu\text{M}$ haemoglobin in 0.1 M bis-Tris, the fraction of dimeric HbCO is 5% at pH 7.2, 15% at pH 6.7 and 40% at pH 6.2. The fraction of dimers was measured as a function of concentration and the curves shown were corrected for the appropriate fraction by extrapolation to infinite concentration. ●, 100% photodissociation, ○, 11% photodissociation, *, 5% photodissociation.

3a). No matter where it is, the sulphhydryl forms no, or only very weak, hydrogen bonds with its neighbours, no such bonds have been observed in crystal structures of small organic compounds, when on SH approaches an oxygen, the H–O distance is the same as the sum of the van der Waals radii— $2.4\ \text{\AA}$ (ref 13). What happens when the cysteine in haemoglobin is replaced by serine? On the basis of their partition coefficients between octanol and water, SH was found to be 25 times more hydrophobic than a hydroxyl group¹⁴. Judged by their effects on the vapour pressure of cysteine and serine in water, the hydration potential of a hydroxyl group was found to be more favourable than that of a sulphhydryl group by $3.8\ \text{kcal mol}^{-1}$ (ref 15). Consequently the side chain of serine is likely to prefer the external, exposed position to the hydrophobic internal one between helices F and H. In the T structure, the OH of serine F9 is so placed that it can donate a hydrogen bond to the unbound terminal oxygen atom of His HC3 β and accept a hydrogen bond from the peptide NH of His HC3 β (Figs 3c and 4). These bonds stabilize the C-terminal salt bridges in the T structure. They would therefore raise the allosteric constant *L*, lower the oxygen binding constant *K_T* and raise the *pK* of His HC3 β . At low pH the hydrogen bonds may also allow His

HC3 β to form a salt bridge with Glu FG1 β in the R structure. If it did, acid pH would lower not only K_T but also K_R . We suggest that the hydrogen bonds formed by Ser F9 β are the prime cause of the Root effect. This hypothesis led Perutz to predict that the Root effect should be absent in fish haemoglobins from which His HC3 β has been enzymatically cleaved. Goss, Parkhurst and Perutz have tested this prediction in carp haemoglobin and found that such cleavage does indeed cause the Root effect to be inhibited and the Bohr effect to be halved (unpublished data).

Variations of the Bohr effect in different species

In human haemoglobin that part of the alkaline Bohr effect that is not due to His HC3 β was found to be linked to anion binding¹⁶. In stripped haemoglobin in 0.1 M chloride it arose from the binding of chloride ions to Val 1 α and Lys EF6 β ¹⁷. In carp haemoglobin that same part is much larger even in deionized solution (~1.8 protons per tetramer, compared to 1.2 in human)^{16,18}. Where does it come from? The amino acid sequence shows that Ser 1 α is acetylated, so that it can contribute no Bohr protons. Val 1 β is free but has never been found to contribute to the Bohr effect of other haemoglobins. Apart from the haem-linked histidines which contribute no Bohr protons and the C-terminal His HC3 β whose contribution we have just discussed, the only histidine present is FG4 β . This is far removed from any other ionizable group, is known not to contribute significantly to the alkaline Bohr effect in human haemoglobin¹⁷ and is present in tadpole haemoglobin which has only a reverse Bohr effect. The structure shows no paired, buried carboxylates which would have pK values in the physiological range. The evidence suggests that the high concentration of cationic groups between the two β chains causes the pair of Lys EF6 β to act as alkaline Bohr groups, as they were found to do in human haemoglobins¹⁷. The position of Lys EF6 is shown in Fig. 5.

In human haemoglobin in 0.1 M chloride the alkaline Bohr effect vanishes at pH 6 and is reversed below that pH. This is known as the acid or reverse Bohr effect. About half of it is contributed by His H21 β , the origin of the other half is unknown¹⁷. In fish where residue H21 β is Arg, the acid Bohr effect is absent.

Xenopus haemoglobin does not exhibit as strong a Root or Bohr effect as do carp and trout IV haemoglobins. For instance, we found that its azide methaemoglobin does not show the

striking transition to higher spin at pH 6 exhibited by the two fish haemoglobins¹⁹. *Xenopus* haemoglobin has conserved the essential Ser F9 β , Glu FG1 β and His HC3 β , and it has Gly rather than Lys in position HC1 β to prevent anchoring of the C-terminus in the R structure (Table 1). On the other hand, it has a Lys at F6 β , one turn of π -helix removed from Glu FG1 β and capable of competing with His HC3 β for the essential salt bridge with that Glu (Fig. 4). This competition may weaken its Root and Bohr effects.

Other amphibian haemoglobins show much weaker alkaline Bohr effects or even none at all. The major haemoglobin component of the large American bullfrog *Rana catesbeiana*, when stripped and in dilute solution, shows a Bohr effect of $\Delta p_{50}/\Delta pH = -0.16$, compared with -0.56 in *Xenopus*²⁰. Position F9 β is occupied by Ser, as in *Xenopus*, but its influence is counteracted by the substitution Gly for Glu in position FG1 β . In consequence His HC3 β cannot have its pK raised in the T structure by the usual strong salt bridge with Glu FG1 β , but can only interact more weakly with Glu F6 β which is one turn of π -helix away from residue FG1 β (Table 1, Fig. 4). His H21 β , which contributes to the acid Bohr effect in human haemoglobin A, is replaced by Lys. Tadpole haemoglobin of *R. catesbeiana* in the absence of phosphates has only a reverse Bohr effect²¹. Here Ser F9 β is replaced by Ala, Glu FG1 by Asn, and Ser 1 α is acetylated, so that the alkaline Bohr effect is inhibited entirely. On the other hand, His H21 β is present, consistent with its role in the acid Bohr effect of human haemoglobin. The two major fractions of the adult haemoglobin of the European frog *Rana esculenta* exhibit only a weak alkaline Bohr effect²². The amino groups of Gly 1 α are free to contribute to it. The sequence of the major component of the β chain is similar to that of *R. catesbeiana*, but position FG1 β is occupied by Asn, so that the strong salt bridge with His HC3 β is inhibited as in *R. catesbeiana*. These are the only amphibian β sequences known.

Haemoglobin of the shark *Heterodontus portusjacksoni*, a cartilaginous fish without a swim bladder, exhibits a weak alkaline Bohr effect²³. Position F9 β is occupied by Ala, residue FG1 β is Glu, which could produce a normal alkaline Bohr effect by forming a strong salt bridge with His HC3 β if it were not for a Lys in position F6 β , one turn of π -helix away, competing with His HC3 β for that salt bridge. The lungfish *Lepidosiren paradoxa* also lacks a swim bladder, its haemoglobin exhibits no Root effect and has an alkaline Bohr effect similar in magnitude to that of human haemoglobin²⁴. It does have Ser at F9 β and Glu at FG1 β , but as in *Xenopus* and in the shark its salt bridge with His HC3 β is weakened by competi-

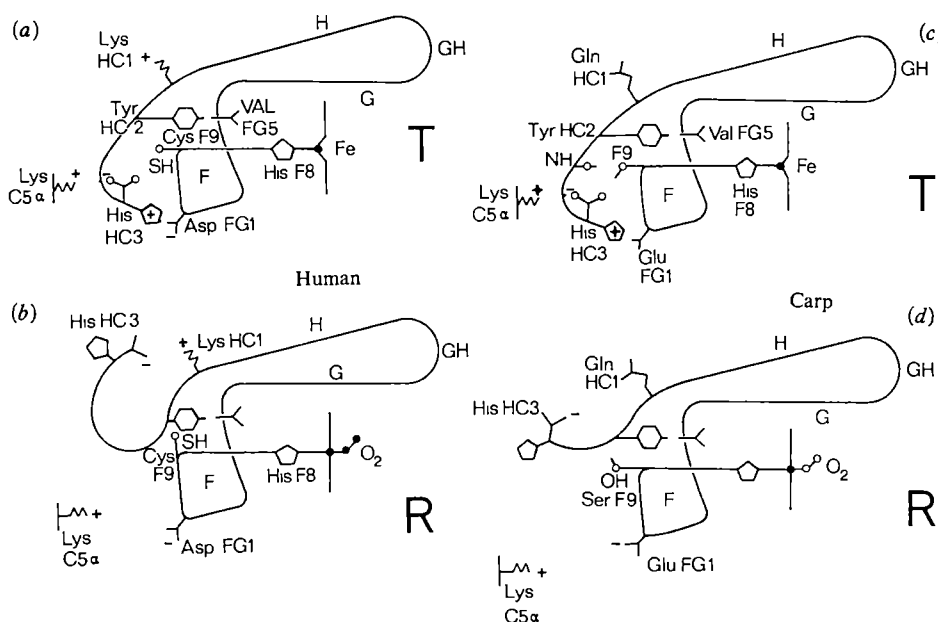
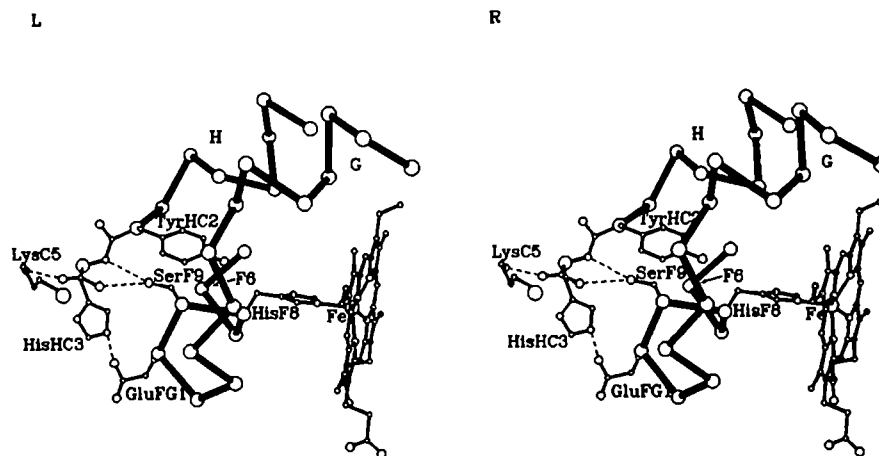


Fig. 3 C-terminal salt bridges and the role of residue F9 in the T and R structures of mammalian and fish haemoglobins. *a*, Human T structure, *b*, human R structure, *c*, carp T structure, *d*, carp R structure. The letters F, G and H denote helical segments, FG, GH and HC denote non-helical segments. The same notation is used in Figs 4 and 5.

Fig. 4 Stereodiagram showing the bonds at the C-terminus of the β chain in the T structure of teleost fish haemoglobin. The amino group of Lys C5 α donates a hydrogen bond to one of the carboxylate oxygens of His HC3 β , and the OH of Ser F9 β donates a hydrogen bond to the other oxygen. The imidazole donates a hydrogen bond to the carboxylate of Glu FG1. The main chain NH of His HC3 donates a hydrogen bond to the lone pair electrons of the OH of Ser F9. Note the direct link from the haem iron via His F8 and Ser F9 to the C-terminus, which would therefore feel the movement of the iron towards the porphyrin that occurs on oxygen binding.



tion from residue F6 β , in this instance a His. Lungfish haemoglobin has an additional residue, a Met, at the amino end of the α chain. It is not clear if this could contribute to the alkaline Bohr effect by binding a chloride ion jointly with Arg HC3 of the opposite α chain, as Val 1 α does in mammals.

Rat haemoglobin

IHP causes the Hill's constant of three of the major components of rat haemoglobin to approach unity at pH 6.²⁵ The only substitutions of polar residues that distinguish rat from human haemoglobin lie on the surface and are not of a kind that would affect the stability of the T structure in the absence of IHP. On the other hand, the dominant fraction III β has a net charge higher by +5 than the human β chain, so that it may bind IHP so strongly as to produce a Root effect. These observations show that a Root effect may be produced by an alternative mechanism to that operating in fish.

The $\alpha_1\beta_2$ contact

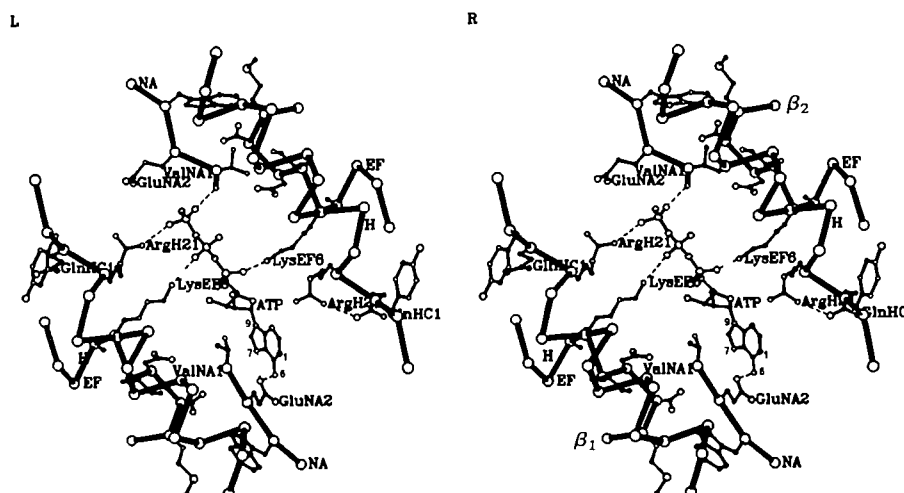
The $\alpha_1\beta_2$ contact works as a snap action switch between the two alternative quaternary structures. In the T structure of all vertebrates a groove formed by Val FG5 β_2 is filled by the side chain of residue C6 α_1 , while in the R structure that same groove is occupied by the side chain of residue C3 α_1 . In mammals C3 α_1 is threonine whose side chain merely interacts with water molecules. In fish C3 α_1 is glutamine whose amide group may either interact with water or form weak hydrogen bonds with Asp G3 β_2 in the T structure and Asp G1 β_2 in the R structure.

In *Xenopus* C3 α_1 is lysine. The atomic models suggest that its amino group would form a salt bridge with Asp G3 β_2 in the T structure, and with Asp G1 β_2 in the R structure. Apart from these differences, the R \rightarrow T switch mechanism is as in human haemoglobin (for illustrations see ref. 26).

ATP and GTP binding sites

Mammals and frogs use D-2,3-diphosphoglycerate (DPG) as an allosteric effector, but teleost fish use ATP, GTP or inositol pentaphosphate.^{27,28} While in mammals DPG lowers the oxygen affinity more than ATP, the opposite holds in teleost fish²⁹, which suggests that the stereochemistry of the binding site must be different. There are three clues to its nature. Carbamylation of Val NA1 β inhibits ATP binding³⁰, mammalian haemoglobins that use DPG as a regulator have a hydrogen donor side chain in position NA2 β (His, Gln or Asn) and they have His in position H21 β . Teleost fish have either Glu or Asp in position NA2 β , and Arg at H21 β . We found that substitution of those side chains in the atomic model of human deoxyhaemoglobin produces a constellation of charged groups stereochemically complementary to strain-free models of ATP or GTP. When ATP is bound, the carboxylate of either Glu or Asp NA2 β_1 accepts a hydrogen bond from the N-6 amino group of adenine, the amino group of Val NA 1 β_2 and the guanidinium group of Arg H21 β_1 , each donate a hydrogen bond to (PO₄)⁻, while Lys EF6 β_1 and β_2 donate hydrogen bonds to either of the other two phosphates, thus neutralizing the four

Fig. 5 Suggested ATP binding site of fish haemoglobins. N-6 of the adenine donates a hydrogen bond to the carboxylate of Glu NA2 whose side chain is oriented so that $\chi_1 = 60^\circ$. The purine is in the *anti* conformation with respect to the ribose. The ribose is C3' *endo* and C5'-05' is *trans*. If ATP is replaced by GTP with the proton bound to N-7, which is unusual, then the purine can remain in the *anti* conformation and N-7 can donate a hydrogen bond to Glu NA2. If the proton is in the usual position on N-1, no hydrogen bond is possible in this conformation. A good hydrogen bond can be made by turning the purine by 180° about the N-9-C-1' bond to the *syn* conformation, and the side chain of Glu NA2 about the C $^\alpha$ -C $^\beta$ bond to $\chi_1 = -60^\circ$. All the hydrogen bonds described here lie in the plane of the purine ring. In human haemoglobin 2,3-diphosphoglycerate (DPG) binds to the same site as shown here, but forming salt bridges with Val NA1, His NA2, Lys EF6 and His H21. Diagrams of the DPG binding site appear in refs 26 and 57.



negative charges of ATP (Fig 5) GTP may bind in two alternative conformations. In the normal tautomer of guanine, which has the proton on N-1, the purine would have to take up the *syn* conformation with respect to the ribose so as to allow N-1 to donate a hydrogen bond to Glu or Asp NA2 β . If the proton were to be transferred to N-7, forming the other tautomer, then the purine could be in the *anti* conformation, as in Fig 5, and N-7 could donate a hydrogen bond to Glu NA2 β . This structure is less likely, because N₇ has never been observed to carry a proton in uncharged guanine. It is intriguing that substitutions at no more than two positions, NA2 and H21, are needed to convert the DPG to an ATP or GTP binding site. In fact, the substitution of Arg for His at H21 may suffice. Lungfish use ATP as an allosteric effector and yet have His at H21. Model building shows that this could accept a hydrogen bond from the adenine NH₂ or donate one to the guanine carbonyl group.

Biological implications

Many fish use the Root effect to secrete oxygen into both the swim bladder and the eye³¹⁻³⁴. Each organ possesses an elaborate vascular network, the rete, which converts a gradient of increasing lactic acid concentration into a gradient of decreasing oxygen saturation by countercurrent circulation³⁵. Frogs do not possess these organs. Why then does *Xenopus* haemoglobin exhibit a Root effect? It is an aquatic frog, and part of its respiratory exchange takes place through capillaries in its skin. Yet this can hardly be the explanation because the same is true for the mainly terrestrial frog *R. esculenta* when it is under water. In both animals about two-thirds of the capillaries for gas exchange are in the lungs and one third is in the skin³⁶, oxygen is taken up mainly through the lungs, while CO₂ is excreted mainly through the skin³⁷. We do not know what, if any, selective advantage the Root effect confers on *Xenopus*, but we have come across one habit unique to *Xenopus* that might give a clue. *Xenopus* lives in muddy pools in Southern Africa. E. M. Deuchar writes "When some of the pools dry up in summer, *Xenopus* has to burrow into the mud to avoid desiccation, and here it remains quiescent, aestivating, until the next rainy season"³⁸. Under these conditions the frog would be short of oxygen. Conceivably the Root effect would then allow a greater fraction of the oxygen stored in the blood to be used by the tissues.

The constellation of polar residues needed to produce the Root effect and the accompanying large Bohr effect in teleost fish seems to consist of Lys EF6, Ser F9, Glu FG1, Arg H21 and His HC3, all on the β chains. We have not found any residues in the α chain that contribute directly, though some may do so indirectly, by biasing the allosteric equilibrium towards the T structure. In many amphibian and fish haemoglobins most or even all these essential polar residues have been conserved even when they lack a Root effect and exhibit only weak Bohr effects. In some instances this happens because their influence is countered by a substitution elsewhere: in *Xenopus* and shark by Val F6 β \rightarrow Lys, and in the lungfish by Val F6 β \rightarrow His, which compete with the C-terminal histidine for the salt bridge with Glu FG1 β . In the adult haemoglobins of the two terrestrial frogs a strong alkaline Bohr effect is inhibited by the substitutions Glu FG1 β \rightarrow Gly or Asn and a weaker one is generated by the substitution Val F6 β \rightarrow Glu. In the tadpole of *R. catesbeiana* the substitutions Ser F9 β \rightarrow Ala and Glu FG1 β \rightarrow Asn seem to abolish the alkaline Bohr effect, even though Glu still occupies the position F6 β , the substitution Lys H21 β \rightarrow His, and possibly others still unknown, introduce a reverse Bohr effect. Trout I haemoglobin shows no response to any heterotropic ligands even though it exhibits normal haem-haem interaction, because all the polar residues involved in both the alkaline and acid Bohr effects and in phosphate binding are replaced by neutral ones. Lys EF6 β is replaced by Leu, Ser F9 β by Ala, Glu FG1 β by Asn, Arg H21 β by Ser and His HC3 β by Phe^{33,38}. Trout I haemoglobin provides the most compelling evidence that heterotropic ligands exert their influence at a small number of specific sites. One cannot help being struck by the beautiful design of the stereochemical mechanism that gives rise to the strong Root and Bohr effects in teleost fish, and by the haphazard way that evolution has chosen to weaken, inhibit and even reverse these effects in a variety of different ways when they are not needed. It is an example of what Jacob calls "evolutionary tinkering"³⁹.

We thank Mr A. Bellelli and Mr S. G. Condo for their technical help, Dr C. Poyart for supplying the P_{50} values of human haemoglobin, Dr S. E. V. Phillips for generating the computer drawings in Figs 4 and 5, and Professor C. Bauer, Professor J. Dumits, Dr A. Klug, Dr R. W. Noble, Dr A. Riggs and Professor K. Winterhalter for helpful comments.

Received 24 May, accepted 23 July 1982

- 1 Root, R. W. *Biol. Bull.* **61**, 427-463 (1931)
- 2 Perutz, M. F. *Nature* **28**, 726-739 (1970)
- 3 Brunori, M. *Curr. Topics cell. Regulation* **9**, 1-36, 1975
- 4 Brunori, M. *et al. Molec. cell. Biochem.* **1**, 189-196 (1973)
- 5 Noble, R. W., Parkhurst, L. J. & Gibson, Q. H. *J. biol. Chem.* **245**, 6628-6633 (1970)
- 6 Tan, A. L., De Young, A. & Noble, R. W. *J. biol. Chem.* **247**, 2493-2498 (1972)
- 7 Imai, K. & Yonetani, T. *J. biol. Chem.* **250**, 2227-2231 (1975)
- 8 Chien, J. C. W. & Mayo, K. H. *J. biol. Chem.* **255**, 9790-9799 (1980)
- 9 Binotti, I. C. *et al. Archs Biochem. Biophys.* **142**, 274-281 (1971)
- 10 Gillen, R. G. & Riggs, A. *J. biol. Chem.* **247**, 6039-6046 (1972)
- 11 *Comp. Biochem. Physiol.* **62A**, No 1 (1979)
- 12 Baldwin, J. M. *J. molec. Biol.* **136**, 103-128 (1980)
- 13 Kerr, K. A., Ashmore, J. P. & Koetzle, T. F. *Acta crystallogr.* **B31**, 2022-2026 (1975)
- 14 Hansch, C. & Leo, A. *Substituent Constants for Correlation Analysis in Chemistry and Biology*, Ch. 4 (Wiley, New York, 1979)
- 15 Wolfenden, K., Anderson, L., Cullis, P. M. & Southgate, C. C. B. *Biochemistry* **20**, 849-885 (1981)
- 16 O'Donnell, S., Mandaro, R., Schuster, T. & Arnone, A. *J. biol. Chem.* **254**, 12204-12208 (1979)
- 17 Perutz, M. F. *et al. J. molec. Biol.* **138**, 649-670 (1980)
- 18 Chien, J. C. W. & Mayo, K. H. *J. biol. Chem.* **255**, 9800-9806 (1980)
- 19 Perutz, M. F. *et al. Biochemistry* **17**, 3640-3652 (1978)
- 20 Aggarwal, S. J. & Riggs, A. *J. biol. Chem.* **244**, 2372-2383 (1969)
- 21 Atha, D. H., Riggs, A., Bonaventura, J. & Bonaventura, C. *J. biol. Chem.* **254**, 3393-3400 (1979)
- 22 Brunori, M. *et al. Comp. Biochem. Physiol.* **24**, 519-526 (1968)
- 23 Nash, A. R., Fisher, W. K. & Thompson, E. O. P. *Aust. J. biol. Sci.* **27**, 607-615 (1974)
- 24 Phelps, C. *et al. Comp. Biochem. Physiol.* **62A**, 139-143 (1979)
- 25 Condo, S. G., Giardina, B., Barra, D., Gill, S. J. & Brunori, M. *Eur. J. Biochem.* **116**, 243-247 (1981)
- 26 Fermi, G. & Perutz, M. F. *Atlas of Molecular Structures in Biology* Vol. 2 (Clarendon, Oxford, 1981)
- 27 Gillen, R. G. & Riggs, A. *Archs Biochem. Biophys.* **183**, 678-685 (1977)
- 28 Isaacks, R. E., Kim, H. D., Bartlett, G. R. & Harkness, G. R. *Life Sci.* **20**, 987-990 (1977)
- 29 Gillen, R. G. & Riggs, A. *Comp. Biochem. Physiol.* **38B**, 585-595 (1971)
- 30 Powers, D. A. & Edmundson, A. B. *J. biol. Chem.* **247**, 6686-6693 (1972)
- 31 Steen, J. B. in *Fish Physiology* Vol. 4 (eds Hoar, W. S., Randall, D. J. & Brett, J. R.) (Academic, New York, 1979)
- 32 Wittenberg, J. B. & Wittenberg, B. A. *Biol. Bull.* **146**, 116-136 (1974)
- 33 Wittenberg, J. B. & Haedrich, R. L. *Biol. Bull.* **146**, 137-156 (1974)
- 34 Farmer, M., Fyhn, H. J., Fyhn, U. E. H. & Noble, R. W. *Comp. Biochem. Physiol.* **62A**, 115-124 (1979)
- 35 Haldane, J. S. in *Respiration*, 250-257 (Yale University Press, 1922)
- 36 Czopek, J. *Acta anat.* **25**, 346-360 (1955)
- 37 Charles, E. *Proc. R. Soc. B107*, 486-503 (1931)
- 38 Barra, D., Bossa, F. & Brunori, M. *Nature* **293**, 587-588 (1981)
- 39 Jacob, F. in *The Possible and the Actual* (University of Washington Press, 1982)
- 40 Dayhoff, M. O. *Atlas of Protein Sequence and Structure* (National Biomedical Research Foundation, Washington, D. C. 1972)
- 41 Garrick, L. M., Sharma, V. S., Macdonald, M. J. & Ranney, H. M. *Biochem. J.* **149**, 245-258 (1975)
- 42 Garrick, L. M., Sloan, R. L., Ryan, T. W., Klonowski, T. J. & Garrick, M. D. *Biochem. J.* **173**, 321-330 (1978)
- 43 Grujic-Injac, B., Braunitzer, G. & Stangl, A. *Hoppe-Seyler's Z. physiol. Chem.* **361**, 1629-1639 (1980)
- 44 Bossa, F. *et al. FEBS Lett.* **64**, 76-80 (1976)
- 45 Bossa, F., Barra, D., Petrucci, R., Martini, F. & Brunori, M. *Biochim. biophys. Acta* **536**, 298-305 (1978)
- 46 Williams, J. G., Kay, R. M. & Patient, R. K. *Nucleic Acids Res.* **8**, 4247-4258 (1980)
- 47 Chauvet, J. P. & Acher, R. *Biochemistry* **11**, 916-927 (1972)
- 48 Baldwin, T. O. & Riggs, A. *J. biol. Chem.* **249**, 6110-6118 (1974)
- 49 Tentori, L., Vivaldi, G., Carta, S., Velani, S. & Zito, R. *Biochim. biophys. Acta* **133**, 177-180 (1967)
- 50 Maruyama, T., Watt, K. W. K. & Riggs, A. *J. biol. Chem.* **255**, 3285-3293 (1980)
- 51 Watt, K. W. K., Maruyama, T. & Riggs, A. *J. biol. Chem.* **255**, 3294-3301 (1980)
- 52 Nash, A. R., Fisher, W. K. & Thompson, E. O. P. *Aust. J. Biol.* **29**, 73-97 (1976)
- 53 Fisher, W. K., Nash, A. R. & Thompson, E. O. P. *Aust. J. Biol.* **30**, 487-506 (1977)
- 54 Rhodewald, K. & Braunitzer, G. *Hoppe-Seyler's Z. physiol. Chem.* (in the press)
- 55 Condo, S. G., Giardina, B., Lunader, M., Ferracini, A. & Brunori, M. *Eur. J. Biochem.* **120**, 323-327 (1981)
- 56 Brunori, M. & Giacometti, G. M. *Meth. Enzym.* **76**, 582-595 (1982)
- 57 Arnone, A. *Nature* **237**, 146-149 (1972)
- 58 Deuchar, E. M. *Xenopus: The South African Clawed Frog* (Wiley, London, 1975)

LETTERS TO NATURE

Neutron oscillation as a source of excess sub-GeV antiprotons in galactic cosmic rays

C. Sivaram & V. Krishan

Indian Institute of Astrophysics, Bangalore-560 034, India

The recent detection^{1,2} of an antiproton/proton (\bar{p}/p) ratio at energies much less than 1 GeV is several orders of magnitude above that predicted for \bar{p} production from primary cosmic ray collisions. It is well recognized that there is no mechanism to explain this sub-GeV (130–320 MeV) \bar{p} excess although many suggestions have been made. For example, Eichler³ considers secondary production in high-energy collisions while Kiraly⁴ *et al.* suggest black hole evaporation as a \bar{p} source. Most of these suggestions have inherent difficulties such as the imposition of severe constraints on the sources to suppress excessive γ -ray production. We postulate here that the phenomenon of neutron–antineutron ($n\bar{n}$) oscillations as a signature of grand unified theories may operate in neutron-rich astrophysical sources such as supernovae to produce the required low-energy galactic antiproton background.

Theoretical predictions of the generation of antiprotons in cosmic rays as a result of collisions of primary protons at relativistic energies would require \bar{p}/p to decrease with decreasing energy, as the threshold for production of \bar{p} from these mechanisms is ~ 2 GeV. This is in contrast with the observations where \bar{p}/p increases at lower energies, the ratio being $>10^{-4}$ at 130–320 MeV. The observation of Buffington *et al.*^{1,2} would imply a \bar{p} energy density of $\sim 10^{-4}$ eV cm⁻³ inside our Galaxy. In some hypotheses the \bar{p} s have been considered to be primary cosmic rays from antigalaxies⁵. But the fact that the reported He/He ratio is significantly lower than the \bar{p}/p ratio would raise difficulties with such models. A recent trend has been to assume the \bar{p} s as secondaries and propose scenarios for decelerating them to sub-GeV energies. For example, \bar{p} s could be produced at a large cosmological redshift and decelerated by the expansion of the Universe. Unfortunately this would imply an energy density in high-energy neutrinos (simultaneously produced in the high-energy collisions) well in excess of the Reines⁶ experimental limit on cosmic neutrino background at $E > 0.5$ GeV. Other models of deceleration of \bar{p} s within the Galaxy also have undesirable features such as excessive γ -ray production. This would require \bar{p} s to be produced only in compact optically thick sources that would reduce the γ -ray flux. Moreover there are constraints on the density of the traversed matter. Clearly a mechanism is needed to account for the excess production of sub-GeV \bar{p} s at the same time without producing γ rays and high-energy neutrinos. Preferably one should have a means of producing the \bar{p} s directly at sub-GeV energies without having to invoke deceleration mechanisms. Obviously, the direct low-energy production of \bar{p} s would violate baryon number conservation. Fortunately recent progress in grand unified theories⁷ has provided for just such a situation. The phenomenon of $n\bar{n}$ oscillation has been suggested as a consequence of grand unification^{8,9}. It has also been invoked to generate the cosmic-ray antiproton flux by the spallation of cosmic-ray nuclei in interstellar space which is, however, low because of the low ${}^4\text{He}/p$ ratio¹⁰.

The $n\bar{n}$ mechanism is expected to be important wherever large fluxes of low-energy neutrons are produced or are present. A supernova explosion, for instance, is expected to release a very large number of neutrons. There are several ways in which the neutrons may be generated, for instance the supernova shell

is sufficiently dense for the heavy nuclei to interact and produce neutrons by breakup or charge exchange. Nuclear statistical equilibrium distributions dominated by extremely neutron-rich nuclei are expected for the large neutron-to-proton ratio characterizing the supernova material. One expects¹¹ that the total ratios of neutrons to protons will reach 2–8. In effect, every supernova explosion might shoot out 10^{57} free neutrons into interstellar space, the rest having been captured. We will now briefly discuss the phenomenon of $n\bar{n}$ oscillations. This transition is a first-order process involving a baryon number change of 2. This is analogous to the well known phenomenon of strangeness oscillation in the neutral K-meson system, that is $K_0 \leftrightarrow \bar{K}_0$, which involves a strangeness change of 2. Several theoretical models have been proposed to estimate the average transition time for the oscillations $n\bar{n}$. The characteristic time of such oscillations is predicted to be between 10^5 and 10^7 s and the associated transition energies ($\Delta\rho$) are of the order of 10^{-20} eV (refs 8, 9). The β decay of the antineutron so formed results in an antiproton. So the net result is the transformation of a neutron into an antiproton and this can take place at low energies. Therefore, this may be an appropriate phenomenon for the production of low-energy \bar{p} s without any of the attendant γ rays which is the weakness of other mechanisms. In the presence of the magnetic field, the $n\bar{n}$ oscillations are inhibited because of magnetic splitting of the neutron energy levels, $\Delta E = g\mu B$, where g is the anomalous gyromagnetic ratio of the neutron, $\mu = (e\hbar/2m_n c)$ and B is the magnetic field strength. Writing the hamiltonian in the presence of the magnetic field, the usual Schrodinger perturbation theory then gives for the transition rate \bar{n}/n as¹⁰

$$\frac{\bar{n}}{n} \approx \frac{1}{2} \left[\frac{\Delta\rho}{\Delta E} \right]^2 \quad (1)$$

where $\Delta\rho = \hbar/\tau \rightarrow 10^{-32}$ erg, τ being the oscillation time of 10^5 s and $\Delta E = 9 \times 10^{-24} B$ erg, where B is in Gs. As \bar{n} subsequently decays to antiprotons, equation (1) also gives the ratio \bar{p}/n . As mentioned above, every supernova explosion shoots out 10^{57} free neutrons into interstellar space where the average magnetic field is known to lie between 10^{-6} and 10^{-7} G. With this value of B in equation (1) then gives for \bar{p}/n ,

$$\frac{\bar{n}}{n} = \frac{\bar{p}}{n} = \left[\frac{10^{-32}}{9 \times 10^{-24}} \right]^2 \frac{1}{(10^{-7})^2} \approx 10^{-4} \quad (2)$$

As observed above $n/p \sim 10$ for supernova matter, thereby giving $\bar{p}/p \sim 10^{-3}$. This would imply that out of the 10^{57} free neutrons shot out of the supernova into the interstellar space, 10^{54} of them would get converted into low energy antiprotons. A cosmic-ray proton density of 1 eV cm⁻³ and a galactic volume of 10^{68} cm³ would give $\sim 10^{59}$ protons. The observed \bar{p}/p ratio would then require 10^{55} antiprotons to be present in the Galaxy (an observed energy density of 10^{-4} eV cm⁻³). We thus see that a few supernova explosions are fully capable of accounting for the background antiproton flux.

The value of 10^{-7} G for the interstellar field used in equation (2) is rather low, a commonly quoted value is $\sim 10^{-6}$ G. This is the value given by equipartition arguments though there is no physical basis for it. It could be different from 10^{-6} G, as discussed by Burbidge¹², in the context of synchrotron radiation from extended galactic and extragalactic sources. The use of 10^{-6} G in equation (2), however, reduces \bar{p}/n to 10^{-6} , which would imply (with $n/p \sim 10$) that each supernova explosion would produce only 10^{52} antiprotons. So, the observed \bar{p} background density of 10^{-4} eV cm⁻³ can be produced only after 1,000 supernova explosions. Assuming a rate of one explosion in 10 yr (ref 13) would require time periods $\sim 10^5$ yr (about the same order as that required for the particles to spread over the Galaxy) for the observed antiproton background to build

up. We can thus trade off a higher value for the magnetic field with more explosions to build up the antiproton background. Thus interstellar fields of a few microgauss can over a period of a few hundred thousand years give rise to an antiproton background of about the observed galactic density.

The effect of solar activity on the background cosmic ray intensity is interesting. It is well known that during flares, the solar wind sweeps away the low energy cosmic rays, resulting in Forbush decrease. On the other hand, the generation of antiprotons through $n\bar{n}$ oscillations occurs additionally during solar flares at which time a large neutron flux is produced¹⁴.

We conclude that the phenomenon of $n\bar{n}$ oscillation occurring in the aftermath of a large neutron release in supernova explosions can account for the observed sub-GeV antiproton flux in cosmic rays. We note that this mechanism does not suffer from the attendant production of large fluxes of unaccountable γ rays or high-energy neutrinos like other scenarios, nor is there any need for deceleration mechanisms, as the antiprotons are produced at MeV energies straightaway.

Received 15 March, accepted 8 June 1982

- 1 Buffington, A. & Schindler, S. M. *Astrophys J Lett* **247**, L105–L109 (1981)
- 2 Buffington, A., Schindler, S. M. & Penypacker, C. R. *Astrophys J* **248**, 1179–1193 (1981)
- 3 Eichies, D. *Nature* **295**, 391–393 (1982)
- 4 Kiraly, P., Szabalki, J., Wdowczyk, J. & Wolfendale, A. W. *Nature* **293**, 126–128 (1981)
- 5 Stocker, F. W. *Nasa Tech Mem* No 82083 (1981)
- 6 Crouch, H. F. *et al Phys Rev D* (1978)
- 7 Glashow, S. L. *Proc Conf Neutrino*, Bergen **1**, 518 (1979)
- 8 Kuzmin, V. A. *JETP Lett* **12**, 228–230 (1978)
- 9 Mahapatra, R. W. & Marshak, R. E. *Phys Rev Lett* **44**, 1316 (1980)
- 10 Sawada, O., Fakugita, M. & Arafune, J. *Astrophys J* **248**, 1162–1165 (1981)
- 11 Turan, J. W. *Supernovae* (ed Schramm, D.) 145 (Reidel, Dordrecht, 1977)
- 12 Burbidge, G. R. *IAU Symp* No 55, 205 (1973)
- 13 Tammann, G. A. *Proc 1976 DUMAND Summer Workshop* (ed Roberts A.) 137 (University of Hawaii, Honolulu 1976)
- 14 Svestka, Z. *Solar Flares* 286 (Reidel, Dordrecht 1976)

Intense $\text{Ly}\alpha$ emission from Uranus

Samuel T. Durrance & H. Warren Moos

Department of Physics, Johns Hopkins University, Baltimore, Maryland 21218, USA

The existence of intense atomic hydrogen $\text{Ly}\alpha$ emission from Uranus is demonstrated here by utilizing the monochromatic imaging capabilities of the International Ultraviolet Explorer (IUE) spectrograph. Our observations show increased emission in the vicinity of Uranus superimposed on the geocoronal/interplanetary background. If resonant scattering of solar $\text{Ly}\alpha$ is the source of the 1.6 ± 0.4 kR disk averaged brightness, then very high column densities of atomic H above the absorbing methane are required. Precipitation of trapped charged particles—aurora—could explain the emissions. This would imply a planetary magnetic field.

The $\text{Ly}\alpha$ line of atomic hydrogen is often the most easily detected UV emission from the upper atmosphere of a planet, in the case of the major planets with largely H_2 atmospheres, the line may be quite bright. The resonant scattering of the intense solar radiation provides a means of estimating the upper atmosphere H column density, which in turn depends on the eddy diffusion transport rate. If a planetary magnetic field is present, precipitating charged particles can produce intense emissions particularly near the polar latitudes.

Darius and Fricke¹ recently described a measurement of the $\text{Ly}\alpha$ brightness of Uranus with the IUE spacecraft, the value was surprisingly high, 1.9 kR. However, two questions caused uncertainty. First, because of the imperfect image quality of the telescope, it was not certain how much of the 3.8 arc planetary disk passed through the nominal 3 arc diameter small aperture. Second, the ratio of the solid angles of the large and small apertures—used to subtract the dominant terrestrial airglow from the total signal—was uncertain. A new and more reliable determination of the $\text{Ly}\alpha$ brightness of Uranus is now

described that uses the IUE spacecraft but with a different technique. In particular, the imaging property of the UV instrumentation was utilized. When the planetary image is placed in the large aperture, an ~ 9 arc s monochromatic image is produced in the focal plane of the low resolution spectrograph at the wavelength of $\text{Ly}\alpha$, the planetary $\text{Ly}\alpha$ emission appears as a feature on top of the larger terrestrial/interplanetary feature which covers an area in the focal plane equivalent to $\sim 16 \times 27$ arc s. As a result, the strength of the planetary emission relative to the geocoronal/interplanetary contribution can be assessed directly and $\text{Ly}\alpha$ emission from Uranus can be demonstrated beyond doubt. In addition, to reduce the geocoronal contribution, the observation was performed on 3 March 1982 when the local spacecraft zenith angle of Uranus was near minimum at the time or orbit apogee. Also a determination² of the variation of the $\text{Ly}\alpha$ emission with IUE orbit parameters enabled us to scale with confidence $\text{Ly}\alpha$ background measurements for the large aperture obtained at other times in the shift so that the terrestrial/interplanetary contribution could be subtracted.

Two 2-h exposures of Uranus (SWP 16468 and SWP 16469) were obtained beginning at 11 h 58 min and 14 h 26 min UT. The planetary disk was 3.7 arc s. This was followed by three exposures of the terrestrial airglow (SWP 16470, SWP 16471 and SWP 16472) 330 arc s south-west of the planet. The exposures began at 16 h 56 min UT and ended at 20 h 51 min UT, their total integrated observing time was 185 min. The line by line spectra—in which a datapoint corresponds to an area 1.1 arc s in the dispersion direction by 2.1 arc s high—were used to obtain a two-dimensional plot of the focal plane flux. Figure 1 shows a projection of the resulting data set at $\text{Ly}\alpha$. Figure 1a shows the sum of the three airglow only exposures whereas Fig. 1b also contains the contribution of Uranus. There seems to be no question that Uranus is a strong emitter, producing a localized hump on top of the flat topped distribution of ~ 1.2 kR of terrestrial/interplanetary airglow. Finally, Fig. 1c shows our best estimate of the Uranus only emission obtained by subtracting Fig. 1a from Fig. 1b and multiplying by a factor of 3. (Note that Fig. 1a has both been corrected for differences in observing times and multiplied by 0.67 to correct for the variation in geocorona with time.) Summing the flux over a circle of 10 arc s diameter and using the standard IUE calibration of Bohlin *et al.*³ implies a uranian disk averaged brightness of 1.6 ± 0.4 kR. The value of the brightness is dependent on measuring the flux in the tail of the distribution. Thus, if one arbitrarily rejects all values outside of a 7 arc s diameter instead of a 10 arc s diameter, the computed value drops to 1.1 kR. Hence, the imaging technique used here is important. As a check on the subtraction, the airglow contribution was increased before subtraction. When the value for Uranus dropped to 1.2 kR, most of the data points in the region of airglow only were negative. Similarly, decreasing the airglow contribution led to an upper limit of 2.0 kR. The effect of absorption by interplanetary H is difficult to ascertain because the line width of the emitted radiation is not known. In general it will raise the value above that reported here.

What is the cause of this strong emission? First, consider resonant scattering from an optically very thick layer of atomic H. Assuming a cosine distribution⁴, the implied uranian subsolar brightness is 2.4 kR. This is to be compared with a subsolar brightness for Jupiter of 8.5 kR obtained in January 1982 (ref. 5). Correcting for the different heliocentric distances gives that the reflectivity of Uranus is 3.8 times higher. Using the calculations of Clarke *et al.*⁶ scaled to a solar $\text{Ly}\alpha$ flux at the Earth 3.6×10^{11} photons $\text{cm}^{-2} \text{s}^{-1}$ (G. J. Rottman, personal communication) implies that the uranian atomic hydrogen column density above the absorbing methane is ≥ 10 times thicker than the case of Jupiter. This would be surprising in that the effect of solar photodissociation to produce H from H_2 is down by a factor of 14, removal of the hydrogen by eddy diffusion transport would have to be two orders of magnitude below the case of Jupiter. The methane density in the high atmosphere may

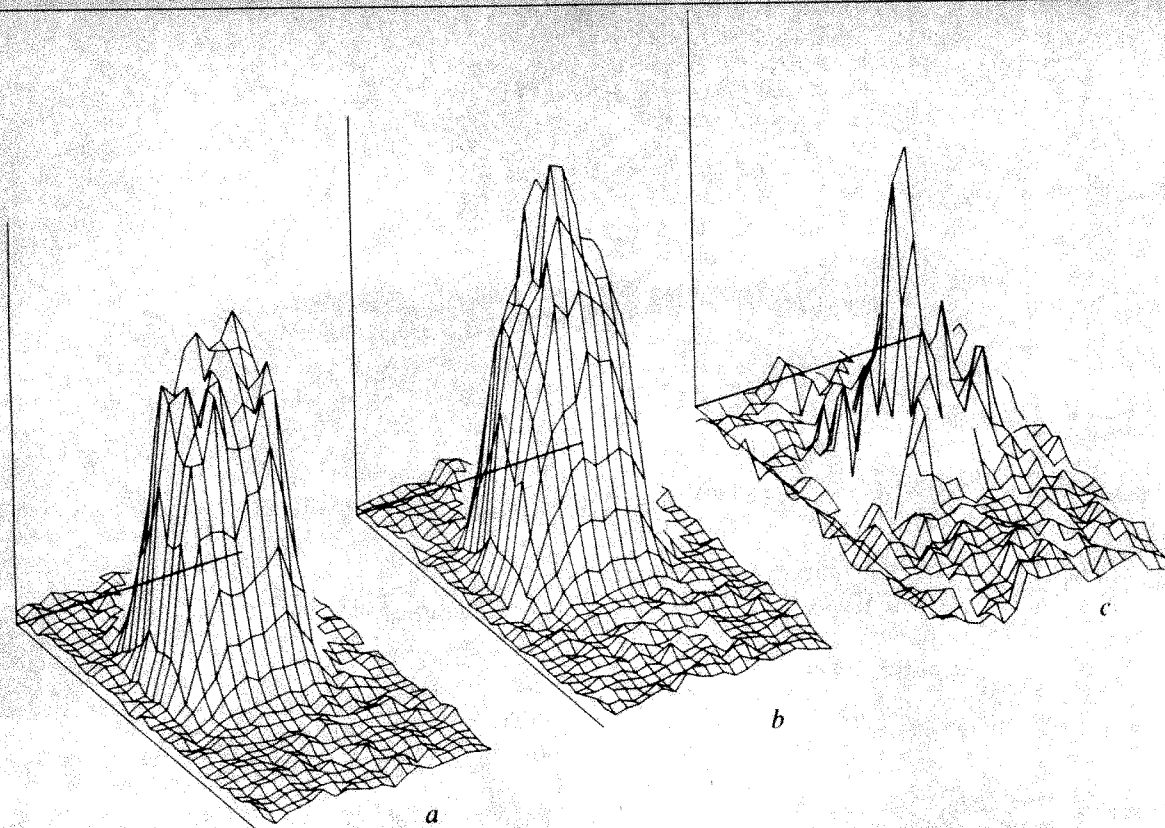


Fig. 1 Projection of the $\text{Ly}\alpha$ flux in the IUE short wavelength spectrograph focal plane showing the $\text{Ly}\alpha$ emission from Uranus. *a*, Sum of three exposures with geocorona only normalized to *b*; *b*, sum of two 2-h exposures with Uranus at the centre of the large entrance aperture; *c*, the uranian $\text{Ly}\alpha$ emission obtained by subtracting the geocoronal contribution from *b* and multiplying the result by 3. The long dimension of the aperture is approximately parallel to the axes pointing upward and to the right. The dispersion direction is approximately parallel to the axes pointing downward and to the right.

be lower than the other major planets⁷ which would increase the depth of the hydrogen column. In any case, the subsolar reflectivity is 60% of that expected from a perfect lambertian surface, a not impossible but quite high value.

An alternative explanation is precipitation of trapped charged particles. Polar aurorae on both Jupiter⁸ and Saturn⁹ have produced $\text{Ly}\alpha$ emissions easily observed by IUE. Uranus had its pole in the ecliptic plane pointing approximately earthwards at the time of the observation. Thus polar aurorae could have contributed substantially to the observed brightness.

At present, we are not able to distinguish between the two sources, although the demands on resonance reradiation of solar $\text{Ly}\alpha$ are so great that it forces a prejudice towards trapped charged particle precipitation. The latter in turn implies a planetary magnetic field. Observational signatures of trapped particle precipitation are temporal variations in the $\text{Ly}\alpha$ brightness and H_2 Lyman/Werner band emission². We plan to extend our observations of Uranus to see if these signatures exist.

We thank T. E. Skinner for helping with the observations, P. D. Feldman and John Caldwell for helpful discussions, and the IUE observatory staff for assistance in the acquisition and reduction of the data. We thank Dr J. T. Clarke for discussing his recent observations of Uranus. This research was supported by NASA under grant NSG 5393 to the Johns Hopkins University.

Received 26 July; accepted 27 August 1982.

1. Darius, J. & Fricke, K. H. *The Universe at Ultraviolet Wavelengths: The First Two Years of IUE*, 85–87 (NASA CP-2171, Washington DC, 1981).
2. Durrance, S. T., Feldman, P. D. & Moos, H. W. *Geophys. Res. Lett.* **9**, 652–655 (1982).
3. Bohlin, R. C., Holm, A. V., Savage, B. D., Sijnders, M. A. J. & Sparks, W. M. *Astr. Astrophys.* **85**, 1–13 (1980).
4. Broadfoot, A. L. *et al. Science* **204**, 979–982 (1979).
5. Skinner, T. E., Durrance, S. T., Feldman, P. D. & Moos, H. W. *Astrophys. J. Lett.* (submitted).
6. Clarke, J. T. *et al. Astrophys. J.* **240**, 696–701 (1980).
7. Gillett, F. C. & Rieke, G. H. *Astrophys. J. Lett.* **218**, L141–L144 (1977).
8. Clarke, J. T., Moos, H. W., Atreya, S. K. & Lane, A. L. *Astrophys. J. Lett.* **241**, L179 (1980).
9. Clarke, J. T., Moos, H. W., Atreya, S. K. & Lane, A. L. *Nature* **290**, 226–227 (1981).

Precambrian endoliths discovered

Susan E. Campbell

Department of Biology, Boston University, 2 Cummington St, Boston Massachusetts 02215, USA

The earliest known microborings have now been found in late Precambrian ooids (Upper Riphean¹/Vendian², 570–700 Myr) of the Eleonore Bay Group of eastern Greenland. The ooids were originally carbonaceous and underwent silicification after boring occurred. The finding establishes that the habit of microbial boring evolved before the appearance of skeleton-bearing metazoans in the geological record.

Microbial endoliths have bored skeletal fragments and carbonate rock³ throughout the Phanerozoic eon⁴. Precambrian ooids were surveyed for early endolithic activity because microbial endoliths are commonly associated with modern ooids⁵, whereas epiliths have a much lower frequency of association with them⁶. Ooids are hard, spherical structures that accrete and form concentric laminae abiotically, that is, without the involvement of carbonate-precipitating microorganisms such as those responsible for stromatolite formation⁵. For these reasons, Precambrian ooids were considered to be microbiologically 'clean' systems in which only endolith fossils were likely to be found.

Twenty-three fossils were found in the thin sections of oolite from level 16 of the Eleonore Bay Group in sample GGU 145426, which corresponds to the no. MGUH 13 807 of the Geological Museum, Copenhagen². The endolithic microfossils (Fig. 1a–d) are present as fillings of boreholes, and thus appear dark against the lighter background of the silica mineralogy of the ooids. Borings in modern ooids (Fig. 1e, f) often become filled with material darker than the white ooidal carbonate

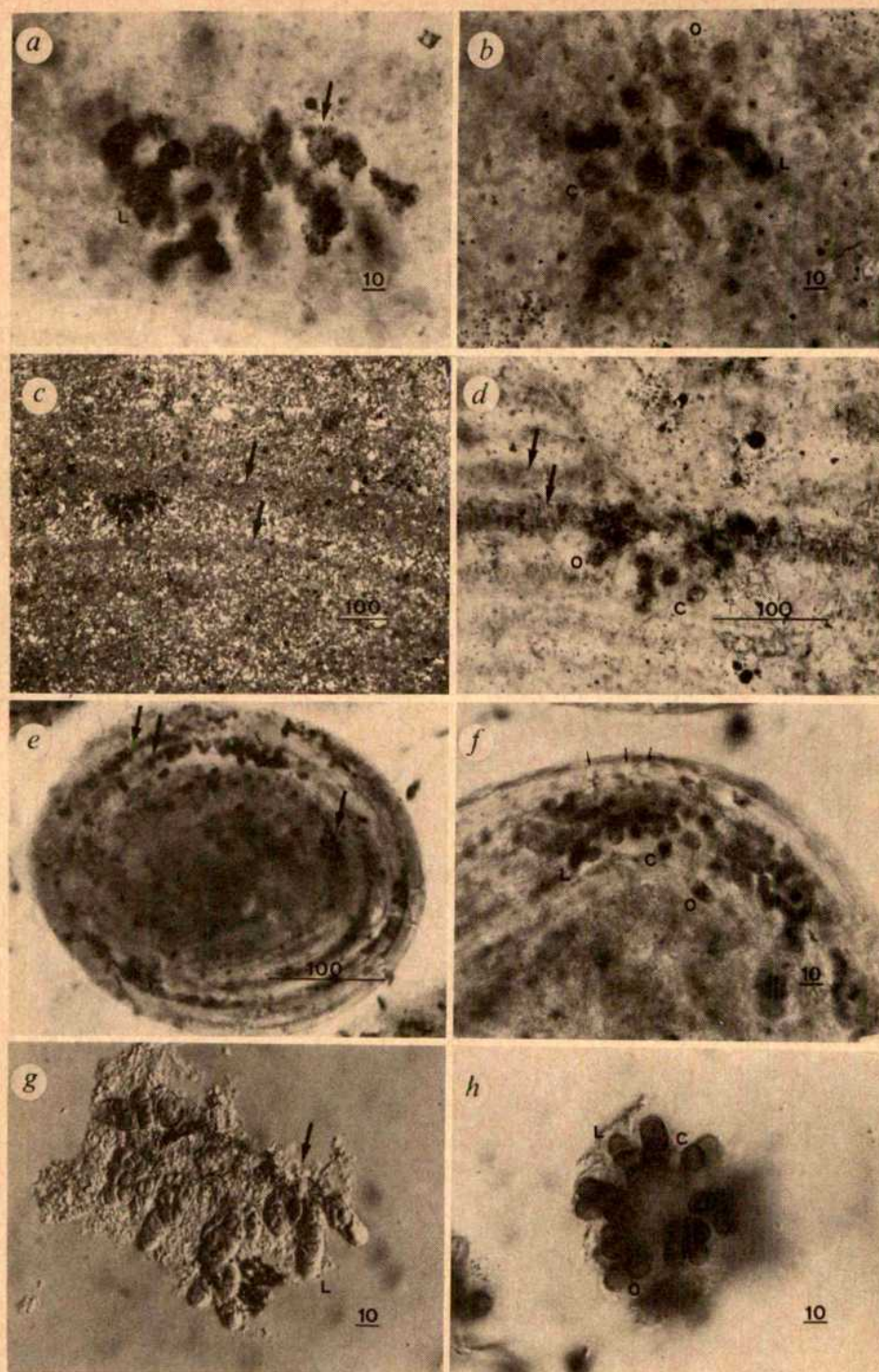


Fig. 1 *a*, Precambrian endolith within a silicified ooid. It is composed of a cluster of short branching filaments (compare with *g*). L = longitudinal section of boring. Arrow indicates surface at the time of boring. Scale bar, 10 μ m. *b*, Precambrian endolith cluster transversely sectioned. Individual borings appear in cross (C), oblique (O) and longitudinal (L) section. Scale bar, 10 μ m. *c*, Fossil in *a* shown in mineralogical context; partial cross-polarized light emphasizes concentric laminae (arrows). Scale bar, 100 μ m. *d*, Precambrian endolith aligned along lamina. Laminae (one-time surfaces of the ooid) shown by arrows. Endolith cluster is cut tangentially (off-centre) while ooid is in radial section. Borings are seen in cross-section (C) and oblique section (O). Scale bar, 100 μ m. *e*, Modern carbonate ooid from Bahamas showing multiple generations of boring along concentric laminae (arrows). Scale bar, 100 μ m. *f*, Empty boreholds are visible at the edge of this modern ooid (small arrows), whereas filled borings are dark against the white ooidal carbonate. Borings in longitudinal section (L), cross-section (C) and oblique section (O). Scale bar, 10 μ m. *g*, Modern decalcified endolithic microorganism *Hyella* (Cyanophyta) in longitudinal view. Arrow indicates the position of substrate surface before the carbonate was dissolved. Scale bar, 10 μ m. *h*, Decalcified *Hyella*, photographed from beneath (optical section), illustrates radiating morphology. Compare with borehole morphology of fossil in *b*. Cells in longitudinal (L), cross (C) and oblique (O) sections. Scale bar, 10 μ m.

(Fig. 1*f*, dark structures), whereas empty boreholes remain clear in transmitted light microscopy (Fig. 1*f*, lacunae in the ooid periphery, small arrows). The fossils (Fig. 1*a-d*) are defined by dark particulate matter of submicrometre size. This material may be finely disseminated pyrite, graphite or bitumen. The sharp outlines of the fossils represent the borehole walls. There are no cellular or extracellular organismal structures present such as those described for other Precambrian microfossils⁷⁻⁹. Thus, the endolithic fossils are actually trace fossils rather than body fossils.

Nearly all the fossils are associated with the concentric laminae of the ooids (Fig. 1*c, d*, arrows). Borings in modern ooids are also preferentially aligned along the laminae (Fig. 1*e*) because the latter represent one-time surfaces of discontinuously growing ooids. Endoliths bore into the ooid after

settling on the surface. Any single ooid may have many laminae containing successive generations of boring (Fig. 1*e*, arrows), or many successive undisturbed laminae containing only isolated borings (Fig. 1*c, d*). The frequency of boring depends on the residence time of individual ooids at the sediment-water interface where boring occurs, or the availability of reproductive propagules of the colonizing endoliths. In the case of the fossil, taphonomic (post-mortem) information loss¹⁰ and diagenetic recrystallization may have removed a portion of the record of endolithic boring.

The morphological features of the fossils are best seen in radial section of the ooid (Fig. 1*a, c*). In this position, the endoliths appear in profile. They are composed of clustered, branching filaments (8–15 μ m diameter), radiating out from the point of entry (at a concentric lamina) in a generally centripetal

direction with respect to the ooid nucleus. The structures are three-dimensional and, as such, cannot be fully represented in a two-dimensional photomicrograph. Drawings made with a camera lucida attachment on the microscope can, however, take three-dimensionality into account by outlining each filament while the microscope is slowly focused up and down. Figure 2 is a camera lucida drawing of the fossil shown in Fig. 1a, c. Filaments branch laterally and dichotomously, and they tend to swell somewhat at their tips. All these are morphological features common to the modern photosynthetic prokaryotic endolith *Hyella* (Cyanophyta, Figs 1g, h).

The ooid in Fig. 1b was cut tangentially during preparation of the thin section. As a result, the cluster of borings was cut transversely. A similar orientation of a cluster of modern *Hyella* is seen in transverse optical section in Fig. 1h. Figure 1d shows a radial section through an ooid. Here, the concentric laminae are visible in their parallel relations (arrows), but the section preparation process ground away all but the tips of the ramifying fossil borings, and they appear both in cross-section (C) and oblique section (O). A similar orientation of borings can be seen in the modern ooid of Fig. 1f. There, small segments of longitudinally sectioned filamentous borings are visible, but most borings have been cut obliquely and in cross-section.

The age of the oldest endoliths has previously been reported to be Cambrian¹¹, and the oldest that were photographically documented were Ordovician¹². S. M. Awramik (personal communication) has found silicified endoliths similar to the modern cyanophyte *Cyanosaccus* in Cambrian rock. The nearly constant association of endoliths with modern ooids is well known⁵ and Harris *et al.*⁶ have compared borings made by several modern endolithic genera with those found in Pleistocene ooids.

The size and morphology of the Precambrian boreholes reported here are most similar to those of the modern endolithic cyanophyte genus *Hyella* (Fig. 1g, h), an organism that bores modern ooids⁶. The only other modern endoliths of comparable size and morphology are the conchosporangial branches of the endolithic stage of the bangiacean rhodophytes (eukaryotes), a group which has been found to have ancient Silurian members¹³. Insufficient evidence exists at present to make closer comparisons between these organisms and the Precambrian fossils. Clearly, however, of all endolithic borehole morphologies known today, only those of photosynthetic endoliths are comparable with the Precambrian ones reported here.

Thus, the earliest known occurrence of microbial endoliths in silicified late Precambrian ooids predates the appearance in the geological record of skeleton-bearing metazoans, whose hard parts were bored from Cambrian time to the present. The morphology of the Precambrian fossils corresponds to that of modern photosynthetic endolithic taxa rather than heterotrophic ones.

The finding of Precambrian microborings in ooids raises a new question for palaeontological evaluations of Precambrian stromatolites, another group of laminated accretional carbonate structures. In his study of modern stromatolites of Shark Bay, Australia, Golubic^{14,15} discussed the importance of endoliths in the destruction of lithified stromatolites. Thus, it must now be recognized that Precambrian stromatolites may have been alternately recolonized by carbonate-precipitating (constructive) microflora, and following lithification events, by carbon-

ate-solubilizing (destructive) ones. This has not been considered in previous interpretations of the Precambrian fossil record. Thus, both past and future reports of silicified microfossils in Precambrian stromatolites need to be evaluated with this distinction in mind.

Research was supported by NASA, NSF and a NATO Post-doctoral Fellowship. I thank J. Billingham for stimulating discussion. R. Caby (collector), J. Bertrand-Sarfati and the Greenland Geological Survey kindly loaned the fossil oolite. L. Simone and G. Carannante provided modern ooid specimens. S. Golubic critically read the paper.

Received 26 April; accepted 22 July 1982.

1. Vidal, G. *Geol. Unders. Rapp.* **78**, 1-18 (1976).
2. Bertrand-Sarfati, J. & Caby, R. *Geol. Unders. Bull.* **119**, 1-51 (1976).
3. Golubic, S., Friedman, I. & Schneider, J. *J. Sedim. Petrol.* **51**, 475-478 (1981).
4. Campbell, S. E. in *Proc. 4th int. Symp. Biomineralization* (eds Westbroek, P. & deJong, E. W.) (Reidel, Dordrecht, in the press).
5. Simone, L. *Earth-Sci. Rev.* **16**, 319-355 (1980/81).
6. Harris, P. M., Halley, R. B. & Lukas, K. J. *Geology* **7**, 216-220 (1979).
7. Golubic, S. & HHHofmann, H. J. *J. Paleont.* **55**, 1074-1082 (1976).
8. Golubic, S. & Barghoorn, E. S. in *Fossil Algae* (ed. Flügel, E.) 1-14 (Springer, New York, 1977).
9. Golubic, S. & Campbell, S. E. *Precamb. Res.* **8**, 201-217 (1979).
10. Knoll, A. H. & Golubic, S. *Precamb. Res.* **10**, 115-151 (1979).
11. James, N. P. & Kobluk, D. R. *Sedimentology* **25**, 1-35 (1978).
12. Hessland, I. *Bull. geol. Inst. Uppsala* **33**, 409-427 (1949).
13. Campbell, S. E. *Phycologia* **19**, 25-36 (1980).
14. Golubic, S. *Dev. Sedim.* **20**, 113-126 (1976).
15. Golubic, S. in *Proc. 4th int. Symp. Biomineralization* (eds Westbroek, P. & deJong, E. W.) (Reidel, Dordrecht, in the press).

Temporal variations in dissolved selenium in a coastal ecosystem

J. J. Wrench*

Marine Ecology Laboratory, Bedford Institute of Oceanography, Dartmouth, Nova Scotia, Canada B2Y 4A2

C. I. Measures

Department of Earth and Planetary Sciences, Massachusetts Institute of Technology, Cambridge, Massachusetts 02139, USA

In oceanic environments biological processes are now known to have a central role in establishing the redox state and spatial distribution of certain dissolved trace elements. Biological effects on the natural cycles of Cr, As, Se, Cd, Ni and Al are inferred from the existence of thermodynamically unfavourable species, from non-conservative vertical profiles or because trace element levels in planktonic debris are such that the subsequent regeneration of material could produce the observed profiles¹⁻⁷. In cases where biological activity has been implicated as a determinant of either redox state or spatial distribution in the oceans no field investigations have yet been made into the relationships between rapid fluctuations of biological parameters and trace element levels and speciation. We now present a temporal study of the response of selenium levels and redox state to pulses of primary productivity in a coastal ecosystem. The sampling time series demonstrated selective assimilation of the lower oxidation state, selenite [Se(IV)]. Ratios of particulate selenium to particulate organic carbon (Se:C) allowed an estimation of the selenium levels in a natural phytoplankton population and the flux of selenium from surface ocean water to deep water.

Selenium is a unique example of a multiple oxidation state trace element in that the thermodynamically unfavourable species, Se(IV), persists throughout the water column in oceanic profiles⁴. This phenomenon may be a result of bioreduction of the dominant higher oxidation state, Se(VI), in surface water and downward transport of the kinetically stable reduced form.

* Present address: Department of Microbiology, University of British Columbia, British Columbia 300 6174 University Boulevard, Vancouver, Canada V6T 1W5.



Fig. 2 Camera lucida drawing of Precambrian endolith in Fig. 1a illustrates its filamentous morphology. The dotted line shows the position of the previous ooid surface. Scale bar, 10 μ m.

The underlying processes which lead to non-conservative behaviour of selenium in the water column can only be investigated in a non-equilibrium context. For this reason we have considered the question of selenium redox chemistry against a background of variations in biological activity in a fjord ecosystem (Bedford Basin, Nova Scotia, Canada) where primary productivity is high and for which a strong biological data base already exists^{8,9}. As this was a pilot study we collected only one sample at 5 m depth at a single station on a weekly basis between 6 January and 28 April 1981. The intentions of this simple scheme were to establish whether (1) such ecosystems produce significant temporal changes in trace element levels; (2) what kind of quantitative data can be obtained from a simple sampling scheme; (3) how further more extensive temporal and spatial sampling schemes should be designed to provide a closed budget for such a system.

Selenium levels in surface waters are typically in the picomolar range. We have therefore applied a recently developed gas-liquid chromatographic (GLC) technique to the accurate resolution of small variations of dissolved selenium species¹⁰. Selenium analyses on the particulate fraction were also carried out by GLC after wet digestion of the particulates retained on a glass fibre filter from 40 l of seawater¹¹. The detection limits and precisions (1σ) at the observed levels are: Se(IV), 10 pmol l^{-1} ($\pm 4\%$); total Se, 10 pmol l^{-1} ($\pm 6\%$); Se(VI) (by difference), 10 pmol l^{-1} ($\pm 10\%$); particulate selenium (PSe) $< 0.1 \text{ pmol l}^{-1}$ ($\pm 7\%$).

The sampling period is characterized by four distinct events in the particulate phase (Fig. 1). Nutrient behaviour (Fig. 2a) during the first of these events centred on 14 January is anomalous in that there is a decrease in dissolved $\text{NO}_3 + \text{NO}_2$ but no significant reduction in PO_4 and SiO_2 . The particulate organic carbon (POC) maximum on 21 April is not associated with any rise in chlorophyll levels. These observations suggest that the first and last biomass maxima are not simple algal blooms and they will therefore not be discussed in any detail.

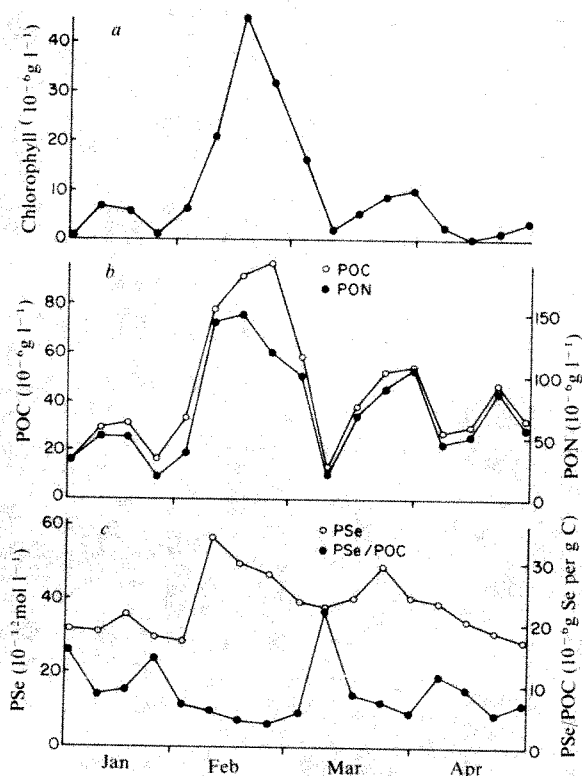


Fig. 1 Temporal changes of biological parameters and selenium in the particulate phase at 5 m depth (Bedford Basin). Samples were taken by Niskin bottle. POC and PON retained on silver filters from 1 l of seawater were quantified using a Perkin Elmer CHN analyser. Chlorophyll was measured by fluorescence spectrometry.

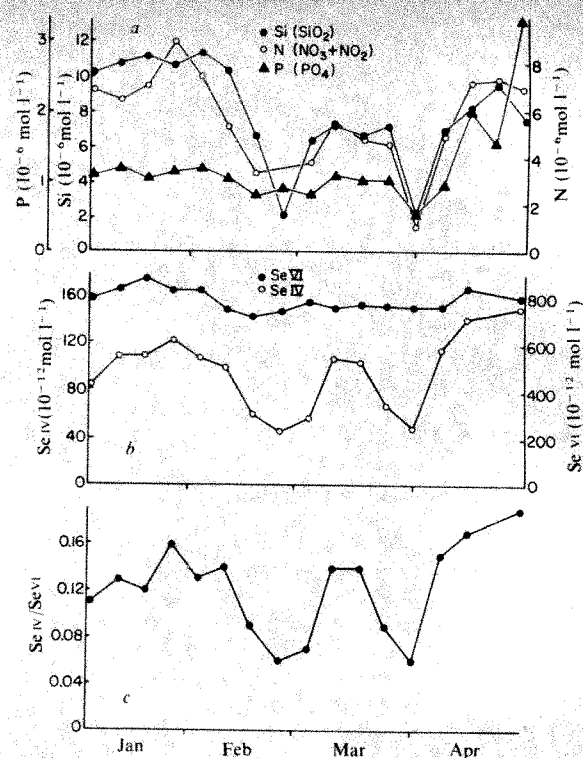


Fig. 2 Temporal changes of nutrients and selenium redox species in the dissolved phase at 5 m (Bedford Basin). Samples were taken by Niskin bottle. Nutrient analyses were carried out on fresh samples using a Technicon autoanalyser.

The second and major event centred between 17 and 24 February is a typical phytoplankton bloom with large increases in POC, particulate organic nitrogen (PON), (PSe) and chlorophyll, and corresponding decreases in SiO_2 , PO_4 , $\text{NO}_3 + \text{NO}_2$, Se(IV) and Se(VI). The decay of this bloom is marked by a rapid regeneration of the dissolved nutrients including Se(IV) (Fig. 2b), with concentrations reaching 65–90% of the pre-bloom levels. Se(VI) does not seem to be regenerated as efficiently as Se(IV) after the bloom.

The third event centred on 31 March is also a characteristic algal bloom but of lower magnitude than the February event. Rises in POC, PON, PSe and chlorophyll levels are mirrored by decreases in the dissolved nutrients and Se(IV) but not Se(VI). The decay of the bloom is again marked by a rapid regeneration of nutrients, including Se(IV) (Fig. 2b), with final concentrations approximately equal to the pre-bloom levels. Over the period of the two blooms both Se(IV) and PSe show significant correlations with both POC and PON with $P < 0.01$ in all cases. After 7 April the nutrients lose their inverse correlation with the particulate phase.

The net effect of the two successive blooms is to cycle Se(IV) rapidly through the biota while apparently removing a small fraction of Se(VI). A single point sampling scheme prevents calculation of a comprehensive budget for selenium or elucidation of the ultimate fate of assimilated Se(VI). At the end of the overall sampling period Se(IV) levels are considerably enhanced over those in early January while Se(VI) values are virtually unchanged. Further interpretation of these observations in terms of cycling between the oxidation states is restricted by three considerations. First, towards the end of the sampling period (7 April) the nutrients lose their inverse correlation with the particulate phase—probably as a result of external inputs, for example, river run-off, which will similarly affect the selenium species. Second, the single point sampling scheme will certainly be unable to account for any vertical flux of selenium which may become important as stratification of the water column develops (historically in early April). Third, the fraction that we call Se(VI) will also by its methodological

definition¹⁰ include any labile dissolved organically bound selenium and thus represents an upper limit for Se(VI). Our own (unpublished) work, however, indicates that selenium in the dissolved organic fraction of seawater collected from Bedford Basin ranges between 87 and 102 pmol l⁻¹ and therefore represents only a minor part of the total dissolved element. In view of these limitations we can make no unique interpretation of the elevated post-bloom Se(IV) levels.

That Se(IV) during the two main blooms is removed from the dissolved phase to a much greater extent than Se(VI) is clearly shown by the inverse relationship of the Se(IV)/Se(VI) ratio (Fig. 2c) to biomass. Preferential assimilation of the lower oxidation state during algal blooms, the main components of which are the diatoms *Thalassiosira nodenskioldi* and *Chaetoceros septentrionalis* and the dinoflagellate *Gymnodinium* sp., could simply reflect a physicochemical selection process, based for example on ionic radius, resulting in non-biochemical incorporation of selenium into diatom tests. However, it is evident that selenium is an essential micronutrient for a wide variety of organisms¹², including phytoplankton¹³, and that the biochemically operational form is selenide. It is therefore probable that microorganisms will select the lowest available oxidation state because less chemical energy is then required for the reductive process linking selenium to organic molecules.

Maximal selenium levels in the particulate fraction precede PON, POC and chlorophyll peaks by 1–2 weeks. Although out of phase with biomass, the PSe maximum occurs when C:N ratios are lowest. This observation suggests a link between selenium metabolism and algal protein synthesis and is consistent with the observation that marine phytoplankton in culture incorporate the majority of assimilated selenium into protein¹⁴.

Temporal changes in the PSe:POC ratio (Fig. 1c) reveal the presence of two distinct pools of organic carbon with different selenium contents. The lower ratios of 3.9 and 5.4 pg per µg C associated with algal blooms reflect that of natural phytoplankton populations while the much higher ratio represents a background or non-living detrital pool. If algal carbon is taken to be 4.0% of wet weight¹⁵ then, using the derived PSe:POC ratios, the selenium content of phytoplankton is estimated to be between 160 and 220 ng per g wet weight. Selenium levels in organisms at higher trophic levels, usually reported to be in the low µg per g range, are significantly greater than the derived value for phytoplankton^{16–19}. For example, a concentration of 530 ng per g wet weight for Arctic pteropods (*Clione limacina*) has recently been obtained by the GLC technique used in the present study¹⁹. These observations suggest that selenium may be accumulated along the food chain.

If annual carbon fixation in the oceans is taken as 2.7×10^{16} g C yr⁻¹ and assuming that 93% of this material is recycled in the euphotic zone²⁰, the biologically mediated flux of selenium from surface water to deep water is estimated to range from 7.4×10^9 to 1.0×10^{10} g Se yr⁻¹. In general terms our results provide direct evidence that biological activity in the euphotic zone can modify both the redox balance and the concentrations of a multiple oxidation state trace element. Similar biological effects may be of critical significance in the cycles of other trace elements in the oceans. Eutrophic coastal ecosystems should prove to be useful models in which new methods of trace analysis can be applied to examine such fundamental biogeochemical processes. While a more extensive sampling scheme will enable budgets to be calculated, a simple single point scheme as outlined here can provide a significant amount of information and at the same time lay a background against which more extensive studies can be designed.

We thank Nancy Campbell and Georgina Phillips for assistance in the collection and analysis of samples, and colleagues at MEL and MIT for critical discussion of the manuscript. C.I.M. was supported by a grant from the Office of Naval Research. J.J.W. acknowledges the support of NSERC of Canada for provision of a visiting fellowship.

Received 29 June; accepted 26 July 1982.

1. Cranston, R. E. & Murray, J. W. *Analyt. chim. Acta* **99**, 275–282 (1978).
2. Andrae, M. O. *Deep-Sea Res.* **25**, 391–402 (1978).
3. Collier, R. W. thesis, Massachusetts Inst. Technol. (1981).
4. Measures, C. I., McDuff, R. E. & Edmond, J. M. *Earth planet. Sci. Lett.* **49**, 102–108 (1980).
5. Hydes, D. J. *Nature* **268**, 136–137 (1977).
6. Boyle, E. A., Slater, F. R. & Edmond, J. M. *Nature* **263**, 42–44 (1976).
7. Slater, F. R., Boyle, E. A. & Edmond, J. M. *Earth planet. Sci. Lett.* **31**, 119–128 (1976).
8. Platt, T. & Irwin, B. *Tech. Rep. No. 247* (Fisheries Research Board of Canada, 1971).
9. Platt, T., Irwin, B. & Subba Rao, D. V. *Tech. Rep. No. 423* (Fisheries Research Board of Canada, 1973).
10. Measures, C. I. & Burton, J. D. *Analyt. chim. Acta* **120**, 177–186 (1980).
11. Cappon, C. J. & Crispin Smith, J. J. *anal. Tox.* **2**, 114–120 (1978).
12. Gamboa Lewis, B. A. in *Environmental Biogeochemistry* (ed. Nriagu, J. O.) 389–409 (Ann Arbor Science, 1976).
13. Lindstrom, K. & Rhode, W. *Mitt. int. Verein. theor. angew. Limnol.* **21**, 168–173 (1978).
14. Wrench, J. J. *Mar. Biol.* **49**, 231–236 (1978).
15. Parsons, T. R., Takahashi, M. & Hargrave, B. *Biological Oceanographic Processes* 2nd edn, 1–332 (Pergamon, Oxford, 1977).
16. Koeman, J. H., van de Ven, W. S. M., Goeij, J. J. M., Tjioe, P. S. & van Haften, J. L. *Sci. Total Envir.* **3**, 279–287 (1975).
17. Mackay, N. J., Kazacos, M. N., Williams, R. J. & Leedow, M. I. *Mar. Pollut. Bull.* **6**, 57–60 (1975).
18. Fowler, S. W. *Nature* **269**, 51–53 (1977).
19. Wrench, J. J. & Campbell, N. C. *Chemosphere* **10**, 1155–1161 (1981).
20. Walsh, J. J., Rowe, G. T., Iverson, R. L. & McRoy, C. P. *Nature* **291**, 196–201 (1981).

Microbial activity and bioturbation-induced oscillations in pore water chemistry of estuarine sediments in spring

Mark E. Hines*‡§, William H. Orem†‡, W. Berry Lyons‡ & Galen E. Jones*§

* Jackson Estuarine Laboratory, and Departments of †Chemistry, ‡Earth Sciences and §Microbiology, University of New Hampshire, Durham, New Hampshire 03824, USA

Temperature increases occurring during the spring in temperate shallow-water marine sediments lead to increased microbial activity, oxygen removal and a decrease in redox potential^{1,2}. These changes cause shifts in the relative importance of specific terminal electron acceptors used in bacterial respiration¹. The decrease in redox potential affects the physicochemical state of redox-sensitive elements such as iron and sulphur². In addition to changing sedimentary chemistry, these variations may affect the overlying water through changes in diffusional fluxes and other processes. Such biogeochemical processes are further complicated when the sediments are subjected to particle reworking and irrigation by bioturbating infauna^{3,4}. In an attempt to clarify the chain of sedimentary events occurring between the relatively oxidizing, inactive winter and the highly reducing, active summer, we examined several chemical and biological parameters in samples of estuarine sediment collected from February to July of 1980. Some of those data are presented here, and we report that the combined effects of increasing microbial activity and the onset of rapid bioturbation produced oscillations in the concentrations of pore water constituents in these sediments.

Sediment box cores were collected from a shallow-water site off the dock of the Jackson Estuarine Laboratory (JEL) in the Great Bay Estuary, New Hampshire. This location has been described previously⁵. Sediments at JEL consisted primarily of clay and silt-sized particles interspersed with fine sand. The upper 8–10 cm of these sediments are bioturbated actively from June to November⁶.

Horizontal sections (2 cm) of sediment were analysed for dissolved iron⁷ and dissolved organic carbon (DOC)⁸ (coefficients of variation of <1.0 and <0.5%, respectively) in conjunction with triplicate radiometric determinations of sulphate reduction^{5,9} and glucose turnover rates^{5,10}. All sediment manipulations and pore water extractions and filtrations (0.4 µm Nuclepore) were carried out under N₂ to prevent oxidation artefacts¹¹.

Temporal changes in the chemical and bacteriological parameters at JEL are presented in Fig. 1. Data points represent averages of the upper 6 cm of sediment to demonstrate the breadth of the variations noted. Dissolved iron concentrations varied more with depth than the other parameters. However, similar temporal trends were noted at each depth⁵.

During winter, sulphate reduction rates were slow, <50 nmol per ml per day. Glucose turnover rates were relatively slow and reported as the sum of radiocarbon recovered as carbon dioxide, particulate material (microbial biomass) and ether-soluble dissolved end products⁵. Iron was nearly absent from solution as a result of its oxidation and precipitation¹². The upper 3–4 cm of these sediments were orange-brown in colour. A previously reported winter increase in sulphate/chloride ratios¹³ demonstrated the generation of sulphate in JEL sediments from the oxidation of iron monosulphides. Concentrations of acid-volatile sulphides in the upper 2 cm increased 12-fold between April ($4.0 \mu\text{mol ml}^{-1}$) and August ($48.0 \mu\text{mol ml}^{-1}$) 1980⁵. Despite the relatively oxidizing state of these surface sediments during winter, sulphate reduction was detected throughout, although at low levels. Winter DOC concentrations were high, an unexplained but common phenomenon in these pore waters (M.E.H., W.H.O. and W.B.L., in preparation).

As the sediment temperature increased in March and April, there was an increase in heterotrophic activity. This was shown, indirectly, by the dissolution of iron. The relative biotic and abiotic contributions to this iron reduction are unknown¹⁴. Glucose turnover rates increased; however, without knowledge of the glucose pool size, this increase is not positive evidence of increased heterotrophy. DOC was consumed rapidly during this period. We have yet to determine if this DOC decrease is due to uptake by bacteria, abiotic mechanisms or a combination of both. In any event, this early spring interval is characterized by rapid changes in sedimentary chemistry.

Sulphate reduction rates remained slow during April even though the temperature had increased. Howarth and Teal¹⁵ reported a similar finding for salt marsh soils.

In May, sulphate reduction activity increased. Dissolved iron was partially removed from solution, undoubtedly due to ferrous sulphide precipitation. DOC concentration increased as a result of sulphate reduction processes¹⁶.

Bioturbation activity increased rapidly in late May–early June (arrows, Fig. 1). This increase was reflected by dramatic changes in the visual and textural character of the sediment such as increased porosity and homogeneity. In addition, previous seasonal X-ray analyses demonstrated this increase in macrofaunal activity⁶. The start of active bioturbation was accompanied by a tripling of sulphate reduction rate, a doubling of the rate of glucose turnover, a five-fold increase in the concentration of dissolved iron and a decrease in DOC.

The dominant active macroorganism in JEL sediments in June is the capitellid polychaete *Heteromastus filiformis*¹⁷. As discussed by others^{3,4,18,19}, bioturbation can increase microbial activity through reworking and irrigation activities while decreasing pore water constituents through facilitated advection. Anaerobic metabolism was enhanced at JEL by the macrofauna-mediated transport of organic material into deeper anoxic regions. The magnitude of this enhancement and other bioturbation-mediated aspects of these sediments will be reported elsewhere.

During summer, bioturbation remained active. DOC concentrations continued to decrease even though anaerobic microbial activity was rapid. Dissolved iron concentrations decreased into July yet remained relatively high at 7–8 mg l^{-1} .

Although bioturbation seemed to enhance sulphate reduction and therefore sulphide production, iron remained in solution during the summer. For comparison, we measured these same parameters in sediments from another site in the Great Bay Estuary located near the mouth of the Squamscott and Lamprey Rivers (SQUAM). These sediments consisted of similar size particles as JEL. However, seasonal X-ray analyses demon-

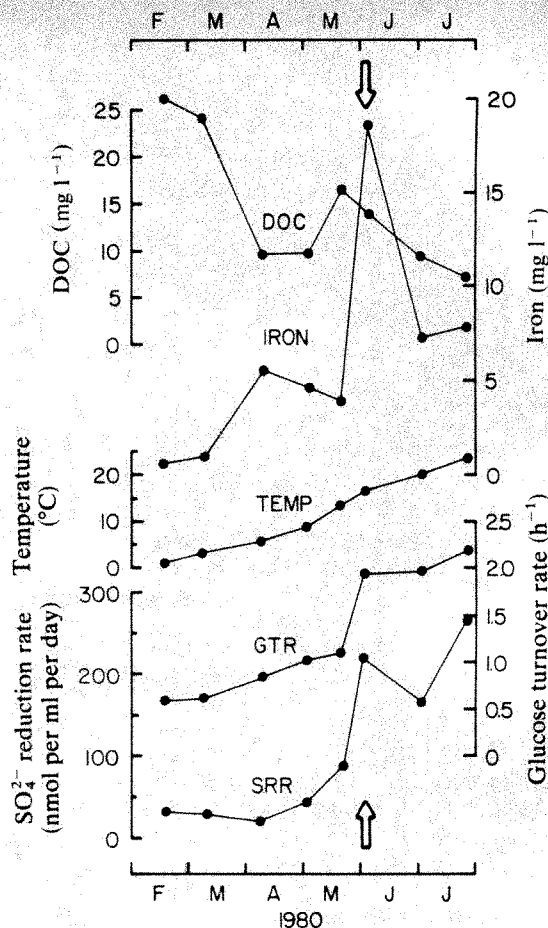


Fig. 1 Variations in sulphate reduction rate (SSR), glucose turnover rate (GTR), temperature (TEMP), dissolved iron and dissolved organic carbon (DOC) in the upper 6 cm of sediments at JEL. Values are averages of replicate determinations from three 2-cm horizontal sections of sediments. Arrows indicate when the start of active bioturbation was observed.

strated that SQUAM sediments are not significantly bioturbated⁶. Dissolved iron concentrations in SQUAM sediments increased from 0.2 to 2.5 mg l^{-1} in May, while DOC decreased from 18 to 10 mg l^{-1} . However, with the onset of sulphate reduction and lack of bioturbation, iron concentrations decreased to near zero in July while DOC increased to 20 mg l^{-1} . These summer values occurred even though sulphate reduction was less than one-third as rapid as in JEL sediments⁵. Therefore, the net effect of bioturbation was the maintenance of high dissolved iron concentrations in JEL sediments even though the removal of DOC was enhanced. As discussed by Aller³, bioturbation may affect iron speciation by the transport of surface Fe^{3+} and the oxidation/reduction of iron sulphides during reworking and irrigation. However, unlike Aller's³ sediments, which were bioturbated most actively in later summer, bioturbation in the JEL sediments began rapidly in June and overwhelmed the changes in iron and DOC concentrations previously initiated by increased sulphate reduction.

Lyons *et al.*² provided evidence that, during April, a large portion of the dissolved iron in JEL sediments is organically associated. This association may have aided in preventing the removal of iron as a sulphide precipitate. However, the pore water iron concentration in June was extremely high (Fig. 1) and the molar ratio of DOC to iron was only 4.1. This ratio was 2.2 in the top 2 cm of the sediment. Hence, organically associated iron is not a likely mechanism for maintaining this quantity of iron in solution in the presence of rapid sulphide production.

The net rate of iron dissolution between late May and early June at JEL was 11 nmol per ml per day (Fig. 1). As these sediments were fairly homogeneous and highly reducing, the

gross rate of iron reduction probably exceeded the sulphide production rate of 100–200 nmol per ml per day. Because other metals often are associated with iron oxyhydroxides²⁰ or may behave similarly to iron, this spring transition period may profoundly affect the speciation and mobility of other elements.

The combined effects of increased microbial activity and bioturbation-mediated sediment reworking, irrigation and enhanced anaerobic processes caused an oscillation in the pore water concentrations of iron and DOC. In addition, dissolved phosphate, ammonium and alkalinity concentrations varied similarly to DOC⁸. The amplitude and wavelengths of these temporal changes would be expected to vary yearly depending on differences in temperature regimes and weather events. Weather-related variations have been noted⁵ and seem to be the result of the removal of infauna by storms. Oscillations in the concentrations of pore water constituents may affect the diffusional flux of material across the sediment–water interface and when combined with bioturbation-enhanced fluxes may have a profound effect on sediment and overlying water processes. Most importantly, metals may undergo rapid speciation changes which could influence the flux of pollutants into the water column and the distribution of sedimentary minerals.

We thank P. B. Armstrong for technical assistance, and R. W. Howarth and H. E. Gaudette for reviews. This work was supported by NSF Oceanography section grants DES-75-04790 and OCE 80-18460.

Received 3 March; accepted 26 July 1982.

1. Sørensen, J., Jørgensen, B. B. & Revsbech, N. P. *Microbial Ecol.* **5**, 105–115 (1979).
2. Lyons, W. B., Gaudette, H. E. & Armstrong, P. B. *Nature* **282**, 202–203 (1979).
3. Aller, R. C. thesis, Yale Univ. (1977).
4. Aller, R. C. *Am. J. Sci.* **278**, 1185–1234 (1978).
5. Hines, M. E. thesis, Univ. New Hampshire (1981).
6. Armstrong, P. B., Fischer, C., Lyons, W. B. & Gaudette, H. E. *5th Biennial Int. Est. Res. Fedn Conf.*, Jekyll Is., Georgia, Abstr. (1979).
7. Stookey, L. L. *Analyt. Chem.* **42**, 779–781 (1970).
8. Orem, W. H. thesis, Univ. New Hampshire (1982).
9. Jørgensen, B. B. *Geomicrobiol. J.* **1**, 29–51 (1978).
10. Christian, R. R. & Wiebe, W. J. *Limnol. Oceanogr.* **23**, 328–336 (1978).
11. Loder, T. C., Lyons, W. B., Murray, S. & McGuinness, H. D. *Nature* **273**, 373–374 (1978).
12. Goldhaber, M. B. & Kaplan, I. R. in *The Sea* Vol. 5 (ed. Goldberg, E. D.) 569–655 (Wiley, New York, 1974).
13. Templeton, G. D. thesis, Univ. New Hampshire (1980).
14. Sørensen, J. *Appl. Envir. Microbiol.* **43**, 319–324 (1982).
15. Howarth, R. W. & Teal, J. M. *Limnol. Oceanogr.* **24**, 999–1013 (1979).
16. Nissenbaum, A. & Kaplan, I. R. in *Advances in Organic Geochemistry* (eds von Gaertner, H. R. & Wehner, H.) 427–440 (Pergamon, Oxford, 1972).
17. Black, L. F. in *Estuarine Perspectives* (ed. Kennedy, V. S.) 389–402 (Academic, London, 1980).
18. Hargrave, B. T. *Limnol. Oceanogr.* **15**, 21–30 (1970).
19. Fenchel, T. M. *Limnol. Oceanogr.* **15**, 14–20 (1970).
20. Elderfield, H. & Hepworth, A. *Mar. Pollut. Bull.* **6**, 85–87 (1975).

Reappraisal of sea-ice distribution in Atlantic and Pacific sectors of the Southern Ocean at 18,000 yr BP

L. H. Burckle, D. Robinson & D. Cooke*

Lamont-Doherty Geological Observatory of Columbia University, Palisades, New York 10964, USA

* Mineral Management Service, Metairie, Louisiana 70003, USA

The question of the distribution of winter and summer sea-ice cover during the last glacial maximum (18,000 yr BP) is important in climatic modelling of the glacial world. We have now compared satellite-derived 5-yr monthly averages of per cent summer sea-ice cover in the Atlantic and Pacific sectors of the Southern Ocean with the distribution of reported sedimentological indicators of sea-ice cover at the sediment–water interface. These data strongly suggest that sediment type cannot be used to identify summer sea-ice limits, neither in Recent sediments nor in sediments of the last glacial maximum. Rather, the data seem to indicate that sediment type can be used to identify spring sea-ice limits for these two time intervals.

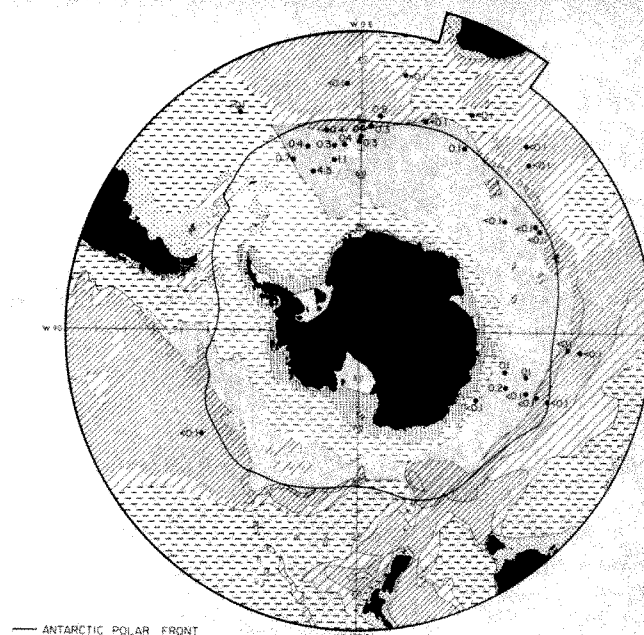


Fig. 1 Distribution of surface sediments around the Antarctic continent. Sediment types from the continent northward are as follows: parallel rows of dots = shelf and coastal deposits; light parallel dashed lines = siliceous silty clay and clayey silt; fine dots = siliceous ooze; oblique solid lines = calcareous ooze; oblique solid lines alternating with fine dots = siliceous and calcareous ooze. Numbers refer to percentage coarse fraction. Data are from ref. 9.

Attempts to define past sea-ice boundaries in the Antarctic began with Philippi¹ but considerable refinements have since been added^{2–5}. Lozano and Hays⁶ and Hays *et al.*⁷ were the first to place the various sediment types within a good chronostratigraphical context. They were able to show that the thin veneer of diatomaceous ooze found in the Southern Ocean was Holocene in age while the underlying silty diatomaceous clay represented glacial conditions. These alternating sediment types were directly linked to the oxygen isotope record and permitted Hays *et al.*⁷ and Cooke and Hays⁸ to devise a chronostratigraphic framework for late Quaternary sediments of the Southern Ocean. These workers have argued that the boundary in surface sediment between the silty diatomaceous clay and the diatomaceous ooze represents the northern edge of summer sea ice (Fig. 1). Further, they argue that this boundary at 18,000 yr BP represents the northern limit of summer sea ice during a glacial maximum. As might be expected, this boundary is considerably north of the present-day boundary and closely approximates present-day winter sea-ice limits. The presence of diatoms within the silty diatomaceous clay is attributed both to leads which opened in the summer sea-ice, resulting in higher phytoplankton productivity, and to occasional summers when sea ice melted back almost to the continent (ref. 8 and J. D. Hays *et al.*, in preparation).

Here we suggest an alternative interpretation of the sediment analysis of Cooke⁹ and Cooke and Hays⁸. We use modern-day sea-ice distribution and compare it with sediment distribution (and particularly sediment type boundaries) in surface sediments and at 18,000 yr BP⁹. Sea-ice cover, derived predominantly from satellite imagery¹⁰, was averaged monthly over a 5-yr period (1973–77) for both the Atlantic and the Pacific sectors (Fig. 2). These data show a seasonally fluctuating ice front with a low percentage of sea-ice cover near the ice margin and higher values ranging between 75 and 100% some 6–7° behind the ice front. The lower values encountered in higher latitudes near the continent represent polynyas where high winds have pushed the sea ice away from the shore and maintained open water, sometimes well into the winter and in early spring.

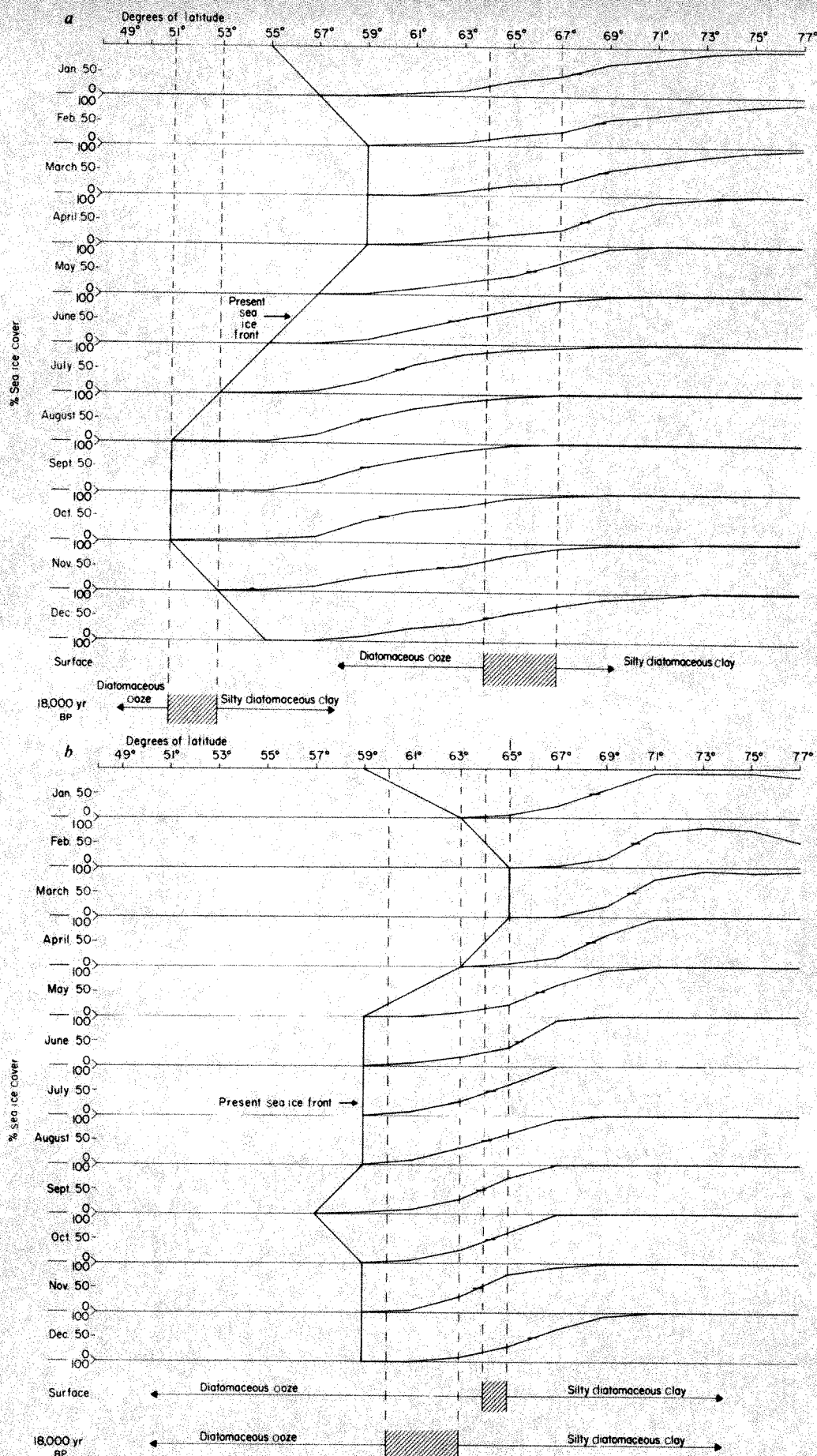


Fig. 2 Satellite-derived 5-yr monthly averages of per cent sea-ice cover for each 2° of latitude in the Pacific (a) and Atlantic (b) sectors of the Southern Ocean. Data on sediment distribution in Recent and at 18,000 yr BP are taken from ref.⁹.

Figure 2 also shows the present-day northern boundary between silty diatomaceous clay and diatom ooze⁹. This boundary is rather irregular but is between 64° and 65° in the Pacific sector and 64° and 67° in the Atlantic sector. If this boundary is projected up through the diagram, it is seen that in the Pacific the range of sea-ice cover is 0–0.1% during the months of February to March. In the Atlantic, on the other hand, the sea-ice concentration during those 2 months ranges over 15–30%. A sea-ice concentration of 0.1% seems insufficient to produce a silty diatomaceous clay on the sea floor. Equally doubtful is the notion that 15–30% sea-ice cover is enough to produce such a sediment type. It seems, therefore, that this sediment boundary cannot represent summer sea-ice limits.

Although we believe that this approach is better than those previously attempted, there are some obvious weaknesses in it. Kukla and Gavin¹⁰, for example, have recently shown that in the 1930s, summer ice conditions were heavier than at present. However, this translates into a change in the position of the sea-ice edge of the order of 1–2° of latitude. Further, as Kukla and Gavin¹⁰ point out, there are periodic variations ranging from a few years to tens of years in duration in oceanic circulation and these would probably affect sea-ice distributions. Heap¹¹ also reported oscillations in ice extent in the Weddell Sea and Palmer Peninsula. Finally, Kukla¹² and Kukla and Gavin¹⁰ report extensive spring sea ice in 1972 and 1973 and again in 1981, with declining spring sea-ice cover in the intervening years. These data suggest, therefore, that the use of sea-ice cover averaged over a 5-yr period or better may be adequate for comparison with surface sediment data.

If not summer sea-ice limits, what event does this sediment boundary record? Figure 2 shows that the biggest drop in ice cover overlying this sediment boundary occurs in the late spring (November–December). In the Pacific, the change is from 60–80% in November to ≤5% in January. In the Atlantic, the change is less dramatic, but the ice cover drops from as much as 90% in November to slightly more than 40% in January. The fact that this ice lingers on into late spring before retreating produces several results. Most important is the fact that the presence of the ice inhibits open-ocean diatom productivity. There are, of course, diatoms living and growing in the underside of the sea ice, but this production is considerably less than in the open ocean. The diatom growing season begins in November north of the Polar Front and moves southward as the spring and summer seasons progress. As has been shown^{13,14}, the southward progression of this productivity maximum is heavily dependent on the melt back of the ice. Thus, sea ice can act to inhibit diatom productivity.

A second important point is the origin and distribution of the silt and clay size particles associated with diatoms in the sediment. Spring peaks in aerosol concentration and condensation nuclei have been recorded in the Antarctic atmosphere^{15,16}, suggesting a Southern Hemisphere similarity with that of Murozumi *et al.*¹⁷, who found terrestrial dust concentrations of Greenland spring snows to be three times larger than those of other seasons. It seems that whereas this dust falls on the open ocean and is dispersed, the sea ice acts as a collector and selectively dumps it in the late spring and summer. This point, combined with the fact that the sea ice may act as an inhibitor of diatom productivity until well into the growing season, seems to be a reasonable mechanism for producing a silty diatomaceous clay on the sea floor.

The lack of additional data both of ice cover and of surface and 18,000 yr BP sediment distribution prevent us from further speculation. However, we feel that the true summer ice limit during the last glacial maximum is more appropriately placed south of all data points. This means that this limit has not been defined for the last glaciation and is a suitable target for study by palaeoceanographers.

The manuscript was reviewed by G. Kukla and D. Lazarus. Research was supported by NSF grants DPP 80-08011 and ATM 80-01470. This is Lamont-Doherty Geological Observatory contribution no. 3361.

Received 6 May; accepted 22 July 1982.

- Philippi, E. *Deutsche Sudpolar-Expedition, 1901–1903* Vol. 2, 415 (1912).
- Schott, W. *Recent mar. Sediments* Vol. 7, 396 (1939).
- Hough, J. L. *J. Sedim. Petrol.* **26**, 301 (1956).
- Lisitzin, A. P. *Deep Sea Res.* **7**, 88 (1960).
- Goodell, H. G. *Antarctic Map Folio Ser.* No. 17 (1973).
- Lozano, J. A. & Hays, J. D. *Investigation of Late Quaternary Paleooceanography and Paleoclimatology*, 303 (Geological Society of America, Washington, DC, 1976).
- Hays, J. D. *et al.* *Investigation of Late Quaternary Paleooceanography and Paleoclimatology*, 337 (Geological Society of America, Washington DC, 1976).
- Cooke, D. W. & Hays, J. D. *Proc. 3rd Symp. Ant. Geol. Geophys.* (in the press).
- Cooke, D. W. thesis, Columbia Univ. (1978).
- Kukla, G. & Gavin, J. *Science* **214**, 497 (1981).
- Heap, J. A. in *Antarctica*, 187 (Praeger, London, 1965).
- Kukla, G. J. *Climatic Change*, 114 (Cambridge University Press, 1978).
- Hart, T. J. *Discovery Rep.* **21**, 261 (1942).
- Burckle, L. H. & Clarke, D. B. *Nova Hedwegia* **54**, 1977 (1977).
- Hogan, A. S., Barnard, S. & Somson, J. *Geophysical Monitoring for Climatic Change*, No. 7, 89 (NOAA Environmental Research Laboratories, 1978).
- Mosley-Thompson, E. *Inst. pol. Stud. Rep.* (1980).
- Murozumi, M., Chow, T. & Patterson, C. *Geochim. cosmochim. Acta* **33**, 1247 (1969).

De-A-steroid ketones and de-A-aromatic steroid hydrocarbons in shale indicate a novel diagenetic pathway

Ger van Graas, F. de Lange, J. W. de Leeuw & P. A. Schenck

Department of Chemistry and Chemical Engineering, Organic Geochemistry Unit, Delft University of Technology, De Vries van Heystplantsoen 2, 2628 RZ Delft, The Netherlands

Recent investigations of Cretaceous black shales have led to the identification of several hitherto unknown steroidal compounds^{1,2}, thus providing information on some diagenetic pathways of steroids. We report here the identification of ring A-degraded steroids in a Cretaceous black shale from the Livello Bonarelli, a carbonate-poor interval deposited at the Cenomanian–Turonian boundary. The ketone fraction of the extract contains a series of compounds which we have identified as 10 α (Me)-de-A-cholestan-5-one and homologues. The presence of mono- and diaromatic de-A-steroid hydrocarbons in the aromatic fraction of the extract is suggested. The occurrence of these degraded steroids can be explained by a degradation pathway similar to that suggested for 3-oxygenated triterpenoids such as β -amyrin and lupeol^{3–7}.

The shale sample was taken from an exposure (43°33' N, 12°41' E) near the cemetery of Moria, a small village near Cagliari, province of Pesaro and Urbino, Italy⁸. The sediment, which has an organic carbon content of 13.3%, was Soxhlet-extracted with toluene/methanol (1:3 v/v; 20 h). The hexane-soluble part of the extract was separated by column chromatography over silica gel. Elution with 50-ml portions of hexane containing increasing amounts of diethyl ether (0, 1, 3, 5, 7, 10, 20%)

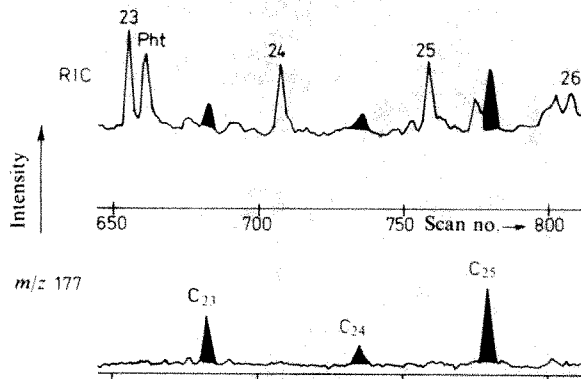


Fig. 1 Part of the reconstructed ion chromatogram (RIC) and part of the mass chromatogram of m/z 177. Numbered compounds in the RIC are n -alkan-2-ones. Pht, phthalate. Temperature programme: 150–300 °C (4 °C min⁻¹).

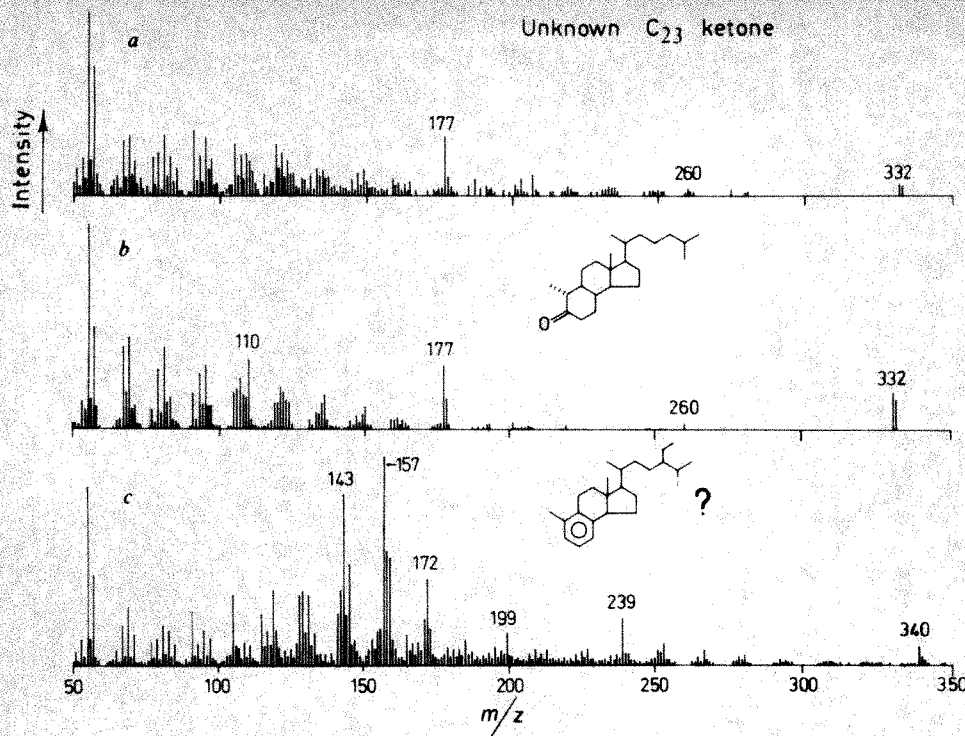


Fig. 2 Mass spectra of *a*, unknown C_{23} ketone; *b*, synthetic $10\alpha(\text{Me})\text{-de-A-cholestan-5-one}$; *c*, C_{25} monoaromatic de-A-steroid hydrocarbon (tentative identification). Spectra *a* and *c* comprise contributions from other compounds.

yielded several fractions including aromatic hydrocarbons (1 and 3% diethyl ether) and ketones (7 and 10% diethyl ether). Gas chromatography-mass spectrometry was performed on a Varian 3700 gas chromatograph equipped with a 25-m fused silica column coated with CP-sil-5, coupled to a MAT 44 quadrupole mass spectrometer operating at 80 eV (mass range m/z 50–500, cycle time 2 s).

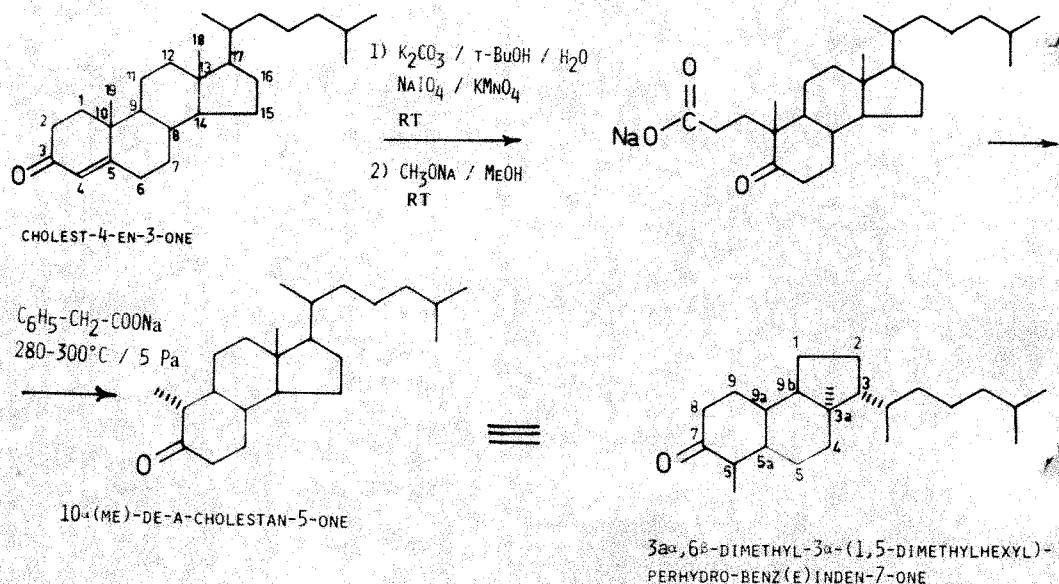
The ketone fraction contains several series of *n*- and isoprenoid alkan-2-ones, steroidal and hopanoid ketones, and a series of three compounds whose mass spectra exhibit a characteristic peak at m/z 177 (Fig. 1). The distribution pattern of these compounds is similar to that often encountered with steroidal compounds. As the main fragment ion at m/z 177 and the molecular ions at m/z 332 (Fig. 2*a*), 346 and 360 of the unknown compounds were 54 mass units lower than the corresponding ions in the mass spectra of C_{27} , C_{28} and C_{29} cholestan-3-ones (m/z 231, 386, 400 and 414 respectively), we assumed that we were dealing with a series of de-A-steroid ketones. To test this hypothesis we synthesized de-A-cholestan-5-one ($3\alpha,6\beta$ -dimethyl- 3α -(1,5-dimethylhexyl)-perhydrobenz(e)inden-7-one) starting from cholest-4-en-3-one (Fig.

3)^{9–11}. During the removal of ring A the orientation of the C-19 methyl group changes from β to the more stable α configuration¹⁰.

The synthetic compound co-eluted with the unknown C_{23} compound on two stationary phases (OV 101 and SE 52). On the basis of this observation and a comparison of the mass spectra (Fig. 2*a,b*), we concluded that the unknown C_{23} compound was identical to $10\alpha(\text{Me})\text{-de-A-cholestan-5-one}$. The unknown C_{24} and C_{25} compounds are probably the 24-methyl- and 24-ethyl-substituted homologues.

The aromatic fraction of the extracts contains C_{23} , C_{24} and C_{25} compounds whose mass spectra resemble those of ring A monoaromatic steroid hydrocarbons [4-methyl-24-ethyl-19-nor-cholesta-1,3,5(10)-triene: m/z 394 (M^+ , 85%), 253 (M^+ -side chain, 5%), 226(13%), 211(100%), 197(8%), 158(66%), 157(32%)]¹, but with a shift of 54 mass units for the prominent ions (Fig. 2*c*). Therefore, we may be dealing with a series of de-A-ster-5,7,9(10)-trienes ($3\alpha,6\beta$ -dimethyl- 3α -(1,5-dimethylhexyl)-2,3,3a,4,5,9b-hexahydrobenz(e)indenes). Also present in the aromatic fraction are compounds with mass spectra having a base peak at m/z 195 and weak molecular

Fig. 3 Preparation of $10\alpha(\text{Me})\text{-de-A-cholestan-5-one}$ from cholest-4-en-3-one^{9–11}. RT, room temperature.



ions (among others at m/z 322 and 336). These compounds could be diaromatic de-A-steroid hydrocarbons. Unambiguous identification of the mono- and diaromatic compounds will only be possible after synthesis of the proper reference compounds.

As ring A-degraded steroidal compounds have not been reported in living organisms, it seems likely that they are formed by diagenetic degradation of steroids. This degradation could proceed along the pathway proposed for 3-oxygenated triterpenoids such as β -amyrin and lupeol³⁻⁷. Cleavage of the C-3/C-4 bond may occur through a photochemical or microbial oxidation yielding 3:4 seco acids⁶. Further steps may involve the

removal of the ring A remains, yielding de-A-triterpanes⁷. The formation of di-^{4,5} and triaromatic³ de-A-triterpenoid hydrocarbons is also possible. The occurrence of ring A-degraded steroids in the sediment investigated is compatible with the degradation pathway described. The likelihood of this pathway in the case of steroids would be greatly enhanced by the identification of 3:4 seco steroidal acids in recent sediments.

This research is supported by the Netherlands Foundation for Earth Science Research (AWON) with financial aid from the Netherlands Organization for the Advancement of Pure Research (ZWO).

Received 1 June; accepted 23 July 1982.

1. Hussler, G., Chappe, B., Wehrung, P. & Albrecht, P. *Nature* **294**, 556-558 (1981).
2. Van Graas, G., de Lange, F., de Leeuw, J. W. & Schenck, P. A. *Nature* **296**, 59-61 (1982).
3. Spyckerelle, C., Greiner, A. G., Albrecht, P. & Ourisson, G. *J. chem. Res. (S)* 330-331, (M) 3746-3777 (1977).
4. Spyckerelle, C., Greiner, A. G., Albrecht, P. & Ourisson, G. *J. chem. Res. (S)* 332-333, (M) 3801-3828 (1977).

5. Laflamme, R. E. & Hites, R. A. *Geochim. cosmochim. Acta* **43**, 1687-1691 (1979).
6. Corbet, B., Albrecht, P. & Ourisson, G. *J. Am. chem. Soc.* **102**, 1171-1173 (1980).
7. Schmitter, J. M., Arpino, P. J. & Guiochon, G. *Geochim. cosmochim. Acta* **45**, 1951-1955 (1981).
8. Wonders, A. A. H. *Utrecht micropaleont. Bull.* **24**, 1-157 (1980).
9. Edward, J. T., Holder, D., Lunne, W. H. & Puskas, I. *Can. J. Chem.* **39**, 599-600 (1961).
10. Edward, J. T. & Lawson, N. E. *J. org. Chem.* **35**, 1426-1430 (1970).
11. Hartshorn, M. P. & Jones, E. R. H. *J. chem. Soc.* 1312-1313 (1962).

Pseudocholinesterase staining in the primary visual pathway of the macaque monkey

Ann M. Graybiel & Clifton W. Ragsdale Jr

Department of Psychology and Brain Science, Massachusetts Institute of Technology, Cambridge, Massachusetts 02139, USA

Cholinesterases in brain tissue are divided into two main classes: 'true' cholinesterases (acetylcholinesterase, AChE, EC 3.1.1.7), which preferentially hydrolyse the neurotransmitter acetylcholine; and 'pseudocholinesterases' (for example, butyrylcholinesterase, BuChE, EC 3.1.1.8), which preferentially hydrolyse higher choline esters¹. AChE is found at peripheral and central cholinergic synapses, is known to be the degradative enzyme of the cholinergic mechanism and may also have other functions in the central nervous system¹⁻³. In contrast to AChE, the pseudocholinesterases have been assigned no certain function in neural transmission and initially were thought to occur mainly in neuroglia, Schwann cells and vascular endothelia^{1,4}. Pseudocholinesterase activity has since been found in neurones and neuropil in several brain regions^{1,4,5}, however, and in the superior cervical ganglion, BuChE has been localized to postsynaptic membranes⁶ and shown to exist in stable molecular forms corresponding to each of the known molecular forms of true cholinesterase⁷. These observations have led to the alternative interpretations that the pseudocholinesterases are either metabolic precursors of AChE⁸ or that they have functions closely related to those of AChE^{5,7} while being independent of true cholinesterases. We have directly compared the distributions of BuChE and AChE in the central visual pathway of the primate, a neural system in which anatomical and functional compartmentalization is well known⁹. We demonstrate here that the histochemical localization of pseudocholinesterase rivals that of AChE in terms of specificity, and that BuChE is independent of AChE both in its normal distribution in the lateral geniculate body and striate cortex and in the response it shows to eye enucleation. We conclude that BuChE or its endogenous substrate may be a neuroactive substance in the primate brain.

In the brains of nine adult rhesus macaque monkeys, we studied the distributions of BuChE and AChE in serially adjoining sections through the lateral geniculate body and pulvinar nuclei of the thalamus and through the striate and peristriate cortex. We related these, in turn, to the distribution of cytochrome oxidase, a histochemical marker for modular tissue arrangements in the visual cortex¹⁰⁻¹². Three of the monkeys had undergone unilateral (left) eye enucleation, 10, 15 and 29

days before death. All brains were fixed by vascular perfusion with 4% paraformaldehyde in 0.1 M PO₄ buffer and cut at 30-50 μ m on a freezing microtome. For the cholinesterase histochemistry we followed modified thiocholine protocols¹³: BuChE sections were incubated with butyrylthiocholine iodide as substrate in the presence of 10^{-3} - 10^{-2} M BW284c51 (Burroughs Wellcome), an AChE inhibitor; AChE sections were incubated with acetylthiocholine iodide as substrate in the presence of a saturated solution of ethopropazine (Parsidol, Warner Chilcott), a pseudocholinesterase inhibitor; and control sections were incubated with either substrate in the presence of 1 mM eserine, a general inhibitor of cholinesterases. Incubations were carried out at room temperature and at 4°C for times ranging from 13 h to 13 days for the BuChE and 4 h to 10 days for the AChE. Cytochrome oxidase sections were prepared according to the protocol described by Wong-Riley¹².

In the normal monkeys there was a striking compartmentalization of BuChE activity in relation to known functional subdivisions of the visual thalamus and cortex. First, the enzyme stain sharply distinguished between the parvocellular and magnocellular layers of the lateral geniculate body: the parvocellular layers were rich in BuChE, the magnocellular layers were nearly devoid of staining (Fig. 1a). Second, the several subnuclei of the pulvinar were stained in a non-uniform way, as we will describe separately. Finally, there was a detailed patterning of BuChE staining in the striate cortex which set it off from surrounding areas (Fig. 2a): layer 4C α was most densely stained and thin dark laminae appeared at the borders of layer 5. Layer 4C β , at least at its base, was only very weakly stained. In the supragranular layers BuChE activity was concentrated in 100-300 μ m wide patches which in tangential sections formed a partly connected gridwork. As shown in Fig. 2, the spacing of the BuChE patches was similar to that of the patches of cytochrome oxidase visible in serially adjoining sections (300-500 μ m centre-to-centre) but the relationship between the two sets of patches was not clear because they were, in the case material, instances of alignment, complementarity and apparent lack of correlation of the two patterns. In the infragranular layers there was also clear periodicity in the BuChE and, especially in layer 6, some prominent BuChE-positive neurones. Vascular staining was notable in the BuChE sections because the walls of the microvessels, but not the larger vessels, showed intense enzyme activity.

Neither in the thalamus nor in the cortex did the distribution of AChE match that just described for BuChE. In the lateral geniculate body all of the cell layers were stained for AChE, the magnocellular layers more intensely than the parvocellular¹⁴ (Fig. 1b). This pattern closely matched that of cytochrome oxidase. Zones of high and low AChE activity also appeared in the pulvinar, but were not sharply different from the BuChE-positive subdivisions. In the striate cortex AChE staining was most pronounced in layers 4A and both 4C α and 4C β , and was

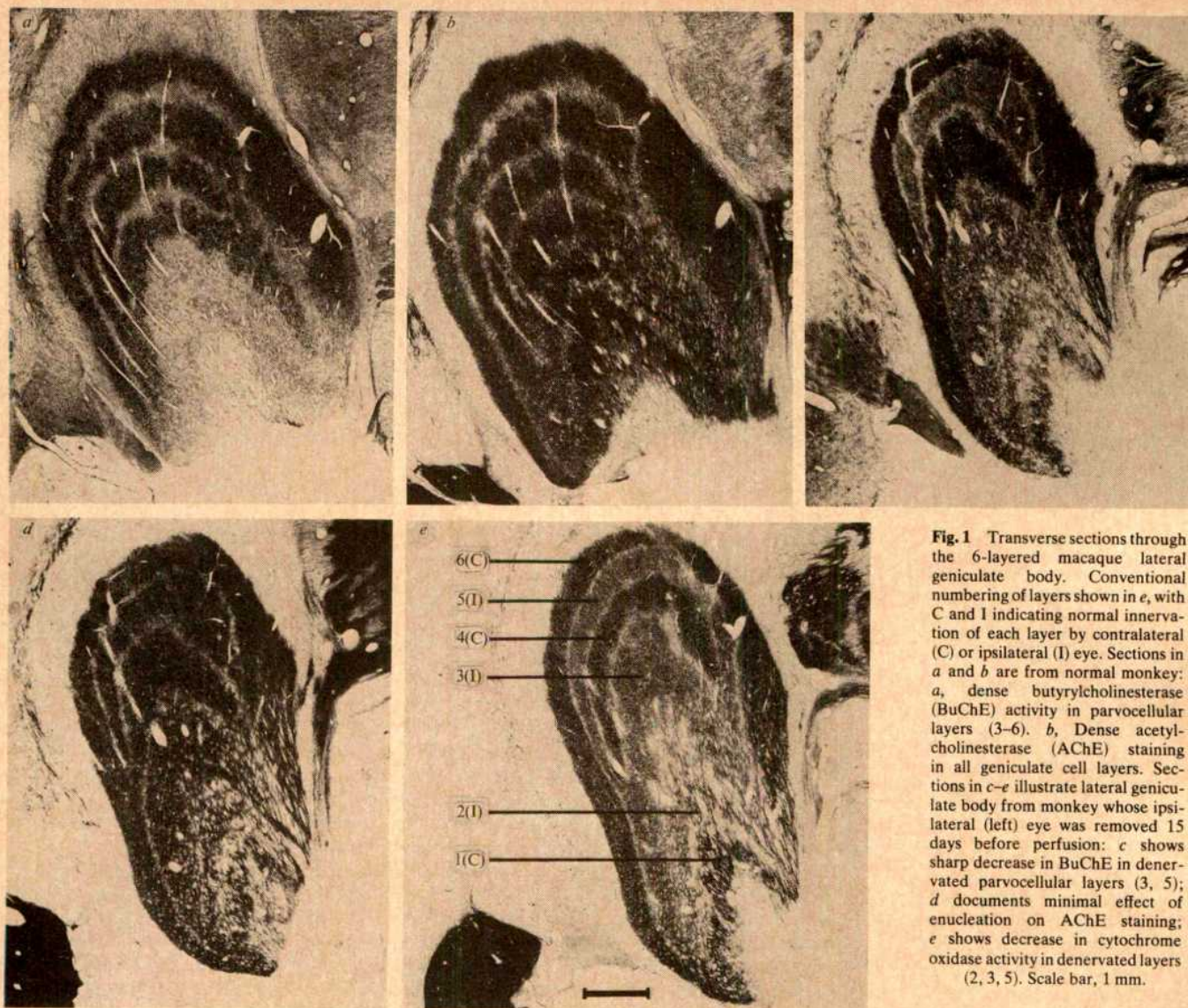


Fig. 1 Transverse sections through the 6-layered macaque lateral geniculate body. Conventional numbering of layers shown in *e*, with C and I indicating normal innervation of each layer by contralateral (C) or ipsilateral (I) eye. Sections in *a* and *b* are from normal monkey: *a*, dense butyrylcholinesterase (BuChE) activity in parvocellular layers (3–6). *b*, Dense acetylcholinesterase (AChE) staining in all geniculate cell layers. Sections in *c–e* illustrate lateral geniculate body from monkey whose ipsilateral (left) eye was removed 15 days before perfusion: *c* shows sharp decrease in BuChE in denervated parvocellular layers (3, 5); *d* documents minimal effect of enucleation on AChE staining; *e* shows decrease in cytochrome oxidase activity in denervated layers (2, 3, 5). Scale bar, 1 mm.

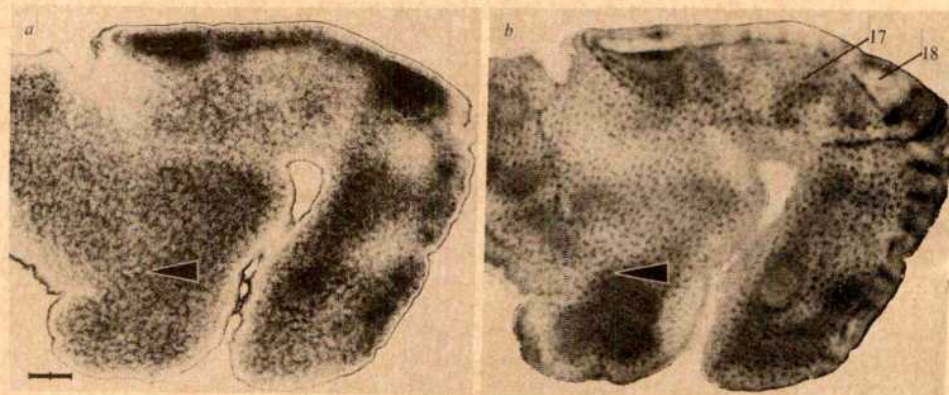
strong in layers 1 and 6 (see ref. 15). Patches were present in the supragranular layers in most preparations and, in sections studied in detail, lay in register with the BuChE patches. They were fuzzy and difficult to see, however, even after prolonged incubations.

Unilateral eye removal resulted in marked changes in these cholinesterase patterns but did not influence the two enzymes in the same way. In the lateral geniculate body there was a blanching of BuChE stain in the parvocellular layers innervated by the enucleated eye (Fig. 1*c*) but the AChE patterns in the geniculate appeared nearly normal, at most a slight weakening

being visible in the denervated layers (Fig. 1*d*). The cytochrome oxidase was decreased in the denervated layers (Fig. 1*e*).

Although AChE activity did not change greatly in the geniculate, it did in the striate cortex, where, as shown for the 10-day eye enucleate in Fig. 3*a*, stripes of high AChE activity alternated regularly with zones of low AChE activity in layer 4C. Changes in BuChE staining were more difficult to detect in transverse sections, but in tangential sections through the base of layer 4 (Fig. 3*b*) and in favourable transverse sections, periodically arranged thin dark stripes could be seen. Even 10 days after enucleation, there also were subtle periodic variations in the

Fig. 2 Adjacent tangential sections cutting through supragranular layers of the visual cortex in a normal macaque monkey. *a*, Supragranular gridwork of BuChE activity in area 17. *b*, Patches of cytochrome oxidase activity in supragranular layers. Tips of arrows touch blood vessel running through the two sections. In this pair of sections many BuChE patches avoid cytochrome oxidase patches. The border between areas 17 and 18 is shown to right and top. Note that both BuChE and cytochrome oxidase are distributed unevenly in area 18 as well as in area 17. Sections 50 μ m thick; scale bar, 2 mm.



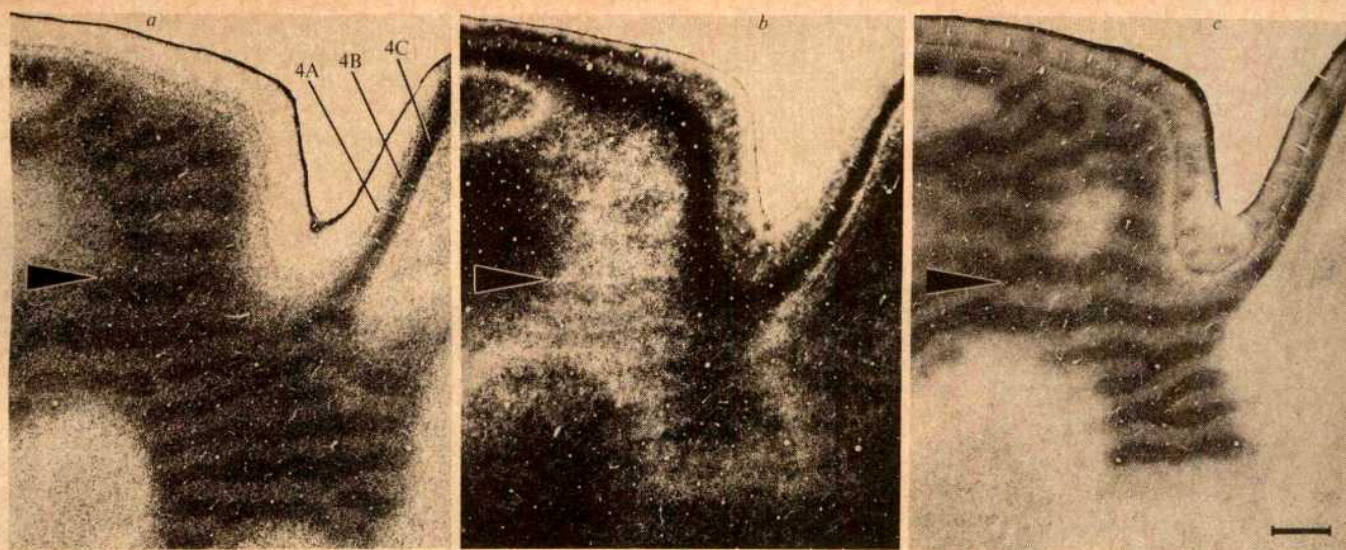


Fig. 3 Serially adjoining 50- μ m thick tangential sections through area 17 of a macaque monkey whose ipsilateral (left) eye was enucleated 10 days before perfusion. *a*, AChE activity; *b*, BuChE activity; *c*, cytochrome oxidase activity. Sections illustrate that, as a result of the eye enucleation, stripes form in layer 4 in all three stains. Similar stripes appeared on the contralateral side. Arrows indicate position common to all sections, located by using blood vessels as fiducial markers. Alignment of the sections shows that the AChE-rich and BuChE-rich stripes in *a* and *b* are in register but that they correspond to the stripes poor in cytochrome oxidase activity in *c*. At the upper right, the plane of section is oblique to the cortical layers, which are numbered according to the scheme of Lund¹⁸. Scale bar, 1 mm.

intensity of Nissl staining in layer 4C and in the supragranular layers (not illustrated; see ref. 16). Alignment of serial sections such as those shown in Fig. 3 demonstrated that the dark BuChE stripes were in register with the dark AChE stripes (and also with the zones of darker Nissl stain). Remarkably, the stripes of high AChE and BuChE activity coincided with stripes of low cytochrome oxidase activity, known from previous work to represent the enucleated eye¹⁰. This finding (see Fig. 3*a-c*) will be described further elsewhere.

The present study demonstrates that BuChE is a sensitive marker for functional subdivisions in the primate visual system. In the lateral geniculate body, high BuChE activity singles out the layers reported to have physiological properties of the X (colour-opponent) type¹⁷. In the cortex, BuChE activity patterns distinguish area 17 from area 18 and within area 17 delimit distinct sublaminae as well as periodic elements in the supragranular and infragranular layers. It is unlikely that the geniculate and cortical patterns of BuChE activity denote a single functional system. For example, the BuChE-rich parvocellular layers of the geniculate project mainly to layers 4A and 4C β ¹⁸, yet in the striate cortex BuChE in layer 4 is densest in the magnocellular-recipient 4C α . Nor is the supragranular patchwork of BuChE activity in area 17 clearly related to geniculate innervation. It did not undergo changes with eye enucleation comparable to those observed in the cytochrome oxidase sections and was not even always aligned with the cytochrome oxidase grid: in some serial sections the two sets of patches were in complementary positions. Thus, in the striate cortex, BuChE may mark fibre systems intrinsic to area 17¹⁹ or systems originating in extrastriate cortex¹⁸ or in the pulvinar²⁰. By virtue of branching of the patches, the BuChE gridwork showed a striking resemblance to 2-deoxyglucose patterns illustrated by Hubel *et al.*²¹ and others²²⁻²⁴. Identification of the BuChE-containing elements may therefore help resolve uncertainty as to the origin of the heightened metabolic activity in the supragranular grid^{10,24,25}.

In the lateral geniculate body the BuChE pattern seemed clearly associated with the primary visual pathway and the systematic decreases in BuChE activity on denervation suggest that BuChE may be a highly specific marker for retinal axon terminals or the neurones which they innervate. An alternative explanation is that BuChE is a marker of functional activity as cytochrome oxidase is thought to be¹², but this is made unlikely by the fact that BuChE activity in the cortex did not decrease in the regions representing the removed eye.

Both the specificity in the distribution of BuChE and its independence of AChE levels emphasize the possibility that the pseudocholinesterases or their substrates may be neuroactive substances in the central nervous system. The present findings suggest that the primate visual pathway may serve as a valuable system in studies designed to identify such endogenous substrates, which, based on previous reports, could include neuropeptides or compounds related to γ -aminobutyric acid metabolism^{5,26}.

In addition to these findings on the distribution of BuChE, a corollary observation of importance in its own right was the sensitivity of cortical AChE to eye enucleation. AChE in the brain stem is known to derive from several sources^{5,15} but in most of the neocortex AChE levels have been reported to depend on the integrity of the nucleus basalis of Meynert, which as part of the substantia innominata is thought to provide the main cholinergic innervation of the neocortical parts of the cerebral hemispheres^{5,27,28}. The implication of the present study is that the cortical fibre systems delimited by the presence of AChE are probably multiple, including at least some that are dependent on activity in the main sensory pathways and possibly, more generally, on thalamic innervation.

This work was supported by NIH grants 5R01-EY-02866 and 5P30-EY-02621. We thank Mr Henry F. Hall for the photography, and Mr Hall, Ms Lisa Metzger and Ms Dianne Sahagian for their help with the histology.

Received 24 May; accepted 28 July 1982.

1. Silver, A. *The Biology of Cholinesterases* (Elsevier, Amsterdam, 1974).
2. Chubb, I. W., Hodgson, A. J. & White, G. H. *Neuroscience* **5**, 2065-2072 (1980).
3. Greenfield, S., Cheramy, A., Leviel, V. & Glowinski, J. *Nature* **284**, 355-357 (1980).
4. Friede, R. L. *Topographic Brain Chemistry* (Academic, New York, 1966).
5. Shute, C. C. D. & Lewis, P. R. *Nature* **199**, 1160-1164 (1963).
6. Davis, R. & Koelle, G. B. *J. Cell Biol.* **78**, 785-809 (1978).
7. Vigny, M., Grisiger, V. & Massoulié, J. *Proc. natn. Acad. Sci. U.S.A.* **75**, 2588-2592 (1978).
8. Koelle, W. A. *et al. J. Neurochem.* **28**, 307-311 (1977).
9. Hubel, D. H. & Wiesel, T. N. *Proc. R. Soc. B* **198**, 1-59 (1977).
10. Horton, J. C. & Hubel, D. H. *Nature* **292**, 762-764 (1981).
11. Hendrickson, A. E., Hunt, S. P. & Wu, J.-Y. *Nature* **292**, 605-607 (1981).
12. Wong-Riley, M. T. T. *Brain Res.* **171**, 11-28 (1979).
13. Geneser-Jensen, F. A. & Blackstad, T. W. *Z. Zellforsch. Mikrosk. Anat.* **114**, 460-481 (1971).
14. Manocha, S. L. & Shantha, T. R. *Macaca Mulatta. Enzyme Histochemistry of the Nervous System*, 115 (Academic, New York, 1970).
15. Fitzpatrick, D. & Diamond, I. T. *J. comp. Neurol.* **194**, 703-719 (1980).
16. Haseltine, E. C., DeBruyn, E. J. & Casagrande, V. A. *Brain Res.* **176**, 153-158 (1979).
17. Schiller, P. H. & Malpeli, J. G. *J. Neurophysiol.* **41**, 788-797 (1978).
18. Lund, J. S. in *The Organization of the Cerebral Cortex* (eds Schmitt, F. O., Worden, F. G. & Dennis, F.) 105-124 (MIT Press, Cambridge, 1981).
19. Rockland, K. S. & Lund, J. S. *Science* **215**, 1532-1534 (1982).

20. Ogren, M. P. & Hendrickson, A. E. *Brain Res.* **137**, 343–350 (1978).
21. Hubel, D. H., Wiesel, T. N. & Stryker, M. P. *J. comp. Neurol.* **177**, 361–380 (1978).
22. Kennedy, C. *et al. Proc. natn. Acad. Sci. U.S.A.* **73**, 4230–4234 (1976).
23. Hendrickson, A. E. & Wilson, J. R. *Brain Res.* **170**, 353–358 (1979).
24. Tootell, R. B. H. & Silverman, M. S. *Neurosci. Abstr.* **7**, 356 (1981).
25. Humphrey, A. L. & Hendrickson, A. E. *Neurosci. Abstr.* **6**, 315 (1980).
26. Holmstedt, B. & Sjöqvist, F. *Biochem. Pharmacol.* **3**, 297–304 (1960).
27. Wenk, H., Bigl, V. & Meyer, U. *Brain Res. Rev.* **2**, 295–316 (1980).
28. Coyle, J. T., McKinney, M. & Johnston, M. V. in *Brain Neurotransmitters and Receptors in Aging and Age-Related Disorders* (eds Enna, S. J. *et al.*) 147–161 (Raven, New York, 1981).

Functional reconnections without new axonal growth in a partially denervated visual relay nucleus

Ulf Th. Eysel

Institut für Physiologie, Universitätsklinikum Essen,
Hufelandstrasse 55, D-4300 Essen 1, FRG

Physiological mapping of the retino-geniculate projections in adult cats which had previously undergone partial retinal lesioning have demonstrated a delayed spread of excitation into regions initially deafferented¹. Anatomical studies in the adult cat^{2–5} and monkey⁶ have, however, not revealed any new axonal growth. The present results demonstrate that the lesion-induced functional reorganization is brought about not by new axonal growth but probably by local changes at the periphery of the dendrites.

In a combined electrophysiological and autoradiographic study of the partially deafferented lateral geniculate nucleus, extracellular recordings were obtained from the light-excitable cells closest to deafferented geniculate zones. The cells were marked by electrolytic lesions, and ³H-proline was then injected into the damaged eye to trace the distribution of surviving retinal afferents to the geniculate cells. After short survival times light-excitable and distribution of autoradiographic label corresponded, but after survival times longer than 30 days light-excitable cells were detected in the unlabelled regions for a distance of up to 150 μ m beyond the boundaries of the autoradiographically labelled zones.

Single-cell recordings obtained from the lateral geniculate nucleus (LGN) of adult cats with long survival times after photocoagulation in the nasal retina have revealed characteristic topographical changes in the border region between normal innervation and deafferentation¹. At 1–20 days after retinal lesions normal retino-geniculate projection columns⁷ were

found at the borders of deafferented regions in layer A (Fig. 1a). After survival times exceeding 25 days, excitation from parts of the retina adjacent to the lesions could be detected in the normal topographical location and also up to 200 μ m inside the initially deafferented zones of layer A¹. This was demonstrated by making recordings from cells in layer A with receptive fields at the border of the retinal lesions which were displaced by up to 4.5° of visual angle with respect to the normal receptive field positions of layer A₁ cells recorded during the same vertical penetrations. In layer A the respective projection columns had expanded asymmetrically into the deafferented region (Fig. 1b).

The time course with which the displaced receptive fields of layer A cells developed was similar to that observed in anatomical studies of axonal sprouting in subcortical structures of the cat central nervous system^{8–10}, but no indications of any long-range axonal sprouting had been found in the adult cat LGN after either monocular enucleations^{2,3} or focal lesions of the retina⁴, while axonal sprouts of 100–200 μ m had not been ruled out. Because sprouting in this range would explain our neurophysiological observations, we tested this possibility in the range of 200 μ m with an autoradiographic experiment.

In five cats a narrow normal retinal strip of constant width (6–8°), bordered by photocoagulator lesions, was created in two stages so that the upper part was bordered by long-established (90–160 days) and the lower part by recent (6 days) lesions (Fig. 1c). The high-intensity lesions destroyed all excitable layers of the retina. In the final experiment, electrolytic lesions were made in the LGN to mark the regions of long- and short-term deafferentation. ³H-proline was injected into the eye to label the axons projecting to the LGN. This allowed an autoradiographic comparison of the projections into long-term and short-term zones of deafferentation in the LGN in the same experiment. If there was axonal growth corresponding to the spread of excitation, the band of label seen in frontal sections of the LGN should be approximately double the width in the region of long-term deafferentation. No change of this magnitude was observed (Fig. 1d). In contrast, the width of the labelled regions was slightly less in the long-term deafferented parts of the LGN (Table 1) due to the continuous decrease of the retino-geniculate magnification factor towards the periphery of the retina. At this stage our electrophysiological demonstration of lesion-induced plasticity in the adult cat LGN¹ seemed to be at clear variance with all anatomical results^{2–5}.

In an attempt to resolve this discrepancy, we investigated the position of the light-excitable cells relative to the distribution of the input fibres. In two cats a long-term lesion (90 and 97 days) in the upper nasal retina was extended 6 days before the final experiments by a second lesion in the lower nasal retina

Fig. 1 The physiologically observed expansion of light-evoked excitation in the LGN (a,b) is not accompanied by spreading of the retino-geniculate axons (d) originating from a narrow strip of retina bordered by photocoagulator lesions (c). a, Schematic drawing of a frontal section through the cat LGN approximately at the projection of the horizontal meridian of the visual field. Projection columns are indicated for 1°, 5°, 20° and 24° of horizontal eccentricity. Between 1 and 20 days after a nasal retinal lesion at 20° in the contralateral eye the black area shows the deafferented part of layer A. The C laminae (stippled) are not included in the present studies. The 20° projection column is normal, the 24° column ends at the A/A₁ border. b, More than 25 days after deafferentation. Conventions as in a. The 20° projection column has expanded in layer A (hatched region) and now includes the region up to the area previously occupied by the 24° column. Layer A₁ remained unchanged. c, Fundus photograph showing long (upper retina) and short (lower retina) survival-time photocoagulator lesions leaving a strip of normal retina with blood vessels and the papilla (below) unaffected. The orientation of the large vessels is tilted by 20° to the left, relative to the vertical meridian. Scale bar, 10° of visual angle. d, Dark-field photomicrographs from frontal sections of the LGN with bands of autoradiographic label in layers A, C₂ and sparing of layers A₁ and C₁. The upper photograph shows a section from the (posterior) short-term deafferented part of the LGN, the lower is from the (anterior) long-term deafferented part. The distance between the sections within the LGN was 96 μ m. Scale bars, 200 μ m.

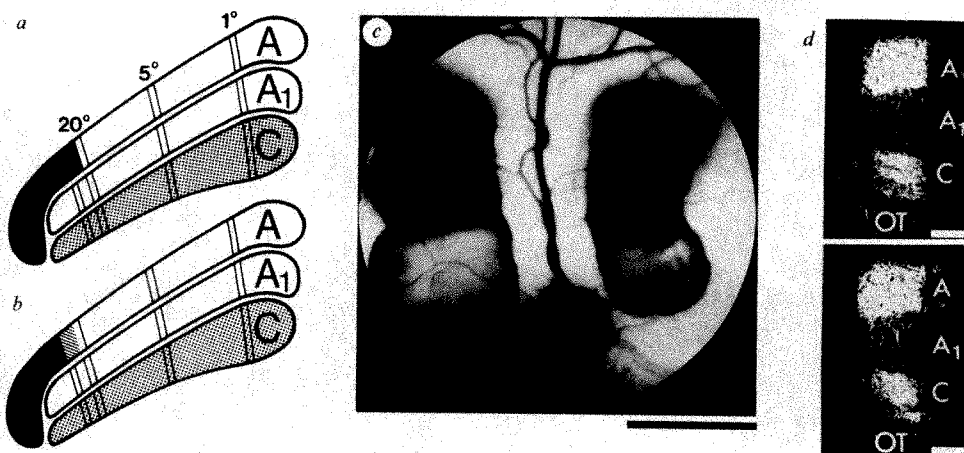
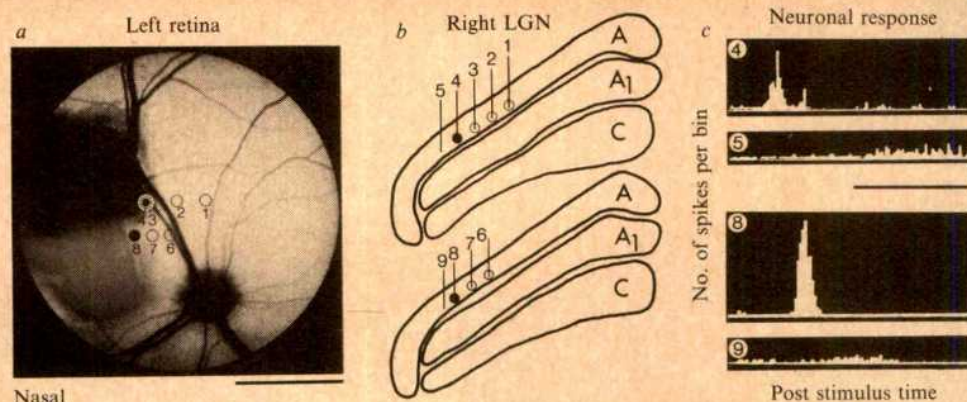


Fig. 2 Receptive field positions (*a*) of neurones, recorded in the LGN (*b*), and responses to flashing lights (*c*) from regions with short- and long-term deafferentation. *a*, Fundus photograph showing the long-term lesion (black) above the short-term lesion (grey). Receptive field positions are marked with numbers. Scale bar, 10° of visual angle. *b*, Line drawings of frontal sections through the contralateral LGN with series of numbered penetrations schematically indicated. Up is dorsal, right is medial. Above, the anterior series of penetrations with correspondingly numbered receptive fields in the upper retina. Below, the series of more posterior penetrations near the zone of short-term deafferentation. Circles indicate detection of light-excitable cells, black dots symbolize electrolytic lesions at the recording sites of the light-excitable cells closest to the deafferented zones. Interpenetration distances were 150–200 μm , except for 100 μm between 8 and 9. *c*, Neuronal responses to flashing lights. ($n = 64$ flashes, repetition rate 4 s^{-1} .) The numbers indicate the penetrations during which the recordings were made. The responses obtained at the positions of electrolytic lesions close to the regions of long-term (4) and short-term (8) visual deafferentation are paired with typical responses of cells in the nearby unresponsive regions. Time calibration, 50 ms; response calibration, 20 spikes per bin.



of the same eye (Fig. 2*a*). The final experiments were made with anaesthetized and immobilized animals. Single cells were recorded with varnished tungsten microelectrodes¹¹ in layer A of the LGN contralateral to the retinal lesions. The receptive field centres of light-excitable LGN cells were drawn on a map together with the back-projected map of the retina with typical landmarks (vessels, papilla) and both the long- and short-term retinal lesions. The receptive field positions were later transferred to fundus photographs of the lesioned eye (Fig. 2*a*). One series of penetrations of the LGN was made to show the light-excitable cells closest to the LGN region with long-term deafferentation caused by destruction of the upper nasal retina. A second, more caudal series of penetrations was aimed to demonstrate the border of light-excitability next to short-term deafferentation in the LGN due to the lower lesion on the retina (Fig. 2*b*).

The region of long-term geniculate deafferentation contained cells with displaced receptive fields¹ located at the border of the long-established lesions (penetration 4 in Fig. 2*b* yielded the same receptive field position as penetration 3, see Fig. 2*a*). An electrolytic lesion (0.5–1.0 μA , 10 s, electrode tip negative) was placed to mark this recording site. The maintained activities and the visual responses of the cells with displaced receptive fields were reduced with respect to those recorded from cells with normal retinotopy¹, but the visual responses could be clearly distinguished from the activity obtained in the visually unresponsive regions (Fig. 2*c*). At the border of the short-term lesions no displaced receptive fields could be found and light-excitability ended when the normal projection of the retinal ganglion cells at the border of the retinal lesion was reached in the LGN (penetration 8 in Fig. 2*b*). An electrolytic lesion was also used to mark this geniculate location. The crucial

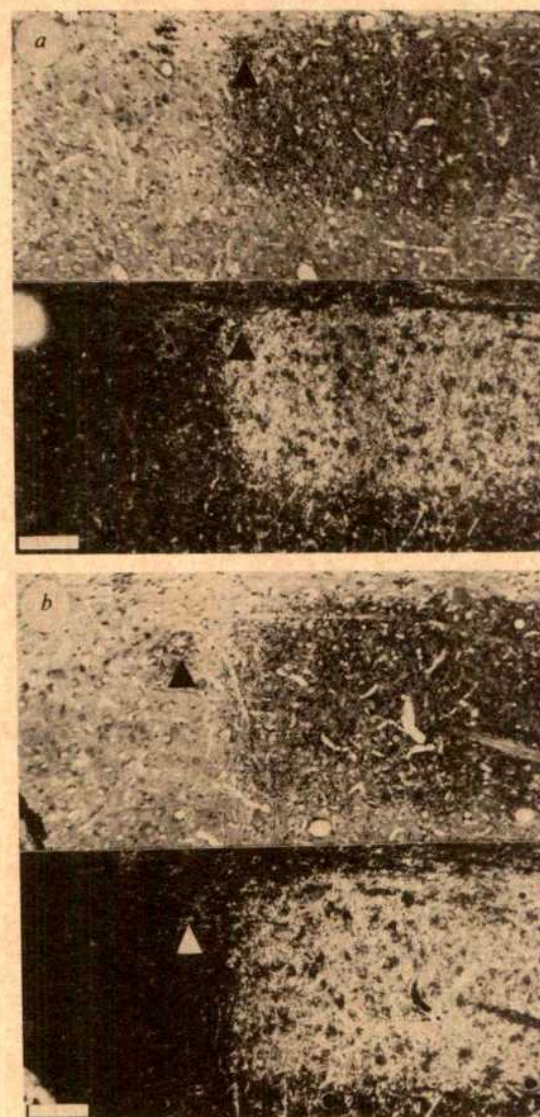


Fig. 3 Autoradiographs of frontal LGN sections with electrolytic lesions at the positions of the light-excitable cells recorded closest to zones of short-term (*a*) and long-term (*b*) deafferentation. *a*, Bright-field and dark-field photomicrographs of layer A. Scale bar, 200 μm . The arrowheads indicate the electrolytic lesion within the labelled region. The lesions were clearly defined in the stained sections by a core of damaged tissue surrounded by gliosis. A second electrode track without electrolytic lesion is visible in the unexcitable deafferented region. *b*, Section anterior to the one in *a*. The electrolytic lesion (arrowhead) is in the deafferented, unlabelled zone. Scale bar, 200 μm .

Table 1 Mediolateral width of the labelled zones in layer A of the LGN between recently deafferented and long-term deafferented regions

Animal	Short-term deafferentation		Long-term deafferentation	
	Width (μm)	s.d. (μm)	Width (μm)	s.d. (μm)
1	372.31	13.30	335.31	11.45
2	388.50	33.09	352.66	22.88
3*	507.59	22.37	326.06	21.22
4	538.81	18.96	511.06	20.12
5	494.88	17.22	389.66	15.80

In each animal measurements were made from 32 adjacent 6- μm frontal sections. Mean values and standard deviations were separately computed for the 16 sections in the short-term and the 16 sections in the long-term deafferented region.

*In this animal the abnormal reduction of width in the long-term deafferented region was caused by damage of the corresponding part of the retina.

difference between the long- and short-term deafferentation then was that there was excitation extending lateral to the normal projection of the border of the retinal lesion in the LGN only in the long-term case¹ (see Fig. 1b).

Thereafter, 1 mCi of ³H-proline in 30 µl saline was injected into the vitreous body of the experimental eye. The animals survived 24 h and were fixed by vascular perfusion with 4% phosphate-buffered paraformaldehyde (pH 7.2). Serial frontal sections (6 µm) were made through the entire paraffin-embedded LGN, processed for autoradiography (Ilford K2 emulsion, 4–6 weeks' exposure time) and counterstained with cresyl violet through the emulsion. The distribution of radioactive label relative to the electrode tracks with electrolytic lesions was compared in the anterior region with penetrations (long-term deafferentation) and the posterior region with penetrations (short-term deafferentation). After short-term deafferentation the light-excitable geniculate cells were confined to the region of autoradiographically labelled retino-geniculate axons (Fig. 3a). After long-term deafferentation, however, light-excitable cells were found in the deafferented, unlabelled zone as much as 150 µm away from the labelled afferents (Fig. 3b). The second animal which had been subjected to the same experimental procedure yielded practically identical results (data not shown).

This result is interpreted as a demonstration of functional reconnection of formerly deafferented cells by a mechanism not involving significant growth of the retino-geniculate axons. The dendrites of cells in the LGN could provide a structural basis for the described lateral excitation without necessarily undergoing additional growth. Our own observations indicate that the cells with displaced receptive fields after long-term deafferentation received fibres of the fast-conducting (Y) type according to stimulus response latency criteria, after electrical stimulation near the optic chiasm, and thus are most probably Y cells¹². These cells have dendrites with comparatively large lateral extent¹³. A mechanism—probably acting at the periphery of the LGN cell dendrites—may have elevated the excitatory power of visual inputs at formerly ineffective synapses from sub- to supra-threshold levels. Some physiological^{14,15} and behavioural^{8,9} observations have led to the postulation of such post-lesion phenomena in other parts of the mature sub-cortical central nervous system at borders between regions of deafferentation and surviving afferents. Although collateral axonal sprouting is one of the most discussed mechanisms, sprouting has not been found in many sensory relay nuclei^{2–6,16–18}. Other possible explanations for the changed excitability of deafferented cells are denervation supersensitivity¹⁹, localized formation of new synaptic junctions without significant axonal growth as observed in the septum nuclei of the rat²⁰, translocation of synapses²¹ over distances below the resolution of the autoradiographic method, or dendritic growth²² into the domain of surviving afferents. The present results show that for the LGN of the adult cat absence of significant axonal extension does not imply an absence of functional reorganization, and that alternative mechanisms must be considered.

This work was supported by the Deutsche Forschungsgemeinschaft (Ey 8/9). We thank U. Neubacher and U. Wolfhard for technical assistance, and Drs R. W. Guillery and G. Raisman for valuable comments on the manuscript.

Received 23 March; accepted 19 July 1982.

1. Eysel, U. T., Gonzalez-Aguilar, F. & Mayer, U. *Brain Res.* **181**, 285–300 (1980); *Expl Brain Res.* **41**, 256–263 (1981).
2. Guillery, R. W. *J. comp. Neurol.* **146**, 407–420 (1972).
3. Hickey, T. L. *J. comp. Neurol.* **161**, 359–382 (1975).
4. Baisden, R. H., Polley, E. H., Goodman, D. C. & Wolf, E. D. *Neurosci. Lett.* **17**, 33–39 (1980).
5. Eysel, U. T., Mayer, U. & Wolfhard, U. *Soc. Neurosci. Abstr.* **7**, 626 (1981).
6. Stelzner, D. J. & Keating, E. G. *Brain Res.* **126**, 201–210 (1977).
7. Sanderson, K. J. *Expl Brain Res.* **13**, 159–177 (1971).
8. McCouch, G. P., Austin, G. M., Liu, C. N. & Liu, C. Y. *J. Neurophysiol.* **21**, 205–216 (1958).
9. Murray, M. & Goldberger, M. E. *J. comp. Neurol.* **158**, 19–36 (1974).
10. Nakamura, Y., Nizuno, N., Konishi, A. & Manabu, S. *Brain Res.* **82**, 298–301 (1974).
11. Hubel, H. D. *Science* **125**, 549–550 (1957).
12. Stone, J. & Hoffmann, K. P. *Brain Res.* **32**, 454–459 (1971).

13. Friedlander, M. J., Lin, C. S. & Sherman, S. M. *Science* **204**, 1114–1117 (1979).
14. Wall, P. D. & Egger, M. D. *Nature* **232**, 542–545 (1971).
15. Millar, J., Basbaum, A. I. & Wall, P. D. *Expl Neurol.* **50**, 658–672 (1976).
16. Kerr, F. W. L. *Brain Res.* **43**, 547–560 (1972).
17. O'Neal, J. T. & Westrum, L. E. *Brain Res.* **51**, 97–124 (1973).
18. Rustioni, A. & Molenaar, I. *Expl Brain Res.* **23**, 1–12 (1975).
19. Bird, S. J. & Aghajanian, G. K. *Brain Res.* **100**, 355–370 (1975).
20. Raisman, G. *Brain Res.* **14**, 25–48 (1969).
21. Lynch, G., Stanfield, B. & Cotman, C. W. *Brain Res.* **59**, 155–168 (1973).
22. Rose, J. E., Malis, L. I., Kruger, L. & Baker, C. P. *J. comp. Neurol.* **115**, 243–296 (1960).

Localization of β -adrenoreceptors in mammalian lung by light microscopic autoradiography

Peter J. Barnes*, Carol B. Basbaum, Jay A. Nadel & James M. Roberts

Cardiovascular Research Institute, Department of Anatomy and Department of Obstetrics and Gynecology and Reproductive Sciences, University of California, San Francisco, California 94143, USA

β -Adrenergic agonists regulate a variety of lung functions including relaxation of airway smooth muscle, secretion of mucus¹, release of surfactant² and modulation of mediator release from mast cells³. Assays of the direct binding of radio-labelled β -adrenergic antagonists to homogenates of whole lung from several species have revealed a very high density of β -adrenoreceptors, but the cellular location of these receptors has not been determined^{4–7}. Using a technique previously used to study distribution of receptors in the brain^{8,9} we report here for the first time the localization of β -receptors in the lung by light microscopic autoradiography. Initial biochemical studies showed that ³H-dihydroalprenolol (³H-DHA) bound to slide-mounted frozen sections of ferret lung with the characteristics expected of interaction with β -receptors. Autoradiograms prepared by apposition of dry emulsion-coated coverslips to these sections showed that the distribution of β -receptors in the lung was widespread. The highest concentration of β -receptors was found in smooth muscle of bronchioles with somewhat lower densities in smooth muscle of large airways. Labelling also occurred in airway epithelium, submucosal glands and vascular smooth muscle. Alveolar walls were heavily labelled and as type II pneumocytes, which are known to have β -receptors, comprise only a small portion of the surface area, β -receptors must also be present on type I cells and/or capillary endothelial cells, although their function is at present unknown.

The lung contains over 40 different cell types and, although radioligand binding assays show the density of β -receptors in whole lung homogenates to be higher than in any other tissue^{4–7}, the localization of β -receptors in the lung has not been possible by assay alone. Previous attempts to study distribution of β -receptors in tissues, including lung, using a fluorescent β -antagonist¹⁰ were unsuccessful, largely because of the low affinity of the fluorescent analogue¹¹. Another method using ³H-DHA given by intravenous injection showed *in vivo* labelling of pulmonary β -receptors, but the ratio of specific to nonspecific binding was low, and interpretation confounded by *in vivo* metabolism, unequal distribution of the radioligand and competition for binding sites by endogenous catecholamines¹². These problems do not arise with slide-mounted sections of lung and detailed biochemical studies of such sections showed that ³H-DHA bound to frozen sections of ferret lung with all the characteristics expected of interactions with β -receptors. Specific binding was defined as that prevented by 1 µM (–)propanolol and accounted for 80–90% of total binding at concentrations of ³H-DHA below 2 nM. Specific binding was saturable and Scatchard analysis showed a single class of binding sites with a maximum binding capacity (B_{max}) of 16.2 ± 3.2 fmol

* To whom correspondence should be addressed at: Cardiovascular Research Institute, 1315-M School of Medicine, University of California, San Francisco, California 94143, USA.

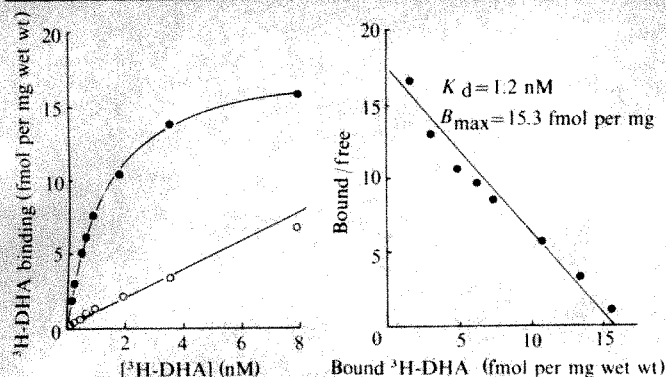


Fig. 1 Equilibrium binding of ³H-DHA to frozen sections of ferret lung. *a*, Saturation curve showing specific (●) and non-specific (○) binding in the presence of 1 μM (–)propranolol. *b*, Scatchard plot showing a single class of binding site. The inverse of the slope determined by linear regression ($r = 0.96$) gives a K_d of 1.2 nM and its intercept with the abscissa shows a B_{max} of 15.3 fmol per mg wet weight of tissue. Each point is the mean of triplicate determinations in one experiment. Separate determinations in other animals gave a K_d of $1.4 \pm 0.27 \text{ nM}$ (mean \pm s.e.m., $n = 4$) with B_{max} of $16.2 \pm 3.2 \text{ fmol per mg wet weight}$. Ferrets (*Mustela putorius*) were anaesthetized with pentobarbitone (35 mg kg^{-1} , intraperitoneally) and the lungs rapidly removed. Individual lobes were cannulated and inflated with saline-diluted OCT embedding fluid (Lab-Tek) then rapidly frozen in freon cooled by liquid nitrogen. Cryostat sections ($8\text{--}16 \mu\text{m}$ thick) were cut at -15°C and thaw-mounted onto gelatinized glass microscope slides. After washing to remove OCT, slides bearing 3 to 4 sections were incubated with 0.1 to 8 nM ³H-DHA (specific activity 101 Ci mol^{-1} NEN) in 50 mM Tris-HCl buffer, pH 7.4 at 25°C for 20 min. Alternate lung sections were incubated with ³H-DHA in the presence of $1 \mu\text{M}$ (–)propranolol to determine nonspecific binding. Slides were washed in buffer at 4°C to remove unbound radioligand. Washing for 10 min gave the greatest specific:nonspecific ratio with a decrease in nonspecific radioactivity of over 90%, but a decrease in specific radioactivity of only 40%. Sections from each slide were then scraped into pre-weighed glass scintillation vials and the wet weight of tissue determined, (approximately 10 mg per vial). After incubation with tissue solubilizer (Protosol, NEN) at 60°C for 6 h, vials were counted in a Beckman liquid scintillation spectrometer at an efficiency of 50%. Specific binding, calculated from the difference in counts between total and non-specific binding, was 80–90% of total counts bound.

per mg wet weight of tissue (mean \pm s.e.m., $n = 4$, Fig. 1). Binding was of high affinity with a K_d of $1.4 \pm 0.27 \text{ nM}$. This was not significantly different from the binding affinity measured in a washed membrane preparation of whole lung from these animals ($K_d = 1.3 \pm 0.15 \text{ nM}$, $n = 5$) determined as previously described¹³, indicating that preparation of the lung sections did not alter binding characteristics. Specific binding was stereoselective with (–)propranolol ($K_i = 1.6 \text{ nM}$) showing over 100 times greater potency than propranolol in inhibiting specific binding (Fig. 2). Amongst agonists, isoprenaline ($K_i = 0.09 \mu\text{M}$) was more potent than adrenaline ($K_i = 0.4 \mu\text{M}$), with noradrenaline ($K_i = 5.2 \mu\text{M}$) having only a weak effect. Pulmonary β -receptors, therefore, seem to be predominantly of the β_2 -subtype. Phentolamine and atropine had no significant inhibitory effect on binding. Specific binding was rapid and had reached equilibrium by 10 min. Washing at 4°C for 10 min was found to reduce nonspecific binding and provided the optimal specific:nonspecific ratio.

Autoradiography revealed that β -receptors were widely distributed throughout the lung. Labelling was confined to cellular regions with no significant elevation of radioactivity above background levels in interstitial spaces, signifying that no diffusion of the radioligand had occurred during processing (Figs 3, 4). Adjacent sections which had been incubated with ³H-DHA in the presence of $1 \mu\text{M}$ (–)propranolol showed relatively few autoradiographic grains that did not coincide with tissue structures in a specific pattern. There was dense labelling of airway smooth muscle and this was greater in small airways

(bronchioles) than in large airways (cartilaginous bronchi). The presence of β -receptors on airway smooth muscle is not surprising as β -agonists are potent bronchodilators. Our study shows that they are likely to cause dilation of all airways because of the widespread distribution of β -receptors in muscle of airways of all sizes. β -Agonists stimulate ion transport and fluid secretion in tracheal epithelium¹⁴ and ³H-DHA binds specifically to isolated tracheal epithelial cells (P.J.B. and J. H. Widdicombe, unpublished observations). The finding of β -receptors on epithelium of all sizes of airway suggests that β -receptors may regulate fluid movement in the intrapulmonary airways as well. This is supported by the demonstration that β -agonists increase mucociliary clearance by the lung¹⁵. β -Receptors were also found in submucosal glands of large airways, which is consistent with the finding that β -agonists stimulate the secretion of airway mucus. There is increasing evidence that β -agonists stimulate secretion primarily from mucous rather than serous cells of airway glands¹⁶, but it was not possible to distinguish these cell types in our cryostat sections. There was almost no specific labelling in connective tissue and it was not possible to identify mast cells. Vascular smooth muscle showed some labelling, consistent with the finding that β -agonists cause relaxation of pulmonary arteries¹⁷, but there was no labelling of endothelial cells of large vessels.

The most surprising finding was the uniformly dense labelling of alveoli. β -Agonists stimulate release of surfactant from alveolar type II pneumocytes² and radioligand binding to isolated type II cells has demonstrated the presence of β -receptors¹⁸. However, type II cells line less than 3% of the alveolar surface, with the alveolar wall being comprised predominantly of type I pneumocytes and capillary endothelial cells¹⁹. The role of β -receptors on type I cells or endothelial cells has not been studied. It is possible that β -receptors may regulate fluid resorption from the alveolar spaces, particularly at birth, as catecholamines are known to reduce fetal alveolar fluid content²⁰. Alternatively, β -receptors on type I cells may have no physiological role but may be present on type I cells as a vestige of their derivation from type II cells. In any case the large number of β -receptors in the alveolar walls explains the very high density of β -receptors found in membrane preparations

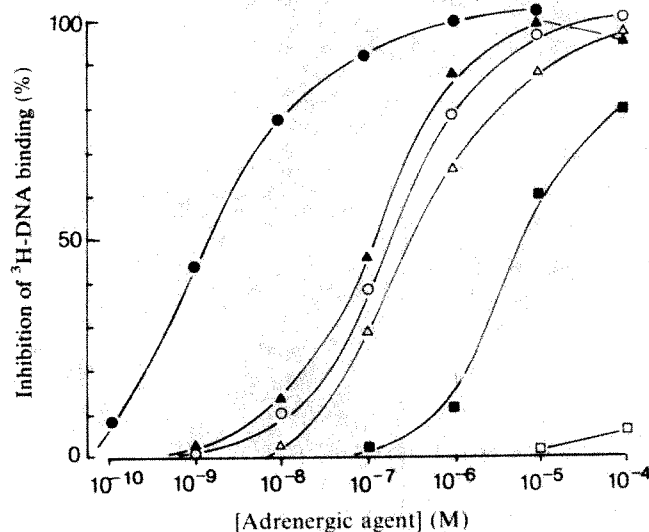


Fig. 2 Inhibition of specific ³H-DHA binding to ferret lung sections by increasing concentration of adrenergic agents. Each point is the mean of three determinations which did not differ by more than 10%. Assays were performed as described in Fig. 1 using 1.5 nM ³H-DHA. The concentration of drug causing 50% inhibition of binding (IC_{50}) was determined, and the inhibitory dissociation constant (K_i) was calculated from the formula $K_i = \text{IC}_{50} / [1 + K_d / (L)]$ where K_d is the dissociation constant of ³H-DHA binding and (L) is the concentration of ³H-DHA used in the assay. ●, (–)Propranolol; ▲, (–)isoprenaline; ○, (+)propranolol; △, (–)adrenaline; ■, (–)noradrenaline; □, phentolamine.

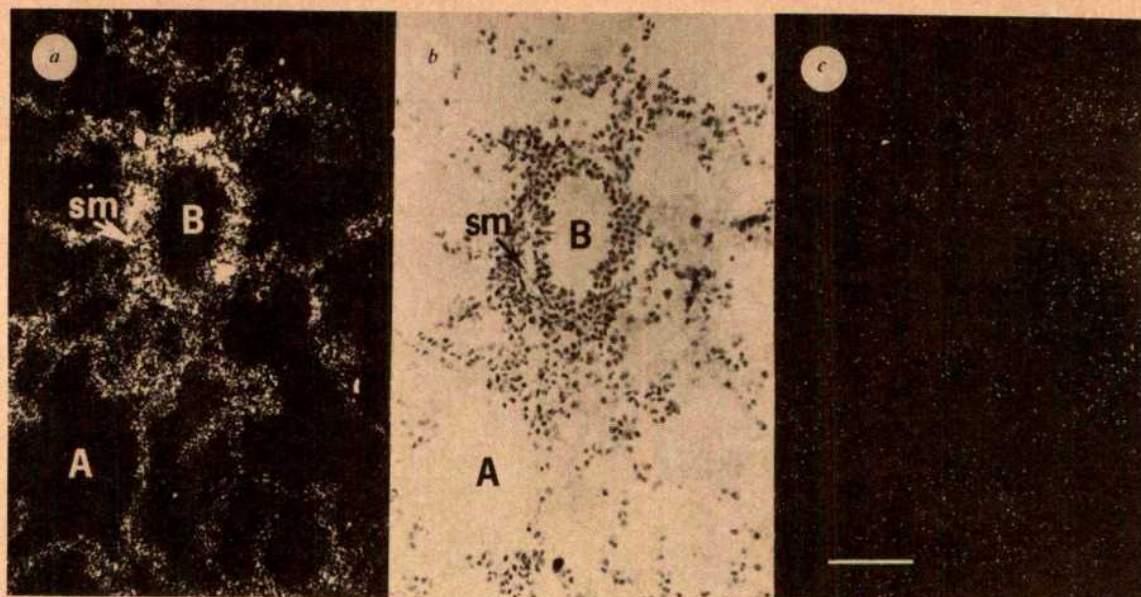


Fig. 3 Distribution of β -receptors in peripheral lung of ferret. *a*, Dark-field photomicrograph of the section shown in *b*, stained with cresyl violet. The section shows a small bronchiole (B) with surrounding alveoli (A). Note the dense labelling of patches of smooth muscle (sm) in the bronchiolar walls and the uniform labelling of alveolar wall. Scale bar, 100 μ m. *c*, Dark-field photomicrograph of an adjacent section, incubated in an identical way but in the presence of 1 μ M (–)propranolol, shows absence of specific labelling. Cryostat sections 8 μ m thick were incubated with 1.5 nM 3 H-DHA at 25 °C for 20 min as described in Fig. 1. After washing, sections were rapidly dried in a stream of cold air then left to dry overnight at 4 °C. Glass coverslips, which had been coated with photographic emulsion (Kodak NTB 2 diluted 1:1 with water) and dried overnight, were then fixed to the slides at the end distant from the section with cyanoacrylate glue and closely applied to the section with binder clips. Slides were stored in light-proof boxes with desiccant capsules at 4 °C for 12 weeks. The coverslips were then removed using a diamond pencil to score and break the glass distal to the glue and developed (Kodak D19 for 3 min at 17 °C). The sections were stained with cresyl violet and dried coverslips reapposed over the tissue using scored guide-lines to reposition exactly. Slides were then examined with a Zeiss microscope equipped for bright-field and dark-field illumination. Grain counts were performed under bright-field illumination using a $\times 40$ objective lens and a calibrated eyepiece grid. Grain densities were expressed as autoradiographic grains per 1,000 μ m² (mean \pm s.e.m.) and were determined from 10 separate fields in 3 different sections. To obtain specific grain densities, nonspecific grain densities in the presence of 1 μ M (–)propranolol (29–39) were subtracted for total grain densities. Specific grain counts: bronchiolar smooth muscle 358 ± 18 , large airway smooth muscle 185 ± 17 , airway epithelium 74 ± 5 , airway gland 109 ± 6 , alveolar wall 263 ± 16 , vascular smooth muscle 78 ± 6 , airway connective tissue 8 ± 2 . A similar pattern of distribution was seen in four separate animals.

from whole lung homogenates as most of the cell membranes of the lung are derived from alveolar cells.

There is considerable variation between species in sympathetic innervation of the lungs²¹. In many species there is an adrenergic nerve supply to blood vessels and airway glands but not to smooth muscle of intrapulmonary airways. Using a fluorescent histochemical technique²² to study distribution of

adrenergic nerve fibres in cryostat sections of ferret lung we found sympathetic innervation of vascular smooth muscle as expected, but also of smooth muscle of intrapulmonary cartilaginous airways. There was no detectable innervation of bronchioles or alveolar walls, the structures having the highest density of β -receptors, indicating that these receptors are probably controlled by circulating catecholamines.

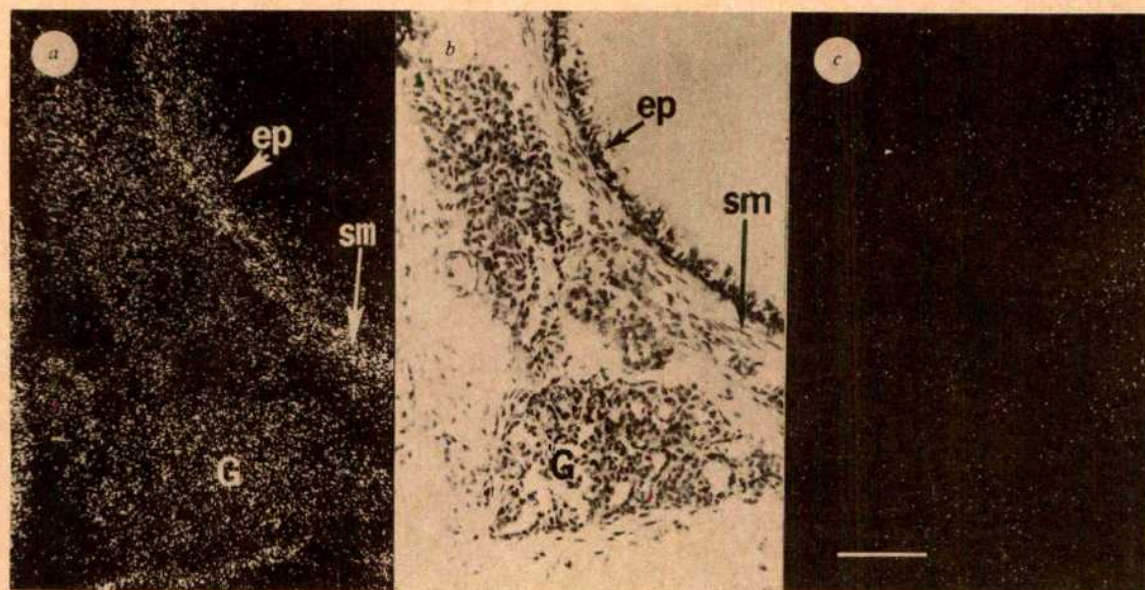


Fig. 4 Distribution of β -receptors in a large airway (segmental bronchus) of ferret. *a*, Dark-field photomicrograph of sections shown in *b*. Note the dense labelling of airway smooth muscle (sm) with lighter labelling of epithelium (ep) and submucosal glands (G). Scale bar, 100 μ m. *c*, The same area in an adjacent section incubated in the presence of 1 μ M (–)propranolol with no specific labelling.

In homogenates of whole lung, changes in the density of β -receptors have been shown during development^{23,24}, with steroid treatment^{23,25} and in an animal model of asthma⁶. It may now be possible to study the cellular location of these changes in pulmonary β -receptor density, leading to further advances in our understanding of the role of β -receptors in the regulation of various lung functions.

This work was supported by NIH Program Project Grant HL-24136. P.J.B. was supported by a MRC Travelling Fellowship, and J.M.R. is the recipient of NIH, RCDA no. 1K04 HD 00267.

Received 30 March; accepted 13 July 1982.

1. Phipps, R. J., Nadel, J. A. & Davis, B. *Am. Rev. resp. Dis.* **121**, 359–365 (1980).
2. Dobbs, L. G. & Mason, R. J. *J. clin. Invest.* **63**, 378–387 (1979).
3. Orange, R. P., Kaliner, M. A., Loraia, P. J. & Austen, K. F. *Fedn Proc.* **30**, 1725–1729 (1971).
4. Rugg, E. L., Barnett, D. B. & Nahorski, S. R. *Molec. Pharmac.* **14**, 996–1005 (1978).
5. Minneman, K. P., Hegstrand, L. R. & Molinoff, P. B. *Molec. Pharmac.* **16**, 34–46 (1979).
6. Barnes, P. J., Dollery, C. T. & McDermott, J. *Nature* **285**, 569–571 (1980).
7. Barnes, P. J., Karlner, J. S. & Dollery, C. T. *Clin. Sci.* **58**, 457–461 (1980).
8. Young, W. S. & Kuhar, M. J. *Brain Res.* **179**, 255–270 (1979).
9. Palacios, J. M. & Kuhar, M. J. *Science* **208**, 1378–1380 (1980).
10. Atlas, D. & Levitski, A. *Proc. natn. Acad. Sci. U.S.A.* **74**, 5290–5294 (1977).
11. Barnes, P. J. *et al. Brain Res.* **181**, 209–213 (1980).
12. Barnes, P. J. & Karlner, J. S. *Pharmacology* **24**, 321–327 (1982).
13. Barnes, P. J., Karlner, J. S., Hamilton, C. & Dollery, C. T. *Life Sci.* **25**, 1207–1214 (1979).
14. Davis, B., Marin, M. G., Yee, J. W. & Nadel, J. A. *Am. Rev. resp. Dis.* **120**, 547–552 (1979).
15. Santa Cruz, R., Landa, J. F., Hirsch, J. & Sackner, M. A. *Am. Rev. resp. Dis.* **109**, 458–463 (1974).
16. Basbaum, C. B., Ueki, I., Brezina, L. & Nadel, J. A. *Cell Tissue Res.* **220**, 481–498 (1981).
17. Boe, J. & Simonsson, B. G. *Eur. J. resp. Dis.* **61**, 195–202 (1980).
18. Sommers Smith, S. K. & Giannopoulos, G. *Fedn Proc.* **40**, 407 (1981).
19. Haies, D. M., Gil, J. & Weibel, E. R. *Am. Rev. resp. Dis.* **123**, 533–541 (1981).
20. Walters, D. V. & Olver, R. E. *Paediat. Res.* **12**, 239–242 (1978).
21. Richardson, J. B. *Am. Rev. resp. Dis.* **119**, 785–802 (1979).
22. Corrodi, H., Jonsson, G. J. *Histochem. Cytochem.* **15**, 65–78 (1967).
23. Cheng, J. B., Goldfine, A., Ballard, P. L. & Roberts, J. M. *Endocrinology* **107**, 1646–1648 (1980).
24. Whitsett, J. A., Manton, M. A., Darovec-Beckerman, C., Adams, K. G. & Moore, J. J. *Am. J. Physiol.* **204**, E351–E357 (1981).
25. Mano, K. A., Akbarzadeh, A. & Townley, R. G. *Life Sci.* **25**, 1925–1930 (1979).

Structural and biological properties of a monoclonal auto-anti-(anti-idiotypic) antibody

Brian A. Pollok*, Ajit S. Bhownt† & John F. Kearney*

*The Cellular Immunobiology Unit of the Tumor Institute, Department of Microbiology, and The Comprehensive Cancer Center, and †Clinical Immunology and Rheumatology, University of Alabama in Birmingham, Birmingham, Alabama 35294, USA

Several studies illustrating idiotype network-directed regulation of the immune response¹ have demonstrated that heterologous anti-(anti-idiotypic) antibodies (1) share variable (V) region antigenic determinants with idiotype-bearing antibodies^{2–5}, (2) lack antigen-binding activity^{3–6} and (3) alter the clonal profile of an immune response by stimulating/suppressing regulatory lymphocyte clones of anti-idiotypic specificity^{2–4,6}. However, the existence and significance of anti-(anti-idiotypic) antibody in natural immunological responses has been questioned because of the artificial immunization procedures used to induce these antibodies. Here we describe a monoclonal mouse anti-(anti-idiotypic) antibody generated in physiological conditions by immunizing BALB/c mice with a pneumococcal vaccine that elicits a humoral anti-phosphorylcholine (PC) response dominated by the T15 idiotype⁷. This antibody recognized an idiotope on a monoclonal anti-T15 antibody, failed to bind PC, did not exhibit detectable idiotypic cross-reactivity with T15⁺ immunoglobulins, utilized V_H and V_L genes distinct from the T15 V gene group⁸, and exerted a suppressive effect on the *in vivo* response to PC in syngeneic mice.

Spleen cells were taken from BALB/c mice 4 days after intravenous (i.v.) immunization with heat-killed *Streptococcus pneumoniae* strain R36A and were fused with the non-secreting myeloma P3×63Ag8.653 (ref. 9). In initial screening of the

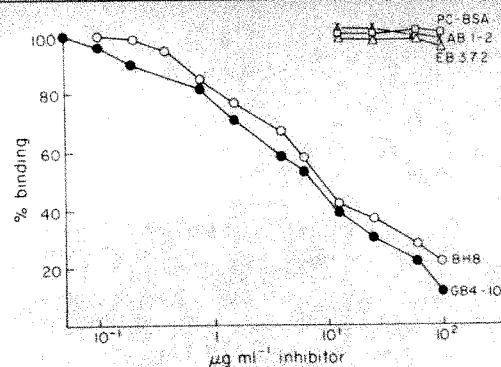


Fig. 1 Determination of binding specificity for MM-60. Various monoclonal antibodies and PC-bovine serum albumin (PC-BSA) were tested for ability to inhibit reactivity between immobilized MM-60 and alkaline phosphatase-conjugated GB4-10 in an enzyme-linked solid phase immunosorbent assay (ELISA)¹⁰. *p*-Nitrophenylphosphate (1 mg ml⁻¹) was used as substrate and reactivity was quantitated using absorbance measurements at 405 nm. Wells containing incubation buffer served as control samples (100% binding). PC-BSA was synthesized by the method of Chesebro and Metzgar²⁴ and immunoglobulins were purified by ion exchange or affinity chromatography. Inhibition values for DB1-1, B24-44, PC12-3, FD5-3 and affinity-purified goat anti-T15 antibody (not shown) are virtually identical to those found for AB1-2 (97–100% binding at 100 μg ml⁻¹ inhibitor). Recognition of PC hapten by MM-60 could not be determined using this assay since binding of GB4-10 to T15⁺ antibody is not inhibited by PC hapten¹⁰. AB1-2, DB1-1 and B24-44 are distinct anti-T15 idiotype antibodies^{10,29}; BH8 is an IgMκ AB1-2⁺, GB4-10⁺ anti-PC antibody; PC12-3 is an IgMκ AB1-2⁺, GB4-10⁺ anti-PC antibody; EB3.7.2 is J558 (α1→3 dextran-binding myeloma) idiotype-specific; and FD5-3 recognizes an idiotope on MOPC 460 (dinitrophenol-binding myeloma).

hybridoma supernatants, one hybridoma (MM-60) produced an antibody (IgMλ) that reacted with the monoclonal A/J anti-T15 idiotype antibody GB4-10 (ref. 10), but did not bind to PC. After subsequent cloning, the specificity of purified MM-60 was tested using a battery of monoclonal BALB/c and A/J antibodies in a solid-phase immunosorbent binding inhibition assay. As shown in Fig. 1, MM-60 was specific for GB4-10 and did not recognize allotypic or isotypic determinants (irrelevant anti-idiotypic hybridoma proteins FD5-3 and EB3.7.2 are of identical allotype and isotype). BH8, an anti-PC hybridoma protein reactive with GB4-10, effectively inhibited binding of MM-60 and GB4-10, providing additional evidence that the recognition of idiotypic determinants was involved. General idiotypic cross-reactivity between MM-60 and T15⁺ immunoglobulin was not observed, as other monoclonal anti-T15 idiotype antibodies and purified heterologous goat anti-T15 idiotype antibody did not inhibit the MM-60/GB4-10 interaction (Fig. 1).

Several observations suggested that MM-60 was anti-(anti-idiotypic), rather than an immunoglobulin that merely expressed the GB4-10-defined idiotope. First, MM-60 did not bind to PC-protein conjugates (Fig. 1 and in direct binding assays), in contrast to all GB4-10-bearing proteins identified so far^{10,11}. Second, MM-60 did not express the heavy chain-associated idiotope DB1-1 (Fig. 1), a characteristic of all GB4-10-bearing immunoglobulins (J.K., unpublished). In addition, it has been demonstrated that the binding of GB4-10 to murine splenic lymphocytes was completely abolished in the presence of soluble PC-protein conjugates (E. J. B. Bast and J.K., unpublished). The apparent restriction in expression of the GB4-10 idiotope among immunoglobulins to the T15⁺ anti-PC group strongly argues that MM-60 is not expressing a 'public' idiotope (that is, GB4-10) on unrelated V regions of different antigen specificity.

Somatic variants of a T15⁺ anti-PC myeloma have been isolated that have lost binding activity for PC-protein conjugates^{12,13}; presumably MM-60 could be such a variant that has

Fig. 2 Comparison of N-terminal V_H sequence for MM-60 and TEPC 15. MM-60 heavy chain was isolated by molecular sieve chromatography after exhaustive reduction and alkylation of the IgM fraction from MM-60 ascites fluid²⁵. Amino acid sequencing was performed by sequential Edman degradation on a modified Beckman 890C automated sequencer²⁶. The TEPC 15 sequence is from Barstad *et al.*²⁷. Sequence differences between MM-60 and TEPC 15 V_H are underlined, invariant residues (for murine heavy chain group III²⁸) are italicized and residues tentatively identified are shown in parentheses.

MM-60	Asx-Val-Gln-Leu-Val-Glu-Ser-Gly-Gly-Gly-Leu-Val-(Gln)-Pro-Gly-Gly-Ser-(Leu)-Lys-Leu-
TEPC 15	Gly-Val-Lys-Leu-Val-Glu-Ser-Gly-Gly-Gly-Leu-Val-Gln-Pro-Gly-Gly-Ser-Leu-Arg-Leu-
	1 5 10 15 20

also lost several T15-associated idiotopes, while retaining the GB4-10 idiotope. MM-60 and T15⁺ immunoglobulins would then utilize identical germ-line V_H and/or V_L genes. However, different V_L genes are used as MM-60 contained λ light chains and all anti-PC antibodies have κ light chains¹⁴. Comparison of the N-terminal heavy chain sequence for MM-60 and the prototype antibody TEPC 15 (Fig. 2) showed at least three sequence differences among framework residues 1 through 20, demonstrating that these two antibodies belong to distinct V_H groups¹⁵. Within this region of the V_H domain, T15⁺ antibodies and their characterized antigen-binding variants exhibit 100% homology¹⁶.

In conjunction with its unique chemical properties, MM-60 was capable of suppressing the *in vivo* response to PC in an idiotype-specific manner (Table 1). CAF₁ (BALB/c \times A/J) mice treated with the anti-(anti-idiotypic) and subsequently challenged with R36A vaccine produce serum anti-PC IgM at 20% of control levels; the T15 component of the response was preferentially affected with only 8% of the normal serum levels of T15⁺ IgM made. MM-60-induced suppression was specific for the PC response (Table 1), was attained using low doses of antibody (variable degrees of suppression were accomplished in a dosage range of 10 ng–100 μ g), and was chronic only for the T15 component of the response (78% suppression in T15⁺ antibody production at 10 weeks after anti-(anti-idiotypic) treatment). Furthermore, a similar pattern of suppression can be effected in BALB/c mice (not shown).

Lymphocytes that express anti-T15 receptors containing the GB4-10 idiotope and that specifically regulate T15⁺ B cells are the probable targets for MM-60 *in vivo*. Several cell populations that could satisfy these requirements have been described; anti-T15 idiotypic B cells¹⁷, suppressor T cells¹⁸ and helper T cells¹⁹. Using a Western blot analysis²⁰ (Fig. 3), we found that MM-60 recognized a determinant on GB4-10 that is dependent

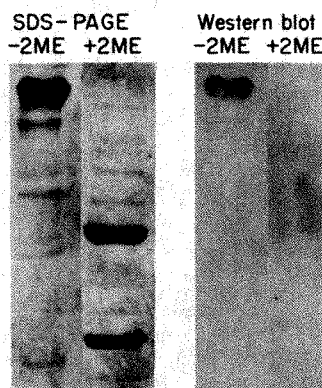


Fig. 3 Expression of the MM-60-defined idiotope requires associated heavy and light chains. SDS-polyacrylamide gel electrophoresis²⁵ was performed on the GB4-10 protein ($\gamma_1\kappa$, equal amounts) in reducing (5% 2-mercaptoethanol) and non-reducing conditions. The Western blotting technique described by Towbin *et al.*²⁰ was followed; electrophoretic transfer of the protein from slab gel to nitrocellulose paper was carried out for 3 h and unreacted sites on the paper were blocked with a 3% BSA (w/v) and 5% carrier mouse serum (v/v) solution in borate-buffered saline. ¹²⁵I-MM-60 (10^5 c.p.m. ml^{-1}) was incubated with the nitrocellulose sheet for 3 h at 37 °C with gentle swirling. After extensive washing, autoradiography of the paper was performed at -70 °C for 30 h. MM-60 reacted only with the intact GB4-10 molecule and no reaction of MM-60 at heavy or light chain bands was observed on increasing exposure time (4 days).

Table 1 MM-60-induced suppression of anti-PC and T15⁺ IgM response

Assay	Serum IgM ($\mu\text{g ml}^{-1} \pm \text{s.e.}$)	
	MM-60-treated	Control
Anti-PC	4.6 \pm 1.4	19.8 \pm 2.7
T15 ⁺		
(a) AB1-2 ⁺	1.3 \pm 1.3	16.8 \pm 3.0
(b) GB4-10 ⁺	1.0 \pm 1.1	17.3 \pm 3.3
Anti- $\alpha 1 \rightarrow 3$ dextran ^a	424 \pm 10.1	392 \pm 11.2

Two groups of five 8-week-old CAF₁ female mice [BALB/cx(A/J)F₁] received either two intraperitoneal (i.p.) injections of 100 μ g MM-60 antibody (purified from tissue culture supernatant by affinity chromatography on a goat anti-mouse column) or two injections of saline (5 days interval). All mice were challenged (i.p.) 3 days later with 2×10^8 heat-killed *S. pneumoniae* strain R36A and bled 5 days afterwards. Serum antibody was quantitated for anti-PC and T15⁺ IgM using an enzyme-linked immunosorbent direct binding assay¹⁰ (AB1-2 and GB4-10 are idiotope markers for T15 expression); linear regression analysis of binding activity over twofold serum dilutions was carried out. Absence of nonspecific immune suppression caused by MM-60 treatment was shown by measuring the response to $\alpha 1 \rightarrow 3$ dextran (Dex) in similarly suppressed CAF₁ mice^a (10 μ g i.p.; Dex and R36A vaccine are classified as T1-2 antigens²³). Mice were bled 7 days later and serum antibody quantitated as before (Dex-BSA used as immobilized antigen for the assay). Statistical comparison of experimental versus control groups using a two-sample rank test gave *P* values <0.02 for anti-PC and T15⁺ assays.

on associated heavy and light chains for its expression. Thus it seems likely that the reactivity of our monoclonal anti-(anti-idiotypic) antibody is limited to anti-idiotypic B cells, as the T-cell antigen receptor apparently lacks light chains²¹ and seems to express only V_H -associated idiotopes²². Indirect fluorescent antibody staining of the GB4-10 hybridoma cell surface confirmed that MM-60 can recognize its respective determinant on membrane-bound immunoglobulin.

Although MM-60 exerted a dampening influence on the appropriate B-cell repertoire, heterogeneous anti-(anti-idiotypic) antibodies in other antigen systems generally potentiate the corresponding humoral response to antigen. This discrepancy has several possible explanations: (1) Many of the autologous anti-(anti-idiotypic) antibodies previously studied correspond to silent idiotypic systems instead of dominant responses like PC/T15. (2) Anti-(anti-idiotypic) antibody generated under intensive immunization regimens might not reflect those anti-(anti-idiotypic) clones which are stimulated during the course of a natural immune response (as to specificity or isotype). And (3) heterologous anti-(anti-idiotypic) antibody preparations can contain idiotype-bearing immunoglobulin⁴ which could possess disparate immunoregulatory activity. However, our results do support the general significance of idiotype network interactions in the regulation of antibody production. Further cloning of lymphocytes that arise at various times during an immune response should help in understanding these reactions.

We thank Drs H. Kubagawa, R. Stohrer and D. Briles for valuable suggestions, Ms M. McCarthy for technical assistance and Ms A. Brookshire for preparation of the manuscript. This work was supported by NIH grants CA 00338, AI 14782, AMO 3555 and RCDA 00338.

Received 25 May; accepted 23 July 1982.

1. Jerne, N. K. *Annls Immun. Inst. Pasteur, Paris* **125C**, 373–389 (1974).
2. Cazenave, P. A. *Proc. natn. Acad. Sci. U.S.A.* **74**, 5122–5125 (1977).

3. Urbain, J., Wilkler, M., Fransen, J. D. & Collignon, C. *Proc. natn. Acad. Sci. U.S.A.* **74**, 5126-5130 (1977).
4. Bona, C., Heber-Katz, E., & Paul, W. J. *exp. Med.* **153**, 951-967 (1981).
5. Wikler, M. *et al.* *J. exp. Med.* **150**, 184-195 (1979).
6. Bona, C., Hooghe, R., Cazenave, P., Leguern, C. & Paul, W. J. *exp. Med.* **149**, 815-823 (1979).
7. Sher, A. & Cohn, M. *Eur. J. Immun.* **2**, 319-326 (1972).
8. Crews, S., Griffin, J., Huang, H., Calame, K. & Hood, L. *Cell* **25**, 59-66 (1981).
9. Kearney, J., Radbruch, A., Liesegang, B. & Rajewsky, K. *J. Immun.* **123**, 1548-1550 (1979).
10. Kearney, J., Barletta, R., Quan, Z., & Quintans, J. *Eur. J. Immun.* **11**, 877-882 (1981).
11. Volanakis, J. & Kearney, J. *J. exp. Med.* **153**, 1604-1614 (1981).
12. Cook, W. D., Rudikoff, S., Giusti, A. M. & Scharff, M. D. *Proc. natn. Acad. Sci. U.S.A.* **79**, 1240-1244 (1982).
13. Rudikoff, S., Giusti, A. M., Cook, W. D. & Scharff, M. D. *Proc. natn. Acad. Sci. U.S.A.* **79**, 1979-1983 (1982).
14. Clafflin, J. L. *Eur. J. Immun.* **6**, 666-668 (1976).
15. Potter, M. *Adv. Immun.* **25**, 141-211 (1977).
16. Gearhart, P. J., Johnson, N. D., Douglas, R. & Hood, L. *Nature* **291**, 29-34 (1981).
17. Cosenza, H., Julius, M., & Augustin, A. *Eur. J. Immun.* **6**, 114-116 (1976).
18. Kim, B. S. & Greenberg, J. *J. exp. Med.* **154**, 809-820 (1981).
19. Cosenza, H., Julius, M., & Augustin, A. *Immun. Rev.* **34**, 3-33 (1977).
20. Towbin, H., Staehelin, T. & Gordon, J. *Proc. natn. Acad. Sci.* **76**, 4350-4354 (1979).
21. Lonai, P., Ben-Neriah, Y., Steinman, L. & Givol, D. *Eur. J. Immun.* **8**, 827-832 (1978).
22. Sy, M.-S. *et al.* *Proc. natn. Acad. Sci. U.S.A.* **78**, 1143-1147 (1981).
23. Slack, J., Der-Balian, G., Nahm, M. & Davie, J. *J. exp. Med.* **151**, 853-862 (1980).
24. Chesebro, B. & Metzgar, H. *Biochemistry* **11**, 760-771 (1972).
25. Kubagawa, H. *et al.* *J. exp. Med.* **150**, 792-807 (1979).
26. Bhowan, A. S. *et al.* *Analyt. Biochem.* **102**, 35-38 (1980).
27. Barstad, P. *et al.* *Science* **183**, 962-964 (1944).
28. Kabat, E. A., Wu, T. & Bilofsky, H. *Sequences of Immunoglobulin Chains* (U.S. Department of Health, Education and Welfare, 1979).
29. Hämmerling, G. & Wallich, R. in *Protides of the Biological Fluids*, Vol. 28 (ed. Peeters, H.) 569-574 (Pergamon, Oxford, 1980).

Chromatin changes accompany immunoglobulin κ gene activation: a potential control region within the gene

Tristram G. Parslow & Daryl K. Granner

Departments of Internal Medicine and Biochemistry, University of Iowa, Iowa City, Iowa 52242, USA

A functional immunoglobulin gene is formed by the fusion of individual coding elements which are widely separated in germ-line DNA. For the mouse κ light chain gene, this is accomplished by DNA rearrangement which brings one of a large repertoire of non-allelic variable region (V_{κ}) genes into apposition with one of four functional (J_{κ}) elements located 2.7-3.9 kilobases (kb) upstream from the κ constant region coding sequence (C_{κ})¹⁻⁴. Transcription is initiated near the 5' end of the rearranged V_{κ} locus, and spans all three coding elements and the large intervening sequence between J_{κ} and C_{κ} , and a smaller intervening sequence within the V_{κ} gene⁵. Little is known of the mechanisms which control the expression of rearranged immunoglobulin genes. We have studied the process of κ light chain gene activation in a mouse leukaemia cell line, 70Z/3, which synthesizes a κ -type light chain protein in response to bacterial lipopolysaccharide (LPS). Here we describe changes in the chromatin structure of the κ genes occurring as a result of LPS treatment, and present evidence that a discrete region located inside the large intervening sequence of the κ transcription unit plays a part in κ gene activation.

Cells of the 70Z/3 line exhibit several features typical of the early stages of B lymphocyte differentiation⁶⁻⁹. The cells constitutively produce cytoplasmic μ heavy chains without detectable light chain synthesis. On exposure to LPS, however, the cells initiate synthesis of κ light chain protein, and begin to express both heavy and light chains on their surfaces. The response of 70Z/3 cells to LPS is rapid and uniform. In the absence of LPS, most cells (>90%) have no light chain protein; after optimal LPS treatment, 70-100% express surface and cytoplasmic κ determinants^{6,7}. Because maximal expression can be achieved within 12 h, this phenotypic change probably does not arise through selection of an endogenous subpopulation. The cells carry a single rearranged κ gene; the excluded κ allele retains the germ-line configuration⁸. Despite extensive restriction enzyme mapping of regions in and around the two κ alleles

of 70Z/3, we have detected no changes in the sequence organization of either gene occurring as a result of exposure to LPS. This observation implies that the light chain produced by 70Z/3 is a product of the constitutively rearranged allele. While untreated 70Z/3 cells contain little or no cytoplasmic κ -specific RNA, exposure to LPS results in an accumulation of 50-100 copies of mature-sized κ mRNA per cell⁹, suggesting that LPS induces transcription of the κ gene. More rigorous evidence for an effect of LPS on κ transcription in 70Z/3 will be presented elsewhere¹⁰.

Several lines of evidence suggest that transcriptional activity is an inherent property of the C_{κ} region, and is imparted to a particular V_{κ} gene only after rearrangement has linked it to an active C_{κ} locus. Thus, while each V_{κ} element in the genome apparently harbours a potential initiation site near its 5' end, unrearranged V_{κ} genes are not transcribed¹¹, and do not show the enhanced accessibility to nuclease digestion characteristic of transcriptionally active chromatin¹². In contrast, unrearranged C_{κ} alleles found in myeloma cells are transcribed^{5,13,14}, and are nuclease-sensitive to a degree comparable with that of rearranged C_{κ} genes¹². It is not known whether transcription is the cause or the result of nuclease sensitivity in these genes.

To characterize the effect of LPS on immunoglobulin gene structure, we first examined the chromatin conformation of the light chain genes of untreated 70Z/3 cells, by determining the susceptibility of these genes to digestion with pancreatic deoxyribonuclease I (DNase I). Nuclei from cells grown in the absence of LPS were subjected to mild digestion with various concentrations of DNase. DNA isolated from these nuclei showed a gradual decrease in mean fragment size with increasing DNase digestion (Fig. 1a). These DNA preparations were then cleaved to completion with selected restriction endonucleases, subjected to agarose gel electrophoresis, and then transferred to nitrocellulose membranes. Specific gene sequences were identified by hybridization to radiolabelled recombinant DNA probes, followed by autoradiography. When undigested 70Z/3 DNA was cleaved with the enzyme *EcoRI* and probed for κ constant region coding sequences (Fig. 1b, lane 1), two bands (labelled K) were observed, corresponding to the germ-line (15 kb) and rearranged (17 kb) C_{κ} alleles⁸. Both these κ -bearing fragments were relatively sensitive to nuclease action, and disappeared rapidly as nuclei were exposed to increasing concentrations of DNase (Fig. 1b, lanes 2-6). In contrast, the λ I light chain genes, which are neither rearranged nor expressed in these cells, were comparatively resistant to DNase digestion (Fig. 1b, unlabelled arrow). Similar results were obtained for DNA preparations probed simultaneously for C_{κ} and albumin gene sequences: both κ alleles were significantly more sensitive than the unexpressed albumin sequences (Fig. 1c). Analysis of these same DNA preparations after combined cleavage with *EcoRI* and *BamHI* gave better resolution of the two C_{κ} -bearing fragments (Fig. 1d) and revealed no difference in nuclease sensitivity between the rearranged (K^+) and germ-line (K^0) alleles.

These findings indicate that the κ constant region genes of untreated 70Z/3 cells exist in a chromatin conformation which renders them preferentially accessible to DNase digestion compared with transcriptionally inactive chromatin, and that this alteration in chromatin structure affects both rearranged and unrearranged C_{κ} genes. Similar observations have been made for the κ genes of mature B lymphocytes and plasma cells¹²; the present findings suggest that this altered chromatin structure may be established at a very early stage in B-cell ontogeny, and can be maintained in the absence of κ gene expression.

Similar analysis of 70Z/3 cells treated with LPS revealed a striking change in the digestion pattern of κ -specific chromatin. Combined *EcoRI* and *BamHI* cleavage of DNA from LPS-treated cells produced the two expected C_{κ} -bearing fragments, which were rapidly digested in nuclei exposed to DNase (Fig. 2). During DNase digestion, however, a prominent 2.1-kb subfragment accumulated. This subfragment was generated by mild DNase treatment, and was eventually degraded after

Fig. 1 Preferential accessibility of inactive κ light chain genes to nuclease digestion. 70Z/3 cells were grown in suspension culture as described elsewhere⁹ in the absence of LPS. The absence of detectable κ gene expression was confirmed by surface fluorescence immunoassay and by RNA blot hybridization²⁶. Nuclei were isolated from washed cells by the method of Jackson and Chalkley²⁷, and suspended at a DNA concentration of 1 mg ml^{-1} in ice-cold 0.25 M sucrose, 10 mM Tris pH 8.0, 10 mM MgCl_2 . Aliquots (0.25 ml) of the nuclear suspension were preincubated at 37°C for 1 min. Pancreatic DNase I (Worthington DPFP grade) was added to a final concentration of $0.4\text{--}4.0 \text{ U ml}^{-1}$, and incubation continued for 2 min. Digestion was stopped by adding 0.1 vol each of 10% SDS and 2 mg ml^{-1} proteinase K. After incubation

at 37°C for 2 h, the reaction mixture was extracted twice with anhydrous ether and adjusted to 0.5 M NaCl. Nucleic acids were precipitated by addition of 2.5 vol ethanol. The precipitate was resuspended in 10 mM Tris pH 8.0, 0.1 mM EDTA, and digested successively with 0.1 mg ml^{-1} ribonuclease A and 0.2 mg ml^{-1} proteinase K for 2 h each at 37°C . The samples were extracted twice with phenol/chloroform (1:1) and twice with anhydrous ether, then adjusted to 0.2 M ammonium acetate and precipitated with ethanol. After digestion with selected restriction enzymes, aliquots of the purified DNA were electrophoresed on 0.6% agarose gels and transferred to nitrocellulose²⁸. Hybridization to radiolabelled probes was carried out for 18 h at 65°C in 0.72 M NaCl, 40 mM sodium phosphate pH 7.0, 4 mM EDTA, and 10% (w/v) dextran sulphate. Filters were washed and autoradiographed as described elsewhere²⁶. Hybridization probes were labelled by nick-translation²⁹ of purified cloned restriction fragments. κ Constant region sequences were detected with a 300-base pair fragment obtained by *HincII*–*HinfI* digestion of a cloned κ complementary DNA (unpublished). The probe for λ constant region sequences was prepared as described elsewhere³⁰ from a recombinant plasmid supplied by A. Bothwell and D. Baltimore. The probe complementary to rat albumin sequences was a gift from J. Taylor³¹. *a*, Purified DNA before restriction digestion: lane D is unincubated DNA; lanes 1–6 are from nuclei incubated with increasing concentrations of DNase, ranging in equal increments from 0 to 4 U ml^{-1} . *b*, *EcoRI* digests ($10 \mu\text{g}$ DNA per lane), probed simultaneously for κ and λ constant region sequences. *c*, *EcoRI* digests ($10 \mu\text{g}$ DNA per lane), probed simultaneously for κ constant region and albumin sequences. *d*, Combined *EcoRI* and *BamHI* digests ($20 \mu\text{g}$ DNA per lane), probed for κ constant region sequences. Corresponding lanes in *a*–*d* are from the same DNA preparation, and therefore can be compared directly. A 50% reduction in the image density of the κ fragments occurred at a DNase concentration of $0.8\text{--}1.6 \text{ U ml}^{-1}$; this value was essentially unaffected by a 60% reduction in the size of the fragments (compare *b* and *d*). A 50% reduction in intensity of the λ and albumin fragments required ~ 2.4 and 3.2 U ml^{-1} , respectively. K denotes the κ genes; K° and K^+ , the embryonic and rearranged κ genes, respectively. Unlabelled arrows indicate λ genes in *b* and albumin sequences in *c*.

further digestion. The subfragment was observed in DNA from digested nuclei after cleavage with any of a variety of restriction endonucleases, and varied in size according to the particular restriction enzyme used. Faint traces of such subfragments were occasionally present in DNA from untreated cells (for example, Fig. 1*d*), consistent with the presence of a small subpopulation of endogenously activated cells in the untreated population^{7,9}.

The occurrence of such a subfragment after mild nucleolytic digestion of chromatin indicates that a specific site in the vicinity

of the C_κ loci in treated cells is unusually sensitive to DNase action, being cleaved by the enzyme with extremely high frequency. We have mapped the position of this hypersensitive site relative to several neighbouring restriction enzyme sites, and have identified its location in the known restriction map

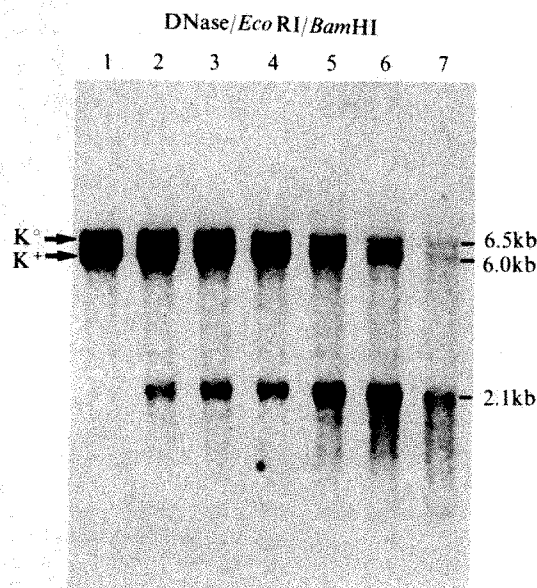


Fig. 2 Nuclease digestion of κ genes from cells treated with LPS. Growth conditions were the same as described in Fig. 1 legend, except that LPS from *Salmonella typhosa* 0901 (Difco) was included ($10 \mu\text{g ml}^{-1}$) for 20 h before collection. These conditions gave maximal expression of surface κ determinants and of κ -specific RNA, but did not affect the doubling time of the cells (12 h). DNA was isolated from nuclei of these cells after treatment with DNase (see Fig. 1 legend). The extent of bulk DNA digestion varied rather between nuclear preparations; the samples shown here were digested to approximately half the extent of corresponding lanes in Fig. 1. After combined *EcoRI*–*BamHI*, the purified DNA was electrophoresed, transferred to nitrocellulose, and probed for κ constant region sequences. K° and K^+ denote the embryonic and rearranged κ loci, respectively.

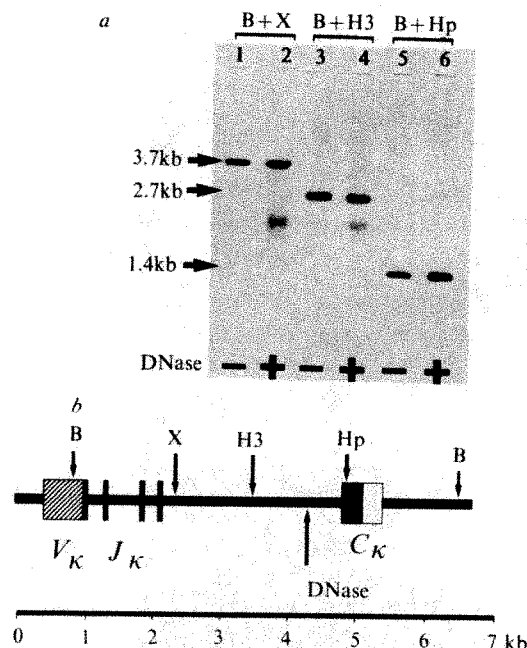


Fig. 3 Location of the LPS-inducible hypersensitive site. DNA was isolated from the nuclei of LPS-treated cells either with or without previous DNase digestion. The DNA was cleaved first with *BamHI*, then with one of several other restriction enzymes, electrophoresed, transferred to nitrocellulose, and probed for κ constant region sequences. *a*, The location of the hypersensitive site was mapped by comparing the sizes of fragments generated with and without DNase for each pair of restriction cleavages. The 2.1-kb subfragment appears in lanes 2 and 4. No differences in the restriction digestion patterns of the two alleles were noted for regions downstream of the J_κ loci. *b*, The map shows the rearranged κ allele; the structure of this gene was determined by analysis of recombinant phage carrying the rearranged κ locus, cloned from 70Z/3 cells³². C_κ , constant coding and 3' untranslated regions; J_κ , joining region coding elements; V_κ , 5' untranslated and variable region coding sequences; B, *BamHI*; H3, *HindIII*; Hp, *HpaI*; X, *XbaI*; DNase, the inducible hypersensitive site.

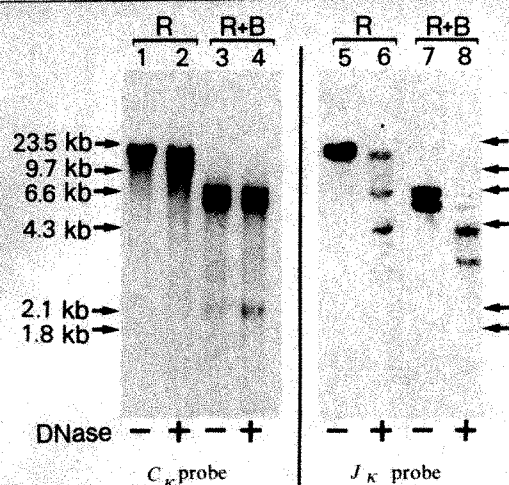


Fig. 4 Boundaries of the inducible hypersensitive site. DNA was isolated from LPS-treated cells either with or without previous DNase digestion of nuclei. After cleavage with either *EcoRI* alone (R) or a combination of *EcoRI* and *BamHI* (R+B), the DNA was electrophoresed, transferred to nitrocellulose, and probed for either κ constant region (lanes 1–4) or J_κ (lanes 5–8) sequences. The J_κ probe was a 2.5-kb *HindIII* fragment of the embryonic κ locus¹⁵, isolated from a recombinant plasmid provided by E. Max and P. Leder. DNase concentrations were 1.0 U ml^{-1} in lanes 2 and 4, and 3.0 U ml^{-1} in lanes 6 and 8. The approximate sizes of the subfragments generated by DNase digestion are: lane 2, 10 kb; lane 4, 2.1 kb; lane 6, 6.5 and 4.2 kb; lane 8, 4.2 and 3.7 kb.

of the C_κ region¹⁵ (Fig. 3). The hypersensitive site lies inside the region which forms the large intervening sequence of a rearranged κ gene, with its 3' boundary 0.5–0.7 kb upstream of the constant region coding sequence. To identify the 5' boundary of the hypersensitive site, restriction digests of DNA from LPS-treated cells were probed for fragments bearing the J_κ region (Fig. 4). Mild DNase digestion always produced two distinct J_κ -bearing subfragments, corresponding to the two κ alleles. Analysis of the sizes of these subfragments indicated that DNase hypersensitivity arises at the same location in both the rearranged and germline κ alleles after exposure to LPS, and is confined to a discrete region not more than 0.5 kb long. The location of this hypersensitivity does not coincide with known sites of transcriptional initiation, DNA recombination^{16,17} or RNA splicing, and serves no other recognized function. Recently, however, the sequence of a short (150-base pair) segment of DNA occupying approximately this same location, has been found to be conserved evolutionarily between the human and mouse κ genes, whereas the remaining intronic sequences on either side have undergone extensive divergence¹⁸. This segment is, in fact, the only conserved noncoding region in the vicinity of the C_κ locus. No additional hypersensitive sites were detected; in particular, there was no evidence of hypersensitivity near the 5' end of the rearranged κ gene. We have detected neither constitutive nor inducible transcripts derived from the germ-line κ locus in these cells, suggesting that hypersensitivity is not simply a consequence of ongoing transcription (data not shown). The factors which prevent coordinate activation of the germ-line allele remain to be elucidated.

Thus, our data indicate that when κ light chain expression is induced by LPS treatment, a discrete DNA region closely linked to the constant region coding sequence becomes extremely sensitive to DNase digestion, presumably as a result of a localized change in chromatin structure. While this region has no identified function, its sequence has apparently been conserved during evolution, whereas adjacent sequences have not. Similar hypersensitive sites have been observed in other genes^{19–25}, where they are frequently (but not exclusively) found near the transcriptional initiation site at the 5' end of the gene. Because the hypersensitivity of certain of the sites correlates with gene activity, it has been argued that these may have a role in the regulation of transcription^{20–25}. By analogy with these sites, it is tempting to speculate that the LPS-inducible hypersensitive site found inside the κ gene may play a part in

transcriptional activation of the gene in response to lipopolysaccharide.

We thank R. P. Perry for providing 70Z/3 cells and for helpful discussion, and J. E. Donelson for reviewing the manuscript. This research was supported by NIH grants AM20858, AM24037 and AM25295 (Diabetes and Endocrinology Research Center), and by VA research funds. T.G.P. received support from Medical Scientist Training grant GM07337. D.K.G. was a VA Medical Investigator.

Received 15 March; accepted 13 July 1982.

- Brack, C., Hiram, M., Lenhard-Schuller, R. & Tonegawa, S. *Cell* **15**, 1–14 (1978).
- Seidman, J. G. & Leder, P. *Nature* **276**, 790–795 (1978).
- Early, P. W., Davies, M. M., Kaback, D. B., Davidson, N. & Hood, L. *Proc. natn. Acad. Sci. U.S.A.* **76**, 857–861 (1979).
- Max, E. E., Seidman, J. G. & Leder, P. *Proc. natn. Acad. Sci. U.S.A.* **76**, 3450–3454 (1979).
- Perry, R. P. *et al.* *Proc. natn. Acad. Sci. U.S.A.* **77**, 1937–1941 (1980).
- Paige, C. J., Kincade, P. W. & Ralph, P. *J. Immun.* **121**, 641–647 (1978).
- Paige, C. J., Kincade, P. W. & Ralph, P. *Nature* **292**, 631–633 (1981).
- Maki, R., Kearney, J., Paige, C. J. & Tonegawa, S. *Science* **209**, 1366–1369 (1980).
- Perry, R. P. & Kelley, D. E. *Cell* **18**, 1333–1339 (1979).
- Parslow, T. G. & Granner, D. K. (in preparation).
- Mather, E. L. & Perry, R. P. *Nucleic Acids Res.* **9**, 6855–6867 (1981).
- Storb, U., Wilson, R., Selsing, E. & Walfield, A. *Biochemistry* **20**, 990–996 (1981).
- Perry, R. P., Kelley, D. E., Coleclough, C. & Kearney, J. F. *Proc. natn. Acad. Sci. U.S.A.* **78**, 247–251 (1981).
- Van Ness, B. G. *et al.* *Cell* **27**, 593–602 (1981).
- Selsing, E. & Storb, U. *Cell* **25**, 47–58 (1981).
- Choi, E., Kuehl, M. & Wall, R. *Nature* **286**, 776–779 (1980).
- Seidman, J. G. & Leder, P. *Nature* **286**, 779–783 (1980).
- Heiter, P. A., Max, E. E., Seidman, J. G., Maizel, J. V. & Leder, P. *Cell* **22**, 197–207 (1980).
- Stalder, J. *et al.* *Cell* **20**, 451–460 (1980).
- Groudine, M. & Weintraub, H. *Cell* **24**, 393–401 (1981).
- Keene, M. A., Corcos, V., Lowenhaupt, K. & Elgin, S. C. R. *Proc. natn. Acad. Sci. U.S.A.* **78**, 143–146 (1981).
- Samal, B., Worcel, A., Louis, C. & Schedl, P. *Cell* **23**, 401–409 (1981).
- Wu, C. & Gilbert, W. *Proc. natn. Acad. Sci. U.S.A.* **78**, 1577–1580 (1981).
- Storb, U., Arp, B. & Wilson, R. *Nature* **294**, 90–92 (1981).
- Elgin, S. C. R. *Cell* **27**, 413–415 (1981).
- Thomas, P. S. *Proc. natn. Acad. Sci. U.S.A.* **77**, 5201–5205 (1980).
- Jackson, V. & Chalkley, R. *Biochemistry* **13**, 3952–3956 (1974).
- Smith, G. E. & Summers, M. D. *Analyt. Biochem.* **109**, 123–129 (1980).
- Rigby, P. W. J., Dieckmann, M., Rhodes, C. & Berg, P. *J. molec. Biol.* **113**, 237–251 (1977).
- Schwartz, R. C., Sonenshein, G. E., Bothwell, A. & Gefter, M. L. *J. Immun.* **126**, 2104–2108 (1981).
- Kioussis, D. *et al.* *Proc. natn. Acad. Sci. U.S.A.* **76**, 4370–4374 (1979).
- Parslow, T. G., Murphy, W., Katzen, C. & Granner, D. K. (in preparation).

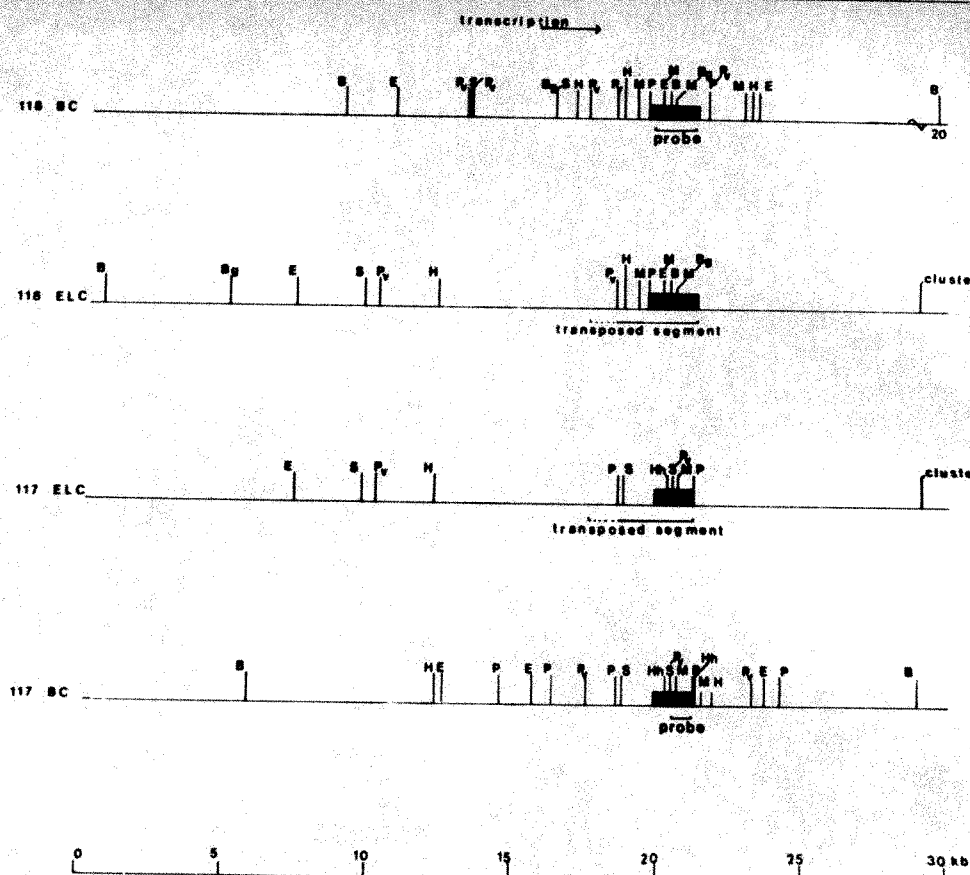
Genomic environment of the expression-linked extra copies of genes for surface antigens of *Trypanosoma brucei* resembles the end of a chromosome

Titia De Lange & Piet Borst

Section for Medical Enzymology and Molecular Biology, Laboratory of Biochemistry, University of Amsterdam, Jan Swammerdam Institute, PO Box 60,000, 1005 GA Amsterdam, The Netherlands

The surface coat of trypanosomes consists essentially of a single protein, the variant surface glycoprotein (VSG)^{1,2}. But more than a hundred different VSGs can be produced³. By switching from the synthesis of one VSG to the next, trypanosomes change the antigenic nature of their surface and thus escape destruction by the host immune system^{4–6}. Each VSG is encoded by a separate gene and expression of some of these genes involves the duplication and transposition of a silent basic copy (BC) into a new genomic environment^{7–9}, where the gene is transcribed^{10,11}. The DNA segment downstream of this transposed expression-linked extra copy (ELC) of the gene has two remarkable properties. It is devoid of restriction endonuclease cutting sites for a stretch of 7 kilobases (kb) which ends abruptly in an apparent cluster of at least 17 restriction endonuclease cutting sites. Here we show that in intact DNA the 'barren' region 3' to two active VSG genes is preferentially attacked by exonuclease *Bal31*. We conclude that the expressed copies of these genes are located adjacent to a discontinuity in the DNA, presumably the end of a chromosome.

Fig. 1 Physical maps of the 117 and 118 VSG genes. Restriction endonuclease cleavage sites in and around the BC and ELC genes for VSGs 117 and 118 in *Trypanosoma brucei* (from ref. 12). The clusters at the 3' ends of the ELC maps indicate small regions where 17 restriction enzymes appear to cut (*EcoRI*, *BamHI*, *PstI*, *MspI*, *HindIII*, *PvuII*, *BglII*, *SalI*, *HhaI*, *HphI*, *TaqI*, *XbaI*, *BspI*, *XhoI*, *AvaI*, *KpnI*, *MboI*). The transposed segment of the BC genes is shown in the ELC maps. The sequences that hybridize to the probes used in the experiments shown in Fig. 2 are indicated underneath the BC genes. Abbreviations: B, *BamHI*; Bg, *BglII*; E, *EcoRI*; Hh, *HhaI*; H, *HindIII*; M, *MspI*; P, *PstI*; Pv, *PvuII*; S, *SalI*.



The physical maps of the BCs and ELCs of VSG genes 117 and 118 are shown in Fig. 1. The regions surrounding both ELCs are indistinguishable and both genes may have been inserted into the same expression site. This site is characterized by long stretches of DNA in which no restriction enzymes cut. These stretches may represent repetitive DNA, but this has not been verified, as all attempts to isolate this DNA as recombinant DNA have failed^{11,12}.

To test whether the apparent restriction site cluster downstream of the ELCs really is a discontinuity in the DNA, we determined whether this site is preferentially attacked by *Bal31* exonuclease in large DNA. DNA with a molecular weight of 50–80 kb was isolated from trypanosome variant antigen types 117 and 118 and incubated with *Bal31* for various periods of time. The DNA was recovered and digested with appropriate restriction endonucleases to examine the effect of *Bal31* digestion on ELC and BC fragments in Southern blots.

Figure 2a shows a Southern blot of 117 DNA treated with *Bal31* and restricted with *PvuII*. The filter-bound DNA was hybridized to the 3' part of a cloned VSG 117 complementary DNA (cDNA) fragment. Two restriction fragments are detected: a 2.7-kb BC gene fragment and a 8.7-kb fragment that represents the ELC gene. The ELC gene fragment is progressively shortened by *Bal31*, whereas the BC gene fragment is unaffected even by the most extensive *Bal31* treatment.

The probe used to visualize the 117 VSG gene fragments is known to cross-hybridize with a family of putative VSG genes, the 117-related genes^{6–8,12}. Even at the high stringency used in this experiment ($0.1 \times \text{SSC}$ at 65°C), 117-related genes are detected. All cross-hybridizing fragments, some of which are larger than the 117 ELC gene fragment, are resistant to *Bal31* digestion, suggesting that the shortening of the 117 ELC gene fragment by *Bal31* nuclease is a specific event, unrelated to the size of the target.

Figure 2b shows the result of an analogous experiment with variant type 118 DNA. After *Bal31* treatment, the DNA samples were cleaved with *BglII* and a Southern blot of this

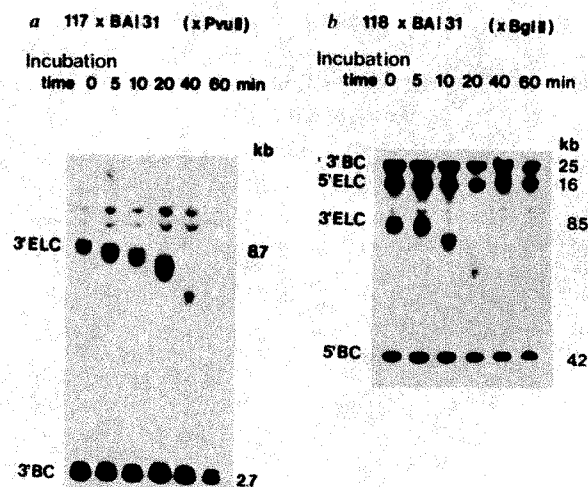


Fig. 2 Autoradiograms showing the preferential sensitivity of the 3' flanking region of the 117 and 118 ELC genes to digestion by *Bal31* nuclease. The DNA from trypanosome variant types 117 and 118 (MITat 1.4 and 1.5) was isolated as described in ref. 11 and digested with 1 U *Bal31* nuclease (Biolabs) per 30 μg DNA, as described in ref. 13, for the times indicated. The DNA was collected by ethanol precipitation after phenol extraction and digested with the restriction enzymes indicated. The restricted DNA was size-fractionated on agarose slab gels, blotted onto nitrocellulose filters and hybridized to nick-translated ^{32}P -labelled VSG cDNA fragments. *a*, Southern blot of 117 DNA treated with *Bal31*, digested with *PvuII* and hybridized to the 3' *SalI*-*PstI* fragment from TcV117-5 (ref. 11). *b*, Southern blot of 118 DNA treated with *Bal31*, digested with *BglII* and hybridized to the *PstI* insert fragment of TcV118-2 (ref. 11). The localization of the genomic sequences that hybridize to the cDNA fragments is shown in Fig. 1. The origin and size of the fragments detected are indicated. The extra hybridizing fragments in *a* represent 117-related genes (see text).

DNA was probed with a cloned VSG 118 cDNA fragment. One of the four *Bgl*II fragments detected is shortened by *Bal*31 nuclease. This 8.5-kb *Bgl*II fragment contains the 3' part of the 118 ELC gene and its flanking region.

The preferential sensitivity to *Bal*31 digestion of the 3'-flanking region of the 117 and 118 ELC genes shows that this region contains a discontinuity. As the *Bal*31 preparations also cleave single-stranded DNA¹⁴, this discontinuity could either be in one DNA strand (nick or gap) or in both DNA strands. The fact that 17 restriction endonucleases appear to cut at this position is compatible only with a discontinuity in both strands. Whether this discontinuity is also present *in vivo* or unmasked by removal of protein or RNA during DNA isolation is not easily tested with trypanosomes, because they lack condensed or polytene chromosomes suitable for cytological (hybridization) analysis.

The ends of the linear DNA molecules found in viruses or chromosomes are known to have unusual properties. A protein may be covalently linked to the end^{15,16} or the two DNA strands may be linked and form a hairpin¹⁷⁻²¹. The presence of a long hairpin (more than 500 base pairs) in the trypanosome DNA was rendered unlikely by running restriction digests of nuclear DNA on an alkaline gel before and after treatment with *S*₁ nuclease, which specifically cuts single-stranded DNA. No shortening of ELC fragments was seen (experiment not shown).

Another unusual feature of chromosome ends is the presence of tandem repeats. These were first detected at the ends of ribosomal DNA molecules, which were shown to contain 20-70 tandem repeats of the hexanucleotide CCCCAA¹⁶. This simple repeated sequence is probably present at most termini of *Tetrahymena* macronuclear DNA²² and analogous short terminal repeats have been found in other ciliates²³⁻²⁵, in the rDNA of the slime mould *Dictyostelium*²⁶ and in linear viral DNAs^{21,27}. The recent finding that the ends of rDNA from *Tetrahymena* can be stably replicated in yeast nuclei as ends of linear plasmids²⁸ suggests that terminal repeats may indeed be a common characteristic of most stable linear nuclear DNAs. The 'barren' regions surrounding the ELCs (Fig. 1) could, therefore, represent analogous short tandem repeats marking the end of a chromosome.

This work was supported by a grant from the Foundation for Fundamental Biological Research (BION), which is subsidized by the Netherlands Organization for the Advancement of Pure Research (ZWO) and the World Health Organization (T16/181/T7/34).

Received 1 June; accepted 9 July 1982.

- Vickerman, K. *J. Cell Sci.* **5**, 163-193 (1969).
- Cross, G. A. M. *Parasitology* **71**, 393-417 (1975).
- Capbern, A., Giroud, C., Baltz, T. & Mattern, P. *Exp. Parasit.* **42**, 6-13 (1977).
- Vickerman, K. *Nature* **273**, 613-617 (1978).
- Marcu, K. B. & Williams, R. O. in *Genetic Engineering* Vol. 3 (eds Setlow, S. K. & Hollaender, A.) 129-155 (Plenum, New York, 1981).
- Borst, P. & Cross, G. A. M. *Cell* **29**, 291-303 (1982).
- Hoelmakers, J. H. J., Frasch, A. C. C., Bernards, A., Borst, P. & Cross, G. A. M. *Nature* **284**, 78-80 (1980).
- Borst, P. *et al.* *Cold Spring Harb. Symp. quant. Biol.* **45**, 935-943 (1981).
- Pays, E., Van Meirvenne, N., Le Ray, D. & Steinert, M., *Proc. natn. Acad. Sci. U.S.A.* **78**, 2673-2677 (1981).
- Pays, E., Lheureux, M. & Steinert, M. *Nature* **292**, 365-367 (1981).
- Bernards, A. *et al.* *Cell* **27**, 497-505 (1981).
- Van der Ploeg, L. H. T., Bernards, A., Rijsewijk, F. A. M. & Borst, P. *Nucleic Acids Res.* **10**, 593-609 (1982).
- Yao, M. C. *Cell* **24**, 765-775 (1981).
- Gray, H. B., Ostrander, D. A., Hodnett, J. L., Legerski, R. J. & Roberson, D. L. *Nucleic Acids Res.* **2**, 1459-1492 (1975).
- Rekosh, D. M. K., Russel, W. C., Bellet, A. J. D. & Robinson, A. J. *Cell* **11**, 283-295 (1977).
- Wimmer, E. *Cell* **28**, 199-201 (1982).
- Geshelin, P. & Berns, K. I. *J. molec. Biol.* **88**, 785-796 (1974).
- Blackburn, E. H. & Gall, J. G. *J. molec. Biol.* **120**, 33-53 (1978).
- Cavalier-Smith, T. *Nature* **250**, 467-470 (1974).
- Bateman, A. J. *Nature* **253**, 379 (1975).
- Baroudy, B. M., Venkatesan, S. & Moss, B. *Cell* **28**, 315-324 (1982).
- Yao, M. C. & Yao, C. H. *Proc. natn. Acad. Sci. U.S.A.* **78**, 7436-7439 (1981).
- Katzen, A. L., Cann, G. M. & Blackburn, E. H. *Cell* **24**, 313-320 (1980).
- Oka, Y., Shiota, S., Nakai, S., Nishida, Y. & Okubo, S. *Gene* **10**, 301-306 (1980).
- Klobutcher, L. A., Swanton, M. T., Donini, P. & Prescott, D. M. *Proc. natn. Acad. Sci. U.S.A.* **78**, 3015-3019 (1981).
- Emery, H. S. & Weiner, A. M. *Cell* **26**, 411-419 (1981).
- Davidson, A. J. & Wilkie, N. M. J. *gen. Virol.* **55**, 315-331 (1981).
- Szostak, J. W. & Blackburn, E. H. *Cell* **29**, 245-255 (1982).

A specific replication origin in the chromosomal rDNA of *Lytechinus variegatus*

Peter M. Botchan* & Andrew I. Dayton*†

* The Wistar Institute of Anatomy and Biology, 36th Street at Spruce, Philadelphia, Pennsylvania 19104, USA

† Department of Biochemistry and Biophysics, University of Pennsylvania, Philadelphia, Pennsylvania 19104, USA

Specific replication origins have been well characterized in prokaryotes^{1,2}, and have been identified in eukaryotic extra-chromosomal DNAs³⁻⁸. The best candidate, until now, for a specific eukaryotic chromosomal replication origin has been found in yeast⁹, but the general existence of such origins is challenged¹⁰ by the finding that SV40 and polyoma DNA fragments lacking the viral replication origin can replicate after injection into *Xenopus* eggs. It has thus been suggested that the origins found on extrachromosomal DNAs exist solely to circumvent the cells' strict requirement for chromosomal DNA to replicate once per cell division. Clearly the disparate views can only be reconciled after the replication of specific chromosomal genes has been studied. To this end, we have studied the replication of the ribosomal genes (rDNA) of the sea urchin *Lytechinus variegatus*. The visualization of replicating rDNA, isolated from rapidly dividing sea urchin gastrula cells, after restriction endonuclease digestion demonstrates that the initiation of replication in these chromosomal genes is sequence-specific, and is most probably confined to a region within the non-transcribed spacer.

After fertilization *L. variegatus* undergoes a rapid cleavage stage during which the embryos divide approximately every half hour. The rDNA genes of *L. variegatus* are present in about 200 copies per genome, and are isolatable as a dense satellite after equilibrium density centrifugation in CsCl^{11,12}. DNA was isolated from sea urchin embryos about 4 h after fertilization. Following the first CsCl equilibrium density gradient, the ribosomal DNA peak was located by hybridization with a cloned ribosomal gene (pUNC220, provided by Dr D. Stafford). The rDNA was then re-centrifuged in a second CsCl gradient and found to band at a density of 1.723 g cm⁻³. The rDNA peak formed a dense satellite well separated from the main band DNA, which has a mean density of about 1.695 g cm⁻³ (ref. 11).

Table 1 Purity of rDNA fractions

Hours	% Chromosomal DNA bound at equilibrium	
	Expt 1	Expt 2
24	17.5	18.4
48	15.7	14.6
72	14.0	14.3

The purity of ribosomal fraction was determined by saturation hybridization: three plasmids with inserts spanning the ribosomal repeat (see Fig. 1) were pooled on an equal weight basis, simultaneously nicked and denatured by treatment with 0.2 M NaOH for 10 min at 65 °C, neutralized and 10 µg applied to each 2.5-cm filter. Filters were cut into four identical pieces and after 1 h at 75 °C in 0.2 × SSC, 0.1% SDS, each was added to 56% (v/v) formamide, 4.6 × SSC, 9.2% dextran sulphate, 0.1% SDS containing about 2 ng ³²P-labelled chromosomal DNA and 0.5 ng ³H-labelled nick-translated 'pooled plasmid' as an internal control. Hybridization was at 42 °C for the indicated times. Binding of the chromosomal probe and the pooled plasmid was found to be invariant over a 40- and 14-fold range, respectively. Results are normalized to the fraction of the ³H-labelled pooled plasmid internal control at each time point. In both experiments, the value at 4 h was 20% but this time is omitted because it is pre-equilibrium. Maximum hybridization of the control was 57% of input for expt 1, 58% of input for expt 2.

The purity of the rDNA fraction was assayed by electron microscopy (EM) and saturation hybridization. When hybridized to a vast excess of cloned rDNA fixed to nitrocellulose, the chromosomal rDNA fraction was judged to be about 18% pure (Table 1). The EM determination is based on the measurement of DNA size after endonuclease restriction with an enzyme which recognizes one site in each rDNA repeat¹¹. Based on the fraction of molecules in the rDNA size range (see below and ref. 1), we estimate that the rDNA fraction was 23% pure.

The rRNA genes have been shown to occur as tandem repeats separated by an untranscribed spacer region in a variety of eukaryotes^{11,13-16}. Since the rDNA gene region usually covers more than 10⁶ base pairs (bp) there is a very great likelihood that some of the gene repeats will contain origins of replication. An additional feature of the gene family is that the repeat unit can vary in size within any one species¹⁷. This is due to the fact that the spacer region between transcription units varies in size. In *L. variegatus*, a spacer size variation of about 2 kilobase pairs (kb) has been reported (D. Stafford, personal communication, and ref. 11) as shown in Fig. 1. We have estimated the range of repeat sizes by restricting rDNA with the single cutter *Kpn*I, sizing the digest by agarose gel electrophoresis and blotting the gel to nitrocellulose. Hybridization of the blot with cloned rDNA shows most of the variation in size to be between 11 and 14 kb (Fig. 2). However, approximately 13% of the DNA has a size of about 9 kb.

To determine the position of the replication origins, the rDNA was restricted with *Kpn*I and visualized by EM. Before restriction, about 2% of the molecules contained eye forms¹⁸. After restriction, less than 1% contained eye forms (Fig. 3). A total of 128 molecules with eye forms were found; of these, 25 were in the ribosomal size range between 10.8 and 13.8 kb. In Fig. 4, the position of the replication bubbles on these molecules is indicated. Each molecule has one end placed at 0 kb, and has been oriented so that the centre of the replication loop (the origin) is to the right of the centre of the molecule.

It is not possible to discern the orientation of a given molecule visualized in the electron microscope by our techniques. However, it is also not possible to orient a series of such molecules to give a tight clustering of replication origins (assuming that the molecules are displayed with one end aligned) if the origins are randomly distributed along the molecules. Thus, if the members of a sufficiently large sample can be oriented to produce a tight distribution of origins, one can conclude that the origins are indeed located specifically with respect to sequence. A broad distribution, on the other hand, would most probably indicate a location random with respect to sequence.

Plots of the distances from the *Kpn*I site to the midpoint of the replication eyes are shown in Fig. 5. When the midpoints are plotted using the long distance to the *Kpn*I site (Fig. 5a), a tight distribution is found. Thus the origins are located specifically with respect to sequence.

The centre of the distribution is 8.4–8.6 kb from the *Kpn*I site. This places it either within the 26S gene, or within the non-transcribed spacer 2 kb from the 3' end of the 26S gene. Should the midpoint occur within the 26S gene, the short distance to the *Kpn*I site would be constant from molecule to molecule and the long distance would vary. Conversely, should the midpoint occur within the spacer, the long distance would

be relatively constant from molecule to molecule and the short distance would vary. In Fig. 5b, the short distance from the midpoint of the eyes to the *Kpn*I site is charted. A broad, random distribution is clearly seen in this case. Thus we tentatively assign the replication origin to the non-transcribed spacer, about 2 kb from the 3' end of the 26S gene (Fig. 1).

We note that several assumptions have been made in our analysis of the data. First, we assume that chromosomal replication is bidirectional. The available evidence indicates that this is a valid assumption¹⁹⁻²¹. Second, we have treated all molecules between 10.8 and 13.8 kb as though they were of ribosomal origin. While undoubtedly some of the molecules are contaminants, it is likely that the large majority are ribosomal, as indicated by the agreement between the saturation hybridiz-

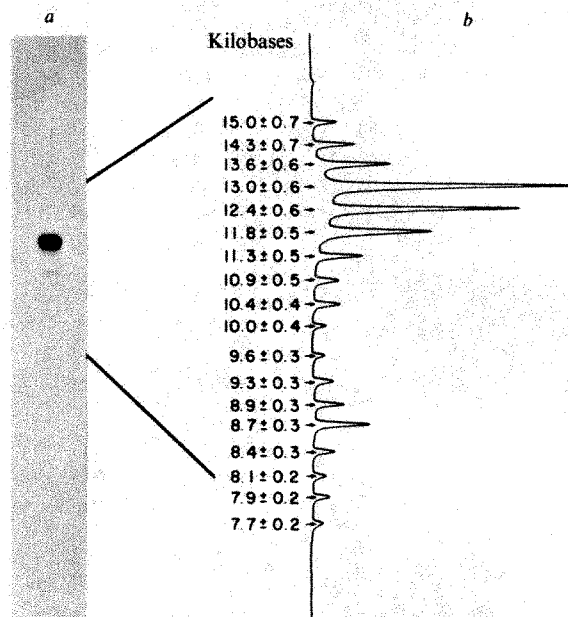


Fig. 2 Gulf Coast *L. variegatus* were obtained from the Gulf Specimen Company, Panacea, Florida, during season (May–June). 6 ml of packed embryos were chilled at the eighth cleavage stage (~4 h after *in vivo* fertilization) and allowed to settle for 25 min at 1 g on ice. After washing in 250 ml ice-cold seawater and resettling, they were added to 50 ml of cold buffer containing 33 g CsCl, 10 mM 2-mercaptoethanol, 20 mM Tris-HCl, pH 8.0, 50 mM EDTA and immediately ruptured by several passes of a dounce homogenizer. The homogenate was adjusted to a density of 1.499 g cm⁻³ and centrifuged for 90 min at 20,000 r.p.m., 20 °C in a SW27 rotor. The protein layer was removed and the remainder was adjusted to a density of 1.6 g cm⁻³, layered on a cushion of CsCl and centrifuged as above for 14 h. Fractions containing DNA were pooled and banded by CsCl equilibrium density centrifugation for 3 days at 20 °C, 35,000 r.p.m. in a Ti60 rotor. Aliquots of each fraction were denatured and bound to nitrocellulose and rDNA detected by hybridization with a nick-translated rDNA clone, pUNC220. The rDNA was then rebanded in a second CsCl gradient. The ribosomal peak was then dialysed overnight against 0.1 M Tris-HCl, pH 8.0, 10 mM EDTA, 10 mM NaCl. Approximately 0.1 µg of purified rDNA was digested with *Kpn*I at 30 °C in the presence of 0.3 µg λ *Hind*III fragments to assess the completeness of the digestion conditions. Samples were electrophoresed in a 0.6% agarose gel containing ethidium bromide. The gel was blotted by Southern's procedure³¹ and hybridized with a nick-translated set of pooled plasmids containing inserts spanning the entire *Lytechinus* ribosomal repeat (pUNC220, pLv147 and pLv128, courtesy of Dr Stafford). The filter was washed in 0.1 M NaCl, 0.1 mM EDTA, 0.1% SDS at 68 °C, cut into consecutive 1-mm slices which were individually autoradiographed and then scanned by densitometry to give a quantitative measure of the length of distribution of the *Kpn*I-digested rDNA unbiased by the spread of ³²P radiation. *a*, Autoradiogram of the intact blot; *b*, densitometer tracings of consecutive 1-mm slices of the blot.

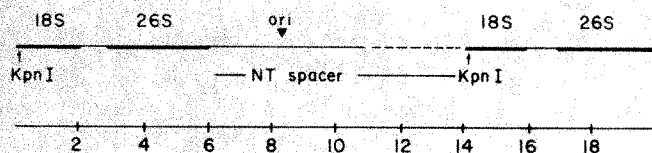
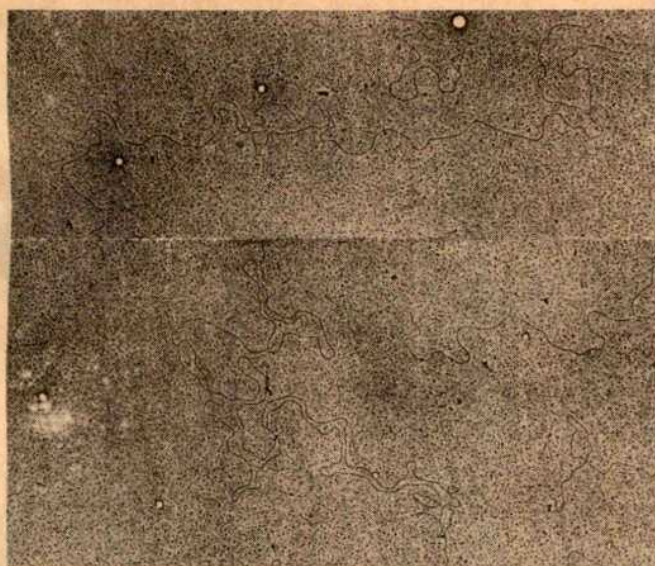
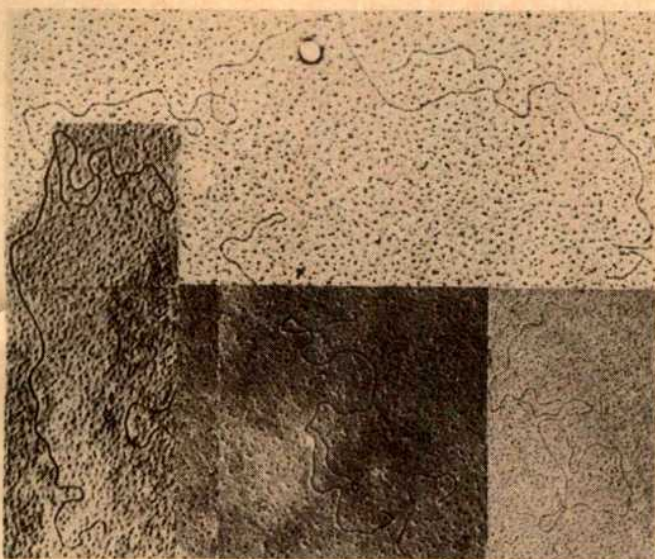


Fig. 1 The rDNA repeat in *L. variegatus*. The dashed line in the non-transcribed spacer region indicates the approximate amount of heterogeneity among the various members of the class, not the location of the heterogeneity, which is spread throughout the non-transcribed spacer region.



a

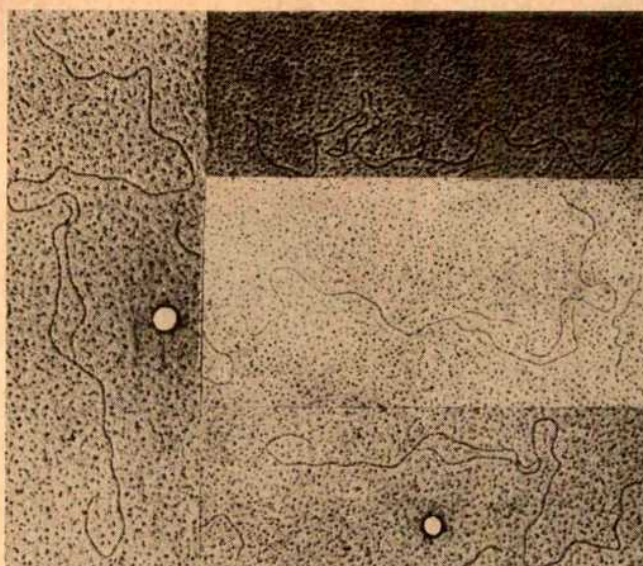


b

ation, 18% and the per cent of total eyes in the right size range, 23%.

It remains to be determined whether every ribosomal gene contains an origin. After fertilization, *L. variegatus* undergoes a rapid cleavage stage during which the embryos divide every half hour. At this stage the entire sea urchin genome is dividing at the rate of *Escherichia coli*, even though it contains several orders of magnitude more DNA. Based on a replication rate of about 3 kb per min per fork, *L. variegatus* should contain about 10,000 forks, or one eye form every 10^5 bp¹³. This translates into about one eye form per 10 ribosomal genes. Theoretically it is possible that only one out of 10 spacers contains an origin or that most spacers contain origins and the ones used are chosen at random.

A second class of molecules with a size distribution of 9 to 10.3 kb has also been found to contain a specific origin of replication (Fig. 4). The replication origin of these molecules maps at about 6.1 kb from one *Kpn*I site (Fig. 5c). About 12% of the total eye forms visualized were on 9–10.3-kb sized molecules. While we have observed rDNA in this size range, it is unlikely that the amount observed can account for 10% of the total eyes seen or almost 50% of the major class of rDNA genes. A possible alternative is that these molecules represent a separate chromosomal region with a defined origin of replication about 6.1 kb from a *Kpn*I site. We note, however, that if this class were ribosomal, the origin would occur exactly



c

Fig. 3 Eye forms before and after *Kpn*I digestion. DNA was spread essentially as described by Davis³². The spreading solution and the hypophase contained, respectively, 40% and 10% formamide. DNA was digested with *Kpn*I as described in Fig. 1 legend and diluted 20–50-fold into spreading solution. pBR322 was added as a molecular weight standard. *a*, Uncut DNA; *b*, eye form in the rDNA size range; *c*, eye form in the 9–10.3 kb size range.

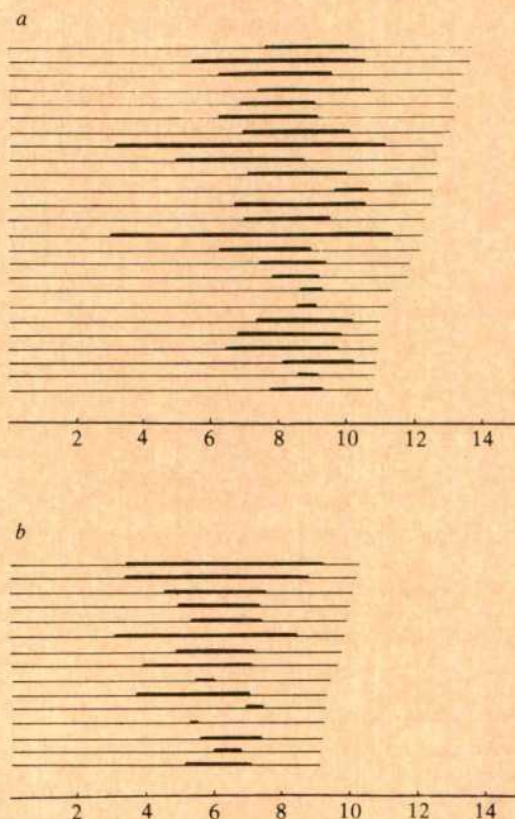


Fig. 4 Position of the eye forms on: *a*, molecules between 10.8 and 13.8 kb; *b*, 9 and 10.3 kb.

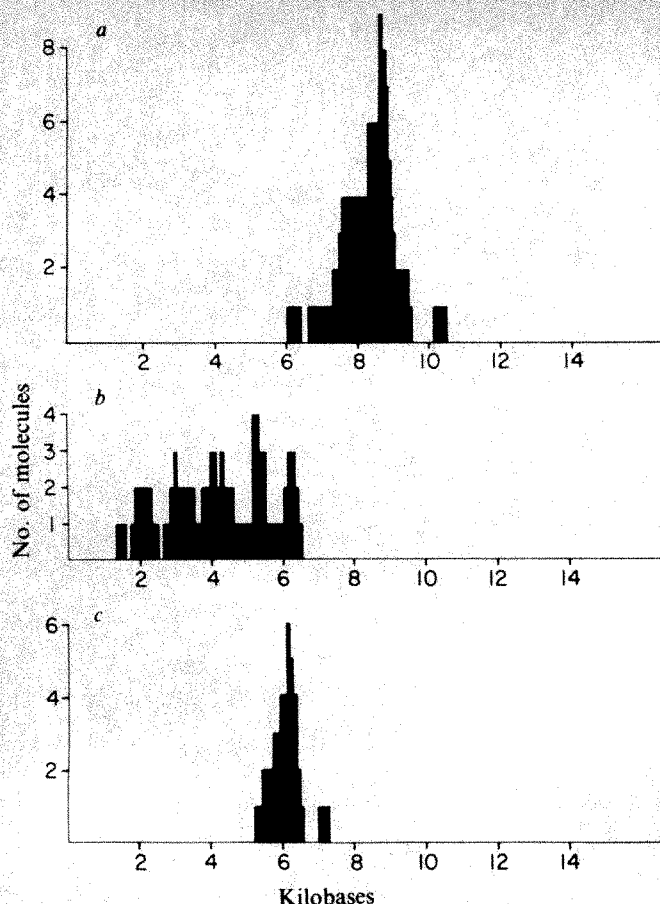


Fig. 5 Mapping of the replication start sites. The distance from the midpoint of the eye forms to the ends of each molecule was measured. A 3% error correction, determined by successive measurements of the standard, pBR322, was incorporated into each determination. *a*, The longer distance from the midpoint of the eyes to the *KpnI* site on molecules between 10.8 and 13.8 kb; *b*, the shorter distance from the midpoint to the *KpnI* site; *c*, the eye midpoint on molecules between 9 and 10.3 kb.

at the boundary between the 26S gene and the non-transcribed spacer, a distance that is 6.15 kb from the *KpnI* site (Fig. 1).

The finding of a specific replication origin for the rDNA genes of *L. variegatus* is consistent with previous work in prokaryotes and the localization of origins in lower eukaryotic extrachromosomal elements. In addition to the finding of specificity, the suggested localization within the rDNA spacer is consistent with the assignment of the other mapped origins to non-transcribed regions. The amplified rRNA genes in *Tetrahymena*^{6,22} and *Physarum*⁷ have specific origins of replication mapping near the middle of the spacer separating the linear, palindromic genes. Using Miller spreads of ribonuclear complexes, the ribosomal genes of *Drosophila* showed a negative correlation between the centre of eye forms and transcription fibrils, suggesting that the origin resides in the spacer region²³. In yeast, autonomously replicating plasmids (ARS) with specific chromosomal inserts have been characterized by a higher transformation frequency than uninserted vectors, a closed circular form, and a high rate of curing^{9,24}. The putative origin of the yeast ARS element containing the *Trp1* gene maps in a non-transcribed region flanking the 3' end of the gene^{25,26}. The origin in *Xenopus* mitochondrial DNA also maps to a region in which no transcripts have been detected²⁷. If origins in general are located in spacer regions, then the compelling need for an RNA primer to accompany replication must be resolved with the absence of spacer transcription. The promoters located in some spacers could serve a replication function²⁸⁻³⁰.

We thank Josef Weibel, Dr L. Peachy, Chris Overton, Carlo Croce, and Steven McKnight for their help, and Laurence Korn

for reading the manuscript. This work was supported by grants IN-143 from the American Cancer Society and GM2700 from the NIH.

Received 2 April; accepted 3 August 1982.

- Jacob, F., Brenner, S. & Cuzin, F. *Cold Spring Harb. Symp. quant. Biol.* **28**, 329-348 (1963).
- Kolter, R. & Helinski, D. R. *A. Rev. Genet.* **13**, 355-391 (1979).
- Nathan, D. & Danna, K. *Nature new Biol.* **236**, 202-212 (1972).
- Crawford, L. V., Syrett, C. & Wilde, A. *J. gen. Virol.* **21**, 515-521 (1973).
- Chalberg, R. & Kelly, T. *J. molec. Biol.* **135**, 988-1012 (1979).
- Robberson, D. L., Clayton, D. A. & Morrow, J. F. *Proc. natn. Acad. Sci. U.S.A.* **71**, 4447-4451 (1974).
- Truett, M. A. & Gall, J. G. *Chromosoma* **64**, 295-303 (1977).
- Vogt, V. M. & Braun, R. *Eur. J. Biochem.* **80**, 557-566 (1977).
- Struhl, K., Stinchcomb, D. T., Scherer, S. & Davis, R. W. *Proc. natn. Acad. Sci. U.S.A.* **76**, 1035-1039 (1979).
- Harland, R. M. & Laskey, R. A. *Cell* **21**, 761-777 (1980).
- Blin, N. *et al. J. biol. Chem.* **254**, 2716-2721 (1979).
- Wilson, F. G., Blin, N. & Stafford, D. C. *Chromosoma* **58**, 247-253 (1976).
- Edenburgh, H. J. & Huberman, J. A. *A. Rev. Genet.* **9**, 255-284 (1975).
- Wellauer, P. K., Dawid, I. B., Brown, D. D. & Reeder, R. H. *J. molec. Biol.* **105**, 461-486 (1976).
- Arneheim, N. & Southern, E. M. *Cell* **11**, 366-370 (1977).
- Dawid, I. B. & Wellauer, P. K. *Cold Spring Harb. Symp. quant. Biol.* **42**, 1185-1194 (1977).
- Long, E. & Dawid, I. B. *A. Rev. Biochem.* **49**, 727-764 (1980).
- Dressler, D., Wolfson, J. & Magazin, M. *Proc. natn. Acad. Sci. U.S.A.* **69**, 998-1002 (1972).
- Huberman, J. A. & Riggs, A. D. *J. molec. Biol.* **32**, 327-341 (1968).
- Kriegstein, J. & Hogness, D. S. *Proc. natn. Acad. Sci. U.S.A.* **71**, 135-139 (1974).
- Weintraub, H. *Nature new Biol.* **236**, 195-197 (1972).
- Cech, T. & Brehm, S. L. *Nucleic Acids Res.* **9**, 3531-3543 (1981).
- McKnight, S. L., Bustin, M. & Miller, O. L. *Cold Spring Harb. Symp. quant. Biol.* **42**, 741-754 (1977).
- Stinchcomb, D. T., Thomas, M., Kelley, J., Selkoe, E. & Davis, R. W. *Proc. natn. Acad. Sci. U.S.A.* **77**, 4559-4563 (1980).
- Tschumper, G. & Carbon, J. *Gene* **10**, 157-166 (1980).
- Stinchcomb, D. T., Struhl, K. & Davis, R. W. *Nature* **282**, 39-43 (1979).
- Rastl, E. & Dawid, I. B. *Cell* **18**, 501-510 (1979).
- Moss, T. & Birnstiel, M. C. *Nucleic Acids Res.* **6**, 3733-3743 (1979).
- Bach, R., Allet, B. & Crippa, M. *Nucleic Acids Res.* **9**, 5311-5330 (1981).
- Runger, D., Acherman, H. & Crippa, M. *Proc. natn. Acad. Sci. U.S.A.* **76**, 3957-3961 (1979).
- Southern, E. M. *J. molec. Biol.* **98**, 503-517 (1975).
- Davis, R. W., Simon, M. & Davidson, N. *Meth. exp. zool.* **21**, 413-428 (1973).

Suppression of an amber mutation by microinjection of suppressor tRNA in *C. elegans*

Judith Kimble, Jonathan Hodgkin, Terry Smith & John Smith

MRC Laboratory of Molecular Biology, Hills Road, Cambridge CB2 2QH, UK

Informational suppression by nonsense suppressor tRNAs has classically been a powerful tool for study of the mechanism of protein synthesis, to obtain conditional mutants and to demonstrate that a gene encodes a given protein product (for reviews see refs 1-3). In the nematode *Caenorhabditis elegans*, two genetically identified suppressors, *sup-5* and *sup-7* (refs 4, 5), have recently been shown to be amber suppressor tRNAs (N. Wills, R. F. Gesteland, J. Karn, L. Barnett, S. Bolten and R. H. Waterston, personal communication). We report here the microinjection of *sup-7* tRNA into the gonad of an animal bearing an amber allele of a maternal-effect mutant affecting sex determination (*tra-3*). We observe phenotypic suppression in the injected parent's offspring. tRNA from wild-type animals does not show this *in vivo* suppressor activity, and *sup-7* tRNA does not cause suppression of a non-amber allele of the same gene. *In vivo* suppression of an amber mutant by microinjection provides a new means of gene manipulation in *C. elegans*.

tRNA was introduced into *C. elegans* embryos by injection into the hermaphrodite gonad (Fig. 1). In this technique, a micropipette penetrates the adult cuticle and body wall to enter the distal arm of the gonadal tube (~400 µm long and 30 µm in diameter, Fig. 1a). This region of the gonad consists primarily of immature germ cells connected by bridges to a central core of cytoplasm⁶ (Fig. 1b). Studies with a fluorescein-tagged D-amino acid dodecapeptide (synthesized and kindly provided by D. Weisblatt) demonstrate that small injected macromolecules

Fig. 1 Introduction of tRNA into embryos by microinjection into the parental gonad. The hermaphrodite gonad consists of two symmetrical and equivalent U-shaped tubes⁶. Each half produces oocytes and sperm; embryos are made in assembly-line fashion as oocytes pass, one by one into the spermatheca to be fertilized, and then enter the uterus to begin embryogenesis. A micropipette (4–6 μ m diameter at the tip) is inserted into the germ-line tissue in the distal arm of the gonad of an animal anaesthetized with 0.01% tetramisole and 0.1% tricaine mounted against the edge of a coverslip under Voltalef oil (BDH), and inspected using a Wild M8 dissecting microscope at $\times 50$ magnification. 5–10 pl tRNA (20 mg ml⁻¹) is injected using an oil-filled syringe connected to the micropipette. Each injected worm is examined after 4–8 h to ensure that the injected half-gonad is still producing embryos. Embryos made by the uninjected half-gonad serve as an internal control.

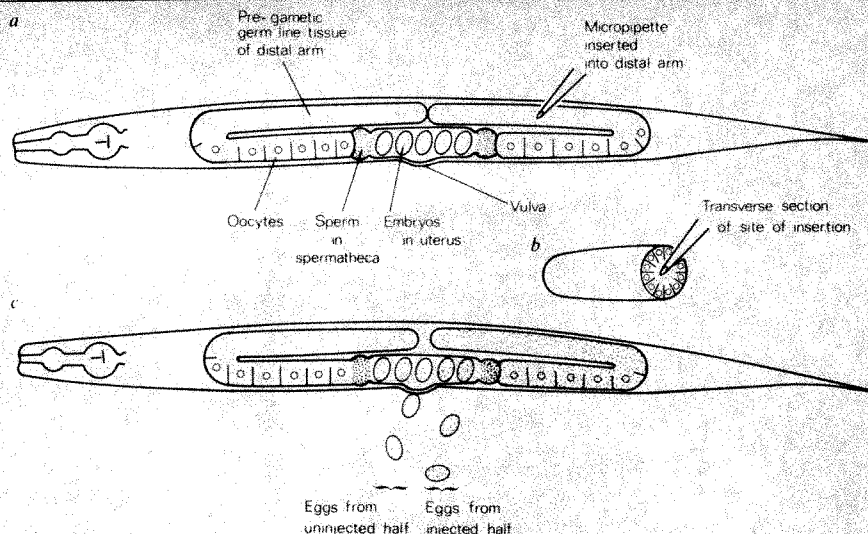
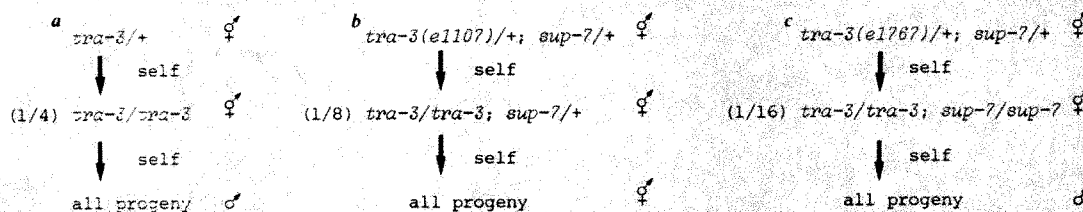


Fig. 2 *a*, Maternal effect of *tra-3*⁷. Homozygous *tra-3/tra-3* XX animals are hermaphrodite (ϕ) if born from a heterozygous *tra-3/+* parent, but are pseudomale (δ) if born from a homozygous *tra-3/tra-3* parent. Thus, expression of the wild-type gene in the heterozygous parent rescues the phenotype of its homozygous progeny. In addition, a wild-type gene introduced by cross-fertilization by a wild-type male produces hermaphrodite cross-progeny, again rescuing the *tra* phenotype. *b*, One allele of *tra-3*, *e1107*, is suppressed. Here, we show that one maternal dose of *sup-7* is sufficient for suppression. Other crosses have shown that one copy of *sup-5* or *sup-7* in either the hermaphrodite parent or the zygote can rescue the *e1107* phenotype. *c*, Another allele of *tra-3*, *e1767*, is not suppressed. Two copies of *sup-7* in both parent and zygote cannot rescue the *e1767* phenotype.



can diffuse within minutes throughout the U-shaped gonadal tube and that oocytes and embryos produced by this tube contain injected tracer (data not shown). Thus, this procedure provides a means of injecting several embryos by a single injection into a target tissue that is large and easy to inject compared with the embryo (Fig. 1c).

The mutation selected for attempted rescue by microinjection of *sup-7* tRNA is in the *tra-3* locus⁷. Normally in *C. elegans*, sex is determined by the X:autosome ratio¹¹. In a wild-type diploid strain, XX animals are self-fertilizing hermaphrodites and XO animals are male. However, recessive mutations in one of three autosomal transformer genes (*tra-1*, *tra-2* and *tra-3*) divert XX animals from the hermaphrodite to the male pathway of development⁷.

tra-3 was chosen for mutant rescue by injection of suppressor tRNA for two reasons. First *tra-3* exhibits a maternal effect (Fig. 2a). The wild-type gene product expressed by a heterozygous (*tra-3/+*) XX hermaphrodite rescues its homozygous (*tra-3/tra-3*) self progeny. The self progeny of these *tra-3/tra-3* hermaphrodites, however, all develop as morphologically distinct pseudomales (Fig. 3a). The first sign of sexual dimorphism is midway during embryogenesis (J. Sulston, personal communication). Thus, the *tra-3* gene product is likely to be present in oocytes, and must function during embryogenesis.

Second, both amber and non-amber alleles of *tra-3* are available. Genetic tests with *sup-5* and *sup-7*, both amber suppressors, have shown that *e1107* is an amber allele of *tra-3* and that *e1767* is not (Fig. 2b,c). (Alleles are given lettered numbers, for example, *e1107*, according to the place and time isolated⁸.) Even a single copy of the *sup-5* gene, the weaker of the two suppressors⁸, is sufficient to rescue the *tra-3* phenotype of *e1107* progeny (Fig. 2b). Conversely, two copies of the stronger suppressor, *sup-7*, do not rescue the *tra-3* phenotype of *e1767* progeny (Fig. 2c).

sup-7 tRNA (for extraction procedure see Table 1 legend) was microinjected into the distal arm of *e1107/e1107* hermaphrodite gonads, and the progeny of each injected parent examined for suppression. The tail, vulva and gonad morphology of a hermaphrodite is easily distinguishable from that of the expected *tra-3* pseudomale. Ten animals continued to produce embryos in the half-gonad injected. Of these, six produced some progeny that were clearly hermaphrodite (Table 1). The presence of any hermaphrodites among progeny of a

Table 1 Results of suppressor tRNA microinjection in *C. elegans*

Allele injected	tRNA injected	No. injected*	No. progeny†	No. hermaphrodites
<i>e1107</i>	<i>sup-7</i>	10	1,023	21
<i>e1767</i>	<i>sup-7</i>	10	1,106	0
<i>e1107</i>	Wild type	13	1,127	0
<i>e1107</i>	—	—	4,000	0

Wild-type (*C. elegans* Bristol strain, N2) and *sup-7*-bearing [RW2108 = *unc-15(e1214)*I; *dpy-18(e364)*III; *sup-7(st5)*X] animals grown in liquid culture⁹ were suspended in 0.05 M disodium naphthalene disulphonate together with an equal volume of phenol saturated with 1% aqueous 8-hydroxyquinoline and disrupted in a French pressure cell at 2,000 p.s.i. RNA was extracted according to the method of Kirby¹⁰ and fractionated on a DEAE-cellulose (Whatman DE52) column. The fraction eluting between 0.25 M and 1.0 M NaCl, containing 4S, 5S and small RNAs, was assayed for tRNAs by aminoacylation with ¹⁴C-labelled amino acids, using a crude nematode aminoacyl tRNA synthetase preparation. Using a mixture of 10 ¹⁴C-labelled amino acids (each 100 cmol⁻¹), 300–500 pmol per A₂₆₀ unit of both wild-type and *sup-7* crude tRNAs were charged.

* Only animals that continue to produce embryos in the half-gonad injected are included.

† Only half the number listed arise from the injected half-gonad.

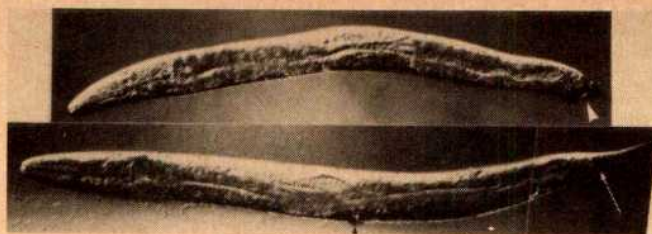


Fig. 3 Comparison of the unrescued *tra-3* phenotype, a pseudomale (a), and a rescued hermaphrodite (b). Both animals were derived from a *tra-3/tra-3* XX hermaphrodite injected with *sup-7* tRNA. The pseudomale possesses a vestigial male tail (white arrowhead); the hermaphrodite has a whip-like tail (arrow). The pseudomale either has no vulva, as shown here, or a grossly malformed vulva; the hermaphrodite has a normal vulva (small black arrowhead). The pseudomale gonad is intersexual; the rescued gonad is indistinguishable from a hermaphrodite gonad, except that oocytes are made later than normal. Only one hermaphrodite has laid eggs, so some defect in the egg-laying system is probable. The injected animal carries a mutation in *dpy-4* (*e1166*) which is closely linked to *tra-3* on chromosome IV; this distinguishes the *tra-3* homozygote among progeny of a heterozygous parent. In addition, the animal is homozygous for a mutation in *nuc-1* (*e1392*), which encodes the major endonuclease.

homozygous *tra-3* animal is particularly striking as no hermaphrodites were observed among the progeny of control animals (see below). Thus, 60% of the injected animals showed the effects of suppression. It is unclear, however, whether the injected RNA acts before or after fertilization. The genotype of the injected animals was confirmed by their production of pseudomales (expected to arise from the uninjected half gonad). The genotype of the rescued hermaphrodite progeny produced after injection was verified in turn by examining their self progeny; in all cases, only *tra-3* pseudomales were produced, confirming that these phenotypic hermaphrodites were homozygous *tra-3* animals.

As controls, *sup-7* tRNA was injected into animals homozygous for the non-amber allele, *e1767*, and wild-type tRNA was injected into animals homozygous for the amber allele, *e1107*. In addition, 4,000 progeny of uninjected *e1107/e1107* hermaphrodites were examined. In both injected and uninjected control animals, no hermaphrodite progeny were produced (Table 1). Therefore, production of hermaphrodites after injection of *sup-7* tRNA into *e1107/e1107* animals must result from *in vivo* suppression.

The small number of hermaphrodites made by each injected parent may result from the relative impurity of the tRNA injected, or it may mean that the injected molecules are concentrated into a few oocytes. Experiments are in progress to determine more precisely when the rescued embryos are made after injection, and what the effects of injecting a more purified tRNA preparation might be on the efficiency of suppression.

In vivo suppression by *sup-7* tRNA provides a convenient means of assaying and manipulating gene function during embryogenesis. Injection of *sup-7* tRNA into individual blastomeres after fertilization should generate precisely engineered genetic mosaics for subsequent analysis of tissue-specific developmental effects. In addition, suppression of *tra-3* or other genes with suppressible alleles may prove useful as a bioassay to detect transcripts of a cloned DNA encoding the *sup-7* gene *in vivo*.

J.E.K. was supported by National Research Service Award 1 F32 GM07774-02.

Received 25 May; accepted 13 July 1982.

1. Gorini, L. A. *Rev. Genet.* **4**, 107-134 (1970).
2. Korner, A. M., Feinstein, S. I. & Altman, S. in *Transfer RNA* (ed. Altman, S.) 105-135 (MIT Press, Cambridge, Massachusetts, 1978).
3. Celis, J. E. & Smith, J. D. (eds) *Nonsense Mutations and tRNA Suppressors* (Academic, London, 1979).
4. Waterston, R. H. & Brenner, S. *Nature* **275**, 715-719 (1978).
5. Waterston, R. H. *Genetics* **97**, 307-325 (1981).
6. Hirsh, D., Oppenheim, D. & Klass, M. *Dev. Biol.* **49**, 200-219 (1976).

7. Hodgkin, J. A. & Brenner, S. *Genetics* **86**, 275-287 (1977).
8. Horvitz, H. R., Brenner, S., Hodgkin, J. & Herman, R. K. *Molec. gen. Genet.* **175**, 129-133 (1979).
9. Sulston, J. E. & Brenner, S. *Genetics* **77**, 95-104, (1974).
10. Kirby, K. S. *Meth. Enzym.* **12B**, 87-98 (1968).
11. Madl, J. E. & Herman, R. K. *Genetics* **93**, 393-402 (1979).

When do carcinogen-treated 10T1/2 cells acquire the commitment to form transformed foci?

J. M. Backer, M. Boerzig & I. B. Weinstein

Division of Environmental Sciences and Cancer Center/Institute of Cancer Research, Columbia University, New York, New York 10032, USA

A major advance in analysing the mechanisms of chemical carcinogenesis has been the development of cell culture systems in which normal rodent cells can be transformed as a result of *in vitro* exposure to specific chemicals or radiation¹⁻⁶. An unexpected finding in these systems is that the frequency of transformation is often much greater than that of induction of drug-resistant mutants^{3,6-10}. In addition, studies using the technique of cell spreading have suggested that the latent period between exposure of cell cultures to carcinogens and the emergence of cells having the heritable ability to form transformed foci is also much greater than that for the induction of drug-resistant mutants^{8,11,12}. In most of the above transformation studies, the cells were exposed to carcinogens at low cell densities and, therefore, mutation-like events that might be induced with a low frequency could have been missed. Thus, we have now analysed the kinetics of cell transformation of C3H 10T1/2 cells when exposed to the potent ultimate carcinogen (±)7β,8α-dihydroxy-9α,10α-epoxy-7,8,9,10-tetrahydrobenzo(a)pyrene (BPDE) in conditions of high cell density. We report here that in these conditions acquisition of the ability to form transformed foci and acquisition of ouabain resistance occur with similar kinetics and within 2 days of carcinogen exposure.

To determine when carcinogen-treated C3H 10T1/2 cells acquire the heritable property of ouabain resistance or the ability to form morphologically transformed foci we used the protocol described in Fig. 1 legend. Replicate plates of cells were trypsinized and replated at the same density at various times after exposure to the carcinogen, and then the secondary plates were incubated and scored for the number of ouabain-resistant clones or the number of foci of transformed cells. The rationale is that if colonies of committed cells have already begun to form on the donor plates, then the individual cells of such colonies will be dispersed on the secondary plates where they will form multiple colonies or foci. Thus, the time after carcinogen treatment at which reseeding expands the number of colonies or foci indicates, approximately, the time at which the treated cells have become committed or clonogenic for the property being measured. Since the plating efficiency during the replating is <100%, the number of colonies or foci on the secondary dishes may actually be a lower limit of the number of committed cells. We used the same initial cell density (50,000 cells per 6 cm plate) to study the induction by BPDE of both ouabain resistance and transformation.

Figure 1a shows representative plates from BPDE-treated and control cultures that were used to select for ouabain-resistant mutants, with or without the replating procedure. It is obvious that replating markedly increases the number of ouabain-resistant colonies. This effect was apparent within 2 days of BPDE treatment and reached a plateau within 5 days, at which time the cells on the primary plates were confluent (Fig. 2a). The replating procedure led to about an eightfold increase in the number of colonies growing in the presence of ouabain. This increase was less than the 16-fold increase one would expect if the cells had undergone approximately four doublings before reaching confluency. This difference may be

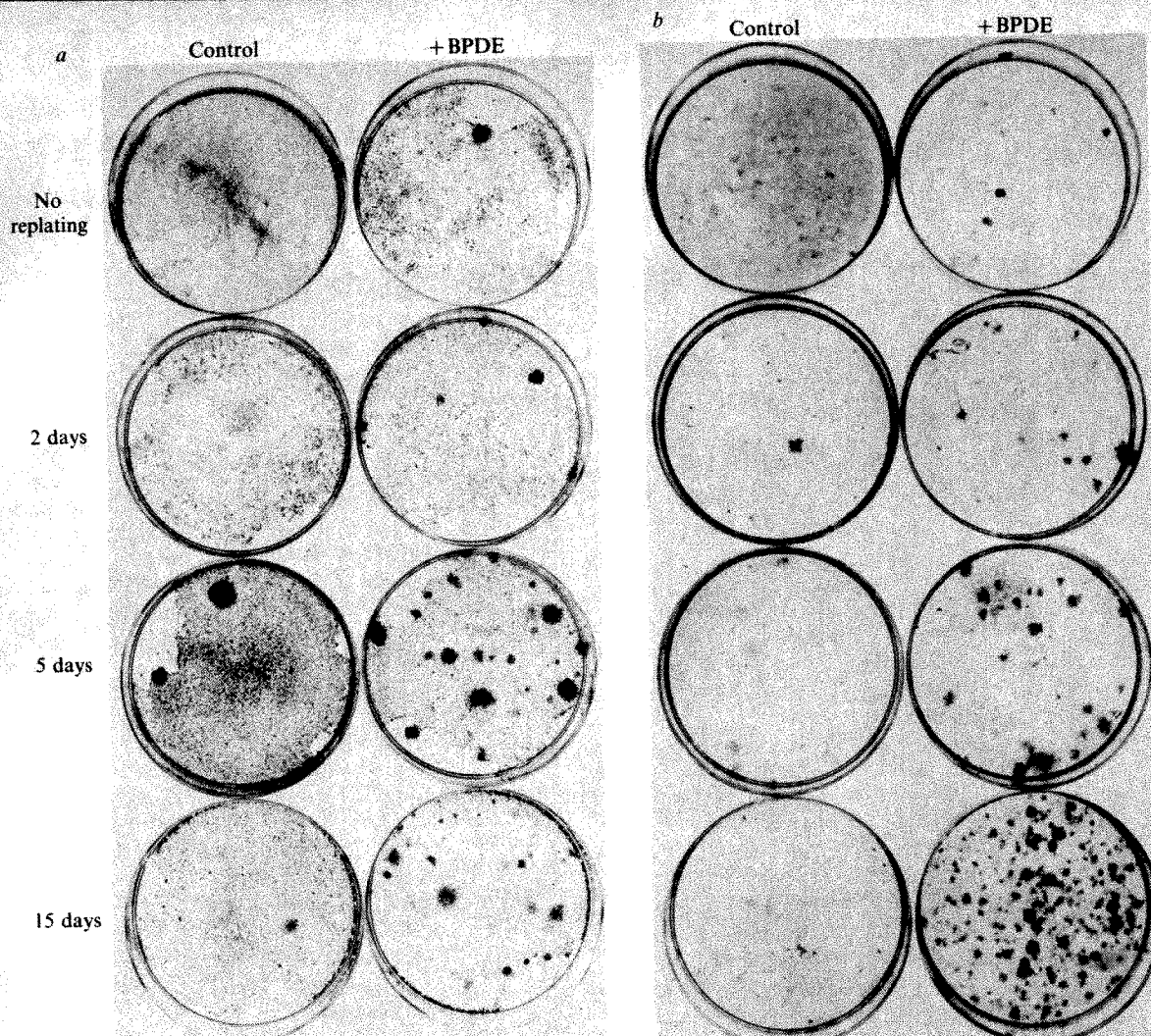


Fig. 1 Effect of replating on the number of ouabain-resistant colonies and the number of transformed foci. *a*, Representative plates of cultures replated at various times after BPDE treatment and stained for ouabain-resistant colonies. *b*, Representative plates stained for transformed foci. C3H 10T1/2 Cl8 (ref. 15) was provided by Dr J. Bertram and grown on plastic tissue culture plates (Nunc, Denmark) in Dulbecco's modified Eagle's medium (DMEM) supplemented with 10% calf serum (GIBCO). 50,000 cells were seeded per 6 cm plate; 24 h later the plates were rinsed with phosphate-buffered saline (PBS) and incubated for 1 h with 2 ml of DMEM containing either BPDE (50 ng ml^{-1}) in 0.01% of tetrahydrofuran (THF) or 0.01% THF (solvent control). The BPDE stock solution in THF was diluted into DMEM immediately before use. After incubation, the plates were rinsed with PBS and 5 ml of DMEM supplemented with 5% calf serum (DMEM-5) were added to each plate; this medium was changed every week. Four to six weeks after the cells reached confluency, either on the primary or secondary plates (see below), they were fixed with 3.7% formaldehyde, stained with Giemsa and the sum of type II and type III foci was determined as previously described¹⁵. For the ouabain resistance mutation assay, the protocol was similar except that DMEM-5 containing 3 mM ouabain was added to the dishes either 62 h after treatment with BPDE or THF, or 24 h after the cells were reseeded onto the secondary plates. Colonies were fixed, stained and counted 2–3 weeks after exposure to ouabain¹³. For the replating studies, at various times after the cells were treated with BPDE, or THF, five replicate plates were dissociated with 0.25% trypsin/versene, the cells were pooled in 25 ml of DMEM-5 and seeded onto five new Petri plates. Thus the densities of cells on the secondary plates were approximately the same as that on the donor primary plates.

due to the known decrease in the number of ouabain-resistant mutants recovered if the expression time (time between treatment and exposure to ouabain) is delayed for several days^{13,14}.

Figure 1b shows representative plates from parallel studies in which BPDE-treated and control cultures were or were not replated at various times after treatment and the plates scored for foci of transformed cells 4–6 weeks after the cells had reached confluency. It is obvious that the replating procedure markedly increased the number of transformed foci that were detected. This increase was apparent within 48 h of BPDE treatment and reached a plateau between 8 and 12 days (Fig. 2b). At this plateau the replating procedure led to about a 16-fold increase in the number of foci, which one would expect if the focus-forming cells had undergone about four doublings before replating.

Three additional experiments using the protocol described in Fig. 1 legend gave results that were qualitatively similar to those shown in Fig. 2a, b. It is of interest that the kinetics of

induction of transformed cells by BPDE were quite similar to those for induction of ouabain-resistant mutants, suggesting that both processes involve similar events. Although the cells on the primary plates became confluent by 5 days after the BPDE treatment, the number of transformed foci observed after replating continued to rise from days 5 to 15 (Figs 1b, 2b). We presume that this is because the cells in the process of transformation continue to replicate on the primary plates, even after the rest of the cell population ceases proliferating. Growth curves revealed that the concentration of BPDE (50 ng ml^{-1}) used in these studies produced negligible cytotoxicity (data not shown).

Thus, it seems that within 48 h of BPDE treatment, variants emerge that have a heritable alteration in both ouabain resistance and morphological transformation. As the doubling time of these cells is 18–24 h (ref. 15), this commitment occurred within one or two doublings after BPDE treatment. In similar experiments using BPDE and replating at the same time

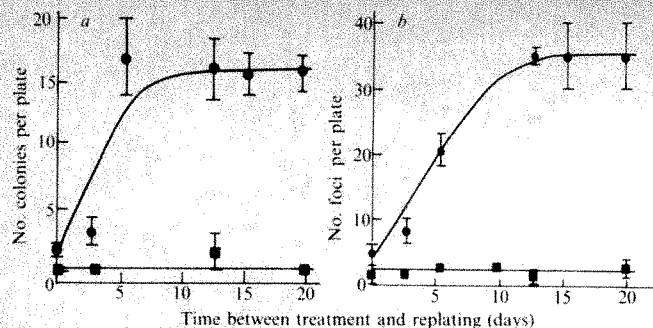


Fig. 2 *a*, Number of ouabain-resistant colonies obtained on the secondary plates when the cultures were treated with BPDE (●) or the solvent (■). *b*, Number of transformed foci obtained on the secondary plates following treatment with BPDE (●) or the solvent (■). The values represent the means and standard deviations of five replicate plates. The complete protocol is given in Fig. 1 legend.

intervals, but where many fewer cells (5,000 per dish) were treated with BPDE, we did not observe an increase in the number of foci (data not shown). This result, as well as similar negative results obtained in replating experiments following the treatment of C3H 10T1/2 cells at low cell density with benzo(a)pyrene¹¹, X rays⁸, or alkylating agents¹², suggest that the replating procedure itself does not act by enhancing the acquisition of the transformed phenotype.

Previous authors^{8,9} have proposed a two-step model to explain the transformation of C3H 10T1/2 cells following exposure of cells at low density to either radiation or chemical carcinogens. The model postulates that the first step occurs with a very high probability on treatment with the carcinogen, and that the second step occurs only after many subsequent cell generations and with a low probability, of about 10^{-6} per generation⁹. With respect to the present studies, the model predicts that early replating of treated cells will not increase the number of foci, simply because cells are not committed to transformation until this late step occurs.

Our observation of an early commitment of cells to form transformed foci when the initial exposure to carcinogen occurs at a high cell density, but not at a low cell density, might be explained by assuming that a high cell density increases the likelihood that the second step occurs more rapidly. Alternatively, it is possible that transformation can also occur via a single mutation-like event, but that this occurs with a low probability, in the range of 10^{-4} to 10^{-5} . Thus this route would be observed only when one exposes about 10^4 or more cells to the carcinogen. If two different routes for cell transformation do exist, then it will be of interest to determine which of them involves random point mutations, genomic rearrangements or epigenetic mechanisms, and whether or not such changes involve protooncogenes or long terminal repeat sequences normally present in the mouse genome^{10,16}. Regardless of the mechanism, the replating procedure described in the present study may be of practical significance because it shortens the lag period and increases the sensitivity of *in vitro* assays for carcinogens in the C3H 10T1/2 cell system.

Received 10 May; accepted 19 July 1982.

- Berwald, Y. & Sachs, L. *J. natn. Cancer Inst.* **35**, 641-661 (1965).
- Chen, T. T. & Heidelberger, C. *Int. J. Cancer* **4**, 166-178 (1969).
- Heidelberger, C. *et al. Mutat. Res.* (in the press).
- DiPaolo, J. A., Donovan, P. J. & Nelson, R. L. *Nature new Biol.* **230**, 240-242 (1971).
- DiPaolo, J. A., Takano, K. & Popescu, N. C. *Cancer Res.* **32**, 2686-2695 (1972).
- Barrett, J. C. & Elmore, E. in *Mutagenesis and Carcinogenesis* (eds Andrews, L. S., Lorentzen, R. J. & Flamm, W. G.) (Springer, Berlin, in the press).
- Parodi, S. & Brambilla, G. *Mutat. Res.* **47**, 53-74 (1977).
- Kennedy, A. R. *et al. Proc. natn. Acad. Sci. U.S.A.* **77**, 7262-7266 (1980).
- Fernandez, A., Mondal, S. & Heidelberger, C. *Proc. natn. Acad. Sci. U.S.A.* **77**, 7272-7276 (1980).
- Weinstein, I. B. *J. supramolec. Struct.* **17**, 99-120 (1981).
- Haber, D. A. *et al. Cancer Res.* **37**, 1644-1648 (1977).
- Peterson, A. R. *et al. Cancer Res.* **41**, 3095-3099 (1981).
- Landolph, J. R. & Heidelberger, C. *Proc. natn. Acad. Sci. U.S.A.* **76**, 930-934 (1979).
- Chan, G. & Little, J. B. *Proc. natn. Acad. Sci. U.S.A.* **75**, 3363-3366 (1978).
- Reznikoff, C. A., Brankow, D. W. & Heidelberger, C. *Cancer Res.* **33**, 3231-3238 (1973).
- Kirschmeier, P. *et al. Proc. natn. Acad. Sci. U.S.A.* **79**, 273-277 (1982).

Cytoplasmic control of preimplantation development *in vitro* in the mouse

Audrey Muggleton-Harris*, D. G. Whittingham* & Lynette Wilson*

MRC Laboratory Animals Centre, Woodmansterne Road, Carshalton, Surrey SM5 4EF, UK

Although the embryos of certain mammals, including man, can be cultured *in vitro* through several cleavage divisions^{1,2}, it is only in the mouse that complete development through the preimplantation period (one-cell to the blastocyst stage³) occurs without affecting subsequent embryonic viability after transfer^{1,4}. But even in the mouse, development *in vitro* from the one-cell to the blastocyst stage is restricted to certain inbred strains and *F*₁ hybrids^{1,3,5,6}. In most randomly bred strains the one-cell embryo becomes blocked at the two-cell stage *in vitro* and it will only continue development if transferred back into the oviduct⁷. Here we present evidence that this so-called 'in vitro two-cell block' can be obviated by injecting small amounts of cytoplasm from embryos which do not exhibit this block.

Fertilized one-cell eggs were obtained from superovulated randomly bred MF1 (OLAC, UK) and *F*₁ (C57BL/6 × CBA/H) hybrid females mated with MF1 males. Intraperitoneal injections of 5 IU pregnant mare serum gonadotropin (PMSG; Organon) and 5 IU human chorionic gonadotropin (HCG; Organon) were given 48 h apart. Fertilized one-cell eggs were recovered from mated females about 19 h after HCG injection. The cumulus cells were dispersed with hyaluronidase (150 U ml^{-1}) and the eggs washed in several changes of HEPES-buffered mouse embryo culture medium, M2 (ref. 8) before setting up for cytoplasmic injections at the one-cell stage or culturing for 24 h for cytoplasmic transfer at the two-cell stage. Cytoplasmic injections were carried out using glass micropipettes ($\sim 4 \mu\text{m}$ diameter at the tip) attached to Agla microsyringes and a De Fonbrune micromanipulator. Before manipulation, groups of eggs were incubated for 15 min at 37°C in mouse embryo culture medium no. 16 (ref. 9) containing cytochalasin D (Sigma) at a concentration of between 0.2 and $0.5 \mu\text{g ml}^{-1}$ (ref. 10). To maintain a stable pH (between 7.2 and 7.4) in air for microinjections, the eggs were transferred to 50–100- μl drops of M2 medium plus cytochalasin D overlaid with paraffin oil, in plastic culture dishes (Falcon). Although exposure of eggs to cytochalasin D during micromanipulation facilitated egg penetration and withdrawal and delivery of the cytoplasm, preliminary experiments showed that the period when such manipulations could be accomplished without affecting the subsequent survival of the egg was critical: between 15 and 45 min after placing eggs in cytochalasin D (our unpublished observations). Care was taken not to withdraw pronuclei or blastomere nuclei when removing cytoplasm from donor eggs. After injection, the eggs were washed and cultured in medium 16. The eggs were observed several hours after incubation to determine the numbers surviving microinjection. Subsequent observations were made every 24 h until development of control embryos had reached the blastocyst stage.

In the first series of experiments (Table 1) cytoplasm from fertilized one-cell *F*₁ (C57BL/6 × CBA/H) eggs was injected into one-cell fertilized eggs of the randomly bred MF1 strain ($\sim 22 \text{ pl}$ of cytoplasm per egg). Over 50% of the eggs survived the injection and some of the eggs seemed to be proceeding further in preimplantation development compared with the uninjected MF1 controls. The injection of equivalent volumes of culture medium had no effect on further development of either strain (our unpublished observations). The inability of uninjected fertilized one-cell MF1 eggs to complete preim-

* Present addresses: Department of Biology and Biotechnology, Worcester Polytechnic Institute, Worcester, Massachusetts 01609, USA (A.M.H.); MRC Mammalian Development Unit, Wolfson House, University College London, 4 Stephenson Way, London NW1 2HE (L.W.). Correspondence should be addressed to D.G.W.

Table 1 *In vitro* development of fertilized one-cell MF1 eggs after injection of cytoplasm from fertilized one-cell F₁ (C57BL/6×CBA/H) eggs

No. of 1-cell eggs injected	No. surviving (%)	No. cleaved (%)	2-Cell	4-Cell	8-Cell	Morula	Blastocyst
105	58 (55)	46 (79)	35	2	4	5	—
Uninjected controls							
	No. of 1-cell eggs						
MF1	43	39 (91)	37	1	1	—	—
F ₁	45	45 (100)	6	1	1	2	35

plantation development *in vitro* confirms all previously reported findings¹.

A second series of experiments was designed to examine the effect of injecting F₁ cytoplasm from two-cell embryos into MF1 eggs at the two-cell stage. For these purposes both F₁ and MF1 two-cell eggs were grown from the one-cell stage *in vitro*. Only one blastomere was injected with cytoplasm (~8 pl), thus the remaining uninjected blastomere provided a within-embryo control. About 70% of the MF1 eggs receiving cytoplasm from F₁ two-cell eggs developed to the morula and blastocyst stages during 72 h in culture but none of the MF1 eggs receiving MF1 cytoplasm developed beyond the four-cell stage (Table 2 and Fig. 1). In most of the MF1 eggs injected with F₁ cytoplasm (~60%) both the uninjected and injected blastomeres divided at the second cleavage division. As the injections were performed when the two-cell embryo was about midway between the first and second cleavages, the cytoplasmic bridge was probably still present, allowing material to pass between the two blastomeres as shown by Lo and Gilula¹¹. A single MF1 egg developed to the blastocyst stage in the uninjected control group, confirming previous observations¹ where a small propor-

tion of randomly bred embryos have been shown to complete preimplantation development from the one-cell stage *in vitro*.

Although the *in vitro* arrest observed in the development of zygotes from certain mouse strains may be due to some artefact of the culture system, our results clearly demonstrate that this block can be overcome by injecting small quantities of cytoplasm (~8 pl—about 4% of the egg volume at the two-cell stage) from two-cell eggs fully capable of completing preimplantation development *in vitro*. The component(s) in the F₁ cytoplasm responsible for initiating further development of the MF1 zygotes *in vitro* are unknown. It is apparent that cytoplasm from the two-cell stage eggs is better able to promote further development *in vitro* than that from one-cell stage eggs. There were marked differences in the nature of the cytoplasm at the one- and two-cell stages after exposure to cytochalasin D (one-cell stage cytoplasm dispersed freely in the culture medium but at the two-cell stage the cytoplasm remained compacted and sausage-shaped) suggesting changes in its structural organization (our unpublished observations). It is possible that either the components added in the cytoplasm injected at the one-cell stage are leached out during culture to the two-cell stage or

Fig. 1 *a*, Two-cell MF1 embryos (grown from the one-cell stage *in vitro*) shortly after injecting F₁ cytoplasm into one-blastomere. *b*, Development of injected two-cell MF1 embryos after a further 24 h incubation *in vitro*. Note the different types of development occurring. The degenerated blastomeres are those which did not receive an injection of cytoplasm. *c*, Uninjected MF1 controls still at the two-cell stage 24 h later. *d*, Injected two-cell MF1 embryos 48 h after injection. These are at the four-cell, morulae and compacted morulae stages of development. *e*, Various developmental stages consisting of compacted morulae, blastocysts and expanded blastocysts, 72 h after injection—that is, after a total of 96 h *in vitro*. Note the oil droplet in one blastomere of the middle embryo on the left. This was injected with cytoplasm into one of the blastomeres at the two-cell stage. *f*, Uninjected MF1 controls after a similar 96-h culture period remain at the two-cell stage of development. ×125.

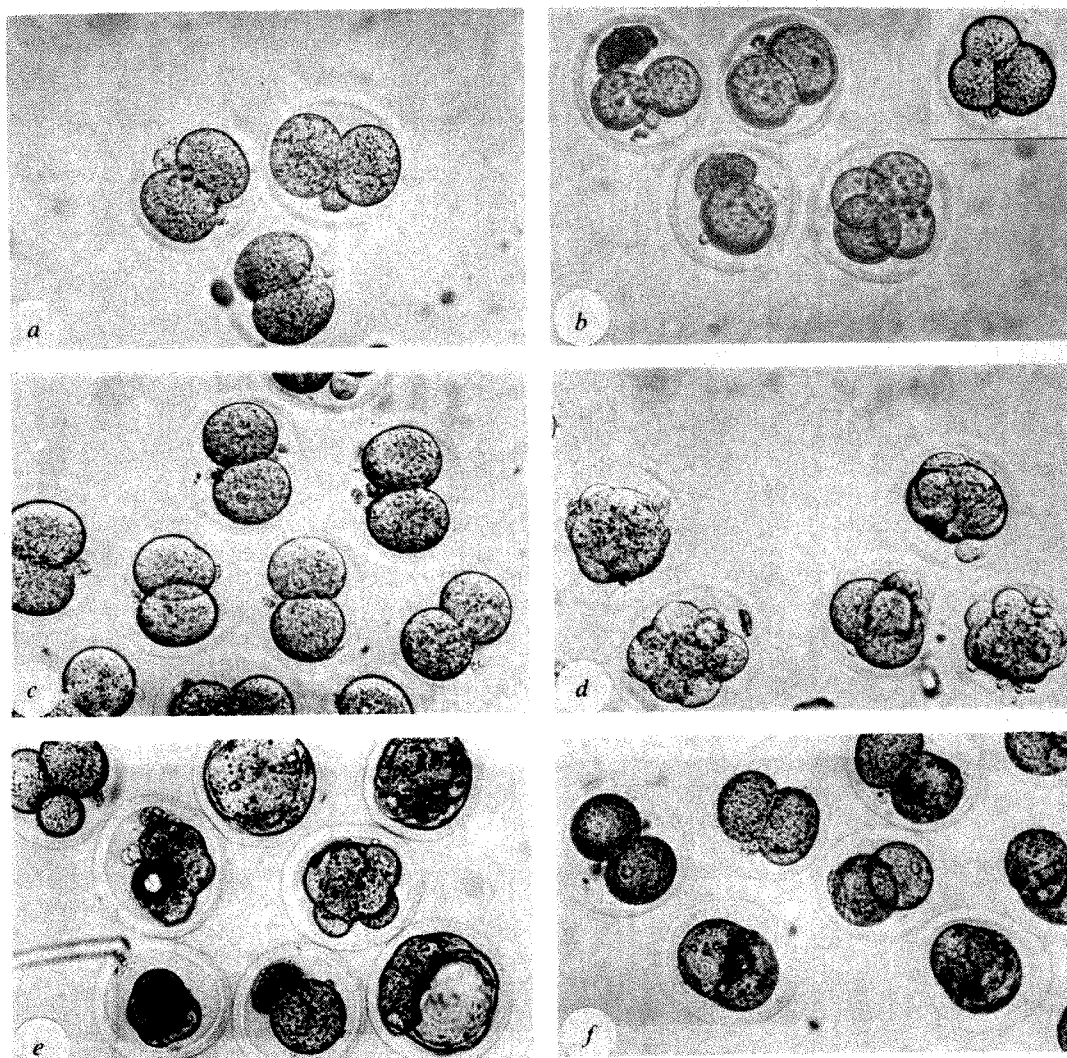


Table 2 *In vitro* development of one-cell MF1 eggs after injection at the two-cell stage with cytoplasm from two-cell stage eggs

Source of cytoplasm	No. of 2-cell eggs injected	No. surviving (%)	Developmental stage after 24 h			Developmental stage reached during subsequent culture for 48 h					
			2-Cell	3-Cell	4-Cell	2-Cell	3-Cell	4-Cell	8-Cell	Morula	Blastocyst
F ₁ hybrid	72	42 (58)	9	8	25	9	2	1	—	13	17
MF1	24	18 (75)	10	6	2	10	6	2	—	—	—
Uninjected controls											
	No. of 1-cell eggs										
MF1	92		79	—	13	79	—	12	—	—	1
F ₁	73		1	—	72	1	—	4	5	4	59

Development *in vitro* of fertilized one-cell MF1 eggs when one of the blastomeres at the two-cell stage was injected with cytoplasm from either two-cell F₁ hybrid (C57BL/6×CBA/H) or two-cell MF1 embryos cultured from the one-cell stage. Both injected and uninjected eggs were grown from the one-cell stage *in vitro*.

the quantity of substance(s) injected is inadequate to overcome the block. Alternatively, new vital components may be present in the cytoplasm at the two-cell stage arising either by transcription from the embryonic genome^{12,13} or by synthesis from maternal messenger RNA¹⁴. Perhaps these processes are not fully initiated during the culture of zygotes from certain strains.

The differences between *in vitro* development of one-cell eggs from various strains may have a genetic basis. Subtle differences in the amount of stored maternal mRNA, the activity of enzymes, the activity of the mitochondria and the structure and permeability characteristics of the egg plasma membrane may all contribute to the successful development of the one-cell embryo *in vitro*. Higher levels of ATP have been found in F₁ hybrid two-cell eggs grown from the one-cell stage *in vitro* compared with similar eggs from a randomly bred

strain¹⁵. Regulation of expression from the embryonic genome may well be controlled by factors in the egg cytoplasm and further studies with nuclear transfers might solve this problem.

Whatever the reasons for the inability of some one-cell mouse embryos to complete preimplantation development *in vitro*, the evidence so far shows that special environmental conditions are required to obtain early development *in vitro*, and these are still unknown for the eggs and embryos of most mammals. Until techniques are available for direct studies of mammalian eggs and embryos *in vivo*, our knowledge of the requirements of these early stages of development depends on biochemical analysis of eggs, embryos and oviduct secretions.

A.M.-H. was supported by USPHS grants 1R01 EY-02523-03 and 1R01 AGO-1212-03.

Received 8 June; accepted 16 August 1982.

- Whittingham, D. G. in *The Early Development of Mammals* (eds Balls, M. & Wild, A. E.) 1–24 (Cambridge University Press, London, 1975).
- Whittingham, D. G. *Br. med. Bull.* **35**, 105–111 (1979).
- Whitten, W. K. & Biggers, J. D. *J. Reprod. Fert.* **17**, 399–401 (1968).
- Hoppe, P. C. & Pitts, S. *Biol. Reprod.* **8**, 420–426 (1973).
- Biggers, J. D. in *The Biology of the Blastocyst* (ed. Blandau, R. J.) 319–327 (University of Chicago Press, 1971).
- Shire, J. G. M. & Whitten, W. K. *Biol. Reprod.* **23**, 369–376 (1980).

- Whittingham, D. G. & Biggers, J. D. *Nature* **213**, 942–943 (1967).
- Fulton, B. & Whittingham, D. G. *Nature* **272**, 149–151 (1978).
- Whittingham, D. G. *J. Reprod. Fert. Suppl.* **14**, 7–21 (1971).
- Siracusa, G., Whittingham, D. G. & De Felici, M. *J. Embryol. exp. Morph.* **60**, 71–82 (1980).
- Lo, C. W. & Gilula, N. B. *Cell* **18**, 399–409 (1979).
- Young, R. J., Sweeney, K. & Bedford, J. M. *J. Embryol. exp. Morph.* **44**, 133–148 (1978).
- Levey, I. L., Stull, G. B. & Brinster, R. L. *Dev. Biol.* **64**, 140–148 (1978).
- Clegg, K. B. & Piko, L. *Nature* **295**, 342–345 (1982).
- Quinn, P. & Wales, R. G. *J. Reprod. Fert.* **35**, 301–309 (1973).

Rearrangement of mammalian chromatin structure following excision repair

Miriam E. Zolan, Charles Allen Smith, Noel M. Calvin & Philip C. Hanawalt

Department of Biological Sciences, Stanford University, Stanford, California 94305, USA

Repair of DNA damage in eukaryotic cells involves local disruption of chromatin structure such that repair-incorporated nucleotides are transiently highly sensitive to digestion by staphylococcal nuclease (SN)^{1–4}. We have examined the dependence of this phenomenon on the initial distribution in chromatin of DNA damage by comparing the repair of pyrimidine dimers, which are distributed randomly in chromatin⁵, with the repair of angelicin photoadducts, which are formed primarily in linker regions of nucleosomes^{6,7}. We find that the transient nuclease sensitivity of repair patches is independent of the initial distribution of DNA damage in chromatin. In addition, our observation that repair patches produced in response to a linker-specific damaging agent become distributed randomly in chromatin implies that nucleosome cores do not necessarily return to their original sites along a DNA strand after the DNA is repaired.

It has been shown that the stretches of new DNA synthesis produced by excision repair in mammalian cells in response to 254 nm UV light or to chemicals that produce DNA damage fairly randomly in chromatin are initially more sensitive to digestion by the enzyme SN than is the bulk DNA, and that this enhanced sensitivity disappears within a few hours^{1–4}. It was originally thought that repair could only be initiated in the linker regions between nucleosome cores, and that nucleosome sliding eventually randomized the positions of repair patches

with respect to core structures¹. Remaining lesions would be moved concomitantly from core to linker regions, where they would be susceptible to repair. The realization that although nucleosome linkers are SN-sensitive, not all SN-sensitive DNA is necessarily linker, has led to the hypothesis that the initial SN sensitivity is due to a loss of native nucleosome structure at sites undergoing repair and that complete restoration of such structures requires several hours^{3,4}. In cases where the damaged sites are nearly random in the chromatin, such restoration of nucleosome cores exactly to their original positions along the DNA would eventually cause repair patches to exhibit the SN sensitivity of bulk DNA.

We have tested this hypothesis more rigorously by taking advantage of the unusual properties of the furocoumarins as DNA-damaging agents. These are conjugated tricyclic compounds which intercalate into DNA and can form covalent adducts to pyrimidines when activated by 360 nm light (UVA). The psoralen furocoumarins have their rings in a linear configuration and can form both monoadducts and bifunctional adducts that cross-link the DNA strands. Other furocoumarins, such as angelicin, have rings in an angular configuration and form only monoadducts in the conditions we have used^{8,9}. It seems that most, if not all, psoralen adducts are formed in linker regions of chromatin^{6,7}. In contrast, the pyrimidine dimers formed after UV irradiation of cells are distributed nearly randomly in chromatin^{5,10}.

To confine the present study to the repair of monoadducts so as to avoid the possible complications of interpreting results in cells containing both monoadducts and cross-links, we have used the furocoumarin angelicin. Although we expected that, like other furocoumarin adducts, those of angelicin would be formed predominantly in SN-sensitive regions of chromatin, we examined this directly. We observed that, in contrast to pyrimidine dimers, angelicin adducts in chromatin were

released by SN with kinetics consistent with their being primarily in SN-sensitive linker DNA (Fig. 1).

We compared the repair of angelicin adducts with that of pyrimidine dimers in human cell line T98G (refs 9, 11) to determine how the distribution of DNA damage in chromatin affects repair replication. The time course for repair synthesis is the same after UV damage as after treatment of cells with angelicin and UVA (Fig. 2). Thus, damage in linker DNA is apparently recognized and repaired with the same kinetics as damage that is randomly distributed in chromatin. This result has also been obtained with human diploid fibroblasts⁹ and African green monkey kidney cells¹².

We also examined the SN sensitivity of DNA synthesized during excision repair of UV or angelicin damage. In both cases, the repair patches were initially more sensitive than the bulk chromatin, and this difference was considerably reduced after a further 24 h incubation of the cells (Fig. 3).

The measurement of the relative amounts of radioisotope incorporated by semi-conservative replication and by repair synthesis is important for interpretation of these data. Even though our experiments were performed on confluent, contact-inhibited cultures, some radioactive precursor was incorporated

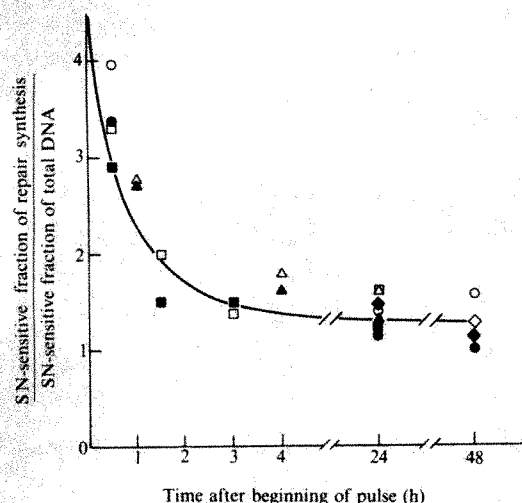


Fig. 1 Sensitivity of angelicin adducts or pyrimidine dimers in chromatin to digestion by SN. Cells were grown for 15 h in ^3H -deoxythymidine ($10 \mu\text{g ml}^{-1}$) and treated with $25 \mu\text{g ml}^{-1}$ angelicin and 7.5 kJ m^{-2} UVA. Nuclei were prepared and either digested with SN as described in Fig. 3 legend, or held on ice. After aliquots had been removed for determination of the extent of digestion, the nuclei were lysed and treated with proteinase K. DNA was extracted with phenol and then chloroform/isoamyl alcohol and precipitated with ethanol. A portion of the purified DNA from nuclei not digested with SN was then treated with SN, the extent of digestion analysed as before and the DNA repurified as above. For analysis of adduct frequencies, the DNAs were digested to mononucleotides with a mixture of DNase II and spleen phosphodiesterase. These digests were analysed by electrophoresis through $0.3 \times 10 \text{ cm}$ tube gels of 30% acrylamide/3% bis-acrylamide, in a continuous-flow collection apparatus. Samples collected from the bottom of the gel were assayed for radioactivity by scintillation spectrometry. The positions of angelicin adducts were determined from experiments with ^3H -labelled angelicin and pure DNA labelled with either ^{32}P or with ^{14}C -thymine. These experiments showed that nearly all adducts were to thymine, which allowed us to calculate adduct frequencies as the fraction of radioactivity loaded onto the gel that appeared in these positions. The per cent adducts remaining was calculated from these frequencies and the fraction of DNA digested. Random distribution of adducts in chromatin would yield the theoretical result shown by the dashed line. ●, Digestion of nuclei from angelicin-treated cells. ○, Digestion of purified DNA from nuclei not treated with SN. For pyrimidine dimers (x), cells were grown in ^3H -deoxythymidine and irradiated with 10 J m^{-2} UV. Nuclei were prepared and digested with SN, then lysed, treated with proteinase K and the DNA was centrifuged through a neutral sucrose gradient in an SW60 rotor in conditions that placed a 175-base pair marker DNA in the centre of the tube. The profile obtained by assaying total radioactivity in aliquots of the fractions allowed both the calculation of the fraction of DNA digested and isolation of the undigested DNA, which was further purified by centrifugation in CsCl gradients. A sample of DNA from nuclei not digested with SN was also prepared by centrifugation in CsCl. The DNAs so obtained were analysed for pyrimidine dimer content by TLC after acid hydrolysis²². In these experiments, the actual adduct frequencies were roughly comparable; the conditions used produced about 25 pyrimidine dimers and about 50 angelicin adducts per 10^6 daltons DNA.

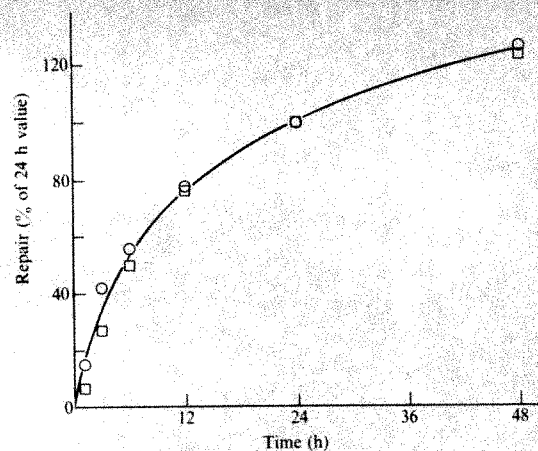


Fig. 2 Time course of the repair replication in T98G cells in response to 10 J m^{-2} UV (○) or $25 \mu\text{g ml}^{-1}$ angelicin and 7.5 kJ m^{-2} UVA (□). Treatment of cells was as in ref. 9 except that DNA-damaging treatments were done at 4°C . Repair synthesis was measured as described in ref. 23. In these conditions, the actual repair synthesis observed per unit DNA for angelicin was about 60% of that with UV.

into DNA synthesized by semi-conservative replication. The radioisotope so incorporated had the same SN sensitivity as bulk chromatin in these digestion conditions (ref. 13 and M.E.Z., unpublished observation). The amount of residual semi-conservative replication in a culture depends on the dose and type of damage, and the condition of the culture, which varied from experiment to experiment. In our experiments, DNA synthesis was always almost completely inhibited by the angelicin and UVA treatment used, but after 10 J m^{-2} UV as much as 30% of the isotope incorporated during a 30 min labelling period was in DNA made by semi-conservative replication. Thus, the apparent increase in the SN sensitivity of repair label relative to the prelabel was smaller after UV damage than after angelicin damage (Fig. 3). To compare experiments done at different times and using different damaging agents, it is necessary to normalize SN digestion data in a manner that corrects for the amount of isotope incorporated into DNA by semi-conservative synthesis. Such a method was developed by Smerdon and co-workers¹³. In their analysis, which has been discussed in detail^{4,13}, the ratio of the fraction of repair label that is SN-sensitive to the fraction of the total genome that is SN-sensitive is determined at various times after a short labelling period.

We analysed the data from several experiments by this method (Fig. 4). In each experiment, we measured directly the amounts of isotope incorporated by replication and repair; some of the cells were incubated with ^3H -bromodeoxyuridine and the DNA synthesized by semi-conservative replication was resolved from parental-density DNA containing repair patches by CsCl density gradient centrifugation as described in ref. 4.

Our analysis showed that the relative SN sensitivity of repair patches was initially high and decreased with time in the same manner after UV or angelicin damage (Fig. 4). The fact that the magnitude of the initial SN sensitivity of repair patches is about the same for repair of the two different adducts does not address the question of the cause of this increased nuclease sensitivity. It merely confirms the notion that all repair patches are initially nuclease-sensitive⁴, whether because they were initiated in linker DNA or because the repair process itself requires dissolution of normal nucleosome structure. However, our observation that the repair patches produced in response to angelicin damage become distributed nearly randomly in chromatin with time indicates that the final distribution of repair patches in chromatin is not the same as the initial, linker-specific distribution of this DNA damage. We have shown previously that the size of repair patches synthesized in response to angelicin and UV damage is about 25 nucleotides⁹, slightly smaller than the average size of nucleosome linkers in human cells¹⁴. A large fraction of the nucleotides in repair patches

made during repair of angelicin damage would remain in linker DNA (and would therefore be SN-sensitive) if nucleosomes re-formed at their original positions after DNA is repaired. However, as repair patches made in response to angelicin damage eventually exhibit the SN sensitivity characteristic of

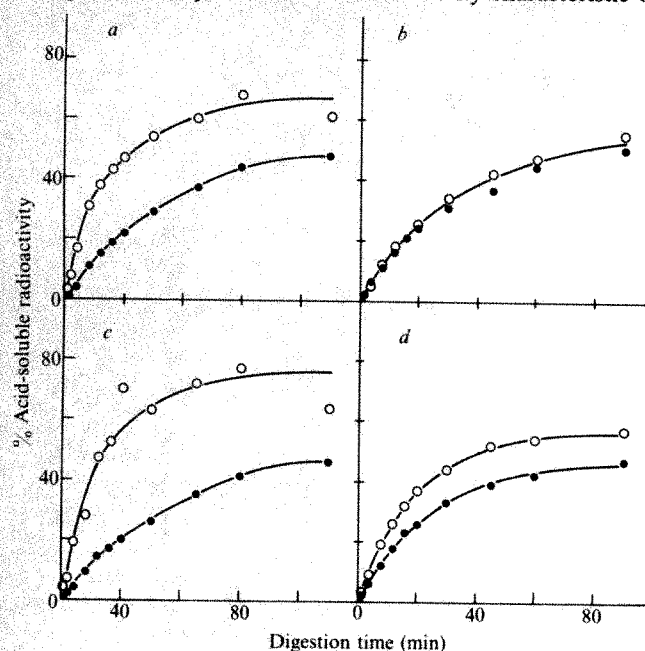


Fig. 3 Digestion of repair-labelled nuclei with SN. T98G cells were treated with UV (a, b) or angelicin and UVA (c, d) as described in Fig. 1 legend and incubated at 37°C for 30 min in conditioned medium containing 10 $\mu\text{Ci ml}^{-1}$ ^3H -deoxythymidine (50 Ci mmol $^{-1}$; NEN). This medium was removed and nuclei were prepared immediately (a, c) or after the cells were incubated for 24 h in medium containing 100 μM non-radioactive deoxythymidine (b, d). To prepare nuclei, cells were first washed twice with 10 mM Tris, pH 8, 1 mM CaCl $_2$. To each dish was added 3 ml of this buffer and the dishes were held on ice for 20 min. The buffer was vigorously pipetted several times against the cell monolayer with a Pasteur pipette to release nuclei which were then pelleted by centrifugation at 2,000 r.p.m. for 10 min in an IEC universal centrifuge. The pellet was washed twice in 10 mM Tris, pH 8, 1 mM CaCl $_2$, 0.25 M sucrose, and resuspended in this buffer at a concentration equivalent to 180 $\mu\text{g ml}^{-1}$ DNA. Samples were incubated at 37°C for 5 min and SN (Millipore) was added to 8 U ml $^{-1}$. At the times shown, 0.1-ml samples were taken and added to an equal volume of ice-cold 2 M NaCl, 2 M perchloric acid 24 . After 10 min on ice, samples were centrifuged for 5 min in a Beckman microfuge B, and 0.15 ml of each supernatant was assayed for radioactivity in 1 ml H $_2\text{O}$ plus 10 ml of a 1:2 mixture of Triton/Omnifluor (NEN). Aliquots of undigested nuclei were assayed for total radioactivity incorporated as described in ref. 13. \circ , ^3H repair label; \bullet , ^{32}P prelabel.

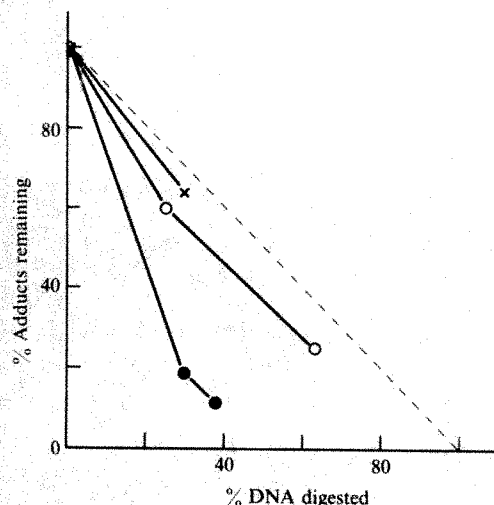


Fig. 4 Change with time of the enhanced SN sensitivity of repair patches synthesized in the first 30 min after treatment of cells with UV (solid symbols) or angelicin and UVA (open symbols). Different symbols represent different experiments. The analysis used was that described by Smerdon *et al.* 13 , except that we measured the relative amounts of radioactivity incorporated by semi-conservative replication and repair as described in the text. The experimental details are described in Fig. 3 legend.

a random distribution in chromatin, we conclude that nucleosome cores do not obligatorily re-form at their original positions after DNA is repaired. Our observations support models of random location of nucleosomes with respect to DNA sequences $^{15-17}$, but they are not sensitive enough to rule out the possibility that nucleosome cores do occupy preferred sites in some regions of the genome $^{18-21}$.

We thank M. Ashwood-Smith for the generous gift of pure angelicin, T. Tlsty and M. Smerdon for helpful discussions concerning the techniques used, M. Defais and D. Okumoto for technical assistance, and M. Philippe, J. Palmer and A. K. Ganesan for reading the manuscript. This work was supported by American Cancer Society grant NP161F, a contract with the US Dept of Energy (DE-AT03-76EV70007) and by National Research Service Award GMO7276 to M.E.Z. for predoctoral training.

Received 12 November 1981; accepted 26 July 1982.

1. Smerdon, M. J. & Lieberman, M. W. *Proc. natn. Acad. Sci. U.S.A.* **75**, 4238-4241 (1978).
2. Bodell, W. J. & Cleaver, J. E. *Nucleic Acids Res.* **9**, 203-212 (1981).
3. Oleson, F. B., Mitchell, B. L., Dipple, A. & Lieberman, M. W. *Nucleic Acids Res.* **7**, 1343-1361 (1979).
4. Lieberman, M. W., Smerdon, M. J., Tlsty, T. D. & Oleson, F. B. in *Environmental Carcinogenesis* (eds Emmelot, P. & Kriek, E.) 345-363 (Elsevier, Amsterdam, 1979).
5. Williams, J. I. & Friedberg, E. C. *Biochemistry* **18**, 3965-3972 (1979).
6. Wiesenbahn, G. P., Hyde, J. E. & Hearst, J. E. *Biochemistry* **16**, 925-932 (1979).
7. Cech, T. & Pardue, M. L. *Cell* **11**, 631-640 (1977).
8. Dall'Acqua, F., Marciani, S., Ciavatta, L. & Rodighiero, G. *Z. Naturf.* **26b**, 561-569 (1971).
9. Kaye, J., Smith, C. A. & Hanawalt, P. C. *Cancer Res.* **40**, 696-702 (1980).
10. Niggli, H. J. & Cerutti, P. A. *Biochem. biophys. Res. Commun.* **105**, 1215-1223 (1982).
11. Stein, G. H. *J. cell. Physiol.* **99**, 43-54 (1979).
12. Zolan, M. E., Cortopassi, G. A., Smith, C. A. & Hanawalt, P. C. *Cell* **28**, 613-619 (1982).
13. Smerdon, M. J., Tlsty, T. D. & Lieberman, M. W. *Biochemistry* **17**, 2377-2386 (1978).
14. Kornberg, R. D. A. *Rev. Biochem.* **46**, 931-954 (1977).
15. Baer, B. W. & Kornberg, R. D. *J. biol. Chem.* **254**, 9678-9681 (1979).
16. Prunell, A. in *Chromatin Structure and Function* (ed. Nicolini, C.) 441-449 (Plenum, New York, 1979).
17. Nelson, P. P., Albright, S. C. & Garrad, W. T. *J. biol. Chem.* **254**, 9194-9199 (1979).
18. Louis, C., Schedl, P., Samal, B. & Worcel, A. *Cell* **22**, 387-392 (1980).
19. Wittig, B. & Wittig, S. *Cell* **18**, 1173-1183 (1979).
20. Gottesfeld, J. M. & Bloomer, L. S. *Cell* **21**, 751-760 (1980).
21. Igo-Kemenes, T., Omori, A. & Zachau, H. G. *Nucleic Acids Res.* **8**, 5377-5390 (1980).
22. Cook, K. H. & Friedberg, E. C. *Analyt. Biochem.* **73**, 411-418 (1976).
23. Smith, C. A., Cooper, P. K. & Hanawalt, P. C. in *DNA Repair: A Laboratory Manual of Research Procedures* Vol. 1 (eds Friedberg, E. C. & Hanawalt, P. C.) 289-305 (Dekker, New York, 1981).
24. Axel, R. *Biochemistry* **14**, 2921-2925 (1975).

Selective reinnervation of adult mammalian muscle by axons from different segmental levels

Donald J. Wigston & Joshua R. Sanes

Department of Physiology and Biophysics, Washington University School of Medicine, St Louis, Missouri 63110, USA

The ability of axons to innervate selectively subsets of a population of largely similar target cells is undoubtedly important for the establishment of ordered patterns of neural connections. Vertebrate skeletal muscle is well suited for studies of factors that account for selective synapse formation as a wealth of information is available about the structure, function and molecular components of its neuromuscular junctions. Furthermore, skeletal muscle is readily reinnervated following nerve damage, permitting study of synaptogenesis in an accessible postembryonic environment. However, although selective synapse formation clearly occurs elsewhere in the adult peripheral nervous system $^{1-10}$, previous attempts to demonstrate selectivity in the reinnervation of mammalian muscles have been disappointing $^{7-15}$. We have now used a novel approach to reinvestigate this issue, and describe here a situation in which two different adult rat muscles are preferentially reinnervated by axons from different spinal segments. Our results suggest that adult muscles differ in some stable quality, perhaps related to their position, which influences the innervation they accept.

Our approach was based on studies of the segmental innervation of sympathetic ganglion cells by autonomic preganglionic axons. The cervical sympathetic trunk, which innervates the

superior cervical ganglion (SCG; Fig. 1), contains populations of preganglionic axons that arise from several segments of the spinal cord^{1-3,16}; axons from each segment can be stimulated separately via the appropriate ventral root¹⁷. Preganglionic axons from different segments preferentially reinnervate different classes of neurones in the SCG^{1,2,7}. In particular, Purves *et al.*³ have shown that ganglia transplanted from the fifth thoracic (T5) level to the neck are reinnervated by a more caudal subset of cervical trunk axons than are reimplanted SCGs. Thus, ganglia from different levels may differ in some quality that biases synapse formation. As sympathetic preganglionic axons can be made to innervate skeletal muscle¹⁸⁻²⁰, and muscles survive free grafting²¹, we were able to investigate whether muscles from different segments are also differentially reinnervated by subpopulations of preganglionic axons.

The muscles we used, the external intercostals, are a set of 12 similar muscles in the thorax, each of which joins two adjacent ribs and is innervated by axons from the corresponding spinal segment²². Pieces of external intercostal muscle were transplanted from either the second (T2) or the eighth (T8) thoracic interspace to the neck of the same rat; the SCG was removed and the proximal cut end of the cervical trunk attached to the implant (Fig. 1). Two to fourteen weeks later, the transplanted muscle, cervical trunk, sympathetic chain and ventral roots were dissected in continuity and mounted in a bath^{2,3}. Individual ventral roots were stimulated with suction electrodes and synaptic potentials were recorded intracellularly from

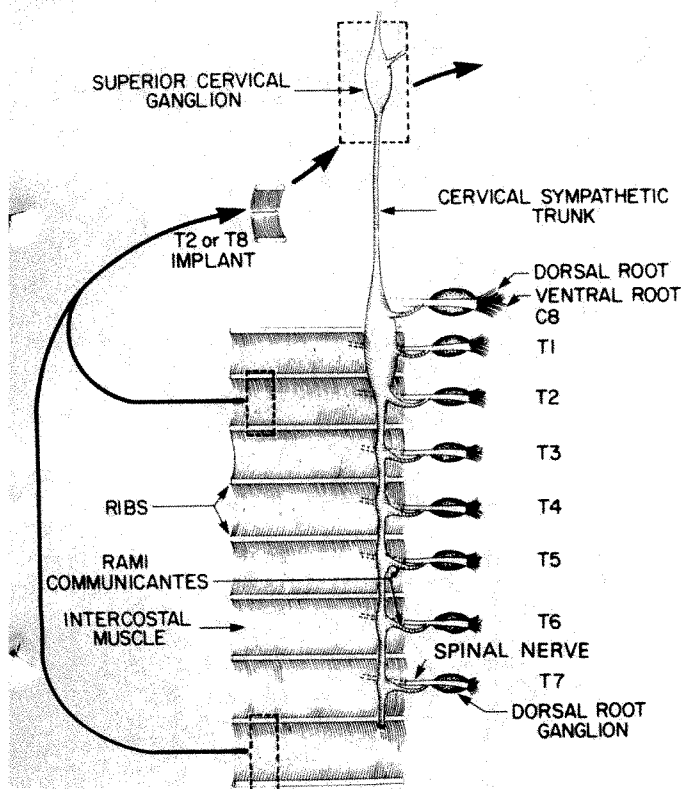


Fig. 1 External intercostal muscles from the second (T2) or eighth (T8) thoracic level were transplanted to the neck where they were reinnervated by axons of the cervical sympathetic trunk. Adult, male rats (Sprague-Dawley; 150–200 g) were anaesthetized with chloral hydrate, and a 2–3 mm wide piece of either the T2 (with second and third ribs attached) or the T8 (with eighth and ninth ribs) intercostal muscle removed. The internal intercostal muscle was peeled away, leaving a sheet of predominantly intact external intercostal muscle fibres attached to ribs at both ends. An incision was then made in the neck and the SCG removed. The external intercostal muscle was sutured by its ribs to the superficial surface of the omohyoid muscle and the cut end of the sympathetic trunk pulled through a small hole near the edge of the implant. For simplicity, muscle and nerve are shown on the same side; in reality, muscle was taken from the left side and transplanted to the right, to avoid inadvertent damage to the sympathetic trunk or ventral roots. Drawing not to scale.

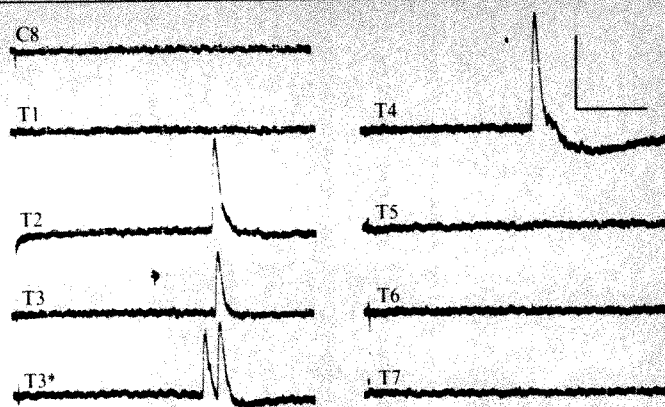


Fig. 2 Synaptic potentials recorded intracellularly from a single fibre in a transplanted intercostal muscle on stimulation of the indicated ventral root. The transplanted muscle, thoracic sympathetic chain, communicating rami and ventral roots were mounted in a bath and superfused with oxygenated Ringer's^{2,3}. The muscle was pinned beyond resting length to minimize its movement. A KCl-filled microelectrode was moved across the implant in small, roughly equal steps, to sample fibres throughout the muscle. For each muscle fibre impaled that had a resting potential of greater than 50 mV (range 50–90 mV) ventral roots C8 to T7 were stimulated in turn with suction electrodes (0.5 ms pulses of ± 5 –50 V at 0.5 Hz). When a response was seen, the strength of the stimulating current was varied to discern multiple inputs from a single ventral root. Reinnervation of the transplanted muscles was often patchy, with nearly all fibres innervated in some areas, and other large areas not innervated at all. However, all muscles tested were reinnervated, and none was excluded on grounds of poor reinnervation. On average, 29 innervated fibres (maximum 35) were studied per muscle. Fibres were generally impaled mid-way along their length, near where the nerve had been implanted, but no other attempt was made to record from near synaptic sites; therefore, synaptic potentials must have been variably attenuated by passive decay. The smallest synaptic potentials we could reliably detect were about 1 mV. Forty-two per cent of unitary inputs were suprathreshold, and gave rise to action potentials. An average of 1.9 inputs (range 1–6) was detected per innervated fibre and 60% of innervated fibres ($n = 941$) received 2 or more inputs. In the fibre illustrated, we recorded four inputs, all of which were subthreshold: one each from T2 and T4 ventral roots, two from T3 (stimulus strength was increased between traces marked T3 and T3*) and none from C8, T1, or T5–7. Calibration bars, 5 mV (vertical) and 50 ms (horizontal).

muscle fibres in the transplant. We thereby compared the segmental origin of inputs to the transplanted T2 and T8 intercostal muscles.

Muscle fibres in both T2 and T8 transplants were reinnervated, often polyneuronally, within 2 weeks (Fig. 2). Figure 3a summarizes the segmental origin of 1,410 inputs to 688 fibres from 11 T2 and 12 T8 muscles studied 2–4 weeks after transplantation. Transplanted T2 and T8 muscles differed in the pattern of the innervation they received: T2 muscles were innervated more effectively by axons from rostral segments, and T8 muscles by axons from caudal segments. Similar results were obtained from muscles examined 10–14 weeks after transplantation (Fig. 3b); thus, neither the existence nor the magnitude of the difference between T2 and T8 muscles is peculiar to an early stage of reinnervation. The ratio of inputs recorded from T2 muscles to inputs recorded from T8 muscle varied progressively from segment to segment (Fig. 3c). Thus, there is a systematic caudal shift in the innervation of T8 compared with T2 muscles.

Because the difference between groups of T2 and T8 transplants was small, it was important to show that the segmental distribution of inputs we observed was a consistent property of individual muscles. We therefore calculated an index of the overall segmental innervation of each transplanted muscle. This index provides a single value equivalent to the average segment of origin of all synaptic inputs recorded; thus, the more caudal the subset of axons that reinnervated a muscle, the higher its

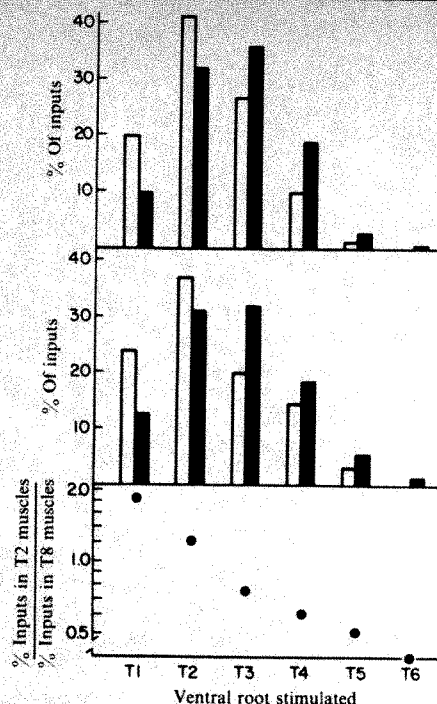


Fig. 3 Reinnervation of transplanted T2 and T8 external intercostal muscles by axons arising from different spinal segments. *a, b*, Per cent of all synaptic inputs recorded from T2 (open bars) or T8 (dark bars) transplants that were evoked by stimulation of the indicated ventral root. *a*, 2–4 weeks after transplantation: 789 inputs recorded from 346 fibres in 11 T2 muscles studied 14–22 days (average 19) after surgery, and 621 inputs from 342 fibres in 12 T8 muscles studied 15–26 days (average 20) after surgery. *b*, 10–14 weeks after transplantation: 235 inputs recorded from 110 fibres in 4 T2 muscles studied 67–97 days (average 79) after surgery, and 331 inputs from 143 fibres in 5 T8 muscles studied 74–96 days (average 80) after surgery. No inputs from C8 or T7 were detected. Segmental distribution of inputs to T2 and T8 muscles differ at $P < 0.001$ in both *a* and *b*, by χ^2 test. *c*, Ratio of inputs recorded from T2 muscle fibres to inputs recorded from T8 muscle fibres, calculated for each segment from the combined data of *a* and *b*.

index of segmental innervation (see Fig. 4 legend). T2 and T8 muscles differed significantly by this index in both the 2–4 ($P < 0.005$) and the 10–14 ($P < 0.05$) week groups (Fig. 4). In 32 experiments, the 10 highest values were all obtained from T8 muscles, and 9 of the 10 lowest values from T2 muscles. Thus, the difference between the innervation of T2 and T8 muscles is reasonably consistent from muscle to muscle.

Many of the synaptic potentials recorded from muscle fibres in the transplants exceeded threshold, initiated propagated action potentials and caused muscle contractions. Forty per cent of inputs to T2 transplants and 44% of inputs to T8 transplants were suprathreshold. An index of segmental innervation calculated using only action potentials showed a difference between T2 and T8 muscles equivalent to that seen when all inputs were considered (Table 1). The difference between T2 and T8 muscles was also demonstrated by visual estimates of the strength of contractions evoked by stimulating individual roots (Table 1). It is possible that the difference between T2 and T8 muscles is reflected in the strength as well as the number of their inputs. However, these results show that the selectivity we observed was neither limited to subthreshold inputs nor influenced by any possible failure to detect small synaptic potentials.

Two further experiments ruled out the possibility that the differential reinnervation of transplanted T2 and T8 muscles was attributable to differences in surgical procedure rather than to intrinsic differences between the muscles. First, in four animals, pieces of both T2 and T8 muscles were removed, but only the T8 muscle was reimplanted. The index of segmental innervation of these transplants (2.77 ± 0.07 ; mean \pm s.e.) was

Table 1 Average segmental innervation of transplanted T2 and T8 intercostal muscles

Measure of reinnervation	Intercostal muscle transplanted	
	T2 ($n = 15$)	T8 ($n = 17$)
All inputs	2.32 ± 0.06	$2.76 \pm 0.07^*$
Action potentials	2.24 ± 0.07	$2.79 \pm 0.12^*$
Strength of contractions	2.49 ± 0.08	$2.80 \pm 0.10^\dagger$

Average segmental innervation as judged by all inputs recorded intracellularly was calculated from data presented in Fig. 4. A similar index was calculated for only those inputs that exceeded threshold and gave rise to muscle action potentials. Strength of contractions evoked by single supramaximal stimuli delivered to each ventral root was estimated visually. Responses were rated from 0 (no twitch seen) to 4 (strongest twitch in a given muscle), and a segmental index calculated for each muscle. Differences between values for T2 and T8 muscles are significant at $P < 0.0005$ (*) or $P < 0.02$ (†) by Student's *t*-test.

indistinguishable from that of eight other T8 transplants (2.72 ± 0.14). (This comparison tests for effects of T2 removal; as can be appreciated from Fig. 1, inadvertent damage to relevant structures would have been far more likely to have resulted from removal of T2 than T8 muscles.) Second, the reinnervation of transplanted intercostal muscles was studied in a series of inbred rats (Wistar-Furth) in which one animal served as donor and another as host; again, the muscles of more rostral origin received stronger innervation from more rostral spinal segments (D.J.W. and J.R.S., in preparation).

The selective reinnervation of transplanted intercostals observed here contrasts with the apparently nonselective reinnervation of adult mammalian muscles in several other situations^{7–15}. However, several features of our experiments may

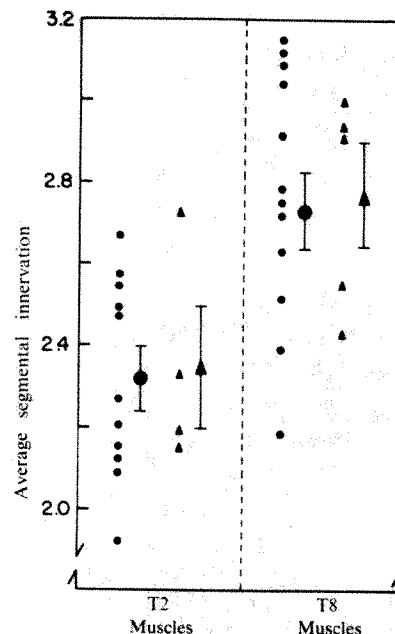


Fig. 4 The average segmental innervation of transplanted T2 and T8 intercostal muscles. This index is the segmentally weighted average of all synaptic inputs recorded from the fibres of a transplanted muscle. For example, a muscle in which we recorded 5 inputs from axons in the T1 ventral root, 20 from T2, 30 from T3, 10 from T4, 5 from T5 and 1 from T6 would be given a value of $(5)1 + (20)2 + (30)3 + (10)4 + (5)5 + (1)6 / 5 + 20 + 30 + 10 + 5 + 1 = 206/71 = 2.90$. Circles represent muscles studied 2–4 weeks after transplantation (see Fig. 3*a*) and triangles represent muscles studied 10–14 weeks after transplantation (see Fig. 3*b*). Small symbols show values for individual muscles, while large symbols show means (\pm s.e.) of groups. The average segmental innervation of the normal superior cervical ganglion, calculated from recordings made by J. Lichtman, is 2.5. Differences between T2 and T8 muscles are significant for both the 2–4 week group ($P < 0.005$) and the 10–14 week group ($P < 0.05$) by Student's *t*-test.

have favoured the detection of selectivity. First, by implanting a single nerve trunk, we ensured that all axons tested had equal and direct access to the target; our results do not depend on the presence or absence of cues on the pathway to the muscle. Second, by transplanting muscles instead of transposing nerves, we were able to compare the reinnervation of nonadjacent muscles. Third, each intercostal is distinct in the segment from which it originates and receives its normal innervation; in contrast, limb muscles used in previous experiments are innervated by^{12,15} and may originate from²³ overlapping sets of segments. Fourth, by comparing inputs from each of several sources (that is, segments) we were able to detect a subtle but systematic difference between the innervation of two muscles. Finally, it is known that preganglionic axons can selectively reinnervate different classes of sympathetic ganglion cells in adults¹⁻⁴; preganglionic axons may reveal differences between adult muscles that motor axons ignore.

We have shown that two adult rat muscles are differentially reinnervated by segmental subsets of a population of autonomic

axons. We conclude that adult muscles can be selectively reinnervated, and predict that T2 and T8 intercostal muscles bear different amounts or types of some factor(s) that contribute to selectivity in synapse formation. In addition, our results raise two possibilities that merit testing. First, the finding that skeletal muscles are selectively innervated by autonomic axons that they normally do not encounter suggests that this selectivity may be based on a recognition system that is widely distributed in the nervous system. Second, the observation that the more rostral of the two muscles we tested is reinnervated by a relatively rostral subset of axons suggests that the basis of the selection could be some positional quality that is shared by nerves and muscles.

We thank D. Purves for helpful contributions to this work, and B. Carlson, J. Lichtman, C. Rovainen and E. Rubin for advice. J.S. is a Sloan Fellow and an Established Investigator of the American Heart Association. D.W. was a Postdoctoral Fellow of the Muscular Dystrophy Association (MDA). This work was supported by MDA and NSF grants.

Received 16 June; accepted 28 July 1982.

1. Langley, J. N. *J. Physiol., Lond.* **18**, 280-284 (1895).
2. Nja, A. & Purves, D. *J. Physiol., Lond.* **272**, 633-651 (1977).
3. Purves, D., Thompson, W. & Yip, J. W. *J. Physiol., Lond.* **313**, 49-63 (1981).
4. Feldman, D. *Neurosci. Abstr.* **5**, 625 (1979).
5. Landmesser, L. & Pilar, G. *J. Physiol., Lond.* **211**, 203-216 (1970).
6. Schmidt, H. & Stefani, E. *J. Physiol., Lond.* **258**, 99-123 (1976).
7. Purves, D. in *Studies in Developmental Neurobiology* (ed. Cowan, W. M.) (Oxford University Press, 1981).
8. Landmesser, L. *A. Rev. Neurosci.* **3**, 279-302 (1980).
9. Mark, R. F. *Physiol. Rev.* **60**, 355-395 (1980).
10. Fambrough, D. M. in *Neuronal Recognition* (ed. Barondes, S. H.) 25-66 (Plenum, New York, 1976).

11. Weiss, P. & Hoag, A. *J. Neurophysiol.* **9**, 413-418 (1946).
12. Bernstein, J. J. & Guth, L. *Expl. Neurol.* **4**, 262-275 (1961).
13. Miledi, R. & Stefani, E. *Nature* **222**, 569-571 (1969).
14. Gerding, R., Robbins, N. & Antosiak, J. *Dev. Biol.* **61**, 177-183 (1977).
15. Brushart, T. M. & Mesulam, M.-M. *Science* **208**, 603-605 (1980).
16. Rando, T. A., Bowers, C. W. & Zigmond, R. E. *J. comp. Neurol.* **196**, 73-83 (1981).
17. Rubin, E. & Purves, D. *J. comp. Neurol.* **192**, 163-174 (1980).
18. Langley, J. N. & Anderson, H. K. *J. Physiol., Lond.* **31**, 365-391 (1904).
19. Hillarp, N.-A. *Acta anat. Suppl.* **4**(1), 1-153 (1946).
20. Bennett, M. R., McLachlan, E. M. & Taylor, R. S. *J. Physiol., Lond.* **233**, 501-517 (1973).
21. Carlson, B. M. *Physiologia bohemoslov.* **27**, 387-400 (1978).
22. Grobstein, C.A. thesis, Univ. Chicago (1980).
23. Chevallier, A. *J. Embryol. exp. Morph.* **49**, 73-88 (1979).

Structural evidence that myosin heads may interact with two sites on F-actin

L. A. Amos*, H. E. Huxley*, K. C. Holmes†, R. S. Goody† & K. A. Taylor‡

*MRC Laboratory of Molecular Biology, Cambridge CB2 2QH, UK
†Max-Planck-Institut für Medizinische Forschung, 6900 Heidelberg, FRG 1

‡Department of Anatomy, Duke University Medical Center, Durham, North Carolina 27710, USA

Analysis of the rigor complex of muscle thin filaments decorated with myosin subfragment-1 (S-1) by three-dimensional image reconstruction from electron micrographs¹ shows S-1 to be a comma-shaped molecule, the broad head of which interacts with F-actin near the groove between the two strands of actin monomers. Increased resolution near the filament axis has allowed us to distinguish separate components more reliably than in an earlier analysis². Using X-ray diffraction data from striated muscle decorated with S-1 molecules³ as a reference, we have now refined the electron microscope data to show the interaction in more detail. We show here that individual S-1 molecules apparently interact with both strands of a filament, straddling the regulatory protein tropomyosin in the long-pitch groove. This double-sided interaction agrees with chemical cross-linking data⁴ and suggests some interesting possibilities for cross-bridge cycling in muscle.

Optical diffraction patterns from electron microscope (EM) images of different filaments show variation in the positions of intensity peaks along the layer lines, presumably because of distortions induced during staining and dehydration. For example, the radial positions of the strongest peaks on the '1st' and '6th' layer lines ranged from 0.055 nm⁻¹ to 0.080 nm⁻¹ and from 0.035 nm⁻¹ to 0.065 nm⁻¹, respectively, even for our five 'best' images of S-1 decorated thin filaments¹. Originally, a simple average of these data gave peaks centred at 0.0685 nm⁻¹ and 0.0442 nm⁻¹ respectively¹. X-ray diffraction data³ now show the radial positions for hydrated specimens to be 0.060 nm⁻¹ and 0.040 nm⁻¹. Our new average includes only those sets of EM data that closely resemble the X-ray data (Fig. 1). Because of the narrower range of variation, the finer features of the averaged image should be less smeared.

The main peaks of density (Fig. 2, shaded regions) are very similar to those in the original averaged image¹. A division of each actin monomer into two domains (Fig. 3, Aa, Ab), detectable in the earlier image, is now more obvious. The curved end of the S-1 'tail' is somewhat strengthened in density and, finally, a connection between S-1 and an actin monomer on the opposite strand from the main interaction can be seen. The latter was detectable in individual reconstructed images of S-1 decorated thin filaments¹ and also in the averaged image of S-1 decorated pure actin filaments¹. However, being absent from the averaged decorated thin filament image, its significance was previously uncertain. It is not apparent in the reconstructed images of other workers^{5,6} but their specimens appear to have suffered worse distortions than most of ours, as the peaks on the 1st and 6th layer lines are at 0.075-0.100 nm⁻¹ and 0.057-0.080 nm⁻¹ respectively. We attribute the unusual preservation of our best filaments to the method of specimen preparation¹; where distortions are minimized by supporting the filaments on holey carbon, the stain films over holes being stabilized by a final light shadowing of carbon. Minimal dose imaging methods help to avoid stain granulation.

The interaction between S-1 and actin in the rigor state thus seems to involve two independent contacts, in agreement with results obtained by carbodiimide cross-linking of the rigor complex⁴ which indicate that independent regions of the 95,000 molecular weight (MW) heavy chain of S-1 contact two adjacent actin monomers. The most extensive contact in our model (Fig. 3, no. 1) is between S-1 and a monomer on the left of the groove as shown. The weaker contact (Fig. 3, no. 2) is with the monomer just below on the opposite strand. Tropomyosin, although not resolved as a separate entity, appears to interact with S-1 in the fork between its two actin-binding sites. S-1 also has a downward-projecting prong, lying close to the putative tropomyosin position (Fig. 3, S-1c), which may have interfaces with one or both of the next two monomers below. An S-1 molecule bound to four actin monomers could explain a 265,000 MW cross-linked complex sometimes found with the main 170,000 MW complex of one S-1 plus two actin molecules⁴. The latter authors' suggestion that the larger complex consists of two S-1 and two actin monomers seems unsatisfactory as two S-1s cannot bind symmetrically to two actin monomers, because of their staggered polar arrangement (Fig. 3).

The structure analysed represents the rigor state, which has been assumed to correspond to the 'end' of an active stroke. However, X-ray scattering data from S-1 in solution is consistent with this shape, suggesting that the conformation on first binding to actin may also be similar⁷. Nothing is known about conformations at intermediate stages of the cycle; these could be quite different. The apparent existence of two or more independent sites of contact between S-1 and F-actin in the rigor state suggests that the interaction during an active stroke might involve a cycle of different S-1 binding configurations.

Extensive movements are required somewhere in the myosin molecule during muscle contraction. According to the estimates of Huxley and Simmons⁸, each active cross-bridge stroke involves an axial shift of 10 to 12 nm, the distance between one actin monomer and the next but one on the same strand. Probably much of the movement occurs within S-1. The myosin head seems to us a more likely location for primary power generating conformational changes than parts of the molecule

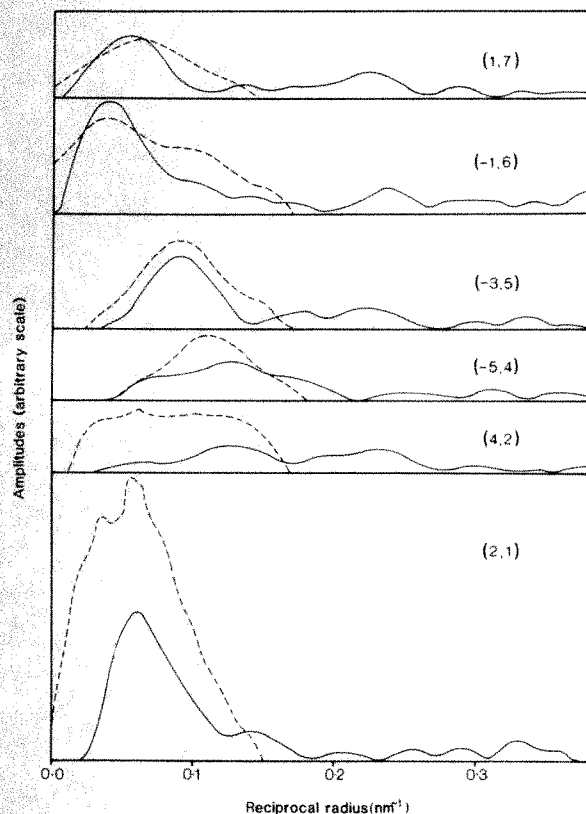


Fig. 1 Layer line amplitudes. The numbers in brackets are n (the Bessel order) and l (the layer line number, based on an axial repeat of $1/39 \text{ nm}^{-1}$ (see ref. 1)). The dashed lines were derived from X-ray diffraction data for insect muscle decorated with papain-cleaved S-1 (ref. 3), the 1st and 2nd layer lines having been folded with a gaussian to remove the Bragg reflections. Data for crab muscle decorated with chymotryptic S-1 are very similar. The solid lines show a new average from EM data derived from nine sides (near and far sides of a helical structure provide nearly independent information in the diffraction pattern¹⁶), including three not used in the original average (ref. 1, Fig. 4). The distribution of peaks remains similar, but there are slight shifts in the positions of the peaks. The corresponding phase changes are also quite subtle. The main differences from the X-ray amplitudes are in the heights and shapes of the peaks on the 1st and 2nd layer lines. If they were weighted up, the main effect would be a strengthening of the tail part of the S-1 molecule. Possibly, the EM reflections are weaker than they should be, owing to disorder at the outermost radii. The additional near-meridional intensities on the X-ray 1st and 2nd layer lines would contribute beyond the radial limits of the EM model. Their presence may reflect some interaction between the S-1 tails and the lattice of thick filaments in the muscle. The equatorial layer line data (not shown) from filaments seen side-on in negative stain are unreliable; nor are these data available from the X-ray patterns because of thick filament interference. A mean radial density distribution for the reconstructed image was therefore calculated by averaging in real space from end-on views of cross-bridges bound to thin filaments. The latter were cut out from computer-filtered images of very thin transverse sections of insect flight muscle (K. A. T., M. K. Reedy and M. Reedy, unpublished data). The result is very similar to the curve deduced from the negatively stained images and used in the original image reconstructions¹.

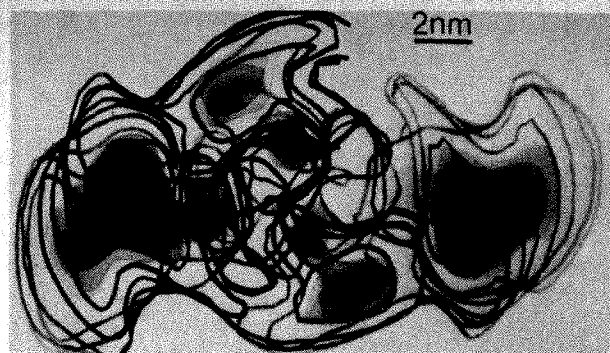


Fig. 2 Part of the three-dimensional reconstructed image, represented by contours drawn on a stack of Perspex sheets. The view is down the filament axis, looking towards the Z-band end. The segment shown includes two actin monomers plus two attached S-1 molecules. The shading indicates the regions of highest stain-excluding density within the reconstructed image. These regions are interpreted in terms of actin, myosin S-1 and tropomyosin as shown in Fig. 3. Actin and S-1 give quite distinct peaks in this view, but tropomyosin is not separately resolved, though its position can be inferred from other evidence¹.

which are distant from the ATP splitting site, or weak (protease sensitive) points such as the S-1/S-2 junction. Evidence from X-ray diffraction is compatible with substantial shape changes in S-1 (ref. 9). A range of different head shapes during contraction could explain the weakening of the actin-based symmetry compared with the rigor state, when a permanent double-sided attachment to actin would stabilize the head in the conformation observed in the EM.

As the regions of strongest density within the reconstructed S-1 structure fall into at least three separate domains (S-1a, S-1b, S-1c), any shape change may primarily involve alterations in angle of 'hinges' covalently connecting different domains, as in tomato bushy stunt virus coat protein where the domains seem relatively rigid¹⁰. There is evidence for one rigid domain at least in the S-1 molecule; Cooke¹¹ has found, using a paramagnetic probe, that the conformation and orientation of an actin-binding domain is unaltered when rigor muscle is stretched. However, other domains may change in internal conformation. So little is known about the structure of S-1 other than in rigor, that ideas on movements during contraction remain purely speculative.

Details of the calcium-regulated control at a molecular level are also unclear. In the active state, tropomyosin occupies a position near the middle of an actin groove^{2,12,13}. In the inhibited state it is probably towards one or other side of the groove^{13,14}, where it could interfere with the interaction between S-1 and actin at either of contact sites 1 or 2. Thus, simple steric blocking is still a possible mechanism. However, Chalovich and Eisenberg¹⁵ have found the association constant of S-1ATP and S-1ADP. P_i with regulated actin to be virtually the same in the

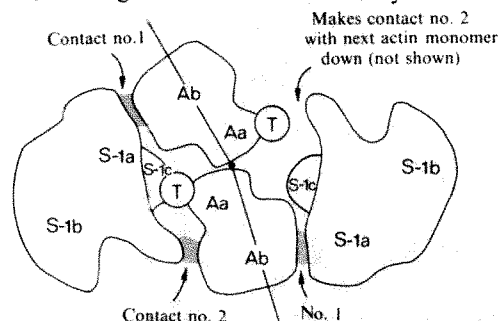


Fig. 3 Diagram of the proposed interactions in the rigor state, between myosin heads (S-1), actin monomers (A) in F-actin and tropomyosin molecules (T) which are thought to lie in the actin helix grooves. Independent sites on S-1 contact two neighbouring actin monomers and there is close contact between S-1 and tropomyosin¹ that may account for the stronger binding of S-1 to regulated than to unregulated actin¹⁷. Each actin monomer consists of two stain-excluding domains, in agreement with other data (for example, ref. 18), S-1 of three such domains. The shape shown here for S-1 gives even better agreement with X-ray scattering data from solutions of the purified protein (R. Mendelson, personal communication) than our earlier model¹.

presence or absence of calcium, although the ATPase rates are very different. They suggest that in the absence of calcium a kinetic step, perhaps release of phosphate, is inhibited. This would also be quite consistent with our model.

Received 12 May; accepted 16 July 1982.

1. Taylor, K. A. & Amos, L. A. *J. molec. Biol.* **147**, 297–324 (1981).
2. Moore, P. B., Huxley, H. E. & DeRosier, D. J. *J. molec. Biol.* **50**, 279–295 (1970).
3. Holmes, K. C., Goody, R. S. & Amos, L. A. *Ultramicroscopy* (in the press).
4. Mornet, D., Bertrand, R., Pantel, P., Audemard, E. & Kassab, R. *Nature* **292**, 301–306 (1981).
5. Wakabayashi, T. & Toyoshima, C. *J. Biochem., Tokyo* **90**, 683–701 (1981).
6. Vibert, P. & Craig, R. *J. molec. Biol.* **157**, 299–319 (1982).
7. Mendelson, R. *Nature* **298**, 665–667 (1982).
8. Huxley, A. F. & Simmons, R. M. *Nature* **233**, 533–583 (1971).
9. Huxley, H. E. *et al. Proc. natn. Acad. Sci. U.S.A.* **78**, 2297–2301 (1981).
10. Harrison, S. C., Olson, A. J., Schutt, C. E., Winkler, F. K. & Bricogne, G. *Nature* **276**, 368–373 (1978).
11. Cooke, R. *Nature* **294**, 570–571 (1981).
12. Spudich, J. A., Huxley, H. E., Finch, J. T. *J. molec. Biol.* **72**, 619–632 (1972).
13. Wakabayashi, T., Huxley, H. E., Amos, L. A. & Klug, A. *J. molec. Biol.* **93**, 477–497 (1975).
14. Seymour, J. & O'Brien, E. *Nature* **283**, 680–682 (1980).
15. Chalovich, J. M. & Eisenberg, E. *J. biol. Chem.* **257**, 2432–2437 (1982).
16. DeRosier, D. J. & Klug, A. *Nature* **217**, 130–134 (1968).
17. Greene, L. E. & Eisenberg, E. *Proc. natn. Acad. Sci. U.S.A.* **77**, 2616–2620 (1980).
18. Suck, D., Kabsch, W. & Mannherz, H. G. *Proc. natn. Acad. Sci. U.S.A.* **78**, 4319–4323 (1981).

Structure of a Zn^{2+} -containing D-alanyl-D-alanine-cleaving carboxypeptidase at 2.5 Å resolution

O. Dideberg*, P. Charlier†, G. Dive‡, B. Jorist†, J. M. Frère† & J. M. Ghuysen†

* Laboratoire de Cristallographie, Institut de Physique, B5, Université de Liège, B-4000 Sart Tilman, Liège, Belgium

† Service de Microbiologie appliquée aux Sciences pharmaceutiques, Institut de Chimie, B6, Université de Liège, B-4000 Sart Tilman, Liège, Belgium

‡ Laboratoire de Chimie analytique, Institut de Pharmacie, F1, Université de Liège, Rue Fusch 3–5, B-4000 Liège, Belgium

Bacteria possess proteases that are specific for the peptide bonds between D-alanine residues, one of which has a free α -carboxyl group. These D-alanyl-D-alanine peptidases catalyse carboxypeptidation and transepeptidation reactions involved in bacterial cell wall metabolism^{1,2}, and are inactivated by β -lactam antibiotics. We have now elucidated the structure, at 2.5 Å resolution, of the penicillin-resistant Zn^{2+} -containing D-alanyl-D-alanine peptidase of *Streptomyces albus* (Zn^{2+} G peptidase)^{3,4}. The enzyme is shown to consist of two globular domains, connected by a single link. The N-terminal domain has three α -helices, and the C-terminal domain has three α -helices and five β -strands. The Zn^{2+} ion is ligated by three histidine residues, and located in a cleft in the C-terminal domain. The mechanism of action of the enzyme may be related to that of other carboxypeptidases, which also contain functional Zn^{2+} ions.

Crystals of the Zn^{2+} G peptidase were grown⁵, using the vapour diffusion technique, from a solution containing 50 mM Tris-HCl pH 8.0, 5 mM MgCl_2 , 10 mM NaN_3 and a protein concentration of 2%. The crystals were prismatic and belonged to the space group $P2_1$ ($a = 51.1$ Å, $b = 49.7$ Å, $c = 38.7$ Å and $\beta = 100.6^\circ$). The asymmetric unit contained one protein molecule. The heavy-atom derivatives were prepared by soaking native crystals in appropriate solutions: 5.6 mM $\text{K}_2\text{Pt}(\text{C}_2\text{O}_4)_2$, 3 mM NaAuCl_4 and 30 mM $\text{K}_3\text{UO}_2\text{F}_5$. X-ray diffraction data were collected on a four-circle diffractometer (Hilger-Watts) with a Ni-filtered $\text{CuK}\alpha$ radiation and an ω -scan procedure. Two equivalent reflections for the native and four for the derivatives, including Bijvoet pairs, were measured in shells of increasing θ values. The heavy-atom sites were located using F^2_{HLE} Patterson functions⁶. Heavy-atom parameters were refined by the F_{HLE} procedure, followed by three cycles of phase refinement. The mean figure of merit was 0.66 for 6,700 reflections. Despite this rather low value, the high quality of the electron density map can be judged from Fig. 1.

The interpretation of the 2.5 Å electron density map of the Zn^{2+} G peptidase was carried out more or less simultaneously

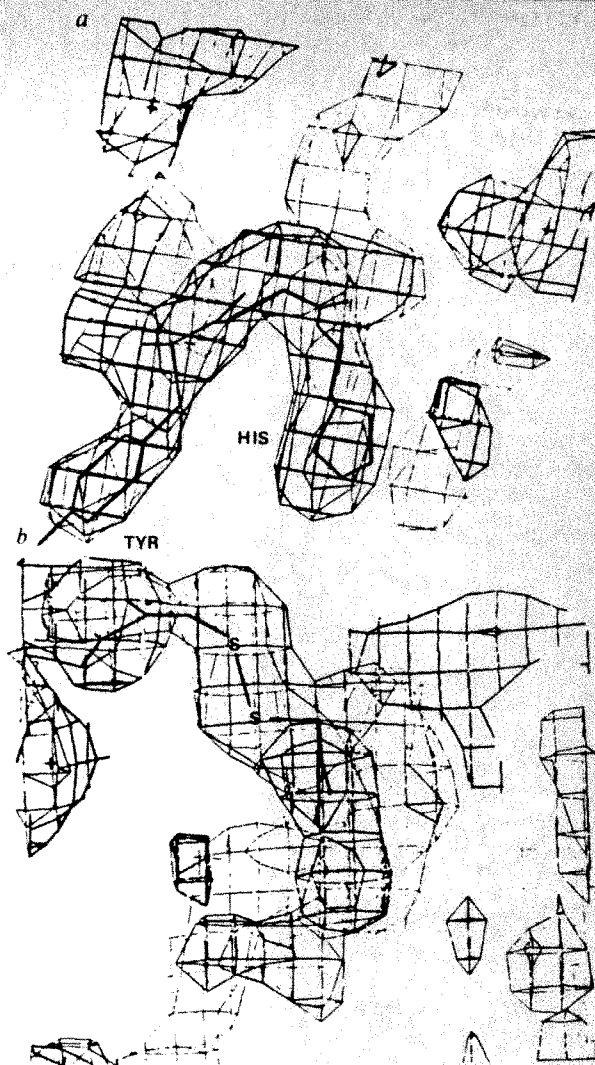


Fig. 1 The electron density map in two different regions of the molecule. a, Two large side chains at the end of the cleft: Tyr 154 and His 156. b, A well defined S—S bridge: Cys 168—Cys 210.

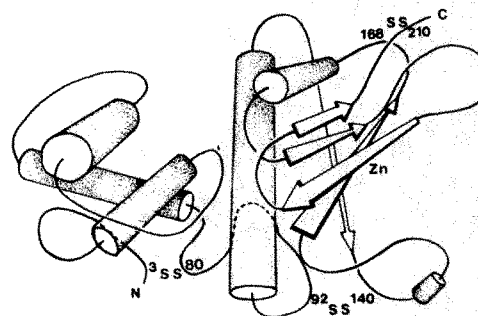


Fig. 2 Schematic drawing of the model of the Zn^{2+} G enzyme built from secondary structure elements. α -Helices and β -strands are represented by cylinders and arrows, respectively. The N and C terminus of the polypeptide chain and the S—S bridges are shown.

with the establishment of its primary structure. Initially, the N-terminal 55 residues and the C-terminal 45 residues could be located directly on the mini-map and six fragments (totalling 84 residues) could be correctly positioned using the Evans-Sutherland graphic system (at the University of London). However, examination of all possible tracings of the polypeptide chain and re-evaluation of the $\text{C}\alpha$ — $\text{C}\alpha$ distances led to the conclusion that a 28-residue fragment was missing. This fragment was subsequently isolated and sequenced so that, at this time, the two techniques are in agreement except for a few residues located outside the catalytic cavity. The complete sequence will be published elsewhere⁷, but Table 1 gives the

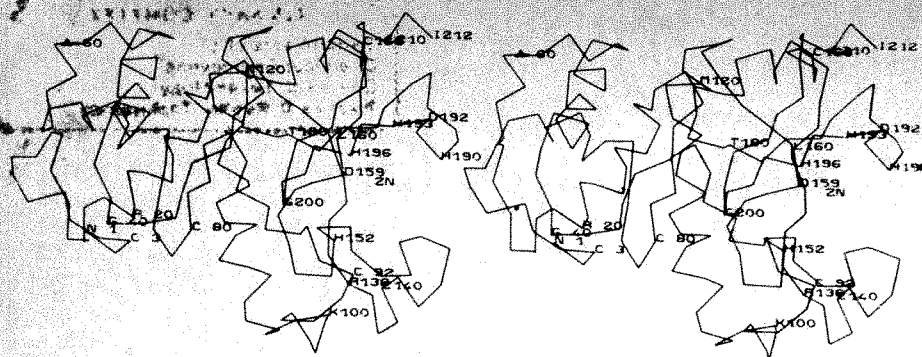


Fig. 3 Stereoscopic views of the main polypeptide chain. The α -carbon positions were derived from the mini-map. Important amino acid residues are labelled using the one-letter code.

positions and proposed functions of some critical amino acid residues.

Besides the Zn^{2+} ion, cysteines 92–140 and 168–210 were the most prominent features of the electron density map. Electron density at the methionine residues was rather weak and the weakest Met 153 was located near an Au-binding site. Tracing the polypeptide chain was easy except for two regions, $\text{C}^{\alpha 76}$ – $\text{C}^{\alpha 82}$ and $\text{C}^{\alpha 90}$ – $\text{C}^{\alpha 95}$, respectively. The enzyme molecule has an overall dimension of $48 \text{ \AA} \times 34 \text{ \AA} \times 28 \text{ \AA}$ and consists of two distinct globular domains of different sizes (Figs 2, 3). The small N-terminal domain (76 residues) contains three α -helices (43%) and is connected to the large C-terminal domain (136 residues) by a single link that exhibits a rather unusual folding. The C-terminal domain belongs to the α/β -type secondary structure⁸, containing three α -helices (34%) and five β -strands (17%). About 38% and 11% of the total number of amino acid residues are comprised of α -helix (80 residues) and β -structure (23 residues), respectively. To our knowledge, such a secondary structure has not been found previously in any other protein.

The five β -strands of the C-terminal domain form a mixed sheet with the usual left-handed twist. The cross-over connection is right-handed, a widely observed rule in protein folding⁹. This sheet constitutes the lining of one side of the catalytic cavity. Other remarkable features of the C-terminal domain are the long, 24-residue-containing helix and, especially, the two loops ($\text{C}^{\alpha 186}$ – $\text{C}^{\alpha 193}$ and $\text{C}^{\alpha 138}$ – $\text{C}^{\alpha 152}$) which, in turn, form the edges of the catalytic cavity. This cavity cuts the C-terminal domain into two parts, with the Zn^{2+} cofactor bound inside coordinated with the three protein ligands His 152, His 193 and His 196. Previous studies at 4.5 \AA resolution¹⁰ have shown this cleft to be the binding site of the two enzyme competitive inhibitors, the dipeptide acetyl-D-Ala-D-Glu and the β -lactam compound *p*-iodo-7- β -phenylacetylaminoccephalosporanic acid. The cavity of the native enzyme was not free of electron density; this might be due either to the presence of ordered solvent molecules or to spurious peaks originating from the heavy-atom binding sites. (In fact, each of the three heavy-atom derivatives studied had at least one binding site inside the cavity.)

A full characterization of the catalytic cavity of the Zn^{2+} G peptidase must await the final fitting of the protein molecule in the Richard's box and crystallographic refinements. Similarly, a full identification of all the residues involved in the binding and catalytic processes must await study at high resolution of various inhibitor (inactivator)–enzyme complexes. Neverthe-

less, at the present stage of the analysis, one may make interesting hypotheses concerning the mechanistic properties of this peptidase. Most likely, Arg 136 is concerned with binding, by charge pairing, of the carboxylate substrate. In addition, two Asp residues (159 and 192) and His 190 are located near the Zn^{2+} cofactor and their side chains have the right orientation to interact with the bound peptide substrate molecule. Contrary to all the other β -lactam compounds tested, β -iodopenicillanate bound irreversibly to the catalytic cavity of the Zn^{2+} G peptidase in rather mild conditions (unpublished results). The difference Fourier synthesis at 2.8 \AA resolution of the complex thus formed showed two peaks in the vicinity of Arg 136 and His 190, respectively. Permanent inactivation of the peptidase may be due to alkylation of this His residue.

In the proposed catalytic mechanism of carboxypeptidase A and thermolysin^{11–14}, the Zn^{2+} ion functions as a negative-charge stabilizer, the side-chain oxygen of a Glu residue as a proton abstractor (with or without a water molecule as the nucleophile), and a His or Tyr residue as a proton donor. By analogy, one may propose that in the Zn^{2+} G peptidase, Asp 159 or Asp 192 also acts as proton abstractor and His 190 as proton donor. Following this view, the Zn^{2+} G peptidase would be mechanistically similar to the usual metalloproteases and its specificity would depend entirely on the shape and structural features of its substrate binding cavity.

Two further comments deserve attention. Contrary to observations on carboxypeptidase A, whose active centre is a closed cavity, that of the Zn^{2+} G peptidase is an open cleft. This feature, which is reminiscent of that of thermolysin, should permit accommodation of extended structures. It might be related to the ability of the Zn^{2+} G peptidase to perform endopeptidase activities effectively on complex peptide substrates (possessing a free carbonyl group in α position to the scissile linkage)¹⁵. Finally, the role of the small N-terminal domain remains unknown.

This work was supported in part by the FRSM, Brussels (3.4501.79), the Belgian Government (Action concertée 79/84-11) and the NIH (2 RO1 13364-05). O.D. thanks EMBO, NATO and the FNRS (contracts 52/5-F6-E20 and 52/5-CG-E47) for financial support. We thank Professor T. L. Blundell for making available his interactive display system, and Professor J. Toussaint, Dr I. Tickle, Dr G. Wistow, Dr J. Lamotte-Brasseur and Mr M. Vermeire for help during this work.

Received 14 April; accepted 23 June 1982.

Table 1 Positions and proposed functions of some critical amino acid residues

Asn–Gly 1–2	N-terminal*
Cystine 3–80	S–S bridge
Cystine 92–140	S–S bridge
Cystine 168–210	S–S bridge
His 152, His 193, His 196	Zn^{2+} ligands
Arg 136	Charge pairing with substrate
Asp 159 or 192	Proton abstractor
His 190	Proton donor
Ile 212	C-terminal

* Partly in the form of a cyclic imide.

1. Ghuyens, J. M. *et al.* in *Topics in Molecular Pharmacology* (eds Burgen, A. S. V. & Roberts, G. C. K.) 63–97 (Elsevier, Amsterdam, 1981).
2. Waxman, D. J., Yocum, R. R. & Strominger, J. L. *Phil. Trans. R. Soc. B* **289**, 257–271 (1980).
3. Frère, J. M. *et al.* *Biochem. J.* **143**, 233–240 (1974).
4. Dideberg, O. *et al.* *FEBS Lett.* **117**, 215–218 (1980).
5. Dideberg, O., Frère, J. M. & Ghuyens, J. M. *J. molec. Biol.* **129**, 677–679 (1979).
6. Matthews, B. W. *Acta crystallogr.* **20**, 82–86 (1966).
7. Joris, B. *et al.* *Eur. J. Biochem.* (submitted).
8. Levitt, H. & Chothia, C. *Nature* **261**, 552–557 (1976).
9. Richardson, J. *Proc. natn. Acad. Sci. U.S.A.* **73**, 2619–2623 (1976).
10. Dideberg, O. *et al.* *FEBS Lett.* **117**, 212–214 (1980).
11. Hartsuck, J. A. & Lipscomb, W. N. in *The Enzymes* Vol. 3, 3rd edn (ed. Boyer, P. D.) 1–56 (Academic, New York, 1971).
12. Kester, W. R. & Matthews, B. W. *J. biol. Chem.* **252**, 7704–7710 (1977).
13. Argos, P., Garavito, R. M., Eventoff, W., Rossmann, M. & Bränden, C. I. *J. molec. Biol.* **126**, 141–158 (1978).
14. Kuo, L. C. & Makinen, M. W. *J. biol. Chem.* **257**, 24–27 (1982).
15. Leyh-Bouille, M. *et al.* *Biochemistry* **9**, 2961–2971 (1970).

BOOK REVIEWS

Dreams of disappointment

John Maddox

PROFESSOR Victor Jakob, theoretical physicist at a small German university that could be anywhere between Heidelberg and Göttingen, is a creature of the compelling imagination of Professor Russell McCormmach, professor of the history of science at Johns Hopkins University. At the end of his career in 1918, Jakob's spirit has been broken by a succession of disasters — the impending defeat of the Kaiser's reich, his personal defeat and humiliation by the head of the physics institute (an experimentalist), by his sense that the classical values of German society had been corrupted by the synthetic patriotism of the twentieth century and by his failure or, rather, his disinclination to come to grips with quantum physics.

The first appearance on the stage that McCormmach has designed for his protagonist is at a patriotic evening arranged by the university and the local Goethe Society, where he is waiting for the Bach to end to give his first-hand account of heroism in the Franco-Prussian War nearly half a century earlier, before finishing, he collapses with what appears to be a minor stroke. By the end of the book Jakob has sadly wandered off into the woods, fallen into a ditch from which he cannot climb but from which the roar of the guns firing near the university can be heard. Whether the old gentleman succeeds in blowing out his brains with the revolver in his pocket is not known.

In between, McCormmach's Jakob is but a vehicle for a stream of unspoken reminiscence, almost free association, guided chiefly by his wish to understand what has become of himself. The shining hopefulness of his student days had long since drained away. But why had his devotion to classical physics failed to bring the reward of discovery that he and his teachers had every reason, at the outset, to expect? "Why", Jakob keeps worrying, "have I so obviously fallen short of what Hertz, Helmholtz, Drude and those great men expected of me?"

So McCormmach's Jakob is more than a device for telling what physics was like in the early decades of this century. It is also a window on the corrosiveness of disappointment, a way of showing how a person such as Jakob can be destroyed by too great a gap between reality and expectations — of himself and of others. McCormmach says that he has "drawn on an approach from fiction" but he could as well have said that he has written a novel, and a good one at that.

Night Thoughts of a Classical Physicist By Russell McCormmach Pp 215 ISBN 0-674-62460-2 (Harvard University Press 1982) \$19.50, £10.50

Jakob's bemusement with his plight is described best by Anna von Helmholtz's account in 1894 of her husband Hermann towards the end of his life.

It is always as if his soul were far, far away, in a beautiful noble sphere where only science and eternal laws rule — and then that does not correspond to anything which surrounds him and he becomes unclear and confused.

Jakob's failure to make a bridge between his internal picture of what the world is like, and the reality outside, is what destroyed him — though reality itself, Jakob as a Jew and as a theoretician, conspired to that end.

Jakob's night thoughts are a moving account of the personal disappointments of academic life in the traditional German academic institute. At the point in his own young career when the next step would have been an appointment as tenured professor (*Ordinarius*), several universities informally enquired of him whether he would be free, but none of them translated this into a formal "call" — the firm offer of a job that, even if declined, could then appear in a *curriculum vitae*. So Jakob soldiered on, becoming indispensable as a teacher (especially when military service dragged away the younger teachers) and was rewarded with the title of honorary professor, an advertisement that he has not quite made the grade.

Before that humiliation, Jakob finds himself being interviewed by the Prussian official Althoff about the prospect of taking over the physical institute in Berlin. Althoff, although only a junior official at the ministry, seems to have established the right to appoint most physics professors at the German universities and to negotiate their terms of service. Among other misdemeanours, he was the principal agent whereby Philip Lenard was foisted on the unwilling faculty at Breslau. Althoff is best known for his complaint that professors are like whores "who go with the one who pays the most". "Each", he is given as saying, "has his price, which is not high".

The account of Jakob's resentment of this interview with the overbearing Althoff is both moving and persuasive, yet it is also one of the points at which McCormmach's technique lets him down. The question why powerful Althoff should be persuading an unsuccessful provincial such as Jakob to

take the post occupied by people such as Helmholtz, Hertz and Drude is a stumbling-block. Worse, at this point the notes tucked away at the back of the book turn out to be as gripping as the narrative.

The most compelling part of Jakob's stream of consciousness is his affection for the great men of German physics — Helmholtz, Hertz, Drude and so on. The tale has it that Jakob's study is decorated with the portraits of his heroes, among whom Maxwell (whom Jakob had never met) and Helmholtz take precedence. But Drude, appointed director of the Berlin institute in 1905, is Jakob's most vivid recollection. A whirlwind of energy, he sought to reorganize the institute but was enmeshed in the tangled bureaucracy of the state — it took endless letters even to change a light-bulb, according to Jakob — so that almost the most tangible of the marks left by Drude on the institute was his habit of keeping his stick of chalk on the left-hand side of the blackboard. Drude himself was driven sick with worry, and to suicide in 1906.

Perhaps predictably, Jakob is better on people than on physics. His stubborn scepticism of the Plancks of his world stems more from aesthetic than from intellectual arguments. He grumbles at the way in which the quantum physicists appear to have been licensed to take any hypothesis as a starting point, making physics seem like mere mathematics. Rather, Jakob argues, just as the study of Latin and Greek is based on the supposed congruence of ancient and modern minds, so classical physics is based on the assumption that at some level there is a congruence between mental and natural processes. But Jakob's refusal to follow Planck, while reinforced by Planck's firm but kind rejection of Jakob's attempt to square the circle of contradiction that had arisen, is at root simply a protest at the way that everything seemed to have changed.

Jakob's stream of reminiscence ends with his fall into the ditch on a hillside high above the university at which his career ended, in the last September of the war. McCormmach, his creator, seems principally concerned to have Jakob describe the social problems of German physics in those stirring days. That his pastiche of a hero should have turned out to be such an appealing down-trodden academic is an uncovenanted benefit, both haunting and memorable. □

John Maddox is Editor of Nature

Acid tests for the Usanovich theory

John Gibson

A New View of Current Acid-Base Theories By Harmon L. Finston and Allen C. Rychtman Pp 216 ISBN 0-471-08472-7 (Wiley 1982) £39.50, \$66.50

MOST chemical reactions and many life processes are carried out in a solvent, and closely connected with the properties of solvents is the behaviour of acids and bases. The acid-base concept has long had a unifying effect in chemistry and in modern times has a great bearing on solvation, compound solubility, the choice of a solvent for chemical synthesis, the understanding of nucleophilic and electrophilic reaction steps, and reaction mechanisms. In their *New View of Current Acid-Base Theories*, Finston and Rychtman review all the old theories, justify them within their limits but finally support the Usanovich theory as the most inclusive, giving experimental evidence for concerted proton and electron transfer, and for the relationship between oxidizing ability and acidity.

The evolution of the acid-base concept over the last three centuries was, at first, a shrinking process, continually reducing the number of substances regarded as acids and bases, it culminated in the restrictive electrolytic dissociation theory of the late nineteenth century, with its emphasis on protons and hydroxide ions in aqueous solution.

Brønsted and Lowry reversed this process in 1923 by omitting water as a requisite solvent and re-defining a base as any substance which can accept a proton. In his book *Valence and the Structure of Atoms and Molecules* published in the same year, G. N. Lewis proposed with complete generality "that a basic substance is one which has a lone pair of electrons which may be used to complete the stable group of another atom." This throwaway line went largely unheeded for 15 years before he supported his alternative ideas in detail. In the meantime the Brønsted-Lowry theory grew strong and an independent theory, the solvent systems theory, became established for aprotic solvents. Only in the late 1930s did Lewis's theory gain currency. Lewis saw no reason for limiting acids to hydrogen-containing compounds and also objected to the over-emphasis of ions in the solvent systems theory. His definition of a base as "have pair, will share" incorporates the Brønsted-Lowry theory but his definition of an acid as an electron pair acceptor continues our enlargement process. The Lewis theory suffers from the disadvantage of being difficult to quantify, but this aspect has attracted attention from Mulliken, Klopman and Hudson, Pearson, Drago, Gutmann and others.

All of this comes over well in Finston and Rychtman's very readable book. Many

comparisons are made between the different theories, but the main message of the book comes in the penultimate chapter. This elaborates the very general definitions of Usanovich who matches the wide definition of base given by Brønsted and Lowry with an equally wide definition of acid, which now becomes capable of splitting off *any* cation. Moreover, since the electron is regarded as a base, redox reactions become a subclass of acid-base reactions. Thus oxidizing agents relate to acids, reducing agents to bases and quantitative comparisons arise through ionization energies and reduction potentials.

The last chapter is rather novel in that the authors describe some of their own experiments which were designed to test the Usanovich theory as applied to aqueous electrolytes. They carried out pH measurements and acid-base titrations to determine the acidity of the aqueous

oxidization agents dichromate, permanganate and ferric ion. Some support was found by analogous transfer mechanisms for protons and electrons. Enhancement of acidity by oxidizing agents, and enhancement of the oxidizing power of a given redox couple with increasing acidity. I think that at this stage the authors would have us believe that our enlargement process is now complete. I take a more conservative view and suggest that some readers might like to repeat these experiments, and perhaps make the obvious extension to non-aqueous solvents, before we can consider the debate finished.

The book is well produced and makes interesting and convincing reading. It would be a good companion to a first-year university lecture course on this subject, but equally would be of interest to researchers in the traditional areas of chemistry and in biochemistry. □

John Gibson is a Senior Lecturer in the Department of Chemistry at Imperial College, University of London.

Unusual chain behaviour

Paul Calvert

Polymers and their Properties Vol 1, Fundamentals of Structure and Mechanics By J. W. S. Hearle Pp 437 US ISBN 0-470-27302-X, UK ISBN 0-85312-033-1 (Halsted/Ellis Horwood 1982) \$94.95, £32.50

IN AN established field the author of a textbook will usually play safe. He will repeat and update the contents of previous books and re-work only those areas which he knows well. Alternative and equally safe techniques are to be abstractly mathematical or to be light and descriptive. Hearle follows none of these courses and has produced a very original and personal book.

He starts with isolated polymer chains and discusses their conformations, energetics and response to stress. The rest of the book then traces the behaviour of the chains in successively more restrained states through melts and solutions, rubbers, glasses and crystals. There is no polymer chemistry, nothing about industrial plastics, no diversions into analytical techniques and not much mathematics, but there is a clear and consistent development of the main theme of chain behaviour. Hearle tries to give simple explanations or analogies for many aspects of chain behaviour and these are accompanied by many rough sketches of chains in various states of distortion.

Some of the questions which he raises have been quietly ignored by most other authors. I think that his explanations are

occasionally wrong but they are usually enlightening. An example is in the discussion of the origin of the β relaxation in polyethylene terephthalate where he draws an analogy between the flexible ethylene moiety and the soft segments of block copolymers. It is a nice idea but β relaxation also occurs in totally rigid molecules and cannot be attributed to a single chain segment.

Also, the final chapter in the book — which tries to relate the morphology of plastics and fibres to their mechanical properties — is not altogether satisfactory. I feel the author fails here because he does not keep a clear distinction between the highly oriented structures of fibres and the isotropic state of plastics where it is no longer fashionable to talk of "fringed micelles". Much of Hearle's own work has been on the structure and properties of fibres, however, so perhaps it is right that the deviations from the mainstream should be greatest here.

I would certainly recommend this book to someone seeking a first course on the physical properties of polymers. It provides a good framework either for more rigorous studies or for understanding the technology and applications of polymers. The small errors can be sorted out later, the overall structure will be of lasting value to a student. □

Paul Calvert is a Lecturer in Polymer Science in the School of Chemistry and Molecular Sciences, University of Sussex.

Immunological individualism

C.A. Janeway, Jr

Idiotypes and Lymphocytes. By Constantin A Bona Pp 211 ISBN 0-12-112950-0 (Academic 1982) £18 60, \$28

IDIOTYPES, which are antigenic determinants unique to antibody molecules binding a particular antigen, have been a central interest of immunologists in recent years. Initial studies defined idiotypic determinants immunochemically, and demonstrated that certain idiotypic determinants could be used to map genes required for idiotype expression in induced antibody responses. These studies showed that some idiotypic determinants behaved as though they were products of germ line genes encoding immunoglobulin heavy and/or light chain variable regions, consistent with the location of these markers.

A second focus has been the use of anti-idiotypic antibodies to probe the nature of lymphocyte receptors for antigen. The precise meaning of such studies is still disputed, but they do support the structural similarity of T and B lymphocyte receptors specific for the same antigen.

Perhaps the most active area of research involving immunoglobulin idiotypes was launched by a theoretical paper published in 1974 by Niels Jerne, in which the immune system was described as a network of interacting idiotypes. The basic premise of the network theory is that immunoglobulins and T cell receptors, since they can specifically recognize virtually any foreign protein, must themselves be as structurally and antigenically diverse as the universe of external or foreign antigens.

It follows from this premise that any foreign antigenic determinant will be mimicked by an internal image antigenic determinant found in the variable domains of an animal's own immunoglobulins and T cell receptors. Furthermore, antibody produced in response to the foreign antigen will also bind to, or be bound by, this internal image set of immunoglobulins and receptors. The circular nature of this interaction has made it difficult to assess its influence on an antibody response, but numerous artificial experiments involving the direct injection of idiotype or anti-idiotypic do suggest that such interactions can affect the expression of idiotype itself.

Because of the extensive interest in idiotype, it would be very helpful to have a current and thorough review of the field, citing major principles and the data that

support them. Unfortunately, Dr Bona has not provided us with such a book. This monograph, though appropriately brief, consists of a good deal of loosely organized data and very little in the way of an enlightening overview. This failing is seen most clearly in the tables and figures, which consist of raw data from Bona's own work. Bona's contributions to this field have indeed been numerous, but valuable data from other laboratories are given short shrift, while those from his own laboratory are presented in detail but without the necessary supporting text, making them virtually impossible to decipher without carefully scrutinizing each table. This greatly weakens the value of the book, as well as using a great deal of space. Furthermore, citations of other authors' research are not very accurate, and, since they are not supported by actual data, the reader seeking information about work by other investigators cannot rely on the text as a source.

This book covers an area of great current interest. But because of its lack of clarity and balance in presentation it can be recommended neither as an introduction to the field nor as a comprehensive treatise intended for the expert. □

C.A. Janeway, Jr is Associate Professor of Pathology at Yale University School of Medicine.

Cell meets cell

David I. Gottlieb

Cell Behaviour. A Tribute to Michael Abercrombie. Edited by Ruth Bellairs, Adam Curtis and Graham Dunn. Pp 615. ISBN 0-521-24107-3 (Cambridge University Press 1982) £45, \$89 50.

PROFESSOR Michael Abercrombie was a pioneer in the study of how vertebrate cells move and respond to each other's presence. That line of inquiry has since broadened into a vigorous branch of cell biology which is a major part of contemporary science. As a memorial to the man and his accomplishments, a group of his friends and colleagues have assembled this collection of essays. They have succeeded in both honouring their friend's memory and producing a volume which will be of great use to other scientists.

The book consists of a posthumous review of cell motility by Professor Abercrombie, 22 scientific essays on related topics and a personal memoir of Michael Abercrombie by D. R. Newth.

More Random Walks in Science

Compiled by Robert L Weber

Another inspired collection from Robert Weber in the same entertaining vein as his outstandingly popular *A Random Walk in Science!*

This new anthology offers yet more fascinating and frequently amusing anecdotes, quotations, illustrations, articles, and reviews which reflect, individually and together, the more lighthearted aspects of the scientific world, and the less serious excursions of the scientific mind. Too often, scientists are taken for men whose intelligence is of a ponderous kind, but Dr Weber, who believes that science should be entertaining as well as enlightening, demonstrates that their humour and wit is never far from the surface, and yet is tempered by wisdom and keen intellect. His anthologies are guaranteed to delight anyone who has a professional or amateur interest in science, and many more besides who do not.

October 1982 xvi + 208pp illus
hardcover 0-85498-040-7 £9 95

Still available, Dr Weber's earlier and ever popular

A Random Walk in Science

a magnificent assemblage of informal writings, comment and historical record. There is not a dull page, wit and stimulation abound. Times Educational Supplement.

1973 xvii + 206pp illus
hardcover 0-85498-027-X £7 95

Published by The Institute of Physics and distributed by Adam Hilger Ltd.

Adam Hilger Ltd
Techno House
Redcliffe Way
Bristol BS1 6NX
England



Evolution from space

Americans now have the opportunity to read Fred Hoyle and Chandra Wickramasinghe's *Evolution from Space*. The book (which was reviewed in *Nature* 294, 489, 1981) has been published in the United States by Simon & Schuster, price \$13 95.

Most of the essays are critical reviews rather than comprehensive updates of the literature, and many succeed in describing accurately the root observations of the field and critically evaluating our current understanding of the phenomena thus revealed. For this reason the volume should be an enduring one.

Contributions focus on several themes. One is the analysis of how isolated cells move on artificial substrata. Movement of fibroblasts is especially well treated. The topic of polarization of the moving cell as seen by light microscope cinematography is prominent, and the ultrastructural correlates of the light microscopic image are given in detail. A good deal of attention is also devoted to the small-scale specializations of the cell surface which seem to be the actual sites of adhesion, namely focal adhesion plaques and close contact zones. The question of which attributes of artificial substrata are necessary for cell movement and adhesion is reviewed in several of the essays, although the problem of the mechanisms which generate the force necessary for cell motility is not extensively treated. The initial interest in fibroblast movement has since been extended to other types of cells, most notably nerve and epithelia, so it is appropriate that three excellent essays deal with the question of nerve growth cone motility and two with epithelia.

A second theme is the reactions that occur when moving cells in tissue culture encounter one another. Abercrombie's essay reviews the original discovery of contact inhibition between cultured embryonic heart fibroblasts and subsequent efforts to analyse the mechanistic basis for this crucial interaction. The theme of cell-cell interactions is carried over to the interactions of nerve cells with each other and of fibroblasts with epithelial cells, the emphasis being on the morphological complexity of such interactions. The natural stage for cell movement and interactions is the organism, cell and tissue movement in embryonic development is particularly well reviewed. Even better is the account of the migration of cells from the neural crest and of entire tissues during gastrulation, topics which receive a clearer and more comprehensive treatment here than any I have seen in recent years.

This is a valuable book because it gives a clear picture of the current intellectual status of an important part of cell biology and embryology. Part of its message is that there is a wealth of interesting facets of cell behaviour which are accessible to investigation. Armed with all the new probes developed over the past few years (monoclonal antibodies, cloned genes, etc.), molecular biologists will be able to read this book and pick their next set of problems. □

David I. Gottlieb is in the Department of Anatomy and Neurobiology, Washington University School of Medicine, St Louis

Ordered and disordered systems in order

Nicolaas Bloembergen

Nuclear Magnetism: Order and Disorder
By A. Abragam and M. Goldman. Pp. 626.
ISBN 0-19-851294-5 (Oxford University Press, 1982) £45, \$69.

PROFESSOR Abragam has scored for the third time in 20 years, thus completing his hat-trick. The assist in this case is credited to Dr Goldman. The sport to which this feat applies is the widely diversified field of magnetic resonance, the goals are major publication events scored on the home grounds of the Clarendon Press, Oxford.

Abragam published his first book, *The Principles of Nuclear Magnetism*, already a classic, in 1961. About a decade later, in 1970, he co-authored *Electron Paramagnetic Resonance of Transition Ions* with Professor Bleaney. The present book follows some ten years after the second one. Aficionados of magnetic resonance will not be disappointed. It is a different ball game in the 1980s and there is virtually no duplication with the earlier volumes, amongst which Dr Goldman's *Spin Temperature and Nuclear Magnetic Resonance in Solids* (Clarendon, 1970) should be included. In fact, both this last book and Abragam's *Nuclear Magnetism* are almost required reading before the present volume can be enjoyed. It is definitely not for beginning students.

The first chapter is called "Epitome of the Theory of Spin Temperature" and is a condensation of Goldman's book, with a concomitant high density of equations. It contains the groundwork for all subsequent chapters, which may be read almost independently of one another.

These remaining chapters fall into two parts. In the first the authors discuss three topics, in which they describe themselves as observers rather than active participants. One is concerned with high resolution spectroscopy in solids. The clever manipulation of nuclear spin systems by pulse sequences and by (de)magnetizations in rotating frames of reference leads to uncanny reversibilities, which defy the application of statistical mechanics to nuclear spin hamiltonians in certain cases. The other two topics, concluding the first half of the book, are nuclear magnetism of solid and liquid He_3 , respectively. The authors have digested the complex literature about these intriguing quantum solids and liquids, and provide a good introduction to the appreciation of the

fundamental role that nuclear magnetic resonance (NMR) has played in the development of this important sub-field of low temperature physics. The large body of NMR work on solid hydrogen and methane is not discussed, because of the wish of the authors "to complete a book of finite size in a finite time". Although the temperature may be in the order of millikelvins in some cases, the nuclear spin systems are still largely disordered, as the Boltzmann energy kT remains large compared to the nuclear spin interactions. Nonetheless, in this first part of the book the authors have put a lot of order into the discussion of these disordered systems.

The second part deals with the ordered systems, where the degree of nuclear spin polarization is significantly different from zero, and may approach unity in some cases. The authors have been leaders in a laboratory group that has made most important contributions to this field, so here they perform as actors instead of spectators. They describe the changes in lineshapes, entropy, susceptibilities and other thermodynamic quantities, when the degree of nuclear spin ordering becomes significant. The method of dynamic polarization is discussed in detail. Neutrons are scattered from ordered nuclear spin systems, and neutron spin resonance is induced by the pseudomagnetic interaction with the precessing nuclear spin polarization. Again, enough background is provided for the non-specialists in neutron physics.

The final chapter deals with the antiferromagnetic and ferromagnetic ordered arrangements in nuclear spin systems. With the exception of solid He_3 (and nuclear spins in heavy elements, which are not discussed), the ordering is determined by a pure dipolar interaction. This chapter should also be of considerable interest to those who work with the more familiar electronic ferro- and antiferromagnetic materials. The NMR data provide illuminating examples for those more technical fields of magnetism.

In this book a close contact between theory, experiment and data is maintained at all times. The high density of equations is in many spots alleviated by glimpses of physical insight. One would, however, look in vain for detailed descriptions of experimental apparatus.

There is a lot of physics to enjoy in this book. It belongs in all major physics research libraries, as well as in the individual libraries of low temperature physicists and of those active in NMR research or in magnetism. If you enjoyed Abragam and you liked Goldman, you will love Abragam and Goldman. □

Nicolaas Bloembergen is Gerhard Gade University Professor at Harvard University.

New in paper

Douglas Heggie's *Megalithic Science* (reviewed in *Nature* 296, 373, 1982) has now appeared in paperback. Published by Thames and Hudson, the book costs £5.95. Also new in a paper edition is *Genesis* by John Gribbin. Publisher is Oxford University Press, price £3.95, for review see *Nature* 294, 491, 1981.

nature

14 October 1982

LIBRARY COMPLEX
 Department of:
 Chemical Engineering
 Chemical Technology
 Plastics & Rubber Technology

What policy for West Germany?

The new government in Bonn was promising last week to keep faith with research and development, which is honourable and even creditable. But it should not forget the problems hitherto ignored.

The new ministers of the federal government of West Germany are still forgivably startled to find themselves where they are. Even though the disintegration of ex-Chancellor Helmut Schmidt's coalition government had been apparent since the Hamburg elections at the end of last year, its final collapse last week could not be accurately predicted. So it is inevitable that the new ministers should begin their spells of office by saying what their party has been saying in opposition. This explains what Dr Heinz Riesenhuber, the new minister of research and technology, was saying in Bonn last week (see page 569). Yes, the role of the large national research establishments must be re-examined, and links with industry must be strengthened. (Technology transfer is the catchword.) Yes, industry itself must shoulder more of the cost of research and of responsibility for its direction, but the federal government will help with tax incentives and by other means. And more of the cost of keeping students at universities will be financed by loans rather than by grants. All this is consistent with what the Christian Democrats have been saying in opposition, but it will be some time before the new government can break new ground, with policies that go beyond the generalities of opposition. Indeed, that time may be postponed by the new Chancellor's promise of general elections in March next year, politically contentious and potentially distracting.

Luckily, West Germany has one important circumstance in its favour: the new government party echoes what the beaten Social Democrats have always said, that strong government support for basic research is essential to future prosperity. The trouble, so far, is that the funds spent on research have been used inefficiently (see page 570). The crucial question now is whether the new government will have the political courage and skill first to acknowledge that reforms are necessary and then to carry them out. People in West Germany, in the research community and elsewhere, have been agonizing for the past several years about the reasons for what appears to be poor productivity in research. All kinds of fanciful explanations have been offered, from the aftermath of the Third Reich to the partition of Germany thirty years ago. The real trouble is too much organization (see *Nature*, 23 May).

One obvious impediment to change is that the ministry in Bonn which has been for the past decade the most powerful influence on science and technology in West Germany has no direct influence on what happens in universities, where the need for change is most urgent (and, on recent form, the ministry has been almost indifferent to the problems of academic research). Another and more serious difficulty is that the federal government has no direct influence on the universities, which are constitutionally the creatures of the *Länder* governments in whose regions they happen to be situated. For the new government to require, as it should, that the traditional autonomy of the select company of tenured professors (*Ordinarien*) should be moderated by, say, peer review, assessment of the use of research funds, or that student numbers should be restricted at the more popular universities, would be to take on a series of dog-fights, especially with the *Länder* governments still in the hands of the Social Democrats. Sooner rather than later, however, these battles must be fought.

Fortunately, the federal government has some levers more immediately in its hands. While the constitutional difficulties would be formidable, a first priority should be an attempt to

engineer a redistribution of university research spending from university subventions by the *Länder* governments, now all short of funds, to central grant-making organizations such as the Deutsche Forschungsgemeinschaft. The result would be a concentration of research in universities and departments with proven track records. Another urgent need is somehow to bridge the long-standing gulf between technically excellent Max Planck institutes and the rest of the academic research system. For while there continue to coexist two constitutionally separate, even if occasionally geographically contiguous, sets of institutes for basic research, the system is bound to be less effective than it could be. Even where Max Planck institutes work closely in collaboration with university researchers (which is not always the case), the fact that the people concerned follow distinct career tracks is a continuing cause of resentment and a source of needless rigidity. Will the new ministers of education and of research have the wit to see what could be accomplished by joint action?

The new government has a more untidy problem in deciding what to do about the major national laboratories that have emerged since the end of the Second World War. The rhetoric of the past few days, like that of the past thirteen years, is that the national laboratories must be judged by the contribution they make to industrial innovation and development. In reality, these federal laboratories are too mixed a bunch for that test to be applicable. Thus the cancer research centre at Heidelberg may in passing be a source of industrial innovations (in the techniques of body scanning, for example), but this is only accidental. Similarly, the heavy-ion establishment at Darmstadt (the laboratory that synthesized an isotope of element 109 a few weeks ago) should not be judged by its immediate contribution to industrial change but as a source of basic research as such (and thus comparable with the accelerator laboratory at Hamburg). What the federal government needs, therefore, is not a uniform policy for persuading these establishments to be more directly of benefit to West German industry but a clear understanding that they have different functions. Some of them could with advantage be managed by the Deutsche Forschungsgemeinschaft rather than the Ministry of Research and Technology, for then their role as parts of the academic research enterprise would be more apparent and more easily developed. Others, the nuclear research establishments at Jülich and Karlsruhe for example, may need more drastic treatment.

The temptation in the next few months will be for the new government to put these claims on its attention to one side, seeking instead ways of implementing its election promises about industrial tax incentives or resisting (as is its political inclination) demands for special help for the electronics industry or some other suffering from overseas competition. The snag is that it is rarely possible in the real world to compensate for the effects of one set of structural defects by devising a different set of institutional regulations. Incentives for industrial research are not to be scorned, in West Germany, although there will be many who would prefer to wait for evidence on the working of the Reagan Administration's schemes, introduced just over a year ago. But it is even more important that the new government should face up to the problems, administrative, legal and even constitutional, that have everybody crying about the disappointments of the past few decades while pretending that the causes are unknown.

London's agony (contd.)

The University of London may surprisingly have become a model of good administration.

The University of London is the British university system in microcosm, but with the added disadvantages that its budget is more vulnerable to the flight of high fee paying students from overseas and that its administration is poorly suited to making decisions, even of the simplest kind. This week, the university has told its constituent parts how much money from the centre they will have to spend in the financial year that began more than two months ago, on 1 August. On this occasion, however, the delay is partially forgivable, for the court of the university, formally responsible for money matters that do not involve questions of academic policy (whatever they may be), has been uncustomarily decisive. In particular, it has broken out of the mould in which it had become trapped of sharing its funds as they had happened to be shared in the previous year, with allowances for special pleading on the side. Even so, much remains to be done.

The university's constitutional difficulty stems from the notional autonomy of the parts of which it is composed. Formally, the university cannot tell one of its constituent colleges how to conduct its affairs except by insisting through a cumbersome network of committees that acceptable academic standards should be followed and by doling out funds in such a way as to encourage or discourage various activities. (In dealings from the centre with individual universities in the United Kingdom, the University Grants Committee responsible for sharing out the government subvention of universities can only command the second weapon, at least in the short term.) Two years ago and then last year, the university somewhat arbitrarily told its colleges what they would have to spend in the succeeding years without explaining how the figures had been decided, except for the still puzzling and unwarrantable decision that courses combining two different lines of study should be discouraged. This year, the university has told its dependants how it has done its sums.

To its credit, the university has also devised an important innovation, and has decided that constituent colleges able to attract substantial amounts of research income should be paid extra on that account. This decision is entirely consistent with all that has been said in recent months about the collapse of what is called the dual-support system, by means of which the general university subvention is meant to cover the overhead cost of carrying out research (but nobody likes the word "overhead"). This is the most tangible way in which the university can substantiate its frequently expressed hope that research will survive all the troubles there have been. The failure to follow such procedures in recent years has unfairly robbed of funds those colleges with strong traditions in research but which for other reasons have been dealt with meanly within the university.

It is also sensible that in this first year, the university should have followed the logic of its conclusion that research requires extra support only part of the way, to the tune of one-third of what will be done two years from now. One of the ironies of the redistribution in the coming year is that the only one of the nine regular undergraduate schools to gain funds as a result, Queen Elizabeth College, is one of those dealt with most severely last year. (Imperial College deals separately with the University Grants Committee, while the London School of Economics has no substantial amount of research in scientific subjects.) The end result of this new arrangement is certain to be that the different parts of the university will have an incentive to improve their research. Should not the British system as a whole now promptly follow suit?

The university has also been sensible in planning for a reduction of the number of its parts. While it remains to be clearly demonstrated that small colleges with only about a thousand or so students are inviable, there is something in the view that concentration would help and might be cheaper. That course of action is at least worth a try. So colleges with plans to merge with

each other are now offered a modest incentive — an increase of combined student numbers — and possibly a share of the pot of money the university is salting away meanwhile. Exactly such incentives would have allowed the University Grants Committee, in its dealing with the British universities collectively, to help rationalize the system without as much pain as there has been. In London, with the university's new-found taste for open government, what remains to be done is to explain exactly why those colleges that will find life even more difficult if they choose to stand alone have been singled out for such a fate, and to make more durable arrangements than now exist for making sure that potential casualties of the rearrangement, people and institutions, are not discarded without thought.

Soviet science not quoted

Why are Soviet papers less often cited by US authors than in the 1970s? Secrecy? Or quality?

Is Soviet science approaching a crisis of quality? Or is the regime becoming more and more secretive about its good science? These questions, which have an important bearing on international science policy and questions of technology transfer, are attracting much attention. Although the data to answer them are scant, some trends are arresting. Thus in the field of mathematics, US scientists have been citing Soviet work less and less; US citations of Soviet mathematics declined by 48 per cent from 1973 to 1979 (see *Nature* 30 September, p.388). More recent unpublished data from the National Science Foundation suggest that the decline is now 53 per cent.

Why would US authors make less and less use of Soviet mathematics — a field in which that country is believed to excel? The principal translators of Soviet mathematical work in the United States are the American Mathematical Society, in Providence, Rhode Island, and Plenum Press in New York. (The latter is a principal source of translating and distributing foreign scientific materials, especially materials from Eastern bloc countries.) Both organizations report that, if anything, they are translating and distributing more Soviet mathematics papers than they did a decade ago. So the decline in citations is not apparently connected with a decline in the amount of material available in translation in the United States. Another explanation has unexpectedly turned up in a study for the US Department of State carried out by Computer Horizons Inc., a New Jersey corporation. Francis Narin, president of the corporation, says that there are two distinctly different groups of highly cited Soviet scientific papers: those describing work of the highest quality which is cited over and over again, and those which are cited often by Soviet scientists but much less often elsewhere. It seems as if Soviet authors look to one group of Soviet mathematicians while Western authors look to another. The study was too preliminary to show whether the work in the two sets of papers is related, but Narin has established that the papers cited by Westerners were not merely translations of those cited most by the Soviet scientists. The results so far are, however, a telling illustration of what citation analysis may eventually accomplish in this important field.

Meanwhile, speculation about the causes of these changes flourishes. To many US academics, it seems natural to account for what is happening as a consequence of Soviet classification policy. The case of computer science and its applications is often mentioned: in the United States, most work not strictly related to defence and commercial development is published freely, while in the Soviet Union the opposite is true. But the past decade has also seen more modest declines in the frequency of US citations of Soviet work in physics and the Earth and space sciences, while US citations of work in these fields by other than Soviet nationals have risen dramatically. So there is again speculation that the Soviet Union may be hiding its best work. For the time being, US academics do not accept that there has been a decline of quality of Soviet research. But they are intrigued at the possibility that citation analysis could help them find out.

Threat to French research directors

Ructions about twelve-year tenure limit

Senior scientists in France were staggered last week to learn that they may remain as research directors — heads of laboratories or research groups — for no more than 12 years. The new regulation, announced by science and industry minister Jean-Pierre Chevènement, will be applied retroactively from 31 December 1985. Hence any director who has now been in post for more than nine years must contemplate resignation by that date.

There have been strong reactions, both positive and negative. Professor Jean Dausset, the Nobel prize-winning immunologist, has described it as "a good measure", mobility being necessary at all levels of research. "Our laboratories are dying of sclerosis", he said. But according to another world-renowned biologist, the measure is "very bad for French science".

In fact, the regulation is not yet law, and may be modified. François Gros, ex-director of the Institut Pasteur and now science adviser to the Prime Minister, Pierre Mauroy, is being urged from all quarters to advise Chevènement against the move.

The chance that such pressure will succeed, however, seems slim. Chevènement has in fact already *hardened* the proposal from the version which originated from the medical research council, INSERM. INSERM probably suffers more than most French research councils from the longevity of its research directors, some of whom have been in the job for between 20 and 25 years. It was generally agreed that the worst should be shaken out, to leave room for new blood. The question was how?

After long debate stimulated by the new director-general of INSERM (Philippe Lazar, who was *rapporteur* for the National Colloquium on Science and Technology last January), it was agreed by the directorate, the scientific council and the trade unions at INSERM that the 250 or so posts of scientific director should be limited to four-year terms, renewable twice (for 12 years in all). After that, all agreed that the director of a group could be re-confirmed in his post "in exceptional circumstances". But when the ministry was consulted about the proposal, it insisted that the 12-year term would be final, and that there would be no exceptions.

According to one leading scientist close to the INSERM directorate, the result is a harsh, bureaucratic solution to a real problem in France: how to make effective evaluations of scientific progress. "It's

true I've never seen a group leader fired", he said. But the imposition of a rigid 12-year rule is not the answer. Rather, there should be proper, expert evaluation, using both French scientists and scientists from abroad. Many existing INSERM directors should go, he felt; but equally others who had been in place 12 years should stay for the good of science such as the neurophysiologist Jacques Glowinski, or Michel Jouvet (a specialist in sleep mechanisms), both threatened by the new rule.

Unfortunately for French science the whole issue is rapidly becoming politicized, with those resisting the move being classed as rightist. However, left-wing scientists also consider the move hypocritical — because it avoids the "democratic" assessment systems set up by the new government. These systems, which involve largely elected committees to make judgements on appointments, grants and so on, are sup-

posed to be "transparent" and avoid the formation of cliques and interest groups. But if they are expected to work, why does the government not make use of them to decide whether a group leader should continue or not? The imposition of a rigid rule reduces the power of the committees, and indicates that the government lacks confidence in their decisions.

Whatever final decision is reached on the 12-year rule, INSERM is at pains to smoothe the highly troubled waters. On Monday it released a statement arguing that very few of its directors would be affected (a medical newspaper in Paris last week estimated that 60–70 positions were under threat); and that the object of the reform was above all "the quality of research". The period between now and the deadline of 31 December 1985 would be one of "intense reflection on how to apply the rule", the statement said.

Robert Walgate

Few changes for West Germany

Heidelberg

The new West German Minister of Research and Technology, Dr Heinz Riesenhuber, gave a good impression last week, after 48 hours in office, of having hit the ground running. Once party spokesman on energy, he was obviously familiar with his role, fielding even questions on the fast breeder with confidence and humour.

Riesenhuber holds a PhD (University of Frankfurt, 1965) for work on lattice distortions in microcrystalline iron phosphate. For eleven years, he has been the technical director of a thriving middle-sized company specializing in industrial polymers. He entered the Bundestag in 1976 and became chairman of the intra-parliamentary committee on energy and environment in 1977.

Last week he stressed the deteriorating national economic situation, the increasing financial burden of the prototype reactors (see *Nature* 30 September, p.384) and the inertia of large projects which limit the immediate possibility of increasing investment and change. But Riesenhuber sees a positive role for his ministry in the implementation of party research and technology policies (*Nature* 23 September, p.289).

Nevertheless, Riesenhuber emphasized his commitment to basic research and to continuing support along the lines of the previous administration. But why, he wondered, is world-class investment in basic research not always matched by research results, as assessed by criteria such as the *Science Citation Index* or Nobel prizes?

The new minister has already carried out an analysis of potential growth areas. Besides microelectronics and biotechnology, materials research, particu-

larly high-temperature polymers, was mentioned. (There are suggestions of a new Max Planck Institute for polymer research.)

To promote these key areas, Riesenhuber will encourage closer collaborations with other ministries, research organizations and industry, so as to create "market push" rather than "government pull". He plans to take a close look at the country's many large research organizations which, despite their solid research achievement, may not be pulling their weight economically.

Riesenhuber also stressed the importance of integrating risk assessment — financial and environmental — at all stages of scientific and technological undertakings. The *post factum* imposition of controls resulted in expense, delays and environmental damage that increased public disquiet about the role of science and technology in a vulnerable world. This, he says, is the only way to restore public trust in science and technology. How far he succeeds in dispelling the environmentalists' fears, the polls will tell.

By contrast with Riesenhuber's bustle, all was peaceful last week at the sister Ministry of Education and Science where Dorothee Wilms has taken over as minister. But the new administration's decision to put student grants on a loan basis will have far-reaching effects. There are no signs of French expansionism, but, although a general cut of 5 per cent in all expenditure is expected, Gerhard Stoltenburg, the new Finance Minister and himself once a forceful minister of scientific research under Kiesinger in the 1969 Christian Democrat government, may yet exempt science and technology and even provide the 5 per cent increase needed to

cover inflation. Playing for safety, however, Riesenhuber plans also to encourage industry to finance more research. He considers that large projects can be better initiated and carried out by industry than by the cameral system of federal government. It remains to be seen how well he succeeds — and what the consequences would be for the government's own research establishments. **Sarah Tooze**

Why the lag?

Why has research in West Germany been a disappointment? Economically, West Germany has been if anything better off than its competitors. But West Germany has problems peculiar to itself, as follows:

- Length of education. Both school and university education take longer in West Germany than elsewhere, so that the average age for beginning a PhD is 27. The results are expense and loss of some of the most creative years.

- The PhD is finished at an age when tenured jobs and stability are more attractive than mobility, so grants for travel are undersubscribed.

- Too few untenured posts. Under German employment laws there must be a reason for ending a job. Despite loopholes and contrivances, mobility within the research community is limited.

- Legal responsibility of the *Ordinarius* (C₄) professors. By law, responsibility for finance and administration is usually vested only in the C₄ professor. This creates a sharply pyramidal hierarchy which deprives other members of staff of responsibility.

- Research budgets of universities are contributed three quarters by the region (*Land*). This money goes automatically to the C₄ professors, who have complete control and who are not subject to review of any kind. Federal money allotted by a normal grant system covers one quarter of university research spending and is the only money allocated subject to review.

- The 1976 university law laid down that all grant money, even when allocated to a specific person for a specific purpose, must be administered by the university. This has spawned a bureaucratic machine which leaves the grant-user trapped in a mesh of regulations and subject to interference. These procedures discourage industry from financing research in the universities.

- Inefficient administration. There is a lack of professionalism in the university administrations and administrators are rarely appointed within university departments to help research staffs and coordinate with the university.

- The numbers of students have soared, but despite overall increased spending, research money per head has fallen.

Sarah Tooze

Polish universities

More signs of latent discontent

"Universities must not turn into an arena for political games", the Polish government newspaper *Rzeczpospolita* warned as the new term opened on 1 October. Government and party officials were evidently worried that the reassembly of some 400,000 young people in the country's 87 universities and higher colleges could provide a focus for further confrontations — particularly in the atmosphere of heightened tension following the enactment of the new law on trade unions which dissolves all existing union structures (including the 11-million strong Solidarity). In the event, the students, whose own Independent Students' Association (NZS) was outlawed last January, reassembled peacefully, and the problem now facing the universities is not so much the threat of student political action but rather of inaction.

Calling for a "climate of normality" in the universities, the party daily *Trybuna Ludu* stated last week that "it will be difficult for the academic milieu to fulfil its task if it does not embark on a dialogue on such issues as the new law on higher education, improvement in upbringing and teaching methods, and the future of the student movement".

The President of the Council of State, Henryk Jablonski, reiterated this theme when conferring professorial diplomas in Warsaw on 6 October. Normal functioning of society will be impossible, he stressed, if citizens are "inactive", and students should therefore be trained to show "initiative, independent thinking and imagination". A conference of university lecturers from Lower Silesia and Opole went so far as to urge encouraging a "creative" approach by students to political and social studies (courses once more obligatory for all).

The students, however, seem reluctant to embark on dialogue with an academic establishment they no longer trust. Some 30 university rectors, elected under the previous democratic procedures have been replaced under martial law, and, under the political "verification" procedures, some 2 per cent of university staff have failed to meet the required criteria, while more than 5 per cent have been re-employed only conditionally, and 2½ per cent have had to take up non-teaching jobs within the universities.

"Internal emigration" — passive non-cooperation with the political and social life of the country — became widespread among Polish intellectual and creative circles under martial law, and has been widely advocated in underground Solidarity literature. In what appears to be a last-ditch stand to "channel" the aspirations of the students, the authorities are now trying to establish a new students' organization, to replace both the banned

NZS and the party-linked Socialist Union of Polish Students (SZSP), a move that many SZSP activists themselves urge as a way to bring the mass of students back into the party fold.

Trade union law, which effectively put an end to hopes for a return to the liberalizations of 1980–81 has already moved some Polish students to consider turning their internal emigration into an external one, and to try to continue their studies abroad. Some Western embassies in Warsaw, the British Embassy in particular, have already foreseen this possibility and are granting visas to students only if financial support is assured by a Western sponsor (see p.574). Such sponsors will not prove easy to find. In the United Kingdom, where a Polish Students' Appeal Fund was set up to help students stranded by the declaration of martial law, universities have been generous with free places, but funds for maintenance and such necessities as textbooks are, in the words of Dr Stanislaw Gomulka of the London School of Economics, "already over-extended".

Vera Rich

Canada's research plans

Holding up

Washington

Canada's ambitious five-year plan for a rapid growth of investment in research and development is in trouble — but it is surviving present economic difficulties more successfully than almost any other government initiative.

This mixed picture emerges from a report just issued by the Canadian National Research Council (NRC), the government's national laboratory. NRC's budget for the 1981–82 fiscal year fell short of the \$304 million it said it needed to carry out even the most restrictive of three alter-

OECD data on research and development expenditure

Country	Year	Expenditure as % of GDP
United States	1980	2.49
Switzerland	1979	2.45
Germany	1979	2.27
United Kingdom	1979	2.20
Japan	1980	2.04
Netherlands	1978	1.97
Sweden	1977	1.90
France	1979	1.79
Belgium	1979	1.40
Norway	1979	1.37
Yugoslavia	1977	1.20
Canada	1981	1.18*
Finland	1979	1.08
Denmark	1979	0.97
Italy	1979	0.82
Turkey	1978	0.59
Portugal	1978	0.32
Greece	1980	0.18

*The OECD figures include social sciences and humanities research. The figures cited in the text (1.07 per cent current and 1.5 per cent goal) do not.

natives in the 1980 five-year plan. That plan is aimed ultimately at doubling the production of technology-intensive industry by 1990.

Even so, the \$296 million that NRC spent in 1981–82 was a 30 per cent increase over the previous year, allowing NRC to go ahead with several new programmes, including the Industrial Materials Research Institute in Boucherville, Quebec, an ice research project in Newfoundland and a small tokamak fusion research programme in cooperation with Hydro-Quebec.

NRC officials are worried, however, that the government will not be able to

sustain the annual 30 per cent increases called for in the plan. Since budget items can be approved by the government throughout the fiscal year, the 1982–83 budget will not be known until the year is over, but officials are predicting that it will fall significantly short of the planned figure. The big worry is that what NRC calls “core support” is going to suffer the most. This is the reserve of expertise and backbone research facilities (analytical chemistry laboratories, for example) that NRC says must be built up if the government is to be able to address problems as they arise.

NRC officials say the tendency has been for immediate needs — such as the recent “fire-fighting” operation on the health-effects of urea-formaldehyde foam insulation — to draw personnel and resources away from the core. This, they say, “jeopardizes the viability of NRC as Canada’s national laboratory”. It seems likely also to jeopardize the nation’s effort to boost its overall research and development by 1985 from 1.07 per cent of gross national (GDP) to 1.5 per cent — and thus to bring it closer in line with the more industrialized countries of Western Europe.

Stephen Budiansky

Bilingual planners disagree

Brussels

Two separate plans to create an advanced electronics industry in Belgium have just been announced, one by the new Flemish regional government and the other by the central government’s Minister for Science, Philip Maystadt. Although there are claims that the two plans complement one another, it seems likely that Belgian research and development policy will again become a source of conflict between the country’s two communities.

Like the French plan and the European Commission’s *Esprit* programme, the new initiatives spring from fears that European industry is in danger of missing the boat for the “Third Industrial Revolution” as the Flemish are calling it.

Since last December, Belgium’s already complex political arena has been further complicated by the delegation of much of central government’s power to two separate regional governments, one for Flanders and the other for Wallonia. The micro-electronics strategy presented by the president of the Flemish “government”, Gaston Geens, is one of the first fruits of this constitutional change.

It will cost some BF 4,000 million (£44 million) over the next four years. Unlike the French plan, it is strongly orientated towards stimulating private industry and differs in its emphasis on the production of customized chips. A large part of the funds will go towards establishing with Bell Telephone (a Belgian affiliate of ITT) a silicon foundry manufacturing customized microchips. The Belgian company is putting up half the cost of BF 2,800 million (£32.5 million) and the Flemish government the remainder.

The second element will be the major expansion of the research facilities at Leuven University, led by Professor Overstraeten, into a laboratory for advanced research into micro-electronics at a cost of some BF 1,500 million. This will be complemented by a programme of grants to engineers already working in industry or finishing doctorates to improve their knowledge of the state of the art of very large-scale integrated chips and other fields. To help industry directly, there will be a consultancy centre where companies

can receive advice on how to computerize either their products or their production.

The Flemish micro-electronics programme has strong backing from the region’s political parties, and industry has organized itself into pressure groups such as FLORA — Flemish companies interested in the development of the information technology industry.

The central government plan, still to be officially adopted, concentrates on creating a receptive environment for companies in the forefront of electronics. Above all, Maystadt proposes to use the public purchasing power of the state in the defence and telecommunications sectors to favour Belgian companies, particularly those seeking their first customer. This is

not strictly permitted under EEC or GATT rules, but Belgium awards more public works contracts to foreign companies than any other EEC country.

BF 200 million will also be set aside for subsidizing research and development work in companies involved in developing customized chips, in the belief that Belgium will never be able to compete with the French or Americans in producing standardized chips. A further BF 240 million will be spent on a study on the sociological impact of micro-electronics in an effort to calm the Walloon trade unions hostile to the changes their use will bring.

The central government’s programme is estimated to cost BF 820 million a year but this figure may be revised in the light of efforts to cut the large government deficit.

Jasper Becker

US medical profession

Fight against anti-trust laws

Washington

The first of October may turn out to have been a decisive date for the medical profession in the United States, ending a shoot-out between the profession and the Federal Trade Commission (FTC), the government agency that seeks to monitor anti-competitive, anti-consumer practices in the medical profession (as well as others).

The issue, according to FTC’s chairman, James C. Miller III, is whether the professions should be immune from the normal inquisitiveness of the agency empowered to protect consumers. “Admission to a profession should be a guarantee of competence, not a guarantee of immunity from the laws the rest of us must obey”, Miller has said.

As long ago as December 1975, FTC issued a complaint against the American Medical Association (AMA), the profession’s powerful umbrella organization, barring it from prohibiting advertising by doctors, among other things. Since then, AMA has fought the complaint in the courts. But when the US Supreme Court was deadlocked on the issue earlier this year, the FTC order automatically became effective on 1 October, the first day of fiscal year 1983.

But AMA has not given up. Having failed in the courts, it seeks relief in Congress by amending FTC’s authorizing legislation to prevent it from proceeding against the professions. The changes stood a good chance of being passed — reflecting AMA’s considerable power in Washington — until Congress went into recess. AMA spokesmen still say they can change the law when Congress returns in November. But Congress’s huge agenda, its lame-duck status and the Reagan Administration’s support for FTC in this matter may combine to frustrate AMA’s plans.

The fight has been long because several interlocking issues are involved: whether professionals can be the subject of anti-trust action, whether FTC has the power to regulate the professions, whether AMA has reformed itself sufficiently in the past seven years to be considered now above reproach. To complicate matters, FTC has issued related orders against the American Dental Association (which agreed to be bound by the outcome of the AMA battle), the ophthalmologists, and several state and local medical societies. All these support AMA in its fight with FTC.

But the central issue is who should determine medical practice locally in the United States. FTC’s position is that state and

local medical societies have enormous influence over doctors and over state legislatures and courts. Thus they can facilitate doctors' boycotts of hospitals that charge too little, prevent physicians from working on a salary instead of the more lucrative fee-for-service basis and decide whether to encourage or to discourage advertising.

Regulation of these professional groups is traditionally the job of the states. But, FTC argues, it is hard for state authorities to rule against these powerful groups. Many consumer groups believe that the influence of these professional associations is connected with their powerful political fund-raising ability. In May, a bill introduced by Thomas A. Luken (Democrat, Ohio) that would place a moratorium on all FTC action against the professions had 155 co-sponsors in the House of Representatives. According to Congress Watch, a public interest group, those 155 co-sponsors had received \$599,000 in campaign contributions from AMA, \$191,000

from the American Dental Association and \$41,000 from the ophthalmologists. By October, the bill had 221 co-sponsors.

A more limited measure was attached to FTC's authorizing legislation last May by the Senate Committee on Commerce, Science and Transportation. It would declare that FTC has no jurisdiction over state-regulated professionals and their professional associations. This measure may well remain in the final Senate bill.

William Rial, president of AMA, is unsparing in his criticism of FTC's allegedly blundering intrusion into the medical profession which, he writes, is "threatening the future of medical practice in this country". The drain on medical societies' resources because of FTC administrative procedures, Rial says, "can hinder these groups from performing their most important functions. . . The standards of quality established by the American Medical Association and other medical societies . . . are being undermined by a federal

agency that possesses no medical qualifications." AMA spokesmen point out that FTC has investigated some professional groups only to find nothing at all wrong after a great expense of time and money. An AMA spokesman in Washington says the profession is already feeling the chill of the FTC order. Local cost-containment groups, he says, are afraid to meet "for fear FTC will investigate them for price-fixing".

But this seems to be just what FTC wants. It cites the case of fees for eye glasses and optometry, where the agency won the right to promote advertising. In a short time, the price of eye glasses and contact lenses fell by as much as a half. The cost of health care in the United States continues to rise in double figures, even though inflation now stands at approximately 6 per cent. FTC is not promising that it can lower the overall costs but it now has a licence to try to do so.

Deborah Shapley

Commonwealth agriculture

More journals mean more food

The Commonwealth Agricultural Bureaux (CAB) are among the first beneficiaries of the British government's new International Organizations' Act passed early last year. Incorporation under the new act has given CAB full international status and thus removed some of the previous obstacles to legal agreements between the bureaux and national governments. Hence a new station for the Commonwealth Institute of Biological Control in Kenya can now go ahead because the Kenyan government has a legal entity with which to sign a contract. The new act also means that CAB member governments, which contribute to the financial upkeep of the bureaux, need no longer fear that part of their contribution will end up in the British exchequer. CAB employees, most of whom work in Britain, no longer pay income tax.

After nearly 30 years gestation, CAB was finally born in 1930, since when it has grown into a major international information service for agricultural scientists. It offers three basic services — identification of biological specimens, advice on biological control and the publication of agricultural abstracts and some primary journals. Three Commonwealth institutes — those of entomology, helminthology and the mycological institute — provide identification services. The Commonwealth Institute of Biological Control, the only CAB institution based outside Britain, provides advice on biological control from its headquarters in Jamaica. The four institutes and a further ten bureaux prepare abstracts of the literature in their own specialities and conduct literature searches for enquirers.

Until 1975, CAB had been largely financed by contributions from member

governments. Since then, however, the publishing activity has been made self-financing by substantially increasing the charge for journals. The biological control service also earns half its keep from contracts. But the identification and taxonomy services are financed from member governments' contributions.

Of the £6 million needed to run CAB each year, £4.5 million is now earned, mainly from journal sales and charges for literature searches. (CAB's abstracts data-

base is now available on-line on the world's major host computers.) The remaining £1.5 million is provided by member governments which contribute roughly according to their means. Thus, Britain makes the largest contribution of about £400,000 (or just 30 per cent of £1.5 million), Canada, Australia and New Zealand come next and many of the smaller Commonwealth nations contribute only a little.

Member nations are entitled to a quota of free journals depending on the size of their contributions, and to a slightly discounted rate for extra journals, on-line services and advice on biological control. Non-member nations may also take advantage of CAB's services — but they must pay slightly over the odds. The identification service, however, is free for all, members and non-members alike.

The United States and Japan, two non-member nations, have in fact made greater use of CAB's services than any other nation. Thus, CAB are open to the criticism that many developing countries are subsidizing services which the developed countries are best equipped to use. That criticism was reinforced when CAB made their abstracts available on-line on the world's major host computers, all of which are in the industrialized north.

At a conference in 1980 to review CAB's work and celebrate their golden jubilee, developing countries expressed a wish for greater access to CAB's services but also their appreciation of them. For although the developed countries may benefit most — Britain as the host country most of all — CAB often provide developing countries with their only access to the world agricultural literature or to advice on agricultural pests. The alternative for developing countries — to finance their own identification and biological control services and establish their own libraries — would in most cases be prohibitively expensive.

Judy Redfearn



This weevil, *Elaeidobius kamerunicus*, should save Malaysian agriculture around \$115 million a year if things go according to plan. The weevil (actual length 4 mm) has been introduced into Malaysia from West Africa and has already greatly increased the fruit production of Malaysia's oil palms and eliminated the need for hand pollination of the trees. Since its introduction in 1981 the weevil has spread throughout the Malaysian peninsula and increases of 20 per cent in yield have been obtained. As a spin-off from this work, based on a study by Dr R.A. Syed of CAB's Commonwealth Institute of Biological Control, growers in West Africa are now keen to find means of controlling oil palm pests biologically — since the continued use of insecticides will inevitably limit the effectiveness of the pollinating weevils.

Nobel prizes 1982

Prostaglandins

The 1982 Nobel Prize for Medicine was awarded this week jointly to Dr John R. Vane of the United Kingdom and Dr Sune Bergström and Dr Bengt Samuelsson of Sweden for their "discoveries concerning prostaglandins and related biologically active substances".

It has taken fifty years for prostaglandins to be deemed worthy of a Nobel prize. They were discovered in semen by the Swede Ulf van Euler who misnamed them prostaglandins believing them to originate from the prostate whereas, in fact, they came from the seminal vesicles. Sune Bergström's interest in prostaglandins stemmed from the early contributions of van Euler who must be counted unlucky not to share in the prize. Bergström, at the Karolinska Institute in Stockholm used newly developed chromatographic methods for the separation of lipids for the first purification of prostaglandins. Bergström and J. Sjövall published the empirical formulae of prostaglandins E and F in *Acta chemica scandinavica* in 1960. Two years later, Bergström and Bengt Samuelsson, produced the first complete chemical structure of a prostaglandin.

The structure suggested that arachadonic acid, an essential fatty acid, was a precursor of prostaglandins. Bergström and Samuelsson proved that point in 1964 but only with the help of David van Dorp of Unilever who provided them with radioactively labelled arachadonic acid; van Dorp published the same result independently but simultaneously. Samuelsson has continued to make important contributions, most notably in determining the structure of the prostaglandin-related thromboxanes and leukotrienes.

Two major contributions are attached to John Vane's name. The first is the discovery, published in *Nature* in 1971, that the anti-inflammatory effects of aspirin and other non-steroidal drugs are related to their ability to inhibit the synthesis of prostaglandins. Vane was then at the Institute of Basic Medical Sciences but later went to the Wellcome Research Laboratories where he discovered prostacyclin, a highly unstable prostaglandin which can inhibit platelet aggregation. The work on prostacyclin was primarily in the hands of Salvador Moncada, first author of the key paper (*Nature* 263, 663; 1976).

Pharmacologically, prostaglandins have marked effects on the contraction of smooth muscle and they are implicated in uterine and blood vessel contraction. They have been used in the induction of labour and abortion in humans and are used widely in veterinary practice to synchronize oestrus prior to artificial insemination of a herd of cows.

Peter Newmark

Biotechnology index

Cool reception for Genex shares

Washington

The Genex Corporation of Rockville, Maryland, one of the larger US biotechnology companies, went public on schedule by offering 2 million shares of stock for public sale on Wednesday 29 September (too late for inclusion in *Nature's* September Biotechnology Index, see table).

As always, the first public stock offering is a major event for a young company as a test of how sound and promising the business community believes it to be. And as the first public offering of a major biotechnology corporation for some time, Genex's debut was closely watched by those concerned with genetic engineering as an investment. Wall Street analysts say that the fact that Genex could soon derive steady income from the artificial sweetener market, and that it has work under way in the interferon field and other promising areas, made the stock trade well. But the lack of a market "hype" or a well-publicized human drug product made the Genex offering lacklustre, in the opinion of some analysts.

Even so, the stock traded quickly at \$9.50 per share and all 2 million shares were sold. Thus, Genex grossed approximately \$19 million, and after fees can now put around \$17 million in the bank.

Genex was founded by J. Leslie Glick, a former senior cancer research scientist at Roswell Park Memorial Institute. Glick had previously, in 1969, founded Associated Biomedic Systems, Inc., which filed for bankruptcy in 1977. In 1977 Glick started Genex with backing from Koppers Company Inc. of Pittsburgh and the Inno-Venn Group of venture capitalists. At the time of the offering, Koppers held 45 per cent of the company's shares. InnoVenn

held 22 per cent, Robert F. Johnston, chairman of the board, held 11 per cent and Glick had 11 per cent. Now, Glick's 1,080,000 shares in Genex have a book value of approximately \$9 million.

The offering also gave the company's founders some inkling of what their shares are worth. Genex has grown steadily and now has 211 employees. Each year, it has increased its income through research contracts. In mid-1982, Genex had eight major research contracts: four with Japanese companies (including work on interferon for Green Cross) and two with Swedish companies. A seventh contract was with Koppers and the eighth was with Bristol-Meyers. The company has a pilot plant producing L-aspartic acid for possible use in producing aspartame (an artificial sweetener considered to have great market potential — see *Nature* 16 September p.199).

The market's calm response to the offer of Genex shares showed that the US business community no longer views genetic engineering as the next best thing to the Midas touch. Genex earlier planned to sell 2.5 million shares for up to \$12 per share, and could have grossed as much as \$33 million. But it was felt that the market would not bear such a price, so the offer was pitched lower and the company's plans scaled back. After a week of trading, Genex stock was selling at about \$8.50 per share. By contrast, in 1980, Genentech, another stable, well-regarded firm, offered its first public stock at \$35 per share and the price rose, in hours of frenetic trading, to \$89 per share. By late September, however, Genentech stock was selling below the original offer price, reflecting the market's calmer mood.

Deborah Shapley

Nature index of biotechnology stocks

1982 high	1982 low	Company	Close previous month	Close 24 Sept	Change
34 1/4	16 1/8	A.B. Fortia (Sweden)	32 3/4	34 1/4 *	+ 1 1/2
8	2	Bio Logicals (Canada)	2	2 1/2	+ 1/2
7	3 5/8	Bio-Response (USA)	4	4 3/4	+ 3/4
14 1/8	8	Cetus (USA)	8 7/8	8 3/4	- 1/8
11	6 1/8	Collaborative Research (USA)	8 7/8	8 5/8	+ 1/4
21 7/8	14	Collagen (USA)	17 5/8	18 1/2	+ 7/8
8 7/8	5 1/4	Damon (USA)	7 7/8	7 1/2	- 1/8
17 1/4	11 1/4	Enzo-Biochem (USA)	12	14 1/2	+ 2 1/2
28	6 5/8	Flow General (USA)	10 5/8	10 7/8	+ 1/4
37 3/4	26	Genentech (USA)	33 3/4	33 1/4	- 1/2
3 1/8	2 1/4	Genetic Systems (USA)	3 1/8	3 1/4	+ 1/8
17 7/8	9 5/8	Hybritech (USA)	14 3/8	13 1/2	- 1/8
10 1/4	6 1/4	Molecular Genetics (USA)	10 3/4	10 3/4 *	0
46 3/4	34 7/8	Novo Industri A/S (Den.)	46 3/4	44	- 2 3/4
12 1/8	8	Monoclonal Antibodies (USA)	9 3/4	8 1/4	- 1 1/2

The *Nature* Biotechnology Index for September 1982 stands at 117.9, compared with 118.1 last month. Base is 100 as of 25 June 1982. Previous indexes appeared *Nature* 12 August p.599 and 9 September p.101. Close-of-month prices are the closing prices on the last Friday of each month. Where stocks are traded over the counter, the price quoted is the bid price. For stocks traded on the American and New York Stock Exchanges, the price quoted is the transaction price. Data from E.F. Hutton, Inc.

*High or low for this calendar year.

CORRESPONDENCE

SERC and South Africa

SIR — The replies to the questionnaire sent out by a working group of the Science and Engineering Research Council (SERC) on the South African Astronomical Observatory (SAAO) should not be taken as representing the balance of opinion among astronomers on whether the United Kingdom should continue to subsidize the SAAO (see *Nature* 23 September, p.291). The questionnaire was not sent to all UK astronomers and was in fact sent mainly to groups who have already used the SAAO. Many of those who refuse to use SAAO on principle did not receive it. The questions asked were all concerned with what facilities should be used, what programmes pursued and what instrumentation required. As there was no question on whether the subsidy to SAAO should continue, I and many others did not reply to the questionnaire, regarding it as an irrelevance to the central issue.

The central issue is a moral one, whether astronomy is so important that it should come before one's duty to the oppressed black majority in South Africa, whose leaders (those who have not been murdered or imprisoned) have repeatedly called for the severing of all international ties with South Africa. This call has been supported by the United Nations, UNESCO and many other international bodies. The agreement maintained by SERC with the South African government on behalf of UK astronomers is probably the last official cultural link between the two countries and is a disgrace to UK science.

Note that I am not trying to prevent individuals with strong stomachs from using telescopes in South Africa or for that matter Chile. The issue is whether a substantial chunk of the UK astronomy budget should go to maintain an official subsidy of SAAO by the United Kingdom.

I ask all concerned scientists, and UK astronomers particularly, to write to the Chairman of the Astronomy, Space and Radio Board, c/o SERC, North Star Avenue, Swindon, calling for an end to this shameful treaty.

MICHAEL ROWAN-ROBINSON
Department of Applied Mathematics,
Queen Mary College,
London E1, UK

How to help Poland

SIR — As a recent and relatively frequent visitor to Poland, I have the unhappy task of reporting to the Western scientific community the particularly unfortunate situation that Polish scientists now find themselves in.

Specifically, they are caught in a pincer between the scientific policies of the Polish and US governments. On the Polish side, in this time of economic crisis during which the average Polish standard of living has already decreased by 25 per cent, it is a fact that the relative decrease in salaries for scientists is far greater than for most other economic groups. For example, under the new system coal miners' earnings are about four times that of professors and more importantly, coal miners have access to stores that have something for

sale other than the most basic foods while professors do not.

The reasons for this especially poor treatment of scientists by the politically captive Polish government are: (1) universities and institutes have generally been organizational centres for Solidarity; (2) the scientific community is generally Western-oriented in its values and has been particularly tainted by extensive contacts and visits to the West; (3) this Western orientation precludes its usefulness to the Eastern bloc defence establishment; (4) the Soviet Union has little intrinsic interest in the cultural value of Polish science.

Salaries, prices and availability of goods have been restructured to the great detriment of scientists. Polish scientists, thanks to money saved during visits to the West, have lived relatively well in the sense of better apartments, clothes and cars. Their Polish salary has only paid for subsistence at a moderate level. The reduced salaries now barely cover monthly expenses in normal markets, where little is available, and are certainly very inadequate on the black market where such luxuries as decent soap, toothpaste and shirts are to be purchased. Clearly the future is economically even more downhill for Polish scientists than it is for the general worker. The second arm of the pincer is the American policy of cutting support for joint US-Polish projects. This money was very important in that it financed travel to Western scientific conferences. The Polish government rarely releases its foreign exchange for such purposes. The US policy is based on the idea that actions which punish Polish science and culture will cause Polish scientific and cultural

groups to apply pressure on the Polish government, thereby affecting its policies.

Sensible as this may seem in countries whose governments serve their people, as we see from the above discussion the policy cannot be effective in Poland. In fact the policy is damaging to Western interests in that it helps destroy one of the most Western-oriented communities in Poland.

Can we in the West do anything to help our Polish colleagues? The answer is yes. This correspondent has already communicated the contents of this letter to the US government at the highest levels. On the economic and intellectual side, invitations to established, as well as young, Polish scientists to come to the West, even for the more easily arranged short visits, can be a great help. It will keep the Poles abreast of Western scientific work. It will also be amazingly effective in helping them survive economically. To appreciate this one must realize that \$100 saved when converted to zloty on the ever present and unofficially tolerated black market (the government wants the dollars) is roughly equal to four to five months salary for a scientist at the beginning of his scientific career. Importantly, it has been my experience that Polish visitors return excellent value for their salaries. They truly value their chance to work in the luxury of Western scientific facilities and because of the limited time they have, they work very hard.

Finally, invitations to visit the West help elevate the spirit of our Polish colleagues who truly live these days under the heavy foot of external oppression.

Name and address
supplied but withheld

No rising trend for IQ in Japan

SIR — R. Lynn¹ reported evidence of IQ levels in Japan and drew some far reaching implications for American and European economies. In his letter, T.B.L. Kirkwood (*Nature* 2 September)² suggested, rather cautiously I thought, that the evidence presented does not entirely support a "rising trend".

Taking the data presented for the mean IQs of the 23 Japanese cohorts, I plotted the cumulative sum chart³ shown in the figure. Without making any statistical test it is clear that there are two "populations" and no

obvious outliers. There is certainly no evidence for a "rising trend" in any part of this data.

As to likely explanations, in the absence of further information regarding the way that the data were gathered, I suggest that the following hypotheses can be advanced:

- (1) There was step change in the ability of the Japanese to do intelligence tests starting with those born after 1946.
- (2) There was a step change in the test applied to those born after 1946.

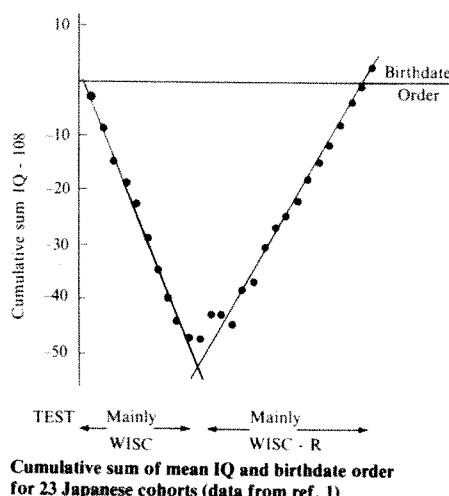
Before getting too involved in the implications of hypothesis (1) it seems prudent to investigate hypothesis (2) more thoroughly, for while it remains open, doubt must be cast on IQ comparisons such as those made by Lynn in his paper, and indeed on the levels themselves.

Whether the Japanese are more intelligent than other nations or whether IQ measures anything that can be related to "economic success", are no doubt fascinating questions. What the Japanese have done is to allow and encourage a broad mass of people to use their intelligence in their ordinary jobs, and in particular by many national training programmes since 1950, to deal with data effectively by means of simple charts and statistical treatments.

E.J. PEARSON

Manchester, UK

1. Lynn R., *Nature* 297, 222-223 (1982).
2. Kirkwood, T. B.L. *Nature* 299, 8 (1982).
3. *Cumulative Sum Techniques* (ICI Monograph No. 3, Oliver and Boyd, Edinburgh, 1964).



NEWS AND VIEWS

Limitations of Maxwell's distribution

A calculation of the evolution of a system of gravitating masses (galaxies) in an expanding universe surprisingly suggests that Maxwell's velocity distribution is not an acceptable end point.

EVERYBODY knows that if you put a collection of massive interacting particles in a box and let them settle down, in due course their velocities will have a maxwellian distribution. The interaction may be only sporadic, physical collision, as in a classical monatomic gas for example, or otherwise be ever-present, as with the long-range forces of gravitation. Either way, the end result is that the chance that the velocity of a particle lies between v and $v + dv$ is proportional to

$$v^2 \exp(-\frac{1}{2}mv^2/kT) dv$$

where m is the particle mass, T the temperature and k is Boltzmann's constant. For what it is worth, the proportionality constant is $4\pi(m/2\pi kT)^{3/2}$. Maxwell's first flawed derivation of this distribution function in 1860 was afterwards recast along the lines of Ehrenfest's much later principle of detailed balancing — at equilibrium, the rate at which particles are removed from some velocity interval will be equal to the rate at which particles with such velocities are produced, by collision or otherwise. By 1878, Boltzmann had put kinetic theory on an analytical basis with his integro-differential equation admitting only permissible distribution functions as solutions. During the First World War, Enskog and then Chapman showed how the maxwellian distribution is the end point in the evolution in time of an arbitrary initial velocity distribution, at least if interactions between the particles dissipate no kinetic energy. So what happens if the interacting massive particles are not atoms of a gas but a collection of galaxies (for simplicity, with equal mass) and if the box into which they are put is the expanding universe?

Certainly not a maxwellian distribution, as can be told from the treatment of this problem by Henry E. Kandrup of the University of California, Santa Barbara, published in an August issue of *Astrophysical Journal* (259, 1; 1982). The problem is of course relevant to the current preoccupation in cosmology with the formation of clusters of galaxies. While many hold to the theory of Zel'dovich and his colleagues that galaxy clusters are formed by the internal coalescence of large pancake-shaped aggregations of matter, recent Monte Carlo simulations of the evolution of gravitating masses suggest that clustering may be a natural outcome of a different starting point — a collection of galaxy-sized objects in an expanding box. Kandrup's study is an attempt at an analytical treatment of the problem hitherto dealt with primarily by numerical modelling. The most striking of his conclusions is that if you put a collection of identical massive objects (galaxies) in an expanding box (universe) and take proper account of their long-range interaction through gravitation, then you find that the total kinetic energy of the massive objects increases monotonically with time. Naturally, the steady increase of kinetic energy must be compensated for somehow — by what Kandrup calls the "generation of negative correlational energy", presumably another name for potential energy. In short, the calculation suggests that clustering should be a natural occurrence, while the steady increase of kinetic energy is a direct proof that a maxwellian distribution is entirely out of court.

On a little reflection, this conclusion should not be as surprising as it seems. For the expanding universe is hardly a system in equilibrium, and since Enskog's inaugural dissertation at the

University of Uppsala in 1917, it has been in principle possible to calculate deviations from simple maxwellian distributions in the many familiar physical circumstances in which equilibrium does not obtain, the transport of heat through a kinetic gas for example, or the transport of momentum as in viscous phenomena. Kandrup acknowledges the way in which Prigogine and his associates have more recently dealt with non-equilibrium systems, showing how circumstances can arise in which a system can be deflected from relaxation towards a maxwellian distribution. With all this said, however, the physical implications of these phenomena are not at all well understood. Is the time ripe for revival of interest in classical kinetic theory?

Kandrup's analysis of his own problem of what happens to a collection of gravitating point masses in an expanding universe contains a further and perhaps deeper surprise. The calculation starts from a time-dependent distribution function for the values of each of the independent variables (space coordinates and velocities) for each of the galactic masses, whereupon it is possible to relate the time-rate of change of the distribution function to the space gradient of the distribution function and to the forces between particles. The procedure is strictly analogous to the direction of Liouville's theorem, and says little more than that probability is conserved. The algebra, however, is complicated by the need to work in an appropriate and moving reference frame. Exactly by analogy with classical kinetic theory, Kandrup nevertheless sets out to calculate a one-particle distribution function by integrating over the coordinates of all other masses and arrives at the equivalent of Boltzmann's equation for the time-rate of change of that same function. Analytical solutions of this equation are for the time being out of reach, if only because of the complications flowing from the $1/r$ form of the gravitational potential, but there are approximations that put the analogue of Boltzmann's equation into barely manageable form. And Kandrup's conclusion is that in these circumstances, a maxwellian distribution of velocities is not a stationary solution of the equation. And, Kandrup insists, this unexpected result "has nothing to do with the fact that the universe is expanding" but is directly a consequence of the long-range character of the gravitational forces between all the particles.

The implications of Kandrup's calculation for the understanding of the clustering of galaxies remain to be seen. The fact that the monotonic increase of kinetic energy which tumbles out of the calculations implies a decrease of potential energy which is at least consistent with the formation of galaxy clusters is of at least more than passing interest. But Kandrup's approximations deserve to be scrutinized with great care by those with an interest in his problem of galaxies in an expanding box as a test of simple classical kinetic theory. Hitherto, attempts to calculate velocity distribution functions in circumstances where particles interact by means of inverse-square law forces — in ionized gases, for example — have tended to be frustrated by the recognition that 'collisions' are not simple binary collisions when such long-range forces are involved. If Kandrup has found a way round this kind of difficulty, he will no doubt be embraced not merely by cosmologists but by plasma physicists as well. □

An immunoregulatory molecular complex with five active sites

from N.A. Mitchison

THE cellular immunology group at Yale University has just published a very important claim¹. It comes in several parts, of which the most important is to have discovered a new suppressive transmitter or 'factor' with five distinct active sites.

Antibody production in the immune response is believed to be regulated in part by a cascade of interacting T cells which produce soluble transmitters that act on others in the chain and ultimately suppress the activity of the helper T cells that induce the proliferation of the antibody-producing B cells. The new transmitter is made by two cells at the end of the suppressor T cell cascade, each of which releases a single peptide chain (or, just possibly, a very stable assembly of chains). The two chains assemble to make up a complex which acts in a suppressive manner on the target of suppression, a helper T cell. Two of the five active sites on this two-chain molecule are necessary for assembly of the chains. One of these sites is a product of the H-2J locus of the major histocompatibility complex, made by a cell which bears the same product on its surface. H-2J is well known as a marker on suppressor T cells and their products, so it is no surprise to find it turning up here. The other site is on the other chain made by an H-2J⁺ cell, and it binds the H-2J product on the H-2J⁺ chain.

The H-2J⁺ chain also has an anti-idiotypic site, which binds to an idiotypic on the surface of the target cell. Idiotypes are antigenic determinants of the antigen-binding sites of antibodies. They can also be detected on T cells where they are believed to be associated with the antigen-binding site of the T cell receptor. Because of their association with the antigen-binding site, they are thought to be the target of antigen-specific regulation of the immune response. However, it is a little surprising to encounter them at the end of the suppressor cascade, since they have more usually been associated with its induction rather than with its final action. (Gershon *et al.* do not use the term idiotypic; I suspect this is because they believe that products similar but not identical to immunoglobulin are involved, which are encoded by a family of related genes on the same chromosome and immediately to the right of the immunoglobulin genes. Whether or not they are correct in this belief, the idiotypic nomenclature seems appropriate and is in general use for markers identified by the mouse strains they use.)

The other chain, in addition to the H-2J-

binding site, carries an antigen-binding site and an effector site that mediates the suppression of the target cell. The antigen-binding site presumably makes a bridge via antigen to the target cell, and thus helps the transmitter find its appropriate target which it then suppresses, Gershon *et al.* suggest, by cleaving to generate a toxic peptide. They have in mind the way diphtheria toxin acts, and more immediately a cleavage mechanism to yield a toxic product which has recently been demonstrated for the products of a T suppressor cell clone².

It is further proposed that this transmitter is only one among a class of similar molecular assemblies, all of which are composed of a pair of chains, one with an anti-idiotypic binding site and the other with effector activity. In another publication³, the Yale group describes another such factor which acts earlier in the suppressor cascade. The function of this one is to induce activity in the terminal cells of the cascade, and accordingly its effector site has an activating rather than a suppressive effect. Thus, as a general rule, the anti-idiotypic chain can be regarded as a 'schlepper' or carrier, targetting the effector activity to the T cell bearing the appropriate antigenic specificity.

The importance and originality of this part of the claim is as follows. In the first place, it provides fresh insight into the linkage between cells within the immunoregulatory circuits and cascades. If transmitters really work through generating active peptides in the way that Cantor, Gershon and their colleagues propose, then a whole new field of cell biology opens up concerning the mode of action of these peptides. It will be reminiscent of the study of bacterial toxins and colicines, but different insofar as it will deal with physiological interactions rather than attack and defence. Furthermore, the idiotypic- and antigen-binding activity of these transmitters makes sense only if they act at a fair distance. It is refreshing to find this kind of evidence at a time when the case for interleukin-2, hitherto the strongest candidate for a long-distance transmitter between T cells, is weakening^{4,5}. What is more generally agreed is that it profits little to debate whether these transmitters operate physiologically or are *in vitro* artefacts. After all, the neurophysiologists have been debating the same question over substance P for the last fifty years, and the molecular biologists seem to be on the point of building enough of these immunologically active transmitters to answer some really decisive questions. This, in fact, is another reason why the present claim is so important: the new idiotypic- and H-2J-binding sites should

provide useful handles for grabbing these polypeptides in transcription experiments.

But surely what is most important is to have brought together the idiotypic- and antigen-recognizing systems. Hitherto authorities such as Sercarz and Janeway (himself a member of the Yale group) have argued that these two activities are mediated by different T cells ('Ts1 and Ts2'), acting independently of one another and converging only at the end of the regulatory cascade. What is now proposed is that within the suppressor cascade at least, the two activities are not separate.

This brings us to the second part of the claim, advanced in the present publication with further details promised later, that the anti-idiotypic repertoire of T cells is acquired in the thymus. Thus the presence of an (A × B) F₁ thymus graft in an A-strain mouse enables its T cells to produce a factor which recognizes immunoglobulin-linked products on B-strain cells under circumstances where normal A-strain T cells would not be able to do so. This again runs contrary to current doctrine, that the T cell receptor repertoire for recognition of idiotypes is largely independent of the thymus.

How convincing are these claims? The idea that a single factor may carry both J- and an antigen-binding site was implicit in the very first work on J, and has been extended recently to include a factor with J-binding and antigen-binding activities⁶. Incidentally, if Zembala *et al.* are correct, the target of the J- and antigen-binding factor is itself still a suppressor cell, not a helper. What is new is that five activities can all go together, including two from distinct chromosomes (H-2J is on chromosome 19, immunoglobulin on chromosome 12) that appear to be on the same chain. The Yale group indeed recognizes this difficulty, and has no solution to offer at present. They cite other work on two-chain suppressor factors, but the analogy is surely misleading since these involve chains separately encoded by chromosomes 12 and 19.

Perhaps the main point is this. There is a further part of this study which is still owing. In the publications which I have so far seen, there is no direct stoichiometry of the proposed molecular assembly. Obviously the two chains need to be characterized separately, and their binding to one another and to appropriate substrates examined, either in solution or on appropriate absorbents. It looks as though some of the data could be acquired rather easily, particularly as significant readings can be made from as little as "three individual calculations from each culture condition". Perhaps the Yale group already has these data. Until they are available, the group's claims should be treated with some caution.

1. Flood, Yamauchi & Gershon *J. exp. Med.* (in the press).
2. Fresno *et al. J. exp. Med.* 153, 1260 (1981).
3. Yamauchi *et al. J. exp. Med.* (in the press).
4. Keene & Forman *J. exp. Med.* 155, 768 (1982).
5. Crispe *et al. Transplant. Proc.* (in the press).
6. Zembala, Asherson & Golizzi *Nature* 297, 411 (1982).

N.A. Mitchison is in the Department of Zoology, University College London, London WC1E 6BT.

Mapping the Local supercluster

from Joseph Silk

WHAT can be learned about the mechanism of galaxy formation from observations of the Local supercluster, the array of some thousands of galaxies, including those of the Virgo cluster, which is the only one easily accessible to astronomers? The question has been made pointed by the now popular view that only large-density fluctuations, containing 10^{14} solar masses and which are therefore perhaps 10^3 times as massive as the Milky Way system, can have survived from the early universe. Studies of the structure of the Local supercluster (confirming, among other things, that there is indeed a structure) have a bearing on this theory, suggesting that the supercluster may be the evolved state of a minimal surviving density fluctuation.

The prevailing view is that in the early universe, small-scale structure was suppressed by the diffusive smoothing due to radiation to which matter was coupled or, if massive neutrinos were dominant, by collisionless phase mixing and damping. Only when matter could move freely and when it first combined into atoms, some 3×10^5 years after the big bang, was gravitational instability effective at enhancing the growth of density.

Pressure gradients would have been negligible at this stage, and Zel'dovich and his colleagues in Moscow have argued that matter in a region of density fluctuation whose magnitude was of order unity over its extent would probably collapse to what would initially be a highly anisotropic pancake-like configuration. Recent numerical simulations suggest that both filamentary and sheet-like structures may be the generic outcome of such collapses, with great voids separating the highly compressed regions to form an almost cellular structure. The characteristic scale is about 5 Mpc if baryonic matter predominates, but may be somewhat larger if massive neutrinos play that role.

On this theory, the dense sheets of compressed gas cool rapidly by radiation and become unstable to further fragmentation. Galaxies form from the fragments, initially in flattened or elongated configurations which are likely to be only transient, because continuing gravitational collapse and infall tends to make the galaxy distribution spherical. However if the universe is open, with a present mean density of about one-tenth the critical value for closure, gravitational forces do not significantly modify the pancakes if the initial collapse is fairly recent, say at a redshift less than 10.

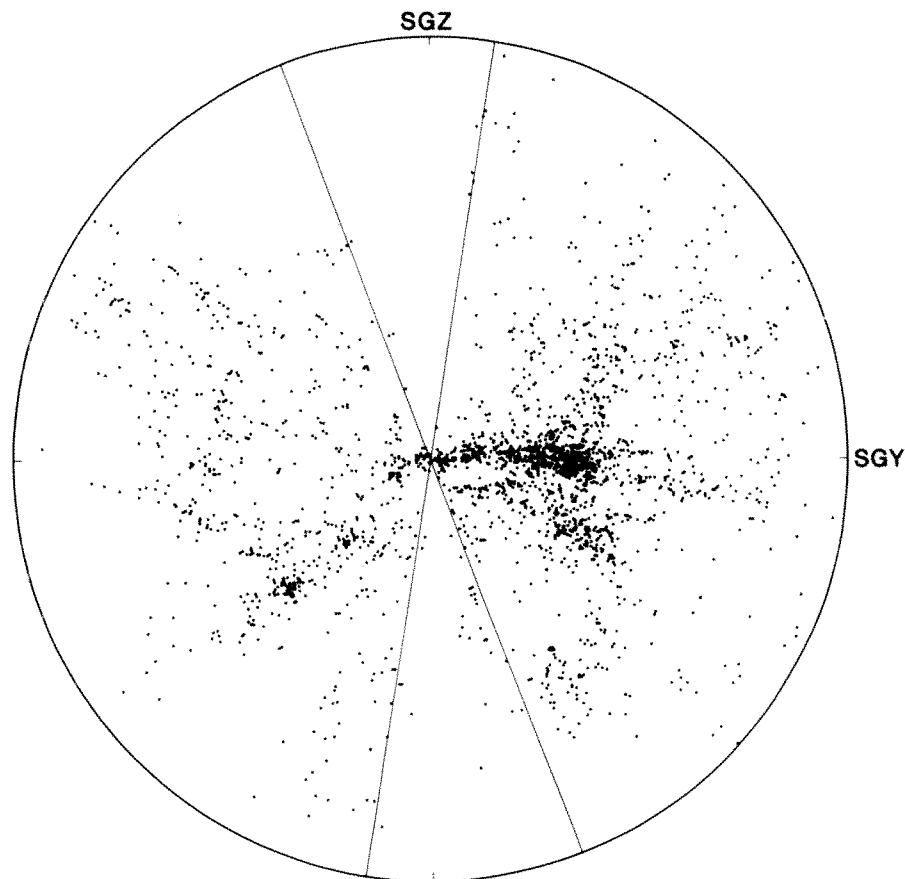
To what extent is this theory consistent with what is known of the distribution of galaxies? Recently, data bearing on the

theory have come from three-dimensional maps of the galaxy distribution and from redshift surveys. There has been a substantial advance on earlier studies of galaxy counts, which yielded only two-dimensional information. Vast regions devoid of luminous galaxies have been discovered, and the galaxies are often distributed in great chains of clusters and superclusters. This is certainly in qualitative agreement with the pancake theory, but it remains difficult to make quantitative comparisons of predictions with observations.

New studies of the galaxy distribution in our immediate neighbourhood are accordingly timely, and may provide the closest and most detailed view of large-scale structure. It has been known for many years that there is a clear excess of nearby galaxies (above background) in a region that extends over 90° or more near the north galactic pole and called by De Vaucouleurs the Local supercluster. The Local Group of galaxies, of which our own Milky Way galaxy and the Andromeda galaxy Messier 31 are the most prominent, lies on the outskirts of the Local supercluster.

The most detailed chart so far of the Local supercluster has been compiled by R. Brent Tully (*Astrophys. J.* 257, 389; 1982), who measured some 2,200 galactic redshifts extending to about three times the distance of the Virgo cluster. He finds that the Local supercluster possesses structure and comprises two distinct components — a thin disk containing sixty per cent of the luminous galaxies with the remainder in an inhomogeneous halo. The thickness of the disk is only 2 Mpc (if the Hubble constant is $100 \text{ km s}^{-1} \text{ Mpc}^{-1}$), whereas its diameter is 12 Mpc. In the halo component, almost all luminous galaxies appear to be in a small number of diffuse clouds, so that most of the halo volume is empty. The more prominent clouds of galaxies are elongated, and their long axes are directed towards the centrally situated Virgo cluster.

To understand this remarkable structure, Tully argues that the disk of the Local supercluster can be so thin only if random motions of galaxies normal to the disk are less than 100 km s^{-1} or if there are very substantial amounts of unseen matter dominating the gravitational attraction within it. The prolate structures found in the halo are suggestive of tidal interactions soon after the halo clouds were formed. The disk thinness is very suggestive of the pancake theory, as is the existence of large volumes devoid of galaxies, but the halo



Inferred positions of 2,175 galaxies projected on a plane roughly coincident with the plane of the Milky Way system. The wedge-shaped regions are the exclusion zones determined by the Milky Way. The dense patch of galaxies to the right of centre includes the Virgo cluster. The radius of the circle, inversely proportional to Hubble's constant, is 30 Megaparsec if Hubble's constant is 100 km s^{-1} . (From Tully *Astrophys. J.* 257, 389; 1982.)

Joseph Silk is Professor of Astronomy at the University of California, Berkeley, California 94720.

clouds pose more of a problem. The mass of a cloud is only about 10^{13} solar masses — uncomfortably low compared with the predicted minimum pancake mass.

The cloud structures could conceivably arise by fragmentation of pancakes. The details of pancake collapse are sensitive to assumptions about the initial distribution of density fluctuations, and only a modest amount of fragmentation is required. But there are more exotic possibilities if gravitinos or other very weakly interacting particles provide the major contribution to the mass density of the universe. One needs particles that are even more weakly interacting than neutrinos: they decouple from the universe at an earlier epoch, when density fluctuations of mass comparable with the horizon size can first grow. In this way, it is possible to have the smallest structures collapse with masses of 10^{13} or even less.

The redshift survey of the Local supercluster, providing information on the velocity field, is also relevant. Aaronson *et al.* (*Astrophys. J.* **258**, 64; 1982) combine data on galaxy redshifts with measurements of IR luminosities and neutral hydrogen line profiles. The Tully-Fisher relation, which expresses the empirical correlation between galaxy luminosity and hydrogen profile width, was used to infer the distances to all galaxies in a restricted sample. The authors thus have independently derived distances and velocities, and so are able to develop a model for the velocity field in the Local

supercluster.

They find that the excess in the local density decelerates galaxies relative to the universal expansion. In addition, the Local Group could have a random component of motion relative to nearby galaxies. The result of fitting the data to the model is a value for the deceleration pattern at the position of the Local Group of about 250 km s^{-1} . This sets an important constraint on the mean cosmological density, which cannot exceed a value of about one-third of the critical density for a closed universe. If the mean density were any larger, a correspondingly larger gravitational acceleration would be experienced by the Local Group than is inferred from the observations.

One surprising result has emerged from the analysis of the velocity field in the Local supercluster. Aaronson *et al.* also examined a model which allowed rotation about the supercluster centre in addition to deceleration from the Hubble flow. A significant effect was found: the rotation velocity at the position of the Local Group is $180 (\pm 60) \text{ km s}^{-1}$. It may be premature to overemphasize the significance of such a rotation, but it would be a relatively natural outcome of the pancake theory in which coherent formation of large-scale structure occurs. It is also worth noting that the concept of rotation loses much of its meaning for the Local supercluster: the Local Group has completed only a small fraction of a single orbit since the formation of the supercluster. □

unique in acting even more potently on the κ opiate receptor sub-type, where its actions are only weakly antagonized by naloxone⁷. This and other evidence led Cavkin, James and Goldstein⁷ to suggest that dynorphin might represent a specific endogenous ligand for the κ opiate receptors, but the recent results of Weber *et al.*³ and those described in an accompanying article by Corbett *et al.*⁸ suggest that at least in brain, this role is more likely to be filled by a smaller fragment of the dynorphin molecule, dynorphin₁₋₈.

Using three highly specific radio-immunoassays which recognized dynorphin₁₋₁₇, dynorphin₁₋₈ and α -neoendorphin respectively, Weber *et al.* found that dynorphin₁₋₈ was present in various areas of rat brain in concentrations which were about ten times higher than those of the complete molecule dynorphin₁₋₁₇ and almost precisely equal to those of α -neoendorphin, suggesting that it may share with α -neoendorphin a common biosynthetic origin². Weber *et al.* presented chromatographic evidence to support the claim that the immunoreactive material measured did indeed correspond to dynorphin₁₋₈, which had previously been described as a naturally occurring peptide in extracts of hypothalamus and pituitary^{9,10}. The regional distribution of the dynorphin-related peptides in brain — with the highest concentrations in striatum and hypothalamus — differs from that of the enkephalins, suggesting they occur in distinct neuronal systems.

Some insight into the possible significance of the existence of dynorphin₁₋₈ in brain is provided by the recent results of Corbett *et al.*⁸ on the pharmacological activities of this and various other dynorphin-related peptides. Using a variety of bioassays and radioligand-binding assays capable of discriminating between the μ , δ and κ receptor sub-types, they show a dramatic difference in the pharmacological profiles of Leu-enkephalin and dynorphin₁₋₈ (Leu-enkephalin-Arg-Arg-Ile). Whereas Leu-enkephalin is a selective δ agonist with only weak activity on κ receptors, dynorphin₁₋₈ is less active as a δ agonist but over 1,000 times more potent than Leu-enkephalin as a κ -receptor agonist. The full-sequence peptide, dynorphin₁₋₁₇, is highly potent on all three types of opiate receptor, but less selective than the octapeptide in its κ -receptor activity.

Corbett *et al.* also find that, like most other short opioid peptides, dynorphin₁₋₈ is much more rapidly metabolized in brain

Yet another opioid peptide?

from L.L. Iversen

THE discovery, some seven years ago, that the brain contains its own morphine-like chemicals — the pentapeptides leucine- and methionine-enkephalin¹ — has aroused enormous interest and is rightly regarded as one of the most significant recent advances in our understanding of brain chemistry. Since then, however, a bewildering variety of other naturally occurring opioid peptides has been described². With almost a dozen such compounds already known, the recent report by Weber *et al.*³ of yet another naturally occurring endorphin in brain might at first sight seem merely to add to the difficulties we face in understanding this group of substances. However, the new peptide, which represents the amino-terminal octapeptide fragment of dynorphin (Fig.1), has some unusual properties.

Dynorphin is a potent opioid peptide first identified by Goldstein and colleagues

in pituitary extracts⁴, containing 17 amino acid residues⁵. It belongs to the third branch of the opioid peptide dynasty², of which the first branch comprises the pentapeptide enkephalins and their various slightly elongated forms, and the second branch β -endorphin and other peptides derived from the pro-opiomelanocortin precursor. Dynorphin₁₋₁₇ and related peptides, such as α -neoendorphin⁶ (Fig.1), all contain Leu-enkephalin as their amino-terminal sequence, but dynorphin has strikingly different pharmacological properties from Leu-enkephalin and other opioid peptides. Although, like the other peptides, it is a potent agonist at both μ and δ opiate receptor sub-types, dynorphin is

Dynorphin-related peptides.

Leu-enkephalin	Tyr-Gly-Gly-Phe-Leu
Dynorphin ₁₋₈	Tyr-Gly-Gly-Phe-Leu-Arg-Arg-Ile
Dynorphin ₁₋₁₇	Tyr-Gly-Gly-Phe-Leu-Arg-Arg-Ile-Arg-Pro-Lys-Leu-Lys-Trp-Asp-Asn-Gln
α -Neoendorphin	Tyr-Gly-Gly-Phe-Leu-Arg-Lys-Tyr-Pro-Lys

L.L. Iversen is Director of the MRC Neurochemical Pharmacology Unit, Hills Road, Cambridge CB2 2QH.

than the full-length dynorphin₁₋₁₇ — thus the potency of the octapeptide was markedly increased when a cocktail of peptidase inhibitors was added to the assay system. This is in keeping with a putative transmitter role for dynorphin₁₋₈, whereas the longer peptide, dynorphin₁₋₁₇, may be more important in a hormonal function, perhaps after secretion from the pituitary. The companion peptide, α -neoendorphin, is pharmacologically similar to dynorphin₁₋₈.

Whether these two peptides represent a distinct new family of endogenous ligands for the κ sites in brain and spinal cord remains to be established, but this is certainly an intriguing possibility. The function of these sites remains obscure, but κ -selective drugs, for example ethylketocyclazocine and bremazocine, are known to be effective analgesics and do not substitute for morphine in preventing with-

drawal symptoms in morphine-dependent animals⁹ (they seem to have only low addiction liability). Drugs with such a profile clearly have therapeutic potential, and a better understanding of the κ -receptors and their endogenous ligands is urgently needed. □

1. Hughes, J. *et al.* *Nature* **258**, 577 (1975).
2. Rossier, J. *Nature* **298**, 221 (1982).
3. Weber, E., Evans, C.J. & Barchas, J.D. *Nature* **299**, 77 (1982).
4. Goldstein, A. *et al.* *Proc. natn. Acad. Sci. U.S.A.* **76**, 6666 (1979).
5. Goldstein, A. *et al.* *Proc. natn. Acad. Sci. U.S.A.* **78**, 7219 (1981).
6. Kangawa, K. *et al.* *Biochem. biophys. Res. Commun.* **99**, 871 (1981).
7. Cavkin, C., James, I.F. & Goldstein, A. *Science* **215**, 413 (1982).
8. Corbett, A.D. *et al.* *Nature* **299**, 79 (1982).
9. Minamino, N. *et al.* *Biochem. biophys. Res. Commun.* **95**, 1475 (1980).
10. Seizinger, B., Holtt, V. & Herz, A. *Biochem. biophys. Res. Commun.* **102**, 197 (1981).

Plasma astrophysics at Santa Barbara

from R. Rosner*, E. Zweibel† and V. Trimble‡

AT the workshop on 'Space and Astrophysical Plasmas' held this summer at the Institute for Theoretical Physics at the University of California, Santa Barbara, three topics held sway: hydromagnetic shocks and particle acceleration, the interaction of hot and cold plasmas, and hydromagnetic flows. A diverse group of theorists from the laboratory plasma, space plasma and astrophysics communities took part.

The possibility that particles can be accelerated to high energies in the vicinity of collisionless shocks — yielding solar and galactic cosmic rays and relativistic particles in extragalactic radio sources — has received wide attention in recent years. The outstanding problems include the structure of collisionless shocks (the mechanisms which produce a shock transition in collisionless plasmas), the 'injection problem' (how thermal particles can be extracted from the background plasma and accelerated to high energy), the shock efficiency and — most difficult — the interaction between the accelerating particle population and the processes determining shock structure and acceleration efficiency.

These difficult issues can be at least partially addressed by observations of the terrestrial bowshock, produced by the interaction between the solar wind and the terrestrial magnetosphere. E. Greenstadt (TRW) showed that while the shock layer is quite thin when the interplanetary magnetic field is nearly normal to the direction of motion of the shock (quasi-perpendicular case), it is highly irregular and quite extended in space in the quasi-

parallel case (magnetic field nearly parallel to the direction of motion of the shock). A fraction of the incoming solar wind particles is reflected back upstream, and these particles excite low-frequency electromagnetic waves which exert a retarding force on the solar wind. A diffuse energetic ion component is also observed. The terrestrial bowshock (and interplanetary shocks) will evidently provide important 'laboratory' constraints on theoretical studies of shock structure and particle acceleration.

The problems of internal shock structure, including the details of ion dynamics, were addressed by a number of theorists by powerful numerical simulations of collisionless shocks. The simulations show reflected ions and short-wavelength electromagnetic turbulence (D. Forslund, Los Alamos), in reasonable agreement with observations, with ions bent back upstream by the enhanced magnetic field in a postshock magnetic overshoot layer (C. C. Goodrich, University of Maryland). However, the need of an electrostatic potential layer to slow down electrons (in quasiparallel shocks) remains unresolved by the present simulations and observations.

The basic model of shock acceleration, the starting point for discussions at the workshop, is a steady-state model in which

cosmic rays diffuse in the vicinity of a high Mach number quasi-parallel shock which is approximated to by a discontinuity in flow speed. Observations of cosmic-ray secondaries ($E \sim 1$ to 100 GeV) constrain the extent to which cosmic rays can be accelerated to high energies by successive passage through interstellar shocks because the volume in which acceleration occurs does not exceed 10 per cent of the confinement volume (W. I. Axford, Max-Planck Institut). The cosmic rays are scattered by magnetic irregularities, which are assumed to be nearly stationary in the frame of the flow; thus, because of the jump in flow speed across the shock, particles are accelerated by a first-order Fermi process as they scatter back and forth across the shock front, with the well known result that the energetic particle spectrum is quite similar to that of galactic cosmic rays.

Some major issues remain unresolved, however. Thus the efficiency of the shock (the fraction of energy which goes into relativistic particles) is not determined, and the properties of the hypothetical scattering centres, which determine the cosmic ray diffusion coefficient, must be specified *ad hoc*. If the scattering mean-free path is not large compared with the width of the shock transition, the detailed fluid velocity profile must determine the acceleration. But the flow itself is modified by the coupling between the cosmic ray momentum flux and pressure and the thermal gas, the modification being highly sensitive to the details of the coupling (D. Eichler, University of Maryland; H. Volk, Max-Planck Institut/University of Chicago).

There is a very different problem in the transfer of energy between hot and cold plasmas. Thus the structure of the transition layer between the solar chromosphere and corona is crucial to an understanding of the energetics of these plasmas, but the construction of valid model atmospheres is complicated by the high degree of spatial inhomogeneity (including the probable existence of unresolved features), flows in the boundary layer region and the general absence of steady-state conditions (R. Rosner, Harvard University). Even if these difficulties were not present, calculations show that the electron distribution function in the transition region (E. Shoub, Stanford University) is significantly non-Maxwellian. The distribution at a given height is 'contaminated' by superthermal particles representative of the temperature of overlying layers, possibly significantly altering the rates of collisional ionization and excitation (and the heat flux). Thus, the diagnostic problem remains a major difficulty in modelling solar thermal boundary layers.

Different problems arise in heat transport in laser-irradiated plasmas (C. Max, Lawrence Livermore). Experiments show the heat flux often to be much less than predicted by classical transport

*Harvard-Smithsonian Center for Astrophysics, Cambridge, Massachusetts 02138.

†University of Colorado, Boulder, Colorado 80309.

‡University of California, Irvine, California 92717.

formulae. The solution may lie in improved classical calculations; in the suppression of heat flux by plasma instabilities (ion acoustic waves, Weibel instabilities and so on) which increase the electron-scattering frequency; or in the inhibition of thermal conduction by strong (megagauss) d.c. magnetic fields (which occur because the isothermal and isodensity surfaces do not coincide, as in the classic Biermann 'battery' dynamo). In any case, the observed heat flux appears to limit at about 3–9 per cent of the free-streaming value, a result which the simulations do not as yet reproduce.

This observation is clearly relevant to models of heat exchange between tenuous hot plasma and much cooler gas in the interstellar medium of galaxies (discussed by C. McKee, University of California, Berkeley, and S. Balbus, MIT). In such models, the crucial parameters controlling the dynamics are the ratio of the thermal electron mean free path to the dimension of the cool plasma embedded in the hotter gas phase; and the dimensionless coefficient marking the reduction of the heat flux below its free-streaming value. Present calculations have now explored the parameter space of the hot electron-cold plasma interaction in some detail; presumably, the 'zoo' of possible solutions must be constrained by observations (which are likely to lend considerable insight into the dominant mechanisms of energy transport across such steep temperature boundary layers) and by the laboratory laser work (which reduces the arbitrariness of assigning a reduction factor to the saturated heat flux).

The discussions on hydromagnetic (MHD) flows indicated that although much is understood in restricted contexts, and there is an appreciation of the connections on the observational level, an integrated theoretical view of the problem (as is now emerging in the above two cases) is not yet at hand. At the very fundamental level, it is apparent that study of equilibria may be of limited usefulness because, for example, one can now show (E. N. Parker, University of Chicago) that 'most' perturbations lead to departures from equilibrium conditions characterized by some symmetry property (these are indeed the only known equilibria). Furthermore, MHD equilibria which have been shown to be stable to (analytical) perturbations have only remote connections with observed magnetic structures (on, for example, the Sun). It is likely that further progress will require sophisticated numerical (MHD) simulations, as experience in laboratory fusion work has indicated.

There is considerable interest in studying the dynamic interaction between hydrodynamic flows and ambient magnetic fields, such as occurs both within the solar wind and in its interaction with planetary magnetospheres (T. Holzer, HAO); and in the interaction between the relativistic plasma and ambient magnetic fields

surrounding pulsars (J. Arons, University of California, Berkeley). In the case of solar wind streams the origin of the high speeds remains a basic question. Observations have now placed stringent constraints on the available wave momentum flux below the solar corona, which seem severely to constrain the popular Alfvén wave-driven models. Another outstanding problem remains the construction of a self-consistent magnetosphere, a problem which is, as pointed out by Arons, very reminiscent of the global terrestrial magnetosphere problem discussed earlier by J. M. Cornwall (University of California, Los Angeles).

In both cases, local theories encounter the difficulty that the current flow is determined by boundary conditions which, in fact, simply reflect global structure. An interesting further example of hydromagnetic flows which seem to be ubiquitous are the 'bi-polar' flows, or jets,

discussed by A. Königl (University of California, Berkeley); these are perhaps best known in the context of radio galaxies and relatively exotic objects such as SS433, but are apparently also associated with protostellar objects. The mechanisms responsible for the initial plasma acceleration and for the high degree of collimation are at the heart of current theoretical studies; Königl focused particular attention on radiative driving and on the beaming resulting from the planar symmetry and stratification of gas in accreting protostellar objects.

On the whole, our impression was that this workshop gave substance to the long-rumoured emergence of plasma astrophysics as a well defined discipline; the discussions indicated that a community of scholars has 'gelled' in at least two of the three principal topics of discussion and that the much-discussed, but often in practice neglected, contact with laboratory and space plasma physics has been made. □

Key structures in transposition

from N. Symonds

It is widely agreed that transposition is normally a replicative process but little is known about the location of replication origins within transposons or the events which herald the initiation or termination of DNA synthesis. Of undoubted importance are the sequences at the ends of transposons which remain constant during transposition and, in nearly all cases, are inverted repeats of one another. It was this symmetry in the structure of transposons, together with a considerable amount of genetic data, which led Shapiro¹ to propose his model for transposition which has become the archetype for the numerous alternative schemes subsequently put forward.

The model involves a symmetric intermediate structure possessing two replication forks for DNA synthesis (Fig. 1a). It has been successful in explaining the properties of such transposons as Tn3 and $\gamma \delta$, but it fits less well with the properties of phage Mu from which most of Shapiro's early genetic data were obtained and which, ironically as it turned out later, seems to be the only transposon lacking inverted repeats at its ends.

As well as discrepancies in the genetic data, earlier electron-microscope studies by Harshey and Bukhari² had indicated that the intermediate structures in Mu transposition were not as predicted from the Shapiro model but consisted of 'keys' having circles of variable size attached to

tails of variable length. This led these authors to propose a modification to the Shapiro model with an intermediate structure essentially as depicted in Fig. 1b. The main innovation is that it contains a single replication fork starting from one end only of the transposon: the second end of the target molecule is left unligated until the last stage in the transposition process and in the interim is held by a protein complex which could be the replication complex itself. Protease treatment of such an intermediate then yields a key molecule with a free end.

To obtain definitive evidence that the key structures are indeed transposition

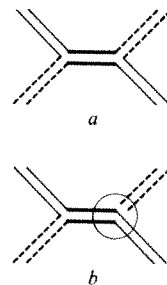


Fig. 1 The initial intermediate structures in transposition according to *a*, the original model of Shapiro (two replication forks); and *b*, the modification of Harshey and Bukhari (one replication fork). Solid lines: donor DNA containing the transposon (heavy lines). Dotted lines: target molecule. The circle represents a protein complex and could be located at the replication fork. Normally the donor and target molecules would be on different circular genomes, or at different locations on the same circular genome.

N. Symonds is in the School of Biological Sciences, The University of Sussex, Falmer, Brighton, Sussex BN1 9QG.

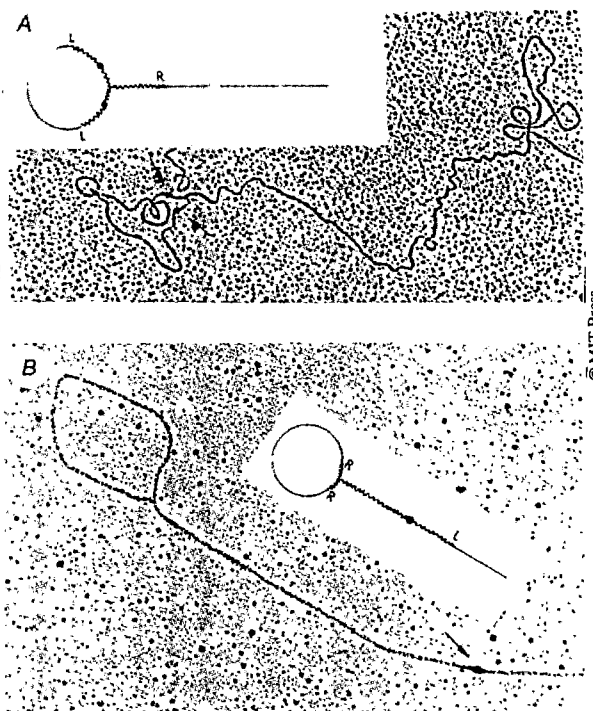
intermediates and to determine from which end of the Mu genome replication is initiated, Harshey and Bukhari³ have recently performed some ingenious experiments using a Mu derivative into which they first engineered a *lac* operator site. After induction, the Mu derivatives were allowed to undergo transposition and the DNA was passed over nitrocellulose filters containing *lac* repressor. All Mu-containing DNA was trapped on the filters by *lac* repressor-operator binding and the *lac* repressor-binding sites were subsequently visualized in the electron microscope by complexing the repressor with ferritin-conjugated antibody (Fig. 2). These experiments, and others employing restriction analysis, have shown unequivocally that key structures contain replicating DNA and so are true transposition intermediates. The experiments also throw an unexpected result into the transposition debate: Mu replication can originate with equal facility from either end of the genome.

As the two ends of Mu possess different DNA sequences it is not altogether surprising that there should be some asymmetry in the initial events of Mu transposition. A first guess would be that one end of Mu was involved in DNA initiation, the other in termination; but the new results show unexpectedly that this is clearly not the case. The role of the two ends of Mu (which do possess certain sequence similarities⁴) in transposition must therefore be more subtle. The deletion of either end of Mu abolishes even the introduction of a single-strand nick in the donor molecule, so the two ends of the genome must presumably act in some co-operative way for transposition to be initiated.

If the end of Mu at which replication commences is not determined by the terminal sequences, then other causes must be sought. Two possibilities are the availability of specific enzymes and the DNA sequences at the target sites. The products of two Mu genes, *A* and *B*, are essential for efficient transposition and the *A* product is known to be present in limiting amounts. Perhaps only a single molecule of *A* product is normally available for a particular Mu genome, and it could bind either to the left or the right end, so triggering off replication from either direction.

With regard to the preference of Mu for particular target sites, few sequence data are available. It is usually said that Mu integration occurs completely at random — certainly Mu phage can integrate at a large number of locations in the bacterial chromosome — but it must be remembered that the integration of phage DNA to form lysogens is not necessarily an identical

Fig. 2 Electron micrographs of Mu DNA undergoing transposition, showing the key structures as transposition intermediates. The *lac* operator appears as an electron-dense ferritin core; L and R, left and right ends of Mu respectively. In *A*, the ferritin cores are equidistant from the junction between the circle and tail, so replication must have taken place, with the replication fork at the junction. The Mu plasmid is 16.5 kb long and the *lac* operator 5 kb from the left end. As the circle in *A* is 12 kb, the key structure must be a result of replication starting at the left end. In *B*, the circle is 8.9 kb and there is one ferritin core on the tail. The key structure could only have arisen from replication starting at the right end.



process to that which goes on in the experiments considered here, which follow Mu transposition in lysogenic cells which have undergone induction. There is indeed some indirect evidence that in these conditions transposition does occur into non-random sites⁴, and these sites in turn could

determine at which end the replication of Mu commences.

There is one afterthought from this discussion. If Mu can transpose so efficiently without having inverted repeats at its ends, why do other transposons all seem to possess them? □

Survival mechanisms in wetland plants

from Peter D. Moore

AN apparently simple problem faces the wetland ecologist when considering how it is that flood-tolerant plants are able to survive anoxic conditions. The roots of wetland plants are often, sometimes permanently waterlogged and thus subject to low oxygen tensions. Below about eight per cent oxygen saturation (about 320–350 mV at pH 5)¹, ferric ions are replaced by ferrous ions and environmental conditions are distinctly reducing, and yet many species of plant can still survive.

In practical terms, the ecologist encounters two main difficulties. The first is that in anoxic conditions, not only does the plant encounter problems of oxygen supply, but it also experiences a build-up of potentially toxic materials², such as ferrous and manganese ions and perhaps even organic compounds produced by incomplete microbial decay³, which may affect its response. The second is the sheer technical difficulty of producing strictly anoxic conditions in order to test the plant's degree of dependence on oxygen supply.

Field experimentation, such as that of Armstrong and Boatman⁴, has shown that different plants have varying tolerance to anoxia. The wetland grass *Molinia caerulea*, for example, was not found in peats with oxidation-reduction potentials below 50–100 mV (no hydrogen sulphide was present at this oxidation level), whereas the bogbean, *Menyanthes trifoliata*, was able to tolerate lower oxygen tensions and free sulphide. Oxygen undoubtedly diffuses from the above-ground structures into the roots of wetland plants, especially those with anatomical air ducts, such as *Menyanthes*⁵, and may even diffuse out of the root to form an oxygen-enhanced sheath^{6,7}. This can produce complex micropatterns of oxygen concentration in the field, making experimentation difficult.

To overcome the complications due to

Peter D. Moore is a Senior Lecturer in the Department of Plant Sciences, University of London King's College, 68 Half Moon Lane, London SE24 9JF.

1. Shapiro *Proc. natn. Acad. Sci. U.S.A.* 76, 1933 (1979).
2. Harshey & Bukhari *Proc. natn. Acad. Sci. U.S.A.* 78, 1090 (1981).
3. Harshey & Bukhari *Cell* 29, 561 (1982).
4. Kamp & Kahmann *Cold Spring Harb. Symp. quant. Biol.* 45, 329 (1981).

oxygen diffusion, Laing^{8,9} supplied aquatic plants with an atmosphere of nitrogen and showed that some species, such as pickerel weed (*Pontederia cordata*), grew well, whereas reedmace (*Typha latifolia*) did not, again confirming the interspecific differences in anoxia tolerance. But the nitrogen supply used by Laing could not be regarded as totally oxygen free, so his results still did not establish how long various plant species could survive in strictly anoxic conditions.

R.M.M. Crawford has long maintained that the tolerance of a plant species to flooding is a function of its metabolic adaptation to the low oxygen tensions in its tissues. One obvious effect of oxygen scarcity on a non-adapted plant is the build-up of ethanol to toxic levels in its cells, this being the end point of glycolysis in anaerobic conditions. Crawford was able to show that flood tolerance involved the control of ethanol production¹⁰ and with McManmon¹¹ he proposed that in anoxic conditions, the glycolytic pathway is diverted to oxaloacetate and (non-toxic) malate which, if the activity of malic enzyme were impaired, would accumulate and a return to pyruvate and ethanol production would be prevented. In flood-

tolerant species such as *Glyceria maxima* and *Iris pseudacorus*, they found that malic enzyme was indeed inactive and malate accumulated. Subsequently, Crawford has shown that in tolerant trees, malate accumulates in response to flooding and ethanol production is controlled¹², and that in pea seedlings anoxic death is closely related to the build-up of ethanol, an internal concentration of 60 μ M being apparently the critical survival threshold¹³.

If the response of a plant species to flooding indeed depends on its metabolic adaptations rather than its efficiency in translocating oxygen from another part of

its body, then one should be able to observe interspecific differences in survival under strictly anoxic conditions. It is precisely this experiment that Barclay and Crawford¹⁴ have now carried out to vindicate the metabolic theory. They have grown a range of species under an oxygen-free nitrogen atmosphere (85 per cent N₂, 10 per cent H₂ and 5 per cent CO₂) in the presence of a palladium catalyst to ensure a total absence of oxygen. They found that some species, for example the bulrushes *Scirpus lacustris* and *S. maritimus*, not only survived but continued to grow over 14 days, whereas others, such as *Phragmites* and *Iris*, survived but showed no growth after 7 days, and another group, for example *Glyceria maxima* and *Juncus effusus*, failed to survive the week. This latter group included, rather surprisingly, rice (*Oryza sativa*) which has previously been regarded as particularly anoxia tolerant.

The capacity of some wetland plants to survive in conditions of strict anoxia, together with the degree of variation found among the species tested, strengthen very considerably the assertion that flood tolerance can, at least in part, be explained at the cellular, metabolic level. □

1. Pearsall, W.H. *J. Ecol.* 26, 298 (1938).
2. Rutter, A.J. *J. Ecol.* 43, 507 (1955).
3. Drew, M.C. *Curr. Adv. Pl. Sci.* 11, 1 (1979).
4. Armstrong, W. & Boatman, D.J. *J. Ecol.* 55, 101 (1967).
5. Coult, D.A. & Vallance, K.B. *J. exp. Bot.* 9, 384 (1958).
6. Jeffery, J.W.O. *J. Soil Sci.* 12, 172 (1961).
7. Jeffery, J.W.O. *J. Soil Sci.* 12, 317 (1961).
8. Laing, H.E. *Am. J. Bot.* 27, 574 (1940).
9. Laing, H.E. *Bot. Gazette* 102, 712 (1941).
10. Crawford, R.M.M. *J. Ecol.* 54, 403 (1966).
11. McManmon, M. & Crawford, R.M.M. *New Phytol.* 70, 299 (1971).
12. Crawford, R.M.M. & Baines, M.A. *New Phytol.* 79, 519 (1977).
13. Barclay, A.M. & Crawford, R.M.M. *J. exp. Bot.* 32, 943 (1981).
14. Barclay, A.M. & Crawford, R.M.M. *J. exp. Bot.* 33, 541 (1982).

100 years ago

NEW OR RARE ANIMALS IN THE ZOOLOGICAL SOCIETY'S LIVING COLLECTION

THE PIGMY HOG (*Porcula salvania*). — Few additions to the Zoological Society's living collection of late years have attracted more attention than the Pigmy Hogs of Nepal, of which the first specimens ever imported into Europe reached the Gardens in May last.

For our first knowledge of the existence of this diminutive form of the pig-family in the sub-Himalayan forests we are indebted to the researches of Mr. Bryan H. Hodgson, formerly Resident at the Court of Nepal, who described the Pigmy Hog so long ago as 1847, in an article published in the *Journal of the Asiatic Society of Bengal*. While the Wild Boar, or a species closely resembling it abounds all over India, the Pigmy Hog is exclusively confined, as Mr. Hodgson tells us, to the deep recesses of the primeval forests of the Terai of Nepal and Bhotan, where it roams about in herds. It is very rarely seen even by the natives. A well-known hunter informed Mr. Hodgson that during fifty years' abode in the Saul forests he had obtained but three or four of these animals to eat, partly owing to their scarcity, and partly to the speed with which the females and young disperse, and to the extraordinary vigour and activity with which the males defend themselves while their families are retreating.

THE CABOT'S TRAGOPAN (*Ceriornis caboti*). — The Tragopans, or Horned Pheasants, constituting the genus *Ceriornis* of naturalists, must be ranked amongst the finest and most brilliantly coloured representatives of the splendid group of Indian game birds. Two of them — the Crimson Tragopan of the Central and Eastern Himalayas, and the Black-headed Tragopan of the Western Himalayas and Cashmere, are well known to Indian Sportsmen, and are familiar objects of pursuit, though we believe, by no means easily procured. The Crimson Tragopan was introduced into Europe by the Zoological Society in 1859, and has frequently bred in their Gardens, as has likewise the Temminck's Tragopan (*Ceriornis temminckii*), first received by the Society in 1864.

Between the furthest known eastern range of the Crimson Tragopan and the frontiers of China a fourth species of *Ceriornis* has its home — Blyth's Tragopan (*C. blythi*).

The fifth and last species of Tragopan, lately acquired by the Zoological Society, is still more rare and little known than the four above-mentioned members of the genus. Cabot's Tragopan, as it is called, was described in 1857 by the late Mr. Gould, and subsequently figured in his great illustrated work on the *Birds of Asia*. Its habitat is South-Eastern China, but little is yet known of its exact range. The only naturalist who has met with it in its native wilds is the celebrated Chinese explorer, M. le Père David. M. David, in his "*Oiseaux de la Chine*," tells us that he found this fine Gallinaceous bird rather common in the wooded mountainous range which separates the provinces of Folien and Kiangsi, when he traversed this district in the autumn of 1873.

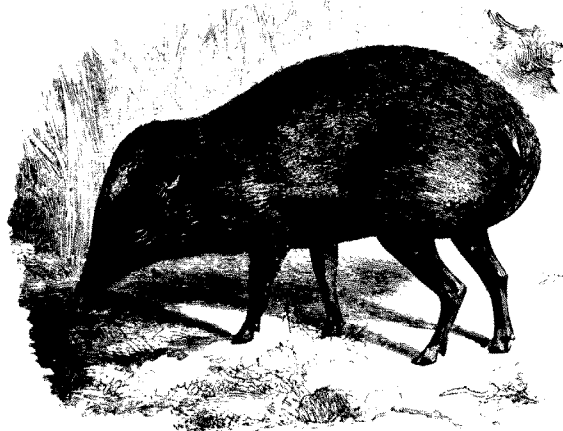


FIG. 23.—The Pigmy Hog.

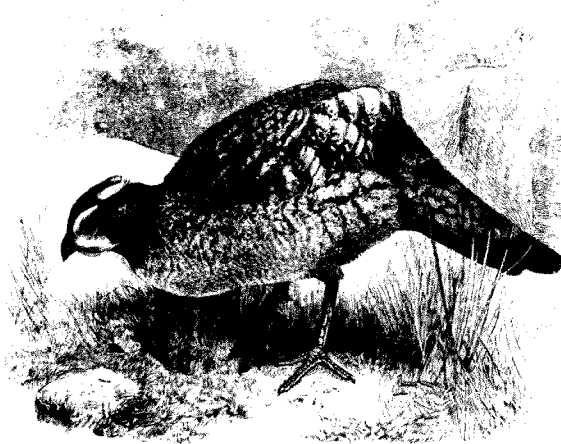


FIG. 24.—The Cabot's Tragopan.

REVIEW ARTICLE

Postnatal development of the visual cortex and the influence of environment

Torsten N. Wiesel*

The following is the lecture delivered by the author in Stockholm on 8 December 1981 when he received the Nobel Prize in Medicine, which he shared with Roger Sperry and David H. Hubel. The article is published here with permission from the Nobel Foundation and will also be included in the complete volume of Les Prix Nobel en 1981 as well as in the series Nobel Lectures (in English) published by Elsevier.

IN the early 'sixties, having begun to describe the physiology of cells in the visual cortex of the adult cat¹, David Hubel and I decided to investigate how the highly specific response properties of cortical cells emerged during postnatal development. We were also interested in examining the role of visual experience in normal development, a question raised and discussed by philosophers since the time of Descartes. The design of these experiments was undoubtedly influenced by the observation that children with congenital cataracts still have substantial and often permanent visual deficits after removal of the cataract and proper refraction². Also, behavioural studies had shown that animals raised in the dark or in an environment devoid of contours have a similar impairment of their visual functions^{3,4}.

Because of the difficulties associated with raising kittens in total darkness, we decided to fuse the lids by suture. This procedure prevented any form vision without completely depriving the animal of light. We expected this to be an effective procedure because cortical cells respond to contours and are insensitive to changes in levels of diffuse light⁵. Initially we raised kittens with only one eye closed, using the other eye as a control. This design turned out to be fortunate because the effects of single eye closure on the visual cortex are more dramatic than the results obtained from animals raised with both eyes occluded or kept in the dark.

Our initial findings were that kittens with an eye occluded by lid suture during the first 3 months of life were blind in the deprived eye and that in the striate cortex the majority of the cells responded only to stimulation of the normal eye⁶. This defect seemed to be localized to the visual cortex, perhaps at the site of interaction between geniculate afferents and cortical cells⁷. From another series of experiments, we found that the properties of orientation specificity and binocularity developed through innate mechanisms⁸. This result, taken together with the monocular deprivation experiment, indicated that neural connections present early in life can be modified by visual experience. Such neural plasticity was not observed in the adult cat, but existed only during the first 3 postnatal months⁹.

The early experiments were done in the cat, but we soon turned our attention to the rhesus monkey. Having demonstrated that cells in the monkey visual cortex also respond selectively to lines of different orientations and often are binocular¹⁰, we showed that the monkey was also susceptible to visual deprivation¹¹, a finding subsequently confirmed and extended¹²⁻¹⁵. Further advances in our understanding of the nature of and mechanism underlying the deprivation phenomena depended on working out some of the functional architecture of the visual cortex. This was done through further physiological experiments in the normal animal and by using

newly developed anatomical methods¹⁶⁻²¹. Over the years, our parallel pursuit of the normal and developmental studies has accelerated our progress in both areas. For example, while the deprivation experiments depended on the understanding of the functional architecture of the normal adult animal, we were alerted to the existence of ocular dominance columns in the cat by experiments we had done in strabismic animals²².

In this lecture I will present our current understanding of the development of the monkey visual cortex and the role of visual experience in influencing neural connections. Rather than attempt to discuss in any detail the now extensive literature in the field, I will emphasize the work carried out in our laboratory²³⁻²⁵. Hubel and I did much of this work in collaboration with Simon LeVay.

Monocular deprivation

The procedure of suturing a monkey's eyelid shut creates a condition similar to a cataract, since though the light reaching the retina through the closed lid is only slightly attenuated (by a factor of 3), the forms of objects are no longer visible. As mentioned above, when the deprived eye is opened after months of deprivation, the animal is unable to see with it: there are no obvious changes in ocular media, the retina or the lateral geniculate nucleus (LGN) that can explain this deficit; instead marked changes have occurred at the level of the primary visual cortex (striate cortex). Even if the ocular media are clear, the occluded eye develops with time a marked axial-length myopia (up to 12 dioptres over a 1-yr period)²⁶.

One way of seeing the change is to record from cells in the striate cortex and determine their ocular preference⁷. In the monkey, there is normally a fairly even balance between cells driven preferentially by one eye and cells driven preferentially by the other¹⁰. In layer 4, most cells are strictly monocular, and outside layer 4 they are usually binocular, although they still tend to respond more strongly to stimulation of one eye than the other. About as many cells prefer stimulation of the left eye as prefer stimulation of the right (Fig. 1a). In conditions of monocular deprivation, however, the great majority of cortical cells are driven exclusively by the nondeprived eye (Fig. 1b)¹¹⁻¹³. One could ask whether this can be accounted for in terms of changes occurring at the level of the LGN. Although the cells lying in the geniculate layers that receive input from the deprived eye are smaller than those in the nondeprived layers (Fig. 2), they are present in normal numbers, respond briskly to stimulation of the deprived eye, and have normal receptive fields. Since geniculate cells are functionally normal and the cortical cells are altered in their properties, there must be some change in the effectiveness of the geniculocortical connections. We were interested in investigating whether there were any structural changes associated with this abnormality.

The first aspect of cortical organization to be examined is the pattern of input of the geniculate afferents to the cortex.

* Department of Neurobiology, Harvard Medical School, Boston, Massachusetts 02115, USA.

This can be done with the autoradiographic technique for tracing neuronal connections, either transynaptically from the eye^{18,21} or by a fibre stain¹⁹. When in the normal monkey the input from the LGN reaches layer 4 of the cortex, the information from the two eyes is still segregated. The input from each eye is distributed into a series of branching and anastomosing bands about 0.5 mm wide, which alternate with similar bands serving the other eye (Fig. 3a). This pattern of innervation forms the anatomical basis for ocular dominance columns. Cells in the superficial and deep layers, while tending to be more binocular than cells in layer 4, are still more strongly influenced by the eye that provides input to the column in which they reside. The relative influence of the two eyes is shown by making tangential electrode penetrations through different cortical layers. Such penetrations in the normal monkey show regular changes in eye preference as expected from the columnar arrangements (Figs 3a, 4a).

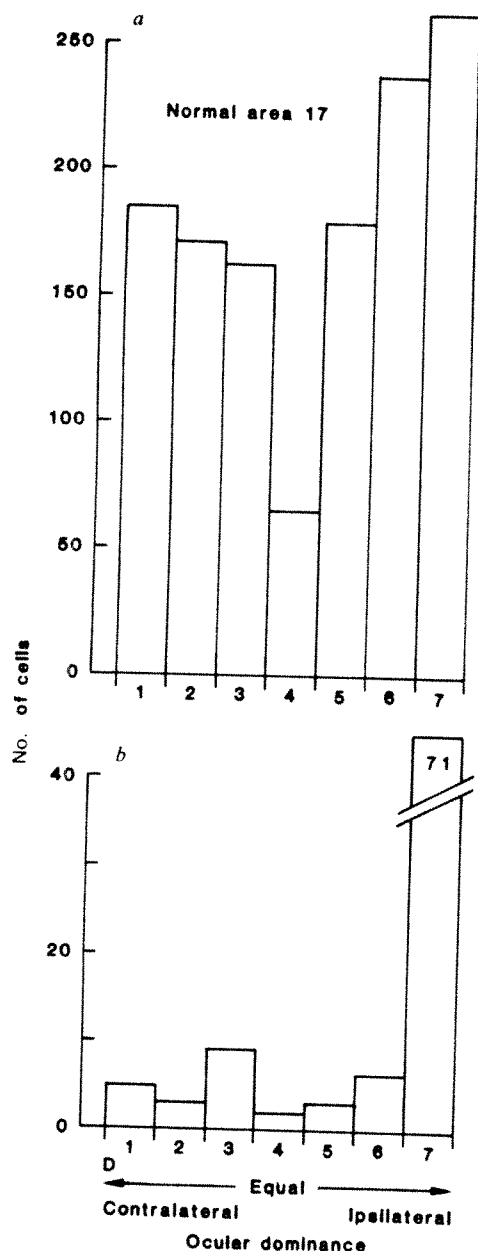


Fig. 1 Ocular dominance histograms in normal and monocularly deprived rhesus macaque monkeys. *a*, Cells (1,256) recorded from area 17 in normal adult or juvenile rhesus monkeys¹³. *b*, Histogram obtained from a monkey in which the right eye was closed at the age of 2 weeks for 18 months¹⁵, showing the relative eye preference of 100 cells recorded from the left hemisphere. The letter D indicates the side of the histogram corresponding to dominance by the deprived eye. Cells in layer 4C are excluded here and in other histograms. Cells in group 1 are driven exclusively from the contralateral eye, those in group 7 from the ipsilateral eye, those in group 4 are equally influenced, and the remaining groups are intermediate.

In an animal that has undergone monocular deprivation, the geniculate terminals with input from the nondeprived eye take over much of the space that would normally have been occupied by terminals from the deprived eye (Fig. 3b)^{13,15}. The input from the deprived eye has shrunk down to occupy the small strips lying between the terminals of the input to the nondeprived eye. Tangential electrode penetrations through cortical layers reveal long expanses of cells driven by the nondeprived eye interrupted by small patches of cells that are either unresponsive or driven by the deprived eye (Fig. 4b). As will be shown below, this expansion of the input from the nondeprived eye occurs at the level of single geniculate afferents. Cells in the deprived layers of the LGN are smaller than normal. One reason for this is that their shrunken cortical arbors may require a smaller soma to maintain them, as originally proposed by Guillery and Stelzner²⁷.

Morphological examination of the LGN in these animals showed a good relationship ($r = 0.91$) between the relative size of normal and deprived cells and the relative size of normal and deprived ocular dominance columns in layer 4C¹⁵. Thus, measuring geniculate cell sizes is yet another means of evaluating the effects of monocular closure.

From the histogram shown in Fig. 1 one cannot tell whether many cells have changed allegiance from the deprived to the nondeprived eye or have simply become unresponsive. The autoradiographic labelling of the afferents in layer 4 (Fig. 3b) shows that a greater proportion of the cells receive direct input from the nondeprived eye. The consequence of this change is that cells at later stages have shifted allegiance from the deprived to the nondeprived eye, rather than become unresponsive. This conclusion is supported by the physiological findings that the large majority of cells in superficial and deep layers respond only to the stimulation of the normal eye (Fig. 4b).

The critical period

Having observed these dramatic effects of monocular suture early in an animal's life, we wanted to determine if there was a period over which the cortex retained its plasticity.

Our experiments in adult cats and monkeys^{6,15} showed that long periods of monocular lid suture did not result in the sort



Fig. 2 Frozen coronal section through the right lateral geniculate nucleus of the monkey with right eye closed at 2 weeks for 18 months (Fig. 1b). Atrophy in the layers receiving input from the deprived eye is indicated by arrows. Stained with cresyl violet (from ref. 13).

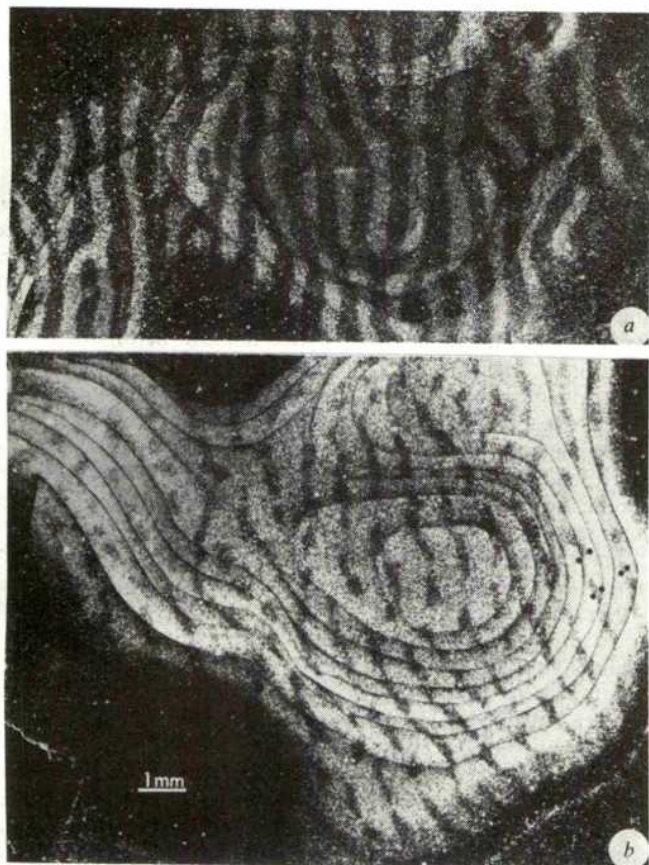


Fig. 3 Dark-field autoradiographs of monkey striate cortex 2 weeks after the injection of ^3H -proline in the vitreous of one eye. *a*, Normal monkey, a montage of a series of tangential sections through layer 4C. The light stripes, representing the labelled eye columns, are separated by gaps of the same width representing the other eye. *b*, Monocularly deprived monkey, again a montage from a series of tangential sections through layer 4C. This is the same monkey shown in Figs 1*a* and 2, which had the right eye closed at 2 weeks for 18 months. The input from the normal eye is in the form of expanded bands which in places coalesce, obliterating the narrow gaps which represent the columns connected to the closed eye.

of changes in the visual cortex described above. Instead, we found that there is a definite period of time, early in life, during which the visual system shows this lability. We termed this the 'critical period'. The permanent visual deficits observed in children with congenital cataracts are therefore most probably a result of changes in the visual cortex that occurred during the critical period. Adult humans suffering from cataracts for many years will have normal vision when the cataracts have been removed, presumably because they are well past their critical period at the onset of the disease.

The critical period in the monkey was estimated by closing one eye at different ages and keeping it closed for several months or longer¹⁵. The deprivation effect was gauged by the relative influence of the two eyes on single cortical cells (ocular dominance distribution), by the distribution of the input from the two eyes in layer 4 (with the autoradiographic technique shown in Fig. 3), and by a comparison of the cell sizes in deprived and nondeprived layers of the LGN. The physiological results in monkeys with one eye closed at 2 weeks of age, 10 weeks, 1 yr and in the adult are illustrated in terms of ocular dominance histograms in Fig. 5. The earliest closure produced the most severe shift of preference towards the normal eye. The same degree of shift could be seen up to an age of 6 weeks. At that age the animal's susceptibility to monocular deprivation began to decline, but it was still pronounced at 10 weeks and was detectable at 1 yr. There were no cortical changes when the closure was done in the adult.

The changes occurring in the geniculocortical innervation were in general agreement with the physiology, though the time course was different (Fig. 6). Animals with a closure at 2 and

5½ weeks showed the expected expansion of the nondeprived geniculate terminals; closure at 10 weeks showed a more moderate expansion, and at 1 yr the pattern was indistinguishable from that in the adult. Geniculate cell sizes in the deprived layers changed in a parallel fashion, showing marked shrinkage at early closures, moderate reduction in closure at 10 weeks, and no change when closed at 1 yr. Since in the closure at 1 yr we observed physiological changes in the absence of a change in the pattern of geniculate innervation, there must presumably be changes at subsequent levels in the cortical circuit^{13,14}. At any rate, in the adult even this higher level of plasticity disappears.

The high degree of susceptibility to deprivation at early ages is also apparent from experiments in which one eye in monkeys was closed for short periods. Before 6 weeks of age, it was sufficient to close an eye for a few days to obtain substantial change in eye preference. The ocular dominance histogram from a monkey with one eye closed for 12 days is shown in Fig. 7*a*. During the subsequent several months a marked change required several weeks of closure, and during the second year any change required months of closure.

From these and similar experiments by us^{13,15} and others^{14,28}, we conclude that the macaque monkey is highly susceptible to monocular deprivation during the first 6 weeks of life, at which age the sensitivity declines progressively, so that at 1½ to 2 years the monkey loses this type of neural plasticity. The length of the critical period varies among species. In cats it is 3–4 months^{9,29}, and clinical observations in humans suggest that it may extend to 5–10 yr, though the susceptibility to deprivation seems most pronounced during the first year and declines with age^{30–32}.

Recovery from deprivation

Monocular closure during the entire critical period in cats and monkeys leads to permanent blindness (refs 33, 34 and T.N.W.,

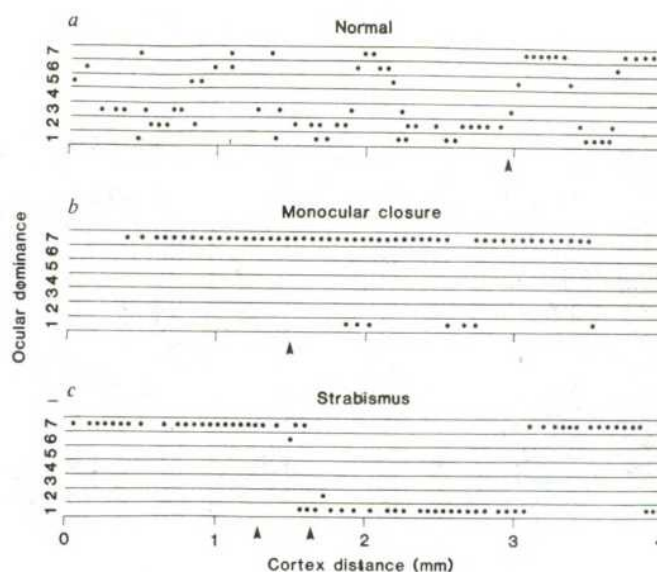


Fig. 4 Eye preference of cells recorded in oblique penetrations through the cortex. Ocular dominance categories 1 to 7 are shown relative to the distance the electrode penetrated through the cortex. *a*, Penetration in a normal monkey showing the sinusoidal shift in eye preference with distance. The arrowhead indicates that the electrode entered layer 4C, in which cells are monocular, and there are abrupt shifts of dominance from one eye to the other. *b*, Oblique penetration in a monkey raised with monocular closure (same monkey as in Figs 1*b*, 2, 3*b*). Outside layer 4, all cells are driven only by the normal eye⁷, and in layer 4C (arrow) there are only short stretches of cells with input from the deprived eye. The overlap of input from left and right eye is not present in the normal monkey. *c*, Oblique penetration in a monkey with a 10° convergent squint produced by sectioning the lateral rectus at 3 weeks (same animal as in Fig. 11*a*). The penetration was made through the striate cortex when the animal was 3½ yr old. Even outside of layer 4, cells were monocular, with equal stretches of cortex dominated by either eye.

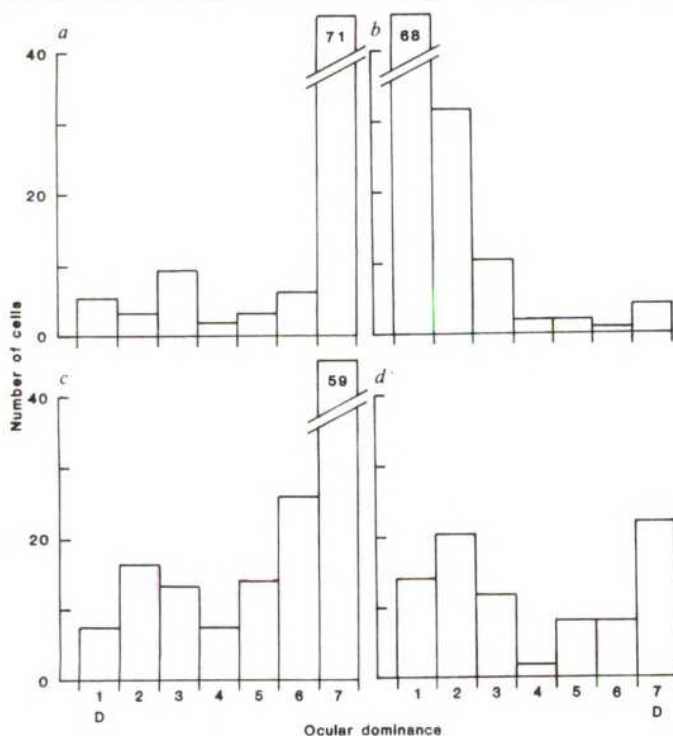


Fig. 5 Ocular dominance histograms of monkeys with one eye occluded by lid suture at different ages and examined after relatively long periods of closure¹⁵. *a*, Same monkey as in Figs 1*b*, 2, 3*b*, 4*b*. The right eye was closed at 2 weeks for 18 months. *b*, A monkey with right eye closed at 10 weeks for 4 months. The strong dominance of normal eye was not as pronounced as at earlier closure. The duration of deprivation was relatively short, but our experience is that at this age the main changes in eye preference occur within the first few months of closure. *c*, A monkey with right eye closed at 1 yr for a period of 1 yr. Preference shifted moderately towards the nondeprived eye, particularly for cells in layers 2 and 3. *d*, Adult monkey (6 yr old) with one eye occluded for 1½ yr. There was no obvious difference in eye preference from that observed in the normal monkey.

unpublished). Presumably there is no recovery of vision after the eye is opened because the pattern of geniculate innervation and the eye preference of cortical cells can no longer be modified. During the period of high susceptibility, partial recovery of vision in the deprived eye is possible after brief periods of monocular closure (refs 15, 35, 36 and T.N.W., unpublished). This was shown in a monkey with one eye closed between days 21 and 30, after which the monkey lived with both eyes open for a period of 4 yr. Initially the animal appeared blind in the deprived eye, but with time it slowly regained the use of the eye; the final acuity in that eye was 20/80 to 100 and in the nondeprived eye, 20/40. The recordings from the striate cortex showed a marked dominance of the nondeprived eye (Fig. 4, right). If there was an increase in the number of cells driven by the once-deprived eye, it was not very obvious. There was a marked narrowing of the deprived columns and a corresponding widening of the nondeprived ones. Thus even if there had been some behavioural recovery, these results demonstrate that a few days of monocular closure had caused clear physiological and anatomical changes in the striate cortex.

These results are relevant to observations in children who have been monocularly deprived for short periods of time. When tested later, some children were found to have reduced acuity in the once-patched eye, the degree of deficit dependent on how young the child was at the time of patching^{37,38}. The experience in children with cataract removal indicates that surgery must be performed very early in the critical period in order to prevent the appearance of any deficit^{39,40}.

A procedure commonly used in children with strabismic amblyopia is to place a patch over the good eye to improve vision in a weak eye. In monocularly deprived animals it was possible to open the sutured eye and close the normal eye⁹, here termed 'reverse suture'. Both in the cat and monkey, reverse suture led to a complete switch in eye preference if it was done within the early part of the critical period^{15,28,29,41}. The geniculate innervation of layer 4C also reversed so that the shrunken regions controlled by the initially closed eye expanded at the expense of the other eye, and consequently the cortical cells switched eye preference in favour of the eye closed first^{15,41,42}. An example is shown in Fig. 8*a*, in which the

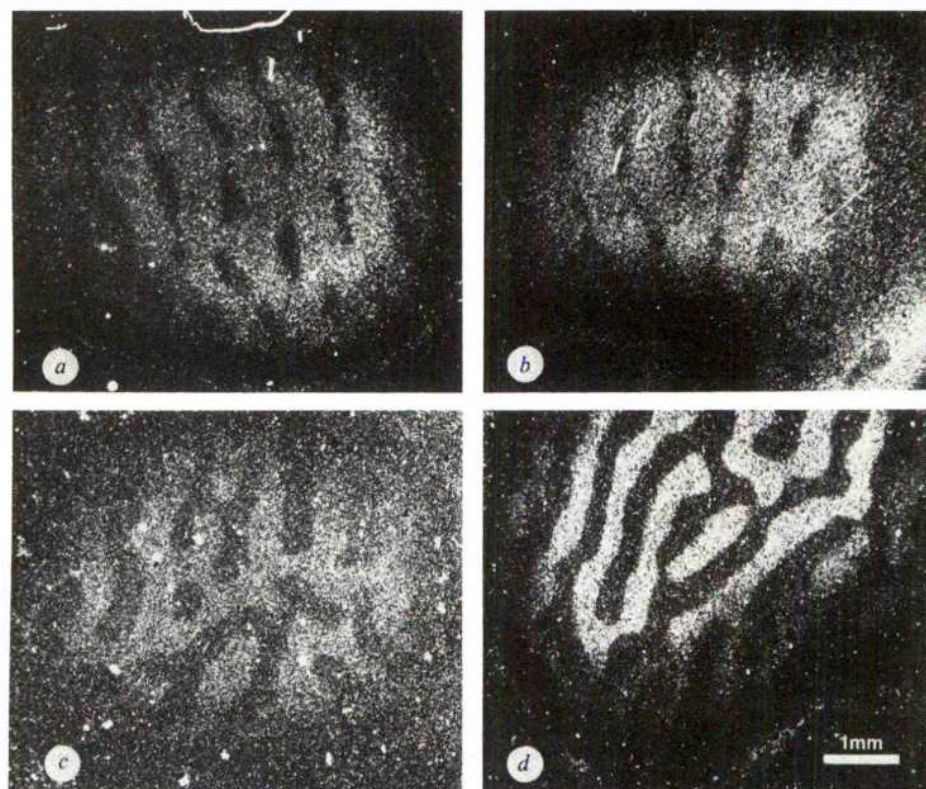


Fig. 6 Autoradiographic labelling patterns from the striate cortex of four monocularly deprived monkeys illustrating the distribution of geniculate terminals in layer 4C after closures at different ages. In all cases the normal (left) eye was injected with ³H-proline, thereby labelling the nondeprived geniculate terminals (from ref. 15). *a*, Right eye closed at 2 weeks for 18 months. Same animal as in Figs 1*b*, 4*b*, 5*a*. *b*, Right eye closed at 5½ weeks for 16 months. *c*, Right eye closed at 10 weeks for 4 months. Same animal as in Fig. 5*b*. *d*, Right eye closed at 14 months for 14 months.

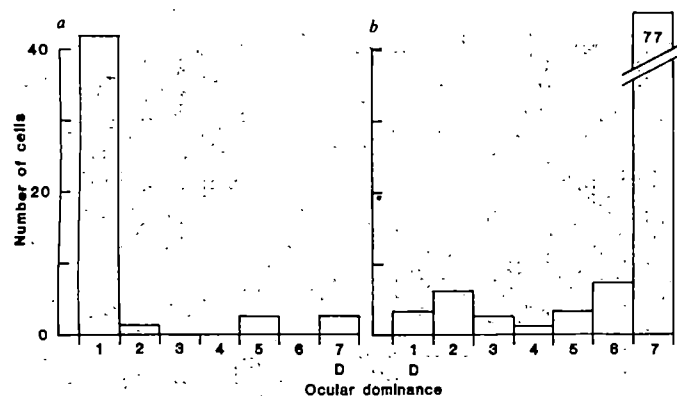


Fig. 7 Ocular dominance histogram for 47 neurones recorded in a 20-day-old monkey whose right eye had been closed since 8 days of age. The physiological picture is similar to that seen after months of deprivation (from ref. 15). *b*, Ocular dominance histogram of 99 cells recorded in a monkey whose right eye was closed from 21 to 30 days of age. Despite a subsequent 4 yr of binocular vision, most cortical neurones were still unresponsive to stimulation of the right eye (from ref. 15).

eye reversal was done at 3 weeks and the recordings 8 months later. The ocular dominance histogram shows that the initially closed eye, which at the time of eye reversal would have influenced very few cortical cells, became strongly dominant. The autoradiography (Fig. 9a) shows a marked expansion in layer 4C β of the initially deprived geniculate terminals. When reversal was done at 6 weeks, the physiology indicated a complete reversal, with a strong dominance of the initially deprived eye (Fig. 8b). Such a marked shift was not reflected in the innervation of layer 4, in which the initially deprived eye had succeeded only in regaining its normal territory (Fig. 9c). This indicates that a significant part of the changes were occurring at the level of intrinsic cortical connections. Finally, reversing at 1 yr failed to restore any of the function of the initially deprived eye (Figs 8c, 9d). Although it is possible to cause changes by monocular deprivation at 1 yr (Fig. 5c), it appears to be more difficult to repair connections that have already been changed once.

Looking more closely at the autoradiography of the geniculate input to layer 4C in the monkey with the reversal at 3 weeks (Fig. 9a, b), one sees a surprising result. The initially deprived eye took over much of the area of innervation of the lower part of layer 4C (4C β), but failed to reverse the dominance of the other eye in the upper part of layer 4C (4C α). Apparently the eye preference of the majority of cortical cells is determined primarily by the cells in layer 4C β (Figs 8a, and 9a, b). Layer 4C β is innervated by cells in the dorsal part of the LGN (parvocellular layers), and layer 4C α by cells in the ventral part of the same nucleus (magnocellular layers). The result of the eye-reversal experiment indicates that the critical period is different for the two cell types. Whereas the critical period is over for the magnocellular input at 3 weeks, the parvocellular input apparently begins to lose its ability to expand at 6 weeks (Fig. 9c), a time when intracortical connections still show considerable plasticity. This result suggests that throughout the brain each functional unit has a unique programme of development.

Mechanism: disuse versus competition

These experiments demonstrate that when a binocular cortical cell is not stimulated by a given eye, the input from that eye

Fig. 8 (Right) Ocular dominance of cortical cells recorded in three monkeys in which reversed suture was done at various ages. *a*, Cells ($n=77$) recorded from the right striate cortex of a monkey with the right eye (D_1) closed at 2 days for 3 weeks and the left eye (D_2) closed at 3 weeks for about 8 months. Nearly all neurones responded only to the initially deprived right eye (D_1). *b*, Neurones ($n=56$) recorded from the left striate cortex. The right eye (D_1) was closed at 3 days for 6 weeks and the left eye (D_2) at 6 weeks for 4½ months. Again, nearly all neurones were driven exclusively by the initially deprived right eye (D_1). *c*, Neurones ($n=74$) recorded from the left striate cortex. The right eye (D_1) was closed at 7 days for 1 yr, and the left eye (D_2) at 1 yr for 2½ yr. In this case the reversal had no effect: nearly all the cells responded only to the initially open eye (from ref. 15).

drops out. Other forms of visual deprivation have shed some light on the mechanism of the effect of monocular deprivation. For example, if disuse were an important factor, one might expect that with both eyes closed, cortical cells would not be driven by either eye. Experiments in cats and monkeys raised in conditions of binocular deprivation showed, however, that cells were readily driven by the two eyes^{29,43,44}. The cortex in the monkey was nonetheless altered substantially, in that very few cells were binocularly responsive⁴⁴. This is illustrated in Fig. 10, in which a monkey had both eyes sutured from birth to 4 weeks of age. Except for the obvious lack of binocular cells, the cortex seemed quite normal. The cells were briskly responsive, showed a high degree of orientation selectivity, and had regular sequences of shifts in orientation preference. From tangential electrode penetrations we were also able to see a

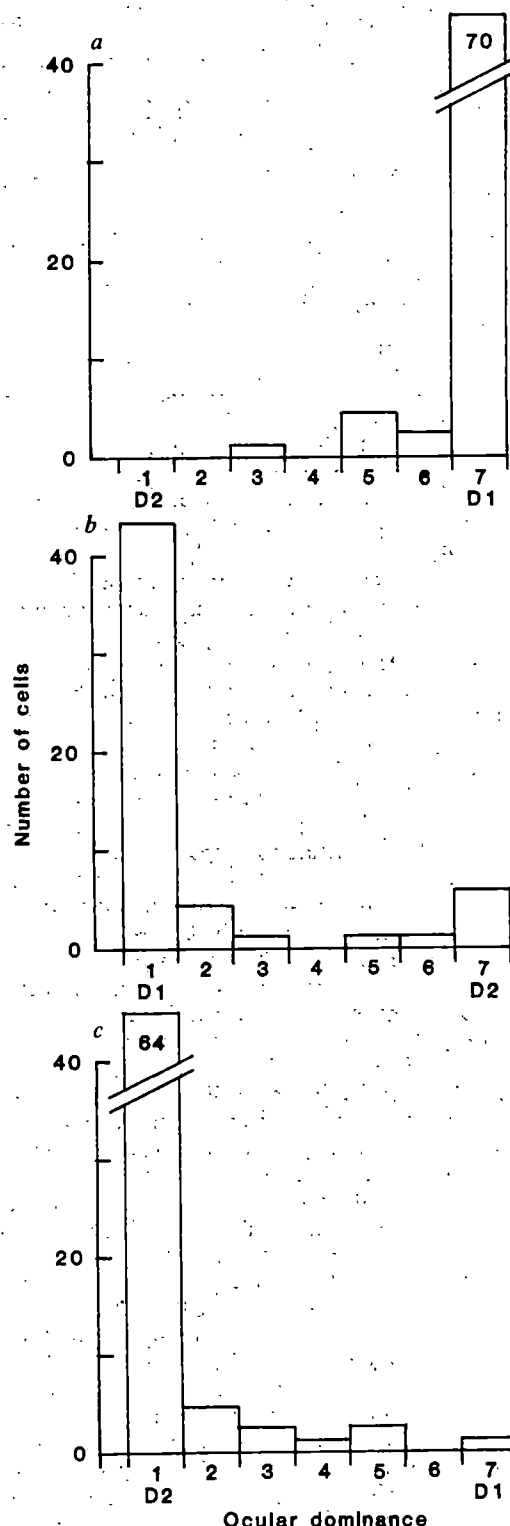
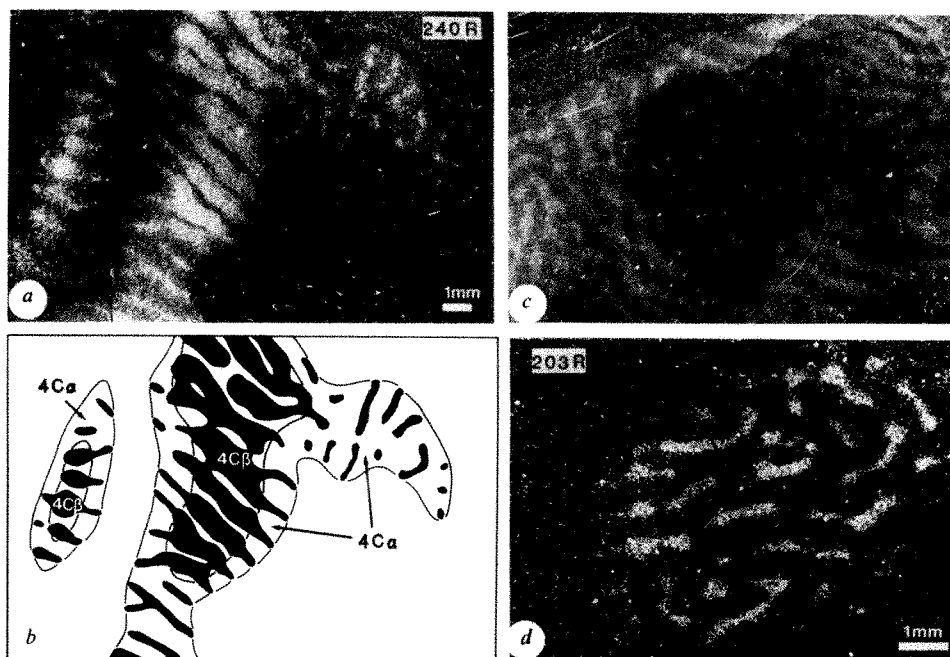


Fig. 9 Effect of reversed suture at various ages on the labelling pattern of geniculate terminals in layer 4C. *a*, Same monkey as in Fig. 8*a*, in which reversed suture was done at 3 weeks of age. The initially deprived (right) eye was injected with ^3H -proline. In the central region of this single tangential section, the labelled bands are expanded. In the surrounding belt the bands are contracted. These two regions correspond to the β and α sublaminae of layer 4C. *b*, Key to *a*, showing the distribution of label (in black) and the boundaries of the sublaminae 4C α and 4C β , traced from an adjacent section stained with cresyl violet. The thin labelled bands in 4C α run into the centres of the enlarged bands in 4C β , meaning that the two sets of bands, although differing in width, are still in register with each other, as they are in normal animals. *c*, The autoradiographic montage of the labelling pattern in a monkey with reversed suture at 6 weeks (compare with Fig. 8*b*). The initially deprived right eye was injected. The labelled bands are of about normal width, indicating a recovery from the effects of the early deprivation, but not a complete reversal. Most of the montage shows layer 4C β . In layer 4C α , the labelled columns remained shrunken (not shown). *d*, Autoradiographic montage from monkey with reverse suture at 1 yr of age (Fig. 8*c*). The labelled columns (for the initially deprived right eye) remain shrunken, indicating that the late reversal did not permit any anatomical recovery.



clear segregation of the cells into unusually distinct ocular dominance columns, even outside layer 4. When monkeys are kept in the binocularly deprived condition for many months, a considerable fraction of the cells are unresponsive or respond only sluggishly, and they often lack orientation preference. Binocular closures in kittens had a similar effect except that neither short- nor long-term deprivation led to an obvious loss of binocular cells^{29,43}.

Evidence for competitive mechanisms has also been found by measurements of geniculate cell sizes in an ingenious set of experiments^{27,45,46}. First, it was demonstrated in kittens with monocular occlusions that deprived cells in the monocular segment of the nucleus were of normal size, whereas those in the binocular segment showed marked shrinkage²⁷. Next, Guilery produced a monocular region in the zone of binocular overlap by making a local retinal lesion in the normal eye of monocularly occluded kittens⁴⁵. Again the deprived geniculate cells with no competitive input from the other eye were of normal size, and those outside the topographical area corresponding to the retinal lesion showed the usual shrinkage. Finally, binocular closure in kittens apparently did not reduce geniculate cell size⁴⁶, as we originally reported⁴³. These experiments support the hypothesis that competitive mechanisms rather than disuse are prime factors in producing the changes observed in conditions of monocular deprivation.

Because many cortical cells are binocular from birth, the loss in the monkey of binocular cells at early times after closure suggests that in order for cortical cells to sustain a binocular input the two eyes must work together. Another situation that interrupts coordinated activity from the two eyes is strabismus⁴⁷. One way of producing experimental strabismus is to section an extraocular muscle. Sectioning the lateral rectus causes the eye to deviate inwards (convergent strabismus), whereas sectioning the medial rectus produces an outward deviation of the eye (divergent strabismus). After surgery, the sectioned muscle usually reattaches behind the original site, so that, except for the misalignment, normal eye movements are restored. In four monkeys with convergent strabismus, the operation was performed between 3 and 5 weeks (T.N.W. and D. H. Hubel, unpublished). When the animals were examined after a year or more, three of them had normal acuity in both eyes but lacked the ability to fuse the images in the two eyes. The striate cortex of these animals had normal single unit activity, but there was a striking absence of binocular cells (Fig. 11*a*).

Tangential penetrations showed that the monocular cells were grouped in the usual regular columnar pattern (Fig. 4*c*), suggesting that binocular cells had lost the input from the nondominant eye. The fourth monkey had low acuity in one eye, and fewer cortical cells were driven from that eye than from the normal one (Fig. 11*b*). When in five additional monkeys a strabismus was produced at later times during the critical period, there was an increase in the proportion of binocularly driven cells. From these results and earlier experiments in cats and monkeys, it seems that the period during which the cortex can be influenced by the artificially induced strabismus is comparable in duration and sensitivity to that observed with monocular deprivation⁴⁸⁻⁵⁰.

The binocular deprivation and strabismus experiments support the notion that competition, rather than disuse, is the main cause of the observed changes⁴³. The right circumstances must exist, however, for the competition to occur, since cells in the normal monkey tend to be dominated by one eye or the other¹⁰, and the dominant eye does not take over the cell completely. The difference between normal and deprived animals is that in normal conditions a cell receives input synchronously from the two eyes, whereas in monocularly deprived animals the two eyes do not act together. The maintenance of a given input may depend on the rate of firing of the postsynaptic cell while

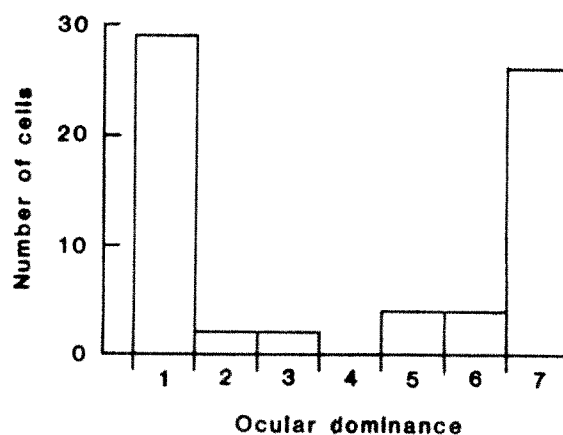


Fig. 10 Ocular dominance histogram of a monkey with binocular lid suture from birth to 30 days of age. The number of binocular cells was low (from ref. 44).

that input is active³ so that in normal animals the nondominant input is maintained by the activity of the dominant input. Carefully designed experiments by Singer *et al.*⁵¹ and Wilson *et al.*⁵² have provided support for the notion that it is crucial to activate the postsynaptic cell in order to change ocular dominance (for a more general discussion of synapse formation and stabilization see refs 53, 54).

In addition to providing insight into the mechanisms of development and plasticity in the visual cortex, the strabismus experiments may be of direct clinical relevance. A common situation in children with strabismus is that they have good vision in both eyes, but cannot fuse the images in the two eyes. These children often use the two eyes alternately, fixating and attending first with one eye and then with the other. The lack of binocular cells in strabismic animals is perhaps the physiological basis of this condition^{12,47}. Another common consequence of strabismus in children is a loss of acuity in one eye (strabismic amblyopia). The physiological mechanism of this condition is less well understood, even if our experiments (Fig. 11*b*) and those of others^{12,55} indicate that one eye has been weakened in its ability to drive cortical cells, as is seen in monocular deprivation.

As mentioned above, the late monocular deprivation in the monkey (Fig. 5*c*) and reversal experiments (Figs 8*b*, 9*c*) altered the cortical circuit at stages subsequent to the input from the LGN. Another series of experiments illustrated this point dramatically. The approach is a variation of the original experiments by Hirsch and Spinelli⁵⁶ and by Blakemore and Cooper⁵⁷ in which kittens were raised viewing only stripes of one orientation. In our experiments we allowed a monkey to see vertical stripes through one eye only (T.N.W., M. Carlson and D. H. Hubel, in preparation). The other eye was deprived by lid suture. This effectively produced a different condition of deprivation for different populations of cortical cells: those with vertical orientation preference were monocularly deprived, and those with horizontal orientation preference were binocularly deprived. We recorded from the striate cortex after 57 h of exposure (between days 12 and 54 after birth) and found normal levels of activity and cells of all orientations with their usual regular columnar arrangement¹⁷. There was an overall domin-

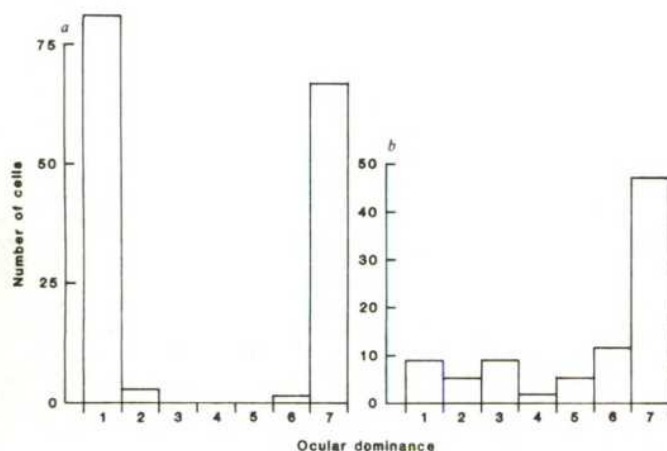


Fig. 11 Ocular dominance histograms of cells recorded in the striate cortex of two strabismic rhesus monkeys. *a*, Eye preference of cells recorded in a 3 yr-old monkey in which the lateral rectus of the right eye was sectioned at 3 weeks of age. Binocular cells are almost completely absent; the cells are driven exclusively either by the right or the left eye. Cells are clustered in a columnar fashion (Fig. 4*c*). The monkey had a 10° convergent strabismus and normal acuity in both eyes, but it could not fuse images presented separately to the two eyes. *b*, A monkey with convergent strabismus resulting from section of the lateral rectus muscle of the right eye at 3 weeks. Behavioural testing showed normal acuity in the left eye (20/30) and lower acuity in the right eye (20/60 to 20/120). There was no difference in refraction between the two eyes. The amblyopic eye influenced fewer neurones in the superficial and deep layers of the striate cortex. The ocular dominance columns in layer 4C had appeared normal when examined in tangential sections stained with a reduced silver method (Liesegang)¹⁹ (T.N.W. and D. H. Hubel, unpublished).

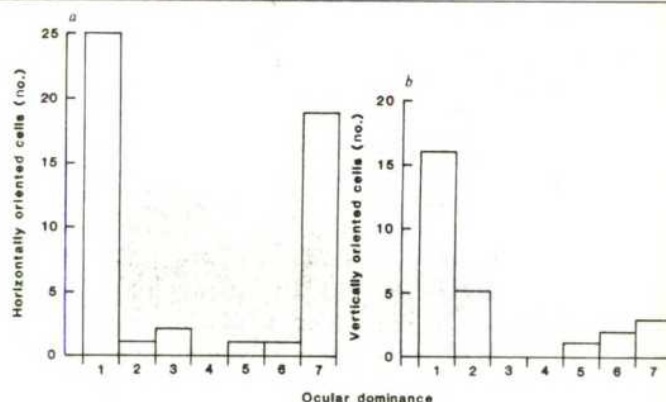


Fig. 12 Ocular dominance histograms of cells recorded from a monkey with the right eye closed at 12 days of age, then kept in the dark except for 57 h of self-exposure to vertical stripes during the subsequent 42 days. *a*, Cells ($n = 48$) recorded in the right striate cortex with preferred orientation within 45° of the horizontal axis. Few binocular cells and a good number of monocular cells responded to stimulation of either the left or the right eye. The distribution of eye preference resembled that seen in binocularly deprived animals (compare with Fig. 10). *b*, Cells ($n = 27$) with preferred orientation within 45° of the vertical axis. The majority of the recorded cells responded to the open eye, producing a histogram similar to that seen after monocular deprivation (T.N.W., M. Carlson and D. H. Hubel, in preparation).

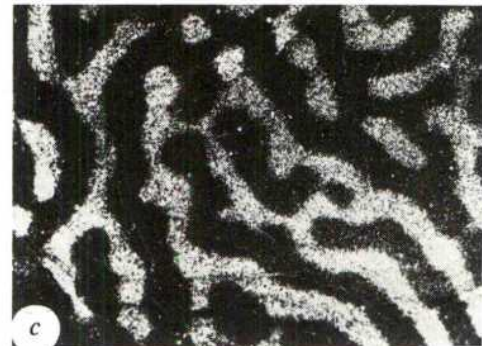
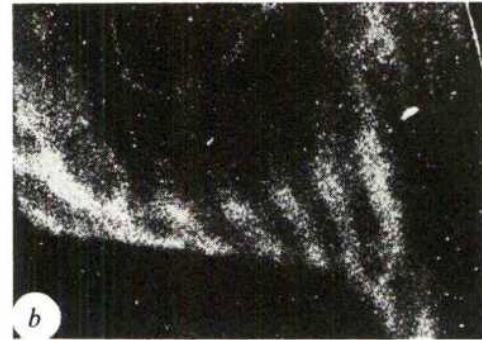
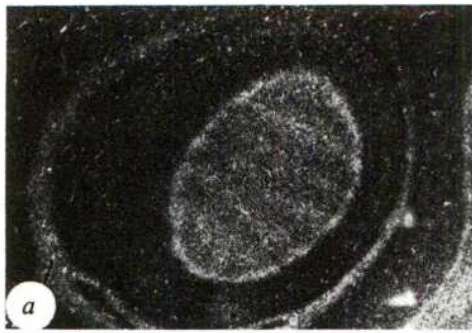
ance of the open eye, but when we produced separate ocular dominance histograms for vertically and horizontally oriented cells (Fig. 12), it became clear that horizontally oriented cells tended to be driven monocularly by either eye (a picture typical of binocular deprivation), and vertically oriented cells tended to be driven monocularly by the exposed eye only (a picture typical of monocular deprivation). Thus these findings again demonstrate that in addition to influencing the thalamocortical input, deprivation can alter the connections in the cortex without changing that input. This question has also been addressed in the kitten by rather different approaches, but with essentially the same results^{58,59}.

In looking at the effects of various forms of deprivation, one gets certain insights into the processes that govern the balance between different inputs, enabling the visual cortex to integrate information in the appropriate manner. We have learned that competition and synchronization of inputs are important factors in forming and maintaining this balance. If these processes are disturbed early in life, the system can be permanently altered.

Normal development

We cannot properly evaluate the experiments on visual deprivation without having detailed knowledge about the normal development of the visual system. To assess the relative importance of the genetic programme and the visual environment, it is necessary to evaluate the capabilities of the visual cortex at birth. The monkey is visually alert at or very soon after birth, and cells in the visual cortex show orientation preference and binocularity as in the adult monkey. This was shown by single-cell recordings in neonatal monkeys with no experience of contours of forms⁴⁴.

Compared with monkeys, kittens are poorly developed at birth; their eyes do not open until the second week, and they spend their first 3 weeks mainly eating and sleeping. In the visual cortex, cells tend to give weak or erratic responses during the early postnatal period and come to respond like adult cells at about 3–4 weeks of age^{9,29,60}. During the same time period, cortical cells differentiate and active synapse formation takes place^{61,62}. Whether cells in the cat visual cortex develop normally without visual experience, as was originally reported for binocularly sutured kittens⁸ was questioned at first⁶³, but subsequently confirmed in several studies^{60,64–66}. Whether in the kitten all cortical cells can develop fully through innate mechanisms is not entirely clear, as animals raised in the dark or with binocular lid closures seem to have a certain fraction of unresponsive or unoriented cortical cells^{60,64,66}.



1 mm

Fig. 13 Dark-field autoradiographs of geniculate afferent terminals in the striate cortex of normal neonatal monkeys in which the right eye had been injected with a radioactive tracer 1 to 2 weeks earlier. *a*, Single section from the left hemisphere of a normal 6-day-old monkey; the section grazes layer 4C tangentially in the central oval region. Silver grains are distributed continuously over the layer 4C, bands of alternating higher and lower grain density indicate that afferents for the two eyes are in the process of columnar segregation. *b*, A single section through layer 4C of the left hemisphere of a normal 3-week-old monkey. The slight blurring of the margin of the labelled bands suggests a modest intermixing of left- and right-eye afferents at the borders of ocular dominance columns. *c*, Autoradiographic montage of the geniculate labelling pattern in layer 4C of the right striate cortex of a 6-week-old normal monkey. The ocular dominance columns appear as sharply defined as they do in the adult monkey (adapted from ref. 15).

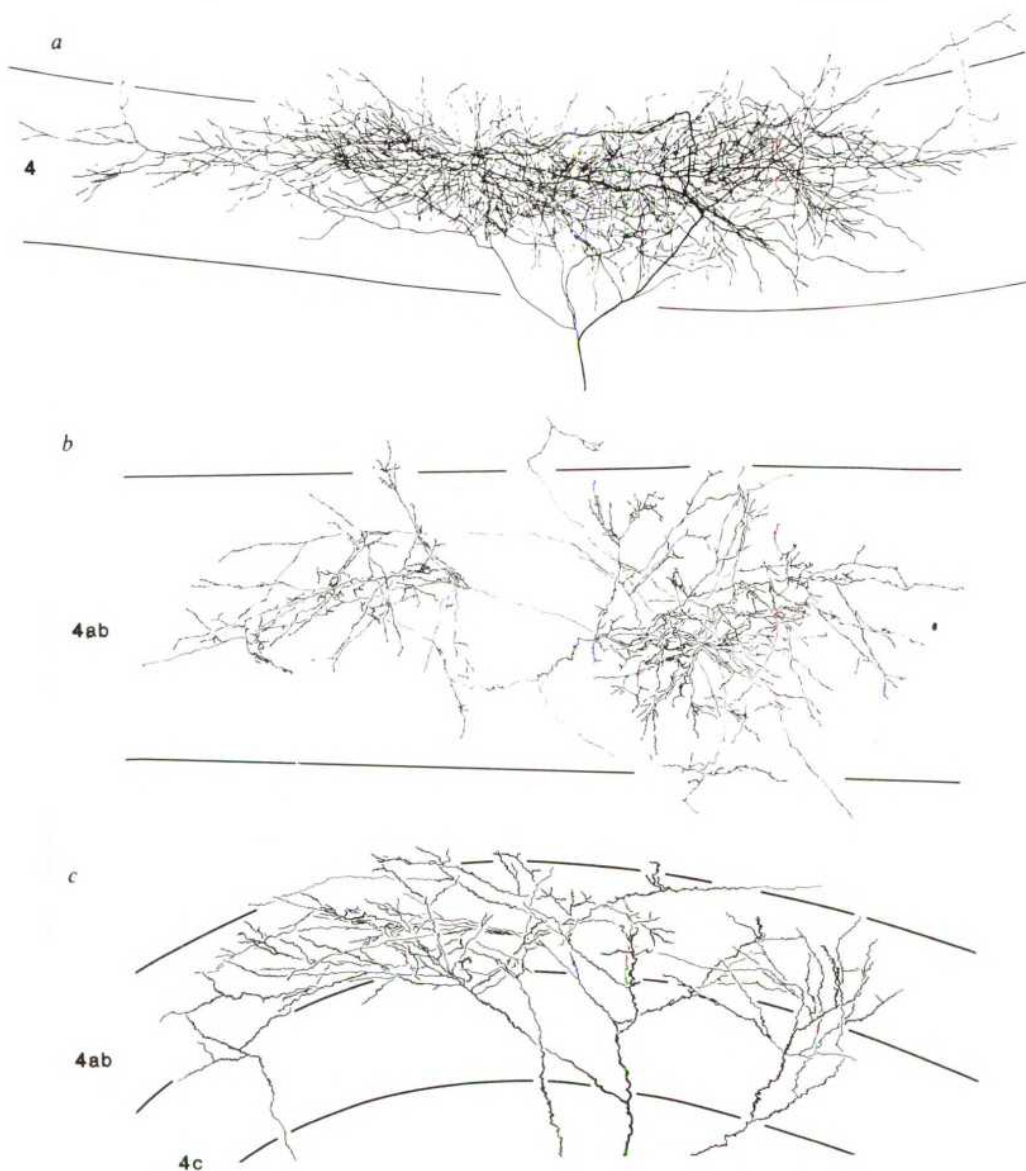


Fig. 14 Patterns of arborization of single geniculate axons in layer 4 of the cat visual cortex. *a*, A 17-day-old kitten. The arborization of a single afferent is shown at an age prior to columnar segregation⁶⁹. The axon, impregnated in its entirety with the rapid Golgi method, arborizes profusely and uniformly over a disk-shaped area more than 2 mm in diameter (from Ref. 71). *b*, Normal adult cat. OFF-centre geniculate afferent (Y-type)⁷⁵ injected intra-axonally with horseradish peroxidase in the striate cortex. The arborization, which is entirely within layer 4 AB, forms two patches separated by a terminal-free gap. Presumably this pattern corresponds to the segregation of the input from the two eyes in a columnar fashion (from ref. 73). *c*, A monocularly deprived cat between 2 weeks and more than 1 yr. The cell is a nondeprived Y-type afferent with an ON-centre receptive field injected intra-axonally with horseradish peroxidase. The arborization is primarily within layer 4 AB, but it does not have the normal patchy distribution of terminals. The absence of a terminal-free region indicates that nondeprived geniculate branches are present in the territory that normally belongs only to the other eye (unpublished observations).

The newborn animal does differ from the adult in one significant respect, relating to the segregation of the afferents from the two eyes in layer 4C. In the newborn monkey we were able to show by injection of ^3H -proline into the eye that the inputs from the two eyes strongly overlap with only a mild fluctuation of eye dominance in a bandlike pattern¹³. Des Rosiers *et al.*⁶⁷ confirmed this observation with the 2-deoxy-D-glucose method. In the monkey fetus, Rakic showed that initially the left- and right-eye afferents overlap completely, and not until a few days before birth do they begin to sort out into ocular dominance columns⁶⁸. We followed this process of segregation postnatally; it was completed by 4–6 weeks of age (Fig. 13)¹³. Recordings also indicated an initial overlap, followed by separation of the inputs from the two eyes in layer 4C, and the time course of the events was similar. The process of segregation did not require visual experience, since it also occurred in an animal raised in the dark¹⁵. In kittens, ocular dominance columns are formed much as they are in monkeys, showing a sequence of initial overlap and segregation during the first few months of life⁶⁹, even though in this species visual experience appears necessary for their normal development⁷⁰.

In the kitten, it has been possible to examine the segregation of ocular dominance columns at the level of single cells. In the early postnatal period, a single geniculate afferent gives off numerous branches innervating without interruption an area covering several future ocular dominance columns (Fig. 14a)⁷¹. As the axon matures, there appears to be a selective loss of branches, so that ultimately it innervates ocular dominance columns serving one eye and leaves gaps for the columns serving the opposite eye (Fig. 14b)^{72,73}. In a cat monocularly deprived during its critical period, a geniculocortical afferent with input from the normal eye is shown in Fig. 14c (unpublished observations). It appears to have innervated an area that normally would have been occupied by the other eye.

Both the autoradiography (Fig. 3) and the single-cell reconstructions (Fig. 14) suggest a mechanism for the expansion and contraction of ocular dominance columns in monocular closure. The terminals with input from the normal eye continue to occupy the territory which they would normally have relinquished, while the deprived terminals are trimmed to an abnormal extent. Another mechanism appears to operate at slightly later stages: when the ocular dominance columns are fully segregated (at 6 weeks of age in the monkey), monocular closure

still causes an expansion and a contraction of the columns similar to that seen after earlier closure (Fig. 6b). This argues for a mechanism of sprouting by one axon into the territory originally occupied exclusively by the deprived eye. Perhaps sprouting occurs from the axon branches that traverse the ocular dominance columns for the other eye (Fig. 14b). Reverse suture experiments also indicate that both trimming and sprouting are involved in plastic changes of the geniculocortical pathway (Fig. 9a–c). We know little of the biochemical mechanisms underlying these changes, except for the intriguing observation of the possible role of noradrenaline in neural plasticity⁷⁴. Since the critical period seems to vary in onset and duration between different brain regions and even between layers of an individual cortical area (compare layers 4C α and 4C β in monkey striate cortex¹⁵ (Fig. 9a, b), the control of plasticity appears to be specific and localized, not a phenomenon controlled by diffuse processes.

Conclusion

Innate mechanisms endow the visual system with highly specific connections, but visual experience early in life is necessary for their maintenance and full development. Deprivation experiments demonstrate that neural connections can be modulated by environmental influences during a critical period of postnatal development. We have studied this process in detail in one set of functional properties of the nervous system, but it may well be that other aspects of brain function, such as language, complex perceptual tasks, learning, memory and personality, have different programmes of development. Such sensitivity of the nervous system to the effects of experience may represent the fundamental mechanism by which the organism adapts to its environment during the period of growth and development.

I thank the staff, faculty and students in the Department of Neurobiology. For more than two decades this has been a unique place because of its blend of scientific excellence and compassion. The late Stephen Kuffler played a very special role in the creation of this environment. I thank both the Johns Hopkins and Harvard Medical Schools for providing me with invaluable opportunities for scientific training and research. I want also to recognize Robert Winthrop who provided the resources for my endowed professorship, and acknowledge the steady and generous support from the National Eye Institute. I thank A. Houdek and C. Gilbert for their help in preparing the manuscript.

- Hubel, D. H. & Wiesel, T. N. *J. Physiol., Lond.* **160**, 106 (1962).
- von Senden, M. *Space and Sight* (The Free Press, Glencoe, 1960).
- Hebb, D. O. *The Organization of Behavior* (Wiley, New York, 1949).
- McCleary, R. A. *Genetic and Experimental Factors in Perception* (Scott Foresman, Glenview, 1970).
- Hubel, D. H. & Wiesel, T. N. *J. Physiol., Lond.* **148**, 574 (1959).
- Wiesel, T. N. & Hubel, D. H. *J. Neurophysiol.* **26**, 1003 (1963).
- Wiesel, T. N. & Hubel, D. H. *J. Neurophysiol.* **26**, 978 (1963).
- Hubel, D. H. & Wiesel, T. N. *J. Neurophysiol.* **26**, 994 (1963).
- Hubel, D. H. & Wiesel, T. N. *J. Physiol., Lond.* **206**, 419 (1970).
- Hubel, D. H. & Wiesel, T. N. *J. Physiol., Lond.* **195**, 215 (1968).
- Wiesel, T. N. & Hubel, D. H. *Symp. Int. Un. of Physiol. Sci. Abstr. P.*, Munich (1971).
- Baker, F. H., Grigg, P. & von Noorden, G. K. *Brain Res.* **66**, 185 (1974).
- Hubel, D. H., Wiesel, T. N. & LeVay, S. *Phil. Trans. Soc. Lond.* **B278**, 377 (1977).
- Blakemore, C., Garey, L. J. & Vital-Durand, F. *J. Physiol., Lond.* **283**, 223 (1978).
- LeVay, S., Wiesel, T. N. & Hubel, D. H. *J. comp. Neurol.* **191**, 1 (1980).
- Hubel, D. H. & Wiesel, T. N. *J. comp. Neurol.* **146**, 421 (1972).
- Hubel, D. H. & Wiesel, T. N. *J. comp. Neurol.* **158**, 267 (1974).
- Wiesel, T. N., Hubel, D. H. & Lam, D. *Brain Res.* **79**, 273 (1974).
- LeVay, S., Hubel, D. H. & Wiesel, T. N. *J. comp. Neurol.* **159**, 559 (1975).
- Hubel, D. H. *Nature* **299**, 515–524 (1982).
- Hubel, D. H. & Wiesel, T. N. *Proc. R. Soc. B198*, 1 (1977).
- Hubel, D. H. & Wiesel, T. N. *J. Neurophysiol.* **28**, 229 (1965).
- Barlow, H. B. *Nature* **258**, 199 (1975).
- Pettigrew, J. D. in *Neuronal Plasticity* (ed. Cotman, C.) 311–330 (Raven, New York, 1978).
- Movshon, J. A. & von Sluyter, R. C. A. *Rev. Psychol.* **32**, 477 (1981).
- Wiesel, T. N. & Raviola, E. *Nature* **266**, 66 (1977).
- Guillery, R. W. & Stelzner, D. J. *J. comp. Neurol.* **139**, 413 (1970).
- Crawford, M. L. J., Blake, R., Cool, S. J. & von Noorden, G. K. *Brain Res.* **84**, 150 (1975).
- Blakemore, C. & von Sluyter, R. C. *J. Physiol., Lond.* **237**, 195 (1974).
- Arden, G. B. & Barnard, W. M. *Trans. ophthalm. Soc. U.K.* **99**, 419 (1979).
- Vaegan, D. T. *Trans. ophthalm. Soc. U.K.* **99**, 432 (1979).
- von Noorden, G. K. *Am. J. ophthalm.* **92**, 416 (1981).
- Dews, P. B. & Wiesel, T. N. *J. Physiol., Lond.* **206**, 437 (1970).
- Ganz, L., Hirsch, H. V. B. & Tieman, S. B. *Brain Res.* **44**, 547 (1972).
- Mitchell, D. E., Cynader, M. & Movshon, J. A. *J. comp. Neurol.* **176**, 53 (1977).
- Olson, C. R. & Freeman, R. D. *J. Neurophysiol.* **41**, 65 (1978).
- Awaya, S., Sugawara, M. & Miyake, S. *Trans. ophthalm. Soc. U.K.* **99**, 447 (1979).
- Odum, J. V., Hoyt, C. S. & Marg, E. *Archs Ophthalm.* **99**, 1412 (1981).
- Beller, R., Hoyt, S., Marg, E. & Odum, J. V. *Am. J. Ophthalm.* **91**, 559 (1981).
- Jacobson, S. G., Mohindra, J. & Held, R. *Br. J. Ophthalm.* **65**, 727 (1981).
- Blakemore, C., Vital-Durand, F. & Garey, J. *Proc. R. Soc. B213*, 399 (1981).
- Swindale, N. V., Vital-Durand, F. & Blakemore, C. *Proc. R. Soc. B213*, 435 (1981).
- Wiesel, T. N. & Hubel, D. H. *J. Neurophysiol.* **28**, 1029 (1965).
- Wiesel, T. N. & Hubel, D. H. *J. comp. Neurol.* **158**, 807 (1974).
- Guillery, R. W. *J. comp. Neurol.* **144**, 117 (1972).
- Guillery, R. W. *J. comp. Neurol.* **148**, 417 (1973).
- Hubel, D. H. & Wiesel, T. N. *J. Neurophysiol.* **28**, 1041 (1965).
- Yinon, U. *Expl Brain Res.* **26**, 151 (1976).
- Crawford, M. L. J. & von Noorden, G. K. *Invest. Ophthalm.* **18**, 496 (1979).
- Jacobson, S. G. & Ikeda, H. *Expl Brain Res.* **34**, 11 (1979).
- Singer, W., Rauschecker, J. & Werth, R. *Brain Res.* **134**, 568 (1977).
- Wilson, J. R., Webb, S. V. & Sherman, S. M. *Brain Res.* **136**, 277 (1977).
- Stent, G. S. *Proc. natn. Acad. Sci. U.S.A.* **70**, 997 (1973).
- Changeux, J.-P. & Danchin, A. *Nature* **264**, 705 (1976).
- Ikeda, H. & Wright, M. J. *Expl Brain Res.* **25**, 63 (1976).
- Hirsch, H. V. B. & Spinelli, D. N. *Science* **168**, 869 (1970).
- Blakemore, C. & Cooper, G. F. *Nature* **228**, 477 (1970).
- Cynader, M. & Mitchell, D. E. *Nature* **270**, 177 (1977).
- Rauschecker, J. P. & Singer, W. *Nature* **280**, 58 (1979).
- Buisseret, P. & Imbert, M. J. *Physiol., Lond.* **255**, 511 (1976).
- Marty, R. *Archs Anat. Microsc. Morphol. Exp.* **52**, 129 (1962).
- Cragg, B. G. *J. comp. Neurol.* **160**, 147 (1975).
- Pettigrew, J. D. *J. Physiol., Lond.* **237**, 49 (1974).
- Blakemore, C. & von Sluyter, R. C. *J. Physiol., Lond.* **248**, 663 (1975).
- Sherk, H. & Stryker, M. P. *J. Neurophysiol.* **39**, 63 (1976).
- Singer, W. & Treutler, F. *J. Neurophysiol.* **39**, 613 (1976).
- Des Rosiers, M. H. *et al. Science* **200**, 447 (1978).
- Rakic, P. *Phil. Trans. R. Soc. B278*, 245 (1977).
- LeVay, S., Stryker, M. P. & Shatz, C. J. *J. comp. Neurol.* **179**, 223 (1978).
- Swindale, N. V. *Nature* **290**, 332 (1981).
- LeVay, S. & Stryker, M. P. *Soc. Neurosci. Symp.* **4**, 83 (1979).
- Ferster, D. & LeVay, S. *J. comp. Neurol.* **182**, 923 (1978).
- Gilbert, C. & Wiesel, T. N. *Nature* **280**, 120 (1979).
- Kasamatsu, T. & Pettigrew, J. D. *J. comp. Neurol.* **185**, 139 (1979).
- Enroth-Cugell, C. & Robson, J. G. *J. Physiol., Lond.* **182**, 923 (1966).

REVIEW ARTICLE

Tapping the immunological repertoire to produce antibodies of predetermined specificity

Richard A. Lerner

Committee for the Study of Molecular Genetics, Research Institute of Scripps Clinic, La Jolla, California 92037, USA

We understand the structure of antibodies in detail, but know little about the molecular basis of the immunogenicity of proteins. Recent experiments have shown that chemically synthesized peptides representative of virtually any part of the surface of a protein can elicit antibodies reactive with the native molecule. Such peptides can serve as synthetic vaccines, and antibodies, useful in the study of changes in protein structure, can be generated. As these antibodies react with regions of the protein known in advance to the experimenter, they can be said to be of predetermined specificity.

THE immune system of a mammal is one of the most versatile systems in the biological kingdom as probably greater than 1.0×10^7 antibody specificities can be produced¹. Indeed, much of contemporary biological and medical research is directed toward tapping this repertoire. As it is so vast, it might appear to be a relatively simple matter to produce antibodies of a particular specificity but until recently this was not the case because of two essential complications. The first problem is that serum antibodies consist of a mixture of molecules of diverse reactivity. As such they are useful for studying whole proteins but an understanding of fine specificity is difficult if not impossible. The development by Köhler and Milstein of the hybridoma methodology has solved this problem by making it possible to obtain in pure form antibodies of a single specificity from those induced during an immune response² but this left a second problem in that during an immune response to an intact protein antibodies are only produced against a very limited set of determinants within the protein molecule. This problem is the one to be discussed here.

Limited response to intact proteins

The key to eliciting antibodies of predetermined specificity is an understanding of what constitutes an immunogenic determinant on a protein. Whereas the term an antigenic determinant simply reflects the ability of a region in a protein to bind to antibodies, an immunogenic determinant is a region capable of inducing antibody. (Here we further define an immunogenic determinant as one that induces antibody reactive with the native protein.)

Previous studies on the nature of antigenic determinants, mostly following immunization with intact proteins, have led to two fundamental conclusions (reviewed in ref. 3, see also refs 4–21). The first is that during an immune response to a native protein, antibody reactivity is confined to only a few regions of the molecule. Studies on enzymatically fragmented proteins suggested that most globular proteins contain fewer than five antigenic sites; as a rough rule, about one site per 5,000 daltons of protein. The second conclusion is that antigenic determinants are dependent on tertiary conformation and are often constructed from discontinuous regions of the protein chain brought into proximity by folding of the molecule. These determinants are called 'conformational' or 'discontinuous'. Thus, by the mid-1970s, a picture of the antigenic profile of a protein had emerged. The determinants are few in number and largely dependent on native conformation (Fig. 1). However, throughout these studies it was tacitly assumed that antigenicity and immunogenicity are equivalent; in other words, the number of antigenic determinants of an intact protein was presumed to set a limit on the number of protein fragments which would carry immunogenic determinants.

The repertoire can be tapped

Needless to say, the above concepts did not bode well for a general method of producing antibodies reactive with most regions of a protein molecule. Our own interest in the problem followed an experiment we carried out to detect a protein potentially encoded by the Moloney leukaemia virus genome. During our sequencing of this genome, we found an open reading frame whose coding capacity did not fit with the known biochemistry of the viral proteins, a problem we have called genotype in search of phenotype. We decided to synthesize chemically a peptide from within the protein predicted by the nucleotide sequence, raise an antibody to it, and see if that antibody reacted with protein(s) in infected cells. Because of uncertainties as to how or if RNA splicing might be taking place, we synthesized a peptide potentially encoded by the 3' end of the reading frame, and thus representative of the C-terminus of the putative protein. Indeed, the anti-peptide antibody precipitated a protein from infected but not normal cells²². Such an approach could be very useful as more and more DNA sequences were generated, but it was far from proven as a general methodology. We had studied the C-terminus of a protein and it seemed possible that the method might be useful only in detecting the ends of proteins. It was thought that the untethered C-terminus of a protein was relatively free to rotate and could be thought of as a kind of hapten carried by the rest of the molecule, a situation which we could have fortuitously duplicated when we coupled the peptide to the carrier protein for immunization.

To test the generality of the method we carried out a study on a protein of known structure. We chose the influenza virus haemagglutinin (HA) because the complete nucleic acid sequence of its gene is available²³ and its crystallographic structure is known at high resolution²⁴. A series of peptides covering 75% of the HA1 chain were chemically synthesized (we have now synthesized additional peptides so that the entire span of the molecule is represented) and antibodies made to each of the peptides. Antibodies to almost all (18 of 20) peptides react with the native molecule²⁵. Because in its folded state the HA1 molecule displays a number of conformations including α -helix, random coil and β -sheets, it is clear that the ability of the anti-peptide antibodies to react with the intact structure is independent of any particular conformation or location in the molecule²⁵. Probably the only requirement for selecting an immunogenic peptide is that a part of the sequence be located on the surface of the molecule so as to be available to antibody. In Fig. 2b, we show the portion of the surface of the HA1 molecule against which we have made antibodies using chemically synthesized peptides as immunogens. In Fig. 2a, we show those areas of the molecule thought to be immunogenic during viral infection or immunization with intact virus or purified viral



Fig. 1 Exposed surfaces of antigenic sites (shown in pink) of hen's egg-white lysozyme. Stereo projections showing the limited number of antigenic sites in the lysozyme molecule and their discontinuous ('conformational') nature. The data are based on Atassi and Lee⁷¹ using the structure of Blake *et al.*⁷² and Imoto *et al.*⁷³. Exposed surfaces based on α -carbon positions using molecular surface computer program of Connolly⁷⁴. The three antigenic sites are constructed by the spatially contiguous residues as follows: (1) Arg 125, Arg 5, Glu 7, Arg 14 and Lys 13; (2) Trp 62, Lys 97, Lys 96, Asn 93, Thr 89 and Asp 87; (3) Lys 116, Asn 113, Arg 114, Phe 34 and Lys 33.

a

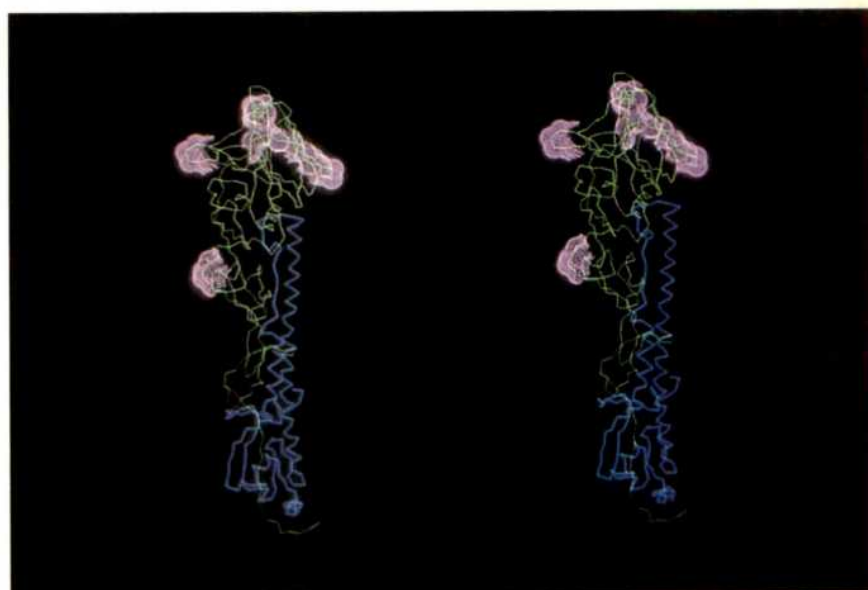
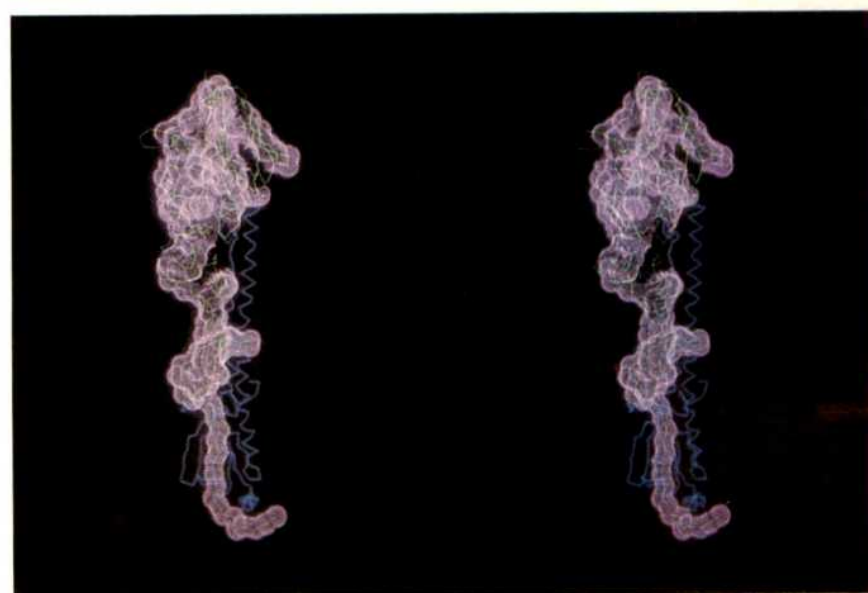


Fig. 2 Antigenic and immunogenic sites (shown in pink) of the influenza virus HA1 molecule. (HA1 shown in green, HA2 shown in blue.) Structure of the molecule based on crystallographic coordinates of Wilson *et al.*³¹. Exposed surfaces based on α -carbon positions using molecular surface computer program of Connolly⁷⁴. *a*, Stereo-pair representing sites eliciting antibodies during the process of infection or immunization with intact virus. *b*, Stereo-pair representing sites against which antibody can be induced by immunization with chemically synthesized peptides.

b



proteins²⁶⁻²⁸. The conclusions from these studies were clear—the immunogenicity of a protein is less than the sum of the immunogenicity of its pieces²⁵ with, however, one caveat. The map in Fig. 2 is based on neutralization data and it is possible that during ordinary immunization, antibodies reactive with other parts of the protein are generated but are not scored because they are not neutralizing. (This problem arises because not all antibodies that bind to viral proteins inhibit the infectivity of the virus.) If this were the case then the collection of anti-virus antibodies would have a reactivity pattern much broader than that observed by neutralization studies. This is, however, probably not the case: we have found that high-titred antibody made against the intact haemagglutinin does not react with any of the synthetic peptides²⁵. We recently carried out a more compelling demonstration of the exclusion of some reactivities in anti-virus sera by taking advantage of the facts that among various influenza strains there are constant and variable regions of the HA1 and HA2 components of the viral haemagglutinin, and that antibody to the native molecule does not widely neutralize across strains. If an anti-peptide antibody to a conserved region neutralized across strains whereas an anti-virus antibody did not, it would indicate that different immunological specificities are generated during the two types of immunization. We therefore studied antibodies to several peptides from conserved portions of the protein structure and showed that even though the anti-virus antibody has a titre against the homologous strain which is about 100-fold higher than that of the anti-peptide antibodies, only the latter neutralizes across strains (S. Alexander and R.A.L., unpublished). Thus, even during a vigorous immune response against virus, the region represented by these synthetic peptides is not immunogenic; hence, by using peptide immunization one can generate antibody specificities that cannot be obtained in any other way.

Antibody of predetermined specificity in biology

The spread of the use of chemically synthesized peptides to generate antibodies of predetermined specificity is indicated by the number and diversity of experiments recently carried out. The antibodies have been designed for a wide variety of uses.

Detection of proteins predicted from nucleic acid sequences:

Anti-peptide antibodies have proved useful in detecting proteins predicted on the basis of nucleic acid sequences to be present in cells. The technology has been particularly successful in discovering DNA and RNA tumour virus proteins implicated in cell transformation. Anti-peptide antibodies have been used to detect the large T antigen of polyoma and SV40 viruses, as well as the cellular transformation-associated protein uniquely expressed in many types of malignant cells²⁹⁻³¹. Green and Brackmann (personal communication) made an anti-peptide antibody that precipitates the 53,000 molecular weight (53K) protein encoded by the adenovirus E1B transcription unit. As expression of the 53K protein is essential for a fully transformed cell, this antibody together with that made to adenovirus E1A products (see below) should be useful in studying the process of cell transformation. A particularly successful use of anti-peptide antibodies has been in defining the proteins encoded by the oncogenes of the rapidly transforming retroviruses including those of the Moloney sarcoma^{32,33}, feline sarcoma³⁴, Rous sarcoma (refs 35, 36 and L. E. Gentry *et al.*, personal communication), avian myeloblastosis³⁷ and Simian sarcoma virus³⁸.

Antibodies against functionally active regions of proteins:

Peptide hormones are often cleaved from larger precursor proteins, which contain multiple hormones. Anti-peptide antibodies have been used to localize the portions of the 31,000-MW γ -melanocyte-stimulating hormone and 17,500-MW calcitonin precursor which correspond to the functional activities of these two hormones^{39,40}.

Schaffhauser *et al.* have used anti-peptide antibodies to perturb the functional activity of proteins⁴¹. The middle T antigen of polyoma virus has been implicated in cell transformation

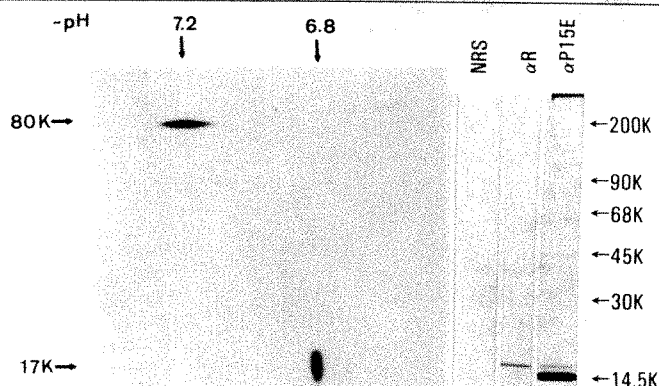


Fig. 3 Studies illustrating the use of anti-peptide antibodies to demonstrate the cleavage of viral protein during virus maturation. Left: immune precipitates of virus infected cells with anti-peptide antibody. Extracts of ³H-leucine-labelled cells were reacted with anti-peptide antibody and the solubilized immune precipitates characterized by two-dimensional gel electrophoresis. The 80K protein is the entire product (Pr80^{env}) of the envelope gene and contains N-gp70-15E-C. The 17K protein (pre-15E) was confirmed by radioactive protein sequencing to be the precursor to the 15E anchor protein⁴⁴. Right: immune precipitates of labeled virus showing that amino acids had been cleaved from the C-terminus of pre-15E during virus maturation to yield viral p15E. Virus labelled with ³⁵S-methionine was reacted with normal rabbit sera (NRS); anti-peptide antibody [here called α R to designate that this serum represents antibody against amino acids predicted by right most (3') possible 15 codons of the viral genome]; and antibody against the mature anchor protein p15E (α P15E). The bulk of the p15E in virus fails to react with α R sera and thus lacks a portion of its C-terminus⁴⁴.

and contains a tyrosine kinase activity that predominantly phosphorylates tyrosine 315 of the middle T protein. They synthesized a nonapeptide corresponding to residues 311–319 of the middle T antigen. This antibody not only precipitates middle T in infected cells but inhibits phosphorylation of the protein *in vitro*. Interestingly, the anti-peptide antibody does not react with the middle T antigen when tyrosine 315 is phosphorylated. Shinnick *et al.*⁴² have also used anti-peptide antibodies to localize and perturb the functions of enzymes encoded by viral genomes. The retroviral *pol* gene is about twice as big as necessary to encode the 80,000-MW reverse transcriptase⁴³. Gene products were sampled by synthesizing peptides at intervals of about 100 amino acids along the predicted *pol* sequence and antibodies against these peptides used to study *pol* gene products in infected cells. Antibodies to peptides predicted from the 5' end of the gene precipitated an 80,000-MW protein and inhibited the reverse transcriptase activity whereas antibodies to peptides from the middle of the gene precipitated a 40,000-MW protein and inhibited the virus-associated endonuclease activity. Antibodies to peptides from the 3' end of the gene precipitate a 20,000-MW protein which according to enzyme inhibition studies seems to be protease. Thus, anti-peptide antibodies are useful not only in detecting the protein product of a gene, but also in identifying its function.

Following protein domains: Anti-peptide antibodies have been used in the difficult problem of following the fate of individual protein domains and have shown that the cleavage and removal of the hydrophilic C-terminus from the retroviral membrane anchor protein takes place during virus maturation⁴⁴. The main envelope glycoprotein, gp70, is anchored into the viral membrane through its attachment by disulphide bonds to the membrane spanning proteins, p15E. Antibody against a synthetic peptide corresponding to the C-terminus of the pre-15E protein was made and used to study the fate of this region of the protein during processing leading to virus formation. In infected cells the antibody detected two proteins of molecular sizes of 80K and 17K corresponding, respectively, to the envelope polyprotein precursor containing gp70 and p15E, and one of the cleavage products (pre-15E) (Fig. 3). However, when the proteins of radioactively labelled virus were studied

with the anti-peptide antibody, it could be seen that the C-terminus predicted from the nucleotide sequence was missing from the mature p15E protein (Fig. 3), thus demonstrating its removal during virus maturation. It remains to be seen if cleavage and processing of C-termini are frequent events which will be found in other systems or if they are peculiar to events involved in viral maturation.

Baron and Baltimore⁴⁵ and Semler *et al.*⁴⁶ used anti-peptide antibodies to follow poliovirus protein domains, by making antibodies to chemically synthesized peptides corresponding to the genome-linked protein (VPg). Since mature poliovirus proteins are generated by a cascade of cleavages starting with a large precursor (NCVPOO), the peptide of interest is located in various positions in the different intermediate cleavage products, ultimately becoming the C-terminus of a 12,000-MW polypeptide from which 22 amino acids are donated to the 5' end of the genomic RNA. In the Baron and Baltimore experiments antibodies raised against the entire 22 amino acids of VPg as well as a peptide corresponding to its 14 most C-terminal amino acids reacted with the peptide when it was present in five different members of the cleavage cascade. As well as providing the solution of a biological problem, these results demonstrate that the reaction of anti-peptide sera with the native protein is relatively independent of the position of the target in the native structure.

Exon usage: A special example of the use of antibodies of predetermined specificity to follow protein domains is in the study of exon usage during gene expression. Shinnick and Blattner⁴⁷ used anti-peptide antibodies to follow exon usage in the immunoglobulin-D system. They synthesized peptides uniquely corresponding to the protein encoded by the exons specific for either the secreted or the membrane-bound form of IgD. Each of the anti-peptide antibodies was shown to be specific for one of the alternative forms of IgD and can now be used to follow the fate of these two proteins in cells. These results, again, demonstrate the production of specific reagents which would be difficult to make by other means. Anti-peptide antibodies have also facilitated the study of exon usage in the adenovirus-2E1A transcription unit. E1A encodes functions which both regulate expression of other early viral genes and have a role in cell transformation⁴⁸⁻⁵¹. The E1A region transcript is processed into at least two overlapping mRNAs (12S and 13S) which share 5' and 3' termini and differ by 138 nucleotides. Since the 12S and 13S mRNAs are in the same reading frame and translation is probably initiated at the common first AUG, it has been assumed that the two proteins encoded by these messages have common N- and C-termini and differ by 46 amino acids unique to the middle of the larger protein⁵². Feldman and Nevins prepared antibody to a 13 amino acid long synthetic peptide predicted from the nucleotide sequence to correspond to a hydrophilic portion of the putative 46 amino acids unique to the larger protein and were able to show that this antibody only reacted with the larger of the two proteins encoded in E1A⁵³. This antibody should be very helpful in defining the role of the different E1A proteins in transformation and control of transcription.

Anti-'wrong' reading frame antibodies: We prepared anti-'wrong' reading frame antibodies to study frameshift mutations in viral proteins (A. Sen and R.A.L., unpublished). We used the nucleotide sequence of several sarcoma virus transforming genes to predict the protein sequence which would correspond to +1 and +2 frameshifts far enough to the 3' end of the genome so that premature terminations would not occur. Using these antibodies we were able to detect frameshifted proteins in infected cells. Coupled with transfection of genes, such anti-'wrong' reading frame antibodies may be very useful in comparing the fate of wild-type and mutant proteins in the same cells.

Antibody of predetermined specificity in medicine

Small molecules were first used in the design of synthetic vaccines in 1938 when Goebel made antibody to the carbo-

hydrate antigen diazotized *p*-aminobenzyl cellobiuronide coupled to horse serum globulin^{54,55}. Mice immunized with the preparation acquired active resistance to infection with virulent type III pneumococci⁵⁴. Anderer, working from the results of denaturation and cleavage experiments and assuming that the immunogenicity of the tobacco mosaic virus protein depends on retention of conformation, studied a C-terminal hexapeptide coupled to bovine serum albumin. He showed that antibody to the hexapeptide would precipitate and neutralize the virus⁵⁶. Working with phage, Langbeheim and his colleagues synthesized two peptides from the coat protein of MS-2 and made rabbit antiserum against them⁵⁷. They were able to show binding by one of the anti-peptide antibodies. In their experiment, addition of the rabbit anti-peptide antibody was followed by addition of antisera against rabbit immunoglobulin, thus obscuring whether the anti-peptide antibody had any primary neutralizing activity.

Before synthetic vaccines could be realistically designed to combat eukaryotic viruses, two things were required: a method for obtaining protein sequences of relatively scarce viral proteins, and constraints of the actual or perceived need for conformational determinants had to be overcome. Advances by Sanger and Gilbert and their colleagues in nucleic acid sequencing technology solved the problem of obtaining reliable amino acid sequences of viral proteins, and chemical synthesis of peptides allowed production of antibodies not necessarily restricted, to reactivity with conformational determinants within native proteins. Recently, peptides corresponding to influenza HA1 (refs 25, 58), the hepatitis B surface antigen (HB_sAg)⁵⁹⁻⁶², the foot-and-mouth disease (FMDV) VPI protein⁶³, and the rabies virus glycoprotein⁶⁴, have been synthesized. One interesting result in the HB_sAg system is that peptides differing in only two residues were capable of inducing antibodies in rabbits and chimpanzees which were capable of distinguishing the y and d subtypes of HB_sAg⁶⁵. It appears that synthetic peptides can duplicate serological markers known to be of significance from classical virological and epidemiological studies. In the influenza⁶⁶ and FMDV systems⁶³, synthetic peptides induced neutralizing antibodies. Further studies using antibodies of predetermined specificity should, in turn, improve our understanding of the process of virus neutralization and thus guide the design of useful peptides. One can envisage that the reason for strain variation in viral proteins is due to selective pressures of the immune system, and thus that the variable regions signal areas available for, and sensitive to, antibody binding. Alternatively, one can aim for invariant regions with functional activities. An additional theoretical issue important to the design of new vaccines is that an intact protein when free may fold differently from when it is part of a virus particle and thus may not confront the immune system in such a way as to induce neutralizing antibodies. In these cases, synthetic peptides may offer advantages over purified viral capsid proteins (so-called subunit vaccines) because they can induce anti-virus antibodies which are independent of protein folding and can be directed to neutralizing sites on the virus surface.

Practical considerations

Given a nucleotide sequence, the problem often is which peptide to synthesize. As so many different peptides have been shown to induce antibodies reactive with the native protein, the only essential point is to choose one which contains hydrophilic amino acids and is thus likely to be exposed on the surface of the intact molecule. Also, peptides containing hydrophilic groups are likely to be soluble, making their handling and coupling to carrier molecules easier. A number of computer programs have been used to predict secondary structures⁶⁷⁻⁶⁹, which indicate regions of proteins located on the surface of the molecule and available to antibody but a simple search of the amino acid sequence for charged residues seems to be equally effective for most studies. In the experiments carried out so far, several different carriers and coupling methods have been used with equally good results, and so this choice does not seem

to be critical as long as an immunogenic carrier is used. However, where cultured cells are used, bovine serum albumin should be avoided as a carrier since it is a component of the growth media to which many cellular proteins bind non-specifically and the presence of antibodies to it can confuse immunoprecipitation studies of radioactively labelled cells.

Another question is that of the titre of an anti-peptide antibody compared with that raised by immunization with the intact protein. The answer, as far as we know, is that sometimes it is greater and sometimes less. However an important point is that by using peptide immunization, one can generate antibody specificities which cannot be obtained in any other way.

The minimum size of the peptide chosen is important and should be larger than six amino acids. We generally synthesize peptides of 15 amino acids. Considerably larger peptides have also proved useful²⁵ but often do not offer any advantage as one risks the problem that they are more likely to assume a fixed conformation distinct from that of the native molecule.

Anti-peptide antibodies can also be used for immunoaffinity purification of rare proteins⁷⁰. The main advantage of anti-peptide antibodies for immunoaffinity purification of proteins is that elution can be accomplished by excess peptide instead of the usual methods of high salt, low pH or chaotropic agents. Since the peptide elution is specific for the antigen-antibody union of interest, the recovered protein is less likely to be contaminated with extraneous proteins which were bound to the column at sites other than the antibody combining site. Also, proteins eluted by peptides are more likely to be recovered in a native state.

Theoretical considerations

The reason anti-peptide antibodies so often react with the native structure seems to be that they can adopt a number of conformations in solution, one of which approximates that adopted in the native molecule. If this is the case anti-peptide antibodies should contain a mixture of reactivities to these various conformations with only a small percentage of them actually reacting with the native structure. There are, however, other theoretical possibilities. One is that a protein molecule perturbed by solvent interactions exists as a statistical ensemble of conformational states with similar backbone structures but with variations in side-chain orientations on the surface of the molecule. In this

situation the anti-peptide antibody could either 'lock in' a particular conformation, induce a conformation, or, in fact, mould its own combining site which for similar reasons would itself be somewhat sterically mutable. That at least some of the latter notions may be true is supported by our studies on monoclonal antibodies to chemically synthesized peptides (H. Niman and R.A.L., unpublished). We selected monoclonal anti-peptide antibodies against an influenza virus HA1 peptide (amino acids 75-111) and then looked at what percentage would react with the native protein. Surprisingly, 14 of 27 reacted in an enzyme-linked immunoabsorbent assay (ELISA) and immunoprecipitation assays with intact HA1, a number much too large to be compatible with a simple model of occasional shared conformations between the free peptide and its counterpart in the protein. If these results can be extended and generalized, one will have to think in terms of flexible structures in protein, antibody molecules, or both. Alternatively, both in solution and as part of protein molecules, peptides may spend the bulk of their time in a limited number of comparable conformations presumably representing the state of lowest free energy.

Future prospects

The ability to make antibodies to defined regions of proteins will, no doubt, open the way to a number of biochemical experiments on the structure-function relationships of proteins as well as help in the immunological prevention and perhaps treatment of disease. Consideration of the theoretical basis for the immunogenicity of small synthetic peptides has led to questions about the fluidity of regions of protein molecules in solution, as well as the possibility that antibodies induce shape changes in proteins. The somewhat surprising results concerning the immunogenicity of peptides may lead to a better understanding of the dynamics of protein molecules in solution. The fact that such a high percentage of monoclonal anti-peptide antibodies react with the native protein already suggests that something unexpected is on the horizon.

I thank the many investigators who allowed me to cite their experiments before publication. I also thank my colleagues Greg Sutcliffe, Tom Shinnick, Nicola Green, Hannah Alexander, Steve Alexander, Richard Houghton, Jim Bittle, John Gerin, Bob Purcell, Dave Rowlands, Fred Brown, Henry Niman and Art Olson for their collaboration.

1. Sigal, N. H. & Klinman, N. R. *Adv. Immun.* **26**, 255 (1978).
2. Köhler, G. & Milstein, C. *Nature* **256**, 495 (1975).
3. Crumpton, M. J. in *The Antigens* (ed. Sela, M.) (Academic, New York, 1974).
4. Benjamini, E., Young, J. D., Shimizu, M. & Leung, C. Y. *Biochemistry* **3**, 1115 (1964).
5. LaPresle, C. & Durieux, J. *Ann. Inst. Pasteur, Paris* **92**, 62 (1957).
6. Cebra, J. J. *J. Immun.* **86**, 205 (1961).
7. Anderer, F. A. Z. *Naturforsch.* **18b**, 1010 (1963).
8. Atassi, M. Z. *Nature* **202**, 496 (1964).
9. Crumpton, M. J. & Wilkinson, J. M. *Biochem. J.* **94**, 545 (1965).
10. Landsteiner, K. *J. exp. Med.* **75**, 269 (1942).
11. Brown, R. K., Delaney, R., Levine, L. & van Vunakis, H. *J. biol. Chem.* **234**, 2043 (1959).
12. Goetzl, E. J. & Peters, J. H. *J. Immun.* **108**, 785 (1972).
13. Arnon, R. & Sela, M. *Proc. natn. Acad. Sci. U.S.A.* **62**, 163 (1969).
14. Arnon, R., Maron, E., Sela, M. & Anfinsen, C. B. *Proc. natn. Acad. Sci. U.S.A.* **68**, 1450 (1971).
15. Parish, C. R., Wistar, R. & Ada, G. L. *Biochem. J.* **113**, 501 (1969).
16. Ichiki, A. T. & Parish, C. R. *Immunochemistry* **9**, 153 (1972).
17. Atassi, M. Z. & Saplin, B. J. *Biochemistry* **7**, 688 (1968).
18. Shinka, S. et al. *Biken's J.* **10**, 89 (1967).
19. Fujio, H., Imanishi, M., Nishioka, K. & Amano, T. *Biken's J.* **11**, 207 (1968).
20. Omenn, G. S., Ontjes, D. A. & Anfinsen, C. B. *Biochemistry* **9**, 313 (1970).
21. Sachs, D. H., Schechter, A. N., Eastlake, A. & Anfinsen, C. B. *J. Immun.* **109**, 1300 (1972).
22. Sutcliffe, J. G., Shinnick, T. M., Green, N., Liu, F.-T., Niman, H. L. & Lerner, R. A. *Nature* **287**, 801 (1980).
23. Min Jou, W. et al. *Cell* **19**, 683 (1980).
24. Wilson, I. A., Skehel, J. J. & Wiley, D. C. *Nature* **289**, 366 (1981).
25. Green, N. et al. *Cell* **28**, 477 (1982).
26. Laver, W. G., Air, G. M., Dopheide, T. A. & Ward, C. W. *Nature* **283**, 454 (1980).
27. Webster, R. G. & Laver, W. G. *Virology* **104**, 139 (1980).
28. Wiley, D. C., Wilson, I. A. & Skehel, J. J. *Nature* **289**, 373 (1981).
29. Walter, G., Hutchinson, M. A., Hunter, T. & Eckhart, W. *Proc. natn. Acad. Sci. U.S.A.* **78**, 4882 (1981).
30. Walter, G., Scheidtmann, K.-H., Carbonek, A., Laudano, A. P. & Doolittle, R. F. *Proc. natn. Acad. Sci. U.S.A.* **77**, 5197 (1980).
31. Luka, J. & Klein, G. (in preparation).
32. Papkoff, J., Lai, M. H.-T., Hunter, T. & Verma, I. M. *Cell* **27**, 109 (1981).
33. Papkoff, J., Verma, I. M. & Hunter, T. *Cell* **29**, 417 (1981).
34. Sen, A. & Sen, S. (in preparation).
35. Wong, T.-W. & Goldberg, A. R. *Proc. natn. Acad. Sci. U.S.A.* **78**, 7412 (1981).
36. Sen, A. & Sen, S. (in preparation).
37. Lukacs, G. & Baluda, M. (in preparation).
38. Robbins, K. C., Devare, S. G., Premkumar, R. & Aaronson, S. A. *Science* (in the press).
39. Shibasaki, T., Ling, N. & Guillemin, R. *Nature* **285**, 416 (1980).
40. Amara, S. G. et al. *J. biol. Chem.* **257**, 2129 (1981).
41. Schaffhausen, B., Benjamin, T. L., Pike, L., Casnellie, J. & Krebs, E. (in preparation).
42. Shinnick, T., Lerner, R. A. & Sutcliffe, J. G. (in preparation).
43. Shinnick, T. M., Lerner, R. A. & Sutcliffe, J. G. *Nature* **293**, 543 (1981).
44. Green, N. et al. *Proc. natn. Acad. Sci. U.S.A.* **78**, 6023 (1981).
45. Baron, M. H. & Baltimore, D. *Cell* **28**, 395 (1982).
46. Semier, B. L., Anderson, C. W., Hanecek, R., Dorner, L. F. & Wimmer, E. *Cell* **28**, 405 (1982).
47. Shinnick, T. M. & Blattner, F. (in preparation).
48. Berk, A. J., Lee, F., Harrison, T., Williams, J. & Sharp, P. A. *Cell* **17**, 935 (1979).
49. Jones, N. & Shenk, T. *Proc. natn. Acad. Sci. U.S.A.* **76**, 3665 (1979).
50. Graham, F. L., Harrison, T. & Williams, J. *Virology* **86**, 10 (1978).
51. Jones, N. & Shenk, T. *Cell* **17**, 583 (1979).
52. Montell, C., Fisher, E. F., Caruthers, M. H. & Berk, A. J. *Nature* **295**, 380 (1982).
53. Feldman, L. & Nevins, J. (in preparation).
54. Goebel, W. F. *Nature* **143**, 77 (1939).
55. Goebel, W. F. *J. exp. Med.* **68**, 469 (1938).
56. Anderer, F. A. *Biochim. biophys. Acta* **71**, 246 (1963).
57. Langbeheim, H., Arnon, R. & Sela, M. *Proc. natn. Acad. Sci. U.S.A.* **73**, 4636 (1976).
58. Müller, G., Shapira, M. & Arnon, R. *Proc. natn. Acad. Sci. U.S.A.* **78**, 3403 (1982).
59. Lerner, R. A., Green, N., Alexander, H., Liu, F.-T., Sutcliffe, J. G. & Shinnick, T. M. *Proc. natn. Acad. Sci. U.S.A.* **78**, 3403 (1981).
60. Dreesmann, G. R. et al. *Nature* **295**, 158 (1982).
61. Vyas, G. N. in *Hepatitis B. Vaccine* (eds Naupias, P. & Guesry, P.) 227 (Elsevier, Amsterdam, 1981).
62. Prince, A. M., Ikram, J. & Hupp, J. P. *Proc. natn. Acad. Sci. U.S.A.* **79**, 579 (1982).
63. Bittle, J. L. et al. *Nature* **298**, 30 (1982).
64. Sutcliffe, J. G. & Koprowski, H. (in preparation).
65. Gerin, J., Purcell, R. & Lerner, R. A. (in preparation).
66. Alexander, S., Alexander, H., Green, N. & Lerner, R. A. (in preparation).
67. Chou, P. Y. & Fasman, G. D. *Adv. Enzym.* **47**, 45 (1978).
68. Kyte, J. & Doolittle, R. F. *J. molec. Biol.* **157**, 105 (1982).
69. Hopp, T. P. & Woods, K. R. *Proc. natn. Acad. Sci. U.S.A.* **78**, 3824 (1981).
70. Walter, G., Hutchinson, M. A., Hunter, T. & Eckhart, W. *Proc. natn. Acad. Sci. U.S.A.* **79**, 4025 (1982).
71. Atassi, Z. & Lee, C.-L. *Biochem. J.* **171**, 429 (1978).
72. Blake, C. C. F., Mair, G. A., North, A. C. T., Phillips, D. C. & Sarma, V. R. *Proc. R. Soc. B167*, 365 (1967).
73. Imoto, T., Johnson, L. N., North, A. C. T., Phillips, D. C. & Rupley, J. A. *Enzymes* **7**, 665 (1972).
74. Connolly, M. *Science* (submitted).

ARTICLES

High dynamic range mapping of strong radio sources, with application to 3C84

J. E. Noordam & A. G. de Bruyn

Radiosterrenwacht, Postbus 2, 7990 AA Dwingeloo, The Netherlands

A new reduction procedure is described to correct data obtained by the Westerbork Synthesis Radio Telescope. The technique allows very high dynamic range mapping of strong radio sources by also using redundant interferometers. The performance is illustrated with 6-cm and 21-cm continuum maps of 3C84, which have a dynamic range of about 10,000:1.

THE continuing improvement of radioastronomical detection systems during the past decade has resulted in the potential ability to detect ever fainter sources of radio emission. Aperture synthesis arrays in particular have been able to take advantage of the new low-noise receivers, to detect and map faint sources of radio emission. However, the synthesis arrays show increasing limitations when studying faint emission in the immediate vicinity of intense radio sources. These limitations are due to the corruption of the visibility amplitudes and phases of the correlated interferometer signals by ionosphere, troposphere, receivers and detectors. The way in which these errors, after Fourier inversion, will distort the source intensity distribution depends, among other things, on the array configuration. In the case of the Westerbork Synthesis Radio Telescope (WSRT) the map distortions tend to appear as (sections of) elliptical rings around and radial spokes emanating from the highest intensity features in the map¹. The dynamic range attained in a standard WSRT observation has previously been limited to 100–1,000, depending both on observing frequency and area of interest in the map. In special cases a technique called kneading² has been used to improve WSRT maps significantly over the result obtainable using standard reduction procedures.

Recently, several new data correction schemes^{3–5} have been introduced in aperture synthesis, and have produced high quality maps. In essence these schemes are all based on the assumption that errors can be traced to individual telescopes, rather than interferometers. In that case, the $N(N-1)/2$ interferometers one can form with N telescopes suffer from only N independent phase and gain errors per integration time (scan). The idea now is to try to adapt the data to a tentative model of the source intensity distribution, by allowing only the independent errors to vary, within specified limits. The fewer independent errors there are, the less freedom the data will have to comply with a wrong model, and it is assumed that the discrepancies will show the way to a better model for the next iteration step. This process has been known to converge to reliable and consistent results in many practical cases, although it seems to discriminate against extended structure. For the best results one needs many telescopes, and all telescopes

should participate in short as well as long baselines. The possibility of using redundant baseline information in the case of the WSRT constitutes an improvement in the sense that the number of independent errors can be reduced dramatically. This has opened the way to producing very high dynamic range maps ($>10,000:1$) of strong radio sources.

The method was tested—and to some extent developed—on the radio source 3C84, one of the strongest extragalactic radio sources at centimetre wavelengths, with total flux densities in 1981 (it varies) of 19 Jy at 21 cm and 60 Jy at 6 cm ($1 \text{ Jy} = 10^{-26} \text{ W m}^{-2} \text{ Hz}^{-1}$). Its emission is dominated by an unresolved inverted spectrum core⁶ whose intensity had previously prevented mapping at centimetre wavelengths the surrounding extended emission.

Use of redundant interferometers

The WSRT consists of 14 telescopes, 4 movable and 10 fixed, configured in a regular east–west array (Fig. 1). In the standard observing mode, 40 interferometers are formed by correlating signals from pairs of movable and fixed dishes. The advent of a new digital backend⁷ made it possible, in principle, to correlate all telescopes with one another, yielding 91 interferometers. However, in the present correlator, polarization information and a factor of 2 in sensitivity have to be traded to achieve this.

Although a minimum-redundant array produces more visibility information per telescope, the extra information provided by the redundant interferometers can be functionally exploited. When the array is positioned in its standard configuration (with separations $9A = AB = CD = 72 \text{ m}$, see Fig. 1), all spacings that carry redundant information, and a reasonably defined signal, can be compared to yield a weighted least-squares solution for all telescope errors. This reduces the number of independent errors per hour-angle scan (usually 2 min long) to only one gain and one phase error! (Because visibilities are compared, absolute intensity and position information are lost; the gain and phase stability of the WSRT, however, is such that these can usually be derived to 2% and 1 arc s, respectively, from the raw uncorrected data.) The corrected scans, which consist of complex visibilities on 38 different spacings, can be

Table 1 Summary of features of 3C84 structure and flux density

Component	Size		Flux density (Jy)	
	Angular	Linear*	1412 MHz	4995 MHz
VLBI core	$\sim 0.008 \times 0.016 \text{ arc s}$	$4 \times 8 \text{ pc}$	$13.2 \pm 0.2^\dagger$	59.6 ± 1.2
'30 arc s component'	$15 \times 40 \text{ arc s}$	$8 \times 21 \text{ kpc}$	2.3 ± 0.2	0.75 ± 0.05
Halo	$> 4 \times 6 \text{ arc min}$	$> 120 \times 180 \text{ kpc}$	> 2.4	?

* Assuming a distance of 106 Mpc, which is based on $V_{\text{sys}} = 5,300 \text{ km s}^{-1}$, $H = 50 \text{ km s}^{-1} \text{ Mpc}^{-1}$.

† In August 1980. One year later the core flux had increased to 14.4 Jy.

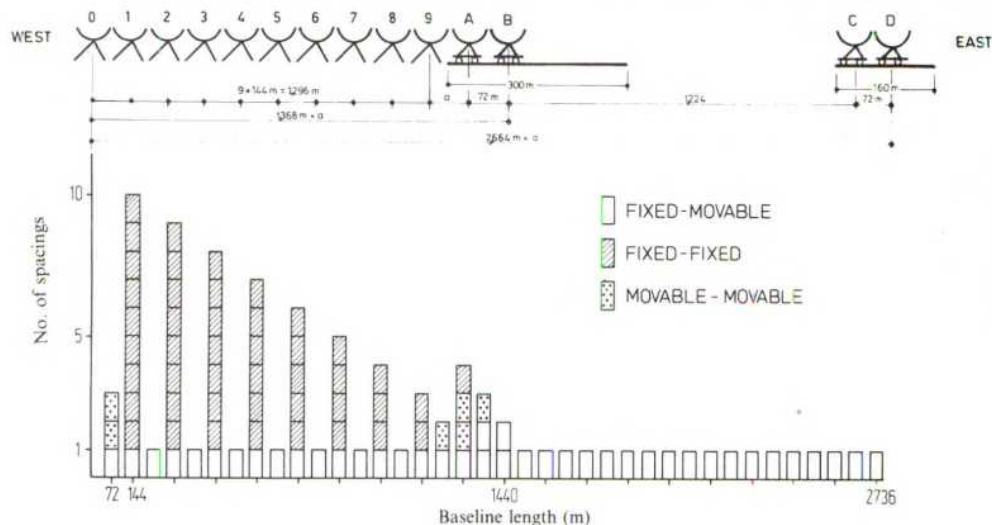


Fig. 1 Top, the geometry of the Westerbork array. The distance a between telescopes 9 and A is variable. In the optimum redundant configuration a is set to 72 m. Bottom, a histogram of the observed interferometer spacings when $a = 9A = 72$ m.

considered perfect internally and will be kept 'rigid' through-out further processing.

The decomposition into telescope errors also provides an r.m.s. measure of the consistency of the input data with the final solution. If telescope errors are indeed the only type of error, the level of inconsistency should be determined by the thermal noise. Down to a level of about 0.1° in phase and 0.2% in amplitude we find this indeed to be the case. Only when observing very intense sources, for example 3C84 at 6 cm, could amplitude and phase errors be detected at a level of 0.1° and 0.2%, which must be ascribed to individual interferometers. These errors, whose origin is still unknown, appear to remain constant during a 12-h observation and can therefore be removed in the reduction process (see below). These errors should be compared with the so-called closure errors in VLBI³ and MERLIN⁵ hybrid mapping.

Alignment of individual scans

Following the redundancy step the scans are perfect and 'rigid', by which we mean that from then on no adjustments of individual amplitudes or phases are allowed (or necessary). The need for alignment stems from several causes. The scans must be phase-aligned to correct for phase gradients over the array that are caused by short- and long-term atmospheric effects (troposphere at 6/21 cm, ionosphere at 21/49 cm). Amplitude-alignment is required to correct for slow variations in the overall system gain, extinction variations (6 cm) and scintillation (49 cm). Typical amplitude adjustments are in the range 1–3%; phase gradient adjustments can be as large as 50 – 100° across the array, but are more typically 10 – 20° .

We have investigated several ways of aligning scans. The preferred method would be to align without knowledge of the

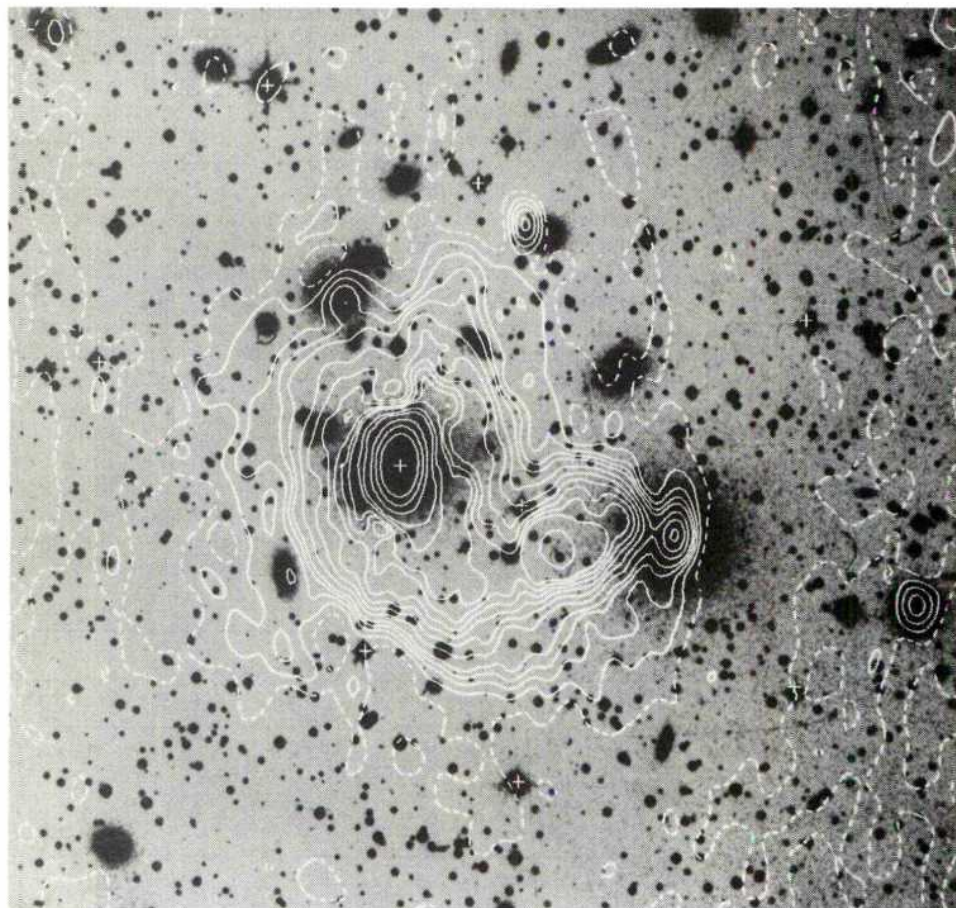


Fig. 2 The convolved 21-cm map of August 1980 superimposed on a deep optical photograph¹⁶. North is up and east to the left; the area shown measures 16.5×18 arc min. The resolution (30×45 arc s FWHM) can be judged from the appearance of the point source in the upper-right quadrant. A point source of flux density 13.2 Jy has been subtracted at the position of the cross centred on NGC1275. The displayed contour levels are $-5, 0, 2.5, 10, 50, 100, 200, 400, 800, 1600, 3200$ and 6400 mJy per beam; the peak brightness is at 2,060 mJy per beam. The true zero level varies slightly across the map but lies at about -2.5 mJy in the inner 10 arc min of the map.

source structure. An elegant way of doing this is to use the fact that the centroid of an extended source should remain at a fixed location irrespective of the hour angle of the scan⁸. By shifting every scan to the projected position of this centroid one does not require a model of the source. A determination of the source centroid and total flux density using, for example, a one-dimensional CLEAN⁹, would suffice. Although this method is clearly easier for the user, the results obtained thus far are still inferior to those obtained using a model for the source. Nevertheless, the results are encouraging (dynamic range $\sim 1,000:1$) and for very extended complex sources, in particular, we expect it to become the preferred method.

At present, in a more conventional approach, the unaligned scans are Fourier inverted to produce a map of the synthesized field and then CLEAN⁹ is used to provide a simple model for the source. The individual scans are then adjusted to agree with the predicted model amplitudes and phases. In the alignment stage the user can specify the range of baselines over which he wants to force agreement between model and data. Depending on the source structure, for which some information can be gained by inspecting the visibility amplitudes, one could decide to align on the shorter or longer baselines. Following the alignment of the scans a better model for the source can be constructed and the alignments refined, if necessary. Here the method is similar to the self-calibration procedures used for VLA and MERLIN data. However, in the case of the WSRT only two parameters per scan need be determined. This, and the near-perfection of the individual scan complex visibilities, are the reasons that the process usually converges in one or two iterations. Finally, corrections can be applied for interferometer errors, if they are important (on sources stronger than several Jy). Following the final alignment corrections the difference between the model visibilities and the observed visibilities, averaged over 12 h, are determined for each interferometer. An incomplete model would only produce slowly varying differences as a function of interferometer baseline length. The misbehaving interferometers can then easily be spotted and corrected.

We have applied the technique to more than 12 sources at wavelengths of 6, 21 and 49 cm. The very high dynamic range attained in nearly all of these cases can, in summary, be attributed to mainly two factors: (1) the excellent design and performance of the correlator, limiting the magnitude of inter-

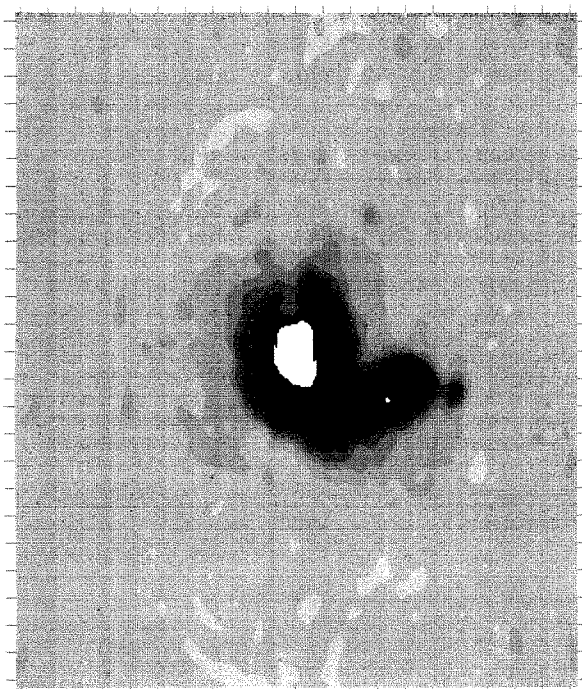


Fig. 3 Grey-scale presentation of the convolved 21-cm map shown in Fig. 2.



Fig. 4 The full resolution 6-cm map made from the April 1981 data is shown superimposed on the narrow band H_{α} photograph taken by Lynds²¹ (courtesy Dr Lynds and the Kitt Peak National Observatory). An unresolved source of 60 Jy was removed at the peak position. The residual peak is about 110 mJy. Contours are $\pm 6, 12, 18, 24$ (12) and 108 mJy per beam (3.5×5.3 arc s FWHM). North is up and east to the left; the region shown measures about 190×150 arc s.

ferometer-based errors; (2) the use of redundant baselines to reduce to only two the number of independent 'errors' per scan.

21-cm results on 3C84

3C84 is associated with NGC1275, the brightest galaxy in the Perseus cluster. Its radio structure is unusually complex and has been mapped previously with the Cambridge and WSRT arrays¹⁰⁻¹³. Two 12-h syntheses were made of the source in the redundant configuration at both 6 and 21 cm wavelength. The 21-cm observations were done on 14 August 1980 and 21 August 1981, and the 6-cm observations on 21 April 1981 and 2 January 1982. In the first 21-cm and both 6-cm observations the system temperature was ~ 90 K and the bandwidth 10 MHz. Feed polarization was linear in position angle 0° . During the more recent 21-cm observation the four movable telescopes were equipped with cooled low-noise receivers¹⁴, resulting in an overall system temperature of 55 K. The amplitude scale was calibrated using 3C286 as the primary flux density standard; it is assumed to have flux densities of 7.41 Jy at 4,995 MHz and 14.77 Jy at 1,412 MHz, which are on the Baars *et al.*¹⁵ scale. The coordinates in the various maps were tied to that of the core source in 3C84: RA = 03 h 16 min 29.57 s, dec. = $+41^{\circ}19$ arc min 51.9 arc s (1950.0).

Figure 2 shows the 21-cm total intensity distribution superimposed on a deep optical photograph¹⁶ of the central part of the Perseus cluster. A smoothed map is shown to bring up the extended halo around NGC1275. The map shows at much greater sensitivity and higher resolution the various structures seen previously^{10,13}. It also revealed the presence of weak discrete radio sources associated with NGC1270, NGC1272 and NGC1278. The dynamic range in this map varies from $\sim 3,000$ close to the source peak to 10,000 further out. 3C84 has three distinct radiation components of widely different angular scales (see Table 1). The most intense one is an unresolved VLBI core which was subtracted from the map. Underneath the core lies the so-called 30 arc s component which we find to be symmetrically extended, contrary to the findings of Miley and Perola¹⁰.

The diffuse emission surrounding the 30 arc s component has a surface brightness more than two orders of magnitude below that of the component itself. The relationship between these two components is unknown. This third component, which we will refer to as the halo, has no apparent boundary. At the lowest significant contour in our map the size is nearly 10 arc min. The brighter part of it, 4×6 arc min is elliptically shaped

and centred on NGC1275. Since our shortest interferometer spacing (72 m) has a fringe separation of 10 arc min we cannot detect any more extended structure. Structure on a scale somewhat greater than 10 arc min was seen at 408 MHz (ref. 12).

An interesting feature of the halo is the bright region about 3 arc min south-west of NGC1275 of which the outermost contours enclose the galaxy NGC1272 which is a radio source in its own right. NGC1272 seems to be connected to NGC1275, through this feature, in a curved bridge of emission. However, we regard this connection as illusionary and attribute it to the superposition of a trail of emission associated with NGC1272 and a symmetrical halo surrounding NGC1275. Gisler and Miley¹³ have suggested that NGC1272 and NGC1275 are a pair of head-tail sources in orbit around each other. The fine structure within the region between the two galaxies, and the structure of the discrete source associated with NGC1272, do not support such a view. Below we discuss an alternative explanation for the enhanced emission features.

Various arguments suggest that NGC1272 is physically close to NGC1275, that is, not only in projection. If so, NGC1272 is moving through the composite thermal/non-thermal halo surrounding NGC1275. Such a trajectory is likely to affect the non-thermal radio emissivity (and, possibly also the thermal X-ray emissivity¹⁷). This scenario is strongly suggested by Fig. 3, which is a grey-scale representation of Fig. 2. A rough calculation supports this hypothesis quantitatively. The power deposited in the wake of a galaxy moving trans-sonically through the cluster medium is $\pi \rho v_g^3 R^2$, where ρ is the cluster density, v_g the galaxy velocity ($\sim 1,000 \text{ km s}^{-1}$) and R some characteristic radius^{18,19}. Where the radio brightness enhancement is highest, the density¹⁷ is $\sim 10^{-2} \text{ cm}^{-3}$. We take R to be 10 kpc, which is the accretion radius of NGC1272 for an adopted mass of $10^{12} M_\odot$. Although this cross-section is uncertain we note that the radio source associated with NGC1272 itself is also ~ 20 kpc diameter transverse to its hypothesized direction of motion. The total pathlength through the halo we estimate to be ~ 100 kpc. During the 10^8 yr taken by NGC1272 to traverse this distance, it deposits $\sim 10^{59}$ erg in the form of turbulent motions. How much of this energy eventually ends up in the form of magnetic and relativistic electron energy is unknown. The minimum (equipartition) energy contained in the 'trail' is $\sim 10^{57}$ erg and a 1% conversion efficiency therefore suffices to explain the emission from the trail. This does not seem implausible.

In the context of the wake hypothesis, the trail emission might also be explained as a mere enhancement of the diffuse halo emission, without invoking *in situ* turbulent acceleration. As can be seen in Figs 2 and 3, the halo surface brightness at the location of the trail was non-zero before the passage of NGC1272. A moderate compression of the halo magnetic field in the wake of NGC1272 will lead to betatron acceleration of the relativistic electrons and with the enhanced field strength this will combine to yield a considerable increase of the synchrotron emissivity. However, the line-of-sight depth through the trail is considerably smaller than that through the halo and it is unlikely that this mechanism could explain the factor 30 enhancement in the surface brightness ~ 50 kpc behind NGC1272 where the wake reaches its peak brightness. If the wake hypothesis is correct, the observations provide direct evidence for turbulence-induced *in situ* particle acceleration in diffuse radio sources, on time scales of $\sim 5 \times 10^7$ yr.

The wake of NGC1272 shows some curvature; this is to be expected due to the dynamical pressure exerted by the gas in the accretion flow—which in the picture by Cowie *et al.*²⁰ rotates around NGC1275 with a period of $\sim 10^9$ yr—during the radiative (and kinematic) lifetime of the trail of $\sim 10^8$ yr. If NGC1272 can leave such an impressive mark, it is conceivable that part or all of the halo emission is due to continuous stirring through passages of other galaxies (see ref. 19). Another feature in the halo that might be interpreted as the remnant of a galactic wake is the spur in PA = 15° , extending out to 4 arc min. However, this is also the direction of the peculiar outlying H α filament²¹.

The 30 arc s component

Figure 4 gives the 6-cm map, which has nearly an order of magnitude higher resolution than the 21-cm map shown in Fig. 2. Although no trace of the halo could be found above a limiting flux density of about 2 mJy per beam area, this is not surprising in view of the steep spectrum¹³ of the halo and its resolved appearance at 21 cm. After subtraction of the intense unresolved core source the 6-cm map becomes dominated by the 30 arc s component referred to earlier. Our resolution is insufficient to decide whether there exists some emission on an arc second scale surrounding the core. The details of the structure within about one beamwidth from the core position therefore remain uncertain. The dynamic range in the 6-cm map varies from nearly 10,000:1 close in to about 50,000:1 further out. This was nicely demonstrated by the detection (independently in both 6-cm data sets), at a level of 4 ± 1 mJy, of the nuclear source in NGC1278, previously seen at 21 cm.

The 30 arc s component is oriented roughly in PA -10° , as first deduced by Miley and Perola¹⁰, and has an axial ratio of about 3:1. As has been noted before, this is also the direction of elongation of the core as deduced from VLBI studies^{6,22}. At the higher intensity levels the structure has some S-type symmetry. The overall dimensions of this component are roughly 15×40 arc s, corresponding to linear dimensions of 8×21 kpc. It is surprising that there is no structural relationship between the radio radiation and the H α filamentation system discovered by Lynds²¹ (Fig. 4). Fabian and Nulsen²³ suggested that the compression flow gave rise to the radio halo around NGC1275. Our 6- and 21-cm maps do not support this suggestion, considering the lack of correspondence between the halo emission and the optical filaments where the compression presumably is largest. However, the accretion flow may have profound effects on the structure of the 30 arc s component. If the rotating accretion flow continues its inflow beyond the stagnation point, which Cowie *et al.*²⁰ place at a radius of ~ 50 kpc, the dynamic pressure of the inflowing matter would eventually be strong enough to halt the relativistic particle flow from the nucleus, which is probably oriented in PA -10° . Transfer of angular momentum from the flow to the relativistic plasma clouds might then be responsible for the S-type symmetry in the 30 arc s component.

We thank Drs J. D. O'Sullivan, J. P. Hamaker, A. Bos and H. W. van Someren Gréve for informative discussions and assistance during the long period from planning to implementation of this reduction method. The Westerbork Synthesis Radio Telescope is operated by the Netherlands Foundation for Radio Astronomy (SRZM) with the financial support of the Organization for the Advancement of Pure Research (ZWO).

Received 28 May; accepted 2 August 1982.

- Hamaker, J. P. in *Image Formation from Coherence Functions in Astronomy* (ed. van Schooneveld, C.) 27–45 (Reidel, Dordrecht, 1979).
- Hamaker, J. P. in *Image Formation from Coherence Functions in Astronomy* (ed. van Schooneveld, C.) 47–53 (Reidel, Dordrecht, 1979).
- Readhead, A. C. S. & Wilkinson, P. N. *Astrophys. J.* **223**, 25–36 (1978).
- Schwab, F. R. *Proc. 1980 Int. Optical Computing Conf.*, SPIE, 230, 18–24 (1980).
- Cornwell, T. J. & Wilkinson, P. N. *Mon. Not. R. astr. Soc.* **196**, 1067–1086 (1981).
- Pauliny-Toth, I. I. K. *et al.* *Nature* **259**, 17–20 (1976).
- Bos, A., Raimond, E. & van Someren Gréve, H. W. *Astr. Astrophys.* **98**, 251–259 (1981).
- O'Sullivan, J. D. *NFRA Internal Note* 240 (1977).
- Högbom, J. A. *Astr. Astrophys. Suppl.* **15**, 417–426 (1974).
- Miley, G. K. & Perola, G. C. *Astr. Astrophys.* **45**, 223–226 (1975).

- Ryle, M. & Windram, M. D. *Mon. Not. R. astr. Soc.* **138**, 1–21 (1968).
- Birkinshaw, M. *Mon. Not. R. astr. Soc.* **190**, 793–799 (1980).
- Gisler, G. R. & Miley, G. K. *Astr. Astrophys.* **76**, 109–119 (1979).
- Casse, J. L., Woestenburger, E. E. M. & Visser, J. J. *IEEE Trans. Microwave Theory Tech.* **30**, 201–209 (1982).
- Baars, J. W. M. *et al.* *Astr. Astrophys.* **61**, 99–106 (1977).
- Arp, H. C. & Bertola, F. *Astrophys. J.* **163**, 195–201 (1971).
- Fabian, A. C., Hu, E. M., Cowie, L. L. & Grindlay, J. *Astrophys. J.* **248**, 47–54 (1981).
- Jaffe, W. *Astrophys. J.* **241**, 925–927 (1980).
- Roland, J. *Astr. Astrophys.* **93**, 407–410 (1981).
- Cowie, L. L., Fabian, A. C. & Nulsen, P. E. J. *Mon. Not. R. astr. Soc.* **191**, 399–410 (1980).
- Lynds, R. *Astrophys. J. Lett.* **159**, L151–154 (1970).
- Unwin, S. C. *et al.* *Astrophys. J.* **256**, 83–91 (1982).
- Fabian, A. C. & Nulsen, P. E. J. *Mon. Not. R. astr. Soc.* **180**, 479–484 (1977).

Molecular structure of r(GCG)d(TATACGC): a DNA–RNA hybrid helix joined to double helical DNA

Andrew H.-J. Wang*, Satoshi Fujii*, Jacques H. van Boom†, Gijs A. van der Marel†, Stan A. A. van Boeckel† & Alexander Rich*

* Department of Biology, Massachusetts Institute of Technology, Cambridge, Massachusetts 02139, USA

† Gorlaeus Laboratory, University of Leiden, 2300 RA Leiden, The Netherlands

The molecule r(GCG)d(TATACGC) is self-complementary and forms two DNA–RNA hybrid segments surrounding a central region of double helical DNA; its molecular structure has been solved by X-ray analysis. All three parts of the molecule adopt a conformation which is close to that seen in the 11-fold RNA double helix. The conformation of the ribonucleotides is partly determined by water molecules bridging between the ribose O2' hydroxyl group and cytosine O2. The hybrid–DNA duplex junction contains no structural discontinuities. However, the central DNA TATA sequence has some structural irregularities.

THE sugar–phosphate backbones of DNA and RNA differ in one fundamental feature—the presence of a 2' hydroxyl group in the RNA backbone, which makes it more reactive and less flexible than the DNA backbone. Hybrid molecules are formed when DNA directs the polymerization of RNA or when RNA is the template for DNA polymerization. The former process occurs during transcription and the latter is found in the action of reverse transcriptase. In DNA replication, Okazaki fragments are initiated by a short primer containing a few ribonucleotides¹. In all these cases, a hybrid helix is found containing an RNA and a DNA strand. Double helical DNA and RNA usually form different types of helices, the B form being common for DNA, and the A form for RNA. Thus, we are interested in understanding how these two types of backbones are accommodated in a hybrid molecule. The formation of a DNA–RNA hybrid helix was first demonstrated with synthetic polynucleotides². Advances in synthetic technique have allowed the synthesis of oligomers which can provide structural information about molecules of this type. In considering this problem, we decided to synthesize a self-complementary decamer containing three ribonucleotide units at the 5' end linked to seven deoxynucleotide units. This can form a molecule which has a DNA–RNA hybrid in the three base pairs at either end of the molecule and a central segment of four base pairs which is a DNA–DNA duplex. The DNA duplex and its attached DNA–RNA hybrid may serve as a model for visualizing the structure of the Okazaki DNA fragment after initiation of replication, as only a small number of ribonucleotides are used as a primer. Here we report crystallization of the decamer r(GCG)d(TATACGC) in a form suitable for X-ray diffraction analysis. We have determined the structure of the crystal and find that the hybrid molecule forms a helix which is of the A type or close to 11-fold RNA³. Further, the presence of an A-type helix in the hybrid portion of the molecule seems to have influenced the conformation of the central four base pairs of DNA, which also assume the same A-DNA conformation.

Crystallization and structure determination

Synthesis of the hybrid decamer has been described previously⁴. The decamer was crystallized in a solution containing 1.5 mM decamer, 30 mM sodium cacodylate buffer (pH 6.0), 8 mM spermine, and 15 mM magnesium chloride; 20 μ l of this solution were placed in the depression of a glass spot plate, which was then enclosed in a sealed box containing a reservoir with 40% 2-methyl-2,4-pentanediol. Crystals were formed by vapour diffusion. After 1 week, thick chunky rods (0.4 \times 0.4 \times 0.7 mm) were observed growing in the solution. The crystals

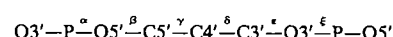
were mounted in sealed glass capillary tubes with a droplet of mother liquor and were found to diffract to a resolution of 1.9 Å. The space group was P2₁2₁2₁ with $a = 24.20$ Å, $b = 43.46$ Å and $c = 49.40$ Å. The asymmetric unit consisted of one decamer duplex containing 20 bases. Data were collected on a Nicolet diffractometer to 2 Å resolution at 0 °C.

Of 3,798 independent reflections, 2,521 were found to be observable over the 1.5 σ (I) level. A rotation–translation search was attempted using A-DNA as a model³. This search produced only moderate agreement using the data from 13 to 5 Å resolution, and the model would not refine further. We believed this might be due to the fact that the molecule has slightly different conformations in the three different segments of the molecule, that is, the two DNA–RNA hybrid segments and the DNA–DNA duplex. Another search was carried out using a model with three different segments covering the two hybrid parts and the DNA duplex. This refinement strategy did not converge, therefore another model was used in which the molecule was broken up into three segments containing four base pairs at either end and two in the middle. An 11-fold

Table 1 Averaged torsional angles* and helical parameters

	DNA–RNA hybrid (this work)	A-DNA ³ (fibre)	A-RNA ³ (11-fold) (fibre)	B-DNA ³ (fibre)
Torsional angle (deg)				
α	–69(31)	–90	–60	–39
β	175(14)	211	175	209
γ	55(22)	47	49	31
δ	82(9)	83	83	157
ϵ	–151(15)	–185	–147	–201
ξ	–75(16)	–45	–78	–99
χ	–162(10)	–153	–167	–95
P	17(15)	14	14	192
Helical parameters				
Rotation per unit (deg)	33(3)	33	33	36
Rise per unit (Å)	2.6(3)	2.6	2.8	3.4
Residues per turn	10.9	11.0	11.0	10.0
Propeller twist angles (deg) in base pairs				
Dihedral angle	14	11	12	1
Roll component	11	–11	–12	1
Tilt component	–2	0	0	0
Adjacent phosphorus atom separation (Å)				
	5.9(2)	5.7	5.7	6.5

Torsional angles are defined as



and χ is the glycosyl torsion angle. P is the phase angle of pseudorotation¹⁹.

* End effects are excluded and the standard deviations are given in parentheses.

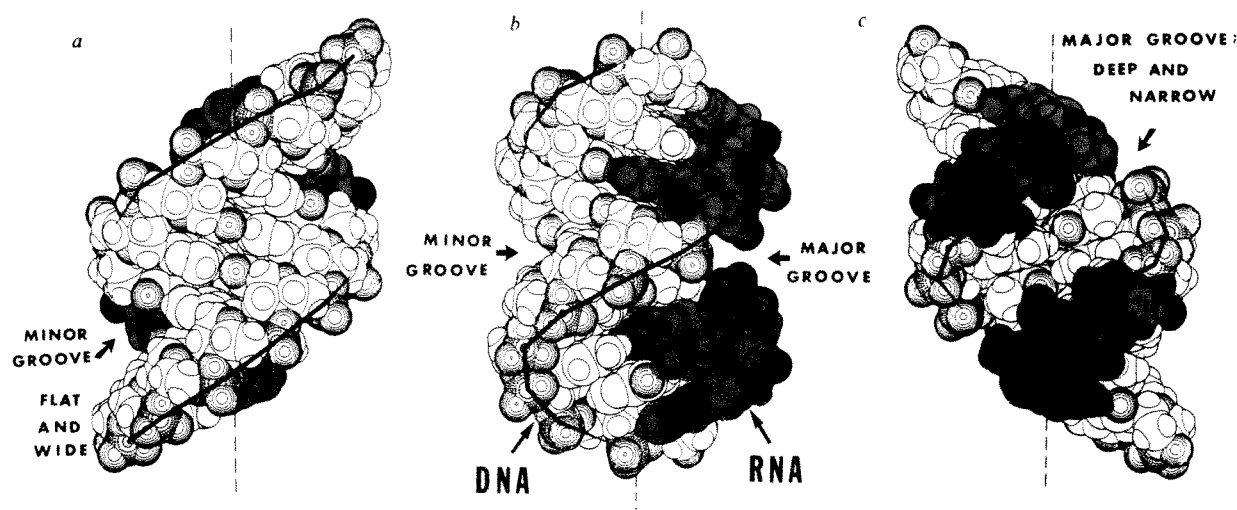


Fig. 1 A space-filling drawing of the molecule is shown in three different orientations 90° apart from each other about the dashed vertical axis. *a*, Looking into the minor groove of the molecule which is broad and flat. The phosphate groups on opposite strands are 8.6 Å apart across the minor groove. The heavy black lines are drawn from phosphate to phosphate to show the flow of the polynucleotide chain. The ribonucleotides are shaded and the ribose 2' oxygen atoms are solid. *b* Diagram shows both the minor groove on the upper part of the molecule and the major groove at the lower right. The shaded ribonucleotide backbone segments on the right are close to each other on either side of the major groove. The bases are tilted 19° from the vertical axis. In this centre view, the tilt reverses itself in going from the upper part to the lower part of the molecule. *c*, Looking into the deep narrow major groove of the molecule. The phosphate groups are 4.7 Å away from each other across this groove. Solid circles, oxygen atoms; stippled circles, nitrogen atoms; spiked circles, phosphorus atoms.

RNA model was then used for all three segments and an additional search was carried out to find local minima. This search was satisfactory, producing an *R* factor of 36% at 5 Å resolution. The model was further refined using the Konnert-Hendrickson restrained refinement program⁵ to a final *R* factor of 0.16. As the molecule gradually refined, a large number of water molecules appeared in the electron density map; at the end, 179 water molecules could be located surrounding each decamer. However, it was not possible to make an unambiguous assignment for either spermine molecules or Mg²⁺ ions in the electron density map even though they have been observed in other oligonucleotide structures which diffracted to higher resolution⁶.

Description of the molecule

Although the asymmetric unit is a 10-base pair (bp) duplex, the molecule possesses a non-crystallographic 2-fold axis with a r.m.s. deviation of 0.95 Å between the two strands of the duplex, by least-square fitting. The two strands thus have almost identical conformations. The molecule has an almost perfect A-type geometry with all the ribose and deoxyribose sugars in the C3' *endo* conformation; this is the conformation normally found in ribonucleotides^{7,8} and in the A-form of DNA³. Three different views of the molecule are shown as van der Waals' diagrams in Fig. 1. To aid in the identification of the ribonucleotides, they have been shaded and the ribose 2' oxygen atoms are black. Figure 1*b* shows both the minor groove on the left side of the molecule and the major groove on the right side. The views of either side of the molecule are obtained by a rotation of 90° about the vertical axis. At the right we are looking into the deep, narrow major groove that has a depth of 8 Å. The view at the left shows the broad, flat minor groove with a depth of only 2–3 Å. The difference between these two surfaces is quite great in the A conformation in contrast to the B-DNA conformation where the two grooves are more equivalent.

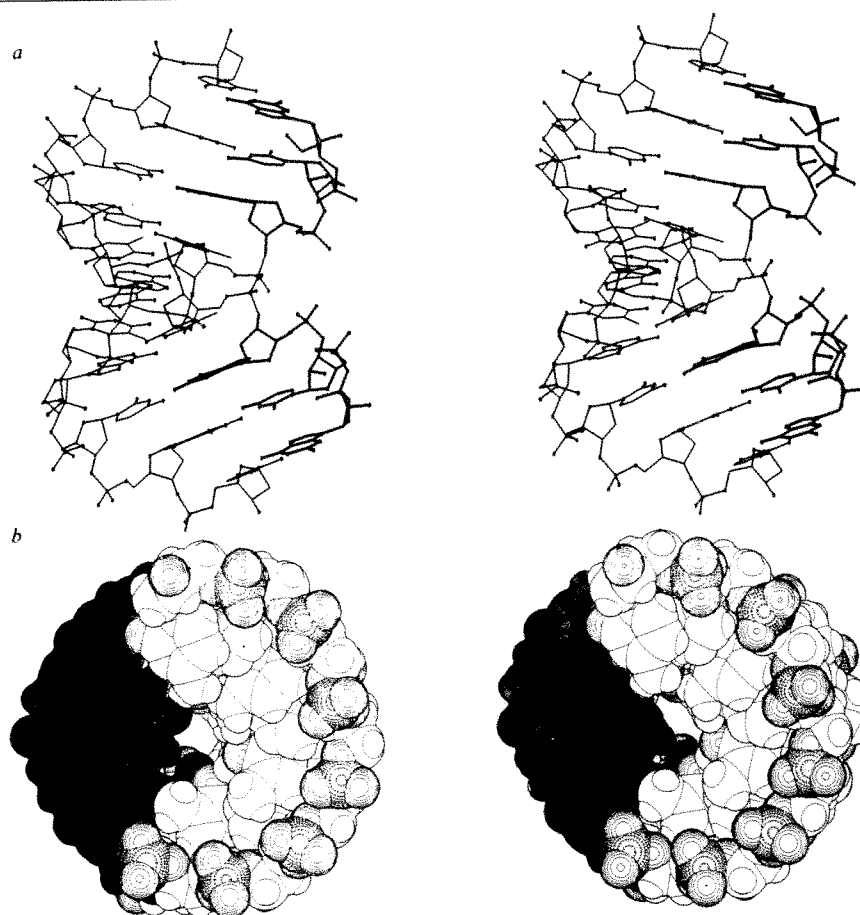
Figure 2*a* is a stereo skeletal side view of the molecule. The base pairs have an average rotation per residue of 33° and a rise along the axis of 2.6 Å. In this helix there are 10.9 residues per turn; we are thus observing just under one complete turn. The base pairs are considerably removed from the axis of the molecule and are tilted at an angle of 20° to the helix axis. Three different crystal structures of DNA oligonucleotides have been reported that assume A-DNA conformations: two octamers^{9,10} and one tetramer¹¹. However, the helical param-

eters of the present molecule are closer to that of the A-type geometry which has been studied extensively in both DNA and RNA fibres (Table 1). This may reflect the influence of the hybrid portions of the molecule. It is interesting that the perfection of the A-type geometry is found not only in the hybrid sections but also in the 4-bp central DNA section. The space-filling stereo view in Fig. 2*b* shows the molecule as viewed down the axis. There is an empty space nearly 2 Å in diameter along the axis of the molecule.

The Watson-Crick base pairs all have a propeller twisting (see Fig. 2*a*), the average dihedral angle of which is 14° excluding the two terminal base pairs which are involved in the intermolecular interactions. The sign of the propeller twisting between the base pairs is the same as that observed in a crystal of a B-DNA dodecamer¹². We have examined the hydrogen bond lengths in the various segments of the molecule. The four A·T base pairs in the DNA-DNA segment of the centre of the molecule have average bond lengths for NH—N of 2.8 Å and for NH—O, 3.12 Å. The six G·C base pairs in the DNA-RNA hybrid portion of the molecule have average hydrogen bond lengths: N—HN, 2.86 Å; N4H—O6, 2.84 Å; and N2H—O2, 2.80 Å. The nucleotide conformations are not identical but fall within a fairly narrow range. The average torsion angles for the sugar-phosphate backbone are listed in Table 1. A detailed listing of the torsion angles for the individual residues will be published elsewhere.

There is considerable interest in the contribution made by the 2' hydroxyl group of the ribose residues to the overall conformation. The 2' hydroxyl stabilizes the C3' *endo* conformation of the sugar¹³. Several model building proposals have been made which involve the ribose 2' hydroxyl group in different types of intramolecular hydrogen bonding to adjacent nucleotides in the chain¹⁴. We have examined the six hydroxyl groups present in this structure. The two hydroxyl groups associated with the pyrimidine residues have a hydrogen bonding interaction with a water molecule located 2.93 Å away. The water is hydrogen-bonded (3.07 Å) to O2 of the same cytosine residue (Fig. 3). The 2' hydroxyl group thus seems to play a significant part in stabilizing the conformation in the ribonucleotide segments of the molecule through the use of a bridging water molecule. Examination of the hydroxyl groups found in the four riboguanosine residues reveals that they also are hydrogen-bonded to water molecules, but the latter are hydrogen-bonded to adjacent molecules in the lattice. An intramolecular bridging water molecule similar to that seen on

Fig. 2 Stereo views of the hybrid helix. *a*, The molecule in the same orientation as that seen in Fig. 1*b*. The ribonucleotide segments are drawn with a thicker line than the deoxyribonucleotide segments. In this stereo view with a skeletal backbone, it can be seen that the base pairs have a propeller twist between them. The propeller twist angle has an average value of 14° throughout the structure, excluding the terminal base pairs. *b*, Stereo view of the molecule drawn with space-filling atoms viewed down the helix axis. The axis of the molecule has an empty space ~ 2 Å in diameter which is not occupied. The base pairs form a prominent right-handed staircase-like arrangement in this view; the phosphate groups have a conformation such that they are tipped into the major groove of the helix, so that they form an interrupted 'railing' for the staircase. The shading of the atoms and the nucleotides is the same as for Fig. 1.



the cytosine residues has been found between the O2' hydroxyl group and the N3 of guanine in the crystal structure of the dinucleoside monophosphate GpC⁸. It is perhaps reasonable to believe that such bridging water molecules could be a constant feature of RNA double helices in solution. Note that bridging water molecules have been found in several nucleic acid structures where they are believed to have a significant role. For example, a water molecule is found bridging between guanine N2 and the phosphate oxygen of the next nucleotide in the left-handed Z-DNA helix⁶; this water molecule stabilizes the *syn* conformation of the deoxyguanosine residue. Another example is found in the interaction of the antibiotic daunomycin with a DNA oligonucleotide, where the acetyl group of the daunomycin molecule is linked to a guanine residue in the base pair adjacent to the intercalative site through the use of a bridging water molecule¹⁵.

Studies have been made of the exchange rate of protons attached to the 2' hydroxyl group of ribonucleotides in a DNA-RNA hybrid model system¹⁶. These protons have a slow exchange rate, which suggests that they might be involved in some kind of stable structural interaction. Interactions with bridging water molecules may be responsible for some of this behaviour.

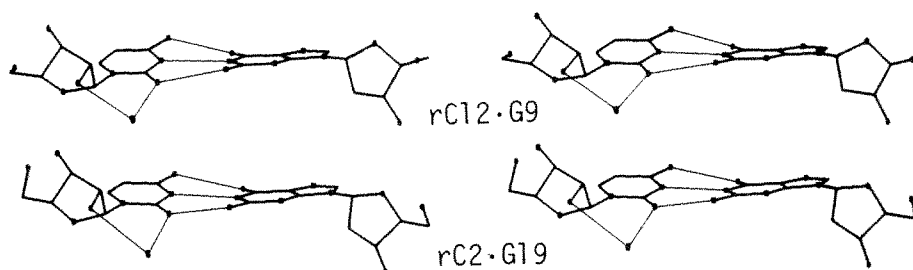
The stacking of successive nucleotides along the helix is similar to that found in a typical A-DNA helix or the similar 11-fold RNA helix³. The stacking interactions at the hybrid-deoxynucleotide interface were found to be similar to those observed in purine-pyrimidine sequences elsewhere in the

molecule. Thus no structural discontinuity is found when the stacking is examined in detail. Note that there are some bends in the helix axis at the TpA steps. The dihedral angles between the TATA base pairs show an interesting discontinuity. The angle between the first two base pairs is 19° , while that of the second step is 16° . In both cases, the opening of the base pairs is always in the direction of the minor groove. This explains the fact that in the structure determination, we obtained a satisfactory rotation-translation search only when the molecule was divided into 4-2-4-bp segments. Note also that the two central A·T base pairs have elongated NH—O hydrogen bonds with lengths averaging 3.23 Å. The distortions associated with the TATA sequence observed in this structure may be a sequence-dependent property of the DNA molecule, and is noteworthy in view of the special role which TATA sequences have in the initiation of transcription by RNA polymerase.

Lattice packing

The lattice is rather tightly packed and contains 33–35% water by mass, an average value for oligonucleotide crystals. The molecules are organized around a series of 2-fold screw axes running through the lattice in three perpendicular directions. The major interactions between the molecules are due to the flat base pairs at both ends which stack on adjacent molecules in the broad, shallow minor groove. The nucleotides are numbered from the 5' to the 3' end on both chains, so that rG1 is paired to C20. Stacking of the terminal base pairs is shown in

Fig. 3 Stereo skeletal drawings of two different guanosine-cytosine pairs in the hybrid helix. (The nucleotides are numbered 1–10 on one chain, 5' → 3', and 11–20 on the other chain in the same 5' → 3' direction.) The figures show a similar conformation of the cytosine ribose residues at the left in both base pairs. A bridging water molecule at the lower left in both diagrams is hydrogen-bonded both to the 2' hydroxyl group of the ribose and the O2 of cytosine. The electron density of the water molecule indicates that it is fully occupied, thus it is possible that this bonding helps to stabilize the orientation of the base relative to the sugar.



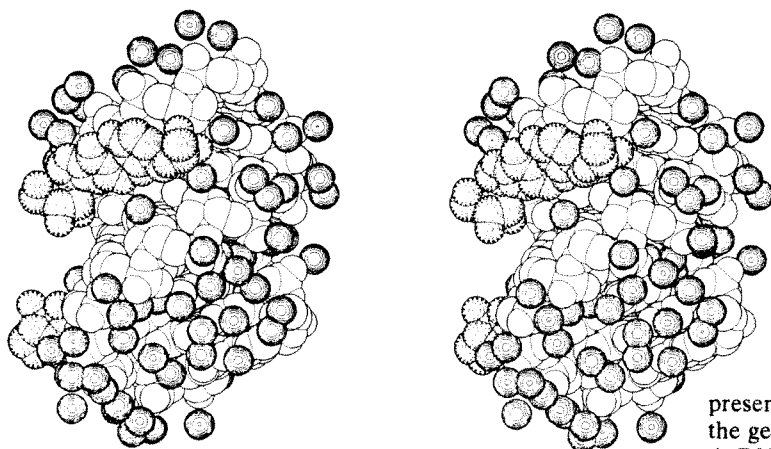


Fig. 4. The base pair rG1-C20 abuts onto nucleotides A7 and C8 of an adjoining molecule. The guanine base of rG1 makes van der Waals' contacts with the adenine A7 (atoms N3, C1' and C2') while the cytosine ring of C20 makes close contacts with the C1' and C2' atoms of the sugar ring of cytosine C8. The long direction of the base pair rG1-C20 lies along the path of the minor groove (Fig. 4).

The contacts at the other end of the molecule involving C10-rG11 have a similar orientation but they differ in detail. A hydrogen bond is found between the oxygen O3' of C10 and N2 of guanine G19. This hydrogen bond may be important in building up the lattice because of its directionality. Another interaction involves the O2' oxygen of rG11 which hydrogen bonds to a bridging water molecule, which in turn donates a proton to atom N3 of the adenine ring on A17. Other close van der Waals' contacts are found between the guanine ring of rG11 and the sugar phosphate chain of C18. The interaction at this end of the molecule is associated with hydrogen bonding as well as a bridging water molecule, in contrast to the strictly van der Waals' interactions found at the opposite end.

The major motif in building up the lattice is the stacking of planar base pairs on the flat minor grooves. The importance of this type of interaction in the lattice formation of A-DNA fragments has been discussed previously⁹. Similar interactions are found in three other lattices which form A-type helices, including the DNA octamers d(GGCCGGCC)⁹ and d(GGTATACC)¹⁰, and the tetramer d(CCGG)¹¹. The prevalence of these interactions in building up lattices is probably due to the fact that the energy is minimized by having the hydrophobic planar purine-pyrimidine base pair stacked on the relatively hydrophobic planar A-DNA minor groove. Neither the B-DNA helix, with a deeper minor groove, nor Z-DNA has a planar surface of this type, thus different types of lattice packing interactions are found in these cases. In Z-DNA crystals⁶ and in the daunomycin-B-DNA crystal complex¹⁵, the planar purine-pyrimidine base pairs at the ends of the molecules stack on themselves to build up a lattice.

Oligonucleotides as models

The mating of ribonucleotide strands with deoxyribonucleotide strands to form a hybrid double helix is one of the principal reactions of the biological information transfer system. DNA-RNA hybrid molecules are found covalently linked to a DNA duplex at the initiation of DNA replication in the Okazaki fragments¹ and are also found in mitochondrial DNA¹⁷. The

Fig. 4 A space-filling stereo diagram of the molecule showing the water molecules (solid circles) which are found in the first hydration sphere. In addition, base pairs from the ends of other molecules are shown stacked in the minor groove (interrupted circles). Fewer water molecules are found in the flat minor groove than in the major groove.

present structure has allowed us to visualize for the first time the geometry of the hybrid helix. We find that the helix has an A-DNA or 11-fold RNA geometry. It consistently uses C3' *endo* puckering of both ribo- and deoxyfuranose rings, so that adjacent phosphate groups are closer together than they are in the B-DNA double helix which uses C2' *endo* puckering. It seems that the RNA backbone has forced its geometry on the DNA backbone in a stable conformation. This may be due to the fact that deoxynucleotides can have either ring pucker, but ribonucleotides favour the C3' *endo* pucker.

It should be noted that the 2' oxygen atoms in the ribonucleotide segment are prominent on the outer surface of the molecule (Fig. 1). As the overall conformation of the residues of both the ribose and the deoxyribose residues is almost the same in the hybrid molecule, the presence of the hydroxyl group on the surface means that proteins or other molecules interacting with this can readily detect the difference between an RNA fragment forming an A-helix and a deoxynucleotide segment having the same conformation.

The central four base pairs of the DNA-DNA duplex also have the A-DNA geometry usually found in the RNA double helix; possibly this is due to the influence of the hybrid segments at either end of the molecule. If this is the case, it would be interesting to know how long a stretch of DNA would be influenced by an A conformation at one point. The answer to this would elucidate the nature of the A-to-B transitions which undoubtedly occur at many points in long DNA molecules.

Another question in this regard is whether the central 4-bp DNA duplex of this molecule would retain an A-DNA conformation in solution. A NMR study of this molecule in solution suggests that it does retain the A-DNA conformation, similar to that seen when the molecule is in the crystal lattice¹⁸. The latter study supports the idea that the A conformation must be due to the ribonucleotide components because the same molecule composed entirely of deoxyribonucleotides shows the typical B-DNA conformation.

The availability of pure fragments of oligonucleotides constructed using both the ribo and the deoxy series may help to further our understanding of the chemical forces which stabilize different conformations. As different conformations are often used in different ways in biological systems, these studies may eventually provide a firm basis for understanding the manner in which the nucleic acids perform their functions.

We thank Dr Gary Quigley for helpful discussions and for the use of his graphic plotting programs. This research was supported by grants from the NIH, NASA, the American Cancer Society and the Netherlands Organization for the Advancement of Pure Research (ZWO).

Received 7 July; accepted 12 August 1982.

- Ogawa, T. & Okazaki, T. A. *Rev. Biochem.* **49**, 421-457 (1980).
- Rich, A. *Proc. natn. Acad. Sci. U.S.A.* **46**, 1044-1053 (1960).
- Arnott, S., Smith, P. J. C. & Chandrasekaran, R. *CRC Handbk Biochem. molec. Biol.* 3rd edn, Vol. 2 (ed. Fasman, G. D.) (CRC, Cleveland, 1976).
- van Boeckel, C. A. A. *et al. Recl Trav. chim. Pays-Bas Belg.* **100**, 389-390 (1981).
- Hendrickson, W. A. & Konnert, J. *Biomolecular Structure, Conformation, Function and Evolution* Vol. 1 (ed. Srinivasan, R.) 43-57 (Pergamon, Oxford, 1979).
- Wang, A. H.-J. *et al. Nature* **282**, 680-686 (1979).
- Seeman, N. C., Rosenberg, J. M., Suddath, F. L., Kim, J. J. P. & Rich, A. *J. molec. Biol.* **104**, 109-194 (1976).
- Rosenberg, J. M., Seeman, N. C., Day, R. O. & Rich, A. *J. molec. Biol.* **104**, 145-167 (1976).
- Wang, A. H.-J., Fujii, S., van Boom, J. H. & Rich, A. *Proc. natn. Acad. Sci. U.S.A.* **79**, 3968-3972 (1982).
- Shakked, Z. *et al. Proc. R. Soc. B* **213**, 479-487 (1981).
- Conner, B. N., Takano, T., Tanaka, S., Itakura, K. & Dickerson, R. E. *Nature* **295**, 294-299 (1982).
- Wing, R. M. *et al. Nature* **287**, 755-758 (1980).
- Davies, D. B. *Prog. nucl. magn. Resonance Spectrosc.* **12**, 135-225 (1978).
- Ts'o, P. O. P., Rappaport, S. A. & Bollum, F. J. *Biochemistry* **5**, 4153-4156 (1966).
- Quigley, G. J. *et al. Proc. natn. Acad. Sci. U.S.A.* **77**, 7204-7208 (1980).
- Selsing, E., Wells, R. D., Early, T. A. & Kearns, D. R. *Nature* **275**, 249-250 (1978).
- Bernicke, A. & Clayton, D. A. *J. biol. Chem.* **256**, 10613-10617 (1981).
- Mellema, J.-R. *et al. Nature* (submitted).
- Altona, C. & Sundaralingam, M. *J. Am. chem. Soc.* **94**, 8205-8212 (1972).

LETTERS TO NATURE

Optical polarization position angle versus radio source axis in radio galaxies

Robert R. J. Antonucci

Lick Observatory, Board of Studies in Astronomy and Astrophysics, University of California, Santa Cruz, California 95064, USA

Optical polarization position angles tend to align with large-scale radio structure in low polarization quasars¹, indicating the existence of a simple geometrical relationship between the inner, optically-emitting region and the outermost, radio-emitting region. However, the meaning of the alignment is unclear because the cause of the optical polarization is unknown. If the polarization is caused by a synchrotron emission process then we are learning the direction of the magnetic field in the optically-emitting region. If it arises from scattering, then the position angle refers to the distribution of scatterers. At Lick Observatory we have been observing some quasars in the Stockman *et al.* sample¹ spectropolarimetrically to distinguish between the two possibilities (J. S. Miller and R. R. J. A. in preparation). If the polarization arises from the continuum emission process, only the continuum is polarized. If due to scattering, some of the line emission is probably polarized too. I have obtained optical spectropolarimetry data and VLA radio maps for a sample of radio galaxies to identify and interpret such alignment effects. The entire data set will be published as part of a study of the relationship between optical and radio properties of radio galaxies (work in preparation). The results show that most radio galaxies with optical nuclear emission are in fact polarized. There is a population showing quasar alignment effect, and unexpectedly there is also a population showing a perpendicular relationship. Emission-line polarizations exhibit various behaviours but in all cases make it very likely that the polarizations of both groups arise from scattering or dust transmission rather than the emission process itself.

Optical spectropolarimetry data for this project were obtained with the Lick 3-m Image Dissector Scanner as modified for simultaneous spectropolarimetry and spectrophotometry². Broadband polarizations presented here were obtained by integrating the spectropolarimetry data. Objects were chosen for polarization measurement by brightness and emission-line strength, consistent with the need to include a variety of optical and radio morphological types.

In most cases the radio position angles were measured from 6-cm radio maps made by E. B. Fomalont and myself with the NRAO Very Large Array. (The exceptions are 4C31.32 (ref. 3) and 3C234 (ref. 4).) The VLA instrument and standard reduction programs have been described previously⁵.

Table 1 shows the absolute value of the difference between the position angle of optical polarization and that of large-scale radio structure. It includes all those with constant polarization position angle and apparently not in danger of contamination by galactic interstellar polarization⁶. The result is that an aligned population analogous to the quasars is present, and unexpectedly there is apparently a group showing a perpendicular relationship. Note from Table 1 that the statistical errors in the polarization position angle are sometimes large; the best observed objects generally show the most precise alignments. For the low-polarization objects, there may be additional errors due to superposed galactic interstellar polarization. The uncertainties in measuring the radio axis position angles are estimated to be 5°.

As a test of the reality of the aligned group, the cumulative binomial probability distribution was computed. A random

distribution of position angle differences would result in at least five objects in the range 0°–20° only 5% of the time.

A similar analysis of the 90° peak does not yield a very high level of significance, but its reality is supported by (1) the fact that the best-observed objects in the peak show the most precise perpendicularity, and (2) the single significantly deviant object, 4C29.06, has an S-shaped radio map⁷, with the inner contours perpendicular to the optical polarization. More recent observations designed to determine whether the inner radio contours are more closely related to the optical polarization indicate that this is likely. Further observations to increase the sample size are under way.

Note that the most geometrically reasonable locations for peaks in the position-angle difference histogram are 0° and 90°. This is because any relationships other than alignment or perpendicularity would be somewhat dependent on viewing aspect and so would be washed out in an observational histogram. Also, in an axially-symmetric geometry, scattering polarization at intermediate angles would cancel out. Axially-symmetric geometries such as optically-thin and optically-thick scattering disks would produce parallel and perpendicular groups, respectively, independent of viewing aspect.

Referring again to Table 1, we see that the perpendicular group members tend to be N-systems. They are generally more highly polarized, more photometrically variable and systematically different in spectral properties when compared to the aligned group.

Spectropolarimetry data indicate that the polarization behaviour in the emission lines is varied for different objects and among the lines of a particular object. However, in all well-observed cases for both the parallel and the perpendicular subgroups, it appears that the polarization arises from a scattering or dust transmission effect rather than from the continuum-emission process. This is true even for the highly polarized object 3C234. In that object the broad H α line is polarized like the neighbouring continuum, while the forbidden [O III] lines have low polarization. The object is also unusual among active objects in that, although the polarization is very high (~10% in the continuum), its polarization is constant in time.

I will discuss the implications of these results elsewhere where the full radio, optical spectroscopic and optical spectropolarimetric data are available. To summarize the observations presented here: (1) most radiogalaxies with optical nuclei are polarized; (2) almost all well-observed objects have optical polarizations aligned with or perpendicular to the associated radio sources; (3) all polarizations are apparently due to scattering or dust transmission.

I thank Dr J. S. Miller for guidance throughout this project; this work was partially supported by NSF grant AST 80-19322. This is Lick Observatory bulletin no. 934.

Table 1 The polarizations are averages of two or more measurements

Object	Optical type	Optical polarization		Radio structure position angle	Difference
3C382	D3	1.29 ± 0.04%	58 ± 1°	54 ± 5	4 ± 5
4C29.41	ED	1.70 ± 0.36	85 ± 6	75	10 ± 8
3C287.1	N	3.10 ± 1.55	73 ± 14	88	15 ± 15
4C31.32	E	0.78 ± 0.30	143 ± 11	161	18 ± 12
3C305	Sa,pec	0.75 ± 0.18	94 ± 7	112	18 ± 9
4C02.39	N	2.11 ± 1.10	56 ± 15	117	61 ± 16
3C79	N	1.42 ± 0.78	172 ± 16	105	67 ± 17
4C29.06	E	1.92 ± 0.27	128 ± 4	57	71 ± 6
3C227	N	1.94 ± 0.28	29 ± 4	125	84 ± 6
3C234	N	7.20 ± 0.25	159 ± 1	68	89 ± 5

Some measurements vary in percent polarization. Objects which vary in polarization position angle have been excluded.

Received 24 May; accepted 12 August 1982.

1. Stockman, H. S., Angel, J. R. P. & Miley, G. K. *Astrophys. J. Lett.* **227**, 55–58 (1979).
2. Miller, J. S., Robinson, L. B. & Schmidt, G. D. *Publ. astr. Soc. Pacif.* **92**, 702–712 (1980).
3. van Breugel, W. J. M. *Astr. & Astrophys.* **81**, 275–281 (1980).
4. Riley, J. M. & Pooley, G. G. *Mem. R. astr. Soc.* **80**, 105–137 (1975).
5. Thompson, A. R., Clark, B. G., Wade, C. M. & Napier, P. J. *Astrophys. J. Suppl.* **44**, 151–167 (1980).
6. Mathewson, D. S. & Ford, V. L. *Mem. R. astr. Soc.* **74**, 139–182 (1970).
7. Katgent-Merkelijn, J., Lari, C. & Padrielli, L. *Astr. Astrophys. Suppl.* **40**, 91–118 (1980).

Distance to Crab-like supernova remnant 3C58

D. A. Green & S. F. Gull

Mullard Radio Astronomy Observatory, Cavendish Laboratory,
Madingley Road, Cambridge CB3 0HE, UK

The radio source 3C58 (G130.7+3.1) marks the probable position of the supernova of AD1181 (ref. 1). In its morphology, apparent size and radio spectrum, it is remarkably similar to the Crab Nebula (SN1054), being a 'filled-centre' supernova remnant (SNR), rather than the more usual shell-type. When comparing the physical properties of 3C58 with the Crab, or other 'filled-centre' remnants, a knowledge of its distance is required, and this has been a long-standing problem. Often, a value, or lower limit, of ~ 8 kpc has been assumed^{2–4}, but this implies that 3C58, although slightly younger than the Crab, is some five times larger. Also, it places 3C58 over 400 pc from the galactic plane, which is very surprising if it, like the Crab, is the remnant of a Type II supernova. The observations presented here show that 3C58 is in fact much closer, at a distance of only 2.6 kpc.

Previous estimates of the distance rest, like ours, on measurements of absorption by interstellar neutral hydrogen, but they all suffer from some drawback. The single-dish measurements² lack sufficient angular resolution to disentangle the complicated filamentary structures in the interstellar medium (ISM), whereas interferometric observations^{3,4} do not provide the information on the large-scale structure that is needed for reliable calibration of the spectrum. These studies have, however, shown that there is very little, if any, absorption ($\tau < 0.1$) of the 3C58 continuum for velocities beyond -35 km s⁻¹.

With this in mind, we observed 3C58 with the Cambridge Half-Mile Telescope (HMT) at 21 cm. Two complete surveys, overlapping in velocity coverage, were made in November 1981. Details of the telescope, receivers and surveys are given in Table 1. Data on the large-scale structure, unobtainable with the HMT, were derived from the Berkeley single-dish survey^{5,6} and were added to the synthesis maps. The continuum emission was subtracted from these 'composite' maps to give final 'channel' maps. Photographic representations of some of these 'channel' maps, made on the Cambridge 'Starlink' node, are shown in Fig. 1. These maps will provide detailed information about the ISM in this direction, but here we restrict ourselves to a discussion of the distance to 3C58, and its consequences.

The absorption and column density profiles for H I along the line of sight to 3C58, for each channel, are shown in Fig. 2. Actual on-axis temperatures for the continuum (T_{cont}), and for each channel (T_{chan}) were taken directly from the continuum and 'channel' maps. The emission temperature (T_{em}) in the direction of 3C58, for each channel, was estimated from the surrounding area on each of the 'channel' maps. The uncertainties in these estimates, ranging from 2 to 6 K, are almost solely due to the complicated structure in the ISM (and are taken to represent 2σ errors). From these temperatures the optical depth (τ) and column density ($N_{\text{H I}}$, m⁻²), were derived for each channel using⁷

$$\tau = \log_e(T_{\text{cont}}/(T_{\text{chan}} - T_{\text{em}}))$$

$$N_{\text{H I}} = 1.823 \times 10^{22} \Delta V T_{\text{em}} \text{ m}^{-2} \quad \text{where } \Delta V = 2.0 \text{ km s}^{-1}$$

Figure 2a shows only two distinct absorption features, one from -14.3 to -17.6 km s⁻¹, corresponding to the edge of the local arm, and another centred at -34.1 km s⁻¹, corresponding to the Perseus arm. It is clear, however, from Fig. 2b and the 'channel' maps that in this direction there are two emission peaks in the Perseus arm. The one with lower velocity coincides with the absorption feature at -34.1 km s⁻¹, where a filament crosses the line of sight (Fig. 1). A minimum is found at -39.1 km s⁻¹, beyond which the emission rises to a further peak at -45.7 km s⁻¹. Because no increase in absorption occurs past -39.1 km s⁻¹ corresponding to this second peak, we must conclude that 3C58 is behind the filament at -34.1 km s⁻¹, but in front of the neutral hydrogen at -39.1 km s⁻¹ and beyond. We can thus place 3C58 as being at a distance equivalent to a velocity of -36.6 ± 2.5 km s⁻¹.

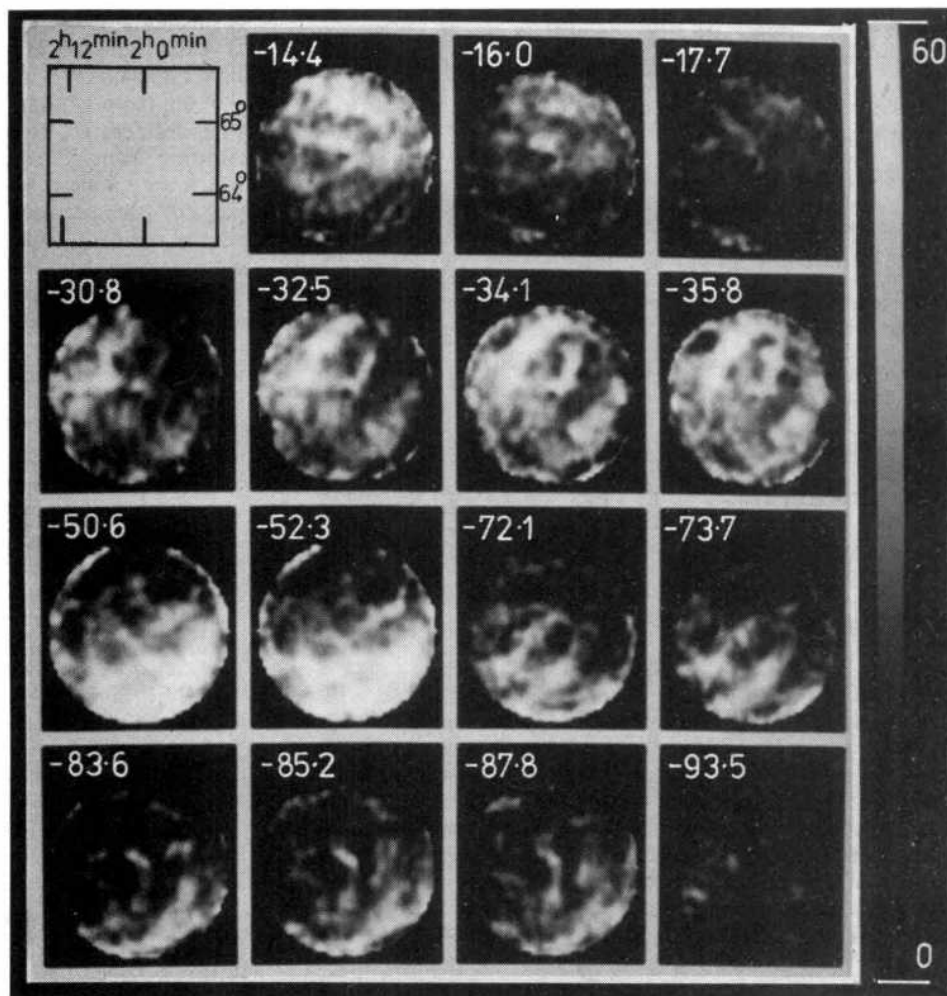
On the basis of the Schmidt rotation model⁸, the distance to 3C58 is then 2.6 ± 0.2 kpc. However, note that any systematic difference from the Schmidt rotation curve would give rise to larger errors. These differences could be due to streaming motions, or any general inadequacy of the Schmidt model. For example, the work of Roberts⁹ would put 3C58 only 2 kpc away, whereas the use of Blitz's rotation curve¹⁰ gives a distance of 3.4 kpc. In the following discussion we have, nevertheless, taken 3C58 to be at a distance of 2.6 ± 0.2 kpc.

Our value for the distance to 3C58 is only a third of the lower limits derived from previous observations, and it is important to understand the reason for such large discrepancy. Consider, for example, Williams' single-dish measurements². He estimated the emission by averaging values at one beamwidth (9 arc min) from the source in four directions. Now it is apparent from Fig. 1 that the ISM shows structure on this scale. If the direction of the source coincides, over a particular velocity range, with a hole in the H I, then the off-axis measurements will give an artificially high value of the emission. This value, combined with the on-axis measurement, will in turn give an artificially high value for the absorption. Bright filaments adjacent to the line of sight will similarly lead to an erroneously high estimate of absorption. This is indeed the case for velocities around -53 , -62 to -75 and -93 km s⁻¹ (Fig. 1), which are just those velocities where Williams finds apparent peaks in absorption. Conversely, a bright filament across the line of sight to the source will mean that the apparent emission and absorption are too low. This again accounts for differences between our results and those of Williams. The effect is particularly noticeable around -85 km s⁻¹ (Fig. 1), where we estimate an emission on the line of sight to 3C58 which is about 10 K higher than that of Williams. This explains why Williams' results shows a drop in absorption to zero in this region, and presumably

Table 1 Specification of the HMT as used for observations in the direction of 3C58

Primary beam	94 arc m in HPBW (field of view shown on Fig. 1 is 80 arc min)
Spatial resolution	7.1 × 7.9 arc min (RA × Dec)
Receiver; wide band	10 MHz, phase switched Stokes parameters observed $I + Q$ and $I - Q$
Receiver; narrow band	Digital cross correlation spectrometer measuring $I + Q$ 80 delay channels/spacing 32 frequency channels for each synthesis Bandwidth 0.25 MHz overall
Noise on synthesis maps	~ 0.4 K
Velocity coverage	-14.3 to -108.4 km s ⁻¹ w.r.t. LSR 58 informative channels
Velocity resolution	2 km s ⁻¹ (to half power points)
Separation of velocity channels	1.65 km s ⁻¹
Position of field (195.0.0)	RA = 02 h 02 min Dec = 64° 35'

Fig. 1 Photographic representations of some of the channel maps. The radio images are positive (bright emission appears white) and cover a range 0–60 K, as shown by the scale on the right. The field of view is sharply cut off at a radius of 80 arc min. The velocity of each channel (w.r.t. the local standard of rest in km s^{-1}) is marked above each map.



enhanced emission was observed. Our results show no significant absorption, nor enhanced emission. The results obtained by Hughes *et al.*³ are based on only one interferometer spacing, and therefore suffer from a lack of information on the large scale structure of the ISM. The interferometric observations of Goss *et al.*⁴ were very poorly sampled both in space and velocity, so detailed comparison with our results is not worthwhile.

3C58, with an assumed distance of around 8 kpc, has been used as a calibrator for several^{11–13} plots of surface brightness (Σ) against linear diameter (D) for SNRs. As most of the calibrators for these plots are shell-types, the relationships derived are representative of idealized shell-type SNRs. There is some theoretical basis¹⁴ for expecting a general evolutionary Σ - D trend for such remnants, although it has been pointed out¹⁵ that young and old remnants should not be considered together. Our revision of the distance to 3C58 will only slightly alter the relations derived, and not at all that of Milne¹⁶, who did not use 3C58 for calibration. On the other hand, the fact that our results, and recent observations^{17,18} of Tycho's SNR (3C10), indicate H I distances much less than was previously thought, must raise doubts concerning other H I distances that have been used for Σ - D calibration. Note^{19,20} that most 'Crab-like' remnants seem to be subluminal compared with an idealized shell-type of the same diameter. Adopting a distance of 2.6 kpc, this is now also true of 3C58, thus strengthening this suggestion.

Our observations give the integrated H I column density between -14.4 km s^{-1} and -36.6 km s^{-1} as $1.0 \pm 0.05 \times 10^{25} \text{ m}^{-2}$. The column density out to -14.4 km s^{-1} can be estimated from Williams' data as $1.55 \pm 0.3 \times 10^{25} \text{ m}^{-2}$, thus the total integrated column density of neutral hydrogen in front of 3C58 is $2.55 \pm 0.3 \times 10^{25} \text{ m}^{-2}$. This is in good agreement with

the value of $2.0 \pm 0.5 \times 10^{25} \text{ m}^{-2}$ recently derived from 'Einstein' X-ray observations²¹.

We can now estimate the optical extinction (A_V) and colour excess ($E(B - V)$) towards 3C58 to deduce its absolute magnitude at maximum ($M_V(\text{max})$). Using

$$N_{\text{tot}}/(6.2 \times 10^{25}) = E(B - V) = A_V/3.2$$

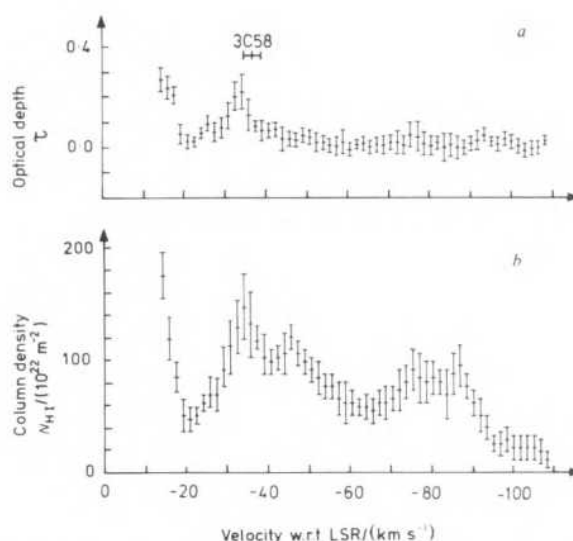


Fig. 2 *a*, Plot of optical depth (τ) against velocity. The velocity of 3C58 is marked. *b*, Plot of column density N_{HI} against velocity. Error bars indicate estimated 2σ errors on both plots.

Table 2 Comparison of the properties of 3C58 and of the Crab Nebula

	3C58	Crab	Refs
Galactic coordinates	G130.7+3.1	G184.6-5.8	
Distance (kpc)	2.6	2.0	This paper, 29*
Angular size (arc min)	10×6	7×5	29*
Linear size (pc)	7.6×4.5	4×3	
Explosion date	AD 1181	AD 1054	1
Mean expansion velocity (km s ⁻¹)	4,600	2,100	
Distance from galactic plane (pc)	140	200	
Total flux density at 1 GHz (Jy)	33	1,000	29*
Surface brightness at 1 GHz (W m ⁻² Hz ⁻¹ sr ⁻¹)	2.6×10 ⁻¹⁹	1.2×10 ⁻¹⁷	16
Spectral index α ($s \propto \nu^{-\alpha}$)	0.09	0.26	29*
Luminosity (W)			
Radio (10 ⁷ –10 ¹¹ Hz)	1.7×10 ²⁷	1.8×10 ²⁸	29*
X-ray (0.1–4 keV)	1.0×10 ²⁷	2.5×10 ³⁰	21*
Absolute magnitude at maximum (mag)	-13.4	-18	This work, 30

* And refs therein.

(refs 22, 23) we obtain $A_V = 1.3 \pm 0.2$ mag and $E(B-V) = 0.40 \pm 0.05$ mag. For a distance of 2.6 ± 0.2 kpc, the distance modulus is then $(m_V - M_V) = 12.1 \pm 0.1$ mag, where the quoted error does not take account of the possible systematic errors noted above. The apparent magnitude of 3C58 at brightest was¹ $m_V(\text{max}) = 0$ mag so, after allowing for absorption, we obtain: $M_V(\text{max}) = -13.4$ mag. The error in this is dominated by the uncertainty of the apparent magnitude at maximum, which is hard to estimate, but it seems unlikely that this value for the absolute magnitude is in error by more than one magnitude. This makes 3C58 substantially subluminal compared with Type II supernovae observed in external galaxies²⁴, but the detection of extra-galactic supernovae is biased towards those of higher luminosity. Supernovae of Type II have, in any case, a wide range of intrinsic luminosities (as is reasonable if they represent the explosions of very massive stars with extended envelopes).

Table 2 gives values of various properties of 3C58, and those of the Crab Nebula for comparison. It can be seen that 3C58 and the Crab, although similar in many respects, are very different in others. The similarities include their radio morphology—both are 'filled-centre' remnants, with filaments seen on high resolution radio maps; their low spectral indices; and their apparent sizes. They also have similar linear sizes, and mean expansion velocities. On the other hand, they seem very different energetically, particularly at other than radio frequencies. The difference between their radio luminosities is only a factor of ~ 10 , whereas for X rays it is $> 2,000$. Optically, there are large differences as the filaments of the Crab can be easily studied but the optical emission from 3C58 is barely visible²⁵. Also, the absolute magnitudes of the supernovae that gave rise to these remnants were very different.

There have been several discussions of the properties of 'Crab-like' remnants, including attempts to derive some evolutionary trends^{21, 26, 27} for this class of object, even though so few have been found and well studied. The discussion of Weiler and Panagia²⁶ rests heavily on the observational properties of just three of this class, the Crab, 3C58 and Vela X. They derive an evolutionary sequence, assuming all three to be in the adiabatic or 'phase II' expansion²⁸, of the form

$$Sd^2 \propto t^{-0.8}$$

where S is the flux density, d the distance and t the age of the remnant. With the revised distance, it is impossible to fit all three remnants on the same sequence. This could mean that some of the observational data is in error, or the theory may be wrong, or not applicable to all three remnants. If the theory

is substantially correct, and if all three remnants are in 'phase II' expansion and are indeed to be placed in the same class, then this class must have a very wide spread of intrinsic properties. On the other hand, Shklovskii²⁷ regards 3C58 as in 'phase I', undecelerated, expansion into the ISM. He compares radio-emitting Type II supernovae with 'filled-centre' remnants, which are taken to be the products of Type II supernovae. In particular he assumes 3C58 to be a more or less typical 'filled-centre' remnant, at a distance of 8 kpc. So the empirical conclusion drawn, that the radio luminosity for Type II supernovae is inversely proportional to age, is no longer valid. The discussion by Becker *et al.*²¹ concerns six filled-centre remnants for which soft X-ray observations are available. They put forward an evolutionary sequence, that with age there is an increase of radio size, and a decrease of both the X-ray luminosity and the ratio of X-ray to radio luminosity. They suggest that the identification of 3C58 with SN1181 is incorrect, and that the probable age is some several thousand years. With a distance of 2.6 kpc for 3C58, this difficulty does not arise.

We thank all those who helped make the observations and reduce the data. D.A.G. thanks the SERC for financial support.

Received 1 June; accepted 30 July 1982.

- Stephenson, F. R. *Q. J. R. astr. Soc.* **12**, 10–38 (1971).
- Williams, D. R. W. *Astr. Astrophys.* **28**, 309–311 (1973).
- Hughes, M. P., Thompson, A. R. & Colvin, R. S. *Astrophys. J. Suppl.* **23**, 323–370 (1971).
- Goss, W. M., Schwarz, U. J., & Wesselius, P. R. *Astr. Astrophys.* **28**, 305–307 (1973).
- Williams, D. R. W. *Astr. Astrophys. Suppl.* **8**, 505–516 (1973).
- Weaver, H. & Williams, D. R. W. *Astr. Astrophys. Suppl.* **8**, 1–504 (1973).
- Verschuur, G. L. in *Galactic and Extra-galactic Radio Astronomy* (eds Verschuur, G. L. & Kellermann, K. I.) 27–47 (Springer, Berlin, 1974).
- Schmidt, M. *Stars and Stellar Systems* Vol. 5 (eds Blaauw, A. & Schmidt, M.) 513–530 (University of Chicago Press, 1965).
- Roberts, W. W. *Astrophys. J.* **173**, 259–285 (1972).
- Blitz, L. *Astrophys. J. Lett.* **231**, L115–L119 (1979).
- Ilovaisky, S. A. & Lequeux, J. *Astr. Astrophys.* **18**, 169–185 (1972).
- Clark, D. H. & Caswell, J. L. *Mon. Not. R. astr. Soc.* **174**, 267–305 (1976).
- Gobel, W., Hirth, W. & Furst, E. *Astr. Astrophys.* **93**, 43–47 (1981).
- Shklovskii, I. S. *Supernovae* (Wiley, New York, 1969).
- Gull, S. F., *Mon. Not. R. astr. Soc.* **161**, 47–69 (1973).
- Milne, D. K. *Aust. J. Phys.* **32**, 83–92 (1979).
- Albinson, J. S. & Gull, S. F. in *Regions of Recent Star Formation* (eds Roger, R. S. & Dewdney, P. E.) 193–199 (Reidel, Dordrecht, 1982).
- Chevalier, R. A., Kirshner, R. P. & Raymond, J. C. *Astrophys. J.* **235**, 186–191 (1980).
- Weiler, K. W. & Shaver, P. A. *Astr. Astrophys.* **70**, 389–397 (1978).
- Lockhart, I. A., Goss, W. M., Caswell, J. L. & McAdam, W. B. *Mon. Not. R. astr. Soc.* **179**, 147–152 (1977).
- Becker, R. H., Helfand, D. J. & Szymkowiak, A. E. *Astrophys. J.* **255**, 557–567 (1982).
- Spitzer, L. *Physical Processes in the Interstellar Medium* (Wiley, New York, 1978).
- Jenkins, E. B. & Savage, B. D. *Astrophys. J.* **187**, 243–255 (1974).
- Tammann, G. A. in *Supernovae* (ed. Schramm, D. N.) 95–116 (Reidel, Dordrecht, 1977).
- van den Bergh, S. *Astrophys. J. Lett.* **220**, L9–L10 (1978).
- Weiler, K. W. & Panagia, N. *Astr. Astrophys.* **90**, 269–282 (1980).
- Shklovskii, I. S. *Soviet Astr. Lett.* **7**, 263–264 (1981).
- Woltjer, L. A. *Rev. Astr. Astrophys.* **10**, 129–158 (1972).
- Wilson, A. S. & Weiler, K. W. *Astr. Astrophys.* **49**, 357–374 (1976).
- Chevalier, R. A. in *Supernovae* (ed. Schramm, D. N.) 53–62 (Reidel, Dordrecht, 1977).

Resolution of controversy concerning the morphology of polyacetylene

James C. W. Chien, Y. Yamashita, J. A. Hirsch, J. L. Fan, M. A. Schen & Frank E. Karasz

Department of Polymer Science and Engineering, Materials Research Laboratory, University of Massachusetts, Amherst, Massachusetts 01003, USA

A free standing film of polyacetylene, first obtained by Ito *et al.*¹, has been shown by electron micrograph (EM) to consist of fibrils with average diameter of 20 nm. The results were confirmed by us² and many other laboratories. To eliminate any morphological changes resulting from post polymerization handling of the specimen, we have developed the technique of direct polymerization onto EM grids^{2,3}. The 20–100 nm thick polyacetylene films thus obtained were found to have 3-nm diameter microfibrils as the ultimate morphological entity which aggregate to form the more abundant 20-nm fibrils. Electron

diffraction showed the polymer chain axis to be along the fibre axis³⁻⁵. In marked contrast Wegner and co-workers⁶⁻¹¹ reported that polyacetylene particles contain irregularly shaped lamellae ~5–20 nm in thickness connected into ribbon-like aggregates with polymer chain axis perpendicular to the aggregate direction^{6,7}, and proposed an irregular chain folded lamellar morphology, highly cross-linked with the average length of linear chain segments of ~20 units. We have resolved this controversial observation by reproducing the work of Wegner *et al.* and show here that such specimens were readily transformed to smooth fibrillar morphology by washing with methanolic-HCl.

The direct polymerization of acetylene onto EM grids with Ziegler–Natta catalyst was as described elsewhere^{2,3}. Acetylene was also polymerized by the $\text{Ti}(\text{O}i\text{Bu})_4/4\text{AlEt}_3$ catalyst in the diluent by stirring. The three concentrations of catalyst used were: low $[\text{Ti}] = 1 \text{ mM}$; medium $[\text{Ti}] = 5 \text{ mM}$, and high $[\text{Ti}] = 40 \text{ mM}$. Only for the highest concentration did free standing film form; the others gave suspended particles of polymer. After washing with toluene, methanol or methanolic-HCl, the polymer was collected with carbon coated grids from the suspension to simulate the technique reported by Wegner *et al.*⁶⁻¹¹.

Direct polymerization of acetylene onto gold EM grids with Luttinger catalyst was carried out as follows. A reactor containing suspended EM grids was evacuated for 14 h, flame dried, filled with Ar and transferred into a dry-box. NaBH_4 (20 mg) in 5 ml ether was added to the reactor and then taken out under Ar. The temperature of the reactor was reduced to -78°C and 1 ml of a 10% $\text{Co}(\text{NO}_3)_2 \cdot 6\text{H}_2\text{O}$ solution in ethanol was added to the NaBH_4 . The colour immediately turned purple. The reactor was degassed quickly and shaken so that drops of catalyst solution were caught on the grid. Acetylene at ~15 torr was admitted to ensure rapid polymerization. Polyacetylene films formed both on the reactor wall and on the grid. The total time of reaction was 5 min and 60 torr of monomer was consumed. In this procedure the catalyst concentration was $[\text{Co}(\text{NO}_3)_2] = 30 \text{ mM}$ and $[\text{NaBH}_4] = 48 \text{ mM}$.

Using Luttinger catalyst of lower concentrations and polymerizing at -30°C produces only suspended polymer particles. For instance, mixtures of $3.5 \times 10^{-4} \text{ M}$ $\text{Co}(\text{NO}_3)_2$ and $5.3 \times 10^{-3} \text{ M}$ NaBH_4 solutions at -30°C was magenta colour which during acetylene polymerization changed to blue, dark blue, and finally black. In 17 min, the reaction consumed ~50 torr of monomer. Doubling the concentration of both catalyst components caused more rapid polymerization of acetylene at

-30°C . Only suspended polymer particles were produced in these conditions.

Figure 1a shows a transmission EM image of $[\text{CH}]_x$ obtained at a low concentration of $[\text{Ti}] = 1.0 \text{ mM}$. The toluene-washed specimen consisted of fibrils, ribbons and a dark spongy mass; no pseudo-lamellae particles were present. After the polymer was washed with methanolic-HCl, clean fibril morphology resulted (Fig. 1b). The spongy material seems to be soluble in methanolic-HCl and the ribbons in Fig. 1a seem to be aggregates of fibrils glued together by methanolic-HCl soluble substances such as catalyst residue or low molecular weight polymers. At a $[\text{Ti}]$ of 40 mM the $[\text{CH}]_x$ after a thorough toluene wash has a major portion of the specimen masked by spongy substance (Fig. 1c). There are also aggregates of irregularly shaped lamellae-like particles, and fibrils with striation. In fact, this micrograph closely resembles those published by Wegner *et al.* (Fig. 1 of ref. 6, Fig. 3 of ref. 11, Fig. 2 of ref. 8, Fig. 4 of ref. 10, and Fig. 2 of ref. 9.) By washing with methanolic-HCl we obtain EM Fig. 1d which contains only $[\text{CH}]_x$ fibrils although the number of fibrils per unit area in this sample is much greater than that of Fig. 1b. This high $[\text{Ti}]$ is still lower than that commonly used in the preparation of $[\text{CH}]_x$ films, which is 0.2 M. At an intermediate catalyst concentration of 5 mM, the toluene-washed sample has EM Fig. 1e which is intermediate between those of Fig. 1a and c). Thus contribution of the catalyst residue to the dirty morphology seems to be established.

Polyacetylene obtained with Luttinger catalyst [0.35 mM $\text{Co}(\text{NO}_3)_2/5.3 \text{ mM NaBH}_4$], washed with ethanol shows definite fibril morphology (Fig. 2a). There were also impurity materials and the fibrils appear to have deposits of foreign materials. Using 10-fold higher catalyst concentration, we observed EMs similar to those reported by Wegner *et al.*⁶⁻¹¹. These are a dense mass fringed with irregularly shaped particles as shown in Fig. 2b. If the polymer was washed with methanolic-HCl, fibrillar morphology is revealed (Fig. 2c). However, much spongy material still remained. It is apparently more difficult to remove contaminants from the polyacetylene obtained with the Luttinger catalyst than in the case of the Ziegler–Natta catalyst.

To show that the two catalyst systems produce truly identical $[\text{CH}]_x$ we have polymerized acetylene directly onto the grid using both the Luttinger (Fig. 3a) and the Ziegler–Natta catalysts (Fig. 3b). The fibrils in the former are smooth, free of foreign substances and have diameters generally greater than in the latter. Electron diffraction patterns of selected areas with parallel bundles of fibrils in both specimens are identical to

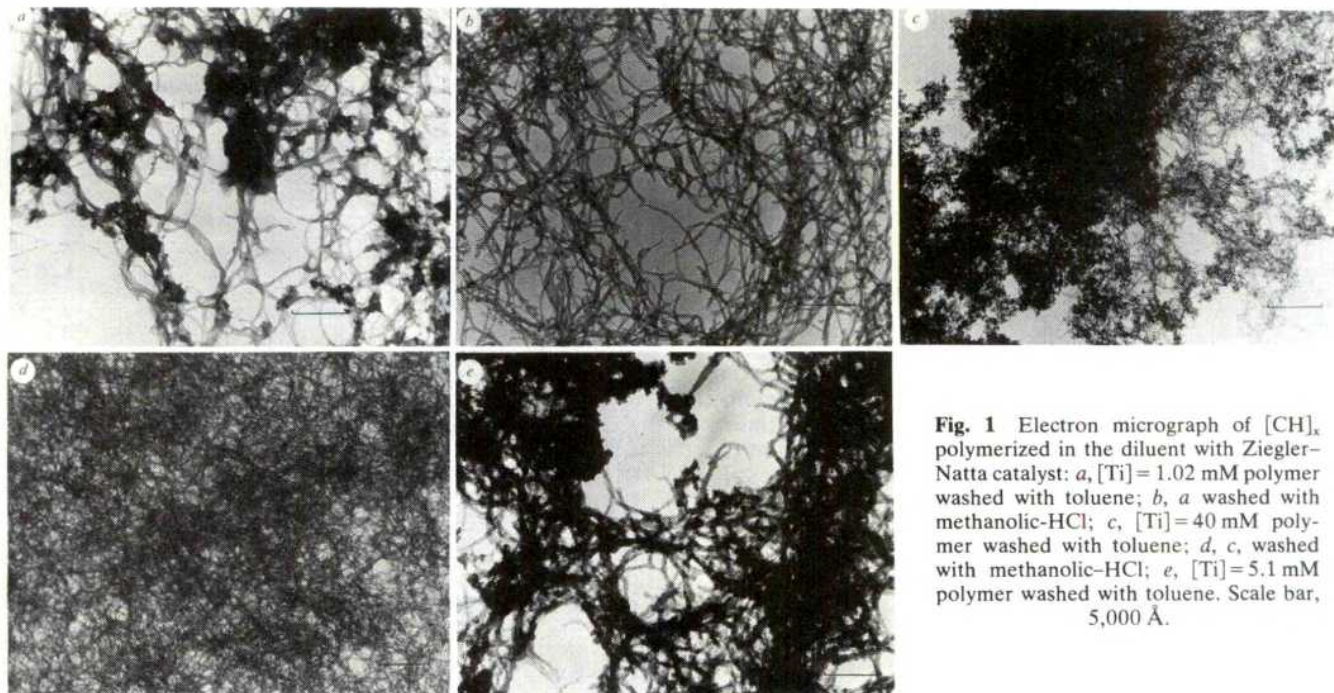


Fig. 1 Electron micrograph of $[\text{CH}]_x$ polymerized in the diluent with Ziegler–Natta catalyst: a, $[\text{Ti}] = 1.02 \text{ mM}$ polymer washed with toluene; b, a washed with methanolic-HCl; c, $[\text{Ti}] = 40 \text{ mM}$ polymer washed with toluene; d, c, washed with methanolic-HCl; e, $[\text{Ti}] = 5.1 \text{ mM}$ polymer washed with toluene. Scale bar, 5,000 Å.

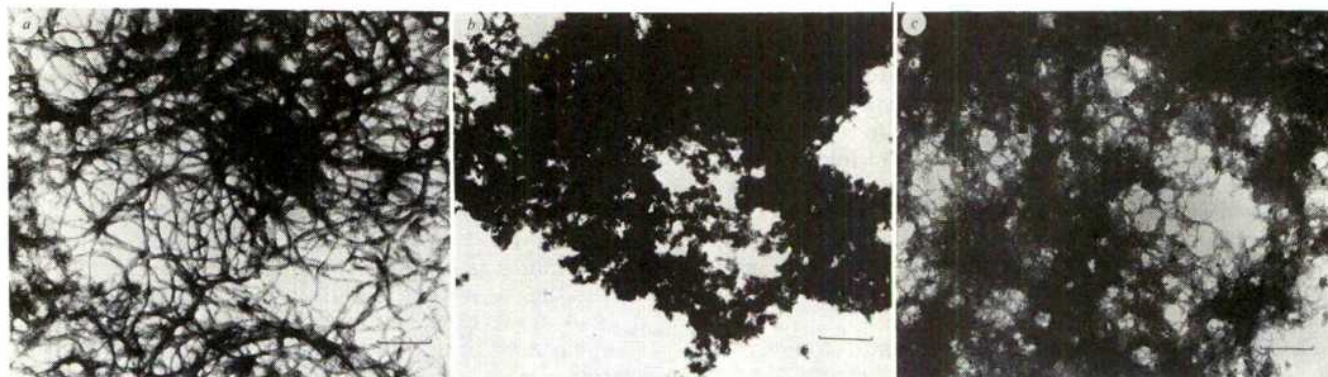


Fig. 2 Electron micrograph of $[\text{CH}]_x$ polymerized in the diluent with Luttinger catalyst: *a*, $[\text{Co}] = 0.35 \text{ mM}$, polymer washed with ethanol; *b*, $[\text{Co}] = 30 \text{ mM}$ polymer washed with ethanol; *c*, *b* washed with methanolic-HCl. Scale bar, $5,000 \text{ \AA}$.

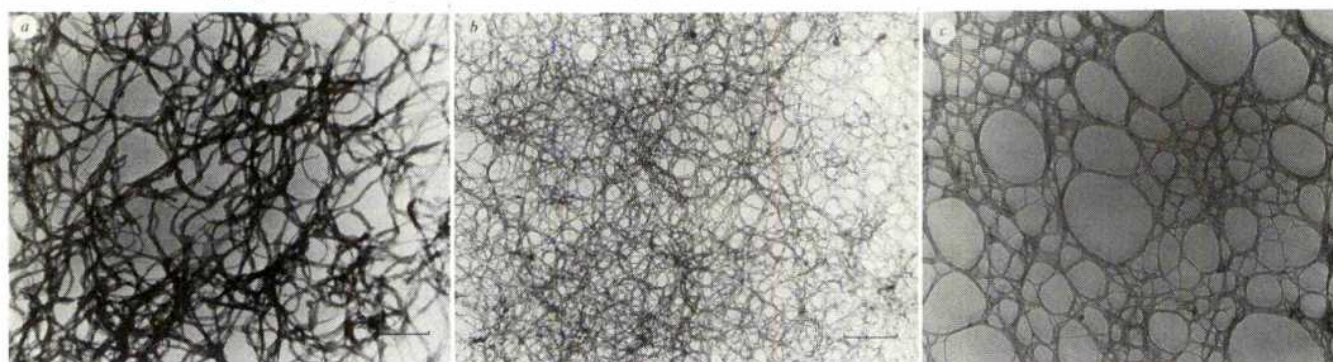


Fig. 3 Electron micrograph of $[\text{CH}]_x$ polymerized directly onto EM grids: *a*, with Luttinger catalyst; *b*, with Ziegler-Natta catalyst; *c*, showing 3-nm diameter microfibrils. Scale bar, $5,000 \text{ \AA}$.

those of *cis*- $[\text{CH}]_x$ described earlier⁵ with the chain axes both along the fibre axis. Furthermore, using low monomer pressure, low Ziegler-Natta catalyst concentration, and short polymerization time, we were able to obtain ultra-thin $[\text{CH}]_x$ specimens which showed an abundance of 3-nm diameter microfibrils (Fig. 3c). These microfibrils are probably the ultimate morphological entity which aggregate to form the more commonly reported 20 nm fibrils.

Meyer¹² reported that low-voltage electron-beam damage and OsO_4 staining revealed fibrils of $[\text{CH}]_x$ with regularly spaced striation. It was interpreted to be lamellae packed like stacks of salami slices. We have also occasionally observed such morphology (Fig. 4) in samples that are always aged and sometimes washed with methanolic-HCl. These striations are probably oxidation- or solvent-induced stress cracking. Such cracks appeared as voids along the original fibril and will be more or less regularly spaced because a crack will release the stress in its vicinity. OsO_4 is certainly too strong an oxidizing agent to be used as a staining agent for $[\text{CH}]_x$. Freshly prepared $[\text{CH}]_x$ specimens show neither striation by EM nor long periodicity in low-angle X-ray scattering. Therefore, in the case of Mayer's work the striations were probably produced by stress cracking due to oxidation by OsO_4 or radiation damage.

Wegner *et al.*^{8,10,11} proposed that polyacetylene becomes highly cross-linked even at low temperatures and in the mildest conditions. This was partly based on the observation that the polymer soon becomes difficult to chlorinate to soluble derivatives. It was stated that the average length of linear chain segments is ~ 20 units. ^{13}C -NMR and ozonolysis results showed that there is $<1\%$ of sp^3 carbon atoms. We have found that electron diffraction patterns of pristine *cis*- $[\text{CH}]_x$ has discrete arcs in the equator but diffuse arcs in the layer lines. Careful isomerization in optimal conditions (175°C for 3 min) yielded *trans*- $[\text{CH}]_x$ having very sharp diffraction layer lines suggesting an annealing effect improving the longitudinal order. If *cis*- $[\text{CH}]_x$ were as highly cross-linked as claimed by Wegner *et al.* all of the above observations would seem inconceivable.

The catalyst concentration used in acetylene polymerization is very much higher than in olefin polymerization.^{13,14} When

acetylene is polymerized with a thin coating of catalyst solution on the wall of the reactor or directly onto EM grid, the catalyst residues can be substantially removed by washing with toluene, pentane or heptane. Even then, the Ti content in the free standing polyacetylene is high (0.022%)¹⁵; it can be reduced to 0.008% by methanolic-HCl washing which is a standard work-up procedure of Ziegler-Natta polymerized polyethylene and polypropylene. Washing with toluene or aliphatic solvent would not be enough to remove the catalyst residues. Furthermore, we have found by radiotagging^{16,17} that there are in the diluent very low molecular weight polymers of ~ 500 whereas the molecular weight of the film on the reactor wall is $\sim 22,000$. The dirty morphology of the specimen collected from suspended particle therefore contains copious amounts of catalyst debris

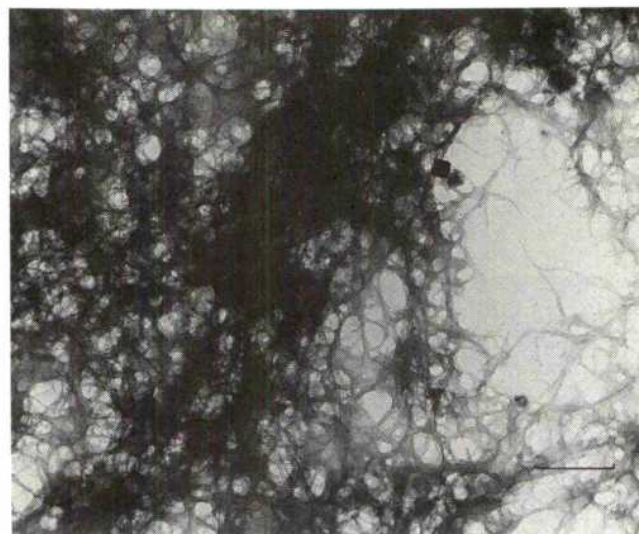


Fig. 4 Electron micrograph of old $[\text{CH}]_x$ specimen showing striations which are probably stress-cracking. Scale bar, $5,000 \text{ \AA}$.

and low molecular weight polymers adhered to the fibrils which can be removed by methanolic-HCl washing.

In conclusion, the basic morphological unit in *cis*-polyacetylene is the 3-nm microfibril which contains about 40 [CH]_n chains based on its crystal structure^{4,5}. Monomers crystallized from polyacetylene are inserted with the chain axis along the fibre axis. There is no evidence for a chain-folded lamellar morphology which would be difficult for a polymer with a stiff back-bone to assume. Striations of the fibrils sometimes observed are not believed to be basic to the polyacetylene morphology.

Received 15 April; accepted 29 July 1982.

1. Ito, T., Shirakawa, H. & Ikeda, S. *J. Polym. Sci. Polym. Chem. Ed.* **12**, 11 (1974).
2. Karasz, F. E. *et al. Nature* **282**, 286 (1979).
3. Shimamura, K., Karasz, F. E., Hirsch, J. A. & Chien, J. C. W. *Makromolek. Chem. Rapid Commun.* **2**, 473 (1981).
4. Chien, J. C. W., Karasz, F. E. & Shimamura, K. *Macromolecules* **15**, 1012 (1982).
5. Shimamura, K., Karasz, F. E., Chien, J. C. W. & Hirsch, J. A. *J. Polym. Sci. Polym. Lett. Ed.* **20**, 97 (1982).
6. Lieser, G., Wegner, G., Müller, W. & Enkelmann, V. *Makromolek. Chem. Rapid Commun.* **1**, 621 (1980).
7. Lieser, G., Wegner, G., Müller, W., Enkelmann, V. & Meyer, W. H. *Makromolek. Chem. Rapid Commun.* **1**, 627 (1980).
8. Enkelmann, V., Lieser, G., Monkenbusch, M., Müller, W. & Wegner, G. *Molec. Cryst. Liq. Cryst.* **77**, 111 (1981).
9. Lieser, G., Monkenbusch, M., Enkelmann, V. & Wegner, G. *Molec. Cryst. Liq. Cryst.* **77**, 169 (1981).
10. Wegner, G. *Angew. Chem. int. Ed.* **20**, 361 (1981).
11. Enkelmann, V., Müller, W. & Wegner, G. *Syn. Metals* **1**, 185 (1979/80).
12. Meyer, W. H. *Mol. Cryst. Liq. Cryst.* **77**, 1237 (1981).
13. Chien, J. C. W. *J. Polym. Sci. A1*, **1**, 425 (1963).
14. Chien, J. C. W., Wu, J. C. & Kuo, C. I. *J. Polym. Sci. Polym. Chem. Ed.*, (in the press).
15. Chien, J. C. W. *et al. Macromolecules* **15**, 614 (1982).
16. Wnek, G. E. *et al. in Conductive Polymers* (ed. Seymour, R. B.) 183-208 (Plenum, New York, 1981).
17. Chien, J. C. W., Capistran, J. D., Karasz, F. E., Dickinson, L. C. & Schen, M. A. *J. Polym. Sci., Polym. Lett. Ed.* (in the press).

Iron in north-east Pacific waters

R. M. Gordon, J. H. Martin & G. A. Knauer

Moss Landing Marine Laboratories, PO Box 223, Moss Landing, California 95039, USA

Although Fe is an element of great biological¹ and geochemical² importance, little is known about its distribution in the sea. The reasons for this are: (1) contamination is extremely difficult to avoid during sampling and laboratory procedures, not only because of man's wide use of this element, but also because it is fourth most abundant element in the Earth's crust (5.63%)³; (2) the chemistry of Fe is very complex, and its form (or forms) in seawater is poorly known, hence whether one preconcentration technique will work for existing species is questionable. Iron also appears to be very insoluble⁴ in oxygenated ocean water, and most (90%)⁵ precipitates out in association with dissolved organics during estuarine mixing processes⁵⁻⁸. Indeed, some argue that truly dissolved Fe does not exist in seawater and that the fraction found in filtrates is totally colloidal⁹. We have been attempting oceanic dissolved Fe measurements for the past four years and report here three vertical Fe profiles (Fig. 1) that have the following features in common: Fe is severely depleted (0.15–0.30 nmol kg⁻¹) in surface waters; Fe maxima (up to 2.6 nmol kg⁻¹) occur in association with oxygen minima; and, Fe levels appear to vary little in mid-depth waters (0.5–1.0 nmol kg⁻¹).

Our data were obtained using the same sampling (Go-Flo bottles on Kevlar line), filtration (0.4 µm Nuclepore), preconcentration (APDC, DDDC/chloroform organic extraction) and analytical (graphite furnace atomic absorption spectrophotometry, AAS) techniques that were developed largely by Bruland and used by us in previous studies¹⁰. Contamination during collection and filtration procedures was estimated indirectly using Zn and Si analyses; because it is very easy to contaminate samples for Zn (ref. 11), any samples with values

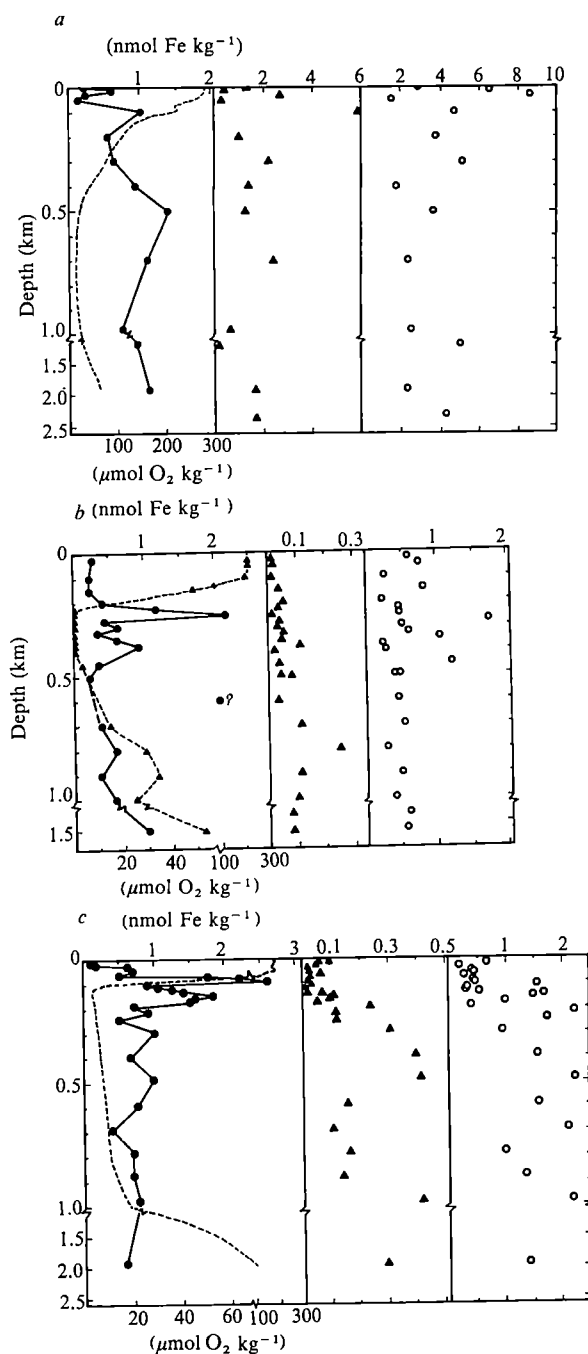


Fig. 1 Dissolved (●), particulate leachable (▲), and particulate refractory (○) Fe versus depth observed: a, off central California (36° 30' N, 123° 05' W) in June 1981; b, hundreds of kilometres west of central Mexico in April 1980; c, 330 km west of Manzanillo, Mexico (18° 00' W, 108° 00' W) in October 1981. (Exact station location of b cannot be given because of contract agreement with Ocean Minerals Corp.)

markedly higher than those expected from Zn/Si ratios (ref. 12) were also assumed to be contaminated with extraneous Fe (Zn/Si data not shown).

Blanks for the organic extraction procedures were ($\bar{x} \pm 1s$) 0.12 ± 0.016 ($n = 7$), 0.13 ($n = 1$) and 0.084 ± 0.023 ($n = 6$) total nmol in the concentrated extract for the data shown in Fig. 1a–c, respectively. Yields for the organic extraction method were estimated in two ways: 95% recovery was obtained using ⁵⁹Fe in the form of Fe³⁺ as a tracer; near 100% recovery was achieved when organic extraction Fe values were compared with those obtained using direct-injection AAS. The latter was possible in low salinity north San Francisco Bay waters where filtrate Fe levels exceeded $0.17 \mu\text{mol kg}^{-1}$ (see Table 1).

Table 1 Filtrate Fe levels in north San Francisco Bay waters

Salinity (%)		Direct injection ($\mu\text{mol kg}^{-1}$)	Organic extraction ($\mu\text{mol kg}^{-1}$)	Organic extraction Direct injection $\times 100$ (%)
2.2	A	0.286	0.252	88
	B	0.176	0.179	102
6.1	A	14.4	13.8	96
	B	8.50	8.15	96
12.3	A	6.36	7.02	110
	B	6.50	7.36	113
$\bar{X} \pm 1s$ 101 \pm 9.4				

Two replicates were analysed using the organic extraction preconcentration technique; precision was generally good, as exemplified by the data presented in Table 2. Iron values estimated using another preconcentration technique (chelex ion exchange at pH 6) are also shown in Table 2. Good agreement between the two preconcentration methods was generally found in the 11 replicates that were checked. This was also true for the Fig. 1a data (chelex values not shown).

Although there are few recent Fe data available for comparison with those we report here, those that do exist are in general agreement. Landing and Bruland¹³ also reported low Fe levels (0.4 nmol kg^{-1}) in surface waters, and maxima in the oxygen minimum ($1\text{--}2 \text{ nmol kg}^{-1}$) at locations in the same vicinity as our Fig. 1a station. Although we failed to find a

mid-depth (750–1,500 m) maximum that they reported, we may have missed this feature, as we only had two samples in this depth range.

Low surface Fe values could be expected for two reasons: (1) Fe is least soluble in oxygen-rich surface waters⁴; and (2) phytoplankton require this nanonutrient^{14,15} and depletion is logical in the euphotic zone. Higher Fe levels in association with oxygen minima are also likely because of increased solubility⁴ in such waters. In this regard, it is interesting that the shape of the profiles shown in Fig. 1b and c are the same as those observed in the Black Sea¹⁶, although the Pacific Fe levels are two orders of magnitude lower.

Why Fe varies little in mid-depth waters is uncertain. Perhaps the lack of variability suggests equilibrium with particulate phases, but our particulate Fe data (Fig. 1) generally give little information in this regard. Two fractions of particulate Fe were analysed: refractory Fe (ref. 17) and weakly leachable (25% acetic acid) Fe (ref. 18). The latter technique is not very suitable for this element, as hydrous oxides are not removed. Obviously, more would be learned if a more appropriate procedure were used to separate hydrous Fe oxide coatings from crystalline Fe (ref. 19). Nevertheless, the particulate Fe data at least illustrate the general insolubility of Fe, as these values usually exceeded those for dissolved Fe. Refractory Fe amounts reflect various levels of suspended aluminosilicates in the water column, and as expected, quantities were higher at the near-shore California location (Fig. 1a) than those in the more oceanic waters (Fig. 1b, c). Leachable Fe quantities showed a consistent trend in only one case; values were lowest where dissolved Fe levels were highest at the top of the oxygen minimum off Mexico (Fig. 1c). The increase in leachable Fe beneath the dissolved Fe maxima suggests that Fe was being removed back onto particles at these depths.

Based on recent experience with several trace elements, it is probable that the $\mu\text{g per kg}$ amounts of dissolved Fe previously reported for seawater resulted from gross sample contamination. The data we present here and those of Landing and Bruland¹³ are an order of magnitude less than the maximum possible dissolved amounts (20 nmol kg^{-1}) estimated by Byrne and Kester²⁰. Thus, it is possible that the Fe we measured was truly dissolved, perhaps in organic complexes^{5–8} or as $\text{Fe}(\text{OH})_3$ (refs 4, 20). Obviously, much remains to be learned about Fe in oceanic waters, and we hope that this report will stimulate research on this topic.

We thank W. W. Broenkow for the CTOD oxygen data, and S. E. Fitzwater for help with sample collection and analyses. This research was supported by grants from the NSF Marine Chemistry (VERTEX, OCE 80-03200) and Biological Oceanography (OCE 79-09431) programmes, the Ocean Minerals Corporation, and the US Environmental Protection Agency (CR 8077110020).

Received 7 April; accepted 29 July 1982.

- Bowen, H. J. M. *Trace Elements in Biochemistry* (Academic, London, 1966).
- Goldberg, E. D. *J. Geol.* **62**, 249–265 (1954).
- Taylor, S. R. *Geochim. cosmochim. Acta* **28**, 1273–1285 (1964).
- Stumm, W. & Morgan, J. J. *Aquatic Chemistry* 2nd edn (Wiley, New York, 1981).
- Boyle, E. A., Edmond, J. M. & Sholkovitz, E. R. *Geochim. cosmochim. Acta* **41**, 1313–1324 (1977).
- Sholkovitz, E. R., Boyle, E. A. & Price, N. B. *Earth planet. Sci. Lett.* **40**, 130–136 (1978).
- Sholkovitz, E. R. *Earth planet. Sci. Lett.* **41**, 77–86 (1978).
- Sholkovitz, E. R. & Copland, D. *Geochim. cosmochim. Acta* **45**, 181–189 (1981).
- Mill, A. J. B. *Envir. Tech. Lett.* **1**, 97–108 (1980).
- Bruland, K. W., Franks, R. P., Knauer, G. A. & Martin, J. H. *Analyt. chim. Acta* **105**, 233–245 (1979).
- Bruland, K. W., Knauer, G. A. & Martin, J. H. *Nature* **271**, 741–743 (1978).
- Bruland, K. W. *Earth planet. Sci. Lett.* **47**, 176–198 (1980).
- Landing, W. M. & Bruland, K. W. *EOS* **62**, 906 (1981).
- Lewin, J. C. & Chen, C. H. *Limnol. Oceanogr.* **16**, 670–675 (1971).
- Menzel, D. W. & Ryther, J. H. *Deep-Sea Res.* **7**, 276–281 (1961).
- Spencer, D. W. & Brewer, P. G. *J. geophys. Res.* **76**, 5877–5892 (1971).
- Eggemann, D. W. & Betzer, P. R. *Analyt. Chem.* **48**, 866–890 (1976).
- Chester, R. & Hughes, M. J. *Chem. Geol.* **2**, 249–262 (1967).
- Gibbs, R. J. *Bull. geol. Soc. Am.* **88**, 829–843 (1977).
- Byrne, R. H. & Kester, D. R. *Mar. Chem.* **4**, 255–274 (1976).

Table 2 Dissolved Fe values found off central Mexico ($18^\circ 00' \text{ N}$, $108^\circ 00' \text{ W}$) in October 1981 (data are also shown in Fig. 1c)

Depth (m)	OE 1	OE 2	\bar{X} OE Fe (nmol kg^{-1})	CX Fe
Surface	0.14	0.13	0.14	0.16
5	0.28*	0.13	0.13	—
10	(3.6)†	(3.8)	(3.7)	—
20	0.16	0.49*	0.16	0.16
30	0.69	0.60	0.64	0.51
40	(1.4)	(1.1)	(1.2)	(1.6)
50	0.73	0.73	0.73	0.61
60	0.49	0.60	0.54	0.64
70	1.6	2.0	1.8	1.7
80	2.2	2.3	2.2	—
90	2.7	2.6	2.6	—
100	0.95	0.89	0.92	—
110	1.2	0.98	1.1	—
120	1.2	1.3	1.3	—
130	1.5	1.5	1.5	—
140	(4.8)	(4.0)	(4.4)	—
150	1.9	1.8	1.8	—
160	1.7	1.4	1.6	—
175	1.7	1.4	1.6	—
195	0.74	0.73	0.74	—
220	1.0	0.82	0.91	—
245	0.66	0.37	0.52	—
295	1.1	0.95	1.0	1.0
395	0.76	0.60	0.68	—
490	0.90	1.0	0.95	—
590	0.92	0.61	0.76	0.86
690	0.50	0.29	0.40	—
785	0.75	0.68	0.72	—
880	0.76	0.65	0.70	0.69
980	0.84	0.76	0.80	—
1,955	0.73	0.46	0.60	0.74

Iron was preconcentrated in 2 replicates (OE 1, OE 2) using organic extraction. Replicate values were averaged (\bar{X} OE Fe) and are compared with those obtained using chelex ion exchange (CX FE) preconcentration at selected depths.

* Not used in \bar{X} .

† () thought to be contaminated (see text).

Radiocaesium and plutonium in intertidal sediments from southern Scotland

A. B. MacKenzie & R. D. Scott

Scottish Universities Research and Reactor Centre, East Kilbride, Glasgow G75 0QU, UK

The dispersion of radionuclides discharged to the Irish Sea from the works of British Nuclear Fuels Ltd at Sellafield (Windscale) is a topic of major importance, attracting considerable interest in recent years. Annual surveys by the Ministry of Agriculture, Fisheries and Food (MAFF) of marine radioactivity^{1,2} supplemented by other work³⁻¹⁷ have defined the major features of this dispersion during the 30 yr of the plant's operation. Two species of radiological concern are radiocaesium isotopes (^{137}Cs , β , γ , $t_{1/2} = 30.25$ yr; ^{134}Cs , β , γ , $t_{1/2} = 2.05$ yr) which constitute the main effluent radioactivity and plutonium isotopes (^{238}Pu , α , $t_{1/2} = 86$ yr; ^{239}Pu , α , $t_{1/2} = 2.44 \times 10^4$ yr; ^{240}Pu , α , $t_{1/2} = 6.58 \times 10^3$ yr) with high radio-toxicities. We present here plutonium and radiocaesium profiles for intertidal sediment cores collected from four sites in southern Scotland (Fig. 1) during October 1979 and discuss the present and longer-term significance of the interaction of Sellafield effluent with such sediments.

Intertidal sediment cores of length 18 cm were extruded immediately on collection and divided into 3-cm sections. The sediments consisted of sand/silt and, with the exception of Westferry, shell fragments. The biological population was restricted to small crustaceans and worms at Westferry but was more varied at the other sites. Dried sediment samples were analysed for radiocaesium¹⁸, plutonium^{19,20}, aluminium, manganese and carbonate, results being presented in Table 1.

Plutonium and radiocaesium arise in the study area from two main sources—Sellafield and nuclear weapons testing fallout. Sellafield effluent has had a $^{134}\text{Cs}/^{137}\text{Cs}$ ratio in the range 0.1–0.25 in recent years⁸ and a $^{238}\text{Pu}/^{239,240}\text{Pu}$ ratio increasing from 0.05 to 0.25 during the period 1966–79^{12,6}. Fallout contains ^{137}Cs but not ^{134}Cs and has a $^{238}\text{Pu}/^{239,240}\text{Pu}$ ratio of about 0.05 (ref. 21). The Sellafield discharge is very much larger than

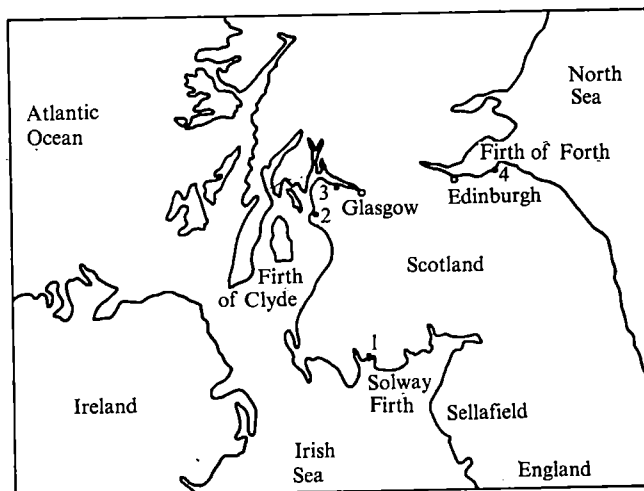


Fig. 1 Map showing locations of sampling sites. 1, Skyreburn Bay; 2, Ardrossan; 3, Westferry; 4, Aberlady Bay.

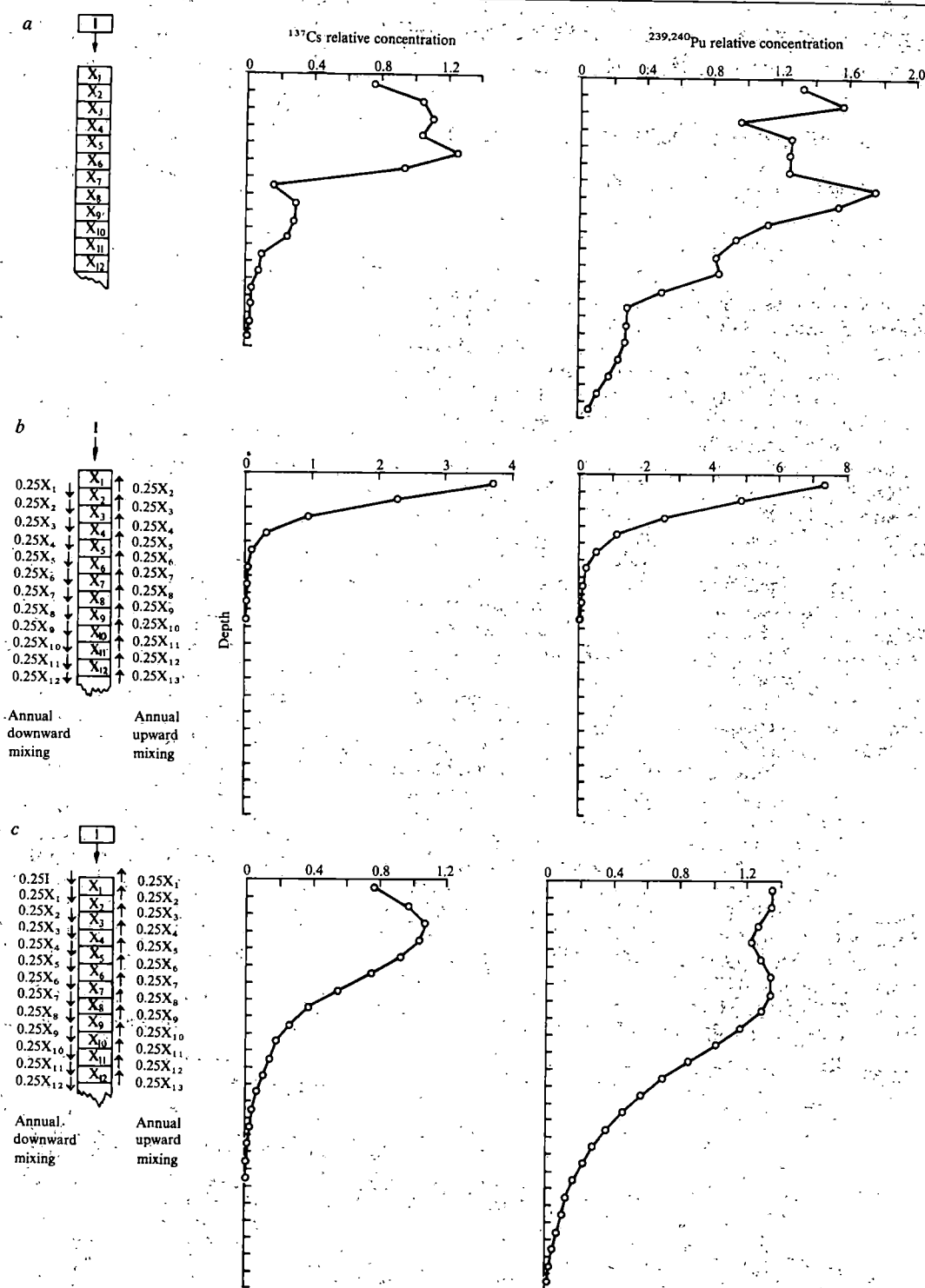
that from any other nuclear facility in the UK and concentrations of manmade radionuclides in the marine environment of south-west Scotland are consequently dominated by Sellafield waste^{1,2,8}. The east coast site will receive a minor input from Dounreay (and possibly La Hague) but the largest source of manmade radionuclides in this section of the North Sea is Sellafield⁷. Consistent with this, it is apparent from Table 1 and the isotope ratios given above that all four sites studied are contaminated to some extent with Sellafield effluent. The Skyreburn Bay concentrations can be almost totally attributed to Sellafield and are in good agreement with MAFF data for nearby sites^{1,2}. The other sites show ^{137}Cs and $^{239,240}\text{Pu}$ contents which are factors of 10 and 10^2 , respectively, lower than those in Skyreburn Bay, reflecting dilution and preferential uptake of Pu by sediments during transit. As the concentrations at the three northerly sites are similar to soil fallout levels, the observed isotope ratios could result from mixtures of either Sellafield effluent and fallout, or wastes discharged from Sellafield at different times. However, the results imply a lower limit of 70–75% for the Sellafield component of the total activity. In attempting to rationalize the observed profiles, it is

Table 1 Analytical results

Location	Depth (cm)	^{137}Cs		$^{239,240}\text{Pu}$		Al concentration (% dry weight)	Mn concentration (% dry weight)	CaCO_3 concentration (% dry weight)
		concentration (mBq g^{-1})	$^{134}\text{Cs}/^{137}\text{Cs}$	concentration (mBq g^{-1})	$^{238}\text{Pu}/^{239,240}\text{Pu}$			
Skyreburn Bay	0–3	478 \pm 5	0.073 \pm 0.004	58 \pm 2	0.23 \pm 0.01	3.8	0.076	4.4
	3–6	657 \pm 5	0.072 \pm 0.003	43 \pm 2	0.22 \pm 0.01	3.5	0.051	4.7
	6–9	762 \pm 5	0.062 \pm 0.003	49 \pm 2	0.23 \pm 0.01	3.7	0.047	4.6
	9–12	950 \pm 7	0.059 \pm 0.002	77 \pm 3	0.22 \pm 0.01	3.5	0.046	5.3
	12–15	793 \pm 6	0.060 \pm 0.003	63 \pm 3	0.21 \pm 0.01	3.4	0.045	5.0
	15–18	742 \pm 5	0.050 \pm 0.003	42 \pm 2	0.25 \pm 0.02	3.8	0.045	5.6
Ardrossan	0–3	30 \pm 2	0.15 \pm 0.08	1.05 \pm 0.04	0.15 \pm 0.02	1.4	0.011	0.6
	3–6	37 \pm 2	0.14 \pm 0.06	0.31 \pm 0.02	0.15 \pm 0.02	1.5	0.011	2.3
	6–9	45 \pm 2	0.08 \pm 0.05	0.68 \pm 0.03	0.15 \pm 0.02	2.1	0.012	2.7
	9–12	48 \pm 2	0.06 \pm 0.05	0.83 \pm 0.03	0.14 \pm 0.02	1.7	0.013	3.3
	12–15	55 \pm 2	0.08 \pm 0.05	1.12 \pm 0.04	0.13 \pm 0.02	1.8	0.013	5.0
	15–18	55 \pm 2	BDL	0.98 \pm 0.04	0.15 \pm 0.02	1.8	0.014	7.4
Westferry	0–3	87 \pm 3	0.09 \pm 0.02	1.22 \pm 0.03	0.18 \pm 0.02	3.3	0.026	<0.4
	3–6	53 \pm 2	0.09 \pm 0.03	0.07 \pm 0.003	0.20 \pm 0.02	4.5	0.026	<0.4
	6–9	25 \pm 2	BDL	0.05 \pm 0.003	0.16 \pm 0.02	4.1	0.028	<0.4
	9–12	12 \pm 1	BDL	0.021 \pm 0.004	BDL	3.7	0.033	<0.4
	12–15	9 \pm 1	BDL	0.015 \pm 0.001	BDL	3.3	0.032	<0.4
	15–18	3 \pm 1	BDL	0.005 \pm 0.002	BDL	4.2	0.023	<0.4
Aberlady Bay	0–3	39 \pm 2	0.06 \pm 0.03	0.53 \pm 0.02	0.13 \pm 0.01	2.6	0.017	3.1
	3–6	26 \pm 2	0.08 \pm 0.03	0.34 \pm 0.02	0.20 \pm 0.02	2.3	0.016	2.2
	6–9	15 \pm 1	BDL	0.24 \pm 0.010	0.15 \pm 0.02	2.1	0.014	0.5
	9–12	11 \pm 1	BDL	0.11 \pm 0.005	0.19 \pm 0.02	1.5	0.008	3.6
	12–15	11 \pm 2	BDL	0.075 \pm 0.008	BDL	1.6	0.011	2.5
	15–18	13 \pm 2	BDL	0.046 \pm 0.003	0.13 \pm 0.02	1.7	0.011	4.2

Radionuclide errors are based on 1σ counting statistics; errors on other results $\sim 3\%$. Al and Mn were determined by instrumental neutron activation analysis; CO_2 were determined by measurement of CO_2 evolved by reaction with acid. BDL, below detection limit.

Fig. 2 Sediment box models and resultant radionuclide profiles relating to the Sellafield discharge of ^{137}Cs (discharge data used for 1964 to 1979 inclusive) and $^{239,240}\text{Pu}$ (discharge data used for 1960 to 1979 inclusive). Relative concentrations can be related between models for one nuclide but cannot be related between ^{137}Cs and $^{239,240}\text{Pu}$. An arbitrary, but constant, depth scale is used in all cases. *a*, 'Accumulation-only' model. An input *I* of the radionuclide, proportional to the Sellafield discharge, is added to the sediment column annually along with a fixed amount of sediment. The sediment column is notionally divided into a series of boxes as shown, each of which contains an amount of sediment equivalent to 1 year's deposition. No mixing occurs between boxes. The radionuclide concentrations in the boxes at the start of a given year are denoted by X_1 , X_2 , etc. and are all zero before the first input of radionuclide. Radioactive decay is applied on an annual basis and no other removal of radionuclides occurs. *b*, 'Mixing-only' model. An input *I* of the radionuclide, proportional to the Sellafield discharge, is added annually to the surface sediment with no addition of new sediment material. The sediment is again notionally divided into a series of boxes and the radionuclide concentrations in the boxes at the start of a given year are again denoted by X_1 , X_2 , etc.



Mixing between boxes occurs and in the example selected, intense mixing involving exchange of 0.25 of the material originally present is assumed to occur annually between contiguous boxes. The amount of exchange between boxes can be varied to simulate different intensities of mixing and varied rates of mixing can also be applied down the sediment column. *c*, 'Mixing-plus-accumulation' model. This model is a direct combination of models *a* and *b*. (More complex models of this type are discussed by Santschi *et al.*²³)

necessary to consider the well defined^{8,10,12} temporal variations in the Sellafield discharge in conjunction with processes which influence the uptake and subsequent behaviour of radionuclides in sediment. Surface sediments are subject to a complex interaction of influences, including physical (for example, mixing, compaction, variable accumulation/erosion), chemical (such as redox reactions, interstitial water processes, sediment heterogeneity) and biological (mixing, irrigation, feeding, excreting) processes²², resulting in severe difficulties in modelling the system. Figure 2 shows three models combining the Sellafield discharge data with varied accumulation and mixing situations. These are examples from a suite of models

and illustrate that 'accumulation-plus-mixing' profiles are similar to those for 'accumulation-only' but with the curve smoothed, variations attenuated and radionuclide penetration to greater depth. Subsurface maxima are retained, even with intense mixing, provided there is also accumulation, but the non-symmetrical maximum for ^{137}Cs can be displaced towards the surface relative to that for $^{239,240}\text{Pu}$.

The Skyreburn Bay and Ardrossan profiles (Fig. 3) conform to the 'accumulation-only' or 'accumulation-plus-mixing' type whereas Westferry and Aberlady Bay relate to the 'mixing-only' model. No correlation is apparent between radionuclide profiles and those for Al (indication of clay content), Mn (indication of

redox processes) and carbonate (shell content), showing that these parameters do not exert a major influence on the radionuclide distributions and that variations in input, sedimentation and mixing are probably the dominant processes. Sellafield radionuclides dispersed by water movements require a transit time of 8 months or less to reach the northern parts of the Clyde Sea area^{8,24}, so a shorter transit time to Skyreburn Bay and Ardrossan can be assumed, as is confirmed by the profiles for these sites, which show trends relating to the Sellafield discharge up to 1979. Sediment mixing by waves, currents and biological activity was observed at both locations so the profiles should be related to the 'accumulation-plus-mixing' model. Relating maxima in the profiles to those in the Sellafield discharge implies 'sedimentation rates' in the range 2.5–3.0 cm yr⁻¹ for these sites. This 'sedimentation' is probably a transient component of a complex, long-term reworking of these sediments because the bays have been stable over long periods^{25–27}. An extended study of Skyreburn Bay, to be reported elsewhere, has shown that cores collected from different parts of the bay show similar profiles, the total depth of radionuclide penetration is ~35 cm and variations in the profiles as a function of time tend to support the above hypothesis of reworking. Distinction between reworking and continuous sedimentation is important because the former would result in retention of the radionuclides in the surface zone of potential radiological significance over much longer timespans.

Several workers have studied sedimentation processes in the River Esk, Ravensglass Estuary, by relating radionuclide concentrations and isotope ratio profiles to the Sellafield discharge^{6,10,12,14,17}, and Clifton and Hamilton present a detailed study of the influence of geochemical parameters, variable sedimentation rates and mixing processes on radionuclide profiles and derived chronologies. Aston and Stanners¹² contend that their ²³⁸Pu/^{239,240}Pu profiles for Ravensglass Estuary sediments, in conjunction with a model deriving a vanishingly small 'apparent diffusion coefficient', demonstrate negligible post-depositional remobilization of plutonium. However, the information which can be derived on this subject either from the present work or from that of Aston and Stanners is subject to considerable uncertainty because: (1) Sellafield discharge ²³⁶Pu/^{239,240}Pu data are not available before 1978; the only data available for comparison with sediment profiles are Hetherington's results for surface sediments from the Ravensglass Estuary for the period 1966–75 and these results have an implicit sampling error of several per cent and an explicit 1σ error on counting statistics of as much as 47%. (2) Mixing of discharges of different ages and isotope ratios in Irish Sea waters and surface sediments leads to uncertainty in relating observed profiles to discharge data. (3) Experimental errors for ²³⁸Pu/^{239,240}Pu ratios are often as large as 10%. (4) Sampling increments are large by comparison with any plausible remobilization movement of plutonium. Thus, while this type of study does provide useful information on the uptake of radionuclides by sediments, it does not provide a sensitive method for study of possible remobilization and removal processes which would be more meaningfully studied by analysis of radionuclide concentrations in interstitial and overlying waters^{6,28}.

Westferry and Aberlady Bay occupy relatively sheltered sites (in contrast to Skyreburn Bay and Ardrossan) and show radionuclide profiles which suggest negligible accumulation with mixing which results in penetration of ¹³⁷Cs and ^{239,240}Pu to depths of at least 18 cm over a period of about 30 yr. ¹³⁷Cs and ^{239,240}Pu have similar distributions in Aberlady Bay, indicating that similar processes influence both species. For Westferry, however, there is pronounced penetration of ¹³⁷Cs to greater depths than ^{239,240}Pu. Livingston and Bowen²⁹ suggest that similar observations for nearshore sediments can be explained by diagenetic remobilization of Pu and this argument could be invoked for the Westferry profiles. However, alternative explanations also exist, for example, preferential downward migration of radiocaesium in interstitial waters, the ambiguity again

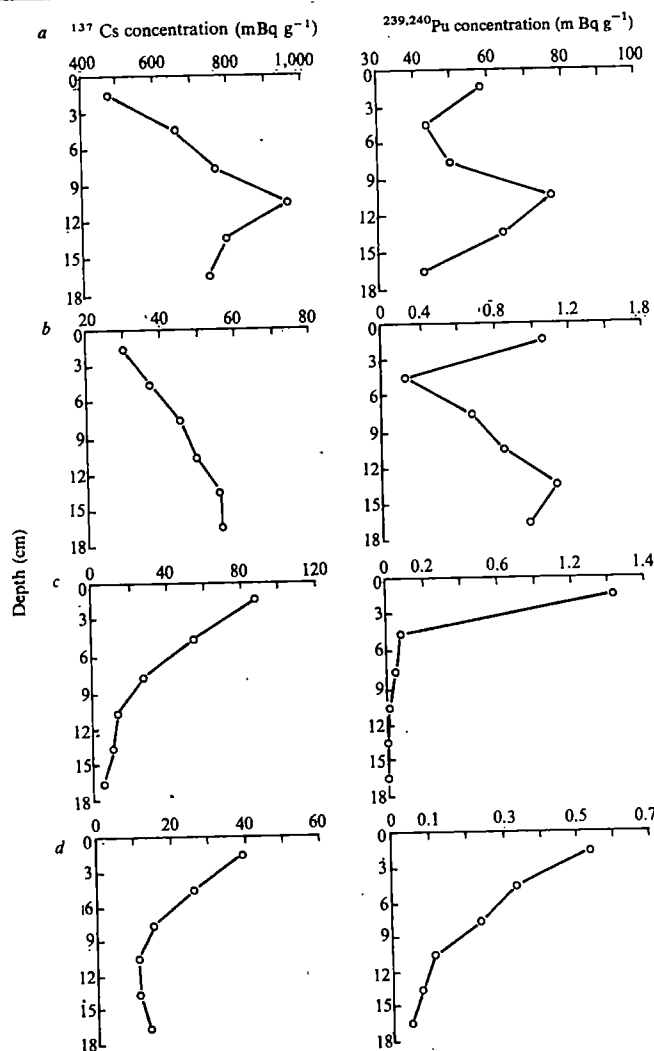


Fig. 3 ¹³⁷Cs and ^{239,240}Pu profiles in intertidal sediments from southern Scotland, October 1979. a, Skyreburn Bay; b, Ardrossan; c, Westferry; d, Aberlady Bay.

illustrating the limitations of bulk sediment analysis in investigating such processes.

Uncertainties concerning possible removal impose a limitation on estimates of long-term variations of radionuclide concentrations in these sediments. However, assuming no removal occurs other than by radioactive decay and that radionuclide concentrations increase in response to a continued discharge from Sellafield at present levels, an (improbably long) operation period of 200 yr would result in ¹³⁷Cs and ^{239,240}Pu inventories increasing by factors of 3 and 10, respectively, relative to 1979 levels. Resultant concentrations at the study sites would then, at highest, equal present levels in Cumbria, the significance of which has been discussed by Hunt^{1,2}. This calculation derives an order of magnitude upper limit and the concentrations which develop will almost certainly be lower than this, as removal by processes other than radioactive decay will occur and the Sellafield discharge will probably decrease as the nuclear power industry evolves and improved chemical procedures (for example, the SIXEP ion exchange plant³⁰) are introduced.

Partial financial support of this work by the International Atomic Energy Agency under research contract no. 2409/RB is gratefully acknowledged. We thank Professor H. W. Wilson for his encouragement.

Received 8 March; accepted 3 August 1982.

1. Hunt G. J. *Aquatic Environment Monitoring Report No. 4* (Ministry of Agriculture Fisheries and Food, Lowestoft, 1980).
2. Hunt G. J. *Aquatic Environment Monitoring Report No. 6* (Ministry of Agriculture Fisheries and Food, Lowestoft, 1981).
3. Jefferies, D. F., Preston, A. & Steele, A. K. *Mar. Pollut. Bull.* 4, 118 (1973).

4. Wilson T. S. R. *Nature* **248**, 125 (1974).
5. Livingston H. D. & Bowen, V. T. *Nature* **269**, 586 (1977).
6. Hetherington, J. A. *Mar. Sci. Commun.* **4**, 239 (1978).
7. Murray, C. N., Kautsky, H., Hoppenheit, M. & Domian M. *Nature* **276**, 225 (1978).
8. Baxter, M. S., McKinley, I. G., MacKenzie, A. B. & Jack, W. *Mar. Pollut. Bull.* **10**, 116 (1979).
9. Murray, C. N., Kautsky, H. & Eicke, H. F. *Nature* **278**, 617 (1979).
10. Aston, S. R. & Stanners, D. A. *Estuar. coastal mar. Sci.* **9**, 529 (1979).
11. McKinley, I. G., Baxter, M. S., Ellett, D. J. & Jack, W. *Estuar. coastal Shelf Sci.* **13**, 69 (1981).
12. Aston, S. R. & Stanners, D. A. *Nature* **289**, 581 (1981).
13. Day, J. P. & Cross, J. E. *Nature* **292**, 43 (1981).
14. Stanners, D. A. & Aston, S. R. *Estuar. coastal Shelf Sci.* **13**, 101 (1981).
15. Stanners, D. A. & Aston, S. R. *Estuar. coastal Shelf Sci.* **13**, 409 (1981).
16. Aston, S. R. & Stanners, D. A. *Estuar. coastal Shelf Sci.* **14**, 167 (1982).
17. Clifton, R. J. & Hamilton, E. I. *Estuar. coastal Shelf Sci.* **14**, 433 (1982).
18. MacKenzie, A. B., Baxter, M. S., McKinley, I. G., Swan, D. S. & Jack, W. *J. radioanalyt. Chem.* **48**, 29 (1979).
19. Coleman, G. R. *The Radiochemistry of Plutonium* (National Academy of Sciences Report NAS-NS 3058, 1965).
20. MacKenzie, A. B. *Analyst. Proc.* (in the press).
21. Cambray, R. S. & Eakins, J. D. *Studies of Environmental Radioactivity in Cumbria Pt 1* (UKAEA report AERE-R-9807, HMSO, London, 1980).
22. Berner, R. A. *Early Diagenesis* (Princeton University Press, 1980).
23. Santschi, P. H., Li, Y. H., Bell, J. J., Trier, R. W. & Kawtaluk, K. *Earth planet. Sci. Lett.* **51**, 248 (1980).
24. McKinley, I. G., Baxter, M. S. & Jack, W. *Estuar. coastal Shelf Sci.* **13**, 59 (1981).
25. *Ordnance Survey Map of Scotland*, Popular Edn, 1" to 1 mile, 3rd revision, 1921-23 (HMSO, London, 1923).
26. *The Atlas of Scotland* (Thomson, Edinburgh, 1832).
27. Ainslie J. *Map Published According to Act of Parliament with Improvements till 1800* (Brown, Edinburgh, 1800).
28. Nelson, D. M. & Lovett, M. B. in *Proc. IAEA conf.*, Vienna 1980 (International Atomic Energy Agency, Vienna, 1981).
29. Livingston, H. D. & Bowen, V. T. *Earth planet. Sci. Lett.* **43**, 29 (1979).
30. British Nuclear Fuels Ltd. *Windscale and Calder Works* (BNFL, Risley, 1981).

Detection of imogolite in soils using solid state ^{29}Si NMR

P. F. Barron*, M. A. Wilson†, A. S. Campbell‡ & R. L. Frost§

* Brisbane NMR Centre, Griffith University, Nathan, Queensland, Australia 4111

† CSIRO Division of Fossil Fuels, PO Box 136, North Ryde, New South Wales, Australia 2113

‡ Department of Soil Science, Lincoln College, Canterbury, New Zealand

§ Queensland Institute of Technology, Brisbane, Australia 4001

High resolution solid state ^{29}Si -NMR has recently been used to examine silicates, and synthetic and natural zeolites¹⁻⁴. This has been possible through the use of dipolar decoupling, magic-angle spinning and cross-polarization techniques which have enabled line narrowing and also considerable signal enhancement for ^{29}Si nuclei in close proximity to protons. It has been found that isotropic ^{29}Si chemical shifts in solids and solutions are generally similar and depend mainly on the degree of condensation of silicon-oxygen tetrahedra¹. For silicates, increasing condensation from single (Q^0 , -66 to -72 p.p.m.) to double tetrahedra (Q^1 , -78 to -82 p.p.m.), to chains (Q^2 , -86 to -88 p.p.m.) and cyclic layered structures (Q^3 , -107 to -109 p.p.m.) leads to increasing diamagnetic shielding. In solid aluminosilicates, the ^{29}Si chemical shift is sensitive to the substitution of aluminium. A further important point was that the ^{29}Si linewidth in aluminosilicates is sensitive to the regularity of aluminium distribution in the lattice. Thus ^{29}Si -NMR has obvious potential for the elucidation of the coordination of silicon in soils and mineral components. We report here the first ^{29}Si -NMR study of the clay mineral imogolite, and show that ^{29}Si -NMR is an excellent analytical technique for the identification of imogolite (or imogolite like materials, that is proto-imogolite) in clay fractions. The observed chemical shift of imogolite (-78 p.p.m.) is consistent with the proposal that imogolite is a tubular hydrated aluminosilicate in which silicon tetrahedra are isolated by coordination through oxygen with three aluminium atoms and one proton.

X-ray diffraction is useful for identifying long range order in materials; that is, order brought about by alignment of large

numbers of atoms such as that existing in the crystalline state. NMR, however, gives information about localized bonding. Largest effects are observed from changes in structure only one or two atoms removed from the nucleus under investigation. The application of ^{29}Si -NMR to the study of mineral and clay chemistry would be expected to have greatest potential in elucidating the structure of those components for which X-ray diffraction gives little structural information, such as the fine clay fractions from volcanic ash soils.

These materials may contain quantities of imogolite⁵⁻¹¹, a hydrated aluminosilicate of tubular structure in which it has been proposed that silicon tetrahedra are isolated by coordination through oxygen with three aluminium atoms and one proton. The external surface of the tube is made up of a gibbsite-like structure, but the internal surface has exposed Si-OH groups which arise from O_3SiOH tetrahedra. Imogolite has been identified by X-ray and electron diffraction patterns, but this requires the presence of bundles of aligned tubes. IR spectroscopy has been used to identify and crudely quantify the presence of imogolite⁵. However, the method is far from satisfactory due to possibility of overlapping bands from other mineral species. There are at present no satisfactory methods for identifying and quantifying the amounts of imogolite in clay fractions.

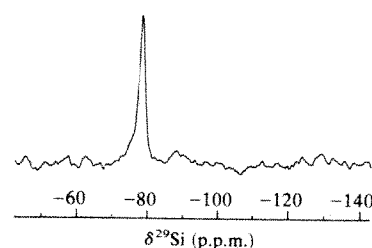


Fig. 1 DD/MAS ^{29}Si -NMR spectrum of imogolite. The chemical shift of imogolite is -78 p.p.m. from TMS.

Previously^{12,13} we reported the characterization of poorly ordered aluminosilicates in a vitric andosol and a spodosol from New Zealand. Imogolite was not identified in any of these samples by electron microscopy, although this may be the result of insufficient resolution. Nevertheless, the samples meet all the defined requirements of allophane¹⁴, and are therefore very suitable for testing the ^{29}Si -NMR analytical method. In the present work the ^{29}Si -NMR spectra of the andosol and spodosol fine clay fractions are investigated and comparison is made with ^{29}Si -NMR spectra of authentic imogolite.

The soils used (Taupo and Bealey) and soil sites have been described elsewhere¹²⁻¹⁵. Chemical properties of the size fractions investigated are shown in Table 1. Authentic imogolite was provided by CSIRO Division of Soils and originated from Kitakami City, Suete Prefecture, Japan and was separated from Kitakami Pumice. ^{29}Si -NMR spectra were obtained at 59.61 MHz on a Bruker CXP-300 spectrometer using cross-polarization with magic angle spinning (CP/MAS) or using a single pulse sequence with dipolar ^1H decoupling (DD/MAS) and B_1 fields of 10 and 50 mT for ^1H and ^{29}Si respectively. The latter experiment can be considered as giving quantitative assessment of the types of ^{29}Si environments present whilst the former experiment should yield information on the presence of hydroxy groups or bound water in close proximity to ^{29}Si nuclei. All the samples were packed into Andrews-type Delrin rotors and spun at speeds of 3-4 kHz. A pulse delay of 20 s was used for DD/MAS experiments. Experiments using a range of pulse delays were performed and showed that delays of 10 s or more would allow quantitative interpretation of DD/MAS spectra. CP/MAS experiments were performed using single 5-ms contacts repeated at 3-s intervals. Contact time dependence experiments were performed for selected samples. Chemical shifts are referenced indirectly to TMS.

The DD/MAS spectrum of the authentic imogolite is shown in Fig. 1. It consists of one peak at -78 p.p.m. According to

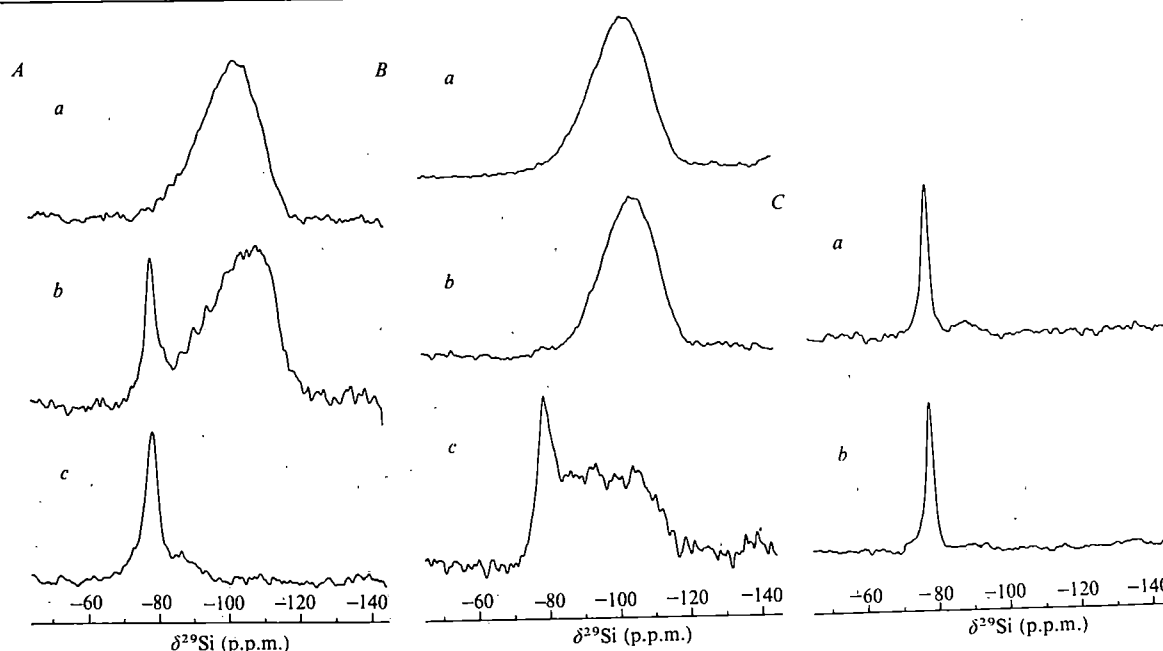


Fig. 2 A, DD/MAS ^{29}Si -NMR spectra of Taupo B horizon fractions. a, 2–150 μm ; b, 0.2–2 μm ; c, 0.2 μm . B, DD/MAS ^{29}Si -NMR spectra of Taupo C horizon fractions. a, 2–150 μm ; b, 0.2–2 μm ; c, <0.2 μm . C, DD/MAS ^{29}Si -NMR spectra of Bealey fractions. a, 0.2–2 μm ; b, <0.2 μm .

the accepted view, imogolite is a $Q^3(3\text{Al})$ aluminosilicate as it consists of trisubstituted silicon tetrahedra. The only published spectra of Q^3 aluminosilicates are those of pyrophyllite ($Q^3(0\text{Al})$) and muscovite ($Q^3(1\text{Al})$) and it is difficult to predict the chemical shift of imogolite from these samples alone. However, Lippmaa¹ has published spectra of a complete range of Q^4 aluminosilicates. The Q^4 samples substituted with three alumina, $Q^4(3\text{Al})$, have chemical shifts at –88 p.p.m. The corresponding Q^4 samples substituted with four silica units and no alumina groups $Q^4(0\text{Al})$ (silica) have a chemical shift (δ) at –107 p.p.m. Thus, the difference in chemical shift between the two samples (Δ) is

$$\begin{aligned}\Delta &= \delta Q^4(0\text{Al}) - \delta Q^4(3\text{Al}) \\ &= (-107) - (-88) = -19 \text{ p.p.m.}\end{aligned}$$

The chemical shift of $Q^3(3\text{Al})$ groups in imogolite can be predicted to a first approximation as

$$\delta Q^3(3\text{Al}) = \delta Q^3(0\text{Al}) - \Delta$$

Chemical shifts of –91 and –95 p.p.m. are observed for $Q^3(0\text{Al})$ tetrahedra in kaolin¹⁶ and pyrophyllite^{1,16} (the second resonance at –91 p.p.m. reported by Lippmaa¹ must be due to the presence of kaolin in the sample studied) respectively. Hence, the expected chemical shift of imogolite is ~–72 to –76 p.p.m. There is thus good agreement between the observed and predicted chemical shift. Our results are therefore in good agreement with the proposed structure of imogolite as a $Q^3(3\text{Al})$ aluminosilicate. That imogolite is a hydroxy aluminosilicate is supported by the signal enhancement obtained using CP/MAS. Contact time dependence experiments showed

maximum enhancement occurring at ~0.75 ms. In contrast, maximum enhancement for kaolin is achieved in the vicinity of 5 ms (ref. 17). The much shorter T_{CH} in imogolite is easily rationalized when the structures are considered. Kaolin contains hydroxyl groups bonded to aluminium in aluminium sheets which are in turn attached to silicon tetrahedral sheets. However, imogolite contains hydroxyl groups directly bound to silicon. Thus, the internuclear ^{29}Si – ^1H separation to nearest protons is probably smaller in imogolite than in kaolin and resulting in more rapid cross-polarization.

DD/MAS ^{29}Si spectra of Taupo B and C horizons, and Bealey soil fractions are shown in Fig. 2 respectively. Each sample was examined by both DD/MAS and CP/MAS techniques. The DD/MAS spectra (Fig. 2A) of the three Taupo B fractions clearly show the variation in the silicate composition with fraction size. The non-clay fraction spectrum exhibits a broad resonance from ~–80 to –110 p.p.m. and centred at ~–100 p.p.m. The unresolved nature of the resonance indicates the presence of an amorphous array of ^{29}Si environments with the shift range, according to Lippmaa's work¹, indicative of both silicates and aluminosilicates. The $\text{SiO}_2/\text{Al}_2\text{O}_3$ ratio of 8.9 previously determined for this fraction indicates that this broad resonance results largely from silicates. Only minor amounts of quartz and cristobalite were previously detected by X-ray analysis and this is consistent with the minor amount of signal in the vicinity of –107 p.p.m. CP/MAS examination of this sample yields very little signal, indicating that silicates containing hydroxy groups or constituent water are not present in significant amounts. The coarse clay fraction spectrum exhibits quite different features. The spectrum shows a resolved

Table 1 Chemical properties of the clay-sized separates of Bealey spodosol and Taupo vitric andosol

	Spodosol			Andosol				
				B horizon		C horizon		
Size fraction (μm)	<0.2	0.2–2		<0.2	0.2–2	2–150	<0.2	0.2–2
Organic carbon (%)	15.3	14.2	13.2	9.4	0.27	6.3	0.94	0.16
Total Si	13.9	16.7	17.5	26.4	29.8	21.6	31.8	34.7
Al	32.4	28.1	25.4	14.7	6.4	21.7	7.6	6.8
Fe	1.2	1.9	7.9	5.8	2.2	6.0	2.3	2.2
$\text{SiO}_2/\text{Al}_2\text{O}_3$ mole ratio	0.82	1.1	1.3	3.5	8.9	1.9	8.0	9.9

See refs 13, 14 for further details.

signal at -78 p.p.m., consistent with the presence of imogolite-like material as well as a broad signal extending from -90 to -115 p.p.m. and centred at -105 p.p.m.

The spectrum of the Taupo B fine clay fraction virtually consists only of the relatively sharp resonance at -78 p.p.m. indicating the high regularity of the material. Only a small amount of unresolved signal is present over the -80 to -110 p.p.m. range. The previously determined $\text{SiO}_2/\text{Al}_2\text{O}_3$ ratio is further reduced to 1.3. A cross-polarization study of this sample was performed which revealed that this signal cross-polarized and achieved maximum enhancement at ~ 0.75 ms. These findings are also consistent with the proposed structure and NMR results for imogolite. However, the linewidth of the -78 p.p.m. resonance is larger than that for imogolite, probably indicating a lesser degree of order of structure.

Comparison of spectra of Taupo C horizon fractions (Fig. 2B) demonstrates a similar but not identical variation in silicon environments. The non-clay fraction for Taupo C yields a ^{29}Si spectrum identical to that of the B horizon in that it consists of a single broad featureless peak centred at ~ -101 p.p.m. consistent with an amorphous silicate/aluminosilicate composition. However, in contrast to the B horizon coarse clay fraction, the C horizon coarse clay fraction spectrum is identical to that of the non-clay fraction, except for a small shift to ~ -105 p.p.m., and this is consistent with its high $\text{SiO}_2/\text{Al}_2\text{O}_3$ ratio of 8.0. There is no sign of highly ordered and regular material as found in the B horizon. For the fine clay fraction of the C horizon, however, the ^{29}Si NMR spectrum does indicate the presence of ordered material. As for the coarse clay B fraction a clearly resolved resonance is present at -78 p.p.m. with a broad resonance extending from -80 to -110 p.p.m. This broad resonance appears to exhibit partially resolved resonances at ~ -92 and -105 p.p.m. Again, this sharper signal exhibited rapid cross-polarization. This fraction has a considerably lower $\text{SiO}_2/\text{Al}_2\text{O}_3$ ratio (1.9) which is again consistent with the proposal that the -78 p.p.m. resonance is due to imogolite.

Only two fractions from the Bealey soil, the coarse ($0.2-2\ \mu\text{m}$) and fine ($<0.2\ \mu\text{m}$) clay fractions, were examined (Fig. 2C). Both gave what could be considered as virtually single line spectra with a sharp resonance at -78 p.p.m. The resonance is in fact considerably sharper than that found in the Taupo fractions with a linewidth close to that obtained for imogolite. The previously determined $\text{SiO}_2/\text{Al}_2\text{O}_3$ ratio for the coarse and fine clays of 1.1 and 0.82 respectively are even lower than that found for the B horizon fine clay. Hence, the silicon species in the Bealey clay fractions consist almost entirely of imogolite or perhaps proto-imogolite. Note that at present we cannot distinguish different physical forms of imogolite.

We have been able to detect quantitatively imogolite in clay fractions when it is present in significant amounts, using ^{29}Si DD/MAS NMR. However, the clay fractions constitute only a few per cent¹² of the total soils and hence imogolite is present at levels of less than a few per cent in the whole soils. Quantitative detection of imogolite in the whole soils using ^{29}Si DD/MAS NMR may be difficult, if not impossible, given the time required to obtain spectra of sufficient signal to noise, and dynamic range and chemical shift overlap problems associated with the expected signal from the large excess of amorphous silicates/aluminosilicates. However, the difference in cross-polarization behaviour between imogolite and other aluminosilicates pointed out earlier, and the non-cross-polarizability of silicates may enable non-qualitative detection of imogolite at low levels in whole soils by ^{29}Si CP/MAS NMR using a suitably short contact time. To demonstrate this, we have been able to detect the presence of imogolite in the whole Taupo B horizon soil using the ^{29}Si CP/MAS technique with a contact time of 1 ms. We are currently investigating the detection limits of this technique.

We conclude therefore that:

(1) ^{29}Si -NMR provides a viable method for the detection of imogolite in soils. It is straightforward to quantify the fraction

of silicon present as ordered imogolite, when present in significant amounts, relative to that present as amorphous silicates/aluminosilicates. Due to the cross-polarization characteristics of imogolite, the non-quantitative detection of the presence of imogolite in small amounts relative to silicates and other aluminosilicates may be feasible.

(2) Imogolite is an important component of several clay fractions of an andosol and spodosol from New Zealand. In some cases, it seems to be the only component containing silicon.

(3) The observed chemical shift of imogolite (-78 p.p.m.) and its cross-polarization behaviour is consistent with the proposal that imogolite consists of isolated silica tetrahedra substituted with three alumina and one hydroxyl unit.

Since submission of this manuscript, it has been pointed out that another $Q^3(3\text{Al})$ aluminosilicate, margarite, has been examined by ^{29}Si -NMR (ref. 17). A single peak at -75.5 p.p.m. was obtained in good agreement with our observations for imogolite.

We thank J. Skjemstad and Mr J. Pickering, CSIRO Division of Soils, for the imogolite sample and M. A. Young for the preparation of some of the clay samples. The Bruker CXP-300 NMR spectrometer is operated by the Brisbane NMR Centre.

Received 4 May; accepted 28 July 1982.

- Lippmaa, E., Magi, M., Samoson, A., Engelhardt, G. & Grimer, A. R. *J. Am. chem. Soc.* **102**, 4889-4893 (1980).
- Lippmaa, E., Magi, M., Samoson, A. & Engelhardt, G. *J. Am. chem. Soc.* **103**, 4992-4996 (1981).
- Klinowski, J., Thomas, J. M., Fyfe, C. A. & Hartman, J. S., *J. phys. Chem.* **85**, 2590-2594 (1981).
- Engelhardt, G., Lippmaa, E. & Magi, M. *JCS chem. Commun.* 712-713 (1981).
- Farmer, V. C., Fraser, A. R., Russell, J. D. & Yoshinaga, N. *Clay Minerals* **12**, 55-57 (1977).
- Cradwick, P. D. G. *et al. Nature phys. Sci.* **240**, 187-189 (1972).
- Farmer, V. C. & Fraser, A. R. in *International Clay Conference 1978* (eds Mortland, M. M. & Farmer, V.) (Elsevier, Amsterdam, 1979).
- Parfitt, R. L. in *Soils with Variable Charge*, 167-179 (N.Z. Soil Bureau, Wellington, New Zealand, 1981).
- Wada, K. & Yoshinaga, N. *Am. Miner.* **54**, 50-71 (1969).
- Wada, K. & Matsubara, I. *Trans. 9th int. Cong. Soil Sci.* **3**, 123-131 (1968).
- Yoshinaga, N. *Soil Sci. Pl. Nutr., Tokyo* **8**, 22-29 (1962).
- Campbell, A. S., Young, A. W., Livingstone, L. G., Wilson, M. A. & Walker, T. W. *Soil Sci.* **123**, 362-368 (1977).
- Young, A. W., Campbell, A. S. & Walker, T. W. *Nature* **284**, 46-48 (1980).
- van Olphen, H. *Science* **177**, 91-97 (1971).
- N.Z. Soil Bureau Bull. **26**, 1-127 (1978).
- Barron, P. F., Skjemstad, J. & Frost, R. L. *Nature* (submitted).
- Magi, M., Samoson, A., Tarmak, M., Englehardt, G. & Lippmaa, E. *Doklady Akad. Nauk. SSSR* **261**, 1169 (1981).

Reduction of molybdate by soil organic matter: EPR evidence for formation of both Mo(V) and Mo(III)

B. A. Goodman & M. V. Cheshire

The Macaulay Institute for Soil Research, Craigiebuckler, Aberdeen AB9 2QJ, UK

The reducing ability of organic fractions extracted from the soil is well known¹⁻³. Here the reduction of Mo(VI) by humic acid and polysaccharide components from peat and soil, respectively, has been studied by electron paramagnetic resonance (EPR) spectroscopy. We report that reduction to Mo(V) species occurred initially, but with the humic acid, we observed reduction of part of the molybdenum to Mo(III). This represents the first definite evidence for Mo(III) formation in natural substances.

The humic acid⁴ was extracted from a raised bog peat overlying parent materials of the Hatton Association⁵. The polysaccharide was extracted with 0.2 M NaOH from a soil of the Countesswells series, Countesswells Association, and isolated by using Polyclar and ethanol precipitation⁶. For the formation of molybdenum complexes, the humic acid (~ 100 mg) was dissolved in 0.2 M NaOH and mixed with sodium molybdate

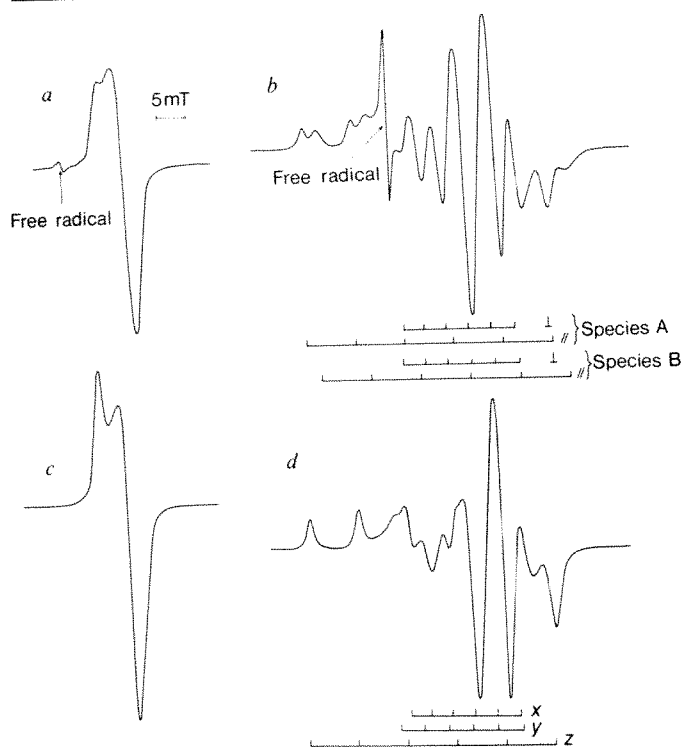


Fig. 1 EPR spectra at ambient temperatures of *a*, the Mo(V)-humic acid complex, with natural isotope ratios for Mo; *b*, the ^{95}Mo (V)-humic acid complex; *c*, the Mo(V)-polysaccharide complex with natural isotope ratios for Mo; and *d*, the ^{95}Mo (V)-polysaccharide complex.

solution (1.7 mg MoO_3 in 0.2 M NaOH). After 30 min the solution was acidified to pH 2 with 6 M HCl and centrifuged. The precipitated humic acid-molybdenum complex was dried in air under reduced pressure. The soil polysaccharide (~100 mg) was dissolved in 10 ml water and mixed with sodium molybdate solution (as above). After 30 min the pH was reduced to 3 with HCl and the mixture was freeze-dried. In a subsequent experiment the solid humic acid-molybdenum complex was washed twice with 0.1 M HCl (50 ml) and dried in air under reduced pressure.

EPR spectra were recorded at ambient temperatures at X-band frequencies on a Varian E 104 spectrometer. In the case of humic acid and molybdenum of natural isotopic abundance, a spectrum was obtained (Fig. 1*a*) which had parameters characteristic of axially symmetric Mo(V) species⁷. A weak peak from the well known humic acid free radical was also observed. The molybdenum peaks in Fig. 1*a* arise from the isotopes with zero spin. Weak hyperfine structure from the ^{95}Mo ($I = 5/2$, 15.7%) and ^{97}Mo ($I = 5/2$, 9.5%) isotopes was also observed (not shown), indicating that more than one type of Mo(V) species was present. Therefore, the experiment was repeated using molybdenum enriched to 97.43% in ^{95}Mo (obtained from AERE, Harwell). This produced a spectrum (Fig. 1*b*) in which two components (A and B) are clearly resolved. The spectral parameters for both species, obtained by computer simulation, are given in Table 1. When the same experiment was performed with the polysaccharide, only one species was obtained (Fig. 1*c*, *d*). In this case the absence of a second component in the spectrum allowed the computer simulation to be performed with greater precision than for the humic acid complexes. The peak positions could not be matched accurately when an axially-symmetric Hamiltonian was used, and the parameters given in Table 1 correspond to the best fit obtained when three independent axes were assumed. The components from the humic acid system were fitted by an axially-symmetric Hamiltonian but, because of appreciable line overlap in the perpendicular region, it is not possible to state with certainty that true axial symmetry

Table 1 EPR parameters for molybdenum complexes with soil organic matter

	g_{\perp}	g_{\parallel}	A_{\perp} (mT)	A_{\parallel} (mT)
Mo(V)-humic acid species A	1.941	1.968	3.6	8.0
Mo(V)-humic acid	1.939	1.953	3.8	8.1
Mo(V) polysaccharide	g_x 1.948	g_y 1.951	g_z 1.979	A_x 3.6
				A_y 4.1
				A_z 8.0
Mo(III)-humic acid	g 1.944		A 4.6	

applies. Nevertheless, it is clear from the magnitudes of the g -values that both of the Mo(V)-humic acid complexes differ from the polysaccharide complex.

In an attempt to alter the relative amounts of the Mo(V)-humic acid complexes, the solid molybdenum-humic acid samples were washed with 0.1 M HCl. The resulting spectra from the natural isotope and ^{95}Mo system are shown in Fig. 2*a* and *b*, respectively. These spectra are dominated by the intense narrow component from the humic acid free radical. The hyperfine structure on the low-field side of the spectra arises from copper porphyrin complexes, which are known to be present in the humic acid⁸. The molybdenum components are on the high-field side of the spectra. The natural isotope system produced a single isotropic peak, which was confirmed as arising from molybdenum by the presence of the hyperfine structure in the spectrum obtained for the sample containing the ^{95}Mo isotope. Of the various molybdenum ions that might be expected to give EPR signals at ambient temperatures, only high-spin

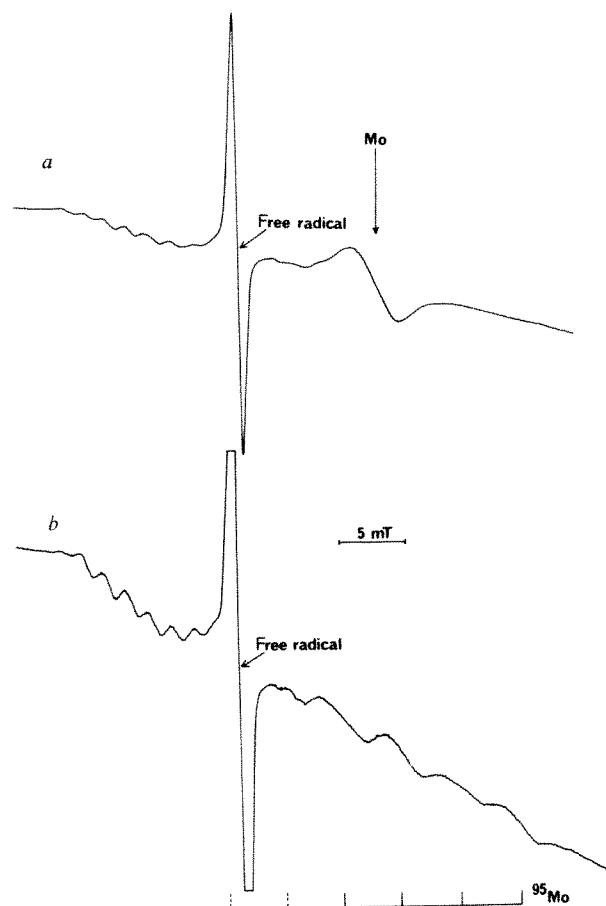


Fig. 2 EPR spectra at ambient temperatures of the Mo(III)-humic acid complex with natural isotopic ratios (*a*) and using ^{95}Mo (*b*).

Mo(I) and Mo(III) would be likely to produce isotropic spectra in the solid state. (Ions with an even number of unpaired electrons, such as Mo(IV), usually require very low temperatures for EPR experiments and even then may not produce a spectrum if the zero-field splitting is large.) While the presence of the former ion would be highly unlikely on chemical grounds, it seems also to be excluded by the EPR parameters because it should have a g -value very close to 2.00, by analogy with other high-spin d^5 ions⁷, and the value of 1.944 (Table 1) obtained from the spectrum is significantly less than this. Thus these EPR results can only be reasonably interpreted as arising from a Mo(III) species.

Note, however, that the intensities of these spectra are very much less (<1%) than those from the initial samples, hence the Mo(III) accounts for only a very small proportion of the molybdenum originally added to the humic acid. Nevertheless, the formation of Mo(III) is highly significant because, although it has been proposed as an intermediate in the reactions of some molybdenum-containing enzymes^{9,10}, there has been little definitive evidence for its formation in natural systems. Also, most complexes of Mo(III) that have been characterized are unstable and readily oxidized by air and mild reducing agents¹¹, but in the present work this ion was formed and remained stable in the solid state even in aerobic conditions. We hope, therefore, that this discovery will provide a stimulus for further searches for the presence of Mo(III) in natural systems.

Received 15 June; accepted 10 August 1982.

1. Beres, T. & Kiraly, I. *Agrokém. Talajt.* **7**, 281–286 (1958).
2. Szilagyi, M. *Soil Sci.* **111**, 233–235 (1971).
3. Goodman, B. A. & Cheshire, M. V. *J. Soil Sci.* **30**, 85–91 (1979).
4. Goodman, B. A. & Cheshire, M. V. *Nature new Biol.* **244**, 158 (1973).
5. Glentworth, R. & Muir, J. W. *Mem. Surv. Scotl.*, Edinburgh (HMSO, 1963).
6. Cheshire, M. V. *et al. J. Soil Sci.* **30**, 315–326 (1979).
7. Goodman, B. A. & Raynor, J. B. *Adv. inorg. Chem. Radiochem.* **13**, 135–362 (1970).
8. Goodman, B. A. & Cheshire, M. V. *J. Soil Sci.* **27**, 337–347 (1976).
9. Ketchum, P. A., Johnson, D., Taylor, R. C., Young, D. C. & Atkinson, A. W. *Adv. Chem. Ser.* **162**, 408–420 (1977).
10. Jacob, G. S. & Orme-Johnson, W. H. in *Molybdenum and Molybdenum-Containing Enzymes* (ed. Coughlan, M.) (Pergamon, New York, 1980).
11. Stiefel, E. I. *Prog. Inorg. Chem.* **22**, 1–223 (1977).

Isotopic variations within a single oceanic island: the Terceira case

Bernard Dupré, Bernard Lambret & Claude J. Allègre

Laboratoire de Géochimie-Cosmochimie (LA 196), Institut de Physique du Globe de Paris et Département des Sciences de la Terre, 4 place Jussieu, 75230 Paris Cedex 05, France

Since the early work of Gast *et al.*¹ it has been recognized that some isotopic variations exist on the scale of a single oceanic island^{2,3}, although the cause of such isotopic heterogeneity remains a matter of debate. For some authors, such as Grant⁴, the variations are related to local contamination in the island. Others, for example, Chase⁵, consider isotopic variation within an oceanic island to reflect mantle heterogeneity, so that it can be used to characterize the mantle and calculate the age of mantle differentiation (mantle isochron). This debate is extremely important in connection with the problem of the isotopic characteristics of the reservoir, the product of which built the oceanic island, and more generally for the structure of the mantle. Terceira is an island of the Azores Archipelago for which we have obtained several kinds of information, including geological⁶, geochronological⁷ and geochemical^{8,9} data, thus enabling us to study its isotopic composition in a well known context. We report here a Sr and Pb isotopic analysis completed on the same samples as were analysed for the major and trace elements¹⁰, and K/Ar dating⁷. Our isotopic results are correlated with the emplacement age of the rocks. This observation is in agreement with a model of mixing between two different mantle components, as has previously been proposed^{2,11,12} for other oceanic islands.

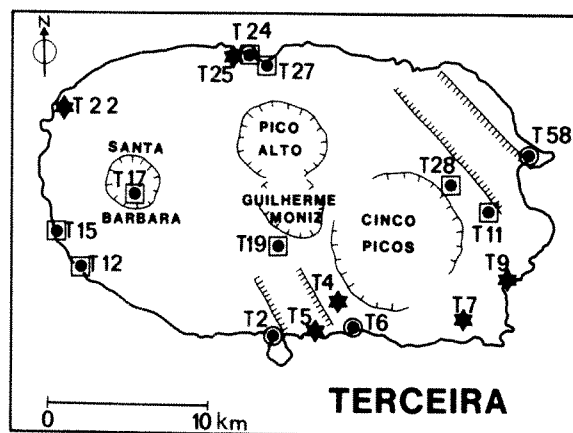


Fig. 1 Localities of samples from Terceira Island. ○, Antecaldera; □, syncaldera; ★, postcaldera.

The volcanic activity on Terceira can be divided into three periods: (1) formation of an antecaldera basaltic shield dated⁷ at 300,000 yr subsequently affected by collapses along a NW–SE orientation; (2) four strato-volcanoes with caldera—Cinco Picos, Santa Barbara, Guilherme Moniz and Pico Alto—were then built; (3) recent volcanic activity produced trachytic domes and basaltic lava flows. The samples analysed are representative of these three units and their location is given in Fig. 1, while Table 1 gives their petrographic characteristics and the Pb and Sr isotopic results. Our results clearly show the existence of important isotopic variations in both Sr and Pb.

The Pb results are plotted on a diagram of $^{206}\text{Pb}/^{204}\text{Pb}$ versus $^{207}\text{Pb}/^{204}\text{Pb}$ (Fig. 3) and show large isotopic variations: $^{206}\text{Pb}/^{204}\text{Pb}$ ratios range from 19.37 to 20.02, $^{207}\text{Pb}/^{204}\text{Pb}$ from 15.57 to 15.64 and $^{208}\text{Pb}/^{204}\text{Pb}$ from 38.95 to 39.35. Sample T27, which is enriched in ^{87}Sr , is not significantly different from the other samples in the Pb diagram.

When examined in a $^{87}\text{Sr}/^{86}\text{Sr}$ versus Sr diagram, the data display isotopic variations of different orders of magnitude: the basalts that are only slightly differentiated exhibit a 4‰ variation (values range from 0.7034 to 0.7038) whereas the highly evolved lavas (pantellerite, trachyte) yield isotopic ratios that are a few % larger than the former (T24 and T27 values are 0.7060 and 0.7075 respectively). Such variation has been observed by Gast *et al.*¹ on Gough and Ascension Islands.

Post-crystallization alteration is often invoked to explain erratic Sr isotopic variations and this has led Dash *et al.*¹³ and O'Nions *et al.*¹⁴ to use leaching techniques to test the influence of this parameter. We have also performed several leaching experiments on the Terceira samples with varying degrees of severity. Our analyses of the residues are listed in Table 2 together with analyses of the leachates which were systemati-

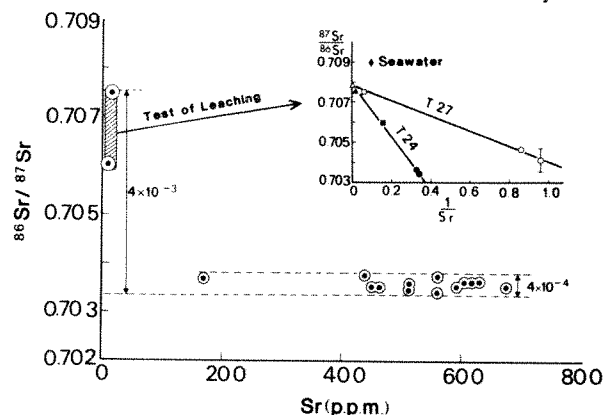


Fig. 2 $^{87}\text{Sr}/^{86}\text{Sr}$ versus Sr diagram: samples with low Sr concentrations yield high Sr-isotopic ratios. Inset: $^{87}\text{Sr}/^{86}\text{Sr}$ versus $1/\text{Sr}$: results of the leaching experiments. T24: ■, whole rocks; ▲, leachates; ●, residues. T27: □, whole rocks; △, leachates; ○, residues.

Table 1 Petrographic characteristics and Pb and Sr isotopic results in samples from Terceira Island

		$^{206}\text{Pb}/^{204}\text{Pb}$	$^{207}\text{Pb}/^{204}\text{Pb}$	$^{208}\text{Pb}/^{204}\text{Pb}$	$^{87}\text{Sr}/^{86}\text{Sr}$	Sr (p.p.m.)	Rb (p.p.m.)	$^{87}\text{Rb}/^{86}\text{Sr}$	
Antecaldera	T2	19.919	15.593	39.07	0.70379 \pm 9	440	12.3	0.079	Basalt
	T6	19.930	15.598	39.24	0.70376 \pm 11				
	T31				0.70370 \pm 12	170	90	1.47	Commendite
	T58				0.70353 \pm 7	593	23	0.110	Basalt
	T77				0.70364 \pm 7	630	27.7	0.124	Hawaiite
Syncaldera	T12	20.022	15.641	39.35	0.70350 \pm 5	452	16.3	0.101	Basalt
	T15	19.861	15.617	39.15					Basalt
	T17	19.973	15.591	39.13	0.70361 \pm 6	618	36	0.162	Andesite
	T19	19.799	15.587	39.13					Commendite
	T11	19.969	15.596	39.23	0.70373 \pm 6	561	30	0.148	Basalt
	T28	19.748	15.605	39.16	0.70340 \pm 9	560	22.3	0.112	Basalt
	T24				0.70600 \pm 10	6.3	138	62	Pantellerite
	T27	19.824	15.625	39.29	0.70752 \pm 15	17	122	20.1	Trachyte
Postcaldera	T22	19.859	15.575	39.08					Commendite
	T4	19.608	15.570	39.05	0.70347 \pm 8	516	24.3	0.132	Basalt
	T25	19.800	15.598	39.15	0.70352 \pm 7	676	30.5	0.127	Andesite
	T7	19.726	15.594	39.08	0.70359 \pm 7	516	14.7	0.070	Basalt
	T9	19.368	15.570	38.95	0.70352 \pm 8	463	21	0.126	Basalte
	T5	19.737	15.575	39.02	0.70362 \pm 6	608	35	0.760	Andesite

Pb-Sr compositions have been measured using the technique described by Manhães *et al.*¹⁷ and Birk and Allègre¹⁸ respectively. The Sr results were obtained in 1978 in the course of a study towards a third cycle doctorate. Values for Terceira can be compared with those obtained for samples from the same location by White and Schilling¹⁹. Analytical errors for the $^{206}\text{Pb}/^{204}\text{Pb}$, $^{207}\text{Pb}/^{204}\text{Pb}$, and $^{208}\text{Pb}/^{204}\text{Pb}$ ratios are 0.02, 0.02 and 0.06 respectively.

cally done when the residue and the whole rock yielded different ratios. These data are presented in Fig. 2 (inset) and display two important points.

First, the high $^{87}\text{Sr}/^{86}\text{Sr}$ ratio values obtained on T24 and T27 may be due to post-crystallization alteration, as the composition of their residue is similar to the composition of the other basalts. The results obtained for the liquid extracted by a weak leaching (ultrasonically processed with cold 6 M HCl) show a Sr isotopic value of 0.708, that is, close to the composition of seawater. Second samples T2, T7 and T17 did not show significant modifications of their isotopic ratios during the leaching experiments, and therefore alteration cannot be invoked in their cases. Furthermore, the existence of a relatively good correlation between Pb and Sr isotopic ratios is another argument against alteration as the cause of the isotopic variations observed among the slightly differentiated basalts (Fig. 3, inset).

During these leaching experiments, we also analysed the lead isotopic composition of the samples and found no significant variation. Post-crystallization alteration thus affects only the end-products of the differentiation in which the Sr concentrations are very low (<10 p.p.m.). The use of the latter to date the volcanic activity of Terceira seems unjustified.

After discarding alteration, we looked for possible correlations between these variations and other parameters, such as the geographical location, differentiation index or age of emplacement.

(1) No correlation can be clearly established between the geographical location and the composition.

(2) We found no clear correlation on plotting the isotopic results against the differentiation index as defined by Allègre *et al.*⁸, Minister *et al.*⁹ and Provost *et al.*¹¹, using either trace or major elements.

The whole series of samples which seems to define a common trend of fractional crystallization have variable isotopic ratio values and must therefore belong to different magmatic series. It is quite surprising, however, that despite these isotopic differences, they define a common chemical evolution; this demonstrates that when the trace or major element compositions of the starting magma are similar, the differentiation processes yield similar chemical evolution trends which overlap and give the impression of a unique trend. This has also been demonstrated through ^{230}Th - ^{238}U systematics, as defined by Condomines *et al.*¹⁵ for Mt Etna.

In the case of Terceira, an extensive study done by M. Jordan (personal communication) showed that the trace element trend is, in fact, split into several trends; this corroborates our analysis.

Since the Pb or Sr isotopic variations do not seem to be correlated with the chemical differentiation of the volcanic series, it is quite logical that the variations are not produced during the differentiation processes.

(3) A clear relationship exists between the isotopic composition and the age of eruption: the isotopic values of recent basalts are significantly lower than those of older basalts. In addition, the Pb and Sr values of the oceanic crust measured on the ridge at the latitude of the Azores (ref. 16 and B. Hamelin, B. D. and C.J.A. in preparation) are close to those obtained on recent rocks from Terceira (Fig. 3).

Table 2 Sr results obtained by the leaching technique

		Leaching intensity			Whole rocks
		6 M HCl, 20 min ultrasonic 30 °C	6 M HCl, 1 h, ultrasonic 30 °C	6 M HCl, 12 h bombs, 130 °C	
T24	Liquid	$^{87}\text{Sr}/^{86}\text{Sr}$ Sr (p.p.m.)	0.70799 \pm 9 465	0.70754 \pm 10 47	0.70600 \pm 10
	Residue	$^{87}\text{Sr}/^{86}\text{Sr}$ Sr (p.p.m.)	0.70358 \pm 16 3.04	0.70344 \pm 9 2.96	
	Liquid	$^{87}\text{Sr}/^{86}\text{Sr}$ Sr (p.p.m.)	0.70785 \pm 14 334	0.70778 \pm 9 165	0.70752 \pm 15
T27	Residue	$^{87}\text{Sr}/^{86}\text{Sr}$ Sr (p.p.m.)	0.70467 \pm 10 1.16	0.70410 \pm 6 1.04	
		$^{87}\text{Sr}/^{86}\text{Sr}$		0.70384 \pm 7	
T2	Residue	Sr (p.p.m.)		159	0.70379 \pm 9 440
		$^{87}\text{Sr}/^{86}\text{Sr}$		0.70362 \pm 6	0.70359 \pm 7 516
	Residue	Sr (p.p.m.)		204	
T17	Residue	$^{87}\text{Sr}/^{86}\text{Sr}$		0.70357 \pm 6	0.70361 \pm 618
		Sr (p.p.m.)			

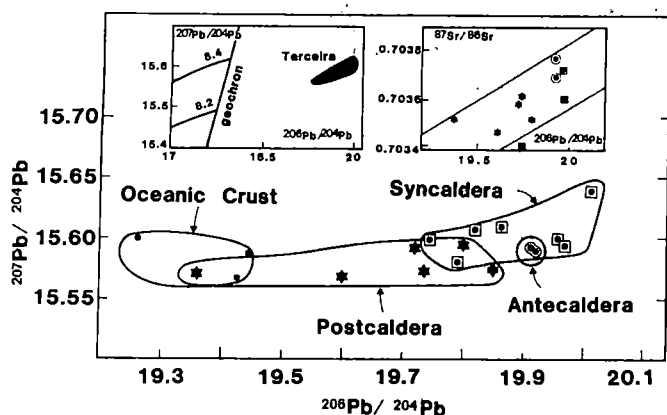


Fig. 3 $^{206}\text{Pb}/^{204}\text{Pb}$ versus $^{207}\text{Pb}/^{204}\text{Pb}$ diagram: the samples are grouped according to their age of eruption. Symbols as in Fig. 1. Upper left corner inset: location of Terceira Island within the (J) field; upper right corner inset: Pb-Sr correlation for Terceira samples.

Such similarities between Pb and Sr isotopic compositions of the oceanic crust and recent alkali basalts and the fact that the isotopic composition changed through time on Terceira indicate that an important exchange occurs between the source of the island basalts and the oceanic crust and/or the source of the oceanic tholeiites. In such a contamination model, the minimum values of the non-contaminated end member-producing Terceira volcanics are 20.05 for $^{206}\text{Pb}/^{204}\text{Pb}$, 15.65 for $^{207}\text{Pb}/^{204}\text{Pb}$ and 39.40 for $^{208}\text{Pb}/^{204}\text{Pb}$ and 0.7038 for $^{87}\text{Sr}/^{86}\text{Sr}$.

As discussed above, the contamination does not seem to occur in the magma chamber, where the chemical differentiation takes place, but rather, in a deeper reservoir. If we admit that blobs (hot spots) are the source material of oceanic islands, it is therefore possible that the contamination occurs during the blob ascension. Similar interpretations have been proposed by Tatsumoto¹² for the Hawaiian Islands and by Sun and Jahn¹¹ for Iceland.

This result is critical because it invalidates the possibility of using the straight lines defined in the $^{207}\text{Pb}/^{204}\text{Pb}$ versus $^{206}\text{Pb}/^{204}\text{Pb}$ diagram to infer the age of the differentiation of the mantle source of these basalts as Chase⁵ has done. These straight lines must be considered as mixing lines with no chronometric significance. The Terceira case is by no means unique and our explanation can be extended to St Helena⁴, the Canaries² and certainly to other oceanic islands. As a consequence, only the least contaminated member may be considered representative of the hot spot source. For Terceira this is most probably on the (J) field in the Pb-Pb diagram, in agreement with the general characteristics of oceanic islands (Fig. 3, inset).

We thank C. Gariépy and C. Mercier for help. This is IGP contribution NS/605.

Received 1 June; accepted 26 July 1982.

- Gast, P. W., Tilton, C. R. & Hedge, C. E. *Science* **145**, 1181 (1964).
- Sun, C. S. *Phil. Trans. R. Soc. A* **297**, 409 (1980).
- Hofmann, A. W. & Hart, S. R. *Earth planet. Sci. Lett.* **38**, 44 (1978).
- Grant, N. K., Powell, J. L., Burkholder, F. R., Walther, J. V. & Coleman, M. L. *Earth planet. Sci. Lett.* **31**, 209 (1976).
- Chase, G. G. *Earth planet. Sci. Lett.* **52**, 277 (1981).
- Zbyszewsky, G. *Mem. Acad. Cienc. Lisboa* **12**, 185 (1968).
- Féraud, G., Kaneoka, I. & Allègre, C. J. *Earth planet. Sci. Lett.* **46**, 275 (1980).
- Allègre, C. J., Treuil, M., Minster, J. F., Minster, B. & Albarède, F. *Contr. Miner. Petrol.* **60**, 57 (1977).
- Minster, J. F., Minster, J. B., Treuil, M. & Allègre, C. J. *Contr. Miner. Petrol.* **61**, 49 (1977).
- Provost, A. & Allègre, C. J. *Geochim. cosmochim. Acta* **43**, 487 (1979).
- Sun, S. S. & Jahn, B. M. *Nature* **255**, 527 (1975).
- Tatsumoto, M. *Earth planet. Sci. Lett.* **38**, 63 (1978).
- Dasch, E. J., Hedge, C. E. & Dymond, J. *Earth planet. Sci. Lett.* **19**, 177 (1973).
- O'Nions, R. K. & Pankhurst, R. J. *Earth planet. Sci. Lett.* **31**, 255 (1976).
- Condomines, M. *Geochim. cosmochim. Acta* (in the press).
- Dupré, B. & Allègre, C. J. *Nature* **286**, 17 (1980).
- Manhes, G., Minster, J. F. & Allègre, C. J. *Earth planet. Sci. Lett.* **39**, 269 (1978).
- Birck, J. L. & Allègre, C. J. *Earth planet. Sci. Lett.* **39**, 37 (1978).
- White, N. M., Schilling, J. G. & Hart, S. R. *Nature* **263**, 659 (1976).

Source of the detrital components of uraniferous conglomerates, Quirke ore zone, Elliot Lake, Ontario, Canada

Andrew Robinson* & Edward T. C. Spooner

Department of Geology, University of Toronto, Toronto, Ontario, Canada M5S 1A1.

Large volumes of pyritic quartz-pebble conglomerate in the Elliot Lake district of Ontario contain at least 300,000 tonnes U_3O_8 recoverable at a grade of 0.1% (ref. 1), with much greater tonnages available at lower recovery grades. The Quirke zone alone contains in excess of 224,000 tonnes U_3O_8 at ~0.1% (refs 2-4) and is, accordingly, one of the world's largest known uranium deposits. Situated 40 km north of the North Channel of Lake Huron, 400 km north-west of Toronto, ore conglomerates occur in the Matinenda Formation, locally the basal unit of the Huronian Supergroup, and, although their age is not well constrained, they are probably close to 2,350 Myr old.⁵ Uraninite, the most important primary ore mineral, occurs as poorly rounded to euhedral grains 0.05-0.2 mm across within the matrix between quartz pebbles. While its chemical and morphological characteristics have led most workers to consider that the uraninite is detrital⁵⁻⁷, there has hitherto been no attempt to characterize its source lithology, a matter of considerable significance as regards mineral exploration. This was the aim of the present study. We have examined the mineral and fluid inclusions observed in the quartz pebbles in the conglomerate and conclude that they were derived from a pegmatitic, potassic (alaskitic) granite. We have also demonstrated that in this source lithology, pebble-sized quartz was spatially associated with radioactive minerals, by inference, uraninite. The postulated characteristics of such a source are remarkably similar in several respects to the uraniferous alaskites of the Rössing deposit in Namibia.

At least three features of clastic sediments can provide clues concerning the nature of their source lithologies: (1) internal textures of detrital grains; (2) sediment bulk mineralogy and chemistry; (3) mineral and fluid inclusions in detrital grains. In each case, it is necessary to distinguish features possibly inherited from source lithologies from those that developed subsequent to deposition and within the sediment. The Elliot Lake conglomerates have been significantly deformed through pressure solution⁷ and although many of the deformation textures displayed by quartz clasts can be demonstrated to have originated after deposition, we have been unable to identify such textures that might have been inherited from a source lithology, as sometimes is possible in undeformed sediments⁸. Table 1 lists the minerals present in the conglomerate along with their presumed origins (that is, detrital or authigenic).^{5,7} The detrital mineral suite suggests, in a general way, a source of alaskitic affinities. However, because clastic components of sediments are frequently derived from more than one precursor, the best method of characterizing the source of any particular mineral is to examine its mineral and fluid inclusions. The uraninite grains themselves occasionally contain inclusions of quartz but these are invariably associated with secondary coffinite and are considered to be mostly intrastratal replacement features. Even if some quartz inclusions are inherited, these cannot be distinguished. We have therefore examined mineral and fluid inclusions in ore horizon quartz.

Mineral inclusions that have been introduced into quartz clasts during pressure solution deformation in the conglomerate are readily identifiable through their concentration around pebble margins or by the 'trail' of sericite left in their lee (Fig.

* Present address: Billiton International Metals, BV, 19 Louis Couperusplein, Box 190, The Hague, The Netherlands.

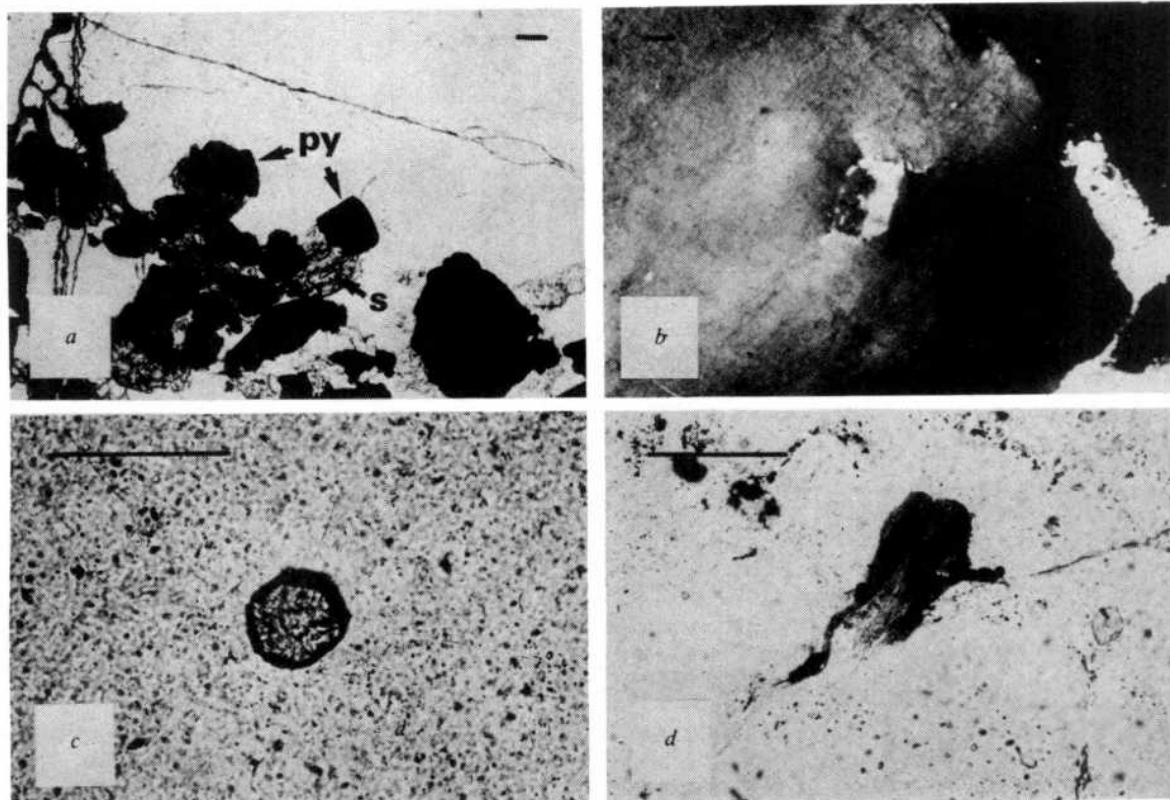


Fig. 1 Mineral inclusions in quartz clasts. *a*, Pyrite euhedra (py) introduced during pressure-solution deformation within the conglomerate. A trail of sericite (s) commonly occurs behind such inclusions. *b*, Euhedral, primary orthoclase inclusion. *c*, Euhedral, primary zircon inclusion. *d*, Altered biotite inclusion. Scale bar, 0.1 mm.

1a). Primary (inherited) inclusions larger than 1–2 μm across are rare. We have identified microcline—the most common, often intergrown with quartz as lithoclasts—orthoclase, zircon and biotite (Fig. 1b–d). In addition, minute yellow needles, abundant in certain clasts, are probably rutile. Although plagioclase has not been recognized as an inclusion, it is very rare as a detrital phase. Neither have uraninite crystals been found in quartz clasts. This mineral suite is very characteristic of alkali-feldspar granites (alaskites) and the grain size of the quartz pebbles (generally <6 cm, but up to 20 cm across) indicates that such a granite would have been in part pegmatitic. In particular, zircon is not known to occur as a hydrothermal mineral in veins, such as have previously been advanced as possible sources for the quartz⁵.

Drawing a distinction between primary and post-depositional features is particularly difficult in the study of fluid inclusions

in quartz and we have therefore subdivided these non-genetically (Table 2). Some type Ia and type IIa inclusions are demonstrably post-depositional in origin as the healed fractures along which they occur can sometimes be traced along their length into other clasts or into sericite-filled fractures. Similarly, the type Ib and IIb inclusions that occur in the rare quartz cement must have been entrapped following sedimentation. The fluid inclusions that are most likely to have been inherited from the source from which the quartz pebbles were eroded are those that contain liquid CO_2 (type IV) and those relatively large (up to 8 μm across) clustered, highly saline inclusions that contain a variety of, and usually several, included mineral phases (type IIb). Although both these types of inclusion are generally rather rare, a suite of this kind is characteristic of granitic rocks in general, including certain pegmatitic alaskites^{9,10}, and is not typical of hydrothermal veins.

The discussion has concentrated on characterizing the lithology that supplied quartz to the conglomerates. This is only relevant to a study of the source of uraninite if it can be demonstrated that the two minerals are co-genetic. A characteristic of ore conglomerates is the common occurrence of smoky quartz pebbles, the smokiness being a feature generally attributed to the formation of free silicon through exposure to radioactive minerals¹¹. Such pebbles are assumed by most workers to have been irradiated after deposition and while this may well have been the case in some instances, several ore samples have been found in which distinctly smoky and milky, or clear, quartz pebbles are juxtaposed (Fig. 2). Serial sections were cut every 8 mm across two such samples from Elliot Lake (Fig. 2a,b) and autoradiographs of the sections revealed, in both cases, no preferential association of radioactivity with the smoky pebble. For comparison, the same experiment was performed on a single similar sample from the Steyn Placer of the Upper Witwatersrand System of South Africa with the same result (Fig. 2c). Smoky quartz pebbles may also occasionally be observed in the very poorly radioactive 'IQ' (intermediate quartzite) between ore reefs. The conclusion that follows is that smokiness

Table 1 The mineralogy of the Elliot Lake conglomerates

Mineral	Abundance	Origin
Quartz	A	D (+ minor cement)
Microcline	A	D
Sericite	A	Au (after feldspar) + some D(?)
Pyrite	A	Au + minor D
Uraninite	C	D
Rutile-brannerite	C	Au (after detrital magnetite-ilmenite)
Monazite	C	D
Zircon	C	D
Uranothorite	R	Au + D
Coffinite	R	Au
Yttrium-uranium-REE-phosphate	R	Au
Chromite	VR	D
+ many other very rare detrital heavy minerals		

A, abundant; C, common; R, rare; VR, very rare; D, detrital; Au, authigenic. Sources: refs 5–7.

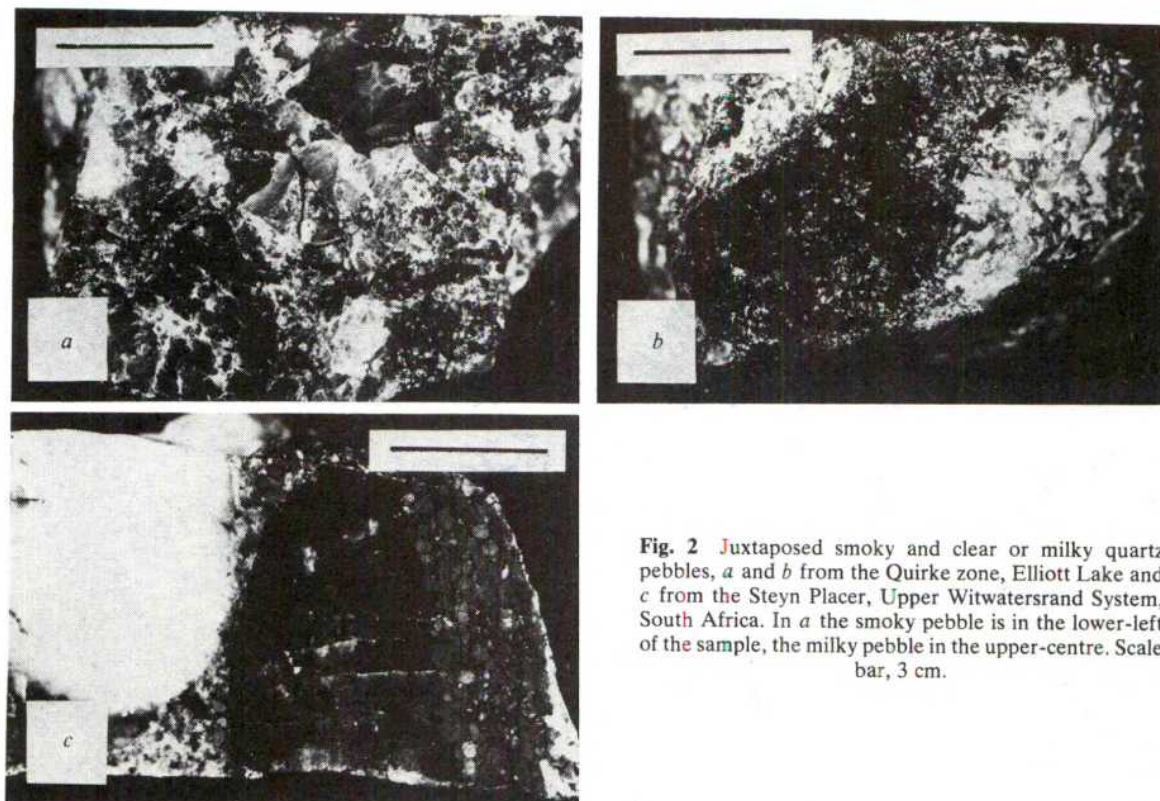


Fig. 2 Juxtaposed smoky and clear or milky quartz pebbles, *a* and *b* from the Quirke zone, Elliott Lake and *c* from the Steyn Placer, Upper Witwatersrand System, South Africa. In *a* the smoky pebble is in the lower-left of the sample, the milky pebble in the upper-centre. Scale bar, 3 cm.

is at least in part a feature inherited from a source lithology in which coarse quartz was associated with radioactive minerals. The most important radioactive detrital mineral preserved in the ore conglomerates is uraninite. (Although monazite may contain substantial amounts of thorium and uranium, these are mainly alteration products that originated during the diagenesis of the conglomerates⁷. Monazite may nonetheless have been fairly radioactive within the source lithology.)

The evidence described above suggests that the major detrital components of the Elliot Lake uraniferous conglomerates were derived from a uraninite-bearing, pegmatitic, alaskitic granite. A comparison can be drawn between this postulated source lithology and the Rössing deposit in Namibia, where Lower Palaeozoic pegmatitic alaskites are being mined for uranium^{12,13}. The pegmatites contain major smoky quartz and perthitic microcline with an overall typical grain size of 0.5–5 cm. There is minor orthoclase, plagioclase and biotite and a

suite of accessory minerals, the most common of which are zircon and monazite. Uraninite, the main primary ore mineral, concentrates with the potassic minerals microcline and biotite. Both its range of grain sizes (0.05–0.1 mm) and its ThO₂ content (~7%) are remarkably similar to the corresponding characteristics of Elliot Lake uraninite grains (grain size 0.05–0.2 mm, ThO₂ content 4–8%)⁶. Clustered, highly saline, as well as CO₂-rich fluid inclusions are characteristic of the smoky quartz in the pegmatites¹⁰. The Rössing deposit contains ~136,000 tonnes U₃O₈ recoverable at a grade of 0.035% (ref. 14). If a deposit of this type and size was eroded and quantitatively deposited as a sediment, a placer uranium deposit with tonnage, grade and petrological characteristics comparable with those of the Quirke zone, Elliot Lake, would have resulted.

A.R. gratefully acknowledges the receipt of a University of Toronto Connaught Scholarship, a Rhodes Scholarship to Canada and an Ontario Graduate Fellowship. E.T.C.S. acknowledges the support of the Natural Sciences and Engineering Research Council of Canada, operating grant A6114. We also thank the staff of the Rio Algom Quirke Mine and the Denison Mine, particularly Russ Gunning; Brian O'Donovan (photographer); and fax (typing services).

Received 13 April; accepted 27 July 1982.

Table 2 Fluid inclusions in quartz in the Elliot Lake conglomerates

Type	Characteristics	Comments
I	H ₂ O ⁺ + small V bubble	Up to 5 µm across; Ia occurs in both detrital and authigenic quartz; Ib most common type in detrital quartz
II	H ₂ O ⁺ + small V bubble + contained mineral(s)	IIa contain a small, usually prismatic daughter mineral and may be cogenetic with most Ia inclusions. Most IIb inclusions are very similar to Ib. Rather rare, clustered, highly saline inclusions with a variety of included solid minerals, up to 8 µm across, are probably not genetically related to type Ib
III	H ₂ O ⁺ + large V bubble	IIIa and IIIb inclusions are very small (2 µm across) and thus very difficult to characterize
IV	CO ₂ ^L ± H ₂ O ⁺ + V bubble ± contained mineral(s)	Up to 8 µm across, variable characteristics. Rather rare
V	Highly irregular	Up to 10 µm long; may represent decrepitated inclusions.

Suffix a after the type number indicates that inclusions are fracture related; suffix b indicates that they are isolated.

- Boyle, R. W. *Geol. Surv. Can. Bull.* **280**, (1979).
- McMillan, R. H. in *Geology, Mining and Extractive Processing of Uranium* (ed. Jones, M. J.) 43–55 (Institute of Mining and Metallurgy, London, 1976).
- Canadian Mines Handbooks 1977–78 to 1981–82* (Northern Miner Press, Toronto, 1977–81).
- Rio Algom Limited Annual Report, 1980 (1981).
- Roscoe, S. M. *Geol. Surv. Can. Pap.* **68–40** (1969).
- Theis, N. J. *Geol. Surv. Can. Bull.* **304** (1979).
- Robinson, A. G. thesis, Univ. Toronto (1982).
- Young, S. W. *J. Sedim. Petrol.* **46**, 595–603 (1976).
- Konnerup-Madsen, J. *Lithos* **12**, 13–23 (1979).
- Cuney, M. *Trans. geol. Soc. S. Afr.* **83**, 39–45 (1980).
- Hurlbut, C. S. & Klein, C. *Manual of Mineralogy*, 19th edn (Wiley, New York, 1977).
- Berning, J., Cooke, R., Hiemstra, S. A. & Hoffman, U. *Econ. Geol.* **71**, 351–368 (1976).
- Von Backström, J. W. & Jacob, R. E. *Phil. Trans. R. Soc. A* **291**, 307–319 (1979).
- Nash, J. T., Granger, H. C. & Adams, S. S. *Econ. Geol.* 75th Anniversary Vol. 63–116 (1981).

Discordant layering relations in the Fongen-Hyllingen basic intrusion

J. R. Wilson & S. Brink Larsen

Department of Geology, University of Aarhus,
8000 Århus C, Denmark

Modal stratification or layering on the scale of centimetres to metres is a common macroscopic feature of many basic intrusions. In some cases this rhythmic layering is accompanied by gradual changes in the composition of mineral solid solutions (cryptic layering) and by the entry and exit of certain minerals (phase layering). These compositional variations, which evidently reflect progressive fractional crystallization, are generally assumed to be orthogonal to rhythmic layering, as predicted by crystal settling models for the origin of layered basic intrusions, and they have been used to establish 'cumulate stratigraphy' of many layered intrusions¹. In the southern part of the synorogenic Fongen-Hyllingen complex², Norway, well developed rhythmic layering is markedly discordant to phase and cryptic layering. Regressions in the cryptic and phase layering that are believed to reflect magma addition are also discordant to the rhythmic layering. These features raise questions as to the stratigraphical significance of phase layering and add to the mounting evidence in favour of *in situ* crystallization for the origin of layered igneous rocks^{3,4}.

The 160 km² Fongen-Hyllingen basic complex² (Fig. 1) is a strongly differentiated layered intrusion situated in the Trondheim region of Norway (11.5° E, 63° N). In spite of being emplaced synorogenically before the culmination of the Caledonian regional deformation and metamorphism⁵, it exhibits sufficient primary features to allow detailed study of the igneous mineralogy and petrology. The present form of the

complex is largely controlled by its proximity to the Tydal synform, a late Caledonian fold⁶ (Fig. 1b).

The intrusive complex consists predominantly of rhythmically layered rocks, sections with thicknesses of ~6,200 and 3,600 m being preserved in the northern (Fongen) and southern (Hyllingen) areas, respectively. The stratigraphically lowest rocks (dunites and troctolites with olivine Fo₈₆ and plagioclase An₈₀) occur in the extreme north. The highest, most evolved rocks (quartz-bearing ferrosyenites with Mg-free mafic minerals and albite) occur in the south along the eastern margin of the Hyllingen area. A broadly tholeiitic parent magma apparently fractionated under moderate, increasing P_{H_2O} , the fractionation trend being broadly intermediate between tholeiitic and calc-alkaline trends^{2,7}. Regressions in cryptic variations and phase layering with stratigraphical height suggest periodic magma addition into a chamber that was probably closed to the removal or exit of magma².

The strike of centimetre-metre scale rhythmic layering in most of the structurally simple Hyllingen area⁸ swings gently from ~N15° E in the north to N25° W in the south, broadly parallel with the lower, western boundary (Fig. 1c). Younging is consistently eastwards and dips average ~40° E. A narrow zone of unlayered, broadly gabbroic rocks occurs along the western margin, whereas in the east, syenitic differentiates vein country rock amphibolites with no intervening marginal facies. The rhythmic layering strikes directly towards the southern margin and there is no evidence of local banking of the layering against the wall of the intrusion. Approaching the southern margin, the intensity of rhythmic layering decreases over a distance of ~150 m until, in the immediate vicinity of the contact, layering is absent. The presence of many country rock hornfels inclusions (pendants?) and zones of ferrodioritic and ferrosyenitic differentiates entirely surrounded by hornfels in the extreme south-east confirm that the original wall and/or roof of the intrusion are preserved here.

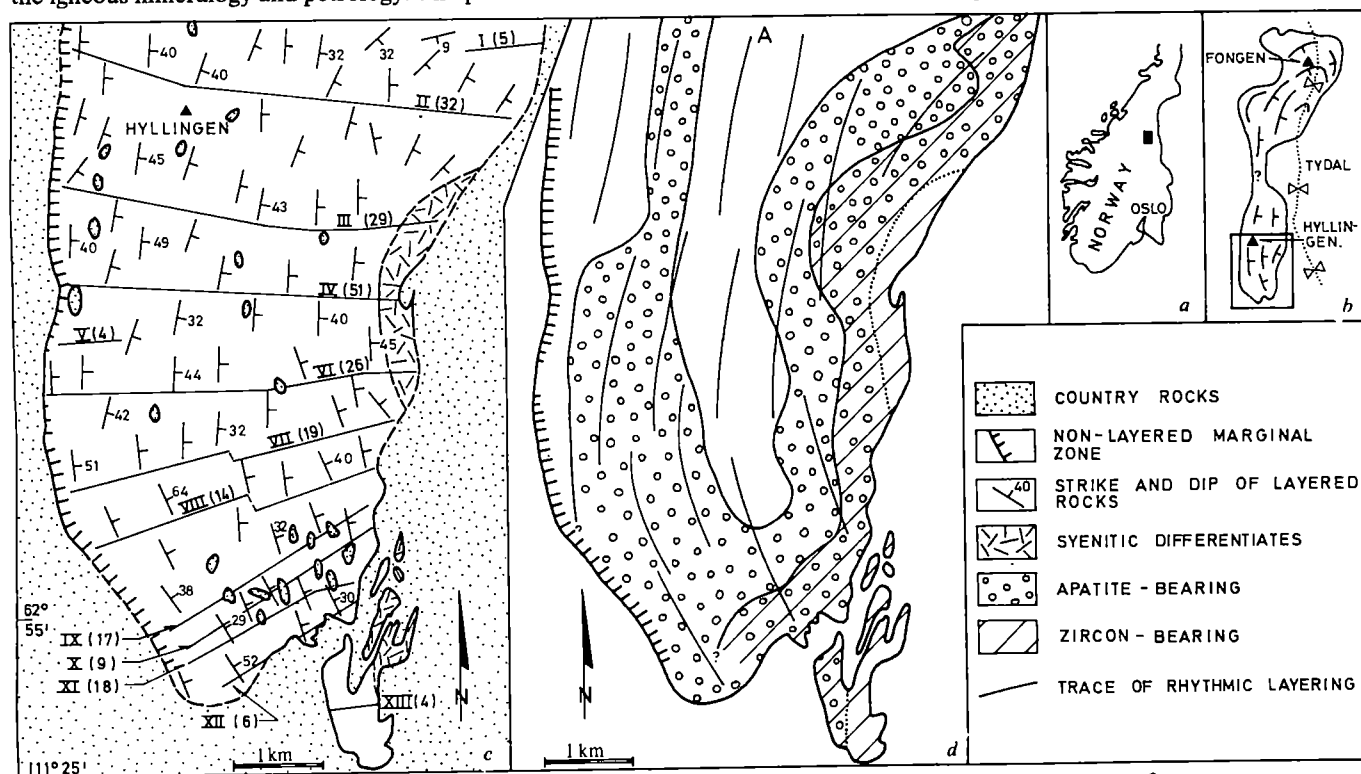


Fig. 1 a, Map showing location of b in Norway. b, Outline map of the Fongen-Hyllingen complex after Wilson *et al.*² showing generalized orientation of the rhythmic layering and the trace of the hinge zone of the Tydal synform. Location of c and d is boxed. c, The southern part of the Fongen-Hyllingen complex. Rhythmic layering strikes directly towards the southern intrusive contact. A thickness of about 2,700 m is exposed in profile IV. Number of samples from each profile is shown in parentheses (total of 234 samples). Average sample density is about 1 per 110 m except for profile IV (1 per 53 m). Profile IV is essentially equivalent to profile IIC in Fig. 3 of ref. 2. Faulting is minor and has no significant influence on the feature described here. d, Distribution of apatite and zircon in the Hyllingen area based on samples from profiles I-XIII in c. Note strong discordance between the curves showing the entry/exit of these phases and the trace of the rhythmic layering. Detailed sampling has shown that apatite is absent in the final differentiates, in the uppermost ~100 m of profile IV. The final, most fractionated liquid must have been almost completely depleted in phosphorus.

In a profile normal to the strike of the rhythmic layering ending in the most fractionated rocks along the eastern margin, such as profile IV in Fig. 1c (which has a stratigraphical thickness of ~2,700 m) the early crystallizing phases in the lowest layered rocks are olivine (Fo₄₀), plagioclase (An₄₅), Ca-poor pyroxene, Ca-rich pyroxene and Fe-Ti oxides. The sequence of entry (+) and exit (-) of early crystallizing phases in this profile is apatite (+), apatite (-), calcic amphibole (+), apatite (+), biotite (+), zircon (+), quartz (+), Ca-poor pyroxene (-), K-feldspar (+), olivine (-), allanite (+) and apatite (-). The areal distribution of certain phases has been established through petrographical study of 234 samples from 13 profiles (Fig. 1c, d). Lines defining the entry and exit of cumulus apatite and cumulus zircon are markedly discordant to the rhythmic layering and appear to be more closely related to the exposed shape of the intrusion. For example, cumulus zircon enters at a stratigraphical level some 1,200 m lower in profile XI than in profile VI, these profiles being from ~2,300 to 3,000 m apart. Following the strike of the rhythmic layering from point A in Fig. 1d southwards, the compositions of plagioclase and olivine change from about An₆₀ and Fo₇₃ in profile II to about An₃₀ and Fo₁₀ in profile XII. Thus the rocks become increasingly differentiated along the strike of the rhythmic layering as the margin is approached. It would appear that differentiation varied from place to place within the intrusion and was probably influenced by the distance from the roof and wall. Consequently concordance between cumulate stratigraphical zones and rhythmic layering, implicit in the use of phase layering as stratigraphically significant, akin to zone fossils in sedimentary sequences, cannot be assumed for layered intrusions. Similar features have been indicated for the Skaergaard intrusion^{3,9} and favour a model involving at least partly diffusion-controlled *in situ* crystallization rather than crystal settling for the origin of the Fongen-Hyllingen complex.

Abrupt regressions in phase and/or cryptic layering are commonly ascribed to the influx of fresh magma. Such a reversal is represented, for example, in the lower part of profile III by the exit of apatite accompanied by composition changes in plagioclase from about An₄₀ to An₅₅ and in olivine from about Fo₂₀ to Fo₅₀ (ref. 2 and unpublished results). However, work in progress has revealed that this major regression is not an abrupt event. After the disappearance of apatite in profile III, the compositions of solid solution minerals gradually become less evolved over a thickness of some 300 m, after which they again begin to evolve to lower temperature compositions. The regression indicated by the exit of apatite appears more or less concordant with the rhythmic layering in the north but becomes increasingly discordant to the south (Fig. 1d).

Discordance between rhythmic layering and the phase and cryptic layering raises the question as to which, if any, of them represents a constant time surface during crystallization. Compared with the time it takes for a large layered intrusion to crystallize, magma replenishment is generally believed to be a relatively rapid process¹⁰. If this is so, then discordant relations between a major reversal and rhythmic layering imply that the plane of rhythmic layering probably does not represent a constant time surface. Alternatively, the nature of this discordance in the southern Hyllingen area (Fig. 1d) could indicate that replenishment was a slow process, the magma chamber being gradually filled from a direction with a northerly component.

The Carlsberg Foundation of Denmark provided financial support for field work. Dr W. J. Wadsworth criticized the manuscript.

Received 26 April; accepted 23 July 1982.

1. Wager, L. R. & Brown, G. M. *Layered Igneous Rocks* (Oliver & Boyd, Edinburgh, 1968).
2. Wilson, J. R., Esbensen, K. H. & Thy, P. *J. Petrol.* **22**, 584-627 (1981).
3. McBirney, A. R. & Noyes, R. M. *J. Petrol.* **20**, 487-554 (1979).
4. Campbell, I. H. *Lithos* **11**, 311-323 (1978).
5. Olesen, N. Ø., Hansen, E. S., Kristensen, L. H. & Thyrsted, T. *Leid. geol. Meded.* **49**, 259-276 (1973).
6. Wilson, J. R. & Olesen, N. Ø. *Norsk. geol. Tidsskr.* **55**, 423-439 (1975).
7. Wilson, J. R., Esbensen, K. H. & Thy, P. *Nature* **290**, 325-326 (1981).
8. Nilsen, O. *Norsk. geol. Tidsskr.* **53**, 213-231 (1973).
9. Naslund, H. R. *Yb. Carnegie Instn. Wash.* **75**, 640-644 (1976).
10. Irvine, T. N. in *Physics of Magmatic Processes* 325-383 (Princeton University Press, 1980).

Arsenic in Napoleon's wallpaper

David E. H. Jones

Department of Physical Chemistry, The University of Newcastle upon Tyne, Newcastle upon Tyne NE1 7RU, UK

Kenneth W. D. Ledingham

Department of Natural Philosophy, University of Glasgow, Kelvin Laboratory, East Kilbride, Lanarkshire G75 0QU, UK

Napoleon's illness and death on St Helena have been the subject of controversy. His symptoms have been compared with those of arsenic poisoning¹⁻³, and arsenic has been found in surviving samples of his hair⁴⁻⁸. During the nineteenth century, many people were accidentally poisoned by arsenical vapours from wallpaper⁹⁻¹¹. Accordingly, it is an intriguing speculation that Napoleon may have ingested arsenic from his wallpaper. After presenting this speculation on a radio broadcast, one of us (D.E.H.J.) was offered an original sample of wallpaper from Napoleon's residence on St Helena. We report here that X-ray fluorescence measurements on this paper reveal enough arsenic to be capable of causing illness but probably not death. So if Napoleon was poisoned by arsenic, it may have come not from deliberate administration but from his wallpaper.

After Napoleon Bonaparte's death in May 1821, autopsy revealed an enlarged liver and a stomach lesion¹². However, later neutron activation analyses of his hair⁴⁻⁸ have found abnormal quantities of arsenic in some (but not all) samples from his period on St Helena. Forshufvud and Weider have argued that he was the victim of a poisoning conspiracy¹⁻³, but arsenic was widely used for many medical, cosmetic and environmental applications during the nineteenth century, so he may have ingested it from some quite innocent source.

One possible source is paint or wallpaper. The green copper arsenite pigments (Scheele's green, and Paris or emerald green) were introduced in about 1780, and were soon widely used in paints and wallpapers. By 1815 they were known to be poisonous, and throughout the nineteenth century many people were made ill or even killed by arsenic from their wallpaper⁹⁻¹¹. Not until 1983 was the mechanism of the process elucidated¹³. On damp wallpaper, many moulds (for example, *S. brevicaulis*) can metabolize arsenic compounds to volatile, poisonous arsenic trimethyl, which is released into the air of the room.

Our sample of Napoleon's wallpaper had been preserved in an old family scrapbook. It measured about 55 × 60 mm, with a beige coating carrying a 40-mm diameter flock-decorated rosette, mainly brownish but with bright green areas (Fig. 1).

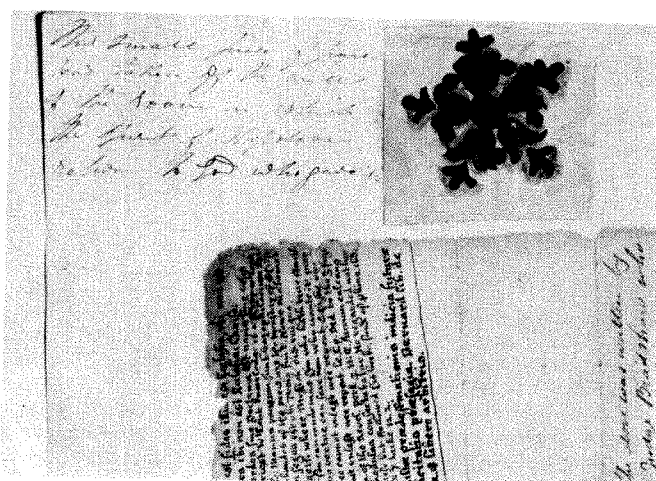


Fig. 1 A sample of Napoleon's wallpaper preserved in an old family scrapbook.

Table 1 Metal content of historical wallpapers, determined by X-ray fluorescence spectroscopy

Element	X-ray observed	Metal content (as the element) (g m^{-2})				
		Napoleon's wallpaper			Craggside papers	
		a	b	c	1	2
Cu	K α	4.6	0.03	0.28	3.8	3.5
As	K α	1.5	0.04	0.12	6.5	6.2
Pb	L β_1	19	0.3	1.3	1.9	0.4
Ca	K α , K β	6.6	14	14	7.5	17
Fe	K α	0.15	0.4	0.4	0.07	0.06

a, Rosette area; b, beige area surrounding rosette; c, mean composition of the original wallpaper, deduced by weighting the compositions of rosettes and beige background according to their relative areas.

It had been removed from the drawing room of Longwood House (the room in which Napoleon died) and pasted into the scrapbook in May or June of 1825. At the time, the room had a cream wallpaper with blue stars¹⁴; the brownish rosette must be one of the stars, faded over the years. For comparison, other samples of nineteenth century wallpapers were sought from the National Trust. Two specimens of 1864, from 'Craggside', Lord Armstrong's country house in Northumberland, proved highly arsenical.

The wallpapers were analysed primarily by X-ray fluorescence spectroscopy (XRF). Our equipment used a ^{147}Pm source of 1.5×10^5 Bq, a Si(Li) detector of area 80 mm^2 , and a 2,000-channel analyser covering the range 0–60 keV; all elements from potassium to lead show either K or L X-ray fluorescence within this range. The spectra of the wallpapers were dominated by peaks due to copper, arsenic, lead, calcium and iron.

The spectra were calibrated by comparing them with those of calibration papers made up to contain known amounts of these metals. Interpretation was complicated by the presence of lead pigments in the papers. The L α line of lead almost coincides with the K α line of arsenic, and the lead components had to be subtracted from the recorded spectra before the arsenic peaks could be measured. Furthermore, a dense layer of lead pigment in the rosette of Napoleon's wallpaper attenuated the radiation from the metal pigments beneath it. They were estimated by reversing the paper in its mount and irradiating it from the back. The final results are shown in Table 1.

Matrix and attenuation effects, inevitable in the XRF analysis of heterogeneous samples, make the results uncertain by ± 20 –30%. Within these limits, the XRF results are supported by neutron and photon activation analyses of pigment flakes detached from Napoleon's wallpaper, and chemical analysis of a section of Craggside 1. The average composition of Napoleon's wallpaper (Table 1) was derived by taking the rosettes to be 12 cm^2 in area, and spaced¹⁴ at one per 225 cm^2 on the beige background. On this basis, the rosettes contribute 0.08 g m^{-2} of arsenic, and the beige background 0.04 g m^{-2} ; a total of 0.12 g m^{-2} .

With this fairly mild arsenic loading, Napoleon's wallpaper could not have posed a serious threat to his life, but it may well have contributed to his illness. In suitably damp and mouldy conditions, highly arsenical wallpapers like Craggside 1 and 2 could cause illness or even death in a few days or weeks^{15–17}, but even much less arsenical papers could cause notable ill-health. In 1893, a detailed study¹¹ showed that wallpapers containing 0.6 – 0.015 g m^{-2} of arsenic could cause illness, and suggested that even 0.006 g m^{-2} could be hazardous. The safety standards of the time¹⁸ recommended 0.001 – 0.005 g m^{-2} as a safe upper limit. Thus, our finding of 0.12 g m^{-2} of arsenic in Napoleon's wallpaper is toxicologically significant, particularly in view of the arsenic found in his hair by several neutron-activation studies.

These studies, on hair samples spanning 1816–21, reported irregularly fluctuating levels of arsenic, as would be expected from a source like damp and mouldy wallpaper. Fluctuations with humidity, temperature, ventilation, and the amount of

time that Napoleon spent in the relevant rooms, would be expected. Longwood was notoriously damp¹⁹, and many of its other inhabitants also suffered from its 'unhealthy atmosphere'¹.

The present sample of Napoleon's wallpaper was only installed¹⁴ in 1819, so cannot have contributed to his arsenic intake before that time. This report does, however, demonstrate that hazardously arsenical wallpaper was available on St Helena during Napoleon's captivity, and in one instance at least was used to decorate his residence. Accordingly, conspiracy theories need not be invoked to explain arsenic found in his hair.

Received 17 May; accepted 10 August 1982.

1. Forshufvud, S. *Who Killed Napoleon?* (Hutchinson, London, 1962).
2. Forshufvud, S. & Weider, B. *Assassination at St Helena* (Mitchell, Vancouver, 1978).
3. Weider, B. & Hapgood, D. *The Murder of Napoleon* (Robson Books, London, 1982).
4. Smith, H., Forshufvud, S. & Wassen, A. *Nature* **194**, 725–726 (1962).
5. Forshufvud, S., Smith, H. & Wassen, A. *Archs Tox.* **20**, 210–219 (1964).
6. Leslie, A.C.D. & Smith, H. *Archs Tox.* **41**, 163–167 (1978).
7. Forshufvud, S., Smith, H. & Wassen, A. *Nature* **192**, 103–105 (1961).
8. Lewin, P. K., Hancock, R. G. V. & Voynovich, P. *Nature* **299**, 627–628 (1982).
9. Challenger, F. *Chem. Rev.* **36**, 315–361 (1945).
10. Hunter, D. *Diseases of Occupation*, 348, 363 (Hodder & Stoughton, London, 1978).
11. Sanger, C. R. *Proc. Am. Acad. Arts Sci.* **29**, 148–177 (1893).
12. Hillemand, P. *Pathologie de Napoleon*, 119–187 (La Palatine, Paris, 1970).
13. Gosio, E. *Archs Ital. Biol.* **18**, 235–298 (1893); *Ber. dt. chem. Ges.* **30**, 1024–1026 (1897).
14. *Longwood Old House* (official pamphlet) 8–9 (1960).
15. Huss, H. Z. *Hyg.* **76**, 361 (1914).
16. Metcalfe, J. B. *Lancet* **ii**, 535–536 (1860).
17. Orton, T. *Lancet*, **ii**, 516–518 (1862).
18. Brunton, T. L. B. *med. J. I*, 1218–1221 (1883).
19. Korngold, R. *The Last Years of Napoleon*, 84–85 (Harcourt, Brace & Co., New York, 1959).

Napoleon Bonaparte—no evidence of chronic arsenic poisoning

Peter K. Lewin, Ronald G. V. Hancock* & Paul Voynovich

The Hospital for Sick Children, Toronto, Ontario, Canada M5G 1X8

* Slowpoke Reactor Facility, University of Toronto, Toronto, Ontario, Canada M5S 1A4

Napoleon Bonaparte died in exile on the island of St Helena in 1821 at the age of 51. An autopsy by his physician, Autommarchi, in the presence of Sir Thomas Reade, some staff officers and eight medical men revealed a cancerous growth of his stomach¹. But mainly on the basis of high levels of arsenic detected in several samples of his hair² it has been suggested, most recently by Hapgood and Weider³, that Napoleon was poisoned by arsenic. We have analysed a different sample of Napoleon's hair and find an almost normal arsenic content but elevated antimony.

A lock of hair was obtained by Major Poppleton, one of the staff officers on St Helena. Major Poppleton gave this hair sample to his uncle, whose relatives retained it until the First World War (Fig. 1). It was then obtained by the late Mr Gilbert William Plenty, who gave it to his son, Mr Albert William Plenty of Toronto, in whose custody it now is. The specimen consists of a well preserved lock of hair, chestnut in colour (Fig. 1). Gross and microscopic examination have revealed no structural abnormalities.

A sample (12 mg) of the hair was placed in a 1 ml polyethylene vial and irradiated in the Slowpoke Nuclear Reactor of the University of Toronto for 16 h at a thermal neutron flux of $2.5 \times 10^{11} \text{ N cm}^{-2} \text{ s}^{-1}$ for neutron activation analysis.

After a 7-h delay to allow short-lived radioisotopes to decay away, the hair was transferred to a clean polyethylene vial and re-weighed. The sample was then analysed for elements producing radioactive half lives of 12.5–67 h (K, Na, As, Br, Au and Sb) by counting the γ rays emitted from the samples with a 12.7% relative efficiency Ge–Li detector coupled to a hardwired 4196 channel (Canberra) multichannel analyser. The Slowpoke

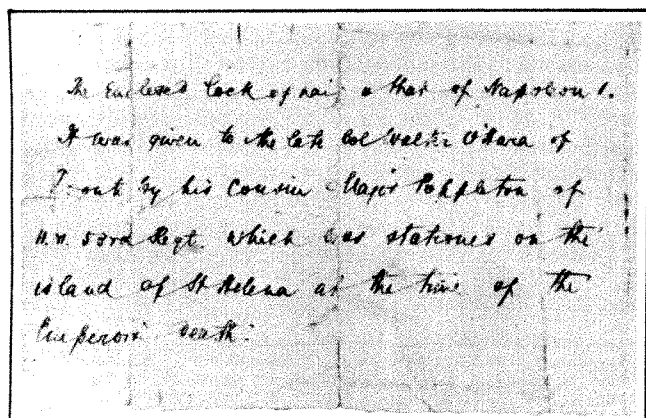


Fig. 1 Lock of hair from Napoleon I, with accompanying note.

reactor has the advantage of maintaining a reproducible and constant ($\pm 1\%$) neutron flux over the long term. The analytical system was calibrated previously with several standard reference materials, including NBS Coal (SRM 1632) and Fly Ash (SRM 1633), and with dilute solutions of arsenic salts. Stability of the specific activity produced by analysing various arsenic standards over nearly 6 yr guaranteed the reliability of the calibration.

The sample was counted for 5–50 min to obtain varying counting statistics. The concentrations of the elements K, Na, As, Br, Au and Sb in the hair were then calculated by comparing the net γ -ray peak areas with standard values. After preliminary counting, the hair was washed four times with absolute ethanol to remove surface contamination and was recounted several times over the next few days. The washing had no apparent effect on the elemental concentrations determined.

Table 1 shows that our sample of Napoleon's hair does not contain high levels of arsenic (maximum control range 0.7–1 p.p.m.), but does contain a moderately increased level of antimony (maximum control range 1–1.5 p.p.m.). Antimony (Sb) is of interest because it was a component of many medications of that time, particularly tartar emetic.

Previous investigations suggested that the maximal levels of arsenic were located 4 to 9 cm from the proximal end of a 13-cm length of hair². The average hair length of our sample, which measured 8 cm, was from the distal end, and therefore may not have recorded recent events. However, it would have contained high average levels of arsenic had there been chronic poisoning.

Improved technology in the past 20 years compared with that used in the original investigations^{2,4} allows us now to clearly separate the radioisotopes of arsenic, antimony and bromine. The previous analytical method used⁴ was not tested for the efficiency of separation of antimony and bromine from arsenic. Lack of such separation would tend to give apparent high

arsenic levels. In addition, our 12 mg hair sample from Napoleon could be a more representative sample, compared with the individual hair samples of less than 0.5 mg reported by Smith *et al.*².

We therefore conclude that Napoleon Bonaparte did not die of chronic arsenic poisoning.

Received 24 May; accepted 10 August 1982.

1. De Bourienne, L. A. F. *Mem. Napoleon Bonaparte* Vol 4, 427–428 (Grolier Society, London, 1885).
2. Smith, H., Forshufvud, S. & Wassen, A. *Nature* **194**, 725–726 (1962).
3. Weider, B. & Haggood, D. *The Murder of Napoleon* (Methuen, New York, 1982).
4. Smith, H. *Analyt. Chem.* **31**, 1361–1363 (1959).
5. Takeuchi, T. *et al. Radioanalyt. Chem.* **70**, 29–55 (1982).

The formation of isomaltulose by immobilized *Erwinia rhapontici*

Peter S. J. Cheetham, Carol E. Imber* & Jamie Isherwood*

Tate & Lyle Group Research & Development, Philip Lyle Memorial Research Laboratory, PO Box 68, Whiteknights, Reading RG6 2BX, UK

Recently the potential of immobilized cells for the production of biochemicals has become recognized^{1,2}. Here we describe a simple, stable, continuous method of converting concentrated sucrose solutions into isomaltulose using columns of *Erwinia rhapontici* cells entrapped in alginate gel pellets, which exemplifies several strategies for maximizing the yield and stability of immobilized cells. This method has been successfully operated on a pilot-plant scale. The isomaltulose has possible applications, which are at present being evaluated by potential users, as a non-cariogenic bulking agent in foodstuffs and pharmaceuticals^{3–5}. Little enzyme activity or viability was lost during immobilization and surprisingly high yields of isomaltulose were obtained. The enzyme associated with the cells was stabilized by immobilizing in alginate rather than other support materials; by using structurally intact non-growing but not necessarily viable cells rather than isolated enzyme, disrupted cells or growing cell preparations; and most dramatically, by using concentrated pure sucrose as substrate and by maintaining complete conversion of the sucrose into isomaltulose. Thus the immobilized cells were about 350 times more stable than free cells, a half life of about 8,600 h being achieved.

Isomaltulose, commonly referred to as palatinose, is a reducing disaccharide (6-O- α -D-glucosylpyranosyl-D-fructofuranose) of about one-third the sweetness of sucrose but which otherwise has very similar physical and organoleptic properties to sucrose. It is believed to be non-cariogenic since very much less acid and glucan are formed by *Streptococcus mutans* from isomaltulose than from sucrose³. Several microorganisms have been reported to form isomaltulose^{6–10}; among them is *E. rhapontici* (NCPB 1578), a cause of crown rot of rhubarb, which we have selected to use on the basis of the stability of its isomaltulose-forming enzyme when the cells are used in a non-growing immobilized form.

The adaptive significance of isomaltulose formation by *E. rhapontici* is unclear. However, this bioconversion may be a method of irreversibly sequestering a carbon and energy source in a form less available to the host plant, and to other organisms that could otherwise compete successfully with the *Erwinia* cells for sucrose. Thus isomaltulose may have a similar useful role to the 3-ketosucrose formed by *Agrobacterium tumefaciens*^{11,12}, and the gluconate and 2-oxoglucose produced by *Pseudomonas aeruginosa*^{13,14}. Such a mechanism would be facilitated by the isomaltulose-forming enzyme being stabilized by sucrose, and by the ability of non-viable cells to continue

Table 1 Element concentration in Napoleon's hair

Element	Isotope	Half life (h)	γ -Ray energy (keV)	Concentration (p.p.m.)	Control ⁵
K	⁴² K	12.5	1,225	750 \pm 100	0.94–310
Na	²⁴ Na	15.0	1,369	1,100 \pm 100	0.4–850
Br	⁸² Br	35.5	777	4.2 \pm 0.6	0.77–490
As	⁷⁶ As	26.4	559	1.4 \pm 0.2	0.079–0.67
Au	¹⁹⁸ Au	64.7	412	0.45 \pm 0.06	0.0006–1.36
Sb	¹²² Sb	67.1	564	5.7 \pm 0.6	0.016–1.30

Standard deviation, 2σ (95% confidence level).

*Present addresses: Searle Pharmaceuticals (G. D. Searle & Co. Ltd), Lane End Road, High Wycombe, Bucks, UK (C.E.I.); Lavender Cottage, 1 Longreach, W. Horsley, Surrey, UK (J.I.).

to produce isomaltulose to the advantage of the remaining viable cells.

Cells were grown in an undefined medium and immobilized¹⁵⁻¹⁷ so as to enable continuous use of the enzyme and to prevent contamination of the product by the cells (Fig. 1). The enzyme associated with the cell is a previously undescribed sucrose-specific, direct glucosyl transferase which was most active at pH 7.0 and 30°C, and had a K_m towards sucrose of 0.35 M. Activity was not enhanced by the presence of nitrogen, trace nutrients or other sugars. CO₂ and H₂, acids and a disaccharide believed to be 1-*O*- α -D-glucosylfructose⁸ were produced as side-products.

Immobilization in alginate stabilized the isomaltulose-synthesizing activity of intact cells and of a cell-free extract of the *Erwinia* cells (Table 1). Alginate was the most desirable support because in addition to its cheapness, lack of toxicity, mechanical strength and the simplicity of the immobilization method the cells lost only 5-10% of their activity on immobilization. Thus, alginate provides a favourable microenvironment for the cells, perhaps because it simulates the natural capsular polysaccharides produced by *Erwinia*, which are thought to have a protective role¹⁸. Of a variety of alternative immobilization techniques that we tested, none approached the combination of half life and efficiency of conversion achieved with alginate.

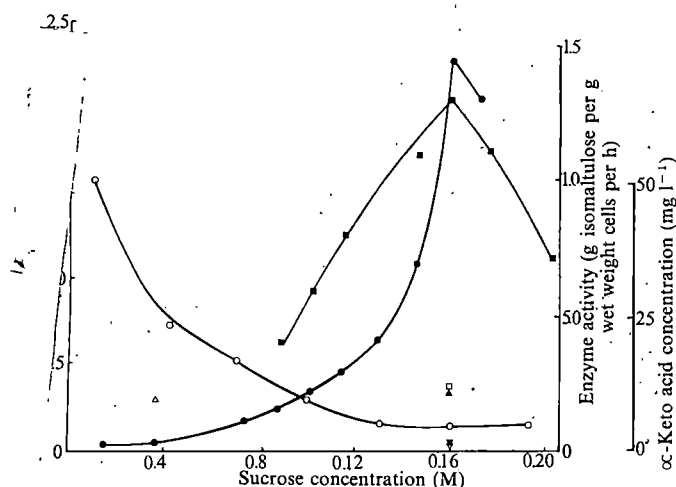


Fig. 1 The effect of sucrose concentration on the activities of free and immobilized *E. raphontici* cells and on the operational stability of the immobilized cells. *Erwinia* cells were grown, immobilized and used in columns as described in Table 1 legend. Immobilized cells (■) were shaken at 30°C with sucrose solutions for initial rate determinations. For the determination of operational stabilities substrate solutions of varying sucrose content were pumped up columns using Watson-Marlow pumps such that an initial degree of conversion of sucrose to total products of 70% was achieved in each column (●) once a steady-state had been reached after 1 day's operation. Each column was run continuously for several months when necessary and half-life values calculated by linear regression analysis. The concentration of isomaltulose in the assay solutions or columns eluates measured at 24-h intervals by assaying the reducing sugar concentration²³, or by HPLC using a Spherisorb 5 μ silica column, which had been treated with acetone/water/tetraethylpentamine (80/20/0.01). This was also used as the eluting solvent. Sugars in the eluate were detected using a refractive index detector (Applied Chromatography Systems Ltd). Viable cells counts were made by grinding the pellets in phosphate-buffered saline (PBS), plating serial dilutions of the PBS extracts onto nutrient agar, incubating at 30°C for 24 h and then counting the numbers of colonies formed. Total cell measurements were calculated from A_{540} readings of the PBS extracts made versus a suitable blank solution. α -Keto acids were measured as pyruvate equivalent by an adaptation of an existing method²⁴ (○). This method had an analytical threshold of 5 mg acids per l of column eluate. On one occasion affination syrup diluted to 1.6 M sucrose with deionized water and adjusted to pH 7.0 was supplied to a column of immobilized cells (□). On another 0.365 M sucrose pH 7.0 buffered with 100 mM HEPES buffer was supplied to a column (Δ). 76% and 95% conversion of the sucrose was achieved respectively. The continuous stirred reactor (▲) consisted of a stirred vessel containing 200 ml of pellets and 300 ml of substrate which was maintained at pH 7.0 by the addition of 0.1 M NaOH using a PHM64 pH meter and TTT60 titration unit (Radiometer). Substrate was pumped into the reactor at a rate of 0.016 l h⁻¹ and samples of the reactor contents pumped out at the same rate.

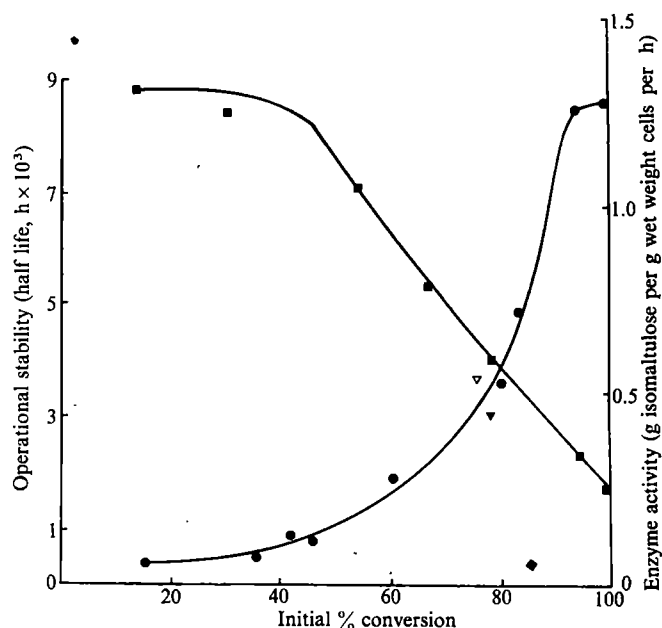


Fig. 2 The effect of the degree of conversion of sucrose into products on the operational stability of columns of immobilized *Erwinia* cells. Columns of immobilized cell pellets were prepared and operated as described in Table 1 and Fig. 1 legends with 1.6 M sucrose pH 7.0 pumped up the columns at various flow rates. The rate of decline in the activity of the immobilized cells was monitored while a constant degree of conversion was maintained by continuously decreasing the flow rate. The stability and activity of the immobilized cells are represented by ● and ■ respectively. Experiments were also carried out in the same manner in which benzylpenicillin (▼) or chloramphenicol (▽) were included in the substrate at concentrations of 500 μ g ml⁻¹.

The immobilized cells were both most active and most stable when high concentrations of sucrose were used, reaching a maximum at 1.6 M (Fig. 1). However, it was only the immobilized and not the free cells that were markedly stabilized by the concentrated sucrose solutions, although similar effects were observed when both high and low degrees of conversion of sucrose into isomaltulose were achieved (Table 1, Fig. 1). The use of concentrated sucrose was also advantageous because the equilibrium between isomaltulose and sucrose favoured the formation of isomaltulose. Also concentrated sucrose reduced the formation of gaseous and acidic side-products (Fig. 1), the growth of contaminant microorganisms and the activity of endogenous proteases, while minimizing the size of equipment and volumes of syrup that had to be manipulated, and the volume of water that had to be removed before crystallization.

The extent of conversion of sucrose into isomaltulose could be maximized (<1% w/v sucrose remaining) by decreasing the flow-rate of substrate up the column, thus increasing its contact time with the cells. Increases in the extent of conversion were accompanied by decreases in activity as the reaction became first order with respect to the substrate concentration, and also by a marked increase in the stability of the immobilized cells (Figs 2, 3). This enhanced stability is probably due to diffusional restrictions on the immobilized enzyme activity especially as stability could be further increased by raising the concentration of entrapped cells.

High yields of isomaltulose were obtained first by screening for an organism resistant to excess substrate and product inhibition. Second, a concentrated substrate lacking nutrients was used, such that substrate was not diverted into cell growth, and other enzymes of the cells that tend to produce side-products such as acids (Fig. 1) are inhibited. Third, the use of packed-bed reactors, in which virtual plug-flow of substrate is achieved by using even-sized, spherical, evenly packed immobilized cell pellets¹⁶, encouraged complete conversion of substrate, plug-flow being impossible with free cells or stirred reactors¹⁹.

In the above conditions the immobilized cell columns yielded around 0.75 g isomaltulose per g of sucrose supplied and had an initial activity of about 0.2 g isomaltulose produced per g

wet weight of cells per h, equivalent to 40 g isomaltulose produced per l column volume per h. The activity decayed very slowly with a half life of 1 yr (Fig. 2, Table 1). Small, white, needle-shaped, but virtually pure crystals of isomaltulose could be recovered by evaporating the column eluate under vacuum at 60 °C until an isomaltulose concentration of 2.0 M was reached, seeding the supersaturated solution as it cooled and collecting the resulting crystals in a basket centrifuge. This purification and recovery of the crystals was greatly facilitated by the use of concentrated sucrose solutions as substrate and by the achievement of high degrees of conversion by the cells.

Rapid loss of the enzyme activities of non-growing microorganisms often limits their useful life as biosynthetic agents, particularly of secondary metabolites. Enzymes vary considerably in stability and very little is understood of the causes of inactivation and of the optimum physiological state of cells when they are to be used in a non-growing form. Nevertheless the stability of the *Erwinia* cells used here is surprisingly high considering that the normal metabolic turnover of enzymes usually rises substantially when growth ceases^{20,21}, and some enzymes disappear at rates greater than the overall rate of protein turnover²². Stabilization is not due to product stabilization by the isomaltulose (Table 1), but may be connected with the cells' low rate of endogenous metabolism as illustrated by the decreased rate of acid formation (Fig. 1), or with their plasmolysis by the high sugar concentrations. The purity of the sucrose used was also important, as both the activity and stabil-

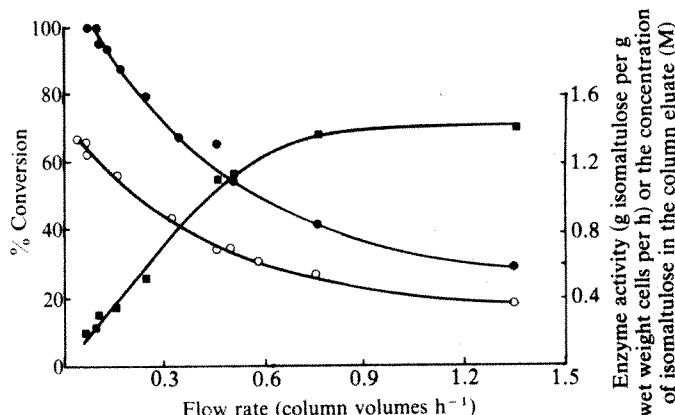


Fig. 3 The influence of the residence time of substrate in the column on the activity of the immobilized *Erwinia* cells (●) and the degree of conversion of sucrose to products (○). *E. rhapsodica* were grown and immobilized, and the columns operated as described in Table 1 legend. The flow rate through the column is expressed as the number of empty column volumes (ecv) of substrate pumped through the column per h where an empty column volume represents the volume of the pellets plus the interstitial fluid. Thus a flow rate of 0.08 ecv h⁻¹ through the 0.035-l columns used in these experiments gives a residence time of 12.5 h. The molar isomaltulose concentration in the column eluate is expressed as ○—○.

Table 1 The operational stabilities of the isomaltulose forming activities of various *E. rhapsodica* preparations

Type of preparation and conditions of use	Stability (half life, h)
Free cells maintained in exhausted growth medium	335
Free cells used batchwise in 0.12 M sucrose	25
Free cells used batchwise in 1.60 M sucrose (28% conversion) [†]	41
Immobilized cells used with 0.12 M sucrose (70% conversion)	55
Immobilized cells used with 1.60 M sucrose (70% conversion)	2,265
Immobilized cells used with 1.60 M sucrose (99% conversion)	8,625*
Immobilized cell debris (45% conversion)	190
A cell-free extract obtained by osmotically shocking cells used batchwise	26
An immobilized cell-free extract (81.5% conversion)	620
Immobilized cells supplied continuously with growth medium (90% conversion)	76
Immobilized cells supplied with 1.02 M isomaltulose	300

Erwinia rhapsodica (NCPBB 1578, ATCC 29283) a Gram-negative facultative anaerobe was grown in shake flasks at 30 °C containing 200-ml aliquots of medium consisting of sucrose (40 g l⁻¹), peptone (10 g l⁻¹) and beef extract (4 g l⁻¹). Once stationary phase had been reached after about 70 h the cells were collected by centrifuging at 23,000g for 20 min at 30 °C. A yield of approximately 7 g wet packed cells per l of medium was obtained (~2 × 10⁹ viable cells per g wet weight). The cells were evenly dispersed as a 20% (wet w cell/v) slurry in a freshly prepared 5% (dry w/v) sodium alginate solution (pH 6.0), which was then immobilized by extruding dropwise, gelation taking place at room temperature in a 0.1 M CaCl₂ solution (pH 6.5) to form even-sized, smooth, spherical pellets with a diameter of 5 mm and consisting of a thin, highly polymerized skin and a core of highly porous gel. Sodium alginate (Protanal LF10/60, BDH) extracted from *Laminaria hyperborea*, which has a high guluronic to mannuronic acid ratio and thus a high mechanical strength, was used in all the experiments, the gel being formed by calcium ions cross-linking guluronic acid residues in adjacent polysaccharide chains. The pellets were packed into columns (20 × 1.5 cm diameter) thermostated at 30 °C and supplied with a sucrose solution adjusted to pH 7.0 with 0.1 M NaOH. The enzymatically active cell-free extract was prepared by suspending 1.5 g (wet weight) cells in 150 ml of ice-cold deionized water for 30 min, followed by centrifugation at 23,000g for 20 min at 30 °C, so as to obtain a clear dilute enzyme solution. The cell-free extract could not be easily concentrated by ultrafiltration but could be permanently immobilized by mixing with 8% w/v alginate and gelling with 1.0 M CaCl₂. *Erwinia* cell debris was prepared by mixing 20 g (wet weight) cells with 20 g dry sand and 20 ml of deionized water and shaking for 20 min at 20 °C in a Mickle-shaker (Chem. Lab. Instruments), so that maximum oscillation of the vials occurred. The growing cell preparation was prepared by immobilizing a 1% (wet weight/v) cell inoculum and pumping medium through the column continuously at a rate of 0.04 empty column volumes per h. Unless otherwise stated preparations were assayed in columns at 30 °C using 1.60 M sucrose pH 7.0 as substrate.

*Stability is more properly quoted as a first order decay constant of 1.95 × 10⁻² per day.

[†]Because of the interdependence of stability and degree of conversion (Fig. 2) where appropriate the degree of conversion is quoted in parentheses above.

ity were greatly reduced when affination syrup, an impure sucrose stream produced during refining, was used (Fig. 1). Loss of activity was not due to the action of contaminant microorganisms, and no enzyme induction or turnover could have occurred in the immobilized *Erwinia* cells considering the purity of the substrate used and as addition of chloramphenicol or benzylpenicillin to the substrate, which inhibit protein and cell wall synthesis respectively, did not affect stability (Fig. 2). Stability was, however, enhanced by the use of buffered substrate (Fig. 1) and by the use of the immobilized cells in packed columns rather than in a continuous stirred reactor maintained at pH 7.0 (Fig. 1), or a fluidized-bed in which the reactants were recycled through the reactor and neutralized after each cycle.

The stability of the immobilized cells was much greater than when a cell-free enzyme extract, mechanically disrupted cells or growing cells were used (Table 1), although the initial activities of these preparations were not appreciably different. Viable cells were not required for isomaltulose formation because whereas the activity of the cells decayed slowly and linearly with time, with a half life of 1 yr (Table 1, Fig. 2), the viable cell count declined rapidly with a half life of 300 h. Some metabolic activity was, however, retained by the non-viable immobilized cells as they continued to produce α -keto acids throughout the useful life of the column, presumably by the mixed acid and 2,3-butanediol pathways, such that typically the column eluate was at pH 4.0–4.5.

In conclusion, we have succeeded in obtaining high yields of isomaltulose, stabilizing the isomaltulose synthesizing activity of the *Erwinia* cells and operating the process on a small pilot-plant scale. The immobilized cells appear to be in a resting state caused by a lack of nitrogenous and trace nutrients and the physical constraints imposed by the alginate gel as they did not grow or autolyse and no involution forms were observed. These experiments demonstrate the potential of immobilized non-growing cells particularly when the enzyme of interest is designed to function when the cells are in a non-growing form. They also illustrate the desirability of using specific, stable catalysts, mild immobilization techniques, high reactant concentrations and of maintaining high degrees of conversion and of developing efficient methods for purifying and recovering the product.

This work is the subject of UK Patent Application GB 2 063 268A.

Received 13 May; accepted 2 August 1982.

- Abbott, B. J. A. *Rep. Ferm. Processes*, 205–235 (1977).
- Cheetham, P. S. J. *Topics Enzym. Ferm. Biotechnol.* 4, 189–238 (1980).

3. Roberts, K. R. & Hayes, M. C. *Scand. J. dent. Res.* **88**, 201–209 (1980).
4. UK Patent Application 2 066 639A assigned to Tate & Lyle PLC.
5. UK Patent Application 2 066 640A assigned to Tate & Lyle PLC.
6. Sharpe, E. S., Stodola, F. H. & Koepsell, H. J. *Am. chem. Soc. Abstr.*, 5-D (1954).
7. Bourne, E. J., Hutson, D. H. & Weigel, H. *Biochem. J.* **79**, 549–553 (1961).
8. Lund, B. M. & Wyatt, G. M. *J. gen. Microbiol.* **78**, 331–336 (1973).
9. Weidenhagen, R. *Zucker* **14**, 456–462 (1961).
10. UK Patent Specification 1 429 334 assigned to the South German Sugar Co.
11. Bernaerts, M. J. & De Ley, J. *Biochim. biophys. Acta* **30**, 661–662 (1958).
12. Hayano, K. & Fukui, S. *J. biol. Chem.* **242**, 3665–3672 (1967).
13. Whiting, P. H., Midgley, M. & Dawes, E. A. *Biochem. J.* **154**, 659–668 (1976).
14. Whiting, P. H., Midgley, M. & Dawes, E. A. *J. gen. Microbiol.* **92**, 304–310 (1976).
15. Kierstan, M. & Bucke, C. *Biotechnol. Bioengng* **19**, 387–397 (1977).
16. Cheetham, P. S. J., Blunt, K. W. & Bucke, C. *Biotechnol. Bioengng* **21**, 2155–2168 (1979).
17. Cheetham, P. S. J. *Enzym. microb. Tech.* **1**, 183–188 (1979).
18. Politis, D. J. & Goodman, R. N. *Appl. Microbiol.* **40**, 596–607 (1980).
19. Lilly, M. D. & Sharpe, A. K. *Chem. Engng. Lond.* **215**, CE12 (1968).
20. Mandelstam, J. *Bact. Rev.* **24**, 289–308 (1960).
21. Trinci, A. P. J. & Thurston, C. F. *Symp. Soc. gen. Microbiol.* **26**, 55–80 (1976).
22. Thurston, C. F. *Process Biochem.*, **7**, (8) 18–23 (1972).
23. Astoor, A. & King, E. J. *Biochem. J.* **56**, XLIV (1954).
24. Sloneker, J. H. & Orentos, D. G. *Nature* **194**, 478–479 (1962).

Changes in muscle stiffness during contraction recorded using ultrasonic waves

Yujiro Tamura, Ichiro Hatta & Takashi Matsuda

Department of Applied Physics, Faculty of Engineering,
Nagoya University, Nagoya 464, Japan

Haruo Sugi* & Teizo Tsuchiya

Department of Physiology, School of Medicine, Teikyo University,
Tokyo 173, Japan

Although it is generally accepted that muscles contract by means of cross-links between the thick and thin filaments^{1,2}, the molecular mechanism of contraction is still a matter for debate and speculation. To investigate the number and state of the cross-links at various stages of muscle contraction, muscle stiffness changes have been studied by applying step or sinusoidal length changes and measuring the resulting force changes^{3–5}, or the propagation of longitudinal mechanical waves^{6,7}. These methods, however, involve relatively large perturbations to the contractile system, and may not be free from the possibility that the state of the contractile system is altered by the measurement procedure. We have developed a technique in which muscle stiffness can be continuously recorded during a single mechanical response in frog skeletal muscle by measuring the propagation velocity of ultrasonic waves with negligibly small perturbations to the contractile system and a high time resolution. Using this technique we have obtained the novel and unexpected result that during contraction muscle stiffness decreased in the transverse direction, though it increased in the longitudinal direction.

For measuring muscle stiffness in the longitudinal direction, the semitendinosus muscle of the bullfrog (*Rana catesbeiana*) was mounted in a Lucite chamber as shown in Fig. 1a; a ceramic piezo-electric transducer, which was a circular plate (8 mm diameter) of $\text{PbZrO}_3\text{--PbTiO}_3$ (ref. 8), was in contact with the muscle at each bent end portion. One transducer was repetitively energized with sinusoidal voltages from a function generator (Wavetek, model 162) to transmit brief trains of ultrasonic waves (1, 3 and 7 MHz) to the muscle. The wave trains propagated longitudinally through the muscle, and were sensed by another transducer.

For measuring muscle stiffness in the transverse direction, the sartorius muscle of the bullfrog was mounted with its lower surface in contact with the bottom of the chamber (Fig. 1b); a ceramic transducer (diameter, 6 mm) was in contact with the upper muscle surface. The ultrasonic wave trains (7 MHz) were transmitted to the muscle by the transducer, propagated across

the muscle, and reflected by the chamber to be sensed, as trains of echo waves, by the transmitting transducer.

For accurate determination of the change in propagation velocity of ultrasonic waves in the muscle, the time interval between the original and the propagated ultrasonic signals was divided into two parts, T and ΔT (Fig. 2). A rectangular pulse of a constant duration T with an accuracy of 9.5 figures was generated by a synthesizer (Rockland, type 5100). The duration ΔT was equal to the time interval between the end of the pulse T and the beginning of the first propagated signals. The pulse with a duration ΔT was integrated by a time-to-amplitude converter to obtain an amplitude signal A proportional to the time ΔT . As the propagation velocity of ultrasonic waves changed with time to give values $\Delta T_1, \Delta T_2, \dots$, the corresponding amplitude signals A_1, A_2, \dots , were successively recorded in a digital-memoryscope (Hitachi, type VC 801). The time resolution of muscle stiffness measurements was limited by the frequency of repetition of ultrasonic wave trains, being 250 μs for the longitudinal stiffness and 30 μs for the transverse stiffness. The amplitude of perturbations produced in the muscle during the application of ultrasonic waves ($\sim 1 \text{ \AA}$) was negligibly small. The experiments were performed at room temperature (20–25 °C).

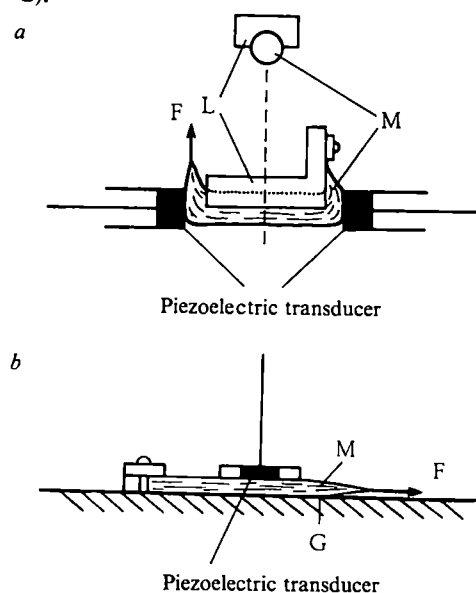


Fig. 1 Methods of recording muscle stiffness changes during isometric contraction. *a*, Experimental arrangement for measuring longitudinal stiffness. The semitendinosus muscle was held by a Lucite block (L) with a cylindrical groove of ~ 5 mm diameter, and bent around the rectangular corner of the block near both ends. Two ceramic transducers were then put in contact with the muscle in such a way that their planes were perpendicular to muscle long axis. The distance between the transducers was 2–2.5 cm. One transducer transmitted ultrasonic waves to the muscle, while the other sensed the propagated waves. *b*, Arrangement for measuring transverse stiffness. The sartorius muscle was placed with its lower surface in contact with the bottom of the chamber (G) serving as a reflecting plane of ultrasonic waves. The transducer was in contact with the upper muscle surface so that its plane was in parallel with the bottom of the chamber. The distance between the transducer and the chamber was 1.5–2 mm. Ultrasonic waves from the transducer propagated across the muscle, and were reflected by the bottom of the chamber to be sensed by the same transducer. In both *a* and *b*, one end of the muscle was fixed in position, while the other end was connected to the strain gauge (Sinko, type UT, F). The muscle was soaked in Ringer solution (NaCl 115 mM, KCl 2.5 mM, CaCl_2 , 1.8 mM, pH 7.3 by Na-phosphate buffer), and each time of stiffness measurement the chamber was drained and the muscle was stimulated maximally with single or repetitive 0.5-ms pulses through a pair of Pt plate electrodes in contact with the muscle surface along its entire length (not shown). To minimize the muscle movement, the initial muscle length was made at 1.2 times slack length. The changes in propagation velocity and isometric force were recorded in a memoryscope, and displayed on a chart recorder.

* To whom correspondence should be addressed.

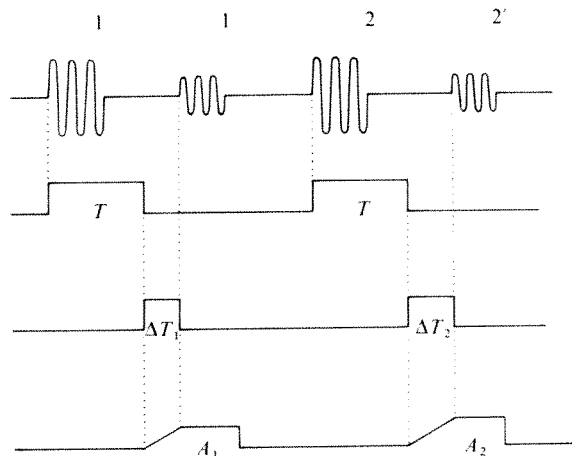


Fig. 2 Diagram illustrating the method for measuring propagation velocity changes. Top record shows two original wave trains (1 and 2) and the corresponding propagated wave signals (1' and 2'). As shown in the two middle records, the interval between the original and the propagated signals was divided into two parts; a rectangular pulse of constant duration (T) and an additional brief pulse of variable duration ΔT . The brief additional pulses (ΔT_1 and ΔT_2) were integrated by the time-to-amplitude converter to give the amplitude signals (A_1 and A_2) in the bottom record.

Figure 3a shows a typical example of the change in propagation velocity of ultrasonic waves along the muscle length during an isometric twitch. On stimulation, the propagation velocity started to increase before the onset of isometric force development, reached a maximum while the isometric force still continued to rise, and then began to decrease to the initial value. The return of propagation velocity to the initial value was complete before the completion of relaxation of isometric twitch. With 3 and 7 MHz waves, the longitudinal propagation velocity was the same within the accuracy of measurements, being $1.61 \pm 0.05 \times 10^3 \text{ m s}^{-1}$ (mean \pm s.d., $n = 20$) in resting muscle. The magnitude of increase in the propagation velocity during twitches was always about 0.9%. Smaller values of propagation velocity was obtained with 1 MHz waves.

A typical example showing the change in propagation velocity in the direction perpendicular to the muscle longitudinal axis during a twitch is shown in Fig. 4a. Unexpectedly, the transverse propagation velocity was found to decrease during a twitch. With 7 MHz waves, the transverse propagation velocity was $1.50 \pm 0.1 \times 10^3 \text{ m s}^{-1}$ (mean \pm s.d., $n = 20$) in resting muscle, and always decreased by about 1% during a twitch. The propagation velocity started to decrease before the onset of isometric force development, and reached a minimum prior to the peak twitch force (Fig. 3a).

In both the longitudinal and transverse propagation velocity, a steady propagation velocity was attained during the plateau of an isometric tetanus. The magnitude of velocity changes during a tetanus was about twice that during a twitch. When the peak twitch force was varied by applying submaximal stimuli of various strengths, the magnitude of both the longitudinal and transverse velocity changes was proportional to the peak twitch force (Figs 3b, 4b).

When mechanical waves with a constant frequency f propagate in muscle, their phase velocity V_f is related to muscle stiffness E_f as:

$$V_f = (E_f/\rho)^{1/2} \quad (1)$$

where ρ is the density of muscle, which may remain unchanged during isometric contraction. Thus, muscle stiffness can be estimated from equation (1) if the measured velocities, which are generally very close to the group velocities, can be regarded as the phase velocities. This condition is satisfied in the range of high enough wave frequencies where the frequency dependence of the propagation velocities is no longer obvious. The similarity of the propagation velocity between 3 and 7 MHz

waves indicates that the measured velocities with waves above 3 MHz are equal to the phase velocities. Moreover, in the case of the longitudinal velocities, the wavelength λ should also satisfy the condition, $a/\lambda > 2.5$, where a is the muscle radius⁹; otherwise, the waves propagate along the muscle fibres with mixed modes to make the measurement of the phase velocity complicated. In the present study, the muscle was nearly circular in cross-section (Fig. 1) with a radius of about 2.5 mm, while the wavelengths of 7, 3 and 1 MHz waves were about 0.2, 0.5 and 1.5 mm respectively.

Therefore, the velocities with waves above 3 MHz can serve as a valid measure of muscle stiffness, and the results shown in Figs 2 and 3 may indicate that, during isometric contraction, longitudinal muscle stiffness increases while transverse muscle stiffness decreases. The linear relation between the magnitude of velocity changes and the peak twitch force may be taken to indicate that the stiffness changes observed are related to the force generating mechanism. Note also that the time course of stiffness changes during the isometric force development resembles that of the intensity ratio of two equatorial reflections ($I_{1,0}/I_{1,1}$)^{10,11}, which is regarded to reflect the radial movement of cross-bridges towards the thin filaments.

Assuming that ρ is 1 g cm^{-3} , the value of longitudinal muscle stiffness for 3 MHz waves was estimated from equation (1) to be about $2.56 \times 10^9 \text{ N m}^{-2}$ in resting muscle, and the increment of muscle stiffness in a tetanus above the resting value was about $6 \times 10^7 \text{ N m}^{-2}$. The high value of resting muscle stiffness results from the fact that, with ultrasonic waves, it is the bulk properties of the muscle that are measured, and therefore it is the increment of stiffness during contraction that is relevant to the cross-bridge properties. We tentatively calculated the increment of muscle stiffness for 3 kHz mechanical waves during contraction from the published data of Truong⁷, and also obtained a value of the order of 10^7 N m^{-2} . A similar value of muscle stiffness is also obtained from the slope of the T_1 curve in the length step experiments of Ford *et al.*³. This suggests

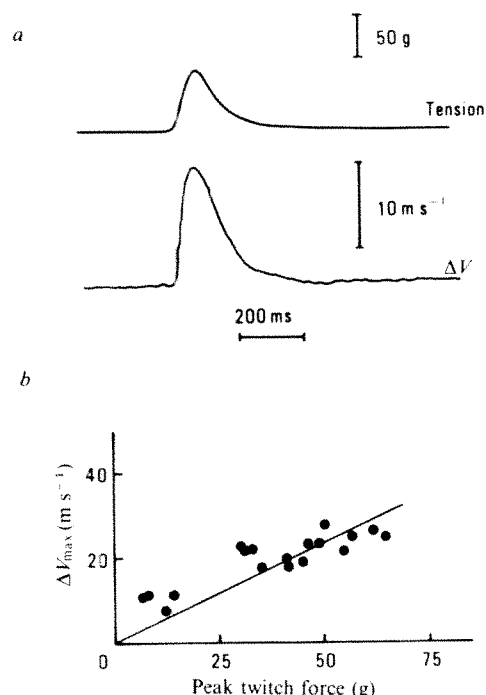


Fig. 3 a, Change in longitudinal propagation velocity of 3 MHz ultrasonic waves (ΔV , lower trace) during an isometric twitch (upper trace). In this and subsequent figures, the upward and downward deflection of the velocity trace indicate an increase and a decrease in propagation velocity respectively. Temperature, 25 °C. b, Relationship between the magnitude of increase in the longitudinal propagation velocity in a twitch (ΔV_{\max} , ordinate) and the peak twitch force (abscissa). Peak twitch forces were varied by applying submaximal stimuli of various strengths. Temperature, 25 °C.

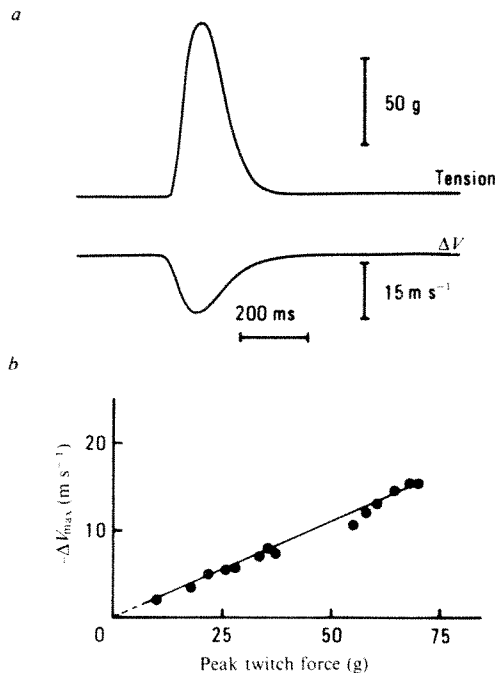


Fig. 4 *a*, Change in transverse propagation velocity (ΔV) of 7 MHz waves during an isometric twitch. Note that the propagation velocity decreases during a twitch. Temperature, 15 °C. *b*, Relation between the magnitude of decrease in the transverse propagation velocity in a twitch ($-\Delta V_{\max}$, ordinate) and the peak twitch force (abscissa). Peak twitch forces were varied by applying submaximal stimuli of various strengths. Temperature, 25 °C.

that the increase in longitudinal muscle stiffness during contraction, which has been observed with different techniques, may result from the formation of an elastic element exhibiting almost constant stiffness values over a wide frequency range of mechanical perturbations. On the other hand, transverse muscle stiffness for 7 MHz waves was about $2.25 \times 10^9 \text{ N m}^{-2}$ in resting muscle, and the decrement of muscle stiffness in a tetanus was about $8 \times 10^7 \text{ N m}^{-2}$. The decrease in transverse stiffness may not result from local segmental shortening introducing an increase in protein density underneath the transducer, as the stiffness decrease was always observed irrespective of the position of the transducer along the entire muscle length. Moreover, our theoretical calculations indicate that an increase in protein density leads to an increase in propagation velocity, an effect opposite to the present results.

A possible mechanism of the decrease in transverse stiffness, which is a novel and unexpected result of the present study, may be that the nature of the cross-links between the filaments is such that the strain in the transverse direction is largely taken up by the deformation of the cross-links to result in softening of the muscle in the transverse direction.

We thank Professor Sir Andrew F. Huxley for his invaluable advice and criticisms during this work.

Received 24 May; accepted 9 August 1982.

1. Huxley, A. F. *Prog. Biophys. biophys. Chem.* **7**, 255–318 (1957).
2. Huxley, H. E. in *The Cell* (eds Brachet, J. & Mirsky, A. E.) 365–481 (Academic, New York, 1960).
3. Ford, L. E., Huxley, A. F. & Simmons, R. M. *J. Physiol., Lond.* **269**, 441–515 (1977).
4. Rüegg, J. C. *et al.* in *Cross-bridge Mechanism in Muscle Contraction* (eds Sugi, H. & Pollack, G. H.) 125–148 (University of Tokyo Press and University Park Press, Baltimore, 1979).
5. Julian, F. J. & Sollins, M. R. *J. gen. Physiol.* **66**, 287–302 (1975).
6. Schoenberg, M., Wells, J. B. & Podolsky, R. J. *J. gen. Physiol.* **64**, 623–642 (1974).
7. Truong, X. T. *Am. J. Physiol.* **226**, 256–264 (1974).
8. Berlincourt, D. A., Curran, D. R. & Jaffe, H. in *Physical Acoustics* Vol. 1, pt A (ed. Mason, W. P.) 169–270 (Academic, New York, 1964).
9. Yu, L. T., Brennan, J. N. & Sauer, J. A. *J. Acoust. Soc. Am.* **27**, 550–555 (1955).
10. Haselgrove, J. C. & Huxley, H. E. *J. molec. Biol.* **77**, 549–568 (1973).
11. Amemiya, Y., Sugi, H. & Hashizume, H. in *Cross-bridge Mechanism in Muscle Contraction* (eds Sugi, H. & Pollack, G. H.) 425–443 (University of Tokyo Press and University Park Press, Baltimore, 1979).

Induction of immortality is an early event in malignant transformation of mammalian cells by carcinogens

Robert F. Newbold, Robert W. Overell
& Jane R. Connell

Chemical Carcinogenesis Division, Institute of Cancer Research,
Pollards Wood Research Station, Nightingales Lane,
Chalfont St Giles, Buckinghamshire HP8 4SP, UK

Limited lifespan in normal diploid mammalian cells in culture is well documented^{1–3} and there is evidence that it is also a property of normal tissues serially transplanted *in vivo*^{4,5}. In contrast, in favourable growth conditions, cells derived from tumours or premalignant tissue often exhibit unlimited proliferative potential (immortality) both *in vitro* and *in vivo*^{2,4,6–10}. Malignant transformation of diploid cells in culture by carcinogens has been clearly demonstrated in several laboratories^{2,11–13}. However, although it has been frequently reported that establishment in culture is one of many alterations in cell behaviour associated with transformation, the induction of immortality and its role in malignancy have not previously been subjected to serious scientific examination. Here, we show that treatment of Syrian hamster cell cultures with carcinogenic chemicals can induce rare immortal variants, the progeny of which then frequently progress to anchorage independence and malignancy after a further period of growth. In addition, by studying the properties of cell lines that are either immortal or anchorage-independent but not both, we have obtained evidence that immortality, although insufficient by itself, may be a prerequisite for malignant transformation.

Rapidly dividing fusiform cells which, in minimal media, dominate cell cultures derived from primary tissue, are generally assumed to be fibroblasts. Even though the precise origin of cells which adapt easily to culture has not been established¹⁴, they have formed the basis of most cell culture transformation systems developed to date. Nevertheless, their use for this purpose can be justified by the fact that malignant tumours can arise *in vivo* from most cells that are capable of division, including those of mesenchymal origin. The cells used in our experiments were obtained from mixed Syrian hamster embryo tissues, newborn hamster dermis and human fetal lung; they were maintained in Dulbecco's modified Eagle's minimal essential medium (DMEM; Gibco) supplemented with 15% fetal calf serum (FCS). Spontaneous malignant transformation is rare in cells derived from Syrian hamster^{11,13} and has never been reported in the case of human fibroblasts from normal donors¹⁵.

The effect of several carcinogenic chemicals on the frequency of appearance of immortal Syrian hamster cell variants is shown in Table 1. Replicate cultures of tertiary embryo or dermal cells were treated with solvent alone (dimethyl sulphoxide, DMSO) or solutions of carcinogens (see Table 1). In controls and some treated cultures a phase of rapid proliferation, necessitating frequent subculture, was followed by a decline in growth rate, leading eventually to a complete loss of division potential. At this point, the cells became greatly enlarged and flattened, and phase-dense stress fibres¹⁶ in the cytoplasm were clearly visible by phase contrast microscopy. These stages in culture lifespan are typical of those described for human fibroblasts by Hayflick and Moorhead¹; the term senescence has since been widely used to denote the final non-proliferative state. In a proportion of cultures treated with benzo(a)pyrene (BP), its ultimate carcinogenic metabolite anti-BP-7,8-dihydrodiol-9,10 oxide (BPDE)¹⁷, and the two methylating agents *N*-methyl-*N*-nitrosourea (MNUA) and dimethylsulphate (DMS)¹⁸, immortal (Sen⁺) cells appeared which gave rise to continuous cell lines. (Treated cells capable of proliferation for

Table 1 Induction of immortal variants in Syrian hamster cell cultures treated with various chemical carcinogens

Expt	Treatment	Dose ($\mu\text{g ml}^{-1}$ medium)	Survival (% control)	No. of immortal cultures obtained/ no. of replicate cultures observed
<i>a, Mixed embryo cultures</i>				
1	BP	1.0	90	8/18
2	BPDE	0.1	81	1/7
	BPDE	0.3	20	2/4
	DMS	12.5	84	1/6
	DMS	25.0	21	2/6
3	BP	1.2	96	18/21
	BPDE	0.2	56	8/19
	DMS	19.0	38	3/21
	MNUA	34.0	73	9/20
Pooled control	DMSO (0.2%)		100	1/101
<i>b, Newborn dermal fibroblasts</i>				
1	BP	1.0	100	3/10
	BPDE	0.06	95	1/10
	BPDE	0.12	82	3/10
2	BP	2.5	95	4/10
	BPDE	0.07	94	2/9
	BPDE	0.15	63	2/9
	MNUA	30.0	60	2/9
Pooled control	DMSO (0.2%)		100	0/50

Primary cell cultures were prepared from trypsinized, minced, eviscerated Syrian hamster embryos (13–14 days of gestation) and collagenase-treated newborn dermis. In the latter case, separation of the epidermis from the dermis was facilitated by floating skins overnight in 0.01% pronase (Sigma) at 4°C as described elsewhere²⁸. Disaggregated cells of both types were seeded at a density of 1.5×10^7 per 175-cm² culture flask (Nunc) and, when almost confluent, were trypsinized and cryopreserved in liquid nitrogen. Samples of cells from each preparation were checked for the presence of mycoplasma by staining with the fluorescent dye, Hoechst 33258. For experiments, ampoules were thawed and the cells returned to 175-cm² flasks. After 3–4 days at 37°C, exponentially growing cultures were trypsinized and 1×10^6 cells seeded in 75-cm² flasks in 20 ml of medium for treatment with carcinogens. Compounds were added directly to the flasks 24 h later as 500× stock solutions in DMSO. Cells were exposed to the agents for 1 h (MNUA, DMS and BPDE) or 48 h (BP) after which the medium was changed. Embryo cells were re-plated 2 h later in replicate 5-cm Petri dishes (Sterilin) at a density of $0.4\text{--}2 \times 10^5$ per dish; dermal cells were allowed to grow to confluence. From this point onwards, cells were subcultured when confluent (embryo cells 1:10 in 5-cm dishes, dermal fibroblasts 1:5 in 9-cm dishes) and the medium replaced regularly every 3 days. Cell survival was determined immediately after treatment by plating 400 cells from each experimental group into 5-cm dishes on a feeder layer of 8×10^4 lethally irradiated homologous cells; colonies were scored after 7–10 days of incubation. Control plating efficiencies ranged from 22 to 34% for both cell types, depending on the cell preparation and the serum batch used. On reaching senescence, mass cultures were subcultured once more if confluent (1:2). The resulting semi-confluent cultures of non-proliferating cells remained visibly healthy for many weeks afterwards, if the medium was replaced regularly. The carcinogen treatments described had no significant effects on the replicative lifespan of cultures which showed no transformation. Transformed cell lines were maintained in culture for at least 100 pd after their emergence and cells were regularly cryopreserved for subsequent studies of their tumorigenicity and anchorage independence.

>100 population doublings (pd) after senescence of the respective controls, were considered immortal.) Transformation or senescence of cultures was found to be highly reproducible when experiments were repeated with replicate samples of cells cryopreserved soon (6–8 pd) after treatment, demonstrating that the system permits efficient recovery of transformants. On the assumption that Sen⁻ variants were monoclonal in origin, we estimated the range of transformation frequencies for the embryo and dermal cells to be $0.9\text{--}7 \times 10^{-5}$ and $1.6\text{--}6 \times 10^{-7}$, respectively, per viable treated cell, depending on the agent and the dose applied. More detailed, quantitative studies are now in progress to determine accurately the relative potencies of these and other carcinogens and mutagens for inducing immortality. We are also examining the validity of the assumption that Sen⁻ lines which emerge in these conditions are clones, by performing experiments with mixtures of male and female cells of known transformability and using C-banding to reveal the presence of the heterochromatic Y-chromosome in transformed cells.

With hamster embryo cells, the appearance of carcinogen-induced Sen⁻ variants occasionally occurred after crisis at the end of the proliferative phase of growth but more often little

or no crisis was observed, indicating that immortal cells had emerged before the cessation of normal cell division. In contrast, Sen⁻ dermal fibroblasts always appeared at the end of the normal culture lifespan as foci of dividing cells on a background of senescent counterparts. Only one Sen⁻ cell line was obtained from over 100 cultures of solvent-treated control embryo cells and this line (S33) has generated no malignant progeny on further subculture; no spontaneous transformation has so far been observed with the dermal cells. Because of their shorter lifespan (15–20 pd compared with 50–60 pd for the hamster embryo cells) and the fact that Sen⁻ transformants can be scored as foci 6–7 weeks after treatment, the dermal cells seem preferable for future studies. When foci of Sen⁻ dermal cells were isolated and grown in mass culture, it was noted that in many lines enlarged, flattened, non-proliferating cells continued to be produced at a variable rate. Indeed, in a few lines, the probability of senescence was so high that their continued maintenance *in vitro* required careful handling at subculture. In contrast, some cell lines were obtained which grew almost exponentially with few senescent cells visible. Thus, the induction of immortality did not seem to be an all-or-none process; rather it appeared to involve different degrees of reduction in the commitment of cells to a non-proliferative state.

When injected subcutaneously or intraperitoneally into syngeneic 1-day-old hamsters, carcinogen-induced Sen⁻ cell lines were not tumorigenic immediately they exceeded the normal lifespan but most (75%) progressed to malignancy after a further period of culture. This period was highly variable and was a characteristic of the individual cell line; some lines remained non-tumorigenic even after prolonged growth (>300 pd) *in vitro*. In many cases, the tumours formed were capable of invasion of surrounding tissues and/or metastasis to other organs. Normal untreated cells did not give rise to tumours in any circumstances. As reported previously¹³, the acquisition of tumorigenic potential was correlated perfectly with the

Table 2 Correlation between anchorage-independent growth and tumorigenicity in immortal Syrian hamster cells

Cell line	Passage tested (approximate pd)	Frequency of Aga ⁺ colonies per seeded cell	No. of animals with tumours/no. surviving	Mean latent period for tumour formation (days)	No. of animals with metastases/no. with tumours
S33	48 (190)	<10 ⁻⁶	0/5	—	—
BP1	54 (215)	<10 ⁻⁶	0/9	—	—
BP30	65 (260)	<10 ⁻⁶	0/5	—	—
DMS11	40 (160)	<10 ⁻⁶	0/5	—	—
BPDE7	44 (175)	<10 ⁻⁶	0/10	—	—
BP9	45 (180)	2.4×10^{-4}	5/6	88	2/5
BP3	49 (195)	4.3×10^{-4}	6/10	111	2/6
BP40	33 (130)	>1%	7/8	55	3/7
BP6	42 (170)	>1%	10/10	69	6/10
BPDE17	45 (180)	>1%	7/7	50	0/7

Immortal hamster embryo cell lines were tested for their ability to form colonies in soft agar medium at the passage number shown. 10^5 cells of each line were seeded in 3 ml DMEM plus 0.33% Noble agar (Difco) and 1 mg ml⁻¹ Bacto-Peptone in each of 10 5-cm dishes containing a 0.6% solidified agar base; these conditions did not permit any proliferation of normal diploid cells (see ref. 29). Colonies of more than ~100 cells were scored after 10–12 days at 37°C and representative examples isolated for subsequent confirmation of the heritability of the Aga⁺ phenotype. The tumorigenicity of lines was established by injecting 1-day-old syngeneic hamsters (5–10 animals per cell line) intradermally with 10^6 cells in 0.1 ml phosphate-buffered saline (PBS); animals were checked three times weekly for signs of tumour growth. When tumours at the site of injection had reached ~2 cm in diameter the animals were killed; both the primary tumours and organs suspected of carrying secondary growths were removed for histology and cell culture. Metastases were evident in a proportion of tumour-bearing animals; these involved mainly the lymph nodes, liver, pancreas and lungs. Invasion and destruction of underlying muscle was common, and occasionally extended to the diaphragm, ovary and kidney; angiogenesis associated with the primary tumour was often marked. Animals were observed for at least 300 days before being scored as negative for tumour growth. Preliminary analysis of the karyotypes of the various Sen⁻ transformants at the time of assay revealed no consistent differences between tumorigenic and non-tumorigenic lines with respect to chromosome numbers. Most lines had diploid modes plus a significant proportion of hyperdiploid cells with 1–4 extra chromosomes. A detailed study of G-banded karyotypes is now being done.

Table 3 Properties of Aga⁺ mammalian cell variants induced by carcinogens independently of immortality

Treatment	Frequency of Aga ⁺ clones per seeded cell	No. of clones isolated	No. of clones re-plated in agar	Re-plated Aga ⁺ frequency × 10 ⁵ (±s.d.)
<i>a, Syrian hamster embryo cells</i>				
DMSO (control)	<5.0 × 10 ⁻⁷	—	—	—
MNUA (30 µg ml ⁻¹)	7.0 × 10 ⁻⁶	8	0*	—
BPDE (0.15 µg ml ⁻¹)	1.3 × 10 ⁻⁵	12	0*	—
<i>b, Human fetal lung fibroblasts</i>				
DMSO (control)	<1.0 × 10 ⁻⁷	—	—	—
BPDE (single treatment, of 0.2 µg ml ⁻¹)	<1.0 × 10 ⁻⁷	—	—	—
BPDE (0.2 µg ml ⁻¹ + 4 sequential treatments of 0.1 µg ml ⁻¹)	2.2 × 10 ⁻⁵	15	3	42 ± 8 (clone A5) 38 ± 11 (clone A7) 29 ± 8 (clone A8)

a, Secondary hamster embryo cells were treated with BPDE and MNUA as described in Table 1 legend, and were then maintained in the exponential phase of growth. Samples of cells from each culture were plated in 0.33% agar medium 3, 7 and 21 days after treatment. For both treated cultures, the maximum yield of agar colonies was obtained with cells which had been allowed 7 days for expression of the Aga⁺ phenotype; these are the values shown. Twenty large, viable colonies were isolated and transferred to 1.5-cm culture wells. *b*, Secondary normal fetal lung fibroblasts were provided by J. J. Roberts, Institute of Cancer Research. At pd 10, replicate cultures of 10⁷ cells in 175-cm² flasks were treated with 0.2 µg ml⁻¹ BPDE. After 2 weeks without subculture, but with medium changes every 3 days, the cells had recovered sufficiently to produce confluent cultures. We detected no Aga⁺ variants at this stage in a total of 10⁷ cells plated in agar. Therefore, some cultures received four additional treatments of BPDE (0.1 µg ml⁻¹) evenly spread over an 8-week period. At pd 38, rare Aga⁺ variants were detected and 15 colonies (A1–A15) were isolated; cells derived from three of these (clones A5, A7 and A8) were re-plated in agar and simultaneously tested for tumorigenicity in nude (*nu/nu*) mice. Groups of four mice were injected intradermally with 5 × 10⁶ cells in 0.1 ml PBS and, as a positive control, animals in one group each received 1 × 10⁶ Sen⁻ Aga⁺ hamster cells. Animals were observed twice a week for signs of tumours.

*Most of the cultures from Aga⁺ hamster clones possessed sufficient residual division potential to form a confluent monolayer. However, all 20 cultures senesced after two subcultures.

appearance of anchorage-independent (Aga⁺) variants in Sen⁻ cell lines (Table 2). So far we have observed no lines having a Sen⁻ Aga⁺ phenotype which are non-tumorigenic, nor have we obtained any tumorigenic lines which do not form colonies in soft agar. Moreover, cells derived from all nine fibrosarcomas that we induced in hamsters by single intradermal injections of BP (100% tumour incidence; tumours excised when ≥2 cm in diameter after 109–167 days) possessed a Sen⁻ Aga⁺ phenotype in culture without entering an obvious crisis after outgrowth from tumour explants.

Several workers^{19–21} have published evidence supporting a mutational mechanism for the induction of anchorage independence. Thus, a possible explanation for the progression of our hamster lines is that rare Aga⁺ variants arise in cultures through spontaneous mutation and that cells with the new phenotype (Sen⁻ Aga⁺) then drift through the population due to a growth advantage²¹. If this is the case, then the variable rates of appearance of Aga⁺ cells could be due to variable spontaneous mutability of the individual cell lines. To test this hypothesis, we are now examining spontaneous mutation rates at the *hprt* locus, in Aga⁺, pre-Aga⁺ and non-progressing Sen⁻ hamster dermal cell lines.

Evidence supporting the notion that immortality is an essential step in malignant transformation was obtained from experiments with secondary hamster embryo cells in which Aga⁺ variants were induced by BPDE and MNUA treatment (Table 3a). Large, viable-looking colonies were picked and transferred to 1.5-cm diameter multi-dish wells (Nunc), and 20 dividing monolayer cultures were established successfully. However, although we were able to transfer the cells to larger culture vessels at least once, all 20 isolates underwent typical senes-

cence before sufficient cells could be accumulated for repeat anchorage independence assays or tumorigenicity studies. To examine the properties of Sen⁻ Aga⁺ cells having a longer residual lifespan, we carried out similar experiments with fibroblasts derived from human fetal lung; in our hands these cells regularly underwent >100 pd in medium supplemented with selected batches of FCS (also found by Pooley *et al.*²²). We were able to induce Aga⁺ variants of these cells after multiple treatments with BPDE (Table 3b). When cells grown from isolated agar colonies were re-plated in agar, their cloning efficiency was invariably more than an order of magnitude higher than that of the original carcinogen-treated mass cultures. Despite this, these Aga⁺ cells were non-tumorigenic in athymic (*nu/nu*) mice in conditions where a Sen⁻ Aga⁺ hamster cell line formed progressively growing tumours at one-fifth of the cell inoculum; in the case of the Aga⁺ human cells we observed only small nodules which appeared after 2–3 weeks and regressed 1–2 weeks later. Moreover, the cells in culture possessed senescence characteristics similar to their Aga⁻ counterparts (see also ref. 23), ceasing proliferation after a further 12–15 pd. Therefore, in both of the above studies, it was possible to induce the Aga⁺ phenotype independently of immortality but this change alone did not endow the cells with the ability to form truly malignant tumours. Numerous attempts by ourselves and others to achieve immortal transformation of human fibroblasts by chemical carcinogens have proved unsuccessful, although two clear cases have been reported^{15,24}.

The most popular interpretation of the biological significance of the limited culture lifespan of fibroblasts is that it represents ageing at the cellular level¹, and the possibility that accumulation of errors in DNA or proteins is responsible²⁵ has received much attention. An alternative idea²⁶ is that, rather than being a manifestation of senescence, finite lifespan *in vitro* may be a process analogous to terminal differentiation. There are, as yet, insufficient data available to support conclusively either theory. Nevertheless, it is clear from our results that normal mammalian cells can be induced to escape from their commitment²⁷ to senescence by exposure to various mutagenic^{17,18} carcinogens, and that the resulting capacity for infinite multiplication precedes (and may be necessary for) malignant transformation. That such a potential for unlimited division provides the basis for the evolution of carcinogen-induced malignancy *in vivo*, by permitting repeated selection of rare variants having increasingly autonomous properties, is, we believe, an appealing hypothesis which warrants further study.

This work was supported by grants from the Cancer Research Campaign/MRC (G80/1094), the US NCI (RO1-CA-25807-04) and Gallaher Ltd. We thank Mrs M. White, Ms J. Amos and Mr T. A. Slade for technical assistance.

Received 21 June; accepted 3 August 1982.

- Hayflick, L. & Moorhead, P. *Expl Cell Res.* **25**, 585–621 (1961).
- Ponten, J. *Biochim. biophys. Acta* **458**, 397–422 (1976).
- Barrett, J. C. *et al.* *J. Cancer Res.* **37**, 3815–3823 (1977).
- Daniel, C. W., Aidells, B. D., Medina, D. & Faulkin, L. J. *Fedn Proc.* **34**, 64–67 (1975).
- Hellman, S., Botnick, L. E., Hannon, E. C. & Vignoulle, R. M. *Proc. natn. Acad. Sci. U.S.A.* **75**, 490–494 (1978).
- Klein, G. *Cancer Res.* **19**, 343–358 (1959).
- DiPaolo, J. A., Nelson, R. L. & Donovan, P. J. *J. natn. Cancer Inst.* **46**, 171–181 (1971).
- Sinkovics, J. G., Gyorkey, F., Kusyk, C. & Siciliano, M. J. *Meth. Cancer Res.* **14**, 243–323 (1978).
- Klein, G. *Proc. natn. Acad. Sci. U.S.A.* **76**, 2442–2446 (1979).
- Rheinwald, J. G. & Beckett, M. A. *Cancer Res.* **41**, 1657–1663 (1981).
- Berwald, Y. & Sachs, L. *J. natn. Cancer Inst.* **35**, 641–661 (1965).
- DiPaolo, J. A., Nelson, R. L. & Donovan, P. J. *Cancer Res.* **31**, 1118–1127 (1971).
- Barrett, J. C. & Ts'o, P. O. P. *Proc. natn. Acad. Sci. U.S.A.* **75**, 3761–3765 (1978).
- Franks, L. M. & Wilson, P. D. *Int. Rev. Cytol.* **48**, 55–139 (1977).
- Kakunaga, T. *Proc. natn. Acad. Sci. U.S.A.* **75**, 1334–1338 (1978).
- Lewis, L. *et al.* *J. Cell Sci.* **53**, 21–36 (1982).
- Newbold, R. F. & Brookes, P. *Nature* **261**, 52–54 (1976).
- Newbold, R. F., Warren, W., Medcalf, A. S. C. & Amos, J. *Nature* **283**, 596–599 (1980).
- Bouck, N. & DiMayorca, G. *Nature* **264**, 722–727 (1976).
- Bellet, A. J. D. & Younghusband, H. B. *J. cell. Physiol.* **101**, 33–48 (1979).
- Marin, G. *Expl Cell Res.* **125**, 31–36 (1980).
- Pooley, J. A., Schuman, R. F. & Pienta, R. J. *In Vitro* **14**, 405–412 (1978).
- Freedman, V. H. & Shin, S. J. *J. natn. Cancer Inst.* **58**, 1873–1875 (1977).
- Namba, M., Nishitani, K. & Kimoto, T. *Japan J. exp. Med.* **48**, 303–311 (1978).
- Orgel, L. E. *Nature* **243**, 441–445 (1973).
- Bell, E. *et al.* *Science* **202**, 1158–1163 (1978).
- Holliday, R., Hushchitscha, L. I. & Kirkwood, T. B. L. *Science* **213**, 1505–1508 (1981).
- Sun, N. *et al.* *Cancer Res.* **41**, 1669–1676 (1981).
- Peehl, D. M. & Stanbridge, E. J. *Proc. natn. Acad. Sci. U.S.A.* **78**, 3053–3057 (1981).

Noradrenaline blocks accommodation of pyramidal cell discharge in the hippocampus

D. V. Madison* & R. A. Nicoll

Departments of Pharmacology and Physiology and *Graduate Program in Neuroscience, University of California, San Francisco, California 94143, USA

The hippocampus, as well as a variety of other brain regions, is known to receive a diffuse projection of noradrenaline (NA) containing fibres which originates in the brain stem¹⁻⁴. Although there is considerable evidence for the involvement of this system in a variety of behaviours⁵⁻⁷, the precise cellular actions of NA are poorly understood. Early studies emphasized the direct inhibitory effects of NA⁸⁻¹²; more recent experiments have shown that at several sites, NA, or stimulation of NA-containing afferents, can also facilitate excitatory synaptic responses¹³⁻¹⁸. This has led to the concept that NA increases the 'signal-to-noise' ratio of neurones¹³, acting as an 'enabling' device⁴ which allows cells to respond more briskly to conventional synaptic excitation. In the olfactory bulb, NA reduces inhibitory postsynaptic potentials by a presynaptic action¹⁹, which could contribute to enhanced excitatory synaptic responses. However, in other systems, NA has been reported to enhance excitatory responses to iontophoretically applied transmitters, and it was proposed that NA increases the sensitivity of the neurone to these excitatory transmitters¹³⁻¹⁵. We report here experiments that could explain such direct effects. We have found that NA and cyclic AMP block the Ca^{2+} -activated K^+ conductance in hippocampal pyramidal cells and that this blockade occurs at a step subsequent to the entry of Ca^{2+} into the neurone. As a consequence, the spike frequency adaptation or accommodation which normally occurs with depolarizing stimuli is severely reduced. Thus, NA greatly increases the number of spikes elicited by a depolarizing stimulus.

Rat hippocampal slices were prepared and superfused as previously described²⁰. The normal superfusion medium consisted of 116.4 mM NaCl, 5.4 mM KCl, 2.5 mM CaCl_2 , 1.3 mM MgSO_4 , 26.2 mM NaHCO_3 , 0.92 mM Na_2HPO_4 and 11 mM glucose. The recording microelectrode, filled with 2 M KMeSO_4 (90–120 M Ω), was placed in the pyramidal cell layer under visual guidance. Pyramidal cells were activated directly by passing depolarizing current through the recording electrode using a bridge circuit. Drugs were applied by addition to the superfusing medium or, in a few experiments, by iontophoresis. Iontophoretic pipettes were filled with either 1 M sodium glutamate (pH 8) or 1 M NA (pH 4.5). The findings reported here are based on recordings from over 100 cells with resting membrane potentials of greater than -55 mV.

We have found that when CA1 pyramidal cells are excited by prolonged (for example, 600 ms) depolarizing current pulses, they respond with an initial burst of spikes, after which the cell remains silent for the duration of the pulse (Fig. 1a). Increasing the stimulus current from threshold increases the number of spikes until a maximum of six to eight spikes is reached. This spike frequency adaptation, or accommodation, is markedly attenuated by the addition of NA (1–10 μM) to the superfusate ($n = 24$). Although little change in either the passive membrane properties of the cell or in the firing threshold usually occurs, NA causes the cell to fire throughout the depolarizing current pulse (Fig. 1a). For strong depolarizing currents, pyramidal cells fired 6.8 ± 1.7 (mean \pm s.d.) spikes to a 650-ms pulse in control conditions, whereas in 10 μM NA the same cells fired 16.8 ± 2.7 spikes ($n = 14$). Because these neurones fire continuously during depolarizing stimuli in the presence of NA, the number of spikes elicited is determined by the duration of the depolarizing pulse. In those few cells which were hyperpolarized by 10 μM NA (see refs 11, 12), the response to threshold depolarizing pulses was inhibited, yet the response to strong current pulses was markedly augmented. The block of accommodation by NA is also seen when pyramidal cells are depolarized by glutamate applied iontophoretically (Fig. 1c). In the presence of NA, the cells fire throughout the depolarization induced by glutamate ($n = 9$).

Fig. 1 Noradrenaline and cadmium block calcium-activated potassium responses and prolong spike discharge in hippocampal pyramidal cells. The responses in a to c are all from the same pyramidal cell. a, Film records of the response of cell to a depolarizing current pulse. The current trace is positioned below the voltage trace. The response in the middle column was obtained 4 min after the addition of 10 μM NA to the bathing solution. The membrane potential did not change during the application of NA. The records in 'Wash' were obtained 30 min after returning to the control solution. b, Simultaneously recorded chart records of the response shown in a (b_1), and response to a short (100 ms) depolarizing current pulse (b_2). c, Film records of response to 30 nA of iontophoretically applied glutamate. Membrane potential, -58 mV. The gain of c is the same as in a. d, Chart records from another cell showing responses to a long (d_1) and short (d_2) depolarizing current pulse recorded at different gains. The calcium antagonist cadmium (0.1 mM) was applied for 8 min. The records in 'Wash' were obtained 32 min after returning to the control bathing solution. The spikes are attenuated by the pen recorder. The time calibration is the same as in b. The gain for d_2 is the same as in b, while d_1 is half the gain of b. Membrane potential, -57 mV.

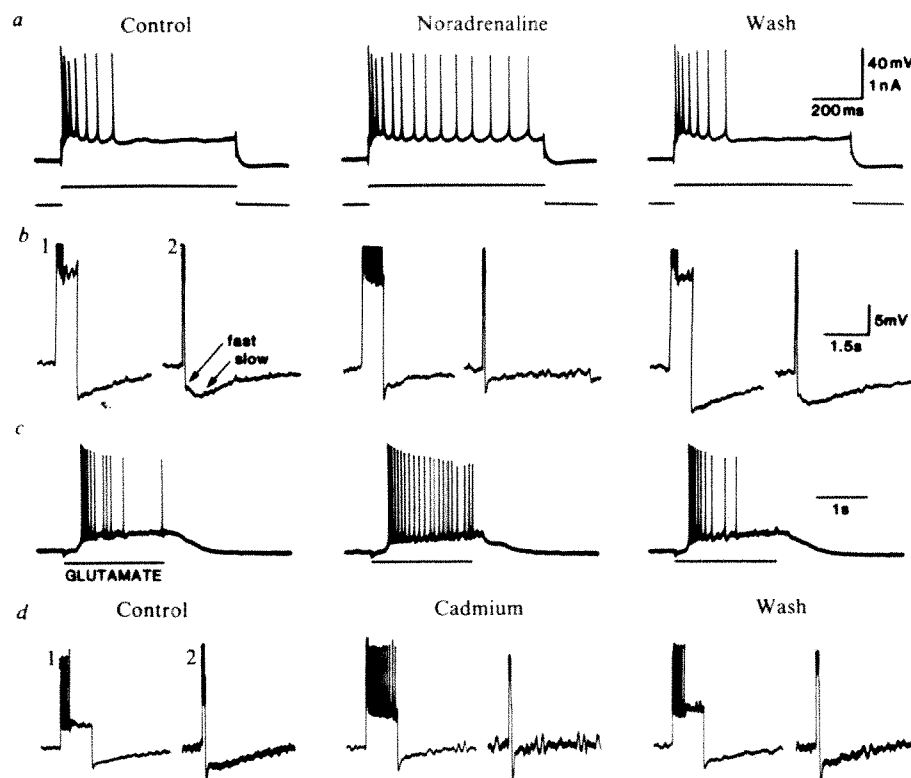
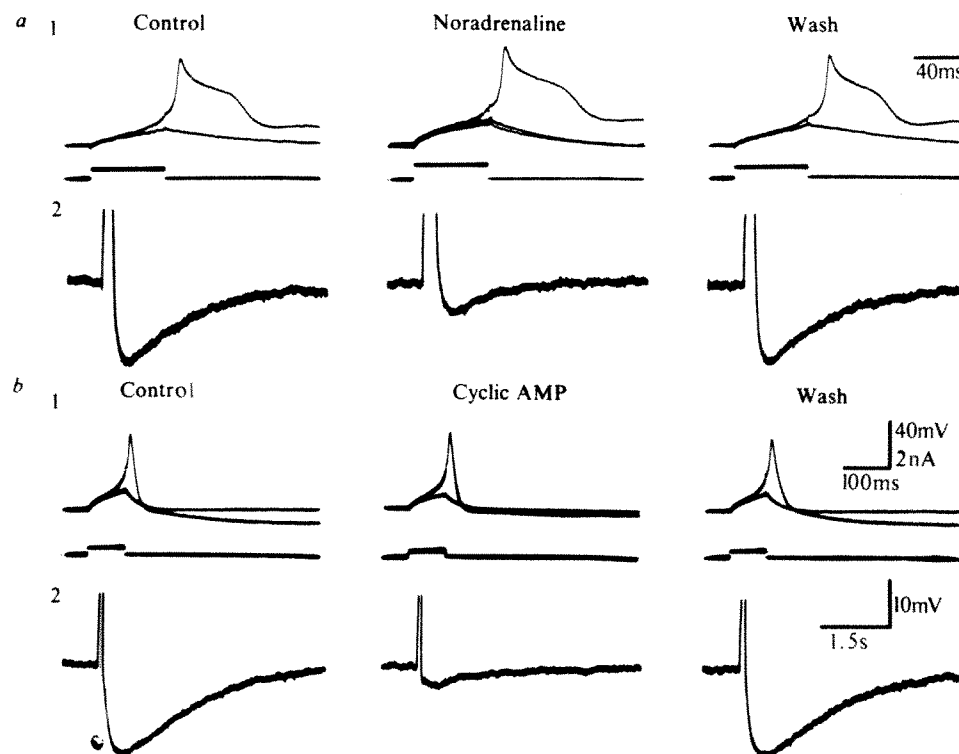


Fig. 2 Noradrenaline and cyclic AMP block calcium-activated potassium responses without reducing calcium spikes. *a*, The top traces (a_1) are film records of the Ca^{2+} spike evoked in a pyramidal cell and the corresponding current pulses. The bottom traces (a_2) are the simultaneously recorded chart records. The preparation was bathed with a solution containing $1\ \mu\text{M}$ tetrodotoxin and $5\ \text{mM}$ tetraethylammonium. The response in the middle column were obtained 7 min after starting the iontophoretic application of NA ($200\ \text{nA}$). In this cell the threshold for spike initiation was slightly increased in NA but this was not a typical finding. The response in 'Wash' was obtained 15 min after termination of NA iontophoresis. Membrane potential $-56\ \text{mV}$. *b* Shows similar responses to those in *a*, but from another cell. The record in the middle column was obtained 9 min after the addition of $1\ \text{mM}$ bromocyclic AMP to the superfusate. The record in 'Wash' was obtained 66 min after returning to the control superfusate. Membrane potential $-62\ \text{mV}$. The calibrations in *a* are the same as in *b* except for the time calibration in a_1 .



We have examined possible mechanisms underlying the ability of NA to block accommodation. A hyperpolarization of a few seconds' duration follows depolarizing current pulses (Fig. 1*b*). This hyperpolarization is due to an initial, fast, K^+ conductance followed by a slow, Ca^{2+} -activated K^+ conductance²¹⁻²³. These two components are most clearly seen in responses to short current pulses (Fig. 1*b*₂). NA reduces the late hyperpolarization but not the initial fast hyperpolarization ($n = 35$). Both the late, Ca^{2+} -activated K^+ conductance and the ability of the cell to accommodate, recover with the same time course following NA washout, suggesting that the failure of the cells to accommodate in the presence of NA is due to block of the Ca^{2+} -activated K^+ conductance. This association is strengthened by experiments in which the Ca^{2+} -activated K^+ conductance was blocked by other means. Thus, like NA, accommodation is attenuated by application of the calcium antagonist cadmium ($0.1\ \text{mM}$, added to control medium; Fig. 1*d*, $n = 10$), or low calcium solution ($2.5\ \text{mM}$ MgCl_2 substituted for CaCl_2 in control medium, $n = 3$), or recording from the cell with an electrode filled with EGTA ($0.2\ \text{M}$ EGTA plus $2\ \text{M}$ KMeSO_4 , $n = 4$). For the experiment using cadmium, in control conditions the cells fired 6.0 ± 2.2 spikes during a large 600-ms pulse, whereas in cadmium they fired 19.0 ± 4.4 spikes ($n = 10$). Furthermore, NA added to cadmium-treated cells had no additional effect.

In sympathetic ganglia, NA blocks the Ca^{2+} -activated K^+ conductance by blocking Ca^{2+} entry into the cell. This effect is mediated by an α -adrenergic receptor²⁴. NA also reduces Ca^{2+} currents in embryonic sensory neurones²⁵. To see if a similar mechanism might explain our results with NA in pyramidal cells, we have examined the effects of NA on Ca^{2+} spikes generated in the presence of tetrodotoxin ($1\ \mu\text{M}$) and tetraethylammonium ($5\ \text{mM}$). NA ($10\ \mu\text{M}$) did not reduce the Ca^{2+} spike, although the subsequent hyperpolarization was severely depressed (Fig. 2*a*). The average reduction of the after-hyperpolarization by $10\ \mu\text{M}$ NA was $87.4\% \pm 18.8$ ($n = 14$). In fact, in the presence of NA, the calcium spike in many cells was prolonged (see Fig. 2*a*), and the cells often fired repetitive Ca^{2+} spikes. These results strongly suggest that NA blocks the Ca^{2+} -activated K^+ conductance at some step that occurs after Ca^{2+} entry into the cell.

The effect of NA on Ca^{2+} -activated K^+ conductance in pyramidal cells is not affected by the α -receptor antagonist

phentolamine ($20\ \mu\text{M}$, $n = 3$), but is antagonized by 10 – $20\ \mu\text{M}$ propranolol, a β -antagonist ($n = 7$). In addition, the β -agonist isoprenaline is approximately 10 times more potent than NA in reducing the Ca^{2+} -activated K^+ conductance ($n = 7$), while the α -agonist phenylephrine is ineffective at $10\ \mu\text{M}$ ($n = 4$). As most β -receptors exert their effects via cyclic AMP, we tested the cyclic AMP analogue, 8-bromo-adenosine 3':5'-cyclic monophosphate (8-bromo-cyclic AMP, 0.1 – $1\ \text{mM}$), and found that its effects mimic exactly those of NA. Thus, it strongly antagonizes the Ca^{2+} -activated K^+ response both in normal medium ($n = 14$) and in medium containing tetrodotoxin and tetraethylammonium (Fig. 2*b*, $n = 4$). This occurs without any reduction of Ca^{2+} spikes (Fig. 2*b*). At a concentration of $1\ \text{mM}$, the average reduction in the Ca^{2+} -activated K^+ response exceeded 80% ($n = 15$). It has recently been reported that 8-bromo-cyclic AMP augments the Ca^{2+} -activated K^+ response in guinea pig hippocampal pyramidal cells²⁶. We have only seen large reductions in this potential and, except for species difference, are unable to explain this discrepancy. 8-Bromo-cyclic AMP also markedly reduces accommodation of cell firing ($n = 5$, not illustrated). In control conditions, the cells fired 7.0 ± 2.0 spikes to strong 600-ms depolarizing pulses, whereas in the presence of $1\ \text{mM}$ of the analogue, the cells fired 16.7 ± 6.7 spikes ($n = 3$). The effect of the cyclic AMP analogue is not mimicked by adenosine ($10\ \mu\text{M}$, $n = 5$), indicating that the effects are not mediated by adenosine receptors. Recording electrodes were also filled with cyclic AMP ($100\ \text{mM}$ in $2\ \text{M}$ KMeSO_4) for intracellular injections. The number of spikes elicited from cells recorded with such electrodes (16.4 ± 2.8 spikes, $n = 5$) is similar to that observed after the extracellular application of the 8-bromo analogue. Forskolin, a diterpene compound which specifically and directly stimulates adenylate cyclase activity in a number of systems²⁷, also mimics the action of NA. In the presence of forskolin ($10\ \mu\text{M}$), a 600-ms depolarizing pulse elicited 18.4 ± 4.3 spikes ($n = 6$). The precise site at which cyclic AMP acts to reduce the Ca^{2+} -activated K^+ conductance is unclear, but it presumably involves some step subsequent to Ca^{2+} entry into the cell. One possible mechanism might be a cyclic AMP-induced alteration in a Ca^{2+} binding protein.

Cyclic AMP or the catalytic subunit of cyclic AMP-dependent protein kinase have been shown to modulate both voltage-sensitive and calcium-activated potassium conductances in a number of invertebrate neurones²⁸⁻³². Our results along with

these others emphasize the importance of both voltage-sensitive and calcium-activated potassium channels as targets for cyclic AMP and transmitter modulation of neuronal excitability.

Thus, our findings show that NA and cyclic AMP profoundly augment the pyramidal cell response to depolarization produced either by current injection or by iontophoresis of glutamate. NA seems to exert this effect by selectively blocking a Ca^{2+} -activated K^{+} conductance. This augmentation can be demonstrated even when NA hyperpolarizes the membrane and depresses the response to threshold current pulses. Such a combined action of suppressing weak inputs and enhancing strong inputs is consistent with the concept advanced by Woodward *et al.*¹³, that NA increases the signal-to-noise ratio in central nervous system neurones. Hippocampal neurones treated with NA thus bear a marked resemblance to the 'quiet readiness' of neurones during arousal³³, a condition associated with an increased firing rate of NA-containing locus coeruleus neurones^{6,7}.

We thank Dr H. Bourne for his interest in this work and for his many helpful suggestions, also Drs Z. Hall and M. P. Stryker for their comments on the manuscript. This work was supported by NIH predoctoral fellowship GM-07449 to D.V.M. and grant NS 15764; RCDA NS 00287 and the Klingenstein Fund to R.A.N.

Received 28 June; accepted 20 August 1982.

- Pickel, V., Segal, M. & Bloom, F. E. *J. comp. Neurol.* **155**, 15–42 (1974).
- Nakamura, S. & Iwama, K. *Brain Res.* **99**, 372–376 (1975).
- Loy, R., Koziell, D. A., Lindsey, J. D. & Moore, R. Y. *J. comp. Neurol.* **189**, 699–710 (1980).
- Moore, R. Y. & Bloom, F. E. *A. Rev. Neurosci.* **2**, 113–168 (1979).
- Mason, S. T. *Prog. Neurobiol.* **16**, 263–303 (1981).
- Aston-Jones, G. & Bloom, F. E. *Neuroscience* **1**, 876–886 (1981).
- Aston-Jones, G. & Bloom, F. E. *Neuroscience* **1**, 887–900 (1981).
- Bloom, F. E. in *Psychopharmacology—A 20 Year Progress Report* (eds Lipton, M. E., Killam, K. C. & Di Mascio, A.) 131–142 (Raven, New York, 1978).
- Hoffer, B. J., Siggins, G. R. & Bloom, F. E. *Brain Res.* **25**, 523–534 (1971).
- Segal, M. & Bloom, F. E. *Brain Res.* **107**, 513–525 (1976).
- Segal, M. *Brain Res.* **206**, 107–128 (1981).
- Langmoen, I. A., Segal, M. & Andersen, P. *Brain Res.* **208**, 349–362 (1981).
- Woodward, D. J., Moises, H. C., Waterhouse, B. D., Hoffer, B. J. & Freedman, R. *Fedn Proc.* **38**, 2109–2116 (1979).
- Rogawski, M. A. & Aghajanian, G. K. *Nature* **287**, 731–734 (1980).
- Waterhouse, B. D., Moises, H. C. & Woodward, D. J. *Neuropharmacology* **20**, 907–920 (1981).
- Kayama, Y., Negi, T., Sugitani, M. & Iwama, K. *Neuroscience* **7**, 655–666 (1982).
- Mueller, A. L., Hoffer, B. J. & Dunwiddie, T. V. *Brain Res.* **214**, 113–126 (1981).
- Moises, H. C., Waterhouse, B. D. & Woodward, D. J. *Brain Res.* **222**, 43–64 (1981).
- Jahr, C. E. & Nicoli, R. A. *Nature* **297**, 227–229 (1982).
- Nicoli, R. A. & Alger, B. E. *J. Neurosci. Meth.* **4**, 153–156 (1981).
- Hotson, J. R. & Prince, D. A. *J. Neurophysiol.* **43**, 409–419 (1980).
- Alger, B. E. & Nicoli, R. A. *Science* **210**, 1122–1124 (1980).
- Schwartzkroin, P. A. & Stafstrom, C. E. *Science* **210**, 1125–1126 (1980).
- Horn, J. P. & McAfee, D. A. *J. Physiol., Lond.* **301**, 191–204 (1980).
- Dunlap, K. & Fischbach, G. D. *J. Physiol., Lond.* **317**, 519–535 (1981).
- Benardo, L. S. & Prince, D. A. *J. Neurosci.* **2**, 415–423 (1982).
- Seamon, K. & Daly, J. W. *J. biol. Chem.* **256**, 9799–9801 (1981).
- Klein, M. & Kandel, E. R. *Proc. natn. Acad. Sci. U.S.A.* **77**, 6912–6916 (1980).
- Deterre, P., Paupardin-Tritsch, D., Bockaert, J. & Gerschenfeld, H. M. *Nature* **290**, 783–785 (1981).
- Adams, W. B. & Levitan, I. B. *Proc. natn. Acad. Sci. U.S.A.* **79**, 3877–3880 (1982).
- Kaczmarek, L. R. & Strumwasser, F. *Neurosci. Abstr.* **7**, 932 (1981).
- DePeyer, J. E., Cachelin, A. B., Levitan, I. B. & Reuter, H. *Proc. natn. Acad. Sci. U.S.A.* **79**, 4207–4211 (1982).
- Livingstone, M. S. & Hubel, D. H. *Nature* **291**, 554–561 (1981).

Retroviruses induce granulocyte-macrophage colony stimulating activity in fibroblasts

Mark J. Koury & Ian B. Pragnell

Beatson Institute for Cancer Research, Garscube Estate, Switchback Road, Bearsden, Glasgow G61 1BD, UK

Murine retroviruses which cause sarcomas also induce abnormal proliferation of haematopoietic cells leading to death in newborn^{1–5} and, in some cases, adult⁶ mice. A murine sarcoma virus is a complex of a replication-defective sarcoma virus and a replication-competent murine leukaemia virus (MuLV). Cloned MuLV isolates also cause abnormal haematopoietic cell proliferations^{6–9}. It is unknown whether such proliferative

responses are direct effects of retroviruses on haematopoietic progenitor cells or indirect effects on other cells, which in turn provide the stimuli for the proliferation of haematopoietic cells. We demonstrate here that specific fibroblastic cell lines produce low levels of granulocyte-macrophage colony stimulating activity (GM-CSA) and that infection of certain fibroblast lines with murine retroviruses results in large increases in GM-CSA. Other cell lines which do not produce detectable CSA when uninfected do not produce it after retroviral infection.

Granulocyte-macrophage colony forming cells (GM-CFC) are haematopoietic progenitor cells which respond to GM-CSA by proliferation and differentiation *in vitro*¹⁰ yielding either pure or mixed colonies of granulocytes and macrophages. Sera of mice having virus-induced leukaemias contain large amounts of GM-CSA compared with sera of uninfected controls^{11,12}. Adult mice injected with myeloproliferative virus (MPSV), one of the sarcoma viruses, develop acute splenomegaly, anaemia and increased numbers of blood granulocytes and granulocytic precursors^{13,14}. These haematological changes are accompanied by fibroblastic proliferation primarily in the bone marrow and

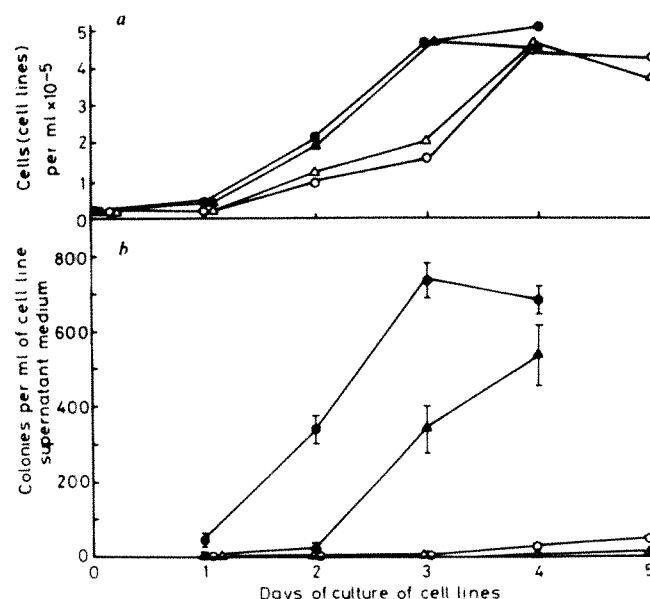


Fig. 1 Effect of sarcoma virus infection on growth and GM-CSA in supernatant medium of cell line cultures. Normal rat kidney (NRK)¹⁵ and mouse embryo (MMCE)¹⁶ cell lines were infected with myeloproliferative virus (MPSV). Infection was confirmed by reverse transcriptase¹⁷ and fibroblast-transforming¹⁸ activities of supernatant culture media. Infected cells and their uninfected controls were cultured in Dulbecco's modified Eagle's minimal essential medium (DMEM) plus 10% fetal calf serum (FCS). Replicate 25-cm² flasks of 1.5×10^5 cells in 7 ml were incubated at 37 °C in 5% CO₂ in air. At daily intervals the medium plus any nonadherent cells of a replicate culture were collected. After centrifugation to pellet any cells, the supernatant medium was filtered through 0.2- μ m² filters and stored at 4 °C. Adherent cells were collected after treatment with trypsin, added to the centrifuged nonadherent cells and total cells were counted. Cell concentrations per ml are shown in *a*. The supernatants were assayed for the presence of GM-CSA with bone marrow cells from 8–12-week-old female BALB/c mice. The assays were done by culturing, in 16-mm diameter wells, 0.5 ml aliquots of 5×10^4 nucleated marrow cells per ml in supplemented DMEM¹⁹. The medium also contained 0.8% methylcellulose, 20% FCS, 100 U ml⁻¹ penicillin, 100 μ g ml⁻¹ streptomycin and 20% cell line supernatant. Colonies of ≥ 50 cells were scored after 7 days incubation at 37 °C in humidified air plus 5% CO₂. Colonies were identical to the types found with spleen cell-conditioned medium as a source of GM-CSA¹⁰. The granulocytes and macrophages were identified by their morphology and by staining with Wright's or Leishman's stain in clotted, fixed cultures²⁰. In cytocentrifuge preparations of washed cultured cells, the morphological studies were confirmed by the staining of the macrophages with α -naphthylacetate esterase and the granulocytes with chloroacetate esterase. CSA per ml of supernatant medium was determined from quadruplicate cultures. (*b*). ●, MPSV-infected NRK; ▲, uninfected NRK; ○, MPSV-infected MMCE; △, uninfected MMCE. All results are ± 1 s.d.

Table 1 Effects of sarcoma virus and MuLV on production of GM-CSA

Cell line/infection	Supernatant activities		
	GM-CFC stimulation (colonies per ml)	Reverse transcriptase	Fibroblast focus formation
NRK			
Uninfected	50 ± 10	—	—
MPSV complex	540 ± 30	+	+
MPSV complex (56 °C)	590 ± 50	—	—
MPSV (NP)	400 ± 50	—	—
ts MPSV (NP) (39 °C)	480 ± 70	—	—
ts MPSV (NP) (33 °C)	550 ± 80	—	—
MuLV-F	280 ± 50	+	—
Moloney complex	390 ± 70	+	+
Moloney (NP)	300 ± 60	—	—
MuLV-Mol	190 ± 40	+	—
Kirsten (NP)	340 ± 30	—	—
SC-1			
Uninfected	110 ± 40	—	—
MPSV complex	590 ± 50	+	+
MPSV complex (56 °C)	540 ± 70	—	—
MuLV-F	470 ± 80	+	—
NIH/3T3			
Uninfected	50 ± 40	—	—
Harvey (NP)	270 ± 40	—	—
FRE			
Uninfected	0	—	—
MPSV complex	0	+	+
MuLV-F	0	+	—
MMCE			
Uninfected	0	—	—
MPSV complex	0	+	+
MuLV-F	0	+	—
Mixed supernatants			
10% FRE (MPSV) + 10% SC-1 (MPSV)	420 ± 50		
10% MMCE (MPSV) + 10% SC-1 (MPSV)	480 ± 30		
10% Culture medium + 10% SC-1 (MPSV)	440 ± 60		
20% Culture medium	0		

Continuous cell lines were infected with sarcoma virus complex, infected with MuLV-F (clone 643/22N; ref. 21), or were isolated containing a defective sarcoma virus component [that is, non-producer cells (NP)]. In the Moloney sarcoma complex the helper virus is Moloney MuLV (MuLV-Mol; ref. 21). Some non-producer lines were superinfected with MuLV-F. Each cell in the cell line cultures was infected as most cell lines were either clones from single infected cells or were chronically infected for at least 2 months before the experiment. The SC-1 and NIH 3T3 cell lines have been described elsewhere^{22,23}. The Fischer rat embryo (FRE) line was a gift from E. Scolnick. The non-producer lines of MPSV, Moloney, Kirsten, and Harvey viruses have been described²¹, as has the temperature sensitive mutant (ts 159/5/1)²⁴. The cells were plated in flasks and cultured as described in Fig. 1 legend. After 2 days of culture when the cells were subconfluent, the medium was changed and they were allowed to grow to confluence for the following 2 days. After the second 2-day period, the supernatant medium was collected, processed, and GM-CSA determined from quadruplicate cultures as described in Fig. 1 legend. Supernatants were collected from cultures having similar numbers of cells. Adjustments for cell numbers were made in the supernatant assays of ts mutants due to altered growth rates at the permissive (33 °C) and nonpermissive (39 °C) temperatures for sarcoma phenotypic expression. Heat-treated samples were raised to 56 °C for 30 min. Reverse transcriptase and focus-forming assays were done on supernatant media (see Fig. 1 legend). All results are ± 1 s.d.

later in the spleen¹³. Sera of mice during these acute stages of MPSV infection show large increases in GM-CSA compared with controls (our unpublished results). However, *in vivo* studies do not reveal the mechanism by which retrovirus infection results in these pathological changes. Because of its effects on fibroblast and granulocyte proliferation and on serum GM-CSA, we initially used MPSV to investigate the relationship between infection of fibroblasts by sarcoma virus and the induction of haematopoietic proliferation.

Cell lines infected with MPSV were compared with uninfected controls for growth and for GM-CSA production (Fig. 1). Similar growth was observed in infected and uninfected cultures (Fig. 1a). During the first two days of culture, the supernatant medium of normal rat kidney (NRK) cells contained slight amounts of GM-CSA, while infected NRK cells had much greater amounts of GM-CSA in their supernatant medium (Fig

1b). Supernatants of infected and uninfected NRK cells cultured for 4 days stimulated the growth of similar numbers of colonies (Fig. 1b), but the colonies stimulated by infected cell supernatants contained several hundred of cells per colony while those stimulated by uninfected cell supernatants contained 50–100 cells. This difference in colony size suggested a greater amount of GM-CSA in the infected cell supernatants. The increased amount of GM-CSA in the 4 day-infected cell supernatants was confirmed by dose titration as shown in Fig. 2. In contrast to NRK cells, a mouse embryo cell line, MMCE, had negligible GM-CSA in the supernatant medium at all times, whether the cells were infected or uninfected (Fig. 1b). This lack of GM-CSA occurred despite MMCE cell growth to concentrations sufficient for large amounts of GM-CSA production by NRK cells.

Other cell lines and viruses were also examined (Table 1). In this study we found that some cell lines had constitutive production of GM-CSA while other lines did not. This ability to produce GM-CSA effective for mouse GM-CFC development was found in fibroblast lines of both adult and fetal origin and in lines of both rat and mouse origin. However, if a cell produced GM-CSA when uninfected, then infection with MPSV, MuLV, or the defective sarcoma virus (that is, non-producer state) resulted in large increases in GM-CSA. A consistent pattern in multiple experiments was that the largest increase in GM-CSA occurred with sarcoma complex infections, with slightly less of an increase for sarcoma non-producers, and the smallest increase with MuLV infections. Moloney, Kirsten, and Harvey sarcoma viruses increased GM-CSA as well as MPSV (Table 1). Conversely, if GM-CSA in the supernatant of an uninfected cell line was not detected, then infection of the line did not induce any GM-CSA after 2 days (Table 1) and even 5 days of culture (data not shown). The lack of GM-CSA in MMCE and FRE supernatants was not due to an inhibitor of colony formation, as shown by mixing experiments (Table 1).

Retroviruses did not directly stimulate colony growth as non-producer cell supernatants (which lack virus particles) and heat-treated supernatants (which have inactivated virus) both showed increased GM-CSA (Table 1). Furthermore,

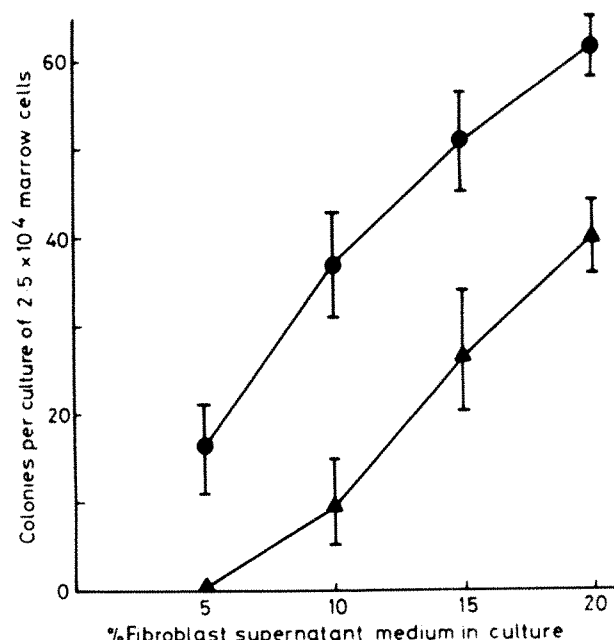


Fig. 2 Titration of GM-CSA in fibroblast line supernatants. The same day 4 supernatants of MPSV-infected and uninfected NRK cells as in Fig. 1 were assayed at various dilutions for GM-CSA. The assay was performed as described in Fig. 1 legend. All data are ± 1 s.d. for quadruplicate cultures. ●, MPSV-infected NRK; ▲, uninfected NRK.

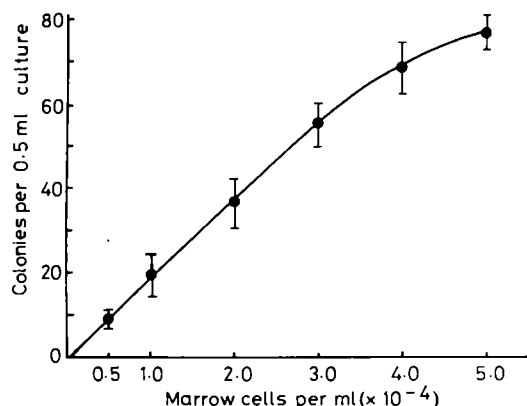


Fig. 3 Effect of decreasing the number of marrow cells on the assay of GM-CSA from infected cells. Supernatant from 2-day cultures of MPSV-infected SC-1 cells comprised 20% of the GM-CSA assay medium as described in Fig. 1 legend. Marrow cell concentrations in the assay were varied as shown. All data are ± 1 s.d. of quadruplicate cultures.

phenotypic expression of the sarcoma genome (that is, morphological transformation) was not necessary for increased GM-CSA production because cells infected with a temperature-sensitive mutant of MPSV had similar GM-CSA production at both permissive and non-permissive temperatures (Table 1). The direct GM-CSA action on GM-CFC is suggested by the linear slope intersecting zero as cell number is decreased in the assay (Fig. 3). Colonies grown with infected NRK or SC-1 cell supernatants were generally 50% macrophage, 25% granulocyte and 25% mixed.

Although it is not known how retroviruses cause the abnormal haematopoietic proliferation found in infected mice, our results suggest that large increases in the production of haematopoietic growth factors by infected fibroblasts may well play a part in the process. This indirect action of the virus on the haematopoietic progenitor cells may be further amplified in the case of the sarcoma viruses. In these infections, sarcomatous growth of fibroblasts or other mesodermal cells could result in an increased number of cells, each producing an increased amount of haematopoietic growth factor.

The studies were funded by grants from the Leukaemia Research Fund, the MRC and the Cancer Research Campaign. We thank Dr W. Ostertag for his advice about and supply of cloned cell lines and viruses and Dr T. M. Dexter for his advice about colony assays.

Received 5 July; accepted 9 August 1982.

- Harvey, J. J. *Nature* **204**, 1104–1105 (1964).
- Perk, K. & Moloney, J. B. *J. natn. Cancer Inst.* **37**, 581–599 (1966).
- Kirsten, W. H. & Mayer, L. A. *J. natn. Cancer Inst.* **39**, 311–335 (1967).
- Chirigos, M. A., Scott, D., Turner, W. & Perk, K. *Int. J. Cancer* **3**, 223–237 (1968).
- Scher, C. D., Scolnick, E. M. & Siegler, R. *Nature* **256**, 225–226 (1975).
- Fischinger, P. J., Moore, C. O. & O'Connor, T. E. *J. natn. Cancer Inst.* **42**, 605–622 (1969).
- Troxler, D. H., Ruscetti, S. K., Linemeyer, D. L. & Scolnick, E. M. *Virology* **102**, 28–45 (1980).
- MacDonald, M. E., Mak, T. N. & Bernstein, A. *J. exp. Med.* **151**, 1493–1503 (1980).
- McGarry, M. P., Steeves, R. A., Eckner, R. J., Mirand, E. A. & Trudel, P. J. *Int. J. Cancer* **13**, 867–878 (1974).
- Burgess, A. W. & Metcalf, D. *Blood* **56**, 947–958 (1980).
- Robinson, W., Metcalf, D. & Bradley, T. R. *J. cell. Physiol.* **69**, 83–91 (1976).
- Metcalf, D. & Foster, R. J. *J. natn. Cancer Inst.* **39**, 1235–1245 (1967).
- LeBousse-Kerdiles, M. C., Smadja-Joffe, F., Klein, B., Caillou, B. & Jasmin, C. *Eur. J. Cancer* **16**, 43–51 (1980).
- Klein, B. *et al. J. natn. Cancer Inst.* **66**, 935–940 (1981).
- Huu, D., Rosenblum, E. N. & Zeigel, R. F. *J. Bact.* **92**, 1133–1140 (1966).
- Rapp, U. R., Keski-Oja, J. & Heine, U. *Cancer Res.* **39**, 4111–4118 (1979).
- Pragnell, I. B., Ostertag, W. & Paul, J. *Exp. Cell Res.* **108**, 268–276 (1977).
- Billette, J. A., Strand, M. & August, J. T. *Proc. natn. Acad. Sci. U.S.A.* **71**, 3234–3238 (1974).
- Kost, T. A., Koury, M. J. & Krantz, S. B. *Virology* **108**, 309–317 (1981).
- McMahon, Y. & Hankins, W. D. *Exp. Hemat.* **8**, 1081–1085 (1980).
- Ostertag, W. *et al. J. Virol.* **33**, 573–582 (1980).
- Hartley, J. W. & Rowe, W. P. *Virology* **65**, 128–134 (1975).
- Todaro, G. J. & Green, H. *J. Cell Biol.* **17**, 299–313 (1963).
- Ostertag, W. *et al. in Expression of Differentiated Functions in Cancer Cells* (ed. Revoltella, R.) 401–416 (Raven, New York, 1981).

Differential expression of cellular oncogenes during pre- and postnatal development of the mouse

Rolf Müller*, Dennis J. Slamon†, Joanne M. Tremblay*, Martin J. Cline† & Inder M. Verma*

* Tumor Virology Laboratory, The Salk Institute, PO Box 85800, San Diego, California 92138, USA

† Division of Hematology/Oncology, Department of Medicine, UCLA Medical Center, Los Angeles, California 92004, USA

The acutely oncogenic retroviruses induce a wide spectrum of malignancies including sarcomas, carcinomas, lymphomas and leukaemias¹. They all contain sequences which are required for neoplastic transformation as an integral part of their genomes^{1–3}. These sequences, termed viral oncogenes (*v-onc*), apparently originated from the normal vertebrate genome. To date, cellular homologues of over a dozen different oncogenes of acutely oncogenic viruses have been identified^{1–4}. Although transcription of some *c-onc* genes has been detected in normal vertebrate cells^{1,5–7}, relatively little is known about their role in normal cell metabolism. We describe here stage- and tissue-specific expression of cellular genes homologous to the oncogenes of FBJ murine osteosarcoma virus, Abelson murine leukaemia virus and Harvey sarcoma virus during mouse prenatal and early postnatal development. Our results suggest participation of cellular oncogenes in normal developmental processes.

The FBJ murine osteosarcoma virus (FBJ-MSV) complex was isolated from a spontaneous tumour in a 260-day-old CF1 mouse⁸. Serial passage of cell-free tumour extracts in newborn mice resulted in a virus stock which induced osteosarcomas with a latency as short as 3 weeks⁹. A 55,000 molecular weight (55K) protein encoded by the FBJ-MuSV transforming gene (*v-fos*) has been described previously¹⁰. The cellular homologue of *v-fos* could be identified in DNA of normal vertebrate cells¹¹.

Relatively high levels of *c-fos*-related sequences were detected in poly(A⁺) RNA prepared from day 6, 7, 8 and 9 conceptuses containing the embryo proper and extraembryonal tissues (Figs 1a, 2a). More than 10-fold lower *fes* expression was observed in embryos of later developmental stages dissected free of extraembryonal tissues (Fig. 1a), as measured by density scanning of the autoradiogram (Fig. 1c). To determine if this dramatic change is due to a stage-specific *c-fos* expression in the embryo proper or rather a consequence of a cell-type-specific expression in an extraembryonal tissue, we analysed poly(A⁺) RNA prepared separately from day 10 embryos, extraembryonal membranes and placenta. Figure 2a shows that *c-fos*-related transcripts were found at considerably higher quantities in the placenta (PL) than in the embryo proper (E) and the extraembryonal membranes (M). Consistent with these observations is the high level of *c-fos* expression in day 18 placenta and the absence of significant amounts of *c-fos*-related transcripts in day 12 extraembryonal membranes. These findings suggest that *c-fos* expression at early developmental stages (days 6–9) probably occurs in cells which give rise to the placenta at later developmental stages. Expression of *c-fos* in the fetus increases about fivefold at later stages of development (after day 16 of gestation, Fig. 1a, c). In an attempt to identify cells expressing *c-fos* transcripts, we analysed poly(A⁺) RNA from various postnatal tissues. Figure 2b shows that low levels of *c-fos* expression were observed in all tissues investigated. However, RNA isolated from 'bone' (sternum, ribs and vertebra of 1–3 day old mice, including bone marrow, muscles and part of the pleura) and 'skin' (including the subcutaneous connective

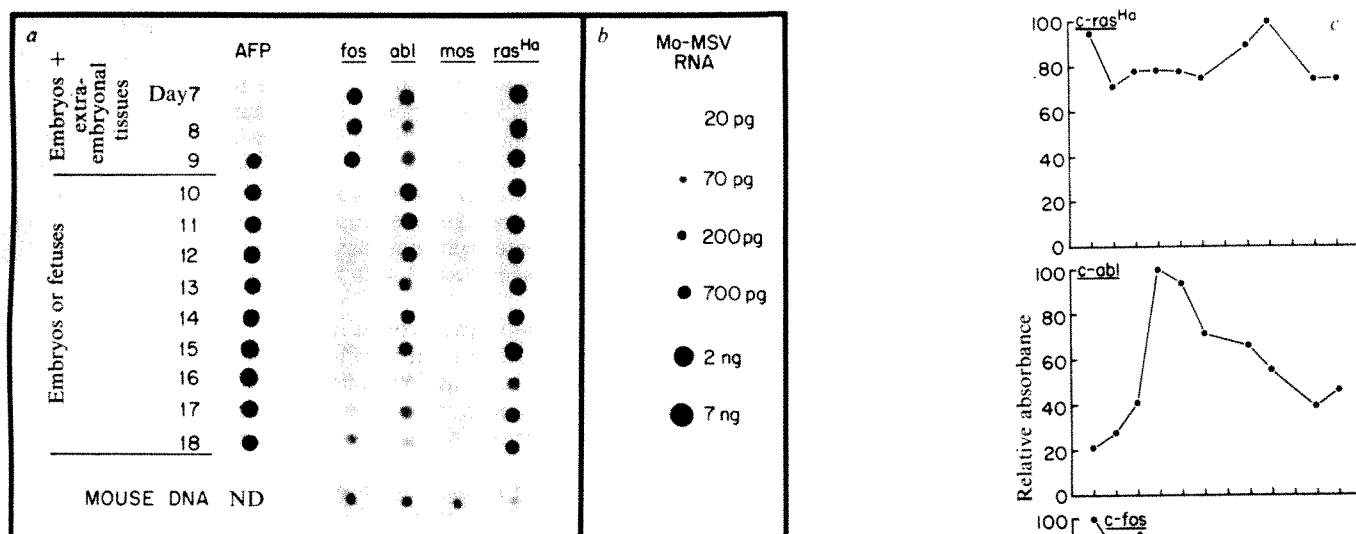


Fig. 1 *a*, Expression of cellular oncogenes during mouse prenatal development. RNA was isolated from Swiss-Webster mouse embryos/fetuses at daily intervals using the guanidine thiocyanate method²⁷. Beginning at day 10 of prenatal development (day of coital plug was taken as day 0 of prenatal development) the embryo proper was separated from the extra-embryonal membranes and placenta. Separation was not performed before this stage because of the very small size of the embryo proper. Therefore, day 6–9 embryos represent the entire conceptus as dissected from the uterine wall. RNA was selected for poly(A⁺) RNA by one cycle of chromatography on oligo(dT)–cellulose columns²⁸. Poly(A⁺) RNA was dissolved in H₂O, boiled, quick-cooled on ice, and 3 μ g (1.5 μ l) applied to sheets of nitrocellulose paper which had previously been equilibrated with 20 \times SSC (1 \times SSC is 0.15 M NaCl, 0.015 M sodium citrate) and air dried. After baking overnight at 80 °C the blots were prehybridized for at least 4 h at 45 °C in a buffer containing 0.75 M NaCl, 0.05 M sodium phosphate (pH 7.5), 0.005 M EDTA, 0.2% SDS, 10 mg per ml glycine, 5 \times Denhard's reagent (1 \times Denhard's reagent is 0.02% each of Ficoll, bovine serum albumin and polyvinylpyrrolidone), 0.25 mg of denatured herring DNA per ml and 50% formamide. Subsequently, the blots were hybridized for ~20 h at 45 °C with 1 \times 10⁶ c.p.m. of nick-translated probe per ml of hybridization buffer (same composition as prehybridization buffer except that the concentration of Denhard's reagent was decreased to 1 \times). The cloned oncogene fragments purified from vector sequences by preparative agarose gel electrophoresis were nick-translated²⁹ in the presence of either [³⁵S]-dATP (500 Ci mmol⁻¹, used for the α -fetoprotein (AFP)-specific probe) or [³²P]-dCTP (3,200 Ci mmol⁻¹, used for all the other probes) to specific radioactivities of ~2 \times 10⁸ c.p.m. per μ g of DNA for ³⁵S-labelled probes and 1–2 \times 10⁹ c.p.m. per μ g of DNA for ³²P-labelled probes, respectively. The following fragments from cloned retroviral genomes were used as *onc*-specific probes: *fos*, *Bgl*II–*Pvu*II (1.3 kbp) or *Pst*I–*Pvu*II (1.0 kbp; ref. 11); *mos*, *Xba*I–*Hind*III (1.1 kbp; ref. 30); *abl*, *Sma*I–*Bgl*II (~1.2 kbp; ref. 31); *ras*^{Ha}, *Bgl*II–*Sal*I (0.46 kbp; ref. 32). After hybridization the blots were washed three times in 1 \times SSC at 50 °C for about 2 h and exposed to X-ray films with intensifying screens at –70 °C for 72 h. Bottom row: hybridization of probes to total mouse genomic DNA. One microgramme of heat-denatured mouse DNA was applied to the same nitrocellulose filters used for RNA analysis and thus subjected to the same hybridization procedure, to assess the relative extent of hybridization of the nick-translated viral oncogene probes to the corresponding mouse homologue in the conditions used. ND, not done. A crucial point of the validity of the present results is the authenticity of RNA samples isolated from embryos/fetuses and extraembryonal tissues at distinct stages of prenatal development. We therefore included in all studies concerning prenatal development a mouse AFP-specific probe (pBR322-AFP2; ref. 33). AFP polypeptide is known to be expressed exclusively in visceral endoderm (starting at around day 7 of prenatal development in a few cells) and at later developmental stages also in fetal liver^{34,35}. We observed absence or very low levels of AFP-related mRNA transcripts in day 6, 7 and 8 conceptuses as compared with embryos/fetuses of later developmental stages as well as relatively low AFP expression in 10-day embryos as compared with, for example, extraembryonal membranes (Figs 1a, 2a). Our findings agree closely with those of previously published studies on protein expression^{34,35}. *b*, Sensitivity of dot blot analysis. The *v-mos*-specific probe was hybridized to varying amounts of sucrose-gradient purified 60/70 Mo-MSV RNA spotted on nitrocellulose paper. The experiment was performed essentially as described above. The detection limit was ~20 pg of Mo-RSV RNA (5.6 kb, equivalent to ~1 RNA transcript of ~3 kb per cell; ~2 μ g of poly(A⁺) RNA applied to filter). Exposure time was 48 h. *c*, Quantitation of *c-osc* expression during mouse prenatal development. The dot blot autoradiogram shown in *a* was evaluated by soft laser density scanning and the relative absorbance was plotted against the stage of development. Values were normalized to 100 for the highest level of expression in the case of each *c-osc*. Day 16 was not considered because the amount of poly(A⁺) RNA applied to the filter (*a*) was considerably lower than for all other developmental stages, as shown by a shorter exposure of the AFP blot (*a*).

tissue, muscles and part of the peritoneum) from 1–3 day old mice showed a 5–20-fold greater hybridization to the *fos*-specific probe than did RNA from all other tissues (Fig. 2b). Little transcriptional activity of *c-fos* could be detected in any haematopoietic tissue (Fig. 2b), including fetal liver (data not shown). Therefore, it appears that those cells exhibiting high levels of *c-fos* expression are not located in the bone marrow. Moreover, elevated levels of *c-fos* expression were also observed in 'skin' (Fig. 2b), suggesting that the enhanced *c-fos* transcription occurs in cells of mesenchymal origin which participate in the formation of serous membranes or connective tissues. A role of the *c-fos* gene in normal bone differentiation would be of particular interest, as its viral homologue (*v-fos*) has been implicated in the induction of osteosarcomas by FBJ-MSV in newborn mice^{8–11}.

To characterize the size of the *c-fos* transcripts, poly(A⁺) RNA isolated from embryos/fetuses of various developmental stages was analysed by agarose gel electrophoresis and Northern blotting on nitrocellulose paper (Fig. 3A). A single transcript of ~2.2 kilobases (kb) was detected in day 7 conceptuses and day 18 fetuses, consistent with the results obtained by dot blot analysis (Fig. 1a). Similarly, a 2.2-kb *c-fos*-specific transcript was observed only in day 10 placenta, not in extraembryonal

membranes (Fig. 3A). In agreement with the dot blot analysis (Fig. 2b), a 2.2-kb transcript was also found in poly(A⁺) RNA isolated from 'bones' and 'skin' of newborn animals (Fig. 3A).

Albion murine leukaemia virus (A-MuLV) induces lymphosarcomas of pre-B-cell origin¹² and T-cell lymphomas¹³ in mice. In virus-transformed cells, a 120K protein (p120^{abl}) encoded by the A-MuLV oncogene (*v-abl*) has been identified¹⁴. In normal cells of murine haematopoietic tissues, a 150K protein (NCP150), which can be immunoprecipitated by an anti-A-MuLV tumour regressor serum, has also been reported¹⁵.

Despite significant transcriptional activity of *c-abl* throughout mouse prenatal development, a differential pattern of expression was observed. RNA transcripts related to *c-abl* were found at three- to fivefold lower concentrations in poly(A⁺) RNA isolated from day 6, 7, 8 and 9 conceptuses containing the embryo proper and extraembryonal tissues than from embryos/fetuses at day 10–11 of prenatal development which are devoid of extraembryonal tissues (Figs 1a, 1c, 2a). Accordingly, *c-abl* is expressed at about threefold higher levels in the embryo proper than in day 10 extraembryonal membranes and placenta (Fig. 2a) as determined by density scanning of the autoradiogram. Based on the dot blot analyses

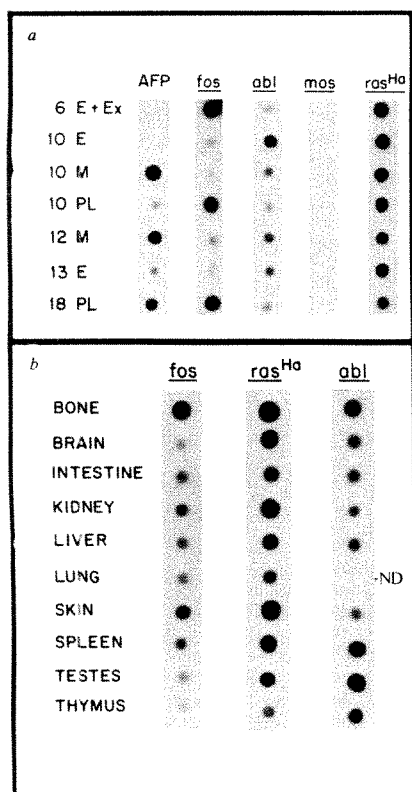


Fig. 2 *a*, Expression of *c-onc* genes in mouse embryos compared with extraembryonal tissues. The embryo proper was surgically separated from the extraembryonal membranes (that is, amnion and visceral yolk sac) and the placenta. Isolation of poly(A⁺) RNA and performance of dot blots were as described in Fig. 1a, legend except that 0.5 μ g of twice poly(A⁺) RNA (selected twice) was spotted onto the nitrocellulose filter in each case. All probes were ³²P labelled. Blots were exposed for 1 h (AFP) and 72 h (all others), respectively. Day 6 embryos containing extraembryonal tissues (6E + Ex); day 10 embryos (10E), membranes (10M) and placenta (10PL); day 12 membranes (12M); day 13 embryo (13E); day 18 placenta (18 PL), containing part of the adherent membranes. *b*, Expression of *c-onc* genes in postnatal mouse tissues. The dot blot analysis of poly(A⁺) RNA (selected once) was carried out exactly as described above. Blots were exposed for 72 h (*fos*) and 24 h (*abl*, *ras*^{Ha}), respectively. All tissues were dissected from 10-day-old mice except for bone, skin (see text) (1–3 day old mice) and testes (3-month-old mice). A potential difficulty with the quantitative evaluation of this blot is the possible variability in mRNA content of various tissues. Thus, equal amounts of poly(A⁺) RNA from different tissues have not necessarily been extracted from equal numbers of cells. Furthermore, the amount of mRNA in poly(A⁺) RNA fractions obtained from different tissues can be subject to considerable variations. Therefore, less than threefold differences on this blot autoradiogram could reflect such variations rather than differences in gene expression.

(Figs 1a, c, 2a), expression of *c-abl* in the fetus seems to decrease after day 11 of prenatal development. These results could suggest transcriptional activity of *c-abl* in various tissues, with at least one cell type expressing *c-abl* at significantly higher levels. This explanation is lent further support by the fact that *c-abl* is expressed in all postnatal mouse tissues examined, with spleen and thymus poly(A⁺) RNA exhibiting a stronger hybridization (~threefold) to the *abl*-specific probe than poly(A⁺) RNA from other tissues (Fig. 2b). By far the highest level of *c-abl* expression was observed in testes of young adult mice (Fig. 2b). Size analysis by agarose gel electrophoresis and Northern blotting revealed two size classes of *c-abl* transcripts of approximately 4.7 and 5.7 kb in day 6, 10 and 13 embryos as well as in postnatal thymus and spleen (Fig. 3B). In adult testes, an additional transcript of 3.7 kb was detected which is considerably more abundant than the 4.7- and 5.7-kb mRNAs (Fig. 3B). This observation may suggest that initiation or termination of *c-abl* transcription or splicing of the *c-abl*-related transcript is a precisely modulated tissue-specific mechanism.

Harvey sarcoma virus (HaSV) causes erythroleukaemia and sarcomas in rodents¹⁶. Its transforming gene (*v-ras*^{Ha}) originated from normal rat cellular sequences¹⁷. A *ras*^{Ha}-encoded protein of molecular weight 21K (p21) has been identified in

both virus-transformed and normal mouse cells^{18,19}. In the present study, *c-ras*^{Ha} was found to be expressed at considerable, but similar levels at all stages of prenatal development, both in the embryo proper and in extraembryonal tissues (Figs 1a, c, 2a). High levels of *c-ras*^{Ha} expression were also observed in various tissues of newborn or 10-day-old mice, particularly in 'bone', brain, kidney and 'skin' (Fig. 2b). Analysis of poly(A⁺) RNA by agarose gel electrophoresis and Northern blotting indicates a heterogeneous class of *c-ras*^{Ha}-related transcripts with an average size of 1.4 kb for all pre- and postnatal tissues (Fig. 3C).

Mo-MSV induces sarcomas in mice²⁰. The oncogene (*v-mos*) of Mo-MSV has a counterpart (*c-mos*) in the genome of normal vertebrate cells. A sustained effort to detect expression of *c-mos* sequences in uninfected mouse cells has proved unsuccessful^{21,22}. No expression of *v-mos* sequences was observed during mouse prenatal development (Figs 1a, 3A). It has recently been suggested that *c-mos* sequences are highly methylated, which may prevent their transcription²². The lack of RNA hybridization to the *v-mos*-specific probe in Fig. 1 shows that nonspecific hybridization is minimal in the dot blot analysis used in the present study.

Embryos and unfractionated tissues consist of a great variety of cell types, which may exhibit considerably different levels of *c-onc* expression. Therefore, studies pertaining to a quantitative evaluation of *c-onc* expression can only yield average values for the heterogeneous cell population of a given tissue or an embryo at a particular developmental stage. However, to obtain an estimation of the order of *c-onc* expression in mouse embryos, transcriptional activity of *c-abl* and *c-ras*^{Ha} in total embryos at day 11 of prenatal development was compared with expression of the corresponding *v-onc* genes in cell lines transformed by A-MuLV or HaSV. Figure 4 shows that the relationship between the amount of RNA applied to the filter and the signal observed on the autoradiogram is approximately linear. The levels of *v-onc* expression in the virus-transformed cell lines were found to be about 10-fold higher than expression of the corresponding *c-onc* genes in the total embryo (Fig. 4). Because one can assume that certain *c-oncs* are expressed at significantly elevated levels only in a limited number of cells, the level of expression in these particular cells is presumably much higher than the observed average value.

Significant expression of the *c-fos* gene has been detected during mouse prenatal development specifically in the placenta (Figs 1a, 2a, 3A). Both fetal and maternal moieties of the mouse placenta—trophoblast and decidua—are very rapidly proliferating tissues. The mouse trophoblast has been considered a 'pseudo-malignant' tissue, because it grows invasively into the uterine epithelium or any other surrounding tissue²³. It will now be of particular interest to determine if these growth properties can be correlated with the expression of a *c-onc* gene like *c-fos*. The pattern of *c-abl* expression in postnatal tissues (Figs 2b, 3B) suggests a physiological role of this *c-onc* gene in the male germ cell lineage, and possibly a different role in development of lymphatic tissues. In day 10–12 embryos, however, cell types exhibiting high levels of *c-abl* expression could not be identified, but apparently are not germ cell precursors, as the testes-specific 3.7 kb *c-abl* transcript does not seem to be present in embryos of any developmental stage (Fig. 3B). The role of *c-ras*^{Ha} in physiological processes remains obscure because it is expressed in embryos/fetuses of all developmental stages as well as in a variety of pre- and postnatal tissues at similar levels (Figs 1a, c, 2, 3C). It has been shown that *c-ras*^{Ha} linked to a retroviral long terminal repeat induces uncontrolled cell proliferation when introduced into a mouse fibroblastic cell line¹⁷. This finding suggests that a role of *c-ras*^{Ha} in normal cell proliferation is possible, but, however, may be confined to particular cell types.

In the present study, as well as in another investigation²⁴ concerned with expression of avian oncogenes, we have demonstrated differential transcriptional activity of *c-onc* genes during pre- and early postnatal development of the mouse. Our

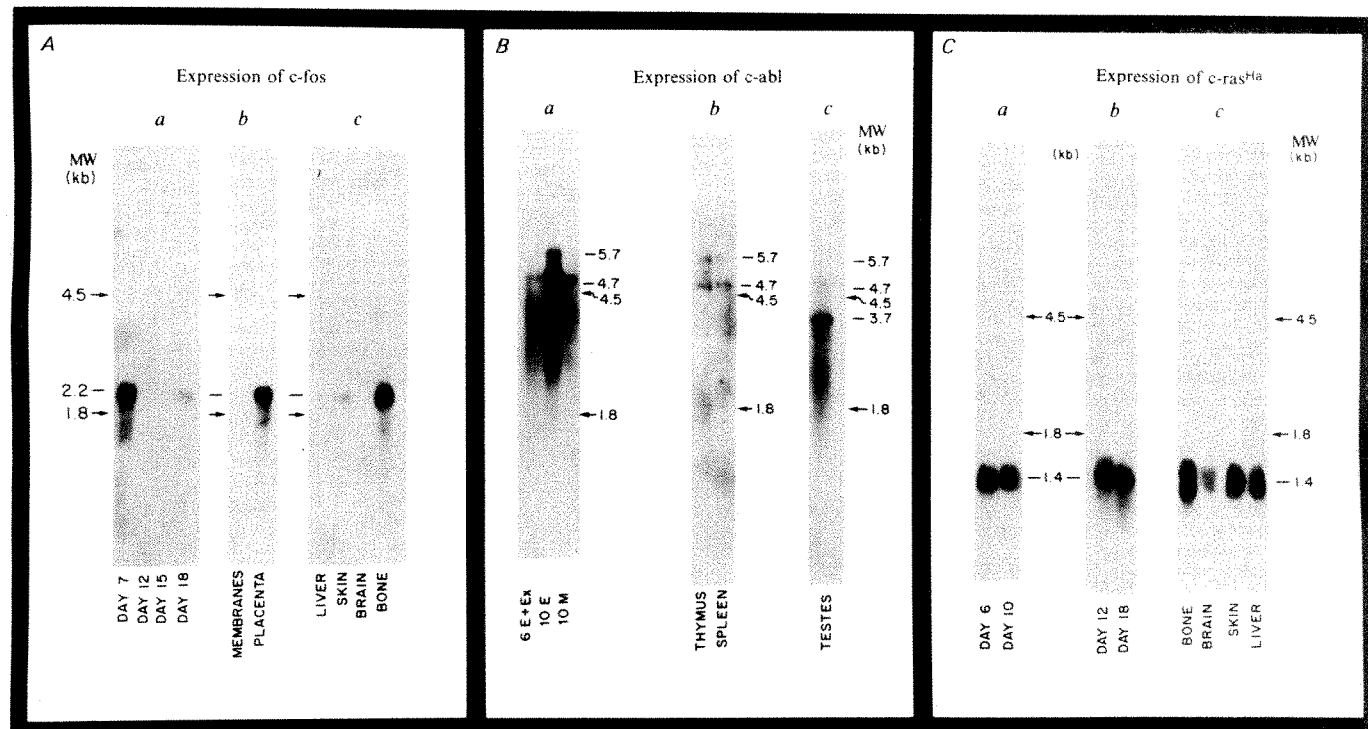


Fig. 3 *A*, *c-fos* Transcripts in total mouse embryos/fetuses and various tissues. Twenty-five microgrammes of poly(A⁺) RNA (selected once; *a*, *c*) or 10 μ g of poly(A⁺) RNA (selected twice; *b*) (isolated as described in Fig. 1a legend) were denatured in the presence of 1 M glyoxal, 20 mM sodium phosphate pH 7.0, for 1 h at 50 °C. The denatured RNA was separated on horizontal 1.1% agarose gels made up and run in 10 mM sodium phosphate buffer pH 7.0 for about 20 h at 35 V, and thereafter blotted on to nitrocellulose paper with 20 \times SSC36. Blots were baked for 3 h at 80 °C and prehybridized, hybridized and washed as described for dot blots in Fig. 1a, except that the hybridization was carried out in the presence of 5 \times 10⁶ c.p.m. of nick-translated probe per ml for 60 h at 45 °C. Blots were exposed for 60 h (*a*) and 18 h (*b*, *c*), respectively. *a*, Day 7 embryos containing extraembryonal tissues; day 12, 15, 18 total embryos/fetuses. *b*, Day 10 membranes and day 10 placenta. *c*, Bone and skin from 1–3-day-old mice; brain and liver from 10-day-old mice. Arrows indicate the positions of 18S/28S ribosomal RNA markers. *B*, *c-abl* Transcripts in total mouse embryos and tissues. Ten microgrammes of poly(A⁺) RNA (selected twice; *a*) or 20 μ g of poly(A⁺) RNA (selected once; *b*, *c*) were electrophoresed and analysed as described above. Blots were exposed for 24 h (*a*, *c*) and 96 h (*b*), respectively. *a*, Total embryos and extraembryonal tissue (see Fig. 2a legend). *b*, *c*, Postnatal mouse tissues (see Fig. 2b legend). *C*, *c-ras^{Ha}* Transcripts in mouse embryos/fetuses and various postnatal mouse tissues. Ten microgrammes of poly(A⁺) RNA (selected twice; *a*) or 20 μ g of poly(A⁺) RNA (selected once; *b*, *c*) were separated by agarose gel electrophoresis and analysed by Northern blotting essentially as described above. Blots were exposed for 24 h. *a*, *b*, RNA from day 6, 10, 12 and 18 embryos/fetuses (day 6 embryos included also extraembryonal tissues). *c*, Various postnatal tissues (see Fig. 2b legend).

findings lend support to the widely held notion that *c-onc* genes are involved in developmental processes like cell proliferation and differentiation^{25,26}.

We thank Drs E. Adamson, A. Berns, T. Curran, T. Hunter, B. Sefton, C. Van Beveren and M. Vogt for critical reading of the manuscript and valuable suggestions, S. Pitts for technical assistance, Drs S. P. Goff, D. R. Lowy and S. M. Tilghman for

recombinant plasmids containing sequences specific for *v-abl*, *v-ras^{Ha}* and AFP respectively and Dr T. Curran for *v-fos*-specific fragment. R.M. is the recipient of a postdoctoral fellowship from the Deutsche Forschungsgemeinschaft. This work was supported by grants from NIH and ACS (to I.M.V.), and from Brown and Williamson, Philip-Morris, Inc., R. J. Reynolds, and U.S. Tobacco Co. (to M.J.C.).

Fig 4 Level of *c-onc* expression in embryos compared with virus-transformed cell lines. 1.5 μ g of poly(A⁺) RNA (selected once) from embryos at day 11 of prenatal development and various amounts of poly(A⁺) RNA from virus-transformed cell lines were spotted on nitrocellulose paper and hybridized to *onc*-specific probes as described above. The blot was exposed for 24 h. Relative absorbances indicate the values measured by density scanning of the autoradiogram normalized to 100 for 0.5 μ g of RNA. * Absorbance readings obtained from autoradiograms exposed for only 6 h; RAW253 (cell line derived from an A-MuLV-induced mouse B-cell lymphoma)³⁷, ANN-1 (NIH/3T3 cell line transformed by A-MuLV *in vitro*)³⁸, 3T3-Ha8-21 (NIH/3T3 cell line transformed by HaSV *in vitro*)³⁹.

RNA (μ g)	<i>abl</i>			<i>ras^{Ha}</i>		
	RAW 253	Relative absorbance	ANN-1	Relative absorbance	3T3-Ha8-21	Relative absorbance
1.5		286*		248*		252*
0.5		100		100		100
0.15		42		36		45
0.05		10		10		10
0.015		< 5		< 5		< 5
0.005		< 5		< 5		< 5

Received 7 June; accepted 12 August 1982.

1. Weiss, A., Teich, N. M., Varmus, H. & Coffin, J. M. (eds) *RNA Tumor Viruses. The Molecular Biology of Tumor Viruses Part III* (Cold Spring Harbor Monograph 10C, Cold Spring Harbor, New York 1982).
2. Bishop, J. M. *Scient. Am.* **246**, 68-78 (1982).
3. Coffin, J. M. *et al. J. Virol.* **40**, 953-957 (1981).
4. Bishop, J. M. *A. Rev. Biochem.* **47**, 35-88 (1978).
5. Chen, J. H. *J. Virol.* **36**, 162-170 (1980).
6. Shibuya, M., Hanafusa, H. & Balduzzi, P. L. *J. Virol.* **42**, 143-152 (1982).
7. Gonda, T. J., Sheiness, D. K. & Bishop, J. M. *Molec. cell. Biol.* **2**, 617-624 (1982).
8. Finkle, M. P., Biskis, B. O. & Jinkins, P. B. *Science* **151**, 698-701 (1966).
9. Finkel, M. P. & Biskis, B. O. *Prog. exp. Tumor Res.* **10**, 72-111 (1968).
10. Curran, T. & Teich, N. M. *J. Virol.* **42**, 114-122 (1982).
11. Curran, T., Peters, G., Van Beveren, C., Teich, N. M. & Verma, I. M. *J. Virol.* (in the press).
12. Abelson, H. T. & Rabstein, L. S. *Cancer Res.* **30**, 2208-2212 (1970).
13. Cook, W. D. *Proc. natn. Acad. Sci. U.S.A.* **79**, 2917-2921 (1982).
14. Witte, O. N. *et al. Proc. natn. Acad. Sci. U.S.A.* **75**, 2488-2492 (1978).
15. Witte, O. N., Rosenberg, N. E. & Baltimore, D. *Nature* **281**, 396-398 (1979).
16. Harvey, J. J. *Nature* **204**, 1104-1105 (1964).
17. DeFeo, D. *et al. Proc. natn. Acad. Sci. U.S.A.* **78**, 3328-3332 (1981).
18. Langbeheim, H., Shih, T. Y. & Scolnick, E. M. *Virology* **106**, 292-300 (1980).
19. Scolnick, E. M. *et al. Molec. cell. Biol.* **1**, 66-74 (1981).
20. Moloney, J. B. *Natn. Cancer Inst. Monogr.* **22**, 139-142 (1966).
21. Frankel, A. E. & Fischinger, P. J. *Proc. natn. Acad. Sci. U.S.A.* **73**, 3705-3709 (1976).
22. Gattoni, S. *et al. Molec. cell. Biol.* **2**, 42-51 (1981).
23. Kirby, D. R. S. in *Early Concepts, Normal and Abnormal* (ed. Park, W. W.) 68-73 (University of St Andrews Press, Edinburgh, 1965).
24. Slamon, D. J., Müller, R., Cline, M. J. & Verma, I. M. *Science* (submitted).
25. Comings, D. E. *Proc. natn. Acad. Sci. U.S.A.* **70**, 3324-3328 (1973).
26. Bishop, J. M. *ICN-UCLA Symp. molec. cell. Biol.* **23**, 515-524 (1981).
27. Chirgwin, J. M., Przybyla, A. E., MacDonald, R. J. & Rutter, W. J. *Biochemistry* **18**, 5294-5299 (1979).
28. Aviv, H. & Leder, P. *Proc. natn. Acad. Sci. U.S.A.* **69**, 1408-1412 (1972).
29. Rigby, P. W. J., Dieckmann, M., Rhodes, C. & Berg, P. *J. molec. Biol.* **113**, 237-251 (1977).
30. Jones, M. *et al. Proc. natn. Acad. Sci. U.S.A.* **77**, 2651-2655 (1980).
31. Goff, S. P., Gilboa, E., Witte, O. N. & Baltimore, D. *Cell* **22**, 777-785 (1980).
32. Ellis, R. W. *et al. J. Virol.* **36**, 408-420 (1980).
33. Tilghman, S. M. *et al. J. biol. Chem.* **254**, 7393-7399 (1979).
34. Wilson, J. R. & Zimmerman, E. F. *Dev. Biol.* **54**, 187-200 (1976).
35. Dziadek, M. & Adamson, E. J. *Embryol. exp. Morphol.* **143**, 289-313 (1978).
36. Thomas, P. S. *Proc. natn. Acad. Sci. U.S.A.* **77**, 5201-5205 (1980).
37. Raschke, W. *Cold Spring Harb Symp. quant. Biol.* **44**, 1187-1194 (1979).
38. Scher, C. D. & Siegel, R. *Nature* **253**, 729-731 (1975).
39. Maisel, J., Scolnick, E. M. & Duesberg, P. H. *J. Virol.* **16**, 749-753 (1975).

Ia invariant chain detected on lymphocyte surfaces by monoclonal antibody

Norbert Koch, Susanne Koch
& Günter J. Hammerling

Institut für Immunologie und Genetik,
Deutsches Krebsforschungszentrum, Im Neuenheimer Feld 280,
D-6900 Heidelberg, FRG

The immune response (I) region of the major histocompatibility complex encodes a set of cell-surface glycoproteins, the Ia antigens, which are probably identical with the products of immune response genes. Chemically, the polymorphic Ia antigens controlled by the I-A and I-E subregions consist of two associated polypeptide chains, α and β (ref. 1). In addition, this α - β complex is noncovalently associated with another chain of 31,000 molecular weight which, because of its non-polymorphic nature, has been designated invariant (I_i) chain². Whereas Ia antigens are known to span the plasma membrane³, the I_i chain has been found in the cytoplasm but not on the surface of lymphocytes². Here we describe a monoclonal antibody detecting free I_i chains on the cell surface which are not associated with Ia antigens.

The belief that I_i chains were not expressed on the cell surface was based on the finding that I_i chains are only observed when metabolically labelled antigens are immunoprecipitated with anti-Ia antibodies and not when surface-iodinated material was investigated⁴. In an attempt to raise monoclonal antibodies against constant parts of murine histocompatibility antigens we have obtained a rat anti-mouse hybridoma, In-1. In a cellular radioimmunoassay, In-1 reacted only with Ia-positive B-cell tumours and spleen cells, but not with Ia-negative T- or B-cell tumours (Table 1). In-1 was positive on spleen cells of all H-2 haplotypes tested so far (H-2^{b,d,f,k,i,r,s}), indicating the non-poly-

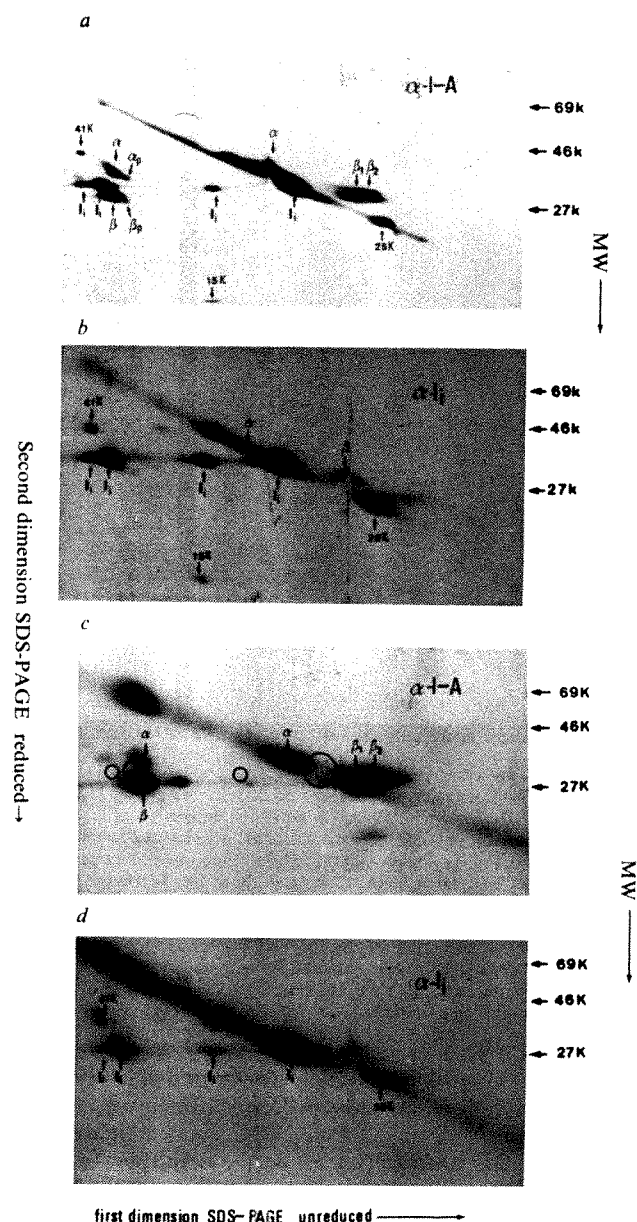


Fig. 1 Two-dimensional SDS-polyacrylamide gel electrophoresis (PAGE) (unreduced-reduced) of Ia and I_i immunoprecipitates. *a, b*, Fluorographs of metabolically (³⁵S-methionine) labelled Ia antigens. 10⁷ blast cells were collected on day 3 after lipopolysaccharide stimulation and labelled for 1 h in the presence of 200 μ Ci ³⁵S-methionine. The *Lens culinaris* binding material was immunoprecipitated with: *a*, monoclonal anti-I-A^k antibody 17/227⁵ or *b*, with In-1 followed by rabbit anti-rat immunoglobulin. Immune complexes were isolated via protein A Sepharose. *c, d*, Autoradiograms of ¹²⁵I surface-labelled (lactoperoxidase) C57BL/6 cells. *c*, *Lens culinaris* binding material was immunoprecipitated using monoclonal anti-I-A^b antibody K25-8.7 (ref. 18). Circles indicate positions where I_i chains usually appear in this type of gel system. This becomes evident when *c* and *d* are superimposed. *d*, C57BL/6 spleen cells were surface labelled with ¹²⁵I. To avoid competition by cold cytoplasmic I_i which is present in excess¹⁰, iodinated cells were incubated with In-1 for 1.5 h. Excess antibody was removed by washing and cells solubilized with 1% NP40. Immune complexes were isolated with rabbit anti-rat immunoglobulin followed by protein A Sepharose.

morphic nature of the determinant recognized. Our failure to block the binding of In-1 to spleen cells by addition of 12 different monoclonal anti-Ia antibodies (refs 5, 18), or by a mixture of these anti-Ia antibodies suggested that the respective determinant did not reside on an Ia antigen.

By immune precipitation of ³⁵S-methionine-labelled spleen cells and separation in one-dimensional 10% SDS gel, a band

with an apparent molecular weight of 31,000 (31K) was observed (not shown). From all these findings, the molecular weight, the non-polymorphic nature and the expression on Ia-positive cells, it seemed that this glycoprotein may be identical with the I_i chain although it is expressed on cell surfaces.

To prove this hypothesis, we used a two-dimensional gel system which allows identification of complexes and their respective subunits⁶. The precipitates are first separated in unreduced form and then, after reduction, in the second dimension. In this type of gel subunits of previously S-S-linked complexes are located in the dimeric region exactly one above each other, whereas components pre-existing as monomers are found on the diagonal. Using this technique we have recently shown that I_i chains occur in at least three different dimeric forms⁷. A typical example of two-dimensional gel analysis of ³⁵S-labelled Ia antigens immunoprecipitated from CBA spleens with monoclonal anti-I-A^k antibody 17/227 (ref. 5) is presented in Fig. 1a. In the dimeric region subunits of the following dimers can be observed (from left to right): (1) I_i plus a component of molecular weight 41K, (2) an I_i homo-dimer, (3) α - β dimers and dimers consisting of their precursors, $\alpha_p\beta_p$, and (4) I_i plus a component of about 15K. Previous alkylation studies have demonstrated that disulphide-linked α - β dimers are formed during solubilization of cells^{7,8}, whereas I_i dimers seem to pre-exist as S-S-linked complexes⁷. The monomeric region shows the characteristic Ia α -polypeptide, single I_i chains, two different forms of β chains which have been described previously⁹, and another component of about 25K molecular weight⁹. The important aspect is that the I_i chain can be identified in three different and characteristic dimeric forms. Two-dimensional peptide analysis demonstrates that the 41K, 25K and 15K components do not share peptides and that they are not structurally related to α or β chains (manuscript in preparation). Figure 1b shows ³⁵S-labelled material immunoprecipitated with In-1. The most prominent spots in Fig. 1b are identical with those for monomeric and dimeric forms of I_i . In addition, traces of α and β chains can be seen in the monomeric but not in the dimeric region. These findings strongly suggest that the antigen recognized by In-1 is identical with the I_i chain. The presence of only small amounts of spots migrating like I-A α and β chains (Fig. 1b) indicates that not all I_i chains, which are in excess in the cytoplasm¹⁰, are associated with Ia. Additional evidence that In-1 is indeed directed against I_i stems from a cell-free translation system in which In-1 precipitated exclusively I_i chains but no other products (J. Lipp *et al.*, manuscript in preparation).

Table 1 Binding of In-1 to Ia positive cells

Cell type	Ref.	H-2	Surface Ia	Surface Ig	Binding of In-1 (c.p.m.)
CH1 tumours	11	a	+	+	3,357 ± 128
WEHI 231 tumours	12	d	+	+	1,319 ± 79
38C13 tumours	13	k	-	+	130 ± 25
EL4 tumours	14	b	-	-	184 ± 47
TL ⁺ tumours	15	k	-	-	167 ± 34
Ag8.653 tumours	16	d	-	±	88 ± 19
CBA spleen		k	+	+	2,805 ± 135

Monoclonal antibody In-1 was obtained by fusion of x63 Ag8.653 myeloma cells and splenocytes from Wistar rats immunized with lymphocytes of strain A.TL followed by injections with B10.A-derived CH1 tumour cells using standard fusion procedures⁵. Hybridoma supernatants were screened on Ia-positive (CH1) and Ia-negative (38C13) B-cell tumours in a cellular binding assay with 20,000 c.p.m. iodinated sheep anti-rat immunoglobulin as a developing reagent which was preabsorbed with mouse immunoglobulin. Data show c.p.m. (±s.e.) bound per 5×10^5 cells. Background with irrelevant monoclonal rat antibody (100–200 c.p.m.) has been subtracted. Ia positivity of CH1 and WEHI 231 was confirmed with monoclonal anti-Ia antibodies in cellular binding assays. In-1 is an IgG2b antibody (G. Moldenhauer, unpublished), and it is not cytotoxic.

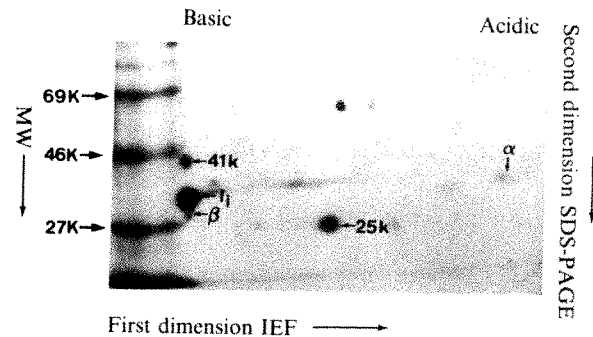


Fig. 2 Two-dimensional IEF gel of I_i immunoprecipitate. Fluorograph of metabolically ³⁵S-methionine labelled Ia antigens. 5×10^6 CH-1 tumour cells were labelled for 1 h in the presence of 100 μ Ci ³⁵S-methionine. *Lens culinaris* binding material was immunoprecipitated with In-1 and rabbit anti-rat immunoglobulin followed by protein A Sepharose. Two-dimensional IEF gels were performed according to O'Farrell¹⁷.

Because cellular binding assays (Table 1) show that In-1 also reacts with antigens expressed on the cell surface, we immunoprecipitated surface-iodinated molecules. When anti-I-A^k antibodies are used for precipitation, mostly iodinated β chains, some α chains and no invariant chains are seen (Fig. 1c). These data, which are in accordance with published results^{2,4}, have been used to argue that I_i chains are not expressed on the cell surface. In contrast, precipitation of surface-iodinated material with In-1 results in the characteristic I_i spots in the dimeric and monomeric regions (see Fig. 1d). No spots corresponding to α and β chains are visible. Further evidence that the antigen recognized by In-1 on the cell surface is the I_i chain is given by two-dimensional SDS-isoelectrofocusing (IEF) gels (Fig. 2) in which the predominant spot is located in approximately the same position ($P_i \sim 7.5$ –8.0) as has been reported by other investigators for I_i (ref. 4).

In conclusion, we have shown that the monoclonal antibody In-1 binds to a glycoprotein which appears identical to the I_i chain. The two surprising findings were that the I_i chain is expressed on the cell surface and that the cell-surface material is not associated with the Ia α and β chains as is the case in the cytoplasm. The lack of association on the cell surface explains why anti-Ia antibodies have not been suitable reagents for the detection of I_i on cell surfaces.

Whereas it has been speculated that intracellular I_i is involved in transport of Ia α and β chains to the cell membrane¹⁶, the biological function of cell-surface bound I_i is not yet understood. Monoclonal antibody In-1 may be useful in addressing this question and also for isolation and studies on structure and genetics of the I_i polypeptide.

We thank Mr K. Meese for technical help and Mrs A. Riedl for preparation of the manuscript. S.K. is the recipient of a research stipend from the German Cancer Research Centre.

Received 24 March; accepted 3 August 1982.

- Cullen, S. E., Freed, J. H. & Nathanson, S. G. *Transplant Rev.* **30**, 236–270 (1976).
- Jones, P. P., Murphy, D. B., Hewgill, D. & McDevitt, H. D. *Immunochemistry* **16**, 51–60 (1978).
- Walsh, F. S. & Crumpton, M. J. *Nature* **269**, 307–311 (1977).
- Suny, E. & Jones, P. P. *Molec. Immun.* **18**, 899–913 (1981).
- Lemke, H., Hämmerling, G. J. & Hämmerling, U. *Immun. Rev.* **47**, 175–206 (1979).
- Springer, T. A., Kaufmann, J. F., Liddoway, L. A., Mann, D. L. & Strominger, J. L. *J. biol. Chem.* **252**, 6201–6207 (1977).
- Koch, N. & Hämmerling, G. J. *J. Immun.* **128**, 1155–1158 (1982).
- Cook, R. G., Uhr, J. W., Capra, J. D. & Vitetta, E. S. *J. Immun.* **121**, 2205–2212 (1978).
- Koch, N. & Hämmerling, G. J. *Immunogenetics* **14**, 437–444 (1981).
- Kvist, S., Wiman, K., Claesson, L., Peterson, P. A. & Dobberstein, B. *Cell* **29**, 61–69 (1982).
- Lynes, M. A., Lanier, L. L., Babcock, G. F., Wettstein, P. J. & Haughton, G. J. *Immun.* **121**, 2352–2357 (1978).
- McKean, D. J. *et al. J. exp. Med.* **154**, 1419–1431 (1981).
- Bergmann, Y. & Haimovich, J. *Eur. J. Immun.* **7**, 413–417 (1977).
- Old, L., Boyse, E. & Stockert, E. *Cancer Res.* **25**, 813–819 (1965).
- Ralph, P. J. *Immun.* **110**, 1470–1475 (1973).
- Kearney, J. F., Radbruch, A., Liesegang, B. & Rajewsky, K. *J. Immun.* **123**, 1548–1550 (1979).
- O'Farrell, P. H. *J. biol. Chem.* **250**, 4007–4021 (1975).
- Koch, N., Hämmerling, G. J., Tada, N., Kimura, S. & Hämmerling, U. *Eur. J. Immun.* (in the press).

uvr Genes function differently in repair of acetylaminofluorene and aminofluorene DNA adducts

Moon-shong Tang* & Michael W. Lieberman

Department of Pathology, Washington University School of Medicine, St Louis, Missouri 63110, USA

Charles M. King

Department of Chemical Carcinogenesis, Michigan Cancer Foundation, Detroit, Michigan 48201, USA

The repair of UV-damaged DNA in *Escherichia coli* is controlled by the *uvr* genes (*A*, *B* and *C*)^{1,2}. These genes are also thought to be involved in the repair of chemically damaged DNA³⁻⁵, however their specific roles in repairing the multiplicity of different adducts that can be produced by chemical carcinogens are not well understood. We have investigated the repair of DNA damaged by different chemical carcinogens and transfected into *E. coli* strains with mutations in different *uvr* genes. The major product of DNA damage by *N*-acetoxy-2-acetylaminofluorene (NA-AAF) is *N*-(guanine-C8-yl)-2-acetylaminofluorene (G-C8-AAF)⁶. Our results suggest that, like UV-induced pyrimidine dimers, the repair of this adduct requires all three *uvr* genes. However, the repair of DNA damaged by *N*-hydroxy-aminofluorene (N-OH-AF, the major adduct of which is *N*-(guanine-C8-yl)-2-aminofluorene, G-C8-AF) seems only to require the *uvrC* gene.

To study the direct biological effect of chemically induced DNA damage and the role of different *uvr* genes in its repair, we have modified ΦX174 RF DNA *in vitro* and used it for transfection of different *E. coli* C strains with a nearly isogenic background (Table 1). This approach is important because chemicals damage a variety of cellular constituents including DNA, RNA, proteins, membranes and small molecules, and the contributions of these various types of damage to toxicity and survival cannot be determined if the whole cell is treated. We have validated our transfection system by studying transfection of wild-type *E. coli* C and the *uvrA*, *uvrB* and *uvrC* strains with UV-irradiated ΦX174 RF DNA. As expected, the transfection frequency of UV-irradiated phage DNA shows the same extent of decrease in all three mutants, as compared with the wild-type cells (Fig. 1a). These three *uvr*⁻ mutants also show significantly lower transfection frequencies than wild-type cells

when NA-AAF-modified ΦX174 RF DNA is used (Fig. 1b).

The lethality of NA-AAF-modified DNA is due mainly to the G-C8-AAF adduct. This conclusion is based on several observations. First, in our conditions, NA-AAF treatment produces at least 85% G-C8-AAF adducts (Fig. 2a). Second, less than two bound carcinogen molecules per molecule of ΦX174 RF DNA are needed to reduce the transfection frequency to 37% (from the Poisson distribution, one lethal hit would reduce survival to 37%, that is, the D₃₇). Thus most of the lethality must result from the G-C8-AAF adduct. In support of this conclusion is the observation that the G-C8-AF adduct is relatively non-lethal (Fig. 1c, see below). These results also demonstrate that all three *uvr* genes are necessary for repair of the G-C8-AAF adduct. The low D₃₇ value for G-C8-AAF is similar to that for pyrimidine dimers (Fig. 1a). This result is consistent with the observation that both dimers and this adduct stall DNA replication near the site of DNA damage⁷.

In contrast, treatment of ΦX174 RF DNA with N-OH-AF results in the formation of only the G-C8-AF adduct (Fig. 2b). Transfection studies with this G-C8-AF-containing DNA reveal two distinct features (Fig. 1c): (1) compared with wild-type *E. coli*, two strains carrying independently derived *uvrC* mutations have significantly lower transfection frequencies, while *uvrA* and *uvrB* cells have the same transfection frequency; (2) compared with G-C8-AAF, about 10 times as many G-C8-AF adducts are needed to reduce the transfection frequency to the same extent. Thus, not only is the G-C8-AF adduct less lethal than the G-C8-AAF adduct, but also its repair occurs independently of *uvrA* and *uvrB* gene function. In addition, these results cannot be accounted for by loss of *alk*⁸ function, since both of our *uvrC* strains are *alk*⁺ (methyl methanesulphonate resistant).

These data suggest that all bulky chemical adducts are not repaired in precisely the same way by the *uvr* system. An attractive hypothesis to explain these data relates to steric alterations in DNA. G-C8-AAF lesions assume a *syn* conformation in the DNA helix and result in a distortion which may be similar to that produced by pyrimidine dimers^{9,10}; hence these lesions may have similar requirements for repair. On the other hand, the G-C8-AF products are preferentially in the *anti* conformation and therefore result in little distortion¹¹; this and similar lesions may require only the *uvrC* gene product for increased survival (repair). Thus, the *uvrC* gene product may be required for the nucleotide excision repair of a wide range of DNA adducts while *uvrA* and *uvrB* gene products may be required only for those which produce a great deal of distortion of the DNA helix. Another implication of our findings is that the *uvrC* gene product can function either as a complex with the *uvrA* and *uvrB* gene products (reviewed in ref. 2) or as an independent entity. In this light it is interesting to consider the relationship of the seven known complementation groups of

* Present address: The University of Texas System Cancer Center, Science Park—Research Division, Smithville, Texas 78957, USA.

Table 1 The bacterial strains used

Strain designation	Repair associated marker	Other markers	Source
MST1	Wt	<i>thr-1</i> , <i>leu-6</i> , <i>proA2</i> , <i>his-4</i> , <i>argE3</i> or <i>arg-49</i> , <i>lacY1</i> , <i>galK2</i> , <i>rpsL31</i> , or <i>rpsL154</i> , <i>supE44</i> An <i>E. coli</i> K-12 × <i>E. coli</i> C hybrid φX sensitive	HF4714, T. Kunkel
MST3	<i>uvrB5</i>	Same as MST1 except Gal ⁺	P1::Tn9c·SR289×HF4714 (select Gal ⁺)
MST8	<i>uvrC34</i>	Same as MST1 except His ⁺	T4GT7·MST5×HF4714 (select His ⁺)
MST13	<i>uvrA6</i>	Same as MST1 except Arg ⁺	P1::Tn9c·SR114×MST11 (select Mal ⁺)
MST14	<i>uvrC56</i>	Same as MST1 except His ⁺	T4GT7·N17-7×MST1 (select His ⁺)
SR289	<i>uvrB5</i>	<i>leuB19</i> , <i>metE70</i> , <i>thyA36</i> , <i>deo(??)</i> , <i>lacZ53</i> , <i>rha-5</i> , <i>rpsL151</i>	W3110, N. Sargentini
SR114	<i>uvrA6</i>	<i>thr-1</i> , <i>leuB6</i> , <i>proA2</i> , <i>his-4</i> , <i>argE3</i> , <i>lacY1</i> , <i>mtl-1</i> , <i>galK2</i> , <i>xyl-5</i> , <i>thi-1</i> , <i>tsx-33</i> , <i>rpsL31</i> , <i>ara-14</i> , <i>supE44</i>	AB1886, N. Sargentini
N17-7	<i>uvrC56</i>	<i>try</i> , <i>gal</i> , <i>sm</i> ⁺	T. Kato
MST5	<i>uvrC34</i>	Same as SR231 except His ⁺	P1 _{kc} ·SR550×SR231 (select His ⁺)
SR231	<i>uvrC34</i>	Same as SR114	N. Sargentini
SR550	Wt	Same as SR289	N. Sargentini
MST11	Wt	Same as MST1 except Arg ⁺ , <i>malB45</i>	This study

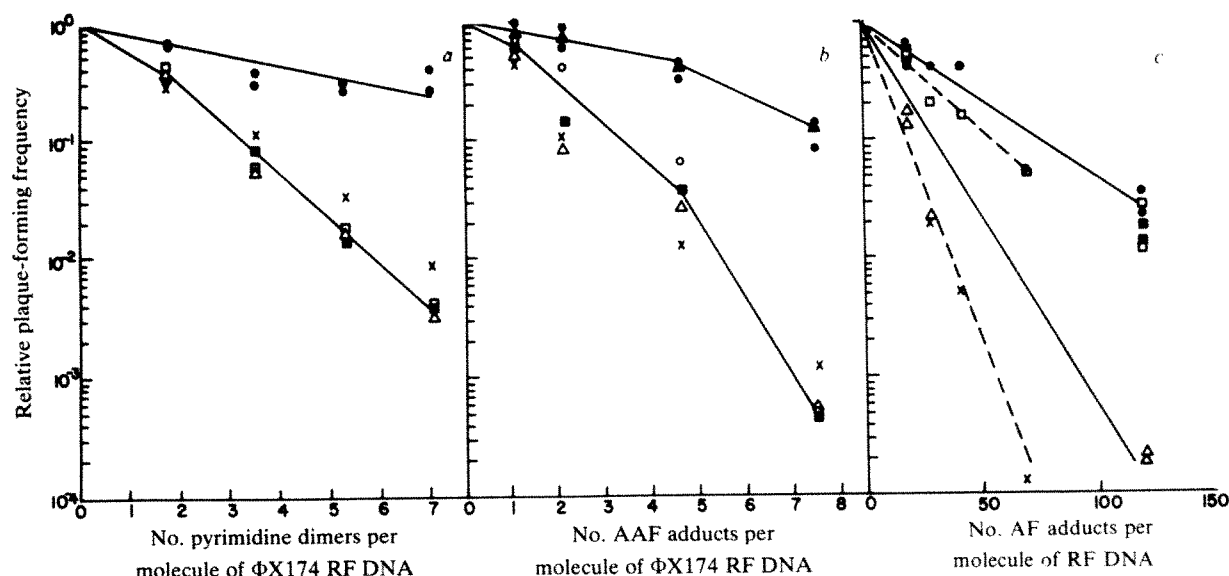


Fig. 1 Relative transfection frequency of Φ X174 am3cs70 RF DNA damaged with: a, UV; b, NA-AAF; c N-OH-AF in different *E. coli* C strains. Φ X174 am3cs70 RF DNA was prepared using the method described by Barnes¹⁵. Different *E. coli* *uvr*⁻ markers (\square , *uvrA6*; \blacksquare , *uvrB5*; \triangle , *uvrC34*; \times , *uvrC56*; are introduced into the same *E. coli* C \times K12 hybrid (HF4714) parental strain (\bullet) by P1 or T4 transduction (Table 1). *E. coli* C *uvrA* 103 strain (\circ) was obtained from Drs T. Kunkel and L. Loeb, and *E. coli* C wild-type strain (\blacktriangle) from Dr D. Berg. Cells were grown to $2-5 \times 10^8$ cells ml⁻¹ in Luria broth (LB; 10 g tryptone, 5 g yeast extract and 15 g NaCl in 1 l of H₂O) with 0.1% glucose and 50 μ g ml⁻¹ thymine. The cells were spun down and resuspended in cold 50 mM CaCl₂ and stored at 4°C overnight. They were concentrated to about 9×10^9 cells ml⁻¹ by centrifugation before transfection. Transfection was carried out by incubating 0.1 ml of chilled DNA in 10 mM Tris, pH 7.5, and 1 mM EDTA with 0.2 ml of CaCl₂-treated cell suspension in an ice water bath for 20 min. At the end of incubation, 3 ml of LB soft agar (6 g agar in 1 l LB broth with 1 mM CaCl₂) were added to the mixture and plated on LB plates (12 g agar in 1 l LB broth). The plates were incubated at 37°C for at least 5 h before counting. The transfection frequency for control DNA ranged from 10^{-5} to 10^{-6} . The relative transfection frequency was calculated by the formula N/N_0 , where N is the number of plaques formed per unit damaged DNA and N_0 the number of plaques formed per unit of control DNA. ³H-(ring-labelled)NA-AAF (in dimethyl sulphoxide) or ³H-N-OH-AF (in ethanol) was reacted with DNA in 10 mM sodium citrate (for N-OH-AF) or sodium acetate (for NA-AAF) at pH 5.5. The unbound labelled carcinogens were removed by multiple extractions with ether, dialysis and precipitation with ethanol (NA-AAF), or by successive extractions with phenol and ether and precipitation with ethanol (N-OH-AF). The number of adducts formed per molecule of Φ X174 RF DNA was calculated from the ³H specific activity of NA-AAF (710 mCi mmol⁻¹) or N-OH-AF (193 or 206 mCi mmol⁻¹) used for treatment and the specific activity of the DNA. The dotted and solid lines in c represent DNA modified by different batches of ³H-N-OH-AF. The number of pyrimidine dimers formed per molecule of Φ X174 RF DNA was calculated using a dimer yield of 2.6×10^{-5} dimers per thymine residue per J per m² (ref. 16).

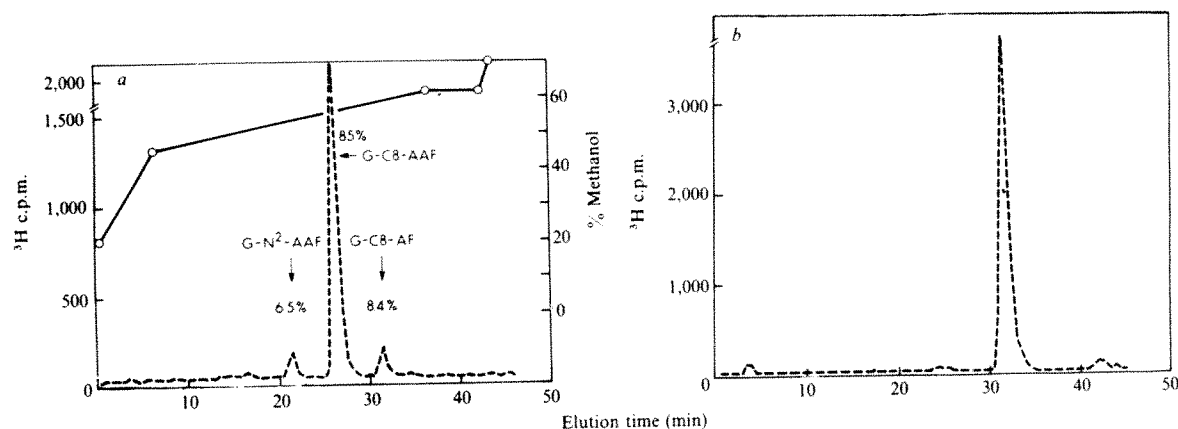


Fig. 2 Chemical analysis of DNA adducts formed in Φ X174 RF DNA after modification by: a, ³H-NA-AAF; or b, ³H-N-OH-AF. NA-AAF-modified Φ X174 RF DNA was hydrolysed by digestion with DNase I, snake venom phosphodiesterase and alkaline phosphatase¹³ and subsequent treatment with trifluoroacetic acid (TFA) at 70°C for 30 min (M.S.T. and M.W.L., in preparation). The DNA modified with N-OH-AF was treated with TFA at 70°C for 30 min directly. The hydrolysed mixture was dried under nitrogen and reconstituted in 30% methanol for HPLC. A 0.1 ml sample was injected into a Varian 8500 HPLC with 10 μ m Alltech-C18 column (300 \times 4 mm). The adducts were eluted with a gradient of 21–70% methanol in 8 mM (NH₄)₂PO₄ (pH 3.8; 20°C) over a 48 min period at a flow rate of 1 ml min⁻¹. Standards (dG-C8-AAF and dG-C8-AF) were added to the mixture as internal markers before adding TFA. A dG-N²-AAF standard was treated with TFA and chromatographed separately, and its position is indicated in the profile. TFA treatment removes deoxyribose from the adducts¹⁷. 0.5 ml samples were counted. The solid line represents the methanol concentration for the elution.

xeroderma pigmentosum in human cells to the repair of chemical damage in these cells.

One plausible explanation for the low lethality of G-C8-AF is that cells tolerate this kind of DNA damage well. In animals or in mammalian cell culture, G-C8-AF has been found to remain in DNA for a long period of time^{12,13}. However, N-OH-AF has been demonstrated to be a very potent mutagen in the Ames' *Salmonella* mutation test¹⁴. These two findings suggest that DNA replication or transcription machinery may be able to read through G-C8-AF without stalling but with poor fidelity.

We thank Dr Frederick A. Beland for the gift of dG-C8-AAF and dG-N²-AAF adducts. This work has been supported by

NIH grants CA 09118 and ES CA 02740 (M.S.T.), CA 20513 (M.W.L.) and CA 23386 (C.M.K.), and by the following companies: Brown & Williamson Tobacco Corporation, Philip Morris Incorporated, R. J. Reynolds Tobacco Company and United States Tobacco Company.

Received March 2; accepted July 26 1982.

- Howard-Flanders, P., Boyce, R. P. & Theriot, L. *Genetics* **53**, 1119–1136 (1966).
- Seeborg, E. *Prog. Nucleic Acid Res. molec. Biol.* **26**, 217–226 (1981).
- Venitt, S. & Tarmy, E. M. *Biochim. biophys. Acta* **287**, 38–51 (1972).
- Ikenaga, M., Ichikawa-Ryo, H. & Kondo, S. *J. molec. Biol.* **92**, 341–356 (1975).
- Hanawalt, P. C., Cooper, P. K., Ganesan, A. K. & Smith, C. A. *A. Rev. Biochem.* **48**, 783–836 (1979).
- Miller, E. C. & Miller, J. A. *Cancer* **47**, 2327–2345 (1981).

7. Moore, P., Bose, K. K., Rabkin, S. D. & Strauss, B. S. *Proc. natn. Acad. Sci. U.S.A.* **78**, 110–114 (1981).
8. Yamamoto, Y., Katsuki, M., Sekiguchi, M. & Otsuji, N. *J. Bact.* **135**, 144–152 (1978).
9. Trifonov, E. N., Shafranovskaya, V. N., Frank-Kamenetskii, M. D. & Lazurkin, Yu. S. *Molec. Biol.* **2**, 698–705 (1968).
10. Fuchs, R. P. P. & Daune, M. P. *Biochemistry* **13**, 4435–4440 (1974).
11. Leng, M., Ptak, M. & Rio, P. *Biochem. biophys. Res. Commun.* **96**, 1095–1102 (1980).
12. Visser, A. & Westra, J. G. *Carcinogenesis* **2**, 737–740 (1981).
13. Howard, P. C., Casciano, D. A., Beland, F. A. & Shaddock, J. G. Jr *Carcinogenesis* **2**, 97–102 (1981).
14. Ames, B. N., Gurney, E. G., Miller, J. A. & Bartsch, H. *Proc. natn. Acad. Sci. U.S.A.* **69**, 3128–3132 (1972).
15. Barnes, W. M. *J. molec. Biol.* **119**, 83–99 (1978).
16. Howard-Flanders, P. A. *Rev. Biochem.* **37**, 175–200 (1968).
17. Westra, J. G. & Visser, A. *Cancer Lett.* **8**, 155–162 (1979).

A protein immunologically related to erythrocyte band 4.1 is found on stress fibres of non-erythroid cells

Carl M. Cohen*†, Susan F. Foley* & Catherine Korsgren*

* Department of Research, Division of Hematology and Oncology, St Elizabeth's Hospital, Boston, Massachusetts 02135, USA

† Departments of Medicine and Molecular Biology, Tufts University School of Medicine, Boston, Massachusetts 02111, USA

Erythrocyte band 4.1 is one of the three major structural proteins of the erythrocyte cytoskeleton, along with spectrin and actin^{1–3}. When bound to the tail-end of the actin-binding protein spectrin, band 4.1 is capable of promoting the formation of stable ternary complexes with spectrin and F-actin^{4–7}, both in solution and on the erythrocyte membrane⁸. Recent work has demonstrated that proteins immunologically and structurally related to spectrin, as well as ankyrin—spectrin's membrane attachment site—are present in a wide variety of non-erythroid cells^{9–13}, although the function of these proteins in such cells is still unclear. It has been reported¹⁴ that band 4.1 is present in platelets and granulocytes. Here we show that a protein immunologically related to band 4.1 is present in a non-erythroid cell, the fibroblast, and appears by immunofluorescent labelling to be distributed uniformly along stress fibres. We suggest that by analogy with erythrocyte band 4.1 this protein may be an accessory actin-binding protein, and may serve to integrate actin filaments and actin-binding proteins.

Antibodies to electrophoretically pure band 4.1 were produced in New Zealand white rabbits by multiple intradermal injection of 60 µg freshly prepared^{4,15} band 4.1. Antisera were tested for reactivity against band 4.1 by immunoperoxidase staining of erythrocyte ghost proteins that had been electrophoresed in a 5–15% acrylamide gel, and transferred electrophoretically to nitrocellulose paper. Anti-band 4.1 IgG was purified by affinity chromatography of serum IgG on a band 4.1 affinity column. Figure 1 shows that reaction of affinity purified anti-4.1 with erythrocyte membrane proteins gave one major band in the position of band 4.1 as well as several minor bands of lower molecular weight (see below) (Fig. 1, lane b).

Although it cannot easily be seen in Fig. 1, in the Laemmli buffer system¹⁶ band 4.1 migrates as a closely spaced doublet (4.1a and b), which has recently been shown by peptide mapping to consist of related phosphoproteins¹⁷. Other electroblots (not shown) clearly demonstrate that our antibody is equally reactive with these two components of band 4.1.

To demonstrate further the identity of the peroxidase stained band with band 4.1, we briefly prestained a separate nitrocellulose strip with Coomassie blue, so that the protein bands could be visualized, and then counterstained by the immunoperoxidase procedure. A distinct brown band appeared exactly on top of the Coomassie blue stained band 4.1, verifying the identity of the reactive protein (not shown). Pretreatment of ghosts or intact erythrocytes with diisopropyl fluorophosphate (DFP), pepstatin, phenylmethyl sulphonyl fluoride (PMSF) or EDTA had no effect on the appearance of the lower molecular weight bands, which are likely to be membrane-

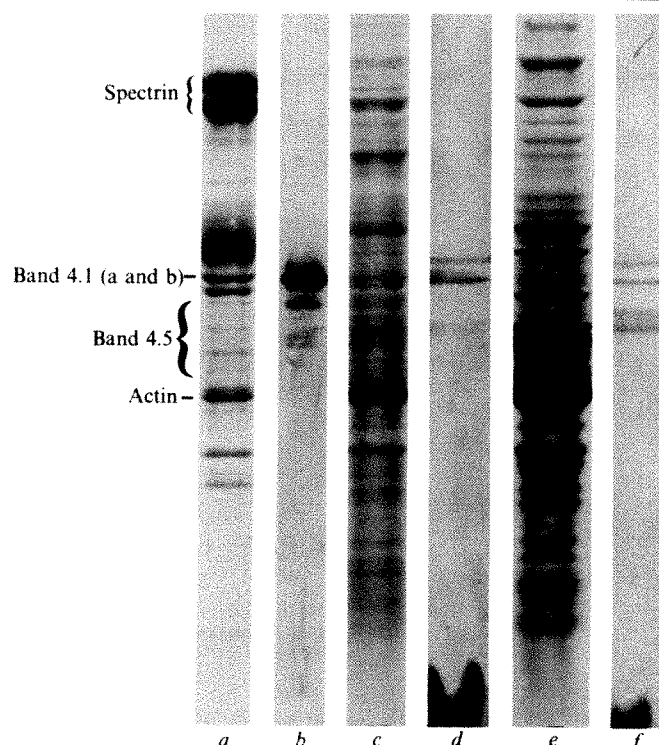


Fig. 1 a, Erythrocyte membrane proteins electrophoresed on a 5–15% acrylamide gradient gel¹⁶ and stained with Coomassie blue. b, Immunoperoxidase stained electroblot of ghost proteins. Erythrocyte membrane proteins electrophoresed in 1.5 mm thick Laemmli slab gels were transferred to nitrocellulose paper (Schleicher & Schuell BA83)²⁴ in a Bio-Rad transblot apparatus at 30 V for 18 h, with cooling. Electroblots were stained with anti-band 4.1 antibody and counterstained with peroxidase conjugated second antibody as described in ref. 25. Coomassie blue staining of the nitrocellulose paper, as well as of the residual proteins on the electroblotted gel, showed that all proteins were transferred with at least 50% efficiency. Affinity purified anti-band 4.1 IgG was prepared from rabbits as follows. Three New Zealand white rabbits received 20–40 subcutaneous injections of purified band 4.1 (total of 60 µg per rabbit) emulsified with an equal volume of Freund's complete adjuvant. After 7 weeks, each of the rabbits produced sera which were positive for anti-band 4.1 activity by the above assay. None of the rabbits' preimmune sera showed any reactivity against red cell membrane proteins. IgG was prepared from sera by two cycles of precipitation at 4 °C with 37% saturated ammonium sulphate. The final precipitate was resuspended in phosphate-buffered saline (PBS) and dialysed for 48 h against 5 mM Na phosphate pH 7.0. After clarification at 32,000g for 15 min the material was passed down a column of Whatman DE 52 equilibrated with 5 mM Na phosphate pH 7.0, and the void volume collected and concentrated by precipitation with 50% saturated ammonium sulphate pH 7.8. The concentrated IgG was dialysed for 48 h against 8 l of ice cold PBS. Electrophoretically pure band 4.1 was coupled to Bio Rad Affigel 10 in 50 mM HEPES pH 7.6 and rabbit IgG was passed over the column and flushed with PBS. Anti-band 4.1 IgG was eluted from the column with 0.2 M glycine pH 2.8 and the fractions were collected into tubes containing sufficient 1 M Na phosphate pH 7.4 for neutralizations²⁶. After recording the A_{280} of the fractions they were stabilized by the addition of 0.02% w/v NaN₃ plus 0.25 mg ml⁻¹ bovine serum albumin and dialysed against PBS. c, High speed pellet of homogenized fibroblasts. Fibroblasts were grown on glass coverslips to about 80% confluency in Dulbecco's minimal essential medium (MEM) plus 10% fetal calf serum and removed by treatment with 0.25% trypsin for 10 min. The cells were washed in PBS containing 2 mM PMSF and suspended to a density of 1×10^7 ml⁻¹ in 0.34 M sucrose, 5 mM EGTA, 10 mM dithiothreitol DTT, 0.5 mM ATP, 2 mM PMSF and 20 mM imidazole-HCl pH 7.0²⁵. The cells were then homogenized in a Teflon-glass homogenizer until >90% of the nuclei were released, as monitored by phase contrast microscopy. The suspension was centrifuged at 140g for 6 min to remove nuclei and unlysed cells and the supernatant was spun at 17,500 r.p.m. for 20 min in a Sorvall SS34 rotor. The resulting pellet (c, d) was solubilized directly into SDS gel solution while the supernatant (e, f) was precipitated with 10% w/v trichloroacetic acid before solubilization. Gel lane c contains ~40 µg of protein. d, Anti-band 4.1 immunoperoxidase staining of fibroblast proteins shown in c transferred to nitrocellulose paper as described for b except that the electroblotting time was increased to 24 h. The staining procedure is identical to that described for erythrocyte membranes except these fibroblast strips were stained with 45 µg affinity purified anti-band 4.1 IgG in 3 ml for 16 h at 37 °C. The lane shown originally contained a total of 170 µg protein. e, Coomassie blue stained gel of high speed supernatant obtained from fibroblast homogenate described in c 60 µg protein. f, Anti-band 4.1 immunoperoxidase stain of supernatant proteins shown in lane e. Electroblotting and staining were done exactly as described in d. The lane shown originally contained 84 µg protein.

bound proteolytic fragments of band 4.1. Purified band 4.1 showed the same pattern of secondary bands as did ghosts. All of these secondary bands lined up with Coomassie blue stained bands visible in the band 4.5 region¹⁸ of ghosts.

Band 4.1 extracted by our standard method^{4,15}, or by an entirely unrelated method using Tween 20¹⁹, appeared homogeneous on overloaded Fairbanks gels¹⁸, but on Laemmli gels revealed a small band (~5% of total protein) migrating just above band 4.1 in addition to the low molecular weight fragments. This band also appeared in ghosts stained by the peroxidase method (Fig. 1, lane *b*), but did not line up with any visible Coomassie blue stained band. While the relationship of this band to band 4.1 is still unclear, preliminary studies

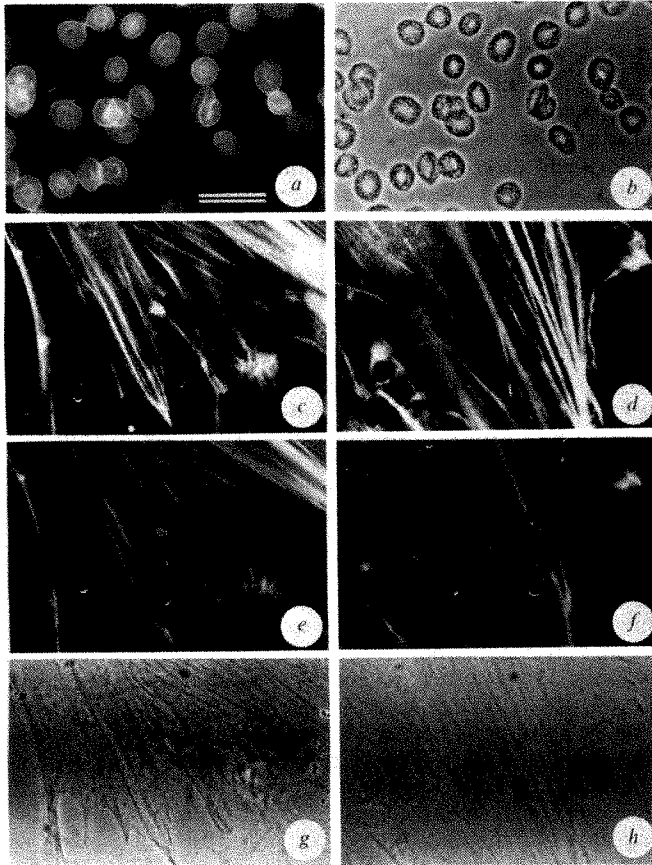


Fig. 2 Phase and immunofluorescent micrographs of fibroblasts and erythrocytes. *a*, Human erythrocytes were washed and diluted in PBS and smeared on a glass slide and allowed to dry. The cells were fixed for 20 min at room temperature in 3.7% formaldehyde in PBS, washed in PBS and dehydrated in acetone at -10°C for 10 min. After rinsing in PBS the fixed cells were incubated with $40\ \mu\text{l}$ of $30\ \mu\text{g ml}^{-1}$ affinity purified anti-band 4.1 antiserum in PBS plus $0.25\ \text{mg ml}^{-1}$ bovine serum albumin for 30 min at 37°C . The slides were rinsed for 30 min in PBS and then $40\ \mu\text{l}$ of 1:30 diluted rhodamine conjugated goat anti-rabbit IgG (Cappel, $5\ \text{mg ml}^{-1}$) was added and incubated for 30 min at 37°C . Slides were washed in 10 changes of PBS over 1 h and coverslips were placed on a drop of 90% glycerol, 10% PBS and sealed with wax. Slides were examined in a Leitz Dialux 20 microscope equipped with a Ploem epifluorescent attachment and a $\times 100$, 1.32 numerical aperture NPL Fluotar lens. Rhodamine fluorescence was viewed with a Leitz N2 fluorescence cube. Scale bar, $2\ \mu\text{m}$. *b*, Erythrocytes from *a* viewed in phase contrast optics. *c, d*, Portion of fibroblasts after staining with affinity purified anti-band 4.1. Fibroblasts were grown as described in Fig. 1 legend on glass coverslips, and were fixed and dehydrated as described above except that they were not allowed to air dry. Coverslips were stained as described for erythrocytes by inverting them on to a $40\text{-}\mu\text{l}$ drop of primary or secondary antibody except that the primary antibody was used at a concentration of $100\ \mu\text{g ml}^{-1}$. Fibroblast in *e, f* were also stained simultaneously for F-actin using NBD-phalloidin. After incubation of cells with primary antibody as described above, the cells were washed and incubated with rhodamine conjugated goat anti-rabbit IgG plus NBD-phalloidin. The phalloidin was added by drying $15\ \mu\text{l}$ of a $2\ \text{ml}$ ($150\ \text{U ml}^{-1}$) stock solution (Molecular Probes, Inc.) in methanol in a glass tube and adding $60\ \mu\text{l}$ of a 1:30 dilution of rhodamine conjugated goat anti-rabbit IgG in PBS. $40\ \mu\text{l}$ of this mixture was then used to stain cells by the procedure described above. *e, f*, F-actin of same cells shown in *c* and *d* viewed by NBD-phalloidin fluorescence using the Leitz I2 fluorescence cube. *g, h*, Phase contrast views of the same cells shown in *2c* and *d* and *2e* and *f* respectively.

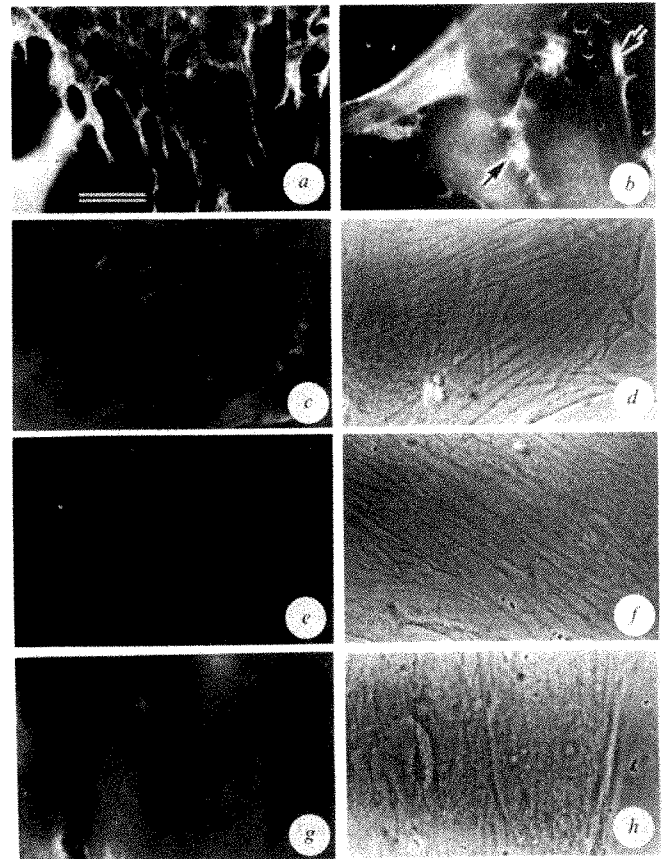


Fig. 3 *a*, Anti-band 4.1 staining of fibroblasts pretreated with $10\ \mu\text{g ml}^{-1}$ cytochalasin B for 60 min at 37°C before fixation and extraction. Cells were treated with affinity purified anti 4.1 as described in Fig. 2 legend. Scale bar, $2\ \mu\text{m}$. *b*, Anti-band 4.1 staining of small poorly spread fibroblasts. Note intense staining in pseudopods and lamellipodia (arrows) but lack of stress fibre staining. *c*, Fibroblasts stained as described in Fig. 2 legend except that $100\ \mu\text{g ml}^{-1}$ normal rabbit IgG was substituted for anti-band 4.1 IgG. *d*, Phase contrast picture of the same cell as in *c* illustrating abundance of stress fibres which were not stained in *c*. *e*, Fibroblasts were stained with $50\ \mu\text{g ml}^{-1}$ anti-band 4.1, washed in PBS and incubated with $40\ \mu\text{l}$ of $100\ \mu\text{g ml}^{-1}$ purified erythrocyte band 4.1 at 37°C for 15 min. The coverslips were washed in PBS and stained with second antibody as described above. *f*, Phase contrast picture of cell in *e*. *g*, Fibroblasts were fixed in formaldehyde but not extracted in acetone, and labelled with primary and secondary antibodies as described for Fig. 2. *h*, Phase contrast picture of cell shown in *g*.

suggest that it is closely related to band 4.1 as it binds to spectrin (unpublished data).

To determine whether band 4.1 was present in a non-erythroid cell we assayed human fibroblasts (ATCC CRL 1139 En Son) grown in culture on glass coverslips, by both immunoperoxidase and immunofluorescence. For the immunoperoxidase method we disrupted fibroblasts in a Dounce homogenizer and after removing nuclei by low speed centrifugation examined the pellet and supernatant produced by subsequent high speed centrifugation for band 4.1. Figure 1, lanes *c, e*, show the Coomassie blue stained gels of the high speed pellet and supernatant, while lanes *d* and *f* show the respective electroblots of these proteins stained by the anti-band 4.1-peroxidase procedure. Both *d* and *f* show a clear peroxidase-stained band which co-migrates exactly with erythrocyte band 4.1, and also a band that migrates just above band 4.1, coincidentally with a similar faint band found in peroxidase-stained erythrocyte membranes mentioned above.

To localize band 4.1 within the cells we examined both fibroblasts and erythrocytes by indirect immunofluorescence using affinity purified anti-band 4.1 IgG. Figure 2*a* shows that staining with anti-band 4.1 IgG resulted in uniform labelling of human erythrocytes. Figure 2*c* and *d* show anti-band 4.1 staining of fibroblasts. The staining appears primarily as bright linear bundles extending to the cell periphery. To determine whether these bundles were identical to stress fibres, we simultaneously stained F-actin in the same cells (Fig. 2*e, f*) using

nitrobenzo oxadiazole (NBD)-phalloidin^{20,21}. Comparison of the band 4.1 and F-actin staining revealed a surprisingly complete correspondence between the two patterns. Further, both sets of patterns coincided well with the appearance of phase dense stress fibres in extracted cells (Fig. 2g, h). Band 4.1 staining seemed particularly intense in ruffles at the leading and upper edge of 'triangular' fibroblasts (Fig. 3b).

To correlate further the distribution of anti-band 4.1 fluorescence with actin, we pretreated the fibroblasts with 10 $\mu\text{g ml}^{-1}$ cytochalasin B before staining. Cytochalasin is known to have profound morphological effects on cells, and leads to the breakdown and disorganization of stress fibres and actin filaments (reviewed in ref. 22). After cytochalasin treatment the cells retracted and began to round up on the coverslips. Figure 3a shows that the pattern of anti-band 4.1 fluorescence was no longer that of linear bundles, but was diffuse and rather disorganized, consistent with the appearance of actin (not shown). Small poorly spread fibroblasts had few or no prominent stress fibres²³, and in these same cells anti-band 4.1 fluorescence was also diffuse (Fig. 3b). Many of these smaller cells had areas of bright anti-band 4.1 staining at their periphery, consistent with band 4.1 being concentrated in lamellapodia or ruffles, as has been reported for actin²³ (arrows, Fig. 3b).

To demonstrate specificity of staining we performed the following controls. (1) Preimmune serum, or non-immune IgG from normal rabbits, gave no reaction with either erythrocyte or fibroblast proteins by the immunoperoxidase method. (2) Pooled normal rabbit IgG gave no fluorescent staining of fibroblasts when substituted for anti-band 4.1 IgG (Fig. 3c). (3) Anti-band 4.1 fluorescence could be displaced or blocked by incubating fibroblasts with purified band 4.1 either during or after antibody labelling (Fig. 3e). (4) No appreciable surface staining was obtained when fixed but non-acetone extracted fibroblasts were reacted with anti-band 4.1 (Fig. 3g).

We conclude that a protein immunologically related to erythrocyte band 4.1 is uniformly distributed along actin filaments in a non-erythroid cell. If the fibroblast protein serves a function similar to erythrocyte band 4.1, then it is possible that it may connect actin filaments to actin-binding proteins and thus to other cellular structures such as plasma or intracellular membranes. Further, by analogy with its interaction with erythrocyte proteins, this protein may be importantly involved in maintaining the elasticity of extended cytoskeletal structures⁷, allowing F-actin-actin binding protein contacts to be made and broken repeatedly without irreversible or long-term cytoskeletal breakdown.

This work was supported by USPHS grant HL 24382 to C.M.C. We thank Dr Deborah K. Smith for many helpful suggestions during this work.

Received 1 July; accepted 23 August 1982.

- Branton, D., Cohen, C. M. & Tyler, J. *Cell* **24**, 24-30 (1981).
- Gratzer, W. B. *Biochem. J.* **198**, 1-8 (1981).
- Sheetz, M. P. *Biochim. biophys. Acta* **557**, 122-134 (1979).
- Tyler, J., Hargreaves, W. & Branton, D. *Proc. natn. Acad. Sci. U.S.A.* **76**, 5192-5196 (1979).
- Ungewickell, E., Bennett, P. M., Calvert, R., Ohanian, V. & Gratzer, W. B. *Nature* **280**, 811-814 (1979).
- Fowler, V. & Taylor, D. L. *J. Cell Biol.* **85**, 361-376 (1980).
- Cohen, C. M. & Korsgren, C. *Biochem. biophys. Res. Commun.* **97**, 1429-1435 (1980).
- Cohen, C. M. & Foley, S. F. *Biochem. biophys. Acta* **688**, 691-701 (1982).
- Goodman, S. R., Zagan, J. S. & Kulikowski, C. R. (1981) *Proc. natn. Acad. Sci. U.S.A.* **78**, 7570-7574.
- Davis, J. & Bennett, V. *J. biol. Chem.* **257**, 5816-5820 (1982).
- Bennett, V. *Nature* **281**, 597-599 (1979).
- Bennett, V. & Davis, J. *Proc. natn. Acad. Sci. U.S.A.* **78**, 7550-7554 (1981).
- Glenney, J. R., Glenney, P., Osborn, M. & Weber, K. *Cell* **28**, 843-854 (1982).
- Spiegel, J. E., Beardsley, D. S. & Lux, S. E. *Fedn Proc.* **41**, 657 (1982).
- Cohen, C. M. & Foley, S. F. *J. Cell Biol.* **86**, 694-698 (1980).
- Laemmli, U. K. *Nature* **227**, 680-685 (1970).
- Goodman, S. R., Yu, J., Whitfield, C. F., Culp, E. N. & Posnak, E. J. *J. biol. Chem.* **257**, 4564-4569 (1982).
- Fairbanks, G., Steck, T. L. & Wallach, D. F. H. *Biochemistry* **13**, 2606-2617 (1971).
- Liljas, L., Lundahl, P. & Hjerten, S. *Biochim. biophys. Acta* **352**, 327-337 (1974).
- Barak, L. S., Yocum, R., Nothnagel, E. A. & Webb, W. W. *Proc. natn. Acad. Sci. U.S.A.* **77**, 980-984 (1980).
- Barak, L. S., Yocum, R. R. & Webb, W. W. *J. Cell Biol.* **89**, 368-372 (1981).
- Pollard, T. D. & Weihing, R. R. *CRC crit. Rev. Biochem.* **2**, 1-65 (1974).
- Herman, I. M., Crisone, N. & Pollard, T. D. *J. Cell Biol.* **90**, 84-91 (1981).
- Towbin, H., Staehelin, T. & Gordon, J. *Proc. natn. Acad. Sci. U.S.A.* **76**, 4350-4354 (1979).
- Yin, H., Albrecht, J. H. & Fattoum, A. *J. Cell Biol.* **91**, 901-906 (1981).
- Fujiwara, K. & Pollard, T. D. *J. Cell Biol.* **71**, 848-875 (1976).

Post-transcriptional control of tubulin biosynthesis during leishmanial differentiation

Michael Wallach, Dunne Fong & Kwang-Poo Chang*

The Rockefeller University, New York, New York 10021, USA

Controls of gene expression can occur at different levels during cell differentiation. Using an *in vitro* culture system¹, we have studied protein biosynthesis during the differentiation of a parasitic protozoan, *Leishmania mexicana*. There are two developmental stages in the life cycle of this and similar parasites: motile extracellular promastigotes in the sandfly gut and non-motile intracellular amastigotes in the mammalian macrophages. Intracellular parasitism by the latter results in human leishmaniasis, diseases still widespread in many parts of the world². During leishmanial differentiation from one stage to the other, we observed changes in tubulin biosynthesis, concomitant with the morphological changes of these parasites in the length of their flagella and subpellicular microtubules³. With few exceptions^{4,5} tubulin biosynthesis is known to be under transcriptional control in other eukaryotic systems⁶⁻¹². Here we have examined the protein synthesis during leishmanial differentiation in *in vitro* translation systems using total cellular poly(A)⁺ RNA from amastigotes and promastigotes. Contrary to our expectations, the results indicate a post-transcriptional control for the tubulin biosynthesis during leishmanial differentiation in our host-parasite culture system.

Total cellular poly(A)⁺ RNA was extracted from the promastigotes by phenol-SDS extraction¹³ and oligo(dT)-cellulose elution¹⁴. RNA was translated in wheat germ¹⁵ and rabbit reticulocyte lysate¹⁶ cell-free systems and the products were compared with *in vivo* metabolically labelled proteins. As shown in Fig. 1, the 55,000-molecular weight (MW) doublet bands, previously identified as tubulins in metabolically labelled parasites³, were also found in the translation products from poly(A)⁺ RNA. Little or no tubulin was translated *in vitro* using promastigote poly(A)⁻ RNA (not shown). The labelling intensity of tubulin bands seemed to vary with the Mg²⁺ concentration. The lower band of the doublet (β -tubulin) had a higher labelling intensity in sub-optimal conditions than the upper one (α -tubulin). Preferential translation of β - over α -tubulin *in vitro* has also been reported with *Tetrahymena* poly(A)⁺ RNA (ref. 17). However, note that β -tubulin contains more methionine residues than α -tubulin¹⁸. It is also possible that mRNAs compete for the available factors in an *in vitro* translation system^{19,20}. In our study with *Leishmania* RNA, we selected the reticulocyte system for further experiments because of its lower background translation activities.

Our previous finding of a pronounced decrease in the tubulin biosynthesis during leishmanial promastigote to amastigote differentiation led us to determine whether there might be a concomitant decrease in the level of translatable tubulin mRNA. Cell-free translation products of promastigote and amastigote poly(A)⁺ RNAs were compared with each other and with the *in vivo* metabolically labelled proteins from the same batch of parasites (Fig. 2). Tubulins were found, as expected, to be the most prominent bands in metabolically labelled promastigotes (a) and in *in vitro* products from promastigote mRNA (b), but not in metabolically labelled amastigotes (c); an unexpected finding was that mRNA from amastigotes translated *in vitro* (c, d) just as much tubulin as that from promastigotes (a, b). Identical results were obtained when the concentrations of mRNA from both stages were varied from 0.1 to 2 μg for the *in vitro* translation experiments (not shown), thereby eliminating mRNA competition as a possible explanation for the results observed.

*To whom correspondence should be addressed.

As the purity of isolated amastigotes has been verified¹, macrophage RNA could not possibly contribute to the *in vitro* translation products observed. To ascertain the identity and quantity of tubulin translated *in vitro* we performed immunoprecipitation of samples using monospecific rabbit antiserum against β -tubulin of *Chlamydomonas flagella*²¹. β -Tubulin bands of equal intensity were specifically precipitated from translation products of total cellular poly(A)⁺ RNA from both promastigotes and amastigotes (Fig. 3). Thus similar amounts of translatable tubulin mRNA are present in the two developmental stages of *Leishmania mexicana*.

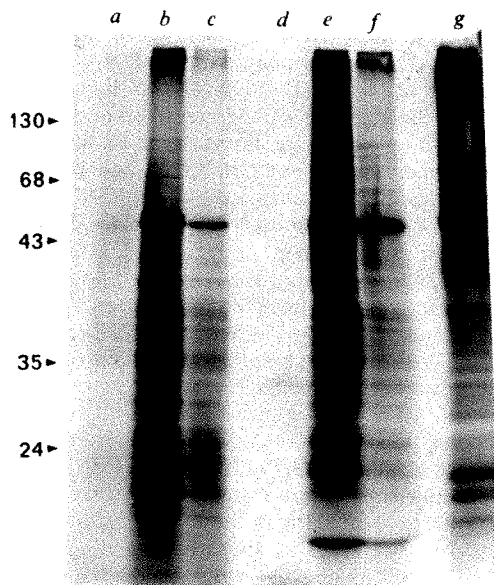
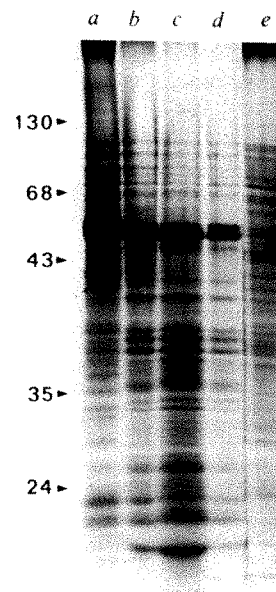


Fig. 1 Translation of promastigote mRNA in the wheat germ and rabbit reticulocyte cell-free systems. *Leishmania mexicana amazonensis* promastigotes were cultured in HEPES buffered Medium 199 plus 10% HIFBS and used after washing three times in Hanks' balanced salt solution by centrifugation. Total RNA was extracted using SDS and phenol¹³ and was chromatographed on an oligo(dT)-cellulose column¹⁴. Total poly(A)⁺ RNA was ethanol precipitated, dried with nitrogen, and dissolved in 10 mM HEPES pH 7.5. Promastigote mRNA was translated in the wheat germ and rabbit reticulocyte cell-free systems (Bethesda Research) as described previously^{15,16}, using ³⁵S-methionine as the labelling substrate. Intact cells were labelled with ³⁵S-methionine for 60 min as previously described³. Total cell-free products were analysed on a 10–15% gradient polyacrylamide gel³. The results using the wheat germ system are as follows: a, no mRNA, 3 mM Mg²⁺; b, promastigote mRNA (1 μ g), 3 mM Mg²⁺; c, promastigote mRNA (1 μ g), 5 mM Mg²⁺. The results using the rabbit reticulocyte system are as follows: d, no mRNA, 3 mM Mg²⁺; e, promastigote mRNA (1 μ g), 3 mM Mg²⁺; f, promastigote mRNA (1 μ g), 5 mM Mg²⁺. Lane g shows the proteins metabolically labelled *in vivo* using the same batch of promastigotes. α - And β -tubulin appear as dense bands in between the 43,000 and 68,000 MW markers. Numbers at the left indicate MW marker proteins: β -galactosidase (130,000), bovine serum albumin (68,000), ovalbumin (43,000), pepsin (35,000) and trypsinogen (24,000).

Our results indicate that the large decrease in tubulin biosynthesis which occurs during leishmanial differentiation from the extracellular promastigote stage to the intracellular amastigote stage is not due to a decrease in the amount of translatable tubulin mRNA. Thus, post-transcriptional regulation must be in operation during cell differentiation of this parasite. It is possible that the tubulin half-lives of promastigotes and amastigotes may be different due to a different level of proteolytic activities between the two stages. It has been reported that protease activities are somewhat higher in the amastigotes than in the promastigotes²². However, this difference between the two stages cannot explain their difference in tubulin proteins, as we have pulse-labelled both for 15–60 min and found no difference in the labelling intensity of the tubulin bands (not shown). It is perhaps more likely that tubulin mRNA of amastigotes may be sequestered, thereby unavailable for the protein biosynthetic machinery. It is known that the masked maternal mRNA has a long half-life during the early development of sea urchin and marine snail embryos^{4,5}. In another trypanosomatid *Crithidia*, about 45% of total translationally competent

Fig. 2 Comparison of proteins synthesized *in vitro* by promastigote and amastigote mRNAs with those metabolically labelled *in vivo*. Promastigotes of *Leishmania mexicana* were obtained and total poly(A)⁺ RNA extracted as described in the legend to Fig. 1. Amastigotes were cultured in cells of the macrophage line J774 and purified by Percoll gradient centrifugation; isolated amastigotes remained viable and free from the contamination of macrophage materials¹. Total amastigote poly(A)⁺ RNA was extracted as described in Fig. 1 legend. Proteins synthesized in the rabbit reticulocyte cell-free system using poly(A)⁺ RNA (1 μ g) and metabolically labelled proteins of intact organisms in the presence of ³⁵S-methionine were analysed by SDS-polyacrylamide gel electrophoresis and autoradiography. a, Proteins synthesized by promastigotes *in vivo*. b, Cell-free products directed by promastigote mRNA. c, mRNA from 9-day-old cultures of amastigotes. d, mRNA from 3-week-old cultures of amastigotes. e, The proteins synthesized by amastigotes *in vivo*. Molecular weight markers are indicated as in Fig. 1.

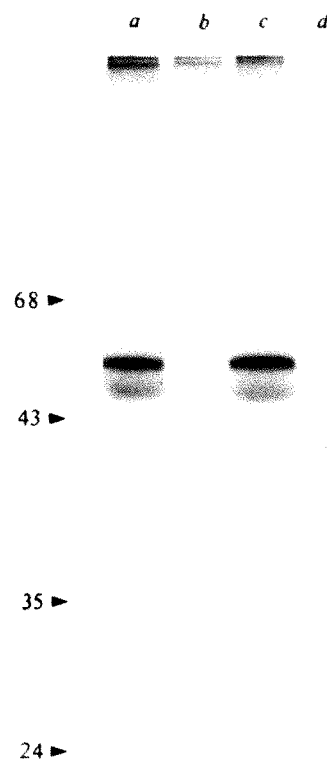


poly(A)⁺ RNA has been found in a non-polysomal compartment²³ and unavailable for translation *in vivo*.

The presence of untranslated tubulin mRNA in amastigotes may have bearings on the evolution of pathogenic *Leishmania* species. Presumably, the promastigote stage in the invertebrates precedes the amastigote stage during the evolution of leishmaniasis²⁴. Retention of tubulin mRNA by amastigotes might be a manifestation of incomplete adaptation of leishmanias in the mammalian host. The presence of abundant tubulin mRNA in the amastigotes could also explain the previous observation that leishmanial differentiation is more rapid from amastigotes to promastigotes than in the reverse direction³.

Thus, we have demonstrated post-transcriptional regulation of tubulin biosynthesis during leishmanial differentiation based on the evidence of *in vitro* translation and β -tubulin

Fig. 3 Immunoprecipitation for β -tubulin of *in vitro* translation products of amastigotes and promastigote mRNAs. Protein samples translated in the reticulocyte system were diluted to about 1.5×10^6 c.p.m. in 50 μ l phosphate-buffered saline (PBS) containing 1% NP40 and incubated for 30 min at 4°C. Each sample was divided into two equal portions; to each was added 10 μ l normal rabbit serum as control or rabbit antiserum against β -tubulin of *Chlamydomonas flagella*²¹. After 18 h at 4°C, each sample received a 50 μ l 33% Protein A-Sepharose 4B in PBS and incubated at 4°C for 2 h under constant agitation. Immunoprecipitates collected in the Protein A beads were extensively washed as previously described³. All samples were subjected to SDS-polyacrylamide gel electrophoresis followed by autoradiography. a and c are immunoprecipitated β -tubulin from amastigote and promastigote samples, respectively. b and d are their respective controls using normal rabbit serum. Note that the 55,000-MW β -tubulin bands immunoprecipitated from amastigotes and promastigote samples are of equal intensity and that there are no protein bands in the controls. The light band below tubulin are artefacts due to the presence of abundant heavy chains of IgG, which is banded at about the same location and brings down some of the radiolabelled tubulins.



immunoprecipitation experiments. This finding can be further studied by using cloned cDNA probes for the analysis of leishmanial tubulin mRNA^{10,11,25}.

We thank Dr Gianni Piperno for the antiserum for β -tubulin of *Chlamydomonas*, Dr A. Kilejian for her support of this project, and Mr J. Stanorski for preparation of this manuscript. M.W. is supported by NIH grant AI-07185 (A.K.); D.F. and K.P.C. are supported by NIH grant AI-15183 and Hirschl Trust (K.P.C.).

Received 21 October 1981; accepted 4 August 1982.

1. Chang, K.-P. *Science* **209**, 1240-1242 (1980).
2. Zuckerman, A. & Lainson, R. in *Parasitic Protozoa* Vol. 1 (ed. Kreier, J. P.) 57-133 (Academic, New York, 1977).
3. Fong, D. & Chang, K.-P. *Proc. natn. Acad. Sci. U.S.A.* **78**, 7624-7628 (1981).
4. Raff, R. A., Colot, H. V., Selvig, S. E. & Gross, P. R. *Nature* **235**, 211-214 (1972).
5. Raff, R. A., Newrock, K. M. & Secrist, R. D. *Dev. Biol.* **44**, 369-374 (1975).
6. Merlino, G. T., Chamberlain, J. P. & Kleinsmith, L. J. *J. Biol. Chem.* **253**, 7078-7085 (1978).
7. Marcaud, L. & Hayes, D. *Eur. J. Biochem.* **98**, 267-273 (1979).
8. Lai, E. Y., Walsh, C., Wardell, D. & Fulton, C. *Cell* **17**, 867-878 (1979).
9. Lefebvre, P. A., Silflow, C. D., Wieben, E. D. & Rosenbaum, J. L. *Cell* **20**, 469-477 (1980).
10. Silflow, C. D. & Rosenbaum, J. L. *Cell* **24**, 81-88 (1981).
11. Minami, S. A., Collis, P. S., Young, E. E. & Weeks, D. P. *Cell* **24**, 89-95 (1981).
12. Raff, E. C. *et al. Cell* **28**, 33-40 (1982).
13. Nienhuis, A. W., Falvey, A. K. & Anderson, W. F. *Meth. Enzym.* **30**, 621-630 (1974).
14. Krystosek, A., Cawthon, M. L. & Kabat, D. J. *biol. Chem.* **250**, 6077-6084 (1975).
15. Roberts, B. E. & Paterson, B. M. *Proc. natn. Acad. Sci. U.S.A.* **70**, 2330-2334 (1973).
16. Pelham, H. R. B. & Jackson, R. J. *Eur. J. Biochem.* **67**, 247-256 (1976).
17. Portier, M. M., Milet, M. & Hayes, D. H. *Eur. J. Biochem.* **97**, 161-168 (1979).
18. Kraus, E. *et al. Proc. natn. Acad. Sci. U.S.A.* **78**, 4156-4160 (1981).
19. Gilmore-Herbert, M. A. & Heywood, S. M. *Biochim. biophys. Acta* **454**, 55-66 (1976).
20. Asselbergs, F. A. M., Meulenber, E., Van Venrooij, W. J. & Bloemendal, H. *Eur. J. Biochem.* **109**, 159-165 (1980).
21. Piperno, G. & Luck, D. J. *J. Biol. Chem.* **252**, 383-391 (1977).
22. Coombs, G. H. *Parasitology* **84**, 149-155 (1982).
23. Rondinelli, E., Soares, M. C. M., de Castro, J. F. & de Castro, F. T. *Archs Biochem. Biophys.* **209**, 349-355 (1981).
24. Wilson, V. C. L. C. & Southgate, B. A. in *Biology of the Kinetoplastida* Vol. 2 (eds Lumsden, W. H. R. & Evans, D. A.) 241-268 (Academic, London, 1979).
25. Cleveland, D. W., Lepata, M. A., Sherline, P. & Kirschner, M. W. *Cell* **25**, 537-546 (1981).

Developmental inactivity of 5S RNA genes persists when chromosomes are cut between genes

J. B. Gurdon*, Colin Dingwall*, Ronald A. Laskey* & Laurence Jay Korn†

* MRC Laboratory of Molecular Biology, Hills Road, Cambridge CB2 2QH, UK

† Department of Genetics, Stanford University, Stanford, California 94305, USA

Xenopus and other amphibians possess two major classes of 5S RNA genes¹. One class, which codes for somatic-type 5S RNA, is expressed in both oocytes and somatic cells². The other class, which is 50 times more abundant and encodes oocyte-type 5S RNA, is expressed in oocytes but not in somatic cells²⁻⁴. The oocyte-type 5S genes are located in tandem arrays of hundreds of genes at the ends of most chromosomes⁵, and it has been postulated that the lack of expression of oocyte-type 5S RNA genes in somatic cells is due to some general characteristic of the chromosomal region which the genes occupy⁶, for example, a folding into heterochromatin or higher-order structures. An alternative possibility is that the inactivity of these genes is controlled individually, and is independent of adjacent genetic material. We have now distinguished between these two possibilities by testing the transcription of oocyte-type 5S RNA genes either in their normal arrangement on intact chromosomes or after each gene has been separated from its neighbours by micrococcal nuclease digestion. Transcription was assayed by injecting intact nuclei, containing the 5S RNA genes as chromatin, into *Xenopus* oocytes⁷. We find that the developmental inactivity of oocyte-type 5S RNA genes is retained after the chromatin is cleaved into fragments the size of individual gene repeats.

Micrococcal nuclease was used to cut the interphase chromosomes of intact somatic nuclei. Digestion was arrested by cooling the nuclear suspension on ice or by adding EDTA to 1 mM. (When nuclear suspensions treated in this way are injected directly into oocytes, no further digestion of DNA takes place

in the oocytes, as shown by analysis of re-extracted DNA; data not shown.) After nuclei had been digested with nuclease for varying lengths of time, DNA was extracted and analysed. Digestion for 2 h is sufficient to reduce most of the nuclear DNA to less than 600 base pairs (bp) in length (Fig. 1a). Moreover, transfer of the digested DNA to nitrocellulose and hybridization with [α -³²P]-labelled 5S DNA shows that the chromatin containing 5S RNA genes is digested to the same extent as total chromatin (Fig. 1b). Although this probe will hybridize to both oocyte- and somatic-type 5S RNA genes, the 50-fold excess of oocyte over somatic genes in the *Xenopus* genome⁸ makes it likely that only the oocyte-type 5S RNA genes are seen in this analysis. Hybridization with specific 5S somatic spacer DNA or 5S oocyte spacer DNA gave identical results except that the signal obtained with the somatic spacer was weaker, reflecting the smaller number of somatic genes (data not shown). Because the oocyte-type 5S RNA genes are arranged in repeats of about 650 bp^{9,10}, and because a 2-h digestion of chromatin reduces most of the DNA to less than 600 bp long, there is, on the average, only one 5S RNA gene (120 bp long) in each fragment of chromatin. We estimate that <1% of the 120 min-digested DNA is long enough to contain three genes (Fig. 1b). We note that even after 2 h of nuclease digestion, the nuclei are still intact, and that while the DNA has been cut into small segments, there could conceivably be some continuity of chromosomal fragments as a result of protein interactions.

The transcription of 5S RNA genes was tested by injecting suspensions of nuclei, treated with nuclease for various lengths of time, into non-activating oocytes⁷, which were then labelled for 2 days with [α -³²P]GTP⁷. In these circumstances, when the chromatin is not digested at all, it has been shown that the somatic-type 5S RNA genes are transcribed but the oocyte-type 5S RNA genes in the nuclei remain transcriptionally inactive⁷. (When oocytes from activating females are used the 5S oocyte-type genes are always activated.) Gel analysis of the transcripts (Fig. 2a) shows that there is no activation of the oocyte-type 5S RNA genes at any level of nuclease digestion. Even when the chromosomes have been cut to a length of DNA too small

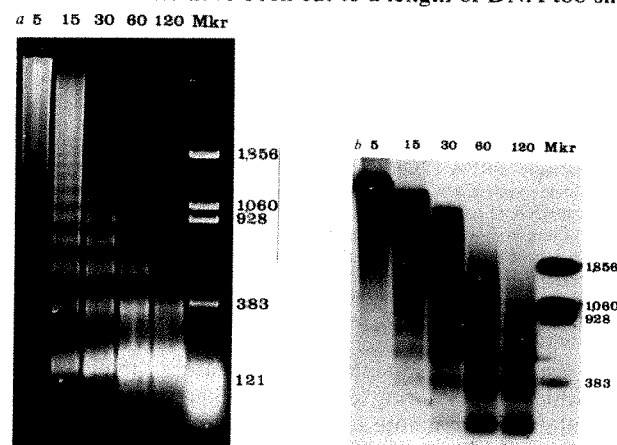


Fig. 1 Agarose gel analysis of DNA extracted from erythrocyte nuclei, after varying times of micrococcal nuclease digestion. *a*, Ethidium bromide stain of total DNA. *b*, Southern transfer of above, hybridized to ³²P-nick-translated pXlo 31, a pBR322 plasmid containing one repeat of *Xenopus laevis* oocyte-type 5S DNA⁹. Lanes marked 5 to 120 are nuclei treated with micrococcal nuclease for 5 to 120 min; Mkr, *Eco*RII digest of pBR322 showing fragment lengths in base pairs. The DNAs used for *b* were from the same samples as for *a*, but were run on a separate agarose gel. *Xenopus* erythrocyte nuclei, prepared by lysolecithin¹⁵, were incubated at 10⁷ nuclei ml⁻¹ in 50 mM Tris-HCl pH 8.0, 1 mM CaCl₂, and 2 U ml⁻¹ of micrococcal nuclease (Worthington Biochemicals) at 37 °C for the times indicated. DNA was prepared from nuclei and analysed on a 1.2% agarose gel. The inefficient transfer of small DNA fragments to nitrocellulose¹⁶ has resulted in a reduced signal from the DNA of mononucleosome length. Note that the 383-bp marker fragment has also transferred inefficiently.

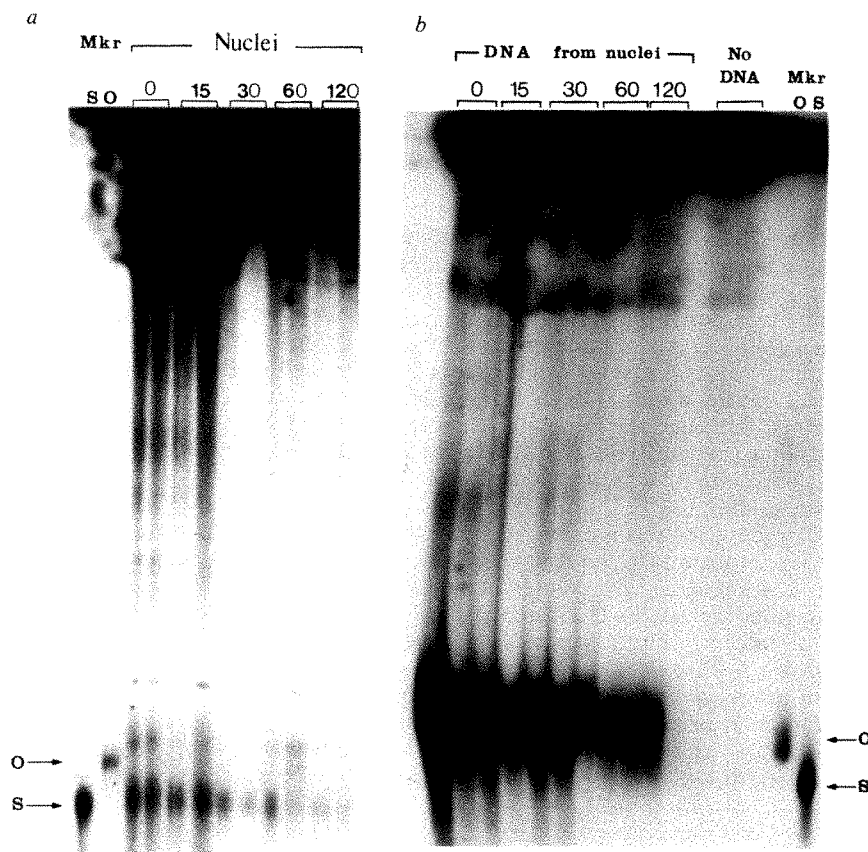


Fig. 2 5S gene transcription from erythrocyte nuclei or DNA injected into *Xenopus* oocytes. *a*, Approximately 500 somatic nuclei (after digestion with micrococcal nuclease for 0–120 min) were injected into individual oocytes, aiming for the germinal vesicle. Preparation of nuclei and nuclease digestions were as for Fig. 1. Oocyte (O) and somatic (S) 5S RNA markers are indicated in the Mkr lanes. *b*, DNA was purified from the same nuclease-treated nuclei as used for *a* and injected into oocytes. All oocytes were subsequently injected with [α - 32 P]GTP and incubated for 2 days. The lane marked 'No DNA' depicts control oocytes not injected with DNA. Labelled RNA was extracted and analysed on non-denaturing polyacrylamide gels⁷. Each track contains the RNA from a single oocyte.

on average to contain more than one gene, the developmental inactivation persists. At each time, the transcription of the somatic-type 5S genes can be seen, though there is less activity at later times. When interpreting this result, it is necessary to recall that there are 50 times more oocyte- than somatic-type genes⁸; a reactivation of oocyte-type genes in only 10% of the injected nuclei would have been readily observed.

One explanation for the non-expression of the oocyte-type 5S genes in nuclease-treated nuclei is that these genes cannot be transcribed as small segments of DNA. Large fragments of 5S DNA injected into oocytes are always transcribed^{11,12}. We have purified DNA from the nuclease-treated nuclei, and injected it into non-activating oocytes. Figure 2*b* shows that oocyte-type 5S RNA is synthesized by DNA from all samples, thus demonstrating that small segments of 5S DNA can be transcribed.

We have shown that the developmental inactivation of 5S RNA genes, once established, can be maintained when chromosomal DNA is cut into pieces containing only one gene. Therefore, although our results do not exclude a need for the tandem arrangement of genes to establish the inactive state initially (see refs 13, 14 for further discussion), they show that the mechanism which maintains the inactive state does not depend on a cooperative effect of many adjacent genes or on distant DNA sequences. Rather, each gene unit must contain regulatory elements sufficient to maintain the inactive state.

We thank S. Whytock for assistance with these experiments, D. Brown for 5S DNA clones, and C. Queen and J. Price for helpful comments on the manuscript. This work was partly supported by NSF grant PCM 8104522 to L.J.K.

Received 23 June; accepted 1 September 1982.

1. Brown, D. D. & Sugimoto, K. *Cold Spring Harb. Symp. quant. Biol.* **38**, 501–505 (1973).
2. Ford, P. J. & Southern, E. M. *Nature new Biol.* **241**, 7–12 (1973).
3. Wegnez, M., Monier, R. & Denis, H. *FEBS Lett.* **25**, 13–20 (1972).
4. Denis, H. & Wegnez, M. *Dev Biol.* **58**, 212–217 (1977).
5. Pardue, M. L., Brown, D. D. & Birnstiel, M. L. *Chromosoma* **42**, 191–203 (1973).
6. Ford, P. J. & Mathieson, T. *Nature* **261**, 433–435 (1976).
7. Korn, L. J. & Gurdon, J. B. *Nature* **289**, 461–465 (1981).
8. Peterson, R. C., Doering, J. L. & Brown, D. D. *Cell* **20**, 131–141 (1980).
9. Federoff, N. V. & Brown, D. D. *Cell* **13**, 701–716 (1978).
10. Carroll, D. & Brown, D. D. *Cell* **7**, 467–475, 477–486 (1976).
11. Brown, D. D. & Gurdon, J. B. *Proc. natn. Acad. Sci. U.S.A.* **74**, 2064–2068 (1977); **75**, 2849–2853 (1978).

12. Gurdon, J. B. & Brown, D. D. *Dev Biol.* **67**, 346–356 (1978).
13. Bogenhagen, D. F., Wormington, W. M. & Brown, D. D. *Cell* **28**, 413–421 (1982).
14. Gottesfeld, J. M. & Bloomer, L. S. *Cell* **28**, 781–791 (1982).
15. Gurdon, J. B. *J. Embryol. exp. Morph.* **36**, 523–540 (1976).
16. Thomas, P. *Proc. natn. Acad. Sci. U.S.A.* **77**, 5201–5205 (1980).

Identification of a potential control region in bacteriophage T7 late promoters

L. K. Jolliffe, A. D. Carter* & W. T. McAllister†

Department of Microbiology, University of Medicine and Dentistry of New Jersey, Rutgers Medical School, PO Box 101, Piscataway, New Jersey 08854, USA

During infection of *Escherichia coli*, bacteriophage T7 encodes a simple RNA polymerase that consists of a single protein species of 883 amino acids^{1,2}. This phage-specified RNA polymerase transcribes the late genes of T7 in two temporal classes (class II and class III)³. The mechanism by which late transcription is regulated is unclear. In general, class II promoters are weaker than class III promoters and *in vitro* the purified phage RNA polymerase discriminates between these classes of promoters as a function of ionic conditions and agents that affect the stability of the DNA helix⁴. Sequence analysis of 17 promoters utilized by the phage RNA polymerase reveals a highly conserved 23 base-pair (bp) consensus sequence that is different from known bacterial promoters⁵. To determine which structural features of the late promoters are important for the regulation of transcription, we have constructed a number of class II/III hybrid promoters and have determined their properties both *in vitro* and *in vivo*. The results reported here indicate that an A + T-rich region that overlaps the upstream end of the promoter has an important role in the control of promoter selection during T7 infection. In addition, changes in the 23-bp conserved promoter sequence may also affect promoter regulation.

* Present address: Laboratory of Biochemistry, National Cancer Institute, Building 37, NIH, Bethesda, Maryland 20205, USA.

† To whom all correspondence should be addressed.

A detailed comparison of promoter structure for the class II and class III promoters (Table 1) reveals a highly conserved region that extends from the +6 position to the -17 position (+1 represents the site at which RNA synthesis is initiated). As a rule, the class III promoters never deviate from the consensus sequence, whereas the class II promoters deviate from the conserved sequence at several locations. Another feature to note is the length of the AT run located between positions -13 and -22. In all class III promoters the AT run extends uninterrupted for 8 to 10 nucleotides. In contrast, the AT run is interrupted by one or more GC base pairs after 4-6 nucleotides in nearly all class II promoters. The exception to this general observation is the promoter located at 27.95 T7 units; this promoter has several mismatches from the conserved sequence but has a long AT run characteristic of the class III promoters. Although this promoter is located in the class II region of the genome, it behaves *in vivo* as a class III promoter when cloned into pBR322 (ref. 6 and F. W. Studier, personal communication).

To determine the relative importance of the various regions of the late promoters in the control of transcription, we have constructed a number of promoter variants (Fig. 1). By taking advantage of the *HinfI* site located at position -10 in nearly all T7 promoters, we have constructed hybrid promoters which contain the A+T-rich region (left of the *HinfI* site) from one class of promoter and the remaining portion (to the right of the *HinfI* site) from the other class of promoter. During the course of these constructions, we also isolated promoter derivatives in which regions downstream from position +12 were

removed from the promoter (pADC10) and in which regions upstream from -23 were removed from the promoter (pLJ1).

To test the behaviour of promoter variants, we first examined their properties *in vitro* by transcribing linearized plasmid DNA that contained the promoters with purified T7 RNA polymerase in the presence of increasing concentrations of KCl. *In vitro*, initiation of transcription by the T7 RNA polymerase at class II promoters in T7 DNA has been observed to be more sensitive to increased ionic strength than is initiation at the class III promoters⁴. As seen in Fig. 2, this is also true of class II and class III promoters that have been removed from T7 DNA and embedded into plasmid DNA sequences. Removal of regions downstream from the +12 position (pADC10) and upstream from position -23 (pLJ1) did not affect the characteristic behaviour of the class III promoters tested.

The class II/III hybrid promoter in pADC5 (which has the AT region from a class II promoter and the initiation region from a class III promoter) behaves as a class II promoter *in vitro*. The class III/II hybrid promoter (in pLJ8) behaves as a class III promoter *in vitro*. These experiments indicate that the A+T-rich region plays a predominant part in determining the salt sensitivity of the late promoters *in vitro*.

During infection of cells carrying recombinant plasmids, T7 late promoters in the plasmids are recognized with similar kinetics as the corresponding late promoters located in the phage genome⁶. This feature makes it possible to examine the properties of the altered promoters *in vivo* by means of a simple hybridization protocol (Fig. 3). In the typical pattern of transcription exhibited by a class II promoter (in pAR95), transcrip-

Table 1 Sequences of promoters for T7 RNA polymerase

Promoter	RNA start site [†]	Nucleotide sequence*
Left end promoter		5' - -35 -20 -15 -10 -5 +1 +5 +10 +15 +20 -3'
φ0L	1.02	TTGTCTTATTAATACAACTCACTATAAGGAGAGA
Class II promoters		
φ1.1A	14.62	TCCGTTCCGCTAACGCCAAATCAATACGACTCACTATAGGGGCAAACTCAAGTCA
φ1.1B	14.81	TTATGATTGACCTTCTCGGTTAATACGACTCACTATAGGAAACCTTAAGGTTAAG
φ1.3	16.02	GACCAATTGAAGGACTGGAACTAATACGACTCACTATAGGGAATGCTTAAGTCCG
φ1.5	19.45	CGTGTGAGTATAGTTAACTGCTAATACGACTCACTAAAGGAGGTACACCATGATGT
φ1.6	19.74	TGATATGCCAGATGGTCCGCTAATACGACTCACTAAAGGAGACACTATATGTTCCGA
φ2.5	22.77	GGTCTTGTGTAGCACCGAATCAATACGACTCACTATAGGGAAGAC
φ3.8	27.95	GTCACTTTCACCGTGGATAATTGAATGAACCTCACTAAAGGGAGACACACGGG
φ4C	31.68	CCGACTGAGCAATCCGACTCACTAAAGAGAGACA
φ4.3	33.35	GTTTGGCTGGAGAGTCCGATTCGAATACGACTCACTAAAGGAGACACCATGTTCAAA
φ4.7	34.78	TAAGTGGTGGCTTCATGAATAATTGCACTCACTATAGGAGATATTACCATGGCTGA
Class III promoters		
φ7	46.50	GATAAACTCAAGGTCCTCAATCAATACGACTCACTATAGGAGATAGGGGCGCTT
φ9	54.40	CGGAATTCAATACGACTCACTATAGGAGACTCACTCT
φ10	57.29	AACTTCTGATAGACTTCGAAATCAATACGACTCACTATAGGAGACACAAACGG
φ13	68.00	TGTGGTGGCTCGAAATCAATACGACTCACTATAGGAGACAATACGACCG
φ17	86.56	AACTTAGGGAGCGTAGCAATCAATACGACTCACTATAGGAGAGGGCAATAA
φOR	98.24	TTACTGAAAGACACGATAAATCAATACGACTCACTATAGGAGAGGAGGACGAAAGG
Cloned promoters [§]		
pAR95	34.78	TAAGTGGTGGCTTCATGAATAATTGCACTCACTATAGGAGATATTACCATGGCTGA
pADC5	II/III hybrid	TAAGTGGTGGCTTCATGAATAATTGCACTCACTATAGGAGATAGGGGCTTACGG
pADC10	46.50	GATAAACTCAAGGTCCTCAATCAATACGACTCACTATAGGAGATAGGGGCTTACGG
pLJ8	III/II hybrid	GATAAACTCAAGGTCCTCAATCAATACGACTCACTATAGGAGATATTACCATGGCTGA
pLJ1	68.00	TTGACAGCTTATCATCGAAATCAATACGACTCACTATAGGAGACAATACGACCG

Sequences for the promoters at 31.68 and 98.3 T7 units were personal communications from J. Dunn and S. Stahl, respectively. Sequences for the remaining promoters have been published previously¹¹⁻¹⁴. The sequence given for the upstream substitution in pLJ1 is the sequence which would result from cloning a *TaqI* fragment into the *ClaI* site of pBR322 (see Fig. 1).

[†] The location given is in T7 units¹².

[‡] The 23-base pair conserved region is enclosed by the box. Mismatches from the consensus sequence are indicated by an asterisk. The AT run in each promoter is underlined. The dashed lines indicate the upstream and downstream substitutions in the appropriate cloned promoters. The *HinfI* cleavage site is marked by an apostrophe.

[§] Promoter constructions are described in Fig. 1. The hybrid promoters were sequenced by the method of Maxam and Gilbert¹⁵.

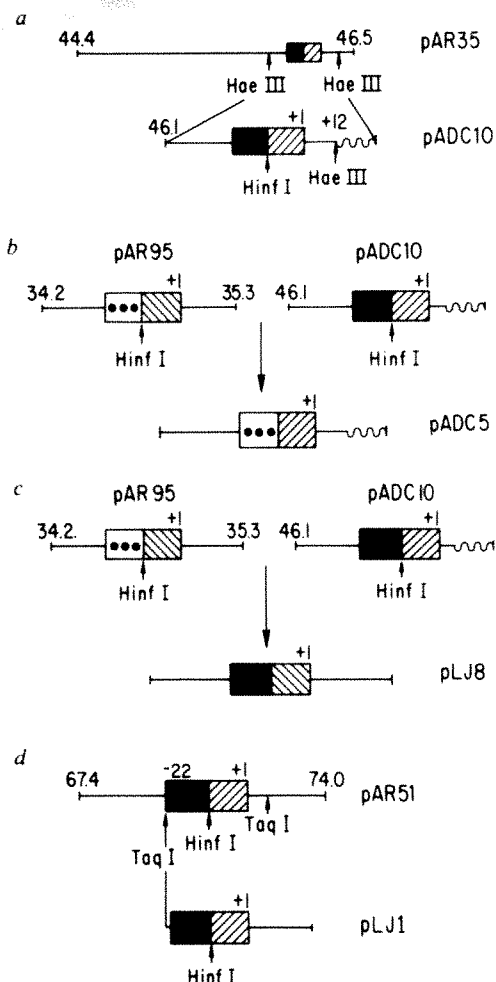


Fig. 1 The constructions described below began with T7 late promoters that had been cloned into pBR322 (ref. 16) using standard procedures¹⁷. Unless otherwise noted, all promoters are inserted into the *Bam*HI site of pBR322. *a*, The class III promoter from 46.5 T7 units (in pAR35; ref. 16) was cloned as a *Hae*III fragment into the *Bam*HI site of pBR322 by ligation of synthetic linkers to give pADC10. During the subcloning, regions downstream from position +12 were substituted by a 51-bp *Hae*III fragment of unknown origin. *b*, The AT run of the class II promoter from 34.7% (in pAR95; ref. 16) was joined to the initiation region of the class III promoter from 46.5% (in pADC10) by ligation at the common *Hinf*I site to obtain a class II/III hybrid promoter (pADC5). *c*, A class III/II hybrid promoter was constructed by joining the left section of the 46.5% promoter (from pADC10) to the right section of the 34.7% promoter (from pAR95) to yield pLJ8. *d*, The upstream flanking regions of the promoter at 68% were removed by digestion of the *Bam*HI insert of pAR51 (ref. 16) with *Taq*I. This fragment was cloned into the *Cla*I site of pBR322. The left portion of class III promoters is indicated by ■; the right portion is denoted by ▨. The left half of a class II promoter is indicated by □; the right half is denoted by ▩. Restriction sites are as indicated. The downstream substitution in pADC10 and pADC5 is indicated by a wavy line. The start site for initiation of RNA synthesis is represented by +1. Sequence analysis of the hybrid promoters confirmed the constructions described above (Table 1).

tion of the plasmid begins early and is markedly reduced by about 10–12 min post infection. In contrast, the class III promoter in pAR35 continues to be used until later in infection. Transcription from the promoter in pADC10 (which has a downstream substitution 12 bp to the right of the initiation site) resembles that of pAR35, indicating that removal of the downstream flanking regions does not affect regulation of this promoter *in vivo*. Similarly, transcription of plasmid sequences controlled by a class III promoter having an upstream substitution 2 bp to the left of the AT run (pLJ1) remains unchanged from that of a class III promoter (that is, pAR35).

The properties of the hybrid promoters were compared with each of the starting promoters by the same techniques (Fig. 3). The behaviour of the class II/III promoter (pADC5) is characteristic of the class II promoter that donated the A+T-rich region (pAR95), whilst the behaviour of the class III/II hybrid promoter (pLJ8) is somewhat intermediate between the class II and class III parent promoters. We conclude from these results that shortening the AT run from 9 to 4 bp is sufficient to cause a class III promoter to be regulated as a class II promoter *in vivo*. However, replacing the short AT run of the class II promoter with the longer AT run of a class III promoter does not seem to overcome completely the effects of changes in the consensus sequence from +2 to +6.

The results of this study enable us to define more precisely the sequences in T7 late promoters that are required for transcription initiation and regulation. Panayotatos and Wells had reported that the region from +33 to –20 bp is sufficient for polymerase binding and initiation *in vitro*⁷. Subsequently, Osterman and Coleman demonstrated that cleavage of the promoter at –10 by *Hinf*I prevented initiation; however, substitution of a nonspecific *Hinf*I fragment of DNA restored initiation of transcription *in vitro*⁸. Although these results suggested that specific T7 sequences to the left of the *Hinf*I site are not required for promoter recognition *in vitro*, note that the nonspecific fragments used to reconstitute the promoter in the latter study resulted in the presence of AT regions of 2–4 bp at the same location as in the native promoter sequences. The possibility that this region might participate in promoter function thus remained open.

To answer these questions, we have examined the effects of changes in promoter structure on promoter use *in vivo* and *in vitro*. Our results demonstrate that the region from +13 to –22 bp is sufficient to allow for initiation of transcription both *in vitro* and *in vivo*. Further, we have shown that the sequence

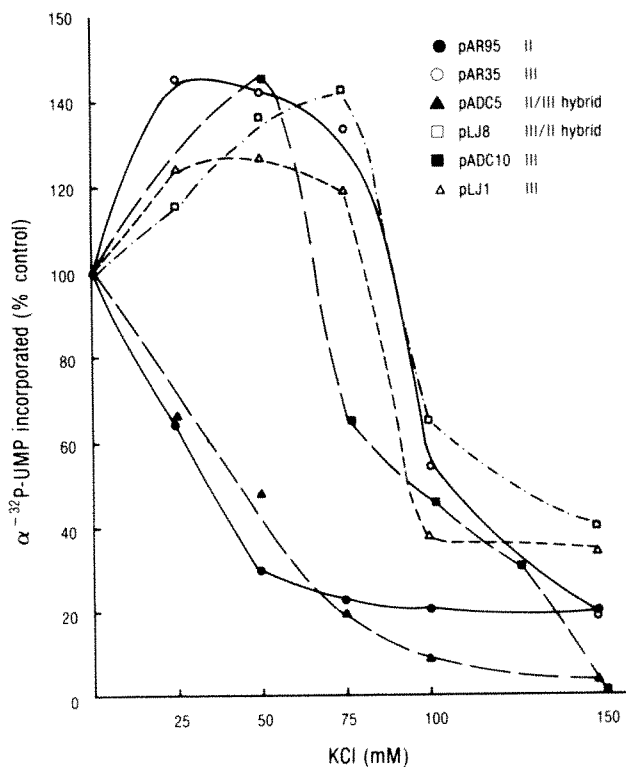


Fig. 2 Plasmids containing T7 promoters linearized by digestion with *Ava*I (which cuts pBR322 only once, and does not cut T7 DNA) were transcribed by purified T7 RNA polymerase in the presence of KCl as indicated. The amount of ³²P-UMP incorporated into acid insoluble products was determined as previously described⁴ and is indicated as per cent of control (in the absence of KCl). The average level of activity in the control samples was 3.1×10^4 c.p.m.

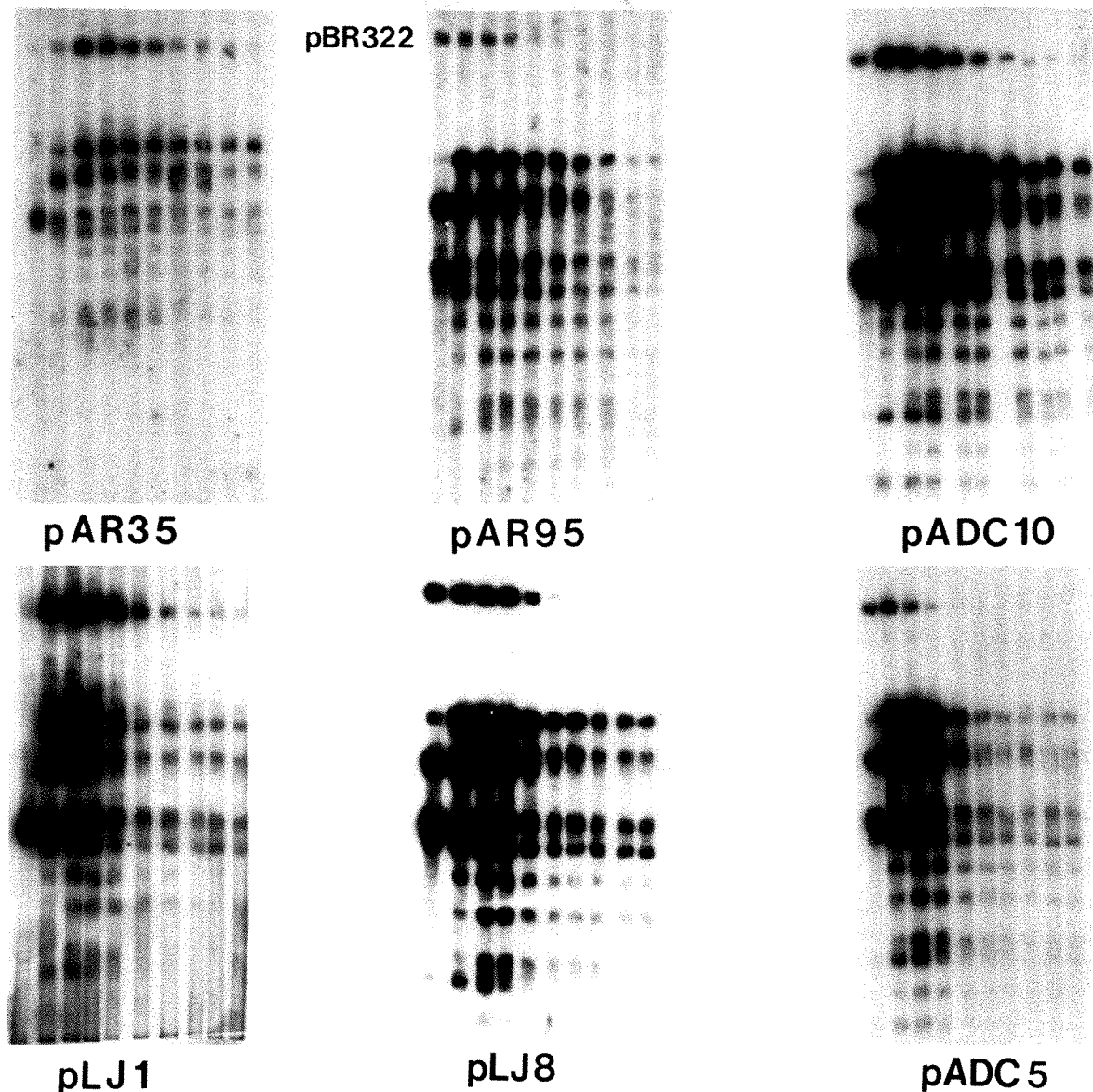


Fig. 3 Bacteria harbouring the plasmids indicated were grown in B2 medium¹⁸ containing thymidine ($20 \mu\text{g ml}^{-1}$) and ampicillin ($20 \mu\text{g ml}^{-1}$), at 37°C to a density of approximately 5×10^8 cell ml^{-1} . The cultures were infected with T7⁺ at a ratio of 10 to 7 phage particles per cell. At intervals following infection, $100 \mu\text{l}$ of culture were removed and added to $\text{H}_3^{32}\text{PO}_4$ ($10 \mu\text{Ci ml}^{-1}$; specific activity, 285 Ci mg^{-1}). Incorporation of label was terminated by the addition of 5 vol. cold $0.01 \text{ mM Na}_2\text{S}_2\text{O}_8$, $75 \text{ mM Na}_2\text{HPO}_4$. The cells were collected by centrifugation and lysed by incubation in lysis buffer (0.02 M sodium acetate, $\text{pH } 5.2$, 1 mM EDTA , 0.5% SDS). Cell lysates were extracted twice with phenol at 65°C to obtain total RNA⁶. The aqueous phase ($25 \mu\text{l}$) was used directly for hybridization to nitrocellulose filter strips containing *Hpa*I fragments of T7 DNA, and pBR322 DNA that had been linearized by digestion with *Eco*RI (ref. 6). Each lane represents successive 2-min pulse intervals beginning at 2 min post infection and ending 22 min post infection. The top band in each panel represents hybridization to plasmid DNA. The bands below the plasmid DNA represent hybridization of labelled RNA to *Hpa*I fragments of T7 DNA. Note that the T7 RNA polymerase does not recognize any promoters in pBR322 and, because host transcription is shut off by 4 min after infection, all transcription of plasmid sequences after that time depends on recognition of the T7 late promoter cloned into the plasmid⁶.

in this region provides the necessary information for appropriate regulation of polymerase activity. Whereas the length of the AT run seems to play a primary part in regulating promoter selection *in vitro*, the results are less clear cut *in vivo* and suggest that in some cases changes in the conserved region (+2 to +6) may also be involved in promoter regulation.

Although we have identified a potential control region in late T7 promoters, the mechanism by which promoter selection is regulated *in vivo* remains unclear. We had previously observed that T7 mutants that are defective in gene 3.5 (lysozyme) show an altered transcription programme in which transcription of the class II genes is not shut off with normal kinetics¹. It has been reported that expression of gene 3.5 results in changes in the permeability of the cell membrane⁹ and release of phage DNA from a membrane bound complex¹⁰. Whether these changes affect the state of the DNA helix or alter the overall transcriptional capacity of the cell such that only the strongest promoters continue to be used remains to be determined.

This work was supported by NIH grant GM21783 and a grant to W.T.M. from the Foundation of the University of

Medicine and Dentistry of the New Jersey (UMDNJ 21-82). L.K.J. and A.D.C. were supported by USPHS Training Grant CA-09069-07. Part of this work was submitted to Rutgers University in fulfillment of the degree requirements of A.D.C.

Received 19 April; accepted 15 July 1982.

1. Chamberlin, M., McGrath, J. & Waskell, L. *Nature* **228**, 227-231 (1970).
2. Stahl, S. J. & Zinn, K. *J. molec. Biol.* **148**, 481-485 (1981).
3. McAllister, W. T. & Wu, H.-L. *Proc. natn. Acad. Sci. U.S.A.* **75**, 804-808 (1978).
4. McAllister, W. T. & Carter, A. D. *Nucleic Acids Res.* **8**, 4821-4837 (1980).
5. Rosenberg, M. & Court, D. A. *Rev. Genet.* **13**, 319-353 (1979).
6. McAllister, W. T., Morris, C., Rosenberg, A. H. & Studier, F. W. *J. molec. Biol.* **153**, 527-544 (1981).
7. Panayotatos, N. & Wells, R. D. *Nature* **280**, 35-39 (1979).
8. Osterman, H. L. & Coleman, J. E. *Biochemistry* **20**, 4884-4892 (1981).
9. Condit, R. C. *J. molec. Biol.* **98**, 45-56 (1975).
10. Silberstein, S., Inouye, M. & Studier, F. W. *J. molec. Biol.* **96**, 1-11 (1975).
11. Carter, A. D. & McAllister, W. T. *J. molec. Biol.* **153**, 825-830 (1981).
12. Dunn, J. J. & Studier, F. W. *J. molec. Biol.* **148**, 303-330 (1981).
13. Rosa, M. D. *Cell* **16**, 815-825 (1979).
14. Oakley, J., Strothkamp, R., Sarris, A. & Coleman, J. *Biochemistry* **18**, 528-537 (1979).
15. Maxam, A. & Gilbert, W. *Meth. Enzym.* **65**, 499-559 (1980).
16. Studier, F. W. & Rosenberg, A. H. *J. molec. Biol.* **153**, 503-525 (1981).
17. Colowick, S. P. & Kaplan, N. O. *Meth. Enzym.* **68**, 1-555 (1979).
18. Studier, F. W. *J. Bact.* **124**, 307-316 (1975).

MATTERS ARISING

Significance of ankle structures in archosaur phylogeny

IN his recent analysis of archosaur phylogeny¹, Chatterjee places great emphasis on the pattern of articulation between the proximal tarsal bones. He takes the distinction between 'normal' and 'reverse' articulations (Fig. 1*d, e*) to reflect a basic dichotomy of archosaur stocks, in each of which there occurred transitions between mesotarsal (MT) and crurotarsal (CT) joints. These joints are distinguished by the course of the 'hinge' through the ankle (Fig. 1*a, c*). Chatterjee's interpretation (Fig. 2*a*) is not entirely satisfactory: it entails reversals in ankle structure and involves morphological changes that are not readily explained in functional terms.

Chatterjee maintains¹ that the CT joint evolved from the MT joint, and vice versa, even though it is difficult^{2,3} or impossible^{4,5} to envisage such changes. Moreover, Chatterjee suggests that these changes constituted at least two reversals (in parallel) during archosaur history: from MT (in primitive 'sprawling' archosaurs) to CT (in archosaurs with 'semi-improved' stance), and back to MT (in advanced archosaurs with 'erect' or 'fully-improved' stance). There are only three ways in which the MT joint might have evolved from the CT joint (or vice versa): (1) by way of a non-functional ankle in adult animals (with calcaneum locked both to crus and to distal tarsals); (2) by way of a non-functional ankle in embryonic archosaurs; (3) by way of a duplex ankle joint (with 'hinges' of the ankle

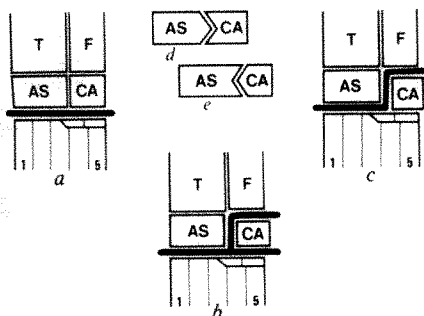


Fig. 1 Block diagrams to illustrate tarsal characters of archosaurs. *a*, Mesotarsal (MT) joint; *b*, duplex (DP) joint; *c*, crurotarsal (CT) joint. In all three cases the left ankle is shown in anterior view, with its principal 'hinge' indicated by a thick line. Bones identified as follows: AS, astragalus; CA, calcaneum; F, fibula; T, tibia; 1, first metatarsal; 5, fifth metatarsal. Both MT and CT joints (*a, c*) might have been derived from the DP joint (*b*) by suppression of appropriate sections of 'hinge' in the latter. *d*, 'Normal' peg-and-socket linkage of proximal tarsals; *e*, 'reverse' peg-and-socket linkage of proximal tarsals.

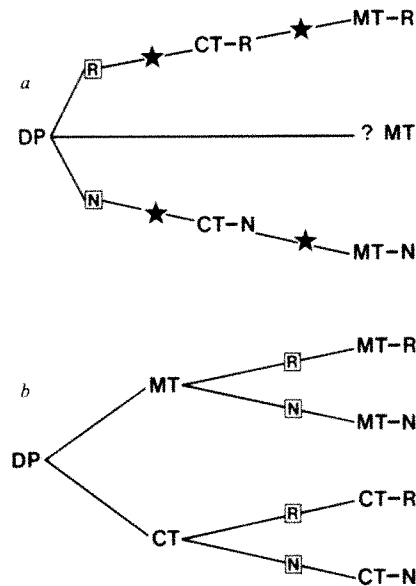


Fig. 2 Distribution of tarsal character-states in *a*, Chatterjee's scheme of archosaur phylogeny¹; and in *b*, alternative scheme proposed here. CT, crurotarsal joint; DP, duplex joint; MT, mesotarsal joint; suffix-N, 'normal' linkage of proximal tarsals; suffix-R, 'reverse' linkage of proximal tarsals; boxed N, development/elaboration of 'normal' linkage; boxed R, development/elaboration of 'reverse' linkage; star, transition from MT joint to CT joint or vice versa.

proximal and distal to the calcaneum; Fig. 1*b*). The first possibility seems unlikely, while the second is untestable. A duplex ankle joint (DP) has been identified in some Triassic archosaurs³, though it has not been regarded as structurally intermediate between MT and CT joints. If the DP joint were intermediate, the scheme proposed by Chatterjee would entail even more complicated reversals: MT → DP → CT → DP → MT.

Peg-and-socket articulation of the proximal tarsals is widespread among Triassic archosaurs^{1,6}, irrespective of the basic ankle joint (whether DP, MT or CT). Vestiges of such articulations ('normal' or 'reverse') persist in the MT ankles of some advanced archosaurs, and rudiments of them ('normal' plus 'reverse') occur in the DP ankles of primitive archosaurs. Development of a peg-and-socket articulation is a relatively minor innovation: it is certainly easy to envisage, and could have occurred in only one of two ways ('normal' or 'reverse'). Such minor features might well have appeared independently in distantly related archosaurs. Nonetheless these features are accorded primary significance in Chatterjee's analysis of archosaur phylogeny; by contrast some much greater and more complicated morphological changes (from

MT joint to CT joint and vice versa) are relegated to secondary importance.

By attaching primary significance to the course of the 'hinge' through the ankle (that is, to DP, MT and CT joints), it is possible to construct a more parsimonious scheme of archosaur phylogeny (Fig. 2*b*). In this scheme MT and CT joints are not derived from one another, but are derived independently from the DP joints of primitive archosaurs. Consequently there are no reversals in ankle structure, and convergences appear only in relatively minor features (the 'normal' and 'reverse' articulations of the proximal tarsals).

RICHARD A. THULBORN

Department of Zoology,
University of Queensland,
St Lucia, Queensland 4067,
Australia

1. Chatterjee, S. *Nature* **295**, 317-320 (1982).
2. Charig, A. J. in *Studies in Vertebrate Evolution* (eds Joysey, K. A. & Kemp, T. S.) 121-155 (Oliver & Boyd, Edinburgh, 1972).
3. Thulborn, R. A. *Alcheringa* **4**, 241-261 (1980).
4. Krebs, B. *Paläont. Z.* **37**, 88-95 (1963).
5. Krebs, B. *Naturwissenschaften* **61**, 17-24 (1974).
6. Cruickshank, A. R. I. *S. Afr. J. Sci.* **75**, 168-178 (1979).

CHATTERJEE REPLIES—Thulborn wants to replace the term 'primitive mesotarsal' (PM) ankle joint¹ with 'duplex' (DP) ankle joint. I prefer the former term because the ankle joint in these groups (proterosuchians) is both functionally mesotarsal^{2,3}, and primitive as 'the astragalus and calcaneum articulate with each other by means of double convex-concave complementary joints'. Both of us agree that the PM (= DP) joint could give rise to the crocodiloid (CN and CR) joint. In his earlier paper⁴, Thulborn did not refute the argument that the AM (= MT) joint, as seen in dinosaurs, could have evolved from the crocodiloid joint, but he now considers that the AM joint was derived directly from a PM joint, not via a crocodiloid joint. In Fig. 1 (ref. 1), I suggested this latter possibility. But there are some dinosaurs which retain the vestiges of peg-and-socket joint, either in CN or CR fashion, indicating a close structural affinity. The origin of dinosaurs from different thecodontian lineages is not clear at this moment, but differences among the tarsi may yet be an important clue to such relationships. It is possible that carnosaurs evolved from two separate stocks of thecodontians (allosaurs from ornithosuchids, and tyrannosaurs from poposaurids), as indicated by the correlation between ankle structure and other anatomical details. In ornithosuchids and poposaurids, the initiation of the ascending process of the

astragalus, so prominent in later carnosaurs, can be seen (Fig. 1)¹. This also implies that the AM joint could have evolved from a crocodiloid joint.

SANKAR CHATTERJEE
The Museum,
Texas Tech University,
Lubbock, Texas 79409, USA

1. Chatterjee, S. *Nature* **295**, 317–320 (1982).
2. Cruickshank, A. R. I. *S. Afr. J. Sci.* **75**, 168–178 (1979).
3. Hughes, B. J. *zool. Res.* **156**, 457–481 (1968).
4. Thulborn, R. A. *Alcheringa* **4**, 241–261 (1980).

Reduction in plasma calcium during exercise in man

RUBEN and Bennett¹ reported increased plasma calcium concentration $[Ca_p]$ following exercise in various species. They suggested that increased $[Ca_p]$ is due to bone resorption, implying an increase in total plasma calcium content (Ca_t). However, the rise in $[Ca_p]$ following exercise might merely result from a reduction

in plasma volume (PV)² with or without change in Ca_t .

We have now investigated the responses of PV, $[Ca_p]$ and Ca_t in 13 men (22 ± 1 yr, 73.9 ± 2.1 kg and mean maximal oxygen uptake of 56.4 ± 2.2 ml kg⁻¹ min⁻¹) who worked on a cycle ergometer at one of three randomly ordered work intensities for 6 min on three different days (Table 1). PV was measured with Evans blue dye², and change in PV was calculated from the haematocrit³. $[Ca_p]$ was analysed by atomic absorption spectrophotometry. Ca_t was calculated from $[Ca_p]$ and per cent change in PV⁴.

These results, from men, show that during exercise, $[Ca_p]$ increased to a constant level while PV and Ca_t decreased progressively with increasing exercise level (Table 1). The rate of decrease in PV was greater than that for Ca_t (Fig. 1). This suggests that the increase in $[Ca_p]$ during exercise can be attributed to a more rapid loss of fluid from the vascular space and does not necessarily require a significant net influx of calcium from extravascular

Table 1 Effect of submaximal and maximal work on plasma volume and calcium ion concentration in humans (from Fig. 5 in ref. 2)

% Work load	% Net change in plasma volume	Ca ² concentration (mmol l ⁻¹)
Rest	—	1.10
43	-8	1.03*
62	-14	1.02*
100	-16	1.20*

* After 10 min exercise.

systematic lactic acid accumulation and pH depression associated with maximal levels of exercise in vertebrates. The plasma volume and calcium concentrations cited by Convertino *et al.* associated with 'heavy' muscular activity (225 W) represent submaximal exercise levels (about 60–65% of capacity) for humans. Thus, it is unlikely that exercise-related hypercalcaemia of the sort we described occurred in their experimental subjects. Significantly, Greenleaf *et al.*² have previously described a dramatic rise in the concentration of calcium ions in plasma immediately following maximal exercise, whereas there is a slight decrease in plasma calcium ion concentration at 43% and 62% work levels (Table 1).

Additionally, haemoconcentration cannot possibly account for the exercise-related hypercalcaemia measured in other species in our study. For haemoconcentration to account for the degree of post-exercise hypercalcaemia present in all non-mammalian osseous species, plasma volume reduction of at least 30% (for fish with acellular bone) and 50% (for fish with cellular bone and reptiles) would have to have occurred. Acute plasma volume losses approaching 20–25% are generally associated with hypovolemic shock. There were no indications that any of our experimental animals experienced such a condition. Moreover, the lack of exercise-related hypercalcaemia in non-osseous species investigated (lamprey, shark) seems particularly noteworthy in this respect.

While haemoconcentration may well be a contributing factor to some of the exercise-related hypercalcaemia we describe, it seems unlikely to be a major factor accounting for the phenomena discussed in our paper.

JOHN A. RUBEN

Zoology Department,
Oregon State University,
Corvallis, Oregon 97331, USA

ALBERT F. BENNETT

Department of Cell and Developmental Biology,
University of California,
Irvine, California 92664, USA

1. Ruben, J. A. & Bennett, A. F. *Nature* **291**, 411–413 (1981).
2. Greenleaf, J. E. *et al.* *J. appl. Physiol.* **43**, 1026–1032 (1977).

Table 1 Effect of light, moderate and heavy muscular activity on PV, $[Ca_p]$ and (Ca_t)

Exercise level (W)	PV (ml)	$[Ca_p]$ (mmol l ⁻¹)	Ca_t (mg)
Rest	3,504 ± 83	2.47 ± 0.03	347 ± 9
Light (100)	3,388 ± 91*	2.53 ± 0.03*	344 ± 9
Moderate (175)	3,208 ± 94*	2.55 ± 0.03*	324 ± 10*
Heavy (225)	3,072 ± 83*	2.57 ± 0.03*	317 ± 9*

Values are mean ± s.e.

* $P < 0.05$ compared with corresponding rest value.

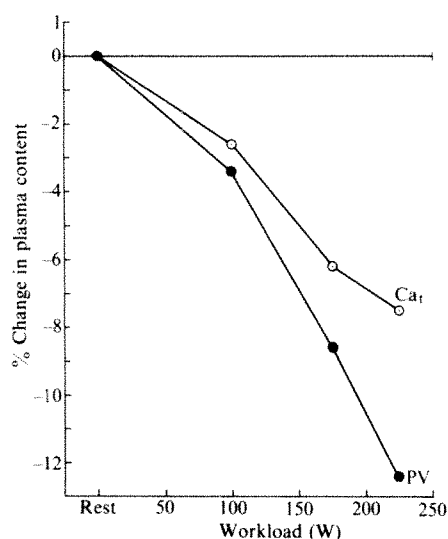


Fig. 1 Proportional changes in PV and Ca_t with graded work intensities of 100, 175 and 225 W. Plotted points are mean values of the percentage change calculated from pre- and post-exercise haematocrit and plasma calcium concentrations⁴.

sources. Thus, the conclusion of Ruben and Bennett¹ should be evaluated cautiously until measurements of vascular fluid and calcium shifts are available.

VICTOR A. CONVERTINO*
EMILY R. MOREY
JOHN E. GREENLEAF

Biomedical Research Division,
NASA Ames Research Center,
Moffett Field, California 94035, USA

1. Ruben, J. A. & Bennett, A. F. *Nature* **291**, 411–413 (1981).
2. Greenleaf, J. E., Convertino, V. A. & Mangseth, G. R. *J. appl. Physiol.* **47**, 1031–1038 (1979).
3. Van Beaumont, W., Greenleaf, J. E. & Juhos, L. *J. appl. Physiol.* **33**, 55–61 (1972).
4. Van Beaumont, W., Strand, J. C., Petrofsky, J. S., Hipkind, S. G. & Greenleaf, J. E. *J. appl. Physiol.* **34**, 102–106 (1973).

RUBEN AND BENNETT REPLY—The values cited above by Convertino *et al.* for blood calcium levels during human exercise are not directly relevant to our previous study¹. We hypothesize that the mechanism resulting in post-exercise hypercalcaemia involves dissolution of a fraction of the crystalline calcium hydroxyapatite compartment of the skeleton. This dissolution is a result of

* Present address: Exercise and Sport Sciences Laboratory, Department of Physical Education, University of Arizona, Tucson, Arizona 85721, USA.

BOOK REVIEWS

Risk and rationality

Stephen Cotgrove

THE debate about risk can generate strong emotions — on both sides. Opponents of nuclear power, for example, are sometimes accused of being short on facts; or worse, they are charged with being emotional and irrational. Indeed, if we look at the risks of dying from various causes, from snake-bite to smoking, there doesn't seem to be much connection between probability and anxiety. One of the most persuasive arguments is that what we need is a calculus of risk — a league table — which will tell us when we should worry, and when to relax.

Such an approach, however, is simplistic in the extreme. Indeed, the two closely written books reviewed here are testament enough to the complexities of deciding on courses of action which have risky consequences. And at the end of the day, it is not surprising that neither comes up with even relatively simple solutions.

Of the two, *Acceptable Risk* is by far the more extensive in its coverage. As its title implies it analyses the processes by which we can arrive at decisions as to what risks are acceptable. Three main strategies are explored. First, there is formal analysis, of which cost-benefit analysis is the most familiar example. Second, there are what the authors call "bootstrapping approaches". In essence, these take the safety levels achieved with old risks as a guide to managing new risks, an example being the natural-standards approach which includes taking natural levels of radiation as the bench mark for judging acceptable levels. Finally, there is reliance on the theoretical judgement of the technical experts who are most knowledgeable in a particular field.

Each of these approaches has advantages and disadvantages, depending on the area of application. In deciding on the adoption of a new technology, for example, the formal approach is more open to evaluation and more politically acceptable than professional judgement. But this latter method is superior for arriving at routine individual decisions. The natural-standards approach assumes that past levels are currently acceptable. Inherent in each of these strategies is a number of generic problems which can be tackled with varying degrees of success. These include uncertainties in defining the problem, and difficulties in assessing the facts, and the relevant values.

Defining the problem includes identifying what consequences are to be taken into account. So, for example, the environmental movement has sought to

Acceptable Risk. By Baruch Fischhoff *et al.* Pp.185. ISBN 0-521-24164-2. (Cambridge University Press: 1982.) £15, \$19.95.

Risk/Benefit Analysis. By Richard Wilson and Edmund Crouch. Pp.218. ISBN US 0-88410-667-5; ISBN UK 0-66-60514-8. (Ballinger/Harper & Row: 1982.) \$23.75, £16.95.

extend the consequences of the impact of new technologies to include consideration of ecological consequences (changes to the balance of ecosystems). Setting the agenda is part of the political process: the definition of the problem reflects the prevailing balance of power. The way in which a problem is defined can even determine the outcome of the decision process.

The view that rational decision-making is mainly a question of getting the facts right also runs into considerable difficulties when we look at the uncertainties surrounding establishing the facts in all but the most straightforward examples. The greatest problems arise where there are insufficient cases to arrive at any reliable assessment of probabilities, though the results may be catastrophic. Where data are inadequate, fault-tree and event-tree analysis may be used to construct a model of a complex system which provides a basis for predicting the results of any one or more of a number of possible failures. In practice, such analyses are prone to a number of faults including failure to consider human errors. The DC-10 failures, for example, were the result of not recognizing the way in which a technological system functions as a whole. The simultaneous breakdown of safety systems designed to be independent (common-mode failure) has also constituted a major unanticipated hazard in several reactor accidents. And these are but a few of the difficulties pin-pointed by the authors.

A brief summary cannot do justice to the depth and breadth of the analysis laid out in *Acceptable Risk*. For example, it is not simply the probable frequency of the hazard, but the characteristics of the hazard which are crucial for understanding responses. Catastrophic risks generate more anxiety than more probable hazards with less disastrous consequences. Similarly, involuntary risks are less acceptable than voluntary.

A crucial factor in any decision on the acceptability of risk is the purpose for which the risk is taken. Where the end or goal is highly valued, such as saving a life, greater risks may be justified than for some

trivial result. Values are at the centre of all decisions entailing risks; but they do not easily lend themselves to quantification. While this question, a central one, is explored in some detail by Fischhoff and his associates, it is practically ignored by Wilson and Crouch.

Of the three strategies, cost-benefit analysis is the least likely to ignore values, but it can only treat economic consequences or those that are quantifiable in monetary terms. Nowhere are the difficulties more obvious than in the attempts to put a monetary value on life itself. Such attempts come up against a fundamental philosophical objection which is not sufficiently explored by the authors. To reduce all values to dollars assumes that this is the ultimate criterion for human conduct. The impossibility of putting a monetary value on human life should be warning enough that there are higher order values which cannot be traded against money. Yet it is no answer to say that because values are elusive and changeable they should be omitted from rational, objective analysis. This is a simple recipe for the uncritical acceptance of the values of the decision takers.

Fischhoff and his associates end their book with a chapter of recommendations for improving acceptable-risk decision making and with one identifying the areas requiring further analysis and research. In all they have achieved a masterly systematization of the many practical, methodological and philosophical problems raised by attempts to answer the question "How safe is safe enough?"

In *Risk/Benefit Analysis*, Wilson and Crouch tackle a more limited brief. They too emphasize the problems inherent in defining, perceiving and estimating risk. They stress the importance of drawing the attention of the decision-makers to the uncertainties in the process and of emphasizing the distinction between decision-making and risk analysis. But the authors explore a more limited range of strategies and lack an awareness of the philosophical presuppositions, political acceptability and underlying assumptions about human behaviour which are such an important element in *Acceptable Risk*. The strength of their book is in its exposition of the practice of risk analysis, and in its actual review of nine case studies, most of which, however, fall far short of the rigorous and systematic approach set out in the text. This book, too, constantly underlines that risk analysis is only an aid to

decision making and not a substitute for it.

Part of the reason for the growing anxiety about risk is obvious enough — modern technology holds out great promise but it carries with it potential for danger. Its benefits and hazards are not equally distributed. Nor is exposure to risk always within the control of the individual, who may choose not to smoke, but has little say in the disposal of toxic waste.

The importance of both books is to emphasize that rational decisions on risk

cannot be reduced largely to a calculus of probabilities. Such an approach would simply brush under the carpet the inescapable political dimensions of many such decisions. But worse, it fails to account for the ways in which reasonable and rational beings in fact seek to cope with the complexities of how to act in the face of potential danger. □

S.F. Cotgrove is Professor of Sociology at the University of Bath.

Dendrochronology by numbers

John Fletcher

Tree-Ring Dating and Archaeology. By M.G.L. Baillie. Pp.274. ISBN UK 0-7099-0613-7; ISBN US 0-226-03630-8. (Croom Helm/University of Chicago Press: 1982.) £16.95, \$25.

THE attraction of using tree-rings for dating buildings and archaeological artefacts lies in the high accuracy — to the year or to within a decade — that can be achieved if the felling date of the timber can be identified. But how often is that feasible? One limitation lies in the relatively few species which have annual growth that can be reliably identified and converted to a chronology. Another is that in temperate areas various ecological factors affect the growth rings of each species, so a range of reference chronologies may be necessary to permit a large fraction of the somewhat different ring-width patterns to be matched. In addition, palaeoclimatologists recognize from climatic swings in the past that the extent of dendroecological zones has not remained constant.

Artefacts from extreme environments are especially suitable for tree-ring dating as stress comes mainly from one factor. Douglass in 1929 was the first to use this to advantage and date ancient cliff dwellings in Arizona and New Mexico from the pines used in building them. In central Europe, first Huber then Hollstein had by the mid-1960s matched sequences of rings from several hundreds of the oaks used in buildings and artefacts in hilly areas, including prehistoric lakeside settlements around the Alps.

In contrast, the diverse stresses which apply to valley and lowland oaks in north-west Europe made the pattern matching of rings impossible in the pre-computer era. In this book Dr Baillie tells of his success, using a computer program devised with his colleague J.R. Pilcher and now widely adopted, in matching Irish samples and a few from south-west Scotland. Archaeological remains of oak are scarce in Ireland, and the items dated number only about thirty. They include cruck houses, the Dublin waterfront, lake dwellings known

as crannogs and the archaeologically interesting horizontal water-mills. The results have enabled Baillie to construct two oak chronologies for the last two millennia (that for fossil timber for carbon-14 calibration goes back much further).

The methodology described is largely that of the Tucson tree-ring laboratory in which ring-widths are converted to indices, thus losing, when plotted, visual features known as indicator years and signatures. (As applied elsewhere in Europe these features are of particular value, for example in matching short sequences with dates known approximately by other evidence.) The author's approach is largely statistical and he displays no interest in the scientific and analytical research which has revealed relevant information about wood structure and tree physiology. Thus the value of a rare abnormality in oak, noticed by Buffon as of chronological significance, is not mentioned.

The book gives a detailed, step-by-step account of the regional application of the author's method to a limited number of widely separated items in the wetter zone which covers much of the western part of the British Isles. As such it will be of interest to departmental libraries and to the enquiring archaeologist. It is not suitable for use as a text-book, however. Some statements are misleading in the context of European dendrochronology, while inaccuracies render parts unsuitable for being quoted. This applies in particular when the author turns from Ireland to write briefly about southern Britain. In this region, not only oak trees but oak artefacts and excavated material are numerous. In the lower and drier zone — which includes rain shadows in the midlands, the east and south-east of England, as well as continental areas around the southern basin of the North Sea — the Irish chronologies rarely apply (and vice versa) while Baillie's method is too limited for success in matching a high proportion of samples. □

John Fletcher is at the Research Laboratory for Archaeology and the History of Art, University of Oxford.

Course of storms

T. N. Krishnamurti

Tropical Cyclones: Their Evolution, Structure and Effects. By Richard A. Anthes. Pp.208. ISBN 0-933876-8. (American Meteorological Society, Boston: 1982.) \$40.

IN TEACHING tropical meteorology courses it is generally necessary to devote about 25 per cent of the course to tropical cyclones: their origin, maintenance and eventual decay. Richard Anthes has provided, for my needs, an important text that covers this area more than adequately.

The monograph deals with the structure, life cycle, physical effects, numerical simulation, storm modification, oceanic responses and weather forecasting aspects of tropical cyclones. The description of structure is based on the best available observations of such storms, mostly provided by the National Hurricane Center in the United States. In the area of physical effects the role of cumulus convection is brought out in considerable depth, and a critical appraisal of the convective heating, the vertical eddy flux of heat, the role of non-convective heating, convergence of eddy flux of moisture and the moistening by cumulus scale motions is presented neatly and clearly. In this area, Anthes discusses a number of recent findings, most notably the role of radiative forcing in the diurnal modulation of tropical cyclones. His breakdown deals with observational as well as modelling aspects, and will be most helpful to students modelling such storms.

The account of modelling covers the state of the art of simulation of idealized as well as real data numerical weather prediction experiments in two and three dimensions. Several examples carry important information on why storms form from incipient disturbances in some cases and not in others; this is largely based on Anthes' own research over many years. The oceanic response is a topic hardly addressed in most other texts or reviews, and is a welcome addition to the completeness of this book. The noteworthy area here is the role of the oceanic stratification.

The final section covers the use of statistical and dynamical methods in operational prediction up to three days from the initial state. Here Anthes summarizes the current ranges for the error statistics in hurricane (typhoon) prediction centres in the United States and elsewhere.

I find this an extremely important book with few areas to dispute in the assessment of our current understanding of hurricanes. No previous text has addressed the wide range of teaching needs covering both observations and theory. It is a blend that is remarkably well done in this monograph.

T.N. Krishnamurti is a Professor in the Department of Meteorology at The Florida State University, Tallahassee.

Antarctica: the geological background to resource assessment

J.F. Lovering

Antarctic Geoscience. International Union of Geological Sciences: Series B, No.4. Edited by Campbell Craddock. Pp.1,172. ISBN 0-299-08410-8. (University of Wisconsin Press: 1982.) \$35, £26.25.

THE last continent — Antarctica — is rapidly assuming a new importance as a resource-hungry world begins to wonder whether it hosts exploitable mineral and fuel deposits and, if it does, who has title to them. Since 1961 the nations signatory to the Antarctic Treaty have quietly been engaged in basic geological and geophysical studies of the continent and its ice blanket. Although their research has not been directed specifically towards resource exploration, it is reasonable to conclude that many programmes have more than a passing relevance to an assessment of Antarctic resource potential.

For these reasons a lot of people, not all of them geoscientists, have been waiting with impatience for this massive volume which contains the papers presented at the Third Symposium on Antarctic Geology, together with a 1:5,000,000 geological map of Antarctica compiled from data available up to 1972. Their impatience is well justified since the symposium was held in Madison, Wisconsin, in August 1977.

In virtually any other scientific field, a symposium volume having a gestation period of five years would, on its birth, be hopelessly out of date. This volume is saved from such a fate by the studied pace with which field studies in Antarctica must proceed — the self-evident climatic constraints limit activity to around three months each austral summer so the rate of data collection is relatively slow. Still, it is difficult to understand why it has taken so long for the book to appear. The editor's preface hints at a multitude of problems and at his growing horror as he gradually recognized the enormity of his task. We should be grateful that he persisted to the bitter end.

Antarctica is the keystone to reconstructions of Gondwana so it is not surprising that many contributions focus on the specific relationships between Antarctica and South America, Africa, India, Australia and New Zealand. Many reconstructions use ocean floor magnetic lineation data which were relatively new at the time of the symposium but are now merely records of the state of the art at that time. Probably the most valuable series of papers in this general area is that concerned with the nature and evolution of the Scotia Arc — that puzzling and highly deformed connection between the margin cordillera in southern-most America and the Antarctic Peninsula. The islands of the Scotia Arc (South Georgia, South Orkney Islands and South Shetland Islands) are shown to have been initiated in Middle

Late Jurassic times on an older metamorphosed "basement" complex, probably in an old re-entrant in Gondwana which formed a physical separation between the Andes and the West Antarctic cordillera. Other contributors, however, suggest that the eastern South Scotia ridge is an intraoceanic island arc.

In view of the recent fracas in the Falkland Islands, and the often-quoted petroleum potential of the sedimentary cover over the Precambrian basement of the area, many readers will be disappointed that only one contribution discusses Jurassic, Cretaceous and Tertiary sequences on the Falkland Plateau. Nonetheless they will be interested to learn of the existence of a sapropelic claystone with an organic content averaging three per cent within the Jurassic sediments near the base of the cover section. These same people will also be intrigued by the records of the first multichannel seismic reconnaissance survey of the thick sedimentary sequence filling the Weddell Sea basin, an area thought to have high petroleum potential on previously rather general grounds. There are enough promising structures and traps indicated on the records to send exploration managers hot foot to their friendly seismic survey contractor.

Another series of papers is concerned with the constitution, geochronology and structural evolution of the East Antarctic Precambrian Shield. These contributions represent a significant advance in our understanding of this important Archaean Shield, but still form only a relatively crude picture of what is a structurally complex but fascinatingly accessible example of a very ancient piece of the Earth's crust. Resource implications of the East Antarctic Shield rocks receive little attention except for one paper on the Precambrian "iron deposits", more realistically termed jaspillites, of the Prince Charles Mountains. With an average iron

oxide content of 43 per cent it will be a long time indeed before anyone looks to Antarctica as a source of supply for the world's steel makers.

Only two other papers are concerned with metallic mineral resources, and both examine the possible association of base metal deposits with the igneous rocks of the Antarctic Peninsula. Although many have suggested the existence of mineral wealth in the Peninsula by analogy with the mineral-rich central Andes, a warning is given that this conclusion may be premature because the two regions have rather different Cenozoic tectonic histories.

There is much that I have not discussed and it is simply impossible to do justice to the rich variety of information contained within this volume — including structural geology and tectonics, crustal structure, palaeontology, marine geology and Precambrian, Palaeozoic and Cenozoic history. I have focused on those studies which have a bearing on the future assessment of Antarctic resources both on- and off-shore, but the ice flow and bedrock information arising from the beautiful data provided by air-borne radio echo-sounding should at least be mentioned.

The confirmed Antarctic geoscientist will need this volume (and, at its remarkably low price, probably buy it); but the book hardly constitutes an easy entry to the subject for the non-specialist. I would like to see a wider group become interested in the geological evolution of the continent since Antarctic geologists and geophysicists comprise a small group largely closed to outsiders who have not braved the rigours of an Antarctic field season. We still badly need an up-to-date and readable monograph on the subject to stimulate this wider interest. □

J.F. Lovering is Professor of Geology and Chairman of the School of Earth Sciences at the University of Melbourne.



Wealth beneath the ice? Heavily glaciated terrain in the Transantarctic Mountains, dividing the East and West Antarctic plates and bordering the Ross Ice Shelf.

David Drewry, Scott Polar Research Institute.

Semiconductors from Bell Laboratories

Andrew Holmes-Siedle

Physics of Semiconductor Devices, 2nd Edn. By S.M. Sze. Pp.868. Hbk ISBN 0-471-05661-8; pbk ISBN 0-471-05983-7. (Wiley: 1982.) Hbk £37.20, \$63.20; pbk £12.91, \$23.30.

THE impending publication of a new edition of a famous textbook is always an occasion for keen anticipation. In the field of semiconductor devices, there have been few textbooks more authoritative or comprehensive than the first edition of *Physics of Semiconductor Devices*, a book which bore the stamp of the author's broad personal experience of device development and the unique aura of Bell Laboratories. That 1969 edition, however, was clearly becoming dated by the rapid advance of integrated semiconductor device technology. The performance and sizes of devices had altered by orders of magnitude, while the principles of device operation had been the subject of over 40,000 research papers. Obviously, the revision of so comprehensive a book would be a huge undertaking.

I can only say that the task has been completed with a thoroughness that leaves me open-mouthed with admiration. All the parts of the first edition which I had earmarked as obsolete have been eradicated, and the structure has been subtly altered to accommodate the changes of the past 15 years. Dr Sze states that over 65 per cent of the references and diagrams are new and 80 per cent of the text has been revised. All this has been done most effectively; the mark of authority again appears in the large amount of new material added.

The first edition was divided into five major sections: Physics; p-n Junction Devices; Interface Devices; Optoelectronic Devices; and Bulk-Effect Devices. In the second edition, the major growth of metal-oxide-semiconductor device technology has been acknowledged by means of a new division of sections between bipolar and unipolar devices. Microwave devices also have their own section, while photo-detectors and solar cells are now rightly given chapters to themselves. The broadening of the treatment of solar cells will prove extremely useful to many students of energy generation: it goes so far as to give some useful data on geographical distribution of solar flux and its spectral properties, relates these to mechanisms of conversion in semiconductors and adds a fascinating account of the new device structures being investigated (for example the textured single-crystal surface, the cascade two-junction cell, thin films etc.).

In the section on metal-oxide-semiconductor devices, the author evidently felt that there was a danger that the immense body of recent information could run away with the book; for instance, there is a notable austerity in the handling of MOS measurement methods. In the section on the myriad forms of the MOS field-effect transistor (the device which has revolutionized computers, watches, entertainment and communications), the new relevance of the submicron device structure is well described. Surprisingly, the author manages to confine the growth of these sections to an increase of about ten pages. At the same time little that is really important has been left out, although (inevitably) details of processing and circuitry have had to be ignored. Real flaws

are rare. The brief treatment of ionizing-radiation effects is not up-to-date; so much has happened since the 1967 references given. Also, it is probably wrong to say that carrier generation in SiO₂ is caused "by breaking Si-O bonds".

While such a concentrated treatment of semiconductors could never be light reading, Dr Sze has certainly taken pains to present his material clearly, with liberal use of line drawings as explanations in their own right. As a result, the book will remain an indispensable companion to the student and research worker. Moreover, I believe it will be illuminating for journalists and others who have to know what this commercially-important field of semiconductors is about. □

Andrew Holmes-Siedle is Consultant in Solid State Physics and Radiation Damage to the Fulmer Research Institute, Stoke Poges, Buckinghamshire.

Fingers on the pulse of the insect

John Brady

Insect Clocks, 2nd Edn. By D.S. Saunders. Pp.409. Hbk ISBN 0-08-028848-0; pbk ISBN 0-08-028847-2. (Pergamon: 1982.) Hbk £45, \$90; pbk £24, \$48.

FEW scientific monographs survive to a second edition, and still fewer get there within six years of the first. It is a measure of the success of *Insect Clocks* as a textbook, and of the general interest in this apparently esoteric corner of biology, that the book has already been given a face-lift.

The interest in insect timekeeping stems from insects' economic importance and the tantalizing hope of distressing their life cycles in our favour by manipulating their clocks. It must be said, however, that basic knowledge of their timekeeping — as evinced by the 1,120 papers Saunders reviews — far outstrips any practical manipulation thereof. This is in marked contrast with the commercial application of false photoperiods to induce plants to flower or poultry to ovulate year in and year out. The unfortunate truth is that 99 per cent of insect pests occur in the open air.

If justification for this second edition were needed it is that since 1976 a number of gaps in our knowledge have been closed. An important one is the apparent reconciliation of "hour-glass" and "circadian" explanations of insect photoperiodic control. The former finds daylength apparently being measured by a single, non-repeated process (like a kitchen timer), the latter that organisms seem sensitive to light at a particular point in their daily cycle, every day (like a 24-hour light-sensitive clock).

One should never expect simple answers

in biology, however, and having argued the reconciliation in depth, Saunders is then forced to largely demolish his case with an added footnote saying that A.D. Lees's latest evidence from his aphids can still best be described as an "hourglass".

That much less is known of the ultimate chemistry and physiology of insect clocks than of those of micro-organisms or molluscs is as apparent in this second edition as it was in the first. Most research over the past six years has been along the same lines as before, dealing with phenomenology and modelling of insect timekeeping, and it is with this that the book's 400 new references are chiefly concerned. Nevertheless the — albeit modest — advances in knowledge of the clock's coupling mechanisms do seem underplayed. The greatest single addition to the book is a long new chapter on multioscillators.

All is admirably explained in Saunders's usual lucid style, and this time he has removed some of the unnecessary algebraic symbols that speckled the first edition. The book does still suffer slightly from its original division into chapters on rhythms in single insects, rhythms in populations and rhythms in physiology, with the result that entrainment, phase response curves and so on have to be dealt with repetitively rather than as the single phenomena they are. *Insect Clocks* is, however, well on the way to becoming a classic, and this new edition should surely find its way onto the shelves of insect physiologists and chronobiologists alike. □

John Brady is Reader in Insect Behaviour in the Department of Pure and Applied Biology, Imperial College, University of London.

● Volume 3 of *Electron Microscopy of Proteins*, edited by James Harris, has recently been published by Academic Press. Price is £27.80, \$57. For review of Vols 1 and 2 see *Nature* 298, 498; 1982.

NEW WAYS WITH MAGNETS

The case for attending to magnets

LIKE the air we breathe, magnets and the materials of which they are made have become ubiquitous but almost unobtrusive. The pages that follow are not meant as a systematic survey of what has happened since the first (probably Mediterranean) navigators used naturally occurring magnets in steering their ships, but as a pointer to the interest of this field in the past few years. For it tends to be forgotten how much things have changed in the years that have followed the Second World War.

Part of the difficulty is that magnetism itself retains some of the mysteriousness that perplexed the old mariners (or should have done). Magnetic forces are non-central. A sufficiently small dipole (say a nuclear spin or an electronic magnetic moment) will neither attract nor repel another like it, but create a torque. And it is not even now surprising that the force on a charged particle travelling in a uniform magnetic field should be perpendicular both to the field and to its own direction of motion? Faraday's description of this unexpected behaviour 150 years ago remains a remarkable exercise in thinking the unthinkable.

In the circumstances, it is not surprising that the most obvious properties of magnetic materials, the ferromagnetism of iron and nickel, for example, should have been explained (and only then phenomenologically) only when an account of the electronic structure of atoms had been completed in the second half of the 1920s. And although it is now natural to look askance at atoms of transition elements in which outer electronic shells have begun to be filled while inner shells are still incomplete, the calculation of the most familiar properties of ferromagnetic materials — say the Curie temperature above which permanent magnetism disappears — remains an empirical art. The best that can be done is to show by model calculations that such a transition is an order-disorder transition or, more accurately, that model lattices such as the Ising lattice can produce behaviour of the required kind. (That the Ising lattice, a set of interacting bi-directional spins at the corners of a two-dimensional square lattice, can be solved exactly has been a powerful but frustrating challenge for those who would solve real models, but has engendered a whole new industry for theoretical physicists.) The consequence, however, is that the search for new magnetic materials has become an empirical process guided only by

enlightened guesswork (see box).

Even so, there have been some important successes. Néel's work on the ferrites twenty years ago is one vivid proof of how phenomenologically-based theory can help to illuminate even problems not exactly calculable. Much the same is true of the way in which the study of magnetic domains, and of the migration of their boundaries when the magnetization of the material that contains them changes, has pointed to the design of materials now almost certain to play an important part in emerging technology.

Exactly the same circumstances obtain in the development of new superconducting materials. That it is even now known that some materials (tin, niobium and so on) literally lose electrical resistance at sufficiently low temperatures is something to be grateful for. But while the essential character of the phenomenon has been understood for the past twenty years, the prediction of the properties as a superconductor of some new alloy remains largely a matter for empirically guided speculation. The underlying difficulty is the complexity of the real world.

None of this has prevented the steady march of magnets in the technology of research and in public use. The dependence of experimental high-energy physics on the improved design of magnets (see page 665) is unsurprising, but it tends to be forgotten that analytical techniques such as mass spectrometry and nuclear magnetic resonance are no better than the magnets around which the instruments are built. Fortunately, in this respect at least, empiricism has almost entirely given way to computation as computers large enough to handle real-life models have arrived.

With all this said, it is surprising that the whole field of magnetism remains as neglected as it is. While the company of those with an interest in designing better magnets, or understanding how existing magnets work, is quite substantial, their preoccupations are not generally shared. The unfamiliarity of the subject is as forbidding as its intrinsic difficulty. (For experimentalists, mere measurement remains a seemingly needless bugbear.)

Yet the way in which the technological applications of magnets in the past few decades have improved the performance of saleable devices, and made others feasible, suggests that the time has come when the research community and its sponsors should take the subject more seriously. An element of science policy in search of a government, perhaps? □

Materials galore

LODESTONE, the archetypal permanent magnet, was probably another name for magnetite (Fe_3O_4), which curiously has been the basis for most recent excitement about the development of magnetic materials. For magnetite has proved to be a literal representation of what the old school textbooks of chemistry say — a molecular compound of two iron oxides (FeO and Fe_2O_3) in which divalent and trivalent iron atoms occupy different kinds of lattice sites. The ferrites are merely lattices like those in which some divalent iron ions are replaced by others with different electronic properties.

The consequences of ferrite revolution are apparent inside any transistor radio. The old metallic magnetic components, in transformer cores for example, have been replaced by cylinders of dullish ceramic material which have in turn been fabricated from raw oxides or carbonates of their component elements. But the same ferrite revolution has helped also to throw light on what makes a material ferro or ferri magnetic, as well as providing Professor Louis Néel with a Nobel for his part in the explanation.

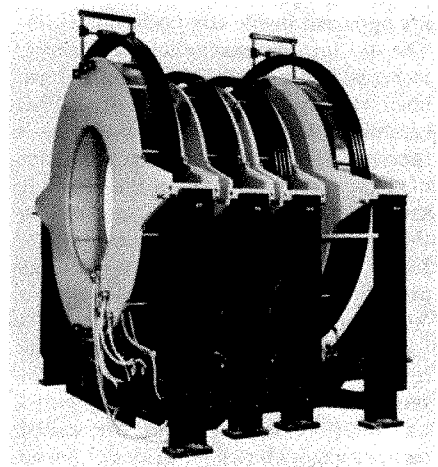
So what can be next? With the ferrite revolution now reduced to the search for small improvements, attention is focused on the potential of what are called metallic glasses based on oxides of boron and phosphorus heavily doped with oxides of iron and nickel. Being amorphous, these materials are free from the hysteresis that arises in crystalline materials because magnetic domains can be smaller than single crystals. The metallic glasses may prove to be easily and cheaply manufactured, leading to even less "lossy" power transformers and magnetic tapes that can be read more faithfully than those now on the market.

The magnetic tape industry seems to provide the chief incentive for another current development — that of alloys of cobalt and chromium with high coercivity. The technical objective is to allow some form of recording information by means of magnetization perpendicular to the plane of the recording tape, and is made possible by the high coercivity (resistance to demagnetization by magnetic fields) of these alloys. The result should be recording tapes with improved sensitivity, a denser packing of information and a more nearly digital representation of it.

Superconducting magnets

No longer are superconducting magnets confined to research laboratories or those which use nuclear magnetic resonance (NMR) machines for more routine measurements. With the development of techniques that, for example, permit the use of NMR in the study of living tissues, it is natural that the body-scanning fraternity should have devised machines intended to provide biochemically based whole-body scans of human beings. This development entails the construction of magnets providing a uniform magnetic field of 2 tesla or so over regions 100 cm in dimension — for practical purposes unattainable without the use of superconducting magnets.

One of the British companies active in the field, Oxford Instruments Limited, has already built a number of magnets of this type. Physiological whole-body scanning is for the time being directed at two objectives — the use of the resonances of ^{31}P as indicators of physiological function,



A 0.15-tesla four-coil resistive magnet for whole-body imaging. Clear-bore access is 800 mm.

and of proton resonances as indicators of where water is more plentiful in the body (which could be an alternative to the use of diagnostic X rays).

Whether large-volume magnetic fields for such purposes will prove to be in great demand will no doubt hang on the outcome of the several clinical studies with prototype machines now being planned. The magnet manufacturers will be overjoyed if it turns out that scanning procedures yielding representations of the structure of cross-sections through a human body (such as may be constructed from suitable proton magnetic resonance measurements) are preferable to the more familiar use of diagnostic X rays. Meanwhile, the supply of large-volume magnets for the prototype machines, at a cost of £100,000 or so each, seems to be a sufficient recompense for the high cost of development.

In the evolution of superconducting magnets for laboratory use, the cutting edge of development seems to be what it

has been for the past twenty years — the improvement of magnets for use in nuclear magnetic resonance. For the higher the value of the magnetic field in which a sample is immersed, the greater the resolution that will ultimately be possible. But the sharpness of the spectral lines that eventually emerge will also be determined by the uniformity of the field over the volume of whatever sample is being used, with the result that stronger fields must also be more uniform.

Standard superconducting magnets with pre-specified field homogeneity can now be bought off the shelf. Central field strengths of these standard products range up to 14 tesla (140,000 gauss), but the magnets themselves may be no more than a foot long. The compactness of the range of superconducting magnets now available is perhaps their most striking characteristic, especially when the imagination is invited to speculate about the bulk of the power supply equipment that would be necessary to generate fields of a tesla (the maximum obtainable with conventional electromagnets).

Cooling problems

The analogous penalty in the use of laboratory superconducting magnetics is, however, the cryostatic equipment needed to maintain the superconductor at liquid helium temperatures. The coils of a superconducting magnet must be immersed in liquid helium or, alternatively, in liquid-helium vapour. Naturally enough, users of superconducting magnets have no wish to double as low-temperature physicists, worrying about the adequacy of the cooling system. Fortunately, most of the suppliers of laboratory magnets have been able to reduce the rate at which helium is lost from their cryostats to the point at which topping up the system with liquid helium is necessary only at intervals of a few months. The ideal is that replenishment can be tied in with routine maintenance visits.

For the rest, the design of a super-

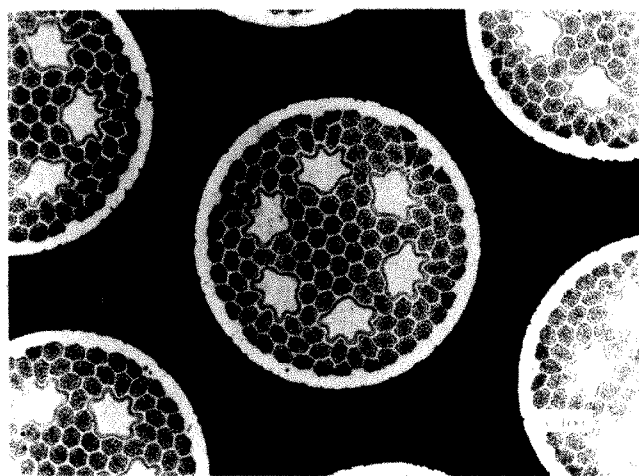
conducting magnet raises few problems not encountered by the traditional designers of electromagnets. The simplest magnets are solenoids. Often it is convenient to split the solenoids in half, on a plane perpendicular to the axis, but at the expense of maximum field strength. Improving the homogeneity of the field, increasing the volume over which irregularities do not exceed some specified percentage, is to some extent a function of the way the coils are wound, but the inclusion of shims of superconducting material is usually also advantageous.

Quite apart from considerations of compactness, the overriding attraction of superconducting magnets over conventional electromagnets is that the maximum field is not limited by the magnetic permeability of the core material, soft iron perhaps. Yet there are limits to the extent to which the field strength of a superconducting magnet can be increased which are themselves determined by the properties of the superconductors used for constructing the coils. The crucial consideration is that the material of which the coils are made should not experience magnetic fields great enough to rob them of the superconducting properties. With existing superconducting alloys (niobium-titanium and niobium-tin) it should be possible to push beyond 17 tesla, the present limit of what is practicable.

The most straightforward way of using this material is to deposit it on layers of a tape of copper and stainless steel (relatively an insulator at liquid helium temperatures, but a means of carrying current if superconducting properties should at any point be lost). More recently, techniques have been developed for forming niobium-tin alloy from filaments of niobium which are annealed with bronze in such a way that the tin component of the bronze preferentially alloys with the niobium. The residual copper serves both as a mechanical support and as a means of conduction should superconducting properties be lost.

Where the design of superconducting magnets will go from here is anybody's guess. The few companies specializing in laboratory-scale magnets (beam-forming

A section through an early 10-tesla solenoid Nb₃Sn section. The amoeba-like "islands" are of pure copper ($\times 100$).



magnets are another business) usually offer custom-built designs intended to suit the needs of people in academic or industrial laboratories in need of some predetermined configuration of magnetic field. As with NMR, from any one of these applications might spring some new range of off-the-shelf superconducting magnets.

Oxford Instruments, one of the principal suppliers, says that it will consider *ad hoc* proposals from potential academic customers, but will not in the first instance produce a detailed estimate of the cost of building a new design. Rather, it will undertake to produce information sufficient to sustain a research grant application, and will produce a final estimate of cost in return for a fee, refundable against a firm order when the application has been successful.

Whether this esoteric business will — or would be — transformed by the development of superconducting materials with transition temperatures substantially above the boiling point of liquid helium is another matter. The chief benefit, as things are, would be quantitative: helium consumption would be reduced. But if somebody were to construct a material superconducting at liquid nitrogen temperatures, a whole new ballpark would be accessible. . . . □

Cold comfort at room temperature

SUPERCONDUCTIVITY is the next best thing to perpetual motion: an electrical current once established in a superconducting circuit will keep going indefinitely. So is it not mere misfortune that the only circumstances in which known materials can be made superconducting are those involving temperatures in the liquid helium range, below 4.1 K or thereabouts?

After the best part of a decade, the hopes first fostered by the empirical discovery that suitably constructed linear polymer materials have electronic conduction bands and are indeed capable of conducting electricity might make possible the design of molecules exhibiting superconductivity at room temperatures. In reality, painful experience has shown that superconductivity is doggedly a low-temperature phenomenon, involving lattice or molecular vibrations (phonons) and electron movement in a cooperative transition from a disordered to an ordered state. Room-temperature superconductivity is likely always to lie in the future.

For practical purposes, it is a sufficient but still daunting goal to find materials

superconducting at the temperature of liquid nitrogen, the common outer refrigerant in superconducting cooling systems.

The record so far is a transition temperature of 21 K for a version of Nb₃Ge in which germanium atoms are partly replaced by atoms of aluminium. (This is a true superconductor of Type II, able to sustain high magnetic fields without losing its essential properties, but metallurgically hard to work with.) As things are, such interest in the search for improved superconductors centres on the sulphides of molybdenum doped with rare-earth elements as substitutes for Mb.

In practice, even unexpectedly rapid progress in the search for superconductors with higher transition temperatures would only slowly transform the technology of making superconducting magnets. In practice the improved superconductors now coming into use are metallurgically almost impossible. They function as planned only if pure and stoichiometrically exact. It will be some time before it is a matter of routine to wind kilometres of wire on some form and call the result a magnet.

High-energy physics rides on flux

THERE is a real sense in which the development of high-energy physics in the past half century has been sustained by the technology of the magnet builders. Although the first important landmark in the artificial manipulation of nuclear structure — the use of 300 MeV protons for the disintegration of nuclei by Cockcroft and Walton in 1931 — was made possible by means of an electrostatic accelerator, E.O. Lawrence was even then building the first cyclotron at Berkeley. By the time, in 1935 or so, that the limits of electrostatic acceleration had been reached, working cyclotrons were all the rage.

The principle of these machines is simple enough. The path of a charged particle travelling in a magnetic field will be curved, but no kinetic energy will be lost. If the magnetic field is sufficiently extensive, the particle will travel in a closed path, thus increasing the length of time for which other means of accelerating it can do their work.

The cyclotrons which in the 1930s followed the Berkeley design were the simplest of all accelerating machines. The principle is simply to construct a substantial volume of uniform magnetic field between the poles of an electromagnet, to provide a source of charged particles at the centre of the arrangement and to arrange for some means of adding to the kinetic energy of the charged particles as they traverse closed orbits between the poles of the source magnet.

Cyclotrons have functioned since the

early 1930s because the frequency with which a charged particle traverses its closed orbit in a magnetic field is independent of the dimensions of the orbit and simply a function of the characteristics of the particle and the strength of the field (B). Thus the frequency of rotation is given by the familiar relationship $eB/2\pi m$, where e and m are the charge and mass of the particles.

Since the beginning, cyclotrons have been no better and no worse than the design of their magnets. Since the first machine at Berkeley, the standard procedure has been to accelerate charged particles by means of alternating electrostatic fields within a pair of semicircular hollow conducting surfaces shaped so that, when put together, they would constitute a hollow pancake-shaped structure — and which, when separate, are known as “dees”. The two halves of this structure are fed with radiofrequency power at the characteristic frequency of the cyclotron (a function only of B and the particle concerned).

One obvious difficulty with which the magnet designers have had since the beginning to contend is the sheer physical problem of shaping the magnetic field appropriately. Since charged particles spiral outwards from the central point at which they are injected, the field must be for practical purposes uniform over the maximal orbits followed by the particles. The construction of electromagnets spanning close on 2 m (such as with the 184-inch cyclotron built at Berkeley after

the Second World War) is a formidable undertaking.

For one thing, the sheer bulk of the magnetic circuit required to provide a return path for the magnetic field between the poles of the electromagnet where the action is is almost a feat of mechanical engineering in its own right. For another, the shaping of the pole pieces (usually machined from cast or forged blocks of soft iron) is a complicated process of balancing the loss of flux through the sides of tapering circular endpieces against the need for uniformity of field.

Throughout the 1930s, the construction of cyclotron magnets was almost a black art. Once a machine had been built, the designers of the magnet would be required to fiddle around with the placing of shims near the poles of the magnets to improve the characteristics of the field, its uniformity in particular. Even the first cyclotrons, however, were blessed with one important built-in benefit — because, between the poles of an electromagnet, flux lines unavoidably become more distant from each other, displacements of circulating charged particles towards one pole or another are discouraged by the mirroring effect thereby produced.

For practical purposes, cyclotrons have been used for accelerating protons and heavier ions, with maximum energy (determined by the area of the space between the pole pieces) measured in tens of MeV. The acceleration of electrons to comparable and greater energies is best accomplished by means of linear accelerators (most spectacularly by the two-mile accelerator at Stanford,

California) but the brief wartime history of the machine called the betatron is a landmark in the ingenious development of accelerating magnets.

The principle of this machine is that particles would be made to travel in strictly circular (and not outward spiralling) orbits, and would be energized by means of a varying magnetic field. In principle, a betatron is a transformer in which the primary winding is the wiring that energizes the electromagnet and the secondary "winding" is the circulating beam of electrons. Betatrons thus exploit the principle of magnetic induction, providing an electric field tangential to the circular orbits of the particles which is itself proportional to the rate of change of the magnetic field.

The evolution of this machine was largely the achievement of D.W. Kerst, who built a 2.3 MeV electron accelerator at the University of Illinois in 1940, who afterwards worked at General Electric on the development of increasingly energetic electron accelerators for use in medicine and other applications and who returned to the University of Illinois to complete (in 1961) a betatron with a maximum energy of 300 MeV. Inevitably, the operation of such machines is limited by the rate of energy loss by radiation from circulating electrons. Technically, the magnet design (at least as practised by Kerst), involving the use of laminated steel to avoid energy loss by means of eddy currents, seems to have been relatively predictable.

The development of high-energy physics has since then been determined entirely by the design of accelerating machines in which particles travel in or near predetermined orbits. The advantages are principally that the volume within which it is necessary to provide a magnetic field is confined to an area small compared with the area covered by the orbit of the accelerating particles. But the magnetic field must be steadily increased as the momentum of the particles is increased, by means of electric fields generated in oscillating radio-frequency resonant cavities for example. The result is a generation of machines called synchrotrons which produce a pulse of

energetic particles after each cycle of pre-programmed increase of the magnetic field around the orbit.

For practical purposes, electron machines such as that at DESY in Hamburg are simpler than those designed for accelerating protons, for provided that the source of particles to be accelerated is already relativistic, the frequency of the source of accelerating energy can be virtually constant. Proton synchrotrons must be designed in such a way that the frequency source has a dynamic range of frequency at least great enough to span the total range of acceleration of the particles.

In the design of accelerators in the past two decades, perhaps the most striking improvements have been made possible by the clever design of magnets so as to focus the circulating beam of particles more precisely on the predetermined orbit. The trick is to alternate around the orbit the gradients of the magnetic fields sensed by the circulating particles in two directions orthogonal to the orbit. The benefits of alternating gradient focusing are not merely the improvement of the quality of the beam but the reduction of the volume of the vacuum chamber which encloses the beam, the reduction of the gap between the poles of the magnets which follows and the simplicity that is as a result effected. One of the most striking visual features of the newer accelerators is the relative unobtrusiveness of their magnets.

Inevitably, the now demonstrated feasibility of superconducting magnets excites the interest of the machine builders, notably at Stanford University (separately from the electron accelerator SLAC) and at other places where particles are accelerated. One possibility is that the ultimate particle energy from existing accelerators might be increased by the replacement of electromagnets with superconducting magnets, while machines such as LEP, on which work has begun at CERN in Geneva, have been designed from the outset to accommodate superconducting magnets at some stage. The benefits of success, at least with closed-orbit machines, is that the civil engineering investment in a tunnel can be used to generate more energetic particles. □

Magnets for detection

THE use of magnets in producing beams of high-energy particles is obviously indispensable, but is similarly essential for their detection. Cosmic-ray physicists have long known this, and magnetic fields have been used as momentum spectrometers since cloud chambers came into common use.

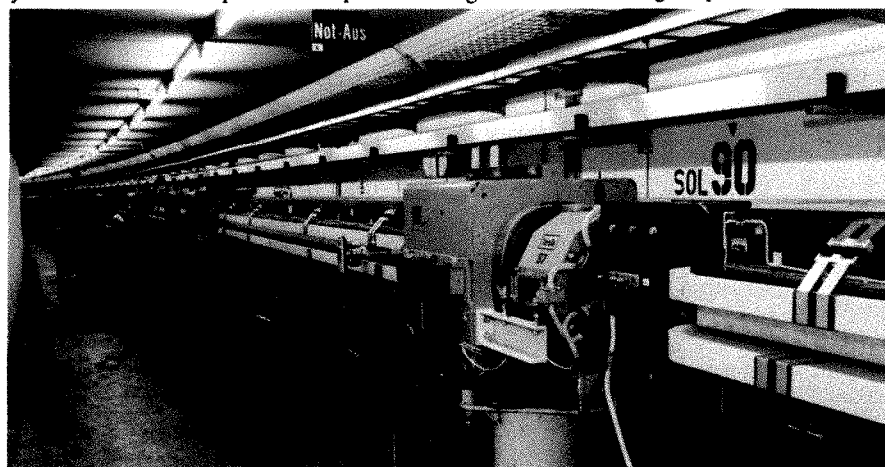
The principle is that of the mass spectrometer except that it is rarely necessary to arrange that all particles of the same mass, whatever their velocity, should be brought to a common focus. It is sufficient that the strength of the magnetic field be known, and the momentum inferred from the observed curvature of a track. The first V-particles, now with hindsight recognized as the first mesons containing a strange quark, were found in 1950 by installing a sensitive cloud chamber and a powerful electromagnet on the Pic du Midi in the Swiss Alps.

Nowadays, the same principle that the deflection of a charged particle in a magnetic field is inversely proportional to its momentum is usually a necessary part of particle detectors. Given that, in spark or bubble chambers for example, particles are "observed" individually, a measurement of momentum provides as much information as could be asked for. But the technology of spanning bubble chambers up to 2 metres in dimension with a more or less uniform magnetic field as strong as possible, remains a challenge.

The intricacies of this technology are perhaps most evident in the "beam switchyard" at the business end of the Stanford linear electron accelerator. Analogous to a shunting yard on a railway system, the hangar in which the system is contained is populated by a variety of electromagnets intended to channel successive bunches of electrons into predetermined vacuum lines.

The main problem the magnet designers face is that of arranging that the insulation between laminations will not be broken down by the accumulated dose of radiation. One common solution is that of coating a glass tape with epoxy-resin loaded with alumina, but the technology of protecting lamellar insulation from radiation damage is in its infancy.

The problem may be economically more significant if working thermonuclear plants ever come to depend more than incidentally on magnetic systems. The most challenging systems are the magnetic mirror machines in which charged particles constituting a hot plasma bounce repeatedly from one end to the other. But here, as in the manipulation of hot plasma in what is otherwise a vacuum, what will matter most is the configuration of the magnetic field.



The magnet line at Petra, the electron synchrotron at DESY, Hamburg.

nature

28 October 1982

 Department of:
 Chemical Engineering
 Chemical Technology
 Plastics & Rubber Technology

14 NOV 1983

Cable in haste, repent at leisure

The British government is exaggerating the benefits of cable television and underestimating the cost. It should urgently investigate the economics of its proposals.

Is a new technology a way of transforming society or merely of inducing people to spend more? These questions are not raised in the advice given recently to the British government by the committee under Lord Hunt, former Secretary to the Cabinet. The Hunt committee, given only six months for its task, dutifully told the government just what it wanted to know: how to provide safeguards for national broadcasting while encouraging the expansion of a national cable system with at least 30 video channels and an interactive facility.

The committee's recommendations would leave cable, by broadcasting standards, virtually free of regulation. Hunt did offer some sensible proposals for allocating franchises without getting into the morass of local government corruption and greed that is slowing down cable's progress in the United States. Briefly, he would all but exclude local government from the franchising process, leaving that to a national cable authority that should itself subsequently supervise cable operators very lightly, with no day to day supervision of programmes or even of fees — Hunt has great faith in market forces — but with the risk that their eight-year franchises will not be renewed.

Debate

Lord Hunt has asked that a debate be begun. This debate is doomed to be a disappointment. Cable is misunderstood and misinterpreted, by those like the broadcasting institutions who feel their survival threatened, and by the government which sees "rewiring Britain" as a handy slogan for the next election to use against reminders of three million unemployed. The British Broadcasting Corporation and the Independent Broadcasting Authority are proclaiming the imminent end of the British tradition of balanced, public service broadcasting, without appreciating that cable television is, by its multi-channelled nature, complementary to and not competitive with national mass-oriented airborne networks. Other custodians of public taste, elected, self-appointed and both, will be up in arms about the prospect that cable television subscribers will be able more cheaply than with their video recorders to watch soft porn. A few judicious compromises in the next few months should give the British government an easy ride through the House of Commons some time next summer for the bill that it will need to let franchise holders dig up the streets, and further to erode the old monopoly powers of British Telecom, as well as the power of local governments to grant wayleaves. The danger is that the debate that will occupy the next few months will disastrously neglect the questions that should be asked — is the British government right in thinking that cable television by itself will bring prosperity, or is it simply economic candy floss?

The government is in no doubt. Under the guidance of its full-time cheerleader, Mr Kenneth Baker, once with the software house Logica but now a minister of state at the Department of Industry, the British government has slipped into the habit of believing that Britain is backward in manufacturing electronic equipment that ordinary people buy (which is true) and must therefore embrace every opportunity to change its ways (which is not true). This is the spirit in which it nominated 1982 as "Information Technology Year" — and in which it has begun complaining that people have not taken it seriously enough. The danger now is that the government may be entirely mistaken in

believing what at least Mr Baker has persuaded himself — that cable television equals prosperity.

American experience shows that cannot be true. If the government can wave its legislative green flag next summer, conveniently ahead of the next general election, there will be plenty of people willing to invest in companies scrambled together to apply for franchises to operate cable systems. At this stage it is impossible to estimate what the total capital cost will be. Much will depend on the technical standards that will not even have been drafted until the spring, and much too on other requirements that may be laid in the path of cabling around Britain which make entrepreneurs judge that the venture will not be worth the risk. The government's (or rather Mr Baker's) own guess is £3,000 million, spread perhaps over five years. By the yardstick of the present level of private investment in British industry and commerce (as distinct from lending to the government) this is small beer — perhaps five per cent of the total over the next five years. But is this the way that a government worried stiff about the survival of manufacturing industry would wish to see industrial investment channelled in the next few years? On the face of things, for a country dependent to the tune of 30 per cent of its Gross National Product on exports, industries capable of making known electronics products more competitively would be better bets. Naturally, if the British government is clever enough to insist in its approval of technical standards that British cable systems are technically just the right distance ahead of comparable systems elsewhere, there could be a short spell in which British manufacturers of transmission and terminal equipment enjoyed an advantage over their competitors. The unhappy snag is that the specification of exacting standards will frighten off investors and their potential subscribers, the danger in the Concorde syndrome (too much too soon). Sceptical taxpayers should have in mind a realistic lower limit of what to expect — the chance that a suddenly increased demand for television signals to put out on cable systems will give more British broadcasters, who appear to have some skill, a greater incentive to sell overseas.

Unemployment

But will not a new investment project on this scale do something to lift the British economy out of its doldrums? For you cannot spend £3,000 million (or, more probably, twice as much) without creating jobs. And the money spent will finish up in the pockets of those concerned, not be buried in trenches in the ground. That seems to be an important part of the government's calculation, but it raises two questions, one of arithmetic and one of principle. At present wage rates, a new investment of even £6,000 million would pay for only one million man-years of work, but since half the investment would probably finish up with the manufacturers of equipment now working well below capacity (and able to increase that only by buying more raw materials from abroad), a five-year programme is unlikely to provide more than 100,000 new jobs. The arithmetical question is whether a special programme to "cable Britain" can be justified by a mere three per cent (or less) reduction of the dole queues. The question of principle is why, if the government is as eager as it seems to give cable television a green light, it should steadfastly have resisted the pleadings of the Confederation of British Industry and of the Trades Union Congress that monetary restraint should be relaxed

(to the tune of £2,000 million and twice as much respectively). The obvious monetarist rejoinder, that it matters whether the money comes from private pockets or from the public revenue, does not cover the objection that the encouragement of cable television, essentially a domestic service industry, will ironically make it harder for manufacturing industry to lay its hands on investment capital just at the time when the government's own demands on the capital markets are at last abating.

None of this implies that the British government should not do the decent thing and fall in with proposals like Hunt's for regulating the development of cable television in Britain, but the case for following such a course stems not from economics but from equity — entrepreneurs wishing to invest in cable systems should be free to do so, and subscribers wishing to subscribe should equally be free to pay their money. For would-be cable operators (and their accountants) the crucial question will be how much of that money there will be. In Britain, the demand curve (what proportion at which price per month) has not yet been drawn. For the government, however, it is more important to know where subscribers' monthly payments to the still non-existent cable television operators' services will come from. Other things being equal, the economists' loose translation of *ceteris paribus*, subscribers will be able to pay their monthly bills only by saving less (which would be bad for the rest of British industry) or by consuming less, which would be good for British industry only if, against recent form, British consumers discriminated against imported goods. In the acrimony about the government's intentions that will occupy the next few months, Mr Baker's little experiment with cable should thus be clearly seen for what it is: not a magic programme for the reinvigoration of British industry but a step in the right (because inevitable) direction taken too fast.

No future for the Greens

The Hamburg elections may show that extremist single-issue parties will not last long.

Ironically, the British would-be equivalent of the West German Greens, a political party dedicated to environmental causes, held its first public meeting last weekend at Bridlington (a small windy coastal town in Yorkshire) while the Greens of Hamburg were reluctantly voting for a new general election in the *Land*. The British party, still in its infancy but conscious that it has to be organized to fight elections within a year or so, is full of dreams but unsure how to make them come true. The West German party, on the other hand, having made a principle of its policy not to form coalitions with conventional political parties, and conscious that nine months of impotence in the Hamburg parliament have weakened its reputation, can only look forward to the next Hamburg election with trepidation. This time, the voters are likely to take the view that politics is too serious to be left to environmentalists. The Hamburg Greens are unlikely to repeat their spectacular success earlier this year.

The moral should be more widely understood than it has been in Hamburg or in Bridlington. Environmental issues are socially important and politically unavoidable. Air pollution standards, or public policies on nuclear power, concern (or should concern) voters, and political parties should know where they stand on them. No doubt from frustration at the deafness of the established parties, the West German Greens have gone off on their own, winning votes by exaggeration but for that reason unable to exercise the power thus derived. They would have been better advised to have pressed more moderate versions of their arguments on the existing parties. The same is true of those who met at Bridlington at the weekend.

American contributors please note

Authors in the United States and Canada are reminded that they should send their manuscripts either direct to London or to the Washington office, whose address is *Nature*, 991 National Press Building, Washington, DC 20045; manuscripts should *not* be sent to New York.

Graduate student choice

The British research councils may yet see the value of manpower planning.

Armies have cannon-fodder, political parties have lobby-fodder and research laboratories have graduate students. This widespread assumption is nowhere more faithfully endorsed than in Britain, where the chief sources of support for graduate education, three of the five research councils, all make a practice of delegating to university departments the responsibility for deciding which graduating students should hold the publicly-supported studentships by which most British graduate students try to keep alive. The standard procedure is that selected university departments will be given a quota of studentships which they may offer (within limits) to would-be graduate students.

Naturally, university and polytechnic departments prize their quotas as jealously as they would a kind of collective Nobel medal. For a quota is at once a guarantee that research will be sustained at some level and a powerful lever in the endless interdepartmental competition for resources. This is one reason why Sir Keith Joseph, the British Secretary of State for Education and Science whom everybody hates to love, will have made more enemies by endorsing last week the notion that the Social Science Research Council should deliberately move away from its quota system. Sir Keith should, however, have gone further.

The proposal that the Social Science Research Council should make fewer awards on the quota system stems from Lord Rothschild's report on the working of the council (see *Nature* 27 May, p.254) and was intended as a way of reconciling the need for some kind of manpower planning with sympathy for small university departments with nil quotas in which, the social sciences being what they are, research can never get off the ground. The Rothschild proposal was that quotas should attach to subjects, not to university departments. Sir Keith wants smaller quotas and more of the available awards put into a pool for competition by all university departments. Why not? And why should the same rule not apply to the Science and Engineering Research Council, which makes 3,250 or so new awards each year to graduate students in science and engineering?

In the face of the inevitable and fierce arguments that no change is best, the case for loosening the present quota system deserves a wider hearing. First, with the British university system now in unprecedented flux, the committees that decide quota allocations can be sure only that these will not match the needs of students and the capabilities of departments. Second, the quota system has the effect of spreading graduate students too widely for the interests of graduate education (and the inclinations of the students): a handful of graduate students in a small department does not constitute a graduate school, however much it may flatter the egos of the department heads involved. Third, with even the best research departments under continuing financial pressure, there are good reasons why the best of them should be given a better chance of survival by competition for some share of a pool. The research councils are always saying that they want to concentrate resources where they can be used effectively. Has not the time come for them to back words with deeds, and money?

But competition for and among would-be graduate students is surely a recipe for anarchy. That is what British university departments used to the quota system will be saying. They will of course be wrong. How else, it must be asked, do the outstanding graduate schools in the United States recruit their students? And there is even a British experiment along these lines — the apparently successful award this summer of a proportion of the graduate studentships available from the Science and Engineering Research Council for graduate students in mathematics. When will the others have the courage to follow suit? If mathematicians have been able to put graduate students up for grabs among them without bringing research to a halt, surely physicists, biochemists and others could take the risk. Equity among universities (rewarding quality) and students requires no less.

Belgian universities hit trouble

Money problem complicated by language split

Brussels

The beginning to the new academic year has been depressing for Belgian academics. Almost all of Belgium's oldest and most renowned universities are having to make sweeping staff cutbacks and to reduce the amount of research work possible for the next seven years. Under the special powers awarded to the present centre-right coalition government at the beginning of the year, the government has been free to take any measures it sees fit to stem Belgium's rising public spending deficit. The universities, at least those running large deficits, were given an ultimatum either to put their own financial houses in order, or to have the government intervening directly.

Anxious to preserve their autonomy, the university authorities have been sharpening the axe themselves and their plans are now being studied by the central government. Defiant talk of forming a united front against the government's demands, despite strikes and occupation of university buildings at the Catholic University of Louvain, has subsided into a grumbling acquiescence.

The truth is that the universities are divided and find themselves in widely differing situations. With the important exception of Ghent, only the Walloon or French-speaking universities are faced with a problem. The Flemish universities are by and large the creation of the 1960s, with a younger staff and a more streamlined and efficient administration.

The older francophone universities, which began to run into trouble towards the end of the 1970s, now have their backs against the wall. According to Hervé Hasquin, rector of the Université Libre de Bruxelles (ULB), his university has seen its budget dwindle by 25 per cent from as far back as 1975.

This year alone, the measures taken by Education Minister Michel Tromont have slashed ULB's budget by BF 300 million (\$6 million) and in the country as a whole savings of around BF 2,000 million (\$40 million) will probably have been achieved by the end of the year.

The government has reduced the payments per student, by which the universities finance themselves, by 25 per cent and has abolished grants for students on postgraduate courses. As in the United Kingdom, foreign students have also been a victim of the cuts and are now required to pay full tuition fees — up to \$5,000 a year

— unless they come from one of the 44 earmarked developing countries.

Against this background, it is surprising that the peculiarly Belgian system of "dedoublement" of maintaining separate university systems for each language, has survived intact. There is thus a Dutch-language university in Brussels (FUB) and a French one each offering roughly the same courses. Similarly there is the old Catholic University of Louvain and the Flemish KUL at an modern campus at Louvain La Neuve. With a few exceptions on the humanities side, no courses are held jointly and teaching posts are awarded on a strictly linguistic basis. A Walloon physics professor would be unlikely to obtain a vacant post at a Flemish university.

The problem is further complicated by the religious requirements until recently in force in some Belgian universities. Filling a chair in, say, astrophysics, with a Dutch-speaking Catholic who happens also to be a reasonably distinguished astrophysicist is not always easy. The feasibility of reorganization within the university system is further complicated by the emergence of separate language-based regional governments, likely to resist moves threatening their "own" universities.

The result is that in post baby-boom Belgium, there are now some 15 universities for a population of 9.9 million. For the 4.4 million French speakers in Belgium, there are nine universities. The Catholic University of Louvain — Dutch speakers need not apply.

dedoublement, says Andre Degroove, president of the administrative council of ULB, is definitely not a cause of the financial problems of Belgian universities, which stem from a drop in the number of students and the need to reduce public spending.

The plans put forward by the affected universities consist chiefly of cutting back on salaries and staff, and the universities have been given *carte blanche* by the government to ignore existing employment contracts. Liège, for instance, will enforce the compulsory retirement of teaching staff at the age of 65 and of other employees at 60 from September 1983. The aim will be to reduce personnel by 60, some 25 per cent of the total, and to cut running costs by 12 per cent. Research assistantships will be particularly badly hit in all the affected universities. At ULB, three out of five jobs will disappear and Degroove predicts that in ten or fifteen years there will be a serious shortage of experienced teaching staff.

Research work will also be badly affected and Belgian universities have not so far been especially successful in winning contracts from industry. "What makes the future look all the more dismal is that nobody knows how long the coalition government and its policies will last. Before the last elections there were six coalitions in four years", said Degroove mournfully.

Jasper Becker



Polish Academy of Sciences

Foreign travel rights restricted

Scholars employed by the Polish Academy of Sciences who wish to travel abroad will from now on need the approval of "the appropriate party secretary". According to a recent circular from Dr Zdzisław Kaczmarek, academic secretary of the academy, this change is designed to prevent the issue of passports to "persons whose socio-political activities and attitudes" are "negative" or "openly aimed against the constitutional, and legal order obtaining in the Polish People's Republic".

The circular forms part of the instructions concerning the process of political "verification", now being implemented in two stages within the academy. The restriction on travel has ostensibly been imposed in order to safeguard the prestige of Polish science abroad and to improve the international image of Poland. It is, however, a marked reversal of recent academy policy on foreign travel. Two years ago, after the signing of the Gdansk accord which inaugurated Solidarity and a nationwide wave of liberalization, the academy demanded that it alone should be the arbiter of whether or not its members and employees should travel abroad. Such a clause it was hoped, would be written into the promised new legislation on the Academy of Sciences; but martial law was imposed last December a few days before the session of the academy that would have debated this and other liberal clauses including proposals to change the role of the academic secretary. Indeed, Dr Kaczmarek's instructions on verification are an ironic reminder of what that session had hoped to achieve. For the academic secretary whose post is of ministerial rank under the present structure of the academy, is responsible, in the first instance, not to the academy members or council but to the prime minister.

The new restrictions on foreign travel — and indeed the whole verification process — could affect members and employees of the academy deeply. In Poland, the Academy of Sciences is organized completely separately from the universities (unlike, for example, the Soviet Union, where academicians also hold university lectureships and since the university purges of 1968, the academy has been a haven for scholars whose political views were considered too suspect for them to be entrusted with the teaching of young people. Indeed, the leading dissident group of the late 1970s, the "Committee for Social Self-Defence" (KOR) included among its 33 members two Academicians (Drs Edward Lipinski and Jan Kielanowski), while several others were employed in various academy institutes.

Objections to the new clampdown on travel could, however, in the current

draconian climate, well be taken as further proof of dissent. A recent attack in the party media alleged that cultural and scientific contacts between Poland and the West had been exploited by Western intelligence agencies. At the end of the 1970s, it is claimed, foreign scholarships were given to persons selected as future opposition leaders, while agents were sent to Poland disguised as "scholarship holders, lecturers, correspondents and experts".

Tera Rich

UK universities

Modest hiring prospect cheers

British universities seem this week to have been enormously cheered by the prospect of recruiting some hundred of younger scientists and engineers to academic posts. The only fly in the ointment is that this prospect is made possible only by the £6 million removed by the Secretary of State for Science and Education, Sir Keith Joseph, from the estimated budget of the Social Science Research Council over the next three years. One research council official confessed earlier this week that the "new blood" money seemed a little like "blood money".

As yet, it seems not to have been decided how much of the £6 million will be available in the coming financial year, a decision that Sir Keith has left to the Social Science Research Council. Nor has it been decided how the funds thus liberated will be shared among the other four research councils, although the Science and Engineering Research Council, the largest and with a direct responsibility for university research, seems certain to get the largest share. The chances are that the funds available will be shared out among disciplines, and that departments will be allowed to compete for the posts available by telling hard-luck stories to the councils.

While the numerical effect of the £6 million that will be available over the next three years remains to be determined, the research councils are already congratulating themselves on having been able to counteract some of the damage done to university research by the financial pressures on university budgets.

Thus the Science and Engineering Research Council has supported at least 23 applications under its Special Replacement Scheme, under which it will pay the salary of a senior researcher for up to five years provided that the university will undertake to appoint a younger researcher to a permanent academic post immediately. Applications under this scheme appear, however, to have tailed off in the past

several months, apparently because of the counter-attractions of the government-backed early retirement scheme.

So far, there appear also to have been few takers for the scheme under which the council will pay the salaries of researchers left stranded by the reorganization of universities involving the closure of departments. Two such awards have so far been made, both of them to casualties of the decision of a year ago that the Department of Biological Sciences at the University of Bradford should be "phased out".

Dr Michael Lord, a biochemist concerned with cell organelles, has joined the chloroplast group at the University of Warwick (now renamed plant biochemistry). The council will pay Dr Lord's salary for the next ten years, while the four members of his group transferred from Bradford will continue to be supported from research council funds. Similarly, Professor M.J. Merrett has moved to the University of Wales at Swansea with the help of a research council subvention to the university.

Cancer research

French change

Jack Ralite, French minister of health and one of the few communist ministers in the Mitterrand government, is contemplating a major reorganization of cancer research and the care of cancer patients, to judge by his moves earlier this month.

First, he has dissolved the "high committee" on cancer, which was only a little over two years old, essentially because it had failed in its task of uniting the two major French cancer charities, the Ligue Nationale Française contre le Cancer and the Association pour le Développement de la Recherche sur la Cancer à Villejuif (ADRCV). These charities control budgets amounting to more than FF 122 million (£10 million), considerably more than government expenditure on cancer research. But because of personality conflicts, the two have never been able to develop complementary research policies. The "high committee", now abandoned, was the previous government's attempt to knock their heads together.

The Ligue and ADRCV may now have only a temporary respite, however. For the minister has also launched a great national enquiry on cancer (the Concertation Nationale sur le Cancer) which is designed to provide the basis for a new politics of cancer.

Through the enquiry, which is addressed to all concerned, the minister will no doubt learn how French cancer research and care is riven by factionalism and the philosophy of the *savant*. He may also be expecting to confirm some other more debatable ideas about research, which come through clearly in the questionnaire which is the basis of the Concertation Nationale.

The questionnaire proposes that of the three principal sectors of researchers in cancer — biologists, clinicians and epidemiologists — the biologists are “very preponderant”. Is it not important today, asks the questionnaire, to reflect on the evolution of this state of affairs “and on the consequences of this primacy given to reductionist approaches?” Biologists tend naturally to choose areas of research as close as possible to fundamental biology, says the questionnaire. “Is this not to the detriment of specific research on cancer?” And, the questionnaire asks, should there not be separate rules for making evaluations of cancer research, so it is not subject to the more fundamental criteria applied by the medical research council (INSERM) and the Centre National de la Recherche Scientifique?

Such questions have been asked before, notably in the United States, but they are still appropriate and they are expected to produce some vigorous replies in France, with sectional interests being defended in every direction. Once the fur is flying, and the political positions of every sector are evident to all, M. Ralite will make “coherent recommendations”. This is democracy.

Robert Walgate

Nuclear war games

No survivors?

Moscow radio last week broadcast a virulent attack on Dr Edward Teller, the American physicist, for having published in *Readers' Digest* an article which suggested that nuclear war would not obliterate all life on this planet.

The broadcast, scripted by the official news agency TASS, alleged that Dr Teller has a vested interest in the arms race, since its “reversal” would deprive him of his “cushy job” as a presidential aide. Teller’s article, TASS alleged, was intended to “dampen the truly immense public interest all over the world” in the Soviet peace proposals tabled at the United Nations.

The Soviet proposal for a total test-ban treaty to create a more favourable atmosphere for arms limitation negotiations ran into considerable opposition from the United States, which maintains that the problems of verifying compliance with any such agreement should be solved before negotiations are started. In fact the Soviet Union put forward a package of verification proposals, including the international exchange of seismic data and the right of signatories to any such treaty to demand an on-site inspection of any suspected explosion in the territory of a fellow signatory. Since the Soviet proposals were backed up by carefully orchestrated panegyrics in the Soviet press the TASS writers may have genuinely assumed that the US rejection of these initiatives has a similar media back-up. Teller’s role as “father of the hydrogen bomb” is stressed and the activities of the

Pugwash movement ignored. His attempts to refute some of the more fantastic myths of what nuclear war would entail, his quoting of instances from Hiroshima and Nagasaki (“bridges were open to traffic a day after the blast, trains ran on the second day and streetcars were operating on the third”), and his suggestions on how to remove radioactive contamination are construed, by TASS, as “cynicism and misanthropy”.

In fact, Teller’s thesis that there would be a significant number of survivors of a war involving nuclear weapons and other “means of mass destruction” has tacitly been accepted by Soviet civil defence

planners. Recent reports of civil defence exercises, including practice evacuation of schools and hospitals, speak of the need for further training in the use of “means of protection against weapons of mass destruction”. A broadcast on Vilnius radio last summer by a civil defence official went into considerable details of the various gamma and neutron radiation monitors available to establish contamination of the population and of livestock, machines and equipment — suggesting precisely the same swift return to quasi-normality after nuclear bombardment for which Teller was castigated by TASS.

Vera Rich

Asbestos hazard

Bankruptcy protects the rich

Washington

The question of liability for the long-term latent occupational diseases of workers has been further muddled by the gigantic Manville Corporation, a mining and manufacturing company that is a pillar of US industry, which has filed for bankruptcy to protect itself from claims from asbestos workers, which the company says, could total as much as \$2,000 million.

The company’s action in August threw into turmoil the question of how US corporations deal with occupational health problems, sending other asbestos companies to their lawyers for advice and making claimants and their advocates suspect a fraud. It will be months before the full implications for the declining US asbestos industry, and for other industries with similar problems, are known.

Manville’s action was an extraordinary use of the US bankruptcy courts; companies normally file for bankruptcy when their debts have become intolerable in order to prevent outright liquidation. In those circumstances, the court takes charge of settling a corporation’s debts, freezing creditors’ claims and other lawsuits and dividends paid to shareholders, while a reorganization plan is being agreed.

But Manville is a relatively healthy corporation, although it reported a loss for the first half of 1982 of \$32 million. Its executives believe that the effect of filing for bankruptcy will be, ironically, to make the company still healthier.

Manville, which is the largest US producer of asbestos products used in building, insulation, brake lining, ship-building and underground pipes, has 16,500 claims outstanding against it. Its decision to file for bankruptcy was prompted by a study indicating that another 32,000 claims might yet be made, with an average settlement cost of \$40,000.

The asbestos industry in general faces a tidal wave of claims, because there are an estimated nine million people in the United States who have worked in an asbestos-related industry and who might claim damages on account of the risk of develop-

ing mesothelioma or asbestosis, maybe many years later.

The law so far has not ruled in favour of the asbestos industry. A lawsuit decided by the Supreme Court of the state of New Jersey last month ruled out as a possible defence a company’s ignorance of possible adverse health effects at the time its workers were exposed to asbestos. Awareness of the health hazards of asbestos has been relatively recent. Manville itself (then known as the Johns-Manville Corporation) lost a case in a California court and was forced to pay damages of \$28,000 to a victim over and above the workman’s compensation.

The Manville Corporation has also disputed for seven years with its insurance agents the point at which their liability should begin: at the time when the workers were exposed, when the disease appeared or from the time when medical hazards existed. As a result of the filing for bankruptcy, claimants will be able to obtain from the corporation data about what it knew and when. One court has already concluded that Manville concealed knowledge of asbestos hazards. Nevertheless, the corporation has spent \$24.5 million lawyers’ fees alone, and has so far paid out \$24 million in damages.

“CONGRATULATIONS! YOU ARE NOW FINANCIALLY AS WELL AS MORALLY BANKRUPT.”



By filing for bankruptcy, the corporation can put off paying existing creditors until the courts decide what should be done. In the meantime, no new claims can be filed. In reorganizing itself,

the Johns-Manville Corporation assigned to the new Manville Corporation only those assets associated with asbestos, thus shielding 74 per cent of its total assets from future litigation. It has even argued that claims against the Johns-Manville Corporation are not valid because that corporation no longer exists.

Other companies have been doing much the same. The Union Asbestos and Rubber Company became Unarco Industries Inc. and then UNR Industries. It has not made asbestos products since 1962, but claims are still pouring in. When it created UNR Industries Inc., it assigned to that company only its pre-1970 assets, which amounted to \$24 million. (Its assets today are \$200 million.) Then UNR Industries Inc. filed for bankruptcy in Chicago on the basis of the intolerable outstanding asbestos claim, so perhaps inspiring the Manville Corporation to do the same. **Deborah Shapley**

NRDC and NEB

Union delayed

The National Research Development Corporation is still coining money from the cephalosporin antibiotics, synthetic pyrethroid insecticides and half a dozen other inventions, but its intended marriage with the National Enterprise Board, announced in July 1981, has been delayed. Sir Freddie Wood, chairman of both organizations (which also now have identical boards of directors), said last week that he hopes to know more about the British government's intentions in a few months, but that legislation is unlikely to see the light of day before the end of the next year-long session of the British Parliament, beginning next week.

Meanwhile, the common opinion is that a formal merger of the two organizations would indeed bring the benefits advertised for it. The corporation, set up in 1949 to exploit inventions arising in the public sector (including universities) has been run principally by technical people, and during its chequered history has been accused of neglecting commercial opportunities. The board, by contrast, is stronger on accountancy and financial management.

The corporation as a single entity seems in good financial shape, to judge from the annual report published a week ago. It earned £26.2 million in the year to 31 March, chiefly from royalties on licensed inventions. Payments to inventors (and their institutions) amounted to £3.53 million, rather less than the sum set aside by the corporation for taxation before reaching its net profit of £5.02 million.

In the years immediately ahead, however, the corporation's income is likely to decline as patents on the cephalosporins run out. The annual report says that synthetic pyrethroids should help bridge the gap, but that these insecticides are unlikely to be as profitable. The cephalosporins stem from research at the University of Oxford, the pyrethroids from the Rothamsted Experimental Station.

During the year, the corporation says that 229 patents were assigned to it, a small increase on the previous year — and a surprisingly small number absolutely. The total of inventions about which the corporation was told amounted to 1,935, well over half from the public sector. Something like 350 inventions were earning money at the end of the year, while £23 million had been committed (or spent) on the development of patented inventions and £48 million to joint development ventures with industrial companies. ●

Celltech eyes Japanese market

Celltech, the British biotechnology company, has concluded a major five-year agreement for exclusive distribution of its alpha-interferon purification and assay products with the Sumitomo Corporation of Japan. The deal also covers Celltech's monoclonal antibody ABO blood grouping reagents, as well as anti-beta and gamma interferons.

Sumitomo, one of Japan's largest trading companies, has been selling Celltech products on an informal basis for several months; now Celltech hopes to reach a dominant position in the Japanese pharmaceutical and diagnostics market, valued at £8,500 million per year. Celltech is planning to develop monoclonal antibodies that can be incorporated into diagnostic kits and also hopes to gain some contract research from the present agreement; other cooperative ventures are not excluded.

The agreement follows closely that between Biogen of Switzerland and Fujisawa for joint development of

Biogen's human tissue plasminogen activator, which has yet to reach the stage of clinical trials. Hopes are high for this anticoagulant protein, which is more specific in its effects than other thrombolytic agents now in use, urokinase for example. It may come to represent a significant fraction of the large Japanese market for such agents. Fujisawa already has agreements with overseas companies for the production of human interferons.

These agreements follow a trend which has become apparent over the past few years in which Japanese firms arrange joint development and distribution deals with European and US companies; such arrangements have been reached between Hoffmann-La Roche, Genentech and Takeda, for example. While the Japanese appear actively to be developing their own expertise in techniques such as the production of monoclonal antibodies and recombinant DNA, they seem also to be encouraging the import of foreign products. **Tim Beardsley**

Astrophysics laboratory

Theoretical gain

Chicago

The Fermi National Accelerator Laboratory (Fermilab) has set up the first theoretical astrophysics group to reside at any of the world's accelerator laboratories. The group will start work in January, and is being supported by the US National Aeronautics and Space Administration to the tune of \$500,000 over three years. By January, Dr Leon M. Lederman, director of Fermilab, expects to have taken on one or two senior researchers and two or three junior workers.

Lederman says: "One of the most exciting parts of particle physics research now is the connection between inner and outer space. Particle physicists look down with their microscopes and astrophysicists look up with their telescopes and find they are looking at some of the same things".

Fermilab's studies are essential to model the evolution of the Universe immediately after the Big Bang, but Lederman says that the behaviour of the early Universe in turn constrains what the particle physicists can expect to find as accelerator energies increase.

The new group, with a huge accelerator readily available, will deal primarily with the connection between particle physics and the early Universe, in which high temperatures and energies were generated by the Big Bang. But current interests in particle physics research, the grand unified theories for example, deal with particle energies around 10^{14} GeV, ten orders of magnitude greater than the energies being dreamed of by today's accelerator builders.

Yet astrophysical theory can extrapolate as far back in time as 10^{-43} seconds after the Big Bang — when the thermal energy would have been 10^{19} GeV. The early Universe is thus an ersatz particle accelerator for extreme energies. The group will also investigate the implications of particle physics theory for astrophysics. Some grand unified theories suggest that the Universe passed through an "inflationary" phase of violent expansions that may explain why the Universe today is isotropic, homogeneous and dynamically "flat".

Lederman says that Fermilab has hitherto only "dabbled" in astrophysics, and he hopes that the new formal collaboration will enable more systematic and fruitful studies to be made. **Larry Arbeiter**

Ciba Foundation

In *Nature* for 30 September, p.383, there was a report of what Dr R.G. Edwards had said at a Galton Lecture and at a meeting organized by the British Medical Journalists' Association; this meeting was sponsored by Ciba-Geigy Pharmaceuticals and not, as reported, by the Ciba Foundation.

Social sciences in France

Few friends on the right

The unsympathetic manner in which Britain's Sir Keith Joseph regards the social sciences has precedents across the Channel, according to a long-awaited report on the social sciences in France. Figures collected by M. Maurice Godelier, a respected left-wing anthropologist and friend of the Mitterrand government, show that Giscard d'Estaing, the previous President of France, slashed social science spending by more than half between 1976 and 1981, and the humanities by nearly a quarter. Now is the time for reconstruction, and the government seems likely to follow M. Godelier's recommendations, although science and industry minister Jean-Pierre Chevènement said on introducing the report that full implementation would be too costly.

According to Godelier, there is much work to do. Giscard caused such a collapse in the human sciences "that the general public would hardly believe it". Libraries and documentation centres were particularly badly hit. The result was that subjects not protected by this or that "mandarin" were smothered. In the scramble for funds, academic standards went by the board. Economics fared best, but only mainstream neoclassical economics. Sociology, tainted with being "leftist", was worse hit.

Godelier is thus starting almost from scratch. He recommends recreating infrastructures destroyed by Giscard (contract research supported by government departments had almost disappeared). He wants buildings repaired, libraries re-equipped, more funds for field studies and for publi-

cations, improved international contacts and more staff.

Nobody is likely to disagree with any of that — except for the size of the bill. But eyebrows have been raised in some quarters by his statement that the "new dynamic" should be founded not only on an increase in funding but also on a different cutting of the cake, in response to "a new evaluation of needs". These, it seems, would in part be turned towards the realities of modern French life, involving the study, for example, of both business and administration — the elite.

Moreover, Godelier has recommended the setting up of many more interdisciplinary studies, and cross-border funding committees — which might threaten the very "mandarins" who survived Giscard. Godelier is thus seen as a personal and political threat in some quarters; and when this is combined with his forthright manner, he finds himself facing considerable opposition.

Thus when Chevènement attempted to make Godelier director of social sciences at the Centre National de la Recherche Scientifique (CNRS) last year, key figures in CNRS resigned over this alleged interference with "academic freedom". But others have pointed out that the man Godelier was to replace (and who did indeed resign, leaving a vacancy still unfilled) was himself a political appointee, a friend of Giscard's prime minister, Raymond Barre. Chevènement's logic was not faulty.

The political problem now is to fill the

hot seat at CNRS, from which the Godelier reforms will be implemented, without creating too much uproar. Some kind of compromise, which might perhaps involve Godelier getting half the job but not the full responsibility, seems to be in the offing.

Robert Walgate

Education in Afghanistan

Russian aid

Afghanistan has embarked on a major programme of expansion of higher and technical education, Mr Sarwar Mangal, the Minister of Higher and Vocational Education, announced recently. Mr Mangal, who became minister at the end of September, was taking part in a series of special broadcasts on Kabul radio in which ministers explain the work of their ministries.

The expansion programme will concentrate on those areas most important to the national economy — in particular engineering and agricultural sciences. Three new agricultural technical institutes will be founded at Mazar-e Sharif, Jalalabad and Baglan, and the agricultural secondary school at Helmand will be upgraded to an agricultural technical college. Major building works are under way at Kabul University (a chemistry institute, classrooms block and accommodation for lecturers and students), Nangarhar University (faculty of education and agriculture school) and Balkh (agricultural school). A new accommodation block for Kabul Polytechnic Institute will be started in the near future. Mr Mangal admitted, however, that there were "deficiencies, shortcomings and improper management" in the building programme.

Higher education in Afghanistan has mushroomed in the past few years. Enrolment in higher education (including the Kabul Polytechnic Institute and the Mangarhar and Kabul medical schools) in the Afghan year 1361 (March 1982–March 1983) was 155, a 250 per cent increase compared with 1355 (1976–77). Entrance examinations were recently standardized, although ex-soldiers are admitted to university without taking the competitive examination. Recruitment to technical-vocational education seems to be going more slowly; Mangal spoke of recent improvements in the vocational sphere, including the launching of poster campaigns and sports contests to attract young people to vocational courses. The first "professional-technical" school, which can train 100 students in the maintenance of vehicles and industrial machinery and which was constructed under a grant-in-aid from the Soviet Union, was opened recently, and a similar television and refrigerator maintenance school, equipped by the Soviet Union, should be ready at the end of this (Afghan) year or the beginning of the next.

Spending low on France's books

A library, to a researcher in the humanities or social sciences, writes Hervé Le Bras, director of research at the Institut National des Etudes Démographiques, is like a telescope to an astronomer. But, claims Le Bras in an appendix to the Godelier report (see adjacent story), French libraries (though never good) are now "catastrophic".

The present state of affairs is illustrated by a comparison between the British Library (based in part at the British Museum) and the French equivalent, the

Bibliothèque Nationale. The table shows, in particular, a lack of French funds, posts and lending.

Some other figures: the Bibliothèque Nationale buys only 3.6 per cent of European titles in languages other than French, and only 2 per cent of North American titles. "The shadow which covers our own history [through lack of texts and documents] also extends to the rest of the world" says Le Bras. French social sciences "must not become provincial" he says.

	British Library (1979–80)	Bibliothèque Nationale (1981–82)
Total budget (FF)*	381,205,000	61,740,766
Conservation budget	24,200,000	11,611,508
Acquisitions of titles	2,100,000	750,000
Accredited readers	18,800	15,600
Staff	1,125	802
Requests for borrowing	2,375,000	24,700
Lending for borrowing	2,375,000	24,700
Lending budget (FF)	22,792,000	250,000
Lending staff	730	54

* (FF 12 = £1)

Higher and professional education is critically dependent on Soviet aid. As well as supplying funds for the professional schools, the Soviet "Progress Publishing Company" is to produce more than 200 university textbooks with a total print-run of 300,000 copies as grant in aid. (These will mostly be translations of existing Soviet texts). Moreover, although postgraduate courses up to master's degree

are now available at the Kabul Polytechnic Institute and will shortly be introduced at Kabul University, most postgraduate training can still take place only in the Soviet Union. This year, some 1,500 graduate students began courses in Moscow, which, compared with the 4,155 freshmen enrolled this year, constitutes a sizeable proportion of the student body.

Vera Rich

FDA on overseas data

US drug market to open up?

Washington

New drugs may be approved for sale in the United States solely on the basis of foreign data under a proposed reorganization of the Food and Drug Administration (FDA) new drug application process. One effect may be to facilitate the entry of drugs developed abroad into the US market.

The proposed changes, published last week, have already provoked some strong reactions. Under current FDA rules, at least one of the clinical studies of a new drug must be conducted within the United States. Critics claim that FDA's proposal, increasing the admissibility of foreign data, flies in the face of evidence that foreign studies are difficult to verify and that standards for protection of human subjects are generally lower outside the United States.

In a discussion that accompanies the new proposal, FDA concedes that there are problems in accepting foreign studies. For one thing, genetic differences between foreign and US populations may render foreign results inapplicable; similarly, differences in medical practice and even in terminology (the definition of "depression", for example, is shaded by cultural differences from country to country) may also be significant. FDA admits, too, that the competence of foreign researchers is more difficult to judge than that of US scientists. FDA's proposed solution is to reject applications based solely on foreign studies when "the calibre of the key clinical investigators and facilities is unknown" or when there is "reason to believe" that genetic, medical or cultural differences affect the applicability of the results to the United States.

But a potentially more serious obstacle to the acceptability of foreign data is the difficulty of auditing foreign clinical trials. A House of Representatives subcommittee found last August (see *Nature* 12 August, p.598) that FDA investigators were unable to gain access to the medical records of a clinical trial in a Canadian hospital because of local confidentiality laws; and an audit of one Mexican study found patients' records destroyed.

FDA says it will reject applications if a "for-cause" inspection is considered necessary and then cannot be carried out

because of such obstacles. But Dan Sigelman, who is on the staff of the House subcommittee that investigated FDA, says that this is a "Catch-22". FDA routinely conducts spot-check audits of domestic studies and these, according to Sigelman, are what normally turn up the cause for further "for-cause" inspections. "On what ground are you going to determine the need for an audit without an audit?" he asks.

Sigelman also questions FDA's assertion that US drug companies will continue to favour US studies so that they can acquaint US physicians with the new drug before it is marketed. "They can sit and argue all they want that drug companies won't go abroad, but if the trade-off is getting a drug on the market more quickly, you're just opening up the floodgates to foreign data", he says.

The change on foreign data had been pressed by the US drug companies' trade group, the Pharmaceutical Manufacturers' Association (PMA). PMA also got its way on another controversial point: FDA is proposing to drop the current requirement that case-report forms from clinical trials be submitted with new drug applications. In place of these forms, which are made out by the clinical investigator on each patient, a tabulation of the raw data would be submitted. Under this proposed change, FDA could still request the case-report forms, but only when a "legitimate need for them exists in order to conduct an adequate review of the application".

The only noticeable tightening of the rules in the FDA proposal concerns the reporting of adverse findings about a drug by its manufacturer. The current rules are vague on how and even whether adverse findings are to be reported to FDA once an application is on file for approval — as the case of Eli Lilly and Co.'s reporting of deaths among Oralflex (benoxaprofen) users demonstrated earlier this year.

FDA's proposal requires drug companies to file a safety report every four months when it has an application on file. FDA is also proposing to tighten its requirements on reporting of adverse effects of drugs already on the market: fatal and life-threatening effects would be reported to FDA within 15 days in "alert reports", other "adverse experiences"

within 30 days.

Critics are calling these changes window dressing, however. Dr Sidney Wolfe of the Ralph Nader Health Research Group says, "my response to this whole stunt is that the more important issue is enforcing existing regulations". Wolfe cites FDA's continued failure to bring criminal charges against Lilly, as recommended by a former FDA investigator, for withholding adverse effect data on Oralflex and three other drugs.

FDA is accepting public comments on its proposed changes until 20 December. After digesting these — and possibly making some alterations — the agency will publish a final rule, probably in early spring. As the proposals stand now, though, it is clear that the big winners are the drug companies, which will be able to file less paper, receive quicker responses and have an easier time introducing drugs already marketed abroad into the United States.

Stephen Budiansky

Halley upstaged?

Washington

The US National Aeronautics and Space Administration (NASA) has set one of its spacecraft on a complex manoeuvring course that will enable it to intercept and study the Giacobini-Zinner comet on 11 September 1985 — six months before Soviet, European and Japanese spacecraft are due to meet Halley's comet.

The Giacobini-Zinner comet, which approaches the Sun every 13 years, will not be visible from the Earth, but the better known Halley's comet has already been detected with the 5-metre Hale telescope on Palomar Mountain.

NASA's plan is to move the International Sun-Earth Explorer (ISEE 3), which has been in a permanent orbit between the Earth and the Sun since 1978, measuring electric and magnetic fields. US scientists have been upset by the Reagan Administration's cancellation of the \$250 million plan for a US spacecraft to Halley's comet. The NASA decision to use ISEE 3 to intercept another comet first may console them, because the United States will thereby be the first to provide valuable data that others can use in analysis of Halley's comet.

ISEE 3 has already been moved to the side of the Earth away from the Sun and on 6 February next year it will be directed on a course that will take it past the Moon. It will then be brought close to the Moon to use its gravity to give the spacecraft a push towards the comet. After the Giacobini-Zinner probe, ISEE 3 may be used to measure the solar wind extending from the Sun towards Halley's comet at the time when the other probes reach that comet early next year.

Deborah Shapley

Nuclear fuel supply

World enrichment over-capacity

Brussels

The Euratom Supply Agency, which has the sole right to negotiate nuclear fuel supply contracts for Euratom's 10 member states, points out in its annual report for 1981 that EEC is in danger of creating an overcapacity of nuclear fuel enrichment services. Last year EEC registered a positive trade balance of 2,200 tonnes SWU (separative work units) compared with its own requirements of 4,500 tonnes. By 1984 the European Community could have a capacity of 11,800 tonnes and an internal demand of 7,400 tonnes.

The over-capacity is likely to become more of an embarrassment, since Japan and Brazil, which until now have been in the market as buyers, have decided to build their own enrichment plants. What is worse is that Australia, which has signed a long-term supply contract with EEC, plans to upgrade locally the uranium it mines, and detailed studies are already under way for the construction of a plant for isotopic separation. This may create political problems as some of Euratom's member states would prefer to keep separate the purchase of natural uranium and enriched uranium for security reasons.

By 1990, according to the Euratom

Supply Agency, world enrichment capacity is likely to be around 49,650 tonnes SWU compared with the 1980 figure of 36,150 tonnes. The United States still dominates the industry with a 27,300 tonne capacity but from 1989 onwards France will be capable of enriching 13,300 tonnes.

The prospect of competition from France may have a significant impact on the costs of enrichment. The price of the US Department of Energy's enrichment services is steadily increasing, reports the Euratom agency. The cost per SWU rose by 27.4 per cent last year (from \$111.75 to \$141.14) and the Department of Energy announced a further price rise for 1982. These price rises have been further exacerbated by the decline in the value of the European Currency Unit (ECU) against the dollar so that enrichment costs at the "front end" of the fuel cycle now exceed 40 per cent of the total cost of operations while the natural uranium component has for the first time fallen to below 40 per cent of the cost. Uranium users have therefore been hanging onto their stocks of natural uranium rather than enriching it prematurely.

The price of plutonium has also fallen, from \$10 to \$4 per gramme of Pu fissile

Uranium enrichment in Euratom nations (tonnes SWU)

Production	Requirement	Balance
1978 —	1,400	-1,400
1979 2,600	3,200	- 600
1980 6,000	3,900	+ 2,100
1981 6,700	4,500	+ 2,200
<i>Capacity</i>		
1984 11,800	7,000	+ 4,800
1985 11,800	7,400	+ 4,400

material, and the Euratom agency predicts that in future the supply of plutonium could considerably exceed that required by fast reactor programmes. Similarly, natural uranium is also likely to remain a buyer's market with an excess of supply over demand. Prices have remained stable, with world stocks of natural and enriched uranium now equivalent to more than three years' consumption. Deliveries of natural uranium to Euratom countries amounted to 13,000 tonnes in 1981 and this is likely to drop to 10,750 tonnes by 1983.

Jasper Becker

French nuclear power

EDF's setbacks

Electricité de France (EDF) is having increasing trouble with some tiny but important parts of its pressurized water nuclear reactors, which were due to provide half of France's electricity by next year. In fact the problem is so worrying that EDF says it will have to close down 20 stations for repair between 1983 and 1984, with a total loss of some 22 operational reactor-months.

The pieces are clips which hold up guide tubes for the control rods — rods which must be driven or dropped into the reactor core to close down the nuclear reactor in case of accident. In January, pieces of one of these clips were found lodged in an emergency cooling pipe in one of the reactors at Gravelines, and since then other broken clips have been detected at Fessenheim and in two reactors at Bugey. The loss of the clips is potentially dangerous — they could block the proper entry of the control rods, or, by circulating in the cooling system they could damage pumps and valves.

Moreover, it seems that the broken clips had no individual faults: the error appears to have come in the choice and treatment of the clip material (which is exposed to high temperatures and radiation levels in the reactor). That is why the clips must be replaced in all 20 reactors where the material was used, at a cost (mostly in lost electricity production) of at least FF 1,000 million.

The incident illustrates one of the dangers of the massive French nuclear programme, which reduced costs by using long series production of a few single designs. If the design is wrong, all fail at once. "This just shows how the French nuclear industry has all its problems yet to come" said one commentator this week. Robert Walgate

Projected world enrichment capacity (tonnes SWU)

	1981	1982	1986	1987	1988	1989	1990
Eurodif (France)	10,000	10,800	10,800	10,800	10,800	10,800	10,800
Urenco	550	750	2,100	2,300	2,700	3,000	3,300
DoE diffusion (US)	26,900	27,100	27,300	27,300	27,300	27,300	27,300
DoE centrifugation (US)	—	—	—	—	1,100	2,200	2,200
Technabexport (USSR)	3,000	3,000	3,000	3,000	3,000	3,000	3,000
PNC (Japan)	—	—	100	100	250	250	250
UCOR (South Africa)	—	—	—	—	100	100	100
Nuclei (Brazil)	—	—	100	200	200	200	200
Coredif (France)	—	—	—	—	—	2,500	2,500
Total	40,450	41,650	43,400	43,700	45,450	49,350	49,650

India embroiled in nuclear politics

Bangalore

After more than three months, negotiations between India and France over the supply of enriched uranium for India's troubled nuclear power station at Tarapur have reached stalemate. France is insisting on operating the safeguards laid down by the International Atomic Energy Agency (IAEA), aimed at limiting the spread of nuclear weapons. To the Indian negotiators, however, such restrictions imposed by Western countries on the supply of nuclear fuel "devalue India's national prestige" by asking for "humiliating terms and conditions".

The negotiations, described by India's Foreign Minister Mr Narashima Rao as "a tortuous process", did see some compromises made by France on the matter of reprocessing spent fuel in India. But these proved insufficient to break the

deadlock, with India being particularly unwilling to comply with France's alleged insistence on a written undertaking that India will not carry out any further testing of nuclear bombs.

The Indian government is also in disagreement with the Soviet Union, having declined a Soviet offer to build a 1,000-MW nuclear plant in India, despite its problems in obtaining enriched uranium for its Tarapur plant. The Soviet offer, made previously when Mr Morarji Desai was Prime Minister, was renewed during Mrs Indira Gandhi's recent visit to Moscow.

Like France, the Soviet Union is insisting on the IAEA safeguards. In the face of restrictions from both East and West, members of India's parliament have called for a speeding up of plans to develop MOX, an indigenous fuel supply.

B. Radhakrishna Rao

CORRESPONDENCE

Ball lightning in the laboratory

SIR — Sir Brian Pippard's account of ball lightning observed outside the Cavendish Laboratory¹ is the latest of many reported sightings of this phenomenon. Unfortunately, Nature is not an obliging wench² and men generally experience her performance no more than once in a lifetime. Thus descriptions garnered from single momentary unexpected glimpses tend to be inexact and unscientific; if the fireball be the angular size of the Moon¹, what is its diameter? I would like therefore to draw attention to the possibility that some photographs we published³ some years ago were in fact of a laboratory version of ball lightning.

The work was a consequence of some peripheral observations we made while developing a streamer chamber⁴ for cosmic ray studies. Originally we discovered a ringing phenomenon superimposed on the Lichtenberg figures that appeared on the insulated bottom of the chamber and centred on the particle tracks⁵. This was with a chamber filled with the noble gas mixture of 70 per cent neon and 30 per cent helium. These dark rings could manifest themselves as dark spaces in a columnar discharge⁶ and the advance of the discharge could be studied by arresting the field and photographing the various stages⁷. It was when we extended the work to air³ that a new effect emerged which may now shed light on the nature of ball lightning.

The photograph shows the electrical discharge resulting from the application of a

avalanches but which here can only move upwards and so some photoionization mechanism must be assumed. The downward velocity of the luminous front is of the order of $5 \times 10^5 \text{ m s}^{-1}$.

The curiosity here is the well-defined luminous cone seen in the photograph (region 3), for which we have seen no counterpart in noble gases. The photomultiplier trace⁸ shows that light is emitted synchronically with the oscillations of the applied voltage — even though the adjacent regions^{2,3} emit essentially only once when the discharge front traverses. The cone is seen to be a stationary, stable, localized fireball maintained by the electric field. If the field oscillations were allowed appropriately to continue for seconds, one might suppose the emission from the plasma cone would similarly continue.

The similarity between the suspended cone of plasma and ball lightning prompts the hypothesis that ball lightning itself is maintained by an oscillatory atmospheric electric field. The reason for the localized containment of the plasma is an unanswered question, but one which is now open to experimental study in the laboratory. Ball lightning moves gently and one must presume that this is in response to the site of the advantageous field conditions itself moving. In that discharge phenomena tend to be a function of the ratio E/p , the higher atmospheric pressure would imply higher electric fields.

P.C. RICE-EVANS

Department of Physics,
Bedford College,
University of London,
London NW1, UK

1. Pippard, A.B. *Nature* **298**, 702 (1982).
2. Tonks, L. *Nature* **187**, 1013 (1960).
3. Rice-Evans, P.C. & Franco, I.J. *J. Phys* **D13**, 1079 (1980).
4. Rice-Evans, P. *Spark Streamer, Proportional and Drift Chambers* (Richelieu, London, 1974).
5. Rice-Evans, P. & Hassairi, I.J. *Phys. Lett.* **38A**, 196 (1972).
6. Rice-Evans, P. & Franco, I.J. *Phys. Lett.* **63A**, 291 (1977).
7. Rice-Evans, P. & Franco, I.J. *Phys. Lett.* **70A**, 20 (1979).
8. Golde, R.H. *Lightning* Vol.1 (Academic, London, 1977).

ICSU matters

SIR — In view of the factual errors in "Doing one's thing" *Nature* 16 September, p. 194, I should be grateful if you would publish the following:

(1) Discussions have been taking place with representatives of the China Association for Science and Technology and the Academy located in Taipei, China, for the past ten years to prepare the terms of an agreement that would be acceptable to all three parties and would make it possible for both organizations to be members of ICSU with the right to vote. These were successfully completed on 15 September, as Vera Rich indicates in your issue of 23 September.

(2) The communication from the Government of Australia to the Australian

Academy is quite specific and does not give "terms of reference wide enough, etc.". It did not add the proviso that "in future it should have a hand in planning conferences of this kind". To which kind of conferences do you refer?

(3) Sir John Kendrew was elected as first Vice-President for two years. He will become President in 1984 for four years.

(4) If ICSU is "short of money" it is because of a general shortage of money in the academic world, which provides most of the funds for ICSU, not because "it is trying to accomplish goals for which it was not created".

Further, in relation to "Academies not international" (23 September, p.288), the argument from which the predecessor of ICSU, the International Research Council (IRC) and ICSU spring is: the coordination of international efforts in the different branches of science and its applications.

Today ICSU's ultimate objectives include "to encourage international scientific activities for the benefit of mankind and so promote the cause of peace and international security throughout the world", and in pursuing these objectives ICSU observes a basic policy of non-discrimination — it affirms "the rights of scientists throughout the world to adhere to or to associate with international scientific activity without regard to race, religion, political philosophy, ethnic origin, citizenship, language or sex". The withdrawal of Taiwan was not an acceptable solution.

ICSU does not have and does not need a UN sponsor. As an organization expands, which ICSU has done in the past three decades (10 new International Scientific Unions, 26 new National Members, 17 new Scientific Associates, 4 new National Associates Biological Programme, the Upper Mantle Programme, the world Scientific and Technical Information Study jointly with Unesco, the Global Atmospheric Research Programme jointly with WMO, etc), paperwork expands . . . as has the number of printed pages about scientific discoveries in the past three decades.

"The state of affairs" about which your article says ICSU should be worrying seems to be pure politics: an area ICSU tries to avoid — "tries" is put purposively because it is not possible for any organization, not even a non-governmental organization, to escape from the effects of politics and governments' policies.

F.W.G. BAKER
(Executive Secretary)

International Council of Scientific Unions,
Paris, France

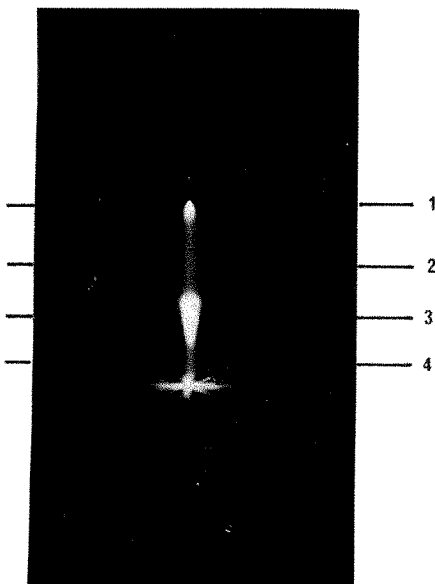
(1) Agreed; we said so twice.

(2) The Australian government has asked the Australian National Academy of Science to consult on future international conferences.

(3) We are grateful for this correction.

(4) A matter of opinion, linked with the question raised in the article "Science not international" of whether ICSU would be more effective in its laudable fight against discrimination if it were organized differently.

EDITOR NATURE



Photograph of the discharge corresponding to the positive high voltage pulse applied to the wire electrode (invisible here).

modulated positive potential to the wire with the lower plate earthed. The initial rise of the impulse causes field emission at the wire tip, and the plasma develops downwards. The precise nature of this advance is not understood; the main agents of discharges are electrons that participate in Townsend

NEWS AND VIEWS

Calculating the strength of wood

A group of mechanical engineers has provided a rational framework for understanding what is known of the strength of all kinds of wood. The methods should be more widely applied.

That wood is in some sense strong has been known since antiquity. Surprisingly, the reasons why have only in the past few weeks been made clear.

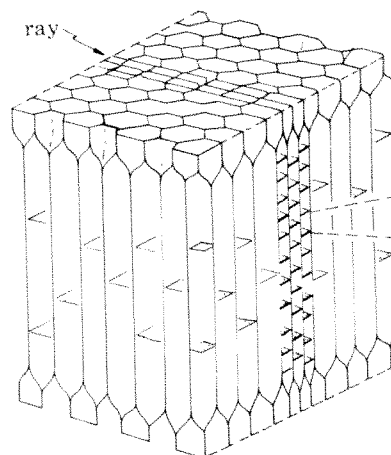
The construction industry probably includes few avid readers of the *Proceedings of the Royal Society*, either series A (physics) or B (biology), which is why something must be done to draw attention to the remarkable circumstances that this most august journal has now published what seems to be the first convincing explanation of the mechanical strength of wood. For what it is worth, the analysis (by K.E. Easterling, R. Harrysson, L.J. Gibson and M.F. Ashby, the first two from the University of Luleå in Sweden and the others from the Department of Engineering at the University of Cambridge) turns up in series A of *Proc. R. Soc.* (383, 31-41, 1982). The paper, which owes something to an earlier study of the structure of cork (L.J. Gibson, K.E. Easterling and M.F. Ashby, *Proc. R. Soc.* 377, 99-117; 1981) and to some newly reported investigations of the cellular structure of balsa wood, is a splendid illustration of what mechanical engineers can accomplish (if they are permitted) for biologists.

Living trees are of course aggregates of cells, most of them filled with cytoplasm, some of them seasonably capable of photosynthesis. The wood derived from trees that is used in the construction industry is, however, best thought of in quite different images, as a three-dimensional structure made from the walls of empty cells, themselves made largely from cellulose with a measured and nearly constant density of about $1.5 \times 10^3 \text{ kg m}^{-3}$, and with tensile strengths and other mechanical properties that can in principle be measured (but which in practice appear to depend on the orientation of the cellulose microfibrils within the cell walls). So, ever since the shapes of wood cells were first described by microscopists, it should have been a relatively simple task for mechanical engineers to figure out just how strong a particular wood should be. Alternatively, just as aeronautical engineers are forever trying to puzzle out what kind of honeycomb structure will provide the most resistance to some specified force (bending, twisting, crushing . . .) for the least use of material, so people should have been on the look-out for wood-cell structures promising desirable mechanical properties.

It will be interesting to see whether an attempt (not yet carried out) to predict the ideally strong wood would point to the cellular structure of a balsa wood now described — a three-dimensional network of cells with hexagonal cross-section with pointed ends and with an aspect ratio (of length to breadth) of about sixteen. In practice, the circumstances (see figure) are more complicated. In balsa wood, bundles of hexagonal needles oriented along the axis of the tree are lumped together around each annual growth ring, but are also separated from each other in blocks by layers of differently shaped cells running out in sheets from the centre of the tree (and which, when seen in the cross-section of a tree, not merely a balsa tree, are called rays). One important complication is that individual cells may have stiffening cellulose membranes perpendicular to the axis of the cell (and of the tree). What Easterling *et al.* have done is to calculate the mechanical properties of such structures.

The results of the analysis are surprisingly straightforward, but consistent with what has been found empirically about the strength of wood. Take, for example, the calculation of the Young's modulus of wood compressed tangentially. The only

way in which the wood cells can be deformed is by the bending of the angles by which the walls are joined, which can be related to the Young's modulus (in that direction) of the materials of which the walls themselves are made. Indeed, the tangential Young's modulus turns out to be the Young's modulus of the cell-wall material multiplied by the factor $4/\sqrt{3}(t/l)^3$ where t is the thickness of the hexagonal cell wall and l the length of the hexagonal side. Simple geometrical arguments lead to the conclusion that the tangential Young's modulus of balsa wood should be proportional to the cube of the physical density of the



Schematic representation of bundles of columnar hexagonal cells within a balsa growth-ring (from Easterling *et al.*) Cell height = 0.6 mm (approx), diameter = 0.035 mm.

way in which the wood cells can be deformed is by the bending of the angles by which the walls are joined, which can be related to the Young's modulus (in that direction) of the materials of which the walls themselves are made. Indeed, the tangential Young's modulus turns out to be the Young's modulus of the cell-wall material multiplied by the factor $4/\sqrt{3}(t/l)^3$ where t is the thickness of the hexagonal cell wall and l the length of the hexagonal side. Simple geometrical arguments lead to the conclusion that the tangential Young's modulus of balsa wood should be proportional to the cube of the physical density of the

wood. The same line of argument suggests that the radial modulus, corresponding to compression along a radius from the centre of the tree, is twice as large, but that the axial modulus should be proportional to the first power of the density of the bulk wood, not to its cube. The remarkable feature of the comparison between prediction and observation now reported is not that the numerical values (calculated and observed) differ by factors which are sometimes as large as four or five but that they are in the same ball-park. Curiously enough, the mechanical engineers seem to be better able to predict the crushing strength of balsa wood, perhaps because the dominant factors in their calculations are estimates of the collapse strength of the exceptional pieces of the cell structure, the hexagonally prismatic pointed ends of balsa wood cells, for example. The outstanding achievement of the argument, however, about which more could with advantage have been said, is that the variation of the mechanical properties of balsa wood with density calculated from first principles provides scaling laws that appear to accommodate not merely this exceptional material but other kinds of wood as well.

That the scaling laws for the strength of wood should have a rational basis is comforting but unsurprising. What else would one expect? The interest of this study, however, is that it shows that in the investigation of biological materials (of which wood is one) even the macroscopic methods of mechanical engineering can be applied successfully to estimate the mechanical properties of microfibrillar structures, bundles of cellulose molecules and the like. Bone is another such material to which attention has now turned. No doubt there will be many others. □

The acetylcholine receptor cloned east and west

from Charles F. Stevens

A NEW era in neurobiology has begun with the successful cloning and sequencing of DNA that codes for subunits of the acetylcholine receptor. The α subunit sequence reported in this issue of *Nature* (p. 793) is another first for Shosaku Numa's group at Kyoto University and the sequence of the γ subunit, the successful cloning of which was announced recently², is expected to appear soon from the group at the Salk Institute, California³. The existence of cloned DNA coding for channel proteins will allow the power of molecular genetic approaches to be applied to the investigation of brain organization and function — it should be possible to categorize and understand the relationships between the numerous channels found in nerve cells and to see how they appear during development as well as to understand the molecular mechanisms of channel formation.

The acetylcholine receptor is one of a rather large family of integral membrane proteins that are responsible for the electrical activity of the nervous system. The proteins, known as channels, regulate the flow of ions across the membranes of excitable cells and can be divided into two broad categories — ligand-gated channels that are opened by the binding, with enzyme-like specificity, of a particular ligand and function in communication between cells, and voltage-gated channels² that are opened by voltage differences across cell membranes and are responsible for nerve impulses and transmission of information along axons. The acetylcholine receptor is a ligand-gated channel responsible for a link in the communication between nerve cells and skeletal muscle in vertebrates.

The acetylcholine receptor is the best understood channel protein, and has been extensively studied from physiological, biochemical and cell-biological viewpoints. It is a pentameric protein with a molecular weight of approximately 250,000 and is composed of four distinct polypeptide chains, with different molecular weights, designated α , β , γ and δ ; the α subunit is responsible for binding acetylcholine, the ligand that regulates ion flow through the channel, and two α subunits are present per channel. The two α subunits are very similar, but may not be identical.

In this age of cloning, what is notable about bugs growing the DNA coding for yet another protein? Three basic things can be done with the cloned DNA: it can be

used as a means for identifying, in hybridization experiments, other RNA or DNA molecules that contain the same, or similar, information; it can be sequenced; and it can be used to instruct cells to make the protein encoded by the DNA, possibly after modifying the DNA by mutations. All three paths are now available for the acetylcholine receptor.

The several dozen different channel species present in nerve cells are currently categorized according to the neurotransmitter ligand that regulates the ionic flow through them or, for the voltage-gated channels, according to the type of ion which passes most readily through. Thus, we speak of acetylcholine-activated channels, serotonin-activated channels, or sodium channels. Everyone believes that some order exists in the various channel types, but we have no way of categorizing channels now. For example, all ligand-gated channels may be related in some sense, or some subclasses, perhaps those activated by the biogenic amines, may be related. Furthermore, all channels that regulate the passage of a particular ion species (calcium or sodium, for example) may share certain structural characteristics. Presumably, then, channels will form one or several large families of molecules.

The key to understanding the relations within and between these families will be analysis of the genes encoding them. These genes, in turn, can only be studied when they can be identified and this is done with hybridization experiments using cloned DNA. Cloning the DNA for the acetylcholine receptor channel, then, is the first step in beginning to unravel the interrelationships between those protein molecules responsible for the electrical activity of the nervous system.

Understanding how the nervous system develops is one of the main challenges for modern neurobiology. Having DNA for receptor molecules also provides a tool for studying such important developmental questions as when receptors begin to be made and which receptors are made at which times during development. In developing muscle cells, for example, a species of acetylcholine receptor is inserted in membranes that is somewhat different from the one found in mature muscles. How and why is this receptor different, and what regulates its expression? Questions like these can be approached in hybridization experiments once receptor DNA is available.

Another group of questions of interest to modern neurobiology relates to the molecular mechanisms of channel function, and answering these questions

depends on sequencing channel DNA. What structural similarities are there between the various channels that permit sodium ions to pass through and excludes potassium ions? The structure of DNA coding for channels can give us the order of amino acids in the channel protein, and this in turn is the first step in relating structure and function.

A third experimental approach involves the manufacture of channel structures that have been modified by specific mutations of the DNA. By techniques similar to those used by McNight and Kingsbury⁴ one could, in principle, systematically alter small protein regions, and study the functional properties of the channel expressed in cultured cells or oocytes.

The Salk Institute group that has cloned the DNA coding for the γ subunit and the Kyoto University group used similar cloning techniques, and both present a sequence that has 5' and 3' non-coding regions and a 5' signal sequence characteristic of membrane proteins.

The structures of the two proteins encoded by the two DNAs are interesting. Protein sequencing data from Hood's laboratory⁵ had already shown that the first 50 or so amino acids in the four different acetylcholine receptor subunits showed strong homologies. The sequences for the α and γ subunits show that homology extends for about the first 150 amino acids and then is no longer evident. Both subunits share a probable site for glycosylation about 140 amino acids from the amino-terminal end. Despite the fact that the bulk of the protein has no apparent direct amino acid homologies, the overall shape predicted for the two polypeptides is remarkably similar: the amino-terminal end, presumed to be on the extracellular side of the membrane, is hydrophilic and is followed — for both subunits — by three hydrophilic sequences of about the same length which presumably loop through the membrane. A hydrophobic region, again possibly membranous, is found just before the carboxy terminus.

Although the overall procedures used by the two laboratories are similar, some differences are instructive. The Salk group used the approach of enriching their mRNA for the desired message, and then screened the cDNA clones by an *in vitro* translation technique. The Kyoto group screened a much larger number of clones with oligonucleotides synthesized from the known amino acid sequence at the amino-terminal end of the protein. This latter technique has the advantage of permitting many more clones to be screened, but the

Charles F. Stevens is in the Department of Physiology, Yale University, New Haven, Connecticut 06510.

1. Noda *et al.* *Nature* **299**, 793 (1982).
2. Ballivet, Patrick, Lee & Heinemann *Proc. natn. Acad. Sci. U.S.A.* **79**, 4466 (1982).
3. Claudio, Ballivet, Patrick & Heinemann *Proc. natn. Acad. Sci. U.S.A.* (in the press).
4. McNight & Kingsbury *Science* **217**, 316 (1982).
5. Rafetery, Huonkapiller, Strader & Hood *Science* **208**, 1454 (1980).
6. Helfman, Feramisco, Fiddes, Thomas & Hughes *Proc. natn. Acad. Sci. U.S.A.* (in the press).

disadvantage of being restricted only to those proteins where a probe sequence is available. It is probable that the use of expression vectors (see for example, ref. 6) will offer a combination of the advantages of the two methods.

Now that the first step has been taken, we can anticipate rapid progress in

contributions by molecular genetics to understanding the organization and functioning of the brain. Quite probably, the first step will come through hybridization experiments that will reveal relationships between channel proteins, and will give us insight into yet another type of order within the nervous system. □

the technology is developed, the search must continue for matrices which permit facile, secure immobilization with good interaction with substrate, and which conform in shape, size and so on to the use for which they are intended. At present all immobilizations are based on considered guesswork which results in a 'hit and miss' type of selection.

Choices must be made whether to immobilize cells by attachment to the surface of the matrix or by entrapment in the matrix. Relevant to this is the problem of molecular size of the substrate — entrapment may be more protective to the cell, but less approachable by the substrate. Entrapment may prevent multiplication of living cells.

In some cases a partial immobilization may be advantageous (as in some of our own work⁷ using hydrous metal oxides as matrix) in which cell density is increased by immobilization, but where the immobilization is reversible under certain conditions, allowing shedding of 'spent' cells as new ones grow. Questions must be asked as to what level of product contamination can be tolerated — after all, as soon as immobilized cells are mentioned, people tend to think of their being used for one enzyme reaction only and forget that cells are living systems which expose more than one type of molecule on the surface to the surrounding milieu and liberate a collection of molecular types and sizes to the surrounding milieu.

It is true that in the early stages of development of a new technology a detailed scrutiny from the viewpoint of economics can prove very discouraging. For immobilized cells to succeed in having a significant impact on certain aspects of our way of life they must either achieve something new and unavailable by other routes, or replace a (more) conventional process by doing it more cheaply. Thus cost considerations must take into account such factors as cell production, matrix type and form, cell immobilization conditions, reactor design, product purification and interactions of the cells with natural tissues. My prophecy for immobilized cell technology is that economic and advantageous processes can be devised but their general industrial adoption will need time and encouragement.

Cheetham and his colleagues have achieved the immobilization of microbial cells with retention of enzyme activity using a very mild technique which involves the formation of gel pellets of alginate in which the cell is in a resting state. The advantages of the use of this very topical support, obtained from seaweed, are not only cheapness, mechanical strength and non-toxicity, but also that the carbohydrate material provides an environment similar to the natural cell-wall polysaccharides produced by the microbial cells. The polysaccharides may assist in the stabilization of the cells.

The development of this system has been

A future for immobilized cell technology

from John F. Kennedy

ENZYMES are nature's catalysts and their ability to catalyse specific reactions under very mild conditions in a highly efficient manner has led to interest in their potential as industrial catalysts. However, enzymes are not always ideal for industrial applications as their instability usually prevents their use in, for example, organic solvents or at high temperatures. One of the major activities in the field of biotechnology over the past fifteen years has been the immobilization of enzymes to provide industrial catalysts that overcome some of these problems.

There have been numerous reports of laboratory-scale preparations of immobilized enzymes but the number of practical industrial systems using such systems has been very limited. Cheetham¹ and his colleagues at Tate and Lyle have just reported in *Nature* (299, 628) the production of a system in which the enzyme was immobilized without previous purification from its natural cell environment and the final catalyst performed under conditions in which the unbound enzyme would not, thereby allowing the development of a pilot-plant scale process which has been tuned to function with high efficiency in the high sugar (sucrose) concentrations required to aid the subsequent recovery of products by evaporation. An added bonus of the system is that the sugar concentration used prevents bacterial contamination of the biocatalyst.

The fundamentals of immobilized enzyme technology have been much discussed²⁻⁴. But what of immobilized cell technology? Is this replacement to be regarded as a repugnant lowering of the standards of purity? Certainly not — immobilized cell in place of immobilized enzyme not only means a shorter and more economic route to producing the immobilized catalyst for a reaction, but opens up a whole vista of additional harnessing and manipulation of biological processes.

Besides asking the basic question: 'Why immobilize cells?', we need to ask ourselves again and again: 'What do we want to achieve by immobilizing cells?' Are we attempting to reproduce processes

normally conducted with free enzymes or free cells, or are we hoping, by using them, to find new processes hitherto undiscovered? In fact, what types of cells do we want to immobilize? Cells with the characteristics, reactions and molecular abilities necessary for the reaction we intend may not exist. Microbial cells⁵ are receiving almost all the attention at the moment simply because they are easily produced and readily multiply in conditions which can be achieved industrially. Plant cell immobilization has made a debut but given some availability of all cell types what will be our future choice, and why? Furthermore, should immobilized cells be 'dead' or alive and able to duplicate?

It seems to me that, because the immobilization of enzymes with retention of activity is a relatively new laboratory technique to which sophisticated chemistry and technology has been and must be addressed, and because the immobilization of cells with retention of cell life is even newer, we are all forgetting that many of the natural life processes depend on at least one of the following: (1) a phase change between substrate and cell — or tissue-bound enzyme (or other macromolecules), (2) interactions of solutes with cell surfaces, and (3) manifestation of chemical reactions by intact cells *per se* rather than release of soluble components from the cell for the purpose of participating in those chemical reactions. Thus, from the general viewpoint many lessons could be learnt from the chemistry of the natural processes of cell immobilization as in the building up of animal and plant tissues. However, such aspects of biological chemistry still need considerable attention and elucidation.

The methods which are used for the actual immobilization processes of cells⁶, as for enzyme immobilization, will necessarily be subjective and of individual choice. Therefore it will not be possible to suggest a universal means of immobilization. One can only say that as

John F. Kennedy is Director of the Research Laboratory for the Chemistry of Bioactive Carbohydrates and Proteins, University of Birmingham, PO Box 363, Birmingham B15 2TT.

taken a stage further than many similar methods by the construction of a pilot-plant scale process and has gone some way to dispel the criticisms of the Spinks report⁸ which concluded that Britain was again failing to take full commercial and industrial advantage of new technologies to which she has contributed so successfully at the primary research level. Not only has a system been reported which has scientific value, but by careful investigation, the industrial production of a naturally occurring disaccharide with great potential as a non-carcinogenic bulking agent for foodstuffs and pharmaceuticals can be realised with very few of the problems of purification and contamination associated with industrial

enzymic methods. It is hoped that this paper will stimulate further investigations into the industrial applications of immobilized cell technology. □

1. Cheetham, P.S.J., Imber, C.E. & Isherwood, J. *Nature* **299**, 628 (1982).
2. Wiseman, A. (ed.) *Handbook of Enzyme Biotechnology* (Ellis Horwood, Chichester, 1975).
3. Trevan, M.D. *Immobilized Enzymes. An Introduction and Applications in Biotechnology* (Wiley, London, 1980).
4. Kennedy, J.F. & Cabral, J.M.S. in *Solid Phase Biochemistry: Analytical and Synthetic Aspects* (ed. Scouten, W.H. (Wiley, New York, in the press).
5. Venkatsubramanian, K. (ed.) *Immobilized Microbial Cells Am. chem. Soc. Symp. Ser.* **106** (1979).
6. Kennedy, J.F. & Cabral, J.M.S. in *Applied Biochemistry and Bioengineering* (eds Wingard, L.B. & Chibata, I. (Academic New York, in the press).
7. Kennedy, J.F., Barker, S.A. & Humphreys, J.D. *Nature* **261**, 242 (1976).
8. *Biotechnology: Report of a Joint Working Party* (HMSO, London, 1980).

Immunoregulation by gamma-interferon?

from Teresa Basham and Thomas C. Merigan

THE potential of interferons as immunoregulatory as well as antiviral and antitumour agents is currently of great interest. With the advent of genetic engineering, pure preparations of biosynthetic interferons are now available for a precise examination of both their effectiveness in clinical trials and their mechanism of action. In this issue of *Nature* (p.833), David Wallach, Marc Fellous and Michel Revel describe a difference between pure recombinant gamma-interferon (IFN- γ) and the other interferons in the induction of the major histocompatibility antigens HLA-A,B,C which they suggest may be related to interferon's immunoregulatory function.

IFN- γ , a lymphokine derived from T lymphocytes, is one of three different types of interferons, each distinguished by protein sequence, antigenicity and physicochemical properties. The other two types are alpha-interferon (IFN- α) from leukocytes and beta-interferon (IFN- β) from fibroblasts. IFN- γ is closely linked to the immune response and can be induced by a wide variety of substances, including mitogens, bacterial and viral antigens, and tumour cells, while IFN- α and IFN- β are induced predominantly by viruses. In addition to antiviral activity, all three have been shown to have cytostatic and immunoregulatory functions, to modify cell structure, membranes and differentiation, and to induce the synthesis of several new proteins¹. The exact mechanism by which the different interferons exert these various activities is not

yet clear, and recent interest has focused on this problem.

Earlier work had shown that in the murine system, impure IFN- γ preparations increased the expression of the histocompatibility antigens (H-2) at doses 100–10,000 times lower than those required using IFN- α (ref. 2), and that IFN- γ is 250 times more potent in immune cell regulation than the other interferons^{3,4}. But these experiments used only partially purified interferons so it was possible the preparations contained other lymphokines. Using purified recombinant IFN- γ Wallach and his colleagues have now confirmed increased potency of IFN- γ in inducing HLA expression. Furthermore, they describe a differential response between the dose of recombinant IFN- γ required for the induction of HLA antigens and the enzyme (2'–5')oligoadenylate synthetase, which inhibits protein synthesis and is related to the antiviral activity of interferon. In contrast, IFN- α and IFN- β induced both of these cellular proteins at the same concentration. Thus Wallach and his associates suggest that the induction of the HLA antigens is not related to the antiviral activity of IFN- γ and that IFN- γ is the most important interferon in immune regulation.

Three recent papers showed that in a variety of cell types, interferon's effect on HLA expression occurs though a corresponding increase in the specific biosynthesis of these antigens^{5,6} and the mRNA pool for the HLA sequences^{6,7}. The optimum dose of interferon required for maximum HLA synthesis and expression varied from one cell line to another. For example, Basham *et al.* found that as low as 50 U ml⁻¹ of IFN- α were sufficient to induce maximum HLA biosynthesis and

expression in human melanoma cell lines sensitive to the antiviral activity of IFN- α but resistant to its antiproliferative action, whereas Burrone *et al.* used 2,000 U ml⁻¹ of IFN- α to induce a similar response in a T-cell line (Molt 4). Therefore, although it is intriguing that IFN- γ can induce HLA expression at a much lower concentration than that required for induction of (2'–5') oligoadenylate synthetase and antiviral activity, it is possible that any or all of these cell surface-related effects vary from one cell line to another, and many well characterized cell lines should be tested before a conclusion is drawn.

The function of the interferon-induced increases in HLA antigens is at present purely speculative but may well be related to cell–cell recognition. The most obvious role is in potentiating the cytotoxic T-cell response of a virally infected host for the elimination of HLA-matched infected cells. Wallach and co-workers suggest that the increase in HLA expression may also protect uninfected host cells from lysis by natural killer cells.

A claim for a role for IFN- γ , rather than the other interferons, in immune regulation would be much stronger if IFN- γ were shown to have a differential effect on the expression of the immune response antigens that are critical in antigen presentation by macrophages to lymphocyte subpopulations. Wallach *et al.* observed no increase in HLA-DR in a human B-cell line (Ramos). In contrast, using different cell types and impure IFN- γ , Sonnenfeld and colleagues² and, more recently, others⁸ found an increase in the human HLA-DR analogue, Ia, on murine cell surfaces. It is possible that Wallach *et al.* missed this effect of IFN- γ on HLA-DR because B-lymphoblastoid cell lines have a higher HLA-DR concentration on their surface initially.

More work on interferon's effects on antigen expression and regulation of the immune response will undoubtedly be done and should eventually clarify their contribution to the biological role of the interferons. □

1. Vilcek, J., Gresser, I. & Merigan, T.C. (eds) *Regulatory Functions of Interferon* (New York Academy of Sciences, New York, 1980).
2. Sonnenfeld, G., Meruelo, D., McDevitt, H.O. & Merigan, T.C. *Cell. Immun.* **57**, 427 (1981).
3. Sonnenfeld, G., Mandel, A.D. & Merigan, T.C. *Cell. Immun.* **34**, 193 (1977).
4. Virelizier, J.L., Chan, E.L. & Allison, A.C. *Clin. exp. Immun.* **30**, 299 (1977).
5. Basham, T.Y., Bourgeade, M.F., Creasey, A.A. & Merigan, T.C. *Proc. natn. Acad. Sci. U.S.A.* **79**, 3265 (1982).
6. Burrone, O.R. & Milstein, C. *EMBO J.* **1**/3, 345 (1982).
7. Fellous, M. *et al. Proc. natn. Acad. Sci. U.S.A.* **79**, 3082 (1982).
8. Steeg, P.S., Moore, R.N., Johnson, H.M. & Oppenheim, J.J. *J. exp. Med.* (in the press).

ADDENDUM

The article 'Glomar Challenger at the Cretaceous-Tertiary boundary' was authored not just by three, but by all 18 of the DSDP leg 86 scientific staff.

Teresa Basham and Thomas C. Merigan are in the Division of Infectious Diseases, Department of Medicine, Stanford University School of Medicine, Stanford, California 94305.

Recent advances in optical bistability

from Y.R. Shen

IN recent years, optical bistability has been a subject of intense research in quantum electronics because of its potential usefulness in optical data processing and all-optical logic and computing systems¹. There has already been a conference on the topic², and at the XIIth International Quantum Electronics Conference held in Munich in June, two sessions were devoted to the subject.

In a system with optical bistability, the relationship of output to input is characterized by hysteresis loops; at a given input, the steady-state output can be either high or low depending on the operation path. These bistable characteristics are the basis of a binary switching element. Indeed, it was earlier predicted and demonstrated that an optical Fabry-Perot (F-P) interferometer filled with a nonlinear medium should exhibit bistability. The principle of the device, including the transient³ and steady-state behaviour¹ and the analogy with the phenomenon of phase transition⁴, is already fairly well understood. The more

recent advances on the subject are mainly in materials and technology.

A most significant advance in the survey of materials for nonlinear F-P interferometers is the discovery of the superiority of the GaAs-GaAlAs superlattice structure⁵. The future applications of optical bistability will require the development of small ($\sim 1 \mu\text{m}$) fast ($\sim \text{ps}$) low-operating-power ($\sim 1 \mu\text{W}$) room-temperature devices. Semiconductors with an excitonic — a positronium-like entity in the solid — line transition appear to be most promising because of their marked nonlinearity and the very low power required to achieve saturation in absorption.

Optical bistability has indeed been demonstrated in a $4.1 \mu\text{m}$ etalon of pure GaAs with an input laser beam at the exciton frequency⁶. Unfortunately, excitons in GaAs dissociate above 120K, while at low temperatures, the bistable switching time is long ($\sim \mu\text{s}$). But recently it has been found that GaAs-Ga_xAl_{1-x} As superlattices grown by molecular beam

epitaxy can have a larger exciton-binding energy than that of pure GaAs because of the quantum-well effect. As a result, excitons can exist in a superlattice even at room temperature. The power required for saturation of the exciton transition at room temperature is also three times less than that for pure GaAs.

These features point towards the possible construction of a small efficient optical bistable device. Indeed, on a $2 \mu\text{m}$ -thick etalon of GaAs (335 \AA)-Ga_{0.73}Al_{0.27}As (401 \AA) superlattice at room temperature, optical bistability can be observed with an $\sim 100 \text{ mW}$ laser at the exciton frequency. The switching time is around 20–40 ns. Further improvement can probably be made by using thinner layers in the superlattice structure.

Y.R. Shen is at the Department of Physics, University of California, Berkeley, and the Materials and Molecular Research Division, Lawrence Berkeley Laboratory, Berkeley, California 94720.



100 Years ago

LETTERS TO THE EDITOR

The Editor does not hold himself responsible for opinions expressed by his correspondents. Neither can he undertake to return or to correspond with the writers of, rejected manuscripts. No notice is taken of anonymous communications.

The Editor urgently requests correspondents to keep their letters as short as possible. The pressure on his space is so great that it is impossible otherwise to ensure the appearance even of communications containing interesting and novel facts.

The Comet

I ENCLOSE a drawing made this morning after a prolonged examination (with a binocular) of the end of the comet's tail. Should you think the peculiar features which I have endeavoured to portray of sufficient interest to reproduce, the drawing is at your service. It is difficult to indicate truly features of this kind without exaggeration, if they are to catch the eye at all; but I am sure the exaggeration is very slight. The tail would seem to be about to end rather suddenly and with a broad end, when, from near the middle, shoots out, at a slight inclination to the general direction of the tail, a cleanly-shaded wisp.

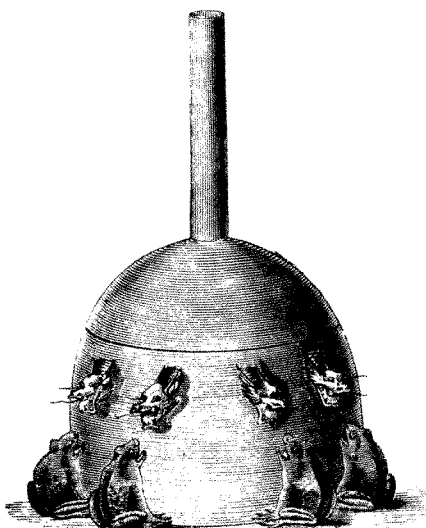
It is surely unusual for such decided features

to present themselves at the very end of a comet's tail.

As a whole, the comet seems to have changed wonderfully little during the three weeks since I first saw it. Its change of place, also, is so moderate that, at this rate, there seems no reason why we should not see it for months yet. What if it should not vanish at all!

J. HERSHCEL

Collingwood, October 23



In a Chinese history called "Gokanjo", we find the following: "In the first year of Yoka (A.D. 136) a Chinese called Chioko invented a seismometer. This instrument consists of a spherically formed copper vessel (Fig. 1), its diameter being 8 'shaku.' It is covered at its top. Its form resembles a wine bottle. Its outer part is ornamented with the figures of different kinds of birds and animals and old peculiar looking letters. In the inner part of this instrument a pillar is so placed that it can move in

eight directions. Also in the inside of this bottle there is an arrangement by which some record of an earthquake is made according to the movement of the pillar. On the outside of the bottle there are eight dragon heads, each of which contains a ball. Underneath these heads there are eight frogs, so placed that they appear to watch the dragon's face, so that they are ready to receive the ball if it should be dropped. All the arrangements which cause the pillars when it moves to knock the ball out of the dragon's mouth are well hidden in the bottle. When an earthquake occurs and the bottle is shaken, the dragon instantly drops the ball, and the frog which receives it vibrates vigorously. Any one watching this instrument can easily observe earthquakes. With this arrangement, although one dragon may drop a ball, it is not necessary for the other seven dragons to drop their balls unless the movement has been in all directions; thus one can easily tell the direction of an earthquake. Once upon a time a dragon dropped its ball without any earthquake, and the people therefore thought that this instrument was of no use, but after two or three days a notice came saying that an earthquake had taken place in Rosei. Hearing of this, those who did not believe about the use of this instrument began to believe in it again. After this ingenious instrument had been invented by Chioko, the Chinese Government wisely appointed a secretary to make observations on earthquakes."

We have here I think not only an account of an earthquake instrument which in principle is identical with many of our modern inventions, but the science has been conjoined with art. The record of the Chinese Government establishing a seismological bureau at a time when America was unknown, and half of Western Europe were living in the woods, is also interesting.

From *Nature* 26, 627; October 26, 1882.

Hitherto, the ray approximation has usually been used in the analysis of optical transmission in the nonlinear F-P interferometer. Because, on this view, different sections of the beam act independently in transmitting through the interferometer, if the beam has a gaussian profile, the switch-up and switch-down intensities would vary with radial position in the beam. But in reality, even in a medium with purely local response, different parts of the beam are coupled through diffraction, most markedly in F-P cavities with large Fresnel numbers. Moreover, the intensity-dependent transverse variation of the induced refractive index can distort the wavefront and lead to self-focusing or defocusing of the beam. Two papers have recently addressed the problem, and have shown by numerical calculation that strong coupling can result in a cooperative switch-up of practically the whole beam, and also in a much faster switching speed. The strong wavefront distortion can also give rise to an output with a multiple-ring pattern.

As a device with positive feedback, the stationary response of a bi-stable optical system may become unstable, leading to periodic oscillation, bifurcation and chaos — a subject of great current interest to many scientists in different disciplines.

Ikeda has recently spelled out, with some help of numerical calculations, the detailed conditions for the instability⁸. Although his theory uses the model of a ring cavity, the results should also apply, at least qualitatively, to the F-P interferometer. Instability, bifurcation and chaos have actually been observed in a F-P interferometer with electronic feed-back controlling the non-linearity of the medium⁹. The experimental results are most useful as a test of the theory of chaos. Chaotic output from an all-optical nonlinear F-P interferometer would be even more interesting, but has not yet been realized. □

1. Gibbs, H.M., McCall, S.L. & Venkatesan, T.N.C. *Opt. Engng* **19**, 463 (1980); Smith, S.D. & Miller, D.A.B. *New Sci.* **85**, 554 (1980); Smith, P.W. & Tomlinson, W.J. *IEEE Spectrum* **18**, 26 (1981).
2. *Optical Bistability* (eds Bowden, C.M., Ciftan, M. & Robl, H.R.) (Plenum, New York, 1981); *IEEE J. Quantum Electron.* **QE-17** (3) (1981).
3. Bischofberger, T. & Shen, Y.R. *Phys. Rev.* **A19**, 1169 (1979).
4. Bonifacio, R. & Lugiato, L.A. in *Pattern Formation by Dynamic Systems and Pattern Recognition* (ed. Haken, H.) (Springer, Berlin, 1979).
5. Gibbs, H.M. *et al. Appl. Phys. Lett.* **41**, 221 (1982); Miller, D.A.B. *et al. Pap. XIIth IQEC* (Munich, 1982).
6. Gibbs, H.M. *et al. Appl. Phys. Lett.* **35**, 451 (1979).
7. Rosanov, N.N. & Semenov, V.E. *Opt. Commun.* **38**, 435 (1981); Moloney, J.V. & Gibbs, H.M. *Phys. Rev. Lett.* **48**, 1607 (1982).
8. Ikeda, K., Daido, H. & Akimoto, O. *Phys. Rev. Lett.* **45**, 709 (1980); **48**, 617 (1982).
9. Gibbs, H.M. *et al. Phys. Rev. Lett.* **46**, 474 (1981).

Snail shells suggest past changes in British chalk vegetation

from Peter D. Moore

IN view of the large proportion of southern Britain lying on chalky substrate and the amount of research effort expended on reconstructing the environmental history of the British Isles, it is surprising that so little is known about changes in the vegetation of the chalk over the past few thousand years. One reason is the scarcity of wetland sites in which lake sediments or peats could have accumulated and which could be suitable for palynological analysis. This is due in part to the pervious nature of the substrate and intense land use. Such palynological data as do exist come mainly, in fact, from sites adjacent to, rather than on, the chalk, suggesting that these calcareous areas were once forested and lost their woodland cover during prehistoric times¹⁻³.

Analyses of plant remains from archaeological sites^{4,5} have provided detailed information concerning crop plants and weed species, and deposits in coombes at the foot of scarp slopes have been analysed for information on phases of erosion^{6,7}.

These sites have proved particularly informative when they contain charcoal fragments which can be carbon-14 dated — for example, the samples at Pitstone, Buckinghamshire dated at 3,910 BP by Valentine and Dalrymple⁸ indicated forest clearance in late Neolithic or early Bronze Age times.

Pollen does not normally survive in calcareous soils, but mollusc shells do and have been used extensively as environmental indicators⁹. For example, Evans¹⁰ has described the snail shells preserved in deposits adjacent to the Pitstone site and shown the replacement of woodland species by open, disturbed habitat species such as *Pomatias elegans*, thus confirming the pedological evidence for forest clearance.

A rather similar sequence has recently been investigated by Burleigh and Kerney¹¹ from the valley below a chalk escarpment at Brook, Kent, which is of particular interest because of its late-glacial sediments¹². As at the Pitstone site, the lower layers are rich in forest species, and then disturbance indicators, including *Pomatias elegans*, become gradually more abundant. In the layers where the transition takes place Neolithic flakes were found and a ¹⁴C date of 4,540 BP was

obtained from charcoal fragments, thus confirming the role of man in the deforestation process.

Burleigh and Kerney attempt to draw some palaeoclimatic conclusions from their snail shells. They find, for example, that the Neolithic *P. elegans* shells were generally larger than those of the present day, having a shell height of 12–18 mm (45 per cent of the population greater than 15 mm) in comparison with living snails which show a range of 11–15 mm. They state that shells higher than 15 mm are rather uncommon in Britain at the present time, although there are records of current populations with 7 per cent of individuals greater than 15 mm and occasional shells over 16 mm (ref. 13). Clearly, however, the Neolithic shells were generally larger than modern ones and Burleigh and Kerney associate the decline in shell size with falling temperature since the climatic optimum. *P. elegans* is a species with a southerly distribution in Britain and has contracted in its ranges since Atlantic times¹⁴.

They also note that 28 per cent of their fossil population of *Cepaea nemoralis* shells lacked banding, whereas only 4.3 per cent of modern *C. nemoralis* are found without bands. Currey and Cain¹⁵ considered that unbanded specimens are favoured by higher temperatures and Jones *et al.*¹⁵ have examined this idea closely and find that unbanded morphs of *C. nemoralis* are more frequent in the Mediterranean areas than in northern Europe. This can be explained in ecological/energetic terms, since unbanded morphs are unlikely to overheat in conditions of high insolation, whereas heavily banded morphs will absorb more radiation, which may be of advantage in cold conditions. On a local scale, other factors, such as predation, influence the balance of the polymorphism, so attempts to use such evidence in palaeoecological reconstructions must be cautious. Coupled with the evidence from *P. elegans*, however, Burleigh and Kerney are able to present a strong case that temperatures were warmer during the Neolithic than at present in this part of Britain.

A final point of interest in Burleigh and Kerney's studies is the use of snail shells as material for radio carbon dating. Normally such shells are avoided because old carbon

1. Thorley A. in *Guide to Sussex Excursions* (ed. Williams, R.B.G.) 47 (IBG Conf., 1971).
2. Godwin, H. *Veroff. Geobot. Inst. Rübel Zurich* **37**, 83 (1962).
3. Brookes, A. Unpublished data from Wellingham, Sussex.
4. Allison, J. & Godwin, H. *New Phytol.* **48**, 253 (1949).
5. Conolly, A.P. *New Phytol.* **40**, 299 (1941).
6. Sparks, B.W. *Geol. Mag.* **89**, 163 (1952).
7. Sparks, B.W. & Lewis, W.V. *Proc. geol. Ass.* **68**, 26 (1957).
8. Vakhtine, K.W.G. & Dalrymple, J.B. *J. Soil Sci.* **27**, 541 (1976).
9. Evans, J.G. *Land Snails in Archaeology* (Seminar, London, 1972).
10. Evans, J.G. *Proc. geol. Ass.* **77**, 347 (1966).
11. Burleigh, R. & Kerney, M.P. *J. archaeol. Sci.* **9**, 29 (1982).
12. Kerney, M.P., Brown, E.H. & Chandler, T.J. *Phil. Trans. R. Soc. B248*, 135 (1964).
13. Moore, C.D. Unpublished data from Shoreham, Kent.
14. Kerney, M.P. *J. Conchology* **27**, 359 (1972).
15. Jones, J.S., Leith, B.H. & Rawlings, P. A. *Rev. Ecol. System.* **8**, 109 (1977).

may have become incorporated into them from the carbonate-rich environment either before or after the death of the animal. Having charcoal fragments, which are regarded as reliable material for dating, found in the same sediments as the shells provided an opportunity to examine their reliability in this respect. Dates from both

Pomatias and *Cepaea* shells were about 400–500 years older than those given by the charcoal. The older date is to be expected and an error of only about 10 per cent is surprisingly small. Although one must still be cautious, this is encouraging since for many studies this order of error is acceptable. □

Chromosome rearrangements in gonococcal pathogenicity

from J.R. Saunders

A STRIKING feature of *Neisseria gonorrhoeae*, the causative agent of gonorrhoea, is its ability to undergo substantial alteration in cell-surface characteristics during both natural infections and laboratory subculture. The most obvious of these changes is the reversible loss of ability to produce pili which confer adhesiveness and increased resistance to host defences^{1,2}. In a recent issue of *Cell*, Thomas Meyer and his colleagues³ show that the expression of pili is determined by rearrangements of the gonococcal genome. *N. gonorrhoeae* thus joins a number of pathogens, including *Salmonella typhimurium*^{4,5} and African trypanosomes^{6,7}, where moveable genetic elements affect the expression of surface antigens.

Single clinical isolates of *N. gonorrhoeae* exhibit several distinct colonial types when grown on the surface of clear agar media^{8–11}. Fresh isolates are invariably of the piliated (P^+) type. During subculture P^+ forms can give rise to non-piliated (P^-) forms and vice versa but after prolonged growth *in vitro* the P^- forms predominate. This suggests that the human host exerts considerable selective pressure on the gonococcus to produce pili.

Gonococcal colonies also vary in opacity, being either opaque (O^+) or translucent (O^-). Opacity is determined by the presence of a family of outer membrane proteins (protein II) that are associated with alterations in the adhesive and antigenic properties of the bacteria^{9,10}. Variation between O^+ and O^- colonial forms occurs reversibly in a similar way to pilus expression.

There is considerable variation in the physical and antigenic properties of pili in different strains of *N. gonorrhoeae*^{12,13}, and even in derivatives of the same strain^{16–18}. For example, variants of *N. gonorrhoeae* strain P9 produce four types of pili- α , β , γ and δ — of subunit molecular weights 19,500, 20,500, 21,000 and 18,500 respectively^{17,18}. The four pilus variants show little antigenic cross-

reactivity and have differential adhesiveness for a number of animal cell types¹⁹. However, they possess similar amino acid compositions and have a number of major peptides in common²⁰. It seems that the first 100 amino acids on the N-terminal end of pilus subunits are conserved among serologically distinct gonococcal pili whereas the C-terminal ends of the proteins are variable^{14,15}.

Variation in the type of pilus and in outer membrane composition may be important in permitting the gonococcus to colonize different sites on the human host during the course of natural infections. Inter- and intra-strain variability would also help a pathogen to avoid host defences.

Analysis of the genetic control of pilus and outer membrane expression in the gonococcus has been hampered by the relative difficulty of performing conventional genetics with a pathogen that exhibits such variation in natural phenotype. Nonetheless, the pilus gene from strain MS11 (ref.3) and the α -pilin gene from strain P9 (ref.21) have recently been cloned in *Escherichia coli*. The gonococcal pilin genes are expressed in *E. coli*, but no mature pili can be detected on the surface of this host^{3,21}. This is perhaps not surprising since several genes are known to be required for pilus production and assembly of other types of pili, for example K88 (ref.22). Even if all the required genes were cloned it is still possible that *E. coli* would be unable to process and insert the pilin molecules into the cell envelope to form an intact pilus.

This cloning of pilus genes has provided probes for the investigation of the molecular switching events involved in alterations in virulence of the gonococcus. Thus Meyer *et al.*³ have used the cloned pilin gene from strain MS11 as a probe in Southern hybridizations of restriction endonuclease-cleaved chromosomal DNA from various derivatives of this strain and shown that the conversion from piliated (P^+O^+ or P^+O^-) to non-piliated (P^-O^+ or P^-O^-) form is accompanied by a chromosomal rearrangement (presumably in the pilus region) of the gonococcal genome. Apparently, the same rearrangement is found after conversion

from P^+O^- to P^+O^+ . It is not yet clear, however, whether this rearrangement actually represents control of both pilus and protein II synthesis by the same genetic element or merely results from a coincidental change in the type of pilus synthesized in this particular experiment. Certainly piliation and opacity characteristics can vary independently^{23,24}. Confirmation or denial of a common controlling element will depend on the use, when it becomes available, of cloned DNA encoding protein II. The hybridizations performed by Meyer *et al.* also indicate that the chromosome of *N. gonorrhoeae* MS11 contains multiple copies of the pilin gene or at least of the constant region (encoding the first 100 amino acids) of that determinant, reflecting the importance of pili to the organism.

The rearrangements of the gonococcal chromosome appear similar to those mediating antigenic phase variation in the flagella of *Salmonella typhimurium*^{4,5}. In this case, a 970-base pair DNA segment containing a promoter for the flagella gene can invert reversibly by site-specific recombination at the ends of the segment. Movement of non-expressing surface antigen genes to new expressing sites also explains antigenic variability in trypanosomes and the ways in which these parasites can evade the host immune response^{6,7}.

The gonococcus apparently possesses both an on-off switch for pilus production and a means of altering the protein composition of the pili it produces. A similar switching system seems to control protein II production. The simplest explanation for these changes would

1. Buchanan, T.M. in *The Gonococcus* (ed. Roberts, R.B.) 255 (Wiley, New York, 1977).
2. Ofek, I., Beachy, E.H. & Bisno, A.L. *J. infect. Dis.* 129, 310 (1974).
3. Meyer, T.M., Mlawer, N. & So, M. *Cell* 30, 45 (1982).
4. Zieg, J., Silverman, M., Hilmen, M. & Simon, M. *Science* 196, 170 (1977).
5. Zieg, J. & Simon, M. *Proc. natn. Acad. Sci. U.S.A.* 77, 4196 (1980).
6. Williams, R.O., Young, J.R. & Majewa, P.A.O. *Nature* 282, 847 (1979).
7. Koejmakers, J.H.J. *et al. Nature* 284, 78 (1980).
8. Kellogg, D.S. *et al. J. Bact.* 85, 1274 (1963).
9. Swanson, J. *Infect. Immun.* 19, 320 (1978).
10. Lambden, P.R., Heckels, J.E., James, L.T. & Watt, P.J. *Gen. Microbiol.* 114, 305 (1979).
11. Penn, C.W., Veale, D.R. & Smith, H. *J. gen. Microbiol.* 100, 147, (1977).
12. Brinton, C.C. *et al. in Immunobiology of Neisseria gonorrhoeae* (ed. Brooks, G.F.) 155 (American Society for General Microbiology, Washington).
13. Buchanan, T.M. *J. exp. Med.* 141, 1470 (1975).
14. Hermodson, M.A., Chen, K.C.S. & Buchanan, T.M. *Biochemistry* 17, 442 (1978).
15. Chen, K.C.S. Cited in ref. 3.
16. Salit, I.E., Blake, M. & Gotschlich, E.C. *J. exp. Med.* 151, 716 (1980).
17. Lambden, P.R., Robertson, J.N. & Watt, P.J. *J. Bact.* 141, 393 (1980).
18. Lambden, P.R., Heckels, J.E., McBride, H. & Watt, P.J. *FEMS microbiol. Lett.* 10, 339 (1981).
19. Heckels, J.E. in *Microbiology 1982* (ed. Schlesinger, J.) (American Society for Microbiology, Washington, in the press).
20. Lambden, P.R. *J. gen. Microbiol.* 128, 2105 (1982).
21. Heighway, J., Graeme-Cook, K.G., Heckels, J.E. & Saunders, J.R. (in preparation).
22. Mooi, F.R., De Graaf, F.K. & van Embden, J.D.A. *Nucleic Acids Res.* 3, 849 (1979).
23. Meyer, L.W. *Infect. Immun.* 37, 481 (1982).
24. Norlander, L., Davies, J., Norqvist, A. & Normark, S. *J. Bact.* 138, 762 (1979).

J.R. Saunders is in the Department of Microbiology, The University of Liverpool, PO Box 147, Liverpool L69 3BX.

involve some sort of transposable genetic element capable on the one hand of allowing or preventing pilus synthesis and on the other of altering the quality of the pilin produced (presumably by altering only the C-terminal end of the pilus protein). It is intriguing that a set of equal-sized (160 base pair) *Hae*III restriction fragments can be detected both within and adjacent to the pilus-coding region of the MS11 genome. Whether these are part of some invertible sequence controlling pilus

expression remains to be seen. It is also unclear whether post-translational modification of envelope components has any role in mediating the changes in gonococcal surface properties.

Nevertheless, the observation that chromosome rearrangements can affect virulence is a very important step towards understanding the extremely complex genetic and phenotypic interactions between this important pathogen and its human host. □

Bacterial toxins and cyclic AMP

from Simon van Heyningen

It has been known for several years that cholera toxin and the very similar protein toxin of some strains of *Escherichia coli* enter intoxicated cells and activate the intracellular adenylate cyclase that catalyses the formation of cyclic AMP from ATP. In cholera patients, this increase in cyclic AMP in gut cells is the chief cause of the massive diarrhoea that is characteristic of the disease. Several recent papers have shown that other toxins also increase the cyclic AMP concentration. In view of the demonstrated connection between adenylate cyclase and cholera, it is surprising that, until recently, little attention had been given to the possibility that the soluble adenylate cyclases secreted by a number of bacteria play a role in virulence. (These cyclases differ from the mammalian enzymes in that they are more active, soluble, heat stable and are not usually regulated by guanine nucleotides.)

A picture is now emerging, however, as a result of recent work, particularly that by Leppla¹, on the toxins of *Bacillus anthracis* which causes anthrax. Three different proteins produced by this organism can be purified: protective antigen (PA or factor II), lethal factor (LF or factor III) and oedema factor (EF factor I). None of these has much biological effect by itself, but combinations of PA with either of the others do: PA and EF produce a skin oedema, and PA and LF are lethal.

Leppla guessed that EF might have a similar action to that of cholera toxin because it has similar effects on vascular permeability in rabbit skin and on the morphology of Chinese Hamster Ovary (CHO) cells. Accordingly, he showed that PA and EF together greatly increased the cyclic AMP concentration in CHO and other cultured cells — however this was not due to increased activity of the adenylate cyclase in the cells, but to enzymatic

activity of EF itself. When EF was tested *in vitro*, it was found to be a highly active cyclase, but only in the presence of a CHO cell lysate. The lysate could be replaced by calmodulin (known to be an activator of many adenylate cyclases) and the activity of the enzyme varied with calcium ion concentration in a manner characteristic of calmodulin-dependent systems. In whole cells, EF was active only in the presence of PA which presumably functions in some way to aid EF entry into the cell. (It must also have this function with the other protein toxin, LF, which is not a cyclase.) EF was thus the first example of a bacterial cyclase that enters eukaryotic cells and is activated by a eukaryotic protein. The relevance of all this to anthrax is not clear — the mixture of PA and LF has generally been thought to be the lethal agent, and they may mask the effects of adenylate cyclase during the disease.

Bacillus anthracis is not the only pathogen that secretes adenylate cyclase. *Bordetella pertussis*, responsible for whooping cough, also produces a highly active adenylate cyclase that is heat stable and stimulated by calmodulin². Confer and Eaton³ have shown that this enzyme can be taken up by phagocytic cells and generate cyclic AMP. Human neutrophils incubated with extracts from *Bordetella* prepared by urea extraction followed by dialysis showed a striking increase in intracellular cyclic AMP concentration, and the cyclase activity in the cells was heat stable, showing that it must have come from the bacterium. How it got into the cells is not clear — purified bacterial cyclase is very active but only with broken cells. A temperature-dependent process is involved, as well as other factors secreted by *Bordetella* (perhaps analogous to the PA of anthrax toxin).

What is the function of the increase in cyclic AMP? It is possible it is used by the invading bacteria to suppress many of the normal functions of phagocytes, including bacterial killing, and so allow the bacteria

to survive longer in a hostile environment. It may also explain the impaired host defence, for example the absence of fever and frequent secondary bacterial pneumonias, found in whooping cough.

Toxin production by *Bordetella pertussis* is complicated and confusing. As well as the extracellular cyclase, the bacterium secretes as many as twenty other antigens. One of these, known as 'pertussis toxin', or islet-activating protein, because there is good evidence that it causes the main harmful effects of whooping cough, has many biological effects, such as potentiation of the immune response, induction of lymphocytosis and sensitization to histamine, which may also be due to an increase in cyclic AMP. However the toxin itself is not a cyclase — it works, like cholera toxin, by activating the cyclase of the intoxicated cell. ATP and NAD⁺ are required in broken cell preparations and, like cholera and diphtheria toxins, pertussis toxin catalyses the transfer of ADP-ribose from NAD⁺ to a receptor protein⁴. This receptor protein has a molecular weight of 41,000 and is presumably part of the adenylate cyclase complex, but it is not the same protein as the one ADP-ribosylated by cholera toxin. Thus *Bordetella pertussis* secretes both an adenylate cyclase of its own and a protein that activates another cyclase. Perhaps the 'toxin' is responsible for the overt symptoms of disease and the cyclase for the ability of the bacteria to survive.

It is remarkable that bacteria can produce proteins that have such similar properties to eukaryotic cyclases and that can be activated by a eukaryotic protein — calmodulin — which is not known to occur in bacteria. It suggests the proteins might have originated in some eukaryotic cyclase which the bacteria have picked up during the course of their evolution.

The same suggestion has been made of the toxins that catalyse ADP-ribosylation. Some recent work suggests that the hormone thyrotropin can increase ADP-ribosylation of several proteins, including the substrate of cholera toxin, in thyroid cell membranes at the same time as adenylate cyclase activity⁵. It seems that the hormone does not catalyse the reaction directly, but increases the activity of endogenous ADP-ribosyl transferases which are known to be present and are presumably part of the normal control process. Cholera, pertussis and other opportunistic toxins are thus subverting this process to their own ends. Since cholera and pertussis toxins ADP-ribosylated different proteins, the system must be a very complicated one. □

Simon van Heyningen is at the Department of Biochemistry, University of Edinburgh Medical School, Edinburgh EH8 9XD.

1. Leppla, S.H. *Proc. natn. Acad. Sci. U.S.A.* **79**, 3162 (1982).
2. Greenlee, D.V., Andreassen, T.J. & Storm, D.R. *Biochemistry* **21**, 2759 (1982).
3. Confer, D.L. & Eaton, J.W. *Science* **217**, 948 (1982).
4. Katada, T. & Ui, M. *Proc. natn. Acad. Sci. U.S.A.* **79**, 3129 (1982); *J. biol. Chem.* **257**, 7219 (1982).
5. Vitti, P., De Wolf, M.J.S., Acquaviva, A.M., Epstein, M. & Kohn, L.D. *Proc. natn. Acad. Sci. U.S.A.* **79**, 1525 (1982).

REVIEW ARTICLE

Hot galactic gas and narrow line quasar absorption systems

T. W. Hartquist & M. A. J. Snijders

Department of Physics and Astronomy, University College London, London WC1E 6BT, UK

Observations of the hot interstellar gas ($T \gg 10^4$ K) are numerous and imply that the temperatures of substantial amounts of the disk gas to be $2-3 \times 10^5$ K and of the halo gas to be 8×10^4 K, but the theoretical models to explain the properties of both the disk and the halo hot gas seem to be in need of some refinement. Observations of the quasar narrow line absorption features suggest that they arise in gas with properties very similar to those of the galactic coronal gas.

WITHIN the past decade the Copernicus and IUE satellites have made possible the detailed study of the hot interstellar gas ($T \gg 10^4$ K) in the galactic disk and in the galactic halo. Additional observations have been made, using rockets, satellites, and manned spacecraft, of soft X-ray and EUV emission in the Galaxy. It is generally believed that some of these soft X rays are emitted by the hot interstellar gas. We now review the UV and soft X-ray observations and argue that the UV data imply that the hot interstellar gas has a very low thermal pressure whereas the soft X-ray data imply a very high pressure. We discuss existing models of the hot disk interstellar gas concluding that the UV and soft X-ray observations are difficult to explain.

The temperature of the observed halo corona gas appears to be considerably lower than that in the disk and to be remarkably uniform. Although models of the halo gas have been published, only recently have any of them been designed to explain the uniform temperature of the halo gas.

The most important consequence of the galactic observations is that they seem to indicate that the temperature of the hot disk gas is $\sim 2-3 \times 10^5$ K and the temperature of the hot halo gas is $\sim 8 \times 10^4$ K. These temperatures are far lower than the value of 10^6 K which has been accepted since 1956 when Spitzer¹ reported on the galactic corona which he postulated to explain the stability of high latitude clouds. Note that Spitzer presented isothermal models of the corona for temperatures ranging over two orders of magnitude and that he discussed the diagnostic utility of absorption features of ions which would be abundant at temperatures below 8×10^4 K to $\sim 10^6$ K. The value 10^6 K seems to have become established because Spitzer quoted the sound speed, the density, and the total mass of his model for 10^6 K apparently just to give some idea of the magnitudes of the physical quantities he was discussing; Spitzer did not argue in any way that $T \approx 10^6$ K.

Many of the ions abundant in the galactic coronal gas are abundant in the narrow line quasar absorption systems. We compare the observational properties of the galactic corona with these systems.

Observations of the hot disk gas

UV absorption observations of several moderately ionized species yield information about the physical conditions in the corona. Table 1 lists several important species, the wavelengths of their absorption features, and the temperatures at which, in the steady state coronal approximation, they reach their maximum concentrations. In Fig. 1 the fractional abundance of these species is plotted as a function of temperature in the steady state coronal approximation. Al^{2+} lies in gas which is not in ionization equilibrium² and is not included in Fig. 1. The silicon results are from Baliunas and Butler³ who were the first to include several important charge transfer processes, and the

C^+ , N^{4+} , and O^{5+} results are those of Shapiro and Moore⁴. We adopted the cosmic abundances given by Allen⁵.

Interstellar O VI was detected⁶⁻⁸ in the directions of several early type stars indicating the presence of interstellar gas at temperatures in excess of 10^5 K. Castor *et al.*⁹ and Weaver *et al.*¹⁰ suggested that the O VI absorption could arise in conduction fronts at the interfaces between shocked interstellar material and stellar winds driving the supersonic expansion of cavities or bubbles around the early type stars towards which the observations were made. However, Jenkins¹¹ has shown that the O VI is not an artefact of the wind-interstellar medium interaction by performing a statistical analysis to find that the column densities of O VI observed against stars of varying distances is in accord with the existence of randomly distributed cells of hot gas having O VI column densities of 10^{13} cm^{-2} . The average spatial number density of O VI is $\sim 2.8 \times 10^{-8} \text{ cm}^{-3}$.

York^{7,12} reported the first detection of interstellar N V, which arises in the same regions as O VI. Towards β Cen and α Ori he found that the N V to O VI abundance ratio was ~ 0.1 while towards HD28497 and μ Col the upper bounds on the ratio were roughly this value. Figure 1 shows that the temperature of the gas would have to be $\leq 3 \times 10^5$ K to be consistent with his results. Smith and Hartquist¹³ published observations of N V in the galactic disk gas towards eight Wolf-Rayet stars which, because of their extremely dense winds, have exceptionally strong broad emission features against which to detect interstellar absorption. Because some of the stars in their study are as much as 3 kpc away the derived average number density

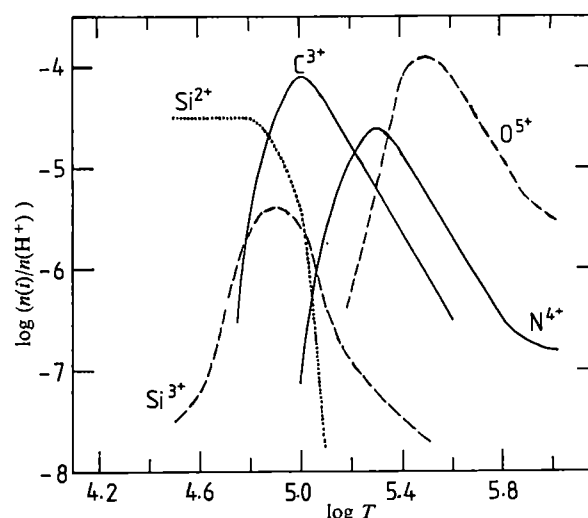


Fig. 1 The fractional abundance of several ionized species as a function of temperature.

of $6-7 \times 10^{-9} \text{ cm}^{-3}$ results from sampling the physical conditions in a large amount of gas. Their results and that of Jenkins¹¹ for the average number density of O VI give $\log T \approx 5.4$. A temperature in this range is also required to explain the narrowness of many of the O VI features¹¹ discussed above. Bruhweiler *et al.*¹⁴ found N V along the line of sight to AO Cas, one of the most distant stars in their sample; the average line of sight density of N^{4+} was comparable with that found by Smith and Hartquist. Bruhweiler *et al.* obtained upper limits for N V in the other directions by assuming that their detection limit was 50 mÅ in all directions. If this limit is correct for the other three most distant stars in their sample the gas in those directions would have to have temperatures higher than that in the AO Cas direction. Black *et al.*¹⁵ and Cowie *et al.*¹⁶ saw N V absorption in about a quarter of the directions in which they looked. The results in these directions too are in harmony with those reported by Smith and Hartquist and the upper limits in the other directions are not very stringent.

From the N V to O VI ratio one can conclude that the temperature of the hot interstellar gas lies in the range $\log T = 5.4 \pm 0.1$. Calculations by Shapiro and Moore⁴ of the N V to O VI ratio in cooling gas indicate that this conclusion is independent of the history of the gas. At $\log T = 5.4$, $\log(n(\text{O}^{5+})/n(\text{H}^+)) = -4.3$ and the product of the hot phase's thermal pressure and its filling factor is $\sim 30 k \text{ erg cm}^{-3}$ where k is Boltzmann's constant. Even if the filling factor of the hot gas is as low as 0.2 (ref. 11) its thermal pressure is an order of magnitude below that of the 'standard' H I clouds¹⁷. Either only H I clouds in high-pressure regions are detected or the H I clouds are confined by some other source of pressure. Turbulent pressure is unlikely to be great enough in the hot phase as the turbulence would have to be supersonic and would dissipate rapidly. Perhaps H I clouds are confined by magnetic pressure¹⁸. As is known from attempts to confine laboratory plasmas¹⁹ the clouds can be confined by field pressure only if the configuration is not subject to the interchange instability²⁰. If some H I clouds are contained by magnetic pressure, they may form initially by thermal instability and collapse along the field lines to a density of $\sim 1 \text{ cm}^{-3}$ and a temperature of around 10^2 K . Draine²¹ has argued that the thermal pressure can be enhanced relative to the magnetic pressure in interstellar material with these physical conditions by the passage of a hydromagnetic shock in which ambipolar diffusion (the motion of the ions, which couple directly to the magnetic field, relative to the neutral particles which are not well coupled to the ions and the magnetic field) occurs.

When O VI lines were first detected it was hoped that measurements of C IV and Si IV might help diagnose the conditions in the hot gas^{6,7}, but much of the C IV and Si IV detected in the disk^{14-16,22} is apparently formed by photoionization in normal H II regions^{15,16}. As shown in Fig. 1 the concentrations of interstellar C IV and Si IV will be far lower than that of N V at temperatures above $2 \times 10^5 \text{ K}$. Black *et al.*¹⁵ and Laurent *et al.*²³ reported the detection of collisionally ionized gas with C IV and Si IV towards the Carina Nebula and Smith *et al.*²² reported similar detections in several other directions in which the intervening gas appears to be disturbed. Cowie *et al.*¹⁶ probably found collisionally ionized gas towards two distant disk stars with an average spatial density of $2 \times 10^{-9} \text{ cm}^{-3}$ for C^{3+} . If C^{3+} has such a large spatial density, it is roughly one-tenth as abundant as O^{5+} . Figure 1 shows that these two abundances can be in that ratio only in a very narrow temperature range around $T = 10^{5.35} \text{ K}$ if the gas is in steady state collisional equilibrium.

The existence of hot interstellar gas has been invoked to explain the origin of the soft X-ray and EUV background^{24-30,93}. Rosner *et al.*²⁶ have argued that much of the flux between 0.28 and 1 keV is produced by M-dwarf stars, and Levine *et al.*²⁷ list known supernova remnants which are localized sources contributing substantially to the soft X-ray and EUV backgrounds. The 0.15–0.28 keV background apparently is not of stellar origin²⁶. From observations between 90 and 140 eV

Levine *et al.*⁹³ concluded that the gas producing soft X rays has a temperature in excess of $6 \times 10^5 \text{ K}$, while Cash *et al.*²⁸ used similar arguments to conclude that the gas must be at temperatures below $3 \times 10^5 \text{ K}$ to produce the high flux at the very longest wavelengths, first observed by Yentis *et al.*²⁹. Interpretation of EUV data obtained from the Apollo-Soyuz mission³⁰ seems to confirm the result of Cash *et al.*²⁸. A temperature of $3 \times 10^5 \text{ K}$ is in harmony with the results of the N V and O VI comparison and the narrow widths of the O VI features, but the high emission measure required by the EUV data restricts the number density of $3 \times 10^5 \text{ K}$ gas to exceeding 10^{-2} cm^{-3} , much larger than the one obtained from the O VI observations.

A 1,350–1,550 Å background at high galactic latitudes may exist³¹. If so its origin may be due to the scattering of stellar radiation by dust grains in high latitude clouds³². The rapid growth of extinction³³⁻³⁶ at 1,000 Å suggests that many grains in diffuse clouds have radii of $\leq 10^{-6} \text{ cm}$ (ref. 17). Possibly, the extinction due to dust is very great at $\lambda \sim 100 \text{ Å}$ and is due to scattering. The diffuse EUV and very soft X-ray backgrounds then could originate in a few localized sources, such as supernova remnants, with high densities. Their radiation would scatter on the intervening clouds. Overbeck³⁷ and Hayakawa³⁸ have discussed the origin of soft X-ray haloes around point sources from such scattering. If the extinction and albedo at 100 Å are high several scatterings will occur before significant numbers of soft X rays are absorbed. Indeed, scatterings may prevent soft X rays from penetrating far enough into neutral clouds for them to suffer much attenuation even though their source is very far away.

Observations of the halo gas

Several moderately ionized species have been detected in absorption towards bright stars in the Magellanic clouds^{39,40}, towards bright stars in the galactic halo^{41,42}, and towards 3C273⁴³. C IV and Si IV were detected towards virtually all sources $>1 \text{ kpc}$ above the disk, and these lines were significantly stronger than those seen towards galactic disk stars. Further the C IV to Si IV ratio in the galactic halo is not typical of that for photoionized gas in H II regions⁴². Hence, it is generally accepted that C^{3+} and Si^{3+} are very abundant in the hot halo interstellar gas. Halo N V has been detected in only one line of sight towards the Small Magellanic Cloud⁴⁴ and towards two halo stars⁴². The latter two lines of sight pass through considerable amounts of disk material as the two background stars are not at very high latitudes and the N V features in those directions may arise in the hot disk gas. The feature seen towards the Small Magellanic Cloud star may arise in an intervening supernova remnant, a few of which may exist in the halo if star formation in high latitude, intermediate and high velocity clouds occur⁴⁵. Typically the observed equivalent widths of the stronger components of the doublet absorption features were 200 mÅ for Si IV and 400 mÅ for C IV. The detections of N V were at the 50-mÅ level.

If the gas, in which C IV and Si IV is seen, is in steady-state collisional equilibrium and if its abundances of carbon and silicon are solar its temperature is $\sim 8 \times 10^4 \text{ K}$. The observed ratios of the features are very uniform and the total possible spread in temperature in the observed regions is only $\sim 1 \times 10^4 \text{ K}$ (ref. 42). At $8 \times 10^4 \text{ K}$, N^{4+} is very scarce; the upper bounds in most directions limit the halo gas temperature to being $<1.5 \times$

Table 1 UV absorption features

Ion	T (max concentration) (K)	Wavelength (Å)
Al III	$10^{4.6}$	1,862.79, 1,854.72
Si III	$10^{4.3-10^{4.8}}$	1,206.51
Si IV	$10^{4.9}$	1,402.77, 1,393.76
C IV	$10^{5.0}$	1,550.77, 1,548.20
N V	$10^{5.3}$	1,242.80, 1,238.82
O VI	$10^{5.5}$	1,037.63, 1,031.94

Table 2 Total column densities along a line of sight perpendicular to the galactic disk

Ion	Disk			Halo			Total $N(10^{13} \text{ cm}^{-2})$
	$n(10^{-9} \text{ cm}^{-3})$	$N(10^{13} \text{ cm}^{-2})$	Refs	$n(10^{-9} \text{ cm}^{-3})$	$N(10^{13} \text{ cm}^{-2})$	Refs	
C^{3+}	≤ 2.0	0.37	16, 23	8.5	15.8	39, 41, 42	16.1
Si^{3+}	0.5	0.09	13	1.9	3.5	39, 42	3.6
N^{4+}	5.0	0.86	13	<1.5	<2.78	39, 42	<3.6
O^{5+}	28.0	5.20	11	?			>5.2

10^5 K . York⁴⁶ has discussed the possibility that the haloes Si^{3+} and C^{3+} are formed by the photoionization of lower ionized species in warm interstellar gas by an intergalactic UV background produced by quasars and other active galaxies. However, the lowest energy photons will be absorbed relatively near the top of the corona. There, the fractional ionization will be high and the charge transfer ionization³ of Si^+ to form Si^{2+} will be rapid and Si^{3+} will be formed by the photoionization of Si^{2+} . Only a bit lower in the halo the fractional ionization will have dropped and the charge transfer recombination of Si^{2+} will be rapid and Si^{3+} will not be formed⁴⁷. The production of Si^{3+} and C^{3+} by photoionization cannot explain their high abundances over a substantial range of heights above the disk.

Estimates for the vertical distribution of the hot halo gas were obtained by observing stars at different heights above the plane^{41,42} and by observing the velocity profile of the features and assuming that the halo gas co-rotates with the disk^{39,40}. Bromage *et al.*⁴¹ and Savage and de Boer^{39,40} found that the scale height is about 2 or 3 kpc which compares with the scale height of 1.4 kpc originally given by Spitzer for 10^5 K gas. Pettini and West⁴², who studied the most extensive sample of objects, reported that while most of the C IV and Si IV absorption occurs within 3 kpc of the plane the number densities of C^{3+} and Si^{3+} may increase between 0.5 and 3 kpc. If so a static plane stratified model of the halo gas may be inappropriate.

The total column density of gas at $8 \times 10^4 \text{ K}$ along a line of sight perpendicular to the disk is $\sim 10^{19} \text{ cm}^{-2}$. If the scale height is 3 kpc its number density at the edge of the disk is 10^{-3} cm^{-3} . A number density of 10^{-3} cm^{-3} , a temperature of 10^5 K , and a filling factor of about 1 correspond to a pressure comparable with that which we derived for the hot disk gas from the N V and O VI data. If f is the true filling factor of the $8 \times 10^4 \text{ K}$ gas it will radiate about $0.1 f^{-1}$ of the total galactic supernova energy⁴⁸. If the $8 \times 10^4 \text{ K}$ gas were embedded in hotter gas the dissipation of energy in the $8 \times 10^4 \text{ K}$ gas would have to be almost unrealistically efficient.

Si III and Al III have also been detected in the hot halo gas⁴⁰. The presence of Si III is expected if the halo gas is at $8 \times 10^4 \text{ K}$, but the Al III feature should be unobservable if all of the gas is at such temperatures. Al^{2+} can be abundant in cooling gas if its initial temperature is $< 5 \times 10^4 \text{ K}$ (ref. 2). Al^{2+} in the halo may form in gas cooler than $5 \times 10^4 \text{ K}$ which is above the $8 \times 10^4 \text{ K}$ gas and is unstable to cloud formation. If this is its origin the presence of Al^{2+} puts restrictions on the coronal fountain models discussed later.

Many absorption features arising in much cooler halo gas also were seen in the UV⁴⁰. Cool predominately neutral high velocity clouds exist at high galactic latitudes⁴⁹. While they undoubtedly lie in the halo little is known about their location or kinematics. If they are moving through $8 \times 10^4 \text{ K}$ halo gas shock heating of the ambient gas occurs. Soft X rays emitted during the subsequent cooling of the gas can serve as diagnostics of their kinematics⁵⁰. The formation of the clouds and the explanation of their kinematics present important challenges to any theory of the hot halo gas.

Twenty-one centimetre studies⁵¹ revealed that warm neutral atomic hydrogen with $T = 1-2 \times 10^3 \text{ K}$ exists at high galactic latitudes. It has been suggested⁵² that such gas can arise at the interface between the more distant edge of molecular cloud and the hot gas. In this model the stability of the gas at $1-2 \times 10^3 \text{ K}$ is due to the presence of molecular hydrogen, which is an efficient coolant.

Theories of coronal heating

Bottcher *et al.*⁵³ made the earliest attempt to construct a self-consistent model of the interstellar medium in the disk taking account of the ionization and heating due to supernova remnants. Since the discovery of O VI absorption⁶ in the interstellar medium other models in which supernova remnants have a role in regulating the balance of the interstellar medium have appeared. Some of the general ideas used in these models in which remnants either tunnel hot channels in the interstellar medium⁵⁴ or overlap before cooling and fill most of the interstellar space⁵⁵ are probably applicable. However, the models face severe difficulties. For example, the model of McKee and Ostriker⁵⁵ has gas pressures too low to explain the origin of the EUV background³⁰. It predicts too much O^{5+} which the authors claim could be hidden if turbulent motions broaden the lines; however, the turbulence would have to be supersonic and would dissipate rapidly and the observed lines are narrow. The model predicts that N V is undetectable^{43,16}. The soft X-ray-EUV, the O VI, and the N V results are the three primary observations of hot interstellar disk gas that a successful model of the interstellar medium must explain.

The hot gas in the Galaxy may be divided into two types. One is that which is close to the plane and near stars among which supernovae do occur. O^{5+} has a density distribution with a scale height of 300 pc (ref. 11) and probably exists in this first type of gas. Gas further from the plane is probably heated by energy generated in the disk by sources including supernova remnants, but the energy is transmitted above the plane by mass flow, cosmic rays, or hydromagnetic waves.

Weisheit and Collins⁵⁶ who calculated the ionization balance for the hot halo gas reviewed the possible heating mechanisms suggested before early 1976. Heating by soft X-ray induced photoionization or by infalling extragalactic material⁵⁷ is insufficient. The conversion of cosmic ray energy by the generation of Alfvén waves which decay rapidly by nonlinear wave-wave interactions⁵⁸⁻⁶⁰ would be a sufficient source of heat. The observation that the detected coronal gas is at $8 \times 10^4 \text{ K}$ may prove valuable in constraining models of galactic cosmic ray propagation.

Chevalier and Gardner⁶¹ and Cox and Smith⁵⁴ suggested that some of the hot gas in the plane escapes and rises into the halo. Chevalier and Oegerle⁶² have argued that such flows probably could not lead to the production of both a galactic wind and the high velocity clouds in our Galaxy. The models of coronal formation which have been received most favourably are the galactic fountain models⁶³⁻⁶⁵ which describe the flow of hot gas from the plane into the halo where it cools radiatively, condenses forming clouds due to thermal instabilities, and falls back to the plane. The advantage of these models is that the high velocity clouds may be identified with the condensations and Bregman⁶⁴ has claimed that by assuming an isothermal corona with a radius dependant density proportional to the total density of neutral hydrogen, the velocity distribution of the high velocity and the intermediate velocity clouds can be understood. He envisages that near the plane the rising gas is accelerated radially by the coronal pressure gradient. Eventually the gas travels high enough above the plane that it has had time to cool to a temperature at which thermal instabilities occur and the clouds, which consequently form, fall like ballistic particles back to the plane after striking it near the point at which the hot gas from which they formed originally left. The

Table 3 Observed frequency of narrow quasar absorption lines

Ion	$\Delta z > 0.1$			$\Delta z < 0.1$		
	Actual detections	Total detections possible	Ratio (%)	Actual detections	Total detections possible	Ratio (%)
C ⁺	19	48	39.6	4	23	17.4
C ³⁺	62	63	98.4	23	24	95.8
N ⁴⁺	4	46	8.7	16	24	66.7
O ⁰	9	43	20.9	2	24	8.3
O ⁵⁺	2	5	40.0	2	3	66.7
Si ⁺	23	61	37.7	5	23	21.7
Si ²⁺	18	37	48.6	7	22	31.8
Si ³⁺	27	55	49.1	14	23	60.9

very major problems with Bregman's model are that the temperature at the base of the corona must lie between 7×10^5 K and 1.6×10^6 K, in conflict with the N V and O VI observations, and that it is very difficult to understand why 8×10^4 K halo gas would be very abundant in such a model as the cooling time is at its shortest near that temperature⁴⁰. Specifically, N V should be more abundant than Si IV if the fountain model were correct.

It is tempting to construct galactic coronal models similar to those used for solar and stellar coronae. However, a major difference between the solar and galactic coronae is that the structure of the solar corona is governed by thermal conductivity while at 8×10^4 K the galactic corona is too cool for conduction to be significant. Recently, Sturrock and Stern⁶⁶ have proposed that the galactic corona is heated by the dissipation of magnetic energy generated by galactic differential rotation. The generation of magnetic energy in the plane produces regions with high magnetic pressure which are buoyant and rise to the halo where field reconnection occurs dissipating the magnetic energy. This model can produce a 10^6 K corona but cannot produce 8×10^4 K gas. Book⁶⁷ has suggested that the work done by the expansion of such magnetic bubbles can heat the solar corona without the need for wave or current dissipation. In the case of the galactic corona the detailed nature of the dissipation of a magnetic bubble's energy will fix the ratio of the bubble formation time and the length of time required to dissipate its energy. If the ratio is nearly unity the corona will be approximately in steady-state.

It has been suggested^{48,68} that the dissipation in the halo gas of Alfvén waves produced in the disk by any source including the expansion and fragmentation of supernova remnants can heat the galactic halo gas. Dissipation can occur through ordinary viscosity or through nonlinear decay into a sound wave and another Alfvén wave. In many cases the latter mechanism may dominate. If it does the heating mechanism turns off rapidly when the temperature becomes too high, because conductive dissipation of sound waves will become rapid preventing them from growing and will lead to a great weakening of the nonlinear wave-wave interaction. For reasonable choices of parameters this rapid turnoff can occur near 8×10^4 K. Such structure in the heating rate probably explains why the gas is thermally stable even though the cooling rate coefficient is structureless between 6×10^4 K and 2×10^5 K (refs 68, 69). Härtquist⁴⁸ has shown that a low density, slow wind, driven by wave pressure will have a temperature which varies slowly with density. It is possible that the galactic corona is a wave-driven fountain. Thermal instability will occur at heights at which the wave energy is no longer large, resulting in cloud formation. As mentioned previously, the Al III data may require that the clouds form from gas with $T \leq 5 \times 10^4$ K, but the Al III also may originate in other cooling gas such as that produced by the collision of two initially cool clumps in high latitude clouds⁴⁵. The velocity dispersion of the clumps is so high that they are not virially stable, but they are probably contained by magnetic pressure. The large scale field strength in the corona required to achieve the containment is comparable with that necessary for the wave heating models to be viable⁴⁵.

Narrow line absorption systems in quasar spectra

The suggestion of Spitzer and Bahcall⁷⁰ that many of the narrow line absorption systems seen in the spectra of quasars may arise in the coronae of intervening galaxies has received observational support^{43,46,71-75}. If the narrow line systems do originate in the intervening galaxies, analysis of them can yield information about the evolution of the interstellar medium and the structure of galaxies. In addition the study of absorption features like those of O VI (λ 1,033 Å and λ 1,037 Å) arising in hot gas and with rest wavelengths which are currently inaccessible, may provide insight into the structure of the corona of our Galaxy.

To provide a further test of the intervening galaxy hypothesis, we have used the observed abundances in the hot galactic disk and halo gas to estimate the column densities of C³⁺, Si³⁺, N⁴⁺ and O⁵⁺ along sight lines through the Galaxy. We used these column densities when trying to understand the observed frequencies of detection of features in quasar absorption line systems. These frequencies of occurrence were determined from a study of all available data obtained with the University College London Image Photon Counting System (IPCS)⁷⁶.

To estimate the column densities observed along a line of sight perpendicular to the disk of our Galaxy we considered two separate contributions. Jenkins¹¹ found that the O⁵⁺ density distribution has a scale height of 300 pc. Hence, for each species we have included a disk contribution given by the average disk abundance multiplied by 600 pc. Observations reporting the average densities of C IV and Si IV in the halo along a number of sight lines were discussed earlier. The density of N V in the halo is uncertain, but excluding three lines of sight, its number density is $< 1.5 \times 10^{-9}$ cm⁻³. Instruments capable of detecting O VI in the halo have not been built. Table 2 summarizes the existing data on these four ions and estimates their total column densities. We have assumed that the halo gas has a scale height of 3 kpc. The densities in Table 2 are averages from several lines of sight. Interstellar material is fairly inhomogeneous. For example, the column densities of material obtained by Savage and de Boer^{39,40} towards the Small Magellanic Cloud are twice those they obtained towards the Large Magellanic Cloud. However, the column densities in Table 2 provide a reasonable data base to compare with QSO absorption data.

Column densities of quasar absorption lines are available for a few exceptionally well studied rich systems. These few column densities are in reasonable agreement with the column densities found in halo material towards the Magellanic cloud stars⁷⁵, but these comparisons were primarily for Si IV, C IV, and features of more lowly ionized species.

Rather than consider column densities, we will concentrate on the frequencies with which features occur. For each absorption line we compared the number of actual detections of a feature with the number of systems for which observations with adequate signal-to-noise have been made in the appropriate wavelength range. With very high quality data a comparison of the equivalent widths of various features seen in a system to that of Si IV would be possible. As such data do not exist,

we are fortunate that, as discussed below, the detection limits are low enough to be comparable with those needed to see Si IV, a moderately abundant ion in our Galaxy and in the absorption line systems. We expect ions less abundant than Si IV to be detected rarely and those much more abundant than Si IV to be detected nearly always. The IPCS data we used were for 30 different quasars^{72,76-90} and show 90 definite absorption systems. For 27 of these systems, the differences, Δz , between their redshift, z_a , and the quasar emission line redshift, z_e , is <0.1 . We treated this group separately as they may be associated with or be near to the quasar so that their ionization structure is influenced by the quasar radiation field. The results of this analysis are presented in Table 3.

The differences between the two groups of systems are striking. It has been noted previously that systems with small Δz often contain N V whereas other systems do not⁹¹. This effect is demonstrated in Table 3. In addition there are few small Δz systems in which C II is detected and the silicon ionization balance in those systems seems to favour more highly ionized species. These trends may be due to the effects of high photoionization rates. Some of the small Δz systems not showing these shifts may be near quasars but shielded by gas in which another absorption line system is formed.

The results in Table 2 can be used to understand the data for the group of absorption lines with $\Delta z > 0.1$. In making this comparison it should be remembered that the smallest detectable equivalent width does vary from quasar to quasar and is a function of wavelength for the systems studied. In addition, it is sometimes difficult to establish unique identifications for lines in the Ly α forest ($\lambda < (1+z_e)1,216 \text{ \AA}$). In particular, for $\Delta z > 0.1$ the N V lines lie in the Ly α forest. Knowing these difficulties, we can still draw a few general conclusions.

Si IV is detected in roughly one half of the $\Delta z > 0.1$ systems, implying that the typical Si^{3+} column density is roughly the minimal detectable one if most systems originate in relatively similar objects. Apparently, Si^{2+} which is also seen in $\sim 50\%$ of the systems has a column density comparable with that of Si^{3+} as is expected in a limited temperature range around 10^5 K . Thus the silicon absorption line data show that the temperature is perhaps marginally higher in most gas seen in absorption against quasars than in the hot galactic halo gas.

Table 2 shows that the N^{4+} column densities may be expected to be as much as five times lower than those of Si^{3+} if N^{4+} exists only in the disks of galaxies. In addition the oscillator strength for the observable transitions of N^{4+} is about 3 times weaker than that of the transitions for Si^{3+} . However, in those few systems in which N V is seen its feature is of at least comparable strength to that of Si IV. Clearly, the N V detections cannot be understood if we assume that the column densities in Table 2 are correct for all intervening galaxies. Smith and Hartquist¹³ found considerable scatter in the disk N V number density, which can be caused by relatively small changes of temperature around $T = 10^{5.4} \text{ K}$. Pettini and West⁴² have also found some scatter in the halo number densities of C IV and Si IV (though little scatter in their ratio). It is probably possible to understand the very few detections in quasar absorption line systems by

assuming that N V exists only in the disks of intervening galaxies and that its density in those disks has a distribution not too different than that in the galactic disk. However, from these data we cannot rule out the presence of interstellar N V in the haloes of the intervening galaxies. Alternatively, the N V absorption features may arise in somewhat unusual regions; perhaps they are in galaxies in their early stages of evolution.

C^{3+} is observed in a high percentage of the absorption line systems. Its column densities in the galactic halo are about 4 times that of Si^{3+} , but the relevant oscillator strength is about 3 times weaker than that of Si^{3+} . For C IV features to be observed in so many systems the density of C^{3+} to Si^{3+} must in general be >4.5 implying as did the Si III to Si IV data that the temperature of the intervening gas is marginally greater than in our galactic halo. An observational bias favouring C IV detection exists: the presence of the C IV doublet is used often to establish the reality of an absorption system.

Data for O VI features are scarce. In our Galaxy the contribution to the O^{5+} column density from the disk gas is greater than the total column density of Si^{3+} , but the relevant oscillator strengths are in the ratio of 1:4. Even if O^{5+} is present only in the disks of our Galaxy and of the intervening galaxies we would expect reasonably frequent detection of it. If the galaxies have densities of O^{5+} in their haloes comparable with that found in the galactic disk, one would expect nearly a 100% detection rate. We cannot draw strong conclusions from the small number of systems observed for O VI, but on the basis of the $\sim 50\%$ detection rate in the $\Delta z > 0.1$ systems, we suspect that our Galaxy has a very low abundance of O^{5+} in its halo interstellar gas.

Future work

The existing UV observations of the galactic corona have provided much information about the physics of the hot interstellar gas. The theoretical explanations of the existing data including the N V and O VI measurements in the disk seem incomplete, and more work is necessary to explain them and the soft X-ray emission. Additional observations of the hot halo gas, whose properties are not fully understood, and of the quasar absorption line regions are desirable. Searches for O VI features in the galactic halo gas will have to wait until the next generation of UV observatories flies, but further optical searches for N V and O VI in quasar absorption line systems are possible. Eventually, they and the future galactic UV O VI observations may contribute significantly to the determination of the origin of the quasar absorption line systems.

Despite the apparent similarity of the physical properties of the galactic coronal gas to the gas in quasar absorption line regions, the question of whether the lines of sight to quasars cross enough galaxies to explain the number of detected absorption systems remains^{82,91} as the hot galactic gas seems to be fairly close to the disk. It is encouraging that the physical properties of the coronal gas of the Large Magellanic Cloud appear to be so similar to the galactic coronal gas⁹² suggesting that galaxies with a very wide range of masses contribute to the absorption by intervening galaxies.

- Spitzer, L. Jr *Astrophys. J.* **124**, 20-34 (1956).
- Hartquist, T. W., Snijders, M. A. J. & West, K. A. *Mon. Not. R. astr. Soc.* (submitted).
- Baliunas, S. L. & Butler, S. E. *Astrophys. J. Lett.* **235**, L45-L48 (1980).
- Shapiro, P. R. & Moore, R. L. *Astrophys. J.* **207**, 460-483 (1976).
- Allen, C. W. *Astrophysical Quantities* 3rd edn (Athlone, London, 1973).
- Jenkins, E. B. & Meloy, D. A. *Astrophys. J. Lett.* **193**, L121-L125 (1974).
- York, D. G. *Astrophys. J. Lett.* **193**, L127-L131 (1974).
- Jenkins, E. B. *Astrophys. J.* **219**, 845-860 (1978).
- Castor, J., McCray, R. & Weaver, R. *Astrophys. J. Lett.* **200**, L107-L110 (1975).
- Weaver, R., McCray, R. & Castor, J. *Astrophys. J.* **218**, 377-395 (1977).
- Jenkins, E. B. *Astrophys. J.* **220**, 107-123 (1978).
- York, D. G. *Astrophys. J.* **213**, 43-51 (1977).
- Smith, L. J. & Hartquist, T. W. *Mon. Not. R. astr. Soc.* **192**, 73P-77P (1980).
- Bruhweiler, F. C., Kondo, Y. & McClusky, G. E. *Astrophys. J.* **237**, 19-25 (1980).
- Black, J. H., Dupree, A. K., Hartmann, L. W. & Raymond, J. C. *Astrophys. J.* **239**, 502-514 (1980).
- Cowie, L. L., Taylor, W. & York, D. G. *Astrophys. J.* **248**, 528-541 (1981).
- Spitzer, L. Jr *Physical Processes in the Interstellar Medium* (Wiley, New York, 1978).
- Chandrasekhar, S. & Fermi, E. *Astrophys. J.* **118**, 113-115 (1953).
- Krall, N. A. & Trivelpiece, A. W. *Principles of Plasma Physics* (McGraw-Hill, New York, 1973).
- Rosenbluth, M. N. & Longmire, C. L. *Ann Phys.* **1**, 120-140 (1957).

- Draine, B. T. *Astrophys. J.* **241**, 1021-1038 (1980).
- Smith, L. J., Willis, A. J. & Wilson, R. *Mon. Not. R. astr. Soc.* **191**, 339-347 (1980).
- Laurent, C., Paul, J. A. & Pettini, M. *Astrophys. J.* **260**, 163-182 (1982).
- Williamson, F. O. et al. *Astrophys. J. Lett.* **193**, L133-L137 (1974).
- Fried, P. M., Nousek, J. A., Sanders, W. T. & Kraushaar, W. L. *Astrophys. J.* **242**, 987-1004 (1980).
- Rosner, R. et al. *Astrophys. J. Lett.* **249**, L5-L10 (1981).
- Levine, A., Rappaport, S., Doxsey, R. & Jernigan, G. *Astrophys. J.* **205**, 226-232 (1976).
- Cash, W., Maline, R. & Stern, R. *Astrophys. J. Lett.* **204**, L7-L11 (1976).
- Yentis, D. J., Novick, R. & Vander Bout, P. *Astrophys. J.* **177**, 365-386 (1972).
- Stern, R. & Bowyer, S. *Astrophys. J.* **230**, 755-767 (1979).
- Paresce, F., McKee, C. F. & Bowyer, S. *Astrophys. J.* **240**, 387-400 (1980).
- Jura, M. *Astrophys. J.* **227**, 798-800 (1979).
- Code, A. D., Davis, J., Bless, R. C. & Hanbury Brown, R. *Astrophys. J.* **203**, 417-434 (1976).
- Nandy, K., Thompson, G. I., Jamar, C., Monfils, A. & Wilson, R. *Astr. Astrophys.* **44**, 195-203 (1975).
- Nandy, K., Thompson, G. I., Jamar, C., Monfils, A. & Wilson, R. *Astr. Astrophys.* **51**, 63-69 (1976).
- Seaton, M. J. *Mon. Not. R. astr. Soc.* **187**, 73P-76P (1978).
- Overbeck, J. W. *Astrophys. J.* **141**, 864-866 (1965).
- Hayakawa, S. *Prog. Theor. Phys.* **43**, 1224-1230 (1970).

39. Savage, B. D. & de Boer, K. S. *Astrophys. J. Lett.* **230**, L77-L82 (1979).
40. Savage, B. D. & de Boer, K. S. *Astrophys. J.* **243**, 460-484 (1981).
41. Bromage, G. E., Gabriel, A. H. & Sciana, D. W. in *2nd European IUE Conf. ESA-SP 157*, 345-351 (1980).
42. Pettini, M. & West, K. A. *Astrophys. J.* (in the press).
43. Ulrich, M.-H. *et al. Mon. Not. R. astr. Soc.* **192**, 561-580 (1980).
44. Savage, B. D. & Fitzpatrick, E. L. *Bull. Am. astr. Soc.* **13**, 895 (1981).
45. Dyson, J. E. & Hartquist, T. W. *Mon. Not. R. astr. Soc.* (submitted).
46. York, D. G. *Ann. Rev. Astr. Astrophys.* **20**, (in the press).
47. Pettini, M., Hartquist, T. W. & Tallant, A. *Mon. Not. R. astr. Soc.* (submitted).
48. Hartquist, T. W. *Mon. Not. R. astr. Soc.* (in the press).
49. Verschuur, G. L. *Ann. Rev. Astr. Astrophys.* **13**, 257-293 (1975).
50. Bone, D., Hartquist, T. W. & Sanford, P. *Astrophys. Spac. Sci.* (in the press).
51. Dickey, J. M., Salpeter, E. E. & Terzian, Y. *Astrophys. J. Lett.* **211**, L77-L81 (1977).
52. Hartquist, T. W., Black, J. H. & Dalgarno, A. *Astrophys. J.* **259**, 591-594 (1982).
53. Bottcher, C., McCray, R. A., Jura, M. & Dalgarno, A. *Astrophys. Lett.* **6**, 237-241 (1970).
54. Cox, D. P. & Smith, B. W. *Astrophys. J. Lett.* **189**, L105-L108 (1974).
55. McKee, C. F. & Ostriker, J. P. *Astrophys. J.* **218**, 148-169 (1977).
56. Weisheit, J. C. & Collins, L. A. *Astrophys. J.* **210**, 299-310 (1976).
57. Sciana, D. *Nature* **240**, 456-457 (1972).
58. Sagdeev, R. Z. & Galeev, A. A. *Nonlinear Plasma Theory* (Benjamin, New York, 1969).
59. Wentzel, D. G. *Astrophys. Lett.* **10**, 167-170 (1972).
60. Wentzel, D. G. *A. Rev. Astr. Astrophys.* **12**, 71-96 (1978).
61. Chevalier, R. A. & Gardner, J. *Astrophys. J.* **192**, 457-463 (1974).
62. Chevalier, R. A. & Oegerle, W. R. *Astrophys. J.* **227**, 398-406 (1979).
63. Shapiro, P. R. & Field, G. B. *Astrophys. J.* **205**, 762-765 (1976).
64. Bregman, J. N. *Astrophys. J.* **236**, 577-591 (1980).
65. Kahn, F. in *Investigating the Universe* (ed. Kahn, F.) 1-28 (Reidel, Dordrecht, 1981).
66. Sturrock, P. A. & Stern, R. *Astrophys. J.* **238**, 98-102 (1980).
67. Book, D. L. *Comments Plasma Phys. Controlled Fusion* **6**, 193-198 (1981).
68. Hartquist, T. W. & Tallant, A. *Mon. Not. R. astr. Soc.* **196**, 527-532 (1981).
69. Summers, H. P. & McWhirter, R. W. P. *J. Phys.* **B12**, 2387-2412 (1979).
70. Bahcall, J. N. & Spitzer, L. Jr *Astrophys. J. Lett.*, **156**, L63-L65 (1969).
71. Boksenberg, A. *Phys. Scr.* **17**, 205-214 (1978).
72. Young, P. J. *et al. Astrophys. J.* **229**, 891-908 (1979).
73. Sargent, W. L. W., Young, P. J., Boksenberg, A., Carswell, R. F. & Whelan, J. A. J. *Astrophys. J.* **230**, 49-67 (1979).
74. Snijders, M. A. J. *ESA SP-157, 2nd European IUE Conf.* lxxi-lxxx (1980).
75. Savage, B. D. & Jeske, N. A. *Astrophys. J.* **244**, 768-776 (1981).
76. Boksenberg, A. & Burgess, D. E. *Proc. Symp. on Astronomical Observations with Television Type Sensors*, British Columbia (eds Glaspey, J. W. & Walker, G. H. A.) 21-30 (1973).
77. Boksenberg, A., Carswell, R. F., Smith, M. G. & Whelan, J. A. J. *Mon. Not. R. astr. Soc.* **184**, 773-782 (1978).
78. Wright, A. E., Morton, D. C., Peterson, B. A. & Jauncey, D. L. *Mon. Not. R. astr. Soc.* **189**, 611-620 (1979).
79. Blades, J. C., Murdoch, H. S. & Hunstead, R. W. *Mon. Not. R. astr. Soc.* **191**, 61-68 (1980).
80. Blades, J. C., Hunstead, R. W. & Murdoch, H. S. *Mon. Not. R. astr. Soc.* **194**, 669-678 (1981).
81. Morton, D. C., Chen, J. S., Wright, A. E., Peterson, B. A. & Jauncey, D. L. *Mon. Not. R. astr. Soc.* **193**, 399-414 (1980).
82. Sargent, W. L. W., Young, P. A., Boksenberg, A. & Tytler, D. *Astrophys. J. Suppl.* **42**, 41-81 (1980).
83. Chen, J. S., Morton, D. C., Peterson, B. A., Wright, A. E. & Jauncey, D. L. *Mon. Not. R. astr. Soc.* **196**, 715-730 (1981).
84. Blades, J. C., Hunstead, R. W., Murdoch, H. S. & Pettini, M. *Mon. Not. R. astr. Soc.* (in the press).
85. Carswell, R. F., Whelan, J. A. J., Smith, M. G., Boksenberg, A. & Tytler, D. *Mon. Not. R. astr. Soc.* **198**, 91-110 (1982).
86. Pettini, M. *et al. Preprint Astrophys. J.* (submitted).
87. Sargent, W. L. W., Young, P. & Boksenberg, A. *Astrophys. J.* **252**, 54-68 (1982).
88. Wright, A. E., Morton, D. C., Peterson, B. A. & Jauncey, D. L. *Mon. Not. R. astr. Soc.* **199**, 81-91 (1982).
89. Young, P., Sargent, W. L. W. & Boksenberg, A. *Astrophys. J.* **252**, 10-31 (1982a).
90. Young, P., Sargent, W. L. W. & Boksenberg, A. *Astrophys. J. Suppl.* **48**, 455-505 (1982b).
91. Weymann, R. J., Carswell, R. F. & Smith, M. G. *A. Rev. Astr. Astrophys.* **19**, 41-76 (1981).
92. de Boer, K. S. & Savage, B. D. *Astrophys. J.* **238**, 86-92 (1980).
93. Levine, A., Rappaport, S., Halpern, J. & Walter, F. *Astrophys. J.* **211**, 215-222 (1977).

ARTICLES

MERLIN observations of superluminal radio sources

I. W. A. Browne, R. R. Clark*, P. K. Moore, T. W. B. Muxlow, P. N. Wilkinson, M. H. Cohen† & R. W. Porcas‡

Nuffield Radio Astronomy Laboratories, Jodrell Bank, Macclesfield, Cheshire SK11 9DL

† Owens Valley Radio Observatory, California Institute of Technology, Pasadena, California 91125, USA

‡ Max Planck Institut für Radioastronomie, Auf dem Hugel 69, D5300 Bonn 1, FRG

Powerful extragalactic radio sources may all be members of a single family in which those showing superluminal behaviour are the ones in which a relativistic jet is directed towards the observer. The superluminal sources are shown to have extended radio structures the form of which is consistent with such a unified scheme. This interpretation requires that the Hubble constant H_0 should be nearer to 100 than to 50 km s⁻¹ Mpc⁻¹.

OBSERVATIONAL evidence for superluminal velocities has so far been found in a small proportion of extragalactic radio sources¹. Only one of these superluminal sources has the steep radio spectrum² and symmetrical outer lobes characteristic of most 'normal doubles'. The emission from the other sources is dominated by flat radio spectrum compact cores. Little is known about the extended radio structure of such sources. We suggest nevertheless, that these flat spectrum core-dominated sources and the steep spectrum normal double sources are closely related. We show that there is extended structure surrounding the cores of most superluminal sources and that its properties are consistent with a unified scheme³ in which the core-dominated type sources happen to be those in which a relativistic jet is directed towards the observer.

We now present hybrid maps made with the Jodrell Bank Multi Element Radio Linked Interferometer Network (MERLIN) of nine superluminal sources and also the core-dominated quasar 4C39.25. The comparatively low observing frequencies of 408 MHz and 1,666 MHz are very suitable for showing up the steep spectrum emission typical of extended parts of radio sources. Maps made, using the techniques described in ref. 4, at 1,666 MHz have a resolution ~0.3 arc s and a dynamic range ~1,000:1, while those at 408 MHz have a resolution ~1 arc s and a dynamic range ~200:1.

The observational results on each source are summarized in Table 1. We take Hubble's constant $H_0 = 100h$ km s⁻¹ Mpc⁻¹ and $q_0 = 0.05$. The factor h allows the results to be scaled for other values of H_0 . The MERLIN maps are displayed in Fig. 1.

Individual sources

NRAO 140: Marscher and Broderick⁵ have three epoch very-long baseline interferometry (VLBI) observations which show this source to be expanding at an angular rate between 0.10 and 0.14 mas yr⁻¹. The MERLIN 408-MHz map shows a weak (0.14 Jy) extended component in position angle (PA) 149°, 7.6 arc s from the 3.57 Jy unresolved core. The source is variable at 408 MHz with mean flux density over the period 1975-79 of 3.12 Jy (ref. 6). There is thus no evidence for extended structure in addition to that visible in our map.

3C120: The latest results on the motion in the core of this Seyfert Type I galaxy are presented by Walter *et al.*⁷. The MERLIN 1,666-MHz map shows a jet with an extended knot 4 arc s from the core. On the 408-MHz map this jet continues a further 10 arc s, bending increasingly to the north as it does so. This jet is visible on the Very Large Array (VLA) maps of Balick *et al.*⁸ and is also just visible on our 1,666-MHz map. The 408-MHz map contains 3.9 Jy compared with a total flux density of ~6.5 Jy (ref. 6). This implies that there is a lot of missing low brightness structure. The VLBI position angle is -108°, that of the 4 arc s knot -99°, and that of the jet -75°.

* Present address: Electrical Engineering Department, University of New Hampshire, Durham, New Hampshire 03824, USA.

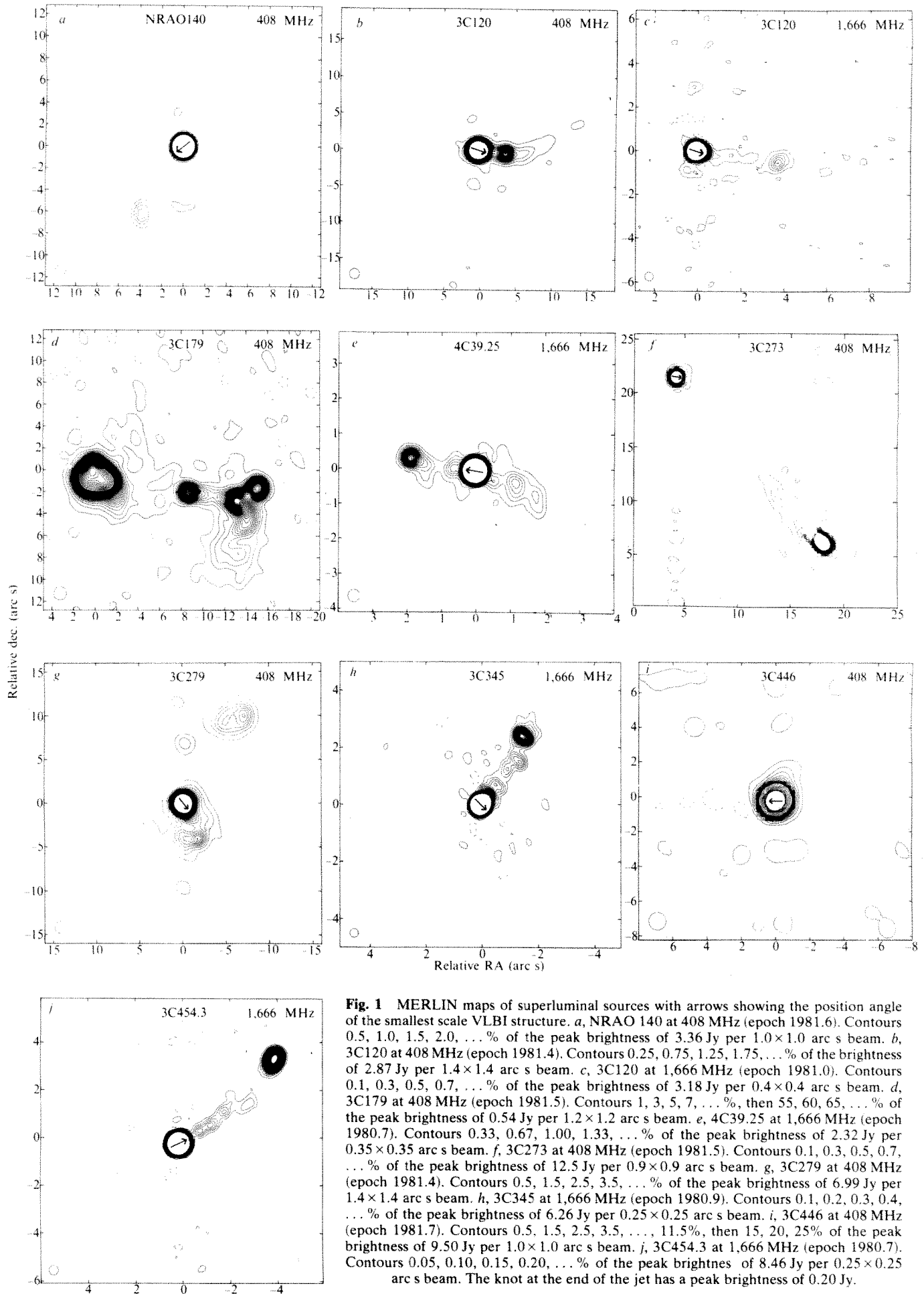


Table 1 Source properties

Name	Identification/redshift	θ (m arc s yr ⁻¹)	v/c	VLBI PA (Refs)	MERLIN PA	Magnetic field direction
NRAO 140	Q/1.258	0.13	$5.4 h^{-1}$	127 (5)	149	138
3C120	G/0.033	1.35	$2.1 h^{-1}$	-108 (7)	-99 to -75	-96
3C179	Q/0.846	0.14	$4.2 h^{-1}$	-88 (2)	-100	-96
4C39.25	Q/0.699	<0.02	$<0.5 h^{-1}$	81 (44)	80	?
3C273	Q/0.158	0.76	$5.3 h^{-1}$	-99 to -138 (45)	-138	-120
3C279	Q/0.538	0.5 or 1.5	(10 or 25) h^{-1}	-142 (7)	-157	-158
3C345	Q/0.595	0.36	$8.2 h^{-1}$	-135 (18) to -57 (45)	-38 to -32	-47
BL Lac	B/0.07	?	?	-170 (22)	—	133 or -47
3C446	Q/0.847	?	?	-90 (24)	-32	-84
3C454.3	Q/0.859	?	?	-65 (28)	-48	-64

The values of θ and v/c are taken from ref. 1 and the magnetic field direction from the intrinsic electric field position angles given by Simard-Normandin *et al.*⁴².

Note that the sense of jet curvature remains the same on all angular size scales.

Direct images of the galaxy have been obtained by Arp⁹ and also by Wlérick *et al.*¹⁰ who describe an optical continuum jet which emerges from the nucleus roughly parallel with the radio jet and which bends north at about the position of the 4 arc-s knot. The bend is in the same sense as the radio but is significantly larger.

Baldwin *et al.*¹¹ have mapped the velocity field of the galaxy and find an axis of symmetry nearly parallel to the VLBI axis. One possible interpretation of their observations is that the emission line gas is rotating about this axis. This is, however, difficult to reconcile with the detection of superluminal motion many explanations of which require the VLBI axis to be close to the line of sight. The true rotation velocities which would be implied if this were the case ($\geq 600 \text{ km s}^{-1}$ for angles to the line of sight $< 30^\circ$) seem unrealistically large for rotating gas in a galaxy. We suggest that the gas is probably not rotating about the VLBI axis. The alternative explanations put forward by Baldwin *et al.* of either infalling or outflowing gas seem more plausible.

3C179: Porcas² finds the central component of this source to be expanding with $v = 4.2c h^{-1}$. The MERLIN 408-MHz map shows strong double lobes and a jet pointing to the western lobe.

3C273: MERLIN 408-MHz observations have been discussed by Conway *et al.*¹². The map presented here is a new one made with all six telescopes.

3C279: This is the first source in which rapid changes in structure were observed¹³ but the details of the structural changes are still not clear. Cohen and Unwin¹ suggest an expansion speed of $10c h^{-1}$, while Pauliny-Toth *et al.*¹⁴ think the expansion rate might be as high as $25c h^{-1}$. The MERLIN 408-MHz map shows the strong core and two extended outer components. On a higher resolution map the extension from the nucleus in PA -145° is clearly seen as a jet (Perley, personal communication). Our map contains virtually all the flux density. The weak component lying ~ 5 arc s due north of the core may be a sidelobe.

3C345: Recent VLBI results are reported in refs 15–17. The MERLIN 1,666-MHz map shows a curved jet starting from the nucleus and ending in a compact knot. Figure 2 shows the position angle of source elongation plotted as a function of

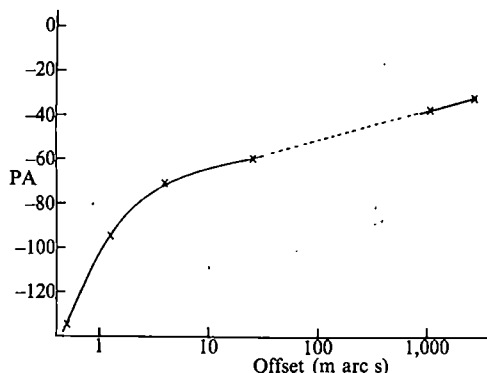


Fig. 2 The bend in 3C345. The position angle of a point in the jet as seen from the core is plotted against the distance of that point from the core. VLBI data are taken from refs 16, 18 and 45.

distance from the core. There are two things to note; first most of the bending occurs in the first 0.1% of the length of the jet well within the region in which the superluminal motion is observed. Second, the sense of curvature on the m arc s scale is retained on the arc s scale. This latter observation suggests that the cause of bending is the same on all scales. Browne *et al.*²⁰ have published a MERLIN 408-MHz map and they point out that 3C345 must have some low brightness emission on a scale of ≥ 5 arc s in addition to the jet.

BL Lac: Mutel *et al.*²¹ and Phillips and Mutel²² report superluminal behaviour in this source. We have no evidence for the source being resolved with MERLIN; at 408 MHz the flux density of any extended structure is $< 2\%$ of that of the core and at 1,666 MHz it is $< 0.5\%$ of the core flux density.

3C446: The MERLIN 408 MHz map shows a strong, unresolved component with a slight extension in PA -32° , in agreement with the 327-MHz lunar occultation results of Joshi and Gopal-Krishna²³. At higher frequencies VLA results²⁴ indicate a resolved component at PA 112° and separation ~ 0.6 arc s from the core. This is more closely aligned with the VLBI structure which is in PA 90° (ref. 24).

3C454.3: No direct structural changes have been observed in this source but rapid low frequency variability provides strong evidence for superluminal behaviour^{25,26}. To first order the VLBI structure consists of an unresolved core with a bright knot 7 m arc s distant in PA -65° (refs 27, 28). There is also some evidence for a weak VLBI component on the opposite side of the core. The MERLIN 1,666-MHz map shows a very weak, slightly curved jet leading to relatively bright component ~ 4 arc s away in PA -48° . The curvature along the MERLIN jet has the same sense as that between the jet and the VLBI nucleus.

4C39.25 (0923+392): This is a quasar whose VLBI structure has been monitored for several years and a limit on the expansion speed $\leq 0.5c h^{-1}$ can be set¹. The MERLIN 1,666-MHz map shows a dominant unresolved core and other complicated extended structure fairly symmetrically disposed about the core. The overall morphology strongly resembles that of 1150+597 (ref. 29) which also has a compact hot spot on one side of a strong core and a more relaxed structure on the other side; both sources also possess a steep spectrum halo^{29,20}. Higher resolution observations of 1150+497 clearly reveal a jet linking the core to the hotspot. Our observations are suggestive of a corresponding jet in 4C39.25 although a higher resolution map will be required to confirm this.

Discussion

Many different models have been proposed to explain the apparent superluminal motion in radio sources. Marscher and Scott³⁰ review most of the theories and find that few are free from conflict with observation. Of the ones that do survive most observational tests, those in which there is bulk relativistic motion of the radiating material are the most widely accepted. We will concentrate on this type of model.

Source morphology

The most obvious thing apparent from our maps is that every source except BL Lac has large scale structure in addition to its compact core. There is clearly great diversity in the struc-

tures; some of them have one-sided jets (3C120, 3C179, 3C273, 3C345 and 3C454.3) and some have extended structure on both sides of the core (3C179, 3C279 and 4C39.25). At least with the present dynamic range, NRAO 140 appears to have a single isolated region of emission well away from the unresolved core. The flat spectrum sources amongst the superluminals have structures very much like other sources with similar spectra^{20,31}, and the only steep spectrum source 3C179 has a fairly normal double structure. Superluminal sources therefore do not look like some completely separate class of exotic object.

Asymmetries

One-sided jets have been observed in extragalactic sources having a wide range of luminosities³². There is considerable evidence that the jets in low luminosity radio galaxies are non-relativistic³³ but the situation is not so clear for the more powerful sources³⁴.

The MERLIN maps of the superluminal sources (except BL Lac) all show a certain degree of asymmetry about the central core component, ranging from a weak jet connecting the core and the western lobe in 3C179 to a totally one sided jet in 3C273. Six of the sources have clearly defined asymmetric VLBI structure (NRAO 140, 3C120, 3C179, 3C273, 3C345 and 3C454.3) and in all these cases the asymmetry in the extended structure is in the same sense. This suggests that the mechanism responsible for the one-sidedness in the VLBI cores is also responsible for that on the arc second scale²⁹. Clearly in the cores there is strong evidence for relativistic velocities which could easily account for the observed one-sidedness even if the sources were intrinsically two-sided. Do the relativistic velocities continue into the arc second jets? Evidence that they do comes from the results discussed by Browne *et al.*²⁰ and P. K. Moore (in preparation) concerning the absence of isolated large-scale jets (that is, those not associated with a strong core). The lack of such jets implies that, if the core emission is Doppler beamed, the jet emission has to be also and so this points towards relativistic jet velocities which continue from the cores to the outer parts of the sources. Doppler beaming is sufficient to explain the observed asymmetries, although relativistic jets which are intrinsically one-sided cannot be ruled out.

Unified scheme

As well as one-sided, sometimes jet-like features, four of the sources have still more extended structure. In 3C179 and 3C279 this takes the form of well defined lobes, but in 3C120 and 3C345 its presence is only betrayed by maximum interferometer visibilities significantly less than unity, even on the shortest baselines. The existence of the extended emission is particularly significant as it is most unlikely to be highly beamed, whereas the core emission might well be. If this is so there should exist a much larger population of unaligned objects dominated by their steep spectrum unbeamed emission. Such considerations led to the proposal of a unified scheme by Orr and Browne³ in which these unaligned counterparts of superluminal sources (and other core-dominated sources) are hypothesized to be normal steep spectrum double sources. Such an idea was dismissed by Scheuer and Readhead³⁵ because they deduced that the Lorentz factor (γ) of the core material was too low ($\gamma < 2$). In fact, Orr and Browne show that the statistical properties of quasars are compatible with a mean core Lorentz factor ~ 5 and therefore such a scheme is viable.

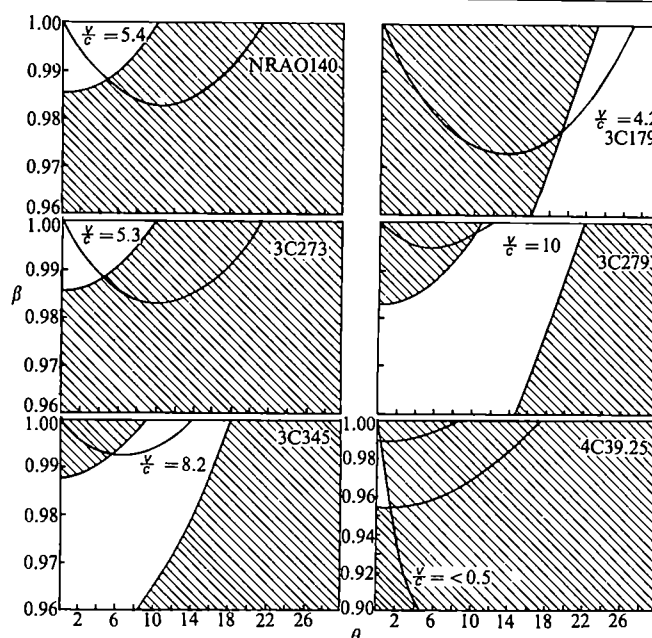


Fig. 3 θ/β diagrams for six sources with measured expansion velocities or limits on expansion velocities. The unified scheme constrains the sources to lie within the unshaded portions of the diagrams. The observed expansion rate means that the source must also lie on the v/c line. The following values of $R(\theta)$ have been used: >100 for NRAO 140, 0.5 for 3C179, >100 for 3C273, 10 for 3C279, 20 for 3C345 and 23 for 4C39.25.

For the sources in the present sample we can make quantitative tests to see if their properties are consistent with the unified scheme. Orr and Browne assume that the intrinsic ratio between the strength of the core and the lobes, defined as

$$R_T = \frac{\text{Core flux density when seen with its axis perpendicular to the line of sight}}{\text{The lobe flux density}}$$

is nearly a constant. The observed ratio $R(\theta)$, which has a very large spread from source to source will, of course, depend on the aspect of the source.

Following van Groningen *et al.*³⁶ we have plotted θ/β diagrams (Fig. 3) for those five quasars with well defined rates of expansion. θ is the angle which the motion in the core makes with the line of sight and βc is the velocity of the radiating component. In relativistic beam models an observed superluminal motion with velocity v requires the material to be moving with speed βc given

$$\beta = \frac{v/c}{\sin \theta + v/c \cos \theta}$$

Each object is constrained by the observed rate of expansion to lie on a line in the θ/β plane given by the above equation. (We assume $h = 1$ for these diagrams; see above.)

If we assume a specific value for R_T we can plot another line in the θ/β plane on which the quasar should lie using the equation³ $R(\theta) = \frac{1}{2}R_T(1 - \beta \cos \theta)^{-2} + \frac{1}{2}R_T(1 + \beta \cos \theta)^{-2}$. However, to allow for some realistic dispersion in R_T we plot two lines corresponding to $R_T = 0.006$ and $R_T = 0.10$. These refer to a frequency of 5 GHz and are respectively a factor of 4 lower and a factor of 4 higher than Orr and Browne's³ preferred value of 0.024. (The range $0.006 < R_T < 0.1$ is small compared with the observed spread in $R(\theta)$.) As can be seen from Fig. 3 in which the line defined by the expansion rate crosses an unshaded area, most of the sources are consistent with the scheme, although in the cases of 3C273 and NRAO 140 this is only by virtue of upper limits to the strength of any lobe-like structure. Should new observations show the lobe strengths very much weaker than the present limits the scheme, at least in its present simple form, would fail. We also note that 3C279 has relatively strong lobes compared with the core and

Table 2 Deprojected linear sizes for six quasars

Source	Observed angular size (arc s)	Allowed angle to the line of sight (deg)	Deprojected linear sizes (kpc)
NRAO 140	7.5	>5	>482
3C179	15.5	19–29	235–160
3C273	21	<4.6	>482
3C279	15	10–12	351–297
3C345	2.8	5.5–14	126–52
4C39.25	4	<1.4	>760

only just fits for the lower of the two possible values of v/c (that is, 10). If $v/c = 25$, as has been suggested by Pauliny-Toth *et al.*¹⁴ then it does not fit.

We can use the θ/β plots in Fig. 3 to define allowable ranges of θ for each source and hence work out limits on their deprojected sizes. We assume that the same value of θ applies to the large scale source structure as to the cores. Such an assumption is probably justified for large values of θ ($\geq 10^\circ$) as the work of

Macklin³⁷ on classical doubles indicates that the average bends in these are $\leq 5^\circ$, but for the sources with small θ our estimates are likely to have large errors. Table 2 lists these deprojected linear size estimates. All the values are within the range known for normal double quasars (≈ 550 kpc (refs 38, 39)) and so angular sizes present no problems for the scheme.

The fact that 3C179 is consistent with the unified scheme is interesting. If in 3C179 the core Lorentz factor is < 10 ($\beta < 0.995$) the scheme requires the angle to the line of sight, θ , to be in the range $19^\circ < \theta < 24^\circ$ giving a deprojected linear size between 167 and 136 kpc. This source illustrates that for not unrealistic Lorentz factors, superluminal motion can be observed in the cores of sources whose angles to the line of sight are quite large. If the unified scheme is correct, many cores of classical doubles should exhibit superluminal motion. That such motion has only been observed in one source is probably a reflection of the practical difficulty of making VLBI observations of weak cores.

Figure 3 also shows a θ/β plot for 4C39.25 using the limit on expansion velocity ($v/c < 0.5 h^{-1}$) given by Cohen and Unwin¹. This source would at first sight appear to be at odds with the scheme but for sufficiently small values of θ such a low apparent expansion speed will be observed even for relatively high values of γ . The probability of finding such a source is low but not prohibitively so; for $\gamma = 5$ the probability that a source selected by its core flux density having an angle to the line of sight $< 0.5^\circ$ is 0.4% (ref. 40). One problem with this interpretation is that the extended structure (Fig. 1) does not resemble a normal double source viewed almost directly along its axis; it appears to be too well collimated. This problem could be alleviated if there is some bending of the source axis which increases the angle to the line of sight of the outer structure. Such an effect would also reduce the deprojected linear size from the 2 Mpc it would be if the angle were truly 0.5° . We conclude that the above explanation for the lack of observed motion in 4C39.25 is not entirely out of the question.

Hubble's constant

Previously we used $H_0 = 100 \text{ km s}^{-1} \text{ Mpc}^{-1}$ ($h = 1$) to plot Fig. 3. If we had used $h = 0.5$ instead this would have increased the values of the expansion rates by a factor of two and hence the required Lorentz factors. As far as the unified scheme is concerned this would make it more difficult to accommodate sources such as 3C279, which has strong extended structure, while making other sources like NRAO 140, 3C273 and 3C446 easier to explain. Individual objects therefore do not put very useful constraints on H_0 . However, a distance-independent average value of γ can be determined using the unified scheme by requiring it to account for the relative numbers of flat and steep spectrum objects. This value, which is well constrained by the observed properties of quasars, should be consistent with the average γ required to explain the observed superluminal motions. The unified scheme requires $\bar{\gamma} \sim 5$ which is only just consistent with the properties of the five known superluminal quasars if $h = 1$ (giving $\bar{\gamma}_{\text{observed}} \approx 7$). Much smaller values of h (such as $h = 0.5$ (ref. 41)) are excluded by the scheme. Conversely, if h is established to be as low as 0.5 the scheme fails.

Component spectra and correlations

Figure 4 shows spectral decompositions for the nine superluminal sources and 4C39.25. From 408 MHz to 50 GHz all the core spectra are relatively flat; the mean core spectral index is 0.01 ± 0.14 . The average spectral index of the extended structure is -0.8 typical of such structure in other powerful radio sources.

We have looked for correlations between the various source properties some of which are listed in Table 1. There is a good correlation between magnetic field direction, inferred from linear polarization measurements⁴² and the position angle of elongation of the whole source. Such an effect has been pointed out before in 3C273, 3C345 and 3C454.3 by Davis *et al.*⁴³ We

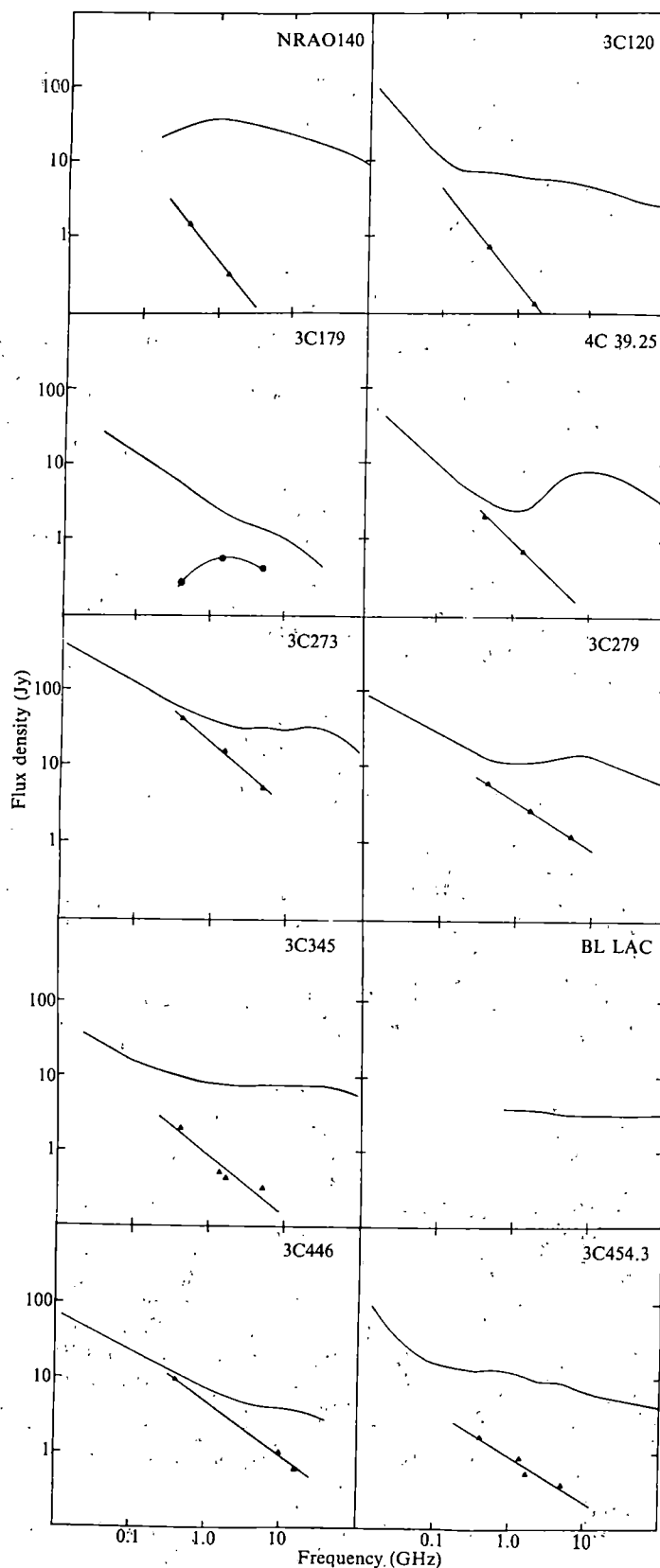


Fig. 4 Radio spectra of the superluminal sources. ▲, Flux density of extended emission. ●, Core flux density.

find that the magnetic field direction is often not perfectly aligned with axis of the dominant VLBI core, but usually has some position angle between that of the smallest and the largest scale structure. This suggests that most of the polarized flux density comes from the VLBI jet, not the core, and that the field direction follows the line of this jet as it does on the arc second scale²⁹.

Conclusions

Superluminal sources nearly all have structures on the scale of a few arc seconds which, although very different from source to source, share common morphological characteristics such as jets and double lobes with other powerful extragalactic objects. Such properties encourage the idea that all such sources are closely related and indeed the properties of most of the superluminal sources are consistent with Orr and Browne's unified scheme³. A consequence of such a scheme is that superluminal

motion should be detectable in most core-dominated sources and many steep spectrum relatively normal doubles like 3C179. A small percentage of core-dominated sources will not show rapid expansion because their angles to the line of sight are very small. 4C39.25 may be one of these.

To make further progress, systematic searches for superluminal motion in a complete sample of sources are essential. The unified scheme which makes well defined predictions for the distribution of apparent expansion velocities would stand or fall by such results.

We thank Tony Foley and Richard Davis for providing a new map of 3C273 and K. J. Johnston, R. A. Perley and G. Wlérick for providing data before publication. P.N.W. acknowledges the receipt of an SERC Advanced Fellowship. M.H.C. is grateful to the Guggenheim Memorial Foundation for a fellowship and to the Institute of Astronomy, Cambridge for their hospitality.

Received 15 June; accepted 11 August 1982.

1. Cohen, M. H. & Unwin, S. C. *IAU Symp.* No. 97, 345-354 (1982).
2. Porcas, R. W. *Nature* **294**, 47-49 (1981).
3. Orr, M. J. L. & Browne, I. W. A. *Mon. Not. R. astr. Soc.* **200**, 1067-1081 (1982).
4. Cornwell, T. J. & Wilkinson, P. N. *Mon. Not. R. astr. Soc.* **196**, 1067-1086 (1981).
5. Marscher, A. P. & Broderick, J. J. *IAU Symp.* No. 97, 359-360 (1982).
6. Fanti, C. et al. *Astr. Astrophys. Suppl.* **45**, 61-78 (1981).
7. Walker, R. C. et al. *Astrophys. J.* **257**, 56-62 (1982).
8. Balick, B., Heckman, T. M. & Crane, P. C. *Astrophys. J.* **254**, 483-488 (1982).
9. Arp, H. C. *Optical Jets in Galaxies* 53-61 (ESO/ESA Workshop 1981).
10. Wlérick, G., Bouchet, P., Cayatte, V. & Michet, D. *Astr. Astrophys.* **102**, L17-L20 (1981).
11. Baldwin, J. A. et al. *Astrophys. J.* **236**, 388-405 (1980).
12. Conway, R. G., Davis, R. J., Foley, A. R. & Ray, T. P. *Nature* **294**, 540-542 (1981).
13. Whitney, A. R. et al. *Science* **173**, 225-230 (1971).
14. Pauliny-Toth, I. I. K. et al. *Astr. J.* **86**, 371-385 (1981).
15. Schraml, J. et al. *Astrophys. J. Lett.* **251**, L57-L60 (1981).
16. Spencer, J. H., Johnston, K. J., Pauliny-Toth, I. I. K. & Witzel, A. *Astrophys. J. Lett.* **251**, L61-L64 (1981).
17. Unwin, S. C. *IAU Symp.* No. 97, 357-358 (1982).
18. Bååth, L. B. et al. *Astrophys. J. Lett.* **243**, L123-L126 (1981).
19. Wilkinson, P. N., Readhead, A. C. S., Anderson, B. & Purcell, G. H. *Astrophys. J.* **232**, 365-381 (1979).
20. Browne, I. W. A. et al. *Mon. Not. R. astr. Soc.* **198**, 673-688 (1982).
21. Mutel, R. L., Allen, H. D. & Phillips, R. B. *Nature* **294**, 236-238 (1981).
22. Phillips, R. B. & Mutel, R. L. *Astrophys. J. Lett.* **257**, L19-L21 (1982).
23. Joshi, M. N. & Gopal-Krishna, *Mon. Not. R. astr. Soc.* **178**, 717-734 (1977).

24. Brown, R. L. et al. *Astrophys. Lett.* **21**, 105-110 (1981).
25. Fanti, R., Ficarra, A., Mantovani, F., Padrielli, L. & Weiler, K. *Astr. Astrophys. Suppl.* **36**, 359-369 (1979).
26. Fisher, J. R. & Erickson, W. C. *Astrophys. J.* **242**, 884-893 (1980).
27. Pearson, T. J., Readhead, A. C. S. & Wilkinson, P. N. *Astrophys. J.* **236**, 714-723 (1980).
28. Cotton, W. D., Geldzahler, B. J. & Shapiro, I. I. *IAU Symp.* No. 97, 301-303 (1982).
29. Perley, R. A. *Optical Jets in Galaxies* 77-81 (ESO/ESA Workshop 1981).
30. Marscher, A. P. & Scott, J. S. *Publ. astr. Soc. Pacif.* **92**, 127-133 (1980).
31. Perley, R. A., Fomalont, E. B. & Johnston, K. J. *Astr. J.* **85**, 649-658 (1980).
32. Bridle, A. H. *IAU Symp.* No. 97, 121-128 (1982).
33. Miley, G. K. *A. Rev. Astr. Astrophys.* **18**, 165-218 (1980).
34. Linfield, R. *Astrophys. J.* **254**, 465-471 (1982).
35. Scheuer, P. A. G. & Readhead, A. C. S. *Nature* **277**, 182-185 (1979).
36. van Groningen, E., Miley, G. K. & Norman, C. A. *Astr. Astrophys.* **90**, L7-L9 (1980).
37. Macklin, J. T. *Mon. Not. R. astr. Soc.* **196**, 967-986 (1981).
38. Hooley, A., Longair, M. S. & Riley, J. M. *Mon. Not. R. astr. Soc.* **182**, 127-145 (1978).
39. Jägers, W. J., van Breugel, W. J. M., Miley, G. K., Schilizzi, R. T. & Conway, R. G. *Astr. Astrophys.* **105**, 278-283 (1982).
40. Moore, P. K., Browne, I. W. A., Daintree, E. J., Noble, R. G. & Walsh, D. *Mon. Not. R. astr. Soc.* **197**, 325-338 (1981).
41. Sandage, A. & Tammann, G. A. *Astrophys. J.* **256**, 339-345 (1982).
42. Simard-Normandin, M., Kronberg, P. P. & Button, S. *Astrophys. J. Suppl.* **45**, 97-111 (1981).
43. Davis, R. J., Stannard, D. & Conway, R. G. *Mon. Not. R. astr. Soc.* **185**, 435-440 (1978).
44. Baath, L. B. et al. *Astr. Astrophys.* **86**, 364-372 (1980).
45. Readhead, A. C. S., Cohen, M. H., Pearson, T. J. & Wilkinson, P. N. *Nature* **276**, 768-771 (1978).

Primary structure of α -subunit precursor of *Torpedo californica* acetylcholine receptor deduced from cDNA sequence

Masaharu Noda*, Hideo Takahashi*, Tsutomu Tanabe*, Mitsuyoshi Toyosato*, Yasuji Furutani*, Tadaaki Hirose†, Michiko Asai†, Seiichi Inayama†, Takashi Miyata‡ & Shosaku Numa*

* Department of Medical Chemistry, Kyoto University Faculty of Medicine, Kyoto 606, Japan

† Pharmaceutical Institute, Keio University School of Medicine, Tokyo 160, Japan

‡ Department of Biology, Kyushu University Faculty of Science, Fukuoka 812, Japan

DNA sequences complementary to the Torpedo californica electroplax mRNA coding for the α -subunit precursor of the acetylcholine receptor were cloned. The nucleotide sequence of the cloned cDNA indicates that the precursor consists of 461 amino acids including a prepeptide of 24 amino acids. Possible sites for acetylcholine binding and antigenic determinants on the α -subunit molecule are discussed.

THE nicotinic acetylcholine receptor that mediates synaptic transmission at the vertebrate neuromuscular junction is the best characterized neurotransmitter receptor from both physiological and biochemical viewpoints (reviewed in refs 1, 2). The acetylcholine receptor from the electroplax of the electric ray *Torpedo californica* is composed of five subunits present in a molar stoichiometry of $\alpha_2\beta\gamma\delta$ (refs 3-5); the apparent molecular weights of the α -, β -, γ - and δ -subunits are 40,000, 50,000, 60,000 and 65,000, respectively⁶⁻¹⁰. The pentameric protein complex is responsible for the binding of agonists,

cholinergic antagonists, α -toxins, histrionicotoxin and local anaesthetics as well as for cation translocation (reviewed in refs 1, 2). The α -subunit contains part or all of the acetylcholine binding site^{6,11,12}. A prerequisite for the understanding of the molecular basis for these various functions is to elucidate the primary structures of the constituent polypeptides of the receptor. Recently, the amino-terminal 54-56 amino acids of all four polypeptides derived from *T. californica* have been sequenced by Raftery et al.⁵, who have found considerable amino acid homology between the subunits, suggesting a common genetic

origin during the evolution of the acetylcholine receptor.

We have now applied recombinant DNA techniques to study the primary structure of the α -subunit of the *T. californica* acetylcholine receptor. DNA sequences complementary to the mRNA coding for this polypeptide have been cloned, and nucleotide sequence analysis of the cloned cDNA has revealed the whole amino acid sequence of the α -subunit precursor. Some structural features of the α -subunit molecule are discussed with respect to acetylcholine binding and immunogenicity.

Isolation of cDNA clones and strategy of DNA sequencing

The approach used to clone cDNA for the α -subunit precursor of the acetylcholine receptor was essentially the same as those described for cloning cDNA for preproenkephalin A (ref. 13) and preproenkephalin B (ref. 14). A library of cDNA clones derived from poly(A)-containing RNA from an electric organ of *T. californica* was constructed using the plasmid DNA vector

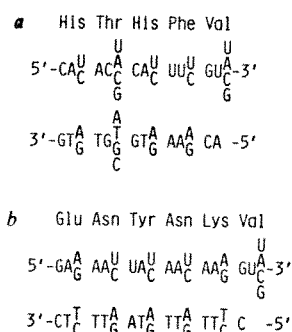


Fig. 1 Synthetic oligodeoxyribonucleotides used for probing cloned cDNA for the α -subunit precursor of the acetylcholine receptor. All possible coding sequences and the corresponding tetradecamers or hexadecamers used are given for the pentapeptide composed of residues 25–29 (a) and the hexapeptide composed of residues 13–18 (b); for the numbering of amino acid residues, see Fig. 3. Probe a was synthesized as two pools that contained A/T or G/C at the position corresponding to the third nucleotide of the Thr codon. Probe b was synthesized as two pools that contained A or G at the position corresponding to the third nucleotide of the left Asn codon (residue 14). For screening cDNA clones, an equimolar mixture of two pools each was used.

elaborated by Okayama and Berg¹⁵. The cDNA library was screened by hybridization with a mixture of 32 oligodeoxyribonucleotides (Fig. 1a) synthesized by the triester method¹⁶. These tetradecamers represented all possible cDNA sequences predicted from the pentapeptide sequence His-Thr-His-Phe-Val (residues 25–29) contained in the amino-terminal region of the α -subunit⁵ (excluding the third nucleotide residue of the Val codon).

Fifty-seven hybridization-positive clones were isolated from $\sim 2 \times 10^5$ transformants and were re-screened by hybridization with a second mixture of 32 oligodeoxyribonucleotides (Fig. 1b) synthesized similarly¹⁶. These hexadecamers corresponded to all possible cDNA sequences predicted from the hexapeptide sequence Glu-Asn-Tyr-Asn-Lys-Val (residues 13–18) present also in the amino-terminal region of the α -subunit⁵ (excluding the second and third nucleotide residues of the Val codon). Thus, 20 clones that hybridized with both probes were isolated. Restriction mapping of these clones with the endonucleases *Pst*I, *Pvu*II, *Rsa*I and *Hin*FI showed the presence of common restriction sites in all clones, suggesting that they represented a single mRNA species. Two of these clones, pACR α 30 and pACR α 44 (carrying the apparently largest cDNA insert), were subjected to nucleotide sequence analysis by the procedure of Maxam and Gilbert¹⁷ according to the strategy indicated in Fig. 2 (see Fig. 2 legend for experimental details of cDNA cloning).

Nucleotide sequence of mRNA and characteristics of the protein sequence deduced

The primary structure of the *T. californica* mRNA encoding the α -subunit precursor of the acetylcholine receptor (Fig. 3) was deduced from the 2,045-nucleotide sequence (excluding the poly(dA)·poly(dT) tract and poly(dG)·poly(dC) tail) determined for the cDNA inserts of clones pACR α 30 and pACR α 44. The nucleotide sequence of the whole protein-coding region was determined with both clones. No nucleotide difference was observed between the sequences determined for the two clones, apparently because the template RNA used for *in vitro* cDNA synthesis was derived from a single electric organ.

The sequence of nucleotide residues 1–162 corresponds precisely to the sequence determined for the amino-terminal 54 amino acids of the acetylcholine receptor α -subunit⁵. The amino acid sequence of the cryptic portion of the α -subunit was

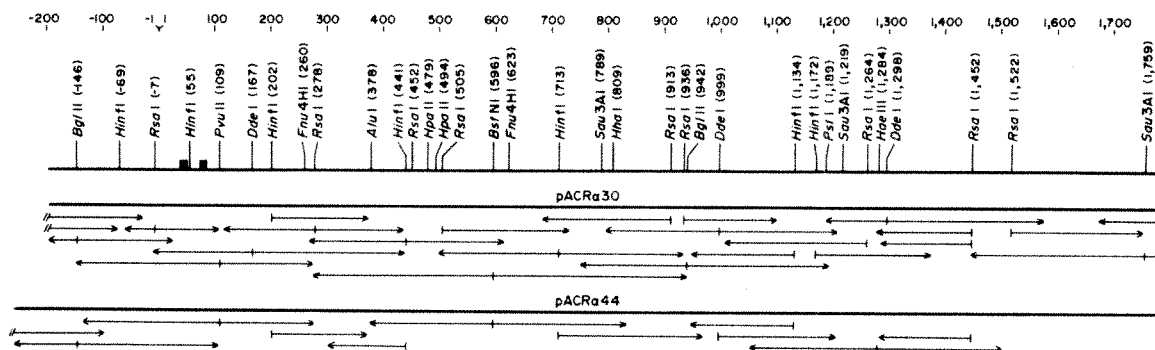


Fig. 2 Strategy for sequencing the cDNA inserts in clones pACR α 30 and pACR α 44. For the isolation of the clones, a cDNA library was constructed by the method of Okayama and Berg¹⁵, using 2.3 μ g of poly(A) RNA from an electric organ of *T. californica* (Pacific Bio-Marine Laboratories) and 1.4 μ g of the vector-primer DNA; avian myeloblastosis virus reverse transcriptase was provided by Dr J.W. Beard. Poly(A) RNA was isolated by subjecting the total RNA extracted³⁷ to oligo(dT)-cellulose chromatography³⁸. *Escherichia coli* χ 1776 (ref. 39) or HB101 (ref. 40) was used for transformation⁴¹, and ampicillin-resistant transformants were screened⁴² by hybridization at 40°C with the oligodeoxyribonucleotide probe a (Fig. 1a) labelled with ³²P at the 5' end. The hybridization-positive clones were re-screened with the oligodeoxyribonucleotide probe b (Fig. 1b) as mentioned above. The restriction map displays only relevant restriction endonuclease sites, which are identified by numbers indicating the 5'-terminal nucleotide generated by cleavage (for the nucleotide numbers, see Fig. 3). The poly(dA)·poly(dT) tract and poly(dG)·poly(dC) tail are not included in the restriction map. The sequences corresponding to the hybridization probes used are indicated by closed boxes. DNA sequencing was carried out by the procedure of Maxam and Gilbert¹⁷. The direction and extent of sequence determinations are shown by horizontal arrows under each clone used; the sites of 5'-end labelling are indicated by short vertical lines at the end of arrows. The slash marks at the end of arrows mean that the site of 5'-end labelling was located on the vector DNA^{15,43} as follows (the numbers in parentheses indicate the distance in nucleotides between the site of labelling and the *Pst*I site (on the 5' side) or *Pvu*II site (on the 3' side) flanking the cDNA insert): *Bst*NI (left upper mark) (45), *Rsa*I (left lower mark) (22) and *Pvu*II (right mark) (0) for pACR α 30; *Bst*NI (45) for pACR α 44. Further details of the sequencing procedures have been described previously⁴⁴.

[illegible]

being involved in poly(A) addition after transcription¹⁸. Computer analysis of the codon usage in the α -subunit precursor mRNA indicates a preference for U (42%) of the third position of the degenerate codons.

We conclude from the mRNA sequence that the α -subunit precursor of the *T. californica* acetylcholine receptor is composed of 461 amino acids, including the amino-terminal 24 amino acids which precede the serine residue at the amino terminus of the known 54-amino acid sequence of the purified α -subunit⁵. The molecular weights of the α -subunit and its precursor are calculated to be 50,116 and 52,738, respectively. The amino-terminal 24-amino acid sequence resembles the signal peptide of secretory proteins¹⁹ in that it contains a large number of hydrophobic amino acids including seven leucine residues (see also Fig. 5). Furthermore, the signal peptide generally contains a region rich in hydrophobic amino acids having large side chains in its central portion, and terminates in a residue with a small neutral side chain²⁰ (for example, alanine, glycine or serine). This is also the case for the

prepeptide of the α -subunit precursor. Thus, it seems likely that this hydrophobic sequence is somehow involved in the translocation of the acetylcholine receptor subunit into the cytoplasmic membrane.

The amino acid composition of the *T. californica* acetylcholine receptor α -subunit predicted from the cDNA sequence agrees fairly well with that determined^{4,10}. However, the predicted molecular weight of the α -subunit (50,116) is considerably larger than the values reported, which range between 39,000 and 48,000 depending on the electrophoresis system and the method of evaluation⁶⁻¹⁰. It is generally recognized that molecular weights estimated by SDS-polyacrylamide gel electrophoresis may be quite inaccurate (for example, see ref. 2). This may hold especially for polypeptides derived from membrane proteins that have higher capacities to bind the detergent due to their larger contents of hydrophobic amino acids²¹⁻²⁴. On the other hand, the possibility that a carboxy-terminal peptide is eliminated by post-translational cleavage cannot be excluded either. Note in this context that the paired basic residues Lys-Arg and Arg-Lys, which generally represent the sites of proteolytic processing^{13,20}, are present at positions 330-331 and 313-314, respectively. Computer analysis of the nucleotide and the amino acid sequence of the α -subunit precursor has not detected such internal homology units as observed for the immunoglobulin polypeptides²⁵.

It has been reported that each subunit of the *T. californica* acetylcholine receptor contains carbohydrate^{4,7,10,11}. The only possible site of *N*-glycosidic linkage in the α -subunit molecule is the asparagine residue in the sequence Asn-Cys-Thr at positions 141-143 (ref. 26). It is possible that *O*-glycosidic carbohydrate units are also present in the α -subunit, because the acetylcholine receptor is known to contain *O*-substituted serine and threonine residues which are probably glycosylated¹⁰.

The α -subunit of the *T. californica* acetylcholine receptor contains seven cysteine residues (excluding the three cysteine residues in the prepeptide). This is consistent with the presence of free sulphhydryls in the receptor molecule^{27,28}. There is evidence that at least two of the cysteine residues in the α -subunit form a disulphide bridge near the acetylcholine binding site^{2,29}. This disulphide can be reduced and alkylated by affinity reagents. Such affinity-labelling studies suggest that, in the acetylcholine binding region, the distance between the negative subsite binding the quaternary ammonium group and one of the sulphhydryl groups formed by reduction is about 1 nm (refs

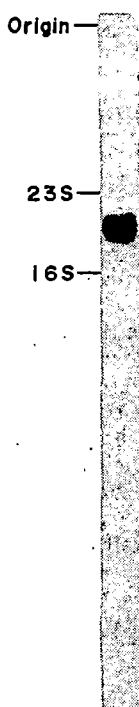


Fig. 4 Autoradiogram of blot hybridization analysis of *T. californica* electroplax RNA with a cDNA probe. Poly(A) RNA (10 μ g) was denatured with 1 M glyoxal and 50% dimethyl sulphoxide⁴⁶, electrophoresed on a 1.5% agarose gel and transferred to diazobenzoylmethyl paper⁴⁷. The hybridization probe used was the 1,088-base pair *Bgl*II fragment (residues -146 to 942) derived from clone pACR α 30; the probe was labelled by nick-translation⁴⁸ with [α -³²P]dCTP. The size markers used were *E. coli* rRNA⁴⁶.

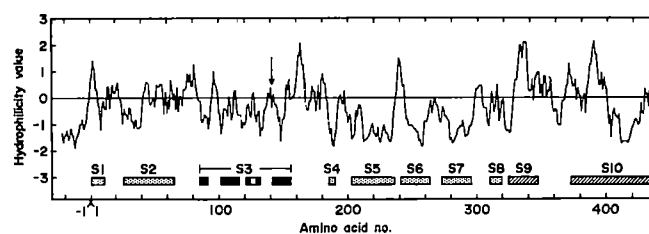


Fig. 5 Predicted secondary structures and hydrophilicity profile of the α -subunit precursor of the acetylcholine receptor. The positions of the predicted structures of α -helix and/or β -sheet (S1-S10) are indicated as follows: shaded boxes, probably α -helix; closed boxes, probably β -sheet; stippled boxes, α -helix or β -sheet; the β -sheet structure corresponding to the open portion in the third box of S3 may partially break. Secondary structure predictions for the prepeptide region are not included. The averaged hydrophilicity value of a hexapeptide composed of amino acid residues $i-2$ to $i+3$ has been plotted against i , where i represents amino acid number (see Fig. 3). The arrow indicates the position of the asparagine residue (residue 141) as a possible site of glycosylation. For the procedures of computer analysis, see refs 33 and 34.

2, 29). In the native unreduced state, a second subsite that is involved in the binding of acetylcholine through hydrophobic interaction or hydrogen bonding is postulated^{2,29}. Because three of the seven cysteine residues present in the α -subunit molecule, that is, residues 222, 412 and 418, are located in predicted secondary structures of strong hydrophobicity (see Fig. 5), it seems improbable that they appear on the outer surface of the membrane or receptor molecule for ready access to affinity reagents. At least two of the remaining four cysteine residues (residues 128, 142, 192 and 193) may take part in the disulphide bridge present in close proximity to the acetylcholine binding site. (The formation of a disulphide bond between the adjacent cysteine residues 192 and 193 is unlikely³⁰.) Because the asparagine residue at position 141 is most probably glycosylated (see above), the region surrounding it would reside on the extracellular surface of the receptor molecule. Moreover, this region encompasses a predicted β -turn structure lying between predicted β -sheet structures which may be tightly packed (see Fig. 5), so that its conformation would be more or less stabilized.

The nucleotide binding site of dehydrogenases occurs at an end of a pleated sheet structure on the outer surface of the molecules³¹. A similar conformation is observed in the hyper-variable regions of the immunoglobulin molecules³². Thus, it is tempting to assume that the acetylcholine binding site is located in the region including the cysteine residues at positions 128 and 142. Measurements on Corey-Pauling-Koltun space-filling models are consistent with the hypothesis that the aspartic acid residue at position 138 (or the glutamic acid residue at position 129) as the negative subsite, together with, for example, the histidine residue at position 134 or a hydrophobic residue in its vicinity as the second subsite, may be involved in the binding of acetylcholine. An alternative possibility is that the aspartic acid residue at position 195 or 200 near the cysteine residues at positions 192 and 193 may act as the negative subsite; the region including these residues also contains a predicted β -turn structure surrounded by predicted secondary structures (see Fig. 5).

The amino acid sequence of the acetylcholine receptor α -subunit precursor was analysed by computer for secondary structure and local hydrophilicity according to the procedures of Chou and Fasman³³ and of Hopp and Woods³⁴, respectively. Figure 5 shows the hydrophilicity profile along the polypeptide chain as well as the predicted structures of α -helix and/or β -sheet which are schematically represented by boxes (S1-S10). The segments that can form secondary structures extend over a wide range of the α -subunit molecule. The structure S10, most likely to be an α -helix, is particularly long (64 amino acid residues) and contains a large hydrophobic region in the middle, probably representing a transmembrane segment. The

structures S5, S6 and S7 also exhibit strong hydrophobicity, presumably being buried in the membrane or being involved in hydrophobic inter-subunit interaction. The structure S3 is composed of a set of four β -sheets which may be closely packed in an antiparallel orientation. This region encompasses a putative acetylcholine binding site as discussed above. The pleated sheet structure would facilitate the generation of a specific conformation for binding the neurotransmitter.

Hopp and Woods³⁴ have reported that the point of highest local hydrophilicity is invariably located in or immediately adjacent to a protein antigenic determinant. This allows us to predict possible candidates for antigenic determinants on the α -subunit molecule, that is, the peptide segments composed of residues 161–166, 330–340 and 387–392. It has been observed that some antigenic determinants are not correlated with hydrophilicity, although there seems to be a correlation of many antigenic determinants with local upspikes of the hydrophilicity profile³⁴. Thus, for example, the residues 1–6 and 237–242 may

also represent possible antigenic determinants. Knowledge of the antigenic determinants on the acetylcholine receptor and its subunits is important because antibodies directed to them are the primary pathological agents in myasthenia gravis and its animal model, experimental autoimmune myasthenia gravis (reviewed in ref. 35). It has been reported that most of the antibodies produced by human patients as well as by experimental animals are directed to the 'main immunogenic region' which is located on the extracellular surface of the α -subunit and is distinct from the acetylcholine binding site³⁶. The possible acetylcholine binding site and antigenic determinants we have proposed are consistent with this finding.

We thank Dr Paul Berg and Dr Hiroto Okayama for providing us with their high-efficiency cloning system, and Dr Tadashi Tanabe for helpful discussions. This investigation was supported in part by research grants from the Ministry of Education, Science and Culture of Japan, the Mitsubishi Foundation and the Japanese Foundation of Metabolism and Diseases.

Received 20 July; accepted 3 September 1982.

- Heidmann, T. & Changeux, J. P. *Rev. Biochem.* **47**, 317–357 (1978).
- Karlin, A. in *Cell Surface Reviews* Vol. 6 (eds Cotman, C. W., Poste, G. & Nicolson, G. L.) 191–260 (North-Holland, Amsterdam, 1980).
- Reynolds, J. & Karlin, A. *Biochemistry* **17**, 2035–2038 (1978).
- Lindstrom, J., Merlie, J. & Yogeewaran, G. *Biochemistry* **18**, 4465–4470 (1979).
- Raftery, M. A., Hunkapiller, M. W., Strader, C. D. & Hood, L. E. *Science* **208**, 1454–1456 (1980).
- Weill, C. L., McNamee, M. G. & Karlin, A. *Biochem. biophys. Res. Commun.* **61**, 997–1003 (1974).
- Raftery, M. A., Vandlen, R. L., Reed, K. L. & Lee, T. *Cold Spring Harb. Symp. quant. Biol.* **40**, 193–202 (1975).
- Hucho, F., Bandini, G. & Suárez-Isla, B. A. *Eur. J. Biochem.* **83**, 335–340 (1978).
- Froehner, S. C. & Rafto, S. *Biochemistry* **18**, 301–307 (1979).
- Vandlen, R. L., Wu, W. C. S., Eisenach, J. C. & Raftery, M. A. *Biochemistry* **18**, 1845–1854 (1979).
- Karlin, A., Weill, C. L., McNamee, M. G. & Valderrama, R. *Cold Spring Harb. Symp. quant. Biol.* **40**, 203–213 (1975).
- Damle, V. & Karlin, A. *Biochemistry* **17**, 2039–2045 (1978).
- Noda, M. *et al. Nature* **295**, 202–206 (1982).
- Kakidani, H. *et al. Nature* **298**, 245–249 (1982).
- Okayama, H. & Berg, P. *Molec. cell. Biol.* **2**, 161–170 (1982).
- Ito, H., Ike, Y., Ikuta, S. & Itakura, K. *Nucleic Acids Res.* **10**, 1755–1769 (1982).
- Maxam, A. M. & Gilbert, W. *Meth. Enzym.* **65**, 499–560 (1980).
- Proudfoot, N. J. & Brownlee, G. G. *Nature* **263**, 211–214 (1976).
- Blöbel, G. & Dobberstein, B. *J. Cell Biol.* **67**, 852–862 (1975).
- Steiner, D. F., Quinn, P. S., Chan, S. J., Marsh, J. & Tager, H. S. *Ann. N.Y. Acad. Sci.* **343**, 1–16 (1980).
- Grefrath, S. P. & Reynolds, J. A. *Proc. natn. Acad. Sci. U.S.A.* **71**, 3913–3916 (1974).
- Robinson, N. C. & Tanford, C. *Biochemistry* **14**, 369–378 (1975).
- Frank, R. N. & Rodbard, D. *Archs Biochem. Biophys.* **171**, 1–13 (1975).
- Miyake, J., Ochiai-Yanagi, S., Kasumi, T. & Takagi, T. *J. Biochem.* **83**, 1679–1686 (1978).
- Hill, R. L., Delaney, R., Fellows, R. E. Jr & Lebovitz, H. E. *Proc. natn. Acad. Sci. U.S.A.* **56**, 1762–1769 (1966).
- Marshall, R. D. *Biochem. Soc. Symp.* **40**, 17–26 (1974).
- Eldefrawi, M. E., Eldefrawi, A. T. & Wilson, D. B. *Biochemistry* **14**, 4304–4310 (1975).
- Chang, H. W. & Bock, E. *Biochemistry* **16**, 4513–4520 (1977).
- Karlin, A. *J. gen. Physiol.* **54**, 245–264s (1969).
- Dayhoff, M. D. in *Atlas of Protein Sequence and Structure* Vol. 5, 77–268 (National Biomedical Research Foundation, Washington DC, 1976).
- Liljas, A. & Rossmann, M. G. *Rev. Biochem.* **43**, 475–507 (1974).
- Poljak, R. J. *et al. Proc. natn. Acad. Sci. U.S.A.* **70**, 3305–3310 (1973).
- Chou, P. Y. & Fasman, G. D. *Rev. Biochem.* **47**, 251–276 (1978).
- Hopp, T. P. & Woods, K. R. *Proc. natn. Acad. Sci. U.S.A.* **78**, 3824–3828 (1981).
- Lindstrom, J. & Dau, P. A. *Rev. Pharmac. Tox.* **20**, 337–362 (1980).
- Tzartos, S. J., Seybold, M. & Lindstrom, J. M. *Proc. natn. Acad. Sci. U.S.A.* **79**, 188–192 (1982).
- Chirgwin, J. M., Przybyla, A. E., MacDonald, R. J. & Rutter, W. J. *Biochemistry* **18**, 5294–5299 (1979).
- Aviv, H. & Leder, P. *Proc. natn. Acad. Sci. U.S.A.* **69**, 1408–1412 (1972).
- Curtiss, R. III *et al. in Recombinant Molecules, Impact on Science and Society* (eds Beers, R. F. & Bassett, E. G.) 45–56 (Raven, New York, 1977).
- Boyer, H. W. & Roulland-Dussoix, D. *J. molec. Biol.* **41**, 459–472 (1969).
- Wahl, G. M., Padgett, R. A. & Stark, G. R. *J. biol. Chem.* **254**, 8679–8689 (1979).
- Hanahan, D. & Meselson, M. *Gene* **10**, 63–67 (1980).
- Reddy, V. B. *et al. Science* **200**, 494–502 (1978).
- Nakanishi, S. *et al. Nature* **278**, 423–427 (1979).
- Sutcliffe, J. G. *Nucleic Acids Res.* **5**, 2721–2728 (1978).
- McMaster, G. K. & Carmichael, G. G. *Proc. natn. Acad. Sci. U.S.A.* **74**, 4835–4838 (1977).
- Alwine, J. C., Kemp, D. J. & Stark, G. R. *Proc. natn. Acad. Sci. U.S.A.* **74**, 5350–5354 (1977).
- Weinstock, R., Sweet, R., Weiss, M., Cedar, H. & Axel, R. *Proc. natn. Acad. Sci. U.S.A.* **75**, 1299–1303 (1978).

Human metallothionein genes—primary structure of the metallothionein-II gene and a related processed gene

Michael Karin* & Robert I. Richards†

* Metabolic Research Unit, Department of Medicine, Biochemistry and Biophysics, University of California, San Francisco, California 94143, USA and Department of Microbiology, University of Southern California School of Medicine, 2025 Zonal Avenue, HMR-401, Los Angeles, California 90033, USA

† Center for Recombinant DNA Research and Department of Genetics, Research School of Biological Sciences, Australian National University, Canberra, ACT 2601, Australia

The complete nucleotide sequence of two of the human metallothionein gene family has been compared. One is a functional metallothionein-II gene, the other a pseudogene, lacking introns, terminating in a poly(A) tail and flanked by two direct repeats. In addition, we have detected a size polymorphism associated with the processed gene in the population examined, and we have observed a region of apparent secondary structure homology between a 5' flanking region of the functional metallothionein-II gene and that of a mouse metallothionein-I gene.

METALLOTHIONEINS (MTs) are a family of low-molecular weight heavy metal binding proteins, unique in their high cysteine content. MTs specifically bind heavy metals, such as zinc, cadmium, copper and mercury. MTs and related heavy metal binding proteins are ubiquitously distributed in the animal and plant kingdoms and are even found in prokaryotes¹. These proteins are inducible in experimental animals and cultured

cells both by exposure to heavy metal ions¹ and glucocorticoid hormone². Their ubiquitous distribution and high inducibility make them an attractive model system to study regulation of gene expression.

Human MTs have been isolated from liver³ and cultured cells^{4,5} where they are present in two major electrophoretically distinguishable forms known as MT-I and MT-II³. The amino

acid sequence of both human MT-I and MT-II have been determined^{1,6}. Although MT-II seems to be a unique protein, MT-I is a mixture of at least three different proteins generating a heterogeneous amino acid sequence.

We have been studying the regulation of MT synthesis in HeLa cells and have shown that either heavy metals or glucocorticoids are primary inducers of MT mRNA⁷. As neither one of them affects the stability of the mRNA⁸, transcriptional control has been suggested. Recently, Palmiter and co-workers have directly demonstrated that either heavy metals or glucocorticoids increase the transcription rate of the mouse MT-I gene^{9,10}. To define the components involved in the molecular mechanisms responsible for the regulation of MT gene expression in man, we isolated and characterized DNA fragments containing the different genes.

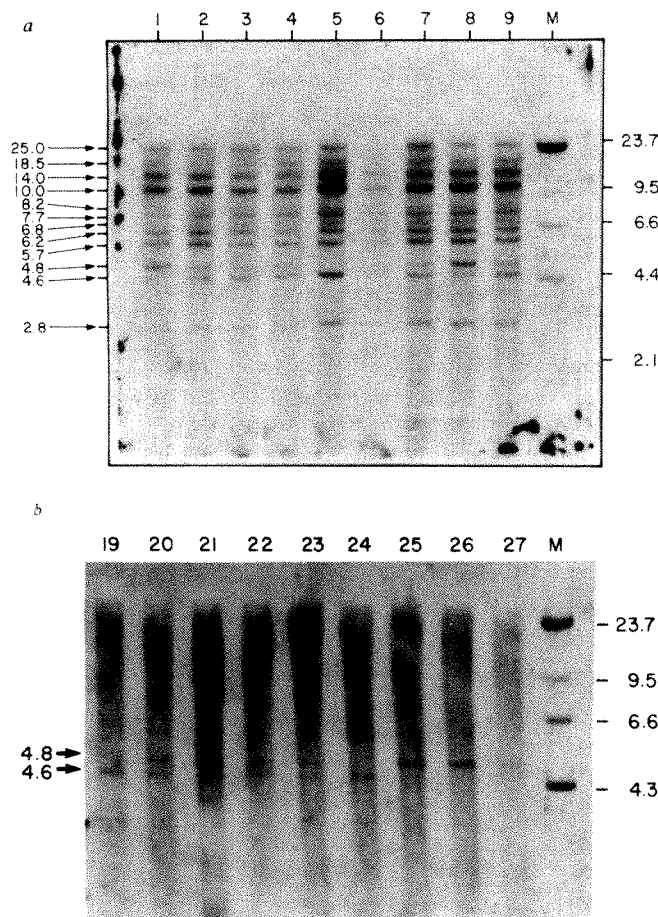


Fig. 1 Detection of MT genes in human genomic DNA. Human genomic DNA was prepared from white blood cells, digested with *EcoRI*, the fragments were separated by electrophoresis on 1% agarose gels and transferred to nitrocellulose filters as described by Bell *et al.*³³. *a*, The *BamHI-PvuII* coding region of phMT-II₃ (ref. 11) was labelled by nick-translation³⁴ using both [α -³²P]dATP and [α -³²P]dCTP. Hybridization was as described by Wahl *et al.*³⁵, with slight modifications. We have included an additional washing step, using 50% formamide, 5×SSC at 42°C for 60 min, before the final wash step, using 0.1×SSC at 42°C was performed (1×SSC=0.15 M NaCl, 0.015 M Na citrate). Individuals are indicated by number above the autoradiogram, the sizes of the hybridizing fragments are on the left and the sizes of the bacteriophage λ *HindIII* fragments, which served as molecular weight markers, are on the right. *b*, To demonstrate more clearly the size polymorphism associated with the MT-II_B pseudogene, an hybridization probe specific for that gene was used. The *EcoRI-BamHI* fragment containing the 5' portion of the MT-II_B gene (see Fig. 2) was labelled by nick-translation³⁴. Hybridization to the blots of *EcoRI*-digested human DNA was as described above. Final washing, using 0.1×SSC, was performed at 60°C.

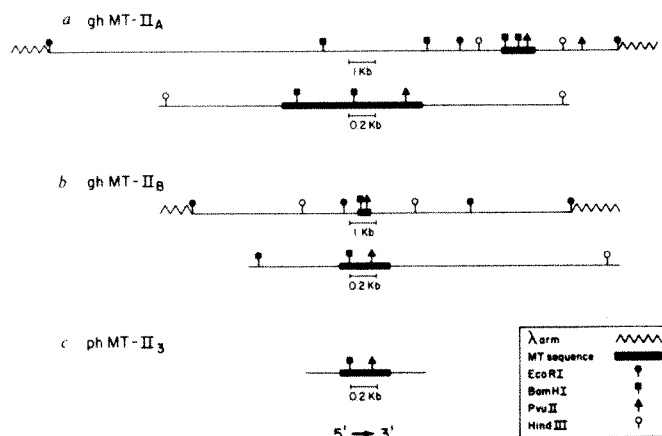


Fig. 2 Restriction maps of the two human MT-II genes. About 1.5×10^6 plaques (10 genome equivalents) of the human genomic library prepared by Lawn *et al.*¹² were screened by the method of Benton and Davis¹⁴ using the *BamHI-PvuII* coding region of phMT-II₃ as a hybridization probe. Of 200 positive plaques detected, 100 were subjected to three cycles of plaque purification which finally resulted in 53 positive clones. Phage DNA was prepared, digested with *EcoRI*, *BamHI* or *PvuII*, the fragments were separated on 1% agarose gels, transferred to nitrocellulose¹³ and the fragments containing MT structural sequences were identified by hybridization to the coding region probe. The genes coding for MT-II were finally identified using the 5' and 3' untranslated regions of phMT-II₃ as hybridization probes. Shown are restriction maps of the largest Charon 4A clones isolated and of subclones of the MT-II_A (*a*) and MT-II_B (*b*) genes. A restriction map of phMT-II₃ (*c*), the cDNA clone coding for MT-II mRNA¹¹, is also shown for comparison.

As described previously¹¹, cDNA clones for the different human MT genes were isolated. Using one of these clones, we screened a human genomic DNA library¹² and isolated phage λ clones containing most of the different MT genes. Here we describe the nucleotide sequence of a functional gene coding for human MT-II and a closely related processed pseudogene.

Metallothioneins are encoded by a large gene family

Previously we obtained a full-length cDNA clone of human MT-II mRNA, phMT-II₃ (ref. 11). The cDNA can be conveniently divided into: (1) 5' untranslated region, from the 5' end of the cDNA to the *BamHI* site; (2) coding region, from the *BamHI* site to the *PvuII* site; and (3), 3' untranslated region, from the *PvuII* site to the 3' end of the cDNA (see Fig. 2). To estimate the number and the sizes of the MT genes in the human genome we have used the *BamHI-PvuII* coding region as a probe, since it is the region most likely to be conserved among the different genes^{1,6}. Human genomic DNA was digested with *EcoRI*, fractionated by electrophoresis on agarose gels and transferred to nitrocellulose filters¹³. At least 11 or 12 different bands hybridizing to the MT-II coding region probe could be detected (Fig. 1). About 15 hybridizing bands can be detected when genomic DNA is digested with *HindIII* (data not shown), suggesting a multiplicity of genes bearing at least 80% homology to the coding region of MT-II. One of the restriction fragments exhibits polymorphism and appears as either a 4.8- or 4.6-kilobase (kb) *EcoRI* band. This fragment corresponds to the MT-II_B pseudogene. The significance of this result is discussed below.

Isolation of the human MT genes

To isolate all the human MT genes, we screened a human genomic library¹² using the *BamHI-PvuII* coding region probe. After screening 1.5×10^6 recombinant phage, 200 positive plaques were detected; 100 of the hybrids were subjected to three cycles of plaque purification¹⁴ which finally yielded 53

positive clones containing fragments hybridizing with the MT-II coding region.

DNA was prepared from each of the 53 positive clones and was analysed by *EcoRI* digestion and Southern blotting. At least 18 different *EcoRI* bands hybridizing to the MT-II coding region probe were detected among the different clones analysed. All but two of the *EcoRI* fragments detected on the genomic blots (Fig. 1) were represented among these bands. The two exceptions were the largest fragments migrating at 25 and 18.5 kb. While most of the λ clones contained a single positively hybridizing *EcoRI* fragment, some of them contained two such fragments. Those clones were found to contain several MT-I genes suggesting close linkage of this subfamily (data not shown). Taken together with the data shown in Fig. 1, the results of the cloning experiment suggest there are about 11 or 12 different human MT genes.

To identify the gene(s) coding for MT-II, the major MT to be expressed in HeLa cells and human liver⁵ *EcoRI*, *BamHI* and *PvuII* restriction enzyme digests of the 53 genomic clones were screened for hybridization with the untranslated region probes. Only three of the genomic clones contained fragments hybridizing to the 5' or 3' untranslated regions of MT-II cDNA. The 5' untranslated region probe hybridized to only two of the *EcoRI* fragments of genomic DNA, containing MT coding regions migrating at 5.8 and 4.8 or 4.6 kb (data not shown). While all the different genes share sequence homology at coding regions, they differ in their 5' and 3' untranslated regions.

Further restriction endonuclease mapping analysis revealed that two of the clones contained some identical DNA fragments and therefore overlapped. The gene contained in these two clones is referred to as ghMT-II_B, while the gene in the third unique clone is referred to as ghMT-II_A. Restriction maps are shown in Fig. 2. Interestingly, the distance between the *BamHI* and *PvuII* restriction sites in ghMT-II_B is approximately 170 base pairs (bp), the same as their relative location in the mRNA sequence¹¹. Since this fragment comprises most of the coding region, which in the mouse contains two intervening sequences¹⁵, it was apparent that no intervening sequences were expected in this gene. The distance between these two sites in ghMT-II_A mapped at 670 bp, suggesting the presence of intervening sequences.

Structure of the MT-II_A gene

We have determined the complete nucleotide sequences of the two genes. ghMT-II_A is the authentic gene coding for the human MT-II protein (Fig. 3). It spans about 900 bp and contains two introns. Both introns obey the GT-AG splicing rule¹⁶ and are located at exactly the same positions within the coding region as the introns in the mouse MT-I gene¹⁵.

The start of transcription of the ghMT-II_A gene was determined by a modification of the S₁ nuclease mapping technique¹⁷. (The experimental protocol is described in Fig. 4 legend.) Three nuclease-resistant bands can be detected corresponding to fragments starting at the *BamHI* site at position +75 and ending at the T at -3, A at +1 and A at +3 (Fig. 4a). (Similar patterns were obtained when S₁ nuclease was used, instead of mung bean nuclease.) The middle start site was determined as position +1, since it seems to be used more frequently.

The sequence of the mouse MT-I gene at the 5' end of the mRNA, GTCACCAGACT, is almost identical to the corresponding region in the human gene, except for two changes: T to C at position -2 and A to C at position 7. In view of this homology we suggest that the start of transcription of the mouse MT-I gene is also at the first A, and not at the G residue at -3, as determined by Glanville *et al.*¹⁵. This discrepancy could be due to strong steric hindrance by the mouse MT-I cap structure which prevents complete digestion by S₁ nuclease. This possibility has actually been raised by Glanville *et al.*¹⁵.

The expression of the mouse MT-I gene is regulated by heavy metals after introduction into human cells¹⁸ and the human

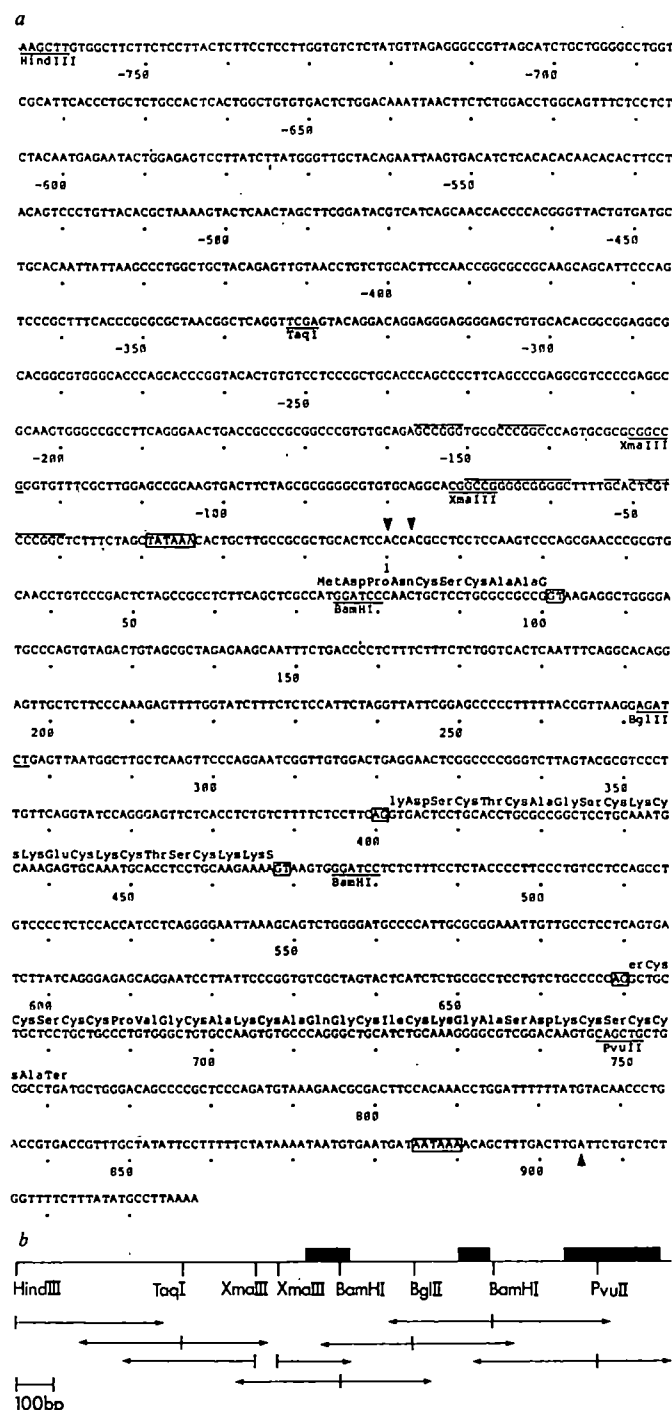


Fig. 3 Primary structure of the human MT-II_A gene. *a*, Nucleotide sequence of the MT-II_A gene. The major cap site (see Fig. 4) is numbered +1. Consensus sequences involved in transcription initiation (-30 to -24) and polyadenylation (886-891) are boxed. Introns run from nucleotides 100-401 and 469-671. The dyad symmetries in the 5' flanking region are underlined; ▽, ▲ indicate transcription initiation and polyadenylation sites, respectively. *b*, Sequencing strategy for the MT-II_A gene. Sequence analysis was performed on DNA isolated from a subclone in plasmid pBR322 (p84H) of the 3.2-kb *HindIII* restriction endonuclease fragment of ghMT-II_A (Fig. 2), by the chemical³⁶ and chain termination³⁷ methods. For the chemical analysis, restriction endonuclease-generated DNA fragments were end-labelled by end-filling³⁸ with [α -³²P]dNTPs (2,000-3,000 Ci mmol⁻¹; Amersham) and AMV reverse transcriptase (W. J. Beard, Life Sciences, Inc.). Modification and cleavage reactions were as described in ref. 36. Chain termination analysis was performed on restriction fragments cloned into bacteriophage M13 (strains mp8 and mp9)³⁹. Sequencing primer (5'-GTTTTCACGTCACGAC-3') was given by Genentech, Inc. ■, Exons of the MT-II_A gene. Arrows indicate the direction and extent of sequencing (each sequence was determined at least twice).

MT-II_A gene is regulated in mouse cells (M.K., unpublished results). Based on the assumption that each of those genes is recognized by the regulatory factors from the other species, it was surprising not to find any extensive required homology in the immediate 5' flanking region of the two genes. Palmiter and co-workers have pointed out two regions of dyad symmetry upstream from the TATA box in the mouse MT-I gene¹⁴ and

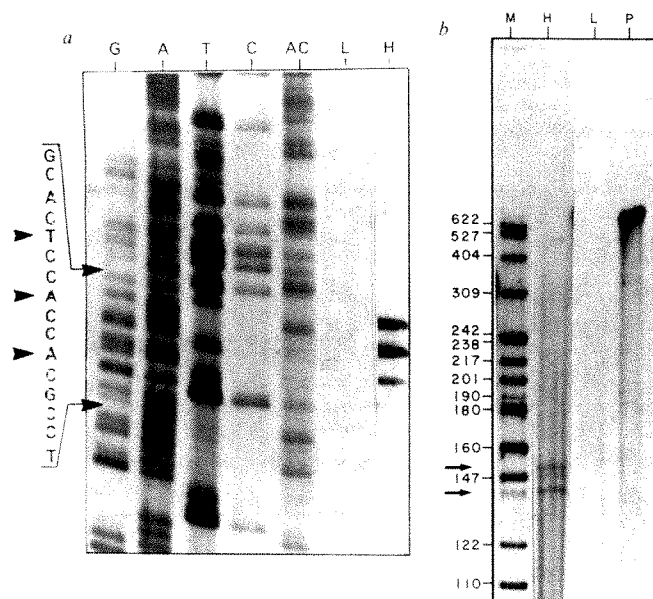


Fig. 4 Identification of the MT-II mRNA transcription start and termination sites. *a*, Plasmid ph84H, a *Hind*III subclone of the MT-II_A gene, was digested with *Bam*HI, 5' end-labelled using T₄ polynucleotide kinase (PL Biochemicals) and [γ -³²P]ATP and subjected to secondary digest with *Hind*III. The labelled *Hind*III-*Bam*HI fragment containing the 5' region of the MT-II_A gene was isolated by electrophoresis on 1% agarose gel and electroelution. Portions of the probe (50,000 c.p.m.) were co-precipitated with 100 μ g of total RNA from cadmium-induced HeLa (H) of LTK⁻ (L) cells, the precipitate was dissolved in 30 μ l of 80% formamide, 0.4 M NaCl, 40 mM PIPES pH 6.5, 1 mM EDTA, and overlaid with paraffin oil. The nucleic acids were denatured for 5 min at 85 °C and allowed to hybridize overnight at 54 °C. The sample was then diluted with 370 μ l of 0.25 M NaCl, 30 mM NaOAc pH 4.6, 1 mM ZnCl₂, 5% glycerol and incubated with 450 units of mung bean nuclease (PL Biochemicals) at 37 °C for 90 min. The digestion was terminated by phenol-CHCl₃ extraction and the nucleic acids were isolated by ethanol precipitation. The RNA was then hydrolysed by 0.2 M NaOH at 45 °C for 60 min, the sample was neutralized and the residual nucleic acids collected by ethanol precipitation. The sample was dissolved in 10 μ l of formamide dye mix³⁶ and 3 μ l of it were loaded on to the sequencing gel. To generate molecular weight size markers, the *Bam*HI-*Hind*III end-labelled fragment was subjected to chemical sequencing reactions and products were displayed on 8% sequencing gel. Lanes A, G, C, T and AC are the sequencing ladders. Lane L, control hybridization between the probe and LTK⁻ cells total RNA; lane H, mung bean nuclease-resistant products generated by hybridization to Cd²⁺-induced HeLa cell RNA. The nucleotide sequence of the sense strand at the region of interest is indicated on the left-hand site, and the putative transcription start sites are indicated by arrows. *b*, Mapping of the termination site. ph84H DNA was digested with *Pvu*II and 3'-labelled using T₄ polymerase (BRL)⁴⁰ and [α -³²P]dCTP > 3,000 Ci mmol⁻¹ (Amersham). The labelled DNA was subjected to secondary digest with *Hind*III, and the *Pvu*II-*Hind*III fragment containing the 3' untranslated and flanking region of the MT-II_A gene was isolated as described above to be used as a probe. Hybridization, digestion and electrophoresis were as described above except for hybridization temperature which was 43 °C. End-labelled *Hpa*II fragments of pBR322 were used as size markers (lane M). Lane H, hybridization to cadmium-induced HeLa cellular RNA. Lane L, hybridization to LTK⁻ cellular RNA. Lane P, undigested probe.

suggested a possible regulatory role for these sequences. The regulatory role of the larger dyad symmetry (centred at position -55 on the MT-I gene) was supported by analysis of deletion mutants at the 5' flanking region of the mouse MT-I gene¹⁹. Deletions extending into this region or completely deleting it, abolish metal inducibility of the mouse gene. Close examination of the human MT-II_A gene at this region reveals similar dyad symmetry regions at almost identical positions to the mouse MT-I gene (Fig. 5).

Although of different composition, such a conserved structure may be of significance in the regulation of MT gene expression. We speculate that regulatory factors, most likely apothionein itself, recognize these secondary structures (possibly forming hairpin loops *in vivo*, as suggested in refs 20 and 21) and not a particular nucleotide sequence *per se*. We are presently constructing mutations at these sites to test this hypothesis.

Our previously obtained MT-II cDNA clone, phMT-II₃, did not end with a poly(A) tract¹¹. We have mapped the polyadenylation site directly by the nuclease protection technique¹⁷. Two major nuclease-resistant fragments could be detected on acrylamide-urea gels. Their sizes are 142 \pm 2 and 153 \pm 2 nucleotides (Fig. 4b). This would place the polyadenylation sites to the A residues at positions 893 and 905 (Fig. 3). It is possible that the observed band at position 893 is an artefact of the nuclease digestion method due to local melting of the hybrid at that region which is A+T-rich (a stretch of 11 A and T residues). The second termination site at 905 is located 15 nucleotides away from the end of the consensus sequence AATAAA, originally suggested by Proudfoot and Brownlee²², to serve as a polyadenylation signal.

Structure of the human MT-II_B gene

The sequence of the MT-II_B gene is shown in Fig. 6, in comparison with the structural sequence of the MT-II_A gene (without the introns). MT-II_B is highly homologous (95%) to an exact cDNA copy of MT-II mRNA. The homology to the MT-II_A gene starts exactly at the major cap site of the later gene and ends at its 3' end. At this point the MT-II_B pseudogene contains a stretch of 15 A residues, a landmark of RNA type processing. The MT-II_B gene is most likely derived from MT-II_A or its ancestor. The two genes share extensive homology in their 5' and 3' untranslated regions. As discussed earlier, the homology between the different MT genes is restricted to the coding region. (We have not detected any other MT-II-like genes among our genomic clones.)

The MT-II_B gene has accumulated several mutations, relative to the MT-II_A gene. Surprisingly, most of the mutations within its coding region are silent changes in the third codon position, only one causing an amino acid change of Gly to Ser. Since the reading frame is maintained and there are no premature termination codons, this gene does probably code for a functional protein although it is not expressed.

The MT-II_B pseudogene is flanked by two long, slightly imperfect, direct repeats which might have been generated by insertion site duplication²³. The 5' and 3' direct repeats are 27 and 25 nucleotides long, respectively, of which 21 nucleotides are identical. The 5' repeat does not flank the gene immediately as expected, but there is actually a trinucleotide spacer between

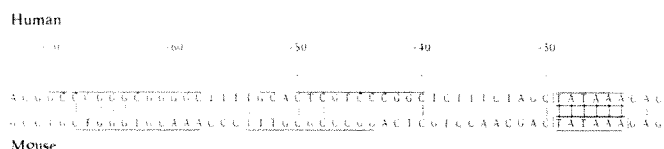


Fig. 5 Putative regulatory sequences in mammalian MT genes. The human MT-II_A and the mouse MT-I¹⁴ gene sequences are aligned, with respect to their TATAA boxes, to show the identical location of dyad symmetry sequences. TATAA sequences are boxed, and the dyad symmetry sequences are underlined. Bases are numbered from the major consensus cap site for each gene (see text). Vertical bars indicate identical bases.

it and the beginning of the pseudogene (the equivalent of the cap site of the authentic MT-II_A gene). The significance of this structure is not yet clear.

The MT-II_B pseudogene is not expressed to any significant extent in HeLa cells, and it is not expressed after introduction into mouse L cells, in experimental conditions that lead to normal expression and regulation of the MT-II_A gene (data not shown). However, such results are not surprising, because of the absence of any structures resembling eukaryotic promoters in the 5' flanking region of the MT-II_B gene.

The nucleotide sequence at the immediate 3' flanking region of the MT-II_B gene is extremely A+T-rich (90%). Such A+T-rich regions are quite prone to breakage and can conceivably generate the staggered break into which the MT-II cDNA integrated to yield the MT-II_B gene.

After re-examination of the human genomic blots shown in Fig. 1a with an MT-II_B specific probe, the polymorphism associated with the processed gene became quite apparent (Fig. 1b). In some individuals it appears as a 4.8-kb *Eco*RI fragment, the same size as the gene isolated from the genomic library, while other individuals are missing this band and instead have a 4.6-kb *Eco*RI fragment. Other individuals seem to have both of these bands, indicating that the MT-II_B pseudogene is present in two allelic forms. Of 36 individuals examined, 22 (61%) were found to be heterozygotes, 6 (17%) were homozygotes for the short form (4.6 kb) and 8 (22%) were homozygotes for the long form (4.8-kb) of the processed gene. This heterogeneity is probably due to either restriction site polymorphism around the gene or a small deletion (about 200 bp) which occurred adjacent to it.

The polymorphism is not due to rearrangement of repetitive DNA sequences near the MT-II_B, since the 4.8-kb *Eco*RI fragment bearing this gene is devoid of such sequences (M.K., unpublished results).

Several processed genes have already been described (refs 24–29 and P. Sharp, personal communication) and what seemed to be a rare event appears to be a more common phenomenon. It is interesting to note that the processed genes from the tissue-specific globin²⁸ and immunoglobulin²⁴ gene families seem to be derived from abnormal transcripts while those from the more ubiquitously transcribed families of metallothionein and tubulin (ref. 29 and P. Sharp, personal communication) are derived from apparently complete, normal transcripts. It is possible that there is a low level or occasional transcription of tissue-specific genes in the germ cells from secondary upstream or downstream promoters^{30–32}. Such aberrant transcripts are probably the precursors of the observed processed genes.

Conclusions

The human MT gene family is more complex than expected, consisting of about 11 closely related members bearing at least 80% nucleotide sequence homology to the MT-II coding region.

Not all of those genes are necessarily functional. So far we have determined the complete nucleotide sequence of two MT-II genes. While the MT-II_A gene is fully functional, the MT-II_B is a processed pseudogene.

Probably the most remarkable feature of the MT-II_A gene sequence is the lack of expected nucleotide homology to the mouse MT-I gene in the immediate 5' flanking region of both genes. Instead, the two genes reveal secondary structure homology. Both of them have dyad symmetry regions, which can form stable hairpin loops at the same positions relative to the TATAA box. So far, in the case of the mouse MT-I gene, there is evidence for the involvement of one of those structures in the metal induction phenomenon¹⁹.

This observation (secondary structure homology) might be valid for other gene systems as well. In such a case, a search for simple nucleotide homologies in the 5' flanking regions of related genes, might not reveal the important regulatory regions.

The MT-II_B pseudogene was probably generated from a normal RNA transcript of the MT-II_A gene. The structure of this and other processed genes suggests that the reversed flow

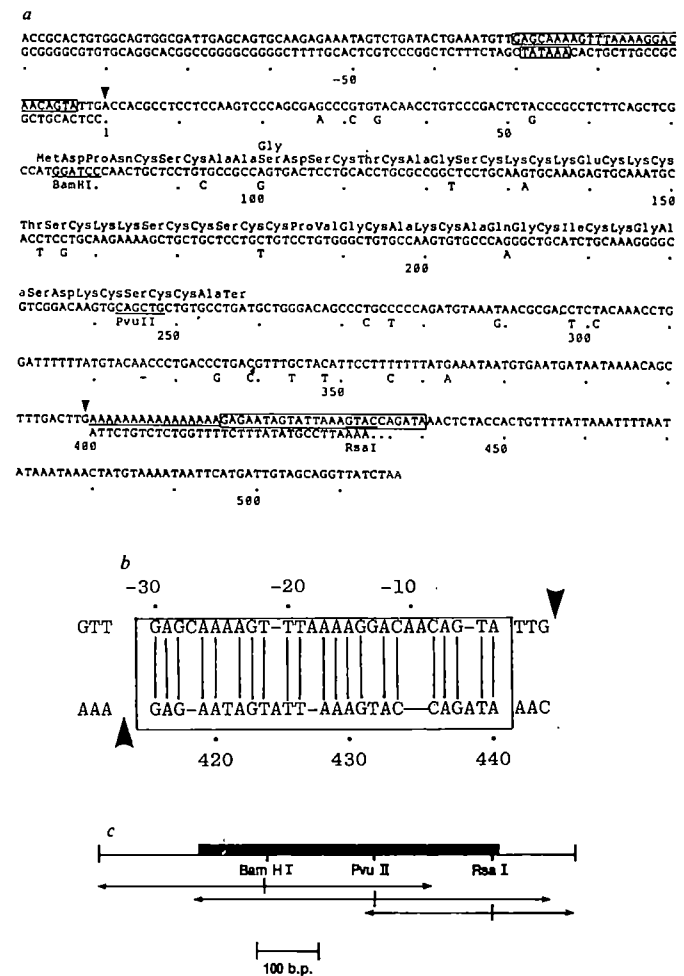


Fig. 6 Primary structure of the human MT-II_B pseudogene. *a*, The DNA sequence of the human MT-II_B pseudogene and flanking regions. Sequence analysis was performed on DNA isolated from a subclone in plasmid pBR322 (p68H) of the 4.3-kb *Hind*III restriction endonuclease fragment of ghMT-II_B. Sequence analysis was as described in Fig. 3 legend. The transcription initiation signal (–30 to –24) of the MT-II_A gene and a putative polyadenylation signal sequence are boxed. Arrows indicate the limits of homology with human MT-II mRNA. Nucleotide differences with the MT-II_A gene sequence (Fig. 3) are indicated below and amino acid differences above the pseudogene sequence. The poly(A) sequence is underlined and sequences flanking the MT-mRNA homology, containing direct repeats, are boxed. *b*, Homology of the direct repeats flanking the MT-II_B processed gene. The region of homology is boxed, identical bases are indicated by vertical bars. Arrows indicate locations of the major cap site and the termination of the poly(A) tract. *c*, Sequencing strategy for the MT-II_B processed gene. The solid box indicates the extent of the MT-II_B processed gene (including the direct repeats). Arrows indicate the direction and extent of sequencing (each sequence was determined at least twice).

of information from RNA to DNA is not limited to retroviruses, but seems to have happened on several occasions in the germ cells of mammals. Such a process might not only be responsible for the generation of non-functional processed pseudogenes, but might have accounted for the generation of functional intronless genes as well.

We thank Drs A. Guiterrez-Hartmann, C. Craik and H. E. Varmus for critical reading of the manuscript, Dr A. Gibbs for assistance with SEQ computer programs, Mr A. J. Mason and Dr. J. Shine for providing information and materials essential to the sequence analysis, Dr G. Bell for samples of human DNA and Dr J. D. Baxter for providing laboratory space. This work was supported in part by grant R-809189 from the Environmental Protection Agency (to M.K.).

Received 15 June; accepted 1 September 1982.

1. Kag, J. H. R. & Nordberg, M. (eds) *Metallothionein* (Birkhauser, Basle, 1979).
2. Karin, M. & Herschman, H. R. *Science* **204**, 176–177 (1979).
3. Pulido, P., Kag, J. H. R. & Vallee, B. L. *Biochemistry* **5**, 1768–1777 (1966).
4. Rudd, C. J. & Herschman, H. R. *Tox. appl. Pharmac.* **47**, 273–278 (1979).
5. Karin, M. & Herschman, H. R. *Eur. J. Biochem.* **107**, 395–401 (1980).
6. Kissling, M. M. and Kag, J. H. R. *FEBS Lett.* **82**, 247–250 (1977).
7. Karin, M. *et al. Nature* **286**, 295–297 (1980).
8. Karin, M., Slater, E. P. & Herschman, H. R. *J. cell. Physiol.* **106**, 63–74 (1981).
9. Durnam, D. M. & Palmiter, R. D. *J. biol. Chem.* **256**, 5712–5716 (1981).
10. Hager, L. J. & Palmiter, R. D. *Nature* **291**, 340–342 (1981).
11. Karin, M. & Richards, R. *Nucleic Acids Res.* **10**, 3165–3173 (1982).
12. Lawn, R. M. *et al. Cell* **15**, 1157–1174 (1978).
13. Southern, E. M. *J. molec. Biol.* **98**, 503–517 (1975).
14. Benton, W. D. & Davis, R. W. *Science* **196**, 180–182 (1977).
15. Glasville, N., Durnam, D. M. & Palmiter, R. D. *Nature* **292**, 267–269 (1981).
16. Breathnach, R. *et al. Proc. natn. Acad. Sci. U.S.A.* **75**, 4853–4857 (1978).
17. Weaver, R. F. & Weissman, C. *Nucleic Acids Res.* **5**, 1175–1193 (1979).
18. Kay, K. E., Warren, R. & Palmiter, R. D. *Cell* **29**, 99–108 (1982).
19. Brinster, R. L. *et al. Nature* **296**, 39–42 (1982).
20. Kingsbury, R. & McKnight, S. L. *Science* **217**, 316–324 (1982).
21. Larsen, A. & Weintraub, H. *Cell* **29**, 609–672 (1982).
22. Proudfoot, N. J. & Brownlee, G. G. *Nature* **263**, 211–214 (1976).
23. Calos, M. P. & Miller, J. H. *Cell* **20**, 579–595 (1980).
24. Hollis, F. G. *et al. Nature* **296**, 321–325 (1982).
25. Leuders, K., Leder, A., Leder, P. & Kuff, E. *Nature* **295**, 426–428 (1982).
26. Van Arsdell, S. W. *et al. Cell* **26**, 11–17 (1981).
27. Jagadeeswaran, P., Forget, B. G. & Weissman, S. M. *Cell* **26**, 141–142 (1982).
28. Nishioka, Y., Leder, A. & Leder, P. *Proc. natn. Acad. Sci. U.S.A.* **77**, 2806–2809 (1980).
29. Wilde, C. D. *et al. Nature* **297**, 83–84 (1982).
30. Shaul, Y., Kaminichik, J. & Aviv, H. *Eur. J. Biochem.* **116**, 461–466 (1981).
31. Perry, R. P. *et al. Proc. natn. Acad. Sci. U.S.A.* **77**, 1937–1941 (1980).
32. Hofer, E. & Darnell, J. E. *Cell* **23**, 585–593 (1981).
33. Bell, G., Karam, J. H. & Rutter, W. J. *Proc. natn. Acad. Sci. U.S.A.* **78**, 5759–5763 (1981).
34. Rigby, P. W. J. *et al. J. molec. Biol.* **113**, 237–251 (1977).
35. Wahl, G. M., Stern, M. & Stark, G. R. *Proc. natn. Acad. Sci. U.S.A.* **76**, 3683–3687 (1979).
36. Maxam, A. & Gilbert, W. *Meth. Enzym.* **65**, 499–559 (1980).
37. Sanger, F., Nicklen, S. & Coulson, A. R. *Proc. natn. Acad. Sci. U.S.A.* **74**, 5463–5468 (1979).
38. Goodman, H. M. *Meth. Enzym.* **65**, 63–64 (1980).
39. Heidecker, G., Messing, J. & Gronenborn, B. *Gene* **10**, 69–73 (1980).
40. O'Farrel, P. *Focus* **3**, 1–3 (1981).

LETTERS TO NATURE

A single quantum cannot be cloned

W. K. Wootters*

Center for Theoretical Physics, The University of Texas at Austin,
Austin, Texas 78712, USA

W. H. Zurek

Theoretical Astrophysics 130–33, California Institute of Technology,
Pasadena, California 91125, USA

If a photon of definite polarization encounters an excited atom, there is typically some nonvanishing probability that the atom will emit a second photon by stimulated emission. Such a photon is guaranteed to have the same polarization as the original photon. But is it possible by this or any other process to amplify a quantum state, that is, to produce several copies of a quantum system (the polarized photon in the present case) each having the same state as the original? If it were, the amplifying process could be used to ascertain the exact state of a quantum system: in the case of a photon, one could determine its polarization by first producing a beam of identically polarized copies and then measuring the Stokes parameters¹. We show here that the linearity of quantum mechanics forbids such replication and that this conclusion holds for all quantum systems.

Note that if photons could be cloned, a plausible argument could be made for the possibility of faster-than-light communication². It is well known that for certain non-separably correlated Einstein–Podolsky–Rosen pairs of photons, once an observer has made a polarization measurement (say, vertical versus horizontal) on one member of the pair, the other one, which may be far away, can be for all purposes of prediction regarded as having the same polarization³. If this second photon could be replicated and its precise polarization measured as above, it would be possible to ascertain whether, for example, the first photon had been subjected to a measurement of linear or circular polarization. In this way the first observer would be able to transmit information faster than light by encoding his message into his choice of measurement. The actual impossibility of cloning photons, shown below, thus prohibits superluminal communication by this scheme. That such a scheme must fail for some reason despite the well-established existence of long-range quantum correlations^{6–8}, is a general consequence of quantum mechanics⁹.

A perfect amplifying device would have the following effect

on an incoming photon with polarization state $|s\rangle$:

$$|A_0\rangle|s\rangle \rightarrow |A_s\rangle|ss\rangle \quad (1)$$

Here $|A_0\rangle$ is the 'ready' state of the apparatus, and $|A_s\rangle$ is its final state, which may or may not depend on the polarization of the original photon. The symbol $|ss\rangle$ refers to the state of the radiation field in which there are two photons each having the polarization $|s\rangle$. Let us suppose that such an amplification can in fact be accomplished for the vertical polarization $|\uparrow\rangle$ and for the horizontal polarization $|\leftrightarrow\rangle$. That is,

$$|A_0\rangle|\uparrow\rangle \rightarrow |A_{\text{vert}}\rangle|\uparrow\uparrow\rangle \quad (2)$$

and

$$|A_0\rangle|\leftrightarrow\rangle \rightarrow |A_{\text{hor}}\rangle|\leftrightarrow\leftrightarrow\rangle \quad (3)$$

According to quantum mechanics this transformation should be representable by a linear (in fact unitary) operator. It therefore follows that if the incoming photon has the polarization given by the linear combination $\alpha|\uparrow\rangle + \beta|\leftrightarrow\rangle$ —for example, it could be linearly polarized in a direction 45° from the vertical, so that $\alpha = \beta = 2^{-1/2}$ —the result of its interaction with the apparatus will be the superposition of equations (2) and (3):

$$|A_0\rangle(\alpha|\uparrow\rangle + \beta|\leftrightarrow\rangle) \rightarrow \alpha|A_{\text{vert}}\rangle|\uparrow\uparrow\rangle + \beta|A_{\text{hor}}\rangle|\leftrightarrow\leftrightarrow\rangle \quad (4)$$

If the apparatus states $|A_{\text{vert}}\rangle$ and $|A_{\text{hor}}\rangle$ are not identical, then the two photons emerging from the apparatus are in a mixed state of polarization. If these apparatus states are identical, then the two photons are in the pure state

$$\alpha|\uparrow\uparrow\rangle + \beta|\leftrightarrow\leftrightarrow\rangle \quad (5)$$

In neither of these cases is the final state the same as the state with two photons both having the polarization $\alpha|\uparrow\rangle + \beta|\leftrightarrow\rangle$. That state, the one which would be required if the apparatus were to be a perfect amplifier, can be written as

$$2^{-1/2}(\alpha a_{\text{vert}}^+ + \beta a_{\text{hor}}^+)^2|0\rangle = \alpha^2|\uparrow\uparrow\rangle + 2^{1/2}\alpha\beta|\uparrow\leftrightarrow\rangle + \beta^2|\leftrightarrow\leftrightarrow\rangle$$

which is a pure state different from the one obtained above by superposition [equation (5)].

Thus no apparatus exists which will amplify an arbitrary polarization. The above argument does not rule out the possibility of a device which can amplify two special polarizations, such as vertical and horizontal. Indeed, any measuring device which distinguishes between these two polarizations, a Nicol prism for example, could be used to trigger such an amplification.

The same argument can be applied to any other kind of quantum system. As in the case of photons, linearity does not forbid the amplification of any given state by a device designed especially for that state, but it does rule out the existence of a device capable of amplifying an arbitrary state.

* Present address: Department of Physics and Astronomy, Williams College, Williamstown, Massachusetts 01267, USA.

Milonni (unpublished work) has shown that the process of stimulated emission does not lead to quantum amplification, because if there is stimulated emission there must also be—with equal probability in the case of one incoming photon—spontaneous emission, and the polarization of a spontaneously emitted photon is entirely independent of the polarization of the original.

It is conceivable that a more sophisticated amplifying apparatus could get around Milonni's argument. We have therefore presented the above simple argument, based on the linearity of quantum mechanics, to show that no apparatus, however complicated, can amplify an arbitrary polarization.

We stress that the question of replicating individual photons is of practical interest. It is obviously closely related to the

quantum limits on the noise in amplifiers^{10,11}. Moreover, an experiment devised to establish the extent to which polarization of single photons can be replicated through the process of stimulated emission is under way (A. Gozzini, personal communication; and see ref. 12). The quantum mechanical prediction is quite definite; for each perfect clone there is also one randomly polarized, spontaneously emitted, photon.

We thank Alain Aspect, Carl Caves, Ron Dickman, Ted Jacobson, Peter Milonni, Marlan Scully, Pierre Meystre, Don Page and John Archibald Wheeler for enjoyable and stimulating discussions.

This work was supported in part by the NSF (PHY 78-26592 and AST 79-22012-A1). W.H.Z. acknowledges a Richard Chace Tolman Fellowship.

Received 11 August; accepted 7 September 1982.

1. Born, M. & Wolf, E. *Principles of Optics* 4th edn (Pergamon, New York, 1970).
2. Herbert, N. *Found. Phys.* (in the press).
3. Einstein, A., Podolsky, B. & Rosen, N. *Phys. Rev.* **47**, 777–780 (1935).
4. Bohm, D. *Quantum Theory*, 611–623 (Prentice-Hall, Englewood Cliffs, 1951).
5. Kocher, C. A. & Commins, E. D. *Phys. Rev. Lett.* **18**, 575–578 (1967).
6. Freedman, S. J. & Clauser, J. R. *Phys. Rev. Lett.* **28**, 938–941 (1972).

7. Fry, E. S. & Thompson, R. C. *Phys. Rev. Lett.* **37**, 465–468 (1976).
8. Aspect, A., Grangier, P. & Roger, G. *Phys. Rev. Lett.* **47**, 460–463 (1981).
9. Bussey, P. J. *Phys. Lett.* **90A**, 9–12 (1982).
10. Haus, H. A. & Mullen, J. A. *Phys. Rev.* **128**, 2407–2410 (1962).
11. Caves, C. M. *Phys. Rev. D* **15**, (in the press).
12. Gozzini, A. *Proc. Symp. on Wave-Particle Dualism* (eds Diner, S., Fargue, D., Lochak, G. & Selleri, F) (Reidel, Dordrecht, in the press).

The Crab Nebula's progenitor

Ken'ichi Nomoto*, Warren M. Sparks†, Robert A. Fesen‡, Theodore R. Gull‡, S. Miyaji‡ & D. Sugimoto*

* Department of Earth Science and Astronomy, University of Tokyo, College of General Education, 3-8-1 Komaba, Meguro, Tokyo 153, Japan

† Group X-5, Mail Stop F669, Los Alamos National Laboratory, Los Alamos, New Mexico 87545, USA

‡ Laboratory for Astronomy and Solar Physics, Goddard Space Flight Center, Greenbelt, Maryland 20771, USA

The study of supernovae is hampered by an insufficient knowledge of the initial stellar mass for individual supernova. Because of large uncertainties in estimating both the total mass of a remnant (including the pulsar or black hole) and any mass loss during the pre-supernova stages, the main sequence mass of the progenitor cannot be accurately determined from observations alone. To calculate an initial mass, one must rely on a combination of both theory and observation. Limits on the progenitor's mass range can be estimated by the presence of a compact remnant and comparison of the observed nebular chemical abundances with detailed evolutionary calculations¹. The Crab Nebula is an excellent choice for investigation because it contains a unique combination of characteristics: a central neutron star (pulsar) and a bright, well studied nebula having little or no swept-up interstellar material. In fact, several studies^{1–4} have suggested an initial mass of $\sim 10 M_{\odot}$ for the Crab progenitor. Recently, Davidson *et al.*⁵, quoting two of us (K.N. and W.M.S.), state that the Crab's progenitor had a mass slightly larger than $8 M_{\odot}$. Here we present in detail the reasoning behind this statement and suggest the explosion mechanism.

Briefly, the Crab consists of a pulsar (assumed here to have a mass of $\approx 1.4 M_{\odot}$) and a nebula mass of $1.2\text{--}3.0 M_{\odot}$ (refs 5, 6) which has a helium overabundance of $1.6 < X_{\text{He}}/X_{\text{H}} < 8$ (where X is an element's mass fraction). The oxygen abundance (X_{O}) is ~ 0.003 (refs 5, 6), which is less than the solar value of 0.007, while the oxygen-to-hydrogen ratio is approximately solar. The carbon-to-oxygen ratio is $0.4 < X_{\text{C}}/X_{\text{O}} < 1.1$ (ref. 5). Nitrogen may be slightly overabundant, while neon, sulphur and iron abundances are uncertain but are probably not greatly over- or underabundant. Because the Crab Nebula is helium-rich but not oxygen-rich, the hydrogen-rich (solar abundances) envelope and the helium layer of the progenitor star were ejected but the oxygen-rich layer below the helium layer was not. The lower layers must have formed the neutron star. The

lower limit of the large helium-to-hydrogen ratio means that at least half of the ejected material must have come from the helium layer.

Arnett (ref. 7 and refs therein) systematically evolved helium cores of various masses (M_{α}) into late stages of evolution. He¹ compared Davidson's⁸ derived abundances of the Crab nebula with calculated abundances from the $M_{\alpha} = 4.0 M_{\odot}$ model, which was his lowest-massed, highly evolved helium core (corresponding to approximately a $15 M_{\odot}$ star). Combining all the material above the helium-burning shell (his case B) with enough interstellar material to obtain $X_{\text{He}}/X_{\text{H}} = 8$, he found good agreement with $X_{\text{N}}/X_{\text{He}}$ and $X_{\text{O}}/X_{\text{He}}$ of Davidson's⁸ 'model 1'. However, the calculated value of $X_{\text{C}}/X_{\text{He}}$ was too large by a factor of 30. At that time, the Crab's carbon abundance had not been directly measured and Arnett suggested several possibilities: the inferred carbon abundance was too low, the carbon was hidden in the filaments, or a lower-mass helium core, $\sim 3 M_{\odot}$, was more appropriate.

Using recent UV observations with the International Ultraviolet Explorer, Davidson *et al.*⁵ have established that the carbon abundance is nearly solar. They also showed that the hydrogen and helium seemed to be fairly well mixed and, as carbon is convectively mixed in the helium layer, this would argue against carbon being hidden in the filaments. However, IR observations by Dennefeld and Andrillat⁹ showed that the strength of [C I] $\lambda 9,850$ relative to [S III] $\lambda 9,069$ varied with position in the Crab. The strongest [C I] line would indicate a rather large carbon abundance if the ionizing flux is constant. Whether the IR observations indicate variation in the carbon abundance, variation in the ionizing flux, or high densities in neutral cores is not known. For the remainder of this report we will assume the carbon abundance as determined by Davidson *et al.*⁵.

The existence of a pulsar in the Crab indicates that the progenitor's mass was larger than the upper mass limit ($8 \pm 1 M_{\odot}$)¹⁰ for degenerate carbon ignition. Degenerate carbon ignition results in carbon deflagration¹¹ which completely disrupts the star, leaving no compact remnant. Lower-mass stars that lose enough mass to avoid degenerate carbon burning eventually become white dwarfs. Stars massive enough ($\geq 8 M_{\odot}$) to burn carbon non-degenerately will eventually undergo a core collapse initiated either by electron capture¹² onto Mg, Ne and O or by burn-out of all the available fuel^{13,14}. When the collapsing core reaches neutron-star densities, stability is regained. Although detailed calculations of the collapse remain inconclusive, it is generally felt that the core will overshoot its equilibrium position and then rebound, initiating a shock wave⁴. This shock wave ejects the outer material but not the core, resulting in both a supernova nebula and a pulsar¹⁵. In more massive stars

the core will continue to collapse down to a black hole, but the stellar mass at which this starts to happen is unknown⁴. Therefore, the presence of a pulsar in the Crab establishes a lower mass limit of $8 \pm 1 M_{\odot}$, but cannot set an upper limit for the progenitor.

We will now investigate the mass constraints due to the chemical abundances of the nebula. Stars more massive than $\sim 10 M_{\odot}$ will undergo an iron core collapse while less massive stars (but more massive than the carbon deflagration supernova) will undergo an electron capture core contraction¹². Let us consider the lowest mass star which undergoes an iron core collapse, that is, $10 M_{\odot}$. Recent evolutionary calculations³ of such a star show that in the late stages there is a $1.5 M_{\odot}$ core, which presumably forms the neutron star, a helium shell of $1.2 M_{\odot}$ and a $7.3 M_{\odot}$ hydrogen-rich envelope. If at least $6 M_{\odot}$ of the hydrogen-rich envelope were lost in pre-supernova stages, the supernova would eject a helium-rich nebula like that of the Crab. In fact, Woosley *et al.*³ and Hillebrandt⁴ suggested this model to fit the Crab. However, the recently observed carbon abundances⁵ also contradict this model. During the late stages of evolution, the helium burning shell becomes so active that it forms a convective region and deposits appreciable amounts of carbon (and oxygen to a less extent) in the helium layer. In this model the convective region included $0.7 M_{\odot}$ of the $1.2 M_{\odot}$ helium layer and contained 0.04 carbon. Thus, if the helium layer were mixed with the maximum allowable amount of hydrogen-rich material ($1.2 M_{\odot}$), the mixture would contain $X_c \sim 0.012$, which is larger than that observed. For somewhat larger-mass stars the mass considerations are similar but the amount of carbon in the helium layer increases even further.

Recently, evolutionary models of the helium cores of stars from 8 to $10 M_{\odot}$ have become available. In addition to the published evolution of helium core masses of 2.6 and $2.8 M_{\odot}$ (ref. 16), one of us (K.N.) has evolved a helium core mass of $2.4 M_{\odot}$. (In these models, the stellar mass is about a factor of 4 times the helium core mass, which is then allowed to increase to simulate the core growth due to the hydrogen-burning shell, and the core mass values quoted are at the end of the central helium burning). Figure 1a shows the chemical evolution for the $2.6 M_{\odot}$ helium core. During the late stages, a large convective region develops above the helium burning shell and deposits a $0.02 M_{\odot}$ of carbon in the helium layer. This is more carbon than the observations allow and a lower-mass helium core is necessary. Another interesting phenomenon occurs slightly later than the development of the helium-burning convective region. As the carbon-burning shell approaches the helium-burning shell, the helium layer expands greatly. This allows the surface convective region to penetrate the helium layer and dredge most of it up.

The dredging-up phase has a more significant role in the $2.4 M_{\odot}$ helium core model, as demonstrated in Fig. 1b. (In this computation, the hydrogen-rich envelope of $1.1 M_{\odot}$ was fitted to the outer edge of the $2.4 M_{\odot}$ helium core; that is, the stellar mass was assumed to have decreased from the initial mass of $\sim 9 M_{\odot}$ to $3.5 M_{\odot}$ by mass loss.) Because of the stronger electron-degeneracy, the penetration of the surface convective region starts earlier than in the $2.6 M_{\odot}$ helium core case. (A similar penetration takes place for a $9 M_{\odot}$ star¹⁷.) Afterwards, the dredge-up of the helium layer proceeds as follows: (1) the first dredge-up reduces the mass of the helium layer from $1.1 M_{\odot}$ to $0.14 M_{\odot}$, (2) a temporal retreat of the surface convection zone during the several carbon shell flashes in the core, (3) a second dredge-up which reduces the helium layer mass to $5 \times 10^{-3} M_{\odot}$, and (4) retreat of the surface convection zone with re-ignition of the hydrogen burning shell. Further evolution of the core mass growth from $1.30 M_{\odot}$ to $1.38 M_{\odot}$ with the hydrogen-helium double shell burnings will be similar to the growth of the carbon-oxygen cores¹⁰.

Between the dredge-up phases, a relatively small helium shell flash occurs and produces $\sim 0.007 M_{\odot}$ carbon. However, the strength of the shell flash has a positive correlation with stellar

mass. If the first phase dredges up more helium, the amount of carbon produced would be smaller. In fact, the amount of carbon produced by the $2.4 M_{\odot}$ helium core model is one-third of that produced by the $2.6 M_{\odot}$ helium core model. Therefore, the carbon abundance not only decreases with decreasing stellar mass but also the abundance has a rather sharp drop-off caused by the presence or absence of the first dredge-up phase. The Crab's observed carbon abundance is consistent with its progenitor's mass being below the critical mass where this sharp drop-off occurs. The exact value of the critical stellar mass at which this occurs must await more detailed evolutionary models, but we estimate it to be $9.5 \pm 0.5 M_{\odot}$.

We therefore believe that the mass of the Crab's progenitor is between the upper limit for carbon deflagration ($8 \pm 1 M_{\odot}$) and the lower limit set by the dredge-up of the helium layer before development of the helium-burning convective region ($9.5 \pm 0.5 M_{\odot}$). According to the latest evolutionary models this mass range falls entirely within the stars that undergo electron capture supernova¹². This would make the Crab the remnant of an electron capture supernova.

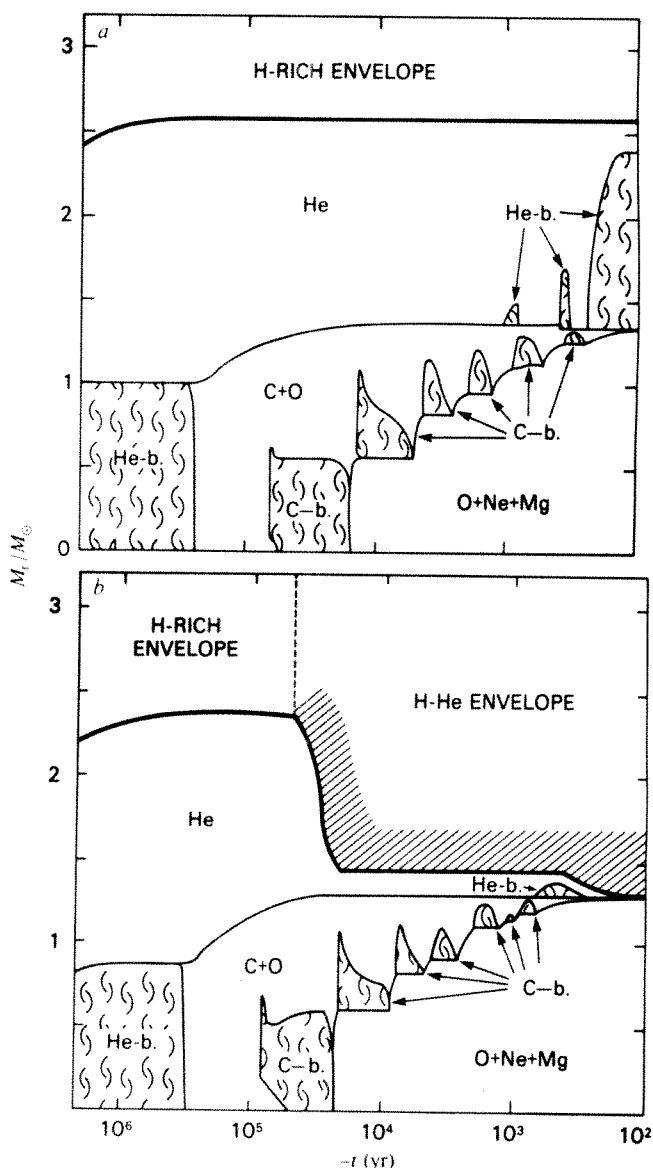


Fig. 1 a, Chemical evolution of the star with a $2.6 M_{\odot}$ helium core. The shaded regions are convective. Time, t , is measured from the onset of the penetration of the surface convection zone into the helium layer. b, Same as a, but for the star with a $2.4 M_{\odot}$ helium core. Time, t , is measured from the stage when the dredge up of the helium layer stops and the hydrogen shell burning is re-ignited.

Based on the above discussion, we propose the following scenario for the Crab's progenitor star as being plausible and most consistent with observations. On the main sequence the star had an initial mass of between 8 and $9.5 M_{\odot}$, and spent 3×10^7 yr, 2×10^6 yr and 6×10^4 yr in hydrogen, helium and carbon burning stages, respectively. During the blue and red supergiant phases, the star lost $5\text{--}6 M_{\odot}$ by a stellar wind, reducing the hydrogen-rich envelope to $0.5\text{--}1.0 M_{\odot}$. During carbon burning the helium layer expanded and allowed the surface convective region to penetrate the helium layer. Most of the helium layer ($\sim 1.2 M_{\odot}$) was dredged up into the hydrogen-rich layer, mixing their compositions. As the degenerate O-Ne-Mg core approached $1.38 M_{\odot}$, electron captures onto Mg, Ne and O reduced the Chandrasekhar's limiting mass to below the core mass, causing a rapid contraction. During the contraction, the remainder of the nuclear fuel in the core burned, and practically all of the energy released escaped as neutrinos. The contracting core finally became free-fall and when it reached neutron-star densities, the core overshot its equilibrium position and then rebounded, creating a shock wave. This shock wave was not strong enough to eject the core, but it was strengthened by the steep density gradient at the core edge enough to eject the loosely bound hydrogen-helium envelope. The $1.38 M_{\odot}$ core was not massive enough to collapse down to a black hole but remained a neutron star, in agreement with the observations. There was little or no nuclear burning in the hydrogen-helium envelope due to the passage of the shock wave. However, the propagation of the shock wave through the extended hydrogen-helium envelope caused the rapid rise and fall in the supernova light curve¹⁸. The ejected hydrogen-helium layer had a mass of $\sim 2 M_{\odot}$, a composition of $X_H \sim 0.2\text{--}0.3$, $X_{He} \sim 0.8\text{--}0.7$, its original solar ratio of X_O/X_H , but slightly enhanced carbon as $X_C/X_O \sim 1$. Because the helium layer was processed via the CNO cycle, the X_N/X_H ratio was ~ 10 times solar. These abundances are in agreement with many of the observations of the Crab nebula. The suggested abundance variations^{6,19} among the filaments could be due to one or more of the following: (1) incomplete mixing during dredge-up, (2) helium shell flashes in the thin, residual layer of helium after the first dredge-up, or (3) mixing with previously ejected hydrogen-rich circumstellar material. It is possible that the rebounding shock strength in the electron-capture supernovae will be weaker than the iron core collapse supernovae because the electron capture core slowly approaches free-fall while the iron core quickly reaches free-fall. Thus, the relatively low kinetic energy of the Crab Nebula may also be consistent.

To establish the correctness of the above scenario, we need actual modelling that shows that the rebounding shock ejects the envelope and gives rise to the supernova light curve. Although most of the recent calculations for the collapse of massive stars ($>15 M_{\odot}$) fail to obtain an explosion¹⁵, the recent calculation of a $10 M_{\odot}$ star explosion by Hillebrandt⁴ is very suggestive. Because a $10 M_{\odot}$ star has a smaller iron core mass than a $15 M_{\odot}$ star, the outgoing shock wave is strengthened by the steep density gradient near the silicon burning shell (or the outer edge of the iron core) and ejects a relatively small amount of core material. In $8\text{--}10 M_{\odot}$ stars, much steeper density gradients exist at the helium burning shell, making it more likely that the shock is strengthened there and thus ejecting only a helium-rich layer.

We cannot be certain whether the mechanism described above applies to other supernova remnants. Although a few objects are considered to be 'Crab-like' remnants (for example, 3C58), this classification has been based largely on their radio emission properties. Until we know more about these remnants (their elemental abundances, total kinetic energies and whether they contain neutron stars), we cannot determine how similar they are to the Crab Nebula. Therefore, although the Crab Nebula was probably the product of an electron capture supernova, it is not yet clear if other Crab-like supernova remnants originated by a similar explosion mechanism.

Received 6 May; accepted 3 August 1982.

- Arnett, W. D. *Astrophys. J.* **195**, 727-733 (1975).
- Gott, J. R., Gunn, J. E. & Ostriker, J. P. *Astrophys. J. Lett.* **160**, L91-L96 (1970).
- Woosley, S. E., Weaver, T. A. & Taam, R. E. in *Type I Supernovae* (ed. Wheeler, J. C.) 96-112 (University of Texas, Austin, 1980).
- Hillebrandt, W. in *Supernovae* (eds Rees, M. J. & Stoneham, R. J.) 123-128 (Reidel, Dordrecht, 1982).
- Davidson, K. *et al. Astrophys. J.* **253**, 696-706 (1982).
- Henry, R. C. & MacAlpine, G. M. *Astrophys. J.* **258**, 11-21 (1982).
- Arnett, W. D. *Astrophys. J. Suppl.* **35**, 145-160 (1977).
- Davidson, K. *Astrophys. J.* **186**, 223-231 (1973).
- Dennefeld, M. & Andriolat, Y. *Astr. Astrophys.* **103**, 44-49 (1981).
- Sugimoto, D. & Nomoto, K. *Space Sci. Rev.* **25**, 155-227 (1980).
- Nomoto, K., Sugimoto, D. & Neo, S. *Astrophys. Space Sci.* **39**, L37-L42 (1976).
- Miyaji, S., Nomoto, K., Yokoi, K. & Sugimoto, D. *Publ. astr. Soc. Japan* **32**, 303-329 (1980).
- Hoyle, F. & Fowler, W. A. *Astrophys. J.* **132**, 565-590 (1960).
- Colgate, S. A. & White, R. H. *Astrophys. J.* **143**, 626-681 (1966).
- Hillebrandt, W. *Astr. Astrophys.* **110**, L3-L6 (1982).
- Nomoto, K. in *Fundamental Problems in the Theory of Stellar Evolution* (eds Sugimoto, D., Lamb, D. Q. & Schramm, D. N.) 295-315 (Reidel, Dordrecht, 1981).
- Weaver, T. A., Axelrod, T. S. & Woosley, S. E. in *Type I Supernovae* (ed. Wheeler, J. C.) 113-154 (University of Texas, Austin, 1980).
- Falk, S. W. & Arnett, W. D. *Astrophys. J. Suppl.* **33**, 515-562 (1977).
- Fesen, R. A. & Kirshner, R. P. *Astrophys. J.* **258**, 1-10 (1982).

Siderophiles in the Brachina meteorite: impact melting?

Graham Ryder

Northrop Services, Inc., Lunar Curatorial Laboratory,
PO Box 34416, Houston, Texas 77034, USA

The published high abundances and unusual ratios of siderophiles in the chassignite Brachina (refs 1, 2 and R. A. Schmitt, personal communication in ref. 1) in comparison with its apparent relatives Chassigny, shergottites, and nakhlites²⁻¹¹, suggest that Brachina might be an impact melt. If so, the projectile was chemically similar to either some iron meteorites¹² or the Eagle Station trio¹³ of pallasites. As contaminants, the latter meteorites would also explain the deviant oxygen isotope ratios¹⁴ of Brachina without recourse to a separate parent planet. We show here that all these meteorites could have formed on Mars, with Brachina ejected as a large tektite-like melt blob, along with shocked and unshocked target rocks. The hypothesis creates predictions which can be tested with data from radiometric ages and dynamic crystallization experiments.

Shergottites, nakhlites and chassignites are distinct from other achondrites, particularly in their higher oxidation states, higher volatile abundances, and young crystallization ages of 1,300 Myr. These meteorites are interesting because of their possible origin as igneous rocks on Mars¹⁵⁻¹⁹. One characteristic apparently not consistent with this is that the ratios of oxygen isotopes of Brachina are distinct from those of all the other shergottites, nakhlites and Chassigny (which fall within error of a mass fractionation line) (Fig. 1), and requires a separate parent planet for Brachina¹⁴. One other feature of Brachina is its texture, which is dominated by fine-grained ($\sim 200 \mu\text{m}$) olivines, which are, however, not quench-textured^{20,21}. The texture is dissimilar to known igneous rocks.

An additional peculiar characteristic of Brachina appears to have passed unnoticed: its extremely high siderophile abundances and their peculiar ratios, unlike shergottites, nakhlites, and Chassigny, or lunar and terrestrial basalts (Table 1). All the abundances for Brachina are high; the most conspicuously different ratios are the high Ni/Co and Ir/Au. The Ni/Co ratio is much closer to chondritic, stony-irons, and irons than to other differentiated silicate materials, for example. Among meteorite groups, the Ir/Au ratio is distinctive (Fig. 2), and the two analyses of Ir and Au for Brachina are remarkably consistent. (However, data for Shergotty and Nakhla are quite varied and inconsistent; Table 1.) These siderophile data, like the oxygen isotopes, demonstrate that Brachina is different in origin from the other shergottites, nakhlites, and chassignites.

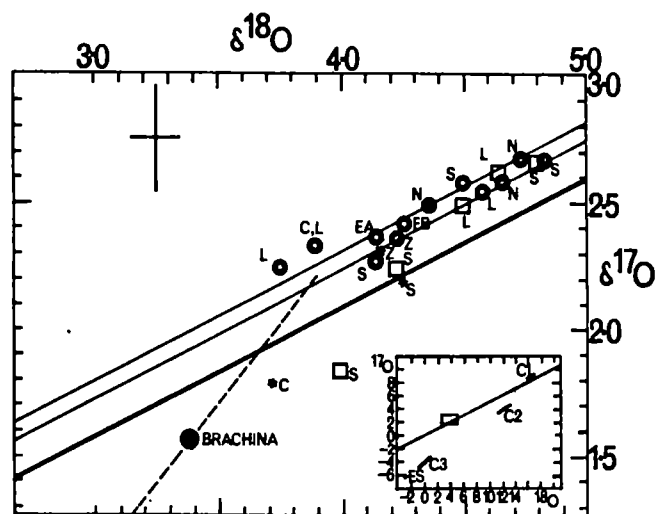


Fig. 1 Oxygen isotope data for Brachina, Chassigny, shergottites, and nakhlites. Heavy diagonal line is terrestrial mass fractionation line; light diagonal lines are reasonable mass fractionation lines for Shergottites, nakhlites, and Chassigny. Dashed line through Brachina connects with Eagle Station trio pallasites. Large cross is precision²³. S, Shergotty; Z, Zagami; L, Lafayette; N, Nakhla; EA, EB, EETA79001; C, Chassigny. Inset shows main diagram area as a rectangle, with Eagle Station trio and carbonaceous chondrite groups for comparison. Data references: stars¹⁴; squares²⁵; asterisks, Clayton (personal communication in ref. 17); Eagle Station and chondrites²³.

One possible explanation of the siderophile data is that Brachina is from the same planet as Chassigny, shergottites, and nakhlites, but that it is an impact melt, contaminated with other siderophile-bearing meteoritic material. For such an hypothesis, by assuming indigenous abundances for Brachina similar to those of Chassigny, one can estimate the abundances resulting from contamination (Table 2); the Ni/Co ratio is similar to most meteorite groups except achondrites. For reasonable amounts of contamination (there is $\leq 10\%$ in the most-siderophile-enriched terrestrial impact melts), stony

meteorites are eliminated because they would require more than 25% contamination and their Ir/Au ratios are too low. Of the remaining meteorites, a few of the iron meteorite groups¹² and the Eagle Station trio pallasites¹³ (Table 2) can reasonably account for the siderophiles. Mesosiderites might account for the siderophiles, but Au data are not available. The Eagle Station trio of pallasites actually have Ni/Ir only half that of the hypothesized contaminant, but the ratio for the contaminant is not precise. Differences in the abundances of sulphide phases between analysed splits of Brachina could account for variations in absolute abundances and ratios in the analyses. The available data have varied nickel concentrations, and suggest that within Brachina, Ni and Ir are not concentrated in a single phase.

Of the contaminant possibilities, the Eagle Station trio of pallasites has unusual oxygen isotope characteristics, and Brachina falls on a mixing line between the Eagle Station trio and a point near Chassigny (Fig. 1). The hypothesized contaminant requires $\sim 2\%$ of Eagle Station trio metal to account for the Ni and Co excess in Brachina, or 1% to account for the Ir and Au. The Eagle Station trio are unusual in having a silicate/metal ratio of 2:1 (ref. 22), thus providing a corresponding 2–4% contamination with silicates. The oxygen isotope data (Fig. 1) require a silicate contamination of 4–11% (from $\delta^{17}\text{O}$) or 5–10% (from $\delta^{18}\text{O}$), according to the isotopic precisions²³, and with a reasonable assumption of the oxygen isotopic composition of the indigenous material. Thus the mixing of about 6 or 7% Eagle Station trio-like material and Chassigny-like material would provide a composition with oxygen isotopes and siderophile abundances and ratios similar to, though not precisely those of, Brachina. The fit would be more exact if (1) Eagle Station trio pallasites actually have a higher silicate/metal ratio than 2:1 (the slab of Eagle Station depicted in ref. 22 appears to have a higher proportion of silicates); or (2) the oxygen isotopic composition of Brachina actually lies slightly closer to the shergottite–nakhlite–chassignite mass fractionation line, which is possible; some other data vary outside of analytical precision, and a duplicate measurement for Brachina is desirable; or (3) Brachina actually has higher abundances of Ir and Au. Contamination with iron meteorites, main

Table 1 Published siderophile element abundances for shergottites, nakhlites, chassignites, lunar basalts and terrestrial basalts

Sample	Ref.	Ni (p.p.m.)	Co (p.p.m.)	Ir (p.p.b.)	Au (p.p.b.)	Ni/Co	Ni/Ir ($\times 10^3$)	Ni/Au ($\times 10^3$)	Ir/Au
Shergotty	2	83	39		16	2.1	(47)	5.2	
	3		63	1.55	88	(1.2)		(0.82)	0.02
	4	56	35			1.6			
	6		62			(1.2)			
	7	80		0.072	0.98	(1.6)	1,111	81	0.07
Zagami	3			0.10	2.10		(670)	(32)	0.05
	4	67	37			1.8			
ALHA 77005	5	320	70			4.6			
Nakhla	2	90	54	<2	2.9	1.7	>45	31	<0.68
	3		81	17	0.55	(1.1)	(5.3)	(163)	31
	6		45	718	2.5	(2)	(<11)	(36)	>3.2
Lafayette	3			0.13	21.0				0.01
	6		44						
Chassigny	2	480	126	2.4	0.9	3.8	200	533	2.7
	9	400	124	6	6	3.2	67	67	1
	10	475	141			3.4			
	11	~600				(~4.6)			
Brachina	2	1,200	234	130	10	5.1	9.2	120	13
	2	4,180	265	111	15	15.8	38	278	7.4
	1	3,600	320			11.3			
Lunar low-Ti basalts	26	40	40	0.01	0.03	1	4,000	1,500	0.33
Terrestrial basalts	27	120	40	0.02	0.02	3	6,300	500	0.08

Values in parentheses use averages of other splits for one parameter. p.p.b., Parts per 10⁹.

Table 2 Composition of hypothetical Brachina contaminant and Eagle Station trio pallasites¹³

	Brachina contaminant	Eagle Station	Itzawisis	Cold Bay
Ni (p.p.m.)	2,500	154,000	147,000	136,000
Co (p.p.m.)	140	8,000	8,100	5,400
Ir (p.p.b.)	115	11,400	16,000	5,800
Au (p.p.b.)	10	980	1,040	870
Ni/Co	18	19.3	18.1	25.2
Ni/Ir ($\times 10^3$)	22	13	9	23
Ni/Au ($\times 10^3$)	250	157	141	156
Ir/Au	11.5	11.6	15.4	6.7

group pallasites, or mesosiderites would have a negligible effect on the oxygen isotopes.

An alternative to the impact melt explanation for the siderophile data is that Brachina is an igneous rock containing cumulate sulphides, bearing Ni, Co, Ir and Au as chalcophile elements. Such an origin could possibly explain generally high siderophile abundances, but probably not explain the Ir/Au ratios. Au and Ir are similarly chalcophile²⁴, and thus the liquid from which Brachina accumulated would be required to have Ir/Au similar to Brachina, hence still unlike shergottites, nakhlites, and Chassigny. Without detailed knowledge of the comparative chalcophilic tendencies of Ir and Au, such an origin cannot be discarded, but does not explain the oxygen isotope data as does the contamination hypothesis.

Brachina (unlike Chassigny) is unshocked, a characteristic expected of an impact melt. Its unusual texture is not unlike some chondrules, for example porphyritic and granular ones. The inclusions^{20,21} in the cores of olivines and plagioclases are not unexpected in impact melts; the effect of these inclusions on nucleation could strongly influence texture. Unfortunately, there are no data from dynamic experiments on appropriate compositions crystallizing with heterogeneous nucleation. Brachina could have formed in a blob of melt ejected from the parent planet in the event which ejected the shergottites, nakhlites, and Chassigny ~180 Myr ago; the blob would be analogous to a large, ejected tektite. If the parent planet is Mars, then it is quite possible that the high S abundance of Brachina is derived from the martian regolith. While Brachina does not have the particularly high chlorine which might be

expected, and the presumed sulphate of the regolith would have to be reduced to the sulphide of Brachina, substantial devolatilization and reduction is normal in the production of terrestrial tektites.

If the hypothesis is correct, Brachina will have a crystallization age of ~180 Myr, apparent in internal isochrons and Ar-Ar ages. There should be no sign of the 1,300 Myr event (shown by its relatives) in the Ar data, but Sm-Nd data should be consistent with a 1,300 Myr event. Rb-Sr whole rock data might be affected by volatilization of Rb during the melting.

The hypothesis that Brachina is a melted mixture of a several per cent Eagle Station trio-like pallasite material and Chassigny-like target material reasonably accounts for both the siderophile and oxygen isotopic data. The challenge for those postulating a purely igneous origin is to explain the high siderophiles and their peculiar ratios, even if one invokes a parent planet separate from that of shergottites, nakhlites and Chassigny to account for the oxygen isotopes. The hypothesis of an origin as an impact melt blob ejected from Mars along with shergottites, nakhlites, and Chassigny is consistent with known data, and can be tested with attainable data, such as Ar-Ar ages, more complete siderophile data for all these meteorites, and experimental reproduction of the textures.

This work was supported by NASA 15425 for the operation of the Lunar Curatorial Laboratory. I thank C. A. Wood and J. Gooding for helpful comments.

Received 20 July; accepted 6 September 1982.

1. Johnson, J. E. *et al. Rec. South Austral. Mus.* **17**, 309-319 (1977).
2. Dreibus, G. *et al. Lunar planet. Sci.* **13**, 186-187 (1982).
3. Lail, J. C. *et al. Geochim. cosmochim. Acta* **36**, 329-345 (1972).
4. Stolper, E. & McSweeney, H. Y. Jr *Geochim. cosmochim. Acta* **43**, 1475-1498 (1979).
5. Ma, M.-S. *et al. Proc. Lunar planet. Sci.* **12B**, 1349-1358 (1981).
6. Schmitt, R. A. *et al. Meteoritics* **7**, 131-214 (1972).
7. Chou, C.-L. *et al. Proc. 7th Lunar Sci. Conf.* 3501-3518 (1976).
8. Ehmann, W. D. *et al. Geochim. cosmochim. Acta* **34**, 493-507 (1970).
9. Boynton, W. V. *et al. Geochim. cosmochim. Acta* **40**, 1439-1447 (1976).
10. Jérôme, D. Y. thesis, Univ. Oregon (1970).
11. Dyakonova, M. I. & Kharitonova, V. Y. *Meteoritika* **18**, 48-67 (1960).
12. Scott, E. R. D. *Earth planet. Sci. Lett.* **37**, 273-284 (1977).
13. Scott, E. R. D. *Geochim. cosmochim. Acta* **41**, 349-360 (1977).
14. Clayton, R. N. & Mayeda, T. K. *Lunar planet. Sci.* **13**, 117-118 (1982).
15. Wasson, J. T. & Wetherill, G. W. in *Asteroids* 926-974 (University of Arizona Press, Tucson, 1979).
16. McSweeney, H. Y. Jr & Stolper, E. *Scient. Am.* **242**(6), 54-63 (1980).
17. Wood, C. A. & Ashwal, L. D. *Proc. Lunar planet. Sci.* **12B**, 1359-1375 (1981).
18. Ashwal, L. D., Warner, J. L. & Wood, C. A. *Proc. Lunar planet. Sci.* **13** (in the press).
19. Nyquist, L. *Proc. Lunar planet. Sci.* **13** (in the press).
20. Nehru, E. C. *et al. Meteoritics* **14**, 493-494 (1979).
21. Floran, R. J. *et al. Geochim. cosmochim. Acta* **42**, 1213-1229 (1978).
22. Mason, B. *Meteorites* (Wiley, New York, 1962).
23. Clayton, R. N. & Mayeda, T. K. *Earth planet. Sci. Lett.* **40**, 168-174 (1978).
24. Greenland, L. P. *Geochim. cosmochim. Acta* **35**, 319-322 (1971).
25. Clayton, R. N. *et al. Earth planet. Sci. Lett.* **30**, 10-18 (1976).
26. Delano, J. W. & Ringwood, A. E. *Proc. 9th Lunar planet. Sci. Conf.* 111-159 (1978).
27. Wolf, R. & Anders, E. *Geochim. cosmochim. Acta* **44**, 2111-2124 (1980).

Terrestrial-type xenon in meteoritic troilite

Golden Hwaung & Oliver K. Manuel

Department of Chemistry, University of Missouri, Rolla, Missouri 65401, USA

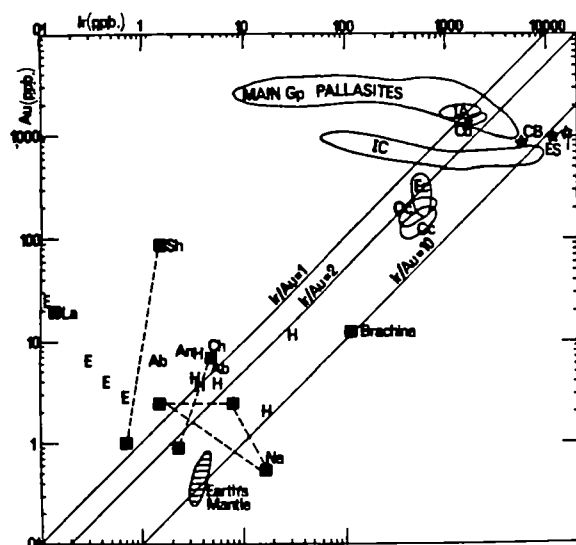


Fig. 2 Au/Ir for several meteorites. Black squares are shergottites, nakhlites, and chassignites (data in Table 1): Sh, Shergotty; Ch, Chassigny; Na, Nakhla; La, Lafayette. Stars are Eagle Station trio pallasites (data from ref. 13): ES, Eagle Station; I, Itzawisis; CB, Cold Bay. Other meteorites (data from many sources): E, Euclites; H, Howardite; Ab, Aubrites; An, Angrite; IA, IC, irons; Cd, Canyon Diablo; Oc, ordinary chondrites; Ec, enstatite chondrites; Cc, Carbonaceous chondrites. p.p.b., parts per 10⁹.

Recently it has been realized that the isotopic composition of Xe in different phases of chondrites is not uniform and that AVCC Xe is a mixture of the different nucleogenetic components trapped in these phases¹⁻⁴. We show here a similar abundance pattern for the nonradiogenic xenon isotopes in air and in meteoritic troilite (FeS), which suggests that the isotopic composition of atmospheric Xe was not produced by unique events in the history of terrestrial material but represents a particular mix of the different nucleogenetic components of Xe that was dominant in a central Fe- and S-rich region of the protoplanetary nebula⁵.

Radiogenic ¹²⁹Xe has been observed in samples from the Earth's mantle, but the abundance pattern of the eight

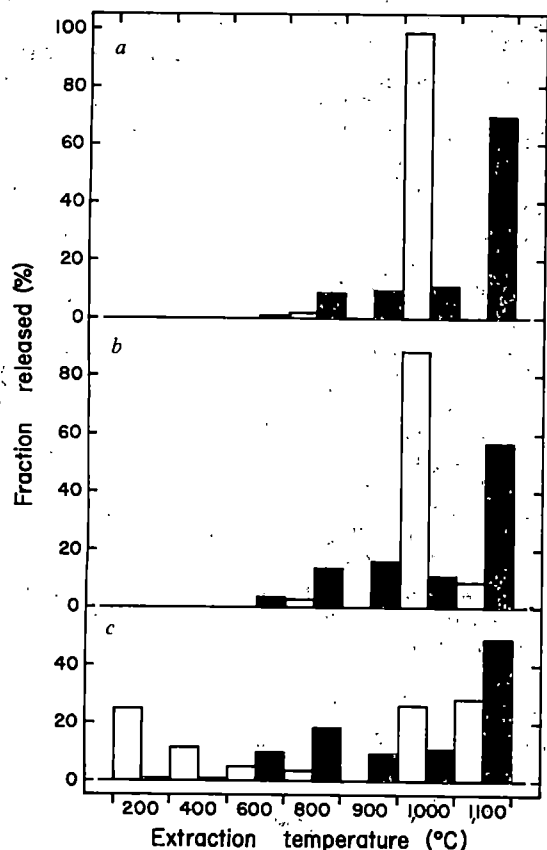


Fig. 1 The per cent of ^{132}Xe (c) and the neutron-capture-produced $^{131*}\text{Xe}$ (b) and $^{83*}\text{Kr}$ (a) released at each extraction temperature from troilite of the Odessa (open bars) and Cape York (black bars) iron meteorites. Note that Cape York is shown on the right and Odessa on the left for each extraction temperature, although the extraction schedules were identical except for the additional 900 °C step used only for Cape York. Values for $^{131*}\text{Xe}$ and $^{83*}\text{Kr}$ are defined by equations (1) and (2), respectively. Extraction temperatures of 200, 400, 600, 800, 900, 1,000 and 1,100 °C were used for both Xe and Kr samples, and an additional gas fraction at 900 °C was collected and analysed from the Cape York sample. The concentrations of ^{132}Xe shown were measured by the peak height method and have uncertainties of $\pm 6\%$. Uncertainties of ± 50 °C are estimated for extraction temperatures above 700 °C.

nonradiogenic isotopes is atmospheric rather than chondritic⁶. 'Terrestrial' Xe will therefore be used instead of 'atmospheric Xe' in referring to the relative abundances of the nonradiogenic xenon isotopes of this planet.

Contamination has been suggested^{4,7} as an explanation for previous observations of terrestrial Xe in meteoritic and lunar material^{4,8-15}. In several cases a spike of terrestrial Xe was observed in the gas released at ≈ 900 –1,100 °C when sulphide separates of chondrites and iron meteorites were subjected to stepwise gas extraction^{4,8,9}. Samples of meteoritic troilite (FeS) were selected for this investigation because (1) this is an abundant sulphide mineral of meteorites and large nodules of troilite are easily recovered from iron meteorites, (2) adsorbed atmospheric gases can be selectively released in the low-temperature fractions when troilite is heated under vacuum, and (3) troilite nodules contain traces of selenium and tellurium, and (n, $\gamma\beta$ -) reactions on ^{82}Se and ^{130}Te have produced excess $^{83*}\text{Kr}$ and $^{131*}\text{Xe}$ within the troilite during the exposure of the meteoroid to cosmic rays. These two stable end products of neutron-capture, $^{83*}\text{Kr}$ and $^{131*}\text{Xe}$, can be used as tracer isotopes to identify the temperature at which gases are released from within the troilite.

For this study, we separated nodules of troilite from two large meteorites, the Odessa Texas coarse octahedrite and the Cape York, West Greenland medium octahedrite. Procedures described elsewhere¹⁶ were used to analyse the isotopic composition of Kr and Xe in each gas fraction as a sample was heated to successively higher temperatures.

Experimental details and the isotopic composition of Xe in each temperature fraction are shown in Table 1 together with those of atmospheric¹⁷ and AVCC¹⁸ xenon. The concentrations and isotopic composition of Kr are given elsewhere¹⁹. Spallation and neutron-capture reactions can account for all observed deviations from the isotopic composition of atmospheric Kr.

To identify the gas component released from within the troilite, the amount of excess $^{131*}\text{Xe}$ from the $^{130}\text{Te}(n, \gamma\beta^-)^{131*}\text{Xe}$ reaction and the amount of excess $^{83*}\text{Kr}$ from the $^{82}\text{Kr}(n, \gamma\beta^-)^{83*}\text{Kr}$ reaction were computed as follows:

$$^{131*}\text{Xe} = [^{132}\text{Xe}] \left(\frac{^{131}\text{Xe}/^{132}\text{Xe}}{^{131}\text{Xe}/^{132}\text{Xe}}_{\text{FeS}} - \left(\frac{^{131}\text{Xe}/^{132}\text{Xe}}{^{131}\text{Xe}/^{132}\text{Xe}}_{\text{Air}} \right) \right] \quad (1)$$

$$^{83*}\text{Kr} = [^{86}\text{Kr}] \left(\frac{^{83}\text{Kr}/^{86}\text{Kr}}{^{83}\text{Kr}/^{86}\text{Kr}}_{\text{FeS}} - \left(\frac{^{83}\text{Kr}/^{86}\text{Kr}}{^{83}\text{Kr}/^{86}\text{Kr}}_{\text{Air}} \right) \right] \quad (2)$$

The release patterns of ^{132}Xe and neutron-capture-produced $^{131*}\text{Xe}$ and $^{83*}\text{Kr}$ for the two troilite samples are shown in Fig. 1.

The total concentration of xenon released from the Cape York troilite, $^{132}\text{Xe} = 1.79 \times 10^{-12} \text{ cm}^3 \text{ STP g}^{-1}$, was appreciably less than that released from the Odessa troilite, $11.5 \times 10^{-12} \text{ cm}^3 \text{ STP g}^{-1}$. Only a small fraction of this gas (1.4%) was released from Cape York troilite below 600 °C, whereas 36.7% of the ^{132}Xe was released from Odessa troilite below 600 °C. The release of significant amounts of xenon from Odessa troilite at low temperatures and the high concentration of ^{132}Xe in this sample seem to be compatible with the earlier finding that Odessa is an agglomeration of heterogeneous material that has not been molten since accretion whereas Cape York had an igneous origin and appears to have undergone an extended period of annealing^{20,21}.

From the release patterns of $^{83*}\text{Kr}$ and $^{131*}\text{Xe}$, we conclude that degassing of troilite is represented by the 1,000 °C fraction of Odessa and the 1,100 °C fraction of Cape York. Figure 1c shows that an appreciable fraction of the total Xe was released when the troilite melted. The amount of Xe in the 1,000 °C fraction of Odessa and the 1,100 °C fraction of Cape York exceeds by more than a factor of 50 the amount of Xe observed in blanks, when the empty crucible was heated to 1,100 °C and the gases collected, cleaned and analysed by the same procedure used for the samples. Adsorbed atmospheric Xe would not be expected to survive the lower extraction temperatures, and the abundance pattern of the nonradiogenic Xe isotopes in the 1,000 °C fraction of Odessa troilite and the 1,100 °C fraction of Cape York troilite can therefore be used to determine the isotopic composition of Xe trapped in these samples.

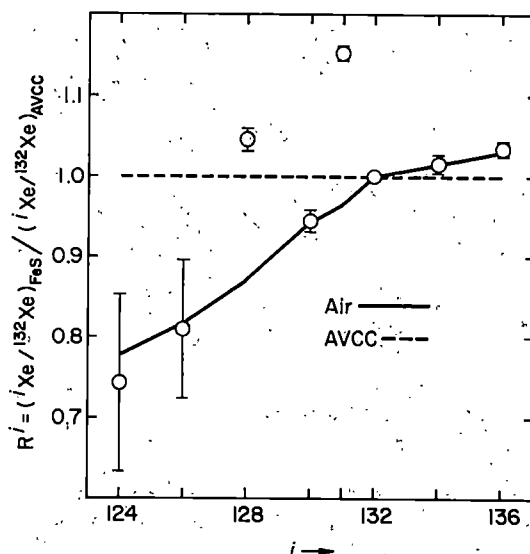


Fig. 2 A comparison of the isotopic composition of Xe in the 1,000 °C fraction of Odessa troilite (O) with that in air and in chondritic meteorites¹⁸, AVCC. AVCC Xe is represented by the dashed line at $R' \approx 1.00$. The isotopic composition of Xe released in this melt fraction of Odessa troilite is identical to that in air, except for excess ^{128}Xe and ^{131}Xe in the troilite. These are the stable end products of neutron-capture on ^{127}I and ^{130}Te .

Table 1 Isotopic composition of xenon and concentration of ^{132}Xe released by stepwise heating of meteoritic troilite

Extraction temperature (°C)	Isotopic composition, (ⁱ Xe/ ¹³² Xe) × 10 ²								¹³² Xe in units of 10 ⁻¹² cm ³ STP g ⁻¹
	i = 124	i = 126	i = 128	i = 129	i = 130	i = 131	i = 134	i = 136	
Odessa troilite									
200				116 ± 3	15.0 ± 0.3	80.7 ± 2.2	39.3 ± 1.3	33.7 ± 0.9	2.89
400	0.361 ± 0.081	0.343 ± 0.051	7.31 ± 0.26	134 ± 2	14.8 ± 0.4	77.9 ± 1.0	38.1 ± 0.6	32.9 ± 0.5	1.31
600	0.546 ± 0.111	0.286 ± 0.173	7.34 ± 0.56	158 ± 3	14.5 ± 0.3	77.3 ± 1.6	38.1 ± 0.7	32.1 ± 0.5	0.57
800	0.553 ± 0.214	0.364 ± 0.110	7.82 ± 0.57	239 ± 3	15.3 ± 0.7	82.5 ± 1.5	38.2 ± 0.7	38.8 ± 0.8	0.41
1,000	0.341 ± 0.050	0.332 ± 0.035	8.58 ± 0.12	325 ± 2	15.2 ± 0.2	94.1 ± 0.6	38.8 ± 0.4	33.2 ± 0.2	3.01
1,100	0.435 ± 0.042	0.385 ± 0.032	9.06 ± 0.15	424 ± 2	15.5 ± 0.2	80.2 ± 0.4	39.9 ± 0.2	33.9 ± 0.2	3.27
Cape York troilite									
200				101 ± 8					0.01
400				122 ± 10					0.01
600				107 ± 4	15.4 ± 0.9	82.5 ± 2.9	39.8 ± 1.2	34.4 ± 1.2	0.18
800			8.53 ± 0.86	127 ± 3	15.1 ± 0.4	88.3 ± 0.8	38.9 ± 0.8	34.0 ± 0.7	0.33
900			8.40 ± 1.25	171 ± 2	14.8 ± 0.6	100.3 ± 2.1	40.2 ± 1.1	34.2 ± 0.5	0.17
1,000			8.97 ± 1.89	144 ± 7	15.2 ± 1.2	91.4 ± 3.7	39.8 ± 1.1	33.7 ± 1.3	0.20
1,100	0.384 ± 0.037	0.385 ± 0.060	7.30 ± 0.38	161 ± 1	15.2 ± 0.4	93.9 ± 1.2	38.9 ± 0.7	33.2 ± 0.6	0.88
Air	0.357	0.335	7.14	98.3	15.17	78.8	38.8	33.0	
AVCC	0.459	0.410	8.20		16.1	81.7	38.2	32.1	

The sample of Cape York troilite was a single piece weighing 2.3236 g and that of Odessa troilite consisted of three pieces weighing 1.5429 g that had been taken from a single nodule.

To compare the isotopic composition of Xe in these two temperature fractions with that seen in chondrites¹⁸, the abundance of each stable isotope of mass, i , is defined by the ratio, R^i , where

$$R^i = (^i\text{Xe}/^{132}\text{Xe})_{\text{sample}} / (^i\text{Xe}/^{132}\text{Xe})_{\text{AVCC}} \quad (3)$$

Values of R^i are shown in Fig. 2 for each xenon isotope in the 1,000 °C fraction of Odessa troilite and in Fig. 3 for those in the 1,100 °C fraction of Cape York troilite.

In both gas fractions, the abundance pattern of the nonradioactive isotopes matches that of terrestrial Xe. The high value of R^{131} indicates the release of neutron-capture-produced $^{131}\text{m}\text{Xe}$, and the high value of R^{128} in the 1,000 °C fraction of Odessa troilite (Fig. 2) probably indicates the release of $^{128}\text{m}\text{Xe}$ from the $^{127}\text{I}(n, \gamma\beta^-)^{128}\text{Xe}$ reaction. The decay product of ^{129}I indicated by $^{129}\text{Xe}/^{132}\text{Xe} = 3.25$ in the 1,000 °C fraction of Odessa troilite also suggests the degassing of sites that contain iodine. A small contribution of spallation-produced Xe may be responsible for the slight enrichment of the light xenon isotopes shown in Fig. 3 for the Cape York troilite.

For xenon released from the troilite samples at most other extraction temperatures, Table 1 shows that values of the $^{136}\text{Xe}/^{132}\text{Xe}$ and $^{134}\text{Xe}/^{132}\text{Xe}$ ratios are generally higher than those of AVCC Xe and that values of the $^{130}\text{Xe}/^{132}\text{Xe}$ ratio are generally lower than that of AVCC Xe. The values of these three ratios are more like those in terrestrial than in AVCC Xe.

Values of the $^{129}\text{Xe}/^{132}\text{Xe}$, $^{128}\text{Xe}/^{132}\text{Xe}$ and $^{131}\text{Xe}/^{132}\text{Xe}$ ratios do not necessarily indicate the isotopic signature of the indigenous component because of *in situ* products from the decay of ^{129}I and from $(n, \gamma\beta^-)$ reactions on ^{128}Te , ^{127}I and ^{130}Te .

There are large uncertainties on the measurements of ^{124}Xe and ^{126}Xe because of their low natural abundance, but measured values of the $^{126}\text{Xe}/^{132}\text{Xe}$ ratio are generally lower than in AVCC Xe. Xenon in the 600, 800 and 1,100 °C fractions of Odessa troilite suggest the possible presence of an excess ^{124}Xe component like that recently reported in the 550–650 °C and 1,400–1,500 °C fractions of troilite-rimmed chondrules and blocky sulphides of the Allende chondrite⁴. Large uncertainties in the measurements of these light isotopes make it impossible to distinguish between spallation products, excess ^{124}Xe and/or a component of AVCC-type Xe. The absence of significant amounts of excess $^{131}\text{m}\text{Xe}$ in the 600, 800 and 1,100 °C fractions of Odessa suggests that ^{124}Xe -enriched xenon is not anyway representative of the bulk Xe trapped within the troilite.

U-Xe, a hypothetical type of xenon recently proposed by Pepin and Phinney²², is characterized by values of the $^{124-131}\text{Xe}/^{132}\text{Xe}$ ratios that are higher than those of AVCC Xe and by values of $^{134-136}\text{Xe}/^{132}\text{Xe}$ ratios that are lower than those of AVCC Xe. Obviously U-Xe cannot explain the isotopic

composition of Xe released from our samples (see Table 1).

To check the melting temperature of troilite under vacuum, a 0.165-g sample of natural terrestrial troilite was heated in an evacuated quartz tube. The troilite was broken from a large single crystal (purchased from Wards Natural Science Establishment). The temperature was increased in 100 °C increments, and melting and partial dissociation was observed at 1,100 °C. The degassing of Odessa troilite at 1,000 °C may indicate crystal imperfections or chemical impurities because Odessa was not exposed to the prolonged annealing of Cape York or terrestrial troilite^{20,21}. However, the uncertainty in the extraction temperature, $\approx \pm 50$ °C, may account for the apparent difference in the melting temperatures of troilite from the Cape York and Odessa meteorites.

The data shown in Figs 1–3 demonstrate the presence of terrestrial Xe trapped in troilite of the Odessa and Cape York iron meteorites. There is growing evidence that the protoplanetary nebula was chemically and isotopically zoned^{5,6} and that the cores of the four inner planets formed in the central

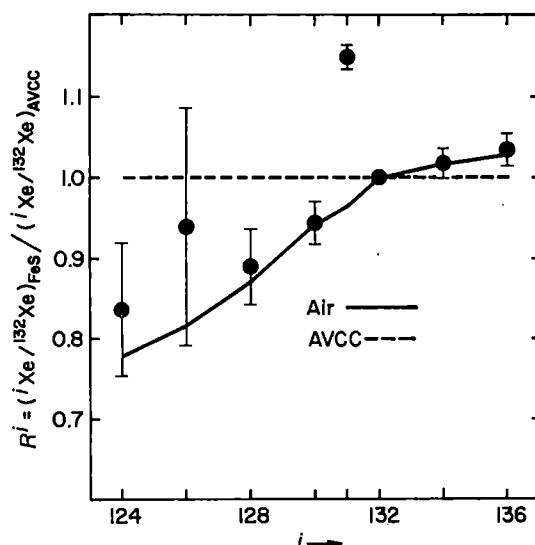


Fig. 3 A comparison of the isotopic composition of Xe in the 1,100 °C fraction of Cape York troilite (●) with that in air and in chondritic meteorites¹⁸, AVCC. The isotopic composition of Xe released from Cape York troilite with the tracer isotope of *in situ* generated $^{131}\text{m}\text{Xe}$ is like that in air, except for a possible component of spallation-produced ^{124}Xe and ^{126}Xe . The isotopic composition of Xe trapped in meteoritic troilite differs from that seen in bulk chondrites¹⁸ across the entire spectrum of stable isotopes.

Fe-rich region^{5,6,23,24}. Since different mixes of nucleogenetic components have been identified in various phases of chondrites¹⁻⁵, the release of terrestrial Xe might also be expected in the melt fraction of troilite separates of chondrites. In fact, terrestrial Xe was reported recently⁴ in the gas released at 900 °C from troilite-rimmed chondrules (no. 20A1) and blocky iron sulphides of the primitive Allende carbonaceous chondrite. The observations were attributed to adsorbed atmospheric Xe, but this interpretation is difficult to reconcile with the release of distinctly non-terrestrial Xe at lower extraction temperatures⁴. Further, the amount of Xe released from the blocky sulphides and the troilite-rimmed chondrules at 900 °C exceeds that released in any other temperature fraction below 1,250 °C. Uncertainties in the extraction temperatures are not given for the Allende study⁴, but the pronounced release of Xe for the temperature fraction labelled 900 °C suggests that this corresponds to the degassing of Xe trapped in, rather than adsorbed on, Allende sulphides.

In air the $^{86}\text{Kr}/^{132}\text{Xe}$ ratio is 8.5, a factor of about 20 higher than that in carbonaceous chondrites. Lower values of Kr/Xe are observed in terrestrial rocks and minerals, and it is uncertain whether preferential retention of Xe by solids can account for its apparent depletion in air⁶. In the troilite samples from Odessa and Cape York the $^{86}\text{Kr}/^{132}\text{Xe}$ ratio is 1.6 and 2.0, respectively, a factor of about 4.7 higher than the $^{86}\text{Kr}/^{132}\text{Xe}$ ratio in carbonaceous chondrites. The higher Kr/Xe ratio in troilite may indicate differences in the value of this ratio in different parts of the protoplanetary nebula or differences in the degree of elemental fractionation by the processes that ultimately incorporated Kr and Xe into carbon and troilite.

Regardless of the mechanism that produced the high Kr/Xe ratio in air, the results shown in Figs 1-3 imply that the isotopic composition of terrestrial Xe represents the particular mix of nucleogenetic components that was dominant in that part of the protoplanetary nebula which contained high concentrations of sulphur and iron. Support for this conclusion can be found in earlier reports of a spike of terrestrial Xe released at ≈ 900 –1,100 °C from iron sulphides of chondrites^{4,8} and iron meteorites⁹.

This research was supported by Weldon Springs Funds of the University of Missouri. We thank Professor Vagn F. Buchwald for providing the sample of Cape York used in this study, Mr Mark Stein for updating our mass spectrometer so that our analyses could be obtained rapidly and reliably by magnetic peak-jumping and computer data acquisition, and Mr Rajeswara Duppatla for writing the computer program used for the acquisition and reduction of output data.

Received 26 April; accepted 11 August 1982.

- Manuel, O. K., Hennecke, E. W. & Sabu, D. D. *Nature* **240**, 99–101 (1972).
- Frick, U. *Proc. 8th Lunar Sci. Conf.* 273–292 (1977).
- Srinivasan, B. & Anders, E. *Science* **201**, 51–56 (1978).
- Lewis, R. S., Hertogen, J., Alaerts, L. & Anders, E. *Geochim. cosmochim. Acta* **43**, 1743–1752 (1979).
- Sabu, D. D. & Manuel, O. K. *Meteoritics* **15**, 117–138 (1980).
- Manuel, O. K. & Sabu, D. D. *Geochim. J.* **15**, 245–267 (1981).
- Niemeyer, S. & Leich, D. A. *Proc. 7th Lunar Sci. Conf.* **2**, 587–597 (1976).
- Merrill, C. J. *geophys. Res.* **71**, 263–313 (1966).
- Niemeyer, S. *Geochim. cosmochim. Acta* **43**, 843–860 (1979).
- Munk, M. N. *Earth planet. Sci. Lett.* **3**, 133–138 (1967).
- Hennecke, E. W. & Manuel, O. K. *Earth planet. Sci. Lett.* **36**, 29–43 (1977).
- Rowe, M. W. & Bogard, D. D. *J. geophys. Res.* **71**, 4183–4188 (1966).
- M. N. Munk, *Earth planet. Sci. Lett.* **3**, 457–465 (1967).
- Edgerley, D. A. & Rowe, M. W. *Geochim. J.* **13**, 103–112 (1979).
- Lightner, B. D. & Marti, K. *Proc. 5th Lunar Sci. Conf.* **2**, 2023–2031 (1974).
- Srinivasan, B., Alexander, E. C. Jr & Manuel, O. K. *J. inorg. Nucl. Chem.* **34**, 2381–2396 (1972).
- Nier, A. O. *Phys. Rev.* **79**, 450–454 (1950).
- Eugster, O., Eberhardt, P. & Geiss, J. *J. geophys. Res.* **71**, 3874–3896 (1969).
- Hwang, C.-Y. G. thesis, Univ. Missouri-Rolla (1982).
- Wasson, J. T. *Geochim. cosmochim. Acta* **34**, 957–964 (1970).
- Scott, E. R. D., Wasson, J. T. & Buchwald, V. F. *Geochim. cosmochim. Acta* **37**, 1957–1983 (1973).
- Pepin, R. O. & Phinney, D. *Components of Xenon in the Solar System* (Preprint, Univ. Minnesota-Minneapolis, 1980).
- Turekian, K. K. & Clarke, R. S. Jr *Earth planet. Sci. Lett.* **6**, 346–348 (1969).
- Vinogradov, A. P. *Geokhimiya* **10**, 1427–1431 (1975).

Phase transition in KOH-doped hexagonal ice

Y. Tajima, T. Matsuō & H. Suga

Department of Chemistry and Chemical Thermodynamics
Laboratory, Faculty of Science, Osaka University, Toyonaka,
Osaka 560, Japan

A few crystals exist which have residual entropy^{1,2}. The most notable of these is hexagonal ice, I_h , the ordinary form of solid H_2O (ref. 3). The structural interpretation of the residual entropy proposed by Pauling and widely accepted ascribes it to positional disorder of the protons in the ice conditions⁴. As such a disordered arrangement of the constituent atom cannot be an equilibrium structure of the crystal at the lowest temperature, there has been great interest in the search for a possible ordering phenomenon in ice crystals. We report here a calorimetric experiment which shows that a first order phase transition takes place in KOH-doped ice crystals and that the transition removes most of the residual entropy of the ice crystal.

The presence of residual entropy implies a lack of thermal equilibrium in the crystal below a certain temperature. In fact, we have observed relaxational heat-capacity anomalies of ~ 100 K for ordinary ice⁵ and ~ 115 K for heavy ice⁶, and have studied the associated enthalpy relaxation by subjecting the ice specimen to rapid quenching and long annealing in an adiabatic calorimeter. The study revealed the relaxational behaviour to be a kind of glass transition in the stable crystal, thus eliminating the previous interpretation⁷ of the corresponding anomalies in dielectric properties as due to the onset of a ferroelectric phase transition. The enthalpy relaxation time became 10^4 s at 105 K

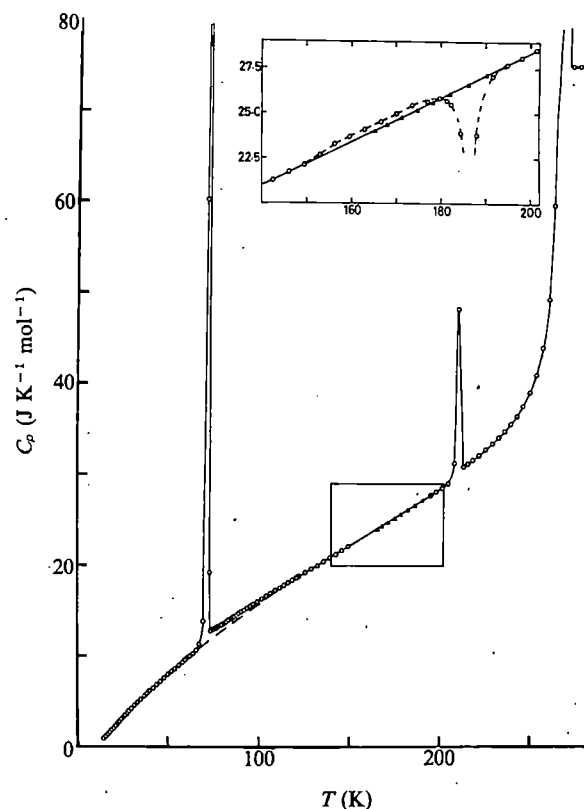


Fig. 1 The heat capacity of H_2O doped with 0.1 mol dm^{-3} KOH. The inset shows the effect of crystallization of the undercooled part of the sample.

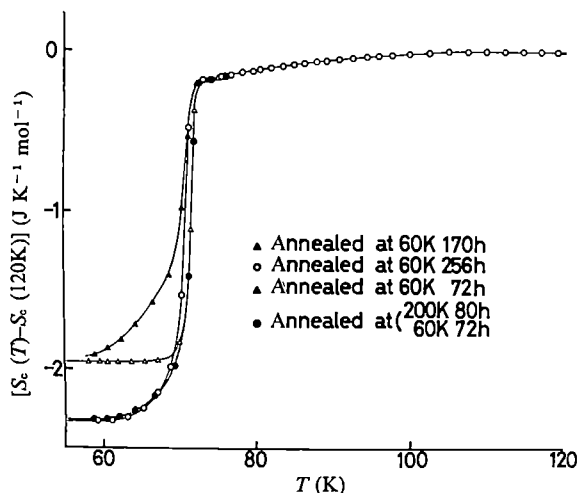


Fig. 2 The anomalous entropy of H_2O doped with 0.1 mol dm^{-3} KOH referred to 120 K. The key follows the order of the measurement.

and 10^6 s at about 87 K. We found that a completely ordered state at the hypothetical transition temperature, 60 K as calculated by Pitzer and Polissar⁸, would require an extremely long time.

Following the proposal by Onsager⁹, we have made heat-capacity measurements on HF-doped ice crystals¹⁰. Doping by this impurity is thought to introduce various kinds of lattice defects, including the Bjerrum fault¹¹, and to accelerate the rate of rearrangement of proton configurations by catalysing proton migration. However, our heat-capacity measurements actually revealed a positive effect of HF-doping, in that it increased the heat-capacity anomaly and thus brought about a more ordered state. The relaxation time was reduced by a factor of 30 at the relevant temperature for the most effective concentration of HF dissolved in the ice specimen, but not enough for a phase transition to take place.

When we doped an ice sample with a small amount of KOH, however, a drastic change occurred in its thermal behaviour. Aqueous solutions of KOH of the desired concentration were prepared by stepwise dilution. The doped water specimen was sealed in a Mylar (polyethylene terephthalate film) bag and put in a calorimeter cell together with 1 atm pressure of He gas as a heat exchanger. The double-jacketed adiabatic calorimeter operating in an intermittent heating mode used in the present study has been described previously¹². The calorimeter cell was made of gold-plated copper and had an internal volume of 8 cm^3 . The temperature of the cell was measured by a platinum resistance thermometer (Minco s1059, Minco Products) along with a precision a.c. double bridge (Automatic System Laboratory Inc., model H8). Resolution of the temperature measurement was better than 0.1 mK in the relevant temperature region. The precision of the heat-capacity data was generally better than 0.1%.

The calorimeter containing 0.1 mol dm^{-3} KOH solution was cooled in the cryostat. The time required for the completion of the crystallization of the 5.5406 g sample was about 15 min as indicated by the duration of the temperature arrest at 273 K. The crystallized sample was cooled to 80 K at 2 K min^{-1} and then to 60–65 K. It was then kept in an adiabatic condition and its temperature recorded. The temperature of the cell increased spontaneously for about 1 week. When the heat evolution ceased, the calorimetric system was cooled to 13 K and the heat-capacity measurement was started. The heat-capacity data are given in Fig. 1 and show three anomalies, at 72, 208 and 273 K. The second anomaly is due to the eutectic melting of the ice and hydrated KOH and the third to the melting of ice into the KOH solution. The anomaly at 72 K is due to the phase transition and is essentially isothermal. The transition

occurs neither in pure ice nor in H_2O doped with HF. The excess heat capacity of the KOH-doped ice over that of pure ice extends over a wide temperature range, up to 40 K above the transition temperature. It is this high-temperature tail of excess heat capacity that we have observed as the relaxational heat capacity in the pure ice crystal. We chose 120 K as the reference temperature for calculating the difference in the entropies between the pure and KOH-doped ices from the heat-capacity data. As Fig. 2 shows, the decrease of the entropy in the phase transition is $2.32 \text{ J K}^{-1} \text{ mol}^{-1}$. Thus, the phase transition removes a substantial fraction ($\approx 70\%$) of the configurational entropy that the ice crystal retains at higher temperatures. In a similar experiment on D_2O the phase transition occurred at 76 K.

As shown in Fig. 2, the magnitude of the entropy removed by the transition depended in a complex manner on the temperature and time of annealing as well as on the previous history of the sample, for example, whether or not it had undergone the phase transition before, or the temperature to which it had been heated after the previous phase transition. However, we simply record here the occurrence of the hysteretic behaviour without going into its analysis, because we are primarily concerned with the determination of the total transition entropy.

We believe that the anomaly is an intrinsic equilibrium property of ice I_h which has previously escaped observation because of its kinetics and which has now been revealed by the catalytic action of KOH. The reasons for this are: (1) the temperature of the heat-capacity peak is independent of the concentration of KOH. In experiments using 10 and 100 times lower concentrations of KOH solution, the transition occurred at the same temperature, as Fig. 3 shows for the $0.001 \text{ mol dm}^{-3}$ specimen. (2) The small amount of KOH (≤ 0.002 by the amount-of-substance fraction) is not expected to change the bulk equilibrium property of the ice to this extent. However, this statement will be tested further by experiments using different dopants such as LiOH, RbOH and $\text{Ba}(\text{OH})_2$.

Use of a polycrystalline sample is justified by the large entropy change of the transition observed, as surface contribu-

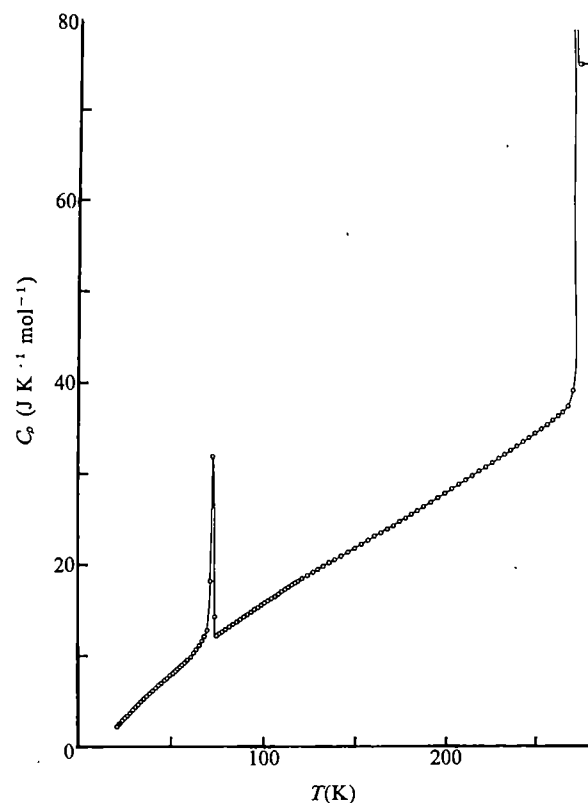


Fig. 3 The heat capacity of H_2O doped with $0.001 \text{ mol dm}^{-3}$ KOH.

tions to the molar entropy for a reasonable crystallite size are much smaller than the observed transition entropy. Both polycrystals and single crystals have been used in calorimetry without any specific surface effects^{3,5,6,13,14}. The crystallite size may influence the rate of the phase transition through the size dependence of the effective dopant concentration in the bulk of the specimen and through surface nucleation of the new phase.

The solubility of HF in ice and characterization of the defects introduced by it have been reported previously^{15,16}. However, very little is known about KOH impurities in ice. The present study shows that the ions are incorporated in the lattice. It would be useful to investigate the properties of the dissolved ions by microscopic methods.

Kawada studied the dielectric properties of doped ices and found a phase transition at 70 K on a KOH-doped specimen¹⁷. The temperature of the dielectric phase transition agrees with the present observation. Theoretical estimates of the transition temperature, depending to different extents on the experimental data, vary between 60 and 73 (refs 8, 18, 19). The agreement between the experimental and theoretical transition temperatures shows that the electrostatic models underlying these calculations are essentially correct. Structural investigation of the low temperature phase in collaboration with a neutron group is being planned.

This is contribution no. 44 from the Chemical Thermodynamics Laboratory.

Received 18 May; accepted 3 August 1982.

- Wilkes, J. *The Third Law of Thermodynamics* (Oxford University Press, 1961).
- Parsonage, N. G. & Staveley, L. A. K. *Disorder in Crystals* (Clarendon, Oxford, 1978).
- Giauque, W. F. & Stout, J. W. *J. Am. chem. Soc.* **58**, 1144–1150 (1936).
- Pauling, L. *J. Am. chem. Soc.* **57**, 2680–2684 (1935).
- Haida, O., Matsuo, T., Suga, H. & Seki, S. *J. chem. Thermodyn.* **6**, 815–825 (1974).
- Haida, O., Suga, H. & Seki, S. *J. Glaciol.* **22**, 155–164 (1979).
- Dengel, O., Eckener, V., Plitz, H. & Riehl, N. *Phys. Lett.* **9**, 291–293 (1964).
- Polissar, J. & Pitzer, K. S. *J. phys. Chem.* **60**, 1140–1142 (1956).
- Onsager, L. in *Ferroelectricity* (ed. Weller, E.) 16–19 (Elsevier, Amsterdam, 1967).
- Ueda, M., Matsuo, T. & Suga, H. *J. Phys. chem. Solids* (in the press).
- Bjerrum, N. *Science* **115**, 385–390 (1952).
- Tatsumi, M., Matsuo, T., Suga, H. & Seki, S. *Bull. chem. Soc. Japan* **48**, 3060–3066 (1975).
- Van den Beukel, A. *Phys. Stat. Solids* **28**, 565–568 (1968).
- Pick, M. A., Wenzel, H. & Engelhardt, H. Z. *Naturforsch.* **26A**, 810–814 (1971).
- Haltenorth, H. & Klinger, J. *J. Solid St. Commun.* **21**, 523–535 (1977).
- Bilgram, J. H., Reos, J. & Gränicher, H. Z. *Phys.* **B23**, 1–9 (1976).
- Kawada, S. *J. phys. Soc. Japan* **32**, 1442 (1972).
- Hentschel, H. G. *Molec. Phys.* **38**, 401–411 (1979).
- Minagawa, I. *J. phys. Soc. Japan* **50**, 3669–3676 (1981).

Influence of cross-diffusion on 'finger' double-diffusive convection

Trevor J. McDougall & J. Stewart Turner

Research School of Earth Sciences, Australian National University, PO Box 4, Canberra 2600, Australia

Structures similar to the oceanic 'salt fingers' that form when warmer more saline water overlies cooler fresher water¹ have recently been observed², in concentrated solutions of polymers in conditions where fingers would not form according to the usual criteria. We here extend previous theories to derive the conditions under which double-diffusive convection can occur in a solution of a pair of solutes with a large coupled diffusion (or cross-diffusion) effect, that is, where a flux of one property is driven by a spatial gradient of another.

Salt fingers have an important role in the mixing of properties in several regions of the ocean³. The fingers form a pattern in which each upward-moving finger is surrounded by downward-moving fingers and vice versa. The downgoing fingers continually lose heat (by horizontal conduction) to the neighbouring upgoing fingers, so making the downgoing fingers more dense

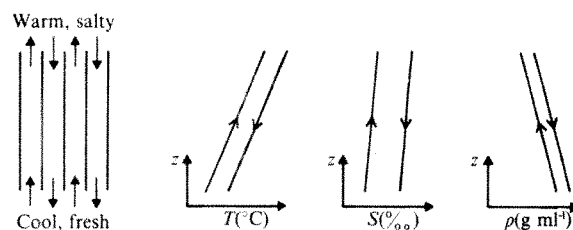


Fig. 1 Up- and down-going salt fingers and their temperatures, salinities and densities. The arrows on the individual profiles distinguish the up from the downgoing fingers. Note that in contrast to Fig. 3, the temperature is plotted here rather than its effect on density.

and the upgoing fingers less dense (Fig. 1). The small width of the fingers (shown by both theory and direct observations to be a few centimetres) allows a significant heat flux to occur by molecular heat conduction, leading to the temperature gradients in the fingers shown in Fig. 1. Because the molecular diffusivity of salt is much less than that of heat, the fingers do not transfer much salt between themselves, so the vertical salinity gradient is small (Fig. 1). Figure 2 is a cross-section through a field of fingers which are growing downwards into a stable temperature gradient set up in a laboratory tank.

Preston *et al.*² have recently produced striking photographs of fingers in studies of the diffusion of macromolecules. In their paper three polymers were used, but in their subsequent work⁴ they have observed fingers at a horizontal interface between an upper dextran solution and a lower, more concentrated dextran solution which also has a small amount of sorbitol added to it. This configuration is not obviously conducive to fingering because both solutes (dextran and sorbitol) are more concentrated in the lower layer. We show here that with a sufficiently large cross-diffusion effect, fingers can form in such a situation.

It is not uncommon, even today, to read in the diffusion literature that convective motion cannot occur at, say, a diffusing horizontal interface between two solutions unless the vertical density gradient ρ_z is positive, that is, unless the fluid is statically unstable. Both types of double-diffusive convection occur, however, in a statically stable density gradient, where $\rho_z < 0$. Wendt⁵ has solved the problem of the diffusion of two properties from an initially sharp interface with two cross-diffusion terms and has shown that such one-dimensional diffusion can lead to a local reversal of the density gradient. This result has been widely used to determine whether convection can be expected in particular situations, often associated with measurements of diffusion coefficients (in, for example, a Gouy diffusimeter) and the testing of the Onsager relations.

Double-diffusive convection developed in the 1960s mainly due to its applications in oceanography but recently it has been realized that it can be important in many other contexts¹. Two recent papers^{6,7} have investigated double-diffusive instabilities



Fig. 2 A field of salt fingers formed by setting up a stable temperature gradient and pouring a little salt solution on top. The downward-moving fingers are made visible by adding fluorescein to the salt solution and lighting through a slit from below.

caused by the Soret effect in the special geometry of a Rayleigh-Bénard convection experiment where a solution is differentially heated from above and cooled below, showing that convective instabilities can and do occur when the density gradient is statically stable. Hurle and Jakeman⁸ have studied the case where the heating and cooling are reversed with the heating occurring at the bottom and the cooling above.

We have incorporated the two cross-diffusion flux terms into the linear stability analysis of double-diffusive convection and we focus our attention on the conditions under which fingers form when *both* components are stably distributed. We consider a solution of two solutes T and S confined between two horizontal porous plates which maintain a fixed contrast in fluid properties between the plates. We parameterize the diffusion and the cross-diffusion fluxes by

$$-\text{Flux of } T = D_{11}\nabla T + D_{12}\nabla S \quad (1)$$

$$-\text{Flux of } S = D_{22}\nabla S + D_{21}\nabla T \quad (2)$$

The density of the fluid ρ is given by the linear relation

$$\rho = \rho_0(1 + \alpha T + \beta S) \quad (3)$$

where α and β are constants, ρ_0 is a reference density and T and S are the concentrations of the two solutes, defined so that $D_{11} > D_{22}$. That is, T has a larger molecular diffusivity than S and we define the ratio D_{22}/D_{11} to be equal to $\tau (< 1)$. On following through the linear stability analysis for small perturbations from linear property gradients and no initial motion, it can be shown⁹ that the finger instability will occur if

$$\left(\frac{\beta D_{21}}{\alpha D_{22}} - 1\right) + \frac{1}{\tau} \frac{\beta S_z}{\alpha T_z} \left(\frac{\alpha D_{12}}{\beta D_{11}} - 1\right) > \frac{27}{4} \frac{\pi^4}{R} \left(1 - \frac{D_{12}D_{21}}{D_{11}D_{22}}\right) \quad (4)$$

This inequality is appropriate to the case where T is distributed in a statically stable fashion (that is if $\alpha T_z < 0$, where z is positive upwards and the subscript denotes differentiation). Here R is the Rayleigh number defined in the usual way and normally it is large in comparison to $27\pi^4/4$ and so the right side of inequality 4 can be taken as zero.

Inequality 4 is the criterion which must be satisfied if fingers are to form when the *in situ* vertical gradients of T and S are T_z and S_z (assumed uniform in the horizontal plane). The normal condition for fingers to form without cross-diffusion is readily recovered from inequality (4). In this case, $D_{12} = D_{21} = 0$, $\beta S_z > 0$, $\alpha T_z < 0$, giving the well known condition $|\beta S_z/\alpha T_z| > \tau$. Hydrostatic instability ($\rho_z > 0$) occurs when $|\beta S_z/\alpha T_z| > 1$ and so this requires a considerably larger gradient of S than is required for the formation of fingers. We postpone further discussion of inequality (4) until after we examine a finite amplitude finger model.

Huppert and Manins¹⁰ have presented a linear model of finite-amplitude steady, very long salt fingers. The nonlinear advective terms in the Navier-Stokes equations are equal to zero because the motion is assumed to be entirely vertical. The vertical velocity W and the deviations T' and S' of the T and S properties from their horizontal averages are assumed to take the form

$$(W, T', S') = (W_0, T_0, S_0) \cos mx \cos ny \quad (5)$$

where x and y are the horizontal coordinates. By substituting equation(s) (5) into the Navier-Stokes equations (significantly simplified by the assumption of purely vertical velocities) we obtain

$$\begin{aligned} -\alpha \bar{T}_z \left(\frac{\beta}{\alpha} D_{21} - D_{22} \right) - \beta \bar{S}_z \left(\frac{\alpha}{\beta} D_{12} - D_{11} \right) \\ = \frac{\nu k^4}{g} (D_{11}D_{22} - D_{12}D_{21}) \end{aligned} \quad (6)$$

where $k^2 = m^2 + n^2$. For fingers to form, k^4 must be positive,

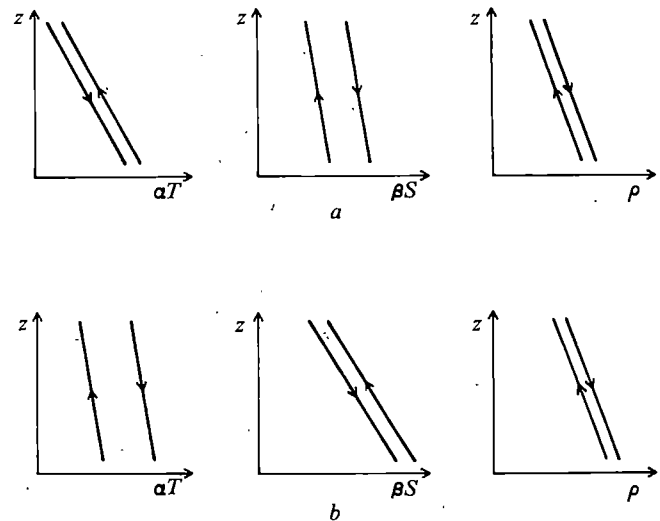


Fig. 3 Sketch of the vertical profiles of αT , βS and ρ in the centres of upgoing and downgoing (indicated by the arrows) fingers for $\bar{T}_z < 0$, $\bar{S}_z < 0$; that is with both T and S stably stratified. Panel *a* has $D_{12} = 0$ and D_{21} satisfies inequality (7) (see text). Panel *b* has $D_{21} = 0$ and D_{12} satisfies inequality (7).

and taking $D_{11}D_{22} > D_{12}D_{21}$ we see that the left hand side of equation (6) must be positive. \bar{T}_z and \bar{S}_z are the vertical gradients of the horizontal average of T and S through the fingers. We concentrate on the case where T is stably stratified ($\alpha T_z < 0$) and from equation (6) we see that finite amplitude fingers will persist if

$$\left(\frac{\beta D_{21}}{\alpha D_{22}} - 1\right) + \frac{1}{\tau} \frac{\beta \bar{S}_z}{\alpha \bar{T}_z} \left(\frac{\alpha D_{12}}{\beta D_{11}} - 1\right) > 0 \quad (7)$$

This inequality looks very similar to inequality (4) but the two relations are derived by very different theoretical methods. Inequality (4) is the result of a linear stability analysis for the onset of fingers in uniform vertical property gradients T_z and S_z , while inequality 7 is the condition for the maintenance of finite amplitude fingers. Apart from the different interpretation of the vertical property gradients in inequalities (4) and (7) the two criteria are the same.

Consider now the situation where both T and S are stably stratified; that is $\alpha T_z < 0$ and $\beta S_z < 0$. We see from inequality 7 that the occurrence of fingers is assisted by large positive values of both D_{12} and D_{21} and that at least one of $\beta D_{21}/\alpha D_{22}$ and $\alpha D_{12}/\beta D_{11}$ must exceed unity.

The driving energy for normal fingering motion comes from the unstably stratified component S and this gravitational potential energy is released by the rapid diffusion of T between the fingers. In the fingering motion we have just described we have shown that even if both components, T and S are distributed in a hydrostatically stable fashion, finger convection can still occur if the cross-diffusion coefficients D_{12} and D_{21} are large enough to satisfy inequality (7). The total gravitational potential energy of the fluid still decreases due to the fingering, but in this case it is the cross-diffusion between the fingers which allows the release of gravitational potential energy even though no separate solute is unstably stratified.

The T , S and ρ profiles in upgoing and downgoing fingers are shown in Fig. 3 for the two special cases when one of the cross-diffusion coefficients is zero. In Fig. 3*a* where $D_{12} = 0$, the T concentration of the downgoing fingers increases due to the diffusion of T from the upgoing into the downgoing fingers. This flux between the fingers occurs in the normal fashion because the T flux is unaffected by coupled diffusion. The flux of S between the fingers is however mainly due to the cross-diffusion flux of S caused by the horizontal spatial gradients of T . Similarly in Fig. 3*b* where $D_{21} = 0$, the flux of S between the

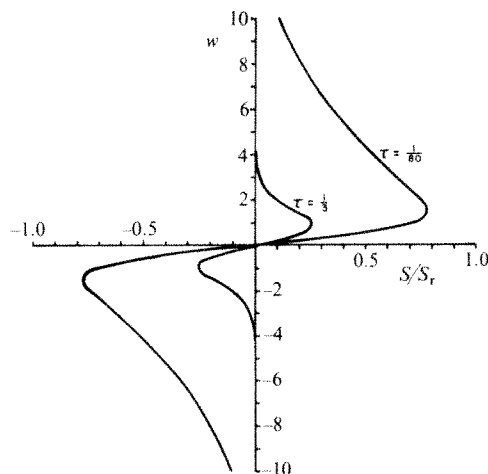


Fig. 4 Vertical profiles of the S concentration at a diffusing interface with $D_{12}=0$ and with the initial contrast in S concentration between the two layers equal to zero. The vertical coordinate w is equal to $z/2\sqrt{D_{22}t}$ and the reference S value S_r is $(\Delta T/2)(D_{21}/D_{22})\tau/(1-\tau)$.

fingers is not affected by coupled diffusion and the flux of T between the fingers is mainly due to the cross-diffusive flux of T caused by the positive value of D_{12} (satisfying inequality (7)) and the S gradient between the fingers. Note that in both *a* and *b* of Fig. 3 the horizontally averaged density gradient is statically stable ($\bar{\rho}_z < 0$) and that the downgoing fingers are more dense than the surrounding upgoing fingers.

The theoretical arguments outlined above have all related to regions in which there are constant vertical gradients of the two diffusing properties. A more common experimental situation, however, is one in which a layer of fluid is placed above another layer of different composition, with initially a sharp interface between them. When two solutions are placed one above the other, the diffusion of the two species T and S across the bounding interface may set up gradients which are favourable for the formation of fingers. Figure 4 shows the profiles of S as a function of $w = z/2\sqrt{D_{22}t}$ when the difference in S concentration between the layers is zero and one of the cross-diffusion coefficients, D_{12} , is also equal to zero. The S gradient is proportional to the cross diffusion coefficient D_{21} and to the difference in the T concentrations between the layers, ΔT . The S gradient is conducive to fingering in this interfacial region where the T gradient maintains the hydrostatic stability. This subject of diffusion at an initially sharp interface is discussed in more detail in ref. 9, including cases where both properties are initially set up in the hydrostatically 'stable' sense.

To test our belief that fingers can form due to cross-diffusion without needing to invoke any other special properties of polymers, we initiated experiments using two layers of sodium chloride solution at different temperatures, the cross diffusion term being now the Soret coefficient. According to published values of the coefficients, the criterion for instability to fingering motions (inequality (4)) could just be satisfied at low temperatures (where D_{21} is positive), with the upper layer a few degrees warmer than the lower. This system was, however, too sensitive to extraneous effects such as heating at the side walls and evaporation at the surface, and we concluded that a definitive experimental test of the theoretical ideas presented here will have to be carried out in a solute-solute system.

Cussler¹¹ lists references to measurements of all four ternary diffusion coefficients in various systems, showing that one of the few substances to exhibit large cross-diffusion fluxes is another polymer, polystyrene, of molecular weight of 190,000. Cussler and Lightfoot¹² used the polystyrene-toluene-cyclohexane combination and found values of $D_{12}/D_{11} < -1$. They also give a simple explanation of the large cross-diffusion effect in terms of the chemical potential as a function of temperature

for the two binary mixtures, polystyrene-toluene and polystyrene-cyclohexane.

In order to understand the mechanism of finger formation in situations such as those discussed by Preston *et al.*^{2,4} we suggest that the next logical step is to endeavour to measure the cross-diffusion fluxes for some of these long chain polymers in the presence of each other.

Received 7 May; accepted 4 August 1982.

- Huppert, H. E. & Turner, J. S. *J. Fluid Mech.* **106**, 299–329 (1981).
- Preston, B. N., Laurent, T. C., Comper, W. D. & Checkley, G. J. *Nature* **287**, 499–503 (1980).
- Williams, A. J. *J. geophys. Res.* **86**, 1917–1928 (1981).
- Comper, W. D. (in preparation).
- Wendt, R. P. *J. phys. Chem.* **66**, 1740–1742 (1962).
- Schechter, R. S., Prigogine, I. & Hamm, J. R. *Phys. Fluids* **15**, 379–386 (1972).
- Velarde, M. G. & Schechter, R. S. *Phys. Fluids* **15**, 1707–1714 (1972).
- Hurle, D. T. J. & Jakeman, E. J. *Fluid Mech.* **47**, 667–687 (1971).
- McDougall, T. J. *J. Fluid Mech.* (in the press).
- Huppert, H. E. & Manins, P. C. *Deep-Sea Res.* **20**, 315–323 (1973).
- Cussler, E. L. *Multicomponent Diffusion* (Elsevier, New York, 1976).
- Cussler, E. L. & Lightfoot, E. N. *J. phys. Chem.* **69**, 1135–1144 (1965).

Cyanophyte calcification and changes in ocean chemistry

Robert Riding

Department of Geology, University College, Cardiff CF1 1XL, UK

Cyanophytes range from at least 2,200 Myr (ref. 1) to the Recent, but they only produced common marine shelly fossils during the Palaeozoic and Mesozoic (570–80 Myr) (Fig. 1). This contrasts with the pattern of metazoan evolution in which rapid diversification near the Precambrian–Cambrian boundary was closely accompanied by skeletonization² which has been retained in marine environments to the Recent. Attempts to explain this unusual geological distribution of marine calcareous cyanophytes cannot be made solely by reference to biological processes because these algae are mainly dependent on environmental conditions for their calcification³. Thus, the presence or absence of calcified cyanophytes may be a general indication of long-term changes in seawater chemistry. This likelihood has been recognized previously⁴ but has not been explored in any detail. Here I outline some possible explanations and suggest that cyanophyte calcification was facilitated by enhancement of marine CaCO_3 precipitation rates in the late Precambrian because of decrease in the $\text{Mg}^{2+}/\text{Ca}^{2+}$ ratio, linked to falling P_{CO_2} levels and extensive dolomite formation. Scarcity of calcareous cyanophytes in Cenozoic marine environments again implicates the $\text{Mg}^{2+}/\text{Ca}^{2+}$ ratio, inferred from oöid mineralogy to have increased in the late Mesozoic⁵, as a factor influencing cyanophyte calcification in the sea.

Calcareous cyanophytes, represented by microscopic fossils such as *Angulocellularia*, *Girvanella* and *Ortonella*, are consistently present in normal marine shelf environments from the Nemakit–Daldyn Horizon of latest Precambrian age in Siberia⁶ until the Jurassic and possibly also Cretaceous⁷. But they have not been reported from Cenozoic marine deposits and the very few records of them in Recent seas indicate that they are extremely rare, are not calcified to the same degree as Palaeozoic and Mesozoic examples, and tend to be limited to marginal marine situations^{8,9}. Similarly, calcareous cyanophytes appear to be absent from most Precambrian rocks despite intensive study of stromatolite microfabrics. The best evidence for Precambrian calcareous cyanophytes is weakly calcified traces of filaments from Upper Riphean and younger rocks in the Soviet Union⁶.

In attempting to account for the paucity of calcareous cyanophytes in the sea during the Precambrian and Cenozoic,

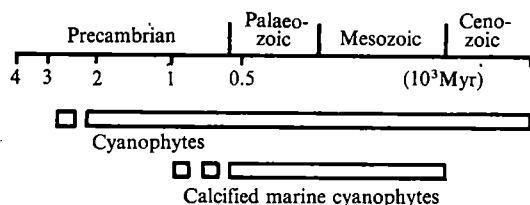


Fig. 1 Precambrian to Recent range of cyanophytes¹ compared with the Palaeozoic–Mesozoic occurrence of marine calcified cyanophytes.

both biological and environmental factors needed to be considered. The possibility that cyanophytes evolved calcification in the latest Precambrian cannot be ruled out, but silicified cyanophytes from the Proterozoic are similar to Recent forms¹⁰ and do not show morphological differences that could account for an absence of calcification. Furthermore, there is no good evidence that cyanophytes capable of calcification either became extinct or were excluded from marine environments in the late Mesozoic. The suggestion that cyanophytes in the sea were outcompeted by red and green algae⁴ is not supported by direct evidence^{11,12}, and it is known that Recent genera which calcify in freshwater can live uncalcified in the sea⁴. Consequently, an environmental control to account for marine cyanophyte calcification is not unreasonable, despite the fact that suggestions of changes in seawater composition near the Precambrian–Cambrian boundary to account for metazoan skeletonization have received little support recently². Mg^{2+}/Ca^{2+} ratio changes near the Precambrian–Cambrian boundary have been suggested in this context¹³, but metazoan skeletonization probably does not share the environmental dependence of cyanophyte calcification. However, it is remarkable that calcification in cyanophytes and metazoans began almost synchronously near 570 Myr.

Thermodynamically, an increase in temperature, partial pressure of CO_2 in buffered seawater, pH, or $a_{Ca^{2+}}$ will enhance the magnitude of $CaCO_3$ precipitation. A decrease in salinity resulting in increases of $\gamma_{Ca^{2+}}$ and $\gamma_{CO_3^{2-}}$ will have the same effect¹⁴. However, these parameters do not necessarily reflect the rate of precipitation of calcareous sediments. In marginal marine embayments it is possible to modify substantially temperature, pH and salinity, but these local changes in restricted environments cannot be invoked as long-term effects on general seawater chemistry. The occurrence of calcareous cyanophytes in reef environments from Cambrian to Jurassic–Cretaceous time⁷ requires modification of normal shelf seawater to be sustained for hundreds of millions of years. The rate of nucleation and growth of calcite, aragonite and dolomite, has been shown to depend on Mg^{2+} ion concentrations and a plausible explanation for changes in cyanophyte calcification can be invoked on the basis of kinetic considerations involving this ion.

The mutual interdependence of P_{CO_2} and the ratio of Mg^{2+}/Ca^{2+} in carbonated buffered seawater is well documented¹⁵. For example, an increase in P_{CO_2} will lead to $CaCO_3$ deposition and thus an increase of the Mg^{2+}/Ca^{2+} ratio. Conversely, any decrease in P_{CO_2} during the Precambrian¹⁶ would thus decrease the Mg^{2+}/Ca^{2+} ratio of seawater. As it has been demonstrated^{17,18} that relative decreases of Mg^{2+} concentrations greatly enhance the rate of nucleation of $CaCO_3$ it might be expected that cyanophyte calcification would be stimulated as a result. Extensive formation of late Precambrian dolomites¹⁹, suggested to be primary²⁰, would also have depressed the Mg^{2+} content of seawater. Reversal of this condition—increased of the Mg^{2+}/Ca^{2+} ratio—in the late Mesozoic has been attributed to widespread deposition of $CaCO_3$ by pelagic microorganisms as calcareous oozes, now preserved as chalks⁵. Hence, changes in the Mg^{2+}/Ca^{2+} ratio can be inferred which correlate with both the appearance of calcareous marine cyanophytes near the Precambrian–Cambrian boundary and their disappearance in the late Mesozoic.

Calcification may have conferred biological advantages on cyanophytes and certainly resulted in important changes in their sedimentological roles, whatever its cause may have been. An environmental control is plausible and implies that cyanophyte calcification could be an index of marine $CaCO_3$ precipitation rates which reflects times when inorganic carbonate production was increased. If this is so then it should also correlate with enhanced ooid formation and subsea cementation in the geological record. The presence of weakly calcified ?cyanophytes in the upper Proterozoic⁶ suggests a period of transition before the abrupt appearance of heavily calcified forms in the Nemakit–Daldyn. More information is required from the late Mesozoic to see whether a similar phase preceded the disappearance of calcareous marine cyanophytes at that time.

This research was supported by the NERC and also by the Humboldt Foundation through a Fellowship at the Technical University, Munich. I thank Peter Williams for advice on carbonate chemistry, and Robin Bathurst, Martin Brasier, Dianne Edwards, and Maurice Tucker for critically reading the manuscript.

Received 28 June; accepted 16 August 1982.

1. Cloud, P. *Paleobiology* 2, 351–387 (1976).
2. Stanley, S. M. *Am. J. Sci.* 276, 56–76 (1976).
3. Golubic, S. in *The Biology of Blue-Green Algae* (eds Carr, N. G. & Whitton, B. A.) 434–473 (Blackwell, Oxford, 1973).
4. Monty, C. L. V. *Ann. Soc. geol. Belg.* 96, 585–624 (1973).
5. Sandberg, P. A. *Sedimentology* 22, 497–538 (1975).
6. Riding, R. & Voronova, L. G. *Naturwissenschaften* (in the press).
7. Wray, J. L. *Developments in Palaeontology and Stratigraphy* Vol. 4 (Elsevier, Amsterdam, 1977).
8. Winland, H. D. & Matthews, R. K. *J. sedim. Petrol.* 44, 921–927 (1974).
9. Golubic, S. & Campbell, S. E. in *Phanerozoic Stromatolites* (ed. Monty, C.) 209–229 (Springer, Berlin, 1981).
10. Schopf, J. W. *Scient. Am.* 239, 85–102 (1978).
11. Gebelein, C. D. in *Developments in Sedimentology* Vol. 20 (ed. Walter, M. R.) 499–515 (Elsevier, Amsterdam, 1976).
12. Stanley, S. M. *Paleobiology* 2, 209–219 (1976).
13. Durov, S. A. *Trudy novozerk. politekh. Inst.* 98, (1960).
14. Garrels, R. M. & Christ, C. L. *Solutions, Minerals and Equilibria* (Harper & Row, New York, 1965).
15. Holland, H. D. *Proc. natn. Acad. Sci. U.S.A.* 53, 1173–1182 (1965).
16. Berkner, L. V. & Marshall, L. C. *Discuss. Faraday Soc.* 37, 122–141 (1964).
17. Pytkowicz, R. M. *J. Geol.* 73, 196–199 (1965).
18. Berner, R. A. *Soc. Econ. Paleont. Miner. Spec. Publ.* 20, 37–43 (1974).
19. Ronov, A. B. *Geokhimiya* 8, 715–743 (1964).
20. Tucker, M. E. *Geology* 10, 1, 7–12 (1982).

Evidence for a central Eurasian source area of Arctic haze in Alaska

G. E. Shaw

Geophysical Institute, University of Alaska, Fairbanks, Alaska 99701, USA

During winter when the polar oceans are frozen, air masses entering Alaska from the Arctic are charged with suspended submicrometre particles whose chemical signatures show evidence of being derived from man-made sources of pollution^{1–3}. Occasionally, the aerosol loading is large enough to reduce visibility and thus the phenomenon has come to be referred to as 'Arctic haze'. We report here three strong episodes of Arctic haze in Alaska which were examined during February–April 1982 and which were found to be possibly associated with air emissions in central Eurasia.

Figure 1 illustrates the episodic nature of Arctic haze in interior Alaska during late winter 1982. The cross-hatched regions are synonymous with incidences of visible haze, which occurred in association with low air temperatures, increased particle concentration for particles near 0.13- μ m diameter (determined with a laser spectrometer) and, as the maps at the

bottom of Fig. 1 show, air trajectories (850 mbar level) coming from Arctic regions west of Alaska.

Particles sampled with impactors and examined with X-ray spectrometry during the time sequence represented in Fig. 1 were found to have very different X-ray spectra, depending on the direction which air masses had taken entering central Alaska. When the air flow had entered from the Gulf of Alaska or from the region of northwestern Canada, the visibility often exceeded 200 km; such times are referred to as 'clean times' and X-ray spectra of the minority (1%) non-sulphate particles taken then were primarily mixtures of Al and Si (crustal) or

ing the incoming air flow was anticyclonic activity over eastern Siberia and a trough over north-central Eurasia. The simultaneous occurrence of such flow conditions (which occur most frequently in the mid-winter months) and the enhanced metal X-ray signatures in aerosol suggest the presence of significant aerosol sources in central Eurasia, particularly around the area of the Taymyr Peninsula (there are no other apparent sources along the transport pathway). A Siberian source region of aerosol has also been deduced for the Canadian Arctic⁴.

Locating the exact geographical region or type of emission in central Eurasia from the back trajectories or from ratios of

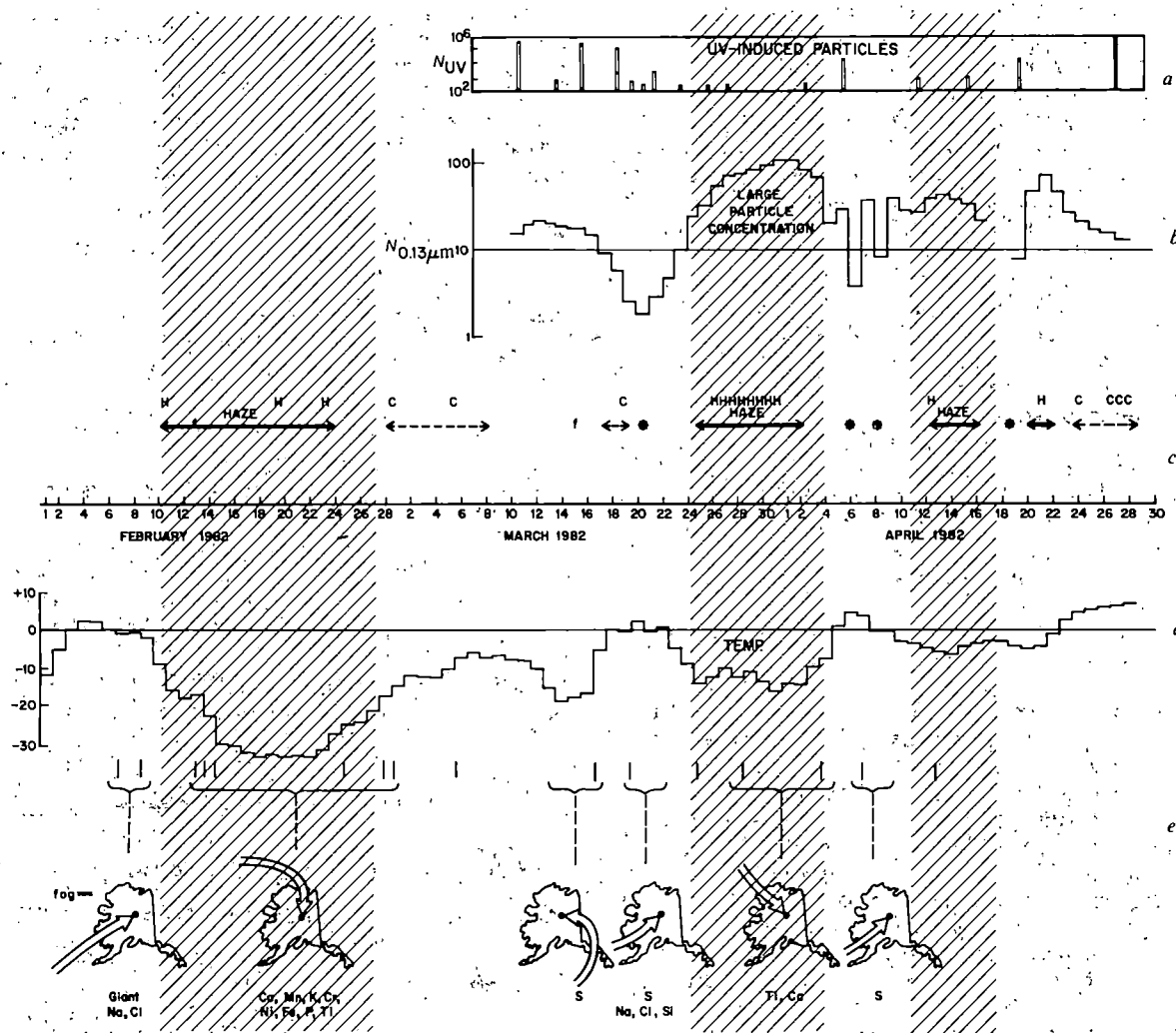


Fig. 1 Parameters associated with Arctic haze in central Alaska. Cross-hatched regions are periods when visibility degraded in central Alaska; they are associated with low air temperature and air masses entering Alaska from the Arctic, west of Alaska (arrows on the maps in *c* show incoming air trajectories). During Arctic haze episodes the concentration of particles in the size range 0.13–0.14 μm diameter (curve *b*) increased. Irradiation of the air samples with the 1,800 Å line of a low pressure Hg discharge lamp nucleated fewer particles (*a*) during Arctic air flow than during air flow from the Pacific Ocean region. H and C refer to visual observation of haze and clear, high visibility periods, respectively.

Na and Cl (marine). When air entered Alaska from the Arctic, the X-ray spectra became very complex showing the presence of various heavy metals including Ti, Cr, Mn, Fe and Ni; additionally the aerosol mass loading increased by several times.

During Arctic haze outbreaks (cross-hatched in Fig. 1) back air trajectories from central Alaska at the 500-mbar level were traced to the central Eurasian sector of the Arctic (Fig. 2). Actual transport of the aerosol material occurs probably at altitudes well below the altitude corresponding to 500 mbar, but the 500-mbar streamlines indicate the large-scale features of the transport pathway. The major synoptic feature controll-

ing the incoming air flow was anticyclonic activity over eastern Siberia and a trough over north-central Eurasia. The simultaneous occurrence of such flow conditions (which occur most frequently in the mid-winter months) and the enhanced metal X-ray signatures in aerosol suggest the presence of significant aerosol sources in central Eurasia, particularly around the area of the Taymyr Peninsula (there are no other apparent sources along the transport pathway). A Siberian source region of aerosol has also been deduced for the Canadian Arctic⁴.

Although there are various pollution sources in central

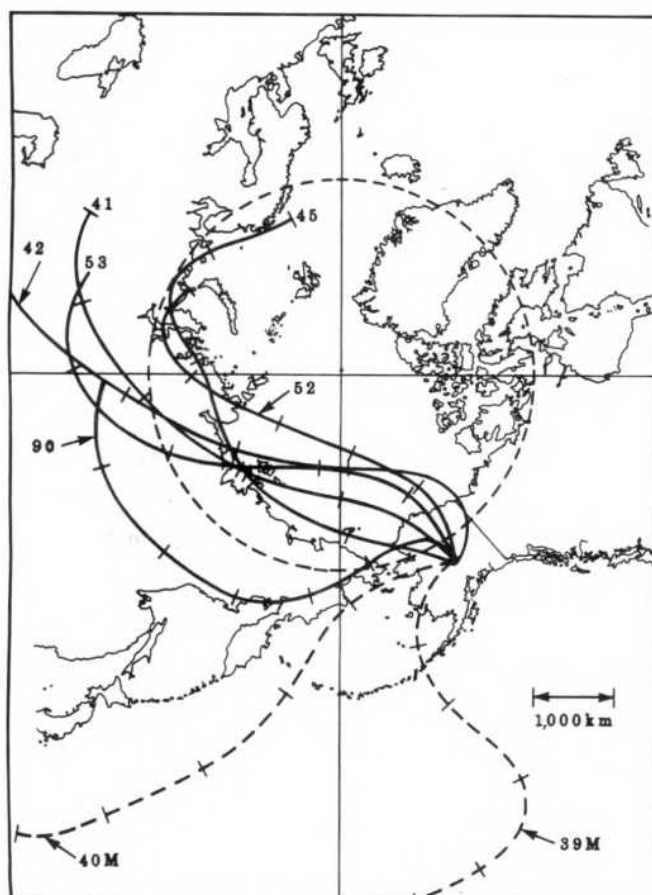
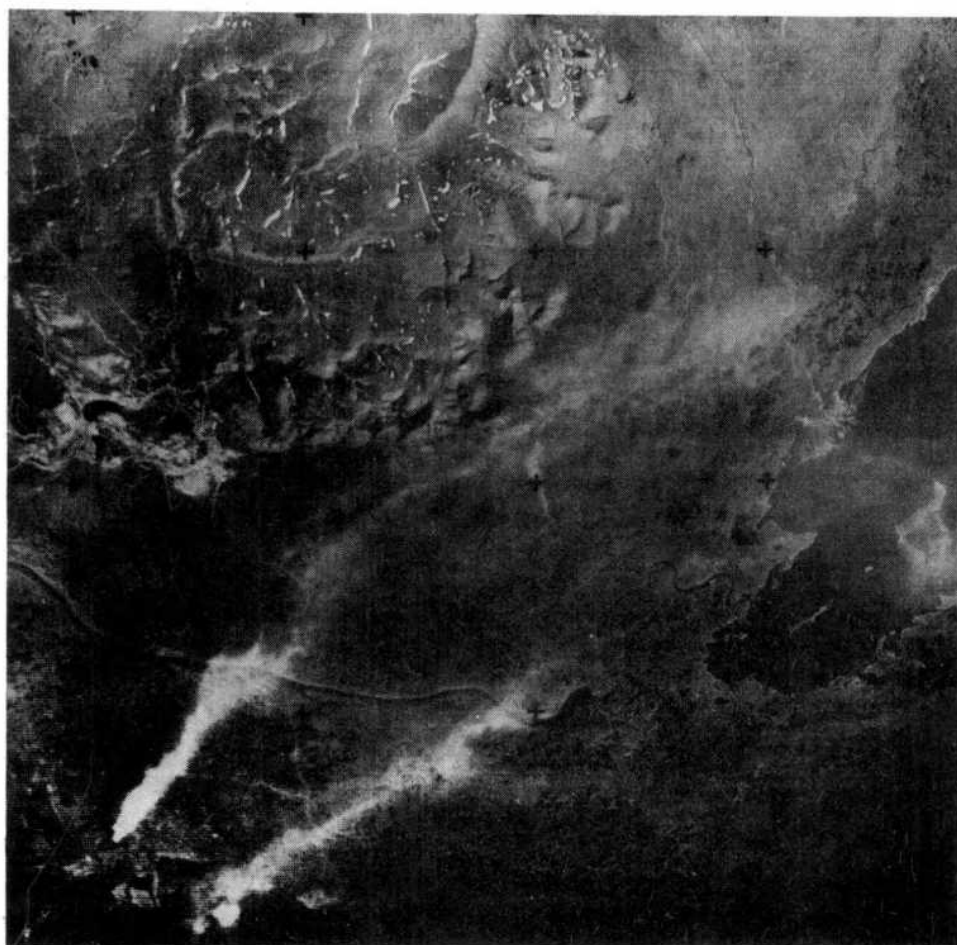


Fig. 2 Five-day back air trajectories to central Alaska at the 500-mbar pressure level. Solid lines, periods when visibility was reduced due to pervasive Arctic haze. Dashed lines, examples of trajectories during clear periods. Numbers refer to the date on which the trajectory reached central Alaska (calendar day, 1982). M indicates that marine elements (Na, Cl) were abundant in aerosol samples. The Arctic Circle is shown for reference. Tick marks on the trajectories refer to sequential 1-day intervals of travel time.

Eurasia, one that may be important is the large polymetallic ore mining-smelting complex at Norilsk (69.4°N, 88.5°E). Satellite photographs of the region (Fig. 3) show the presence of two large plumes, which can be traced for up to 40 km and which emanate from smelters processing rich sulphide Ni-Cu ores.

From the growth rate⁸ and nickel output at Norilsk in the mid-1970s⁹, the present production is estimated at 0.5 million tons of Cu and Ni annually. SO₂ emissions from roasting and reverberatory furnaces and converters at this size operation (scaled from the Sudbury Ni plant in Ontario¹⁰, which has similar ores) would be substantial, probably $\approx 10 \text{ kg SO}_2 \text{ s}^{-1}$, some portion of which would convert to submicrometre particles during transport along a pathway of several thousand kilometres¹¹. If the secondary particles have residence in the atmosphere long enough to be conserved in the travelling plume, the sulphate particle loading from Norilsk in a plume 200 km wide¹² entering Alaska is calculated to be $\sim 4 \mu\text{g m}^{-3}$ (assuming complete conversion of SO₂, which may not occur), compared with several $\mu\text{g m}^{-3}$ sulphate mass loading actually observed in Alaska during the haze episodes. The assumption of a long residence time, say 4–7 days, is consistent with our observation (with diffusion batteries) that most particles of Arctic haze were in a mode of $\sim 0.2 \mu\text{m}$ diameter, a size too small to be efficiently removed by inertial processes and too

Fig. 3 Landsat image of Norilsk mining smelting region (14 August 1981; 0516 GMT). Distance between marks is 11 km. North is up. Two plumes from polymetallic ore refineries can be traced for 30–50 km.



large to be removed efficiently in diffusive-controlled processes¹³.

Of course, the mass loading values obtained with a simple first-order model can only be used to make order of magnitude judgements and it is not justifiable to assert that smelting activities at Norilsk are responsible for Arctic haze in Alaska. The numbers and back trajectories do suggest, however, that air emissions associated with combined industrial activity in central Eurasia may constitute a so far undetermined, but seemingly significant, portion of Arctic haze observed in the American Arctic.

We thank T. Armstrong, J. Roederer and T. Shabad for helpful comments. This research was sponsored by ONR grant N-00014-C-0435 and NSF grant DPP79-19816.

Received 7 July; accepted 24 August 1982.

1. Kerr, R. A. *Science* **205**, 290–293 (1979).
2. Kerr, R. A. *Science* **212**, 1013–1014 (1981).
3. Rahn, K. A. *Atmos. Environ.* **15**, 1447–1455 (1981).
4. Barrie, L. A., Hoff, R. M. & Daggupaty, M. *Atmos. Environ.* **15**, 1407–1419 (1981).
5. Rahn, K. A. *Atmos. Environ.* **15**, 1457–1464 (1981).
6. Armstrong, J. T. *Scanning Electron Microscopy* Vol. 1, 455–466 (SEM/NC, AMF O'Hare, Illinois, 1978).
7. Carlson, T. N. *Atmos. Environ.* **15**, 1473–1478 (1982).
8. Shabad, T. & Mote, U. L. *Gateway to Siberian Resources* (Wiley, New York, 1977).
9. Central Intelligence Agency *Polar Regions Atlas* (GC 78-10040) (US Government Printing Office, Washington DC, 1979).
10. Scheider, W. A., Jeffries, D. S. & Dillon, P. J. *Atmos. Environ.* **15**, 945–956 (1981).
11. Eatough, D. J. *et al. Atmos. Environ.* **16**, 1001–1015 (1982).
12. Hage, K. D. in *Handbook of Environmental Control*, Vol. 1 (eds Bond, R. G., Straub, C. P. & Prober, R.) (CRC, Cleveland, 1972).
13. Twomey, S. *Atmos. Aerosols* (1977).

Female choice selects for extreme tail length in a widowbird

Malte Andersson

Department of Zoology, University of Gothenburg, PO Box 25059, S-400 31 Gothenburg, Sweden

Darwin's¹ hypothesis that male secondary sexual ornaments evolve through female preferences is theoretically plausible^{2–7}, but there is little experimental field evidence that such preferences exist^{8–10}. I have studied female choice in relation to male tail length in the long-tailed widowbird, *Euplectes progne*, and report here that males in which the tail was experimentally elongated showed higher mating success than males having normal or reduced tails. The possibility that intrasexual competition among males maintains the long tail was not supported: males with shortened tails held their territories as long as did other males. These results suggest that the extreme tail length in male long-tailed widowbirds is maintained by female mating preferences.

Male long-tailed widows have the most extreme sexual ornaments among *Euplectes*, an African genus of polygynous weaverbirds (the Ploceidae)¹¹. Reproductive adult males are black except for a red epaulet on the wing, but the most conspicuous feature is the tail: 6–8 of the 12 tail feathers are ~0.5 m long, the rest being one- to two-thirds as long. The tail during flight display is expanded vertically into a deep, long keel below the male as he flies with slow wingbeats 0.5–2 m above the territory. Displaying long-tailed widows are visible from over 1 km distance on their 0.5–3-hectare territories. The territories lie in open grassland on the Kinangop plateau, Kenya, where *E. progne* is one of the most common birds, and where the present study was performed between November 1981 and March 1982. Females are inconspicuous, being mottled brown, with short tails (~7 cm). They build their nests on the territories of the males, in the upper third of the 0.5–0.8 m-high grass, *Eleusine jaegeri*, and raise their young (2–3) unaided by the male. These features make the long-tailed widow

suitable for a test of the theory of intersexual selection of male ornaments.

Darwin¹ and Fisher² suggested that further evolution of an ornament ceases when it becomes so large that it reduces survival enough to exactly balance the mating advantage. For this to be so, females must prefer larger than normal-sized ornaments; otherwise there can be no balance between the two selection pressures. In the present experiment, females chose from males with shortened, normal or elongated tails. The Darwin–Fisher theory therefore predicts that mating success should be highest among males with elongated tails, and lowest among males with shortened tails.

The experiment included nine groups, each containing four individually colour-ringed males, of similar initial tail length and territory quality. Territory boundaries were determined by plotting on maps the locations of male displays and attacks, using cattle fences, streams and vegetation features as landmarks. In each matched group, the following treatments were randomly allocated among the four males. The tail was cut to ~14 cm in one of them; each removed feather was then attached with rapidly (~1 s) hardening cyanoacrylate glue to the corresponding feather in another male, whose tail was thus prolonged by an average of 25 cm. About 3 cm of each removed feather was first cut off and glued back on to its counterpart in the 'shortened' male, which hence was manipulated in a similar manner to the 'elongated' male. The two remaining males were controls; one was ringed only. To check whether the cut-and-glue operation influenced male behaviour or female choice, the tail of the second control male was cut off at the midpoint; each feather was then glued back on again. This operation shortened the tail by only 1 cm (~2%), which is probably not noticeable by females. Uneven joints or ends of glued feathers were trimmed with a scalpel. The joints were difficult to see from more than 1 m.

As capture and manipulation might influence subsequent behaviour, which could confound interpretation, flight displays and territorial disputes were counted in each male for 30 min 1–5 days before, and 10–14 days after the treatment.

Male mating success was estimated by the number of active nests (containing eggs or young) on each territory, for which I searched for about 1 h just after treatment of the male, and at weekly intervals for 1 month afterwards. No new clutches were laid after early January. To avoid bias, I searched each territory in proportion to its area of nesting habitat (tall, rank grass). The first count provided a standard with which to compare male mating success after tail treatment, estimated by the number of clutches laid during the remainder of the breeding season, after the day on which the male was manipulated. This use of each male as his own control reduces the importance of differences in territory quality, which influences female choice of mate in the long-tailed widow (M.A., in preparation). Counts spanned 1 month, so a few nests might represent re-laying, but this should not bias the result as treatments were randomized within each group.

Euplectes females usually seem to mate with the male on whose territory they nest^{12,13}. The possibility that a female might mate with one male and nest on the territory of another should not produce bias favouring the Darwin–Fisher prediction but should reduce the likelihood of detecting female mating preferences in the present study. Whereas attractive males in such cases receive more matings, some of their females may build on the less crowded territories of less attractive males. Group defence against nest predators is poorly developed, and there is no other evidence that female long-tailed widows would benefit from clumped breeding; the nests are well dispersed within a territory.

Females will be selected to respond to a character only if it varies among potential mates¹⁰. This is the case in long-tailed widows: the fully grown tails (no blood quills) of seven territorial males had a mean length of 49.6 cm, with c.v. = 9.4%. There was no significant correlation between male tail length and number of nests on the territory before the experiment.

However, the present randomized block design is unsuitable for detecting such a correlation; it was used to make the experiment maximally sensitive to any importance of tail length.

The two types of control males (I, cut and restored; II, only ringed—see Fig. 1) did not differ significantly in tail length, display rate or any other measured character. Therefore, they should be equivalent from a female perspective, so I have treated them as one category below, with two representatives in each group of four males.

Before tail treatments, there were only minor differences in mating success between 'shortened', control and 'elongated' males (Fig. 1a). After treatment, however, mating success changed as predicted by the female choice hypothesis, with lowest success for males having shortened tails, and highest

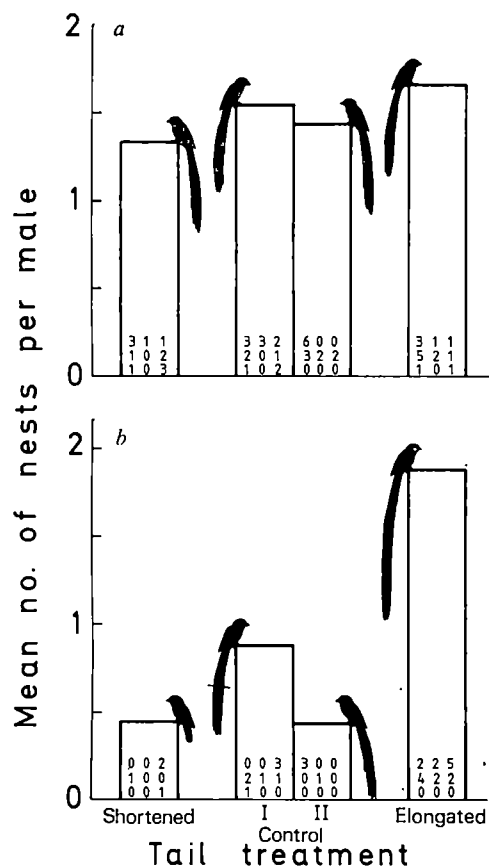


Fig. 1 Mating success in male long-tailed widows subjected to different tail treatments. *a*, Mean number of active nests per territory for the nine males of the four treatment categories, before the experiment. Numbers of nests for the nine males in each of the four categories are given at the bottom of the bars, always in the same order of matched 4-group. *b*, Number of new active nests in each territory after treatment of males. The following procedure was used to test for differences in mating success between the treatment categories. For each male I calculated the difference between the number of new active nests on his territory during the remainder of the breeding season after tail treatment, and the original number of nests on the territory before tail treatment. (Subtraction of the original number of nests reduces the influence of initial variation among males and territories.) These differences were used for matched comparisons (with respect to each group of four males) between shortened, control and elongated males. As predicted by the Darwin-Fisher theory of sexual selection, males with elongated tails became significantly more successful (as measured above, compared with before the tail treatment) than shortened males and control males II ($P < 0.05$ in both cases, paired randomization tests). For the four categories tested together, there was a significant trend of increasing mating success as tail length increased from shortened via control to elongated males ($P = 0.03$, Pitman randomization test¹⁸ adapted to the present experimental design; no standard test fits this situation, with two different treatments (shortened and prolonged tails) and two control categories, and an alternative hypothesis which predicts a specified trend).

success for males with elongated tails (Fig. 1b). Hence, tail length apparently did influence mate choice: females preferred those males having the longest tails. As the main difference was between 'elongated' males and other males (including controls), the difference did not result from possible destruction of species-specific features in males having shortened tails.

Another possible explanation is that 'shortened' males became less active in their courtship behaviour, or that males with elongated tails became more active. However, the only indication of a difference was the reverse of this (but not significant: $P > 0.95$, Friedman two-way analysis of variance). Males having reduced tails increased their average rate of flight display slightly (from 9.2 to 10.3 displays per 30 min), whereas control males showed a decrease (from 10.3 to 6.9), as did males with elongated tails (from 10.8 to 7.8). Therefore, changes in male behaviour were probably not responsible for the higher success of elongated males.

In choosing her mate, a female should respond to the quality of his territory, on which she nests^{10,14}. However, due to the randomization within each group of four males and the use of each male as his own control, territory differences cannot explain the higher mating success of males with elongated tails. As behavioural differences were also excluded, I conclude that the changes in male tail length caused the differences in the attraction for females.

As is implicit in the Darwin-Fisher theory of sexual selection, females preferred males having tails that were longer than normal. This is expected if females are attracted by 'supernormal stimuli'^{14,6,8}. Such a preference can evolve if asymmetrical selection shapes female responsiveness^{4,15}. One possibility is that a male's sexual ornaments reflect his overall phenotypic and genotypic quality, so that females choosing highly ornamented males bear offspring having high expected fitness⁹. However, it is unknown whether fitness in nature is heritable enough to influence female choice of mate.

Highly adorned males can be favoured by active mate choice, where females compare males before accepting one, but also by easier detection¹⁶. This latter advantage may have contributed to the evolution of the long tail and the flight display in the long-tailed widow. The lateral surface of the displaying male is enlarged 2–3 times by the tail, making him correspondingly easier to discover from a distance in the open habitat. However, neighbouring males often display simultaneously, and females sometimes visit several males in rapid succession with ample opportunity for comparisons. The long tail is therefore probably maintained at least partly through active female discrimination among males.

Alternatively, ornaments may be favoured by intrasexual selection among males competing for territories or hierarchy ranks^{9,10,17}. This hypothesis predicts that males having shortened tails are least efficient at holding a territory, and that males with elongated tails are most efficient; this was not supported. Most males remained on their territories until February, when the nesting was over, and territory tenacity did not differ among treatment categories ($P > 0.6$, Pitman randomization test). There was no evidence of increased territory size in males having elongated tails. Males with shortened tails took off and defended their territories more often than other males but the difference was not significant ($P > 0.1$, Friedman two-way analysis of variance); this may indicate more intrusions on their territories. However, 'shortened' males also increased their rate of flight display (see above), usually performed when the male is alone on the territory, or is visited by females. Easier flight in these males relieved of the unwieldy tail, which is carried only during the breeding season, may explain their higher rate of territory defence as well as flight display (insofar as the non-significant differences are real).

The results presented here support Darwin's¹ hypothesis that certain male ornaments are favoured by female mate choice, and probably evolved through it.

I thank the Office of the President, Nairobi, for permission to do field work in Kenya; Derek Pomeroy for assistance with

the study; Kuria Mwaniki and Uno Unger for help in the field, Björn Rosander for statistical advice; and Conny Askenmo, John Maynard Smith, and Peter O'Donald for comments on the manuscript. The study was supported by the Swedish Natural Sciences Research Council.

Received 21 June; accepted 2 September 1982.

1. Darwin, C. *The Descent of Man, and Selection in Relation to Sex* (John Murray, London, 1871).
2. Fisher, R. A. *The Genetical Theory of Natural Selection* (Clarendon, Oxford, 1930).
3. Maynard Smith, J. in *A Century of Darwin* (ed. Barnett, S. A.) 231–245 (Heinemann, London, 1958).
4. O'Donald, P. *Theor. Populat. Biol.* **12**, 298–334 (1977).
5. O'Donald, P. *Genetic Models of Sexual Selection* (Cambridge University Press, 1980).
6. Lande, R. *Proc. natn. Acad. Sci. U.S.A.* **79**, 3721–3725 (1981).
7. Kirkpatrick, M. *Evolution* **36**, 1–12 (1982).
8. Halliday, T. R. in *Behavioural Ecology, An Evolutionary Approach* (eds Krebs, J. R. & Davies, N. B.) 180–213 (Blackwell, Oxford, 1978).
9. Andersson, M. *Biol. J. Linn. Soc.* **17**, 375–393 (1982).
10. Searcy, W. A. *A. Rev. Ecol. Syst.* **13** (in the press).
11. Craig, A. J. F. K. *J. Orn.* **121**, 144–161 (1980).
12. Lack, D. *Ibis* **77**, 817–836 (1935).
13. Craig, A. J. F. K. *Ostrich* **45**, 149–160 (1974).
14. Orians, G. H. *Am. Nat.* **103**, 589–603 (1969).
15. Staddon, J. E. R. *Am. Nat.* **109**, 541–545 (1975).
16. Parker, G. A. in *Current Problems in Sociobiology* (Cambridge University Press, in the press).
17. Borgia, G. in *Sexual Selection and Reproductive Competition in Insects* (eds Blum, M. S. & Blum, N. A.) 19–80 (Academic, New York, 1979).
18. Bradley, J. V. *Distribution-free Statistical Tests* (Prentice-Hall, Englewood Cliffs, 1968).

Self-pituitary grafts are not rejected by frogs deprived of their pituitary anlagen as embryos

Louise A. Rollins-Smith & Nicholas Cohen

Division of Immunology, Department of Microbiology, School of Medicine and Dentistry, University of Rochester, Rochester, New York 14642, USA

In the present study, we have adopted the model of Triplett¹ to reinvestigate the timing of development of immunological tolerance to self-organ-specific antigens. We have removed pituitary or eye² anlagen from frog embryos before development of the immune system and returned them at a later time as differentiated organ implants to their now immunocompetent larval or adult original owners. If immunological tolerance to these putative organ-specific self-antigens occurs at an early and fixed time period, then organ-deprived hosts, lacking the opportunity to become tolerant, would be expected to reject such implants¹. Our results show that self-implants were never rejected whereas control allogeneic implants were usually rejected by larval hosts and were always rejected by adult hosts. These data, which contrast with those reported by Triplett, suggest that frogs, and perhaps other higher vertebrates, can become tolerant to self-organ-specific antigens throughout life.

We recently reported² experiments in which eye anlagen were removed from *Rana pipiens* and *Xenopus laevis* (*X. laevis* and *X. laevis-gilli* hybrid clones³) embryos. When the enucleated embryos developed into immunocompetent larvae, they were implanted with either their own (previously parked) or an isogeneic (cloned) differentiated eye. All self-grafts in intact hosts or enucleated hosts survived in almost perfect condition for as long as they were observed (>100 days; Fig. 3a, b). In contrast, allogeneic eyes were rejected by about half of the intact larval *Xenopus* and *Rana* hosts.

Because only some of the larval hosts rejected allogeneic eyes², and because other studies had demonstrated a greater degree of tolerance of skin allografts in larval than adult hosts⁴, we enucleated cloned (LG15) *Xenopus* embryos (Nieuwkoop and Faber⁵ stages 26–32) and implanted them with an isogeneic eye 2 months after they metamorphosed. In such postmetamorphic *Xenopus*, all allogeneic eye implants were rejected vigorously and rapidly (most within 20 days), whereas isogeneic implants on intact or embryonically enucleated hosts survived for as long as they were observed (2–24 months, Figs 1, 3c). Examination of serially sectioned isogeneic implants fixed at

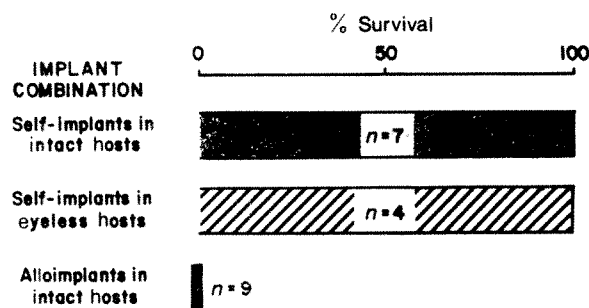


Fig. 1 Per cent survival of self- (▨) and allogeneic (■) eye implants in intact postmetamorphic *Xenopus* and of self-implants in embryonically enucleated postmetamorphic *Xenopus* (▨) at 90 days post-implantation. The number of frogs in each group is indicated within the bars. All enucleations were performed during stage 26–32. One animal, however, developed a partial regenerated eye that was re-extirpated at about stage 43.

1–2 yr post-implantation revealed no lymphocytic infiltration or other evidence of immune destruction.

To minimize the criticism that the eye may not be a good model organ to study development of unresponsiveness to organ-specific antigens and to determine the generality of our observations with the eye, we used the pituitary as a test organ. Triplett reported that most (10/13) self-pituitary implants were rejected by their embryonically hypophysectomized larval tree frog hosts with a mean graft survival time of ~40 days. This study suggested that the pituitary has organ-specific transplantation antigens, and provided experimental support for the idea that unresponsiveness to these antigens must develop in a fixed early time period relative to lymphocyte ontogeny. In our studies, pituitary anlagen were extirpated from Shumway⁶ stage 17–18 *R. pipiens* embryos and 'parked' orthotopically on previously hypophysectomized stage 17–18 sibling hosts. After 50–60 days, we dissected the now differentiated pituitaries free from the brain of the 'parking' host and implanted them in the dorsal tail-fins of the original hosts. The hypophysectomized hosts were pale and their growth was retarded (Fig. 3d). After implantation of either a self- or an allogeneic pituitary, they began to darken due to melanophore stimulating hormone (MSH) release by the implanted gland, and their growth rate increased. Six of nine allogeneic pituitaries were rejected within 20 days. Recipients of these implants again became pale. In marked contrast, all recipients of the self-pituitaries remained dark for as long as they were observed (three for >90 days, Figs 2, 3e). Examination of serially sectioned heads of the hypophysectomized hosts showed no identifiable anterior pituitary cells in association with the brain of any of the six larvae examined (compare Fig. 3f and g). Thus, the darkening of pituitary implanted animals seemed to result from MSH production by the self-implant rather than from any anterior pituitary tissue remaining after embryonic ablation.

Three technical differences between our pituitary grafting experiments and those of Triplett may bear on our discordant observations. First, our experiments were done with *R. pipiens* while his were done with *Hyla regilla*. Thus, although the anlagen were extirpated at comparable stages of embryonic development, and the differentiated organs were reimplanted after about the same time lag, we cannot exclude the possibility that there are species-specific differences in the maturation of immunity and a narrower period in *Hyla* in which self-tolerance may occur.

A second experimental difference was the site in which the pituitary anlagen differentiated. In our experiments, the anlagen were 'parked' orthotopically in previously hypophysectomized age-matched sibling embryos. In contrast, Triplett 'parked' the anlagen under the ectoderm in the tail region in rather older nonsibling larvae¹. In this site, the graft induced formation of a heavily pigmented host-derived fibrous connective tissue capsule that was always transplanted together with the pituitary¹.

Our implants were free of host-derived connective tissue. Whether this allogeneic contaminant (an estimated 20% of the mass of the transplant; E. L. Triplett, personal communication) contributed to the destruction of the self-pituitary graft, is conjectural. Triplett, in fact, attempted to control for allocontamination in a set of experiments in which he removed, 'parked' and then returned a partial gland. Although he observed that all seven partial self-grafts survived, he also reported the survival of four of six allogeneic pituitaries in partially hypophysectomized recipients. This finding, which is consistent with the high frequency of allotolerance observed in larval *Xenopus*⁴ and *Rana*², makes the data from the partial-hypophysectomy experiment difficult to interpret.

A third technical difference is that Triplett supplemented the diet of completely hypophysectomized animals with beef thyroid powder "about 60 days" after hypophysectomy. Our hypophysectomized frogs never received exogenous hormone and did not progress beyond Taylor-Kollros⁷ stage III until after they had received a pituitary implant. That exogenous thyroxine treatment might reveal a net self-cytotoxic rather than tolerogenic response in *Hyla* cannot be excluded. However, it must be pointed out that in our experiments with eye implants, enucleated frogs had an intact endocrine system and self-cytotoxicity was not the net result following implantation of a self-eye. Further, at least alloreactivity of hypophysectomized frogs can develop without addition of exogenous thyroxine, as more than half of the hypophysectomized recipients of allogeneic pituitary grafts in our experiments were capable of rejecting those grafts. Perhaps a better understanding of the relationships between the developing endocrine and immune systems in amphibians might shed light on our discordant data.

Our failure to confirm Triplett's observation may mean that tolerance to organ-specific antigens can occur throughout larval life and, at least in the case of the eye, during adult life. Alternatively, because it was Triplett's original observation of self-rejection that suggested the existence of pituitary-specific antigens, our failure to confirm his observation of rejection may mean either that such antigens do not exist in *R. pipiens* or that they are of such a distribution or immunogenicity as to be incapable of evoking a net destructive response. Reports of eye-specific antigens in other species⁸ and of autoimmune responses directed against the mammalian pituitary^{9,10} do provide independent evidence of pituitary- and eye-specific antigens; a rigorous demonstration of their existence in amphibians awaits further study.

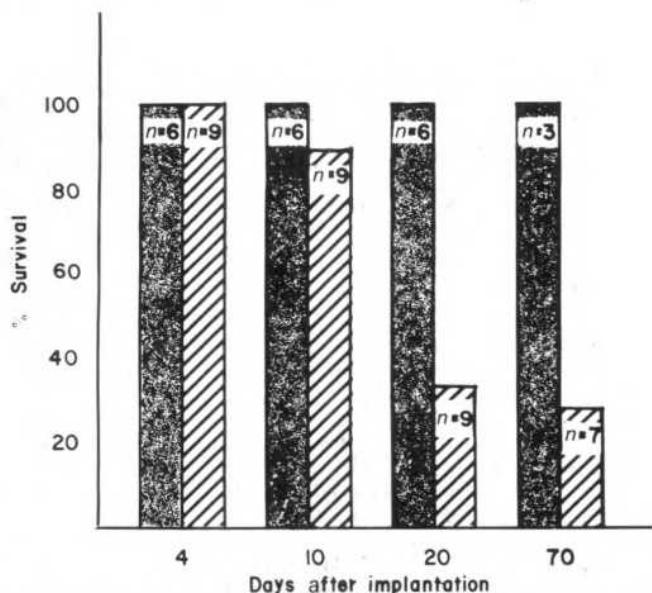


Fig. 2 Per cent survival of self- (■) and allogeneic (▨) pituitary implants in embryonically hypophysectomized *Rana* larvae. The number of larvae in each group is indicated within the bars.

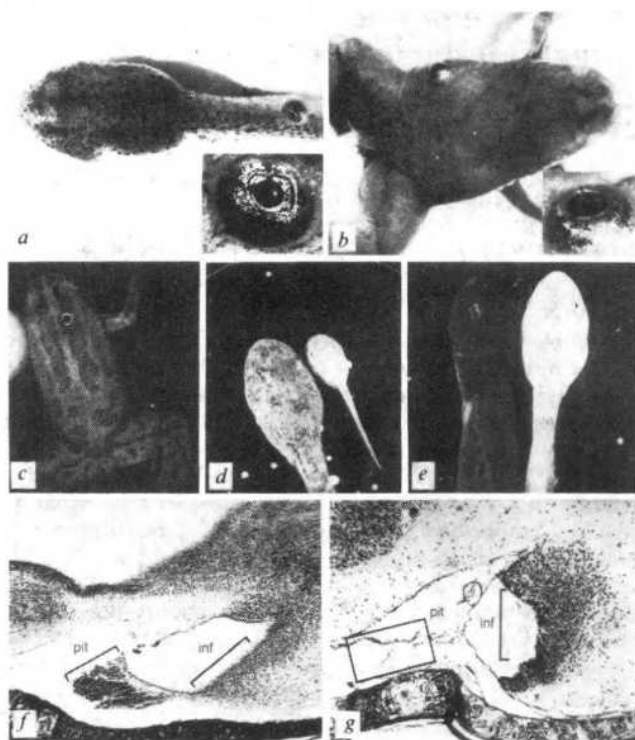


Fig. 3 a, *Rana pipiens* tadpole, enucleated as an embryo and grafted during larval life with a self-eye. Photographed 75 days after implantation ($\times 1.9$), insert ($\times 8.9$) (modified from ref. 2). b, Postmetamorphic *Xenopus laevis*, enucleated as an embryo, with self-eye implant placed during larval life. Photograph taken about 1 yr after implantation ($\times 1.4$), insert ($\times 6.2$) (from ref. 2). c, Postmetamorphic *Xenopus laevis-gilli*, enucleated as an embryo, with isogeneic eye implanted 2 months after metamorphosis. Photograph taken about 1½ yr after implantation ($\times 1.4$). d, *Rana pipiens* tadpoles, 41 days after they had been hypophysectomized as embryos. Tadpole on the left was hypophysectomized and served as the 'parking host' for the pituitary of the tadpole on the right. Note that the 'parking host' is of normal size and pigmentation while the hypophysectomized tadpole is small and pale ($\times 1.4$). e, *Rana pipiens* tadpoles. Tadpole on left was hypophysectomized as an embryo, implanted with its self-pituitary 60 days later, and photographed about 60 days after implantation. This tadpole survived with an intact implant 91 days post-implantation. Note the abnormally dark pigmentation due to unregulated MSH production by the implanted gland. The tadpole on the right shows normal pigmentation of a tadpole about 3 months of age. The animal appears to be blanched because the photograph was underexposed to reveal the detail of the darkly pigmented frog with the self-pituitary implant ($\times 1.0$). f, Sagittal section through the brain of a normal tadpole (stage IX) indicating the infundibulum (inf) of the diencephalon and the pituitary (pit) ($\times 66.8$). g, Sagittal section through the brain of an embryonically hypophysectomized tadpole that received a self-pituitary implant (tadpole pictured on left in e). The truncated infundibulum (inf) is indicated and the empty black rectangle indicates the approximate location of the pituitary (pit) had it not been removed ($\times 66.8$).

This research was supported by USPHS grants F32 CA06375, HD 07901 and AI 18319. We acknowledge the animal care given by Deborah Sussman, Eleanor Berger and Nancy Effrige.

Received 19 March; accepted 1 September 1982.

1. Triplett, E. L. *J. Immun.* **89**, 505-510 (1962).
2. Rollins, L. A. & Cohen, N. in *Development and Differentiation of Vertebrate Lymphocytes* (ed. Horton, J.) 203-214 (Elsevier, Amsterdam, 1980).
3. Kobel, H. R. & Du Pasquier, L. *Immunogenetics* **2**, 87-91 (1975).
4. DiMarzo, S. & Cohen, N. *Immunology* **45**, 39-48 (1982).
5. Nieuwkoop, P. D. & Faber, J. *Normal Table of Xenopus laevis (Daudin)*, 1-252 (North-Holland, Amsterdam, 1967).
6. Shumway, W. *Anat. Rec.* **78**, 139-147 (1940).
7. Taylor, A. C. & Kollros, J. J. *Anat. Rec.* **94**, 7-23 (1946).
8. Rahi, A. H. S. & Garner, A. *Immunopathology of the Eye*, 1-343 (Blackwell Scientific, London, 1976).
9. Asa, S. L., Bilbao, J. M., Kovacs, K., Josse, R. G. & Kreines, K. *Ann. intern. Med.* **95**, 166-171 (1981).
10. Topliss, D. J. & Volpe, R. *Ann. intern. Med.* **95**, 227-229 (1981).

Clonal interaction in tumours

M. F. A. Woodruff*, J. D. Ansell, G. M. Forbes*,
J. C. Gordon*, D. I. Burton & H. S. Micklem

*Medical Research Council Clinical and Population Cytogenetics Unit, Western General Hospital, Crewe Road, Edinburgh EH4 2XU, UK
Department of Zoology, University of Edinburgh, The Kings Buildings, West Mains Road, Edinburgh EH9 3JT, UK

The development of cancer is contingent on the emergence of at least one clone of transformed cells. One method used to investigate whether human tumours are monoclonal depends on the mosaicism in the normal tissues of women heterozygous for the two forms of the enzyme glucose-6-phosphate dehydrogenase (G-6-PD)¹. This mosaicism results from the inactivation of one X chromosome in all somatic cells and should not exist in a monoclonal population. Following the discovery² in feral mice of an electrophoretic variant (A) of the X-coded enzyme phosphoglycerate kinase (PGK-1) which differs from the form (B) found in common laboratory mouse strains it was reported³ that fibrosarcomas induced chemically in hybrids of

feral and laboratory-bred mice expressed both enzyme phenotypes, but the conclusion that both were expressed by neoplastic cells was based solely on morphological evidence. The development of histocompatible substrains of mice homozygous for one or other alloenzyme has made it possible to study the clonal composition of tumours under experimental conditions in which the neoplastic status of subpopulations of cells can be verified by transplantation. The experiments we now report, while confirming that murine fibrosarcomas are often pleoclonal, show that the clonal composition may change markedly during tissue culture and on transplantation to congenic hosts. These changes presumably reflect changes in the growth kinetics of differentiating subpopulations of the tumour. Cloned sublines are less readily transplantable than uncloned tumour cell populations, and some sublines are less readily transplantable than others; this suggests that sublines resistant to a host's attack are selected on transplantation or that some sublines require the cooperation of others to survive. We postulate that changes in clonal composition occur also during tumour development, metastasis and recurrence.

Fibrosarcomas were induced in adult female CBA backcross mice heterozygous at the PGK locus⁴ (*Pgk-1^a/Pgk-1^b*, abbreviated to AB) by subcutaneous (s.c.) injection of methylcholanthrene (MC) dissolved in tricaprillin (S tumours) or s.c.

Table 1 PGK-1 alloenzyme assays of uncloned cultures

No. of tumours	Reference numbers of tumours	Results	Interpretation (types of neoplastic clones)
19	S1, 6, 7, 8, 9, 11, 15; D6, 7, 9, 12, 16, 17	A in all cultures; B in none	A only
	D1, 5, 8, 18	A in all cultures, B trace to 10% in some primary cultures	A only
	S3; D2	A in all cultures; B trace to 10% in some primary and 2nd generation cultures	A only
1	S5	B in all cultures; A 50% falling to 20% in primary cultures only	B only
2	S12, 14	A in all cultures; B increased from trace in primary to 20% in 3rd generation cultures, then disappeared	A only or A and B
2	D4, 14	B in all cultures; A increased from trace in early primary to 20% in 3rd gen. cultures, then disappeared	B only or A and B
10	S13; D15	A in all cultures; B 30–50% in primary and 2nd generation cultures, then declined and disappeared	A and B
	S4	A in all cultures; B 80% in primary culture, then declined and disappeared	A and B
	S2; D10	A in all cultures, B 50% in early primary cultures, persisted to 4th to 6th culture generation in amounts which varied from trace to 50% and then disappeared	A and B
	D13	A with trace B in primary and early 2nd generation cultures; B only, or with trace to 20% A in all subsequent cultures (to 8th generation)	A and B
	D3	B in all cultures; A increased during primary cultures from trace to 50%, persisted to 5th culture generation in amounts which varied from 10–60% and then disappeared	A and B
	S10	B in all cultures; A absent in primary but increased in 2nd generation to 50% and persisted in all subsequent cultures in amounts which varied from 20–50%	A and B
	D11	A and B in substantial amounts in all cultures, A being the larger component in some and B in others	A and B
	D19	A and B in equal amounts in primary culture; subcultures did not grow	A and B

Fibrosarcomas were induced by s.c. injection of 0.5 mg methylcholanthrene (MC) dissolved in tricaprillin (S tumours) or s.c. implantation of a disk (6 mm diameter) of Millipore membrane (0.22 µm pore diam.) impregnated with 0.1 mg MC (D tumours). Sarcomas developed within 9 months in 35 out of 38 mice and were numbered in accordance with the time they took to develop. Cell suspensions were prepared with Dispase⁶ from tumours collected 113–211 days after carcinogen administration, washed, and resuspended in Ham's F10 medium with 10% fetal calf serum (FCS). As a rule the hosts were killed, but in a few animals the tumour-bearing hind limb was removed surgically and in two of these the tumour recurred at the site of amputation. Tissue culture flasks (Falcon 75 cm²) were seeded with 10⁷ viable cells and incubated at 37 °C in an atmosphere containing 5% CO₂. After culture for 18 h to 20 days, non-adherent cells were discarded and adherent tumour cells detached by brief exposure to trypsin (0.07%) and EDTA (0.027%) were used to set up subcultures. This procedure eliminates nearly all the leucocytes (which are non-adherent) and macrophages (which are strongly adherent), but not fibroblasts. Samples from primary cultures and subcultures, and usually also of suspensions prepared from the whole tumour and from host liver, were frozen and thawed in lytic buffer, and the approximate proportions of the two alloenzymes were determined by gel electrophoresis, using a modification of the linked enzyme assay developed by Buchet *et al.*⁸, the production of NADPH being visualized by the reduction of a tetrazolium dye, thiazolyl blue, to its formazan derivative.

implantation of a disk of Millipore membrane impregnated with MC⁵ (D tumours). The relative amounts of the two alloenzymes were determined in whole tumour suspensions⁶ and uncloned cultures after gel electrophoresis (Table 1). As expected, both A and B components were found more often in whole tumour suspensions (17 out of 24 studied) than in primary cultures of the same tumour (11 out of 24), which should contain fewer normal cells. With many tumours the A/B ratio fluctuated greatly during culture. Contrary to the earlier finding of Reddy and Fialkow³, there was a marked preponderance of tumours with an A component; this is not surprising, however, because the *Pgk-1* locus is closely linked to another locus, *Xce*, which determines the probability of the X-chromosome being inactivated⁷; the resulting ratio of A cells to B cells in the normal tissues of AB mice of our CBA stock is about 70:30.

Clones were isolated from 10 tumours, and samples from cloned and uncloned cultures were injected into homozygous females (*Pgk-1^b/Pgk-1^b*, abbreviated to BB) or hemizygous males (*Pgk-1^a/Y*, abbreviated to AY); when tumours developed these were assayed in the same way as the primary tumours (Table 2). Other samples were used for karyotyping and determination of the cellular DNA content by automated scanning⁹ of Feulgen-stained preparations (1,500–4,000 cells).

With four tumours (D11, D13, D15, S10), we have formal proof of the existence of both A and B neoplastic components, since on transplantation to BB mice each gave rise to some tumours with only an A component and others with no detectable A component. In the case of D11 and S10, many A clones and B clones have been isolated and shown to be polyploid. Two A clones from D11 (Nos 6 and 10) had a modal chromosome number of 98, and automated scanning of one of these showed a mean DNA content 2.6 times that of normal diploid cells; one B clone (no. 12) had a modal chromosome number of 79 and mean DNA content 1.9 times that of normal cells. Clones 6 and 10 gave rise to A tumours, and clone 12 to a B tumour, when transplanted to BB mice. With tumour D15 the B neoplastic component disappeared in the course of tissue culture. Tumour S10 is unusual in that we have isolated A clones, B clones, and 'clones' expressing both A and B. Six of the latter were harvested from 192 wells seeded with, on average, 1 cell; and since no colonies developed in 139 wells the mean number of clonogenic cells seeded (assuming a Poisson distribution) was probably about 0.3 per well. It seemed just possible that these supposed clones were mixtures, but on recloning at the same and more extreme dilution we have obtained 19 'subclones' which still express both A and B, 20 which express only B and none which express only A. While the possibility of mixed populations of cells growing in symbiosis is still not formally excluded, it seems likely that AB clones have arisen from hybrid cells formed by fusion, either in the mouse or in tissue culture, of an A cell and a B cell, at least one of which had undergone transformation, and that disappearance of the A component in some cases on recloning was due to chromosome loss. An alternative possibility is that there has been reactivation of the inactive X chromosome in a cell which prior to transformation expressed only A or B. Preliminary observations based on flow cytometry of cells stained with the dye Hoechst 33342 have shown a higher proportion of diploid cells in suspensions from the original tumour and primary cultures than from later cultures. This may be due entirely to selection, but raises the question of whether some of the tetraploid and hypertetraploid clones we have found in other tumours may also have developed from hybrid cells formed during tissue culture. Karyotypic analysis and studies with new tumours may resolve some of these uncertainties.

Clones from five tumours (D11, D13, D14, S2, S10) which transplanted readily in the form of uncloned cultures were transplanted to normal BB mice, and in some cases also to thymectomized, irradiated BB mice protected with cytosine arabinoside¹⁰, by s.c. injection of 1.5×10^6 viable cells. Only 4 out of 21 clones grew in the normal mice, whereas 6 out of 6 which had failed to grow in the normal mice grew in the

Table 2 Characterization of clones, transplants and recurrent tumours

No. of tumour	No. and type of clones isolated	Transplants		Recurrence of primary tumour
		Material transplanted	Neoplastic components proved	
D17	6A			
S3	12A			
S5		Primary tumour	B*	B
D4	60B	Primary tumour	B*†	
D14	16B	Primary tumour	B*	
		B clone	B*†	
S13				A
D15		Primary tumour	A†B*	
		1st generation transplant	A*†	
		2nd generation transplant	A†	
S4		Primary tumour	A†	
		1st generation transplant	A*	
		2nd generation transplant	A*†	
S2	20A‡	A clone	A†	
D10	15A			
D13	1A, 6B	Uncoloned culture	B*†	
		A clone	A†	
D3	78B	Primary tumour	B*	
S10	A, B, AB§	A clone	A†	
		B clone	B*	
		AB clone	A†B*†	
D11	21A, 36B	Primary tumour	B*	
		A clone	A†	
		A clone	A†	
		B clone	B*	

Clones were isolated either in wells of microtest plates (Falcon 30401) seeded with 0.2 ml of a suspension containing tumour cells and irradiated (60 Gy) human fibroblasts which yielded on average 1, 2 or 5 tumour cells and 2,000 fibroblasts per well, or by ring cloning in small (25 cm²) flasks.

* Proof based on development of tumours with A component *only* in AY mice or B component *only* in BB mice.

† Proof based on development of tumours with A component in BB mice or B component in AY mice.

‡ One apparent clone of type B was isolated but on transplantation this yielded only A tumours in AY mice. On retesting, the 'clone' was found to contain a trace of A in addition to the main B component.

§ See text.

|| These clones grew only in, or after passage in, thymectomized, irradiated mice.

thymectomized mice. After passage in thymectomized mice, 5 of the 6 tumours grew when retransplanted to normal mice. These preliminary findings suggest that clones with a high capacity for survival are selected when pleoclonal populations are transplanted; in addition, some clones may require the cooperation of others to survive. The successful transplantation of five clones to normal mice after passage in thymectomized, irradiated mice suggests further that cells resistant to surveillance may emerge when tumours grow under conditions in which surveillance is impaired. The features which favour survival of a clone have not been elucidated, but possibilities to be considered include lack of strong rejection-inducing antigens; failure, despite the presence of such antigens, to evoke an effective immune response; and relative insensitivity to surveillance mediated by NK cells and macrophages.

Our results highlight the problems involved in assessing the clonality of tumours with X-linked markers, whether in man or mouse, and lend support to the view that tumours of pleoclonal origin may appear, at a particular time, to be monoclonal because all clones except one have been competitively eliminated or reduced to the point of being undetectable.

It seems likely^{12,13} that clonal interaction plays a significant role in the life history of pleoclonal tumours in general. At

present we do not have sufficient data to construct models of the cell population kinetics of such tumours, but it is possible to suggest some general principles on which these might be based: (1) The number of clones present at any given time will depend on the number of cells originally transformed and the growth rate of each clone. The number of cells transformed will depend *inter alia* on the nature and dose of the carcinogen. The growth rate of each clone may be influenced by inherent properties of the transformed cells, the host reaction, and interaction between the clone in question and other clones of transformed or initiated cells. (2) If growth rates remain constant the clone with the greatest growth rate will eventually outgrow all others, but this does not necessarily exclude the persistence of small numbers of very slowly growing or dormant cells. (3) Growth rates may change suddenly, and dormant cells may resume cycling. Such changes may be influenced by treatment but may also occur for no apparent reason. Clones which grow slowly or remain dormant in primary tumours may grow rapidly in metastases or locally recurrent tumours. (4) The symbiotic relationship between different clones may be antagonistic, neutral or mutualistic.

We thank Drs James Tucker, Daryll Green and John Hay, respectively, for undertaking automated scanning and flow cytometry, and preparing thymectomized irradiated mice. M.F.A.W., G.M.F. and J.C.G. are indebted to Professor H. J. Evans for the privilege of working in his unit, and to the MRC for a project grant. H.S.M. and J.D.A. thank the Melville Trust for a grant. D.I.B. is supported by an MRC studentship.

Received 1 June; accepted 3 August 1982.

1. Fialkow, P. J. *Adv. Cancer Res.* **15**, 191–226 (1972).
2. Nielsen, J. T. & Chapman, V. M. *Genetics* **87**, 319–327 (1977).
3. Reddy, A. L. & Fialkow, P. J. *J. exp. Med.* **150**, 878–887 (1979).
4. Burton, D. I., Ansell, J. D., Gray, R. A. & Micklem, H. S. *Nature* **298**, 562–563.
5. Woodruff, M. F. A., Bard, J., Ross, A. & Forbes, G. M. *Proc. R. Soc. B* **211**, 269–286 (1981).
6. Matsumura, T., Yamanaka, T., Hashizume, S., Irie, Y. & Nitta, K. *Jap. J. exp. Med.* **45**, 377–382 (1975).
7. Johnston, P. G. & Cattanaach, B. M. *Genet. Res.* **37**, 151–160 (1981).
8. Bücher, T., Bender, W., Fundele, R., Hofner, H. & Linke, I. *FEBS Lett.* **115**, 319–324 (1980).
9. Tucker, J. H. *J. Histochem. Cytochem.* **27**, 613–620 (1979).
10. Steel, G. G., Courtenay, V. D. & Rostom, A. Y. *Br. J. Cancer* **37**, 224–230 (1978).
11. Woodruff, M. F. A. *The Interaction of Cancer and Host—Its Therapeutic Significance*, 123–133 (Grune and Stratton, New York, 1980).
12. Poste, G., Doll, J. & Fidler, I. J. *Proc. natn. Acad. Sci. U.S.A.* **78**, 6226–6230 (1981).
13. Woodruff, M. F. A. *Br. J. Cancer* **46**, 313–322.

Dihydroouabain is an antagonist of ouabain inotropic action

T. Godfraind, J. Ghysel-Burton & A. De Pover

Laboratoire de Pharmacodynamie Générale et de Pharmacologie,
Université Catholique de Louvain, UCL 7350,
Avenue Emmanuel Mounier, 73, B-1200 Bruxelles, Belgium

The Na^+ , K^+ -pump controls a wide variety of cellular systems and its inhibition by cardiac glycosides modifies important physiological functions and evokes several pharmacological effects (refs 1, 2 and refs therein). However, not all the actions of cardiac glycosides can be attributed to Na^+ , K^+ -pump inhibition and several observations show that, at low doses, cardiac glycosides stimulate the pump^{3–5}. It has been proposed that their positive inotropic effect could be the sum of two processes: the inhibition of the pump and a still unknown additional inotropic mechanism⁶. In guinea pig heart, low doses of ouabain interact with high-affinity binding sites, which differ from the lower-affinity sites responsible for Na^+ , K^+ -pump inhibition^{3,7–9}. It has been suggested that ouabain interaction with these high-affinity sites could be responsible for the additional inotropic

mechanism⁶. The existence of two classes of ouabain-binding sites has been documented not only in guinea pig heart, but also in dog¹⁰, rat^{11,12} and human heart¹³. Dihydroouabain, a derivative of ouabain in which the lactone ring is saturated, is about 50-fold less potent than ouabain as an inhibitor of Na^+ , K^+ -pump and does not stimulate the pump at low doses⁷. Its inotropic effect can be entirely accounted for by the inhibition of the pump^{6,14}. We have examined the pharmacological action of ouabain in the presence of dihydroouabain and report here that dihydroouabain reduces ouabain inotropic action but not Na^+ , K^+ -pump inhibition.

Figure 1 shows the inhibition of $(\text{Na}^+ + \text{K}^+)\text{ATPase}$ activity (Fig. 1a) and of specific ^3H -ouabain binding (Fig. 1b) in guinea pig heart microsomes as a function of ouabain or dihydroouabain concentration. With both glycosides, the slope of the Hill plot was equal to 1 for $(\text{Na}^+ + \text{K}^+)\text{ATPase}$ inhibition. In contrast, the slope was 0.64 ± 0.001 for the displacement of ^3H -ouabain. This confirms the previously reported heterogeneity of ouabain binding sites^{4,15} and shows that dihydroouabain competed with ^3H -ouabain at both high- and low-affinity sites. In view of this finding, we have examined whether dihydroouabain could interact with the action of ouabain.

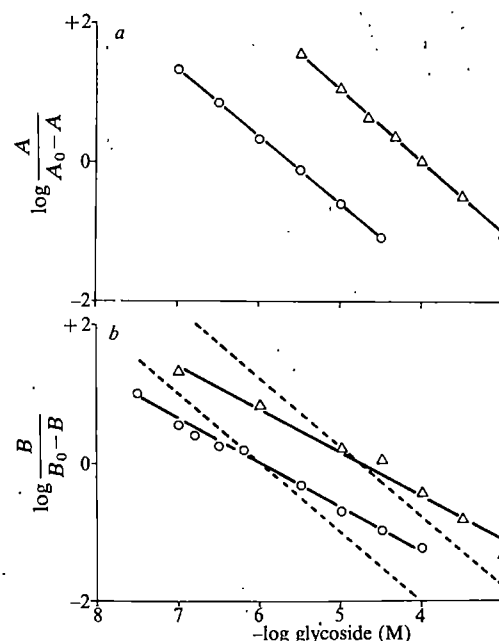


Fig. 1 Interaction of ouabain and dihydroouabain with guinea pig heart microsomes. The methods for microsomal $(\text{Na}^+ + \text{K}^+)\text{ATPase}$ preparation and assay²⁰, and for ^3H -ouabain assay¹³ have been described elsewhere. *a*, $(\text{Na}^+ + \text{K}^+)\text{ATPase}$ inhibition by cardiac glycosides. About 0.01 mg protein was incubated for 120 min in 2 ml medium containing 100 mM NaCl, 10 mM KCl, 3 mM MgCl_2 , 3 mM ATP, 1 mM EGTA, 20 mM Tris-maleate (pH 7.4, 37 °C) and various concentrations of glycoside. The released inorganic phosphate was measured by colorimetry²⁰. ATP hydrolysis was <15%. Ordinate: $\log(A/(A_0 - A))$ where A_0 is the control $(\text{Na}^+ + \text{K}^+)\text{ATPase}$ activity and A the activity in the presence of ouabain (○) or dihydroouabain (△). Abscissa: $-\log$ glycoside concentration. *b*, Displacement by ouabain or dihydroouabain of the specific ^3H -ouabain binding. About 0.24 mg protein was incubated in the conditions described above. The incubation medium was supplemented with 10^{-8} M ^3H -ouabain (19 Ci mmol^{-1} ; Amersham), and with 0.01 mM NaVO_3 , 5 mM inorganic phosphate, 3 mM creatine phosphate and 0.01 mg creatine kinase (25 U per mg) to limit ATP hydrolysis and keep the conditions constant⁶. The reaction was stopped by filtration on Whatman GF/F glass fibre filters. The filters were washed with 10 ml of chilled 0.25 M sucrose solution. The radioactivity trapped by the filters was measured as described previously¹³. The nonspecific binding was estimated in the presence of 1 mM ouabain and subtracted from the total. Ordinate: $\log(B/(B_0 - B))$ where B_0 is the control binding and B the binding in the presence of ouabain (○) or dihydroouabain (△). Abscissa: $-\log$ glycoside concentration. The dashed lines represent theoretical curves with slope equal to 1. The points are means from three experiments. The departure from parallelism between experimental and theoretical curves was checked by a comparison of difference in slopes between the two curves (for ouabain, $t = 5.2$, $P < 0.001$; for dihydroouabain, $t = 8.30$, $P < 0.001$).

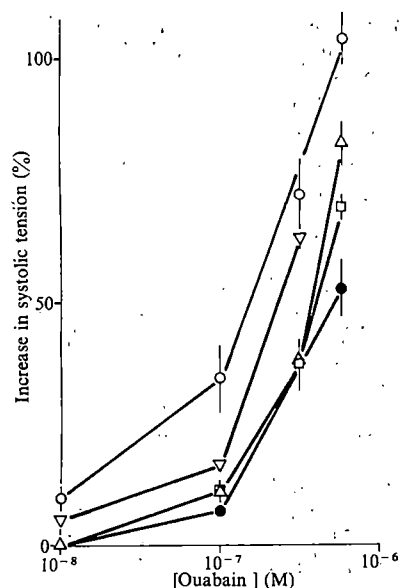


Fig. 2 Inotropic effect of ouabain in the presence or the absence of dihydroouabain. Adult albino guinea pigs (Dunkin Hartley strain, Hacking and Churchill Ltd) weighing 300–400 g were stunned and bled, their chests were opened and their hearts quickly excised. Left atria were dissected and suspended in an organ bath between platinum electrodes, under a preload tension of 500 mg. The physiological Tyrode solution contained (mM): NaCl, 137; KCl, 6; CaCl₂, 1.82; MgCl₂, 1.0; NaH₂PO₄, 0.417; NaHCO₃, 11.9; glucose, 5.5. It was equilibrated at 30 °C with 95% O₂/5% CO₂. The atria were stimulated with rectangular 10-ms pulses (strength at least twice threshold) at a rate of 3.3 Hz. Recordings of the contractile activity were made by isometric lever using two strain gauges as part of a balanced bridge, the output of which was fed into a potentiometric recorder. After 30 min incubation in the absence (○) or the presence of dihydroouabain at concentrations of 10⁻⁸ M (▽), 10⁻⁷ M (Δ), 3 × 10⁻⁷ M (□) or 10⁻⁶ M (●), ouabain was added to the medium. The inotropic effect was recorded at its maximum for each concentration of ouabain, that is, between 20 and 40 min after glycoside addition. The contractility of controls was not modified by dihydroouabain, except for a 10% increase with 10⁻⁶ M. The limits of s.e.m. are shown when they exceed the diameter of the symbol (*n* = 3–5). Ordinate: increase in systolic tension (%). Abscissa: ouabain concentration. Statistical analysis: difference in systolic contraction between randomized groups was checked by variance analysis before and after drug treatment. No statistical significance could be found before treatment. The effect of ouabain was analysed using a paired *t*-test. In the absence of dihydroouabain, ouabain at 10⁻⁸ M (*n* = 5) evoked a small but significant inotropic effect (0.02 < *P* < 0.05); at higher concentrations, ouabain effect was highly significant (*P* < 0.001). The influence of dihydroouabain pretreatment has been estimated by comparing the mean increase in contractility (expressed in g or in per cent of initial values) between groups treated by ouabain with or without different concentrations of the dihydro derivative. The *t*-test analysis showed the following results: ouabain 10⁻⁸ M (*n* = 5) + dihydroouabain 10⁻⁸ M (*n* = 3) not significant (NS), 10⁻⁷ M (*n* = 4) the response to ouabain was abolished; ouabain 10⁻⁷ M (*n* = 11) + dihydroouabain 10⁻⁸ M (*n* = 3) NS, 10⁻⁷ M (*n* = 6), 0.01 < *P* < 0.02, 10⁻⁶ M (*n* = 5), 0.001 < *P* < 0.01; ouabain 3 × 10⁻⁷ M (*n* = 10) + dihydroouabain 10⁻⁸ M (*n* = 3) NS, 10⁻⁷ M (*n* = 6), 0.001 < *P* < 0.01; 10⁻⁶ M (*n* = 5), 0.001 < *P* < 0.01; ouabain 6 × 10⁻⁷ M (*n* = 6) + dihydroouabain 10⁻⁷ M (*n* = 5), 0.02 < *P* < 0.05, 3 × 10⁻⁷ M (*n* = 4), 0.01 < *P* < 0.02, 10⁻⁶ M (*n* = 4), 0.02 < *P* < 0.05.

The experiments were performed on whole left atria stimulated by field electrodes in a medium containing 1.8 mM CaCl₂ so as to observe the action of low ouabain concentrations¹⁶. We compared the increase in atrial contractile force evoked by ouabain added after a preincubation with dihydroouabain concentrations varying from 10⁻⁷ M to 10⁻⁶ M, with that observed without this pretreatment. Figure 2 illustrates the relationship between ouabain concentration and the inotropic response of atria measured at its maximum and expressed as a percentage of controls, before glycoside. It shows how the ouabain inotropic effect was depressed by increasing the dihydroouabain concentration.

We have examined the action of ouabain on the Na⁺, K⁺-pump activity by measuring ⁴²K uptake in atria treated by ouabain in the presence or absence of dihydroouabain.

Figure 3 shows the relationship between the inhibition of ⁴²K uptake and the positive inotropic effect evoked by ouabain,

dihydroouabain or the combination of the two drugs. It confirms our previous report⁶ that for a given inhibition of active ⁴²K uptake, the inotropic effect of ouabain is higher than that evoked by dihydroouabain. The latter is directly related to Na⁺, K⁺-pump inhibition^{6,14}. For ouabain at 10⁻⁸, 10⁻⁷ and 3 × 10⁻⁷ M in the presence of 10⁻⁷ M dihydroouabain (which was without effect on ouabain inhibition of ⁴²K uptake), the relationship between the inhibition of ⁴²K uptake and the inotropic effect was similar to that observed with dihydroouabain at doses equiactive on ⁴²K uptake. This indicates that dihydroouabain did not antagonize the positive inotropic effect resulting from Na⁺, K⁺-pump inhibition, but only antagonized the additional mechanism believed to be specific to ouabain action. Figure 3 further illustrates how the antagonism exerted by dihydroouabain was surmounted by increasing ouabain concentrations.

It has been reported¹⁷ that (Na⁺ + K⁺)ATPase forms a complex with dihydroouabain that is less stable than the complex formed with ouabain. The higher stability of the ouabain-enzyme complex has been attributed¹⁸ to a two-point attachment of the lactone ring to the receptor: (1) through hydrogen bonding and (2) through an ionic bond between a partial positive charge at C-20 and an anionic group of the receptor. Ionic bonding does not occur with dihydroouabain because its lactone ring does not contain conjugated double bonds. This feature seems to be required for the intrinsic activity of ouabain at high-affinity sites that have been proposed to be responsible for the stimulation of the Na⁺, K⁺-pump.

In conclusion, the present results show that dihydroouabain reduces the inotropic action of ouabain but does not modify its inhibitory action on the Na⁺, K⁺-pump. As the inhibitory action of dihydroouabain on ouabain inotropy was overcome by increasing concentrations of this glycoside and as this action was observed at dihydroouabain concentrations devoid of direct pharmacological action, dihydroouabain can be considered as an antagonist of ouabain. The present results are consistent

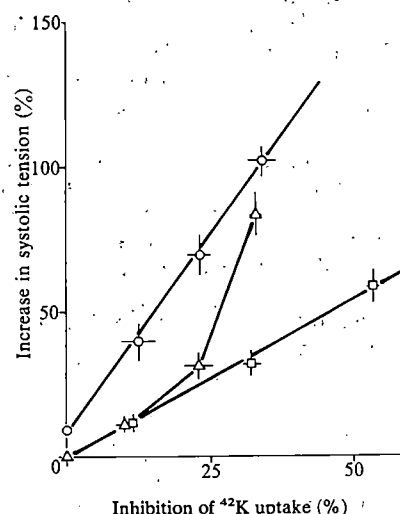


Fig. 3 Relationship between the inhibition of ⁴²K uptake and the increase in systolic tension of guinea pig atria. After incubation in the presence or absence of the glycosides as described in Fig. 2 legend, ⁴²K (Amersham) was added to the solution (5–10 nCi ml⁻¹); 10 min later, the atria were dipped for 5 s in a nonradioactive solution, blotted onto filter paper and pressed three times with a roller weighing 350 g. After weighing, each atrium was transferred to 0.2 ml of a solution composed of equal volumes of perchloric acid (37%, w/v) and H₂O₂. The tissue was dissolved by heating at 75 °C for 30 min. After cooling, 5 ml of Aqualuma (Lumac) was added and the radioactivity of the samples was measured in a liquid scintillation counter. Inhibition of the ouabain-sensitive ⁴²K uptake, estimated as previously reported⁶, was evoked by: ○, ouabain at 10⁻⁸, 10⁻⁷, 3 × 10⁻⁷ and 6 × 10⁻⁷ M (*n* = 6); □, dihydroouabain at 10⁻⁶, 3 × 10⁻⁶ and 10⁻⁵ M (*n* = 8); Δ, a mixture of 10⁻⁷ M dihydroouabain preincubated 30 min before ouabain addition and the ouabain concentrations as stated above (*n* = 8). The limits of s.e.m. are shown when they exceed the diameter of the symbol. Ordinate: increase of systolic tension as % of the control. Abscissa: % inhibition of ouabain-sensitive ⁴²K uptake.

with previous reports that ouabain inotropic action cannot be entirely^{5-7,19} accounted for by the glycoside-evoked changes in Na^+ and K^+ gradients.

In preliminary experiments, these observations have been extended to other preparations (sometimes dihydroouabain 3×10^{-6} M being required). Such experiments could contribute

Received 15 February; accepted 2 September 1982.

1. Bonting, S. L. in *Membrane and Ion Transport* (ed. Bittar, E. E.) 257-363 (Wiley-Interscience, London, 1970).
2. Schwartz, A., Lindenmayer, G. E. & Allen, J. C. *Pharmac. Rev.* **27**, 1-134 (1975).
3. Godfraind, T. & Ghysel-Burton, J. *Nature* **265**, 165-166 (1977).
4. Langer, G. A. *Biochem. Pharmac.* **30**, 3261-3264 (1981).
5. Browning, D. J., Guarnieri, T. & Strauss, H. C. *J. clin. Invest.* **68**, 942-956 (1981).
6. Godfraind, T. & Ghysel-Burton, J. *Proc. natn. Acad. Sci. U.S.A.* **77**, 3067-3069 (1980).
7. Ghysel-Burton, J. & Godfraind, T. *Br. J. Pharmac.* **66**, 175-184 (1979).
8. Godfraind, T., De Pover, A. & Tona Lutete, D. *Biochem. Pharmac.* **29**, 1195-1199 (1980).
9. De Pover, A., Godfraind, T. & Tona Lutete, D. *Br. J. Pharmac.* **72**, P513-P514 (1981).

to a better understanding of the role of the inhibition of the Na^+ , K^+ -pump in the pharmacological action of ouabain.

We thank Dr M. Wibo for reading the manuscript, Mr A. Goffin for technical assistance and Mr P. Simon for the drawings. This work was supported by grant 3'9001.79 of Fonds de la Recherche Scientifique Médicale (Belgium).

10. Wellsmith, N. V. & Lindenmayer, G. E. *Circulation Res.* **47**, 710-720 (1980).
11. Erdmann, E., Philipp, G. & Scholz, H. *Biochem. Pharmac.* **29**, 3219-3229 (1980).
12. Schwartz, A. et al. *Proc. 3rd int. Conf. Na, K-ATPase* (Academic, New York, in the press).
13. De Pover, A. & Godfraind, T. *Biochem. Pharmac.* **28**, 3051-3056 (1979).
14. Lee, C. O., Kang, D. H., Sokol, J. H. & Lee, K. S. *Biophys. J.* **29**, 315-330 (1980).
15. Pocock, G. J. *Physiol., Lond.* **307**, 38P (1980).
16. Grupp, G., Grupp, I. L., Ghysel-Burton, J., Godfraind, T. & Schwartz, A. *J. Pharmac. exp. Ther.* **220**, 145-151 (1982).
17. Clark, A. F., Swanson, P. D. & Stahl, W. L. *J. biol. Chem.* **250**, 9355-9359 (1975).
18. Thomas, R., Boutagy, J. & Gelbart, A. *J. Pharmac. exp. Ther.* **191**, 219-231 (1974).
19. Noble, D. *Cardiovasc. Res.* **14**, 495-514 (1980).
20. Godfraind, T., De Pover, A. & Verbeke, N. *Biochim. biophys. Acta* **481**, 202-211 (1977).

Hydrogen ion currents and intracellular pH in depolarized voltage-clamped snail neurones

R. C. Thomas & R. W. Meech

Department of Physiology, University of Bristol, University Walk, Bristol BS8 1TD, UK

Until now the only reported effect of depolarization on the intracellular pH (pH_i) of excitable cells is an acidification of the cell cytoplasm^{1,2}. It seems unlikely that this could be a direct effect of membrane potential because pH_i is known to be regulated by an electroneutral mechanism^{3,4} and in most cells H^+ ions are not in equilibrium with the membrane potential (E_m). In any case the membrane conductance to H^+ ions would be expected to be small because they are at such low concentrations on either side of the cell membrane. But it is possible that the H^+ ion permeability of the membrane increases on depolarization just like that of other ions in the bathing medium (Na^+ , K^+ and Ca^{2+} for example). To test this idea we have made pH_i measurements on molluscan neurones under voltage-clamp. Our findings, presented here, provide evidence for a large increase in H^+ ion permeability in depolarized cells. We suggest that this increase in proton conductance may be the basis for the 'nonspecific' currents previously described in perfused molluscan neurones^{5,6} and we assess the physiological significance of this newly discovered pathway.

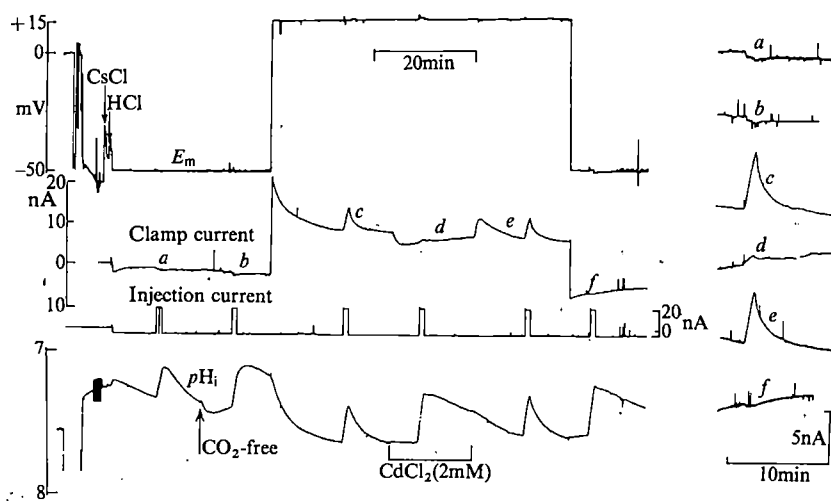
Experiments were done on exposed cells in isolated sub-oesophageal ganglia from the snail, *Helix aspersa*. The neuronal cell body was penetrated with four microelectrodes. The first was to measure pH_i . The second was a reference liquid ion-exchanger electrode to measure E_m ⁸. The third, a micropipette

filled with 3 M KCl, CsCl or $(\text{Cs})_2\text{SO}_4$, supplied feedback current to voltage-clamp the cell⁹. The fourth was for iontophoretic HCl injection. The preparation was superfused with saline buffered to pH 7.5 either with HEPES alone or with HEPES and 4 mM NaHCO_3 . The bicarbonate saline was equilibrated with 0.5% CO_2 in air.

Figure 1 shows an experiment in which HCl was injected at two different holding potentials, -50 mV and +15 mV. After the first injection, at -50 mV, pH_i recovered within 10 min. This pH_i recovery involves a mechanism which exchanges external Na^+ and HCO_3^- ions for internal Cl^- and H^+ ions³. It was inhibited by changing the bathing medium to a bicarbonate-free saline. The next HCl injection produced a slightly larger decrease in pH_i because the buffering capacity of the cytoplasm is smaller in CO_2 -free saline^{10,11}. Recovery from the injection was slow and before it was complete we depolarized the cell to +15 mV. This caused a rapid unexpected increase in pH_i to a steady level of 7.6. (The normal pH_i is between 7.3 and 7.5.) After a third HCl injection the pH_i rapidly returned to this new steady level. Despite the lack of bicarbonate the recovery was faster than the control in normal saline. In other experiments normal pH_i regulation was abolished by using Na-free saline or the inhibitor SITS (4-acetamide-4'-isothiocyanatostilbene-2,2'-disulphonic acid) and the cell was depolarized either under voltage-clamp or with isotonic KCl ¹². In each case there was a rapid recovery of pH_i following an acid load.

At depolarized potentials pH_i recovers from acid injections by a mechanism clearly different from that operating normally. Further evidence for this is that in depolarized cells pH_i recovery is sensitive to heavy metals in the bathing medium. Figure 1 shows that the recovery of pH_i following an acid load at +15 mV was slowed by 2 mM CdCl_2 . When the Cd^{2+} ions were removed there was a significant increase in the rate of pH_i recovery. Preliminary tests with other heavy metals showed that 1 mM CuCl_2 or 1 mM LaCl_3 had a similar effect.

Fig. 1 The effect of HCl injections on the intracellular pH (pH_i) and clamp current of a voltage-clamped snail neurone. The four traces are pen-recordings of membrane potential (E_m), clamp current, injection current and pH_i . Enlargements of the clamp current during the six acid injections are shown at the right. The general experimental procedures have been described previously^{3,7,11}. The clamp time constant was such that the cell could fire action potentials at the resting potential⁹ while at positive potentials there was good voltage control. But the cells survived equally well with a rapidly responding clamp, that is, when there were no action potentials at any potential. In most experiments the voltage-clamp current electrode was filled with CsCl or Cs_2SO_4 so that Cs^+ ions were injected when the cell was depolarized. Intracellular Cs reduces the outward K^+ current and hence gives improved voltage control. The arrows above the E_m record indicate the point at which the current microelectrodes were inserted.



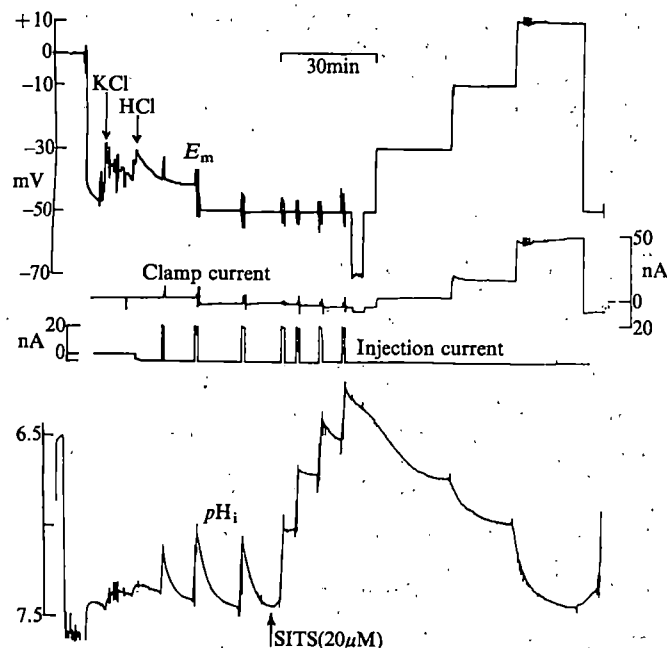


Fig. 2 The intracellular pH (pH_i) at different membrane potentials (E_m) in a voltage-clamped cell. After the first three injections the normal pH_i regulating system was blocked by SITS. The voltage-clamp current electrode was filled with KCl.

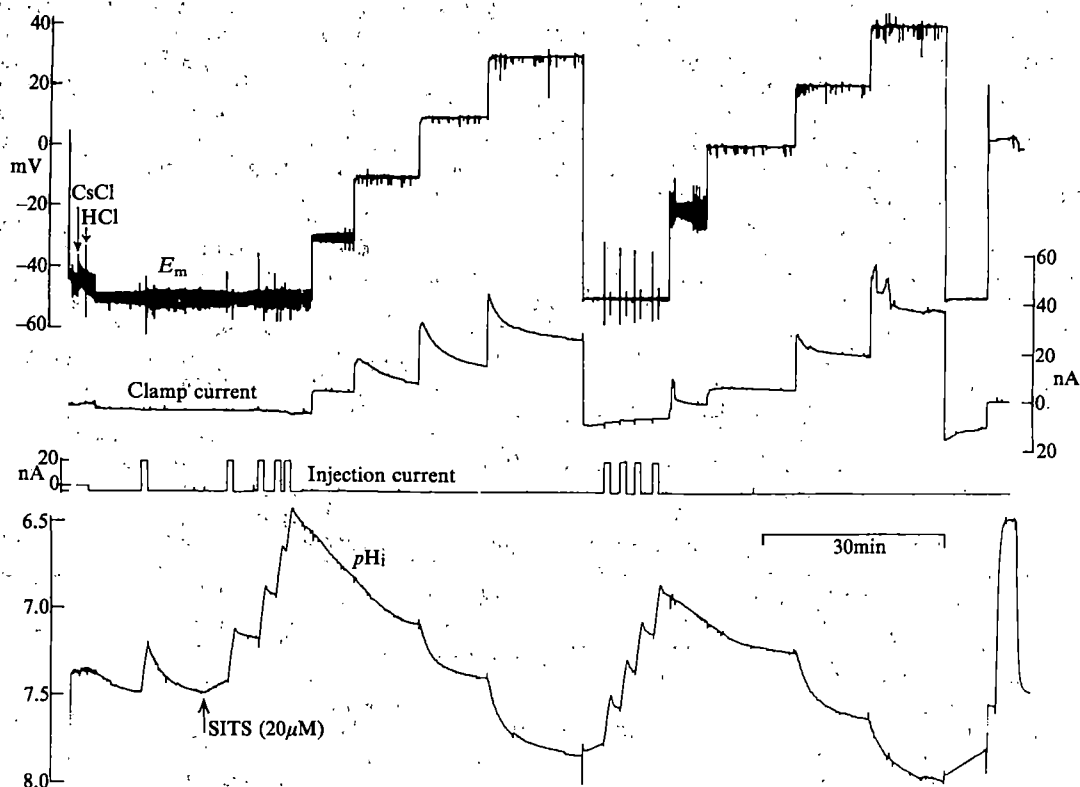
We tested the way in which the membrane potential level influenced the pH_i recovery in the experiment shown in Fig. 2. In this cell pH regulation was first abolished by bathing the cell in saline containing $20 \mu\text{M}$ SITS. Then four separate iontophoretic injections of HCl took pH_i to 6.23. Note that as pH_i was made more acid its rate of recovery increased, but never approached that of the control. The pH_i recovery was unaffected by hyperpolarizing the membrane to -70 mV for 5 min, but its rate increased when the membrane was depolarized to -30 mV . After about 36 min the pH_i reached a steady level at pH 6.74 but a further 20 mV depolarization produced a further increase in pH_i until it reached another steady level at 6.98. At $+10 \text{ mV}$

pH_i became steady at pH 7.44. Heavy metals inhibit these potential-dependent pH_i shifts (not illustrated). In preliminary tests we find that they are blocked by CdCl_2 , LaCl_3 , ZnCl_2 (1 mM) or CoCl_2 (10 mM) and that they are slower in 4 mM Ruthenium red.

In experiments of this kind using KCl-filled micropipettes we were unable to test the effect of depolarizations beyond about $+20 \text{ mV}$ because the cells did not survive for long enough. When we used CsCl the outward currents were greatly reduced and, perhaps as a consequence, the cells survived for longer periods. In the experiment shown in Fig. 3 the membrane potential was increased to $+37.5 \text{ mV}$ in 20-mV steps. With each step beyond -10 mV , there was a rapid pH_i increase to a steady level such that the H^+ ion equilibrium potential also changed by about 20 mV . The relationship between E_m and the steady pH_i level is shown in Fig. 4. The solid line drawn through the points shows the slope expected if pH_i changes by 1 pH -unit for a 58-mV change in E_m . The interrupted line shows the expected result if the membrane potential was at the hydrogen ion equilibrium potential, E_H . If this were the case pH_i would equal the external pH (that is, pH 7.5) when the membrane potential was held at 0 mV . In fact, as Fig. 4 shows, pH_i is close to 7.3 at 0 mV . In four experiments the average difference between the internal and external pH at 0 mV was 0.33 ± 0.09 ($\pm \text{s.d.}$) pH unit. In the absence of SITS the difference was 0.07 ± 0.04 pH unit ($n = 4$). It is possible that this is because of unstirred layers near the cell membrane.

A satisfactory explanation for the potential dependence of pH_i seen at depolarized potentials is that the membrane becomes so highly permeable to H^+ (and/or OH^-) ions that their concentration inside the cell is determined simply by the external pH and the potential across the cell membrane. H^+ ions leave the cell cytoplasm until their gradient across the cell membrane is in equilibrium with E_m . It is likely that most of the H^+ ions leave the cytoplasm by crossing the cell membrane and if so, it may be possible to detect a large outward current. Indeed, such a current can be seen in the clamp current trace in Fig. 1. Injections *a*, *b* and *f* which were carried out at -50 mV produced no obvious changes in the current trace but *c* and *e* produced a large outward current which declined in an exponential fashion once the injection was terminated. The presence of 2 mM Cd^{2+} , which blocked rapid pH_i recovery, also blocked

Fig. 3 Relationship between membrane potential (E_m) and intracellular pH (pH_i) in a neurone injected with Cs. After the first HCl injection the normal pH_i regulating system was blocked by SITS. At the end of the experiment the pH electrode response to calibration with pH 6.5 saline is shown. The apparent noise on the E_m record is caused by action potentials, which are greatly reduced by the long time constant of the pen-recorder and are prolonged by Cs^+ injection under voltage-clamp.



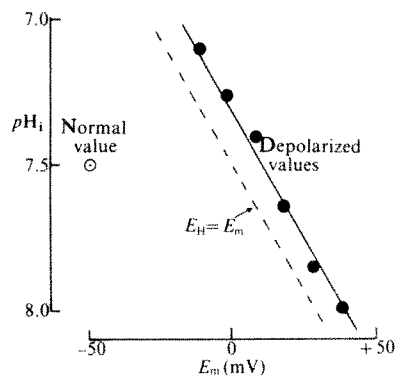


Fig. 4 Graph showing the relationship between membrane potential (E_m) and steady-state intracellular pH (pH_i) from the experiment of Fig. 3. ●, Steady pH_i values taken after the cell had been treated with SITS and depolarized. Solid line drawn by eye with slope of 58 mV per pH unit to give best fit to points. Dashed line shows relationship expected of pH_i determined by purely passive distribution of H^+ ions across cell membrane with no surface charges or net flux of H^+ , OH^- or HCO_3^- ions.

the appearance of the outward current (see injection *d*). The time constant of the decline in the injection dependent current is about 1.4 min, which is half the time constant of the associated pH_i recovery. One possible reason for this difference is that our measurements of pH_i changes are limited by the response time of the pH electrode, and its location in the cell.

If all the injected H^+ (and OH^-) ions leave the cell by crossing the cell membrane and there are no other ion movements, then the injection-induced charge movement should equal the charge used to inject the H^+ ions in the first place. The charge movement generated by injection *c* was 5.97×10^{-7} C which was about 66% of the charge used to inject HCl (assuming a transport number for H^+ of 0.94¹⁰). It is possible that the H^+ movement is coupled to the movement of other ions or that up to a third of the injected H^+ ions are taken into intracellular organelles¹³. Potential-dependent shifts in pH_i could be produced even after 80 min in saline containing *n*-methylglucamine methane sulphonate and HEPES buffer only.

Does this newly discovered H^+ ion permeable pathway operate during the normal activity of the cell? To be of any physiological significance the ions would have to move during the short time that the membrane potential is more positive than about -20 mV during an action potential. If they do it should be possible to identify an outward H^+ current during brief depolarizing pulses. Just like the HCl injection-induced current (Fig. 1), it should be blocked by many of the agents which block calcium channels (Cd^{2+} , Co^{2+} , La^{3+} etc., see ref. 14 for review), it would be expected to reverse near 0 mV and should be sensitive to changes in external pH. Byerly and Hagiwara⁶ have recently described an apparently 'nonspecific' outward current in perfused *Limnaea* neurones which has all these characteristics. A similar outward current has been described in perfused *Helix* neurones⁵. In this case its current-voltage characteristic curve shifts by +15 mV for a unit change in external pH¹⁵. Both currents are rapidly activated. If the nonspecific current is an outward H^+ current as we suggest it could have a significant effect on pH values close to the membrane in actively firing cells and may partly compensate for the rapid acidification described by Ahmed and Connor¹.

The H^+ currents we describe could perhaps be nonspecific in the sense that they flow through several different types of activated channel. For this reason it seems worthwhile to test for pH sensitivity the nonspecific calcium-dependent single channel currents which have been recently described in heart muscle cells¹⁶. H^+ channels may be more widespread than hitherto suspected.

This work was supported by the MRC and by the Wellcome Trust. Preliminary experiments by R.W.M. were carried out in the Physiology Department, University of Utah, supported by

NIH grant EY 02290 and by R.C.T. in the Physiology Department of Yale University partly supported by USPHS grant AM 17322. We thank Michael Rickard and Toni Gillett for technical help, and Bruce Matthews and Sandy Harper for comments on the manuscript.

Received 19 July; accepted 1 September 1982.

1. Ahmed, Z. & Connor, J. A. *J. gen. Physiol.* **75**, 403-426 (1980).
2. Abercrombie, R. F. & Roos, A. *J. Physiol., Lond.* **319**, 65P-66P (1981).
3. Thomas, R. C. *J. Physiol., Lond.* **273**, 317-338 (1977).
4. Roos, A. & Boron, W. F. *Physiol. Rev.* **61**, 296-434 (1981).
5. Kostyuk, P. G. & Krishtal, O. A. *J. Physiol., Lond.* **270**, 545-568 (1977).
6. Byerly, L. & Hagiwara, S. *J. Physiol., Lond.* **322**, 503-528 (1982).
7. Thomas, R. C. *Ion-Sensitive Intracellular Microelectrodes* (Academic, London, 1978).
8. Thomas, R. C. & Cohen, C. J. *Pflügers Arch. ges. Physiol.* **390**, 96-98 (1981).
9. Thomas, R. C. *J. Physiol., Lond.* **201**, 495-514 (1969).
10. Thomas, R. C. *J. Physiol., Lond.* **255**, 715-735 (1976).
11. Meech, R. W. & Thomas, R. C. *J. Physiol., Lond.* **298**, 111-129 (1980).
12. Thomas, R. C. *J. Physiol., Lond.* **296**, 77P (1979).
13. Mitchell, P. & Moyle, J. *Biochem. J.* **104**, 588-600 (1967).
14. Hagiwara, S. & Byerly, L. A. *Rev. Neurosci.* **4**, 69-125 (1981).
15. Doroshenko, P. A., Kostyuk, P. G. & Tsyndrenko, A. Ya. *Neirofizyologiya* **10**, 645-653 (1978). (Translated in *Neurophysiology* **10**, 470-477, 1978).
16. Colquhoun, D., Neher, E., Reuter, H. & Stevens, C. F. *Nature* **294**, 752-754 (1981).

Intracellular Cl^- accumulation reduces Cl^- conductance in inhibitory synaptic channels

Michael R. Gold & A. R. Martin

Department of Physiology, School of Medicine, University of Colorado Health Sciences Center, Denver, Colorado 80262, USA

Glycine increases Cl^- conductance in neurones of the lamprey central nervous system and mimics the natural inhibitory transmitter pharmacologically^{1,2}. We have used current noise produced by glycine to examine in more detail the characteristics of inhibitory channels in Müller cells in the brain stem reticular formation. The channels have large conductances and mean open times consistent with large amplitudes and long durations of spontaneously occurring inhibitory synaptic currents³. We now show that, unlike any post-junctional channels reported so far, their conductance decreases rapidly with increasing intracellular concentration of the permeant ion. This surprising behaviour is inconsistent with constant field theory^{4,5} and also with a single-site pore model such as proposed for cationic channels at the motor endplate⁶, both of which predict an increase in conductance with concentration. In addition, the decrease in conductance cannot be explained quantitatively by a two-site, single-file pore model such as proposed for K^+ channels⁷ and Na^+ channels⁸ in nerve and for gramicidin channels⁹. This property of the inhibitory channel may be functionally important in preventing intracellular Cl^- accumulation during periods of intense synaptic activity when inhibition might otherwise convert progressively to excitation as the Cl^- equilibrium potential became more and more positive.

Brains were isolated from adult lampreys (*Petromyzon marinus* or *Lampetra lamottenii*) anaesthetized with tricaine methylsulphonate (0.5 g l⁻¹), then superfused with an oxygenated saline solution containing (mM): 104.5 NaCl, 2.0 KCl, 5.0 CaCl₂, 5.0 MgCl₂, 4.0 glucose, 2.0 HEPES, and adjusted to pH 7.4. Tetrodotoxin (1.0 μM) and 4-aminopyridine (1.0 mM) were added to prevent spontaneous activity and to reduce delayed rectification. The bathing solution was cooled to ~4 °C. Müller cells were impaled with two electrodes for voltage-clamping. Both the voltage and current electrodes were filled with either 3 M K^+ -acetate or 3 M KCl and had resistances in the range 20-30 MΩ. The voltage-clamp amplifier had a bandpass of 0-1.8 kHz and a maximum gain of 10,000. Glycine

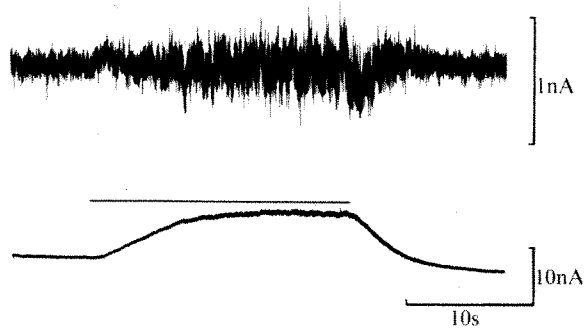


Fig. 1 Example of current noise produced by a 20-s pulse of glycine to a Müller cell. Agonist application (bar) produced a peak outward current of 6.9 nA (lower trace). The accompanying increase in baseline noise is shown in the upper trace at higher gain through an a.c. amplifier with a bandpass of 0.75–140 Hz (half-power points).

was applied to the cells near the base of the dendrites by pressure pulses to a third pipette filled with a 0.2–1.0 M solution of the agonist; the resulting membrane currents were amplified by a low gain d.c. and higher gain a.c. amplifier and stored on two channels of an FM tape recorder for later analysis. Membrane potentials were clamped 10–20 mV away from the reversal potential for the glycine response in either the positive or negative direction.

Figure 1 shows a typical cell response to glycine. Application of the agonist for 20 s produced an outward current of ~10 nA (lower trace) and a marked increase in baseline noise (upper trace). The magnitudes of the frequency components of this excess noise, as represented by their spectral density distribution, were used to determine the conductance and mean open time of the glycine-activated channels¹⁰. Spectral distributions were calculated as the Fourier transforms of 1,024-point samples from the experimental records digitized at 512 or 1,024 points s⁻¹. Spectra of baseline fluctuations before glycine application were subtracted from those obtained during a steady-state response, and 8–32 such difference spectra were averaged to obtain a final distribution. All spectra were consistent with a single distribution of the form $S(f) = S(0)[1 + (f/f_c)^2]^{-1}$, suggesting that glycine opened channels whose lifetimes were distributed exponentially with a mean duration $\tau = 1/2\pi f_c$. The individual channel conductance (γ) was calculated as $\gamma = S(0)/4\pi I\Delta V$, where I is the mean current through the membrane, ΔV the difference between the reversal potential and the holding potential and $S(0)/4\pi$ the area under the distribution (that is, the total variance due to the agonist action).

Spectral distributions from two cells are shown in Fig. 2. The results in Fig. 2a were obtained with acetate-filled electrodes. The reversal potential for the response was -72 mV and the membrane was clamped at -87 mV. Channel conductance was calculated to be 94 pS and the mean channel open time 29 ms. In 14 experiments of this type, the overall mean channel conductance was 73 ± 15 pS (mean \pm s.d.) and the mean channel open time 33 ± 9 ms. The average reversal potential was 66 ± 7 mV. Neither conductance nor open time was significantly dependent on membrane potential. When Cl⁻-filled electrodes were used, the mean channel conductance was markedly less than with acetate electrodes, apparently as a result of loading the cell with Cl⁻. An example of the spectral density distribution from one such cell is shown in Fig. 2b: the reversal potential for the response was -44 mV, reflecting the increase in intracellular Cl⁻, and the membrane was clamped at -54 mV. Mean channel conductance was calculated to be 22 pS and channel open time 35 ms. In 10 such experiments, reversal potentials ranged from -35 to -60 mV and channel conductances from 7 to 43 pS. In four additional experiments acetate electrodes were used and intracellular Cl⁻ was increased in a different way, that is, by increasing extracellular K⁺ concentration². This

again resulted in a positive shift in mean reversal potential (to -47 mV) and channel conductance was reduced to a mean of 30 ± 9 pS. In contrast to the marked changes in γ , τ was unaffected by intracellular Cl⁻ concentration.

The reversal potential for the glycine response was used to calculate internal Cl⁻ concentration, assuming that the response reversed at the Cl⁻ equilibrium potential. The resulting relationship between channel conductance and intracellular Cl⁻ concentration is plotted in Fig. 3. The filled circles represent the results obtained with acetate electrodes, the crosses with Cl⁻ electrodes and the open circles with acetate electrodes and increased external K⁺. Clearly, the channel conductance varies inversely with some function of the internal Cl⁻ concentration, $[Cl]_i$. If we arbitrarily assume an inverse power function, $\gamma = \alpha[Cl]_i^{-n}$, then $n = 1.5$ gives a reasonable fit to the results (solid line). This result is inconsistent with constant field theory^{4,5} and with a single-site pore model⁶, both of which predict an increase in conductance with concentration. Two-site, single-file pore models, however, do predict a decrease in conductance as ionic concentrations increase on either side of the membrane⁷⁻⁹. However, when such models are examined in detail it can be shown that the relationship between conductance and concentration at the high concentration limit assumes the form

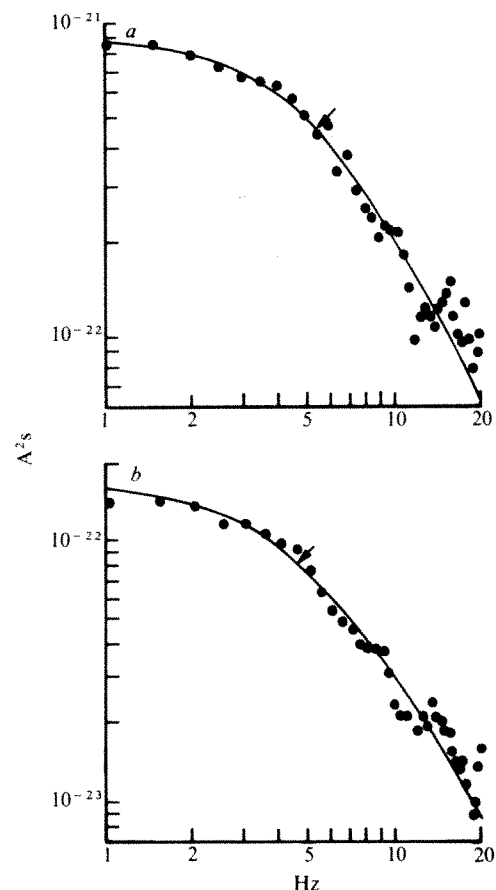


Fig. 2 Power density ($A^2 s$) as a function of frequency (Hz) for two different experimental conditions. Smooth curves are of the form $S(f) = S(0)[1 + (f/f_c)^2]^{-1}$ where $S(f)$ is the power density and f the frequency. These were fitted to the results by eye by selecting asymptotic power density, $S(0)$ and corner frequency, f_c . *a*, Experiment in normal solution with acetate electrodes. Points are the means of 16 difference spectra smoothed by weighted averaging of adjacent points in groups of five. Reversal potential -72 mV, holding potential -87 mV, mean current 5.5 nA. Curve fit with $S(0) = 9 \times 10^{-22} A^2 s$, $f_c = 5.5$ Hz. Estimated channel conductance $\gamma = 94$ pS, mean open time $\tau = 29$ ms. *b*, Average of 32 difference spectra from experiment with Cl⁻-filled electrodes (increased internal Cl⁻). Reversal potential -44 mV, holding potential -54 mV, mean current 4.8 nA. $S(0)$ selected as $1.5 \times 10^{-22} A^2 s$, $f_c = 4.5$ Hz; γ and τ estimated as 22 pS and 35 ms, respectively.

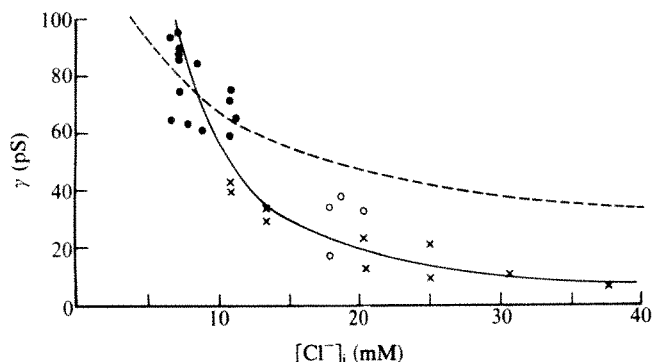


Fig. 3 Relationship between channel conductance (γ) and internal Cl^- concentration, $[\text{Cl}^-]_i$. $[\text{Cl}^-]_i$ was calculated from the reversal potential for the glycine response, E_r , according to the Nernst relation $[\text{Cl}^-]_i = [\text{Cl}^-]_o \exp(E_r F/RT)$, where $[\text{Cl}^-]_o$ is the external Cl^- concentration and R , T and F have their usual meanings. With normal solution and acetate electrodes (●), mean internal Cl^- was 8.4 mM and mean channel conductance 73 pS. The solid curve is drawn through this point according to the relation $\gamma = \alpha[\text{Cl}^-]^{-1.5}$; the broken line is the relationship predicted by a two-site, single-file model of the Cl^- channel (see text). ×, Points obtained with Cl^- -filled electrodes; ○, experiments with acetate electrodes and increased (10 mM) external K^+ .

$\gamma = \beta(C_i C_o)^{-0.5}$, where C_i and C_o are internal and external ionic concentrations, respectively, and β is a constant. Thus, with respect to changes in internal concentration, we would expect the relationship to be an inverse power function with $n = 0.5$. This type of relation (broken line in Fig. 3), is clearly inconsistent with the present results. Studies of additional models are under way. Note that an apparent reduction in channel conductance can be obtained due to receptor saturation by the agonist¹⁰. This was not the case in the present experiments as the estimated conductances were independent of steady-state currents (and hence of glycine concentration at the receptors) over the range of currents used.

The behaviour reported here for individual channel conductances has also been observed with spontaneously occurring inhibitory synaptic currents—these become smaller as internal Cl^- concentration increases³. Thus the reduction in conductance is related specifically to postsynaptic channels. The functional consequence of such behaviour is that any Cl^- accumulation within the cells will result in a decrease in inhibitory conductance and a consequent reduction in further Cl^- entry. Although inhibitory synaptic activity alone would be expected to lead to very little such entry (the membrane simply being hyperpolarized to near the Cl^- equilibrium potential), combined excitatory and inhibitory activity could, in theory, lead to a considerable increase in internal Cl^- concentration. The negative feedback of concentration on conductance may be important in limiting such accumulation. Otherwise inhibitory inputs might, over a period of time, invert to become excitatory as the Cl^- equilibrium potential became more and more positive.

This work was supported by research grant NS-09660 and fellowship NS-06283 from the NIH.

Denervation of newborn rat muscles does not block the appearance of adult fast myosin heavy chain

Gillian S. Butler-Browne*, Lawrence B. Bugaisky*, Sylvia Cuénoud*, Ketty Schwartz† & Robert G. Whalen*

* Département de Biologie Moléculaire, Institut Pasteur, 25 rue du Dr Roux, 75724 Paris, France

† INSERM Unit 127, Hôpital Lariboisière, 41 Bd. de la Chapelle, 75010 Paris, France

Several observations, both *in vivo* and *in vitro*, have indicated that the development and maturation of mammalian skeletal muscle fibres is influenced by nerve-muscle interactions. Morphological maturation of newly regenerated adult mouse muscle fibres in an organotypic nerve-muscle culture system depends on the presence of spinal cord neurones¹. Sciatic nerve transection in newborn rats has been shown to modify the development of the histochemical and contractile properties of the denervated muscles²⁻⁴. In addition, neural influences are important for the appearance of certain of the myosin small subunits^{5,6}. It has been proposed that the nerve also controls the changes in myosin heavy chain isozymes appearing during development^{5,7-9}. One such transition occurs in rat muscle where the neonatal form of myosin heavy chain is replaced by the adult form during the second post-natal week⁸. Here we demonstrate that innervation of the rat gastrocnemius muscle (a fast-contracting muscle in the adult) is not required for the appearance of the adult form of myosin heavy chain.

Muscles of the lower hind leg were denervated by removing a 4–5 mm piece of the sciatic nerve of rats 1 week after birth. The presence of the various myosin heavy chain isozymes was assessed by an immunocytochemical technique using antibodies specific for the various isozymes. In the gastrocnemius muscle of 7–8 day control (unoperated) rats, no reactivity is seen with the anti-fast serum whereas anti-neonatal immunoglobulins stain all fibres that react histochemically as type II (alkali-stable ATPase) (results not shown). From about 2 weeks after birth the number of fibres that stain with the anti-neonatal immunoglobulin begins to decrease, either in control muscles of unoperated rats or in the innervated muscles of operated rats. At 3 weeks of age, in a region of the innervated muscle composed mainly (>90%) of type II fibres, staining serial sections with antibodies against fast and neonatal myosin reveals that about 50% of the fibres react with either fast (~25%) or neonatal (~25%) antibodies whereas ~40% react with both (Fig. 1a, b). By 4–5 weeks after birth in the innervated muscle of operated rats, the percentage of fibres staining with anti-neonatal immunoglobulin alone decreases considerably to <10% and the percentage staining with anti-fast serum alone increases to ~80%.

In the denervated muscle of 22-day old animals (2 weeks after denervation), there is variation in fibre size, with many atrophic fibres. Most fibres irrespective of their diameter react with both fast and neonatal antibodies (Fig. 1c, d), in contrast to the innervated muscles (Fig. 1a, b). By 35 days of age, the staining for neonatal myosin is considerably decreased in the denervated muscle while staining with the anti-fast myosin serum is still present (Fig. 1e, f). A population of small fibres is also seen (Fig. 1f) which reacts strongly with the anti-neonatal immunoglobulin; these small fibres are not seen in control muscles nor in the innervated muscles of operated rats (not shown).

As shown by others¹⁰, many fibres in the fetal (18–20 days gestation) and newborn rat EDL muscle (a future fast-contracting muscle) react with an antibody to slow myosin. In these studies the possible cross-reactivity of the anti-slow immunoglobulin with embryonic or neonatal myosin was not

Received 29 June; accepted 6 September 1982.

- Homma, S. & Rovainen, C. M. *J. Physiol., Lond.* **279**, 231–252 (1978).
- Matthews, G. & Wickelgren, W. O. *J. Physiol., Lond.* **293**, 393–415 (1979).
- Gold, M. R. & Martin, A. R. *Proc. physiol. Soc.*, 16–17 July (1982).
- Goldman, D. E. *J. gen. Physiol.* **27**, 37–60 (1943).
- Hodgkin, A. L. & Katz, B. *J. Physiol., Lond.* **108**, 37–77 (1949).
- Lewis, C. A. *J. Physiol., Lond.* **286**, 417–445 (1979).
- Hille, B. & Schwarz, W. J. *gen. Physiol.* **72**, 409–422 (1978).
- Begenisch, T. B. & Cahalan, M. D. *J. Physiol., Lond.* **307**, 217–242 (1980).
- Urban, B. W., Hlacky, S. B. & Haydon, D. A. *Biochim. biophys. Acta* **602**, 331–354 (1980).
- Anderson, C. R. & Stevens, C. F. *J. Physiol., Lond.* **235**, 655–691 (1973).

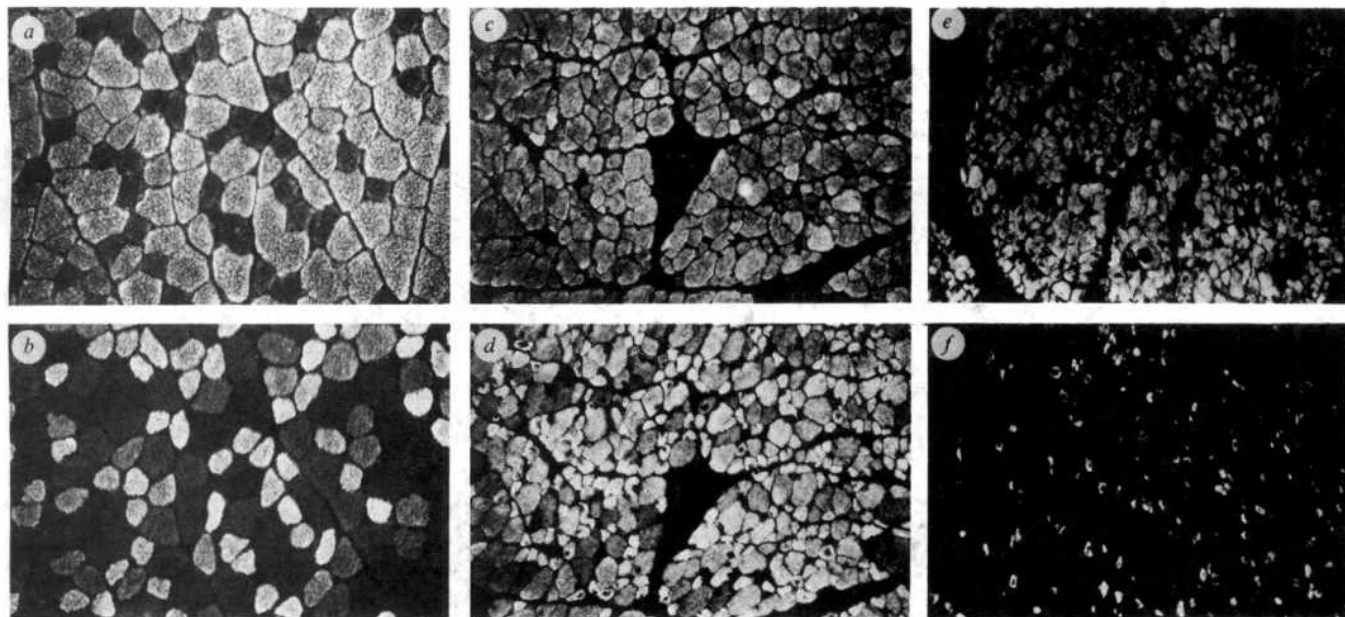


Fig. 1 Indirect immunofluorescence using antibodies to adult fast and neonatal myosin on cryostat sections of denervated and contralateral innervated rat gastrocnemius muscles. The antiserum to adult fast myosin was prepared by injecting guinea pigs with SDS-denatured heavy meromyosin²⁰ prepared from adult rabbit myosin as described previously²¹. When tested in complement fixation assays²¹, this antiserum gave one peak of reactivity using adult fast myosin from either rabbits or rats as test antigen. Antibodies cross-reacting with slow and neonatal myosin were removed by absorption against myosins prepared from the adult rat soleus muscle and from muscle of 8-day old rats. The myosins and antiserum were mixed in 0.4 M NaCl, 30 mM Tris-HCl (pH 7.4) and incubated for 1 h at 4 °C. The mixture was then dialysed at the same temperature against 30 mM NaCl, 20 mM Tris-HCl (pH 7.4) to precipitate the myosin and myosin-antibody complexes⁸. The specificity of the antibody remaining in the supernatant was verified by indirect immunofluorescence; the absorbed anti-fast serum did not react with fibres containing slow myosin in adult rat muscles nor did it react with neonatal muscle. The absorbed serum retained reactivity with adult fast fibres⁸. An antiserum to neonatal myosin was prepared by injecting rabbits with SDS-denatured neonatal heavy meromyosin (from 8-day old rats). The serum was passed over a Sepharose 4B column to which native neonatal myosin had been covalently attached; the bound immunoglobulins were then eluted with 3 M MgCl₂ and the eluate was dialysed against phosphate-buffered saline (PBS) and then against 30% glycerol in PBS. The purified immunoglobulins were absorbed against adult fast myosin, adult slow myosin and embryonic myosin (prepared from cultured L6 cells, see ref. 14) as described above. The specificity of the antibody was again verified by indirect immunofluorescence. The antisera from which both of these antibodies were made recognize the myosin heavy chain subunit as determined by their reaction on nitrocellulose sheets²² after transfer of myosin previously separated by SDS-gel electrophoresis. Immunoelectron microscopy was also used to show that the purified anti-neonatal myosin immunoglobulins react with myosin-containing thick filaments but not with thin filaments in myofibrils prepared from muscles of 7-day old rats (I. Pinset-Härström *et al.*, unpublished observations). Denervation of the lower right hind limb muscles of rats was performed 7–8 days after birth by removing a 4–5-mm piece of the sciatic nerve. At 4 weeks after denervation, electrical stimulation of the sciatic nerve proximal to the point at which it had been severed did not evoke contractions in the muscles of the lower leg. The wet weight of the denervated muscles at this time was about half that of the contralateral leg. The gastrocnemius muscles were removed at various times after denervation, mounted for immunocytochemistry and histochemistry and frozen in isopentane maintained in liquid nitrogen. Cryostat sections 10 µm thick were cut at –20 °C and allowed to dry in air. Incubations with the antibodies to myosin were carried out at 37 °C for 1 h or at 4 °C for 16–20 h. Incubation with the fluorescein-labelled second antibodies (Nordic) was at 37 °C for 30 min. Sections were mounted in Gelvatol (Monsanto). The contralateral innervated muscle of 22-day old operated rats (*a*, *b*), the 2-week-denervated muscle from 22-day old rats (*c*, *d*), and the 4-week-denervated muscle from 35-day old rats (*e*, *f*). The antibody against adult fast myosin was used in *a*, *c* and *e*; the antibody against neonatal myosin was used in *b*, *d* and *f*. For each pair of photos, the same region of two serial sections is shown. It is thus possible to determine the staining of the same fibre with each of the two antibodies. ×170.

determined. Using a specific anti-slow myosin serum, we have found that the gastrocnemius muscle of 1-week old rats does contain regions composed of up to 40–50% slow myosin-containing fibres (results not shown). These fibres are therefore present at the time when the denervation is carried out. In the gastrocnemius muscle that had been denervated for 2 weeks, regions are found in which large-diameter fibres react with the anti-slow serum (Fig. 2*a*). It is thus possible that these slow myosin-containing fibres did not develop in the absence of innervation but rather were those present at the time of denervation. Almost all the fibres in this region of the denervated muscle now also react with fast myosin antibody (Fig. 2*b*), similar to the result shown in Fig. 1*c*. Neonatal myosin immunoglobulins stain all the fibres, although the slow myosin-containing fibres are less intensely stained (Fig. 2*c*). Finally, the embryonic myosin antibody gives a weak but significant staining on some fibres (Fig. 2*d*).

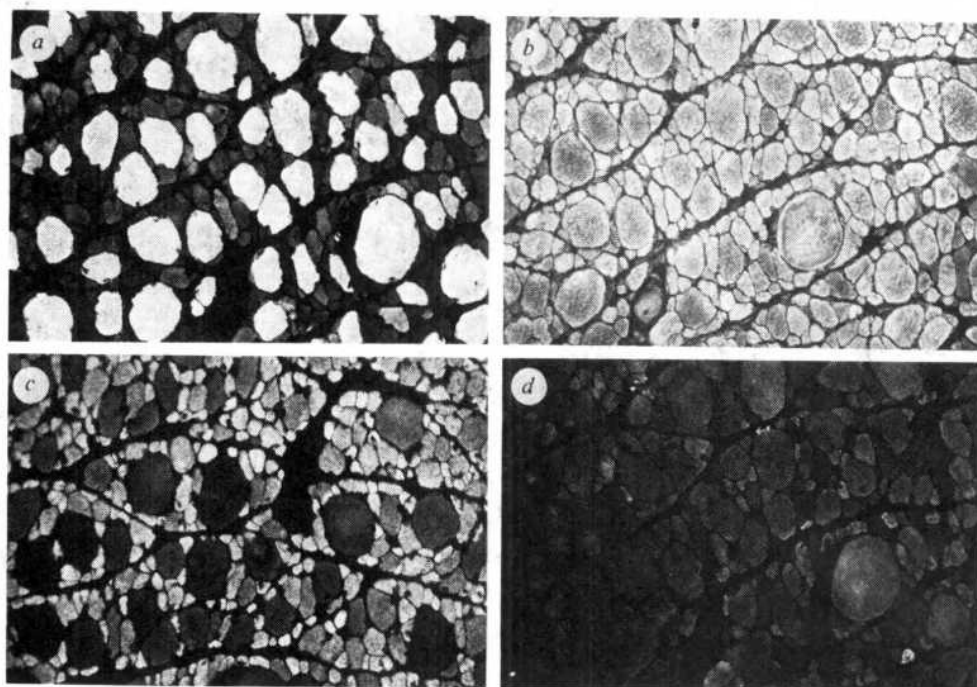
To confirm the appearance of adult fast myosin in the denervated muscles, we analysed the myosin present in extracts of control (unoperated) or denervated muscles by electrophoresis in native conditions^{11,12}. As shown in Fig. 3, the bands corresponding to neonatal myosin⁸ were predominant up to 10 days after birth; three bands were seen at this time, probably because of the isoenzymes formed by the different combinations of light chains, as has been shown for adult fast myosin¹³. By 13 days after birth, fast myosin isoenzymes begin to appear in control and denervated muscles and by 16–22 days the adult fast forms are predominant in both (Fig. 3). At no time does the slow

myosin band represent a major component; it is seen as a minor species in control muscles and some of the denervated ones (Fig. 3). These results indicate that the kinetics of appearance of adult fast myosin are quite similar to those of the control muscles; analysis of myosin isoenzymes in the innervated muscles of operated rats also shows a similar time course (not shown). Bands corresponding to the neonatal myosin isoenzymes are very faint in the 22-day denervated sample (Fig. 3). The staining of the denervated muscles with the neonatal antibody (Figs 1, 2) may therefore indicate that neonatal myosin is present as a minor component.

Polypeptide mapping^{8,14} was also used to examine the heavy chain form found in the denervated muscles. Myosins were prepared from 6-day old control rats and from several denervated and contralateral innervated muscles, and the purified proteins were denatured with SDS. After partial proteolysis in the presence of SDS with one of three proteases (chymotrypsin, *Staphylococcus aureus* protease or subtilisin)^{8,14}, the polypeptides were analysed by SDS-gel electrophoresis (Fig. 4). For each enzyme, neonatal myosin (*a*, *b*, *c*) gave a cleavage pattern different from either the denervated (*a'*, *b'*, *c'*) or contralateral innervated (*a''*, *b''*, *c''*) muscle myosins; the latter two were indistinguishable in this analysis.

All of the results presented here indicate that the myosin found in the gastrocnemius muscle of 3-week old rats, whose sciatic nerve had been sectioned 1 week after birth, is indistinguishable from adult fast myosin by immunological, electrophoretic and protein chemical criteria. The continued

Fig. 2 Indirect immunofluorescence using antibodies against adult fast, adult slow, neonatal and embryonic myosin on cryostat sections of a 2-week-denervated gastrocnemius muscle from 22-day old rats. The antibodies to adult fast and neonatal myosin were those described in Fig. 1 legend. The antibody reacting with adult slow myosin was prepared by injecting guinea pigs with SDS-denatured adult rat cardiac heavy meromyosin^{20,21}. This antiserum cross-reacts strongly with adult rat slow myosin, as determined by microcomplement fixation^{14,21} or by indirect immunofluorescence on control rat muscles containing slow fibres (results not shown). The antiserum was absorbed with neonatal myosin as described in Fig. 1 legend; indirect immunofluorescence showed that the absorbed serum did not react with either control adult fast fibres or with those neonatal fibres reacting with antibody to neonatal myosin. The antibody against embryonic myosin was prepared by injecting rabbits with SDS-denatured myosin heavy chain prepared from L6 myotube cultures¹⁴. Immunoglobulins were purified from this antiserum by affinity chromatography on a column of L6 myosin. When used in indirect immunofluorescence, this immunoglobulin preparation stained fetal muscle strongly but did not react with fibres of neonatal (7 days post-natal) or adult animals. The antisera from which these two antibodies were made also recognize the myosin heavy chain subunit, determined as described in the legend to Fig. 1. This figure shows a region of the denervated gastrocnemius muscle rich in large, hypertrophied fibres. The antibodies used were: *a*, anti-adult slow; *b*, anti-adult fast; *c*, anti-neonatal; *d*, anti-embryonic. All are of the same region in four serial cryostat sections; the staining of the same fibres with each of the four antibodies can thus be evaluated. *a*, *b* and *d* are easily compared; note, however, that the central part of *c* corresponds to the upper part of *a*, *b* and *d*. $\times 170$.



presence of the nerve did not therefore seem to be required for the heavy chain isoenzyme transitions which normally occur during this period. Previous biochemical studies of denervated newborn rat muscle had examined only the myosin light chains^{5,6}. These subunits are the same in newborn fast muscles and the adult muscles⁵, and thus no transition takes place.

Although the kinetics of appearance of fast myosin were not markedly altered by nerve section, denervation did seem to slow down the disappearance of anti-neonatal myosin staining which in innervated muscles has occurred in 20–30% of the fibres by 22 days after birth (Fig. 1*b*). This resulted in a double staining of almost all fibres of the denervated muscle with antibodies to both fast and neonatal myosin at this time (Figs 1*c*, *d*, 2). However, adult fast myosin was the predominant protein accumulated (Figs 3, 4). Neonatal myosin gradually disappeared from most of the denervated fibres, as seen by

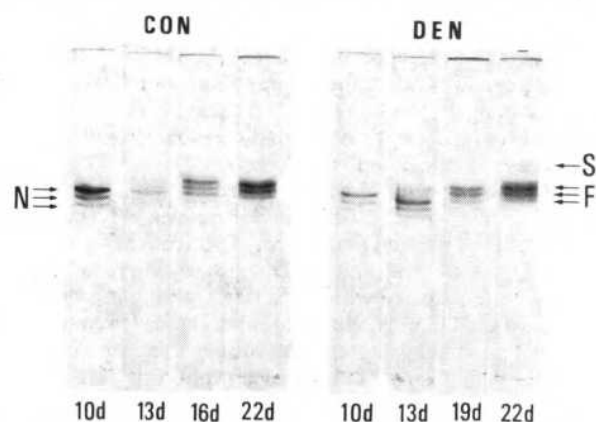


Fig. 3 Electrophoresis of native myosin in non-dissociating conditions. Crude extracts from denervated gastrocnemius muscles (DEN) and from control gastrocnemius muscles from unoperated rats (CON) were analysed by electrophoresis on polyacrylamide gels in the presence of sodium pyrophosphate buffer as previously described⁸. The times indicated are days after birth, denervation having been performed at day 7. Arrows indicate the positions of the bands corresponding to neonatal myosin (N), adult fast myosin (F) and adult slow myosin (S).

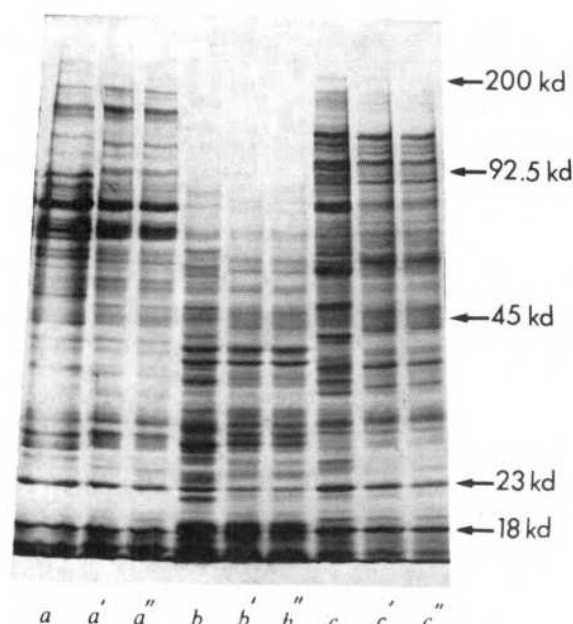


Fig. 4 Polypeptide mapping of the myosin heavy chain. Myosins were prepared by a protocol described previously²¹ from the hind leg muscle of 6-day old rats, and from the denervated and contralateral innervated gastrocnemius muscles of 22-day old rats that had been denervated for 2 weeks. The myosin from the ammonium sulphate fractionation was further purified by passage over a Sepharose 2B column²³. The purest fractions were pooled, placed in dialysis sacks and concentrated against dry Ficoll (Pharmacia). Proteolytic digestion of the myosin was carried out in the presence of 0.5% SDS as described¹⁴ using chymotrypsin (*a*, *a'*, *a''*), *S. aureus* V8 protease (*b*, *b'*, *b''*) or subtilisin (*c*, *c'*, *c''*) at final concentrations of 50 $\mu\text{g ml}^{-1}$, 40 $\mu\text{g ml}^{-1}$ and 0.2 $\mu\text{g ml}^{-1}$ respectively. Lanes *a*, *b*, *c* are myosin prepared from the 6-day old muscles, lanes *a'*, *b'*, *c'* are myosin from the denervated muscles and lanes *a''*, *b''*, *c''* are myosin from the contralateral innervated muscles. Electrophoresis was performed on SDS-polyacrylamide slab gels composed of 12.5% acrylamide and 0.1% bisacrylamide. Molecular mass markers (BioRad) are myosin heavy chain (200,000 (20K)), phosphorylase (92.5K), ovalbumin (45K). The two lowest molecular weight markers are the rat myosin light chains LC1F (23K) and LC2F (18K).

staining at 35 days after birth (Fig. 1e,f). At 35 days the neonatal myosin staining in the denervated muscles is localized to small fibres (Fig. 1f).

It has not been possible to determine, in the experiments shown here, whether development of fibres containing slow myosin is blocked by denervation as others have suggested based on myosin light chain analysis^{5,6}. The fibres staining with the slow myosin antiserum in the denervated gastrocnemius muscle (Fig. 2) were very possibly those slow myosin-staining fibres present at the time of denervation. These observations could explain the contradictory claims concerning slow muscle development after neonatal denervation^{2,5}.

From the results presented here it would appear that the lack of a nerve-imposed activity pattern^{15,16} or the absence of trophic substances¹⁷ secreted by the nerve does not inhibit the accumulation of adult fast myosin in the denervated muscle. This absence of a controlling influence of the nerve might suggest

that initiation of the neonatal myosin → fast myosin transition is an endogenously programmed event in the muscle fibre. It remains possible, however, that the influence already exerted by the nerve by post-natal days 7–8 (when denervation was carried out) is sufficient to initiate the transition. Alternatively, some extrinsic factors could operate in the manner of a hormone. Indeed the level of circulating thyroid hormone seems to influence the myosin types present in adult skeletal¹⁸ and cardiac¹⁹ muscle. Perhaps similar factors affect skeletal muscle development.

We thank Dr Marion Ecob for comments, Dr Pierre Benoit for experimental help, Mrs C. Wisniewsky for technical assistance, and Professor François Gros for support. G.S.B.-B. and L.B.B. were the recipients of Muscular Dystrophy Association postdoctoral fellowships. This work was supported by the CNRS, INSERM and the Muscular Dystrophy Association of America.

Received 26 May; accepted 10 August 1982.

1. Ecob, M. S. *J. neurol. Sci.* (in the press).
2. Engel, W. K. & Karpati, G. *Dev. Biol.* **17**, 713–723 (1968).
3. Shafiq, S. A., Asiedu, S. A. & Milhorat, A. T. *Expl Neurol.* **35**, 529–540 (1972).
4. Brown, M. D. *Nature* **244**, 178–179 (1973).
5. Rubinstein, N. A. & Kelly, A. M. *Dev. Biol.* **62**, 473–485 (1978).
6. Ishiura, S., Nonaka, I., Sugita, H. & Mikawa, T. *Expl Neurol.* **73**, 487–495 (1981).
7. Gauthier, G. F., Lowey, S. & Hobbs, A. W. *Nature* **274**, 25–29 (1978).
8. Whalen, R. G. *et al. Nature* **292**, 805–809 (1981).
9. Whalen, R. G. *Adv. physiol. Sci.* **5**, 63–69 (1981).
10. Rubinstein, N. A. & Kelly, A. M. *J. Cell Biol.* **90**, 128–144 (1981).
11. Hoh, J. F. Y., McGrath, P. A. & White, R. I. *Biochem. J.* **157**, 87–95 (1976).
12. d'Albis, A., Pantaloni, C. & Bechet, J.-J. *Eur. J. Biochem.* **99**, 261–272 (1979).
13. Lowey, S., Benfield, P. A., Silberstein, L. & Lang, L. M. *Nature* **282**, 522–524 (1979).
14. Whalen, R. G., Schwartz, K., Bouveret, P., Sell, S. M. & Gros, F. *Proc. natn. Acad. Sci. U.S.A.* **76**, 5197–5201 (1979).
15. Salmons, S. & Henriksson, J. *Muscle Nerve* **4**, 94–105 (1981).
16. Jolesz, F. & Sreter, F. A. *A. Rev. Physiol.* **43**, 531–552 (1981).
17. Gutmann, E. A. *Rev. Physiol.* **38**, 177–216 (1976).
18. Johnson, M. A., Mastaglia, F. L., Montgomery, A. G., Pope, B. & Weeds, A. G. *FEBS Lett.* **110**, 230–235 (1980).
19. Hoh, J. F. Y., McGrath, P. A. & Hale, P. T. *J. molec. cell. Cardiol.* **10**, 1053–1076 (1978).
20. Lompré, A.-M., Bouveret, P., Leger, J. & Schwartz, K. *J. immun. Meth.* **28**, 143–148 (1979).
21. Schwartz, K., Lompré, A.-M., Bouveret, P., Wisniewsky, C. & Swynghedauw, B. *Eur. J. Biochem.* **104**, 341–346 (1980).
22. Tobin, H., Staehelin, T. & Gordon, J. *Proc. natn. Acad. Sci. U.S.A.* **76**, 4350–4354 (1979).
23. Whalen, R. G., Butler-Browne, G. S. & Gros, F. *J. molec. Biol.* **126**, 415–431 (1978).

Preferential effect of γ interferon on the synthesis of HLA antigens and their mRNAs in human cells

David Wallach, Marc Fellous* & Michel Revel

Department of Virology, The Weizmann Institute of Science, Rehovot, Israel

*Unité d'immunogénétique Humaine, Institut Pasteur, 75015 Paris, France

Interferons produce a variety of biological effects on cells. They induce resistance to virus proliferation^{1,2}, inhibit cell growth³, modify cell structure and differentiation^{4–5}, stimulate some immune functions and inhibit others⁶. However, the different interferon (IFN) species may vary in their mechanism of action and, hence, in their relative efficiency for inducing each of the effects. IFN- γ (type II) appears to show stronger immunoregulatory^{7–9} and growth inhibitory effects^{10–12} than antiviral effects¹³, but this conclusion has been challenged in other reports¹⁴. The aim of the present work is to compare the action of IFN- γ and other (type I) interferons on the induction of (2'–5') oligo(A) synthetase which is probably part of the antiviral response^{15,16} and the induction of the histocompatibility HLA-A, -B, -C antigens^{17–19}. We have shown previously that the induction of both proteins is regulated by interferons at the mRNA level^{20,21}, but show here that IFN- γ from stimulated human lymphocytes²² and from monkey cells transfected by cloned human IFN- γ cDNA²³ induced the HLA-A, -B, -C and β_2 -microglobulin mRNAs or proteins at concentrations over 100 times lower than those needed to induce the (2'–5') oligo(A) synthetase and the antiviral state. This difference was not found with IFN- α and - β (type I).

The experiment in Fig. 1a and b compares the effects of IFN- β and IFN- γ on the amounts of cell surface HLA, on the (2'–5') oligo(A) synthetase and on the inhibition of vesicular stomatitis virus (VSV) replication measured simultaneously on the same human fibroblastoid SV80 cells. As the activities of interferons vary from one cell line to another, it was essential to first compare the antiviral potency of IFN- β and IFN- γ on the same cells. This was done by using a radioimmunoassay for

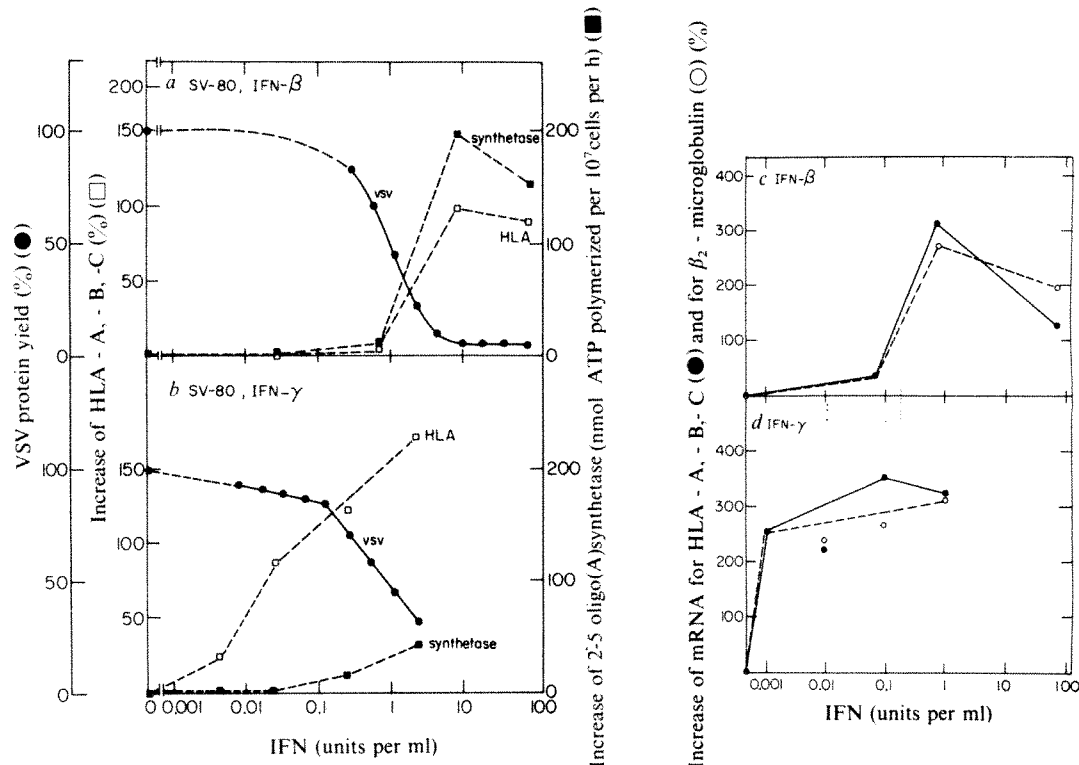
VSV proteins that we have developed for the accurate quantitation of interferon's antiviral effect^{24,25}. The concentration of each IFN required to reduce the yield of VSV proteins on the SV80 cells by 50% was determined (Fig. 1a, b) and is by definition 1 unit per ml on SV80 cells. This corresponds to about 10 units per ml of IFN- β titrated on human diploid fibroblasts, and 100 units per ml of IFN- γ titrated on Wish cells. The (2'–5') oligo(A) synthetase was measured by mixing cytoplasmic extracts of the treated cells with poly(rI)·(rC)-agarose beads, incubating the beads with [α -³²P]ATP and purifying the (2'–5') oligo(A) synthetase formed on alumina columns²⁶. The cell surface HLA was quantitated by the binding

Table 1 Comparison of the effect of α , β and γ interferons on HLA proteins and (2'–5') oligo(A) synthetase in Ramos cells

IFN	U ml ⁻¹	(2'-5')oligo(A) synthetase (nmol per 10 ⁷ cells per h)	HLA-DR	HLA-A,-B,-C	
		c.p.m.	c.p.m.	Increase (%)	
None		6.6	5,000	5,000	
α	100 (on MDBK)	37.1	-	9,200	84
	400 (on MDBK)	52.0	5,100	11,100	122
β	50 (on FS-11)	19.2	-	8,700	74
	200 (on FS-11)	34.3	5,400	9,500	90
γ	40 (on WISH)	7.5	-	8,900	78
	200 (on WISH)	8.3	5,000	10,300	105

The cells used were lymphoblastoid cell line Ramos grown as before²¹ to 2×10^6 cells per ml in RPMI 1640 (10% fetal calf serum, FCS) and treated with each IFN species for 16 h at 37°C. The cells were washed and counted, and the activity of the (2'–5') oligo(A) synthetase as well as the amount of cell-surface HLA-A, -B, -C and HLA-DR antigens were measured as in Fig. 1. The IFNs were prepared as follows: (1) leukocyte IFN- α subspecies $\beta 3^{25}$, also designated IFN- α B³⁶ was purified to electrophoretic homogeneity by HPLC²⁵ starting from IFN induced by Sendai virus in human myelogenous leukaemia cells (Institut Merieux). This purified IFN- α (a gift from Dr M. Rubinstein) titred 2×10^6 units per mg protein on bovine MDBK cells and 5×10^8 units per mg on human FS-11 fibroblasts. (2) Fibroblast IFN- β was purified by a modification of the Cibacron blue Sepharose procedure³⁷ from IFN superinduced by poly(rI)·(rC) in human foreskin fibroblasts FS-11²⁴ (InterYeda). Its titre was over 5×10^7 units per mg on FS-11 cells. (3) IFN- γ was prepared as described^{9,22,31} from human peripheral blood mononuclear cells isolated on Ficoll-Hypaque (Pharmacia) and incubated for 48 h with concanavalin A (Con A, 30 μ g ml⁻¹) and phorbol myristate acetate (5 ng ml⁻¹) in RPMI 1640–2% FCS. The IFN- γ was partially purified on controlled pore glass²² and its antiviral activity (10^5 units per mg) was measured by inhibition of VSV growth in Wish cells. The activities of IFN- α and β were also determined with VSV by comparison to International Reference Standards

Fig. 1 Comparison of the effects of IFN- β and IFN- γ on HLA-A, -B, -C antigens and mRNAs and on the (2'-5')oligo(A) synthetase in SV80 cells. *a, b*, The human fibroblastoid cell line SV80 was grown as before²¹ in Dulbecco's modified Eagle's medium with 10% fetal calf serum (FCS) at 37°C. Confluent monolayers were treated for 16 h with a large range of concentrations of IFN- β (*a*) or IFN- γ (*b*) prepared as in Table 1. The antiviral effect of each IFN on SV80 was measured by infecting one set of cultures with VSV (10 PFU per cell) and measuring after 18 h the yield of VSV proteins in the lysed cells by a radioimmunoassay using rabbit antibodies against purified VSV, followed by ¹²⁵I-protein A as described^{24,25}. The VSV protein yield is shown as per cent of that in cells not treated by IFN (6,000 c.p.m.). One unit per ml of each IFN was defined by the concentration reducing the VSV yield by 50%. In another set of SV80 cultures 16 h after IFN addition, the cells were briefly



trypsinized, washed twice with medium-10% FCS and the cell-surface antigens were quantitated as before²¹. In short, 2.5×10^5 cells were washed with RPMI 1640, 0.5% bovine serum albumin, 0.1% Na azide and mixed in this medium with saturating amounts (50 μ l) of mouse monoclonal antibodies W6/32 specific for HLA-A, -B, -C, or M18 specific for β_2 -microglobulin, or L116 specific for HLA-DR. After 1 h at 4°C, the cells were washed as above, incubated for 1 h at 4°C with 10^5 c.p.m. ¹²⁵I-protein A, washed and counted. The per cent increase in HLA-A, -B, -C is shown relative to the level in cells not treated by IFN (11,500 c.p.m.). For the (2'-5')oligo(A) synthetase assay, 2×10^7 cells were mixed with 1 ml Nonidet P40 extraction buffer²⁶ and 10 μ l of the extracts were used to measure the enzyme activity as detailed before^{26,38}. The synthetase activity is expressed as ³²P-(2'-5') (Ap)nA formed per h and 10^7 cells. Extracts of SV80 cells not treated by IFN gave 0.1 nmol per 10^7 cells per h. *c, d*, SV80 cells were exposed to the same concentrations of (c) IFN- β and (d) IFN- γ as in *a* and *b*, but for 10 h. Poly(A)⁺RNA was prepared from 6×10^8 cells by the LiCl procedure as described²¹. After agarose gel electrophoresis and blotting onto nitrocellulose, the specific mRNAs were quantitated by hybridization to ³²P-labelled cloned cDNA probes as reported in detail before²¹. The HLA probe used here was a HLA-B cDNA clone given by Dr S. M. Weissman²⁹, while the β_2 -microglobulin cDNA clone was a gift from Dr K. Itakura³⁰. Quantitation of the radioactivity hybridized to the mRNA bands was done by spectrophotometric scanning of the autoradiographs. The per cent increase in HLA-A, -B, -C (●) and β_2 -microglobulin (○) mRNAs is shown relative to the level of these mRNAs in untreated cells.

of monoclonal antibodies recognizing a monomorphic determinant of HLA-A, -B, -C²⁷ followed by binding of ¹²⁵I-protein A (ref. 21). Figure 1*a* shows that synthetase and HLA-A, -B, -C were both induced at concentrations of IFN- β which produce the antiviral effect. In contrast, Fig. 1*b* shows that IFN- γ increased the amounts of cell surface HLA-A, -B, -C already at concentrations 100 times lower than those required for the antiviral state. The same was observed for β_2 -microglobulin (not shown). Induction of (2'-5')oligo(A) synthetase by IFN- γ could, however, be detected only in the range of concentrations giving the antiviral effect.

Similar observations were made in other cell types such as the lymphoblastoid line Ramos. Table 1 shows that in these cells, IFN- α and IFN- β both produced a dose-dependent increase in the (2'-5')oligo(A) synthetase as well as in cell-surface HLA-A, -B, -C. Again, IFN- γ increased the HLA-A, -B, -C antigens in conditions where synthetase induction was barely detectable. In all cases, cell-surface HLA-DR remained unchanged as reported^{19,28}. The differential effects of IFN- γ do not depend on the actual titres of IFN used but on the comparison between the relative concentrations at which these effects occur. In Wish cells, for example, which are most sensitive to the antiviral effect of IFN- γ , the concentration of IFN- γ needed to increase the cell-surface HLA antigens was again 30 times lower than that needed to inhibit VSV growth (not shown).

We have shown²¹ that the increase in cell-surface HLA-A, -B, -C induced by type I IFNs is preceded by an even larger increase in the amount of cytoplasmic mRNA coding for these proteins. We therefore compared the effects of IFN- γ and IFN- β on the levels of HLA mRNAs in SV80 cells as described in Fig. 1 legend. The mRNAs were quantitated by hybridization of electrophoretic blots of total cell poly(A)⁺ RNA to a cloned

HLA-B cDNA probe which detects all three HLA-A, -B, -C mRNAs²⁹ and to a cloned β_2 -microglobulin cDNA probe³⁰. Figure 1*c* and *d* shows that IFN- γ induces already maximum (fourfold) increases in HLA and β_2 -microglobulin mRNAs at much lower concentrations than does IFN- β . By comparison with Fig. 1*b*, it can be seen that IFN- γ diluted 1,000 times more than the concentration needed to inhibit VSV growth, is able to fully induce the HLA antigen mRNAs. At these low concentrations, IFN- γ did not induce the (2'-5')oligo(A) synthetase mRNA (not shown).

It is very likely that the increase in HLA mRNAs is responsible for the increase in the antigens. To measure directly the rate of HLA protein synthesis, we labelled the SV80 cells with ³⁵S-methionine for 1 h, lysed the cells and immunoprecipitated the β_2 -microglobulin together with their associated HLA-A, -B, -C chains using polyclonal antibodies against β_2 -microglobulin. The proteins were separated by gel electrophoresis and the labelling of HLA-A, -B, -C and β_2 -microglobulin chains was quantitated. Figure 2 shows that IFN- β and IFN- γ induced a marked 4- to 5-fold increase in the rate of synthesis of the HLA proteins, but with the same difference in the amount of each IFN needed for maximum induction as that seen in Fig. 1 for cell-surface HLA. The stimulation of HLA synthesis by IFN- β required concentrations sufficient to induce the antiviral state (Fig. 2*a*), while IFN- γ stimulated HLA synthesis at much lower concentrations (Fig. 2*b*). A comparison of Figs 1 and 2 also shows that the synthesis of HLA proteins is, like their mRNAs²¹, stimulated by IFNs to a higher extent than the cell-surface HLA antigens.

The striking dissociation between IFN- γ 's antiviral effect on VSV and the (2'-5')oligo(A) synthetase induction on the one hand, and on HLA-A, -B, -C and β_2 -microglobulin induction

on the other hand, raises the question of whether or not it is the same molecule of IFN- γ which produces both effects. As partially purified IFN- γ preparations from stimulated lymphocytes could contain lymphokines or other IFNs¹⁴, we examined this possibility by inducing IFN- γ by two different methods in human white blood cells. Figure 3a and b show that with both preparations the HLA-inducing and the antiviral activity clearly co-purify on Ultrogel Aca 54 or on Sephacryl S-200 and elute as a single peak, separated from the bulk of proteins and corresponding to the characteristic high molecular weight position of IFN- γ ³¹. No HLA-inducing factor other than IFNs is known, and none could be detected in experiments such as that of Fig. 3.

Recently, the cDNA which codes for human IFN- γ has been cloned²³. Monkey kidney fibroblasts of the COS-7 cell line,

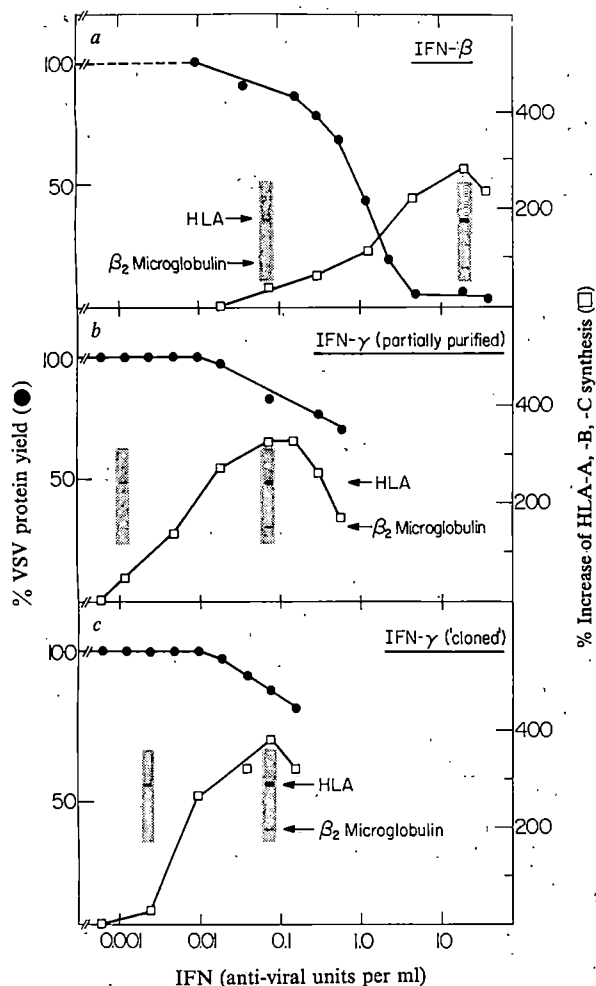


Fig. 2 Comparison of the effects of IFN- β and IFN- γ on the synthesis of HLA-A, B, C proteins in SV80 cells. Cultures of SV80 cells were treated for 18 h as in Fig. 1 with (a) IFN- β and (b) IFN- γ prepared as in Table 1 or (c) IFN- γ produced in COS-7 monkey cells transfected by the pSV- γ -69 plasmid DNA containing the human IFN- γ cDNA under the control of the SV40 late promoter²³. The antiviral effect of each IFN on VSV growth was measured and compared on SV80 cells as in Fig. 1 (●). To measure the rate of HLA protein synthesis, the cells were washed with methionine-free medium and incubated for 1 h with 0.5 mCi ml⁻¹ ³⁵S-methionine (800 Ci mmol⁻¹; Amersham) in this medium-2% FCS. The cells were washed in cold phosphate-buffered saline, and extracted with 0.5% Nonidet P40 in 0.15 M NaCl, 10 mM Tris-HCl pH 7.4, 5 mM MgCl₂, 1 mM phenylmethylsulphonyl fluoride (PMSF), 1 mM 1-tosylamide 2-phenylethyl chloromethyl ketone (TPCK). After centrifugation, the cytoplasmic extracts were incubated for 1 h at 4°C with polyclonal antibodies against β_2 -microglobulin (DAKO) and with 20 mM EDTA. Protein A-Sepharose CL-4B beads (Pharmacia) were added for 1 h at 4°C with stirring. The beads were washed repeatedly in 0.15 M NaCl, 10 mM Tris-HCl pH 7.5, 5 mM EDTA, 0.5% Nonidet P40, 0.5 mg bovine serum albumin and the bound proteins were solubilized in dodecyl sulphate before electrophoresis on a 10-20% polyacrylamide gradient gel. After autoradiography, the radioactivity in the HLA-A, B, C and β_2 -microglobulin bands was quantitated by scanning. The per cent increase in the HLA-A, B, C band is shown (□) relative to the level in cells not treated by IFN. Examples of the autoradiography are shown for a few indicated IFN concentrations.

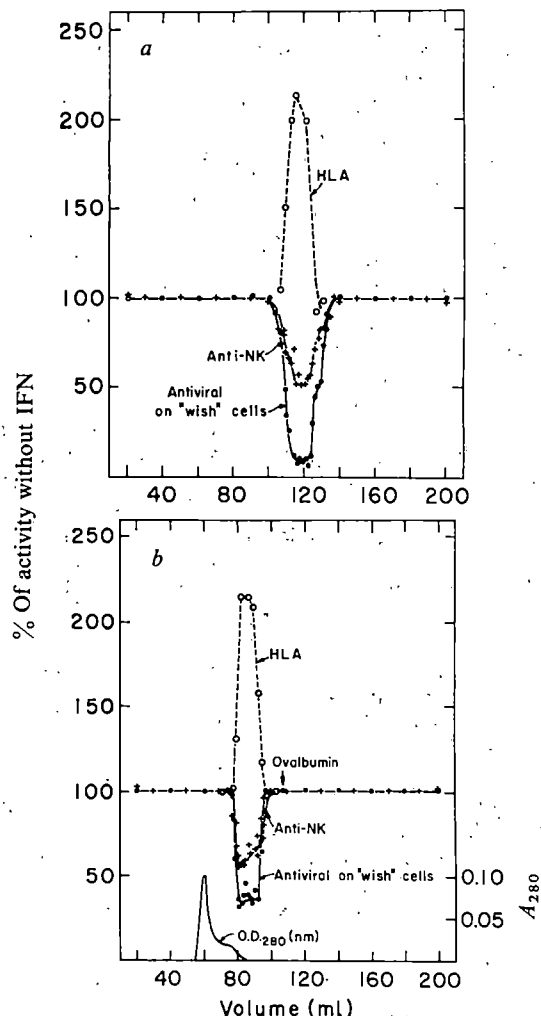


Fig. 3 Co-purification of the HLA-inducing, anti-NK and antiviral activities of IFN- γ . Two preparations of IFN- γ were induced as described in Table 1, with either (a) 3 μ g ml⁻¹ phytohaemagglutinin (PL Biochemicals) or (b) 30 μ g ml⁻¹ Con A in the presence of 5 ng ml⁻¹ phorbol myristate acetate. After adsorption and elution from controlled pore glass²², samples of 0.7 ml were applied to a 1.7 \times 110 cm column of either Ultrogel Aca 54 (LKB) (a) or Sephacryl S-200 (b) (Pharmacia), and eluted with 1 M NaCl, 20 mM Na phosphate buffer pH 7.4 and ethylene glycol (25% in a and 40% in b). Fractions of 1 ml were collected in 1% FCS and used at a final dilution of 1:40 to measure by radioimmunoassay²⁴ the inhibition of VSV growth in Wish cells (antiviral effect) and the HLA-A, B, C inducing activity in SV80 cells (as in Fig. 1). The anti-NK effect was measured as before^{9,34} by ⁵¹Cr release from prelabelled HeLa cells treated by the IFN- γ fractions and incubated for 3 h with non-adherent human peripheral blood leukocytes which had been pretreated for 18 h with 500 units per ml IFN- β . The leukocyte to HeLa cell ratio was 40:1. Without IFN- γ , 34% of the HeLa cells were killed in a and 60% in b. The three IFN- γ activities are shown as per cent decreases in VSV proteins (●), increase in HLA antigens (□) or decrease in specific chromium release (+) relative to controls without IFN. Ovalbumin (molecular weight 44,000) was used as marker in b.

transfected by the recombinant pSV-Y-69 DNA produce mature IFN- γ ²³, which is free of the contaminants found in IFN- γ prepared from human blood cells. When tested for the stimulation of HLA synthesis, as shown in Fig. 2c, this IFN- γ was identical to the partially purified human blood cell IFN- γ used in Fig. 2b. A strong stimulation of HLA synthesis in SV80 cells was seen at concentrations much lower than those needed to produce the antiviral effect, in sharp contrast to the behaviour of fibroblast IFN- β (Fig. 2a). The more efficient HLA-inducing activity was, therefore, transferred to the monkey cells by the IFN- γ cDNA, demonstrating that this is a genuine property of the recently identified IFN- γ molecule, whose amino acid sequence is very different from that of type I IFNs (ref. 23).

With regard to the biological function of the preferential effect of IFN- γ on HLA antigen synthesis in non-immune cells, IFN- γ might enhance the presentation of viral antigens on the surface of virus-infected cells thereby increasing their destruc-

tion by cytotoxic lymphocytes³². For the same antiviral activity, IFN- γ is also much more active than type I IFNs in making human cells resistant to natural killer (NK) cells⁹. This anti-NK effect may be important in protecting some cells against indiscriminate killing by NK cells³³. By analogy with HLA induction, this anti-NK effect of IFN- γ was seen in SV80 and HeLa cells at concentrations much lower than those needed to inhibit VSV growth^{9,34}. Figure 3 shows that this anti-NK activity elutes together with the HLA-inducing and antiviral activities of IFN- γ . Moreover, the IFN- γ produced by the cloned cDNA also induced the anti-NK effect at very low concentrations (not shown). At least one immunoregulatory function is, therefore, induced by IFN- γ in non-immune cells with the same efficiency as the HLA antigens are induced, and much more efficiently than the (2'-5')oligo(A) synthetase or the antiviral state⁹.

These results confirm that IFN- γ and type I IFNs share the ability to induce (2'-5')oligo(A) synthetase and HLA proteins but in the case of IFN- γ there is a dissociation between the two effects and HLA synthesis is stimulated at concentrations much lower than those needed for the synthetase induction. Such a difference may explain some of the biological effects of IFN- γ , although there are probably other cellular proteins which could be differentially induced by type I and type II IFNs¹². The differential effect of IFN- γ may result from the presence of cell-surface receptors distinct from those of type I IFNs³⁹. Many cells are poorly sensitive to the antiviral effect of IFN- γ ¹⁴, and the induction of HLA synthesis could be a more sensitive assay for IFN- γ in such cells.

We thank Dr S. M. Weissman and K. Itakura for gifts of the HLA and β_2 -microglobulin cDNA clones, Dr M. Rubinstein and S. Cimbalista for gifts of IFNs, and Dr P. Gray and D. V. Goeddel (Genentech) for the gift of IFN- γ produced by cloned cDNA. We thank R. Schluskel, U. Nir, G. Merlin and F. Rosa for their collaboration and Ms S. Budilovsky for technical assistance. This work was supported in part by a grant from NCRD (Israel) and GSF (München, Germany).

Received 8 March; accepted 26 August 1982.

- Isaacs, A. & Lindenmann, J. *Proc. R. Soc. B* **147**, 258-267 (1957).
- Friedman, R. M. & Chang, E. H. in *Interferons and Their Actions* (ed. Stewart, W. E. II) 145-152 (CRC Press, Ohio, 1977).
- Gresser, I. & Tovey, M. G. *Biochim. biophys. Acta* **516**, 231-247 (1978).
- Pfeffer, L. M., Wang, E. & Tamm, I. *J. cell. Biol.* **85**, 9-17 (1980).
- Luftig, R. B. et al. *J. Virol.* **23**, 799-810 (1977).
- De Maeyer, E. in *The Biology of the Interferon System* (eds De Maeyer, E., Galasso, G. & Schellekens, H.) 203-209 (Elsevier, Amsterdam, 1981).
- Sonnenfeld, G., Mandel, A. D. & Merigan, T. C. *Cell. Immun.* **34**, 193-206 (1977).
- Virelizier, J. L., Chan, E. L. & Allison, A. C. *Clin. exp. Immun.* **30**, 299-304 (1977).
- Wallach, D. in *Human Lymphokines, Biological Immune Response Modifiers* (eds Khan, A. & Hill, N. O.) 435-449 (Academic, New York).
- Salvin, S. B., Younger, J. S., Nishio, J. & Netar, R. J. *natn. Cancer Inst.* **55**, 1233-1235 (1975).
- Crane, J. L., Glasgow, L. A., Kern, E. & Younger, J. S. *J. natn. Cancer Inst.* **61**, 871-874 (1978).
- Rubin, B. Y. & Gupta, S. L. *Proc. natn. Acad. Sci. U.S.A.* **77**, 5928-5932 (1980).
- Dianzani, F., Salter, L., Fleischmann, W. R. Jr & Zucca, M. *Proc. Soc. exp. Biol. Med.* **159**, 94-97 (1978).
- Epstein, L. B. in *Interferon 3* (ed. Gresser, I.) 13-44 (Academic, New York, 1981).
- Knight, M. et al. *Nature* **288**, 189-191 (1980).
- Revel, M. in *Interferon 1* (ed. Gresser, I.) 101-163 (Academic, New York, 1979).
- Lindahl, P., Leary, P. & Gresser, I. *Eur. J. Immun.* **4**, 779-794 (1974).
- Heron, I., Hokland, M. & Berg, K. *Proc. natn. Acad. Sci. U.S.A.* **75**, 6215-6219 (1978).
- Fellous, M., Kamoun, M., Gresser, I. & Bono, R. *Eur. J. Immun.* **9**, 446-452 (1979).
- Shulman, L. & Revel, M. *Nature* **287**, 98-100 (1980).
- Fellous, M. et al. *Proc. natn. Acad. Sci. U.S.A.* **79**, 3082-3086 (1982).
- Yip, Y. K., Pang, R. H. L., Urban, C. & Vilcek, J. *Proc. natn. Acad. Sci. U.S.A.* **78**, 1601-1605 (1981).
- Gray, P. W. et al. *Nature* **295**, 503-508 (1982).
- Weissenbach, J. et al. *Proc. natn. Acad. Sci. U.S.A.* **77**, 7152-7156 (1980).
- Wallach, D. et al. *J. Interferon Res.* (submitted).
- Merlin, G., Revel, M. & Wallach, D. *Analyt. Biochem.* **110**, 190-196 (1981).
- Barnstable, C. J. et al. *Cell* **14**, 9-31 (1978).
- Vignaux, F. & Gresser, I. *J. Immun.* **118**, 721-723 (1977).
- Sood, A. K., Pereira, D. & Weissmann, S. M. *Proc. natn. Acad. Sci. U.S.A.* **78**, 616-620 (1981).
- Suggs, S. V., Wallace, R. B., Hirose, T., Kawashima, E. H. & Itakura, K. *Proc. natn. Acad. Sci. U.S.A.* **78**, 6613-6617 (1981).
- Vilcek, J. et al. *Miami Winter Symp.* **18**, 331-340 (1981).
- Zinkernagel, R. M. & Doherty, P. C. *Adv. Immun.* **27**, 96 (1979).
- Trichieri, G. & Santoli, D. J. *exp. Med.* **147**, 1314-1333 (1978).
- Wallach, D. *J. Interferon Res.* **2** (in the press).
- Rubinstein, M. et al. *Archs Biochem. Biophys.* **210**, 307-318 (1981).
- Goeddel, D. V. et al. *Nature* **290**, 20-26 (1981).
- Knight, E. Jr & Fahey, D. J. *biol. Chem.* **265**, 3609-3611 (1981).
- Schattner, A. et al. *Lancet* **ii**, 497-500 (1981).
- Branca, A. A. & Baglioni, C. *Nature* **294**, 768-770 (1981).

Direct evidence of homology between human DC-1 antigen and murine I-A molecules

M. Rosa Bono & Jack L. Strominger

Department of Biochemistry and Molecular Biology, Harvard University, Cambridge, Massachusetts 02138, USA

The nature of the interactions between cells of the immune system has been shown to be directly related to a group of antigens present on the surface of B lymphocytes¹. These antigens are under genetic control of the HLA-D/DR region of the human major histocompatibility complex (MHC) located on chromosome 6². DR antigens (the products of the *HLA-DR* locus within this region), have been defined by serological studies. Recently another antigen, DC-1, has been serologically defined^{3,4}. In the mouse, the I region, analogous to the HLA-D/DR region in man, has been subdivided into at least five subregions (A, B, J, E and C) and specific functions and cell populations associated with each of the subregions⁵. Although in man the HLA-D/DR region cannot at present be subdivided, limited NH₂-terminal amino acid sequence data have shown that the DR molecule is homologous to the I-E molecule of the mouse^{6,7}. Furthermore, evidence that DC-1 is not homologous to I-E (and might therefore be homologous to I-A) has been reported⁸. We now report that, using immunoadsorbents prepared with monoclonal antibodies specific for DR or DC-1 antigens, these two human alloantigens were purified from a human lymphoblastoid cell line (LB) and the chains were separated. The NH₂-terminal amino acid sequence of the heavy chain of DC-1 antigen shows great structural homology with the murine I-A molecules, thus providing direct evidence of homology of DC-1 to murine I-A.

DR antigens, like the corresponding murine I region encoded antigens, are carried on molecules composed of two glycoprotein chains (α or heavy chain and β or light chain) of apparent molecular weights 34,000 and 29,000. The response to a certain antigen or susceptibility to certain diseases have been related to the expression of a particular allele of DR and I region encoded antigens⁹. Ten alleles of the *HLA-DR* locus have been identified by serological studies¹⁰. DC 1 (identical to MB 1, MT 1 or LB 12) has been identified as having the same cell distribution and a similar molecular structure to the DR antigen. It appears to be immunogenetically associated with the specificities DR 1, 2 and w6 (ref. 3). However, the DC-1 antigen is expressed on a separate molecule from the

Table 1 Amino acid analysis of the α - and β -chains of DR and DC-1 (values in mol per cent)

	α -DR	α -DC-1	β -DR	β -DC-1
Asp	10.0	9.2	10.9	9.3
Thr	4.9	5.0	7.5	7.0
Ser	10.3	9.2	10.8	8.3
Glu	10.4	11.3	15.7	13.1
Pro	4.9	5.5	5.8	6.4
Gly	16.4	14.8	15.4	10.1
Ala	6.9	7.4	7.1	6.6
Val	4.9	4.8	7.3	6.2
Met	1.0	0.7	0.8	0.6
Ile	2.8	2.7	2.6	3.0
Leu	5.6	6.8	7.8	7.3
Tyr	2.0	2.5	3.1	2.9
Phe	3.7	2.8	4.1	3.0
Lys	5.4	5.7	4.5	4.2
His	6.0	7.0	4.4	4.6
Arg	5.1	5.3	7.7	7.8

Values are the average of two separate preparations.

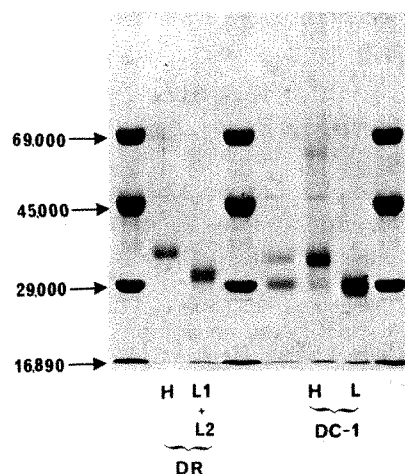


Fig. 1 SDS-polyacrylamide (12%) gel electrophoresis of purified DR and DC-1 antigens. The antigens were obtained from a homozygous B lymphoblastoid cell line, LB, typed as DRw6, w6 and DC-1-positive. Detergent-solubilized membrane proteins were prepared by incubation of frozen cells for 30 min at 4 °C in a buffer solution containing 2% Nonidet P-40, 0.01 M Tris pH 7.8, 0.14 M NaCl, 1 mM MgCl₂ and 0.1 mM PMSF (1 g cells per 4 ml lysis solution). The lysate was centrifuged at 150,000g for 1 h, and the supernatant recovered and centrifuged for an additional 40 min at 12,000g. Before purification of specific antigens, the bulk of actin contaminant was removed by passing the lysate through a Sepharose-4B CL column to which normal rabbit serum was coupled. Purification of DR and DC-1 antigens was done by using immunoabsorbents prepared with a monoclonal antibody L243 to purify DR antigen (obtained from Dr L. Lampson¹³) and Genox 3.53 to obtain the DC-1 antigen (from Dr F. Brodsky¹⁴). Immunoabsorbents were prepared by the method of March *et al.*¹⁹ to give a concentration of 3 mg of protein coupled to 1 ml of Sepharose, then stabilized by cross-linking with a solution of 0.1% glutaraldehyde²⁰. The best yields were obtained when the lysates were first depleted of DR antigens, before purification of DC-1 antigen (yield increased by ~20%). The whole process was done at 4 °C. Lysate corresponding to 20 g of cells was cycled through a 20 ml column of either L243 or Genox 3.53 immunoabsorbent for at least 24 h at a flow rate of 5 ml h⁻¹. Columns were washed with no more than five column bed volumes of a buffer containing 0.14 NaCl, 0.1% DOC and 0.01 M Tris pH 8.0. Elution of the columns was carried out using a buffer of 0.5% DOC, 5% glycerol and 0.1 M Tris pH 11.5. Analysis of the eluted fraction was done by SDS-PAGE. Fractions containing either DR or DC-1 antigen were prepared for amino acid sequencing (Table 2) by extensive dialysis against 0.1% SDS, 1 mM Tris pH 8.0 solution, lyophilization, acetone precipitation (5 volumes) and finally resuspension in a 0.1% SDS solution.

DR antigens^{3,4}. Immunogenetic studies¹¹ also suggest that MB 2 (associated with DR 3 and 7) and MB 3 (associated with DR 4, 5 and 8) are alleles of DC-1 and recently MB 2 has also been shown to be on a molecule distinct from DR 7 and similar to the DC-1 (MB 1) antigen¹².

Detergent-solubilized membranes of the LB cell line (DRw6, w6; DC-1) were passed over an immunoabsorbent column prepared with the DR-specific monoclonal antibody L243 (ref. 13). The bound material was eluted at pH 11.5 and subjected to SDS-polyacrylamide gel electrophoresis (PAGE) (Fig. 1). The unbound material was passed over a second column prepared with the DC-1-specific monoclonal antibody Genox 3.53 (refs 4, 14). The bound material was again eluted at high pH and subjected to SDS-PAGE (Fig. 1).

The DR molecule is composed of heavy chain (H) of apparent molecular weight (MW) 34,000 and two light chains of MWs 29,000 (L1) and 28,000 (L2). The DC-1 molecule contains a heavy chain (H) of MW 32,000 and a light chain (L) of MW 27,000. Note also that the light chain of DC-1 has a larger gel mobility than the L2 chain of DR, from which it can also be distinguished by other methods¹². The best yields from 20 g of LB cells were approximately 3 mg of DR antigens and 1 mg of DC-1 antigen.

The individual chains were then separated by hydroxylapatite chromatography (Fig. 2) to study their amino acid compositions and sequences. With this procedure the heavy chain (H) of the DR antigen was separated from the two light chains (L1 + L2) and the H chain of DC-1 was also separated from its L chain. Amino acid analyses showed significant differences between all four of these preparations (Table 1).

The NH₂-terminal amino acid sequences of the α -chains (H) of DR and DC-1 are shown in Table 2. For comparison, data available for the α -chain of the I-A and I-E molecules of the mouse^{1,6,7,12,15} are also shown. Homologous residues between the α -chains of DR and I-E molecules and between the α -chains of DC-1 and the I-A molecules have been underlined. Only 12 residues are available for comparison in the α -chain of I-E. Ten of these are identical in the DR molecule. These data agree with previous results indicating homology between these two antigens^{6,7}. Only eight positions are available for comparison in the α -chain of I-A. Five of these are identical in the DC-1 α -chain if a gap is inserted at the beginning of the DC-1 sequence. A similar gap was introduced to compare the sequence of the α -chain of the I-A molecule of the marmoset to that of the mouse¹⁶. In addition, conservative substitutions are present at two of the three additional positions compared and two additional valine residues are homologous to valines in the marmoset I-A α -chain sequence. The monoclonal antibody which recognizes the marmoset I-A molecule was also shown to react with an HLA-DR-like antigen in a human cell line, although no direct chemical information about this material was reported¹⁶. Four attempts to obtain an NH₂-terminal amino acid sequence of the β -chain of DC-1 yielded no sequence information, suggesting that this chain is blocked at its NH₂-terminus. Treatment with the enzyme which removes pyrrolidone carboxylic acid did not unblock the sequence. Attempts to obtain sequence information by other methods are in progress.

These data are direct evidence that the α -chain of DC-1 is the molecule analogous to the α -chain of the I-A molecule of the mouse. Although DC-1 and DR have similar molecular weights and nearly identical isoelectric points (in contrast to

Table 2 NH₂-terminal amino acid sequence comparisons between the heavy chains of murine I-A and I-E and human DR and DC-1 molecules

Chain	1	2	3	4	5	6	7	8	9	10	11	12	13	14	15	16	17	18	19	20	21	22	23	24	25	26	27	28
DR α	I	K	E	E	H	V	I	I	Q	A	E	F	Y	L	N	P	D	Q	S	G	E	F	M	F	D	F	D	G
I-E α	I	K			H	T	I	I		A		F	Y	L	L	P		R			F							
DC-1 α	E	D	I	V	A	D		V	A	Q	L	G	V	N	L	Y	Q	F	Y	L/G	P		G	Q	Y/F			E
I-A α			I	*	A			V		V	Y		*		V	Y												

The NH₂-terminal sequences of the DR and DC-1 α -chains were obtained on a Beckman 890-C sequencer with a Quadrol program. The thiazoline derivatives from each sequence step were converted to phenylthiohydantoin (PTH) amino acids and analysed by HPLC. All of the blanks in the DC-1 α chain are either Ser, Arg or His. The murine sequences are from the references cited in the text. Homologous residues are shown in bold type.

* V residues are found at these two positions in the marmoset I-A α sequence.

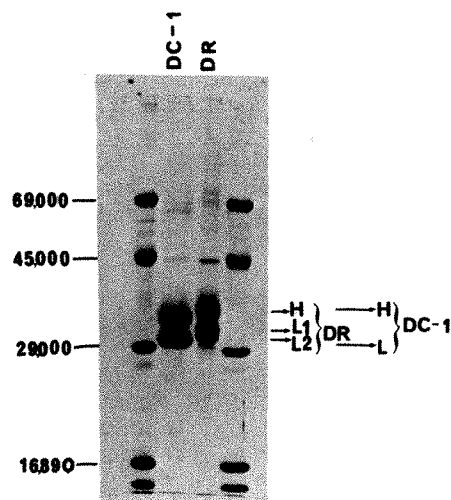


Fig. 2 Polyacrylamide gel electrophoresis of the separate α - and β -chains of DR and DC-1 antigens. Separation was achieved by chromatography on a hydroxylapatite column in the presence of 0.1% SDS and 1 mM dithiothreitol, using a linear phosphate gradient between 0.1 mM and 0.5 M for DR antigen (J. Kaufman, personal communication) and between 0.1 M and 0.3 M for DC-1 antigen. Fractions containing the separated subunits were identified by running an aliquot on SDS-PAGE (12%) and pooled for sequence analysis.

I-A and I-E whose isoelectric points are quite different) and may share some antigenic determinants, they do not present any similarity in the region studied. More sequencing data is necessary to examine a possible common evolutionary origin. It is quite likely that these similar molecules have distinct functions.

We thank Deborah Shackelford, David Andrews and William Lane for advice and assistance. This work was supported by NIH grant AI-10736.

Note added in proof: The amino acid sequence of residues 17–232 of the DC α -chain has been obtained from a cDNA clone¹⁷ and, together with the data reported here, provides the complete sequence. This chain is highly homologous to the DR α -chain, with a notable exception at the N-terminus. Its α 2 region is a typical immunoglobulin-like domain. Moreover, amino acid sequence data have been presented which substantiate the conclusion that an I-A homologue is present on a DR 7 homozygous human cell line¹⁸.

Received 9 June; accepted 1 September 1982.

1. Strominger, J. L. et al. in *The Role of the Major Histocompatibility Complex in Immunobiology* (ed. Dorf, M. E.) 115–171 (Garland, New York, 1981).
2. McKusick, V. A. & Ruddle, F. H. *Science* **196**, 390 (1977).
3. Tosi, R., Tanigaski, N., Centis, N., Ferrara, G. B. & Pressman, D. J. *exp. Med.* **148**, 1592–1611 (1978).
4. Shackelford, D. A., Mann, D. L., van Rood, J. J., Ferrara, G. B. & Strominger, J. L. *Proc. natn. Acad. Sci. U.S.A.* **78**, 4566–4570 (1981).
5. Shreffler, D. C., David, C. S., Cullen, S. E., Frelinger, J. A. & Neiderhuber, J. E. *Cold Spring Harb. Symp. quant. Biol.* **41**, 477 (1976).
6. McMillan, J., Cecka, J. M., Murphy, D. B., McDevitt, H. O. & Hood, L. *Proc. natn. Acad. Sci. U.S.A.* **74**, 5135–5139 (1977).
7. Allison, J. P. et al. *Proc. natn. Acad. Sci. U.S.A.* **75**, 3953–3956 (1978).
8. Corte, G. et al. *Nature* **292**, 357–360 (1981).
9. Batchelor, J. R. & Morris, P. J. in *Histocompatibility Testing 1977*, 205–258 (Munksgaard, Copenhagen, 1978).
10. Terasaki, P. I. in *Histocompatibility Testing 1980*, 18–20 (UCLA Press, Los Angeles, 1980).
11. Duquesnoy, R., Marrari, M. & Vieira, J. in *Histocompatibility Testing 1980*, 861–863 (UCLA Press, Los Angeles, 1980).
12. Shackelford, D. A., Kaufman, J. F., Korman, A. J. & Strominger, J. L. *Immun. Rev.* **66**, 133–187 (1982).
13. Lampson, L. A. & Levy, R. J. *Immun.* **125**, 293–299 (1980).
14. Brodsky, F. M., Parham, P. & Bodmer, W. F. *Tissue Antigens* **16**, 30–48 (1980).
15. Silver, J., Cecka, J. M., McMillan, M. & Hood, L. *Cold Spring Harb. Symp. quant. Biol.* **41**, 369 (1977).
16. Goyert, S. M. & Silver, J. *Nature* **294**, 266–268 (1981).
17. Aufray, C., Korman, A. J., Roux-Dosseto, M., Bono, R. & Strominger, J. L. *Proc. natn. Acad. Sci. U.S.A.* **79** (in the press).
18. Goyert, S. M., Shively, J. E. & Silver, J. J. *exp. Med.* **156**, 550–566 (1982).
19. March, S. C., Parikh, I. & Cuatrecasas, P. *Analyt. Biochem.* **60**, 149–152 (1974).
20. Kowal, R. & Parsons, R. *Analyt. Biochem.* **102**, 72–76 (1980).

Differential expression of steroid sulphatase locus on active and inactive human X chromosome

Barbara R. Migeon*, Larry J. Shapiro†, Robert A. Norum‡, Thuluvancheri Mohandas†, Joyce Axelman* & Rebecca L. Dabora*

* Department of Pediatrics, The Johns Hopkins University School of Medicine, Baltimore, Maryland 21205, USA

† Division of Medical Genetics, Harbor-UCLA Medical Center, Torrance, California 90509, USA

‡ Department of Medicine, Henry Ford Hospital, Detroit, Michigan 48202, USA

The X chromosome in mammalian somatic cells is subject to unique regulation—usually genes on a single X chromosome are expressed while those on other X chromosomes are inactivated¹. The X-locus for steroid sulphatase (STS; EC 3.1.6.2), the microsomal enzyme that catalyses the hydrolysis of various 3β -hydroxysteroid sulphates, is exceptional because it seems to escape inactivation. Evidence for this comes from fibroblast clones in females heterozygous for mutations that result in a severe deficiency of this enzyme in affected males; all clones from these heterozygotes have STS activity, and enzyme-deficient clones that are expected if the locus were subject to inactivation², have not been found³. Further evidence that the STS locus escapes inactivation is that the human inactive X chromosome contributes STS activity to mouse-human hybrid cells⁴. On the basis of these hybrid studies^{5,6} the STS locus has been mapped to the distal half of the short arm (p22–pter) of the human X chromosome. Although the STS locus on both X chromosomes in human female cells is expressed, quantitative measurements of STS activity in males and females do not accurately reflect the sex differences in number of X chromosomes^{7–13} (Table 1). The ratio of mean values for normal females to that of normal males is greater than 1:1 but less than the ratio of 2:1 expected if STS loci on all X chromosomes were equally expressed. The incomplete dosage effect suggests that the STS locus on the inactive X chromosome might not be fully expressed. To test this hypothesis, we examined two heterozygotes for X-linked STS deficiency who were also heterozygous for the common electrophoretic variants of glucose-6-phosphate dehydrogenase (G6PD A and B). Studies of fibroblast clones from these females provide evidence, presented here, for differential expression of STS loci on the active and inactive X chromosome.

The affected males in the pedigree shown in Fig. 1 have X-linked ichthyosis¹³ and complete deficiency of microsomal STS activity, based on assays using cholesterol sulphate and dehydroepiandrosterone sulphate (DHEAS) as steroid substrates (Tables 2, 3). Heterozygotes II-4, II-7 and II-8 are obligate carriers of the mutant gene as their brother and sons are affected. Heterozygotes II-4 and II-7 are also heterozygous

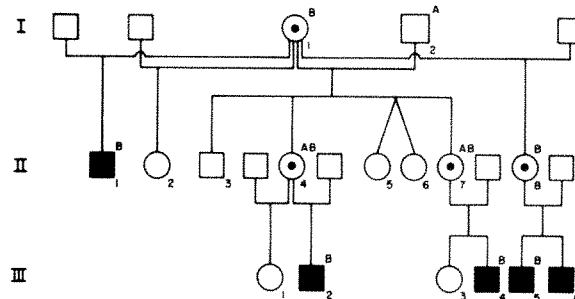


Fig. 1 Pedigree showing segregation of X-linked steroid sulphatase deficiency and G6PD variants. ■, Males with STS deficiency and X-linked ichthyosis. □, Normal male. ○, Carrier of STS deficiency. A, B indicate G6PD genotype.

Table 1 Comparison of specific activity of steroid sulphatase in male and female cells from reported studies

Tissue assayed	No. of specimens		Female: male activity ratio	Ref.
	Female	Male		
Fibroblasts	10	10	1.7	7
Fibroblasts	9	9	1.4	8
Fibroblasts	12	8	1.64	9
Placenta	18	18	1.8	10
Placenta	24	30	1.38	9
Lymphocytes	10	10	1.3	7
Leukocytes	25	12	1.3	11
Hair roots	9	8	1.04	12

Assays were carried out using ^3H -dehydroepiandrosterone sulphate.

for G6PD, having received the A allele from their father and the B allele from their mother. Therefore, in both females the STS mutation is on the same chromosome that carries the G6PD B allele.

Fibroblast cultures were established from skin biopsies of affected males and heterozygotes, and were maintained in Eagle's minimal essential medium supplemented with 15% fetal calf serum and non-essential amino acids. Control cultures included fibroblasts that had been similarly established from two females heterozygous for G6PD A, but normal with regard to the STS locus. Clonal cultures were established² from cells in their second subculture. Ten cells were plated into each of a series of 60-mm Petri dishes. Colonies were isolated 10 days later with cloning cylinders, transferred to establish clonal cultures and each clone was then assayed for G6PD phenotype by cellulose acetate gel electrophoresis¹⁴. Several clones of each G6PD type were transferred to flasks and delivered quickly to Torrance where steroid sulphatase was measured using ^3H -cholesterol sulphate¹⁵; determinations were carried out using two different amounts of cell extract in duplicate for each specimen to ensure linearity of the assay. For some specimens, aryl sulphatase A was assayed¹⁶ in the same lysate used for the STS and protein assays, while control assays of X-linked G6PD and the autosomal enzyme 6-phosphogluconate dehydrogenase (6PGD) were done¹⁴ on replicate cultures in Baltimore. Cultures were collected 10–11 days after plating and cell pellets were maintained at -20°C until assayed for sulphatases. The G6PD and 6PGD assays were carried out on fresh cell extracts. In each case, quantitative determinations were done without knowledge of origin or G6PD phenotype of the specimens.

In contrast to cells from the three affected males that had no detectable STS activity, all the clones from heterozygotes II-4 and II-7 showed STS activity (Table 2, Fig. 2), confirming observations in other heterozygotes³. However, the quantity of STS activity differed significantly in the two populations of clones from these double heterozygotes. The clones of G6PD B phenotype in each heterozygote had less activity than the G6PD A clones, and less activity than any of the clones from

the female controls. Although a few G6PD A clones in heterozygote II-4 had low STS activity, most were in the range of values for clones from the normal female, whereas all the G6PD B clones for II-4 had <4 pmol per mg protein per h of cholesterol sulphatase activity (Fig. 2). The results were similar when additional clones from heterozygote III-7 were assayed using ^3H -DHEAS as the steroid substrate (Table 3); the G6PD B clones had approximately half the activity of the G6PD A clones.

This differential activity was limited to the STS locus as activities for G6PD, 6PGD and aryl sulphatase A did not differ significantly between the two populations of clones in heterozygote II-4 (Table 2, Fig. 2). Because the activity of other enzymes is similar in both populations of clones, the differences in STS activity that we observed cannot be attributed to nonspecific differences in the metabolic activity of these cells. As the activity of STS is reduced in only one population of clones (those expressing G6PD B in both heterozygotes), it is unlikely that the decreased expression results from feedback inhibition of enzyme activity. The most probable explanation for our observations is that in both heterozygotes, the clones expressing G6PD B in fact produce less STS activity than clones that express G6PD A.

As there is no measurable enzyme activity for either steroid substrate in affected males (Tables 2, 3), the mutant locus in these individuals does not produce STS activity. Because the STS mutation in both heterozygotes is carried on the same chromosomes as the G6PD B allele, the active X chromosome in the G6PD B clones does not contribute STS activity. Therefore, all the STS activity in these clones must come from the normal allele on the inactive X chromosome. Furthermore, as G6PD B clones have less STS activity than G6PD A clones, it is clear that the normal STS allele produces less enzyme when it is on the inactive X, than on the active X chromosome.

Although our experimental observations are limited to heterozygous females from one family, we believe that they are representative of heterozygotes in other families also. The STS values for clones from heterozygotes reported previously (see Fig. 1 of ref. 3) are variable and their distribution is compatible with differential expression of the two X chromosomes in these females. Moreover, reduced expression of the STS locus on the inactive X chromosome is consistent with the incomplete dosage effect observed at this locus in normal individuals (see Table 1).

The reduced expression of the STS locus on the inactive X chromosome may reflect merely the influence of neighbouring genes that are subject to inactivation. Presumably, the gene is transcribed at a time when the inactive X chromosome has little if any other transcriptional activity, and is morphologically recognized as heterochromatin. Proximity to inactive X chromatin has been shown to inactivate neighbouring autosomal genes^{17–19}. On the other hand, differential expression at

Table 2 Enzyme activity in fibroblasts from normal females, affected males and heterozygotes for X-linked STS deficiency

Subject	Cloning efficiency	Specimen (no.)	Cholesterol sulphatase (pmol per mg per h)	Aryl sulphatase A (nmol per mg per h)	G6PD ($\mu\text{mol per mg per min}$)	6PGD ($\mu\text{mol per mg per min}$)
T. W., normal ♀	0.72	G6PD A clones (6)	15.3 \pm 2.1	408 \pm 75	0.175	0.038
		G6PD B clones (6)	15.5 \pm 6.3	491 \pm 146	0.187	0.036
		G6PD A clones (10)	11.0 \pm 6.2	413 \pm 137	0.169 \pm 0.03	0.036 \pm 0.00
		G6PD B clones (10)	2.4 \pm 1.0	352 \pm 76	0.201 \pm 0.03	0.035 \pm 0.01
W. K., normal ♀	0.36	G6PD A clones (6)	6.7 \pm 1.0			
		G6PD B clones (6)	9.4 \pm 2.2			
		G6PD A clones (8)	8.2 \pm 2.9			
		G6PD B clones (10)	3.4 \pm 0.6			
II-1, Affected ♂	0.39	G6PD B clones (8)	0.01 \pm 0.0*			
II-1, Affected ♂		G6PD B, uncloned (3)	0.0*	320 \pm 84		
III-4, Affected ♂		G6PD B, uncloned (2)	0.0	482		
III-5, Affected ♂		G6PD B, uncloned (2)	0.0	289		

Values of enzyme activity are mean \pm s.d., or mean of two specimens if no s.d. is given. Cloning efficiency, clones obtained/cells plated. Brackets indicate specimens assayed simultaneously.

* Note that the absence of activity in affected males indicates that cholesterol sulphate is a specific substrate for STS.

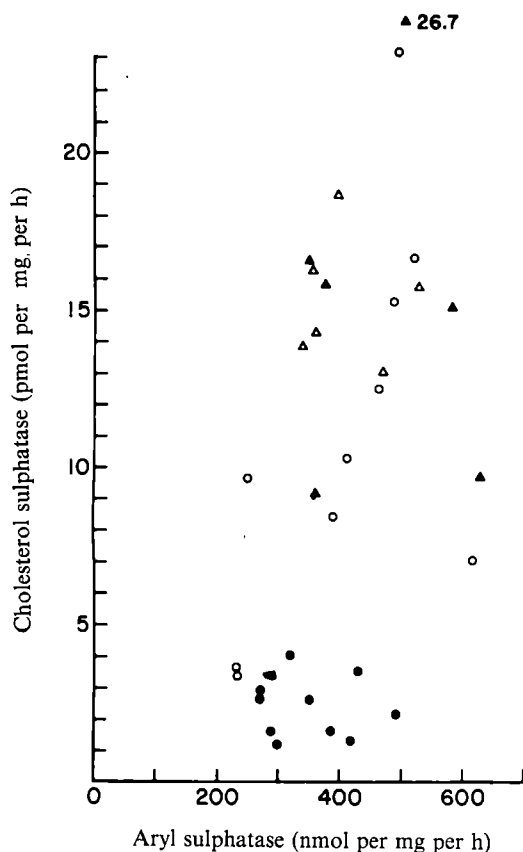


Fig. 2 STS values for individual clones as a function of aryl sulphatase A activity. ○, G6PD A and ●, G6PD B clones from heterozygote II-4; △, G6PD A and ▲, G6PD B clones from T.W., the normal female control.

the *STS* locus could be due to other mechanisms regulating the expression of genes on the X chromosome. Having a single active X chromosome in mammalian cells of both sexes serves to equalize the expression of X-linked genes in male and female somatic cells, but results in an effective monosomy for these genes. The method of X chromosome dosage compensation in *Drosophila* avoids this problem because sexual equality is achieved by increasing the transcriptional activity of the single X in the male²⁰ rather than by inactivating one of the two X chromosomes in the female. Thus, males as well as females have effectively two doses of each X gene. Like the dipteran chromosome, the mammalian X chromosome carries many genes having functions similar to those on autosomes. As monosomy is usually detrimental for mammals, it is possible that mechanisms have evolved to compensate for the single copy of X genes, by enhancing the product output of the active X chromosome²¹⁻²³. The greater activity of the *STS* locus on the active X chromosome observed here could be attributable to gene duplication²² (inconsistent with genetic evidence) or to increased output of the active X locus through enhanced transcription or processing.

Further evidence for greater activity of active X loci comes from studies of normal human fibroblasts, heterozygous for

G6PD A, that have undergone spontaneous derepression of the G6PD locus on the inactive X chromosome²⁴. Electrophoretic analysis of these cells indicates that the reactivated locus on the inactive X contributes half as many subunits as that on the active one. Therefore, it seems that the output of X loci that escape inactivation early in normal development or that are expressed following derepression, is significantly less than that of corresponding loci on the active X. Although compatible with some mechanism that down-regulates expression of the inactive locus, the differential activity may reflect increased expression of the active one. In either case, our observations indicate additional complexity in the regulation of X-chromosomal loci in man.

This work was supported by NIH grants HD 05465 (B.R.M.) and HD 12178 (L.J.S.) and March of Dimes Birth Defects Foundation grant 1-639 (L.J.S.).

Received 28 May; accepted 2 September 1982.

1. Lyon, M. F. *Biol. Rev.* **47**, 1-35 (1972).
2. Migeon, B. R. *et al. Proc. natn. Acad. Sci. U.S.A.* **78**, 5066-5070 (1981).
3. Shapiro, L. J., Mohandas, T., Weiss, R. & Romeo, G. *Science* **204**, 1224-1226 (1979).
4. Mohandas, T., Sparkes, R. S., Hellkuhl, B., Grzeschik, K. H. & Shapiro, L. J. *Proc. natn. Acad. Sci. U.S.A.* **77**, 6759-6763 (1980).
5. Mohandas, T., Shapiro, L. J., Sparkes, R. S. & Sparkes, M. C. *Proc. natn. Acad. Sci. U.S.A.* **76**, 5779-5783 (1979).
6. Müller, C. R., Westerveld, A., Migl, B., Franke, W. & Ropers, H. H. *Hum. Genet.* **54**, 201-204 (1980).
7. Müller, C. R., Migl, B., Traupe, H. & Ropers, H. H. *Hum. Genet.* **54**, 197-199 (1980).
8. Ropers, H. H. *et al. Hum. Genet.* **57**, 354-356 (1981).
9. Bedin, M., Weil, D., Fournier, T., Cedard, L. & Frezal, J. *Hum. Genet.* **59**, 256-258 (1981).
10. Lykkesfeldt, G., Bock, J. E. & Lykkesfeldt, A. E. *Lancet* **ii**, 255-256 (1981).
11. Epstein, E. H. Jr & Leventhal, M. E. *J. clin. Invest.* **67**, 1257-1262 (1981).
12. Dancis, J., Jansen, V. & Hutzler, J. *Pediatr. Res.* **14**, 521 (1980).
13. Shapiro, L. J., Weiss, R., Webster, D. & France, J. T. *Lancet* **i**, 70-72 (1978).
14. Marenzi, C. & Migeon, B. R. *Am. J. hum. Genet.* **33**, 752-761 (1981).
15. Shapiro, L. J. *et al. Lancet* **ii**, 756-757 (1978).
16. Baum, H., Dodgson, K. S. & Spencer, B. *Clinica chim. Acta* **4**, 453-455 (1959).
17. Cattanaach, B. M. Z. *VererbLehre* **92**, 165-182 (1961).
18. Eichler, E. *Adv. Genet.* **15**, 175-259 (1970).
19. Mohandas, T., Sparkes, R. S. & Shapiro, L. J. *Am. J. hum. Genet.* (in the press).
20. Belote, J. M. & Lucchesi, J. C. *Nature* **285**, 573-575 (1980).
21. Ohno, S. *Sex Chromosomes and Sex-linked Genes*, 99 (Springer, New York, 1967).
22. Lyon, M. F. *Proc. R. Soc. B* **187**, 243-268 (1974).
23. Lucchesi, J. C. *Science* **202**, 711-716 (1978).
24. Migeon, B. R., Wolf, S. F., Marenzi, C. & Axelman, J. *Cell* **29**, 595-600 (1982).
25. Hameister, H. *et al. Hum. Genet.* **46**, 199-207 (1979).

Structure of the S-layer of *Sulfolobus acidocaldarius*

K. A. Taylor*, J. F. Deatherage & L. A. Amos

MRC Laboratory of Molecular Biology, Hills Road, Cambridge CB2 2QH, UK

The outermost component of many bacterial cell envelopes is a two-dimensional crystalline array of protein molecules, termed the S-layer¹. Despite considerable effort to investigate its structure and composition, its precise function remains uncertain. We report here the first determination of the three-dimensional structure of an S-layer, that from the thermophilic bacterium, *Sulfolobus acidocaldarius*. Our map shows a complex and strongly interconnected structure, penetrated by numerous channels which appear to provide little barrier to anything but rather large molecules. The external surface is fairly smooth, but the cellular side is sculpted with large cavities and protruding 'pedestals'. The protein substructure consists of three types of globular domain, connected by narrow bridges. We suggest that these may be flexible 'hinges', allowing the S-layer to form a curved surface, and that the multidomain structure allows the S-layer to maintain strong connectivity as it grows with the bacterium.

S. acidocaldarius is a facultative sulphur-oxidizing autotroph whose natural habitat is hot acidic springs². Cells are roughly spherical, 0.8-1.0 µm in diameter, and are often lobed. When

Table 3 Steroid sulphatase activity in fibroblasts assayed with DHEAS as substrate

Subject	Specimen (no.)	DHEAS sulphatase (pmol per mg per h)
II-7, Heterozygote	G6PD A clones (4)	2,665 ± 433
	G6PD B clones (4)	1,518 ± 432
III-2, Affected ♂	Uncoloned	0
	Uncoloned	3,650

Cells were washed, pelleted and suspended in buffer with sodium lauryl sulphate¹⁵ and disrupted by sonication (15 s). The reaction was carried out according to Hameister²⁵ in duplicate at two substrate concentrations using ³H-DHEAS (22.1 Ci mmol⁻¹; NEN) in a final concentration of 6.3 × 10⁻⁶ M at 37 °C for 2 h. The desulphated substrate was recovered after two benzene extractions¹¹.

* Present address: Department of Anatomy, Duke University Medical Center, Durham, North Carolina 27710, USA.

grown in autotrophic conditions with elemental sulphur as an energy source, the cells attach to sulphur crystals by means of pili³. Like other members of the Archaeobacteria, they have a simple cell wall, consisting essentially of the S-layer attached to the plasma membrane⁴. The S-layer consists of a single glycoprotein with an apparent molecular weight (MW) of 140,000–170,000, as determined by SDS-gel electrophoresis⁵. In the electron microscope, untilted specimens of purified S-layer show a hexagonal lattice, two-sided plane group p6, with a 220 Å unit cell dimension (Fig. 1a).

The three-dimensional model (Fig. 2) is more complex than would be expected from direct inspection of the two-dimensional projection of the structure (Fig. 1b), which apparently shows fairly simple dimer units arranged to form a series of hexagonal and triangular holes. In fact, although the three-dimensional structure is very open, with protein occupying just 30% of the volume within the ~100 Å-thick layer, only the holes on the 6-fold axes pass directly through. One side of the layer is relatively smooth, the other deeply indented. Shadowing of intact cells⁴ and isolated S-layers⁵ has shown that the smooth side is the exterior surface. The structure consists essentially of three types of oligomeric globular domains which we have named the diad (D), triad (T) and 6-fold ring (R) regions (Fig. 2). Six large D domains around each ring form a domed chamber on the cellular side of each 6-fold axis (Fig. 2b). At the top of the dome is a hole of 50 Å diameter. On the 3-fold axes, around the rims of the chambers, are the pedestal-like T domains, which presumably bind the S-layer to the cell surface. Published micrographs⁶ suggest that these features are in contact with the surface of the membrane, rather than being in the lipid bilayer.

At this resolution, it is impossible to determine molecular boundaries. At least two monomers must contribute to the D domain, at least three to the T domain and six to the ring. The simplest possible molecular shape (illustrated in Fig. 2) is nevertheless complicated in terms of intermolecular connections, making a total of eight separate contacts with six different neighbours. Indeed, the division into separate polypeptides is likely to be more complex and the number of intermolecular interactions even greater.

Whatever the shape of the individual monomer, it is useful to consider the assembled structure in terms of the morphological features and their interactions. Connecting the D and T domains is a relatively narrow waist (H1) which we believe could function as a flexible hinge. Similarly, two different types of narrow waists (H2, H3) connect the D and R domains. Until the shape of the S-layer monomer is known, it is impossible to determine whether either of the latter connections is a non-covalent intermolecular interface as opposed to a covalent link or hinge. The outer surface is made up of R domains, which terminate in numerous small knobs. Adjacent R domains are linked by a fourth kind of narrow connecting region (H4), which is long and has two sharp bends. Flexing of these bends would allow the distance between adjacent rings to vary, concertina-fashion, and accommodate the distortions necessary for lobe formation (see below).

An analogous multidomain structure connected by hinges has been found for the coat protein subunit of tomato bushy stunt virus (TBSV), which consists of two domains (P and S) connected by a hinge⁷. The TBSV subunit occupies three quasi-equivalent positions in the virus shell, yet the polypeptide chain foldings within the three different kinds of P and S domains are almost identical, the major differences between quasi-equivalent subunits being the angle between the domains. This seems likely to be a common feature of allosteric structural proteins, although as yet there is little evidence as so few structural proteins have been studied at sufficiently high resolution. An S-layer built on this principle could combine strength and flexibility having rigid domains connected by covalently-bonded hinges. Molecules could thus assume a range of similar but not identical conformations as the S-layer curves around the bacterial surface.

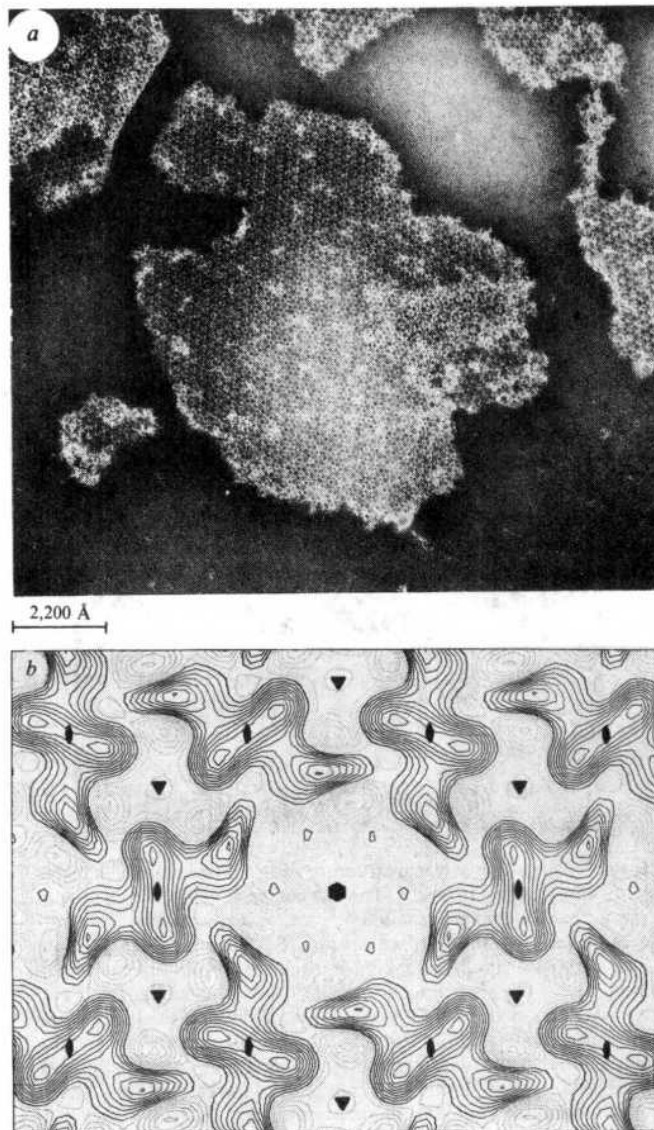


Fig. 1 *a*, Cell wall sacculi were isolated from *S. acidocaldarius*, strain 98-3, by procedures described elsewhere⁵. These were broken into small flat sheets by brief sonication. Specimens for electron microscopy were prepared on glow-discharged carbon support films using potassium phosphotungstate, pH 7.0 as negative stain and observed in a Philips EM 400 electron microscope equipped with goniometer stage and low dose kit for minimizing electron exposure. A specimen in fairly thick stain is shown here for good contrast (most of the images processed were more lightly stained). The relative sizes of the apparent holes in 3-fold and 6-fold positions varies according to the depth of stain. *b*, In-plane projection of a small part of the *Sulfobolus* S-layer. Dark contours represent protein, light contours negative stain. There are apparently large holes in the 6-fold positions and smaller holes in 3-fold positions. The unit cell size is 220 Å.

On a curved surface, the subunits must either move more closely together on the inside or farther apart on the outside, compared with the flat structure we have solved. The former possibility is the more likely, as having the T-domain pedestals spread well apart on the membrane side would prevent them from interfering with one another if the spacing were reduced. At junctions between lobes, the wall would curve the other way, with the T domains spreading farther apart than in a flat structure.

However, a single crystalline S-layer cannot form a closed surface simply by bending. Closure could be achieved in crystalline shells by the introduction of edge dislocations⁸, examples of which have been shown in various other species^{9,10}. In the case of layers having hexagonal symmetry, however, Caspar and Klug¹¹ have discussed the possibility that closed containers may be formed by introducing pentagons instead of hexagons,

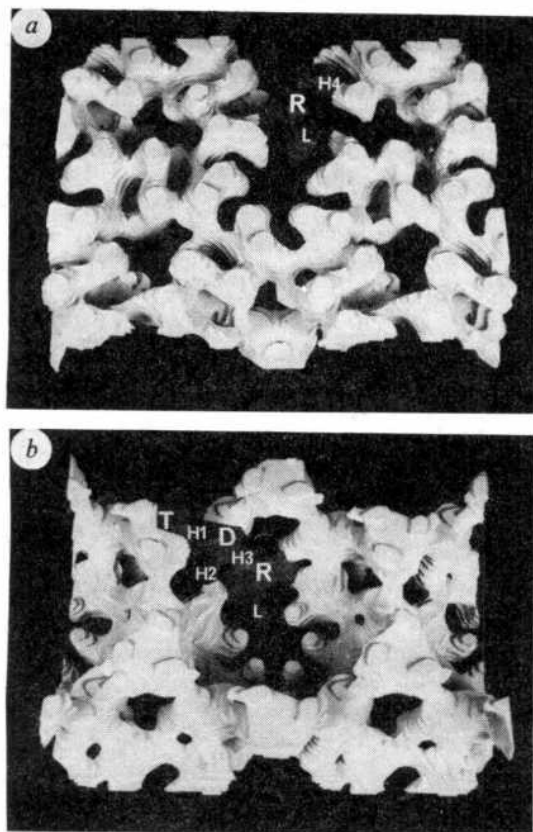


Fig. 2 Three-dimensional structure of the S-layer of *Sulfolobus*. Note the striking porosity. The darker regions of the structure represent the simplest possible molecular shape, an almost linear arrangement of one-third of a triad (T), half of a diad (D) and one-sixth of a ring (R) domain, but there are numerous possible alternatives to this. *a*, View of the balsa wood model from the extracellular side. There are two kinds of hole on this side. One, 50 Å in diameter, in the R domain on the 6-fold axis, opens into a large domed chamber on the plasma membrane side. The second kind of hole, 45 Å in diameter on the 3-fold axes, splits into three crystallographically identical channels of ~25 Å diameter, which open into the sides of the large chamber. *b*, View from the plasma membrane side. The chamber on the 6-fold axis is ~185 Å wide, measured between T domains, and ~80 Å deep. The three-dimensional structure was determined using procedures similar to those of Henderson and Unwin¹⁹, except that both phases and amplitudes were obtained from the computed Fourier transforms of the images. Data from three 10-member tilt series, to angles as high as 60°, and 12 fixed-angle views between 72° and 78° were combined. The resulting three-dimensional model contains almost all the data to 17 Å resolution with the exception of the F(00L) and part of the F(10L). The average phase residual for the three-dimensional origin refinement was 15–25.3 degrees. Variation in density across flat negatively stained areas is 6–10% of the variation across stained protein boundaries. Further details of the data processing will be published elsewhere²⁰. The cut-out model has 95% of the volume predicted for a monomer of MW 170,000.

to give a quasi-equivalent arrangement analogous to that obtained with icosahedral viruses. Edge dislocations are then unnecessary and a stronger wall with no unsatisfied contacts may be achieved without them. To close the spherical shell in this manner requires a minimum of 12 pentagons. By extending this principle we believe that the phenomenon of lobe formation in *S. acidocaldarius* may be explained through the insertion of additional pentagons and compensating heptagons into the surface lattice. Note that surface lattices involving mixtures of pentagons, hexagons and heptagons have been demonstrated, indeed they have been observed at various stages in coated pit formation¹².

The basket-like network raised away from the membrane on pedestals is one of the most striking features of the reconstruction. Several lines of evidence suggest that this may be a fairly

general property of S-layers: for example, the model proposed for the S-layer of *Spirillum serpens*¹³ has similar features, although it is formed in an entirely different fashion. Moreover, edge-on views of negatively stained S-layers, as observed for *Acinetobacter*¹⁴ and profiles viewed in thin section from such species as *Pelodictyon clathratiforme*¹⁵ and *Methylomonas agile*¹⁶ also suggest a similar feature in their three-dimensional structure.

Several physiological functions have been proposed for bacterial S-layers¹. Protection and support of the cell are obvious possibilities. This seems particularly likely in the case of the Archaeobacteria, in which the S-layer seems to be the only component of the cell wall. In *S. acidocaldarius*, it may be essential for providing support against the low osmotic pressure in hot acid springs. In this case, the strength of the S-layer would need to be maintained during cell growth, even while additional molecules are being inserted into the layer. The need to provide a constant framework of support, while allowing a degree of flexibility and porosity, may explain why the subunits are so complex and make so many separate intermolecular contacts. Extra rows of molecules might be inserted by a multi-step process, whereby different sets of bonds would be broken and transferred to the new subunits in separate stages, so that at no time would there be a complete break in the S-layer. By an elaboration of this insertion process, involving the introduction of additional pentagons and compensating heptagons, the S-layer could adapt to lobe formation or to cell division without weakening.

A possible function attributed to the S-layer is that of a selective permeability barrier. Stewart and co-workers^{17,18} have recently suggested, on the basis of projected views of the S-layers from *Aquaspirillum putridiconchylium* and *Sporosarcina ureae*, that they might function as molecular sieves, allowing the passage of small essential metabolites but not proteins. However, the channels we observe in our three-dimensional model of the *Sulfolobus* S-layer seem too large to be selective in this way. This S-layer may be designed simply to provide the cell with as much access to the medium as possible, while still maintaining its supportive function. It may also be relevant that the diameter of the channel through the S-layer on the 6-fold axis is very similar to the size of the pili which attach the bacterium to sulphur crystals¹.

We have found the S-layer of *S. acidocaldarius* to be an excellent specimen for three-dimensional image reconstruction. We hope, therefore, that similar studies on other examples will provide further clues to the mode of assembly and function of cell walls.

We thank H. Michael for providing *S. acidocaldarius* cell sacculi and R. Henderson and all those who participated in the EMBO course on 'Three-Dimensional Structure Analysis by Electron Microscopy', held in Cambridge in 1980, for their help and encouragement. K.A.T. was supported by NIH grant R01 GM/AM 28224 and was assisted by a Research Travel Grant from the Burroughs-Wellcome Fund.

Received 24 May; accepted 20 August 1982.

1. Sleytr, U. B. *Int. Rev. Cytol.* **53**, 1–64 (1978).
2. Brock, T. D. *Thermophilic Microorganisms and Life at High Temperatures*, 117–179 (Springer, New York, 1978).
3. Weiss, R. L. *J. gen. Microbiol.* **77**, 501–507 (1973).
4. Weiss, R. L. *J. Bact.* **118**, 275–284 (1974).
5. Michel, H., Neugebauer, D.-Ch. & Oesterhelt, D. in *Electron Microscopy at Molecular Dimensions* (eds Baumeister, W. & Vogell, W.) 27–35 (Springer, New York, 1980).
6. Brock, T. D., Brock, K. M., Belly, R. T. & Weiss, R. L. *Arch. Mikrobiol.* **84**, 54–68 (1972).
7. Harrison, S. C., Olson, A. J., Schutt, C. E., Winkler, F. K. & Bricogne, G. *Nature* **276**, 368–373 (1978).
8. Harris, W. F. & Scriven, L. E. *Nature* **228**, 827–829 (1970).
9. Watson, S. W. & Remsen, C. C. *Science* **163**, 685 (1969).
10. Sleytr, U. B. & Glauber, A. M. *J. ultrastruct. Res.* **50**, 103–116 (1975).
11. Caspar, D. L. D. & Klug, A. *Cold Spring Harbor. Symp. quant. Biol.* **27**, 1–24 (1962).
12. Heuser, J. J. *Cell Biol.* **84**, 560–583 (1980).
13. Glaeser, R. M., Chiu, W. & Grano, D. J. *ultrastruct. Res.* **66**, 235–242 (1979).
14. Thorne, K. J. *J. Biol. Rev.* **52**, 219–234 (1977).
15. Cohen-Bazire, G., Kunisawa, R. & Pfennig, N. *J. Bact.* **100**, 1049–1061 (1969).
16. Wilkinson, J. F. *Symp. Soc. gen. Microbiol.* **21**, 15–46 (1971).
17. Stewart, M. & Beveridge, T. J. *J. Bact.* **142**, 302–309 (1980).
18. Stewart, M., Beveridge, T. J. & Murray, R. G. E. *J. molec. Biol.* **137**, 1–8 (1980).
19. Henderson, R. & Unwin, P. N. T. *Nature* **257**, 28–32 (1975).
20. Deatherage, J. F., Taylor, K. A. & Amos, L. A. *J. molec. Biol.* (submitted).

BOOK REVIEWS

Lemurs, dead and alive

R.D. Martin

THE prosimians, commonly referred to as "lower primates", can be loosely regarded as representing a primitive grade closer to the ancestral primate condition than the modern monkeys and apes. For this reason, any study of primate evolutionary biology is particularly dependent upon an understanding of the prosimians (lemurs; lorises; tarsiers). Yet, until quite recently, the prosimians were relatively neglected in the primate literature, though several recent publications have done much to fill this gap.

Among the prosimians, the Madagascar lemurs comprise by far the largest assemblage of living species and provide a remarkable example of adaptive radiation on an isolated land-mass. Until now, however, there has been no really comprehensive treatise on the Madagascar lemurs available in the English language; most of the relevant publications are in French. Now, at long last, a highly readable and authoritative English-language reference work on the lemurs has been provided in the form of Ian Tattersall's *The Primates of Madagascar*. This (by today's standards) reasonably priced and attractively presented book is a must for libraries and research workers concerned with primate evolutionary biology.

After providing a neat and illuminating historical survey of the discovery and early description of Madagascar's lemurs, Tattersall goes on to consider the general biogeographical background, giving due reference to continental drift. It now seems to be well established that Africa was the primary source of the original mammal fauna which colonized Madagascar and that this large oceanic island has existed as such for at least the past 65 million years. Adaptive radiation of the lemurs to yield the modern array of a score or so species undoubtedly took place largely or exclusively within Madagascar. These living lemur species are effectively reviewed by Tattersall, who provides standard measurements from his comprehensive survey of major museum collections and body weights wherever possible, as well as providing useful distribution maps incorporating actual locality records in addition to the customary expanses of hopeful shading.

It is a sad fact that until historical times Madagascar's lemur fauna was almost twice as rich in species as it is now, including numerous forms which were markedly bigger than most extant lemurs,

The Primates of Madagascar. By Ian Tattersall. Pp.382. ISBN 0-231-04704-5. (Columbia University Press: 1982.) \$52.

such as the ape-sized *Megaladapis* and the monkey-like *Archaeolemur*. These large-bodied lemurs are known only as subfossils and Tattersall has performed a particularly valuable task in providing a chapter with the clearest available general review of the subfossil lemurs. He also gives a balanced discussion of conflicting explanations for the recent extinction of these animals (human intervention versus climatic change).

The remaining chapters provide very useful syntheses of information on behaviour and ecology, general morphology and adaptation, and phylogeny and classification. The thoughtful concluding chapter ends, as it should, with a strong statement about increasing threats to the survival of the remaining lemur species.

Tattersall's central research interest has been the phylogenetic relationships of the lemurs, and he provides a fairly comprehensive survey of relevant information and conflicting interpretations. His conclusions, however, are somewhat controversial. In agreement with several other authors, he cites morphological evidence (essentially from the auditory bulla and internal carotid circulation) suggesting that certain lemurs (family Cheirogaleidae) diverged from a common ancestry with the Afro-Asian loris group (family Lorisidae) post-dating the initial radiation of the lemurs. Serological evidence, on the other hand, supports the alternative view that the lemurs of Madagascar constitute a self-contained (monophyletic) group.

Tattersall dismisses the biochemical and chromosomal evidence without proper discussion, and this — along with a general reluctance to emphasize quantification — is one of the few shortcomings of an otherwise well-balanced book. It is, of course, impossible to cover everything in a single text, but the principle must be recognized that any overall assessment of lemur phylogeny must eventually integrate biochemical and chromosomal data. The hypothesis of a later link between the Cheirogaleidae and the Lorisidae automatically requires at least two crossings of the Mozambique Channel by early lemurs. Tattersall goes still further than this in postulating, on craniodental grounds, specific relationships between Eocene fossil adapids and certain extant lemurs

(*Notharctus* + *Lepilemur*; *Adapis* + *Hapalemur*). This would require not only multiple crossings of the Mozambique Channel but also a very early origin for the Madagascar lemur radiation. The dental similarities between the Eocene fossils and modern lemurs are, indeed, striking; but parallel evolution would seem to be a strong possibility. Nonetheless, Tattersall's views on lemur phylogeny are thought-provoking and will doubtless fuel further research in this area.

Overall, *The Primates of Madagascar* performs an excellent service in providing an up-to-date review of a wide range of material on the Madagascar lemurs, together with a comprehensive bibliography. It will undoubtedly become a standard reference work for future studies of these unique primates. □

R.D. Martin is Professor of Physical Anthropology at University College London.

Grains of evidence

A.T. Grove

Environmental History of East Africa: A Study of the Quaternary. By A.C. Hamilton. Pp.328. ISBN 0-12-321880-2. (Academic: 1982.) £24, \$44.50.

STUDIES of Late Quaternary environmental history in East Africa exploit the opportunities afforded by the sedimentary record and old shorelines in the rift basins, and by glaciation features on the high mountains. Pollen preserved in the sediments of the rift and in cirque basins, and also in peats in the higher and wetter areas, is an indicator of former plant distributions. It is with the last subject that Hamilton is mainly concerned in this book. Extraction, identification and counting of the pollen grains is testing and time-consuming; interpretation requires a good general knowledge of plant geography. It remains, I suspect, an art as well as a science.

Hamilton has reduced some of the uncertainties of interpretation in East Africa by examining surface pollen samples in relation to current vegetation patterns and drawing conclusions as to the production and mobility of different types of pollen. This has enabled him to

Essential information at your fingertips Every month!

The British Journal of Clinical Pharmacology is the leading authoritative journal presenting results of clinical pharmacological research.

Published monthly on behalf of the British Pharmacological Society the journal:

- ★ Bridges the gap between medical professions, clinical research and the Pharmaceutical industry.

- ★ Contains papers and reports on all aspects of drug action in man, in both health and disease.

- ★ Prints letters and short communications which allow immediate discussion of urgent observations.

Subscribers to British Journal of Clinical Pharmacology receive, free of charge, the proceedings of selected symposia on new methods, new drugs, and new approaches to treatment. Some past symposia have been on narcotic antagonists and antagonist analgesics, labetalol, clobazam, mianserin, temazepam and the relationship between angina pectoris and hypertension.

Why not join the growing number of clinical pharmacologists, clinicians and others who rely on the British Journal of Clinical Pharmacology as their information medium.

For a sample copy write to: Felicity Parker, Scientific & Medical Division, Macmillan Publishers Ltd., Houndmills, Basingstoke, Hampshire, RG21 2XS.

Circle No.63 on Reader Service Card.

reinterpret early pollen diagrams as well as to interpret his own more effectively. The results confirm the conclusions reached by other methods as to the Late Quaternary climatic succession in the region — a cool, dry Late Pleistocene period from about 20,000 to 12,000 BP being preceded and followed by wetter millennia, and current climates becoming established about 4,000 BP.

The significance of Late Quaternary climatic change for the history of the equatorial rain forest has been underlined by J.R. Flenley in *The Equatorial Rain Forest: A Geological History* (Butterworths, 1979). Flenley's field experience was mainly in south-east Asia, however, and evidence of such effects is greater in Africa. Hamilton has worked, on and off, for the last 16 years in East Africa and knows the highland areas intimately from his own field studies made, in recent years, in collaboration with R.A. Perrott.

In this book he considers the altitude zonation of the vegetation and presents, with interpretations, pollen diagrams from Elgon, Cherangani, Mount Kenya, Kilimanjaro, Badda and Bale in Ethiopia, Ruwenzori and the Rukiga Highlands in Uganda, the Kamiranzovu swamp in Rwanda and the dambos of the Nyika Plateau in Malawi (the last by M.E. Meadows). A feature of many of the cores is the absence of peat for some millennia before 4,000 BP; Hamilton explains this in terms of greater surface wash under the wetter conditions of the Early Holocene; but could it rather be the result of wastage accompanying desiccation about 4,000 to 4,500 BP?

Hamilton argues that the key to an understanding of the evolutionary processes in East African vegetation is the recognition of core areas of limited extent where rain forest survived the dry periods of the Quaternary. From these core areas in west Africa, Cameroun-Gabon, eastern Zaire and the Usumbara and Uluguru mountains near the east African coast the diversity of species diminishes outwards. He briefly reviews the past and probable future effects of man on the east African environment and recommends that conservation of the core areas should receive special attention.

This is a welcome addition to the literature on environmental change in low latitudes by one of the most active and experienced researchers in the field. Hamilton presents the botanical evidence bearing on the Quaternary history of East Africa clearly and simply enough to allow the non-specialist to appreciate the implications of the pollen records and see them within a more general setting. Earth scientists and ecologists at both the undergraduate and research level will find his study useful and stimulating. □

A.T. Grove is a Geographer at Downing College and Director of the African Studies Centre, University of Cambridge.

Old space dust

David W. Hughes

Interplanetary Dust. By P.W. Hodge. Pp.280. ISBN 0-677-03620-5. (Gordon & Breach: 1982.) \$38.

DUST gets everywhere and this is certainly true of the interplanetary variety. As it orbits the Sun, it scatters radiation, resulting in a cone of light extending along the ecliptic known as zodiacal light. It collides with the Earth, is brought to a halt in the atmosphere and drifts down to the surface where it can be recovered from deep-sea sediments, in Antarctic and Arctic ice, and as a component of airborne dust. It can be sampled using balloons, rockets and high-flying aircraft. Interplanetary dust continuously bombards the lunar surface producing microcraters in exposed glasses and rocks. It can be measured using satellite-borne instruments and was once regarded as a serious hazard to space missions. In the interplanetary context any particle smaller than 100 µm, about a millionth of a gram, is regarded as dust.

The history of dust investigation is fascinating. It is a science that got off to a bad start. Early satellite experiments both in the United States and the USSR agreed well — and fitted rocket data — but all produced results which were a factor of 10⁶ wrong. Microphones were detecting the creaking of spacecraft and not the impact of dust. Contamination has always been a problem; in airborne dust less than one particle in 10⁹ is extraterrestrial.

P.W. Hodge, the author of this book, played an important part in many of the early dust studies and has produced a short (about 45,000 word) summary of the subject — published in a camera-ready format. His book is easy to read, and provides a reasonable overview of the early days of the subject. I stress "early days" because the references tail off sharply after 1976. The standard of coverage is patchy and the concentrations of technicalities occur in the areas of micrometeorites, fossil dust collection and particles around meteorite craters — all subjects on which Hodge has worked. The illustrations are of a rather mixed quality and many of the photographs of the particles are printed without scales.

This is the sort of book I might recommend a research student to read if he had nothing to do for an afternoon. But I would then insist that he spent much, much longer with, for example, the IAU Symposium 90 report (*Solid Particles in the Solar System*, edited by I. Halliday and B.A. McIntosh and published by Reidel in 1980) to give him an up-to-date overview of the subject, a feel for the excitement of the work of the cosmic dust men and a taste for the potential avenues of research. □

David W. Hughes is a Lecturer in Astronomy and Physics at The University of Sheffield.

Endocrinology through the changes

J.G. Phillips

Hormones in Development and Aging. Edited by Antonia Vernadakis and Paola S. Timiras. Pp.686. ISBN 0-85200-560-1. (MTP Press: 1982.) £50.25.

REVIEW books on important and topical areas of biomedical research are always to be welcomed. Such a reception should greet *Hormones in Development and Aging*. Vernadakis and Timiras, the editors, have assembled an impressive group of authors to review the literature, highlight current concepts and anticipate developments in an area of endocrinology which holds great current interest both in its fundamental aspects and in its impact on clinical practice.

The overall approach has been to provide detailed coverage of the events running from fertilization through to differentiation, development, maturation and ageing, as well as of the role hormones play in organizing cellular expression and regulating metabolic events. Rightly central in the thinking of the authors has been the underscoring of the interrelationship of the endocrine and nervous systems, as both are crucially involved in the processes of growth and adaptation, puberty, rhythms of biological importance, the onset and ageing of reproductive functions, general ageing and neoplasia.

The secondary aim has been to consider the effects of hormones on brain development, both normal and abnormal, and to examine their influence on behaviour throughout the life span. This longitudinal approach allows each of the contributors to describe the basic aspects of changes in endocrinology during development and ageing, as well as pathological alterations which subtract from the optimum conditions for good health and the capacity to maintain vigour into "old age".

The authors have also seized upon the opportunity to propose interventive approaches wherever possible. This emphasis is in tune with the widely held view that, by finding means of strengthening physiological function, there will be a swing away from the current clinical practice of finding the cure for the disease towards the elaboration of a set of well understood guidelines which, when followed, will possibly serve to maintain adaptability and vigour throughout the whole life span. The clinical potential of such procedures is self-evident.

The impact of the book is unfortunately diminished by numerous errors in the text, a lack of consistency in presentation of data, poor photographs and an amazing paucity of very recent papers — indeed, it is explicitly stated that Ramaley's chapter, "Neuroendocrinology of Puberty", was written five years ago! On balance, however, this is a valuable compilation of

reviews which must find its way into libraries and onto the desks of gerontologists, geriatricians and developmental biologists. □

J.G. Phillips is Director of the Wolfson Institute at the University of Hull.

Before Einstein

Stephen G. Brush

Energy, Force, and Matter: The Conceptual Development of Nineteenth-Century Physics. By P.M. Harman. Pp.182. Hbk ISBN 0-521-24600-8; pbk ISBN 0-521-28812-6. (Cambridge University Press: 1982.) Hbk £13.20, \$27.50; pbk £5.50, \$8.95.

IT IS NO easy task to give a concise, accurate and readable account of nineteenth-century physics. Yet someone must undertake it if students and general readers are to gain an understanding of the background for the spectacular theories and discoveries of the twentieth century. In his contribution to the distinguished *Cambridge History of Science Series*, P.M. Harman (formerly Heimann) has satisfied the first two criteria admirably, the third passably. He has condensed an amazing amount of material into fewer than 200 pages (including a valuable bibliographic essay and a useful index); his facts and interpretations are in accord with the best modern scholarship; but his style is not lively enough to attract a reader who is not already convinced of the importance of the subject. It is probably the best textbook currently available for the first part of a course on the history of modern physics, as long as the instructor can motivate students to struggle through Harman's densely-written prose.

Following a rapid survey of imponderable fluids, the ether concept, Fourier's heat theory and the discovery of energy-conversion processes in the first half of the century, Harman gives a thorough treatment of the development of thermodynamics and field theories of electricity and magnetism. An account of Hertz's discovery of electromagnetic waves, the Michelson-Morley experiment and Lorentz's electrodynamics prepares the reader for the introduction of relativity; but, as a professional historian striving to avoid the Whig interpretation (judging the past only as progress towards the present), Harman carefully refrains from mentioning Einstein's theory at this point. Instead, he jumps back to Dalton's chemical atomic theory and traces

molecular physics through Clausius, Maxwell and Boltzmann. A final chapter ties together the late nineteenth-century critiques of atomism and the difficulties in ether theory accompanying the decline of the mechanical world view. Having pointed out the continuity between these trends of the 1890s and the revolutionary ideas of Planck and Einstein, the author ends his story just before the conflicts in his plot are resolved.

Readers familiar with current writings in the history of science will perhaps regret that Harman has chosen to minimize the philosophical, social and psychological aspects of physics; we find here no mention of Kuhnian paradigms, Lakatosian research programmes, or (a more recent fad) Mary Douglas's grid-group categories. This is probably just as well, however, since the instructors or the more sophisticated readers will probably prefer their own version of such schemes to whatever the author might present, and it is always useful to have one straightforward account of the basic technical developments.

For me, a more serious omission is the mathematical basis of physical theories. Incredible as it might seem to a physicist, Harman manages to discuss all the above-mentioned topics without using a single equation or mathematical symbol. While this policy may succeed in making the book appear accessible to a larger audience, I doubt if a phrase such as "Lagrangian formalism" will mean much to the reader who lacks knowledge of theoretical physics. On the other hand there is a definite advantage in having a mathematics-free text if the missing equations are presented and explained in a separate chapter at the end, so that those readers who wish to know, for example, what Maxwell's field equations are and how they explain the propagation of light, can find out.

For those authors who have been frustrated by the refusal of publishers to print discursive footnotes (as opposed to endnotes), the most exciting aspect of this book may be Harman's innovative use of figure captions. He displays admirable ingenuity in adding to these captions not only technical details about the experiments being illustrated, but also sociological comments and other interesting digressions that would have disrupted the flow of ideas in the text. In fact, as the caption to a reproduction of Maxwellian postcards shows (Fig. 4.5), one can even use this format to give brief explanations of important equations. As a reader who sometimes enjoys an author's footnotes more than his text, I look forward to a new era of scholarly publishing in which the most fascinating parts of a book will be found underneath its illustrations. □

Stephen G. Brush is a Professor in the Department of History and the Institute for Physical Science and Technology at the University of Maryland, College Park.

Population modelling: how are large mammals different?

Hans Kruuk

Dynamics of Large Mammal Populations. Edited by Charles W. Fowler and Tim D. Smith. Pp.477. ISBN 0-471-05160-8. (Wiley: 1982.) £33.25, \$56.55.

FOR several decades population models have been generally successfully used in the rational exploitation of fish stocks. Such models focus on productivity, and each involves only a single species. In *Dynamics of Large Mammal Populations* the editors argue that large mammals are different from other animals in their population characteristics; reading through the various chapters, however, it appears that often the approach to population research is the same as in fisheries. Many of the species discussed are being "harvested", and population models are directed towards maximum sustainable yield, with many of the characteristics of fisheries models.

However, as pointed out by G. Caughley in this volume, single-species models may serve exploitation but they do not explain ecological relationships. It is in the relationships with their environment that large mammals differ from other organisms, as argued in the chapter by R.M. Laws (to whom the book is dedicated); as a group they show similarity in feeding strategies, social behaviour, reproduction and demographic parameters. These aspects of large mammal biology have evolved together and it is dangerous to focus on merely the last of them.

The book contains 23 chapters, many with detailed single-species population models, and several general sections on modelling and management. On the whole the contributions are slanted towards marine species, especially seals; several chapters deal with terrestrial carnivores, but the many studies on herbivores (African bovines; deer, sheep) are poorly represented. Generally, there is little cross-reference between chapters, even to the extent that two different sections on models of the Pribilof fur-seal exploitation hardly refer to each other at all. There are no summaries, which makes reading of this kind of material cumbersome.

Highlights amongst the contributions are a section "What we don't know about

the dynamics of large mammals", which details the complexity of even the simplest herbivore-plant interaction in terms of populations; there is also a good comparison of population characteristics of three species of bear, an excellent evaluation of management policies of gray seals and a clearly written decision-making framework for population management. Inevitably there are weak points, too; some of the models presented in the single-species sections make assumptions which are either hopelessly unrealistic or so general as to make the model useless and recommendations impractical. Thus, a model of wolf-moose interactions recommends an optimal moose harvest under conditions whereby wolves are either left alone or controlled only when there are few of them; even the authors were unhappy with that conclusion.

With a few notable exceptions the papers on population dynamics of specific mammals are inward-looking, single-species studies. The often-used concept of density-dependence hides possible dependence on restricted resources in the animal's environment; in the last, theoretical chapter, for instance, it is found after a long and involved argument that density-dependent changes occur in populations close to carrying capacity. Clearly, there is no true density-dependence in such cases, but dependence on, for example, populations of food species.

In all the editors have missed the opportunity to push studies of large mammal populations further along by at least attempting to integrate papers dealing with exploitation with others on resource limitations and utilization. If one is interested in managing the productivity of large mammal populations, however, this volume does provide a great deal of food for thought. □

Hans Kruuk is a Principal Scientific Officer at the Institute of Terrestrial Ecology, Banchory, Scotland.

Resolving problems in spectroscopy

Norman Sheppard

High Resolution Spectroscopy. By J. Michael Hollas. Pp.638. ISBN 0-408-10605-0. (Butterworths: 1982.) £45, \$115.

DURING the past decade the subject of molecular spectroscopy has been revitalized by the development of a wide range of new techniques. Michael Hollas's book represents a timely attempt to provide a comprehensive and balanced account of both these and the more established principles of the subject.

In the preface the author states that "In general . . . the sample is assumed to be in the gas or vapour phase"; indeed, an alternative and more accurate, if perhaps less eye-catching, title for the book could have been *Molecular Spectroscopy of Gases*. Under this rubric the exclusion of the magnetic resonance spectroscopies (little applied to gases) and the inclusion — for very good pedagogical reasons — of photoelectron spectra of gases would have been naturally assumed. Under the present title these two aspects of the book seem to be very anomalous, for the magnetic resonance spectroscopies are of very high resolution, and photoelectron spectra are much less so than others.

Naturally, a particularly interesting section of the book is concerned with those newer developments that are not, or are little, covered in existing comprehensive spectroscopy textbooks. The last two chapters — some 160 pages — are mainly devoted to such topics, including the laser and photoelectron spectroscopies, and provide a welcome and well-balanced

account of the recent advances. The earlier chapters cover more familiar ground but also provide up-to-date treatments of the subject-matter.

The book covers both experimental and theoretical/interpretational aspects of the molecular spectroscopies and has well-chosen spectral illustrations. In general the writing is well-planned and clear, careful attention has been paid to detail and there are some nice historical touches. The occasional helpful footnote shows that the author is a naturally skilled teacher.

Perfection is not to be expected in a book of such wide coverage. For example, as a vibrational spectroscopist, I note that it is a mistake to use the phrase "near-infrared" to cover all that is not "far-infrared". The normal usage of the former phrase is restricted to the high frequency overtone region — the intervening region of fundamental vibrations is nowadays termed the "mid-infrared". I was also surprised to find a comment to the effect (p.176) that the use of rotational contours in infrared vibration spectra is not a "standard" technique for identifying (the symmetries of) fundamentals — it most certainly is, despite some complications.

These are, however, minor criticisms of what is overall a very successful text. The book deserves wide usage by its intended readership of undergraduates specializing in spectroscopy, and postgraduate students and teachers of the subject. □

Norman Sheppard is a Professor in the School of Chemical Sciences at the University of East Anglia.

Pergamon journals

Incorrect dollar subscription rates were quoted for four Pergamon journals in the recent New Journals review issue of *Nature* (299, pp.507, 510, 511 and 514).

Correct prices (for 1983) are: *Insect Science and Its Application* \$85; *Chinese Astronomy and Astrophysics* \$200; *PhysicoChemical Hydrodynamics* \$120; *Bulletin of Science, Technology and Society* \$85.

nature

Author Index for Volume 299

September — October 1982

Issue no.	Issue date	Page nos
5878	2 September	1-94
5879	9 September	95-192
5880	16 September	193-286
5881	23 September	287-380
5882	30 September	381-474
5883	7 October	475-566
5884	14 October	567-666
5885	21 October	667-764
5886	28 October	765-846

- Abbott L. F. and Gavela M. B. Absence of thermal effects on photon mass measurements, *matters arising*, 299, 187
- Able K. P. Skylight polarization patterns at dusk influence migratory orientation in birds, 299, 550
- Abraham A. French Nobels, *correspondence*, 299, 294
- Abraham A. and Goldman M. Nuclear Magnetism: Order and Disorder, *book review by Bloembergen N.*, 299, 474
- Acheson E. D., Winter P. D., Hadfield E. and Macbeth R. G. Is nasal adenocarcinoma in the Buckinghamshire furniture industry declining? 299, 263
- Ackerman M., Lippens C., Muller C. and Vignault P. Blue sunlight extinction and scattering by dust in the 60-km altitude atmospheric region, 299, 17
- Adelman N. E. *see under Steinman L.*, 299, 738
- Aitken R. J. and Chisholm G. D. Journal of Andrology/International Journal of Andrology/The Prostate, *Journal review*, 299, 499
- Akeroyd F. M. Narrative style please, *correspondence*, 299, 674
- Alan A. *see under Gupta C. M.*, 299, 259
- Allègre C. J. *see under Dupré B.*, 299, 620
- Allègre C. J. and Condomines M. Basalt genesis and mantle structure studied through Th-isotopic geochemistry, 299, 21
- Allison A. C. *book review of ISI Atlas of Science: Biochemistry and Molecular Biology 1978/80*, 299, 190
- Amos L. A., Huxley H. E., Holmes K. C., Goody R. S. and Taylor K. A. Structural evidence that myosin heads may interact with two sites on F-actin, 299, 467
- Andersson P. J. *see under McBurney M. W.*, 299, 165
- Andersson M. Female choice selects for extreme tail length in a widow bird, 299, 818
- Ando T. *see under Ohtani T.*, 299, 86
- Andrews P. W. and Goodfellow P. N. Analysing the mouse *T/t* complex, *news and views*, 299, 296
- Ansell J. D. *see under Woodruff M. F. A.*, 299, 822
- Antes R. A. Tropical Cyclones: Their Evolution, Structure and Effects, *book review by Krishnamurti T. N.*, 299, 660
- Antonucci R. R. J. Optical polarization position angle versus radio source axis in radio galaxies, 299, 605
- Arculus R. J. *book review of Andesites: Orogenic Andesites and Related Rocks*, (Thorpe R. S. editor), 299, 377
- Arnold F. Ion nucleation — a potential source for stratospheric aerosols, 299, 134
- Aronson P. S., Nee J. and Suhm M. A. Modifier role of internal H^+ in activating the Na^+H^+ exchanger in renal microvillus membrane vesicles, 299, 161
- Asai M. *see under Noda M.*, 299, 793
- Atkins P. W. International Reviews in Physical Chemistry, *Journal review*, 299, 513
- Atrash B. *see under Szekle M.*, 299, 555
- Atsma B. Which war? 299, 294
- Axelmann J. *see under Migeon B. R.*, 299, 838
- Axford W. I. *see under Nielsen E.*, 299, 238
- Axon D. J., Bailey J. and Hough J. H. Discovery of a very red nucleus in the radio elliptical IC5063 (PKS2048-57), 299, 234
- Backer J. M., Boerzig M. and Weinstein I. B. When do carcinogen-treated 10T1/2 cells acquire the commitment to form transformed foci? 299, 458
- Bailey J. *see under Axon D. J.*, 299, 234
- Baillie M. G. L. Tree-ring Dating and Archaeology, *book review by Fletcher J.*, 299, 660
- Baker C. K., Unsworth M. H. and Greenwood P. Leaf injury on wheat plants exposed in the field in winter to SO_2 , 299, 149
- Baker F. W. G. ICSU matters, *correspondence*, 299, 774
- Baker J. R. Human conception, *correspondence*, 299, 674
- Ballado T. *see under Quinto C.*, 299, 724
- Balzer W. *see under Wefer G.*, 299, 145
- Bancroft G. M., Metson J. B., Kanetkar S. M. and Brown J. D. Surface studies on a leached sphene glass, 299, 708
- Barchas J. D. *see under Weber E.*, 299, 77
- Barnes P. J., Basbaum C. B., Nadel J. A. and Roberts J. M. Localization of β -adrenoreceptors in mammalian lung by light microscopic autoradiography, 299, 444
- Barnstable C. J. Journal of Neuroimmunology, *Journal review*, 299, 504
- Barrantes F. J. *see under Zingsheim H. P.*, 299, 81
- Barron P. F., Wilson M. A., Campbell A. S. and Frost R. L. Detection of imogolite in soils using solid state ^{29}Si NMR, 299, 616
- Barrow J. Journal of Astrophysics and Astronomy/Chinese Astronomy and Astrophysics, *Journal review*, 299, 510
- Basbaum C. B. *see under Barnes P. J.*, 299, 444
- Basham T. and Merigan T. C. Immunoregulation by γ -interferon? *news and views*, 299, 778
- Basu T. K. and Schorah C. J. Vitamin C in Health and Disease, *book review by Rivers J.*, 299, 760
- Batchelor G. K. Physicochemical Hydrodynamics, *Journal review*, 299, 511
- Baylor D. A. *see under Nunn B. J.*, 299, 726
- Behringer D., Birdsall T., Brown M., Cornuelle B., Heinmiller R., Knox R., Metzger K., Munk W., Spiesberger J., Spindel R., Webb D., Worcester P. and Wunsch C. A demonstration of ocean acoustic tomography, 299, 121
- Bellairs A. d'A. Amphibia-Reptilia, *Journal review*, 299, 507
- Bellairs R., Curtis A. and Dunn G. Editors, Cell Behaviour: A Tribute to Michael Abercrombie, *book review by Gottlieb D. I.*, 299, 473
- Beller D. I. *see under Snyder D. S.*, 299, 163
- Benesch R. *see under Benesch R. E.*, 299, 231
- Benesch R. E., Kwong S. and Benesch R. The effects of α chain mutations *cis* and *trans* to the β mutation on the polymerization of sickle cell haemoglobin, 299, 231
- Bennett A. F. *see under Ruben J. A.*, 299, 658
- Bennett V., Davis J. and Fowler W. E. Brain spectrin, a membrane-associated protein related in structure and function to erythrocyte spectrin, 299, 126
- Berger A. J. *see under Sears T. A.*, 299, 728
- Berger M., Sperk G. and Hornykiewicz O. Serotonergic denervation partially protects rat striatum from kainic acid toxicity, 299, 254
- Berger N. A., Berger S. J. and Catino D. M. Abnormal NAD^+ levels in cells from patients with Fanconi's anaemia, 299, 271
- Berger S. J. *see under Berger N. A.*, 299, 271
- Bertram B. *book review of East African Mammals: An Atlas of Evolution in Africa*, (Kingdon J.) 299, 189
- Bevan M. Crown gall tumours and plant growth regulators — any connection? *news and views*, 299, 299
- Beyenbach K. W. Direct demonstration of fluid secretion by glomerular renal tubules in a marine teleost, 299, 54
- Bhown A. S. *see under Pollok B. A.*, 299, 447
- Bird D. M. The American kestrel as a laboratory research animal, *news and views*, 299, 300
- Birdsall T. *see under Behringer D.*, 299, 121
- Blajchman M. A., Heddle N., Naipul N. and Singal D. P. HLA-restricted lymphoproliferative responses to MN blood group determinants, 299, 67
- Blaxter J. H. S. Aquatic Toxicology/Marine Ecology/Biological Oceanography, *Journal review*, 299, 508
- Blobel G. *see under Walter P.*, 299, 691
- Bloembergen N. *book review of Nuclear Magnetism: Order and Disorder*, (Abraham A. and Goldman M.) 299, 474
- Bloom F. E. *see under Staunton D. A.*, 299, 72
- Blumenthal G. R., Pagels H. and Primack J. R. Galaxy formation by dissipationless particles heavier than neutrinos, 299, 37
- Blundell D. J. *see under Smythe D. K.*, 299, 338
- Bodmer W. F. *see under Heisterkamp N.*, 299, 747
- see under Lee J. S.*, 299, 750
- Boerzig M. *see under Backer J. M.*, 299, 458
- Bojesen E. Diversity of cholesterol exchange explained by dissolution into water, 299, 276
- Bollum F. J. Molecular and Cellular Biology/Comments on Molecular and Cellular Biophysics/Bioscience Reports/Biochemistry International/The Journal of Biosciences, *Journal review*, 299, 497
- Bona C. A. Idiotypes and Lymphocytes, *book review by Janeway C. A. Jr*, 299, 473
- Bono M. R. and Strominger J. L. Direct evidence of homology between human DC-1 antigen and murine I-A molecules, 299, 836
- Booth R. S. *see under Norris R. P.*, 299, 131
- Borrieres N., Goldreich P. and Tremaine S. Sharp edges of planetary rings, 299, 209
- Borst P. *see under De Lange T.*, 299, 451
- Botchan P. M. and Dayton A. I. A specific replication origin in the chromosomal rDNA of *Lytechinus variegatus*, 299, 453
- Bourne W. R. and Howe S. Monstrous outrage, *correspondence*, 299, 294
- Bowen D. Q. Rapid environmental and climatic changes, *news and views*, 299, 206
- Brackman J. H., Levell B. K., Martin J. H., Potter T. L. and van Vliet A. Late Palaeozoic Gondwana glaciation in Oman, 299, 48
- Brady J. *book review of Insect Clocks*, (Saunders D. S.) 299, 662
- Brand C. R. *book review of The Biology of Human Conduct: East-West Models of Temperament and Personality*, (Mangan G. L.) 299, 377
- Branigan K. The unacceptable face of Minoan Crete? *news and views*, 299, 201
- Breemen N. van, Burrough P. A., Velthorst E. J., Dobben H. F. van, Wit T. de, Ridder T. B. and Reijnders H. F. R. Soil acidification from atmospheric ammonium sulphate in forest canopy throughfall, 299, 548
- Brewer J. A. *see under Smythe D. K.*, 299, 338
- Briggs D. TrAC (Trends in Analytical Chemistry), *Journal review*, 299, 514
- Bright S. W. J., Keuh J. S. H., Franklin J., Rognes S. E. and Milfin B. J. Two genes for threonine accumulation in barley seeds, 299, 278
- Britten S. On dotted letters, *correspondence*, 299, 102
- Brookes P. Mutation Research Letters/Teratogenesis, Carcinogenesis, and Mutagenesis, *Journal review*, 299, 501
- Brown A. M., Camerer H., Kunze K. L. and Lux H. D. Similarity of unitary Ca^{2+} currents in three different species, 299, 156
- Brown F. H. *see under Cerling T. E.*, 299, 216
- Brown F. H. and Cerling T. E. Stratigraphical significance of the Tulu Bor Tuff of the Kooibi Formation, 299, 212
- Brown J. D. *see under Bancroft G. M.*, 299, 708
- Brown L., Klein J., Middleton R., Sacks I. S. and Tera F. ^{10}Be in island-arc volcanoes and implications for subduction, 299, 718
- Brown M. *see under Behringer D.*, 299, 121
- Brown S. A. *see under Murray R. D. H.*, 299, 285
- Browne I. W. A., Clark R. R., Moore P. K., Muxlow T. W. B., Wilkinson P. N., Cohen M. H. and Porcas R. W. MERLIN observations of superluminal radio sources, 299, 788
- Brownlee G. G. *see under Choo K. H.*, 299, 178
- Brunori M. *see under Perutz M. F.*, 299, 421
- Brush S. G. *book review of Energy, Force, and Matter: The Conceptual Development of Nineteenth-Century Physics*, (Harrman P. M.) 299, 845
- Bugaisky L. B. *see under Butler-Browne G. S.*, 299, 830
- Burckle L. *see under Wright A.*, 299, 208
- Burckle L. H., Robinson D. and Cooke D. Reappraisal of sea-ice distribution in Atlantic and Pacific sectors of the Southern Ocean at 18,000 yr BP, 299, 435
- Burniston Brown G. Retarded Action-at-a-Distance: The Change of Force with Motion, *book review by Clarke C. J.*, 299, 191
- Burrough P. A. *see under Breemen N. van*, 299, 548
- Burton D. I. *see under Woodruff M. F. A.*, 299, 822
- Buseck P. R. *see under Tomeoka K.*, 299, 326
- see under Tomeoka K.*, 299, 327
- Butler-Browne G. S., Bugaisky L. B., Cuénoud S., Schwartz K. and Whalen R. G. Denervation of newborn rat muscles does not block the appearance of adult fast myosin heavy chain, 299, 830
- Cairns J. *see under Foster P. L.*, 299, 365
- Calvert P. *book review of Polymers and their Properties. Vol. 1, Fundamentals of Structure and Mechanics*, (Hearle J. W. S.) 299, 472
- Calvin N. M. *see under Zolan M. E.*, 299, 462
- Camardo J. S. *see under Siegelbaum S. A.*, 299, 413
- Camerer H. *see under Brown A. M.*, 299, 156
- Campbell A. S. *see under Barron P. F.*, 299, 616
- Campbell R. Making sense of journal publishing, *Journal review*, 299, 491
- Campbell S. E. Precambrian endoliths discovered, 299, 429
- Capron A. *see under Haque A. F.*, 299, 361
- Cardon F., Gomes W. P. and Dekeyser W. Editors, Photovoltaic and Photo-electrochemical Solar Energy Conversion, *book review by Wilson J. I. B.*, 299, 378
- Carey J. *see under Lee J. S.*, 299, 750
- Carr M. H. The Surface of Mars, *book review by Veverka J.*, 299, 761
- Carritt B. *see under Heisterkamp N.*, 299, 747
- Carriveau G. W. Image processing in the analysis of art, *news and views*, 299, 487
- Carter A. D. *see under Jolliffe L. K.*, 299, 653
- Casnellie J. E. *see under Nairn A. C.*, 299, 734
- Catino D. M. *see under Berger N. A.*, 299, 271
- Cattaneo R. *see under Will H.*, 299, 740
- Cebra J. J. *see under Hurwitz J. L.*, 299, 742

- Cerling T. E. *see under* Brown F. H., 299, 212
- Cerling T. E. and Brown F. H. Tuffaceous marker horizons in the Koobi Fora region and the Lower Omo Valley, 299, 216
- Chapin G. *see under* Wasserstrom R., 299, 482
- Chapman R. F. Insect Science and Its Application, *Journal review*, 299, 507
- Charlier P. *see under* Dideberg O., 299, 469
- Chater K. F. *Streptomyces* in the ascendant, *news and views*, 299, 10
- Chatterjee S. Significance of ankle structures in archosaur phylogeny—Reply, *matters arising*, 299, 657
- Cheetham A. K., Eddy M. M., Jefferson D. A. and Thomas J. M. A study of Si,Al ordering in thallium zeolite-A by powder neutron diffraction, 299, 24
- Cheetham P. S. J., Imber C. E. and Isherwood J. The formation of isomaltulose by immobilized *Erwinia rhapsodica*, 299, 628
- Chen E. Y., Howley P. M., Levinson A. D. and Seeburg P. H. The primary structure and genetic organization of the bovine papillomavirus type 1 genome, 299, 529
- Chenoy-Marchais D. A. C¹⁴ conductance activated by hyperpolarization in *Aplysia* neurones, 299, 359
- Cheshire M. V. *see under* Goodman B. A., 299, 618
- Chiba T. *see under* Miyachi T., 299, 168
- Chien J. C. W., Yamashita Y., Hirsch J. A., Fan J. L., Shen M. A. and Karasz F. E. Resolution of controversy concerning the morphology of polyacetylene, 299, 608
- Chiesa S. *see under* Gillot P.-Y., 299, 242
- Chisholm G. D. *see under* Aitken R. J., 299, 499
- Chiu L.-T. G. and Kron R. G. A possible CH subunit, 299, 702
- Choo K. H., Gould K. G., Rees D. K. and Brownlee G. G. Molecular cloning of the gene for human anti-haemophilic factor IX, 299, 178
- Christensen A. C. and Young E. T. T4 late transcripts are initiated near a conserved DNA sequence, 299, 369
- Clark D. A. American Journal of Reproductive Immunology, *Journal review*, 299, 504
- Clark G. F. *see under* Whatmore R. W., 299, 44
- Clark R. R. *see under* Browne I. W. A., 299, 788
- Clarke C. J. S. *book review* of Retarded Action-at-a-Distance: The Change of Force with Motion, (Burniston Brown G.), 299, 191
- Claverie A., Isaak G. R., McLeod C. P., van der Raay H. B., Pallé P. L. and Roca Cortes T. Solar core rotation, 299, 704
- Clayton C. E., Murphy D., Lovett M. and Rigby P. W. J. A fragment of the SV40 large T-antigen gene transforms, 299, 59
- Clayton R. N. and Huhtaniemi I. T. Absence of gonadotropin-releasing hormone receptors in human gonadal tissue, 299, 56
- Clifford H. T. *see under* Dahlgren R. M. T., 299, 92
- Cline M. J. *see under* Müller R., 299, 640
- Cohen C. M., Foley S. F. and Korsgren C. A protein immunologically related to erythrocyte band 4.1 is found on stress fibres of non-erythroid cells, 299, 648
- Cohen D. Psychoneuroendocrinology: The Journal of Psychophysical Systems, *Journal review*, 299, 505
- Cohen M. H. *see under* Browne I. W. A., 299, 788
- Cohen N. *see under* Rollins-Smith L. A., 299, 820
- Cohn M. *see under* Collins J. L., 299, 169
- Cole A. J., Kilkenny J. D., Rumsby P. T., Evans R. G., Hooker C. J. and Key M. H. Measurement of Rayleigh-Taylor instability in a laser-accelerated target, 299, 329
- Coleman J. L. *see under* Skirrow R., 299, 142
- Collins J. L., Patek P. Q. and Cohn M. *In vivo* surveillance of tumorigenic cells transformed *in vitro*, 299, 169
- Collins F. H. *see under* Zavala F., 299, 737
- Condomines M. *see under* Allègre C. J., 299, 21
- Conn E. E. *see under* Stumpf P. K., 299, 762
- Connell J. R. *see under* Newbold R. F., 299, 633
- Connolly J. S. Editor, Biocatalytic Conversion and Storage of Solar Energy, *book review* by Wilson J. I. B., 299, 378
- Convertino V. A., Morey E. R. and Greenleaf J. E. Reduction in plasma calcium during exercise in man, *matters arising*, 299, 658
- Cook R. E. and Robinson P. J. Perchlorate hazard, *correspondence*, 299, 674
- Cooke D. *see under* Burckle L. H., 299, 435
- Cooke H. B. S. *book review* of Crustal Evolution of Southern Africa: 3.8 Billion Years of Earth History, (Tankard A. J. et al.), 299, 93
- Corbett A. D., Paterson S. J., McKnight A. T., Magnan J. and Kosterlitz H. W. Dynorphin-8 and dynorphin-9 are ligands for the κ -subtype of opiate receptor, 299, 79
- Cornuelle B. *see under* Behringer D., 299, 121
- Cotgrove S. *book review* of Acceptable Risk, (Fischhoff B. et al.), 299, 659
- Cotterill R. M. J. and Madsen J. U. Crystal instability and melting—Reply, *matters arising*, 299, 188
- Counsell J. N. and Hornig D. H. Editors, Vitamin C (Ascorbic Acid), *book review* by Rivers J., 299, 760
- Coutinho A. *see under* Fornli L., 299, 173
- Cowling G. Synthetase U-turns, *news and views*, 299, 13
- Cox B. Journal of Vertebrate Paleontology, *Journal review*, 299, 508
- Cox J. P. A new type of pulsating star, *news and views*, 299, 402
- Craddock C. Editor, Antarctic Geoscience, *book review* by Lovering J. F., 299, 661
- Craik C. S., Sprang S., Fletcher R. and Rutter W. J. Intron-exon splice junctions map at protein surfaces, 299, 180
- Crocker V. S. Journal of Fusion Energy/Nuclear Technology Fusion, *Journal review*, 299, 512
- Crombie L. *book review* of The Natural Coumarins: Occurrence, Chemistry and Biochemistry, (Murray R. D. H., Mendez J., Brown S. A.), 299, 285
- Crouch E. *see under* Wilson R., 299, 659
- Crounoud S. *see under* Butler-Browne G. S., 299, 830
- Curtin W. A. *see under* O'Sullivan V. R., 299, 102
- Curtis A. *see under* Bellairs R., 299, 473
- Dabora R. L. *see under* Migeon B. R., 299, 838
- Dahlgren R. M. T. and Clifford H. T. The Monocotyledons: A Comparative Study, *book review* by Moore P. D., 299, 92
- Dale B. *see under* Ozanne B., 299, 744
- Darai G. *see under* Will H., 299, 740
- Davies J. What's news in biotechnology? *Journal review*, 299, 493
- Davis J. *see under* Bennett V., 299, 126
- Dayton A. I. *see under* Botchan P. M., 299, 453
- de Bruyn A. G. *see under* Noordam J. E., 299, 597
- de la Vega H. *see under* Quinto C., 299, 724
- de Lange F. *see under* van Graas G., 299, 437
- De Lange T. and Borst P. Genomic environment of the expression-linked extra copies of genes for surface antigens of *Trypanosoma brucei* resembles the end of a chromosome, 299, 451
- de Leeuw J. W. *see under* van Graas G., 299, 437
- De Pover A. *see under* Godfraind T., 299, 824
- de Vaucouleurs G. Five crucial tests of the cosmic distance scale using the Galaxy as fundamental standard, 299, 303
- Dean C. R. Weapons treaties, *correspondence*, 299, 8
- Deatherage J. F. *see under* Taylor K. A., 299, 840
- Deinhardt F. *see under* Will H., 299, 740
- Dekeyser W. *see under* Cardon F., 299, 378
- Delmas R. J. Antarctic sulphate budget, *news and views*, 299, 677
- Detre J. A. *see under* Nairn A. C., 299, 734
- Di Capua E. *see under* Stasiak A., 299, 185
- Diamond P. J. *see under* Norris R. P., 299, 131
- Dideberg O., Charlier P., Dive G., Joris B., Frère J. M. and Ghysen J. M. Structure of a Zn²⁺-containing D-alanyl-D-alanine-cleaving carboxypeptidase at 2.5 Å resolution, 299, 469
- Diehl V. *see under* Schwab U., 299, 65
- Dingwall C. *see under* Gurdon J. B., 299, 652
- Dive G. *see under* Dideberg O., 299, 469
- Dixon A. F. American Journal of Primatology, *Journal review*, 299, 506
- Dixon A. F. and George L. Prolactin and parental behaviour in a male New World primate, 299, 551
- Dobben H. F. *see under* Breemen N. van, 299, 548
- Dobinson A. *see under* Smythe D. K., 299, 338
- Dodd G. *see under* Persaud K., 299, 352
- Doherty P. and Simpson E. Murine models of multiple sclerosis, *news and views*, 299, 106
- Doolittle W. F. *see under* Sapienza C., 299, 182
- Doolittle W. F. *see under* Walker W. F., 299, 723
- Douglas W. W. *see under* Taraskevich P. S., 299, 733
- Dover G. Molecular drive: a cohesive mode of species evolution, *review article*, 299, 111
- Duderstadt J. J. and Moses G. A. Inertial Confinement Fusion, *book review* by Evans R. G., 299, 93
- Dunn G. *see under* Bellairs R., 299, 473
- Dupré B., Lambret B. and Allègre C. J. Isotopic variations within a single oceanic island: the Terceira case, 299, 620
- Durrance S. T. and Moos H. W. Intense Ly α emission from Uranus, 299, 428
- Dutta G. P. *see under* Gupta C. M., 299, 259
- Dworetzky M. M. *see under* Jacobs J. M., 299, 535
- Eddy M. M. *see under* Cheetham A. K., 299, 24
- Edwards M. K. S. *see under* McBurney M. W., 299, 165
- Egan T. M. *see under* Williams J. T., 299, 74
- Eisen H. N. *see under* Elliott B. W. Jr., 299, 559
- Eisenberg D., Weiss R. M. and Terwilliger T. C. The helical hydrophobic moment: a measure of the amphiphilicity of a helix, 299, 371
- Eisenstadt E. *see under* Foster P. L., 299, 365
- Elliott B. W. Jr., Eisen H. N. and Steiner L. A. Unusual association of V, J and C regions in a mouse immunoglobulin λ chain, 299, 559
- Ellis J. Promiscuous DNA — chloroplast genes inside plant mitochondria, *news and views*, 299, 678
- Emson P. Regulatory Peptides/Neuro-peptides/Peptides, *Journal review*, 299, 503
- Erickson R. P. *see under* Tres L. L., 299, 752
- et al. *see under* Fischhoff B., 299, 659
- Ettinger K. V. Nuclear Medicine Communications/Radiation Protection Dosimetry/Clinical Physics and Physiological Measurement, *Journal review*, 299, 509
- Evans C. J. *see under* Weber E., 299, 77
- Evans D. R., Romig J. H., Hord C. W., Simmons K. E., Warwick J. W. and Lane A. L. The source of Saturn electrostatic discharges, 299, 236
- Evans R. G. *book review* of Inertial Confinement Fusion, (Duderstadt J. J. and Moses G. A.), 299, 93
- et al. *see under* Cole A. J., 299, 329
- Fan J. L. *see under* Chien J. C. W., 299, 608
- Fantes P. A. *see under* Mitchison J. M., 299, 92
- Faulkner P. A novel class of wasp viruses and insect immunity, *news and views*, 299, 489
- Favera R. D., Wong-Staal F. and Gallo R. C. *onc* gene amplification in promyelocytic leukaemia cell line HL-60 and primary leukaemic cells of the same patient, 299, 61
- Fejfar O. *see under* Repenning C. A., 299, 344
- Fellous M. *see under* Wallach M. D., 299, 833
- Fernández L. *see under* Quinto C., 299, 724
- Fersht A. R. *see under* Winter G., 299, 756
- Fesen R. A. *see under* Nomoto K., 299, 803
- Field M. *see under* Manning D. C., 299, 256
- Finston H. L. and Rychman A. C. A New View of Current Acid-Base Theories, *book review* by Gibson J., 299, 472
- Fischhoff B. et al. Acceptable Risk, *book review* by Cotgrove S., 299, 659
- Fisher L. M. DNA unwinding in transcription and recombination, *news and views*, 299, 105
- Fisher S. B. *see under* Harbottle J. E., 299, 139
- Fletcher J. *book review* of Tree-ring Dating and Archaeology, (Baillie M. G. L.), 299, 660
- Fletcher R. *see under* Craik C. S., 299, 180
- Flores M. *see under* Quinto C., 299, 724
- Flower M. F. J. Cryptocumulate tholeiite as evidence for magma mixing at an intermediate-rate spreading axis, 299, 542
- Foley S. F. *see under* Cohen C. M., 299, 648
- Fonash S. J. Solar Cell Device Physics, *book review* by Wilson J. I. B., 299, 378
- Fong D. *see under* Wallach M. D., 299, 833
- Forbes G. M. *see under* Woodruff M. F. A., 299, 822
- Fornli L. and Coutinho A. The production of membrane or secretory forms of immunoglobulins is regulated by C-gene-specific signals, 299, 173
- Foster P. L., Eisenstadt E. and Cairns J. Random components in mutagenesis, 299, 365
- Fowler C. W. and Smith T. D. Dynamics of Large Mammal Populations, *book review* by Kruuk H., 299, 846
- Fowler W. E. *see under* Bennett V., 299, 126
- Francis T. J. G. Thermal expansion effects in deep-sea sediments, 299, 334
- Frank J. *see under* Zingsheim H. P., 299, 81
- Franklin J. *see under* Bright S. W. J., 299, 278
- Frère J. M. *see under* Dideberg O., 299, 469
- Fritz W. J. *see under* Harrison S., 299, 720
- Frost R. L. *see under* Barron P. F., 299, 616
- Fujii S. *see under* Wang A. H.-J., 299, 601
- Furutani Y. *see under* Noda M., 299, 793
- Gallo R. C. *see under* Favera R. D., 299, 61
- Galvan M. *see under* Gustafsson B., 299, 252
- Ganic C. J. A. BVP models of nerve membrane, *matters arising*, 299, 375
- Garcia-Mata C. as I was saying, *correspondence*, 299, 8
- Gavala M. B. *see under* Abbott L. F., 299, 187
- Gebbie H. A., Llewellyn-Jones D. T. and Knight R. J. Zenith atmospheric attenuation measurements, *matters arising*, 299, 280
- George L. *see under* Dixon A. F., 299, 551
- Gerdies J. *see under* Schwab U., 299, 65
- Ghysen J. M. *see under* Dideberg O., 299, 469
- Ghysel-Burton J. *see under* Godfraind T., 299, 824
- Gibson J. *book review* of A New View of Current Acid-Base Theories, (Finston H. L. and Rychman A. C.), 299, 472
- Gilbert T. D. *see under* Philip R. P., 299, 245
- Gillett J. D. Ball of fire, *correspondence*, 299, 294
- Gillies G. E., Linton E. A. and Lowry P. J. Corticotropin releasing activity of the new CRF is potentiated several times by vasopressin, 299, 355
- Gillot P.-Y., Chiesa S., Pasquaré G. and Vezzoli L. < 33,000-yr K-Ar dating of the volcano-tectonic horst of the Isle of Ischia, Gulf of Naples, 299, 242
- Gjelsvik T. Polish deflection, *correspondence*, 299, 390
- Goddard P. A. *see under* Whatmore R. W., 299, 44
- Godfraind T., Ghysel-Burton J. and De Pover A. Dihydroouabain is an antagonist of ouabain inotropic action, 299, 824
- Gold M. R. and Martin A. R. Intracellular Cl⁻ accumulation reduces Cl⁻ conductance in inhibitory synaptic channels, 299, 828
- Goldman M. *see under* Abragam A., 299, 474
- Goldman-Rakic P. S. *see under* Schwartz M. L., 299, 154
- Goldreich P. *see under* Borderies N., 299, 209
- Golub E. S. Connections between the nervous, haematopoietic and germ-cell systems, *news and views*, 299, 483
- Gomes W. P. *see under* Cardon F., 299, 378
- Goodfellow P. N. *see under* Andrews P. W., 299, 296
- et al. *see under* Heisterkamp N., 299, 747
- Goodhart C. V. Cancer trends, *correspondence*, 299, 674
- Goodman B. A. and Cheshire M. V. Reduction of molybdate by soil organic matter: EPR evidence for formation of both Mo(V) Mo(III), 299, 618
- Goody R. S. *see under* Amos L. A., 299, 467
- Goorwine E., Webb C. G. and Sachs L. Participation of myeloid leukaemic cells injected into embryos in haematopoietic differentiation in adult mice, 299, 63
- Gordon J. C. *see under* Woodruff M. F. A., 299, 822
- Gordon R. M., Martin J. H. and Knauer G. A. Iron in north-east Pacific waters, 299, 611
- Gordon S. *see under* Vaux D. J. T., 299, 70
- Gottlieb D. I. *book review* of Cell Behaviour: A Tribute to Michael Abercrombie, (Bellairs R., Curtis A., Dunn G. editors), 299, 473
- Gottlieb M. S. *see under* Groopman J. E., 299, 103
- Gould K. G. *see under* Choo K. H., 299, 178
- Grafe P. *see under* Gustafsson B., 299, 252
- Gramer D. K. *see under* Parslow T. G., 299, 449
- Graybiel A. M. and Ragsdale C. W. Jr. Pseudocholinesterase staining in the primary visual pathway of the macaque monkey, 299, 439
- Green D. A. and Gull S. F. Distance to Crab-like supernova remnant 3C58, 299, 606
- Green M. A. Solar Cells: Operating Principles, Technology, and System Applications, *book review* by Wilson J. I. B., 299, 378
- Greengard P. *see under* Nairn A. C., 299, 734
- Greenleaf J. E. *see under* Convertino V. A., 299, 658
- Greenspan R. J. *see under* Hall J. C., 299, 761
- Greenwood P. J. *see under* Baker C. K., 299, 149
- Gregory J. Solar-terrestrial influences on weather and climate, *news and views*, 299, 401
- Grime J. P. and Mowforth M. A. Variation in genome size — an ecological interpretation, 299, 151
- Groffen J. *see under* Heisterkamp N., 299, 747
- Groopman J. E. and Gottlieb M. S. Kaposi's sarcoma: an oncologic looking glass, *news and views*, 299, 103
- Grosfeld F. *see under* Lee J. S., 299, 750
- Grove A. T. *book review* of Environmental History of East Africa, (Hamilton A. C.), 299, 844
- Gull S. F. *see under* Green D. A., 299, 606
- Gull T. R. *see under* Nomoto K., 299, 803
- Gupta C. M., Alam A., Mathur P. N. and Dutta G. P. A new look at nonparasitized red cells of malaria-infected monkeys, 299, 259
- Gurdon J. B., Dingwall C., Laskey R. A. and Korn L. J. Developmental inactivity of SS RNA genes persists when chromosomes are cut between genes, 299, 652
- Gustafsson B., Galvan M., Grafe P. and Wigström H. A transient outward current in a mammalian central neurone blocked by 4-aminopyridine, 299, 252
- Gwads R. W. *see under* Zavala F., 299, 737
- Hadfield E. *see under* Acheson E. D., 299, 263
- Hager B. H. The geoid and geodynamics, *news and views*, 299, 104
- Haj-Ahmad Y. and Hickey D. A. A molecular explanation of frequency-dependent selection in *Drosophila*, 299, 350
- Hall A. *see under* Marshall C. J., 299, 171
- Hall C. Behaviour Analysis Letters, *Journal review*, 299, 506
- Hall J. C., Greenspan R. J. and Harris W. A. Genetic Neurobiology, *book review* by Lawrence P. A., 299, 761
- Hallett A. *see under* Szelke M., 299, 555
- Hamilton A. C. Environmental History of East Africa, *book review* by Grove A. T., 299, 844
- Hämmerling G. J. *see under* Koch N. E., 299, 644
- Hanawalt P. C. *see under* Zolan M. E., 299, 462
- Hancock R. G. V. *see under* Lewin P. K., 299, 627

- Hänicke W. *see under* Zingsheim H. P., 299, 81
 Hanyu T. *see under* Matsumoto G., 299, 52
 Haque A. and Capron A. Transplacental transfer of rodent micro-
 filariae induces antigen-specific tolerance in rats, 299,
 361
 Harbottle J. E. and Fisher S. B. Copper sulphide Cu_2S (Dige-
 nite I) precipitation in mild steel, 299, 139
 Harman P. M. Energy, Force, and Matter: The Conceptual
 Development of Nineteenth-Century Physics, *book review*
 by Brush S. G., 299, 845
 Harris T. *In vitro* mutagenesis, *news and views*, 299, 298
 Harris W. A. *see under* Hall J. C., 299, 761
 Harrison S. and Fritz W. J. Depositional features of March
 1982 Mount St Helens sediment flows, 299, 720
 Hartquist T. W. and Snijders M. A. J. Hot galactic gas and
 narrow line quasar absorption systems, *review article*, 299,
 783
 Haseloff J., Mohamed N. A. and Symons R. H. Viroid RNAs of
 cadang-cadang disease of coconuts, 299, 316
 Hattai I. *see under* Tamura Y., 299, 631
 Hawkesworth C. J. *see under* Rogers N. W., 299, 409
 Hayakawa S. *see under* Tawara Y., 299, 38
 Hearle J. W. S. Polymers and their Properties. Vol. 1, Funda-
 mentals of Structure and Mechanics, *book review by*
 Calvert P., 299, 472
 Heath R. *see under* Wright A., 299, 208
 Hedde N. *see under* Blajchman M. A., 299, 67
 Helmenau U. and Saenger W. Specific protein-nucleic acid
 recognition in ribonuclease T1-2'-guanylic acid complex:
 an X-ray study, 299, 27
 Heinmiller R. *see under* Behringer D., 299, 121
 Heisterkamp N., Groffen J., Stephenson J. R., Spurr N. K.,
 Goodfellow P. N., Solomon E., Carrith B. and Bodmer W. F.
 Chromosomal localization of human cellular homologues
 of two viral oncogenes, 299, 747
 Henckes G., Vannier F., Seiki M., Ogasawara N., Yoshikawa H.
 and Seror-Laurent S. J. Ribosomal RNA genes in the
 replication origin region of *Bacillus subtilis* chromosome,
 299, 268
 Hennig G. J., Herr W., Weber E. and Xirotriris N. I. Petralona
 Cave dating controversy—Reply, *matters arising*, 299, 280
 Herr W. *see under* Hennig G. J., 299, 280
 Hickey D. A. *see under* Haj-Ahmad Y., 299, 350
 Hill T. L. The linear Onsager coefficients for biochemical
 kinetic diagrams as equilibrium one-way cycle fluxes, 299,
 84
 Hindmarsh J. L. and Rose R. M. BVP models of nerve
 membrane—Reply, *matters arising*, 299, 375
 Hines M. E., Orem W. H., Lyons W. B. and Jones G. E.
 Microbial activity and bioturbation-induced oscillations in
 pore water chemistry of estuarine sediments in spring, 299,
 433
 Hinuma Y. *see under* Yamamoto N., 299, 367
 Hirose T. *see under* Noda M., 299, 793
 Hirsch J. A. *see under* Chien J. C. W., 299, 608
 Hodes R. J. Immunology Today, *Journal review*, 299, 503
 Hodge P. W. Interplanetary Dust, *book review by* Hughes D.
 W., 299, 844
 Hodgkin J. *see under* Kimble J., 299, 456
 Holdgate M. W., Kassas M. and White G. F. Editors, The
 World Environment 1972-1982: A Report by the United
 Nations Environment Programme, *book review by*
 O'Riordan T., 299, 91
 Hollas J. M. High Resolution Spectroscopy, *book review by*
 Sheppard N., 299, 846
 Holmes K. C. *see under* Amos L. A., 299, 467
 Holmes-Siedle A. *book review of* Physics of Semiconductor
 Devices, (Sze S. M.) 299, 662
 Hooker C. J. *see under* Cole A. J., 299, 329
 Horai K. A satellite altimetric geoid in the Philippine Sea, 299,
 117
 Hord C. W. *see under* Evans D. R., 299, 236
 Hornig D. H. *see under* Counsell J. N., 299, 760
 Hornykiewicz O. Brain catecholamines in schizophrenia — a
 good case for noradrenaline, *news and views*, 299, 484
see under Berger M., 299, 254
 Hough J. H. *see under* Axon D. J., 299, 234
 Howe S. *see under* Bourne W. E. Y., 299, 294
 Howley P. M. *see under* Chen E. Y., 299, 529
 Hubel D. H. Exploration of the primary visual cortex, 1955-78,
review article, 299, 515
 Hughes D. W. *book review of* Interplanetary Dust, (Hodge P.
 W.) 299, 844
 The first meteorite stream, *news and views*, 299, 14
 Huhtaniemi I. T. *see under* Clayton R. N., 299, 56
 Hunt J. M. *see under* Whelan J. K., 299, 50
 Hurwitz J. L. and Cebra J. R. Rearrangements between the
 immunoglobulin heavy chain gene J_H and C_H regions
 accompany normal B lymphocyte differentiation *in vitro*,
 299, 742
 Huttner W. B. Sulphation of tyrosine residues — a widespread
 modification of proteins, 299, 273
 Huxley H. E. *see under* Amos L. A., 299, 467
 Hwaung G. and Manuel O. K. Terrestrial-type xenon in meteoric
 troilite, 299, 807
 Hyams J. Cell Motility, *Journal review*, 299, 498
 Iino T. *see under* Ohtani T., 299, 86
 Iitaka Y. *see under* Nakamura K. T., 299, 564
 Ikeya M. *see under* Pouloukas A. N., 299, 280
 Imber C. E. *see under* Cheetham P. S. J., 299, 628
 Inayama S. *see under* Noda M., 299, 793
 Inoue Y. *see under* Mikoshiba K., 299, 357
 Intriligator D. S. *see under* Pérez-de-Tejada H., 299, 325
 Irving J. A. China syndrome, *correspondence*, 299, 200
 Isaacs A. *book review of* The McGraw-Hill Encyclopedia of
 Science and Technology, (Parker S. P. editor) 299, 283
 Isaak G. R. *see under* Claverie A., 299, 704
 Isherwood J. *see under* Cheetham P. S. J., 299, 628
 Ish-Horowitz D. Transposable elements, hybrid incompatibility
 and speciation, *news and views*, 299, 676
 Ishizaka S. and Möller G. Lithium chloride induces partial
 responsiveness to LPS in nonresponder B cells, 299, 363
 Iversen L. L. Yet another opioid peptide? *news and views*, 299,
 578
 Iwabuchi M. *see under* Ohtani T., 299, 86
 Iwahashi K. *see under* Nakamura K. T., 299, 564
 Jacobs G. H. Comparative Color Vision, *book review by* Muntz
 W. R. A., 299, 284
 Jacobs J. M. and Dworetzky M. M. Bismuth abundance anoma-
 ly in a Hg-Mn star, 299, 535
 Janeway C. A. Jr. *book review of* Idiotypes and Lymphocytes,
 (Bona C. A.) 299, 473
 Jeanloz R. Oxygen in the Earth's metallic core? *news and views*,
 299, 108
 Jefferson D. A. *see under* Cheetham A. K., 299, 24
 Jenkins J. *see under* Lee J. S., 299, 750
 Jolliffe L. K., Carter A. D. and McAllister W. T. Identification
 of a potential control region in bacteriophage T7 late
 promoters, 299, 653
 Jones D. E. H. and Ledingham K. W. D. Arsenic in Napoleon's
 wallpaper, 299, 626
 Jones D. M. *see under* Szelke M., 299, 555
 Jones E. J. W. and Ramsay A. T. S. Volcanic ash deposits of
 early Eocene age from the Rockall Trough, 299, 342
 Jones G. E. *see under* Hines M. E., 299, 433
 Jones J. S. Of cannibals and kin, *news and views*, 299, 202
 Jones T. B. Generation and propagation of acoustic gravity
 waves, *news and views*, 299, 488
 Jones-Villeneuve E. M. V. *see under* McBurney M. W., 299,
 165
 Joris B. *see under* Dideberg O., 299, 469
 Jouzel J., Merlivat L. and Lorius C. Deuterium excess in an
 East Antarctic ice core suggests higher relative humidity at
 the oceanic surface during the last glacial maximum, 299,
 688
 Kaar G. F. *see under* O'Sullivan V. R., 299, 102
 Kachur J. F. *see under* Manning D. C., 299, 256
 Kahn C. R. Autoimmunity and the aetiology of insulin-
 dependent diabetes mellitus, *news and views*, 299, 15
 Kandel E. R. *see under* Siegelbaum S. A., 299, 413
 Kanetkar S. M. *see under* Bancroft G. M., 299, 708
 Karasz F. E. *see under* Chien J. C. W., 299, 608
 Karin M. and Richards R. I. Human metallothionein genes —
 primary structure of the metallothionein-II gene and a
 related processed gene, 299, 777
 Karn J. *see under* McLachlan A. D., 299, 226
 Kassas M. *see under* Holdgate M. W., 299, 91
 Katze M. G. *see under* Signis C., 299, 175
 Kearney J. F. *see under* Pollak B. A., 299, 447
 Kelk B. *see under* Smythe D. K., 299, 338
 Kennedy G. L., Lajoie K. R. and Wehmiller J. F.
 Aminostratigraphy and faunal correlations of late Quaternary
 marine terraces, Pacific Coast, USA, 299, 545
 Kennedy J. S. A future for immobilized cell technology, *news*
and views, 299, 777
 Kent D. V. Apparent correlation of palaeomagnetic intensity
 and climatic records in deep-sea sediments, 299, 538
 Keuh J. S. H. *see under* Bright S. W. J., 299, 278
 Kew O. *see under* Minor P. D., 299, 109
 Key M. H. *see under* Cole A. J., 299, 329
 Kilkenny J. D. *see under* Cole A. J., 299, 329
 Kimble J., Hodgkin J., Smith T. and Smith J. Suppression of an
 amber mutation by microinjection of suppressor tRNA in
C. elegans, 299, 456
 King A. J. *see under* Palmer A. R., 299, 248
 King C. M. *see under* Moon-shong Tang, 299, 646
 King S. R. Falling stock, *correspondence*, 299, 390
 Kingdon J. East African Mammals: An Atlas of Evolution in
 Africa, *book review by* Bertram B., 299, 189
 Kirchner H. *see under* Schwab U., 299, 65
 Kirkwood T. B. L. IQ jump or trend? *correspondence*, 299, 8
 Klein J. *see under* Brown L., 299, 718
 Klemes V. Cold war, *correspondence*, 299, 200
 Klinger J. A possible resurfacing mechanism for icy satellites,
 299, 41
 Klysik J. *see under* Singleton C. K., 299, 312
 Knaus G. A. *see under* Gordon R. M., 299, 611
 Knight R. J. *see under* Gebbie H. A., 299, 280
 Knox R. *see under* Behringer D., 299, 121
 Koch H.-G. *see under* Will H., 299, 740
 Koch N., Koch S. and Hämmerling G. J. Ia invariant chain
 detected on lymphocyte surface by monoclonal antibody,
 299, 644
 Koch S. *see under* Koch N., 299, 644
 Köhler P. *see under* Seifritz W., 299, 390
 Komarneni S. and Roy R. Use of γ -zirconium phosphate for Cs
 removal from radioactive waste, 299, 707
 Koob G. F. *see under* Staunton D. A., 299, 72
 Korn L. J. *see under* Gurdon J. B., 299, 652
 Korsgren C. *see under* Cohen C. M., 299, 648
 Korteling R. G. *see under* Ku T. L., 299, 240
 Kosterlitz H. W. *see under* Corbett A. D., 299, 79
 Koury M. J. and Pragnell I. B. Retroviruses induce granulocyte-
 macrophage colony stimulating activity in fibroblasts,
 299, 638
 Koyanagi Y. *see under* Yamamoto N., 299, 367
 Krishan V. *see under* Sivaram C., 299, 427
 Krishnamurti T. N. *book review of* Tropical Cyclones: Their
 Evolution, Structure and Effects, (Anthes R. A.) 299, 660
 Kron R. G. *see under* Chiu L.-T. G., 299, 702
 Kruuk H. *book review of* Dynamics of Large Mammal Popula-
 tions, (Fowler C. W. and Smith T. D.) 299, 846
 Ku T. L. *see under* Kusakabe M., 299, 712
 Ku T. L., Kusakabe M. and Nelson D. E., Southon J. R., Korteling
 R. G., Vogel J. and Nowkow I. Constancy of oceanic depo-
 sition of ^{10}Be as recorded in manganese crusts, 299, 240
 Kunieda H. *see under* Tawara Y., 299, 38
 Kunze K. L. *see under* Brown A. M., 299, 156
 Kusakabe M. *see under* Ku T. L., 299, 240
 Kusakabe M., Ku T. L., Vogel J., Southon J. R., Nelson D. E.
 and Richards R. ^{10}Be profiles in seafloor, 299, 712
 Kuszniir N. J. and Park R. G. Intraplate lithosphere strength and
 heat flow, 299, 540
 Kwang-Poo Chang *see under* Wallace M., 299, 650
 Kwong S. *see under* Benesch R. E., 299, 231
 Lachmann P. J. and Peters D. K. Editors, Clinical Aspects of
 Immunology, *book review by* Rosen F. S., 299, 94
 Lajoie K. R. *see under* Kennedy G. L., 299, 545
 Lakhani K. H. Trophic structure of a grassland insect commu-
 nity, *matters arising*, 299, 375
 Lamb P. J. Persistence of Subsaharan drought, 299, 46
 Lambrecht B. *see under* Dupré B., 299, 620
 Lane A. L. *see under* Evans D. R., 299, 236
 Larsen S. B. *see under* Wilson J. R., 299, 625
 Laskey R. A. *see under* Gurdon J. B., 299, 652
 Lawrence P. A. *book review of* Genetic Neurobiology, (Hall J.
 C., Greenspan R. J., Harris W. A.) 299, 761
 Leckie B. *see under* Szelke M., 299, 555
 Ledingham K. W. D. *see under* Jones D. E. H., 299, 626
 Lee J. S., Trowsdale J., Travers P. J., Carey J., Grosfeld F.,
 Jenkins J. and Bodmer W. F. Sequence of an HLA-DR
 α -chain cDNA clone and intron-exon organization of the
 corresponding gene, 299, 750
 Lemke H. *see under* Schwab U., 299, 65
 Lerner R. A. Tapping the immunological repertoire to produce
 antibodies of predetermined specificity, *review article*, 299,
 592
 Levell B. K. *see under* Braakman J. H., 299, 48
 Lever A. F. *see under* Szelke M., 299, 555
 Levine R. B. and Truman J. W. Metamorphosis of the insect
 nervous system: changes in morphology and synaptic
 interactions of identified neurones, 299, 250
 Levinson A. D. *see under* Chen E. Y., 299, 529
 Lewin P. K., Hancock R. G. V. and Vovnovich P. Napoleon
 Bonaparte — no evidence of chronic arsenic poisoning,
 299, 627
 Lewis R. A. and Segall R. L. Pressure dependence of glass disso-
 lution and nuclear waste disposal, 299, 140
 Liang E. P. Emission mechanism and source distances of γ -ray
 bursts, 299, 321
 Lieberman M. W. *see under* Moon-shong Tang, 299, 646
 Lieberzeit G. *see under* Wefer G., 299, 145
 Linton E. A. *see under* Gillies G. E., 299, 355
 Lippens C. *see under* Ackerman M., 299, 17
 Liritzis Y. *see under* Pouloukas A. N., 299, 280
 Llewellyn-Jones D. T. *see under* Gebbie H. A., 299, 280
 Lockwood J. P. T. and McAndrew S. J. Eukaryotic ribosomes can
 recognize preproinsulin initiation codons irrespective of
 their position relative to the 5' end of mRNA, 299, 221
 Lonsdale D. M. *see under* Stern D. B., 299, 698
 Lorius C. *see under* Jouzel J., 299, 688
 Lovering J. F. *book review of* Antarctic Geoscience, (Craddock
 C. editor) 299, 661
 Lorett M. *see under* Clayton C. E., 299, 59
 Lowe C. R. Applied Biochemistry and Biotechnology/Journal of
 Applied Biochemistry, *Journal review*, 299, 497
 Lowenstein A. M., Molleson T. and Washburn S. L. Pildown
 jaw confirmed as orang, *correspondence*, 299, 294
 Lowenstein J. M. Twelve wise men at the Vatican, *news and*
views, 299, 395
 Lowry P. J. *see under* Gillies G. E., 299, 355
 Lowy J. and Poulsen F. R. Time-resolved X-ray diffraction
 studies of the structural behaviour of myosin heads in a
 living contracting unstriated muscle, 299, 308
 Lux H. D. *see under* Brown A. M., 299, 156
 Lyons L. Proton decays and high-energy speculation, *news and*
views, 299, 295
 Lyons W. B. *see under* Hines M. E., 299, 433
 McAllister W. T. *see under* Jolliffe L. K., 299, 653
 McAndrew S. J. *see under* Lomedico P. T., 299, 221
 Macbeth R. G. *see under* Acheson E. D., 299, 263
 McBurney M. W., Jones-Villeneuve E. M. V., Edwards M. K. S.
 and Anderson P. J. Control of muscle and neuronal differen-
 tiation in a cultured embryonal carcinoma cell line, 299,
 165
 McCormmach R. Night Thoughts of a Classical Physicist, *book*
review by Maddox J., 299, 471
 McDevitt H. O. *see under* Steinman L., 299, 738
 Macdonald R. L. *see under* Werz M. A., 299, 730
 McDougall T. J. and Turner J. S. Influence of cross-diffusion on
 'finger' double-diffusive convection, 299, 812
 MacKenzie A. B. and Scott R. D. Radioactive and plutonium
 in intertidal sediments from southern Scotland, 299, 613
 McKnight A. T. *see under* Corbett A. D., 299, 79
 McLachlan A. D. and Karn J. Periodic charge distributions in
 the myosin rod amino acid sequence match cross-bridge
 spacings in muscle, 299, 226
 McLeod C. P. *see under* Claverie A., 299, 704
 McNamara L. F. *see under* Wright C. S., 299, 42
 McNamara L. F. and Wright C. S. Disappearing solar filaments
 and geomagnetic activity, 299, 537
 McQuillin R. *see under* Smythe D. K., 299, 338
 Maddox J. *book review of* Night Thoughts of a Classical Physi-
 cist, (McCormmach R.) 299, 471
 Madison D. V. and Nicoll R. A. Noradrenaline blocks accom-
 modation of pyramidal cell discharge in the hippocampus,
 299, 636
 Madsen J. U. *see under* Cotterill R. M. J., 299, 188
 Magistretti P. J. *see under* Staunton D. A., 299, 72
 Magnan J. *see under* Corbett A. D., 299, 79
 Mahy B. W. J. Antiviral Research/Journal of Interferon Re-
 search, *Journal review*, 299, 500
 Majiwa P. A. O. *see under* Williams R. O., 299, 417
 Makino F. *see under* Tawara Y., 299, 38
 Mangan G. L. The Biology of Human Conduct: East-West
 Models of Temperament and Personality, *book review by*
 Brand C. R., 299, 377
 Mann K. H. Ecology of Coastal Waters: A Systems Approach,
book review by Steele J. H., 299, 191
 Manning D. C., Snyder S. H., Kachur J. F., Miller R. J. and
 Field M. Bradykinin receptor-mediated chloride secretion
 in intestinal function, 299, 256
 Manuel O. K. *see under* Hwaung G., 299, 807
 Marshall C. J., Hall A. and Weiss R. A. A transforming gene
 present in human sarcoma cell lines, 299, 171
 Martin A. R. *see under* Gold M. R., 299, 828
 Martin J. B. Huntington's disease: genetically programmed cell
 death in the human central nervous system, *news and*
views, 299, 205
 Martin J. H. *see under* Braakman J. H., 299, 48
see under Gordon R. M., 299, 611
 Martin R. D. *book review of* The Primates of Madagascar,
 (Tattersall I.) 299, 843
 Maruyama Y. and Petersen O. H. Single-channel currents in
 isolated patches of plasma membrane from basal surface of
 pancreatic acini, 299, 159
 Mathur P. N. *see under* Gupta C. M., 299, 259
 Matsuda T. *see under* Tamura Y., 299, 631
 Matsumoto G., Torii T. and Hanyu T. High abundance of algal
 24-ethylcholesterol in Antarctic lake sediment, 299, 52
 Matsumoto T. *see under* Yamamoto N., 299, 367
 Matsuo T. *see under* Tajima Y., 299, 810
 Matthews D. H. *see under* Smythe D. K., 299, 338
 May J. *see under* May R. M., 299, 11
 May R. M. and May J. Stamp watching and bird collecting,

- news and views, 299, 11
- Measures C. I. see under Wrench J. J., 299, 431
- Meech R. W. see under Thomas R. C., 299, 826
- Megie G. see under Pelon J., 299, 137
- Mellman I. Multiple pathways of membrane transport, *news and views*, 299, 301
- Mendez J. see under Murray R. D. H., 299, 285
- Merigan T. C. see under Basham T., 299, 778
- Merlivi L. see under Jouzel J., 299, 688
- Metson J. B. see under Bancroft G. M., 299, 708
- Metzger K. see under Behringer D., 299, 121
- Michie D. Computer chess and the humanization of technology, *Commentary*, 299, 391
- Micklem H. S. see under Woodruff M. F. A., 299, 822
- Middleton R. see under Brown L., 299, 718
- Mifflin B. J. see under Bright S. W. J., 299, 278
- Migeon B. R., Shapiro L. J., Norum R. A., Mohandas T., Axelman J. and Dabora R. L. Differential expression of steroid sulphatase locus on active and inactive human X chromosome, 299, 838
- Mikoshiba K., Yokoyama M., Inoue Y., Takamatsu K., Tsukada Y. and Nomura T. Oligodendrocyte abnormalities in shiverer mouse mutant are determined in primary chimaeras, 299, 357
- Miller D. W. and Miller L. K. A virus mutant with an insertion of a copia-like transposable element, 299, 562
- Miller L. K. see under Miller D. W., 299, 562
- Miller R. J. The Journal of Neuroscience/Cellular and Molecular Neurobiology, *Journal review*, 299, 504
- see under Manning D. C., 299, 256
- Minor P. D., Kew O. and Schild G. C. Poliomyelitis — epidemiology, molecular biology and immunology, *news and views*, 299, 109
- Mitchison J. M. and Fantes P. A. book review of *The Molecular Biology of the Yeast Saccharomyces: Life Cycle and Inheritance*, (Strathern J. N. et al. editors) 299, 92
- Mitchison N. A. An immunoregulatory molecular complex with five active sites, *news and views*, 299, 576
- Mitsui Y. see under Nakamura K. T., 299, 564
- Miyaji S. see under Nomoto K., 299, 803
- Miyata T. see under Noda M., 299, 793
- Miyauchi T., Yonezawa S., Takamura T., Chiba T., Teijima S., Ozawa M., Sato E. and Muramatsu T. A new fucosyl antigen expressed on colon adenocarcinoma and embryonal carcinoma cells, 299, 168
- Mohamed N. A. see under Haseloff J., 299, 316
- Mohandas T. see under Migeon B. R., 299, 838
- Möller G. see under Ishizaka S., 299, 363
- Molleson T. see under Lowenstein A. M., 299, 294
- Moon-shong Tang, Lieberman M. W. and King C. M. *uvr* Genes function differently in repair of acetylaminofluorene and aminofluorene DNA adducts, 299, 64
- Moore P. D. Nordic Journal of Botany, *Journal review*, 299, 508
- Snail shells suggest past changes in British chalk vegetation, *news and views*, 299, 780
- Survival mechanisms in wetland plants, *news and views*, 299, 581
- book review of *The Monocotyledons: A Comparative Study*, (Dahlgren R. M. T. and Clifford H. T.) 299, 92
- The sunflower seed protection business, *news and views*, 299, 207
- Moore P. K. see under Browne I. W. A., 299, 788
- Moos H. W. see under Durrance S. T., 299, 428
- Moran J. M. see under Rodriguez L. F., 299, 323
- Morey E. R. see under Convertino V. A., 299, 658
- Morgan M. J. and Watt R. J. Mechanisms of interpolation in human spatial vision, 299, 553
- Moriarty F. European Applied Research Reports: Environment and Natural Resources Section/Environmental Monitoring and Assessment, *Journal review*, 299, 506
- Moseley R. Bulletin of Science, Technology and Society, *Journal review*, 299, 514
- Moses G. A. see under Duderstadt J. J., 299, 93
- Mowforth M. A. see under Grime J. P., 299, 151
- Muggleton-Harris A., Whittingham D. G. and Wilson L. Cytoplasmic control of preimplantation development *in vitro* in the mouse, 299, 460
- Muller C. see under Ackerman M., 299, 17
- Müller P. J. see under Wefel G., 299, 145
- Müller R., Slamon D. J., Tremblay J. M., Cline M. J. and Verma I. M. Differential expression of cellular oncogenes during pre- and postnatal development of the mouse, 299, 640
- Munk W. see under Behringer D., 299, 121
- Muntz W. R. A. book review of *Comparative Color Vision*, (Jacobs G. H.) 299, 284
- Muramatsu T. see under Miyauchi T., 299, 168
- Murphy D. see under Clayton C. E., 299, 59
- Murray R. D. H., Mendez J. and Brown S. A. The Natural Coumarins: Occurrence, Chemistry and Biochemistry, *book review* by Crombie L., 299, 285
- Musgrave D. L. and Reeburgh W. S. Density-driven interstitial water motion in sediments, 299, 331
- Muxlow T. W. B. see under Browne I. W. A., 299, 788
- Nadel J. A. see under Barnes P. J., 299, 444
- Nagase F. see under Tawara Y., 299, 38
- Najpal N. see under Blajchman M. A., 299, 67
- Nairn A. C., Detre J. A., Casnellie J. E. and Greengard P. Serum antibodies that distinguish between the phospho- and dephospho-forms of a phosphoprotein, 299, 734
- Nakamura K. T., Iwashashi K., Yamamoto Y., Iitaka Y., Yoshida N. and Mitsui Y. Crystal structure of a microbial ribonuclease, RNase St, 299, 564
- Nanji M. S. To the point, *correspondence*, 299, 200
- Nee J. see under Aronson P. S., 299, 161
- Neisser U. Memory Observed: Remembering in Natural Contexts, *book review* by Sutherland S., 299, 759
- Nelson D. E. see under Ku T. L., 299, 240
- see under Kusakabe M., 299, 712
- Nesbitt H. W. and Young G. M. Early Proterozoic climates and plate motions inferred from major element chemistry of lites, 299, 715
- Neugebauer D.-Ch. see under Zingsheim H. P., 299, 81
- Newbold R. F., Overell R. W. and Connell J. R. Induction of immortality is an early event in malignant transformation of mammalian cells by carcinogens, 299, 633
- Nicoll R. A. see under Madison D. V., 299, 636
- Nielsen E., Sofko G. and Axford W. I. STARE observations of long discrete echoes, 299, 238
- Noble S. and Woodhill J. M. Vitamin C. The Mysterious Redox-System — A Trigger of Life? *book review* by Rivers J., 299, 760
- Noda M., Takahashi H., Tanabe T., Toyosato M., Furutani Y., Hirose T., Asai M., Inayama S., Miyata T. and Numa S. Primary structure of α -subunit precursor of Torpedo californica acetylcholine receptor deduced from cDNA sequence, 299, 793
- Nomoto K., Sparks W. M., Fesen R. A., Gull T. R., Miyaji S. and Sugimoto D. The Crab Nebula's progenitor, 299, 803
- Nomura T. see under Mikoshiba K., 299, 357
- Noordam J. E. and de Bruyn A. G. High dynamic range mapping of strong radio sources, with application to 3C84, 299, 597
- Norris R. P., Diamond P. J. and Booth R. S. MERLIN spectral line observations of circumstellar shells around two OH/IR stars, 299, 131
- North R. A. see under Williams J. T., 299, 74
- Norum R. A. see under Migeon B. R., 299, 838
- Nowikow I. see under Ku T. L., 299, 240
- Numa S. see under Noda M., 299, 793
- Nunn B. J. and Baylor D. A. Visual transduction in retinal rods of the monkey *Macaca fascicularis*, 299, 726
- Nussenzweig R. S. see under Zavala F., 299, 737
- Nussenzweig V. see under Zavala F., 299, 737
- Ogasawara N. see under Henckes G., 299, 268
- Ohtani T., Shibata T., Iwabuchi M., Watabe H., Iino T. and Ando T. ATP-dependent unwinding of double helix in closed circular DNA by RecA protein of *E. coli*, 299, 86
- Okada H. see under Okada N., 299, 261
- Okada N., Yasuda T. and Okada H. Restriction of alternative complement pathway activation by sialosylglycolipids, 299, 261
- Okihana H. and Ponnamperna C. A protective function of the coacervates against UV light on the primitive Earth, 299, 347
- Oliver J. Changes at the crust-mantle boundary, *news and views*, 299, 398
- Oliver S. Journal of Molecular and Applied Genetics, *Journal review*, 299, 502
- Orem W. H. see under Hines M. E., 299, 433
- O'Riordan T. book review of *The World Environment 1972-1982: A Report by the United Nations Environment Programme*, (Holdgate M. W., Kassas M., White G. F. editors) 299, 91
- O'Sullivan V. R., Curtin W. A. and Kaar G. F. Units rule OK? *correspondence*, 299, 102
- Overell R. W. see under Newbold R. F., 299, 633
- Ozanne B., Wheeler T., Zack J., Smith G. and Dale B. Transforming gene of a human leukaemia cell is unrelated to the expressed tumour virus related gene of the cell, 299, 744
- Ozawa M. see under Miyauchi T., 299, 168
- Pagels H. see under Blumenthal G. R., 299, 37
- Pain R. H. The evolution of enzyme activity, *news and views*, 299, 486
- Palacios R. see under Quinto C., 299, 724
- Pallé P. L. see under Claverie A., 299, 704
- Palmer A. R. and King A. J. The representation of auditory space in the mammalian superior colliculus, 299, 248
- Park R. G. see under Kuznir N. J., 299, 540
- Parker S. P. Editor, *The McGraw-Hill Encyclopedia of Science and Technology*, *book review* by Isaacs A., 299, 283
- Parslow T. G. and Granner D. K. Chromatin changes accompanying immunoglobulin x gene activation: a potential control region within the gene, 299, 449
- Pasquaré G. see under Gillot P.-Y., 299, 242
- Patek P. Q. see under Collins, J. L., 299, 169
- Paterson S. J. see under Corbett A. D., 299, 79
- Pattison I. H. Scapine a "gene"? *correspondence*, 299, 200
- Pearson E. J. No rising trend for IQ in Japan, *correspondence*, 299, 574
- Pelon J. and Megie G. Ozone vertical distribution and total content using a ground-based active remote sensing technique, 299, 137
- Pérez-de-Tejada H., Intrilligator D. S. and Russel C. T. Orientation of planetary O⁺ fluxes and magnetic field lines in the Venus wake, 299, 325
- Pérez-Tomé J. M. and Toro M. A. Competition of similar and non-similar genotypes, 299, 153
- Persaud K. and Dodd G. Analysis of discrimination mechanisms in the mammalian olfactory system using a model nose, 299, 352
- Persson H. see under Signés C., 299, 175
- Perutz M. F. and Brunori M. Stereochemistry of cooperative effects in fish and amphibian haemoglobins, 299, 421
- Peters D. K. see under Lachmann P. J., 299, 94
- Petersen O. H. book review of *Calcium and Cellular Secretion*, (Rubin R. P.) 299, 285
- see under Maruyama Y., 299, 159
- Petri W. Transgenic organisms and development, *news and views*, 299, 399
- Phillipson L. see under Signés C., 299, 175
- Phillips J. G. book review of *Hormones in Development and Aging*, (Vernadakis A. and Timiras P. S. editors) 299, 845
- Phillipson E. A. see under Sears T. A., 299, 728
- Philp R. P. and Gilbert T. D. Unusual distribution of biological markers in an Australian crude oil, 299, 245
- Pickles H. Clinical Physiology/Journal of Cerebral Blood Flow and Metabolism/International Journal of Clinical Pharmacology Research/Pediatric Pharmacology/Developmental Pharmacology and Therapeutics/The Clinical Biochemist: Reviews, *Journal review*, 299, 499
- Pirt S. J. book review of Prescott and Dunn's *Industrial Microbiology*, (Reed G. editor) 299, 379
- Poirier J. P. Rheology of ices: a key to the tectonics of the ice moons of Jupiter and Saturn, 299, 683
- Pollok B. A., Bhowan A. S. and Kearney J. F. Structural and biological properties of a monoclonal auto-anti-(anti-idiotypic) antibody, 299, 447
- Ponnamperna C. see under Okihana H., 299, 347
- Porcas R. W. see under Browne I. W. A., 299, 788
- Posthumus M. A. see under Priestley D. A., 299, 148
- Potter T. L. see under Braakman J. H., 299, 48
- Poulanos A. N., Liritzis Y. and Ikeya M. Petralona Cave dating controversy, *matters arising*, 299, 280
- Poulsen F. R. see under Lowy J., 299, 308
- Pragnell I. B. see under Koury M. J., 299, 638
- Priestley D. A. and Posthumus M. A. Extreme longevity of lotus seeds from Pulantien, 299, 148
- Primack J. R. see under Blumenthal G. R., 299, 37
- see under Sher M. A., 299, 187
- Pye K. Thermoluminescence dating of sand dunes, *matters arising*, 299, 376
- Quinto C., de la Vega H., Flores M., Fernández L., Ballado T., Soberón G. and Palacios R. Reiteration of nitrogen fixation gene sequences in *Rhizobium phaseoli*, 299, 724
- Radke I. F. Sulphur and sulphate from Mt Erebus, 299, 710
- Ragsdale C. W. Jr see under Graybiel A. M., 299, 439
- Ramsay A. T. S. see under Jones E. J. W., 299, 342
- Reeburgh W. S. see under Musgrave D. L., 299, 331
- Reed G. Editor, Prescott and Dunn's *Industrial Microbiology*, *book review* by Pirt S. J., 299, 379
- Rees D. J. G. see under Choo K. H., 299, 178
- Reijnders H. F. R. see under Breemen N. van, 299, 548
- Repenning C. A. and Fejfar O. Evidence for earlier date of Ubeidiya, Israel, hominid site, 299, 344
- Revel M. see under Wallach D., 299, 833
- Rice-Evans P. C. Ball lightning in the laboratory, *correspondence*, 299, 774
- Rich A. see under Wang A. H.-J., 299, 601
- Richards G. see under Kusakabe M., 299, 712
- Richards R. I. see under Karin M., 299, 797
- Richards W. G. Theochem/Journal of Computational Chemistry, *Journal review*, 299, 513
- Ridder T. B. see under Breemen N. van, 299, 548
- Riding R. Cyanophyte calcification and changes in ocean chemistry, 299, 814
- Rigby P. W. J. see under Clayton C. E., 299, 59
- Rivers J. Appetite, *Journal review*, 299, 502
- book review of *Vitamin C. The Mysterious Redox-System — A Trigger of Life?* (Noble S. and Woodhill J. M.) 299, 760
- book review of *Vitamin C in Health and Disease*, (Basu T. K. and Schorah C. J.) 299, 760
- book review of *Vitamin C (Ascorbic Acid)*, (Counsell J. N. and Hornig D. H. editors) 299, 760
- Roberts J. M. see under Barnes P. J., 299, 444
- Robinson A. and Spooner E. T. C. Source of the detrital components of uraniferous conglomerates, Quirke ore zone, Elliot Lake, Ontario, Canada, 299, 622
- Robinson D. see under Burckle L. H., 299, 435
- Robinson P. J. see under Cook R. E., 299, 674
- Roca Cortes T. see under Claverie A., 299, 704
- Rodriguez L. F. and Moran J. M. Neutral hydrogen associated with the planetary nebula NGC6302, 299, 323
- Rogers G. C. Oceanic plateaus as meteorite impact signatures, 299, 341
- Rogers N. W. and Hawkesworth C. J. Proterozoic age and cumulate origin for granulite xenoliths, Lesotho, 299, 409
- Rognes S. E. see under Bright S. W. J., 299, 278
- Rollins-Smith L. A. and Cohen N. Self-pituitary grafts are not rejected by frogs deprived of their pituitary anlagen as embryos, 299, 820
- Romig J. H. see under Evans D. R., 299, 236
- Rose M. R. see under Sapienza C., 299, 182
- Rose R. M. see under Hindmarsh J. L., 299, 375
- Rosen F. S. book review of *Clinical Aspects of Immunology*, (Lachmann P. J. and Peters D. K. editors) 299, 94
- Rosner R. Activity in red-dwarf stars, *news and views*, 299, 680
- Rosner R., Zweibel E. and Trimble V. Plasma astrophysics at Santa Barbara, *news and views*, 299, 579
- Rowan-Robinson M. SERC and South Africa, *correspondence*, 299, 574
- Roy R. see under Komarneni S., 299, 707
- Ruben J. A. and Bennett A. F. Reduction in plasma calcium during exercise in man—Reply, *matters arising*, 299, 658
- Rubery P. book review of *The Biochemistry of Plants: A Comprehensive Treatise*, (Stumpf P. K. and Conn E. E. editors) 299, 762
- Rubin R. P. Calcium and Cellular Secretion, *book review* by Petersen O. H., 299, 285
- Rumsby P. T. see under Cole A. J., 299, 329
- Russel C. T. see under Pérez-de-Tejada H., 299, 325
- Rutter W. J. see under Craik C. S., 299, 180
- Rychtmann A. C. see under Finston H. L., 299, 472
- Ryder G. Siderophiles in the Brachina meteorite: impact melting? 299, 805
- Sachs L. see under Gootwine E., 299, 63
- Sacks I. S. see under Brown L., 299, 718
- Saenger W. see under Heinemann U., 299, 27
- Salemme F. R. Cooperative motion and hydrogen exchange stability in protein β -sheets, 299, 754
- Sanes J. R. see under Wigston D. J., 299, 464
- Sapienza C., Rose M. R. and Doolittle W. F. High-frequency genomic rearrangements involving archaeobacterial repeat sequence elements, 299, 182
- Sato E. see under Miyauchi T., 299, 168
- Saunders D. S. Insect Clocks, *book review* by Brady J., 299, 662
- Saunders J. R. Chromosomal rearrangements in gonococcal pathogenicity, *news and views*, 299, 781
- Schaadt M. see under Schwab U., 299, 65
- Schaller H. see under Will H., 299, 740
- Schellekens H. see under Will H., 299, 740
- Schenck P. A. see under van Graas G., 299, 437
- Schild G. C. see under Minor P. D., 299, 109
- Schindel D. E. Deme histories are not species' histories, *news and views*, 299, 490
- Schoch R. M. Gaps in the fossil record: Fossils and stratigraphy, *news and views*, 299, 490
- Schorah C. J. see under Basu T. K., 299, 760
- Schuster T. M. see under Steckert J. J., 299, 32
- Schwab U., Stein H., Gerdes J., Lemke H., Kirchner H., Schaadt M. and Diehl V. Production of a monoclonal antibody specific for Hodgkin and Sternberg-Reed cells of Hodgkin's disease and a subset of normal lymphoid cells, 299, 65
- Schwartz K. see under Butler-Browne G. S., 299, 830
- Schwartz M. L. and Goldman-Rakic P. S. Single cortical neurons have axon collaterals to ipsilateral and contralateral cortex in fetal and adult primates, 299, 154
- Scott R. D. see under MacKenzie A. B., 299, 613
- Sears T. A., Berger A. J. and Phillipson E. A. Reciprocal tonic activation of inspiratory and expiratory motoneurons by chemical drives, 299, 728
- Seeburg P. H. see under Chen E. Y., 299, 529
- Segall J. Disarmament ideas, *correspondence*, 299, 102
- Segal R. L. see under Lewis R. A., 299, 140

- Seifritz W., Köhler P. and Stepanek J. Tanks are unsafe, *correspondence*, 299, 390
- Seiki M. *see under* Henckes G., 299, 268
- Selwyn M. J. *book review of* Mitochondria, (Tzagoloff A.) 299, 190
- Sen G. Composition of basaltic liquids generated from a partially depleted ilmenite at 9 kbar pressure, 299, 336
- Seror-Laurent S. J. *see under* Henckes G., 299, 268
- Shapiro L. J. *see under* Migeon B. R., 299, 838
- Shaw G. E. Evidence for a central Eurasian source area of Arctic haze in Alaska, 299, 815
- Shen M. A. *see under* Chien J. C. W., 299, 608
- Shen Y. R. Recent advances in optical bistability, *news and views*, 299, 779
- Sheppard N. *book review of* High Resolution Spectroscopy, (Hollas J. M.) 299, 846
- Sher M. A. and Primack J. R. Absence of thermal effects on photon mass measurements—Reply, *matters arising*, 299, 187
- Shibata T. *see under* Ohtani T., 299, 86
- Shimizu H. *see under* Yano M., 299, 557
- Shimotohno K. and Temin H. M. Loss of intervening sequences in genomic mouse α -globin DNA inserted in an infectious retrovirus vector, 299, 265
- Shoemaker W. J. *see under* Staunton D. A., 299, 72
- Shibatani A. Japanese IQ, *correspondence*, 299, 102
- Siegelbaum S. A., Camardo J. S. and Kandel E. R. Serotonin and cyclic AMP close single K⁺ channels in *Aplysia* sensory neurones, 299, 413
- Signas C., Katze M. G., Persson H. and Philipson L. An adenovirus glycoprotein binds heavy chains of class I transplantation antigens from man and mouse, 299, 175
- Silk J. Mapping the Local supercluster, *news and views*, 299, 577
- Simmmons K. E. *see under* Evans D. R., 299, 236
- Simpon E. *see under* Doherty P., 299, 106
- Singal D. P. *see under* Blajchman M. A., 299, 67
- Singhi A. K. Thermoluminescence dating of sand dunes—Reply, *matters arising*, 299, 376
- Singleton C. K., Klysk J., Stirling S. M. and Wells R. D. Left-handed Z-DNA is induced by supercoiling in physiological ionic conditions, 299, 312
- Sivaram C. and Krishan V. Neutron oscillation as a source of excess sub-GeV antiprotons in galactic cosmic rays, 299, 427
- Skirrow R. and Coleman M. L. Origin of sulphur and geothermometry of hydrothermal sulphides from the Galapagos Rift, 86°W, 299, 142
- Skojles J. R. Preventing wars, *correspondence*, 299, 482
- Slamon D. J. *see under* Müller R., 299, 640
- Slocum A. H. Sequences on-line *correspondence*, 299, 482
- Smith C. A. *see under* Zolan M. E., 299, 462
- Smith D. J. H. Applied Catalysis, *Journal review*, 299, 513
- Smith G. *see under* Ozanne B., 299, 744
- Smith J. *see under* Kimble J., 299, 456
- Smith P. J. Sub-oceanic heat-flow from above, *news and views*, 299, 679
- Smith T. *see under* Kimble J., 299, 456
- Smith T. D. *see under* Fowler C. W., 299, 846
- Smythe D. K., Dobinson A., McQuillan R., Brewer J. A., Matthews D. H., Bundell D. J. and Kelk B. Deep structure of the Scottish Caledonides revealed by the MOIST reflection profile, 299, 338
- Snijders M. A. J. *see under* Hartquist T. W., 299, 783
- Snyder D. S., Beller D. I. and Unanue E. R. Prostaglandins modulate macrophage Ia expression, 299, 163
- Snyder S. H. *see under* Manning D. C., 299, 256
- Soberón G. *see under* Quinto C., 299, 724
- Sofko G. *see under* Nielsen E., 299, 238
- Solomon E. *see under* Heisterkamp N., 299, 747
- Southon J. R. *see under* Ku T. L., 299, 240
- see under* Kusakabe M., 299, 712
- Sparks W. M. *see under* Nomoto K., 299, 803
- Sperk G. *see under* Berger M., 299, 254
- Spiesberger J. *see under* Behringer D., 299, 121
- Spindel R. *see under* Behringer D., 299, 121
- Spooner E. T. C. *see under* Robinson A., 299, 622
- Sprang S. *see under* Craik C. S., 299, 180
- Spray J. G. Mafic segregations in ophiolite mantle sequences, 299, 524
- Spurr N. K. *see under* Heisterkamp N., 299, 747
- Sriram S. *see under* Steinman L., 299, 738
- Stark S. J. No to quangos, *correspondence*, 299, 200
- Stasiak A. and Di Capua E. The helicity of DNA in complexes with RecA protein, 299, 185
- Staunton D. A., Magistretti P. J., Koob G. F., Shoemaker W. J. and Bloom F. E. Dopaminergic supersensitivity induced by denervation and chronic receptor blockade is additive, 299, 72
- Steckert J. J. and Schuster T. M. Sequence specificity of trinucleotide diphosphate binding to polymerized tobacco mosaic virus protein, 299, 32
- Steele J. H. *book review of* Ecology of Coastal Waters: A Systems Approach, (Mann K. H.) 299, 191
- Stein H. *see under* Schwab U., 299, 65
- Steiner L. A. *see under* Elliott B. W. Jr., 299, 559
- Steinman L., Sriram S., Adelman N. E., Zamvil S., McDewitt H. O. and Ulrich H. Murine model for pertussis vaccine encephalopathy: linkage to H-2, 299, 738
- Stepanek J. *see under* Seifritz W., 299, 390
- Stephenson J. R. *see under* Heisterkamp N., 299, 747
- Stern D. B. and Lonsdale D. M. Mitochondrial and chloroplast genomes of maize have a 12-kilobase DNA sequence in common, 299, 698
- Stevens C. S. The acetylcholine receptor cloned, *news and views*, 299, 776
- Stirling S. M. *see under* Singleton C. K., 299, 312
- Strathern J. N. et al. Editors. The Molecular Biology of the Yeast *Saccharomyces*: Life Cycle and Inheritance, *book review by* Mitchison J. M., Fantes P. A., 299, 92
- Strominger J. L. *see under* Bono M. R., 299, 836
- Stumpf P. K. and Conn E. E. Editors. The Biochemistry of Plants: A Comprehensive Treatise, *book review by* Rubery P., 299, 762
- Sueiras J. *see under* Szelke M., 299, 555
- Suess E. *see under* Wefer G., 299, 145
- Suga H. *see under* Tajima Y., 299, 810
- Sugi H. *see under* Tamura Y., 299, 631
- Sugimoto D. *see under* Nomoto K., 299, 803
- Suhm M. A. *see under* Aronson P. S., 299, 161
- Sutherland S. Cognition and Brain Theory, *Journal review*, 299, 505
- book review of* Memory Observed: Remembering in Natural Contexts, (Neisser U.) 299, 759
- Symonds N. Key structures in transposition, *news and views*, 299, 580
- Symons R. H. *see under* Haseloff J., 299, 316
- Sze S. M. Physics of Semiconductor Devices, *book review by* Holmes-Siedle A., 299, 662
- Szelke M., Leckie B., Hallett A., Jones D. M., Sueiras J., Atrash B. and Lever A. F. Potent new inhibitors of human renin, 299, 555
- Tajima Y., Matsuo T. and Suga H. Phase transition in KOH-doped hexagonal ice, 299, 810
- Takahashi H. *see under* Noda M., 299, 793
- Takamatsu K. *see under* Mikoshiba K., 299, 357
- Takamura T. *see under* Miyachi T., 299, 168
- Tallon J. L. Crystal instability and melting, *matters arising*, 299, 188
- Tamura Y., Hatta I., Matsuda T., Sugi H. and Tsuchiya T. Changes in muscle stiffness during contraction recorded using ultrasonic waves, 299, 631
- Tanabe T. *see under* Noda M., 299, 793
- Tanaka Y. *see under* Yamamoto N., 299, 367
- Tankard A. J. et al. Crustal Evolution of Southern Africa: 3.8 Billion Years of Earth History, *book review by* Cooke H. B. S., 299, 93
- Tanner B. K. *see under* Whatmore R. W., 299, 44
- Tarafa M. E. *see under* Whelan J. K., 299, 50
- Tarashkevich P. S. and Douglas W. W. GABA directly affects electrophysiological properties of pituitary pars intermedia cells, 299, 733
- Tarling D. H. A Proterozoic Pangaea? *news and views*, 299, 207
- Tattersall I. The Primates of Madagascar, *book review by* Martin R. D., 299, 843
- Tawara Y., Hayakawa S., Kunieda H., Makino F. and Nagase F. Discovery of 0.5-s oscillations in long flat top bursts from the Rapid Burster, 299, 38
- Taylor J. B. A classical derivation of the Meissner effect? *news and views*, 299, 681
- Taylor J. H. *book review of* Theory and Experiment in Gravitational Physics, (Will C. M.) 299, 284
- Taylor K. A. *see under* Amos L. A., 299, 467
- Taylor K. A., Deatherage J. F. and Amos L. A. Structure of the S-layer of *Sulfolobus acidocaldarius*, 299, 840
- Tajima S. *see under* Miyachi T., 299, 168
- Temin H. M. *see under* Shimotohno K., 299, 265
- Tera F. *see under* Brown L., 299, 718
- Terwilliger T. C. *see under* Eisenberg D., 299, 371
- Th Eysel U. Functional reconnections without new axonal growth in a partially denervated visual relay nucleus, 299, 442
- Thatcher W. Seismic triggering and earthquake prediction, *news and views*, 299, 12
- Thomas J. M. *see under* Cheetham A. K., 299, 24
- Thomas R. C. and Meech R. W. Hydrogen ion currents and intracellular pH in depolarized voltage-clamped snail neurones, 299, 826
- Thorpe R. S. Editor. Andesites: Orogenic Andesites and Related Rocks, *book review by* Arculus R. J., 299, 377
- Thulborn R. A. Significance of ankle structures in archosaur phylogeny, *matters arising*, 299, 657
- Timiras P. S. *see under* Vernadakis A., 299, 845
- Tomeoka K. and Buseck P. R. An unusual layered mineral in chondrules and aggregates of the Allende carbonaceous chondrite, 299, 327
- Intergrown mica and montmorillonite in the Allende carbonaceous chondrite, 299, 326
- Toril T. *see under* Matsumoto G., 299, 52
- Toro M. A. *see under* Pérez-Tomé J. M., 299, 153
- Townsend R. P. Zeolites: The International Journal of Molecular Sieves, *Journal review*, 299, 512
- Toyosato M. *see under* Noda M., 299, 793
- Travers P. J. *see under* Lee J. S., 299, 750
- Tremaine S. *see under* Borderies N., 299, 209
- Tremblay J. M. *see under* Müller R., 299, 640
- Tres L. L. and Erickson R. P. Electron microscopy of t-allele synaptonemal complexes discloses no inversions, 299, 752
- Trigg G. L. Chinese Physics, *Journal review*, 299, 510
- Trimble V. *see under* Rosner R., 299, 579
- Trowsdale J. *see under* Lee J. S., 299, 750
- Truman J. W. *see under* Levine R. B., 299, 250
- Tsuchiya T. *see under* Tamura Y., 299, 631
- Tsukada Y. *see under* Mikoshiba K., 299, 357
- Turner J. S. *see under* McDougall T. J., 299, 812
- Tzagoloff A. Mitochondria, *book review by* Selwyn M. J., 299, 190
- Unanue E. R. *see under* Snyder D. S., 299, 163
- Ungerer C. A. *see under* Wefer G., 299, 145
- Unsworth M. H. *see under* Baker C. K., 299, 149
- Ulrich H. *see under* Steinman L., 299, 738
- van Boeckel S. A. A. *see under* Wang A. H.-J., 299, 601
- van Boom J. H. *see under* Wang A. H.-J., 299, 601
- van Bruggen E. F. J. Haemocyanins to haemerythrins, *news and views*, 299, 107
- van den Bergh S. In search of the Hubble parameter, *news and views*, 299, 297
- van der Marel G. A. *see under* Wang A. H.-J., 299, 601
- van der Raay H. B. *see under* Claverie A., 299, 704
- van Eerd P. M. C. A. *see under* Will H., 299, 740
- van Graas G. de Lange F., de Leeuw J. W. and Schenck P. A. De-A-steroid ketones and de-A-aromatic steroid hydrocarbons in shale indicate a novel diagenetic pathway, 299, 437
- van Heyningen S. Bacterial toxins and cyclic AMP, *news and views*, 299, 782
- van Vliet A. *see under* Braakman J. H., 299, 48
- Vannier F. *see under* Henckes G., 299, 268
- Varmus H. E. A growing role for reverse transcription, *news and views*, 299, 204
- Vaux D. J. T. and Gordon S. Monoclonal antibody defines a macrophage intracellular Ca²⁺-binding protein which is phosphorylated by phagocytosis, 299, 70
- Velthorst E. J. *see under* Breemen N. van, 299, 548
- Verma I. M. *see under* Müller R., 299, 640
- Vermeij G. J. Phenotypic evolution in a poorly dispersing snail after arrival of predator, 299, 349
- Vernadakis A. and Timiras P. S. Editors. Hormones in Development and Aging, *book review by* Phillips J. G., 299, 845
- Veverka J. *book review of* The Surface of Mars, (Carr M. H.) 299, 761
- Vezzoli L. *see under* Gillot P.-Y., 299, 242
- Vogel J. *see under* Ku T. L., 299, 240
- see under* Kusakabe M., 299, 712
- Voyovich P. *see under* Lewin P. K., 299, 627
- Vrignault P. *see under* Ackerman M., 299, 17
- Walker W. F. and Doolittle W. F. Rediviving the basidiomycetes on the basis of 5S rRNA sequences, 299, 723
- Wallach D., Fellous M. and Revel M. Preferential effect of γ interferon on the synthesis of HLA antigens and their mRNAs in human cells, 299, 833
- Wallach M., Fong D. and Kwang-Poo Chang Post-transcriptional control of tubulin biosynthesis during leishmanial differentiation, 299, 650
- Wallis M. South African link, *correspondence*, 299, 674
- Walter P. and Blobel G. Signal recognition particle contains a 7S RNA essential for protein translocation across the endoplasmic reticulum, 299, 691
- Wang A. H.-J., Fujii S., van Boom J. H., van der Marel G. A., van Boeckel S. A. A. and Rich A. Molecular structure of r(GCG)d(TATACGC): a DNA-RNA hybrid helix joined to double helical DNA, 299, 601
- Warwick J. W. *see under* Evans D. R., 299, 236
- Washburn S. L. *see under* Lowenstein A. M., 299, 294
- Wasserstrom R. and Chapin G. Malaria resurgence, *correspondence*, 299, 482
- Watabe H. *see under* Ohtani T., 299, 86
- Watson D. H. Soviet Progress in Virology, *Journal review*, 299, 501
- Watt R. J. *see under* Morgan M. J., 299, 553
- Webb C. G. *see under* Gootwine E., 299, 63
- Webb D. *see under* Behringer D., 299, 121
- Weber E. *see under* Hennig G. J., 299, 280
- Weber E., Evans C. J. and Barchas J. D. Predominance of the amino-terminal octapeptide fragment of dynorphin in rat brain regions, 299, 77
- Wefer G., Suess E., Balzer W., Liebezeit G., Müller P. J., Ungerer C. A. and Zenk W. Fluxes of biogenic components from sediment trap deployment in circumpolar waters of the Drake Passage, 299, 145
- Wehmiller J. F. *see under* Kennedy G. L., 299, 545
- Weinstein I. B. *see under* Backer J. M., 299, 458
- Weiss R. The myc oncogene in man and birds, *news and views*, 299, 9
- Weiss R. A. *see under* Marshall C. J., 299, 171
- Weiss R. M. *see under* Eisenberg D., 299, 371
- Wells R. D. *see under* Singleton C. K., 299, 312
- Werz M. A. and Macdonald R. L. Heterogeneous sensitivity of cultured dorsal root ganglion neurones to opioid peptides selective for μ - and δ -opioid receptors, 299, 730
- Whalen R. G. *see under* Butler-Browne G. S., 299, 830
- Whatmore R. W., Goddard P. A., Tanner B. K. and Clark G. F. Direct imaging of travelling Rayleigh waves by stroboscopic X-ray topography, 299, 44
- Wheeler T. *see under* Ozanne B., 299, 744
- Whelan J. K., Tarafa M. E. and Hunt J. M. Volatile C₁-C₈ organic compounds in macroalgae, 299, 50
- White G. F. *see under* Holdgate M. W., 299, 91
- Whittingham D. G. *see under* Muggleton-Harris A., 299, 460
- Wiesel T. N. Postnatal developmental of the visual cortex and the influence of environment (Nobel Lecture), *review article*, 299, 583
- Wigley T. M. L. Journal of Climatology, *Journal review*, 299, 511
- Wigston D. J. and Sanes J. R. Selective reinnervation of adult mammalian muscle by axons from different segmental levels, 299, 464
- Wigström H. *see under* Gustafsson B., 299, 252
- Williams R. O., Young J. R. and Majiwa P. A. O. Genomic environment of T. brucei VSG genes: presence of a minichromosome, 299, 417
- Wilkinson A. J. *see under* Winter G., 299, 756
- Wilkinson P. N. *see under* Browne I. W. A., 299, 788
- Will C. M. Theory and Experiment in Gravitational Physics, *book review by* Taylor J. H., 299, 284
- Will H., Cattaneo R., Koch H.-G., Darai G., Schaller H., Schellekens H., van Eerd P. M. C. A. and Deinhardt F. Cloned HBV DNA causes hepatitis in chimpanzees, 299, 740
- Williams J. T., Egan T. M. and North R. A. Enkephalin opens potassium channels on mammalian central neurones, 299, 74
- Wilson J. I. B. *book review of* Photochemical Conversion and Storage of Solar Energy, (Connolly J. S. editor) 299, 378
- book review of* Photovoltaic and Photo-electrochemical Solar Energy Conversion, (Cardon F., Gomes W. P., Dekeyser W. editors) 299, 378
- book review of* Solar Cells: Operating Principles, Technology, and System Applications, (Green M. A.) 299, 378
- book review of* Solar Cell Device Physics, (Fonash S. J.) 299, 378
- Wilson J. R. and Larsen S. B. Discordant layering relations in the Fongren-Hyllingen basic intrusion, 299, 625
- Wilson L. *see under* Muggleton-Harris A., 299, 460
- Wilson M. A. *see under* Barron P. F., 299, 616
- Wilson R. and Crouch E. Risk Benefit Analysis, *book review by* Cotgrove S., 299, 659
- Winter G., Fersht A. R., Wilkinson A. J., Zoller M. and Smith M. Redesigning enzyme structure / by site-directed mutagenesis: tyrosyl tRNA synthetase and ATP binding, 299, 756
- Winter P. D. *see under* Acheson E. D., 299, 263
- Wit T. *see under* Breemen N. van, 299, 548
- Wong-Staal F. *see under* Favara R. D., 299, 61
- Woodhill J. M. *see under* Noble S., 299, 760
- Woodruff M. F. A., Ansell J. D., Forbes G. M., Gordon J. C., Burton D. I. and Micklem H. S. Clonal interaction in tumours, 299, 822
- Wooters W. K. and Zurek W. H. A single quantum cannot be cloned, 299, 802
- Worcester P. *see under* Behringer D., 299, 121
- Wrench J. J. and Measures C. I. Temporal variations in dissolved selenium in a coastal ecosystem, 299, 431
- Wright A., Heath R. and Burckle L. Glomar Challenger at the Cretaceous-Tertiary boundary, *news and views*, 299, 208
- Wright C. S. *see under* McNamara L. F., 299, 537
- Wright C. S. and McNamara L. F. Flare induced geomagnetic activity and orientation of the photospheric magnetic field,

- 299, 42
 Wunsch C. *see under* Behringer D., 299, 121
 Xiroitiris N. I. *see under* Hennig G. J., 299, 280
 Yamamoto N., Matsumoto T., Koyanagi Y., Tanaka Y. and Hinuma Y. Unique cell lines harbouring both Epstein-Barr virus and adult T-cell leukaemia virus, established from leukaemia patients, 299, 367
 Yamamoto Y. *see under* Nakamura K. T., 299, 564
see under Yano M., 299, 557
 Yamashita Y. *see under* Chien J. C. W., 299, 608
 Yano M., Yamamoto Y. and Shimizu H. An actomyosin motor, 299, 557
 Yasuda T. *see under* Okada N., 299, 261
 Yokoyama M. *see under* Mikoshiba K., 299, 357
 Yonezawa S. *see under* Miyauchi T., 299, 168
 Yoshida N. *see under* Nakamura K. T., 299, 564
 Yoshikawa H. *see under* Henckes G., 299, 268
 Young E. T. *see under* Christensen A. C., 299, 369
 Young G. M. *see under* Nesbitt H. W., 299, 715
 Young J. R. *see under* Williams R. O., 299, 417
 Zack J. *see under* Ozanne B., 299, 744
 Zamvil S. *see under* Steinman L., 299, 738
 Zavala F., Gwadz R. W., Collins F. H., Nussenzweig R. S. and Nussenzweig V. Monoclonal antibodies to circumsporozoite proteins identify the species of malaria parasite in infected mosquitoes, 299, 737
 Zenk W. *see under* Wefer G., 299, 145
 Zingsheim H. P., Barrantes F. J., Frank J., Hänicke W. and Neugebauer D.-Ch. Direct structural localization of two toxin-recognition sites on an ACh receptor protein, 299, 81
 Zolan M. E., Smith C. A., Calvin N. M. and Hanawalt P. C. Rearrangement of mammalian chromatin structure following excision repair, 299, 462
 Zoller M. and Smith M. *see under* Winter G., 299, 756
 Zurek W. H. *see under* Wootters W. K., 299, 802
 Zweibel E. *see under* Rosner R., 299, 579

Nature Author Indexes are published bimonthly for each volume. Issues containing this year's Author Indexes are:

Volume	Date
295	18 March
296	20 May
297	15 July
298	16 September
299	18 November

"A unique guide to biological laboratory products."

The Directory of Biologicals offers life scientists a comprehensive listing of what is on the market and where researchers can order these materials for their work. Designed to meet the day-to-day needs of active biologists searching for the right product to use in the laboratory, its simple alphabetical listings cover all of modern life science research. Clear and easy to use, it lists more than 2,000 products commercially available, with the names and addresses of companies throughout the world that offer them for sale. Telex and telephone numbers give users direct access to sales offices in your area. Company entries also briefly describe each supplier's specialization. A separate section lists products by trade name or registered trademark, keyed to the companies in the guide.

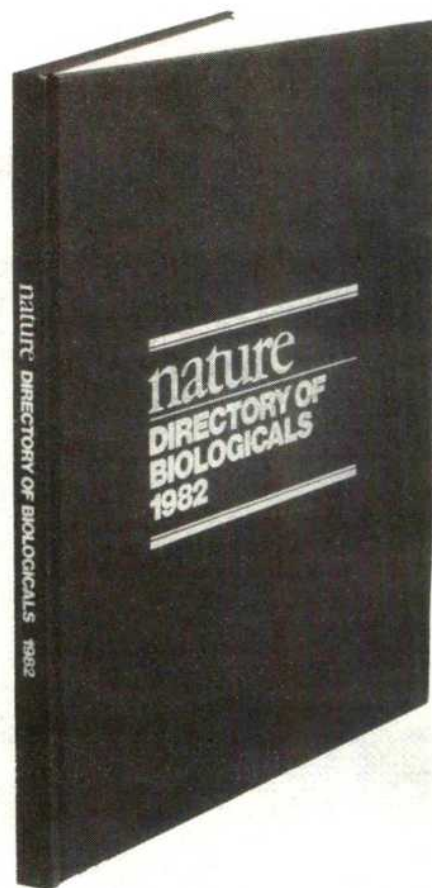
Helpful essays on how to use the directory, safety procedures, how to purchase biological materials, and the future of modern biology, make this the most useful directory ever published for biological research workers.

All subscribers to *Nature** automatically receive a handsome paperbound version of the directory. **But if you think you need a copy to stand up against constant use in your laboratory or your library, or if you are not a subscriber, you can purchase the deluxe hardcover edition.** (No paperback editions will be available after subscribers receive their free copy.) To order a hardcover edition, all you need do is fill out the form and mail it today.

297x210mm

232 pages

ISBN 0 222 33222 4



U.S. and Canada: *Nature*, 15 East 26th Street, New York, NY 10010

U.K. and Rest of World: *Nature*, Canada Road, Byfleet, Surrey KT14 7JL, England.

☐ **Send me _____ copies of the deluxe, hardcover edition of the Directory of Biologicals @ \$45/£22.50 each. (P&P free).** (Tax: N.Y. State Residents, please add sales tax.) (I understand that as a subscriber to *Nature* I will receive a free copy of the paperbound edition as part of my subscription.★)

Name _____

Address _____

City _____ State _____ Zip _____

Country _____

☐ I enclose \$ _____ / £ _____ ☐ I prefer to use my credit card account

Account No. _____ Expiry Date _____

☐ Visa ☐ Access/Mastercard

☐ American Express Signature _____

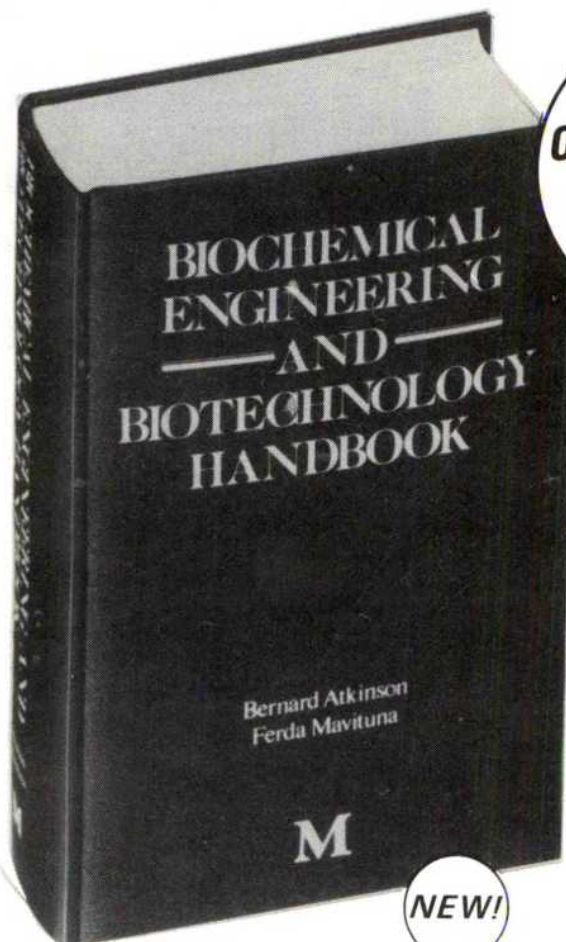
In the U.S. you may make your order by telephone, using our toll-free number. Our operators are on duty 7 days a week, 24 hours a day.

Call toll-free now: (800) 824-7888. Ask for operator 130 (Dept. TNA)

In California: (800) 852-7777. Ask for operator 130 (Dept. TNA)

Please allow 6 weeks for delivery.

*If your subscription was in effect on November 30, 1981, you automatically receive a paperbound copy of the 1982 Directory of Biologicals. Those who entered subscriptions after that date will receive the 1983 Directory of Biologicals next spring.



**EXAMINE
ON APPROVAL
FOR 30 DAYS
WITHOUT
RISK.**

NEW!

The first ever biochemical engineering handbook - packed with authoritative facts and data.

Published in association with The Institution of Chemical Engineers and The Science and Engineering Research Council.

Here is all the information you need:

★ quantities ★ temperature ★ coefficients ★ viscosity ★ diffusion ★ sterilisation ★ heat transfer ★ separation ★ recovery — and more.

Compiled by two outstanding experts in the field — Professor Bernard Atkinson and Dr. Ferda Mavituna.

Allows scientists and engineers:

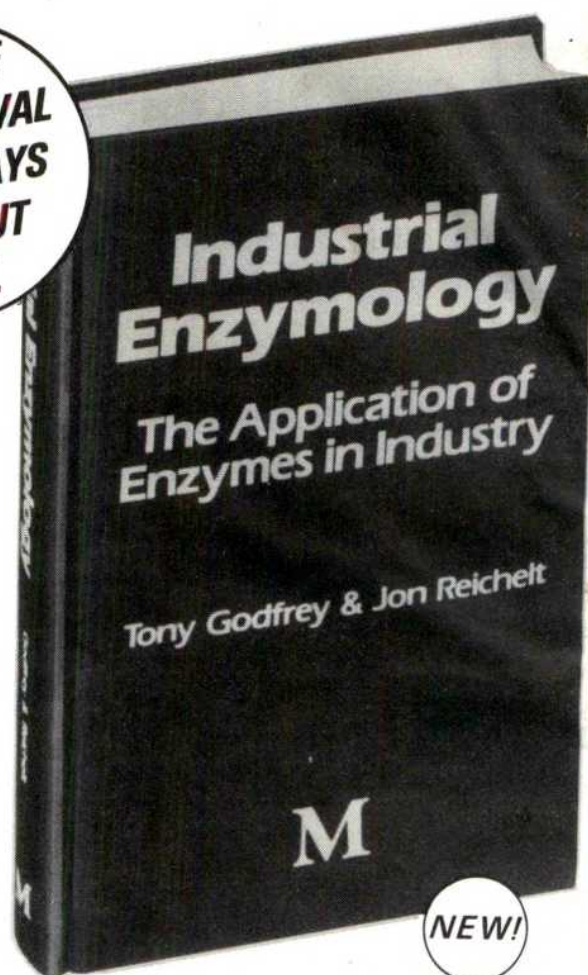
★ to ensure research and development meets process objectives.
★ to estimate possibilities for research to make uneconomic processes profitable
★ to establish the appropriate methodology for process development.
★ to identify equipment needs.

Macmillan Hardcover November 1982
1100pp ISBN 0 333 33274 1 £50.00/\$97.00

GLOBE
BOOK SERVICES LTD

Canada Road, Byfleet,
Surrey, KT14 7JL England.
Tel: Byfleet (09323) 40397

A MEMBER COMPANY OF MACMILLAN PUBLISHERS LTD.



NEW!

A unique collection of practical data covering the sources, performance and applications of enzymes used in major industrial processes.

Practical kinetics of enzymes, legislation and regulations, industrial safety, characteristics of enzymes, suppliers of industrial and development enzymes throughout the world, and up-to-date tabulated lists of permitted enzymes for many countries, including the USA GRAS listings, and the recently published list of enzymes approved in the UK — just some of the diverse subjects conveniently linked by this new book's unique cross-reference system.

The editors, Tony Godfrey and Jon Reichelt, are senior managers of two of the foremost manufacturers of industrial enzymes in the world.

Contents:

- 1 Introduction
- 2 Practical Kinetics
- 3 Legislation and Regulations
- 4 Industrial Practice. Addendum: Biotechnical Specialities
- 5 Comparison of key characteristics of industrial enzymes by type and source
- 6 Data Indexes

Macmillan Hardcover November 1982
736pp ISBN 0 333 32354 8 £40.00/\$77.00

30 DAYS NO-RISK ON-APPROVAL ORDER FORM

To: Ian Jacobs, Globe Book Services Ltd.,
FREEPOST, Canada Road, Byfleet,
Surrey KT14 7BR. England.
The Nature Press,
15 E 26 Street, New York,
N.Y. 10010. Credit card callers call toll-
free 800-221-2123 (or in New York:
212-532-4811)

(Please tick books required)

Please send me _____ copies of ☐ Industrial
Enzymology at £40.00/\$77.00 each and/or
_____ copies of ☐ Biochemical Engineering and Bio-
technology Handbook at £50.00/\$97.00 each.

Free Postage & Packing

When I send cash with my order, postage and packing are FREE. Otherwise there is a standing P&P charge for each book ordered of: UK Subscribers £2. (Overseas £3.) US Subscribers \$1.50.

No-risk money back guarantee

I may examine the book(s) I have selected for 30 days and, if not completely satisfied, can return the book(s) within that period for a full refund.

Tick preferred method of payment

☐ Enclosed is cheque for £/\$ _____

☐ Charge my credit card on publication £/\$ _____

☐ Visa ☐ Access/Mastercharge ☐ Am. Express ☐ Diners

Card No. _____ Expiry Date _____

☐ Bill me. I need send no money now.

Signature _____
(Orders cannot be accepted without a signature)

Name _____
(PLEASE PRINT)

Address _____

Postcode/Zip Code _____
Books will be delivered to you on publication.

**POST TODAY - NO STAMP NEEDED
(UK SUBSCRIBERS)**